



CERTIFICATE OF MAILING  
37 C.F.R. 1.8

I hereby certify that this correspondence is being deposited with the U.S. Postal Service with sufficient postage as First Class Mail in an envelope addressed to: Commissioner for Patents, P. O. Box 1450, Alexandria, VA 22313-1450, on the date below:

September 29, 2005  
Date

*Monica De La Paz*  
Monica A. De La Paz

PATENT

IN THE UNITED STATES PATENT AND TRADEMARK OFFICE

In re Application of:  
Yang *et al.*

Serial No.: 09/599,152

Filed: June 21, 2000

For: ETHYLENEDICYSTEINE (EC)-DRUG  
CONJUGATES, COMPOSITIONS AND  
METHODS FOR TISSUE SPECIFIC  
DISEASE IMAGING

Group Art Unit: 1616

Examiner: Jones, D.

Atty. Dkt. No.: UTSC:664

**BRIEF ON APPEAL**

MS Appeal Brief-Patents  
Commissioner for Patents  
P.O. Box 1450  
Alexandria, VA 22313-1450

BEST AVAILABLE COPY

10/04/2005 MBLANCO 00000016 09599152

02 FC:2402

250.00 OP

# TABLE OF CONTENTS

	Page
I. REAL PARTIES IN INTEREST .....	1
II. RELATED APPEALS AND INTERFERENCES .....	1
III. STATUS OF THE CLAIMS .....	1
IV. STATUS OF AMENDMENTS .....	2
V. SUMMARY OF CLAIMED SUBJECT MATTER .....	2
VI. GROUNDS OF REJECTION TO BE REVIEWED ON APPEAL .....	3
VII. ARGUMENT .....	3
A. Rejection of Claims 2-4, 6, 8-10, 15, 23, 30, 31, 33-35, and 37-41 under 35 U.S.C. §112, First Paragraph .....	4
1. The Same Language Rejected in the Present Case has been Found Acceptable by the Examiner in Appellants' Companion Case, U.S. Patent 6,692,724.....	4
2. The Examiner has Failed to Meet her Burden of Establishing a Factual Basis to Support the Rejection of Claims 2-4, 6, 8, 10, 15, 23, 30, 31, 33-35, and 37-41 under 35 U.S.C. §112, First Paragraph.....	5
3. Undue Experimentation is Not Needed to Practice the Invention of Claims 2-4, 6, 8, 10, 15, 23, 30, 31, 33-35, and 37-41 .....	6
a) The Art Related to the Claimed Invention was Well Developed at the Time of the Priority Date and Skill in the Art was High .....	6
b) The Specification Provides Sufficient Guidance to One of Skill in the Art for the Purpose of Selecting a Targeting Agent.....	7
c) The Specification Provides Sufficient Guidance to One of Skill in the Art for Purposes of Identifying the Necessary Conjugation Chemistry .....	8
d) The Specification Provides Substantial Guidance Regarding Routine Imaging and Distribution studies.....	9
4. Declaration of Jerry L. Bryant, M.S. Further Establishes that the Claimed Invention is Enabled by the Specification.....	9
a) Claims Pertaining to Anticancer Agents.....	11
b) Claims Pertaining to Tumor Markers .....	12
c) Claims Pertaining to Folate Receptor Targeting Ligands.....	13
d) Claims Pertaining to Tumor Apoptotic Cell Targeting Ligands.....	14



**TABLE OF CONTENTS**  
(continued)

	<b>Page</b>
e)    Claims Pertaining to Tumor Hypoxia Targeting Ligands.....	16
f)    Claims Pertaining to Agents that Mimic Glucose.....	17
g)    Conclusion .....	18
5.    Conclusion .....	19
B.    Rejection of Claims 2-4, 6, 8-10, 15, 23, 30, 31, 33-35, and 37-41 under 35 U.S.C. §112, Second Paragraph.....	19
1.    Rejection of Claims 2-4, 6, 8, 10, 15, 23, 30, 31, 33-35, and 37-41 .....	19
a)    Declaration of Jerry L. Bryant, M.S .....	19
(1)    Claims Drawn to Anticancer Agents .....	20
(2)    Claims Drawn to Tumor Markers .....	21
(3)    Claims Pertaining to Folate Receptor Targeting Ligands.....	21
(4)    Claims Pertaining to Tumor Apoptotic Cell Targeting Ligands .....	22
(5)    Claims Pertaining to Tumor Hypoxia Targeting Ligands.....	23
(6)    Claims Pertaining to Agents that Mimic Glucose.....	24
(7)    Conclusion .....	25
b)    Breadth of a Claim is not to be Equated with Indefiniteness.....	26
c)    Conclusion .....	27
2.    Rejection of Claim 32 .....	27
VIII. CONCLUSION.....	29
APPENDIX 1: Claims Appendix	
APPENDIX 2: Evidence Appendix	
APPENDIX 3: Related Proceedings Appendix	



Appellants hereby submit an original and two copies of this Appeal Brief in response to the Final Office Action dated May 20, 2005. This Brief is filed pursuant to the Notice of Appeal mailed on July 28, 2005.

The fee for filing this Appeal Brief is attached hereto. No additional fees are believed due in connection with the instant paper. However, should any other fees be due, or the attached fee be deficient or absent, the Commissioner is authorized to withdraw the appropriate fee from Fulbright & Jaworski L.L.P. Deposit Account No. 50-1212/UTSC:664. Please date stamp and return the enclosed postcard to evidence receipt of this document.

**I. REAL PARTIES IN INTEREST**

The real parties in interest is the Board of Regents, The University of Texas System (assignee).

**II. RELATED APPEALS AND INTERFERENCES**

There are currently no related appeals or interferences.

**III. STATUS OF THE CLAIMS**

The application was filed with original claims 1-51. Claims 1, 5, 33, 36, 42-51, and 54 were canceled during prosecution without prejudice or disclaimer. New claims 52-61 were added during prosecution. Claims 56-61 were withdrawn by the Examiner, who has taken the position that the claims are directed to "independent or distinct" subject matter. Appellants have separately petitioned the withdrawal of claims 56-61.

Thus, claims 2-4, 6-35, 37-41, 52-53, and 55 are currently pending. Of these, claims 2-4, 6-35, 37-41 and 52-55 are subject to the present appeal, with the subject matter of each of these claims being free of the prior art. The Examiner has indicated in the Office Action dated May 20, 2005, that claims 7, 11-14, 16-22, 24-29, 52, 53, and 55 are allowed.

A copy of the appealed claims is attached as a Claims Appendix.

#### **IV. STATUS OF AMENDMENTS**

No amendments were sought to the pending claims following receipt of the most recent Office Action (the Office Action dated May 20, 2005), a non-final Office Action.

#### **V. SUMMARY OF CLAIMED SUBJECT MATTER**

The present invention provides a new radiolabeling strategy to target tissues for imaging. Specification, page 4, lines 11-12. More particularly, the present invention is generally directed to methods of synthesizing a radiolabeled ethylenedicysteine (EC) derivative for imaging, involving the steps of obtaining a tissue specific ligand, admixing the ligand with EC to obtain an EC-tissue specific ligand derivative, and admixing the EC-tissue specific ligand derivative with a radionuclide and a reducing agent to obtain a radionuclide labeled EC-tissue specific ligand derivative, wherein the EC forms an  $N_2S_2$  chelate with the radionuclide. Specification, page 7, lines 5-13.<sup>1</sup> The present invention is also generally directed to methods of labeling a tissue specific ligand for imaging, involving the steps of obtaining a tissue specific ligand, admixing the tissue specific ligand with EC to obtain an EC-ligand conjugate, and reacting the conjugate with  $^{99m}Tc$  in the presence of a reducing agent to form an  $N_2S_2$  chelate between the EC (with or without linker) and the  $^{99m}Tc$ . Specification, page 7, lines 15-20. Exemplary tissue-specific ligands include an anticancer agent, a tumor marker, a folate receptor targeting ligand, a tumor apoptotic cell targeting ligand, a tumor hypoxia targeting ligand, glutamate pentapeptide, and an agent that mimics glucose. Specification, page 5, lines 5-14. Exemplary radionuclides include  $^{99m}Tc$ ,  $^{188}Re$ ,  $^{186}Re$ ,  $^{183}Sm$ ,  $^{166}Ho$ ,  $^{90}Y$ ,  $^{89}Sr$ ,  $^{67}Ga$ ,  $^{68}Ga$ ,  $^{111}In$ ,  $^{183}Gd$ ,  $^{59}Fe$ ,  $^{225}Ac$ ,  $^{212}Bi$ ,  $^{211}At$ ,  $^{64}Cu$  and  $^{62}Cu$ . Specification, page 6, lines 21-28.

---

<sup>1</sup> Appellants note that citations to the Specification identify exemplary support for the claimed invention. Other support in the Specification can be found and relied upon if necessary.

The present invention also pertains to methods of imaging a site within a mammalian body involving the steps of administering an effective diagnostic amount of a composition comprising a <sup>99m</sup>Tc labeled EC-tissue specific ligand conjugate and detecting a radioactive signal from the <sup>99m</sup>Tc localized at the site. Specification, page 7, line 25 through page 8, line 2.

## **VI. GROUNDS OF REJECTION TO BE REVIEWED ON APPEAL**

This appeal presents the following issues:

- a) whether the subject matter of claims 2-4, 6, 8-10, 15, 23, 30, 31, 33-35, and 37-41 is adequately enabled by the subject specification as required by 35 U.S.C. §112, first paragraph;
- b) whether claims 2-4, 6, 8-10, 15, 23, 30, 31, 33-35, and 37-41 are indefinite under 35 U.S.C. §112, second paragraph; and
- c) whether claim 32 is indefinite under 35 U.S.C. §112, second paragraph.

## **VII. ARGUMENT**

As an initial matter, Appellant notes that findings of fact and conclusions of law by the U.S. Patent and Trademark Office must be made in accordance with the Administrative Procedure Act, 5 U.S.C. § 706(A), (E), 1994. *Dickinson v. Zurko*, 527 U.S. 150, 158 (1999). Moreover, the Federal Circuit has held that findings of fact must be supported by "substantial evidence" within the record. *In re Gartside*, 203 F.3d 1305, 1315 (Fed. Cir. 2000). In *In re Gartside*, the Federal Circuit stated that "the 'substantial evidence' standard asks whether a reasonable fact finder could have arrived at the agency's decision." *Id.* at 1312. Accordingly, it necessarily follows that an Examiner's position on Appeal must be supported by "substantial evidence" within the record in order to be upheld by the Board of Patent Appeals and Interferences.

**A. Rejection of Claims 2-4, 6, 8-10, 15, 23, 30, 31, 33-35, and 37-41 under 35 U.S.C. §112, First Paragraph**

The Action rejects claims 2-4, 6, 8, 10, 15, 23, 30, 31, 33-35, and 37-41 under 35 U.S.C. §112, first paragraph, as not being enabled for the full scope of the claimed invention, in particular, methods of synthesizing EC conjugates of anticancer agents, tumor markers, folate receptor targeting ligands, tumor apoptotic cell targeting ligands, tumor hypoxia targeting ligands, or agents that mimic glucose. Appellants respectfully traverse.

35 U.S.C. §112, first paragraph, states in part that “[t]he specification shall contain a written description of the invention, and of the manner and process of making and using it, in such full, clear, concise, and exact terms as to enable any person skilled in the art to which it pertains, or with which it is most nearly connected, to make and use the same.” 35 U.S.C. §112, first paragraph. It is permissible for some experimentation to be required to practice the claimed invention, so long as it is not undue. *Atlas Powder Co. v. E.I. DuPont De Nemours & Co.*, 750 F.2d 1569, 1576 (Fed. Cir. 1984). Appellants also note that “[a]s long as the specification discloses at least one method for making and using the claimed invention that bears a reasonable correlation to the entire scope of the claims, then the enablement requirement is satisfied.” *MPEP* §2164.01(b) citing *In re Fisher*, 427 F.2d 833, 839, 166 USPQ 18, 24 (CCPA 1970).

**1. *The Same Language Rejected in the Present Case has been Found Acceptable by the Examiner in Appellants’ Companion Case, U.S. Patent 6,692,724***

Appellants were somewhat surprised to find that this rejection has been maintained in the present case. In Appellants’ companion case being examined by the same Examiner, USSN 09/434,313, the same language rejected in the present case has been found acceptable based on essentially the same specification. Indeed, the ‘313 application has recently issued as U.S. Patent 6,692,724, copy enclosed (Exhibit A), and was allowed and issued subsequent to the entry of the

rejections in the present case. This issued patent is, of course, presumed valid and the claim language presumed to be enabled and fully described in the specification. As such, the '724 patent is strong evidence that the claims here satisfy both requirements. Appellants therefore assert that the rejections are improper.

**2. *The Examiner has Failed to Meet her Burden of Establishing a Factual Basis to Support the Rejection of Claims 2-4, 6, 8, 10, 15, 23, 30, 31, 33-35, and 37-41 under 35 U.S.C. §112, First Paragraph***

Appellants observe that the Examiner has provided no factual basis to rebut the teachings of the specification or support the premise that one skilled in the art would have to undertake undue experimentation to “obtain a tissue specific ligand, wherein the tissue specific ligand is an anti-cancer agent, a tumor marker, a folate receptor targeting ligand, a tumor apoptotic cell targeting ligand, a tumor hypoxia targeting ligand, or an agent that mimics glucose...admixing said ligand with ethylenediceysteine (EC) to obtain an EC-tissue specific ligand derivative; and...admixing said EC-tissue specific ligand derivative with a radionuclide and a reducing agent to obtain a radionuclide labeled EC-tissue specific ligand derivative, wherein the EC forms an  $N_2S_2$  chelate with the radionuclide.” “A specification disclosure which contains a teaching of the manner and process of making and using the invention . . . must be taken as in compliance with the enabling requirement of the first paragraph of §112 unless there is reason to doubt the objective truth of the statements contained therein which must be relied on for enabling support.” *Rasmusson v. Smithkline Beecham Corp.*, 413 F.3d 1318 (Fed. Cir. 2005), quoting *In re Brana*, 51 F.3d 1560 (Fed. Cir. 1995), quoting *In re Marzocchi*, 439 F.2d 220, 223, 169 U.S.P.Q. 367, (CCPA 1971). Because the Examiner has failed to provide any factual evidence to doubt the sufficiency of Appellants’ disclosure, the rejection is improper.

In contrast, Appellants have presented substantial factual support in their responses to the last two Office Actions, in accordance with the factors of *In re Wands*, to which the Examiner has not responded. Appellants below summarize the previous factual presentation, including the Declaration of Jerry L. Bryant, M.S., which, as discussed below, provides a detailed demonstration of the enablement of the claims.

**3. *Undue Experimentation is Not Needed to Practice the Invention of Claims 2-4, 6, 8, 10, 15, 23, 30, 31, 33-35, and 37-41***

In light of the teachings of the specification and the level of skill in the art, undue experimentation is *not needed* for one of ordinary skill in the art to synthesize a tissue specific ligand-EC conjugate (EC-ligand conjugate) as claimed. Factors to be considered include (1) the nature of the invention, (2) state of the prior art (3) level of one of ordinary skill in the art, (4) level of unpredictability in the art, (5) amount of direction and guidance provided by the inventor (6) existence of working examples (7) breadth of the claims and (8) the quantity of experimentation needed to make or use the invention based on the content of the disclosure. *In re Wands*, 858 F.2d 731, 8 USPQ2d 1400 (Fed. Cir. 1988).

**a) *The Art Related to the Claimed Invention was Well Developed at the Time of the Priority Date and Skill in the Art was High***

The nature of the invention is directed to methods of synthesizing EC-tissue specific ligand complexes. The state of the art is one in which radiolabeling of other chelates was known. Also known in the art were synthetic methods for conjugating imaging agents to targeting agents based on the available functional groups of the targeting agent, *see* U.S. Patent 5,517,993, column 7, line 53 to column 8, line 26 (Exhibit B). Thus, one of ordinary skill in the art of imaging agent synthesis possessed a high level of skill in conjugating imaging agents to targeting agents.

**b)      *The Specification Provides Sufficient Guidance to One of Skill in the Art for the Purpose of Selecting a Targeting Agent***

One of ordinary skill in the art, in light of the specification, could have readily selected a targeting agent to be used in the claimed methods for synthesizing an EC-tissue specific ligand conjugate. Appellants' specification provide guidance to the skilled artisan by means of a number of examples illustrating the coupling of EC to a representative number of tissue specific ligands. The tissue specific ligands described in the specification are representative of the various classes of tissue specific agents, including anti-cancer agents (specification, page 5, line 16-18), tumor markers (specification, page 5, line 18-21), folate receptor targeting ligands (specification, page 5 line 23), tumor apoptotic and tumor hypoxia cell targeting ligands (specification, page 5, line 24-25), and agents that mimic glucose (specification, page 5, Line 29 to page 6, line 2).

In further support, Appellants have cited scientific literature to demonstrate that one of skill in the art, based on the teachings of the specification, would be able to readily identify and select a tissue specific ligand of the invention. There are a variety of methods known in the art for the identification of ligands and the characterization of the identified ligand as an anticancer agent (Yamori *et al.*, 1999 ( Exhibit C) – *in vitro* and *in vivo* growth inhibition assays), a tumor marker (Hibi *et al.*, 1999 ( Exhibit D); Becker *et al.*, 1999 ( Exhibit E) – northern blotting western blotting and immunohistochemistry), a folate receptor targeting ligand (Sudimack and Lee, 2000 ( Exhibit F) – radiolabeled ligand binding), a tumor apoptotic cell targeting ligand (Takamizawa *et al.*, 2000 ( Exhibit G) – RNase protection and western blotting assays), a tumor hypoxia targeting ligand (Garayoa *et al.*, 2000 ( Exhibit H) – northern blotting, immunohistochemistry, and luciferase reporter assays), or an agent that mimics glucose (Kanazawa *et al.*, 1997 ( Exhibit I) – *in vivo* distribution studies and NMR analysis).



The specification identifies various anticancer agents in Table 2 on pages 34-41. In addition, page 4043 of Yamori *et al.* ( Exhibit C), describe methods that exemplify the identification of anticancer agents by analysis of cell growth inhibition and antitumor activity against nude mouse xenografts. Hibi *et al.* ( Exhibit D) describe using northern blot, western blot, and immunohistochemical analysis of various cancer cells and non-cancer cells to identify the tumor marker PGP9.5. Becker *et al.* ( Exhibit E) describe the use of a monoclonal antibody as a tumor marker to identify tumor cells expressing an aberrant form of E-cadherin.

Detection of folate receptor targeting is exemplified in Sudimack and Lee ( Exhibit F) on page 151 to 152 where localization of a folate receptor ligand is accomplished by *in vitro* and *in vivo* radiolabeled ligand studies. An example of tumor apoptotic cell targeting ligand identification is provided in Takamizawa *et al.* ( Exhibit G) where the expression of proapoptotic proteins is assayed by RNase protection and western blotting assays. A tumor hypoxia targeting ligand may be identified by using northern blotting, immunohistochemistry, and luciferase reporter assays in conjunction with hypoxic cell culture as described in Garayoa *et al.* ( Exhibit H) Kanazawa *et al.* ( Exhibit I) identify the tumor localization of glucose mimics or analogs by using *in vivo* distribution studies and NMR analysis. Any of these methods in combination with the guidance provided by the specification could be used for identifying a tissue specific ligand of the invention.

**c)      *The Specification Provides Sufficient Guidance to One of Skill  
in the Art for Purposes of Identifying the Necessary  
Conjugation Chemistry***

The specification provides a detailed description of the conjugation chemistry of the conjugates of the present invention. Appellants refer the Board to at least page 6, lines 4-18; page 22, line 18 to page 23, line 23; FIG. 1-3, 7, 8A, 16, 21, 36, 49, 54, and 59 for a detailed description of the chemistry and functional groups underlying the conjugation of EC to

representative tissue specific ligands. Of particular interest is Table 1 on page 23 of the specification that illustrates exemplary linkers that can be used to conjugate EC to a variety of functional groups. One of skill in the art is capable of identifying a functional group(s) of a tissue specific ligand that is useful for the synthetic methods claimed.

***d) The Specification Provides Substantial Guidance Regarding Routine Imaging and Distribution studies***

Once an EC-conjugate is synthesized according to the present invention, one of skill can readily confirm its imaging capabilities through the application of imaging studies such as the cellular uptake and distribution studies exemplified throughout the examples section, pages 32-68 of the specification. In particular, cellular uptake studies are exemplified throughout the examples section and in FIGs. 46-48, 55-58, 69-73, and 76-80; whereas distribution studies are exemplified throughout the examples section and in FIGs. 6, 11, 12, 14, 15, 17-20, 25, 26, 28-35, 37, 81-86. No undue experimentation is needed to carry out the teachings of the specification and perform the claimed methods for synthesizing imaging conjugates.

In light of the foregoing, undue experimentation is *not required* to practice the methods for synthesizing an EC-tissue specific ligand conjugate in view of the state of the art, and the ample information pertaining to the invention set forth in the specification.

***4. Declaration of Jerry L. Bryant, M.S. Further Establishes that the Claimed Invention is Enabled by the Specification***

As set forth above, the Examiner has failed to meet his burden of coming forward with factual evidence that would raise a “doubt as to the objective truth of the statements” contained in the application regarding enablement. See, *e.g.*, *In re Marzocchi*, 169 U.S.P.Q. 367, 370 (CCPA 1971). Nevertheless, as set forth above, Appellants have provided ample evidence of enablement.

Appellants have provided even further evidence of enablement by submitting, as Exhibit J, the Declaration of Jerry L. Bryant, M.S. It should be noted that in accordance with *MPEP* §2164.05, “Appellants may submit factual affidavits or cite references to show what one skilled in the art knew at the time of filing the application.” *MPEP* §2164.05. “A Declaration or affidavit is, itself, evidence that must be considered.” *MPEP* §2164.05 (emphasis added).

Mr. Bryant has expertise in the synthesis and use of radionuclide imaging agents. His expertise includes employment as Chief Technology Officer of several business entities that are involved with research directed to the synthesis and use of radionuclide imaging agents, a co-inventorship on three patent applications pertaining to novel radionuclide imaging agents and imaging technologies, involvement in funded studies pertaining to the development of radionuclide imaging agents and their use in imaging, and authorship of numerous reference materials pertaining to the synthesis of radionuclides and their use as imaging agents. See paragraphs 1-3 of Exhibit J. Mr. Bryant has reviewed the present patent application and the Office Actions dated September 29, 2003 and June 25, 2004, and he has an understanding of the rejections that have been set forth by the Examiner. See paragraphs 4-6 of Exhibit J.

As a scientist who has expertise in the synthesis and use of radionuclides, Mr. Bryant sets forth in his Declaration his belief that the invention set forth in the present application provides for novel diagnostic and therapeutic radiopharmaceuticals that can be broadly applied by scientists and clinicians, and that the chemistry of the technology is such that those of ordinary skill in the synthesis of radiolabeled imaging agents will be able to make and use the claimed radiolabeled imaging agents without an undue amount of experimentation. See paragraphs 7 and 8 of Exhibit J. Furthermore, Mr. Bryant has declared that “[w]ithout reservation, I believe that if a skilled expert had the foresight to invent and develop this technology many years ago, it would

be in routine use by scientists in the laboratory and clinicians in the hospital.” Paragraph 9 of Exhibit J.

Mr. Bryant has declared that one skilled in the imaging and use of radionuclide imaging agents would have been enabled to make and use the claimed invention when presented with the information provided in the specification, and the specification, with its numerous working examples, provides sufficient guidance to predictably identify the targeting ligands and EC-targeting ligand complexes without an undue amount of experimentation. See paragraphs 10-11 of Exhibit J. In support of his statements pertaining to enablement, he sets forth summaries of information pertaining to support provided in the specification and reference materials available at around the priority date of the instant invention that would support enablement. This information, that is detailed in his Declaration, is summarized as follows.

*a) Claims Pertaining to Anticancer Agents*

Mr. Bryant has declared that the entire specification provides a substantial amount of information regarding embodiments of the claimed invention wherein the tissue specific ligand is an anticancer agent, the conjugation chemistry of anticancer agents as targeting ligands, and information pertaining to the preparation of EC-anticancer agent derivatives. See paragraphs 12-14 of Exhibit J. For example, he indicates that exemplary anticancer agents are set forth in Table 2 of the specification. See paragraph 12, Exhibit J. Exemplary radiolabeled ligands wherein the targeting ligand is an anticancer agent are also set forth in the specification, such as on page 6, line 30 through page 7, line 4, and Table 1, page 23. See paragraph 14 of Exhibit J.

Furthermore, Mr. Bryant declares that around the time of the priority date, numerous anticancer agents were known and widely used in the treatment of cancer, and that the phrase “anticancer agent” would have been readily understood to refer to agents such as chemotherapeutic drugs that had been widely used by scientists and clinicians for many years.

See paragraph 15 of Exhibit J. Furthermore, the use of anticancer agents as targeting ligands was well-known at around the time the application was filed in the context of unrelated inventions, and he has identified numerous examples wherein anticancer agents were known to be used as targeting ligands. See paragraph 16 of Exhibit J. Furthermore, Mr. Bryant describes the state-of-the-art around the time of filing pertaining to use of anticancer agents as targeting ligands in conjugates for imaging. See paragraph 17, Exhibit J. For example, he has cited publications of the present inventors, including Zareneyrizi *et al.*, 1999 (Exhibit 18 of Exhibit J), which describes the use of <sup>99m</sup>Tc-EC-colchicine for imaging studies, and Yang *et al.*, 1999a (Exhibit 19 of Exhibit J) which describes the synthesis of <sup>111</sup>In-labeled DTPA-methotrexate for use in imaging. See paragraph 17 of Exhibit J. Thus, the state-of-the-art pertaining to anticancer agents and their use as targeting ligands was well-developed in the context of unrelated inventions.

In view of the above, Mr. Bryant has concluded that one skilled in the synthesis and use of radiolabeled imaging agents would have understood, from reading the specification, that an “anticancer agent” is a phrase used to refer to a member of a specific group of agents that can readily identified by *in vitro* and/or *in vivo* studies, that anticancer agents can be used as targeting ligands, and that the science related to this area was highly developed at around the priority date. See paragraph 18, Exhibit J. As a result, he declares that “one of ordinary skill in the synthesis and use of radionuclide imaging agents, upon reading the specification of the present application, would have been able to make and use the claimed radionuclide-labeled anticancer agents without an undue amount of experimentation.” Paragraph 18, Exhibit J.

**b)                      *Claims Pertaining to Tumor Markers***

Mr. Bryant has identified a substantial amount of information in the specification pertaining to claims that include a tumor marker as the tissue-specific ligand. See paragraph 19

of Exhibit J. Exemplary sections include page 5, lines 5-14 and page 5, line 22. See paragraph 19 of Exhibit J. Furthermore, he has indicated that the specification provides substantial guidance regarding the synthesis of EC-tumor marker derivatives. See paragraph 20 of Exhibit J. For example, information regarding conjugation chemistry of ligands such as tumor markers can be found on page 22, line 18 through page 23, line 21. See paragraph 20 of Exhibit J. Furthermore, Mr. Bryant has indicated that around the time of the priority date of the referenced patent application, the state-of-the-art pertaining to tumor markers and their use as targeting ligands was well-established. See paragraph 21 of Exhibit J. Numerous examples of tumor markers are set forth in paragraph 21 of Exhibit J, and numerous examples of tumor markers used as targeting ligands are set forth in paragraph 22 of Exhibit J. Furthermore, he was aware of a publication of the inventors that described an imaging agent that included a tumor marker as a targeting ligand. See paragraph 22 of Exhibit J, citing Kim *et al.*, 2000 (Exhibit 30 of Exhibit J). Thus, in view of the information known to those of ordinary skill in the art, Mr. Bryant declares that “one of ordinary skill in the synthesis and use of radiolabeled imaging conjugates, upon reading the specification, would have been able to make and use the claimed radiolabeled conjugates without an undue amount of experimentation.” Paragraph 22 of Exhibit J. Furthermore, one skilled in the synthesis and use of radionuclide imaging agents would have understood that a tumor marker refers to a member of a group of agents that can be readily identified by techniques commonly used by those of ordinary skill in the art. See paragraph 23 of Exhibit J.

**c)      *Claims Pertaining to Folate Receptor Targeting Ligands***

Mr. Bryant has identified detailed information in the specification pertaining to folate receptor targeting ligands and the preparation of radiolabeled folate receptor targeting ligands. See paragraph 24 of Exhibit J. Exemplary folate receptor targeting ligands are set forth on page

5, line 23 and page 6, lines 4-19. See paragraph 24 of Exhibit J. Mr. Bryant has also found that the specification provides substantial guidance pertaining to the preparation of EC-targeting ligand derivatives, including, for example, page 7, lines 5-13 and page 20, lines 7-15. See paragraph 25 of Exhibit J. Furthermore, he has declared that around the priority date of the present patent application, there was a substantial amount of information pertaining to folate receptors and folate receptor targeting ligands that was known in the art in the context of unrelated inventions. See paragraph 26 of Exhibit J. In addition, folate analogs were used in various contexts as targeting ligands, and numerous such examples are disclosed in paragraph 27 of Exhibit J. Regarding the development and use of radiolabeled agents for imaging, Mr. Bryant was aware that  $^{99m}\text{Tc}$ -EC-folate had been described as a new tumor imaging agent in a publication of the inventors. See paragraph 28 of Exhibit J, citing Ilgan *et al.*, 1998 (Exhibit 40 of Exhibit J).

In view of the information known in the art at the time of the priority date of the instant invention, Mr. Bryant has declared that one of ordinary skill in the art would have been able to make and use the claimed radionuclide-labeled folate receptor targeting ligand conjugates without an undue amount of experimentation, and that the skill in the art as to folate receptor targeting was very high at the time of the priority date. See paragraphs 28 and 29 of Exhibit J. Furthermore, he notes that one of ordinary skill in the synthesis and use of radionuclide imaging agents would have understood that a “folate receptor targeting agent” refers to a member of a group of agents that can be readily identified using techniques well-known to those of ordinary skill in the art. See paragraph 29 of Exhibit J.

***d) Claims Pertaining to Tumor Apoptotic Cell Targeting Ligands***

Mr. Bryant has reviewed the specification, and has found that it provides substantial guidance regarding aspects of the invention that pertain to radiolabeled conjugates wherein the

targeting ligand is a tumor apoptotic cell targeting ligand. See Paragraph 30 of Exhibit J. This support includes exemplary tumor apoptotic targeting ligands, information pertaining to the conjugation chemistry of tumor apoptotic targeting ligands, information pertaining to the imaging of tumor apoptotic cells, and a working example pertaining to a radiolabeled conjugate that includes annexin-V, and guidance pertaining to the preparation of EC-targeting ligand conjugates and radiolabeling of EC-targeting ligand derivatives. See paragraphs 30 and 31 of Exhibit J.

In addition, Mr. Bryant has indicated that around the time of the priority date of the present application, it was well-established that apoptosis plays a critical role in the pathophysiology of cancer, and that markers of apoptosis had been identified and were the subject of active investigation in the context of unrelated inventions. See paragraphs 32 and 33 of Exhibit J. Tumor apoptotic cell targeting ligands, exemplified by annexin V, would have been known to refer to a very limited number of specific compounds which are capable of detecting the death of tumor cells. See paragraph 34 of Exhibit J. The state-of-the-art related to apoptotic cell targeting ligands was well-established. See paragraph 34 of Exhibit J.

Therefore, in view of the above, Dr. Bryant declares that “one of ordinary skill in the synthesis and use of radionuclide imaging agents, upon reading the specification, would have been able to make and use the claimed radionuclide-labeled apoptotic cell targeting ligand conjugates without an undue amount of experimentation.” Paragraph 35 of Exhibit J. Furthermore, “one of ordinary skill in the synthesis and use of radionuclide imaging agents would have understood that an ‘apoptotic cell targeting ligand’ refers to a member of a specific group of agents that can be readily identified” using techniques well-known to those of ordinary skill in the art. Paragraph 35 of Exhibit J.



*e) Claims Pertaining to Tumor Hypoxia Targeting Ligands*

Upon review of the specification, Mr. Bryant has found that there is substantial support in the specification for methods of the invention that involve tumor hypoxia targeting ligands and conjugates involving tumor hypoxia targeting ligands. See paragraph 36 of Exhibit J. This information includes exemplary tumor hypoxia targeting ligands, information pertaining to the conjugation chemistry of such targeting ligands, and information pertaining to the preparation of EC-tumor hypoxia targeting ligand conjugates, including a working example pertaining to the synthesis and stability of  $^{99m}\text{Tc}$ -EC-metronidazole. See paragraph 36 of Exhibit J.

Mr. Bryant has declared that around the time of filing of the present patent application, there was substantial information available regarding tumor hypoxia targeting ligands. See paragraph 38 of Exhibit J. Exemplary tumor hypoxia targeting ligands, including use of one such targeting ligand in imaging, are set forth in paragraph 38 of Exhibit J. Dr. Bryant also indicates that Yang *et al.* (Exhibit 57 of Exhibit J, a publication of the inventors), had developed a  $^{99m}\text{Tc}$ -labeled metronidazole using EC as a chelator and determined that it was feasible to use this agent to image tumor hypoxia. See paragraph 39 of Exhibit J.

Therefore, Dr. Bryant has declared that “[o]ne of ordinary skill in the synthesis and use of radionuclide imaging agents, upon reading the specification, would have been able to make and use the claimed radionuclide-labeled tumor hypoxia targeting ligand conjugates without an undue amount of experimentation.” Paragraph 40 of Exhibit J. Furthermore, “[o]ne of ordinary skill in the synthesis and use of radionuclide imaging agents would have understood that a ‘tumor hypoxia targeting ligand’ refers to a member of a specific group of agents that can be readily identified, and that the claims of the invention particularly point out and distinctly claim the subject matter that is the invention.” Paragraph 40 of Exhibit J.

*f) Claims Pertaining to Agents that Mimic Glucose*

Mr. Bryant has reviewed the specification, and has found that aspects of the present invention that include agents that mimic glucose as the tissue specific ligand are discussed throughout the specification. See paragraph 41 of Exhibit J. For example, the specification includes information pertaining to exemplary agents that mimic glucose, information pertaining to the conjugation chemistry of targeting ligands that can be applied to agents that mimic glucose, information pertaining to tumor glycolysis targeting, and two working examples pertaining to the synthesis of  $^{99m}\text{Tc}$ -EC-neomycin and  $^{99m}\text{Tc}$ -EC-deoxyglucose and their evaluation as imaging agents. See paragraph 41 of Exhibit J. The specification has also been found to provide substantial guidance pertaining to the preparation of EC-targeting ligand conjugates that can be applied to conjugates of EC with agents that mimic glucose, as well as information pertaining to the radionuclide labeling of these conjugates. See paragraph 42 of Exhibit J.

Mr. Bryant also notes that the phrase “an agent that mimics glucose” would have been understood to refer to specific compounds which target glucose metabolism, and that a substantial amount of information pertaining to such compounds was available around the priority date of the present patent application in the context of unrelated inventions. See paragraph 42 of Exhibit J. Exemplary agents that mimic glucose are set forth in paragraphs 43 and 44 of Exhibit J, and include  $[^{14}\text{C}]$ deoxyglucose and  $^{18}\text{F}$ -FDG. Certain of these agents, such as FDG, had been widely used in nuclear medicine for cancer diagnosis. See paragraph 44 of Exhibit J. Aminoglycosides were known as agents that mimic glucose, and their use as ligands was well known. See paragraph 45 of Exhibit J.

In view of the above, Mr. Bryant has concluded that “a person of ordinary skill in the synthesis and use of radionuclide imaging agents, upon reading the specification, would have

been able to make and use the claimed radionuclide-labeled conjugates incorporating agents that mimic glucose without an undue amount of experimentation.” Paragraph 46 of Exhibit J. Furthermore, “one of ordinary skill in the synthesis and use of radionuclide imaging agents would have understood that an ‘agent that mimics glucose’ refers to a member of a specific group of agents that can be readily identified.”

*g) Conclusion*

Mr. Bryant has declared that in view of the above, “claims 2-4, 6, 8-10, 15, 23, 30, 31, 33-35, and 37-41 of the above referenced patent application contains subject matter which was described in the specification of the above-referenced patent application in such a way as to enable one of ordinary skill in the synthesis and use of radionuclide imaging agents to make and use the invention.” Paragraph 47 of Exhibit J. Furthermore, Mr. Bryant has declared that “[t]he description of the invention provided in the specification is sufficiently clear and concise such that one of ordinary skill in the synthesis and use of radionuclide imaging agents would be able to make the claimed agents and practice the claimed methods without an undue amount of experimentation.” Paragraph 47 of Exhibit J. In addition, he has found that each of the groups set forth by the phrases “anticancer agent,” “tumor marker,” “folate receptor targeting ligand,” “tumor apoptotic cell targeting ligand,” “tumor hypoxia targeting ligand,” and “an agent that mimics glucose” are limited, and members of these groups “can be identified using techniques known to those of ordinary skill in the synthesis and use of radionuclide imaging agents.” Paragraph 47 of Exhibit J. He also notes that “the art pertaining to the synthesis and use of EC-targeting ligand complexes was highly advanced at the time of filing of the application, and determining which types of targeting ligand complexes would bind EC and generate results would not have required an undue amount of experimentation.” Paragraph 47 of Exhibit J. As a

result, he observes, there would be predictability in practicing the claimed invention, particularly in view of the guidance provided by the working examples. See paragraph 47 of Exhibit J.

## **5. Conclusion**

In view of the argumentation and evidence set forth above, Appellants respectfully request that the Board reverse the enablement rejections under 35 U.S.C. §112, first paragraph.

### **B. Rejection of Claims 2-4, 6, 8-10, 15, 23, 30, 31, 33-35, and 37-41 under 35 U.S.C. §112, Second Paragraph**

#### **1. Rejection of Claims 2-4, 6, 8, 10, 15, 23, 30, 31, 33-35, and 37-41**

Claims 2-4, 6, 8, 10, 15, 23, 30, 31, 33-35, and 37-41 have been rejected based on the premise that the phrases “anticancer agent,” “tumor marker,” “folate receptor targeting ligand,” “tumor apoptotic cell targeting ligand,” “tumor hypoxia targeting ligand,” and “an agent that mimics glucose” are “unlimited.” Appellants respectfully traverse.

The phrases “anticancer agent,” “tumor marker,” “folate receptor targeting ligand,” “tumor apoptotic cell targeting ligand,” “tumor hypoxia targeting ligand,” and “an agent that mimics glucose” are terms used to refer to specific classes of targeting ligands. Each class of targeting ligand, when taken in light of the description provided in the specification, is readily discernable to one of ordinary skill in the art.

#### **a) Declaration of Jerry L. Bryant, M.S.**

Appellants refer to the preceding discussion pertaining to the Declaration of Mr. Jerry Bryant (Exhibit J), herein specifically incorporated into this section, related to ability of one of skill in the art to readily identify and/or obtain tissue specific ligands as described in the specification and in the art. As set forth in the Declaration, Mr. Bryant has an understanding of the nature of the present rejection pertaining to indefiniteness. See paragraph 6 of Exhibit J. He

has declared that “[t]he information provided in the specification would have permitted one skilled in the synthesis and use of radiolabeled imaging agents to understand that the phrases ‘anticancer agent,’ ‘tumor marker,’ ‘folate receptor targeting ligand,’ ‘tumor apoptotic cell targeting ligand,’ ‘tumor hypoxia targeting ligand,’ and ‘an agent that mimics glucose’ are generally accepted phrases that are used to refer to specific, defined classes of targeting ligands.” Paragraph 10 of Exhibit J. In support of this conclusion, Mr. Bryant cites relevant sections of the specification and reference materials pertaining to unrelated inventions that were available at or around the time of the priority date. These sections of the specification and reference materials are discussed above in the response pertaining to the enablement rejections, and the discussion is herein specifically incorporated to apply to this section of the response. Additional detail is provided as follows.

(1) Claims Drawn to Anticancer Agents

Regarding claims drawn to “anticancer agents” as targeting ligands for use in the present invention, Mr. Bryant, as set forth in the previous section, has cited relevant sections of the specification that disclose substantial information pertaining to anticancer agents, including numerous exemplary agents, such as those set forth in Table 2 of the specification. See paragraphs 12-14 of Exhibit J. He has also cited relevant reference material from unrelated inventions that was available at around the time of the priority date, including information pertaining to numerous anticancer agents that were known in the art, and their use as targeting ligands in unrelated inventions. See paragraphs 15-17 of Exhibit J. In view of this information, Mr. Bryant has declared that “[t]he phrase ‘anticancer agent’ [in the specification] would have been understood [by one of ordinary skill in the synthesis and use of radiolabeled imaging agents] to refer to agents such as chemotherapeutic drugs such as methotrexate, paclitaxel or tamoxifen, which had been widely used by scientists and clinicians for many years.” Paragraph

15 of Exhibit J. Consequently, the claims of the invention “particularly point out and distinctly claim the subject matter that is the invention.” Paragraph 18 of Exhibit J.

(2) Claims Drawn to Tumor Markers

Regarding claims drawn to “tumor markers,” Mr. Bryant, as set forth above, has identified substantial support in the specification pertaining to “tumor markers” as the tissue specific ligand for use in the present invention. Paragraphs 19-20 of Exhibit J. He has also, as set forth above, identified a substantial amount of reference material pertaining to tumor markers and their use as targeting ligands from around the time of the priority date of the above-referenced patent application in the context of unrelated inventions. Paragraph 21 of Exhibit J. Numerous tumor markers were known to exist in the art at around the time of the priority date (see paragraph 21 of Exhibit J), tumor markers were known to be used as targeting ligands in the context of unrelated inventions (see paragraph 22 of Exhibit J). In view of this information, Mr. Bryant has declared that “[o]ne of ordinary skill in the synthesis and use of radionuclide imaging agents would have understood that a ‘tumor marker’ refers to a member of a group of agents that can be readily identified by techniques such as Northern blot analysis, Western Blot analysis, and immunohistochemistry, and that the claims of the invention particularly point out and distinctly claim the subject matter that is the invention.” See paragraph 23 of Exhibit J.

(3) Claims Pertaining to Folate Receptor Targeting Ligands

Mr. Bryant, as previously detailed, has identified substantial support in the specification pertaining to folate receptor targeting ligands and the preparation of radiolabeled folate receptor targeting ligands. See paragraphs 24-25 of Exhibit J. This support includes exemplary folate receptor targeting ligands, as set forth on page 5, line 23 through page 7, line 1 of the specification. See paragraph 24 of Exhibit J.

Furthermore, as discussed above, Mr. Bryant has set forth in his Declaration a summary pertaining of the state-of-the-art regarding folate receptor targeting ligands that was known on or about the time of the priority date of the present patent application in the context of unrelated inventions. See paragraph 27 of Exhibit J. Exemplary folate receptor targeting ligands that were known in the art at or around the priority date of the referenced patent application included folic acid, folinic acid, pteropolyglutamic acid, and folate receptor-binding pteridines such as tetrahydropterins, dihydrofolates, tetrahydrofolates, and their deaza and dideaza analogs. Paragraph 27 of Exhibit J, citing column 7, lines 28-34 of U.S. Patent 5,108,921 (Exhibit 35 of Exhibit J). Furthermore, folate had been used as a targeting ligand in a new tumor imaging agent. See paragraph 28 of Exhibit J. The information available pertaining to folate receptor targeting ligands demonstrates that “skill in the art was very high” in the context of unrelated inventions. Paragraph 28 of Exhibit J.

Mr. Bryant has declared that “[i]n view of the disclosure in the specification, one of ordinary skill in the synthesis and use of radionuclide imaging agents would have understood that a ‘folate receptor targeting ligand’ refers to a member of a group of agents that can be readily identified, and that the claims of the invention particularly point out and distinctly claim the subject matter that is the invention.” Paragraph 29 of Exhibit J.

#### (4) Claims Pertaining to Tumor Apoptotic Cell Targeting Ligands

As set forth above, Mr. Bryant has reviewed the instant specification, and has identified substantial guidance regarding aspects of the present invention that include a tumor apoptotic cell targeting ligand. See paragraph 30 of Exhibit J. For example, examples of tumor apoptotic cell targeting ligands can be found on page 5, lines 24-25, and a detailed discuss regarding the imaging of tumor apoptotic cells that includes exemplary tumor apoptotic cell targeting ligands

such as annexin V can be found on page 28, lines 14-20 and page 29, lines 19-23. Furthermore, Example 4 of the specification pertains to the synthesis, biodistribution, and imaging studies of a radiolabeled conjugate that includes annexin V. See paragraph 30 of Exhibit J.

In addition, as set forth above, the state-of-the-art pertaining to tumor apoptotic cell targeting ligands in the context of unrelated inventions was well-established, and markers for apoptosis were actively under investigation. See paragraphs 32-33 of Exhibit J. Mr. Bryant declares that in view of the state-of-the-art, “[t]he phrase ‘tumor apoptotic cell targeting ligand’ would have been and should be well understood to refer to a very limited number of specific compounds which are capable of detecting the death of tumor cells.” Paragraph 34 of Exhibit J. Exemplary tumor apoptotic cell targeting ligands were known in the art, such as PK11195 and annexin V. See paragraph 34 of Exhibit J.

Based on the state-of-the-art at or around the time of the priority date, “one of ordinary skill in the synthesis and use of radionuclide imaging agents would have understood that an ‘apoptotic cell targeting ligand’ refers to a member of a specific group of agents that can be readily identified using techniques such as those set forth above, and that the claims of the invention particularly point out and distinctly claim the subject matter that is the invention.” Paragraph 35 of Exhibit J.

#### (5) Claims Pertaining to Tumor Hypoxia Targeting Ligands

As discussed in the response set forth above pertaining to enablement, Mr. Bryant has identified in-depth information in the specification pertaining to tumor hypoxia targeting ligands, and conjugates that include these types of targeting ligands. See Paragraph 36 of Exhibit J. As set forth in his Declaration, Mr. Bryant has identified exemplary tumor hypoxia targeting ligands in the specification, such as those set forth on page 5, lines 24-25 of the specification. See paragraph 36 of Exhibit J. In addition, the specification includes a detailed discussion pertaining



to the assessment of tumor hypoxia by imaging, information pertaining to the imaging of hypoxia due to stroke using  $^{99m}\text{Tc}$ -EC-metronidazole, and information regarding the preparation of EC-tumor hypoxia targeting ligand conjugates. See paragraphs 36 and 37 of Exhibit J.

Furthermore, as set forth above, the state-of-the-art pertaining to tumor hypoxia targeting ligands was well-established in the context of unrelated inventions. See paragraph 38 of Exhibit J. A number of hypoxia-selective antitumor agents had been identified, such as bis(nitroimidazolyl)alkanecarboxamides, adrenomedullin, and fluorine-18-fluoromisonidazole. See paragraph 28 of Exhibit J. Furthermore, Yang *et al.*, 1999b (Exhibit 57 of Exhibit J, a publication of the inventors) had developed a  $^{99m}\text{Tc}$ -labeled metronidazole using EC as a chelator, and determined that it was feasible to use this agent to image tumor hypoxia. See paragraph 39 of Exhibit J. Thus, the “use of tumor markers as targeting ligands was well-established, and the level of expertise of those in this field was high.” Paragraph 39 of Exhibit J.

In view of the state-of-the-art pertaining to tumor hypoxia targeting ligands, upon reading the specification, “[o]ne of ordinary skill in the synthesis and use of radionuclide imaging agents would have understood that a ‘tumor hypoxia targeting ligand’ refers to a member of a specific group of agents that can be readily identified, and that the claims of the invention particularly point out and distinctly claim the subject matter that is the invention.” Paragraph 40 of Exhibit J.

#### (6) Claims Pertaining to Agents that Mimic Glucose

As set forth previously, Mr. Bryant has reviewed the specification and has identified information pertaining to agents that mimic glucose and their use as targeting ligands throughout the specification. For example, exemplary agents that mimic glucose can be found on page 5, line 29 through page 6, line 3. See paragraph 41 of Exhibit J. The specification also includes detailed information pertaining to the conjugation chemistry of these targeting ligands, a

discussion regarding tumor glycolysis targeting, and working examples pertaining to  $^{99m}\text{Tc}$ -EC-neomycin and  $^{99m}\text{Tc}$ -EC-deoxyglucose. See paragraphs 41-42 of Exhibit J.

Furthermore, as set forth above, Mr. Bryant has reviewed the state-of-the-art pertaining to agents that mimic glucose on or about the priority date of the referenced patent application in the context of other inventions, and has determined that the state-of-the-art in this area was well-established. See paragraph 43 of Exhibit J. Agents that mimic glucose were established agents in the diagnosis and treatment of cancer. See paragraph 43 of Exhibit J. Exemplary agents that mimic glucose that were known in the art included  $[14\text{C}]$ deoxyglucose,  $^{18}\text{F}$ -FDG, glucose-6-phosphate, 2-deoxyglucose-6-phosphate, glucosamine-6-phosphate, N-acetylglucosamine-6-phosphate, and aminoglycosides. See paragraph 44 of Exhibit J.

Therefore, a person of ordinary skill in the synthesis and use of radionuclide imaging agents, upon reading the specification, would have understood that ‘an agent that mimics glucose’ refers to a member of a specific group of agents that can be readily identified, and that the claims of the invention particularly point out and distinctly claim the subject matter that is the invention.” Paragraph 46 of Exhibit J.

#### (7) Conclusion

Based on his review of the specification and in view of the reference material available at or around the priority date of the patent application pertaining to the phrases “anticancer agent,” “tumor marker,” “folate receptor targeting ligand,” “tumor apoptotic cell targeting ligand,” “tumor hypoxia targeting ligand,” and “an agent that mimics glucose,” Mr. Bryant declares that “the present claims particularly point out and distinctly claim the subject matter that the inventors believe is the invention.” Paragraph 48 of Exhibit J. He further declares that “the phrases ‘anticancer agent,’ ‘tumor marker,’ ‘folate receptor targeting ligand,’ ‘tumor apoptotic cell targeting ligand,’ ‘tumor hypoxia targeting ligand,’ and ‘an agent that mimics glucose’ are

not confusing, nor are they unlimited in their scope,” and that “someone skilled in the art would not and should not be confused by what these phrases mean.” Paragraph 48 of Exhibit J. He further declares that “these phrases are definite because they refer to specific classes of targeting ligands whose members can be identified using techniques well-known to those who have an understanding of the synthesis and use of radionuclide imaging agents.” Paragraph 48 of Exhibit J.

**b)      *Breadth of a Claim is not to be Equated with Indefiniteness***

By indicating that the phrases “anticancer agent,” “tumor marker,” “folate receptor targeting ligand,” “tumor apoptotic cell targeting ligand,” “tumor hypoxia targeting ligand,” and “an agent that mimics glucose” are unlimited, the Examiner appears to be equating breadth of the claim to indefiniteness. However, “[b]readth of a claim is not to be equated with indefiniteness.” *MPEP* §2173.04, citing *In re Miller*, 441 F.2d 689, 169 USPQ 597 (CCPA 1971). If the scope of the subject matter embraced by the claims is clear, and if Applicants have not otherwise indicated that they intend the invention to be of a scope different from that defined in the claims, then the claims comply with 35 U.S.C. §112, second paragraph. As per the above argumentation and evidence, Appellants have demonstrated that the scope of the subject matter embraced by the claims is sufficiently clear such that the claims particularly point out and distinctly claim the subject matter that is the invention. As discussed above, the phrases at issue in this rejection pertain to different classes of targeting ligands that can be identified using techniques that were generally available to those of ordinary skill in the synthesis and use of radionuclide imaging agents, and thus are not unlimited in scope.

**c) Conclusion**

Definiteness of claim language must be analyzed, not only based on the content of the particular application disclosure and teachings of the prior art, but also on “[t]he claims interpretation that would be given by one possessing the ordinary level of skill in the pertinent art at the time the invention was made.” *MPEP* §2173.02. Based on the Declaration of Jerry L. Bryant, M.S. set forth herein, the phrases “anticancer agent,” “tumor marker,” “folate receptor targeting ligand,” “tumor apoptotic cell targeting ligand,” “tumor hypoxia targeting ligand,” and “an agent that mimics glucose” are clear, and set forth defined subsets of tissue-specific ligands. Further, Appellants have not otherwise indicated that they intend the invention to be of a scope different from that defined in the claims.

In view of the argumentation and evidence set forth above, Appellants respectfully request that the Board reverse the rejection of claims under 35 U.S.C. §112, second paragraph.

**2. Rejection of Claim 32**

According to the Examiner, the term “octreotide” renders claim 32 indefinite because octreotide can be both an anti-cancer agent and a peptide. Appellants respectfully traverse.

Appellants find this line of argumentation to make no sense. The following examples put this into perspective:

Consider the term “knife” in a claim (*e.g.*, A device suitable for slicing food, comprising a knife, ...). A “knife” can belong to more than one subgenus. For example, a “knife” can be defined by its composition. For example, the knife can be “a metal object.” Alternatively, a knife can be defined by its function. For example, the knife might be “a device suitable for cutting steak.” According to the Examiner’s argument, use of the term “knife” in the claim renders the claim ambiguous because a knife can be defined both as “a metal object” and “a device suitable for cutting steak.”

Here is a second example. Consider a particular “antibody.” The antibody is a protein. The antibody might also be “an agent capable of modulating an immune response.” Consider a claim “A method of treating disease X comprising administering an antibody; wherein the antibody comprising SEQ ID NO:Y.” According to the Examiner’s standard, use of the term “antibody” in this claim would render it indefinite because “antibody” can have more than one meaning – for example, it can be both a protein and an agent that modulates an immune response. Appellants find this line of argumentation nonsensical.

Whether any claim term, such as “octreotide,” can be defined as belonging to more than one subgenus is not dispositive on the issue of whether the term renders a claim indefinite under the standard of 35 U.S.C. §112, second paragraph. The Examiner has cited no support for her assertion. Regarding indefiniteness, the standard to be considered by the Examiner is whether the claim apprises one of ordinary skill in the art of its scope and, therefore, serves the notice function required by 35 U.S.C. §112, second paragraph. See, *e.g.*, *Solomon v. Kimberly-Clark Corp.*, 216 F.3d 1372, 1379, 55 USPQ2d 1279, 1283 (Fed. Cir. 2000).

The Examiner has presented no information to suggest that one of ordinary skill in the art would not sufficient apprise one of ordinary skill in the art of the scope of the claimed subject matter.

In contrast, Appellants have established that octreotide is a well-known anti-cancer agent (see product description, attached as Exhibit K). Appellants have also set forth that octreotide is addressed in the instant specification. Table 2 of the specification (page 34, line 22 through page 42, line 2) is entitled “DRUGS OF CHOICE FOR CANCER CHEMOTHERAPY.” “Octreotide” is specifically listed in Table 2 as an anticancer agent. Specification, page 36. In

addition, page 6, lines 14-17 sets forth octreotide as an example of a tissue-specific ligand that can be conjugated to a linker.

Contrary to the Examiner's assertion, it is of no consequence whether or not "octreotide" is considered a peptide. Appellants are not required to set forth on the record whether they consider "octreotide" to be "peptide" or an "anticancer agent" for purposes of overcoming this rejection. What *is* of consequence is that Appellants have clearly established on the record that octreotide is a well-known anti-cancer agent, and that their specification contemplates octreotide as a tissue-specific ligand. This information is more than sufficient to apprise one of ordinary skill in the art of the scope of claim 32, and the term "octreotide."

The Examiner states that art was previously cited against peptides. Appellants are unaware to what the Examiner refers. However, the relevancy of this assertion to the present §112, second paragraph, rejection is unclear. There is no question that the term "octreotide" is sufficiently clear and unambiguous.

In view of the argumentation and evidence set forth above, Appellants respectfully request that the Board reverse the rejection of claims under 35 U.S.C. §112, second paragraph.

## **VIII. CONCLUSION**

Appellants have provided arguments that overcome the pending rejections. Appellants respectfully submit that the Office Action's conclusions that the claims should be rejected are unwarranted. It is therefore requested that the Board overturn the Action's rejections.

Please date stamp and return the enclosed postcard to evidence receipt of this document.

Respectfully submitted,

A handwritten signature in black ink, appearing to read "Monica De La Paz", with a stylized flourish at the end.

Monica A. De La Paz

Reg. No. 54,662

Attorney for Appellants

FULBRIGHT & JAWORSKI  
600 Congress Avenue, Suite 240  
Austin, Texas 78701  
(512) 536-4598

Date: September 29, 2005

## APPENDIX 1

### CLAIMS APPENDIX

2. (Previously presented) The method of claim 33, wherein said tissue specific ligand is conjugated to said ethylenedicysteine on both acid arms of the ethylenedicysteine.
3. (Previously Presented) The method of claim 33, wherein said radionuclide is  $^{99m}\text{Tc}$ ,  $^{188}\text{Re}$ ,  $^{186}\text{Re}$ ,  $^{183}\text{Sm}$ ,  $^{166}\text{Ho}$ ,  $^{90}\text{Y}$ ,  $^{89}\text{Sr}$ ,  $^{67}\text{Ga}$ ,  $^{68}\text{Ga}$ ,  $^{111}\text{In}$ ,  $^{183}\text{Gd}$ ,  $^{59}\text{Fe}$ ,  $^{225}\text{Ac}$ ,  $^{212}\text{Bi}$ ,  $^{211}\text{At}$ ,  $^{64}\text{Cu}$  or  $^{62}\text{Cu}$ .
4. (Previously Presented) The method of claim 3, wherein said radionuclide is  $^{99m}\text{Tc}$ .
6. (Previously Presented) The method of claim 33, wherein said tissue specific ligand is an anticancer agent.
8. (Previously Presented) The method of claim 33, wherein said tissue specific ligand is a tumor marker.
9. (Previously presented) The method of claim 8, wherein said tumor marker is PSA, ER, PR, CA-125, CA-199, CEA AFP, interferons, BRCA1, HER-2/neu, cytoxan, p53, endostatin, a monoclonal antibody or an antisense tumor marker.
10. (Previously Presented) The method of claim 33, wherein the tissue specific ligand is a folate receptor targeting ligand.
15. (Previously Presented) The method of claim 33, wherein the tissue specific ligand is a tumor apoptotic cell targeting ligand or a tumor hypoxia targeting ligand.
23. (Previously Presented ) The method of claim 33, wherein the tissue specific ligand is an agent that mimics glucose.



30. (Previously Presented) The method of claim 2, further comprising a linker conjugating EC to said tissue specific ligand.

31. (Previously Presented) The method of claim 30, wherein the linker is a water soluble peptide, glutamic acid, aspartic acid, bromo ethylacetate, ethylene diamine or lysine.

32. (Previously presented) The method of claim 31, wherein the tissue specific ligand is topotecan, paclitaxel, raloxifen, etoposide, doxorubicin, mitomycin C, endostatin, annexin V, LHRH, octreotide, methotrexate or folic acid.

33. (Previously Presented) A method of synthesizing a radiolabeled ethylenedicysteine derivative for imaging comprising the steps:

- a) obtaining a tissue specific ligand, wherein the tissue specific ligand is an anticancer agent, a tumor marker, a folate receptor targeting ligand, a tumor apoptotic cell targeting ligand, a tumor hypoxia targeting ligand, glutamate pentapeptide, or an agent that mimics glucose;
- b) admixing said ligand with ethylenedicysteine (EC) to obtain an EC-tissue specific ligand derivative; and
- c) admixing said EC-tissue specific ligand derivative with a radionuclide and a reducing agent to obtain a radionuclide labeled EC-tissue specific ligand derivative, wherein the EC forms an  $N_2S_2$  chelate with the radionuclide.

34. (Previously Presented) The method of claim 33, wherein said reducing agent is a dithionite ion, a stannous ion or a ferrous ion.

35. (Previously presented) A method for labeling a tissue specific ligand for imaging, comprising the steps:

- a) obtaining a tissue specific ligand, wherein the tissue specific ligand is an anticancer agent, a tumor marker, a folate receptor targeting ligand, a tumor apoptotic cell targeting ligand, a tumor hypoxia targeting ligand, glutamate pentapeptide, or an agent that mimics glucose;
- b) admixing the tissue specific ligand with ethylenedicysteine (EC) to obtain an EC-ligand conjugate; and
- c) reacting the conjugate with  $^{99m}\text{Tc}$  in the presence of a reducing agent to form an  $\text{N}_2\text{S}_2$  chelate between the ethylenedicysteine (with or without linker) and the  $^{99m}\text{Tc}$ .

37. (Previously Presented) The method of claim 35, wherein the reducing agent is a dithionite ion, a stannous ion or a ferrous ion.

38. (Previously Presented) A method of imaging a site within a mammalian body comprising the steps of administering an effective diagnostic amount of a composition comprising a  $^{99m}\text{Tc}$  labeled ethylenedicysteine-tissue specific ligand conjugate and detecting a radioactive signal from the  $^{99m}\text{Tc}$  localized at the site, wherein the tissue specific ligand is an anticancer agent, a tumor marker, a folate receptor targeting ligand, a tumor apoptotic cell targeting ligand, a tumor hypoxia targeting ligand, glutamate pentapeptide, or an agent that mimics glucose.

39. (Original) The method of claim 38, wherein the site is a tumor.

40. (Original) The method of claim 38, wherein the site is an infection.

41. (Original) The method of claim 38, wherein the site is breast cancer, ovarian cancer, prostate cancer, endometrium, heart, lung, brain, liver, folate (+) cancer, ER (+) cancer, spleen, pancreas, or intestine.

## APPENDIX 2

### EVIDENCE APPENDIX

- Exhibit A: U.S. Patent 6,692,724, cited in the response to the Office Action dated June 25, 2004, that was mailed on Dec. 23, 2004.
- Exhibit B: U.S. Patent 5,517,993, cited in response to the Office Action dated June 25, 2004, that was mailed on Dec. 23, 2004.
- Exhibit C: Yamori *et al.*, *Cancer Research* 59:4042-4049, 1999, cited in response to the Office Action dated June 25, 2004, that was mailed on Dec. 23, 2004.
- Exhibit D: Hibi *et al.*, *Am. J. Pathology* 155(3):711-715, 1999, cited in response to the Office Action dated June 25, 2004, that was mailed on Dec. 23, 2004.
- Exhibit E: Becker *et al.*, *Am. J. Pathology* 155(6):1803-1809, 1999, cited in response to the Office Action dated June 25, 2004, that was mailed on Dec. 23, 2004.
- Exhibit F: Sudimack and Lee, *Advanced Drug Delivery Reviews* 41:147-162, 2000, cited in response to the Office Action dated June 25, 2004, that was mailed on Dec. 23, 2004.
- Exhibit G: Takamizawa *et al.*, *J. Pediatric Surgery* 35(2):390-395, 2000, cited in response to the Office Action dated June 25, 2004, that was mailed on Dec. 23, 2004.
- Exhibit H: Garayoa *et al.*, *Molecular Endocrinology* 14(6):848-862, 2000, cited in response to the Office Action dated June 25, 2004, that was mailed on Dec. 23, 2004.
- Exhibit I: Kanazawa *et al.*, *NMR in Biomedicine* 10:35-41, 1997, cited in response to the Office Action dated June 25, 2004, that was mailed on Dec. 23, 2004.
- Exhibit J: Declaration of Jerry L. Bryant, M.S, cited in response to the Office Action dated June 25, 2004, that was mailed on Dec. 23, 2004.

Exhibit K: Product Description of Octreotide, cited in response to the Office Action dated June 25, 2004, that was mailed on Dec. 23, 2004.

## Potent Antitumor Activity of MS-247, a Novel DNA Minor Groove Binder, Evaluated by an *in Vitro* and *in Vivo* Human Cancer Cell Line Panel<sup>1</sup>

Takao Yamori,<sup>2</sup> Akio Matsunaga, Shigeo Sato, Kanami Yamazaki, Akiko Komi, Kazuhiro Ishizu, Izumi Mita, Hajime Edatsugi, Yasuhiro Matsuba, Kimiko Takezawa, Osamu Nakanishi, Hiroshi Kohno, Yuki Nakajima, Hironori Komatsu, Toshio Andoh, and Takashi Tsuruo

Division of Experimental Chemotherapy, Cancer Chemotherapy Center, Japanese Foundation for Cancer Research, Tokyo 170-8455 [T. Y., S. S., K. Y., A. K., K. I.]; Life Sciences Laboratory, Mitsui Chemical Inc., Chiba 297-0017 [A. M., H. K., Y. N., H. K.]; Institute of Biological Science, Mitsui Pharmaceuticals, Inc., Chiba 297-0017 [I. M., H. E., Y. M., K. T., O. N.]; Faculty of Engineering, Soka University, Tokyo 192-0003 [T. A.]; and Institute of Molecular and Cellular Biosciences, University of Tokyo, Tokyo 113-0032 [T. T., Japan]

### ABSTRACT

We synthesized a novel anticancer agent MS-247 (2-[[N-[1-methyl-2-[5-[N-[4-[N,N-bis(2-chloroethyl) amino] phenyl]] carbamoyl]-1H-benzimidazol-2-yl] pyrrol-4-yl] carbamoyl] ethyldimethylsulfonium di-*p*-toluenesulfonate) that has a netropsin-like moiety and an alkylating residue in the structure. We evaluated antitumor activity of MS-247 using a human cancer cell line panel coupled with a drug sensitivity database and subsequently using human cancer xenografts. The average MS-247 concentration required for 50% growth inhibition against a panel of 39 cell lines was 0.71  $\mu$ M. The COMPARE analysis revealed that the differential growth inhibition pattern of MS-247 significantly correlated with those of camptothecin analogues and anthracyclins, indicating that MS-247 and the two drug groups might have similar modes of action. MS-247 exhibited remarkable antitumor activity against various xenografts. A single i.v. injection of MS-247 significantly inhibited the growth of all 17 xenografts tested, which included lung, colon, stomach, breast, and ovarian cancers. In many cases, MS-247 was more efficacious than cisplatin, Adriamycin, 5-fluorouracil, cyclophosphamide, VP-16, and vincristine and was almost comparable with paclitaxel and CPT-11; these are the most clinically promising drugs at present. MS-247 was noticeably more effective than paclitaxel (in HCT-15) and CPT-11 (in A549, HBC-4, and SK-OV-3). The toxicity of MS-247, indicated by body weight loss, was reversible within 10 days after administration. The MS-247 mode of action showed DNA binding activity at the site where Hoechst 33342 bound, inhibited topoisomerases I and II (as expected by the COMPARE analysis) blocked the cell cycle at the G<sub>2</sub>-M phase, and induced apoptosis. These results indicate that MS-247 is a promising new anticancer drug candidate to be developed further toward clinical trials.

### INTRODUCTION

DNA minor groove binders are an attractive source of novel antitumor agents. As a whole, they induce a huge range of mutations from simple base sequence changes to deletions and ploidy changes (reviewed in Ref. 1). The recent increased interest in this group of compounds stems from their ability to interact in a sequence-selective fashion at quite long DNA binding sites, suggesting the possibility of targeting specific DNA sequences within the genome (2-6). Several DNA minor groove binders proved to have potent antitumor activity in preclinical studies and are now under clinical phase studies. They include duocarmycin derivatives adozelesin (7-9), carzelesin (10, 11), bizelesin (12, 13) and KW-2189 (14), and a distamycin A-derivative tallimustine (15). However, their clinical efficacies have not been established yet (16-19).

Received 3/23/99; accepted 6/8/99.

The costs of publication of this article were defrayed in part by the payment of page charges. This article must therefore be hereby marked *advertisement* in accordance with 18 U.S.C. Section 1734 solely to indicate this fact.

<sup>1</sup> This work was supported in part by a Grant-in-Aid for Scientific Research on Priority Area "Cancer" from the Ministry of Education, Science, Sports and Culture, Japan, as well as by a grant from the Organization for Pharmaceutical Safety and Research of Japan.

<sup>2</sup> To whom requests for reprints should be addressed, at Cancer Chemotherapy Center, Japanese Foundation for Cancer Research, 1-37-1 Kami-Ikebukuro, Toshima-ku, Tokyo 170-8455, Japan. Phone: 81-3-3918-0111, extension 4453; Fax: 81-3-3918-3716.

We attempted to develop a new DNA minor groove binder that has the more promising antitumor activity. We synthesized compounds that have two moieties in the structure. One is a netropsin-like moiety (Fig. 1) to acquire DNA minor groove binding activity, and another is an *N,N*-bis(2-chloroethyl) amino residue for DNA alkylation. Netropsin is one of the polypyrrolicarboxamides, like distamycin A, and binds to DNA minor grooves at the A-T-rich region (20). After screening a number of synthetic compounds, we selected MS-247<sup>3</sup> (Fig. 1). It had shown significant cytotoxicity in several murine tumor cell lines and strong *in vivo* antitumor activity against murine tumor models in our preliminary study.

The present study was designed to evaluate the antitumor activity of MS-247 against various human cancers *in vitro* and *in vivo* and to elucidate its mode of action. We report here that MS-247 indicated potent antitumor activity against all 17 human xenografts tested, and that MS-247 bound to the DNA minor groove, inhibited topoisomerases I and II, blocked the cell cycle at G<sub>2</sub>-M phase, and induced apoptosis.

### MATERIALS AND METHODS

**Chemicals.** MS-247 was synthesized in the Life Sciences Laboratory Mitsui Chemicals, Inc. (Chiba, Japan). MS-247 was dissolved in *N,N*-dimethylformamide (Tokyo Kasei Kogyo, Tokyo, Japan) before use. CPT-11 was kindly supplied by Yakult Honsha (Tokyo, Japan). Other anticancer drugs and chemicals were purchased as follows: ADM and 5-FU, Kyowa Hakko Kogyo (Tokyo, Japan); cisplatin and VP-16, Nippon Kayaku (Tokyo, Japan); CPM, Shionogi Pharmaceuticals (Osaka, Japan); VCR, Eli Lilly Japan (Kobe, Japan); paclitaxel, camptothecin, calf thymus DNA, RNase A, and propidium iodide, Sigma (St. Louis, MO.); Hoechst 33342, Molecular Probes (Eugene, OR); Proteinase K, Boehringer Mannheim (Mannheim, Germany); and  $\phi$ X174/*Hae*III, Toyobo (Tokyo, Japan).

**Cell Lines.** Human breast cancer MDA-MB-231 and leukemia HL-60 were purchased from American Type Culture Collection (Rockville, MD). Murine leukemia L1210, P388, and the following human cancer cell lines (21) were generously distributed by the National Cancer Institute (Frederick, MD): lung cancer, NCI-H23, NCI-H226, NCI-H522, NCI-H460, DMS273 and DMS114; colon cancer, HCC-2998, KM-12, HT-29, WiDr, HCT-15, and HCT-116; ovarian cancer, OVCAR-3, OVCAR-4, OVCAR-5, OVCAR-8, and SK-OV-3; breast cancer, MCF-7; renal cancer, RXF-631 L and ACHN; melanoma, LOX-IMVI; and brain tumor, U251, SF-295, SF-539, SF-268, SNB-75, and SNB-78. Human stomach cancer, MKN-1, MKN-7, MKN-28, MKN-45, MKN-74, and St-4, and human breast cancer BSY-1, HBC-4, and HBC-5 were described elsewhere (22, 23). The cells were cultured in RPMI 1640 supplemented with 5% fetal bovine serum, penicillin (100 units/ml), and streptomycin (100 mg/ml) at 37°C in humidified air containing 5% CO<sub>2</sub>.

**A Human Cancer Cell Line Panel and the Database.** To evaluate drugs for the cell growth inhibition profile, we established a human cancer cell line

<sup>3</sup> The abbreviations used are: MS-247, 2-[[N-[1-methyl-2-[5-[N-[4-[N,N-bis(2-chloroethyl) amino] phenyl]] carbamoyl]-1H-benzimidazol-2-yl] pyrrol-4-yl] carbamoyl] ethyldimethylsulfonium di-*p*-toluenesulfonate; ADM, Adriamycin; 5-FU, 5-fluorouracil; CPM, cyclophosphamide; VCR, vincristine; VP-16, etoposide; GI<sub>50</sub>, concentration required for 50% growth inhibition; PBS(-), calcium- and magnesium-free PBS.

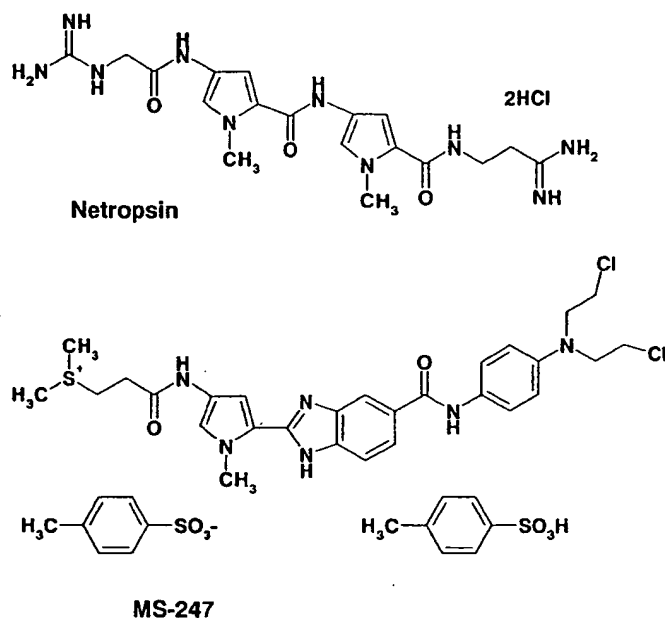


Fig. 1. Chemical structure of netropsin and MS-247. MS-247 has a netropsin-like moiety and an alkylating residue in the structure.

panel combined with a database. The system as a whole was developed according to the method of the National Cancer Institute (24–26), with modification. The cell line panel consisted of 38 human cancer cell lines, described above, and 1 murine leukemia (P388). With this system, we have examined the antiproliferative effect of more than 200 standard compounds, including various anticancer drugs, and established a new database, as described below.

**Measurements of Cell Growth Inhibition and Data Analysis.** The details of measuring cell growth inhibition are described elsewhere (26, 27). Briefly, the cells were plated at proper density in 96-well plates in RPMI 1640 with 5% fetal bovine serum and allowed to attach overnight. The cells were exposed to drugs for 48 h. Then, the cell growth was determined according to the sulforhodamine B assay, described by Skehan *et al.* (28). Data calculations were made according to the method described previously (26). Absorbance for the control well ( $C$ ) and the tests well ( $T$ ) were measured at 525 nm. Moreover, at time 0 (addition of drugs), absorbance for the test well ( $T_0$ ) was also measured. Using these measurements, cell growth inhibition (percentage of growth) by each concentration of drug was calculated as: % growth =  $100 \times [(T - T_0)/(C - T_0)]$ , when  $T > T_0$  and % growth =  $100 \times [(T - T_0)/T]$ , when  $T < T_0$ . By using the computer to process % growth values, the 50% growth inhibition parameter ( $GI_{50}$ ) was determined. The  $GI_{50}$  was calculated as  $100 \times [(T - T_0)/(C - T_0)] = 50$ . The mean graph, which shows the differential growth inhibition of the drug in the cell line panel, was drawn based on a calculation using a set of  $GI_{50}$  (24, 25). To analyze the correlation between the mean graphs of drug A and drug B, the COMPARE computer algorithm was developed according to the method described by Paull *et al.* (25). Pearson correlation coefficients were calculated using the following formula:  $r = (\sum(x_i - x_m)(y_i - y_m))/(\sum(x_i - x_m)^2 \sum(y_i - y_m)^2)^{1/2}$ , where  $x_i$  and  $y_i$  are log  $GI_{50}$  of drug A and drug B, respectively, against each cell line, and  $x_m$  and  $y_m$  are the mean values of  $x_i$  and  $y_i$ , respectively.

**Animals.** Female nude mice with BALB/c genetic backgrounds were purchased from Charles River Japan, Inc. (Kanagawa, Japan). They were maintained under specific pathogen-free conditions and provided with sterile food and water *ad libitum*. Seven-week-old mice weighing 16–22 g were used for this study.

**Drugs and Administration.** Drug administration was done i.v. We selected an administration schedule of single shot for MS-247, according to the results in animal tumor models.<sup>4</sup> We first determined the maximum tolerable dose of MS-247 in the schedule, which was 30 mg/kg. To evaluate the

antitumor effect, MS-247 was given to tumor-bearing nude mice at doses of 30, 25, and 21 mg/kg for lung cancer xenografts and at a dose of 25 mg/kg for other xenografts. The reference drugs chosen were CPT-11, paclitaxel, cisplatin, ADM, 5-FU, CPM, VP-16, and VCR. Each reference drug was given at the maximum tolerable dose in the optimal schedule.

**Antitumor Activity against Xenografts.** Six lung cancers (NCI-H23, NCI-H226, NCI-H460, A549, DMS114, and DMS273), four stomach cancers (MKN-1, MKN-7, MKN-74, and St-4), three colon cancers (HCC-2998, HCT-116, and HCT-15), two breast cancers (HBC-4 and MDA-MB-231), and two ovarian cancers (SK-OV-3 and OVCAR-8) were used to evaluate antitumor activity of MS-247. They were grown as s.c. tumors in nude mice. Nude mice were inoculated s.c. with a  $3 \times 3 \times 3$ -mm tumor fragment. When the tumor reached 100–300 mm<sup>3</sup> in volume, animals were divided randomly into test groups consisting of six mice per group (day 0). Drugs were administered from day 0 according to the dose schedules indicated. The mice were weighed twice each week up to days 24–31 to monitor the toxic effects. The length ( $L$ ) and width ( $W$ ) of the tumor mass were measured twice a week up to days 24–31, and the tumor volume ( $TV$ ) was calculated as:  $TV = (L \times W^2)/2$ . The tumor volume at day  $n$  was expressed as relative tumor volume ( $RTV$ ), according to the following formula:  $RTV = TV_n/TV_0$ , where  $TV_n$  is the tumor volume at day  $n$ , and  $TV_0$  is the tumor volume at day 0. Tumor regression ( $T/C\%$ ) on day 14 was determined by calculating  $RTV$  as:  $T/C\% = 100 \times (\text{mean } RTV \text{ of treated group})/(\text{mean } RTV \text{ of control group})$ . Statistical evaluations of  $RTV$  were performed using the Mann-Whitney  $U$  test.

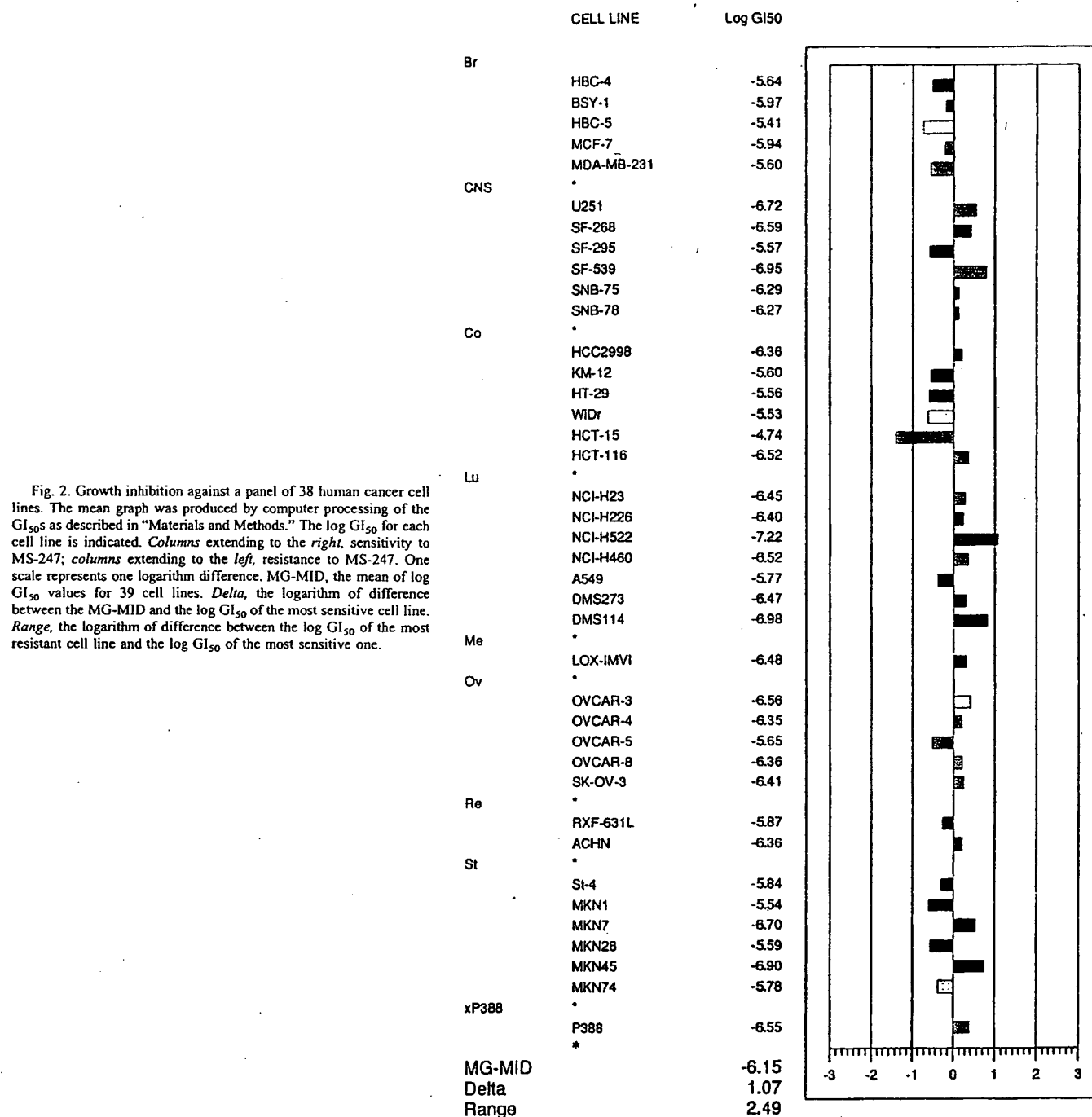
**Measurement of Fluorescence of DNA-bound Hoechst 33342.** In the cell free system, 1  $\mu$ g of calf thymus DNA and 0.8  $\mu$ g of Hoechst 33342 were mixed in 0.2 ml of PBS(–) and preincubated for 10 min at room temperature in a 96-well plate. Then, MS-247 was added at final concentrations of 0.01–30  $\mu$ g/ml. After another 10-min incubation, the fluorescence derived from the Hoechst 33342 bound to DNA was measured with a fluorometer (excitation wavelength, 355 nm; and emission wavelength, 460 nm). In the cellular system, L1210 cells ( $4 \times 10^5$  cells in 1 ml of culture medium) were preincubated with Hoechst 33342 (4  $\mu$ g/ml) at 37°C for 20 min. Then, MS-247 was added at final concentrations of 0.01–100  $\mu$ g/ml. After another 20-min incubation, the cells were washed once with ice-cold PBS(–), resuspended in ice-cold PBS(–), and transferred into a 96-well plate. Fluorescence was measured as described above.

**Cell Cycle Analysis.** Cell cycle analysis was performed using flow cytometry, as described previously (29). The L1210 cells were exposed to MS-247 for 3–48 h. The cells were harvested, washed with ice-cold PBS(–), and fixed in 70% ethanol. The cells were washed twice with ice-cold PBS(–) again, treated with RNase (0.25  $\mu$ g/ml) at 37°C for 1 h, and stained with propidium iodide (50  $\mu$ g/ml). The DNA content of the cells was analyzed using an EPICS ELITE flow cytometer (Coulter, Hialeah, FL).

**Topoisomerase Activity Assays.** Topoisomerase I enzyme activity was measured by DNA relaxation assay using the Topoisomerase I Drug Screening kit (TopoGEN, Columbus, OH). Briefly, supercoiled DNA (0.25  $\mu$ g) was suspended in a standard reaction mixture [10 mM Tris-HCl (pH 7.9), 1 mM EDTA, 150 mM NaCl, 0.1% BSA, 0.1 mM spermidine, and 5% glycerol]. MS-247 was added to the mixture before the reaction was started by topoisomerase I enzyme addition. After a 30-min incubation at 37°C, the reaction was stopped by adding 0.1 volume of 10% SDS. The DNA-bound protein (topoisomerase I) was digested by proteinase K (41.7  $\mu$ g/ml) at 37°C for 30 min. The proteinase K was removed by chloroform:isoamylalcohol (24:1, v/v) treatment. DNA samples were then analyzed by 1% agarose gel electrophoresis.

**DNA Fragmentation Assay.** DNA fragmentation was analyzed by agarose gel electrophoresis. The HL-60 cells ( $5 \times 10^5$ ) were treated with 0.2 or 2  $\mu$ M MS-247 or 20 nM camptothecin at 37°C for 20 h. The drug-treated cells were harvested and then suspended in TNE buffer [10 mM Tris-HCl (pH 7.6), 140 mM NaCl, and 1 mM EDTA]. Subsequently, it was lysed by incubation at 37°C for 30 min in the TNE buffer containing 0.2 mg/ml of RNase A, 0.2 mg/ml of Proteinase K, and 0.83% SDS. DNA extraction was performed as described previously (30), and extracted DNA was resuspended in TNE buffer, then treated with RNase A (0.2 mg/ml) at 37°C for 30 min, after Proteinase K (0.2 mg/ml) digestion at 37°C for 30 min. The purified DNA was resolved by electrophoresis in 2% agarose gels, stained with ethidium bromide, and visualized under UV light.

<sup>4</sup> Unpublished results.



## RESULTS

**Growth Inhibition against a Panel of 38 Human Cancer Cell Lines.** We have established a new human cancer cell line panel coupled with a drug sensitivity database, which is similar to the one developed by the National Cancer Institute (24–26). This panel consists of 38 human cancer cell lines and murine leukemia P388. Thus far, we have used this panel to evaluate more than 200 standard agents, most of which are anticancer drugs and various types of inhibitors. We have also added the growth-inhibitory parameters to the database. We compared standard drugs with each other for the mean graph pattern using COMPARE analysis and confirmed that drugs sharing a certain mode of action clustered together, as described

previously (24, 25). The patterns in the mean graphs of drugs with common modes of action resembled one another.

Using the human cancer cell line panel, we investigated the cell growth inhibition profile of MS-247. Fig. 2 shows the mean graph of MS-247 based on the growth inhibition parameter of  $GI_{50}$ . MS-247 showed differential growth inhibition, and it seemed to be more effective against lung cancer cell lines. The mean  $\log GI_{50}$  of MS-247 was  $-6.15$  ( $0.71 \mu M$ ), which fell in the middle of the range of presently used anticancer drugs in the panel (Fig. 3). The COMPARE analysis of the mean graph revealed that MS-247 significantly correlated with two main groups of anticancer agents (Table 1). The first was a camptothecin analogue group, including CPT-11, SN-38 (active

# ANTITUMOR ACTIVITY OF MS-247 AGAINST XENOGRAPHS

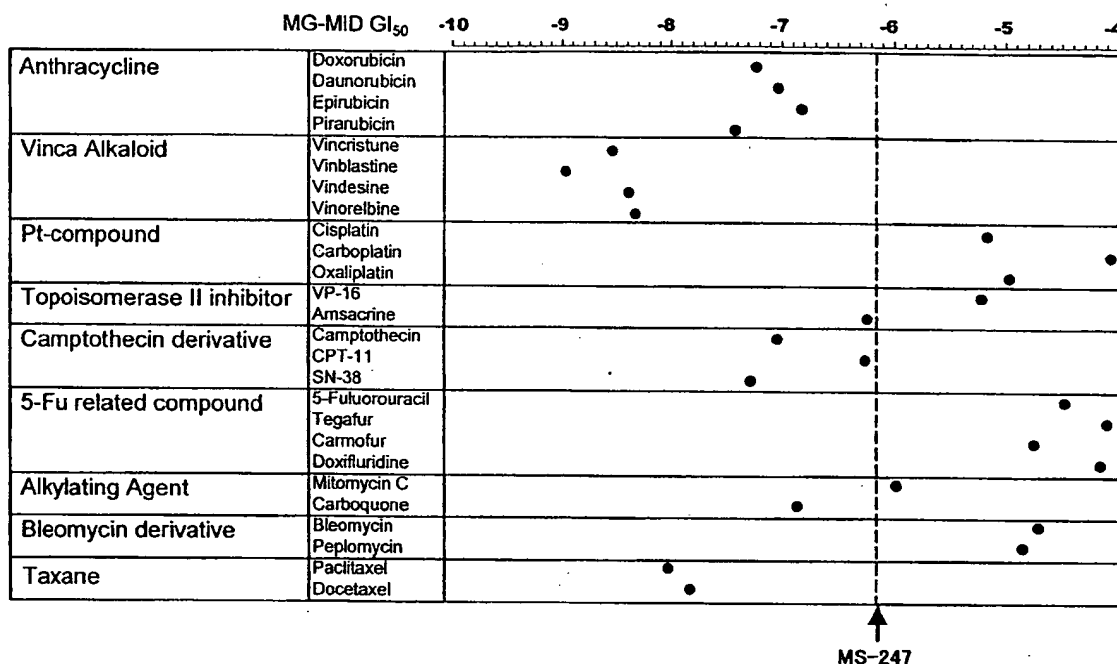


Fig. 3. Comparison of MS-247 with clinically active anticancer agents for the mean log  $GI_{50}$  against 39 cell lines. The  $GI_{50}$  of each drug to 39 cell lines was determined as described in "Materials and Methods." ●, mean log  $GI_{50}$  of each drug.

metabolite of CPT-11), and camptothecin. The second was an anthracycline group, including epirubicin, ADM, mitoxantrone, KW-2170, and daunorubicin. These results indicate that MS-247 may share some modes of action with both groups.

**Antitumor Activity of MS-247 against Human Cancer Xenografts.** To evaluate the antitumor activity of MS-247, we developed various human cancer xenografts by s.c. injecting 17 cell lines of the panel into nude mice. We examined the antitumor activity and the toxicity of MS-247 using six lung cancer xenografts (Fig. 4). The four lung cancer cell lines, NCI-H23, NCI-H226, NCI-H460, and A549, were originally non-small cell lung cancers, and others, DMS273 and DMS114, were small cell lung cancers. A single i.v. administration of MS-247 on day 0 significantly inhibited tumor growth at all of the dosages, 30, 25, and 21 mg/kg (Fig. 4, upper panels). There were not major differences in the efficacy within a dose range, indicating that MS-247 was effective in a rather wide dose range. It is remarkable that MS-247 induced tumor regression during a certain period in NCI-H23, NCI-H226, DMS273, and DMS114. As for toxicity, the body weight of the tumor-bearing mice decreased by day 10 after the administration, but it was recovered afterward (Fig. 4, lower panels). These results demonstrated the therapeutic efficacy of MS-247 in the nude mice bearing lung cancer xenografts.

Then, we examined MS-247 for activity against 10 other xenografts including colon, stomach, breast, and ovarian cancers, and we compared MS-247 with eight major anticancer drugs, paclitaxel, CPT-11, cisplatin, ADM, 5-FU, CPM, VP-16, and VCR (Table 2). A single injection of 25 mg/kg MS-247 showed significant antitumor activity against all 17 xenografts tested. MS-247 was more effective in most xenografts than cisplatin, ADM, 5-FU, CPM, VP-16, or VCR. MS-247 was comparable to paclitaxel and CPT-11, presently the most promising drugs. Noticeably, MS-247 was more effective than paclitaxel in HCT-15 and than CPT-11 in A549, HBC-4, and SK-OV-3; therefore, it showed a higher response rate than paclitaxel and CPT-11.

**DNA Binding of MS-247.** Hoechst 33342 is a fluorochrome that binds to the DNA minor groove and generates specific fluorescence

(31, 32). To confirm MS-247 binding to DNA, we observed the effect of MS-247 on the fluorescence generated by DNA-bound Hoechst 33342. In a cell free system, the fluorescence of DNA-bound Hoechst 33342 was quenched after MS-247 was added in a dose-dependent manner (Fig. 5A). Similar results were obtained when fluorescence was measured in the cellular system where MS-247 was exogenously added to L1210 cells that had been preincubated with Hoechst 33342 (Fig. 5B). These results indicated that MS-247 may have displaced the DNA-bound Hoechst 33342 on the DNA.

**Inhibition of Topoisomerase I by MS-247.** Some of the DNA minor groove binders reportedly inhibit topoisomerases (1). In addition, the COMPARE analysis of the mean graph of MS-247 suggested that the mode of action of MS-247 was similar to camptothecin analogues and anthracyclins, which inhibit topoisomerases I and II, respectively. Therefore, we examined whether MS-247 inhibited topoisomerases (Fig. 6). Topoisomerase I converted supercoiled DNA to nicked and relaxed DNA. MS-247 inhibited the process in a dose-dependent manner. These results demonstrated that MS-247 had topoisomerase I inhibitory activity at concentrations of 50–100  $\mu$ g/ml. MS-247 also inhibited topoisomerase II activity at the same concentration range (data not shown).

Table 1 The COMPARE analysis of MS-247

The mean graph of MS-247 was compared with those of 200 standard compounds using the COMPARE analysis. Drugs were ordered according to the correlation coefficient. Drugs with correlation coefficients higher than 0.5 ( $P < 0.001$ ) were included.

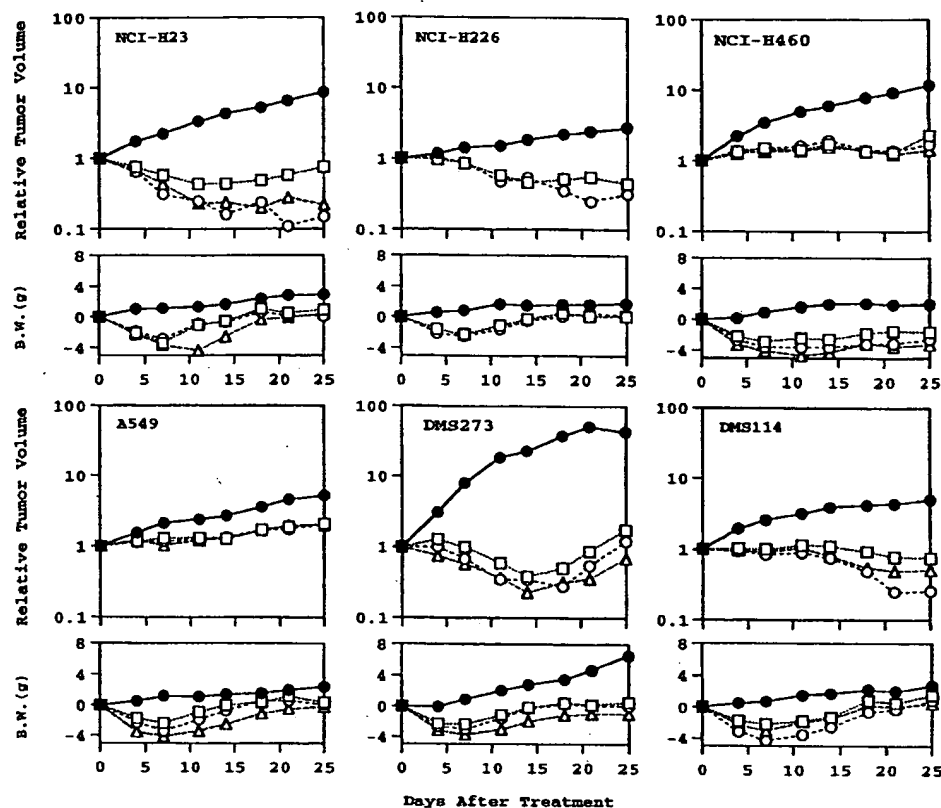
Ranking order	Drug	$r^a$
1	SN-38	0.688
2	CPT-11	0.683
3	Epirubicin	0.636
4	ADM	0.602
5	Mitoxantrone	0.596
6	KW2170	0.588
7	Melphalan	0.579
8	DMDC	0.575
9	Camptothecin	0.557
10	Daunorubicin	0.516

<sup>a</sup> Pearson correlation coefficient.



## ANTITUMOR ACTIVITY OF MS-247 AGAINST XENOGRAPHS

Fig. 4. Effect of MS-247 on the tumor growth and the body weight change in nude mice bearing human lung cancer xenografts. Tumor inoculation was carried out as described in "Materials and Methods." MS-247 was administered on day 0 at doses of 30 ( $\Delta$ ), 25 (O), 21 ( $\square$ ), and 0 mg/kg ( $\bullet$ , control). Each curve represents the average of six mice.



**Effects of MS-247 on the Cell Cycle.** We investigated the effect of MS-247 on cell cycle progression in L1210 cells (Fig. 7). The cells were exposed to 10, 30, and 100 ng/ml of MS-247 for 3–48 h. The cell population in  $G_2$ -M phase increased time dependently at each con-

centration, indicating that MS-247 blocked the cell cycle at the  $G_2$ -M phase.

**Apoptosis Induced by MS-247.** We tested the apoptosis-inducing ability of MS-247 in HL-60 cells by DNA fragmentation assay. As

Table 2. Antitumor activity of MS-247 against human cancer xenografts

Nude mice were each inoculated s.c. with a  $3 \times 3 \times 3$ -mm tumor fragment. When tumors reached 100–300 mm<sup>3</sup> in volume, animals were divided randomly into test groups of six each (day 0). Drugs were administered from day 0 according to the dose schedules indicated. Tumor regression (T/C %) on day 14 was determined.

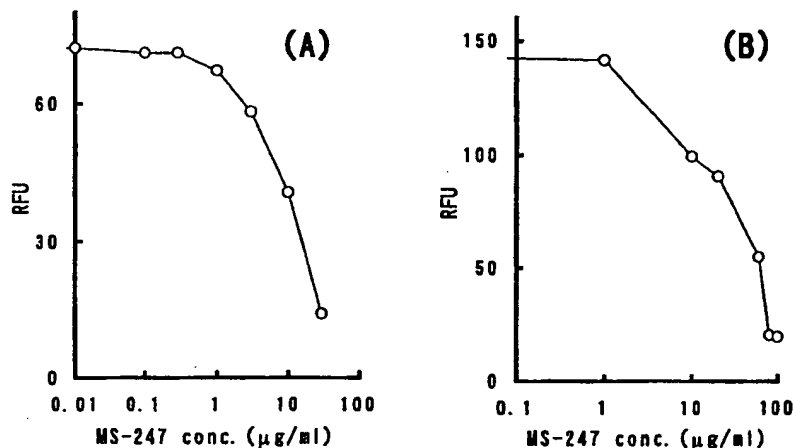
Drug dose (mg/kg) <sup>a</sup> schedule <sup>b</sup>	T/C (%)								
	MS247 25 qd $\times$ 1	Cisplatin 10 qd $\times$ 1	Paclitaxel 28 qd $\times$ 5	CPT-11 100 q4d $\times$ 3	ADM 12 qd $\times$ 1	5-Fu 50 q4d $\times$ 3	CPM 260 qd $\times$ 1	VP-16 12 qd $\times$ 5	VCR 1.6 qd $\times$ 1
<b>Lung cancer</b>									
NCI-H23	4 <sup>c</sup>	10 <sup>c</sup>	4 <sup>c</sup>	8 <sup>c</sup>	43 <sup>c</sup>	63	21 <sup>c</sup>	67	67
NCI-H226	29 <sup>c</sup>	71	6 <sup>c</sup>	14 <sup>c</sup>	40 <sup>c</sup>	70	89	78	24 <sup>c</sup>
NCI-H460	32 <sup>c</sup>	45 <sup>c</sup>	22 <sup>c</sup>	35 <sup>c</sup>	45 <sup>c</sup>	41	60	66	81
A 549	50 <sup>c</sup>	78	29 <sup>c</sup>	75	78	111	88	76	73
DMS 114	19 <sup>c</sup>	69	27 <sup>c</sup>	20 <sup>c</sup>	52	63	9 <sup>c</sup>	61	20 <sup>c</sup>
DMS 273	2 <sup>c</sup>	33 <sup>c</sup>	1 <sup>c</sup>	5 <sup>c</sup>	71	70	43 <sup>c</sup>	137	27 <sup>c</sup>
<b>Stomach cancer</b>									
MKN-1	42 <sup>c</sup>	63	46 <sup>c</sup>	49 <sup>c</sup>	41	55	74	103	88
MKN-7	32 <sup>c</sup>	60	11 <sup>c</sup>	41 <sup>c</sup>	58	75	79	68	66
MKN-74	35 <sup>c</sup>	78	16 <sup>c</sup>	28 <sup>c</sup>	78	76	69	134	82
St-4	24 <sup>c</sup>	62	22 <sup>c</sup>	42 <sup>c</sup>	66	55	95	86	87
<b>Colon cancer</b>									
HCC-2998	28 <sup>c</sup>	52	1 <sup>c</sup>	16 <sup>c</sup>	72	42	71	76	73
HCT-1116	30 <sup>c</sup>	78	5 <sup>c</sup>	11 <sup>c</sup>	60	48 <sup>c</sup>	53	64	57
HCT-15	46 <sup>c</sup>	54	78	10 <sup>c</sup>	73	61	53	66	104
<b>Breast cancer</b>									
HBC-4	24 <sup>c</sup>	56	37 <sup>c</sup>	54	46 <sup>c</sup>	49 <sup>c</sup>	41 <sup>c</sup>	86	46 <sup>c</sup>
MDA-MB-231	18 <sup>c</sup>	28 <sup>c</sup>	13 <sup>c</sup>	50 <sup>c</sup>	86	83	25 <sup>c</sup>	56	32 <sup>c</sup>
<b>Ovarian cancer</b>									
SK-OV-3	39 <sup>c</sup>	72	45 <sup>c</sup>	80	53	75	105	100	85
OVCR-8	36 <sup>c</sup>	69	17 <sup>c</sup>	18 <sup>c</sup>	58	76	78	74	80
<b>Positive rate</b>	17/17	4/17	16/17	14/17	4/17	2/17	5/17	0/17	5/17

<sup>a</sup> Each drug was administered at MTD in the schedule indicated.

<sup>b</sup> The administration schedules were abbreviated as: qd  $\times$  1, a single injection; qd  $\times$  5, five daily injections; q4d  $\times$  3, 3 injections with a 4-day interval.

<sup>c</sup>  $P < 0.01$  by Mann Whitney  $U$  test as compared with respective control.

Fig. 5. Quenching of the fluorescence of DNA-bound Hoechst 33342 by MS-247. The fluorescence of DNA-bound Hoechst 33342 was measured under the following conditions: A, calf thymus DNA was preincubated with Hoechst 33342 and then incubated with MS-247; B, L1210 cells were preincubated with Hoechst 33342 and then incubated with MS-247. The fluorescence derived from DNA-bound Hoechst 33342 decayed when MS-247 was added to the two systems.



shown in Fig. 8, MS-247 at concentrations around  $IC_{50}$  induced a DNA ladder in HL-60 cells. These results demonstrated that MS-247 induced apoptosis.

## DISCUSSION

MS-247 is a synthetic compound with a netropsin-like moiety and an alkylating residue in its structure. We found MS-247 by screening about 300 similar compounds, based primarily on the activity of tumor cell growth inhibition, and selected MS-247 for extensive evaluation because of its significant antitumor activity against murine tumors, L1210 and colon 26, and its higher stability.<sup>4</sup>

In the present study, we evaluated the antitumor activity of MS-247 by an *in vitro* and *in vivo* human cancer cell line panel. The mean  $log_{50}$  of MS-247 was  $-6.15$  ( $0.71 \mu M$ ), which fell in the middle of the range of anticancer drugs presently in use. The COMPARE analysis indicated that the differential growth inhibition pattern of MS-247 (the mean graph) significantly correlated with those of camptothecin analogues and anthracyclins, suggesting that the modes of action are similar. The most remarkable feature of MS-247 was its efficacy

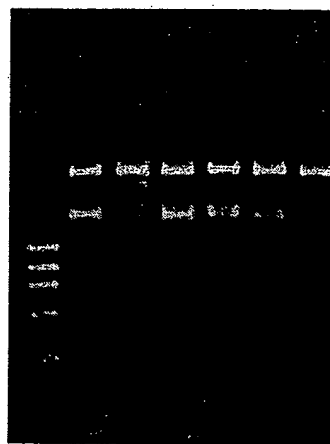
against human xenografts. A single 25 mg/kg injection of MS-247 showed significant antitumor activity against all 17 xenografts tested, which included lung, colon, stomach, breast, and ovarian cancers. In comparison with the clinically active drugs, MS-247 was more effective than cisplatin, ADM, 5-FU, CPM, VP-16, and VCR, in most cases, and moreover, was almost comparable with paclitaxel and CPT-11, the most clinically promising drugs at the present. These results demonstrated the broad anticancer spectrum of MS-247. It is noticeable that MS-247 was more effective than paclitaxel in HCT-15 and than CPT-11 in A549, HBC-4, and SK-OV-3. On the other hand, the toxicity of MS-247, indicated by the body weight loss, was reversible within 10 days after the administration. In our preliminary study, the dose-limiting toxicity of MS-247 was bone marrow suppression. Our results suggest that MS-247 is a promising anticancer drug candidate for further research and development toward clinical investigation.

We also investigated the mode of action of MS-247. We confirmed its binding to DNA by the fact that MS-247 displaced DNA-bound Hoechst 33342 both in the cell-free system and in the cellular system. Hoechst 33342 is a fluorochrome that binds to AT-rich sites in the DNA minor groove and covers four bp, AATT (31, 32). Therefore, it seems correct to consider MS-247 as a DNA minor groove binder, as expected, and that it shares sequence specificity at least with Hoechst 33342.

MS-247 proved to have inhibitory activity against topoisomerases I and II. This was reasonable to expect because several DNA minor groove binders reportedly inhibit topoisomerases. For example, Hoechst 33342, Hoechst 33258, distamycin A, berenil, netropsin, and tallimustine inhibited topoisomerase I (33–35), and distamycin A and tallimustine inhibited topoisomerase II (34, 36). The inhibitory activity against topoisomerase I and II was also expected because the results of the COMPARE analysis suggested that the mode of action of MS-247 was similar to those of camptothecin analogues (topoisomerase I inhibitors) and anthracyclins (topoisomerase II inhibitors). Therefore, topoisomerases I and II are at least the molecular targets of MS-247. Moreover, there might be other possible targets, such as other enzymes, involved in DNA metabolism and/or transcription factors because their activities were inhibited by some DNA minor groove binders (34, 37, 38).

MS-247 blocked the cell cycle at the  $G_2$ -M phase and induced apoptosis. The  $G_2$ -M blockage is the common feature of DNA minor groove binders (1, 39). However, subsequent induction of apoptosis by this type of drug has not been studied, except for apoptosis induced by Hoechst 33342 (40, 41). We showed here the induction of apoptosis by MS-247, which possibly contributes to *in vivo* efficacy, at

Drug	—	—	CPT	MS-247		
Conc. ( $\mu M$ )	—	—	5	100	50	10
Topo I	—	+	+	+	+	+



← Nicked DNA  
← Supercoiled DNA

Fig. 6. Inhibition of topoisomerase I by MS-247. Supercoiled DNA was mixed with an indicated concentration of MS-247 or camptothecin before topoisomerase I was added. After a 30-min incubation at 37°C, the reaction mixture was treated as described in "Materials and Methods," and the DNA was analyzed by 1% agarose gel electrophoresis. MS-247 inhibited the topoisomerase I-induced DNA relaxation at concentrations of 50 and 100  $\mu M$ . Camptothecin was used as a positive control.

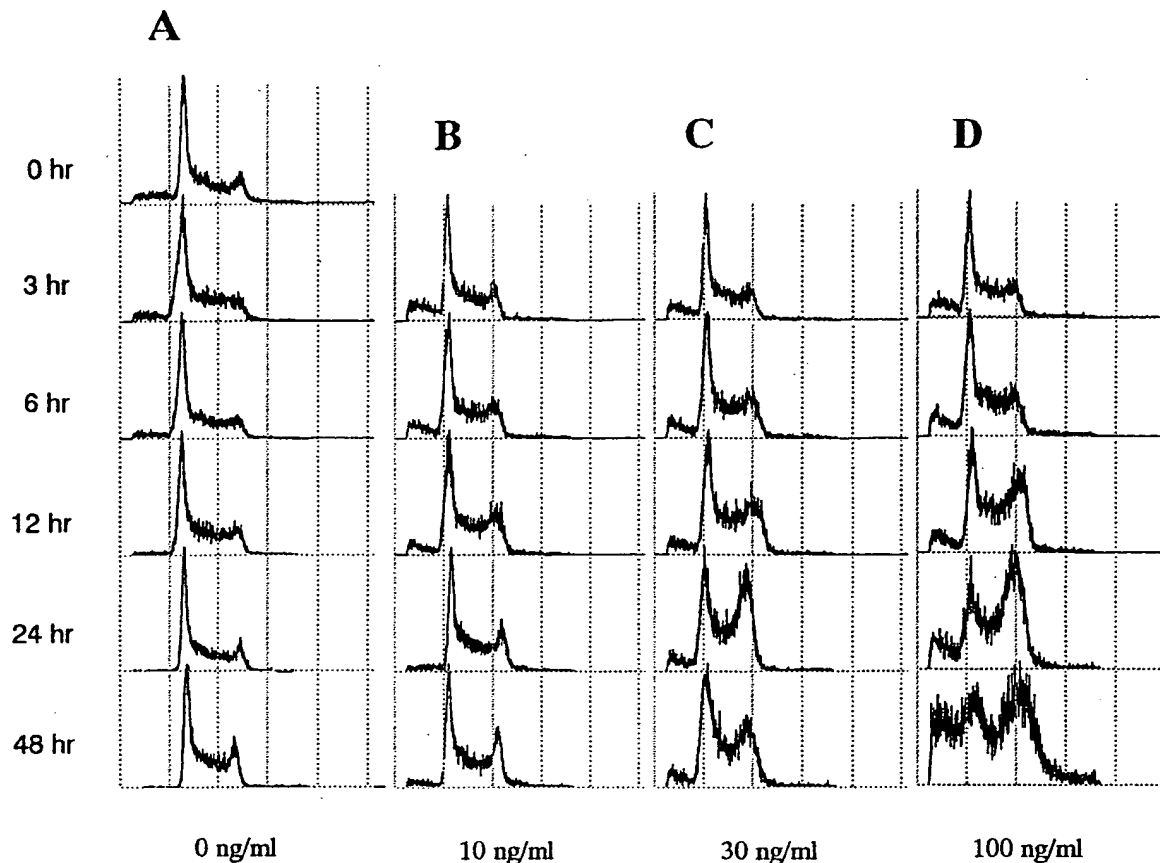


Fig. 7. Effect of MS-247 on cell cycle. L1210 cells were exposed to 0 (A), 10 (B), 30 (C), and 100 ng/ml (D) of MS-247 for 3–48 h. Then, the DNA content of the cells was analyzed by a flow cytometer as described in "Materials and Methods." When exposed to MS-247, the cell population in the G<sub>2</sub>-M phase significantly increased.

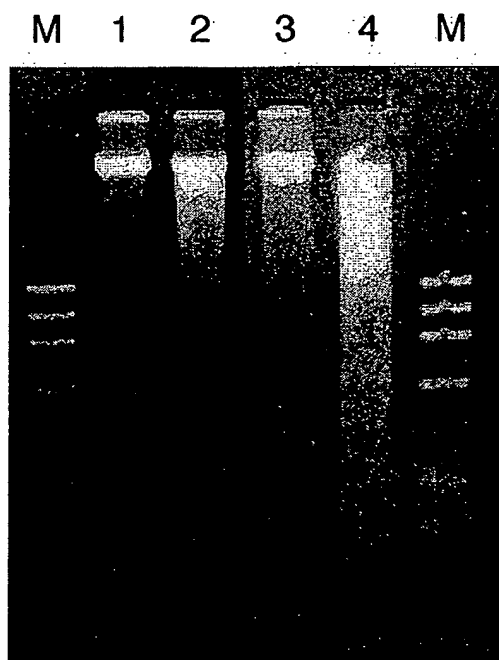


Fig. 8. Apoptosis induced by MS-247. Total DNA was extracted from HL-60 cells treated with nothing (Lane 1), 2  $\mu$ M MS-247 (Lane 2), 0.2  $\mu$ M MS-247 (Lane 3), or 20 nM camptothecin (Lane 4). Then, DNA fragmentation was measured by electrophoresis, as described in "Materials and Methods." Camptothecin was used as a positive control. Lane M, DNA size markers ( $\phi$ x174/HaeIII).

least in part. Recently, the analysis of the apoptotic cascade induced by anticancer drugs has been studied (42). It seems an important next step to analyze the mechanism of apoptosis induced by MS-247 and to compare MS-247 with other antitumor agents.

Tallimustine, a derivative of distamycin A, has the closest structural relationship to MS-247 of the DNA minor groove binders that were developed as anticancer drugs. Although tallimustine was subjected to clinical trials, its efficacy has not yet been demonstrated (17, 18). It may be important to compare MS-247 and tallimustine in a preclinical study. In our preliminary study, the sequence specificity of DNA binding between the two is slightly different, suggesting that MS-247 is different from tallimustine in biological activity.

We report here our synthesis of a novel DNA minor groove binder, MS-247, and have demonstrated its strong antitumor activity against several human cancer xenografts. We see that MS-247 binds to DNA, inhibits topoisomerases and other possible targets around DNA, blocks the cell cycle at G<sub>2</sub>-M, and induces apoptosis. MS-247 is a promising new anticancer drug for further development toward clinical investigation.

#### ACKNOWLEDGMENTS

We thank Dr. R. H. Shoemaker and Dr. K. D. Paull (Developmental Therapeutics Program, Division of Cancer Treatment, National Cancer Institute) for their helpful discussions during the development of the human cancer cell line panel and the database system.

#### REFERENCES

1. Turner, P. R., and Denny, W. A. The mutagenic properties of DNA minor-groove binding ligands. *Mutat. Res.*, 355: 141–169, 1996.

2. Hartley, J. A., Lown, J. W., Mattes, W. B., and Kohn, K. W. DNA sequence specificity of antitumor agents. *Oncogenes as possible targets for cancer therapy*. *Acta. Oncol.*, 27: 503-510, 1988.
3. Lown, J. W. DNA recognition by lexitropsins, minor groove binding agents. *J. Mol. Recognit.* 7: 79-88, 1994.
4. Marchini, S., Cozzi, P., Beria, I., Geroni, C., Capolongo, L., D'Incalci, M., and Broggin, M. Sequence-specific DNA alkylation of novel tallimustine derivatives. *Anticancer Drug Des.*, 13: 193-205, 1998.
5. Brooks, N., Lee, M., Wright, S. R., Woo, S., Centioni, S., and Hartley, J. A. Synthesis, DNA binding, cytotoxicity and sequence specificity of a series of imidazole-containing analogs of the benzoic acid mustard distamycin derivative tallimustine containing an alkylating group at the C-terminus. *Anticancer Drug Des.*, 12: 591-606, 1997.
6. Yoon, J. H., and Lee, C. S. Sequence selectivity of DNA alkylation by adozelesin and carzelesin. *Arch. Pharmacol. Res. (Seoul)*, 21: 385-390, 1998.
7. Bhuyan, B. K., Smith, K. S., Adams, E. G., Wallace, T. L., Von Hoff, D. D., and Li, L. H. Adozelesin, a potent new alkylating agent: cell-killing kinetics and cell-cycle effects. *Cancer Chemother. Pharmacol.*, 30: 348-354, 1992.
8. Burris, H. A., Dieras, V. C., Tunca, M., Earhart, R. H., Eckardt, J. R., Rodriguez, G. I., Shaffer, D. S., Fields, S. M., Campbell, E., Schaaf, L., Kasunic, D., and Von Hoff, D. D. Phase I study with the DNA sequence-specific agent adozelesin. *Anticancer Drugs*, 8: 588-596, 1997.
9. Foster, B. J., LoRusso, P. M., Poplin, E., Zalupski, M., Valdivieso, M., Wozniak, A., Flaherty, L., Kasunic, D. A., Earhart, R. H., and Baker, L. H. Phase I trial of adozelesin using the treatment schedule of daily  $\times 5$  every 3 weeks. *Invest. New Drugs*, 13: 321-326, 1996.
10. Li, L. H., DeKoning, T. F., Kelly, R. C., Krueger, W. C., McGovren, J. P., Padbury, G. E., Petzold, G. L., Wallace, T. L., Ouding, R. J., Prairie, M. D., and Gebhard, I. Cytotoxicity and antitumor activity of carzelesin, a prodrug cyclopropylpyrrolindole analogue. *Cancer Res.*, 52: 4904-4913, 1992.
11. Houghton, P. J., Cheshire, P. J., Hallman, J. D. N., and Houghton, J. A. Therapeutic efficacy of the cyclopropylpyrrolindole, carzelesin, against xenografts derived from adult and childhood solid tumors. *Cancer Chemother. Pharmacol.*, 36: 45-52, 1995.
12. Carter, C. A., Waud, W. R., Li, L. H., DeKoning, T. F., McGovren, J. P., and Plowman, J. Preclinical antitumor activity of bizelesin in mice. *Clin. Cancer Res.*, 2: 1143-1149, 1996.
13. Walker, D. L., Reid, J. M., and Ames, M. M. Preclinical pharmacology of bizelesin, a potent bifunctional analog of the DNA-binding antibiotic CC-1065. *Cancer Chemother. Pharmacol.*, 34: 317-322, 1994.
14. Kobayashi, E., Okamoto, A., Asada, M., Okabe, M., Nagamura, S., Asai, A., Saito, H., Gomi, K., and Hirata, T. Characteristics of antitumor activity of KW-2189, a novel water-soluble derivative of duocarmycin, against murine and human tumors. *Cancer Res.*, 54: 2404-2410, 1994.
15. Pezzoni, G., Grandi, M., Biasoli, G., Capolongo, L., Ballinari, D., Giuliani, F. C., Barbieri, B., Pastori, A., Pesenti, E., Mongelli, N., and Spreafico, F. Biological profile of FCE 24517, a novel benzoyl mustard analogue of distamycin A. *Br. J. Cancer*, 64: 1047-1050, 1991.
16. Verweij, J. New promising anticancer agents in development: what comes next? *Cancer Chemother. Pharmacol.*, 38 (Suppl.): S3-S10, 1996.
17. Viallet, J., Stewart, D., Shepherd, F., Ayoub, J., Cormier, Y., DiPietro, N., and Stewart, W. Tallimustine is inactive in patients with previously treated small cell lung cancer. A Phase II trial of the National Cancer Institute of Canada Clinical Trials Group. *Lung Cancer*, 15: 367-373, 1996.
18. Punt, C. J., Humblet, Y., Roca, E., Dirix, L. Y., Wainstein, R., Polli, A., and Corradino, I. Tallimustine in advanced previously untreated colorectal cancer, a Phase II study. *Br. J. Cancer*, 73: 803-804, 1996.
19. Alberts, S. R., Erlichman, C., Reid, J. M., Sloan, J. A., Ames, M. M., Richardson, R. L., and Goldberg, R. M. Phase I study of the duocarmycin semisynthetic derivative KW-2189 given daily for five days every six weeks. *Clin. Cancer Res.*, 4: 2111-2117, 1998.
20. Tabernero, L., Verdager, N., Coll, M., Fita, I., van der Marel, G. A., van Boom, J. H., Rich, A., and Aymami, J. Molecular structure of the A-tract DNA dodecamer d(CGAAATTTGCG) complexed with the minor groove binding drug netropsin. *Biochemistry*, 32: 8403-8410, 1993.
21. Stinson, S. F., Alley, M. C., Kopp, W. C., Fiebig, H. H., Mullendore, L. A., Pittman, A. F., Kenney, S., Keller, J., and Boyd, M. R. Morphological and immunocytochemical characteristics of human tumor cell lines for use in a disease-oriented anticancer drug screen. *Anticancer Res.*, 12: 1035-1053, 1992.
22. Satoh, A., Takayama, E., Kojima, K., Ogawa, H., Yamori, T., Sato, S., Kawaguchi, T., Tsuruo, T., Yoshimoto, K., Kine, T., and Matsumoto, I. Expression of carbohydrate-binding protein p33/41 human tumor cell lines. *J. Biochem.*, 119: 346-353, 1996.
23. Motoyama, T., Hojo, H., and Watanabe, H. Comparison of seven cell lines derived from human gastric carcinomas. *Acta. Pathol. Jpn.*, 36: 65-83, 1986.
24. Boyd, M. R. Status of the National Cancer Institute preclinical antitumor drug discovery screen: implications for selection of new agents for clinical trial. In: V. T. Devita, Jr., S. Hellman, and S. A. Rosenberg (eds.), *Cancer: Principles and Practice of Oncology Update*, Vol. 3, pp. 1-12. Philadelphia: Lippincott, 1989.
25. Paull, K. D., Shoemaker, R. H., Hodes, L., Monks, A., Scudiero, D. A., Rubinstein, L., Plowman, J., and Boyd, M. R. Display and analysis of patterns of differential activity of drugs against human tumor cell lines: development of mean graph and COMPARE algorithm. *J. Natl. Cancer Inst.*, 81: 1088-1092, 1989.
26. Monks, A., Scudiero, D., Skehan, P., Shoemaker, R., Paull, K., Vistica, D., Hose, C., Langley, J., Cronise, P., Vaigro-Wolff, A., Gray-Goodrich, M., Campbell, H., Mayo, J., and Boyd, M. Feasibility of a high-flux anticancer drug screen using a diverse panel of cultured human tumor cell lines. *J. Natl. Cancer Inst.*, 83: 757-766, 1991.
27. Yamori, T., Sato, S., Chikazawa, H., and Kadota, T. Anti-tumor efficacy of paclitaxel against human lung cancer xenografts. *Jpn. J. Cancer Res.*, 88: 1205-1210, 1997.
28. Skehan, P., Storeng, R., Scudiero, D., Monks, A., McMahon, J., Vistica, D., Warren, J. T., Bokesch, H., Kenney, S., and Boyd, M. R. New colorimetric cytotoxicity assay for anticancer-drug screening. *J. Natl. Cancer Inst.*, 82: 1107-1112, 1990.
29. Goldwasser, F., Shimizu, T., Jackman, J., Hoki, Y., O'Connor, P. M., Kohn, K. W., and Pommier, Y. Correlations between S and G2 arrest and the cytotoxicity of camptothecin in human colon carcinoma cells. *Cancer Res.*, 56: 4430-4437, 1996.
30. Ishizawa, M., Kobayashi, Y., Miyamura, T., and Matsuura, S. Simple procedure of DNA isolation from human serum. *Nucleic Acids Res.*, 19: 5792, 1991.
31. Sriram, M., van der Marel, G. A., Roelen, H. L., van Boom, J. H., and Wang, A. H. Conformation of B-DNA containing O<sup>6</sup>-ethyl-G-C base pairs stabilized by minor groove binding drugs: molecular structure of d(CGCG[e6G]AATTCGCG) complexed with Hoechst 33258 or Hoechst 33342. *EMBO J.*, 11: 225-232, 1992.
32. Robinson, H., Gao, Y. G., Bauer, C., Roberts, C., Switzer, C., and Wang, A. H. 2'-Deoxyisoguanosine adopts more than one tautomer to form base pairs with thymidine observed by high-resolution crystal structure analysis. *Biochemistry*, 37: 10897-10905, 1998.
33. Chen, A. Y., Yu, C., Gatto, B., and Liu, L. F. DNA minor groove-binding ligands: a different class of mammalian DNA topoisomerase I inhibitors. *Proc. Natl. Acad. Sci. USA*, 90: 8131-8135, 1993.
34. Montecucco, A., Fontana, M., Focher, F., Lestingi, M., Spadari, S., and Ciarrocchi, G. Specific inhibition of human DNA ligase adenylation by a distamycin derivative possessing antitumor activity. *Nucleic Acids Res.*, 19: 1067-1072, 1991.
35. Wang, Z., Zimmer, C., Lown, J. W., and Knippers, R. Effects of bifunctional netropsin-related minor groove-binding ligands on mammalian type I DNA topoisomerase. *Biochem. Pharmacol.*, 53: 309-316, 1997.
36. Fesen, M., and Pommier, Y. Mammalian topoisomerase II activity is modulated by the DNA minor groove binder distamycin in simian virus 40 DNA. *J. Biol. Chem.*, 264: 11354-11359, 1989.
37. Bendorini, M., Moncollin, V., D'Incalci, M., Mongelli, N., and Mantovani, R. Distamycin A and tallimustine inhibit TBP binding and basal *in vitro* transcription. *Nucleic Acids Res.*, 23: 1657-1663, 1995.
38. Broggin, M., and D'Incalci, M. Modulation of transcription factor-DNA interactions by anticancer drugs. *Anticancer Drug Des.*, 9: 373-387, 1994.
39. Erba, E., Mascellani, E., Pifferi, A., and D'Incalci, M. Comparison of cell-cycle phase perturbations induced by the DNA-minor-groove alkylator tallimustine and by melphalan in the SW626 cell line. *Int. J. Cancer*, 62: 170-175, 1995.
40. Zhang, X., and Kiechle, F. L. Hoechst 33342 induces apoptosis and alters TATA box binding protein/DNA complexes in nuclei from BC3H-1 myocytes. *Biochem. Biophys. Res. Commun.*, 248: 18-21, 1998.
41. Zhang, X., and Kiechle, F. L. Mechanism of Hoechst 33342-induced apoptosis in BC3H-1 myocytes. *Ann. Clin. Lab. Sci.*, 28: 104-114, 1998.
42. Kamesaki, H. Mechanisms involved in chemotherapy-induced apoptosis and their implications in cancer chemotherapy. *Int. J. Hematol.*, 68: 29-43, 1998.

## Short Communication

### PGP9.5 As a Candidate Tumor Marker for Non-Small-Cell Lung Cancer

Kenji Hibi,\* William H. Westra,\*† Michael Borges,†  
Steve Goodman,‡ David Sidransky,\*‡ and  
Jin Jen\*‡

From the Department of Otolaryngology-Head and Neck Surgery,  
Division of Head and Neck Cancer Research,\* and the  
Departments of Pathology<sup>†</sup> and Oncology,<sup>‡</sup> Johns Hopkins  
University School of Medicine, Baltimore, Maryland

PGP9.5 is a neurospecific peptide that functions to remove ubiquitin from ubiquitinated proteins and prevents them from targeted degradation by proteasomes. Using the serial analysis of gene expression method (SAGE), we observed that the PGP9.5 transcript was highly expressed in primary lung cancers and lung cancer cell lines but was not detectable in the normal lung. Here we examined the expression of PGP9.5 protein in normal lung epithelium, lung tumor cell lines, and 98 resected primary non-small-cell lung carcinomas (NSCLCs). We found PGP9.5 reactivity in normal lung in a pattern compatible with K-cells of the diffuse neuroendocrine system. However, the PGP9.5 was present in both small-cell lung cancer (SCLC) and NSCLC cell lines (22/24) independent of neuronal differentiation. In primary NSCLCs, 54% (53/98) of the cases had positive PGP9.5 staining, and the expression of protein was strongly associated with pathological stage of the cancer. It was present in 44% (29/66) of stage I NSCLCs and in 75% (24/32) of stage II and IIIA NSCLCs ( $p = 0.0032$ ). These results suggest that the increased expression of PGP9.5 is specifically associated with lung cancer development and may serve as a potential marker for the detection of lung cancer. (*Am J Pathol* 1999, 155:711-715)

Lung cancer is the second most common malignancy worldwide and is the leading cause of cancer death in men.<sup>1</sup> Accumulating evidence indicates that a series of genetic changes in dominant oncogenes such as *myc* and *ras* are involved in the pathogenesis of human lung cancer.<sup>2,3</sup> Several other candidate oncogenes have also been implicated.<sup>4,5</sup> It is now clear that the accumulation of multiple genetic changes in a tumor leads to major

differences involving altered expression of many genes.<sup>6</sup> Recently, using the serial analysis of gene expression (SAGE) method, we showed that the PGP9.5 (protein gene product 9.5) gene had no detectable expression in normal lung tissues but was frequently overexpressed in primary non-small-cell lung tumors.<sup>7</sup>

PGP9.5 is a ubiquitin hydrolase widely expressed in neuronal tissues at all stages of neuronal differentiation.<sup>8,9</sup> Ubiquitination of cellular proteins and targeting them for subsequent degradation via ubiquitin-mediated proteolysis is potentially an important mechanism that regulates cell cycle genes.<sup>10,11</sup> In tumors, increased deubiquitination of cyclins by PGP9.5 could contribute to the uncontrolled growth of somatic cells.<sup>12</sup>

To better characterize the role of PGP9.5 in lung cancer, we first studied PGP9.5 expression in normal lung and a panel of lung cancer cell lines with defined neuroendocrine (NE) differentiation. Next, we examined the expression of PGP9.5 in 98 resected primary non-small-cell lung cancers (NSCLCs), using immunohistochemistry and correlated PGP9.5 expression in tumors with the clinicopathological features of affected patients.

#### Materials and Methods

##### Tissue Specimens

All lung cancer cell lines were obtained from the American Type Culture Collection (ATCC) and propagated according to the provided instructions.<sup>13</sup> Formalin-fixed and paraffin-embedded tumor samples from consecutive patients who had undergone resections of NSCLCs with curative intent were retrieved from the Surgical Pathology files of the Johns Hopkins Hospital (JHH). Information regarding tumor stage, tumor recurrence, and patient

Supported in part by National Institutes of Health grant CA06973, Lung SPOR CA58184, and an award to J. Jen from the V Foundation.

Accepted for publication May 22, 1999.

Address reprint requests to Dr. Jin Jen, Department of Otolaryngology-Head and Neck Surgery, Division of Head and Neck Cancer Research, Johns Hopkins University School of Medicine, 824 Ross Research Building, 720 Rutland Avenue, Baltimore, MD 21205-2196. E-mail: jenjin@jhmi.edu.

survival was obtained from the medical records, including the JHH Tumor Registry files.

### *Northern Blot Analysis*

Cell lines used for Northern blot analysis were collected after trypsinization and lysed immediately in Trizol reagent (GIBCO BRL, Gaithersburg, MD). Normal lung total RNA was extracted by the GuSCN method and purified by CsCl gradient ultracentrifugation as described.<sup>7</sup> Ten micrograms of RNA was separated on a 1.5% denaturing agarose gel and transferred to Gene Screen membrane (DuPont, Boston, MA). A PGP9.5 cDNA probe was isolated from an EST clone (no. 268107) obtained from Genome Systems (Huntsville, AL). Northern blot hybridization using the PGP9.5 cDNA probe was performed as described.<sup>7</sup>

### *Western Blot Analysis*

Twenty micrograms of cell lysates was separated on a 4–20% sodium dodecyl sulfate gradient gel and transferred to a polyvinylidene difluoride membrane (Micron Separations, Westborough, MA). After the nonspecific sites were blocked by incubation in phosphate-buffered saline + 5% nonfat dry milk (NFDM), the blot was incubated with the polyclonal rabbit antiserum against PGP9.5 (Biogenesis, Sandown, NH) at 1:400 dilution for 2 hours at room temperature. After washing, an ECL kit (Amersham, Arlington Heights, IL) was used to visualize the antibody binding to PGP9.5 protein.

### *Immunohistochemical Analysis*

Six- $\mu$ m sections were made from paraffin tissue blocks, and the slides were dried at 60°C for 30 minutes, treated with xylenes, and then dehydrated in alcohol. Endogenous peroxidase was blocked with 0.3% H<sub>2</sub>O<sub>2</sub>. Microwave treatment was performed for 4 minutes in Antigen Retrieval Glyca solution (Biogenex, San Ramon, CA), because it has been shown that the immunoreactivity of PGP9.5 was markedly enhanced by this method.<sup>14</sup> After blocking with normal goat serum, the slides were incubated with the polyclonal rabbit antiserum against PGP9.5 (Biogenesis) at 1:1000 dilution for 2 hours at room temperature. Vectastain ABC Kit and DAB Substrate Kit (Vector, Burlingame, CA) were used to visualize the antibody binding, and the sections were counterstained with hematoxylin.

Immunohistochemical staining for PGP9.5 was interpreted by an experienced pathologist (W.H.W.). For control studies, HeLa and H157 lung cancer cell lines were used as negative and positive controls. The PGP9.5 status of these two cell lines was confirmed by Northern and Western analysis<sup>7</sup> (data not shown). Optimized conditions were then used for the immunostaining of primary lung cancer specimens. In all cases, small nerves in the tissue sections served as a positive internal control, and desmoplastic stroma served as a negative internal control for PGP9.5 staining. Only cytoplasmic staining above

background levels was regarded as specific staining. All immunohistochemical slides were initially reviewed to assess the range of this PGP9.5 immunoreactivity with respect to intensity and distribution of staining. Two patterns were recognized: 1) the tumor was uniformly nonimmunoreactive; or 2) moderate to strong immunoreactivity approaching the intensity seen in the internal control (ie, nerves) was uniformly present throughout most (ie, >70%) of the tumor. Accordingly, tumors were subsequently scored as either negative or positive, based on the total absence or generalized presence of specific staining. To correlate the distribution of the scattered PGP9.5-positive cells in the normal bronchial epithelium with the distribution of the neuroendocrine K-cells, lung sections from two independent cases were incubated with a monoclonal antibody against chromogranin (Boehringer Mannheim, Indianapolis, IN; 1:2000 dilution).

### *Statistical Analysis*

The  $\chi^2$  test was used to examine the association between the PGP9.5 expression status and clinicopathological features.

## *Results*

### *Expression of PGP9.5 Protein in Normal Lung Tissues*

We have previously observed that the PGP9.5 message was frequently detected in lung carcinomas, but was not detectable in normal lung by Northern analysis or reverse transcription-polymerase chain reaction methods.<sup>7</sup> This result suggested that PGP9.5 protein expression could potentially be used as a marker for lung cancer. To better characterize the cell type origin and the timing of PGP9.5 expression, an immunohistochemical approach was used to localize PGP9.5 protein expression in the normal lung and the tumor samples. As shown in Figure 1A, the majority of the normal lung epithelial cells were negative by PGP9.5 staining. In sections of nonneoplastic lung, PGP9.5 staining was restricted to nerves and a few isolated cells scattered throughout the bronchial epithelium. The positive staining of neurons is consistent with the fact that PGP9.5 is a neuron-specific peptide widely expressed in neuronal tissue.<sup>8</sup> The PGP9.5-positive cells scattered throughout the nonneoplastic bronchial epithelium were reminiscent of the neuroendocrine K-cells, based on their morphological appearance and pattern of distribution.<sup>15</sup>

To determine the histological origin of these scattered PGP9.5-positive cells, we stained parallel sections from two cases with chromogranin, a well-characterized marker of neuroendocrine differentiation.<sup>16</sup> As shown in Figure 1B, chromogranin-positive cells showed the same location and tissue distribution as the PGP9.5-positive cells. This result suggests that, in nonneoplastic lung, PGP9.5 protein expression is restricted to cells of the dispersed NE system.

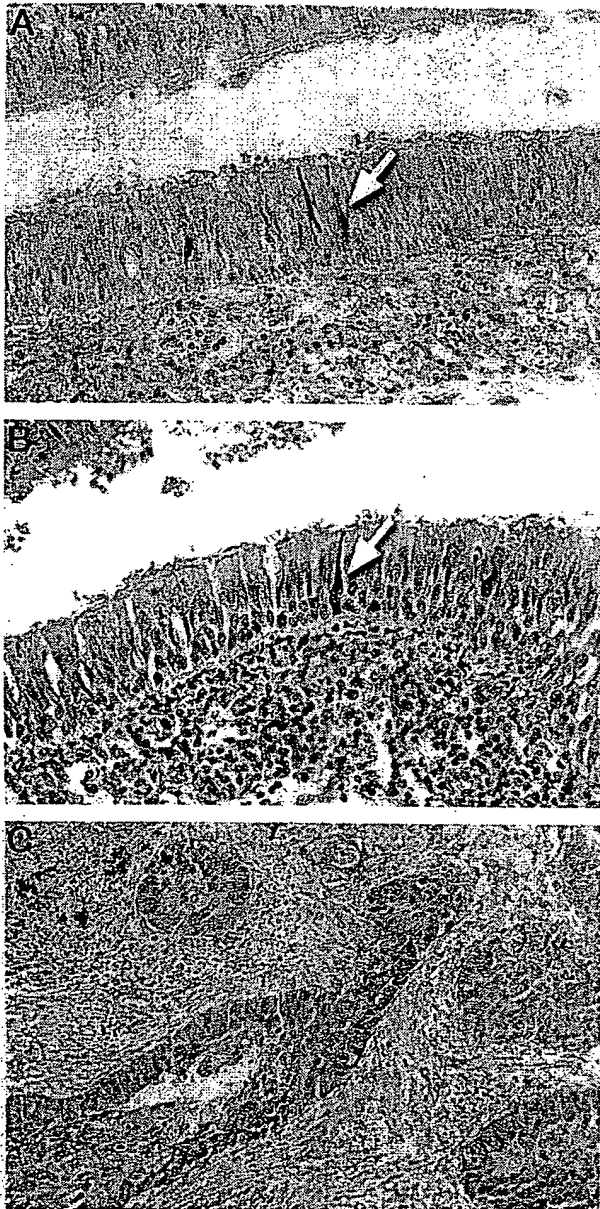


Figure 1. Immunohistochemical staining of lung tumor and adjacent lung tissue for PGP9.5 and chromogranin. A: PGP9.5 staining is present in isolated cells dispersed throughout the normal bronchial mucosa (arrow). B: Chromogranin staining is present in the compatible population of cells as seen in A (arrow). C: Example of PGP9.5 staining in lung cancer.

### PGP9.5 Expression Is Independent of *hASH1* Status in Lung Cancers

Because a majority of small-cell lung cancers and a portion of the NSCLCs often exhibit features of NE differentiation, we next tested whether PGP9.5 overexpression was associated with lung cancers of NE lineage. A panel of established lung cancer cell lines with *hASH1* status was used for this study. *hASH1* is a transcription factor essential for the NE development of the human lung.<sup>17</sup> As shown in Figure 2 (upper panel), PGP9.5 message was abundantly detected in both small-cell lung cancer (SCLC) and NSCLC cell lines regardless of *hASH1* status.

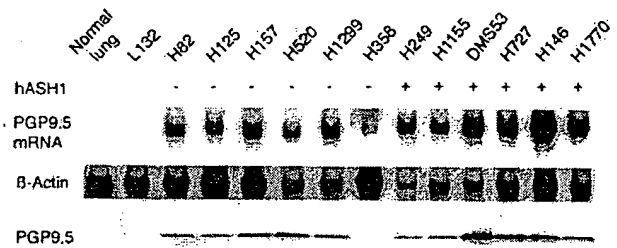


Figure 2. PGP9.5 expression in lung cancer cell lines with defined *hASH1* status. PGP9.5 transcript was not detectable in either normal lung or an embryonic lung cell line (L132) but was expressed in all lung cancer cell lines. The *hASH1* status is indicated at the top. H358 had a weak PGP9.5 message compared to other cell lines. The lower panel shows a Western blot using the anti-PGP9.5 antibody. Note that all tumor cell lines except H358 had PGP9.5 protein. The  $\beta$ -actin control was used to normalized sample loading. The histological subtypes of the cell lines are: L132, embryonic lung; H82, H249, DMS53, and H146, small cell carcinoma; H125, adenocarcinoma; H157 and H520, squamous cell carcinoma; H1299 and H1155, large cell carcinoma; H358, bronchoalveolar carcinoma; H727, carcinoid; H1770, neuroendocrine carcinoma.

Similarly, the PGP9.5 protein was detected in nearly all cell lines that expressed the gene (Figure 2, lower panel). Although there was a faint message in H358 by Northern analysis, no PGP9.5 protein was detectable for this sample. Furthermore, no PGP9.5 product was obtained by reverse transcription-polymerase chain reaction in this case, indicating that the message was probably rearranged or unstable and could not serve as a template for protein translation. Thus the expression of PGP9.5 appears to be present in NSCLC in the absence of NE differentiation, as well as SCLC frequently derived from NE cells of the lung.

### Association of PGP9.5 Expression with Pathological Stage in NSCLC

To seek the role of PGP9.5 expression in NSCLC, we examined the presence of PGP9.5 protein in the tumors of 98 NSCLC patients, using immunohistochemistry. The clinicopathological features of the patients and the results of PGP9.5 staining are shown in Table 1. Overall, 54% (53/98) of NSCLCs were positive by PGP9.5 staining, and the intensity of the staining was uniform and consistent for almost all cases (Figure 1C). Seventy-two percent (26/36) of squamous cell carcinomas were stained positive for PGP9.5, whereas only 41% (22/54) of adenocarcinomas had positive PGP9.5 staining ( $p = 0.0066$ ). These results are consistent with previous reports which showed that squamous cell carcinomas were more likely to be PGP9.5-positive than adenocarcinomas of the lung.<sup>18,19</sup> However, when the clinical stage of the patients was considered, the PGP9.5-positive rate for stage II and IIIA patients was significantly higher than those with stage I disease ( $p = 0.0074$ ) (Table 1).

### Discussion

PGP9.5 was first isolated as a specific cytoplasmic marker for neurons and NE cells.<sup>20,21</sup> About 10–15% NSCLCs demonstrate NE features by electron micros-

Table 1. Clinicopathological Features and PGP9.5 Expression in Primary NSCLC

Clinicopathological feature	Variable	No. of cases	PGP9.5 expression		p value*
			+	-	
Sex	Male	61	37 (61%)	24 (39%)	0.14
	Female	37	16 (43%)	21 (57%)	
Histology	Adenocarcinoma	55	22 (41%)	32 (59%)	<0.01†
	Squamous cell carcinoma	36	26 (72%)	10 (28%)	
	Others	8	5 (63%)	3 (37%)	
Tumor stage	I	66	29 (44%)	37 (56%)	<0.01
	II and IIIA	32	24 (75%)	8 (25%)	
Vital status	Alive	26	11 (42%)	15 (58%)	0.24
	Dead	72	42 (58%)	30 (42%)	
Median follow-up time	41 months				
Total		98	53 (54%)	45 (46%)	

\* $\chi^2$  test.

†PGP9.5 expression in adenocarcinoma versus squamous cell carcinoma.

copy or immunohistochemistry, despite the absence of NE features by light microscopy. Therefore, it was possible that PGP9.5 expression in these cancers may have simply reflected their NE status. Indeed, PGP9.5 had been used as a marker of NE differentiation for lung tumors. However, discordant staining patterns between PGP9.5 and other neuroendocrine markers have often been observed.<sup>18,19</sup> In our study, *hASH1* was used as a marker of neuroendocrine differentiation, because homozygous disruption of the *hASH1* gene in mouse prevents the development of pulmonary NE cells.<sup>17</sup> However, most lung tumor cell lines expressed high levels of PGP9.5, regardless of *hASH1* gene expression. Therefore, our results suggested that expression of PGP9.5 in lung cancers is independent of NE differentiation.

Functionally, PGP9.5 belongs to the ubiquitin carboxyl-terminal hydrolase (UCH) family.<sup>8</sup> The UCH family has conserved Cys and His domains common to yeast and mammalian ubiquitin hydrolases.<sup>22,23</sup> It is becoming increasingly clear that these enzymes are a part of the cellular proteolytic pathway that regulates many cellular processes, including cell cycle progression and cell death.<sup>12</sup> Several other studies have shown that some UCH family members are overexpressed in different tumors and can potentially be oncogenic. For example, the *tre-2* gene was identified as one of the UCH family proteins. The expression of *tre-2* is not detectable in normal tissues but becomes elevated in a variety of tumor cells.<sup>24</sup> Another UCH family gene, *Unph*, was isolated as a human homolog of the murine *Unp* protooncogene.<sup>25</sup> Overexpression of murine *Unp* gene leads to oncogenic transformation of NIH3T3 cells, and the expression level of this gene is also elevated in lung tumors.<sup>25,26</sup> The results of our current study also suggest that the expression of PGP9.5 in lung cancer may play a causative role in the oncogenic transformation of human lung epithelial cells, because 1) PGP9.5 shares conserved domains with the members of ubiquitin hydrolase family, several of which are potential oncogenes; 2) PGP9.5 expression is not present in the normal lung epithelium, but becomes activated sometimes during the course of neoplastic transformation; and 3) expression of PGP9.5 is closely associated with advanced stages of NSCLC.

Although further studies will be needed to elucidate the downstream target of deubiquitination by PGP9.5 and to better understand the molecular mechanism of PGP9.5 overexpression in lung cancer development, the frequent occurrence of PGP9.5 expression in NSCLC makes it a potential marker for the detection of this disease.

### Acknowledgments

We thank Dr. Stephen Baylin for helpful discussions about the project and Mrs. Janice Pulley for assistance with the manuscript preparation.

### References

1. American Cancer Society: Cancer Facts and Figures—1997. Atlanta, American Cancer Society, 1997
2. Rodenhuis S, van de Wetering ML, Mooi WJ, Evers SG, van Zandwijk N, Bos JL: Mutational activation of the K-ras oncogene. A possible pathogenetic factor in adenocarcinoma of the lung. *N Engl J Med* 1987; 317:929-935
3. Nau MM, Brooks BJ, Battey J, Sausville E, Gazdar AF, Kirsch IR, McBride OW, Bertness V, Hollis GF, Minna JD: L-myc, a new myc-related gene amplified and expressed in human small cell lung cancer. *Nature* 1985; 318:69-73
4. Hibi K, Takahashi T, Sekido Y, Ueda R, Hida T, Ariyoshi Y, Takagi H, Takahashi T: Coexpression of the stem cell factor and the c-kit genes in small-cell lung cancer. *Oncogene* 1991; 6:2291-2296
5. Hibi K, Yamakawa K, Ueda R, Horio Y, Murata Y, Tamari M, Uchida K, Takahashi T, Nakamura Y, Takahashi T: Aberrant upregulation of a novel integrin  $\alpha$  subunit gene at 3p21.3 in small cell lung cancer. *Oncogene* 1994; 9:611-619
6. Kinzler KW, Vogelstein B: Landscaping the cancer terrain. *Science* 1998; 280:1036-1037
7. Hibi K, Liu Q, Beaudry GA, Madden SL, Westra WH, Wehage SL, Yang SC, Heitmiller RF, Bertelsen AH, Sidransky D, Jen J: Serial analysis of gene expression in non-small cell lung cancer. *Cancer Res* 1998; 58:5690-5694
8. Wilkinson KD, Lee KM, Deshpande S, Duerksen-Hughes P, Boss JM, Pohl J: The neuron-specific protein PGP9.5 is a ubiquitin carboxyl-terminal hydrolase. *Science* 1989; 246:670-673
9. Schofield JN, Day IN, Thompson RJ, Edwards YH: PGP9.5, a ubiquitin C-terminal hydrolase; pattern of mRNA, and protein expression during neural development in the mouse. *Brain Res Dev Brain Res* 1995; 85:229-238
10. Hochstrasser M: Ubiquitin-dependent protein degradation. *Annu Rev Genet* 1996; 30:405-439



11. Diehl JA, Zindy F, Sherr CJ: Inhibition of cyclin D1 phosphorylation on threonine-286 prevents its rapid degradation via the ubiquitin-proteasome pathway. *Genes Dev* 1997, 11:957-972
12. Spataro V, Norbury C, Harris AL: The ubiquitin-proteasome pathway in cancer. *Br J Cancer* 1998, 77:448-455
13. Phelps RM, Johnson BE, Ihde DC, Gazdar AF, Carbone DP, McClintock PR, Linnoila RI, Matthews MJ, Bunn PA Jr, Carney D, Minna JD, Mulshine JL: NCI-Navy Medical Oncology Branch cell line data base. *J Cell Biochem Suppl* 1996, 24:32-91
14. McQuaid S, McConnell R, McMahon J, Herron B: Microwave antigen retrieval for immunocytochemistry on formalin-fixed, paraffin-embedded post-mortem CNS tissue. *J Pathol* 1985, 176:207-216
15. McDowell EM, Barrett LA, Trump BF: Observations on small granule cells in adult human bronchial epithelium and in carcinoid and oat cell tumors. *Lab Invest* 1976, 34:202-206
16. Wilson BS, Lloyd RV: Detection of chromogranin in neuroendocrine cells with a monoclonal antibody. *Am J Pathol* 1984, 115:458-468
17. Borges M, Linnoila RI, van de Velde HJ, Chen H, Nelkin BD, Mabry M, Baylin SB, Ball DW: An achaete-scute homologue essential for neuroendocrine differentiation in the lung. *Nature* 1997, 386:852-855
18. Dhillon AP, Rode J, Dhillon DP, Moss E, Thompson RJ, Spiro SG, Corrin B: Neural markers in carcinoma of the lung. *Br J Cancer* 1985, 51:645-652
19. Addis BJ, Hamid Q, Ibrahim NB, Fahey M, Bloom SR, Polak JM: Immunohistochemical markers of small cell carcinoma and related neuroendocrine tumours of the lung. *J Pathol* 1987, 153:137-150
20. Jackson P, Thompson RJ: The demonstration of new human brain-specific proteins by high-resolution two-dimensional polyacrylamide gel electrophoresis. *J Neurol Sci* 1981, 49:429-438
21. Day IN, Thompson RJ: Molecular cloning of cDNA coding for human PGP9.5 protein. A novel cytoplasmic marker for neurones and neuroendocrine cells. *FEBS Lett* 1987, 210:157-160
22. Baker RT, Tobias JW, Varshavsky A: Ubiquitin-specific proteases of *Saccharomyces cerevisiae*: Cloning of Ubp2 and Ubp3, and functional analysis of the Ubp gene family. *J Biol Chem* 1992, 267:23364-23375
23. Papa FR, Hochstrasser M: The yeast DOA4 gene encodes a deubiquitinating enzyme related to a product of the human tre-2 oncogene. *Nature* 1993, 366:313-319
24. Nakamura T, Hillova J, Mariage-Samson R, Onno M, Huebner K, Cannizzaro LA, Boghosian-Sell L, Croce CM, Hill M: A novel transcriptional unit of the tre oncogene widely expressed in human cancer cells. *Oncogene* 1992, 7:733-741
25. Gray DA, Inazawa J, Gupta K, Wong A, Ueda R, Takahashi T: Elevated expression of Unph, a proto-oncogene at 3p21.3, in human lung tumors. *Oncogene* 1995, 10:2179-2183
26. Gupta K, Chevrette M, Gray DA: The Unp proto-oncogene encodes a nuclear protein. *Oncogene* 1994, 9:1729-1731

## Short Communication

### Analysis of E-Cadherin in Diffuse-Type Gastric Cancer Using a Mutation-Specific Monoclonal Antibody

Karl-Friedrich Becker,<sup>\*†</sup> Elisabeth Kremmer,<sup>‡</sup>  
Manfred Eulitz,<sup>§</sup> Ingrid Becker,<sup>\*</sup>  
Gabriele Handschuh,<sup>†</sup> Christoph Schuhmacher,<sup>¶</sup>  
Wolfram Müller,<sup>||</sup> Helmut E. Gabbert,<sup>||</sup>  
Atsushi Ochiai,<sup>\*\*</sup> Setsuo Hirohashi,<sup>\*\*</sup> and  
Heinz Höfler<sup>\*†</sup>

From the Technische Universität München, Klinikum rechts der Isar, Institut für Pathologie\* and Chirurgische Klinik,<sup>†</sup> München, Germany; the GSF-Forschungszentrum für Umwelt und Gesundheit, Institut für Molekulare Immunologie,<sup>‡</sup> Institut für Klinische Molekularbiologie,<sup>§</sup> and Institut für Pathologie,<sup>¶</sup> Neuberg, Germany; the Institut für Pathologie,<sup>||</sup> Heinrich-Heine Universität, Düsseldorf, Germany; and the Pathology Division,<sup>\*\*</sup> National Cancer Center Research Institute, Tokyo, Japan

In-frame deletions from the E-cadherin mRNA, coding for a homophilic cell adhesion molecule, are characteristic for diffuse-type gastric carcinomas. Using immunohistochemical analysis the mutant form cannot be distinguished from normal E-cadherin, making results difficult to interpret. In this study, a rat monoclonal antibody, designated E-cad delta 9-1, was generated against a peptide spanning the fusion junction region between exons 8 and 10. This new epitope is present in an E-cadherin variant that lacks exon 9 from the mRNA due to different splice-site gene mutations. Using Western blotting and immunohistochemistry of E-cadherin-transfected cells, we demonstrate that E-cad delta 9-1 specifically reacts with E-cadherin lacking exon 9 but not with the wild-type protein. No immunoreactivity was observed in 31 nontumorous and embryonal tissues analyzed. In gastric carcinoma specimens known to express mutant E-cadherin mRNA lacking exon 9, E-cad delta 9-1 targets exclusively tumor cells in routine formalin-fixed and paraffin-embedded material from biopsies, primary tumors, and lymph node metastases. In a retrospective series of 172 diffuse-type gastric carcinomas expressing E-cadherin, E-cad delta 9-1 reacted with 22 tumors (13%). This new tumor marker-

monoclonal antibody system could open novel avenues for selective diagnosis and specific therapy of a subgroup of diffuse-type gastric cancer patients. (*Am J Pathol* 1999, 155:1803-1809)

The calcium-dependent homophilic cell adhesion molecule E-cadherin and associated catenins, cytoplasmic plaque proteins, link polarized epithelial cells and maintain the structural integrity of an epithelial monolayer. Moreover, the cadherin/catenin multiprotein complex is implicated in developmental processes and cell signaling.<sup>1-3</sup> Because in carcinomas the tissue architecture is often disorganized, E-cadherin expression has been analyzed in various tumor types typically using immunohistochemistry.<sup>4</sup> It could be demonstrated that E-cadherin immunoreactivity is often reduced or lost in less differentiated and invasive carcinomas.<sup>5</sup> However, in diffuse-type gastric cancer, in which tumor cells generally have lost homophilic cell-to-cell contacts and invade surrounding tissues as single cells, E-cadherin immunoreactivity was detected in many cases,<sup>6-8</sup> whereas in others it was found to be completely absent.<sup>9</sup> The reason for this discrepancy was unknown. The selection of the cases or the use of different antibodies may, at least in part, explain these results.

Recently, E-cadherin gene mutations that may also have contributed to variable immunoreactivity have been identified in tumor cell lines, primary tumors, and lymph node metastases from gastric cancer patients.<sup>10-14</sup> Remarkably, in 50% of diffuse-type gastric cancer patients E-cadherin mutations were identified that typically re-

---

K.-F. B. is a recipient of a Foreign Research Fellow Award from the Foundation for Promotion of Cancer Research, Tokyo.

Accepted for publication August 5, 1999.

A. Ochiai's present address is Pathology Division, National Cancer Center Research Institute East, 6-5-1, Kashiwa City, Chiba 277-0882, Japan.

Address reprint requests to Dr. Karl-Friedrich Becker, Technische Universität München, Klinikum rechts der Isar, Institut für Pathologie, Ismaninger Strasse 22, D-81675 München, Germany. E-mail: kf.becker@lrz.tum.de.

sulted in in-frame deletions removing partial or complete exon sequences from the extracellular portion of the transmembrane protein or point mutations resulting in amino acid substitutions.<sup>15</sup> Complete deletion of exon 9 from the E-cadherin mRNA is a mutational hot spot in diffuse-type gastric cancer which was detected in 14% (10/70) of the patients analyzed using reverse transcription-polymerase chain reaction (RT-PCR) and sequencing.<sup>11-13</sup> A variety of somatic splice-site gene mutations were identified that lead to in-frame skipping of exon 9 from the E-cadherin mRNA. Although alternative splicing mechanisms are generally possible, they have not been detected for E-cadherin and do not account for the frequent loss of exon 9. In addition, E-cadherin in-frame deletion mutations were exclusively associated with malignant tissues and never seen in nontumorous gastric epithelium from the same patients.

Because E-cadherin mRNA deletion mutations identified in primary gastric tumors and lymph node metastases do not interrupt the reading frame,<sup>15</sup> the mutated protein may still be integrated into the plasma membrane although parts of its extracellular domain are altered. These structurally changed portions of the molecule could serve as possible targets for monoclonal antibodies. Numerous monoclonal antibodies have been generated against E-cadherin.<sup>16,17</sup> However, using current antibodies, it was impossible to differentiate between normal or altered forms of the expressed E-cadherin protein. Here we report the generation and characterization of E-cad delta 9-1, a rat monoclonal antibody that specifically reacts with mutant E-cadherin lacking exon 9 and that does not recognize the wild-type protein. In a multicenter study we determined the frequency of this mutation in archival diffuse-type gastric carcinomas using E-cad delta 9-1.

## Materials and Methods

### Peptide Synthesis and Generation of Monoclonal Antibodies

A 13-mer peptide (Pro-Ile-Phe-Asn-Pro-Thr-Thr-Gly-Leu-Asp-Phe-Glu-Ala) was synthesized that spans the fusion junction between exon 8 and exon 10 from mutant E-cadherin lacking exon 9 and subsequently coupled to Keyhole limpet hemocyanin (KLH) using standard methods. Approximately 50  $\mu$ g of KLH-coupled peptide dissolved in phosphate buffered saline and emulsified with Freund's complete adjuvant were injected both intraperitoneally (i.p.) and subcutaneously (s.c.) into Lou/C rats. After a 4-week interval a final boost without adjuvant was given i.p. and s.c. 3 days before fusion. Fusion of the myeloma cell line P3X63-Ag8.653 with the rat immune spleen cells was performed essentially as described.<sup>18</sup> Hybridoma supernatants were tested in a solid-phase immunoassay using bovine serum albumin-coupled peptide (10  $\mu$ g/ml) adsorbed to polystyrene microtiter plates. Solid-phase enzyme-linked immunosorbent assay (ELISA) on microtiter plates coated with mouse anti-rat Ig antibodies was used to determine the immunoglobulin

type with rat Ig class (anti-IgM; Zymed) and IgG subclass-specific mouse monoclonal antibodies.<sup>19</sup>

### Cells and cDNA Transfection

Wild-type and mutant E-cadherin cDNA used for transfection were generated by RT-PCR from normal or malignant gastric tissue, respectively, and cloned into the expression vector pBAT (a gift from Prof. Takeichi; inserts are under the control of a chicken  $\beta$ -actin promoter). The coding regions of both cDNA constructs were confirmed by sequencing either to be unaltered (wild-type; sequence identical to the one deposited in the EMBL/GenBank database libraries, accession number Z 13009) or to contain an in-frame deletion of exon 9 as the only sequence change (exon 9 deletion). The human mammary carcinoma cell line MDA-MB-435S (ATCC) was transfected by the calcium phosphate coprecipitation method with either wild-type or mutant E-cadherin cDNA lacking exon 9 together with a plasmid for neomycin resistance. Cloning and transfection of wild-type and

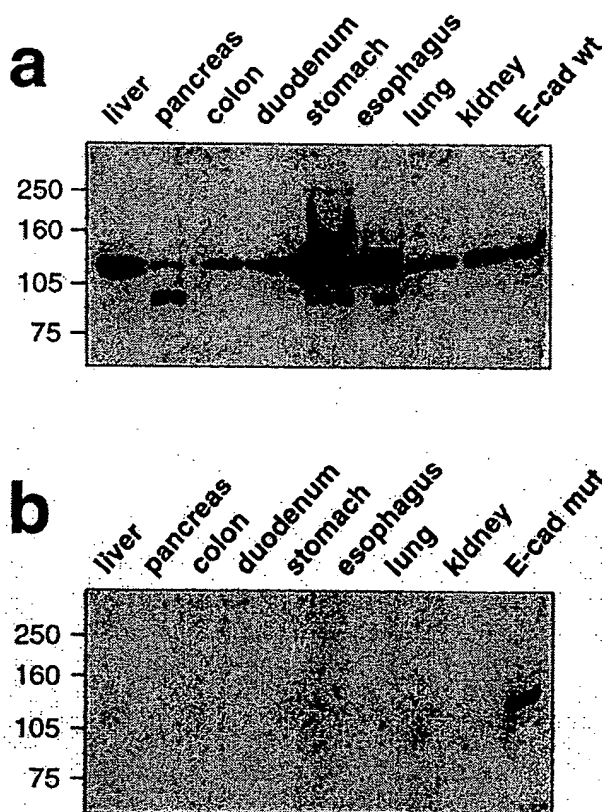


**Figure 1.** Western blot analysis. **a:** Cell extracts from various normal tissues (liver, pancreas, colon, duodenum, stomach, esophagus, lung, kidney) were analyzed using monoclonal antibody AEC (Anti-E-Cadherin, clone 36, Transduction Lab, Lexington, KY). An extract from MDA-MB-435S mammary carcinoma cells that were transfected with wild-type E-cadherin (E-cad wt) was used as a control. AEC reacts with a protein of approximately 120 kD, corresponding to normal E-cadherin, in all lanes. **b:** The same tissues as in **a** were analyzed with the mutation-specific monoclonal antibody E-cad delta 9-1. No cross-immunoreactivity with these tissues was seen. An extract from MDA-MB-435S cells transfected with mutant E-cadherin lacking exon 9 (E-cad mut) was used as a positive control. Molecular weight in kD is indicated on the left.

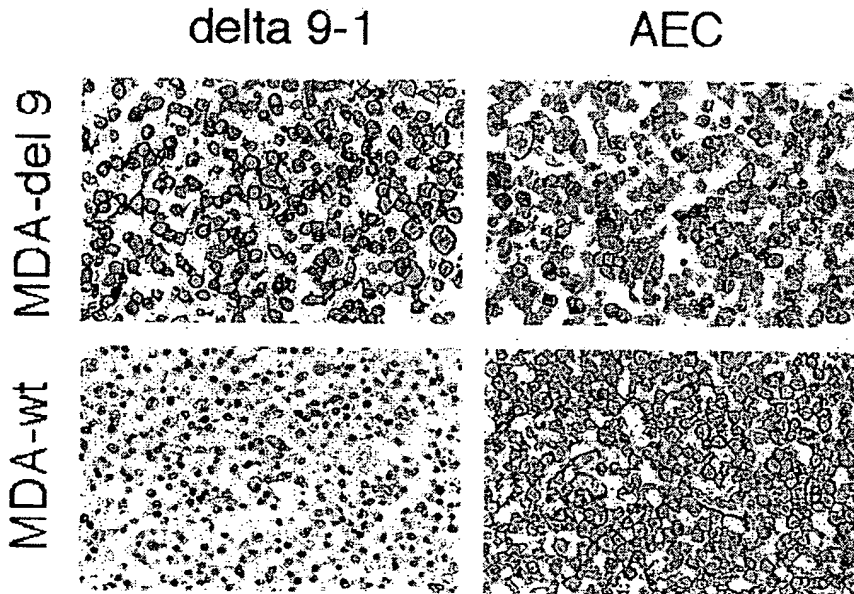


**Figure 2.** Immunoreactivity of formalin-fixed and paraffin-embedded MDA-MB-435S cells. The cells were transfected with mutant E-cadherin lacking exon 9 (MDA-del9) or with the wild-type cDNA (MDA-wt). E-cad delta 9-1 specifically reacts with cells transfected with mutant but not with cells transfected with wild-type E-cadherin cDNA (left panel). Monoclonal antibody AEC reacts with cells expressing mutant and wild-type E-cadherin (right panel).

mutant E-cadherin cDNA has been described in detail elsewhere.<sup>20</sup>

#### Western Blot Analysis

Extracts from E-cadherin (wild-type/mutant) transfected MDA-MB-435S cells and fresh frozen samples from liver, pancreas, colon, duodenum, stomach, esophagus, lung, and kidney were prepared according to a method previously published<sup>21</sup> and used for Western blot analysis. To detect E-cadherin protein the monoclonal antibody AEC (Anti-E-Cadherin, clone 36, Transduction Laboratories, Lexington, KY) and the mutation-specific antibody E-cad delta 9-1 (clone 7E6) were used. Detection was performed using a peroxidase-coupled secondary antibody (ECL-Western, Amersham).

#### Immunohistochemical Analysis

To proof mutation-specific E-cad delta 9-1 immunoreactivity, 5- $\mu$ m sections of formalin-fixed and paraffin-embedded MDA-MB-435S mammary carcinoma cells transfected with either wild-type or mutant E-cadherin cDNA (see above) were analyzed. In addition, routine formalin-fixed and paraffin-embedded material from four gastric cancer patients confirmed to express mutant E-cadherin mRNA lacking exon 9 in malignant tissues<sup>11</sup> were analyzed. After microwave-based antigen retrieval with citric acid pretreatment,<sup>22</sup> sections were incubated in 1% hydrogen peroxide for 15 minutes to block endogenous peroxidase. For detection of E-cadherin specific immunoreactivity, the specimens were incubated with either monoclonal antibody AEC (diluted 1:1000) or E-cad delta 9-1 (undiluted hybridoma supernatant) at room temperature for 2 hours. Bound antibodies were detected using the avidin-biotin-complex (ABC) peroxidase method (ABC Elite Kit, Vector, Burlingame, CA). Final staining was developed with the Sigma FAST DAB peroxidase

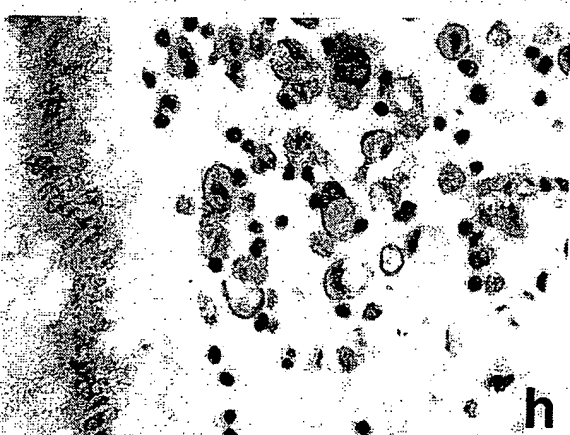
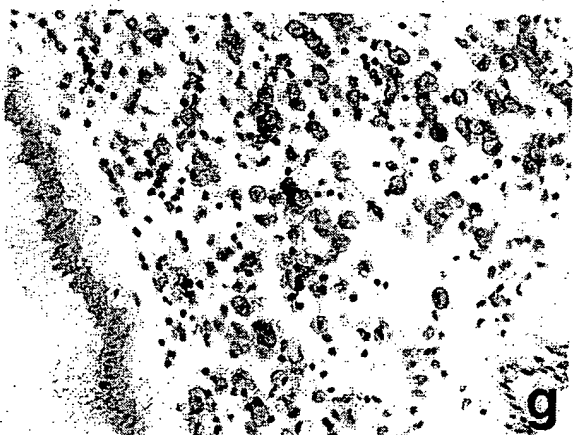
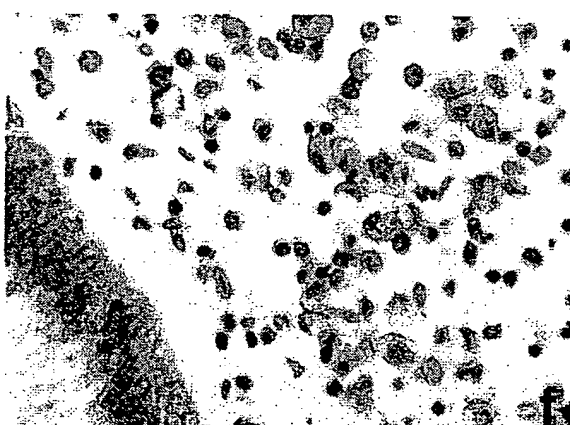
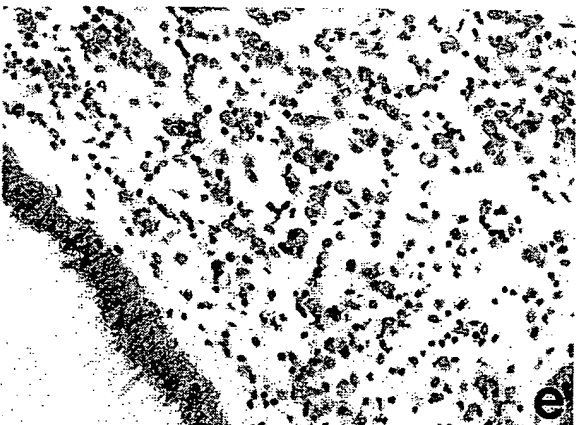
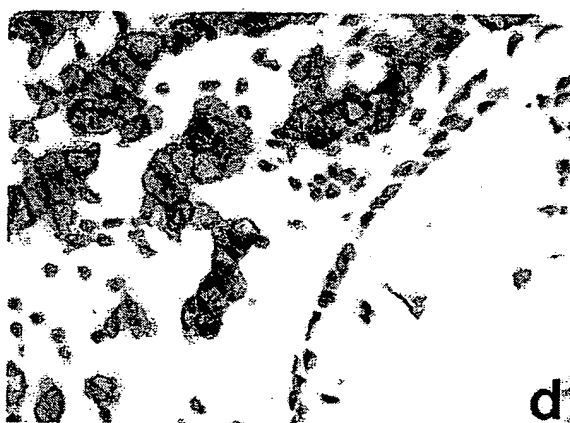
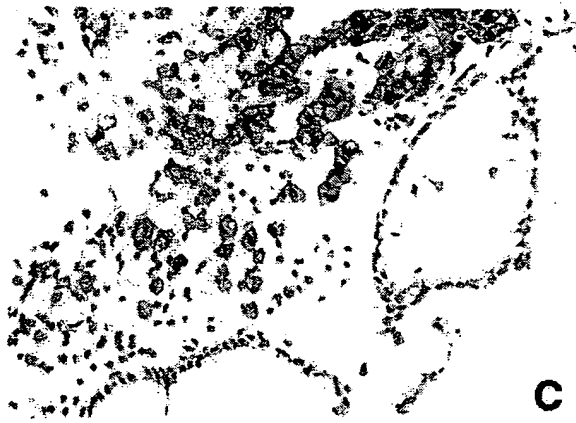
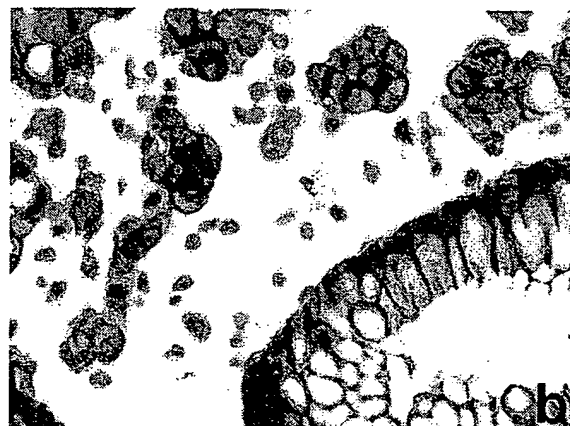
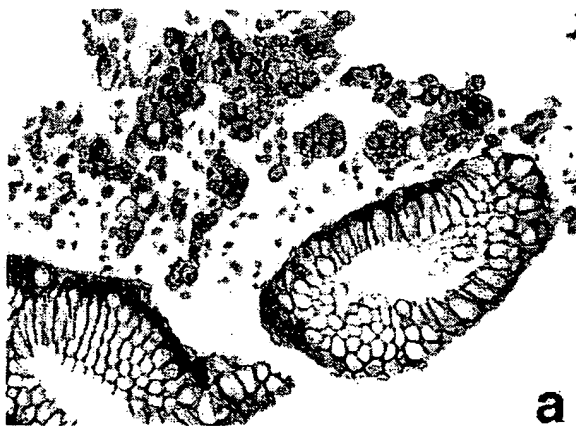
substrate kit (Sigma, Deisenhofen, Germany). Hemalaun was used for counterstaining. Nontumorous adult tissues (lung, heart, thyroid, placenta, salivary gland, bone marrow, lymph nodes, adipose tissue, skin, peripheral nerve, connective tissue, skeletal muscle, breast, pituitary, cerebellum, cerebral cortex, esophagus, stomach, small intestine, duodenum, colon, liver, pancreas, uterine endometrium, uterine cervix, ovary, tube, prostate, seminal vesicle, testis, epididymis) and embryonal tissues (13th week of pregnancy; umbilical cord, spinal cord, kidney, uterus, cartilage, skin, connective tissue, adipose tissue, colon, placenta, chorion) were analyzed in the same way to examine potential cross-reactivity of E-cad delta 9-1 monoclonal antibody. A series of 322 diffuse-type gastric cancer samples from Munich ( $n = 97$ ), Düsseldorf ( $n = 117$ ), and Tokyo ( $n = 108$ ) were subsequently analyzed with E-cad delta 9-1. From these 322 carcinomas, 205 tumors derived from Munich and Tokyo were analyzed using both AEC and E-cad delta 9-1. All tumor sections contained nontumorous epithelium as control.

#### Results

E-cadherin mutation-specific monoclonal antibodies were produced in rats against a peptide that spans the fusion junction generated by direct adjoining of exon 8 and 10. Hybridoma supernatants were tested in a solid phase immunoassay using the specific peptide coupled to bovine serum albumin. Hybridoma E-cad delta 9-1 (clone 7E6) of rat IgG1 subclass was selected for further analysis.

#### Western Blot

To confirm specificity of the selected hybridoma and to determine potential cross-reactivity with nontumorous tissues Western blot analysis was performed. Extracts from



MDA-MB-435S mammary carcinoma cells transfected with either wild-type or exon 9-deleted E-cadherin and extracts from various fresh-frozen nontumorous tissues (liver, pancreas, colon, duodenum, stomach, esophagus, lung, kidney) were analyzed using monoclonal antibody AEC and E-cad delta 9-1. The epitope reacting with AEC is located within the intracellular domain of E-cadherin. AEC revealed a major protein band at approximately 120 kd corresponding to wild-type E-cadherin in all tissues that was also present in MDA-MB-435S cells transfected with wild-type E-cadherin (Figure 1a). Faster migrating bands most likely correspond to degradation products. No immunoreactivity in these tissues, however, was seen using E-cad delta 9-1; a protein band corresponding to mutant E-cadherin was detected only in extracts from MDA-MB-435S cells transfected with mutant E-cadherin cDNA (Figure 1b). A protein band of identical molecular weight was seen using AEC, confirming E-cadherin specificity (not shown).

### Immunohistochemistry

After having demonstrated antibody specificity by Western blot we tested whether antibody E-cad delta 9-1 may react with formalin-fixed, paraffin-embedded E-cadherin transfected cells: E-cad delta 9-1 strongly stained mutant E-cadherin expressing cells, preferentially at the cell membrane, while wild-type expressing cells were not stained. In contrast, antibody AEC reacted with wild-type E-cadherin as well as with mutant E-cadherin expressing cells (Figure 2). These results indicate that the epitopes reacting with both antibodies are successfully unmasked by the procedures used.

In subsequent immunohistochemical analysis of four diffuse-type gastric carcinomas (routine formalin-fixed, paraffin-embedded material) in which the expression of mutant E-cadherin mRNA lacking exon 9 was previously demonstrated by RT-PCR and direct sequencing,<sup>11</sup> monoclonal antibody AEC reacts with nontumorous epithelial cells as well as with tumor cells in biopsies (Figure 3, a and b). However, the mutation-specific monoclonal antibody delta 9-1 exclusively labels tumor cells on serial sections from the same material, whereas nontumorous epithelial cells were not stained (Figure 3, c and d). Furthermore, tumor cells expressing mutant E-cadherin can be identified in the primary tumors (Figure 3, e and h). Because virtually all tumor cells were stained, the mutation, at least in these cases, is most likely clonal. In addition, E-cad delta 9-1 reacts strongly with tumor cells in lymphatic vessels and in lymph node metastases (not shown). Our results indicate that mutant E-cadherin protein can, for the first time, be specifically detected on tumor cells from gastric cancer patients.

To further examine potential cross-reactivity of antibody E-cad delta 9-1 with nontumorous cells, we analyzed normal tissue specimens from adults as well as from an embryo. We have not observed any cross-reactivity of E-cad delta 9-1 in the normal tissues listed in Materials and Methods.

After a rigorous demonstration that antibody E-cad delta 9-1 reacts only with mutant E-cadherin, even in archival material, the incidence of the E-cadherin variant lacking exon 9 in gastric cancer was determined. We analyzed 322 primary gastric carcinomas of the diffuse type from Germany and Japan. We found that 25 of them (8%) showed a clear reaction with delta 9-1 (Munich, 9/97; Düsseldorf, 3/117; Tokyo, 13/108). The immunoreactivity was detected mainly at the cell membrane as described above. In 205 cases immunohistochemical analysis with AEC was also performed. E-cadherin immunoreactivity with AEC was seen in 84% (172/205) of these cases. From the E-cadherin-positive tumors as determined using AEC, 13% (22/172) also reacted with E-cad delta 9-1.

### Discussion

The E-cadherin exon 9 deletion variant was previously detected in 14% (10/70) of diffuse-type gastric cancer patients using RT-PCR and sequencing.<sup>11-13</sup> The generation and characterization of monoclonal antibody E-cad delta 9-1 now enabled us to easily screen a large series of gastric cancer patients specifically for the exon 9-deletion mutation. We detected 25/322 tumors expressing exon 9 deleted E-cadherin. The lower incidence of E-cad delta 9-1-positive tumors observed in the cases derived from Düsseldorf may be due to the fact that exclusively surgically R0 resected tumors were analyzed whereas in the Munich and Tokyo groups R0, R1, and R2 resected tumors were examined. The incidence of 8% is lower compared to the results using RT-PCR (14%) in a smaller series.<sup>11-13</sup> Possibly, RT-PCR is more sensitive than immunohistochemistry, or the half-life of mutant mRNA and protein may be different. Furthermore, proteins interacting with E-cadherin, catenins, may be altered, potentially resulting in degradation of mutant E-cadherin. In some cases precursor processing or posttranslational modification may be abnormal, resulting in instability of the protein without affecting mRNA stability. However, when the incidence of the mutation was related to immunoreactivity of E-cadherin, as determined by staining with AEC, a monoclonal antibody reacting with the intracellular portion of E-cadherin, we found that 13% (22/172) of the tumors expressing E-cadherin were E-cad delta 9-1-positive (the three missing cases were not included in the

**Figure 3.** Immunohistochemical analysis. This signet ring cell gastric carcinoma was previously confirmed to express mutant E-cadherin mRNA lacking exon 9 due to a somatic splice-site gene mutation.<sup>11</sup> **a-d:** Biopsy. Using monoclonal antibody AEC as primary antibody, both tumor cells and normal epithelial cells are stained (**a, b**); differentiation between cells expressing mutant or wild-type E-cadherin protein is not possible. In contrast, monoclonal antibody E-cad delta 9-1 exclusively stains tumor cells. Nontumorous cells, including E-cadherin-expressing epithelial cells, are not stained (**c, d**). **e-h:** Primary tumor. AEC reacts with normal epithelial cells as well as with tumor cells expressing mutant E-cadherin (**e, f**). Only tumor cells expressing abnormal E-cadherin are stained using E-cad delta 9-1 (**g, h**). Original magnifications: **a, c, e, and g**,  $\times 100$ ; **b, d, f, and h**,  $\times 200$ .

series of cases stained with AEC). Because AEC reacts with E-cadherin's cytoplasmic portion, a potential cross-reactivity with another member of the cadherin superfamily showing homology to this domain, P-cadherin, is conceivable. However, using a different E-cadherin- and a P-cadherin-specific monoclonal antibody, only 1 out of 28 (4%) diffuse-type gastric carcinomas was found to express P-cadherin but not E-cadherin.<sup>6</sup> Thus, E-cadherin-negative tumors that express P-cadherin seem to be rare in this type of cancer and may not significantly interfere with our approximations.

With our study E-cadherin lacking exon 9 has now been confirmed to be expressed exclusively in malignant tissues since no other tissue analyzed showed E-cad delta 9-1 immunoreactivity. The fact that this mutation is frequently found in gastric cancer patients in Europe and Japan suggests that it may play a crucial role in tumorigenesis. Data from a functional analysis using a cell culture approach are in line with this hypothesis. We could demonstrate that mutant E-cadherin has dramatic effects on calcium-dependent cell adhesion, aggregation, cell morphology, and motility, indicating that mutant E-cadherin contributes to the malignant phenotype. Interestingly, the mutation not only results in loss of E-cadherin's cell-to-cell adhesion function, but also can act in a *trans*-dominant negative manner altering the function of other cadherins, eg, N-cadherin.<sup>20</sup>

Detectable immunoreactivity of E-cadherin in gastric cancer specimens using currently available antibodies may not in every case indicate the presence of a normal protein. Our mutation-specific antibody may help to resolve the discrepancy between detection of E-cadherin in the absence of homophilic cell-to-cell adhesion. Moreover, other malignant tissues besides stomach carcinoma could be identified to express mutant E-cadherin protein. E-cadherin gene mutations have been identified so far in invasive lobular breast carcinoma,<sup>23-25</sup> diffuse sclerosing variant of papillary thyroid carcinoma,<sup>26</sup> and endometrial and ovarian carcinoma.<sup>27</sup> Interestingly, an exon 9 splice-site mutation was described in a breast carcinoma cell line,<sup>28</sup> although in-frame deletion mutations are rare in breast cancer.<sup>15</sup>

Mutation-specific monoclonal antibodies reacting with abnormal cell surface molecules found exclusively on tumor cells due to somatic gene mutations may open novel clinical avenues for a more specific diagnosis and therapy of gastric cancer: a humanized version of E-cad delta 9-1 could be applied to stimulate the patient's immune system or, after conjugating to radioisotopes, toxins, or drugs, it could be used to specifically target malignant cells in minimal residual cancer. With the mutation-specific monoclonal antibody E-cad delta 9-1 in hand, rapid screening of potential E-cadherin exon 9 deletion mutations in routine biopsies can now easily be performed on large populations, because this antibody works excellently with formalin-fixed, paraffin-embedded material. Cancer patients who may profit from a potential immunotherapy using modified E-cad delta 9-1 monoclonal antibody can be easily and quickly identified.

## Acknowledgments

We wish to acknowledge Professor Masatoshi Takeichi for providing the expression vector pBAT and Professor Martin Werner and Dr. Thomas Richter for providing us with tissue specimens. We thank Christina Schott and Yuko Yamauchi for excellent technical assistance.

## References

- Huber O, Bierkamp C, Kemler R: Cadherins and catenins in development. *Curr Opin Cell Biol* 1996, 8:685-691
- Peifer M:  $\beta$ -catenin as oncogene: the smoking gun. *Science* 1997, 275:1752-1753
- Takeichi M: Cadherin cell adhesion receptors as a morphogenetic regulator. *Science* 1991, 251:1451-1455
- Hirohashi S: Inactivation of the E-cadherin-mediated cell adhesion system in human cancers. *Am J Pathol* 1998, 153:333-339
- Birchmeier W, Behrens J: Cadherin expression in carcinomas: role in the formation of cell junctions and the prevention of invasiveness. *Biochem Biophys Acta Rev Cancer* 1994, 1198:11-26
- Shimoyama Y, Hirohashi S: Expression of E- and P-cadherin in gastric carcinomas. *Cancer Res* 1991, 51:2185-2192
- Matsui S, Shiozaki H, Inoue M, Tamura S, Doki Y, Kadowaki T, Iwazawa T, Shimaya K, Nagafuchi A, Tsukita S, Mori T: Immunohistochemical evaluation of  $\alpha$ -catenin expression in human gastric cancer. *Virchows Arch* 1994, 424:375-381
- Gabbert HE, Mueller W, Schneiders A, Meier S, Moll R, Birchmeier W, Hommel G: Prognostic value of E-cadherin expression in 413 gastric carcinomas. *Int J Cancer* 1996, 69:184-189
- Mayer B, Johnson JP, Leiti F, Jauch KW, Heiss MM, Schildberg FW, Birchmeier W, Funke I: E-cadherin expression in primary and metastatic gastric cancer: down-regulation correlates with cellular dedifferentiation and glandular disintegration. *Cancer Res* 1993, 53:1690-1695
- Oda T, Kanai Y, Oyama T, Yoshiura K, Shimoyama Y, Birchmeier W, Sugimura T, Hirohashi S: E-cadherin gene mutations in human gastric carcinoma cell lines. *Proc Natl Acad Sci USA* 1994, 91:1858-1862
- Becker KF, Atkinson MJ, Reich U, Becker I, Nekarda H, Siewert JR, Höfler H: E-cadherin gene mutations provide clues to diffuse type gastric carcinomas. *Cancer Res* 1994, 54:3845-3852
- Tamura G, Sakata K, Nishizuka S, Maesawa C, Suzuki Y, Iwaya T, Terashima M, Saito K, Satodate R: Inactivation of the E-cadherin gene in primary gastric carcinomas and gastric carcinoma cell lines. *Jpn J Cancer Res* 1996, 87:1153-1159
- Muta H, Noguchi M, Kana Y, Ochiai A, Nawata H, Hirohashi S: E-cadherin gene mutations in signet ring cell carcinoma of the stomach. *Jpn J Cancer Res* 1996, 87:843-848
- Machado JC, Soares P, Carneiro F, Rocha A, Beck S, Blin N, Bex G, Sobrinho-Simoes M: E-cadherin gene mutations provide a genetic basis for the phenotypic divergence of mixed gastric carcinomas. *Lab Invest* 1999, 79:459-465
- Bex G, Becker K-F, Höfler H, van Roy F: Mutations of the human E-cadherin (CDH1) gene. *Hum Mutat* 1998, 12:226-237
- Frixen UH, Behrens J, Sachs M, Eberle G, Voss B, Warda A, Lochner D, Birchmeier W: E-cadherin-mediated cell-cell adhesion prevents invasiveness of human carcinoma cells. *J Cell Biol* 1991, 113:173-185
- Shimoyama Y, Hirohashi S, Hirano S, Noguchi M, Shimozato Y, Takeichi M, Abe O: Cadherin cell-adhesion molecules in human epithelial tissues and carcinomas. *Cancer Res* 1989, 49:2128-2133
- Kremmer E, Kranz BR, Hille A, Klein K, Eulitz M, Hoffmann-Fezer G, Feiden W, Herrmann K, Delecluse H-J, Delsol G, Bornkamm GW, Mueller-Lantzsch N, Grässert FA: Rat monoclonal antibodies differentiating between the Epstein-Barr virus nuclear antigens 2A (EBNA2A) and 2B (EBNA2B). *Virology* 1995, 208:336-342
- Springer TA, Bhattacharya A, Cardoza JT, Sanchez-Madrid F: Monoclonal antibodies specific for rat IgG1, IgG2a, and IgG2b subclasses, and kappa chain monotypic and allotypic determinants: reagents for use with rat monoclonal antibodies. *Hybridoma* 1982, 1:257-273
- Handschuh G, Candidus S, Lubert B, Reich U, Schott C, Oswald S,

- Becke H, Hutzler P, Birchmeier W, Höfler H, Becker KF: Tumor-associated E-cadherin mutations alter cellular morphology, decrease cellular adhesion, and increase cellular motility. *Oncogene* 1999, 8:4301-4312
21. Cunningham BA, Leutzing Y, Gallin WJ, Sorkin BC, Edelman GM: Linear organization of the liver cell adhesion molecule L-CAM. *Proc Acad Sci USA* 1984, 81:5787-5791
22. Shi S-R, Key M, Kalra K: Antigen retrieval in formalin-fixed, paraffin-embedded tissues: an enhancement method for immunohistochemical staining based on microwave oven heating of tissue sections. *J Histochem Cytochem* 1991, 39:741-748
23. Berx G, Cleton Jansen AM, Nollet F, de Leeuw WJ, van de Vijver M, Cornelisse C, van Roy F: E-cadherin is a tumour/invasion suppressor gene mutated in human lobular breast cancers. *EMBO J* 1995, 14: 6107-6115
24. Berx G, Cleton-Jansen A-M, Strumane K, de Leeuw W, Nollet F, van Roy F, Cornelisse C: E-cadherin is inactivated in a majority of invasive human lobular breast cancers by truncation mutations throughout its extracellular domain. *Oncogene* 1996, 13:1919-1925
25. Kanai Y, Oda T, Tsuda H, Ochiai A, Hirohashi S: Point mutation of the E-cadherin gene in invasive lobular carcinoma of the breast. *Jpn J Cancer Res* 1994, 85:1035-1039
26. Soares P, Berx G, van Roy F, Sobrinho-Simoes M: E-cadherin gene alterations are rare events in thyroid tumors. *Int J Cancer* 1997, 70:32-38
27. Risinger JI, Berchuck A, Kohler MF, Boyd J: Mutations of the E-cadherin gene in human gynecologic cancers. *Nat Genet* 1994, 7:98-102
28. Hiraguri S, Godfrey T, Nakamura H, Graff J, Collins C, Shayesteh L, Doggett N, Johnson K, Wheelock M, Herman J, Baylin S, Pinkel D, Gray J: Mechanisms of inactivation of E-cadherin in breast cancer cell lines. *Cancer Res* 1998, 58:1972-1977





ELSEVIER

Advanced Drug Delivery Reviews 41 (2000) 147–162

advanced  
drug delivery  
reviews

www.elsevier.com/locate/drugdeliv

## Targeted drug delivery via the folate receptor

Jennifer Sudimack B.A., Robert J. Lee PhD\*

*Division of Pharmaceutics and Pharmaceutical Chemistry, College of Pharmacy, The Ohio State University, Rm 542 LM Parks Hall,  
500 W. 12th Ave., Columbus, OH 43210, USA*

Received 19 July 1999; accepted 15 October 1999

### Abstract

The folate receptor is a highly selective tumor marker overexpressed in greater than 90% of ovarian carcinomas. Two general strategies have been developed for the targeted delivery of drugs to folate receptor-positive tumor cells: by coupling to a monoclonal antibody against the receptor and by coupling to a high affinity ligand, folic acid. First, antibodies against the folate receptor, including their fragments and derivatives, have been evaluated for tumor imaging and immunotherapy clinically and have shown significant targeting efficacy in ovarian cancer patients. Folic acid, a high affinity ligand of the folate receptor, retains its receptor binding properties when derivatized via its  $\gamma$ -carboxyl. Folate conjugation, therefore, presents an alternative method of targeting the folate receptor. This second strategy has been successfully applied in vitro for the receptor-specific delivery of protein toxins, anti-T-cell receptor antibodies, interleukin-2, chemotherapy agents,  $\gamma$ -emitting radiopharmaceuticals, magnetic resonance imaging contrast agents, liposomal drug carriers, and gene transfer vectors. Low molecular weight radiopharmaceuticals based on folate conjugates showed much more favorable pharmacokinetic properties than radiolabeled antibodies and greater tumor selectivity in folate receptor-positive animal tumor models. The small size, convenient availability, simple conjugation chemistry, and presumed lack of immunogenicity of folic acid make it an ideal ligand for targeted delivery to tumors. © 2000 Elsevier Science B.V. All rights reserved.

**Keywords:** Drug delivery systems; Folate receptor; Endocytosis; Immunotherapy; Gene therapy; Protein toxins; Radioimaging; Liposomes

### Contents

1. Introduction .....	148
2. Overexpression of folate receptors in human tumors .....	148
3. Delivery of radiopharmaceuticals .....	150
3.1. Delivery of radionuclides utilizing MOv18 .....	150
3.2. Delivery of radionuclides utilizing low molecular weight folate conjugates .....	151
4. Delivery of liposomal drug carriers .....	153
5. Delivery of gene transfer vectors .....	154
5.1. Viral vectors .....	154
5.2. Non-viral vectors .....	155
5.3. Anionic liposome-entrapped polyplexes (LPDII) .....	155

\*Corresponding author. Tel.: +1-614-292-4172; fax: +1-614-292-7766.

E-mail address: lee.1339@osu.edu (R.J. Lee)

0169-409X/00/\$ – see front matter © 2000 Elsevier Science B.V. All rights reserved.  
PII: S0169-409X(99)00062-9

6. Delivery of protein toxins .....	157
6.1. Delivery of immunotherapy agents .....	158
7. Summary .....	158
References .....	159

## 1. Introduction

Targeted drug delivery systems promise to expand the therapeutic windows of drugs by increasing delivery to the target tissue as well as the target–non-target tissue ratio. This will in turn lead to a reduction in the minimum effective dose of the drug and the accompanying drug toxicity, and an improvement in therapeutic efficacy at equivalent plasma concentrations. Given the often limited number of targeted receptor sites on any given target tissue, targeted delivery is a particularly attractive approach for agents with narrow therapeutic windows and/or are active at very low concentrations.

For targeted delivery to tumor, the cellular target often consists of a membrane-bound tumor-associated antigen (TAA). The receptor for vitamin folate has been identified as a marker for ovarian carcinomas and has also been found to be frequently overexpressed in a wide range of other types of tumors, therefore, presents an attractive target for tumor-selective drug delivery [1–9].

## 2. Overexpression of folate receptors in human tumors

Folate receptor (FR), also known as the high affinity membrane folate-binding protein, is a glycosylphosphatidylinositol (GPI)-linked membrane glycoprotein with an apparent molecular weight of 38–40 kDa [10]. Two membrane-bound isoforms of FR have been identified in humans, designated  $\alpha$  and  $\beta$ . FRs bind folic acid (an oxidized form of folate) with high affinity. FR  $\alpha$ -isoform has a dissociation constant ( $K_d$ ) for folic acid of  $\sim 0.1$  nM, which is approximately 10-fold lower than its  $K_d$  for reduced folates (e.g., 5-methyltetrahydrofolate) [11,12]. The role of FR in cellular folate transport is not well understood, although a “potocytosis” model has been proposed [13]. FRs were found to be clustered in non-coated membrane regions called caveolae.

Localization of FRs in caveolae and receptor internalization can be induced by receptor crosslinking and is regulated by cholesterol [13,14]. Rather than the FR, an anion transporter with a  $K_t$  in the micromolar range and sensitivity to the anion transporter inhibitor probenecid appeared to be responsible for the transmembrane cellular transport of physiological forms of the folate coenzyme, 5-methyltetrahydrofolate [15].

While elevated expression of FR has frequently been observed in various types of human cancers, the receptor is generally absent in most normal tissues with the exceptions of choroid plexus, placenta, and low levels in lung, thyroid and kidney [8]. Although FR type  $\beta$  has been found on CD34+ cells, the receptor curiously lack affinity for [ $^3$ H] folic acid and various folate derivatives [9]. FR type  $\alpha$  is frequently overexpressed in tumor cells in culture and epithelial lineaged tumors such as ovarian carcinomas. Several studies show that over 90% of ovarian carcinomas overexpress the FR [4,7]. Expression of the receptor is mostly homogeneous in ovarian cancer tissue samples [4]. In a recent study, a monoclonal antibody against the type  $\alpha$  receptor, LK26, was used to determine the frequency of FR overexpression in human tumors by indirect immunohistochemical staining [4]. High frequencies of receptor overexpression were found in many types of tumors, including ovarian (52 of 56 cases tested), endometrial (10 of 11), colorectal (6 of 27), breast (11 of 53), lung (6 of 18), renal cell (9 of 18) carcinomas, brain metastases derived from epithelial cancers (4 of 5), and neuroendocrine carcinomas (3 of 21) [4]. In a separate study, quantitative reverse transcription polymerase chain reaction (RT-PCR) analysis was used to determine the mRNA transcript levels of both subtypes of the FR in various human tumor tissues, and [ $^3$ H] folic acid binding was also used to determine the FR ligand binding capacity in these tissues [7]. Highly elevated levels of the FR were detected in choriocarcinomas, meningiomas, uterine sarcomas, osteosarcomas, non-Hodgkin's

lymphomas, and promyelocytic leukemias [7]. FR type  $\beta$  is frequently overexpressed in non-epithelial lineaged tumors such as sarcomas and acute myeloid leukemias but not in established cell lines of the same origin [16]. The causes of FR overexpression in cancers are unclear. Transfection and expression of FR on NIH/3T3 cells provides cells with the ability to survive in low folate medium and increased cell growth both in vitro and in vivo [17,18]. However, another study showed that transfection of cervical carcinoma cells with FR cDNA led to a

decrease in the rate of cellular proliferation rather than an increase, suggesting FR expression may not provide a growth advantage to rapidly dividing cells in all cases [19]. Studies also show that high levels of FR expression are associated with increased biological aggressiveness of ovarian carcinomas as shown by a higher percentage of S-phase cells and increased resistance to chemotherapeutic agents [20]. Thus FR elevation may be a useful prognostic factor.

The prevalence of FR overexpression among human tumors makes it a good marker for targeted drug delivery to these tumors. Two strategies have been developed for FR-specific drug targeting: (1) coupling to monoclonal antibodies (e.g., MOv18) against the FR; and (2) coupling to folic acid, in which folic acid functions as the targeting ligand. High affinity FR binding is retained when folate (Fig. 1) is covalently linked via its  $\gamma$ -carboxyl group to a foreign molecule. The general model for the cellular uptake of drug conjugates targeted to the FR is illustrated in Fig. 2.

This review summarizes recent studies on the

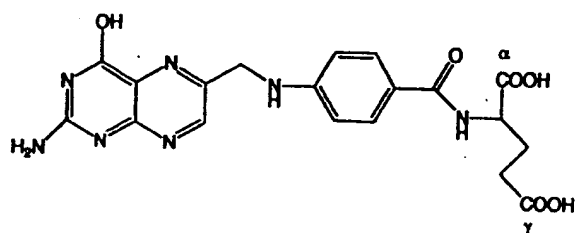


Fig. 1. The structure of folic acid. The  $\alpha$  and  $\gamma$  carboxyl groups are labeled.

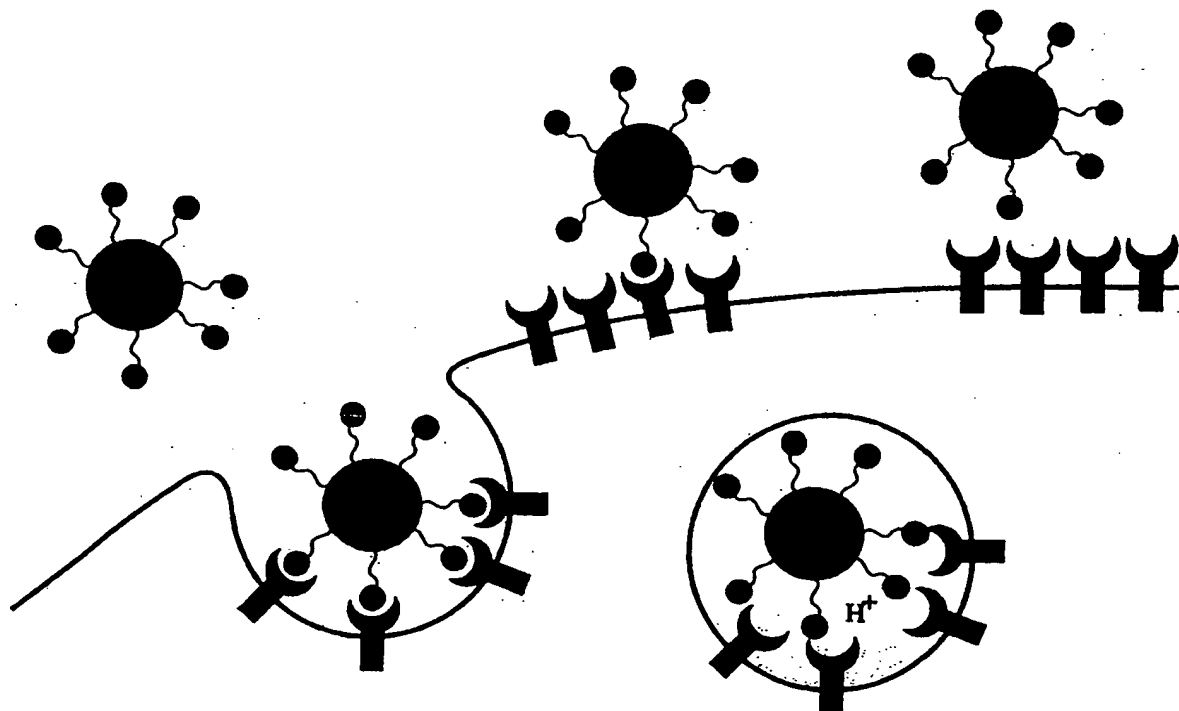


Fig. 2. A schematic diagram of the folate receptor-mediated endocytosis pathway.

diagnostic and therapeutic applications of targeting the FR in vitro and in vivo using either folate or monoclonal antibodies against the FR. The drugs or drug carriers evaluated include liposomes, protein toxins, plasmid DNA complexes, imaging, chemotherapeutic, and immunotherapeutic agents [27,28]. Targeted drug delivery via the FR has been reviewed in several recent articles [21–26].

### 3. Delivery of radiopharmaceuticals

Radioactive tracer techniques are widely used in the diagnostic imaging of tumors due to their ability to non-invasively probe for tissue pathophysiology. The development of new and improved tumor-selective radiopharmaceuticals is clinically desirable as a means of: (i) detecting and/or confirming the presence and location of primary and metastatic lesions; (ii) probing biochemical features of neoplastic tissue that have implications for tumor staging and/or subsequent treatment planning; and (iii) monitoring tumor response to treatment. Photon emitting radiopharmaceuticals that can be used to generate planar and/or tomographic (SPECT) images comprise the cornerstone of current nuclear medicine practice due to the widespread availability of appropriate radionuclides (e.g.,  $^{99m}\text{Tc}$ ,  $^{123}\text{I}$ ,  $^{67}\text{Ga}$ , and  $^{111}\text{In}$ ), FDA-approved radiopharmaceuticals, and the required imaging equipment. Actively targeted  $\gamma$ -emitting radiopharmaceuticals promise to greatly improve the specificity and sensitivity of scintigraphy imaging procedures. If sufficient tumor specificity can be achieved, radiopharmaceuticals labeled with an appropriate  $\alpha$ - or  $\beta$ -emitting radionuclide can also provide an attractive means for site-selective radiation therapy. Criteria for radionuclide selection in the development of diagnostic or therapeutic radiopharmaceuticals include the physical and biological half-lives of the radionuclide, presence or absence of particulate emissions and conversion electrons, as well as the pharmacokinetic and biodistribution properties of the radiopharmaceutical.

Monoclonal antibodies have been evaluated clinically for the tumor-selective delivery of radionuclides for both therapeutic and diagnostic purposes through techniques including radioimmunoscinigraphy (RIS), single-photon-emission computed

tomography (SPECT) and radioimmunotherapy (RIT). Radiolabeled MOv18, a monoclonal antibody against the FR, and its fragments were used in clinical studies in ovarian cancer patients.

#### 3.1. Delivery of radionuclides utilizing MOv18

Radiolabeled antibodies against the FR have been used in the immunohistochemical detection of tissue FR expression, in planar or tomographic (SPECT) imaging, as well as in radioimmunotherapy treatment of ovarian carcinomas.

In a recent clinical study,  $^{131}\text{I}$ -MOv18 was administered either intravenously (i.v.) or intraperitoneally (i.p.) to 30 patients with ovarian carcinoma. Radioimmunoscinigraphy (RIS) was carried out in this study to compare the two routes of administration. A more favorable tumor to non-target (T/NT) ratio (2.8 vs. 1.9) and tumor uptake (1.3% vs. 0.8%) resulted when the  $^{131}\text{I}$ -MOv18 was delivered intraperitoneally. For diagnostic applications, the i.p. route of administration was not very practical. However, the significant increase in targeting ratio achieved via the i.p. route compared to the i.v. route suggests that it may be more appropriate for certain therapeutic applications. The average sensitivity of this method was shown to be 73% (55 tumors detected out of a total of 75 tumors) and the specificity was 100% [29].

In a separate clinical study, 16 patients with minimal residual disease of ovarian cancer were treated by radioimmunotherapy (RIT) with a single i.p. dose of  $^{131}\text{I}$ -MOv18. Complete response (CR) was observed in five patients, no change (NC) in six patients, and progressive disease (PD) in five patients [30]. Furthermore, one patient exhibited long-term CR in a follow-up exam [30].

In single-step radioimmunoimaging protocols, patients are exposed to radiation for a relatively long period of time since it was shown to take approximately 48–72 h for the optimal T/NT ratios to be reached following radiotracer administration [29]. In order to minimize patient radiation exposure, a two-step method was developed. In a two-step protocol, an initial i.p. injection of biotinylated MOv18 was followed by a waiting period, which allows the MOv18 to localize in tumors, and then an i.p. injection of  $^{111}\text{In}$ -streptavidin was administered.

SPECT was then performed for tumor imaging. The mean T/NT ratio obtained was higher (9 vs. 2.8) than when the conventional one-step method was utilized [31]. The improvement in tumor targeting was due to the reduced size and accelerated systemic clearance of the radiotracer  $^{111}\text{In}$ -streptavidin in comparison with the radiolabeled whole antibody. However, this method has limited appeal for clinical imaging applications due to the requirement for repeated i.p. injections at various time intervals and the potential immunogenicity of the streptavidin.

Finally, a three-step method was developed where patients were administered biotinylated MOv18, avidin, followed by  $^{111}\text{In}$ -labeled biotin. The T/NT ratio obtained was 1.7, in contrast to 9 for the two-step method. The relatively poor contrast of this procedure was due to the internalization of the antibody/antigen complexes induced by avidin crosslinking [32]. The receptor-bound avidin, therefore, is no longer accessible to the radiolabeled biotin derivative. While detrimental to tumor imaging, this mechanism of cellular internalization may be exploited for FR-mediated delivery of certain therapeutic agents.

### 3.2. *Delivery of radionuclides utilizing low molecular weight folate conjugates*

Radiolabeled low molecular weight folate conjugates compared to radiolabeled antibody have greatly reduced size, therefore, much faster systemic clearance. This in turn leads to increased tumor to background ratios. The radionuclides which have been evaluated as folate conjugates include  $^{67}\text{Ga}$ ,  $^{111}\text{In}$ , and  $^{99\text{m}}\text{Tc}$ . The results are summarized as follows:

$^{67}\text{Ga}$  and  $^{111}\text{In}$  are  $\gamma$ -emitting radionuclides commonly used in medical imaging procedures with half-lives of 78 h and 68 h, respectively. When administered as a citrate complex,  $^{67}\text{Ga}$  forms a high affinity complex with circulating transferrin. Since the transferrin receptor is frequently overexpressed in various types of tumors, the  $^{67}\text{Ga}$ -transferrin complex preferentially localizes in the tumor, which allows for tumor imaging [33–35]. Deferoxamine is a commonly used chelator that forms a stable complex with Ga.  $^{67}\text{Ga}$ -labeled deferoxamine (DF) conjugates have been frequently used in positron

emission tomography (PET) and gamma scintigraphy [36–38]. For FR imaging, folate was conjugated to deferoxamine via its amino group [39]. The resulting conjugate, deferoxamine-folate (DF-folate), was efficiently labeled with  $^{67}\text{Ga}$  [39].  $^{67}\text{Ga}$ -DF-folate was shown to have 100 times greater uptake in FR-positive oral carcinoma KB cells than the non-targeted  $^{67}\text{Ga}$ -DF [39]. Further, KB cell binding was completely blocked by excess free folate, indicating that binding was specific for the FR [39].  $^{67}\text{Ga}$ -DF-folate was then evaluated for its tumor localizing properties in athymic mice, on a folate free diet, carrying xenograft implants derived from subcutaneously injected KB cells [40,41]. The tumor to blood ratio obtained at 4 h post i.v. injection reached 409 to 1, which was far superior than various controls including  $^{67}\text{Ga}$ -DF and  $^{67}\text{Ga}$ -citrate. Only, the tumor and the kidneys accumulated high levels of the radionuclide conjugate. Radioactivity clearance from the tumor and the kidneys was slower than from other organs, resulting in even higher tumor to blood ratios ( $>1000$ ) at 24 h post injection [40]. The undesirable radionuclide accumulation in the kidneys was likely due to the presence of FRs in the kidney proximal tubules. Targeting efficacy was much poorer in mice on the folate-enriched regular rodent diet or when excess free folate was pre-administered as a receptor blocking agent [40]. In addition, the superb imaging property exhibited by  $^{67}\text{Ga}$ -DF-folate was primarily attributable to its rapid blood clearance kinetics.

An  $^{111}\text{In}$ -labeled diethylenetriaminepentaacetic acid (DTPA)-folate was also synthesized and evaluated both in vitro and in vivo using the KB xenograft tumor model, as described for  $^{67}\text{Ga}$ -DF-folate [42]. The tumor to blood ratios obtained at 4 h post i.v. administration was 82 to 1 [43]. Overall the data obtained with  $^{111}\text{In}$ -DTPA-folate was very similar to those for  $^{67}\text{Ga}$ -DF-folate. There was, however, a significant reduction in hepatobiliary clearance of this agent compared to  $^{67}\text{Ga}$ -DF-folate. The overall clearance kinetics of this agent, therefore, was more rapid and more favorable for tumor imaging.  $^{111}\text{In}$ -DTPA-folate is currently being developed as a clinical imaging agent. A phase I/II radioimaging clinical study on  $^{111}\text{In}$ -DTPA-folate is being conducted at the University of Texas MD Anderson Cancer Center in ovarian cancer patients.

Compared to  $^{111}\text{In}$  and  $^{67}\text{Ga}$ ,  $^{99\text{m}}\text{Tc}$  is considered to be a more favorable radionuclide for radioimaging applications due to its short half-life of 6 h, a 140 keV  $\gamma$ -radiation energy, which is optimal for available imaging equipment, and low cost. A novel folate conjugate of a Tc-chelating ligand, 6-hydrazinonicotinamido-hydrazido (HYNIC)-folate, was recently synthesized in our laboratory (Fig. 3). HYNIC-folate was radiolabeled with  $^{99\text{m}}\text{Tc}$  using tricine and trisodium triphenylphosphine-3,3',3"-trisulfonate (TPPTS) as co-ligands. The receptor binding property of  $^{99\text{m}}\text{Tc}$ -HYNIC-folate was studied in cultured KB cells. FR-mediated uptake was  $\sim 300$  times the non-specific binding in the presence of 1 mM free folic acid (Fig. 4).  $^{99\text{m}}\text{Tc}$ -HYNIC-folate was further evaluated in a C57BL/6 mouse model carrying syngeneic solid tumor grafts derived from 24JK-FBP cells, a methylcholanthrene-induced sarcoma

cell line transfected with the human FR type alpha [44]. Tumor to blood ratios reached 55 and 81 at 4 h and 24 h post i.v. injection of the radiotracer, respectively [45]. Tumor uptake of the radioconjugate was blocked by the co-injection of 100  $\mu\text{g}$  of free folic acid, indicating the role of the FR in tumor localization. Tumors were clearly identifiable in gamma-camera images (Fig. 5). Two other  $^{99\text{m}}\text{Tc}$ -labeled folate conjugates have been synthesized and evaluated for gamma-imaging, including  $^{99\text{m}}\text{Tc}$ -DTPA-folate and  $^{99\text{m}}\text{Tc}$ -ethylenedicysteine-folate, each showing good tumor selectivity [46,47].

Regardless of the specific radionuclide chelate-folate conjugate used, high levels of the radiotracers were consistently found in the kidneys besides the tumors. This poses a potential challenge for application of low molecular weight folate conjugates in targeted radiotherapy. However, the high selectivity

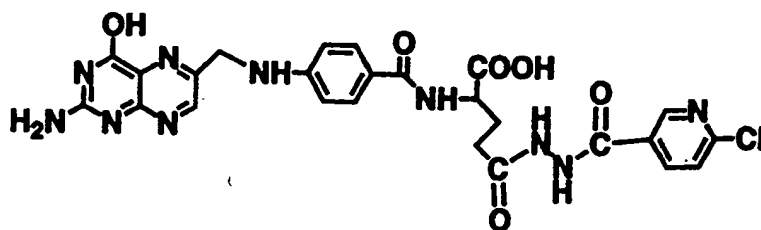


Fig. 3. Structure of 6-hydrazinonicotinamido-hydrazido (HYNIC)-folate.

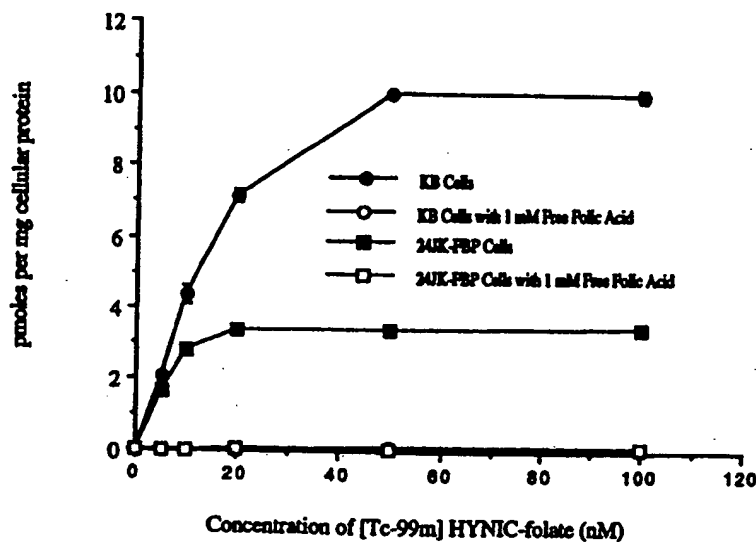


Fig. 4.  $^{99\text{m}}\text{Tc}$ -HYNIC-folate uptake by culture tumor cells.

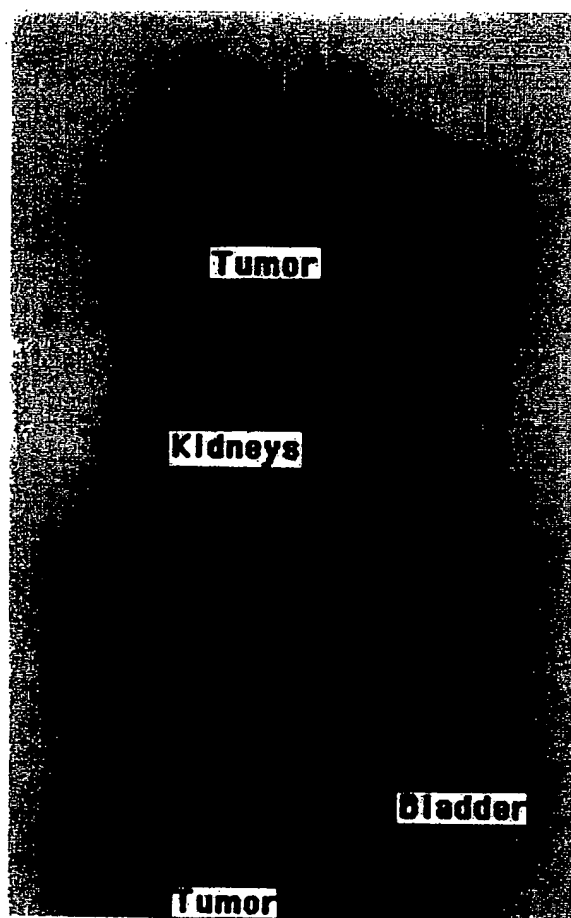


Fig. 5. Gamma camera image of a mouse treated with  $^{99m}\text{Tc}$ -HYNIC-folate.

and the rapid clearance kinetics of these conjugates make them ideal candidates for development as imaging agents for the detection of FR positive tumors.

#### 4. Delivery of liposomal drug carriers

Liposomes are phospholipid bilayer vesicles. As drug carriers, liposomes possess the following properties: (1) the ability to entrap hydrophilic drug molecules in its aqueous interior and/or incorporate hydrophobic molecules in its bilayer(s); (2) long systemic circulation time; (3) efficient uptake by the reticuloendothelial system (RES); and (4) preferen-

tial accumulation in solid tumors due to increased endothelial permeability and reduced lymphatic drainage [48–51]. Low liposome encapsulation efficiency is a limiting factor for delivery of hydrophilic drugs and has been addressed in the delivery of an antitumor agent doxorubicin through the recent development of the “remote-loading” method [52]. Modification of the liposome surface with polyethyleneglycol (PEG) has resulted in reduced RES uptake and further prolonged circulation time [53–60].

The therapeutic efficacy of drug carrying liposomes can potentially be greatly improved if they could be targeted selectively to the tumor. Monoclonal antibodies and their fragments have been attached to the liposome surface to construct immunoliposomes [54–57]. The clinical potential of immunoliposomes is limited because: (1) the targeting ligand is immunogenic. The elicitation of a human-antimouse IgG antibody (HAMA) response precludes repeated administration of immunoliposomes; (2) covalent attachment of a protein to a liposome is technically challenging. The conjugation chemistry for attaching antibodies to lipids is cumbersome and may result in partial denaturation of the targeting ligand; (3) proteinaceous ligands are prone to denaturation upon exposure to organic solvent, limiting the methods available for liposome preparation; (4) immunoliposomes are often unstable and tend to lose immunoreactivity upon storage and/or become rapidly cleared upon injection via  $F_c$  receptor-mediated RES uptake; and (5) few tumor-specific antibodies are available in quantities needed for drug targeting.

For effective targeting of liposomes, folate has to be attached via a long PEG spacer (e.g., PEG  $M_r$  3350) to overcome the steric hindrance encountered at the cell surface [61]. In cultured KB cells, liposome uptake appeared to saturate at  $\sim 2.5 \times 10^5$  sites/cell [61]. The cellular uptake of folate-PEG-liposomes was saturable and could be blocked with a high concentration (1 mM) of free folic acid [60]. The requirement for high concentrations of free folate for effective receptor blocking indicated that folate-targeted liposomes had very high affinity for receptor-bearing tumor cells, possibly due to its capacity to interact with cellular FRs via multivalent interaction [61,62]. Folate-targeted liposomes encap-

sulating a fluorescent dye, calcein, were shown to be taken up by cultured KB cells via receptor-mediated endocytosis and displayed punctate fluorescence pattern when examined under a fluorescence microscope [61]. Folate-PEG-liposomes entrapping doxorubicin were evaluated in cultured KB cells for its uptake and cytotoxicity [63]. Cellular doxorubicin uptake following incubation with these liposomes was 45-fold higher than that of non-targeted liposomes and 1.6 times higher than free doxorubicin, and the cytotoxicity of these liposomes was 86 times and 2.7 times higher, respectively [63]. The cellular uptake of the folate-PEG-liposomes was unaffected by the presence of physiological concentrations of folate in the culture medium [63].

Folate-targeted liposomes have also been used to deliver an antisense oligodeoxyribonucleotide, which inhibits the expression of epidermal growth factor receptor (EGFR) [64]. The main obstacles to the therapeutic application of antisense oligodeoxyribonucleotides were poor cellular uptake, short plasma half-life, and lack of tissue specificity. Folate-PEG-liposome-encapsulated oligonucleotides were efficiently delivered as indicated by increased cellular uptake. These liposomal oligos were also shown to effectively suppress the expression of EGFR in KB cells and to inhibit cell growth [64].

Folate conjugates and folate-targeted liposomes were shown to be internalized into a low-pH endosomal compartment by FR-bearing cells via receptor-mediated endocytosis. The rates of liposome content release following endocytosis and cytosolic drug delivery are effected by the environmental pH and intraliposomal buffer strength [65]. Further, the rate of endosomal release of liposome-entrapped drug molecules could be greatly increased by the utilization of a pH-sensitive lipid composition or attachment of pH-sensitive fusogenic peptides to the surface of liposomes [66,67].

Folate offers many unique advantages as a targeting ligand for liposomes over antibodies. It is non-immunogenic, is not prone to denaturation, has good stability, has simple and defined conjugation chemistry, is highly specific for tumors, is available in large quantities, and is compatible with the use of organic solvent during preparation. Due to the relative large size (50–200 nm in diameter) of liposomes and their tendency to passively accumulate in tumor tissues, it

is difficult to predict whether the incorporation of a targeting ligand could further improve liposome uptake by solid tumors in terms of overall tumor accumulation. Previous studies with immunoliposomes were sparse and results have been mixed. While there was generally very limited increase in tumor accumulation due to targeting based on percent injected dose per gram of tumor tissue, significantly improved therapeutic efficacy has been observed in some cases. For example, intravenously administered anti-HER2 immunoliposomes carrying doxorubicin have shown significantly improved tumor penetration, intracellular accumulation, and antitumor activity compared with non-targeted control liposomes, which primarily accumulated in the interstitial space [57]. Therefore, beneficial effects of liposome targeting are likely found at the cellular and subcellular levels.

## 5. Delivery of gene transfer vectors

Gene therapy presents a promising approach for the treatment of human diseases. A series of potential therapeutic DNA constructs for cancer gene therapy have been developed including those coding for suicide genes, cytokines, tumor-suppressor genes, antisense genes/oligonucleotides, and ribozymes. The clinical application of gene therapy, however, has been limited by the availability of suitable gene transfer vectors. An ideal gene transfer vector should be safe, stable, cost-effective to produce in clinically relevant quantities, and capable of efficient and tissue-specific gene delivery.

### 5.1. Viral vectors

Most of the gene transfer vectors currently under clinical evaluation are based on genetically engineered replication-defective viruses, e.g., retroviral vectors, adenoviral vectors, and adeno-associated viral vectors. While often quite efficient in gene transfer, viral vectors suffer from oncogenic risks associated with random insertion into the host genome (for retro- and adeno-associated viruses) and elicitation of a host immune response, resulting in the elimination of the transduced cells and preventing repeated use of the vector due to induction of



neutralizing antibodies (for adenoviruses). There is also the risk of genetic recombination inside the cell that leads to the generation of infectious viral particles. Viral vectors are also limited in gene-carrying capacity and are challenging to manufacture and purify in clinically relevant quantities. Due to these limitations, there has been considerable interest in the development of non-viral vectors based on synthetic components. Viral vectors can be targeted through attachment of a ligand. Douglas et. al. showed that folate coupled to  $F_{ab}$  fragments against the adenoviral fiber was able to redirect the viral vector to specifically transfect cells that are positive for the FR [80].

### 5.2. Non-viral vectors

Existing synthetic non-viral vectors often consist of DNA complexes of cationic liposomes and/or cationic polymers [68,69]. They have the common advantages of being non-immunogenic, easy to produce, and non-restrictive on the size of the DNA molecule it carries. The structure and gene transfer activity of these complexes is dependent on both vector composition and the formulation method. Monovalent cationic lipids form a different type of DNA complex (lipoplexes) than cationic lipids with a multivalent cationic head group or when cationic lipid is used in conjunction with a polycation (lipopolyplexes). Under freeze-fracture electron microscopy, monovalent cationic lipid/DNA complexes (lipoplexes) often appears as “spaghetti-like” structures consisting of lipid-coated DNA double helix strands. The multivalent cationic lipid/DNA complexes and lipopolyplexes are often more compact in size and more active in gene transfer (in the absence of serum) [70]. However, the transfection activity of these complexes is usually highly sensitive to the presence of serum in the culture media. The gene transfer efficiencies of non-viral vectors are often much lower than viral vectors, especially when administered in vivo. Also, the performance of these vectors is quite variable depending on the route of injection. Major problems with existing non-viral vectors are vector aggregation, non-specific tissue uptake, rapid systemic clearance, and undesirable organ distribution patterns determined by the first-pass effect.

A common flaw in the design of positively charged DNA complexes for gene transfer is that the formulations are usually optimized for gene transfer in vitro. In tissue culture, cellular uptake of the DNA complexes is mediated by charge interaction between the positively charged DNA complexes and the negatively charged cellular membrane. This interaction further induces cellular internalization via endocytosis of the DNA complexes. However, when administered into the blood stream, the DNA complexes are placed in an environment rich in negatively charged plasma proteins and circulating blood cells. The positive charge of the complex is instantly neutralized and the complexes aggregated and accumulate in the lung by pulmonary embolism and/or by the liver due to first pass effect. Since the positive charge of the DNA complexes is primarily contributing to the extent of vector aggregation and is not likely to be available for target cell interaction, negatively charged DNA complexes and naked DNA are often found to be more active than the in vitro optimized gene transfer formulations, which invariably are positively charged. The fate of the DNA complexes is also highly dependent on the route of administration. Intranasal, intraperitoneal, and intratumoral administration expose the vector to different biological environments, therefore, different vector formulations may be needed for optimal gene delivery efficiency for differing methods of injection.

Attachment of a targeting ligand and/or components that promote endosome escape has shown to greatly improve the gene transfer efficiency of nonviral vectors [71–76]. In addition, studies showed that folate-conjugated polylysine coupled to inactivated viral particles mediated efficient receptor-specific gene delivery in vitro [75,76].

### 5.3. Anionic liposome-entrapped polyplexes (LPDII)

Neutral or anionic liposomes have also been evaluated for plasmid DNA delivery. However, they suffer from low DNA entrapment efficiency (usually less than 20%) due to the large molecular size and heavy negative charge of plasmid DNA. Protocols for DNA entrapment into these liposomes are often cumbersome and require the use of high lipid concentrations for high DNA entrapment, which also

leads to the generation of a large number of empty vesicles. Although anionic pH-sensitive immunoliposomes have been shown to deliver DNA into lymphoma ascites tumors, their practical usefulness in gene therapy has yet to be demonstrated.

In the LPDII system, DNA is first complexed to polylysine to form a cationic complex and then mixed with anionic pH-sensitive liposomes carrying a receptor targeting ligand to form liposome-entrapped polyplex particles by a charge-mediated self-assembly process [77]. Folic acid has been used as the targeting ligand for the receptor-mediated gene delivery to tumor cells.

Folate-targeted pH-sensitive liposomes entrapping polyplexes (folate-LPDII) were capable of highly efficient and receptor-specific gene transfer. Folate-LPDII particles were prepared by mixing anionic liposomes composed of dioleoylphosphatidylethanolamine (DOPE)/cholesteryl hemisuccinate (CHEMS)/folate-PEG-DOPE (60:40:0.1, m/m) and the cationic DNA/polylysine (1:0.75, w/w) complexes. Vector self-assembly was mediated by charge interactions. The resulting vector particles were spherical and had a mean diameter of 70–80 nm as determined by negative-stain electron microscopy. The vector particles could be formulated at a variety of anionic lipid/DNA polyplex charge ratios. At low lipid/polyplex ratios, the overall charge of the vector was positive, cellular uptake and transfection were mediated by non-specific charge interaction. Meanwhile, at high lipid/polyplex ratios, the vector was negatively charged and required the presence of a targeting ligand and transfected only cells that express the corresponding receptor. The negatively charged particles were particularly interesting due to their potential for improved compatibility with blood components and tissue-specific targeted gene delivery.

Folate-targeted LPDII vectors carrying a firefly luciferase reporter gene driven by the Rous sarcoma viral promoter (pRSVL) have been evaluated for their *in vitro* gene transfer activity in cultured KB cells. DNA/polylysine polyplexes alone showed very little transfection activity. High transfection activities were observed with folate-LPDII vectors formed at lipid/DNA ratios of 4, 6, 10, and 12 [77]. But the transfection activity of only vectors formed at high lipid/DNA ratios (10 and 12) could be

partially blocked by 1 mM free folic acid [77]. Complete free folate blocking was not expected since these vectors, similar in size to large unilamellar liposomes, are likely to interact with FR-bearing cells via multivalent binding, resulting in much greater cellular affinity. These data suggest that tumor cell transfection by folate-LPDII is mediated by the FR at lipid/DNA ratios that give anionic particles but not at ratios that produce cationic particles, due to the presence of overriding charge mediated cellular uptake. The transfection activity correlates well with the level of  $^{125}\text{I}$ -labeled DNA uptake by these same cells [77]. The role of the FR was further confirmed by duplicating the above studies in the receptor-negative CHO cells, where transfection was only observed with cationic folate-LPDII vectors where uptake is mediated by charge interaction [77].

The study further showed that the pH-sensitive liposomal composition was essential for the observed transfection pattern. pH-sensitive liposomes are generally composed of a fusogenic lipid, usually DOPE, and a pH-sensitive component that is anionic at extracellular pH but becomes charge neutral at the acidic endosomal pH, such as CHEMS. DOPE is a cone-shaped lipid molecule that favors the transition from bilayer to hexagonal II phase thereby facilitating membrane fusion and/or disruption. This lipid phase transition is blocked by the presence of the negatively charged CHEMS. Upon protonation at endosomal pH, CHEMS becomes uncharged, therefore, can no longer stabilize the bilayer structure and allows for DOPE-mediated membrane fusion. Replacing DOPE with the cylindrical lipid DOPC completely abolishes transfection activity of the folate-LPDII vectors [77]. Also, replacing CHEMS with DOPS, a lipid that does not become extensively protonated at endosomal pH, eliminates transfection activity at high lipid/DNA ratios where negatively charged vectors formed [77].

The structure of folate-targeted LPDII has been studied by negative-stain electron microscopy. The vector particles appeared spherical and consist of a high electron density core representing the DNA polyplex, and a low electron density coat representing lipidic components. When dual isotopically labeled folate-LPDII particles were fractionated on a sucrose gradient, most of the lipid (labeled with  $^3\text{H}$ )

co-migrates with the plasmid DNA (labeled with  $^{125}\text{I}$ ) as an intermediate density band (DNA polyplexes have high density and liposomes have low density).

Under optimal in vitro conditions, negatively charged folate-LPDII vectors are more efficient in transfection than lipoplexes and are specific for receptor-positive tumor cells. The plasmid DNA in LPDII particles is also more optimally condensed compared to cationic liposome lipoplexes resulting in the formation of smaller and colloiddally more stable particles. The negatively charged LPDII particles should also be more compatible with the in vivo environment, which is abundant with negatively charged components. Compared to anionic liposomes containing passively entrapped DNA, LPDII formulation has the advantage of quantitative DNA incorporation and having high transfection activity without the contamination of empty lipid vesicles. The main limitation of existing LPDII formulation is the high level of serum sensitivity. A possible explanation is that the fusogenic activity of DOPE is inhibited by the presence of serum. Further improvements are needed for LPDII formulations to be used for in vivo gene transfer. For in vivo applications, a potential limitation is clearance by the reticuloendothelial system (RES); however, this may be partially overcome by coating vector particles with polyethyleneglycol (PEG). This strategy has previously been applied to produce longcirculating sterically stabilized liposomes.

Folate has also been conjugated to polyethylenimine (PEI, branched polymer,  $M_r \sim 60$  kDa) via a PEG linker. Polyethylenimine (PEI), linear or branched, is a cationic polymer ideally suited for the formation of compact charge complexes with plasmid DNA. In addition to its DNA condensing properties, this polymer also possess endosomolytic activities due to its strong buffering capacity at endosomal acidic pH. In this study, folate conjugates of polyethylenimine were synthesized and evaluated for their ability to mediate receptor-specific gene transfer in vitro. The transfection efficiency of the folate-PEG-PEI/DNA complexes was highly dependent on the PEI nitrogen to DNA phosphate (N/P) ratio, and was partially receptor-dependent [78,79]. This conjugate is simpler than the LPDII system and produces DNA complexes of smaller sizes, therefore,

may be potentially useful for in vivo tumor cell-specific gene delivery.

Furthermore, antisense oligodeoxynucleotides have been specifically delivered to tumor cells in vitro via direct conjugation to folate [81]. Folate was attached to the 3' terminus of an anti-c-fos oligodeoxynucleotide. The cellular uptake in cells, which overexpress the FR, was determined to be approximately eightfold higher with the folate-conjugated oligo compared to the oligo alone. The folate-conjugated oligo also exhibited a much greater tumor inhibitory effect.

## 6. Delivery of protein toxins

Protein toxin, including plant ribosome inactivating proteins and bacterial toxins, have been conjugated to folate and shown to be effectively kill cells overexpressing the FR without damaging the surrounding normal cells [82]. This approach is attractive due to the extreme potency of these toxins to cause cell death. Usually, delivery of a few hundred molecules per cell is sufficient to ensure cellular death. This is very important for targeted delivery systems where the capacity for targeting is limited by the number of receptors on the target cell.

Momordin, a ribosome-inactivating toxin, was conjugated to folate and was utilized in a co-culture with malignant and normal cell lines in vitro [83,84]. The momordin-folate treatment resulted in the selective killing of the malignant cells without damaging the normal cells. The  $\text{IC}_{50}$  for the folate conjugates was reduced to  $10^{-9}$  M. In addition, the momordin-folate did not significantly affect the rate of proliferation of the normal cells at the concentrations tested [84].

Other folate-conjugates, including folate-truncated *Pseudomonas* exotoxin and folate-truncated diphtheria toxin, have also been shown to selectively kill malignant cell lines in co-cultures [85]. LysPE38-folate (a truncated *Pseudomonas* exotoxin-folate) conjugate killed malignant cells 6 times faster and 10 times more potent than the momordin-folate conjugate [85]. This is due to the presence of a translocation domain, which allows for the efficient endosomal escape of the folate conjugates following receptor binding and endocytosis.

Folate conjugated protein toxins are significantly smaller than the corresponding immunotoxins. This should lead to more favorable pharmacokinetics and reduced immunogenicity.

### 6.1. Delivery of immunotherapy agents

Immunotherapy via receptor targeting presents yet another promising approach for the treatment of tumors. A number of strategies are currently being explored, including the use of humanized anti-FR antibody, chimeric anti-FR transfected tumor-infiltrating lymphocytes, bispecific antibodies against the T-cell receptor, and interleukin-2 fusion protein.

Monoclonal antibodies directed against tumor-associated antigens have been shown to mediate lysis of tumor cells by effector immunocytes, such as macrophages, natural killer cells or monocytes. Humanized chimeric antibodies are often used instead of murine antibodies due to the variable Fc receptor affinity and undesirable human anti-mouse antibody (HAMA) response associated with the use of murine antibodies.

Humanized chimeric MOv18 and MOv19 monoclonal antibodies were generated and evaluated for lytic activity against FR-positive tumor cells [86]. An equal amount of lysis of the target ovarian cancer cell line (IGROV1) resulted when murine MOv19 was compared to the chimeric MOv19. Chimeric MOv18 resulted in higher levels and more consistent tumor lysis than murine MOv18. The chimeric analogs were found to bind FR with similar affinity and only one chimeric antibody was required per FR to achieve effective cell kill [86].

A chimeric MOv18 antibody/T-cell receptor construct, which consists of T-cell receptor-transmembrane and signaling chains fused to the variable domains from the MOv18 monoclonal antibody, was also evaluated for tumor immunotherapy [44]. C57BL6 mice carrying FR transfected 24JK-FBP cells were treated with tumor-infiltration lymphocytes transfected with the above chimeric construct [44]. A significant increase in survival resulted in mice treated with MOv-TIL (tumor-infiltrating lymphocytes) over those treated with saline, nontransduced TIL, or TIL transduced with a control antitritonphenol chimeric receptor gene. MOv-TIL

treatment also resulted in fewer lung metastases in mice injected intravenously with tumor cells [44].

MOv18-derived bispecific antibodies have also been investigated for potential use in tumor immunotherapy. Bispecific antibody OC/TR were constructed using MOv18 (recognizing the FR) and a monoclonal antibody against the T cell receptor (recognizing CD3). T lymphocytes retargeted using  $F_{(ab')_2}$  fragments of the bispecific monoclonal antibody OC/TR have been shown to lyse ovarian carcinoma cells [87,88]. In a clinical trial, the treatment of in vitro-activated autologous peripheral blood T lymphocytes retargeted with OC/TR combined with IL-2 were evaluated in 19 patients with ovarian cancer for potential therapeutic efficacy. Complete response, complete intraperitoneal response, stable disease, and progressive disease was shown in 3, 1, 7, and 5 patients, respectively. Complete responses lasted from 18 up to 26 months. In addition, the HAMA response was evident at the end of treatment in 21 of 25 patients; however, tumor regression was evident in this study when the bi-specific antibody-retargeted T lymphocytes were used [88].

Folate conjugated anti-T-cell receptor antibody fragment has been evaluated as an alternative to bispecific antibodies. The folate conjugate is smaller in size, easier to prepare, and is highly potent in mediating the lysis of tumor cells, which express either FR isoform [89,90]. The affinity of these folate/anti-T-cell receptor conjugates is found to be only one-tenth of the affinity of free folate [90].

Finally, interleukin 2 (IL-2) has been fused to a single-chain Fv of MOv19. This construct has been shown to specifically accumulate in tumors in a mouse tumor model and exhibit significant antitumor activity [91]. This approach provides local delivery of IL-2 without causing systemic toxicity.

## 7. Summary

In addition to the above mentioned areas, folate has been used in the targeting of chemotherapeutic agents [92] and paramagnetic magnetic resonance imaging contrast agents [91] with very promising results.

Efficacy of targeted drug delivery is greatly affected by the size of the drug conjugate or drug carrier. Larger constructs are often immunogenic, prone to RES uptake, have prolonged systemic circulation time, slow to extravasate, and exhibit significant passive targeting effects in solid tumors. Therefore, in order to achieve high tumor to normal tissue ratios, low molecular weight conjugates are greatly preferred. For the targeted delivery of large particles such as liposomes and gene transfer vectors, it is often difficult to demonstrate a significant increase in overall tumor accumulation. Targeting nonetheless may be beneficial at the cellular and/or subcellular level.

Folate as a targeting ligand offers many potential advantages over macromolecules such as monoclonal antibodies. These include: (1) small size of the targeting ligand, which often leads to favorable pharmacokinetic properties of the folate conjugates and reduced probability of immunogenicity thus allowing for repeated administration; (2) convenient availability and low cost; (3) relatively simple and defined conjugation chemistry; (4) high receptor affinity and lack of normal tissue receptor expression, thus high tumor tissue specificity; (5) the receptor/ligand complex can be induced to internalize via endocytosis, which may facilitate the cytosolic delivery of therapeutic agents, and (6) high frequency of overexpression among human tumors thus a wide range of tumor targets. Therefore, folate-based targeting systems show great potential for future clinical diagnostic and therapeutic applications.

## References

- [1] I.G. Campbell, T.A. Jones, W.D. Foulkes, J. Trowsdale, Folate-binding protein is a marker for ovarian cancer, *Cancer Res.* 51 (1991) 5329–5338.
- [2] L.R. Coney, A. Tomasetti, L. Carayannopoulos et al., Cloning of a tumor-associated antigen: MOv18 and MOv19 antibodies recognize a folate-binding protein, *Cancer Res.* 51 (1991) 6125–6132.
- [3] W.A. Franklin, M. Waintrub, D. Edwards et al., New anti-tumor antibody cluster 12 reacts with human folate receptors present on adenocarcinoma, *Int. J. Cancer* 8 (1994) 89–95.
- [4] P. Garin-Chesa, I. Campbell, P. Saigo, J. Lewis, L. Old, W. Rettig, Trophoblast and ovarian cancer antigen LK26. Sensitivity and specificity in immunopathology and molecular identification as a folate-binding protein, *Am. J. Path.* 142 (1993) 557–567.
- [5] J. Holm, S.I. Hansen, M. Hoier-Madsen, K. Sondergaard, M. Bzorek, Folate receptor of human mammary adenocarcinoma, *APMIS* 102 (1994) 413–419.
- [6] W. Rettig, P. Garin-Chesa, H. Beresford, H. Oettgen, M. Melamed, L. Old, Cell-surface glycoproteins of human sarcomas: differential expression in normal and malignant tissues and cultured cells, *Proc. Natl. Acad. Sci. USA* 85 (1988) 3110–3114.
- [7] J.F. Ross, P.K. Chaudhuri, M. Ratnam, Differential regulation of folate receptor isoforms in normal and malignant tissues in vivo and in established cell lines – Physiologic and clinical applications, *Cancer* 73 (1994) 2432–2443.
- [8] S.D. Weitman, R.H. Lark, L.R. Coney et al., Distribution of the folate receptor GP38 in normal and malignant cell lines and tissues, *Cancer Res.* 52 (1992) 3396–3401.
- [9] J.A. Reddy, L.S. Haneline, E.F. Srouf, A.C. Antony, D.W. Clapp, P.S. Low, Expression and functional characterization of the beta-isoform of the folate receptor on CD34+ cells, *Blood* 93 (1999) 3940–3948.
- [10] A.C. Antony, Folate receptors, *Ann. Rev. Nutr.* 16 (1996) 501–521.
- [11] X. Wang, F. Shen, J.H. Freisheim, L.E. Gentry, M. Ratnam, Differential stereospecificities and affinities of folate receptor isoforms for folate compounds and antifolates, *Biochem. Pharmacol.* 44 (1992) 1898–1901.
- [12] K.M. Maziarz, H.L. Monaco, F. Shen, M. Ratnam, Complete mapping of divergent amino acids responsible for differential ligand binding of folate receptors alpha and beta, *J. Biol. Chem.* 274 (1999) 11086–11091.
- [13] R.G.W. Anderson, B.A. Kamen, K.G. Rothberg, S.W. Lacey, Potocytosis: sequestration and transport of small molecules by caveolae, *Science* 255 (1992) 410–411.
- [14] E.J. Smart, C. Mineo, R.G. Anderson, Clustered folate receptors deliver 5-methyltetrahydrofolate to cytoplasm of MA104 cells, *J. Cell Biol.* 134 (1996) 1169–1177.
- [15] S. Miotti, M. Bagnoli, F. Ottone, A. Tomasetti, M.I. Colnaghi, S. Canevari, Simultaneous activity of two different mechanisms of folate transport in ovarian carcinoma cell lines, *J. Cell. Biochem.* 65 (1997) 479–491.
- [16] J.F. Ross, H. Wang, F.G. Behm et al., Folate receptor type beta is a neutrophilic lineage marker and is differentially expressed in myeloid leukemia, *Cancer* 85 (1999) 348–357.
- [17] F. Bottero, A. Tomasetti, S. Canevari, S. Miotti, S. Menard, M.I. Calnagi, Gene transfection and expression of the ovarian carcinoma marker folate binding protein on NIH/3T3 cells increases cell growth in vitro and in vivo, *Cancer Res.* 53 (1993) 5791–5796.
- [18] C.A. Luhrs, C.A. Raskin, R. Durbin et al., Transfection of a glycosylated phosphatidylinositol-anchored folate-binding protein complementary DNA provides cells with the ability to survive in low folate medium, *J. Clin. Invest.* 90 (1992) 840–847.
- [19] X.L. Sun, B.R. Murphy, Q.J. Li et al., Transduction of folate receptor cDNA into cervical carcinoma cells using recombi-

- nant adeno-associated virions delays cell proliferation in vitro and in vivo, *J. Clin. Invest.* 96 (1995) 1535–1547.
- [20] G. Toffoli, C. Cerniglio, A. Russo, A. Gallo, M. Bagnoli, M. Boiocchi, Overexpression of folate binding protein in ovarian cancers, *Int. J. Cancer* 74 (1997) 193–198.
  - [21] R.J. Lee, P.S. Low, Folate-targeted liposomes for drug delivery. Forum on liposome targeting, *J. Liposome Res.* 7 (1997) 455–466.
  - [22] R.J. Lee, P.S. Low, Folate as a targeting device for protein utilizing folate receptor-mediated endocytosis, drug targeting, in: G.E. Francis, C. Delgado (Eds.), *Series on Methods in Molecular Medicine*, 25 (1999).
  - [23] S. Wang, P.S. Low, Folate-mediated targeting of antineoplastic drugs, imaging agents, and nucleic acids to cancer cells, *J. Control. Rel.* 53 (1998) 39–48.
  - [24] J.A. Reddy, P.S. Low, Folate-mediated targeting of therapeutic and imaging agents to cancers, *Crit. Rev. Ther. Drug Carrier Syst.* 15 (1998) 587–627.
  - [25] B.A. Gruner, S.D. Weitman, The folate receptor as a potential therapeutic anticancer target, *Invest. New Drugs* 16 (1998) 205–219.
  - [26] T.M. Trippett, J.R. Bertino, Therapeutic strategies targeting proteins that regulate folate and reduced folate transport, *J. Chemother.* 11 (1999) 3–10.
  - [27] C.P. Leamon, P.S. Low, Delivery of macromolecules into living cells: a method that exploits folate receptor endocytosis, *Proc. Natl. Acad. Sci. USA* 88 (1991) 5572–5576.
  - [28] C.P. Leamon, P.S. Low, Membrane folate-binding proteins are responsible for folate-protein conjugate endocytosis into cultured cells, *Biochem. J.* 291 (1993) 855–860.
  - [29] F. Crippa, G.L. Buraggi, E. Di Re et al., Radioimmunoscinigraphy of ovarian cancer with the MOv18 monoclonal antibody, *Eur. J. Cancer* 27 (1991) 724–729.
  - [30] F. Crippa, G. Bolis, E. Seregini et al., Single-dose intraperitoneal radioimmunotherapy with the murine monoclonal antibody 1-131 MOv18: clinical results in patients with minimal residual disease of ovarian cancer, *Eur. J. Cancer* 31A (1995) 686–690.
  - [31] G. Paganelli, C. Belloni, P. Magnani et al., Two-step tumour targeting in ovarian cancer patients using biotinylated monoclonal antibodies and radioactive streptavidin, *Eur. J. Nucl. Med.* 19 (1992) 322–329.
  - [32] P. Casalini, E. Luison, S. Menard, M.I. Colnaghi, G. Paganelli, S. Canevari, Tumor pretargeting: role of avidin/streptavidin on monoclonal antibody internalization, *J. Nucl. Med.* 38 (1997) 1378–1381.
  - [33] D. Front, O. Israel, The role of Ga-67 scintigraphy in evaluating the results of therapy of lymphoma patients, *Semin. Nucl. Med.* 25 (1995) 60–71.
  - [34] A.E. van Leeuwen-Stok, A.M. Drager, G.J. Schuurhuis, A.W. Platier, G.J. Teule, P.C. Huijgens, Gallium 67 in the human lymphoid cell line U-715: Uptake, cytotoxicity, and intracellular localization, *Int. J. Radiat. Biol.* 64 (1993) 749–759.
  - [35] M.H. Sohn, B.J. Jones, J.H.J. Whiting, F.L. Datz, R.E. Lynch, K.A. Morton, Distribution of gallium-67 in normal and hypotransferrinemic tumor-bearing mice, *J. Nucl. Med.* 34 (1993) 2135–2143.
  - [36] D.R. Vera, Gallium-labeled deferoxamine-galactosyl-neoglycoalbumin: A radiopharmaceutical for regional measurement of hepatic receptor biochemistry, *J. Nucl. Med.* 33 (1992) 1160–1166.
  - [37] M.A. Green, Metal radionuclides in diagnostic imaging by positron emission tomography (PET), *Adv. Metals Med.* 1 (1993) 75–114.
  - [38] P.M. Smith-Jones, B. Stolz, C. Bruns et al., Gallium-67/gallium-68-[DFO]-octreotide – a potential radiopharmaceutical for PET imaging of somatostatin receptor-positive tumors: Synthesis and radiolabeling in vitro and preliminary in vivo studies, *J. Nucl. Med.* 35 (1994) 317–325.
  - [39] S. Wang, R.J. Lee, C.J. Mathias, M.A. Green, P.S. Low, Synthesis, purification, and tumor cell uptake of <sup>67</sup>Ga-deferoxamine-folate, a potential radiopharmaceutical for tumor imaging, *Bioconj. Chem.* 7 (1996) 56–62.
  - [40] C.J. Mathias, S. Wang, R.J. Lee, D.J. Waters, P.S. Low, M.A. Green, Tumor-selective radiopharmaceutical targeting via receptor-mediated endocytosis of gallium-67-deferoxamine-folate, *J. Nucl. Med.* 37 (1996) 1003–1008.
  - [41] C.J. Mathias, S. Wang, D.J. Waters, P.S. Low, M.A. Green, Receptor-mediated targeting of Ga-67-deferoxamine-folate to folate receptor positive human KB tumor xenografts, *Nucl. Med. Biol.* 26 (1999) 23–25.
  - [42] S. Wang, J. Luo, D.A. Lantrip et al., Design and synthesis of In-111-DTPA-folate for use as a tumor-targeted radiopharmaceutical, *Bioconj. Chem.* 8 (1997) 673.
  - [43] C.J. Mathias, S. Wang, D.J. Waters, J.J. Turek, P.S. Low, M.A. Green, Indium-111-DTPA-folate as a potential folate-receptor-targeted radiopharmaceutical, *J. Nucl. Med.* 39 (1998) 1579–1585.
  - [44] P. Hwu, J.C. Yang, Y.R. Cowherd et al., In vivo antitumor activity of T cells redirected with chimeric antibody/T-cell receptor genes, *Cancer Res.* 55 (1995) 3369–3373.
  - [45] W. Guo, G.H. Hinkle, R.J. Lee, <sup>99m</sup>Tc-HYNIC-folate a novel receptor-based targeted radiopharmaceutical for tumor imaging, *J. Nucl. Med.* 40 (1999) 1563–1569.
  - [46] S. Ilgan, D.J. Yang, T. Higuchi et al., Tc-99m-ethylenedicycysteine-folate: a new tumor imaging agent. Synthesis, labeling and evaluation in animals, *Cancer Biother. Radiopharm.* 13 (1998) 427–435.
  - [47] C.J. Mathias, D. Hubers, D.P. Trump, P.S. Low, M.A. Green, Synthesis of Tc-99m-DTPA-folate and preliminary evaluation as a folate receptor-targeted radiopharmaceutical, in: *Soc. Nucl. Med. 44th Ann. Meeting*, San Antonio, TX, 1997.
  - [48] D. Lichtenberg, Liposomes: Preparation, characterization, and preservation, *Methods Biochem. Anal.* 33 (1988) 337–462.
  - [49] G. Gregoriadis, A.T. Florence, Liposomes in drug delivery-clinical, diagnostic and ophthalmic potential, *Drugs* 45 (1993) 15–28.
  - [50] N. Garelli, P. Vierling, Incorporation of new amphiphilic perfluoroalkylated bipyridine platinum and palladium complexes into liposomes: Stability and structure-incorporation relationships, *Biochim. Biophys. Acta* 1127 (1992) 41–48.
  - [51] D.C. Litzinger, L. Huang, Phosphatidylethanolamine liposomes: Drug delivery, gene transfer and immunodiagnostic applications, *Biochim. Biophys. Acta* 1113 (1992) 201–227.

- [52] L.D. Mayer, L.C.L. Tai, D.S.C. Ko et al., Influence of vesicle size, lipid composition, and drug-to-lipid ratio on the biological activity of liposomal doxorubicin in mice, *Cancer Res.* 49 (1989) 5922–5930.
- [53] A. Gabizon, R. Catane, B. Uziely et al., Prolonged circulation time and enhanced accumulation in malignant exudates of doxorubicin encapsulated in polyethylene-glycol coated liposomes, *Cancer Res.* 54 (1994) 987–992.
- [54] L.D. Leserman, J.N. Weinstein, R. Blumenthal, W.D. Terry, Receptor-mediated endocytosis of antibody-opsonized liposomes by tumor cells, *Proc. Natl. Acad. Sci. USA* 77 (1980) 4089–4093.
- [55] N. Berinstein, K.K. Matthey, D. Papahadjopoulos, R. Levy, B.I. Sikic, Antibody-directed targeting of liposomes to human cell lines: Role of binding and internalization on growth inhibition, *Cancer Res.* 47 (1987) 5954–5959.
- [56] P.G. Milhaud, P. Machy, B. Lebleu, L. Leserman, Antibody targeted liposomes containing poly(rI)·poly(rC) exert a specific antiviral and toxic effect on cells primed with interferons alpha/beta or gamma, *Biochim. Biophys. Acta* 987 (1989) 15–20.
- [57] J.W. Park, K. Hong, D.B. Kirpotin, O. Meyer, D. Papahadjopoulos, C. Benz, Anti-HER2 immunoliposomes for targeted therapy of human tumors, *Cancer Lett.* 118 (1997) 153–160.
- [58] D.C. Litzinger, L. Huang, Biodistribution and immunotargetability of ganglioside-stabilized dioleoylphosphatidylethanolamine liposomes, *Biochim. Biophys. Acta* 1104 (1992) 179–187.
- [59] A.L. Klivanov, K. Maruyama, A.M. Beckerleg, V.P. Torchilin, L. Huang, Activity of amphipathic poly(ethylene glycol)5000 to prolong the circulation time of liposomes depends on the liposome size and is unfavorable for immunoliposome binding to target, *Biochim. Biophys. Acta* 1062 (1991) 142–148.
- [60] D. Liu, L. Huang, pH-sensitive, plasma-stable liposomes with relatively prolonged residence in circulation, *Biochim. Biophys. Acta* 1022 (1990) 348–354.
- [61] R.J. Lee, P.S. Low, Delivery of liposomes into cultured KB cells via folate receptor-mediated endocytosis, *J. Biol. Chem.* 269 (1994) 3198–3204.
- [62] A. Gabizon, A.T. Horowitz, D. Goren et al., Targeting folate receptor with folate linked to extremities of poly(ethylene glycol)-grafted liposomes: in vitro studies, *Bioconj. Chem.* 10 (1999) 289–298.
- [63] R.J. Lee, P.S. Low, Folate-mediated tumor cell targeting of liposome-entrapped doxorubicin in vitro, *Biochim. Biophys. Acta* 1233 (1995) 134–144.
- [64] S. Wang, R.J. Lee, G. Cauchon, D.G. Gorenstein, P.S. Low, Delivery of antisense oligodeoxynucleotides against the human epidermal growth factor receptor into cultured KB cells with liposomes conjugated to folate via polyethylene glycol, *Proc. Natl. Acad. Sci. USA* 92 (1995) 3318–3322.
- [65] R.J. Lee, P.S. Low, Delivery of liposomes into cultured KB cells via folate receptor-mediated endocytosis, *J. Biol. Chem.* 269 (1994) 3198–3204.
- [66] R.J. Lee, S. Wang, M.J. Turk, P.S. Low, The effects of pH and intraliposomal buffer strength on the rate of liposome content release and intracellular drug delivery, *Biosci. Rep.* 18 (1998) 69–78.
- [67] N.K. Subbarao, R.A. Parente, F.C. Szoka, L. Nadasdi, K. Pongracz, pH-dependent bilayer destabilization by an amphipathic peptide, *Biochemistry* 26 (1987) 2964–2972.
- [68] K. Vogel, S. Wang, R.J. Lee, J. Chmielewski, P.S. Low, Peptide-mediated release of folate-targeted liposome contents from endosomal compartments, *J. Am. Chem. Soc.* 118 (1996) 1581–1586.
- [69] P.L. Felgner, T.R. Gadek, M. Holm et al., Lipofection: A highly efficient, lipid-mediated DNA-transfection procedure, *Proc. Natl. Acad. Sci. USA* 84 (1987) 7413–7417.
- [70] E. Wagner, M. Zenke, M. Cotten, H. Beug, M.L. Birnstiel, Transferrin-polycation conjugates as carriers for DNA uptake into cells, *Proc. Natl. Acad. Sci. USA* 87 (1990) 3410–3414.
- [71] J.P. Behr, B. Demeneix, J.P. Loeffler, J.P. Mutul, Efficient gene transfer into mammalian primary endocrine with lipopolyamine-coated DNA, *Proc. Natl. Acad. Sci. USA* 86 (1989) 6982.
- [72] E. Wagner, K. Zatloukal, M. Cotten, H. Kirkappos, K. Mechtler, D.T. Curiel, Coupling of adenovirus to transferrin-polylysine/DNA complexes greatly enhances receptor-mediated gene delivery and expression of transfected genes, *Proc. Natl. Acad. Sci. USA* 89 (1992) 6099–6103.
- [73] D.T. Curiel, E. Wagner, M. Cotten, M.L. Birnstiel, S. Agarwal, C.M. Li, High-efficiency gene transfer mediated by adenovirus coupled to DNA-polylysine conjugates, *Hum. Gene Ther.* 3 (1992) 147–154.
- [74] R.J. Cristiano, L.C. Smith, S.L.C. Woo, Hepatic gene therapy: Adenovirus enhancement of receptor-mediated gene delivery and expression in primary hepatocytes, *Proc. Natl. Acad. Sci. USA* 90 (1993) 2122–2126.
- [75] R.J. Cristiano, L.C. Smith, M.A. Kay, B.R. Brinkley, S.L. Woo, Hepatic gene therapy: Efficient gene delivery and expression in primary hepatocytes utilizing a conjugated adenovirus-DNA complex, *Proc. Natl. Acad. Sci. USA* 90 (1993) 11548–11552.
- [76] K.A. Mislick, J.D. Baldeschwieler, J.F. Kayyem, T.J. Meade, Transfection of folate-polylysine DNA complexes: Evidence for lysosomal delivery, *Bioconj. Chem.* 6 (1995) 512–515.
- [77] S. Gottschalk, R.J. Cristiano, L.C. Smith, S.L.C. Woo, Folate receptor mediated DNA delivery into tumor cells: potosomal disruption results in enhanced gene expression, *Gene Ther.* 1 (1994) 185–191.
- [78] R.J. Lee, L. Huang, Folate-targeted, anionic liposome-entrapped polylysine-condensed DNA for tumor cell-specific gene transfer, *J. Biol. Chem.* 271 (1996) 8481–8487.
- [79] R.J. Lee, L. Huang, Lipidic vector systems for gene transfer, *Crit. Rev. Ther. Drug Carrier Syst.* 14 (1997) 173–206.
- [80] W. Guo, R.J. Lee, Targeted gene delivery via the folate receptor, in: *Annu. Natl. Meeting of Am. Chem. Soc.*, Anaheim, CA, March, 1999, Abstract.
- [81] J.T. Douglas, B.E. Rogers, M.E. Rosenfeld, S.I. Michael, M. Feng, D.T. Curiel, Targeting gene delivery by tropism-modified adenoviral vectors, *Nat. Biotech.* 14 (1996) 1574–1578.

- [82] S. Li, H.M. Deshmukh, L. Huang, Folate-mediated targeting of antisense oligodeoxynucleotides to ovarian cancer cells, *Pharm. Res.* 15 (1998) 1540–1545.
- [83] A.E. Frankel, Immunotoxin therapy of cancer, *Oncology* 7 (1993) 69–78.
- [84] C.P. Leamon, P.S. Low, Selective targeting of malignant cells with cytotoxin-folate conjugates, *J. Drug Targeting* 2 (1994) 101–112.
- [85] C.P. Leamon, P.S. Low, Cytotoxicity of momordin-folate conjugates in cultured human cells, *J. Biol. Chem.* 267 (1992) 24966–24971.
- [86] C.P. Leamon, I. Pastan, P.S. Low, Cytotoxicity of folate-pseudomonas exotoxin conjugates toward tumor cells, *J. Biol. Chem.* 268 (1993) 24847–24854.
- [87] L.R. Coney, D. Mezzanzanica, D. Sanborn, P. Casalini, M.I. Colnaghi, V.R. Zurawski, Chimeric murin-human antibodies directed against folate binding receptor are efficient mediators of ovarian carcinoma cell killing, *Cancer Res.* 54 (1994) 2448–2455.
- [88] S. Canevari, G. Stoter, F. Arienti et al., Regression of advanced ovarian carcinoma by intraperitoneal treatment with autologous T lymphocytes retargeted by a bispecific monoclonal antibody, *J. Natl. Cancer Inst.* 87 (1995) 1463–1469.
- [89] S. Canevari, D. Mezzanzanica, A. Mazzoni et al., Bispecific antibody targeted T cell therapy of ovarian cancer: Clinical results and future directions, *J. Hematother.* 4 (1995) 423–427.
- [90] D.M. Kranz, T.A. Patrick, K.E. Brigle, M.J. Spinella, E.J. Roy, Conjugates of folate and anti-T-cell-receptor antibodies specifically target folate receptor-positive tumor cells for lysis, *Proc. Natl. Acad. Sci. USA* 92 (1995) 9057–9061.
- [91] C.A. Ladino, R.V. Charm, L.A. Bourret, N.L. Kedersha, V.S. Goldmacher, Folate-maytansinoids: target-selective drugs of low molecular weight, *Int. J. Cancer* 73 (1997) 859–864.
- [92] C. Melani, M. Figini, D. Nicosia et al., Targeting of interleukin 2 to human ovarian carcinoma by fusion with a single-chain Fv of antifolate receptor antibody, *Cancer Res.* 58 (1998) 4146–4154.



# Differential Apoptosis Gene Expression in Pediatric Tumors of the Kidney

By Shigeru Takamizawa, Shinya Okamoto, Warren Bishop, Judy Wen, Ken Kimura, and Anthony Sandler  
Iowa City, Iowa

**Background/Purpose:** Apoptosis, or programmed cell death, is essential in maintaining normal homeostasis of tissues. The process of apoptosis is controlled by numerous pro- and antiapoptotic factors. Variations in expression of such factors may account for some variations in tumor behavior. This study evaluates the expression of apoptotic mRNA species in pediatric renal tumors to determine whether a pattern of differential apoptosis gene expression correlates with tumor grade and type.

**Methods:** Twenty-five frozen tissue specimens were obtained from patients undergoing biopsy or resection of pediatric renal tumors before chemotherapy: Wilms' tumor stage II (WT-II,  $n = 4$ ); Wilms' tumor stage III/IV (WT-III/IV,  $n = 4$ ); clear cell sarcoma of the kidney stage III (CCSK,  $n = 2$ ); rhabdoid tumor of the kidney stage III/IV (RTK,  $n = 4$ ); and normal kidney (NK,  $n = 11$ ). An RNase Protection Assay (RPA) was performed for 19 pro- and antiapoptotic mRNA species to detect and quantify expression (percentage of GAPDH expressed). Expression of specific mRNAs of interest were confirmed by Western Blot (WB).

**Results:** The expression of apoptotic mRNA species varied markedly between tumors. WT-II expressed greater amounts

of proapoptotic receptor mRNA than CCSK or RTK. (Fas,  $17.0 \pm 2.7\%$  v  $2.5 \pm 0.5\%$  v  $3.3 \pm 0.9\%$ ;  $P < .02$ ; DR5,  $77.0 \pm 8.8\%$  v  $13.5 \pm 0.5\%$  v  $27.0 \pm 4.8\%$ ;  $P < .001$ ; TNF-R,  $71.3 \pm 17.0\%$  v  $21.0 \pm 4.0\%$  v  $29.0 \pm 5.0\%$ ;  $P < .07$ , respectively). Surprisingly, antiapoptotic factors (eg, *bcl-2* and *bcl-xl*) were not overexpressed in poor prognostic tumors (CCSK, RTK) compared with those with good prognosis (WT). Expression of TRAIL (a ligand for DR4 and DR5) was significantly lower in CCSK and RTK than in normal kidney ( $9.5 \pm 1.5\%$  v  $56.1 \pm 10.1\%$ ;  $P = .01$ ).

**Conclusions:** Proapoptotic receptors are expressed at greater levels in good prognostic tumors, and this finding is compatible with their clinical behavior. Knowledge of differential apoptotic gene expression is of potential value in predicting prognosis and treating such tumors with targeted ligands. *J Pediatr Surg* 35:390-395. Copyright © 2000 by W.B. Saunders Company.

**INDEX WORDS:** Wilms' tumor, clear cell sarcoma of the kidney, rhabdoid tumor of the kidney, apoptosis, pediatric renal tumors.

**W**ILMS' TUMOR is the most common primary malignant renal tumor of childhood and accounts for 5% to 6% of all childhood cancers in the United States. The survival rate of Wilms' tumor stage II and stage III/IV are 92.2% and 73%, respectively.<sup>1</sup> Clear cell sarcoma of the kidney (CCSK) and rhabdoid tumor of the kidney (RTK) are other malignant pediatric renal tumors that show aggressive behavior and poor prognoses. The 6-year relapse-free survival rate of CCSK is about 60%,<sup>2</sup> and only 10% of patients with RTK survive despite aggressive antitumor therapy.<sup>3</sup>

Apoptosis, or programmed cell death, is the process by which activated cells undergo a suicide program that

results in individual cell death. This is a highly orchestrated process in which cells neatly commit suicide by destroying themselves in a regulated fashion. Apoptosis is a normal physiological process that occurs in the developing embryo as well as in mature animals during tissue turnover and during down-regulation of an immune response. Proper regulation of this process is essential for normal homeostasis and tissue development.<sup>4,5</sup> An aberration in the process of apoptosis may contribute to the pathogenesis of cancer.

A depletion of proapoptotic (death) factors or an abundance of antiapoptotic (survival) mediators, could result in failure of dividing cells to undergo apoptosis and contribute to tumorigenicity. Proapoptotic proteins such as Fas, Fas-L, TNFR, TRAIL, DR4, DR5, Bax, Bix, Bak, and Bcl-xs induce apoptosis by either signaling for the activation of proteolytic enzymes called caspases that destroy the cell, or by blocking inhibitors of apoptosis.<sup>6</sup> Antiapoptotic proteins such as Bcl-2, Bcl-xl, and mcl-1 inhibit adapter molecules needed for activation of caspases during apoptosis and hence prolong cell survival.<sup>7</sup>

The balance between pro- and antiapoptotic genes may be critical to the behavior and survival of tumor cells.

From the Department of Surgery and Pediatrics, University of Iowa Hospitals & Clinics, Iowa City, IA.

Presented at the 30th Annual Meeting of the American Pediatric Surgical Association, Rancho Mirage, California, May 16-19, 1999.

This work was supported by a grant from the Children's Miracle Network, sponsored by The University of Iowa.

Address reprint requests to Anthony D. Sandler MD, Department of Surgery, Section of Pediatric Surgery, The University of Iowa Hospitals and Clinics, 200 Hawkins Dr, Iowa City, IA 52242.

Copyright © 2000 by W.B. Saunders Company  
0022-3468/00/3502-0047\$03.00/0

Variations in expression of such factors may account for some of the variations in tumor behavior observed clinically. This study evaluates the expression of apoptotic mRNA species in pediatric renal tumors to determine whether a pattern of differential apoptosis gene expression correlates with tumor stage and type.

## MATERIALS AND METHODS

### Tissue Collection

Twenty-five frozen tissue kidney biopsy or resection specimens were obtained from pediatric patients with renal tumors before chemotherapy at the University of Iowa Hospitals & Clinics and from the National Wilms Tumor Study Group (NWTSG) tissue bank. Tissue specimens were grouped according to clinical stage of disease and tumor type: Wilms' tumor stage II (WT-II,  $n = 4$ ), Wilms' tumor stage III/IV (WT III/IV,  $n = 4$ ), clear cell sarcoma stage III (CCSK,  $n = 2$ ), rhabdoid tumor of the kidney stage III/IV (RTK,  $n = 4$ ), and normal adjacent kidney (NK,  $n = 11$ ). All protocols and tissues harvested were approved by our Institutional Review Board.

### RNase Protection Assay

RNase Protection Assay (RPA) is a highly sensitive and specific procedure that allows for simultaneous detection and quantification of multiple mRNA species. RPA was used to detect and quantify 19 different mRNA apoptotic species expression with 2 human template probe sets, hApo-2 and hApo-3c. (The RiboQuant Multi-probe protection assay system; Pharmingen, San Diego, CA). The probe set hApo-2 includes 8 *bcl-2*-related gene templates including *bcl-x1*, *bcl-xs*, *bfl-1*, *bik*, *bak*, *bax*, *bcl-2*, and *mcl-1*. The hApo-3c probe set includes 11 proapoptotic and tumor necrosis factor family-related gene templates, namely, caspase-8, *Fas-L*, *Fas*, *DCR1*, *DR3*, *DR5*, *DR4*, *TRAIL*, *TNFRp55*, *TRADD*, and *RIP*.

After isolating RNA from the tissues of interest, the antisense RNA probe was hybridized in excess to target RNA in-solution. Free probe and nonhybridized single stranded RNA are digested with RNases. Phosphorus P32-labeled antisense RNA was transcribed using T7 RNA polymerase (Pharmingen) and [ $\alpha$ -<sup>32</sup>P]UTP (Amersham Life Science, England). Total RNA was extracted from tissue using TRIzol (Gibco Life Technologies, MD). Fourteen to 16  $\mu$ g of total RNA was hybridized with the <sup>32</sup>P-labeled RNA probes, which were transcribed from hApo-2 or hApo-3c multiprobes (DNA templates) at 56°C overnight, followed by digestion with a 1:417 dilution of RNase "cocktail" (RNase A:T1 mixture; Pharmingen) for 45 minutes at 30°C. Single-stranded and unhybridized excess mRNA was digested by the RNase cocktail. The protected double-stranded RNA pellets were dried and resuspended in 5  $\mu$ L of 1 $\times$  loading buffer (Pharmingen), and electrophoretically resolved on 5% polyacrylamide, 8 mol/L urea gel. The polyacrylamide-urea gel was dried on blotting paper for 1 hour at 80°C. The labeled probes were then quantified by autoradiography by exposing the blotting paper to BIO MAX FILM (Kodak, NY) with an intensifying screen (Kodak) for 20 hours at 80°C.

### Radioanalytic Imaging

For comparative analysis, we quantified mRNA species expression as a percentage of mRNA GAPDH expression. Radioactivity of each band in the sample was quantified, standardized, and compared with GAPDH expression of that sample. Radioactivity of each template was quantified directly from the gel by a radioanalytic imaging system (AMBIS 4000, AMBIS Inc, San Diego, CA) equipped with AMBIS QuantProbe Software Version 3.0 for 1,000 minutes. Net counts were obtained from each template (band), including GAPDH, and the radioactive ratio of each mRNA to GAPDH was calculated.

### Western Blot for Fas Receptor Protein Expression

The standard technique of Western Blot (WB) was performed.<sup>8</sup> Briefly, tissue lysate proteins from WT stage II ( $n = 2$ ), RTK ( $n = 1$ ), and NK ( $n = 2$ ) were isolated by solubilizing in RIPA buffer (1% Triton X-10, 1% Deoxycholate [DOC], 0.1% sodium dodecyl sulfate [SDS], 50 mmol/L Tris-HCl [pH 7.4], 150 mmol/L NaCl, 0.5 mmol/L Na<sub>3</sub>VO<sub>4</sub>, 5 mmol/L EDTA), and protease inhibitors; leupeptin (20  $\mu$ g/mL RIPA), phenylmethylsulfonyl fluoride (PMSF 20  $\mu$ g/mL RIPA). The protein content was equilibrated between samples by using the Lowry protein assay to quantify protein isolated.<sup>9</sup> Subsequently, 120  $\mu$ g of total protein from each specimen was electrophoretically resolved on SDS-containing 8% polyacrylamide gels. Separated proteins were then transferred to a nitrocellulose membrane at 210 mAmps for 4 hours. Membranes were blocked using 5% skim milk in Tris-buffered saline (TBS), supplemented with 0.1% Tween-20 (TBS-T), overnight at 4°C. The nitrocellulose membrane was rinsed with TBS-T and incubated for 1 hour at room temperature in a sealed bag with 1.0  $\mu$ g/mL of the antihuman Fas rabbit polyclonal antibody (Santa Cruz Biotechnology Inc, Santa Cruz, CA) in 5 mL of 5% dry milk in TBS-T. Bound antibody was detected with a 1:2500 dilution of horseradish peroxidase (HRP)-labeled goat antirabbit IgG secondary antibody (SIGMA, MO). Bands denoting Fas expression were viewed after developing on radiographic plates by enhanced chemiluminescence (ECL; Amersham, Arlington Heights, IL).

### Data Analysis

Percent gene expression was compared between the groups using one-way analysis of variance (ANOVA) for *Fas*, *DR4*, *DR5*, *TNFR*, *TRAIL* and *Bcl-2*. The square root transformation was applied to *Fas* and *TNFR*, and the natural logarithm transformation was applied to *Bcl-2* and *TRAIL* before analysis to stabilize the variance among the groups or to normalize the data distribution. A nonparametric test (Kruskal-Wallis test) was applied to *Bax* and *Bcl-xL* because no suitable transformation was found. If the one-way ANOVA F-test or the Kruskal-Wallis test was significant, pairwise comparisons between the groups were performed. To adjust for the multiple tests, Bonferroni's method was used, and the adjusted *P* values less than .05 were considered statistically significant.

## RESULTS

To determine if an association between apoptosis genes and tumor stage and type existed, we categorized the apoptosis mRNA species studied into 2 groups, namely proapoptosis and antiapoptosis species. Comparisons were made between the different tumor types and clinical stages of disease (WT II [ $n = 4$ ] v WT III/IV [ $n = 4$ ] v CCSK III [ $n = 2$ ] v RTK III/IV [ $n = 4$ ] v NK [ $n = 11$ ]) and between groups of tumors (WT [ $n = 8$ ] v CCSK/RTK [ $n = 6$ ] v NK [ $n = 11$ ]).

### Proapoptosis Genes

Concerning the proapoptosis mRNA species, all 15 (*bcl-xs*, *bik*, *bak*, *bax*, *caspase-8*, *Fas-L*, *Fas*, *DCR1*, *DR3*, *DR5*, *DR4*, *TRAIL*, *TNFRp55*, *TRADD*, and *RIP*) were detected in all samples at different intensities (Fig 1). Six species of interest reflecting the proapoptotic pathways were selected for statistical analysis based on their gross differences in expression (*bax*, *Fas*, *DR5*, *DR4*, *TRAIL*, and *TNFRp55*).

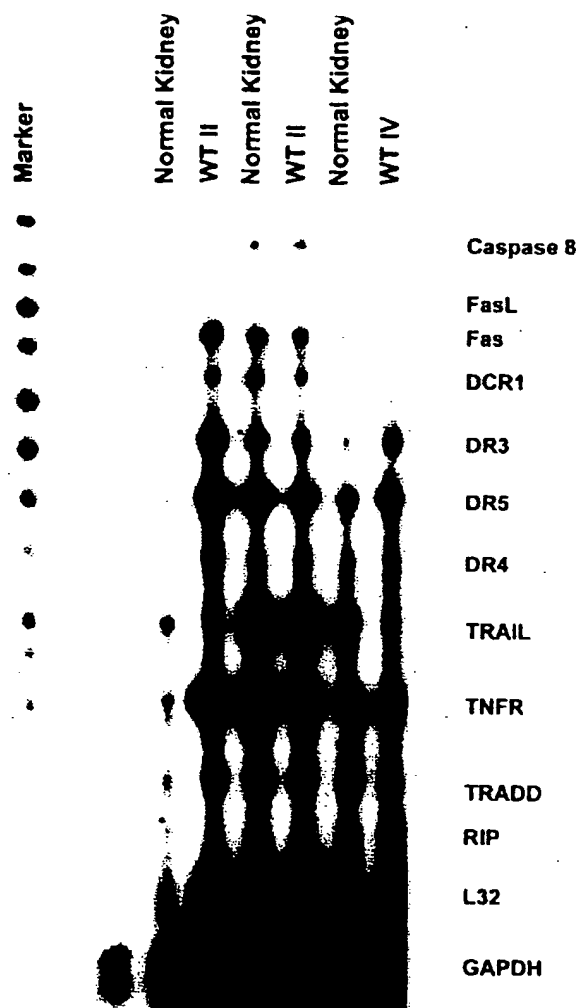


Fig 1. Sample RPA of tissues evaluating proapoptotic (TNF related family) mRNA species. The radioactivity of each band (mRNA specie) is calculated and quantified as a percent of GAPDH expressed.

**Fas.** WT stage II/III/IV showed greater expression ( $13.1 \pm 2.8\%$ ) compared with CCSK/RTK ( $3.0 \pm 0.6\%$ ;  $P = .01$ ) and tended to be greater than NK ( $5.6 \pm 0.9\%$ ;  $P = .09$ ). WT-II, had the greatest expression of Fas mRNA ( $17.0 \pm 2.7\%$ ) compared with WT III/IV ( $9.3 \pm 4.3\%$ ;  $P = .2$ ), CCSK ( $2.5 \pm 0.5\%$ ;  $P = .015$ ), RTK ( $3.3 \pm 0.9\%$ ;  $P = .004$ ) and NK ( $5.6 \pm 0.9\%$ ;  $P = .008$ ).

**DR5.** WT stage II/III/IV expressed greater amounts ( $59.1 \pm 8.1\%$ ) compared with CCSK/RTK ( $22.5 \pm 4.2\%$ ;  $P = .008$ ) and NK ( $25.8 \pm 4.3\%$ ;  $P = .004$ ). WT-II had the greatest expression of DR5 mRNA ( $77.0 \pm 8.8\%$ ) compared with WT-III/IV ( $41.3 \pm 3.6\%$ ;  $P = .019$ ), CCSK ( $13.5 \pm 0.5\%$ ;  $P = .0003$ ), RTK ( $27.0 \pm 4.8\%$ ;  $P = .0005$ ) and NK ( $25.8 \pm 4.3\%$ ;  $P < .0001$ ).

**TNFRp55.** WT-II tended to have the greatest expres-

sion ( $71.3 \pm 16.9\%$ ) compared with CCSK ( $21.0 \pm 4.0\%$ ;  $P = .058$ ) and RTK ( $29.0 \pm 5.0\%$ ;  $P = .07$ ).

**TRAIL.** The expression of TRAIL mRNA (proapoptotic ligand) was significantly lower in CCSK/RTK ( $9.5 \pm 1.5\%$ ) compared with NK ( $56.1 \pm 10.1\%$ ;  $P = .01$ ). Normal kidney adjacent to benign mesoblastic nephroma or normal kidney with unrelated disease had lower TRAIL expression ( $13.7 \pm 3.7\%$ ) than normal kidney adjacent to CCSK and RTK ( $74.0 \pm 13.0\%$ ;  $P = .02$ ).

**Bax.** CCSK/RTK had greater expression of Bax ( $39.8 \pm 6.7\%$ ) compared with NK ( $12.9 \pm 2.0\%$ ;  $P = .003$ ). WT-II ( $32.3 \pm 5.4\%$ ;  $P = .049$ ) and RTK ( $41.8 \pm 10.2\%$ ;  $P = .009$ ) had significantly greater expression of Bax mRNA compared with NK ( $12.9 \pm 2.0\%$ ).

**DR4.** There was no difference in mRNA DR4 expression. (WT stage II,  $19.0 \pm 2.1\%$ ; WT stage III/IV,  $15.8 \pm 1.5\%$ ; CCSK,  $6.0 \pm 1\%$ ; RTK,  $12.8 \pm 3.0\%$ ; and NK,  $13.8 \pm 2.1\%$ ;  $P = .1$ ).

In general, these results show that proapoptotic mediators are more abundantly expressed in tumors with a better stage and prognosis. These findings imply that such tumors have the machinery in place that will allow for the process of apoptosis (Fig 2).

#### Antiapoptosis Genes

All 4 antiapoptosis gene mRNA species (*bcl-xl*, *bfl-1*, *bcl-2* and *mcl-1*) were detected in all samples at different intensities and of those, *bcl-xl* and *bcl-2* were compared (Fig 3).

**bcl-2.** Surprisingly, this inhibitor of apoptosis was expressed at significantly lower levels in poor prognostic tumors (CCSK/RTK  $8.5 \pm 2.1\%$ ) compared with NK ( $14.5 \pm 0.5\%$ ;  $P = .03$ ). RTK also had significantly lower expression of *bcl-2* mRNA ( $5.3 \pm 0.9\%$ ) compared with WT II ( $15.0 \pm 3.6\%$ ;  $P = .02$ ), WT III/IV

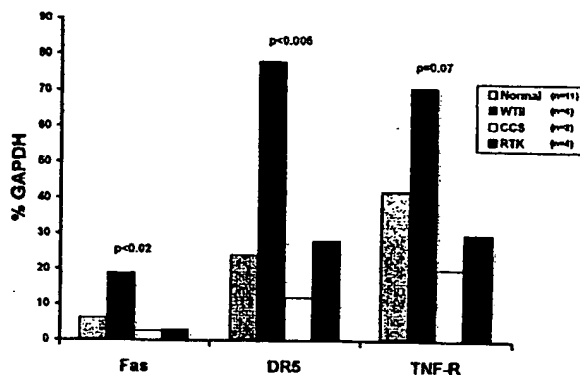


Fig 2. Differences in Fas, DR5 and TNF-R mRNA expression in normal kidney (Normal), Wilms' tumor Stage II (WTII), Clear cell Sarcoma Stage III (CCSK), and Rhabdoid tumor of the kidney stage III/IV (RTK). Note that in each case, WT has the greatest expression of the mRNA of interest.

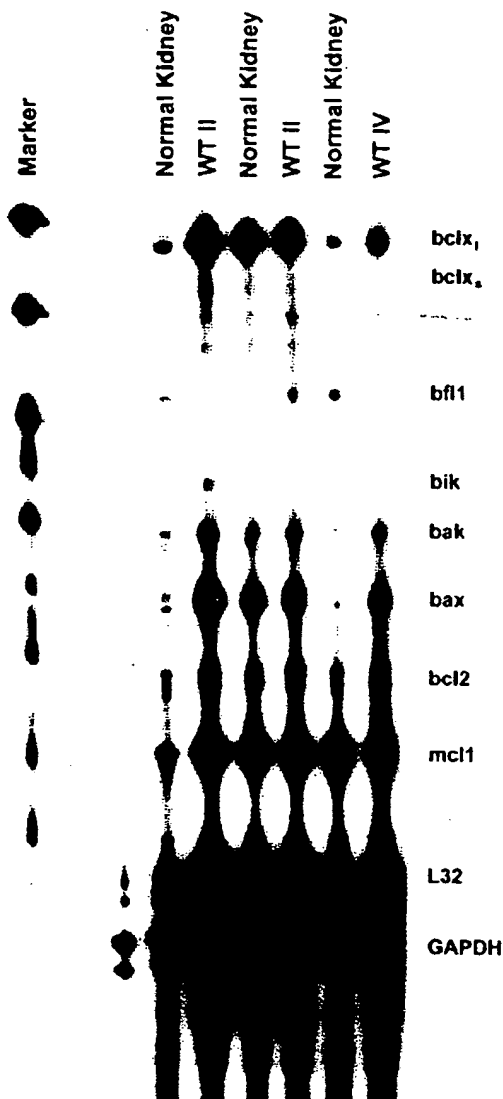


Fig 3. Sample RNase Protection Assay (RPA) of tissues evaluating *bcl-2*-related family mRNA species. The radioactivity of each band (mRNA species) is calculated and quantified as a percent of GAPDH expressed.

( $13.8 \pm 2.3\%$ ;  $P = .024$ ), CCSK ( $15.0 \pm 0.0\%$ ;  $P = .04$ ), and NK ( $14.5 \pm 0.5\%$ ;  $P = .001$ ).

*bcl-xl*. There was no difference in *bcl-xl* mRNA expression between the various stages or type of renal tumors ( $P = .2$ ). The lower expression of the antiapoptotic factor Bcl-2 in RTK (which carries the worst prognosis) was initially surprising considering previous literature reports.<sup>10</sup> However, in the absence of significant levels of proapoptotic gene expression, the need for abundant expression of antiapoptotic factors may be redundant.

#### Western Blot for Fas and Bcl-xl Proteins

To determine if greater mRNA expression detected by RPA translated into greater protein expression, we selec-

tively performed WB of Fas expression from NK, WTII, and RTK. WB showed a positive Fas band at 45 kDa in WTII, which was far brighter than expression in NK or RTK. This helped in verifying the accuracy of RPA analysis (Fig 4).

#### DISCUSSION

Apoptosis gene expression may contribute to the viability of tumors and may account for their varied clinical behavior. If such a concept were true, predicting the prognosis of tumors would be dependent on their biology, and treatment could be tailored to block or stimulate specific apoptotic factors of interest. The current study was undertaken to explore whether variations in apoptotic gene expression correlate with stage and type of pediatric renal tumors.

Despite the relatively small numbers in this study, it was clear that WT-stage II (in general a good prognostic tumor) expressed proapoptotic mRNA species more abundantly than CCSK or RTK, 2 tumors of worse prognosis. Specifically, Fas, DR5 and TNF-R, representing a family of "death receptors," were all expressed at greater levels in Wilms' tumor stage II. These cell surface receptor proteins bind to specific ligands (Fas-L, TRAIL, and TNF, respectively) that induce activation of proteolytic enzymes called caspases. The caspase cascade disassembles and ultimately destroys the cell.<sup>6</sup> Relating prognosis to expression of proapoptotic receptors is an appealing theory, because both cytotoxic T lymphocytes (CTL) and natural killer (NK) immune surveillance cells use such ligands for killing of target cells.<sup>11,12</sup> Furthermore, TNFR-1, Fas, DR3, and DR4 are activated on overexpression in a ligand-independent manner and may spontaneously induce apoptosis.<sup>13-16</sup>

The mRNA of DR5 is detected in several normal human tissues, and the amount of DR5 transcription is reported to be 100-fold more in most tumor cell lines than in normal tissues.<sup>17</sup> The expression of DR4 or DR5 in tumors of poor prognosis was no different to that of normal kidney in the current study, whereas expression of DR5 in WT II was about 3-fold greater. The ligand for DR4 and DR5 (TRAIL, TNF related apoptosis-inducing

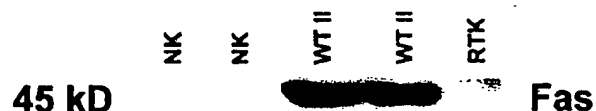


Fig 4. Western Blot (WB) analysis of selected samples looking at Fas protein expression. The differential expression of protein detected by WB correlated with the differential expression of mRNA detected by RPA. Note the absence of Fas bands in the normal kidney (NK) and rhabdoid tumor of the kidney (RTK) lanes, with bright bands in the Wilms tumor stage II (WTII) lanes. This observation verifies the accuracy of RPA results.

ligand) is shown to induce killing of several tumor cell lines, thus expression of these receptors may have therapeutic implications.<sup>18</sup>

The balance between expression of apoptosis-inducing receptors and their ligands may regulate cell susceptibility to undergoing apoptosis.<sup>19</sup> We have shown that overexpression of Fas-L induces apoptosis in Fas-expressing HepG2/C3A hepatoblastoma cell lines by inducing cell suicide (Unpublished data). Fas-L was barely detectable in any of the tumor specimens examined, thus, this suicide effect is probably inconsequential. However, TRAIL, along with its receptors, was expressed in many of the tumors at relatively high levels. The balance between TRAIL and DR4/DR5 receptors potentially could have a regulatory effect on apoptosis in these tumors. It is of interest to note that normal kidney had a nearly 10-fold greater expression of TRAIL than adjacent CCSK or RTK. Although purely conjectural, this phenomenon may be a defensive response of the normal kidney to invasion of the adjacent tumor. Comparatively high levels of expression were not seen in normal kidney biopsied from unrelated disease or when benign mesoblastic nephroma was the adjacent tumor.

Bcl-2 and Bcl-xL are antiapoptosis proteins localized to the outer mitochondrial membrane, endoplasmic reticulum, and nuclear membranes of cells. These factors suppress apoptosis and allow proliferation and prolonged survival that may explain tumor cell viability. Although *bcl-2* is one of the most noted antiapoptosis genes, the correlation between *bcl-2* overexpression and tumor behavior is uncertain. Conflicting studies are reported in neuroblastoma, a childhood malignancy of neurogenic origin. Overexpression of *bcl-2* is said to correlate with tumor progression, poor prognosis, and unfavorable histology,<sup>10,20</sup> whereas another study suggests that *bcl-2* expression is associated with favorable histology.<sup>21</sup> Despite these reports, the expression of *bcl-2* or *bcl-xL* mRNA did not show any correlation between renal tumor

type, stage of disease or normal kidney in our study. The lower expression of the antiapoptotic factor Bcl-2 in RTK (which carries the worst prognosis) seems inconsistent, but in the absence of significant levels of proapoptotic gene expression, the need for abundant expression of antiapoptotic factors may be redundant.

Proapoptosis (*bax*, *bik*, *bak* and *bcl-xs*) and antiapoptosis (*bcl-2*, *bcl-xL*, *bfl-1*, *mcl-1*) activity is different among *bcl-2* gene-related family members.<sup>22</sup> However, there was no association between the ratio of pro- to antiapoptotic *bcl-2*-related mRNA species in the tumors studied. Bcl-2 inhibits apoptosis induced by the tumor suppressor gene *p53*.<sup>23,24</sup> Consequently, the role of *bcl-2* in such tumors cannot be completely understood without studying the associated expression of *p53*.

To determine whether differences in mRNA expression detected by RPA translated into differences in actual protein expression, we examined Fas protein expression by WB and compared its expression with RPA results for several tumors and normal kidney. The differences noted between tumors and normal tissue by RPA were confirmed in that we found Fas followed the same differential pattern of protein expression. This finding helped verify the accuracy of the results obtained by RPA analysis.

In general, these findings show that proapoptosis genes are expressed at greatest levels in good prognostic renal tumors, whereas expression is less in normal kidney and lowest in poor prognostic tumors. This suggests that good prognostic tumors may readily undergo apoptosis, whereas diminished expression of apoptosis genes in normal mature tissue may reflect a state of senescence. Poor prognostic tumors are rapidly proliferating, independent of proapoptotic mediators.

#### ACKNOWLEDGMENTS

The authors thank Paul Grundy and the National Wilms Tumor Study Group (NWTSG) for supplying many of the specimens used in this study.

#### REFERENCES

1. D'Angio GJ, Breslow N, Beckwith JB, et al: Treatment of Wilms' tumor. Results of the third National Wilms' Tumor Study. *Cancer* 64:349-360, 1989
2. Green DM, Breslow N, Beckwith JB, et al: Treatment of children with clear-cell sarcoma of the kidney: A report from national Wilms' Tumor Study Group. *J Clin Oncol* 12:212-217, 1994
3. Palmer NF, Sutow W: Clinical aspect of the rhabdoid tumor of the kidney: A report of the National Wilms' Tumor Study Group. *Med Pediatr Oncol* 11:242-245, 1983
4. Miller L, Marx J: Apoptosis. *Science* 281:1301, 1998
5. Steller H: Mechanisms and genes of cellular suicide. *Science* 267:1445-1449, 1995
6. Ashkenazi A, Dixit VM: Death receptors: Signaling and modulation. *Science* 281:1305-1308, 1998
7. Adams JM, Cory S: The Bcl-2 protein family: Arbiters of cell survival. *Science* 281:1322-1326, 1998
8. Fogh J, Fogh JM, Orfeo T: One hundred and twenty-seven cultured human tumor cell lines producing tumors in nude mice. *J Natl Cancer Inst* 59:221-226, 1977
9. Lowry O, Rosebrough NJ, Farr AL, et al: Protein measurement with folinphenol reagent. *J Biol Chem* 193:265, 1951
10. Castle VP, Heidelberger KP, Bromberg J, et al: Expression of the apoptosis-suppressing protein *bcl-2*, in neuroblastoma is associated with unfavorable histology and N-myc amplification. *Am J Pathol* 143:1543-1550, 1993
11. Liston P, Roy N, Tamal K, et al: Suppression of apoptosis in mammalian cells by NAIP and a related family of IAP genes. *Nature* 379:349-353, 1996
12. Deveraux QL, Takahashi R, Salvesen GS: X-linked IAP is a direct inhibitor of cell-death proteases. *Nature* 388:300-304, 1997
13. Muzio M, Chinnaiyan AM, Kischkel FC, et al: FLICE, a novel FADD-homologous ICE/CED-3-like proteins, is recruited to the CD95(Fas/Apo-1) death-inducing signaling complex. *Cell* 85:817-827, 1996

14. Chinnaiyan AM, O'Rourke, Yu GL, et al: Signal transduction by DR3, a death domain-containing receptor related to TNFR-1 and CD95. *Science* 274:990-992, 1996
15. Kitson J, Raven T, Jiana YP, et al: A death-domain-containing receptor that mediates apoptosis. *Nature* 384:372-375, 1996
16. Pan G, O'Rourke K, Chinnaiyan AM, et al: The receptor for the cytotoxic ligand TRAIL. *Science* 276:111-113, 1997
17. MacFarlane M, Ahmad M, Srinivasula SM, et al: Identification and molecular cloning of two novel receptors for the cytotoxic ligand TRAIL. *J Biol Chem* 272:25417-25420, 1997
18. Walczak H, Miller RE, Ariail K, et al: Tumoricidal activity of tumor necrosis factor-related apoptosis-inducing ligand in vivo. *Nat Med* 5:157-163, 1999
19. Muller M, Strand S, Hug H, et al: Drug-induced apoptosis in hepatoma cells is mediated by the CD95(APO-1/Fas) receptor/ligand system and involves activation of wild-type p53. *J Clin Invest* 99:403-413, 1997
20. Hoehner J, Hedborg F, Wiklund HJ, et al: Cellular death in Neuroblastoma: In situ correlation of apoptosis and bcl-2 expression. *Int J Cancer* 62:19-24, 1995
21. Krajewski S, Chatten J, Handa H, et al: Immunohistochemical analysis of the Bcl2 oncoprotein in human neuroblastoma. *Lab Invest* 72:42-54, 1995
22. D'sa-Eipper C, Subramanian T, Chinnadurai G, et al: bfl-1, a bcl-2 homologue, suppresses p53-induced apoptosis and exhibits potent cooperative transforming activity. *Cancer Res* 56:3879-3882, 1996
23. Miyashita T, Krajewski S, Krajewski M, et al: Tumor suppressor p53 is a regulator of bcl2 and bax gene expression in vitro and in vivo. *Oncogene* 9:1799-1805, 1994
24. Brambilla E, Negoescu A, Grazzini S, et al: Apoptosis-related factors p53, bcl2, and Bax in neuroendocrine lung tumors. *Am J Pathol* 149:1941-52, 1996

# Hypoxia-Inducible Factor-1 (HIF-1) Up-Regulates Adrenomedullin Expression in Human Tumor Cell Lines during Oxygen Deprivation: A Possible Promotion Mechanism of Carcinogenesis

Mercedes Garayoa, Alfredo Martínez, Sunmin Lee, Rubén Pío,  
Won G. An, Len Neckers, Jane Trepel, Luis M. Montuenga,  
Heather Ryan, Randall Johnson, Max Gassmann, and  
Frank Cuttitta

Department of Cell and Cancer Biology (M.G., A.M., S.L., R.P.,  
W.G.A., L.N., J.T., F.C.)  
National Cancer Institute  
National Institutes of Health  
Bethesda, Maryland 20892

Department of Histology and Pathology (L.M.M.)  
University of Navarra  
31080 Pamplona, Spain

Department of Biology (H.R., R.J.)  
University of California San Diego  
La Jolla, California 92093

Institute of Physiology (M.G.)  
University of Zürich-Irchel  
CH-8057, Switzerland

Little is known about the molecular mechanisms that control adrenomedullin (AM) production in human cancers. We demonstrate here that the expression of AM mRNA in a variety of human tumor cell lines is highly induced in a time-dependent manner by reduced oxygen tension (1% O<sub>2</sub>) or exposure to hypoxia mimetics such as desferrioxamine mesylate (DFX) or CoCl<sub>2</sub>. This AM expression seems to be under hypoxia-inducible factor-1 (HIF-1) transcriptional regulation, since HIF-1 $\alpha$  and HIF-1 $\beta$  knockout mouse cell lines had an ablated or greatly reduced hypoxia AM mRNA induction. Similarly, inhibition or enhancement of HIF-1 activity in human tumor cells showed an analogous modulation of AM mRNA. Under hypoxic conditions, immunohistochemical analysis of tumor cell lines revealed elevated levels of AM and HIF-1 $\alpha$  as compared with normoxia, and we also found an increase of immunoreactive AM in the conditioned medium of tumor cells analyzed by RIA. AM mRNA

stabilization was shown to be partially responsible for the hypoxic up-regulated expression of AM. In addition, we have identified several putative hypoxia response elements (HREs) in the human AM gene, and reporter studies with selected HREs were capable of enhancing luciferase expression after exposure to DFX. Furthermore, transient co-expression of HIF-1 $\alpha$  resulted in an augmented transactivation of the reporter gene after DFX treatment. Given that most solid human tumors have focal hypoxic areas and that AM functions as a mitogen, angiogenic factor, and apoptosis-survival factor, our findings implicate the HIF-1/AM link as a possible promotion mechanism of carcinogenesis. (Molecular Endocrinology 14:848-862, 2000)

## INTRODUCTION

Adrenomedullin (AM) is a recently discovered hypotensive peptide isolated from a human pheochromocytoma (1). The cDNAs for human, rat, mouse, pig, and cow AM have been cloned and the genomic organi-

zation profile for human and mouse identified (2, 3). This peptide has been shown to mediate a multifunctional response in cell culture and animal systems that includes regulation of cardiovascular tone, bronchodilation, modulation of central brain function, natriuretic and diuretic action, antimicrobial activity, inhibition of hormone release, growth regulation, apoptosis survival, and induction of angiogenesis (see review in Refs. 4–6).

Several prior reports have demonstrated AM and its corresponding receptor (AM-R) to be ubiquitously expressed during embryogenesis and carcinogenesis. Early in both mouse and rat fetal development AM/AM-R are first detected in the heart, and then they appear progressively in other anatomical sites during organogenesis (7, 8). Maternal decidual cells and embryonic cells (fetal cytotrophoblast giant cells) of the ectoplacental cone, a site that mimics the invasion process of carcinogenesis, also show abundant expression of AM/AM-R (8, 9). After its initial identification in a human pheochromocytoma, further studies have demonstrated increased AM expression in tumor tissue of ganglioneuroblastoma, neuroblastoma, and adrenocortical carcinomas (10, 11). In addition, AM plasma levels are elevated in patients with gastrointestinal or lung cancer (12). Our group has shown that AM and AM-R are expressed in human tumor cell lines of the lung, breast, colon, ovary, prostate, brain, cartilage, and blood (13). In several of these lines, AM functioned as an autocrine proliferation factor whose effect could be inhibited by a neutralizing monoclonal antibody (MoAb-G6) causing growth cessation *in vitro* (13). Recently, it has been shown that hypoxic conditions or exposure to  $\text{CoCl}_2$  (a transition metal that mimics hypoxia) induces an increase in AM mRNA expression and protein production in a human colorectal carcinoma cell line, DLD-1 (14).

Focal areas of low oxygen tension ( $\leq 2.0\% \text{ O}_2$ ) are inherent to the biological processes of embryogenesis, wound repair, and carcinogenesis (15–17). A state of diminished free oxygen availability results when regional growth demands exceed the oxygen supply of the capillary bed (15). Under such conditions, an oxygen-sensing mechanism activates a transcription factor known as hypoxia-inducible factor-1 (HIF-1), which in turn up-regulates a series of genes that support the cell to compensate for the potentially lethal microenvironment (18). HIF-1 is a heterodimer composed of HIF-1 $\alpha$  and HIF-1 $\beta$ /ARNT (aryl hydrocarbon receptor nuclear translocator) subunits, both representing members of the PAS (Per, ARNT, Sim) basic-helix-loop-helix family (18). Transcription/translation products of HIF-1 $\alpha$  and HIF-1 $\beta$  are constitutively expressed; however, the HIF-1 $\alpha$  protein contains an oxygen-dependent degradation domain that is rapidly cleaved by the ubiquitin-proteasome pathway under normoxic conditions, thus enabling the modulation of HIF-1 activity in an oxygen-dependent manner (19). Genes transactivated by HIF-1 include aldolase A, enolase 1, erythropoietin (Epo), glucose transporter 1,

heme oxygenase 1, inducible nitric oxide synthase, lactate dehydrogenase A, phosphofructokinase L, phosphoglycerate kinase 1, transferrin (Tf), vascular endothelial growth factor (VEGF), and endothelin-1 (ET-1) (18, 20). Low oxygen tension is known to play a critical role in embryonic development, causes the emergence of drug/radiation-resistant tumor cells, enhances mutagenesis of neoplastic lesions, and elevates metastatic potential of the tumor (15, 21–24).

The way AM gene expression is regulated in human tumors is not yet known, but a decrease in oxygen tension could be a major cause for the induction of this molecule. In our present study we actually demonstrate the ability of hypoxia and hypoxia mimetics to up-regulate the AM message and protein expression in a variety of human tumor cell lines. We also made use of both molecular and biochemical characterization approaches to support that this induction is mediated by transactivation of the AM promoter by HIF-1 transcription factor as well as posttranscriptional mRNA stabilization.

## RESULTS

### AM mRNA Induction in Human Tumor Cell Lines under Hypoxic Treatments

Northern analysis for AM mRNA expression in a variety of human tumor cell lines (cancers of the lung, breast, colon, ovary, prostate, bone, and blood) demonstrated a consistent increase in message induced by exposure to  $1\% \text{ O}_2$ , desferrioxamine (DFX), or  $\text{CoCl}_2$ . All 17 cell lines evaluated in this manner showed inducible AM expression, and Fig. 1 illustrates a representative example of the observed responses to our test conditions (6 h exposure to  $100 \mu\text{M} \text{ CoCl}_2$ , 6 h exposure to  $260 \mu\text{M} \text{ DFX}$  or 12 h exposure to  $1\% \text{ O}_2$ ). Interestingly, although there is variability of expression in the basal AM mRNA levels between cell lines [the two pulmonary cancer cell lines NCI-H1264 (adenocarcinoma) and NCI-H157 (squamous cell carcinoma) being the opposing extremes], all tumor cell lines show increases in AM message expression on exposure to our hypoxic test conditions, with calculated test/basal ratios ranging from 1.3- to 25-fold.

We have used MCF7 (breast adenocarcinoma) as our standard human cancer cell line for all time course studies with exposures to  $\text{CoCl}_2$ , DFX, or  $1\% \text{ O}_2$ . Figure 2, A–C, demonstrates the induction of AM message at different time increments over a 24–48 h exposure series. Note that although  $\text{CoCl}_2$  exposure causes AM mRNA levels to reach a maximum at 8 h, both DFX and  $1\% \text{ O}_2$  induced an AM message zenith at 12 h, indicating a potential mechanistic difference between test reagents. Induced maximum levels of AM message are maintained with all the hypoxia treatments tested at 24 h of exposure, and even elevated levels are still observed at 48 h of exposure to  $1\% \text{ O}_2$ .



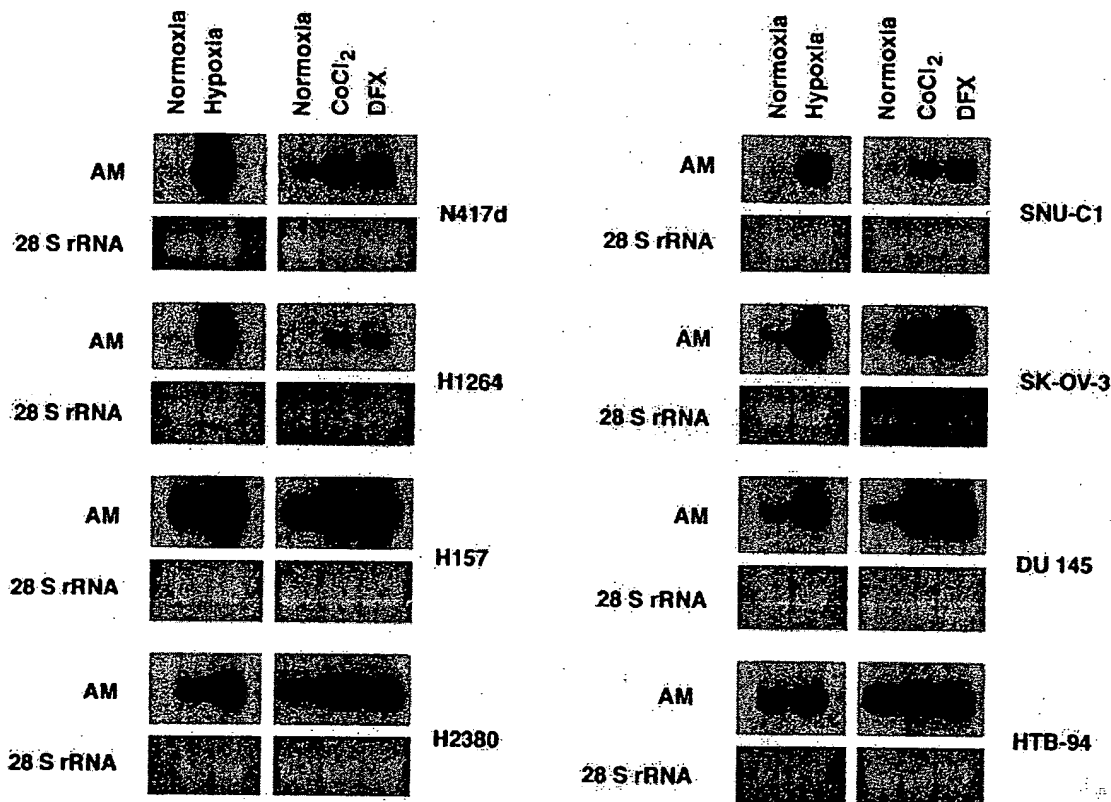


**Fig. 1. Up-Regulation of AM mRNA in Several Human Tumor Cell Lines under Hypoxic Treatments**

Northern blot analysis for AM of cells exposed either to hypoxia mimetics (100  $\mu$ M  $\text{CoCl}_2$ , 260  $\mu$ M DFX) for 6 h, or to a hypoxic atmosphere (1%  $\text{O}_2$ , 5%  $\text{CO}_2$ , 94%  $\text{N}_2$ ) for 12 h, as compared with untreated cells. Cell lines shown here were selected from a total of 17 cell lines tested and also chosen as representatives of the main human tumor types: carcinomas of the lung (N417d, H1264, H157), breast (H2380), colon (SNUC-1), ovary (K-OV-3), prostate (DU 145), or chondrosarcoma (HTB-94). Fifteen micrograms of total RNA were loaded per lane, and ethidium bromide staining of 28 S rRNA was used to check for equal loading and RNA integrity.

Of the three treatments, exposure to 1%  $\text{O}_2$  is the one that shows a steeper induction of AM mRNA over time, and also more dramatic increases between the basal and the maximum induction are observed (>25-fold increase between maximum induction and baseline levels).

We have also performed a parallel analysis for HIF-1 $\alpha$  mRNA in MCF7 cells throughout the hypoxic studies. HIF-1 $\alpha$  transcript levels remained constant or showed a slight decline over time in the  $\text{CoCl}_2$  and 1%  $\text{O}_2$  time course studies (Fig. 2, A and C). This observation is in accordance with other reports indicating that HIF-1 $\alpha$  is mainly regulated not at the transcriptional level but by protein stabilization in hypoxia, whereas the protein is rapidly degraded by the ubiquitin-proteasome pathway during normoxic conditions (19, 25).

#### Under Hypoxic Conditions, AM Is Also Induced at the Protein Level

To address whether the induction of AM mRNA was accompanied by an increase in the production of AM

protein, the presence and cellular localization of AM and HIF-1 $\alpha$  in tumor cell lines at normoxic or hypoxic conditions were studied using double immunofluorescence followed by confocal microscopy. A typical image is shown in Fig. 3, in which prostate carcinoma DU 145 cells are immunostained for both AM (green fluorescence) and HIF-1 $\alpha$  (red fluorescence). At normoxic conditions (Fig. 3, A and B), both AM and HIF-1 $\alpha$  are moderately expressed in the cytoplasm and nucleus of the cells. After 12 h exposure to 260  $\mu$ M DFX, the cells showed a marked increase of AM staining in the cytoplasm and nucleus (Fig. 3C); in agreement with our previous results (26) HIF-1 $\alpha$  immunoreactivity is primarily elevated in the nucleus of the cells (Fig. 3D). Similar patterns of staining were obtained with H157, MCF7, and SNUC-1 cell lines (data not shown).

Since we and other investigators have reported a rapid secretion of the bioactive processed AM peptide by human tumor cells and endothelial cells (13, 27), we also examined the presence of AM in the conditioned medium of MCF7 under hypoxic conditions. As is shown in Fig. 4, a significant increase in immunoreactive AM (IR-AM) was observed for MCF7 cells treated

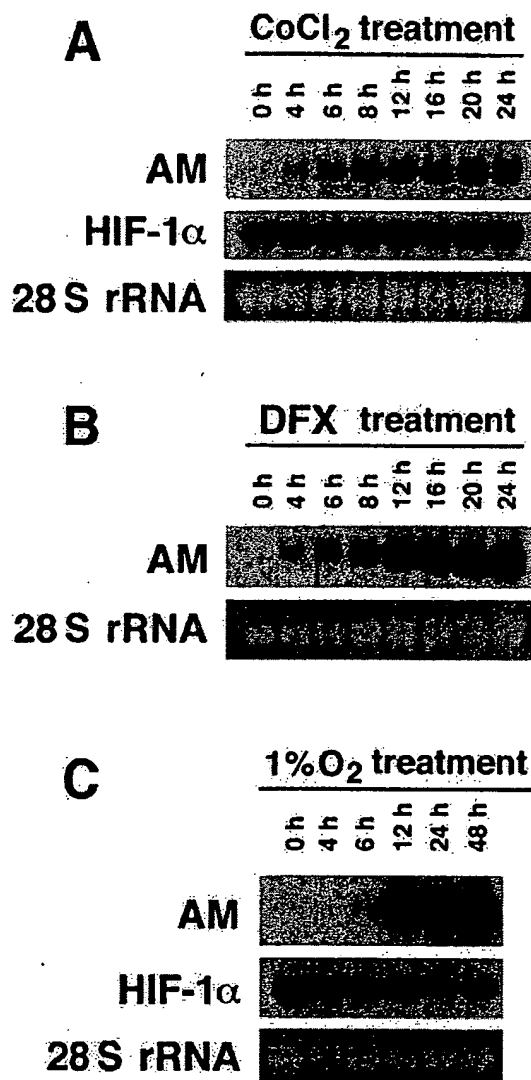


**Fig. 2.** Time Course Analysis of AM Expression

Northern blot analysis of MCF7 cells cultured under 100  $\mu$ M CoCl<sub>2</sub> (A), 260  $\mu$ M DFX (B), or 1% O<sub>2</sub> (C) for the indicated times. Fifteen micrograms of total RNA were loaded per lane and hybridized subsequently with human AM and human HIF-1 $\alpha$  cDNA probes. Equal loading was monitored by ethidium bromide staining of 28 S rRNA for each blot.

with 1% O<sub>2</sub> at various times as compared with the cells maintained in normoxic conditions. Increasing values of accumulated IR-AM in the conditioned media of this cell line were also observed for the CoCl<sub>2</sub> or DFX treatments (data not shown).

#### The Hypoxic Induction of AM mRNA Is Dependent on HIF-1

To determine whether the hypoxic up-regulation of AM mRNA was driven by HIF-1, we used cell lines derived from HIF-1 $\alpha$  or HIF-1 $\beta$  knockout mice to evaluate AM induction capabilities as compared with those of their

wild-type counterparts under hypoxic treatments. Figure 5A illustrates an experiment designed to compare AM mRNA levels in these cell lines when subjected to 6 h treatment of CoCl<sub>2</sub> or DFX. It is shown that HIF-1 $\alpha$  null (–/–) mouse fibroblast cells failed to induce AM expression in these conditions, while the wild-type HIF-1 $\alpha$  (+/+) fibroblasts showed an inducible response. Similarly, normal HIF-1 $\beta$  (+/+) mouse embryonic stem (ES) cells demonstrated an inducible response, whereas HIF-1 $\beta$  null (–/–) ES cells showed a 32% and a 60% reduced induction when compared with the wild-type control, depending on the test reagent examined.

In addition, when HIF-1 $\alpha$  +/+ and HIF-1 $\alpha$  –/– cell lines were exposed to a hypoxia (1% O<sub>2</sub>) time course study (Fig. 5B), the hypoxic induction of AM mRNA was not detectable on the cells with the null mutation, although it was present in the wild-type cells. We also analyzed the levels of HIF-1 $\alpha$  message expression in this experiment. Note that HIF-1 $\alpha$  mRNA remained constant through the hypoxia treatment; however, HIF-1 $\alpha$  transcripts in HIF-1 $\alpha$  –/– cells present a higher molecular size than in the corresponding wild-type cells, since the null mutation was obtained by replacement of the helix-loop-helix domain of HIF-1 $\alpha$  with a neomycin resistance cassette (28).

Furthermore, artificial manipulation of HIF-1 activity with appropriate biochemical reagents was also used to elucidate the role of this transcription factor in AM message regulation under hypoxia. In this sense, the nitric oxide donor sodium nitroprusside (SNP) as well as genistein (a tyrosine kinase inhibitor), are known to inhibit HIF-1 activity by blocking the synthesis of HIF-1 subunits and/or interfering with HIF-1 DNA binding activity in hypoxia (29, 30). MCF7 cells were cultured for 12 h in normoxic or hypoxic conditions, with or without the appropriate biochemical reagents, and AM mRNA expression was analyzed comparing the treated vs. the nontreated cells (control). As is shown in Fig. 6, addition of 100  $\mu$ M SNP completely inhibited the induced expression of AM mRNA after 12 h of hypoxia (1% O<sub>2</sub>) treatment, while genistein at 100  $\mu$ M was a less potent suppressor of the AM mRNA induction mediated by low oxygen tension. Thus, the inhibited activity of HIF-1 with SNP and genistein is correlated with a suppressive effect on the AM mRNA hypoxic induction. Conversely, it has been reported that the CO scavenger hemoglobin (Hb) enhances HIF-1 activity by increasing HIF-1 DNA binding (31). Treatment of MCF7 cells with 50  $\mu$ M Hb was shown to further increase AM mRNA expression under hypoxic conditions by approximately 1.7-fold (Fig. 6).

#### Stabilization of AM Transcripts under Hypoxia

Hypoxia-induced up-regulation of gene expression can be mediated both by *de novo* synthesis of mRNA and by stabilization of the normally labile mRNAs under hypoxic conditions. To test whether the latter possibility was involved in the induced response of AM to

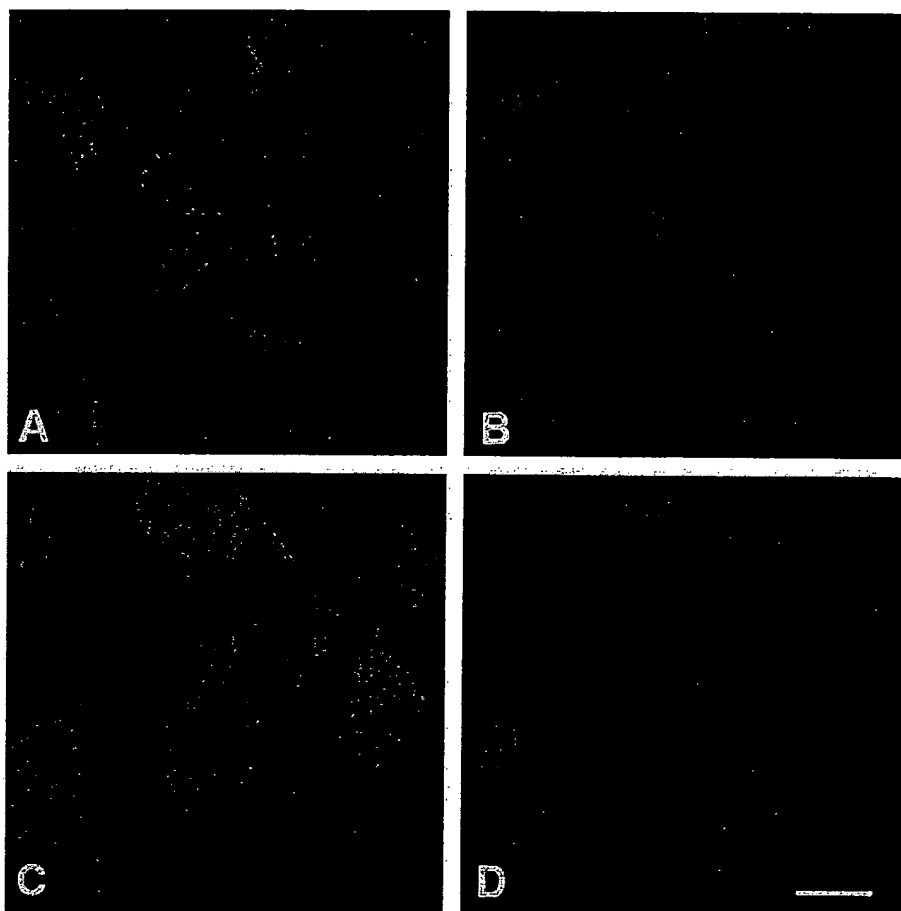


**Fig. 3.** Double Immunostaining for AM and HIF-1 $\alpha$  on DU 145 Cells Analyzed by Confocal Microscopy  
Cells were grown on glass slides, left under normoxic conditions (A and B), or treated with 260  $\mu$ M DFX for 12 h (C and D), and then immunostained for AM and HIF-1 $\alpha$ . Equal microscope settings and exposures were maintained on images from normoxic/DFX-treated cells, to compare expression under both conditions. Both AM (A and C) and HIF-1 $\alpha$  (B and D) become markedly overexpressed after 12 h of DFX treatment. Bar = 5  $\mu$ m.

hypoxia, we examined the half-life of AM transcripts under normoxic and hypoxic conditions in the presence of actinomycin D, a compound known to inhibit RNA synthesis. MCF7 cells were maintained under hypoxic (1% O<sub>2</sub>) conditions for 12 h to sufficiently induce the expression of AM transcripts, and AM mRNA level at this point was considered the standard to which the rest of the samples were compared. After the initial hypoxic induction, actinomycin D was added at 4  $\mu$ g/ml, and the cells were further maintained at normoxic or hypoxic (1% O<sub>2</sub>) conditions from 1 to 4 h. As shown in Fig. 7, AM mRNA clearly decayed more rapidly under normoxic than under hypoxic conditions, thus indicating a stabilization process in hypoxia.

Densitometry analysis of the degradation of AM mRNA under normoxia and hypoxia in this experiment was performed, and the pooled data resulted in a calculated half-life of the AM mRNA of 1.7 h under normoxia and of 2.5 h under hypoxia. Our data thus indicate that the hypoxia-induced expression of AM

transcripts is at least partially dependent upon stabilization of AM mRNA.

#### Identification of Putative Hypoxia-Response Element (HRE) Sites in the Human AM Gene

Since it is known that HIF-1 mediated gene transactivation involves its binding to distinct nucleic acid motifs, namely HREs, we used GCG computer software from Genetics Computer Group (Madison, WI) to analyze the human and mouse AM genes (GenBank accession nos. D43639 and D78349, respectively) for appropriate HRE sequences. In this analysis we followed the HRE consensus motif proposed by Wenger and Gassmann (18, 32): (T,G,C) (A,G) CGTG (C,G,A) (G,T,C) (G,T,C) (C,T,G), which has been constructed from the nucleotide sequence of HIF-1 binding sites of 13 oxygen-dependent genes, and allowed for no more than a single base mismatch outside the CGTG core sequence. We have analyzed not only the 5'-promoter region but also the 3'-flanking region, introns/exons,

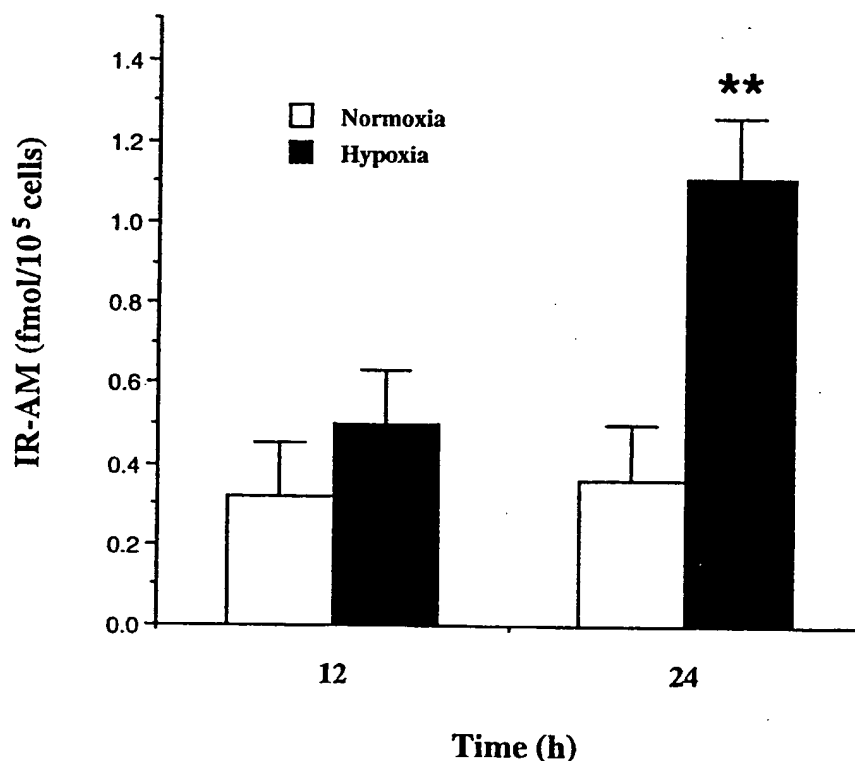


Fig. 4. RIA of IR-AM in the Conditioned Media of MCF7 Cells Cultured under Normoxia or 1% O<sub>2</sub> Atmosphere

After 12 h treatment, levels of AM detected in the conditioned medium of cells in both conditions are similar; however, at 24 h, values of accumulated IR-AM in cultured media of 1% O<sub>2</sub> treated cells were significantly higher than those from normoxic cells (\*\*,  $P = 0.004$ ). Values are the mean  $\pm$  SEM.

and looked for consensus motifs in both sense and antisense strands, since these genomic areas have been previously shown to have functional HRE sites in other HIF-1-inducible genes (18, 20, 33). With these premises, eight putative HRE sites at the 5'- and six sites at the 3'-untranslated flanking sequences of the human AM gene were found, together with putative HRE sequences in the first intron and in exon 3 and exon 4 (see Fig. 8). Similar analysis of the mouse AM gene identified three putative HRE sites in the antisense strand of the 5'-promoter region (positions: -1143, [AACTCACGgA]; -98, [CAAGCACGct]; and -62, [tGACCACGCC]), and another three on the sense orientation: one in intron 1 (position 533, [CGCGTGCTGa]), one in intron 2 (position 727, [GcCGTGCTTT]), and finally one at exon 4 (position: 1960, [GACGTGAaTG]).

#### Luciferase Reporter Assays for the Human AM Promoter Region under Hypoxia

To determine whether these HRE sites were actually involved in the regulation of AM mRNA expression, luciferase reporter studies were performed for different regions of the 5'-flanking region of the human AM gene. MCF7 cells were transiently transfected with the empty parental plasmid (pGL2basic) or with con-

structs comprising one, two, four, or eight putative HREs of the AM promoter (see Fig. 9A). A cotransfected  $\beta$ -galactosidase expression vector served as internal control for transfection efficiency and extract preparation. After the transfection, cells were left under normoxic conditions or exposed to 260  $\mu$ M DFX for 24 h, and luciferase activity was determined. No significant increase for the luciferase activity in the DFX-treated cells/normoxic cells was obtained when transfections were performed with constructs containing the one or two putative HREs closest to the TATA box (Fig. 9A). However, when cells were transfected with constructs containing four or eight putative HREs sites at the 5'-end of the TATA box, a significant ( $P < 0.01$ ) 1.5- and 1.7-fold increase in luciferase activity was observed when comparing DFX-treated vs. normoxic cells.

To test whether we could potentiate the increase in luciferase activity for the DFX treated/normoxic cells, we performed transient expression experiments using the HIF-1 $\alpha$  expression vector pCMV $\beta$ -HA-HIF-1 $\alpha$  (34). This expression vector was cotransfected into MCF7 cells together with the empty parental vector or plasmid constructs containing four or eight HREs from the AM promoter (pGL2basic, pGL2b-4, or pGL2b-8), and the normalization  $\beta$ -galactosidase plasmid. A repre-

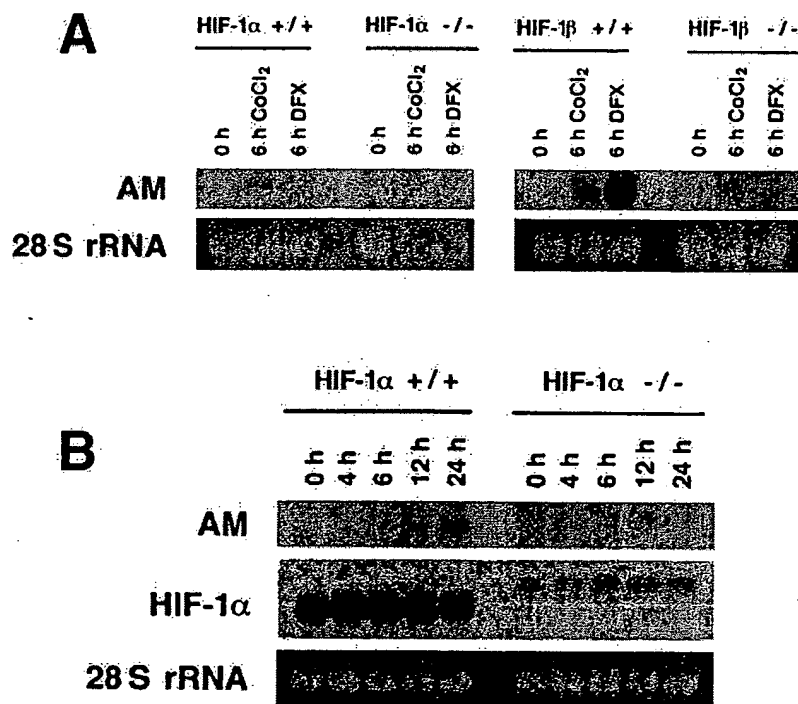


**Fig. 5.** Northern Blot Analysis on HIF-1α and HIF-1β Knockout Mouse Cell Lines

Fifteen micrograms of total RNA were loaded per lane, and equal loading and integrity of RNA were monitored by ethidium bromide staining of 28S rRNA. A, AM mRNA induction is suppressed in fibroblast HIF-1α -/- cells or reduced in ES HIF-1β -/- cells treated with CoCl<sub>2</sub> or DFX for 6 h as compared with their wild-type counterparts. B, Hypoxia (1% O<sub>2</sub>) time course study on HIF-1α wild-type (+/+) and HIF-1α null cells (-/-) probed for mouse AM and HIF-1α. Note that HIF-1α null cells fail to induce AM mRNA expression.

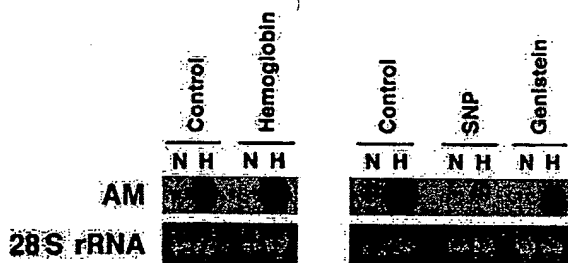


**Fig. 6.** Expression of AM mRNA in MCF7 Cells Treated with Reagents That Modulate HIF-1 Activity

Northern blot analysis was performed on MCF7 cells cultured for 12 h in a normoxic or hypoxic (1% O<sub>2</sub>) fashion with or without 50 μM Hb, 100 μM SNP, or 100 μM genistein. The hypoxic induction of AM transcripts in hypoxia was further augmented with Hb (a reagent that enhances HIF-1 activity), whereas SNP and genistein (known to inhibit HIF-1 activity) had a suppressive effect on that induction.

sentative experiment is shown in Fig. 9B, in which the transient overexpression of HIF-1α augmented the luciferase reporter activity after DFX treatment up to 2.9-fold when four HREs were present, and up to 4.8-fold with eight HREs as compared with the values of transfected cells in normoxic conditions; no significant increase was observed when the HIF-1α expression vector was cotransfected with the pGL2basic empty vector.

## DISCUSSION

Oxygen availability is known to play a key role in the growth-regulatory process underlying carcinogenesis (15). Seminal work by Semenza and collaborators (35, 36) demonstrated the general involvement of HIF-1 in the transcriptional response to hypoxia. Since then, several established growth modulation factors, including Epo, VEGF, Tf, ET-1, and insulin-like growth factor binding protein 1 (IGFBP-1), have been shown to be under HIF-1 transcriptional control (18, 20, 33). Based on previous reports showing that AM functions as an autocrine growth factor for certain human tumor cell lines (13), we began a comprehensive study to determine whether hypoxia could influence the expression of AM via HIF-1 in human tumor cell lines as an *in vitro* approach for similar conditions occurring in solid human cancers.

Our initial analysis by Northern blot in a variety of human tumor cell lines clearly demonstrates that hypoxia increases mRNA levels in these cells as compared with the untreated controls. Interestingly, there is a considerable variation in the basal levels of AM mRNA observed in normoxic conditions. High levels of basal AM mRNA may arise from the constitutive expression of HIF-1α protein in certain cells, a condition that has been previously reported for primary cultures of human pulmonary arterial smooth muscle cells (37).

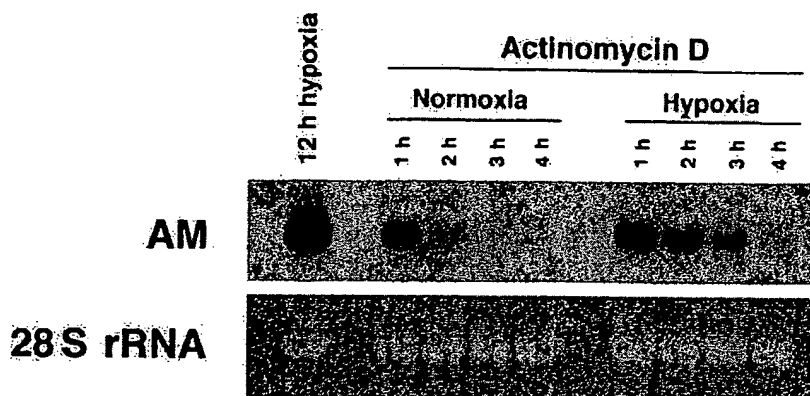


Fig. 7. Stabilization of AM Transcripts under Hypoxia

MCF7 cells were treated with 1% O<sub>2</sub> for 12 h to induce the expression of AM mRNA. After addition of actinomycin D at 4 µg/ml, cells were further maintained in normoxic or hypoxic conditions for the indicated times. Fifteen micrograms of total RNA were then loaded in each lane for Northern blot analysis of AM transcripts. AM mRNA levels at each point were compared with levels observed at 12 h hypoxia (previous to the addition of actinomycin D), and the half-life for AM transcripts under normoxic and hypoxic conditions was estimated.

In the time course experiments using MCF7 cells subjected to an hypoxic environment, we also demonstrate that the AM mRNA induction is paralleled by a somewhat delayed increased secretion of AM peptide from the cells to the conditioned media. Given our prior finding that endogenous AM functions as an autocrine growth factor for MCF7 (13), the demonstration that hypoxia augments bioactive AM production and secretion in these cells suggests that a similar scenario may take place in tissue neoplasms. The production and secretion of AM at the hypoxic areas present in tumors (15) could establish an autocrine/paracrine-mediated proliferation event leading to tumor growth. In addition, since AM has angiogenic and vasodilator capabilities (1, 6), the secreted AM could induce neovascularization and facilitate nutritional supplementation to the tumor cells. Finally, AM also has been shown to protect cells from apoptosis (5), and this feature could selectively rescue tumor cells from programmed cell death and might even predispose tumors to a more malignant phenotype (15).

The data obtained with the HIF-1 $\alpha$  and HIF-1 $\beta$  knockout mouse cell lines, together with those from the HIF-1 biochemical modulation studies performed on MCF7 cells, provide consistent evidence supporting the major involvement of HIF-1 in the transcriptional activation of AM by hypoxia and suggest that AM could be considered a new member of the growing family of HIF-1-targeted genes. The absence of inducible AM mRNA expression in HIF-1 $\alpha$  null mouse fibroblast cell line under hypoxia seems to highlight the critical importance of the HIF-1 $\alpha$  subunit in the transactivation of AM mRNA. Recent studies with HIF-1 $\alpha$  knockout mice have shown this genetic deletion to be an embryonic lethal event in the later stages of fetal development (28, 38). In addition, tumors derived from mouse ES cells with HIF-1 $\alpha$  null genotype have retarded growth, reduced VEGF expression, and less angiogenesis than their wild-type counterparts (28).

Given that AM is also highly expressed during embryogenesis (8), it would be interesting to evaluate whether there are modifications in the AM distribution patterns in early HIF-1 $\alpha$  null embryos. HIF-2 $\alpha$ , a hypoxia-inducible transcription factor sharing homology with HIF-1 $\alpha$ , has recently been shown to be essential in embryonic vascularization and catecholamine production (39); we cannot exclude a possible role of HIF-2 $\alpha$  in AM transactivation in endothelial and catecholamines-producing cells of embryos as well as catecholamines-producing tumors. In contrast to HIF-1 $\alpha$  knockout cell lines, ES HIF-1 $\beta$  null cells under hypoxia showed a diminished AM mRNA induction as compared with their wild-type counterparts, which may reflect the ability of other basic helix-loop-helix family members (e.g. ARNT 2 and ARNT 3) to compensate for the loss of HIF-1 $\beta$  in the formation of a functional heterodimer with HIF-1 $\alpha$ , albeit at lower efficiency (40, 41).

Prior studies have demonstrated the ability of reduced oxygen tension to mediate elevations in AM message/protein expression in several animal and cell systems. In this sense, hypoxia was shown to induce AM gene expression and secretion in cultured human umbilical vein endothelial cells (42); focal ischemic regions of the rat brain show high AM mRNA expression (43), and patients with chronic obstructive pulmonary disease involving tissue hypoxia have elevated AM plasma levels (44). Nakayama and colleagues (14) have demonstrated that hypoxia can elevate AM mRNA and protein expression in a single human colorectal carcinoma cell line, DLD-1; however, these investigators did not identify any HRE motifs in the 5'-upstream flanking region of the human AM gene and suggested the possible involvement of AP-1 in the hypoxia elevation they observed. Given that the AM promoter has several AP-1 binding motifs and that hypoxia can elevate *c-fos*, which in turn can activate AP-1 expression (45, 46), their supposition had a log-

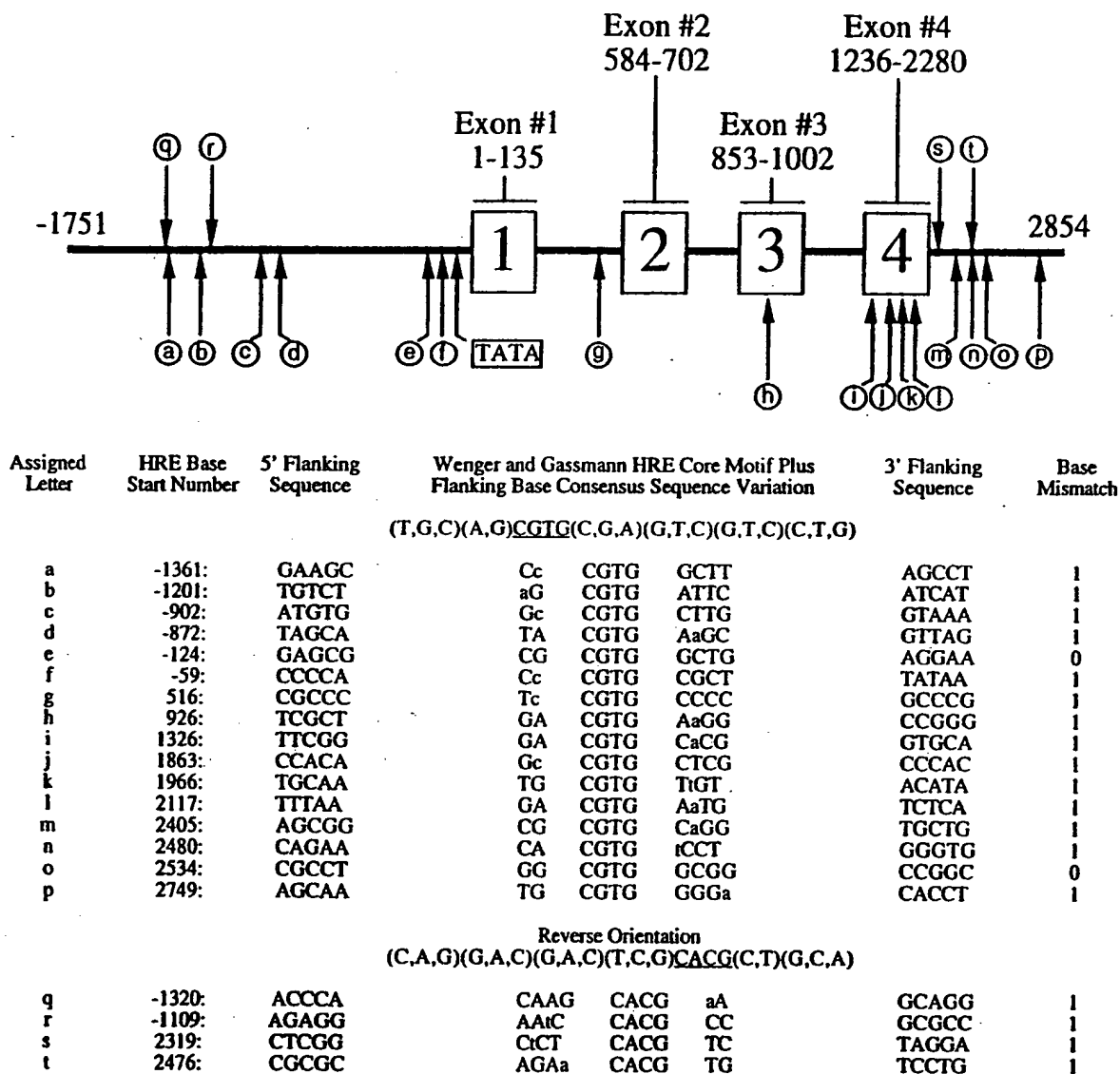


Fig. 8. Schematic Drawing of Potential HRE Motifs in the Human AM Gene

Genomic structure was taken from GenBank accession no. D43639. Identification of putative HIF-1 binding sites is derived from the HRE consensus sequence model of Wenger and Gassmann (18, 32), which represents the deca base region (T,G,C)(A,G)CGTG(C,G,A)(G,T,C)(G,T,C)(C,T,G), and allowing for only one base mismatch outside the CGTG core structure. HRE sites in the schematic drawing are indicated by lowercase letters within circles. GCG analysis was performed in both sense and antisense orientation, and nucleotide positioning of HRE sites was based on the AM transcriptional start site as +1. Accompanying chart identifies numerical positioning of HRE, single mismatched base, and 5'- and 3'-flanking sequences.

ical basis and may in fact work in concert with our observed HIF-1-driven AM expression. Recently, it was also reported that the hypoxic expression of AM in rodent cardiomyocytes is under HIF-1 control (47); although Cormier-Regard and colleagues clearly demonstrate the induction of AM mRNA under hypoxia, no experimental data confirming a similar relationship for AM peptide were shown.

In our luciferase reporter studies, MCF7 cells were transfected with reporter plasmid constructs containing one, two, four, or eight of the putative HRE con-

sensus sequences that we identified in the human AM promoter. Only when four or eight potential HREs were present, a statistically significant fold increase in luciferase expression was observed on exposure to DFX over that of untreated controls. Although the luciferase induction observed in our test conditions is modest, it is within the range observed for the mouse AM gene (47) and human Tf (48). For the human VEGF gene, it has been reported that the increase in transcription rate cannot account for all the observed increase in the steady-state VEGF mRNA levels induced by hypoxia

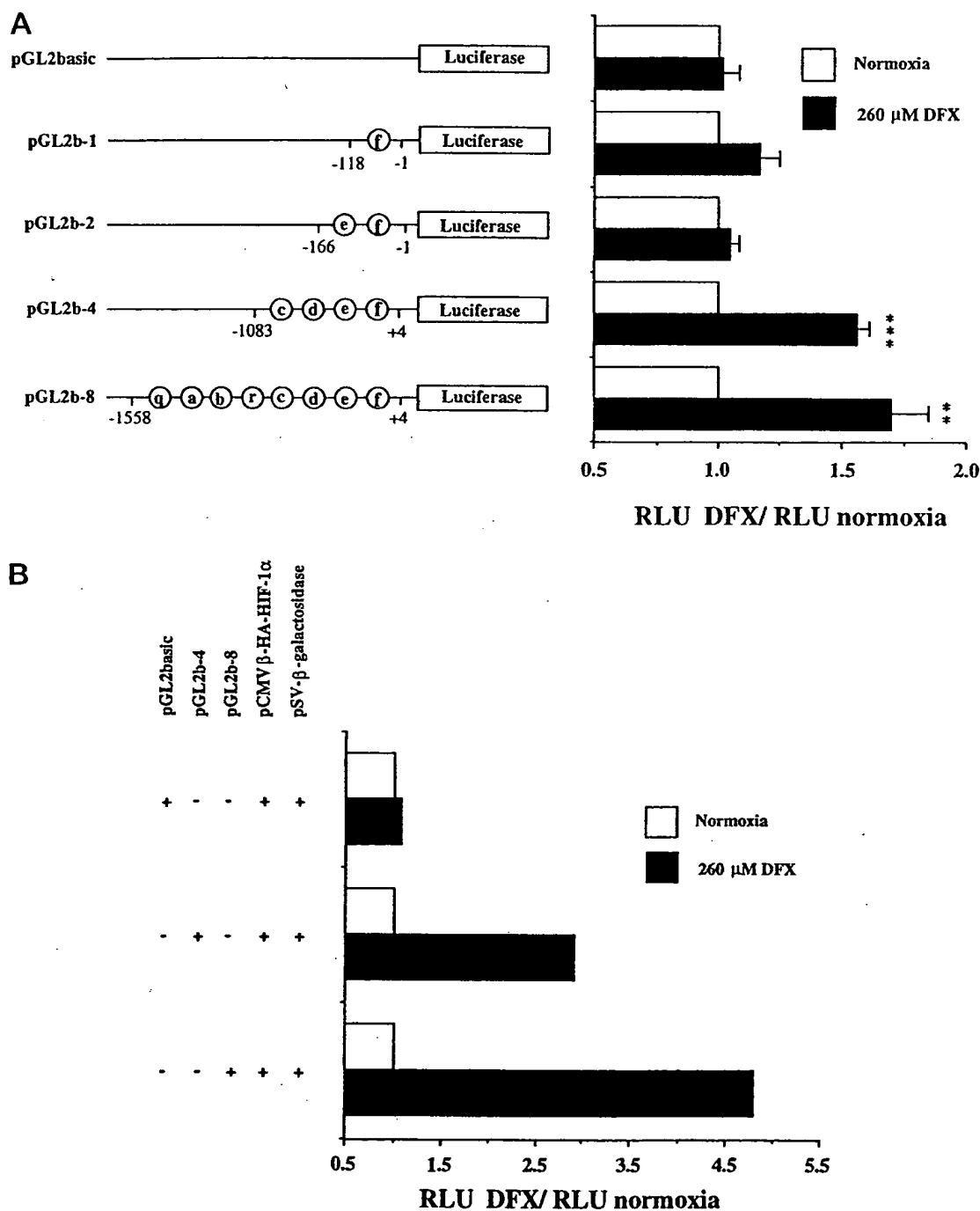


**Fig. 9.** Evaluation of HRE Activity by Luciferase Reporter Assay

**A**, Hypoxia responsiveness of the human AM 5'-flanking region. Schematic diagrams of the luciferase plasmids used in this study, containing one, two, four, or eight putative HREs are shown on the left. The HRE sites are named in the same way as in Fig. 8, and numbering refers to the region of the AM promoter inserted into the parental pGL2basic vector relative to the AM transcription start site as +1. MCF7 cells were transiently transfected with one of the mentioned luciferase plasmids and a pSV-β-galactosidase control vector. After normoxic or 260 μM DFX exposure for 24 h, luciferase activity was determined by normalization to the corresponding β-galactosidase values. For each construct tested, fold increase of luciferase activities with 260 μM DFX vs. luciferase values in normoxia (arbitrarily defined as 1) are represented. Means ± SEM of three to five independent experiments are shown; \*\*,  $P < 0.01$ , \*\*\*,  $P < 0.001$ . **B**, Transient expression of HIF-1α potentiates the enhanced luciferase activity after exposure to DFX. MCF7 cells were transiently cotransfected with the HIF-1α expression vector (pCMVβ-HA-HIF-1α) and the plasmid constructs shown at the left of the figure. After normoxic or 24 h DFX (260 μM) treatment, the luciferase activity was determined, corrected for transfection efficiency according to the β-galactosidase activity, and in each case normalized to the luciferase value in normoxic conditions arbitrarily defined as 1.



(49), and important posttranscriptional regulation events mediated by mRNA stabilization do, in fact, take place (50). A similar situation could also be depicted for the human AM gene, since not only transcriptional activation but also, as we have shown, RNA stabilization events contribute to the AM mRNA up-regulation under hypoxic conditions. We cannot exclude, however, the possibility of major functional HRE sites at the 3'-flanking region of the human AM gene, a location that has been shown for HREs in the human and mouse Epo gene (51, 52). Furthermore, when MCF7 cells were cotransfected with a HIF-1 $\alpha$  expression vector and plasmid constructs containing four or eight HREs of the 5'-flanking region of the human AM gene, the increase in luciferase activity was remarkably potentiated as compared with the increase obtained with the pGL2-4 or pGL2-8 plasmids alone. This stimulated luciferase reporter activity with the transient overexpression of HIF-1 $\alpha$  has also been reported for the human Tf, VEGF, and Epo genes (48, 53). These data further support that the transcriptional activation of AM in hypoxic conditions is driven by HIF-1 and not through other transcriptional factors activated by hypoxia; additionally, they give stronger evidence that at least some of the selected potential HRE sites in the 5'-flanking region of the human AM gene are functional in the up-regulation of AM transcription under hypoxia.

Based on our actinomycin D studies, we clearly demonstrate AM mRNA stabilization mediated by hypoxic conditions. Recent studies on RNA degradation mechanisms have identified hypoxia-inducible proteins that bind to adenylate-uridylylate (AU)-rich elements of the 3'-untranslated region (3'-UTR) of short half-life RNA (i.e. VEGF, c-Myc, c-fos) and suppress ribonuclease degradation (54, 55). One such stabilizing RNA-binding protein, HuR, has been shown to interact with AUUUA or AUUUUA base sequences in the 3'-UTR of the VEGF mRNA and to extend its half-life under hypoxic conditions (55). Interestingly, the 3'-UTR of both human and mouse AM mRNA have AUUUA and AUUUUA sequences that could possibly augment message survival during reduced oxygen tension through a similar HuR or HuR-like interaction. In addition, tumor cell lines that have a mutated von Hippel-Lindau (VHL) tumor suppressor gene contain constitutively stabilized VEGF mRNA and also have constitutively expressed stabilizing RNA-binding proteins (54). Considering these reports and the recent discovery by Ratcliffe and co-workers that the VHL gene product controls the degradation of HIF-1 $\alpha$  protein (25), it will be interesting to determine the status of the VHL suppressor gene in those human tumor cell lines that have an elevated basal expression of AM message under normoxic conditions (i.e. H157), to determine whether this feature relates to an increased half-life of AM mRNA mediated by constitutive expression of stabilizing RNA-binding proteins.

In conclusion, we have shown evidence in favor of hypoxia as an inducer of AM mRNA and protein ex-

pression in human tumor cell lines. The data obtained from HIF-1 knockout mouse cell lines, biochemical modulation of HIF-1 activity, and transfection experiments give solid proof for the involvement of HIF-1 in the up-regulation of AM mRNA under hypoxic conditions. In addition to HIF-1 transcriptional activation, increased hypoxic mRNA stability also accounts for AM induction based on our actinomycin D assays. Our collective data, taken together with previous reports that most solid human tumors have common hypoxic regions (15) and that AM can function as a mitogen/angiogenic factor/apoptotic survival factor (5, 6, 13), implicate HIF-1/AM as members of a potential promotion mechanism of carcinogenesis and identify a possible biological target for intervention strategies against malignant disease.

## MATERIALS AND METHODS

### Cell Lines, Hypoxia Treatments, and Reagents

Cell lines used in this study were selected to represent an array of the most widely distributed human cancer types. In particular, we used representatives of carcinomas (CA) or carcinoids of the lung [N417d (small cell CA), H1264 (adenocarcinoma), H157 (squamous cell CA), H720 (carcinoid)], breast (H2380, MCF7, SK-BR-3, ZR-75), colon (H630, H716, SNUC-1), ovary (OVCAR-3, SK-OV-3), prostate (DU 145, PC-3-M), chondrosarcoma (HTB-94) or promyelocytic leukemia (HL-60). All cell lines were obtained from the National Cancer Institute-Navy Medical Oncology Branch or purchased through the American Type Culture Collection (ATCC, Manassas, VA). All tumor cell lines were cultured in RPMI 1640 or DMEM media supplemented with 10% heat inactivated FBS, 2 mM L-glutamine, 10 mM HEPES buffer, 100 U/ml penicillin, and 100  $\mu$ g/ml streptomycin (all tissue culture reagents purchased from Life Technologies, Inc., Gaithersburg, MD). The development, characterization, and maintenance of embryonic stem cell lines from HIF-1 $\beta$  knockout mice have been previously described (56). The HIF-1 $\alpha$  (-/-) fibroblast cell line was generated from HIF-1 $\alpha$  null mice (28) via SV-40 transformation of embryonic fibroblast cells; HIF-1 $\alpha$  (-/-), and (+/+) fibroblast cell lines were maintained with the same media as specified for the human tumor cell lines.

Cells were cultured at 37 C in 20% O<sub>2</sub>, 5% CO<sub>2</sub>, 75% N<sub>2</sub> for normoxic conditions, and new media were added 12 h before the beginning of each hypoxia experiment. The hypoxia induction was achieved either by hypoxia mimetics: 100  $\mu$ M CoCl<sub>2</sub>, 260  $\mu$ M DFX mesylate (both from Sigma, St. Louis, MO), or by culturing cells in a hypoxia chamber at 37 C with 1% O<sub>2</sub>, 5% CO<sub>2</sub>, 94% N<sub>2</sub> atmosphere. The hypoxia chamber was fabricated from a Labconco seamless fiberglass vacuum desiccator (Fisher Scientific, Pittsburgh, PA) fitted with two stainless steel angle ball valves having serrated hose connectors (Washington Valve & Fitting Co., Frederick, MD), which allowed for chamber equilibration to hypoxic environment via venting with gas mixture (Roberts Oxygen Co., Gaithersburg, MD). The chamber was tested for leaks under positive pressure using a bubble-forming agent (SNOOP, Nupro Co., Willoughby, OH) and was shown to hold a 3 psi charge for 48 h.

In the HIF-1 modulating studies, different agents were added to the culture media, and then the cells were incubated under normoxic conditions or in the hypoxia chamber for 12 h at 37 C. SNP (a NO donor), and genistein (a tyrosine kinase inhibitor), were used at 100  $\mu$ M to inhibit HIF-1 activity (29, 30). Hemoglobin (Hb), which acts as a CO scavenger, was

used at a final concentration of 50  $\mu$ M to up-regulate HIF-1 activity (31); Hb was prepared by treatment with excess reducing agent sodium dithionite (57). All reagents were purchased from Sigma.

For the AM mRNA stabilization studies, cells were initially exposed to 12 h hypoxia, after which actinomycin D was added at a final concentration of 4  $\mu$ g/ml (Sigma); cells were subsequently maintained from 1 h to 4 h under normoxic or hypoxic conditions.

### Northern Blot Analysis

Immediately after treatment for the indicated times, cells were washed once in PBS, and total RNA was extracted using the guanidine isothiocyanate and cesium chloride method (58). Fifteen micrograms of RNA were loaded per lane, run in 1% agarose gels containing 2.2 M formaldehyde, blotted by capillarity onto nitrocellulose membranes (Schleicher & Schuell, Inc., Keene, NH), and baked for 2 h at 80°C. Equal loading and integrity of RNA were monitored by ethidium bromide staining of the 28 S subunit of rRNA.

The human AM cDNA probe used in this study was generated as an RT-PCR product (831 bp) obtained using oligonucleotide primers: 5'-TACCTGGGTTGCTCGCCTTCTA-3' (sense, bp 184–207) and 5'-CTCCGGGGGTCTCAGCATTCATTT-3' (antisense, bp 991–1014). The human HIF-1 $\alpha$  cDNA probe was also produced by RT-PCR (1308-bp product) using oligonucleotide primers: 5'-CGGCGCGAAGCAAGAAAAAGAT-3' (sense, bp 43–66) and 5'-TCGTTGGGTGAGGGGAGCATTACA-3' (antisense, bp 1327–1350). Numbering of the nucleotide base positioning was taken from the GenBank profile accession no. D14874 (human AM mRNA) and U22431 (human HIF-1 $\alpha$  mRNA). All RT-PCR products were sequenced to validate base integrity of the probes. The mouse AM cDNA 550-bp probe was a gift from Dr. Sonia Jakowlew (59).

Probes were labeled with [ $\alpha$ -<sup>32</sup>P]dCTP (3000 Ci/mmol; NEN Life Science Products, Boston, MA) by random priming, and unincorporated nucleotides were removed by Probe-Quant G-50 Micro Columns (Amersham Pharmacia Biotech, Piscataway, NJ). Hybridization was carried out overnight at 42°C in a hybridization buffer containing 40% formamide (58). After stringency washes, blots were exposed to XAR film (Eastman Kodak Co., Rochester, NY) at –80°C for varying times. Densitometry of the autoradiograms was performed using a Chemilmager 4000 (Alpha Innotech Corp., San Leandro, CA). The half-life of the endogenous AM mRNA was calculated using Prism 3.0 software.

### Confocal Immunofluorescence for AM and HIF-1 $\alpha$

Cells were grown on glass slides, treated with 260  $\mu$ M DFX for 12 h, and fixed in Bouin's fluid (Sigma) for 10 min at room temperature. Slides were blocked with normal goat serum (1:30 in PBS) for 30 min and then incubated overnight at 4°C in a mixture of both antibodies: mGc3 antihuman HIF-1 $\alpha$  monoclonal antibody (60) at 1:500 dilution and rabbit antihuman AM 22–52 antibody (13) at 1:1,000 dilution. The second layer consisted on a mixture of Rhodamine-antimouse and Bodipy-antirabbit IgGs (Molecular Probes, Inc., Eugene, OR) at a final concentration of 1:200 each. The cells were observed with a Carl Zeiss Laser Scanning Microscope 510, equipped with four lasers. Images from cells subjected to DFX treatment and normoxic controls were taken with exactly the same microscope settings and exposures, to compare expression of AM and HIF-1 $\alpha$  in both conditions.

### RIA of Immunoreactive AM

Concentrations of AM in culture media of MCF7 cells under hypoxia or mimetics treatment were measured by double

antibody RIA. Samples of culture media (1 ml) were mixed with an equal volume of 0.1% alkali-treated casein in PBS, pH 7.4, and applied to reverse-phase Sep-Pak C-18 cartridges (Waters Corp., Milford, MA). The proteins were eluted with 3 ml of 80% isopropanol containing 0.125 N HCl and lyophilized. Extracts were reconstituted in 0.4 ml of RIA buffer (10 mM phosphate, 50 mM EDTA, 135 mM NaCl, 5 mM NaHCO<sub>3</sub>, 0.05% Triton X-100, 0.1% Tween-20, 0.1% alkali-treated casein, 20 mg/l phenol red, pH 7.4), and spun to remove any solid matter. After a 24-h preincubation of 0.1 ml of sample with 0.1 ml of antihuman AM antibody (Phoenix Pharmaceuticals, Inc., Mountain View, CA) at 4°C, 0.1 ml of <sup>125</sup>I-labeled AM (Phoenix Pharmaceuticals, Inc.) was added (10,000 cpm) and the mixture was incubated at 4°C overnight. Bound tracer was separated by polyethylenglycol-facilitated precipitation with goat antirabbit IgG and normal rabbit serum. After centrifugation, the supernatant was discarded, and the radioactivity in the pellets was determined in a  $\gamma$ -counter. Data were statistically evaluated by a two-tailed Student's *t* test using Prism 3.0 software. Differences were regarded as significant at a value of *P* < 0.05.

### Reporter Plasmid Constructs

A PCR product of 118 bp (–118, –1) containing the putative HRE site closest to the transcription start site in the 5'-flanking region of the AM gene (named HRE f in Fig. 8) was generated using human genomic DNA as template and the following oligonucleotide primers: sense, 5'-GCTGAGGAAAGAAAGGGAAG-3' and antisense, 5'-TGTCACCAAGAAACCACTGA-3'. Similarly, primers: sense, 5'-AGCCCCAAAGGAAGCAATGC-3' and antisense, 5'-TGTCACCAAGAAACCACTGA-3' were used to generate a PCR product of 166 bp (–166, –1) comprising the two potential HREs closest to the transcription start site of the AM promoter (HREs named e and f in Fig. 8). Each of the resulting 118-bp and 166-bp DNA fragments were ligated into the pCR2.1 vector (Invitrogen, Carlsbad, CA) to generate pCR2.1–118 and pCR2.1–166. These plasmids were then digested with *Hind*III and *Xho*I, and the resulting DNA fragments were cloned into the same sites of a promoterless luciferase reporter pGL2basic (Promega Corp., Madison, WI) to generate pGL2b-1 and pGL2b-2, respectively.

The entire 5'-flanking region of the human AM gene was amplified by standard PCR from human genomic DNA using primers: sense, 5'-GAATTCAGGTCCGCTCAGGTGACTCCTTCC-3' and antisense, 5'-GAGCTCGTAGCCAGTGTACCAAGAAACC-3' (the antisense primer introduced a *Sac*I site [underlined] and an *Nhe*I site [bolded]). The resulting 1755 bp (–1751, +4) product was ligated into the pCR2.1 vector to generate pCR2.1–1755. An *Nhe*I/*Nhe*I fragment from pCR2.1–1755 was subcloned into the same site of pGL2basic generating pGL2b-4 (which carries 4 putative HREs from the 5'-end of the AM promoter, namely c, d, e, and f in Fig. 8). In the same way, a *Sac*I/*Sac*I fragment from pCR2.1–1755 was also subcloned into the *Sac*I site of pGL2basic, generating pGL2b-8, which encompasses the 8 putative HREs in the 5'-flanking region of the AM gene (HREs a, b, c, d, e, f, q, and r in Fig. 8). The fidelity of all PCR-derived sequences was verified by sequence analysis. All positions are referred relative to the transcription start site of the AM gene (+1; see Fig. 8).

The HIF-1 $\alpha$  expression vector (pCMV $\beta$ -HA-HIF-1 $\alpha$ ) (34) was generously provided by Dr. D. Livingstone (Dana Farber Cancer Institute).

### Transient Transfections and Luciferase Reporter Assay

Approximately 20 h before transfection 1.5  $\times$  10<sup>5</sup> MCF7 cells were seeded onto 60-mm plates. Each dish was then transfected for 4 h in the presence of lipofectAMINE and OptiMem medium I (Life Technologies, Inc.) with 1  $\mu$ g of pSV- $\beta$ -galac-

tosidase control vector (Promega Corp.) and 3  $\mu$ g of one of the following plasmids: pGL2basic, pGL2b-1, pGL2b-2, pGL2b-4, or pGL2b-8. For the HIF-1 $\alpha$  transient overexpression assays, 5  $\mu$ g of the pCMV $\beta$ -HA-HIF-1 $\alpha$  vector were cotransfected with an equal amount of one of the following plasmids: pGL2basic, pGL2b-4, or pGL2b-8, together with 1  $\mu$ g of pSV- $\beta$ -Galactosidase control vector (quantities referred per dish). All transfections were carried out in duplicate with aliquots of transfection mixture from a single pool. After transfection, cells were incubated in RPMI 1640 medium supplemented with 10% FBS and were either treated with DFX at 260  $\mu$ M for 24 h or left under normoxic conditions for the same time. Cells were then collected in EBC lysis buffer with protease inhibitors (40 mM Tris, pH 8.0, 120 mM NaCl, 0.5% NP-40, 1 mM AEBSF, 10  $\mu$ g/ml aprotinin, 1 mM NaVO<sub>4</sub>, 10  $\mu$ g/ml leupeptin), and luciferase and  $\beta$ -galactosidase activities were determined according to the manufacturer's instructions using a TopCount NXT Packard luminometer and a Bio-Rad Laboratories, Inc. 3550 Microplate Reader. Luciferase readings were normalized by the  $\beta$ -galactosidase values to correct for differences in transfection efficiency and extract preparation. For each construct transfectants, data were expressed as fold increase of the luciferase value obtained with the DFX treatment as compared with the luciferase value obtained in normoxic conditions, which was arbitrarily defined as 1. Data were statistically evaluated by a two-tailed one-sample Student's *t* test using Prism 3.0 software. Differences were regarded as significant at a value of *P* < 0.05.

## Acknowledgments

We thank Dr. J. A. Calera (Georgetown University Medical Center) for his help in the construction of plasmids as well as for useful comments on the manuscript. We are indebted to Dr. G. Camenish for his gift of mGc3 HIF-1 $\alpha$  antibody, and to Dr. R. H. Wenger for critical reading of the manuscript (Institute of Physiology, University of Zürich-Irchel). We gratefully acknowledge Dr. Y. Ward (Department of Cell and Cancer Biology, National Cancer Institute) for her expertise in confocal microscopy. Authors are also thankful to Drs. E. Maltepe and C. Simon (Howard Hughes Medical Institute, University of Chicago) for the HIF-1 $\beta$  knockout mouse cell line, and to Dr. D. Livingstone (Dana Farber Cancer Institute) for the pCMV $\beta$ -HA-HIF-1 $\alpha$  vector.

Received November 23, 1999. Revision received February 1, 2000. Accepted March 1, 2000.

Address requests for reprints to: Dr. Mercedes Garayoa, Cell and Cancer Biology Department, National Cancer Institute, National Institutes of Health, Building 10/12N226, 9000 Rockville Pike, Bethesda, Maryland 20892-1906. E-mail: garayoa@bprb.nci.nih.gov.

M. Garayoa was supported by a postdoctoral fellowship from the Dirección General de Enseñanza Superior, Ministerio de Educación y Cultura, Spain (PF96 0029138440). R. Pío was recipient of a fellowship from the Instituto de Salud Carlos III, Ministerio de Sanidad y Consumo, Spain (Grant 98/9172). This work was also supported in part by the Swiss National Science Foundation (3100-56743.99).

## REFERENCES

1. Kitamura K, Kangawa K, Kawamoto M, Ichiki Y, Nakamura S, Matsuo H, Eto T 1993 Adrenomedullin: a novel hypotensive peptide isolated from human pheochromocytoma. *Biochem Biophys Res Commun* 192:553-560
2. Barker S, Wood E, Clark AJ, Corder R 1998 Cloning of bovine preproadrenomedullin and inhibition of its basal expression in vascular endothelial cells by staurosporine. *Life Sci* 62:1407-1415
3. Kitamura K, Kangawa K, Matsuo H, Eto T 1998 Structure and function of adrenomedullin and PAMP. In: Martínez A, Cuttitta F (eds) *Adrenomedullin*. IOS Press/Ohmsha Ltd., Amsterdam, Tokyo, pp 27-39
4. Cuttitta F, Miller MJ, Montuenga LM, Garayoa M, Elsasser T, Walsh T, Unsworth E, Martínez A 1998 Adrenomedullin: *terra incognita*. In: Martínez A, Cuttitta F (eds) *Adrenomedullin*. IOS Press/Ohmsha Ltd., Amsterdam, Tokyo, pp 1-26
5. Kato H, Shichiri M, Marumo F, Hirata Y 1997 Adrenomedullin as an autocrine/paracrine apoptosis survival factor for rat endothelial cells. *Endocrinology* 138:2615-2620
6. Zhao Y, Hague S, Manek S, Zhang L, Bicknell R, Rees MC 1998 PCR display identifies tamoxifen induction of the novel angiogenic factor adrenomedullin by a non estrogenic mechanism in the human endometrium. *Oncogene* 16:409-415
7. Martínez A, Cuttitta F, Teitelman G 1998 Expression pattern for adrenomedullin during pancreatic development in the rat reveals a common precursor with other endocrine cell types. *Cell Tissue Res* 293:95-100
8. Montuenga LM, Martínez A, Miller MJ, Unsworth EJ, Cuttitta F 1997 Expression of adrenomedullin and its receptor during embryogenesis suggests autocrine or paracrine modes of action. *Endocrinology* 138:440-451
9. Morish DW, Linetsky E, Bhardwaj D, Li H, Dakour J, Marsh RG, Paterson MC, Godbout R 1996 Identification by subtractive hybridization of a spectrum of novel and unexpected genes associated with *in vitro* differentiation of human cytotrophoblast cells. *Placenta* 17:431-441
10. Liu J, Kahri AI, Heikkilä P, Voutilainen R 1997 Adrenomedullin gene expression and its different regulation in human adrenocortical and medullary tumors. *J Endocrinol* 155:483-490
11. Satoh F, Takahashi K, Murakami O, Totsune K, Sone M, Ohneda M, Abe K, Miura Y, Hayashi Y, Sasano H, Ouri T 1995 Adrenomedullin in human brain, adrenal glands and tumor tissues of pheochromocytoma, ganglioneuroblastoma and neuroblastoma. *J Clin Endocrinol Metab* 80:1750-1752
12. Ehlenz K, Koch B, Preuss P, Simon B, Koop I, Lang RE 1997 High levels of circulating adrenomedullin in severe illness: correlation with C-reactive protein and evidence against the adrenal medulla as site of origin. *Exp Clin Endocrinol Diabetes* 105:156-162
13. Miller MJ, Martínez A, Unsworth EJ, Thiele CJ, Moody TW, Elsasser T, Cuttitta F 1996 Adrenomedullin expression in human tumor cell lines. Its potential role as an autocrine growth factor. *J Biol Chem* 271:23345-23351
14. Nakayama M, Takahashi K, Murakami O, Shirato K, Shibahara S 1998 Induction of adrenomedullin by hypoxia and cobalt chloride in human colorectal carcinoma cells. *Biochem Biophys Res Commun* 243:514-517
15. Brown JM, Giaccia AJ 1998 The unique physiology of solid tumors: opportunities (and problems) for cancer therapy. *Cancer Res* 58:1408-1416
16. Genbacev O, Zhou Y, Ludlow JW, Fisher SJ 1997 Regulation of human placental development by oxygen tension. *Science* 277:1669-1672
17. LaVan FB, Hunt TK 1990 Oxygen and wound healing. *Clin Plast Surg* 17:463-472
18. Wenger RH, Gassmann M 1997 Oxygen(es) and the hypoxia-inducible factor-1. *Biol Chem* 378:609-616
19. Huang LE, Gu J, Schau M, Bunn HF 1998 Regulation of hypoxia-inducible factor 1 $\alpha$  is mediated by an O<sub>2</sub>-dependent degradation domain via the ubiquitin-proteasome pathway. *Proc Natl Acad Sci USA* 95:7987-7992

20. Hu J, Discher DJ, Bishopric NH, Webster KA 1998 Hypoxia regulates expression of the endothelin-1 gene through a proximal hypoxia-inducible factor-1 binding site on the antisense strand. *Biochem Biophys Res Commun* 245:894-899
21. Dachs GU, Chaplin DJ 1998 Microenvironmental control of gene expression: implications for tumor angiogenesis, progression, and metastasis. *Semin Radiat Oncol* 8:208-216
22. Gassmann M, Fandrey J, Bichet S, Wartenberg M, Marti HH, Bauer C, Wenger RH, Acker H 1996 Oxygen supply and oxygen-dependent gene expression in differentiating embryonic stem cells. *Proc Natl Acad Sci USA* 93:2867-2872
23. Hasan NM, Adams GE, Joiner MC, Marshall JF, Hart IR 1998 Hypoxia facilitates tumour cell detachment by reducing expression of surface adhesion molecules and adhesion to extracellular matrices without loss of cell viability. *Br J Cancer* 77:1799-1805
24. Yuan J, Glazer PM 1998 Mutagenesis induced by the tumor microenvironment. *Mutat Res* 400:439-446
25. Maxwell PH, Wiesener MS, Chang GW, Clifford SC, Vaux EC, Cockman ME, Wykoff CC, Pugh CW, Maher ER, Ratcliffe PJ 1999 The tumour suppressor protein VHL targets hypoxia-inducible factors for oxygen-dependent proteolysis. *Nature* 399:271-275
26. Chilov D, Camenisch G, Kvietikova I, Ziegler U, Gassmann M, Wenger RH 1999 Induction and nuclear translocation of hypoxia-inducible factor-1 (HIF-1): heterodimerization with ARNT is not necessary for nuclear accumulation of HIF-1 $\alpha$ . *J Cell Sci* 112:1203-1212
27. Isumi Y, Shoji H, Sugo S, Tochimoto T, Yoshioka M, Kangawa K, Matsuo H, Minamino N 1998 Regulation of adrenomedullin production in rat endothelial cells. *Endocrinology* 139:838-846
28. Ryan HE, Lo J, Johnson RS 1998 HIF-1 $\alpha$  is required for solid tumor formation and embryonic vascularization. *EMBO J* 17:3005-3015
29. Sogawa K, Numayama-Tsuruta K, Ema M, Abe M, Abe H, Fujii-Kuriyama Y 1998 Inhibition of hypoxia-inducible factor 1 activity by nitric oxide donors in hypoxia. *Proc Natl Acad Sci USA* 95:7368-7373
30. Wang GL, Jiang BH, Semenza GL 1995 Effect of protein kinase and phosphatase inhibitors on expression of hypoxia-inducible factor 1. *Biochem Biophys Res Commun* 216:669-675
31. Liu Y, Christou H, Morita T, Laughner E, Semenza GL, Kourembanas S 1998 Carbon monoxide and nitric oxide suppress the hypoxic induction of vascular endothelial growth factor gene via the 5' enhancer. *J Biol Chem* 273:15257-15262
32. Wenger RH, Gassmann M 1999 HIF-1 and the molecular response to hypoxia in mammals. In: Storey KB (ed) *Environmental Stress and Gene Regulation*. BIOS Scientific Publishers Ltd., Oxford, UK, pp 25-45
33. Tazuke SI, Mazure NM, Sugawara J, Carland G, Faessen GH, Suen LF, Irwin JC, Powell DR, Giaccia AJ, Giudice LC 1998 Hypoxia stimulates insulin-like growth factor binding protein 1 (IGFBP-1) gene expression in HepG2 cells: a possible model for IGFBP-1 expression in fetal hypoxia. *Proc Natl Acad Sci USA* 95:10188-10193
34. Eckner R, Ewen ME, Newsome D, Gerdes M, DeCaprio JA, Lawrence JB, Livingston DM 1994 Molecular cloning and functional analysis of the adenovirus E1A-associated 300-kD protein (p300) reveals a protein with properties of a transcriptional adaptor. *Genes Dev* 8:869-884
35. Semenza GL, Roth PH, Fang HM, Wang GL 1994 Transcriptional regulation of genes encoding glycolytic enzymes by hypoxia-inducible factor 1. *J Biol Chem* 269:23757-23763
36. Wang GL, Semenza GL 1993 Characterization of hypoxia-inducible factor 1 and regulation of DNA binding activity by hypoxia. *J Biol Chem* 268:21513-21518
37. Yu AY, Frid MG, Shimoda LA, Wiener CM, Stenmark K, Semenza GL 1998 Temporal, spatial, and oxygen-regulated expression of hypoxia-inducible factor-1 in the lung. *Am J Physiol* 275:L818-826
38. Iyer NV, Kotch LE, Agani F, Leung SW, Laughner E, Wenger RH, Gassmann M, Gearhart JD, Lawler AM, Yu AY, Semenza GL 1998 Cellular and developmental control of O<sub>2</sub> homeostasis by hypoxia-inducible factor 1 $\alpha$ . *Genes Dev* 12:149-162
39. Tian H, Hammer RE, Matsumoto AM, Russell DW, McKnight SL 1998 The hypoxia-responsive transcription factor EPAS1 is essential for catecholamine homeostasis and protection against heart failure during embryonic development. *Genes Dev* 12:3320-3324
40. Hirose K, Morita M, Ema M, Mimura J, Hamada H, Fujii H, Saijo Y, Gotoh O, Sogawa K, Fujii-Kuriyama Y 1996 cDNA cloning and tissue-specific expression of a novel basic helix-loop-helix/PAS factor (Arnt2) with close sequence similarity to the aryl hydrocarbon receptor nuclear translocator (Arnt). *Mol Cell Biol* 16:1706-1713
41. Takahata S, Sogawa K, Kobayashi A, Ema M, Mimura J, Ozaki N, Fujii-Kuriyama Y 1998 Transcriptionally active heterodimer formation of an Arnt-like PAS protein, Arnt3, with HIF-1 $\alpha$ , HLF, and clock. *Biochem Biophys Res Commun* 248:789-794
42. Ogita T, Hashimoto E, Nakaoka T, Okabe F, Kira Y, Matsuo K, Fujita T 1997 Hypoxia induces adrenomedullin gene expression and secretin in cultured human umbilical vein endothelial cells. *Circulation* 96:962
43. Wang X, Yue TL, Barone FC, White RF, Clark RK, Willette RN, Sulpizio AC, Aiyar NV, Ruffolo Jr RR, Feuerstein GZ 1995 Discovery of adrenomedullin in rat ischemic cortex and evidence for its role in exacerbating focal brain ischemic damage. *Proc Natl Acad Sci USA* 92:11480-11484
44. Cheung B, Leung R 1997 Elevated plasma levels of human adrenomedullin in cardiovascular, respiratory, hepatic and renal disorders. *Clin Sci (Colch)* 92:59-62
45. Ishimitsu T, Kojima M, Kangawa K, Hino J, Matsuo H, Kitamura K, Eto T, Matsuo H 1994 Genomic structure of human adrenomedullin gene. *Biochem Biophys Res Commun* 203:631-639
46. Mishra RR, Adhikary G, Simonson MS, Cherniack NS, Prabhakar NR 1998 Role of c-fos in hypoxia-induced AP-1 cis-element activity and tyrosine hydroxylase gene expression. *Brain Res Mol Brain Res* 59:74-83
47. Cormier-Regard S, Nguyen SV, Claycomb WC 1998 Adrenomedullin gene expression is developmentally regulated and induced by hypoxia in rat ventricular cardiac myocytes. *J Biol Chem* 273:17787-17792
48. Roffs A, Kvietikova I, Gassmann M, Wenger RH 1997 Oxygen-regulated transferrin expression is mediated by hypoxia-inducible factor-1. *J Biol Chem* 272:20055-20062
49. Levy AP, Levy NS, Wegner S, Goldberg MA 1995 Transcriptional regulation of the rat vascular endothelial growth factor gene by hypoxia. *J Biol Chem* 270:13333-13340
50. Dibbets JA, Miller DL, Damert A, Risau W, Vadas MA, Goodall GJ 1999 Hypoxic regulation of vascular endothelial growth factor mRNA stability requires the cooperation of multiple RNA elements. *Mol Biol Cell* 10:907-919
51. Beck I, Ramirez S, Weinmann R, Caro J 1991 Enhancer element at the 3'-flanking region controls transcriptional response to hypoxia in the human erythropoietin gene. *J Biol Chem* 266:15563-15566
52. Pugh CW, Tan CC, Jones RW, Ratcliffe PJ 1991 Functional analysis of an oxygen-regulated transcriptional enhancer lying 3' to the mouse erythropoietin gene. *Proc Natl Acad Sci USA* 88:10553-10557
53. Blagosklonny MV, An WG, Romanova LY, Trepel J, Fojo T, Neckers L 1998 p53 inhibits hypoxia-inducible factor-stimulated transcription. *J Biol Chem* 273:11995-11998
54. Levy AP, Levy NS, Goldberg MA 1996 Hypoxia-inducible protein binding to vascular endothelial growth factor

- mRNA and its modulation by the von Hippel-Lindau protein. *J Biol Chem* 271:25492-25497
55. Levy NS, Chung S, Furneaux H, Levy AP 1998 Hypoxic stabilization of vascular endothelial growth factor mRNA by the RNA-binding protein HuR. *J Biol Chem* 273: 6417-6423
56. Maltepe E, Schmidt JV, Baunoch D, Bradfield CA, Simon MC 1997 Abnormal angiogenesis and responses to glucose and oxygen deprivation in mice lacking the protein ARNT. *Nature* 386:403-407
57. Martin W, Villani GM, Jothianandan D, Furchgott RF 1985 Selective blockade of endothelium-dependent and glyceryl trinitrate-induced relaxation by hemoglobin and by methylene blue in the rabbit aorta. *J Pharmacol Exp Ther* 232:708-716
58. Davis LG, Kuehl WM, Battey JM 1994 *Basic Methods in Molecular Biology*, ed. 2. Appleton & Lange, Norwalk, CT
59. Montuenga LM, Mariano JM, Prentice MA, Cuttitta F, Jakowlew SB 1998 Coordinate expression of transforming growth factor- $\beta$ 1 and adrenomedullin in rodent embryogenesis. *Endocrinology* 139:3946-3957
60. Camenisch G, Tini M, Chilov D, Kvietikova I, Srinivas V, Caro J, Spielmann P, Wenger RH, Gassmann M 1999 General applicability of chicken egg yolk antibodies: the performance of IgY immunoglobulins raised against the hypoxia-inducible factor 1 $\alpha$ . *FASEB J* 13:81-88



# <sup>19</sup>F NMR of 2-Deoxy-2-fluoro-D-glucose for Tumor Diagnosis in Mice. An NDP-Bound Hexose Analog as a New NMR Target for Imaging

Yoko Kanazawa,<sup>1\*</sup> Keiko Umayahara,<sup>1</sup> Toshiyuki Shimmura<sup>1</sup> and Tsuneo Yamashita<sup>2</sup>

<sup>1</sup> Faculty of Pharmaceutical Sciences, Kyushu University, Fukuoka 812-82, Japan

<sup>2</sup> Daikin Industries, Nishi-ichitsuya, Settsu 566, Japan

A well-known radiopharmaceutical 2-deoxy-2-fluoro-D-glucose widely used for positron emission tomography diagnosis in terms of glucose utilization, was re-evaluated here as a nuclear magnetic resonance pharmaceutical for cancer detection. The uptake and metabolism of FDG in the experimental tumor, MH134, transplanted to the peritoneum of C3H mice as an ascitic tumor was studied extensively by *ex vivo* <sup>19</sup>F NMR. Prolonged retention of FDG and its metabolites over 2 days was confirmed in the tumor cells as well as in the heart. In these tissues, the 6-phosphate of the injected compound was converted reversibly to its epimer 2-deoxy-2-fluoro-D-mannose and further to their NDP bound forms. The metabolites were almost cleared within a day from the other healthy organs where the formation of NDP-2-deoxy-2-fluoro-D-mannose was low. Thus, the <sup>19</sup>F NMR signal of NDP-FDM detected 1 day after the FDG injection could be used as a target signal for tumor detection. Through the use of *in vivo* <sup>19</sup>F NMR spectra and <sup>19</sup>F chemical shift images, the feasibility of this proposal was demonstrated. It was concluded that FDG-NMR has a potential for tumor diagnosis in animals. © 1997 by John Wiley & Sons, Ltd.

*NMR in Biomed.* 10, 35–41 (1997) No. of Figures: 8 No. of Tables: 0 No. of References: 23

**Keywords:** chemical shift imaging; tumour diagnosis; 2-deoxy-2-fluoro-D-glucose; 2-deoxy-2-fluoro-D-mannose; <sup>19</sup>F NMR; mouse

Received 19 December 1996; revised 13 January 1997; accepted 13 January 1997

## INTRODUCTION

2-Deoxy-2-[<sup>18</sup>F]fluoro-D-glucose (FDG) has been developed as a radio-pharmaceutical for *in vivo* determination of regional glucose utilization in positron emission tomography (PET),<sup>1</sup> particularly for the measurement of brain activity.<sup>2</sup> Later, cancer has become one of the important research targets<sup>3–5</sup> along with brain activity and cardiac muscles. The metabolic trap of FDG-6 phosphate (FDG-6-P) in tissue has been the established principle of <sup>18</sup>F uptake. Thus, PET-FDG data are analyzed by the model of reversible rate processes of tissue incorporation and 6-phosphorylation.<sup>6</sup> Increased glucose metabolism and diminished activity of glucose-6-phosphatase are thought to explain the image contrast between malignant and healthy tissues in the cancer studies.<sup>3,5</sup> Further metabolic pathways have been less emphasised in the study of <sup>18</sup>F radio-pharmaceuticals which have a lifetime of 110 min.

In nuclear magnetic resonance (NMR) studies of <sup>19</sup>F FDG in mice, the metabolism of FDG beyond FDG-6-P has been observed in most organs.<sup>7–9</sup> The reversible epimerization of FDG-6-P to 2-deoxy-2-fluoro-D-mannose-6 phosphate (FDM-6-P)<sup>8</sup> takes place by the action of phosphoglucose isomerase (PGI), and is observed in almost every tissue.<sup>7–10</sup> The formation of FDM-6-P is fastest in brain, followed by heart<sup>7–9,11</sup> and cancer cells.<sup>10</sup> In basic studies of PET-FDG,<sup>1,3,4</sup> these organs have been found to retain <sup>18</sup>F radioactivity longer than the others and are the subjects of recent FDG-PET studies, and retention of F-compound over

2 days has been confirmed in the heart and tumor using the <sup>19</sup>F NMR method.<sup>7–10</sup> In the proton-coupled tissue spectra obtained 1 day after FDG injection, the signal intensity in the region of FDM relative to that of FDG exceeded the equilibrium ratio between FDM-6-P and FDG-6-P attained by the catalysis of PGI.<sup>8–10</sup> By high-resolution spectroscopy of tissue extracts, we have shown that FDG-6-P and FDM-6-P are metabolized further to their nucleotide-bound forms, NDP-FDG and NDP-FDM, in brain, heart and several other organs as in Fig. 1.<sup>9</sup> We suspected, therefore, that the formation of NDP-bound hexoses could be the source of unusual intensity ratio of FDG and FDM in heart and tumors, and it was proved in the study reported herein.

Chemical shift imaging has long been expected to be an ideal method for visualizing regional tissue characteristics through the metabolism of intrinsic compounds of physiological importance or of specifically designed NMR pharmaceuticals. Due to the inherent low sensitivity of the NMR method, however, metabolic imaging has been applied only to limited systems.<sup>12,13</sup> NMR imaging *in vivo*, by using a stable signal of FDG metabolites beyond FDG-6-P, that is characteristic to tumor cells, was considered to be a powerful technique for the detection and investigation of proliferative tissues. A high field imaging instrument was employed here to observe the unique metabolite of FDG in tumors.

We report here the potential of FDG as an NMR pharmaceutical for cancer diagnosis by *in vivo* NMR measurement. Prolonged retention of FDG metabolites in tumor cells was accompanied by an effective FDG-FDM conversion followed by the synthesis and intensive accumulation of NDP-FDM. The <sup>19</sup>F NMR signals of FDG

\* Correspondence to: Y. Kanazawa.

Contract grant sponsor: Ministry of Education, Japan.

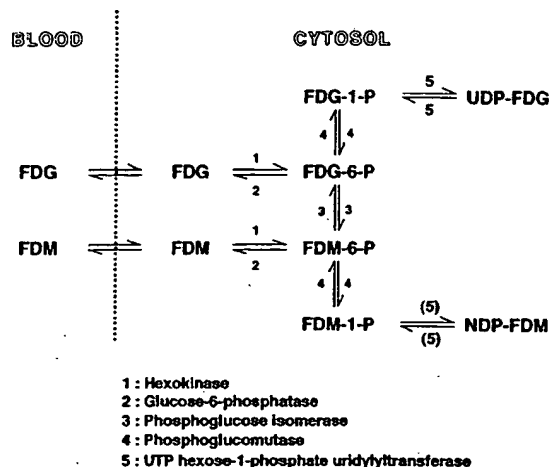


Figure 1. Metabolic pathway of fluorohexoses in tumors and organs.

metabolites were observable in simple *in vivo* NMR spectroscopy and imaging. The feasibility of metabolic imaging of tumor by using NDP-FDM as the target signal was demonstrated.

## MATERIALS AND METHODS

### Materials

FDG was prepared according to the method of Haradahira *et al.*<sup>14</sup> The main impurity, FDM, was determined by <sup>19</sup>F NMR to be below 0.8%.

### Animal experiments

Female C3H mice were supplied from the Animal Center of Kyushu University at 5 weeks of age and kept for 2–4 weeks in the animal room at the Faculty of Pharmaceutical Sciences (23±1 °C). About 5×10<sup>5</sup> cells of MH134 hepatoma were transplanted into peritoneal cavities of the mice 7–9 days prior to the NMR experiments. FDG was injected as a saline solution through the tail vein after 16 h of fasting. The dose for *ex vivo* study was 100 mg/kg which was the amount where no apparent sign of behavioral disturbance was observed.<sup>9</sup> It was doubled for *in vivo* <sup>19</sup>F NMR to give a better signal-to-noise ratio.

### Quantification of metabolites

Immediately after the mouse was killed by cervical dislocation, tumor cells were collected from ascitic fluids by repeated centrifugation (400–900 g) and washed three times with ice-cold saline. Healthy organs (brain, heart, liver, muscle, intestine) were excised on an ice bath, washed with cold saline to remove most of the blood, wiped with filter paper, and packed into a 10 mm NMR tube. The intestine was cut into 1–2 cm lengths to remove the contents. The cells and organs in the NMR tubes were heated in boiling water for 3 min for enzyme deactivation, and the air in the tube was replaced with Ar gas to prevent oxidation.

### Metabolite identification

After the NMR measurements of whole organs or cells for quantification at 94 MHz, the metabolites were extracted with water for detailed analysis by high resolution NMR. Tumor cells and organs were homogenized with a teflon homogenizer (WEATON) with distilled and deionized water and centrifuged for 30 min at 18 500 g. The supernatant was added with the aliquot used to rinse the pellet, and with D<sub>2</sub>O as the NMR lock signal source. The extracted residue was also packed in a 10 mm NMR tube for the evaluation of extraction efficiency.

### NMR measurements

**Spectral assignments and quantification.** The <sup>19</sup>F NMR spectra of water extracts were obtained by JEOL GSX-270WB operated at 254 MHz under proton decoupling conditions. For the spectral analysis, the conditions were: spectral band width of 20 kHz, pulse width of 8 μs (45°), *TR* 450 ms. Spectral assignment was made by referring to the <sup>19</sup>F NMR data of authentic samples<sup>9,15</sup> measured from an external standard of hexafluorobenzene in benzene (1/400, v/v, abbreviated as HFB) with and without proton decoupling. The concentration of fluorine compounds in organs was determined using the <sup>19</sup>F NMR spectrum of the individual whole organ in a 10 mm NMR tube with a JEOL FX-100 spectrometer operated at 93.7 MHz and 23±1 °C with a spectral band width of 40 kHz, pulse width of 16 μs (45°) and *TR* 180 ms. The intensities of the three main peaks from whole organs, the FDG-group ( $\alpha$ -,  $\beta$ -FDG, FDG-6-P, FDG-1-P and NDP-FDG) at -36 ppm from HFB, the  $\alpha$ -FDM-group (FDM, FDM-6-P, FDM-1-P and NDP-FDM) at -41 ppm, and the  $\beta$ -FDM-group (FDM and FDM-6-P) at -59 ppm<sup>9</sup> were measured. The quantification was done by the published method<sup>7,9</sup> using an average *T*<sub>1</sub> determined with deactivated tissues by a standard inversion recovery method using the same spectrometer, a JEOL FX-100: 0.9 s for the FDG group and 0.8 s for the FDM groups in ascitic cells, and 0.7 s for the FDG group and 0.6 s for the FDM group compounds in the other organs, respectively.

***In vivo* spectra.** <sup>19</sup>F spectra of the mice bearing ascitic MH134 tumors were taken with a one-turn surface coil of 12 mm diameter placed on the lower abdomen using a JEOL GSX-270WB spectrometer under halothane anesthesia (0.5% halothane in air). The signal positions of halothane, more than 120 ppm downfield from the FDG-group signals, were too far distant to interfere with the spectral region of interest. The spectra were collected for 15 min under the acquisition conditions of 8 μs pulse (22° at a depth of 3 mm, 11° at 6 mm) 200 ms pulse repetition time and 80 kHz spectral bandwidth. Spectra were obtained at 1, 6, 24 and 48 h after the injection of 200 mg FDG/kg.

**<sup>19</sup>F imaging.** The images of FDG and its metabolites were obtained using a Varian Unity 400plus with a 9.4 T vertical magnet of bore size 89 mm. The image probe, used both for *in vivo* spectra and imaging, was equipped with a <sup>1</sup>H/<sup>19</sup>F tunable bird-cage type rf coil of 40 mm inner diameter and 45 mm height, and shielded gradient coils. FDG (200 mg/kg, i.v.) was injected after 16 h fasting. Thirty minutes before imaging, the mouse was placed in the animal container under pentobarbital anesthesia (50 mg/kg, i.p.). <sup>19</sup>F chemical shift-selected images were obtained at

376 MHz with a simple spin-echo: a chemical shift-selection of 1 kHz band width by a gaussian pulse.  $TR=1$  s,  $TE=4$  ms,  $64 \times 16$  data points, field of vision (FOV) of  $6 \text{ cm} \times 4 \text{ cm}$  without slice selection, and a data accumulation time of 40–160 min. Images were obtained on the first and second days of FDG injection. The mice were fed freely in their cages during the interval between *in vivo* NMR experiments. The ascitic cells and heart were collected immediately after the *in vivo* NMR experiments for quantification.

## RESULTS

### *Ex vivo* $^{19}\text{F}$ spectrum

$^{19}\text{F}$  NMR spectra of packed ascitic cells (93.4 MHz) and a proton decoupled spectrum of the water extracts observed at 254 MHz are shown in Fig. 2. The spectral separation of the FDM groups from the FDG group was sufficient in the whole packed cells without  $^1\text{H}$  decoupling. The increase in the  $\alpha$ -FDM group towards 24 h was clearly shown in a low resolution spectrum at 93.4 MHz. The  $^1\text{H}$  decoupled spectrum of tumor extracts at 254 MHz indicated that NDP-FDM was the main component of the  $\alpha$ -FDM group signal 1 day after FDG injection. The total concentration of fluorine compounds determined from 93.7 MHz NMR spectrum was used as the uptake value of FDG in Fig. 3. In the early period, between 30 and 120 min after the injection

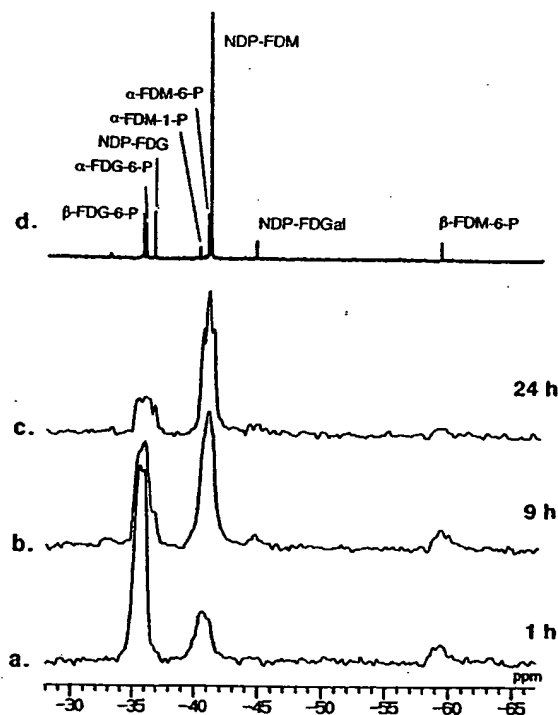


Figure 2.  $^{19}\text{F}$  NMR spectra of MH134 ascitic cells collected at the indicated times after 100 mg/kg i.v. injection. (a)–(c) Packed ascitic cells at 1, 9, and 24 h after injection, observed at 93.4 MHz; (d) proton-decoupled spectrum of water extracts of ascitic cells collected immediately after the observation of (c), at 254 MHz. The chemical shift standard was hexafluorobenzene in benzene (1/400, v/v). The FDG-group (FDG),  $\alpha$ -FDM-group ( $\alpha$ -FDM) and  $\beta$ -FDM-6-P ( $\beta$ -FDM) were distinguishable.

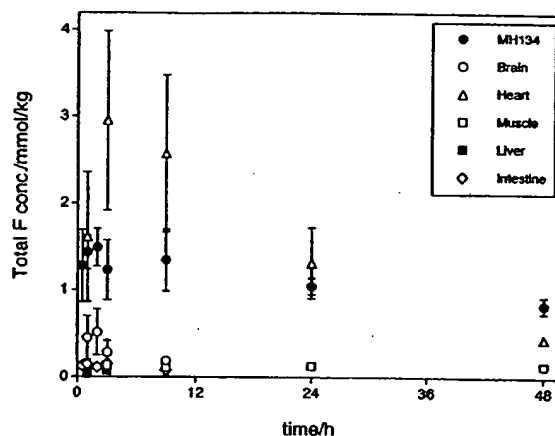


Figure 3. Uptake of FDG in collected ascitic cells and normal organs of 100 mg/kg FDG injected mice. Concentrations were determined from 93.4 MHz  $^{19}\text{F}$  NMR spectra. Most of the points are the averages of  $n$ =two to four points + standard deviation. The data at 48 h are the averages of one to two points.

of 100 mg FDG/kg, uptake was in the order: heart > packed ascitic cells > brain  $\approx$  muscle and the other organs. The order of uptake after 9 h was changed as follows: heart = packed ascitic cells  $\gg$  other organs. The remarkably long retention of FDG and its metabolites reported in the previous work, in the heart of healthy male ddY mouse<sup>7,9</sup> and in the ascitic cells of Sarcoma 180 bearing male ddY mice,<sup>10</sup> was reproduced with female C3H mice bearing MH134 tumors in the present study. The contribution from the FDM group to the total uptake is shown in Fig. 4. It increased to 67% of the total uptake value 24 h after and to 72% 48 h after FDG injection in ascitic cells, which is comparable to our previous observation of 73% in the ascitic cells of Sarcoma 180-bearing ddY mice collected 48 h after 200 mg/kg FDG injection.<sup>10</sup> The ratio FDM-group/total uptake was also high in heart, 66–70% at 24 and 48 h, which was similar to the value of 70–74% in the healthy ddY mice.<sup>7</sup> High values were also obtained in the brain and muscle.

The NMR spectra of the extraction residue indicated that the efficiency of the water extraction of metabolites from each organ was higher than 80% of visible signals, and it was nearly constant through the metabolites: FDG,  $\alpha$ -FDM,

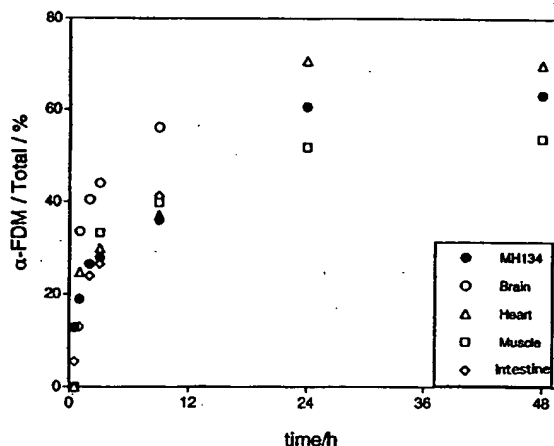


Figure 4. Concentrations of the FDM-group of metabolites found in MH134 ascitic cells and organs of MH134 bearing mice injected with 100 mg/kg FDG, relative to total uptake value. The data of organs without detectable signals were not included.



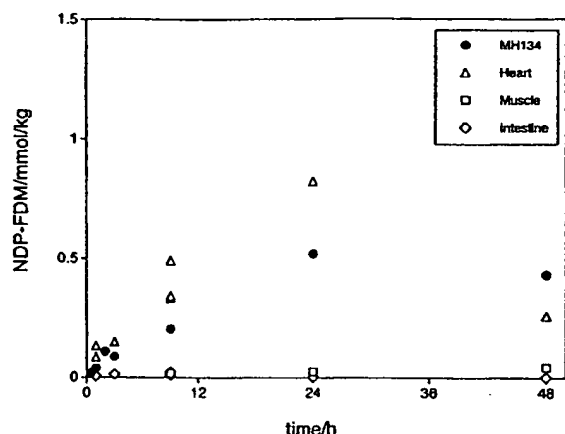


Figure 5. Concentrations of NDP-FDM found in the water extracts of MH134 ascitic cells and organs of 100 mg/kg FDG injected mice.

and  $\beta$ -FDM groups in the phosphates or NDP bound forms. Thus, the composition of metabolites was evaluated from the  $^1\text{H}$  decoupled spectra of water extracts (as in Fig. 2(d)). The contribution of NDP-FDM to the FDM signal in Fig. 4 and consequently to the total uptake was found to be dominant in tumor and heart 1 day after injection, as seen in Fig. 5.

The rate of conversion from FDG to the FDM-group was evaluated in two ways. In the early period after FDG injection, when the reaction was limited to the epimerization from FDG-6-P to FDM-6-P, typically within 1 h, the rate could be estimated by the half time in approaching the equilibrium ratio of these two compounds, when FDM-6-P formed 42.9% of the total metabolites.<sup>11</sup> From the data of Fig. 4, it was evaluated to be 0.6 h for brain and heart, 0.7 h for MH134 cells and 0.5–1 h for muscle, and much slower values for intestine (2 h) and liver (4 h). The next step, the approach to the final state where the dominant metabolite was NDP-FDM, was a very slow process. The half times of approach to the maximum value of NDP-FDM specific to the organs as evaluated from the data of Fig. 5 were of the order of 12 h, e.g. ascitic cells (12 h), heart (10 h) and

muscle (16 h). In the organs such as brain, liver and intestine where the metabolites became almost undetectable in 1 day, the contribution from NDP-FDM was much less. This suggested a correlation between retention and the amount of NDP-FDM formed. Although FDG metabolism in tumor cells were slow, of the order of 0.7 h from FDG-6-P to FDM-6-P and 12 h from FDM-6-P to NDP-FDM at a dose of 100 mg/kg, the rate of excretion from tumor cells was even smaller as seen in Fig. 3. Since the excretion rate was an order of magnitude lower than the rates of these reactions, we were able to measure the time courses of the reactions themselves by the NMR method with low time resolution.

### In vivo spectrum

*In vivo* spectra of the mice bearing ascitic hepatomas, taken immediately after the injection of 200 mg/kg of FDG and at some subsequent intervals, are shown in Fig. 6. The time course of FDG dynamics determined from *in vivo* spectra is depicted in Fig. 7. The profile of conversion from the FDG group to the FDM group was in good agreement with the one obtained *ex vivo*. The rate of washout at the initial stage was larger compared to the *ex vivo* data (Fig. 3). The reason is probably the higher dose used for this *in vivo* observation, which was greater by a factor of two than that for the *ex vivo* study. The spectrum of the last *in vivo* observation (in Fig. 6(a)), had essentially same relative intensities as the excised cells (Fig. 5(b)) and the water extract (Fig. 5(c)), which indicated the equal visibility of F signals *in vivo* and in the high resolution NMR probe, and confirms the efficiency of water extraction from tumor cells.

### $^{19}\text{F}$ images

$^{19}\text{F}$  NMR chemical shift selected images were constructed from the signal of the FDG-group, starting at 5 h after the 200 mg FDG/kg injection and accumulated for 107 min,

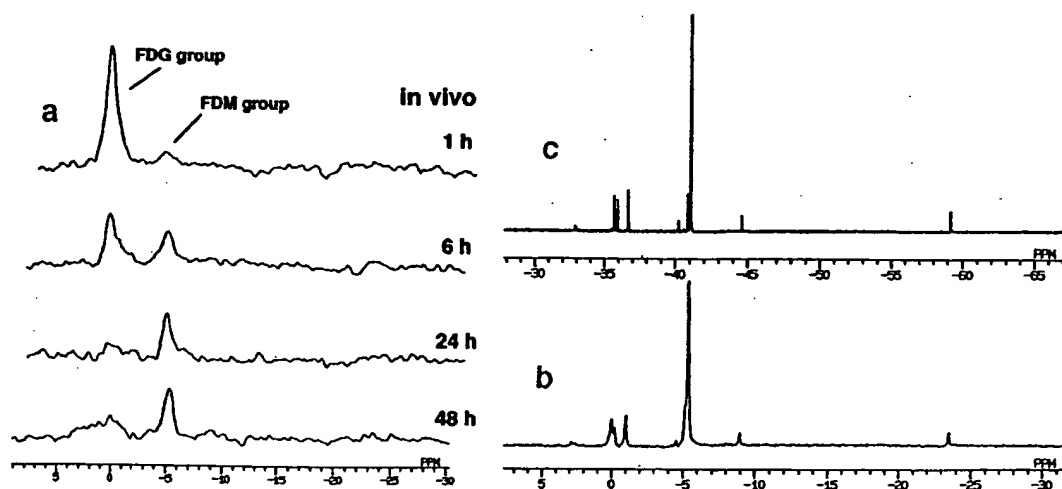
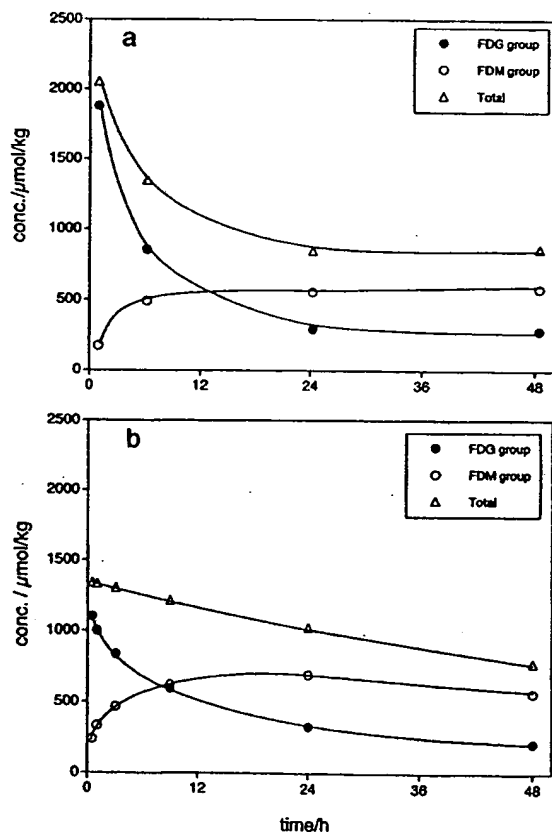


Figure 6.  $^{19}\text{F}$  NMR spectra (254 MHz) of a 200 mg/kg FDG injected mouse. (a) *In vivo* spectra of the lower abdomen, obtained by a 12 mm surface coil under halothane (0.5%) anesthesia, with 15 min data accumulations. The starting time is shown in the figure. (b) Proton-decoupled spectrum of packed ascitic cells immediately after the *in vivo* observation. (c) Proton decoupled spectrum of water extracts of collected cells used for (b).

and of the FDM-group starting at 25 h after the injection and accumulated for 160 min. They are shown in Fig. 8 with the respective  $^1\text{H}$  scout images and  $^{19}\text{F}$  spectra obtained by the same  $^{19}\text{F}/^1\text{H}$  tunable volume coil. In the  $^{19}\text{F}$  FDG-selected image, the signal of the FDG-group was observed mainly at the position in the lower abdomen where ascitic cells were expected. A strong signal was observed at the position of the bladder during this period. The region of tumor cells was visualized in the FDM-group selected image 1 day after FDG injection as well as the position of bladder. A  $^{19}\text{F}$  spectrum taken at 28 h with a 12 mm surface coil as a receiver with a 43  $\mu\text{s}$  pulse at the lower abdomen was also shown in Fig. 8. The spectral pattern was essentially the same as that which we obtained from the whole body at 25 h. The concentrations of metabolites determined immediately after the last spectral measurement were as follows: FDG-group, 220  $\mu\text{mol/kg}$ ;  $\alpha$ -FDM-group, 430  $\mu\text{mol/kg}$ ;  $\beta$ -FDM-group, 30  $\mu\text{mol/kg}$  in collected ascitic cells; FDG-group, 210  $\mu\text{mol/kg}$ ; and FDM-group, 690  $\mu\text{mol/kg}$  in heart. Taking account of the fact that the ascitic cells are in fluid at a concentration of 1/4–1/3, v/v, the *in vivo* concentration of the FDM-group used for the last  $^{19}\text{F}$  image should be below 150  $\mu\text{mol/kg}$ . No such images were obtained from healthy mice 1 day after FDG injection.



**Figure 7.** (a) The time course of FDG dynamics determined from the data of Fig. 6. The concentrations at 24 h was determined from the spectrum of collected cells, which was used with the relative intensities of *in vivo* spectra to determine the concentration at each time, assuming that the sensitivity in each experiment was the same. (b) The FDG dynamics from the *ex vivo* data of excised ascitic cells in Fig. 3. (a) and (b) are essentially the same except for the initial stage where the effect of the doubled dose used for the *in vivo* observations was significant.

## DISCUSSION

The retention of FDG metabolites in heart and tumor tissue over 2 days was confirmed in female C3H mice by  $^{19}\text{F}$  NMR. It generalized our previous observations of their long retention in heart<sup>7</sup> and tumor<sup>10</sup> using mice of different strains and gender, healthy or with tumor cells of different origin.

The main metabolite found in the ascitic cells 1 day after FDG injection was NDP-FDM, which formed 0.5 mmol/kg of packed cells at the dose of 100 mg/kg body weight. The formation of NDP-FDG and NDP-FDM in living systems has been reported in yeast and chick-embryo cells using  $^3\text{H}$ -labeled FDG and FDM and  $^{14}\text{C}$ -labeled GTP and UTP by the method of radioactive gas-liquid chromatography.<sup>16</sup> The products of C2-epimerization such as GDP-FDM from FDG have been found in yeast cells.<sup>16</sup> The  $^{18}\text{F}$ -activity found in the nucleotide derivatives of  $^{18}\text{F}$ FDG in rat tumor has been shown to be proportional to that of  $^{18}\text{F}$ FDG-6-P.<sup>17</sup> However, this is probably the first report of the formation of NDP-FDM from FDG as the dominant metabolite in heart and tumor cells.

The slow washout of FDG from cancer cells has been explained by the low activity of glucose 6-phosphatase,<sup>3,5,17</sup> which also accounts for high rate of uptake in brain.<sup>2,6</sup> A decreased activity of glucose-6-phosphatase in Morris hepatomas has been reported.<sup>18</sup> In the present work, however, the half washout time of FDG metabolites in brain of ca. 4 h was much shorter than those of heart of 1 day and tumor which was over 2 days. In spite of very low initial uptake, retention over 2 days was also observed in muscle (Fig. 3), where the formation of the FDM group was not small (Fig. 4). A strong correlation was found between the retention of FDG metabolites and the formation of NDP-FDM. These results suggest the presence of many factors in addition to the modified activity of glucose-6-phosphatase on the glucose analogs FDG-6-P and FDM-6-P as the mechanism of slow FDG clearance. Nor have we any evidence to determine whether the long life of metabolites in these cells was due to the formation of NDP-FDM or whether the regional retention caused the accumulation of this compound. In order to understand the mechanism of retention over 2 days more work will be required, including the determination of the base species in NDP-FDM. The knowledge of such metabolites will contribute to the elucidation of the FDG accumulation mechanism. At least, we can propose here that FDG could be used as an NMR pharmaceutical for tumor diagnosis for both *in vivo* spectroscopy and imaging since the signal of NDP-FDM can be used as a marker of tumor, with almost the only exception being the heart.

A mouse tumor has been visualized by using the unique metabolite of FDG as the target signal for chemical shift selected  $^{19}\text{F}$  NMR imaging. Besides the proof of the new principle of FDG metabolism in tumor, we achieved a  $^{19}\text{F}$  chemical shift image of a metabolite at a concentration below 150  $\mu\text{mol/kg}$  in a small animal. The success in the chemical shift imaging at such a low concentration in mice was in part due to the slow rate of reaction and even slower rate of clearance of this pharmaceutical, and in part to the use of the high field, 9.4 T. Imaging with a vertical type magnet has the advantage of large  $B_0$  within a limited hardware cost and laboratory space, while being applicable to both *in vivo* study and high-resolution observations.

The use of FDG for tumor diagnosis was originally

proposed using the PET method, and has been established as a standard procedure in that field. Most of the protocols for FDG-PET tumor diagnosis are different from those used for brain activity measurements based on the original principle of FDG-6-P trapping; data acquired 45 min or more after FDG injection are known to have a better tumor to background contrast.<sup>3-5,19</sup> Recently, single photon emission tomography (SPECT) for FDG imaging<sup>20,21</sup> has been seen as a promising method for meeting the wider need for cancer diagnosis due to its better accessibility than PET. It is of interest that the data acquisition periods for the clinical SPECT study are set in the range of 60–150 min after <sup>18</sup>F-DG injection, which is later than the paired PET measurement and the standard FDG-PET protocol.<sup>20</sup> The image contrast for tumors seems to be attained at the latest period allowed for the detection of <sup>18</sup>F because of its limited lifetime. Recent progress in PET technology enables creation of a whole body map<sup>22</sup> which is suitable for searching for metastasis. However, a problem has been found in the accumulation of FDG in healthy muscle which obscures the small target tumor.<sup>22</sup> This result is in good agreement with our finding of low but long muscle retention: a signal source in low concentration but large volume can easily mask a small target with higher

concentration if the imaging method has low spatial resolution. Fukuda *et al.*<sup>23</sup> proposed <sup>18</sup>FDM as a pharmaceutical for PET-tumor imaging. Our results from this NMR study support FDM as a precursor compound for synthesizing NDP-FDM *in vivo*. So far, the results of studies using the radioactive pharmaceutical FDG and those with <sup>19</sup>F NMR are in good agreement, irrespective of the order of magnitude difference in the dose employed, and suggest the importance of elucidating the mechanism of FDG retention in tumors. The combination of molecular information from the NMR study with the abundant clinical and experimental FDG-PET data will lead to that goal.

## CONCLUSION

(1) Prolonged retention of FDG metabolites over 2 days in the heart and in tumors, mainly in the form of NDP-FDM, has been shown for the first time, whereas most metabolites were cleared from the other organs within 1 day.

(2) *Ex vivo* and *in vivo* <sup>19</sup>F NMR spectra of FDG and its products were consistent, confirming *in vivo* NMR detectability of FDG metabolites and the reliability of

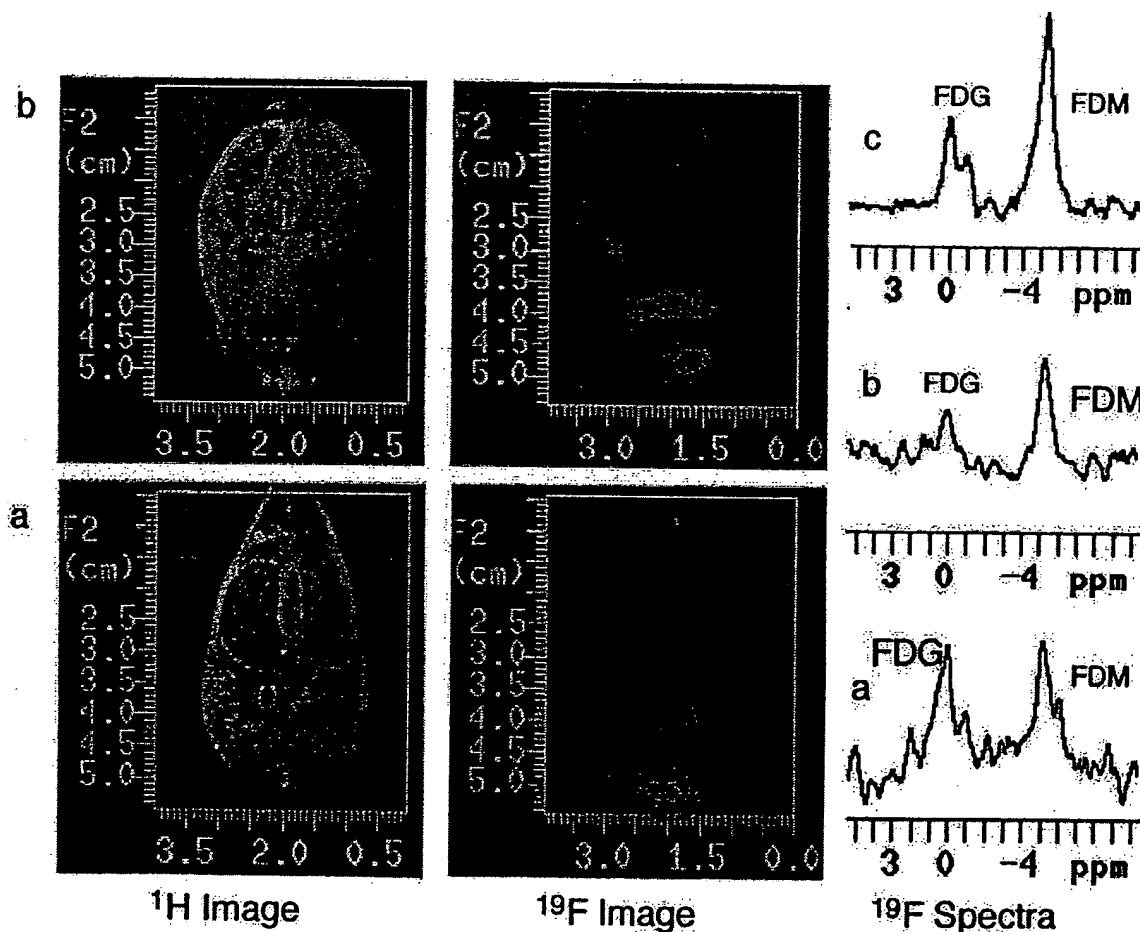


**Figure 8.** Chemical shift selected <sup>19</sup>F coronal images (376 MHz) of a 200 mg/kg FDG injected into an ascites-bearing mouse under pentobarbital anesthesia with corresponding <sup>1</sup>H scout images and the <sup>19</sup>F spectra taken immediately before the <sup>19</sup>F image. (a) Data acquisition started at 5 h after the FDG injection and accumulated for 107 min. The FDG-group was selected for the <sup>19</sup>F image. (b) Data acquisition started at 25 h after the injection of FDG, and accumulated for 160 min. The  $\alpha$ -FDM-group was selected. The image intensity of (b) was doubled compared with that of image (a). <sup>19</sup>F images were processed as follows: zero-filled to 256 × 128 data points, subjected to a gaussian filter of 500 Hz bandwidth, and displayed at 1.2 times intensity steps. (c) <sup>19</sup>F spectrum from the lower abdomen with a 12 mm surface coil.

quantification.

(3) The <sup>19</sup>F NMR signal of the FDM-group of metabolites, mainly from NDP-FDM, was shown to be a good target for *in vivo* spectroscopy and imaging, to assist in tumor detection.

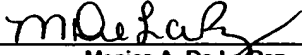
(4) The applicability of chemical shift imaging to the study of metabolites at low concentration in small animals by high field magnetic resonance has been demonstrated.

## Acknowledgements

This work was partly supported by the Grant in Aid for Scientific Research from the Ministry of Education, Japan. We would like to thank Professor Kouji Masuda of Kyushu University, Faculty of Medicine for the use of a GSX-270 spectrometer. MH134 cells were the gift of Taiho Pharmaceutical Co. Ltd. Part of this work was presented at the 2nd International Symposium on PET in Oncology, 1993, Sendai, 12th annual meeting of SMRM (1993) and 2nd meeting of SMR (1994).

## REFERENCES

- Gallagher, B. M., Ansari, A., Atkins, J., Casella, V., Christman, D. R., Fowler, J. S., Ido, T., MacGregor, R. R., Som, P., Wan, C. N., Wolf, A. P., Kuhl, D. E. and Reivich, M. Radiopharmaceuticals XXVII. <sup>18</sup>F-labeled 2-deoxy-2-fluoro-D-glucose as a radiopharmaceutical for measuring regional myocardial glucose metabolism *in vivo*: tissue distribution and imaging studies in animals. *J. Nucl. Med.* **18**, 990-996 (1977).
- Reivich, M., Kuhl, D., Wolf, A., Greenberg, J., Phelps, M., Ido, T., Casella, V., Fowler, J., Hoffman, E., Alavi, A., Som, P. and Sokoloff, L. The [<sup>18</sup>F]fluorodeoxyglucose method for the measurement of local cerebral glucose utilization in man. *Circ. Res.* **44**, 127-137 (1979).
- Yonekura, Y., Benua, R. S., Brill, A. B., Som, P., Yeh, S. D. J., Kemeny, N. E., Fowler, J. S., MacGregor, R. R., Stamm, R., Christman, D. R. and Wolf, A. P. Increased accumulation of 2-deoxy-2-[<sup>18</sup>F]fluoro-D-glucose in liver metastases from colon carcinoma. *J. Nucl. Med.* **23**, 1133-1137 (1982).
- Strauss, R. W. and Conti, P. S. The applications of PET in clinical oncology. *J. Nucl. Med.* **32**, 623-648 (1991).
- Wahl, R. L., Hutchins, G. D., Buchsbaum, D. J., Liebert, M., Grossman, H. B. and Fisher, S. <sup>18</sup>F-2-Deoxy-2-fluoro-D-glucose uptake into human tumor xenographs. *Cancer* **67**, 1544-1550 (1991).
- Sokoloff, L., Reivich, M., Kennedy, C., Des Rosiers, M. H., Patlak, C. S., Pettigrew, K. D., Sakurada, O. and Shinohara, M. The [<sup>14</sup>C]deoxyglucose method for the measurement of local cerebral glucose utilization: theory, procedure, and normal values in the conscious and anesthetized albino rat. *J. Neurochem.* **28**, 897-916 (1977).
- Kanazawa, Y., Momozono, Y., Yamane, H., Haradahira, T., Maeda, M. and Kojima, M. Metabolic pathway of 2-deoxy-2-fluoro-D-glucose studied by F-19 NMR. *Life Sci.* **39**, 737-742 (1986).
- Kanazawa, Y., Momozono, Y., Yamane, H., Haradahira, T., Maeda, M. and Kojima, M. NMR evidence for the unexpected interconversion of 2-deoxy-2-fluoro-D-glucose and 2-deoxy-2-fluoro-D-mannose in mice. *Chem. Pharm. Bull.* **35**, 895-898 (1987).
- Kanazawa, Y., Yamane, H., Shinohara, S., Kuribayashi, S., Momozono, Y., Yamato, Y., Kojima, M. and Masuda, M. 2-Deoxy-2-fluoro-D-glucose as a functional probe for NMR: the unique metabolism beyond its 6-phosphate. *J. Neurochem.* **66**, 2113-2120 (1996).
- Kojima, M., Kuribayashi, S., Kanazawa, Y., Haradahira, T., Maehara, Y. and Endo, H. Metabolic pathway of 2-deoxy-2-fluoro-D-glucose and 2-deoxy-2-fluoro-D-mannose in mice bearing Sarcoma 180 studied by fluorine-19 nuclear magnetic resonance. *Chem. Pharm. Bull.* **36**, 1194-1197 (1988).
- Shinohara, S., Kanazawa, Y. and Kojima, M. Evaluation of energy metabolism in brain using epimerization of 2-deoxy-2-fluoro-D-glucose by <sup>19</sup>F NMR: the effect of anesthesia. *Magn. Reson. Med.* **21**, 191-196 (1991).
- Nakada, T., Kwee, I. L., Card, P. J., Matwiyoff, N. A., Griffey, B. V. and Griffey, R. H. Fluorine-19 NMR imaging of glucose metabolism. *Magn. Reson. Med.* **6**, 307-313 (1988).
- Brix, G., Bellman, M. E., Haberkorn, U., Gerlach, L., Bachert, P. and Lorenz, W. J. Mapping of biodistribution and catabolism of 5-fluorouracil in tumor-bearing rats by chemical-shift selective <sup>19</sup>F imaging. *Magn. Reson. Med.* **34**, 302-307 (1995).
- Haradahira, T., Maeda, M., Kai, Y. and Kojima, M. A new high yield synthesis of 2-deoxy-2-fluoro-D-glucose. *J. Chem. Soc. Chem. Commun.* **1985**, 364-365 (1985).
- Kanazawa, Y., Kuribayashi, S. and Kojima, M. A <sup>19</sup>F NMR study of 2-deoxy-2-fluoro-D-galactose in mice. *Chem. Pharm. Bull.* **36**, 4213-4216 (1988).
- Schmidt, M. F. G., Biely, P., Kratzky, Z. and Schwarz, T. Metabolism of 2-deoxy-2-fluoro-D-[<sup>3</sup>H]glucose and 2-deoxy-2-fluoro-D-[<sup>3</sup>H]mannose in yeast and chick-embryo cells. *Eur. J. Biochem.* **87**, 55-68 (1978).
- Suolinna, E.-L., Haaparana, M., Paul, R., Harkonen, P., Solin, O. and Sipila, H. Metabolism of 2-[<sup>18</sup>F]fluoro-2-deoxyglucose in tumor bearing rats: chromatographic and enzymatic studies. *Nucl. Med. Biol.* **13**, 577-581 (1986).
- Xiao, Q., Jaspers, I., Matthew, E. and Lea, M. A. Changes in the glucose-6-phosphatase complex in hepatomas. *Mol. Cell. Biochem.* **122**, 17-24 (1993).
- Zasadny, K. R. and Wahl, R. L. Enhanced FDG-PET tumor imaging with correlation-coefficient filtered influx-constant images. *J. Nucl. Med.* **37**, 371-374 (1996).
- Martin, W. M., Delbeke, D., Patton, J. A., Hendrix, B., Weinfeld, Z., Ohara, I., Kessler, R. M. and Sandler, M. P. FDG-SPECT: correlation with FDG-PET. *J. Nucl. Med.* **36**, 988-995 (1995).
- Holle, L.-H., Tranpert, L., Lung-Kurt, S., Villena-Heinsen, C. E., Puschel, W., Schmidt, S. and Oberhausen, E. Investigations of breast tumors with fluorine-18-fluorodeoxyglucose and SPECT. *J. Nucl. Med.* **37**, 615-622 (1996).
- Engel, H., Steinert, H., Berthold, T., Boni, A. H. and von Schulthess, G. K. Whole-body PET: physiological and artificial fluorodeoxyglucose accumulation. *J. Nucl. Med.* **37**, 441-446 (1996).
- Fukuda, H., Matsuzawa, T., Abe, Y., Endo, S., Yamada, K., Kubota, K., Hatazawa, J., Sato, T., Ito, M., Takahashi, T., Iwata, R. and Ido, T. Experimental study for cancer diagnosis with positron-labeled fluorinated glucose analogs: [<sup>18</sup>F]-2-fluoro-2-deoxy-D-mannose: a new tracer for cancer diagnosis. *Eur. J. Nucl. Med.* **7**, 294-297 (1982).

CERTIFICATE OF MAILING 37 C.F.R. 1.8	
I hereby certify that this correspondence is being deposited with the U.S. Postal Service with sufficient postage as First Class Mail in an envelope addressed to: Commissioner for Patents, P. O. Box 1450, Alexandria, VA 22313-1450, on the date below:	
12/23/04 Date	 Monica A. De La Paz

**PATENT**

**IN THE UNITED STATES PATENT AND TRADEMARK OFFICE**

In re Application of:  
Yang, *et al.*

Serial No.: 09/599,152

Filed: June 21, 2000

For: ETHYLENEDICYSTEINE (EC)-DRUG  
CONJUGATES, COMPOSITIONS AND  
METHODS FOR TISSUE SPECIFIC  
DISEASE IMAGING

Group Art Unit: 1619

Examiner: Jones, D.

Atty. Dkt. No.: UTXC:664

**DECLARATION OF JERRY L. BRYANT, M.S., UNDER 37 C.F.R. §1.132**

MS AF  
Commissioner for Patents  
P. O. Box 1450  
Alexandria, VA 22313-1450

I, Jerry L. Bryant, M.S., do declare that:

1. I am a United States citizen residing at 6861 Staffordshire St. Houston, TX 77030.
2. I currently hold the position of Chief Technology Officer, Head of Scientific Evaluation, Division of Business Development, Cell>Point, LLC, 7120 E. Orchard Road, Suite 350, Englewood, CO 80111. A copy of my curriculum vitae, including a list of my publications, is attached as Appendix A.

3. I am skilled in the synthesis and use of radionuclide-labeled imaging agents, as evidenced by the following:
- I have worked as Chief Technology Officer of Cell>Point, LLC since 2001.
  - I have been employed as the Director of Research Development of VeriMed Research Corporation in Houston, TX, from 2002-2004.
  - My duties at Cell>Point and VeriMed include participation in the development of novel radiopharmaceuticals for different diseases, such as cancer, cardiovascular disease, and diabetes. I have also been involved with studies directed to the synthesis and use of radionuclides, and studies directed to understanding the mechanism and biochemistry of the agents as it pertains to the pharmacokinetics and biodistribution of the agents in animals and humans. In addition, I have been involved in the evaluation of new technologies for the treatment of cancer, cardiovascular disease, and diabetes.
  - I was employed as Chief Scientific Officer of Allcure, Inc., in Houston, TX, from May, 2001-May, 2002. My duties at Allcure included designing and marketing *in vitro* and *in vivo* services to drug and bio-tech companies for evaluating compounds of interest (nuclear medicine, SCID mouse *in vivo* service and mechanism studies).
  - I have experience as a Research Assistant II in the Department of Nuclear Medicine, the Division of Diagnostic Imaging, of the University of Texas M.D. Anderson Cancer Center, from October, 2002 to June, 2003.
  - I am a co-inventor of three patent applications that pertain to imaging technology, including USSN 10/703,405 ("Ethylenedicysteine (EC)-Drug Conjugates, Compositions, and Methods for Tissue Specific Disease Imaging," Yang *et al.*); USSN 10/942,615 ("Mechanism-Based Targeted Pancreatic Beta Cell Imaging and Therapy," Yang *et al.*);

and USSN 10/732,919 (N2S2 Chelate-Targeting Ligand Conjugates,” Yang *et al.*). See page 6 of Appendix A.

- I have been involved in funded studies pertaining to the development and evaluation of imaging agents during the past five years, including: (1) a study of CT and MRI functional agent development and evaluation supported by VeriMed Research Corporation; (2) a study of 99m-Tc-Ethylenedicysteine (EC)-Drug Conjugates for Tissue Specific Disease Imaging supported by Cell>Point, LLC; and (3) a study to compare Tc-99m-EC-deoxyglucose (EC-DG) and FDG-PET scans for the evaluation of patients suspected of having persistent/recurrent squamous cell carcinoma of the larynx after definitive treatment with radiation therapy and the evaluation of primary lung cancer patients, sponsored by Cell>Point, LLC. See page 7 of Appendix A.
  - I am a co-author of seven articles and numerous abstracts pertaining to the evaluation and testing of radiolabeled imaging agents. See pages 9-14 of Appendix A.
  - I am also a co-author of two book chapters pertaining to radiolabeled imaging agents and their uses in chemistry and nuclear medicine. See page 14 of Appendix A.
  - Regarding my formal education, I have a Master of Science degree (1991) in Microbiology & Cell Science and Molecular Biology from the University of Florida, and a B.S. degree (1987) in Chemistry and Biochemistry from Tennessee State University.
  - I have extensive experience in cell and molecular biology, as delineated in my curriculum vitae. See pages 2-3, Appendix A.
4. I have reviewed the above-referenced application, as well as the Office Actions to the above-referenced application that are dated September 29, 2003, and June 25, 2004. I understand that the above-referenced application was filed on or about June 21, 2000.

5. I understand that the Examiner has rejected claims 2-4, 6, 8-10, 15, 23, 30, 31, 33-35, and 37-41 of the above-referenced application because the Examiner believes the claims contain subject matter that was not described in the specification in such a way as to enable a skilled expert in the synthesis of radionuclide-labeled imaging agents to make and use the invention. I understand that the Examiner believes this to be true because she considers the potential number of EC-targeting ligand complexes to be too vast since the phrases "anticancer agent," "tumor marker," "folate receptor targeting ligand," "tumor apoptotic cell targeting ligand," "tumor hypoxia targeting ligand," and "an agent that mimics glucose" are said to be unlimited. I also understand that the Examiner believes the art pertaining to the synthesis of ethylenedicycysteine (EC)-targeting ligand complexes is highly unpredictable, and determining which types of targeting ligands would bind EC and generate results would require an undue amount of experimentation such that there would be little predictability in practicing the claimed invention. In addition, the examples presented in the specification are considered by the Examiner to be insufficient to enable the public to prepare the claimed EC-targeting ligand complexes. I respectfully disagree for the reasons set forth below.

6. I also understand that the Examiner has rejected claims 2-4, 6, 8-10, 15, 23, 30, 31, 33-35, and 37-41 of the above-referenced application because the Examiner believes that the claims are indefinite because they do not particularly point out and distinctly claim the subject matter that the inventors believe is their invention. In particular, the Examiner is of the opinion that the claims are confusing because the phrases "anticancer agent," "tumor marker," "folate receptor targeting ligand," "tumor apoptotic cell targeting



ligand,” “tumor hypoxia targeting ligand,” and “an agent that mimics glucose” are considered unlimited. I again respectfully disagree for the reasons set forth below.

7. As a scientist who has worked in translational medicine, the technology disclosed in the above-referenced patent application will serve as the foundation for the development of novel diagnostic and therapeutic radiopharmaceuticals. A single technology with the capability to simplify the ease of radiolabeling of an array of tissue specific ligands has not been available to scientists and clinicians who work in the field of nuclear oncology, nuclear cardiology and infectious disease. It is important to note that the chemistry of the claimed technology is such that a skilled expert in the synthesis of radionuclide-labeled imaging agents, with the availability of the present specification, will be able to make and use the invention without undue experimentation.
8. The beauty of this technology is its ease of use. Even the most average of skilled experts should have no difficulty making and using the invention when presented with the information in the present specification. It is well known that scientists and clinicians working in oncology, cardiology and infectious disease have had a very keen interest in tissue specific radiolabeled ligands that can be used to identify specific tissue type(s) in an *in vivo* model.
9. Without reservation, I believe that if a skilled expert had the foresight to invent and develop this technology many years ago, it would be in routine use by scientists in the laboratory and clinicians in the hospital. With access to the information set forth in the present specification, I have no doubt that a skilled expert in the synthesis of

radionuclide-labeled imaging agents can easily and conveniently make and use the invention for their specific field of interest.

10. One skilled in the synthesis and use of radionuclide imaging agents would have been enabled to make and use the claimed invention when presented with the information provided in the specification. The information provided in the specification would have permitted one skilled in the synthesis and use of radiolabeled imaging agents to understand that the phrases “anticancer agent,” “tumor marker,” “folate receptor targeting ligand,” “tumor apoptotic cell targeting ligand,” “tumor hypoxia targeting ligand,” and “an agent that mimics glucose” are generally accepted phrases that are used to refer to specific, defined classes of targeting ligands. One skilled in the synthesis and use of radionuclide imaging agents would have no difficulty making and using the claimed invention when presented with the information provided in the specification. By utilizing the claimed technology, a skilled expert would be able to build upon their existing knowledge to develop better radiolabeled imaging agents for genetic diseases and other human diseases. Therefore, the specification, with its numerous working examples, provides sufficient guidance to one of skill in the synthesis of radionuclide imaging agents to predictably identify the EC-targeting ligand complexes of the invention without an undue amount of experimentation.
11. The cited sections of the specification and reference materials set forth beginning with paragraph 12 below provide facts in support of my assessment. In particular, these cited sections of the specification and reference materials support my conclusions regarding the general use and understanding of the phrases “anticancer agent,” “tumor marker,”

“folate receptor targeting ligand,” “tumor apoptotic cell targeting ligand,” “tumor hypoxia targeting ligand,” and “an agent that mimics glucose,” and the fact that EC-targeting ligands of the present invention that incorporate an “anticancer agent,” a “tumor marker,” a “folate receptor targeting ligand,” a “tumor apoptotic cell targeting ligand,” a “tumor hypoxia targeting ligand,” or “an agent that mimics glucose” can be made and used without an undue amount of experimentation.

12. Claims Pertaining to Anticancer Agents

*Support in the Specification*

The entire specification provides a substantial amount of detail regarding embodiments of the claimed invention where the tissue specific ligand is an anticancer agent. Particular sections of the specification that are exemplary include page 5, lines 16-18, which provides examples of anticancer agents to be used in the claimed EC-targeting ligand complexes and page 9, lines 18-24 which indicates that examples of anticancer agents include chemotherapeutic agents used in the treatment of cancer. A listing of exemplary anticancer drugs is provided in Table 2 (page 34, line 24 through page 42, line 2).

13. Information pertaining to the conjugation chemistry of anticancer agents and additional examples of anticancer agents for use in the invention are provided on page 6, lines 4-16 and on page 22, lines 18 through page 23, line 21. The specification also provides substantial guidance pertaining to the preparation of EC-targeting ligand derivatives (see, e.g., page 7, lines 5-13 and page 20, lines 7-15), and the radionuclide labeling of these EC-targeting ligand derivatives (see, e.g., page 7, lines 15-20 and page 7, line 17 through

page 22, line 16; page 21, line 6 through page 22, line 16; page 23, line 23 through page 24, line 16).

14. Examples of radiolabeled ligands of the present invention where the targeting ligand is an anticancer agent are provided on page 6, line 30 through page 7, line 4, and Table 1, page 23. Information pertaining to the synthesis, biodistribution, and imaging properties of  $^{99m}\text{Tc}$ -EC-methotrexate and  $^{99m}\text{Tc}$ -EC-tomodex are discussed in Example 1 (page 32, line 10 through page 45, line 7) and FIGS. 2 and 3. Information pertaining to the synthesis, biodistribution, and imaging properties of  $^{99m}\text{Tc}$ -EC-colchicine is discussed in Example 5 (page 56, line 11 through page 60, line 17), FIGS. 21-27, and Tables 6 and 7.

15. *Reference Materials Available Around the Time of the Priority Date*

Around the time of the priority date, numerous anticancer agents were known and widely used in the treatment of cancer. See, e.g., review in Connors, 1996 (Exhibit 1). *In vitro* studies, animal protocols, and clinical trials, were evaluation tools commonly used to assist in the identification of anticancer agents. Reviewed in Connors, 1996 (Exhibit 1). Exemplary *in vitro* studies that were known to be useful in the identification of anticancer agents included cancer cell growth inhibition studies (see, e.g., Jiang *et al.* (Exhibit 2), 1983; Jiang *et al.*, 1998 (Exhibit 3); Palyi *et al.*, 1999 (Exhibit 4), and Yoshinari *et al.*, 1999 (Exhibit 5); U.S. Patent 5,356,793 (Exhibit 6); Yamori *et al.*, 1999 (Exhibit 7)). *In vivo* studies to evaluate anticancer agents ranged from human cancer xenografts in nude mice (see, e.g., Cammisuli *et al.*, 1996 (Exhibit 8) and Hjarnaa *et al.*, 1999 (Exhibit 9); Yamori *et al.*, 1999 (Exhibit 7)) and other tumor-bearing animal studies (see, e.g., Cafaggi *et al.*, 1992; Exhibit 10) to clinical trials involving patients afflicted

with cancer (reviewed in Connors, 1996 (Exhibit 1); see, *e.g.*, Foa *et al.*, 1994 (Exhibit 11)). The chemical and physical properties of many of these agents were well-understood. See, *e.g.*, Pavlik *et al.*, 1983 (Exhibit 12). Thus, one of skill in the synthesis and use of radionuclide agents for imaging would have understood that numerous anticancer agents were known to be in existence, and numerous commonly available laboratory and clinical investigative techniques were available to assist in the identification of new anticancer agents. The phrase "anticancer agent" would have been understood to refer to agents such as chemotherapeutic drugs such as methotrexate, paclitaxel or tamoxifen, which had been widely used by scientists and clinicians for many years.

16. Furthermore, the use of anticancer agents as targeting ligands was well-known at around the time the application was filed in the context of unrelated inventions. For example, WO98/08859 (Exhibit 13) described bioconjugates of a bioactive agent and an organocobalt complex, where certain aspects of the invention involved an anticancer agent as the bioactive agent. See abstract. In Chakrabarti *et al.*, 1998 (Exhibit 14), the antitumor antibiotic chromomycin A3 was reported to be a "DNA-binding ligand." See abstract. Immunoconjugates that included an antibody fragment covalently bound to a diagnostic or therapeutic agent, such as an anticancer agent, were described in U.S. Patent 5,635,603 (Exhibit 15). Conjugation of the anticancer agent gemcitabine to agents that target peripheral benzodiazepine receptors in tumors was described by Guo and Gallo (1999) (Exhibit 16).

17. I am aware of publications of the present inventors wherein anticancer agents were used as targeting ligands in conjugates for imaging. For example, Inoue *et al.* (1999) (Exhibit 17) disclosed  $^{111}\text{In}$ -DTPA-paclitaxel conjugates for use in scintigraphy. Zareneyrizi *et al.*, 1999 (Exhibit 18) described the use of  $^{99\text{m}}\text{Tc}$ -EC-colchicine for imaging studies, and Yang *et al.*, 1999a (Exhibit 19) described synthesis of  $^{111}\text{In}$ -labeled DTPA-methotrexate for use in imaging studies. One of ordinary skill in the synthesis and use of radiolabeled imaging agents would have understood that paclitaxel, colchicine, and methotrexate are exemplary anticancer agents that can be incorporated as targeting ligands into the conjugates of the claimed invention. Furthermore, one of ordinary skill in the art would have understand that these publications, which pertain to the synthesis of radiolabeled conjugates, would provide background information to one of ordinary skill in the art which would enable a person of skill in the art, upon reading the specification, to practice the claimed invention without an undue amount of experimentation.
18. Therefore, one skilled in the synthesis and use of radiolabeled imaging agents would have understood, from reading the specification, that an "anticancer agent" is a phrase used to refer to a member of a specific group of agents that can be readily identified by *in vitro* and/or *in vivo* studies, such as the examples set forth above. In addition, one of ordinary skill in the synthesis of radionuclide imaging agents would have also understood that "anticancer agents" can be used as ligands. The cited references demonstrate that the state-of-the-art pertaining to the use of "anticancer agents" as ligands was highly-developed. As a result, one of ordinary skill in the synthesis and use of radionuclide imaging agents, upon reading the specification of the present application, would have been able to make and use the claimed radionuclide-labeled anticancer agents without an

undue amount of experimentation. Consequently, the claims of the invention particularly point out and distinctly claim the subject matter that is the invention.

19. Claims Pertaining to Tumor Markers

*Support in the Specification*

Aspects of the present invention that include a tumor marker as the tissue-specific ligand are addressed throughout the specification. For example, a general discussion concerning the use of tumor markers as tissue specific ligands can be found on page 5, lines 5-14. A list of examples of tumor markers can be found on page 5, lines 22, where it is noted that “[i]t is envisioned that any other known tumor marker or any monoclonal antibody will be effective for use in conjunction with the invention.” Additional examples of tumor markers for use in the conjugates of the present invention are included in claim 9.

20. The specification provides substantial guidance regarding the synthesis of radiolabeled EC-targeting ligand derivatives. In particular, information concerning the conjugation chemistry of ligands such as tumor markers of the present invention can be found on page 22, line 18 through page 23, line 21. The specification also provides substantial guidance pertaining to the preparation of EC-targeting ligand derivatives (see, *e.g.*, page 7, lines 5-13 and page 20, lines 7-15), and the radionuclide labeling of these EC-targeting ligand derivatives (see, *e.g.*, page 7, lines 15-20 and page 7, line 17 through page 22, line 16; page 21, line 6 through page 22, line 16; page 23, line 23 through page 24, line 16). Information pertaining to the synthesis, biodistribution, and imaging properties of exemplary <sup>99m</sup>Tc-EC-targeting ligand derivatives is found in Examples 1-7 (page 32, line 10 through page 68, line 12).

21. *Reference Materials Available Around the Time of the Priority Date*

Around the time of the priority date of the referenced patent application, the state-of-the-art pertaining to tumor markers and their use as targeting ligands was a developing area of technology in the context of unrelated inventions. In particular, numerous tumor markers had been identified. For example, identification of a candidate tumor marker, PGP9.5, was described in Hibi *et al.*, 1999 (Exhibit 20). Experimental techniques used to identify tumor markers in Hibi *et al.* (Exhibit 20) included Northern blot analysis, Western blot analysis, and immunohistochemical staining. In Becker *et al.*, 1999 (Exhibit 21), *in vitro* studies using Western blotting and immunohistochemistry of E-cadherin transfected cells were employed to identify a mutated E-cadherin gene as a tumor marker. In Pavicevic *et al.*, 1998 (Exhibit 22), enzyme immunoassays were used to identify CYFRA 21-1 as a serum tumor marker in lung cancer. Immunohistochemistry was also used to identify the association of matrix metalloproteinase-1 with poor prognosis in esophageal cancer (Murray *et al.*, 1998; Exhibit 23), and the association of tryptophan hydroxylase antibodies with carcinoid (Meyer *et al.*, 1998; Exhibit 24).

22. Prior to the priority date, tumor markers were used in various contexts as targeting ligands. U.S. Patent 4,988,496 (Exhibit 25) disclosed chelate-targeting agent conjugates wherein the targeting agent ligand is a monoclonal antibody directed against an antigen on a tumor cell. See claims 3, 5, 6, and 7 of Exhibit 25. U.S. Patent 4,824,659 (Exhibit 26) disclosed modified antibodies that can bind a ligand, wherein the ligand in certain aspects of the invention is a marker which is produced by or associated with a tumor or a pathological lesion. (see claim 5). U.S. Patent 5,877,289 (Exhibit 27), which pertained to



methods and compositions for use in the coagulation of blood vessels, described agents that "bind to a tumor cell" as targeting ligands. Page 5, column 1, lines 10-14. U.S. Patent 5,013,556 (Exhibit 28) disclosed compositions of liposomes with enhanced circulation times, which in certain embodiments included surface-bound targeting ligands that could be specific antibodies directed against tumor-specific antigens. See claims 15 and 29. Lundberg *et al.* (1999) (Exhibit 29) described the conjugation of an anti-B-cell lymphoma monoclonal antibody to the surface of lipid-emulsion globules using a novel coupling agent. I am aware that a publication of the inventors, Kim *et al.*, 2000 (Exhibit 30) disclosed  $^{99m}\text{Tc}$ -EC-polyglutamate in an effort to target glutamate receptors, which were known to be overexpressed in certain tumors. One of ordinary skill in the synthesis and use of radiolabeled imaging agents would have understood, from reading Kim *et al.*, 2000 (Exhibit 30) that polyglutamate is an example of a tumor marker ligand that could be incorporated into the conjugates of the claimed invention. In view of the background information provided in publications such as Kim *et al.*, 2000 (Exhibit 30) and the other publications set forth above, one of ordinary skill in the synthesis and use of radiolabeled imaging conjugates, upon reading the specification, would have been able to make and use the claimed radiolabeled conjugates without an undue amount of experimentation. It would follow that one of ordinary skill in the synthesis and use of radiolabeled contrast agents would have understood that tumor markers were actively used as targeting ligands at around the time of the priority date, and the state-of-the art was well-established.

23. In view of the information provided in the specification, one of ordinary skill in the synthesis and use of radionuclide imaging agents would have been able to make and use the claimed radionuclide-labeled tumor marker conjugates of the present invention

without an undue amount of experimentation. One of ordinary skill in the synthesis and use of radionuclide imaging agents would have understood that a “tumor marker” refers to a member of a group of agents that can be readily identified by techniques such as Northern blot analysis, Western Blot analysis, and immunohistochemistry, and that the claims of the invention particularly point out and distinctly claim the subject matter that is the invention.

24. Claims Pertaining to Folate Receptor Targeting Ligands

*Support in the Specification*

The specification provides detailed information pertaining to folate receptor targeting ligands and the preparation of radiolabeled folate receptor targeting ligands. Exemplary folate receptor targeting ligands are provided on page 5, line 23 and page 7, line 1. Information regarding the conjugation chemistry of targeting ligands, including folate receptor targeting ligands, is provided on page 6, lines 4-19 and page 22, line 18 through page 23, line 21. A detailed discussion pertaining to folate receptor targeting can be found on page 25, line 28 through page 26, line 27.

25. The specification also provides substantial guidance pertaining to the preparation of EC-targeting ligand derivatives (see, *e.g.*, page 7, lines 5-13 and page 20, lines 7-15), and the radionuclide labeling of these EC-targeting ligand derivatives (see, *e.g.*, page 7, lines 15-20 and page 7, line 17 through page 22, line 16; page 21, line 6 through page 22, line 16; page 23, line 23 through page 24, line 16) that can be applied in the preparation of radiolabeled EC-folate receptor targeting ligand derivatives. In addition, Example 1 and FIGS. 1-6 includes information regarding the synthesis, biodistribution and imaging

studies pertaining to  $^{99m}\text{Tc}$ -EC-folate,  $^{99m}\text{Tc}$ -EC-MTX, and  $^{99m}\text{Tc}$ -EC-TDX. Page 32, line 10 through page 45, line 7.

26. *Reference Materials Available Around the Time of the Priority Date*

Around the priority date of the referenced patent application, there was a substantial amount of information pertaining to folate receptors and folate receptor targeting ligands in the context of unrelated inventions. The structure of the folate receptor, molecular and biochemical aspects of the folate receptor, and transport of agents across the folate receptor were established areas of research. Reviewed in Antony, 1996 (Exhibit 31); see also Holm *et al.*, 1994 (Exhibit 32), pertaining to the folate receptor of human mammary adenocarcinoma and Westerhof *et al.*, 1991 (Exhibit 33) pertaining to membrane transport of natural folates and antifolate compounds in murine leukemia cells. It was known that marked overexpression of folate receptors in some malignant cells suggested that the folate receptor may be an important target for diagnostic or therapeutic exploitation.

27. In addition, folate analogs were used in various contexts as targeting ligands. In particular, Sudimack *et al.*, 2000 (Exhibit 34) addressed mechanisms of targeted drug delivery via the folate receptor, including “coupling [of the drug] to a high affinity ligand, folic acid.” Abstract, page 147. The abstract notes that folic acid is “a high affinity ligand of the folate receptor,” and “folate conjugation, therefore, presents an alternative method of targeting the folate receptor.” Abstract, page 147. U.S. Patent 5,108,921 (Exhibit 35), U.S. Patent 5,416,016 (Exhibit 36), and U.S. Patent 5,820,847 (Exhibit 37) described methods of enhanced transmembrane transport of molecule complexes of an

agent and a targeting ligand, where, in certain embodiments, the targeting ligands are folate analogs and other folate receptor-binding ligands. See Abstract and claim 1 in these patents. Examples of folate receptor targeting ligands presented in these patents include folic acid, folinic acid, pteropolyglutamic acid, and folate receptor-binding pteridines such as tetrahydropterins, dihydrofolates, tetrahydrofolates, and their deaza and dideaza analogs. See, *e.g.*, column 7, lines 28-34 of U.S. Patent 5,108,921 (Exhibit 35). U.S. Patent 5,891,468 (Exhibit 38) pertains to fusogenic liposome compositions that in certain aspects include, in certain embodiments, a targeting ligand such as folate attached to a hydrophilic polymer chain. See abstract and claims 1, 8, and 9. U.S. Patent 6,033,884 (Exhibit 39) pertains to nucleic acid transporter systems for delivery of nucleic acid to a cell, where the transporter system contains a binding molecule covalently linked to a surface targeting ligand, such as folate. See abstract and claims 1, 3, and 4.

28. Regarding the development and use of radiolabeled agents for imaging, in 1998,  $^{99m}\text{Tc}$ -ethylenedicycysteine-folate was described as a new tumor imaging agent in a publication of the inventors. Ilgan *et al.*, 1998 (Exhibit 40). One of ordinary skill in the art would have understood that in view of the background information provided in Ilgan *et al.* and the other publications set forth above, one of ordinary skill in the synthesis and use of radiolabeled imaging conjugates, upon reading the specification, would have been able to make and use the claimed imaging conjugates without an undue amount of experimentation. These publications demonstrate that the state of the art as to folate receptor targeting and use of folate receptor as targeting ligands was well-developed, and skill in the art was very high.

29. In view of the disclosure in the specification, one of ordinary skill in the synthesis and use of radionuclide imaging agents, upon reading the specification, would have been able to make and use the claimed radionuclide-labeled folate receptor targeting ligand conjugates of the present invention without an undue amount of experimentation. One of ordinary skill in the synthesis and use of radionuclide imaging agents would have understood that a "folate receptor targeting ligand" refers to a member of a group of agents that can be readily identified, and that the claims of the invention particularly point out and distinctly claim the subject matter that is the invention.

30. Claims Pertaining to Tumor Apoptotic Cell Targeting Ligands

*Support in the Specification*

The specification provides substantial guidance regarding aspects of the invention that include a tumor apoptotic cell targeting ligand. In particular, page 5, lines 24-25 provide specific examples of the tumor apoptotic cell targeting ligands. Information pertaining to the conjugation chemistry of ligands, including tumor apoptotic cell targeting ligands, is provide on page 22, line 18 through page 23, line 21. A discussion regarding the imaging of tumor apoptotic cells, which includes an example of tumor apoptotic cell targeting ligands (annexin V), can be found on page 28, lines 14-20 and page 29, lines 19-23. Example 4 (page 54, line 24 through page 56, line 8) and FIGS. 18-20 provide information pertaining to the synthesis, biodistribution, and imaging studies of a radiolabeled conjugate that includes annexin-V, a tumor apoptotic cell targeting ligand.

31. The specification also provides substantial guidance pertaining to the preparation of EC-targeting ligand conjugates (see, e.g., page 7, lines 5-13 and page 20, lines 7-15), and the

radionuclide labeling of these EC-targeting ligand derivatives (see, *e.g.*, page 7, lines 15-20 and page 7, line 17 through page 22, line 16; page 21, line 6 through page 22, line 16; page 23, line 23 through page 24, line 16). This information can be directly applied in the synthesis of radiolabeled EC-tumor apoptotic cell targeting ligand conjugates.

32. *Reference Materials Available Around the Time of the Priority Date*

At around the time of the priority date of the present patent application, it was well-established that apoptosis plays a critical role in the physiology of cancer. Reviewed in Thompson, 1995 (Exhibit 41). The cascade of cellular events that occur during apoptosis, and the search for markers for apoptosis was an established area of research. Reviewed in Blankenberg *et al.*, 1998 (Exhibit 42).

33. Markers for apoptosis were actively under investigation in the context of unrelated inventions. For example, *in vitro* assays had been developed that use annexin V to detect apoptosis in a wide variety of cell types (see, *e.g.*, Boersma *et al.*, 1996 (Exhibit 43); Reutelingsperger and van Heerde, 1997 (Exhibit 44)). Using the RNase protection assays and western blotting assays, Takamizawa *et al.*, 2000 (Exhibit 45), investigated the expression of apoptotic proteins by evaluating apoptotic mRNA species in tumor specimens.

34. The phrase "tumor apoptotic cell targeting ligand" would have been and should be well understood to refer to a very limited number of specific compounds which are capable of detecting the death of tumor cells. A number of apoptotic cell targeting ligands had been identified. For example, PK11195, a ligand of the mitochondrial benzodiazepine

receptor, was found to facilitate the induction of apoptosis of cells *in vitro* (Hirsch *et al.*, 1998; Exhibit 46). Annexin V, certainly the most well known and widely used tumor apoptotic ligand, had been identified as an apoptotic targeting ligand for radioimaging by Blankenberg *et al.* (1998) (Exhibit 42), who demonstrated that <sup>99m</sup>Tc-hydrazinonicotinamide-annexin V could be used to detect and serially image tissues and organs undergoing programmed cell death.. Parallel work by van den Eijnde *et al.*, 1997 (Exhibit 47), supported the use of annexin V for *in situ* detection of apoptotic cells in developing embryos using immunohistochemical techniques. Scientists around the world had been working with annexin V for a number of years as of the priority date. Furthermore, studies using cell culture techniques were underway to elucidate the role of Fas ligand in anticancer drug-mediated apoptosis. (see, *e.g.*, Tolomeo *et al.*, 1998 (Exhibit 48); McGahon *et al.*, 1998 (Exhibit 49)). Therefore, the state-of-the-art related to apoptotic cell targeting ligands was well-established. U.S. Patent 5,834,266 (Exhibit 50) and U.S. Patent 6,054,436 (Exhibit 51) pertain to methods of initiating apoptosis in genetically engineered cells using chimeric proteins capable of cross-linking ligands. See abstract and claim 1 in both patents.

35. Based on the above, one of ordinary skill in the synthesis and use of radionuclide imaging agents, upon reading the specification, would have been able to make and use the claimed radionuclide-labeled apoptotic cell targeting ligand conjugates without an undue amount of experimentation. Furthermore, one of ordinary skill in the synthesis and use of radionuclide imaging agents would have understood that an "apoptotic cell targeting ligand" refers to a member of a specific group of agents that can be readily identified

using techniques such as those set forth above, and that the claims of the invention particularly point out and distinctly claim the subject matter that is the invention.

36. Claims Pertaining to Tumor Hypoxia Targeting Ligands

*Specification*

The specification provides in-depth information pertaining to aspects of the invention that include tumor hypoxia targeting ligands. Information concerning the benefits of imaging based on hypoxia is discussed on page 2, line 25 through page 3, line 25. Examples of tumor hypoxia targeting ligands are disclosed on page 5, lines 24-25. Information pertaining to the conjugation chemistry of these ligands is provided on page 6, line 4-19. A discussion pertaining to the assessment of tumor hypoxia by imaging can be found on page 29, line 26 through page 30, line 4. Imaging hypoxia due to stroke using  $^{99m}\text{Tc}$ -EC-metronidazole is discussed on page 30, line 22 through page 31, line 15. Example 2 and FIGS. 7-15 disclose information pertaining to the synthesis and stability of  $^{99m}\text{Tc}$ -EC-metronidazole, and imaging studies using this agent. Page 45, line 9 through page 53, line 13.

37. The specification also provides substantial guidance pertaining to the preparation of EC-targeting ligand conjugates (see, *e.g.*, page 7, lines 5-13 and page 20, lines 7-15), and the radionuclide labeling of these EC-targeting ligand derivatives (see, *e.g.*, page 7, lines 15-20 and page 7, line 17 through page 22, line 16; page 21, line 6 through page 22, line 16; page 23, line 23 through page 24, line 16). This information can be directly applied in the synthesis of radiolabeled EC-tumor hypoxia targeting ligand conjugates.



38. *Reference Materials Available Around the Priority Date of the Patent Application*

At the time of filing of the patent application, there was substantial information available regarding tumor hypoxia targeting ligands in the context of unrelated inventions. A number of hypoxia-selective antitumor agents had been identified. For example, Hay *et al.* (1994) (Exhibit 52) identified bis(nitroimidazolyl)alkanecarboxamides as a new class of hypoxia-selective antitumor agents using *in vitro* and *in vivo* cytotoxicity and hypoxic cell radiosensitization assays. Garayoa *et al.*, 2000 (Exhibit 53), identified adrenomedullin as a tumor hypoxia marker using hypoxic cell culture techniques, Northern blot analysis, confocal immunohistochemistry, and luciferase reporter assays. Fluorine-18-fluoromisonidazole had been identified as an agent that can bind selectively to hypoxic cells *in vitro* and *in vivo* (Rasey *et al.*, 1989, Exhibit 54); Rasey *et al.*, 1990, Exhibit 55). U.S. Patent 5,688,487 (Exhibit 56) described particular complexes of a metal, a hypoxia-localizing moiety, and a complexing ligand for use in imaging, where in certain embodiments the hypoxia-localizing group is a hypoxia-mediated nitro-heterocyclic group. The phrase “tumor hypoxia targeting ligand” would have been understood to refer to a limited number of specific compounds that can detect the presence of hypoxia in tumors. For many years, scientists have been working with the development and use of [F-18]Fluoromisonidazole in the laboratory setting for the detection and measurement of tumor hypoxia in animals.

39. Regarding the incorporation of bioactive compounds into the radiolabeled agents, Yang *et al.*, 1999b (Exhibit 57), one of the publications of the present inventors, developed a <sup>99m</sup>Tc-labeled metronidazole (MN) using EC as a chelator and determined that it was feasible to use this agent to image tumor hypoxia. Thus, use of tumor hypoxia markers

as targeting ligands was well-established, and the level of expertise of those in this field was high.

40. One of ordinary skill in the synthesis and use of radionuclide imaging agents, upon reading the specification, would have been able to make and use the claimed radionuclide-labeled tumor hypoxia targeting ligand conjugates without an undue amount of experimentation. One of ordinary skill in the synthesis and use of radionuclide imaging agents would have understood that a “tumor hypoxia targeting ligand” refers to a member of a specific group of agents that can be readily identified, and that the claims of the invention particularly point out and distinctly claim the subject matter that is the invention. I believe the claimed technology will provide the critical linkage necessary for the development and successful clinical study of new tumor hypoxia targeting agents.

41. Claims Pertaining to Agents that Mimics Glucose

*Specification*

Aspects of the present invention that include agents that mimic glucose as the tissue-specific ligand are discussed throughout the specification. For instance, examples of agents that mimic glucose are discussed on page 5, line 29 through page 6, line 3. Information pertaining to the conjugation chemistry of these ligands can be found in the specification on page 6, lines 4-19 and page 22, lines 18-28. A discussion regarding tumor glycolysis targeting is found on page 31, lines 20-29. Example 6 and FIGS. 40-48 pertain to tumor glycolysis targeting and the development of  $^{99m}\text{Tc}$ -EC-neomycin. Page 60, line 23 through page 64, line 26. In addition, tumor metabolic imaging with  $^{99m}\text{Tc}$ -

EC-deoxyglucose is addressed in Example 7 and FIGS. 66-86. Page 65, line 4 through page 68, line 12.

42. Furthermore, the specification provides substantial guidance pertaining to the preparation of EC-targeting ligand conjugates (see, *e.g.*, page 7, lines 5-13 and page 20, lines 7-15), and the radionuclide labeling of these EC-targeting ligand derivatives (see, *e.g.*, page 7, lines 15-20 and page 7, line 17 through page 22, line 16; page 21, line 6 through page 22, line 16; page 23, line 23 through page 24, line 16). This information can be directly applied in the synthesis of radiolabeled conjugates that include agents that mimic glucose.

43. *Reference Materials Around the Priority Date of the Patent Application*

The phrase “an agent that mimics glucose” would have been understood to refer to specific compounds which target glucose metabolism. Around the priority date of the patent application at issue, it was known that the propensity to catabolize glucose at elevated rates was among the most common biochemical characteristics of cancer cells. Reviewed in Fanciulli *et al.*, 1994 (Exhibit 58). This feature of cancer cells led to investigation to identify agents that mimic glucose that could be applied in the diagnosis and treatment of cancer in the context of other inventions. For many years, scientists had been working with compounds such as [14C]deoxyglucose, which are agents that mimic glucose

44. For over three decades, <sup>18</sup>F-FDG has been studied by scientists throughout the world and during the past fifteen years, it has grown to be widely used in nuclear medicine in the

context of other inventions. FDG is an agent that mimics glucose. Kanazawa *et al.* (1997) (Exhibit 59) reported on the potential of 2-deoxy-2-[<sup>18</sup>F] fluoro-D-glucose (FDG), as an NMR pharmaceutical for cancer diagnosis. *In vivo* and *ex vivo* NMR studies were employed in Kanazawa *et al.* to identify FDG as an NMR pharmaceutical for cancer diagnosis. U.S. Patent 4,789,542 (Exhibit 60) described radioiodinated branched carbohydrates for tissue imaging that include a glucose analogue and a vinyl functional group. See abstract and claim 1. Examples of glucose analogues disclosed in the '542 patent include those analogues shown in claims 2 and 3. U.S. Patent 5,643,883 (Exhibit 61) disclosed methods of inhibiting the import of glucose-6-phosphate into the endoplasmic reticulum of a cell, comprising the step of administering a pharmacologically effective dose of a glucose analogue to said cell. Abstract and claim 1. The glucose analogues disclosed in the '883 patent included competitive inhibitors of glucose-6-phosphate uptake, including 2-deoxyglucose-6-phosphate, glucosamine-6-phosphate and N-acetylglucosamine-6-phosphate. Column 5, lines 53-64.

45. Much information was available regarding the structure and function of aminoglycosides, which are agents that mimic glucose (see, *e.g.*, review by Wright *et al.*, 1998, Exhibit 62). U.S. Patent 4,279,992 (Exhibit 63) describes use of aminoglycosides as targeting ligands that can be used to practice the invention directed to a homogeneous specific binding assay method for determining a ligand in a liquid medium. See claims 1 and 11-14. In a study evaluating interactions between RNA and ligands, 3D-SAR analysis was used to study the bound conformations of aminoglycoside ligands with Rev-binding element

RNA (LeClerc and Cedergren, 1998, Exhibit 64). Thus, aminoglycosides were in active use as targeting ligands around the priority date of the application.

46. Therefore, a person of ordinary skill in the synthesis and use of radionuclide imaging agents, upon reading the specification, would have been able to make and use the claimed radionuclide-labeled conjugates incorporating agents that mimic glucose without an undue amount of experimentation. One of ordinary skill in the synthesis and use of radionuclide imaging agents would have understood that an "agent that mimics glucose" refers to a member of a specific group of agents that can be readily identified, and that the claims of the invention particularly point out and distinctly claim the subject matter that is the invention.
47. In conclusion, claims 2-4, 6, 8-10, 15, 23, 30, 31, 33-35, and 37-41 of the above-referenced patent application contain subject matter which was described in the specification of the above-referenced application in such a way as to enable one of ordinary skill in the synthesis and use of radionuclide imaging agents to make and use the invention. The description of the invention provided in the specification is sufficiently clear and concise such that one of ordinary skill in the synthesis and use of radionuclide imaging agents would be able to make the claimed agents and practice the claimed methods without an undue amount of experimentation. The potential number of EC-targeting ligand complexes is not vast and unlimited. Rather, each of the groups set forth by the phrases "anticancer agent," "tumor marker," "folate receptor targeting ligand," "tumor apoptotic cell targeting ligand," "tumor hypoxia targeting ligand," and "an agent that mimics glucose" are limited, and targeting ligands belonging to each of these groups

can be identified using techniques known to those of ordinary skill in the synthesis and use of radionuclide imaging agents. As set forth above, the art pertaining to the synthesis and use of EC-targeting ligand complexes was highly advanced at the time of filing of the application, and determining which types of targeting ligand complexes would bind EC and generate results would not have required an undue amount of experimentation. As a result, there would be predictability in practicing the claimed invention. Furthermore, the working examples presented in the specification are sufficient to enable the public to prepare the claimed radionuclide labeled complexes.

48. In addition, based on my review of the specification and in view of the above-cited literature pertaining to the phrases “anticancer agent,” “tumor marker,” “folate receptor targeting ligand,” “tumor apoptotic cell targeting ligand,” “tumor hypoxia targeting ligand,” and “an agent that mimics glucose,” the present claims particularly point out and distinctly claim the subject matter that the inventors believe is the invention. In particular, the phrases “anticancer agent,” “tumor marker,” “folate receptor targeting ligand,” “tumor apoptotic cell targeting ligand,” “tumor hypoxia targeting ligand,” and “an agent that mimics glucose” are not confusing, nor are they unlimited in their scope. The phrases referenced above are not unlimited in scope and someone skilled in the art would not and should not be confused by what such phrases mean. Rather, these phrases are definite because they refer to specific classes of targeting ligands whose members can be identified using techniques well-known to those who have an ordinary understanding of the synthesis and use of radionuclide imaging agents.

49. I hereby declare that all statements made herein of my knowledge are true and that all statements made on information and belief are believed to be true; and further that these statements were made with the knowledge that willful false statements and the like so made are punishable by fine or imprisonment, or both, under Section 1001 of Title 18 of the United States Code and that such willful false statements may jeopardize the validity of the application or any patent issued thereon.

Date

12/22/2004

  
Jerry L. Bryant, Jr., M.S.

## **APPENDIX A**



**CURRICULUM VITAE**

**NAME:** Jerry L. Bryant, M.S.

**TITLE/AFFILIATION:**

**(a) Primary Appointment:** Chief Technology Officer Present  
Head of Scientific Evaluation  
Division of Business Development  
Cell>Point, LLC

**(b) Joint/Adjunct Appointment:** Research Assistant II Oct. 2002-June, 2003  
Department of Experimental Nuclear Medicine  
Division of Diagnostic Imaging  
University of Texas M.D. Anderson Cancer Center  
Houston, TX

Director of Research and Development Present  
Verimed Research Corporation  
Houston, TX 77098

**BIRTHDATE/PLACE:** August 27, 1966, Louisiana

**CITIZENSHIP:** U.S. Citizen

**HOME ADDRESS:** 6861 Staffordshire Blvd. **TELEPHONE:** 713-797-6689  
Houston, Texas 77030

**OFFICE ADDRESS:** Cell>Point, LLC **TELEPHONE:** 303-689-9693  
Division of Business Dev **FAX:** 303-689-0198  
7120 East Orchard Rd., Suite 350  
Englewood, CO 80111  
e-mail: cellpoint@swbell.net

**MARITAL STATUS:** Married

**LICENSURES-ACTIVE:** None

**EDUCATION:**

**GRADUATE:** University of Florida, M.S.  
Microbiology & Cell Science w/Molecular Biology,  
January, 1990-December, 1991, Gainesville, FL

**UNDERGRADUATE:** Tennessee State University, B.S.  
Chemistry w/Biochemistry  
June, 1984-May, 1987, Nashville, Tennessee

**POSTGRADUATE TRAINING:** None

**SPECIALITY BOARDS:** None

**MILITARY/GOVERNMENT:** None

**ACADEMIC & PROFESSIONAL APPOINTMENTS:**

Chief Technology Officer  
Division of Business Development  
Cell>Point, LLC  
(2001-present)

Research Assistant  
Department of Experimental Nuclear Medicine  
Division of Diagnostic Imaging  
University of Texas M. D. Anderson Cancer Center,  
(2002-2003)

Director of Research and Development  
Division of Business Development,  
Verimed Research Corporation  
Houston, TX  
(2002-2004)

Chief Scientific Officer  
Division of Business Development  
Allcure, Inc.  
Houston, TX  
(May, 2001-May, 2002)

President/Board Director  
Allcure JEMA Medicine Services, Inc.  
Medical and Research Supply Distributor  
Houston, TX  
(January, 1996-April, 2001)

Research Assistant II  
Department of Medicine  
Division of Pathology  
Molecular Pathology  
The University of Texas M.D. Anderson Cancer Center  
Houston, TX  
(November, 1994-March, 1999)

Volunteer Technician  
Department of Anesthesiology  
University of Florida  
Gainesville, FL  
(July, 1994-September, 1994)

Research Assistant  
Department of Anesthesiology  
University of Florida  
Gainesville, FL  
(August, 1992-June, 1994)

Research Associate  
Department of Medicine  
Division of Cardiology  
Cardiovascular Disease  
VA Medical Center  
University of Florida  
Gainesville, FL  
(November, 1993-February, 1994)

Research Associate  
Department of Medicine  
Division of Cardiology  
Cardiovascular Disease  
University of Florida  
Gainesville, FL  
(October, 1991-March, 1992)

Research Technician  
Department of Pediatric Hematology and Oncology  
University of Florida  
Gainesville, FL  
(October, 1991-March, 1992)

Teaching Assistant  
Department of Microbiology and Cell Science  
University of Florida  
Gainesville, FL  
(January, 1991-May, 1991)

Research Assistant  
Department of Microbiology and Cell Science/Molecular Biology  
University of Florida  
Gainesville, FL  
(August, 1989-August, 1991)

Graduate Student  
Department of Microbiology and Cell Science/Molecular Biology  
University of Florida  
Gainesville, FL  
(August, 1989-August, 1991)

Summer Miniorty Graduate Program  
University of Florida  
Gainesville, FL  
(June, 1989-August, 1989)

**a) Consultantships**

Board of Director Member  
Cell>Point, LLC  
Englewood, CO  
(May, 2001-Present)

Advisory Scientific Board Member  
Cell>Point, LLC  
Englewood, CO  
(March, 2003-Present)

Board of Director Member  
Verimed Research Corporation  
Houston, TX  
(August, 2002-Present)

**ADMINISTRATIVE APPOINTMENTS AND RESPONSIBILITIES:**

Director of Clinical Trial Research Protocol  
Sponsor by Cell>Point, LLC  
Department of Nuclear Medicine & Radiation Oncology  
Division of Diagnostic Imaging  
(June, 2002-present)

Director of a Pilot Biodistribution and Pharmacokinetics Study of  
99mTc-EC-Annexin V in patients with Breast Cancer  
Sponsor by Cell>Point, LLC  
Department of Breast Medical Oncology & Division of Diagnostic  
Imaging  
(April, 2003-May, 2004)

Director of a Pilot Imaging study of COX-2 expression with  
99mTc-Celecoxib Spectro-Computer Tomography in Colorectal  
Cancer  
Sponsor by Cell>Point, LLC  
Department of Gastrointestinal Medical Oncology & Division of  
Diagnostic Imaging  
(April, 2003-present)

**COMMITTEE MEMBERSHIPS:**

**a) M.D. Anderson Committee Memberships/Chairmanships:**

Member of the Core Logistics Committee for Clinical Trial Project  
The University of Texas MD Anderson Cancer Center  
(March, 2003-present)

**b) Society Memberships with Offices held:**

Member, American Association for Cancer Research,  
(January, 2003-Present)

Member, M. D. Anderson Associates,  
(October, 2002-Present)

Member, Society of Nuclear Medicine,  
(June, 2002-Present)

Member, American Association for the Advancement of Science,  
(August, 2001-Present)

Member, American Association of Microbiology,  
(January, 1990-Present)

Member, American Chemical Society,  
(June, 2002-Present)

**EDITORSHIPS AND EDITORIAL BOARD MEMBERSHIPS:**

**Journal Reviewer:**

None

**HONORS AND AWARDS:**

None

**LECTURESHIPS AND VISITING PROFESSORSHIPS:**

The 42<sup>nd</sup> American College of Cardiology Annual Scientific  
Session  
Anaheim, CA  
(March, 14-18, 1993)

**ORGANIZATION OF NATIONAL OR INTERNATIONAL CONFERENCES**

**International:**

None

**PATENTS PENDING AND GRANTED:**

1. Yang, D.J., Yu, D-F, Oh, C-S, and Bryant, J.: Ethylenedicycysteine (EC)-Drug Conjugates Compositions and Methods for Tissue Specific Disease Imaging , US patent S/N 10/703,405. UTMDACC:02-073 (UTXC:758USP1), 11/7/2003 filed, US Patent (pending).
2. Yang, D.J., Oh, C-S, Kohanim, S., Yu, D-F, Azhdarinia, A. and Bryant, J.: Mechanism-based Targeted Pancreatic Beta Cell Imaging and Therapy, US patent S/N. UTMDACC/VeriMed Research Corporation: (10/942,615 and IPA# PCT/US04/30374), 9/10/03 filed, US patent (pending).
3. Yang, D.J., Yu, D-F, Oh, C-S, and Bryant, J.: N2S2 Chelate-Targeting Ligand Conjugates, US patent S/N 10/732,919. UTSC:841US-MDA02-073, 12/10/2003 filed, US patent (pending).

**GRANT/CONTRACT SUPPORT: (last 5 years)**

CT and MRI functional agents development and evaluation (SR 2002-00007147SM). Director: **Bryant, J.L.** P.I. Yang, D.J. Supported by VeriMed Research Corporation (Houston, TX). August, 2002-August 1, 2007, \$1,000,000 (\$200,000/year).

<sup>99m</sup>Tc-Ethylenedicysteine (EC)-Drug Conjugates for Tissue Specific Disease Imaging (LS01-212), Director: **Bryant, J.L.** P.I. Yang, D.J. Supported by Cell> Point, LLC (Englewood, CO). June 15, 2001-June 15, 2006, \$1,000,000 (\$200,000/year).

"Human Malignant Lymphoma Models in Immune Deficient Mice" (LS01-123), Director: **Bryant, J.L.**, P.I. Ford, R.J. Supported by VeriMed Research Corporation (Houston, TX). July, 2001-July, 2006, \$1,280,000 (\$256,000/year).

Assessment of Tumor Factors with <sup>99m</sup>Tc-EC-Deoxyglucose for effective imaging Guided Therapy and by utilizing the EC-Technology for Targeting Specific Regulatory Functions (-01), P.I.: **Bryant, J.L.**, NIH-NCI (R21/R33) June 21, 2003-September 30, 2006, \$1,572,249 (Submitting).

Director "**Bryant, J.L.**", of Clinical Trial Research Protocol "Comparison of Tc-<sup>99m</sup>-EC-Deoxyglucose (EC-DG) and FDG-PET Scans for 1) the Evaluation of Patients Suspected of Having Persistent/Recurrent Squamous Cell Carcinoma of the Larynx after Definitive Treatment with Radiation Therapy and 2) the Evaluation of Primary Lung Cancer Patients", Sponsor by Cell>Point, LLC, March 10, 2003- March 10, 2005, Funding \$560,000 for two years.

Director "**Bryant, J.L.**" of a Pilot Biodistribution and Pharmacokinetics Study of "<sup>99m</sup>Tc-EC-Annexin V in patients with Breast Cancer", Sponsor by Cell>Point, LLC, Activated May 1, 2003-May 1, 2004, Funding \$25,000 for one year.

Director "**Bryant, J.L.**" of a Pilot Imaging study of COX-2 expression with "<sup>99m</sup>Tc-Celecoxib Spectro-Computer Tomography in Colorectal Cancer", Sponsor by Cell>Point, LLC, Activated June 1, 2003-June 1, 2004, Funding \$25,000 for one year.

**TEACHING EXPERIENCES:**

**Courses Taught:**

*Microbiology Laboratory*, University of Florida, Nursing Students  
January, 1991-May, 1991.

**Training Programs:** None

**Other Educational Programs:** None

**SUPERVISORY TEACHING**

**Advisory Committees:** None

**Supervisory committees:** None

**Students/Postgraduates directly supervised:** None

**Clinical Fellows:** None

**Medical/Undergraduate Students:** None

**INVITATIONS TO NATIONAL OR INTERNATIONAL CONFERENCES:** None

## **BIBLIOGRAPHY**

### **PUBLISHED ARTICLES IN REFERRED JOURNALS**

1. **Bryant JL Jr., Mehta P, Von der Porten A, Mehta, JL:** Co-Purification of 130 kD nitric oxide synthase and a 22 kD link protein from human neutrophils. *Biochemical and Biophysical Research Communications* 189: 558-564, 1992.
2. **Mehta JL, Bryant JL Jr., Mehta P:** Reduction of Nitric oxide synthase activity in human neutrophils by oxidized low-density lipoproteins. *Biochemical Pharmacology*, Vol.50,No. 8,pp. 1181-1195, 1995.
3. **Yang BC, Bryant JL Jr., Saldeen TGP, Mehta JL:** Dietary fish oil protects against ischemia-reperfusion induced myocardial dysfunction and alters vascular response without affecting nitric oxide synthesis in rats. *American Heart Journal*, 1993.
4. **Mehta JL, Lopez LM, Bryant JL, Cox G:** Salutary effect of antihypertensive therapy with celiprolol on nitric oxide synthase activity, superoxide anion generation and platelet aggregation in hypertensive subjects. *Circulation*, 1993.
5. **B.C. Yang, T.G.P. Saldeen, J.L. Bryant, W.W. Nichols and J.L. Mehta:** Long-term dietary fish oil supplementation protects against ischemia-reperfusion-induced myocardial dysfunction in isolated rat hearts. *American Heart Journal*, 126: 1287-92, 1993.
6. **Bryant, J., Pham, L., Yoshimura, L., Tamayo, A., Ordonez, N. and Ford, R.J.** Development of intermediate-grade (mantle cell) and low-grade (small lymphocytic and marginal zone) human non-Hodgkin's lymphomas xenotransplanted in severe combined immunodeficiency mouse models. *Laboratory Investigation*, 80:557-573, 2000.



7. Yang, D.J., Kim, K-D, Schechter, N.R., Yu, D-F, Wu, P., Azhdarinia, A., Roach, J.S., Kohanim, S., Ozaki, K., Fogler, W.E., Bryant, J.L., Herbst R.S., Abbruzzes J., Kim, E.E., and Podoloff, D.A. Assessment of Antiangiogenic Effect Using  $^{99m}\text{Tc}$ -EC-Endostatin. *Cancer Biotherapy and Radiopharmaceuticals*. 17(2): 233-246, 2002.
8. Schechter, N.R., Yang, D.J., Azhdarinia, A., Kohanim, S., Wendt, R., Oh, C-S, Hu, M., Yu, D-F, Bryant, J., Ang, K.K., Forster, K.M., Kim, E.E., and Podoloff, D.A. Assessment of EGF receptors with  $^{99m}\text{Tc}$ -ethylenedicysteine-C225 monoclonal antibody. *Anti-Cancer Drugs*, 14: 49-56, 2003.
9. Yang, D.J., Kim, C-G, Schechter, N.R., Azhdarinia, A., Yu, D-F, Oh, C-S, Bryant, J.L., Won, J.J., Kim, E. E., Podoloff, D.A. Imaging with  $^{99m}\text{Tc}$ -EC-DG Targeted at the Multifunctional Glucose Transport System: Feasibility study with rodents. *Radiology*, 226: 465-473, 2003.
10. Yang DJ, Bryant J, Chang JY, Mendez R, Oh C-S, Yu D-F, Ito M, Azhdarinia A, Kohanim S, Kim EE, Lin E, Podoloff DA. Assessment of COX-2 expression with  $^{99m}\text{Tc}$ -labeled celebrex. *Anti-Cancer Drugs* 15:255-263, 2004.
11. Yang DJ, Yukihiro M, Oh C-S, Kohanim S, Azhdarinia A, Yu D-F, Kim C-G, Ito M, Bryant JL, Kim EE, Podoloff DA. Assessment of Therapeutic Tumor Response Using  $^{99m}\text{Tc}$ -Ethylenedicysteine-Glucosamine. *Cancer Biotherapy and Radiopharm*. 19(4):444-458, 2004.
12. Yang DJ, Ozaki K, Oh C-S, Azhdarinia A, Ito M, Greenwell AC, Bryant JL, Kohanim S, Kim EE.  $^{99m}\text{Tc}$ -EC-Guanine: assessment of tumor growth using  $^{99m}\text{Tc}$ -EC-guanine. *Chemotherapy* 2004 (submitted).
13. Yang DJ, Oh C-S, Kohanim S, Ito M, Bryant JL, Yu D-F, Azhdarinia A, Greenwell AC, Kim JH, Kim EE. Imaging pancreas beta-cell sulfonylurea receptors with  $^{99m}\text{Tc}$ -DTPA-sulfonylurea receptor agents. *Diabetes* 2004 (submitted).

#### Articles Submitted:

1. Bryant JL Jr., Von der Porten A, Nicolini FA, Mehta P, Mehta JL: Oxidized low density lipoprotein decrease superoxide radical generation and increase platelet-inhibitory activity in human neutrophils.
2. Mehta P, Bryant JL Jr., Mehta JL: The effect of oxidized low density lipoproteins on nitric oxide synthase in human neutrophils.

3. **Bryant JL Jr., Mehta P, Mehta JL:** Identification of calcium-dependent nitric oxide synthase in human neutrophil membrane.

**Published Abstracts:**

1. **Bryant JL Jr., Yang BC, Mehta P, Saldeen TGP, Mehta JL:** Dietary fish oil decreases superoxide radical generation without affecting nitric oxide synthase activity: a mechanism of vasorelaxation. *Journal of the American College of Cardiology* 21 430A, 1993.
2. **Lopez LM, Bryant JL Jr., Mehta JL:** Effect of combined beta and alpha-adrenergic blockade on nitric oxide synthase activity, superoxide generation and platelet aggregation in patients with hypertension. *Proceeding of the American College of Clinical Pharmacology*, 1993.
3. **Lopez LM, Bryant JL Jr., Mehta JL:** Effects of therapy with celiprolol on nitric oxide synthase activity, superoxide generation and platelet aggregation in patients with hypertension. *Journal of the American College of Cardiology*, 1994.
4. **Ford, R.J., Bryant, J., Claypool, K. and Cabanillas, F:** Human lymphoma models in SCID mice: Non-Hodgkin and Hodgkin's. *Blood*, 87, 1996.
5. **Ford, R.J., Luthra R., Bryant, J., Tamayo, A., Curiel, T:** In vitro and in vivo models for mantle cell lymphoma. *Blood*, 92:314a, 1998.
6. **A. Azhdarinia, D.J. Yang, S., Zakko, M., Yukihiro, D-F Yu, J.L. Bryant, S. Kohanim, E.E. Kim, D.A., Podoloff.** Targeted tumor imaging using <sup>99m</sup>Tc-EC-deoxyglucose in comparison with <sup>18</sup>F-FDG. Presented at the 49<sup>th</sup> Annual Meeting of the Society of Nuclear Medicine, Los Angeles, CA, June 15-19, 2002.
6. **A. Azhdarinia, M. Yukihiro, D.J. Yang, J.L. Bryant, C-G Kim, D-F Yu, S. Kohanim, E.E. Kim, D.A. Podoloff.** Imaging angiogenesis using <sup>99m</sup>Tc-EC-endostatin. Presented at the 49<sup>th</sup> Annual Meeting of the Society of Nuclear Medicine, Los Angeles, CA, June 15-19, 2002.
7. **N.R. Schechter, D.J. Yang, K. Ang, D-F Yu, L.W. Tansey, J.L. Bryant, E.E. Kim, D.A. Podoloff.** Preliminary Tumor EGF Receptor imaging with <sup>99m</sup>Tc-EC-C225. Presented at the 49<sup>th</sup> Annual Meeting of the Society of Nuclear Medicine, Los Angeles, CA, June 15-19, 2002.
8. **D.J. Yang, H.A. Macapinlac, D-F. Yu, A. Azhdarinia, S. Kihanim, J.L. Bryant, E.E. Kim, D.A. Podoloff.** Glucosamine pathway imaging using <sup>99m</sup>Tc-EC-deoxyglucose in comparison with <sup>18</sup>F-FDG. Presented at the 49<sup>th</sup> Annual Meeting of the Society of Nuclear Medicine, Los Angeles, CA, June 15-19, 2002.

9. C-S Oh, D.J. Yang, C-G Kim, D-F Yu, M. Yukihiro, S. Kohanim, A. Azhdarinia, **J.L. Bryant**, E.E. Kim, D.A. Podoloff. <sup>99m</sup>Tc-labeled nitroimidazole analogues for assessment of tumor hypoxia. Presented at the 49<sup>th</sup> Annual Meeting of the Society of Nuclear Medicine, Los Angeles, CA, June 15-19, 2002.
10. M. Yukihiro, D.J. Yang, T. Inoue, D-F Yu, S. Kohanim, A. Azhdarinia, **J.L. Bryant**, E.E. Kim, D.A. Podoloff. In vitro cellular uptake and in vivo biodistribution of <sup>99m</sup>Tc-EC-Angiostatin. Presented at the 49<sup>th</sup> Annual Meeting of the Society of Nuclear Medicine, Los Angeles, CA, June 15-19, 2002.
11. Schechter, N. R., Yang, D. J., Ang, K., Yu, D-F, Tansey, L.W., **Bryant, J. L.**, Kim, E. E., Podoloff, D. A. Preliminary tumor egf receptor imaging with <sup>99m</sup>Tc-EC-C225. Presented at the 49<sup>th</sup> Annual Meeting of the Society of Nuclear Medicine, Los angeles, CA June 15-19, 2002. J. Nucl. Med. 43 (5): 269, 2002 (Abstract 1088).
12. Azhdarinia, A., Yang, D. J., Zakko, S., Yukihiro, M., Yu, D-F, **Bryant, J. L.**, Kohanim, S., Kim, E. E., Podoloff, D. A. Targeted tumor imaging using <sup>99m</sup>Tc-EC-deoxyglucose in comparison with <sup>18</sup>F-FDG. Presented at the 49<sup>th</sup> Annual Meeting of the Society of Nuclear Medicine, Los angeles, CA June 15-19, 2002. J. Nucl. Med. 43 (5): 273, 2002 (Abstract 1102).
13. Azhdarinia, A., Yukihiro, M., Yang, D. J., **Bryant, J. L.**, Kim, C-G, Yu, D-F, Kohanim, S., Kim, E. E., Podoloff, D. A. Imaging angiogenesis using <sup>99m</sup>Tc-EC-endostatin. Presented at the 49<sup>th</sup> Annual Meeting of the Society of Nuclear Medicine, Los angeles, CA June 15-19, 2002. J. Nucl. Med. 43 (5): 121, 2002 (Abstract 435).
14. Yang, D. J., Macapinlac, H.A., Yu, D-F, Azhdarinia, A., Kohanim, S., **Bryant, J. L.**, Kim, E. E., Podoloff, D. A. Glucosamine pathway imaging using <sup>99m</sup>Tc-EC-deoxyglucose in comparison with <sup>18</sup>F-FDG. Presented at the 49<sup>th</sup> Annual Meeting of the Society of Nuclear Medicine, Los angeles, CA June 15-19, 2002. J. Nucl. Med. 43 (5): 368, 2002 (Abstract 1478).
15. Azhdarinia, A., Yang, D. J., Schechter, N. R., Yu, D-F, **Bryant, J.**, Kohanim, S., Kim, E.E., Podoloff, D.A. <sup>99m</sup>Tc-EC-C225: An EGFR Targeting Tracer To Assess Angiogenesis. Presented at the 6th International Symposium on Technetium, Rhenium and other Metals in Chemistry and Nuclear Medicine,, Bressanone, Italy, September 4-7, 2002 (Abstract # CP5).
16. Azhdarinia, A., Yang, D. J., Yukihiro, M., Yu, D-F, **Bryant, J.**, Kim, E.E., Podoloff, D.A. <sup>99m</sup>Tc- Labeled Endostatin and Angiostatin for Angiogenesis Imaging. Presented at the 6th International Symposium on Technetium, Rhenium and other Metals in Chemistry and Nuclear Medicine, Bressanone, Italy, September 4-7, 2002 (Abstract # BP1).
17. **Jerry Bryant**, David J. Yang, Ali Azhdarinia, Edward Lin, Edmund E. Kim, Donald A. Podoloff. Radiosynthesis, Biodistribution and Planar Scintigraphy of

- 99mTc-Labeled Celebrex in DMBA-induced tumor bearing rats: Presented at the 94<sup>th</sup> American Association for Cancer Research 2003 Annual Meeting, Toronto, Canada, April 5-9. (Abstract # 107933).
18. M. Yukihiro, D.J. Yang, A. Azhdarinia, D-F Yu, C-G Kim, S. Kohanim, **J.L. Bryant**, E.E. Kim, D.A. Podoloff. Assessment of Tumor Growth with 99mTc-EC-Glucosamine: Presented at the 50<sup>th</sup> Annual Meeting of the Society of Nuclear Medicine, New Orleans, Louisiana, June 21-25, 2003. J. Nucl. Med. 43 (5): 368, 2002 (Abstract 1478).
  19. A. Azhdarinia, D. J. Yang, M. Yukihiro, **J. L. Bryant**, D-F Yu, S. Kohanim, E. E. Kim, D. A. Podoloff. Imaging, Dosimetry and Acute Toxicity with 99mTc-EC-Deoxyglucose in Tumor-Bearing Animals. Presented at the 50<sup>th</sup> Annual Meeting of the Society of Nuclear Medicine, New Orleans, Louisiana, June 21-25, 2003. J. Nucl. Med. 43 (5): 368, 2002 (Abstract 1478).
  20. A. Azhdarinia, D. J. Yang, M. Yukihiro, C. K. S. Chao, D-F Yu, **J. L. Bryant**, E. E. Kim, D. A. Podoloff. 99mTc-Labeled Endostatin and Angiostatin for Angiogenesis Imaging. Presented at the 50<sup>th</sup> Annual Meeting of the Society of Nuclear Medicine, New Orleans, Louisiana, June 21-25, 2003. J. Nucl. Med. 43 (5): 368, 2002 (Abstract 1478).
  21. R. Mendez, C-S Oh, A. Azhdarinia, D. J. Yang, D-F Yu, M. Yukihiro, **J. L. Bryant**, E. E. Kim, D. A. Podoloff. In-Vitro and In-Vivo evaluation of 99mTc-EC-Doxorubicin as a marker of Mdr to Doxorubicin. Presented at the 50<sup>th</sup> Annual Meeting of the Society of Nuclear Medicine, New Orleans, Louisiana, June 21-25, 2003. J. Nucl. Med. 43 (5): 368, 2002 (Abstract 1478).
  22. C-S Oh, D. J. Yang, M. Yukihiro, A. Azhdarinia, D-F Yu, C-G Kim, S. Kohanim, **J. L. Bryant**, E. E. Kim, D. A. Podoloff. Synthesis and evaluation of adenosine analogue in tumor-bearing rodents for assessment of tumor cell proliferation. Presented at the 50<sup>th</sup> Annual Meeting of the Society of Nuclear Medicine, New Orleans, Louisiana, June 21-25, 2003. J. Nucl. Med. 43 (5): 368, 2002 (Abstract 1478).
  23. S. Kohanim, C. Sharma, M. Yukihiro, D. J. Yang, A. Azhdarinia, D-F Yu, **J. L. Bryant**, E. E. Kim, D. A. Podoloff. Targeting Lipid metabolism with 99mTc-EC-TML: A carnitine Analogue. Presented at the 50<sup>th</sup> Annual Meeting of the Society of Nuclear Medicine, New Orleans, Louisiana, June 21-25, 2003. J. Nucl. Med. 43 (5): 368, 2002 (Abstract 1478).
  24. D. J. Yang, A. Azhdarinia, M. Yukihiro, D-F Yu, C-S Oh, **J. L. Bryant**, S. Zakko, E. E. Kim, D. A. Podoloff. Assessment of tumor growth using angiogenic and apoptotic agents. Presented at the 50<sup>th</sup> Annual Meeting of the Society of Nuclear Medicine, New Orleans, Louisiana, June 21-25, 2003. J. Nucl. Med. 43 (5): 368, 2002 (Abstract 1478).
  25. A. Azhdarinia, D. J. Yang, **J. L. Bryant**, M. Yukihiro, D-F Yu, C-S Oh, S. Kohanim, E. E. Kim, D. A. Podoloff. Radiosynthesis, Biodistribution and Planar Scintigraphy of

- <sup>99m</sup>Tc-EC-Coxi in tumor bearing animal models. Presented at the 50<sup>th</sup> Annual Meeting of the Society of Nuclear Medicine, New Orleans, Louisiana, June 21-25, 2003. J. Nucl. Med. 43 (5): 368, 2002 (Abstract 1478).
26. A. Azhdarinia, D.J. Yang, D-F Yu, C. Chao, E. Lin, J. Bryant, E.E. Kim, D.A. Podoloff. <sup>99m</sup>Tc-EC-COXi: Biodistribution and planar scintigraphy in mammary tumor-bearing animal models. Presented at the 2003 Annual Meeting of American Society of Clinical Oncology, Chicago, Illinois, May 31-June 3, 2003.
  27. Yukihiro M, Yang DJ, Azhdarinia A, Yu D-F, Kim C-G, Kohanim S, Bryant JL, Kim EE, Podoloff DA. Assessment of tumor growth with <sup>99m</sup>Tc-EC-glucosamine. J Nucl Med 44 (5):299, 2003 (Abstract 1071).
  28. Azhdarinia A, Yang DJ, Yukihiro M, Chao CKS, Yu D-F, Bryant JL, Kim EE, Podoloff DA. <sup>99m</sup>Tc-labeled endostatin and angiostatin for angiogenesis imaging. J Nucl Med 44 (5): 302, 2003 (Abstract 1082).
  29. Azhdarinia A, Yang DJ, Yukihiro M, Bryant JL, Yu D-F, Kohanim S, Kim EE, Podoloff DA. Imaging, dosimetry and acute toxicity with <sup>99m</sup>Tc-EC-deoxyglucose in tumor-bearing animals. J Nucl Med 44 (5):323, 2003 (Abstract 1158).
  30. Kohanim S, Sharma C, Yukihiro M, Yang DJ, Azhdarinia A, Yu D-F, Bryant JL, Kim EE, Podoloff DA. Targeting lipid metabolism with <sup>99m</sup>Tc-EC-TML: a carnitine analogue. J Nucl Med 44 (5):301, 2003 (Abstract 1077).
  31. Oh C-S, Yang DJ, Yukihiro M, Azhdarinia A, Yu D-F, Kim C-G, Kohanim S, Bryant JL, Kim EE, Podoloff DA. Synthesis and evaluation of adenosine analogue in tumor-bearing rodents for assessment of tumor cell proliferation. J Nucl Med 44 (5):301, 2003 (Abstract 1078).
  32. Mendez R, Oh C-S, Azhdarinia A, Yang DJ, Yu D-F, Yukihiro M, Bryant JL, Kim EE, Podoloff DA. *In vitro* and *in vivo* evaluation of <sup>99m</sup>Tc-EC-doxorubicin as a marker of MDR to doxorubicin. J Nucl Med 44 (5): 303, 2003 (Abstract 1084).
  33. Ito M, Yang DJ, Azhdarinia A, Mendez R, Kohanim S, Oh C-S, Yu D-F, Bryant JL, Chao CKS, Kim EE. PET and planar imaging of tumor hypoxia with radiolabeled metronidazole. . Proceedings of the AACR 45:104, 2004 (Abstract 946).
  34. Mendez R, Bryant J, Yang DJ, Lin E, Chang JY, Ito M, Azhdarinia A, Kim EE, Podoloff DA. Imaging COX-2 expression with <sup>99m</sup>Tc-labeled celebrex. Proceedings of the AACR 45:104, 2004 (Abstract 948).
  35. Rollo FD, Bryant JL, Yang DJ, Bai C, Kim EE, Yu DF, Ye J, Durbin MK, Garrard DJ, Shao L. The Complementary Role of FDG and Tc-99m ECDG for Tumor Imaging. Proceedings of the Society of Nuclear Medicine 51st Annual Meeting, June, 2004. (Abstract No. 1062)
  36. Azhdarinia A, Yang DJ, Yu DF, Oh C, Kohanim S, Mendez R, Ito M, Bryant JL, Kim EE, Podoloff DA. Local Regional Chemotherapy and Radiotherapy using an *In Situ* Hydrogel and Planar Imaging for Assessment of Tumor Growth. Proceedings of

the Society of Nuclear Medicine 51st Annual Meeting, June, 2004. (Abstract No. 1222)

37. Yang DJ, Chang JY, Mendez R, Bryant J, Azhdarina A, Oh C, Kohanim S, Ito M, Kim EE, Lin E, Podoloff DA. <sup>99m</sup>Tc-Labeled Celebrex: Synthesis, In Vitro and In Vivo Assessment of Cox-2 Expression. Proceedings of the Society of Nuclear Medicine 51st Annual Meeting, June, 2004. (Abstract No. 1406)
38. Oh C, Ozaki K, Yang DJ, Zakko S, Inoue T, Azhdarina A, Bryant JL, Kim CG, Kohanim S, Kim EE, Podoloff DA. Assessment of Tumor Cell Proliferation with <sup>99m</sup>Tc-Labeled Adenosine and Guanine Analogues. Proceedings of the Society of Nuclear Medicine 51st Annual Meeting, June, 2004. (Abstract No. 1407)
39. Yang DJ, Oh C, Yu DF, Kohanim Azhdarina A, Ito M, Mendez R, Chanda M. Bryant JL, Kim EE, Podoloff DA. Imaging Sulfonylurea Receptors on the Pancreas Beta-cell using Tc-99m Labeled Sulfonylurea Agents. Proceedings of the Society of Nuclear Medicine 51st Annual Meeting, June, 2004. (Abstract No. 1435)
40. Bai, C, Shao, J, Durbin, MK, Da Silva, AJ, Rollo FD, Garrard DJ, Forster, KM and Bryant, J. SPECT/CT Imaging with three-dimensional detector response correction and CT-based attenuation correction to improve SPECT Oncology. Proceedings of the Society of Nuclear Medicine 51st Annual Meeting, June, 2004. (Abstract No. 10..)

#### INVITED ARTICLES IN JOURNALS: None

#### BOOKS AND CHAPTERS:

#### BOOKS EDITED AND WRITTEN:

#### BOOK CHAPTERS:

1. Azhdarina, A., Yang, D. J., Schechter, N. R., Yu, D-F, Bryant, J., Kohanim, S., Kim, E.E., Podoloff, D.A. <sup>99m</sup>Tc-EC-C225: An EGFR Targeting Tracer To Assess Angiogenesis. *In: M. Nicolini and U. Mazzi (eds), Technetium, Rhenium and other Metals in Chemistry and Nuclear Medicine*, pp. 665-667, Padova, Italy, Servizi Grafici Editoriali snc, 2002.
2. Azhdarina, A., Yang, D. J., Yukihiro, M., Yu, D-F, Bryant, J., Kim, E.E., Podoloff, D.A. <sup>99m</sup>Tc- Labeled Endostatin and Angiostatin for Angiogenesis Imaging. *In: M. Nicolini and U. Mazzi (eds), Technetium, Rhenium and other Metals in Chemistry and Nuclear Medicine*, pp. 387-389, Padova, Italy, Servizi Grafici Editoriali snc, 2002.

## REFERENCES

***Richard J. Ford, M.D., Ph.D.***

Professor of Hematopathology  
UT MD Anderson Cancer Center  
1515 Holcombe Blvd., Box 72  
Houston, TX 77030 Tel. 713/792-3121

***David J. Yang, Ph.D.***

Associate Professor and Associate Chemist of Nuclear Medicine  
Department of Nuclear Medicine  
UT MD Anderson Cancer Center  
1515 Holcombe Blvd., Box 59  
Houston, TX 77030 Tel. 713/794-1053

***E. Edmund Kim, M.D.***

Professor of Radiology & Medicine  
Division of Nuclear Medicine  
UT MD Anderson Cancer Center  
1515 Holcombe Blvd., Box 59  
Houston, TX 77030 Tel. 713/794-1052

***F. David Rollo, M.D., Ph.D***

Chief Medical Officer  
Philips Medical Systems  
540 Alder Drive  
Milpitas, CA 95035 Tel. 408/468-3634

# The Oncologist

## Commentary

## Anticancer Drug Development: The Way Forward

TOM CONNORS

Research Division of the European Organisation for Research and Treatment of Cancer, London, United Kingdom

Cancer chemotherapy celebrated its fiftieth anniversary last year. It was in 1945 that wartime research on the nitrogen mustards, which uncovered their potential use in the treatment of leukaemias and other cancers, was first made public. Fifty years later, more than sixty drugs have been registered in the USA for the treatment of cancer, but there are still lessons to be learnt.

One problem, paradoxically, is that many anticancer agents produce a response in several different classes of the disease. This means that once a new agent has been shown to be effective in one cancer, much effort is devoted to further investigations of the same drug in various combinations for different disorders. While this approach has led to advances in the treatment of many childhood cancers and some rare diseases, a plethora of studies on metastatic colon cancer, for example, has yielded little benefit. 5-fluorouracil continues to be used in trials, yet there is no evidence for an increase in survival. The lesson to be learnt is that many common cancers are not adequately treated by present-day chemotherapy, and most trials of this sort are a waste of time. Significant increases in survival will only occur if the selectivity of present-day anticancer agents can be increased or new classes of more selective agents can be discovered. There are two fundamental problems in drug development: a lack of suitable laboratory tests and the difficulty of conducting early clinical trials. Firstly, no existing laboratory method can accurately predict which chemical will be effective against a particular class of human cancer. At best, tests can demonstrate a general 'anticancer' property. This is well exemplified by the discovery of cisplatin. The fact that cisplatin caused regression in a number of transplanted rodent tumours created no great excitement amongst chemotherapists. It was only later when it was tested clinically against ovarian cancer that results were sufficiently positive to encourage others to investigate. Only then was it discovered that metastatic teratoma was extraordinarily sensitive to the drug. This finding was made as a result of phase II trials and no laboratory model could have

predicted it. The lesson to be learnt is that new drugs should be tested extensively in phase II trials before they are discarded.

The second problem concerns early clinical trials. Because new drugs can only be tested against advanced and usually heavily pretreated disease, it is unlikely that dramatic responses will occur. The methods used to detect responses in solid tumours and metastases are crude, and it is likely that many useful drugs are missed. New techniques are needed to detect small but important responses.

In addition to these technical problems, clinical trials are expensive and the time required for preclinical pharmacology and toxicology is lengthy. In the early days, drugs could enter clinical trials after fairly simple toxicological studies. The thalidomide disaster in the 1960s, however, led to the setting up of regulatory bodies to scrutinize drugs before clinical trials. This proved detrimental for cancer drug development because a series of fairly long-term tests is now required. These must be carried out in both rodents and one other species, usually the dog. This approach was probably a good thing for most medicines where a large margin of safety is required between the therapeutic dose and the dose which causes side effects, but was inappropriate for anticancer agents which are tested at the maximum possible dose which gives manageable side effects. These new regulations meant that the cost of one clinical trial after the 1970s was equivalent to the cost of ten before that time.

Solutions to these problems are available, although to put them into practice would require the cooperation of government regulatory authorities, the pharmaceutical industry and other organisations such as the US National Cancer Institute (NCI), the UK Cancer Research Campaign (CRC) and the European Organisation for Research and Treatment of Cancer (EORTC). Firstly, it is important to switch from clinical trials of analogues and combinations of standard drugs to trials of new classes of anticancer agents. Further, an international effort should be launched whereby

*Correspondence: Tom Connors, M.D., Chairman, Research Division of the European Organisation for Research and Treatment of Cancer, CPT, School of Pharmacy, Brunswick Sq., London, WC1W 4AY, United Kingdom. Telephone: 441-71-753-5932; Fax: 441-71-753-5931; e-mail: EZCRCC@ULCC.AC.UK ©AlphaMed Press 1083-7159/96/\$5.00/0*



these new agents can be rapidly tested in phase II trials against common solid cancers using new techniques to detect small but significant tumour responses. Lead chemicals discovered in this way could then be taken back to the laboratory for further development. There is no shortage of new drugs which act by mechanisms quite different from present-day agents, and new approaches can greatly increase the amount of cytotoxic agents delivered to solid tumours.

As long ago as 1980, the CRC introduced protocols which enabled early clinical trials to be carried out rapidly and with minimal cost. These procedures used short-term tests only in rodents to determine a safe starting dose. The test can be completed within six months and around fifty clinical trials using this protocol have been successfully carried out in collaboration with the EORTC. Despite this, the American Food and Drug Administration (FDA), regulatory authorities in many other countries and many drug companies still insist on using a second animal species before a phase I clinical trial is permitted instead of using the money spent to develop several agents with minimal toxicology testing. The EORTC and CRC also plan to introduce positron emission tomographic scanning into early clinical trials as a highly sensitive method of measuring tumour response.

Cancer mortality has changed little over the past forty years, mainly because of our failure to develop curative chemotherapy for the common solid cancers. The way forward is to carry out extensive phase I and II clinical trials of the many new types of anticancer agent that have become available as a result of increased knowledge about cancer cells and how they differ from normal tissues. In order to do this, the regulatory authorities must recognize that minimal toxicology protocols are adequate, and drug companies must be persuaded to give more emphasis to the search for new chemotherapeutic agents. A coordinated effort to achieve these aims would be a wonderful way to mark the fiftieth anniversary of modern chemotherapy. Unfortunately the regulatory authorities find it less risky to stick with extensive safety testing rather than to use shortcuts, however well-validated clinically. Many but not all drug companies, mindful of profits, prefer the easy way out and concentrate on analogues, while most clinicians opt for trials of combinations of known agents, being aware that they are worth a publication or two.

Reprinted with permission from *Helix*, Volume V, Issue 1, 1996, pp. 20-21.

## Antitumor Activity of Didemnin B in the Human Tumor Stem Cell Assay

T. L. Jiang, R. H. Liu, and S. E. Salmon

The University of Arizona, Cancer Center, Tucson, Arizona 85724, USA

**Summary.** *In vitro* studies of the schedule dependency and cytotoxicity of didemnin B, a novel depsipeptide isolated from a Caribbean tunicate (*Didemnidae*), were carried out in fresh tumor cells obtained from biopsies from 39 cancer patients using the human tumor stem cell assay. Two schedules of drug exposure were examined (1 h and continuous exposure in the agar). Tumor cells from nine of 26 patients (34.6%) showed reduced survival of tumor-colony forming units to 30% of control or less at the 0.01  $\mu\text{g}$  level in the continuous exposure studies. Cells from eight of 17 patients (47%) showed a similar degree of sensitivity to didemnin after a 1-h exposure to 0.1  $\mu\text{g}$  prior to plating. The median  $\text{ID}_{50}$  values were  $4.2 \times 10^{-3}$   $\mu\text{g}/\text{ml}$  and  $46 \times 10^{-3}$   $\mu\text{g}/\text{ml}$  for continuous and 1-h exposures, respectively. A clear dose-response relationship was observed with both dosage schedules. Comparison of the slopes of the continuous and 1-h exposures and of the  $\text{ID}_{50}$  of the drug schedules suggests that didemnin is a cell-cycle-non-specific cytotoxic agent. Significant *in vitro* antitumor activity was observed at low concentrations against carcinomas of the breast, ovary, and kidney, and also mesothelioma and sarcoma. These results can provide pharmacologic goals to be achieved in phase I clinical trial. Further *in vitro* testing should help select tumor types for study in phase II trials of this very promising new anticancer drug.

### Introduction

Didemnins, a new class of depsipeptide agents, were isolated from Caribbean tunicates (*Didemnidae*) (ascidian, sea squirt) [5]. The depsipeptide didemnins represent novel ring-peptide structures containing hydroxyisovalerylpropionate and a new stereoisomer of the highly unusual amino acid statine (Fig. 1) [7]. Recently, Rinehart et al. [7, 8] and Weinheimer et al. (personal communication) found that didemnins, especially didemnin B (NSC 325319), could inhibit the growth of KB cells, L1210 and P388 leukemias, and B16 melanoma *in vitro* and *in vivo*. The  $\text{LD}_{10}$  of didemnin B is in the range of 160  $\mu\text{g}/\text{kg}$ , given IP, with significant antitumor activity observed in B16 melanomas *in vivo* at that dosage when administered on days 1-9 (lifespan extended to 160% of control) (J. Venditti, personal communication). Didemnins also inhibit replication of several DNA and RNA viruses *in vitro*. We thought it would be of interest to test this agent on

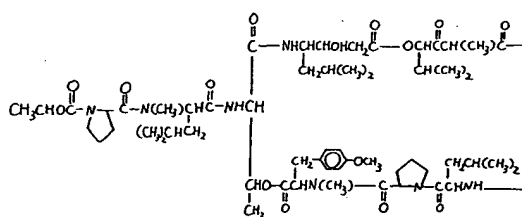


Fig. 1. Structure of didemnin B (NSC 325319)

clonogenic human tumor cells, as this novel agent has recently been approved by the NCI's decision network for toxicology testing and subsequent entry into phase I clinical trials (J. Venditti, personal communication).

The *in vitro* human tumor stem cell assay developed by Hamburger and Salmon [3] has proven useful for testing new anticancer drugs for potential phase II activity [12] and for predicting clinical response to individual chemotherapeutic drugs in individual patients [9, 10, 13]. Therefore, it might prove to be a very effective tool for new drug screening and development. In this paper the results of our initial antitumor studies of didemnin B in the human tumor stem cell assay are presented. Our data may prove useful for further experimental studies and in relation to future phase I-II clinical trials of this agent.

### Materials and Methods

**Drugs.** Purified didemnin B (NSC 325319) was kindly provided by the Natural Products Branch, Division of Cancer Treatment, NCI and Dr A. J. Weinheimer, University of Houston, Texas, USA. Stock solutions of didemnin B were prepared in 100% ethanol, then diluted with 0.9% sterile NaCl, and stored at  $-80^{\circ}\text{C}$  in aliquots sufficient for individual assays. Subsequent dilutions for incubation with cells were made with saline. The final concentration of ethanol in the incubation was 0.4% for 1-h exposure and 0.16% for continuous exposure.

**Preparation of Tumor Cell Samples.** A variety of types of malignant tumors from 39 patients were used for evaluating anticancer activity of didemnin B in these studies. The tumor types were as follows: ovarian, 11; breast, five; lung, three; cervical, three; endometrial, three; sarcoma, three; mesothelioma, two; malignant peritoneal or pleural effusion with

unknown original sites, four; and cancer of kidney, skin, stomach, pancreas, and melanoma, one each.

Cell suspensions were prepared mechanically according to techniques reported previously [9]. Solid tumors were minced into small pieces with scissors, then enzymatically disaggregated with 0.8% collagenase and 0.002% DNase on a magnetic stirrer at room temperature for 30 min. After the suspension had been passed through a gauze to remove clumps, the single cell suspension was washed twice with serum-free medium and adjusted to a final concentration of  $3 \times 10^6$  cells/ml in McCoy's 5A medium with 10% FCS.

**In vitro Exposure to Drug.** Two procedures were used for exposure of human tumor cells to drugs. One-hour exposure: Tumor cells incubated with didemnin B in 0.4% ethanol or 0.4% ethanol alone for 1 h at 37° C in McCoy's 5A with 10% FCS. The cells were then washed twice and prepared for culture. Continuous contact: Didemnin B was incorporated into the upper layer of the culture system for the duration of the culture.

For the initial dose finding, in each of the first 14 tumors tested didemnin B was tested at a single concentration (2.5, 1.0, or 0.1 µg/ml by continuous exposure). Subsequently, tumors were tested with three concentrations of the drug (0.1, 0.01, 0.001 µg/ml by continuous exposure or 1.0, 0.1, 0.01 µg/ml for 1 h).

**Tumor Stem Cell Assay.** The clonogenic assay system utilized was the method of Hamburger and Salmon [3]. In brief, cells to be tested were suspended in 0.3% agar in enriched CMRL 1066 medium to yield a final concentration of  $0.5 \times 10^6$  cells/ml. Of this mixture, 1 ml was pipetted into each of three 35-mm petri dishes containing 1 ml 0.5% agar in enriched McCoy's 5A medium, but without conditioned medium. All drug assays were done in triplicate along with six simultaneous controls incorporating the ethanol solvents.

Plates were incubated at 37° C in a humidified atmosphere containing 6% CO<sub>2</sub> for 7–30 days (average: 18 days). Only specimens with good in vitro growth are reported. The number of colonies on control and drug-treated plates was determined with an automated image analysis system (Bausch and Lomb Omnicon Fas II). At least 30 tumor colonies per control plate,

each with at least 60 µm diameter, were required for a drug experiment to be considered evaluable for measurement of drug effect. As it was set up, the FAS II counted 52% of the total colony growth area in the agar, so that in the reported experiments the minimum number of colonies per plate in controls was approximately 60. In this study, the median number of colonies counted by the FAS II was 64 per control plate.

**Data Analysis.** Colony counts for the triplicate plates for a particular drug concentration were averaged to obtain each data point and the standard error was calculated. The percent survival of tumor colony-forming units (TCFU) in the treated plates was calculated from the formula:

$$\% \text{ Survival} = \frac{\text{No. of colonies in treated plates}}{\text{No. of colonies in control plates}} \times 100$$

Reduction in survival to 30% of control or less was applied as the criterion of in vitro sensitivity to didemnin B. To compare the activity between different drugs or different exposure procedures, the concentration of didemnin B required to reduce survival to 50% of the control TCFU (ID<sub>50</sub>) was determined from dose-response curves with the Lagrange interpolation function and the Newtonian iteration method.

## Results

### Effects of Didemnin B on Clonogenic Human Tumor Cells

#### Continuous Exposure

Table 1 and Fig. 2 summarize the in vitro response to didemnin B of more than 12 different types of tumors from 39 patients. In the initial experiments with drug concentrations of 1.0 and 2.5 µg/ml in continuous contacts, the TCFU survival was less than 15% in all samples tested, with means of  $5.8 \pm 2.9\%$  and  $5.1 \pm 2.3\%$ , respectively (means  $\pm$  SE). There was less than 1% survival of TCFU in three tumors. The mean percent survival rose progressively with decreasing doses of didemnin B. Thus, the mean survival of TCFU was  $30.6 \pm 5.8\%$

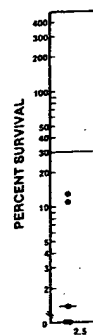


Fig. 2. In vitro response of human tumor cells to didemnin B. The percent survival of tumor colony-forming units (TCFU) in the treated plates was calculated from the formula:

at 0.1 µg/ml, the percent survival was approximately 30%. At 0.01 µg/ml, the percent survival was approximately 50%. At 0.001 µg/ml, the percent survival was approximately 70%.

#### One-Hour Exposure

In the one-hour exposure experiments, the percent survival of TCFU was less than 15% in all samples tested, with means of  $5.8 \pm 2.9\%$  and  $5.1 \pm 2.3\%$ , respectively (means  $\pm$  SE). There was less than 1% survival of TCFU in three tumors. The mean percent survival rose progressively with decreasing doses of didemnin B. Thus, the mean survival of TCFU was  $30.6 \pm 5.8\%$

## Discussion

In the present study, we have shown that didemnin B is a potent inhibitor of human tumor cell growth in vitro. The percent survival of TCFU was less than 15% in all samples tested, with means of  $5.8 \pm 2.9\%$  and  $5.1 \pm 2.3\%$ , respectively (means  $\pm$  SE). There was less than 1% survival of TCFU in three tumors. The mean percent survival rose progressively with decreasing doses of didemnin B. Thus, the mean survival of TCFU was  $30.6 \pm 5.8\%$

Table 1. Sensitivity of human tumor stem cells to didemnin B in 1-h and continuous exposure experiments

	Continuous contact concentration (µg/ml)					1-h exposure concentration (µg/ml)		
	2.5	1.0	0.1	0.01	0.001	1.0	0.1	0.01
Ovarian			6/9 <sup>a</sup>	2/10	0/10	3/8	3/8	0/8
Breast	1/1	2/2	2/2	1/1	0/1	1/1	1/1	0/1
Lung			1/3	1/3	1/3	1/2	0/2	0/2
Cervical		1/1		0/2	1/2			
Endometrial	3/3							
Sarcoma			3/3	2/3	2/3	2/3	2/3	2/3
Mesothelioma			0/1	0/1	0/1	1/1	1/1	1/1
Renal			1/1	1/1	0/1	1/1	1/1	0/1
Skin			0/1	0/1	0/1			
Stomach	1/1							
Pancreatic		1/1						
Melanoma		1/1						
Others			0/1	2/4	0/3	0/1	0/1	0/1
Total	5/5	5/5	13/21	9/26	4/25	9/17	8/17	3/17

<sup>a</sup> No. of sensitive cultures/no. tested. Sensitivity = survival  $\leq$  30% of control TCFU (see Methods)

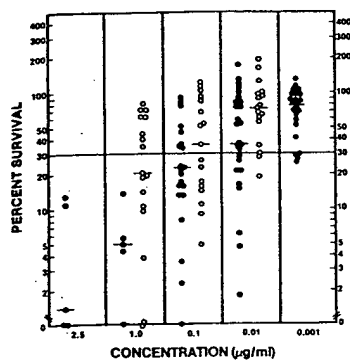


Fig. 2. In vitro activity of didemnin B against tumor colony-forming cells from 39 patients. Each point (● continuous exposure; ○ 1-h exposure) represents an individual tumor sample tested. The horizontal bars represent the median percent survival for all tumors at the concentration tested

at 0.1  $\mu\text{g/ml}$ ,  $58.0 \pm 8.4\%$  at 0.01  $\mu\text{g/ml}$ , and  $75.0 \pm 5.9\%$  at 0.001  $\mu\text{g/ml}$ . Nevertheless, there were four instances in which the percent survival was less than 10% at 0.1  $\mu\text{g/ml}$ , and four additional cases (2 sarcoma, 1 lung, 1 renal carcinoma) where survival was less than 20% of control at the 0.01  $\mu\text{g/ml}$  concentration. The survival curves for tumors tested at multiple doses were similar and showed a clear dose-response relationship. In the continuous exposure studies, approximately 62% of tumor specimens tested were sensitive to didemnin at the concentration of 0.1  $\mu\text{g/ml}$ , 34% at 0.01  $\mu\text{g/ml}$ , and 16% at 0.001  $\mu\text{g/ml}$ .

#### One-Hour Exposure

In the 1-h exposure experiments 17 tumors were tested against didemnin B at three concentrations. A clear dose-response relationship was observed. The mean percent survival was  $33.2 \pm 6.6\%$  at 1.0  $\mu\text{g/ml}$ ,  $50.6 \pm 9.8\%$  at 0.1  $\mu\text{g/ml}$ , and  $80.7 \pm 11.2\%$  at the 0.01  $\mu\text{g/ml}$  concentration. Of the tumors tested, 53% were sensitive to the drug at the concentration of 1.0  $\mu\text{g/ml}$ , 47% at 0.1  $\mu\text{g/ml}$ , and 18% at 0.01  $\mu\text{g/ml}$ , respectively. Less than 10% survival was observed with one sarcoma and renal carcinoma at the concentration of 0.1  $\mu\text{g/ml}$ . Three ovarian carcinomas and one additional sarcoma had survival reduced to less than 20% at that dose level.

The  $\text{ID}_{50}$  of didemnin B in the 1-h and continuous exposure studies was calculated for 11 tumors which provided sufficient cells to carry out both types of drug exposure simultaneously on replicate aliquots. The mean  $\text{ID}_{50}$  was  $0.0042 \pm 0.0010 \mu\text{g/ml}$  for continuous exposure and  $0.0462 \pm 0.0130 \mu\text{g/ml}$  for the 1-h exposure. However, the median  $\text{ID}_{50}$ s were 0.0035  $\mu\text{g/ml}$  and 0.0168  $\mu\text{g/ml}$ , respectively. The  $\text{ID}_{50}$  ratio (1 h/continuous) had a mean rate of 11 and a median of 4.8.

#### Discussion

In these studies of the new antitumor agent didemnin B, we have used the soft agar human tumor stem cell assay to study its potential antineoplastic potency and spectrum against clonogenic human tumor cells. Our results in 39 fresh human tumors indicate that low doses of didemnin B can significantly reduce the ability of a variety of human tumor types to form colonies in soft agar. The human tumor stem cell assay has previously been applied to testing clonogenic human tumor

cells against a variety of standard and new anticancer drugs [2, 6, 10–12, 14, 15]. Correlative clinical trials from several centers have indicated that in vitro sensitivity in this assay system can predict clinical response with 60%–70% accuracy and failure of response to therapy with 95% accuracy [9, 10, 13]. True positive clinical correlations (observe clinical response) have been obtained when standard cytotoxic drugs reduce survival of TCFU to 30% of control or less after a 1-h exposure to doses that are 10% of the peak plasma concentration or concentration-time product or less [1]. True negative clinical correlations (failure of response) have been observed when survival of TCFU is greater than 30% at such doses, and particularly when greater than 50% survival is observed with the agent tested in vitro. Available data on various new agents tested in this assay system suggest that in vitro analysis can pinpoint tumor types that may prove sensitive to the agent, and thereby serve as a type of 'in vitro phase II trial' [12, 14, 15]. In view of the positive results observed with various murine tumors in vivo, and with our in vitro observations in human tumors, it is reasonable to project that didemnin will have significant antitumor activity in clinical practice, assuming that excessive toxicity is not observed with didemnin in phase I clinical trials, and that clinically achievable plasma concentrations are at least ten times higher than the in vitro concentrations utilized in the 1-h exposure studies in which sensitivity (survival  $\leq 30\%$  of control) was observed. Thus we predict that this agent will prove useful if peak plasma concentrations or concentration-time products can be obtained in vivo in the range of 0.1–1.0  $\mu\text{g} \cdot \text{h/ml}$ . Inasmuch as pharmacokinetic and toxicologic data have yet to be obtained in man, these projections remain conjectural, but nonetheless they should provide a useful level to set as a pharmacokinetic goal for phase I studies of didemnin. We have previously used the comparison of patterns of dose-survival curves and  $\text{ID}_{50}$  values in 1-h and continuous exposure experiments to gain some knowledge of the mechanism of action and schedule dependency of anticancer drugs [1, 4]. When the slope of the survival-concentration curves is much steeper in the continuous exposure studies than the 1-h studies, and the ratio of  $\text{ID}_{50}$  values (1 h/continuous) is very high (e.g., 200–300), then the drug tested has a high likelihood of being schedule-dependent or cell-cycle-specific. Conversely, when 1-h and continuous exposure curves are parallel, and the ratio of  $\text{ID}_{50}$  values is in the range of 10 or lower, then it is likely that the agent is a cell-cycle-non-specific drug. We recognize that our approach to assessing cell cycle activity or schedule dependency of a new drug (by comparing 1-h and continuous exposure data) is only a first approximation. It is generally recognized that even cycle-non-specific drugs often have higher lethality against cycling than against resting cells, but the differential effect is of far lesser magnitude than is observed with drugs that kill only cycling cells. Thus, in our prior studies of doxorubicin and camptothecin (two cycle-non-specific agents), the ratio of  $\text{ID}_{50}$  values was in the range of 10 [4], whereas for drugs such as bleomycin [1] and VP-16, schedule-dependent in vitro toxicity is observed in the clonogenic assay, effective doses in the continuous exposure experiments being less than 1% of those required in the 1-h studies. The results of such comparisons for didemnin suggest that it is a cell-cycle-non-specific cytotoxic agent, as its  $\text{ID}_{50}$  ratio was in the range of 10. The molecular mechanism of action remains to be determined, but is likely to be novel, as this agent does not bear any apparent structural similarities to alkylating agents or other cycle-non-specific agents.

As the major objective of this *in vitro* study was to define dosage exposures and schedule dependency of didemnin, our experience with regard to its antitumor spectrum is still preliminary. The data summarized in Table 1 lends encouragement to the view that this agent will have a broad spectrum of action, as significant antitumor activity was observed at relatively low doses (0.1  $\mu\text{g/ml}$  for 1 h) in ovarian, breast, and renal carcinomas, as well as in mesothelioma and sarcoma. Additional *in vitro* investigation (with 1-h exposure) against a larger spectrum and number of tumors is clearly warranted for didemnin, so that additional tumor types with a high likelihood of clinical response can be more definitively identified and thereby help provide goals for phase II clinical trials with this promising new anticancer drug. It is important to point out that didemnins have a molar potency similar to that of actinomycin; therefore, even 1-h exposure dosages of 0.1  $\mu\text{g/ml}$  may overestimate potential clinical activity for didemnins, and *in vitro* studies with even lower dosage levels may prove necessary.

**Acknowledgements.** We thank Dr Al Weinheimer for bringing didemnin to our attention and for providing us with an initial sample of the drug, and Dr John Douros of the Natural Products Branch, Division of Cancer Treatment, National Cancer Institute for providing us with subsequent supplies of didemnin (NSC 325319) for *in vitro* testing; and Dr John Venditti, Drug Evaluation Branch, NCI for providing us with relevant preclinical testing data observed by the NCI. Research by Sydney E. Salmon was supported by Grants CA 21839, CA 17094, CA 23074, and a contract CM 17497 from the National Cancer Institute, Bethesda, MD 20205. T. L. Jiang was a visiting scholar from the Institute of Chinese Materia Medica, Academy of Traditional Chinese Medicine, Beijing, China.

## References

1. Alberts DS, Salmon SE, Chen H-SG, Moon TE, Young L, Surwit EA (1981) Pharmacologic studies of anticancer drugs using the human tumor stem cell assay. *Cancer Chemother Pharmacol* 6: 253-264
2. Bradley EC, Ruscetti FW (1981) Effect of fibroblast, lymphoid, and myeloid interferons on human tumor colony formation *in vitro*. *Cancer Res* 41: 244-249
3. Hamburger AW, Salmon SE (1977) Primary bioassay of human tumor stem cells. *Science* 197: 461-463
4. Jiang TL, Salmon SE, Liu RH (1983) Activity of camptothecin, harringtonin, cantharidin and curcuma in the human tumor stem cell assay. *Eur J Cancer* 19: 263-270
5. Li LH, Renis HE, McGovern JP, Rinehart KL Jr (1981) Didemnins - Novel antitumor and antiviral depsipeptides from the sea. *Proc Am Assoc Cancer Res* 22: 255
6. Meyskens FL, Salmon SE (1979) Inhibition of human melanoma colony formation by retinoids. *Cancer Res* 39: 4055-4057
7. Rinehart KL Jr, Gloer JB, Cook JC Jr, Mizesak ST, Seahill TA (1981a) Structures of the didemnins, antiviral and cytotoxic depsipeptides from a Caribbean tunicate. *J Am Chem Soc* 103: 1857-1859
8. Rinehart KL Jr, Gloer JB, Hughes RG Jr, Rebus HE, McGovern JP, Swynenberg EB, Stringfellow DA, Kuentzel SL, Li LH (1981b) Didemnins: Antiviral and antitumor depsipeptides from a Caribbean tunicate. *Science* 212: 933-935
9. Salmon SE (ed) (1980) Cloning of human tumor stem cells. Alan R. Liss, New York
10. Salmon SE, Hamburger AW, Soehnlen B, Durie BGM, Alberts DS, Moon TE (1978) Quantitation of differential sensitivity of human tumor stem cells to anticancer drugs. *N Engl J Med* 298: 1321-1327
11. Salmon SE, Liu RH, Casazza AM (1981a) Evaluation of a new anthracycline analogs with the human tumor stem cell assay. *Cancer Chemother Pharmacol* 6: 103-110
12. Salmon SE, Meyskens FL Jr, Alberts DS, Soehnlen B, Young L (1981b) New drugs in ovarian cancer and malignant melanoma: *In vitro* phase II screening with the human tumor stem cell assay. *Cancer Treat Rep* 65: 1-12
13. Von Hoff DD, Casper J, Bradley E, Jones D, Makuch R (1981a) Association between human tumor colony-forming assay results and response of an individual patient's tumor to chemotherapy. *Am J Med* 70: 1027-1032
14. Von Hoff DD, Coltman CA Jr, Forseth B (1981b) Activity of 9-10-anthracene-dicarboxaldehyde bis [(4,5-dihydro-1 H-imidazol-2-yl) hydrazone] dihydrochloride (CL 216, 942) in a human tumor cloning system. Leads for phase II trials in man. *Cancer Chemother Pharmacol* 6: 141-144
15. Von Hoff DD, Coltman CA Jr, Forseth B (1981c) Activity of mitoxantrone in a human tumor cloning system. *Cancer Res* 41: 1853-1855

Received March 29, 1982/Accepted July 1, 1982

## Blood Labell in Car

H. Sharm  
S. Owens

<sup>1</sup> Departm

<sup>2</sup> Cancer F

<sup>3</sup> Departm

<sup>4</sup> Regional

<sup>5</sup> Paterson

## Summary

1,1-cyclo  
were deter  
injection  
serial blo

The t  
intermedi  
respective  
the first 6  
for cispl  
excreted t  
for CHII  
The  
account j

## Introduc

Cisplatin  
of a vari  
cisplatin  
tubular  
otherwise  
CBI  
The age

Table 1.

Patient  
Age  
Sex

Blood cl

$t_{1/2}$  Fast  
A%

$t_{1/2}$  Inter  
B%

$t_{1/2}$  Slow  
C%

Reprint

# 3-(Iodoacetamido)-benzoylurea: A Novel Cancericidal Tubulin Ligand that Inhibits Microtubule Polymerization, Phosphorylates *bcl-2*, and Induces Apoptosis in Tumor Cells<sup>1</sup>

Jian-Dong Jiang, Ashley S. Davis, Kim Middleton, Yi-He Ling, Roman Perez-Soler, James F. Holland, and J. George Bekesi<sup>2</sup>

T. J. Martell Laboratory for Leukemia, Cancer and AIDS Research, Department of Medicine, Mount Sinai School of Medicine, New York, New York 10029 [J.-D. J., J. F. H., J. G. B.]; Cytoskeleton, Inc., Denver, Colorado 80206 [A. S. D., K. M.]; and Kaplan Comprehensive Cancer Center, New York University Medical Center, New York, New York 10016 [Y.-H. L., R. P.-S.]

## ABSTRACT

3-(Iodoacetamido)-benzoylurea (3-IAABU) is a newly synthesized anti-tubulin compound with a molecular weight of 347. 3-IAABU exhibited anticancer activity in a variety of tumor cell lines with  $ID_{50}$  in the range of 0.015–0.29  $\mu$ M for leukemic cells and 0.06–0.92  $\mu$ M for solid tumors. Higher selectivity against malignant cells was observed with 3-IAABU than that with vinblastine and paclitaxel. It inhibits microtubule assembly in tubulin systems either with or without microtubule-associated proteins ( $ID_{50}$  was 0.1  $\mu$ M and 1.2  $\mu$ M, respectively) and microtubule depolymerization was not affected, indicating an inhibition of polymerization by binding of 3-IAABU to the heterodimeric subunit of tubulin. 3-IAABU was shown to inhibit the binding of colchicine, a subunit binding compound, but did not inhibit binding of vinblastine and guanosine 5'-triphosphate/guanosine 5'-diphosphate, indicating that colchicine site corresponds to the site that 3-IAABU locates. Tumor cells treated with 3-IAABU showed scattered chromosomes in metaphase. Normal microtubule architecture or spindle apparatus was absent in these cells; instead, punctuated aggregates of tubulin were found by an immunofluorescent staining. Cell cycle analyses showed an accumulation of tumor cells at M phase after a 4-h treatment with 3-IAABU. The phosphorylated *bcl-2* representative of an inactivated form of the oncoprotein was found in the cells 12 h after treatment with 3-IAABU. These cells progressed to apoptosis within 16 h. As a new tubulin ligand, 3-IAABU could be a promising agent in cancer chemotherapy.

## INTRODUCTION

Microtubules are highly dynamic assemblies of  $\alpha\beta$ -tubulin. One essential function of microtubules is to partition duplicated chromosomes equally into two daughter cells in cell division. When cells enter mitosis, microtubule dynamics increased up to 100-fold (1), as compared with that in interphase, and the half-times of exchanging spindle tubulin with tubulin in the free tubulin pool is about 10 s (2). This high-speed dynamic is very sensitive to interferences and is, therefore, a moving target in tumor cells for many chemotherapeutic agents, such as *Vinca* alkaloids, nocodolones, and paclitaxel (3, 4). The primary action of these agents is to bind to the sites on tubulin or microtubules, as reflected by their aptitude to cause alteration of microtubule architecture, dynamics and, subsequently, mitotic blocking (5). Recent investigations showed that disruption of microtubules by any of the microtubule-active agents resulted in a phosphorylated form of *bcl-2* (6–8), which was without activity (9) and failed to bind to bax (6). This process leads the *bcl-2*-positive tumor cells to apoptosis (6). These

observations suggest that tumor-related gene products, such as *bcl-2* and *Raf-1* (7), seem to be the secondary molecular targets of the microtubule-active compounds.

We have recently synthesized a group of small MW<sup>3</sup>-compounds highly active in the inhibition of microtubules assembly (10). The biological activity of these compounds can be regulated by changing moieties on the structure. Of more than 73 modifications, 3-IAABU (Fig. 1) exhibited the strongest inhibitory activity in microtubule assembly (10). In this communication, information of 3-IAABU in microtubule assembly inhibition, binding site on tubulin dimer, effect on mitotic spindle and cell cycle, and phosphorylation of *bcl-2*, as well as the induction of apoptosis, are displayed. These molecular mechanisms render 3-IAABU a promising anticancer potential for future development.

## MATERIALS AND METHODS

**Reagents.** 3-IAABU was synthesized in our laboratory (patent pending). The details of the synthesis and confirmation of the compound were reported elsewhere (10). The compound was dissolved in a mixture of N,N-dimethyl acetamide, propylene glycol, and Tween 80 (v/v/v, 1:2:1) and was further diluted in medium before use. Paclitaxel, vinblastine sulfate, colchicine, and mebendazole (Aldrich Chemical Co., Milwaukee, WI) were dissolved in DMSO.

**Cells.** Cell lines used are listed in Table 1. Tumor lines are all from human tumors. All cell lines, except SP biphenotypic leukemic cells (11, 12) and DND-1A melanoma (provided by Dr. T. Ohnuma, Mount Sinai School of Medicine), were obtained from the American Tissue Culture Collection (Manassas, VA). HL60, U937, NB40, Daudi, PC3, KB, and DND-1A cells were cultivated in RPMI 1640 supplemented with 10% FBS, penicillin (250 units/ml), and streptomycin (250 units/ml); CEM was a suspension in Iscove's Modified Dulbecco's Medium with 10% heat-inactivated FBS and antibiotics. MOT, HeLa, and BT-483 cells were cultured in DMEM with 10% heat-inactivated FBS. SP cells were in Minimum Eagle's Medium plus 10% FBS. Normal human lymphocytes were isolated from the blood of healthy individuals using Ficoll-Hypaque gradients and cultured in RPMI 1640 plus 10% FBS.

**Cytotoxicity Determination.** Cells were distributed into 96-well plates (Falcon, Oxnard, CA) with  $10^5$  cells/well, followed by treatment with 3-IAABU or candidate compounds at concentrations between 0–10  $\mu$ M at 37°C for 48 h. Cell viability was determined by trypan blue staining. For the monolayer cultures, cells were seeded at  $5 \times 10^4$  cells/well in the presence or absence of drugs and incubated at 37°C for 48 h. The supernatants were removed gently, and the cells were digested with EDTA-Trypsin.  $ID_{50}$  and  $ID_{90}$  were drug concentrations killing 50 or 90% of cells in comparison with untreated controls and calculated by regression analysis.

**Microtubule Polymerization and Depolymerization Assay.** The CytoDYNAMIX Microtubule Polymerization Screens 1 and 2 (CDS01 and CDS02) from Cytoskeleton, Inc. (Denver, CO) were used to determine the

Received 8/18/98; accepted 10/5/98.

The costs of publication of this article were defrayed in part by the payment of page charges. This article must therefore be hereby marked advertisement in accordance with 18 U.S.C. Section 1734 solely to indicate this fact.

<sup>1</sup> Supported by the T. J. Martell Foundation for Leukemia, Cancer, and AIDS Research and NIH Small Business Innovative Research Grant GM-53696-03.

<sup>2</sup> To whom requests for reprints should be addressed, at Department of Medicine, Division of Neoplastic Diseases, Box 1131, Mount Sinai School of Medicine, New York, NY 10029. Phone: (212) 241-7549; Fax: (212) 996-9801.

<sup>3</sup> The abbreviations used are: MW, molecular weight; 3-IAABU, 3-(iodoacetamido)-benzoylurea; FBS, fetal bovine serum; MAP, microtubule-associated protein; AMM, 2-amino-6-mercapto-7-methylpurine; AMMR, AMM riboside; MOT, myocardial cell; CEM, leukemic cell; GDP, guanosine 5'-diphosphate; GTP, guanosine 5'-triphosphate; RT, room temperature; PGP, P-glycoprotein.

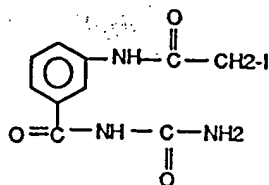


Fig. 1. Structure of 3-IAABU.

potency of 3-IAABU to inhibit microtubule polymerization with MAP-rich tubulin and purified tubulin, respectively. Lyophilized protein was resuspended (120  $\mu$ g/well) in the wells of a 96-well plate with 125  $\mu$ l of G-PEM [80 mM PIPES buffer (pH 6.9), 1.0 mM MgCl<sub>2</sub>, 0.5 mM EGTA and 1.0 mM GTP] containing the test compound. The absorbance was read (Spectromax 250; Molecular Devices, Inc., Sunnyvale, CA) at 340 nm once/min for 60 min. Temperature was set at 24°C for CDS01 and 37°C for CDS02. OD is proportional to the concentration of polymerized tubulin. The MAP-rich system (CDS01) is approximately 10 times more sensitive than the purified tubulin system (CDS02) for polymerization inhibitors because the latter system contains four times the concentration of tubulin and 5% (v/v) glycerol, which promote polymerization. For disassembly assays, the methods have been reported (13). The solvents didn't affect polymerization or depolymerization at concentrations <1% (v/v), as used in the experiments.

**Tubulin Ligand Binding Assays.** Competitive binding assays were performed on the colchicine, vinblastine, and GTP/GDP binding sites. The colchicine site reporter was fluorescein-colchicine, and the vinblastine site was probed with BODIPY-vinblastine; all fluorescent conjugates were purchased from Molecular Probes Inc. (Eugene, OR). The GTP/GDP site was probed using the endogenous bound nucleotide. Greater than 99% purified bovine brain tubulin (Cytoskeleton, Inc., Denver, CO) was diluted to 1.1 mg/ml in PEM buffer and placed on ice. Binding reactions were composed of 100  $\mu$ g tubulin, 2.0–20  $\mu$ M fluorescent conjugate, 5.0–60  $\mu$ M 3-IAABU, 0.1 mM GTP plus 1% (v/v) DMSO, and 1% 3-IAABU solvent (see "Reagents") in 100  $\mu$ l of PEM buffer. The two most common tubulin ligand binding techniques, DEAE filter binding method (14) and the size exclusion chromatography method (15), were compared using the nonradioactive conjugates. The gel filtration method (15) allowed greater sensitivity because greater amounts of tubulin could be used in each condition. Reactions were incubated for 1 h at 37°C and passed over a 2.0-ml G-25-size exclusion column equilibrated in PEM. Column elution took <2 min, hence, reducing ligand dissociation to a minimum. Ten fractions were collected from each column and analyzed for fluorochrome and protein molarity. Fluorochrome molarity was determined by absorbance at 455 and 504 nm for fluorescein-colchicine (MW, 747) and BODIPY-vinblastine (MW, 1043), respectively. Protein concentration was determined with the Bio-Rad protein assay kit (Bio-Rad, Hercules, CA). The stoichiometry of fluorochrome binding was determined by dividing the fluorochrome molarity by the tubulin protein molarity based on MW of  $M_r$  110,000. The fluorescent conjugates were determined to bind to the correct site by competition with the appropriate parent ligand. Vinblastine at 5  $\mu$ M was shown to increase fluorescein-colchicine binding to tubulin as observed previously for colchicine binding (16, 17). This phenomena was used to stabilize and enhance the signal obtained from fluorescein-colchicine binding.

**Tubulin GTPase Assays.** Tubulin GTPase assays were developed previously (18) using the phosphate detection assay (19). For the endogenous subunit tubulin GTPase activity the reaction contained 100  $\mu$ g/ml of greater than 99% purified tubulin in PEM buffer containing 5–40  $\mu$ M 3-IAABU, 100  $\mu$ M GTP, 300  $\mu$ M AMMR and 1 unit/ml purine nucleoside phosphorylase. In this system, phosphate, generated from tubulin-induced hydrolysis of GTP to GDP, reacts with AMMR by purine nucleoside phosphorylase catalysis, AMMR phosphate breaks down to form ribose-1-phosphate and AMM. The absorbance maximum for AMMR is 330 nm and that for AMM is 360 nm; therefore, phosphate can be related to the absorbance increase at 360 nm. A similar system was used to measure microtubule-associated GTPase activity with the following exceptions: (a) the tubulin concentration was raised to 1 mg/ml; (b) the concentration of

test compound was set to the  $ID_{50}$  for tubulin polymerization; and (c) the reaction was initiated with 1.6 nM of microtubules (assuming the MW of tubulin  $M_r$  110,000 and 1650 dimers/ $\mu$ m; Ref. 20).

**Morphology.** Cell samples on slides were prepared using a Cytospin centrifuge (Shandon Southern Products Ltd., Sewickley, PA) and stained with Giemsa (Harleco, Gibbstown, NJ) as described before (13). Mitosis was identified by the appearance of chromosomes and disappearance of nuclear membranes. Apoptosis was recognized by the criteria described previously (21, 22).

**Immunofluorescent Detection of Mitotic Spindles.** The method was reported previously (13). In brief, cells on slides were air dried and fixed with methanol at –20°C for 20 min, followed by incubation with PBS containing 1% BSA at 37°C for 30 min. After washing, samples on the slides were incubated with 30  $\mu$ l (4  $\mu$ g/ml) antihuman  $\beta$ -tubulin monoclonal antibody (Accurate Antibody, Westbury, NY) in a humid chamber at RT for 60 min. After three times washing, 10  $\mu$ l of FITC-labeled goat antimouse antibody (Coulter Electronics, Hialeah, FL) was applied on the samples and cultured in a humid chamber at RT for 1 h. The stained cells were visualized under a fluorescence microscope (Zeiss, Jena, Germany).

**Cell Cycle.** DNA content was measured using a Cycle TEST kit (Becton Dickinson, San Jose, CA). Light-scattering and DNA luminescence of individual cells were examined with a FACScan flow cytometer using Cellfit software for gating analysis (Becton Dickinson).

**Detection of *bcl-2* Phosphorylation.** Cells were treated with different concentrations of drugs for the time range between 6 and 72 h. Aliquots of cells were taken and lysed with lysis buffer containing 50 mM Tris-HCl (pH 7.4), 0.1% Triton X100, 1% SDS, 250 mM NaCl, 15 mM MgCl<sub>2</sub>, 1 mM DTT, 2 mM EDTA, 2 mM EGTA, 25 mM NaF, 1 mM PMSF, 10  $\mu$ g/ml leupeptin, and 10  $\mu$ g/ml aprotinin. The protein concentration was determined by a DC protein assay kit (Bio-Rad). Equal amounts of lysate were subjected to electrophoresis in a 0.1% SDS, 10% polyacrylamide gel. The blots were transferred onto nitrocellulose membrane. After blocking with 5% nonfat milk in TBST buffer at RT for 1 h, *bcl-2* protein was probed with anti-*bcl-2* mAb (PharMingen, San Diego, CA) as described (23).

**DNA Fragmentation.** DNA samples were extracted by a previously reported method (24). Briefly, cells were incubated in 1 ml of lysis buffer [0.01 M Tris-HCl (pH 8.0), 0.01 M NaCl, 0.01 M EDTA (pH 8.0), and 5% SDS] containing 1  $\mu$ g/ml protease K for 1 h at 50°C. DNA was extracted with phenol and chloroform:isoamylalcohol (v/v, 24:1), and precipitated with ethanol. The dry pellet of samples was resuspended in 10 mM Tris-HCl/1 mM EDTA solution. The DNA (4  $\mu$ g/lane), after treatment with RNase (Sigma Chemical Co., St. Louis, MO) at a final concentration of 0.1  $\mu$ g/ $\mu$ l at 37°C for 20 min, were analyzed in 1.5% agarose gel having 1% ethidium bromide.

## RESULTS

**Cancericidal Activity and Selectivity.** The potential of 3-IAABU as an anticancer compound was examined in 11 human tumor cell lines (Table 1).  $ID_{90}$  of 3-IAABU were in the range of 0.06–0.92  $\mu$ M for solid tumor lines and 0.015–0.29  $\mu$ M for leukemia or lymphoma

Table 1 Cancericidal activity of 3-IAABU

Tissue type	Cells	$ID_{50}$ ( $\mu$ M)	$ID_{90}$ ( $\mu$ M)
Human cancer			
MDS <sup>a</sup>	SP	0.014 $\pm$ 0.003	0.29 $\pm$ 0.05
Acute T-cell leukemia	CEM	0.004 $\pm$ 0.001	0.015 $\pm$ 0.002
Lymphoma	Daudi	0.017 $\pm$ 0.004	0.058 $\pm$ 0.07
Histiocytic lymphoma	U937	0.010 $\pm$ 0.001	0.046 $\pm$ 0.05
Promyelocytic leukemia (M3)	NB4	0.014 $\pm$ 0.004	0.066 $\pm$ 0.009
Promyelocytic leukemia	HL60	0.012 $\pm$ 0.003	0.072 $\pm$ 0.012
Breast cancer	BT-483	0.011 $\pm$ 0.001	0.3 $\pm$ 0.04
Melanoma	DND-1A	0.007 $\pm$ 0.001	0.06 $\pm$ 0.009
Cervical carcinoma	Hela	0.04 $\pm$ 0.003	0.09 $\pm$ 0.017
Prostate cancer	PC3	0.130 $\pm$ 0.02	0.92 $\pm$ 0.07
Nasopharyngeal carcinoma	KB	0.25 $\pm$ 0.06	0.79 $\pm$ 0.12
Nonmalignant cells			
Myocardial fibroblast (rat)	MOT	0.8 $\pm$ 0.1	2.16 $\pm$ 0.21
Normal lymphocyte (human)	Lymphocytes	1.1 $\pm$ 0.12	2.5 $\pm$ 0.34

<sup>a</sup> Myelodysplasia syndrome.

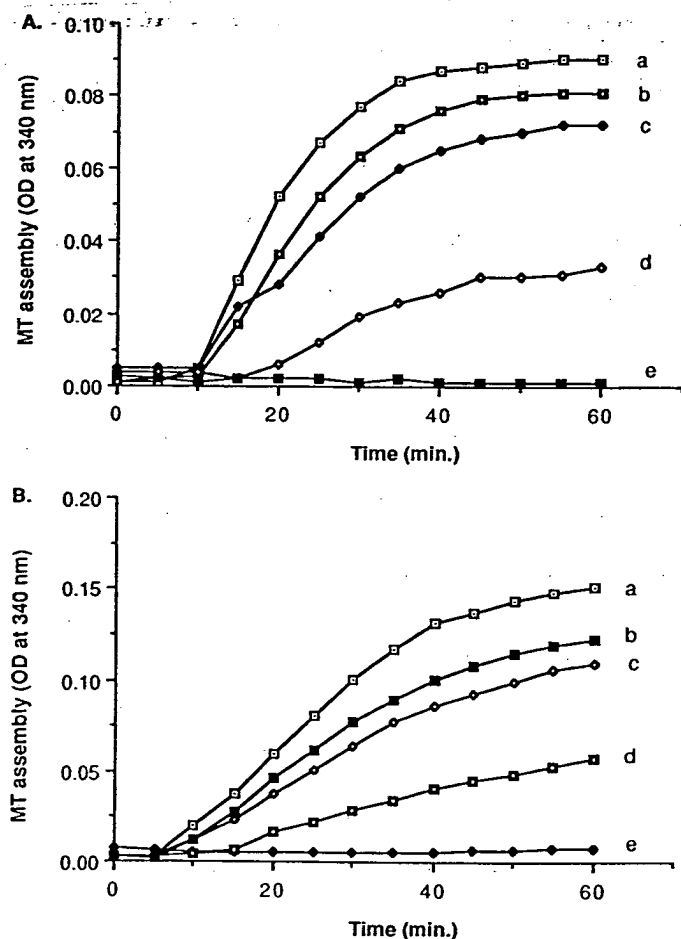


Fig. 2. Effect of 3-IAABU on microtubule polymerization. A, curves a-e represent the MAP-rich tubulin incubated with 3-IAABU (24°C) at concentrations of 0 (control), 0.015, 0.05, 0.15, and 0.5  $\mu\text{M}$ , respectively; B, curves a-e are the purified tubulin treated with 3-IAABU (37°C) at 0 (control), 0.15, 0.5, 1.5, and 5.0  $\mu\text{M}$  respectively. The level of the polymerization was measured by absorbance at 340 nm, and the SD ( $\pm$ ) values for each time points were within 0.001–0.0045 range. MT, microtubule.

cell lines. In contrast,  $\text{ID}_{90}$  of 3-IAABU in nonmalignant proliferating MOTs was 2.2  $\mu\text{M}$ , 150 times of that in CEMs. Comparison of 3-IAABU with vinblastine or paclitaxel in MOTs (doubling time of which was 18–22 h in culture) and CEMs showed that the ratio of  $\text{ID}_{90}$  (MOT)/ $\text{ID}_{90}$  (CEM) of 3-IAABU (*i.e.*, 150) was higher than that of paclitaxel (*i.e.*, 118) and vinblastine (*i.e.*, 73).

**Microtubule Polymerization Inhibition.** The ability of 3-IAABU to inhibit tubulin polymerization *in vitro* was assessed using two systems, MAP-rich tubulin and the purified tubulin. In the MAP-rich system, tubulin polymerization was inhibited with an  $\text{ID}_{50}$  of 0.1  $\mu\text{M}$  (Fig. 2A), whereas the purified tubulin system was inhibited with an  $\text{ID}_{50}$  of 1.2  $\mu\text{M}$  (Fig. 2B). The microtubule disassembly was not interfered with 3-IAABU even at the concentration as high as 50  $\mu\text{M}$ .

**GTPase Activity of Tubulin Subunit and Microtubules.** To know whether the inhibition of polymerization by 3-IAABU was due to an activation of GTPase, the enzyme activity was measured. The activities of tubulin subunit GTPase and microtubule GTPase were not interfered by paclitaxel, but, on the other extreme, completely inhibited by vinblastine (Fig. 3, A and B). In the presence of 3-IAABU, tubulin subunit GTPase activity was reduced by 60% over the control value (0.055 GTPase/subunit/min), which was greater than the inhibition by mebendazole and colchicine (34 and 30% respectively; Fig. 3A). The microtubule GTPase was reduced by 40% over the control, a value that was similar to that of mebendazole and colchicine reactions (Fig. 3B).

**Determination of Binding Site of 3-IAABU on Tubulin.** BODIPY-vinblastine and Fluorescein-colchicine conjugates were tested for their ability to bind to the vinblastine and colchicine sites, respectively. BODIPY-vinblastine at 5  $\mu\text{M}$  was inhibited 65% by 100  $\mu\text{M}$  vinblastine (Fig. 4A). BODIPY-vinblastine binding to tubulin was not affected by 3-IAABU (Fig. 4A). Fluorescein-colchicine binding at 5  $\mu\text{M}$  was inhibited 75% by 100  $\mu\text{M}$  colchicine and about 50% by 100  $\mu\text{M}$  3-IAABU (Fig. 4B). GTP levels in tubulin subunit were determined with and without the presence of 40  $\mu\text{M}$  3-IAABU (Fig. 4C). There was no difference in the amount of GTP/GDP bound to tubulin after size exclusion chromatography. Therefore, 3-IAABU does not interfere with GTP/GDP binding.

**Mitotic Arrest.** Microscopic examination showed that the treatment of CEMs with 3-IAABU (0.015  $\mu\text{M}$ ) for 24 h induced about 90% of the cells to arrest in metaphase (Fig. 5B) with chromosomes

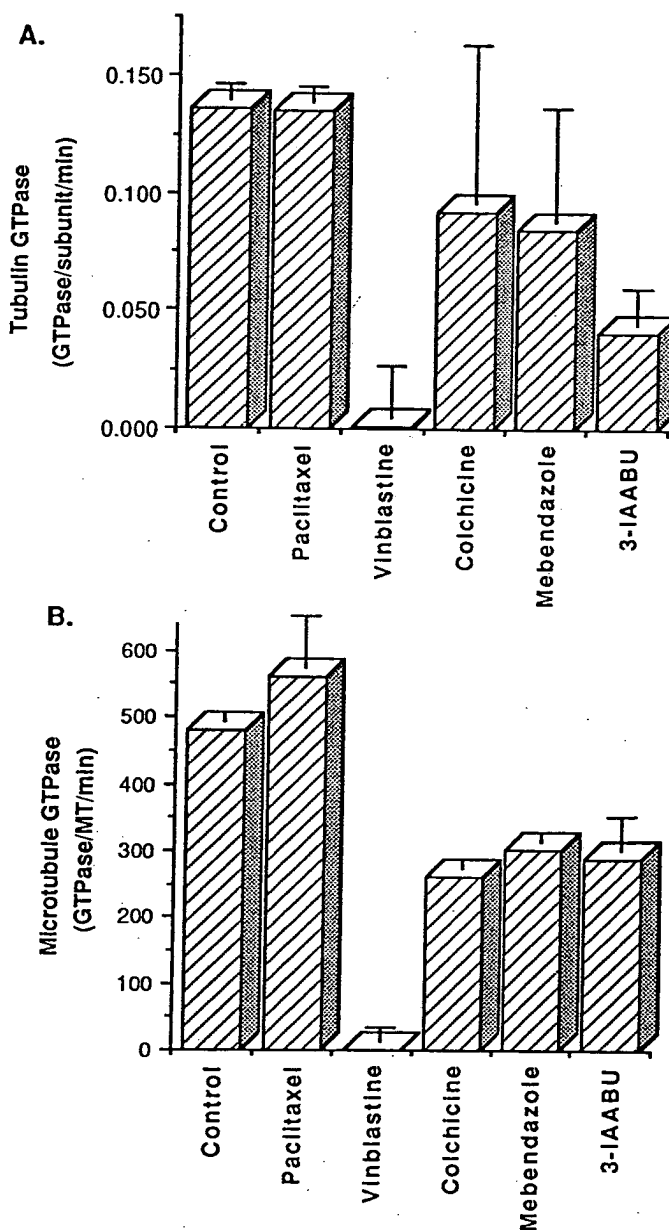
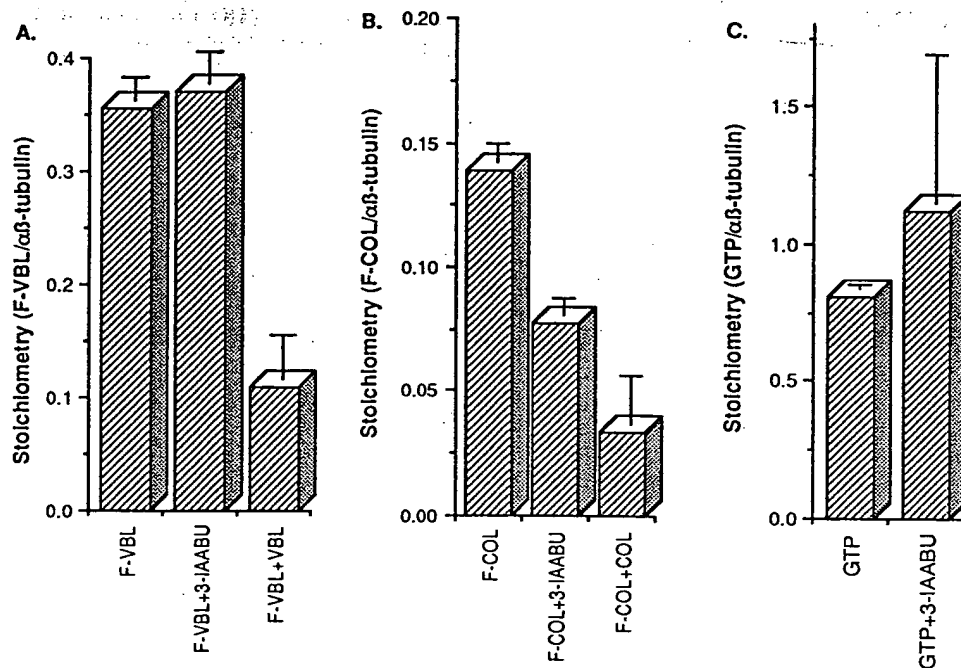


Fig. 3. Effect of 3-IAABU on GTPase. The activity of tubulin GTPase (A) and microtubule GTPase (B) were measured at 360 nm, as described in "Materials and Methods." The concentrations of paclitaxel, vinblastine, colchicine, mebendazole, and 3-IAABU for tubulin GTPase and microtubule experiments were all 20  $\mu\text{M}$  and 5  $\mu\text{M}$ , respectively. MT, microtubule.



Fig. 4. Binding site of 3-IAABU on tubulin. A, competitive binding of 3-IAABU (40  $\mu$ M) with F-VBL (5  $\mu$ M) as compared with VBL (100  $\mu$ M). B, competitive binding of 3-IAABU (100  $\mu$ M) with F-COL (5  $\mu$ M) as compared with COL (100  $\mu$ M). C, competitive binding of 3-IAABU (40  $\mu$ M) with GTP (5  $\mu$ M). VBL, vinblastine; F-VBL, fluorescein-VBL; COL, colchicine; F-COL, fluorescein-COL.



dispersed in the cytoplasm. Immunofluorescent staining showed punctuated  $\beta$ -tubulin aggregates scattered in the cytoplasm (Fig. 5B, insert). Normal microtubule spindle of mitotic cells (Fig. 5A, insert) or microtubular network of interphase cells were not seen in 3-IAABU treated cells.

To have a quantitative view of mitotic arrest, 3-IAABU treated CEMs were analyzed for the cell cycle using flow cytometry. As shown in Fig. 6,  $G_2$ -M peak increased at 4 h, and most cells accumulated at  $G_2$ -M 8 h after 3-IAABU (0.015  $\mu$ M) treatment, paralleled with which was the significant reduction of the  $G_0$ - $G_1$  peak. The shift from  $G_0$ - $G_1$  to  $G_2$ -M became even more striking at 16 h, when 61% of the cells were blocked in  $G_2$ -M phase and only 17% were left in  $G_0$ - $G_1$  phase, forming an inverted distribution in respect to the untreated control (Fig. 6).

**bcl-2 Phosphorylation.** The change of *bcl-2* in response to 3-IAABU was examined. CEMs treated with 3-IAABU at 0.03  $\mu$ M or above clearly showed *bcl-2* phosphorylation characterized as the slower-migrating bands in Fig. 7A (9). The earliest phosphorylation was observed 12 h after treatment (Fig. 7B). Vinblastine- and paclitaxel-treated CEMs were used as positive controls in the experiments. HL60, HeLa, and KB cells treated with 3-IAABU exhibited similar results (data not shown).

**Apoptosis.** The consequences of inactivation of *bcl-2* is, in many cases, apoptotic cell death in *bcl-2*-positive tumor cells (6, 7). Preliminary microscopic examination found chromatin condensation and nuclear fragmentation in 3-IAABU-treated cells, indicating an apoptotic process. To confirm the morphological finding, DNA was extracted from treated CEMs. Gel analyses (Fig. 8) exhibited classical internucleosomal DNA fragmentation after 16 h of treatment. The intensity of the multiple-unit DNA ladder increased with time, and the strongest signal was detected after 24 and 48 h exposure to 3-IAABU. Similar results were obtained in other tumor cells such as U937, KB, and PC-3.

## DISCUSSION

3-IAABU was selected from a group of novel synthetic compounds with small MWs and targeting at tubulin-microtubule equi-

librium in tumor cells (10). Antimicrotubule activity of 3-IAABU were tested in tubulin systems, either with or without MAP. Microtubule assembly was significantly inhibited by 3-IAABU in both systems, whereas microtubule disassembly was not altered. There was a difference in sensitivity between the two polymerization systems, which is most likely due to the difference in concentration of tubulin and glycerol in the two systems. This has been shown to be the case for a number of tubulin ligands (25, 26). For example, nocodazole has an  $ID_{50}$  of 0.1  $\mu$ M in the MAP-rich system and an  $ID_{50}$  of 1.5  $\mu$ M in the purified tubulin system. The inhibition of assembly in MAP-containing tubulin reveals that the target of 3-IAABU is contained in this system; inhibition of assembly in purified tubulin further clearly tells us that 3-IAABU directly targets at tubulin protein. In the presence of 3-IAABU, polymerization is inhibited in a similar manner to nocodazole, in that nucleation, polymerization rate and maximum absorbance are reduced. This indicates that the mechanism of inhibition is similar to that of nocodazole (27), which interacts with tubulin at a similar site to that of colchicine (27).

Microtubule-active compounds could be classified into categories based on their binding domains. *Vinca* alkaloids, rhizoxin, dolastatins, and spongistatin obligate to "vinblastine" domain; colchicine, nocodazole, podophyllotoxin, steganacin, and curacin A bind to "colchicine" domain (26, 27); and paclitaxel interacts with the 31 amino acids at NH<sub>2</sub>-terminal of tubulin (28). It is interesting to see whether 3-IAABU can fit in those domains related to microtubule assembly.

Experiments concerning the binding site of 3-IAABU strongly favor the colchicine site, not the vinblastine site and the GTP site. Nocodazole and mebendazole also bind at this site, and their activity on tubulin polymerization is similar to that of 3-IAABU (data not shown). Although nocodazole binds to two sites on subunit tubulin (29), we do not know whether this is the case for 3-IAABU. It has been reported that colchicine binds at a stoichiometry of 0.3:1.0 to 1.8:1.0/tubulin subunit (14) and probably is 2.0:1.0 (30). One site is thought to be a higher affinity site on  $\beta$ -tubulin, and the other a lower affinity site on  $\alpha$ -tubulin (31).

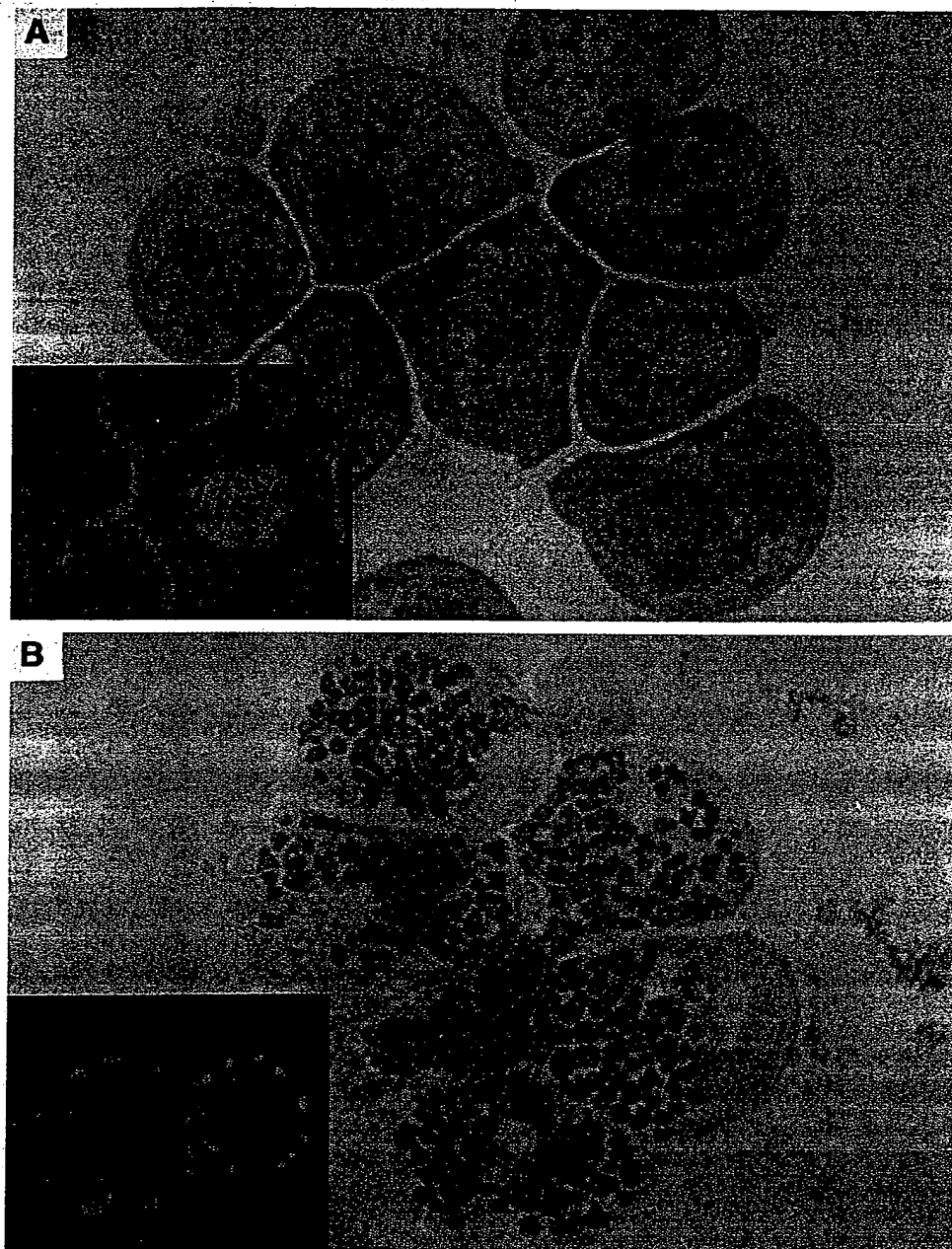


Fig. 5. Morphological observation of CEMs arrested at mitosis by 3-IAABU. A, untreated CEMs (Giemsa;  $\times 400$ ) with normal mitotic spindle in dividing cells (*inset*); B, CEMs blocked at mitosis by 3-IAABU ( $0.014 \mu\text{M}$  Giemsa;  $\times 400$ ) and punctuated aggregates of  $\beta$ -tubulin in cytoplasm (*inset*).

Because of the concentration of fluorescein on colchicine is less than the  $K_{\text{aff}}$  for the lower affinity site, we would expect that 3-IAABU interacts at the high affinity site only, or both sites. Another aspect of binding site inhibition is competitive or non-competitive inhibition, further studies will determine which type of inhibition relates 3-IAABU to colchicine. The effect of 3-IAABU on tubulin subunit and microtubule GTPase activity was similar to that of colchicine and mebendazole, a reduction of activity.

*bcl-2* is an integral membrane protein that functions as an apoptosis suppressor (32, 33) through formation of heterodimer with bax, an apoptosis enhancer (34). The overexpression of *bcl-2* is considered to be responsible, in part, for the survival advantage of tumor cells (35–37) and for the mechanisms of drug-resistance in cancer chemotherapy (38, 39). Antisense oligonucleotides to *bcl-2* mRNA inhibit CEM growth (40), indicating its potential of being a molecular target for antitumor drugs. Recent reports showed that almost all microtubule-active drugs (*Vinca* alkaloids, paclitaxel, podophyllotoxin, colchicine, epothilones, and nocodo-

zole) induce phosphorylation of *bcl-2* protein resulting in inactivation of *bcl-2*, whereas DNA-damaging drugs, antimetabolites, and alkylating agents do not (6–9, 41). The posttranslational modification (phosphorylation) made *bcl-2* incapable of forming heterodimers with bax (6) and drive the *bcl-2*-positive cells toward apoptosis (42). In this study, 3-IAABU inhibited microtubule assembly by binding to the colchicine site on tubulin and caused mitotic arrest via interference of the formation of normal spindle in  $M_1$  phase cells. This was followed by phosphorylation of *bcl-2* and subsequently by the onset of apoptosis. The results strongly support the model that *bcl-2* phosphorylation following disruption of microtubular architecture serves as a signaling cascade mediating apoptosis for antimicrotubule agents. Results obtained with microscopy, flow cytometry, *bcl-2* protein analysis, and DNA electrophoresis were consistent with respect to the timing of these events. A significant increase of  $G_0$ -M phase was first observed 4 h after treatment. The earliest visible *bcl-2* phosphorylation was observed between 6 and 12 h, and the detectable fragmented DNA

appeared at 16 h. The 180–200-bp ladder of DNA represents the length of each oligonucleosome, indicating the break of double-stranded DNA at the linker region between nucleosomes and the involvement of endonucleases in this process (43).

The onset of apoptosis induced by 3-IAABU was observed in a variety of tumor cells, although there is a variation of sensitivity among the cell lines. The results regarding drug selectivity show significant difference in cytotoxicity of 3-IAABU between malignant and nonmalignant cells.  $ID_{50}$  of 3-IAABU in the proliferative nonmalignant cells was about 150 times higher than those for leukemia or lymphoma cells, showing a selective cytotoxicity of 3-IAABU higher than that of paclitaxel and vinblastine. The different susceptibilities of tumor and nontumor cells to microtubule-active agents could be possibly due to: (a) inactivation (phosphorylation) of Raf-1/bcl-2 after disruption of microtubule, as we discussed above; (b) abrogated function of G1 microtubule-dependent checkpoint in transformed cells (44); (c) deficiency of p53 and pRb tumor suppressor genes (45); and (d) structural differences of microtubule or MAP in normal and tumor cells (46, 47). Importantly, in the drug-resistance studies, we found that 3-IAABU seems not to be a PGP substrate because the susceptibility to 3-IAABU between Daudi/PGP(–) and Daudi/PGP(+) cells as well as between KB/PGP(–) and KB/PGP(+) cells were virtually same. Also, the attempts to induce resistance in solid

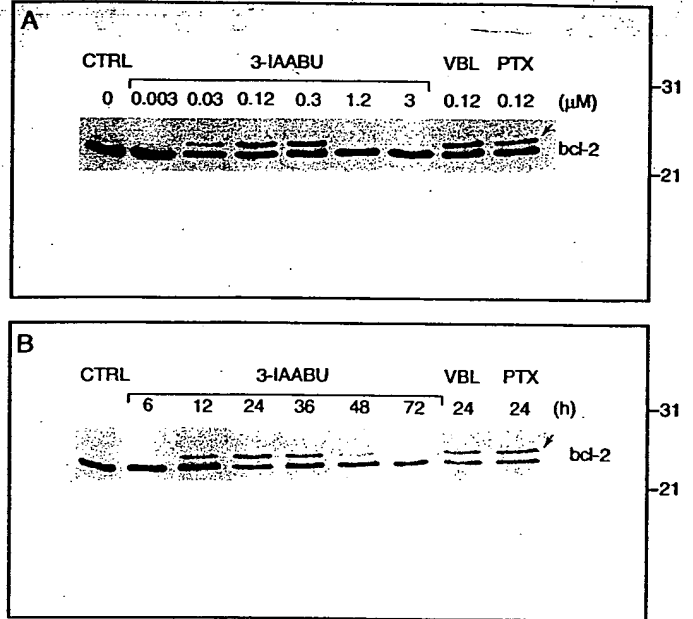


Fig. 7. 3-IAABU induced phosphorylation of *bcl-2* in CEMs. A, CEMs were treated with 3-IAABU for 24 h at concentrations of 0, 0.003, 0.03, 0.12, 0.3, 1.2, and 3  $\mu$ M respectively; B, CEMs were incubated in the absence (CTRL) or presence of 3-IAABU (0.12  $\mu$ M) for 6, 12, 24, 36, 48, and 72 h. Vinblastine and Paclitaxel (0.12  $\mu$ M, 24 h for both) were used as controls. Phosphorylated *bcl-2* is shown by an arrow.

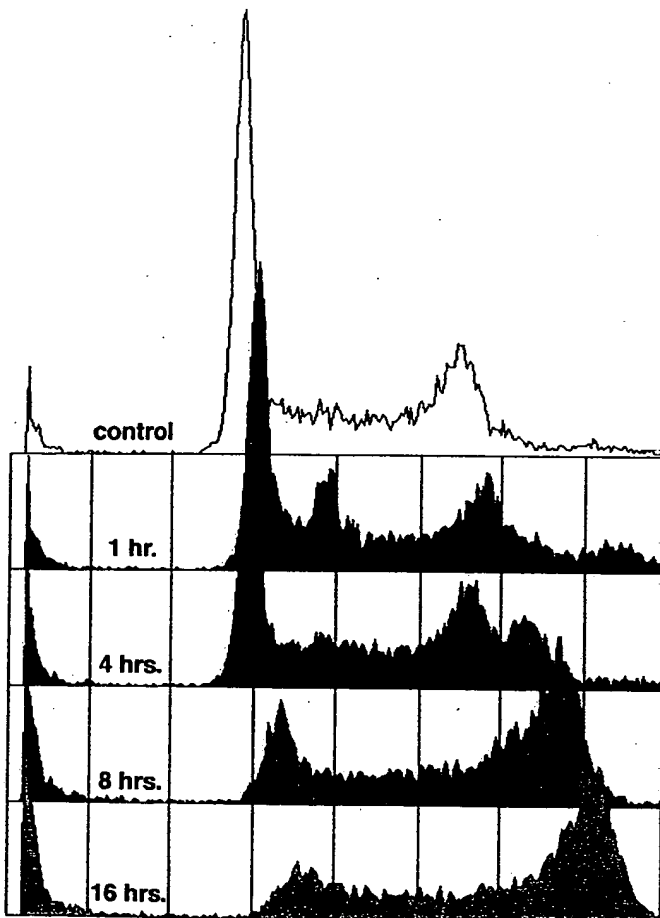


Fig. 6. Blocking cell cycle at  $G_2$ -M phase in CEMs treated with 3-IAABU. Using flow cytometry cell cycle analysis was done in CEMs incubated without (control) or with 3-IAABU (0.014  $\mu$ M) for 1, 4, 8, or 16 h. The majority of the cells were suspended at  $G_2$ -M phase at 8 h.

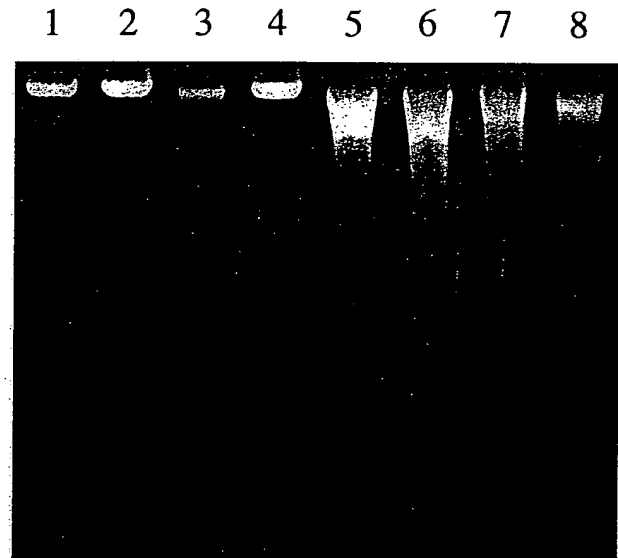


Fig. 8. Apoptosis in CEMs treated with 3-IAABU. CEMs were treated with 3-IAABU (0.014  $\mu$ M) for 1, 4, 8, 16, 24, and 48 h (Lanes 2–7). Apoptotic DNA ladder was evidenced at and after 16 h. Lanes 1 and 8 are the untreated CEM control and molecular marker, respectively.

tumor cells failed after 7 months of culture with low-dose 3-IAABU.<sup>4</sup>

Collectively, 3-IAABU is a newly synthesized antimicrotubule agent with a much smaller MW than those isolated from natural sources. The primary action of the compound is to bind at or near to the colchicine site of tubulin. As a consequence, it inhibits microtubule assembly, blocks cell cycle at mitosis and causes phosphorylation of *bcl-2* in target cells. The end of the process is apoptosis, which is

<sup>4</sup> Unpublished observations.

selectively sensitive in tumor cells. We suggest 3-IAABU as a new tubulin ligand attractive to anticancer chemotherapy.

## REFERENCES

- Wilson, L., and Jordan, M. A. Microtubule dynamics: taking aim at a moving target. *Chem. Biol. (Lond.)*, 2: 569-573, 1995.
- Hyams, J. S., and Lloyd, C. W. Microtubules. New York: Wiley-Liss, Inc., 1994.
- Rowinsky, E. K., and Donehower, R. C. The clinical pharmacology and use of antimicrotubule agents in cancer chemotherapeutics. *Pharmacol. Ther.*, 52: 35-84, 1991.
- Tishler, R. B., Lamppu, D. M., Park, S., and Price, B. D. Microtubule-active drugs Taxol, vinblastine, and nocodazole increase the levels of transcriptionally active p53. *Cancer Res.*, 55: 6021-6025, 1995.
- Jordan, M. A., and Wilson, L. Microtubules and actin filaments: dynamic targets for cancer chemotherapy. *Curr. Opin. Cell Biol.*, 10: 123-130, 1998.
- Halder, S., Chintapalli, J., and Croce, C. M. Taxol-induced bcl-2 phosphorylation and death of prostate cancer cells. *Cancer Res.*, 56: 1253-1255, 1996.
- Blagosklonny, M. V., Giannakakou, P., el-Deiry, W. S., Kingston, D. G., Higgs, P. I., Neckers, L., and Fojo, T. Raf-1/bcl-2 phosphorylation: a step from microtubule damage to cell death. *Cancer Res.*, 57: 130-135, 1997.
- Halder, S., Basu, A., and Croce, C. M. Bcl-2 is the guardian of microtubule integrity. *Cancer Res.*, 57: 229-233, 1997.
- Halder, S., Jena, N., and Croce, C. M. Inactivation of bcl-2 by phosphorylation. *Proc. Natl. Acad. Sci. USA*, 92: 4507-4511, 1995.
- Jiang, J. D., Roboz, J., Weisz, I., Deng, L., Ma, J. H., Holland, J. F., and Bekesi, G. J. Synthesis, anticancer and antimicrotubule activities of 3-(haloacetamido)-benzoylureas. *Anticancer Drug Des.*, in press, 1998.
- Banerjee, R., Bekesi, J. G., Tarcsafalvi, A., Sperber, K., Deak, G., Choi, H. S. H., Paronetto, F., Holland, J. F., and Acs, G. Productive non-lytic HIV-1 replication in a newly established human leukemic cell line. *Proc. Natl. Acad. Sci. USA*, 89: 9996-10000, 1992.
- Bekesi, G. J., Banerjee, R., Jiang, J. D., Roboz, J. P., Tarcsafalvi, A., Holland, J. F., and Acs, G. Translocation of cytoplasmic antigen markers in a biphenotypic cell line derived from a patient with myelodysplastic syndrome. *Mol. Cell. Differ.*, 3: 111-123, 1995.
- Jiang, J. D., Wang, Y., Roboz, J., Strauchen, J., Holland, J. F., and Bekesi, J. G. Inhibition of microtubule assembly in tumor cells by 3-bromoacetamido benzoylurea, a new anticancer compound. *Cancer Res.*, 58: 2126-2133, 1998.
- Hains, F. O., Dickerson, R. M., Wilson, L., and Owellen, R. J. Differences in the binding properties of vinca alkaloids and colchicine to tubulin by varying protein sources and methodology. *Biochem. Pharmacol.*, 27: 71-76, 1978.
- Wilson, L., Creswell, C. R., and Chin, D. The mechanism of action of vinblastine. Binding of [acetyl-<sup>3</sup>H] vinblastine to embryonic chick brain tubulin and tubulin from sea urchin sperm tail outer doublet microtubules. *Biochemistry*, 14: 5586-5592, 1975.
- Wilson, L., Bamburg, J. R., Mizel, S. B., Grisham, L., and Creswell, K. M. Interaction of drugs with microtubule proteins. *Fed. Proc.*, 33: 158-166, 1974.
- Kralovic, R. C., and Voeltz, H. Vinblastine enhanced colchicine binding to tubulin in mouse fibroblasts. *Exp. Cell Res.*, 106: 205-210, 1977.
- Melki, R., Fievez, S., and Carlier, M. F. Continuous monitoring of  $\pi$  release following nucleotide hydrolysis in action or tubulin assembly using 2-amino-6-mercapto-7-methylpurine ribonucleoside and purine nucleoside phosphorylase as an enzyme link assay. *Biochemistry* 35: 12038-12045, 1996.
- Webb, M. R. A continuous spectrophotometric assay for inorganic phosphate and measuring phosphate release kinetics in biological systems. *Proc. Natl. Acad. Sci. USA*, 87: 4884-4887, 1992.
- Amos, L. A., and Klug, A. Arrangement of subunits in flagellar microtubules. *J. Cell Sci.*, 14: 523-527, 1974.
- Wyllie, A. H., Kerr, J. F. R., and Currie, A. R. Cell death: the significance of apoptosis. *Int. Rev. Cytol.*, 68: 251-306, 1980.
- Kerr, J. F. R., Winterford, C. M., and Harmon, B. V. Apoptosis. Its significance in cancer and cancer therapy. *Cancer (Phila.)*, 73: 2013-2026, 1994.
- Blagosklonny, M. V., Schulte, T. W., Nguyen, P., Mimnaugh, E. G., Trepel, J., and Neckers, L. Taxol induction of p21<sup>WAF1</sup> and p53 requires c-raf-1. *Cancer Res.*, 55: 4623-4626, 1995.
- Roboz, J., Jiang, J. D., Holland, J. F., and Bekesi, J. G. Selective tumor apoptosis by MF13, L-prolyl-L-m-[bis(chloroethyl)amino]-phenylalanyl-L-norvaline ethyl ester, a new sarcosyls containing tripeptide. *Cancer Res.*, 57: 4795-4802, 1997.
- Bai, R., Paull, K. D., Herald, C. L., Malspeis, L., Pettit, G. R., and Hamel, E. Halichondrin B and homohalichondrin B, marine natural products binding in the vinca domain of tubulin. *J. Biol. Chem.*, 266: 15882-15889, 1991.
- Smith, C. D., and Zhang, X. Q. Mechanism of action of cryptophycin. *J. Biol. Chem.*, 271: 6192-6198, 1996.
- Hoebeke, J., Van Nijen, G., and Brabander, D. Interaction of nocodazole (R17934), a new anti-tumoral drug, with rat brain tubulin. *Biochem. Biophys. Res. Commun.*, 69: 319-324, 1976.
- Rao, S., Krauss, N. E., Heerding, J. M., Swindell, C. S., Ringel, I., Orr, G. A., and Horwitz, S. B. 3'-(p-azidobenzamido) taxol photolabels the N-terminal 31 amino acids of  $\beta$ -tubulin. *J. Biol. Chem.*, 269: 3132-3134, 1994.
- Head, J., Lee, L. Y., Fielf, D. J., and Lee, J. C. Equilibrium and rapid kinetic studies on nocodazole-tubulin interaction. *J. Biol. Chem.*, 260: 11060-11066, 1985.
- Floyd, L. J., Bames, L. D., and Williams, R. F. Photoaffinity labeling with (2-nitro-4-azidophenyl) deacetylcolchicine: direct evidence for two colchicine binding sites. *Biochemistry*, 28: 8515-8525, 1989.
- Wolff, J., Knipling, L., and Palumbo, G. Direct photoaffinity labeling of tubulin with colchicine. *Proc. Natl. Acad. Sci. USA*, 88: 2820-2824, 1991.
- Hengartner, M. O., and Horvitz, H. R. *C. elegans* cell survival gene ced-9 encodes a functional homolog of the mammalian proto-oncogene bcl-2. *Cell*, 76: 665-676, 1994.
- Chen-Levy, Z., Nourse, J., and Cleary, M. L. The bcl-2 candidate proto-oncogene is a 24-kilodalton integral-membrane protein highly expressed in lymphoid cell lines and lymphomas carrying the t(14;18) translocation. *Mol. Cell. Biol.*, 9: 701-710, 1989.
- Miyashita, T., and Reed, J. C. Tumor suppressor p53 is a direct transcriptional activator of the human bax gene. *Cell*, 80: 293-299, 1995.
- Henderson, S., Rowe, M., Gregory, C., Croom-Carter, D., Wang, F., Longnecker, R., Kieff, E., and Rickinson, A. Induction of bcl-2 expression by Epstein-Barr virus latent membrane protein 1 protects infected B cells from programmed cell death. *Cell*, 65: 1107-1115, 1991.
- Reed, J. C. Regulation of apoptosis by bcl-2 family proteins and its role in cancer and chemoresistance. *Curr. Opin. Oncol.*, 7: 541-546, 1995.
- Korsmeyer, S. J. Regulators of cell death. *Trends Genet.*, 11: 101-105, 1995.
- Miyashita, T., and Reed, J. C. Bcl-2 oncoprotein blocks chemotherapy-induced apoptosis in a human leukemia cell line. *Blood*, 81: 151-157, 1993.
- Fisher, T. C., Milner, A. E., Gregory, C. D., Jackman, A. L., Aherne, G. W., Hartley, J. A., Dive, C., and Hickman, J. A. Bcl-2 modification of apoptosis induced by anticancer drugs: resistance to thymidylate stress is independent of classical resistance pathways. *Cancer Res.*, 53: 3321-3326, 1993.
- Reed, J. C., Stein, C. Y., Subasinghe, C., Halder, S., Croce, C., Yum, S., and Cohen, J. Antisense mediated inhibition of bcl-2 protooncogene expression and leukemic cell growth and survival: comparison of phosphodiester and phosphorothioate oligodeoxynucleotides. *Cancer Res.*, 50: 6529-6579, 1990.
- Halder, S., Basu, A., and Croce, C. M. Serine-70 is one of the critical sites for drug-induced bcl-2 phosphorylation in cancer cells. *Cancer Res.*, 58: 1609-1615, 1998.
- Yang, E., Zha, J., Jockel, J., Boise, L. H., Thompson, C. B., and Korsmeyer, S. J. Bad, a heterodimeric partner for Bcl-X<sub>L</sub> and Bcl-2, displaces bax and promotes cell death. *Cell*, 80: 285-291, 1995.
- Khodarev, N. N., and Ashwell, J. D. An inducible lymphocyte nuclear Ca<sup>2+</sup>/Mg<sup>2+</sup>-dependent endonuclease associated with apoptosis. *J. Immunol.*, 156: 922-931, 1996.
- Trielli, M., Andreasson, P. R., Lacroix, F. B., and Margolis, R. L. Differential taxol-dependent arrest of transformed and nontransformed cells in the G<sub>1</sub> phase of the cell cycle, and specific-related mortality of transformed cells. *J. Biol. Chem.* 135: 689-700, 1996.
- Di Leonardo, A., Khan, S., Linke, S., Greco, V., Seidita, G., and Wahl, G. DNA rereplication in the presence of mitotic spindle inhibitors in human and mouse fibroblasts lacking either p53 or pRb function. *Cancer Res.*, 57: 1013-1019, 1997.
- Fromes, Y., Gounon, P., Veitia, R., Bissery, M. C., and Fellous, A. Influence of microtubule-associated proteins on the differential effects of Paclitaxel and Docetaxel. *J. Protein Chem.*, 15: 377-388, 1996.
- Garcia, P., Braguer, D., Carles, G., El Khyari, S., Barra, Y., de Ines, C., Barasoain, I., and Briand, C. Comparative effects of taxol and Taxotere on two different human carcinoma cell lines. *Cancer Chemother. Pharmacol.*, 34: 335-343, 1994.

## Preclinical paper

# Effects of methylacetylenic putrescine, an ornithine decarboxylase inhibitor and potential novel anticancer agent, on human and mouse cancer cell lines

István Pályi, Tibor Kremmer, Adrienn Kálnay, Gizella Turi, Rudolf Mihalik,<sup>1</sup>  
Katalin Bencsik and Mariann Boldizsár

Research Center of Oncology, National Institute of Oncology, 1525 Budapest, Hungary. <sup>1</sup>Institute of Hematology and Blood Transfusion, 1502 Budapest, Hungary.

Sensitivity of several human and mouse cancer cell lines to methylacetylenic putrescine (MAP) was evaluated using clonogenic, sulforhodamine B and cell counting assays. The effects of MAP on cell morphology, cell cycle phase distribution and changes in polyamine metabolism of xenografted MCF-7 and MDA-MB-231 human mammary tumor cells were also investigated. On the basis of IC<sub>50</sub> values, BHT-101 human thyroid carcinoma cells were the most sensitive (9 µg/ml), followed by P388 mouse lymphoma (32 µg/ml), MCF-7 (48 µg/ml) and MDA-MB-231 (110 µg/ml) human breast carcinoma cell lines. MAP treatment led to accumulation of P388 cells in G<sub>1</sub> phase. At higher doses, the cytoplasm of the cells became vacuolated followed by apoptosis. The foamy cytoplasm may suggest a rare type of cell death (Clarke III type) called non-apoptotic programmed cell death. MAP treatment resulted in a total inhibition of ornithine decarboxylase (ODC) activity with a concomitant decrease of intracellular polyamine (mostly putrescine and spermidine) content in the breast cancer cells, whilst the spermine concentration was shown to increase. MAP proved at least 10 times more potent than the formerly studied DL-α-difluoromethylornithine making it an attractive candidate for clinical testing. [© 1999 Lippincott Williams & Wilkins.]

**Key words:** Cell cycle, *in vitro* sensitivity, methylacetylenic putrescine, non-apoptotic cell death, ODC activity, polyamine metabolism.

## Introduction

Natural poly(oligo)amines are highly basic, with rather

simple structures which exhibit definite biological activity. Cumulative data indicate the ubiquitous role of putrescine (Pu), spermidine (Spd), spermine (Spn) and agmatine (Agm) in the regulation and/or modulation of the most basic biosynthetic and reproductive functions (e.g. proliferation, differentiation, etc.) in all living cells under physiological and pathological conditions.<sup>1-5</sup> According to their particular importance in the malignant processes high intracellular Pu and Spd levels have been measured in various experimental and human tumors depending on the rate of cell proliferation.<sup>2,6-13</sup> Due to the high biosynthetic activity of malignant tissues elevated serum concentrations and urinary excretion of polyamines have been reported in cancer patients and regarded as a useful biochemical tumor marker.<sup>7,8,11,14</sup>

Depletion of cellular polyamines using various ornithine and Pu analogs, potential inhibitors of ornithine decarboxylase (ODC, EC 4.1.1.17), the first key enzyme of the polyamine biosynthetic pathway, has opened new perspectives in enzyme-regulated anticancer chemotherapy.<sup>4,9,15-21</sup> Among several active derivatives DL-α-difluoromethylornithine (DFMO, Eflornithine<sup>TM</sup>) has been shown to inhibit cell proliferation and tumor growth *in vitro* and *in vivo*,<sup>13,22-30</sup> and has also been introduced into clinical therapy of human cancers.<sup>17,20,21,31,32</sup> Recently, a promising Pu analog, (2R,5R)-6-heptyne-2,5-diamine (methylacetylenic putrescine, MAP), has been synthesized and reported to be 10-50 times more active than DFMO.<sup>28,33-38</sup> Both DFMO and MAP altered cell cycle phase distributions by accumulating cells in G<sub>1</sub> phase.<sup>21,26,28</sup> However, both cytostatic and cytotoxic effects were demonstrated depending on the cell line studied.<sup>39</sup> Polyamine analogs were considered to

Correspondence to I Pályi, Research Center of Oncology, National Institute of Oncology, Ráth György str 7-9, 1525 Budapest, Hungary.

Tel: (+36) 1 224-8786; Fax: (+36) 1 224-8786 or (+36) 1 224-8620;

E-mail: palyi@oncol.hu

induce apoptotic cell death, as shown first using a new Spn derivative.<sup>40</sup>

In the present study the effects of MAP on the clonogenicity of P388 mouse lymphoma and of some human cancer cell lines, as well as on the cell cycle distribution and the intracellular polyamine levels of P388 cells were evaluated *in vitro*. Morphological alterations observed in human tumor cell lines, suggesting a special type of programmed cell death, are also described.

## Materials and methods

### Cell cultures

P388 mouse lymphoma was obtained from I Wodinsky (Arthur D Little, Cambridge, MA) and was established in suspension culture.<sup>41</sup> MCF-7 estrogen receptor (ER)-positive and MDA-MB-231 ER-negative human breast cancer and PC3 prostatic cancer cell lines were obtained from the ATCC (Rockville, MD). BHT-101 human thyroid anaplastic cell line was established in our laboratory.<sup>42</sup>

### Drug solutions

MAP was generously supplied by Merrell Research Institute (Strasbourg, France). Fresh MAP solution was made by dissolving the compound in saline or in medium before the experiments.

### Clonogenic assay

Cloning efficiency of monolayer cultures was performed as previously described.<sup>42</sup> Briefly, known numbers of exponentially growing cells were plated into triplicate 35 mm Petri dishes (Nunc, Roskilde, Denmark). On the following day the cultures were exposed to different doses of MAP and the MAP was left in contact with the cells throughout the study, and the cultures were incubated in a CO<sub>2</sub> incubator (Heraeus, Hanau, Germany) at 37°C for 10–12 days. The cultures were then rinsed with saline and stained with crystal violet. Colonies containing at least 50 cells were counted. Cloning efficiency of cells growing in suspension was determined as published.<sup>41</sup> The cell suspension, containing the appropriately diluted MAP, was solidified with 0.25% final concentration of agar (Difco, Detroit, MD). Three-dimensional colonies were counted after 10–12 days of incubation under a dissecting microscope.

Absolute cloning efficiency of untreated control cultures was normalized as 100%. Survival of treated cultures was expressed as a fraction of the survival of the control cultures. IC<sub>50</sub> is the inhibitory drug concentration needed to decrease the survival by 50%.

### Antiproliferation studies

The effect of MAP on cell proliferation has been determined by comparing the changes in cell numbers of control and MAP-treated cell populations. MDA-MB-231 or MCF-7 ( $2-3 \times 10^5$ ) cells were seeded into 50 mm Petri dishes and on the following day were exposed to 100–500 µg/ml MAP. The cells were trypsinized on day 2 and the cell numbers were determined using a Neubauer-type hemocytometer.

### Flow cytometry

Samples were prepared according to Shapiro.<sup>43</sup> Briefly,  $5 \times 10^5$  cells were fixed in 70% ethanol and stored at –20°C for a few days. The samples were then centrifuged and washed in phosphate-buffered saline (PBS) solution. After repeated centrifugation, cell pellets were diluted with 1 ml PBS containing 20 µg propidium iodide (PI) (Sigma, St Louis, MO) and 100 µg RNase (Sigma), and were incubated on room temperature for 30 min before measurements. Cell cycle phase distributions were analyzed by measurements of relative DNA content of individual cells using a Cytoron Absolute flow cytometer (Ortho, Raritan, NJ). The quality of the setup was checked by lysed, propidium iodide-stained normal human lymphocytes. The data were analyzed on Cell Cycle software (Ortho).

### Cell morphology

MDA-MB-231, BHT-101 and PC3 cells were seeded into Petri dishes, and the morphology of the MAP-treated and control cultures was examined and compared using an Olympus inverted phase contrast microscope. In some cases, fixed and hematoxylin & eosin-stained preparations were also prepared.

### Determination of cellular polyamines and ODC activity

Simultaneous determinations of ODC, EC 4.1.1.14 activity and base polyamine levels in cell homogenates were performed by the method of Kvannes and

Flatmark,<sup>44</sup> as modified previously.<sup>45</sup> Polyamines (Pu, Spd and Spn) were extracted from the enzyme reaction and blank (base line level) samples with ice-cold perchloric acid and measured as dansyl derivatives by reversed-phase high-performance liquid chromatography (RP-HPLC). ODC activity was calculated from the amount of putrescine formed in the enzymatic reaction and given in nmol Pu/h/10<sup>6</sup> cells.

## Results

### Dose survival studies (clonogenic assay)

The effect of MAP on the clonogenicity of P388 mouse lymphoma and BHT-101 human thyroid cancer cells is shown in Figure 1. The first region of the dose-response curves is steep followed by a nearly horizontal 'plateau' portion. Above 75  $\mu\text{g/ml}$ , both curves decline. The IC<sub>50</sub> values of the P388 and BHT-101 cells were 32 and 9  $\mu\text{g/ml}$ , respectively. The dose-response curves of the two breast cancer lines (Figure 2) are rather different in shape from those of Figure 1. IC<sub>50</sub> values of MCF-7 and MDA-MB-231 cells were 48 and about 110  $\mu\text{g/ml}$ , respectively. Of the four cell lines studied, the BHT-101 cells were the most sensitive and the MDA-MB-231 cells the least sensitive to MAP. IC<sub>50</sub> values are summarized on Table 1.

### Effect of MAP on cell proliferation

The effect of MAP on the proliferation of ER-positive

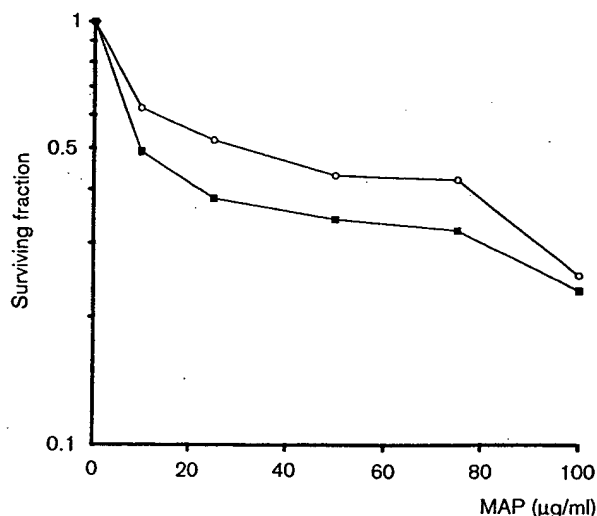


**Figure 1.** Dose-response curves of P388 mouse lymphoma (○) and BHT-101 human thyroid carcinoma (■) cells treated with MAP continuously.

### In vitro effects of methylacetylenic putrescine

MCF-7 and ER-negative MDA-MB-231 human breast cancer cell lines was determined by cell counting. No significant retardation of cell proliferation was achieved below 100  $\mu\text{g/ml}$  MAP. The results summarized in Table 2 show a dose-dependent rate of growth retardation, with MCF-7 cells proving more sensitive than MDA-MB-231 cells.

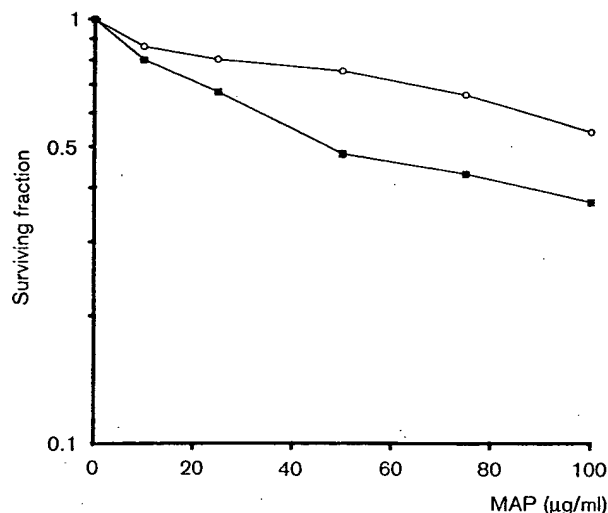


**Figure 2.** Dose-response curves of MDA-MB-231 (○) and MCF-7 (■) human mammary carcinoma cells treated with MAP continuously.

**Table 1.** IC<sub>50</sub> values (mean  $\pm$  SEM) obtained by treatment with MAP of tumor cell lines in clonogenic assays

Cell line	IC <sub>50</sub> value ( $\mu\text{g/ml}$ )
P388	32 $\pm$ 3
BHT-101	9 $\pm$ 1
MCF-7	48 $\pm$ 4
MDA-MB-231	~110 $\pm$ 10

**Table 2.** Effect of MAP on proliferation of MCF-7 and MDA-MB-231 cells

Doses ( $\mu\text{g/ml}$ )	Rate of inhibition (%)	
	MCF-7	MDA-MB-231
100	36 $\pm$ 5 <sup>a</sup>	21 $\pm$ 3
200	42 $\pm$ 6	22 $\pm$ 3
500	66 $\pm$ 8	53 $\pm$ 6

<sup>a</sup>Mean values  $\pm$  SEM at 48 h after treatment.

## Effect of MAP on the cell cycle

Concentrations between 10 and 50  $\mu\text{g/ml}$  caused only minimal changes in cell cycle distribution, while those of 75 or 100  $\mu\text{g/ml}$  MAP altered the ratio of cell cycle phases considerably, both at 24 and 48 h following MAP addition (Figure 3 and Table 3). The percent of  $G_1$  phase cells increased from 34 to 47 and 55% at the expense of  $G_2/M$  cells. The ratio of S phase cells showed an increase at 24 h and a decrease at 48 h, parallel with the higher concentrations.

## Effect of MAP treatment on cell morphology

No characteristic cytomorphological changes were observed below 250  $\mu\text{g/ml}$  MAP. The most typical alteration was vacuolization of the cytoplasm ('foamy cytoplasm') which began to appear in some cells at 250  $\mu\text{g/ml}$  and the vacuoles were small. All cells became heavily vacuolated exposed to 500  $\mu\text{g/ml}$  and the vacuoles were of different sizes. Confluency of the cells ceased and they showed a tendency to

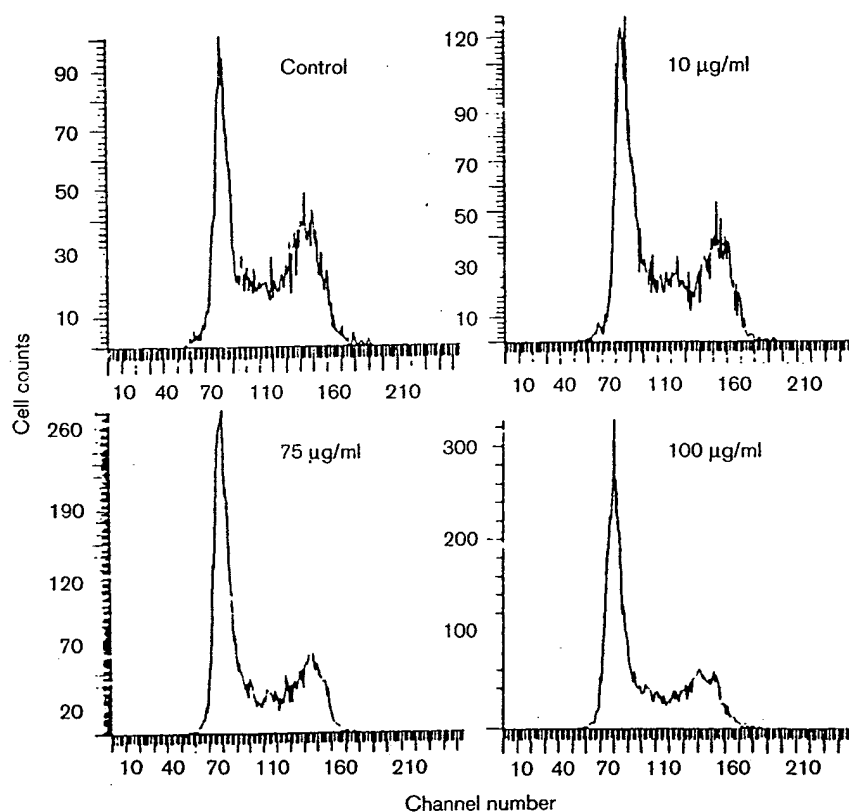


**Figure 3.** Changes in the cell cycle phase distribution of P388 cells 48 h after exposure to 10, 75 and 100  $\mu\text{g/ml}$  of MAP. The major peak in channel 80 corresponds to  $G_1$  cells.

**Table 3.** Effect of MAP on the cell cycle phase distribution of P388 mouse lymphoma cells

Doses ( $\mu\text{g/ml}$ )	Phase distribution (%)					
	24 h			48 h		
	$G_1$	S	$G_2$	$G_1$	S	$G_2$
Control	34	33	23	34	38	28
10	38	43	19	36	39	25
25	32	45	23	43	34	23
50	34	43	23	42	35	23
75	47	36	17	55	27	18
100	41	41	18	55	27	18



round up. A fraction of the cells showed signs of apoptosis, e.g. bleb formation and pyknosis (Figure 4a-c). Long and thin cytoplasmic processes were characteristic by 72 h. At even higher concentrations of MAP (1000  $\mu\text{g/ml}$ ), all cells rounded up, began to disintegrate and formed coalesced groups (Figure 4d-f).

Effect of MAP treatment on the ODC activity and polyamine content of MCF-7 and MDA-MB-231 human breast carcinoma cells

Changes in ODC activity and in polyamine content of MCF-7 and MDA-MB-231 human breast cancer cell lines

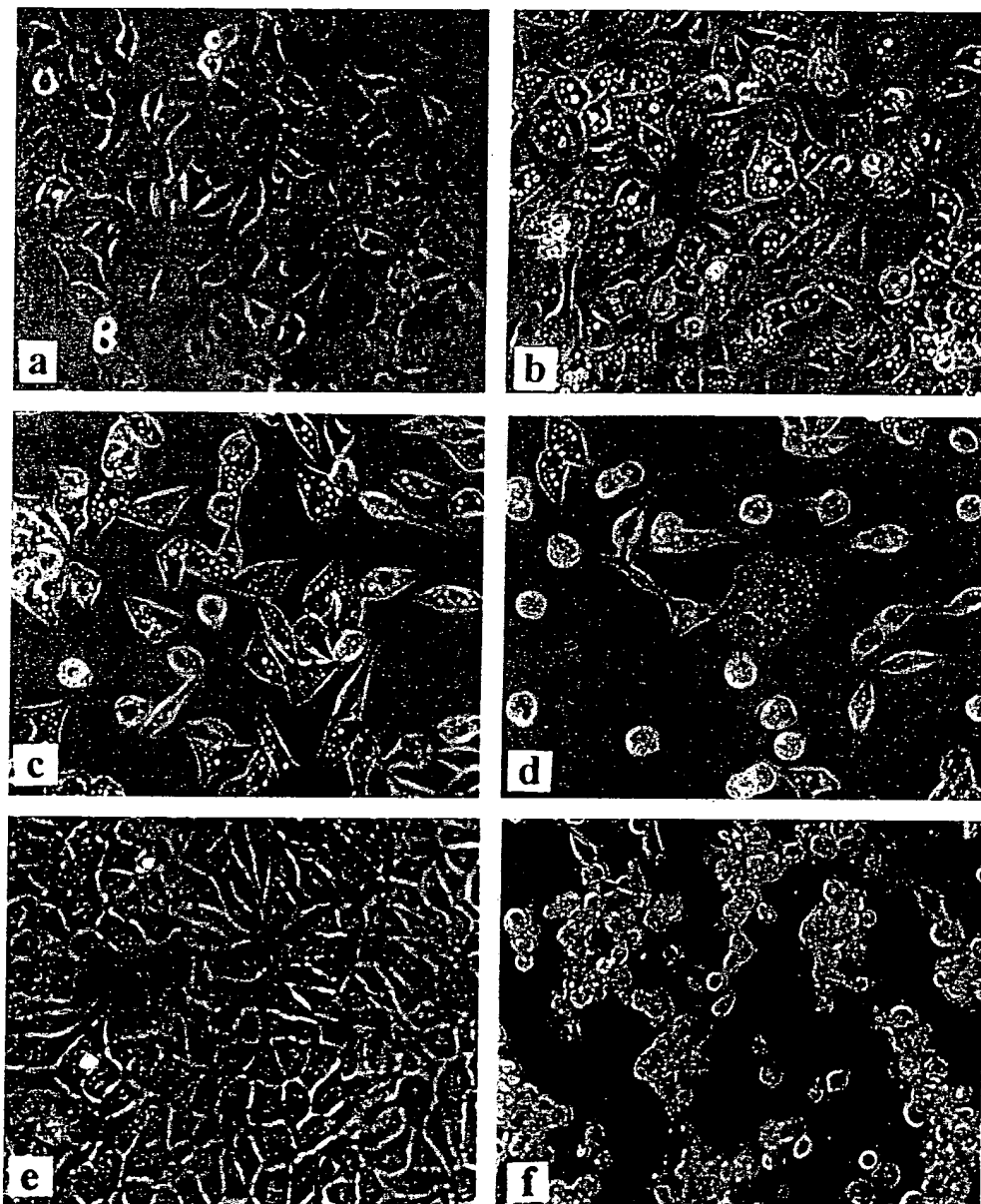


**Figure 4.** Effect of MAP on cell morphology. (a) Untreated MDA-MB-231 cells with regular morphology and mitotic figures. (b) Cells treated with 500  $\mu\text{g/ml}$  MAP for 24 h. Note the heavily vacuolated cytoplasm and the loose arrangement of the cells. (c) PC3 cells treated with 500  $\mu\text{g/ml}$  MAP for 24 h. The cytoplasm of the cells is filled with vacuoles. Some cells are rounded up, others have long filaments. (d) PC3 cells treated with 1000  $\mu\text{g/ml}$  MAP for 24 h. Most cells rounded up, others have long processes and one giant cell is full of vacuoles. (e) Untreated BHT-101 cells with regular morphology. (f) Cells treated with 1000  $\mu\text{g/ml}$  MAP for 24 h. All cells rounded up producing clusters. Some single cells show apoptosis with bleb formation and freely floating apoptotic bodies are seen. Phase contrast picture of living cells. Magnification:  $\times 160$ .

induced by a 24 h exposure to 250  $\mu\text{g/ml}$  MAP are summarized in Figure 5. MAP treatment resulted in practically total inhibition of ODC activity in both cell lines. Simultaneously, a decrease in total intracellular polyamine content (mostly in terms of Pu and Spd levels) and a relative increase in Spn concentration was observed. We have found significant differences between the total polyamine base levels of these two cell lines, indicating a higher biosynthetic activity in MDA-MB-231 cells and a higher sensitivity to MAP treatment, first of all, in relation to the changes in Spd content. Retention of Spn induced by MAP in MCF-7

cells also showed a marked contrast to that noted in the MDA-MB-231 line. Similar changes were observed depending on either the MAP concentration (50–500  $\mu\text{g/ml}$ ) applied or the time of *in vitro* exposure (24, 48 or 72 h).

## Discussion

Our results presented here demonstrate that all cell lines tested were sensitive to MAP. Their sensitivity was, however, dependent on the ER content (MCF-7 versus MDA-MB-231) or on the organ they originated from. The MDA-MB-231 breast cancer cells were the least sensitive, while the BHT-101 thyroid tumor cells were the most sensitive to MAP treatment. This observation supports the significance of the histio-specific toxicity and the disease-oriented anticancer drug discovery screen.<sup>46</sup> In comparison of MAP with the ODC inhibitor DFMO, the former proved to be more potent against malignant human and mouse cell lines. Namely,  $\text{IC}_{50}$  values of DFMO were 60, 625 and 300  $\mu\text{g/ml}$  for MCF-7, MDA-MB-231 and P388 cells, respectively.<sup>29,30</sup> It means that the difference between DFMO and MAP ranged from slight (20%) to big (10 times). According to other observations, MAP was 20–100,<sup>37</sup> 10–30<sup>33</sup> or 50–300 times<sup>36</sup> more potent than DFMO, depending on the choice of end point, assay and cell type. Bakic *et al.*<sup>28</sup> found only a minimal difference using HL-60 cells and a clonogenic assay. The enhanced growth-inhibitory activity could be due to increased cellular uptake of MAP. The difference in sensitivity to MAP among the various cell lines could also be due to the difference in their doubling times.<sup>36</sup> According to the classic viewpoint, sensitivity is dependent on the rate of proliferation ('proliferation-dependent cytotoxicity'),<sup>47</sup> although we have shown that this view may not be universally valid.<sup>41</sup> Indeed, the slower growing BHT-101 thyroid carcinoma cells were more sensitive to MAP than the fast-growing P388 cells. There was a difference in sensitivity between the two breast cancer cell lines as well, both against DFMO<sup>30</sup> and MAP, with the ER-positive MCF-7 cells being more sensitive. According to Davidson *et al.*<sup>48</sup> there was no clear relationship between either the ER status or the proliferation rate and sensitivity to the spermine analog BESpm. MAP induced an accumulation of cells in  $G_1$  and a decrease of cells in  $G_2$  using P388 mouse lymphoma cells. Similar changes in cells cycle phase distribution following DFMO or MAP treatment were described by several authors.<sup>22,26,37,38,49</sup> This effect can be a consequence of polyamine depletion. The shape of the dose-

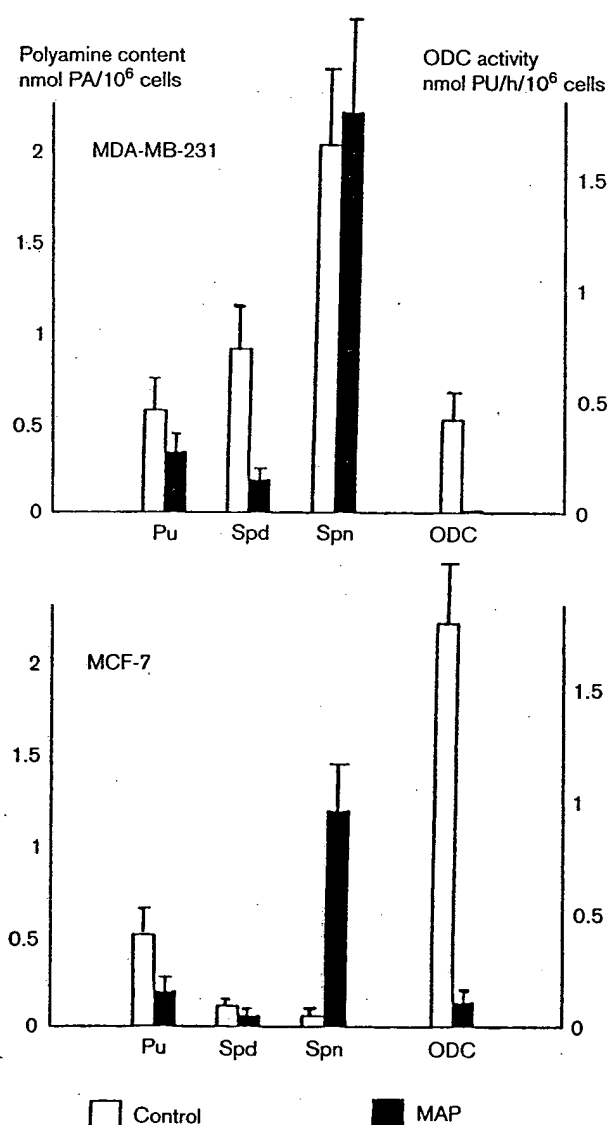


Figure 5. Changes in polyamine content and ODC activity of MCF-7 and MDA-MB-231 breast cancer cells following treatment with 250  $\mu\text{g/ml}$  MAP for 24 h.

response curves, e.g. the plateau portion, also suggested phase-specific effects of the ODC inhibitors.<sup>50</sup> Both compounds exerted cytostatic<sup>39</sup> rather than cytotoxic effects, although the latter were also observed.<sup>24</sup> Whether the effect is cytostatic or cytotoxic is dependent on the cell line employed.<sup>39</sup> In our opinion, it may be concentration dependent as well. At high MAP concentrations, a specific cytomorphological effect appeared in most cell lines, the cytoplasm became heavily vacuolated, 'foamy', followed by cell death. This phenomenon suggests a rare type of programmed cell death as described by Clarke<sup>51</sup> and called non-apoptotic programmed cell death (Clarke III type). Foamy cytoplasm induced by high doses of tyrphostin, a tyrosine kinase inhibitor,<sup>52</sup> has been observed.<sup>53</sup> Programmed cell death induced by a polyamine analog, CPENSp<sub>m</sub>, was first described by McCloskey *et al.*<sup>40</sup> No other data on programmed cell death elicited by either DFMO or MAP have so far been published. The role of ODC in c-Myc-induced apoptosis has been reviewed by Packham and Cleveland.<sup>54</sup> Polyamines are associated with cell death and the precise regulation of ODC activity in cells has been suggested as preventing polyamine associated cytotoxicity.<sup>55,56</sup> ODC inhibitors are potential anticancer drugs. DFMO has been introduced into clinical trials.<sup>17,20,21</sup> In conclusion, superiority for MAP as a new anticancer drug in comparison to DFMO is expressed in its higher biological activity, its histio-specific selectivity and its induction of programmed cell death.

## Acknowledgments

The excellent technical assistance of Vilma Pályi, Judit Szász, Irén Nemes and Edit Szoke is greatly acknowledged.

## References

- Heby O. Role of polyamines in the control of cell proliferation and differentiation. *Differentiation* 1981; 19: 1-20.
- Tabor CW, Tabor H. Polyamines. *Annu Rev Biochem* 1984; 53: 749-90.
- Seiler N. Polyamines. *J Chromatogr* 1986; 379: 157-76.
- Pegg AE. Polyamine metabolism and its importance in neoplastic growth and as a target for chemotherapy. *Cancer Res* 1988; 48: 759-64.
- Seiler N, Delcros JG, Moulinoux JP. Polyamine transport in mammalian cells. An update. *Int J Biochem Cell Biol* 1996; 28: 843-61.
- Scalabrino G, Ferioli ME. Polyamines in mammalian tumors. *Adv Cancer Res* 1981; 35: 151-268.
- Horn Y, Beal SL, Walach N, Lubich WP, Spigel I, Marton LJ. Further evidence for the use of polyamines as biochemical markers for malignant tumors. *Cancer Res* 1982; 42: 3248-51.
- Russell DH. Clinical relevance of polyamines. *CRC Crit Rev Clin Lab Sci* 1983; 18: 261-311.
- Bondy PK, Canellakis ZN. Polyamines and neoplasia: a review of present knowledge of their function and therapeutic potential. In: Davis W, Maltoni C, Tanneberger ST, eds. *The control of tumour growth and its biological bases*. Berlin: Akademie-Verlag 1983: 258-68.
- Kremmer T, Selmeci L, Bardócz S, Holczinger L, Bálint S. Polyamine metabolism in P388 leukemia cells and in ascites tumor bearing mice. *Exp Cell Biol* 1984; 52: 279-85.
- Horn Y, Beal SL, Walach N, Lubich WP, Spigel I, Marton LJ. Relationship of urinary polyamines to tumor activity and tumor volume in patients. *Cancer Res* 1984; 44: 4675-8.
- Seiler N, Knödgen B, Bartholeyns J. Polyamine metabolism and polyamine excretion in normal and tumor bearing rodents. *Anticancer Res* 1985; 5: 371-8.
- Seiler N, Sarhan S, Graufferl C, Jones R, Knödgen B, Moulinoux JP. Endogenous and exogenous polyamines in support of tumor growth. *Cancer Res* 1990; 50: 5077-83.
- Russell DH, Durie BGM. Polyamines as tumor markers. In: Boelsma E, Rümke Ph, eds. *Tumor markers: impact and prospects, applied methods in oncology 2*. Amsterdam: Elsevier-North Holland 1979: 45-60.
- Heby O, Oredsson SM, Kanje M. Polyamine biosynthetic enzymes as targets in cancer chemotherapy. *Adv Enz Reg* 1984; 22: 243-64.
- McCann PP, Pegg AE, Sjoerdsma A, eds. *Inhibition of polyamine metabolism. Biological significance and basis for new therapies*. New York: Academic Press 1987.
- Levin VA, Chamberlain MC, Prados MD, *et al.* Phase I-II study of eflornithine and mitoguazone combined in the treatment of recurrent primary brain tumor. *Cancer Treat Rep* 1987; 75: 459-64.
- Heston WDW. Prostatic polyamines and polyamine targeting as a new approach to therapy of prostatic cancer. *Cancer Surv* 1991; 11: 217-38.
- Quemener V, Blanchard Y, Chamaillard L, Havouis R, Cipolla B, Moulinoux JPh. Polyamine deprivation: a new tool in cancer treatment. *Anticancer Res* 1994; 14: 443-8.
- Meyskeris FL Jr, Emerson SS, Pelot D, *et al.* Dose-de-escalation chemoprevention trial of  $\alpha$ -difluoromethylornithine in patients with colon polyps. *J Natl Cancer Inst* 1994; 86: 1122-30.
- Meyskens F, Gerner E, Pelot D, *et al.* A randomized double-blind placebo-controlled phase IIb trial of difluoromethylornithine (DFMO) for colon cancer prevention. *Proc Am Ass Cancer Res* 1997; 38: 528.
- Seidenfeld J, Gray JW, Laurence JM. Depletion of 9L rat brain tumor cell polyamine content by treatment with DL- $\alpha$ -difluoromethylornithine inhibits proliferation and the G<sub>1</sub> to S transition. *Exp Cell Res* 1981; 131: 209-16.

23. Sunkara PS, Chiang CC, Prakash NJ, Lachmann PJ. Effect of inhibition of polyamine biosynthesis by DL- $\alpha$ -difluoromethylornithine on the growth and melanogenesis of B16 melanoma *in vitro* and *in vivo*. *Cancer Res* 1985; 45: 4067-70.
24. Luk GD, Baylin SB. Anchorage dependency effects of difluoromethylornithine cytotoxicity in human lung carcinoma cells. *Cancer Res* 1986; 46: 1844-8.
25. Luk GD, Abeloff MD, McCann PP, Sjoerdsma A, Baylin SB. Long-term maintenance therapy of established human small cell variant lung carcinoma implants in athymic mice with a cyclic regimen of difluoromethylornithine. *Cancer Res* 1986; 46: 1849-53.
26. Seidenfeld J, Block AL, Komar KA, Naujokas MF. Altered cell cycle phase distributions in cultured human carcinoma cells partially depleted polyamines by treatment with difluoromethylornithine. *Cancer Res* 1986; 46: 47-53.
27. Kremmer T, Boldizsár M, Holczinger L. *In vivo* effect of DL- $\alpha$ -difluoromethylornithine (DFMO) on the polyamine and nucleotide phosphate metabolism in P388/S leukemia cells. *Exp Cell Biol* 1986; 54: 8-15.
28. Bakic M, Chan D, Freireich EJ, Marton LJ, Zwelling LA. Effect of polyamine depletion by  $\alpha$ -difluoromethylornithine or (2R,5R)-6-heptyne-2,5-diamine on drug-induced topoisomerase II-mediated DNA cleavage and cytotoxicity in human and murine leukemia cells. *Cancer Res* 1987; 47: 6437-43.
29. Kremmer T, Pályi I, Holczinger L, et al. Changes in the polyamine and nucleotide metabolism of P388 leukemia cells treated with DL- $\alpha$ -difluoromethylornithine in culture. *Exp Cell Biol* 1988; 56: 131-7.
30. Kremmer T, Pályi I, Daubner D, et al. Comparative studies on the polyamine metabolism and DFMO treatment of MCF-7 and MDA-MB-231 breast cancer cell lines and xenografts. *Anticancer Res* 1991; 11: 1807-14.
31. Lipton A, Harvey HA, Glenn J, et al. A phase I study of hepatic arterial infusion using difluoromethylornithine. *Cancer* 1989; 63: 433-7.
32. Boiko I, Mitchell MF, Hu W, Malpica A, Pandey D, Hittelman WN. High mean DNA content and EGFR expression predict poor response of CIN 3 lesions to chemoprevention by difluoromethylornithine (DFMO). *Proc Am Ass Cancer Res* 1997; 38: 262.
33. Danzin G, Casara P, Claverie N, Metcalf BW, Jung MJ. (2R,5R)-6-heptyne-2,5-diamine, an extremely potent inhibitor of mammalian ornithine decarboxylase. *Biochem Biophys Res Commun* 1983; 116: 237-43.
34. Bartholeyns J, Mamont P, Casara P. Antitumor properties of (2R,5R)-6-heptyne-2,5-diamine, a new potent enzyme-activated irreversible inhibitor of ornithine decarboxylase in rodents. *Cancer Res* 1984; 44: 4972-7.
35. Mamont PS, Siat M, Joder-Ohlenbusch AM, Bernhardt A, Casara P. Effects of (2R,5R)-6-heptyne-2,5-diamine, a potent inhibitor of L-ornithine decarboxylase, on rat hepatoma cells cultured *in vitro*. *Eur J Biochem* 1984; 142: 457-63.
36. Pera PJ, Kramer DL, Sufrin JR, Porter CW. Comparison of the biological effect of four irreversible inhibitors of ornithine decarboxylase in two murine lymphocytic leukemia cell lines. *Cancer Res* 1986; 46: 1148-54.
37. Milam KM, Deen DF, Marton LJ. Cell proliferation and polyamine metabolism in 9L cells treated with (2R,5R)-6-heptyne-2,5-diamine or  $\alpha$ -difluoromethylornithine. *Cell Tissue Kinet* 1989; 22: 269-77.
38. Adlakha RC, Ashorn C, Wagle J, Nishioka K, Freireich EJ. Differential effects of (2R,5R)-6-heptyne-2,5 diamine, a potent inhibitor of polyamines on the cell cycle traverse of normal and transformed cells. *Proc Am Ass Cancer Res* 1989; 30: 586.
39. Sunkara PS, Baylin SB, Luk GD. Inhibitors of polyamine biosynthesis: cellular and *in vivo* effects of tumor proliferation. In: McCann PP, Pegg AE, Sjoerdsma A, eds. *Inhibition of polyamine metabolism*. Orlando: Academic Press 1987: 121-140.
40. McCloskey DE, Casero RA Jr, Woster PM, Davidson NE. Induction of programmed cell death in human breast cancer cells by an unsymmetrically alkylated polyamine analogue. *Cancer Res* 1995; 55: 3233-6.
41. Pályi I. Survival responses to new cytostatic hexitols of P388 mouse and K562 human leukemia cells *in vitro*. *Cancer Treat Rep* 1986; 70: 279-84.
42. Pályi I, Péter I, Daubner D, Vincze B, Lorincz I. Establishment, characterization and drug sensitivity of a new anaplastic thyroid carcinoma cell line (BHT-101). *Virchows Archiv B Cell Pathol Mol Pathol* 1993; 63: 263-9.
43. Shapiro HM. *Practical flow cytometry*. New York: Alan R Liss 1988.
44. Kvannes J., Flatmark T. Rapid and sensitive assay of ornithine decarboxylase activity by high-performance liquid chromatography of the o-phthalaldehyde derivative of putrescine. *J Chromatogr* 1987; 419: 291-5.
45. Kremmer T, Boldizsár M, Paulik E. Application of high-performance liquid chromatographic methods in the monitoring of enzyme-targeted chemotherapy. *Chromatographia* 1988; 26: 423-8.
46. Shoemaker RH, Monks A, Alley MC, et al. Development of human tumor cell line panels for use in disease-oriented drug screening. In: Hall T, ed. *Prediction of response to cancer chemotherapy*. New York: Alan R Liss 1988: 265-85.
47. Van Putten LM. Are cell kinetic data relevant for the design of tumour chemotherapy schedules? *Cell Tissue Kinet* 1974; 7: 493-504.
48. Davidson NE, Mank AR, Prestigiacomo LJ, Bergeron RJ, Casero RA Jr. Growth inhibition of hormone-responsive and -resistant human breast cancer cell in culture by  $N^1$ ,  $N^{12}$ -Bis(ethyl)spermine. *Cancer Res* 1993; 53: 2071-5.
49. Ask A, Persson L, Oredsson SM, Heby O. Synergistic antileukemic effect of two polyamine synthesis inhibitors. Host survival and cell-cycle kinetic analysis. *Int J Cancer* 1986; 37: 465-70.
50. Bruce WR, Meeker BE, Valeriote FA. Comparison of the sensitivity of normal hematopoietic and transplanted lymphoma colony-forming cells to chemotherapeutic agents administered *in vivo*. *J Natl Cancer Inst* 1966; 37: 233-45.
51. Clarke PGH. Developmental cell death: morphological diversity and multiple mechanisms. *Anat Embryol* 1990; 181: 195-213.
52. Levitzki G, Gazit A. Tyrosine kinase inhibition: an approach to drug development. *Science* 1995; 267: 1782-8.

*In vitro effects of methylacetylenic putrescine*

53. Szende B, Kéri Gy, Szegedi Zs, *et al.* Tyrphostin induces non-apoptotic programmed cell death in colon tumor cell. *Cell Biol Int* 1995; 19: 903-11.
54. Packham G, Cleveland JL. C-Myc and apoptosis. *Biochim Biophys Acta* 1995; 1242: 11-28.
55. Coffino P, Poznanski A. Killer polyaminase? *J Cell Biochem* 1991; 45: 54-8.
56. Morris DR. New perspectives on ornithine decarboxylase regulation: Prevention of polyamine toxicity is the overriding theme. *J Cell Biochem* 1991; 46: 102-5.

(Received 23 July 1998; revised form accepted 18 August 1998)

## Mode of Action of a New Indolocarbazole Anticancer Agent, J-107088, Targeting Topoisomerase I

Tomoko Yoshinari, Mitsuru Ohkubo, Kazuhiro Fukasawa,<sup>1</sup> Shin-ichirou Egashira, Yoshikazu Hara, Mami Matsumoto, Kiyoshi Nakai, Hiroharu Arakawa, Hajime Morishima, and Susumu Nishimura

Banyu Tsukuba Research Institute in collaboration with Merck Research Laboratories, Tsukuba 300-2611, Japan

### ABSTRACT

**J-107088** [6-*N*-(1-hydroxymethyl-2-hydroxy)ethylamino-12,13-dihydro-2,10-dihydroxy-13-( $\beta$ -D-glucopyranosyl)-5*H*-indolo[2,3-*a*]-pyrrolo[3,4-*c*]-carbazole-5,7(6*H*)-dione] is a new derivative of NB-506, an indolocarbazole antitumor agent. J-107088 induced single-strand DNA cleavage only in the presence of topoisomerase I (top1) more effectively than NB-506 or camptothecin. The preferable sequences of the DNA cleaved by J-107088 were C/T  $\downarrow$  G as in the case of NB-506. This base-preference of J-107088 in top1-mediated cleavage was different from that of camptothecin, which was T  $\downarrow$  G/A. top1 poisons stabilize the complex between DNA and top1 (cleavable complex). This cleavable complex is released on addition of a high concentration of monovalent cation or removal of top1 poisons. The complex induced by J-107088 was quite stable; it was scarcely released on the addition of NaCl or dilution of J-107088, contrary to the case with camptothecin and NB-506. J-107088-inducing complexes were also stable in cultured cells, when the compound was added to the culture medium. These unique *in vitro* activities of J-107088 on top1 that differed from those of camptothecin and NB-506 may be relevant to its more potent *in vivo* antitumor efficacy in a human tumor xenografted nude mouse model.

### INTRODUCTION

DNA top1<sup>2</sup> is a very important anticancer target. The top1 poisons irinotecan and topotecan have been used for the treatment of several types of human cancers, and 9-aminocamptothecin and 9-nitrocamptothecin are now in Phase II/III tests. In addition to these camptothecin analogues, new indolocarbazole compounds have been reported as top1 poisons. Among them, NB-506 is one of the most potent top1 poisons showing significant antitumor activity *in vitro* and *in vivo* (1, 2). Whereas camptothecin and its analogues selectively enhance DNA cleavage at a T  $\downarrow$  G/A site, NB-506 enhances cleavage at a C/T  $\downarrow$  G site (3). Because NB-506 shows a very wide chemotherapeutic spectrum against both murine tumors and human tumor xenografts in mice (2), Phase I studies were conducted on it at the National Cancer Center Hospital East, Chiba, Japan in 1993-1995.

During the course of clinical trials of NB-506, we continued to synthesize derivatives of NB-506, to obtain more potent compounds. Among several hundred compounds thus far synthesized, J-107088 turned out to be superior to NB-506 for targeting top1. J-107088 contains an alcohol group instead of the formyl group in NB-506 at position N-6 and two hydroxyl substitutions at positions 2 and 10, instead of positions 1 and 11 (Fig. 1). J-107088 showed greater inhibitory activity than NB-506 against top1, unique characteristics of its mode of action on top1 stronger cytotoxicity. Here we report the top1 inhibitory activity of J-107088 and its antitumor activity *in vitro*.

### MATERIALS AND METHODS

**Cells and Enzymes.** PSN-1 and HCT116 cells were gifts from Dr. M. Terada and Dr. N. Shindo-Okada, respectively, of the National Cancer Center Research Institute (Tokyo, Japan). MCF-7 and their multidrug resistant cells MCF-7 AdrR were provided from National Cancer Institute (Bethesda, MD). LX-1 cells were provided by Dr. K. Komiyama of Kitasato Institute (Tokyo, Japan). MKN-45 and PC-13 cells were purchased from Immuno Biological Laboratories (Gunma, Japan). Other cell lines were purchased from the American Type Culture Collection (Rockville, MD). All of the cells were cultured in DMEM or RPMI 1640 supplemented with 10% fetal bovine serum.

Recombinant mouse top1 containing six histidine residues at the NH<sub>2</sub>-terminal was produced in *Spodoptera frugiperda* (Sf9) cells using a baculovirus expression system. Histidine-fused Top1 was purified from the cell extracts on a hydroxyapatite column and a Ni-NTA column (QUIAGEN; Hilden, Germany; Ref. 3). One unit of these enzymes was defined as the activity that completely relaxed 0.4  $\mu$ g of supercoiled pBR322 DNA.

**J-107088 and Other Anticancer Drugs.** J-107088 (Fig. 1), 6-*N*-(1-hydroxymethyl-2-hydroxy)ethylamino-12,13-dihydro-2,10-dihydroxy-13-( $\beta$ -D-glucopyranosyl)-5*H*-indolo[2,3-*a*]-pyrrolo[3,4-*c*]carbazole-5,7(6*H*)-dione and NB-506 were synthesized in our institute by the method reported previously (4). Etoposide, Adriamycin and camptothecin were purchased from Sigma Chemical Co. [Methyl-(<sup>3</sup>H)]thymidine and [ $\alpha$ -<sup>32</sup>P]dCTP were purchased from Amersham-Pharmacia Biotech.

**Topoisomerase-mediated DNA Cleavage and Religation.** The DNA cleavage reaction by top1 was carried out as reported previously (1). Briefly, 50 units of top1 were incubated in reaction mixtures [0.4  $\mu$ g of pBR322 plasmid DNA, 50 mM Tris-HCl (pH 7.9), 120 mM KCl, 0.5 mM DTT, 0.5 mM EDTA, and 30  $\mu$ g/ml BSA in a total volume of 20  $\mu$ l] with top1 poisons at 30°C for 15 min. For measurement of the religation rate of DNA at high salt concentration, NaCl was added at 0.35 M after the cleavage reaction, and the reaction mixture was further incubated at 30°C for 15 min. For experiments on the dilution of top1 poisons, the reaction mixture without a top1 poison was added to the cleavage reaction to reduce the concentration of top1 poison to one-tenth of its initial concentration. Then the diluted reaction mixtures were incubated at 30°C for 15 min. After each incubation, aliquots were taken at the indicated times and mixed with stop solution (0.65% SDS). The denatured proteins were digested with 1 mg/ml proteinase K. Cleaved DNA was separated by 1% agarose gel electrophoresis in the presence of 0.5  $\mu$ g/ml of ethidium bromide, and measured using a densitometer.

**Cleavage Site Induced by top1.** A synthetic oligonucleotide containing the *Tetrahymena*'s top1 binding sequence (5, 6) was inserted into the *HindIII*-*EcoRI* site of pBR322. The DNA was digested with *Bam*HI and the 3' end of the fragment was labeled with [ $\alpha$ -<sup>32</sup>P]dCTP and the Klenow fragment. After digestion with *EcoRI*, the 258-bp fragment was used as a substrate for cleavage site analysis (3). A sample of 0.1 pmol of the 3'-end-labeled fragment was incubated with 500 units of top1 in 20  $\mu$ l of reaction mixture [50 mM Tris-HCl (pH 7.9), 120 mM KCl, 0.5 mM DTT, 0.5 mM EDTA, and 30  $\mu$ g/ml BSA]. After incubation for 15 min at 30°C, the reaction was stopped by the addition of 3  $\mu$ l of 5% SDS and the denatured enzyme was digested with 1 mg/ml proteinase K. The cleaved fragments were analyzed by denaturing 6% PAGE.

**Cleavable Complex Formation in Cultured Cells.** Aliquots of  $2.5 \times 10^4$  HCT116 human colon cancer cells were prelabeled by incubation with DMEM-10% fetal bovine serum containing [<sup>3</sup>H]thymidine [1 mCi/mmol; 0.5  $\mu$ Ci/ml] at 37°C and 5% CO<sub>2</sub> for 18 h in a total volume of 0.1 ml. The cells were washed with fresh medium and then incubated with top1 inhibitors for the indicated times. For analysis of the amount of cleavable complex after the removal of top1 poisons, cells that had been incubated with the drugs for 60 min were washed once with fresh medium and cultured further in drug-free

Received 3/3/99; accepted 7/7/99.

The costs of publication of this article were defrayed in part by the payment of page charges. This article must therefore be hereby marked *advertisement* in accordance with 18 U.S.C. Section 1734 solely to indicate this fact.

<sup>1</sup> To whom requests for reprints should be addressed, at Banyu Tsukuba Research Institute, Okubo 3, Tsukuba 300-2611, Japan.

<sup>2</sup> The abbreviation used is: top1, topoisomerase I.

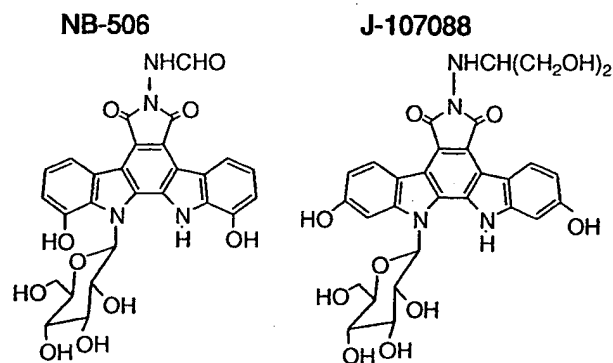


Fig. 1. Structures of J-107088 [6-*N*-(1-hydroxymethyl-2-hydroxy)ethylamino-12,13-dihydro-2,10-dihydroxy-13-( $\beta$ -D-glucopyranosyl)-5*H*-indolo[2,3-*a*]-pyrrolo[3,4-*c*]carbazole-5,7(6*H*)-dione] and NB-506.

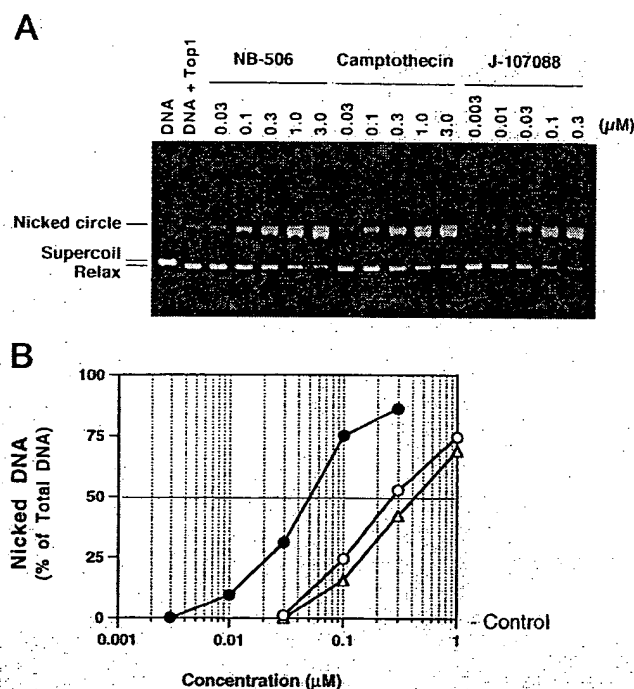


Fig. 2. Top1 mediated DNA cleavages induced by J-107088, NB-506, and camptothecin. pBR322 plasmid DNA was incubated with top1 in the presence of test compounds. **A**, top1-mediated DNA cleavage. **B**, densitometric analysis of top1-mediated DNA cleavage. ●, J-107088; ○, NB-506; Δ, camptothecin. Control shows the amount of DNA cleaved by topoisomerases in the absence of topoisomerase poisons.

medium for 5, 15, 30, 60, and 120 min. After incubation, the cells were lysed with 1.5% SDS-5 mM EDTA solution and subjected to  $K^+$ /SDS precipitation assay as described previously (7).

**Antitumor Spectrum *In Vitro*.** Samples of  $1 \times 10^3$  cells were plated in 96-well plates 1 day before the start of the assay. Then, sequentially diluted test compounds were added to each well, and incubation was continued for 72 h. Growth of cells was estimated by a sulforhodamine B dye-staining method (8).

## RESULTS

**Induction of top1-mediated DNA cleavage.** J-107088 induced single-strand cleavage in pBR322 plasmid DNA only in the presence of top1. The  $EC_{50}$  values of J-107088, NB-506, and camptothecin were 0.05, 0.27, and 0.42  $\mu$ M, respectively (Fig. 2). As reported about many indolocarbazoles including NB-506 (1, 9), J-107088 did not induce double-strand DNA cleavage in the presence of topoisomerase

II (data not shown). And J-107088 does not belong to the staurosporine family of kinase inhibitors (data not shown). Therefore, the mechanism by which J-107088 inhibited top1 was similar to, but more potent than, those of NB-506 and camptothecin.

DNA, cleaved by incubation with top1 poisons, was found to be religated by increasing concentrations of NaCl or decreasing concentrations of top1 poisons in an *in vitro* system. When 0.35 M NaCl was added to the DNA cleavage reaction, camptothecin-induced DNA nicking rapidly decreased to almost completely religated within 5 min (Fig. 3A). In contrast, DNA cleavage induced by J-107088 remained almost unchanged even 15 min after the addition of NaCl. The cleavable complex formed with NB-506 showed intermediate stability between those with camptothecin and those with J-107088. When the concentration of top1 poisons was decreased by dilution, the cleavable complex dissociated and, consequently, the level of nicked DNA was reduced (Fig. 3B). The speed of release of the J-107088-induced cleavable complex was much slower than that of NB-506 or camptothecin. These results suggested that the cleavable complex formed by J-107088 tended to be more stable than that formed by NB-506 or camptothecin.

**Nucleotide Sequence of Preferable Cleavage Sites.** The cleavage sites that are preferentially enhanced by J-107088 were analyzed using a 3' end-labeled 258-bp DNA fragment. J-107088 did not enhance DNA cleavage in the absence of top1 (Fig. 4, Lane 14). There were some common sites at which J-107088, NB-506, and campto-

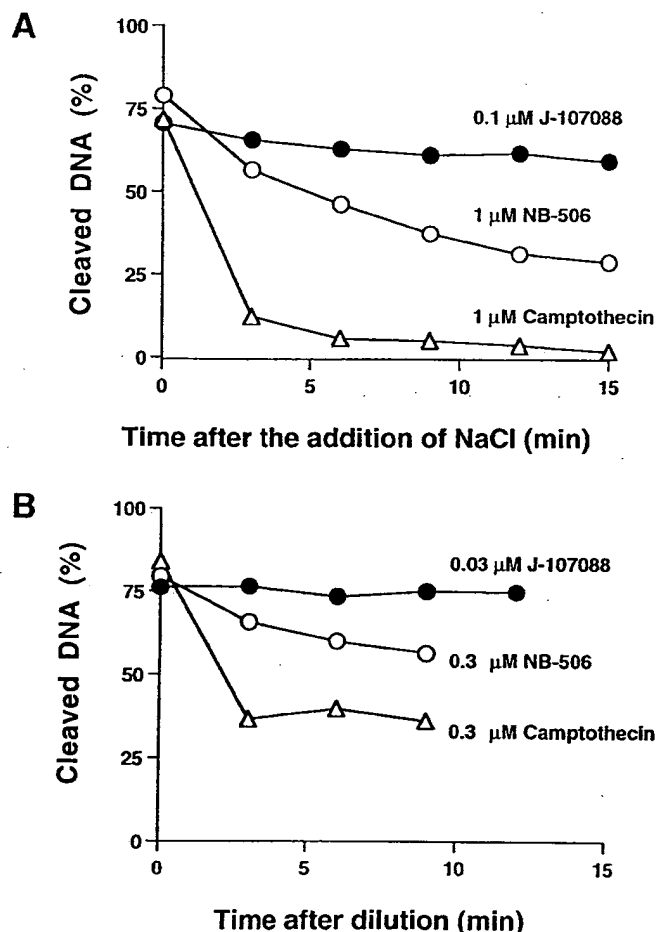


Fig. 3. Religation of DNA cleaved on addition of NaCl (**A**) or dilution of test compounds (**B**). The ordinate indicates the time after addition of NaCl or dilution of test compounds. The abscissa indicates the amount of cleaved DNA remaining. ●, J-107088; ○, NB-506; Δ, camptothecin.

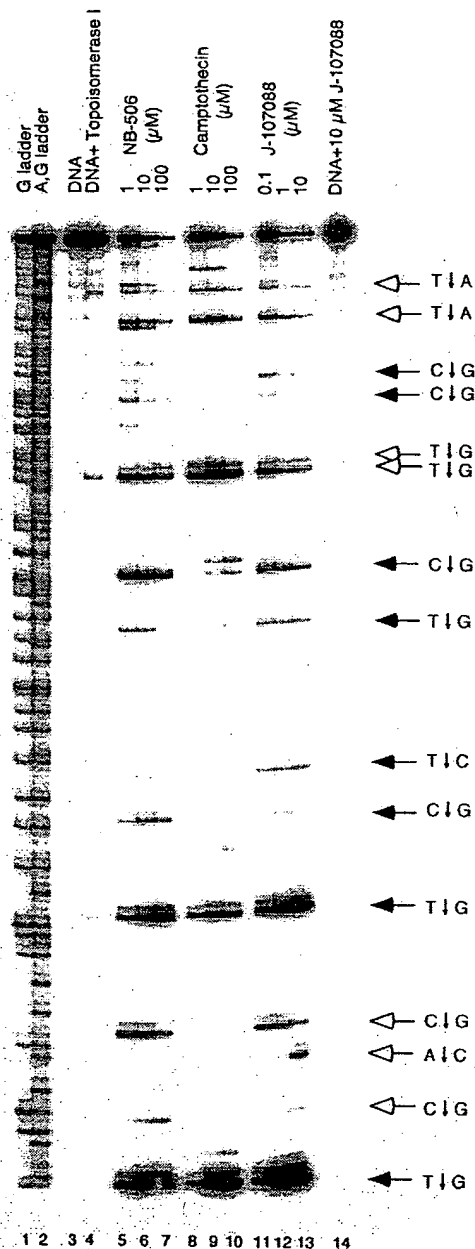


Fig. 4. Preferable cleavage sites of DNA induced by J-107088 in the presence of top1. The DNA ladders of G (Lane 1) and A+G (Lane 2) were prepared by the Maxam-Gilbert reaction and treatment with bacterial alkaline phosphatase. The cleavage sites enhanced by J-107088 and camptothecin were analyzed using a 3'-end-labeled 258-bp DNA fragment and 500 units of top1 (Lanes 4–13). Open arrowheads, sites cleaved by both J-107088 and camptothecin. Closed arrowheads, sites cleaved by J-107088 but not camptothecin. Letters next to these arrowheads, the bases at -1 and +1 positions of cleavage sites.

thein enhanced DNA cleavage (Fig. 4, open arrowhead). Most of these common sites had T and G at the -1 and +1 position, respectively, of the cleavage sites. In addition to these common sites, J-107088 and NB-506 enhanced the cleavage at several specific sites (Fig. 4, closed arrowhead). These J-107088 and NB-506-specific sites had C and G at the -1 and +1 position, respectively, of the cleavage sites. The pattern of cleavage by J-107088 was almost the same as that by NB-506. There were no other apparent rules of base preference of cleavage sites except for the bases at the -1 and +1 positions.

**DNA-Protein Complex Formation in Cells.** J-107088 increased formation of the DNA-protein complex in a time-dependent manner

for up to 3 h. When J-107088 was removed from the medium, the amount of protein-linked DNA in cells decreased very slowly, and two-thirds of the complex still remained 2 h after drug removal (Fig. 5A). In contrast, the DNA-protein complex formed by camptothecin increased immediately on addition of the drug and rapidly decreased on withdrawal of the drug (Fig. 5C). Results with NB-506 were intermediate between those with J-107088 and camptothecin; the complex increased gradually and was saturated 1 h after exposure to the drug. The complex in the cells was gradually decreased after withdrawal of NB-506, disappearing almost completely after 2 h (Fig. 5B). Thus, the DNA-protein complex induced by J-107088 persisted for longer after removal of the drug from the culture medium than those formed by NB-506 and camptothecin.

**Antitumor Spectrum of J-107088 on Various Human Cancers *in Vitro*.** The cytotoxic activities of J-107088 on various human cancer cells were measured by a 72-h continuous exposure assay, and the results were compared with those for NB-506, camptothecin, Adriamycin, etoposide, and cisplatin (Table 1). The  $IC_{50}$  values of

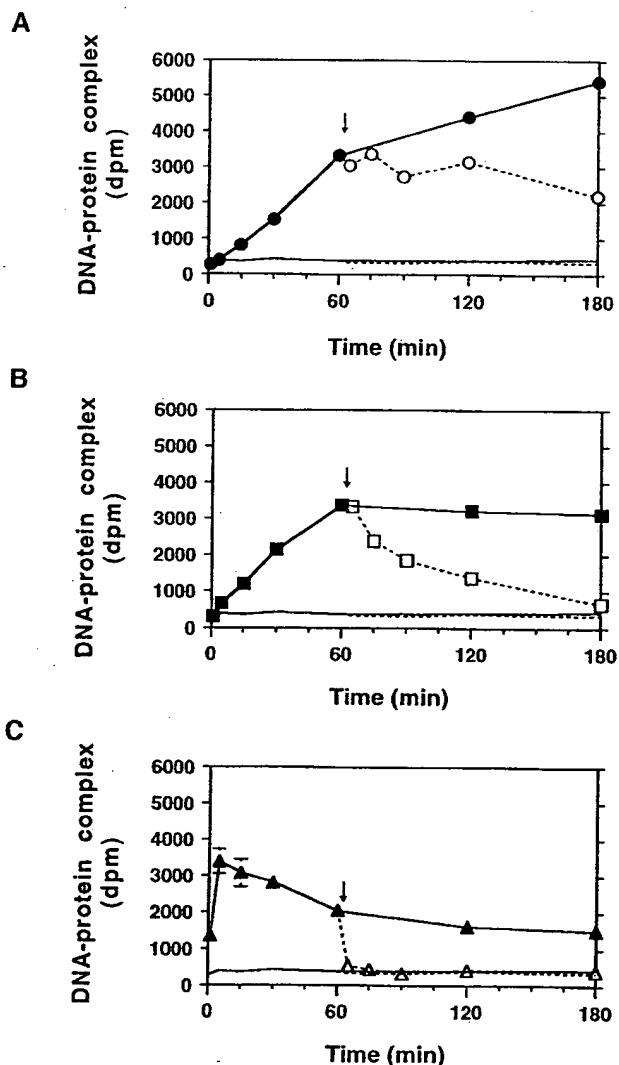


Fig. 5. DNA-protein complex remaining after removal of top1 inhibitors. HCT116 human colon cancer cells were incubated with top1 inhibitors, and the amounts of DNA-protein complexes were measured by  $K^+$ /SDS assay after incubation for the indicated times. Solid line with closed symbols, the amount of DNA-protein complex; broken line with open symbols, the amount of the complex after removal of drugs; line without symbols, control. ● and ○ (A), 0.6  $\mu$ M J-107088; ■ and □ (B), 4.0  $\mu$ M NB-506; ▲ and △ (C), 0.3  $\mu$ M camptothecin.



Table 1 Cytotoxicities of J-107088, NB-506, and other anticancer agents against various human cancer cell lines

Cell line <sup>a</sup>	IC <sub>50</sub> (μM)					
	J-107088	NB-506	Camptothecin	Adriamycin	Etoposide	Cisplatin
UM-UC-3	0.0015	0.35	0.015	0.043	0.57	1.4
FaDu	0.0028	0.15	0.013	0.024	0.53	2.5
SK-HEP-1	0.0058	0.20	0.012	0.0063	0.20	3.0
MKN-45	0.0075	0.61	0.018	0.21	3.9	2.3
HT-1080	0.025	1.3	0.018	0.031	0.60	1.1
PC-13	0.025	1.3	0.065	0.11	0.13	>5.0
ACHN	0.031	1.4	0.021	0.022	0.40	2.3
C32	0.17	11	0.033	0.11	1.7	2.0
DLD-1	0.19	3.4	0.080	0.13	0.46	>5.0
HT-29	0.21	12	0.041	0.10	4.5	5.0
BxPC-3	0.23	3.2	0.056	0.17	7.3	1.9

<sup>a</sup> The origins of the human cancer cell lines were as follows: UM-UC-3, bladder; FaDu, pharynx; SK-HEP-1, liver; MKN-45, stomach; HT-1080, fibrosarcoma; PC-13, lung; ACHN, renal; C32, melanoma; DLD-1, colon; HT-29, colon; BxPC-3, pancreas.

J-107088 on the 11 cell lines ranged from 0.0015 to 0.23 μM. The antitumor spectrum of J-107088 was similar to that of NB-506 but far higher against all of these cell lines. The spectrum of J-107088 was quite different from those of the other anticancer agents tested. MCF-7 AdrR were 40- and 200-fold more resistant than parental MCF-7 cells to Adriamycin and Taxol, respectively. In contrast, MCF-7 AdrR cells showed only 1.6-fold and 2.7-fold greater resistance than the parental cells to J-107088 and NB-506, respectively (Table 2). Thus, we concluded that J-107088 was effective against cancer cells that acquired resistance to Adriamycin or Taxol because of overexpression of p-glycoprotein (gp-170).

## DISCUSSION

J-107088 was categorized as a top1 poison that is a cleavable complex-forming inhibitor because it inhibited top1 through stabilization of the DNA-enzyme complex and enhanced single-strand DNA cleavage. In this characteristic, J-107088 resembled camptothecins. However, the potency, the stability of the cleavable complex, and the preferable sequence of cleavage sites of J-107088 were quite different from those of camptothecins.

Enhancement of topoisomerase-mediated DNA cleavage is likely to be caused by the following two mechanisms; acceleration of the cleavage process and suppression of the resealing process (9, 10). Because the addition of NaCl inhibits the cleavage reaction by blocking the association of top1 with DNA, the effect on the resealing process can be highlighted at a high salt concentration (11). J-107088-induced DNA cleavage was not resealed on addition of NaCl. This result suggested that the inhibitory effect of J-107088 on the resealing process was quite potent. It is also known that restoration of cleavage is caused by the removal of top1 inhibitors. When the concentration of J-107088 was decreased by diluting the reaction mixture, the decreasing speed of nicked DNA was obviously slower than those of NB-506 and camptothecin. These results demonstrated that the cleavable complexes formed by J-107088 were more stable than those of complexes with NB-506 and camptothecin.

In analyses using cultured cells, J-107088 increased the DNA-protein complexes time-dependently during incubation, and considerable amounts of the complexes remained after withdrawal of

J-107088. In contrast, the DNA-protein complex formed by camptothecin rapidly disappeared after removal of the drug. The rate of formation of J-107088-induced cleavable complex in cells was much slower than that of camptothecin. The level of DNA-protein complex was higher with camptothecin as compared with J-107088 for short incubation times (e.g., < 30 min.), although J-107088 showed higher potency to purified top1 than camptothecin. The reason for this discrepancy is not clear. The amount of complex was probably determined by the concentrations of the drug in the cells and the potency of the top1 poisons. There are at least two possibilities. One is that the uptake of J-107088 to cells may be very much slower than camptothecin. Another possibility is that J-107088 inhibits the formation of cleavable complex because J-107088 intercalates to DNA (data not shown). The amount of complex remaining after the removal of drugs was probably determined by the concentrations of the drug remaining in the cells and the stability of the cleavable complexes. Although, the cellular concentration of J-107088 was not investigated, the high stability of the J-107088-induced cleavable complex possibly contributed to the duration of stability of its intracellular complex.

J-107088 showed a very different antitumor spectrum *in vitro* pattern from those of camptothecin, Adriamycin, etoposide, and cisplatin. J-107088 was also effective against multidrug resistance cell lines which overexpress gp170. Previously, we demonstrated that the cytotoxic effects of NB-506 were determined by its accumulation level in cells (1). Although the level of J-107088 in each cell has not yet been investigated, the accumulation of J-107088 may play crucial roles in its activity and selectivity against various tumors as in the case of NB-506.

J-107088 differs from NB-506 by two substitutions (Fig. 1). Although both modifications are necessary to increase the top1 inhibition and cytotoxicity, the shift of OH groups is likely to be more critical. Similar to the result reported by Zembower *et al.* (12), the shift of OH groups of NB-506 from 1,11 to 2,10 positions considerably increased the potency of top1 inhibition and cytotoxicity.<sup>3</sup> Furthermore, Bailly *et al.* in collaboration with us showed that the position of OH groups of NB-506-type drugs affected the DNA binding activities and potency of top1 inhibition (13). The shift of OH groups from 1,11 to 2,10 without the change of substituent at the 6-N position of NB-506 abolished the DNA binding activity and changed its preferable sequence of DNA cleavage from C/T ↓ G to T ↓ G. J-107088 was bound to DNA (data not shown), and its preferable sequence of DNA cleavage was C/T ↓ G (Fig. 4). The replacement of NHCHO of NB-506 to NHCH(CH<sub>2</sub>OH)<sub>2</sub> without the change of

Table 2 Cytotoxic activities of J-107088 and other agents against parent and multidrug resistant cell lines

Cell line	Cytotoxicity (IC <sub>50</sub> , μM)			
	J-107088 <sup>a</sup>	NB-506	Adriamycin	Taxol
MCF-7	0.057 (1.0)	1.8 (1.0)	0.030 (1.0)	0.0017 (1.0)
MCF-7 AdrR	0.091 (1.6)	4.8 (2.7)	1.2 (40)	0.34 (200)

<sup>a</sup> ( ), relative resistance.

<sup>3</sup> M. Ohkubo, T. Nishimura, T. Honma, I. Nishimura, S. Ito, T. Yoshinari, H. Arakawa, H. Suda, H. Morishima, and S. Nishimura. Synthesis and biological activity of NB-506 analogues: effect on the position of two hydroxyl groups at the indole rings, manuscript in preparation.

position of OH groups increased the potency of top1 inhibition, DNA binding, and cytotoxicity (14, 15). Thus, the potency of top1 inhibition, DNA binding activity, and cytotoxicity of NB-506-type drug may be determined by the combination of the position of OH groups and substituent at the 6-*N* position.

All of these *in vitro* data suggest that J-107088 is a new type of top1 inhibitor with different and superior characters to other anticancer drugs currently used clinically. These finding are supported by the superior *in vivo* efficacy of J-107088 in a human tumor xenograft nude mouse model (16).

## ACKNOWLEDGMENTS

We thank A. Oliff of Merck Research Laboratories (West Point, PA) for providing MCF-7 AdR cells. We thank N. Sakaizumi, H. Komatani, and E. Yoshida of our institute for technical assistance and advice.

## REFERENCES

1. Yoshinari, T., Matsumoto, M., Arakawa, H., Okada, H., Noguchi, K., Suda, H., Okura, A., and Nishimura, S. Novel antitumor indolocarbazole compound 6-*N*-formylamino-12,13-dihydro-1,11-dihydroxy-13-( $\beta$ -D-glucopyranosyl)-5*H*-indolo[2,3-*a*]pyrrolo[3,4-*c*]carbazole-5,7-(6*H*)-dione (NB-506): induction of topoisomerase I-mediated DNA cleavage and mechanism of cell line-selective cytotoxicity. *Cancer Res.*, 55: 1310-1315, 1995.
2. Arakawa, H., Iguchi, T., Morita, M., Yoshinari, T., Kojiri, K., Suda, H., and Okura, A., and Nishimura, S. Novel antitumor indolocarbazole compound 6-*N*-formylamino-12,13-dihydro-1,11-dihydroxy-13-( $\beta$ -D-glucopyranosyl)-5*H*-indolo[2,3-*a*]pyrrolo[3,4-*c*]carbazole-5,7-(6*H*)-dione (NB-506): Its potent antitumor activity in mice. *Cancer Res.*, 55: 1316-1320, 1995.
3. Fukasawa, K., Komatani, H., Hara, Y., Suda, H., Okura, A., Nishimura, S., and Yoshinari, T. Sequence-selective DNA cleavage by topoisomerase I poison, NB-506. *Int. J. Cancer*, 75: 145-150, 1998.
4. Ohkubo, M., Nishimura, T., Jona, H., Honma, T., and Morishima, H. Practical synthesis of indolopyrrolocarbazoles. *Tetrahedron*, 52: 8099-8112, 1996.
5. Bonven, B. J., Gocke, E., and Westergaard, O. A high affinity topoisomerase I binding sequence is clustered at DNase I hypersensitive sites in *Tetrahymena* r-chromatin. *Cell*, 41: 541-551, 1985.
6. Christiansen, K., Bonven, B. J., and Westergaard, O. Mapping of sequence-specific chromatin proteins by a novel method. *J. Mol. Biol.*, 193: 517-525, 1987.
7. Okura, A., Arakawa, H., Oka, H., Yoshinari, T., and Monden, Y. Effect of genestein on topoisomerase activity and on the growth of [VAL 12]Ha-ras-transformed NIH 3T3 cells. *Biochem. Biophys. Res. Commun.*, 157: 183-189, 1988.
8. Skehan, P., Storeng, R., Scudiero, D., Monks, A., MaMahon, J., Vistica, D., Warren, J. T., Bokesch, S., and Boyd, M. R. New colorimetric cytotoxicity assay for anticancer-drug screening. *J. Natl. Cancer Inst.*, 82: 1107-1112, 1990.
9. Pommier, Y., Pourquier, P., Fan, Y., and Strumberg, D. Mechanism of action of eukaryotic DNA topoisomerase I and drugs targeted to the enzyme. *Biochim. Biophys. Acta*, 1400: 83-106, 1998.
10. Champoux, J. J. Mechanistic aspect of type I topoisomerases. In: J. C. Wang and N. R. Cozarelli (eds.), *DNA Topology and Its Biological Effects*, pp. 217-242. Cold Spring Harbor, NY: Cold Spring Harbor Laboratory, 1990.
11. Svejstrup, J. Q., Christiansen, K., Gromova, I. I., Andersen, A. H., and Westergaard, O. New technique for uncoupling the cleavage and religation reaction of eucariotic topoisomerase I. *J. Mol. Biol.*, 222: 669-678, 1991.
12. Zembower, D. E., Zhang, H., Lineswala, J. P., Kuffel, M., Aytes, S. A., and Ames, M. M. Indolocarbazole poisons of human topoisomerase I: regioisomeric analogues of ED-110. *Bioorg. Med. Chem. Lett.*, 9: 145-150, 1999.
13. Bailly, C., Dassonneville, L., Colson, P., Houssier, C., Fukasawa, K., Nishimura, S., and Yoshinari, T. Intercalation into DNA is not required for inhibition of topoisomerase I by indolocarbazole antitumor agents. *Cancer Res.*, 59: 2853-2860, 1999.
14. Ohkubo, M., Kojiri, K., Kondo, H., Tanaka, S., Kawamoto, H., Nishimura, T., Nishimura, I., Yoshinari, T., Arakawa, H., Suda, H., Morishima, H., and Nishimura, S. Synthesis and biological activities of topoisomerase I inhibitors, 6-*N*-amino analogues of NB-506. *Bioorg. Med. Chem. Lett.*, 9: 1219-1224, 1999.
15. Bailly, C., Qu, X., Chaires, J. B., Colson, P., Houssier, C., Ohkubo, M., Nishimura, S., and Yoshinari, T. Top1tion at F-ring *N*-imide of the indolocarbazole antitumor drug NB-506 increases the cytotoxicity, DNA binding and topoisomerase I inhibition activities. *J. Med. Chem.*, in press, 1999.
16. Arakawa, H., Morita, M., Koda, T., Okura, A., Ohkubo, M., Morishima, H., and Nishimura, S. *In vivo* antitumor activity of a novel indolocarbazole compound, J-107088, on murine and human tumors transplanted into mice. *Jpn. J. Cancer Res.*, in press, 1999.



US005356793A

**United States Patent** [19]

Koezuka et al.

[11] **Patent Number:** 5,356,793[45] **Date of Patent:** Oct. 18, 1994[54] **METHOD FOR TESTING THE SENSITIVITY OF ANTICANCER DRUG**[75] **Inventors:** Masahiro Koezuka, Nara; Naohito Kondo, Osaka; Sachiko Oda, Osaka; Hisayuki Kobayashi, Osaka; Masayuki Yasutomi, Osaka, all of Japan[73] **Assignee:** Nitta Gelatin Inc., Osaka, Japan[21] **Appl. No.:** 649,526[22] **Filed:** Feb. 1, 1991[30] **Foreign Application Priority Data**

Mar. 15, 1990 [JP] Japan ..... 2-66328

Oct. 3, 1990 [JP] Japan ..... 2-267343

[51] **Int. Cl.<sup>5</sup>** ..... C12M 1/00; C12M 3/00; C12N 5/06; C12N 5/00[52] **U.S. Cl.** ..... 435/32; 435/240.1; 435/240.2; 435/240.23; 435/240.25; 435/808; 435/284; 364/924.2; 382/6; 382/10; 382/25[58] **Field of Search** ..... 435/240.2, 240.23, 240.25, 435/240.243, 240.1, 808, 4, 29, 32, 284; 364/924.2, 924; 382/6, 10, 25[56] **References Cited****U.S. PATENT DOCUMENTS**

3,493,772 2/1970 Daughters et al. .... 250/222

4,637,053 1/1987 Schalkowsky ..... 435/291

**OTHER PUBLICATIONS**

Koezuka et al, "Tissue Culture Research Communications", vol. 6, No. 1, Jun. 1987.

Arii T., et al., J Electron Microscopy vol. 36, No. 4, pp. 177-195 (1987).

Kawamura K., et al Proc Japan Acad 62 Ser B. (1986).

Enami J., et al. Dokkyo J of Medical Sciences vol. 12, pp. 25-30 (1985).

Bodin et al, Methods in Laboratory Investigation "Study of Living Single Cells in Culture: Automated Recognition of Cell Behavior" vol. 39, No. 1, pp. 137-143, 1988.

Jaggi et al, The Design and Development of an Optical Scanner for Cell Biology, 27-30 Sep. 1985, pp. 980-985. Koezuka et al Biosis #38091394 Biological Abstracts (1990).

Blystone et al Biosis #40020455 Biological Abstracts (1991).

**Primary Examiner**—Michael G. Wityshyn**Assistant Examiner**—Jane A. Williams**Attorney, Agent, or Firm**—Lowe, Price, LeBlanc & Becker[57] **ABSTRACT**

The present invention relates to a method of testing the sensitivity of cancer drugs with cancer cells cultured in vitro. Cancer cells are cultured in a collagen gel substrate. A wide variety of human cancer cell types readily proliferate in the collagen gel substrate, however, fibroblast cells proliferate as well. The measurement of the growth of the cancer cells is hindered by the presence of the fibroblast cells. The present invention solves this problem by counting the number of colonies with an image processor which selectively extracts the image signals of cancer cells and their colonies. In a second embodiment, the growth of cancer cells is determined by measuring the volume of colonies with the image signals of cancer cells and their colonies selectively extracted. The results can be obtained effectively within a short period of time.

**6 Claims, 11 Drawing Sheets**

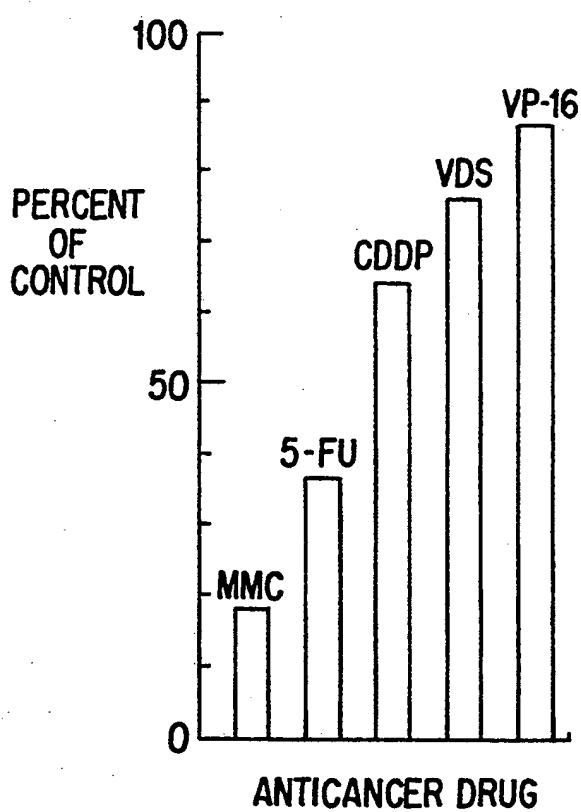


FIG. 1

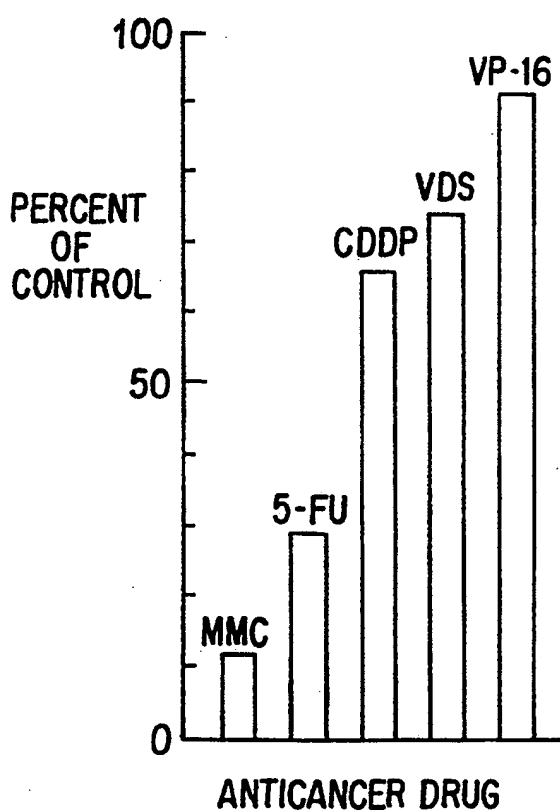
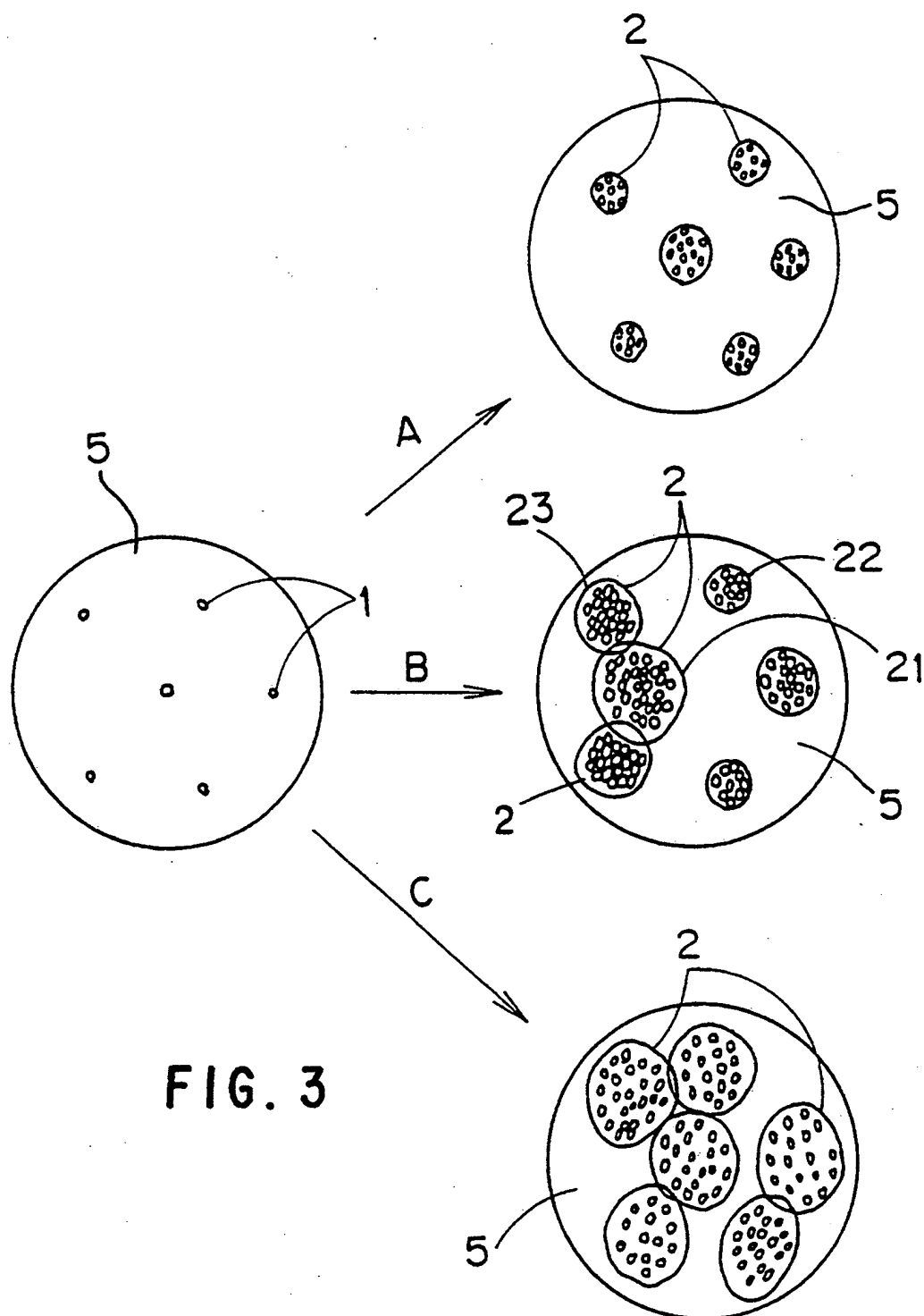
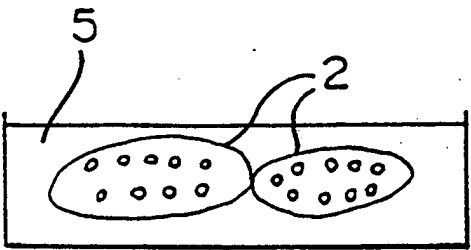
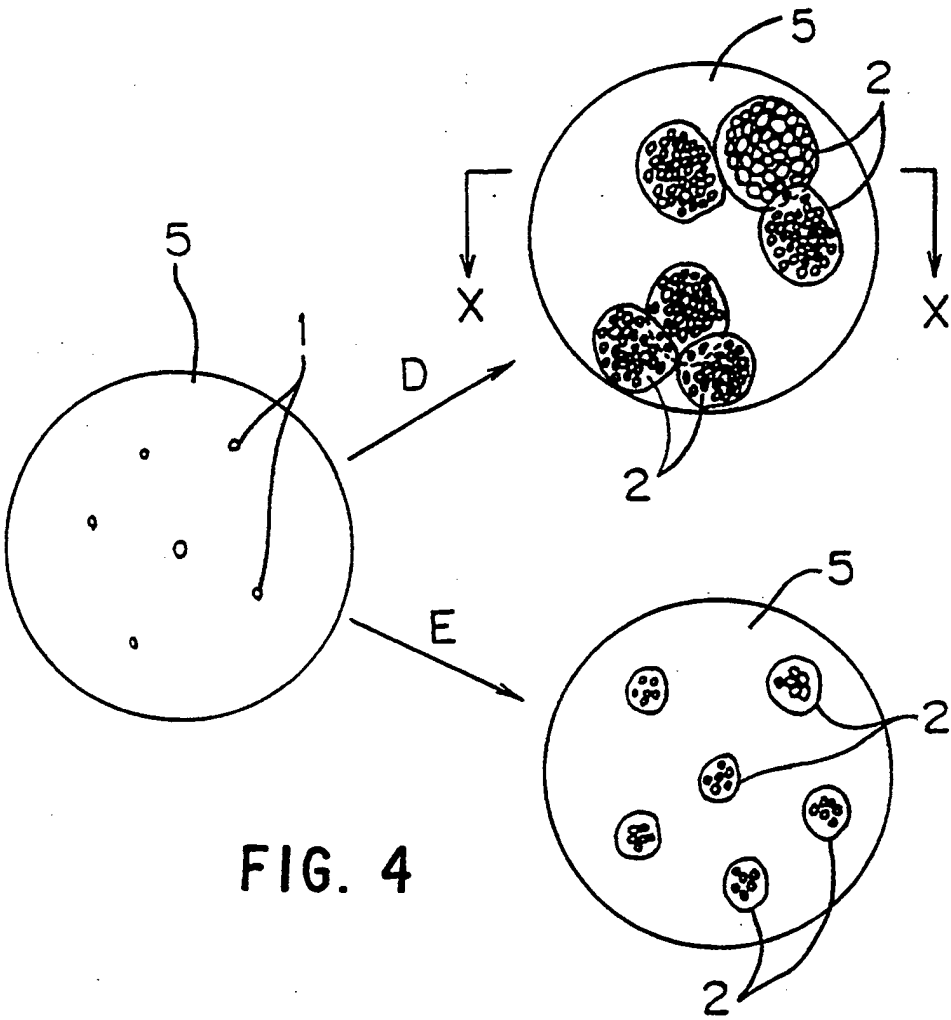


FIG. 2





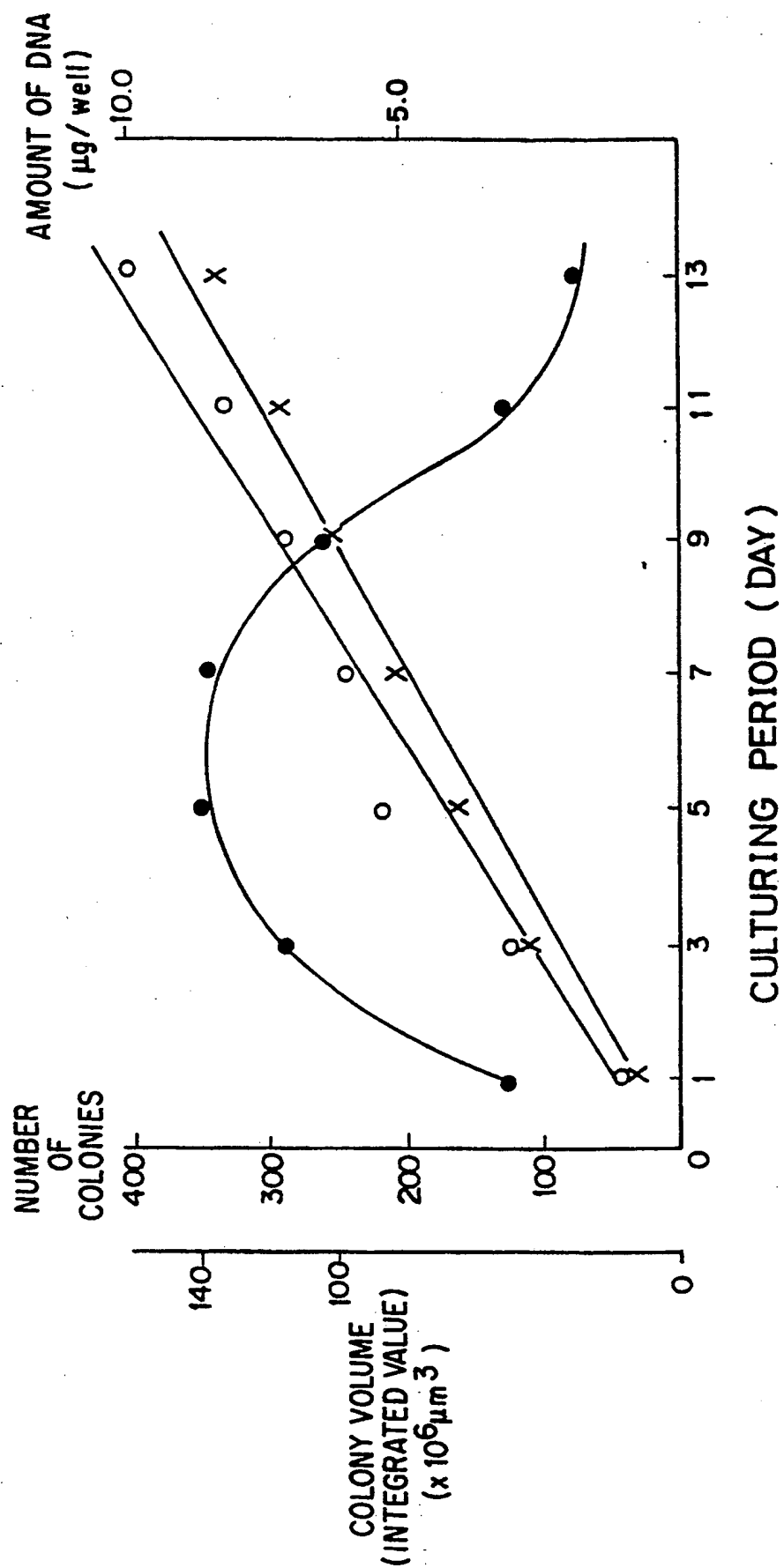





FIG. 6

 : METHOD OF MEASURING COLONY VOLUME (V)  
 : METHOD OF COUNTING COLONY NUMBER (C)  
 : NUDE MOUSE METHOD (N)

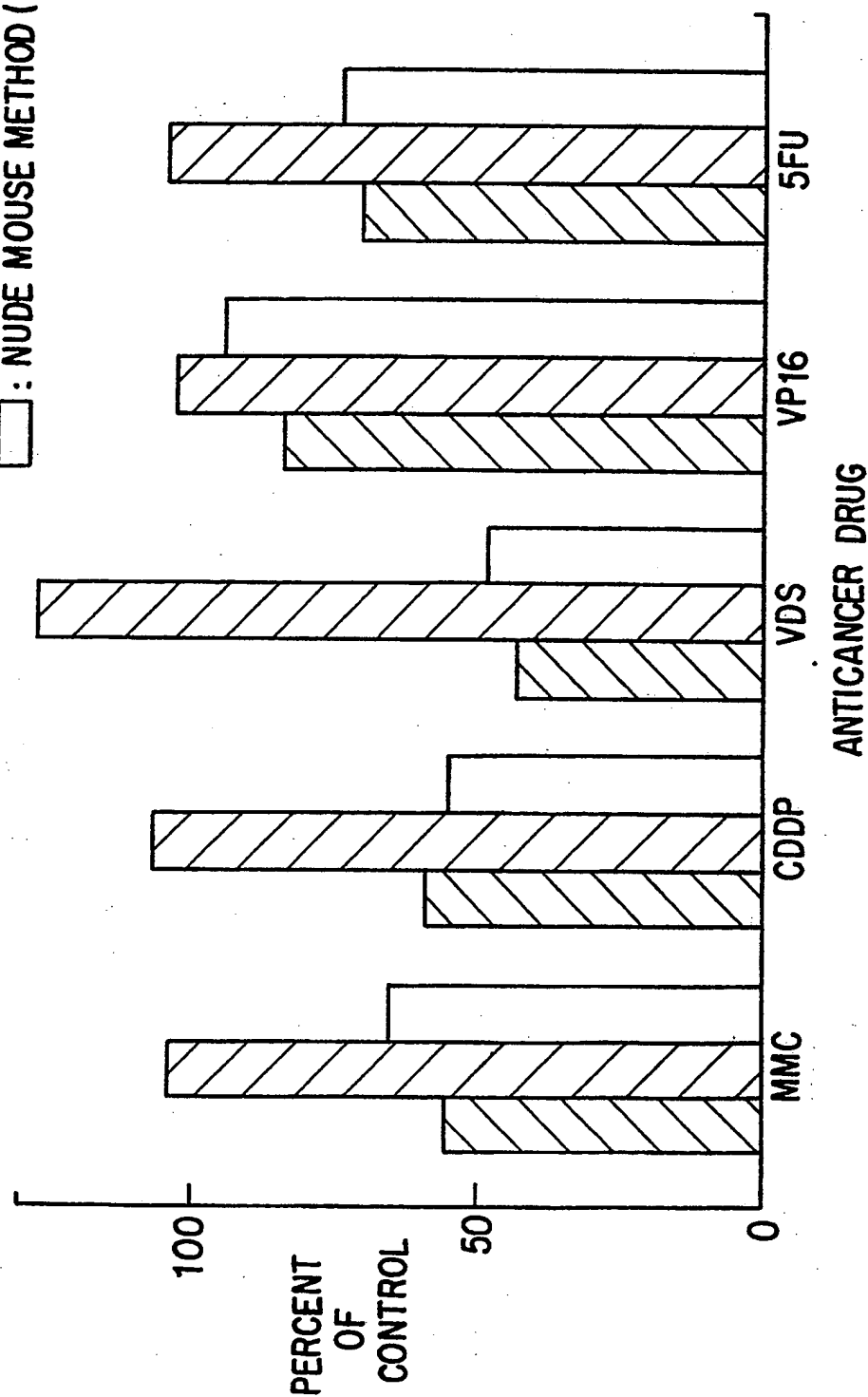


FIG. 7



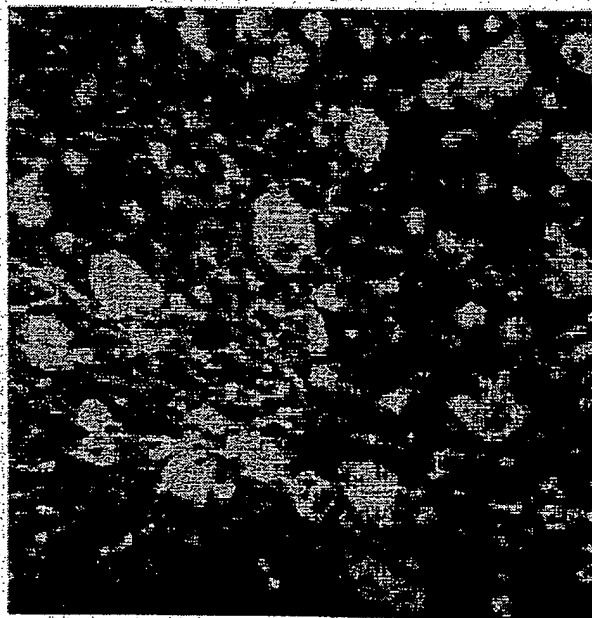


FIG. 8

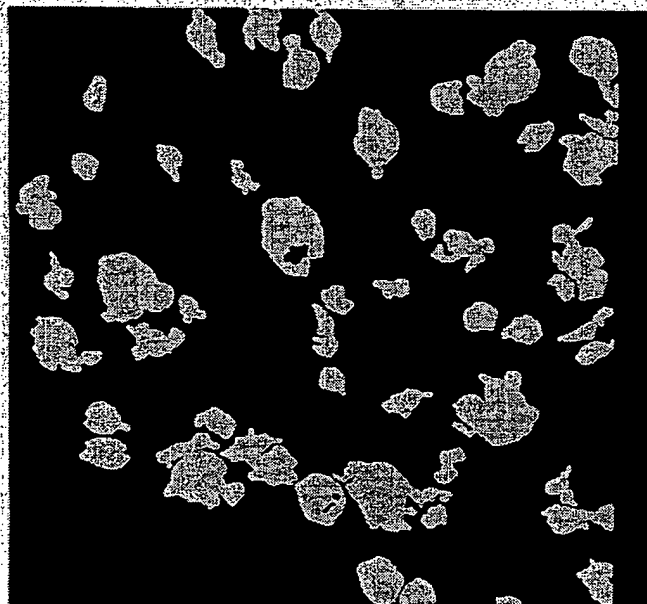


FIG. 9

1 DAY



FIG. 10

3 DAY

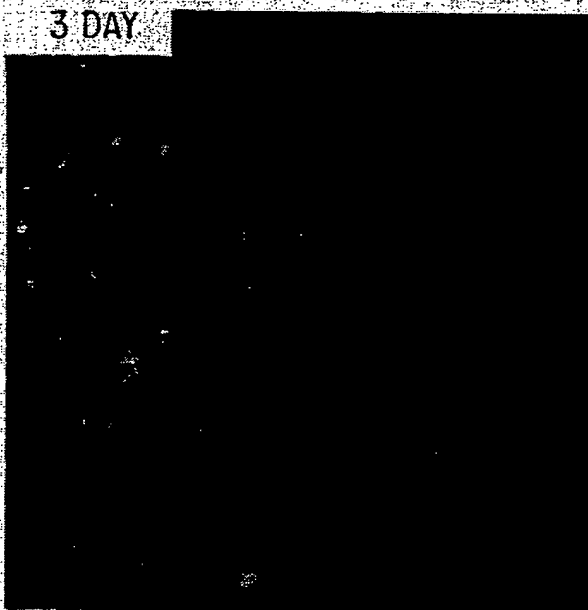
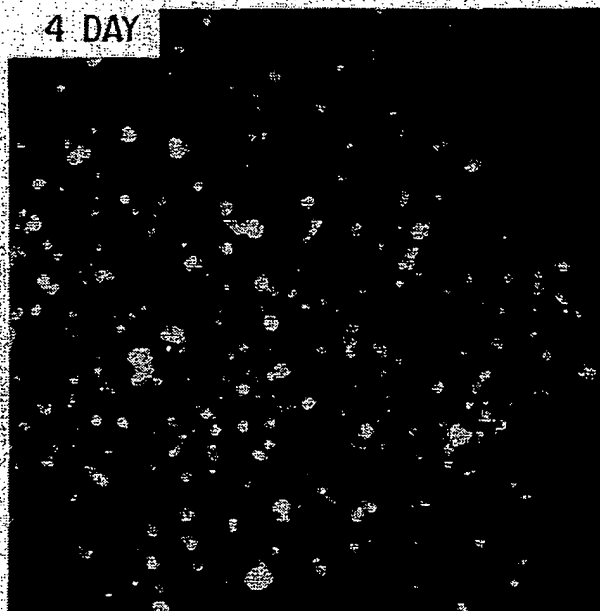


FIG. 11

4 DAY



*FIG. 12*

5 DAY

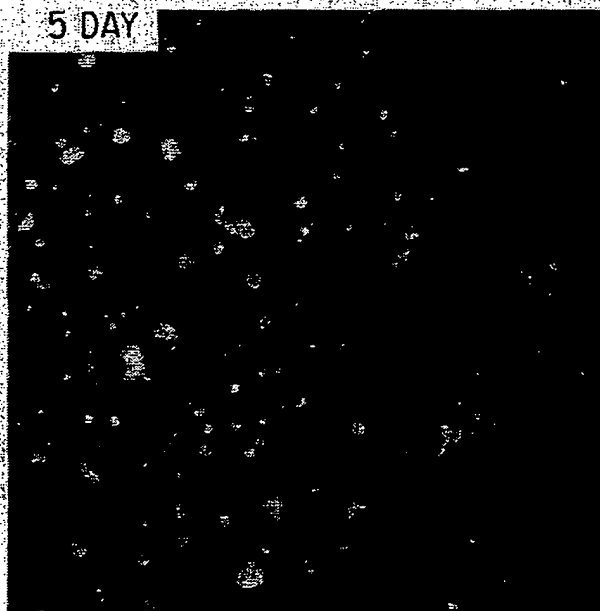


*FIG. 13*



FIG. 14

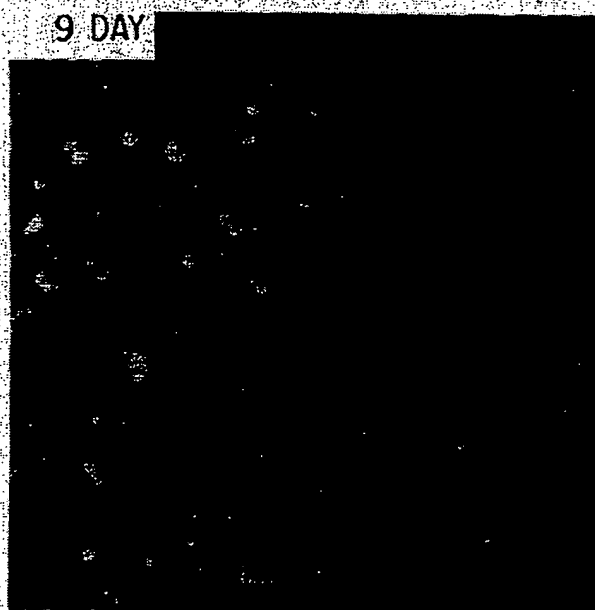


FIG. 15

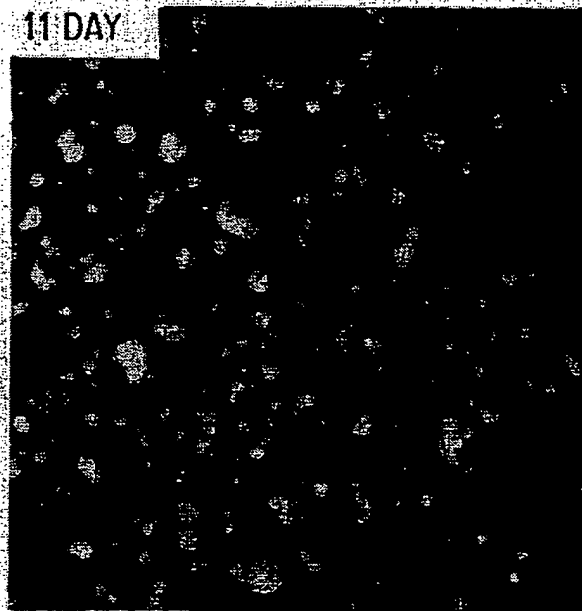


FIG. 16

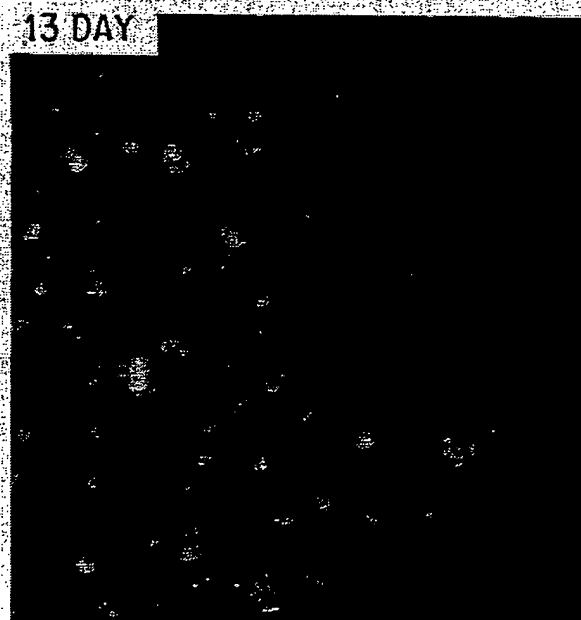


FIG. 17

19 DAY

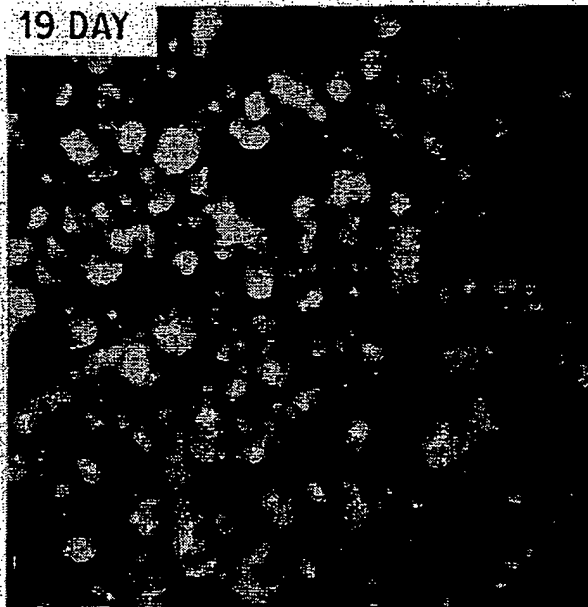


FIG. 18

25 DAY

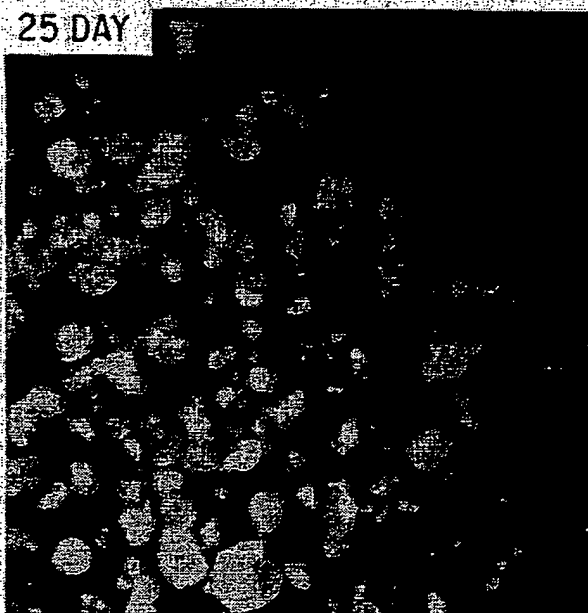


FIG. 19

## METHOD FOR TESTING THE SENSITIVITY OF ANTICANCER DRUG

### BACKGROUND OF THE INVENTION

The present invention relates to a testing method for sensitivity of anticancer drugs and, in detail, relates to a method in which the sensitivity of cancer cells to anticancer drugs is tested with cancer cells cultured in vitro.

There have been known the following methods for determining the therapeutic efficacy of anticancer drugs, or for the drug-sensitivity test: a clinical testing method in which anticancer drugs are dosed to cancer patients and the change in cancer tissue is examined by diagnostic examination; an in vivo (animal) testing method in which anticancer drugs are dosed to animals to whom human cancer tissue is transplanted; a cell culture testing method in which cancer cells are taken from cancer patients, brought in contact with anticancer drugs and then cultured by using an adequate substrate, or the cells are brought in contact with the drug while cultivating, and after a definite period of time, the growth of cancer cells is measured; and other methods.

It is as usual that after confirmation of the anticancer efficacy of newly developed anticancer drugs by using the cell culture or in vivo-testing methods, the drugs are tested clinically to confirm the efficacy in a final stage, because they can not be applied to the clinical testing method from the first stage of their development. The in vivo-testing method suffers disadvantages of difficulties in controlling animals for experiments such as nude mice etc. and low success rate in the transplantation of human cancer cells, and also requires a long period of time before obtaining experimental results. In contrast, a cell culture testing method has advantages that it is performed by using a relatively simple equipment and by a relatively simple procedure and provides the experimental results in a short period of time. Therefore, an anticancer drug sensitivity test by a cell culture testing method plays a very important role in the development of new anticancer drugs.

Hitherto, as a typical cell culture testing method, a method which is called as the HTCA (Human Tumor Clonogenic Assay) method has been known. According to the method, a single cell suspension is prepared from cancer tissue obtained from a living body and brought in contact with an anticancer drug, and the cancer cells are then cultured in a soft agar substrate. Subsequently, the number of the cancer cell colonies formed after cultivating for a definite period of time is counted to evaluate the inhibition rate on the colony formation by the anticancer drug and thereby the anticancer drug sensitivity is tested. The counting of colonies is performed with eye measurement or by using a colony counter. As alternatives, there are methods in which cells are cultured by using a monolayer culture technique followed by evaluating the efficacy of anticancer drugs against cancer cells using an isotope method and a DNA-measuring method and others.

However, the HTCA method which is the most typical anticancer drug sensitivity testing method in the cell culture methods has the following problems.

First, although the cell culture method using soft agar substrata has an advantage of depressing proliferation of fibroblasts, it requires a large number of cells for culture because of the low colony formation rate of cancer cells. Therefore, the number of tests being carried out

with the limited quantity of obtained cells is smaller. Second, there is a problem that the kinds of cancer cells capable of being cultured are limited. That is, the cancer cells variously differ in kind and character due to a tissue difference etc. in a diseased part so that among these variously different kinds of cancer cells only a few kinds of cells can be cultured in a soft agar substrate.

The present inventors, therefore, examined a new anti-cancer drug-sensitivity test, in which a collagen gel substrate was used in place of a soft agar substrate, in a primary culture system using human cancer cells. As a result, we found that even the human cancer cells which did not proliferate in a soft agar substrate were able to proliferate steadily in collagen gel substrate (refer to Koezuka et. al., "Tissue Culture Research Communications", Vol. 6, No. 1, 1987). From the results, the collagen gel culture method made it possible for the cell culture testing method to greatly spread the range of adaptability. Furthermore, the method has been found to have advantages of that the number of cells required for culture is small because cancer cells are proliferated more effectively in collagen gel than in soft agar etc., and that the test results can be obtained effectively within a short period of time.

Generally, when collagen gels are used as substrata, the DNA of cells proliferated in collagen gels is measured for determination of the growth of cancer cells.

However, when cancer cells are cultured in a collagen gel substrate, the collagen gel culture creates a problem that fibroblasts which are contained in cancer tissues also proliferate together with the cancer cells, depending on the kind of the cancer tissue. Since the fibroblasts also possess DNA similarly to the cancer cells, the method for measuring the growth of cancer cells by the above-mentioned quantitative determination of DNA can not be used. Therefore, in such a case the formed cancer cell colonies have to be counted by eye measurement or by means of a colony counter. However, when the measurement is carried out by eye measurement using a stereoscopic microscope, selective counting of the cultured cancer cells alone requires a great deal of labor, and the measurement varies from observer to observer, resulting in inaccurate results. It is also actually impossible to distinguish exactly between the cultured cancer cells and fibroblasts by means of a conventional colony counter. In most human cancer tissues obtained from a surgery material, fibroblasts and cancer cells proliferate simultaneously in collagen gel substrata, and hence it is very difficult to examine the sensitivity of anticancer drugs against human cancer cells cultured in the substrate unless both the fibroblasts and cancer cells are separated. Although several techniques such as the cis-hydroxyproline(Oxyprolin) method, the D-valine method, the citrulline method, and the like have hitherto been proposed as methods for depressing the proliferation of fibroblasts without depressing proliferation of cancer cells, none of these techniques is practically useful because they are effective for only a few, limited kinds of fibroblast.

### SUMMARY OF THE INVENTION

An object of the present invention is to provide a testing method for testing the sensitivity of anticancer drugs, which has not only the advantage of collagen gel substrate capable of cultivating cancer cells effectively, but also capability of simply and accurately measuring the growth of cancer cells alone, even if the fibroblast

proliferation simultaneously occurs that is up to present a defect of the collagen gel substrate.

To solve said object, the present invention provides a testing method for testing the sensitivity of anticancer drugs, wherein cancer cells are proliferated by using a collagen gel as a substrate and an image processor is used as a means for measuring the growth of cancer cells. Thus, image signals of the cancer cells and their colonies are selectively extracted from those of a sample obtained with imaging and the growth of cancer cells is determined with the thus-obtained image information of the cells and colonies to assay the anticancer drug sensitivity.

According to one embodiment in the present invention, the growth of cancer cells is determined by counting the number of colonies with the image signals of cancer cells and their colonies selectively extracted.

According to another embodiment in the present invention, the growth of cancer cells is determined by measuring the volume of colonies with the image signals of cancer cells and their colonies selectively extracted.

The collagen used as a substrate may be capable of gelation, and type I collagen which shows high gel strength is further preferred. Additionally, since an optical measurement is being carried out, it is preferable that the collagen used in the present invention is such that it exhibits transparency for light having the wavelength used for the measurement, and further that it has an optically uniform character in the gel form. Furthermore, collagen which does not cause any optical quality-change due to time-passage during culturing is desired.

Also, the process in which cancer cells are cultured in a substrate composed of collagen gel is carried out according to hitherto-known, various kinds of tissue-culture methods using collagen gel. The time when an anticancer drug is brought in contact with cancer cells may be properly set, for example, it may be just before inoculating cancer cells taken from a patient (primary cancer cells) into a collagen gel substrate; before inoculating cells treated with subculture of the primary cancer cells into the substrate; immediately after inoculating them into the substrate; or after several days' cultivation of cells inoculated. There is no special limitation about the time.

An image processor is used as a means which measures a change in the growth of cancer cells. The image processor is connected with an optical instrument such as a microscope etc. and image signals obtained thereof are converted into numerical image information followed by arithmetic processing and, thus the processor is used in order to obtain clear and accurate information of an object. Thus, the processor is equipped with an image processing mechanism such as a microcomputer, etc.; a memory mechanism for the image derived from a fixed disk device, etc.; and an outputting mechanism such as a monitor television or a video printer for outputting the image information processed.

The microscope used may be similar to a microscope which has hitherto been used for measuring cancer cells with eye measurement. Measurement performance and measurement accuracy can be elevated by properly selecting the conditions such as the magnification of a microscope that is largeness of a visible scope, depth of a focus, distance of a subject, an equipping structure of culturing vessels, and an illuminating apparatus etc. The microscope may be equipped with an inputting device

such as a TV camera in order to input the sample image signals into the image processor.

Setting of a culture sample at an observing position of a microscope can be performed by hand, but if a continuous transfer mechanism which is able to send a culture sample continuously to the observing position or to take out the sample is equipped, an attempt to raise efficiency of measurement may be achieved.

In the present invention, a TV camera of the image processor receives gray images of a cultured sample. For the sample images received, there is a case where only the images of cancer cells and their colonies (hereinafter referred to as "cancer cells") exist and a case where the images of those and images of the above-mentioned fibroblasts exist as a mixture. The image processor undergoes processing for removing unnecessary images such as those of fibroblasts etc. other than the cancer cells from the sample images. To separate the images of cancer cells from the other unnecessary images and remove the latter images, a function for separating the gray levels and shapes in the image processor is employed. The cancer cells form a solid image having a certain degree of size as well as a profile and a gray level by that a large number of cells gather together, that is a colony, whereas the fibroblasts take a fine fibrous shape or a twig shape as suggested by the name. Therefore, the cancer cells and fibroblasts can be distinctly distinguished by the shape difference as well by differences in the gray levels of images. Thus, the image processor recognizes as cancer cells only the images in which the shape, area, gray level, and color difference etc. fulfill definite conditions, and also recognizes the images, which does not fulfill said condition, as unnecessary images of fibroblasts etc. and thus, the images other than the images of cancer cells are removed and the remaining cancer cell images can be taken out. Then, when the shapes of individual images being shown in the cancer cell images undergo arithmetic processing and are evaluated, a change in the growth of cancer cells, that is a proliferating extent, can be measured.

In order to evaluate the sensitivity of anticancer drugs, for example, a pair of cancer cells, one of which is brought in contact with an anticancer drug or with different anticancer drugs of two or more kinds and the other of which is not brought in contact with any anticancer drug as a control experiment, are cultured under identical conditions, and change in the growth of cancer cells measured with said image processor is compared.

To determine a growth extent of cancer cells with the images of cancer cells selectively extracted, as described above, there are, for example, the following two kinds of procedure. One is to count the number of colonies in the images of cancer cells. The other is to measure the volume of colonies in the images of cancer cells.

According to the first procedure, for example, the number of colonies obtained by culturing cancer cells which have been brought in contact with an anticancer drug and that obtained by culturing cancer cells without the contact (control experiment) are determined by automatic counting for comparison.

According to the other procedure, for example, the volume of colonies obtained by culturing cancer cells which have been brought in contact with an anticancer drug and that obtained by culturing cancer cells without the contact (control experiment) are derived for



comparison. Here, the derivation of the volume is, for example, carried out as the undermentioned, but it is not limited within it.

With culturing of cancer cells in the collagen gel substrate, the kind of cancer cells being cultured increases the application region of the cell culture testing method enlarges, and also the growth of cancer cells proceeds smoothly and the test results can be obtained surely and promptly.

By that the amount of colonies formed with cancer cells is measured and analysed by means of an image processor, the effect of fibroblasts which proliferate together with cancer cells can be eliminated. That is, in an image of a cultured sample, the cancer cell image shows a block shape and a dark image, while the fibroblast shows a light image of a fine fibrous shape, so that the cancer cell and fibroblast are distinctly different in the shape and gray level. In the image processor, only the images having a shape and a grey level of definite conditions can be taken out from inputted images, so that the images of cancer cells and those of fibroblasts are separated to take only the images of cancer cells. Also, besides the fibroblasts, the images of unnecessary objects having a grey level and a profile different from those of cancer cells, can be separated from the images of cancer cells. When the amount of colonies being formed with cancer cells is measured with the cancer cell images taken out, a change in the growth of only the cancer cells which do not involve the fibroblasts can be measured.

The measurement by an image processor, for example, when it is compared with that by the nude eye under a microscope, is capable of measuring a complex amount more effectively and precisely and within a far shorter period of time, and also the measurement can be carried out under definite conditions avoiding scattering of results and possibility of erroneous measurement which results from a different skill etc. of measuring workers, so that the test results are stable.

Additionally, since the present method is a nondestructive method, the measurement of an identical sample can be carried out with passage of time and, in a case of that a change in amount of the object, that is cancer cells, is measured, such measurement accuracy as that can not be obtained from a destructive method may be easily realized. Furthermore, the process which is necessary for analyses may be automated inside the image processor and, if it is linked to a continuous measuring mechanism, the time and labor necessary for measurement can be reduced and rationalized.

If measurement of a growth extent of cancer cells is carried out by number-counting of colonies with the cancer cell images selectively extracted, precise results were obtained with an inexpensive image processor only in cases wherein the colonies do not come in contact with one another.

Also, if measurement of a growth extent of cancer cells is carried out by volume measurement of colonies with the cancer cell images selectively extracted, when colonies came into contact with one another or overlapped, more precise results were obtained compared with the above number-counting.

#### BRIEF DESCRIPTION OF THE DRAWINGS

FIG. 1 is a graphic diagram which shows results obtained from the measurement of sensitivities of anticancer drugs in the examples of the present invention.

FIG. 2 is a graphic diagram which shows results obtained from the measurement of sensitivities of anticancer drugs in the examples for comparison.

FIG. 3 is a diagram which explains three examples for proliferating extents in culturing cancer cells.

FIG. 4 is a diagram which shows, in culturing cancer cells, one example of cases where treatment with an anticancer drug was not carried out (a control experiment group) and one example of cases where the treatment was carried out.

FIG. 5 is a cross-sectional view for the X—X in FIG. 4 and shows one example of cases where the colonies come in contact.

FIG. 6 is the graph which shows a correlation between the colony number and colony volume with the DNA amount.

FIG. 7 is a graph which shows the sensitivity-measuring results by each anticancer drug in the example 2 and example for comparison 2.

FIGS. 8-19 are photographs of monitor television pictures referred.

#### DESCRIPTION OF THE PREFERRED EMBODIMENTS

The examples of the present invention are explained in detail, but this invention is not limited within the undermentioned examples.

#### EXPERIMENT 1

##### Comparison of Collagen Gel Culture With Other Kinds of Culture

Initially, it was confirmed by experiments that the collagen gel substrate employed in this invention was superior to the so far known soft agar gel substrates for the culture of human cancer cells.

Table 1 presented below shows the results obtained from the culture of various kinds of human cancer cells in collagen gel substrate and so far known soft agar substrate.

The culture method used in the so far-known HTCA method was used for the soft agar substrate in the table. Upon observation of the cultured samples after culturing, if the number of colonies of cancer cells exceeded 20, the culture was evaluated as successful. The numerical values in each column of the table show the number of success in the culture versus the number of total experiments. The number of cells inoculated were  $5 \times 10^4$  for 1 ml of collagen gel substrate and  $5 \times 10^5$  for 1 ml of soft agar substrate.

TABLE 1

Kinds of cancer cells	Collagen gel substrate	Soft agar substrate
Colon cancer-1	5/5	0/5
Colon cancer-2	5/5	4/5
Colon cancer-3	1/5	0/5
Rectal cancer-1	5/5	2/5
Lung cancer-1	5/5	0/5
Lung cancer-2	0/1	1/1
Total	21/26	7/26

As seen from said results, it was proved that, when a collagen gel substrate is used, many more kinds of cancer cells were successfully cultured as compared to when a soft agar substrate is used.

## EXAMPLE 1

According to the undermentioned procedure, the anticancer drug sensitivity tests in the present invention were carried out to compare the effects of plural anticancer drugs.

## Culture of Cancer Cells

The culture of cancer cells being supplied to image processing was carried out.

The cancer cells used were human cancer cells separated from nude mouse-xenografted human colon cancer by a stepwise enzyme-treatment using collagenase and pronase. The obtained cells were embedded in collagen gels and cultured.

The embedding was carried out as follows: to 8 volumes of Cellmatrix Type I-A (0.3% acid-soluble collagen solution, made by Nitta Gelatin Inc., Japan) were added 1 volume of 10 times concentrated Ham's F12 medium(not containing  $\text{NaHCO}_3$ ), 1 volume of a reconstitution buffer(aqueous 50 mM sodium hydroxide solution containing 260 mM of  $\text{NaHCO}_3$  and 200 mM of HEPES), and 1 volume of FBS(fetal bovine serum), and to the mixture thus-obtained were added and mixed well the human cancer cells which were obtained from said enzyme-treatment, and the mixture thus-prepared was kept in ice. One ml of the collagen-cell mixture solution was pipetted into each Petri dish of 35 mm diameter. The cell number was  $5 \times 10^4$  cells/ml. This mixture solution was then warmed to  $37^\circ \text{C}$ . in a carbon dioxide incubator to form collagen gel substrata containing the human cancer cells.

The resulting collagen gel substrata were overlaid with 1 ml of a culture medium containing each of anticancer drugs and allowed to stand for 24 hours at  $37^\circ \text{C}$ . in the carbon dioxide incubator to bring the cells in contact with drugs. Hereafter, the medium which contained drugs was removed by suction, and 2 ml of a culture medium which does not contain anticancer drugs were added and shaken in the carbon dioxide incubator to wash the collagen gel substrata. This washing was repeated 10 times at 10 minutes intervals to remove drugs from the substrata. In the control experiment a culture medium which does not contain anticancer drugs is used and the contact of human cancer cells with anticancer drugs is not carried out.

Next, 2 ml of a culture medium was added and cancer cells were cultured for 10 days at  $37^\circ \text{C}$ . in the carbon dioxide incubator. The culture medium was changed at 1 to 2 day intervals. After culturing, each collagen gel substrate containing cells was fixed by using 10% aqueous formalin to prepare the samples.

The culture medium used in the above procedure was composed of DME, 10% of FBS, Insulin (1  $\mu\text{g}/\text{ml}$ ), and an EGF culture medium (10 ng/ml); where the DME is Dulbecco's Modified Eagle's culture medium (made by Nissui Seiyaku Co.), FBS is Fetal Bovine Serum (made by Gibco Co.), Insulin is insulin (from Sigma Co.), and EGF is Epidermal Growth Factor (made by Collaborative Co.).

Anticancer drugs used herein were the following five kinds: mitomycin (MMC made by Kyowa Hakko Kogyo Co., Ltd., Tokyo), 5-fluorouracil (5-FU made by Kyowa Hakko Kogyo Co., Ltd.), Vindecine sulfate (VDS made by Shionogi Pharmaceutical Co., Ltd., Tokyo), Etoposide (VP-16 made by Nippon Kayaku Co., Ltd.), and Cisplatin (CDDP made by Bristol-Myers Co., Ltd., Tokyo).

The concentration for use of each anticancer drug which was brought in contact with cells was equivalent to one-tenth of the highest concentration achievable in blood among various concentrations of the drug for clinical use(concentration in tumor tissue). They were 0.1  $\mu\text{g}/\text{ml}$  for MMC, 1.0  $\mu\text{g}/\text{ml}$  for 5-FU, 0.005  $\mu\text{g}/\text{ml}$  for VDS, 0.1  $\mu\text{g}/\text{ml}$  for VP-16, and 0.2  $\mu\text{g}/\text{ml}$  for CDDP.

## Image Processing

Both the pictures of the colonies of the human cancer cells, which were proliferated in collagen gel substrata, and fibroblasts, which were proliferated simultaneously with the cancer cells, in the fixed samples prepared as mentioned above, were taken with a TV camera through a stereoscopic microscope, whereby the images obtained were inputted as image signals into an image processor (LUZEX III U, made by Nikon Co., Ltd.)

Specifications of the image processor are as follows. Control processor: Intel 80386/7 32 bits processor  
Memory unit: 40 megabytes fixed disk drive

Image processing circuit: image area and density, maximum  $1024 \times 1024$  pixel  $\times (8+1)$  bit, image array processor

Image inputting device: TV camera, Chalnicon camera tube, optical microscope

Image outputting device: digital/analog RGB monitor, video printer

The image signals inputted into the image processor were digitized into picture elements and the concentrations corresponding to each element of the image were converted into numerals and then, taking the images of colonies of cancer cells and those of fibroblasts as the objects, processing to separate them from the original images was carried out. The processing for separating the object images enhanced a feature in the gray level of the objects by a logical operation. For this operation, a high-frequency component extracting operation, a gray level-classifying operation, and a noise removal were used in combination. Only the images of the objects were extracted from the obtained, enhanced images, according to a definite standard value relating to the gray level. At this stage, the numbers of colonies due to only human cancer cells were counted with a difference in the gray levels or a difference in a changing rate of the gray levels. In the images after the image processing being carried out, the colonies of cancer cells of the present object are only enhanced and the unnecessary images of fibroblasts etc. has been removed, so that counting the number of colonies is easy.

## Examination of Measurement Results Obtained by Image Processing

As described above, from the images after the image processing being carried out, the measurement results of colonies of only human cancer cells are compared with the results which are obtained from similar measurements without the image processing.

When a formalin-fixed sample which has not been brought in contact with an anticancer drug is seen with a stereoscopic microscope, there exist in a mixture the colonies of cancer cells having a sphere shape and the fibroblasts being formed in a bipolar linear shape.

Under these conditions, when only colonies of a sphere shape, that are the colonies of cancer cells, were carefully and with time-taking measured with counting by the naked eye, the number were 52 pieces per 1.4

square millimeters (one visual field). The counting was carried out under a condition of a high extent of enlargement by a stereoscopic microscope.

When a picture-taken image of the same sample was counted in a stage previous to the image processing by a colony counter which is usually employed, the colony number was 1024 pieces per 1.4 square millimeters, so that precise counting of colonies of cancer cells was not possible by an influence of fibroblasts.

Next, the counting result of colony number for the image in a stage of that said image processing (a high frequency component extracting operation and a gray level-classifying operation) which had already been carried out was 51 pieces per 1.4 square millimeter, which is almost the same result as the counting-measurement result by said naked eye. Therefore, it was proved that the counting of the colony number resulting from the image processing has sufficient accuracy. Also, the colony number-counting for the image in a stage of that said image processing was already carried out was far simpler than the counting of only the cancer cell colonies in a fibroblasts etc.-coexisting mixture.

#### Result of Counting of Colony Numbers After Image Processing

Table 2 below-presented shows results of image processing as described above followed by counting the colony numbers concerning samples which were brought in contact with anticancer drugs. In order to raise the measurement accuracy the counting of colony numbers was carried out with a low extent of enlargement (one visual field of 2.8 mm×2.8 mm).

TABLE 2

Anticancer drug	Colony number/2.8 mm × 2.8 mm
(-)	206
MMC	37
5-FU	74
VP-16	181
VDS	159
CDDP	113

In Table 2, the symbol (-) indicates a case where any anticancer drug is not used (a control experiment) and, the anticancer drug for the sample having a smaller number of colonies in comparison with this control, that is the sample in which the growth of cancer cells has been depressed, indicates higher sensitivity.

#### EXPERIMENT 2

##### Comparison with Previous Method

To confirm the reliability of the method of the example in this invention for an anticancer drug sensitivity test, the obtained results were compared with the measurement results from the nude mouse method which at present has been recognized as a method showing the best clinical correlation in anti tumor effect.

First, from the counting results of the colony numbers obtained from said example, the percentages of the numbers of colonies formed when treated with each anticancer drug against those when untreated (control experiment) were derived with calculation as "percent of control". Results are shown as graphs in FIG. 1.

Next, the anticancer drug sensitivity test using nude mice (Example for comparison 1) was carried out as undermentioned. The nude mouse-xenografted human colon cancer, which was used in the forementioned "Culture of cancer cells", was minced into fragments of approximately 2 mm in cubic size and, subsequently,

transplanted subcutaneously into nude mice. Then, when the estimated weight of the tumors(cancers) reached approximately 100 mg, each of 3 mg/kg of said MMC, 50 mg/kg of 5-FU, 25 mg/kg of VP-16, 5 mg/kg of CDDP, and 3 mg/kg of VDS was injected 4 times weekly into the abdominal cavity of 5 nude mice in each group and an, additional one group was served as controls for which the anticancer drug is not injected. The estimated weights of tumors were calculated by measuring the length (L mm) and width (W mm) of the tumors and using a formula  $L \times W^2/2$ . Then, at one week later than the final injection, the estimated weights of tumors were again measured, and the percentages of the mean tumor weights in the case of that treatment with each drug was carried out against those in the case untreated with a drug (control) were calculated similarly as "percent of control". The results are illustrated in FIG. 2.

When FIG. 1 showing the measurement results of the examples in this invention which comprises a combination of collagen gel culture and an image processing is compared with FIG. 2 showing the measurement results obtained from the nude mice method, an excellent correlation was obtained for all the cancer drugs. It was thus proved that the method of this invention has been highly practical as an in vitro alternative method for the in vivo nude mouse method. Furthermore, it was proved that although the nude mouse method required more than one month in period of experiment, the method of the present examples were able to provide reliable results of high accuracy within short period of time of approximately 10 days.

When the growth of cancer cells is measured by number-counting of colonies, an exact growth of cells is sometimes not obtained depending upon the proliferating mode of cells. For example, as seen in FIG. 3, when six pieces of single cancer cell 1 are cultured in collagen gel 5, in a case of that the growth is uniform and small as shown by the arrow A, the six colonies 2 of almost similar size are formed, so that there is no each other's overlapping of colonies. In this case the automatic counting gives a result of six for the colony number. However, in a case of that the growth is non-uniform as shown by the arrow B in FIG. 3, or in a case of that the growth is large as shown by the arrow C in FIG. 3, plural colonies 2 in a neighborhood are overlapped, so that essentially, plural colonies are determined as one by automatic counting. For example, in the proliferating case as shown by the arrow B, the automatic counting gives a result of four colonies and, in the proliferating case as shown by the arrow C, the automatic counting gives a result of two colonies (in both cases, the exact number of colonies is six). To solve an error of these kinds, there have been considered;

① a method in which the number of inoculating cells (cell density) is lowered (for example,  $1 \times 10^4$  cells/ml or less); or

② a method in which measurement finishes before the colony overlapping takes place.

However, in a majority of primary cancer cells, observation of the colonies is only possible in a high density of culturing such as  $5 \times 10^4$  cells/ml or more of cell density, so that according to the method ①, an exact judgment for the effects of anticancer drugs is not possible. Also, since the growth of cancer cells differs depending upon each cancer cell, the measurement in said ② method is finished before difference between the measurement and a control experiment as well as before

difference in the effects of differing anticancer drugs sufficiently appears. Thus, the exact effects of anticancer drugs can not be obtained with the method (2).

As the forementioned, if the growth of cancer cells is not exactly measured, great inconvenience occurs in actual anticancer drug sensitivity testing methods. For example, as seen in FIG. 4, when six pieces of single cancer cell 1 are cultured in the collagen gel 5, in a case where the cancer cell is not treated with an anticancer drug as shown by the arrow D, six pieces of large colonies 2 are formed, but if three each among these colonies is each other overlapped or come in contact, the automatic counting gives a result of two for the colony number. In contrast, in a case where the cancer cell is treated with an anticancer drug as shown by the arrow E, if six pieces of small colonies 2 are formed and each other separated, the automatic counting, gives a result of six for the colony number. In general, the effect of an anticancer drug (an inhibition extent for growth) is derived from a percent ratio in the following equation:

$$\frac{\left( \begin{array}{l} \text{colony number by culturing cancer} \\ \text{cells treated with anticancer drug} \end{array} \right)}{\left( \begin{array}{l} \text{colony number of a control group} \\ \text{(by culturing cancer cells not} \\ \text{treated with anticancer drug)} \end{array} \right)} \times 100(\%)$$

and, therefore, if an anticancer drug is effective, the ratio must be less than 100%. However, in the example in FIG. 4, the ratio is 300% [(6/2) × 100%].

The reason why such a unreasonable result was obtained in a case where the growth of cancer cells is measured with the number of colonies is a result of contact of colonies and/or overlapping of colonies.

Therefore, in the present invention it is preferred to measure the growth of cancer cells by determination of the volume of colonies. In this case, the effect of an anticancer drug (an inhibiting extent for growth) is derived from a percent ratio in the following equation:

$$\frac{\left( \begin{array}{l} \text{colony volume by culturing cancer} \\ \text{cells treated with anticancer drug} \end{array} \right)}{\left( \begin{array}{l} \text{colony volume of a control group} \\ \text{(by culturing cancer cells not} \\ \text{treated with anticancer drug)} \end{array} \right)} \times 100(\%)$$

and, therefore, if an anticancer drug is effective, the ratio must be less than 100%. As seen in FIG. 5 too, neighboring colonies (for example, two pieces of colonies) 2 and 2 are each other in contact, the volume of these colonies is the same to a total volume of (two) separate colonies. In other words, in the contacting case, there is little effect or no effect on a total volume of a plural colony. Also, in a case of the overlapping, since the overlapping part is very small in volume, there is no significant effect on the total volume. Therefore, an exact measurement of the growth of cells is always possible with determination of the colony volume, but it is not always possible with determination of the colony number by an automatic counting.

As mentioned above, in measuring the growth of cancer cells with image processing, even if the growth can not be measured with determination of the colony number, exact measurement of the growth is possible

with determination of an estimated colony volume. This fact was confirmed by comparison with an measured DNA amount in the following experiment. This experiment differs from said experiment in use of a human cancer cell strain not containing fibroblasts. Because of this, the measurement of the human cancer cell strain growth is exactly confirmed with measurement of the DNA amount.

## EXPERIMENT 3

### Culture of Cancer Cells

Using a human lung cancer cell strain, in a manner same to the control experiment in the above-mentioned example 1, a collagen gel-embedded culture was carried out without treating with an anticancer drug.

### Image Processing

Picture of the human lung cancer cell strain cultured with embedding in a collagen gel substrate was, as carried out before, taken to input into the image processor as image signals. An original image inputted was, as carried out before, processed by image processing and only the image of cancer cell colonies was extracted (but in this case, since tile fibroblasts are not contained, removing-processing for them is unnecessary). Then, the colony number was counted in from the image as carried out before and, at the same time, an integrated value of the three-dimensional volume estimated from the colony image is determined. A procedure of the volume determination was carried out as follows.

1. A binary image which is a projected image of colonies is defined as an original image.

2. Separately, a picture frame capable of representing the grey level is defined as a storage-image plane.

3. The original image is copied onto the storage-image plane by setting the grey level as 1.

4. A picture element which composes a peripheral line of the projected image, is removed from the original image.

5. The projected image, which was reduced with removal of the picture elements composing the peripheral line, is defined as a new original image.

6. This new original image is copied onto the storage-image plane, to which one grey level is added.

7. The processing of 4. to 6. is repeated until the projected image disappears. By doing this, a three-dimensional image of a mountain style is obtained, in which a bottom face is a face surrounded with the peripheral line of the first projected image, and which needs not to be a real image.

8. A product of the length of a picture element with a grey level which is stored in each picture element in the storage-image plane is defined as the height.

9. The height of each picture element in the storage-image plane is integrated. With this, a volume of the three-dimensional image of a mountain style is obtained.

10. By assuming the real body of a colony as symmetrical in the surface and reverse side with respect to the projected image, a value obtained by a double of the integrated value is assigned as a volume of the colonies. Why the above assuming is carried out is due to consideration of that a form same to the form expanding broadwise in a three-dimensional culture will also expand upward and downward.

11. In cases of necessity, the outputting is carried out.

The number and volume of colonies obtained from the above-mentioned image processing as well as the measurement results of DNA amounts are summarized in Table 3 and FIG. 6.

TABLE 3

Culturing period (day)	1	3	5	7	9	11	13	19	25	Symbols in FIG. 6
Number of colonies* (piece)	126	287	347	343	256	124	69	45	39	●
Colony volume* (Integrated value) ( $\times 10^6 \mu\text{m}^2$ )	14	44	67	82	97	116	134	205	235	X
Amount of DNA ( $\mu\text{g}/\text{well}$ )	1.04	2.94	5.29	6.03	7.26	8.19	9.77	13.58	16.21	○

(Note) \*A numeral value per a 4 mm  $\times$  4 mm visual field.

As seen with the DNA amounts in the results of Table 3 and FIG. 6, the cells proliferate with a culturing period of days. Although the colony number counted is in consistent with the change in the DNA amount until the fifth day of the culturing, a peak of the colony number is observed on from the fifth to the seventh day and, after these days, a decrease is observed. This indicates that, as a result of the cell growth, the cell density becomes so high causing overlapping of cells and, therefore, an exact counting of the colony number is not achieved. On the other hand, the colony volume is well correlated with the change in the DNA amount from an initial stage of the culturing until a long period of culturing. It is thus understood that the volume-measuring method is very suitable for measuring the growth of cells, in particular, for measuring it for a long period.

Further, the number-counting measurement of colonies has the following problems. That is, the growth of cancer cells differs depending upon an individual cell (refer to the cell colonies indicated by the arrow B in FIG. 3). Since each of the colonies 21, 22, and, 23 differs in size, the number of cells contained differs, but according to number-counting of the colonies, each of the colonies 21, 22, and 23 is determined as one piece. On the other hand, in measuring the volume of colonies the colonies 21, 22, and 23 have different volume.

#### EXAMPLE 2

In the "Culturing of cancer cells" in the example 1, the procedure of example 1 was repeated for culturing cancer cells except that a nude mouse-xenografted human lung cancer was used instead of a nude mouse-xenografted human colon cancer, whereby a sample obtained was processed with image processing as carried out for the example 1 in order to extract only the image of colonies.

From the image obtained, the number of colonies was counted as carried out for the example 1 and a value by integrating the volume of colonies was determined as carried out for the experiment 3.

#### EXAMPLE FOR COMPARISON 2

To examine the results from the example 2, by using the cells same to those used in the forementioned example 2, an anticancer drug sensitivity test by a nude mouse method is carried out in a manner same to said example for comparison 1 at the same time.

For the results obtained from the respective examples, the percents of control were derived as carried out before and shown as the graphs in FIG. 7.

As seen in FIG. 7, a very good correlation for any anticancer drug was obtained between the results from both the nude mouse method (N) and the method of measuring colony volume (V). On the other hand, the

results from the method of counting colony number (C) show abnormal values. This indicates that the cells used here show high growth and, in particular, in a case where the cells are not treated with an anticancer drug

(a control experiment), the proliferating cells are overlapped as explained above so that the number-counting of colonies does not show the exact growth, while the volume-measuring of colonies shows the exact growth even in a case of this kind.

That is, in a case of actively proliferating cells or in a case where the cell density is heightened during a period of culturing, it was proved that the colony-volume measurement carried out after proliferation is an effective method for measuring the growth.

#### Illustration of Photographs of Monitor Television (TV) Picture Frames in Reference

Photographs of monitor TV picture frames (FIGS. 8 and 9), as explained before, show the results of that the images of a sample (a control experiment), with which human cancer cells were cultured using a collagen gel substrate, were outputted onto a monitor TV at the stages of before (FIG. 8) and after (FIG. 9) the image processing. The visual scope of images is 1.4 mm in the whole width between the right and left.

In the image of FIG. 8, there appears a condition under which the colonies of cancer cells having a sphere shape or a block shape and the fibroblasts having a bipolar linear shape exist in a mixing condition. The number-counting of cancer cell colonies by a nude eye so far used has been carried out under an image condition of this FIG. 8.

In the image of FIG. 9, there appears only the colonies of cancer cells after removing unnecessary images of fibroblasts etc. In the present invention, the colony number of cancer cells is counted by the images shown in FIG. 9.

A series of photographs, from FIG. 10 to FIG. 19, as explained before, are the photographs of picture frames obtained by that a sample (control) is given by culturing human lung cancer cells with embedding them by using a collagen gel substrate, culturing conditions of the sample varying with the passage of culturing days are processed by image processing, and the images thus-obtained are outputted onto a monitor TV. The visual scope of images is 4 mm in the whole width between the right and left.

The photographs from FIG. 10 to FIG. 19 are the images, each of which is obtained in sequence with the passage of following culturing days; one day, three days, four days, five days, seven days, eleven days, thirteen days, nineteen days, and twenty-five days. The cancer cell colonies which are shown with a white or bluish gray color are gradually varying from a small spot type to a large block type and one another coming in contact or overlapping. The growth is not uniform

and differs with an individual cell. In the present invention the growth of cancer cells is measured by the colony number or colony volume, for example, with the images which are shown in anyone of Photographs from FIG. 10 to FIG. 19. Beside, as the forementioned, it is possible to trace the growth with the passage of culturing periods of days.

According to the forementioned anticancer drug sensitivity-testing method in the present invention, since a collagen gel is used as a substrate for culturing cancer cells, a variety of cancer cells of such kinds that the culturing is impossible in hitherto-known soft agar substrate and the like can be cultured.

The effects of fibroblasts etc., which proliferate together with cancer cells in a case where the cancer cells are cultured in the collagen gel substrate, can be eliminated by measuring the growth of cancer cells by image processing, so that the testing results are obtained accurately and quickly.

In the image processing of the growth of cancer cells, the measurement of colony volume gives more reliable results than the counting of the colony number, and gives results of the growth for a longer period.

With the results forementioned, it can be said that a sensitivity-testing method useful for development of anticancer drugs is provided which, compared with a testing method so far used, has much wider applicability for many kinds of cancer cells, is much simpler in handling, and is capable of providing the test results promptly and accurately.

What is claimed is:

1. A method for testing the sensitivity of anticancer drugs comprising the steps of:

- (a) proliferating cancer cells in a collagen gel substrate after contacting the cells with an anticancer drug, wherein fibroblast cells which are contained in cancer tissues proliferate together with the cancer cells of step (a),
- (b) proliferating cancer cells for a control in a collagen gel substrate without contacting with the anticancer drug, wherein fibroblast cells which are contained in cancer tissues proliferate together with the cancer cells of step (b),
- (c) obtaining a picture image for the cancer cells of step (a) and a control picture image for the cancer cells of step (b), each picture image comprising first images of proliferated cancer cells and colonies composed of the proliferated cancer cells, and second images of proliferated fibroblast cells, and
- (d) measuring the growth of the cancer cells proliferated in said substrates of step (a) and step (b) by:
  - (1) inputting both picture images after growth into an image processor,
  - (2) selectively extracting the first images, respectively, from said both picture images using the image processor, and
  - (3) determining the colony count or volume of said cancer cells using the image processor and using the selectively extracted first images from said picture image for the cancer cells of step (a) and the selectively extracted first picture images from said control picture image for the cancer cells of step (b) to compare the colony count or volume of the cancer cells of step (a) with the

colony count or volume of the cancer cells of step (b).

2. The method as claimed in claim 1, wherein the step of selectively extracting the first images using the image processor comprises the steps of:

- (a) digitizing the picture image into picture elements,
- (b) converting into numerals, the concentrations of each picture element of the digitized picture image,
- (c) selecting, according to a value of said numerals, the objects to be processed,
- (d) processing said objects on the basis of at least one of the differences in shape and said value of said numerals to remove the second images from said digitized picture image.

3. The method as claimed in claim 2, wherein the numerals refer to gray levels of said picture elements.

4. The method as claimed in claim 3, wherein the measurement of the growth of the cancer cells is determined by counting the number of said first images.

5. The method as claimed in claim 3, wherein the measurement of the growth of the cancer cells is carried out by calculating the total volume of said selectively extracted first images using the image processor.

6. The method as claimed in claim 5, wherein the calculation of the total volume of the selectively extracted first images using the image processor comprises the steps of:

- (a) providing binary images of the selectively extracted first images,
- (b) processing said binary images to form the corresponding three-dimensional images of a mountain style of which the bottom face is a face surrounded with the peripheral line of each of said binary images by:
  - (1) providing a storage-image plane to represent a gray level,
  - (2) copying said binary images onto the storage-image plane, the copied binary images having a gray level of 1,
  - (3) removing the picture elements forming the peripheral lines of said binary images from the binary images to form reduced binary images,
  - (4) providing the reduced binary images of step (3) in place of said binary images,
  - (5) copying the reduced binary images of step (3) over the corresponding copied binary images of step (2) on said storage-image plane to form stored images, the copied, reduced binary images having a gray level of 1, and
  - (6) repeating steps (3), (4) and (5) until said reduced binary images disappear, so that said stored images form said corresponding three-dimensional images of a mountain style, and
- (c) calculating the total volume of the selectively extracted first images by:
  - (1) providing, as a height, the product of the length of a picture element with the corresponding gray level stored on each picture element on the storage-image plane,
  - (2) integrating the height on each picture element to obtain the volume of each three-dimensional image of a mountain style, and multiplying the volume by two to obtain the total volume of said first images.

\* \* \* \* \*

## Potent Antitumor Activity of MS-247, a Novel DNA Minor Groove Binder, Evaluated by an *in Vitro* and *in Vivo* Human Cancer Cell Line Panel<sup>1</sup>

Takao Yamori,<sup>2</sup> Akio Matsunaga, Shigeo Sato, Kanami Yamazaki, Akiko Komi, Kazuhiro Ishizu, Izumi Mita, Hajime Edatsugi, Yasuhiro Matsuba, Kimiko Takezawa, Osamu Nakanishi, Hiroshi Kohno, Yuki Nakajima, Hironori Komatsu, Toshio Andoh, and Takashi Tsuruo

Division of Experimental Chemotherapy, Cancer Chemotherapy Center, Japanese Foundation for Cancer Research, Tokyo 170-8455 [T. Y., S. S., K. Y., A. K., K. I.]; Life Sciences Laboratory, Mitsui Chemical Inc., Chiba 297-0017 [A. M., H. K., Y. N., H. K.]; Institute of Biological Science, Mitsui Pharmaceuticals, Inc., Chiba 297-0017 [I. M., H. E., Y. M., K. T., O. N.]; Faculty of Engineering, Soka University, Tokyo 192-0003 [T. A.]; and Institute of Molecular and Cellular Biosciences, University of Tokyo, Tokyo 113-0032 [T. T.], Japan

### ABSTRACT

We synthesized a novel anticancer agent MS-247 (2-[[[N-[1-methyl-2-[5-[N-[4-[N,N-bis(2-chloroethyl) amino] phenyl]] carbamoyl]-1H-benzimidazol-2-yl] pyrrol-4-yl] carbamoyl] ethyldimethylsulfonium di-*p*-toluenesulfonate) that has a netropsin-like moiety and an alkylating residue in the structure. We evaluated antitumor activity of MS-247 using a human cancer cell line panel coupled with a drug sensitivity database and subsequently using human cancer xenografts. The average MS-247 concentration required for 50% growth inhibition against a panel of 39 cell lines was 0.71  $\mu$ M. The COMPARE analysis revealed that the differential growth inhibition pattern of MS-247 significantly correlated with those of camptothecin analogues and anthracyclins, indicating that MS-247 and the two drug groups might have similar modes of action. MS-247 exhibited remarkable antitumor activity against various xenografts. A single i.v. injection of MS-247 significantly inhibited the growth of all 17 xenografts tested, which included lung, colon, stomach, breast, and ovarian cancers. In many cases, MS-247 was more efficacious than cisplatin, Adriamycin, 5-fluorouracil, cyclophosphamide, VP-16, and vincristine and was almost comparable with paclitaxel and CPT-11; these are the most clinically promising drugs at present. MS-247 was noticeably more effective than paclitaxel (in HCT-15) and CPT-11 (in A549, HBC-4, and SK-OV-3). The toxicity of MS-247, indicated by body weight loss, was reversible within 10 days after administration. The MS-247 mode of action showed DNA binding activity at the site where Hoechst 33342 bound, inhibited topoisomerases I and II (as expected by the COMPARE analysis) blocked the cell cycle at the G<sub>2</sub>-M phase, and induced apoptosis. These results indicate that MS-247 is a promising new anticancer drug candidate to be developed further toward clinical trials.

### INTRODUCTION

DNA minor groove binders are an attractive source of novel antitumor agents. As a whole, they induce a huge range of mutations from simple base sequence changes to deletions and ploidy changes (reviewed in Ref. 1). The recent increased interest in this group of compounds stems from their ability to interact in a sequence-selective fashion at quite long DNA binding sites, suggesting the possibility of targeting specific DNA sequences within the genome (2-6). Several DNA minor groove binders proved to have potent antitumor activity in preclinical studies and are now under clinical phase studies. They include duocarmycin derivatives adozelesin (7-9), carzelesin (10, 11), bizelesin (12, 13) and KW-2189 (14), and a distamycin A-derivative tallimustine (15). However, their clinical efficacies have not been established yet (16-19).

Received 3/23/99; accepted 6/8/99.

The costs of publication of this article were defrayed in part by the payment of page charges. This article must therefore be hereby marked *advertisement* in accordance with 18 U.S.C. Section 1734 solely to indicate this fact.

<sup>1</sup> This work was supported in part by a Grant-in-Aid for Scientific Research on Priority Area "Cancer" from the Ministry of Education, Science, Sports and Culture, Japan, as well as by a grant from the Organization for Pharmaceutical Safety and Research of Japan.

<sup>2</sup> To whom requests for reprints should be addressed, at Cancer Chemotherapy Center, Japanese Foundation for Cancer Research, 1-37-1 Kami-Ikebukuro, Toshima-ku, Tokyo 170-8455, Japan. Phone: 81-3-3918-0111, extension 4453; Fax: 81-3-3918-3716.

We attempted to develop a new DNA minor groove binder that has the more promising antitumor activity. We synthesized compounds that have two moieties in the structure. One is a netropsin-like moiety (Fig. 1) to acquire DNA minor groove binding activity, and another is an *N,N*-bis(2-chloroethyl) amino residue for DNA alkylation. Netropsin is one of the polypyrrrolecarboxamides, like distamycin A, and binds to DNA minor grooves at the A-T-rich region (20). After screening a number of synthetic compounds, we selected MS-247<sup>3</sup> (Fig. 1). It had shown significant cytotoxicity in several murine tumor cell lines and strong *in vivo* antitumor activity against murine tumor models in our preliminary study.

The present study was designed to evaluate the antitumor activity of MS-247 against various human cancers *in vitro* and *in vivo* and to elucidate its mode of action. We report here that MS-247 indicated potent antitumor activity against all 17 human xenografts tested, and that MS-247 bound to the DNA minor groove, inhibited topoisomerases I and II, blocked the cell cycle at G<sub>2</sub>-M phase, and induced apoptosis.

### MATERIALS AND METHODS

**Chemicals.** MS-247 was synthesized in the Life Sciences Laboratory Mitsui Chemicals, Inc. (Chiba, Japan). MS-247 was dissolved in *N,N*-dimethylformamide (Tokyo Kasei Kogyo, Tokyo, Japan) before use. CPT-11 was kindly supplied by Yakult Honsha (Tokyo, Japan). Other anticancer drugs and chemicals were purchased as follows: ADM and 5-FU, Kyowa Hakkō Kogyo (Tokyo, Japan); cisplatin and VP-16, Nippon Kayaku (Tokyo, Japan); CPM, Shionogi Pharmaceuticals (Osaka, Japan); VCR, Eli Lilly Japan (Kobe, Japan); paclitaxel, camptothecin, calf thymus DNA, RNase A, and propidium iodide, Sigma (St. Louis, MO.); Hoechst 33342, Molecular Probes (Eugene, OR); Proteinase K, Boehringer Mannheim (Mannheim, Germany); and  $\phi$ X174/HaeIII, Toyobo (Tokyo, Japan).

**Cell Lines.** Human breast cancer MDA-MB-231 and leukemia HL-60 were purchased from American Type Culture Collection (Rockville, MD). Murine leukemia L1210, P388, and the following human cancer cell lines (21) were generously distributed by the National Cancer Institute (Frederick, MD): lung cancer, NCI-H23, NCI-H226, NCI-H522, NCI-H460, DMS273 and DMS114; colon cancer, HCC-2998, KM-12, HT-29, WiDr, HCT-15, and HCT-116; ovarian cancer, OVCAR-3, OVCAR-4, OVCAR-5, OVCAR-8, and SK-OV-3; breast cancer, MCF-7; renal cancer, RXF-631 L and ACHN; melanoma, LOX-IMVI; and brain tumor, U251, SF-295, SF-539, SF-268, SNB-75, and SNB-78. Human stomach cancer, MKN-1, MKN-7, MKN-28, MKN-45, MKN-74, and St-4, and human breast cancer BSY-1, HBC-4, and HBC-5 were described elsewhere (22, 23). The cells were cultured in RPMI 1640 supplemented with 5% fetal bovine serum, penicillin (100 units/ml), and streptomycin (100 mg/ml) at 37°C in humidified air containing 5% CO<sub>2</sub>.

**A Human Cancer Cell Line Panel and the Database.** To evaluate drugs for the cell growth inhibition profile, we established a human cancer cell line

<sup>3</sup> The abbreviations used are: MS-247, 2-[[[N-[1-methyl-2-[5-[N-[4-[N,N-bis(2-chloroethyl) amino] phenyl]] carbamoyl]-1H-benzimidazol-2-yl] pyrrol-4-yl] carbamoyl] ethyldimethylsulfonium di-*p*-toluenesulfonate; ADM, Adriamycin; 5-FU, 5-fluorouracil; CPM, cyclophosphamide; VCR, vincristine; VP-16, etoposide; GI<sub>50</sub>, concentration required for 50% growth inhibition; PBS(-), calcium- and magnesium-free PBS.



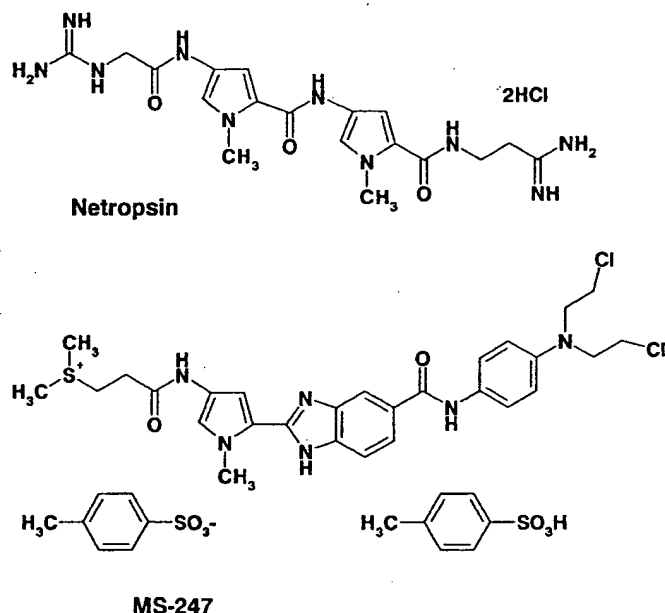


Fig. 1. Chemical structure of netropsin and MS-247. MS-247 has a netropsin-like moiety and an alkylating residue in the structure.

panel combined with a database. The system as a whole was developed according to the method of the National Cancer Institute (24–26), with modification. The cell line panel consisted of 38 human cancer cell lines, described above, and 1 murine leukemia (P388). With this system, we have examined the antiproliferative effect of more than 200 standard compounds, including various anticancer drugs, and established a new database, as described below.

**Measurements of Cell Growth Inhibition and Data Analysis.** The details of measuring cell growth inhibition are described elsewhere (26, 27). Briefly, the cells were plated at proper density in 96-well plates in RPMI 1640 with 5% fetal bovine serum and allowed to attach overnight. The cells were exposed to drugs for 48 h. Then, the cell growth was determined according to the sulforhodamine B assay, described by Skehan *et al.* (28). Data calculations were made according to the method described previously (26). Absorbance for the control well (C) and the tests well (T) were measured at 525 nm. Moreover, at time 0 (addition of drugs), absorbance for the test well ( $T_0$ ) was also measured. Using these measurements, cell growth inhibition (percentage of growth) by each concentration of drug was calculated as: % growth =  $100 \times [(T - T_0)/(C - T_0)]$ , when  $T > T_0$  and % growth =  $100 \times [(T - T_0)/T]$ , when  $T < T_0$ . By using the computer to process % growth values, the 50% growth inhibition parameter ( $GI_{50}$ ) was determined. The  $GI_{50}$  was calculated as  $100 \times [(T - T_0)/(C - T_0)] = 50$ . The mean graph, which shows the differential growth inhibition of the drug in the cell line panel, was drawn based on a calculation using a set of  $GI_{50}$  (24, 25). To analyze the correlation between the mean graphs of drug A and drug B, the COMPARE computer algorithm was developed according to the method described by Paull *et al.* (25). Pearson correlation coefficients were calculated using the following formula:  $r = (\sum(x_i - x_m)(y_i - y_m))/(\sum(x_i - x_m)^2 \sum(y_i - y_m)^2)^{1/2}$ , where  $x_i$  and  $y_i$  are log  $GI_{50}$  of drug A and drug B, respectively, against each cell line, and  $x_m$  and  $y_m$  are the mean values of  $x_i$  and  $y_i$ , respectively.

**Animals.** Female nude mice with BALB/c genetic backgrounds were purchased from Charles River Japan, Inc. (Kanagawa, Japan). They were maintained under specific pathogen-free conditions and provided with sterile food and water *ad libitum*. Seven-week-old mice weighing 16–22 g were used for this study.

**Drugs and Administration.** Drug administration was done i.v. We selected an administration schedule of single shot for MS-247, according to the results in animal tumor models.<sup>4</sup> We first determined the maximum tolerable dose of MS-247 in the schedule, which was 30 mg/kg. To evaluate the

antitumor effect, MS-247 was given to tumor-bearing nude mice at doses of 30, 25, and 21 mg/kg for lung cancer xenografts and at a dose of 25 mg/kg for other xenografts. The reference drugs chosen were CPT-11, paclitaxel, cisplatin, ADM, 5-FU, CPM, VP-16, and VCR. Each reference drug was given at the maximum tolerable dose in the optimal schedule.

**Antitumor Activity against Xenografts.** Six lung cancers (NCI-H23, NCI-H226, NCI-H460, A549, DMS114, and DMS273), four stomach cancers (MKN-1, MKN-7, MKN-74, and St-4), three colon cancers (HCC-2998, HCT-116, and HCT-15), two breast cancers (HBC-4 and MDA-MB-231), and two ovarian cancers (SK-OV-3 and OVCAR-8) were used to evaluate antitumor activity of MS-247. They were grown as s.c. tumors in nude mice. Nude mice were inoculated s.c. with a  $3 \times 3 \times 3$ -mm tumor fragment. When the tumor reached 100–300 mm<sup>3</sup> in volume, animals were divided randomly into test groups consisting of six mice per group (day 0). Drugs were administered from day 0 according to the dose schedules indicated. The mice were weighed twice each week up to days 24–31 to monitor the toxic effects. The length (L) and width (W) of the tumor mass were measured twice a week up to days 24–31, and the tumor volume (TV) was calculated as:  $TV = (L \times W^2)/2$ . The tumor volume at day  $n$  was expressed as relative tumor volume (RTV), according to the following formula:  $RTV = TV_n/TV_0$ , where  $TV_n$  is the tumor volume at day  $n$ , and  $TV_0$  is the tumor volume at day 0. Tumor regression (T/C%) on day 14 was determined by calculating RTV as:  $T/C\% = 100 \times (\text{mean RTV of treated group})/(\text{mean RTV of control group})$ . Statistical evaluations of RTV were performed using the Mann-Whitney *U* test.

**Measurement of Fluorescence of DNA-bound Hoechst 33342.** In the cell free system, 1  $\mu$ g of calf thymus DNA and 0.8  $\mu$ g of Hoechst 33342 were mixed in 0.2 ml of PBS(–) and preincubated for 10 min at room temperature in a 96-well plate. Then, MS-247 was added at final concentrations of 0.01–30  $\mu$ g/ml. After another 10-min incubation, the fluorescence derived from the Hoechst 33342 bound to DNA was measured with a fluorometer (excitation wavelength, 355 nm; and emission wavelength, 460 nm). In the cellular system, L1210 cells ( $4 \times 10^5$  cells in 1 ml of culture medium) were preincubated with Hoechst 33342 (4  $\mu$ g/ml) at 37°C for 20 min. Then, MS-247 was added at final concentrations of 0.01–100  $\mu$ g/ml. After another 20-min incubation, the cells were washed once with ice-cold PBS(–), resuspended in ice-cold PBS(–), and transferred into a 96-well plate. Fluorescence was measured as described above.

**Cell Cycle Analysis.** Cell cycle analysis was performed using flow cytometry, as described previously (29). The L1210 cells were exposed to MS-247 for 3–48 h. The cells were harvested, washed with ice-cold PBS(–), and fixed in 70% ethanol. The cells were washed twice with ice-cold PBS(–) again, treated with RNase (0.25  $\mu$ g/ml) at 37°C for 1 h, and stained with propidium iodide (50  $\mu$ g/ml). The DNA content of the cells was analyzed using an EPICS ELITE flow cytometer (Coulter, Hialeah, FL).

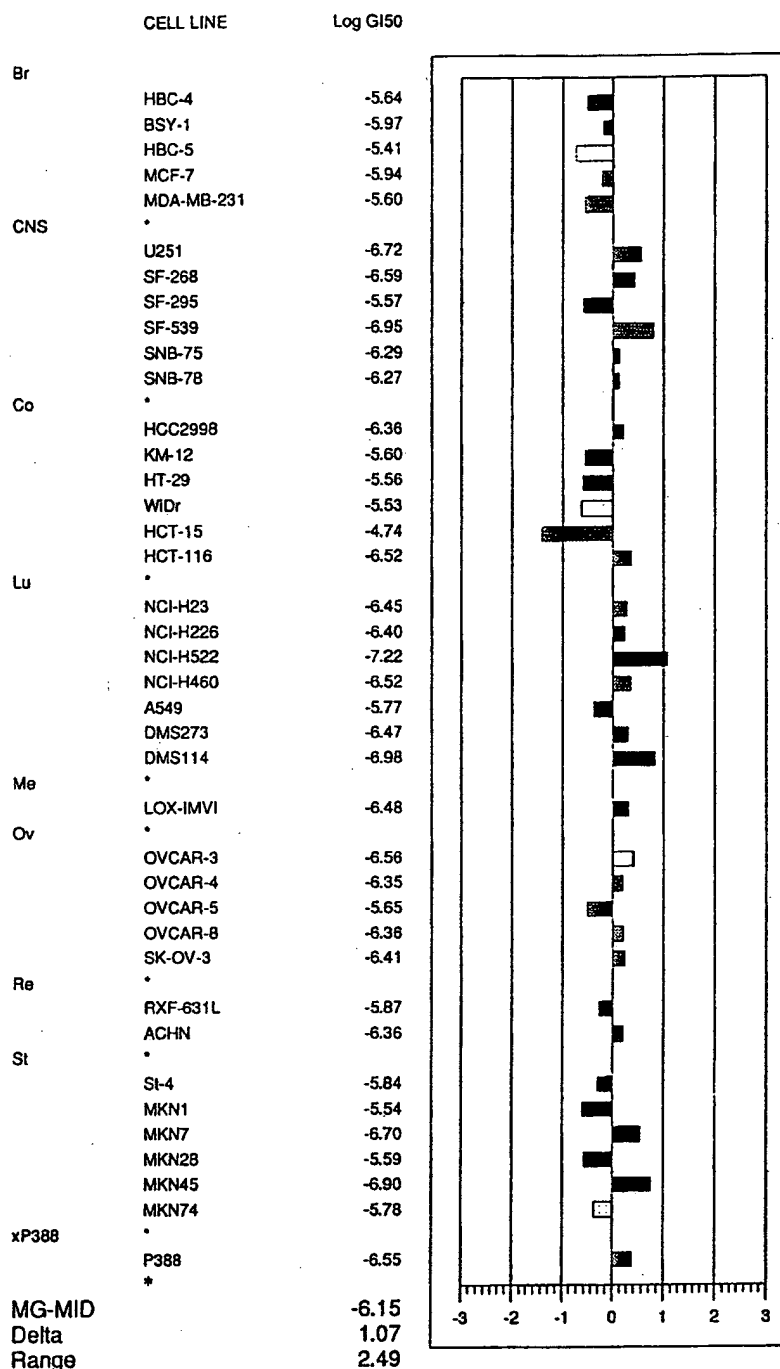
**Topoisomerase Activity Assays.** Topoisomerase I enzyme activity was measured by DNA relaxation assay using the Topoisomerase I Drug Screening kit (TopoGEN, Columbus, OH). Briefly, supercoiled DNA (0.25  $\mu$ g) was suspended in a standard reaction mixture [10 mM Tris-HCl (pH 7.9), 1 mM EDTA, 150 mM NaCl, 0.1% BSA, 0.1 mM spermidine, and 5% glycerol]. MS-247 was added to the mixture before the reaction was started by topoisomerase I enzyme addition. After a 30-min incubation at 37°C, the reaction was stopped by adding 0.1 volume of 10% SDS. The DNA-bound protein (topoisomerase I) was digested by proteinase K (41.7  $\mu$ g/ml) at 37°C for 30 min. The proteinase K was removed by chloroform:isoamylalcohol (24:1, v/v) treatment. DNA samples were then analyzed by 1% agarose gel electrophoresis.

**DNA Fragmentation Assay.** DNA fragmentation was analyzed by agarose gel electrophoresis. The HL-60 cells ( $5 \times 10^5$ ) were treated with 0.2 or 2  $\mu$ M MS-247 or 20 nM camptothecin at 37°C for 20 h. The drug-treated cells were harvested and then suspended in TNE buffer [10 mM Tris-HCl (pH 7.6), 140 mM NaCl, and 1 mM EDTA]. Subsequently, it was lysed by incubation at 37°C for 30 min in the TNE buffer containing 0.2 mg/ml of RNase A, 0.2 mg/ml of Proteinase K, and 0.83% SDS. DNA extraction was performed as described previously (30), and extracted DNA was resuspended in TNE buffer, then treated with RNase A (0.2 mg/ml) at 37°C for 30 min, after Proteinase K (0.2 mg/ml) digestion at 37°C for 30 min. The purified DNA was resolved by electrophoresis in 2% agarose gels, stained with ethidium bromide, and visualized under UV light.

<sup>4</sup> Unpublished results.



Fig. 2. Growth inhibition against a panel of 38 human cancer cell lines. The mean graph was produced by computer processing of the  $GI_{50}$ s as described in "Materials and Methods." The  $\log GI_{50}$  for each cell line is indicated. Columns extending to the right, sensitivity to MS-247; columns extending to the left, resistance to MS-247. One scale represents one logarithm difference. MG-MID, the mean of  $\log GI_{50}$  values for 39 cell lines. Delta, the logarithm of difference between the MG-MID and the  $\log GI_{50}$  of the most sensitive cell line. Range, the logarithm of difference between the  $\log GI_{50}$  of the most resistant cell line and the  $\log GI_{50}$  of the most sensitive one.



## RESULTS

**Growth Inhibition against a Panel of 38 Human Cancer Cell Lines.** We have established a new human cancer cell line panel coupled with a drug sensitivity database, which is similar to the one developed by the National Cancer Institute (24–26). This panel consists of 38 human cancer cell lines and murine leukemia P388. Thus far, we have used this panel to evaluate more than 200 standard agents, most of which are anticancer drugs and various types of inhibitors. We have also added the growth-inhibitory parameters to the database. We compared standard drugs with each other for the mean graph pattern using COMPARE analysis and confirmed that drugs sharing a certain mode of action clustered together, as described

previously (24, 25). The patterns in the mean graphs of drugs with common modes of action resembled one another.

Using the human cancer cell line panel, we investigated the cell growth inhibition profile of MS-247. Fig. 2 shows the mean graph of MS-247 based on the growth inhibition parameter of  $GI_{50}$ . MS-247 showed differential growth inhibition, and it seemed to be more effective against lung cancer cell lines. The mean  $\log GI_{50}$  of MS-247 was  $-6.15$  ( $0.71 \mu M$ ), which fell in the middle of the range of presently used anticancer drugs in the panel (Fig. 3). The COMPARE analysis of the mean graph revealed that MS-247 significantly correlated with two main groups of anticancer agents (Table 1). The first was a camptothecin analogue group, including CPT-11, SN-38 (active

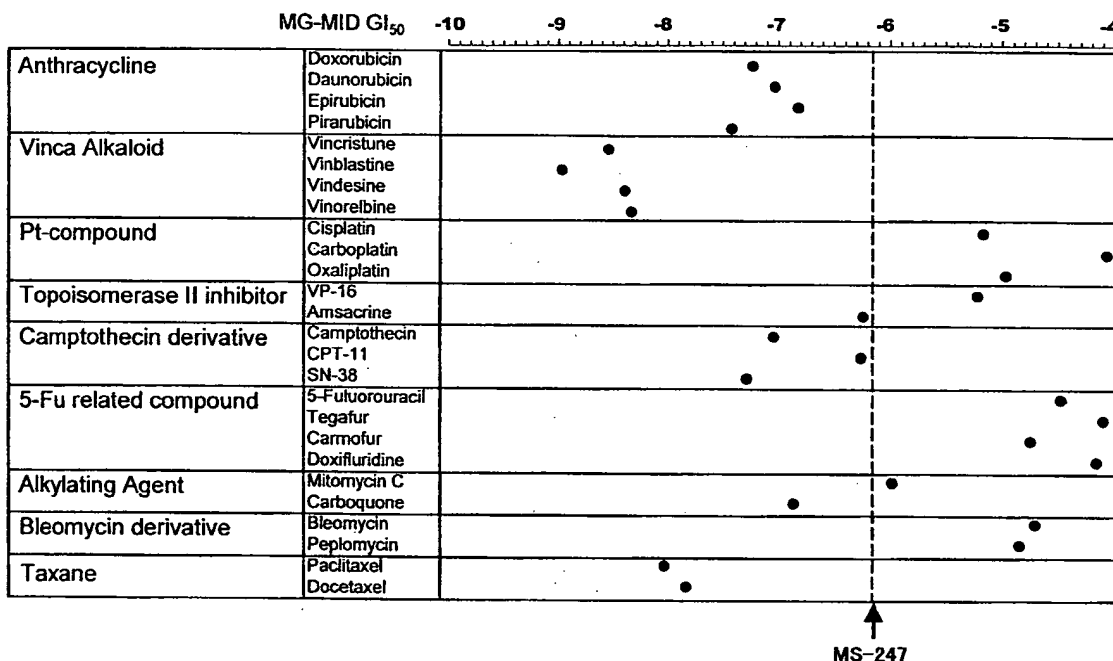


Fig. 3. Comparison of MS-247 with clinically active anticancer agents for the mean log  $GI_{50}$  against 39 cell lines. The  $GI_{50}$  of each drug to 39 cell lines was determined as described in "Materials and Methods." ●, mean log  $GI_{50}$  of each drug.

metabolite of CPT-11), and camptothecin. The second was an anthracycline group, including epirubicin, ADM, mitoxantrone, KW-2170, and daunorubicin. These results indicate that MS-247 may share some modes of action with both groups.

**Antitumor Activity of MS-247 against Human Cancer Xenografts.** To evaluate the antitumor activity of MS-247, we developed various human cancer xenografts by s.c. injecting 17 cell lines of the panel into nude mice. We examined the antitumor activity and the toxicity of MS-247 using six lung cancer xenografts (Fig. 4). The four lung cancer cell lines, NCI-H23, NCI-H226, NCI-H460, and A549, were originally non-small cell lung cancers, and others, DMS273 and DMS114, were small cell lung cancers. A single i.v. administration of MS-247 on day 0 significantly inhibited tumor growth at all of the dosages, 30, 25, and 21 mg/kg (Fig. 4, upper panels). There were not major differences in the efficacy within a dose range, indicating that MS-247 was effective in a rather wide dose range. It is remarkable that MS-247 induced tumor regression during a certain period in NCI-H23, NCI-H226, DMS273, and DMS114. As for toxicity, the body weight of the tumor-bearing mice decreased by day 10 after the administration, but it was recovered afterward (Fig. 4, lower panels). These results demonstrated the therapeutic efficacy of MS-247 in the nude mice bearing lung cancer xenografts.

Then, we examined MS-247 for activity against 10 other xenografts including colon, stomach, breast, and ovarian cancers, and we compared MS-247 with eight major anticancer drugs, paclitaxel, CPT-11, cisplatin, ADM, 5-FU, CPM, VP-16, and VCR (Table 2). A single injection of 25 mg/kg MS-247 showed significant antitumor activity against all 17 xenografts tested. MS-247 was more effective in most xenografts than cisplatin, ADM, 5-FU, CPM, VP-16, or VCR. MS-247 was comparable to paclitaxel and CPT-11, presently the most promising drugs. Noticeably, MS-247 was more effective than paclitaxel in HCT-15 and than CPT-11 in A549, HBC-4, and SK-OV-3; therefore, it showed a higher response rate than paclitaxel and CPT-11.

**DNA Binding of MS-247.** Hoechst 33342 is a fluorochrome that binds to the DNA minor groove and generates specific fluorescence

(31, 32). To confirm MS-247 binding to DNA, we observed the effect of MS-247 on the fluorescence generated by DNA-bound Hoechst 33342. In a cell free system, the fluorescence of DNA-bound Hoechst 33342 was quenched after MS-247 was added in a dose-dependent manner (Fig. 5A). Similar results were obtained when fluorescence was measured in the cellular system where MS-247 was exogenously added to L1210 cells that had been preincubated with Hoechst 33342 (Fig. 5B). These results indicated that MS-247 may have displaced the DNA-bound Hoechst 33342 on the DNA.

**Inhibition of Topoisomerase I by MS-247.** Some of the DNA minor groove binders reportedly inhibit topoisomerases (1). In addition, the COMPARE analysis of the mean graph of MS-247 suggested that the mode of action of MS-247 was similar to camptothecin analogues and anthracyclins, which inhibit topoisomerases I and II, respectively. Therefore, we examined whether MS-247 inhibited topoisomerases (Fig. 6). Topoisomerase I converted supercoiled DNA to nicked and relaxed DNA. MS-247 inhibited the process in a dose-dependent manner. These results demonstrated that MS-247 had topoisomerase I inhibitory activity at concentrations of 50–100  $\mu$ g/ml. MS-247 also inhibited topoisomerase II activity at the same concentration range (data not shown).

Table 1 The COMPARE analysis of MS-247

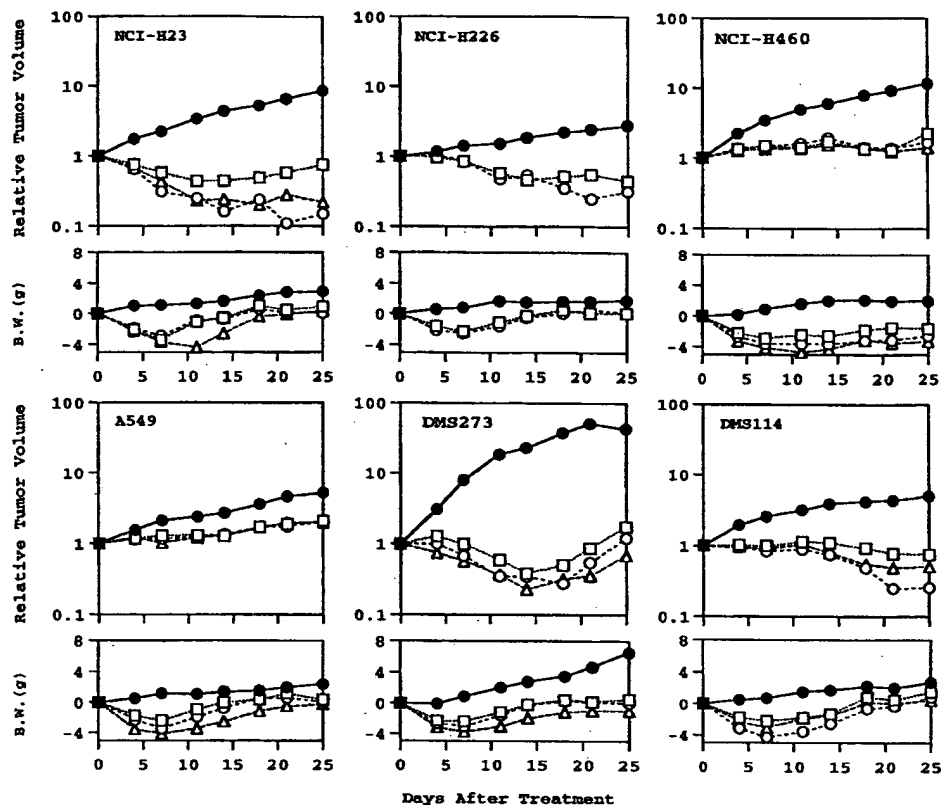
The mean graph of MS-247 was compared with those of 200 standard compounds using the COMPARE analysis. Drugs were ordered according to the correlation coefficient. Drugs with correlation coefficients higher than 0.5 ( $P < 0.001$ ) were included.

Ranking order	Drug	$r^2$
1	SN-38	0.688
2	CPT-11	0.683
3	Epirubicin	0.636
4	ADM	0.602
5	Mitoxantrone	0.596
6	KW2170	0.588
7	Melphalan	0.579
8	DMDC	0.575
9	Camptothecin	0.557
10	Daunorubicin	0.516

<sup>a</sup> Pearson correlation coefficient.

## ANTITUMOR ACTIVITY OF MS-247 AGAINST XENOGRAPHS

Fig. 4. Effect of MS-247 on the tumor growth and the body weight change in nude mice bearing human lung cancer xenografts. Tumor inoculation was carried out as described in "Materials and Methods." MS-247 was administered on day 0 at doses of 30 ( $\Delta$ ), 25 ( $\circ$ ), 21 ( $\square$ ), and 0 mg/kg ( $\bullet$ , control). Each curve represents the average of six mice.



**Effects of MS-247 on the Cell Cycle.** We investigated the effect of MS-247 on cell cycle progression in L1210 cells (Fig. 7). The cells were exposed to 10, 30, and 100 ng/ml of MS-247 for 3–48 h. The cell population in  $G_2$ -M phase increased time dependently at each con-

centration, indicating that MS-247 blocked the cell cycle at the  $G_2$ -M phase.

**Apoptosis Induced by MS-247.** We tested the apoptosis-inducing ability of MS-247 in HL-60 cells by DNA fragmentation assay. As

Table 2. Antitumor activity of MS-247 against human cancer xenografts

Nude mice were each inoculated s.c. with a  $3 \times 3 \times 3$ -mm tumor fragment. When tumors reached 100–300 mm<sup>3</sup> in volume, animals were divided randomly into test groups of six each (day 0). Drugs were administered from day 0 according to the dose schedules indicated. Tumor regression (T/C %) on day 14 was determined.

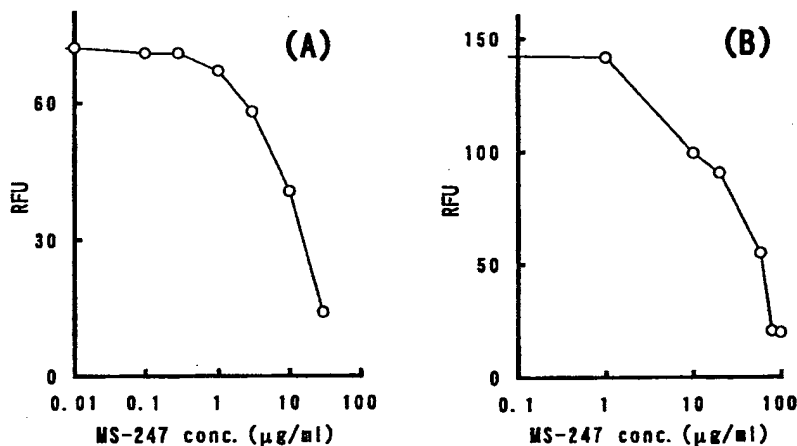
Drug dose (mg/kg) <sup>a</sup> schedule <sup>b</sup>	T/C (%)								
	MS247 25 qd $\times$ 1	Cisplatin 10 qd $\times$ 1	Paclitaxel 28 qd $\times$ 5	CPT-11 100 q4d $\times$ 3	ADM 12 qd $\times$ 1	5-Fu 50 q4d $\times$ 3	CPM 260 qd $\times$ 1	VP-16 12 qd $\times$ 5	VCR 1.6 qd $\times$ 1
Lung cancer									
NCI-H23	4 <sup>c</sup>	10 <sup>c</sup>	4 <sup>c</sup>	8 <sup>c</sup>	43 <sup>c</sup>	63	21 <sup>c</sup>	67	67
NCI-H226	29 <sup>c</sup>	71	6 <sup>c</sup>	14 <sup>c</sup>	40 <sup>c</sup>	70	89	78	24 <sup>c</sup>
NCI-H460	32 <sup>c</sup>	45 <sup>c</sup>	22 <sup>c</sup>	35 <sup>c</sup>	45 <sup>c</sup>	41	60	66	81
A 549	50 <sup>c</sup>	78	29 <sup>c</sup>	75	78	111	88	76	73
DMS 114	19 <sup>c</sup>	69	27 <sup>c</sup>	20 <sup>c</sup>	52	63	9 <sup>c</sup>	61	20 <sup>c</sup>
DMS 273	2 <sup>c</sup>	33 <sup>c</sup>	1 <sup>c</sup>	5 <sup>c</sup>	71	70	43 <sup>c</sup>	137	27 <sup>c</sup>
Stomach cancer									
MKN-1	42 <sup>c</sup>	63	46 <sup>c</sup>	49 <sup>c</sup>	41	55	74	103	88
MKN-7	32 <sup>c</sup>	60	11 <sup>c</sup>	41 <sup>c</sup>	58	75	79	68	66
MKN-74	35 <sup>c</sup>	78	16 <sup>c</sup>	28 <sup>c</sup>	78	76	69	134	82
St-4	24 <sup>c</sup>	62	22 <sup>c</sup>	42 <sup>c</sup>	66	55	95	86	87
Colon cancer									
HCC-2998	28 <sup>c</sup>	52	1 <sup>c</sup>	16 <sup>c</sup>	72	42	71	76	73
HCT-1116	30 <sup>c</sup>	78	5 <sup>c</sup>	11 <sup>c</sup>	60	48 <sup>c</sup>	53	64	57
HCT-15	46 <sup>c</sup>	54	78	10 <sup>c</sup>	73	61	53	66	104
Breast cancer									
HBC-4	24 <sup>c</sup>	56	37 <sup>c</sup>	54	46 <sup>c</sup>	49 <sup>c</sup>	41 <sup>c</sup>	86	46 <sup>c</sup>
MDA-MB-231	18 <sup>c</sup>	28 <sup>c</sup>	13 <sup>c</sup>	50 <sup>c</sup>	86	83	25 <sup>c</sup>	56	32 <sup>c</sup>
Ovarian cancer									
SK-OV-3	39 <sup>c</sup>	72	45 <sup>c</sup>	80	53	75	105	100	85
OVCR-8	36 <sup>c</sup>	69	17 <sup>c</sup>	18 <sup>c</sup>	58	76	78	74	80
Positive rate	17/17	4/17	16/17	14/17	4/17	2/17	5/17	0/17	5/17

<sup>a</sup> Each drug was administered at MTD in the schedule indicated.

<sup>b</sup> The administration schedules were abbreviated as: qd  $\times$  1, a single injection; qd  $\times$  5, five daily injections; q4d  $\times$  3, 3 injections with a 4-day interval.

<sup>c</sup>  $P < 0.01$  by Mann Whitney  $U$  test as compared with respective control.

Fig. 5. Quenching of the fluorescence of DNA-bound Hoechst 33342 by MS-247. The fluorescence of DNA-bound Hoechst 33342 was measured under the following conditions: A, calf thymus DNA was preincubated with Hoechst 33342 and then incubated with MS-247; B, L1210 cells were preincubated with Hoechst 33342 and then incubated with MS-247. The fluorescence derived from DNA-bound Hoechst 33342 decayed when MS-247 was added to the two systems.



shown in Fig. 8, MS-247 at concentrations around  $\text{IC}_{50}$  induced a DNA ladder in HL-60 cells. These results demonstrated that MS-247 induced apoptosis.

## DISCUSSION

MS-247 is a synthetic compound with a netropsin-like moiety and an alkylating residue in its structure. We found MS-247 by screening about 300 similar compounds, based primarily on the activity of tumor cell growth inhibition, and selected MS-247 for extensive evaluation because of its significant antitumor activity against murine tumors, L1210 and colon 26, and its higher stability.<sup>4</sup>

In the present study, we evaluated the antitumor activity of MS-247 by an *in vitro* and *in vivo* human cancer cell line panel. The mean  $\log \text{GI}_{50}$  of MS-247 was  $-6.15$  ( $0.71 \mu\text{M}$ ), which fell in the middle of the range of anticancer drugs presently in use. The COMPARE analysis indicated that the differential growth inhibition pattern of MS-247 (the mean graph) significantly correlated with those of camptothecin analogues and anthracyclins, suggesting that the modes of action are similar. The most remarkable feature of MS-247 was its efficacy

against human xenografts. A single 25 mg/kg injection of MS-247 showed significant antitumor activity against all 17 xenografts tested, which included lung, colon, stomach, breast, and ovarian cancers. In comparison with the clinically active drugs, MS-247 was more effective than cisplatin, ADM, 5-FU, CPM, VP-16, and VCR, in most cases, and moreover, was almost comparable with paclitaxel and CPT-11, the most clinically promising drugs at the present. These results demonstrated the broad anticancer spectrum of MS-247. It is noticeable that MS-247 was more effective than paclitaxel in HCT-15 and than CPT-11 in A549, HBC-4, and SK-OV-3. On the other hand, the toxicity of MS-247, indicated by the body weight loss, was reversible within 10 days after the administration. In our preliminary study, the dose-limiting toxicity of MS-247 was bone marrow suppression. Our results suggest that MS-247 is a promising anticancer drug candidate for further research and development toward clinical investigation.

We also investigated the mode of action of MS-247. We confirmed its binding to DNA by the fact that MS-247 displaced DNA-bound Hoechst 33342 both in the cell-free system and in the cellular system. Hoechst 33342 is a fluorochrome that binds to AT-rich sites in the DNA minor groove and covers four bp, AATT (31, 32). Therefore, it seems correct to consider MS-247 as a DNA minor groove binder, as expected, and that it shares sequence specificity at least with Hoechst 33342.

MS-247 proved to have inhibitory activity against topoisomerases I and II. This was reasonable to expect because several DNA minor groove binders reportedly inhibit topoisomerases. For example, Hoechst 33342, Hoechst 33258, distamycin A, berenil, netropsin, and tallimustine inhibited topoisomerase I (33–35), and distamycin A and tallimustine inhibited topoisomerase II (34, 36). The inhibitory activity against topoisomerase I and II was also expected because the results of the COMPARE analysis suggested that the mode of action of MS-247 was similar to those of camptothecin analogues (topoisomerase I inhibitors) and anthracyclins (topoisomerase II inhibitors). Therefore, topoisomerases I and II are at least the molecular targets of MS-247. Moreover, there might be other possible targets, such as other enzymes, involved in DNA metabolism and/or transcription factors because their activities were inhibited by some DNA minor groove binders (34, 37, 38).

MS-247 blocked the cell cycle at the  $G_2$ -M phase and induced apoptosis. The  $G_2$ -M blockage is the common feature of DNA minor groove binders (1, 39). However, subsequent induction of apoptosis by this type of drug has not been studied, except for apoptosis induced by Hoechst 33342 (40, 41). We showed here the induction of apoptosis by MS-247, which possibly contributes to *in vivo* efficacy, at

Drug	—	—	CPT	MS-247		
Conc. ( $\mu\text{M}$ )			5	100	50	10
Topo I	—	+	+	+	+	+

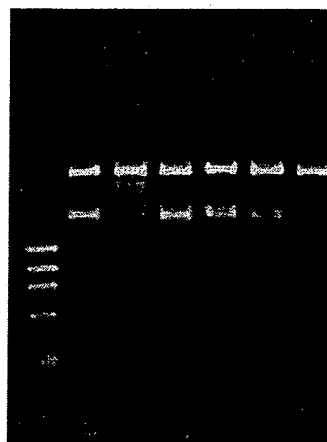


Fig. 6. Inhibition of topoisomerase I by MS-247. Supercoiled DNA was mixed with an indicated concentration of MS-247 or camptothecin before topoisomerase I was added. After a 30-min incubation at  $37^\circ\text{C}$ , the reaction mixture was treated as described in "Materials and Methods," and the DNA was analyzed by 1% agarose gel electrophoresis. MS-247 inhibited the topoisomerase I-induced DNA relaxation at concentrations of 50 and  $100 \mu\text{M}$ . Camptothecin was used as a positive control.

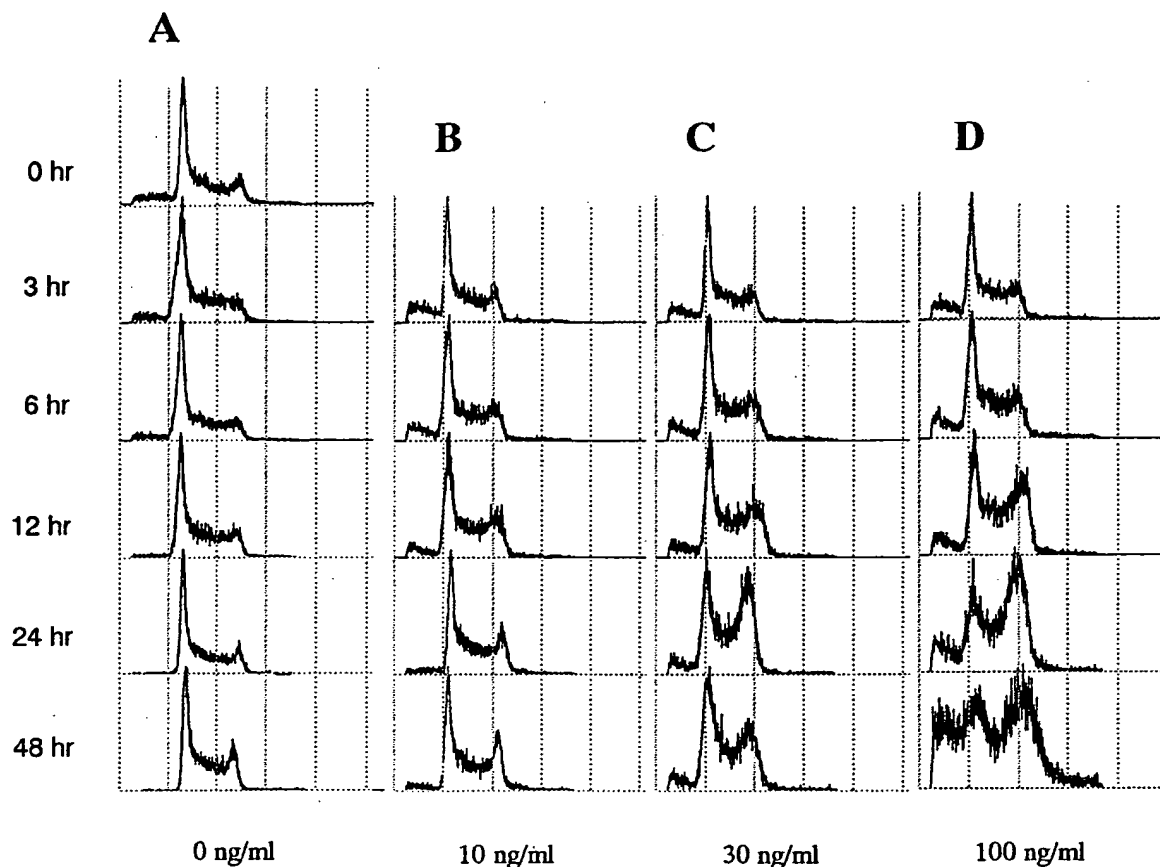


Fig. 7. Effect of MS-247 on cell cycle. L1210 cells were exposed to 0 (A), 10 (B), 30 (C), and 100 ng/ml (D) of MS-247 for 3–48 h. Then, the DNA content of the cells was analyzed by a flow cytometer as described in "Materials and Methods." When exposed to MS-247, the cell population in the G<sub>2</sub>-M phase significantly increased.

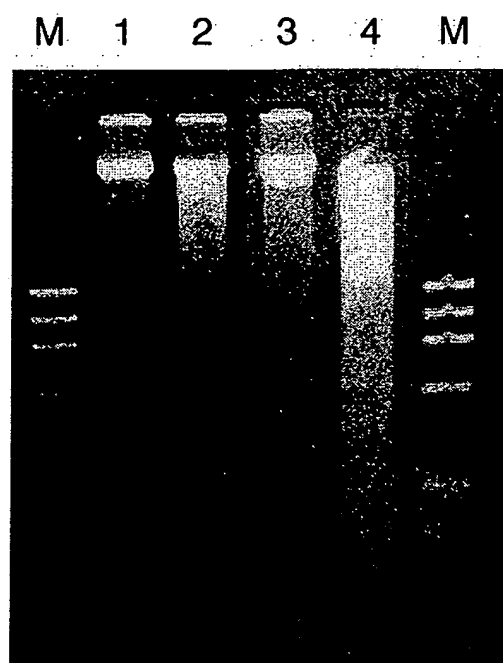


Fig. 8. Apoptosis induced by MS-247. Total DNA was extracted from HL-60 cells treated with nothing (Lane 1), 2  $\mu$ M MS-247 (Lane 2), 0.2  $\mu$ M MS-247 (Lane 3), or 20 nM camptothecin (Lane 4). Then, DNA fragmentation was measured by electrophoresis, as described in "Materials and Methods." Camptothecin was used as a positive control. Lane M, DNA size markers ( $\phi$ X174/HaeIII).

least in part. Recently, the analysis of the apoptotic cascade induced by anticancer drugs has been studied (42). It seems an important next step to analyze the mechanism of apoptosis induced by MS-247 and to compare MS-247 with other antitumor agents.

Tallimustine, a derivative of distamycin A, has the closest structural relationship to MS-247 of the DNA minor groove binders that were developed as anticancer drugs. Although tallimustine was subjected to clinical trials, its efficacy has not yet been demonstrated (17, 18). It may be important to compare MS-247 and tallimustine in a preclinical study. In our preliminary study, the sequence specificity of DNA binding between the two is slightly different, suggesting that MS-247 is different from tallimustine in biological activity.

We report here our synthesis of a novel DNA minor groove binder, MS-247, and have demonstrated its strong antitumor activity against several human cancer xenografts. We see that MS-247 binds to DNA, inhibits topoisomerases and other possible targets around DNA, blocks the cell cycle at G<sub>2</sub>-M, and induces apoptosis. MS-247 is a promising new anticancer drug for further development toward clinical investigation.

#### ACKNOWLEDGMENTS

We thank Dr. R. H. Shoemaker and Dr. K. D. Paull (Developmental Therapeutics Program, Division of Cancer Treatment, National Cancer Institute) for their helpful discussions during the development of the human cancer cell line panel and the database system.

#### REFERENCES

1. Turner, P. R., and Denny, W. A. The mutagenic properties of DNA minor-groove binding ligands. *Mutat. Res.*, 355: 141–169, 1996.

2. Hartley, J. A., Lown, J. W., Mattes, W. B., and Kohn, K. W. DNA sequence specificity of antitumor agents. Oncogenes as possible targets for cancer therapy. *Acta. Oncol.*, 27: 503-510, 1988.
3. Lown, J. W. DNA recognition by lexitropsins, minor groove binding agents. *J. Mol. Recognit.* 7: 79-88, 1994.
4. Marchini, S., Cozzi, P., Beria, I., Geroni, C., Capolongo, L., D'Incalci, M., and Broggin, M. Sequence-specific DNA alkylation of novel tallimustine derivatives. *Anticancer Drug Des.*, 13: 193-205, 1998.
5. Brooks, N., Lee, M., Wright, S. R., Woo, S., Centioni, S., and Hartley, J. A. Synthesis, DNA binding, cytotoxicity and sequence specificity of a series of imidazole-containing analogs of the benzoic acid mustard distamycin derivative tallimustine containing an alkylating group at the C-terminus. *Anticancer Drug Des.*, 12: 591-606, 1997.
6. Yoon, J. H., and Lee, C. S. Sequence selectivity of DNA alkylation by adozelesin and carzelesin. *Arch. Pharmacol. Res. (Seoul)*, 21: 385-390, 1998.
7. Bhuyan, B. K., Smith, K. S., Adams, E. G., Wallace, T. L., Von Hoff, D. D., and Li, L. H. Adozelesin, a potent new alkylating agent: cell-killing kinetics and cell-cycle effects. *Cancer Chemother. Pharmacol.*, 30: 348-354, 1992.
8. Burris, H. A., Dieras, V. C., Tunca, M., Earhart, R. H., Eckardt, J. R., Rodriguez, G. I., Shaffer, D. S., Fields, S. M., Campbell, E., Schaaf, L., Kasunic, D., and Von Hoff, D. D. Phase I study with the DNA sequence-specific agent adozelesin. *Anticancer Drugs*, 8: 588-596, 1997.
9. Foster, B. J., LoRusso, P. M., Poplin, E., Zalupski, M., Valdivieso, M., Wozniak, A., Flaherty, L., Kasunic, D. A., Earhart, R. H., and Baker, L. H. Phase I trial of adozelesin using the treatment schedule of daily  $\times 5$  every 3 weeks. *Invest. New Drugs*, 13: 321-326, 1996.
10. Li, L. H., DeKoning, T. F., Kelly, R. C., Krueger, W. C., McGovren, J. P., Padbury, G. E., Petzold, G. L., Wallace, T. L., Oudine, R. J., Prairie, M. D., and Gebhard, I. Cytotoxicity and antitumor activity of carzelesin, a prodrug cyclopropylpyrrolindole analogue. *Cancer Res.*, 52: 4904-4913, 1992.
11. Houghton, P. J., Cheshire, P. J., Hallman, J. D. N., and Houghton, J. A. Therapeutic efficacy of the cyclopropylpyrrolindole, carzelesin, against xenografts derived from adult and childhood solid tumors. *Cancer Chemother. Pharmacol.*, 36: 45-52, 1995.
12. Carter, C. A., Waud, W. R., Li, L. H., DeKoning, T. F., McGovren, J. P., and Plowman, J. Preclinical antitumor activity of bizelesin in mice. *Clin. Cancer Res.*, 2: 1143-1149, 1996.
13. Walker, D. L., Reid, J. M., and Ames, M. M. Preclinical pharmacology of bizelesin, a potent bifunctional analog of the DNA-binding antibiotic CC-1065. *Cancer Chemother. Pharmacol.*, 34: 317-322, 1994.
14. Kobayashi, E., Okamoto, A., Asada, M., Okabe, M., Nagamura, S., Asai, A., Saito, H., Gomi, K., and Hirata, T. Characteristics of antitumor activity of KW-2189, a novel water-soluble derivative of duocarmycin, against murine and human tumors. *Cancer Res.*, 54: 2404-2410, 1994.
15. Pezzoni, G., Grandi, M., Biasoli, G., Capolongo, L., Ballinari, D., Giuliani, F. C., Barbieri, B., Pastori, A., Pesenti, E., Mongelli, N., and Spreafico, F. Biological profile of FCE 24517, a novel benzoyl mustard analogue of distamycin A. *Br. J. Cancer*, 64: 1047-1050, 1991.
16. Verweij, J. New promising anticancer agents in development: what comes next? *Cancer Chemother. Pharmacol.*, 38 (Suppl.): S3-S10, 1996.
17. Viallet, J., Stewart, D., Shepherd, F., Ayoub, J., Cormier, Y., DiPietro, N., and Steward, W. Tallimustine is inactive in patients with previously treated small cell lung cancer. A Phase II trial of the National Cancer Institute of Canada Clinical Trials Group. *Lung Cancer*, 15: 367-373, 1996.
18. Punt, C. J., Humblet, Y., Roca, E., Dirix, L. Y., Wainstein, R., Polli, A., and Corradino, I. Tallimustine in advanced previously untreated colorectal cancer, a Phase II study. *Br. J. Cancer*, 73: 803-804, 1996.
19. Alberts, S. R., Erlichman, C., Reid, J. M., Sloan, J. A., Ames, M. M., Richardson, R. L., and Goldberg, R. M. Phase I study of the duocarmycin semisynthetic derivative KW-2189 given daily for five days every six weeks. *Clin. Cancer Res.*, 4: 2111-2117, 1998.
20. Tabernero, L., Verdager, N., Coll, M., Fita, I., van der Marel, G. A., van Boom, J. H., Rich, A., and Aymami, J. Molecular structure of the A-tract DNA dodecamer d(CGCAAAATTGCG) complexed with the minor groove binding drug netropsin. *Biochemistry*, 32: 8403-8410, 1993.
21. Stinson, S. F., Alley, M. C., Kopp, W. C., Fiebig, H. H., Mullendore, L. A., Pittman, A. F., Kenney, S., Keller, J., and Boyd, M. R. Morphological and immunocytochemical characteristics of human tumor cell lines for use in a disease-oriented anticancer drug screen. *Anticancer Res.*, 12: 1035-1053, 1992.
22. Satoh, A., Takayama, E., Kojima, K., Ogawa, H., Yamori, T., Sato, S., Kawaguchi, T., Tsuruo, T., Yoshimoto, K., Kine, T., and Matsumoto, I. Expression of carbohydrate-binding protein p33/41 human tumor cell lines. *J. Biochem.*, 119: 346-353, 1996.
23. Motoyama, T., Hojo, H., and Watanabe, H. Comparison of seven cell lines derived from human gastric carcinomas. *Acta. Pathol. Jpn.*, 36: 65-83, 1986.
24. Boyd, M. R. Status of the National Cancer Institute preclinical antitumor drug discovery screen: implications for selection of new agents for clinical trial. In: V. T. Devita, Jr., S. Hellman, and S. A. Rosenberg (eds.), *Cancer: Principles and Practice of Oncology*. Update, Vol. 3, pp. 1-12. Philadelphia: Lippincott, 1989.
25. Paull, K. D., Shoemaker, R. H., Hodes, L., Monks, A., Scudiero, D. A., Rubinstein, L., Plowman, J., and Boyd, M. R. Display and analysis of patterns of differential activity of drugs against human tumor cell lines: development of mean graph and COMPARE algorithm. *J. Natl. Cancer Inst.*, 81: 1088-1092, 1989.
26. Monks, A., Scudiero, D., Skehan, P., Shoemaker, R., Paull, K., Vistica, D., Hose, C., Langley, J., Cronise, P., Vaigro-Wolff, A., Gray-Goodrich, M., Campbell, H., Mayo, J., and Boyd, M. Feasibility of a high-flux anticancer drug screen using a diverse panel of cultured human tumor cell lines. *J. Natl. Cancer Inst.*, 83: 757-766, 1991.
27. Yamori, T., Sato, S., Chikazawa, H., and Kadota, T. Anti-tumor efficacy of paclitaxel against human lung cancer xenografts. *Jpn. J. Cancer Res.*, 88: 1205-1210, 1997.
28. Skehan, P., Storeng, R., Scudiero, D., Monks, A., McMahon, J., Vistica, D., Warren, J. T., Bokesch, H., Kenney, S., and Boyd, M. R. New colorimetric cytotoxicity assay for anticancer-drug screening. *J. Natl. Cancer Inst.*, 82: 1107-1112, 1990.
29. Goldwasser, F., Shimizu, T., Jackman, J., Hoki, Y., O'Connor, P. M., Kohn, K. W., and Pommier, Y. Correlations between S and G2 arrest and the cytotoxicity of camptothecin in human colon carcinoma cells. *Cancer Res.*, 56: 4430-4437, 1996.
30. Ishizawa, M., Kobayashi, Y., Miyamura, T., and Matsuura, S. Simple procedure of DNA isolation from human serum. *Nucleic Acids Res.*, 19: 5792, 1991.
31. Sriram, M., van der Marel, G. A., Roelen, H. L., van Boom, J. H., and Wang, A. H. Conformation of B-DNA containing  $O^6$ -ethyl-G-C base pairs stabilized by minor groove binding drugs: molecular structure of d(CGC[e6G]AATTCGCG) complexed with Hoechst 33258 or Hoechst 33342. *EMBO J.*, 11: 225-232, 1992.
32. Robinson, H., Gao, Y. G., Bauer, C., Roberts, C., Switzer, C., and Wang, A. H. 2'-Deoxyisoguanosine adopts more than one tautomer to form base pairs with thymidine observed by high-resolution crystal structure analysis. *Biochemistry*, 37: 10897-10905, 1998.
33. Chen, A. Y., Yu, C., Gatto, B., and Liu, L. F. DNA minor groove-binding ligands: a different class of mammalian DNA topoisomerase I inhibitors. *Proc. Natl. Acad. Sci. USA*, 90: 8131-8135, 1993.
34. Montecucco, A., Fontana, M., Focher, F., Lestingi, M., Spadari, S., and Ciarrocchi, G. Specific inhibition of human DNA ligase adenylation by a distamycin derivative possessing antitumor activity. *Nucleic Acids Res.*, 19: 1067-1072, 1991.
35. Wang, Z., Zimmer, C., Lown, J. W., and Knippers, R. Effects of bifunctional netropsin-related minor groove-binding ligands on mammalian type I DNA topoisomerase. *Biochem. Pharmacol.*, 53: 309-316, 1997.
36. Fesen, M., and Pommier, Y. Mammalian topoisomerase II activity is modulated by the DNA minor groove binder distamycin in simian virus 40 DNA. *J. Biol. Chem.*, 264: 11354-11359, 1989.
37. Bellorini, M., Moncollin, V., D'Incalci, M., Mongelli, N., and Mantovani, R. Distamycin A and tallimustine inhibit TBP binding and basal *in vitro* transcription. *Nucleic Acids Res.*, 23: 1657-1663, 1995.
38. Broggin, M., and D'Incalci, M. Modulation of transcription factor-DNA interactions by anticancer drugs. *Anticancer Drug Des.*, 9: 373-387, 1994.
39. Erba, E., Mascellani, E., Pifferi, A., and D'Incalci, M. Comparison of cell-cycle phase perturbations induced by the DNA-minor groove alkylator tallimustine and by melphalan in the SW626 cell line. *Int. J. Cancer*, 62: 170-175, 1995.
40. Zhang, X., and Kiechle, F. L. Hoechst 33342 induces apoptosis and alters TATA box binding protein/DNA complexes in nuclei from BC3H-1 myocytes. *Biochem. Biophys. Res. Commun.*, 248: 18-21, 1998.
41. Zhang, X., and Kiechle, F. L. Mechanism of Hoechst 33342-induced apoptosis in BC3H-1 myocytes. *Ann. Clin. Lab. Sci.*, 28: 104-114, 1998.
42. Kamesaki, H. Mechanisms involved in chemotherapy-induced apoptosis and their implications in cancer chemotherapy. *Int. J. Hematol.*, 68: 29-43, 1998.



## SDZ 281-977: A MODIFIED PARTIAL STRUCTURE OF LAVENDUSTIN A THAT EXERTS POTENT AND SELECTIVE ANTIPROLIFERATIVE ACTIVITIES *IN VITRO* AND *IN VIVO*

Salvatore CAMMISULI<sup>1</sup>, Anthony WINISKI<sup>2</sup>, Peter NUSSBAUMER<sup>2</sup>, Peter HIESTAND<sup>1</sup>, Anton STÜTZ<sup>2</sup> and Gisbert WECKBECKER<sup>1,3</sup>

<sup>1</sup>Preclinical Research, Sandoz Pharma Ltd., CH-4002 Basle, Switzerland; and <sup>2</sup>Department of Dermatology, Sandoz Research Institute, A-1235 Vienna, Austria.

The chemical derivatization of biologically active microbial metabolites continues to be a promising approach to the identification of new drugs. We recently synthesized the novel antiproliferative compound SDZ 281-977, 5-[2-(2,5-dimethoxyphenyl)ethyl]-2-hydroxy-benzoic acid methylester, a derivative of the EGF receptor tyrosine kinase inhibitor lavendustin A. Here we report on our studies of the anticancer efficacy and the mode of action of SDZ 281-977. The growth of both the human pancreatic tumor cells MIA PaCa-2 and the human vulvar carcinoma cells A431 was inhibited in the low micromolar range. Tumors from these cells were induced in nude mice and were shown to respond to orally or intravenously administered SDZ 281-977. In contrast, no antitumor effect was detected in rats bearing dimethylbenzanthracene-induced mammary tumors. Studies in mice indicated that SDZ 281-977 was neither immunosuppressive nor hematosuppressive at doses effectively inhibiting tumor growth. Surprisingly, the mode of action of SDZ 281-977 apparently does not involve inhibition of EGF receptor tyrosine kinase, because, in contrast to lavendustin A, SDZ 281-977 failed to inhibit this enzyme in a cell-free assay. The mechanism of the antiproliferative effect can be explained on a cellular level by the ability of the compound to arrest cells in mitosis. SDZ 281-977 is thus the first example of an antimitotic agent derived from the potent tyrosine kinase inhibitor lavendustin A. The therapeutic potential of SDZ 281-977 is enhanced by the fact that it is not subject to multidrug resistance, because tumor cells expressing the multidrug resistance phenotype were as sensitive to SDZ 281-977 as their nonresistant counterparts. In conclusion, SDZ 281-977 represents a novel lavendustin A derivative with potent antiproliferative properties *in vitro* and *in vivo* that may be explained on the basis of its antimitotic effects. SDZ 281-977 may be a candidate drug for the treatment of selected cancers, including those expressing the multidrug resistance phenotype.

© 1996 Wiley-Liss, Inc.

Tyrosine kinases have been identified as promising targets for the development of new anticancer drugs (Bishop, 1987; Hunter, 1987; Lyall *et al.*, 1989; Geissler *et al.*, 1990; Yuan *et al.*, 1990; Yoneda *et al.*, 1991; Marx, 1994). Therefore, we selected the tyrosine kinase inhibitor lavendustin A, a microbial secondary metabolite (isolated from *Streptomyces griseolavendus*) as a lead structure for the development of new antiproliferative drugs. Lavendustin A strongly inhibits the EGF receptor tyrosine kinase in A431 cell-free extracts by binding at the ATP site, but it is inactive in inhibiting EGF receptor autophosphorylation in intact A431 cells and inhibiting cellular proliferation (Onoda *et al.*, 1989). This lack of activity in intact cells was attributed to poor cell penetration (Onoda *et al.*, 1990).

A series of esterified derivatives of lavendustin A was prepared with the idea that such lipophilic lavendustin A analogs might be cell-permeable inhibitors of the EGF receptor tyrosine kinase and, thus, inhibit tumor cell proliferation (Nussbaumer *et al.*, 1994a,b). SDZ 281-977 was demonstrated to be the most potent antiproliferative agent of this series when tested against a large panel of tumor cell lines *in vitro* (Nussbaumer *et al.*, 1994a).

In this study, we focused on the antitumor effects in nude mouse tumor models and the potential mechanism underlying the antiproliferative action of SDZ 281-977.

### MATERIAL AND METHODS

#### Material

Fluorouracil, mitomycin C, colchicine, growth factors, tyrosylpeptide and supplements for substrate phosphorylation assays were purchased from Sigma (Zürich, Switzerland). IGF I was supplied by KabiGen (Stockholm, Sweden). SDZ 281-977 was prepared as published (Nussbaumer *et al.*, 1994a). For *in vitro* studies, SDZ 281-977 was dissolved either in DMSO or ethanol containing 10% Tween 80. This stock solution was prepared and then diluted into culture medium immediately before use. In all cases, at the concentrations used, there was no detectable solvent effect. Media and FCS were supplied by Flow (Irvine, UK). Cell culture plates were supplied by Falcon (Dietikon, Switzerland).

#### Cells and animals

The cell lines were obtained from the ATCC (Rockville, MD) and, of these, only cells with low passage numbers (<10–20) were used. They were cultured in the recommended media without antibiotics and antifungal agents. The absence of Mycoplasma was checked by use of bisbenzimidazole staining and the GenProbe hybridization assay (San Diego, CA). OF<sub>1</sub> female mice weighing 20–25 g and virgin female OFA rats (130–160 g) were purchased from BRL (Basle, Switzerland). Female nude mice (nu/nu IFFA C BALB A) weighing 20–23 g were purchased from IFFA Credo (Lyon, France).

#### Assay of cell proliferation

Tumor cell lines were grown at 37°C under optimal medium and cell concentration conditions in the absence of antibiotics. At the time of exponential growth for tumor cell lines growing in suspension or at the time of 60–90% confluence for adherent cell lines, cells were harvested (adherent cell lines were trypsinized), suspended in fresh growth medium and seeded into 96-well cell culture plates at concentrations ranging between 1000 and 5000 cells/well. Cells were grown at optimal initial concentration for 3–4 days in a final volume of 0.2 ml/well in the presence of graded concentrations of test compounds. Extent of cellular proliferation was measured by a colorimetric assay using 3-[4,5-dimethylthiazol-2-yl]-2,5-diphenyltetrazolium bromide (MTT) (Alley *et al.*, 1988) for cells growing in suspension or by sulforhodamine B (SRB) (Skehan *et al.*, 1990) for adherent cells.

<sup>3</sup>To whom correspondence and reprint requests should be sent, at Preclinical Research, Sandoz Pharma, 386/627, CH-4002 Basle, Switzerland. Fax: 41-61-324 3576.

**Abbreviations:** BSA, bovine serum albumin; DAPI, 4',6-diamidino-2-phenylindole; DMBA, 7,12-dimethylbenz[*a*]anthracene; FCS, fetal calf serum; MDR, multidrug resistant; PBS, phosphate-buffered saline; PFC, plaque forming cells; SRBC, sheep red blood cells; TCA, tricarboxylic acid.

### Tumor models with nude mice

The animal tumor models have essentially been described previously (Weckbecker *et al.*, 1992a,b). In these studies we used the human cancer cell lines MIA PaCa-2 (undifferentiated pancreatic tumor), A431 (epidermoid carcinoma of the vulva) and MDA-MB-231 (estrogen-independent breast carcinoma cells). Female nude mice (*nu/nu* IFFA C BALB A) weighing 20–23 g were kept as groups of 5 animals in macrolon cages (16 × 22 × 11 cm) placed in ventilated closed cabinets (IFFA Credo) at 24 ± 1°C. The animals had free access to drinking water and a pathogen-free rodent diet (Diet A, Kliba, Basle). The tumors were initiated from cultured tumor cell lines by injecting *ca.* 10<sup>7</sup> cells subcutaneously into nude mice. Once the tumors had reached approximately 1 cm in diameter, they were excised, cut into small pieces of approximately 4 × 3 mm and transplanted subcutaneously into both flanks of nude mice. All operations were done on chloral hydrate-anesthetized animals (470–520 mg/kg/5 ml i.p. chloral hydrate).

The passage number of the tumors used in the experiments was between 10 and 16. One and 2 weeks subsequent to transplantation, the size of the tumors was determined by use of a caliper. For calculation of the tumor volume, the equation "volume (ellipsoid) = length × depth × height × 0.52" was applied. Animals with growing tumors were randomized into control and treatment groups with identical mean tumor burden per mouse. For i.v. studies, SDZ 281-977 (10 mg) was dissolved in 1 ml Vepesid solvent (3250 mg PEG 300, 10 mg citric acid, 400 mg Tween 80 and 1205 mg ethanol). This solution was diluted with saline or Vepesid solvent/saline 1:10 so that all animals intravenously received 0.2 ml of 1:10 Vepesid solvent containing 1, 3 and 10 mg SDZ 281-977/kg. Higher doses were not given due to limited solubility. The compound was injected into the tail vein 3 or 4 times a week. For oral testing, the compound was dissolved in Placebo G (18% ethanol, 43% Labrafil M2125CS and 39% corn oil) and 0.2 ml was given orally with a gavage. Control animals were treated with the vehicle only. For the comparative experiments, standard anticancer drugs were dissolved in saline containing 1% Tween 80 and water, respectively, and were injected i.p. once a day for 4 days in a row (Nielsen *et al.*, 1992). Treatment started 2 days after animals had been randomized.

At weekly intervals, the animals were weighed and the tumor volumes were determined as described above and expressed as mean tumor volume per animal (mm<sup>3</sup>). Data were evaluated with the statistics program of RS/1 (BBN Software Products, Cambridge, MA), and tests including Student's *t*-test and the Mann-Whitney *U*-test were applied.

### DMBA-induced mammary carcinomas in rats

Virgin female OFA rats (130–160 g) were kept in groups of 4 or 5 animals per cage (macrolon, 54 × 32 × 19 cm) (Weckbecker *et al.*, 1992b). The rats had free access to water and a standard rodent diet (NAFAG cubes). To induce mammary tumors, animals were given a single dose of 20 mg DMBA (Fluka, Buchs, Switzerland) p.o. as a finely dispersed suspension in 4 ml sesame oil/water (1:1). Approximately 8 weeks following DMBA administration (*ca.* 1 week before tumors became palpable), animals were randomized to control and treatment groups.

### Primary antibody response to sheep erythrocytes

Groups of 2 month old OF1 female mice were immunized on day 0 i.v. with 10<sup>8</sup> SRBC suspended in 0.2 ml isotonic saline and treated with drug on 4 consecutive days (0–3). Spleen cell suspensions were prepared on day 4 after immunization, and the SRBC-specific plaque forming cells were counted using the haemolytic plaque assay (Jerne *et al.*, 1974).

### Hematological effects

When SDZ 281-977, mitomycin-C and 5-fluorouracil were compared for their antitumor activity in the A431 tumor mouse model, the potential hematological side effects of these drugs were also analyzed. Groups of 5 mice were treated intravenously for 4 consecutive days post A431 tumor-transplantation with: (1) vehicle, (2) 5-fluorouracil (25 mg/kg), (3) mitomycin-C (1.5 mg/kg) or (4) SDZ 281-977 (10 mg/kg), and observed for 3 weeks for tumor growth. Following the last observation, mice were treated for 2 more days with the same drug doses used at the beginning of the experiments. After a further 2 day rest, mice were anesthetized with forene and then bled by retroorbital puncture. The numbers of leukocytes (millions/ml), platelets (millions/ml) and erythrocytes (billions/ml) were assessed by differential counting using a Technicon H1 Analyzer. Immediately after being bled, mice were killed by cervical dislocation while under anesthesia. The femurs were dissected and their contents of bone marrow cells were isolated by flushing the bone diaphyses with 1 ml of RPMI 1640 containing 50 IU of heparin. Bone marrow nucleated cells were stained for viability with ethidium bromide and acridine orange and counted by standard fluorescence microscopy. Two to 4 hemocytometer fields, for a total of 100–300 cells/field, were counted for each individual preparation. Cell numbers are expressed as millions/femur.

### EGF receptor tyrosine kinase assay

The assay mixture (30 µl total) contained 0.3 µM mouse EGF, solubilized EGF receptors from A431 human vulva carcinomas, 5 µM ATP, *ca.* 10<sup>6</sup> cpm <sup>32</sup>P-ATP, 12 mM MgCl<sub>2</sub>, 2 mM MnCl<sub>2</sub>, 0.1 mM Na-orthovanadate, 0.02 mM *p*-nitrophenylphosphate, 0.3 mM tyrosylpeptide substrate (Arg-Arg-Leu-Ile-Glu-Asp-Ala-Glu-Tyr-Ala-Ala-Arg-Gly) and graded concentrations of the test compounds dissolved at 100 mM in ethanol/Tween 80 (9:1) and appropriately diluted in assay buffer (=0.1% Triton X-100, 10% glycerol, 150 mM NaCl, 50 mM Hepes, pH 7.6). The kinase was activated on ice by a 20 min preincubation with EGF prior to the addition of substrates to start the phosphorylation of the tyrosylpeptide (8 min). Following termination of the reaction by incubation with TCA (10%) and BSA (1%) for 30 min on ice, the protein was pelleted by centrifugation, and the phosphorylated peptide in the supernatant was adsorbed to P81 paper (2 × 2 cm) (Whatman, Zürich, Switzerland). This paper was thoroughly washed (3 times) in 75 mM phosphoric acid containing 10 mM Na-pyrophosphate, followed by a final wash using acetone. Adsorbed radioactivity was quantified in Cerenkov mode using a Tri-Carb 2000CA analyzer (Canberra-Packard, Zürich, Switzerland).

### Measurement of mitotic indices

Cells were seeded into 8-well Lab-Tek plastic chamber slides (Permanox, Nunc, Vienna, Austria) at a final density of 24,000 cells/0.4 ml/well. After 24 hr, the medium was replaced with fresh medium containing graded concentrations of the test compound. After various incubation times, the medium was removed from each slide chamber, and 90% acetone was added for 5 min at room temperature to fix the cells. DNA was stained with DAPI in PBS (0.5 µg/ml for 1 hr at room temperature). Fluorescence microscopy was performed with a Zeiss IM microscope equipped with epifluorescence optics. Cells arrested in metaphase were scored for each sample and the mitotic index (100% × number of mitotic cells/number of total cells) determined. At least 300 cells were counted at each drug concentration tested.

### Immunofluorescence microscopy

For immunofluorescence studies, cells were seeded and treated with SDZ 281-977 as for the measurement of mitotic indices. However, the cells were fixed as in Jordan *et al.* (1992).



Briefly the cells were fixed in PBS containing 10% formalin and 2 mM EGTA for 10 min. This solution was replaced by cold 99.6% methanol, 2 mM EGTA and incubated at  $-20^{\circ}\text{C}$  for 10 min. Three 5-min washes in PBS were followed by a blocking step in 20% normal goat serum (15 min). This was followed by a 1 hr incubation with a 1:1 mixture of mouse monoclonal anti- $\alpha$ - and anti- $\beta$ -tubulin antibodies (Amersham N-356 and N-357, Zürich, Switzerland) each at 1:2000 dilution. After three 5 min rinses in PBS, the cells were incubated for 1 hr with rhodamine-conjugated goat anti-mouse IgG (Accurate Chemicals, Vienna, Austria) used at 1:100 dilution. After 3 rinses with PBS, the cells were stained with DAPI (0.1  $\mu\text{g}/\text{ml}$ , 6 min), followed by 3 more rinses and mounting on a glass coverslip with Bacto FA mounting fluid (Difco, Vienna, Austria). All dilutions and rinses were in PBS containing 1% BSA, and all steps were performed at room temperature unless stated otherwise. Photomicrographs were taken with a Zeiss Axiovert 10 microscope equipped with epifluorescence optics and a 63 $\times$  objective. Kodak TMAX film was used.

## RESULTS

### *Anticancer effects of SDZ 281-977*

We investigated the anticancer profile of SDZ 281-977 in nude mice bearing the human tumor cell lines A431 (vulvar carcinoma cells), MIA PaCa-2 (pancreatic tumor cells) and MDA-MB-231 (breast carcinoma cells). These cell lines were selected because of their *in vitro* sensitivity for SDZ 281-977. The  $\text{IC}_{50}$  values for inhibition of *in vitro* growth of A431, MIA PaCa-2 and MDA-MB-231 cells were 0.21  $\mu\text{M}$ , 0.29  $\mu\text{M}$  and 0.43  $\mu\text{M}$ , respectively (data not shown).

Nude mice bearing A431 human vulvar carcinomas received intravenous injections of SDZ 281-977 (1–10 mg/kg) for 4 weeks. This treatment resulted in a dose-dependent inhibition of tumor growth (Fig. 1a). Orally administered SDZ 281-977 (30 mg/kg) induced a 54% inhibition of A431 tumor growth after 3 weeks of treatment (Fig. 1b). The above regimens were well tolerated. No significant change in body weight occurred during treatment.

Repeated intravenous injection of SDZ 281-977 (10 mg/kg) potentially inhibited the growth of human pancreatic tumors (MIA PaCa-2) in nude mice (Fig. 2a). Moreover, a 4 week oral treatment with SDZ 281-977 (30 mg/kg) also resulted in a significant, 53%, inhibition of MIA PaCa-2 tumor growth (Fig. 2b). No overt drug-related toxicity was seen.

The antitumor effect of SDZ 281-977 was compared with the action of 5-fluorouracil and mitomycin C, which were administered at doses identical or close to the maximum tolerated dose for nude mice (Inaba, 1989; Nielsen *et al.*, 1992). A comparable degree of tumor growth inhibition was achieved with SDZ 281-977 and mitomycin C when these compounds were given i.v. to A431 tumor-bearing nude mice 4 times in the 1st week (Fig. 3). Effects of these drugs on the hematological parameters of these nude mice are reported below. 5-Fluorouracil and mitomycin C were also shown to exert significant tumor growth-inhibitory effects on MIA PaCa-2 pancreatic tumors. The degree of inhibition was comparable to that of SDZ 281-977 in separate experiments (data not shown).

In the MDA-MB-231 xenograft model, the compound showed significant activity (complete inhibition of tumor growth) only in the 1st week of treatment, with quick recovery of tumor growth thereafter despite continued treatment (10 mg/kg given i.v. 4 times a week during weeks 1, 3 and 5; data not shown). The compound was further evaluated in OFA rats bearing DMBA-induced mammary tumors. When DMBA-treated rats received intraperitoneal injections of SDZ 281-977 (30 mg/kg, thrice per week for 10 weeks), tumor growth, tumor multiplicity and weight gain were not different between control animals and rats treated with SDZ 281-977 (data not shown).

These data show that SDZ 281-977, applied via the intravenous or the oral route, exerts potent anticancer effects in some but not all animal cancer models examined.

### *Hematopoiesis and humoral immune response in vivo*

In the experiment comparing the anticancer activity of SDZ 281-977, 5-fluorouracil and mitomycin C (Fig. 3), we also characterized a potential myelo- or leukosuppressive effect of these drugs. At doses that produce clear anticancer effects, SDZ 281-977 treatment did not significantly affect peripheral blood cell count (leukocytes, platelets and erythrocytes) and bone-marrow nucleated cell numbers (data not shown). On the other hand, the antimetabolite 5-fluorouracil and the alkylating drug mitomycin C induced significant hematological changes. 5-Fluorouracil strongly reduced the blood leukocyte counts (29% of control) and moderately decreased the bone-marrow counts (69% of control) while not affecting blood erythrocyte or platelet numbers. Mitomycin C strongly reduced the blood leukocyte count (46% of control) without affecting bone-marrow cell, erythrocyte or platelet numbers.

Potential immunologic side effects of SDZ 281-977 were studied using the primary anti-sheep erythrocyte antibody model in OF1 mice. SDZ 281-977, at therapeutic doses, was devoid of immunosuppressive activity and had no leukotoxic effect on mouse spleen (Table I). This further confirms its lack of hematological side effects *in vivo* in this dose range.

### *Studies on the mechanism of the antiproliferative effect of SDZ 281-977*

Since lavendustin A is a potent tyrosine kinase inhibitor, it was of interest to establish whether SDZ 281-977 had retained this inhibitory activity. The EGF receptor tyrosine kinase-catalyzed phosphorylation of a tyrosine-containing peptide substrate was measured in the presence of SDZ 281-977 and the standard inhibitor lavendustin A. Enzyme activity was determined using a membrane preparation from A431 tumor cells. Whereas lavendustin A potently suppressed EGF receptor tyrosine kinase activity in a concentration-dependent manner, SDZ 281-977 was inactive (Fig. 4).

A clue to the mechanism of action was the accumulation of rounded cells in cultures treated with SDZ 281-977, suggesting a block in the cell cycle in mitosis. This was confirmed via DNA staining with the fluorescent dye DAPI to determine mitotic indices. An excellent correlation between inhibition of cell growth and accumulation of cells in mitosis was seen for SDZ 281-977 in A431 tumor cells (Fig. 5). Immunofluorescence studies demonstrated that SDZ 281-977 disrupted the mitotic spindle apparatus at concentrations where cells were blocked in mitosis (Winiski and Meingassner, 1994; Fig. 6). Untreated cells (Fig. 6a) exhibited well-defined mitotic spindles with the chromosomes lined up neatly between the spindle poles at the metaphase plate (Fig. 6b). Mitotic spindles in cells treated with SDZ 281-977 (Fig. 6c) were obviously perturbed. The spindle poles were less defined with fewer interpolar microtubules. The interpolar distance was also clearly shorter than in untreated mitotic spindles. The aberrant chromosomal distribution in treated cells was also quite apparent, with many chromosomes located at 1 or both spindle poles (Fig. 6d). The effects of SDZ 281-977 on the spindle apparatus were seen within 2 hr after drug addition, indicating that SDZ 281-977 quickly penetrated into cells to affect those cells just entering mitosis. The number of cells exhibiting abnormal mitosis increased with drug incubation time, as expected for a cell-cycle-related effect. The magnitude of the effects was concentration-dependent, as reported for other antimitotic agents (Jordan *et al.*, 1992): at higher concentrations the spindle apparatus was progressively fragmented into small aggregates. Another characteristic of antimitotic agents is their ability to induce the formation of micronuclei resulting from abortive mitoses (Rieder and Palazzo, 1992). SDZ 281-977 also exhibited this

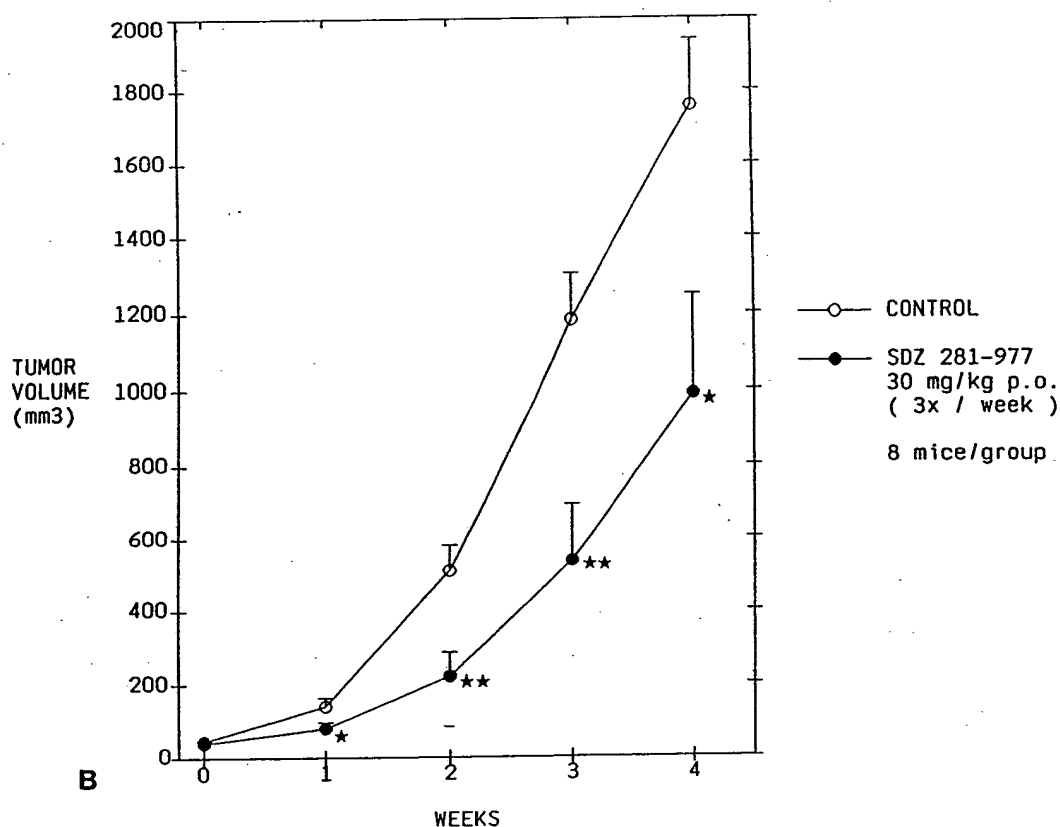
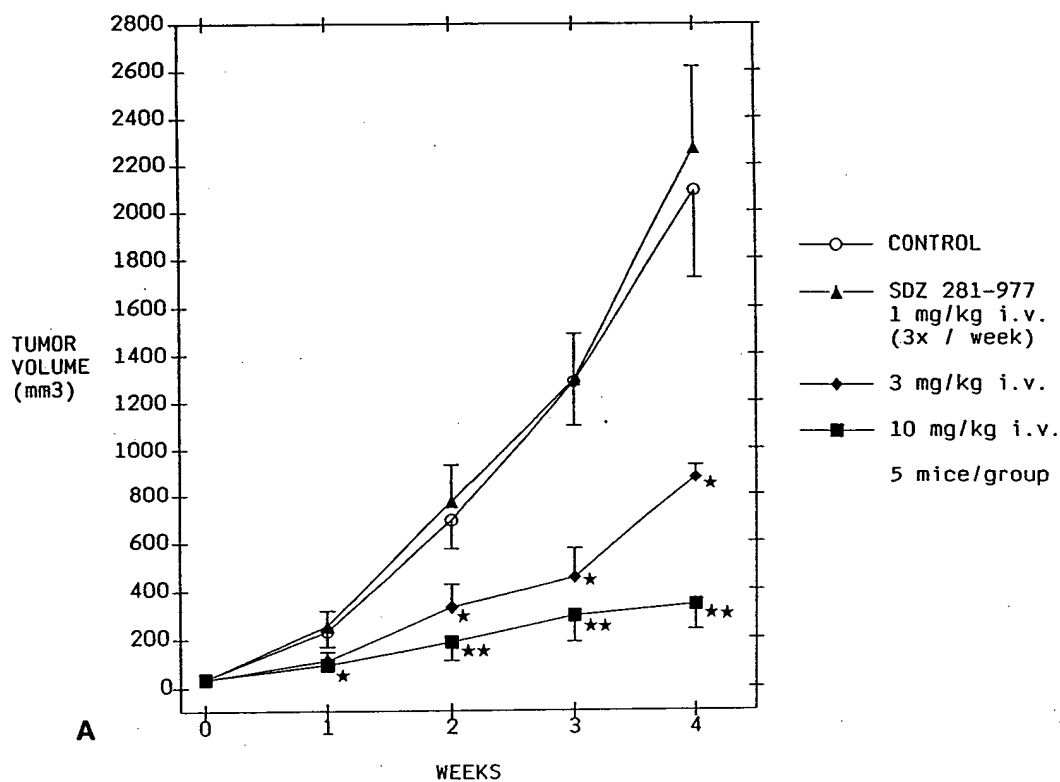


FIGURE 1 - (a) Effect of intravenous treatment with SDZ 281-977 on the growth of human vulvar tumors (A431) in nude mice. Doses were 1, 3 and 10 mg/kg given 3 times a week into the tail vein. Points, mean of 10 tumors in 5 animals/group; bars, SE. \* $p < 0.05$ ; \*\* $p < 0.01$ . (b) Oral treatment with SDZ 281-977 (30 mg/kg 3 times a week). Points, mean of 16 tumors in 8 animals/group; bars, SE. \* $p < 0.05$ ; \*\* $p < 0.01$ .

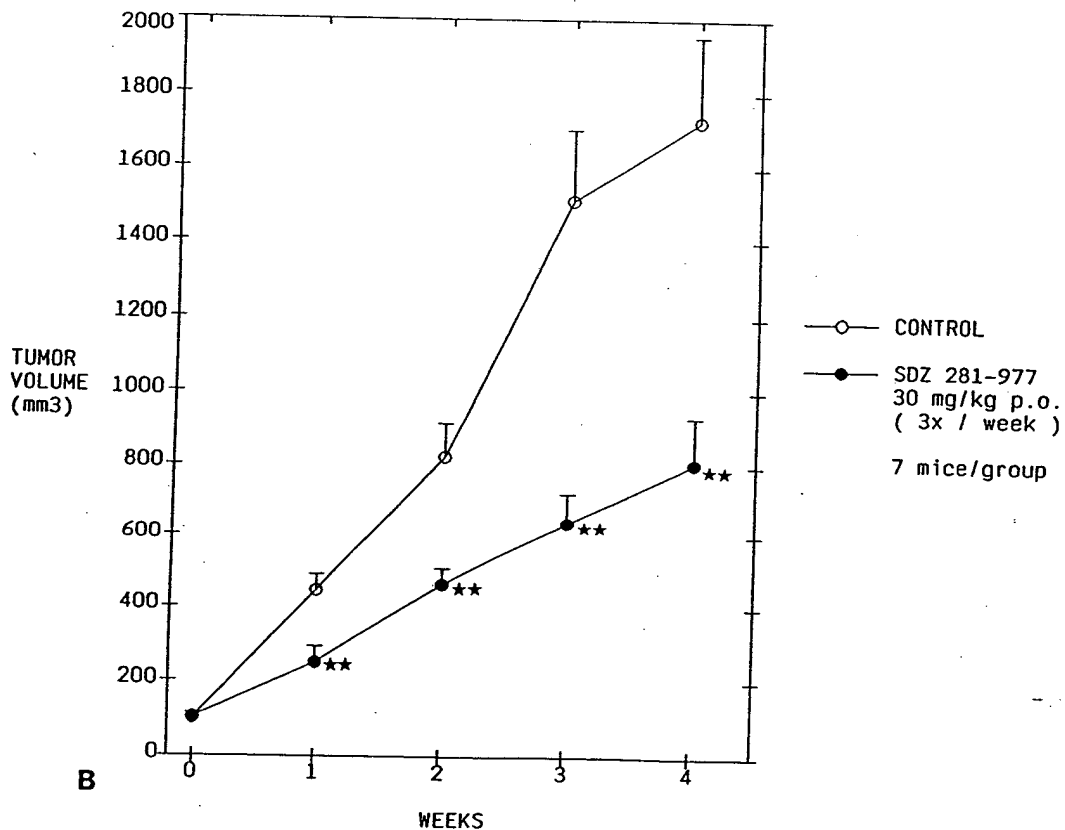
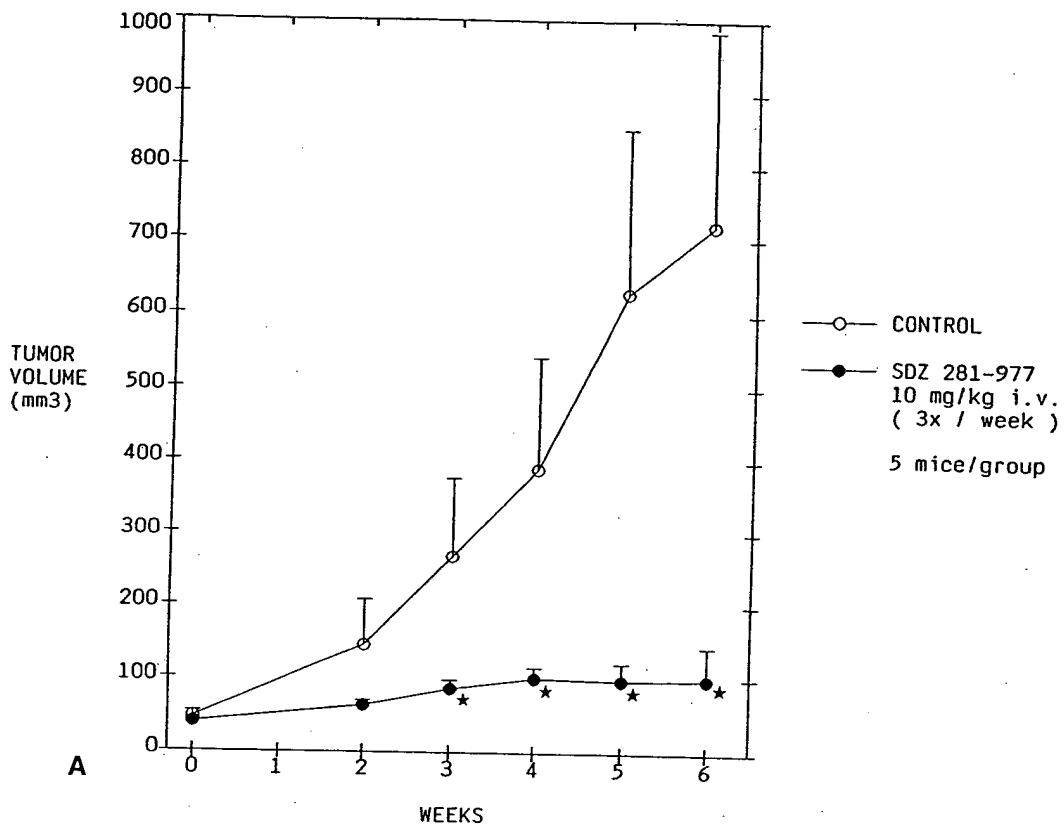


FIGURE 2 - (a) Inhibition of the growth of xenotransplanted human MIA PaCa-2 pancreatic tumors in nude mice. Effects of intravenous administration of SDZ 281-977 (10 mg/kg, 3 times a week). Points, mean of 10 tumors in 5 mice/group; bars, SE. \* $p < 0.05$ . (b) Effect of oral treatment with SDZ 281-977 (30 mg/kg, 3 times a week). Points, mean of 14 tumors in 7 animals/group; bars, SE. \*\* $p < 0.01$ .

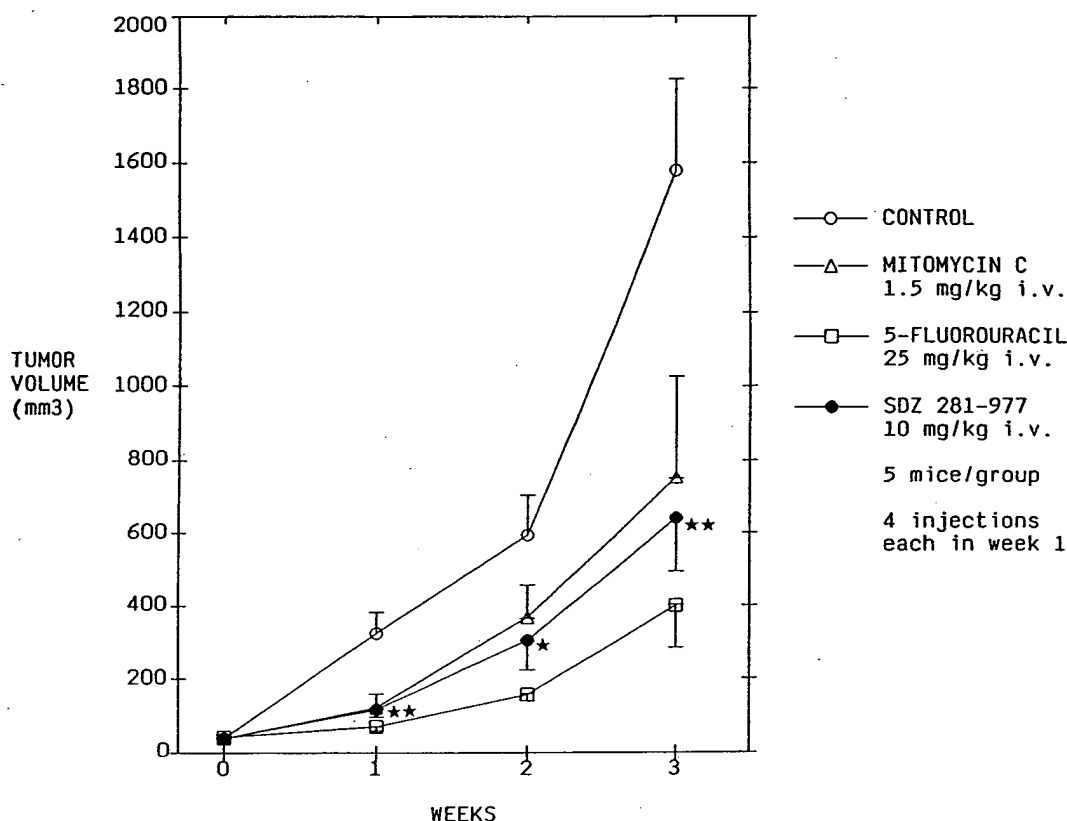


FIGURE 3 – Inhibition of A431 tumor growth in nude mice treated with SDZ 281-977 or standard anticancer drugs. 5-Fluorouracil (25 mg/kg), mitomycin C (1.5 mg/kg) or SDZ 281-977 (10 mg/kg) were administered i.v. 4 days in a row in week 1. Points, mean of 10 tumors in 5 animals/group; bars, SE. \* $p < 0.05$ ; \*\* $p < 0.01$ .

TABLE I – EFFECTS OF SDZ 281-977 ON THE PRIMARY ANTI-SRBC HUMORAL RESPONSE IN OF<sub>1</sub> MICE<sup>1</sup>

Treatment	Dose (mg/kg)	Cells/spleen ( $10^6$ )	Anti-SRBC PFC ( $10^3$ /spleen)
Vehicle	i.v.	231 $\pm$ 54	286 $\pm$ 66
SDZ 281-977	10 i.v.	251 $\pm$ 95	286 $\pm$ 126
SDZ 281-977	30 i.v.	218 $\pm$ 38	237 $\pm$ 110
Cyclosporin A	75 p.o.	228 $\pm$ 57	47 $\pm$ 24

<sup>1</sup>Female OF<sub>1</sub> mice were inoculated i.v. with SRBC. Mice were treated with drug for 4 consecutive days and the SRBC-specific PFC were counted.

phenomenon: large numbers of cells containing micronuclei were observed after 1 day of incubation.

#### Effects on MDR cells

The growth-inhibitory action of SDZ 281-977 was investigated in 2 pairs of MDR cell lines (L1210 vs. L1210-MDR and K562 vs. K562-MDR). The MDR-negative cell lines (L1210 and K562) were as susceptible to SDZ 281-977 as their MDR counterparts (Table II). As expected, the antiproliferative action of colchicine was greater in non-MDR cells as compared to its effects on the resistant variants (17-fold with L1210 and 11-fold with K562). Thus, the antiproliferative activity of SDZ 281-977 is not reduced in cells expressing the MDR phenotype.

#### DISCUSSION

We have established the oncopharmacological profile of the novel antiproliferative agent SDZ 281-977. This compound is a

modified, lipophilic analog of the tyrosine kinase inhibitor lavendustin A that is inactive in whole cells, probably due to poor cellular uptake (Onoda *et al.*, 1989, 1990). The antiproliferative effects previously seen with SDZ 281-977 *in vitro* (Nussbaumer *et al.*, 1994a) have now been confirmed in nude mice bearing human tumors. Intravenously injected SDZ 281-977 was more potent at exerting antiproliferative effects than orally given drug. However, mere existence of oral efficiency represents a major advantage over most commonly used anticancer agents that require parenteral use. In both the pancreatic (MIA PaCa-2) and the epidermoid (A431) carcinoma models, SDZ 281-977 appears to exert a cytostatic effect, because treated tumors exhibit a decrease in growth rate but not shrinkage.

In comparative *in vivo* studies, using intravenous administration in the A431 model, we found the anticancer action of the standard drugs 5-fluorouracil and mitomycin C to be in a range similar to that of SDZ 281-977 (Fig. 3). These standard agents, however, are known to exert severe toxic effects; in particular, they interfere with bone-marrow function and maturation of blood cells. It was thus of interest to study the potential side effects of SDZ 281-977 at therapeutic doses.

We have found that, under conditions where mice treated with 5-fluorouracil and mitomycin C exhibit clear hematological alterations, anticancer treatment with efficacious doses of SDZ 281-977 was not associated with such side effects. Moreover, at doses that are effective in retarding tumor growth in mice, SDZ 281-977 was totally ineffective in inhibiting the primary anti-SRBC response or decreasing spleen cellularity in mice (Table I). Apart from the apparent lack of untoward effects on the immune and hematopoietic systems, SDZ

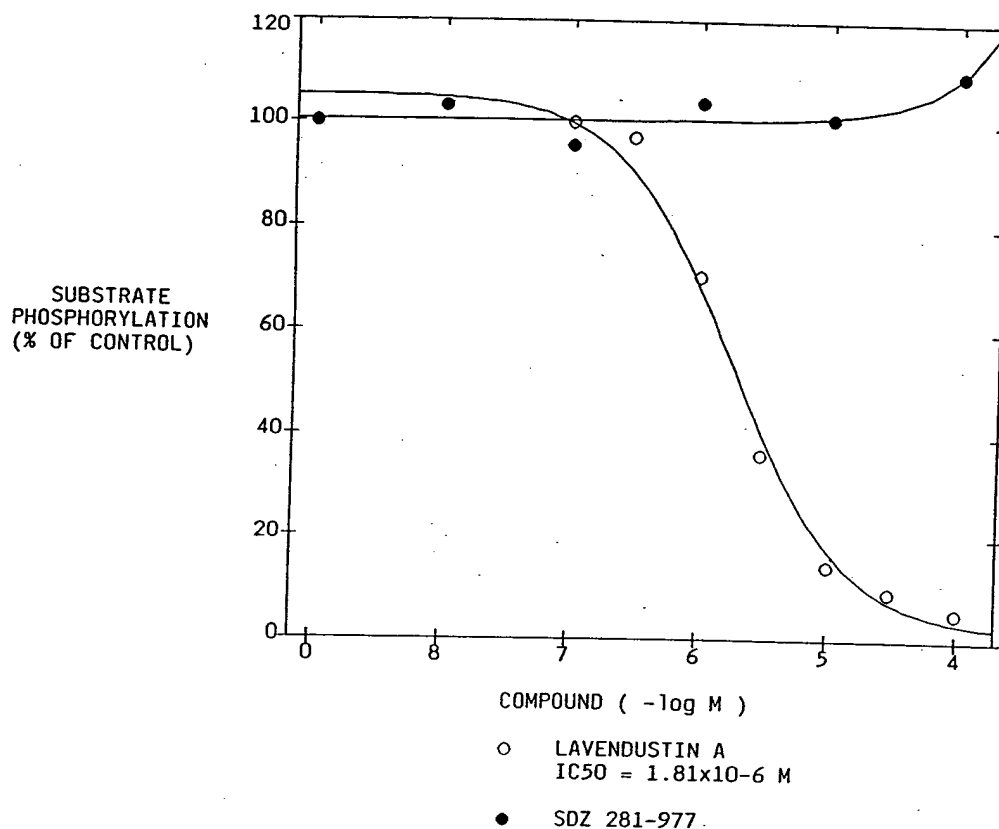


FIGURE 4 – Effects of lavendustin A and its derivative SDZ 281-977 on the activity of the EGF receptor tyrosine kinase in broken cells. Points, mean of duplicate determinations.

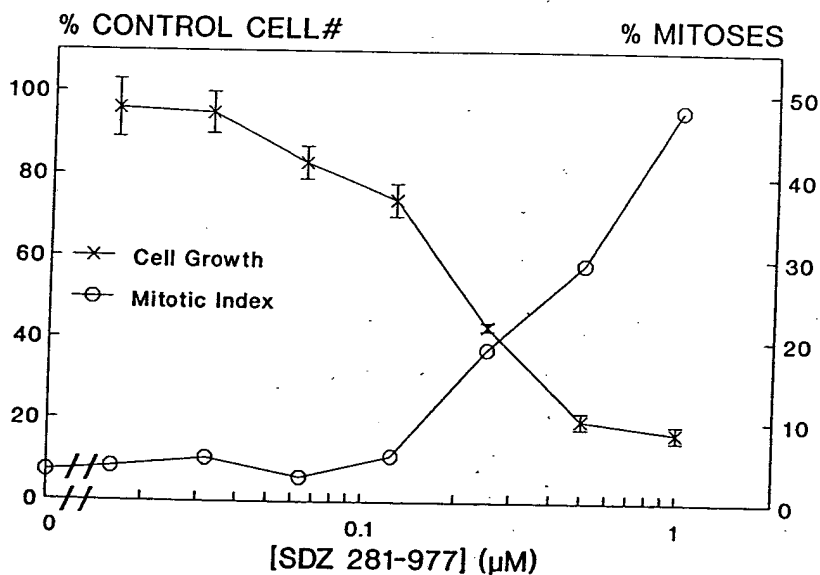


FIGURE 5 – Effect of SDZ 281-977 on the growth and mitotic index of A431 tumor cells determined after 3 days and 8 hr using the SRB colorimetric assay and DAPI staining of DNA, respectively. Points, mean of triplicate determinations; bars, SD.

281-977 was well tolerated by nude mice, as indicated by the fact that the body weight of the animals was not significantly affected by treatment with therapeutic drug doses. The potent antitumor effects combined with good tolerability make SDZ 281-977 an interesting new anticancer agent that warrants further oncopharmacological studies.

The interest in this compound is further based on its very distinct antiproliferative profile, in that it exhibits a high degree of selectivity for certain cell and tumor types. Cells that are not growth inhibited by SDZ 281-977 *in vitro* and *in vivo* include normal cells such as hematopoietic progenitor cells and certain cancer cells. Our preliminary studies demon-

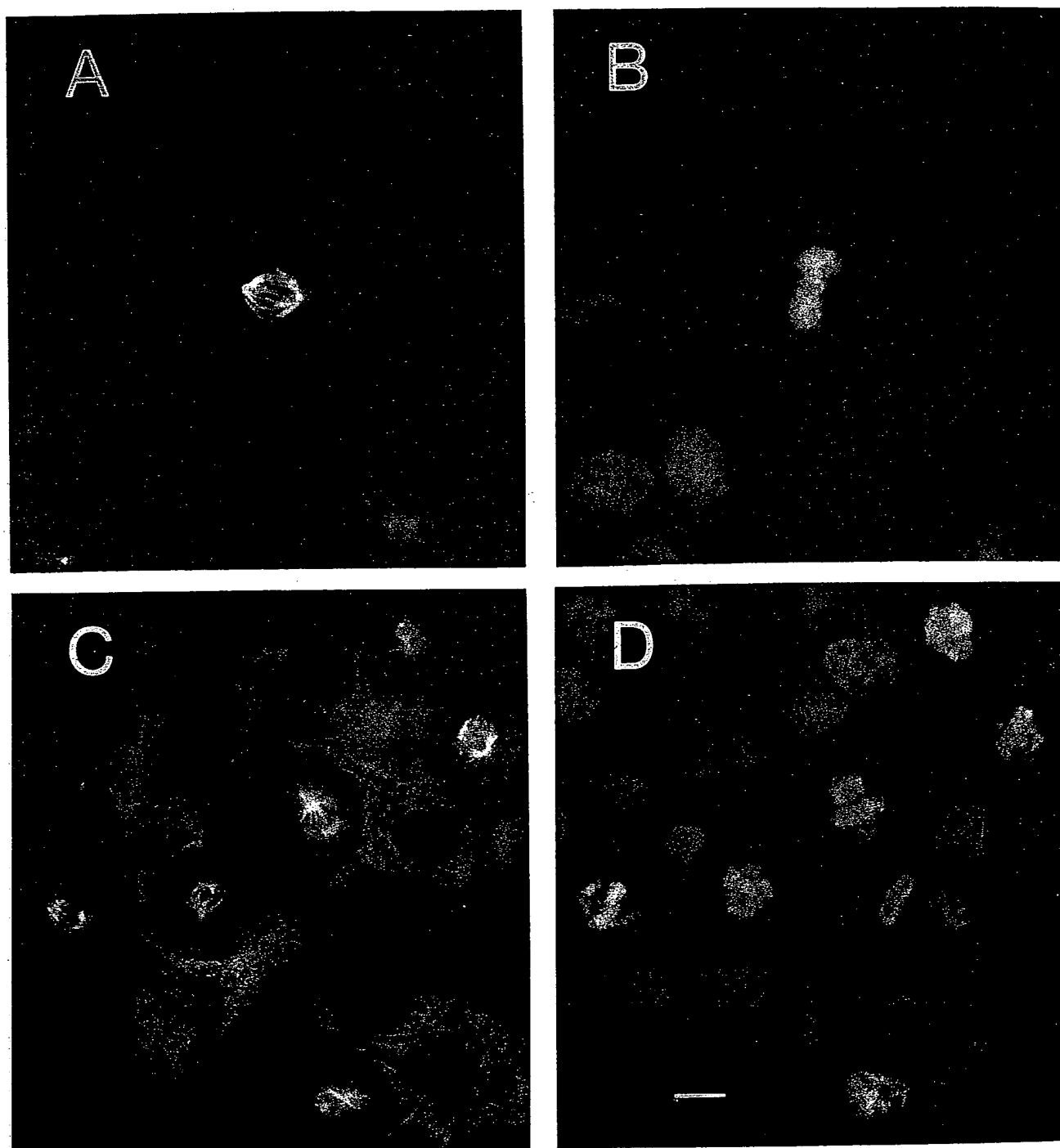


FIGURE 6 - Microtubule and chromosomal distribution in A431 cells incubated with or without SDZ 281-977 for 8 hr. (a, b) No drug added; (c, d) 0.5  $\mu$ M. (a, c) Antitubulin immunofluorescence; (b, d) DAPI stain of chromosomes. Bar = 10  $\mu$ m.

strated that DMBA-induced mammary carcinomas fail to respond to this agent and that MDA-MB 231 breast xenografts were only weakly and transiently inhibited. Understanding the mode of action of SDZ 281-977 is important, because this may explain the observed *in vitro* and *in vivo* selectivities. The different sensitivities of various cells is apparently unrelated to P-glycoprotein mediated mechanisms of resistance. SDZ 281-977 inhibited the proliferation of MDR tumor cell lines and their sensitive parental counterparts with the same potency

(Table II). Therefore, SDZ 281-977 may be a promising drug for the treatment of MDR tumors. Multidrug resistance due to tumoral expression of the multidrug transporter P-glycoprotein is an important mechanism responsible for treatment failure in various types of cancer (Gottesmann and Pastan, 1988; Lum *et al.*, 1993). The efficacy of SDZ 281-977 in MDR tumor cells implies that this compound is not a substrate for P-glycoprotein. At the clinical level, the challenge will be to identify those types of cancer that respond to treatment with SDZ 281-977.

TABLE II - ANTIPROLIFERATIVE EFFECTS OF COLCHICINE AND SDZ 281-977 ON MDR+ TUMOR CELL LINES<sup>1</sup>

Tumor cell	IC <sub>50</sub> (nM)	
	Colchicine	SDZ 281-977
L1210	14.7 ± 11.0	415.0 ± 7.1
L1210-MDR	252.5 ± 53.0	232.5 ± 24.8
K562	14.1 ± 4.1	217.5 ± 31.8
K562-MDR	152.5 ± 31.8	215.0 ± 49.5

<sup>1</sup>Results represent means ± standard deviation of 2 independent experiments run in triplicate.

We have started to investigate the mechanism of action of SDZ 281-977. SDZ 281-977 is derived from a compound, lavendustin A, that potentially inhibits the activity of the isolated EGF receptor tyrosine kinase. Thus, the growth inhibitory action of SDZ 281-977 was expected to be based on the inhibition of tyrosine kinases, in particular the EGF receptor tyrosine kinase. In contrast to lavendustin A, SDZ 281-977 failed to inhibit the activity of the EGF receptor tyrosine kinase when studied in a cell-free assay system (Fig. 4). While the possibility that SDZ 281-977 interferes with other (tyrosine) kinases cannot be excluded, the antimitotic effect of this compound strongly suggests that either tubulin or microtubule-associated proteins are the molecular target (Fig. 6). An

examination of the effects on tubulin polymerization *in vitro* should address this issue. In any case, SDZ 281-977 is the first example of an antimitotic agent derived from the potent tyrosine kinase inhibitor lavendustin A.

In conclusion, SDZ 281-977 is a novel chemical entity endowed with selective antiproliferative activity against certain tumor cells. The mechanism of the antiproliferative effect can be explained on a cellular level by the ability of SDZ 281-977 to induce mitotic arrest. Orally and intravenously administered SDZ 281-977 exerts antiproliferative effects *in vivo* in 2 human tumor models. Importantly, SDZ 281-977 is active in cells exhibiting the multidrug resistance phenotype. In contrast to classical anticancer drugs, it does not suppress hematopoiesis, and it is not immunosuppressive at concentrations that interfere with tumor cell growth. These characteristics indicate that SDZ 281-977 may be an innovative anticancer drug.

#### ACKNOWLEDGEMENTS

The authors express their gratitude to Drs. V. Quesniaux, B. Fagg and M. Kammüller for participating in hematologic investigations and for carefully reviewing the manuscript. The authors thank Mrs. L. Baboulène, Mr. N. v. Jeney and Mr. L. Tolcsvai for excellently performing cell culture and tumor xenograft studies.

#### REFERENCES

- ALLEY, M.C., SCUDIERO, D.A., MONKS, A., HURSEY, M.L., CZERWINSKI, M.J., FINE, D.L., ABBOTT, B.J., MAYO, J.G., SHOEMAKER, R.H. and BOYD, M.R., Feasibility of drug screening with panels of human tumor cell lines using a microculture tetrazolium assay. *Cancer Res.*, **48**, 589-601 (1988).
- BISHOP, J.M., The molecular genetics of cancer. *Science*, **235**, 305-311 (1987).
- GEISSLER, J.F., TRAXLER, P., REGENASS, U., MURRAY, B.J., ROESSEL, J.L., MEYER, J., MCGLYNN, E., STORNI, A. and LYDON, N.B., Thiazolidine-diones. Biochemical and biological activity of a novel class of tyrosine protein kinase inhibitors. *J. Biol. Chem.*, **265**, 22255-22261 (1990).
- GOTTESMANN, M.M. and PASTAN, I., Resistance to multiple chemotherapeutic agents in human cancer cells. *Trends Pharmacol. Sci.*, **9**, 54-58 (1988).
- HUNTER, T., A thousand and one protein kinases. *Cell*, **50**, 823-829 (1987).
- INABA, M., Revaluation of the human tumor/nude mouse system as a screening model for antitumor agents. In: B.-q. Wu and J. Zheng (eds.), *Immune-deficient animals in experimental medicine*, pp. 245-253, Karger, Basel (1989).
- JERNE, N.R., HENRY, C., NORDIN, A.A., FUJI, H., KOROS, A.M.C. and LEFKOVITS, I., Plaque forming cells: methodology and theory. *Transplantation Rev.*, **18**, 130-191 (1974).
- JORDAN, M.A., THROWER, D. and WILSON, L., Effects of vinblastine, podophyllotoxin and nocodazole on mitotic spindles. Implications for the role of microtubule dynamics in mitosis. *J. Cell Sci.*, **102**, 401-416 (1992).
- LUM, B.L., FISHER, G.A., BROPHY, N.A., YAHANDA, A.M., ADLER, K.M., KAUBISCH, S., HALSEY, J. and SIKIC, B.I., Clinical trials of modulation of multidrug resistance. Pharmacokinetic and pharmacodynamic considerations. *Cancer*, **72**, 3502-3514 (1993).
- LYALL, R.M., ZILBERSTEIN, A., GAZIT, A., GILON, C., LEVITZKI, A. and SCHLESSINGER, J., Typhostins inhibit epidermal growth factor (EGF)-receptor tyrosine kinase activity in living cells and EGF-stimulated cell proliferation. *J. Biol. Chem.*, **264**, 14503-14509 (1989).
- MARX, J., How cells cycle toward cancer. *Science*, **263**, 319-321 (1994).
- NIELSEN, L.L., GURNANI, M. and TYLER, R.D., Evaluation of the wip-ras transgenic mouse as a model system for testing anticancer drugs. *Cancer Res.*, **52**, 3733-3738 (1992).
- NUSSBAUMER, P., WINISKI, A.P., CAMMISULI, S., HIESTAND, P., WECKBECKER, G. and STÜTZ, A., Novel antiproliferative agents derived from lavendustin. *Amer. J. med. Chem.*, **37**, 4079-4084 (1994a).
- NUSSBAUMER, P., WINISKI, A.P., MEINGASSNER, J.G., CAMMISULI, S., WECKBECKER, G. and STÜTZ, A., SDZ LAP 977: a novel antiproliferative agent derived from the tyrosine kinase inhibitor lavendustin A. SID Meeting, Baltimore, MD. *J. Invest. Dermatol.*, **102**, 565 (1994b).
- ONODA, T., IINUMA, H., SASAKI, Y., HAMADA, M., ISSHIKI, K., NAGANAWA, H. and TAKEUCHI, T., Isolation of a novel tyrosine kinase inhibitor, lavendustin A, from *Streptomyces griseolavendus*. *J. nat. Prod.*, **52**, 1252-1257 (1989).
- ONODA, T., ISSHIKI, K., TAKEUCHI, T., TATSUTA, K. and UMEZAWA, K., Inhibition of tyrosine kinase and epidermal growth factor receptor internalization by lavendustin A methyl ester in cultured A431 cells. *Drugs exp. clin. Res.*, **16**, 249-253 (1990).
- RIEDER, C.L. and PALAZZO, R.E., Colcemid and the mitotic cycle. *J. Cell Sci.*, **102**, 387-392 (1992).
- SKEHAN, P., STORENG, R., SCUDIERO, D., MONKS, A., MCMAHON, J., VISTICA, D., WARREN, J.T., BOKESCH, H., KENNEY, S. and BOYD, M.R., New colorimetric cytotoxicity assay for anticancer-drug screening. *J. nat. Cancer Inst.*, **82**, 1107-1112 (1990).
- WECKBECKER, G., LIU, R., TOLCSVAI, L. and BRUNS, C., Antiproliferative effects of the somatostatin analog octreotide (SMS 201-995) on ZR-75-1 human breast cancer cells *in vivo* and *in vitro*. *Cancer Res.*, **52**, 4973-4978 (1992a).
- WECKBECKER, G., TOLCSVAI, L., LIU, R. and BRUNS, C., Preclinical studies on the anticancer activity of the somatostatin analog octreotide (SMS 201-995). *Metabolism*, **41**(Suppl. 2), 99-103 (1992b).
- WINISKI, A.T. and MEINGASSNER, J.G., A novel antiproliferative agent derived from the tyrosine kinase inhibitor lavendustin A: mechanism of action. *J. invest. Dermatol.*, **102**(abstract 251), 565 (1994).
- YONEDA, T., LYALL, R.M., ALSINA, M.M., PERSONS, P.E., SPADA, A.P., LEVITZKI, A., ZILBERSTEIN, A. and MUNDY, G.R., The antiproliferative effects of tyrosine kinase inhibitors typhostins on a human squamous cell carcinoma *in vitro* and in nude mice. *Cancer Res.*, **51**, 4430-4435 (1991).
- YUAN, C.J., JAKES, S., ELLIOTT, S. and GRAVES, D.J., A rationale for the design of an inhibitor of tyrosyl kinase. *J. Biol. Chem.*, **265**, 16205-16209 (1990).

## CHS 828, a Novel Pyridyl Cyanoguanidine with Potent Antitumor Activity *in Vitro* and *in Vivo*

Pernille-Julia Vig Hjarnaa, Elin Jonsson, Scilla Latini, Sumeer Dhar, Rolf Larsson, Erik Bramm, Torsten Skov, and Lise Binderup<sup>1</sup>

Leo Pharmaceutical Products, DK-2750 Ballerup, Denmark [P.-J. V. H., S. L., E. B., T. S., L. B.], and Division of Clinical Pharmacology, University Hospital, Uppsala University, S-751 85 Uppsala, Sweden [E. J., S. D., R. L.]

### ABSTRACT

A new class of recently discovered antineoplastic agents, the pyridyl cyanoguanidines, exert a potent antitumor activity in rodents after oral administration. Optimization *in vitro* and *in vivo* has resulted in the selection of the lead candidate CHS 828 (*N*-(6-chlorophenoxyhexyl)-*N'*-cyano-*N'*-4-pyridylguanidine). CHS 828 was found to exert potent cytotoxic effects in human breast and lung cancer cell lines, with lesser effects on normal fibroblasts and endothelial cells. In a study using a panel of cell lines with different resistance patterns, the effects of CHS 828 showed a low correlation with the activity patterns of known anticancer agents, and no sensitivity to known mechanisms of multidrug resistance was observed. In nude mice bearing human tumor xenografts, CHS 828, at doses from 20 to 50 mg/kg/day p.o., inhibited the growth of MCF-7 breast cancer tumors and caused regression of NYH small cell lung cancer tumors. Oral administration of CHS 828 once weekly improved efficacy without increasing toxicity. CHS 828 was found to compare favorably with established chemotherapeutic agents such as cyclophosphamide, etoposide, methotrexate, and paclitaxel. In mice with NYH tumors, long-term survival (>6 months) was observed after treatment with CHS 828 was stopped. In conclusion, CHS 828 is an effective new antitumor agent, with a potentially new mechanism of action. CHS 828 is presently being tested in Phase I clinical trials in collaboration with the European Organization for Research and Treatment of Cancer.

### INTRODUCTION

Chemotherapy is the mainstay of therapy for a large number of malignant tumors, especially in the metastatic setting. Although for certain tumor types this modality of treatment has been shown to produce impressive results including cures, the majority of human solid tumors is considerably less responsive. Today more than 50 established cytotoxic drugs are available for treatment of human malignant tumors in the Western world. The majority of these drugs act directly or indirectly on the DNA by inhibiting its synthesis, or they can also act at the level of microtubuli by interfering with mitosis, cell motility, or intracellular transport. They are mostly derived from natural products, they have to be parenterally administered, and they easily induce MDR<sup>2</sup> in the clinical setting.

In the search for new low molecular weight synthetic inhibitors of tumor cell growth, we unexpectedly discovered that a number of pyridyl cyanoguanidines showed antitumor activity after oral administration in a routine screening program in rats (1). Some pyridyl cyanoguanidines are known as potassium channel openers. Among these, pinacidil (*N*-1,2,2-trimethylpropyl-*N'*-cyano-*N'*-4-pyridylguanidine) is a structural prototype with potent antihypertensive activity

(2). Replacement of the side chain of pinacidil by longer aryl-containing side chains gave rise to compounds with increasing antitumor activity but without hypotensive activity. Monosubstitution in the terminal phenoxy group with a chloro group and optimization of the side chain length with regard to antitumor activity resulted in the selection of a drug candidate, CHS 828 (*N*-(6-chlorophenoxyhexyl)-*N'*-cyano-*N'*-4-pyridylguanidine; Ref. 1).

The data presented here comprise *in vitro* and *in vivo* studies with CHS 828. Cytotoxic activity and inhibition of cell proliferation were studied *in vitro*, using established cancer cell lines, cell lines resistant to known antineoplastic agents, and normal cells.

*In vivo*, CHS 828 was investigated in nude mice with various human tumor cell xenografts and in rats with transplanted tumors in a series of studies focusing on dose-response and schedule-dependent effects of CHS 828, on its antitumor activity in established tumors, and on comparison with reference chemotherapeutic agents.

### MATERIALS AND METHODS

#### Compounds

***In Vitro* Experiments.** For DNA synthesis and cytotoxicity experiments, CHS 828 (Department of Chemical Research, Leo Pharmaceutical Products), daunorubicin and paclitaxel (both from Sigma Chemical Co., St. Louis, MO) were dissolved at 10 mM in DMSO and stored at -20°C. Dilutions were made with DMSO.

In the activity profile study, fluorescein diacetate (Sigma Chemical Co.) was dissolved in DMSO and stored at -20°C as a stock solution protected from light. Reference drugs were obtained from commercial sources and were dissolved according to the guidelines from the manufacturers. The Pgp-blocker SDZ PSC 833 was obtained from Novartis, Stockholm, Sweden, MIBG from Sigma Chemical Co., and MGBG from the Drug Synthesis and Chemistry Branch, National Cancer Institute (Bethesda, MD).

***In Vivo* Experiments.** CHS 828 was formulated as a suspension in 2% carboxymethyl cellulose in 0.9% NaCl solution. Cyclophosphamide (Sendoxan, Asta Medica, Frankfurt am Main, Germany) was dissolved in distilled water. Etoposide (Vepesid, Bristol-Myers Squibb, Syracuse, NY) and paclitaxel (Taxol, Bristol-Myers Squibb) were dissolved in 0.9% NaCl solution.

**Cells.** The human cancer cell lines used for the studies of DNA synthesis and cytotoxicity included NYH SCLC cells (Rigshospitalet, Copenhagen, Denmark) and MCF-7 breast cancer cells (ATCC, Rockville, MD). MRC-5 fetal lung fibroblasts (European Collection of Cell Cultures, Salisbury, United Kingdom) and HUVEC cells (ATCC) were used as normal human reference cells.

NYH cells were grown as partly floating cultures. Floating and loosely adherent cells were passaged once a week in RPMI 1640 with the addition of 10% FCS, 2 mM glutamine, 100 IU/ml penicillin, and 100 µg/ml streptomycin. Fresh growth medium was added every 2nd or 3rd day.

MCF-7 cells were cultured as monolayer cultures. Monolayers were passaged once a week in DMEM deprived of phenol red and supplemented with 5% FCS, 2 mM glutamine, 100 IU/ml penicillin, and 100 µg/ml streptomycin. The growth medium was changed every 2nd or 3rd day.

MRC-5 cells were cultured as monolayer cultures. Monolayers were passaged once a week in DMEM with 10% FCS, 2 mM glutamine, 100 IU/ml penicillin, and 100 µg/ml streptomycin. The growth medium was changed every 2nd or 3rd day.

HUVEC cells were cultured as monolayer cultures. Monolayers were pas-

Received 3/31/99; accepted 9/15/99.

The costs of publication of this article were defrayed in part by the payment of page charges. This article must therefore be hereby marked *advertisement* in accordance with 18 U.S.C. Section 1734 solely to indicate this fact.

<sup>1</sup> To whom requests for reprints should be addressed, at Leo Pharmaceutical Products, Industriparken 55, DK-2750 Ballerup, Denmark.

<sup>2</sup> The abbreviations used are: MDR, multidrug resistance; ATCC, American Type Culture Collection; AUC, area under the curve; FMCA, fluorometric microculture cytotoxicity assay; GSH, glutathione; HUVEC, human umbilical vein endothelial cells; MGBG, methylglyoxal bis(guanyldiazotone); MIBG, *m*-iodobenzylguanidine; MRP, MDR-associated protein; MTT, 3-(4,5-dimethylthiazolyl)-2,5-diphenyl tetrazolium bromide; Pgp, P-glycoprotein; SCLC, small cell lung cancer; SI, survival index.



saged once a week in M199 medium supplemented with 10% FCS, 0.1 mg/ml heparin, 30  $\mu$ g/ml endothelial cell growth supplement, 2 mM glutamine, 100 IU/ml penicillin, and 100  $\mu$ g/ml streptomycin. The growth medium was changed every 2nd or 3rd day.

For the activity profile studies, a human tumor cell line panel consisting of four sensitive parental cell lines, five drug resistant sublines, representing different mechanisms of resistance, and one cell line with primary resistance was used (3). The cell lines included the myeloma cell line RPMI 8226/S and its sublines 8226/Dox40 and 8226/LR-5 (W. S. Dalton, University of Arizona, Tucson, AZ), the lymphoma cell lines U-937 GTB and U-937-Vcr (4, 5), the SCLC cell line NCI-H69 and its subline H69AR (ATCC, Rockville, MD), the renal adenocarcinoma cell line ACHN (ATCC), and the leukemic cell line CCRF-CEM and its subline CEM/VM-1 (W. T. Beck, University of Tennessee, Memphis, TN).

The 8226/Dox40 was selected for doxorubicin resistance and shows the classical MDR phenotype with overexpression of Pgp 170 (6). The 8226/LR-5 was selected for melphalan resistance, proposed to be associated with increased levels of GSH (7, 8). The U-937-Vcr was selected for vincristine resistance, proposed to be tubulin-associated (5). The H69AR, selected for doxorubicin resistance, expresses a MDR phenotype proposed to be mediated by MRP (9, 10). The CEM/VM-1, selected for teniposide resistance, expresses an atypical MDR, which is proposed to be topoisomerase II (11, 12). The exact mechanism of resistance for the primary resistant ACHN cell line is not known and may be multifactorial (13).

The cell lines were grown in RPMI 1640 with 10% FCS, 2 mM glutamine, 50  $\mu$ g/ml streptomycin, and 60  $\mu$ g/ml penicillin. The 8226/Dox40 was treated once a month with doxorubicin at 0.24  $\mu$ g/ml and the 8226/LR-5 with melphalan at 1.53  $\mu$ g/ml at each change of medium. The U-937-Vcr was continuously cultured in the presence of 10 ng/ml of vincristine, and the H69AR was alternately fed with drug-free medium and medium containing 0.46  $\mu$ g/ml of doxorubicin. The CEM/VM-1 cell line was cultured in drug-free medium without any loss of resistance for a period of 6–8 months. The resistance patterns of the cell lines were routinely confirmed in control experiments.

In the xenograft studies, MCF-7 breast cancer cells (Clone L, N. Br  nner, Rigshospitalet, Copenhagen, Denmark), NYH SCLC cells (P. Buhl Jensen, Rigshospitalet, Copenhagen, Denmark), and H-460 non-SCLC cells (ATCC, Rockville, MD) were used. The cells used in the rodent tumor studies included rat Yoshida hepatosarcoma cells (Finsen Institutet, Copenhagen, Denmark), and rat Walker 256 mammary carcinoma cells (Deutsche Krebsforschungszentrum, Heidelberg, Germany).

### Cell Line Experiments

**DNA Synthesis.** The ability of CHS 828 to inhibit DNA synthesis was determined by the incorporation of tritiated thymidine. Paclitaxel and daunorubicin were used as reference compounds.

The MCF-7 and NYH cells were seeded in tissue culture vessels at the concentration of  $7.5 \times 10^3$  cells/ml, the test compounds were added 2 h after plating, and the cells were cultured with the test compounds for 96 h (MCF-7 cells) or 144 h (NYH cells). MRC-5 fibroblasts were seeded in tissue culture vessels at the concentration of  $2.5 \times 10^3$  cells/ml, the test compounds were added 2 h after plating, and the cells were cultured with the test compounds for 144 h. Endothelial cells were seeded at the concentration of  $25 \times 10^3$  cells/ml in multidish plates in M199 medium without heparin and endothelial cell growth supplement and were incubated for 24 h. Then the test compounds were added, and the cells were incubated for an additional 96 h with 1 ng/ml vascular endothelial growth factor and with 2% FCS.

Tritiated thymidine (5 Ci/mmol, Amersham, Denmark) was added to the cultures at the concentration of 1  $\mu$ Ci/ml, and the cells were incubated for an additional 4 h. The incorporated thymidine was measured with a  $\beta$ -counter. Each drug concentration was tested in triplicate.

**Cytotoxicity.** The ability of CHS 828 to induce cytotoxic effects was determined by the conversion of MTT to formazan by mitochondrial dehydrogenases. The cells were seeded in tissue culture vessels at the concentration of  $2.5 \times 10^3$  cells/ml, were incubated for 2 h, and were then exposed to the test compounds for 96 h (MCF-7 cells) or 120 h (NYH cells). Then, MTT was added at the concentration of 5 mg/ml, and the cells were incubated for 4 h. To solubilize the formazan product, 5% SDS was added to the cultures overnight.

The absorbance of the solubilized formazan was then determined with an ELISA reader. Each drug concentration was tested in triplicate.

**Activity Profile Studies.** The FMCA is based on measurement of fluorescence generated from the hydrolysis of fluorescein diacetate to fluorescein by cells with intact plasma membranes and has been described in detail previously (14). Briefly, 180  $\mu$ l of cell suspension were seeded into the wells of 96-well microtiter plates prepared with drugs. Cell density ranged from  $5$  to  $20 \times 10^3$  cells/well. Each drug concentration was tested in triplicate. Six wells with cells but without drugs served as control and six wells with only culture medium as blank.

The plates were incubated for 72 h. At the end of the incubation period, the plates were centrifuged, and the medium was removed. The cells were washed once and 100  $\mu$ l/well of fluorescein diacetate (10  $\mu$ g/ml) was added. The plates were incubated for 45 min, and the generated fluorescence from each well was measured at 538 nm in a 96-well scanning fluorometer (Fluoroscanner II, Lab-systems OY, Helsinki, Finland).

To evaluate the schedule dependency of drug activity, RPMI 8226S cells were exposed to the drug for 2 or 72 h followed by washing and the addition of new culture medium, after which FMCA was performed at 72 h.

### Animal Models

**Animals and Animal Welfare.** All of the animal experiments were conducted according to the guidelines and ethical standards of the Danish Committee for Animal Experiments. Female NMRI nu/nu mice 6 weeks of age were purchased from M&B (Ry, Denmark). Female outbred Sprague Dawley rats, 4–6 weeks old, and female inbred Lewis rats, 9–11 weeks old, were obtained from M&B (Ejby, Denmark). The nude mice were housed under specific pathogen-free conditions, whereas the rats were maintained under standard laboratory conditions.

**MCF-7 Xenografts.** Oophorectomized 17 $\beta$ -estradiol-substituted NMRI nu/nu mice were inoculated with  $1$ – $1.5 \times 10^7$  MCF-7 cells in both flanks, and the tumor growth was measured twice weekly for 8 weeks (15). The tumor area was used as expression of the tumor size and was calculated from two perpendicular diameters measured with a digital caliper (16). CHS 828 was given by oral gavage from day 21 when the mean tumor size  $\pm$  SE was  $29 \pm 3$  mm<sup>2</sup>. Each treatment group consisted of five to seven mice.

Two treatment schedules with CHS 828 were used:

- (a) 20, 50, or 100 mg/kg once daily for 8 weeks; and
- (b) 100 or 250 mg/kg once weekly for 8 weeks.

**NYH Xenografts.** NMRI nu/nu mice were injected with  $1 \times 10^7$  NYH cells s.c. in both flanks (17, 18). The tumor size was measured as described for the MCF-7 model. CHS 828 was given by oral gavage from day 14, when the tumor size was 30–130 mm<sup>2</sup>. The tumor size doubled two to three times in 2 weeks. For this reason, vehicle-treated mice had to be euthanized between week 4 and 6. Each treatment group consisted of 6 to 15 mice.

Two treatment schedules with CHS 828 were used:

- (a) 1, 3, 10, 20, or 30 mg/kg once daily for 2 weeks; and
- (b) 100 or 250 mg/kg once weekly for 3 weeks.

To ascertain long treatment efficacy, the treated animals were observed for 6 months after the last dose.

CHS 828 at 20 mg/kg was compared with etoposide, paclitaxel, cyclophosphamide, and methotrexate using a once-daily schedule (from day 14 to day 28).

**H-460 Xenografts.** NMRI nu/nu mice were injected with  $5 \times 10^5$  H-460 non-SCLC cells in both flanks and treated from the day of inoculation with p.o. doses of CHS 828 ranging from 20 to 100 mg/kg daily for 2 weeks.

**Rat Tumors.** In the Yoshida ascites hepatosarcoma model,  $2 \times 10^7$  ascites cells were injected i.p. into inbred female Lewis rats (19, 20), and treatment with CHS 828 was started 3 days after tumor inoculation. CHS 828 was given p.o. at 20–100 mg/kg once daily for a maximum of 21 days. Each treatment group consisted of six rats.

The Walker 256 breast carcinosarcoma tumor was grown by weekly passage in female outbred Sprague Dawley rats (21). Tumor pieces were mechanically disrupted, and a tumor cell suspension of  $1 \times 10^7$  cells was injected s.c. into the inguinal region. Animals were treated with CHS 828 at a daily oral dose of 20 mg/kg from the day of tumor injection to day 9, when the tumors were dissected and weighed. Each treatment group consisted of 6 animals.

### Statistical Methods

In the DNA synthesis and cytotoxicity studies, the  $IC_{50}$  values were calculated from the dose-response curves and were expressed as the mean  $\pm$  SD of two to three independent experiments.

In the activity profile study, tumor cell survival was presented as the SI, defined as the fluorescence in experimental wells expressed in per cent of that in control wells, with blank values subtracted. The concentration-response data were expressed as the mean  $\pm$  SE obtained from three independent experiments.  $IC_{50}$  values obtained in the cell line panel were used for comparing the activity of CHS 828 with other compounds using Pearson's correlation coefficient as previously described (22). Curve fitting and parameter estimation in Fig. 1 were performed with the Graphpad Prism software (Graphpad Software, Inc., San Diego, CA), using nonlinear regression and a standard sigmoidal concentration-response model with variable slope. CHS 828 exposure (AUC) was calculated as the CHS 828 concentration multiplied by the exposure time, as the drug was shown to be stable under assay conditions.

In the animal models, tumor sizes were expressed as the mean  $\pm$  SE of tumor areas for the animals alive at the time of measurement. Comparison with controls was expressed as  $T/C$  % (median tumor area in the treated group  $\div$  median tumor area in the vehicle group  $\times$  100). Significance was tested with the Mann-Whitney  $U$  test.

## RESULTS

### DNA Synthesis and Cytotoxicity

**NYH SCLC Cells and Lung Fibroblasts.** The potency of CHS 828 in NYH SCLC cells measured by the thymidine incorporation assay and by the MTT assay was in the same range as that of paclitaxel and daunorubicin (Table 1). In normal fetal lung fibroblasts, CHS 828 was about 100 times less active than in NYH cells. In contrast, paclitaxel and daunorubicin potently inhibited thymidine incorporation in both NYH cells and lung fibroblasts.

**MCF-7 Breast Cancer Cells and Endothelial Cells.** Measured by the thymidine incorporation assay, the potency of CHS 828 in breast

Table 1 DNA synthesis and cytotoxicity in NYH SCLC cells and normal lung fibroblasts: effects of CHS 828, paclitaxel, and daunorubicin

Results are expressed as the mean  $IC_{50}$  concentration  $\pm$  SD of two to three experiments.

	NYH SCLC ( $IC_{50}$ nM)		Lung fibroblasts ( $IC_{50}$ nM)
	$^3H$ -TdR inc. <sup>a</sup>	MTT	$^3H$ -TdR inc.
CHS 828	2.7 $\pm$ 2.0	0.5 $\pm$ 0.0	188 $\pm$ 130
Paclitaxel	4.3 $\pm$ 3.3	7.0 $\pm$ 1.7	6.2 $\pm$ 1.5
Daunorubicin	3.9 $\pm$ 0.9	8.3 $\pm$ 1.7	5.8 $\pm$ 0.9

<sup>a</sup> Incorporation of tritiated thymidine.

cancer cells was in the same range as that of daunorubicin, whereas paclitaxel was 6 times more potent (Table 2). Measured by the cytotoxicity MTT assay, paclitaxel and daunorubicin showed the same potency as in the thymidine incorporation studies, whereas CHS 828 was about 4 times more potent. In HUVEC cells, CHS 828 was markedly less active than in tumor cells. Paclitaxel and daunorubicin had  $IC_{50}$  values more similar to those obtained with tumor cells.

### Activity Profile

To further study the antiproliferative activity profile of CHS 828, a panel of 10 cell lines with different resistance patterns was chosen. Clear differences in the potency of CHS 828 were observed among the 10 cell lines with respect to both  $IC_{50}$  and maximal effect ( $E_{max}$ ), and the concentration-response curves were typically plateau-shaped at higher concentrations (Fig. 1A). At 100  $\mu$ M, the drug was highly cytotoxic against all of the cell lines with SI values  $<10\%$  (data not shown). The U937 cell lines were the most sensitive, whereas the ACHN cell line was the most resistant cell line in terms of  $IC_{50}$  (Fig. 1B). When the overall activity pattern was compared with the corresponding activity data for 10 standard drugs and 2 clinically used guanidine compounds (MIBG and MGBG), low-to-moderate correlation coefficients were observed (Table 3). When this comparison was extended to 100 other investigational cytotoxic or antiproliferative compounds, all of the correlation coefficients obtained were less than 0.65 (range,  $-0.45$  to  $0.65$ ), except for eosinophilic cationic protein (ECP), for which the correlation was 0.79 (data not shown).

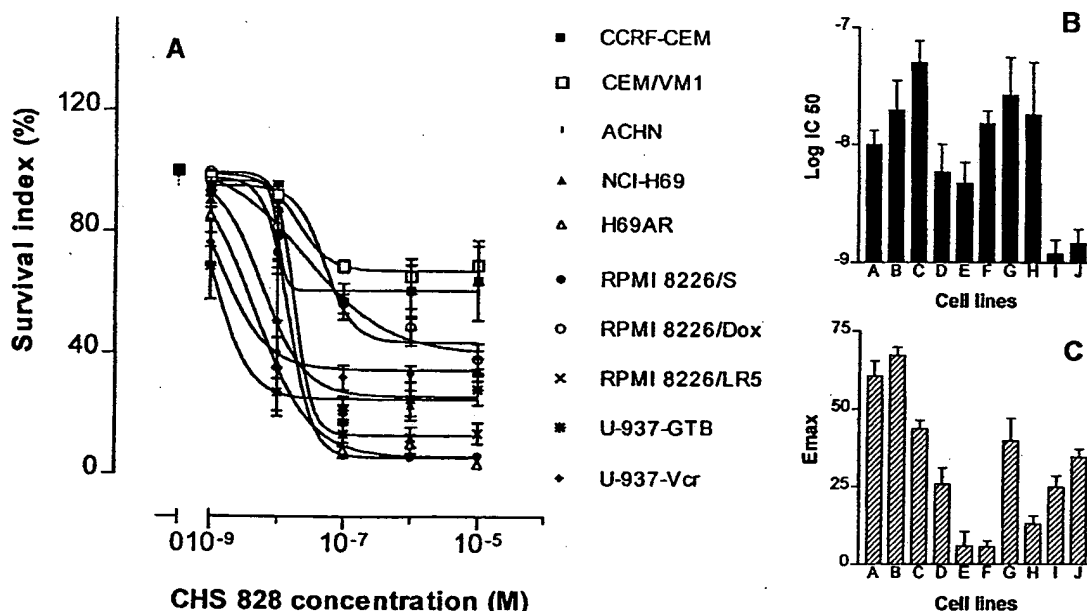


Fig. 1. Cytotoxic activity of CHS 828 in a panel of 10 human tumor cell lines measured by the FMCA after a 72-h incubation with continuous exposure (A). Calculated  $\log IC_{50}$ s are shown in B and the maximum effect ( $E_{max}$ ) in C. Curve fitting and parameter estimation were performed with a standard sigmoidal concentration-response model with variable slope. The results are presented as mean values  $\pm$  SE obtained from three independent experiments.

From the concentration-effect graphs in Fig. 1, A and C, it is apparent that CHS 828 showed a diminished activity ( $E_{max}$ ) against the Pgp-expressing subline compared with the parental one. Addition of the Pgp-blocker SDZ PSC 833 at 1–3  $\mu\text{g}/\text{ml}$  to RPMI 8226/Dox40 cells only marginally increased the sensitivity to CHS 828, and the effect was of similar magnitude in the parental line. At these concentrations, SDZ PSC 833 produced a near complete reversal of doxorubicin resistance (data not shown). In addition, CHS 828 was shown not to interfere with the function of the Pgp in Pgp-overexpressing MCF-7<sub>adr</sub> cells, in the standard chemosensitizer assay performed by Panlabs, Inc. (Bothell, WA; data not shown). No significant sensitivity to MRP, GSH, or tubulin-associated MDR, was apparent when comparing the concentration-response curves of the parental cell lines and their resistant sublines (Fig. 1, A–C).

To investigate the time dependency of the induction of the cytotoxic effects of CHS 828, RPMI 8226/S cells were incubated with the drug for 2 and 72 h, respectively. Continuous exposure for 72 h, compared with 2 h, produced a left-shifted dose-response curve (Fig. 2A). However, when the SI was plotted against the AUC (concentration  $\times$  h), the difference between the two incubation schedules disappeared (Fig. 2B).

### Animal Models

**MCF-7 Xenografts in Nude Mice.** CHS 828 was administered daily at 20, 50, or 100 mg/kg p.o. to mice with established tumors from day 21 to 70 after inoculation (Fig. 3A). The dose of 20 mg/kg tended to delay tumor growth for the first 3 weeks of treatment, but, thereafter, tumor growth resumed. The dose of 50 mg/kg arrested tumor growth, but two mice died during the experiment. The remaining mice showed no sign of toxicity (no weight loss). The highest dose of CHS 828 (100 mg/kg/day) was toxic to all of the mice. CHS 828 was next administered once weekly at 100 or 250 mg/kg/week (Fig. 3B). At 100 mg/kg, no significant effect on tumor regression was observed. Mice that were given 250 mg/kg had tumor regression

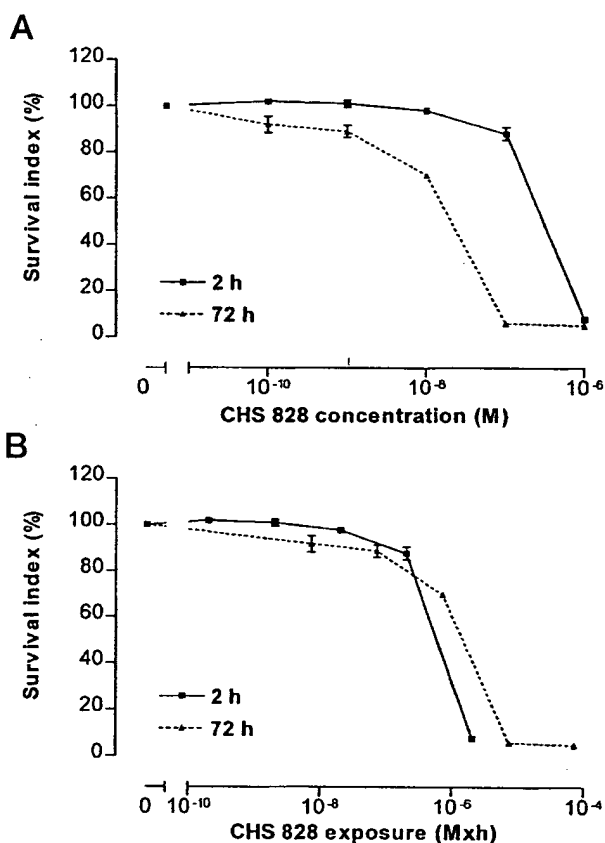


Fig. 2. Dependency of exposure time in CHS 828-induced cytotoxicity. RPMI 8226/S cells were cultured for 72 h, CHS 828 was present for 2 h (■) or for 72 h (▲). In A, the drug concentration is shown on the X-axis, whereas in B, the total drug exposure (AUC = drug concentration  $\times$  exposure time) is used. The results are presented as mean values  $\pm$  SE obtained from three independent experiments.

Table 2 DNA synthesis and cytotoxicity in MCF-7 breast cancer cells and endothelial cells: effects of CHS 828, paclitaxel, and daunorubicin

Results are expressed as the mean  $IC_{50}$  concentration  $\pm$  SD of two to four experiments.

	MCF-7 breast cancer cells ( $IC_{50}$ nM)		Endothelial cells ( $IC_{50}$ nM) $^3\text{H-TdR}$ inc.
	$^3\text{H-TdR}$ inc. <sup>a</sup>	MTT	
CHS 828	31.0 $\pm$ 24.0	7.3 $\pm$ 3.3	5650 $\pm$ 212
Paclitaxel	4.9 $\pm$ 0.8	8.6 $\pm$ 0.3	5.3 $\pm$ 0.2
Daunorubicin	39.0 $\pm$ 4.9	38.5 $\pm$ 36.0	45.0 $\pm$ 1.0

<sup>a</sup> Incorporation of tritiated thymidine.

Table 3 Activity pattern of CHS 828: correlation with chemotherapeutic agents with various mechanisms of action and with two structurally related guanidines, MIBG and MGBG

Drugs	Mechanistic class	$R^a$
Etoposide	Topo II inhibitor	0.57
MIBG	Other	0.30
Daunorubicin	Topo II inhibitor	0.20
MGBG	Other	0.16
Cladribine	Antimetabolite	-0.01
Paclitaxel	Tubulin-active	-0.03
Vincristine	Tubulin-active	-0.06
Topotecan	Topo I inhibitor	-0.19
5-Fluorouracil	Antimetabolite	-0.28
4-Hc <sup>b</sup>	Alkylating agent	-0.29
Cisplatin	Alkylating agent	-0.32
Cytarabine	Antimetabolite	-0.34

<sup>a</sup>  $R$ , Pearson's correlation coefficient.

<sup>b</sup> 4-Hc, hydroperoxy-cyclophosphamide (active metabolite of cyclophosphamide); Topo II, topoisomerase II.

already in the week after the first dose. One mouse died during this experiment, whereas the remaining mice showed no loss of body weight after 7 weeks of dosing.

**NYH Xenografts in Nude Mice.** CHS 828 was administered daily at 3, 10, 20, and 30 mg/kg p.o. to mice with established tumors from day 14 to 28 after inoculation (Fig. 4A). The dose of 3 mg/kg was without effect, whereas tumor growth arrest was observed with 10 mg/kg. Twenty and 30 mg/kg caused regression of tumors. No weight loss was observed in any of the treatment groups.

Once-a-week administration of 100 mg/kg or 250 mg/kg of CHS 828 on day 14, 21, and 28 caused rapid regression of tumors (Fig. 4B). Regression of tumors continued throughout the observation period, which lasted for more than 6 months after cessation of treatment (Fig. 4B). In the group treated with 250 mg/week, regression was observed after the first dose, and at the end of the experiment, no tumors persisted. All of the mice survived, and no loss of body weight was observed in any of the mice.

The effects of CHS 828 were compared with those of reference chemotherapeutic agents in the NYH xenograft model (Table 4). CHS 828, etoposide, methotrexate, and cyclophosphamide were administered p.o., whereas paclitaxel was given s.c. All of the reference compounds were used at the maximally tolerated dosages. Of these, only paclitaxel showed significant activity with a  $T/C$  value of 48%. CHS 828 was extremely efficient, having a  $T/C$  value of 0%, at doses below the maximum tolerated dose.

**H-460 Xenografts in Nude Mice.** CHS 828 was administered daily at doses ranging from 20 to 100 mg/kg p.o. for 2 weeks from the day of the inoculation of tumor cells. No effect of CHS 828 was

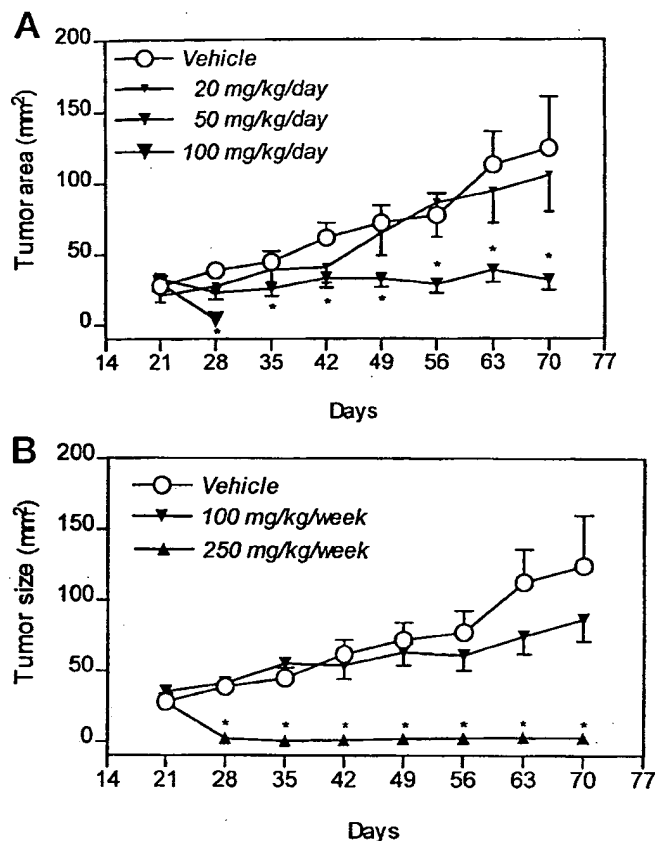


Fig. 3. Effects of CHS 828 in nude mice with MCF-7 breast cancer tumors. Ovariectomized and estrogen-substituted female mice were inoculated with  $5 \times 10^6$  MCF-7 cells in both flanks. CHS 828 was administered p.o. from day 21 to day 70. A, effects on tumor size after treatment once daily; B, effects after treatment once weekly.

observed on tumor growth in this model of non-SCLC (data not shown).

**Rat Tumors.** In rats with i.p. implanted Yoshida hepatosarcoma cells, CHS 828 was found to prolong survival time by more than 100%, when administered at doses ranging from 20 to 50 mg/kg p.o. (given once daily or once every second day). In rats with s.c. Walker 256 breast carcinosarcomas, CHS 828 at 20 mg/kg p.o. once daily reduced tumor weight by 80%, compared with control tumors (data not shown).

## DISCUSSION

CHS 828 is a recently discovered antitumor drug candidate, belonging to a group of pyridyl cyanoguanidines that hitherto have attracted pharmacological interest as hypotensive agents because of their activity as potassium channel openers. This activity is, however, not associated with the antitumor activity, and CHS 828 has no potassium channel-opening activity (1). Pyridyl cyanoguanidines have not previously been shown to exert antitumor effects, but two structurally related benzylguanidines (MIBG and MGBG) have shown cytotoxic effects in cultured cancer cells and antitumor responses in animals (23, 24). MIBG is a structural and functional analogue of epinephrine, and its radio-iodinated form has been used for scintigraphic detection and radiotherapy of tumors derived from adrenergic tissues (24). MIBG and MGBG were included as reference compounds in our cell line activity pattern studies, but no significant correlation with the profile of CHS 828 was observed.

In the present study, the antiproliferative and cytotoxic effects of

CHS 828 were studied in MCF-7 human breast cancer cells and in NYH human SCLC cells—the two cell types that were also used for the *in vivo* tumor studies in nude mice. The MCF-7 cells are broadly used as a representative of a classic estrogen-dependent tumor, with an intact p53-dependent repair mechanism (25). The NYH cells are aggressive SCLC cells that have lost several tumor suppressor proteins such as pRB and p130 (26). The NYH cells are resistant to the alkylating agent 1,3-bis-(2-chloroethyl)-1-nitroso-urea (18).

*In vitro*, CHS 828 displayed a potency similar to that of the reference cytotoxic agents daunorubicin and paclitaxel. Comparative studies with normal cells were performed using fetal lung fibroblasts as normal counterparts for the SCLC cells. The choice of a normal cell type for comparative studies with the MCF-7 breast cancer cells was more difficult. We decided to use human endothelial cells stimulated by vascular endothelial growth factor, which, in addition, allowed us to gain information on the possible effects of CHS 828 on angiogenesis. In contrast to daunorubicin and paclitaxel, CHS 828 was found to have considerably less antiproliferative activity against the normal cell types than against the tumor cells. The results suggest a decreased risk of toxicity against normal tissues but also indicate that CHS 828 does not exert antiangiogenic effects at the level of endothelial cell proliferation.

The mechanism for induction of cell death by CHS 828 remains to be clarified. The assays used for the determination of the antiproliferative and cytotoxic effects of CHS 828 do not distinguish between

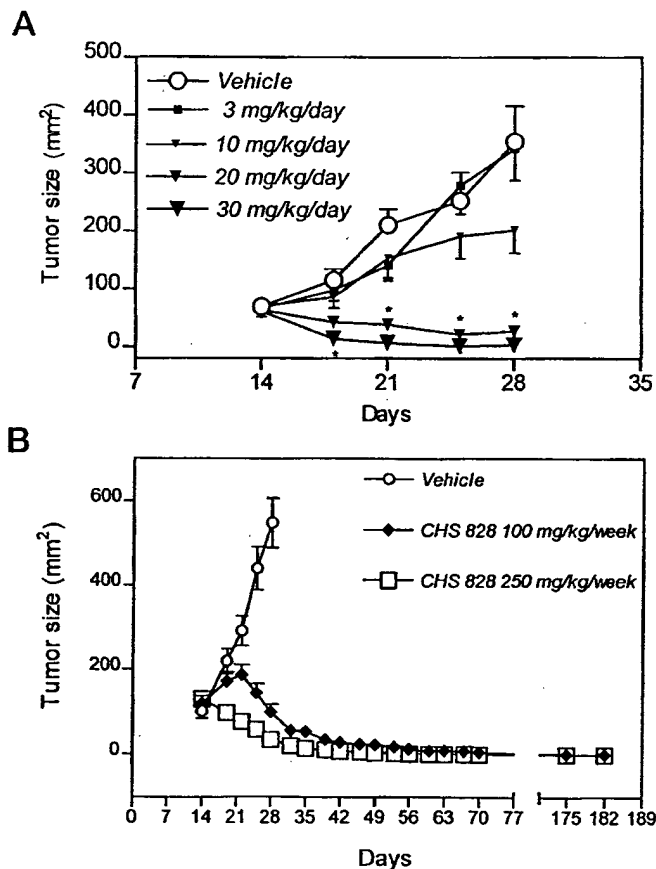


Fig. 4. Effects of CHS 828 in nude mice with NYH SCLC tumors. Female mice were inoculated with  $1 \times 10^7$  NYH cells in both flanks. CHS 828 was administered p.o. from day 14 to day 28. A, effects on tumor size after treatment once daily; B, effects after treatment once weekly. Tumor growth was monitored for 6 months after the cessation of treatment (B).

Table 4 Effects of CHS 828 in nude mice with NYH SCLC tumors: comparison with reference antineoplastic compounds

Compound	CHS 828	Etoposide	Paclitaxel	Methotrexate	Cyclophosphamide
Dose (once daily)	20 mg/kg	20 mg/kg	10 mg/kg	5 mg/kg	10 mg/kg
Route	p.o.	p.o.	s.c.	p.o.	p.o.
T/C % <sup>a</sup>	0%	64%	48%	67%	86%
	$P < 0.05$	ns <sup>b</sup>	$P < 0.05$	ns	ns

<sup>a</sup> T/C %: Median tumor area in the treated group/median tumor area in the vehicle group after 14 days of treatment (from day 14 to day 28). (Statistics by Mann Whitney U-test).

<sup>b</sup> ns, not significant.

necrotic and apoptotic cell death. Additional studies, including DNA fragmentation and caspase 3 activity studies, have been undertaken.<sup>3</sup>

When the activity pattern of CHS 828 in a human cell panel (consisting of four sensitive parental cells lines, five drug-resistant sublines with different mechanisms of resistance, and one cell line with primary resistance) was correlated with the activity data from standard chemotherapeutic agents, correlation coefficients were low to medium. Previous studies using this system have shown that anticancer agents with closely related mechanisms of action generally show high correlation coefficients ( $>0.85$ ; Refs. 3, 27, 28, 29). These results suggest a potentially new mechanism of action for CHS 828.

The studies in the drug-resistant cell lines indicated no sensitivity of CHS 828 to drug resistance mediated by MRP, GSH, topoisomerase II, or tubulin-associated MDR. CHS 828 was less cytotoxic against the Pgp-overexpressing RPMI 8226/Dox40 cell line than against the parental RPMI 8226/S line. This finding suggested a role for Pgp in protecting the cells from the effects of CHS 828. However, the lack of reversibility of CHS 828 resistance by Pgp-blockers indicates that this is not the case. Measurements of the rate of proliferation during the incubation time showed a slightly reduced rate of proliferation in the doxorubicin-resistant subline compared with the parental cell line, which might, at least to some extent, contribute to the observed difference in sensitivity to CHS 828.

Studies in the RPMI 8226/S cell line showed that CHS 828 induced less cytotoxicity when present in the incubation for only 2 h compared with continuous presence for 72 h. This difference disappeared after taking AUC (concentration  $\times$  time) into account; the AUC indicated that the effect of CHS 828 was dependent on the total exposure rather than on exposure time alone. The fact that even a 2-h incubation with CHS 828 resulted in the induction of cytotoxicity after 72 h of incubation suggests that the activation of cell death pathways by CHS 828 is an early event that does not require prolonged exposure. These results together with the *in vivo* data also suggest that single or intermittent dosing schedules may be sufficient to obtain tumor responses in the clinical setting, at least from a strictly pharmacodynamic point of view.

CHS 828 was tested *in vivo* in a number of animal models, including nude mice xenografted with human cancer cells and rats with transplanted rodent tumors. CHS 828 was active after oral administration in most of the models. In the MCF-7 breast cancer model, a weekly dose of 250 mg/kg had a significant antitumor effect after the first dose, leading to regression of established tumors. The lower weekly dose of 100 mg/kg was less efficient. The daily dosing schedule was associated with significant toxicity at doses that were able to induce tumor regression. Long-term observation of treated animals was not performed because of mortality in both the vehicle- and the drug-treated groups after the depletion of the estrogen content of the implanted pellets, which occurred after day 60.

MCF-7 cells seem to be generally refractory to standard chemotherapy when grown as xenografts in nude mice. In a study of drug

activity in xenograft models from the National Cancer Institute (30), a panel of 12 standard drugs encompassing alkylating agents, DNA binders, antimetabolites, and mitotic inhibitors were tested. None of the 12 drugs was found to induce tumor regression in the MCF-7 model.

In accordance with the differences in sensitivity observed *in vitro* between the MCF-7 and NYH cells, NYH tumors in mice were more sensitive to CHS 828 than the MCF-7 tumors were. The weekly dosing schedule was again the most efficient one. A weekly dose of 250 mg/kg induced immediate tumor regression and, in contrast to the MCF-7 tumors, NYH tumors were also very sensitive to 100 mg/kg. Continued regression and no tumor regrowth were seen during a 6-month observation period after the third (and last) dose of CHS 828. No toxic effects of CHS 828 were noted in these experiments. These results are particularly interesting because the NYH xenograft model does not seem to be very sensitive to standard drugs. As shown in the present study, all of the reference chemotherapeutic drugs, including paclitaxel, induce little or no growth inhibition in this model despite being tested at their maximum tolerated doses. The significant tumor regression induced by CHS 828 in these xenograft models is, therefore, encouraging.

CHS 828 was also tested in nude mice bearing H-460 non-small cell lung tumors. These cells had previously shown sensitivity to CHS 828 *in vitro*, comparable with that seen with the MCF-7 cells (results not shown). Surprisingly, no effect of CHS 828 was seen on H-460 tumor growth in the nude mice. The reason for this treatment failure is not clear, but it may be associated with the aggressive growth rate of the tumors, which severely limits the life span of the animals and reduces the treatment time to a few weeks (starting at the time of inoculation of the tumor cells).

CHS 828 showed a substantial antitumor activity against rodent tumors, both in the form of i.p.-implanted Yoshida hepatosarcoma cells (ascitic tumors) and s.c.-growing Walker 256 breast carcinosarcomas.

The toxicological profile of CHS 828 is currently under investigation in rodents and dogs. The predominant toxicity seems to be gastrointestinal irritation with mucositis, diarrhea, and vomiting. In genotoxicity tests, CHS 828 has not shown any mutagenic or clastogenic effects.

In conclusion, CHS 828 is a new antineoplastic agent with a broad spectrum of activity against a variety of human cancer cells, including multidrug resistant cells. The mechanism of action of CHS 828 is still unknown, but it seems to be different from that of currently used chemotherapeutic agents. CHS 828 is presently in Phase I clinical studies.

## REFERENCES

- Schou, C., Ottosen, E. R., Björklund, F., Latini, S., Hjarnaa, P. V., Bramm, E., and Binderup, L. Novel cyanoguanidines with potent oral antitumor activity. *Bioorg. & Med. Chem. Lett.*, 7: 3095-3100, 1997.
- Petersen, H. J., Kargaard Nielsen, C., and Arrigoni-Martelli, E. Synthesis and hypotensive activity of *N*-alkyl-*N'*-cyano-*N'*-pyridylguanidines. *J. Med. Chem.*, 21: 773-781, 1978.
- Dhar, S., Nygren, P., Csoka, K., Botling, J., Nilsson, K., and Larsson, R. Anti-cancer drug characterisation using a human cell line panel representing defined types of drug resistance. *Br. J. Cancer*, 74: 888-896, 1996.

<sup>3</sup> P. Martinsson, G. Liminga, E. Jonsson, S. Ekelund, J. Gullbo, S. Dhar, A. Lukinius, M. De La Torre, L. Binderup, and R. Larsson. A novel cyanoguanidine compound with potent anti-tumor activity induces programmed cell death with unusual features, manuscript in preparation.

4. Sundström, C., and Nilsson, K. Establishment and characterisation of a human histiocytic lymphoma cell line (U-937). *Int. J. Cancer*, **17**: 565-577, 1976.
5. Botling, J., Liminga, G., Larsson, R., Nygren, P., and Nilsson, K. Development of vincristine resistance and increased sensitivity to cyclosporin A and verapamil in the human U-937 lymphoma cell line without overexpression of the 170kDa P-glycoprotein. *Int. J. Cancer*, **58**: 269-274, 1994.
6. Dalton, W. S., Durie, B. G., Alberts, D. S., Gerlach, J. H., and Cress, A. E. Characterization of a new drug-resistant human myeloma cell line that expresses P-glycoprotein. *Cancer Res.*, **46**: 5125-5130, 1986.
7. Bellamy, W. T., Dalton, W. S., Gleason, M. C., Grogan, T. M., and Trent, J. M. Development and characterization of a melphalan-resistant human multiple myeloma cell line. *Cancer Res.*, **51**: 995-1002, 1991.
8. Mulcahy, R. T., Bailey, H. H., and Gipp, J. J. Up-regulation of  $\gamma$ -glutamylcysteine synthetase activity in melphalan-resistant human multiple myeloma cells expressing increased glutathione levels. *Cancer Chemother. Pharmacol.*, **34**: 67-71, 1994.
9. Cole, S. P., Bhardwaj, G., Gerlach, J. H., Mackie, J. E., Grant, C. E., Almquist, K. C., Stewart, A. J., Kurz, E. U., Duncan, A. M., and Decley, R. G. Overexpression of a transporter gene in a multidrug-resistant human lung cancer cell line. *Science (Washington DC)*, **258**: 1650-1654, 1992.
10. Mirski, S. E., Gerlach, J. H., and Cole, S. P. Multidrug resistance in a human small cell lung cancer cell line selected in Adriamycin. *Cancer Res.*, **47**: 2594-2598, 1987.
11. Danks, M. K., Schmidt, C. A., Cirtain, M. C., Suttle, D. P., and Beck, W. T. Altered catalytic activity of and DNA cleavage by DNA topoisomerase II from human leukemic cells selected for resistance to VM-26. *Biochemistry*, **27**: 8861-8869, 1988.
12. Danks, M. K., Yalowich, J. C., and Beck, W. T. Atypical multidrug resistance in a human leukemic cell line selected for resistance to teniposide (VM-26). *Cancer Res.*, **47**: 1297-1301, 1987.
13. Nygren, P., and Larsson, R. Verapamil and cyclosporin A sensitize human kidney tumor cells to vincristine in absence of membrane P-glycoprotein and without apparent changes in the cytoplasmic free  $Ca^{2+}$  concentration. *Biosci. Rep.*, **10**: 231-237, 1990.
14. Larsson, R., Kristensen, J., Sandberg, C., and Nygren, P. Laboratory determination of chemotherapeutic drug resistance in tumor cells from patients with leukemia, using a fluorometric microculture cytotoxicity assay (FMCA). *Int. J. Cancer*, **50**: 177-185, 1992.
15. Brünner, N., Bronzert, D., Vindeloev, L. L., Spang-Thomsen, M., and Lippmann, M. E. Effect on growth and cell cycle kinetics of estradiol and tamoxifen on MCF-7 human breast cancer cells grown *in vitro* and in nude mice. *Cancer Res.*, **49**: 1515-1520, 1989.
16. Tomayko, M. M., and Reynolds, C. P. Determination of subcutaneous tumor size in athymic (nude) mice. *Cancer Chemother. Pharmacol.*, **24**: 148-154, 1989.
17. Aabo, K., Vindeloev, L. L., and Spang-Thomsen, M. Clonal dominance between subpopulations of mixed small cell lung cancer xenografts implanted ectopically in nude mice. *Eur. J. Cancer*, **31A**: 222-229, 1995.
18. Aabo, K., Roed, H., Vindeloev, L. L., and Spang-Thomsen, M. A dominated and resistant subpopulation causes regrowth after response to 1,3-bis(2-chloroethyl)-1-nitrosurea treatment of a heterogeneous small cell lung cancer xenograft in nude mice. *Cancer Res.*, **54**: 3295-3299, 1994.
19. Marusic, M., Allegretti, N., and Culo, F. The timing of cyclophosphamide therapy in tumor-bearing rats affects the resistance to tumor challenge in survivors. *Experientia*, **34**: 1355-1356, 1978.
20. Fujita, H., Sakurai, T., and Toyoshima, S. New antitumor amino acid derivative, A-748, evaluated in rat ascites hepatomas. *Cancer Treat. Rep.*, **63**: 223-224, 1979.
21. Minne, H. W., Raue, F., Bellwinkel, S., and Ziegler, R. The hypercalcaemic syndrome in rats bearing the Walker carcinosarcoma 256. *Acta Endocrinol.*, **78**: 613-624, 1975.
22. Boyd, M. R., and Paull, K. D. Some practical considerations and applications of the National Cancer Institute *in vitro* anticancer drug discovery screen. *Drug Dev. Res.*, **34**: 91-109, 1995.
23. Smets, L. A., Bout, B., and Wisse, J. Cytotoxic and antitumour effects of the norepinephrine analogue *meta*-iodo-benzylguanidine (MIBG). *Cancer Chemother. Pharmacol.*, **21**: 9-13, 1988.
24. Loesberg, C., Van Rooij, H., Romijn, J. C., and Smets, L. A. Mitochondrial effects of the guanidino group-containing cytostatic drugs, *m*-iodobenzylguanidine and methylglyoxal bis (guanyldrazone). *Biochem. Pharmacol.*, **42**: 793-798, 1991.
25. Thompson, A. M., Steel, C. M., Chetty, U., Hawkins, R. A., Miller, W. R., Carter, D. C., Forrest, A. P., and Evans, H. J. *p53* gene mRNA expression and chromosome 17p allele loss in breast cancer. *Br. J. Cancer*, **61**: 74-78, 1990.
26. Helin, K., Holm, K., Niebuhr, A., Eiberg, H., Tommerup, N., Hougaard, S., Poulsen, H. S., Spang-Thomsen, M., and Nørgaard, P. Loss of the retinoblastoma protein-related p130 protein in small cell lung carcinoma. *Proc. Natl. Acad. Sci. USA*, **94**: 6933-6938, 1997.
27. Fridborg, H., Nygren, P., Dhar, S., Csoka, K., Kristensen, J., and Larsson, R. *In vitro* evaluation of new anticancer drugs, exemplified by vinorelbine, using the fluorometric microculture cytotoxicity assay on human tumour cell lines and patient biopsy cells. *J. Exp. Ther. Oncol.*, **1**: 286-295, 1996.
28. Jonsson, E., Fridborg, H., Csoka, K., Dhar, S., Sundström, C., Nygren, P., and Larsson, R. Cytotoxic activity of topotecan in human tumour cell lines and primary cultures of human tumour cells from patients. *Br. J. Cancer*, **76**: 211-219, 1997.
29. Dhar, S., Nygren, P., Liminga, G., Sundström, C., de la Torre, M., Nilsson, K., and Larsson, R. Relationship between cytotoxic drug response patterns and activity of drug efflux transporters mediating multidrug resistance. *Eur. J. Pharmacol.*, **346**: 315-322, 1998.
30. Plowman, J., Dykes, D. J., Hollingshead, M., Simpson-Herren, L., and Alley, M. C. Human Tumor Xenograft Models in NCI Drug Development. In: B. A. Teicher (ed.), *Anticancer Drug Development Guide*, pp. 101-125. New Jersey: Humana Press, 1997.

## Synthesis and Antitumor Activity of a New Cis-Diammineplatinum (II) Complex Containing Procaine Hydrochloride

SERGIO CAFAGGI<sup>1</sup>, MAURO ESPOSITO<sup>2</sup>, BRUNELLA PARODI<sup>1</sup>, MARIA O. VANNOZZI<sup>2</sup>, MAURIZIO VIALE<sup>2</sup>, CATERINA PELLECCIA<sup>2</sup>, ROSA ANNA FULCO<sup>2</sup>, FRANCO MERLO<sup>3</sup>, ANTONIO ZICCA<sup>4</sup>, ANGELA CADONI<sup>4</sup> and GAETANO BIGNARDI<sup>1</sup>

<sup>1</sup>Istituto di Analisi e Tecnologie Farmaceutiche dell'Università di Genova; <sup>2</sup>Servizio di Farmacologia Tossicologica and

<sup>3</sup>Servizio di Epidemiologia Ambientale e Biostatistica, Istituto Nazionale per la Ricerca sul Cancro, Genova;

<sup>4</sup>Istituto di Anatomia Umana dell'Università di Genova, Genova, Italy

**Abstract.** This paper refers to some of the chemical and biological properties of a new platinum (II) complex where the aromatic amino group of procaine is involved in the coordination with platinum and whose structure was defined by UV, IR, <sup>1</sup>H-NMR, and elemental analysis. This new cationic platinum-triamine complex (DPR) displays excellent solubility (> 50 mg/ml) and stability in water. DPR has significant in vitro cytotoxicity against murine P388 leukemic cell line; human K562 erythroleukemic cell line and human Jurkat T cell line. The in vitro cytotoxic effects of DPR on P388 and Jurkat leukemic cells were comparable to those of cis-diamminedichloroplatinum (II) (DDP), while its activity on K562 cells was significantly better than that of DDP [ $IC_{50} = 1.07 \pm 0.36$  (SD)  $\mu$ M vs  $2.62 \pm 0.23$  (SD)  $\mu$ M,  $P < 0.01$ ]. The in vitro Pt accumulation rate for P388 cells was twice as rapid after DPR than after DDP exposure, while no difference in cellular platinum efflux was observed. The antitumor activity of DPR was tested in vivo against P388 leukemic cells in BDF1 mice and gave a % ILS value (75%) similar to that of the maximum tolerated dose (MTD) of DDP (8 mg/Kg). A comparative study of plasma urea nitrogen (PUN) levels and kidney morphological analysis in tumor-bearing mice receiving the LD<sub>50</sub> dose of both drugs (39.3 mg/Kg and 16.5 mg/Kg for DPR and DDP, respectively), showed DPR to be less nephrotoxic than DDP. These results indicate that this new cationic platinum-triamine complex containing primary amine ligand is surprisingly active both in vitro and in vivo. In summary, the good characteristics of DPR in terms of high solubility, encouraging anticancer activity and absence of nephrotoxic effects make DPR a promising new platinum anticancer agent for preclinical development.

cis-Diamminedichloroplatinum (II) (DDP) is well recognized as a useful antitumor drug in the treatment of several human cancers (1-3). However its side effects, e.g. nephrotoxicity, ototoxicity, neurotoxicity and gastrointestinal symptoms, together with the evidence that some tumors are totally refractory to DDP, have emerged as factors that compromise its clinical effectiveness.

The occurrence of these limiting factors has stimulated attempts to reduce the dose-limiting toxic side effects of DDP by the co-administration of various compounds (4-10) or the synthesis of many chemically-modified DDP analogues with better solubility and reduced nephrotoxicity than DDP (11-14). Research in this field has produced a new series of platinum compounds which are cationic triamine complexes with chemical and biological properties that are quite different from those of DDP (15). On this basis, along with the evidence that procaine hydrochloride (P.HCl) improves the therapeutic index of DDP (16), the feasibility of preparing a platinum (II) complex containing an amine ligand derived from P.HCl was investigated. The antitumor effects of this new platinum triamine cation were tested both *in vitro*, against human and murine leukemic cell lines, and *in vivo* against P388 leukemia in mice. Its nephrotoxicity was compared with that of DDP.

### Materials and Methods

**Drugs.** DDP was purchased from Janssen Chimica (Belgium) and used without further purification. P.HCl was purchased from BDH Chemicals Ltd Poole (England) and used as received. Chromatographic solvents and other chemicals were of HPLC grade (BDH). Water used in HPLC was glass double distilled, deionized and Millipore filtered.

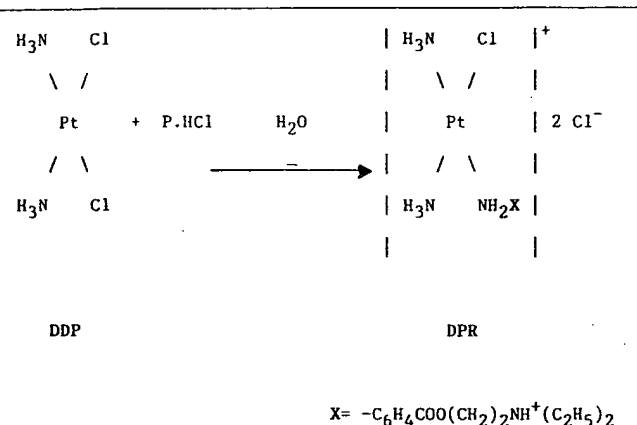
**Animals.** Female BDF1 mice (18-22 g, Charles River Laboratories, Calco, Italy) were allowed at least a 7-day period before use. Standard food (4RF-25 Italiana Mangimi, Settimo Milanese, Italy) and water were available to the mice at all times.

**Physical methods.** The IR spectra (KBr, 4000-200  $cm^{-1}$ ) were measured with a Perkin Elmer 683 spectrophotometer, and the <sup>1</sup>H-NMR spectra [60 MHz, solvent D<sub>2</sub>O, 3-(trimethylsilyl) propionic-d<sub>4</sub> acid sodium salt as internal standard] were recorded with an Hitachi R-600 instrument. The

Correspondence to: Dr. Mauro Esposito, Servizio di Farmacologia Tossicologica, Istituto Nazionale per la Ricerca sul Cancro, IST, Viale Benedetto XV, 10, 16132 Genova, Italy.

**Key Words:** cis-Diamminedichloroplatinum (II), procaine hydrochloride, synthesis, antitumor activity.

Scheme I



<sup>195</sup>Pt-NMR spectrum was recorded at 22° C on a Bruker spectrometer (42.9 MHz) under full proton decoupling using a 5 mm "reverse" probe with outer coils tunable in the range <sup>109</sup>Ag-<sup>31</sup>P. A 13 μs pulse (70°) was employed; the acquisition time for 8192 data points over a spectral width of 50000 Hz was 82 ms. A line broadening factor of 50 Hz was applied before the Fourier transform. The <sup>195</sup>Pt chemical shift was compared to an external sample of K<sub>2</sub>PtCl<sub>6</sub>.

Ultraviolet spectra were measured with a Perkin Elmer Lambda 3 spectrometer in aqueous solution, while the elemental analysis was carried out on a Carlo Erba mod. 1106 analyzer. The melting point was determined with a Buchi 500 apparatus and it is uncorrected.

Thin-layer chromatography (TLC) was carried out in ascending technique with RP 18 precoated glass plates and silica gel and cellulose aluminum sheets (5 × 10 cm, with fluorescence indicator, from Merck, Darmstadt). The preparative low pressure LC was performed using a chromatographic system from Pharmacia LKB (Sweden): a Varioprepex II 2120 peristaltic pump, a KX (72 × 1.6 cm) column with Sephadex G10 as stationary phase, a LKB 2138 Uvicord S spectrophotometer detector working at 206 nm (cell length = 5 cm, ABS range = 1), a LKB 2210 potentiometric recorder (input range = 100 mV, chart drive = 1 mm/min) and a LKB 2111 Multirac fraction collector (collection time = 2 min). The analytical low pressure LC was carried out by the same apparatus as above, with the following modifications: SR column (17 × 1 cm), ABS = 0.1, chart drive = 0.2 mm/min. HPLC analyses were conducted using a Hewlett-Packard Series 1050 LC with a 1040 M detector (diode array detector), HP-300 PC and HP 9153 disk drive. This system possesses the capability of instant UV-VIS spectral scanning and storing-retrieving chromatographic data. Columns from Supelco Inc. (USA) were used.

**Synthesis of cis-[PtCl(NH<sub>3</sub>)<sub>2</sub>](Procainium)]Cl<sub>2</sub> (DPR).** DPR was synthesized by reaction of DDP with P.HCl (molar ratio 1:3) in H<sub>2</sub>O, at 55° C, under constant stirring for 48 h (Scheme I). The starting concentration of DDP was 1 mg/ml. The reaction mixture (30 ml) was concentrated to about 2 ml in a rotating evaporator, under reduced pressure, at 60° C and injected into the preparative LC system using H<sub>2</sub>O as eluent with a flow rate of 1.6 ml/min. Eluate fractions of 3.2 ml (24 -36) containing the complex were collected and evaporated, under reduced pressure, at 40° C. The solid residue was then dissolved in methanol (10 ml); by adding diethyl ether (10 ml) a white precipitate was obtained within 1 h. Through filtration and washing with methanol/diethyl ether 1:1, 25 mg of product were obtained (yield about 42%). Recrystallization from the same solvent gave the elemental analysis product (mp = 173-176° C, with decomposition).

**Chemical analysis.** The purity and stability of the compound were evaluated by several methods. 1) By TLC, through the following systems: a) tetraethylammonium chloride 0.1 M/methanol 20:10 (RP 18); b) potassium hydrogen phthalate 0.01 M (Cellulose); c) acetone/toluene/water 76:20:4 (Silica gel). The zones were located by irradiation at 254 nm and by dipping the plate into an ethanolic solution of p-nitroso-N, N-dimethylaniline, followed by heating at 120° C for 15 min (17). 2) By HPLC, employing a Nucleosil C18 column (15 × 0.46 cm, 5 μm) with ammonium carbonate 0.4% plus tetraethylammonium chloride 0.1% / acetonitrile 50:50 as eluent, at flow rate of 1 ml/min, sample volume 10 μl (0.150 mg/ml). Absorbance was monitored at 210 nm. 3) By HPLC, using the same column as in 2) and with ammonium carbonate 0.1% + tetraethylammonium chloride 0.05% / acetonitrile 80:20 as eluent. Flow rate was 1 ml/min and absorbance was monitored at 210 nm. Sample volume 10 μl (2 mg/ml), t<sub>r</sub>(DDP) = 1.3 min. 4) By HPLC using a Hisep column (C<sub>18</sub>, 15×0.46 cm, 5 μm) with precolumn and ammonium acetate 0.18 M as an eluent at flow rate of 1.5 ml/min. Absorbance was monitored at 243 nm (DPR, tr = 3 min) and 289 nm (procaine, tr = 5 min). On this column direct injection of serum samples for analysis of unbound drug was possible. 5) By analytical low pressure LC, using NaCl 2 mM as an eluent, at flow rate of 1 ml/min. Sample volume 0.5 ml (0.6 mg/ml), t<sub>r</sub>(DDP) = 18 min.

The method proposed by Arpalahti and Lippert (18) was used to check the geometric purity of the compound.

#### In vitro studies

**Cell lines.** Murine P388 leukemic cells, human K562 erythroleukemic cells and human Jurkat T cells were seeded respectively at 2.5, 10<sup>4</sup> and 10<sup>4</sup> × 10<sup>3</sup> cells/well in round-bottomed microtiter plates in a final volume of 200 μl of RPMI 1640 medium containing glutamine (2 mmol/L), gentamycin (100 μg/ml), non-essential aminoacids (2% vol/vol) and 10% fetal calf serum (FCS) (complete medium).

**Cytotoxicity of platinum complexes on P388 leukemic cells.** Cells were exposed to equimolar concentrations (0.52, 1.04, 2.07, 4.15, 8.3, and 16.6 μM) of DPR and DDP for 4 h or 24 h (continuous drug exposure) at 37° C. After 4 h exposure, cells were washed twice with complete medium, counted and seeded. Eighteen hours later, cells were pulsed for 6 h with 0.5 μCi of [<sup>3</sup>H]-thymidine and then harvested and counted in a B counter. The concentration of drug producing 50% inhibition of cell growth (IC<sub>50</sub>) compared to untreated controls was obtained by plotting the results, as percentage of control cultures, in a diagram using the probit transformation of data.

**Cytotoxicity of the platinum complexes on human leukemic cell lines.** Sensitivity to DPR and DDP of the human K562 erythroleukemic cell line and the human Jurkat T cell line was assessed by [<sup>3</sup>H]-thymidine incorporation in a 24 h assay. Both cell lines were treated with doses of 0, 1.04, 2.07, 4.15, 8.3, and 16.6 μM drug for 24 h (continuous drug exposure). After 18 h cells were pulsed for 6 h with 0.5 μCi of [<sup>3</sup>H]-thymidine and then harvested and counted in a B counter.

**Clonogenic assay.** K562 cells were used in a clonogenic assay where cells were plated in 6-well plate dishes at 5 × 10<sup>2</sup> cells/well in alpha medium containing 0.3% agar, 100 μg/ml gentamicin, 2% (vol/vol) sodium pyruvate, 2 mmol/L L-glutamine, 1% (vol/vol) non essential aminoacids and 10% FCS. Plates were incubated for 14 days in a humidified atmosphere of 5% CO<sub>2</sub> at 37° C. Chemosensitivity was determined by continuous exposure of cells to equimolar concentrations of drugs over the entire period of culture (19). The number of colonies (i.e., more than 40 cells) was evaluated microscopically. Results were plotted as percentage of control cultures (probits transformation) and IC<sub>50</sub> values determined from the dose/response curves so obtained.

**Measurement of cellular drug accumulation.** In one set of experiments, P388 leukemic cells were treated with DDP and DPR at equimolar



Table I. Elemental analysis of cis-diamminechloro-[2-(diethylamino)ethyl 4-amino-benzoate, N<sup>4</sup>]-chlorideplatinum (II) monohydrochloride monohydrate (DPR).

Formula	Found (%)			Calculated (%)		
	C	H	N	C	H	N
C <sub>13</sub> H <sub>27</sub> Cl <sub>3</sub> N <sub>4</sub> O <sub>2</sub> Pt.H <sub>2</sub> O	26.58	4.95	9.36	26.43	4.95	9.48

Table II. UV, IR and <sup>1</sup>H-NMR data of DPR and P.HCl.

Compound	λ <sub>max</sub> , nm (logε)	wn (cm <sup>-1</sup> )
DPR	202(4.22) 244(4.13)	3500-3400 (m) (OH); 3300-3080 (s, broad structured band) (NH); 2700-2600 (m) (NH <sup>+</sup> ); 1710(vs)(C=O); 1600(s) (C=C); 1270(s) (C-O); 1210(m) (C-NH <sub>2</sub> ); 575(w), 495(vw), 460(vw), 410(vw); 330(w) (Pt-Cl).
P.HCl	194 (4.32), 220 (3.94), 289 (4.28)	3350(m), 3310(m) (NH), 3200(m) (NH <sub>2</sub> ); 2700-2400 (m) (NH <sup>+</sup> ); 1685 (vs) (C=O) 1640(m) (NH <sub>2</sub> ); 1600(s) (C=C); 1270(s) (C-O)
	δ (ppm)	
DPR	8.10 (d, J=8 Hz, 2 H ar, meta-NH <sub>2</sub> ); 7.45 (d, J=8 Hz, 2 H ar, ortho-NH <sub>2</sub> ); 3.65 (m, -CO-O-CH <sub>2</sub> -CH <sub>2</sub> -); 3.35 (q, J=7.4 Hz, 2 CH <sub>3</sub> -CH <sub>2</sub> -); 1.35 (t, J=7.4 Hz, 2 CH <sub>3</sub> -CH <sub>2</sub> -).	
P.HCl	7.85 (d, J=8 Hz, 2 H ar, meta-NH <sub>2</sub> ); 6.85 (d, J=8 Hz, 2 H ar, ortho-NH <sub>2</sub> ); 4.60 (m, -CO-O-CH <sub>2</sub> -CH <sub>2</sub> -); 3.60 (m, -CO-O-CH <sub>2</sub> -CH <sub>2</sub> -); 3.35 (q, J=7.4 Hz, 2 CH <sub>3</sub> -CH <sub>2</sub> -); 1.35 (t, J=7.4 Hz, 2 CH <sub>3</sub> -CH <sub>2</sub> -).	

Abbreviations: wn = wavenumber, vs = very strong, s = strong, m = medium, w = weak, vw = very weak, ar = aromatic.

concentrations of 0, 1.04, 2.07, 4.15, 8.3, or 16.6 μM for 2 h and 4 h at 37° C. After drug exposure, cells were collected by centrifugation and washed twice with 0.9% NaCl to remove extracellular drug. Cells were counted and those collected were treated with 1 ml of conc. HNO<sub>3</sub> at 120° C. The mixture was digested until HNO<sub>3</sub> was evaporated and the digested cells were dissolved with 10 mM HNO<sub>3</sub> (0.2 ml). Platinum concentrations were determined by flameless atomic absorption spectroscopy (Atomic Absorption Spectrophotometer, Hitachi Model Z-9000 simultaneous spectrophotometer, W. Pabish Instrument, Milano, Italy) under the following conditions: drying 30s at 80-120° C, 15s at 120-200° C, 10s at 200° C; ashing 45s at 200-1100° C, 20s 1100° C; atomization 10s at 3000° C; clean 5s at 3000° C. Total cellular drug accumulation was measured as nanograms of platinum per 10<sup>5</sup> cells.

**Measurement of cellular drug efflux.** P388 leukemic cells were treated with DDP and DPR at an equimolar dose of 8.3 μM and exposed to each drug for 4 h. After a 4 h exposure, cells were harvested at the following time points: 30 min, 60 min, 120 min, and 240 min after drug removal. Total cellular efflux of the two drugs was compared by assigning the value of 100% to the drug level achieved after 4 h exposure, and assessing all other values relative to the 100% value.

**In vivo antitumor activity.** Female BDF1 mice (18-22 g) were implanted i.p. with 10<sup>5</sup> P388 leukemic cells on day 0 and DPR was administered i.p. dissolved in water (0.1-0.2 ml) 24 h later (day 1). Tests were conducted using groups of 6 mice for each dose, with a control group of 10 mice receiving only tumor cells and 0.1 ml of water. A positive control group received tumor cells and 8 mg/Kg of DDP dissolved in normal saline (the

Table III. IC<sub>50</sub> values of platinum compounds in P388 leukemic cells<sup>a</sup>.

Complexes	4 h exposure <sup>b</sup>	24 h exposure
DDP	0.65 ± 0.22	0.40 ± 0.11
DPR	0.70 ± 0.28	0.43 ± 0.06

<sup>a</sup>IC<sub>50</sub> = concentration of drug (μM) producing 50% inhibition of cell growth compared to untreated controls, and evaluated by [<sup>3</sup>H]-Thymidine incorporation in a 24 h assay from a 4 h and 24 h exposure (continuous exposure) to the platinum complexes as described in "Materials and Methods". <sup>b</sup>Values are expressed as Mean ± SD from 3-6 separate experiments.

maximum tolerated dose without the occurrence of toxic deaths, corresponding to approximately 50% acute LD<sub>50</sub> for a single treatment) or in distilled water. The test was terminated after 3 times the median survival time (MST) of the normal control group, and surviving mice were counted as dying on the day. Activity was determined based on the percent increase in MST of test mice over controls (% ILS). An ILS of >30% indicates activity in this tumor.

**Toxicological testing.** Preliminary toxicity testing was performed in groups of 8 normal female BDF1 mice by observing daily for signs of toxicity and survival following a single i.p. injection of the test compound. A sufficient number of doses were tested for DPR to allow calculation of the LD<sub>10</sub>, LD<sub>50</sub>, and LD<sub>90</sub> by probit analyses using deaths up to 14 days after drug administration. Mice were administered the calculated LD<sub>50</sub>, and 4 or 7 days later blood was collected by orbital-sinus puncture, using heparinized Pasteur pipettes. Plasma urea nitrogen (PUN) levels were determined according to the Beckman Liquid STAT test-combination (Beckman Instruments, Inc., Fullerton, CA). The kidneys were removed and treated for morphological analyses as previously described (16). As a measure of renal toxicity, PUN levels and renal tubular histopathological changes were investigated in animals receiving the test compound at the LD<sub>50</sub> dose (39.3 mg/Kg). PUN and kidney morphological analyses were also performed on a separate group of mice receiving a single i.p. injection of the calculated LD<sub>50</sub> of DDP in normal saline [16.5 ± 1.4 (SD) mg/Kg].

**Statistical analysis.** The significance of the differences between DDP and DPR treatments was assessed according to Student's t test.

## Results

**Chemical characterization.** The complex DPR showed a sole spot on TLC systems 1a), 1b) and a single peak with a retention time of about 6 min in the HPLC chromatogram (method 2). The difficulty of obtaining a DDP free product was overcome by a chromatography on the LC low pressure system, before crystallization. The residual DDP was less than 0.2% in the first crystallization product, as detected by chromatographic techniques (method 1c, 3 and 5). After thiourea (tu) treatment no *trans*-[Pt(tu)<sub>2</sub>(NH<sub>3</sub>)<sub>2</sub>]Cl<sub>2</sub> was detected, unlike what would be expected if *trans*-DPR was present, on the analogy of the compound [Pt(NH<sub>3</sub>)<sub>3</sub>Cl]Cl that gives the mentioned derivative as a sole product (18). The solubility of DPR in water was > 50 mg/ml. The elemental analysis values for carbon, hydrogen and nitrogen were in good agreement with those calculated for the proposed formula (Table I). These data showed a 1:1 molar ratio of platinum to P.HCl. The compound structure was inferred

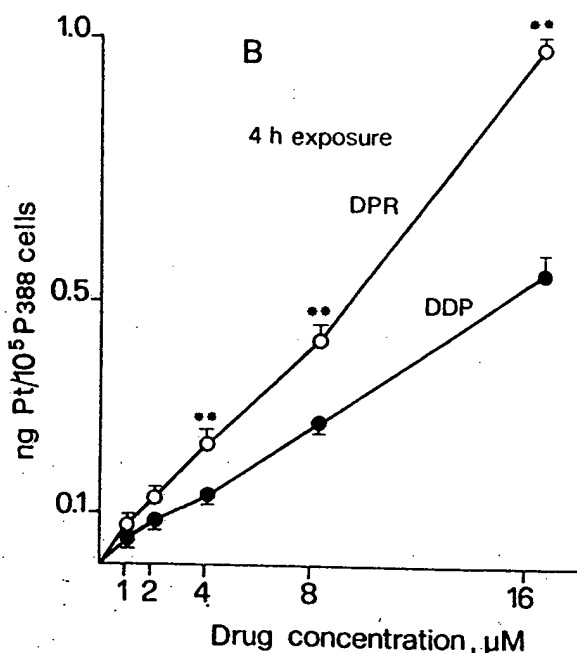
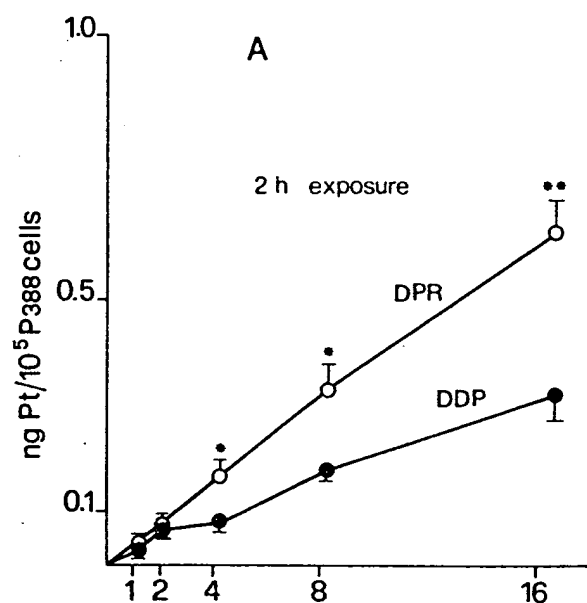


Figure 1. In vitro cellular uptake of DPR (○) and DDP (●) in P388 leukemic cells. Cells were exposed to equimolar concentrations of drugs for 2 h (A) or 4 h (B) at 37° C. At each time point, cells were collected and washed free of drug and cellular uptake of platinum was determined by atomic absorption spectroscopy as described in "Materials and Methods". Each experimental point represents the mean of 3-5 replicate experiments. Bars, SE.

(\*)  $P < 0.05$ ; (\*\*)  $P < 0.02$ .

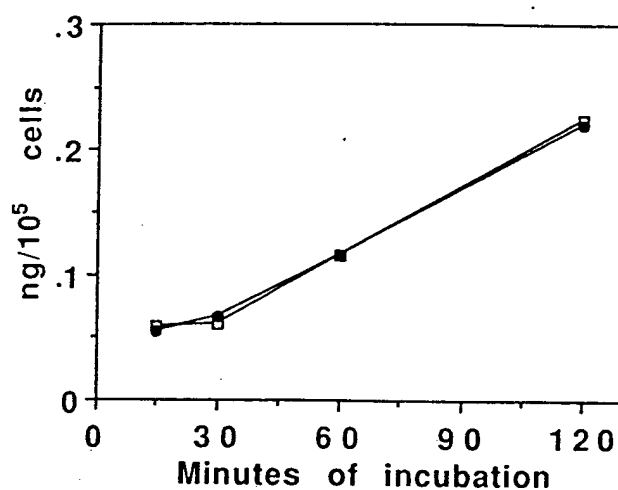


Figure 2. In vitro cellular uptake of Pt after P388 leukemic cells exposure to 16.6 μM DDP (□) and DDP + P.HCl at a 1:1 molar ratio (●). SD < 15%.

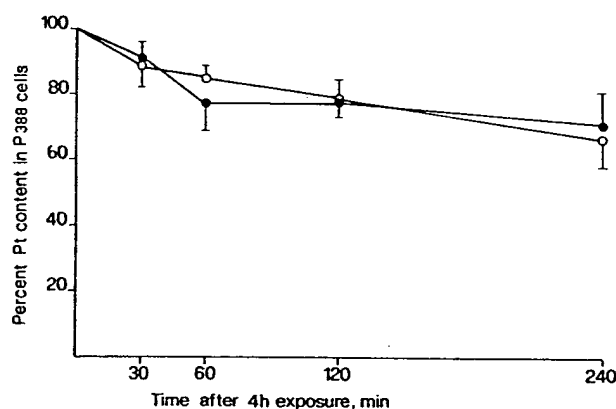


Figure 3. In vitro cellular efflux of DPR (○) and DDP (●) determined in P388 leukemic cells after 8.3 μM drug exposure for 4 h. Cells were treated as described in the text. Each data point is the mean of 3-7 separate determinations. Bar, SE.

from spectral data analyses (Table II). In the IR spectrum the  $\nu(\text{N-H})$  vibrations of the primary amino group are shifted to lower frequencies when compared to the parent P.HCl (from 3350-3200  $\text{cm}^{-1}$  to 3300-3080  $\text{cm}^{-1}$ , together with the stretching bands of the  $\text{NH}_2$  groups of the parent DDP). The  $\nu(\text{C=O})$  band, at 1685  $\text{cm}^{-1}$ , in free P.HCl, is moved to 1710  $\text{cm}^{-1}$  in DPR. The band at 1640  $\text{cm}^{-1}$  ( $\text{NH}_2$  bending vibration) in P.HCl disappears in the complex, probably shifted to about 1600  $\text{cm}^{-1}$  and overlapped by the  $\text{C=C}$  stretching band, whereas a new signal at 1210  $\text{cm}^{-1}$  is observable and can be assigned to the  $\text{C-NH}_2$  stretching absorption. These data emphasize the role of the aromatic amino group of P.HCl in the formation of the complex, as they can be considered to be due to a  $\text{Pt-NH}_2$  bonding with consequent removal of conjugation with the carbonyl group. Several weak bands are

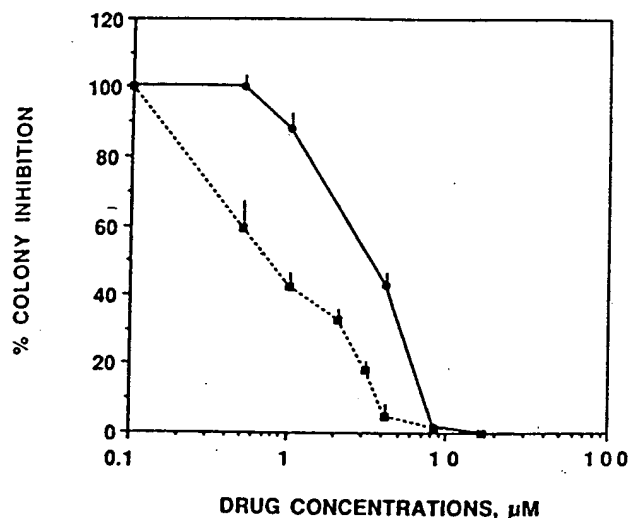


Figure 4. Effect of treatment with DPR (■) and DDP (●) on colony-forming ability of K562 cells. Survival is based on colony count expressed as percentage of the untreated control. Cells were exposed to various concentrations of drugs over the entire period of culture as described in "Materials and Methods". Each data point is the mean of three separate experiments. Bars, SD.

$IC_{50}$  values:  $3.87 \pm 0.21 \mu M$  for DDP and  $0.79 \pm 0.27 \mu M$  for DPR,  $P < 0.001$ .

observed in the  $\nu$  (Pt-N) region, but they may be due in part to the librational modes of the crystalline water (20, 21). The last important feature in the IR spectrum is one  $\nu$  (Pt-Cl) band at  $330 \text{ cm}^{-1}$ , whose presence is, again, in agreement with the proposed structure (20). The UV spectrum of the compound is drastically changed by complexation compared to that of P.HCl: only a maximum absorption at 244 nm is present in the 220-350 nm region, whereas the UV spectrum of P.HCl shows two absorption maxima at 220 and 289 nm. This hypsochromic shift is consistent with that of the carbonyl in the IR spectrum.

In the  $^1\text{H-NMR}$  spectrum the resonances of the aromatic protons in the ortho and meta position to the amino group in the complex are shifted downfield with respect to the parent P.HCl (about 0.6 and 0.3 ppm, respectively); these shifts further indicate that the primary amino group of P.HCl is involved in the coordination with platinum (22). The  $^{195}\text{Pt}$  chemical shift of DPR was  $-2373 \text{ ppm}$ .

**Stability of DPR in water, in normal saline (NS), in phosphate buffer (PB) 150 mM, and in fetal calf serum (FCS) at  $37^\circ \text{C}$ .** The HPLC (method 4) signals of DPR and procaine were used for monitoring the disappearance and decomposition of the complex in these media. The complex ( $0.5 \text{ mg/ml}$ ) loses  $\approx 5\%$  and  $\approx 20\%$  in water and NS ( $T_{90} = 10 \text{ h}$ ), respectively, over a 24 h period. A correspondent production of procaine was measured. By monitoring the HPLC of DPR as a function of time, the half-life of this complex was determined to be 4 h in PB, pH 7.3, and no measurable degradation to

Table IV. Growth-inhibiting effect of DPR evaluated by [ $^3\text{H}$ ]-Thymidine incorporation in a 24 h assay on human leukemic cell lines.

Leukemic cell lines	$IC_{50}^a$ ( $\mu M$ )	
	DPR	DDP
Jurkat	$0.86 \pm 0.16$	$1.04 \pm 0.23$
K562	$1.07 \pm 0.36^b$	$2.62 \pm 0.23$

<sup>a</sup> $IC_{50}$  = concentration of drug producing 50% inhibition of cell growth compared to untreated controls. Values are expressed as Mean  $\pm$  SD from three experiments. All experiments were performed with continuous drug exposure for 24 h (see Materials and Methods).

<sup>b</sup> $P < 0.01$  compared with cells exposed to DDP.

procaine was observed at this time. A small amount of procaine ( $\approx 2\%$  of the initial DPR concentration) was detected after 20 h incubation. These data, along with the new HPLC signals revealed, suggest that DPR undergoes transformation by reaction with phosphate, without involving the Pt-P.HCl bond. Filterable DPR showed a  $T_{50} = 1 \text{ h}$  in FCS, while the concomitant procaine formation rate was similar to that observed in NS ( $T_{90} = 10 \text{ h}$ ). Since a  $T_{90} = 4 \text{ h}$  was determined for procaine after incubation of P.HCl alone in FCS, the quantitation of procaine in the medium containing DPR alone can be taken as a measure of the complex decomposition with a good approximation. This suggests that a very small amount of DPR degrades to P.HCl in FCS and that the decrease in DPR concentration can be regarded as consequence of its serum protein-binding or transformation occurring without loss of the P.HCl ligand.

**Cytotoxic activity on P388 cells in vitro.** P388 cells were exposed to DDP and DPR for 4 and 24 h (continuous drug exposure), and  $IC_{50}$  values evaluated after overall 24 h incubation. As summarized in Table III, no significant differences were noted in the cytotoxic activity of DDP and DPR in the two different culture conditions used. The  $IC_{50}$  values of DDP and DPR after 4 h [ $0.65 \pm 0.22$  (SD)  $\mu M$  vs  $0.70 \pm 0.28$  (SD)  $\mu M$ ] or 24 h [ $0.40 \pm 0.11$  (SD)  $\mu M$  vs  $0.43 \pm 0.06 \mu M$ ] exposure of cells shows that the growth of P388 cells in culture is significantly inhibited by DDP and DPR treatment and that the cytotoxicity of both drugs tends to increase with the length of exposure.

**Cellular uptake studies.** As shown in Figure 1, the relationship between drug dose and total cellular accumulation inside P388 cells approached linearity for both DDP and DPR. The uptake of platinum by P388 cells occurs more rapidly through cell membrane after DPR than after DDP exposure. In the cells exposed to DPR, the linear regression equations were  $y = 0.038x - 0.0014$ ,  $r = 0.99$ , for 2 h exposure, and  $y = 0.058x + 0.0023$ ,  $r = 0.99$ , for 4 h exposure; in the cells treated with DDP the equations were  $y = 0.019x + 0.0076$ ,  $r = 0.99$ , for 2 h exposure, and  $y = 0.032x + 0.0094$ ,  $r = 0.99$ , for 4 h exposure (Figure 1A, B). Based on the slopes of the linear

Table V. Antitumor activity of DPR administered as a single i.p. injection<sup>a</sup>.

Complex	Dose (mg/Kg)	MST <sup>b</sup> (days)	%ILS <sup>c</sup>	Survivors at day 11	% change in weight at day 7	36-day survivors
DPR (water)	37	Toxic <sup>d</sup>	Toxic	2/6	- 5.2	0/6
	30	19	58	6/6	- 4.4	1/6
	28	19	58	6/6	+ 2.0	1/6
	21	21	75	6/6	+ 4.5	1/6 -
	14	17	42	6/6	+ 4.9	0/6
DDP (saline)	8	21	75	6/6	-10.6	2/6
(water)	8	19	58	5/6	-18.7	0/6

<sup>a</sup>BDF1 mice were inoculated i.p. with 10<sup>5</sup> P388 cells and were administered the test complex the next day as a single i.p. injection. <sup>b</sup>MST = median survival time. <sup>c</sup>%ILS = per cent increase in life span of test mice over controls. <sup>d</sup>Toxicity: < 4/6 mice alive on day 11 [MST of untreated tumour-bearing mice (n = 10) is 12 ± 0.6 days].

portion of the curves, about 50% less DPR is needed to attain the same levels of DDP accumulation in P388 leukemic cells after 2 h and 4 h exposure. In a separate experiment, where the P388 leukemic cells were exposed to DDP (16 µM) and DDP + P.HCl (molar ratio 1:1), no differences in platinum uptake were observed (Figure 2).

**Cellular efflux studies.** P388 cells treated with DPR demonstrated similar efflux as compared to those treated with DDP. After 4 h, about 30% of accumulated cellular platinum had been removed from P388 leukemic cells exposed to DPR and DDP for 4 h at 37° C (Figure 3).

**Cytotoxic activity on human leukemic cell lines.** The cytotoxic activity of DPR was tested on K562 and Jurkat leukemic cell lines. In the human leukemic cell lines DPR showed a strong inhibition of [<sup>3</sup>H]-thymidine incorporation. The specific cytotoxic activity of DPR, evaluated by the IC<sub>50</sub>s after continuous exposure for 24 h, was similar to, or higher (in K562 cells), than that of DDP (Table IV). To define further DPR cytotoxic activity on K562 human cell line, these cells were also tested in a clonogenic assay. Data obtained in 3 experiments confirmed that the activity of DPR was better than that of DDP on this cell line (IC<sub>50</sub>s: 0.79 ± 0.27 vs 3.87 ± 0.21 µM, P < 0.001) (Figure 4).

**In vivo antitumor activity.** The antitumor activity of DDP and DPR following a single i.p. injection is shown in Table V. In the P388 leukemia experiments *in vivo* DPR proved to be very active, displaying antitumor activity comparable to that obtained with the maximum tolerated dose (MTD) of DDP. However, DPR was found to be less toxic than DDP in terms of percent change in weight (+4.5% and -10.6%, respectively) at the dose producing the highest increase in life span (ILS% = 75%, Table V).

**Toxicological studies.** When DPR was administered as a single i.p. injection to female BDF1 mice, the LD<sub>10</sub>, LD<sub>50</sub> and LD<sub>90</sub> calculated values were 26.3 ± 1.02, 39.3 ± 4.1, and 58.7 ± 1.08 mg/Kg, respectively.

Table VI. PUN values (mg/100 ml) after treatment<sup>a</sup>.

Complex	Dose (mg/Kg)	PUN	
		Day 4	Day 7
Control (saline)	-	20 ± 2 <sup>b</sup>	21 2
DDP (saline)	16.5	57 ± 12	68 ± 8
DPR (water)	39.3	20 ± 3 <sup>c</sup>	22 ± 2 <sup>c</sup>

<sup>a</sup>Normal female BDF1 mice were administered a single i.p. injection of the calculated LD<sub>50</sub>s for DDP (16.5 mg/Kg) and DPR (39.3 mg/Kg). PUN levels were determined 4 and 7 days later. <sup>b</sup>Mean ± SD (n = 8). <sup>c</sup>P < 0.01 compared with DDP.

No significant changes in PUN values were observed in mice receiving DPR, while the equitoxic dose of DDP produced elevated PUN values (Table VI). Whereas degenerative changes localized to the murine proximal tubules were clearly evident after i.p. administration of 16.5 mg/Kg of DDP, kidneys from DPR treated mice did not show any difference in tubular damage (Figure 5) when compared to normal control kidneys.

## Discussion

In the present study DPR and DDP efficacy against i.p. implanted P388 leukemia and cytotoxic effects *in vitro* on some leukemic cell lines were compared. Over the dosage range used, DPR appeared to have good activity in both *in vivo* and *in vitro* experimental studies. These results indicate that this platinum complex increases the life span of P388 tumor-bearing mice as does the maximum tolerated dose of DDP (8 mg/Kg). Furthermore, at equimolar doses its cytotoxic effect was the same as that of DDP in the P388 and Jurkat cell lines, and even better in the K562 cell line. In addition, BDF1 mice toxicity studies failed to detect PUN elevation and kidney lesions over the 7-day examination

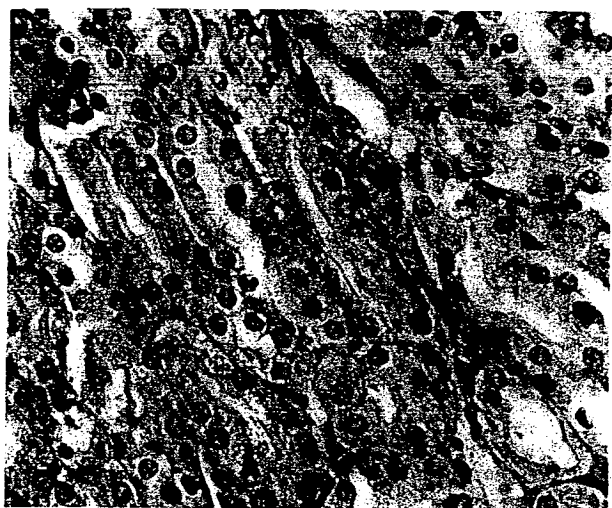


Figure 5. Light micrograph of cortical parenchyma from mouse kidney following single treatment with 39.3 mg/Kg DPR (i.e.,  $LD_{50}$  dose). Mice were killed on day 7. The cortical parenchyma shows tubules with normal morphology, particularly as far as the striated border of the proximal convoluted tubules. (Original magnification  $\times 400$ ).

period when DPR was given at  $LD_{50}$  value, suggesting that this complex is much less nephrotoxic than DDP. It is also noteworthy that DPR is highly water soluble as compared to DDP ( $> 50$  mg/ml vs 1 mg/ml). These findings indicate that DPR, compared to DDP, has a similar or stronger cytotoxic effect on leukemic cells and a lower nephrotoxicity. These results are particularly relevant, since all DDP analogues that have been synthesized to reduce DDP renal toxicity and other side effects and to increase water solubility have been shown to be less nephrotoxic but also less cytotoxic.

As regards the chemical characteristics, DPR is peculiar both for its structure and antitumor activity. The majority of the amine analogues of DDP are in the form  $cis-(PtA_2X_2)$ , where A is an amine ligand and X is an anionic leaving group (15, 23). Generally, the active DDP analogues are neutral complexes which bind to DNA in a bidentate fashion (24, 25). Recent studies by Hollis *et al* (15, 26) showed that cationic platinum-triamine analogues also display activity against murine tumors, although they are expected to bind to DNA in a monodentate fashion. Our results indicate that the primary amino group of P.HCl is involved in the coordination with platinum and that this new cationic platinum-triamine complex also displays good cytotoxic and antitumor activity in both *in vitro* and *in vivo* experiments. The  $^{195}Pt$  chemical shift value for DPR (-2373 ppm) is comparable to those presented by Hollis *et al* (15) for a series of Pt-triamine complexes, suggesting that the ligand has a good donor strength despite the low basicity of the aromatic amino group of P.HCl. The question of whether DPR remains intact in medium and cells or whether it may degrade to its parent forms was investigated in biological media. The findings suggest that, while DPR is highly stable in water, the complex

could react in the presence of chloride or phosphate ions. DPR loses  $\approx 20\%$  over a 24 h period in normal saline and a correspondent production of procaine was measured. This amount of procaine was too low to account for the observed protective effect exerted by P.HCl on DDP toxicity (16). In fetal calf serum the half-life of DPR was about 1 h, a sufficient time to hypothesize that the cells could be exposed to intact DPR following administration *in vivo*. Interestingly, in the phosphate buffer medium at a concentration of 150 mM (similar to that found inside the cell), the compound was transformed in uncharacterized Pt-complexes without any relevant loss ( $\approx 2\%$ ) of P.HCl ligand. These findings indicate that P.HCl in the complex can be viewed as a ligand of moderate (normal saline, fetal calf serum) or quite low lability (water, phosphate buffer solution). Although DPR cannot be considered in every respect a triamine-platinum complex of the type described by Hollis *et al* (15, 26), these findings suggest that DPR has its own pharmacological activity.

The present study demonstrates that the *in vitro* cellular uptake of DPR is increased considerably after both 2 and 4 h exposure compared to DDP in P388 cells. Cellular uptake is not necessarily related to cytotoxicity which mainly depends on binding with DNA and interaction with other intracellular targets. In the case of 4 h exposure, indeed,  $IC_{50}$  values were similar for DPR and DDP, although significantly higher amounts of Pt-uptake from DPR treated cells and no differences between DPR and DDP in cellular efflux were noted. However, the fact that no difference in Pt uptake was noted between cells exposed to DDP and DDP+P.HCl (molar ratio 1:1) eliminates the mechanistic possibility that DPR influences the cellular uptake of platinum and exhibits activity only after decomposition into its parent forms.

While detailed studies are required to investigate the mechanism of action of DPR at the cellular and molecular level, our results indicate that DPR may be a promising new platinum anticancer agent for preclinical development.

#### Acknowledgements

The authors are grateful to Dr. C.A. Gandolfi for his helpful discussions and to Dr. T. Beringhelli (Istituto di Chimica Inorganica, Università di Milano) for the  $^{195}Pt$ -NMR analyses.

#### References

- 1 Prestaiko AW, Crooke ST and Carter SK (eds): *Cisplatin, Current Status and New Developments*. New York, Academic Press, 1980.
- 2 Holland JF, Bruckner HW, Cohen CJ, Wallech RC, Brusberth SB, Greenspan EM and Goldberg J: *Cisplatin Therapy of Ovarian Cancer*. New York, Academic Press, 1980.
- 3 Loeher PJ and Einhorn LH: Drugs five years later: Cisplatin. *Ann Intern Med* 100: 704-713, 1984.
- 4 Ross DA and Gale GR: Reduction of the renal toxicity of cis-dichlorodiammineplatinum (II) by probenecid. *Cancer Treat Rep* 63: 781-787, 1979.
- 5 Howell SB and Taetle R: Effect of sodium thiosulfate on cis-dichlorodiammineplatinum (II) toxicity and antitumor activity in L1210 leukemia. *Cancer Treat Rep* 64: 611-616, 1980.
- 6 Yuhás JM and Culo F: Selective inhibition of the nephrotoxicity of

- cis-dichlorodiammineplatinum (II) by WR-2721 without altering its antitumor properties. *Cancer Treat Rep* 64: 57-64, 1980.
- 7 Bodenner DL, Dedon PC, Keng PC, Katz JC and Borsch RF: Selective protection against cis-diamminedichloroplatinum (II) - induced toxicity in kidney, gut, and bone marrow by diethyldithiocarbamate. *Cancer Res* 46: 2751-2755, 1986.
  - 8 Baldew GS, McVie JG, van der Valk MA, Los G, de Goeij JJM and Vermeulen NPE: Selective reduction of cis-diamminedichloroplatinum (II) nephrotoxicity by ebelen. *Cancer Res* 50: 7031-7036, 1990.
  - 9 Di Re F, Bohm S, Oriana S, Spatti GB and Zunino F: Efficacy and safety of high-dose of cisplatin and cyclophosphamide with glutathione protection in the treatment of bulky advanced epithelial ovarian cancer. *Cancer Chemother Pharmacol* 25: 355-360, 1990.
  - 10 Jacobs C, Kaubisch S, Halsey J, Lum BL, Gosland M, Coleman CN and Sikic BI: The use of probenecid as a chemoprotector against cisplatin nephrotoxicity. *Cancer* 67: 1518-1524, 1991.
  - 11 Harrap KR: Platinum analogues criteria for selection. In: Muggia FM (ed), *Cancer Chemotherapy*, Vol 1, Boston, Martinus Nijhoff, 1983, pp 171-217.
  - 12 Hacker MP, Khokhar AR, Brown DB, McCormack JJ and Krakoff IH: Ascorbate (1,2-diaminocyclohexane): platinum (II) complexes, a new series of water-soluble antitumor drugs. *Cancer Res* 45: 4748-4753, 1985.
  - 13 Rahman A, Roth JK, Wolpert-DeFilippes MK, Goldin A, Venditti JM and Wooley PV: Therapeutic and pharmacological studies of tetra-chloro(d,l-trans) 1,2-diaminocyclohexane platinum (IV) (tetraplatin), a new platinum analogue. *Cancer Res* 48: 1745-1752, 1988.
  - 14 Hirano T, Inagaki K, Fukai T, Alink M, Nakahara H and Kidani Y: Cytotoxicity of asymmetric platinum complexes against L-1210 cells. Effect of bulky substituents. *Chem Pharm Bull* 38: 2850-2852, 1990.
  - 15 Hollis LS, Amudsen AR and Stern EW: Chemical and biological properties of a new series of cis-diammineplatinum (II) antitumor agents containing three nitrogen donors: cis-[Pt(NH<sub>3</sub>)<sub>2</sub>(N-donor)Cl]<sup>+</sup>. *J Med Chem* 32: 128-136, 1989.
  - 16 Esposito M, Fulco RA, Collecchi P, Zicca A, Cadoni A, Merlo F, Rosso R and Sobrero A: Improved therapeutic index of cisplatin by procaine hydrochloride. *J Natl Cancer Inst* 82: 677-684, 1990.
  - 17 De Spiegeleer B, Slegers G, Van den Bossche W and De Moerloose P: Quantitative analysis of cis-dichlorodiammineplatinum (II) by high-performance thin-layer chromatography. *J Chromatog* 315: 481-487, 1984.
  - 18 Arpalahti J and Lippert B: An alternative HPLC method for analysing mixtures of isomeric platinum (II) diammine compounds. *Inorg Chim Acta* 138: 171-173, 1987.
  - 19 Shoemaker RH, Wolpert-DeFilippes MK, Kern DH, Lieber MM, Makuch RW, Melnick NR, Miller WT, Salmon SE, Simon RM, Venditti JM and Von Hoff DD: Application of a human tumor colony-forming assay to new drug screening. *Cancer Res* 45: 2145-2153, 1985.
  - 20 Jungbauer MAJ and Curran C: Infrared spectra of complexes of aniline with metal (II) halides. *Spectrochim Acta* 21: 641-648, 1965.
  - 21 Hiraishi J, Nakagawa I and Shimanouchi T: Far-infrared spectra and force constants of ammine complexes of Pt(IV), Pd(II). *Spektrochim Acta* 24A: 819-832, 1968.
  - 22 Foulds GA and Thornton DA: Application of spectroscopic techniques to substituted aniline derivatives of Zeise's salt. *J Mol Struct* 98: 309-314, 1983.
  - 23 Hydes PC: Synthesis and Testing of Platinum Analogues- An Overview. In: Hacher MP, Douple EB and Krakoff IH, (eds), *Platinum Coordination Complexes in Cancer Chemotherapy*. Boston, Martinus Nijhoff, 1984, pp 216-227.
  - 24 Pinto AL and Lippard SJ: Binding of the antitumor drug cis-diamminedichloroplatinum (II) (cisplatin) to DNA. *Biochem Biophys Acta* 780: 167-180, 1985.
  - 25 Roberts JJ, Knox RJ, Friedlos F and Lydall DA: DNA as the target for the cytotoxicity and antitumor action of platinum coordination complexes: comparative *in vitro* and *in vivo* studies of cisplatin and carboplatin. In: McBrien DCH and Slater TS (eds), *Biochemical Mechanisms of Platinum Antitumor Drugs*, Oxford, England, IRL Press, 1986, pp 29-64.
  - 26 Hollis LS, Sundquist WI, Burstyn JN, Heiger-Bernays WJ, Bellon SF, Ahmed KJ, Amudsen AR, Stern EW and Lippard SJ: Mechanistic studies of a novel class of trisubstituted platinum (II) antitumor agents. *Cancer Res* 51: 1866-1875, 1991.

Received August 18, 1992  
Accepted October 13, 1992

Ele

Abstract  
ly untrea  
late synt  
tumors,  
correlati  
doxorub  
TS-positi  
the 27 T  
group c  
chemoth  
platinum  
clinically  
TS-nega.  
(p<0.05  
TS nega  
positive  
patients  
TS-positi  
ion of T  
clinical c  
carcinom

The mo  
over the  
patients  
patients  
These d  
which is  
To d  
have be  
of P-gly  
regulati

Correspc  
schungsz  
Germany

Key Wo  
thymidyl

VOLUME XXIV · 1994

A 21037 F

---

INTERNATIONAL JOURNAL OF CLINICAL & LABORATORY

---

EXHIBIT 11



**Springer**

INTERNATIONAL

## Reviews

# Taxol (paclitaxel): a novel anti-microtubule agent with remarkable anti-neoplastic activity

Robin Foa<sup>1</sup>, Larry Norton<sup>2</sup>, and Andrew D. Seidman<sup>2</sup>

<sup>1</sup> Dipartimento di Scienze Biomediche e Oncologia Umana, Sezione Clinica, Via Genova 3, I-10126 Turin, Italy

<sup>2</sup> Breast and Gynecological Cancer Medicine Service, Division of Solid Tumor Oncology, Department of Medicine, Memorial Sloan-Kettering Cancer Center, New York, NY 10021, USA

**Summary.** Taxol (paclitaxel), an anti-microtubule agent extracted from the needles and bark of the Pacific yew tree *Taxus brevifolia*, has shown a remarkable anti-neoplastic effect in human cancer in phase I studies and early phase II and III trials thus far conducted. This has been reported primarily in advanced ovarian and breast cancer, although significant activity has also been documented in small-cell and non-small-cell lung cancer, head and neck cancers, and with lower activity in metastatic melanoma. The clinical utilization of Taxol had been previously somewhat restricted by its limited availability, a limitation that has recently been overcome by combined efforts of pharmaceutical, agricultural, and governmental agencies. In this review we shall address the pre-clinical data which have led to the use of Taxol in man, the main clinical results thus far obtained, the toxicities associated with its use, current ongoing trials and future clinical directions of this promising agent.

**Key words:** Taxol (paclitaxel) – Anti-neoplastic activity – Ovarian and breast cancer

## Introduction

Since the introduction of the anthracyclines and cisplatin, the identification of new agents with significant activity in cancer has been slow. Taxol is arguably the most important and novel new addition to the chemotherapeutic armamentarium this decade. As can be the case for many promising developments in clinical oncology, the initial extent and tone of media coverage regarding Taxol's utility may misrepresent its eventual clinical utility. However, there is certainly reason for much optimism, although not unbridled enthusiasm.

Correspondence to: R. Foa

Taxol is a novel diterpenoid plant product derived from the needles and bark of the Western yew *Taxus brevifolia* [1], which has subsequently been found in the leaves, stems, and roots of other *Taxus* species. Interest in this compound goes back to the 1960s when a National Cancer Institute-sponsored study on over 35,000 plant species led to the discovery that bark extracts from the *Taxus brevifolia* yew displayed anti-neoplastic activity against different experimental tumors [1, 2]. Despite its remarkable activity, several concomitant factors contributed to limit its development and possible clinical exploitation. These included formulation obstacles, due to the aqueous insolubility of Taxol, and hypersensitivity reactions that occurred when the agent was solubilized in the suitable vehicle Cremophor. They also involved public policy decisions regarding the difficulties in extracting large amounts of this natural product from trees found in forests in the Pacific Northwest region of the United States.

Interest in Taxol was revitalized by the recognition of its unique biological properties and anti-tumor mode of action [3-5]. Despite difficulties in obtaining sufficient quantities of Taxol and serious conservation issues posed by the need to harvest mature bark, sustained efforts continue in the development of this compound. Recent public policy initiatives coupled with intensive efforts from the pharmaceutical and agricultural industries strive to ensure an adequate supply of Taxol. Efforts continue toward procuring adequate amounts of a synthetic or semi-synthetic form of this complex organic molecule. Its increased availability has enabled the performance of necessary pre-clinical and toxicological studies, and conduct of clinical investigations, including phase III clinical trials in different neoplastic conditions.

In the present review we shall briefly discuss the mechanism of action of Taxol, the pre-clinical screening studies, the early clinical results obtained following its *in vivo* use in advanced tumors, the initial phase II trials, and, finally, the ongoing studies and future perspectives for this promising anti-cancer agent.



## Mode of action

Taxol is directed against microtubules, ubiquitous cellular structures which play a key role in the initiation of DNA synthesis, mitosis, and other critical interphase functions, such as motility, maintenance of shape, intracellular transport, and signal transduction [6]. Much of the *in vitro* pre-clinical work which has enabled elucidation of the mode of action of Taxol has been performed at the Albert Einstein College of Medicine in New York [3, 5–7]. These researchers demonstrated that Taxol binds preferentially to microtubules and that its binding site is different from that of other anti-microtubule agents, such as colchicine, vinca alkaloids, and podophyllotoxin [4, 7, 8]. In fact, the overall effect of Taxol, that of binding to tubulin and of promoting the assembly of microtubules with stabilization against depolymerization [3, 7, 8], is different from that of other anti-microtubule products, which induce disassembly or prevent proper assembly of microtubules.

Taxol induces the formation of microtubule polymerization by shifting the tubulin dimer-polymer equilibrium in favor of polymer assembly and by eliminating the lag period prior to tubulin assembly. Cells treated with Taxol give rise to abundant disorganized microtubules, often in the form of parallel bundles [9]. These occur during all phases of the cell cycle. Microtubules become stable and this leads to an inhibition of the normal process of dynamic reorganization of the microtubule compartment. Following exposure to Taxol, there is an arrest in the growth of the murine P388 leukemia, as well as of HeLa cells and BALB/c mouse fibroblasts in the G<sub>2</sub> and M phases of the cell cycle [10]. This observation has led to studies evaluating the role of Taxol as a potential radiation sensitizer [11].

## Pre-clinical studies

The possibility that this compound could have a role in the management of cancer patients was suggested by extensive pre-clinical studies at the National Cancer Institute (Bethesda, Md., USA) which allowed the demonstration of its activity against a variety of tumors [11, 12]. This was largely promoted by the impressive anti-tumor activity shown against the murine B16 melanoma cells. Remarkable anti-tumor efficacy was also recorded against the human MX-1 mammary tumor xenograft. Moderate s.c. activity was shown against the human CX-1 colon and LX-1 lung tumor cell lines and against i.p. implanted P388 and L1210 murine leukemia cell lines. In contrast, Taxol proved ineffective against the s.c. implanted murine Cd8F<sub>1</sub> mammary and colon 38 carcinomas and the i.v. implanted Lewis lung carcinoma. Other studies have shown the potentially important activity of Taxol against a variety of tumors. Tumor regression has been reported in nude mice implanted with human breast carcinoma cells, as well as *in vivo* growth delays for human endometrial, ovarian, brain, tongue, and lung tumors.

## Clinical investigation

### Single agent trials

**Phase I.** In view of its aqueous insolubility, Taxol has had to be dissolved in a diluent, Cremophor EL, a mixture of 50% ethanol and 50% polyoxyethylated castor oil. This vehicle alone is capable of inducing significant hypersensitivity reactions in dogs [13]. The first phase I clinical trials were initiated back in the early 1980s and over the years different schedules of administration have been attempted. These include daily continuous i.v. infusions every 14 or, more frequently, 21 days over a 1-, 3-, 6-, or 24-h period. The possibility of administering lower doses of Taxol i.v. in 1 or 6 h over 5 consecutive days every 3 weeks has also been contemplated. The continuation of the early trials was jeopardized by some severe side effects [14]. These consisted largely of acute hypersensitivity reactions, which could at least in part have been related to the vehicle formulation. Since the side effects were more frequent and severe when Taxol was administered over a short time period (<6 h), the subsequent phase I studies were carried out to assess whether a 6- or 24-h i.v. infusion could lead to a more acceptable toxicity profile. These studies demonstrated that the use of a more prolonged infusion time (24 h) and the concomitant use of prophylactic steroids and histamine receptor antagonists as anti-allergic pre-medication could decrease the incidence and severity of acute hypersensitivity reactions.

While the problem of unacceptable early toxicity could be solved by adopting pre-medication and a different schedule of administration, numerous other side effects have been observed with Taxol treatment, sometimes independently of the schedule and dose employed. These, which will be discussed in more detail later, have not hampered continuation of further clinical trials.

Overall, the early phase I studies allowed the National Cancer Institute to put forward initial recommendations for the clinical use of Taxol: i.e., a safe schedule of administration (by continuous i.v. infusion over a 24-h period every 21 days, with anti-allergic pre-medication) and dose range (170–250 mg/m<sup>2</sup> body surface area, depending upon extent of prior exposure to cytotoxic therapy). Furthermore, these studies demonstrated the potential anti-neoplastic activity of this compound, with responses observed in several types of human malignancies.

As dose-limiting toxicity at higher Taxol doses consisted predominantly of neutropenia, phase I trials of Taxol alone and in combination with other cytotoxic agents in conjunction with hematopoietic growth factor support have been performed. In a phase I study conducted at the National Cancer Institute, Taxol could be safely dose escalated from the standard 175 mg/m<sup>2</sup> every 21 days (58.3 mg/m<sup>2</sup> per week dose intensity) to 250 mg/m<sup>2</sup> every 21 days (83.3 mg/m<sup>2</sup> per week) in 15 patients with platinum-refractory recurrent advanced-stage ovarian cancer, with the concurrent administration of granulocyte-colony-stimulating factor (G-CSF) at 10 µg/kg per day by s.c. injection [15]. Since a steep dose-response relationship has been observed for cisplatin in ovarian cancer [16], the concomitant use of G-CSF may allow for a

similar evaluation of the role of dose intensity of Taxol in this and other malignancies. A summary of the phase I single-agent clinical trial data is shown in Table 1.

**Phase II–III.** The early phase II trials, initially restricted by the quantities of Taxol available, were conducted on limited numbers of patients with selected neoplastic conditions. With an increased supply of Taxol, the last 2 years have witnessed a rapid expansion of both phase II and phase III studies. Phase II trials have thus far been conducted in ovarian carcinoma, breast cancer, small-cell and non-small-cell lung cancer, head and neck cancer, metastatic melanoma, colon cancer, cervical cancer, prostate cancer, and renal cell carcinoma. Trials are presently ongoing in other adult solid and hematological malignancies, including gastric, esophageal, pancreatic, hepatocellular, endometrial, germ cell, and bladder carcinomas, sarcoma, myeloma, acute leukemia and lymphoma, as well as in pediatric malignancies. Table 2 summarizes the phase II clinical trials of Taxol as monotherapy to date [14, 17–32]. The most impressive results have thus far been observed in advanced ovarian cancer.

Four independent groups – the Johns Hopkins Oncology Center, the Gynecology Oncology Group, the Medicine Branch of the National Cancer Institute, and the Albert Einstein College of Medicine – have published that objective responses may be expected in 20%–50% of patients [17–20]. It is important to note that responses were observed in patients who had had extensive prior chemotherapy, including patients with platinum-resistant carcinoma. A dose-response relationship has been suggested for Taxol in ovarian cancer in a multicenter European-Canadian randomized phase III clinical trial addressing the issue of dose and readdressing the issue of infusion duration [33]. In this bifactorial trial design, patients were randomized to receive Taxol at 135 or 175 mg/m<sup>2</sup>, by either a 3- or 24-h infusion. With 298 evaluable patients, responses were observed in 24% of patients treated on the higher dose arm, and in 13% of patients on the lower dose arm. The duration of drug infusion is presently an area of renewed interest in the light of evidence for the safety of a 3-h infusion in two large European-Canadian randomized trials [33, 34] and the more convenient administration of the shorter infusion.

Another exciting area in which early data show a high level of anti-tumor activity for Taxol is in the treatment of breast cancer. In the initial phase II study carried out in 25 women with metastatic breast cancer who had received only one previous chemotherapy regimen, an objective response rate of 56% has been reported [22]. Although neutropenia was the dose-limiting factor, neutropenic fever occurred in only 5% of 232 courses administered. Data accumulated at the Memorial Sloan-Kettering Cancer Center, in a confirmatory phase II trial of Taxol in metastatic breast cancer patients, show that the addition of prophylactic recombinant G-CSF, while shortening the duration of neutropenia and allowing retreatment every 21 days, did not allow for increasing the Taxol dose above 250 mg/m<sup>2</sup> [23]. Objective responses were observed in 62% of patients who had not received

**Table 1.** Phase I trials of Taxol

Investigator/ institution	Schedule (mg/m <sup>2</sup> )	MTD	DLT
MDACC	1 h i.v. 5 days every 3 weeks	40	Leukopenia
UWisc	1 h or 6 h i.v. 5 days every 4 weeks	30	Leukopenia
DFCC	24 h continuous i.v. 5 days every 3–4 weeks	30	Leukopenia
MSKCC	3 h i.v. 1 day every 3 weeks	–	Hyper-sensitivity
JHOC	1 h or 6 h i.v. 1 day every 3 weeks	265	Leukopenia
Einstein	1–6 h i.v. 1 day every 3 weeks	275	Leukopenia
	24 h continuous i.v. 1 day every 3 weeks	275	Neuropathy
Mount Sinai	24 h continuous i.v. every 3 weeks	300	Leukopenia
JHOC	24 h continuous i.v. every 3 weeks	390	Mucositis
UT-S.A.	6 h i.v. every 3 weeks	275	Leukopenia
NCI	24 h continuous i.v. every 3 weeks (+G-CSF)	250	Neuropathy

MTD, Maximally tolerated dose; DLT, dose-limiting toxicity; MDACC, M.D. Anderson Cancer Center; MSKCC, Memorial Sloan-Kettering Cancer Center; JHOC, Johns Hopkins Oncology Center; NCI, National Cancer Institute (USA); UT-S.A., University of Texas–San Antonio; DFCC, Dana Farber Cancer Center; G-CSF, granulocyte-colony-stimulating factor

**Table 2.** Phase II trials of Taxol

Tumor	Investigator/institution	Activity	Reference
Ovarian	McGuire/JHOC	+++	[17]
	Einzig/Einstein	+++	[18]
	Thippen/GOG	+++	[19]
	Sarosy/NCI	+++	[20]
Renal	Einzig/ECOG	–	[21]
Breast	Holmes/MDACC	+++	[22]
	Reichman/MSKCC	+++	[23]
Cervical	McGuire/GOG	–	–*
Colon	Einzig/ECOG	–	–*
Gastric	Einzig/ECOG	–	[24]
Head and neck	Forastiere/ECOG	++	[25]
Lymphoma	Wilson/NCI	++	[26]
Melanoma	Einzig/ECOG	+	[27]
	Legha/MDACC	+	[28]
NSCLC	Chang/ECOG	++	[29]
	Murphy/MDACC	++	[30]
Pancreas	Brown/UT-SA	–	[31]
Prostate	Roth/ECOG	–	[14]
SCLC	Ettinger/ECOG	++	[32]

NSCLC, Non-small-cell lung carcinoma; SCLC, small-cell lung carcinoma; GOG, Gynecology Oncology Group; ECOG, Eastern Cooperative Oncology Group

\* Unpublished information

**Table 3.** Randomized trials of Taxol in breast cancer

Group/study	Trial design
European/Canadian (BMS-048)	175 vs. 135 mg/m <sup>2</sup> , 3 h
European (BMS-071)	175 mg/m <sup>2</sup> → MTD, 3 vs. 24 h
CALGB	250 mg/m <sup>2</sup> + G-CSF vs. 175 mg/m <sup>2</sup> , 3 h
NSABP	250 mg/m <sup>2</sup> + G-CSF, 3 vs. 24 h
ECOG	Taxol 175 mg/m <sup>2</sup> (24 h) vs. doxorubicin 60 mg/m <sup>2</sup> vs. Taxol 150 mg/m <sup>2</sup> + doxorubicin 50 mg/m <sup>2</sup> + G-CSF
NCI (TRC 9301)	Taxol 175 mg/m <sup>2</sup> (3 h) every 3 weeks vs. vinblastine 5.5 mg/m <sup>2</sup> every week

CALGB, Cancer and Leukemia Group B; NSABP, National Surgical Adjuvant Breast Project

prior chemotherapy for metastatic breast cancer, mirroring the results of Holmes et al. [22].

Significant activity and tolerability have also been documented in patients receiving Taxol after failure of prior chemotherapy for advanced breast cancer. In a trial of Taxol at 200 mg/m<sup>2</sup> via a 24-h continuous infusion every 3 weeks with G-CSF, partial responses were observed in 25 of 76 pre-treated patients (33%, 95% confidence interval 23%–45%) [35]. In a subset of 51 patients receiving Taxol after at least two prior chemotherapy regimens for stage IV disease, partial responses were observed in 14 (27.5%, 95% confidence interval 16%–42%). Quality of life measurements have been performed in parallel with this study to more comprehensively assess the impact of Taxol in this setting [36]. An ongoing trial at M.D. Anderson Cancer Center in Houston, Texas (USA) is also presently evaluating the activity of Taxol in more heavily treated metastatic breast cancer patients [37].

Activity observed in the initial phase II trials have provided the impetus for randomized phase III studies which address the issue of optimal dose and infusion duration, among others. A summary of ongoing and planned phase III trials of Taxol in breast cancer is listed in Table 3. In an interim analysis of 245 patients in a large European-Canadian study comparing Taxol at 135 and 175 mg/m<sup>2</sup>, both via a 3-h infusion, 22% and 29% responded, respectively [34]. Treatment was well tolerated by these patients who had received either adjuvant therapy alone (31%), metastatic therapy alone (37%), or both (32%). At 175 mg/m<sup>2</sup>, responses were observed as frequently in patients who were refractory to anthracycline as in those patients who were sensitive. Results from the other trials listed have not yet been reported.

Based on clinical results obtained thus far, which clearly demonstrate the significant anti-tumor activity of Taxol in the treatment of metastatic breast cancer, a clinical trial incorporating Taxol into an adjuvant regimen for the post-operative management of high risk stage II–III resectable breast cancer is ongoing at Memorial Sloan-Kettering Cancer Center. Additionally, Taxol will be evaluated in the neoadjuvant setting for locally advanced stage III breast cancer at other centers. Finally, phase I trials evaluating Taxol with doxorubicin with the

hematopoietic support of G-CSF have been performed, and phase II trials of Taxol in combination with cisplatin and G-CSF are ongoing.

A phase II study has been conducted in metastatic melanoma patients who had not received prior chemotherapy [27]. Three complete and one partial response, with an overall response rate of 14%, were recorded in 34 treated patients. Two of the three complete responses have been durable. Legha et al. [28] reported a similar experience in metastatic melanoma, indicating that Taxol may be an active agent for a modest proportion of patients with malignant melanoma. No objective responses have been registered in patients with untreated renal cell carcinoma [21]. Taxol was found to be similarly inactive in colorectal cancer and cervical cancer.

### Combination trials

**Phase I.** The ability to develop effective combination regimens of Taxol with other active chemotherapeutic agents remains a challenge for this decade. The impetus for clinical studies aimed at assessing the efficacy of Taxol in combination with cisplatin derives largely from the evidence that Taxol has proven to be active in patients pre-treated with cisplatin, including cisplatin-resistant cases. Rowinsky et al. [38] have evaluated Taxol and cisplatin in sequence at the Johns Hopkins Oncology Center (Baltimore, USA) in minimally pre-treated patients with solid tumors. Despite the combined use of two potentially neurotoxic agents, mild to modest neurotoxicity occurred in only 27% of the 42 patients treated. Neutropenia was the main toxic side effect and was dose dependent. The use of cisplatin before Taxol caused a more profound neutropenia compared with the reverse sequence iteration. Interestingly, pharmacokinetic studies have demonstrated delayed Taxol clearance when administered *after* cisplatin. Objective responses were documented in melanoma, non-small-cell lung, ovarian, breast, head and neck, colon, and pancreatic carcinomas, suggesting that phase II/III studies with Taxol and cisplatin should be considered. Higher escalating dose protocols are to be considered only in conjunction with hematopoietic growth factors. A phase I trial of Taxol followed by cisplatin with G-CSF in patients with solid tumors found neuropathy to be dose limiting at 300 mg/m<sup>2</sup> of Taxol with 75 mg/m<sup>2</sup> cisplatin [39].

A phase I trial of the combination of doxorubicin and Taxol with the hematopoietic support of recombinant human G-CSF in patients without previous chemotherapy for metastatic breast cancer unexpectedly found stomatitis and neutropenia to be dose limiting at modest doses of both agents [40]. At a doxorubicin dose of 60 mg/m<sup>2</sup> (over 48 h on days 2 and 3) with Taxol at 125 mg/m<sup>2</sup> by 24-h continuous i.v. infusion on day 1, 4 patients experienced grade 3 stomatitis or neutropenia with infection, requiring dose reduction of doxorubicin to 48 mg/m<sup>2</sup>. In the reverse sequence iteration, the maximally tolerated doses of doxorubicin and Taxol were 60 mg/m<sup>2</sup> and 180 mg/m<sup>2</sup>, respectively; ongoing pharmacokinetic studies may explain the sequence-dependent

toxicity of these agents, similar to the cisplatin/Taxol combination (F. Holmes, personal communication). Another phase I trial designed to determine the maximally tolerated doses of Taxol and doxorubicin administered concurrently by 72-h continuous infusion with recombinant human G-CSF support found gastrointestinal toxicity (typhlitis) and leukopenia to be dose limiting at 75 mg/m<sup>2</sup> of doxorubicin and 180 mg/m<sup>2</sup> of Taxol [41, 42]. Further clinical and pharmacological studies may provide clues to the optimal dose, schedule, and sequence of these two agents.

Other phase I trials are presently evaluating various "doublet" combinations of Taxol, some with and some without growth factor support. Agents that are already in, or may soon be in, combination trials with Taxol include edatrexate (10-ethyl-deaza-aminopterin), carboplatin, ifosfamide, etoposide, topotecan, and cyclophosphamide [43], among others. In addition, the combination of Taxol plus cyclophosphamide plus cisplatin with G-CSF is presently under evaluation [44].

*Phase II–III.* Presently ongoing phase II/III trials involving Taxol in combination with other agents include those combining Taxol with cisplatin, carboplatin, or cyclophosphamide in ovarian cancer, with cisplatin in non-small-cell lung cancer and head and neck cancer, and with doxorubicin in metastatic breast cancer. A phase III study of the Gynecology Oncology Group randomizing previously untreated stage III–IV ovarian cancer patients to cyclophosphamide 750 mg/m<sup>2</sup> plus cisplatin 75 mg/m<sup>2</sup> or to Taxol 135 mg/m<sup>2</sup> 1 day prior to cisplatin 75 mg/m<sup>2</sup>, both recycled every 21 days for six cycles, has shown a higher response proportion and longer progression-free survival for the latter protocol [45]. A phase II trial assessing the feasibility of sequential doxorubicin, Taxol, and high-dose cyclophosphamide for breast cancer patients in the high-risk adjuvant setting is ongoing, based on promising prior experience at Memorial Sloan-Kettering Cancer Center [46].

## Toxicity

### *Allergic hypersensitivity reactions*

During the earlier trials of Taxol in the mid 1980s, infrequent episodes of hypotension, urticaria, wheezing, and dyspnea were noted. These often occurred within 2–3 min of the initiation of the infusion, and most were noted within the first 30–90 min after the infusion began. Based on the successful reduction in similar reactions related to iodinated contrast materials, the National Cancer Institute recommended prophylactic anti-allergic pre-medication with dexamethasone 20 mg i.v. or orally 14 and 7 h before Taxol treatment, and diphenhydramine 50 mg i.v. with cimetidine or ranitidine, 300 mg or 50 mg i.v. 30 min before Taxol. Weiss et al. [47] noted 16%, 13%, and 7% incidence rates of these apparent type I hypersensitivity reactions after 3-, 6-, and 24-h infusions of Taxol, respectively. The majority of 24-h infusions were administered after pre-medication with dexamethasone,

diphenhydramine, and cimetidine; thus, the relationship between infusion duration and the incidence of these reactions was unclear. More recent data from two large randomized trials suggest that there is no significant difference in the incidence of significant hypersensitivity reactions between 3- and 24-h Taxol infusions, when both are delivered with anti-allergic pre-medication [33, 34], with a low incidence observed with either 3- or 24-h schedules at 135 and 175 mg/m<sup>2</sup> dose levels.

The relative contribution of Taxol itself versus the Cremophor EL vehicle in the etiology of these reactions remains unclear. Similar histamine-mediated reactions related to Cremophor have been noted in dogs [13], and with other drugs solubilized in Cremophor and administered to humans (cyclosporine, teniposide, didemnin B, vitamin K) [48]. Despite the lack of a clear understanding of whether Taxol itself or Cremophor is causative in these reactions, due to the apparent lower incidence of these reactions observed with anti-allergic pre-medication, the aforementioned regimen has become standard before the administration of Taxol. Interestingly, with slower infusion rates of Taxol, allergic reactions are uncommon, and prophylactic anti-allergic pre-medication may be unnecessary [26]. The ability to retreat patients with Taxol after major hypersensitivity reactions has been shown [49], and may be at least in part related to a slower infusion rate.

### *Hematological toxicity*

Hematological toxicity due to myelosuppression consists mainly of neutropenia, which occurs in the great majority of patients and is the main dose-limiting factor. Pharmacokinetic studies have demonstrated a relationship between Taxol AUC (area under the time versus concentration curve) and the severity of leukopenia [50]. The severity of the neutropenia is also related to the extent of prior cytotoxic chemotherapy and to the extent of radiation in marrow-bearing sites. This may contribute to the occurrence of febrile neutropenic episodes, not infrequently encountered in Taxol-treated patients. In vitro studies have also shown that Taxol is capable of affecting the function of neutrophils by inhibiting both their locomotion and bacterial killing [51]. In contrast, anemia and thrombocytopenia are usually not as pronounced.

### *Neurotoxicity*

Taxol has been noted to cause a predominantly sensory peripheral neuropathy, most commonly characterized by numbness and paraesthesias in the feet and hands ("glove-and-stockings neuropathy") [52]. This phenomenon appears to be dose related, with a high incidence at doses in excess of 275 mg/m<sup>2</sup>, and a much lower incidence at doses below 170 mg/m<sup>2</sup>. Symptoms can occur within several days after Taxol, usually resolving within 5–7 days. Neurotoxicity can be cumulative and progressive, but usually resolves completely within several weeks to months after discontinuation of Taxol.

Neurological examination often initially reveals diminished deep tendon reflexes, with subsequent sensory deficits in distal extremities. Sensory abnormalities evaluated in symptomatic patients by electrophysiological testing show changes consistent with axonal degeneration and demyelination [52], findings similar to those observed in murine systems [53, 54]. One important issue relates to the possibility that the frequency and intensity of neurotoxicity following the administration of Taxol could be greater in patients who have been previously treated with cisplatin or with vinca alkaloids. Results thus far reported have, however, failed to conclusively document this. Early studies of Taxol in combination with cisplatin, that have included careful neurological monitoring, have shown a higher incidence of neurotoxic events than reported with either agent used singly [38].

### *Cardiac arrhythmias*

Taxol administration has been associated with a variety of cardiac rhythm disturbances, which have been well described in a prior review by Rowinsky et al. [55]. Cardiac toxicity led the National Cancer Institute to publish a letter in 1990 alerting investigators of this possible complication, particularly for patients receiving cisplatin and Taxol. This includes, most commonly, asymptomatic bradycardia, which has not precluded the use of Taxol. Other conduction abnormalities, including varying degrees of A-V nodal block and even transient asystole in 1 patient, have been observed. Additionally, ventricular ectopy and tachycardia have been noted during Taxol infusions in a phase I study of Taxol with cisplatin [38]. The broader experience with Taxol as a single agent when administered by 24-h infusion in many phase II trials would indicate that these events are particularly infrequent, although patient eligibility for these trials has generally excluded patients with a history of significant conduction abnormalities, arrhythmias, and those taking medication known to affect the cardiac conduction system (e.g.,  $\beta$ -blockers, digitalis).

### *Gastrointestinal effects*

Taxol-induced mucositis has been uncommon in clinical trials in patients with solid tumors, although it has been observed as a dose-limiting toxicity in a previous study in patients with leukemia [56], at doses in excess of those now commonly employed in clinical trials. Pathophysiological correlation has demonstrated Taxol-induced microtubular aster formation in damaged epithelial cells, suggesting mitotic arrest of proliferating mucosal cells [57]. Occasionally, esophagitis may be observed, in addition to oral mucosal ulceration. As previously mentioned, typhlitis (cecal inflammation) has been observed in a phase I trial combining Taxol and doxorubicin via simultaneous 72-h infusion [42].

Taxol administration is occasionally associated with nausea and vomiting, although these side effects are uncommon. Prophylactic anti-emetics are not routinely

administered due to the low incidence of nausea and vomiting. Diarrhea has also been reported.

### *Alopecia*

Reversible total/near-total hair loss is almost universally observed in Taxol-treated patients. Scalp hair loss usually begins within 2–4 weeks of the initial dose. Hair loss may include eyebrows and lashes, and also axillary, pubic, and extremity hair. Hair regrowth has been observed in several patients who continue to receive Taxol at doses of 150–180 mg/m<sup>2</sup> in a phase-II trial in metastatic breast cancer (A. D. Seidman, unpublished data).

### *Other side effects*

Fatigue and malaise have been reported, particularly in patients who have had extensive prior therapy and in whom these symptoms can be rather pronounced. Myalgias and arthralgias have been noted and are usually successfully managed with non-narcotic analgesics, such as acetaminophen or non-steroidal anti-inflammatory agents. Additionally, headache, taste alterations, and atypical chest pain have been reported, as have minor elevations in liver and renal function tests. The contribution of Cremophor to any of these side effects is unclear.

### *i.p. Taxol*

Apart from its activity in advanced and platinum-resistant ovarian cancer when administered systemically, Taxol's large structure and physicochemical characteristics make it an ideal candidate for i.p. delivery. A phase I investigation performed by Markman et al. [58] evaluated the i.p. administration of Taxol in heavily pre-treated patients. At doses in excess of 125 mg/m<sup>2</sup> administered every 3–4 weeks, severe abdominal pain became dose limiting [58]. Pharmacokinetic studies demonstrated a high ratio of i.p. systemic exposure (AUC), with i.p. Taxol concentrations in the range previously shown to be necessary for in vitro activity. Preliminary phase I and pharmacological data suggest an advantage for weekly i.p. administration [59].

### *Taxotere (docetaxel)*

In an effort to procure a readily available source of Taxol or a related active analog, a collaboration between the French Centre National de la Recherche Scientifique and Rhone-Poulenc Rorer has led to the development of Taxotere (docetaxel). Taxotere is a semi-synthetic analog of Taxol derived from a common precursor molecule (baccatin III) extracted from the needles of the European yew, *Taxus baccata*. Since this process is not dependent upon bark, trees can therefore be harvested without being destroyed, and thus a renewable and readily available source for this compound is possible.

**Table 4.** Phase II trials of taxotere (docetaxel): preliminary results

Tumor type	Center	No. of patients evaluated	Prior Rx.	RR (95% CI)
Ovary	EORTC (CSG)	34	+	35% (20–54)
	MDACC	20	+	35% (15–59)
Breast	MSKCC <sup>a</sup>	29	–	76% (57–90)
	ECTC	24	+	54% (33–74)
	EORTC (CSG)	32	–	72% (53–86)
	NCIC CTG <sup>a</sup>	34	–	65% (47–80)
	MDACC	6	–	67% (22–96)
NSCLC	EORTC (ECTG)	24	–	33% (16–55)
	UT-S.A.	29	±	21% (8–40)
	MSKCC	18	–	28% (10–54)

<sup>a</sup> Updated from Proc Am Soc Clin Oncol 12:63, 1993

EORTC (CSG), European Organization for Research and Treatment of Cancer (Clinical Screening Group); ECTG, Early Clinical Trials Group; NCIC CTG, National Cancer Institute of Canada Clinical Trials Group; RR, remission rate; Rx, Radiotherapy; CI, confidence interval

In vitro, Taxotere inhibits microtubule disassembly, as does Taxol, and may be more active than Taxol as a promoter of tubulin polymerization in pre-clinical systems [60]. This agent was found to have anti-neoplastic activity against a variety of transplantable murine solid tumors, including pancreatic ductal adenocarcinoma P03, colon adenocarcinoma C38 and 51, and the B16 melanoma [61]. The EORTC CASSG group recently reported superior activity of Taxotere over Taxol in head and neck cancer, sarcoma, ovarian, colon, and breast cancer cell lines [62]. Phase I and pharmacokinetic studies have been performed in man, utilizing various dose schedules. The dose of Taxotere chosen for broad phase II testing was 100 mg/m<sup>2</sup> delivered i.v. over 1 h.

Phase II trials in various malignancies have been recently initiated in the United States and Europe. Anti-tumor activity in phase II clinical trials has thus far been reported in breast, ovarian, and non-small-cell lung cancer (Table 4). Similar to Taxol, neutropenia has been the predominant dose-limiting toxicity in these trials. A more unique toxicity characterized by edema, fluid retention, and the development of pleural effusions, suggestive of a capillary-leak syndrome, has been reported in most of these initial trials, and appears to be related to the cumulative dose received. Further clinical investigation will be necessary to determine ways of circumventing this phenomenon.

### Conclusions and perspectives

The results thus far obtained have clearly shown that Taxol displays in many tumors a marked anti-neoplastic activity that makes this novel anti-microtubule agent the most interesting new drug in the management of patients with cancer. As mentioned earlier, the effectiveness of Taxol is well documented in ovarian and breast cancer, and significant activity has also been observed in non-small-cell lung cancer and head and neck tumors. Fortunately, the increased availability of the compound has

permitted the recent expansion of clinical trials to a broad spectrum of malignancies, and has allowed the performance of larger randomized trials.

Future studies will be directed at clarifying some areas of uncertainty. Optimal doses and schedules of administration (i.e., infusion duration) are questions being addressed in current ongoing clinical trials. As previously noted, the primary limiting factor has been neutropenia, which, although usually short lived, may give rise to infectious complications, particularly in heavily pre-treated patients. Along these lines, the impact of hemopoietic growth factors given with higher doses of Taxol and with combinations should be better appreciated. Evaluation of Taxol in combination regimes for various malignancies, with attention to sequence-dependent differences in toxicity, activity, and pharmacokinetics, will enable optimal combination regimens to be developed. Ongoing trials in other solid and hematological malignancies should better define the full spectrum of Taxol's anti-tumor activity. Drug supply remains a concern, although less so with the further development of potential alternative sources of Taxol. Current clinical development of Taxotere and investigation with other newer taxane analogues may yield other clinically useful compounds.

Taxol represents the first of a new class of chemotherapeutic agents with a unique and novel mechanism of anti-neoplastic action. The optimal integration of this unique and promising agent into the treatment of a variety of human malignancies is certain to be a focus of active investigation for years to come.

**Acknowledgements.** R.F. was partly supported during his stay at Memorial Sloan-Kettering Cancer Center by the "American-Italian Foundation for Cancer Research", New York. A.D.S. is the recipient of a Career Development Award from the American Society of Clinical Oncology.

### References

1. Wani MC, Taylor HL, Wall ME, et al, Plant antitumor agents. VI. The isolation and structure of Taxol, a novel antileukemic and antitumor agent from *Taxus brevifolia*. *J Am Chem Soc* 93:2325, 1991
2. Rowinsky EK, Cavenave LA, Donehower RC, Taxol: a novel investigational antimicrotubule agent. *J Natl Cancer Inst* 82:1247, 1990
3. Schiff PB, Fant J, Horwitz SB, Promotion of microtubule assembly in vitro by Taxol. *Nature* 277:665, 1979
4. Kumar N, Taxol-induced polymerization of purified tubulin. Mechanism of action. *J Biol Chem* 256:10435, 1981
5. Manfredi JJ, Horwitz SB, Taxol: an antimetabolic agent with a new mechanism of action. *Pharmacol Ther* 25:83, 1984
6. Rao S, Horwitz SB, Ringel I, Direct photoaffinity labeling of tubulin with Taxol. *J Natl Cancer Inst* 84:785, 1992
7. Parness J, Horwitz SB, Taxol binds to polymerized tubulin in vitro. *J Cell Biol* 91:479, 1981
8. Dustin P, Microtubules. *Sci Am* 243:66, 1980
9. Roberts JR, Rowinsky EK, Donehower RC, et al, Demonstration of the cell cycle positions for Taxol-induced "asters" and "bundles" by sequential measurements of tubulin immunofluorescence, DNA content, and autoradiographic labeling of Taxol-sensitive and resistant cells. *J Histochem Cytochem* 37:1659, 1989
10. Taxol clinical brochure. National Cancer Institute, Bethesda, 1983

11. Choy H, Rodriguez FF, Koester S, et al, Investigation of Taxol as a potential radiation sensitizer. *Cancer* 71:3774, 1993
12. Investigational Drug Branch, National Cancer Institute, Taxol (NSC 125973) clinical brochure. National Cancer Institute, Bethesda, 1990
13. Lorenz W, Reimann HJ, Schmal A, et al, Histamine release in dogs by Cremophor EL and its derivatives: oxyethylated oleic acid is the most effective constituent. *Agents Actions* 7: 63, 1977
14. Roth B, Yeap B, Wilding G, et al, Taxol (NSC 125973) in advanced, hormone-refractory prostate cancer: an ECOG phase II trial. *Proc Am Soc Clin Oncol* 11: 196, 1992
15. Sarosy G, Kohn E, Stone DA, et al, Phase I study of Taxol and granulocyte colony-stimulating factor in patients with refractory ovarian cancer. *J Clin Oncol* 10: 1165, 1992
16. Levin L, Hryniuk W, The application of dose intensity to problems in chemotherapy of ovarian and endometrial cancer. *Semin Oncol* 5: 756, 1987
17. McGuire WP, Rowinsky EK, Rosenheim NB, et al, Taxol: a unique antineoplastic agent with significant antitumor activity in advanced ovarian epithelial neoplasms. *Ann Intern Med* 111: 273, 1989
18. Einzig AI, Wiernik P, Sasloff J, et al, Phase II study and long-term follow-up of patients treated with Taxol for advanced ovarian adenocarcinoma. *J Clin Oncol* 10: 1748, 1992
19. Thippen T, Blessing J, Ball H, et al, Phase II trial of Taxol as second-line therapy for ovarian carcinoma: a Gynecologic Oncology Group study. *Proc Am Soc Clin Oncol* 9: 604, 1990
20. Sarosy G, Kohn E, Link C, et al, Taxol dose intensification in patients with recurrent ovarian cancer. *Proc Am Soc Clin Oncol* 11: 226, 1992
21. Einzig AI, Gorowski E, Sasloff J, et al, Phase II trial of Taxol in patients with metastatic renal cell carcinoma. *Cancer Invest* 9: 133, 1991
22. Holmes FA, Frye D, Theriault RS, et al, Phase II trial of Taxol, an active drug in the treatment of metastatic breast cancer. *J Natl Cancer Inst* 83: 1797, 1991
23. Reichman BS, Seidman AD, Crown JPA, et al, Taxol and recombinant granulocyte colony stimulating factor as initial chemotherapy for metastatic breast cancer. *J Clin Oncol* (in press)
24. Einzig AL, Wiernik PH, Lipsitz S, et al, Phase II trial of Taxol in patients with adenocarcinoma of the upper gastrointestinal tract (UGIT). *Proc Am Soc Clin Oncol* 12: 194, 1993
25. Forastiere AA, Neuberg D, Taylor IV SG, et al, Phase II evaluation of Taxol in advanced head and neck cancer: an Eastern Cooperative Oncology Group trial. *Proc Am Soc Clin Oncol* 12: 277, 1993
26. Wilson WH, Berg S, Kang Y-K, et al, Phase I/II study of taxol 96-hour infusion in refractory lymphoma and breast cancer: pharmacodynamics and analysis of multidrug resistance (mdr-1). *Proc Am Soc Clin Oncol* 12: 134, 1993
27. Einzig AI, Hochster HH, Wiernik PH, et al, Phase II trial of Taxol in patients with metastatic melanoma. *Invest New Drugs* 9: 54, 1991
28. Legha SS, Ring S, Papadopoulos N, A phase II trial of Taxol in metastatic melanoma. *Cancer* 65: 2478, 1990
29. Chang AY, Kim K, Glick J, et al, Phase II study of Taxol, Merbarone, and Piroxantrone in stage IV non-small-cell lung cancer: the Eastern Cooperative Oncology Group results. *J Natl Cancer Inst* 85: 388, 1993
30. Murphy WK, Fossella FV, Winn RJ, et al, Phase II study of Taxol in patients with untreated advanced non-small-cell lung cancer. *J Natl Cancer Inst* 85: 384, 1993
31. Brown T, Tangen C, Fleming T, et al, A phase II trial of Taxol and granulocyte colony stimulating factor (G-CSF) in patients with adenocarcinoma of the pancreas. *Proc Am Soc Clin Oncol* 12: 200, 1993
32. Ettinger DS, Finkelstein DM, Sarma R, et al, Phase II study of Taxol in patients with extensive-stage small cell lung cancer (SCLC): an Eastern Cooperative Oncology Group Study. *Proc Am Soc Clin Oncol* 12: 1095, 1993
33. Swenerton K, Eisenhauer E, Bokkel Huinink W ten, et al, Taxol in relapsed ovarian cancer: high vs low dose and short vs long infusion. *Proc Am Soc Clin Oncol* 12: 256, 1993
34. Nabholz JM, Gelmon K, Bontenbal M, et al, Randomized trial of two doses of Taxol in metastatic breast cancer: an interim analysis. *Proc Am Soc Clin Oncol* 12: 60, 1993
35. Seidman AD, Crown JPA, Reichman BS, et al, Lack of clinical cross-resistance of Taxol with anthracycline in the treatment of metastatic breast cancer. *Proc Am Soc Clin Oncol* 12: 63, 1993
36. Seidman AD, McCarthy J, Anthony V, et al, Pain and quality of life assessment in patients receiving Taxol and recombinant human granulocyte colony stimulating factor for metastatic breast cancer. *Proceedings of the 2nd National Cancer Institute Workshop on Taxol and Taxus* September 23-24, 1992
37. Holmes FA, Valero V, Theriault RL, et al, Phase II trial of Taxol in metastatic breast cancer refractory to multiple prior treatments. *Proc Am Soc Clin Oncol* 12: 94, 1993
38. Rowinsky EK, Gilbert MR, McGuire WP, et al, Sequences of Taxol and cisplatin: a phase I and pharmacologic study. *J Clin Oncol* 9: 1692, 1991
39. Forastiere AA, Rowinsky E, Chaudry V, et al, Phase I trial of Taxol (T) and cisplatin (C) + G-CSF in solid tumors. *Proc Am Soc Clin Oncol* 289: 1992
40. Holmes FA, Frye D, Valero V, et al, Phase I study of Taxol (T) and doxorubicin (D) with G-CSF in patients without prior chemotherapy (CT) for metastatic breast cancer (MBC). *Proc Am Soc Clin Oncol* 11: 60, 1992
41. Fisherman J, McCabe M, Hillig M, et al, Phase I study of Taxol and doxorubicin (DOX) with G-CSF in previously untreated metastatic breast cancer (MBC). *Proc Am Soc Clin Oncol* 11: 57, 1992
42. Pestalozzi BC, Sotos GA, Choyke PL, et al, Typhlitis resulting from treatment with Taxol and doxorubicin in patients with metastatic breast cancer. *Cancer* 71: 1797, 1993
43. Kennedy MJ, Donehower RC, Sartorius SE, et al, Sequences of Taxol and cyclophosphamide: a phase I and pharmacologic study in doxorubicin resistant metastatic breast cancer. *Proc Am Soc Clin Oncol* 12: 165, 1993
44. Kohn E, Reed E, Link C, et al, A pilot study of Taxol, cisplatin, cyclophosphamide, and G-CSF in newly diagnosed stage III/IV ovarian cancer patients. *Proc Am Soc Clin Oncol* 12: 257, 1993
45. McGuire WP, Hoskins WJ, Brady MF, et al, A phase III trial comparing cisplatin/cytosine (PC) and cisplatin/taxol (PT) in advanced ovarian cancer (AOC). *Proc Am Soc Clin Oncol* 12: 255, 1993
46. Hudis C, Lebwahl D, Crown J, et al, Feasibility of dose-intensive cyclophosphamide with G-CSF after doxorubicin in women with high risk stage II/III resectable breast cancer. *Proc Am Soc Clin Oncol* 11: 55, 1992
47. Weiss R, Donehower RC, Cates AE, et al, Hypersensitivity reactions from Taxol. *J Clin Oncol* 8: 1263, 1990
48. National Cancer Institute Clinical Brochure: Taxol (NSC 125973). Division of Cancer Treatment, National Cancer Institute, Bethesda, 1991
49. Peereboom DM, Donehower RC, Eisenhauer A, et al, Successful re-treatment with Taxol after major hypersensitivity reactions. *J Clin Oncol* 11: 885, 1993
50. Brown T, Havlin K, Weiss G, Cagnola J, Koeller J, Kuhn J, Rizzo J, Craig J, Phillips J, Von-Hoff D, A phase I trial of Taxol given by a 6-hour intravenous infusion. *J Clin Oncol* 9: 1261, 1991
51. Roberts RL, Nath J, Friedman MM, Gallin JI, Effects of Taxol on human neutrophils. *J Immunol* 129: 2134, 1982
52. Lipton RB, Apfel SC, Dutcher JP, et al, Taxol produces a predominantly sensory neuropathy. *Neurology* 39: 368, 1989
53. Masurovsky EB, Peterson ER, Crain SM, et al, Morphological alterations in dorsal root ganglion neurons and supporting cells of organotypic mouse spinal cord-ganglion cultures exposed to Taxol. *Neuroscience* 10: 491, 1983
54. Letourneau PC, Shattuck TA, Ressler AH, et al, Branching of sensory and sympathetic neurites in vitro is inhibited by treatment with Taxol. *J Neurosci* 6: 1912, 1986



55. Rowinsky EK, McGuire WP, Guarnieri T, et al, Cardiac disturbances during the administration of Taxol. *J Clin Oncol* 9:1704, 1991
56. Rowinsky EK, Burke PJ, Karp JE, et al, Phase I and pharmacodynamic study of Taxol in refractory acute leukemias. *Cancer Res* 49:4640, 1989
57. Hruban RH, Yardley JH, Donehower RC, et al, Taxol toxicity: epithelial necrosis in the gastrointestinal tract associated with polymerized microtubule accumulation and mitotic arrest. *Cancer* 63:1944, 1989
58. Markman MM, Rowinsky E, Hakes T, et al, Phase I trial of intraperitoneal Taxol: a Gynecologic Oncology Group study. *J Clin Oncol* 9:1485, 1992
59. Francis P, Rowinsky E, Hakes T, et al, Phase I trial of weekly intraperitoneal (IP) Taxol in patients with residual ovarian carcinoma. *Proc Am Soc Clin Oncol* 12:257, 1993
60. Ringel I, Horwitz SB, Studies with RP 56976 (Taxotere): a semi-synthetic analogue of Taxol. *J Natl Cancer Inst* 83:288, 1991
61. Bissery M-C, Guenard D, Gueritte-Voegelein F, Lavelle F, Experimental antitumor activity of Taxotere (RP 56976, NSC 628503), a Taxol analogue. *Cancer Res* 51:4845, 1991
62. Aapro M, Braakhuis B, Dietel M, et al, Superior activity of Taxotere (Ter) over Taxol (Tol) in vitro. *Proc Am Assoc Cancer Res* 33:516, 1992



## Properties of Anticancer Agents Relevant to *in vitro* Determinations of Human Tumor Cell Sensitivity

Edward J. Pavlik<sup>1,2</sup>, Daniel E. Kenady<sup>3</sup>, John R. van Nagell<sup>1</sup>, Kathryn Keaton<sup>3</sup>, Michael B. Hanson<sup>1</sup>, Elvis S. Donaldson<sup>1</sup>, Ward O. Griffen<sup>3</sup>, and Robert C. Flanigan<sup>4</sup>

<sup>1</sup> The Lexington Veterans' Administration Hospital and Departments of Obstetrics and Gynecology

<sup>2</sup> Biochemistry

<sup>3</sup> Surgery

<sup>4</sup> Urology, University of Kentucky College of Medicine, Lexington, Kentucky 40536, USA

**Summary.** The physical properties of 59 anticancer agents have been examined with respect to solubility in tissue culture media, binding to ultrafiltration materials, and molecular absorbance and fluorescence behavior. Methods for dissolving these agents, which are compatible with *in vitro* sensitivity testing of human tumor cells to anticancer agents, are reported in this paper. The potential for anticancer agent binding to cellulose nitrate/cellulose acetate and teflon membrane ultrafilters was documented, and quantitation of these anticancer agents based upon absorbance and fluorescence spectroscopy was performed. Post-filtration quantitation of anticancer agents was found to be a reliable method for determining the actual drug concentrations available in tumor cell sensitivity testing *in vitro*. The properties documented herein are pharmacologically relevant parameters related to *in vitro* determinations of human tumor cell sensitivity to anticancer agents.

### Introduction

Recently, a fundamental new approach in cancer treatment has resulted from the realization that chemotherapy can be individualized on the basis of determinations which assess the sensitivity in cell culture of tumor cells, prepared from individual cancer patients, to various anticancer agents [5, 6, 8–10, 13]. At present, this type of approach has been more successful in identifying those chemotherapeutic agents which will be ineffective in the patient than in predicting those anticancer agents that will be effective *in vivo*. Specifically, this method has been reported to identify drug resistance with a predictive accuracy of 96%–99% and drug sensitivity with a predictive accuracy of 60%–70% [11, 13].

It should be obvious that a drug must be in solution when presented to tumor cells in the test determination; moreover, the means used to achieve drug solvation must not interfere with tumor cell replication. If a drug is not in solution, its precipitation presents a potential mechanism for concentrating drug onto tumor cells, which can lead to false-positive indications of tumor cell sensitivity. Conversely, if drug is allowed to precipitate at some stage prior to introduction to the test determination, the available drug concentration in the test will be much lower than expected and false resistance may be predicted. Often it is necessary to use membrane filtration to remove potential biocontaminants from drug solutions prepared for test determinations. Drug interaction with filtration

materials has the potential for moderating the apparent cytotoxic drug activity by reducing the effective drug concentration.

At present there is no comprehensive source of information on anticancer agent solubility in tissue culture media or on drug interaction with filtration materials, although significant information does exist on the clinical formulation of anticancer agents [4, 12]. Moreover, it is conceptually advantageous to operate within a uniform test background so that only drug-related effects are compared, from test to test, rather than some complex permutation of drug together with buffer, extender, preservative, carrier, solvent, etc.

For these reasons, we report here on the compatibility of anticancer drug solvation with the tissue culture environment and document the potential for solvent-mediated effects, as well as anticancer agent binding to filtration materials.

### Materials and Methods

All determinations on chemotherapeutic agents were performed on pure compounds in the absence of preservatives, stabilizers or extenders. Actinomycin D, bleomycin, cyclophosphamide, progesterone, retinoic acid, and retinol were obtained from Sigma Chemical, St. Louis, USA. *cis*-Diamminedichloroplatinum II, *cis*-dichloro-ethylenediamineplatinum, cordycepin, 5-fluorouracil, and mitomycin C were obtained from Boehringer Mannheim, Indianapolis, Indiana, USA. Doxorubicin was generously provided by Adria Laboratories, Columbus, OH, USA; an alternative batch was obtained from Aldrich Chemical Company, Milwaukee, Wisc., USA. Methotrexate and Thio-TEPA were provided by Lederle Laboratories, Pearl River, NY, USA. Bisanthrene hydrochloride ('Orange Crush' or 9,10-antracenedicarboxaldehyde bis-[(4,5-dihydro-1H-imidazol-1-yl) hydrazone] was provided by American Cyanamid, Pearl River, NY, USA. Cytarabine, medroxyprogesterone acetate, and streptozocin were provided by the Upjohn Company, Kalamazoo, MI, USA. Etoposide ('Vp 16–213'), *cis*-platinum, and prednimustine were generously supplied by Bristol Laboratories, Syracuse, NY, USA. Finally, the Investigational Drug Branch of the National Cancer Institute provided the following: aclacinomycin, amasacrine, anguidine, azapicyl, aziridinylbenzoquinone ('AZQ'), Baker's antifol, bruceatin, camptothecin, carboquone, chlorozotocin, cyclocytidine, daunorubicin, dibromodulcitol, dichloroally lawsone, dichloromethotrexate, dihydroxyanthracenedione, etoposide, gallium nitrate, hexa-



Aclacinomycin  
(<sup>14</sup>C)

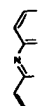
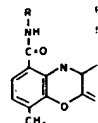


Fig. 1

meth-  
ide, l-  
melp-  
foxid-  
lone,  
rafur

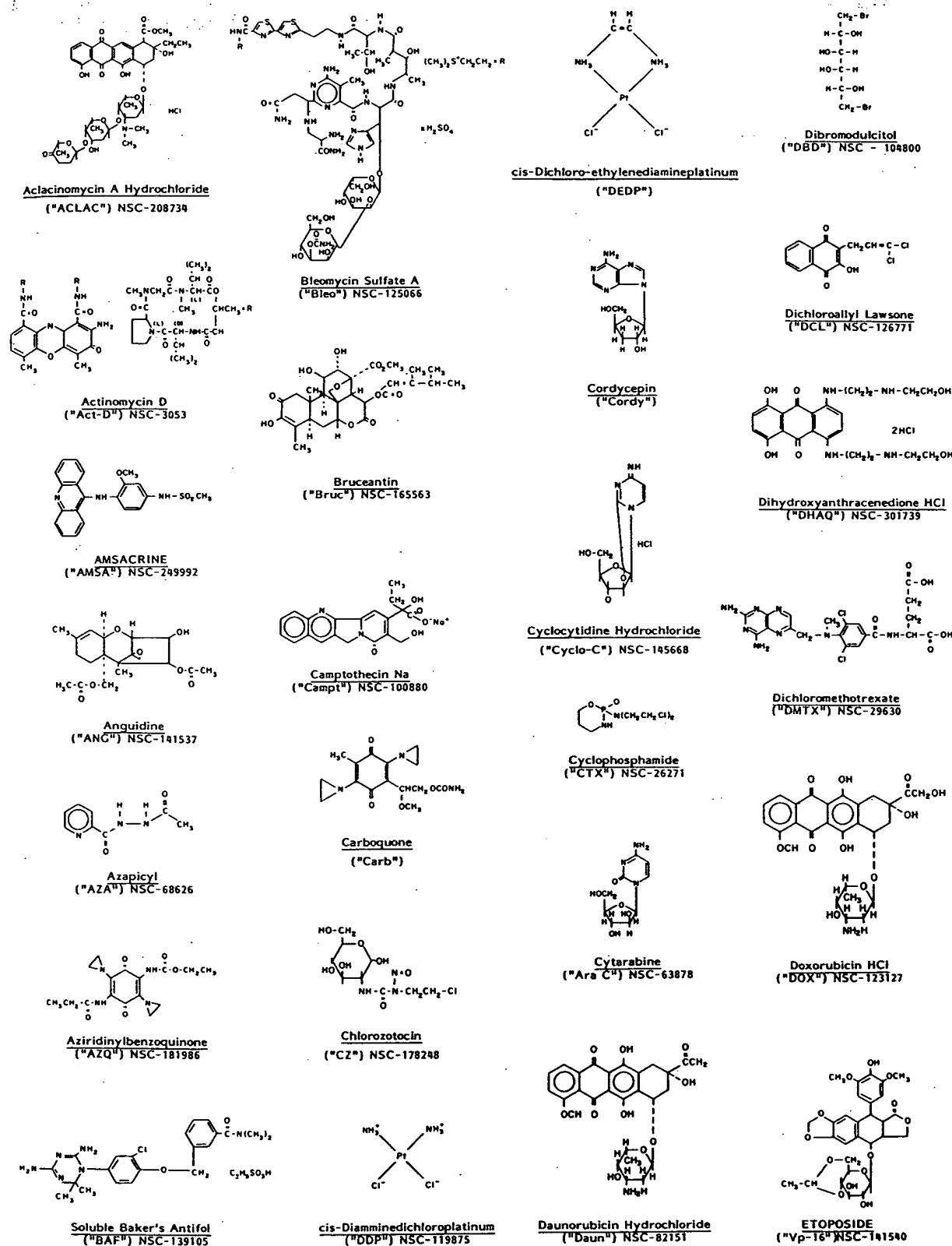


Fig. 1: Chemical structures, National Service Center Identifiers, and abbreviated designations of selected anticancer agents

methylmelamine, ICRF-159 (Razoxane), ICRF-187, ifosfamide, leucovorin, levamisole, lomustine (CCNU), maytansine, melphalan, 5-methyltetrahydrohomofolate, mitoguazone, nafoxidine, PALA, PCNU, pentamethylmelamine, prednisolone, semustine (methyl-CCNU), streptonigrin, tegafur (Ftorafur), and teniposide ("VM-26"). Drugs dissolved in water

were used in absorbance and filter-binding determinations, while drugs dissolved in saline were used in fluorescence determinations. A DU-8 spectrophotometer (Beckman Instruments) was used for absorbance determinations, while an Aminco Bowman Spectrophotofluorometer fitted with a high-intensity Xenon lamp was used in fluorescence determi-

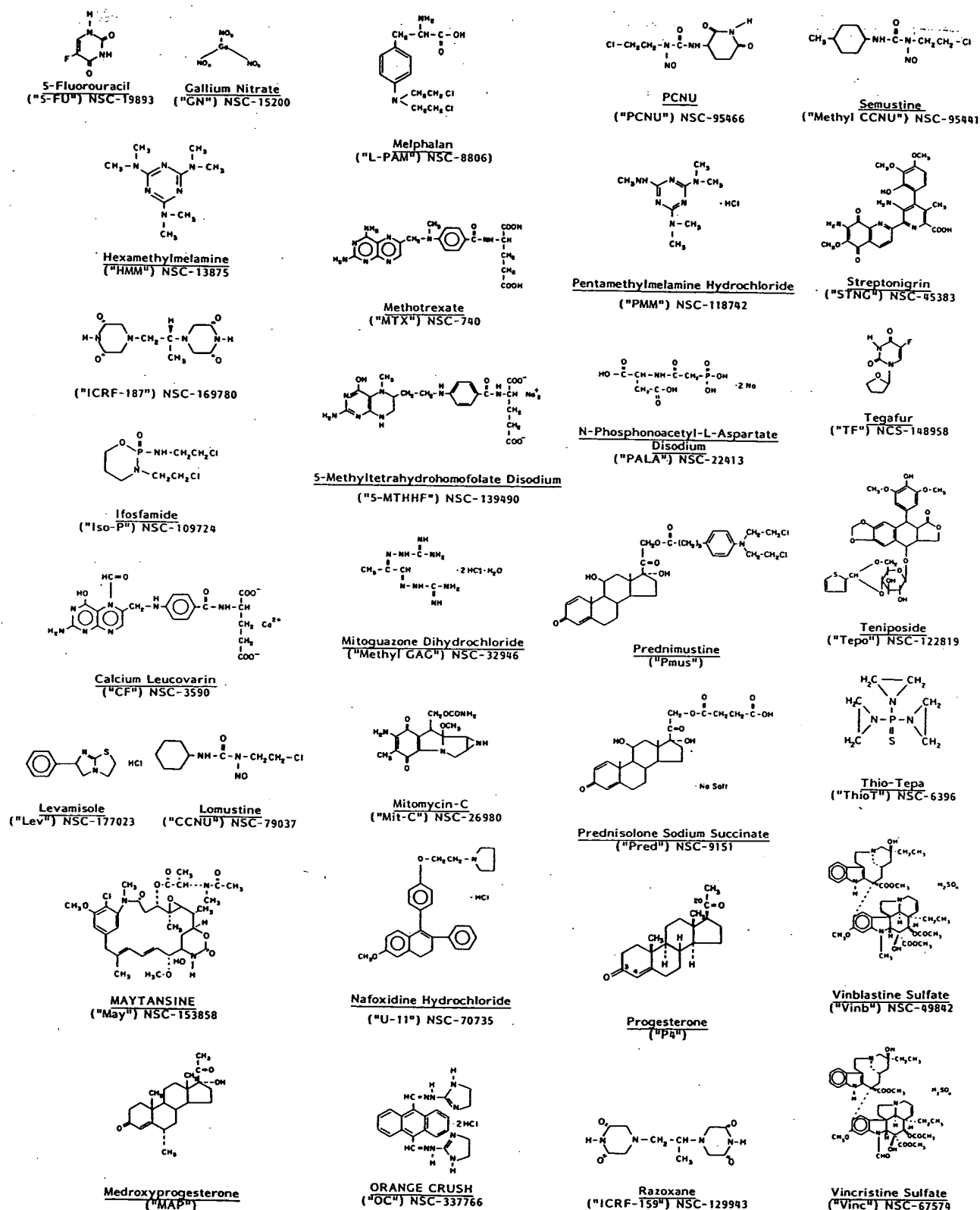


Fig. 1. (continued)

nations. Scans were performed over the range 200–800 nm. Fluorescence determinations were performed in quartz cuvettes (2 ml) with drug fluorescence determined before and after incubation with tumor cells (American Type Culture Collection Cell Line CCL2; 1 h, 37° C). Drugs were dissolved at 1 mg/ml and progressive dilutions were made to identify

concentration ranges which remained linear with respect to absorbance or fluorescence. At least eight different concentrations were examined in duplicate over the linear range, and these concentrations were quantitatively reexamined after filtration in 1-ml volumes. Sterile disposable filtration units (27 mm diameter) were used: Millex-OR, 0.22  $\mu$ m pore and

Millex-  
USA.  
An  
study,  
Center  
nations

Results  
Chemical  
are Pro  
of Anti

Agents

Two p  
determ  
that (1  
and (2)  
variabl  
covaria  
preser  
cludes  
rarely

Table

Agent

Aclaci  
Actinc  
Angui  
Azapi  
(Solut  
Bleorr  
Camp  
Chlor  
cis-DI  
cis-pl  
Cyclo  
Cyclo  
Cytar  
Daun  
Dihyc  
Doxo  
5-Flu  
Galli  
ICRF  
Ifosfa  
Leuco  
Leva  
Mayt  
5-Me  
Mito  
Mito  
"Ora  
PAL  
Pent  
Strej  
Tega  
Thio  
Vint  
Vinc  
\* TI

Millex-FG, 0.2  $\mu$ m pore (Millepore Corp., Bedford, Mass, USA).

An alphabetic listing of the compounds considered in this study, together with the corresponding National Service Center numbers, chemical structures and abbreviated designations is presented in Fig. 1.

## Results

### *Chemical Solubilities and Filter Binding Characteristics are Properties that can Moderate the Activity of Anticancer Agents in vitro*

#### *Agents with Aqueous Solubilities*

Two prerequisites which must be accommodated by test determinations for in vitro sensitivity to anticancer agents are that (1) agents remain soluble in the cell culture environment and (2) a uniform test background is employed so that the only variable from test to test is drug alone, rather than some covariant combination of drug together with buffer, extender, preservative, carrier, and solvent. The latter condition precludes the use of sterile pharmaceutical preparations, which rarely contain drug alone; moreover, most investigational

drugs are more prudently evaluated by methods that can be dissociated from a preliminary formulation which may not ultimately be clinically optimal. As a consequence, it becomes necessary to remove potential biocontaminations from dissolved anticancer preparations by membrane ultrafiltration.

A large number of anticancer agents are water-soluble and hence soluble in tissue culture media (Dulbecco's MEM, RPMI (1640), McCoy's and CMRL) as identified in Table 1. Vinblastine sulfate differs somewhat from the other agents in Table 1 in that its solubility in tissue culture media requires slight acidification with dilute HCl. We have adopted two criteria for effective solubility in tissue culture media: first, no visible precipitate should form after incubation at 37° C for up to 5 h and second, the spectral profiles, which are unique to each agent, should also persist after incubation. All the agents in Table 1 meet both these criteria, except for anguidine and cyclophosphamide which, while not demonstrating any absorbance properties, did not form visible precipitates at concentrations of up to 500  $\mu$ g/ml.

The agents in Table 1 have been dissolved in a working stock solution of up to 1 mg/ml. Dilutions of the working stock solution are made and used for in vitro determinations of tumor cell sensitivity to anticancer agents. As a consequence, the working stock solutions for all the agents in Table 1 could be diluted and quantitated by absorbance spectroscopy, except

Table 1. Properties of selected water-soluble anticancer agents

Agent	Molecular weight	Absorbance maxima (nm)*	Linear absorbance range: $\mu$ g/ml	Millex OR binding	Millex FG binding
Aclacinomycin	884.4	203, <u>228</u> , 258, <u>435</u>	10–100	—	—
Actinomycin-D	1255.5	211, <u>241</u> , 318, <u>440</u>	4–50	> 95%	50%–60%
Anguidine	366	no absorbance	—	—	—
Azapicyl	179.17	<u>236</u> , 275	10–100	< 5%	—
(Soluble) Baker's antifol	539	<u>245</u>	10–100	—	—
Bleomycin	1400	<u>249</u>	10–300	—	—
Camptothecin	388.4	<u>217</u> , <u>252</u> , <u>294</u> , 367	10–200	< 5%	—
Chlorozotocin	313.7	<u>231</u> , <u>248</u> , <u>387</u>	10–300	5%–10%	—
cis-DED-platinum	326.1	<u>224</u> , <u>292</u>	75–300	—	—
cis-platinum	300.0	<u>223</u> , <u>301</u> , 356, 362	10–300	—	—
Cyclocytidine	261.5	<u>244</u>	10–100	—	—
Cyclophosphamide	261.1	no absorbance	—	—	—
Cytarabine	243.22	<u>241</u>	10–100	—	—
Daunorubicin	564	239, <u>251</u> , <u>289</u> , <u>481</u>	10–100	5%–10%	10%–15%
Dihydroxyanthracenedione	517.4	<u>241</u> , <u>275</u> , <u>319</u> , <u>608</u> , <u>661</u>	10–200	50%–60%	10%–20%
Doxorubicin	579.99	<u>233</u> , <u>252</u> , <u>299</u> , <u>453</u> , <u>494</u>	1–30	> 95%	30%–50%
5-Fluorouracil	130.1	<u>244</u>	10–75	< 5%	—
Gallium nitrate	256	<u>229</u>	25–300	—	—
ICRF-187	268	<u>229</u> , 319	10–300	~ 20%	—
Ifosfamide	261	<u>203</u> , 285	Nonlinear to 300 $\mu$ g/ml	—	—
Leucovorin	483	<u>242</u> , 313, 325	10–300	5%–10%	—
Levamisole	241	<u>243</u>	10–100	15%	10%–20%
Maytansine	692	<u>210</u> , <u>232</u> , <u>252</u> , 279, 296	0.5–5	50%–70%	60%–90%
5-Methyltetrahydro-homofolate	517.5	<u>244</u> , 313, 335	10–300	15%–20%	—
Mitoguazone dihydrochloride	275	<u>243</u> , <u>262</u> , 313, 337	10–300	—	—
Mitomycin C	334	<u>225</u> , <u>373</u> , 554	10–75	< 5%	—
"Orange crush"	471.4	<u>236</u> , <u>246</u> , <u>255</u> , 273, <u>408</u>	10–100	—	—
PALA	299	<u>216</u>	10–300	—	—
Pentamethylmelamine	232.7	<u>244</u> , <u>249</u> , <u>256</u>	10–75	—	—
Streptozocin	265	<u>242</u> , 390	10–200	—	—
Tegafur	200	<u>244</u>	10–300	5%–10%	—
ThioTEPA	189	<u>217</u>	10–300	—	—
Vinblastine	909.1	<u>230</u> , <u>247</u> , <u>251</u> , 313, <u>323</u>	10–300	—	—
Vincristine	923.1	<u>243</u> , 313	10–200	10%–15%	10%–15%

\* The major absorbance wavelengths are underlined; the concentration curves were determined at the major absorbance wavelength

for the two nonabsorbing agents and ifosfamide. Quantitation by absorbance spectroscopy was used to determine drug concentration before and after membrane filtration, to determine whether any agents would bind to the filtration materials. Assessments of filter binding were run at five different drug concentrations over the linear absorbance range. All agents were evaluated for binding to both the cellulose nitrate/cellulose acetate-based Millex OR filters and the teflon-based Millex FG filters. Drug binding estimates were related to the highest linear concentration tested when post-filtration determinations remained linear with a reduced slope. When post-filtration determinations become asymptotically nonlinear, drug binding estimates related the asymptotic extrapolated value to the highest linear concentration tested. Drug binding to the cellulose nitrate/cellulose acetate filters was very significant with actinomycin D, dihydroxyanthracenedione, doxorubicin and maytansine, while some binding occurred with chlorozotocin, daunorubicin, ICRF-187, leucovorin, levamisole, 5-methyltetrahydro-homofolate, tegafur, and vincristine. In general, binding to the teflon-based filters was equivalent to or less than binding to the cellulose nitrate/cellulose acetate filters; however, maytansine was observed to be bound significantly better by the teflon filters (Table 1). Orange Crush (i.e., OC or bisantrene) presents a solubility problem because the introduction of this agent (dissolved in distilled water) into several media (DME, RPMI, McCoy's, CMRL) and buffers (saline, buffered saline, HBSS) results in immediate precipitation. Spectrophotometric determinations revealed that subsequent filtration clears virtually all the bisantrene from the preparation.

A limited number of agents can be solubilized as salts generated with NaOH (20 mM) (Table 2). These agents remain soluble after introduction into media maintained at pH 7.4 for up to 5 h at 37° C, as evidenced by a lack of visible precipitates and the persistence of individualized spectral profiles. Only one of these agents (ICRF-159) was significantly bound by cellulose nitrate/cellulose acetate filters, and this interaction could be reduced by the use of teflon filters.

**Agents with Nonaqueous Solubilities.** A number of agents cannot be directly solubilized in water or liquid media. These agents are soluble in the organic solvents, ethanol, and *N,N*-dimethylacetamide, both of which must be used at concentrations that do not perturb cellular replication in the *in vitro* test system. Several primary tumor cell preparations, as well as established tumor cell lines, have been exposed to increasing concentrations of these solvents (data not shown). Some tumor cells have greater sensitivity to these solvents and can be used to establish the lower limits of tolerance for ethanol and *N,N*-dimethylacetamide, as shown in Fig. 2. In

contrast, tumor cell preparations, which demonstrate an exceptional tolerance to these solvents, continue unperturbed replication at up to 10–12  $\mu$ l/ml ethanol or 1–1.5  $\mu$ l/ml *N,N*-dimethylacetamide, and should be considered more unusual than common. From a solvent toxicity standpoint, ethanol is better tolerated and consequently has greater solvent utility than *N,N*-dimethylacetamide.

As a consequence of solvent-mediated effects on replication, it becomes necessary to prepare very high concentrations of certain agents in either ethanol or *N,N*-dimethylacetamide to deliver modest, nontoxic amounts of solvent to cell culture test determinations. Agents that can be dissolved in ethanol at concentrations high enough to enable the great dilution required to avoid solvent mediated effects are listed in Table 3A, while agents which must be dissolved in *N,N*-dimethylacetamide are listed in Table 3B. It should be noted that AZQ (aziridinylbenzoquinone) is much more highly soluble in *N,N*-dimethylacetamide. (Organization of agents in Table 3A

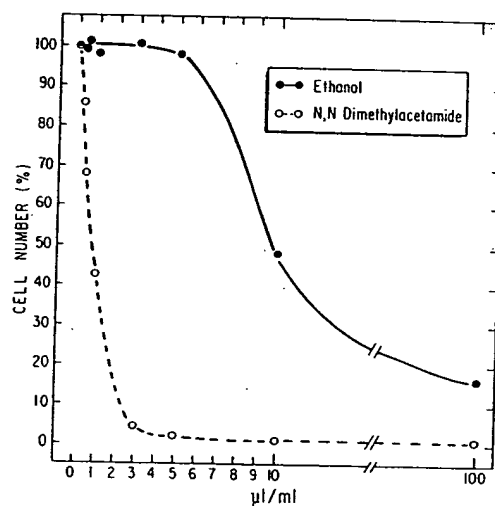


Fig. 2. Solvent-related effects on tumor cell replication. Double glass distilled solvents were obtained from Burdick and Jackson Chemical Company. Tumor cells (ATCC CCL2) were plated in the presence of concentrations of solvent as indicated, and were allowed to replicate for 10 days. Cells were grown in Dulbecco's Modified Eagle's Medium with bicarbonate and HEPES buffering (10 mM) at a final supplementation of 10% fetal calf serum and 100 U/ml penicillin/streptomycin. Cells plated in plastic tissue culture vessels ( $4 \times 10^3$  cells/cm<sup>2</sup>) were nourished with a single change of medium (0.5 ml/cm<sup>2</sup>) and increased to  $64 \times 10^3$  cells/cm<sup>2</sup> (i.e., 100%) in 10 days. Cells were released to single-cell suspensions by exposure to Hank's balanced salt solution containing EDTA (2 mM, pH 7.4) and were counted electronically using a Model ZF Coulter Counter. All determinations were run in triplicate.

Table 2. Properties of selected anticancer agents that are soluble as salts generated with NaOH (20 mM)

Agent	Molecular weight	Absorbance maxima (nm)*	Linear absorbance range: $\mu$ g/ml	Millex OR binding	Millex FG binding
Cordycepin	251.2	215, 260	10–100	< 5%	—
Dichloromethotrexate	559.4	251, 255, 317, 371	10–100	—	—
ICRF-159	268	206, 229	10–50	30%	—
Methotrexate	454.9	231, 250, 313, 320, 372	10–100	—	—
Streptonigrin	506	244, 313, 389, 554	10–100	—	—

\* Parameters are as described in Table 1

Table 3. I in ethanol being int

#### Agent

A. Solub  
Amsacrin  
AZQ<sup>a</sup>  
Buceatir  
Carboque  
Dibromo  
Dichloro  
Hexamet  
Lomustir  
Medroxy  
Melphal  
Nafoxidi  
PCNU  
Prednim  
Predniso  
Progeste  
Retinoic  
Retinol  
Semustir

B. Solub  
AZO  
Etoposic  
Tenipos

<sup>a</sup> Must  
<sup>b</sup> Acid  
<sup>c</sup> Hot,

and 3F  
by pri  
Heatir  
of ho  
solubi  
delive  
absen  
absorl  
37° C.  
*N,N*-c  
becom  
E  
be de  
envir  
aceta  
introc  
CMR  
delive  
deter  
achie

#### Fluoi

In ge  
has a  
wher  
wher  
co-at  
cenci  
meas  
and

**Table 3.** Preparations of select anticancer agents which are solubilized in ethanol (A) or *N,N*-dimethylacetamide (B) and remain soluble after being introduced in liquid media

Agent	Molecular weight	Absorbance Maxima: (nm)*
<b>A. Soluble in ethanol</b>		
Amsacrine	393.5	248, 408
AZQ <sup>a</sup>	364.4	241, <u>355</u> , 472
Bruceatin	548	<u>232</u>
Carboquone	321.24	<u>243</u> , 313, <u>373</u> , 541, 554, 565
Dibromodulcitol <sup>c</sup>	308	<u>212</u>
Dichloroallyl lawsone	283.1	<u>236</u> , 276, 313, <u>355</u> , 377, 555
Hexamethylmelamine	210.3	<u>241</u>
Lomustine	234	<u>241</u> , 383, 398, 415
Medroxyprogesterone	344.48	<u>256</u> , <u>253</u>
Melphalan <sup>b</sup>	305	<u>215</u> , <u>255</u> , 258, 301
Nafoxidine <sup>a</sup>	461.5	<u>245</u> , <u>282</u> , 313, 325
PCNU	262.7	<u>216</u> , <u>233</u>
Prednimustine <sup>b</sup>	646.6	<u>262</u> , <u>300</u>
Prednisolone <sup>b</sup>	482.5	<u>248</u> , 354
Progesterone	314.5	<u>248</u> , <u>250</u> , <u>260</u> , 308, 316
Retinoic acid	300.42	<u>208</u> , <u>240</u> , <u>348</u>
Retinol	286.5	241, 298, <u>306</u> , 313, <u>341</u>
Semustine	248	<u>242</u> , 383, 398, 415
<b>B. Soluble in <i>N,N</i>-dimethylacetamide</b>		
AZO	364.4	241, <u>355</u> , 472
Etoposide	588	<u>246</u> , <u>279</u> , 289, 410
Teniposide	656	<u>285</u>

\* Must be heated

<sup>b</sup> Acid ethanol: 0.6% HCl in ethanol

<sup>c</sup> Hot, acid ethanol

and 3B is based upon minimizing solvent-related toxicity given by priority to the use of ethanol over *N,N*-dimethylacetamide. Heating of agents is limited to warming the vial under a stream of hot tap water.) The previously discussed criteria for solubility can be satisfied by using these two organic solvents to deliver the agents to aqueous environments; namely, in the absence of visible precipitates unique and individualized absorbance profiles can be obtained even after incubation at 37° C. Finally, it should be noted that both ethanol and *N,N*-dimethylacetamide are microcidal so that ultrafiltration becomes unnecessary.

Except for the agent AZQ, all agents listed in Table 3 can be delivered in soluble form to an aqueous tissue culture environment. AZQ (dissolved in ethanol or *N,N*-dimethylacetamide) was observed to precipitate immediately when introduced into tissue culture media (DME, RPMI, McCoy's, CMRL). Thus, with the present systems for drug solvation, the delivery of dissolved AZQ and Orange Crush to tissue culture determinations for tumor cell sensitivity remains unachieved.

#### Fluorescent Properties of Selected Anticancer Agents

In general, quantitation based upon fluorescence spectroscopy has a greater sensitivity than absorbance spectroscopy. Hence, whenever dilute drug concentrations must be determined or whenever absorbance quantitation is confounded by multiple co-absorbing components, quantitation based upon fluorescence may be useful. Most of the agents demonstrated some measurable fluorescence properties (52 of 59 agents, Table 4), and quantitation based upon a linear relationship between

concentration and fluorescence was observed to be possible for 25 of 59 agents, including anguidine, which had not produced sufficient detectable absorbance. In addition, eight agents that were not fluorescent alone in solution formed fluorescent complexes after incubation with cells; these agents were amsacrine, azapicyl, *cis*-DED-platinum, cyclophosphamide, dischloromethotrexate, ICRF-159, levamisole, and mitoguanzone dihydrochloride. This type of fluorescence, which occurs only after interaction with cells, may result from quantum coupling interactions between cellular components and drug. Nevertheless, these observations must be regarded at present as largely phenomenological. Finally, only daunorubicin and doxorubicin (1–5 mg/ml) could be used to visualize tumor cells under the fluorescent microscope after incubation for 1 or 2 h at 37° C.

#### Discussion

When the *in vitro* sensitivities of primary tumor cell preparations to anticancer agents are to be evaluated, it is rather obviously necessary that the anticancer agents remain in solution during the test determinations. In this report we have described how 59 anticancer agents may be solubilized for introduction to tissue culture media; moreover, we have described the limits of solvent concentrations which adversely affect tumor cell replication in culture. The occurrence of stable spectroscopic profiles after incubation at 37° C and the absence of observable precipitation are criteria which most pertinently relate to the *dissolved* status of these compounds; moreover, these criteria do not insure that the absorbing species retains the unaltered active drug form or that the biological activity has not changed. In addition, since it is often necessary to remove potential biocontaminants from preparations of anticancer agents by membrane ultrafiltration, we have examined drug binding to ultramembranes and have observed the potential for interaction between different anticancer agents and filtration materials. This phenomenon involving the binding or adsorption of compounds onto insoluble polymeric materials has long been recognized [1–3, 7]. In general, drugs binding to cellulose nitrate/cellulose acetate filters were found to bind less to teflon filters; however, exceptions can occur (i.e., maytansine) and post-filtration drug quantitation should be performed to unambiguously define the actual drug concentrations in cell culture determinations of sensitivity to anticancer agents. All the drugs considered in this study can be quantitated by either absorbance or fluorescence spectroscopy, except for cyclophosphamide. Nevertheless, it may be possible to quantitate cyclophosphamide on the basis of the fluorescence generated after limited interaction with tumor cells.

Finally, we suggest that the *in vitro* cytotoxic activity of anticancer agents can be moderated by reduced drug concentrations which result from inadequate solvation or by binding to ultrafiltration materials. For the agents listed in this paper, this moderation can be remedied by the appropriate selection of solvents and filters and the use of post-filtration quantitation.

**Acknowledgements.** The authors appreciate the diligence of Brenda Smithson in manuscript preparation and the assistance of Kay Ramey with graphics.

This work was supported by a grant from the Bertha LeBus Educational and Charitable Trust and the Veterans' Administration. Certain agents used in this work were obtained from the Drug

Table 4. Fluorescent properties of selected anticancer agents

Agent	Agent alone			Agent and cells		
	Excitation $\lambda$ (nm)	Emission $\lambda$ (nm)	Linear fluorescence range: $\text{ml} \times 10^{-6}$	Excitation $\lambda$ (nm)	Emission $\lambda$ (nm)	Linear fluorescence range: $\text{ml} \times 10^{-6}$
Aclacinomycin	340	530	6-60	455	530	3-60
Actinomycin-D	340	525	4-40	340	515	4-30
Amsacrine	300	430	—	360	430	0.2-1.5
Anguidine	340	430	180-600	340	430	300-600
Azapicyl	325	435	—	325	355	1,900-5,600
AZQ	300	340	—	280	340	—
(soluble) Baker's Antifol	300	410	0.6-1.9	350	435	0.9-1.9
Bleomycin	315	375	—	315	390	—
Bruceatin	326	380	—	275	340, 380	—
Camptothecin	346	450	0.003-0.030	372	450	0.005-0.025
Carboquone	300	400	—	300	400	—
Chlorozotocin	325	440	0.4-3.2	358	440	0.4-3.2
cis-DED-platinum	350	405	—	350	405	1,100-3,300
cis-platinum	—	—	—	—	—	—
Cordycepin	350	415	—	350	415	—
Cyclocytidine	300	390	420-3,820	300	390	760-3,820
Cyclophosphamide	300	410	—	360	440	770-3,830
Cytarabine	323	380	370-4,100	323	380	310-4,100
Daunorubicin	300	570	4-50	300	570	4-50
Dibromodulcitol	300	340	—	280	340, 415	—
Dichloroallyl lawsone	—	—	—	—	—	—
Dichloromethotrexate	420	480	—	420	480	0.9-1.8
Dihydroxyanthracenedione	—	—	—	—	—	—
Doxorubicin	300	560	4-50	275	560	4-50
Etoposide	300	—	—	282	405	—
5-Fluorouracil	300	385	—	300	385	—
Gallium nitrate	—	—	—	—	—	—
Hexamethylmelamine	272	340	—	272	340	—
ICRF-159	340	395	—	340	395	6-20
ICRF-187	350	420	8-40	350	420	8-40
Ifosfamide	367	450	—	367	450	—
Leucovorin	327	450	4-20	352	450	4-20
Levamisole	320	375	—	278	360	2,070-4,150
Lomustine	334	390	—	334	390	—
Maytansine	370	440	110-1,450	370	440	110-480
Medroxyprogesterone	293	340	—	275	340	—
Melphalan	353	415, 580	6-16	353	415	6-16
Methotrexate	375	450	7-22	375	450	7-22
5-Methyltetrahydrohomofolate	367	450	10-20	367	450	6-20
Mitoquazone dihydrochloride	375	425	—	375	425	400-730
Mitomycin C	410	505	—	410	505	—
Nafoxidine	350	425	5-10	350	425	5-10
Orange crush	325	520	200-1,060	325	550	200-2,120
PALA	—	—	—	—	—	—
PCNU	310	375	20-40	325	375	20-40
Pentamethylmelamine	442	560	—	442	560	—
Prednomustine	300	355	—	300	355	—
Prednisolone	344	405, 500	4-10	344	405, 500	2-10
Progesterone	280	340, 410	5-16	275	340	8-16
Retinoic acid	—	—	—	—	—	—
Retinol	325	475	0.8-7.0	325	475	1.4-7.0
Semustine	300	340	—	275	340	—
Streptonigrin	300	350	—	270	350	—
Streptozocin	320	395	420-3,800	320	395	750-3,800
Tegafur	450	500	—	450	500	—
Teniposide	300	400	—	300	400	—
Thiotepa	362	430, 505	—	362	430, 505	—
Vinblastine	325	360	6-60	325	360	10-60
Vincristine	318	365	120-1,100	318	365	120-1,100

<sup>a</sup> Agent was incubated with cells in balanced saline for 1 h at 37°C

Synthesis  
while oth  
of Cance  
Professor

Referen

1. Berg  
low-r  
Phar.
2. Chio  
solut
3. Chio  
comr  
itativ
4. Doon  
Else
5. Livir  
DN/  
ther:
6. Pavl  
DE,  
Stan  
sens

Synthesis and Chemistry Branch, Division of Cancer Treatment, NCI, while others were provided by the Natural Products Branch, Division of Cancer Treatment, NCI. JRVN is the American Cancer Society Professor of Clinical Oncology.

## References

1. Berg HF, Guess WL, Autian J (1965) Interaction of a group of low-molecular-weight organic acids with soluble polyamides. *J Pharm Sci* 54:79
2. Chiou WL (1975) Possibility of errors in using filter paper for solubility determination. *Can J Pharm Sci* 10:112
3. Chiou WL, Smith LD (1970) Adsorption of organic compounds by commercial filter papers and its implication of quantitative-qualitative chemical analysis. *J Pharm Sci* 59:843
4. Door RT, Fritz WL (1980) *Cancer chemotherapy handbook*. Elsevier, New York, p 1
5. Livingston RB, Titus GA, Heibren LK (1980) In vitro effects on DNA synthesis as a predictor of biological effect from chemotherapy. *Cancer* 40:2209
6. Pavlik EJ, van Nagell JR Jr, Hanson MB, Donaldson ES, Kenady DE, Powell DE (1982) Sensitivity to anticancer agents in vitro: Standardizing the cytotoxic response and characterizing the sensitivities of a reference cell line. *Gynecol Oncol* 14:243
7. Saad HY, Higuchi WI (1965) Water solubility of cholesterol. *J Pharm Sci* 54:1205
8. Salmon SE (1980) Cloning of human tumor stem cells. AR Liss, New York, p 1
9. Salmon SE, von Hoff DD (1981) In vitro evaluation of anticancer drugs with the human tumor stem cell assay. *Semin Oncol* 8:377
10. Salmon SE, Hamburger AW, Soehnlen BN, Durie BG, Alberts DS, Moon TE (1978) Quantitation of differential sensitivity of human tumor stem cells to anticancer drugs. *N Eng J Med* 298:1321
11. Salmon SE, Alberts DS, Meyskens FL, Durie BGM, Jones SE, Soehnlen B, Young L, Chen H-SG, Moon TE (1980) Cloning of human tumor stem cells. AR Liss, New York, p 223
12. Trissel LA, Davignon JP, Kleinman LM, Craddock JC, Flora KP (1980) NCI Investigational drugs, pharmaceutical data 1981. U.S. Department of Health and Human Services, Washington (NIH publication no 81-2141)
13. von Hoff DD, Casper J, Brandley E, Sandbach J, Jones D, Makuch R (1981) Association between human tumor colony-forming assay results and response to an individual patient's tumor to chemotherapy. *Am J Med* 70:1027

Received September 24, 1982/Accepted April 16, 1983





PCT

WORLD INTELLECTUAL PROPERTY ORGANIZATION  
International Bureau

## INTERNATIONAL APPLICATION PUBLISHED UNDER THE PATENT COOPERATION TREATY (PCT)

<b>(51) International Patent Classification <sup>6</sup> :</b> <b>C07H 21/02, 21/04, 23/00, G01N 33/15,</b> <b>A61K 31/525, 39/00, 39/44, 35/00, 49/00</b>		<b>A1</b>	<b>(11) International Publication Number:</b> <b>WO 98/08859</b> <b>(43) International Publication Date:</b> 5 March 1998 (05.03.98)
<b>(21) International Application Number:</b> PCT/US97/14140 <b>(22) International Filing Date:</b> 22 August 1997 (22.08.97) <b>(30) Priority Data:</b> 60/024,430 27 August 1996 (27.08.96) US 60/025,036 27 August 1996 (27.08.96) US <b>(60) Parent Applications or Grants</b> <b>(63) Related by Continuation</b> US 60/024,430 (CIP) Filed on 27 August 1996 (27.08.96) US 60/025,036 (CIP) Filed on 27 August 1996 (27.08.96) <b>(71) Applicant (for all designated States except US):</b> UNIVERSITY OF UTAH RESEARCH FOUNDATION [US/US]; Suite 170, 421 Wakara Way, Salt Lake City, UT 84108 (US). <b>(72) Inventors; and</b> <b>(75) Inventors/Applicants (for US only):</b> GRISSOM, Charles, B. [US/US]; 2740 E. Comanche Drive, Salt Lake City, UT 84108 (US). WEST, Frederick, G. [US/US]; 998 South 1500 East, Salt Lake City, UT 84105 (US). HOWARD, W., Allen,			<b>Jr. [US/US];</b> 2250 Melbourne Avenue #1407, Dexter, MI 48130 (US). <b>(74) Agent:</b> IHNEN, Jeffrey, L.; Rothwell, Figg, Ernst & Kurz, P.C., Suite 701 East Tower, 555 Thirteenth Street, N.W., Washington, DC 20004 (US). <b>(81) Designated States:</b> AL, AM, AT, AU, AZ, BB, BG, BR, BY, CA, CH, CN, CZ, DE, DK, EE, ES, FI, GB, GE, HU, IS, JP, KE, KG, KP, KR, KZ, LK, LR, LS, LT, LU, LV, MD, MG, MK, MN, MW, MX, NO, NZ, PL, PT, RO, RU, SD, SE, SG, SI, SK, SL, TJ, TM, TR, TT, UA, UG, US, UZ, VN, YU, ARIPO patent (GH, KE, LS, MW, SD, SZ, UG, ZW), Eurasian patent (AM, AZ, BY, KG, KZ, MD, RU, TJ, TM), European patent (AT, BE, CH, DE, DK, ES, FI, FR, GB, GR, IE, IT, LU, MC, NL, PT, SE), OAPI patent (BF, BJ, CF, CG, CI, CM, GA, GN, ML, MR, NE, SN, TD, TG). <b>Published</b> <i>With international search report.</i> <i>Before the expiration of the time limit for amending the claims and to be republished in the event of the receipt of amendments.</i>
<b>(54) Title:</b> BIOCONJUGATES AND DELIVERY OF BIOACTIVE AGENTS <b>(57) Abstract</b> <p>The present invention relates to bioconjugates and the delivery of bioactive agents which are preferably targeted for site-specific release in cells, tissues or organs. More particularly, this invention relates to bioconjugates which comprise of bioactive agent and an organocobalt complex. The bioactive agent is covalently bonded directly or indirectly to the cobalt atom of the organocobalt complex. The bioactive agent is released from the bioconjugate by the cleavage of the covalent bond between the bioactive agent and the cobalt atom in the organocobalt complex. The cleavage may occur as a result of normal displacement by cellular nucleophiles or enzymatic action, but is preferably caused to occur selectively at a predetermined release site by application of an external signal. The external signal may be light or photoexcitation, i.e. photolysis, or it may be ultrasound, i.e. sonolysis. Further, if the photolysis takes place in the presence of a magnetic field surrounding the release site, the release of the bioactive agent into surrounding healthy tissue is minimized.</p>			

**FOR THE PURPOSES OF INFORMATION ONLY**

Codes used to identify States party to the PCT on the front pages of pamphlets publishing international applications under the PCT.

AL	Albania	ES	Spain	LS	Lesotho	SI	Slovenia
AM	Armenia	FI	Finland	LT	Lithuania	SK	Slovakia
AT	Austria	FR	France	LU	Luxembourg	SN	Senegal
AU	Australia	GA	Gabon	LV	Latvia	SZ	Swaziland
AZ	Azerbaijan	GB	United Kingdom	MC	Monaco	TD	Chad
BA	Bosnia and Herzegovina	GE	Georgia	MD	Republic of Moldova	TG	Togo
BB	Barbados	GH	Ghana	MG	Madagascar	TJ	Tajikistan
BE	Belgium	GN	Guinea	MK	The former Yugoslav	TM	Turkmenistan
BF	Burkina Faso	GR	Greece		Republic of Macedonia	TR	Turkey
BG	Bulgaria	HU	Hungary	ML	Mali	TT	Trinidad and Tobago
BJ	Benin	IE	Ireland	MN	Mongolia	UA	Ukraine
BR	Brazil	IL	Israel	MR	Mauritania	UG	Uganda
BY	Belarus	IS	Iceland	MW	Malawi	US	United States of America
CA	Canada	IT	Italy	MX	Mexico	UZ	Uzbekistan
CF	Central African Republic	JP	Japan	NE	Niger	VN	Viet Nam
CG	Congo	KE	Kenya	NL	Netherlands	YU	Yugoslavia
CH	Switzerland	KG	Kyrgyzstan	NO	Norway	ZW	Zimbabwe
CI	Côte d'Ivoire	KP	Democratic People's	NZ	New Zealand		
CM	Cameroon		Republic of Korea	PL	Poland		
CN	China	KR	Republic of Korea	PT	Portugal		
CU	Cuba	KZ	Kazakhstan	RO	Romania		
CZ	Czech Republic	LC	Saint Lucia	RU	Russian Federation		
DE	Germany	LI	Liechtenstein	SD	Sudan		
DK	Denmark	LK	Sri Lanka	SE	Sweden		
EE	Estonia	LR	Liberia	SG	Singapore		

TITLE OF THE INVENTION

## BIOCONJUGATES AND DELIVERY OF BIOACTIVE AGENTS

This invention was made in part with Government support under Grant No. ES05728 awarded  
5 by the National Institutes of Health, Bethesda, Maryland. The United States Government has  
certain rights in the invention.

BACKGROUND OF THE INVENTION

The present invention relates to bioconjugates and the delivery of bioactive agents which  
10 are preferably targeted for site-specific release in cells, tissues or organs. More particularly, this  
invention relates to bioconjugates which comprise a bioactive agent and an organocobalt  
complex. The bioactive agent is covalently bonded directly or indirectly to the cobalt atom of  
the organocobalt complex. The bioactive agent is released from the bioconjugate by the  
cleavage of the covalent bond between the bioactive agent and the cobalt atom in the  
15 organocobalt complex. The cleavage may occur as a result of normal displacement by cellular  
nucleophiles or enzymatic action, but is preferably caused to occur selectively at a  
predetermined release site by application of an external signal. The external signal may be light  
or photoexcitation, i.e. photolysis, or it may be ultrasound, i.e. sonolysis. Further, if the  
photolysis takes place in the presence of a magnetic field surrounding the release site, the release  
20 of the bioactive agent into surrounding healthy tissue is minimized.

The publications and other materials used herein to illuminate the background of the  
invention, and in particular, cases to provide additional details respecting the practice, are  
incorporated by reference, and for convenience are referenced in the following text by author  
and date and are listed alphabetically by author in the appended bibliography.

25 The focus of a substantial body of research has been the development of a system  
whereby a pharmaceutical agent can be selectively delivered to a desired anatomic location;  
namely the site in need of treatment. In spite of the great progress which has been achieved in  
this regard, many pharmaceutical delivery systems for the treatment of various diseases or health  
risks, e.g., the treatment of cancer, impart substantial risk to the patient. With respect to the  
30 treatment of cancer, drugs which are effective in attacking malignant cells to destroy them, or at  
least limit their proliferation, have a tendency to attack benign cells also. Therefore, it is highly  
desirable to limit the location of their action to that of the malignancy, and to ensure that at any  
particular time effective, but not excessive, amounts of such drugs are used.

Although it is desired to concentrate a cytotoxic agent at a targeted site, current cancer treatment protocols for administering these cytotoxic agents typically call for repeated intravenous dosing, with careful monitoring of the patient. The drugs are often used in combination to exert a multi-faceted assault on neoplastic cells. The dose is selected to be just  
5 below the amount that will produce acute (and sometimes chronic) toxicity that can lead to life-threatening cardiomyopathy, myelotoxicity, hepatic toxicity, or renal toxicity. Alopecia (hair loss), mucositis, stomatitis, and nausea are other common, but generally not life-threatening, side effects at these doses. Since many of these compounds are potent vesicants, tissue necrosis will occur if localized extravasation (loss of the drug from blood to the  
10 surrounding tissue) occurs. These effects occur since the blood generally attains a specified concentration of that drug before becoming effective. Because the blood is transported throughout the body of the host being treated, so is the pharmaceutical agent. Following this technique provides an even distribution of the drug throughout the body, rather than concentrating it at the treatment site. Moreover, such systemic treatment methods expose the  
15 healthy cells to the cytotoxic agent concurrent with the treatment of the unhealthy or diseased cells besides limiting the concentration of the drug at the site where it is most needed.

Previous attempts to administer such drugs by direct injection into the location of the organ having the malignancy are only partially effective, because of migration of the drug from that location and as a result of extensive tissue necrosis from extravasation. Such dispersion  
20 cannot be totally prevented, with the result that excessive quantities of drug need to be administered to attain a desired result. Although careful clinical monitoring may prevent extensive damage or loss of viable tissue, the providing of a pharmaceutical agent-carrier system which is actively transported through standard biological systems to the treatment site prior to activation of the pharmaceutical agent would be highly desirable not only in optimizing  
25 utilization of the drug but also in the reduction of side effects and/or the minimization of the destruction of healthy cells. The direct injection of cytotoxic agents into solid tumors of the breast, bladder, prostate and lung using conventional cytotoxic chemotherapeutic agents as adjuvants to surgery and/or radiotherapy has been of limited success in prolonging the lives of patients. This is partially due to the dose limitations imposed by the acute and chronic toxicity  
30 to tissues or organ systems beyond those that are targeted.

As it relates to the administration of cytotoxic or antineoplastic drugs, the effective resolution of concerns relating to modes of administration, to the limitation of dosage size and frequency of administration, and to side effects would certainly be of benefit to the treatment of cancer.

5       Oligonucleotides that specifically interfere with gene expression at the transcriptional or translational levels have the potential to be used as therapeutic agents to control the synthesis of deleterious proteins associated with viral, neoplastic or other diseases. It is possible to select single-stranded oligonucleotides that recognize and bind to the major groove of a stretch of double-stranded DNA in a sequence-specific manner to form a triple helix (Le Doan et al., 1987; 10 Moser and Dervan, 1987). Triple helix-forming oligonucleotides targeted to the promoter region of certain genes have been used to physically block RNA synthesis in cell-free transcription assays (Cooney et al., 1988; Postel et al., 1992; Skoog et al., 1993; Rando et al., 1994). Similarly, *in vitro* translation assays have been used to demonstrate that antisense oligonucleotides can bind mRNA targets and prevent protein synthesis (Uhlmann and Peyman, 15 1990; Cohen and Hogan, 1994).

Although antisense oligonucleotides have shown great efficacy in the selective inhibition of gene expression (Stein and Cohen, 1988; Szczylik et al., 1991; Gray et al., 1993), the therapeutic applications of such antisense oligonucleotides are currently limited by their low physiological stability, slow cellular uptake, and lack of tissue specificity. The instability 20 obstacles have been largely overcome by use of backbone-modified oligonucleotides that are more resistant to nucleases. Methylphosphonates, protein-nucleic acid conjugates, and phosphorothioates all appear to resist enzymatic digestion better than the corresponding natural oligonucleotides (Chang and Miller, 1991; Wickstrom et al., 1992; Letsinger, 1993; Zon, 1993).

Problems with cellular uptake of antisense oligonucleotides have been more difficult to 25 solve. Endogenous uptake pathways that rely on pinocytosis and related processes generally have insufficient capacity to deliver the quantities of antisense oligonucleotides required to suppress gene expression (Vlassov et al., 1994). Hydrophobic modifications have also been undertaken to improve membrane permeability, but such derivatization strategies are most useful only for short oligonucleotides (Vlassov et al., 1994). Although complexes of antisense constructs 30 with cationic liposomes or immunoliposomes (Gao and Huang, 1991; Bennett et al., 1992, Ma and Wei, 1996) and polylysine (Trubetskoy et al., 1992; Bunnell et al., 1992) have significantly

enhanced intracellular delivery, they have simultaneously introduced new disadvantages of their own. Thus, both methods exhibit some carrier cytotoxicity, and like other protocols, neither strategy allows for any tissue or cell targeting. In short, intracellular delivery and tissue specificity remain major obstacles to the implementation of antisense drugs in the treatment of human disorders.

Other techniques for the delivery of oligonucleotides to cells include the use of: (a) folate-PEG-liposome constructs for the delivery of antisense DNA against growth factor receptor (Wang et al., 1995); (b) folic acid-polylysine constructs for the delivery of c-myc antisense DNA (Ginobbi et al., (1997); (c) tris(N-acetylgalactosamine aminohexyl glycoside) amide of tyrosyl(glutamyl)-glutamate (YEE(GalNAcAH)<sub>3</sub>) linked to polylysine for the delivery of DNA to cells via the asialoglycoprotein receptor (Merwin et al., 1994); and (d) water-soluble block polycations (Kabanov et al., 1995).

It has been known for some time that a pharmaceutically active agent can be attached to a carrier or molecule. The term "prodrug" is often associated with such systems wherein the active agent is bonded to another molecule for purposes of administration. The drug is usually inactive in the prodrug state and the bond is later cleaved releasing the drug at a site where it can be effective. However, such systems are not as useful as might be desired for various reasons, site specificity being one. Also, the release of the drug from its carrier requires the presence of some agent or event to separate the active drug from its carrier or molecule and, as such, may rely on factors such as the presence of a specific enzyme, pH conditions, time release and the like, which may be variable from host to host and which may not be effectively implemented.

For example, transmembrane transport of nutrient molecules is a critical cellular function. Because practitioners have recognized the importance of transmembrane transport to many areas of medical and biological science, including drug therapy, peptide therapy and gene transfer, there have been significant research efforts directed to the understanding and application of such processes. Thus, for example, transmembrane delivery of nucleic acids has been encouraged through the use of protein carriers, antibody carriers, liposomal delivery systems, electroporation, direct injection, cell fusion, viral carriers, osmotic shock, and calcium-phosphate mediated transformation. However, many of those techniques are limited both by the types of cells in which transmembrane transport is enabled and by the conditions of use for successful transmembrane transport of exogenous molecular species. Further, many of these

known techniques are limited in the type and size of exogenous molecule that can be transported across a membrane without loss of bioactivity.

One method for transmembrane delivery of exogenous molecules having a wide applicability is based on the mechanism of receptor-mediated endocytotic activity. Unlike many other methods, receptor-mediated endocytotic activity can be used successfully both *in vivo* and *in vitro*. Receptor-mediated endocytosis involves the movement of ligands bound to membrane receptors into the interior of an area bounded by the membrane through invagination of the membrane. The process is initiated or activated by the binding of a receptor-specific ligand to the receptor. Many receptor-mediated endocytotic systems have been characterized, including those recognizing galactose, mannose, mannose 6-phosphate, transferrin, asialoglycoprotein, transcobalamin (Vitamin B<sub>12</sub>),  $\alpha$ -2-macroglobulins, insulin, and other peptide growth factors such as epidermal growth factor (EGF).

Receptor-mediated endocytotic activity has been utilized for delivering exogenous molecules such as proteins and nucleic acids to cells. Generally, a specified ligand is chemically conjugated by covalent, ionic or hydrogen bonding to an exogenous molecule of interest (i.e. the exogenous compound), forming a conjugate molecule having a moiety (the ligand portion) that is still recognized in the conjugate by a target receptor. Using this technique, the phototoxic agent psoralen has been conjugated to insulin and internalized by the insulin receptor endocytotic pathway (Gasparro, 1986); the hepatocyte-specific receptor for galactose terminal asialoglycoproteins has been utilized for the hepatocyte-specific transmembrane delivery of asialoorosomucoid-poly-L-lysine non-covalently complexed to a DNA plasmid (Wu, 1987); the cell receptor for epidermal growth factor has been utilized to deliver polynucleotides covalently linked to EGF to the cell interior (Myers, 1988); the intestinally situated cellular receptor for the organometallic Vitamin B<sub>12</sub>-intrinsic factor complex has been used to mediate delivery to the circulatory system of a vertebrate host a drug, hormone, bioactive peptide or immunogen complexed with Vitamin B<sub>12</sub> and delivered to the intestine through oral administration (Russell-Jones et al., 1995); the mannose-6-phosphate receptor has been used to deliver low density lipoproteins to cells (Murray and Neville, 1980); the cholera toxin binding subunit receptor has been used to deliver insulin to cells lacking insulin receptors (Roth and Maddox, 1983); the human chorionic gonadotropin receptor has been employed to deliver a ricin a-chain coupled to HCG to cells with the appropriate HCG receptor in order to kill the cells (Oeltmann and Heath,

1979); the transferrin receptor has been used to deliver mitomycin C to sarcoma cells (Tanaka et al., 1996) or to deliver doxorubicin to multidrug-resistant cells (Fritzer et al., 1996); the biotin receptor has been employed to deliver hypoxanthine-guanine phosphoribosyl transferase (HGPRT) by biotinylating the HGPRT to restore growth to HGPRT deficient cells (Low et al., 1995); and the folic acid receptor has been used to deliver antisense DNA to src-transformed fibroblast cells (Low et al., 1995).

Russell-Jones et al. (1995), describes a system which involves the formation of a covalent bond between the pharmaceutical agent one wishes to deliver and a modified Vitamin B<sub>12</sub> to form a conjugate molecule. The conjugate is orally administered and is then transported from the intestinal lumen to the circulation. Importantly, the pharmaceutical agent and the vitamin are bound through an amide linkage which is prone to acid hydrolysis. Russell-Jones et al. found that many biologically active pharmaceutical agents can be bound to B<sub>12</sub> for facilitating the introduction of the drug into the blood stream through oral administration. Importantly, no method was provided whereby the drug-B<sub>12</sub> bond could be selectively cleaved, nor could location of the active pharmaceutical agent be controlled once activated. Instead, Russell-Jones et al. relied on biochemical degradation of the drug-B<sub>12</sub> bond to release the drug in its active form. Importantly, under this method the drug could be released in its active form anywhere within the circulation system, diminishing the importance of the active transport of B<sub>12</sub> into cancer tissue. Moreover, the conjugates formed under this method require the modification of the structure of the corrin ring of the B<sub>12</sub> molecule, which modification can have serious effects on receptor interactions.

Thus, there exists a need for a drug delivery system which can be utilized for the delivery of bioactive agents, including pharmaceuticals, peptides and oligonucleotides. There is also a need for a drug delivery system which can be used for site-specific release of the bioactive agent in the cells, tissues, or organs in which a therapeutical effect is desired to be effected.

#### SUMMARY OF THE INVENTION

The present invention relates to bioconjugates and the delivery of bioactive agents which are preferably targeted for site specific release in cells, tissues or organs. More particularly, this invention relates to bioconjugates which comprise a bioactive agent and an organocobalt complex. The bioactive agent is covalently bonded directly or indirectly to the cobalt atom of



the organocobalt complex. The bioactive agent is released from the bioconjugate by the cleavage of the covalent bond between the bioactive agent and the cobalt atom in the organocobalt complex, as described herein.

The bioactive agent is any agent which is desired to be delivered to cells, tissues or  
5 organs for nutrient or therapeutic effects. In accordance with the present invention, bioactive agents include, but are not limited to, nutrients, pharmaceuticals, drugs, peptides and oligonucleotides.

The organocobalt complex is any organic complex containing a cobalt atom having bound thereto 4-5 nitrogen and/or chalcogens such as oxygen, sulfur, etc., as part of a multiple  
10 unsaturated heterocyclic ring system. In accordance with the present invention, suitable organocobalt complexes include, but are not limited to, cobalamin, Co[SALEN], organo-(pyridine)bis(dimethylglyoximate)cobalt, corrinoids, derivatives thereof and analogues thereof. The organocobalt complexes may be unsubstituted or substituted with conventional organic functional groups which will not alter the basic nature of the organocobalt complex. The basic  
15 nature of the organocobalt complex is to directly or indirectly bind the bioactive agent covalently to the cobalt such that the cobalt-bioactive agent bond is readily cleavable as described herein. The organocobalt complex may also be covalently bound directly or indirectly to a targeting molecule. The targeting molecule is a molecule for which the desired cell, tissue or organ has a requirement or a receptor, as described herein.

20 The bioconjugate according to the present invention is administered to a subject in need of therapeutic treatment. The bioconjugate concentrates in a targeted cell, tissue or organ site as a result of the organocobalt complex. As an example, a bioconjugate containing a chemotherapeutic is administered to a patient and the bioconjugate concentrates in neoplastic cells where the active chemotherapeutic is released from the bioconjugate by cleavage.  
25 Similarly, other pharmaceuticals, drugs, peptides or oligonucleotides are administered to a subject as part of the bioconjugate which is concentrated in the desired cells, tissues or organs. The pharmaceuticals, drugs, peptides or oligonucleotides are released by cleavage. In one embodiment, the cleavage may occur as a result of normal displacement by cellular nucleophiles or enzymatic action. In a second embodiment, the cleavage is caused to occur selectively at the  
30 release site by an external signal. The external signal may be light or photoexcitation, i.e. photolysis, or it may be ultrasound, i.e. sonolysis. Further, if the photolysis takes place in the

presence of a magnetic field surrounding the release site, the release of the drug, such as a cytotoxic agent, into surrounding healthy tissue can be minimized.

#### BRIEF DESCRIPTION OF THE DRAWINGS

5        Figure 1 shows the structure and absorption spectrum of methylcobalamin ( $B_{12}$ ).

Figure 2 shows the structure and absorption spectrum of ethyl-Co[SALEN] (cobalt-bis-[salicylidene]-ethylenediamine).

Figure 3A shows a sequential absorption spectra of aqueous  $CH_3-Cbl^{III}$  as a function of anaerobic sonolysis (pH 7.38, 100 mM Hepes, saturating Ar).

10        Figure 3B shows the change in absorbance spectra following aerobic sonolysis in the absence of organic buffer.

Figure 4A shows a sequential absorption spectra of aqueous compound 3 (Example 6) as a function of anaerobic sonolysis at pH 7.4, 100 mM Hepes, saturating Ar.

15        Figure 4B shows the change in absorbance spectra following aerobic sonolysis of a compound 3 (Example 6) solution containing phosphate buffer.

Figure 5 shows the effect of a chlorambucil bioconjugate on cell viability for the HCT-116 cell line. The results are shown for chlorambucil (■), the chlorambucil bioconjugate with photolysis (○), the chlorambucil bioconjugate with no photolysis (▲) and the chlorambucil bioconjugate plus 10 equivalents of hydroxycobalamin with photolysis (∇).

20        Figure 6 shows the effect of a chlorambucil bioconjugate on cell viability for the HL-60 cell line. The results are shown for chlorambucil (■), the chlorambucil bioconjugate with no photolysis (▲) and the chlorambucil bioconjugate plus 10 equivalents of hydroxycobalamin with no photolysis (∇).

25        Figure 7 shows the effect of a chlorambucil bioconjugate on cell viability for the B-16 cell line. The results are shown for chlorambucil (■), the chlorambucil bioconjugate with photolysis (○), the chlorambucil bioconjugate with no photolysis (▲) and the chlorambucil bioconjugate plus 10 equivalents of hydroxycobalamin with photolysis (∇).

30        Figure 8 shows the effect of a chlorambucil bioconjugate on cell viability for the Meth-A cell line. The results are shown for chlorambucil (■), the chlorambucil bioconjugate with photolysis (○), the chlorambucil bioconjugate with no photolysis (▲) and the chlorambucil bioconjugate plus 10 equivalents of hydroxycobalamin with photolysis (∇).

Figure 9 shows the effect of a chlorambucil bioconjugate on cell viability for the RD-995 cell line. The results are shown for chlorambucil (■), the chlorambucil bioconjugate with photolysis (○), the chlorambucil bioconjugate with no photolysis (▲) and the chlorambucil bioconjugate plus 10 equivalents of hydroxycobalamin with photolysis (∇).

5

#### DETAILED DESCRIPTION OF THE INVENTION

The present invention relates to bioconjugates and the delivery of bioactive agents which are preferably targeted for site-specific release in cells, tissues or organs. More particularly, this invention relates to bioconjugates which comprise a bioactive agent and an organocobalt complex. The bioactive agent is covalently bonded directly or indirectly to the cobalt atom of the organocobalt complex. The bioactive agent is released from the bioconjugate by the cleavage of the covalent bond between the bioactive agent and the cobalt atom in the organocobalt complex. The cleavage may occur as a result of normal displacement by cellular nucleophiles or enzymatic action, but is preferably caused to occur selectively at a predetermined release site by application of an external signal. The external signal may be light or photoexcitation, i.e. photolysis, or it may be ultrasound, i.e. sonolysis. Further, if the photolysis takes place in the presence of a magnetic field surrounding the release site, the release of the bioactive agent into surrounding healthy tissue is minimized.

The bioconjugate according to the present invention is administered to a subject in need of therapeutic treatment. The bioconjugate concentrates in a targeted cell, tissue or organ site as a result of the organocobalt complex. The bioactive agent is released from the bioconjugate by cleavage. In one embodiment, the cleavage may occur as a result of normal displacement by cellular nucleophiles or enzymatic action. In a second embodiment, the cleavage is caused to occur selectively at the release site by an external signal. The external signal may be light or photoexcitation, i.e. photolysis, or it may be ultrasound, i.e. sonolysis. Further, if the photolysis takes place in the presence of a magnetic field surrounding the release site, the release of the drug, such as a cytotoxic agent, into surrounding healthy tissue is minimized.

As one example, the bioconjugate contains a chemotherapeutic agent and is administered to a patient having cancer. In this example, a therapeutically effective amount of the bioconjugate is administered intravenously to a patient such that the bioconjugate concentrates in the neoplastic cells. The chemotherapeutic agent is released from the bioconjugate by natural

means (e.g., cellular nucleophiles or enzymatic action) or preferably by means of an external signal (e.g., light or ultrasound).

As a second example, the bioconjugate contains a cytotoxic agent and is administered to a patient having psoriasis. In this example, a therapeutically effective amount of the bioconjugate is administered to an afflicted skin site. The cytotoxic agent is released by natural means or  
5 preferably by means of an external signal.

As a third example, the bioconjugate contains the enzymatic domain of diphtheria toxin (Nichols et al., 1997) and is administered to a patient having cancer. In this example, a therapeutically effective amount of the bioconjugate is administered intravenously to a patient  
10 such that the bioconjugate concentrates in the neoplastic cells. The enzymatic domain of diphtheria toxin is released from the bioconjugate by natural means (e.g., cellular nucleophiles or enzymatic action) or preferably by means of an external signal (e.g., light or ultrasound) and proceeds to kill the cancer cells.

As a fourth example, the bioconjugate contains an antisense oligonucleotide against  
15 hepatitis B virus (Yao et al., 1996; Madon and Blum, 1996) and is administered to a subject having hepatitis B. In this example, a therapeutically effective amount of the bioconjugate is administered intravenously to a patient such that the bioconjugate concentrates in the liver. The antisense oligonucleotide is released from the bioconjugate by natural means (e.g., cellular nucleophiles or enzymatic action) or preferably by means of an external signal (e.g., light or  
20 ultrasound) and proceeds to inhibit gene expression and replication of hepatitis B virus.

The present invention employs the following definitions:

**Bioactive agent:** any agent which is desired to be delivered to cells, tissues or organs for modulating or otherwise modifying cell function, including for therapeutic effects. In accordance  
25 with the present invention, bioactive agents include, but are not limited to, pharmaceutically active compounds or diagnostic compounds. Bioactive agents include, but are not limited to, peptides, oligopeptides, proteins, apoproteins, glycoproteins, antigens and antibodies or antibody fragments thereto, receptors and other membrane proteins, retro-inverso oligopeptides, protein analogs in which at least one non-peptide linkage replaces a peptide linkage, enzymes,  
30 coenzymes, enzyme inhibitors, amino acids and their derivatives, hormones, lipids, phospholipids, liposomes, ricin or ricin fragments; toxins such as aflatoxin, digoxin,

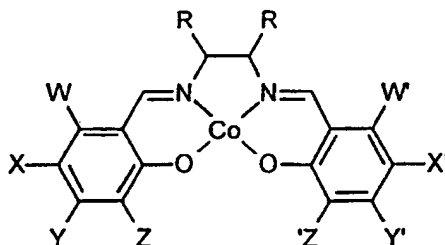
xanthotoxin, rubratoxin; antibiotics such as cephalosporins, penicillin and erythromycin; analgesics such as aspirin, ibuprofen and acetaminophen, bronchodilators such as theophylline and albuterol; beta-blockers such as propranolol, metoprolol, atenolol, labetalol, timolol, penbutolol and pindolol; antimicrobial agents such as those described above and ciprofloxacin, cinoxacin and norfloxacin; antihypertensive agents such as clonidine, methyldopa, prazosin, verapamil, nifedipine, aptopril and enalapril; cardiovascular agents including antiarrhythmics, cardiac glycosides, antianginals and vasodilators, central nervous system agents including stimulants, psychotropics, antimanics and depressants; antiviral agents; antihistamines such as chlorpheniramine and brompheniramine; cancer drugs including chemotherapeutic agents, such as chlorambucil, carboplatin, derivatives of busulfan, doxorubicin, etoposide, topotecan (TPT); tranquilizers such as diazepam, chlordiazepoxide, oxazepam, alprazolam and triazolam, antidepressants such as fluoxetine, amitriptyline, nortriptyline and imipramine; H-2 antagonists such as nizatidine, cimetidine, famotidine and ranitidine, anticonvulsants; antinauseants; prostaglandins; muscle relaxants; anti-inflammatory substances; stimulants; decongestants; antiemetics; diuretics; antispasmodics; antiasthmatics; anti-Parkinson agents; expectorants; cough suppressants, mucolytics; vitamins; and mineral and nutritional additives. Other molecules include nucleotides; oligonucleotides; polynucleotides; and their art-recognized and biologically functional analogs and derivatives including, for example, methylated polynucleotides and nucleotide analogs having phosphorothioate linkages; plasmids, cosmids, artificial chromosomes, other nucleic acid vectors; antisense polynucleotides including those substantially complementary to at least one endogenous nucleic acid or those having sequences with a sense opposed to at least portions of selected viral or retroviral genomes; promoters; enhancers; inhibitors; other ligands for regulating gene transcription and translation. In addition, the bioactive agent can be any other biologically active molecule that can form a conjugate with an organocobalt complex. The bioactive agent may further contain a spacer which provides a covalent bond with the cobalt atom of the organocobalt complex, but which does not adversely affect the biological activity of the bioactive agent.

**Bioconjugate:** a conjugate containing a bioactive agent and an organocobalt complex in which the bioactive agent is covalently bound directly to the cobalt atom or is covalently bound indirectly to the cobalt atom via a spacer.

**Non-reactive atom:** an atom in the bioactive agent that will not lead to rearrangement or destruction of the bioactive agent under conditions of ligand exchange during receptor-mediated endocytosis, but that instead will reproduce the original form of the bioactive agent (or bioactive agent and spacer) and thereby unmask an active bioactive agent. The non-reactive atom may be a carbon atom, a nitrogen atom, an oxygen atom, a sulfur atom, a selenium atom or a silicon atom. A carbon atom (e.g. from an alkyl, acyl or aryl group) is particularly preferred. Such non-reactive atoms are also used in forming the covalent bond between the cobalt and the spacer.

**Organocobalt complex:** an organic complex containing a cobalt atom having bound thereto 4-5 calcogens as part of a multiple unsaturated heterocyclic ring system. In accordance with the present invention, suitable organocobalt complexes include, but are not limited to, cobalamin (coenzyme B<sub>12</sub>), Co[SALEN] (which is a cobalamin analogue), organo(pyridine)-bis(dimethylglyoximate)cobalt, corrinoids (such as disclosed by Brown et al., 1996) and derivatives or analogues of any of the preceding, as well as pharmaceutically acceptable salts. The organocobalt complexes may be unsubstituted or substituted with conventional organic functional groups which will not alter the basic nature of the organocobalt complex. The basic nature of the organocobalt complex is to bind the bioactive agent covalently to the cobalt such that the cobalt-bioactive agent bond is readily cleavable as described herein. Examples of substituents which may be found on the organocobalt complex include amino, nitro, halogen (bromine, chlorine), sulfito, C<sub>2-6</sub>-alkene and C<sub>2-6</sub> alkyne. For example, the organocobalt complex can be formed having a nitro and/or halo (e.g., bromo) derivative of the corrin ring or having an extended conjugation with exocyclic olefin or alkylene groups. Other derivatives include cobalamin lactone, cobalamin lactame and those in which the benzimidazole ring (e.g., of cobalamin, green corrinoid, and the like) are substituted with e.g., one or more halogen (bromine, chlorine), hydroxy or C<sub>1-6</sub> alkyl. Such substituents are useful for increasing the  $\lambda_{\text{max}}$  to be used for cleavage of the bioconjugate as described herein. Further derivatives include anilide, ethylamide, mono-, di- or tri-carboxylic acid or proprionamide derivatives of cobalamin of Vitamin B<sub>12</sub>. In one embodiment, the organocobalt complex is any organic complex containing cobalt which is bound by transcobalamin and transported into a cell by a receptor-mediated process involving transcobalamin. In a second embodiment, the organocobalt complex may also be covalently bound directly or indirectly (through a spacer) to a targeting molecule, wherein said targeting molecule is bound by its receptor and the complex is transported into a

cell by a receptor-mediated process. Co[SALEN] and its derivatives or analogues can be represented by the general formula



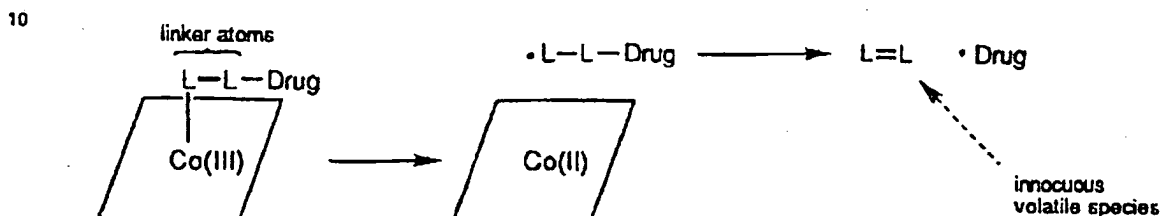
- wherein the substituents may be included or omitted to modulate physical properties of the molecule, e.g., water solubility, stability or  $\lambda_{\max}$  -- the wavelength at which the complex absorbs. Thus, the substituents are as follows: R is H, a group which increases water solubility and/or stability or a group for attachment of a targeting molecule and W, W', X, X', Y, Y', Z and Z' are independently H, a group which increases water solubility and/or stability, a group for attachment of a targeting molecule or a group for modified absorbance of energy, or W and X together and W' and X' together are a 4-6 member cyclic or heterocyclic ring, or Y and Z together and Y' and Z' together are a 4-6 member cyclic or heterocyclic aromatic ring. Examples of groups for enhancing water solubility include amino,  $C_{1-6}$  alcohol,  $C_{1-6}$  carboxyl for any substituent, or also  $SO_3^-$  for the substituents other than R. Examples of groups for attachment of a targeting molecule include amino,  $C_{1-6}$  alcohol and  $C_{1-6}$  carboxyl for any substituent. Examples of groups for modifying absorbance include  $CH_2OH$ ,  $CO_2H$ ,  $SO_3^-$ , amino and nitro for the substituents other than R. Such groups are useful for increasing the wavelength of light to be used for cleavage of the bioconjugate as described herein, while targeting molecules are useful in selectively targeting the bioconjugate to the desired tissue.
- Therefore, when used in the context of the present application, the term organocobalt complex, unless specifically identified, shall be inclusive of  $B_{12}$  in all its embodiments, including coenzyme  $B_{12}$ , Co[SALEN] and other  $B_{12}$  or  $B_{12}$ -like molecules, the organocobalt complexes defined herein, as well as any derivatives and analogues thereof.

**Spacer:** an atom or molecule which covalently binds together two components. In the present invention, a spacer is intended to include atoms and molecules which can be used to covalently bind a bioactive agent to the cobalt atom of an organocobalt complex or to covalently bind a targeting molecule to an organocobalt complex. The spacer must not prevent the binding of the organocobalt complex or the targeting molecule with its appropriate receptor.

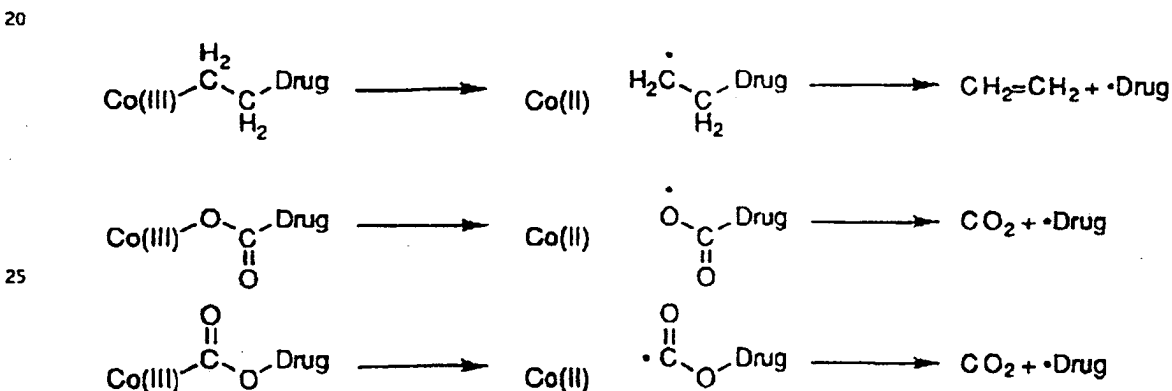
-14-

Examples of suitable spacers include, but are not limited to, polymethylene  $[-(\text{CH}_2)_n]$ , where  $n$  is 1-10], ester [bioactive agent attached to O and Co to  $\text{C}=\text{O}$ ], carbonate, ether, acetal or any combination of two or more of these units. A skilled artisan will readily recognize other spacers which can be used in accordance with the present invention.

Several of these spacers are useful as a "self-destructing" linker group. That is, some or all of the linkage would be consumed in a fragmentation reaction. This means that, following cleavage of the C-Co bond by photolysis or sonolysis, an additional cleavage will take place several bonds away, leading to the formation of a small, unsaturated (and typically volatile) molecule made up of atoms of the former linker. This is shown schematically below:



15 The most typical scenario is the subsequent cleavage of a second bond, two bonds removed from the first. Thus, most self-destructive linkers would contain a two-atom unit whose extrusion as a small, gaseous molecule is favorable. Another design feature is to have the new radical species which is generated after the second cleavage step be an especially stable kind of radical. Examples of self-destructing linkers are shown below:



**Targeting Molecule:** a molecule which is bound by a receptor and transported into a cell by a receptor-mediated process. Examples of suitable targeting molecules include, but are not limited to, glucose, galactose, mannose, mannose 5-phosphate, transferrin.



-15-

asialoglycoprotein,  $\alpha$ -2-macroglobulins, insulin, a peptide growth factor, cobalamin, folic acid or derivatives, biotin or derivatives, YEE(GalNAcAH)<sub>3</sub> or derivatives, albumin, texaphyrin, metallotexaphyrin, porphyrin, any vitamin, any coenzyme, an antibody, an antibody fragment (e.g., Fab) and a single chain antibody variable region (scFv). A skilled artisan will readily  
5 recognize other targeting molecules (ligands) which bind to cell receptors and which are transported into a cell by a receptor-mediated process. The present invention is intended to include all such targeting molecules.

The present invention takes advantage of the cellular properties of cobalamin and cobalamin analogues or derivatives, as well as the cellular properties of other targeting  
10 molecules. For example, studies have shown that the absorption of physiological amounts of vitamin B<sub>12</sub> by the gut requires that it be complexed with a naturally occurring transport protein known as intrinsic factor (IF). (Castle, 1953; Fox and Castle, Allen and Majerus, 1972b). This protein is released into the lumen of the stomach by parietal cells in the fundus. Once bound to  
15 intrinsic factor, the B<sub>12</sub>-IF complex interacts with a membrane bound receptor for IF located on the terminal ileum of the small intestine. The receptor-IF-B<sub>12</sub> complex is then internalized by a process of receptor-mediated endocytosis (RME). Allen and Majerus demonstrated that it is possible to chemically modify B<sub>12</sub>, couple it to a resin and use the B<sub>12</sub>-resin to affinity purify IF  
(Allen and Majerus, 1972a). This finding suggests the possibility of coupling a large  
20 macromolecule (such as the resin used by Allen and Majerus, 1972a) to B<sub>12</sub> while still preserving its ability to interact specifically with intrinsic factor and thus be part of the active transport system. By coupling molecules to B<sub>12</sub> in such a way as to preserve the ability of B<sub>12</sub> to  
interact with intrinsic factor, it was found that the natural uptake mechanism for orally  
administered B<sub>12</sub> could be used to deliver various proteins, drugs or other pharmaceutically  
active molecules from the intestinal lumen to the circulation. It has been found that B<sub>12</sub> is  
25 naturally concentrated in cancer tissue through a similar transport mechanism.

In mammals, B<sub>12</sub> is transported in the blood by transcobalamin proteins TC-I, TC-II, and TC-III. The major form of B<sub>12</sub> in the blood is methylcobalamin and the largest store of B<sub>12</sub> is adenosylcobalamin in the liver. Rapidly dividing cells, including cancer cells, require coenzyme  
30 B<sub>12</sub> for thymidine production during DNA synthesis. It has been reported by Carmel (1975) that in some patients with tumors, up to 50-fold increases in the major cobalamin transport proteins TC-I and TC-II have been observed. Waxman et al. (1972), report the finding of tumor specific

B<sub>12</sub> binding proteins that circulate in the blood. In each instance, these increases in TC transport proteins and the corresponding systemic depletion of B<sub>12</sub> were not the result of megaloblastosis, granulocyte proliferation, or any other pathogenic B<sub>12</sub> deficiency.

In a second example of receptor-mediated endocytosis, folate receptors that mediate  
5 endocytotic activity have previously been identified in bacterial cells (Kumar et al., 1987) and used for delivery of biologically active materials (Low et al., 1995). Folic acid, folinic acid, pteropolyglutamic acid, and folate receptor-binding pteridines such as tetrahydropterins, dihydrofolates, tetrahydrofolates and their deaza and dideaza analogs are useful as targeting molecules in accordance with the present invention. The terms "deaza" and "dideaza" analogs  
10 refer to the art-recognized analogs having a carbon atom substituted for one or two nitrogen atoms in the naturally-occurring folic acid structure. For example, the deaza analogs include the 1-deaza, 3-deaza, 5-deaza, 8-deaza, and 10-deaza analogs. The dideaza analogs include, for example, 1,5-dideaza, 5,10-dideaza, 8,10-dideaza, and 5,8-dideaza analogs. The foregoing folic acid derivatives are conventionally termed "folates," reflecting their capacity to bind with folate-  
15 receptors, and such ligands when complexed with exogenous molecules are effective to enhance trans-membrane transport. Other folates useful as complex forming ligands for this invention are the folate receptor binding analogs aminopterin, amethopterin (methotrexate), N<sup>10</sup>-methylfolate, 2-deamino-hydroxyfolate, deaza analogs such as 1-deazamethopterin or 3-deazamethopterin, and 3'5'-dichloro-4-amino-4-deoxy-N<sup>10</sup>-methylpteroyl-glutamic acid  
20 (dichloromethotrexate). Other suitable ligands capable of binding to folate receptors to initiate receptor-mediated endocytotic transport of the complex include anti-idiotypic antibodies to the folate receptor. An exogenous molecule in complex with an anti-idiotypic antibody to a folate receptor is used to trigger trans-membrane transport of the complex. Such molecules are used in accordance with the present invention as a targeting molecule.

25 In a further example of receptor-mediated endocytosis, biotin receptors have been used to mediate endocytotic activity (Low et al., 1995). Biotin analogs such as biocytin, biotin sulfoxide, oxybiotin and other biotin receptor-binding compounds are ligands that may also be used as suitable targeting molecules to promote the trans-membrane transport of exogenous molecules in accordance with this invention. Other compounds capable of binding to biotin  
30 receptors to initiate receptor-mediated endocytotic transport of the complex are also contemplated. These can include other receptor-binding ligands such as, for example, anti-idiotypic

antibodies to the biotin receptor. An exogenous molecule complexed with an anti-idiotypic antibody to a biotin receptor could be used to trigger trans-membrane transport of the complex. Such molecules are used in accordance with the present invention as a targeting molecule.

Other examples of targeting molecules include glucose, galactose, mannose, mannose 6-phosphate, hormones (e.g., insulin, growth hormone, and the like), growth factors or cytokines (e.g., TGF- $\beta$ , EGF, insulin-like growth factor, and the like), YEE(GalNAcAH)<sub>3</sub> or derivatives, cobalamin,  $\alpha$ -2 macroglobulins, asialoglycoprotein, albumin, texaphyrin, metallotexaphyrin, antibodies, antibody fragments (e.g., Fab), single-chain antibody variable region (scFv), transferrin, any vitamin and any coenzyme.

As previously described, a bioconjugate of the present invention comprises a bioactive agent conjugated directly or indirectly via a covalent bond to the cobalt atom of an organocobalt complex. The bioactive agent is conjugated directly to the cobalt atom through a non-reactive atom in the bioactive agent or is conjugated indirectly to the cobalt atom through the use of a spacer. Therefore, in contrast to the conjugates formed under U.S. Patent 5,428,023, the attachment of a bioactive agent to the cobalt atom in the axial position does not interfere with receptor-mediated endocytosis from the blood into cells.

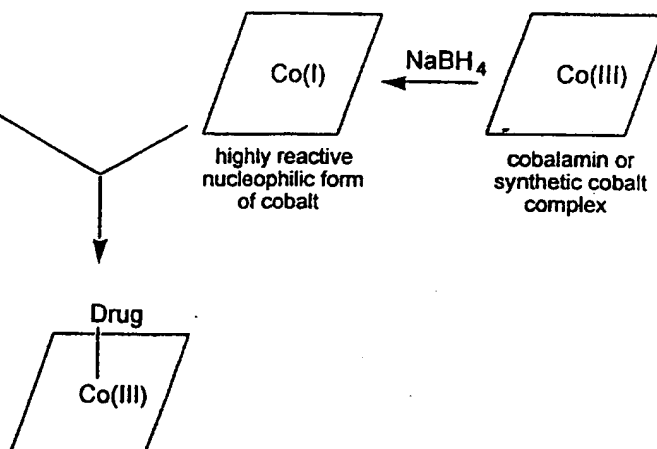
The unusually weak cobalt-non-reactive atom bond (e.g., C-Co bond) of the bioconjugate provides a readily addressable trigger for the controlled *in vivo* release of the bioactive agent from the organocobalt complex. The bond dissociation energy (BDE) of Co-non-reactive atom bond in the bioconjugate is in the range of 30 to 50 kcal/mol (e.g., 30-40 kcal/mol range for a Co-C bond) which make them among the weakest covalent bonds known, yet the bond is relatively stable in aqueous solution.

A common strategy will employ the modification of the anticancer drug so that it possesses an electrophilic site which can react with the highly nucleophilic Co(I) intermediate generated upon treatment of hydroxycobalamin with NaBH<sub>4</sub>. This structural modification will be sufficiently far removed from the active site (pharmacophore) to preclude any interference with the desired biological activity. Approaches used in the case of chlorambucil are typical: the carboxylic acid group of chlorambucil is converted to either an acid chloride or a bromoethyl ester, either of which can be efficiently coupled with cob(I)alamin.

## General Strategy:

Drug  $\longrightarrow$  Drug-X

(X=electrophilic site, such as alkyl halide, acid halide, epoxide, Michael acceptor, etc.)



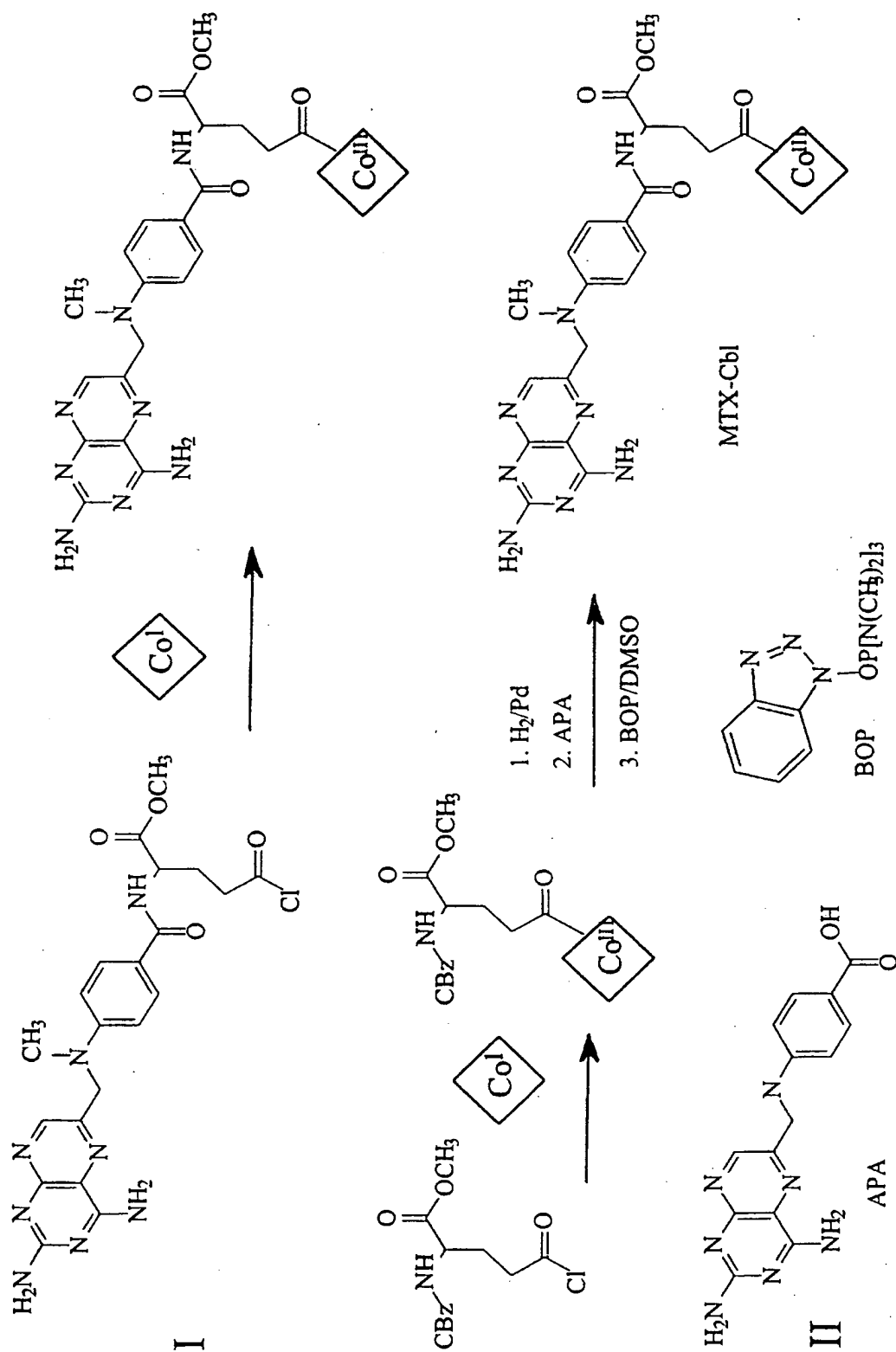
For example, reduced  $\text{Cbl}^I$  is prepared by  $\text{NaBH}_4$  or zinc dust reduction, e.g. of hydroxocob(III)alamin. In the above scheme, the drug can be a cytotoxic agent, other drug or other bioactive agent as described herein. In other schemes, a spacer containing a carbon atom or other atom such as that specified for the non-reactive atom for binding to the cobalt atom and which also contains a reactive grouping, e.g.  $-\text{OH}$  or  $-\text{CN}$ , which is further reacted with the bioactive agent, is introduced. Other reactive groups, e.g.  $-\text{NH}_2$ ,  $-\text{SH}$ ,  $-\text{COOH}$ , etc., can also be utilized for coupling to a bioactive agent. It is important to note that, in some cases (e.g., chlorambucil, doxorubicin), the small organic molecule released is not the parent drug, but rather retains some of the modification installed to allow coupling. In other cases (e.g., topotecan), the structure of the released drug may correspond to the parent molecule.

More specific details of the synthesis of representative bioconjugates according to the present invention are as follows, using a "drug" which can be replaced by any suitable bioactive agent and cobalamin which can be replaced by any suitable organocobalt complex. In this synthesis, all procedures are under argon. Hydroxocob(III)alamin is dissolved in aqueous  $\text{CH}_3\text{OH}$  (1:1 v/v) at  $25^\circ\text{C}$ . A 2-10 fold excess of  $\text{NaBH}_4$  is added. The solution slowly changes color from red to brown and gradually green ( $\text{Cbl}^I$ ). After approximately 15 min. the electrophilic drug ligand (dissolved in the same deoxygenated solvent) is added, e.g., as an alkyl, acyl or aryl chloride. Strictly anaerobic conditions are maintained and the reaction mixture is stirred gently at  $25^\circ\text{C}$ . The color gradually changes back to red as  $\text{Cbl}^I$  is converted to alkyl-, acyl-, or aryl- $\text{Cbl}^{\text{III}}$ . After about 1.5 h, the solution is acidified to pH 3.0 with dilute  $\text{HCl}$ . Methanol is removed under reduced pressure by rotary evaporation at less than  $40^\circ\text{C}$ . The

resulting aqueous solution is diluted with an equal volume of H<sub>2</sub>O and loaded onto a Dowex AG-50-X2 (200-400 mesh) cation exchange column. The column is washed sequentially with H<sub>2</sub>O and 0.1 M NaOAc, pH 6.4. Fractions containing drug-cob(III)alamins appear red and are collected appropriately. Unreacted hydroxocob(III)alamin is retained on the column. Combined  
5 fractions of drug-cob(III)alamin are extracted with phenol and concentrated by rotary evaporation. Drug-cob(III)alamins can often be crystallized by the addition of acetone to a concentrated aqueous solution. Characterization of the alkyl-, acyl-, or aryl-cobalamin conjugates is by NMR, mass spectrometry (FAB, CI, or electrospray), and IR methods.

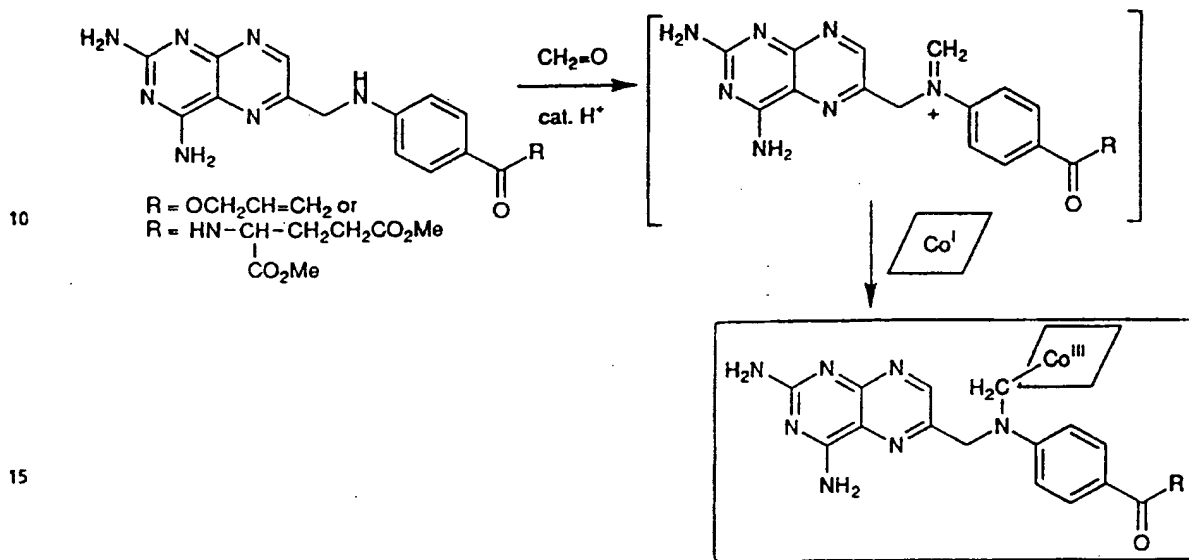
10 A methotrexate-containing bioconjugate can be synthesized by the following methods.

In method one utilizing the above procedure, methotrexate (MTX) is converted to its corresponding acyl chloride and reacted with cobalamin and/or Co(III)[SALEN] and/or other disclosed organocobalt complexes to yield methotrexate-cobalamin and methotrexate-Co(III)[SALEN] according to the following reaction scheme I. In the alternative method two,  
15 the C-Co bond is first formed from an acyl chloride having a protected amino group. The amino group is then deprotected, followed by formation of the amide bond to an aminobenzoylpterin according to the following reaction scheme II.



-21-

An aminopterin-containing bioconjugate can be synthesized by the following method. The des-methyl derivative of methotrexate (aminopterin) is coupled to cobalt as shown by the following reaction formula, in which the iminium ion is either reacted with Co(I) directly, or the iminium ion is converted to the aminonitrile and then slowly unmasked to reveal the iminium cation.



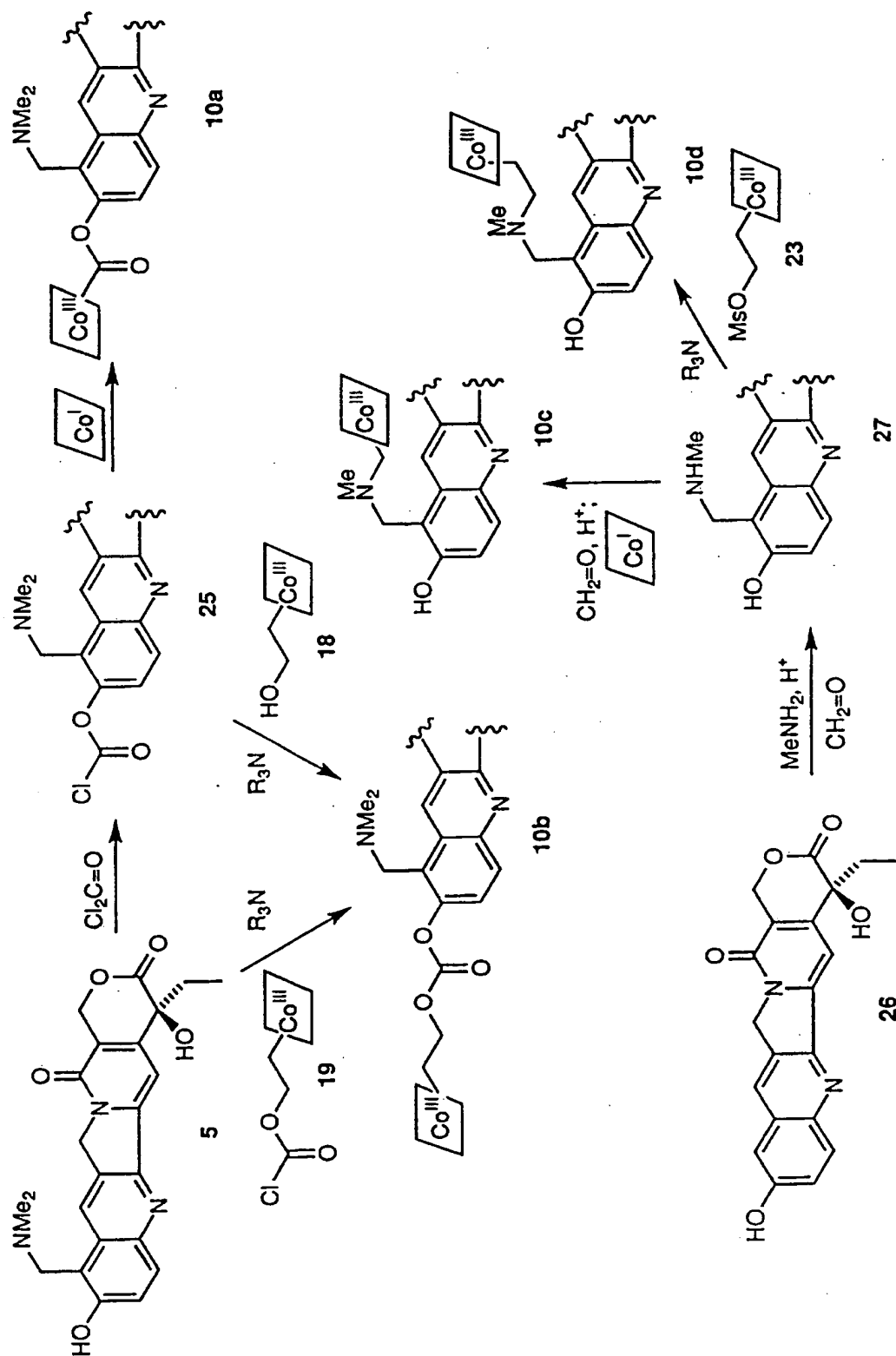
A topotecan-containing bioconjugate can be synthesized by the following method. The cytotoxic activity of topotecan (TPT) or camptothecin (CPT) arises from their ability to freeze topoisomerase I-DNA "cleavable complexes." (Pommier et al., 1995) Since some tumor types display greatly elevated levels of topo I (Giovannella et al., 1989), topoisomerase poisons of this type are likely to have a higher therapeutic index in the treatment of those cancers. However, treatment with camptothecin derivatives could be made more general if used in conjunction with the targeted delivery approach.

25 Topotecan is conjugated to cobalamin, Co[SALEN] and other organocobalt complexes according to the following reaction schemes. Camptothecin is conjugated in a similar manner. Preparation of 10a and 10b involves similar chemistry to that discussed above for 8a,b. Selective generation of the phenyl chloroformate (25) of topotecan (5) and acylation of Co(I) gives 10a. Exposure of 25 to 18 or treatment of 5 with the previously discussed chloroformate 19 furnishes 10b. Conjugates 10c,d will require somewhat longer routes, as they cannot be prepared directly from 5. However, the established synthetic route for conversion of the natural

30

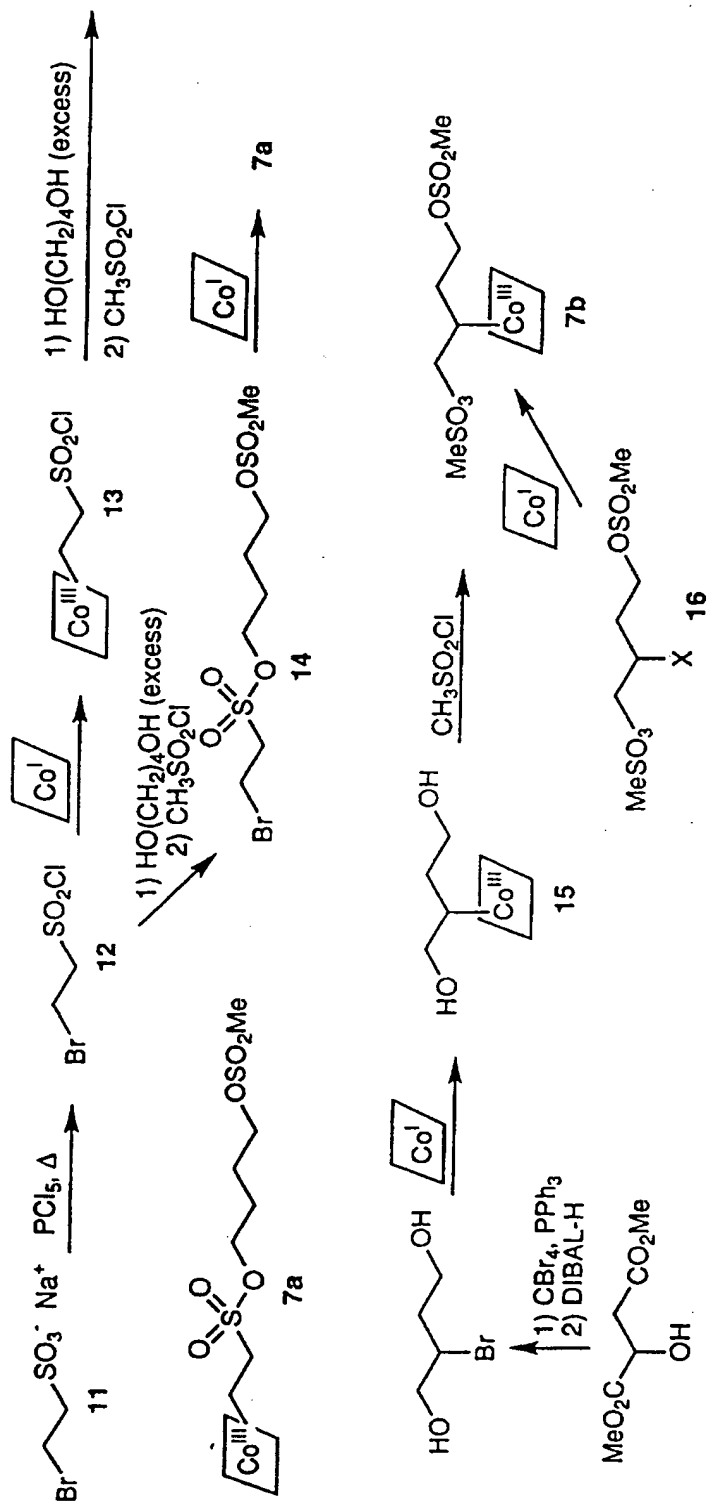
product camptothecin to 5 can be modified at the appropriate point to allow for attachment of the cobalt complex. The first three steps to prepare phenolic intermediate 26 are known (Mulliez et al., 1994). Mannich-type substitution with formaldehyde/dimethylamine then gives 5. Use of methylamine gives the corresponding secondary amine 27. At this point, linkage to Co via a methylene to give 10c is possible via Co(I) trapping of a second, *in situ* generated imminum salt. Alternatively, N-alkylation with 23 gives 10d. Cleavage of 10a and 10b provides 5 directly via fragmentative pathway or indirectly via other products. Cleavage of 10c with hydrogen extraction yields 5. Cleavage of 10d yields the product 5 having an ethylmethylamino group in place of the dimethylamino group.





A busulfan-containing bioconjugate can be synthesized by the following method. Busulfan is an alkylating agent used therapeutically against chronic myelogenous leukemia (CML). The preferred point for attaching busulfan to the organocobalt complex is on one of the alkanesulfonate units. A slight change in the structure of the sulfonate portion of the ester is will  
5 not exert a large effect on the ability of the released drug to crosslink DNA. Cleavage of 7a followed by hydrogen abstraction furnishes the mixed ethanesulfonate/methanesulfonate 2b. Trapping of the carbon radical under oxidative conditions produces mixed bis(sulfonate) 2c, which is also a competent crosslinking agent. Cleavage of 7b results in the release of the parent drug 2a after hydrogen abstraction.

10 Bis-methylsulfonate busulfan is conjugated to cobalamin, Co[SALEN] and other organocobalt complexes according to the following reaction schemes. For the preparation of 7a, the commercially available sodium salt of bromoethanesulfonic acid (11) serves as the starting point. Heating with phosphorus pentachloride furnishes the corresponding sulfonyl chloride 12 as a distillable liquid. Treatment with Co(I) leads to preferential displacement of the bromide to  
15 furnish 13, which is converted to 7a by sequential treatment with 1,4-butanediol and mesyl chloride. The order of the final three steps can be changed; for example, treatment of 12 with excess butanediol, followed by mesyl chloride gives the mixed bis(sulfonate) 14. Selective displacement of the primary bromide by Co(I) then gives 7a. In the case of conjugate 7b, treatment of 2-bromobutane-1,4-diol (which is readily available from malic acid diester) with  
20 Co(I) gives adduct 15. Bis(mesylation) gives 7b. Alternatively, 7b is prepared from 16 (X = Br or I) with selective displacement of the halide.

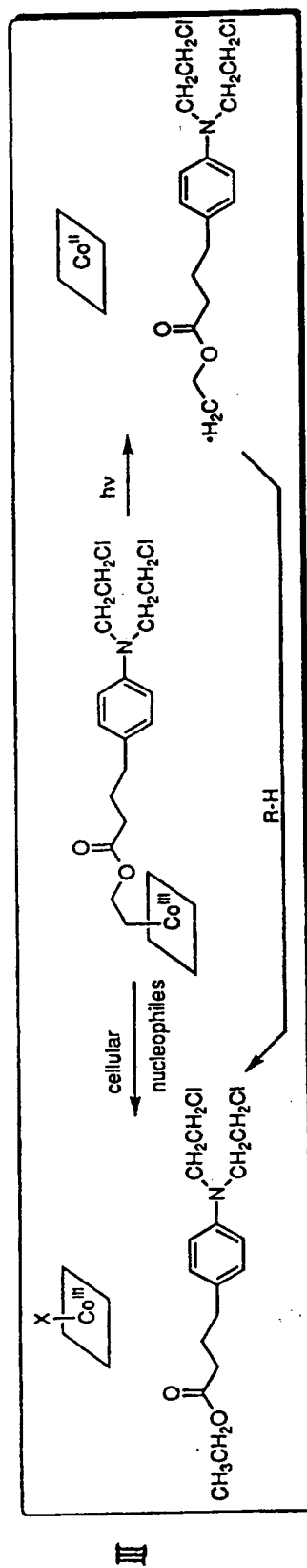
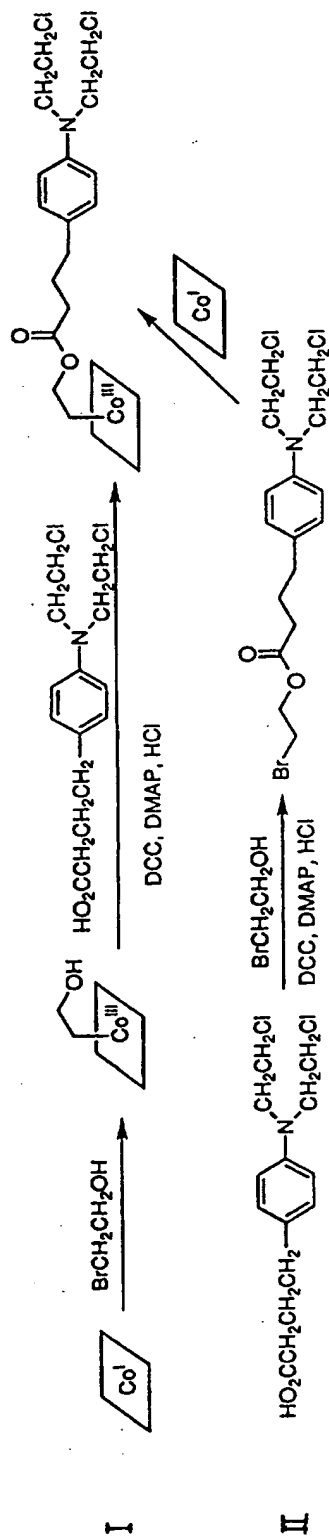


A chlorambucil-containing bioconjugate can be synthesized by the following methods. Chlorambucil is a relatively stable nitrogen mustard with attenuated alkylating ability, presumably as a consequence of the less-basic aniline nitrogen.

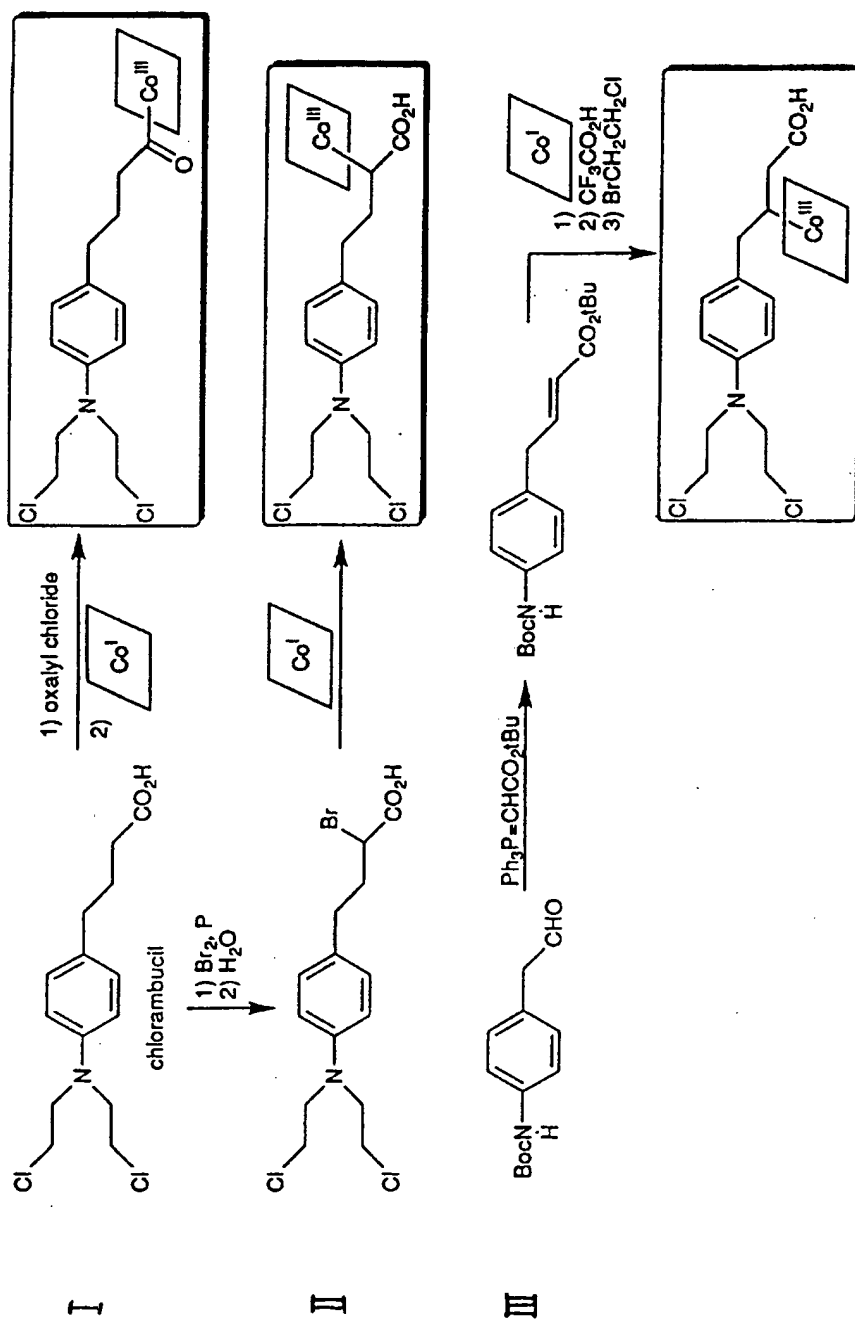
Method One: In this procedure, chlorambucil is converted to the acid chloride followed  
5 by reaction with cob(I)alamin or Co(I)[SALEN] according to reaction sequence I. In situations where the acyl linkage to the organocobalt complex is too labile towards serum nucleophiles, two alternate bioconjugation procedures can be utilized.

Method Two: The procedure involves bromination of a carbon atom adjacent to the  
10 carboxyl group under standard Hell-Vollhardt-Zelinski conditions to permit attachment of the Co complex in the  $\alpha$ -position according to reaction sequence II. In scheme II, replacement of the C-Co with C-H provides chlorambucil. The reactant stoichiometry, temperature, and dilutions conditions can be manipulated to avoid competing displacement of one of the chloroethyl groups, or of the C1 by  $S_N2$  attack.

Method Three: The BOC-protected p-aminophenylacetaldehyde can be conjugated to the  
15 Co moiety, followed by formation of the active nitrogen mustard product according to the following reaction sequence III.



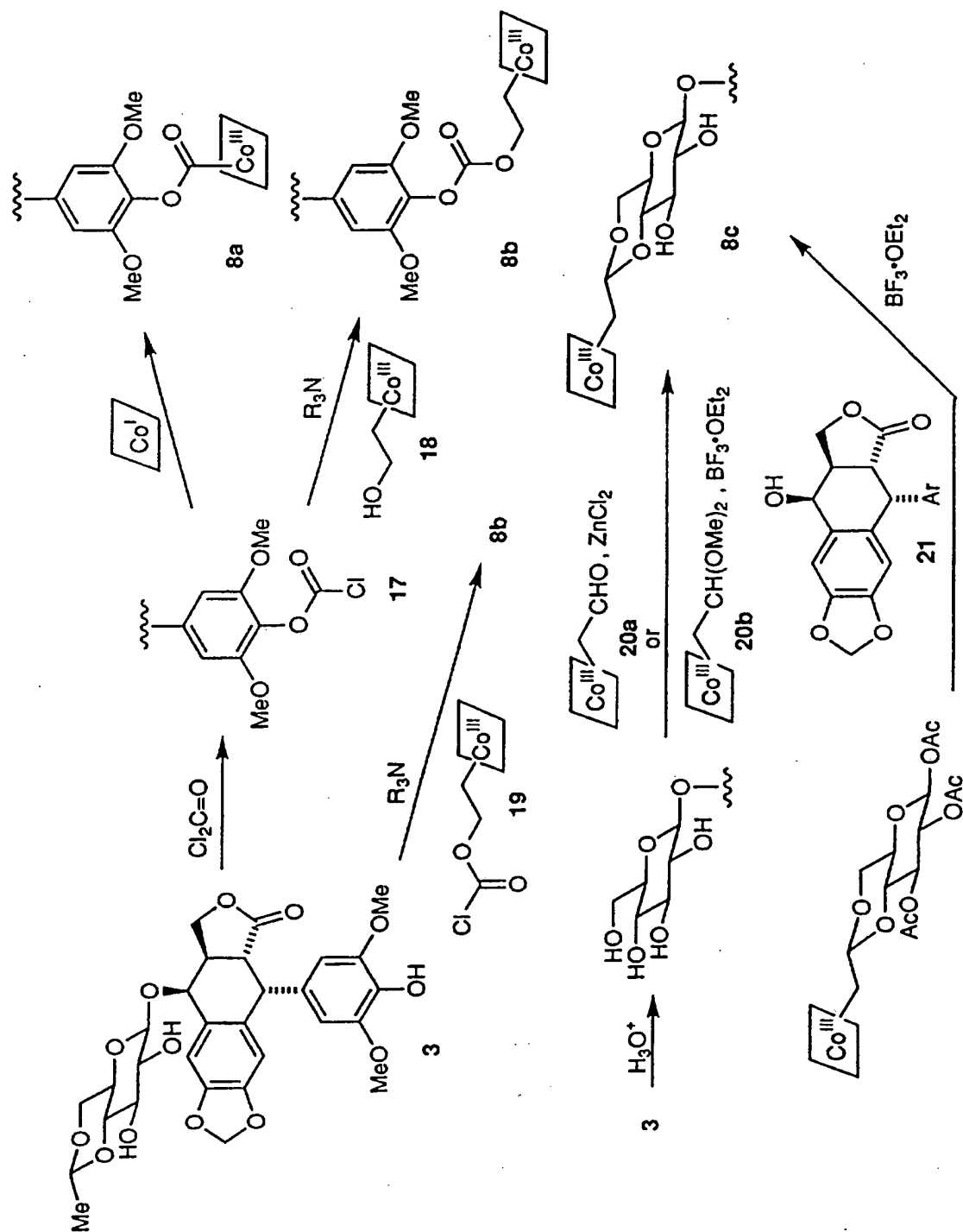
A chlorambucil, ethyl ester-containing bioconjugate can be synthesized by the following methods. When conjugating a drug via a carboxyl group, as in the case of chlorambucil, linking the drug to the cobalamin via a hydroxyethyl tether may be desirable. This can be accomplished by one of two convenient routes, both of which are schematically illustrated below. First, 5 2-hydroxyethyl-cob(III)alamin can be readily prepared from cob(I)alamin and bromoethanol. Esterification is carried out under standard conditions, i.e. by reaction of a carboxylic acid (chlorambucil) with an alcohol (2-hydroxyethylcob(III)alamin) in the presence of dicyclohexylcarbodiimide (DCC) (or water-soluble derivatives such as EDCI) and a catalytic amount of 4-N,N-dimethylaminopyridine (DMAP) and its hydrochloride salt (DMAP-HCl) in 10 dichloromethane or toluene. Alternatively, the ester-linked conjugate can be prepared by first forming the 2-bromoethyl ester of chlorambucil and then reacting the ester with cob(I)alamin to provide the same product. The reaction schemes (I, II) are shown below. With this mode of attachment, cleavage from the bioconjugate leads to release of the ethyl ester of chlorambucil according to reaction scheme III.



An etoposide-containing bioconjugate can be synthesized by the following method. Etoposide is a semisynthetic derivative of the natural product epipodophyllotoxin that is widely used against a variety of tumors, especially small cell lung carcinoma and germ cell tumors (De Jong et al., 1995). It has also shown considerable promise in the treatment of refractory cases of ovarian and breast cancer. Etoposide appears to function as a topoisomerase II poison.

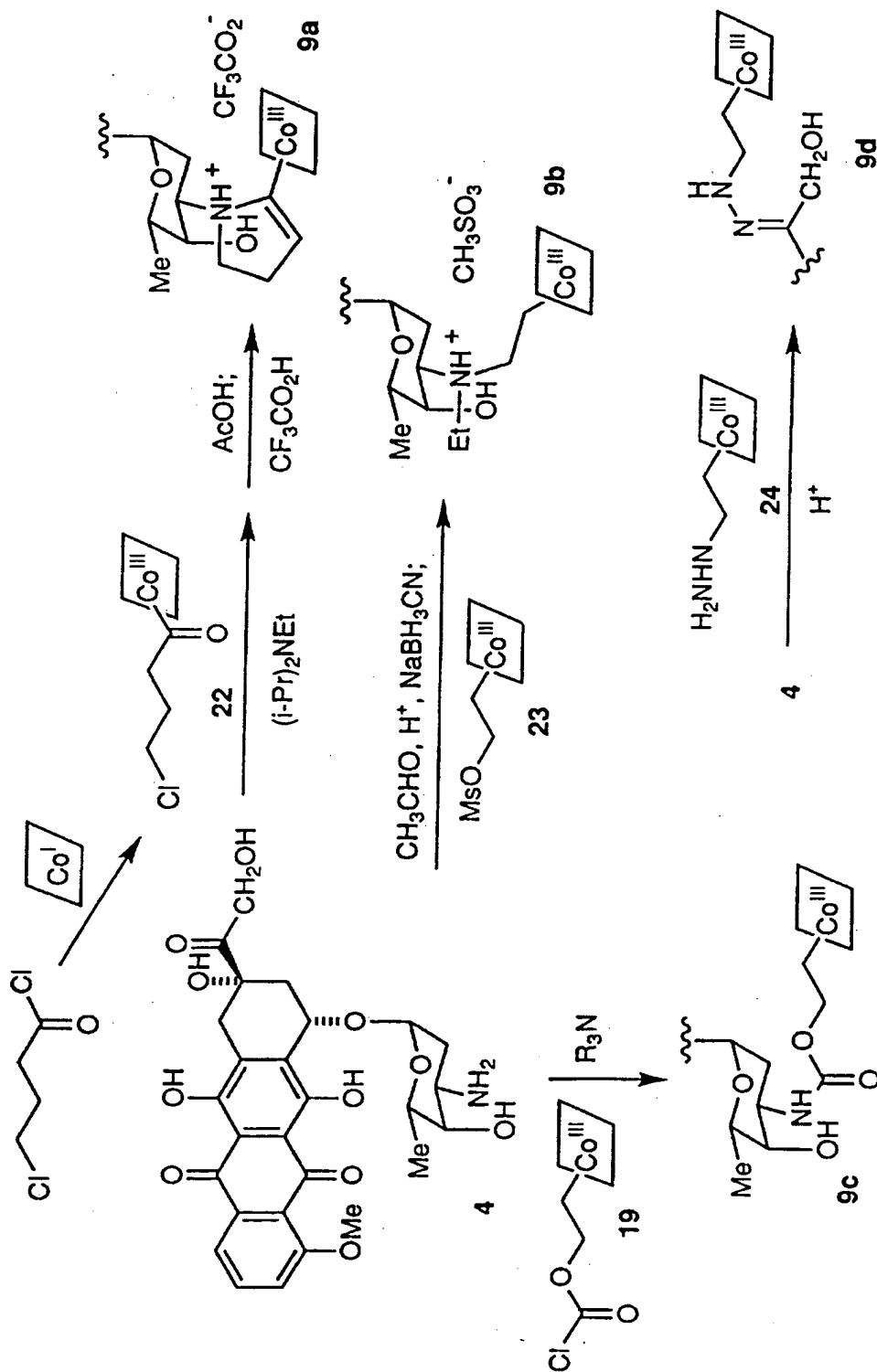
Etoposide is conjugated to cobalamin, Co[SALEN] and other organocobalt complexes according to the following reaction schemes. Bioconjugates **8a** and **8b** require conversion of the free phenol of etoposide (**3**) to the corresponding chloroformate **17**. Direct acylation with Co(I) gives acylCo(III) derivative **8a**, while treatment with the previously described hydroxyethylCo(III) derivative **18** furnishes carbonate **8b**. This derivative is also available via acylation of **3** with the chloroformate **19** derived from **18**. Preparation of acetal-modified conjugate **8c** may be more challenging. The ethylene acetal of **3** can be hydrolyzed and then the acetal reformed using aldehyde **20a** or dimethyl acetal **20b** (Keller-Jusl et al., 1971). Compound **20a** may also be accessed via careful, selective oxidation of **18**, while **20b** should be available via alkylation of the Co(I) derivative with commercially available bromoacetaldehyde dimethyl acetal. In addition, the acetal of glucose can be formed and then the secondary alcohol of **21** can be glucosylated. Cleavage of **8a** or **8b** either give **3** directly via fragmentative pathways, or furnish products which can undergo eventual hydrolysis to **3**. Trapping with H• following homolysis of **8c** would then furnish **3**.

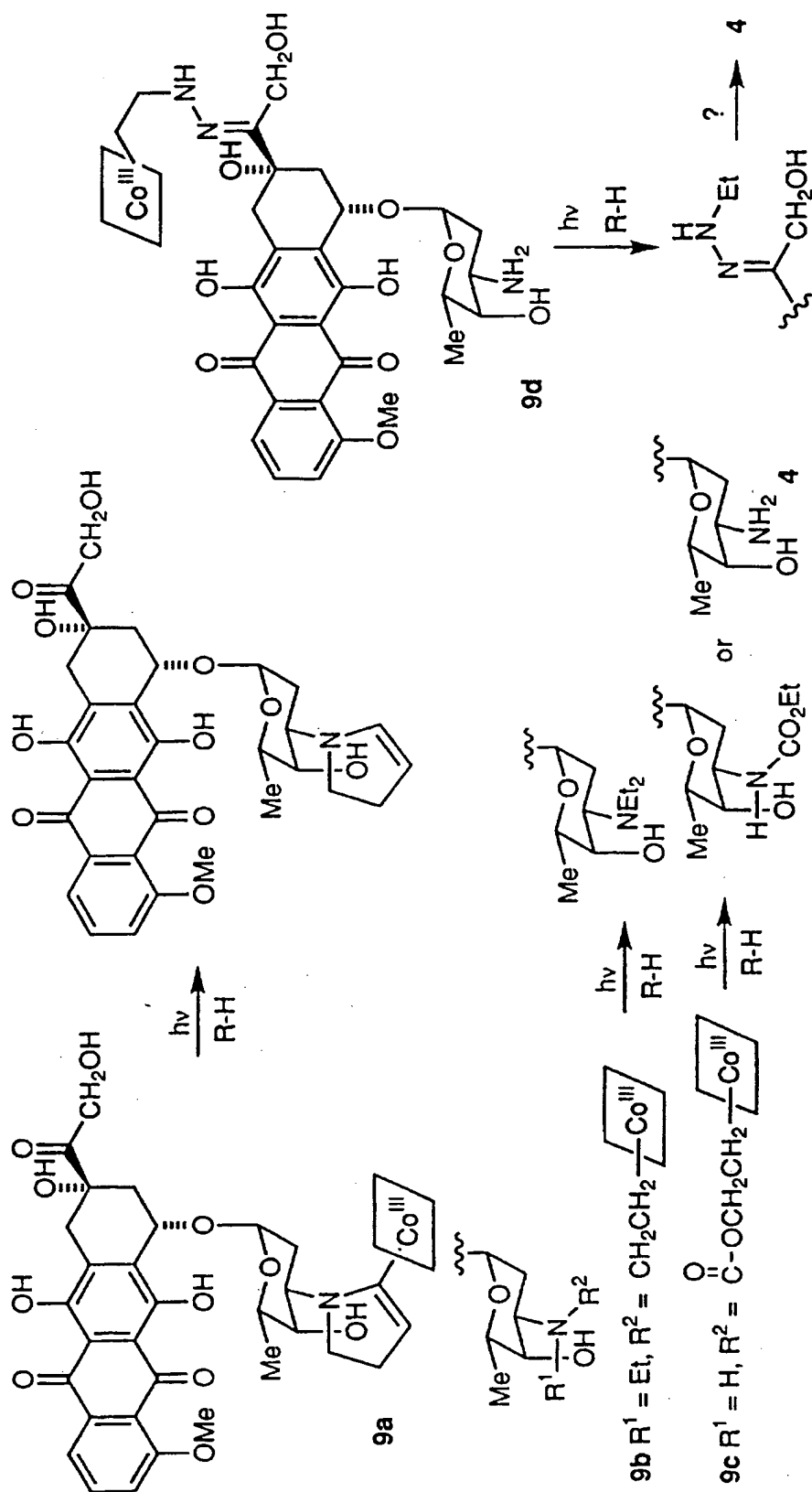




A doxorubicin-containing bioconjugate can be synthesized by the following method. Doxorubicin (4) is the most widely used of the anthracycline antibiotics, and is clinically useful against a broad spectrum of solid and hematological tumors. Like etoposide, doxorubicin appears to target topoisomerase II, ultimately leading to growth arrest and nonapoptotic cell death (Fornari et al., 1996; Ling et al., 1996). The clinical usefulness of doxorubicin is limited by nonspecific toxicity, especially cardiotoxicity. Thus, it would appear to be a particularly good candidate for selective delivery. This is confirmed by its frequent use in liposome-based methods (Hu et al., 1996; Longman et al., 1995; Hosada et al., 1995), as part of immunoconjugates (Johnson et al., 1995; Sivam et al., 1995), or in prodrug approaches (Svensson et al., 1995).

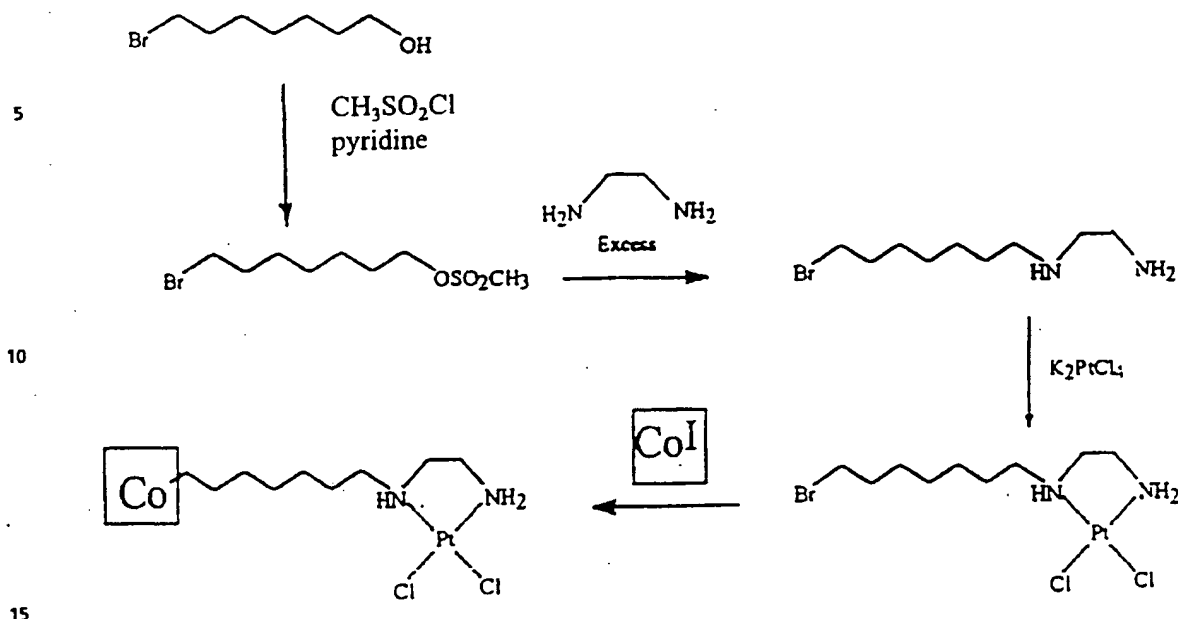
Doxorubicin conjugated to cobalamin, Co[SALEN] and other organocobalt complexes according to the following reaction schemes. For the synthesis bioconjugate 9a, the condensation of the daunosamine amino group with acyl-Co(III) complex 22 is performed. This reaction forms the 2-pyrroline ring in analogy to published routes using 4-iodobutyraldehyde and 5-iodo-2-pentanone.(9b) The acyclic tertiary amine derivative 9b is available from 4 via initial reductive amination with acetaldehyde, then alkylation of the resulting secondary amine with the mesylate 23 derived from 18. Alternatively, treatment of 4 with chloroformate 19 provides carbamate 9c. If alternative points of attachment are desired, hydrazone-linked derivatives such as 9d can be used using simple cobalamin alkyl hydrazides such as 24, obtainable from 23. The cleavage of these bioconjugates is shown in the reaction scheme below.





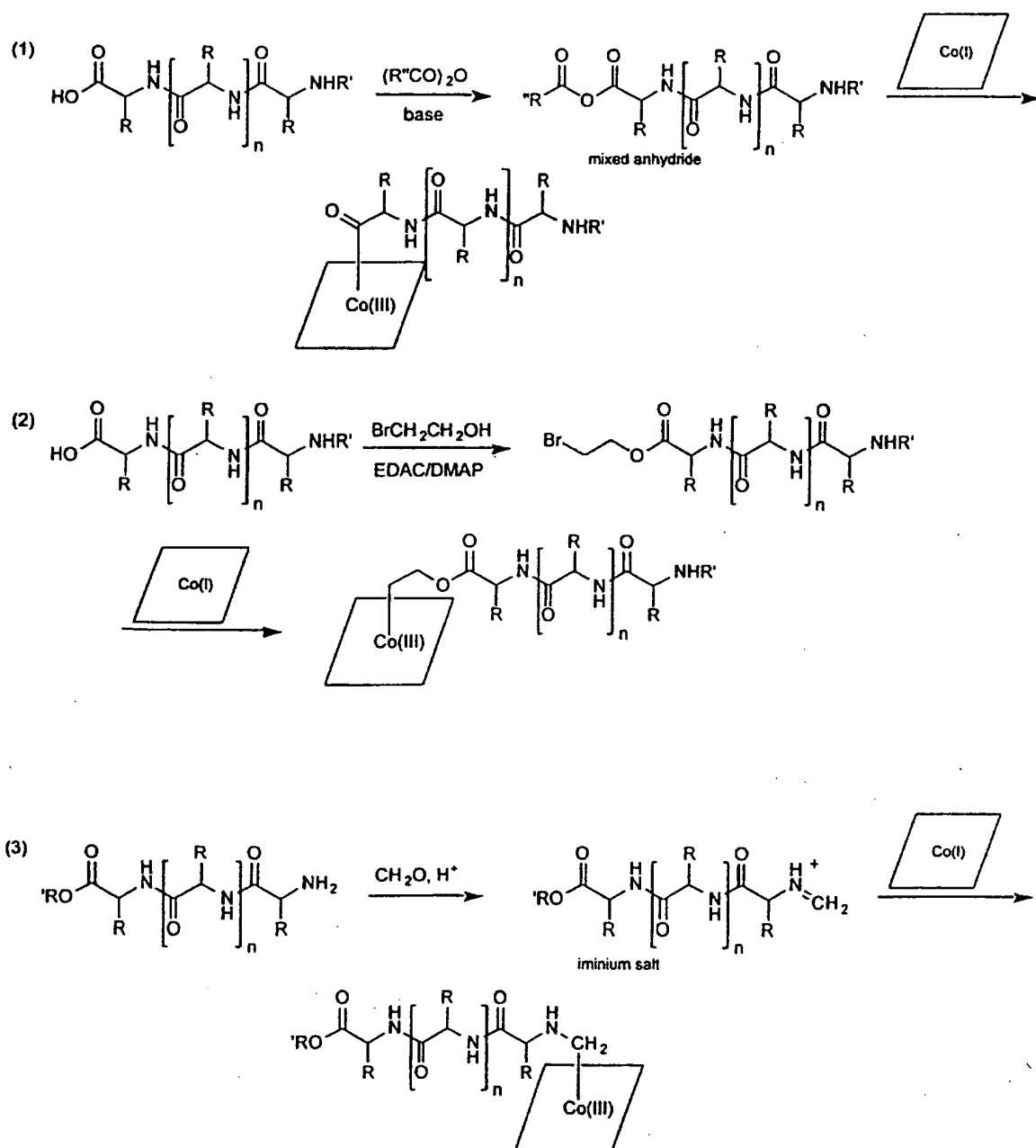
-35-

A carboplatin containing bioconjugate can be synthesized as shown in the following reaction scheme.

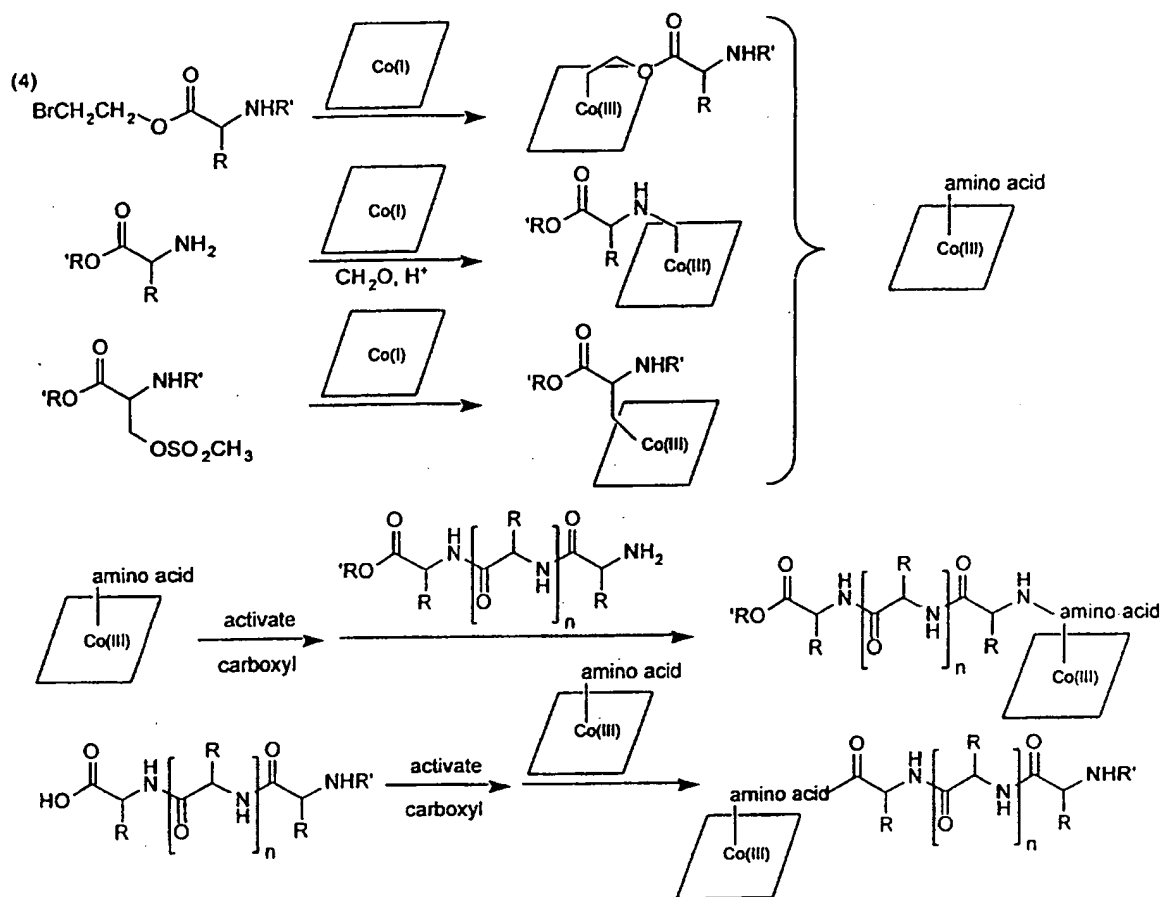


A peptide-containing bioconjugate can be synthesized by the following methods: (1) The C-terminal carboxyl group of the peptide can be activated and used to acylate Co(I), in analogy to the acylation of Co with chlorambucil acid chloride. (2) The C-terminal carboxyl group can be esterified with bromoethanol, in analogy to the other chlorambucil route, and the bromide displaced with Co(I). (3) The N-terminal amino group of the peptide can be treated with  $\text{CH}_2=\text{O}$  and Co(I) to form a Co(III)- $\text{CH}_2\text{-NH-peptide}$  linkage, in analogy to the synthesis of the topotecan bioconjugate. (4) A Co(III)-amino acid complex can be prepared, and used in a coupling step with the remainder of the peptide. These methods can involve attachment of the Co at either the N- or C-terminus, or via a side-chain. A longer linker may be employed in any of these routes, if it is desirable to keep the cobalt complex further removed from the peptide chain.

-36-

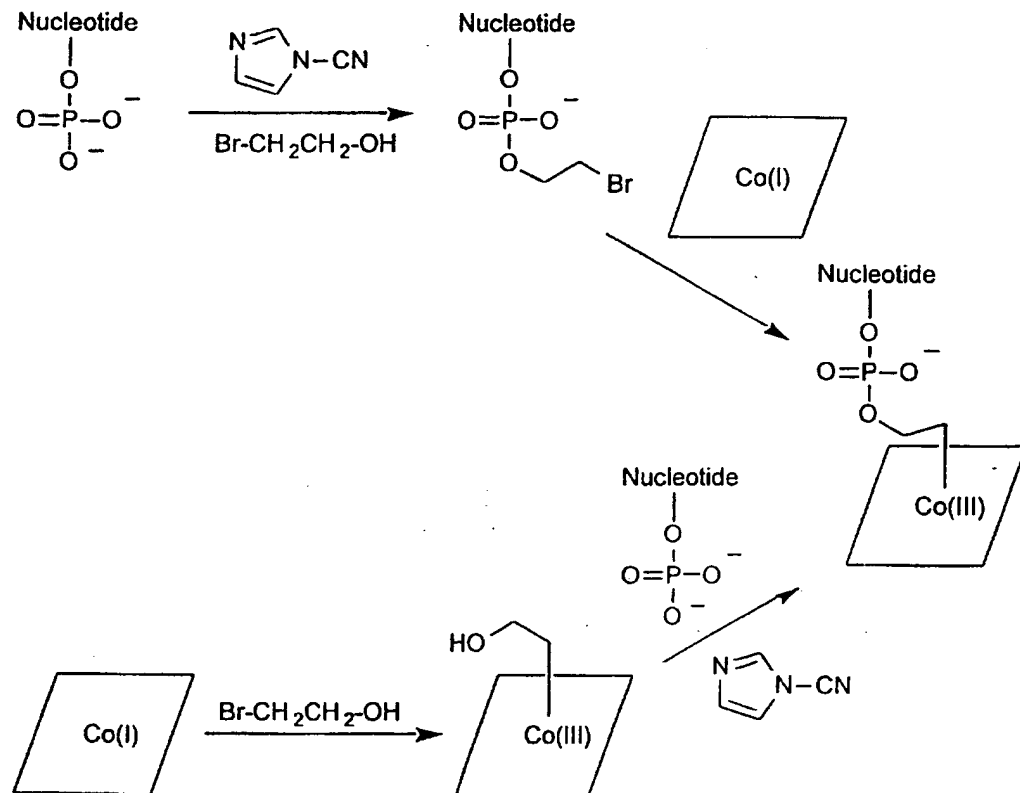


-37-



An oligonucleotide or nucleic acid containing bioconjugate can be synthesized by the following methods. In both methods, a phosphate ester is used to link the end of the nucleotide and a hydroxyethyl-Co group. This linkage can be accomplished by either directly coupling Co-CH<sub>2</sub>CH<sub>2</sub>-OH and Nucl-OPO<sub>3</sub><sup>2-</sup>, or by esterifying Nucl-OPO<sub>3</sub><sup>2-</sup> with Br-CH<sub>2</sub>CH<sub>2</sub>-OH, then displacing the Br with Co(I), as above.

-38-

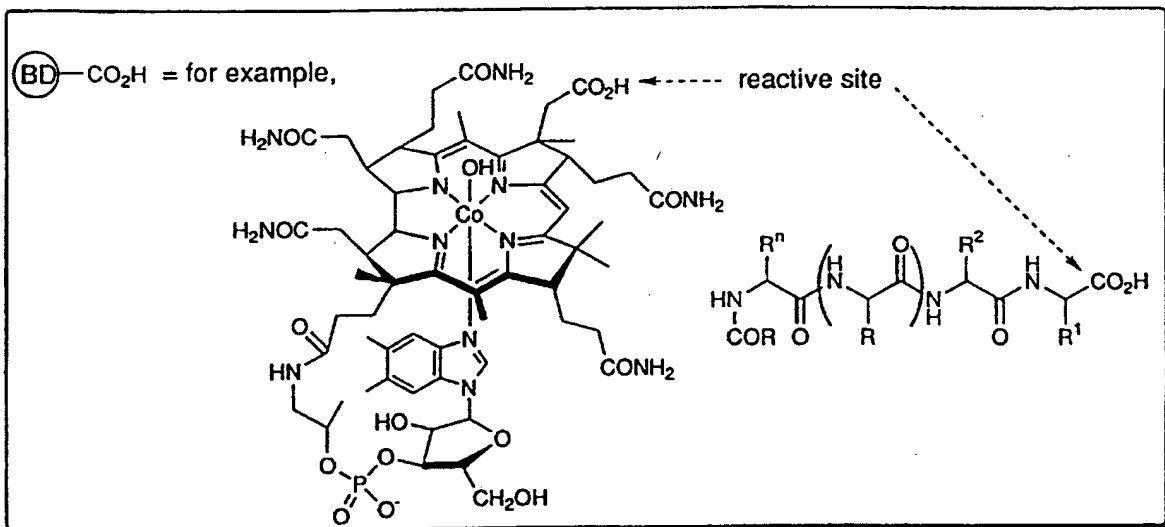
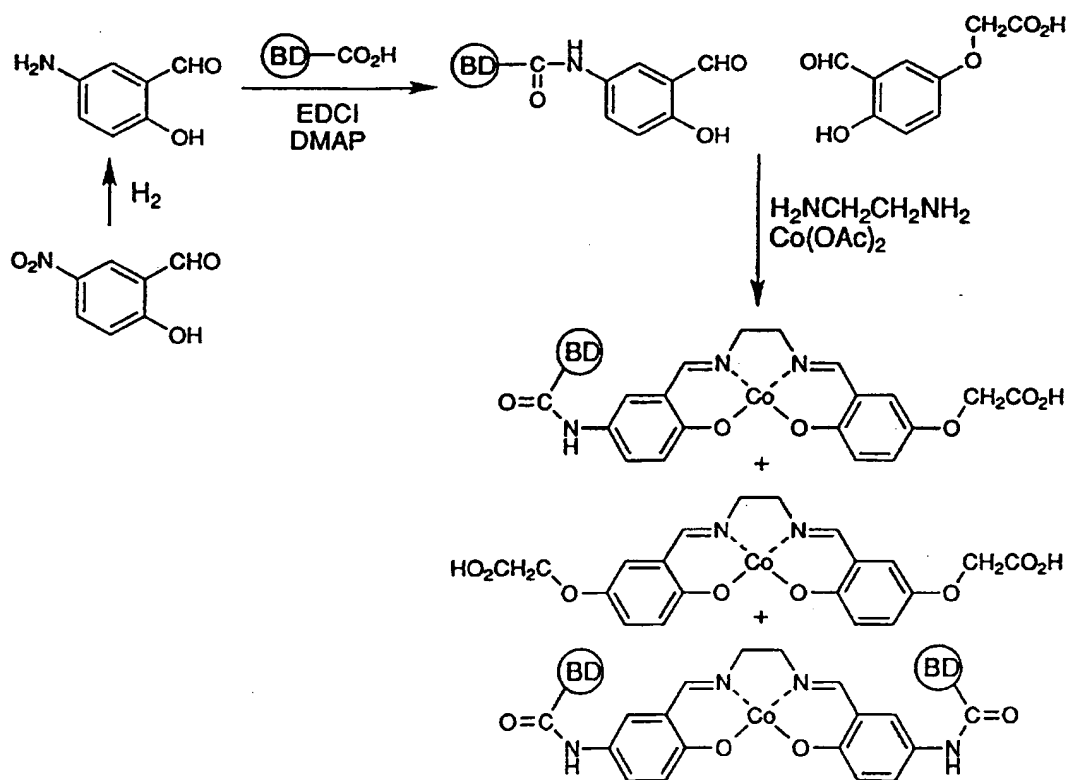


An unsymmetrically substituted Co[SALEN] complex can be prepared from 5-amino-salicylaldehyde and the glycolate ether of 2,5-dihydroxybenzaldehyde. The amino group, which is prepared from commercially available 5-nitrosalicylaldehyde, functions as the attachment for the targeting molecule (binding domain, BD) by way of EDCI-catalyzed amide formation. The other molecule has a carboxylic acid unit attached for solubility enhancement. Coupling of these two molecules with ethylenediamine and Co(II) acetate furnishes a mixture of three complexes: the two symmetrical complexes and the mixed one. All of these are useful, although the one lacking a BD-unit attached to either side of the SALEN is less preferred.

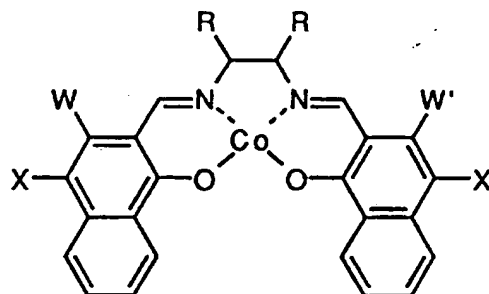
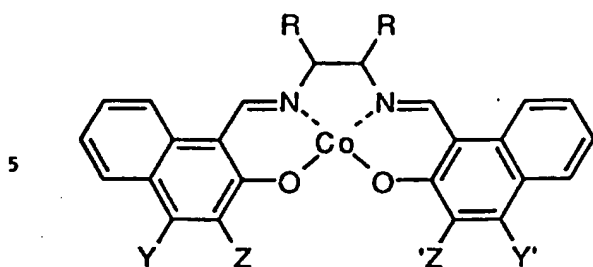
With regard to binding domains, two possibilities are shown: a cobalamin derivative, and a peptide. In the former case, the known carboxylic acid is used to attach cobalamin to the amino group of the SALEN. This bioconjugate still uses cobalamin-based receptor-mediated endocytosis to get into the cell, but the drug is attached through the SALEN instead of the cobalamin. The latter case uses a peptide known to bind to cell surface receptors of tumor cells (e.g., a fragment of epidermal growth factor), with the carboxyl terminus attached to the amino group on the SALEN. Alternatively, one of the glutamate carboxyl groups of folate is used to



obtain a folate-based bioconjugate. In addition to connecting the binding domain via an amide linkage, one could use reductive amination if the targeting molecule contained an aldehyde (BD-CHO + SALEN-NH<sub>2</sub> + NaBH<sub>4</sub>), or one could use the carboxyl group on the other piece to form an amide or ester linkage. Many other approaches (e.g., ether formation, olefination by Wittig  
5 reaction, attachment via a diester or diamide linker, etc.) are also possible.

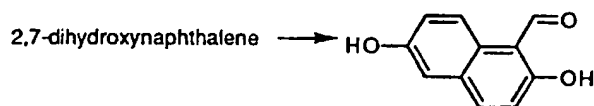
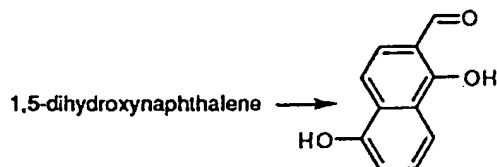


Extended benzenoid systems of the SALEN ligands are shown below.

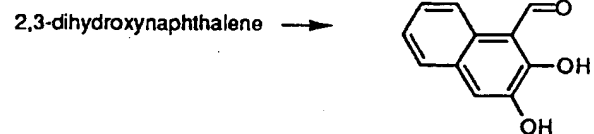
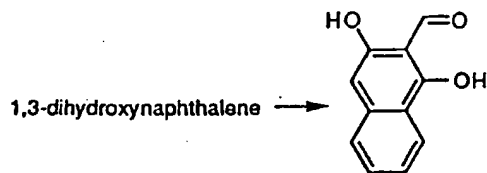


As a starting point in their synthesis, any of the commercially available naphthalene diols  
 10 can be used. The diols undergo formylation reactions to furnish the molecules shown below. These molecules are then be coupled with Co(II) acetate and various diamines to give the extended Co[SALen] complexes. The OH groups on the second ring can be left intact, used to attach the binding domain, or modified to enhance water solubility through attachment of a polar group, such as polyamine, polycarboxylic acid, or carbohydrate moiety.

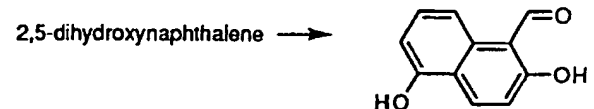
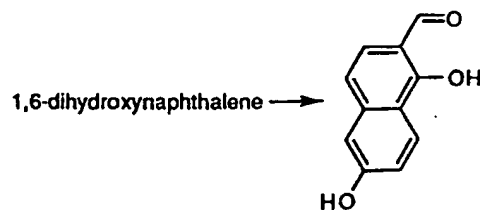
15



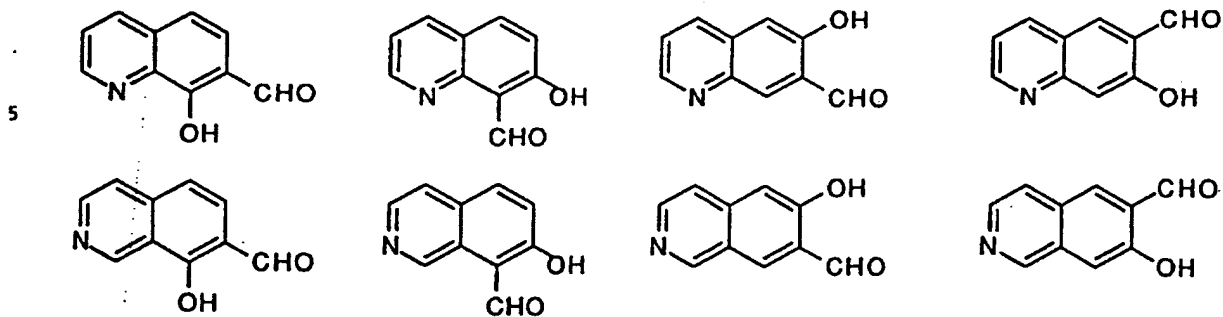
20



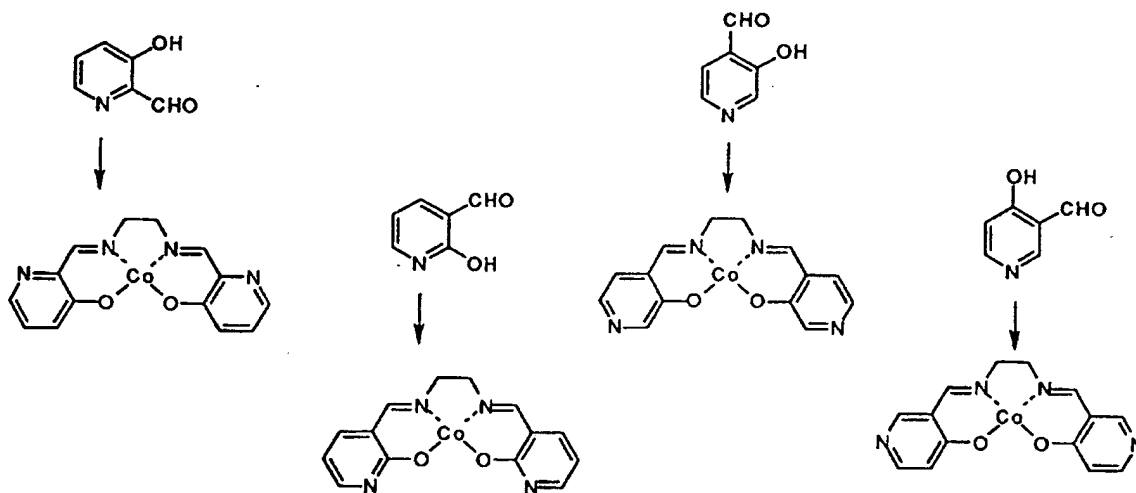
25



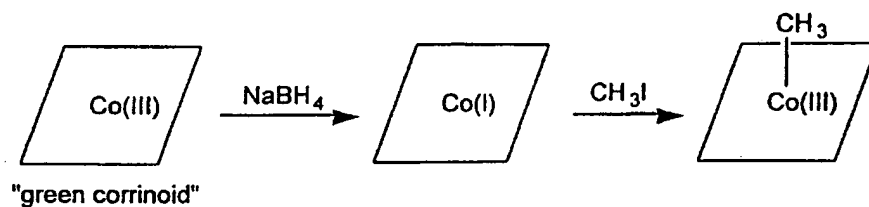
Modification of quinolines and isoquinolines are also carried out to give pyridine-fused SALENs.



10 Along similar lines, SALENs derived from monocyclic heterocyclic hydroxyaldehydes are made, examples of which are shown below.



A bioconjugate containing the "green corrinoid" (Brown et al., 1996) can be synthesized as follows. The "green corrinoid" can be reduced in analogy to cobalamin, and that the reduced corrinoid will react with iodomethane to form the methylCo(III) corrinoid. Since the methylCo(III) corrinoid exhibits similar behavior to natural cobalamin, similar conjugation  
 5 procedures with the electrophilic drug derivatives described above can be carried out.



The bioconjugates of the present invention have the improved property of being capable of targeted, selective release of the bioactive agent from the bioconjugate. The bioactive agent is  
 10 is released from the bioconjugate by cleavage. In one embodiment, the cleavage may occur as a result of normal displacement by cellular nucleophiles or enzymatic action. In a second embodiment, the cleavage is caused to occur selectively at the release site by an external signal. The external signal may be light or photoexcitation, i.e. photolysis, or it may be ultrasound, i.e. sonolysis. Further, if the photolysis takes place in the presence of a magnetic field surrounding  
 15 the release site, the release of the drug, such as a cytotoxic agent, into surrounding healthy tissue can be minimized.

Although it is desired to cause the bioactive agent to be released at the desired cells, tissue or organs, e.g., at the site of the tumor or other cancer cells, it is also desirable to protect adjacent tissues from the negative side effects of such potent agents. The bioactive agent is  
 20 released from the bioconjugate at the targeted site preferably by application of an external signal, such as light or ultrasound. The photolysis of the bioconjugates of the present invention occurs through cleavage of the Co-C bond to produce a solvent-caged radical pair consisting of Co(II) and the bioactive agent radical ( $\text{R}\cdot$ ). Lott et al. (1995) demonstrate that alkylcob(III)alamin photolysis can undergo magnetic field dependent recombination. A magnetic field application of  
 25 100-3000 gauss can be used to enhance radical pair recombination in surrounding tissue where drug release from the conjugate is not desired, leading up to at least a 2-fold decrease in photochemically-triggered drug release in such surrounding healthy tissue.

The sonolysis of the bioconjugates of the present invention occurs through cleavage of the Co-non-reactive atom bond in aqueous solution to produce the bioactive agent and a Co(II) (e.g., cob(II)alamin ( $\text{Cbl}^{\text{II}}$ )) under anaerobic conditions or the bioactive agent and aquoCo-(III) (e.g., aquocob(III)alamin ( $\text{H}_2\text{O}-\text{Cbl}^{\text{III}}$ )) under aerobic conditions. In either event, sonolysis from the focused application of ultrasound, results in Co-non-reactive atom bond cleavage and the irreversible release of the bioactive agent from the organocobalt complex.

The bioconjugates of the present invention can undergo natural cleavage as follows. Bioconjugates may be cleaved by natural means such as by serum nucleophiles. Once inside the cell, cobalamin-drug bioconjugates (utilized here only as an example and not intended to limit the invention) can undergo cleavage by a variety of mechanisms. Standard  $\text{B}_{12}$  ligand exchange mechanisms permit the displacement of the drug. Alternatively, cellular nucleophiles can attack at either the carbon or the cobalt atoms of the Co-C bond. Cyanide is the most common example of a nucleophile which attacks at cobalt, leading to cyanocob(III)alamin and a free drug in which the former C-Co bond has been replaced with a C-H bond. Thiols (such as are found in cysteine or glutathione) can attack at carbon, leading to a reduced cob(I)alamin and a free drug which incorporates the former thiol group. (e.g.,  $\text{R}-\text{Co}[\text{III}] + \text{R}'\text{-SH} + \text{base} \rightarrow \text{R-S-R}' + \text{Co}[\text{I}] + \text{base-H}$ .) Hydroxide and other basic agents can also cleave organic ligands from Co(III) complexes, although this typically occurs via an elimination process which alters the structure of the ligand through incorporation of a new double bond. In addition,  $\text{B}_{12}$  metabolic enzymes present in cells can result in the cleavage of the bioactive agent from the co-atom.

The bioconjugates of the present invention can undergo cleavage by photoactivation or photolysis as follows. The photochemical release of the bioactive agent from the organocobalt complex can be triggered by the application of visible light at 400-800 nm. It is preferred to use organocobalt complexes which require longer wavelengths of visible light (600-800 nm), more preferably red light (600 to 750 nm). When photolysis is utilized for the release of the bioactive agent from the bioconjugate, it is particularly preferred that the non-reactive atom of the bioactive agent or the atom of the spacer bound to the cobalt atom be a carbon atom.

The vitamin  $\text{B}_{12}$  cofactor occurs naturally in two forms: adenosylcob(III)alamin. ( $\text{AdoCbl}^{\text{III}}$ ), also known as coenzyme  $\text{B}_{12}$ , and methylcob(III)alamin ( $\text{CH}_3\text{Cbl}^{\text{III}}$ ). The remarkably weak C-Co bond from the corrin ring to the 5'-deoxyadenosyl or methyl ligand imparts a most unusual chemistry to cobalamins. The C-Co bond energy in  $\text{AdoCbl}^{\text{III}}$  and  $\text{CH}_3\text{Cbl}^{\text{III}}$  is

estimated to be as low as 31 and 37 kcal/mole, respectively. This makes the C-Co bond one of the weakest covalent bonds known and allows photocleavage of the bond by visible light. The initial product of the photocleavage of  $\text{AdoCbl}^{\text{III}}$  is the geminate radical pair  $\{\text{CH}_2\text{-Ado} : \text{Cbl}^{\text{II}}\}$ . Brackets  $\{ : \}$  indicate the radical pair is *geminate* (born of the same parent molecule) and held in close proximity by solvent interactions. Picosecond laser flash photolysis experiments of  $\text{AdoCbl}^{\text{III}}$  have shown this to be a reversible process with a geminate recombination rate constant of  $k_{\text{rec}} \approx 1 \times 10^9 \text{ s}^{-1}$ , following photolysis. Recent nanosecond laser flash photolysis studies have probed a slower radical pair recombination that occurs in the solvent and is limited by diffusion.

The  $\pi\text{-}\pi^*$  electronic transition of the corrin ring of cobalamin produces a long wavelength absorption maximum at 525 nm, as shown by Figure 1. Irradiation of alkylcobalamins at this wavelength leads to cleavage of the C-Co bond with a photolysis quantum yield of 0.1-0.3. The *in vivo* photolysis of bioconjugates according to the present invention is preferably accomplished by delivering the light with a fiber optic probe because of the strong absorption of hemoglobin near this wavelength. To avoid potential problems with the absorption spectrum of cobalamin while maintaining a photolabile C-Co bond,  $\text{Co}[\text{SALEN}]$ , which is a five-coordinate analogue of coenzyme  $\text{B}_{12}$ , can be used. Alkyl- $\text{Co}[\text{SALEN}]$  complexes have absorption maxima near 650 nm, with significant absorption beyond 700 nm as shown by Figure 2. This is a distinct advantage for photoactivatable drug release, as human tissue becomes increasingly transparent above 610 nm. Other synthetic or naturally occurring  $\text{B}_{12}$  derivatives are, or may become, available that have absorption maxima above 600 nm. For example, a green cobalt corrinoid having an absorption maximum at about 624 nm is reported by Brown et al. (1996). Human tissue becomes transparent to depths of up to about 5.7 cm at wavelengths of between about 600 and 800 nm. The use of longer wavelengths enables the more selective irradiation of limited portions of a subject's body, with consequent release in a small target region.

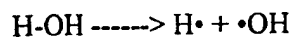
The bioconjugates of the present invention can undergo cleavage by photoactivation or photolysis in the presence of a magnetic field as follows. The use of the magnetic field further limits the release of the bioactive agent to the desired site. For example, because of the toxicity of antineoplastic agents to healthy tissues, it is incumbent upon any effective site specific delivery system to limit damage to cells other than at the site of activity. In the photohomolysis cleavage reaction, the electrons in the broken covalent bond start out with their spins paired  $\uparrow\downarrow$  (singlet state) from having participated in the covalent bond. During the early lifetime of the

radical pair, the spins retain their original orientation  $R\uparrow + \downarrow R'$  until the electron spins randomize over time. During the time the spins are paired, the radicals can recombine and revert to the starting material. If either of these paired radical spins should intersystem cross (ISC) to the triplet spin state ( $R\uparrow + \uparrow R'$ ) they can no longer recombine until their spins are once again paired. That situation is preferred to release the bioactive agent from the bioconjugate. However, in healthy tissue, it is desired to prevent, or at least minimize, the cleavage of the conjugate. If that event, it is desirable to alter the rate of ISC by introducing an external magnetic field that increases the gap between the triplet state energy levels, thus encouraging the recombination of the original bioconjugate in the healthy tissues.

The recombination rate can be increased by application of a magnetic field in the range of 100-3000 gauss to the healthy tissues leading to a net decrease in the photochemical quantum yield and a decrease in drug release into healthy tissues by a factor of at least 2. Application of about 300 to 1000 gauss is considered to be optimal. See, Grissom (1995).

The bioconjugates of the present invention can undergo cleavage by ultrasound or sonolysis as follows. Although any non-reactive atom can be bound to the cobalt atom in the bioconjugate and cleaved by sonolysis, it is preferred that the atom be a carbon atom. The vitamin B<sub>12</sub> cofactor occurs naturally in two forms: adenosylcob(III)alamin, (AdoCbl<sup>III</sup>), also known as coenzyme B<sub>12</sub> and methylcob(III)alamin, (CH<sub>3</sub>Cbl<sup>III</sup>). The remarkably weak C-Co bond from the corrin ring to the 5'-deoxyadenosyl or methyl ligand imparts a most unusual chemistry to cobalamins. The C-Co bond energy in AdoCbl<sup>III</sup> and CH<sub>3</sub>Cbl<sup>III</sup> is estimated to be as low as 31 and 37 kcal/mole, respectively. This makes the C-Co bond one of the weakest covalent bonds known and allows sonolysis of the bond by the application of ultrasound in the range of about 20 kHz - 500 MHz, preferably 20 kHz - 100 MHz, more preferably 20 kHz to 10 MHz.

Sonolysis of aqueous solutions produces a high concentration of hydroxyl radicals and hydrogen atoms according to the equation:



These reactive oxidizing and reducing species are responsible for initiating most reactions in aqueous solvents. Ultrasound irradiation and sonochemistry are often not described as high-energy processes, but during sonolysis, the development, growth and implosion of bubbles in a liquid create extreme reaction environments on a microscopic scale. The collapse of cavitation



bubbles produces pressures >500 atm. and temperatures >5000°C. The radicals formed survive the collapse of the bubbles. The formation of hydroxyl radicals *in vivo* has been the focus of several investigations because of the potentially deleterious effects of oxidizing free radicals in human tissue. However, such radicals do not present an unacceptable health risk, as clinical  
5 experience has demonstrated that diagnostic ultrasound is a benign procedure. The ability to form these radicals by sonolysis *in vivo* provides a mechanism for the triggered release of active neoplastic and other agents from conjugation with B<sub>12</sub>, Co[SALEN] or other suitable cobalamin or cobalamin like substrates.

In the sonolysis of drug-B<sub>12</sub> conjugates (utilized here only as an example and not  
10 intended to limit the invention), the C-Co bond is cleaved in aqueous solution to produce the drug and a cob(II)alamin (Cbl<sup>II</sup>) under anaerobic conditions or the drug and aquocob(III)alamin (H<sub>2</sub>O-Cbl<sup>III</sup>) under aerobic conditions. The cleavage is not a direct breaking of the C-Co bond. Rather, under anaerobic conditions the predominant pathway for C-Co bond cleavage by sonolysis is through reduction of drug-Cbl<sup>III</sup> to the labile drug-Cbl<sup>II</sup> by H•, followed by  
15 dissociation to the closed-shell drug and Cbl<sup>II</sup>. The reaction of HO• with drug-Cbl<sup>II</sup> leads to H<sub>2</sub>O-Cbl<sup>III</sup>, as well as degradation of the corrin ring. Under aerobic conditions, the pathway for the C-Co bond cleavage by sonolysis is through reduction of the drug-Cbl<sup>III</sup> to produce drug and Cbl<sup>II</sup>, but O<sub>2</sub> oxidizes Cbl<sup>II</sup> to H<sub>2</sub>O-Cbl<sup>III</sup>. In either event, sonolysis from the focused application of ultrasound, results in C-Co bond cleavage and the irreversible release of the drug from the  
20 cobalamin. Therefore, sonolysis-triggered release can occur under aerobic and hypoxic conditions alike.

The present invention is useful in the treatment of (including, but not limited to) cancer, hepatitis, psoriasis and other localized diseases, as well as for gene therapy and peptide therapy.  
25 The bioconjugates according to the present invention can be administered by any route, including intravenously, parenterally, orally, intramuscularly, intrathecally or as an aerosol. The mode of delivery will largely depend on the biological effect desired to be achieved. A skilled artisan will readily know the best route of administration for a particular treatment in accordance with the present invention. The appropriate dosages will depend on the route of administration  
30 and the treatment indicated, and can be readily determined by a skilled artisan, such as by extrapolation from current treatment protocols. If the organocobalt complex of the bioconjugate

is cobalamin or derivative or analogue, it is preferred to administer orally a bolus of vitamin B<sub>12</sub> prior to administration of the bioconjugate to reduce or eliminate potential hepatotoxicity which might otherwise result from the administration of the bioconjugate. The oral dose of B<sub>12</sub> will saturate the enterohepatic shuttle system and load hepatocytes with cobalamin. It is preferred that 0.1 mg to 100 mg, more preferably 1.0 mg to 10 mg, of vitamin B<sub>12</sub> be administered prior to the administration of the bioconjugate containing cobalamin. In addition, vitamin B<sub>12</sub> can be administered, preferably intravenously, following the selective cleavage of bioconjugate to wash out all bioconjugate which has not been cleaved, and thus further reduce potential systemic effects. It is preferred that 0.1 mg to 100 mg, more preferably 10 mg to 100 mg, of vitamin B<sub>12</sub> in saline be administered intravenously over 4-5 hrs. Finally, prior to the administration of a cobalamin-based bioconjugate, nitrous oxide can be administered to the subject in order to deplete body stores of cobalamin in its various forms, such as methylcobalamin. Administration of nitrous oxide has the effect of creating a greater body deficit of cobalamin before administration of the cobalamin-based bioconjugate.

Pharmaceutical compositions containing a compound of the present invention as the active ingredient can be prepared according to conventional pharmaceutical compounding techniques. See, for example, *Remington's Pharmaceutical Sciences*, 17th Ed. (1985, Mack Publishing Co., Easton, PA). Typically, an antagonistic amount of active ingredient will be admixed with a pharmaceutically acceptable carrier. The carrier may take a wide variety of forms depending on the form of preparation desired for administration, e.g., intravenous, oral, parenteral, intrathecal, transdermal, or by aerosol.

For oral administration, the compounds can be formulated into solid or liquid preparations such as capsules, pills, tablets, lozenges, melts, powders, suspensions or emulsions. In preparing the compositions in oral dosage form, any of the usual pharmaceutical media may be employed, such as, for example, water, glycols, oils, alcohols, flavoring agents, preservatives, coloring agents, suspending agents, and the like in the case of oral liquid preparations (such as, for example, suspensions, elixirs and solutions); or carriers such as starches, sugars, diluents, granulating agents, lubricants, binders, disintegrating agents and the like in the case of oral solid preparations (such as, for example, powders, capsules and tablets). Because of their ease in administration, tablets and capsules represent the most advantageous oral dosage unit form, in which case solid pharmaceutical carriers are obviously employed. If desired, tablets may be sugar-coated or enteric-coated by

standard techniques. The active agent must be stable to passage through the gastrointestinal tract. If necessary, suitable agents for stable passage can be used, and may include phospholipids or lecithin derivatives described in the literature, as well as liposomes, microparticles (including microspheres and macrospheres).

5 For parenteral administration, the compound may dissolved in a pharmaceutical carrier and administered as either a solution or a suspension. Illustrative of suitable carriers are water, saline, dextrose solutions, fructose solutions, ethanol, or oils of animal, vegetative or synthetic origin. The carrier may also contain other ingredients, for example, preservatives, suspending agents, solubilizing agents, buffers and the like. When the compounds are being administered intracerebroventricularly  
10 or intrathecally, they may also be dissolved in cerebrospinal fluid.

In the treatment of cancer (sarcomas, carcinomas or leukemias), a distinction can be made between the types of systemic adjuvant chemotherapies that are typically used in concert with the more extreme methods of surgical excision and radiation therapy. There are two broad classes of chemotherapeutic adjuvants: (1) endocrine and antivasogenic therapeutic agents which  
15 are aimed at altering the body's physiology; and (2) cytotoxic chemotherapeutic agents which are typically administered systemically to kill or inhibit the growth of transformed cells.

Cytotoxic or antineoplastic agents are represented by a number of drug classes. Alkylating agents undergo chemical reactions that generate highly reactive electrophilic carbocations that readily form covalent linkages (alkylate) with various nucleophilic  
20 biologically important moieties such as nucleic acid bases and phosphate, amine, sulfhydryl, hydroxyl, carboxyl and imidazole groups. These agents, among other functions, have cytotoxic actions that disturb the fundamental mechanisms concerned with cell growth, mitotic activity, differentiation and function. Chlorambucil, modified busulfan, cyclophosphamide, ifosfamide and cisplatin and its structural analogs are representative alkylating agents.

25 Antimetabolites such as folic acid analogs (e.g. methotrexate) and pyrimidine analogs (e.g. fluorouracil and fluorodeoxyuridine) exert cytotoxic activity by blocking or preventing metabolic pathways leading to neoplastic cell destruction. Methotrexate is also known to be useful in the treatment of psoriasis by inhibiting the proliferation of epidermal cells.

Another potent cytotoxic class is mitotic inhibitors such as the paclitaxel or the alkaloids  
30 camptothecin, vincristine and vinblastine.

Also, certain antibiotics, such as doxorubicin and daunorubicin, (tetracyclic aglycone glycosides), intercalate with DNA and inhibit nucleic acid synthesis.

In accordance with the present invention, bioconjugates for the treatment of cancer are formed preferably using chemotherapeutics selected from the group consisting of alkylating agents, antimetabolites and mitotic inhibitors. For example, methotrexate is an antimetabolite; 5 chlorambucil, cisplatin and modified busulfan are alkylating agents, and camptothecin and its derivatives are alkaloids. The bioconjugates formed from these cytotoxic agents can be administered intravenously for the treatment of the specific classes of cancer for which they are known to be effective, e.g. cancer of the colon, lung, kidney, breast, prostate, melanoma, 10 nasopharyngeal, T-cell leukemia, myelogenous leukemia, lymphocytic leukemia and the like. When delivered intravenously to the blood stream and the bioconjugates contain cobalamin, the natural affinity of cancer cells for B<sub>12</sub> will target the bioconjugates to these tissues or cell sites. Alternatively, the bioconjugates can be engineered to be selective for the delivery of the chemotherapeutic agent to the desired cancer cell by the incorporation of a suitable targeting 15 molecule (such as those set forth above) on the organocobalt complex.

In accordance with the present invention, solid tumors are treated as follows, with use of a drug-B<sub>12</sub> bioconjugate as an example. This example is not intended to limit the present invention in any manner, and a skilled artisan could readily determine other bioconjugates of the present invention which could be utilized for the treatment of solid tumors. The drug-B<sub>12</sub> 20 bioconjugate is administered, preferably intravenously, to a cancer patient to target metastatic cancer when the cancer cell has a significant requirement for cobalamin. This propensity of cobalamins to migrate to the cancer cells significantly reduces cardiotoxicity, myelotoxicity, hepatotoxicity and similar side effects that limit the size and frequency of effective dosing of antineoplastic agents. Furthermore, problems associated with toxicity to non-targeted cells is 25 minimized. Delivery is further enhanced by the triggering of the release of the antineoplastic agent from the bioconjugate by the mechanism of photolysis or sonolysis which provides for a high degree of spatial and temporal control of the drug release at a localized area over a short time. The application of a magnetic field with photolysis further serves to protect health cells by recombination of the bioconjugate and limit the release of active agent to the specific cancer 30 cell-containing site(s).

-51-

Although chemotherapy is generally reserved for targeting metastasized cells after the surgical excision of the primary tumor mass, the triggered release of a bioactive agent drawn to the tumor site allows for treatment of the primary tumor, as well as metastatic neoplasms that have spread to a limited and known area. The bioconjugate dosage, length of treatment, degree of photoactivation, and other treatment parameters can be determined by one skilled in the art based on the type of cancer, antineoplastic agent administered, specific cobalamin used, condition of the patient and other factors which are variable and best determined on a case-by-case basis.

In accordance with the present invention, leukemia is treated as follows, with use of a drug-B<sub>12</sub> bioconjugate as an example. This example is not intended to limit the present invention in any manner, and a skilled artisan could readily determine other bioconjugates of the present invention which could be utilized for the treatment of leukemia. At least two forms of leukemia, chronic myeloid leukemia (CML) and acute promyelocytic leukemia (APL), produce high levels of B<sub>12</sub> binding proteins that result in a 3- to 36-fold increase in the unsaturated B<sub>12</sub> binding capacity in the blood. The increased concentration of B<sub>12</sub> binding proteins is consistent with the rapid turnover of immature blood cells and provides an opportunity to target the delivery of antileukemic drugs, such as bis-alkylating agents derived from busulfan, to the transformed hematopoietic cells responsible for the leukemic condition. The bioconjugates of this invention provide a means for the effective administration of such alkylating agents to cell sites from which the active agent can be released from the conjugate. This targeted delivery and release provides a significant advance in the treatment of CML and APL, for which current chemotherapy methods sometimes provide incomplete remission.

The present invention is also useful for the treatment of psoriasis. Psoriasis is a prime target for the transdermally or orally controlled delivery of antimetabolites activated by photolytically induced cleavage. Although not life-threatening, psoriasis can significantly diminish the quality of life of patients who experience severe exfoliation associated with psoriatic and rheumatoid arthritis. Antimetabolites, such as methotrexate and 5-fluorouracil, are effective in controlling severe cases of skin proliferation. Effective oral therapy is limited by hepatotoxicity in spite of low dosing, and the risk of cumulative liver damage requires such therapy to be reserved for only the most severe episodes during a patient's life. The delivery of

such agents to the skin improves the appearance and psychological quality of life of patients whose lives have been dominated by severe psoriasis.

The present invention is further useful for peptide therapy. One example of peptide therapy is as a cytotoxic agent, for example as an antineoplastic agent. In this example, a  
5 bioconjugate containing the enzymatic domain of diphtheria toxin (DT) is administered to a subject such as described above for solid tumors or leukemia. The targeted release of the DT peptide results in the inhibition of protein synthesis and eventual cell death.

The present invention is also useful for gene therapy. One example of gene therapy is the delivery of an antisense oligonucleotide to inhibit viral gene expression and viral replication.  
10 In this example, a bioconjugate containing an antisense oligonucleotide against hepatitis B virus is administered to a patient having a hepatitis B infection. The accumulation of the bioconjugate and release of the antisense oligonucleotide in the liver inhibits hepatitis B virus gene expression and replication.

15 The present invention is further described by reference to the following Examples, which are offered by way of illustration and are not intended to limit the invention in any manner. Standard techniques well known in the art or the techniques specifically described below were utilized.

## 20 EXAMPLE I

### Photolysis of $B_{12}$ and Co[SALEN] Bioconjugates

A protocol for a typical anaerobic continuous-wave photolysis of methylcob(III)alamin or  $CH_3Cbl^{III}$  is as follows. An aqueous solution of 200  $\mu M$   $CH_3Cbl^{III}$  and 50 mM  $K^+$  Hepes pH 7.3 is placed in a 1 cm quartz cuvette. Samples that are to be photolyzed under anaerobic  
25 conditions are either subjected to repeated freeze-pump-thaw cycles, or purged with Ar for 40 minutes immediately prior to photolysis and sealed. Continuous-wave visible light irradiation is accomplished at the desired wavelength with an  $Ar^+$  pumped dye laser. The incident light on the face of the cuvette is reduced to 12 mW  $cm^{-2}$  with neutral density filters. The light flux is determined by potassium ferrioxalate actinometry and by a Scientech surface-reading thermopile.  
30 The cuvette is placed in a thermostated cell holder at 25-37°C. For quantum yield measurements as a function of magnetic field, the cuvette is placed in the gap of a GMW Associates

-53-

electromagnet with 7.5 cm diameter cylindrical poles. The magnetic field within the area of the cuvette is homogeneous to within 2% and the long term stability is better than 0.5% as monitored by a transverse Hall probe and digital teslameter.

Absorption spectra from 300-600 nm are recorded in one second with a diode array spectrophotometer at variable time intervals from 10 seconds to 2 minutes (depending upon the fluence of the photolyzing light source) for a total of 3  $\tau_{1/2}$ . Exposure to light during analysis is kept to a minimum. The concentration of  $\text{CH}_3\text{Cbl}^{\text{III}}$  is determined using the measured absorbance at 350 or 520 nm by the method of Chen and Chance (1993). The plot of  $[\text{CH}_3\text{Cbl}^{\text{III}}]$  vs. time (t) appears zero-order in all cases.

Selection of Photolysis Wavelength: The absorption spectra for  $\text{CH}_3\text{Cbl}^{\text{III}}$  and ethyl-Co[SALEN] are shown in Figures 1 and 2. For  $\text{CH}_3\text{Cbl}^{\text{III}}$  the  $\pi$ - $\pi^*$  electronic transitions that lead to cleavage of the C-Co bond are maximal at 377 and 528 nm. Much preliminary work with  $\text{B}_{12}$  photolysis has been carried out with 514 nm light from an Argon-ion ( $\text{Ar}^+$ ) laser. This is close to the long-wavelength maximum absorbance and gives a quantum yield of about 0.3 for  $\text{CH}_3\text{Cbl}^{\text{III}}$ .

The absorbance of blood and tissue is significant at this optimal wavelength for cob(III)alamin excitation. Blood has a low (partial) transmittance window near 514 nm. This absorbance is sufficient to quickly pyrolyze whole bovine blood placed in the light path of a 20  $\text{W}/\text{cm}^2$  beam of 514 nm light.

It would therefore be beneficial to provide a cobalamin for conjugation wherein the  $\pi$ - $\pi^*$  electronic transitions that lead to cleavage of the C-Co bond are maximal at a wavelength where there is minimal or no interference. Above about 610 nm blood becomes partially transparent and losses beyond 50% transmittance are largely due to light scattering from the erythrocytes. Heparinized bovine blood placed in the light path of a 20  $\text{W}/\text{cm}^2$  beam of 630 nm light shows only minor heating over long exposure times. There is also demonstrated a high transmittance of tissue at 610-800 nm.

This suggests the use of an organocobalt complex for conjugation having an absorption wavelength where tissue and blood are relatively transparent. Figure 2 shows that ethyl-Co[SALEN] complexes have absorption maximums near 650 nm, with significant absorption beyond 700 nm. An  $\text{Ar}^+$ -pumped dye laser or a Krypton-ion ( $\text{Kr}^+$ ) laser can be a suitable high-intensity source of photons in the region of 610+ nm.  $\text{Ar}^+$ -pumped dye lasers are

often used for photodynamic therapy with hematoporphyrins. Also, an inexpensive He-Ne laser, having a principal line at 633 nm might be used. However, such lasers are typically limited to 50 mW maximum output.

There are laser dyes in the 600-700 nm region that can achieve energy conversion efficiencies of up to 45%. This means that a 6 W  $\text{Ar}^+$  pump laser can yield nearly 3 W of spatially-coherent monochromatic light in the region of 610-750 nm. The exact wavelength can be chosen to optimize the continuous-wave quantum yield and still maintain a reasonable degree of tissue penetration. In tests with alkyl-Co[SALEN] complexes it has been found that 690 nm light from an  $\text{Ar}^+$ -pumped dye laser operating with rhodamine 6-G dye is satisfactory. Optimization can be determined depending on the specific cobalamin chosen for animal and/or clinical trials of the bioconjugates. In addition, high-power diode lasers that emit red light of the desirable wavelength are commercially available. These diode lasers have the advantage of providing up to 100 watts of optical power in a narrow region of the optical spectrum that is useful for triggering cleavage of the bioconjugates.

15

## EXAMPLE 2

### Sonolysis of $\text{B}_{12}$ and Co[SALEN] Bioconjugates

Sonolysis was carried out with a Branson ultrasonic bath (model 3200) operating at 47 kHz. The correct placement of the reaction vessel at a focal point of high- intensity ultrasound was determined by the oxidation of iodide to iodine in the presence of starch (Mason, 1991) and the temperature of the bath was maintained at 21° C by a constant temperature circulator. Aerobic sonolysis was typically carried out in a test tube or Erlenmeyer flask, whereas anaerobic sonolysis was carried out in a closed reaction vessel fitted with a sidearm and quartz cuvette. Anaerobic conditions were produced by sparging with Ar for 30 min prior to sonolysis. In some experiments, the pH was buffered by the use of 100 mM phosphate (aerobic experiments) or 100 mM *N*-(2-hydroxyethyl)piperazine-*N*-2-ethanesulfonate (Hepes) (anaerobic experiments), as specified. All procedures were carried out in the absence of light to prevent photolytic cleavage of the Co-C bond. Absorption spectra were recorded on a diode array spectrophotometer (HP 8452A). The solutions were transferred to a quartz cuvette with a 1 cm light path for all optical measurements and care was exercised to ensure that insignificant photolysis occurred during the 1 s measurement time.

30



Sonolysis of Methylcob(III)alamin: Sequential absorption spectra of aqueous  $\text{CH}_3\text{-Cbl}^{\text{III}}$  as a function of anaerobic sonolysis (pH 7.38, 100 mM Hepes, saturating Ar) are shown in Figure 3A. The absorbance at 340, 374, and 520 nm decreases linearly as a function of sonolysis time and the absorbance at 316 and 420 nm increases linearly, thereby indicating the reaction is zero order in substrate concentration. The isosbestic points at 336, 390, and 585 nm are in agreement with those obtained through anaerobic photolysis of  $\text{CH}_3\text{-Cbl}^{\text{III}}$ . Under the conditions of sonolysis, an additional isosbestic point occurs at 476 nm, rather than at 486 nm, as typically observed in the course of photolysis. This slight shift in the isosbestic point is caused by a minor product that has an absorbance maximum near 490 nm. This may be cob(I)alamin that has a sufficient lifetime ( $t_{1/2} = 22$  min at pH 6) to be observed spectrophotometrically. The absorption band at 374 nm is characteristic of a C-Co bond, and its disappearance unambiguously indicates displacement of the axial carbon ligand.

Under aerobic conditions, molecular oxygen scavenges  $\text{H}\cdot$  and prevents the reduction of  $\text{CH}_3\text{-Cbl}^{\text{III}}$  via the equation



In the absence of an organic buffer with abstractable hydrogen atoms, reaction via  $\text{HO}\cdot$  remains to be a viable process.

Figure 3B shows the change in absorbance spectra following aerobic sonolysis in the absence of organic buffer. The decrease in absorbance at 340 and 374 nm is linear with increasing sonolysis time indicating the reaction is zero order in substrate concentration, but the unexpected increase in absorbance at 520 nm indicates the stable product of cobalamin sonolysis is not hydroxocob(III)alamin, as would be expected if molecular oxygen were to reoxidize cob(II)alamin to cob(III)alamin. Aerobic photolysis under the same conditions shows the expected decrease in absorbance at 374 nm but no change at 520 nm. This difference suggests that  $\text{HO}\cdot$  is able to displace the alkyl ligand from  $\text{Co}^{\text{III}}$ , but other  $\text{HO}\cdot$  reactions also occur (perhaps through the secondary products  $\text{HOO}\cdot$  and  $\cdot\text{O}_2$ ) to oxidize the corrin ring. Similar absorbance spectra are obtained from sonolysis of an aerated aqueous solution containing 100 mM phosphate buffer.

A similar result is seen in the reaction of  $\text{CH}_3\text{-Cbl}^{\text{III}}$  with  $\text{H}\cdot$  and  $\text{HO}\cdot$  when these radical species are generated by pulse radiolysis (Blackburn et al., 1972). Reducing species  $\text{H}\cdot$  reacts to produce the same spectral changes as shown in Figure 3A. Multiple oxidizing species ( $\text{HOO}\cdot$

and  $\cdot\text{O}_2^-$ ) can react with  $\text{CH}_3\text{-Cbl}^{\text{III}}$  to cleave the Co-C bond, but these species also lead to the irreversible degradation of the corrin ring, as evidenced by the spectral changes similar to those seen in Figure 3B. A precedent for irreversible oxidation of the corrin ring exists in the photooxygenolysis of alkylcobalamins by singlet oxygen (Krautler and Stepanek, 1985).

5        Aerobic sonolysis of solutions containing 100 mM Hepes or 100 mM *t*-butyl alcohol produces no change in the absorption spectra over comparable time. This is because molecular oxygen quenches the  $\text{H}\cdot$  reaction pathway, and *t*-butyl alcohol quenches the  $\text{HO}\cdot$  reaction pathway. Although Hepes has not previously been reported to be a scavenger of  $\text{HO}\cdot$ , many reports indicate that organic solute molecules such as formate, can inhibit the reaction of  $\text{HO}\cdot$   
10        (Weissler, 1962). The absence of any spectral changes under these conditions suggests that direct sonolysis of the Co-C bond is not an important reaction pathway.

### EXAMPLE 3

#### Biological Testing Against NCI Human Tumor Cell Lines

15        The efficacy of the bioconjugates is tested against tumor cell lines using existing protocols for assessing the effectiveness of targeted coenzyme  $\text{B}_{12}$  antineoplastic agent-containing bioconjugates. Representative cell lines tested include HCT 116 (human colon tumor), A549 (human lung), ACHN (human kidney), MCF7 (human breast), human prostate, SK5-mel (human melanoma), KB (human nasopharyngeal), CCRF-CEM (human T-cell  
20        leukemia), HL-60 (human promyelocytic leukemia), RD-995 (mouse fibrosarcoma), B-16 (mouse melanoma) and Meth-A (mouse carcinoma). Drug screening is carried out with a colorimetric cell viability assay in a 96-well plate.

      Additionally, selected bioconjugates are radiolabeled with  $^{14}\text{C}$  or  $^3\text{H}$  to assess the level of uptake by human tumor cells. As noted above, the prior art reports that some tumor and  
25        leukemia cells produce high levels of  $\text{B}_{12}$  binding proteins in the serum and sequester  $\text{B}_{12}$  in high concentrations of up to 50 fold.

Tumor Cell Line Testing Protocol: The drug bioconjugates, synthesized under procedures described herein or adaptations thereof, are diluted over 5 orders of magnitude (approximately 0.005 to 50  $\mu\text{g/mL}$ ). Four hours after seeding of the cell in the plate, the cells  
30        are treated with the appropriate drug dissolved in isotonic buffered solution. In control experiments, without photolysis triggered drug release, the drug is left on the cells for three

days, as in the normal basic cancer screen. In the wells for triggered drug release, the laser output is focused on selected wells for varying times and with varying intensity. Alternatively, a matrix of light-emitting diodes (LEDs) is used. The cells are incubated under standard mammalian tissue culture conditions under the proper CO<sub>2</sub> balanced atmosphere. After three  
5 days, the cells are re-fed and the colorimetric dye 3-[4,5-dimethylthiazol-2-yl]-2,5-diphenyltetrazolium bromide (MTT) is added. The reduction of the MTT to purple formazan product is quantified in a 96 well plate reader. The concentration of the purple formazan dye is correlated with the number of viable cells. The reduction in cell survival at a given dose rate and photolysis exposure give a quantitative estimation of cell death and drug delivery effectiveness.  
10 Care is taken not to expose portions of the plate to photolysis conditions through adventitious spillover of radiation. This is accomplished by using 96 well plates with an opaque mask (Fisher cat# 07-200-565) for photolysis.

Uptake of Drug-B<sub>12</sub> and Drug-Co[SALEN] Bioconjugates: The uptake of drug-B<sub>12</sub> and drug-Co[SALEN] bioconjugates by cultured tumor cells is monitored by radiolabeling the drug  
15 or cobalamin during synthesis. <sup>3</sup>H-Labeled 5-fluorouracil, methotrexate and chlorambucil are purchased from DuPont/NEN (New England Nuclear). These drug bioconjugates, as well as <sup>14</sup>C-labeled methylcob(III)alamin (synthesized from Cob(I)alamin and <sup>14</sup>CH<sub>3</sub>I) provide an indication of receptor-mediated uptake by the various tumor cell lines. In this study, the cells are exposed to the radiolabeled drug as described in the preceding section, except no MTT is added at the end  
20 of the three-day incubation period. Since all of the cell lines except the leukemia cells grow while attached to the bottom of the microtiter plate well, the growth medium is aspirated to remove the unincorporated radiolabeled drug, followed by several washes with fresh medium. The labeled cells are detached from the bottom of the wells and the radioactivity quantified by scintillation counting. Growth of non-attached leukemia cell takes place in round-bottom  
25 microtiter plates such that centrifugation sediments the cells and allows washing with fresh growth medium before solubilizing the cells and quantifying the incorporated radiolabeled drug by scintillation counting.

## EXAMPLE 4

Synthesis of Co[SALEN]Synthesis of N,N'-bis(salicylidene)ethylenediamine.

To a stirred solution of salicylaldehyde (12.21 g/10.62 mL) in 70°C ethanol (100 mL) was added ethylenediamine (3.01 g/3.33 mL). A yellow crystalline material immediately formed, and the reaction mixture was allowed to cool to room temperature with stirring. The solution was filtered, and the crystals were washed with cold ethanol. The ethanol layers were combined and reduced to approximately 20 mL and allowed to stand at 0°C overnight. The resulting crystals were collected by vacuum filtration and washed with water. The collected solids were dried *in vacuo* to obtain 13.15 g (98%) N,N'-bis(salicylidene)ethylenediamine as yellow platelets with a melting point of 126°C (literature value (24) 127-128°C). <sup>1</sup>H NMR (DMSO-d<sub>6</sub>) δ 8.57 (s 2H, HC=N), 7.42 (d, 2H aromatic, J=7.3 Hz), 7.31 (t, 2H, aromatic, J=9.0 Hz), 6.88 (t, 4H, aromatic, J=8.3, 16.1 Hz), 3.89 (s, 4H, CH<sub>2</sub>). <sup>13</sup>C NMR (DMSO-d<sub>6</sub>) δ 166.94 (2C, CO), 160.57 (2C, HC+N), 132.38 (2C, aromatic), 131.69 (4C, aromatic), 118.59 (2C, aromatic), 116.51 (2C, aromatic), 58.88 (2C, CH<sub>2</sub>).

Synthesis of N,N'-bis(salicylidene)ethylenediaminecobalt(II) (Co[SALEN]).

To a hot (100°C) deoxygenated solution of the above product (2.68 g) in dimethylformamide (25 mL) was added via cannula needle an aqueous solution (10 mL) of cobalt (II) acetate tetrahydrate (2.49 g). The red precipitate which formed was collected by vacuum filtration, washed with cold dimethylformamide, and dried *in vacuo* to obtain 2.6 g (80%) of N,N'-bis(salicylidene)ethylenediaminecobalt (II) as red crystals.

## EXAMPLE 5

Synthesis of Modified Co[SALEN]

The diglycolate ether of Co[SALEN] is prepared as described in Example 4, using the glycolate ether of 2,5-dihydroxybenzaldehyde in place of salicylaldehyde. An unsymmetrically substituted (glycolate ether/amide) complex is prepared as described in Example 4 by using a mixture of the glycolate ether of 2,5-dihydroxybenzaldehyde and 5-aminosalicylaldehyde in place of salicylaldehyde.

## EXAMPLE 6

Synthesis of Chlorambucil-Cobalamin Bioconjugates

Synthesis of 1-bromo-2-[4-(4'-[bis-(2-chloroethyl)amino]phenyl)butyroxyl]ethane.

Twenty-five mL of freshly distilled  $\text{CH}_2\text{Cl}_2$ , 0.343 g dicyclohexylcarbodiimide (1.66 mmol), 0.305 g 4-dimethylaminopyridine (2.5 mmol), and 0.263 g 4-dimethylamino-pyridinium chloride (1.66 mmol) were added to a flame-dried 50 mL round bottom flask equipped with a stir bar, reflux condenser, and Ar inlet (Boden and Keck, 1985). The solution was purged with argon and brought to reflux. While refluxing, a solution of 0.304 g chlorambucil (1.0 mmol) and 0.125 g 2-bromoethanol (1.0 mmol) in 5 mL  $\text{CH}_2\text{Cl}_2$  (purged under argon for 30 min.) was transferred via cannula to the refluxing solution over a period of 30 min. After addition was complete, the reaction mixture was stirred for 2 h at room temperature. Precipitated dicyclohexylurea was removed by filtration and the solution was concentrated by rotary evaporation. The resulting residue was taken up in  $\text{CH}_2\text{Cl}_2$ , filtered, and purified by flash silica column chromatography. The desired product was eluted using 1:9 ethyl acetate:hexanes (v/v) to give 0.374 g of a yellow oil in 91% yield (ester 2).  $^1\text{H}$  NMR ( $\text{CDCl}_3$ , 300 MHz)  $\delta$  7.06 (d, 2H,  $J=8.4$  Hz), 6.60 (d, 2H,  $J=8.7$  Hz), 4.35 (t, 2H,  $J=6.15$  Hz), 3.56-3.72 (m, 8H), 3.48 (t, 2H,  $J=6.15$  Hz), 2.56 (t, 2H,  $J=7.65$  Hz), 2.35 (t, 2H,  $J=7.35$  Hz), 1.91 (quintet, 2H,  $J=7.58$  Hz).  $^{13}\text{C}$  NMR ( $\text{CDCl}_3$ , 75 MHz  $^1\text{H}$  decoupled)  $\delta$  173.05, 144.35, 130.37, 129.75 (2), 112.12 (2), 63.68, 53.55 (2), 40.60 (2), 33.94, 33.41, 29.05, 26.72.

Synthesis of 2-[4-(4'-[bis-(2-chloroethyl)amino]phenyl)butyroxyl]ethylcob(III)alamin (3).

Two hundred mg of hydroxocob(III)alamin (0.15 mmol) was dissolved in 10 mL water and purged with Ar while stirring (Brown and Peck, 1988). The exiting gas was conducted in sequence through: (1) a flask containing 0.025 g  $\text{NaBH}_4$  (0.66 mmol); (2) a flask containing 5 mL  $\text{H}_2\text{O}$ ; and (3) a flask containing 0.226 g ester 2 (0.55 mmol) in 5 mL  $\text{CH}_3\text{OH}$ . After deaerating for 1 h, the water from flask (2) was transferred to flask (1) containing  $\text{NaBH}_4$  via cannula and swirled to promote dissolution. This solution was transferred via cannula to the aqueous cobalamin solution. Reduction was allowed to proceed for 20 min, after which the chlorambucil bromoethylester was added to the solution. The reaction mixture was allowed to stir for an additional 5 min. and then 0.2 mL acetone was added to destroy the excess borohydride. The solution was concentrated to approximately 2 mL by rotary evaporation and

the resulting solution was applied to a 2.5 X 30 cm column of Amberlite XAD-2 resin. The column was washed with 1 L H<sub>2</sub>O to desalt and the cobalamin was eluted with 50% aqueous acetonitrile (v/v). The eluent was reduced to approximately 2 mL by rotary evaporation and the solution was applied to a 1 X 40 cm column of SP-Sephadex C25 (Na<sup>+</sup> form). Elution with  
5 water removed the major red band which was reduced to a minimal volume. Acetone was added until faint turbidity persisted after swirling. The solution was allowed to stand for 1 h at 0°C and excess acetone was added to promote further crystallization. The crystals were collected by vacuum filtration and dried *in vacuo*. 3 was obtained as red crystals (122.5 mg) with a yield of 53%. MS (FAB+) calcd for C<sub>68</sub>H<sub>112</sub>N<sub>14</sub>O<sub>16</sub>CoPCl<sub>2</sub>, 1541; found 1541.

10 4-[4'-(bis-[2-chloroethyl]amino)phenyl]butyroylcob(III)alamin (4) was synthesized in a similar manner starting with the acid chloride of chlorambucil and reacting it with hydroxocob(III)alamin as above.

Synthesis of 2-[4-(4'-(bis-(2-chloroethyl)amino)phenyl)butyroxyl]ethyl-Co[SALEN] and 4-[4'-(bis-[2-chloroethyl]amino)phenyl]butyroyl-Co[SALEN] are synthesized in a similar manner  
15 using Co[SALEN] in place of hydroxocob(III)alamin.

Synthesis of 2-[4-(4'-(bis-(2-chloroethyl)amino)phenyl)butyroxyl]ethyl-(Co[SALEN]-folate) and 4-[4'-(bis-[2-chloroethyl]amino)phenyl]butyroyl-(Co[SALEN]-folate) are synthesized in a similar manner using Co[SALEN]-folate in place of hydroxocob(III)alamin.

Synthesis of 2-[4-(4'-(bis-(2-chloroethyl)amino)phenyl)butyroxyl]ethyl-(green corrinoid)  
20 and 4-[4'-(bis-[2-chloroethyl]amino)phenyl]butyroyl-(green corrinoid) are synthesized in a similar manner using CH<sub>3</sub>-Co(III) corrinoid (prepared by reacting methyl iodide with the green corrinoid of Brown et al. (1996) after it had been reduced with NaBH<sub>4</sub>) in place of hydroxocob(III)alamin.

#### EXAMPLE 7

25 Sonolysis of 2-[4-(4'-(bis-(2-chloroethyl)amino)phenyl)butyroxyl]ethylcob(III)alamin (3)

The products released by exhaustive sonolysis, as described in Example 2, of compound 3 (prepared in Example 6) were isolated by reverse-phase HPLC (Rainin Microsorb C-18). Elution and separation of the sonolysis products were carried out with an increasing gradient of acetonitrile (A) and 0.05 M phosphoric acid (B): initial condition 5% A: 95% B, increased  
30 linearly for 10 min to 30% A and 70% B, maintained for 2 min; followed by a linear increase to

70% A and 30% B over 10 min (Rinchik et al., 1993). The solvent was evaporated from each fraction and the products were extracted with  $\text{CH}_2\text{Cl}_2$  and characterized by  $^1\text{H}$  and  $^{13}\text{C}$  NMR.

Sequential absorption spectra of aqueous 3 as a function of anaerobic sonolysis at pH 7.4, 100 mM Hepes, saturating Ar, are shown in Figure 4A. The absorbance at 374 and 520 nm decreases linearly as a function of sonolysis time, and the absorbance at 316 and 420 nm increases linearly, thereby indicating the reaction is zero order in substrate concentration. The isosbestic points at 336, 390, 486 and 585 nm are in agreement with those obtained through anaerobic photolysis of  $\text{CH}_3\text{-Cbl}^{\text{III}}$ . The absorption band at 374 nm is characteristic of a Co-C bond, and its disappearance unambiguously indicates displacement of the axial carbon ligand.

Figure 4B shows the change in absorbance spectra following aerobic sonolysis of a 3 solution containing phosphate buffer. Different stable products are obtained under aerobic conditions. Because of the presence of molecular oxygen, the released product was shown by NMR to be 2-[4-(4'-[bis-(2-chloroethyl)amino]phenyl)butyroxyl]ethan-1-al.  $^1\text{H}$  NMR ( $\text{CDCl}_3$ , 300 MHz) 9.59 (s, 1H), 7.08 (d, 2H,  $J=2.9$  Hz), 6.62 (d, 2H,  $J=2.9$  Hz), 4.67 (s, 2H), 3.73-3.59 (m, 8H), 2.60 (t, 2H,  $J=7.5$  Hz), 2.45 (t, 2H,  $J=7.4$  Hz), 1.95 (quintet, 2H,  $J=7.4$ );  $^{13}\text{C}$  NMR ( $\text{CDCl}_3$ , 75 MHz  $^1\text{H}$  decoupled) 195.85, 173.09, 144.54, 130.43, 129.92 (2), 112.29 (2), 68.73, 53.74 (2), 40.69 (2), 33.99, 33.13, 26.79. The decrease in absorbance at 374 nm is linear with increasing sonolysis time indicating the reaction is zero order in substrate concentration.

The Co-C bond of  $\text{CH}_3\text{-Cbl}^{\text{III}}$  can be cleaved by sonolysis in aqueous solutions to produce the alkane and cob(II)alamin under anaerobic conditions or to produce the aldehyde and hydroxocob(III)alamin under aerobic conditions. Unlike photolysis and thermolysis that lead to direct Co-C bond cleavage, the predominant pathway for Co-C bond cleavage by sonolysis is through  $\text{H}\cdot$  mediated reduction of  $\text{CH}_3\text{-Cbl}^{\text{III}}$  to the labile  $19\text{e}^- \text{CH}_3\text{-Cbl}^{\text{II}}$  species followed by dissociation to the closed-shell alkane and  $\text{Cbl}^{\text{II}}$ , or through the reaction of  $\text{HO}\cdot$  with  $\text{CH}_3\text{-Cbl}^{\text{III}}$  that leads to formation of hydroxocob(III)alamin as well as degradation of the corrin ring.

A parallel exists between the reactions of alkylcob(III)alamin under the conditions of sonolysis and pulse radiolysis, (Blackburn et al., 1972) but without the need for expensive equipment. Although the violent cavitation during sonolysis has sufficient energy to break the Co-C bond to produce the  $\{\text{R}\cdot \text{Cbl}^{\text{II}}\}$  radical pair by a dissociative pathway analogous to the photolysis of  $\text{CH}_3\text{-Cbl}^{\text{III}}$ , (Endicott and Netzel, 1979; Chagovetz and Grissom, 1993; Natarajan and Grissom, 1996), alkylcob(III)alamins are not sufficiently volatile to be found in the extreme

environment of the collapsing bubbles. Therefore, *direct* Co-C bond cleavage by sonolysis is not possible in spite of the more than 80 kcal/mol difference in bond-dissociation energy between Co-C and H-OH.

Anaerobic sonolysis of the Co-C bond is irreversible because a closed-shell alkane is formed. Under aerobic conditions, the rate of  $H^\bullet$  reaction with  $O_2$  is on the same order of magnitude as the reaction of  $H^\bullet$  with  $CH_3$ , thereby suggesting the closed-shell alkane,  $CH_4$ , should be one of the end products of  $CH_3-Cbl^{III}$  sonolysis (Buxton et al., 1988; Baulch et al., 1992). In contrast, Co-C bond cleavage of  $CH_3-Cbl^{III}$ , *via* anaerobic photolysis, is reversible from the  $\{CH_3^\bullet \cdot Cbl^{II}\}$  radical pair.

In summary, the ability to form cob(II)alamin and the closed-shell alkane without the use of chemical reductants and without the use of electrochemical, photochemical, or pulse radiolysis equipment may be a useful method to promote activation of drug-cobalamin complexes *in vivo*.

## EXAMPLE 8

### Materials and Methods for *in vitro* Assays of Bioconjugate Activity

#### Media Preparation

All media were purchased from Sigma and materials used to supplement the media were purchased from Atlanta Biologicals. The HL-60 cell culture was grown in an  $\alpha$ -MEM media. The media was completed prior to inoculation by the addition of reagents to bring the final media concentration to 7.5% w/v sodium bicarbonate, 10% fetal calf serum, 100  $\mu$ g/mL penicillin and streptomycin, and 50 units/mL nystatin. McCoy's media, with sodium bicarbonate buffer, was used for HCT-116 cell culture. It was completed in the same manner with 8% newborn calf serum and 2% fetal calf serum. Completed media could be stored at 4°C for several weeks. The culture medium was warmed to 37°C before inoculation with cells.

#### Stock Culture Preparation and Maintenance

Stock cell cultures were started from ATCC cell lines. The original ATCC cell line was aliquoted in 10% DMSO and stored in liquid nitrogen. Stock cultures of 40 mL were grown and maintained in collagen-treated, sterile 75 mL culture flasks purchased from Corning. The cultures were incubated at 37°C in a 5%  $CO_2$  environment to maintain a pH of 7.1. Humidity within the



incubator was maintained to prevent hypertonicity in the media by placing an open pan of water in the bottom of the incubator.

The concentration of cells within the stock culture was controlled and cell concentrations were estimated in several ways. The media became more purple and subsequently orange as a result of cell metabolism and metabolic byproducts that accumulated in the media. The cells were also visually observed under microscope at 40X and 100X power. Normal HCT-116 cells appeared rounded, flat, and adhered strongly to the walls of the culture flask. When the cells almost covered the bottom of the flask, the cell concentration was reduced. Normal HL-60 cells appeared round, but were well differentiated and easily suspended in the media. Changes in cell morphology were often indicative of bacterial or fungal contamination. For the accurate determination of cell concentrations, a Coulter Cell Counter™ was employed. Stock cultures were not allowed to grow to greater than 100,000 cells/mL. Both of the cell lines were observed to have a doubling time of about 24 hrs.

#### 15 Assay Preparation

The assays were performed in collagen-treated, sterile 96-well plates that were purchased from Corning. HL-60 cells were grown in round-bottomed wells (Corning catalog #25850) and HCT-116 cells were grown in flat-bottomed wells (Corning catalog #25860). Cell concentrations were measured by a Coulter Cell Counter™. Cells were diluted in bulk and loaded onto the plates with 200 µL in each well. The assays were performed using approximately 25,000 HL-60 cells/well and 40,000 HCT-116 cells/well.

Since HL-60 cells grow in suspension, the cell concentration was measured and diluted directly. HCT-116 cells, however, adhere to the walls of the flask and must be suspended by treatment with trypsin. A 0.025 mg/mL trypsin solution was thawed immediately before use. The bulk culture medium was removed by aspiration and 2mL of the cold trypsin solution were added to the flask. The flask was agitated periodically to promote suspension of the cells. Care was taken to limit cell exposure to the trypsin solution to less than five minutes, since prolonged exposure will damage the cell membrane. When the cells were suspended, as observed by a microscope, 8 mL of media were added to inactivate the trypsin. The cell concentration in the resulting suspension was measured, the suspension diluted appropriately, and loaded onto the

96-well plates. Once on the plates, the cells were allowed to adhere for 3 hrs before treatment with SFU or one of the derivatives.

#### Cell Growth and MTT Determination of Cell Viability

5 HL-60 cells were treated and placed in the incubator for 24 hrs. The plates were centrifuged and the supernatant was carefully aspirated without disturbing the cell pellet. A 200  $\mu$ L aliquot of media was added immediately. The cells were allowed to grow for 48 hrs. HCT-116 cells were treated and allowed to grow undisturbed for 72 hrs. The culture medium was removed by aspiration (after centrifugation in the case of HL-60 cells). 100 mL of McCoy's  
10 media and 11  $\mu$ L MTT dye were added. The cells were incubated at 37°C for 3 hrs. During this time, viable cells reduce the MTT dye to purple formazan by the action of alcohol dehydrogenase. The cells were lysed by the addition of 100  $\mu$ L of a solution 1.2M Hcl in 60% ethanol, thereby releasing the reduced dye into solution. The absorbance at 405 nm was measured for each well using a BIO-RAD Microplate Reader (Model 450)™/

15

### EXAMPLE 9

#### *In Vitro* Activity of Chlorambucil-Cobalamin Bioconjugates

##### Thermal Stability of Bioconjugates in Media

It was noted that the chlorambucil bioconjugates 3 and 4 (prepared in Example 6) have  
20 thermal lability. Thus, they are expected to thermally decompose during the assay, perhaps before entering the cells or before release by photolysis. Thermal decomposition of both bioconjugates was monitored by a UV-vis diode array spectrophotometer (HP8452) at 37°C in water, cell-free media, and filtered media in which HCT-116 cells had been grown to a concentration of about 100,000 cells/mL. Spectra were taken hourly for a total of 8 hrs. The  
25 presence of intact bioconjugate was then determined by photolysis, 20 min, with a high-pressure mercury lamp. If photolysis had no effect on the spectrum, all of the bioconjugate was assumed to have decomposed.

##### *In Vitro* Assays of 3 and 4 Activity

30 Both bioconjugates were assayed against HCT-116, HL-60, B-16, Meth-A, and RD-995 cell lines. The assays were performed in the same manner as described in Example 8 as

modified herein. The B-16, RD-995 and Meth-A cells lines are all Balb/c derived carcinoma lines which were provided by Dr. R. Daynes of the University of Utah. These cell lines were grown in RPMI media which was completed with 5% fetal bovine serum and other media components as previously described. Both the B-16 and RD-995 cell lines were suspended in trypsin, as in the case of HCT-116 cells. The Meth-A cells loosely adhere to the walls of the flask and grow both attached to the flask and suspended in solution. These cells could be completely suspended by successive washing of the flask wall with media.

Assays were performed at cell concentrations of about 40,000 cells per well, with the exception of the HL-60 assay which was performed at 25,000 cell per well. The HCT-116, B-16 and RD-995 cells were assayed in flat bottomed, 96-well plates, while the HL-60 and Meth-A cells were assayed in round bottomed plates. Chlorambucil, unconjugated, was tested prior to the bioconjugates. The cells were treated with the bioconjugates in both non-photolytic and photolytic conditions. The cells were incubated for three days (media was aspirated and replaced after 24 h. in the case of the HL-60 cells) and the resulting viability measured by an MTT assay.

The MTT assay was somewhat altered for this experiment. The culture medium was aspirated after 72 hrs. The Meth-A and HL-60 cells were centrifuged prior to aspiration. Then, 100  $\mu$ L of McCoy's media and 11  $\mu$ L of the MTT solution were added as before. At the end of 4 hours, the culture medium was aspirated a second time (following centrifugation in the case of HL-60 and Meth-A cells) and 100  $\mu$ L of DMSO was added. The DMSO lysed the cells releasing the MTT dye into solution. The absorbance of each well at 450 nm was measured as before. The HCl/ethanol solution previously used has a tendency to precipitate proteins from the resulting solution, which may give falsely increased absorbance measurements. The replacement of DMSO avoids this problem.

The concentration of chlorambucil and the bioconjugates were varied from 0.04  $\mu$ M to 400  $\mu$ M within the assay. The cells were treated with the bioconjugates under dim, red lights to avoid photolysis. Non-photolytic conditions were maintained by wrapping the 96 well plates with foil during the incubation periods. Photolysis was performed in black plates with flat, clear bottomed wells (Costar catalog number: 3603). These plates are sterile, collagen treated, and made of optically clear plastic. Growth of the cells in these plates did not show any differences to those grown in the normal clear plastic plates. Photolysis was achieved by an array of high

intensity green LEDs (Hewlett Packard catalog number: 782-6124). The array was constructed from one of the black plates in which one LED was placed in each well. The LEDs could be turned on and off as vertical rows. In each assay, two rows of cells were left untreated as growth controls. One of these rows was not photolyzed by the LEDs to demonstrate any unexpected effects of photolysis; irradiation did not demonstrate any effects on the untreated control cells. An empty plate was placed between the array and the assay plate to avoid heating the cells. Ten minutes of irradiation produced complete photolysis for the bioconjugate in cell-free media. The cells were irradiated for 10 min during the assay. The time of irradiation, following treatment with drug, was determined by a timecourse assay. The entire plate was treated with one of the bioconjugates at a concentration equal to the  $IC_{50}$  of chlorambucil in that cell line. The rows were irradiated separately one half hour after treatment and then hourly.

Irradiation at 1 h after treatment demonstrated the greatest bioconjugate activity in all of the cell lines. Further assays were performed with irradiation one hour after treatment. In the case of the Meth-A cell line, the cells were transferred from the round-bottomed plate into the black plate for photolysis and then returned to the round bottomed plate. The HL-60 cell line could not be tested under these photolytic conditions.

### Results and Discussion

Both bioconjugates show significant thermal decomposition in both water and cell free media at 37°C. At the end of 8 hrs, photolysis has no effect on the spectrum, indicating that all of the bioconjugate has decomposed. In the HCT-116 cell media both bioconjugates show fast initial decomposition and are significantly stabilized at subsequent time. Haptocorrin, a cobalamin binding protein is known to stabilize alkylcobalamins by several orders of magnitude. This protein is present in the cell-free media from the added bovine serum. However, most of this protein in serum is saturated with cobalamin, so binding to the bioconjugates may be inhibited. It is known that several types of tumor cells secrete high amounts of cobalamin binding proteins, especially haptocorrin. Thus, media in which cells have been growing has a higher concentration of apo-haptocorrin. The initial fast decomposition of the bioconjugates represents the amount remaining after the saturation of haptocorrin in the media. The bound bioconjugates are significantly stabilized by haptocorrin and the haptocorrin complex associates and dissociates in a dynamic fashion in solution, especially in the presence of significant

concentrations of other cobalamins in the media. Thus, the bioconjugates are still susceptible to decomposition when not bound to haptocorrin. While haptocorrin does stabilize the bioconjugates by several orders of magnitude, slow decomposition is still seen during the assay. However, this assay does indicate that the bioconjugates are stabilized such that a significant amount is still intact during the time of uptake and photolysis.

The data from the photolysis timecourse and activity assays are summarized in Figures 5-9 for compound 3 in each of the cell lines tested. Similar results were seen for compound 4. In general, both bioconjugates showed similar uptake and photolysis behavior in the photolysis timecourse assay. The maximal photolytically induced toxicity is seen one hour after treatment with either of the bioconjugates. In all cases, photolysis of the bioconjugate demonstrated increased toxicity over that of unconjugated chlorambucil. Figure 5 shows that the chemotherapeutic drug, chlorambucil, has an LD<sub>50</sub> of about 2  $\mu$ M with respect to the HCT-116 cell line, whereas the bioconjugate shows no substantial toxicity at concentrations approaching 100  $\mu$ M. If cells treated with the bioconjugate are subjected to brief irradiation with red light 12 hours after dosing, the LD<sub>50</sub> decreases by a factor of 25 to 0.08  $\mu$ M. If a 10-fold excess of vitamin B<sub>12</sub> is added to saturate the cell surface receptors, the bioconjugate is not taken into the cells and photolysis triggers release of the active chlorambucil in the cell culture medium. The released chlorambucil now enters the cell by passive diffusion and an LD<sub>50</sub> of 2  $\mu$ M is observed — in close agreement with the value for chlorambucil standard.

Figure 6 shows that in cell line HL-60, the unconjugated chlorambucil standard exhibits an LD<sub>50</sub> of 0.5  $\mu$ M, but the bioconjugate is at least 2-fold better with an LD<sub>50</sub> of 0.2  $\mu$ M. The cytotoxicity of MC-121 against the leukemia cell line is still a dramatic result when compared with the absence of toxicity when the cellular uptake of the conjugate is out-competed by the addition of 10 equivalents of vitamin B<sub>12</sub>. Similar results were obtained with Meth-A cells. The HL-60 and Meth-A cells have a high turnover rate, and in the case of Meth-A divide more rapidly than the other cell lines. These cells may, in fact, metabolize cobalamin at a faster rate than the other cell lines and thus release the chlorambucil in significant concentrations without photolysis. In order for this to be practical, however, cobalamin metabolism must occur before significant hydrolysis of chlorambucil moiety. It is reported that HL-60 cells are able to convert vitamin B<sub>12</sub> into the other cobalamin forms efficiently (more quickly than normal lymphocytes) (Quadros and Jacobsen, 1995) and thus, would be able to efficiently release the conjugated

chlorambucil. In the other cell lines, however, the bioconjugates are essentially not toxic in non-photolytic conditions, which is a promising indication that these bioconjugates may not be toxic in normal somatic cells or healthy hematopoietic cells. IC<sub>50</sub> values of the bioconjugates in both non-photolytic and photolytic conditions are summarized in Table 1.

5

TABLE 1

IC<sub>50</sub> values (μM)

<i>Cell Line</i>	<i>HCT-116</i>	<i>HL-60</i>	<i>B-16</i>	<i>Meth-A</i>	<i>Rd-995</i>
Chlorambucil	20.8	5.8	1.4	1.8	1.1
<u>Photolysis</u>					
3	1.7		0.6	0.2	0.2
4	1.1		0.3	0.3	0.3
<u>No Photolysis</u>					
3		3.2		210.1	
4		8.9		84.2	

10 It will be appreciated that the methods and compositions of the instant invention can be incorporated in the form of a variety of embodiments, only a few of which are disclosed herein. It will be apparent to the artisan that other embodiments exist and do not depart from the spirit of the invention. Thus, the described embodiments are illustrative and should not be construed as restrictive.

15

LIST OF REFERENCES

- 20 Allen, R. H. and Majerus, P. W. (1972a). *J. Biol. Chem.* 247:7695-7701.
- Allen, R. H. and Majerus, P. W. (1972b). *J. Biol. Chem.* 247:7709-7717.
- Baulch, D. L., et al., (1992). *J. Phys. Chem. Ref. Data* 21:411.
- 25 Bennett, C.F., et al. (1992). *Mol. Pharmacol.* 41:1023-1033.
- Blackburn, R., et al. (1972). *J. Chem. Soc. Faraday I*, 1687.
- Boden, E.F. and Keck, G.E. (1985). *J. Org. Chem.* 50:2394.
- 30 Brown, K.L. and Peck, S. (1988). *Organomet. Syn.* 4:304.

- Brown et al. (1996). *J. Inorg. Chem.* 35:3442.
- Bunnell, B.A., et al. (1992). *Somatic Cell Mol. Genet.* 18:559-569.
- 5 Buxton, G. V., et al., (1988). *J. Phys. Chem. Ref. Data* 17:513.
- Carmel (1975). *New Engl. J. Med.* 292:282-284.
- 10 Castle, W. B. (1953). *N. Engl. J. Med.* 24:603-611.
- Chagovetz, A. M. and Grissom, C. B. (1993). *J. Am. Chem. Soc.* 115:12152.
- Chang, E.H. and Miller, P.S. (1991). In *Prospects for Antisense Nucleic Acid Therapy of*  
15 *Cancer and AIDS*, ed. Wickstrom, E., Wiley-Liss, New York, pp. 115-124.
- Chen and Chance (1993). *Biochem.* 32:1480-1487.
- Cohen, J.S. and Hogan, M.E. (1994). *Sci. Am.* 76-82.
- 20 Cooney, M., et al. (1988). *Science* 241:456-459.
- Endicott, J. F. and Netzel, T. L. (1979). *J. Am. Chem. Soc.* 101:4000.
- 25 Fornari, F.A., et al. (1996). *Biochem. Pharmacol.* 51:931-940.
- Fox, H. J. and Castle, W. B. (??). *Am. J. Med. Sci.* 203:18-26.
- Fritzer, M., et al. (1996). *Biochem. Pharmacol.* 51:489-493.
- 30 Gao, X. and Huang, L. (1991). *Biochem. Biophys. Res. Commun.* 179:280-285.
- Gasparro (1986). *Biochem. Biophys. Res. Commun.* 141:502-509.
- 35 Ginobbi, P., et al. (1997). *Anticancer Res.* 17:29-36.
- Grissom, C.B. (1995). *Chem. Rev.* 95:3-25.
- Hosada, J., et al. (1995). *Biol. Pharm. Bull.* 18:1234-1237.
- 40 Howard, W.A., et al. (1997). *Bioconj. Chem.* 8:498-502.
- Hu, Y.-P., et al. (1996). *Cancer Chemother. Pharmacol.* 37,556-560.
- 45 Johnson, D. A., et al. (1995). *Anticancer Res.* 15:1387-1394.
- Kabanov, A.V., et al. (1995). *Bioconjugate Chem.* 6:639-643.

- Krautler, B. and Stepanek, R. (1985). *Angew. Chem. Int. Ed. Engl.* **24**:62.
- Kumar et al. (1987). *J. Biol. Chem.* **262**:7171-7179.
- 5 Le Doan, T., et al. (1987). *Nucl. Acids Res.* **15**:7749-7760.
- Ling, Y.-L., et al. (1996). *Mol. Pharmacol.* **49**:832-841.
- 10 Letsinger, R.L. (1993). *Nucl. Acids Symp. Ser.* **29**:1-2.
- Longman, S. A., et al. (1995). *Cancer Chemother. Pharmacol.* **36**:91-101.
- Lott et al., (1995). *J. Am. Chem. Soc.* **117**:12194-12201.
- 15 Low, P.S. et al. (1995). U.S. Patent No. 5,416,016.
- Ma, D.D.F. and Wei A-Q. (1996). *Leukemia Res.* **20**:925-930.
- 20 Madon, J. and Blum, H.E. (1996). *Hepatology* **24**:474-481.
- Mason, T. J. (1991). *Practical Sonochemistry: Users Guide to Applications in Chemistry and Chemical Engineering* Horwood, New York.
- 25 Merwin, J.R., et al. (1994). *Bioconjugate Chem.* **5**:612-620.
- Moser, H.E. and Dervan, P.B. (1987). *Science* **238**:645-650.
- Murray, G.J. and Neville, D.M. (1980). *J. Biol. Chem.* **255**:11942-11948.
- 30 Myers (1988). European Patent Application No. 86810614.7
- Natarajan, E. and Grissom, C. B. (1996). *Photochem. Photobiol.* **64**:286.
- 35 Nichols, J., et al. (1997). *Eur. J. Cancer* **33** Suppl. 1:S34-S36
- Oeltmann and Heath (1979). *J. Biol. Chem.* **254**:1028.
- Postel, E.H. (1992). *Ann. N.Y. Acad. Sci.* **660**:57-63.
- 40 Quadros, E. V. and Jacobsen, D. W. (1995). *Biochim Biophys. Acta.* **1244**:395-403.
- Rando, R., et al. (1994). *Nucl. Acids Res.* **22**:678-685.
- 45 Rinchik, E.M., et al. (1993). *Bioessays* **12**:831-836.
- Roth and Maddox (1983). *J. Cell. Phys.* **115**:151



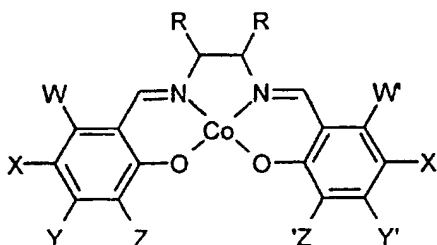
- Russell-Jones, G.J. et al. (1995). U.S. Patent 5,428,023.
- Sivam, G. P., et al. (1995). *Cancer Res.* 55:2352-2356.
- 5 Skoog, J.U. and Maher, L.J., III (1993). *Nucl. Acids Res.* 21:2131-2138.
- Stein, C.A. and Cohen, J.S. (1988). *Cancer Res.* 48:2659-2688.
- 10 Svensson, H. P., et al. (1995). *Cancer Res.* 55:2357-2365.
- Szczylik, C., et al. (1991). *Science* 261:562-565.
- Tanaka, T., et al. (1996). *Biol. Pharm. Bull.* 19:774-777.
- 15 Trubetskoy, V.S., et al. (1992). *Biochim. Biophys. Acta* 1131:311-313.
- Uhlmann, E. and Peyman, A. (1990). *Chem. Rev.* 90:543-584.
- 20 Vlassov, V.V., et al. (1994). *Biochim. Biophys. Acta* 1197:95-108.
- Wang, S., et al. (1995). *Proc. Natl. Acad. Sci. USA* 92:3318-3322.
- Waxman, et al. (1972). *Clin. Res.* ??:572.
- 25 Weissler, A. (1962). *Nature* 193:1070.
- Wickstrom, E., et al. (1992). *Cancer Res.* 52:6741-6745.
- 30 Wu, G.Y. (19887). *J. Biol. Chem.* 262:4429-4432.
- Yao, Z., et al. (1996). *J. Viral Hepat.* 3:19-22.
- Zon, G. (1993). *Methods Mol. Biol.* 20:165-189.
- 35

WHAT IS CLAIMED IS:

1. A bioconjugate of a bioactive agent and an organocobalt complex wherein the bioactive agent is covalently conjugated to the cobalt atom through a non-reactive atom in the bioactive agent molecule.  
5
2. The bioconjugate of claim 1, wherein said non-reactive atom is selected from the group consisting of a carbon atom, a nitrogen atom, an oxygen atom, a sulfur atom, a selenium atom or a silicon atom.  
10
3. The bioconjugate of claim 1, wherein said non-reactive atom is a carbon atom.
4. The bioconjugate of claim 3, wherein the non-reactive carbon atom is a carbon atom from an alkyl, acyl or aryl group that will not lead to rearrangement or destruction of the bioactive agent under conditions of ligand exchange during receptor-mediated endocytosis.  
15
5. The bioconjugate of any one of claims 1-4, wherein said bioactive agent is covalently bound directly to the cobalt atom of the organocobalt complex.  
20
6. The bioconjugate of any one of claims 1-4, wherein said bioactive agent is covalently bound indirectly to the cobalt atom of the organocobalt complex via a spacer.
7. The bioconjugate of claim 6, wherein said spacer is a self-destructing linker.  
25
8. The bioconjugate of any one of claims 1-6, wherein said bioactive agent is a diagnostic compound.
9. The bioconjugate of any one of claims 1-6, wherein said bioactive agent is a pharmaceutically active compound.  
30

-73-

10. The bioconjugate of claim 9, wherein said pharmaceutically active compound is an anticancer agent.
11. The bioconjugate of any one of claims 1-6, wherein said bioactive agent is a peptide or peptide analogue.
12. The bioconjugate of any one of claims 1-6, wherein said bioactive agent is a protein or protein analogue.
13. The bioconjugate of any one of claims 1-6, wherein said bioactive agent is a nucleic acid or a nucleic acid analogue.
14. The bioconjugate of claim 13, wherein said nucleic acid or nucleic acid analogue is a polynucleotide.
15. The bioconjugate of claim 14, wherein said nucleic acid or nucleic acid analogue is an oligonucleotide.
16. The bioconjugate of claim 13, wherein said nucleic acid is antisense DNA or RNA.
17. The bioconjugate of any one of claims 1-16, wherein said organocobalt complex is cobalamin, a cobalamin derivative or a cobalamine analogue.
18. The bioconjugate of any one of claims 1-16, wherein said organocobalt complex is a compound having the following formula:



wherein the substituents may be included or omitted to modulate physical properties of the molecule, e.g., water solubility, stability or  $\lambda_{\max}$  -- the wavelength at which the complex absorbs.

- 5 19. The bioconjugate of claim 18, wherein said targeting molecule is selected from the group consisting of glucose, galactose, mannose, mannose 6-phosphate, transferrin, cobalamin, asialoglycoprotein,  $\alpha$ -2-macroglobulins, insulin, a peptide growth factor, folic acid or derivatives, biotin or derivatives, YEE(GalNAcAH)<sub>3</sub> or derivatives, albumin, texaphyrin, metallotexaphyrin, a vitamin, a coenzyme, an antibody, an antibody fragment and a  
10 single-chain antibody variable region (scFv).
20. The bioconjugate of any one of claims 1-16, wherein said organocobalt complex is selected from the group consisting of organo(pyridine)bis(dimethylglyoximate)cobalt, a corrinoid, derivatives thereof and analogues thereof.
- 15 21. A method of administering a bioactive agent to cells of a targeted tissue site of a subject which comprises administering to said subject an effective amount of said bioactive agent as the bioconjugate of any one of claims 1-20.
- 20 22. The method of claim 20, wherein said cells of said targeted tissue site have an affinity for the organocobalt complex portion of said bioconjugate.
23. The method of claim 20, wherein said cells of said targeted tissue site have an affinity for the targeting molecule of the organocobalt complex portion of said bioconjugate.
- 25 24. The method of any one of claims 21-23, wherein said bioconjugate is administered intravenously.
25. The method of any one of claims 21-23, wherein said bioconjugate is administered  
30 parenterally.

26. The method of any one of claims 21-23, wherein said bioconjugate is administered orally.
27. The method of any one of claims 21-23, wherein said bioconjugate is administered intramuscularly.
28. The method of any one of claims 21-23, wherein said bioconjugate is administered intrathecally.
29. The method of any one of claims 21-23, wherein said bioconjugate is administered as an aerosol.
30. The method of any one of claims 17-28, wherein said bioconjugate is actively transported into said cells of said targeted tissue site and accumulates in an inactive form until activated by cleavage of the bioactive agent from the organocobalt complex.
31. The method of claim 30, wherein the cleavage occurs as the result of cellular displacement.
32. The method of claim 30, wherein the cleavage occurs as the result of cellular B<sub>12</sub> metabolic enzymes.
33. The method of claim 30, wherein the cleavage is caused by an external signal.
34. The method of claim 33, wherein said external signal is applied to the targeted tissue site.
35. The method of claim 33 or 34, wherein said external signal is visible light of a wavelength which causes photolysis of said bioconjugate.
36. The method of claim 35, wherein said visible light has a wavelength of 400-800 nm.

37. The method of claim 35, wherein said visible light has a wavelength of 600-800 nm.
38. The method of claim 38, wherein said visible light has a wavelength of 600-750 nm.
- 5 39. The method of any one of claims 35-38, wherein said visible light is delivered by fiber optics.
40. The method of any one of claims 35-39, wherein the area surrounding said targeted tissue site is subjected to a magnetic field which serves to encourage recombination of  
10 photolyzed bioconjugate outside the targeted tissue site and thereby reduce the amount of bioactive agent available to healthy tissues.
41. The method of claim 33 or 34, wherein said external signal is ultrasound of a frequency which causes sonolysis of said bioconjugate.
- 15 42. The method of claim 41, wherein said ultrasound has a frequency in the range of between about 20 kHz to 500 MHz.
43. The method of claim 41, wherein said ultrasound has a frequency in the range of between  
20 about 20 kHz to 100 MHz.
44. The method of claim 41, wherein said ultrasound has a frequency in the range of between about 20 kHz to 10 MHz.
- 25 45. The method of any one of claims 21-44, wherein said targeted tissue site is neoplastic tissue and said bioactive agent is an anticancer agent.
46. The method of claim 45, wherein said neoplastic tissue is tissue of a sarcoma.
- 30 47. The method of claim 45, wherein said neoplastic tissue is tissue of a carcinoma.

48. The method of claim 45, wherein said neoplastic tissue is tissue of a leukemia.
49. The method of any one of claims 21-44, wherein said targeted tissue site is tissue afflicted with psoriasis and said bioactive agent is a cytotoxic agent or anti-metabolite.
50. The method of any one of claims 21-44, wherein said targeted tissue site is tissue for the application of gene therapy and said bioactive agent is an oligonucleotide or a polynucleotide.
51. The method of claim 50, wherein said oligonucleotide is antisense DNA or RNA.
52. The method of any one of claims 21-44, wherein said targeted tissue site is tissue for the application of peptide therapy and said bioactive agent is a peptide or protein.
53. The method of any one of claims 21-52, wherein a bolus of vitamin B<sub>12</sub> is administered prior to administration of said bioconjugate.
54. The method of any one of claims 21-52, wherein vitamin B<sub>12</sub> is administered intravenously after cleavage of the bioconjugate to wash out uncleaved bioconjugate.
55. The method of any one of claims 21-54, wherein nitrous oxide is administered first to deplete body stores of vitamin B<sub>12</sub>.

1/9

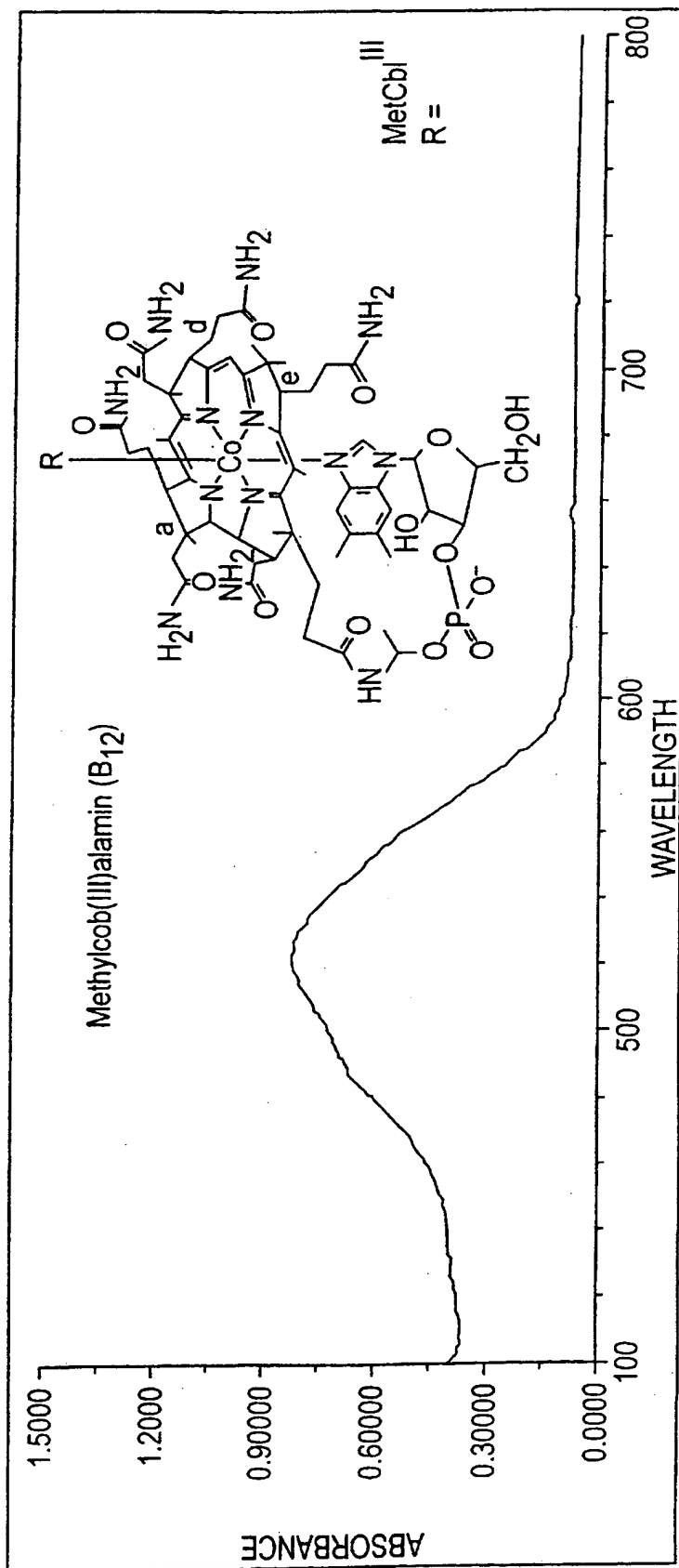


FIG. 1



2/9

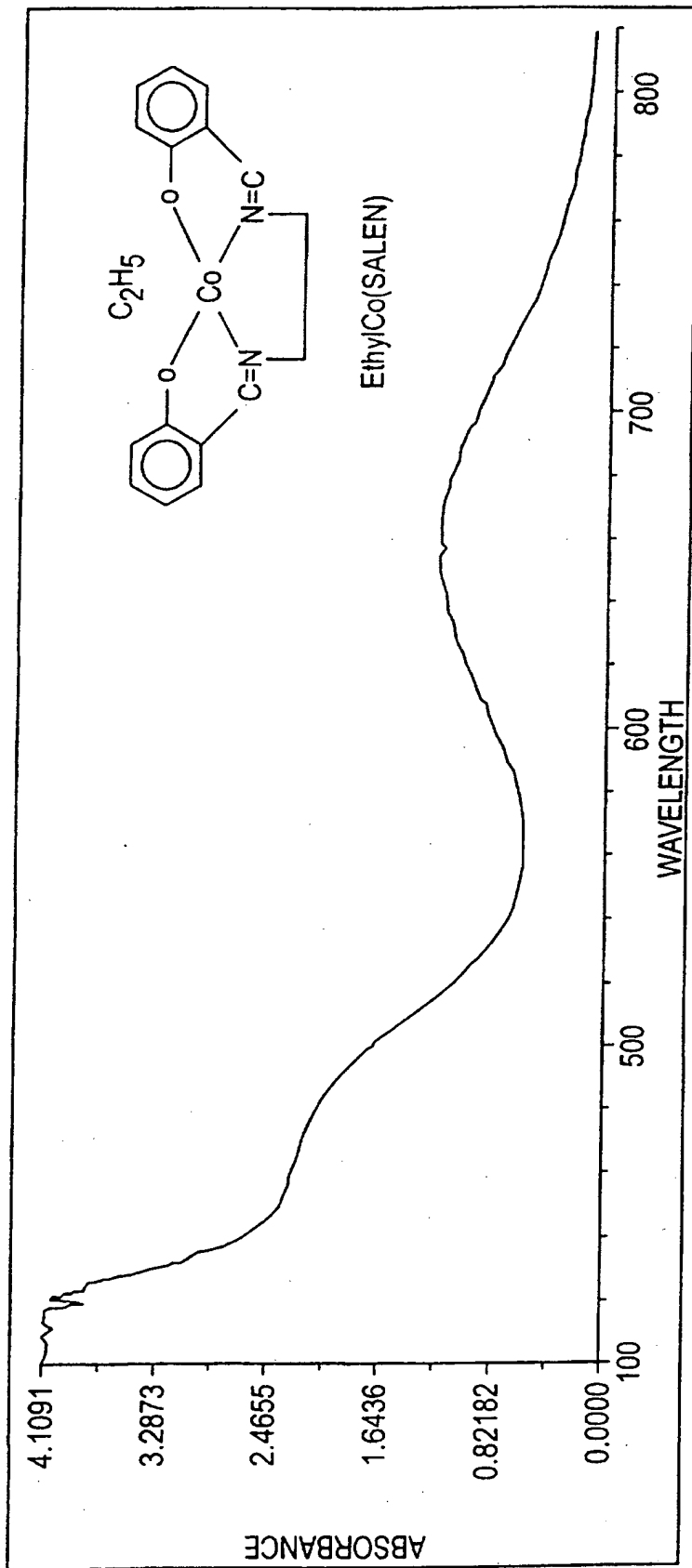


FIG. 2

3/9

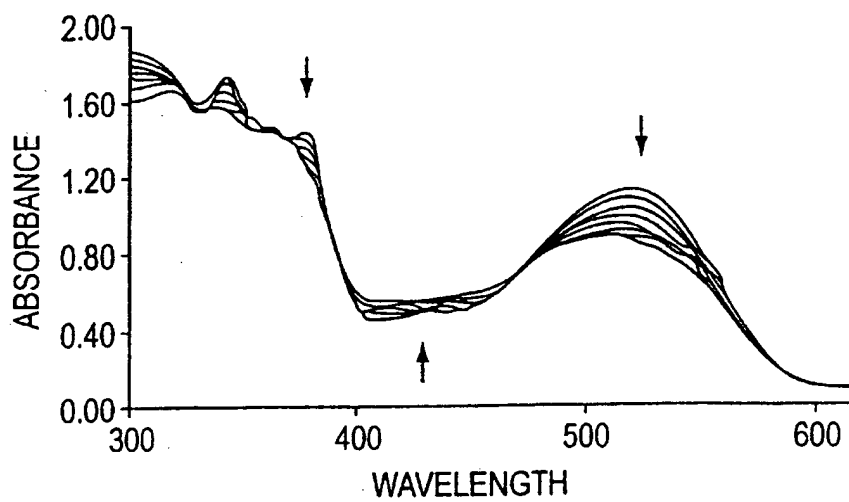


FIG. 3A

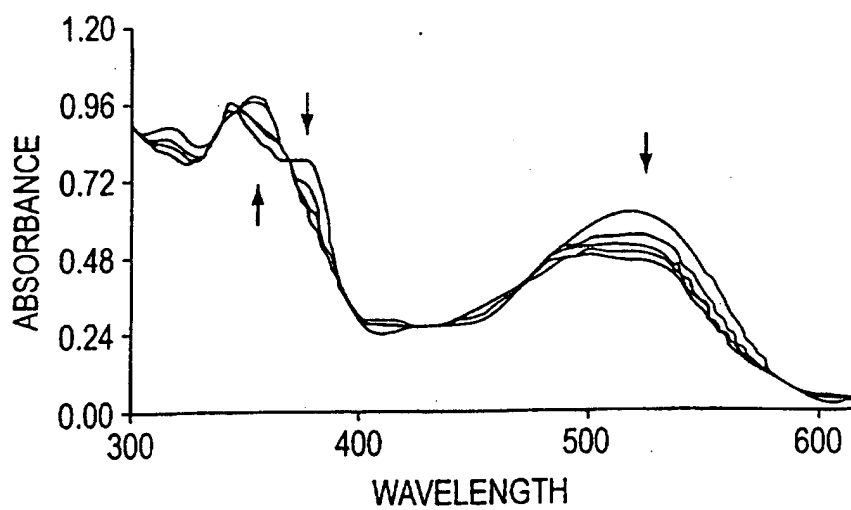


FIG. 3B

4/9

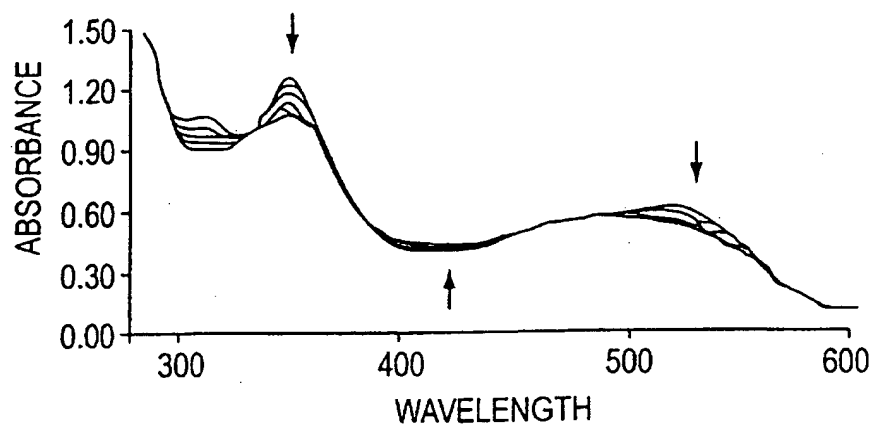


FIG. 4A

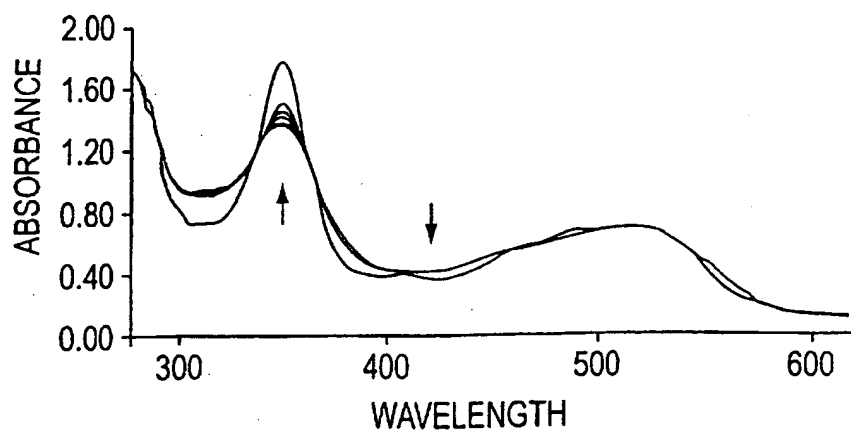


FIG. 4B

5/9

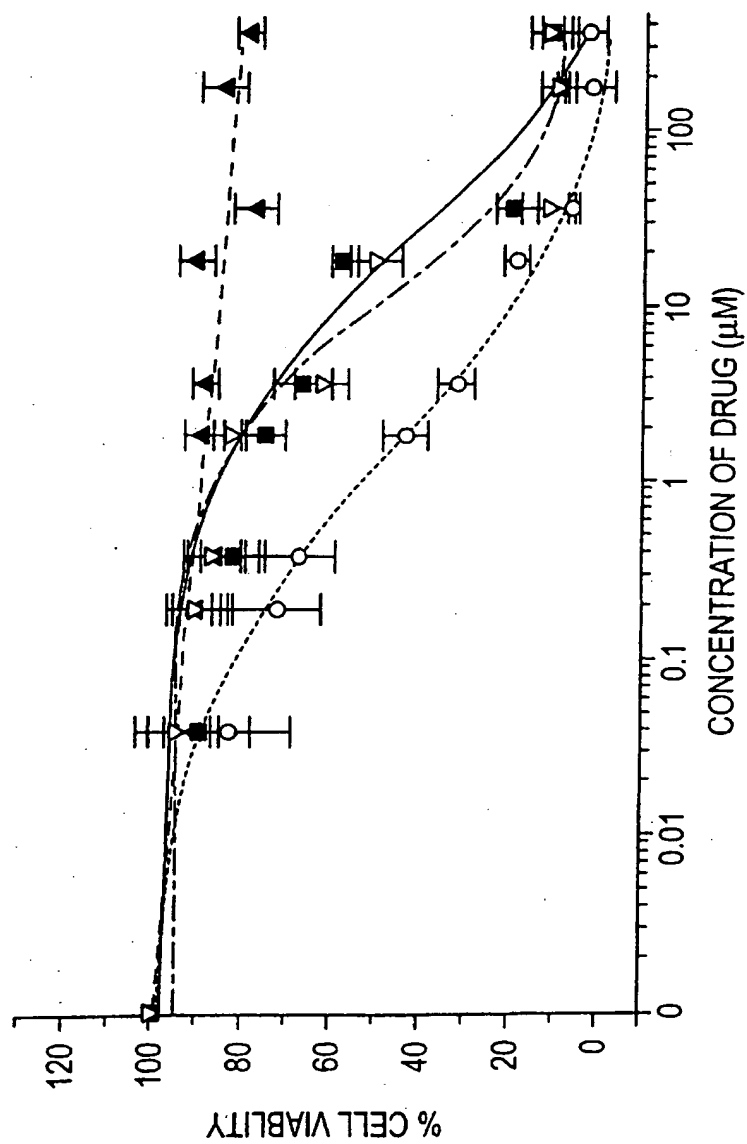


FIG. 5

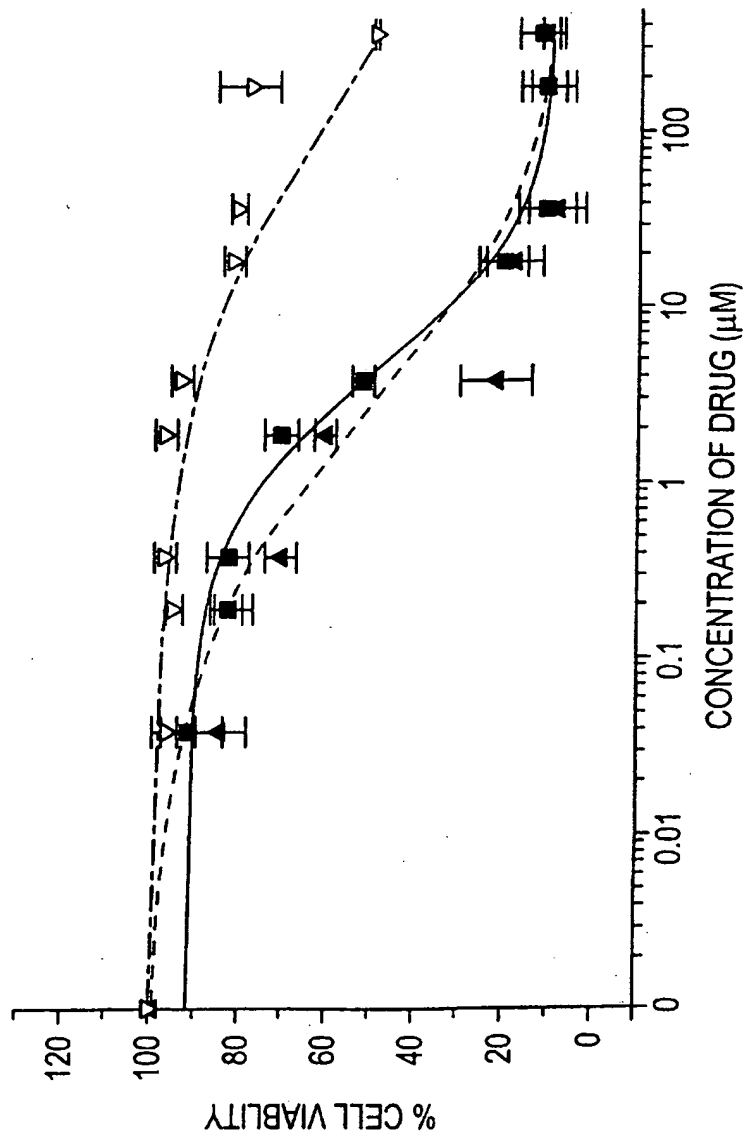


FIG. 6

7/9

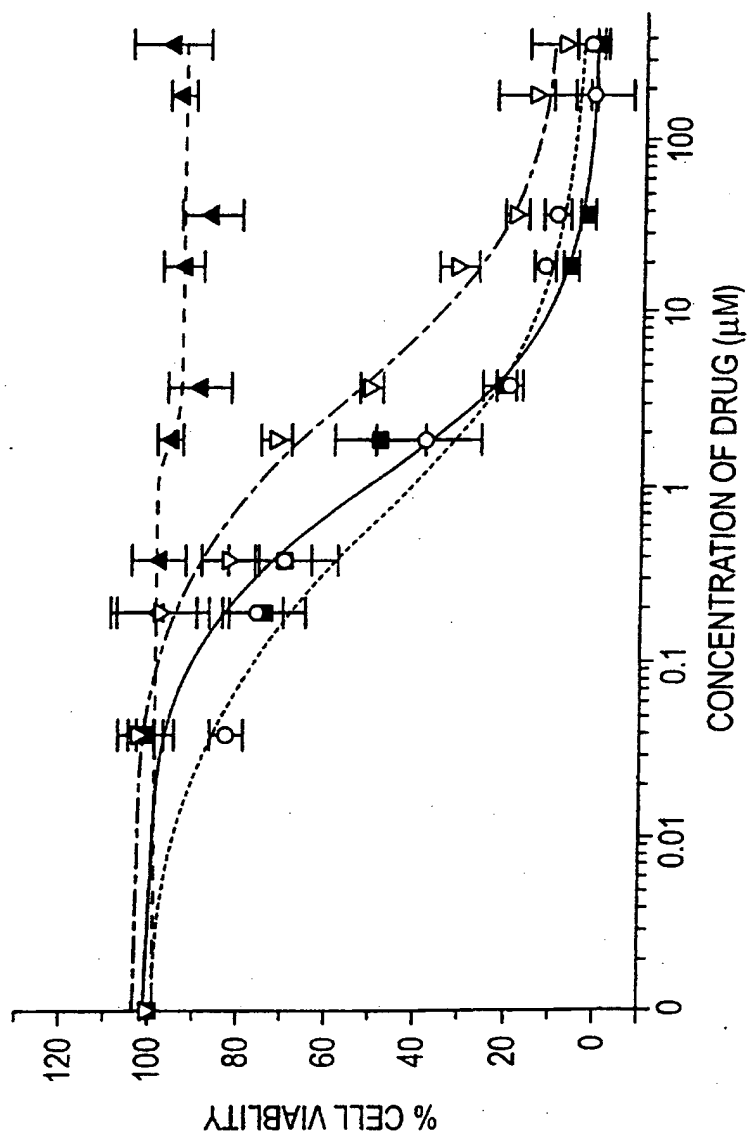


FIG. 7

8/9

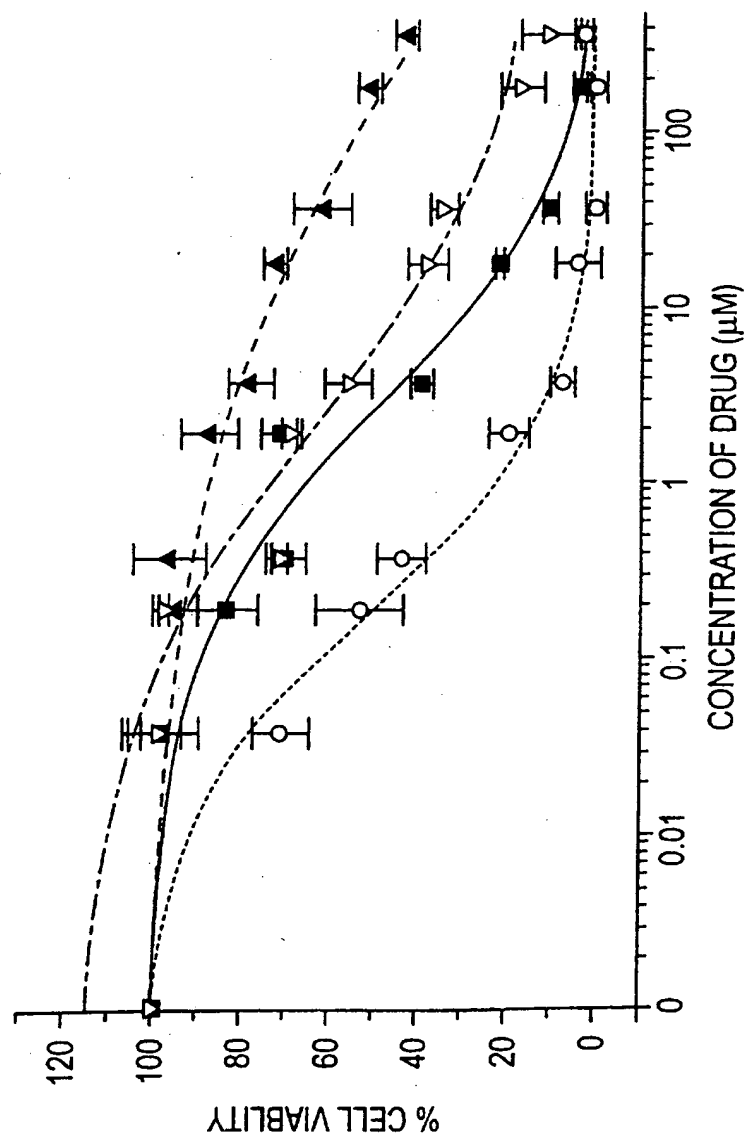


FIG. 8

9/9

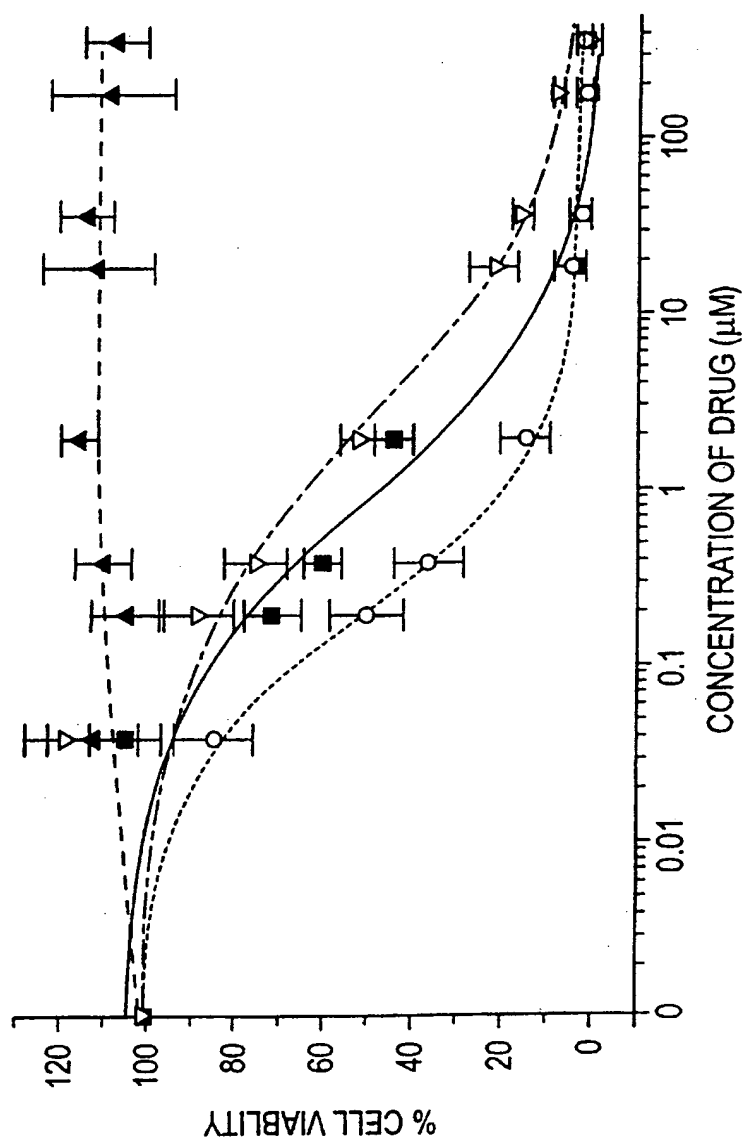


FIG. 9



## INTERNATIONAL SEARCH REPORT

International application No.  
PCT/US97/14140

<b>A. CLASSIFICATION OF SUBJECT MATTER</b> IPC(6) : Please See Extra Sheet. US CL : Please See Extra Sheet. According to International Patent Classification (IPC) or to both national classification and IPC		
<b>B. FIELDS SEARCHED</b> Minimum documentation searched (classification system followed by classification symbols) U.S. : 536/23.1; 424/9.1, 178.1, 179.1, 181.1, 184.1, 193.1, 604, 646; 514/6, 12, 21, 251, 501  Documentation searched other than minimum documentation to the extent that such documents are included in the fields searched None  Electronic data base consulted during the international search (name of data base and, where practicable, search terms used) Please See Extra Sheet.		
<b>C. DOCUMENTS CONSIDERED TO BE RELEVANT</b>		
Category*	Citation of document, with indication, where appropriate, of the relevant passages	Relevant to claim No.
A	US 5,428,023 A (RUSSELL-JONES et al.) 27 June 1995, entire document.	1-7, 10, 14-16, 19, 21-23, 30-34, 36-38, 41-44, 46-48
A	US 5,512,443 A (SCHLOM et al.) 30 April 1996, entire document.	1-7, 10, 14-16, 19, 21-23, 30-34, 36-38, 41-44, 46-48
Y	US 5,589,463 A (RUSSELL-JONES et al.) 31 December 1996, entire document.	1-7, 10, 14-16, 19, 21-23, 30-34, 36-38, 41-44, 46-48
<input checked="" type="checkbox"/> Further documents are listed in the continuation of Box C. <input type="checkbox"/> See patent family annex.		
* "A" "E" "L" "O" "P"	Special categories of cited documents: document defining the general state of the art which is not considered to be of particular relevance earlier document published on or after the international filing date document which may throw doubts on priority claim(s) or which is cited to establish the publication date of another citation or other special reason (as specified) document referring to an oral disclosure, use, exhibition or other means document published prior to the international filing date but later than the priority date claimed	*T* later document published after the international filing date or priority date and not in conflict with the application but cited to understand the principle or theory underlying the invention *X* document of particular relevance; the claimed invention cannot be considered novel or cannot be considered to involve an inventive step when the document is taken alone *Y* document of particular relevance; the claimed invention cannot be considered to involve an inventive step when the document is combined with one or more other such documents, such combination being obvious to a person skilled in the art *A* document member of the same patent family
Date of the actual completion of the international search 10 DECEMBER 1997		Date of mailing of the international search report 06 JAN 1998
Name and mailing address of the ISA/US Commissioner of Patents and Trademarks Box PCT Washington, D.C. 20231 Facsimile No. (703) 305-3230		Authorized officer: P. ACHUTAMURTHY Telephone No. (703) 308-0196

**INTERNATIONAL SEARCH REPORT****International application No.**  
**PCT/US97/14140****C (Continuation). DOCUMENTS CONSIDERED TO BE RELEVANT**

Category*	Citation of document, with indication, where appropriate, of the relevant passages	Relevant to claim No.
Y, P	UA 5,608,046 A (COOK et al.) 04 March 1997, entire document.	1-7, 10, 14-16, 19, 21-23, 30-34, 36-38, 41-44, 46- 48

# INTERNATIONAL SEARCH REPORT

International application No.  
PCT/US97/14140

## A. CLASSIFICATION OF SUBJECT MATTER:

IPC (6):

C07H 21/02, 21/04, 23/00; G01N 33/15; A61K 31/525, 39/00, 39/44, 35/00, 49/00

## A. CLASSIFICATION OF SUBJECT MATTER:

US CL :

536/23.1; 424/9.1, 178.1, 179.1, 181.1, 184.1, 193.1, 604, 646; 514/6, 12, 21, 251, 501

## B. FIELDS SEARCHED

Electronic data bases consulted (Name of data base and where practicable terms used):

APS, CASONLINE

search terms: organocobalt, complexes, cobalamin, vitamin-b12, corrinoids, bioactive agents, biocides, bioconjugates, peptides, nucleotides, DNA, RNA



# Interaction of the Antitumor Antibiotic Chromomycin A<sub>3</sub> with Glutathione, a Sulfhydryl Agent, and the Effect upon Its DNA Binding Properties

Sukanya Chakrabarti,\* Pulak Roy and Dipak Dasgupta†

BIOPHYSICS DIVISION, SAHA INSTITUTE OF NUCLEAR PHYSICS, CALCUTTA-700 037, INDIA

**ABSTRACT.** Chromomycin A<sub>3</sub> (CHR), an anticancer antibiotic, blocks macromolecular synthesis via reversible interaction with DNA only in the presence of divalent cations like Mg<sup>2+</sup>. In the absence of DNA, the antibiotic forms a dimer: Mg<sup>2+</sup> complex [(CHR)<sub>2</sub>Mg<sup>2+</sup>]. It is the DNA-binding ligand. The antibiotic has potential reactive centers that could interact with GSH, the most abundant non-protein thiol in eukaryotic cells and a putative cofactor involved in the activation of many antibiotics *in vivo*. To understand the mode of action of CHR *in vivo*, we studied the interactions of CHR and the (CHR)<sub>2</sub>Mg<sup>2+</sup> complex with GSH and the association of the resultant complexes with DNA by means of absorption, fluorescence, and circular dichroism spectroscopy. The novel finding was that GSH interacts non-covalently with CHR without a chemical modification of the antibiotic. The interaction was reversible in nature. The results are reported in two parts: the interaction of CHR with GSH in the absence and presence of Mg<sup>2+</sup>, and the effect of this interaction on the DNA-binding properties of the antibiotic. CHR forms a single type of complex with GSH. In contrast, (CHR)<sub>2</sub>Mg<sup>2+</sup> forms two different types of complexes with GSH: a low GSH complex at ~ 12 mM GSH and a high GSH complex at ≥ 16 mM GSH. Binding and thermodynamic parameters for the reversible association of the complexes with DNA demonstrated that they bind differently to the same DNA. The thermodynamic parameters indicate that the presence of GSH alters the mode of binding of the (CHR)<sub>2</sub>Mg<sup>2+</sup> complex with DNA. The (CHR)<sub>2</sub>Mg<sup>2+</sup> complex binds to DNA via an entropy-driven process, whereas in the presence of GSH the association is enthalpy-driven. The significance of these results in the understanding of the molecular basis of action of the antibiotic is discussed. *BIOCHEM PHARMACOL* 56;11:1471–1479, 1998. © 1998 Elsevier Science Inc.

**KEY WORDS.** anticancer antibiotic; chromomycin A<sub>3</sub>; glutathione; DNA binding; chromomycin A<sub>3</sub> dimer-Mg<sup>2+</sup> complex; absorbance, fluorescence and circular dichroism spectroscopy

CHR‡ (Fig. 1) is an antitumor antibiotic produced from *Streptomyces griseus* [1]. It reversibly binds to double-stranded DNA and blocks its function as a template for DNA and RNA polymerases [2]. Studies using optical and NMR spectroscopy [3, 4], and enzymatic and chemical footprinting [5, 6] demonstrated that the antibiotic binds via the minor groove with a GC base specificity. It was attributed to H-bonding between potential sites in the antibiotic, such as the OH group at C8 with the NH2 and N3 group of the guanine base [7]. The reversible interaction with DNA requires the presence of a divalent metal ion

such as Mg<sup>2+</sup>. We showed that in the absence of DNA the antibiotic forms two types of complexes with Mg<sup>2+</sup>. These complexes are DNA-binding ligands [8]. The complexes, I (with 1:1 stoichiometry in terms of drug: Mg<sup>2+</sup>) and II (with 2:1 stoichiometry in terms of drug: Mg<sup>2+</sup>), bind differently to the same DNA, as indicated from the values of the binding stoichiometry and thermodynamic parameters [9, 10]. Complex II, i.e. (CHR)<sub>2</sub>Mg<sup>2+</sup>, is the plausible species formed at a millimolar level of intracellular Mg<sup>2+</sup>.

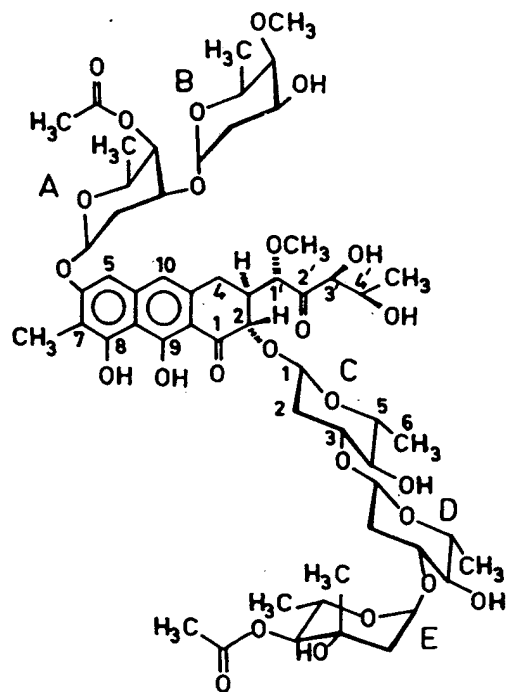
Not much is known about the mode of action of the antibiotic *in vivo* except that it binds reversibly to DNA in the process of blocking its function as a template. The antibiotic has potential reactive centers such as the carbonyl group in the aglycone ring (see Fig. 1) for redox reactions with appropriate cytosolic components. Assessment of such interactions will be relevant in understanding the mode of action of the antibiotic *in vivo*, because the drug will encounter them during its transport to the nucleus. An important cytosolic component is GSH. GSH along with its oxidized form forms a very potent redox system (E° = -240 mV) [11], which often detoxifies the

\* Present address: Chemistry Department, Seth Anandram Jaipuria College, 10, Raja Naba Krishna St., Calcutta-700 005, India.

† Corresponding author: Dr. Dipak Dasgupta, Biophysics Division, Saha Institute of Nuclear Physics, 37, Belgachhia Road, Calcutta-700 037, India. Tel. (91)-(33)-556-5611; E-mail: dipak@biop.saha.ernet.in

‡ Abbreviations: A.U., arbitrary units; AUFS, absorbance unit full scale; CD, circular dichroism; CHR, chromomycin A<sub>3</sub>; CT DNA, calf thymus DNA; and poly(dA-dT), double-stranded poly(dA-dT) · poly(dA-dT).

Received 11 February 1998; accepted 28 July 1998.



### CHROMOMYCIN A<sub>3</sub>

FIG. 1. Structure of chromomycin A<sub>3</sub>.

cell via radical intermediate formation. These intermediates cause DNA damage and increase the cytotoxicity of the antibiotics. GSH is present at a relatively high concentration in the normal cell (0.5 to 10 mM) [12], the levels of which may go up further in the presence of carcinogens or in tumor cells [13, 14]. It interacts reductively with a number of antibiotics such as neocarzinostatin, calicheamicin, and bleomycin, generating active radical intermediates [15, 16]. On the other hand, the cytotoxicity of several covalently binding antibiotics like cisplatin, melphalan, and Adriamycin® is reduced considerably in the presence of GSH by its potential to scavenge free radicals inside the cell [17]. The presence of GSH in the cell also increases the radioresistance of the cell [18]. In view of these results, we have examined in this study the interaction of GSH with CHR under *in vitro* conditions. The effect of the binding of GSH upon the DNA-binding property of the antibiotic also has been followed because DNA is the major cellular target of the antibiotic. This part of the study had two objectives: (1) identifying any possible *in vivo* modification of the antibiotic by GSH, and (2) accounting for the high cytotoxicity of the antibiotic.

A significant result from the present studies was the finding that the antibiotic bound reversibly to GSH in the absence and presence of  $Mg^{2+}$ . There was no covalent modification of the antibiotic. This finding is novel and hitherto unreported for any other antibiotic. We have divided our results into two parts. The first part describes the interaction between CHR and the  $(CHR)_2Mg^{2+}$  com-

plex formed at a millimolar concentration of  $Mg^{2+}$  [8, 9] with GSH. The second part reports the DNA-binding properties of the GSH-bound  $(CHR)_2Mg^{2+}$  complex. Thermodynamic parameters for DNA binding were determined for GSH-bound forms of  $(CHR)_2Mg^{2+}$  to characterize the mode of binding.

All studies were carried out at pH 8.0 where a homogeneous population of negatively charged drug ( $pK_a$  7.0) exists [19]. GSH is also negatively charged at this pH. CT DNA was chosen as the natural DNA model because it consists of comparable percentages of AT and GC base pairs.

### MATERIALS AND METHODS

Chromomycin A<sub>3</sub>, Tris, magnesium chloride solution (4.9 M), and CT DNA were from the Sigma Chemical Co. Poly(dA-dT), Sephadryl S-1000, and agarose were from Pharmacia Biotech Ltd. GSH, methanol, acetic acid, ammonium acetate, and sodium chloride were from the Sisco Research Laboratory. The purity of GSH was checked. Unless mentioned otherwise, studies were done in 20 mM Tris-HCl plus 100 mM NaCl buffer, pH 8.0. All buffers were prepared in deionized, all quartz distilled water. Absorption, fluorescence, and CD spectra were recorded with an Hitachi U-2000 spectrophotometer, a Shimadzu RF-540 spectrofluorometer, and a Jasco 720 spectropolarimeter, respectively. We determined the concentration of the antibiotic, DNA samples, and polynucleotides from their known molar extinction coefficients. The concentration of GSH, estimated by the enzymatic assay [20], was standardized against the dry weight of the chemical. GSH was stored under anhydrous conditions in the dark at a low temperature. A fresh solution of GSH was prepared as needed, just prior to use.

CT DNA was deproteinized by the chloroform-phenol extraction method and precipitated with ethanol. Then it was redissolved in 20 mM Tris-HCl buffer, pH 8.0, dialyzed extensively against the same buffer containing 5 mM EDTA to remove metal ions, and finally dialyzed against the buffer minus EDTA to remove EDTA.

The pARC035 plasmid was isolated from its host strain, JM101, by alkali lysis method [21]. Final purification of the supercoiled plasmid DNA from RNA and relaxed plasmid DNA was done by Sephadryl S-1000 column chromatography. Purity of the circular DNA was checked by agarose gel electrophoresis.

Fluorescence measurements for the antibiotics and the  $(CHR)_2Mg^{2+}$  complex in the presence and absence of GSH were carried out at an excitation wavelength of 470 nm instead of the absorption maximum at 405 nm, to avoid photodegradation [9]. Optical density of the samples at 470 nm did not exceed 0.02. Therefore, we did not correct the emission intensity for an optical filtering effect. Background emission (<5% of maximum) was corrected for by subtracting signals from blank buffer, or GSH plus buffer samples. CD values are expressed as observed ellipticity ( $\theta_{obs}$ ) in millidegrees. CD spectra were measured in a 10-mm path-length cuvette as an average of two runs. They

were subtracted from buffer blank or GSH plus buffer samples, and smoothed within permissible limits by the inbuilt software of the instrument.

An LKB Superpac Cartridge column (4 × 125 mm), Spherisorb ODS2 (3 μm) was used for reversed-phase HPLC. The GSH complex was prepared by mixing 50 μM CHR with 16 mM GSH in 20 mM Tris-HCl plus 100 mM NaCl, pH 8.0, and incubated in the dark for 30 min. Fifty microliters of this sample was loaded into the column. The elution buffer was a gradient running from 100 to 0% methanol in the aqueous phase, 10 mM NH<sub>4</sub>Ac/Ac buffer, pH 6.2. Eluted fractions were detected for CHR from fluorescence emission at 540 nm ( $\lambda_{ex}$  = 470 or 405 nm).

Supercoiled plasmid DNA was incubated with GSH-bound (CHR)<sub>2</sub>Mg<sup>2+</sup> and run on a gel to detect any change in the DNA topology caused by ligand-induced relaxation or nicks [22]. The (CHR)<sub>2</sub>Mg<sup>2+</sup> complex (formed by mixing 196.3 μM CHR with 20 mM MgCl<sub>2</sub> in the dark for 1 hr) was incubated separately with 12.3 and 18.0 mM GSH for 30 min in the dark at 25°, in 20 mM Tris-HCl, plus 100 mM NaCl, pH 8.0. Then GSH-bound complex was incubated with 193 μM plasmid DNA for a period of 4 hr, under the same conditions. The total sample volume of 12 μL was mixed with 2 μL of bromophenol blue dye and run on a 0.7% agarose gel. This was followed by ethidium bromide staining to detect any change in the migration of the complex-bound DNA with respect to the free DNA or DNA plus GSH, which were also loaded as controls.

### Analysis of Binding Data

The binding isotherms were obtained by incubating the GSH plus (CHR)<sub>2</sub>Mg<sup>2+</sup> complex with DNA in the buffer at different ratios of DNA and drug at a particular temperature, and monitoring the change in emission intensity at 540 nm ( $\lambda_{ex}$  = 470 nm) due to binding with the DNA. The spectrofluorometric titration data of the GSH-bound (CHR)<sub>2</sub>Mg<sup>2+</sup> complexes with CT DNA were analyzed by two methods: curve fitting and Scatchard analysis.

In the model-independent curve-fitting method, the apparent binding constant was determined from the dissociation constant that fitted best to the experimentally obtained points. Here the ligand-DNA reaction was considered according to the following equilibrium: L + D = L·D. At a fixed concentration of the ligand and increasing concentrations of DNA, the titration profile shows the increase in the fluorescence intensity of the ligand as it binds to DNA. For an initial concentration "a" of the ligand and an input concentration "b" of DNA, the concentration of L·D is given by "x," such that the dissociation constant  $K_d$  takes the form,  $K_d = (a - x) \cdot (b - x)/x$ . Replacing "x" by the spectroscopic signal "S," the above equation takes the form:

$$K_d = [a - (\Delta S_{obs}/\Delta S_{max}) \cdot a] \cdot [b - \Delta S_{obs}/\Delta S_{max} \cdot a] / [(\Delta S_{obs}/\Delta S_{max}) \cdot a],$$

where  $\Delta S_{obs} = (S_{obs} - S_0)$ ,  $\Delta S_{max} = (S_{max} - S_0)$ , and  $S_0$  is the initial signal value of ligand when no DNA has been added. A program determines the value of  $K_d$  for each experimental value of  $b$  and  $\Delta S_{obs}$ .  $\Delta S_{max}$  was determined from the double-reciprocal plot [23]. Finally, a theoretical curve was constructed using the best fit value for  $K_d$  ( $= 1/K_{app}$ ).

The Scatchard plot is given by the equation  $r/C_f = K_0 (n - r)$ , where  $r = C_b/C_p$  ( $C_b$  is the concentration of the bound ligand and  $C_p$  is the concentration of the DNA);  $n$  is the binding stoichiometry in terms of the number of drug molecules bound per nucleotide, and  $K_0$  is the intrinsic binding constant. The apparent binding constant  $K_{app}$  is given by  $K_0 \cdot n$ . The dequenching of the fluorescence of the ligand as a function of added concentration of DNA was analyzed to construct the binding isotherm according to the Scatchard method.  $C_b$  was calculated as follows:  $C_b = Q/Q_{max} \cdot C_{tot}$ , where  $C_{tot}$  is the initial input concentration of the ligand,  $Q$  is the fractional dequenching during titration, and  $Q_{max}$  is the fractional dequenching when the ligand is totally bound to DNA [24].  $Q$  is determined from the relation  $Q = (I - I_0)/I_0$ , where  $I_0$  and  $I$  are the emission intensities of the free ligand and DNA bound ligand, respectively;  $Q_{max} = (I_{max} - I_0)/I_0$ , where  $I_{max}$  is obtained from a plot of  $1/(I - I_0)$  against  $1/(C_p - C_b)$ , for which the intercept yields the value of  $1/(I_{max} - I_0)$  [23]. This approach is based on the assumption of a linear relation between emission intensity and the concentration of the ligand, which was found to be valid for the concentration range of 5–50 μM of the ligand employed. The experimental points for the binding isotherm were subjected to least squares analysis with a view to getting a best-fit straight line.

The two methods were employed to analyze the binding data in order to check the internal consistency. This is particularly necessary when the affinity constant values are in the moderate range and the ligands are bulky.

The thermodynamic parameters  $\Delta H$  (van't Hoff enthalpy),  $\Delta S$  (entropy), and  $\Delta G$  (free energy) were determined using the following equations: in  $K_{app} = -\Delta H/RT + \Delta S/R$  and  $\Delta G = \Delta H - T\Delta S$ , where  $R$  and  $T$  are the universal gas constant and absolute temperature, respectively [25].  $K_{app}$  was determined at four temperatures: 20°, 25°, 30°, and 35°, respectively, to evaluate  $\Delta H$  and  $\Delta S$ , and these values were incorporated in the equation to obtain the value of  $\Delta G$  at room temperature.

## RESULTS

### Interaction of CHR and Its (CHR)<sub>2</sub>Mg<sup>2+</sup> Complexes with GSH

Changes in the absorbance and CD spectrum showed that CHR and (CHR)<sub>2</sub>Mg<sup>2+</sup> complex bound to GSH (Fig. 2 and 3). The absorption spectra for GSH-bound CHR and (CHR)<sub>2</sub>Mg<sup>2+</sup> complex are shown in Fig. 2a and 3a, respectively. Common features for the change in the absorption spectra were broadening, a red shift of the peak, and hypochromicity when they were compared with the spectrum for

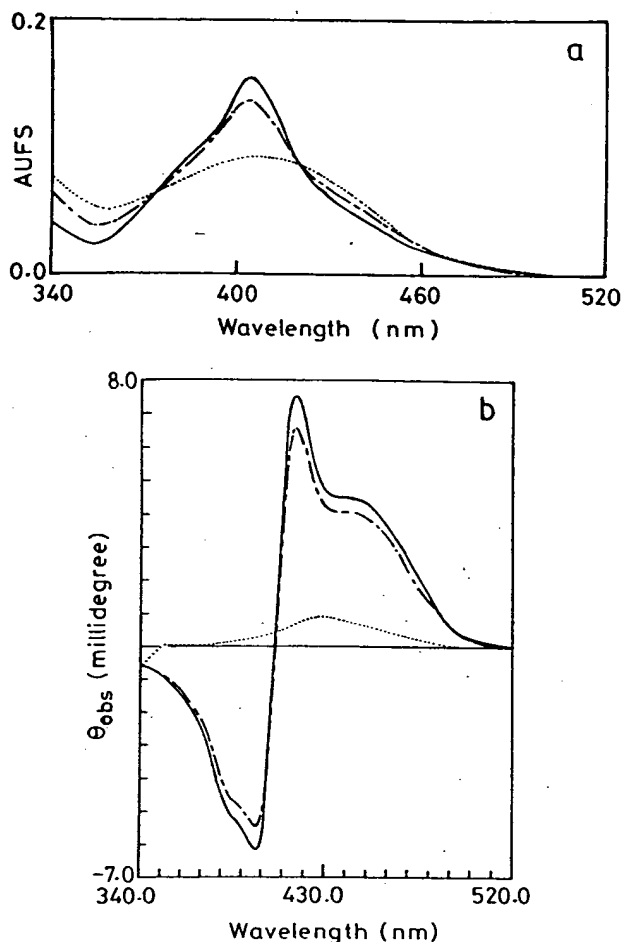


FIG. 2. (a) Absorption spectra of CHR under different conditions in 20 mM Tris-HCl plus 100 mM NaCl buffer, pH 8.0, at 25°: (1) CHR (15.0  $\mu$ M) alone (—); and (2) CHR (15.0  $\mu$ M) in the presence of GSH [10.3 mM (---) and 17.4 mM (.....)]. The reference cuvette contained the above buffer and GSH at the same concentration as in the sample cuvette. (b) CD spectra (340–520 nm) of CHR under different conditions in 20 mM Tris-HCl plus 100 mM NaCl buffer, pH 8.0, at 25°: (1) CHR (15.0  $\mu$ M) alone (—); and (2) CHR (15.0  $\mu$ M) in the presence of GSH [10.7 mM (---) and 16.0 mM (.....)].

the free CHR. The spectrum of GSH-bound  $(\text{CHR})_2\text{Mg}^{2+}$  complex showed a blue shift with respect to that of free  $(\text{CHR})_2\text{Mg}^{2+}$  complex. CD spectral change of CHR provided further evidence in favor of its association with GSH (Fig. 2b). There was a sharp decrease in the intensity of the CD bands when the input concentration of GSH changed from 10.7 to 16 mM. While the change in CD spectra indicated the interaction of  $(\text{CHR})_2\text{Mg}^{2+}$  complex with GSH, the nature of the change as a function of the input concentration of GSH was remarkably different from the previous example (Fig. 3b). The addition of GSH led to an initial increase in the ellipticity around 450 nm. It continued until ~12 mM GSH, when the peak became relatively broad. At a higher GSH concentration (~18 mM), the ellipticity decreased with a concomitant broadening of the spectrum. It suggests that in the concentration range of 10 to 12 mM GSH, a different

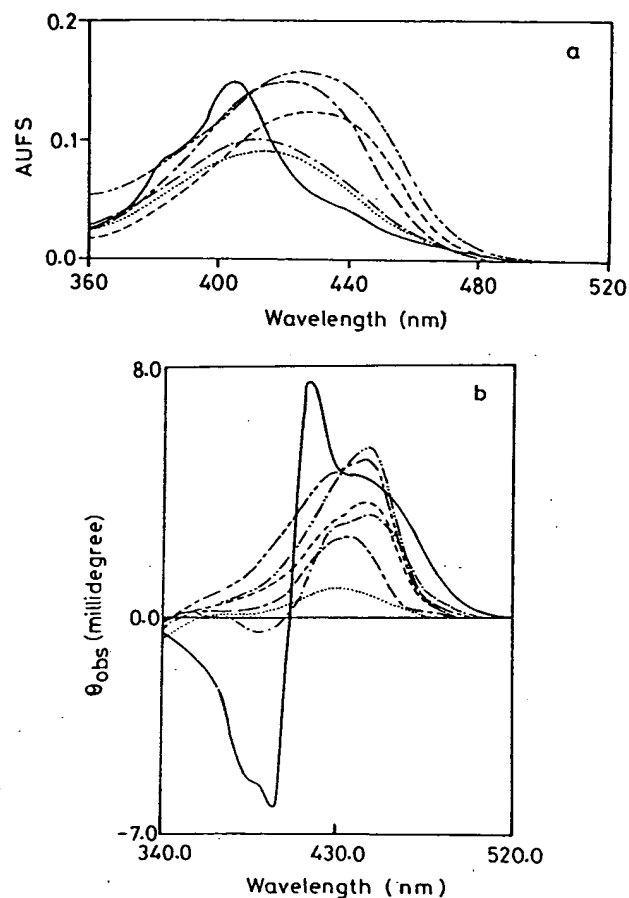


FIG. 3. (a) Absorption spectra of CHR,  $(\text{CHR})_2\text{Mg}^{2+}$  complex, and the low and the high complexes of GSH alone and in the presence of the different concentrations of CT DNA in 20 mM Tris-HCl plus 100 mM NaCl buffer, pH 8.0, at 25°: (1) CHR (15.7  $\mu$ M) alone (—); (2)  $(\text{CHR})_2\text{Mg}^{2+}$  complex containing 15.7  $\mu$ M CHR and 12.0 mM  $\text{MgCl}_2$  (---); (3) low GSH complex [ $(\text{CHR})_2\text{Mg}^{2+}$  complex plus GSH (12.0 mM, - · - ·)]; (4) low GSH complex in the presence of CT DNA (314  $\mu$ M, - - - -); (5) high GSH complex [ $(\text{CHR})_2\text{Mg}^{2+}$  complex plus GSH (18.0 mM, .....)]; and (6) high GSH complex in the presence of CT DNA (750  $\mu$ M, - - - - -). (b) CD spectra (340–520 nm) of CHR,  $(\text{CHR})_2\text{Mg}^{2+}$  complex, and the low and high GSH complexes alone and in the presence of different concentrations of CT DNA in 20 mM Tris-HCl plus 100 mM NaCl buffer, pH 8.0, at 25°. For comparison, the spectra for the  $(\text{CHR})_2\text{Mg}^{2+}$  complex in the presence of a saturating concentration of CT DNA is also given: (1) CHR (15.0  $\mu$ M) alone (—); (2)  $(\text{CHR})_2\text{Mg}^{2+}$  complex containing 15.0  $\mu$ M CHR and 12.0 mM  $\text{MgCl}_2$  (---); (3) low GSH complex [ $(\text{CHR})_2\text{Mg}^{2+}$  complex plus GSH (12.3 mM, - · - ·)]; (4) low GSH complex in the presence of CT DNA (330  $\mu$ M, - - - -); (5) high GSH complex [ $(\text{CHR})_2\text{Mg}^{2+}$  complex plus GSH (18.9 mM, .....)]; (6) high GSH complex in the presence of CT DNA (600  $\mu$ M, - - - - -); and (7)  $(\text{CHR})_2\text{Mg}^{2+}$  complex in the presence of CT DNA (220  $\mu$ M, - · - · -).

species is formed in the case of the  $(\text{CHR})_2\text{Mg}^{2+}$  complex. Absorption spectroscopy did not indicate the formation of such an intermediate complex. Illustrative titration profiles for the binding of  $(\text{CHR})_2\text{Mg}^{2+}$  complex to GSH using two different spectroscopic techniques are shown in Fig. 4. The

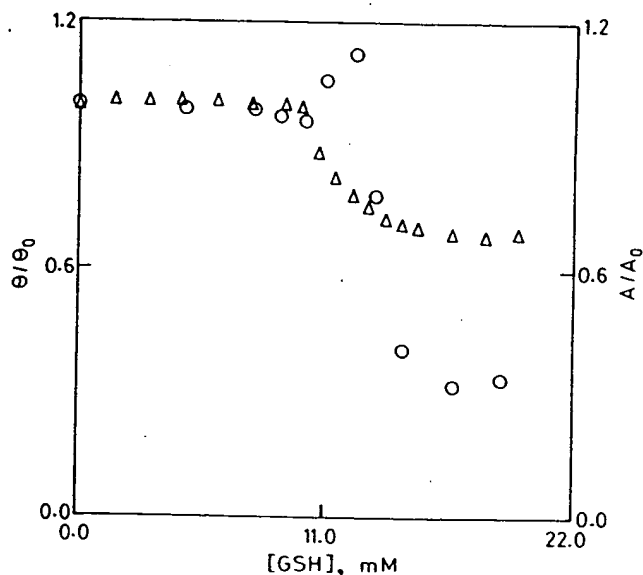


FIG. 4. Titration profiles for the binding of  $(\text{CHR})_2\text{Mg}^{2+}$  complex to GSH obtained from different spectroscopic techniques in 20 mM Tris-HCl plus 100 mM NaCl buffer, pH 8.0, at 25°: (1) CD,  $\theta/\theta_0$ , at 440 nm as a function of GSH concentration (O); and (2) absorption,  $A/A_0$ , at 405 nm as a function of GSH concentration ( $\Delta$ ). In the  $(\text{CHR})_2\text{Mg}^{2+}$  complex, concentrations of CHR and  $\text{MgCl}_2$  were 15.0  $\mu\text{M}$  and 12 mM, respectively.  $\theta$  is the ellipticity observed after each addition of GSH, and  $\theta_0$  is the observed ellipticity in the absence of GSH. Likewise,  $A$  and  $A_0$  represent the absorbance after each addition of GSH and in the absence of GSH, respectively.

profiles bring out the differences in the nature of the change observed from absorbance and CD spectroscopy. The second methodology showed the formation of two types of complexes with GSH, when  $(\text{CHR})_2\text{Mg}^{2+}$  complex bound to it. We did not observe any difference in the nature of the titration profiles in the case of free drug (data not shown). Therefore, we assume that it forms only a single type of complex with GSH.

Henceforth, the complex that was formed at the lower concentration of GSH (12 mM) is referred to as the **low GSH complex** of  $(\text{CHR})_2\text{Mg}^{2+}$  and the one formed at the higher concentration of GSH ( $\geq 16$  mM), as the **high GSH complex**, respectively.

The reversible nature of the binding of CHR and  $(\text{CHR})_2\text{Mg}^{2+}$  complex with GSH was established as follows. A comparison of the reversed-phase HPLC profiles of the drug (or its  $\text{Mg}^{2+}$  complex) and its equilibrium mixture with GSH showed that the free as well as the GSH-bound CHR eluted at the same place, thereby indicating the reversibility of the interaction and the absence of formation of a covalent complex with GSH (data not shown).

#### DNA Binding Potential of the GSH-Bound Antibiotic and $(\text{CHR})_2\text{Mg}^{2+}$ Complex

Since the antibiotic is established as a DNA-binding inhibitor of replication and transcription, we examined the

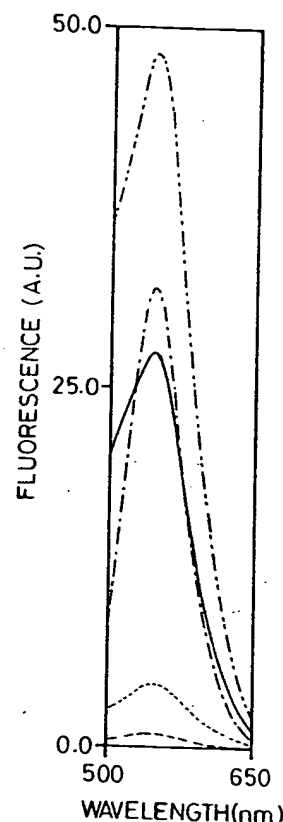


FIG. 5. Fluorescence emission spectra of CHR,  $(\text{CHR})_2\text{Mg}^{2+}$  complex, and the high complex of GSH under different conditions in 20 mM Tris-HCl plus 100 mM NaCl buffer, pH 8.0, at 25°: (1) CHR (15.0  $\mu\text{M}$ ) alone (---); (2)  $(\text{CHR})_2\text{Mg}^{2+}$  complex containing 15.0  $\mu\text{M}$  CHR and 12.0 mM  $\text{MgCl}_2$  (.....); (3)  $(\text{CHR})_2\text{Mg}^{2+}$  complex in the presence of GSH (18.0 mM, ----), i.e. high GSH complex; and (4) high GSH complex in the presence of CT DNA (150  $\mu\text{M}$ , —) and (750  $\mu\text{M}$ , — · —).

DNA-binding properties of the GSH-bound CHR in the absence and presence of  $\text{Mg}^{2+}$ .

Absorption, fluorescence, and CD studies showed that the spectrum of the GSH-bound antibiotic did not change upon the addition of DNA in the absence of  $\text{Mg}^{2+}$  (data not shown). On the other hand, absorbance, CD, and fluorescence spectra of both low and high GSH complexes underwent a considerable change upon the addition of DNA (Fig. 3 and 5), thereby showing that they bind to DNA. It also indicated that the obligatory requirement of a divalent metal ion for the association of the antibiotic with DNA [9] is maintained for its GSH-bound form. GSH-bound  $(\text{CHR})_2\text{Mg}^{2+}$  complexes did not bind to poly (dA-dT) as verified by the absence of change in the absorption spectra of the ligands upon the addition of the polynucleotide. This suggests that GC base specificity is not altered upon association with GSH. Experiments with supercoiled plasmid DNA pARC035 showed the absence of a new band corresponding to relaxed DNA, when the supercoiled DNA was incubated with the high GSH complex of  $(\text{CHR})_2\text{Mg}^{2+}$  for a period of about 4 hr. This indicates that the DNA remains in the same topological



form. This observation eliminates the possibility of the GSH complexes causing a nick in the DNA strand.

An analysis of spectral changes such as those shown in the figures mentioned above indicates the following general trends. A red shift compared with the unbound ligand, and an increase in the molar extinction value near the 400–440 nm region ensue the binding of the ligand(s) to DNA (Fig. 3a). An increase in the fluorescence emission intensity and a blue shift of the emission peak relative to that of the free ligand are the two features in the fluorescence spectra characterizing the binding of the complexes to DNA (Fig. 5). This is in contrast to the red shift of the fluorescence peak for the  $(\text{CHR})_2\text{Mg}^{2+}$  complex when it binds to DNA [9]. CD spectral changes upon addition of DNA provided further evidence for the binding of high and low GSH complexes with DNA. The most general feature was the increase in the CD band intensity around 440 nm. The resultant spectrum in the presence of DNA was not overlapping with that obtained upon the addition of DNA to the  $(\text{CHR})_2\text{Mg}^{2+}$  complex in the absence of GSH (Fig. 3b). It indicates that the overall nature of the DNA-bound ligands is different in both cases. Thus, the addition of DNA does not lead to a dissociation of GSH from the  $(\text{CHR})_2\text{Mg}^{2+}$  complex.

A representative binding isotherm is shown in Fig. 6a. From the binding isotherms, analysis was done to determine the apparent affinity constants,  $K_{\text{app}}$ , as described under Materials and Methods. The non-cooperative nature of the binding isotherm led us to a Scatchard analysis of the data (shown in Fig. 6b). The relevant binding parameters are summarized in Table 1. The results of the analysis by the two methods were found to be self-consistent within the limits of experimental errors. Since there was no significant deviation of the points in the Scatchard plot from linearity near the abscissa, McGhee–Von Hippel analysis of the binding was not attempted. The single temperature values of the affinity parameters for DNA binding of the different GSH complexes show that the DNA-binding affinity for the drug dimer was relatively higher than for the low and high GSH complexes. The affinity was lowest in the case of the high GSH complex. The stoichiometries were comparable for the binding of all the different ligands to DNA (6–7 bases/drug).

Since the enthalpy–entropy compensation may lead to comparable free energy changes, these parameters were determined to characterize the DNA-binding properties of the two GSH complexes. They were evaluated from the measurement of apparent binding constants at four temperatures. A plot of  $\ln K_{\text{app}}$  against  $1/T$  was constructed from which the values of  $\Delta H$  (from the slope) and  $\Delta S$  (from the intercept) were determined (Fig. 6c). Then the values of  $\Delta G$  were calculated from these values (see Materials and Methods). The stoichiometry of binding did not alter with the temperature. The estimated values are summarized in Table 2, and the following features emerge from a scrutiny of this information. Both high and low GSH complexes of  $(\text{CHR})_2\text{Mg}^{2+}$  bind to DNA via an enthalpy-driven process. On the other hand, past results from our laboratory showed that the  $(\text{CHR})_2\text{Mg}^{2+}$  complex binds to DNA in an

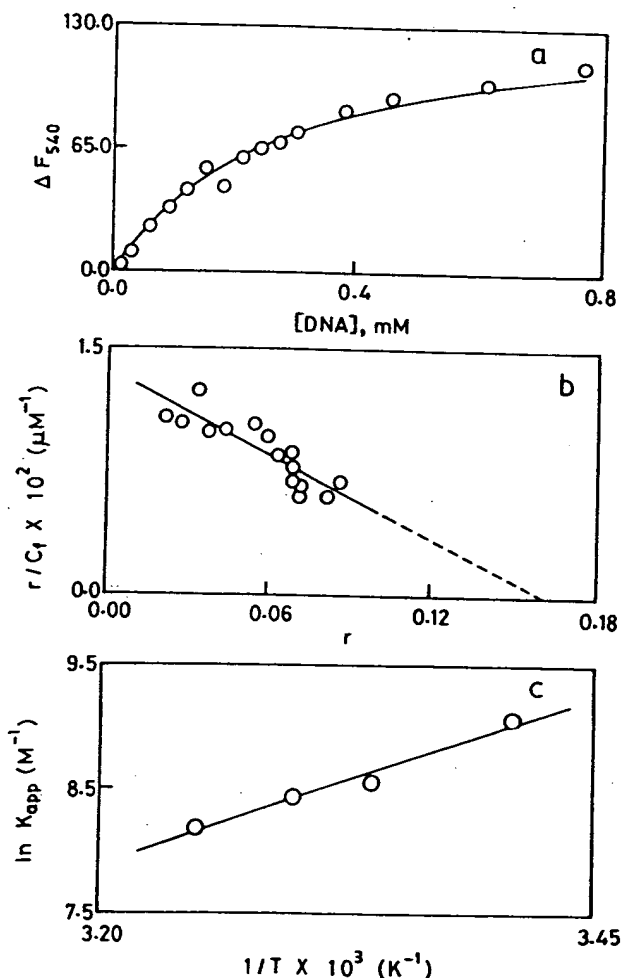


FIG. 6. (a) Binding isotherm (fluorescence emission intensity  $\Delta F_{540}$  of ligand as a function of DNA concentration) obtained by the curve-fitting method for the interaction of high GSH complex of  $(\text{CHR})_2\text{Mg}^{2+}$  with DNA in 20 mM Tris–HCl plus 100 mM NaCl buffer, pH 8.0, at 35°. Experimental points (○) are fitted with the theoretical best-fit curve. In the  $(\text{CHR})_2\text{Mg}^{2+}$  complex, the concentrations of CHR and  $\text{MgCl}_2$  were 15.3  $\mu\text{M}$  and 12.0 mM, respectively. The high GSH complex contained 18.0 mM GSH. (b) Scatchard plot for the interaction of low GSH complex of  $(\text{CHR})_2\text{Mg}^{2+}$  with CT DNA in 20 mM Tris–HCl plus 100 mM NaCl buffer, pH 8.0, at 30°. In the  $(\text{CHR})_2\text{Mg}^{2+}$  complex, the concentrations of CHR and  $\text{MgCl}_2$  were 15.0  $\mu\text{M}$  and 12.0 mM, respectively; and the low GSH complex contained 12.0 mM GSH. (c) van't Hoff plot for the interaction of high GSH complex of  $(\text{CHR})_2\text{Mg}^{2+}$  with CT DNA in 20 mM Tris–HCl plus 100 mM NaCl buffer, pH 8.0.

entropy-driven manner [9]. These observations are significant because they demonstrate that the presence of GSH perturbs the association of the  $(\text{CHR})_2\text{Mg}^{2+}$  complex with DNA and lend support to our previous observation that the addition of DNA does not lead to dissociation of GSH from  $(\text{CHR})_2\text{Mg}^{2+}$  complex.

## DISCUSSION

The above experimental results show that reduced GSH binds reversibly to the free CHR and  $(\text{CHR})_2\text{Mg}^{2+}$  com-

**TABLE 1.** Binding parameters for the interaction of GSH-bound (CHR)<sub>2</sub>Mg<sup>2+</sup> Complex with CT DNA at 20 mM Tris-HCl plus 100 mM NaCl, pH 8.0, at 30°\*

Complex type	$K_{app} (\times 10^4 \text{ M}^{-1})^\dagger$	$K_{app} (\times 10^4 \text{ M}^{-1})^\ddagger$	$n^\ddagger$
(CHR) <sub>2</sub> Mg <sup>2+</sup>	2.1	4.3	0.17
Low complex ([GSH] = 12.0 mM)	0.9	1.2	0.15 ± 0.01
High complex ([GSH] = 18.0 mM)	0.5	0.8	0.15 ± 0.01

\* (CHR)<sub>2</sub>Mg<sup>2+</sup> complex was prepared by incubating 15 μM CHR with 12 mM MgCl<sub>2</sub> for 1 hr. This was followed by the addition of GSH (the concentration is mentioned in the parentheses) and incubation for 30 min. The values were obtained by spectrofluorometric titration as shown in Fig. 5, where separate aliquots of the prepared complex were incubated with increasing concentrations of CT DNA, for 4 hr. Each incubation was done in the dark at 30°. Fluorescence signals (λ<sub>ex</sub> = 470 nm) of the incubated samples were noted at 540 nm.

† Binding constants were determined using the best-fitted theoretical curve method, as described in Materials and Methods.

‡ Binding constant,  $K_{app}$  (M<sup>-1</sup>), and binding stoichiometry,  $n$  (drug molecules bound per nucleotide), were determined using a Scatchard plot as described in Materials and Methods. The value of  $n$  is an average of three independent sets of experiments; ± values denote standard error.

plex. The reversible nature of the interaction is the feature that distinguishes it from other antibiotics such as enediyne or bleomycins. These complexes could be formed under *in vivo* conditions also, because the intracellular concentration of GSH lies in the range of 0.5 to 10 mM [12]. The possibility further increases in tumor cells where the GSH level goes up [13, 14]. The moderate salt concentration used in the buffer (100 mM NaCl) eliminates the possibilities of non-specific association involving negatively charged GSH at pH 8.0 in our studies.

There is an important difference between CHR and (CHR)<sub>2</sub>Mg<sup>2+</sup> complex in the nature of the association with GSH. It forms two types of complexes with the drug dimer, (CHR)<sub>2</sub>Mg<sup>2+</sup>. The difference in the molecular nature of the GSH-bound complexes of the free drug and the (CHR)<sub>2</sub>Mg<sup>2+</sup> complexes is indicated from their spectroscopic properties such as absorbance and CD, and their DNA-binding properties as well.

The experimental results are discussed as follows: interaction of CHR and its (CHR)<sub>2</sub>Mg<sup>2+</sup> complex with GSH and association of the GSH-bound (CHR)<sub>2</sub>Mg<sup>2+</sup> complexes with CT DNA.

#### Interaction of Chromomycin A<sub>3</sub> and the (CHR)<sub>2</sub>Mg<sup>2+</sup> Complex with GSH

The binding of the antibiotic and its Mg<sup>2+</sup> complexes to reduced GSH is characterized by changes in the absorbance

**TABLE 2.** Thermodynamic parameters for the interaction of GSH-bound (CHR)<sub>2</sub>Mg<sup>2+</sup> Complex with CT DNA, in 20 mM Tris-HCl plus 100 mM NaCl, pH 8.0\*

Complex type	$\Delta H$ (kcal/mol)	$\Delta S$ (e.u.)	$\Delta G^\ddagger$ (kcal/mol)
(CHR) <sub>2</sub> Mg <sup>2+</sup>	8.1†	46.3‡	-5.9
Low complex ([GSH] = 12.0 mM)	-12.6	-23.6	-5.4
High complex ([GSH] = 18.0 mM)	-10.8	-19.1	-5.0

\*Complex preparation and titration with CT DNA was done as described in the legend to Table 1 at four different temperatures: 20°, 25°, 30°, and 35°. The thermodynamic parameters were determined by the van't Hoff method, as stated in Materials and Methods. A representative example is shown in Fig. 6c.

†ΔG values were determined at 30°.

‡From Ref. 9.

and chiro-optical properties of the antibiotic. In general, change in the absorption spectrum of free drug or (CHR)<sub>2</sub>Mg<sup>2+</sup> complex upon binding to GSH could be attributed to an alteration in the local electronic environment of the aglycone chromophore. The presence of negatively charged GSH is a potential source for such perturbation in an electronic environment. The hypochromic effect in the absorption spectra originates from the stacking of the chromophores in the aggregated CHR or (CHR)<sub>2</sub>Mg<sup>2+</sup> complex. A similar trend was also noticed when the antibiotic underwent self-association at a higher concentration (unpublished results). Therefore, it may be suggested that complex formation with GSH leads to self-association of the drug. However, the self-associated forms are different in the case of CHR and (CHR)<sub>2</sub>Mg<sup>2+</sup> complex, as apparent from the non-overlapping nature of the final spectra in the presence of GSH (compare Figs. 2a and 3a). The cooperative nature of the binding profiles (Fig. 4) provides further evidence in support of aggregation of the antibiotic when it binds to GSH.

CD spectral changes provide more information about the physical process associated with the binding because it originates from the optical asymmetric properties of the aglycone ring in the GSH-bound antibiotic. They show a major difference in the GSH-binding properties of CHR and (CHR)<sub>2</sub>Mg<sup>2+</sup> complex, namely, the formation of a second species at an intermediate GSH concentration (~12 mM) for the (CHR)<sub>2</sub>Mg<sup>2+</sup> complex. In this case, the CD titration profile is multiphasic in nature (Fig. 4). The increase in ellipticity at an intermediate concentration of GSH is a characteristic property in the presence of Mg<sup>2+</sup>, which induces a certain conformational change of the GSH-bound species. The nature of the CD spectrum at ~12 mM GSH (Fig. 3b) originates from an ordered structure. Such enhanced ellipticity is the feature of a regular structure, permitting a helical flow of charge [26]. Mg<sup>2+</sup> reduces the electrostatic repulsion between the negatively charged drug and GSH molecules, thereby favoring the formation of an ordered structure. Direct or water-mediated H-bond formation involving different potential loci in the tripeptide and (CHR)<sub>2</sub>Mg<sup>2+</sup> complex might also give rise to such an ordered structure [27].

On the other hand, in the high GSH complex formed at a relatively higher concentration of GSH ( $\geq 16$  mM), the above ordered structure is perturbed due to ionic contributions from negatively charged GSH and hydrophobic interactions between the chromophores of the antibiotic. It leads to a disordered structure of the chromophores in CHR or its  $\text{Mg}^{2+}$  complex. Such aggregation would result in a decrease in CD band intensity of the high GSH complex relative to  $(\text{CHR})_2\text{Mg}^{2+}$  complex (Fig. 3b).

#### Interaction of the GSH-bound $(\text{CHR})_2\text{Mg}^{2+}$ Complexes with CT DNA

DNA-binding properties of the GSH-bound  $\text{Mg}^{2+}$  complexes of the antibiotic were examined, because DNA is the prime cellular target. The differences between the low and the high complex of GSH as DNA-binding ligands were checked and compared with that for  $(\text{CHR})_2\text{Mg}^{2+}$  complex in the absence of GSH.

DNA-binding properties of the antibiotic characterized in the absence of GSH are retained even in its presence, e.g. the obligatory requirement of a divalent metal ion and GC base specificity. The possibility of the formation of any covalent interaction between the high and low GSH complex and DNA appears remote, from the absence of any nick in the supercoiled DNA. Similarly, we did not notice any change in the binding when the studies were carried out in a nitrogen atmosphere. It suggests that oxygen does not affect the binding, thereby further reducing the possibility of a covalent interaction via a free radical mechanism, as reported in the case of other antibiotic-GSH interaction [12, 13].

A comparison of the affinity parameters among  $(\text{CHR})_2\text{Mg}^{2+}$  and its low and high GSH complexes for association with DNA showed that the first one has the highest affinity, binding stoichiometry being comparable for all of them. These results suggest that under *in vivo* conditions, either of the GSH complexes has the potential to bind to DNA. A change in the mode of recognition of DNA by the  $(\text{CHR})_2\text{Mg}^{2+}$  complex due to its association with GSH is established from the thermodynamic parameters. The effect of GSH upon the DNA-binding properties of the low and high complex of  $(\text{CHR})_2\text{Mg}^{2+}$  is clearly indicated when we compare the thermodynamic parameters associated with the binding of different ligands to DNA, as shown in Table 2. The presence of GSH changes the entropy-driven interaction of  $(\text{CHR})_2\text{Mg}^{2+}$  complex with DNA to an enthalpy-driven interaction. The thermodynamic parameters associated with the binding to DNA are not much different among the low and high GSH complexes. In an earlier report, we proposed an alteration of the DNA structure at the binding site of the  $(\text{CHR})_2\text{Mg}^{2+}$  complex in order to account for the positive enthalpy change [10]. In the absence of any direct evidence, it may be surmised that anionic GSH may be involved in the formation of a noncovalent bond, such as an H-bond, when low and high GSH complexes bind to DNA. It may lead to

a favorable enthalpy change, thereby making the interaction enthalpy-driven. The negative change in entropy is another distinctive feature for the association of  $(\text{CHR})_2\text{Mg}^{2+}$  complex with DNA in the presence of GSH. Insufficient data prevent us from identifying the origin of the above change, which could result from the ordering of the solvent molecules and counterions when the low and high GSH complexes bind to DNA. The negative value of the entropy change for the GSH complexes may, therefore, be attributed to the reorientation of the  $(\text{CHR})_2\text{Mg}^{2+}$  in the individual complexes prior to binding to DNA. This would lead to a more constrained arrangement of ligand and solvent. In the above processes, the possibility of negatively charged GSH interacting directly with DNA is distant, because it does not bind to DNA at this range of concentration. The differences in the values of the thermodynamic parameters are not significant enough to suggest that the high and low GSH complexes are different DNA-binding ligands. However, the non-overlapping nature of the DNA-bound spectra (absorption and CD) for the GSH complexes of  $(\text{CHR})_2\text{Mg}^{2+}$  (Fig. 3, a and b) suggest that their DNA-bound forms have different molecular structures.

GSH is a reducing agent that covalently modifies many antibiotics, culminating in damage of DNA by these modified antibiotics, thus enhancing their cytotoxicity. From our results, such a possibility in the case of CHR appears very remote. The reason for the high cytotoxicity of the aureolic acid group of antibiotics may be ascribed to their interaction at some other cellular site, e.g. a recent report has shown that a structurally related drug, mithramycin, binds to the cytoskeletal protein spectrin [28].

S. C. wishes to thank Professor (Dr.) B. Sinha, Director of the S.I.N.P., for his permission to allow her to work in the Biophysics Division. We also thank Professor S. K. Ghosh of the Crystallography & Molecular Biology Division of our Institute for making available a Jasco J-720 spectropolarimeter.

#### REFERENCES

1. Gause GF, Olivomycin, chromomycin and mithramycin. In: *Antibiotics III, Mechanism of Action of Antimicrobial Antitumor Agents* (Eds. Corcoran JW and Hahn FE), Vol. II, pp. 197–202. Springer, Berlin, 1975.
2. Chabner BA, Allegra CJ, Curt GA and Calabresi P, Antineoplastic agents. In: *Goodman & Gilman's The Pharmacological Basis of Therapeutics* (Eds. Hardman JG, Limbird LE, Molinoff PB, Ruddon RW and Gilman AG), 9th Edn, pp. 1233–1287. McGraw-Hill, New York, 1996.
3. Sastry M, Fiala R and Patel DJ, Solution structure of mithramycin dimers bound to partially overlapping sites on DNA. *J Mol Biol* 251: 674–689, 1995.
4. Keniry MA, Banville DL, Simmonds PM and Shafer RH, Nuclear magnetic resonance comparison of the binding sites of mithramycin and chromomycin on the self-complementary oligonucleotide d(ACCCGGGT)<sub>2</sub>. *J Mol Biol* 231: 753–767, 1993.
5. van Dyke MW and Dervan PB, Chromomycin, mithramycin and olivomycin binding sites on heterogeneous deoxyribonu-

- cleic acid. Footprinting with (methidiumpropyl-EDTA)iron (II). *Biochemistry* 22: 2373-2377, 1983.
6. Stankus A, Goodisman J and Dabrowiak JC, Quantitative footprinting analysis of the chromomycin A<sub>3</sub>-DNA interaction. *Biochemistry* 31: 9310-9318, 1992.
  7. Goldberg IH and Friedman PA, Antibiotics and nucleic acids. *Annu Rev Biochem* 40: 775-810, 1971.
  8. Aich P, Sen R and Dasgupta D, Interaction between antitumor antibiotic chromomycin A<sub>3</sub> and Mg<sup>2+</sup>. I. Evidence for the formation of two types of chromomycin A<sub>3</sub>-Mg<sup>2+</sup> Complexes. *Chem Biol Interact* 83: 23-33, 1992.
  9. Aich P, Sen R and Dasgupta D, Role of magnesium ion in the interaction between chromomycin A<sub>3</sub> and DNA: Binding of chromomycin A<sub>3</sub>-Mg<sup>2+</sup> complexes with DNA. *Biochemistry* 31: 2988-2997, 1992.
  10. Majee S, Sen R, Guha S, Bhattacharyya D and Dasgupta D, Differential interactions of the Mg<sup>2+</sup> complexes of chromomycin A<sub>3</sub> and mithramycin with poly(dG-dC) · poly(dC-dG) and poly(dG) · poly(dC). *Biochemistry* 36: 2291-2299, 1997.
  11. Gilbert HF, Thiol/disulfide exchange equilibria and disulfide bond stability. *Methods Enzymol* 251 (Part A): 8-28, 1995.
  12. Meister A and Anderson ME, Glutathione. *Annu Rev Biochem* 52: 711-760, 1983.
  13. Cook AJ and Mitchell JB, Measurement of thiols in cell population from tumor and normal tissue. *Methods Enzymol* 251 (Part A): 203-212, 1995.
  14. Hormas RA, Andrews PA, Murphy MP and Burns CP, Glutathione depletion reverses cisplatin resistance in murine L1210 leukemia cells. *Cancer Lett* 34: 913, 1987.
  15. Gao X, Stassinopoulos A, Rice JR and Goldberg IH, Structural basis for the sequence-specific DNA strand cleavage by the Eneidyne neocarzinostatin chromophore. Structure of the post-activated chromophore-DNA complex. *Biochemistry* 34: 40-49, 1995.
  16. Myers AG, Cohen SB and Kwon BM, A study of the reaction of calicheamicin  $\gamma$ 1 with glutathione in the presence of double-stranded DNA. *J Am Chem Soc* 116: 1255-1271, 1994.
  17. Glover D, Fox KR, Weiler C, Kligerman MM, Turrisi A and Glock JH, Clinical treats of WR-2721 prior to alkylating agent chemotherapy and radiotherapy. *Pharmacol Ther* 39: 3-7, 1988.
  18. Révész L and Modig H, Cysteamine-induced increase of cellular glutathione-level: A new hypothesis of the radioprotective mechanism. *Nature* 207: 430-431, 1965.
  19. Nayak R, Sirsi M and Podder SK, Role of magnesium ions on the interaction between chromomycin A<sub>3</sub> and deoxyribonucleic acid. *FEBS Lett* 30: 157-162, 1973.
  20. Anderson ME, Determination of glutathione and glutathione disulfide in biological samples. *Methods Enzymol* 113 (Part A): 548-555, 1985.
  21. Sambrook J, Fritsch EF and Maniatis T, Plasmid vectors. In: *Molecular Cloning* (Ed. Nolan C), Vol. 1, 2nd Edn, pp. 1.33-1.39. Cold Spring Harbor Laboratory Press, Cold Spring Harbor, NY, 1989.
  22. Cobuzzi RJ, Kotsopoulos SK, Otani T and Beerman TA, Effects of the enediyne C-1027 on intracellular DNA targets. *Biochemistry* 34: 583-592, 1995.
  23. Wang JL and Edelman GM, Fluorescence probe for conformational states of proteins. IV. The pepsinogen-pepsin conversion. *J Biol Chem* 246: 1185-1191, 1971.
  24. Hård T, Hsu V, Sayre MH, Geiduschek EP, Appelt K and Kearns DR, Fluorescence studies of a single tyrosine in a type II DNA binding protein. *Biochemistry* 28: 396-406, 1989.
  25. Castellan GW, Chemical reactions and the entropy of the universe. In: *Physical Chemistry* (Indian Student edition), 3rd Ed, pp. 799-815. Addison-Wesley, Reading, MA, U.S.A. and Narosa Publishing House, New Delhi, 1989.
  26. Cantor CR and Schimmel PR, Other optical techniques. In: *Biophysical Chemistry*, Part III, pp. 409-480. Freeman, San Francisco, 1980.
  27. Reinemer P, Dirr HW and Huber R, X-Ray structure methods for glutathione binding. *Methods Enzymol* 251 (Part A): 243-254, 1995.
  28. Majee S and Chakrabarti A, A DNA-binding antitumor antibiotic binds to spectrin. *Biochem Biophys Res Commun* 212: 428-432, 1995.

## United States Patent [19]

Hansen et al.

[11] Patent Number: 5,635,603

[45] Date of Patent: Jun. 3, 1997

[54] PREPARATION AND USE OF  
IMMUNOCONJUGATES

[75] Inventors: **Hans J. Hansen**, Mystic Island;  
**Shui-on Leung**, Madison; **Jerry Shevitz**, Livingston; **Gary L. Griffiths**, Morristown; **Seregulam V. Govindan**, Summit, all of N.J.

[73] Assignee: **Immunomedics, Inc.**, Morris Plains, N.J.

[21] Appl. No.: 352,715

[22] Filed: Dec. 5, 1994

## Related U.S. Application Data

[63] Continuation-in-part of Ser. No. 162,912, Dec. 8, 1993, Pat. No. 5,443,953.

[51] Int. Cl.<sup>6</sup> ..... A61K 39/395; C07K 16/00

[52] U.S. Cl. .... 530/391.5; 424/172.1;  
435/696; 435/172.1

[58] Field of Search ..... 424/1.49, 1.53,  
424/9, 178.1, 179.1, 180.1, 181.1, 182.1;  
435/7.1, 7.2, 7.23, 69.6, 172.1; 530/387.3,  
391.3, 391.5, 391.7, 391.9; 558/256, 251,  
291; 540/474; 564/501

## [56] References Cited

## U.S. PATENT DOCUMENTS

4,867,973 9/1989 Goers et al. .... 424/183.1  
5,057,313 10/1991 Shih et al. .... 424/85.91  
5,443,593 8/1995 Hansen et al. .... 424/1.49

## FOREIGN PATENT DOCUMENTS

90/10700 9/1990 WIPO.

## OTHER PUBLICATIONS

Tomalia, et al. 1990 Angew Chem Int Ed Engl 29: 138-175.  
Wu et al., 1994 Bioorgan & Med. Chem Lett vol. 4 No. 3: 449-454.

Camera et al 1994 J. Nucl Med vol. 35 No. 5: 882-889.

Roberts et al 1990 Bio Conjugate Chem. vol. 1 No. 5:305-308.

Better et al Methods Enzym. 1989 vol. 178: 476-496.

Brown, "Clinical Use Of Monoclonal Antibodies", *Co-linical Use Of Monoclonal Antibodies*, pp. 227-250 (1991).

Goldenburg et al., "Targeting, Dosimetry, and Radioimmunotherapy of B-Cell Lymphomas With Iodine-131-Labeled LL2 Monoclonal Antibody", *Journal of Clinical Oncology*, vol. 9:548-564, (1991).

Kanellos et al., "Studies Of Methotrexate-Monoclonal Antibody Conjugates For Immunotherapy", *Jnci.*, vol. 75:319-329, (1985).

Kreitman et al., "Cytotoxicity of Conjugates Between LL2 And Derivatives Of Pseudomonas Exotoxin Toward B-Cell Non-Hodgkin's Lymphoma", *Immunology*, vol. 33-344, (1992).

Kulkarni et al., "Covalent Binding Of Methotrexate To Immunoglobulins And The Effect Of Antibody-Linked Drug On Tumor Growth In Vivo", *Cancer Research*, vol. 41:2700-2706, (1981).

Murthy et al., "Lymphoma Imaging With A New Technetium-99m Labelled Antibody, LL2", *Nuclear Medicine*, pp. 394-401, (1992).

Orlandi et al., "Cloning Immunoglobulin Variable Domains For Expression By The Polymerase Chain Reaction", *Proc. Natl. Acad. Sci. USA*, vol. 86:3833-3837, (1989).

Pawlak-Byczkowska et al., "Two New Monoclonal Antibodies, EPB-1 and EPB-2 Reactive With Human Lymphoma", *Cancer*, vol. 49:4568-4577, (1989).

Shih et al., "Site-Specific Linkage Of Methotrexate To Monoclonal Antibodies Using An Intermediate Carrier", *Int. J. Cancer*, vol. 41:832-839, (1988).

Shih et al., "A Fluorouridine-Anti-CEA Immunoconjugate Is Therapeutically Effective In A Human Colonic Cancer Xenograft Model", *Int. J. Cancer*, vol. 46:1101-1106, (1990).

Shih et al., "Anthracycline Immunoconjugates Prepared By A Site-Specific Linkage Via Amino-Dextran Intermediate Carrier", *Cancer Research*, vol. 51:4192-4198, (1991).

Co et al., "Chimeric And Humanized Antibodies With Specificity For The CD33 Antigen", *The Journal Of Immunology*, vol. 148:1149-1154, (1992).

Vaughan et al., "Limitations To The Killing Of Tumours Using Radiolabelled Antibodies", *The British Journal Of Radiology*, vol. 60:567-578, (1987).

Wallick et al., "Glycosylation Of A V<sub>H</sub> Residue Of A Monoclonal Antibody Against  $\alpha(1\rightarrow6)$  Dextran Increases Its Affinity For Antigen", *J. Exp. Med.*, vol. 168:1099-1109, (1988).

Wright et al., "Antibody Variable Region Glycosylation: Position Effects On Antigen Binding And Carbohydrate Structure", *The EMBO Journal*, vol. 10:2717-2723, (1991).  
J.R. Couto et al, Hybridoma, 12, 485-498, 1993.

Primary Examiner—Lila Feisee

Assistant Examiner—Julie E. Reeves

Attorney, Agent, or Firm—Foley & Lardner

## [57] ABSTRACT

The present invention relates to immunoconjugates comprising an antibody fragment which is covalently bound to a diagnostic or therapeutic principle through a carbohydrate moiety in the light chain variable region of the antibody fragment. The invention also relates to immunoconjugates comprising an antibody moiety that is an intact antibody containing a glycosylation site in the light chain variable domain which has been introduced into the antibody by mutating the nucleotide sequence encoding the light chain. The resultant immunoconjugates retain the immunoreactivity of the antibody fragment or intact antibody, and target the diagnostic or therapeutic principle to a target tissue where the diagnostic or therapeutic effect is realized. Thus, the invention contemplates the use of such immunoconjugates for diagnosis and immunotherapy. The invention further relates to methods for preparing such immunoconjugates.

12 Claims, No Drawings

## PREPARATION AND USE OF IMMUNOCONJUGATES

This application is a continuation-in-part of U.S. patent application Ser. No. 08/162,912 (filed Dec. 8, 1993), issued as U.S. Pat. No. 5,443,953 on Aug. 22, 1995.

### BACKGROUND OF THE INVENTION

#### 1. Field of the Invention

This invention is directed to novel immunoconjugates that are useful for diagnosis and therapy. In particular, this invention is directed to immunoconjugates comprising an antibody fragment which is covalently bound to a diagnostic or therapeutic principle through a carbohydrate moiety in the light chain variable region of the antibody fragment. This invention is also directed to immunoconjugates comprising an antibody moiety that is an intact antibody containing a glycosylation site in the light chain variable domain which has been introduced into the antibody by mutating the nucleotide sequence encoding the light chain. This invention is further directed to methods for preparing such immunoconjugates. This invention also is directed to methods of diagnosis and therapy using such immunoconjugates.

#### 2. Related Art

Monoclonal antibodies can be conjugated to a variety of agents to form immunoconjugates for use in diagnosis and therapy. These agents include chelates, which allow the immunoconjugate to form a stable bond with radioisotopes, and cytotoxic agents such as toxins and chemotherapy drugs. For example, cytotoxic agents that normally would be too toxic to patients when administered in a systemic fashion can be coupled to anti-cancer antibodies in such a manner that their toxic effects become directed only to the tumor cells bearing the target antigens. The diagnostic or therapeutic efficacy of immunoconjugates depends upon several factors. Among these factors, the molar ratio of the diagnostic or therapeutic principle to antibody and the antibody binding activity of the immunoconjugate are of major concern.

Researchers have found that the maximum number of diagnostic or therapeutic principles that can be directly linked to an antibody is limited by the number of modifiable sites on the antibody molecule and the loss of immunoreactivity of the antibody. For example, Kulkarni et al., *Cancer Research* 41:2700-2706 (1981), have reported that there is a limit to the number of drug molecules that can be incorporated into an antibody without significantly decreasing antigen-binding activity. Kulkarni et al., found that the highest incorporation obtained for methotrexate was about ten methotrexate molecules per molecule of antibody, and that attempts to increase the drug-antibody molar ratio over about ten decreased the yield of immunoconjugate and damaged antibody activity. Kanellos et al., *JNCI* 75:319-329 (1985), have reported similar results.

In order to achieve a high substitution level of drug-immunoconjugate without significantly impairing antigen-binding activity, researchers have investigated the use of a water-soluble polymeric molecule as an intermediary for the indirect conjugation of the drug. Such polymers include oxidized dextran (Arnon et al., *Immunol. Rev.* 62:5-27 (1982)), poly-glutamic acid (Greenfield et al., *Antibody Immunoconjugates and Radiopharmaceuticals* 2:201-216 (1989)), human serum albumin (Baldwin et al., *NCI Monographs* 3:95-99 (1987)), and carboxymethyl-dextran (Schechter et al., *Cancer Immunol. Immunother.* 25:225-230 (1987)).

Shih et al., *Int. J. Cancer* 41:832-839 (1988), have described a site-specific linking method in which methotrexate was linked to the carbohydrate moiety in the constant, or "Fc," region of an antibody via amino-dextran, resulting in an immunoconjugate with high substitution ratio and retention of immunoreactivity. More recently, Shih et al., *Int. J. Cancer* 46:1101-1106 (1990), demonstrated the efficacy of an immunoconjugate comprising 5-fluorouridine conjugated via amino-dextran to the carbohydrate moiety in the Fc region of a monoclonal antibody. In both studies, Shih et al. found that the immunoconjugate contained approximately 30-50 molecules of drug per molecule of immunoglobulin. Thus, indirect conjugation of a diagnostic or therapeutic principle to a carbohydrate moiety in the Fc region of an antibody provides a means to obtain immunoconjugates with functional antigen binding activity and a high substitution level.

An advantage of using the carbohydrate moiety in the Fc region as a site-specific attachment site is that antibodies of all subtypes typically contain a glycosylated Fc region. In general, antibody molecules are glycosylated in their Fc regions at characteristic positions according to their isotype. For example, carbohydrate is typically present at amino acid 297 in the C<sub>H</sub>2 domain in the Fc region of IgG molecules. Conjugating a diagnostic or therapeutic principle to the carbohydrate group at this position, which is far away from the antigen binding site, should produce a minimal effect on the immunoreactivity of the resultant immunoconjugate, as demonstrated by Shih et al.

However, a disadvantage of using the carbohydrate moiety in the Fc region as an attachment site is that the entire antibody is required for the immunoconjugate. The use of antibody fragments, particularly Fab, Fab' and F(ab')<sub>2</sub>, provide an advantage over the use of an entire antibody because such fragments are better able to diffuse out of capillaries and into target tissues. For example, see Brown, "Clinical Use of Monoclonal Antibodies," in *BIOTECHNOLOGY AND PHARMACY*, Pezzuto et al., eds. Chapman & Hall, pp.227-249 (1993). Moreover, antibody fragments will clear from blood and normal tissues more readily than an entire antibody. For example, intact murine IgG has a blood half-life of approximately 30 hours, while F(ab')<sub>2</sub> and Fab/Fab' have half-lives of approximately 20 hours and 2 hours, respectively. Id. Thus, it is advantageous to use antibody fragments for constructing immunoconjugates. Antibody fragments are particularly advantageous in radioimmunotherapy and radioimmunodiagnosis applications in which the exposure of normal tissues to radioisotopes must be minimized.

Antibody variable regions occasionally contain carbohydrate groups which provide potential attachment sites for the preparation of immunoconjugates from antibody fragments. For example, asparagine-linked carbohydrate acceptor sequences have been identified in approximately 15-25% of murine variable regions. Kabat et al. *SEQUENCES OF PROTEINS OF IMMUNOLOGICAL INTEREST*, 5th ed. U.S. Department of Health and Human Services (1990). In the case of the anti-dextran family of antibodies, glycosylation sites reside in the complementarity-determining regions (CDRs), particularly CDR2, of the heavy chain variable regions. Id. The presence of Asn-linked carbohydrates in the CDRs of these antibodies appeared to enhance antigen binding. Wallick et al., *J. Exp. Med.* 168:1099-1109 (1988); Wright et al., *EMBO J.* 10:2717-2723 (1991). However, introduction of additional carbohydrate attachment sites in CDR2 by site-directed mutagenesis resulted in either the enhancement or reduction of affinity for antigen,

depending on the position where the glycosylation site was introduced. Wright et al., *supra*. Thus, the feasibility of attaching a diagnostic or therapeutic principle to a carbohydrate moiety in the VH CDR region is uncertain.

Studies by the present inventors on carbohydrate conjugation demonstrated a high conjugation efficiency with the IgG antibody, LL2, which is a murine monoclonal antibody described by Pawlak-Byczkowska et al. (*Cancer Res.* 49:4568-4577 (1989)) and Goldenberg et al. (*J. Clin. Oncol.* 9:548 (1991)). Analysis of LL2 conjugates using sodium dodecyl-sulfate polyacrylamide gel electrophoresis (SDS-PAGE) under reducing conditions indicated the existence of a glycosylation site in the light chain variable (VL) region of the LL2 antibody. After cloning the VL region of LL2, an Asn-linked glycosylation site at position 18-20 of the framework-1 (FR1) sequence of the VL region was found.

These studies suggested a possible preferential conjugation at a carbohydrate moiety within the VL region. This unexpected finding may be explained by an improved accessibility in the VL region. We used site-directed mutagenesis to remove the Asn-linked glycosylation site and found that the resulting protein exhibited similar immunoreactivity compared with the original antibody. This result is in agreement with the inventors' computer modeling studies which suggested negligible or minimal interaction between the light chain FR1 carbohydrate moiety and the antigen binding site. Thus, these studies indicate that conjugation of a diagnostic or therapeutic principle to a carbohydrate moiety in the FR1 sequence of the VL region provides a means to obtain immunoconjugates of antibody fragments with functional antigen binding activity.

The present invention provides a method for preparing novel immunoconjugates comprising a diagnostic or therapeutic principle which is attached to an intact antibody, or antigen-binding fragment thereof, via a carbohydrate moiety of the light chain variable region.

#### SUMMARY OF THE INVENTION

The present invention is directed to a mutated recombinant antibody or antibody fragment having a non-natural Asn-glycosylation site at about position 18 of the light chain of said antibody or antibody fragment.

The present invention is also directed to a method for preparing a glycosylated mutated recombinant antibody or antibody fragment, comprising the steps of:

- (a) culturing transformed host cells which express and glycosylate a mutated antibody or antibody fragment comprising a mutated light chain and a heavy chain, said host cells being transformed with an expression vector into which is cloned a mutated DNA molecule encoding a mutated light chain containing a nonnatural Asn-glycosylation site at about amino acid position 18; and
- (b) recovering expressed and glycosylated mutated antibody or antibody fragment from said cultured host cells.

The present invention is further directed to a soluble immunoconjugate, comprising:

- (a) a glycosylated antibody fragment, wherein the antibody fragment is selected from the group consisting of Fab, Fab', F(ab)<sub>2</sub>, and F(ab')<sub>2</sub>, and wherein the antibody fragment comprises a light chain variable region and a carbohydrate moiety attached at about amino acid position 18 of the light chain variable region; and
- (b) an intermediate conjugate, comprising a polymer carrier having at least one free amine group and a

plurality of drug, toxin, chelator, boron addend or detectable label molecules covalently bound to the polymer carrier, wherein the intermediate conjugate is covalently bound through at least one free amine group of the polymer carrier to the carbohydrate moiety of the antibody fragment, and wherein the immunoconjugate retains the immunoreactivity of the antibody fragment.

In addition, the present invention is directed to a soluble immunoconjugate, comprising:

- (a) a glycosylated antibody fragment, wherein the antibody fragment is selected from the group consisting of Fab, Fab', F(ab)<sub>2</sub>, and F(ab')<sub>2</sub>, and wherein the antibody fragment comprises a light chain variable region and a carbohydrate moiety attached at about amino acid position 18 of the light chain variable region; and
- (b) a non-antibody moiety selected from the group consisting of a drug, a toxin, a chelator, a polyethylene glycol, a boron addend and a detectable label molecule, wherein the non-antibody moiety is covalently bound to the carbohydrate moiety of the antibody fragment, and wherein the immunoconjugate retains the immunoreactivity of the antibody fragment.

The present invention is further directed to a soluble immunoconjugate, comprising:

- (a) a mutated antibody, wherein the mutated antibody comprises a light chain variable region and a carbohydrate moiety attached at about amino acid position 18 of the light chain variable region; and
- (b) a non-antibody moiety selected from the group consisting of a drug, a toxin, a chelator, a polyethylene glycol, a boron addend and a detectable label molecule, wherein the non-antibody moiety is covalently bound to the carbohydrate moiety of the mutated antibody, and wherein the immunoconjugate retains the immunoreactivity of the mutated antibody.

The present invention is also directed to a soluble immunoconjugate, comprising:

- (a) an antibody component, wherein the antibody component is selected from the group consisting of an Fv and a single chain antibody, and wherein the antibody component comprises a light chain variable region and a carbohydrate moiety attached at about amino acid position 18 of the light chain variable region; and
- (b) an intermediate conjugate, comprising a polymer carrier having at least one free amine group and a plurality of drug, toxin, chelator, boron addend or detectable label molecules covalently bound to the polymer carrier,

wherein the intermediate conjugate is covalently bound through at least one free amine group of the polymer carrier to the carbohydrate moiety of the antibody component, and wherein the immunoconjugate retains the immunoreactivity of the antibody component.

The present invention is further directed to a soluble immunoconjugate, comprising:

- (a) an antibody component, wherein the antibody component is selected from the group consisting of an Fv and a single chain antibody, and wherein the antibody component comprises a light chain variable region and a carbohydrate moiety attached at about amino acid position 18 of the light chain variable region; and
- (b) a non-antibody component selected from the group consisting of a drug, a toxin, a chelator, a polyethylene glycol, a boron addend and a detectable label molecule,



wherein the non-antibody component is covalently bound to the carbohydrate moiety of the antibody component, and wherein the immunoconjugate retains the immunoreactivity of the antibody component.

The present invention is also directed to a method for preparing an immunoconjugate, comprising the steps of:

- (a) introducing an Asn-glycosylation site at about position 18 of the light chain of an antibody by mutating the nucleotide sequence of a DNA molecule encoding the light chain;
- (b) cloning the mutated DNA molecule into an expression vector;
- (c) transforming host cells with the expression vector, and recovering transformed host cells which express a mutated antibody comprising a mutated light chain and a heavy chain;
- (d) culturing the transformed host cells and recovering the mutated antibody from the cultured host cells;
- (e) preparing an antibody fragment from the recovered antibody, wherein the antibody fragment is selected from the group consisting of Fab, Fab', F(ab)<sub>2</sub>, and F(ab')<sub>2</sub>, and wherein the antibody fragment contains a carbohydrate moiety in the mutated light chain of the antibody fragment; and
- (f) covalently binding an intermediate conjugate to the carbohydrate moiety of the antibody fragment, wherein the intermediate conjugate comprises a polymer carrier having at least one free amine group and a plurality of drug, toxin, chelator, boron addend or detectable label molecules covalently bound to the polymer carrier, wherein the intermediate conjugate is covalently bound through at least one free amine group of the polymer carrier to the carbohydrate moiety of the antibody fragment, and wherein the immunoconjugate retains the immunoreactivity of the antibody fragment.

The present invention is also directed to a method for diagnosing the presence of a disease in a mammal, comprising the steps of:

- (a) preparing an immunoconjugate comprising a detectable label and an antibody fragment having a carbohydrate moiety attached at about position 18 of the light chain of the antibody fragment, wherein the detectable label is conjugated to the carbohydrate moiety of the antibody fragment, and wherein the antibody fragment is capable of binding to an antigen which is associated with the disease;
- (b) administering a composition comprising the immunoconjugate and a pharmaceutically acceptable carrier to the mammal; and
- (c) using in vivo imaging to detect the presence of the immunoconjugate at disease sites.

The present invention is further directed to a method for treating a disease in a mammal, comprising the steps of:

- (a) preparing an immunoconjugate comprising an antibody fragment having a carbohydrate moiety attached at about position 18 of the light chain of the antibody fragment and a non-antibody moiety selected from the group consisting of a drug, a toxin, a chelator, a boron addend and a radioisotope, wherein the non-antibody moiety is covalently bound to the carbohydrate moiety of the antibody fragment, and wherein the antibody fragment is capable of binding to an antigen which is associated with the disease; and
- (b) administering a composition comprising the immunoconjugate and a pharmaceutically acceptable carrier to the mammal.

Also included in the present invention are improved methods of in vitro immunoassay and in situ detection of antigen in histological specimens using the immunoconjugates of the invention.

There are also provided suitable polymer carriers, chelates, detectable label molecules, and linking moieties suitable for use in preparing the immunoconjugates of the invention.

## DETAILED DESCRIPTION

### 1. Overview

This invention is directed to immunoconjugates comprising an intact antibody, or antigen-binding fragment thereof, which is covalently bound to a diagnostic or therapeutic principle through a carbohydrate moiety in the light chain variable region of the antibody moiety. This invention further relates to methods for preparing such immunoconjugates. The invention also contemplates the use of such immunoconjugates for diagnosis and immunotherapy.

### 2. Definitions

In the description that follows, a number of terms are utilized extensively. Definitions are herein provided to facilitate understanding of the invention.

**Antibody.**

As used herein, "antibody" includes monoclonal antibodies, such as murine, chimeric, or humanized antibodies, as well as antigen-binding fragments thereof. Such fragments include Fab, Fab', F(ab)<sub>2</sub>, and F(ab')<sub>2</sub>, which lack the Fc fragment of an intact antibody. Such fragments also include isolated fragments consisting of the light chain variable region, "Fv" fragments consisting of the variable regions of the heavy and light chains, and recombinant single chain polypeptide molecules in which light and heavy variable regions are connected by a peptide linker.

### 3. Mutated Antibody.

As used herein, a mutated antibody is an intact antibody, or antigen-binding fragment thereof, having an Asn-linked glycosylation site at about amino acid position 18 in the light chain, which has been introduced into the light chain by altering the corresponding nucleotide sequence. Methods of mutating the nucleotide sequence encoding a light chain include the polymerase chain reaction, site-directed mutagenesis, and gene synthesis using the polymerase chain reaction with synthetic DNA oligomers.

### 4. Diagnostic or Therapeutic Principle.

As used herein, a diagnostic or therapeutic principle is a molecule or atom which is conjugated to an antibody to produce an immunoconjugate which is useful for diagnosis and for therapy. Examples of diagnostic or therapeutic principles include drugs, toxins, chelators, boron compounds, and detectable labels.

### 5. Immunoconjugate.

As used herein, an immunoconjugate is a molecule comprising an antibody and a diagnostic or therapeutic principle. An immunoconjugate retains the immunoreactivity of the antibody, i.e., the antibody moiety has roughly the same, or only slightly reduced, ability to bind the antigen after conjugation as before conjugation.

### 6. Structural gene.

A DNA sequence that is transcribed into messenger RNA (mRNA) which is then translated into a sequence of amino acids characteristic of a specific polypeptide.

### 7. Promoter.

A DNA sequence which directs the transcription of a structural gene to produce mRNA. Typically, a promoter is located in the 5' region of a gene, proximal to the start codon of a structural gene. If a promoter is an inducible promoter,



then the rate of transcription increases in response to an inducing agent. In contrast, the rate of transcription is not regulated by an inducing agent if the promoter is a constitutive promoter.

#### Enhancer.

A promoter element. An enhancer can increase the efficiency with which a particular gene is transcribed into mRNA irrespective of the distance or orientation of the enhancer relative to the start site of transcription.

#### Complementary DNA (cDNA).

Complementary DNA is a single-stranded DNA molecule that is formed from an mRNA template by the enzyme reverse transcriptase. Typically, a primer complementary to portions of mRNA is employed for the initiation of reverse transcription. Those skilled in the art also use the term "cDNA" to refer to a double-stranded DNA molecule consisting of such a single-stranded DNA molecule and its complement.

#### Expression.

Expression is the process by which a polypeptide is produced from a structural gene. The process involves transcription of the gene into mRNA and the translation of such mRNA into polypeptide(s).

#### Cloning vector.

A DNA molecule, such as a plasmid, cosmid, or bacteriophage, which has the capability of replicating autonomously in a host cell and which is used to transform cells for gene manipulation. Cloning vectors typically contain one or a small number of restriction endonuclease recognition sites at which foreign DNA sequences may be inserted in a determinable fashion without loss of an essential biological function of the vector, as well as a marker gene which is suitable for use in the identification and selection of cells transformed with the cloning vector. Marker genes typically include genes that provide tetracycline resistance or ampicillin resistance.

#### Expression vector.

A DNA molecule comprising a cloned structural gene encoding a foreign protein which provides the expression of the foreign protein in a recombinant host. Typically, the expression of the cloned gene is placed under the control of (i.e., operably linked to) certain regulatory sequences such as promoter and enhancer sequences. Promoter sequences may be either constitutive or inducible.

#### Recombinant Host.

A recombinant host may be any prokaryotic or eukaryotic cell which contains either a cloning vector or expression vector. This term is also meant to include those prokaryotic or eukaryotic cells that have been genetically engineered to contain the cloned gene(s) in the chromosome or genome of the host cell. For examples of suitable hosts, see Sambrook et al., *MOLECULAR CLONING: A LABORATORY MANUAL*, Second Edition, Cold Spring Harbor Laboratory, Cold Spring Harbor, N.Y. (1989).

Methods for Introducing an Asn-glycosylation Site in an Antibody Light Chain by Mutating the DNA Sequence Encoding the Protein

#### A. Antibody Structure and Asn-linked Glycosylation

Antibody molecules are composed of two identical copies of heavy chains and light chains, which are covalently interconnected by disulfide bonds. For a general discussion, see Schultz et al., "Proteins II: Structure-Function Relationship of Protein Families," in *TEXTBOOK OF BIOCHEMISTRY WITH CLINICAL CORRELATIONS*, 3rd Ed., T. M. Devlin (ed.), Wiley & Sons, pp. 92-134 (1992); Turner et al., "Antigen Receptor Molecules," in *IMMUNOLOGY*, 3rd Ed., Roitt et al. (eds.), Mosby, pp. 4.1-4.20 (1993). In

the most common type of antibody, IgG, the two heavy chains each have approximately 440 amino acids, while the two light chains each have about 220 amino acids. The carboxyl-terminal one-half of light chains and the carboxyl-terminal three-quarters of heavy chains are highly conserved in amino acid sequence among antibodies with different antigen specificities. These conserved regions in the light and heavy chains are termed "constant regions" and are designated as CL and CH, respectively. The CH regions determine whether a particular antibody belongs to the antibody class IgG, IgA, IgD, IgE, or IgM. The CH regions within a class of antibodies are homologous but differ significantly from the amino acid sequence of the CH regions of other antibody classes.

In contrast, the amino acid sequences of the amino-terminal one-half of the light chains and the amino-terminal of one-quarter of the heavy chains are highly variable among antibodies with different antigen specificities. Particular regions within these variable segments are "hypervariable" and have been designated as "complementarity determining regions" (CDRs) because these regions form the antigen binding site (ABS) that is complementary to the topology of the antigen structure.

Each heavy chain is associated with a light chain such that the amino-terminal ends of both chains are near each other and comprise an antigen binding site. Proteolytic cleavage can be used to fragment an antibody into small, functional units. For example, proteolytic cleavage of an IgG molecule with papain results in the cleavage of the antibody in the hinge peptide of each heavy chain. One product of papain digestion is the carboxyl-terminal one-half of the heavy chains which are bound covalently in a "crystallizable fragment" (Fc). The Fc fragment does not bind antigen. The other cleavage products are identical and consist of an amino-terminal segment of a heavy chain which is associated with an entire light chain. These amino-terminal, or "antigen binding fragments" (Fab) can bind antigen with an affinity similar to that of the intact antibody molecule.

The object of the present invention is to covalently attach a diagnostic or therapeutic principle to an Asn-linked carbohydrate moiety of the light chain variable region of an intact antibody, or antigen-binding fragment thereof. Asn-linked glycosylation, also referred to as "N-linked glycosylation," is a form of glycosylation in which sugar residues are linked through the amide nitrogen of asparagine residues. Intracellular biosynthesis of Asn-linked oligosaccharides occurs in both the lumen of the endoplasmic reticulum and following transport of the protein to the Golgi apparatus. Asn-linked glycosylation occurs at the glycosylation sequence: Asn-X-Thr/Ser, where X may be any amino acid except proline or aspartic acid. Thus, there are 36 possible sequences of three amino acids which code for Asn-linked glycosylation. Considering the degeneracy of the genetic code, there are over a thousand possible nucleotide sequences which encode the glycosylation signal sequences. B. Mutagenesis

The particular nucleotide sequence which is used to introduce an Asn-linked glycosylation sequence into positions 18-20 will depend upon the naturally-occurring nucleotide sequence. As described below, the introduction of an Asn-linked glycosylation site into the PKAPPA(11)24 protein can be achieved by an alteration of codon 18 from AGG to AAC. Such a mutation of the nucleotide sequence can be accomplished by methods well-known to those in the art.

For example, an Asn-linked glycosylation site can be introduced at positions 18-20 using oligonucleotide-directed mutagenesis and a cloned antibody light chain. In

this procedure, a single-stranded DNA template containing the antibody light chain sequence is prepared from a dut<sup>-</sup> ung<sup>-</sup> strain of *E. coli* in order to produce a DNA molecule containing a small number of uracil residues in place of thymidine. Such a DNA template can be obtained by M13 cloning or by in vitro transcription using an SP6 promoter. See, for example, Ausubel et al. (eds.), *CURRENT PROTOCOLS IN MOLECULAR BIOLOGY*, John Wiley & Sons (1987). An oligonucleotide that contains the mutated sequence is synthesized using well-known methods. Id. The oligonucleotide is annealed to the single-stranded template, and T4 DNA polymerase and T4 DNA ligase are used to produce a double-stranded DNA molecule. Transformation of wild-type (dut<sup>+</sup> ung<sup>+</sup>) *E. coli* cells with the double-stranded DNA molecule provides an efficient recovery of mutated DNA.

Detailed protocols for oligonucleotide-directed mutagenesis and related techniques for mutagenesis of cloned DNA are well-known. For example, see Ausubel et al., *supra*; Sambrook et al., *supra*.

Alternatively, an Asn-linked glycosylation site can be introduced into an antibody light chain using an oligonucleotide containing the desired mutation as a primer and DNA clones of the variable regions for the antibody light chain, or by using RNA from cells that produce the antibody of interest as a template. Such techniques include, for example, the polymerase chain reaction, as illustrated in Example 1. Also see, Huse, "Combinatorial Antibody Expression Libraries in Filamentous Phage," in *ANTIBODY ENGINEERING: A PRACTICAL GUIDE*, C. Borrebaeck (ed.), W. H. Freeman and Company, pp. 103-120 (1992). Site-directed mutagenesis can be performed, for example, using the TRANSFORMER™ Site-Directed Mutagenesis Kit (Clontech; Palo Alto, Calif.) according to the manufacturer's instructions.

Alternatively, a glycosylation site can be introduced into an immunoglobulin light chain by synthesizing a light chain gene with mutually priming oligonucleotides in which one of the oligonucleotides contains the desired mutation. Techniques for the construction of large synthetic genes are well known to those in the art. See, for example, Uhlmann, *Gene* 71:29-40 (1988); Wosnick et al., *Gene* 60:115-127 (1988); Ausubel et al., *supra*.

In summary, an Asn-linked glycosylation site can be introduced at about amino acid position 18 in the light chain of any antibody if two requirements are met. First, the nucleotide sequence surrounding and including the codons for amino acid positions 18-20 of the light chain of the antibody of interest must be available in order to design a complementary oligonucleotide containing the desired mutation. Second, there must be access to either cloned antibody DNA or cells that produce the antibody of interest. Given these two restrictions, the present invention encompasses immunoconjugates comprising murine, humanized, or chimeric antibodies, wherein a diagnostic or therapeutic principle is attached to the antibody component via a carbohydrate moiety located at about amino acid position 18 of the light chain variable region. Such antibodies include intact antibodies and the antigen-binding fragments, Fab, Fab', F(ab)<sub>2</sub>, and F(ab')<sub>2</sub>.

Moreover, the present invention contemplates the production of immunoconjugates comprising Fv fragments or single chain antibodies. As discussed above, Fv fragments comprise a non-covalent association of heavy and light chain variable regions. In contrast, single-chain antibodies comprise heavy and light polypeptide chains from the variable region of a given antibody which are connected by a

peptide linker. See, for example, Bird et al., *Science* 242:423-426 (1988); Ladner et al., U.S. Pat. No. 4,946,778; and Pack et al., *Bio/Technology* 11:1271-1277 (1993).

Generally, Fv fragments and single chain antibodies lack a site for attaching certain diagnostic or therapeutic principles, such as radiometals. However, the introduction of an Asn-linked glycosylation site into a light chain variable region of an Fv fragment or single chain antibody provides a carbohydrate moiety for the attachment of a variety of diagnostic or therapeutic principles, as described below. Although Fv fragments and single chain antibodies are typically produced by prokaryotic host cells, eukaryotic host cells are preferred host cells. In particular, insect cells, yeast cells, and mammalian cells are preferred eukaryotic hosts. Mammalian cells are the most preferred host cells.

Although the present invention provides a method for introducing an Asn-linked glycosylation site at about amino acid position 18-20 of the light chain variable region, it will be understood that the present invention is not so limited. It will occur to those of ordinary skill in the art that it is possible to introduce glycosylation sites at alternative positions of the light chain variable region, or even in the heavy chain variable region. Immunoconjugates of the present invention can be prepared using intact antibodies, antibody fragments, or single chain antibodies which contain a carbohydrate moiety attached at such an alternate glycosylation site as long as the mutated antibodies or fragments retain antigen-binding activity. Suitable alternative glycosylation sites can be identified using molecular modeling techniques that are well-known to those of skill in the art. See, for example, Lesk et al., "Antibody Structure and Structural Predictions Useful in Guiding Antibody Engineering," in *ANTIBODY ENGINEERING: A PRACTICAL GUIDE*, C. Borrebaeck (ed.), W. H. Freeman and Company, pp. 1-38 (1992); Cheetham, "Engineering Antibody Affinity" Id. at pp. 39-67.

#### 4. Methods for Expressing and Isolating the Protein Product of a Mutated Antibody DNA Sequence

##### A. Methods for Expressing a Mutated Antibody

After mutating the nucleotide sequence, mutated DNA is inserted into a cloning vector for further analysis, such as confirmation of the DNA sequence, as illustrated in Example 1. To express the polypeptide encoded by the mutated DNA sequence, the DNA sequence must be operably linked to regulatory sequences controlling transcriptional expression in an expression vector and then, introduced into either a prokaryotic or eukaryotic host cell. In addition to transcriptional regulatory sequences, such as promoters and enhancers, expression vectors include translational regulatory sequences and a marker gene which is suitable for selection of cells that carry the expression vector.

Suitable promoters for expression in a prokaryotic host can be repressible, constitutive, or inducible. Suitable promoters are well-known to those of skill in the art and include promoters capable of recognizing the T4, T3, Sp6 and T7 polymerases, the P<sub>R</sub> and P<sub>L</sub> promoters of bacteriophage lambda, the trp, recA, heat shock, and lacZ promoters of *E. coli*, the  $\alpha$ -amylase and the  $\sigma^{28}$ -specific promoters of *B. subtilis*, the promoters of the bacteriophages of *Bacillus*, Streptomyces promoters, the int promoter of bacteriophage lambda, the bla promoter of the  $\beta$ -lactamase gene of pBR322, and the CAT promoter of the chloramphenicol acetyl transferase gene. Prokaryotic promoters are reviewed by Glick, *J. Ind. Microbiol.* 1:277-282 (1987); Watson et al., *MOLECULAR BIOLOGY OF THE GENE*, 4th Ed., Benjamin Cummings (1987); Ausubel et al., *supra*, and Sambrook et al., *supra*.

An especially preferred prokaryotic host is *E. coli*. Preferred strains of *E. coli* include Y1088, Y1089, CSH18, ER1451, and ER1647 (see, for example, Brown (Ed.), *MOLECULAR BIOLOGY LABFAX*, Academic Press (1991)). An alternative preferred host is *Bacillus subtilis*, including such strains as BR151, YB886, MI119, MI120, and B170 (see, for example, Hardy, "Bacillus Cloning Methods," in *DNA CLONING: A PRACTICAL APPROACH*, Glover (Ed.), IRL Press (1985)).

Methods for producing antibody fragments in *E. coli* are well-known to those in the art. See, for example, Huse, "Combinatorial Antibody Expression Libraries in Filamentous Phage," in *ANTIBODY ENGINEERING: A PRACTICAL GUIDE*, C. Borrebaeck (Ed.), W. H. Freeman and Company, pp. 103-120 (1992); Ward, "Expression and Purification of Antibody Fragments Using *Escherichia coli* as a Host," *Id.* at pp. 121-138 (1992). Those skilled in the art also know methods for producing in *E. coli* Fv fragments, which consist of variable regions of heavy and light chains. *Id.* Also, see Whitlow et al., "Single-Chain Fv Proteins and their Fusion Proteins," in *NEW TECHNIQUES IN ANTIBODY GENERATION, Methods 2(2)* (1991).

Moreover, expression systems for cloning antibodies in prokaryotic cells are commercially available. For example, the IMMUNO ZAP™ Cloning and Expression System (Stratagene Cloning Systems; La Jolla, Calif.) provides vectors for the expression of antibody light and heavy chains in *E. coli*.

Since the expression of a mutated DNA sequence in prokaryotic cells will require subsequent in vitro glycosylation, the present invention preferably encompasses the expression of a mutated DNA sequence in eukaryotic cells, and especially mammalian, insect, and yeast cells. Especially preferred eukaryotic hosts are mammalian cells. Mammalian cells provide post-translational modifications to the cloned polypeptide including proper folding and glycosylation. For example, such mammalian host cells include COS-7 cells (ATCC CRL 1651), non-secreting myeloma cells (SP2/0-AG14; ATCC CRL 1581), Chinese hamster ovary cells (CHO-K1; ATCC CCL 61), rat pituitary cells (GH<sub>1</sub>; ATCC CCL 82), HeLa S3 cells (ATCC CCL 2.2), and rat hepatoma cells (H-4-II-E; ATCC CRL 1548).

For a mammalian host, the transcriptional and translational regulatory signals may be derived from viral sources, such as adenovirus, bovine papilloma virus, and simian virus. In addition, promoters from mammalian expression products, such as actin, collagen, or myosin, can be employed. Alternatively, a prokaryotic promoter (such as the bacteriophage T3 RNA polymerase promoter) can be employed, wherein the prokaryotic promoter is regulated by a eukaryotic promoter (for example, see Zhou et al., *Mol. Cell. Biol.* 10:4529-4537 (1990); Kaufman et al., *Nucl. Acids Res.* 19:4485-4490 (1991)). Transcriptional initiation regulatory signals may be selected which allow for repression or activation, so that expression of the genes can be modulated.

In general, eukaryotic regulatory regions will include a promoter region sufficient to direct the initiation of RNA synthesis. Such eukaryotic promoters include the promoter of the mouse metallothionein I gene (Hamer et al., *J. Mol. Appl. Gen.* 1:273-288 (1982)); the TK promoter of Herpes virus (McKnight, *Cell* 31:355-365 (1982)); the SV40 early promoter (Benoist et al., *Nature (London)* 290:304-310 (1981)); the Rous sarcoma virus promoter (Gorman et al., *supra*); the cytomegalovirus promoter (Foecking et al., *Gene* 45:101 (1980)); the yeast gal4 gene promoter (Johnston, et al., *Proc. Natl. Acad. Sci. (USA)* 79:6971-6975 (1982);

Silver, et al., *Proc. Natl. Acad. Sci. (USA)* 81:5951-5955 (1984)); and the IgG promoter (Orlandi et al., *Proc. Natl. Acad. Sci. USA* 86:3833-3837 (1989)).

Strong regulatory sequences are the most preferred regulatory sequences of the present invention. Examples of such preferred regulatory sequences include the SV40 promoter-enhancer (Gorman, "High Efficiency Gene Transfer into Mammalian cells," in *DNA CLONING: A PRACTICAL APPROACH*, Volume II, Glover (Ed.), IRL Press pp. 143-190 (1985)), the hCMV-MIE promoter-enhancer (Bebbington et al., *Bio/Technology* 10:169-175 (1992)), and antibody heavy chain promoter (Orlandi et al., *Proc. Natl. Acad. Sci. USA* 86:3833-3837 (1989)). Also preferred are the kappa chain enhancer for the expression of the light chain and the IgH enhancer (Gillies, "Design of Expression Vectors and Mammalian Cell Systems Suitable for Engineered Antibodies," in *ANTIBODY ENGINEERING: A PRACTICAL GUIDE*, C. Borrebaeck (Ed.), W. H. Freeman and Company, pp. 139-157 (1992); Orlandi et al., *supra*).

The mutated antibody-encoding sequence and an operably linked promoter may be introduced into eukaryotic cells as a non-replicating DNA molecule, which may either be a linear molecule or, more preferably, a closed covalent circular molecule. Since such molecules are incapable of autonomous replication, the expression of the protein may occur through the transient expression of the introduced sequence. Preferably, permanent expression occurs through the integration of the introduced sequence into the host chromosome.

Preferably, the introduced sequence will be incorporated into a plasmid or viral vector that is capable of autonomous replication in the recipient host. Several possible vector systems are available for this purpose. One class of vectors utilize DNA elements which provide autonomously replicating extra-chromosomal plasmids, derived from animal viruses such as bovine papilloma virus, polyoma virus, adenovirus, or SV40 virus. A second class of vectors relies upon the integration of the desired genomic or cDNA sequences into the host chromosome. Additional elements may also be needed for optimal synthesis of mRNA. These elements may include splice signals, as well as transcription promoters, enhancers, and termination signals. The cDNA expression vectors incorporating such elements include those described by Okayama, *Mol. Cell. Biol.* 3:280 (1983), Sambrook et al., *supra*, Ansel et al., *supra*, Bebbington et al., *supra*, Orlandi et al., *supra*, and Fouser et al., *Bio/Technology* 10:1121-1127 (1992); Gillies, *supra*. Genomic DNA expression vectors which include intron sequences are described by Orlandi et al., *supra*. Also, see generally, Lerner et al. (Eds.), *NEW TECHNIQUES IN ANTIBODY GENERATION, Methods 2(2)* (1991).

In order to obtain mammalian cells that express intact antibody, the expression vector comprising the mutated antibody light chain can be co-transfected into mammalian cells with an antibody heavy chain expression vector. See, for example, Orlandi et al., *supra*. Alternatively, mammalian cells containing a heavy chain expression vector can be transfected with an expression vector comprising the mutated antibody light chain, and mammalian cells containing an expression vector comprising a mutated light chain can be transfected with a heavy chain expression vector. Moreover, mammalian cells can be transfected with a single expression vector comprising DNA fragments that encode the mutated antibody light chain, as well as DNA fragments that encode antibody heavy chain. See, for example, Gillies, *supra*; Bebbington et al., *supra*. Any of these approaches will produce transfected cells that express whole antibody mol-

ecules which have the mutated antibody light chain. Standard transfection techniques are well known in the art. See, for example, Sambrook et al., supra; Ausubel et al., supra. B. Methods for Isolating a Mutated Antibody from Transfected Cells

Transfected cells that carry the expression vector are selected using the appropriate drug. For example, G418 can be used to select transfected cells carrying an expression vector having the aminoglycoside phosphotransferase gene. Southern et al., *J. Mol. Appl. Gen.* 1:327-341 (1982). Alternatively, hygromycin-B can be used to select transfected cells carrying an expression vector having the hygromycin-B-phosphotransferase gene. Palmer et al., *Proc. Natl. Acad. Sci. USA* 84:1055-1059 (1987). Alternatively, aminopterin and mycophenolic acid can be used to select transfected cells carrying an expression vector having the xanthine-guanine phosphoribosyltransferase gene. Mulligan et al., *Proc. Natl. Acad. Sci. USA* 78:2072-2076 (1981).

Transfected cells that produce the mutated antibody can be identified using a variety of methods. For example, any immunodetection assay can be used to identify such "transfectomas." Example 1 provides an illustration of the use of an enzyme-linked immunosorbent assay (ELISA) for such a purpose.

After transfectomas have been identified, the cells are cultured and antibodies are isolated from culture supernatants. Isolation techniques include affinity chromatography with Protein-A Sepharose (for intact antibodies), size-exclusion chromatography, and ion-exchange chromatography. For example, see Coligan et al. (eds.), *CURRENT PROTOCOLS IN IMMUNOLOGY*, John Wiley & Sons (1991), for detailed protocols.

#### 5. Methods for Preparing Immunoconjugates

##### A. Preparation of Antibody Fragments

The present invention contemplates the preparation of immunoconjugates from intact mutated antibodies or from antigen-binding antibody fragments. Antibody fragments can be obtained from transfectomas, by proteolytic cleavage of intact mutant antibodies produced by transfectomas, or by proteolytic cleavage of intact antibodies that have naturally-occurring Asn-linked glycosylation sites at position 18-20 of the light chain.

Antibody fragments can be obtained directly from transfectomas by transfecting cells with a heavy chain structural gene that has been mutated. For example, transfectomas should produce Fab fragments if a stop codon was inserted following the sequence of the CH1 domain. Alternatively, transfectomas should produce Fab' or F(ab')<sub>2</sub> fragments if a stop codon was inserted after the sequence encoding the hinge region of the heavy chain.

Alternatively, antibody fragments can be prepared from intact antibodies using well-known proteolytic techniques. For example, see, Coligan et al., supra. As an illustration, Example 2 provides a method to obtain Fab fragments using papain. Moreover, F(ab')<sub>2</sub> fragments can be obtained using pepsin digestion of intact antibodies. Divalent fragments can be cleaved to monovalent fragments using conventional disulfide bond reducing agents, e.g., cysteine, dithiothreitol (DTT), and the like.

##### B. Methods of Conjugation

###### (i) Indirect conjugation

Immunoconjugates can be prepared by indirectly conjugating a diagnostic or therapeutic principle to an intact antibody, or antigen-binding fragment thereof. Such techniques are described in Shih et al., *Int. J. Cancer* 41:832-839 (1988); Shih et al., *Int. J. Cancer* 46:1101-1106 (1990); and Shih et al., U.S. Pat. No. 5,057,313. The general method

involves reacting an antibody component having an oxidized carbohydrate portion with a carrier polymer that has at least one free amine function and that is loaded with a plurality of drug, toxin, chelator, or boron addends, or with detectable labels. This reaction results in an initial Schiff base (imine) linkage, which can be stabilized by reduction to a secondary amine to form the final conjugate.

The carrier polymer is preferably an aminodextran or polypeptide of at least 50 amino acid residues, although other substantially equivalent polymer carriers can also be used. Preferably, the final immunoconjugate is soluble in an aqueous solution, such as mammalian serum, for ease of administration and effective targeting for use in diagnosis or therapy. Thus, solubilizing functions on the carrier polymer will enhance the serum solubility of the final immunoconjugate. Solubilizing functions also are important for use of immunoconjugates for in vitro immunoassay and in situ detection, as described below. In particular, an aminodextran will be preferred.

The process for preparing an immunoconjugate with an aminodextran carrier typically begins with a dextran polymer, advantageously a dextran of average molecular weight of about 10,000-100,000. The dextran is reacted with an oxidizing agent to effect a controlled oxidation of a portion of its carbohydrate rings to generate aldehyde groups. The oxidation is conveniently effected with glycolytic chemical reagents such as NaIO<sub>4</sub>, according to conventional procedures.

The oxidized dextran is then reacted with a polyamine, preferably a diamine, and more preferably, a mono- or polyhydroxy diamine. Suitable amines include ethylene diamine, propylene diamine, or other like polymethylene diamines, diethylene triamine or like polyamines, 1,3-diamino-2-hydroxypropane, or other like hydroxylated diamines or polyamines, and the like. An excess of the amine relative to the aldehyde groups of the dextran is used to insure substantially complete conversion of the aldehyde functions to Schiff base groups.

A reducing agent, such as NaBH<sub>4</sub>, NaBH<sub>3</sub>CN or the like, is used to effect reductive stabilization of the resultant Schiff base intermediate. The resultant adduct can be purified by passage through a conventional sizing column to remove cross-linked dextrans.

Other conventional methods of derivatizing a dextran to introduce amine functions can also be used, e.g., reaction with cyanogen bromide, followed by reaction with a diamine.

The aminodextran is then reacted with a derivative of the particular drug, toxin, chelator, boron addend, or label to be loaded, in an activated form, preferably, a carboxyl-activated derivative, prepared by conventional means, e.g., using dicyclohexylcarbodiimide (DCC) or a water soluble variant thereof, to form an intermediate adduct.

Alternatively, polypeptide toxins such as pokeweed antiviral protein or ricin A-chain, and the like, can be coupled to aminodextran by glutaraldehyde condensation or by reaction of activated carboxyl groups on the protein with amines on the aminodextran.

Chelators for radiometals or magnetic resonance enhancers are well-known in the art. Typical are derivatives of 1,4,7,10-tetraazacyclododecanetetraacetic acid (DOTA), ethylenediaminetetraacetic acid (EDTA), and diethylenetriaminepentaacetic acid (DTPA). These chelators typically have groups on the side chain by which the chelator can be attached to a carrier. Such groups include, e.g., benzylisothiocyanate, by which the DOTA, DTPA or EDTA can be coupled to the amine group of a carrier. Alternatively,

carboxyl groups or amine groups on a chelator can be coupled to a carrier by activation or prior derivatization and then coupling, all by well-known means.

Labels such as enzymes, fluorescent compounds, electron transfer agents, and the like can be linked to a carrier by conventional methods well known to the art. These labeled carriers and the immunoconjugates prepared from them can be used for in vitro immunoassays and for in situ detection, as described below.

Boron addends, such as carboranes, can be attached to antibody components by conventional methods. For example, carboranes can be prepared with carboxyl functions on pendant side chains, as is well known in the art. Attachment of such carboranes to a carrier, e.g., aminodextran, can be achieved by activation of the carboxyl groups of the carboranes and condensation with amines on the carrier to produce an intermediate conjugate. Such intermediate conjugates are then attached to antibody components to produce therapeutically useful immunoconjugates, as described below.

As an alternative to aminodextran, a polyamidoamine dendrimer may be used as a carrier polymer. Dendrimer molecules of a suitable type can be prepared, for example, by the method of Tomalia et al., *Angew. Chem. Int. Ed. Engl.* 29:138-175 (1990). Dendrimers prepared by this method exhibit uniform size, shape and charge, and carry a known number of primary amine groups on the surface of the molecule, all of which may be used for conjugation purposes. Polyamidoamine dendrimers also bear tertiary amine groups which will be protonated in aqueous solution at physiological pH, conferring aqueous solubility on the carrier molecule.

A polypeptide carrier can be also used instead of aminodextran or a polyamidoamine dendrimer, but the polypeptide carrier must have at least 50 amino acid residues in the chain, preferably 100-5000 amino acid residues. At least some of the amino acids should be lysine residues or glutamate or aspartate residues. The pendant amines of lysine residues and pendant carboxylates of glutamine and aspartate are convenient for attaching a drug, toxin, chelator, or boron addend. Examples of suitable polypeptide carriers include polylysine, polyglutamic acid, polyaspartic acid, copolymers thereof, and mixed polymers of these amino acids and others, e.g., serines, to confer desirable solubility properties on the resultant loaded carrier and immunoconjugate.

Conjugation of the intermediate conjugate with the antibody component is effected by oxidizing the carbohydrate portion of the antibody component and reacting the resulting aldehyde (and ketone) carbonyls with amine groups remaining on the carrier after loading with a drug, toxin, chelator, boron addend, or label. Alternatively, an intermediate conjugate can be attached to an oxidized antibody component via amine groups that have been introduced in the intermediate conjugate after loading with the diagnostic or therapeutic principle. Oxidation is conveniently effected either chemically, e.g., with  $\text{NaIO}_4$ , or other glycolytic reagent, or enzymatically, e.g., with neuraminidase and galactose oxidase. In the case of an aminodextran carrier, not all of the amines of the aminodextran are typically used for loading a diagnostic or therapeutic principle. The remaining amines of aminodextran condense with the oxidized antibody component to form Schiff base adducts, which are then reductively stabilized, normally with a borohydride reducing agent.

Analogous procedures are used to produce other immunoconjugates according to the invention. The stoichiometry between the carrier molecule and the diagnostic or therapeutic

principle is adjusted such that loaded dendrimer and polypeptide carriers preferably have free amine residues remaining for condensation with the oxidized carbohydrate portion of an antibody component. Carboxyls on the polypeptide carrier can, if necessary, be converted to amines by, e.g., activation with DCC and reaction with an excess of a diamine.

The final immunoconjugate is purified using conventional techniques, such as size-exclusion chromatography on Sephacryl S-300 or similar matrices.

Indirect conjugation to an antibody fragment is illustrated in Example 4.

#### (ii) Direct conjugation

Alternatively, immunoconjugates can be prepared by directly conjugating an antibody component with a diagnostic or therapeutic principle. The general procedure is analogous to the indirect method of conjugation except that a diagnostic or therapeutic principle is directly attached to an oxidized antibody component. The direct conjugation of chelators to an antibody fragment is illustrated in Example 3. A particular advantage of preparing immunoconjugates via coupling to the oxidized light chain carbohydrate is that the oxidation reaction provides multiple sites for attachment of diagnostic or therapeutic principles. Since the light chain carbohydrate moiety does not impinge on the antigen binding site, this method therefore provides a means of directly attaching multiple diagnostic or therapeutic principles to an antibody fragment, without the use of a polymeric carrier, to increase antibody loading capacity. This is advantageous in circumstances where the presence of a charged intermediate carrier molecule is associated with unfavorable pharmacokinetics of the immunoconjugate.

It will be appreciated that other diagnostic or therapeutic principles can be substituted for the chelators described below. Those of skill in the art will be able to devise conjugation schemes without undue experimentation.

In addition, those of skill in the art will recognize numerous possible variations of the conjugation methods. In one example, the carbohydrate moiety can be used to attach polyethyleneglycol (PEG) in order to alter the pharmacokinetic properties of an intact antibody, or antigen-binding fragment thereof, in blood, lymph, or other extracellular fluids. This is particularly advantageous for the use of antibody fragments labeled with radiometals, and in particular  $^{99m}\text{Tc}$ , in radioimmunodiagnosis (RAID).

$^{99m}\text{Tc}$  is a particularly attractive radioisotope for therapeutic and diagnostic applications, as it is readily available to all nuclear medicine departments, is inexpensive, gives minimal patient radiation doses, and has ideal nuclear imaging properties. It has a half-life of six hours which means that rapid targeting of a technetium-labeled antibody is desirable. Consequently, antibody fragments such as  $\text{F(ab')}_2$  and  $\text{F(ab)}_2$ , and especially Fab and  $\text{Fab'}$ , which show more rapid targeting kinetics than whole immunoglobulin, are preferred for RAID applications with  $\text{Tc-}^{99m}$  labeling. A major drawback to the use of  $\text{Tc-}^{99m}$ -labeled fragments for imaging is the relatively high uptake and retention of radioactivity in the kidney, which leads to imaging difficulties in the area of this organ. It has been found that conjugation of PEG to  $\text{Tc-}^{99m}$ -labeled antibody fragments causes a pronounced decrease in the amount of renal uptake and retention of the fragments. See U.S. patent application Ser. No. 08/309,319, which is herein incorporated by reference in its entirety.

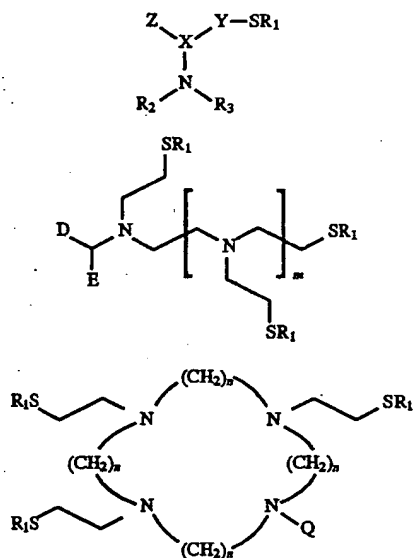
To couple PEG to light chain carbohydrate, the carbohydrate moiety can be oxidized with periodate and coupled with a PEG derivative bearing a nucleophilic moiety by

methods well known in the art. For example, PEG hydrazide (Shearwater Polymers, Inc., Huntsville, Ala.) is mixed with the antibody fragment to form a hydrazone. Alternatively a PEG-amine can be reacted with the oxidized carbohydrate to form a Schiff's base, which is then reduced by treatment with sodium cyanoborohydride to form a stable secondary amine linkage. Conjugation of PEG to a Fab antibody fragment is illustrated in Example 8.

In a preferred embodiment, once the antibody fragment has been conjugated to PEG it can be treated with a reducing agent under controlled conditions to produce free thiol groups which allow direct labeling of the fragment with Tc-99m. Methods for the controlled reduction of antibody fragments are well known to those of ordinary skill in the art. See, for example, U.S. Pat. No. 5,128,119 which is hereby incorporated by reference in its entirety. In another preferred embodiment free thiol groups can be generated on the PEG-conjugated antibody fragment in a non-site specific manner by reaction with a thiolating agent such as Traut's reagent, or as described in U.S. patent application Ser. No. 08/253,772, followed by direct labeling with Tc-99m.

In another embodiment, amine-terminating bifunctional chelating reagents (BFC) are linked to the oxidized light chain carbohydrate of the antibody or antibody fragment. These bifunctional reagents contain pendant thiol and amine groups which are suitably disposed to tightly bind radioactive metals such as  $^{186}\text{Re}$ ,  $^{188}\text{Ag}$ ,  $^{111}\text{Ag}$ , and  $^{67}\text{Cu}$ . Conjugation of the BFC to the antibody is achieved through amine or hydrazine functions on the BFC, which can respectively form imine or hydrazone linkages to the aldehyde functions on the oxidized carbohydrate. Imine linkages can be stabilized by reduction with a reducing agent such as sodium cyanoborohydride. During the conjugation step the thiol group of the chelator moiety is masked as a thiol ester or disulfide, and is deprotected after the preparation of the conjugate.

The BFCs can be described by the general structures Ia, Ib, and Ic:

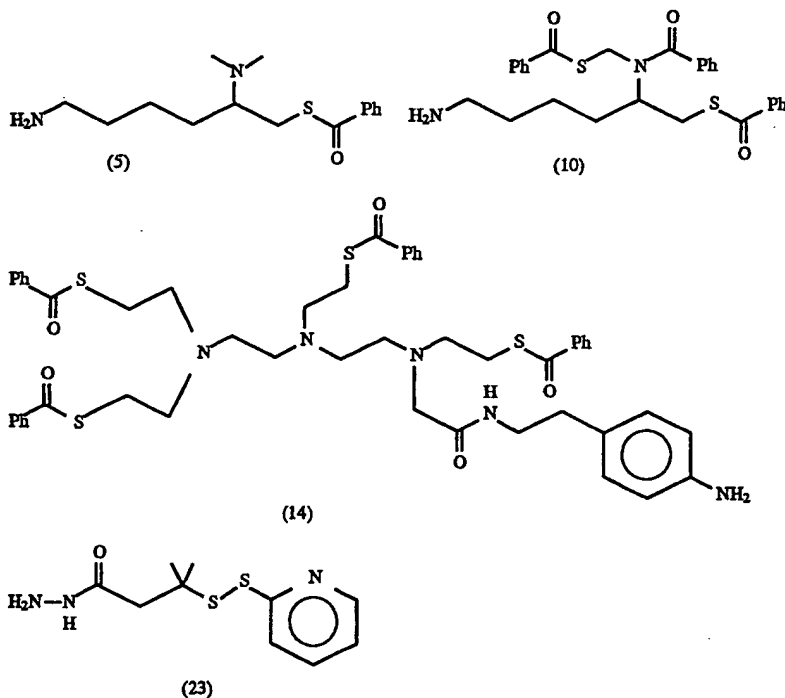


In general structure Ia, X is CH, or X and Z taken together can be CO; Y is CR<sub>4</sub>R<sub>5</sub>, CH<sub>2</sub>CR<sub>4</sub>R<sub>5</sub>, or (CH<sub>2</sub>)<sub>2</sub>CR<sub>4</sub>R<sub>5</sub>, where R<sub>4</sub> and R<sub>5</sub> are the same or different and are selected from the group consisting of hydrogen and alkyl, substituted alkyl, aryl or substituted aryl groups; Z can be any group capable of reacting and/or complexing with the oxidized carbohydrate groups on the protein, or Z can be H; R<sub>1</sub> is a thiol protecting group which can be removed under conditions which do not significantly diminish the immunoreactivity of the protein; R<sub>2</sub> and R<sub>3</sub> can be the same or different, and each represent an acyl group or a substituted acyl group, or hydrogen, alkyl, aryl, substituted alkyl, or substituted aryl, where the substituents on the alkyl or aryl groups are metal-ligating groups selected from the group consisting of sulfhydryl, amine and carboxylic acid or their protected derivatives; R<sub>2</sub> and R<sub>3</sub> also can be any group capable of reacting and/or complexing with the oxidized carbohydrate groups on the protein.

In formula (II) D is H or CH<sub>2</sub>SR<sub>1</sub>; E can be any group capable of reacting and/or complexing with the oxidized carbohydrate groups on the protein; R<sub>1</sub> is a thiol protecting group which can be removed under conditions which do not significantly diminish the immunoreactivity of the protein, and m is 0, 1, 2, or 3.

In formula (III) Q can be any group capable of reacting and/or complexing with the oxidized carbohydrate groups on the protein; R<sub>1</sub> is a thiol protecting group which can be removed under conditions which do not significantly diminish the immunoreactivity of the protein; and each n independently is 2 or 3.

Representative examples of Ia, Ib, and Ic are shown below. In some of these, the antibody-binding group is shown as, but not limited to, a hydrazide. Only the thiol-protected versions of the structures are shown (with 'R' being acyl, benzoyl or 2-thiopyridyl), although metal-complexation will involve thiol-deprotected conjugates. The synthesis of the BFCs can be achieved by methods that are well known in the art. Representative syntheses of some BFCs and methods of conjugation are shown in Examples 9-14.



The thiol protecting group used in the BFC can be any organic or inorganic group which is readily removed under mild conditions to regenerate the free sulfhydryl in the presence of the protein without substantially altering the activity of the protein. Examples of suitable protecting groups include thiol esters, thiocarbamates and disulfides. In a preferred embodiment the thiol protecting group is a benzoate thioester. Those skilled in the art are familiar with the procedures of protecting and deprotecting thiol groups. For example, benzoate thioesters may be deprotected under mild and selective conditions using hydroxylamine. However, when the amine is a hydrazide, the thiol group is most preferably protected as a disulfide, for example with the 'R' function as a 2-pyridylthio group.

In another embodiment of the invention, the oxidized carbohydrate can be used to conjugate groups for pretargeting of the antibody. The pretargeting of monoclonal antibodies is useful for "decoupling" the antibody targeting step and the radiodiagnostic/radiotherapeutic delivery step in antibody-based agents. By reducing the amount of radioisotope in circulation, while maintaining a high uptake of antibody at its target, a reduction in radiation dose to blood and blood-forming tissues, and higher target:non-target ratios of radioisotope are possible. Typical examples of the pretargeting approach are: the use of antibody-avidin (or antibody-streptavidin) conjugates in a prelocalization step, followed by delivery of an isotope conjugated to a biotin moiety; the use of antibody-biotin conjugates in a prelocalization step followed by delivery of an isotope conjugated to an avidin (or streptavidin) moiety; or the use of antibody-biotin conjugates in a prelocalization step followed by delivery of an avidin (streptavidin) moiety and subsequent delivery of an isotope conjugated to a biotin moiety. Other pairs of agents which may find similar use as secondary targeting vectors are, for example: two complimentary sequences of single-stranded nucleic acids; an enzyme together with its specific substrate; or a protein together with its specific ligand, such as intrinsic factor and vitamin B<sub>12</sub>.

Additional targeting steps are also feasible and the use of more than one radiolabeled species are also possible as described in U.S. patent application Ser. No. 08/051,144, issued as U.S. Pat. No. 5,482,698, which is herein incorporated by reference in its entirety. Other approaches to achieving a higher amount of therapeutic at the antibody target site include the incorporation of, for example, an antibody-biotin(avidin)-radioisotope conjugate as a later-step isotope delivery vehicle, directed to a target pretargeted with antibody-avidin(biotin). In this example the antibody-biotin(avidin)-radioisotope conjugate has two sites, i.e. antigen and avidin(biotin), which can be targeted. See, for example, U.S. patent application Ser. No. 08/409,960 which is hereby incorporated by reference in its entirety.

The presence of light-chain carbohydrate on antibody fragments allows for site-specificity of conjugation of suitable pretargeting reagents to antibody fragments such as F(ab')<sub>2</sub>. Additionally, in the case of Fab' fragments bearing free thiol groups the presence of both the carbohydrate and thiol functions allows site-specific conjugation of two different moieties, each of which can have distinct chemical properties.

Examples of schemes for preparing pretargeting conjugates (italicized) are shown below:

- (Avidin-thiol) plus (maleimide-L-hydrazide) forms (Avidin-L-hydrazide)
- 2(Avidin-L-hydrazide) plus (CHO-Fab'-S-S-Fab'-CHO) forms (Avidin)<sub>2</sub>-F(ab')<sub>2</sub>
- (Avidin)<sub>2</sub>-F(ab')<sub>2</sub> reduced with 2-mercaptoethanol forms 2X Avidin-fab'-SH
- Avidin plus (succinimide-L-maleimide) forms (avidin-L-maleimide)
- (Avidin-L-maleimide) plus (Avidin-Fab'-SH) forms (Avidin)<sub>2</sub>-fab'
- (Avidin-CHO) plus (hydrazide-L-hydrazide) forms (Avidin-L-hydrazide)
- 2(Avidin-L-hydrazide) plus (CHO-Fab'-S-S-Fab'-CHO) forms (Avidin)<sub>2</sub>-F(ab')<sub>2</sub>



(Avidin)<sub>2</sub>-F(ab')<sub>2</sub> reduced with 2-mercaptoethanol forms 2(Avidin-fab'-SH)

Avidin-Fab'-SH plus (Avidin-maleimide) forms (Avidin)<sub>2</sub>-fab'

n(Biotin-L-hydrazide) plus (CHO-Fab'-S-S-Fab'-CHO) forms (Biotin)<sub>n</sub>-f(ab')<sub>2</sub>

where n is an integer, usually from 1 to about 30; L designates a linker, hydrocarbon, alkyl, acyl or a combination which separates two distinct reactive functionalities, and which encompasses commercially available protein cross-linking agents. Streptavidin may be used in place of avidin in the examples described above. Carbohydrate moieties can be oxidized to produce aldehydes and disulfide bonds reduced to generate free thiols, when indicated, using standard reagents such as sodium periodate and 2-mercaptoethanol, respectively. Thiol groups may be introduced onto avidin by use of known thiolating agents such as 2-iminothiolane. Free thiol groups on the avidin (streptavidin)-Fab' conjugates optionally may be blocked, for instance with iodoacetamide, prior to their use. Alternatively, the free thiol group may be used as a reactive group for further modification, for example by radiolabeling with Tc-99m, or by conjugation with an agent such as a poly(ethylene glycol) (PEG) derivative activated via a maleimide reaction for subsequent coupling to free thiol groups.

The F(ab')<sub>2</sub>-based streptavidin/avidin conjugates retain two non-sterically compromised antigen-binding sites and all eight biotin-binding sites, and monovalent Fab' units carry one or two streptavidin/avidin units per Fab' with full retention of biotin-binding ability. Use of the carbohydrate means that several biotin units can be coupled to each fragment molecule via the oxidized carbohydrate without interfering with the fragment's antigen-binding capability.

In another embodiment of the invention, conjugation to light-chain carbohydrate residues that are distant from the antigen binding site ensures that interference of binding of a subsequently-administered clearing second antibody will not take place if the second antibody is an antiidiotypic antibody. In this instance, the second antibody will bind to the circulating antibody through its antigen binding site, and the targeting antibody will clear via the liver. Use of this system has the advantage that none of the targeting antibody's secondary sites (e.g. avidins or biotins) are blocked during the clearing step.

In another embodiment of the invention, chelates bearing radioactive nuclides can be linked to the oxidized light-chain carbohydrate via metabolizable linkages. A problem frequently encountered with the use of antibody fragments in radiotherapeutic and radiodiagnostic applications is a potentially dangerous accumulation of the radiolabeled antibody fragments in the kidney. When the conjugate is formed using an acid- or base-labile linker, cleavage of the radioactive chelate from the antibody can advantageously occur. If the chelate is of relatively low molecular weight, it is not retained in the kidney and is excreted in the urine, thereby reducing the exposure of the kidney to radioactivity.

Low molecular weight chelates suitable for this application include, for example, the bifunctional chelates described above, and DOTA or DTPA-type chelates. Each of these molecules can be modified, by standard methods known in the art, to provide reactive functional groups which can form acid-labile linkages with carbonyl groups on the oxidized carbohydrate of the antibody fragment. Examples of suitable acid-labile linkages include hydrazone and thiosemicarbazone functions. These are formed by reacting the oxidized carbohydrate with chelates bearing hydrazide, thiosemicarbazide, and thiocarbazide functions,

respectively. The preparation and conjugation of a thiocarbazide derivative of DTPA is demonstrated in Example 15.

Alternatively, base-cleavable linkers, which have been used for the enhanced clearance of bifunctional chelate-<sup>99</sup>Tc-labeled fragments from the kidneys, can be used. See, for example, Weber et al. *Bioconjug. Chem.* 1:431 (1990). The coupling of a bifunctional chelate to light-chain carbohydrate via a hydrazide linkage can incorporate base-sensitive ester moieties in a linker spacer arm. Such an ester-containing linker unit is exemplified by ethylene glycolbis(succinimidyl succinate), (EGS, available from Pierce Chemical Co., Rockford, Ill.), which has two terminal N-hydroxysuccinimide (NHS) ester derivatives of two 1,4-dibutyric acid units, each of which are linked to a single ethylene glycol moiety by two alkyl esters. One NHS ester may be replaced with a suitable amine-containing BFC (for example 2-aminobenzyl DTPA), while the other NHS ester is reacted with a limiting amount of hydrazine. The resulting hydrazide is used for coupling to the light-chain carbohydrate of an antibody or antibody fragment, forming an antibody-BFC linkage containing two alkyl ester functions. Such a conjugate is stable at physiological pH, but readily cleaved at basic pH.

In another embodiment of the invention, it is possible to construct a "divalent immunoconjugate" by attaching a diagnostic or therapeutic principle to a carbohydrate moiety and to a free sulfhydryl group. Such a free sulfhydryl group may be located in the hinge region of the antibody component.

## 6. Use of Immunoconjugates for Diagnosis and Therapy

### A. Use of Immunoconjugates for Diagnosis

The method of diagnostic imaging with radiolabeled monoclonal antibodies is well known. See, for example, Srivastava (ed.), *RADIOLABELED MONOCLONAL ANTIBODIES FOR IMAGING AND THERAPY*, Plenum Press (1988); Chase, "Medical Applications of Radioisotopes," in *REMINGTON'S PHARMACEUTICAL SCIENCES*, 18th Edition, Gennaro et al. (eds.) Mack Publishing Co., pp. 624-652 (1990); and Brown, "Clinical Use of Monoclonal Antibodies," in *BIOTECHNOLOGY AND PHARMACY*, Pezzuto et al. (eds.), Chapman & Hall, pp. 227-249 (1993). This technique, also known as immunoscintigraphy, uses a gamma camera to detect the location of gamma-emitting radioisotopes conjugated to monoclonal antibodies. Diagnostic imaging can be used to diagnose cardiovascular disease and infectious disease. Brown, *supra*.

The present invention contemplates the use of immunoconjugates to diagnose cardiovascular disease. For example, immunoconjugates comprising anti-myosin fragments can be used for imaging myocardial necrosis associated with acute myocardial infarction. Immunoconjugates comprising antibody fragments that bind platelets and fibrin can be used for imaging deep-vein thrombosis. Moreover, immunoconjugates comprising antibody fragments that bind to activated platelets can be used for imaging atherosclerotic plaque.

Immunoconjugates of the present invention also can be used in the diagnosis of infectious diseases. For example, immunoconjugates comprising antibody fragments that bind specific bacterial antigens can be used to localize abscesses. In addition, immunoconjugates comprising antibody fragments that bind granulocytes and inflammatory leukocytes can be used to localize sites of bacterial infection.

Numerous studies have evaluated the use of monoclonal antibodies for scintigraphic detection of cancer. See, for example, Brown, *supra*, and references therein. Investigations have covered the major types of solid tumors such as



melanoma, colorectal carcinoma, ovarian carcinoma, breast carcinoma, sarcoma, and lung carcinoma. Thus, the present invention contemplates the detection of cancer using immunoconjugates comprising antibody fragments that bind tumor markers to detect cancer. Examples of such tumor markers include carcinoembryonic antigen, alpha-fetoprotein, oncogene products, tumor-associated cell surface antigens, and necrosis-associated intracellular antigens.

In addition to diagnosis, monoclonal antibody imaging can be used to monitor therapeutic responses, detect recurrences of a disease, and guide subsequent clinical decisions.

For diagnostic imaging, radioisotopes may be bound to antibody fragments either directly or indirectly by using an intermediary functional group. Such intermediary functional groups include DOTA, DTPA and EDTA. The radiation dose delivered to the patient is maintained at as low a level as possible. This is accomplished through the choice of isotope for the best combination of minimum half-life, minimum retention in the body, and minimum quantity of isotope which will permit detection and accurate measurement. Examples of radioisotopes which can be bound to antibodies and are appropriate for diagnostic imaging include  $^{99}\text{Tc}$  and  $^{111}\text{In}$ .

Studies indicate that antibody fragments, particularly Fab and Fab', provide advantageous tumor/background ratios. Brown, supra. Thus, the use of Fab and Fab' antibody fragments for the preparation of immunoconjugates is a preferred embodiment of the invention. However, the retention of divalency when using a  $\text{F(ab)}_2$  or a  $\text{F(ab')}_2$  targeting vector leads to higher absolute amounts of antibody at the target compared to monovalent fragments, and can lead to better target:non-target ratios in some tissues.

The immunoconjugates useful in the invention also can be labeled with paramagnetic ions for purposes of in vivo diagnosis. Elements which are particularly useful for magnetic resonance imaging include  $\text{Gd}^{III}$ , Mn, Dy, and Fe ions.

In one embodiment of the invention, multiple chelate molecules, such as DTPA, are directly conjugated to the oxidized light chain carbohydrate of the antibody fragment, allowing the chelation of a large number of paramagnetic ions without the need for an intermediate carrier. The use of some types of intermediate carrier has been observed to have deleterious effects on the magnetic resonance imaging results achieved with metal chelates. See, for example, Wiener, et al., *Magnetic Resonance in Medicine* 31:1-8 (1994). Direct conjugation of chelates in this way therefore eliminates such problems.

In another embodiment of the invention, the immunoconjugate uses a polyamidoamine dendrimer as an intermediate carrier for attachment of a chelating moiety such as DTPA. Such dendrimers have been shown to possess several advantages over other molecules for use as carriers of paramagnetic ions for magnetic resonance imaging. See, for example, Wiener, et al., supra.

The present invention also contemplates the use of immunoconjugates to detect the presence of particular antigens in vitro. In such immunoassays, the immunoconjugates may be utilized in liquid phase or bound to a solid-phase carrier. For example, an intact antibody, or antigen-binding fragment thereof, can be attached to a polymer, such as aminodextran, in order to link the antibody component to an insoluble support such as a polymer-coated bead, plate, or tube.

Alternatively, the immunoconjugates of the present invention can be used to detect the presence of particular antigens in tissue sections prepared from a histological specimen. Such in situ detection can be accomplished by applying a detectably-labeled immunoconjugate to the tissue sections.

In situ detection can be used to determine the presence of a particular antigen and to determine the distribution of the antigen in the examined tissue. General techniques of in situ detection are well known to those of ordinary skill. See, for example, Ponder, "Cell Marking Techniques and Their Application," in *MAMMALIAN DEVELOPMENT: A PRACTICAL APPROACH*, Monk (ed.), IRL Press, pp. 115-138 (1987); Coligan et al., supra.

Detectable labels such as enzymes, fluorescent compounds, electron transfer agents, and the like can be linked to a carrier by conventional methods well known to the art. These labeled carriers and the immunoconjugates prepared from them can be used for in vitro immunoassays and for in situ detection, much as an antibody conjugate prepared by direct attachment of the labels to antibody. However, the loading of the immunoconjugates according to the present invention with a plurality of labels can increase the sensitivity of immunoassays or histological procedures, where only a low extent of binding of the antibody, or antibody fragment, to target antigen is achieved.

#### B. Use of Immunoconjugates for Therapy

Immunoconjugates can be used to treat viral and bacterial infectious diseases, cardiovascular disease, autoimmune disease, and cancer. Brown, supra. The objective of such therapy is to deliver cytotoxic doses of radioactivity, toxin, or drug to target cells, while minimizing exposure to non-target tissues.

As discussed above, a radioisotope can be attached to an intact antibody, or antigen-binding fragment thereof, directly or indirectly, via a chelating agent. For example,  $^{67}\text{Cu}$ , considered one of the more promising radioisotopes for radioimmunotherapy due to its 61.5 hour half-life and abundant supply of beta particles and gamma rays, can be conjugated to an antibody component using the chelating agent, p-bromoacetamidobenzyl-tetraethylaminetetraacetic acid (TETA). Chase, supra. Alternatively,  $^{90}\text{Y}$ , which emits an energetic beta particle, can be coupled to an intact antibody, or antigen-binding fragment thereof, using diethylenetriaminepentaacetic acid (DTPA), or more preferably, tetraazacyclododecane tetraacetic acid (DOTA) as described herein.

Use of the light chain carbohydrate moiety of an antibody fragment for direct conjugation of multiple molecules of a chelator offers an attractive potential solution to a problem associated with the use of DOTA as a chelator for  $^{90}\text{Y}$ . It has been shown that DOTA is the preferred chelating agent for  $^{90}\text{Y}$ , due to the high binding constant and very slow rate of dissociation of the  $^{90}\text{Y}$ -DOTA complex. See, for example, Camera et al., *J. Nucl. Med.* 35:882-888 (1994). It is difficult, however, to attain high incorporations in  $^{90}\text{Y}$  labeling of DOTA immunoconjugates, due to the very slow kinetics of metal binding. See, for example, Wu et al., *Bioorg. Med. Chem. Lett.* 4:449-454 (1994). Wu et al, supra, recently described the use of a polyamidoamine dendrimer intermediate to conjugate 10-11 DOTA molecules, via non site-specific methods, to intact antibodies, and showed that this increased the rate of  $^{90}\text{Y}$  coordination to raise the specific activity of the conjugate to acceptable levels. In the present invention, similarly high numbers of DOTA molecules can be directly conjugated to the light chain carbohydrate of antibody fragments, increasing the rate of  $^{90}\text{Y}$  coordination, and allowing the preparation of conjugates of high incorporations without the use of an intermediate conjugate. Additionally, on an IgG which bears both types of carbohydrate, the light-chain carbohydrate may be used together with the heavy-chain carbohydrate as a site for loading haptens, thus allowing for increased hapten-bearing capacity of the immunoconjugate.

Alternatively, dendrimers similar to those used by Wu et al. can be used as intermediate carriers, allowing the conjugation of even greater numbers of DOTA molecules, and the attainment of still higher incorporations of  $^{90}\text{Y}$  in immunoconjugates. Wu et al., using non site-specific conjugation methods, achieved only a 1:1 ratio of dendrimer to antibody. In the present invention the presence of large number of sugar residues on the light chain carbohydrate, all of which are potential conjugation sites, will allow carrier:antibody ratios of greater than unity. Moreover, since the carbohydrate does not impinge upon the antigen binding site, the immunoreactivity of the immunoconjugate will not be significantly reduced.

Alternatively, boron addends, such as carboranes, can be attached to intact antibodies, or antigen-binding fragments thereof. Carboranes can be prepared with carboxyl functions on pendant side chains, as is well known in the art. Attachment of carboranes to a carrier, such as aminodextran, can be achieved by activation of the carboxyl groups of the carboranes and condensation with amines on the carrier. The intermediate conjugate is then conjugated to the antibody component. After administration of the immunoconjugate, a boron addend is activated by thermal neutron irradiation and converted to radioactive atoms which decay by  $\alpha$ -emission to produce highly toxic, short-range effects.

Moreover, immunoconjugates can be prepared in which the therapeutic principle is a toxin or drug. Useful toxins for the preparation of such immunoconjugates include ricin, abrin, pokeweed antiviral protein, gelonin, diphtherin toxin, and *Pseudomonas* endotoxin. Useful chemotherapeutic drugs for the preparation of immunoconjugates include doxorubicin, daunorubicin, methotrexate, melphalin, chlorambucil, vinca alkaloids, 5-fluorouridine, and mitomycin-C.

#### C. Administration of Immunoconjugates

Generally, the dosage of administered immunoconjugate will vary depending upon such factors as the patient's age, weight, height, sex, general medical condition, and previous medical history. Typically, it is desirable to provide the recipient with a dosage of immunoconjugate which is in the range of from about 1 pg/kg to 10 mg/kg (amount of agent/body weight of patient), although a lower or higher dosage may also be administered. For example, many studies have demonstrated successful diagnostic imaging with doses of 0.1 to 1.0 milligram, while other studies have shown improved localization with doses in excess of 10 milligrams. Brown, supra.

For therapeutic applications, about 10–200 milligrams of immunoconjugate will be administered, normally daily for a period of several days. To reduce patient sensitivity, it may be necessary to reduce the dosage and/or use antibodies from other species and/or use hypoallergenic antibodies, e.g., hybrid human or primate antibodies.

Administration of immunoconjugates to a patient can be intravenous, intraarterial, intraperitoneal, intramuscular, subcutaneous, intrapleural, intrathecal, by perfusion through a regional catheter, or by direct intralesional injection. When administering immunoconjugates by injection, the administration may be by continuous infusion, or by single or multiple boluses.

Immunoconjugates of boron addend-loaded carrier for thermal neutron activation therapy will normally be effected in similar ways. However, it will be advantageous to wait until non-targeted immunoconjugate clears before neutron irradiation is performed. Such clearance can be accelerated by the use of a second antibody, as is known from, e.g., U.S. Pat. No. 4,624,846.

The immunoconjugates of the present invention can be formulated according to known methods to prepare pharmaceutically useful compositions, whereby immunoconjugates are combined in a mixture with a pharmaceutically acceptable carrier. A composition is said to be a "pharmaceutically acceptable carrier" if its administration can be tolerated by a recipient patient. Sterile phosphate-buffered saline is one example of a pharmaceutically acceptable carrier. Other suitable carriers are well-known to those in the art. See, for example, REMINGTON'S PHARMACEUTICAL SCIENCES, 18th Ed. (1990).

For purposes of immunotherapy, an immunoconjugate and a pharmaceutically acceptable carrier are administered to a patient in a therapeutically effective amount. A combination of an immunoconjugate and a pharmaceutically acceptable carrier is said to be administered in a "therapeutically effective amount" if the amount administered is physiologically significant. An agent is physiologically significant if its presence results in a detectable change in the physiology of a recipient patient.

Additional pharmaceutical methods may be employed to control the duration of action of an immunoconjugate in a therapeutic application. Control release preparations can be prepared through the use of polymers to complex or adsorb an immunoconjugate. For example, biocompatible polymers include matrices of poly(ethylene-co-vinyl acetate) and matrices of a polyanhydride copolymer of a stearic acid dimer and sebacic acid. Sherwood et al., *Bio/Technology* 10:1446–1449 (1992). The rate of release of an immunoconjugate from such a matrix depends upon the molecular weight of the immunoconjugate, the amount of immunoconjugate within the matrix, and the size of dispersed particles. Saltzman et al., *Biophysical J.* 55:163–171 (1989); and Sherwood et al., supra. Other solid dosage forms are described in REMINGTON'S PHARMACEUTICAL SCIENCES, 18th Ed. (1990).

Having now generally described the invention, the same will be more readily understood through reference to the following Examples which are provided by way of illustration, and are not intended to be limiting of the present invention, unless specified.

#### EXAMPLE 1

##### Preparation of Immunoconjugates Using Monoclonal Antibodies Which Lack a Naturally-occurring Asn-glycosylation Site in the FR1 Region of the Light Chain Variable Domain

##### (a) Introduction of an Asn-glycosylation Site by Mutagenesis

An Asn-glycosylation site is introduced at amino acid position 18 of the FR1 region of the light chain variable domain of a monoclonal antibody by altering the nucleotide sequence which codes for amino acid residues 18–20. As an illustration, the amino acid sequence, Arg<sub>18</sub>Val<sub>19</sub>Ser<sub>20</sub>, is found in the framework-1 sequence of the light chain variable region of the murine monoclonal antibody, PKAPPA(11)24, which is produced by MPC-11 cells. Rabbitts et al., *Can. J. Biochem.* 58:176–187 (1980); Kabat et al., *SEQUENCES OF PROTEINS OF IMMUNOLOGICAL INTEREST*, U.S. Department of Health and Human Services (1983). The Arg residue at position 18 is encoded by the sequence AGG. Id. Therefore, the objective of the mutagenesis technique is to alter the nucleotide sequence from AGG to AAC, which encodes Asn.

The polymerase chain reaction (PCR) technique is used to introduce the Asn-glycosylation site following the general

procedure of Orlandi et al., *Proc. Natl. Acad. Sci. USA* 86:3833-3837 (1989). In this procedure, total cellular RNA is prepared from about  $5 \times 10^8$  MPC-11 cells (ATCC CCL 167), and mRNA is selected from total RNA on oligo (dT)-cellulose, using standard procedures. First-strand cDNA synthesis is performed using the VK1FOR primer, which is a VK region 3' primer described by Orlandi et al. A 50  $\mu$ l reaction mixture containing 10  $\mu$ g of mRNA, 20 pmol of VK1FOR primer, 250  $\mu$ M of each dNTP, 10 mM dithiothreitol, 100 mM Tris-HCl (pH 8.3), 10 mM MgCl<sub>2</sub>, and 140 mM KCl are incubated at 70° C. for 10 minutes and then, cooled. Reverse transcriptase (46 units) is added and the mixture is incubated at 42° C. for one hour. The reaction is terminated by heating the reaction mixture at 90° C. for 5 minutes.

Alternatively, first strand cDNA is synthesized from total cellular RNA from MPC-11 cells using the SUPERSCRIPT™ preamplification system (Gibco/BRL; Gaithersburg, Md.) with the VK1FOR primer.

The VK sequences are amplified using a 5' primer which encodes the first 20 amino acids of the VK domain, with the exception that amino acids 18-20 encode an Asn-glycosylation site. In this example, amino acid residue at position 18 is encoded by AAC, as discussed above. PCR reaction mixtures contain 10  $\mu$ l of the first-strand cDNA product, 9  $\mu$ l of 10 $\times$ PCR buffer (500 mM KCl, 100 mM Tris-HCl (pH 8.3), 15 mM MgCl<sub>2</sub>, and 0.01% (w/v) gelatin), 5  $\mu$ l of the VK1FOR and 5' primers, and 5 units of AMPLI-TAQ™ DNA polymerase (Perkin Elmer Cetus; Norwalk, Calif.). The mixtures are overlaid with paraffin oil and subjected to 30 rounds of temperature cycling with a programmable heating block. A typical cycle consists of: denaturation at 94° C. for one minute, annealing at 50° C. for 1.5 minutes, and polymerization at 72° C. for 1.5 minutes.

The DNA sample is extracted twice with ether, once with phenol, once with phenol/chloroform and then, precipitated with ethanol. Alternatively, the DNA sample can be purified following electrophoresis through an agarose gel.

Amplified VK fragments are purified on a 2% agarose gel, using standard techniques. The approximately 300 base pair VK fragments are then digested with the restriction enzymes PvuII and BglII, and ligated into the complementary restriction sites of a cloning vector. Various cloning vectors are commercially available. For example, pGEM™ vectors (Promega; Madison, Wis.) and ZAP EXPRESS™ vectors (Stratagene Cloning Systems; La Jolla, Calif.) are useful for cloning the VK fragment. Alternatively, a vector can be used which contains an appropriate immunoglobulin promoter and leader sequence. For example, see Orlandi et al., supra. The ligated DNA is transformed into DH5 $\alpha$  competent *E. coli* cells using a standard calcium chloride method.

To analyze cloned DNA, transformants are grown overnight at 37° C. in SOC (2% Bacto-tryptone, 0.5% Bacto-yeast extract, 10mM NaCl, 2.5 mM KCl, 10mM MgCl<sub>2</sub>, 10mM MgSO<sub>4</sub> and 20 mM glucose). The SOC medium contains the appropriate antibiotic to select for the growth of bacteria containing the vectors. For example, the SOC medium contains 50  $\mu$ g/ml ampicillin to select for the growth of bacteria carrying a pGEM™ vector. Mini-plasmid DNA preparations of the colonies are prepared using standard techniques and subjected to restriction digest analysis. DNA from positive colonies are sequenced using the dideoxy method of Sanger et al., *Proc. Natl. Acad. Sci. USA* 75:5463-5467 (1977). The results of DNA sequence determination are used to confirm that no undesirable mutations are introduced by the PCR reaction and that the mutation(s) in the 18-20 region was introduced.

#### (b) Transfection of Mammalian Cells

Restriction enzymes are used to excise the DNA fragment which contains the VK sequence having an Asn-glycosylation site at position 18 from the staging vector. The DNA fragment is then cloned into an appropriate mammalian expression vector. Such an expression vector should contain the coding sequence of the constant region, an immunoglobulin enhancer, a kappa enhancer and a drug selection marker (e.g., the hygromycin resistance gene). For example, see Orlandi et al., supra.

Approximately 10  $\mu$ g of the linearized light chain expression vector containing the mutated VK region and 20-30  $\mu$ g of linearized heavy chain expression vector are co-transfected by electroporation into mammalian cells, using standard techniques. For example, about  $10^6$  SP2/OAG14 non-secreting myeloma cells (ATCC CRL 1581) are transfected using the technique of Co et al., *J. Immunol.* 148:1149-1154 (1992), or using similar techniques described in either Sambrook et al., supra, or CURRENT PROTOCOLS IN MOLECULAR BIOLOGY, Ausubel et al., eds., John Wiley & Sons (1989). After transfection, cells are grown in 96-well microtiter plates in complete Hybridoma Serum-Free Medium (GIBCO/BRL) at 37° C. in 5% carbon dioxide. Two days later, the selection process is initiated by the addition of medium containing the appropriate selection drug (e.g. hygromycin). Typically, colonies emerge two to three weeks following electroporation. Colonies are transferred to 24-well trays for expansion.

#### (c) Assay for Antibody-secreting Transfectoma Clones

An ELISA assay is used to select antibody-secreting transfectoma clones. Briefly, supernatants from confluent wells are diluted and 100  $\mu$ l of each dilution are added in triplicate to ELISA microtiter plates which have been pre-coated with sheep anti-mouse IgG-specific antibody (The Binding Site Ltd.; San Diego, Calif.). After incubating the microtiter plates for one hour at room temperature, unbound proteins are removed by washing the plates three times with wash buffer (PBS with 0.05% polysorbate-20). Bound antibodies are allowed to react with peroxidase-conjugated goat anti-mouse IgG-specific antibody (HyClone Laboratories; Logan, Utah) After washing the plate three times with wash buffer, 100  $\mu$ l of substrate solution (3.3 mg/ml of orthophenylenediamine and 0.12% hydrogen peroxide in 0.02M citrate buffer (pH 5.0)) are added to each well. Color is allowed to develop in the dark for 30 minutes and the reaction is stopped by the addition of 50  $\mu$ l of 4M HCl per well. An automated ELISA plate reader (Bio-Tek Instrument; Winooski, Vt.) is used to measure absorbance at 490 nm.

Alternatively, chimeric or humanized mutant antibodies can be detected by coating ELISA microtiter plates with goat anti-human Fab or kappa-specific antibody (Jackson ImmunoResearch; West Grove, Pa.), and detecting bound antibody with peroxidase-conjugated goat anti-human Fc-specific antibody (Jackson ImmunoResearch; West Grove, Pa.).

#### (d) Antibody Purification and Analysis

Transfectomas are grown as 500 ml cultures in serum-free medium until confluent. Cultures are centrifuged to pellet cells and the supernatants are filtered through a 0.2 micron membrane. Antibodies are isolated by passing supernatants through a three milliliter protein A column by gravity at a rate of 0.5-1 ml/min. The column is then washed with 20 ml of PBS and bound antibodies are eluted with 10 ml of a solution containing 0.1M glycine and 10 mM EDTA (pH 3.5). One milliliter solution fractions are collected in the presence of 10  $\mu$ l of 3M Tris (pH 8.6). The presence of antibodies is detected by measuring absorbance at 280 nm

and eluant fractions exhibiting absorbances above background are pooled, filtered, dialyzed against PBS and concentrated with a Centricon 30 (Amicon; Beverly, Mass.). The final concentrations of antibody are determined by ELISA and antibody concentrations are adjusted to 1 mg/ml in PBS containing 0.01% (w/v) sodium azide.

Light chain glycosylation is confirmed by electrophoresis of the purified antibodies or antibody fragments on a gradient 4–20% SDS-polyacrylamide gel under reducing conditions, using standard techniques. For example, see CURRENT PROTOCOLS IN IMMUNOLOGY, Coligan et al., eds., John Wiley & Sons (1991). The presence of light chain glycosylation is indicated by a higher apparent molecular weight and by the presence of multiple light chain bands.

#### (c) Preparation of Conjugates

The direct or indirect methods can be used to obtain immunoconjugates, as described below.

### EXAMPLE 2

#### Preparation of Antibody Fragments

Fab, Fab', F(ab)<sub>2</sub>, or F(ab')<sub>2</sub> fragments can be obtained from transfectomas by mutating the heavy chain structural gene in the heavy chain expression vector. Fab expression is accomplished by inserting a stop codon following the sequence of the CH1 domain. In contrast, Fab' or F(ab')<sub>2</sub> expression is accomplished by inserting a stop codon after the sequence encoding the hinge region of the heavy chain. Antibody fragments are purified from transfectoma culture supernatants by size exclusion chromatography, ion-exchange chromatography, or affinity chromatography as described in Coligan et al., supra. Alternatively, a commercially-available purification system is used to purify fragments, such as a Quick MAB Column (Sterogen; Santa Clara, Calif.).

Alternatively, antibody fragments can be prepared from intact antibodies by proteolysis. These techniques are well-known to those of skill in the art. For example, see Coligan et al., supra, at pp. 2.8.1–2.8.10. Also see Stanworth et al. "Immunochemical Analysis of Human and Rabbit Immunoglobulins and Their Subunits," in HANDBOOK OF EXPERIMENTAL IMMUNOLOGY, Vol. 1, D. M. Weir, ed., Blackwell Scientific pp 12.1–12.46 (1986) and Parham, "Preparation and Purification of Active Fragments from Mouse Monoclonal Antibodies," Id at pp. 14.1–14.23.

As an example, preactivated papain can be used to prepare F(ab)<sub>2</sub> fragments from IgG1 or Fab fragments from IgG2a and IgG2b, as follows. Papain is activated by incubating 2 mg/ml papain (2×recrystallized suspension, Sigma #P3125) and 0.05M cysteine (free-base, crystalline; Sigma #C7755) for 30 minutes in a 37° C. water bath. To remove cysteine, the papain/cysteine mixture is applied to a PD-10 column (Pharmacia #G-25), which has been equilibrated with 20 ml of acetate/EDTA buffer (0.1M acetate with 3 mM EDTA, pH 5.5). Fractions are assayed by measuring absorbance at 280 nm, and the two or three fractions that contain protein are pooled. The concentration of preactivated papain is determined by using the formula: (absorbance at 280 nm)/2.5 = mg. preactivated papain/ml.

To prepare antibody for digestion, 10 mg. of antibody in 2 to 5 ml of PBS are dialyzed against acetate/EDTA buffer. Five hundred micrograms of preactivated papain are added to the dialyzed antibody solution, and the mixture is vortexed. After a 6–12 hour incubation in a 37° C. water bath, papain is inactivated by adding crystalline iodoacetamide

(Sigma #I6125) to a final concentration of 0.03M. The mixture is then dialyzed against 1 liter of PBS (pH 8.0) at 4° C. for 6–12 hours.

To remove undigested antibody and Fc fragments, the mixture is applied to a protein A-Sepharose column which has been equilibrated in PBS (pH 8.0). Unbound fractions are collected in 2 ml aliquots and pooled. After concentrating the pool to a total volume of 5 ml or less, protein is fractionated by size-exclusion chromatography and the results are analyzed by SDS-PAGE.

### EXAMPLE 3

#### Direct Conjugation at the Carbohydrate Moiety of the FR1 Region of the Light Chain Variable Domain of F(ab')<sub>2</sub> Fragments

##### (a) Conjugation of the Murine LL2 F(ab')<sub>2</sub> Fragment with Chelator

LL2 is a murine monoclonal antibody that has been shown to be effective for the diagnosis and treatment of non-Hodgkins B-cell lymphoma. Goldenberg et al., *J. Clin. Oncol.* 9:548–564 (1991); Murthy et al., *Eur. J. Nucl. Med.* 19:394–401 (1992); The LL2 F(ab')<sub>2</sub> fragment was conjugated with either aminobenzyl DTPA (DTPA) or a derivative of DTPA containing the long-chain linker, —CSNH(CH<sub>2</sub>)<sub>10</sub>NH<sub>2</sub> (LC-DTPA). Briefly, LL2 F(ab')<sub>2</sub> fragment (2.5 mg) in about 1 ml of 50 mM acetate-buffered 0.9% saline (ABS; pH 5.3) was oxidized in the dark by treatment with sodium metaperiodate (210 µl of a 5.68 mg/ml solution) at 0° C. for one hour. The reaction mixture was treated with ethylene glycol (20 µl) to decompose the unreacted periodate and the oxidized antibody fragment was purified using a Sephadex G-50/80 column (Pharmacia; Piscataway, N.J.) equilibrated in PBS (pH 6.1). The oxidized fragment was then reacted with excess DTPA or LC-DTPA. After 40 hours at room temperature, the Schiff base was reduced by NaBH<sub>3</sub>CN. Conjugated antibody was purified using a centrifuged size-exclusion column (Sephadex G-50/80) equilibrated in 0.1M acetate (pH 6.5). The concentrations of antibody conjugates were determined by measuring absorbance at 280 nm.

The ratio of chelator molecules per molecule of antibody fragment was determined by a metal-binding assay. The assay was performed by mixing an aliquot of LL2 F(ab')<sub>2</sub>-chelator conjugate with 0.1M ammonium acetate (pH 7) and 2M triethanolamine, and incubating the mixture at room temperature with a known excess of cobalt acetate spiked with <sup>57</sup>cobalt acetate. After 30 minutes, EDTA (pH 7) was added to a final concentration of 10 mM. After a further 10 minute incubation, the mixture was analyzed by instant thin layer chromatography (ITLC) using 10mM EDTA for development. The fraction of radioactivity bound to antibody was determined by counting sections of ITLC strips on a gamma counter. The results indicated that there were about 6 molecules of DTPA per antibody fragment and about 5 molecules of LC-DTPA per antibody fragment.

##### (b) Determination of the Immunoreactivity of LL2 F(ab')<sub>2</sub>-chelator Conjugates

The immunoreactivities of the LL2 F(ab')<sub>2</sub>-DTPA and LL2 F(ab')<sub>2</sub>-LC-DTPA conjugates were determined using an ELISA assay. The results demonstrated that LL2 F(ab')<sub>2</sub> and the DTPA and LC-DTPA conjugates exhibited similar binding activity toward an LL2 anti-idiotypic antibody.

In addition, the immunoreactivities of the LL2 F(ab')<sub>2</sub>-DTPA and LL2 F(ab')<sub>2</sub>-LC-DTPA conjugates were examined in a binding competition assay. In these experiments, a human chimeric LL2 (IgG/kappa) was used to compete with

LL2 F(ab')<sub>2</sub> or its conjugates for binding to Raji lymphoma cells (ATCC CCL 86). Raji cells were cultured in DMEM medium, supplemented with 10% fetal calf serum and 2mM L-glutamine. Cells were maintained at 37° C. in 5% carbon dioxide. Cell medium and components were obtained from Gibco/BRL (Gaithersburg, Md.).

In these studies, 1 µg of the chimeric LL2 (IgG/kappa) was incubated with 5×10<sup>5</sup> Raji cells in the presence of various concentrations of LL2 F(ab')<sub>2</sub> or its conjugates in a final volume of 100 µl of PBS supplemented with 1% fetal calf serum and 0.01% (w/v) sodium azide (PBS-FA). The mixtures were incubated for 30 minutes at 4° C., and then washed three times with PBS to remove unbound antibodies. The extent of residual binding by chimeric LL2 after competition was determined by adding 100 µl of a solution containing a goat anti-human Fc-specific antibody labeled with fluorescein isothiocyanate (20×diluted stock solution in PBS-FA), and incubating for 30 min at 4° C. After washing the mixture three times with PBS, fluorescence intensity was measured using a FACSCAN fluorescence activated cell sorter. The results of these studies demonstrated that LL2 F(ab')<sub>2</sub> and its conjugates exhibited similar binding to Raji cells.

Thus, these studies demonstrate that both conjugates were immunoreactive and exhibited binding activities comparable to unconjugated LL2 F(ab')<sub>2</sub> fragments.

#### (c) Labeling with <sup>111</sup>Indium

The LL2 F(ab')<sub>2</sub>-chelator conjugates were labeled with <sup>111</sup>Indium as follows. <sup>111</sup>Indium chloride was buffered at pH 5.5 using ammonium acetate such that the final acetate concentration was about 0.2M. <sup>111</sup>Indium acetate was added to a solution of LL2 F(ab')<sub>2</sub>-conjugate in 0.1M acetate (pH 6.5), and the mixture was incubated for about one hour. Reaction mixtures contained either 9.7 µg of LL2 F(ab')<sub>2</sub>-DTPA and 72.6 µCi of <sup>111</sup>Indium, or 10 µg of LL2 F(ab')<sub>2</sub>-LC-DTPA and 126.7 µCi of <sup>111</sup>Indium.

The extent of <sup>111</sup>indium incorporation was analyzed by incubating the labeling mixture with 10 mM EDTA for ten minutes, followed by ITLC examination using 10 mM EDTA for development. In this assay, unbound <sup>111</sup>indium moves to the solution front, while antibody-bound <sup>111</sup>indium remains at the origin. The presence of any colloidal <sup>111</sup>indium was assayed by ITLC (co-spotted with human serum albumin) using a water:ethanol:ammonia (5:2:1) solution for development. In this system, the fraction of radioactivity at the origin represents colloidal <sup>111</sup>indium. In addition, all labeling mixtures were analyzed using radio-high pressure liquid chromatography (radio-HPLC).

The results of these studies indicated that <sup>111</sup>indium-labeled LL2 F(ab')<sub>2</sub>-DTPA had a specific activity of 7.47 µCi/µg protein, and that <sup>111</sup>indium was incorporated by 97.4%, as determined by ITLC, or 92.5%, as determined by radio-HPLC. Moreover, <sup>111</sup>indium-labeled LL2 F(ab')<sub>2</sub>-LC-DTPA had a specific activity of 12.67 µCi/µg protein, and <sup>111</sup>indium was incorporated by 95.6%, as determined by ITLC, or 94%, as determined by radio-HPLC. The amount of colloidal <sup>111</sup>indium is typically about 1 to 3%.

#### (d) Labeling with <sup>90</sup>Yttrium

LL2 F(ab')<sub>2</sub>-chelator conjugates were prepared as described above. The conjugates were labeled with <sup>90</sup>yttrium, as follows. Briefly, commercially available <sup>90</sup>yttrium chloride (DuPont NEN; 17.68 µl; 5.63 mCi) was buffered with 35.4 µl of 0.5M acetate (pH 6.0). The solution was allowed to stand for 5–10 minutes at room temperature, and then used for radiolabeling.

<sup>90</sup>Yttrium-labeled LL2 F(ab')<sub>2</sub>-DTPA was prepared by mixing <sup>90</sup>yttrium acetate (128.7 µCi) with LL2 F(ab')<sub>2</sub>-

DTPA (30 µg; 8.3 µl), incubating at room temperature for one hour, and diluting with 90 µl of 0.1M acetate (pH 6.5). <sup>90</sup>Yttrium-labeled LL2 F(ab')<sub>2</sub>-LC-DTPA was prepared by mixing <sup>90</sup>yttrium acetate (109.5 µCi) with LL2 F(ab')<sub>2</sub>-LC-DTPA (30 µg; 7.6 µl), incubating at room temperature for one hour, and diluting with 90 µl of 0.1M acetate (pH 6.5). The result of the labeling procedure was tested by ITLC in two solvent systems, and by HPLC, as described above.

<sup>90</sup>Yttrium-labeled LL2 F(ab')<sub>2</sub>-DTPA had a specific activity of 4.29 µCi/µg protein, while <sup>90</sup>yttrium-labeled LL2 F(ab')<sub>2</sub>-LC-DTPA had a specific activity of 3.65 µCi/µg protein. Radio-HPLC analysis indicated that <sup>90</sup>yttrium was incorporated in LL2 F(ab')<sub>2</sub>-DTPA by 96%, while <sup>90</sup>yttrium was incorporated in LL2 F(ab')<sub>2</sub>-LC-DTPA by 90%.

### EXAMPLE 4

#### Indirect Conjugation at the Carbohydrate Moiety of the FR1 Region of the Light Chain Variable Domain of F(ab')<sub>2</sub> Fragments

##### (a) Preparation of the Intermediate Conjugate

The murine LL2 F(ab')<sub>2</sub> fragment was conjugated with doxorubicin via dextran, using the method of Shih et al., *Int. J. Cancer* 41:832–839 (1988). Briefly, amino dextran was prepared by dissolving one gram of dextran (m.w. 18 kD; Sigma Chemical Co.; St. Louis, Mo.) in 70 ml of water. The dextran was partially oxidized to form polyaldehyde dextran by adding 0.5 gram of sodium metaperiodate, and stirring the solution at room temperature overnight. After concentrating the mixture with an Amicon cell (YM10 membrane; MWCO=10,000), the polyaldehyde dextran was purified by Sephadex G-25 chromatography and lyophilized to give about 900 grams of white powder. Polyaldehyde dextran was then treated with two equivalents of 1,3-diamino-2-hydroxypropane in aqueous phase for 24 hours at room temperature. The resultant Schiff base was stabilized by addition of sodium borohydride (0.311mmol per 2.15 mmol of 1,3-diamino-2-hydroxypropane) to the mixture. The mixture was allowed to incubate at room temperature for six hours. Amino dextran was purified using a Sephadex G-25 column.

Doxorubicin (Sigma Chemical Co.; St. Louis, Mo.) was activated by adding one milliliter of anhydrous DMF to 0.1 mmole of doxorubicin in a dried Reacti-vial, followed by a solution of N-hydroxysuccinimide (23 mg, 0.2 mmole; Sigma) in 750 µl of anhydrous DMF and a solution of 1,3-dicyclohexylcarbodiimide (41.5 mg, 0.2 mmol; Sigma) in 750 µl of anhydrous DMF. The reaction mixture was stirred in the dark at room temperature for 16 hours under anhydrous conditions. The side product, i.e., the urea derivative, did not precipitate well in this solvent system. The precipitate was centrifuged and the solution was stored in a sealed bottle at –20° C.

Doxorubicin-dextran intermediate conjugate was prepared by dissolving aminodextran (18 kD; 10 mg) in two milliliters of PBS (pH 7.2) and gradually adding 0.7 ml of the above N-hydroxy-succinimide-activated doxorubicin solution. Thus, 50 moles of doxorubicin were present per mole of aminodextran. The solution was stirred at room temperature for five hours and after removing any precipitate, the conjugate was purified using a Sephadex G-25 column. Doxorubicin-dextran conjugate was characterized by a doxorubicin/dextran ratio of 14.

Alternatively, doxorubicin-dextran conjugate was prepared by reacting doxorubicin with 1-ethyl-3(3-dimethylaminopropyl)-carbodiimide, as described by Shih

et al., *Int. J. Cancer* 41:832-839 (1988). Also, see Shih et al., *Cancer Research* 51:4192-4198 (1991).

(b) Site-specific Attachment of the Intermediate Conjugate to LL2 F(ab')<sub>2</sub>

LL2 F(ab')<sub>2</sub> fragment (25 mg) in 5 ml of PBS (pH 5.5) was oxidized in the dark by treatment with sodium metaperiodate (800 µl of a 21.5 mg/ml solution) at room temperature for 60 minutes. The reaction mixture was treated with ethylene glycol (50 µl) to decompose the unreacted periodate and the oxidized antibody fragment was purified using a Sephadex G-25 column equilibrated in 0.05M HEPES (pH 7.4). The oxidized fragment was then concentrated to 5 mg/ml in 0.05M HEPES (pH 7.4) and reacted with the doxorubicin-dextran conjugate (22 mg). After 24 hours at room temperature, the Schiff base was reduced by NaBH<sub>3</sub>CN. Conjugated antibody was purified using a Sepharose CL-6B column.

Using this procedure, an average of about nine doxorubicin molecules can be coupled to each LL2 F(ab')<sub>2</sub> fragment at the carbohydrate site of the FR1 region of the light chain variable domain. This ratio was determined by measuring the concentration of doxorubicin (A<sub>482</sub>) and protein (A<sub>280</sub>). The conjugate retains 80% of the immunoactivity of the unconjugated LL2 F(ab')<sub>2</sub> fragment, as determined by the flow cytometry method described above.

#### EXAMPLE 5

##### Introduction of an Asn-linked Glycosylation Site in the VK FR1 Region of Humanized MN14

An Asn-glycosylation site was introduced into the VK FR1 region of humanized MN14, which is an antibody that binds carcinoembryonic antigen. Briefly, the nucleotide sequence encoding Arg<sub>18</sub> was mutated to a nucleotide sequence encoding Asn<sub>18</sub> using the PCR method described in Example 1. In this case, DNA from the light chain expression vector for humanized MN14 was used as a template for PCR. The VKFOR1 primer of Orlandi et al. was used as the 3' primer. The 5' primer consisted of a 57-mer encoding the first 20 amino acids of the MN14 VK domain, with the exception that the codon at position 18 encoded Asn. The approximately 300 base pair PCR product was digested with PvuII and BglII, and ligated into complementary sites in a staging or cloning vector. DH5α competent cells were transformed with the staging or cloning vector using a standard calcium chloride method. For example, see, Ausubel et al., *supra*.

The DNA fragment containing the humanized MN14 VK sequence with an Asn-glycosylation site at amino acid position 18 was subcloned into a pSVhyg-based light chain expression vector. SP2/0-AG14 non-secreting myeloma cells were co-transfected by electroporation with the linearized light chain expression vector and with a linearized heavy chain expression vector. Transfectomas were selected using hygromycin-B and cultured to produce antibody.

Antibody was purified and analyzed on an SDS-PAGE reducing gel. The light chain of the glycosylated humanized MN14 migrated as multiple bands and ran at a higher molecular weight, compared to non-glycosylated MN14 light chain. This result indicates that the new Asn-linked glycosylation site was used for carbohydrate addition.

Significantly, the MN14 blocking activities of the glycosylated MN14 antibody and the non-glycosylated MN14 antibody were found to be substantially the same. Thus, glycosylation at the VK FR1 region of humanized MN14 does not affect immunoreactivity.

#### EXAMPLE 6

##### Direct Conjugation of DOTA at the Carbohydrate Moiety of the FR1 Region of the Light Chain Variable Domain of F(ab')<sub>2</sub> Fragments

##### (a) Conjugation of the Murine RS7 F(ab')<sub>2</sub> Fragment with DOTA

The MAb RS7 is a rapidly internalizing antibody that is reactive with carcinomas of the lung, stomach, bladder, breast, ovary, uterus and prostate (Stein et al., 1990, *Cancer Res.*, 50, 1330-1336). Using procedures described above, a glycosylation site, NVT, is introduced at positions 18-20 of the VK domain of RS7. The glycosylated RS7 is expressed in SP2/0-AG14 myeloma cells, and the F(ab')<sub>2</sub> prepared as described above.

To 2 mg of the F(ab')<sub>2</sub> fragment of RS7 in 1 ml of 0.1M phosphate buffered 0.9% sodium chloride solution, pH 7.2 (PBS), is added 400 µl of 2.84 mg/ml sodium metaperiodate. The reaction mixture is stirred in the dark at room temperature for 90 min., and 20 µl of ethylene glycol is added to stop the oxidation reaction. The oxidized antibody fragment is purified on a Sephadex G-25 size-exclusion column (Pharmacia; Piscataway, NJ.) equilibrated in PBS (pH 6.1). The antibody is reconcentrated to 2 mg/ml with a Centricon 30 (Amicon; Beverley, Mass.) and treated with an excess of 2-p-aminobenzyl-1,4,7,10-tetraazacyclododecanetetraacetic acid (NH<sub>2</sub>-Bz-DOTA). The mixture is allowed to react at 4° C. for 48 hr. The Schiff base is reduced in situ by the addition of a 10-fold molar excess (to antibody) of sodium cyanoborohydride, with subsequent stirring for 30 min. The DOTA-F(ab')<sub>2</sub> conjugate is purified using a centrifuged size-exclusion column (Sephadex G-50/80) equilibrated in 0.1M acetate-buffered 0.9% sodium chloride solution (ABS, pH 6.5), prepared with acid-washed components and metal-free buffer media. The concentration of the antibody conjugate is determined by its absorbance at 280 nm, and the ratio of chelates per mole of antibody determined by cobalt-57 binding assay as in Example 3.

Commercially available yttrium-90 chloride (8.9 mCi, 27 µl) is treated with 81 µl of 0.5M ABS, pH 6, and the solution mixed by vortex. It is allowed to stand for 15 min. and then used in the labeling below.

To the DOTA-labeled RS7 F(ab')<sub>2</sub> conjugate (1 mg, 73 µl) in an acid-washed plastic vial, is added yttrium-90 acetate (4.94 mCi, 60 µl) in ABS. The vial contents are mixed gently with a vortex, and allowed to stand at room temperature for 1 hr. Then, 850 µl of 0.1M ABS was added to the labeling vial with mixing. The labeling result is tested by instant thin-layer chromatography in two solvent systems, and by high-performance liquid chromatography, as described in Example 3.

#### EXAMPLE 7

##### Indirect Conjugation using a polyamidoamine dendrimer as the intermediate carrier at the Carbohydrate Moiety of the FR1 Region of the Light Chain Variable Domain of F(ab')<sub>2</sub> Fragments

##### (a) Preparation of the Intermediate Conjugate

The murine RS7 F(ab')<sub>2</sub> fragment, oxidized as described above, was conjugated with DOTA via a generation 2 polyamidoamine dendrimer. The dendrimer was prepared by the method of Tomalia et al., *Angew. Chem. Int. Ed. Engl.* 29:138-175 (1990). The dendrimer (10 µM in 8 ml water) was reacted with 150 µM 2-(p-isothiocyanatobenzyl)-1,4,7,10-tetraazacyclododecyl tetraacetic acid at 40° C., pH 9 for



35

24 h, with periodic additions of 0.2M NaOH to maintain the solution pH at 9.0. Unreacted ligand was removed by ultrafiltration using a stirred cell (Amicon, MA) fitted with a 3000 MW cut-off filter. After lyophilization, the dendrimer-chelator conjugate was resuspended in ABS, and conjugated to the RS7 F(ab')<sub>2</sub> fragment as described in Example 6.

## EXAMPLE 8

Conjugation of Hz-PEG (methoxy polyethylene glycol hydrazide) to F(ab')<sub>2</sub> light chain carbohydrate.

## Conjugation protocol (a).

IMMU-LL2-F(ab')<sub>2</sub> carbohydrate moiety was oxidized with sodium periodate (20 mM final concentration) at pH 6 for 90 min at 0° C. The oxidized fragment was separated from excess periodate by centrifuged spin-column technique, Sephadex G-50-80 in PBS pH 6.0. The hydrazone linkage was obtained through addition of methoxy-PEG hydrazide (MW 5000, Shearwater Polymers, Inc., Huntsville, Ala.) in molar excess (50× and 300×) to the purified oxidized intermediate. The reaction was allowed to proceed for two hours at room temperature. The products were purified with a centrifuged spin-column, containing Sephadex G-50-80, 0.1M sodium phosphate pH 7 and analyzed by size-exclusion HPLC using a BioSil SEC-400 column eluting with 0.2M sodium phosphate, 0.02% sodium azide, pH 6.8.

The results showed 16% unmodified for the reaction with 50×molar excess and only 2.3% unmodified F(ab')<sub>2</sub> for the reaction with 300×molar excess of Hz-PEG.

## Conjugation protocol (b).

IMMU-LL2 F(ab')<sub>2</sub>, 200 μl (2.1 mg, 2.1×10<sup>-8</sup> mol) was oxidized with 29.4 μl of 0.5M NaIO<sub>4</sub>, (700×2.1×10<sup>-8</sup> mol) for 45 min at 26° C. The oxidized fragment was separated from excess NaIO<sub>4</sub> on two consecutive 2.4 ml centrifuged spin columns, Sephadex G-50-80 in 0.1M sodium phosphate, pH 7.

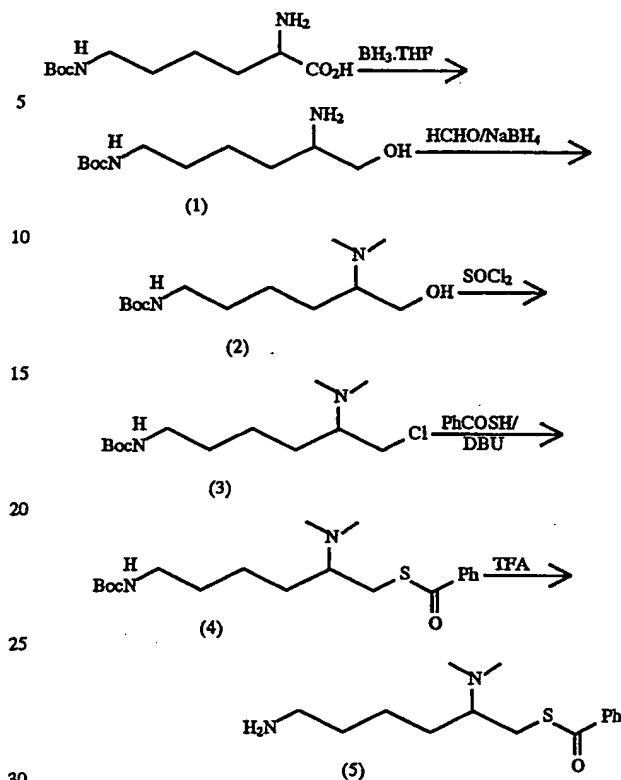
Conjugation of methoxy-Hz-PEG to the oxidized fragment was accomplished by incubating 205 μl (1.52 mg, 1.52×10<sup>-8</sup> mol) of oxidized IMMU-LL2F(ab')<sub>2</sub> with 22.8 mg (300×1.52×10<sup>-8</sup> mol) of methoxy-Hz-PEG (MW5000) at 25° C. for 1 hr. The conjugate was purified on spin-column (4 consecutive 2.4 ml) of Sephadex-G-50-80, eluted with 0.1M sodium phosphate, pH 7. HPLC analyses on a size-exclusion column of BioSil 400 eluted with 0.2M sodium phosphate, 0.15M sodium chloride, 0.02% sodium azide pH 6.8, showed two new peaks, at 7.4 (16.9%) and 8.3 min (83.1%).

## EXAMPLE 9

## Preparation of Bifunctional Chelating Agent (5)

The following example illustrates a method of preparing a particularly preferred bifunctional chelating agent for use in the present invention. Radiolabeling proteins or antibodies having pendant sulfhydryl groups using the bifunctional chelating agents prepared in this example, and using the radiolabeled proteins or antibodies in radioimmunoimaging or radioimmunotherapy methods is within the skill of those skilled in the art. The reaction sequence is shown below.

36



(a). To a stirred solution of N-ε-(t-butoxycarbonyl)lysine in tetrahydrofuran (THF), cooled to 4° C. under argon, is added dropwise borane-tetrahydrofuran complex (1 equivalent). After 2 h, excess borane was decomposed by careful addition of aqueous THF. The reaction mixture was then refluxed with 5M sodium hydroxide for 10-18 h to decompose the borate esters. The aqueous solution was thoroughly extracted with chloroform, washed with brine, dried over anhydrous sodium sulfate, and concentrated to dryness on a rotary evaporator, giving 2-amino-6-N-(t-butoxycarbonyl)amino-1-hexanol (1).

(b). Compound (1) is dissolved in ethanol at 4° C. and formaldehyde gas (prepared by heating paraformaldehyde in a stream of argon) is passed into the solution for 10 min. Sodium borohydride (10 equivalents) is then added slowly, maintaining the temperature at 4° C. The mixture is evaporated to dryness, and 0.1M HCl added dropwise to the residue followed quickly by saturated sodium bicarbonate solution. The solution is extracted with ethyl acetate, washed with brine, and the organic layer dried over anhydrous sodium sulphate and concentrated to dryness. The produce is treated again with formaldehyde and sodium borohydride as above, to give 2-(N,N-dimethylamino)-6-[N-(t-butoxycarbonyl)amino]-1-hexanol, (2).

(c). To a solution of (2) in dichloromethane at 4° C. is added anhydrous potassium carbonate (20 eq.), and the suspension vigorously stirred while excess thionyl chloride was added dropwise. After 1 h, solvent and excess thionyl chloride is removed on a rotary evaporator and the residue extracted with ethyl acetate. Evaporation to dryness affords 1-(N,N-dimethylamino)-5-(t-butoxycarbonyl)amino-1-chloromethylpentane, (3), which may be further purified by chromatography on silica gel if necessary.

(d). To a solution of (3) in toluene is added 1,8-diazabicyclo[5.4.0]undec-7-ene (2.2 eq.), followed by

thiobenzoic acid (1.1 eq.), and the solution heated under reflux. Progress of the reaction is monitored by thin-layer chromatography (TLC) on silica gel plates, visualized with 5% phosphomolybdic acid in ethanol. When reaction is complete, the organic extract is evaporated to dryness and the residue redissolved in chloroform, washed once with water, dried over anhydrous sodium sulphate, and evaporated to obtain crude S-benzoyl-2-(N,N-dimethylamino)-5-(t-butoxycarbonyl)aminomercaptan, (4). This compound is further purified by flash chromatography.

(e). To a stirred solution of (4) in dichloromethane at room temperature is added trifluoroacetic acid (10 eq.). After 2 h the solvent is evaporated to dryness to give (5), which is used directly for conjugation to the oxidized carbohydrate of the antibody fragment.

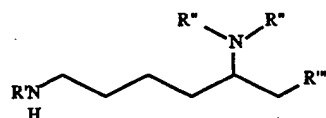
#### EXAMPLE 10

##### Coupling of Bifunctional Chelating Agent (5) to an oxidized antibody.

LL2 F(ab')<sub>2</sub> fragment (2.5 mg) in about 1 ml of 50 mM acetate-buffered 0.9% saline (ABS; pH 5.3) is oxidized in the dark by treatment with sodium metaperiodate (210  $\mu$ l of a 5.68 mg/ml solution) at 0° C. for one hour. The reaction mixture is treated with ethylene glycol (20  $\mu$ l) to decompose the unreacted periodate and the oxidized antibody fragment is purified using a Sephadex G-50/80 column (Pharmacia; Piscataway, N.J.) equilibrated in PBS (pH 6.1). The oxidized fragment is then reacted with an excess of chelating agent (5). After 40 hours at room temperature, the Schiff base is reduced by NaBH<sub>3</sub>CN. Conjugated antibody is purified using a centrifuged size-exclusion column (Sephadex G-50/80) equilibrated in 0.1M acetate (pH 6.5). The concentrations of antibody conjugates are determined by measuring absorbance at 280 nm.

#### EXAMPLE 11

##### Preparation of Bifunctional Chelating Agent (10).



- (6) R' = Boc, R'' = CH<sub>2</sub>CO<sub>2</sub>Bu, R''' = OH  
 (7) R' = Boc, R'' = (CH<sub>2</sub>)<sub>2</sub>OH, R''' = OH  
 (8) R' = Boc, R'' = (CH<sub>2</sub>)<sub>2</sub>Cl, R''' = Cl  
 (9) R' = Boc, R'' = (CH<sub>2</sub>)<sub>2</sub>SCOPh, R''' = SCOPh

(a). To a stirred solution of 2-amino-6-N-(t-butoxycarbonyl)amino-1-hexanol (1) in anhydrous acetonitrile was added anhydrous sodium carbonate, followed by t-butyl bromoacetate (2.2 eq.). The mixture was stirred under reflux for 6–10 h after which the mixture was extracted with ethyl acetate. This solution was evaporated to dryness and purified by chromatography on silica gel to afford (6) in 68–75% yield.

(b). To a stirred solution of (6) in dichloromethane at room temperature was added trifluoroacetic acid (10 eq.) After 1 h the solvent was removed in vacuo and the residue dissolved in dry THF. The solution was cooled to 4° C., and borane-THF complex (3 eq.) was added dropwise over 15 min. After stirring for 2 h, excess borane was decomposed with aqueous THF, and the borate ester was decomposed by refluxing with 5M aqueous sodium hydroxide for 10–18 h. The mixture was extracted with ethyl acetate and the organic

solution was washed with brine, dried over anhydrous sodium sulphate and evaporated to dryness in vacuo. The residue was taken up in THF:water (1:1) and the pH adjusted to 10 with 0.1M NaOH. Di-t-butyl dicarbonate (2.2 eq.) was added in portions, maintaining the pH at 9–10 by addition of 0.1M NaOH as required. One hour after completion of the addition the solution was extracted with ethyl acetate and the organic layer dried and evaporated in vacuo. The residue was chromatographed on silica gel to give (7).

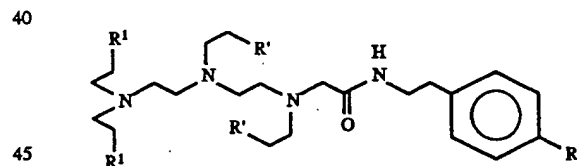
(c). To a solution of (7) in chloroform cooled to 4° C. was added anhydrous potassium carbonate (20 eq.), and the suspension vigorously stirred while excess thionyl chloride was added dropwise. After 1 h, solvent and excess thionyl chloride was removed on a rotary evaporator and the residue extracted with ethyl acetate. Evaporation to dryness afforded (8).

(d). To a solution of (8) in toluene was added 1,8-diazabicyclo[5.4.0]undec-7-ene (1.8 eq./chloride group), followed by thiobenzoic acid (1.4 eq./chloride group), and the solution heated under reflux. Progress of the reaction was monitored by thin-layer chromatography (TLC) on silica gel plates, visualized with 5% phosphomolybdic acid in ethanol. When reaction was complete, the organic extract was evaporated to dryness and the residue redissolved in chloroform, washed once with water, dried over anhydrous sodium sulphate, and evaporated in vacuo to give crude (9), which is further purified by flash chromatography. The <sup>1</sup>H NMR spectrum (400MHz) of (9) showed signals at: 7.95 (m, 6H), 7.55 (t, 3H, J=8), 7.42 (m, 6H), 3.25–2.75 (m, 13H), 1.6–1.2 (m, 6H), 1.44 (s, 9H).

(e). To a stirred solution of (9) in dichloromethane at room temperature was added trifluoroacetic acid (10 eq.). After 2 h the solvent was evaporated to dryness to give (10) which is used directly for conjugation, as described in Example 10, above.

#### EXAMPLE 12

##### Preparation of Bifunctional Chelating Agent (14).



- (11) R' = OH, R'' = NO<sub>2</sub>  
 (12) R' = OH, R'' = NHBoc  
 (13) R' = SCOPh, R'' = NHBoc  
 (14) R' = SCOPh, R'' = NH<sub>2</sub>

(a). To a solution of diethylenetriamine-pentaacetic acid (DTPA) dianhydride in DMF is added triethylamine (1 eq.), followed by 4-nitrophenethylamine (0.25 eq.). After stirring for 2 h, 0.1M NaOH (excess) is added. After 1 h the solution is acidified with 0.1M HCl and the solution evaporated in vacuo. The organic residue is taken up in anhydrous THF, dried over magnesium sulfate, filtered, and cooled to 4°. Borane-THF complex (6 eq.) is added dropwise over 15 min. After stirring for 2 h, 0.1M HCl is added to decompose borate esters. Excess saturated sodium bicarbonate solution is added, and the mixture extracted with ethyl acetate. The organic solution is washed with brine, dried over anhydrous sodium sulphate and evaporated to dryness in vacuo to give (11).

(b). To a stirred solution of (11) in methanol is added palladium on charcoal catalyst (0.1 eq.). The suspension is



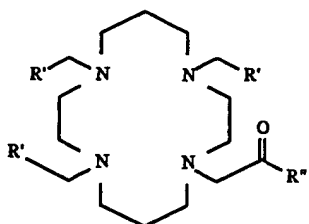
placed under an atmosphere of hydrogen and the reduction allowed to proceed until TLC indicates an absence of (11). The reaction mixture is flushed with argon three times, filtered to remove catalyst, and evaporated to dryness. The residue is taken up in THF:water (1:1) and the pH adjusted to 10 with 0.1M NaOH. Di-*t*-butyl dicarbonate (2.2 eq.) is added in portions, maintaining the pH at 9–10 by addition of 0.1M NaOH as required. One hour after completion of the addition the solution is extracted with ethyl acetate and the organic layer dried and evaporated in vacuo. The residue is chromatographed on silica gel to give (12).

(c). To a solution of (12) in chloroform at 4° C. is added anhydrous potassium carbonate (20 eq.), and the suspension vigorously stirred while excess thionyl chloride is added dropwise. After 1 h, solvent and excess thionyl chloride is removed on a rotary evaporator and the residue extracted with ethyl acetate. The solvent is removed in vacuo to and the residue taken up in toluene. 1,8-diazabicyclo[5.4.0]undec-7-ene (2.2 eq.) is added, followed by thiobenzoic acid (1.1 eq.), and the solution heated under reflux. After 5 h the organic extract is evaporated to dryness and the residue redissolved in chloroform, washed once with water, dried over anhydrous sodium sulphate, and evaporated in vacuo to give crude (13), which is further purified by flash chromatography.

(d). To a solution of (13) in dichloromethane at room temperature is added trifluoroacetic acid (10 eq.). After 2 h the solvent is evaporated to dryness and the residue used directly for conjugation as described in Example 10, above.

#### EXAMPLE 13

##### Preparation of Bifunctional Chelating Agent (19).



- (15) R' = CO<sub>2</sub>tBu, R'' = O<sup>+</sup>tBu  
 (16) R' = CH<sub>2</sub>OH, R'' = NH(CH<sub>2</sub>)<sub>2</sub>-p-C<sub>6</sub>H<sub>4</sub>NO<sub>2</sub>  
 (17) R' = CH<sub>2</sub>OH, R'' = NH(CH<sub>2</sub>)<sub>2</sub>-p-C<sub>6</sub>H<sub>4</sub>NHBoc  
 (18) R' = CH<sub>2</sub>SCOPh, R'' = NH(CH<sub>2</sub>)<sub>2</sub>-p-C<sub>6</sub>H<sub>4</sub>NHBoc  
 (19) R' = CH<sub>2</sub>SCOPh, R'' = NH(CH<sub>2</sub>)<sub>2</sub>-p-C<sub>6</sub>H<sub>4</sub>NH<sub>2</sub>

(a). To a solution of 1,4,8,11-tetraazacyclotetradecane in anhydrous acetonitrile is added anhydrous sodium carbonate, followed by *t*-butyl bromoacetate (6 eq.). The mixture is heated under reflux for 6–10 h, after which the mixture was extracted with ethyl acetate. The solution is evaporated to dryness and purified by chromatography on silica gel to afford (15).

(b). To a solution of (15) in dichloromethane at room temperature is added trifluoroacetic acid (10 eq.). After 2 h the solvent is evaporated to dryness and the residue dissolved in a minimum volume of DMF. The solution is cooled to 4° C. and thionyl chloride (excess) is added. After 2 h the solution is evaporated in vacuo to remove excess thionyl chloride and triethylamine (10 eq.) is added, followed by 4-nitrophenethylamine (0.25 eq.). Powdered sodium borohydride is added in portions to reduce the remaining acid chloride groups, followed by addition of 0.1M HCl. The solution is extracted with ethyl acetate and the organic

solution washed with brine and evaporated in vacuo. The residue is chromatographed on silica gel to yield pure (16).

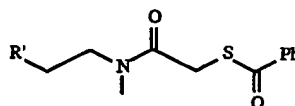
(c). To a stirred solution of (16) in methanol is added palladium on charcoal catalyst (0.1 eq.). The suspension is placed under an atmosphere of hydrogen and the reduction allowed to proceed until TLC indicates an absence of (16). The reaction mixture is flushed with argon three times, filtered to remove catalyst, and evaporated to dryness. The residue is taken up in THF:water (1:1) and the pH adjusted to 10 with 0.1M NaOH. Di-*t*-butyl dicarbonate (2.2 eq.) is added in portions, maintaining the pH at 9–10 by addition of 0.1M NaOH as required. One hour after completion of the addition the solution is extracted with ethyl acetate and the organic layer dried and evaporated in vacuo. The residue is chromatographed on silica gel to give (17).

(d). To a solution of (17) in chloroform at 4° C. is added anhydrous potassium carbonate (20 eq.), and the suspension vigorously stirred while excess thionyl chloride is added dropwise. After 1 h, solvent and excess thionyl chloride is removed on a rotary evaporator and the residue extracted with ethyl acetate. The solvent is removed in vacuo to and the residue taken up in toluene. 1,8-diazabicyclo[5.4.0]undec-7-ene (1.8 eq./chloride group) is added, followed by thiobenzoic acid (1.4 eq./chloride), and the solution heated under reflux. After 5 h the organic extract is evaporated to dryness and the residue redissolved in chloroform, washed once with water, dried over anhydrous sodium sulphate, and evaporated in vacuo to give crude (18), which is further purified by flash chromatography.

(e). To a solution of (18) in dichloromethane at room temperature is added trifluoroacetic acid (10 eq.). After 2 h the solvent is evaporated to dryness to give (19), which is used directly for conjugation as described in Example 10, above.

#### EXAMPLE 13

##### Preparation of Bifunctional Chelating Agent (21).



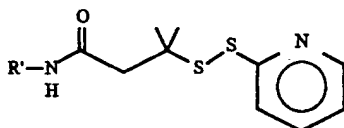
- (20) R' = NHBoc  
 (21) R' = NH<sub>2</sub>

(a). To a solution of N-Boc N'-methylethylenediamine in dichloromethane cooled to 4° C., is added triethylamine (10 eq.) followed by chloroacetyl chloride (1.1 eq.). After stirring for 30 min, water is added and the organic layer separated, dried and concentrated to dryness in vacuo. The residue is taken up in toluene and 1,8-diazabicyclo[5.4.0]undec-7-ene (2.2 eq.) is added, followed by thiobenzoic acid (1.1 eq.), and the solution heated under reflux. After 5 h the organic extract is evaporated to dryness and the residue redissolved in chloroform, washed once with water, dried over anhydrous sodium sulphate, and evaporated in vacuo to give crude (20), which is further purified by flash chromatography.

(b). To a solution of (20) in dichloromethane at room temperature is added trifluoroacetic acid (10 eq.). After 2 h the solvent is evaporated to dryness to give (21), which is used directly for conjugation as described in Example 10, above.

## EXAMPLE 14

## Preparation of Bifunctional Chelating Agent (23).



(22) R' = NHBoc

(23) R' = NH<sub>2</sub>

(a). To a solution of N-Boc-hydrazine in dichloromethane cooled to 4° C., is added triethylamine (10 eq.) followed by dimethylacryloyl chloride (1.1 eq.). After stirring for 30 min, water is added and the organic layer separated, dried and concentrated to dryness in vacuo. The residue is taken up in toluene and 1,8-diazabicyclo[5.4.0]undec-7-ene (2.2 eq.) is added, followed by thiobenzoic acid (1.1 eq.), and the solution heated under reflux. After 5 h the organic extract is evaporated to dryness and the residue redissolved in chloroform, washed once with water, dried over anhydrous sodium sulphate, and evaporated in vacuo to give crude (22), which is further purified by flash chromatography. The thiol group was deprotected with sodium methoxide in methanol, and the thiol was reprotected as a 2-pyridylthio entity.

(b). To a solution of (22) in dichloromethane at room temperature is added trifluoroacetic acid (10 sq.). After 2 h the solvent is evaporated to dryness to give (23), which is used directly for conjugation as described in Example 10, above, but omitting the reduction step.

## EXAMPLE 15

Preparation of a semicarbazide derivative of DTPA and conjugation and radiolabeling to produce an immunoconjugate with an acid-labile linkage.

(a) Preparation of p-(thiosemicarbazidyl)benzyl-DTPA  
p-(Isothicyanato)benzyl DTPA (19.7 μmol) in 0.5 mL of water was mixed with 6.6 μL of a 55% aqueous solution of hydrazine hydrate (6 equiv.), and the pH of the solution was adjusted to 9.13 using solid sodium carbonate. The clear reaction mixture was incubated at 37° C. for 4 h. The pH was then raised to 12.8, and water was removed using a high vacuum pump. The residue was extracted twice with isopropanol to remove residual hydrazine, and dissolved in 0.3 mL of water. The pH was adjusted to 6.5 to yield an aqueous solution of the requisite product at a concentration of 60 μmol/mL.

(b) Coupling of p-(thiosemicarbazidyl)benzyl-DTPA to oxidized carbohydrate portion of antibody fragment LL<sub>2</sub>-F(ab')<sub>2</sub>

The LL<sub>2</sub> F(ab')<sub>2</sub> fragment (0.8 mL; 1.95 mg/mL) in 50 mM acetate buffered saline, pH 5.3, was treated with sodium metaperiodate at a final concentration of 14.3 mM, and incubated at 0° C. (ice-bath) for 1 h. Excess periodate was decomposed using glycerol (20 μL), and the oxidized antibody was purified on a centrifuged size-exclusion column equilibrated in 0.1M phosphate buffer, pH7.

The solution of oxidized antibody was made 150 mM with respect to sodium chloride, the pH was adjusted to 6.2 (using solid sodium phosphate, monobasic), and then treated with a 300-fold molar excess of p-(thiosemicarbazidyl) benzyl DTPA. The reaction mixture was vortexed, and incubated in the dark at room temperature for 18 h. The conjugate was purified on centrifuged size-exclusion col-

umn equilibrated in 0.1M acetate, pH 6.5, and concentrated on Centricon 30 concentrator.

HPLC analysis of the conjugate revealed a single peak, at an identical retention time with that of unmodified antibody.

(c) Determination of number of chelates per LL<sub>2</sub>-F(ab')<sub>2</sub>

40 μg of the above conjugate was labeled with an excess of cobalt acetate, spiked with 50–200,000 cpm of cobalt-57 radioisotope. After 30 minutes, the labeling mixture was made 10 mM in EDTA, and analyzed for incorporation of cobalt into antibody (using ITLC on silica-gel-impregnated glass-fiber strips and 10mM EDTA for chromatogram development). From the fraction of radioactivity bound to the antibody, and the relative molar amount of conjugate and Co/<sup>57</sup>Co solutions used, the number of chelates per antibody fragment was determined to be 1.25.

(d) Radiolabeling of the conjugate with Y-90

5 μL (50 μg) of the solution of the p-(thiosemicarbazonyl) benzyl-DTPA-F(ab')<sub>2</sub> conjugate in 0.1M sodium acetate (pH 6.5) was mixed with 4 μL of Y-90 acetate (95.5 uCi) and incubated for 1 h. The solution was then diluted with 9 μL of 0.1M sodium acetate, and analyzed for incorporation. Instant thin-layer chromatographic analysis was performed on an aliquot of the labeling mixture after incubation with 10 mM EDTA for 10 minutes. Y-90 incorporation was 77.3%, with 1.2% of radioactivity present in the form of colloids. Radio-HPLC showed an incorporation of 64%.

(e) Radiolabeling of the conjugate with In-111

60 μg of the solution of the p-(thiosemicarbazonyl) benzyl-DTPA-F(ab')<sub>2</sub> conjugate was mixed with 124 uCi of In-111 acetate (In-111 chloride buffered with 0.22M ammonium acetate), and left at room temperature for 45 min. Analysis of an aliquot of the labeling mixture, after incubation with 10mM EDTA, showed an In-111 incorporation into conjugate of 86%. The sample was diluted to 90 μL with 0.1M acetate, and incubated for 10 min with 10 μL of 0.1M DTPA solution (pH 7). Two successive purifications by centrifuged size-exclusion chromatography yielded the In-111 labeled conjugate.

Although the foregoing refers to particular preferred embodiments, it will be understood that the present invention is not so limited. It will occur to those of ordinary skill in the art that various modifications may be made to the disclosed embodiments and that such modifications are intended to be within the scope of the present invention, which is defined by the following claims.

All publications and patent applications mentioned in this specification are indicative of the level of skill of those in the art to which the invention pertains. All publications and patent applications are herein incorporated by reference to the same extent as if each individual publication or patent application were specifically and individually indicated to be incorporated by reference in its entirety.

What is claimed is:

1. A soluble immunoconjugate, comprising:

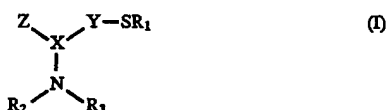
(a) a glycosylated antibody fragment selected from the group consisting of Fab, Fab', F(ab')<sub>2</sub>, F(ab')<sub>2</sub>, Fv and single chain Fv, which comprises a light chain variable region having a carbohydrate moiety attached at about amino acid position 18 of said light chain variable region; and

(b) a loaded polyamidoamine dendrimer carrier, having at least one free amine group and a plurality of chelator molecules covalently bound to said polyamidoamine dendrimer carrier,

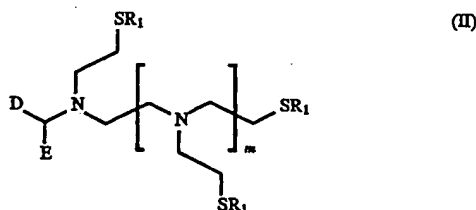
wherein said loaded polyamidoamine dendrimer carrier is covalently bound through said at least one free amine group of said polyamidoamine dendrimer carrier to said carbohydrate moiety of said antibody fragment,

43

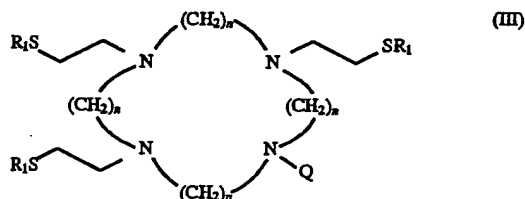
wherein said immunoconjugate retains the immunoreactivity of said antibody fragment,  
and wherein said chelator is selected from the group consisting of compounds represented by formula (I)



where X is CH, or X and Z taken together can be CO;  
Y is CR<sub>4</sub>R<sub>5</sub>, CH<sub>2</sub>CR<sub>4</sub>R<sub>5</sub> or (CH<sub>2</sub>)<sub>2</sub>CR<sub>4</sub>R<sub>5</sub> where R<sub>4</sub>  
and R<sub>5</sub> are the same or different and are selected  
from the group consisting of hydrogen and alkyl,  
substituted alkyl, aryl or substituted aryl groups; Z  
can be any group capable of reacting with said  
carbohydrate moiety of said antibody fragment, or Z  
can be H; R<sub>1</sub> is a thiol protecting group which can be  
removed under conditions which do not significantly  
diminish the immunoreactivity of said protein; R<sub>2</sub>  
and R<sub>3</sub> can be the same or different, and each  
represents an acyl group or a substituted acyl group,  
or hydrogen, alkyl, aryl, substituted alkyl, or substi-  
tuted aryl, where the substituents on the alkyl or aryl  
groups are metal-ligating groups selected from the  
group consisting of sulfhydryl, amine and carboxylic  
acid or their protected derivatives; R<sub>2</sub> and R<sub>3</sub> also  
can be any group capable of reacting with said  
carbohydrate moiety of said antibody fragment,  
compounds represented by formula (II)



where D is H or CH<sub>2</sub>SR<sub>1</sub>; E can be any group capable  
of reacting with said carbohydrate moiety of said  
antibody fragment; R<sub>1</sub> is a thiol protecting group  
which can be removed under conditions which do  
not significantly diminish the immunoreactivity of  
said protein; and m is 0, 1, 2, or 3, and  
compounds represented by formula (III)



where Q can be any group capable of reacting with said  
carbohydrate moiety of said antibody fragment; R<sub>1</sub> is  
a thiol protecting group which can be removed under  
conditions which do not significantly diminish the  
immunoreactivity of said protein; and n is 2 or 3.

2. The soluble immunoconjugate of claim 1 wherein said  
chelator is covalently bound to said polyamidoamine den-  
drimer carrier via an acid-labile linker selected from the  
compounds consisting of a thiosemicarbazide and a  
hydrazide.

3. The soluble immunoconjugate of claim 1, wherein said  
antibody fragment is a mutated antibody fragment having a

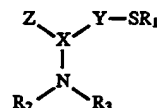
44

non-natural Asn-glycosylation site at about amino acid posi-  
tion 18 of the light chain of said antibody fragment.

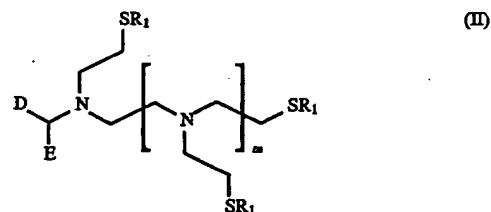
4. A soluble immunoconjugate comprising:

(a) a glycosylated antibody fragment selected from the  
group consisting of Fab, Fab', F(ab')<sub>2</sub>, F(ab')<sub>2</sub>, Fv, and  
single chain Fv, which comprises a light chain variable  
region having a carbohydrate moiety attached at about  
amino acid position 18 of said light chain variable  
region; and

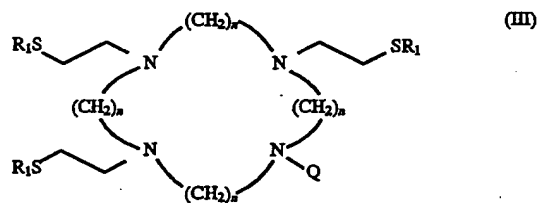
(b) at least one chelator, wherein said chelator is selected  
from the group consisting of compounds represented by  
formula (I)



consisting of hydrogen and alkyl, substituted alkyl, aryl  
or substituted aryl groups; Z can be any group capable  
of reacting with said carbohydrate moiety of said  
antibody fragment, or Z can be H; R<sub>1</sub> is a thiol  
protecting group which can be removed under condi-  
tions which do not significantly diminish the immu-  
noreactivity of said protein; R<sub>2</sub> and R<sub>3</sub> can be the same  
or different, and each represent an acyl group or a  
substituted acyl group, or hydrogen, alkyl, aryl, substi-  
tuted alkyl, or substituted aryl, where the substituents  
on the alkyl or aryl groups are metal-ligating groups  
selected from the group consisting of sulfhydryl, amine  
and carboxylic acid or their protected derivatives; R<sub>2</sub>  
and R<sub>3</sub> also can be any group capable of reacting with  
said carbohydrate moiety of said antibody fragment,  
compounds represented by formula (II)



where D is H or CH<sub>2</sub>SR<sub>1</sub>; E can be any group capable  
of reacting with said carbohydrate moiety of said  
antibody fragment; R<sub>1</sub> is a thiol protecting group  
which can be removed under conditions which do  
not significantly diminish the immunoreactivity of  
said protein; and m is 0, 1, 2, or 3, and  
compounds represented by formula (III)

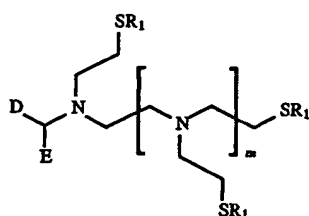


where Q can be any group capable of reacting with said  
carbohydrate moiety of said antibody fragment; R<sub>1</sub> is  
a thiol protecting group which can be removed under  
conditions which do not significantly diminish the  
immunoreactivity of said protein; and n is 2 or 3, and  
wherein each chelator is covalently bound to said  
carbohydrate moiety of said antibody fragment,

where X is CH<sub>3</sub>, or X and Z taken together can be CO; Y is CR<sub>4</sub>R<sub>5</sub>, CH<sub>2</sub>CR<sub>4</sub>R<sub>5</sub> or (CH<sub>2</sub>)<sub>2</sub>CR<sub>4</sub>R<sub>5</sub>, where R<sub>4</sub> and R<sub>5</sub> are the same or different and are selected from the group consisting of hydrogen and alkyl; substituted alkyl, aryl or substituted aryl groups; Z can be any group capable of reacting with said carbohydrate moiety of said antibody fragment, or Z can be H; R<sub>1</sub> is a thiol protecting group which can be removed under conditions which do not significantly diminish the immunoreactivity of said protein; R<sub>2</sub> and R<sub>3</sub> can be the same or different, and each represent an acyl group or a substituted acyl group, or hydrogen, alkyl, aryl, substituted alkyl, or substituted aryl, where the substituents on the alkyl or aryl groups are metal-ligating groups selected from the group consisting of sulfhydryl, amine and carboxylic acid or their protected derivatives; R<sub>2</sub> and R<sub>3</sub> also can be any group capable of reacting with said carbohydrate moiety of said antibody fragment,

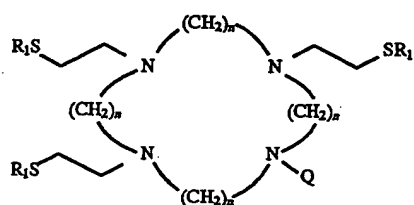
47

compounds represented by formula (II)



where D is H or  $\text{CH}_2\text{SR}_1$ ; E can be any group capable of reacting with said carbohydrate moiety of said antibody fragment;  $\text{R}_1$  is a thiol protecting group which can be removed under conditions which do not significantly diminish the immunoreactivity of said protein; and m is 0, 1, 2, or 3, and

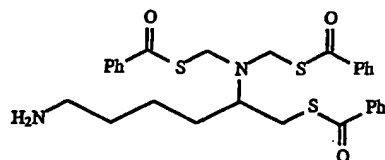
compounds represented by formula (III)



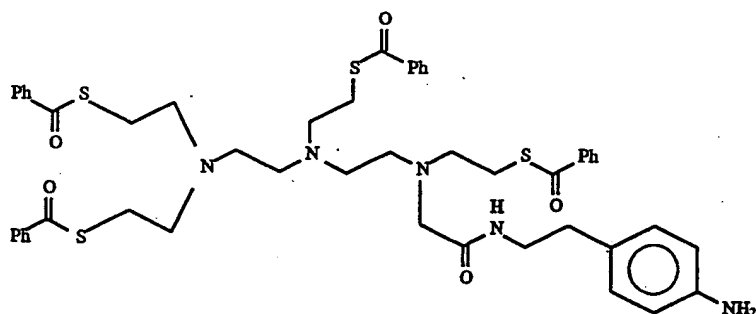
where Q can be any group capable of reacting with said carbohydrate moiety of said antibody fragment;  $\text{R}_1$  is a thiol protecting group which can be removed under conditions which do not significantly diminish the immunoreactivity of said protein; and n is 2 or 3,

48

10. A soluble immunoconjugate of claim 1, wherein said chelator is



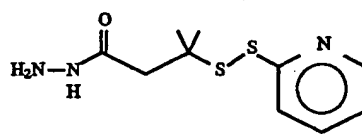
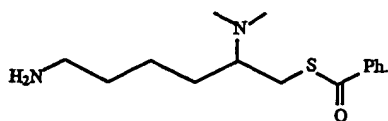
11. A soluble immunoconjugate of claim 1, wherein said chelator is



12. A soluble immunoconjugate of claim 1, wherein said chelator is

and wherein said immunoconjugate retains the immunoreactivity of said antibody fragment.

9. A soluble immunoconjugate of claim 1, wherein said chelator is



\* \* \* \* \*

# Selective Protection of 2',2'-Difluorodeoxycytidine (Gemcitabine) EXHIBIT 16

Zhi-wei Guo and James M. Gallo\*

Department of Pharmacology Fox Chase Cancer Center 7701 Burholme Avenue,  
Philadelphia, Pennsylvania 19111

Received July 12, 1999

Gemcitabine (**1**) is a promising new anticancer agent used in pancreatic cancer. Improvement in the selective targeting of compound **1** and other cytotoxic agents to solid tumors may be enhanced by conjugation to ligands that target peripheral benzodiazepine receptors (PBRs) located on mitochondria and known to be overexpressed in human brain tumors. Development of such chemical conjugates requires selective protection on 4-NH<sub>2</sub>, 3'-OH, and 5'-OH of compound **1**. All three monoprotected and three diprotected gemcitabine derivatives (**2** to **7**) were synthesized in good yield by employing a single commonly used protecting reagent, di-*tert*-butyl dicarbonate, under different conditions. Consequently, the three mono-ligand-gemcitabine conjugates coupled at 4-NH<sub>2</sub>, 3'-OH, and 5'-OH respectively (**14** to **16**) were synthesized in high yield using the PBR ligand PK11195. This selective protection/deprotection strategy offers a relatively straightforward means to modify other nucleosides.

## Introduction

Gemcitabine (2',2'-difluorodeoxycytidine, dFdC) (**1**) is a promising antineoplastic drug approved for use in pancreatic cancer. In comprehensive preclinical and clinical studies,<sup>1</sup> it has shown activity against a wide spectrum of human solid tumors including nonsmall cell lung, pancreatic, colon, breast, bladder, ovarian, head and neck, cervical and hepatocellular cancers. The hydrochloride of compound **1** (GEMZAR) (**1a**) is now marketed in many countries.<sup>1</sup>

Selective drug delivery to solid tumors continues to be a problem that can be addressed by the development of chemical conjugates that bind receptors overexpressed in tumors. Peripheral benzodiazepine receptors (PBRs) located on the outer membrane of mitochondria may serve as such a target as they are overexpressed in brain tumors relative to normal brain.<sup>2</sup> A host of PBR ligands are known that can bind to human PBRs (i.e., PK11195) and rat PBR (i.e., Ro 5 4864 and PK11195).<sup>2</sup> Compound **1** is an attractive candidate for development as a PBR ligand drug conjugate since its uptake into brain is expected to be limited because of its hydrophilicity. An immunoglobulin conjugate of compound **1** has been reported.<sup>3</sup> The PBR ligand–drug conjugates are unique in that they are of low molecular weight and target an intracellular receptor as opposed to the more common cell surface receptor sought in other drug delivery systems.

PBR ligands may be covalently coupled to compound **1** at 4-NH<sub>2</sub>, 3'-OH, and 5'-OH positions directly or via a linker. All conjugates linked at these different positions are potentially interesting because they may possess different PBR binding affinities and cytotoxicity. Many different protection/deprotection strategies of nucleoside monomers have been established.<sup>4</sup> In those strategies, however, multiple protecting reagents were employed to reach the goal. We disclose here that the *tert*-butoxycarbonyl (Boc) group serves as an useful selective protecting group in gemcitabine derivative synthesis. All three monoprotected and three diprotected gemcitabine derivatives (**2**–**7**) were prepared, respectively, in good yield by employing one single commonly used protecting reagent di-*tert*-butyl dicarbonate (DBDC) under different conditions. The usefulness of this strategy was demonstrated by the synthesis of three PBR ligand–gemcitabine conjugates coupled at 4-NH<sub>2</sub>, 3'-OH, and 5'-OH, respectively (**14** to **16**), in high yield and in a relatively simple manner.

## Results and Discussion

When DBDC was added to a solution of **1a** in dioxane–aqueous NaOH, three products formed in 10 min, and the product profile changed over time. The structures of the three products were determined in separate experiments as 3'-*O*-Boc-gemcitabine (**2**), 3'-*O*-5'-*O*-di-Boc-gemcitabine (**3**), and 5'-*O*-Boc-gemcitabine (**4**). Thus, various conditions and procedures were studied to achieve selective protection of **1** in good yield. The results are shown in Scheme 1. Under condition a with 1 equiv of DBDC, **2** was obtained in 85% isolated yield, and the same product

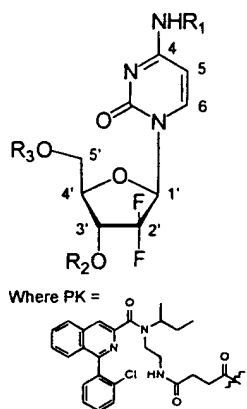
\* Corresponding author. Tel: 215 728-2461. Fax: 215 728-4333.  
E-mail: jm.gallo@fccc.edu.

(1) (a) Hertel, L. W.; Kroin, J. S.; Misner, J. W.; Tustin, J. M. *J. Org. Chem.* 1988, 53, 3: 2406–2409. (b) Postmus, P. E.; Schramel, F. M.; Smit, E. F. *Semin. Oncol.* 1998, 25 (4 Suppl 9), 79–82. (c) Carmichael, J. B. *J. Cancer* 1998, 78 (Suppl 3), 21–25. (d) Graziadei, I.; Kelly, T.; Schirmer, M.; Geisen, F. H.; Vogel, W.; Konwalinka, G. *J. Hepatol.* 1998, 28, 504–509. (e) Aapro, M. S.; Martin, C.; Hatty, S. *Anti-Cancer Drugs* 1998, 9, 191–201.

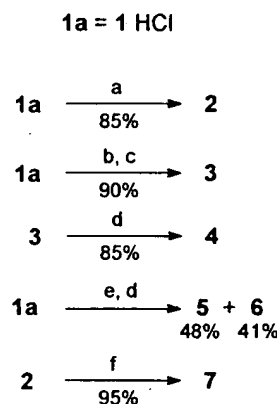
(2) (a) Starosta-Rubinstein, S.; Ciliax, B. J.; Penney, J. B.; McKeever, P.; Young, A. B. *Proc. Natl. Acad. Sci. U.S.A.* 1987, 84, 891–895. (b) Black, K.; Ikezaki, K.; Santori, E.; Becker, D.; Vinters, H. *Cancer* 1990, 65, 93–97. (c) Kupczyk-Subotkowska, L.; Siahaan, T. J.; Basile, A. S.; Friedman, H. S.; Higgins, P. E.; Song, D.; Gallo, J. M. *J. Med. Chem.* 1997, 40, 1726–1730. (d) Guo, Z. W.; Ma, J. G.; Adams, A.; Gallo, J. M. *Proc. Am. Assoc. Cancer Res.* 1999, 40, 585.

(3) Koppel, G. A.; Kennedy, G. D.; Armour, H. K.; Scott, W. L. Eur. Patent 0272891A2, 1987.

(4) (a) Greene, T. W. *Protective groups in organic synthesis*; John Wiley & Sons: New York; pp 50–71 and 223–248. (b) Bhat, B.; Sanghvi, Y. S. *Tetrahedron Lett.* 1997, 38, 8811–8814. (c) Sinha, N. D.; Davis, P.; Schultze, L. M.; Upadhyay, K. *Tetrahedron Lett.* 1995, 36, 9277–9280. (d) Hayakawa, Y.; Kato, H.; Uchiyama, M.; Kajino, H.; Noyori, R. *J. Org. Chem.* 1986, 51, 2400–2402. (e) Ti, G. S.; Gaffney, B. L.; Jones, R. A. *J. Am. Chem. Soc.* 1982, 104, 1316–1319. (f) Ishido, Y.; Nakazaki, N.; Sakairi, N. *J. Chem. Soc., Perkin Trans. 1* 1979, 2088–2098. (g) Beaucage, S. L.; Ogilvie, K. K. *Tetrahedron Lett.* 1977, 20, 1691–1694.

Scheme 1<sup>a</sup>

	R1	R2	R3
1	H	H	H
2	H	Boc	H
3	H	Boc	Boc
4	H	H	Boc
5	Boc	H	Boc
6	Boc	H	H
7	Boc	Boc	H
8	Boc	Boc	Boc
11	PK	Boc	Boc
12	Boc	PK	Boc
13	Boc	Boc	PK
14	PK	H	H
15	H	PK	H
16	H	H	PK



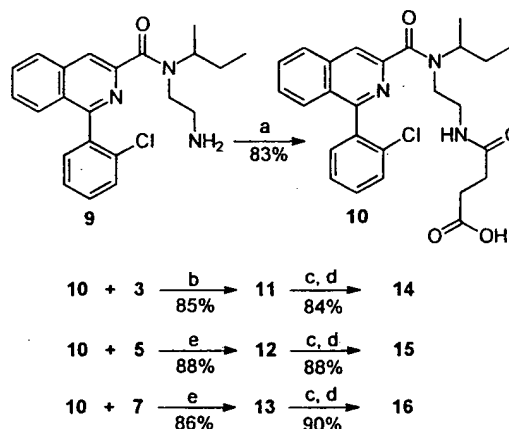
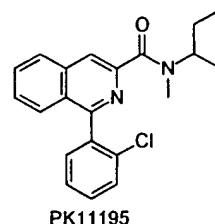
<sup>a</sup> (a) Dioxane–water (4/1), Na<sub>2</sub>CO<sub>3</sub>, DBDC (1–5 equiv); (b) dioxane–1 M aqueous KOH (1/1), DBDC (excess); (c) dioxane, DBDC (excess), then 1 M aqueous KOH (1/1 to dioxane); (d) MeOH–1 M aqueous Na<sub>2</sub>CO<sub>3</sub> (1/1); (e) dioxane, TEA, DMAP, DBDC (excess); (f) dioxane, DBDC (excess), 37 °C.

Table 1. Chemical Shift Data (ppm)<sup>a</sup>

	5	6	1'	3'	4'	5'A	5'B
1	5.98	7.85	6.25	4.35	3.95	3.95	3.82
2	5.96	7.75	6.33	5.32	4.21	3.95	3.82
3	5.98	7.62	6.34	5.28	4.42	4.52	4.45
4	6.01	7.62	6.33	4.33	4.17	4.53	4.38
5	7.27	8.04	6.32	4.36	4.24	4.54	4.42
6	7.23	8.31	6.27	4.54	4.02	4.02	3.86
7	7.27	8.20	6.37	5.36	4.30	4.00	3.86
8	7.28	8.02	6.38	5.32	4.50	4.55	4.50

<sup>a</sup> The 600 MHz <sup>1</sup>H NMR spectra were obtained in acetone-*d*<sub>6</sub> with 2% D<sub>2</sub>O. The position numbers are as indicated in Scheme 1.

profile was obtained with 5 equiv of DBDC based on TLC analysis. Excess DBDC was used for all the following experiments. A 1:1 mixture of 2 and 3 was obtained under condition b with excess DBDC, and the crude product mixture was converted into 3 under condition c to give 90% overall yield. Compound 3 was partially deprotected under condition d to give 4 in 85% isolated yield and recovered 1 in 10%. When 1a was treated under forced condition e with excess DBDC, a mixture of two nonpolar products formed based on TLC analysis. The structure of the major product was determined in a separate experiment as 4-*N*-3'-*O*-5'-*O*-tri-Boc-gemcitabine (8). The minor product was less polar than 8 by TLC, and its structure was not determined. If pyridine was used instead of dioxane, a similar product profile was obtained based on TLC analysis. The product mixture was partially deprotected under condition d to give 4-*N*-5'-*O*-di-Boc-gemcitabine (5) in 48% isolated yield plus 4-*N*-Boc-gemcitabine (6) in 41% isolated yield. Finally, 4-*N*-3'-*O*-Boc-gemcitabine (7) was obtained in 95% isolated yield by using 2 as the starting material under condition f. Interestingly, compound 8 was not detected by TLC analysis under this condition. If triethylamine or diisopropylethylamine was added, a mixture of 7 and 8 formed. When 1a was used instead of 2' under condition f, no reaction occurred after 48 h based on TLC analysis, most likely because 1a is practically insoluble in dry dioxane. The structure determination of compounds 2 thru 8 was based on <sup>1</sup>H NMR and ESI MS. The chemical shift data are listed in Table 1.

Scheme 2<sup>a</sup>

<sup>a</sup> (a) Succinic anhydride, DIEA; (b) DCC, 1-hydroxybenzotriazole; (c) TFA; (d) NaHCO<sub>3</sub>; (e) DCC, DMAP.

PK11195 is a model human PBR ligand<sup>5</sup> and served as the PBR ligand to synthesize conjugates 14, 15, and 16 by coupling compound 10 with di-protected gemcitabine derivatives (3, 5, and 7) followed by deprotection using TFA as shown in Scheme 2. Compound 10 was synthesized from succinic anhydride and compound 9, which was prepared as described in the literature.<sup>5</sup> To assign the <sup>1</sup>H NMR spectrum of compound 10, it was compared to the spectrum of an authentic sample of PK11195 [Research Biochemical, Natick, MA 01760]. Both spectra indicated slow rotation about the amide C–N bond. The structure determination of conjugates 14, 15, and 16 was based on <sup>1</sup>H 1D and 2D NMR, and FAB

(5) (a) Newman, A. H.; Lueddens, H. W. M.; Skolnick, P.; Rice, K. C. *J. Med. Chem.* 1987, 30, 1901–1905; (b) Walsh, D. A.; Sancilio, L. F.; Reese, D. L. *J. Med. Chem.* 1978, 21, 582–585.

HRMS. All NMR spectra of compounds 11–16 also indicated slow rotation about the amide bond and are available as Supporting Information with detailed peak assignment. The three mono-PBR ligand–gemcitabine conjugates were obtained in high yield, demonstrating the usefulness of the selective protection/deprotection strategy disclosed here. This strategy may be applied to other PBR ligand–nucleoside conjugates, and generally to other types of chemical conjugates involving nucleosides in which a selective linkage is required.

## Experimental Section

Gemcitabine hydrochloride (1a) was obtained from Eli Lilly and Co. All other reagents were commercially available. ACROS silica gel (35–70  $\mu$ m) was used for flash chromatography. 600 MHz 1D  $^1\text{H}$ , 2D  $^1\text{H}$ – $^1\text{H}$  COSY NMR spectra were obtained in acetone- $d_6$  with 2%  $\text{D}_2\text{O}$ . Coupling constants are reported in hertz.

**3'-O-(tert-Butoxycarbonyl)gemcitabine (2).** To a stirred mixture of 1a (60 mg, 0.2 mmol) and  $\text{Na}_2\text{CO}_3$  (106 mg), in 4 mL of dioxane and 1 mL of water was added DBDC (44 mg, 0.2 mmol), and the resulting mixture stirred at 24  $^\circ\text{C}$  for 48 h. After 2 mL of water was added, the mixture was extracted with 2  $\times$  30 mL of EtOAc. The organic extracts were washed with water (5 mL) and brine (5 mL), dried over  $\text{Na}_2\text{SO}_4$ , and concentrated to dryness under reduced pressure. The residue was subjected to flash chromatography ( $\text{CH}_2\text{Cl}_2$ –acetone–EtOH 1:1:0.02) to give 2 (62 mg, 85%), homogeneous by TLC ( $\text{CH}_2\text{Cl}_2$ –acetone–EtOH 5:4:1).  $^1\text{H}$  NMR data are shown in Table 1 except a singlet ( $\delta$  1.49, 9H). ESI MS  $m/z$  364 [positive, (M + H)], 362 [negative, (M – H)].

**3',5'-O-Bis(tert-Butoxycarbonyl)gemcitabine (3).** To a stirred solution of 1a (600 mg, 2 mmol) in 40 mL of 1 M aqueous KOH was added DBDC (4.36 g, 20 mmol) dropwise to 40 mL of dioxane over 20 min. The reaction mixture was then stirred at 24  $^\circ\text{C}$  for an additional 40 min and extracted with EtOAc (3  $\times$  80 mL). The organic extracts were washed with brine (2  $\times$  10 mL), dried over  $\text{Na}_2\text{SO}_4$ , and concentrated to dryness under reduced pressure. The residue was a mixture of 2 and 3 (about 1:1 by TLC). To a stirred clear solution of the above residue and DBDC (4.36 g) in 40 mL of dioxane at 24  $^\circ\text{C}$  was added 40 mL of 1 M aqueous KOH. The reaction progress was followed by TLC. After 30 min, the reaction was nearly complete to give only one major product 3 that was extracted by a similar procedure as described above. Flash chromatography ( $\text{CH}_2\text{Cl}_2$ –acetone–EtOH 5:4:1) gave 3 (833 mg, 90%), homogeneous by TLC ( $\text{CH}_2\text{Cl}_2$ –acetone–EtOH 5:4:1).  $^1\text{H}$  NMR data are shown in Table 1 except two singlets ( $\delta$  1.50, 9H; 1.47, 9H). ESI MS  $m/z$  464 [positive, (M + H)], 462 [negative, (M – H)].

**5'-O-(tert-Butoxycarbonyl)gemcitabine (4).** To a stirred solution of 3 (833 mg) in 40 mL of MeOH was added 40 mL of 1 M aqueous  $\text{Na}_2\text{CO}_3$  at 24  $^\circ\text{C}$ . The reaction progress was followed by TLC. After 4 h, the reaction was complete to give one major product 4 and a small amount of 1. A similar workup procedure as stated above for 2 gave 4 (555 mg, 85%), homogeneous by TLC ( $\text{CH}_2\text{Cl}_2$ –acetone–EtOH 5:4:1).  $^1\text{H}$  NMR data are shown in Table 1 except a singlet ( $\delta$  1.47, 9H). ESI MS  $m/z$  364 [positive, (M + H)], 362 [negative, (M – H)]. The aqueous portions during the extraction were combined and dried under reduced pressure at 50  $^\circ\text{C}$ . The residue was treated with acetone (2  $\times$  20 mL). The acetone filtrate was then concentrated. Flash chromatography on a short column ( $\text{CH}_2\text{Cl}_2$ –acetone–EtOH 1:2:0.1) gave 1 (48 mg, 10%), and the  $^1\text{H}$  NMR data are shown in Table 1.

**4-N-5'-O-Bis(tert-Butoxycarbonyl)gemcitabine (5) and 4-N-(tert-Butoxycarbonyl)gemcitabine (6).** To a stirred solution of 1a (90 mg, 0.3 mmol) and DMAP (5 mg) in 5 mL of dioxane and 5 mL of TEA was added DBDC (655 mg, 3 mmol). The reaction mixture was stirred at 24  $^\circ\text{C}$  for 18 h. Solvents were removed under reduced pressure. The residue was treated with 100 mL of EtOAc, washed with 5%  $\text{NaHCO}_3$  and

brine, dried over  $\text{Na}_2\text{SO}_4$ , and then concentrated to dryness. Flash chromatography on a short column ( $\text{CH}_2\text{Cl}_2$ –acetone 4:1) gave a nonpolar product mixture. To a stirred solution of the above mixture in 20 mL of MeOH was added 20 mL of aqueous 1 M  $\text{Na}_2\text{CO}_3$  at 24  $^\circ\text{C}$ . The reaction progress was followed by TLC, and after 4 h was completed. A similar extraction procedure as stated above gave a mixture of two products 5 and 6 that were subjected to flash chromatography ( $\text{CH}_2\text{Cl}_2$ –acetone–EtOH 2:1:0 to 1:1:0.02) to give compounds 5 [(66 mg, 48%), homogeneous by TLC ( $\text{CH}_2\text{Cl}_2$ –acetone–EtOH 5:4:1).  $^1\text{H}$  NMR data are shown in Table 1 except two singlets ( $\delta$  1.51, 9H; 1.49, 9H). ESI MS  $m/z$  486 [positive, (M + Na)], 462 [negative, (M – H)] and 6 [(45 mg, 41%), homogeneous by TLC ( $\text{CH}_2\text{Cl}_2$ –acetone–EtOH 5:4:1).  $^1\text{H}$  NMR data are shown in Table 1 except a singlet ( $\delta$  1.51, 9H). ESI MS  $m/z$  386 [positive, (M + Na)], 362 [negative, (M – H)].

**4-N-3'-O-Bis(tert-Butoxycarbonyl)gemcitabine (7).** To a stirred solution of 2 (73 mg, 0.2 mmol) in 8 mL of dioxane was added DBDC (436 mg, 2 mmol). The reaction mixture was maintained at 37  $^\circ\text{C}$ , 250 rpm, in a rotary shaker for 70 h at which time the solvent was removed under reduced pressure. The residue was washed with 2 mL of water. The solids were dried and subjected to flash chromatography ( $\text{CH}_2\text{Cl}_2$ –acetone 9:1 to 4:1) to give 7 (88 mg, 95%), homogeneous by TLC ( $\text{CH}_2\text{Cl}_2$ –acetone–EtOH 5:4:1).  $^1\text{H}$  NMR data are shown in Table 1 except two singlets ( $\delta$  1.51, 9H; 1.50, 9H). ESI MS  $m/z$  464 [positive, (M + H)], 462 [negative, (M – H)].

**4-N-3'-O-5'-O-Tris(tert-Butoxycarbonyl)gemcitabine (8).** In a separate experiment under similar condition as the first step for the preparation of 5 and 6, 8 was isolated from the product mixture by flash chromatography ( $\text{CH}_2\text{Cl}_2$ –acetone 9:1), homogeneous by TLC ( $\text{CH}_2\text{Cl}_2$ –acetone 4:1).  $^1\text{H}$  NMR data are shown in Table 1 except three singlets ( $\delta$  1.51, 9H; 1.50, 9H; 1.49, 9H). ESI MS  $m/z$  564 [positive, (M + H)], 562 [negative, (M – H)].

**( $\pm$ )-1-(2-Chlorophenyl)-N-(1-methylpropyl)-N-[2-[N-(2-hydroxycarbonyl-ethylcarbonyl)aminoethyl]-3-isoquinolinecarboxamide (10).** To a solution of dihydrochloride of 9 (1.36 g, 3 mmol) in  $\text{CH}_2\text{Cl}_2$  (60 mL) and DIEA (2.09 mL), was added succinic anhydride (600 mg, 6 mmol), and the reaction mixture was stirred at 24  $^\circ\text{C}$  for 1 h. An additional 60 mL of  $\text{CH}_2\text{Cl}_2$  was added to the mixture that was then washed with 1 M HCl (2  $\times$  20 mL) and brine (20 mL), dried over  $\text{MgSO}_4$ , and concentrated to dryness. Flash chromatography ( $\text{CH}_2\text{Cl}_2$ –acetone–HOAc 9:1:0 to 3:1:0.04) produced compound 10 (1.20 g, 83%), homogeneous by TLC ( $\text{CH}_2\text{Cl}_2$ –acetone–HOAc 3:1:0.1).  $^1\text{H}$  NMR  $\delta$  8.20–8.10 (m, 2H), 7.90–7.86 (m, 1H), 7.73–7.55 (m, 6H), 4.1–3.9 (m, 1H), 3.7–3.2 (m, 4H), 2.6–2.3 (m, 4H), 2.0–1.4 (m, 2H), 1.37–1.21 (m, 3H), 0.97–0.73 (m, 3H). 2D NMR was in agreement with the structure. ESI MS  $m/z$  (relative intensity) 482/484 [3/1, positive, (M + H)], 480/482 [3/1, negative, (M – H)].

**3'-O-5'-O-Bis(tert-Butoxycarbonyl)-4-N-[2-[N-(1-methylpropyl)-N-[1-(2-chlorophenyl)-isoquinoline-3-carboxamido]ethylaminocarbonyl]ethylcarbonyl]gemcitabine (11).** A reaction mixture of 3 (93 mg, 0.2 mmol), 10 (96 mg, 0.2 mmol), DCC (83 mg, 0.4 mmol), and 1-hydroxybenzotriazole hydrate (27 mg, 0.2 mmol) in  $\text{CH}_2\text{Cl}_2$  (10 mL) was stirred at 24  $^\circ\text{C}$  for 20 h. After an additional 50 mL of  $\text{CH}_2\text{Cl}_2$  was added, it was washed with water (10 mL) and brine (2  $\times$  10 mL), dried over  $\text{Na}_2\text{SO}_4$ , and concentrated to dryness. The residue was stirred in 20 mL acetone for 1 h. The white solids were removed by filtration after cooled in an ice-bath. The filtrate was concentrated and subjected to flash chromatography ( $\text{CH}_2\text{Cl}_2$ –acetone 4:1 to 2:1) to give 11 (158 mg, 85%), homogeneous by TLC (EtOAc).  $^1\text{H}$  NMR  $\delta$  8.23–8.11 (m, 2H), 8.03 (d, 7.6, 1H), 7.86 (m, 1H), 7.73–7.54 (m, 6H), 7.42 (m, 1H), 6.38 (m, 1H), 5.33 (m, 1H), 4.6–4.4 (m, 3H), 4.2–3.9 (m, 1H), 3.8–3.2 (m, 4H), 2.9–2.5 (m, 4H), 2.0–1.4 (m, 2H, overlap with the following two singlets), 1.50 (s, 9H), 1.47 (s, 9H), 1.37–1.21 (m, 3H), 0.96–0.73 (m, 3H). ESI MS  $m/z$  (relative intensity) 927/929 [3/1, positive, (M + H)], 925/927 [3/1, negative, (M – H)].

**4-N-5'-O-Bis(tert-Butoxycarbonyl)-3'-O-[2-[N-(1-methylpropyl)-N-[1-(2-chlorophenyl)isoquinoline-3-carbo-**



**nyl]amino]ethylaminocarbonyl]ethylcarbonyl]-gemcitabine (12).** To a stirred solution of **5** (46 mg, 0.1 mmol), **10** (48 mg, 0.1 mmol), and DCC (42 mg, 0.2 mmol) in 5 mL of  $\text{CH}_2\text{Cl}_2$  was added 2 mg of DMAP, and the resulting mixture was stirred at 24 °C for 2 h. After an additional 55 mL of  $\text{CH}_2\text{Cl}_2$  was added, it was washed with 20 mM, pH 7 phosphate buffer (2 × 20 mL) and brine (2 × 20 mL), dried over  $\text{Na}_2\text{SO}_4$ , and concentrated to dryness. The residue was stirred in 12 mL acetone for 1 h. The white solids were removed by filtration after being cooled in an ice-bath. The filtrate was concentrated and subjected to flash chromatography (EtOAc–acetone 1:0 to 9:1) to give **12** (82 mg, 88%), homogeneous by TLC (EtOAc).  $^1\text{H}$  NMR  $\delta$  8.2–8.02 (m, 3H), 7.88 (m, 1H), 7.80–7.54 (m, 6H), 7.28 (d, 7.6, 1H), 6.40 (m, 1H), 5.48 (m, 1H), 4.6–4.4 (m, 3H), 4.1–3.9 (m, 1H), 3.8–3.2 (m, 4H), 2.8–2.4 (m, 4H), 2.0–1.4 (m, 2H, overlap with the following two singlets), 1.51 (s, 9H), 1.47 (s, 9H), 1.37–1.21 (m, 3H), 0.96–0.73 (m, 3H). ESI MS  $m/z$  (relative intensity) 949/951 [3/1, positive, (M + Na)], 925/927 [3/1, negative, (M – H)].

**4-N-3'-O-Bis(tert-Butoxycarbonyl)-5'-O-[2-[2-[N-(1-methylpropyl),N-[1-(2-chlorophenyl)isoquinoline-3-carbonyl]amino]ethylaminocarbonyl]ethylcarbonyl]-gemcitabine (13).** To a stirred solution of **7** (46 mg, 0.1 mmol), **10** (48 mg, 0.1 mmol), and DCC (42 mg, 0.2 mmol) in 5 mL of  $\text{CH}_2\text{Cl}_2$  was added 2 mg of DMAP. The resulting mixture was stirred at 24 °C for 2 h. After an additional 55 mL of  $\text{CH}_2\text{Cl}_2$  was added, it was washed with 20 mM, pH 7 phosphate buffer (2 × 20 mL) and brine (2 × 20 mL), dried over  $\text{Na}_2\text{SO}_4$ , and concentrated to dryness. The residue was stirred in 12 mL of acetone for 1 h. The white solids were removed by filtration after cooled in an ice-bath. The filtrate was concentrated and subjected to flash chromatography ( $\text{CH}_2\text{Cl}_2$ –acetone 9:1 to 4:1) to give **13** (80 mg, 86%), homogeneous by TLC ( $\text{CH}_2\text{Cl}_2$ –acetone 4:1).  $^1\text{H}$  NMR  $\delta$  8.22–8.10 (m, 3H), 7.88–7.56 (m, 7H), 7.36–7.28 (m, 1H), 6.39 (m, 1H), 5.38 (m, 1H), 4.61–4.36 (m, 3H), 4.1–3.9 (m, 1H), 3.7–3.2 (m, 4H), 2.8–2.3 (m, 4H), 2.0–1.4 (m, 2H, overlap with the following two singlets), 1.49 (s, 9H), 1.48 (s, 9H), 1.36–1.20 (m, 3H), 0.95–0.72 (m, 3H). ESI MS  $m/z$  (relative intensity) 949/951 [3/1, positive, (M + Na)], 925/927 [3/1, negative, (M – H)].

**4-N-[2-[2-[N-(1-Methylpropyl),N-[1-(2-chlorophenyl)isoquinoline-3-carbonyl]amino]ethylaminocarbonyl]ethylcarbonyl]-gemcitabine (14).** To a stirred solution of **11** (130 mg) in 10 mL of  $\text{CH}_2\text{Cl}_2$  at 0 °C was added 10 mL of TFA. The reaction reached completion in 1 h at the same temperature. The solvents were evaporated, and the residue was treated with EtOAc (2 × 30 mL) and 10 mL of 5% aqueous  $\text{NaHCO}_3$ . The organic extract was washed with 10 mL of  $\text{NaHCO}_3$  and brine (2 × 10 mL), dried over  $\text{Na}_2\text{SO}_4$ , and concentrated. Crystallization from EtOAc gave **14** (85 mg, 84%) in two portions, homogeneous by TLC ( $\text{CH}_2\text{Cl}_2$ –acetone–EtOH 5:4:1).  $^1\text{H}$  NMR  $\delta$  8.31 (d, 7.6, 1H), 8.23–8.12 (m, 2H), 7.87 (m, 1H), 7.75–7.55 (m, 6H), 7.48 (m, 1H), 6.27 (t, 7.3, 1H), 4.43 (m, 1H), 4.15–3.70 (m, 4H), 3.6–3.2 (m, 4H), 2.9–2.5 (m,

4H), 2.1–1.4 (m, 2H), 1.36–1.20 (m, 3H), 0.96–0.72 (m, 3H). 2D NMR was in agreement with the structure. ESI MS  $m/z$  (relative intensity) 727/729 [3/1, positive, (M + H)], 725/727 [3/1, negative, (M – H)]. FAB HRMS [M + H] calcd for  $\text{C}_{35}\text{H}_{38}\text{ClF}_2\text{N}_6\text{O}_7$  727.2459, found 727.2447.

**3'-O-[2-[2-[N-(1-Methylpropyl),N-[1-(2-chlorophenyl)isoquinoline-3-carbonyl]amino]ethylaminocarbonyl]ethylcarbonyl]-gemcitabine (15).** To a stirred solution of **12** (80 mg) in 5 mL of  $\text{CH}_2\text{Cl}_2$  at 0 °C, 5 mL TFA was added. The reaction reached completion in 1.5 h at the same temperature. The solvents were evaporated, and the residue was treated with EtOAc (50 mL) and 5 mL of 5% aqueous  $\text{NaHCO}_3$ . The organic extract was washed with 5 mL of  $\text{NaHCO}_3$  and brine (2 × 5 mL), dried over  $\text{Na}_2\text{SO}_4$ , and concentrated. Crystallization from EtOAc gave **15** (55 mg, 88%), homogeneous by TLC ( $\text{CH}_2\text{Cl}_2$ –acetone–EtOH 5:4:1).  $^1\text{H}$  NMR  $\delta$  8.24–8.11 (m, 2H), 7.90–7.80 (m, 2H), 7.75–7.56 (m, 6H), 6.35 (m, 1H), 6.03 (d, 7.4, 1H), 5.49 (m, 1H), 4.26–3.75 (m, 4H), 3.7–3.2 (m, 4H), 2.8–2.3 (m, 4H), 2.0–1.42 (m, 2H), 1.37–1.19 (m, 3H), 0.96–0.73 (m, 3H). 2D NMR was in agreement with the structure. ESI MS  $m/z$  (relative intensity) 727/729 [3/1, positive, (M + H)], 725/727 [3/1, negative, (M – H)]. FAB HRMS [M + H] calcd for  $\text{C}_{35}\text{H}_{38}\text{ClF}_2\text{N}_6\text{O}_7$  727.2459, found 727.2443.

**5'-O-[2-[2-[N-(1-Methylpropyl),N-[1-(2-chlorophenyl)isoquinoline-3-carbonyl]amino]ethylaminocarbonyl]ethylcarbonyl]gemcitabine (16).** To a stirred solution of **13** (68 mg) in 5 mL of  $\text{CH}_2\text{Cl}_2$  at 0 °C was added 5 mL of TFA. The reaction reached completion in 12 h at the same temperature. The solvents were evaporated, and the residue was treated with EtOAc (50 mL) and 5 mL of 5% aqueous  $\text{NaHCO}_3$ . The organic extract was washed with 5 mL of  $\text{NaHCO}_3$  and brine (2 × 5 mL), dried over  $\text{Na}_2\text{SO}_4$ , and concentrated. Crystallization from EtOAc gave **16** (48 mg, 90%), homogeneous by TLC ( $\text{CH}_2\text{Cl}_2$ –acetone–EtOH 5:4:1).  $^1\text{H}$  NMR  $\delta$  8.24–8.11 (m, 2H), 7.91–7.56 (m, 8H), 6.30 (brs, 1H), 6.11–5.90 (m, 1H), 4.55–4.3 (m, 3H), 4.14 (m, 1H), 4.08–3.92 (m, 1H), 3.6–3.3 (m, 4H), 2.7–2.4 (m, 4H), 1.96–1.42 (m, 2H), 1.37–1.19 (m, 3H), 0.97–0.72 (m, 3H). 2D NMR was in agreement with the structure. ESI MS  $m/z$  (relative intensity) 727/729 [3/1, positive, (M + H)], 725/727 [3/1, negative, (M – H)]. FAB HRMS [M + H] calcd for  $\text{C}_{35}\text{H}_{38}\text{ClF}_2\text{N}_6\text{O}_7$  727.2459, found 727.2461.

**Acknowledgment.** NMR spectra obtained by Fox Chase Cancer Center's Spectroscopy Support Facility. Partial funding provided by NIH Core grant CA-06927.

**Supporting Information Available:** 1D  $^1\text{H}$  NMR spectra of compounds **2**–**8** and **10**–**16**, and 2D  $^1\text{H}$ – $^1\text{H}$  NMR spectra of compounds **10** and **14**–**16**. This material is available free of charge via the Internet at <http://pubs.acs.org>.

JO9911140

## Evaluation of In-111 DTPA-paclitaxel scintigraphy to predict response on murine tumors to paclitaxel

Tomio INOUE,\*,\*\*\*\* Chun LI,\*\* David J. YANG,\* Tetsuya HIGUCHI,\*\*\*\*\* Noboru ORIUCHI,\*\*\*\*\*  
Dongfang YU,\* Luka MILAS,\*\*\* Nancy HUNTER,\*\*\* Sidney WALLACE,\*\*  
E. Edmund KIM\* and Donald A. PODOLOFF\*

Departments of \*Nuclear Medicine, \*\*Diagnostic Radiology, and \*\*\*Experimental Radiotherapy,  
The University of Texas, M.D. Anderson Cancer Center, Houston, USA  
\*\*\*\*Department of Nuclear Medicine, Gunma University School of Medicine, Japan

Our goal was to determine whether scintigraphy with  $^{111}\text{In}$ -DTPA-paclitaxel could predict the response to chemotherapy with paclitaxel. *Methods:* Ovarian carcinoma (OCA 1), mammary carcinoma (MCA-4), fibrosarcoma (FSA) and squamous cell carcinoma (SCC VII) were inoculated into the thighs of female C3Hf/Kam mice. Mice bearing 8 mm tumors were treated with paclitaxel (40 mg/kg). The growth delay, which was defined as the time in days for tumors in the treated groups to grow from 8 to 12 mm in diameter minus the time in days for tumors in the untreated control group to reach the same size, was measured to determine the effect of paclitaxel on the tumors. Sequential scintigraphy in mice bearing 10 to 14 mm tumors was conducted at 5, 30, 60, 120, 240 min and 24 hrs postinjection of  $^{111}\text{In}$ -DTPA-paclitaxel (3.7MBq) or  $^{111}\text{In}$ -DTPA as a control tracer. The tumor uptakes (% injection dose/pixel) were determined. *Results:* The growth delay of OCA 1, MCA-4, FSA and SCC VII tumors was 13.6, 4.0, -0.02 and -0.28 days, respectively. In other words, OCA 1 and MCA-4 were paclitaxel-sensitive tumors, whereas FSA and SCC VII were paclitaxel-resistant tumors. The tumor uptakes at 24 hrs postinjection of In-111 DTPA paclitaxel of OCA 1, MCA-4, FSA and SCC VII were  $1.0 \times 10^{-3}$ ,  $1.6 \times 10^{-3}$ ,  $2.2 \times 10^{-3}$  and  $9.0 \times 10^{-3}$  % injection dose/pixel, respectively. There was no correlation between the response to chemotherapy with paclitaxel and the tumor uptakes of  $^{111}\text{In}$ -DTPA-paclitaxel. *Conclusions:* Scintigraphy with  $^{111}\text{In}$ -DTPA-paclitaxel could not predict the response to paclitaxel chemotherapy. Although there was significant accumulation of the paclitaxel in the tumor cells, additional mechanisms must be operative for the agent to be effective against the neoplasm.  $^{111}\text{In}$ -DTPA-paclitaxel activity is apparently different from that of paclitaxel with Cremophor.

**Key words:** In-111 DTPA-paclitaxel, paclitaxel, chemotherapy

### INTRODUCTION

IT HAS LONG BEEN THE HOPE that scintigraphy would be useful for therapeutic drug monitoring (TDM), which is now conducting by measuring the concentration in blood<sup>1</sup> but the concentration of an anti-cancer agent does not

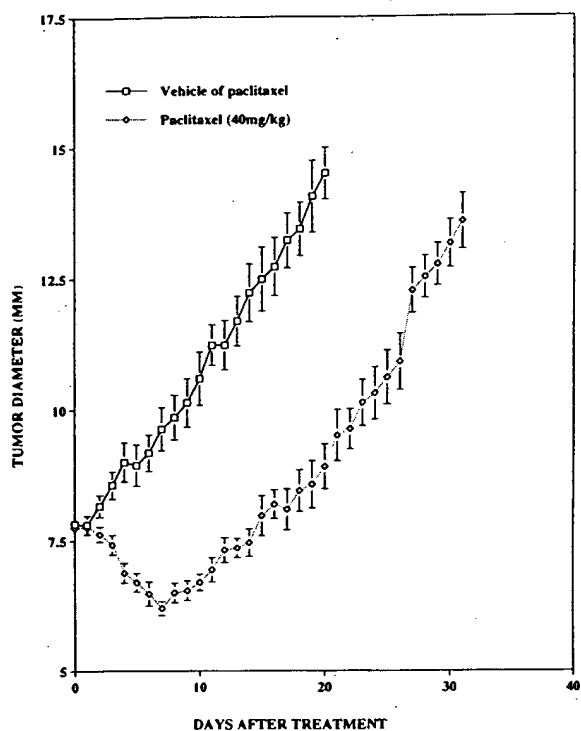
predict the effect on tumor cells. Scintigraphy with radiopharmaceuticals demonstrates the *in vivo* biodistribution of an anti-cancer drug as well as the characteristics of drug resistance.<sup>2</sup> Can we expect a good response if a radiolabeled cytotoxic agent shows signs of high tumor uptake on scintigraphy?

Paclitaxel exerts its cytotoxic effects through its interference with microtubule assembly,<sup>3,4</sup> and is active against a broad range of cancers that are considered to be refractory to conventional chemotherapy.<sup>5,6</sup> If radiolabeled paclitaxel could predict the response to paclitaxel and select those patients to be treated, much expense and time would be saved.

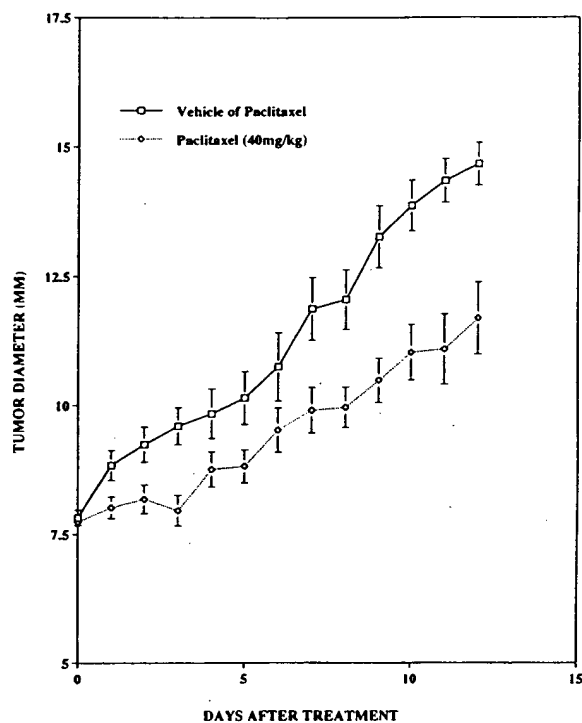
Received November 25, 1998, revision accepted March 9, 1999.

For reprint contact: Tomio Inoue, M.D., Department of Nuclear Medicine, Gunma University School of Medicine, 3-39-22 Showamachi, Maebashi, Gunma 371-8511, JAPAN.

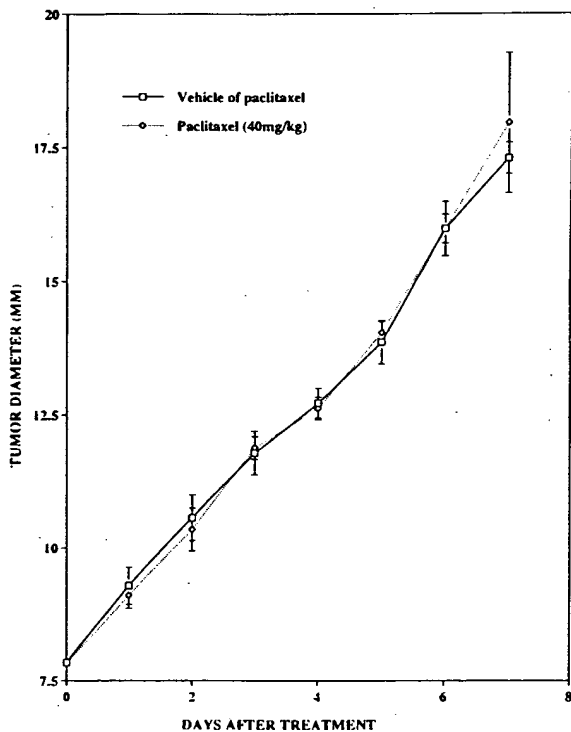
E-mail: tomioi@akagi.sb.gunma-u.ac.jp



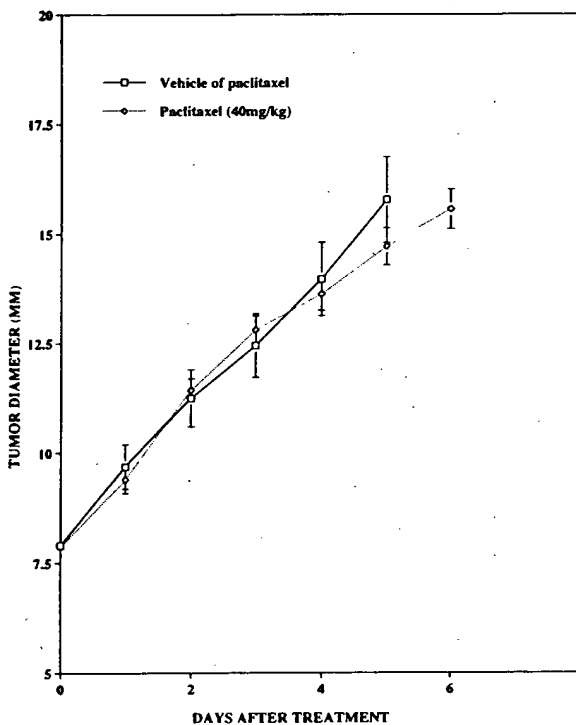
a



b



c



d

Fig. 1 The growth curves in mice treated and untreated with paclitaxel (40 mg/kg). OCA 1 (a) and MCA-4 (b) tumors responded to paclitaxel but FSA (c) and SCC VII (d) tumors did not have sensitivity to paclitaxel.

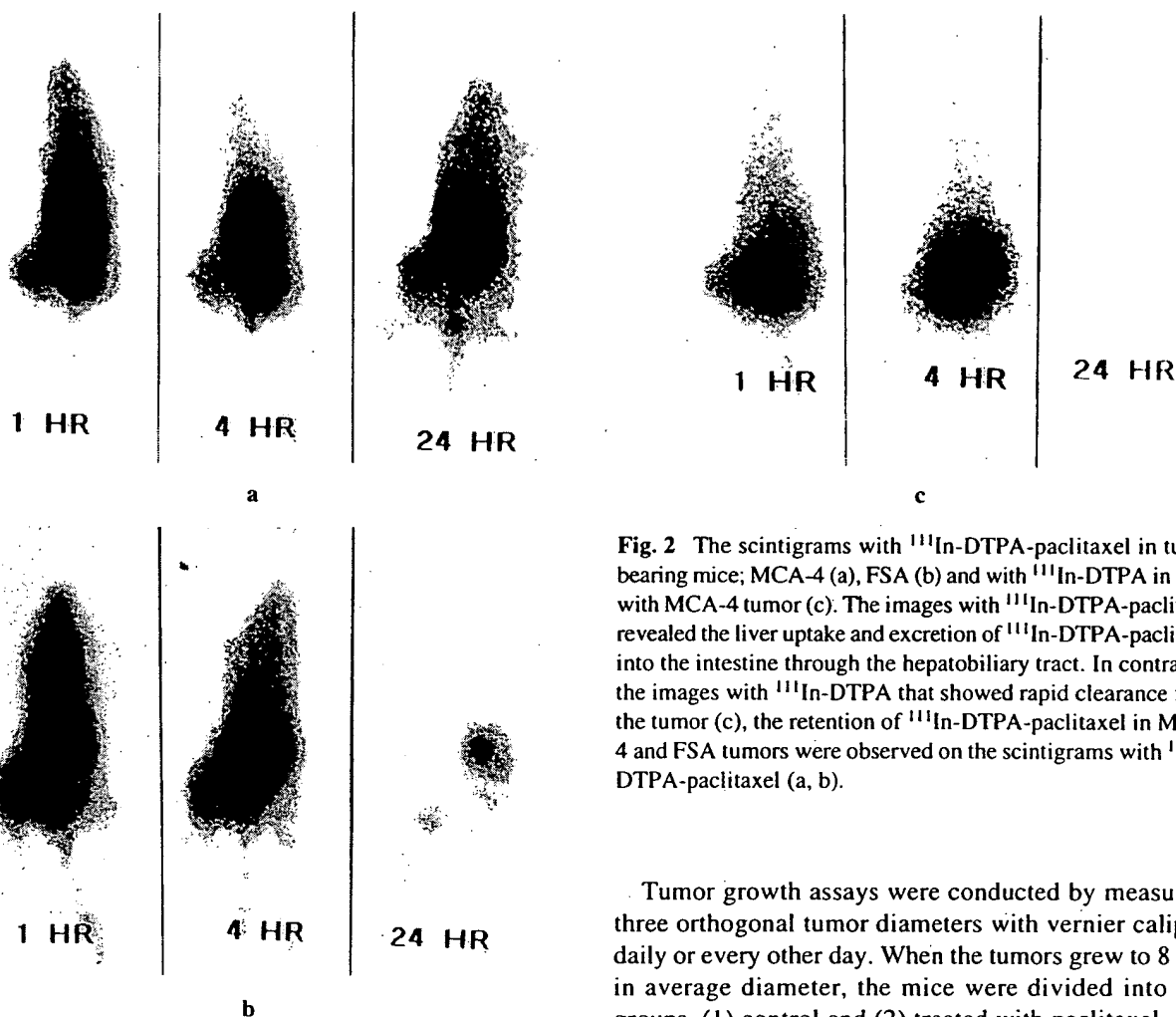


**Fig. 2** The scintigrams with  $^{111}\text{In}$ -DTPA-paclitaxel in tumor bearing mice; MCA-4 (a), FSA (b) and with  $^{111}\text{In}$ -DTPA in mice with MCA-4 tumor (c). The images with  $^{111}\text{In}$ -DTPA-paclitaxel revealed the liver uptake and excretion of  $^{111}\text{In}$ -DTPA-paclitaxel into the intestine through the hepatobiliary tract. In contrast to the images with  $^{111}\text{In}$ -DTPA that showed rapid clearance from the tumor (c), the retention of  $^{111}\text{In}$ -DTPA-paclitaxel in MCA-4 and FSA tumors were observed on the scintigrams with  $^{111}\text{In}$ -DTPA-paclitaxel (a, b).

We developed  $^{111}\text{In}$ -DTPA-paclitaxel at the University of Texas, M.D. Anderson Cancer Center<sup>7</sup> and present preliminary data in the evaluation of tumor uptake of the agent correlated with response to therapy in various tumor cell lines in mice.

## MATERIALS AND METHODS

C3Hf/Kam female mice (20–25 g), bred and maintained in a pathogen-free mouse colony in the Department of Experimental Radiotherapy of the University of Texas, M.D. Anderson Cancer Center, were used.<sup>8</sup> The mice were 3 months old at the beginning of the experiments and were housed 4–5 per cage. The animal models studied in this experiment were the fourth generation isografts of mammary carcinoma (MCA-4 tumors), the seventh generation isografts of ovarian carcinoma (OCA 1), the fifth generation isografts of fibrosarcoma (FSA) and squamous cell carcinoma (SCC VII).<sup>8–10</sup> Tumor cells were implanted in the muscle of the right thigh of mice by the inoculation of  $5 \times 10^5$  viable tumor cells confirmed by trypan blue exclusion and phase microscopy.

Tumor growth assays were conducted by measuring three orthogonal tumor diameters with vernier calipers daily or every other day. When the tumors grew to 8 mm in average diameter, the mice were divided into two groups, (1) control and (2) treated with paclitaxel, of 5 mice each. A single dose of paclitaxel was given intravenously at a dose of 40 mg equiv. paclitaxel/kg body weight. Paclitaxel was first dissolved in absolute ethanol with an equal volume of cremophor. This stock solution (30 mg/ml) was further diluted (1 : 4 by volume) with sterile physiological solution within 10 min of injection. In the control groups, absolute alcohol/cremophor 1 : 1 diluted with saline (1 : 4) was used. After treatment, tumor growth was followed up until the average tumor size reached at least 12 mm in diameter.

The effect on tumor regrowth was expressed as the absolute growth delay, defined as the time in days for tumors treated with paclitaxel to grow from 8 to 12 mm minus the time in days for tumors in the control group to grow from 8 to 12 mm in diameter.

Into a solution of paclitaxel (100 mg, 0.117 mmol) in dry DMF (2.2 ml) was added 210 mg diethylenetriamine-pentaacetic acid (DTPA anhydride, 0.585 mmol). The reaction mixture was stirred at 0°C overnight. The suspension was filtered to remove unreacted DTPA anhydride. The filtrate was poured into distilled water, stirred at room temperature for 20 min, and the precipitate of DTPA-paclitaxel was collected.

Into a 2 ml V-vial were added successively 40  $\mu\text{l}$  0.6 M

sodium acetate (pH 5.3) buffer, 40  $\mu$ l 0.06 M sodium citrate buffer (pH 5.5), 20  $\mu$ l paclitaxel-DTPA solution in methanol (2% w/v) and 20  $\mu$ l  $^{111}\text{InCl}_3$  solution (37 MBq) in sodium acetate buffer (pH 5.5). After an incubation period of 30 min at room temperature, the  $^{111}\text{In}$  labeled paclitaxel-DTPA was collected in a methanol wash. After methanol was evaporated by passing through nitrogen gas, the labeled product was reconstituted in a suitable volume of saline.

HPLC was used to analyze the reaction mixture and the purity of  $^{111}\text{In}$ -DTPA paclitaxel: The system consisted of a LDC binary pump and a 100 mm  $\times$  8 mm (i.d.) Waters column filled with ODS 5  $\mu$ m silica gel. The column was eluted at a flow rate of 1 ml/min with a gradient mixture of water and methanol (gradient from 0% to 85% methanol over 15 min). The gradient system was monitored with a NaI crystal detector and a Spectra-Physics UV/Vis detector.

When the tumors had grown to 12–14 mm in diameter, the mice each bearing a tumor (OCA 1, MCA-4, FSA and SCC VII tumor) were divided into two groups to assess the tumor uptakes of  $^{111}\text{In}$ -DTPA-paclitaxel or  $^{111}\text{In}$ -DTPA as a control tracer. The mice were anesthetized by i.p. injection of sodium pentobarbital, followed by i.v. injection of 3.7 MBq of either  $^{111}\text{In}$ -DTPA-paclitaxel or  $^{111}\text{In}$ -DTPA. Anterior planar images of the whole body were obtained at 5 min, 1, 2, 4 and 24 hrs postinjection of radiotracer with a single-head gamma camera equipped with a parallel-hole medium-energy collimator and connected to a computer. At all times, images were made with a 5-min preset time and stored in a 128  $\times$  128 matrix. A symmetrical 20% energy window was used for both the 173 and 247 keV energy peaks.

Regions of interest (ROIs) were drawn over the tumor manually on the images obtained to measure the tumor uptakes of radiotracers and over the whole body on the image obtained at 5 min postinjection to define the total injection dose of radioactivity. The tumor uptake was defined as a percent of the injected dose per pixel (% ID/pixel). The results were expressed as the mean  $\pm$  standard error of the mean (SEM).

The non-parametric Mann-Whitney U test was used to analyze data. A two-tailed p value less than 0.05 was considered to be a statistically significant difference.

## RESULTS

Purification with a Sep-Pak cartridge removed most of the  $^{111}\text{In}$ -DTPA which had a retention time of 2.7 min. A radiochromatogram of  $^{111}\text{In}$ -DTPA-paclitaxel correlated well with its corresponding UV chromatogram, indicating that the peak at 12.3 min was indeed the target compound. Paclitaxel had a retention time of 17.1 min under the same chromatographic conditions. The radiochemical purity of the final preparation was 90% and the radiochemical yield was 84%.

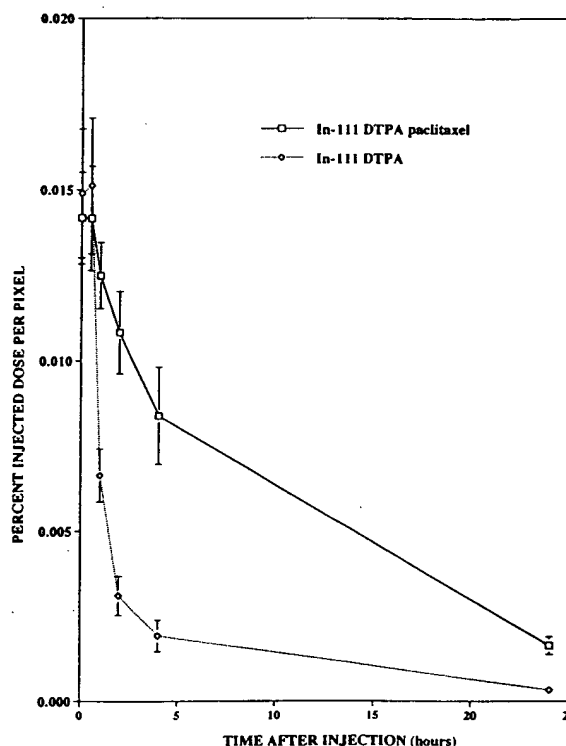


Fig. 3 The time activity curves of  $^{111}\text{In}$ -DTPA-paclitaxel and  $^{111}\text{In}$ -DTPA in MCA-4 tumor. The tumor uptakes of  $^{111}\text{In}$ -DTPA-paclitaxel decreased along with time after the injection but the wash-out from tumors were slower than that of  $^{111}\text{In}$ -DTPA.

Table 1 Results of tumor growth delay assay

Tumor type	Treatment	Growth delay date	Statistics
MCA-4	Vehicle of Paclitaxel	8.80 $\pm$ 1.30	p < 0.01
	Paclitaxel	12.76 $\pm$ 1.29	
OCA 1	Vehicle of Paclitaxel	13.48 $\pm$ 1.55	p < 0.001
	Paclitaxel	27.12 $\pm$ 0.85	
FSA	Vehicle of Paclitaxel	3.24 $\pm$ 0.24	N.S.
	Paclitaxel	3.22 $\pm$ 0.25	
SCC VII	Vehicle of Paclitaxel	2.70 $\pm$ 0.47	N.S.
	Paclitaxel	2.42 $\pm$ 0.22	

Each group included 5 mice. Growth delays were given as the duration when tumor regrew from 8 to 12 mm in diameter. Data were expressed as mean and SEM. Statistics: Student's t-test or non parametric analysis (if SD is significant difference)

Paclitaxel exerted a significant antitumor effect on OCA 1 and MCA-4 but was ineffective against FSA and SCC VII tumors (Table 1). The absolute growth delay of OCA 1, MCA-4, FSA and SCC VII tumors was 13.6, 4.0, -0.02 and -0.28 days, respectively. Tumor regrowth curves are shown in Figure 1.

The scintigrams in tumor bearing mice revealed liver uptake and excretion of  $^{111}\text{In}$ -DTPA-paclitaxel into the intestines through the hepatobiliary tract (Fig. 2). Although the images with  $^{111}\text{In}$ -DTPA showed rapid clear-

Table 2 Results of uptake of  $^{111}\text{In}$ -DTPA-paclitaxel and  $^{111}\text{In}$ -DTPA

Tumor		Times after injection				
		0.5 hr	1 hr	2 hr	4 hr	24 hr
MCA-4	Paclitaxel*	$14.2 \pm 3.7^\dagger$	$12.5 \pm 2.4^\dagger$	$10.8 \pm 1.2^\dagger$	$8.4 \pm 1.4^\dagger$	$1.6 \pm 0.3^\dagger$
	n	6	6	6	6	6
	DTPA <sup>§</sup>	$15.1 \pm 3.4$	$6.6 \pm 0.7$	$3.1 \pm 1.3$	$1.9 \pm 0.5$	$0.3 \pm 0.1$
OCA 1	n	3	5	5	5	3
	Paclitaxel	$8.5 \pm 0.6^\dagger$	$6.7 \pm 5.4$	$5.8 \pm 0.4^\dagger$	$4.3 \pm 1.3^\dagger$	$1.0 \pm 0.2^\dagger$
	n	7	7	7	7	7
FSA	DTPA	$4.9 \pm 1.2$	$4.5 \pm 1.7$	$3.2 \pm 0.7$	$1.2 \pm 0.3$	$0.3 \pm 0.1$
	n	7	7	7	7	7
	Paclitaxel	$16.6 \pm 1.3$	$15.3 \pm 1.3^\dagger$	$12.8 \pm 0.1$	$9.9 \pm 1.7$	$2.2 \pm 0.3^\dagger$
SCC VII	n	6	6	6	6	6
	DTPA	$18.5 \pm 2.5$	$10.7 \pm 0.6$	not done	$4.6 \pm 1.7$	$0.6 \pm 0.0$
	n	4	4		4	4
SCC VII	Paclitaxel	$16.4 \pm 1.3$	$17.3 \pm 1.4$	$18.4 \pm 2.0$	$19.1 \pm 2.8$	$9.0 \pm 2.0^\dagger$
	n	7	7	7	5	3
	DTPA	$21.1 \pm 7.0$	$19.3 \pm 6.5$	$18.2 \pm 6.7$	$16.2 \pm 6.0$	$1.2 \pm 0.2$
	n	5	5	5	4	3

\*  $^{111}\text{In}$ -DTPA-paclitaxel,  $^\dagger$  % injection dose per pixel  $\times 10^{-3}$ ; Data are given as mean  $\pm$  standard error of mean

$^\dagger$  significant difference from tumor uptake of  $^{111}\text{In}$ -DTPA ( $p < 0.05$ ),  $^\S$   $^{111}\text{In}$ -DTPA

ance from the tumor, the retention of  $^{111}\text{In}$ -DTPA paclitaxel was observed in tumors (Fig. 2).

The uptake of  $^{111}\text{In}$ -DTPA-paclitaxel in OCA 1, MCA-4, FSA and SCC VII tumors decreased with time after the injection but wash-out from the tumors was slower than that of  $^{111}\text{In}$ -DTPA (Table 2, Fig. 3). Uptakes at 24 hrs postinjection of  $^{111}\text{In}$ -DTPA-paclitaxel in OCA 1, MCA-4, FSA and SCC VII tumor were  $1.0 \times 10^{-3}$ ,  $1.6 \times 10^{-3}$ ,  $2.2 \times 10^{-3}$  and  $9.0 \times 10^{-3}$  % injection dose/pixel, respectively, which were significantly higher than those with  $^{111}\text{In}$ -DTPA as a control radiotracer (Table 2). Although OCA 1 was the tumor most sensitive to paclitaxel, tumor uptake in OCA 1 tumor at 1, 4 and 24 hrs postinjection of  $^{111}\text{In}$ -DTPA-paclitaxel was significantly lower than that in MCA-4, FSA and SCC VII tumor. There was no correlation between the response to chemotherapy with paclitaxel and tumor uptake of  $^{111}\text{In}$ -DTPA-paclitaxel (Tables 1 and 2).

## DISCUSSION

Assessment of the functional characteristics of the tumor is important in planning treatment. Anatomical information provided by newer imaging methods such as ultrasonography (US), computed tomography (CT) and magnetic resonance imaging (MRI) is not adequate. The nuclear medicine imaging with SPECT and PET can be used to monitor tumor therapy,<sup>11,12</sup> to evaluate tumor metabolism, nucleic acid synthesis and drug uptake.<sup>13</sup> Various radiolabeled anticancer drugs have been developed in the hope of predicting the response to chemotherapy,<sup>14-17</sup> but the results and mechanisms predicting the response to chemotherapy with radiolabeled anticancer

cer drugs were in conflict.

At first we expected that tumors with high uptake of  $^{111}\text{In}$ -DTPA-paclitaxel may respond to chemotherapy with paclitaxel because paclitaxel caused a dose-dependent decrease in the lag time for microtubule assembly.<sup>4</sup> This was also suggested by an *in vitro* study showing that the paclitaxel-resistant cells, J1.T1 cell line, which have a multidrug-resistance (MDR) phenotype, accumulated only 10% of  $^3\text{H}$  labeled paclitaxel found in the paclitaxel sensitive cells.<sup>18,19</sup> All 4 tumor cell lines used in our study showed specific uptakes of  $^{111}\text{In}$ -DTPA-paclitaxel, and in general there was no difference between paclitaxel sensitive OCA 1 and MCA-4 tumors and paclitaxel resistant SCC VII and FSA tumors in the uptake of  $^{111}\text{In}$ -DTPA-paclitaxel. The antineoplastic mechanism of paclitaxel mainly stabilizes tubulin polymerization resulting in the arrest of mitosis and apoptotic death of tumor cells. Since paclitaxel has a binding site on the microtubules, this may be the mechanism of  $^{111}\text{In}$ -DTPA-paclitaxel tumor uptake.<sup>7</sup> Although modification of the chemical structure of paclitaxel by labeling  $^{111}\text{In}$  and DTPA may cause a change in the mechanism of paclitaxel tumor uptake, we have confirmed that DTPA paclitaxel has antineoplastic action on OCA 1 and MCA-4 tumors like paclitaxel (unpublished data). Paclitaxel-resistant tumors (SCC VII tumor) also exhibited mitotic arrest after injection of paclitaxel although it did not have an antitumor action after mitotic arrest,<sup>20</sup> which is consistent with a significant uptake of  $^{111}\text{In}$ -DTPA-paclitaxel in SCC VII tumors. The accumulation of paclitaxel in the tumor cells is undoubtedly a prerequisite but not sufficient for successful treatment. Tumor uptake of  $^{111}\text{In}$ -DTPA-paclitaxel reflects the accumulation of paclitaxel by tumor cells, but the degree of

accumulation does not reflect the tumor cell sensitivity. It is quite possible that some cellular factors determine whether paclitaxel will be cytotoxic to tumor cells.

Although scintigraphy with  $^{111}\text{In}$ -DTPA-paclitaxel failed to predict tumor response to the chemotherapy with paclitaxel, it may be useful in predicting drug toxicity as does  $^{123}\text{I}$ -labeled digoxin.<sup>21</sup> In contrast to the lipophilic characteristics of paclitaxel,  $^{111}\text{In}$ -DTPA paclitaxel is water soluble and may therefore provide different biodistribution than paclitaxel. There was high liver uptake and hepatobiliary excretion, similar to paclitaxel metabolism and its excretion route. Although hepatic metabolism, biliary excretion and fecal elimination appear to be responsible for most of the systemic clearance, the optimal dose of paclitaxel for patients with liver dysfunction has not been determined.<sup>3</sup> Even if the same race of tumor bearing mice, C3H/Kam female mice, was employed in this study, there was a significant difference in liver uptake at 24 hr postinjection (Fig. 2a, b).<sup>7</sup> Scintigraphy may help to optimize chemotherapy for patients with hepatic dysfunction by monitoring the hepatobiliary clearance of  $^{111}\text{In}$ -DTPA-paclitaxel.

Further study to assess the mechanism of tumor uptake of  $^{111}\text{In}$ -DTPA-paclitaxel is needed to determine the usefulness of scintigraphy with this compound. It is speculated that there would be no therapeutic effect of paclitaxel if there is no significant uptake of  $^{111}\text{In}$ -DTPA-paclitaxel in tumors.

## REFERENCES

1. Evans WE, Relling MV. Clinical pharmacokinetics-pharmacodynamics of anticancer drugs. *Clin Pharmacokinet* 16: 327-336, 1989.
2. Moretti JL, Caglar M, D-Cordobes M, Morere JF. Can nuclear medicine predict response to chemotherapy? *Eur J Nucl Med* 22: 97-100, 1995.
3. Rowinsky EK, Donehower RC. Paclitaxel (Taxol). *New Engl J Med* 332: 1004-1014, 1995.
4. Schiff PB, Fant J, Horwitz SB. Promotion of microtubule assembly *in vitro* by taxol. *Nature* 277: 665-667, 1979.
5. Holmes FA, Walters RS, Theriault RL, Forman AD, Newton LK, Raber MN, et al. Phase II trial of taxol, an active drug in the treatment of metastatic breast cancer. *J Natl Cancer Inst* 83: 1797-1805, 1991.
6. Thigpen JT, Blessing JA, Ball H, Hummel SJ, Barrett RJ. Phase II trial of paclitaxel in patients with progressive ovarian carcinoma after platinum-based chemotherapy. A Gynecological Oncology Group study. *J Clin Oncol* 12: 1748-1753, 1994.
7. Li C, Yu DF, Inoue T, Yang DJ, Tansey W, Liu CW, et al. Synthesis, biodistribution and imaging properties of indium-111-DTPA-paclitaxel in mice bearing mammary tumors. *J Nucl Med* 38: 1042-1047, 1997.
8. Milas L, Hunter NR, Mason KA, Kurdoglu B, Peters LJ. Enhancement of tumor radioresponse of a murine mammary carcinoma by paclitaxel. *Cancer Res* 54: 3506-3510, 1994.
9. Stone HB, Milas L. Modification of radiation response of murine tumors by misonidazole (Ro 07-0582), host immune capability, and *Corynebacterium parvum*. *J Natl Cancer Inst* 60: 887-893, 1978.
10. Stephens LC, Ang KK, Shultheiss TE, Milas L, Meyn RE. Apoptosis in irradiated murine tumors. *Radiat Res* 127: 308-316, 1991.
11. Kubota K, Ishiwata K, Kubota R, Yamada S, Tada M, Sato T, et al. Tracer feasibility for monitoring tumor radiotherapy: a quadruple tracer study with fluorine-18-fluorodeoxyglucose or fluorine-18-fluorodeoxyuridine, L-[methyl- $^{14}\text{C}$ ]methionine, [6- $^3\text{H}$ ]thymidine, and gallium-67. *J Nucl Med* 32: 2118-2123, 1991.
12. Ichiya Y, Kuwabara Y, Otsuka M, Tahara T, Yoshikai T, Fukumura T, et al. Assessment of response to cancer therapy using fluorine-18-fluoro-deoxyglucose and positron emission tomography. *J Nucl Med* 32: 1655-1660, 1991.
13. Sasaki Y. Monitoring tumor radiotherapy. *J Nucl Med* 32: 2124-2125, 1991.
14. Philip P, Bagshawe K, Searle F, Green AJ, Begent RHJ, Newlands ES, et al. *In vivo* uptake of  $^{131}\text{I}$ -5-iodo-2-deoxyuridine by malignant tumors in man. *Br J Cancer* 63: 134-135, 1991.
15. Sapir EE, Bettman L, Iosilevsky G, Milshtein D, Frenkel A, Kolodny GM, et al. SPECT quantification of cobalt-57-bleomycin to predict treatment response and outcome of patients with lung cancer. *J Nucl Med* 35: 1129-1133, 1994.
16. Shani J, Wolf W. A model for prediction of chemotherapy response to 5-fluorouracil based on the differential distribution of 5-[ $^{18}\text{F}$ ]fluorouracil in sensitive versus resistant lymphocytic leukemia in mice. *Cancer Res* 37: 2306-2308, 1977.
17. Young D, Vine E, Ghanbarpour A, Shani J, Siesmen JK, Wolf W. Metastatic and distribution studies with radiolabeled 5-fluorouracil. *J Nucl Med* 21: 1-7, 1982.
18. Horwitz SB, Cohen D, Rao S, Ringel I, Shen H, Yang CH. Taxol: Mechanism of action and resistance. *Monogr Natl Cancer Inst Monogr* 15: 55-61, 1993.
19. Roy SN, Horwitz SB. A phosphoglycoprotein associated with taxol-resistance in J774.2 cells. *Cancer Res* 45: 3856-3863, 1985.
20. Saito Y, Milross CG, Hittleman WN, Li D, Jibu T, Peters LJ, et al. Effect of radiation and paclitaxel on p53 expression in murine tumors sensitive or resistant to apoptosis induction. *Int J Rad Oncol Biol Phys* 38: 623-631, 1997.
21. Fujibayashi Y, Takemura Y, Matsumoto K, Wada K, Yonekura Y, Konishi J, et al. High myocardial accumulation of radioiodinated digoxin derivatives: a possible Na,K-ATPase imaging agent. *J Nucl Med* 33: 545-549, 1992.

## Preclinical study

# Synthesis of [ $^{99m}\text{Tc}$ ]ethylenedicysteine-colchicine for evaluation of antiangiogenic effect

Fereshteh Zareneyrizi, David J Yang, Chang-Sok Oh, Seyfettin Ilgan, Dong-Fang Yu, Wayne Tansey, Chun-Wei Liu, E Edmund Kim and Donald A Podoloff  
Divisions of Diagnostic Imaging, University of Texas MD Anderson Cancer Center, Houston, TX 77030, USA.

Angiogenesis is in part responsible for tumor growth and the development of metastasis. Radiolabeled angiogenesis inhibitors would be useful to assess tumor microvasculature density. Colchicine (COL), a potent antiangiogenic agent, is known to inhibit microtubule polymerization and cell arrest at metaphase. This study aimed to develop  $^{99m}\text{Tc}$ -labeled COL (EC-COL) using ethylenedicysteine (EC) as a chelator to assess tumor microvascular density. EC was conjugated to trimethylcolchicinic acid using *N*-hydroxysuccinimide and 1-ethyl-3-dimethylaminopropyl carbodiimide as coupling agents with a yield of 50–60%. *In vivo* stability was analyzed in rabbit serum at 0.5–4 h. Tissue distribution and planar imaging studies of [ $^{99m}\text{Tc}$ ]EC-COL were evaluated in breast tumor-bearing rats at 0.5, 2 and 4 h. The data was compared to that using [ $^{99m}\text{Tc}$ ]EC (control). The radiochemical yield of [ $^{99m}\text{Tc}$ ]EC-COL was greater than 95%. [ $^{99m}\text{Tc}$ ]EC-COL was stable in rabbit serum. *In vivo* biodistribution of [ $^{99m}\text{Tc}$ ]EC-COL in breast tumor-bearing rats showed increased tumor-to-blood ( $0.52 \pm 0.12$  to  $0.72 \pm 0.07$ ) and tumor-to-muscle ( $3.47 \pm 0.40$  to  $7.97 \pm 0.93$ ) ratios as a function of time. Conversely, tumor-to-blood values showed a time-dependent decrease with [ $^{99m}\text{Tc}$ ]EC over the same time period. Planar images confirmed that the tumors could be visualized clearly with [ $^{99m}\text{Tc}$ ]EC-COL from 0.5 to 4 h. [ $^{99m}\text{Tc}$ ]EC-COL may be useful to assess antiangiogenic and therapeutic effects during chemotherapy. © 1999 Lippincott Williams & Wilkins.]

**Key words:** Antiangiogenesis, colchicine, [ $^{99m}\text{Tc}$ ]ethylenedicysteine, tumor imaging.

## Introduction

Angiogenesis is in part responsible for tumor growth and the development of metastasis. Antimitotic compounds are antiangiogenic and are known for

their potential use as anticancer drugs. These compounds inhibit cell division during the mitotic phase of the cell cycle. Microtubules are involved during the biochemical process of cellular functions, such as cell division, cell motility, secretion, ciliary and flagellar movement, intracellular transport, and the maintenance of cell shape. It is known that antimitotic compounds bind with high affinity to microtubule proteins (tubulin), disrupting microtubule assembly and causing mitotic arrest of the proliferating cells. Thus, antimitotic compounds are considered as microtubule inhibitors or as spindle poisons.<sup>1</sup>

Many classes of antimitotic compounds control microtubule assembly-disassembly by binding to tubulin. Compounds such as colchicinoids interact with tubulin on the colchicine (COL) binding sites and inhibit microtubule assembly.<sup>2,3</sup> Among colchicinoids, COL is an effective anti-inflammatory drug used to treat prophylaxis of acute gout. COL is also used in chronic myelocytic leukemia. Although colchicinoids are potent against certain types of tumor growth, the clinical therapeutic potential is limited due to inability to separate the therapeutic and toxic effects.<sup>1</sup> However, COL may be useful as a biochemical tool to assess cellular functions. Therefore, we developed a radio-labeled COL for the assessment of biochemical process on tubulin functions.

Due to favorable physical characteristics as well as extremely low price,  $^{99m}\text{Tc}$  have been preferred to label radiopharmaceuticals. Several compounds have been labeled with  $^{99m}\text{Tc}$  using nitrogen and sulfur chelates.<sup>4–7</sup> Bis-aminoethanethiol tetradentate ligands, also called diaminodithiol compounds, are known to form very stable  $\text{Tc(V)O}$  complexes on the basis of efficient binding of the oxotechnetium group to two thiolsulfur and two amine nitrogen atoms.  $^{99m}\text{Tc}$ -L-ethylenedicysteine ([ $^{99m}\text{Tc}$ ]EC) is a recent and successful example of  $\text{N}_2\text{S}_2$  chelates. EC can be labeled

Correspondence to DJ Yang, Department of Nuclear Medicine, University of Texas MD Anderson Cancer Center, 1515 Holcombe Boulevard, Houston, TX 77030, USA.  
Tel: (+1) 713 745-3368; Fax: (+1) 713 794-5456;  
E-mail: dyang@rpisun1.mdacc.tmc.edu



with  $^{99m}\text{Tc}$  easily and efficiently with high radiochemical purity and stability, and is excreted through the kidney by active tubular transport.<sup>8,9</sup>

In this report, synthesis and breast tumor imaging potential using a new [ $^{99m}\text{Tc}$ ]EC-COL were evaluated.

## Materials and methods

The nuclear magnetic resonance (NMR) and mass spectral analysis were conducted at the University of Texas Health Science Center (Houston, TX). NMR spectra were recorded on a Bruker 200 MHz Spectrometer. The mass data were obtained by fast atom bombardment on a Kratos MS 50 instrument (England). Sulfo-*N*-hydroxysuccinimide (Sulfo-NHS) and 1-ethyl-3-(3-dimethylaminopropyl) carbodiimide-HCl (EDC) were purchased from Pierce (Radford, IL). All other chemicals were purchased from Aldrich (Milwaukee, WI). Silica gel coated thin-layer chromatography (TLC) plates were purchased from Whatman (Clifton, NJ).  $^{99m}\text{Tc}$ -pertechnetate was obtained from a commercial  $^{99}\text{Mo}/^{99m}\text{Tc}$  generator (Ultratechnekow FM; Mallinckrodt Diagnostica, Holland).

### Synthesis of L,L-ethylenedicysteine (EC)

EC was prepared in a two-step synthesis according to the previously described methods.<sup>4,5</sup> The precursor, L-thiazolidine-4-carboxylic acid, was synthesized (m.p. 195°C, reported 196–197°C). EC was then prepared (m.p. 237°C, reported 251–253°C). The structure was confirmed by  $^1\text{H}$ -NMR and mass spectroscopy (FAB-MS)  $m/z$  268 ( $\text{M}^+$ , 100).

### Synthesis of (amino analog of COL) COL-NH<sub>2</sub>

The demethylated amino and hydroxy analog of COL was synthesized according to the previously described methods.<sup>10</sup> Briefly, COL (4 g) was dissolved in 100 ml of water containing 25% sulfuric acid. The reaction mixture was heated for 5 h at 100°C. The mixture was neutralized with sodium carbonate. The product was filtered and dried over a freeze dryer, and yielded 2.4 g (70%) of the desired amino analog (m.p. 153–155°C, reported 155–157°C). Ninhydrin (2% in methanol) spray indicated the positivity of the amino group of COL-NH<sub>2</sub>. The structure was confirmed by  $^1\text{H}$ -NMR and mass spectroscopy (FAB-MS).  $^1\text{H}$ -NMR ( $\text{CDCl}_3$ )  $\delta$  8.09 (s, 1H), 7.51 (d, 1H,  $J=12$  Hz), 7.30 (d, 1H,  $J=12$  Hz), 6.56 (s, 1H), 3.91 (s, 6H), 3.85 (m, 1H), 3.67

(s, 3H), 2.25–2.52 (m, 4H).  $m/z$  308.2 ( $\text{M}^+$ , 20), 307.2 (100).

### Synthesis of EC-COL

Sodium hydroxide (2 N, 0.2 ml) was added to a stirred solution of EC (134 mg, 0.50 mmol) in water (5 ml). To this colorless solution, sulfo-NHS (217 mg, 1.0 mmol) and EDC (192 mg, 1.0 mmol) were added. COL-NH<sub>2</sub> (340 mg, 2.0 mmol) was then added. The mixture was stirred at room temperature for 24 h. The mixture was dialyzed for 48 h using a Spectra/POR molecular porous membrane with cut-off at 500 (Spectrum Medical Industries, Houston, TX). After dialysis, the product was frozen dried using a lyophilizer (Labconco, Kansas City, MO). The product weighed 315 mg (yield 55%).  $^1\text{H}$ -NMR ( $\text{D}_2\text{O}$ )  $\delta$  7.39 (s, 1H), 7.20 (d, 1H,  $J=12$  Hz), 7.03 (d, 1H,  $J=12$  Hz), 6.78 (s, 1H), 4.25–4.40 (m, 1H), 3.87 (s, 3H, -OCH<sub>3</sub>), 3.84 (s, 3H, -OCH<sub>3</sub>), 3.53 (s, 3H, -OCH<sub>3</sub>), 3.42–3.52 (m, 2H), 3.05–3.26 (m, 4H), 2.63–2.82 (m, 4H), 2.19–2.25 (m, 4H). FAB MS  $m/z$  580 (sodium salt, 20). The synthetic scheme of EC-COL is shown in Figure 1.

### Radiolabeling of EC-COL and EC with $^{99m}\text{Tc}$

Radiosynthesis of [ $^{99m}\text{Tc}$ ]EC-COL was achieved by adding the required amount of  $^{99m}\text{Tc}$ -pertechnetate into a home-made kit containing the lyophilized residue of EC-COL (5 mg),  $\text{SnCl}_2$  (100  $\mu\text{g}$ ),  $\text{Na}_2\text{HPO}_4$  (13.5 mg), ascorbic acid (0.5 mg) and NaEDTA (0.5 mg). The final pH of the preparation was 7.4. [ $^{99m}\text{Tc}$ ]EC was also obtained by using a home-made kit containing the lyophilized residue of EC (5 mg),  $\text{SnCl}_2$  (100  $\mu\text{g}$ ),  $\text{Na}_2\text{HPO}_4$  (13.5 mg), ascorbic acid (0.5 mg) and NaEDTA (0.5 mg) at pH 10. The final pH of the preparation was then adjusted to 7.4. Radiochemical purity was determined by TLC (ITLC SG; Gelman Sciences, Ann Arbor, MI) eluted with ammonium acetate (1 M) in water:methanol (4:1). Radio-TLC (Bioscan, Washington, DC) was used to analyze the radiochemical purity for both radiotracers.

### Stability of assay of [ $^{99m}\text{Tc}$ ]EC-COL

The stability of labeled [ $^{99m}\text{Tc}$ ]EC-COL was tested in serum samples. Briefly, 740 kBq of 5 mg [ $^{99m}\text{Tc}$ ]EC-

COL was incubated in the rabbit serum (500  $\mu\text{l}$ ) at 37°C for 4 h. The serum samples were diluted with 50% methanol in water, and radio-TLC repeated at 0.5, 2 and 4 h as described above.

Tissue distribution studies

The animal experiments were approved by The University of Texas MD Anderson Institutional Animal

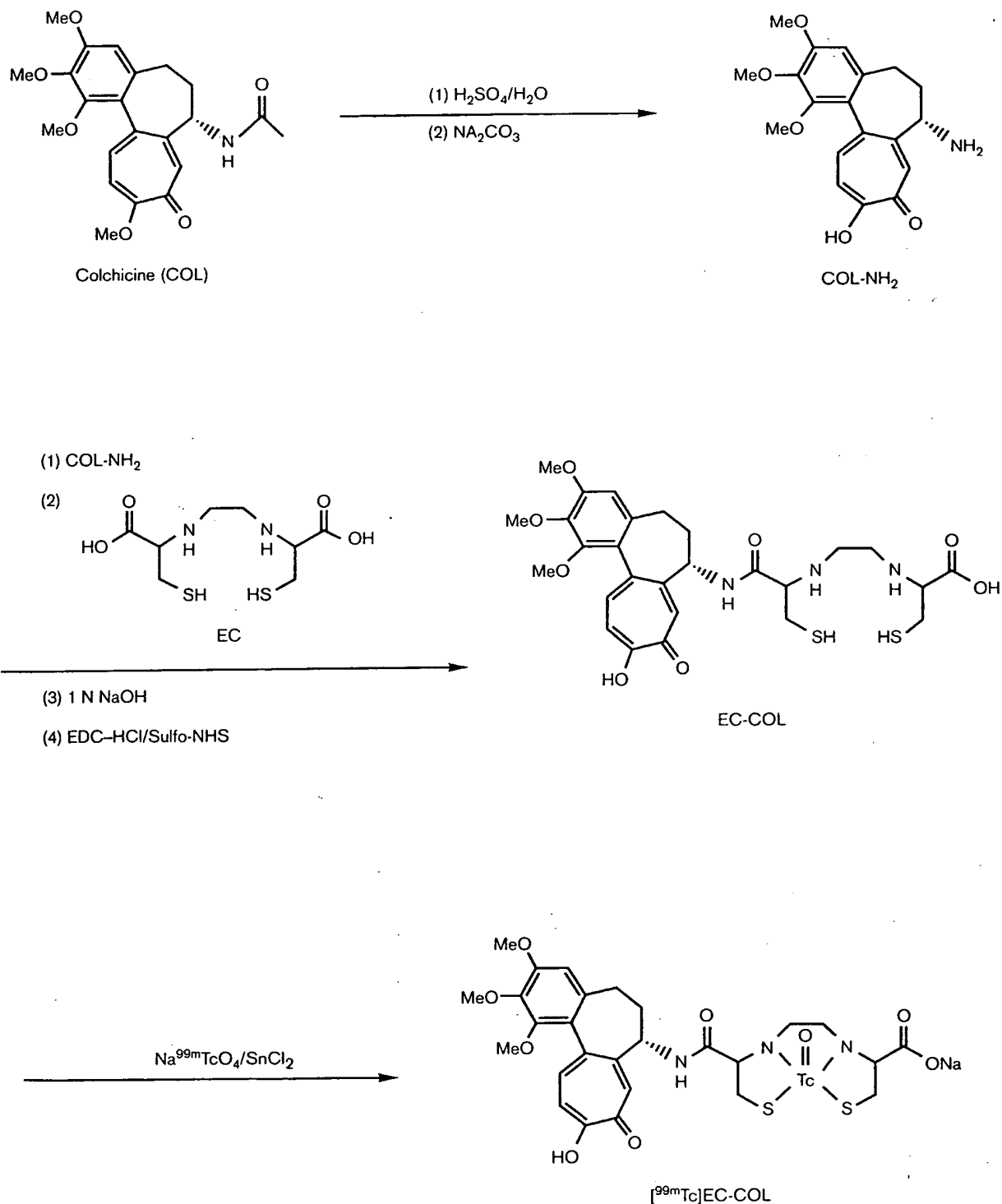


Figure 1. Synthetic scheme of [ $^{99\text{m}}\text{Tc}$ ]EC-COL.

Care and Use Committee (IACUC). Female Fischer 344 rats ( $150 \pm 25$  g) (Harlan Sprague-Dawley, Indianapolis, IN) were inoculated s.c. with 0.1 ml of mammary tumor cells from the 13762 tumor cell line suspension ( $10^6$  cells/rat, a tumor cell line specific to Fischer rats) into the hind legs using 25-gauge needles. Studies were performed 14-17 days after implantation when tumors reached approximately 1 cm diameter. Rats were anesthetized with ketamine (10-15 mg/rat, i.p.) before each procedure.

In tissue distribution studies, each animal was injected i.v. with 370-550 KBq of [ $^{99m}\text{Tc}$ ]EC-COL or [ $^{99m}\text{Tc}$ ]EC ( $n=3$ /time point). The injected mass of [ $^{99m}\text{Tc}$ ]EC-COL was 10  $\mu\text{g}$  per rat. At 0.5, 2 and 4 h following administration of the radiotracers, the rats were sacrificed, and the selected tissues were excised, weighed and counted for radioactivity. The biodistribution of tracer in each sample was calculated as percentage of the injected dose per gram of tissue wet weight (%ID/g). Tumor/non-target tissue count density ratios were calculated from the corresponding %ID/g values. Student's *t*-test was used to assess the significance of differences between groups.

## Scintigraphic imaging studies

Scintigraphic images, using a  $\gamma$ -camera (Siemens Medical Systems, Hoffman Estates, IL) equipped with a low-energy, parallel-hole collimator, were obtained 0.5, 2 and 4 h after i.v. injection of 300  $\mu\text{Ci}$  of [ $^{99m}\text{Tc}$ ]EC-COL and [ $^{99m}\text{Tc}$ ]EC. A computer outlined region of interest (ROI) was used to quantitate (counts per pixel) the tumor uptake versus normal muscle uptake.

## Results

### Radiosynthesis and stability of [ $^{99m}\text{Tc}$ ]EC-COL

Radiosynthesis of EC-COL with  $^{99m}\text{Tc}$  was achieved with high (>95%) radiochemical purity (Figure 2). [ $^{99m}\text{Tc}$ ]EC-COL was found to be stable at 0.5, 2 and 4 h in rabbit serum samples. No degradation products were observed.

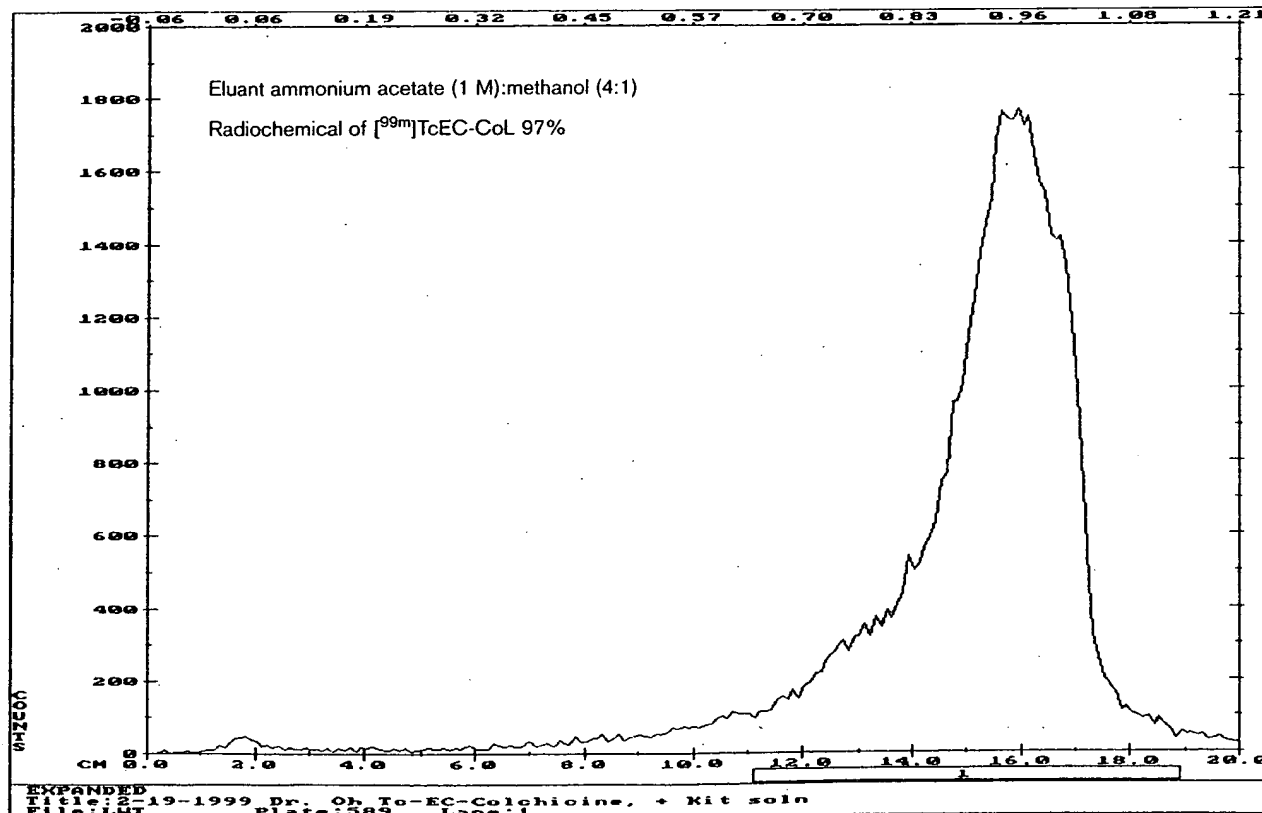


Figure 2. Radio-TLC of [ $^{99m}\text{Tc}$ ]EC-COL.

# *In vivo* biodistribution

The *in vivo* biodistribution of [ $^{99m}\text{Tc}$ ]EC-COL and [ $^{99m}\text{Tc}$ ]EC in breast tumor bearing rats is shown in

**Table 1.** Biodistribution of [ $^{99m}\text{Tc}$ ]EC-COL in breast tumor bearing rats<sup>a</sup>

	30 min	2 h	4 h
Blood	0.837 ± 0.072	0.606 ± 0.266	0.307 ± 0.022
Lung	0.636 ± 0.056	0.407 ± 0.151	0.194 ± 0.009
Liver	1.159 ± 0.095	1.051 ± 0.213	0.808 ± 0.084
Spleen	0.524 ± 0.086	0.559 ± 0.143	0.358 ± 0.032
Kidney	9.705 ± 0.608	14.065 ± 4.007	11.097 ± 0.108
Muscle	0.129 ± 0.040	0.071 ± 0.032	0.028 ± 0.004
Stomach	0.484 ± 0.386	0.342 ± 0.150	0.171 ± 0.123
Uterus	0.502 ± 0.326	0.343 ± 0.370	0.133 ± 0.014
Thyroid	3.907 ± 0.997	2.297 ± 0.711	1.709 ± 0.776
Tumor	0.436 ± 0.089	0.395 ± 0.154	0.221 ± 0.006

<sup>a</sup>Each rat received [ $^{99m}\text{Tc}$ ]EC-COL (10  $\mu\text{Ci}$ , i.v.). Each value is the percent of injected dose per gram tissue weight ( $n=3$ )/time interval. Each data represents mean of three measurements with SD.

**Table 2.** Biodistribution of [ $^{99m}\text{Tc}$ ]EC in breast tumor bearing rats<sup>a</sup>

	30 min	2 h	4 h
Blood	0.435 ± 0.029	0.211 ± 0.001	0.149 ± 0.008
Lung	0.272 ± 0.019	0.144 ± 0.002	0.120 ± 0.012
Liver	0.508 ± 0.063	0.286 ± 0.073	0.234 ± 0.016
Spleen	0.118 ± 0.008	0.075 ± 0.002	0.067 ± 0.003
Kidney	7.914 ± 0.000	9.116 ± 0.053	7.834 ± 1.018
Muscle	0.060 ± 0.006	0.028 ± 0.009	0.019 ± 0.001
Stomach	0.136 ± 0.060	0.038 ± 0.027	0.043 ± 0.001
Uterus	0.218 ± 0.036	0.076 ± 0.000	0.074 ± 0.020
Thyroid	0.219 ± 0.036	0.106 ± 0.003	0.083 ± 0.005
Tumor	0.342 ± 0.163	0.115 ± 0.002	0.097 ± 0.005

<sup>a</sup>Each rat received [ $^{99m}\text{Tc}$ ]EC (10  $\mu\text{Ci}$ , i.v.). Each value is the percent of injected dose per gram tissue weight ( $n=3$ )/time interval. Each data represents mean of three measurements with SD.

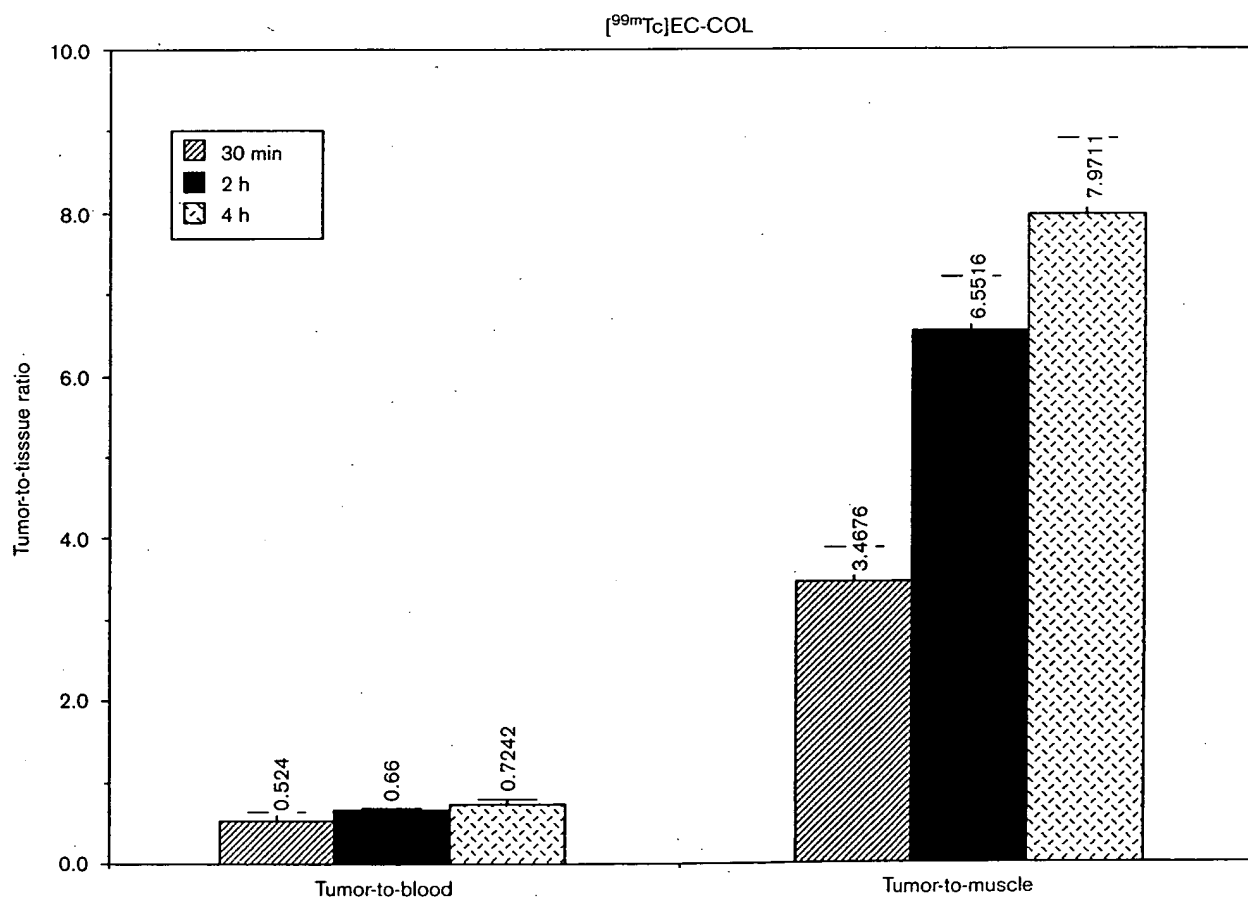


**Figure 3.** Tumor-to-blood and tumor-to-muscle count density ratios of [ $^{99m}\text{Tc}$ ]EC-COL in breast tumor bearing rats as a function of time. Data are expressed as the mean  $\pm$  SE for  $n=3$  rats per group.

and  $0.097 \pm 0.005$ , respectively (Table 2). Increased tumor-to-blood ( $0.52 \pm 0.12$  to  $0.72 \pm 0.07$ ) and tumor-to-muscle ( $3.47 \pm 0.40$  to  $7.97 \pm 0.93$ ) ratios as a function of time were observed in [ $^{99m}\text{Tc}$ ]EC-COL group (Figure

3). Conversely, tumor-to-blood and tumor-to-muscle values showed a time-dependent decrease with [ $^{99m}\text{Tc}$ ]EC when compared to the [ $^{99m}\text{Tc}$ ]EC-COL group over the same time period (Figure 4).

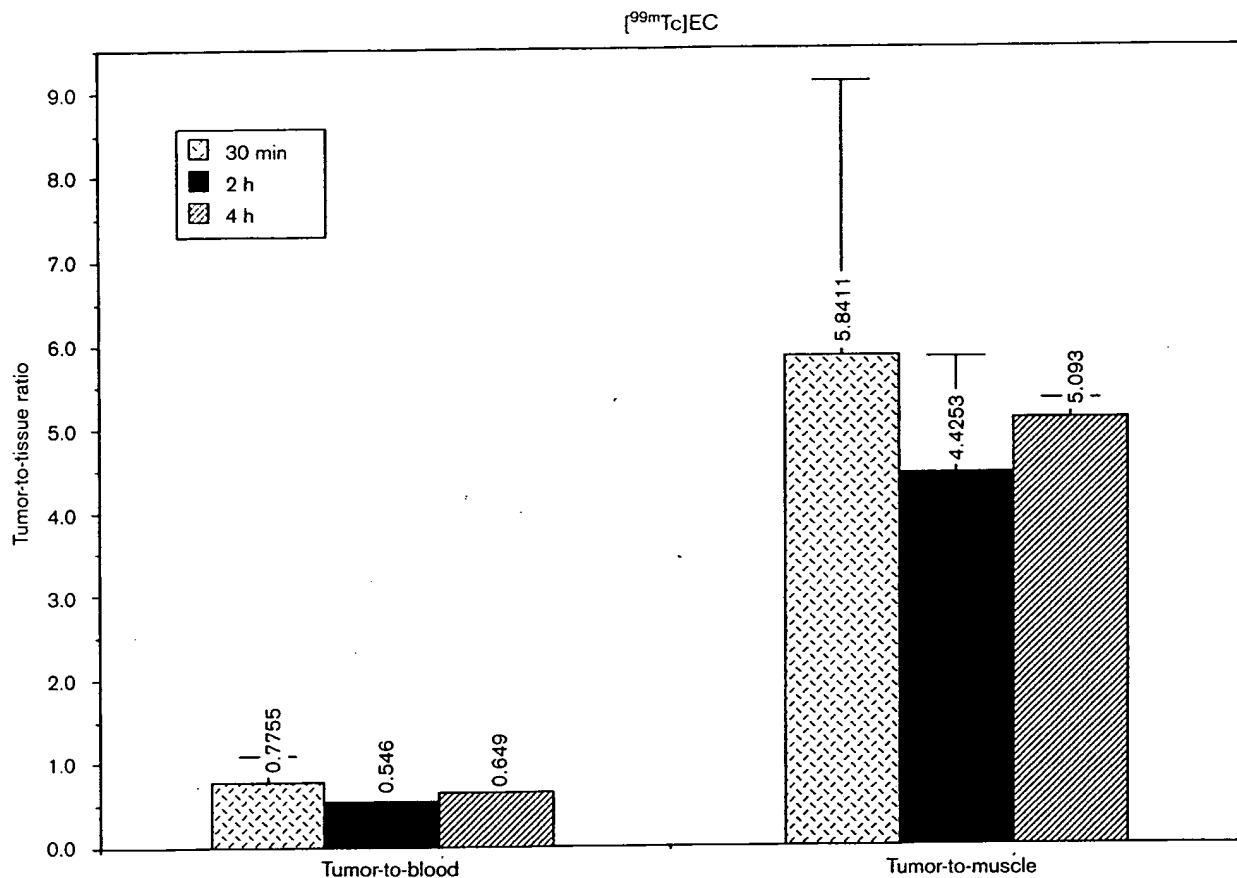


**Figure 4.** Tumor-to-blood and tumor-to-muscle count density ratios of [ $^{99m}\text{Tc}$ ]EC in breast tumor bearing rats as a function of time. Data are expressed as the mean  $\pm$  SE for  $n=3$  rats per group.

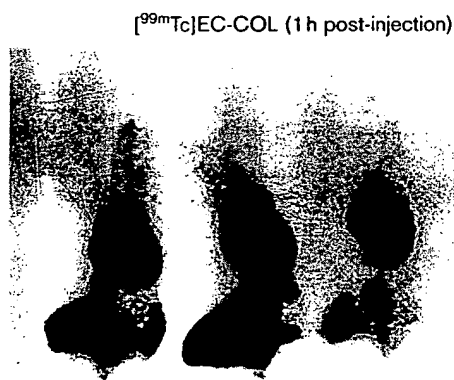


**Figure 5.** Anterior view of breast tumor bearing rats receiving [ $^{99m}\text{Tc}$ ]EC-COL (300  $\mu\text{Ci}$ , i.v.) showed that there was tumor uptake at 1 h post-injection.

[ $^{99m}\text{Tc}$ ]EC-COL (control) (1 h post-injection)

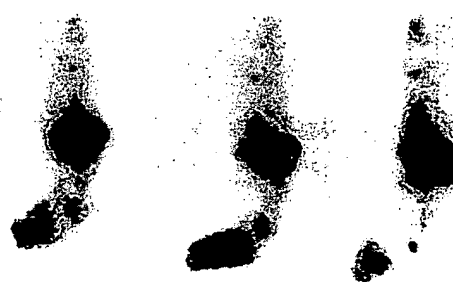


**Figure 6.** Anterior view of breast tumor bearing rats receiving [ $^{99m}\text{Tc}$ ]EC (300  $\mu\text{Ci}$ , i.v.) showed that there was less tumor uptake at 1 h post-injection compared to [ $^{99m}\text{Tc}$ ]EC-COL.

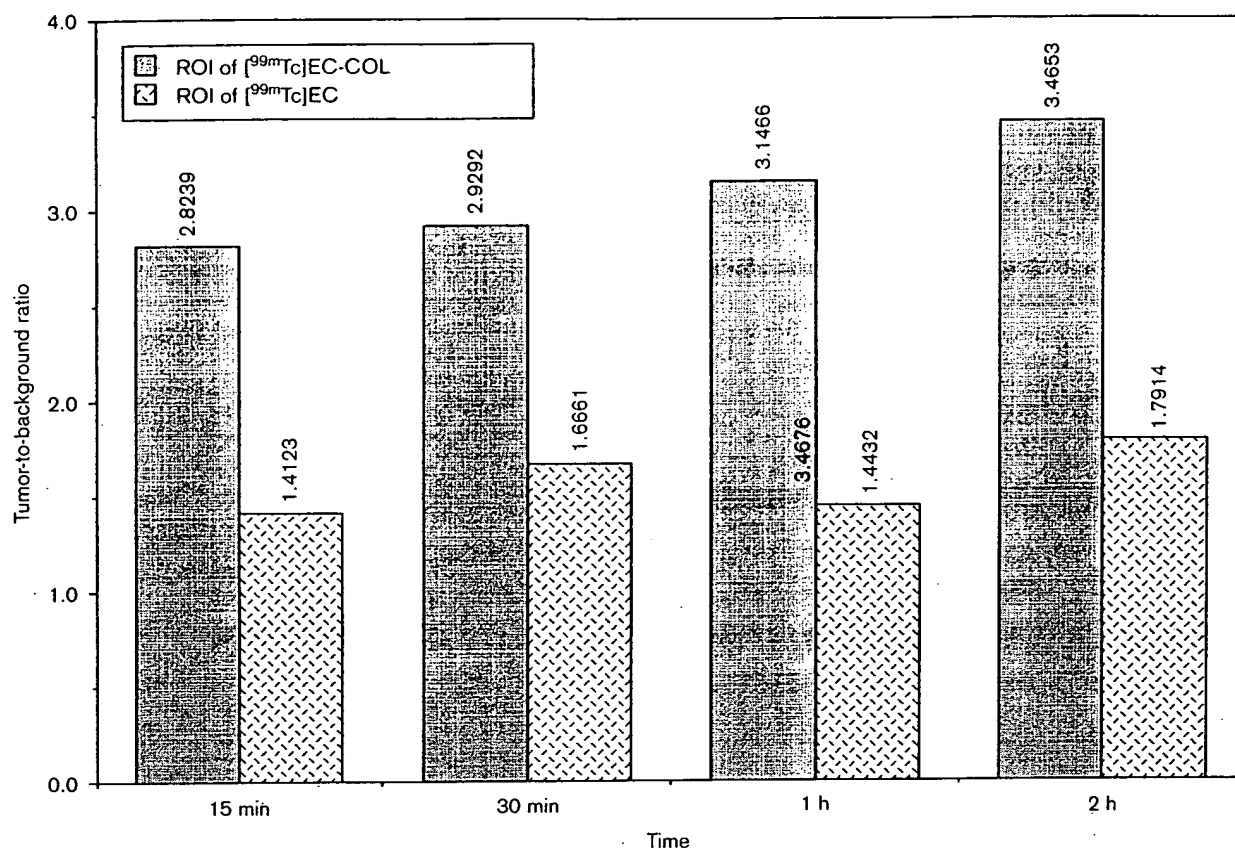


**Figure 7.** Computer outlined ROI comparison of tumor-to-background ratios between [ $^{99m}\text{Tc}$ ]EC-COL and [ $^{99m}\text{Tc}$ ]EC in breast tumor bearing rats.

#### Gamma scintigraphic imaging of [ $^{99m}\text{Tc}$ ]EC-COL in breast tumor bearing rats

*In vivo* imaging studies in three breast tumor bearing rats at 1 h post-administration indicated that the tumor could be visualized well with the [ $^{99m}\text{Tc}$ ]EC-COL group (Figure 5), whereas less tumor uptake in the [ $^{99m}\text{Tc}$ ]EC group was observed (Figure 6). The computer outlined ROI showed that tumor/background ratios in the [ $^{99m}\text{Tc}$ ]EC-COL group were significantly higher than the [ $^{99m}\text{Tc}$ ]EC group (Figure 7).

#### Discussion

Due to better imaging characteristics and lower price, attempts are made to replace the  $^{123}\text{I}$ ,  $^{131}\text{I}$ ,  $^{67}\text{Ga}$ - and  $^{111}\text{In}$ -labeled compounds with corresponding  $^{99m}\text{Tc}$ -labeled compounds when possible. Verbruggen *et al.* reported that EC can be labeled with  $^{99m}\text{Tc}$  very easily

and efficiently at room temperature with high radiochemical purity, and the preparation remains stable for at least 8 h.<sup>7</sup> Because of the reported labeling capacity and rapid renal clearance, EC was selected to synthesize a new  $^{99m}\text{Tc}$ -labeled COL. EC-COL was prepared using a relatively simple and fast chemistry. A labeling kit was also developed. Radio-TLC results with the [ $^{99m}\text{Tc}$ ]EC-COL kit confirm the high radiochemical purity and stability in serum.

In the tissue distribution studies, although no significance difference of tumor-to-blood uptake between [ $^{99m}\text{Tc}$ ]EC-COL and [ $^{99m}\text{Tc}$ ]EC groups was observed, there was a significantly increased tumor-to-tissue uptake ratio as a function of time within the [ $^{99m}\text{Tc}$ ]EC-COL group. Planar imaging of [ $^{99m}\text{Tc}$ ]EC-COL demonstrated the feasibility to image tumors at 1 h post-injection.

The development of new ligands to assess the anti-tubulin effect is clinically desirable for the assessment of treatment outcome. Microtubules are involved in the biochemical process of cellular functions. Microtubulin is associated with cell mitosis and angiogen-

esis. Antimitotic compounds such as vincristine and COL bind with high affinity to microtubule proteins (tubulin), disrupting microtubule assembly and causing mitotic arrest of the proliferating cells. In addition to disrupted microtubule depolymerization, COL also induced apoptotic cell death.<sup>11-18</sup> Apoptosis (programmed cell death) occurs during the treatment of cancer with chemotherapy and radiation. Assessment of apoptosis would be useful to evaluate the efficacy of therapy such as disease progression or regression.

In summary, this study demonstrates the feasibility of using [<sup>99m</sup>Tc]EC-COL for *in vivo* imaging of breast tumors. The findings support further studies on determining treatment outcome by monitoring disease progression using [<sup>99m</sup>Tc]EC-COL and correlating histopathological findings associated with apoptosis.

## Acknowledgments

The authors wish to thank Dianne Perez for her secretarial support. This work was supported in part by the John S Dunn Foundation and Pioneer Pharmaceutical Research Fund.

## References

1. Lu MC. Antimitotic agents. In: Foye WO, ed. *Cancer chemotherapeutic agents*. Washington, DC: American Chemical Society 1995: 345-68.
2. Goh EL, Pircher TJ, Lobie PE. Growth hormone promotion of tubulin polymerization stabilizes the microtubule network and protects against colchicine-induced apoptosis. *Endocrinology* 1998; 139: 4364-72.
3. Wang TH, Wang HS, Ichijo H, et al. Microtubule-interfering agents activate c-Jun N-terminal kinase/stress-activated protein kinase through both Ras and apoptosis signal-regulating kinase pathways. *J Biol Chem* 1998; 273: 4928-36.
4. Ratner S, Clarke HT. The action of formaldehyde upon cysteine. *J Am Chem Soc* 1937; 59: 200-6.
5. Blondeau P, Berse C, Gravel D. Dimerization of an intermediate during the sodium in liquid ammonia reduction of 1-thiazolidine-4-carboxylic acid. *Can J Chem* 1967; 45: 49-52.
6. Davison A, Jones AG, Orvig C, Sohn M. A new class of oxotechnetium(+5) chelate complexes containing a TcON<sub>2</sub>S<sub>2</sub> core. *Inorg Chem* 1981; 20: 1629-32.
7. Verbruggen AM, Nosco DL, Van Nerom CG, et al. Tc-99m-1,1-ethylenedicycysteine: a renal imaging agent. I. Labelling and evaluation in animals. *J Nucl Med* 1992; 33: 551-7.
8. Van Nerom CG, Bormans GM, De Roo MJ, Verbruggen AM. First experience in healthy volunteers with Tc-99m-1,1-ethylenedicycysteine, a new renal imaging agent. *Eur J Nucl Med* 1993; 20: 783-46.
9. Surma MJ, Wiewiora J, Liniecki J. Usefulness of Tc-99m-N,N'-ethylene-1-dicycysteine complex for dynamic kidney investigations. *Nucl Med Commun* 1994; 15: 628-35.
10. Raffauf RF, Farren AL, Ulliot GE. Colchicine. Derivatives of trimethylcolchicinic acid. *J Am Chem Soc* 1953; 75: 5292-4.
11. Suzuki Y, Takeda M, Obara N, Suzuki N. Colchicine-induced cell death and proliferation in the olfactory epithelium and vomeronasal organ of the mouse. *Anat Embryol* 1998; 198: 43-51.
12. Ceccatelli S, Ahlborn E, Diana A, Zhivotovsky B. Apoptosis in rat hippocampal dentate gyrus after intraventricular colchicine. *Neuroreport* 1997; 8: 3779-83.
13. Bumbasirevic V, Skaro-Milik A, Mircic A, Djuricic B. Apoptosis induced by microtubule disrupting drugs in normal murine thymocytes *in vitro*. *Scan Microsc* 1995; 9: 509-16.
14. Bonfoco E, Ceccatelli S, Manzo L, Nicotera P. Colchicine induces apoptosis in cerebellar granule cells. *Exp Cell Res* 1995; 218: 189-200.
15. Lindenboim L, Haviv R, Stein R. Inhibition of drug induced apoptosis by survival factors in PC12 cells. *J Neurochem* 1995; 64: 1054-63.
16. Nakagawa-Yagi Y. Induction of apoptotic cell death in differentiating neuroblastoma SH-SY5Y cells by colchicine. *Biochem Biophys Res Commun* 1994; 199: 807-17.
17. Tsukidate K, Yamamoto K, Snyder JW, Farber JL. Microtubule antagonists activate programmed cell death in cultured rat hepatocytes. *Am J Pathol* 1993; 143: 918-25.
18. Takano Y, Okudaira M, Harmon BV. Apoptosis induced by microtubule disrupting drugs in cultured human lymphoma cells. *Pathol Res Pract* 1993; 189: 197-203.

(Received 30 March 1999; accepted 2 June 1999)

## IMAGING TUMOR FOLATE RECEPTORS USING RADIOLABELED FOLATE AND METHOTREXATE

D.J. Yang, <sup>1</sup>S. Zakko, <sup>1</sup>J. Boulfelfel, <sup>1</sup>H.A. Shamsi, S. Ilgan, D-F Yu,  
L.W. Tansey, C-W Liu, F. Zare, E. E. Kim, D.A. Podoloff

University of Texas M.D. Anderson Cancer Center, Houston, TX and  
<sup>1</sup>Dubai Hospital, Dubai, U.A.E.

Key Words: folate receptor, imaging, Tc-99m, In-111

It is known that membrane folic acid receptors are responsible for cellular accumulation of folate and folate analogs such as methotrexate and overexpressed on various tumor cells. However, these receptors are highly restricted in normal differentiated tissues. (1-3) Results of limited in vitro and in vivo animal studies suggest that folate receptors could be a potential target for tumor imaging. This study aimed to develop a <sup>99m</sup>Tc-labeled folic acid using ethylenedicysteine (EC) as a chelator and an In-111 labeled DTPA-methotrexate (DTPA-MTX) to image tumor folate receptors in vivo.

EC was prepared in a two-step synthesis according to the previously described methods. (4-6) EC was then conjugated to 5-aminoethylamino folic acid (7) using water soluble carbodiimide. Tissue distribution of <sup>99m</sup>Tc-EC-folate was determined in breast tumor-bearing rats at 20 min, 1, 2, and 4 h (n=3/time interval, 370 KBq/rat, i.v.). Blocking study was employed to determine receptor-mediated process; <sup>99m</sup>Tc-EC-folate was co-administrated with 50 and 150  $\mu$ mol/kg of cold folic acid to tumor-bearing rats. Planar imaging and whole-body autoradiograms were performed. The data was compared to that using <sup>99m</sup>Tc-EC (control). In animal studies, tumor/blood count density ratios at 20 min-4 h increased from  $0.81 \pm 0.09$  to  $1.23 \pm 0.13$  with <sup>99m</sup>Tc-EC-folate. Conversely, these values showed time-dependent decrease from  $0.77 \pm 0.32$  to  $0.65 \pm 0.01$  with <sup>99m</sup>Tc-EC in the same time period. Tumor/muscle and tumor/blood count density ratios significantly decreased with folic acid co-administrations. Planar images and autoradiograms confirmed that the tumors could be visualized clearly with <sup>99m</sup>Tc-EC-folate.

DTPA-MTX was synthesized by reacting ethylenediamine with MTX, yielded 82%. The resulting amino analogue of MTX was reacted



with DTPA dianhydride in basic aqueous solution followed by dialysis (cut-off M.W. 500), yielded 85%. Tissue distribution was conducted in breast tumor-bearing rats (induced by 13762 cell line,  $10^6$  cells/rat, s.c. at hind legs) at 0.5, 2, 24 and 48 hours ( $n=3$ /time interval,  $10 \mu\text{Ci/rat}$ , iv). Planar imaging and autoradiograms were performed at 0.5, 24 and 48 hours. The data was compared to  $^{111}\text{In}$ -DTPA (control). Preliminary clinical trial was conducted in a patient with bone fracture. In animal studies, tumor/blood count density ratio at 0.5-48 hours was ranged  $0.8 \pm 0.32$  to  $2.2 \pm 0.41$  for  $^{111}\text{In}$ -DTPA-MTX; and  $0.56 \pm 0.10$  to  $1.19 \pm 0.69$  for  $^{111}\text{In}$ -DTPA, respectively. Tumor uptake value (% ID/g) of  $^{111}\text{In}$ -DTPA-MTX at 0.5 hour was  $0.3 \pm 0.13$ . Planar images and autoradiograms demonstrated that the tumors could be visualized well.

Preliminary clinical study in a patient with bone fracture showed high uptake with  $^{99m}\text{Tc}$ -MDP and no uptake with  $^{201}\text{Tl}$  chloride and  $^{111}\text{In}$ -DTPA-MTX. High uptake in kidneys was observed both in animals and human. This could be due to folate reabsorption in the renal proximal tubules. Our findings indicate the feasibility of using  $^{99m}\text{Tc}$ -EC-folate and  $^{111}\text{In}$ -DTPA-MTX to image tumors through a folate receptor-mediated process.

#### References

1. Campbell I.G., Jones T.A., Foulkes W.D., and Trowsdale J. *Cancer Res* **51**:5329 (1991).
2. Weitman S.D., Weinberg A.G., Coney L.R., Zurawski V.R., Jennings D.S., and Kamen B.A. *Cancer Res* **52**:6708 (1992).
3. Holm J., Hansen S.I., Hoier-Madsen M., Sondergaard K, and Bzorek M. *APMIS* **102**:413 (1994).
4. Surma M.J., Wiewiora J., and Liniecki J. *Nucl. Med. Comm.* **15**:628 (1994).
5. Ratner S., and Clarke H.T. *J. Am. Chem. Soc.* **59**:200 (1937).
6. Blondeau P., Berse C., and Gravel D. *Can. J. Chem.* **45**:49 (1967).
7. Luo J., Smith M.D., Lantrip D.A., Wang S., Fuchs P.L. *J. Am. Chem. Soc.* **119**:10004-10013 (1997).

# Short Communication

## PGP9.5 As a Candidate Tumor Marker for Non-Small-Cell Lung Cancer

Kenji Hibi,\* William H. Westra,\*\* Michael Borges,†  
 Steve Goodman,‡ David Sidransky,\*\* and  
 Jin Jen\*\*

*From the Department of Otolaryngology-Head and Neck Surgery,  
 Division of Head and Neck Cancer Research,\* and the  
 Departments of Pathology† and Oncology,\*\* Johns Hopkins  
 University School of Medicine, Baltimore, Maryland*

PGP9.5 is a neurospecific peptide that functions to remove ubiquitin from ubiquitinated proteins and prevents them from targeted degradation by proteasomes. Using the serial analysis of gene expression method (SAGE), we observed that the PGP9.5 transcript was highly expressed in primary lung cancers and lung cancer cell lines but was not detectable in the normal lung. Here we examined the expression of PGP9.5 protein in normal lung epithelium, lung tumor cell lines, and 98 resected primary non-small-cell lung carcinomas (NSCLCs). We found PGP9.5 reactivity in normal lung in a pattern compatible with K-cells of the diffuse neuroendocrine system. However, the PGP9.5 was present in both small-cell lung cancer (SCLC) and NSCLC cell lines (22/24) independent of neuronal differentiation. In primary NSCLCs, 54% (53/98) of the cases had positive PGP9.5 staining, and the expression of protein was strongly associated with pathological stage of the cancer. It was present in 44% (29/66) of stage I NSCLCs and in 75% (24/32) of stage II and IIIA NSCLCs ( $p = 0.0032$ ). These results suggest that the increased expression of PGP9.5 is specifically associated with lung cancer development and may serve as a potential marker for the detection of lung cancer. (*Am J Pathol* 1999, 155:711-715)

Lung cancer is the second most common malignancy worldwide and is the leading cause of cancer death in men.<sup>1</sup> Accumulating evidence indicates that a series of genetic changes in dominant oncogenes such as *myc* and *ras* are involved in the pathogenesis of human lung cancer.<sup>2,3</sup> Several other candidate oncogenes have also been implicated.<sup>4,5</sup> It is now clear that the accumulation of multiple genetic changes in a tumor leads to major

differences involving altered expression of many genes.<sup>6</sup> Recently, using the serial analysis of gene expression (SAGE) method, we showed that the PGP9.5 (protein gene product 9.5) gene had no detectable expression in normal lung tissues but was frequently overexpressed in primary non-small-cell lung tumors.<sup>7</sup>

PGP9.5 is a ubiquitin hydrolase widely expressed in neuronal tissues at all stages of neuronal differentiation.<sup>8,9</sup> Ubiquitination of cellular proteins and targeting them for subsequent degradation via ubiquitin-mediated proteolysis is potentially an important mechanism that regulates cell cycle genes.<sup>10,11</sup> In tumors, increased deubiquitination of cyclins by PGP9.5 could contribute to the uncontrolled growth of somatic cells.<sup>12</sup>

To better characterize the role of PGP9.5 in lung cancer, we first studied PGP9.5 expression in normal lung and a panel of lung cancer cell lines with defined neuroendocrine (NE) differentiation. Next, we examined the expression of PGP9.5 in 98 resected primary non-small-cell lung cancers (NSCLCs), using immunohistochemistry and correlated PGP9.5 expression in tumors with the clinicopathological features of affected patients.

### Materials and Methods

#### Tissue Specimens

All lung cancer cell lines were obtained from the American Type Culture Collection (ATCC) and propagated according to the provided instructions.<sup>13</sup> Formalin-fixed and paraffin-embedded tumor samples from consecutive patients who had undergone resections of NSCLCs with curative intent were retrieved from the Surgical Pathology files of the Johns Hopkins Hospital (JHH). Information regarding tumor stage, tumor recurrence, and patient

Supported in part by National Institutes of Health grant CA06973, Lung SPORE CA58184, and an award to J. Jen from the V Foundation.

Accepted for publication May 22, 1999.

Address reprint requests to Dr. Jin Jen, Department of Otolaryngology-Head and Neck Surgery, Division of Head and Neck Cancer Research, Johns Hopkins University School of Medicine, 824 Ross Research Building, 720 Rutland Avenue, Baltimore, MD 21205-2196. E-mail: jenjin@jhmi.edu.

survival was obtained from the medical records, including the JHH Tumor Registry files.

### *Northern Blot Analysis*

Cell lines used for Northern blot analysis were collected after trypsinization and lysed immediately in Trizol reagent (GIBCO BRL, Gaithersburg, MD). Normal lung total RNA was extracted by the GuSCN method and purified by CsCl gradient ultracentrifugation as described.<sup>7</sup> Ten micrograms of RNA was separated on a 1.5% denaturing agarose gel and transferred to Gene Screen membrane (DuPont, Boston, MA). A PGP9.5 cDNA probe was isolated from an EST clone (no. 268107) obtained from Genome Systems (Huntsville, AL). Northern blot hybridization using the PGP9.5 cDNA probe was performed as described.<sup>7</sup>

### *Western Blot Analysis*

Twenty micrograms of cell lysates was separated on a 4–20% sodium dodecyl sulfate gradient gel and transferred to a polyvinylidene difluoride membrane (Micron Separations, Westborough, MA). After the nonspecific sites were blocked by incubation in phosphate-buffered saline + 5% nonfat dry milk (NFD), the blot was incubated with the polyclonal rabbit antiserum against PGP9.5 (Biogenesis, Sandown, NH) at 1:400 dilution for 2 hours at room temperature. After washing, an ECL kit (Amersham, Arlington Heights, IL) was used to visualize the antibody binding to PGP9.5 protein.

### *Immunohistochemical Analysis*

Six- $\mu$ m sections were made from paraffin tissue blocks, and the slides were dried at 60°C for 30 minutes, treated with xylenes, and then dehydrated in alcohol. Endogenous peroxidase was blocked with 0.3% H<sub>2</sub>O<sub>2</sub>. Microwave treatment was performed for 4 minutes in Antigen Retrieval Glycine solution (Biogenex, San Ramon, CA), because it has been shown that the immunoreactivity of PGP9.5 was markedly enhanced by this method.<sup>14</sup> After blocking with normal goat serum, the slides were incubated with the polyclonal rabbit antiserum against PGP9.5 (Biogenesis) at 1:1000 dilution for 2 hours at room temperature. Vectastain ABC Kit and DAB Substrate Kit (Vector, Burlingame, CA) were used to visualize the antibody binding, and the sections were counterstained with hematoxylin.

Immunohistochemical staining for PGP9.5 was interpreted by an experienced pathologist (W.H.W.). For control studies, HeLa and H157 lung cancer cell lines were used as negative and positive controls. The PGP9.5 status of these two cell lines was confirmed by Northern and Western analysis<sup>7</sup> (data not shown). Optimized conditions were then used for the immunostaining of primary lung cancer specimens. In all cases, small nerves in the tissue sections served as a positive internal control, and desmoplastic stroma served as a negative internal control for PGP9.5 staining. Only cytoplasmic staining above

background levels was regarded as specific staining. All immunohistochemical slides were initially reviewed to assess the range of this PGP9.5 immunoreactivity with respect to intensity and distribution of staining. Two patterns were recognized: 1) the tumor was uniformly nonimmunoreactive; or 2) moderate to strong immunoreactivity approaching the intensity seen in the internal control (ie, nerves) was uniformly present throughout most (ie, >70%) of the tumor. Accordingly, tumors were subsequently scored as either negative or positive, based on the total absence or generalized presence of specific staining. To correlate the distribution of the scattered PGP9.5-positive cells in the normal bronchial epithelium with the distribution of the neuroendocrine K-cells, lung sections from two independent cases were incubated with a monoclonal antibody against chromogranin (Boehringer Mannheim, Indianapolis, IN; 1:2000 dilution).

### *Statistical Analysis*

The  $\chi^2$  test was used to examine the association between the PGP9.5 expression status and clinicopathological features.

## *Results*

### *Expression of PGP9.5 Protein in Normal Lung Tissues*

We have previously observed that the PGP9.5 message was frequently detected in lung carcinomas, but was not detectable in normal lung by Northern analysis or reverse transcription-polymerase chain reaction methods.<sup>7</sup> This result suggested that PGP9.5 protein expression could potentially be used as a marker for lung cancer. To better characterize the cell type origin and the timing of PGP9.5 expression, an immunohistochemical approach was used to localize PGP9.5 protein expression in the normal lung and the tumor samples. As shown in Figure 1A, the majority of the normal lung epithelial cells were negative by PGP9.5 staining. In sections of nonneoplastic lung, PGP9.5 staining was restricted to nerves and a few isolated cells scattered throughout the bronchial epithelium. The positive staining of neurons is consistent with the fact that PGP9.5 is a neuron-specific peptide widely expressed in neuronal tissue.<sup>8</sup> The PGP9.5-positive cells scattered throughout the nonneoplastic bronchial epithelium were reminiscent of the neuroendocrine K-cells, based on their morphological appearance and pattern of distribution.<sup>15</sup>

To determine the histological origin of these scattered PGP9.5-positive cells, we stained parallel sections from two cases with chromogranin, a well-characterized marker of neuroendocrine differentiation.<sup>16</sup> As shown in Figure 1B, chromogranin-positive cells showed the same location and tissue distribution as the PGP9.5-positive cells. This result suggests that, in nonneoplastic lung, PGP9.5 protein expression is restricted to cells of the dispersed NE system.

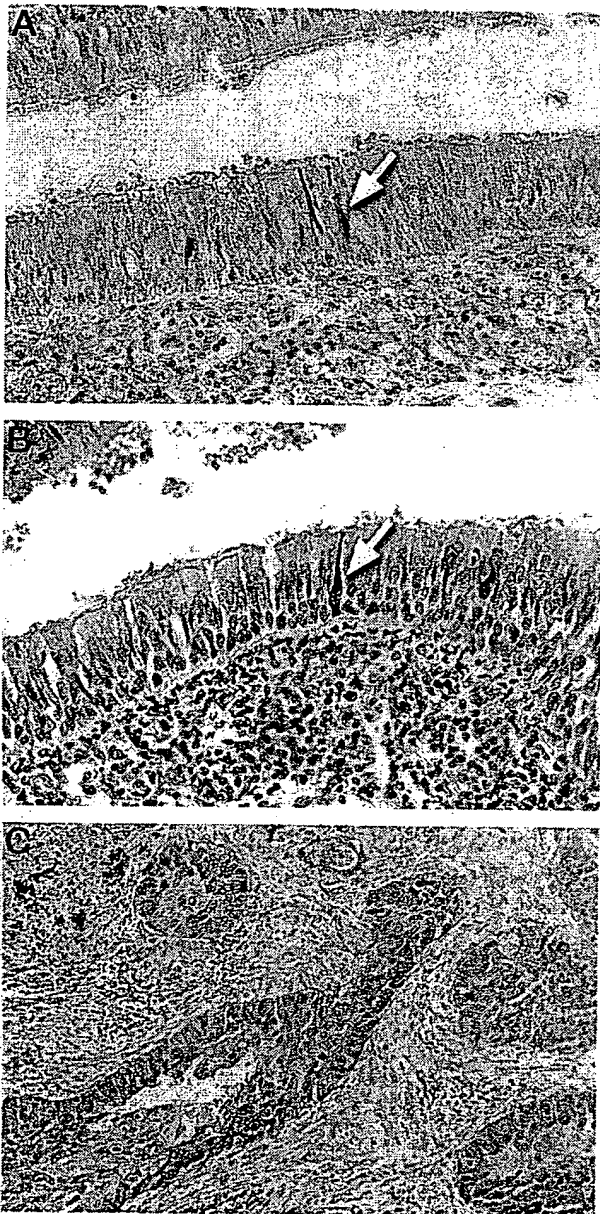


Figure 1. Immunohistochemical staining of lung tumor and adjacent lung tissue for PGP9.5 and chromogranin. A: PGP9.5 staining is present in isolated cells dispersed throughout the normal bronchial mucosa (arrow). B: Chromogranin staining is present in the compatible population of cells as seen in A (arrow). C: Example of PGP9.5 staining in lung cancer.

### PGP9.5 Expression Is Independent of *hASH1* Status in Lung Cancers

Because a majority of small-cell lung cancers and a portion of the NSCLCs often exhibit features of NE differentiation, we next tested whether PGP9.5 overexpression was associated with lung cancers of NE lineage. A panel of established lung cancer cell lines with *hASH1* status was used for this study. *hASH1* is a transcription factor essential for the NE development of the human lung.<sup>17</sup> As shown in Figure 2 (upper panel), PGP9.5 message was abundantly detected in both small-cell lung cancer (SCLC) and NSCLC cell lines regardless of *hASH1* status.

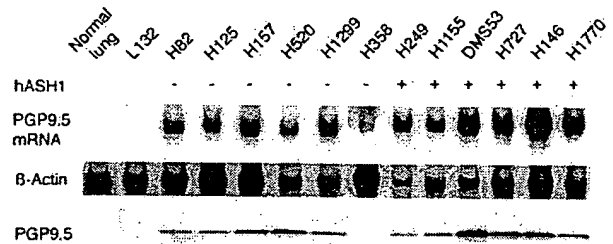


Figure 2. PGP9.5 expression in lung cancer cell lines with defined *hASH1* status. PGP9.5 transcript was not detectable in either normal lung or an embryonic lung cell line (L132) but was expressed in all lung cancer cell lines. The *hASH1* status is indicated at the top. H358 had a weak PGP9.5 message compared to other cell lines. The lower panel shows a Western blot using the anti-PGP9.5 antibody. Note that all tumor cell lines except H358 had PGP9.5 protein. The  $\beta$ -actin control was used to normalized sample loading. The histological subtypes of the cell lines are: L132, embryonic lung; H82, H249, DMS53, and H146, small cell carcinoma; H125, adenocarcinoma; H157 and H520, squamous cell carcinoma; H1299 and H1155, large cell carcinoma; H358, bronchoalveolar carcinoma; H727, carcinoid; H1770, neuroendocrine carcinoma.

Similarly, the PGP9.5 protein was detected in nearly all cell lines that expressed the gene (Figure 2, lower panel). Although there was a faint message in H358 by Northern analysis, no PGP9.5 protein was detectable for this sample. Furthermore, no PGP9.5 product was obtained by reverse transcription-polymerase chain reaction in this case, indicating that the message was probably rearranged or unstable and could not serve as a template for protein translation. Thus the expression of PGP9.5 appears to be present in NSCLC in the absence of NE differentiation, as well as SCLC frequently derived from NE cells of the lung.

### Association of PGP9.5 Expression with Pathological Stage in NSCLC

To seek the role of PGP9.5 expression in NSCLC, we examined the presence of PGP9.5 protein in the tumors of 98 NSCLC patients, using immunohistochemistry. The clinicopathological features of the patients and the results of PGP9.5 staining are shown in Table 1. Overall, 54% (53/98) of NSCLCs were positive by PGP9.5 staining, and the intensity of the staining was uniform and consistent for almost all cases (Figure 1C). Seventy-two percent (26/36) of squamous cell carcinomas were stained positive for PGP9.5, whereas only 41% (22/54) of adenocarcinomas had positive PGP9.5 staining ( $p = 0.0066$ ). These results are consistent with previous reports which showed that squamous cell carcinomas were more likely to be PGP9.5-positive than adenocarcinomas of the lung.<sup>18,19</sup> However, when the clinical stage of the patients was considered, the PGP9.5-positive rate for stage II and IIIA patients was significantly higher than those with stage I disease ( $p = 0.0074$ ) (Table 1).

### Discussion

PGP9.5 was first isolated as a specific cytoplasmic marker for neurons and NE cells.<sup>20,21</sup> About 10–15% NSCLCs demonstrate NE features by electron micros-

Table 1. Clinicopathological Features and PGP9.5 Expression in Primary NSCLC

Clinicopathological feature	Variable	No. of cases	PGP9.5 expression		p value*
			+	-	
Sex	Male	61	37 (61%)	24 (39%)	0.14
	Female	37	16 (43%)	21 (57%)	
Histology	Adenocarcinoma	55	22 (41%)	32 (59%)	<0.01†
	Squamous cell carcinoma	36	26 (72%)	10 (28%)	
	Others	8	5 (63%)	3 (37%)	
Tumor stage	I	66	29 (44%)	37 (56%)	<0.01
	II and IIIA	32	24 (75%)	8 (25%)	
Vital status	Alive	26	11 (42%)	15 (58%)	0.24
	Dead	72	42 (58%)	30 (42%)	
Median follow-up time	41 months				
Total		98	53 (54%)	45 (46%)	

\* $\chi^2$  test.

†PGP9.5 expression in adenocarcinoma versus squamous cell carcinoma.

copy or immunohistochemistry, despite the absence of NE features by light microscopy. Therefore, it was possible that PGP9.5 expression in these cancers may have simply reflected their NE status. Indeed, PGP9.5 had been used as a marker of NE differentiation for lung tumors. However, discordant staining patterns between PGP9.5 and other neuroendocrine markers have often been observed.<sup>18,19</sup> In our study, *hASH1* was used as a marker of neuroendocrine differentiation, because homozygous disruption of the *hASH1* gene in mouse prevents the development of pulmonary NE cells.<sup>17</sup> However, most lung tumor cell lines expressed high levels of PGP9.5, regardless of *hASH1* gene expression. Therefore, our results suggested that expression of PGP9.5 in lung cancers is independent of NE differentiation.

Functionally, PGP9.5 belongs to the ubiquitin carboxyl-terminal hydrolase (UCH) family.<sup>8</sup> The UCH family has conserved Cys and His domains common to yeast and mammalian ubiquitin hydrolases.<sup>22,23</sup> It is becoming increasingly clear that these enzymes are a part of the cellular proteolytic pathway that regulates many cellular processes, including cell cycle progression and cell death.<sup>12</sup> Several other studies have shown that some UCH family members are overexpressed in different tumors and can potentially be oncogenic. For example, the *tre-2* gene was identified as one of the UCH family proteins. The expression of *tre-2* is not detectable in normal tissues but becomes elevated in a variety of tumor cells.<sup>24</sup> Another UCH family gene, *Unph*, was isolated as a human homolog of the murine *Unp* protooncogene.<sup>25</sup> Overexpression of murine *Unp* gene leads to oncogenic transformation of NIH3T3 cells, and the expression level of this gene is also elevated in lung tumors.<sup>25,26</sup> The results of our current study also suggest that the expression of PGP9.5 in lung cancer may play a causative role in the oncogenic transformation of human lung epithelial cells, because 1) PGP9.5 shares conserved domains with the members of ubiquitin hydrolase family, several of which are potential oncogenes; 2) PGP9.5 expression is not present in the normal lung epithelium, but becomes activated sometimes during the course of neoplastic transformation; and 3) expression of PGP9.5 is closely associated with advanced stages of NSCLC.

Although further studies will be needed to elucidate the downstream target of deubiquitination by PGP9.5 and to better understand the molecular mechanism of PGP9.5 overexpression in lung cancer development, the frequent occurrence of PGP9.5 expression in NSCLC makes it a potential marker for the detection of this disease.

### Acknowledgments

We thank Dr. Stephen Baylin for helpful discussions about the project and Mrs. Janice Pulley for assistance with the manuscript preparation.

### References

1. American Cancer Society: Cancer Facts and Figures—1997. Atlanta, American Cancer Society, 1997
2. Rodenhuis S, van de Wetering ML, Mooi WJ, Evers SG, van Zandwijk N, Bos JL: Mutational activation of the K-ras oncogene. A possible pathogenetic factor in adenocarcinoma of the lung. *N Engl J Med* 1987, 317:929–935
3. Nau MM, Brooks BJ, Battey J, Sausville E, Gazdar AF, Kirsch IR, McBride OW, Bertness V, Hollis GF, Minna JD: L-myc, a new myc-related gene amplified and expressed in human small cell lung cancer. *Nature* 1985, 318:69–73
4. Hibi K, Takahashi T, Sekido Y, Ueda R, Hida T, Ariyoshi Y, Takagi H, Takahashi T: Coexpression of the stem cell factor and the c-kit genes in small-cell lung cancer. *Oncogene* 1991, 6:2291–2296
5. Hibi K, Yamakawa K, Ueda R, Horio Y, Murata Y, Tamari M, Uchida K, Takahashi T, Nakamura Y, Takahashi T: Aberrant upregulation of a novel integrin  $\alpha$  subunit gene at 3p21.3 in small cell lung cancer. *Oncogene* 1994, 9:611–619
6. Kinzler KW, Vogelstein B: Landscaping the cancer terrain. *Science* 1998, 280:1036–1037
7. Hibi K, Liu Q, Beaudry GA, Madden SL, Westra WH, Wehage SL, Yang SC, Heitmiller RF, Bertelsen AH, Sidransky D, Jen J: Serial analysis of gene expression in non-small cell lung cancer. *Cancer Res* 1998, 58:5690–5694
8. Wilkinson KD, Lee KM, Deshpande S, Duerksen-Hughes P, Boss JM, Pohl J: The neuron-specific protein PGP9.5 is a ubiquitin carboxyl-terminal hydrolase. *Science* 1989, 246:670–673
9. Schofield JN, Day IN, Thompson RJ, Edwards YH: PGP9.5, a ubiquitin C-terminal hydrolase; pattern of mRNA, and protein expression during neural development in the mouse. *Brain Res Dev Brain Res* 1995, 85:229–238
10. Hochstrasser M: Ubiquitin-dependent protein degradation. *Annu Rev Genet* 1996, 30:405–439

11. Diehl JA, Zindy F, Sherr CJ: Inhibition of cyclin D1 phosphorylation on threonine-286 prevents its rapid degradation via the ubiquitin-proteasome pathway. *Genes Dev* 1997, 11:957-972
12. Spataro V, Norbury C, Harris AL: The ubiquitin-proteasome pathway in cancer. *Br J Cancer* 1998, 77:448-455
13. Phelps RM, Johnson BE, Ihde DC, Gazdar AF, Carbone DP, McClintock PR, Linnoila RI, Matthews MJ, Bunn PA Jr, Carney D, Minna JD, Mulshine JL: NCI-Navy Medical Oncology Branch cell line data base. *J Cell Biochem Suppl* 1996, 24:32-91
14. McQuaid S, McConnell R, McMahon J, Herron B: Microwave antigen retrieval for immunocytochemistry on formalin-fixed, paraffin-embedded post-mortem CNS tissue. *J Pathol* 1985, 176:207-216
15. McDowell EM, Barrett LA, Trump BF: Observations on small granule cells in adult human bronchial epithelium and in carcinoid and oat cell tumors. *Lab Invest* 1976, 34:202-206
16. Wilson BS, Lloyd RV: Detection of chromogranin in neuroendocrine cells with a monoclonal antibody. *Am J Pathol* 1984, 115:458-468
17. Borges M, Linnoila RI, van de Velde HJ, Chen H, Nelkin BD, Mabry M, Baylin SB, Ball DW: An achaete-scute homologue essential for neuroendocrine differentiation in the lung. *Nature* 1997, 386:852-855
18. Dhillon AP, Rode J, Dhillon DP, Moss E, Thompson RJ, Spiro SG, Corrin B: Neural markers in carcinoma of the lung. *Br J Cancer* 1985, 51:645-652
19. Addis BJ, Hamid Q, Ibrahim NB, Fahey M, Bloom SR, Polak JM: Immunohistochemical markers of small cell carcinoma and related neuroendocrine tumours of the lung. *J Pathol* 1987, 153:137-150
20. Jackson P, Thompson RJ: The demonstration of new human brain-specific proteins by high-resolution two-dimensional polyacrylamide gel electrophoresis. *J Neurol Sci* 1981, 49:429-438
21. Day IN, Thompson RJ: Molecular cloning of cDNA coding for human PGP9.5 protein. A novel cytoplasmic marker for neurones and neuroendocrine cells. *FEBS Lett* 1987, 210:157-160
22. Baker RT, Tobias JW, Varshavsky A: Ubiquitin-specific proteases of *Saccharomyces cerevisiae*: Cloning of Ubp2 and Ubp3, and functional analysis of the Ubp gene family. *J Biol Chem* 1992, 267:23364-23375
23. Papa FR, Hochstrasser M: The yeast DOA4 gene encodes a deubiquitinating enzyme related to a product of the human tre-2 oncogene. *Nature* 1993, 366:313-319
24. Nakamura T, Hillova J, Mariage-Samson R, Onno M, Huebner K, Cannizzaro LA, Boghosian-Sell L, Croce CM, Hill M: A novel transcriptional unit of the tre oncogene widely expressed in human cancer cells. *Oncogene* 1992, 7:733-741
25. Gray DA, Inazawa J, Gupta K, Wong A, Ueda R, Takahashi T: Elevated expression of Unph, a proto-oncogene at 3p21.3, in human lung tumors. *Oncogene* 1995, 10:2179-2183
26. Gupta K, Chevrette M, Gray DA: The Unp proto-oncogene encodes a nuclear protein. *Oncogene* 1994, 9:1729-1731

## Short Communication

### Analysis of E-Cadherin in Diffuse-Type Gastric Cancer Using a Mutation-Specific Monoclonal Antibody

Karl-Friedrich Becker,<sup>\*,†</sup> Elisabeth Kremmer,<sup>‡</sup>  
 Manfred Eulitz,<sup>§</sup> Ingrid Becker,<sup>\*</sup>  
 Gabriele Handschuh,<sup>†</sup> Christoph Schuhmacher,<sup>‡</sup>  
 Wolfram Müller,<sup>||</sup> Helmut E. Gabbert,<sup>||</sup>  
 Atsushi Ochiai,<sup>\*\*</sup> Setsuo Hirohashi,<sup>\*\*</sup> and  
 Heinz Höfler<sup>\*†</sup>

*From the Technische Universität München, Klinikum rechts der Isar, Institut für Pathologie\* and Chirurgische Klinik,<sup>‡</sup> München, Germany; the GSF-Forschungszentrum für Umwelt und Gesundheit, Institut für Molekulare Immunologie,<sup>§</sup> Institut für Klinische Molekularbiologie,<sup>||</sup> and Institut für Pathologie,<sup>‡</sup> Neuherberg, Germany; the Institut für Pathologie,<sup>||</sup> Heinrich-Heine Universität, Düsseldorf, Germany; and the Pathology Division,<sup>\*\*</sup> National Cancer Center Research Institute, Tokyo, Japan*

In-frame deletions from the E-cadherin mRNA, coding for a homophilic cell adhesion molecule, are characteristic for diffuse-type gastric carcinomas. Using immunohistochemical analysis the mutant form cannot be distinguished from normal E-cadherin, making results difficult to interpret. In this study, a rat monoclonal antibody, designated E-cad delta 9-1, was generated against a peptide spanning the fusion junction region between exons 8 and 10. This new epitope is present in an E-cadherin variant that lacks exon 9 from the mRNA due to different splice-site gene mutations. Using Western blotting and immunohistochemistry of E-cadherin-transfected cells, we demonstrate that E-cad delta 9-1 specifically reacts with E-cadherin lacking exon 9 but not with the wild-type protein. No immunoreactivity was observed in 31 nontumorous and embryonal tissues analyzed. In gastric carcinoma specimens known to express mutant E-cadherin mRNA lacking exon 9, E-cad delta 9-1 targets exclusively tumor cells in routine formalin-fixed and paraffin-embedded material from biopsies, primary tumors, and lymph node metastases. In a retrospective series of 172 diffuse-type gastric carcinomas expressing E-cadherin, E-cad delta 9-1 reacted with 22 tumors (13%). This new tumor marker-

**monoclonal antibody system could open novel avenues for selective diagnosis and specific therapy of a subgroup of diffuse-type gastric cancer patients.**  
*(Am J Pathol 1999, 155:1803-1809)*

The calcium-dependent homophilic cell adhesion molecule E-cadherin and associated catenins, cytoplasmic plaque proteins, link polarized epithelial cells and maintain the structural integrity of an epithelial monolayer. Moreover, the cadherin/catenin multiprotein complex is implicated in developmental processes and cell signaling.<sup>1-3</sup> Because in carcinomas the tissue architecture is often disorganized, E-cadherin expression has been analyzed in various tumor types typically using immunohistochemistry.<sup>4</sup> It could be demonstrated that E-cadherin immunoreactivity is often reduced or lost in less differentiated and invasive carcinomas.<sup>5</sup> However, in diffuse-type gastric cancer, in which tumor cells generally have lost homophilic cell-to-cell contacts and invade surrounding tissues as single cells, E-cadherin immunoreactivity was detected in many cases,<sup>6-8</sup> whereas in others it was found to be completely absent.<sup>9</sup> The reason for this discrepancy was unknown. The selection of the cases or the use of different antibodies may, at least in part, explain these results.

Recently, E-cadherin gene mutations that may also have contributed to variable immunoreactivity have been identified in tumor cell lines, primary tumors, and lymph node metastases from gastric cancer patients.<sup>10-14</sup> Remarkably, in 50% of diffuse-type gastric cancer patients E-cadherin mutations were identified that typically re-

K.-F. B. is a recipient of a Foreign Research Fellow Award from the Foundation for Promotion of Cancer Research, Tokyo.

Accepted for publication August 5, 1999.

A. Ochiai's present address is Pathology Division, National Cancer Center Research Institute East, 6-5-1, Kashiwa City, Chiba 277-0882, Japan.

Address reprint requests to Dr. Karl-Friedrich Becker, Technische Universität München, Klinikum rechts der Isar, Institut für Pathologie, Ismaninger Strasse 22, D-81675 München, Germany. E-mail: kf.becker@lrz.tum.de.

sulted in in-frame deletions removing partial or complete exon sequences from the extracellular portion of the transmembrane protein or point mutations resulting in amino acid substitutions.<sup>15</sup> Complete deletion of exon 9 from the E-cadherin mRNA is a mutational hot spot in diffuse-type gastric cancer which was detected in 14% (10/70) of the patients analyzed using reverse transcription-polymerase chain reaction (RT-PCR) and sequencing.<sup>11-13</sup> A variety of somatic splice-site gene mutations were identified that lead to in-frame skipping of exon 9 from the E-cadherin mRNA. Although alternative splicing mechanisms are generally possible, they have not been detected for E-cadherin and do not account for the frequent loss of exon 9. In addition, E-cadherin in-frame deletion mutations were exclusively associated with malignant tissues and never seen in nontumorous gastric epithelium from the same patients.

Because E-cadherin mRNA deletion mutations identified in primary gastric tumors and lymph node metastases do not interrupt the reading frame,<sup>15</sup> the mutated protein may still be integrated into the plasma membrane although parts of its extracellular domain are altered. These structurally changed portions of the molecule could serve as possible targets for monoclonal antibodies. Numerous monoclonal antibodies have been generated against E-cadherin.<sup>16,17</sup> However, using current antibodies, it was impossible to differentiate between normal or altered forms of the expressed E-cadherin protein. Here we report the generation and characterization of E-cad delta 9-1, a rat monoclonal antibody that specifically reacts with mutant E-cadherin lacking exon 9 and that does not recognize the wild-type protein. In a multicenter study we determined the frequency of this mutation in archival diffuse-type gastric carcinomas using E-cad delta 9-1.

## Materials and Methods

### Peptide Synthesis and Generation of Monoclonal Antibodies

A 13-mer peptide (Pro-Ile-Phe-Asn-Pro-Thr-Thr-Gly-Leu-Asp-Phe-Glu-Ala) was synthesized that spans the fusion junction between exon 8 and exon 10 from mutant E-cadherin lacking exon 9 and subsequently coupled to Keyhole limpet hemocyanin (KLH) using standard methods. Approximately 50  $\mu$ g of KLH-coupled peptide dissolved in phosphate buffered saline and emulsified with Freund's complete adjuvant were injected both intraperitoneally (i.p.) and subcutaneously (s.c.) into Lou/C rats. After a 4-week interval a final boost without adjuvant was given i.p. and s.c. 3 days before fusion. Fusion of the myeloma cell line P3X63-Ag8.653 with the rat immune spleen cells was performed essentially as described.<sup>18</sup> Hybridoma supernatants were tested in a solid-phase immunoassay using bovine serum albumin-coupled peptide (10  $\mu$ g/ml) adsorbed to polystyrene microtiter plates. Solid-phase enzyme-linked immunosorbent assay (ELISA) on microtiter plates coated with mouse anti-rat Ig antibodies was used to determine the immunoglobulin

type with rat Ig class (anti-IgM; Zymed) and IgG subclass-specific mouse monoclonal antibodies.<sup>19</sup>

### Cells and cDNA Transfection

Wild-type and mutant E-cadherin cDNA used for transfection were generated by RT-PCR from normal or malignant gastric tissue, respectively, and cloned into the expression vector pBAT (a gift from Prof. Takeichi; inserts are under the control of a chicken  $\beta$ -actin promoter). The coding regions of both cDNA constructs were confirmed by sequencing either to be unaltered (wild-type; sequence identical to the one deposited in the EMBL/GenBank database libraries, accession number Z 13009) or to contain an in-frame deletion of exon 9 as the only sequence change (exon 9 deletion). The human mammary carcinoma cell line MDA-MB-435S (ATCC) was transfected by the calcium phosphate coprecipitation method with either wild-type or mutant E-cadherin cDNA lacking exon 9 together with a plasmid for neomycin resistance. Cloning and transfection of wild-type and

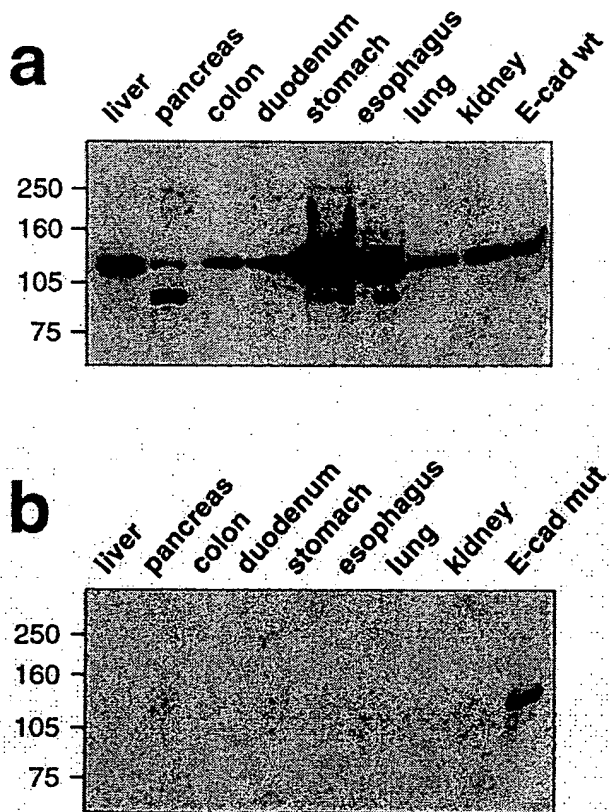


**Figure 1.** Western blot analysis. **a:** Cell extracts from various normal tissues (liver, pancreas, colon, duodenum, stomach, esophagus, lung, kidney) were analyzed using monoclonal antibody AEC (Anti-E-Cadherin, clone 36, Transduction Lab, Lexington, KY). An extract from MDA-MB-435S mammary carcinoma cells that were transfected with wild-type E-cadherin (E-cad wt) was used as a control. AEC reacts with a protein of approximately 120 kD, corresponding to normal E-cadherin, in all lanes. **b:** The same tissues as in **a** were analyzed with the mutation-specific monoclonal antibody E-cad delta 9-1. No cross-immunoreactivity with these tissues was seen. An extract from MDA-MB-435S cells transfected with mutant E-cadherin lacking exon 9 (E-cad mut) was used as a positive control. Molecular weight in kD is indicated on the left.



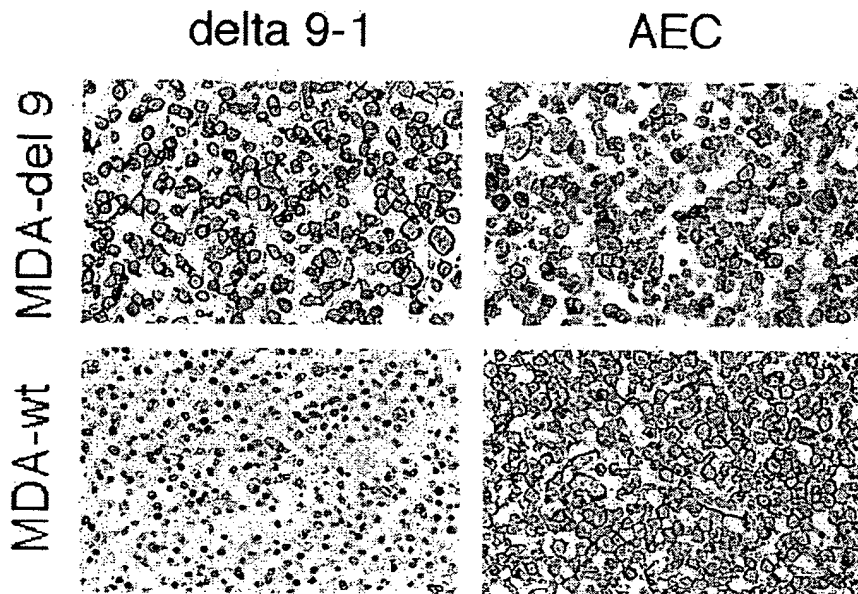


**Figure 2.** Immunoreactivity of formalin-fixed and paraffin-embedded MDA-MB-435S cells. The cells were transfected with mutant E-cadherin lacking exon 9 (MDA-del9) or with the wild-type cDNA (MDA-wt). E-cad delta 9-1 specifically reacts with cells transfected with mutant but not with cells transfected with wild-type E-cadherin cDNA (**left panel**). Monoclonal antibody AEC reacts with cells expressing mutant and wild-type E-cadherin (**right panel**).

mutant E-cadherin cDNA has been described in detail elsewhere.<sup>20</sup>

### Western Blot Analysis

Extracts from E-cadherin (wild-type/mutant) transfected MDA-MB-435S cells and fresh frozen samples from liver, pancreas, colon, duodenum, stomach, esophagus, lung, and kidney were prepared according to a method previously published<sup>21</sup> and used for Western blot analysis. To detect E-cadherin protein the monoclonal antibody AEC (Anti-E-Cadherin, clone 36, Transduction Laboratories, Lexington, KY) and the mutation-specific antibody E-cad delta 9-1 (clone 7E6) were used. Detection was performed using a peroxidase-coupled secondary antibody (ECL-Western, Amersham).

### Immunohistochemical Analysis

To proof mutation-specific E-cad delta 9-1 immunoreactivity, 5- $\mu$ m sections of formalin-fixed and paraffin-embedded MDA-MB-435S mammary carcinoma cells transfected with either wild-type or mutant E-cadherin cDNA (see above) were analyzed. In addition, routine formalin-fixed and paraffin-embedded material from four gastric cancer patients confirmed to express mutant E-cadherin mRNA lacking exon 9 in malignant tissues<sup>11</sup> were analyzed. After microwave-based antigen retrieval with citric acid pretreatment,<sup>22</sup> sections were incubated in 1% hydrogen peroxide for 15 minutes to block endogenous peroxidase. For detection of E-cadherin specific immunoreactivity, the specimens were incubated with either monoclonal antibody AEC (diluted 1:1000) or E-cad delta 9-1 (undiluted hybridoma supernatant) at room temperature for 2 hours. Bound antibodies were detected using the avidin-biotin-complex (ABC) peroxidase method (ABC Elite Kit, Vector, Burlingame, CA). Final staining was developed with the Sigma FAST DAB peroxidase

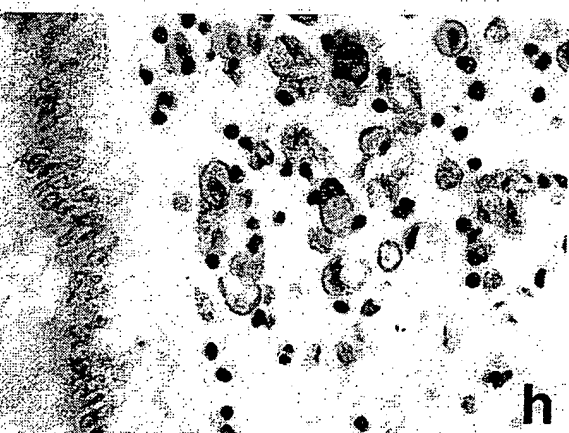
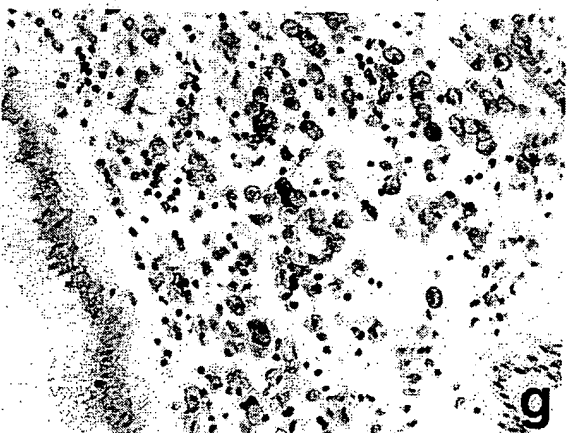
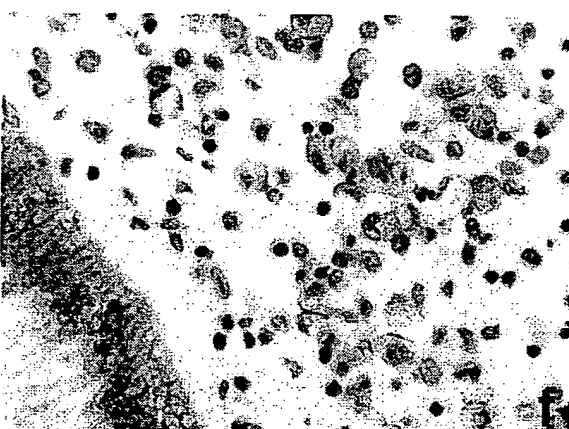
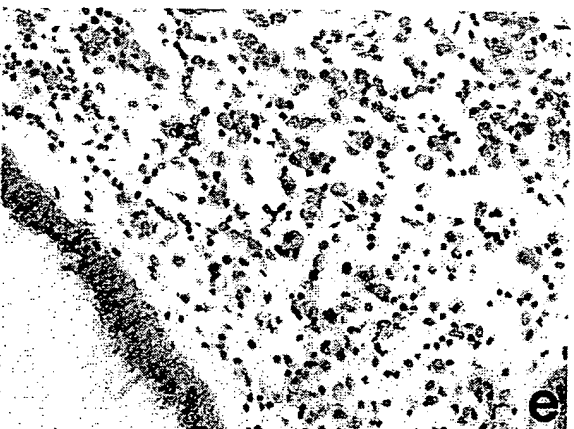
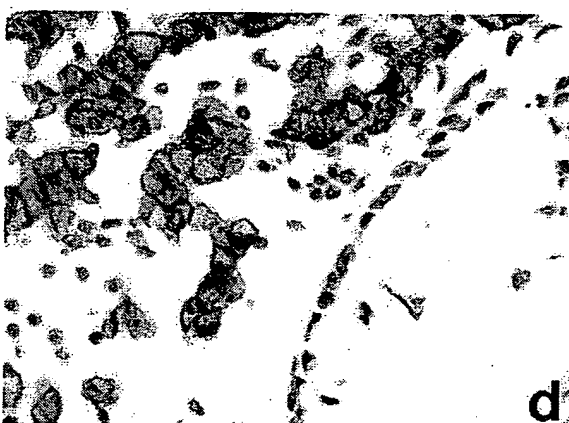
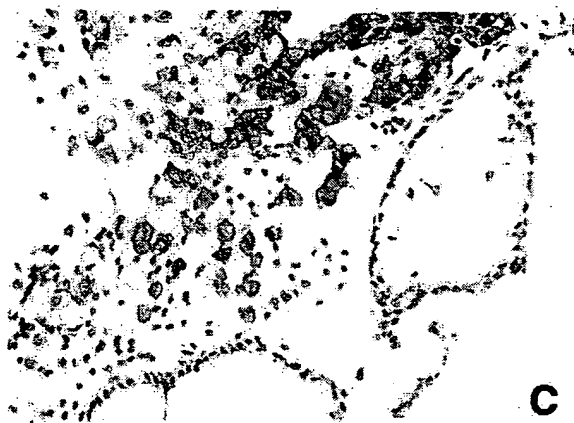
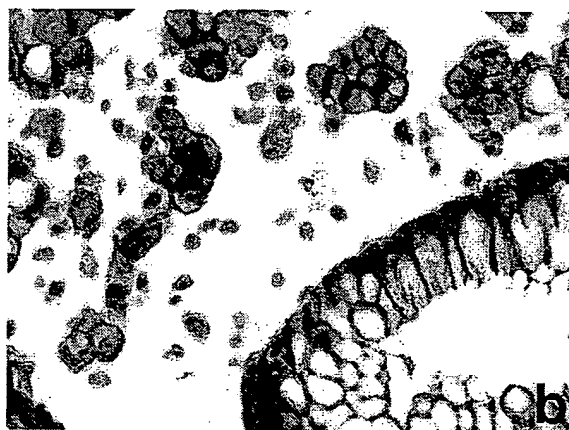
substrate kit (Sigma, Deisenhofen, Germany). Hemalaun was used for counterstaining. Nontumorous adult tissues (lung, heart, thyroid, placenta, salivary gland, bone marrow, lymph nodes, adipose tissue, skin, peripheral nerve, connective tissue, skeletal muscle, breast, pituitary, cerebellum, cerebral cortex, esophagus, stomach, small intestine, duodenum, colon, liver, pancreas, uterine endometrium, uterine cervix, ovary, tube, prostate, seminal vesicle, testis, epididymis) and embryonal tissues (13th week of pregnancy; umbilical cord, spinal cord, kidney, uterus, cartilage, skin, connective tissue, adipose tissue, colon, placenta, chorion) were analyzed in the same way to examine potential cross-reactivity of E-cad delta 9-1 monoclonal antibody. A series of 322 diffuse-type gastric cancer samples from Munich ( $n = 97$ ), Düsseldorf ( $n = 117$ ), and Tokyo ( $n = 108$ ) were subsequently analyzed with E-cad delta 9-1. From these 322 carcinomas, 205 tumors derived from Munich and Tokyo were analyzed using both AEC and E-cad delta 9-1. All tumor sections contained nontumorous epithelium as control.

### Results

E-cadherin mutation-specific monoclonal antibodies were produced in rats against a peptide that spans the fusion junction generated by direct adjoining of exon 8 and 10. Hybridoma supernatants were tested in a solid phase immunoassay using the specific peptide coupled to bovine serum albumin. Hybridoma E-cad delta 9-1 (clone 7E6) of rat IgG1 subclass was selected for further analysis.

### Western Blot

To confirm specificity of the selected hybridoma and to determine potential cross-reactivity with nontumorous tissues Western blot analysis was performed. Extracts from



MDA-MB-435S mammary carcinoma cells transfected with either wild-type or exon 9-deleted E-cadherin and extracts from various fresh-frozen nontumorous tissues (liver, pancreas, colon, duodenum, stomach, esophagus, lung, kidney) were analyzed using monoclonal antibody AEC and E-cad delta 9-1. The epitope reacting with AEC is located within the intracellular domain of E-cadherin. AEC revealed a major protein band at approximately 120 kd corresponding to wild-type E-cadherin in all tissues that was also present in MDA-MB-435S cells transfected with wild-type E-cadherin (Figure 1a). Faster migrating bands most likely correspond to degradation products. No immunoreactivity in these tissues, however, was seen using E-cad delta 9-1; a protein band corresponding to mutant E-cadherin was detected only in extracts from MDA-MB-435S cells transfected with mutant E-cadherin cDNA (Figure 1b). A protein band of identical molecular weight was seen using AEC, confirming E-cadherin specificity (not shown).

### Immunohistochemistry

After having demonstrated antibody specificity by Western blot we tested whether antibody E-cad delta 9-1 may react with formalin-fixed, paraffin-embedded E-cadherin transfected cells. E-cad delta 9-1 strongly stained mutant E-cadherin expressing cells, preferentially at the cell membrane, while wild-type expressing cells were not stained. In contrast, antibody AEC reacted with wild-type E-cadherin as well as with mutant E-cadherin expressing cells (Figure 2). These results indicate that the epitopes reacting with both antibodies are successfully unmasked by the procedures used.

In subsequent immunohistochemical analysis of four diffuse-type gastric carcinomas (routine formalin-fixed, paraffin-embedded material) in which the expression of mutant E-cadherin mRNA lacking exon 9 was previously demonstrated by RT-PCR and direct sequencing,<sup>11</sup> monoclonal antibody AEC reacts with nontumorous epithelial cells as well as with tumor cells in biopsies (Figure 3, a and b). However, the mutation-specific monoclonal antibody delta 9-1 exclusively labels tumor cells on serial sections from the same material, whereas nontumorous epithelial cells were not stained (Figure 3, c and d). Furthermore, tumor cells expressing mutant E-cadherin can be identified in the primary tumors (Figure 3, e and h). Because virtually all tumor cells were stained, the mutation, at least in these cases, is most likely clonal. In addition, E-cad delta 9-1 reacts strongly with tumor cells in lymphatic vessels and in lymph node metastases (not shown). Our results indicate that mutant E-cadherin protein can, for the first time, be specifically detected on tumor cells from gastric cancer patients.

To further examine potential cross-reactivity of antibody E-cad delta 9-1 with nontumorous cells, we analyzed normal tissue specimens from adults as well as from an embryo. We have not observed any cross-reactivity of E-cad delta 9-1 in the normal tissues listed in Materials and Methods.

After a rigorous demonstration that antibody E-cad delta 9-1 reacts only with mutant E-cadherin, even in archival material, the incidence of the E-cadherin variant lacking exon 9 in gastric cancer was determined. We analyzed 322 primary gastric carcinomas of the diffuse type from Germany and Japan. We found that 25 of them (8%) showed a clear reaction with delta 9-1 (Munich, 9/97; Düsseldorf, 3/117; Tokyo, 13/108). The immunoreactivity was detected mainly at the cell membrane as described above. In 205 cases immunohistochemical analysis with AEC was also performed. E-cadherin immunoreactivity with AEC was seen in 84% (172/205) of these cases. From the E-cadherin-positive tumors as determined using AEC, 13% (22/172) also reacted with E-cad delta 9-1.

### Discussion

The E-cadherin exon 9 deletion variant was previously detected in 14% (10/70) of diffuse-type gastric cancer patients using RT-PCR and sequencing.<sup>11-13</sup> The generation and characterization of monoclonal antibody E-cad delta 9-1 now enabled us to easily screen a large series of gastric cancer patients specifically for the exon 9-deletion mutation. We detected 25/322 tumors expressing exon 9 deleted E-cadherin. The lower incidence of E-cad delta 9-1-positive tumors observed in the cases derived from Düsseldorf may be due to the fact that exclusively surgically R0 resected tumors were analyzed whereas in the Munich and Tokyo groups R0, R1, and R2 resected tumors were examined. The incidence of 8% is lower compared to the results using RT-PCR (14%) in a smaller series.<sup>11-13</sup> Possibly, RT-PCR is more sensitive than immunohistochemistry, or the half-life of mutant mRNA and protein may be different. Furthermore, proteins interacting with E-cadherin, catenins, may be altered, potentially resulting in degradation of mutant E-cadherin. In some cases precursor processing or posttranslational modification may be abnormal, resulting in instability of the protein without affecting mRNA stability. However, when the incidence of the mutation was related to immunoreactivity of E-cadherin, as determined by staining with AEC, a monoclonal antibody reacting with the intracellular portion of E-cadherin, we found that 13% (22/172) of the tumors expressing E-cadherin were E-cad delta 9-1-positive (the three missing cases were not included in the

**Figure 3.** Immunohistochemical analysis. This signet ring cell gastric carcinoma was previously confirmed to express mutant E-cadherin mRNA lacking exon 9 due to a somatic splice-site gene mutation.<sup>11</sup> **a-d:** Biopsy. Using monoclonal antibody AEC as primary antibody, both tumor cells and normal epithelial cells are stained (**a, b**); differentiation between cells expressing mutant or wild-type E-cadherin protein is not possible. In contrast, monoclonal antibody E-cad delta 9-1 exclusively stains tumor cells. Nontumorous cells, including E-cadherin-expressing epithelial cells, are not stained (**c, d**). **e-h:** Primary tumor. AEC reacts with normal epithelial cells as well as with tumor cells expressing mutant E-cadherin (**e, f**). Only tumor cells expressing abnormal E-cadherin are stained using E-cad delta 9-1 (**g, h**). Original magnifications: **a, c, e, and g**,  $\times 100$ ; **b, d, f, and h**,  $\times 200$ .

series of cases stained with AEC). Because AEC reacts with E-cadherin's cytoplasmic portion, a potential cross-reactivity with another member of the cadherin superfamily showing homology to this domain, P-cadherin, is conceivable. However, using a different E-cadherin- and a P-cadherin-specific monoclonal antibody, only 1 out of 28 (4%) diffuse-type gastric carcinomas was found to express P-cadherin but not E-cadherin.<sup>6</sup> Thus, E-cadherin-negative tumors that express P-cadherin seem to be rare in this type of cancer and may not significantly interfere with our approximations.

With our study E-cadherin lacking exon 9 has now been confirmed to be expressed exclusively in malignant tissues since no other tissue analyzed showed E-cad delta 9-1 immunoreactivity. The fact that this mutation is frequently found in gastric cancer patients in Europe and Japan suggests that it may play a crucial role in tumorigenesis. Data from a functional analysis using a cell culture approach are in line with this hypothesis. We could demonstrate that mutant E-cadherin has dramatic effects on calcium-dependent cell adhesion, aggregation, cell morphology, and motility, indicating that mutant E-cadherin contributes to the malignant phenotype. Interestingly, the mutation not only results in loss of E-cadherin's cell-to-cell adhesion function, but also can act in a *trans*-dominant negative manner altering the function of other cadherins, eg, N-cadherin.<sup>20</sup>

Detectable immunoreactivity of E-cadherin in gastric cancer specimens using currently available antibodies may not in every case indicate the presence of a normal protein. Our mutation-specific antibody may help to resolve the discrepancy between detection of E-cadherin in the absence of homophilic cell-to-cell adhesion. Moreover, other malignant tissues besides stomach carcinoma could be identified to express mutant E-cadherin protein. E-cadherin gene mutations have been identified so far in invasive lobular breast carcinoma,<sup>23-25</sup> diffuse sclerosing variant of papillary thyroid carcinoma,<sup>26</sup> and endometrial and ovarian carcinoma.<sup>27</sup> Interestingly, an exon 9 splice-site mutation was described in a breast carcinoma cell line,<sup>28</sup> although in-frame deletion mutations are rare in breast cancer.<sup>15</sup>

Mutation-specific monoclonal antibodies reacting with abnormal cell surface molecules found exclusively on tumor cells due to somatic gene mutations may open novel clinical avenues for a more specific diagnosis and therapy of gastric cancer: a humanized version of E-cad delta 9-1 could be applied to stimulate the patient's immune system or, after conjugating to radioisotopes, toxins, or drugs, it could be used to specifically target malignant cells in minimal residual cancer. With the mutation-specific monoclonal antibody E-cad delta 9-1 in hand, rapid screening of potential E-cadherin exon 9 deletion mutations in routine biopsies can now easily be performed on large populations, because this antibody works excellently with formalin-fixed, paraffin-embedded material. Cancer patients who may profit from a potential immunotherapy using modified E-cad delta 9-1 monoclonal antibody can be easily and quickly identified.

## Acknowledgments

We wish to acknowledge Professor Masatoshi Takeichi for providing the expression vector pBAT and Professor Martin Werner and Dr. Thomas Richter for providing us with tissue specimens. We thank Christina Schott and Yuko Yamauchi for excellent technical assistance.

## References

- Huber O, Bierkamp C, Kemler R: Cadherins and catenins in development. *Curr Opin Cell Biol* 1996, 8:685-691
- Peifer M:  $\beta$ -catenin as oncogene: the smoking gun. *Science* 1997, 275:1752-1753
- Takeichi M: Cadherin cell adhesion receptors as a morphogenetic regulator. *Science* 1991, 251:1451-1455
- Hirohashi S: Inactivation of the E-cadherin-mediated cell adhesion system in human cancers. *Am J Pathol* 1998, 153:333-339
- Birchmeier W, Behrens J: Cadherin expression in carcinomas: role in the formation of cell junctions and the prevention of invasiveness. *Biochem Biophys Acta Rev Cancer* 1994, 1198:11-26
- Shimoyama Y, Hirohashi S: Expression of E- and P-cadherin in gastric carcinomas. *Cancer Res* 1991, 51:2185-2192
- Matsui S, Shiozaki H, Inoue M, Tamura S, Doki Y, Kadowaki T, Iwazawa T, Shimaya K, Nagafuchi A, Tsukita S, Mori T: Immunohistochemical evaluation of  $\alpha$ -catenin expression in human gastric cancer. *Virchows Arch* 1994, 424:375-381
- Gabbert HE, Mueller W, Schneiders A, Meier S, Moll R, Birchmeier W, Hommel G: Prognostic value of E-cadherin expression in 413 gastric carcinomas. *Int J Cancer* 1996, 69:184-189
- Mayer B, Johnson JP, Leiti F, Jauch KW, Heiss MM, Schildberg FW, Birchmeier W, Funke I: E-cadherin expression in primary and metastatic gastric cancer: down-regulation correlates with cellular dedifferentiation and glandular disintegration. *Cancer Res* 1993, 53:1690-1695
- Oda T, Kanai Y, Oyama T, Yoshiura K, Shimoyama Y, Birchmeier W, Sugimura T, Hirohashi S: E-cadherin gene mutations in human gastric carcinoma cell lines. *Proc Natl Acad Sci USA* 1994, 91:1858-1862
- Becker KF, Atkinson MJ, Reich U, Becker I, Nekarada H, Siewert JR, Höfler H: E-cadherin gene mutations provide clues to diffuse type gastric carcinomas. *Cancer Res* 1994, 54:3845-3852
- Tamura G, Sakata K, Nishizuka S, Maesawa C, Suzuki Y, Iwaya T, Terashima M, Saito K, Satodate R: Inactivation of the E-cadherin gene in primary gastric carcinomas and gastric carcinoma cell lines. *Jpn J Cancer Res* 1996, 87:1153-1159
- Muta H, Noguchi M, Kana Y, Ochiai A, Nawata H, Hirohashi S: E-cadherin gene mutations in signet ring cell carcinoma of the stomach. *Jpn J Cancer Res* 1996, 87:843-848
- Machado JC, Soares P, Carneiro F, Rocha A, Beck S, Blin N, Bex G, Sobrinho-Simoes M: E-cadherin gene mutations provide a genetic basis for the phenotypic divergence of mixed gastric carcinomas. *Lab Invest* 1999, 79:459-465
- Bex G, Becker K-F, Höfler H, van Roy F: Mutations of the human E-cadherin (CDH1) gene. *Hum Mutat* 1998, 12:226-237
- Frixen UH, Behrens J, Sachs M, Eberle G, Voss B, Warda A, Lochner D, Birchmeier W: E-cadherin-mediated cell-cell adhesion prevents invasiveness of human carcinoma cells. *J Cell Biol* 1991, 113:173-185
- Shimoyama Y, Hirohashi S, Hirano S, Noguchi M, Shimosato Y, Takeichi M, Abe O: Cadherin cell-adhesion molecules in human epithelial tissues and carcinomas. *Cancer Res* 1989, 49:2128-2133
- Kremmer E, Kranz BR, Hille A, Klein K, Eulitz M, Hoffmann-Fezer G, Feiden W, Herrmann K, Delecluse H-J, Delsol G, Bornkamm GW, Mueller-Lantzsch N, Grässert FA: Rat monoclonal antibodies differentiating between the Epstein-Barr virus nuclear antigens 2A (EBNA2A) and 2B (EBNA2B). *Virology* 1995, 208:336-342
- Springer TA, Bhattacharya A, Cardoza JT, Sanchez-Madrid F: Monoclonal antibodies specific for rat IgG1, IgG2a, and IgG2b subclasses, and kappa chain monotypic and allotypic determinants: reagents for use with rat monoclonal antibodies. *Hybridoma* 1982, 1:257-273
- Handschuh G, Candidus S, Lubert B, Reich U, Schott C, Oswald S,

- Becke H, Hutzler P, Birchmeier W, Höfler H, Becker KF: Tumor-associated E-cadherin mutations alter cellular morphology, decrease cellular adhesion, and increase cellular motility. *Oncogene* 1999, 8:4301-4312
21. Cunningham BA, Leutzinger Y, Gallin WJ, Sorkin BC, Edelman GM: Linear organization of the liver cell adhesion molecule L-CAM. *Proc Acad Sci USA* 1984, 81:5787-5791
22. Shi S-R, Key M, Kalra K: Antigen retrieval in formalin-fixed, paraffin-embedded tissues: an enhancement method for immunohistochemical staining based on microwave oven heating of tissue sections. *J Histochem Cytochem* 1991, 39:741-748
23. Bex G, Cleton Jansen AM, Nollet F, de Leeuw WJ, van de Vijver M, Cornelisse C, van Roy F: E-cadherin is a tumour/invasion suppressor gene mutated in human lobular breast cancers. *EMBO J* 1995, 14: 6107-6115
24. Bex G, Cleton-Jansen A-M, Strumane K, de Leeuw W, Nollet F, van Roy F, Cornelisse C: E-cadherin is inactivated in a majority of invasive human lobular breast cancers by truncation mutations throughout its extracellular domain. *Oncogene* 1996, 13:1919-1925
25. Kanai Y, Oda T, Tsuda H, Ochiai A, Hirohashi S: Point mutation of the E-cadherin gene in invasive lobular carcinoma of the breast. *Jpn J Cancer Res* 1994, 85:1035-1039
26. Soares P, Bex G, van Roy F, Sobrinho-Simoes M: E-cadherin gene alterations are rare events in thyroid tumors. *Int J Cancer* 1997, 70:32-38
27. Risinger JI, Berchuck A, Kohler MF, Boyd J: Mutations of the E-cadherin gene in human gynecologic cancers. *Nat Genet* 1994, 7:98-102
28. Hiraguri S, Godfrey T, Nakamura H, Graff J, Collins C, Shayesteh L, Doggett N, Johnson K, Wheelock M, Herman J, Baylin S, Pinkel D, Gray J: Mechanisms of inactivation of E-cadherin in breast cancer cell lines. *Cancer Res* 1998, 58:1972-1977

# Serum Tumor Marker CYFRA 21-1 in the Diagnostics of NSCLC Lung Cancer

R. Pavićević, J. Miličić, G. Bubanović and S. Šupe

## ABSTRACT

*Cytokeratins are epithelial markers whose expression is not lost during malignant transformation. The level of soluble cytokeratin fragment 19 was measured with an enzyme immunoassay method developed by Boehringer Mannheim (Enzymum-test CYFRA 21-1) in the serum of 200 male and 50 female patients with NSCLC (Non Small Cell Lung Cancer) lung cancer (120 planocellulare and 80 adenocarcinoma in males; 22 planocellulare and 28 adenocarcinoma in females). The comparative group comprised 50 young healthy males and 50 females without any clinical proof for malignancy or any other lung disease.*

*The aim of this investigation was to find out if any possible statistical difference exists in the serum level of CYFRA 21-1 between patients with lung cancer and healthy controls, and also between different types of lung cancers.*

*The mean value of serum CYFRA 21-1 in NSCLC (6.25 ng/ml) was significantly higher than in healthy controls (1.26 ng/ml) ( $p < 0.001$ ). Sensitivity for CYFRA 21-1 (using 3.3 ng/ml, a cut-off value corresponding to a 98% specificity for healthy controls) in NSCLC was 60.5%. Positive CYFRA 21-1 levels were significantly higher in patient with carcinoma planocellulare (66.2%) than in adenocarcinoma (52.1%). CYFRA 21-1 levels were significantly different between squamous cell carcinoma (6.52 ng/ml) and adenocarcinoma (5.86 ng/ml) ( $p < 0.05$ ). Our results indicate that CYFRA 21-1 may be a useful tumor marker in NSCLC, especially in carcinoma planocellulare. CYFRA 21-1 may also be useful in identification of the preoperative stages of diseases and the postoperative monitoring of NSCLC.*

## Introduction

The most frequent cause of death in male over 35 years of age among malig-

nant illnesses is lung cancer. In Croatia the rate of patients suffering of lung cancer has risen in males from 39.0/100,000 in 1970 to 85.1/100,000 in 1996 or 237%,

TABLE 1  
THE INCREASE IN THE NUMBER OF DEATHS CAUSED BY BRONCHOPULMONARY  
CARCINOMA IN 1970, 1980, 1990, 1994 AND 1996 IN CROATIA

Year	M		F		Total	
	No	Rate/ 100,000	No	Rate/ 100,000	No	Rate/ 100,000
1970	834	39.0	141	6.2	975	22.0
1980	1369	61.5	258	10.9	1627	35.4
1990	1944	83.8	341	13.8	2285	47.8
1994	1893	81.6	346	14.0	2239	46.8
1996	1973	85.1	417	16.9	2390	50.0
Percentage rise (1996/1970)	237%		296%		245%	

and in females from 6.2/100,000 in 1970 to 16.9/100,000 in 1996 or 296% (Table 1)<sup>1</sup>. In spite of all diagnostic and therapeutic methods a five year survival is more a hope than a rule. Considering the prognostic and therapeutic viewpoint squamous cell carcinoma, adenocarcinoma and large-cell carcinoma behave similar, and are all pooled into a group named non small cell lung cancer (NSCLC)<sup>2</sup>. The squamous cell carcinoma comprises 40 – 50% of all cases of lung cancer. The treatment is primarily surgical and its prognosis have remained almost unchanged over the recent years. The longitudinal follow up of marker values, the stage of the disease and response to the therapy will significantly contribute to future treatment of lung cancer.

Cytokeratins are one of the main families of intermediate filaments which make up the cytoskeleton. Cytokeratins, and particularly CK 19, are strongly expressed by lung cancer tissue<sup>3</sup>. Although cytokeratins are part of the cytoskeleton, some fragments might be released in the serum owing to cell lysis or tumor necrosis. Cytokeratins can be detected both in normal as well as in malignant tissues of epithelial origin<sup>4</sup>. A tumor marker assay CYFRA 21-1 which uses two monoclonal antibodies (ks19-1 and KS 19-21) against

epitopes of a water-soluble fragment of CK 19, was recently introduced<sup>4-8</sup>.

CYFRA 21-1 is a cytokeratin 19 fragment that is soluble in serum, and seems to be most sensitive and specific tumor marker for lung cancer<sup>8,11</sup>, and show its dominant value in squamous cell carcinoma type<sup>5-11</sup>. It is very important to evaluate the diagnostic specificity of the assay CYFRA 21-1 to define the threshold of upper limit for normality in the examined healthy population groups, in patients suffering of different types of lung cancer, as well as in patients with different stage of lung cancer<sup>12-14</sup> and also in pre and post operative monitoring<sup>8,13,18,20-23</sup>.

Analysing several data obtained from different countries there is a set of different values derived as cut-off values. Defined as 95% specificity was set at 3.6 ng/ml for cytokeratin 19 fragment CYFRA 21-1<sup>6,7</sup>; 3.5 ng/ml<sup>18</sup>; 3.3 ng/ml proposed by Boehringer Mannheim (for group of 526 patients suffering from benign chest diseases)<sup>5,11</sup>; 3.0 ng/ml<sup>12</sup>; 2.5 ng/ml<sup>13</sup>; 2.2 ng/ml<sup>14</sup>; 1.2 ng/ml (among healthy individuals n = 711) and 2.95 ng/ml, (in a group of patients with benign lung disease n = 546,<sup>15,16</sup> and 0.91 ng/ml (SD = 0.47 ng/ml; range 0.05 – 2.90 ng/ml), a threshold of 1.9 ng/ml was cho-

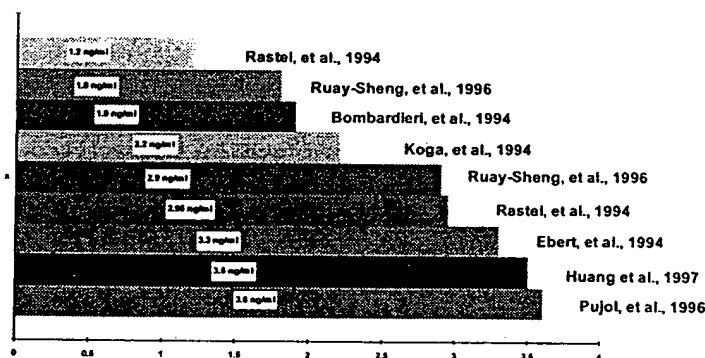


Fig. 1. Different reference range of CYFRA 21-1 values for healthy controls.

sen as the upper limit of normality<sup>17</sup> for the group of healthy blood donors (Figure 1).

### Study objective

The aims of this study were therefore to: 1.) confirm sensitivity and specificity of CYFRA 21-1 in detecting non-small cell lung cancer (NSCLC), especially the squamous cell subtype; 2.) define a cut-off value for our examined population group; and 3.) evaluate whether there is any correlation between tumor stage and serum level of CYFRA 21-1.

### Material and methods

A blood sample was obtained from 200 male and 50 female patients with histologically confirmed NSCLC lung cancer (in males: 120 with squamous cell carcinoma; 80 with adenocarcinoma and in females: 22 with squamous cell carcinoma and 28 with adenocarcinoma), treated from December 15<sup>th</sup>, 1997 to April 1<sup>st</sup>, 1998 at the Department of Thoracic Surgery, »Jordanovac« Pulmonary Hospital Zagreb. Besides biomarker assays, all patients underwent a physical examination, fibre-optic bronchoscopy, chest radiography and computed tomographic scan of the chest, brain and liver. NSCLC was staged according to the International Un-

ion Against Cancer (UICC) TNM classification<sup>23</sup>. One month after surgery we repeated tests on 127 patients. The comparative group comprised 50 young healthy males and 50 females without any clinical prove for malignancy or any other lung disease.

Enzyme-immunological test for the quantitative determination of soluble cytokeratin 19 fragment in vitro was performed using the methodology of Boehringer Mannheim (Enzymum-test CYFRA 21-1) and ES 300 immunodiagnos-

### Results

A soluble cytokeratin 19 fragment useful for assessing circulating tumor antigen in sera was tested in 200 patients suffering from NSCLC lung cancer, at the time of their first diagnosis and after the surgical treatment, using a Enzymum-test CYFRA 21-1: In 100 healthy controls the mean value for CYFRA 21-1 was 1.26 ng/ml in the range of 0.01 ng/ml to 2.03 ng/ml. The univariate analysis showed that the mean value of serum CYFRA 21-1 level in NSCLC (6.25 ng/ml) was significantly higher than in healthy controls (1.26 ng/ml) ( $p < 0.001$ ). Sensitivity for CYFRA 21-1, using 3.3 ng/ml, a cut-off value corresponding to a 98% specificity for healthy controls<sup>5,11</sup>, in NSCLC was



60.5%. Positive CYFRA 21-1 level was significantly higher 66.2% in patients with squamous cell carcinoma than 52.1% in adenocarcinoma. The mean level of CYFRA 21-1 were significantly different between squamous cell carcinoma (6.52 ng/ml) and adenocarcinoma (5.86 ng/ml) ( $p < 0.05$ ).

The patients were classified depending on the type of carcinoma and the stage of diagnosis (Table 2). From 142 patients suffering from squamous cell carcinoma: in 120 males 99 had a stage I and II, and 21 stage IIIa, while from 22 females 16 of them had stage I and II, and 6 had stage IIIa. In 108 patients suffering from adenocarcinoma in 80 males 64 had a stage I and II, and 16 stage IIIa and in 28 females 22 had stage I and II, and 6 has stage IIIa. In our investigation the ratio of incidence in squamous cell carcinoma between males and females is 5.5 : 1 but in adenocarcinoma 2.8 : 1.

Before the surgery patients with I and II stage of carcinoma had an increased level of CYFRA 21-1 in squamous cell carcinoma 69/115 (60.0%) and in adenocarci-

noma 35/86 (40.7%), all other values of CYFRA 21-1 were around the reference range 3.3 ng/ml or slightly lower (Table 3). At the time of diagnosis almost all examinees in stage IIIa (46/49, 93.9%) had a high level of CYFRA 21-1 and the values varied from 10 ng/ml to 55 ng/ml. Three patients with the highest level of CYFRA 21-1 (over 50 ng/ml) died during the first month after surgery.

One month after the surgery the level of CYFRA 21-1 was tested in 74 patients with squamous cell carcinoma (62 males and 12 females) and in 53 patients with adenocarcinoma (39 males and 14 females). We observed the decrease of level of CYFRA 21-1 under the reference range 3.3 ng/ml in 114/127 (89.76 %) patients.

### Discussion

In our series, using the Enzymum-test CYFRA 21-1 (Boehringer Mannheim) using 3.3 ng/ml cut-off values, the best results were for NSCLC (60.5%). Positive CYFRA 21-1 levels were significantly

TABLE 2  
NUMBER OF PATIENTS DEPENDING ON TYPE OF LUNG CANCER, STAGE AND SEX

	Squamous cell carcinoma		Adenocarcinoma	
	Males	Females	Males	Females
Stage I and II	99	16	64	22
Stage IIIa	21	6	16	6
Total	120	22	80	28
Patients tested after surgery	62	12	39	14

TABLE 3  
SERUM CYFRA 21-1 LEVEL IN PATIENTS WITH LUNG CANCER ACCORDING TO CLINICAL STAGE

	Squamous cell carcinoma		Adenocarcinoma	
	No. of cases ( $> 3.3$ ng/ml)	Percent	No. of cases ( $> 3.3$ ng/ml)	Percent
Stage I and II	69/115	60.0%	35/86	40.7%
Stage III a	25/27	92.6%	21/22	95.5%
Total	94/142	66.2%	56/108	52.1%

higher in patient with squamous cell carcinoma (66.2%) than in adenocarcinoma (52.1%).

This study confirms that CYFRA 21-1 has a good specificity in NSCLC but the lack of sensitivity in the early stages is a main limit for clinical applicability. The cut-off values 3.3 ng/ml proposed by Boehringer Mannheim seems to be too high for our population but also for the other populations as well<sup>12-17</sup>. These findings highlight the need to re-evaluate the cut-off values for examined population group. The reference range in 100 healthy controls was 1.26 ng/ml, between 0.01 ng/ml and 2.03 ng/ml, and need to be confirmed using a greater number of healthy controls. The different cut-off values for a group of patients with benign respiratory diseases (pulmonary tuberculosis, interstitial pneumonia etc.) must also be considered<sup>5,11,15,16</sup>.

The serum level and sensitivity of CYFRA 21-1 were well correlated with staging and tumor size in squamous cell carcinoma<sup>20-22</sup>. One of the main drawbacks of serum tumor markers is that the highest level of CYFRA 21-1 are usually found when disease is at an advanced stage. In our results examinees in stage IIIa had a high level of CYFRA 21-1 (between 10 ng/ml and 55 ng/ml). We can conclude that in advanced tumors (IIIa to IV), when the serum level of CYFRA 21-1 is higher than 50 ng/ml, there is a high level risk of surgical treatment failure (in our cases all of them died soon after surgery). On the other hand a high percent of sur-

gically treated patients show decreased level of CYFRA 21-1 and it seems to have a good survival prognosis.

Our results indicate:

1.) That CYFRA 21-1 may be a useful tumor marker in NSCLC, especially in squamous cell carcinoma.

2.) However for our population group it is necessary to define the reference range on the higher number of healthy controls and it is probably lower than 3.3 ng/ml.

3.) CYFRA 21-1 may also be useful in the identification of preoperative stages of the disease and the postoperative monitoring of NSCLC.

4.) Finally, for further decisions we need to confirm our results on a greater number of patients, and also the cut-off values on a greater number of controls. We need more time for a longitudinal study and postoperative monitoring.

### Acknowledgements

This study was supported by the Boehringer Mannheim Immunodiagnostics, Vienna, Austria (Enzymum-test CYFRA 21-1) and Ministry of Science and Technology of Republic of Croatia through Project 01960101, conducted by Professor Pavao Rudan, Director of the Institute for Anthropological Research. Authors wish to thank Ljubomir Pavelić, Ph.D., Director of the Department of Thoracic Surgery, »Jordanovac« Pulmonary Hospital Zagreb, Croatia.

### REFERENCES

1. PAVIĆEVIĆ, R., J. MILIČIĆ, M. STRNAD, L. PAVIĆEVIĆ: The 14th International Congress of anthropological and ethnological sciences Williamsburg, USA. (Abstracts, 1998). — 2. CARNEY, D. N., L. D. LEIJ, Oncol., 15. (1988) 199. — 3. BROERS, J. L., F. C. RAMAEKERS, M. K. ROT, O. OSTENDORPT, A. HUYSMANS, G. N. VAN MUIJEN, S. S.

- WAGENAAR, G. P. VOOLJS, Cancer Res., 48. (1988) 3221. — 4. MOLL, R., W. FRANKE, D. L. SHILLER, B. GEIGER, R. KREPLER, Cell, 31. (1982) 11. — 5. BODENMULLER, H., B. OFENLOCH-HAHNLE, E. B. LANE, A. DESSAUER, V. BOTTGER, F. DONIE, Int. J. Biol. Markers, 9 (1994) 75. — 6. PUJOL, J. L., J. GRENIER, P. RAY, V. GAUTIER, M. D. AOUTA, F.

- B. MICHEL, Presse Medicale, 22 (1993) 1039. — 7. PUJOL, J. L., J. GRENIER, E. PARRAT, M. LEHMANN, T. LAFONTAINE, X. QUANTIN, F. B. MICHEL, Am. J. Respir. Crit. Care Med., 154 (1996) 725. — 8. NIKLINSKI, J., M. FURMAN, T. BURZKOWSKI, L. CHYCZEWSKI, J. LAUDANSKI, E. CHYCZEWSKI, M. RAPELLINO, Brit. J. Cancer, 74 (1996) 956. — 9. STIEBER, P., H. DIENEMANN, U. HASHOLZNER, P. G. FABRICIUS, C. SCHAMBECK, M. WEINZIERL, S. POLEY, W. SAMTLEBEN, K. HOFMANN, W. MEIER, Int. J. Biol. Markers, 9 (1994) 82. — 10. NIKLINSKI, J., M. FURMAN, M. RAPELLINO, L. CHYCZEWSKI, J. LAUDANSKI, A. OLIARO, E. RUFFINI, J. Cardiovasc. Surgery, 36 (1995) 501. — 11. EBERT, W., H. DIENEMANN, A. FATEH MOGHADAM, M. SCHEULEN, N. KONIETZKO, T. SCHLEICH, E. BOMBARDIERI, Eur. J. Clin. Chem. Clin. Biochem., 32 (1994) 189. — 12. C. SCHAMBECK, M. WEINZIERL, S. POLEY, W. SAMTLEBEN, K. HOFMANN, W. MEIER, Int. J. Biol. Markers, 9 (1994) 82. — 13. NIKLINSKI, J., M. FURMAN, M. RAPELLINO, L. CHYCZEWSKI, J. LAUDANSKI, A. OLIARO, E. RUFFINI, J. Cardiovasc. Surgery, 36 (1995) 501. — 14. K. EGUCHI, T. SHINKAI, T. TAMURA, Y. OHE, F. OSHITA, N. SAJO, H. KONDO, K. OKI, H. OKURA, Jpn. J. Clin. Oncol., 24 (1994) 263. — 15. RASTEL, D., A. RAMAIOLI, F. CORNILLIE, B. THIRION, Eur. J. Cancer, 30 (1994) 601. — 16. LAI, R. S., H. K. HSU, J. Y. LU, L. P. GER, N. S. LAI, Chest, 109 (1996) 995. — 17. BOMBARDIERI, E., E. SEREGNI, A. BOGNI, S. ARDIT, S. BELLOLI, A. BUSETTO, B. CANIELLO, M. CASTELLI, A. CIANETTI, M. CORREALE, Int. J. Biol. Markers, 9 (1994) 89. — 18. HUANG, M. S., S. B. JONG, M. S. TSAI, M. S. LIN, I. W. CHONG, H. C. LIN, J. J. HWANG, Respir. Med., 91 (1997) 135. — 19. MORO, D., D. VILLEMAIN, J. P. VUILLEZ, C. A. DELORD, C. BRAMBILLA, Lung Cancer, 13 (1995) 169. — 20. WIESKOPF, B., C. DEMANGEAT, A. PUROHIT, R. STENGER, P. GRIES, H. KREISMAN, E. QUOIX, Chest, 108 (1996) 163. — 21. MURAKI, M., Y. TOHDA, T. IWANAGA, H. UEJIMA, Y. NAGASAKA, S. H. NAKAJIMA, Cancer, 77 (1996) 1274. — 22. HAMZAOU, A., P. THOMAS, O. CASTELNAU, N. ROUX, J. P. KLEISBAUER, Lung Cancer, 16 (1997) 191. — 23. SOBIN, L. H., P. HERMANEK, R. V. P. HUTTER: TNM classification of malignant tumors. (4th ed.) (International Union Against Cancer, Geneva, 1987). — 24. PAONE, G., G. De ANGELIS, L. PORTALONE, S. GRECO, S. GIOSUE, A. TAGLIENTI, A. BISETTI, F. AMEGLIO, Brit. J. Cancer, 75 (1997) 448.

R. Pavićević

Department of Thoracic Surgery, »Jordanovac« Pulmonary Hospital, Jordanovac 104, 10000 Zagreb, Croatia

## SERUMSKI TUMORSKI MARKER CYFRA 21-1 U DIJAGNOSTICI NSCLC RAKA PLUĆA

### SAŽETAK

Citokeraini su epitelni markeri čija se ekspresija ne gubi za vrijeme maligne transformacije. Nivo topivog citokeratinskog fregmenta 19 mjerio se pomoću enzimskih testova metodom Boehringer Mannheim (Enzymum-test CYFRA 21-1) u serumu od 200 muškaraca i 50 oboljelih žena od NSCLC (Non Small Cellulare Lung Cancer) raka pluća od čega 120 muškaraca s planocelularnim karcinomom, 80 muškaraca s adenokarcinomom, te 22 žene s planocelularnim karcinomom i 28 žena s adenokarcinomom. Komparativnu skupinu sačinjavalo je 50 zdravih muškaraca i 50 zdravih žena bez kliničkog dokaza bilo kakve maligne ili druge bolesti pluća.

Cilj je ovog istraživanja bio utvrditi postoje li statistički značajne razlike u nivou CYFRA 21-1 u serumu između zdravih osoba i bolesnika oboljelih od raka pluća, te između bolesnika oboljelih od različitih tipova raka pluća.

Srednja vrijednost nivoa CYFRA 21-1 u serumu bolesnika s NSCLC iznosila je 6,25 ng/ml i statistički je značajno različita nego u zdrave populacije 1,26 ng/ml ( $p < 0,001$ ).

Osjetljivost markera CYFRA 21-1 (koristeći graničnu vrijednost od 3,3 ng/ml koja odgovara 98% specifičnosti za zdravu populaciju) u NSCLC je iznosila 60,5%. Povišeni nivo CYFRA 21-1 markera je zapažen u 66,2% bolesnika s planocelularnim karcinomom i 52,1% bolesnika s adenokarcinomom. Razlika između nivoa tumorskog markera CYFRA 21-1 je statistički značajno različita između bolesnika oboljelih od planocelularnog karcinoma (6,25 ng/ml) i u bolesnika oboljelih od adenokarcinoma (5,86 ng/ml)  $p < 0,05$ . Naši rezultati ukazuju da je CYFRA 21-1 koristan tumorski marker u NSCLC, naročito kad je u pitanju planocelularni karcinom. CYFRA 21-1 može biti koristan identifikator preoperativnog stadija, kao i postoperativnog praćenja bolesti.

# MATRIX METALLOPROTEINASE-1 IS ASSOCIATED WITH POOR PROGNOSIS IN OESOPHAGEAL CANCER

GRAEME I. MURRAY<sup>1</sup>\*, MARGARET E. DUNCAN<sup>2</sup>, PAULINE O'NEIL<sup>1</sup>, JUDITH A. MCKAY<sup>1</sup>, WILLIAM T. MELVIN<sup>2</sup> AND JOHN E. FOTHERGILL<sup>2</sup>

<sup>1</sup>Department of Pathology, University of Aberdeen, Aberdeen, AB25 2ZD, U.K.

<sup>2</sup>Department of Molecular and Cell Biology, University of Aberdeen, Aberdeen, AB25 2ZD, U.K.

## SUMMARY

The matrix metalloproteinases (MMPs) are a family of closely related proteolytic enzymes which are involved in the degradation of different components of the extracellular matrix. There is increasing evidence to indicate that individual MMPs have an important role in tumour invasion and tumour spread. Monoclonal antibodies specific for MMP-1, MMP-2, or MMP-9 have been produced, using as immunogens peptides selected from the amino acid sequences of individual MMPs. The presence of MMP-1, MMP-2, and MMP-9 in oesophageal cancer was investigated by immunohistochemistry on formalin-fixed, wax-embedded sections of oesophageal cancers. The relationship of individual MMPs to prognosis and survival was determined. MMP-1 was present in 24 per cent of oesophageal cancers, while MMP-2 and MMP-9 were present in 78 and 70 per cent of tumours, respectively. The presence of MMP-1 was associated with a particularly poor prognosis (log rank test 8.46,  $P < 0.004$ ) and was an independent prognostic factor ( $P = 0.02$ ). The identification of individual MMPs in oesophageal cancer provides a rational basis for use in the treatment of oesophageal cancer of MMP inhibitors which are currently undergoing clinical trial. © 1998 John Wiley & Sons, Ltd.

J. Pathol. 185: 256-261, 1998.

KEY WORDS—collagenase; interstitial collagenase; matrix metalloproteinase; neoplasm; oesophagus

## INTRODUCTION

Cancer of the oesophagus is one of the commonest malignant tumours of the alimentary tract, with a worldwide distribution. Oesophageal cancer is characterized by a late clinical presentation, rapid progression, and very poor survival.<sup>1</sup> The reason for this poor prognosis is that at the time of diagnosis, oesophageal cancer usually shows extensive local tumour invasion and frequent spread to metastatic sites, particularly regional lymph nodes. Spread of malignant tumours is a multi-step process and many of the stages of tumour invasion require degradation or breakdown of the extracellular matrix and connective tissue surrounding tumour cells.<sup>2,3</sup> The matrix metalloproteinases (MMPs) are a family of zinc-containing enzymes<sup>4,5</sup> which are involved in the degradation of different components of the extracellular matrix, and there is considerable evidence to indicate that individual MMPs have an important role in tumour invasion and tumour spread.<sup>5-9</sup>

The MMPs have been classified into collagenases, gelatinases, and stromelysins, based on the *in vitro* substrate specificity of individual MMPs.<sup>4,10</sup> These MMPs are secreted as inactive precursors which are activated by cleavage of an N-terminal pro-peptide. With the exception of matrilysin (MMP-7), which has only a catalytic domain, the activated MMPs all have an

N-terminal catalytic domain, which has structural similarities with the N-terminal domains of thermolysin and other zinc endopeptidases such as astacin,<sup>11,12</sup> and a C-terminal domain which has homology with haemopexin.<sup>5,13</sup> The three-dimensional structure of the C-terminal domain in porcine synovial collagenase has been shown to be a four-bladed  $\beta$ -propeller, each blade of which contains four anti-parallel  $\beta$ -strands.<sup>14</sup> The catalytic and C-terminal domains of the MMPs are joined by a linker of varying length. The gelatinases (MMP-2 and MMP-9), which are also known as type IV collagenases, have an additional fibronectin-like, collagen binding domain inserted into the catalytic domain, and in MMP-9 the linker between the catalytic and C-terminal domains is especially long. More recently, several MMPs have been identified in tumour cells which are not secreted but are membrane-bound by means of a trans-membrane domain; these have been designated membrane-type MMPs.<sup>15,16</sup>

The gelatinases, particularly MMP-2, appear to be important in the initial stages of tumour invasion,<sup>17</sup> as they degrade components of the basement membrane, including type IV collagen. In addition, cleavage of one component of the extracellular matrix, laminin-5, by MMP-2 promotes cell migration.<sup>18</sup> Local invasion of tumours is facilitated by degradation of the extracellular matrix and this can be performed by several MMPs, particularly MMP-1.<sup>5</sup> Metastatic spread of tumour cells involves invasion into lymphatic and blood vessels and this process requires breakdown of the basement membrane surrounding these vessels. When tumour cells reach a metastatic site the process of invasion is

repe:  
sels  
All  
indiv  
In  
whic  
(inte  
and  
cer.  
asso  
prog

Tiss  
C  
for  
ran  
unc  
mei  
Pat  
for  
wer  
On  
im  
tiss  
on  
U.  
ade  
oes  
sta  
tur

© 1

\*Correspondence to: Dr Graeme I. Murray, Department of Pathology, University of Aberdeen, Foresterhill, Aberdeen, AB25 2ZD, U.K. E-mail: g.i.murray@abdn.ac.uk

Contract grant sponsor: Scottish Hospital Endowments Research Trust.

TED  
NCERIN<sup>2</sup> AND

degradation of  
important role  
duced, using as  
and MMP-9 in  
al cancers. The  
ageal cancers,  
associated with  
dentification of  
MMP inhibitors

uctural simi-  
molysin and  
1,11,12 and a  
with haemo-  
ure of the  
collagenase  
opeller, each  
 $\beta$ -strands.<sup>14</sup>  
the MMPs  
e gelatinases  
known as  
fibronectin-  
1 into the  
ker between  
s especially  
en identified  
ed but are  
s-membrane  
nbrane-type

appear to be  
vasion,<sup>17</sup> as  
membrane.  
vage of one  
minin-5, by  
invasion of  
extracellular  
ral MMPs.  
umour cells  
vessels and  
ment mem-  
umour cells  
invasion is

25 June 1997  
March 1998

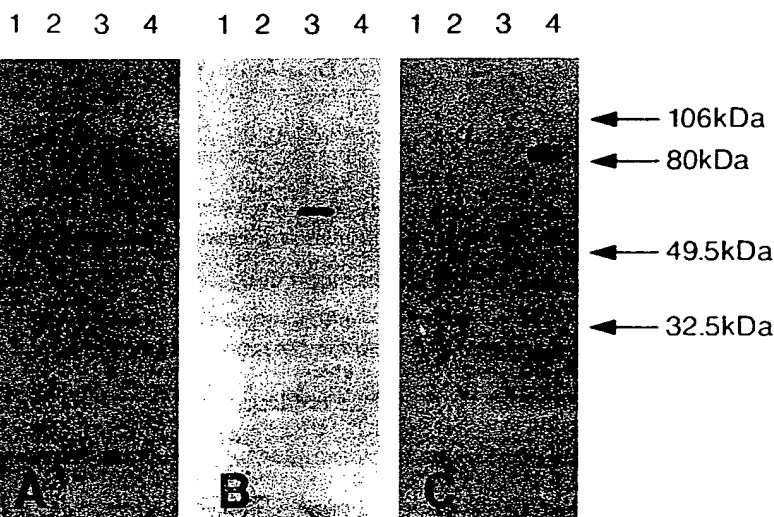


Fig. 1—Immunoblot showing the specificity of the anti-MMP-1, anti-MMP-2 and anti-MMP-9 antibodies. Individual MMP pro-enzymes (0.4  $\mu$ g of purified protein per lane) were subjected to SDS-PAGE and then electrophoretically transferred to PVDF membrane. (A) The membrane was immunostained with the MMP-1 antibody; (B) the membrane was immunostained with the MMP-2 antibody; (C) the membrane was immunostained with the MMP-9 antibody. Lane 1, MMP-1; lane 2, MMP-2; lane 3, MMP-3; lane 4, MMP-9

repeated, with basement membrane degradation of vessels followed by breakdown of the extracellular matrix.<sup>2</sup> All of these steps in the metastatic cascade involve individual MMPs.<sup>2,5,17</sup>

In this study we raised specific monoclonal antibodies which allowed us to investigate the presence of MMP-1 (interstitial collagenase), MMP-2 (72 kD gelatinase), and MMP-9 (92 kD gelatinase) in oesophageal cancer. We have shown that the presence of MMP-1 is associated with poor prognosis and is an independent prognostic factor.

## MATERIALS AND METHODS

### Tissue

Oesophageal tumour samples ( $n=46$ ) were obtained from oesophagectomy specimens from patients (age range 34–70 years; 29 males and 17 females) who had undergone surgery for oesophageal cancer. All specimens which had been submitted to the Department of Pathology, University of Aberdeen had been fixed in formalin and embedded in wax. Histologically, there were 19 squamous carcinomas and 27 adenocarcinomas. One block of tumour from each case was used for immunohistochemical analysis of individual MMPs, and tissue sections (4  $\mu$ m in thickness) were cut and mounted on aminopropyltriethoxysilane (Sigma, Poole, Dorset, U.K.)-coated slides to ensure section adherence. The adenocarcinomas had occurred in areas of Barrett's oesophagus. TNM staging of the tumours showed 15 stage 2a tumours, four stage 2b tumours, 26 stage 3 tumours, and one stage 4 tumour. All the patients had

survived for at least 1 month following surgery and were followed up for 24–60 months.

### Monoclonal antibodies

Monoclonal antibodies to MMP-1, MMP-2 and MMP-9 were produced using synthetic peptides corresponding to a region in the multiple alignment of the MMP sequences where unique sequences were present in the MMP-1, MMP-2, and MMP-9. The amino acid sequences used were SSFGFPRTVKH (MMP-1), TSLGLPPDVQRVD (MMP-2), and KLGLGADVQVT (MMP-9). The peptides were synthesized at the Krebs Institute, University of Sheffield, Sheffield, and were checked by amino acid sequence analysis and mass spectrometry in the Protein Facility, University of Aberdeen. The sequences of 11, 12, or 13 amino acid residues were situated in the C-terminal domain of the MMPs, and homology modelling showed that they formed an external loop between the second and third blade of the  $\beta$ -propeller.<sup>14</sup> This region is distant from the active site of the enzymes and the pro-peptide domains, and its positions on the outside of the molecule makes it likely that anti-peptide antibodies would recognize the intact protein. The peptides were linked at their N-termini to hen ovalbumin as carrier protein, using glutaraldehyde for the MMP-2 and MMP-9 peptides<sup>19</sup> and *m*-maleimidobenzonic acid *N*-hydroxysuccinimide ester for the MMP-1 peptide, which had an N-terminal cysteine residue included to allow conjugation by this reagent.<sup>20</sup> The conjugates were used to immunize BALB-c mice for the generation of monoclonal antibodies by standard methods.<sup>21,22</sup> The peptides, linked to bovine serum albumin (BSA) by the above methods,

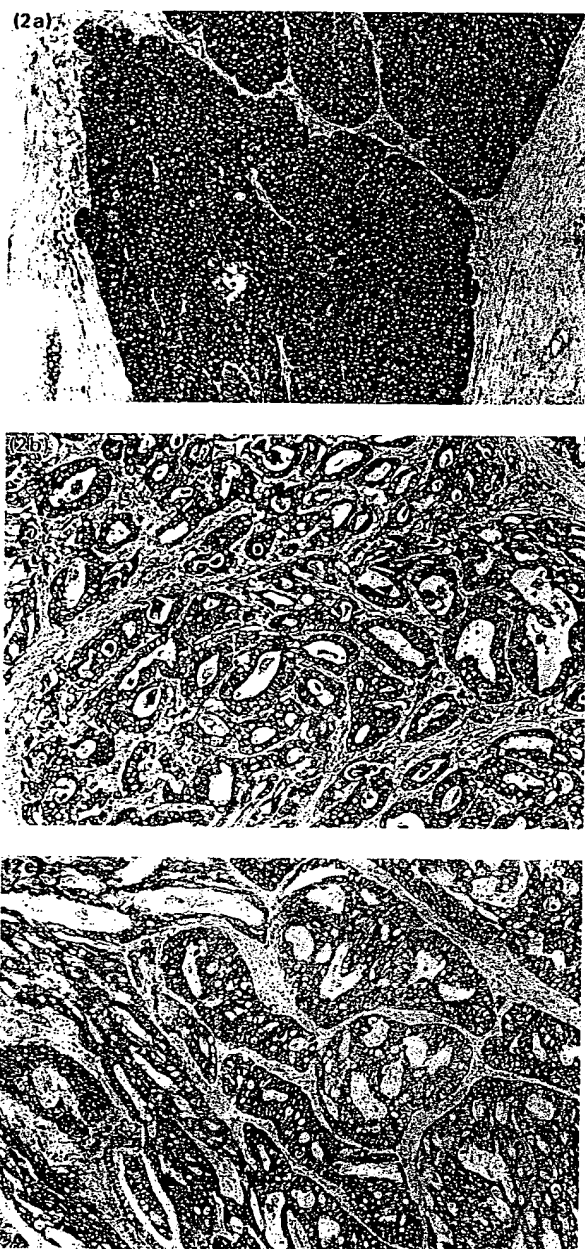


Fig. 2—Immunoreactivity for (a) MMP-1, (b) MMP-2, and (c) MMP-9 in oesophageal cancer. The tumour in a is a poorly differentiated squamous carcinoma, while the tumours in b and c are moderately differentiated adenocarcinomas. Immunoreactivity is found evenly distributed over all the tumour cells

were used for initial antibody screening. The BSA conjugates were bound to an ELISA plate by incubation overnight at 4°C in 50 mM sodium carbonate/bicarbonate buffer, pH 9.6, and the ELISA was performed as described previously.<sup>23</sup>

The specificity of the monoclonal antibodies was demonstrated by immunoblotting against purified MMP pro-enzymes (MMP-1, MMP-2, MMP-3, MMP-9). Natural human MMP-1 and recombinant human MMP-2, MMP-3, and MMP-9 were a kind gift from Dr

Alan Galloway, British Biotech plc. Individual MMPs (0.4 µg of purified protein per lane) were subjected to SDS-PAGE (10 per cent acrylamide) and then electrophoretically transferred to PVDF (Problott, Applied Biosystems, Warrington, U.K.) membrane. The membrane was then divided into three identical sections and each section incubated with one of the MMP antibodies. Antibody which had reacted with antigen on the membrane was detected using alkaline phosphatase-conjugated goat anti-mouse IgG (Fc specific, Sigma) with the detection system 5-bromo-4-chloro-3-indolyl phosphate/nitro blue tetrazolium (BCIP/NBT; Sigma). The antibodies were isotyped with an Isostrip kit (Boehringer Mannheim, Lewes, Sussex, U.K.) used according to the manufacturer's instructions.

### Immunohistochemistry

Sections of oesophageal tumours were immunostained with monoclonal antibodies to MMP-1 (clone 3B6), MMP-2 (clone 4D3), and MMP-9 (clone 2C3). Immunohistochemistry for the individual MMPs was performed using an alkaline phosphatase anti-alkaline phosphatase technique.<sup>24</sup> Tissue sections were subjected to an antigen retrieval step by microwave treatment of the sections for 10 min (MMP-1 and MMP-9) or 5 min (MMP-2) in 0.01 M sodium citrate buffer, pH 6.0, in a microwave (Proline<sup>®</sup>) operated at full power (950 W). The sections were allowed to cool to room temperature before application of the individual MMP antibodies as undiluted tissue culture supernatants. Following incubation with the monoclonal antibodies, sections were sequentially incubated with rabbit anti-mouse immunoglobulin (1/100; Dako, High Wycombe, Berks, U.K.) and monoclonal alkaline phosphatase anti-alkaline phosphatase (1/100; Dako). Following each antibody application, sections were washed in 0.05 M Tris-HCl buffered saline, pH 7.6 (TBS). Alkaline phosphatase was demonstrated using BCIP/NBT. After incubating the sections for 30 min at room temperature, the reaction was stopped by washing the sections for 5 min in hot tap water. The slides were then air-dried and mounted in glycerine jelly. When the immunohistochemistry was complete, the sections were examined microscopically. The MMP status of the tumours was assessed as positive if any of the tumour cells showed significant immunostaining.<sup>25</sup> Negative controls were done by replacing the primary antibody with TBS and by liquid phase pre-absorption of primary antibody with the corresponding immunogen at 10 nmol/ml antibody. The positive control for MMP-1 was colonic adenocarcinoma which had previously been shown to be positive for MMP-1,<sup>24</sup> while the positive controls for both MMP-2 and MMP-9 were lung containing intra-alveolar macrophages.

Survival data were obtained after the assessment of the presence of MMPs in the oesophageal cancers were complete. Statistical analysis was performed using the computer program SPSS for Windows<sup>®</sup>. Cumulative patient survival was assessed by the method of Kaplan-Meier, and comparison of the MMP-positive and MMP-negative survival curves was carried out using the

log-rank  
was per-  
tators. T  
variate  
histolo-  
MMPs

The  
bodies  
not cr-  
phore-  
lane c-  
had b-  
sistent  
MMP  
of IgC  
All  
section  
ity fo-  
cells (  
almo-  
of M-  
types  
II. T  
of ir-  
and  
prese  
MM-  
in 3-  
MM-  
MM-  
tumc  
ing  
oeso-  
for  
show  
show  
St  
was  
11 p-  
by 2  
were

Table I—The presence of MMPs in different stages of oesophageal cancer

	Tumour stage				Total
	2a	2b	3	4	
MMP-1					
Positive	2 (4%)	2 (4%)	6 (14%)	1 (2%)	11 (24%)
Negative	13 (28%)	2 (4%)	20 (44%)	0	35 (76%)
MMP-2					
Positive	13 (28%)	4 (10%)	18 (39%)	1 (2%)	36 (79%)
Negative	2 (4%)	0	8 (17%)	0	10 (21%)
MMP-9					
Positive	13 (28%)	3 (7%)	15 (33%)	1 (2%)	32 (70%)
Negative	2 (4%)	1 (2%)	11 (24%)	0	14 (30%)

log-rank test. Multi-variate analysis using Cox's method was performed to identify independent prognostic factors. The variables which were included in the multi-variate analysis were age, sex of patients, tumour stage, histological type of tumour, and status of individual MMPs.

## RESULTS

The immunoblots showed that the monoclonal antibodies were specific for the appropriate MMP and did not cross-react with other MMPs (Fig. 1). The electrophoretic mobility of the slightly lower band visible in the lane containing MMP-1 of panel A after the membrane had been incubated with the MMP-1 antibody is consistent with that expected for the activated form of MMP-1. All three monoclonal antibodies had an isotype of IgG<sub>1</sub>κ.

All the antibodies were effective on formalin-fixed sections after an antigen retrieval step. Immunoreactivity for each MMP was detected in oesophageal tumour cells (Fig. 2): when staining was present, it was found in almost all the tumour cells. Summaries of the occurrence of MMPs in different stages and different histological types of oesophageal cancer are shown in Tables I and II. There were no significant differences in the presence of individual MMPs between squamous carcinoma and adenocarcinoma. MMP-2 and MMP-9 were both present in the majority of oesophageal tumours, with MMP-2 present in 36 (78 per cent) tumours and MMP-9 in 32 (70 per cent) tumours, respectively. Only one MMP-9-positive tumour did not also express MMP-2. MMP-1 was detected in 11 (24 per cent) oesophageal tumours, with all but two of these tumours also containing MMP-2: all but one contained MMP-9. Normal oesophageal epithelium did not show immunoreactivity for any of the MMPs, while fibroblasts consistently showed MMP-1 immunoreactivity and macrophages showed immunostaining for MMP-2 and MMP-9.

Survival analysis showed that the presence of MMP-1 was associated with more rapid progression and that all 11 patients whose tumours contained MMP-1 were dead by 29 months, while nine of the patients whose tumours were MMP-1-negative remained alive at 60 months.

Table II—The presence of individual MMPs in different histological types of oesophageal cancer

	Histological type		Total
	Squamous carcinoma	Adenocarcinoma	
MMP-1			
Positive	3 (7%)	8 (17%)	11 (24%)
Negative	16 (35%)	19 (41%)	35 (76%)
MMP-2			
Positive	14 (30%)	22 (48%)	36 (78%)
Negative	5 (11%)	5 (11%)	10 (22%)
MMP-9			
Positive	11 (24%)	21 (46%)	32 (70%)
Negative	8 (17%)	6 (13%)	14 (30%)

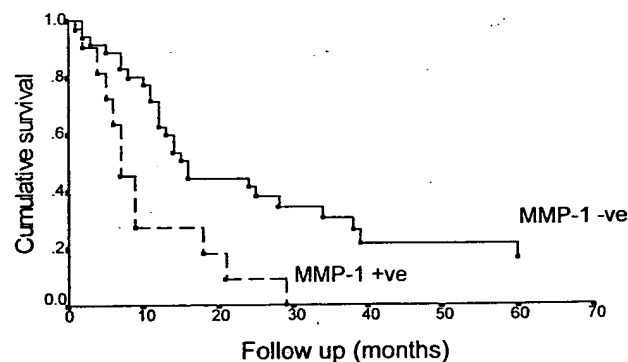


Fig. 3—Cumulative survival of oesophageal cancer patients whose tumours were either positive or negative for MMP-1

The median survival in the MMP-1-positive group was 7 months; while the median survival in the MMP-1-negative group was 16 months (Fig. 3). The difference in survival was significant between the MMP-1-positive and MMP-1-negative groups (log-rank test 8.46,  $P=0.004$ ). There were no significant survival differences between those patients whose tumours were MMP-2-positive or -negative: the same was true for MMP-9. Multi-variate analysis showed that MMP-1 was an independent prognostic factor ( $P=0.02$ ). The most significant prognostic factor was tumour stage ( $P=0.005$ ).



while other factors (patient age, sex of patient, histological type of tumour, MMP-2 and MMP-9 status) were all non-significant.

## DISCUSSION

Improved survival for patients with oesophageal cancer needs the development of new treatment strategies, and this requires the identification of prognostic factors which can be targeted by therapeutic intervention. The MMPs are one group of molecules which are potential targets for novel anti-cancer drugs. There is an increasing amount of evidence to indicate that matrix degradation by MMPs is an important part of the multi-step process of tumour invasion and spread.<sup>3</sup> As the MMPs are a group of closely related enzymes, it is important to have antibodies specific for individual MMPs, and we have demonstrated that this is the case for the antibodies which we have developed. Because of the location of the epitopes on an external loop of the individual MMPs at a site remote from the active site and the pro-peptide domain, it is likely that they recognize the activated forms as well as the pro-enzymes. These monoclonal antibodies, which recognize individual MMPs and are effective on formalin-fixed tissue sections, will greatly facilitate the evaluation of MMPs in tumours.

Very few studies of MMPs in tumours have correlated the presence of individual MMPs to prognosis and survival. The first stage in the invasion of malignant tumour cells is the degradation of basement membrane. Type IV collagen is the major component of the basement membrane and degradation of this is mainly achieved by MMP-2 and possibly by MMP-9.<sup>5,17</sup> Further tumour invasion requires the action of other MMPs, such as MMP-1, which can degrade more components of the extracellular matrix. The majority of oesophageal cancers showed the presence of MMP-2 and this is consistent with the study of Shima *et al.*,<sup>26</sup> who also showed the presence of MMP-2 in oesophageal cancer cells. That study, which also localized MMP-1 and MMP-3 to oesophageal tumour cells, represents the only previous investigation of MMPs in oesophageal cancer.

In oesophageal cancer, as in colorectal cancer,<sup>25</sup> MMP-1 appears to be important in facilitating further tumour spread. In our study, the presence of MMP-1 was associated with a particularly poor prognosis and was an independent prognostic factor. Stage of oesophageal tumour was the most important prognostic factor, while patient age, sex, MMP-2 status, MMP-9 status, and histological type of oesophageal tumour were not significant factors in influencing survival. All the patients who were included in the study had survived for at least 1 month following surgery, thereby excluding bias that post-operative mortality might introduce to survival analysis. Although two main types of oesophageal cancer are recognized histologically, both tumour types invade and spread in a similar manner and have an equally poor prognosis.

Low molecular weight inhibitors of MMPs have been shown to prevent tumour spread in human tumour

xenografts<sup>27,28</sup> and are being developed for clinical use at least one MMP inhibitor (Marimastat) is currently undergoing clinical trials.<sup>29</sup> In view of this, it is important to have objective markers that could potentially be used to identify those patients who are most likely to benefit from anti-MMP therapy. Interstitial collagenase (MMP-1)-activated 5-fluoro-uracil pro-drugs<sup>30</sup> could also be appropriately used in those patients whose tumours contain MMP-1. The MMP status of oesophageal tumours can readily be assessed using immunohistochemistry on formalin-fixed, wax-embedded sections of tumours.

## ACKNOWLEDGEMENTS

We thank the Scottish Hospital Endowments Research Trust for financial support and Mr Bryan Dunbar and Mr Ian Davidson of the University of Aberdeen Protein Facility for amino acid sequence analysis and mass spectrometry.

## REFERENCES

1. Morson BC, Dawson IMP, Day DW, Jass JR, Price AB, Williams GT. Morson and Dawson's Gastrointestinal Pathology. 3rd edn. Oxford: Blackwell Scientific Publications, 1990; 53-70.
2. Hart IR, Saini A. Biology of tumour metastasis. *Lancet* 1992; 339: 1453-1457.
3. Kohn EC, Liotta LA. Molecular insights into cancer invasion: strategies for prevention and intervention. *Cancer Res* 1995; 55: 1856-1862.
4. Murphy G, Docherty AJP. The matrix metalloproteinases and their inhibitors. *Am J Respir Cell Mol Biol* 1992; 7: 120-125.
5. Stetler-Stevenson WG, Liotta LA, Klierer DE. Extracellular matrix 6: role of matrix metalloproteinases in tumor invasion and metastasis. *FASEB J* 1993; 7: 1434-1441.
6. Davies B, Waxman J, Wasan H *et al.* Levels of matrix metalloproteinases in bladder cancer correlate with tumor grade and invasion. *Cancer Res* 1993; 53: 5365-5369.
7. Boag AH, Young ID. Increased expression of the 72-kd type IV collagenase in prostate adenocarcinoma. *Am J Pathol* 1994; 144: 585-591.
8. Muller D, Wolf C, Abecassis J *et al.* Increased stromelysin 3 gene expression is associated with increased local invasiveness in head and neck squamous cell carcinoma. *Cancer Res* 1993; 53: 165-169.
9. Urbanski SJ, Edwards DR, Hershfield N *et al.* Expression pattern of metalloproteinases and their inhibitors changes with the progression of human sporadic colorectal neoplasia. *Diagn Mol Pathol* 1993; 2: 81-89.
10. Woessner JF. Matrix metalloproteinases and their inhibitors in connective tissue remodelling. *FASEB J* 1991; 5: 2145-2154.
11. Bode W. The X-ray crystal structure of the catalytic domain of human neutrophil collagenase inhibited by a substrate analogue reveals the essentials for catalysis and specificity. *EMBO J* 1994; 13: 1263-1269.
12. Lovejoy B, Cleasby A, Hassell AM *et al.* Structure of the catalytic domain of fibroblast collagenase complexed with an inhibitor. *Science* 1994; 263: 375-377.
13. Hunt LT, Barker WC, Chen HR. A domain structure common to hemopexin, vitronectin, interstitial collagenase and a collagenase homolog. *Prot Seq Data Anal* 1987; 1: 21-26.
14. Li J, Brick P, O'Hare MC *et al.* Structure of full-length porcine synovial collagenase reveals a C-terminal domain containing a calcium linked four-bladed  $\beta$ -propeller. *Structure* 1995; 3: 541-549.
15. Sato H, Seiki M. Membrane-type matrix metalloproteinases (MT-MMPs) in tumor metastasis. *J Biochem* 1996; 119: 209-215.
16. Sato H, Takino T, Okada Y *et al.* A matrix metalloproteinase expressed on the surface of invasive tumour cells. *Nature* 1994; 370: 61-65.
17. Tryggvason K, Höyhtä M, Pyke M. Type IV collagenases in invasive tumors. *Breast Cancer Res Treat* 1993; 24: 209-218.
18. Giannelli G, Falk-Marzillier J, Schiraldi O, Stetler-Stevenson WG, Quaranta V. Induction of cell migration by matrix metalloproteinase-2 cleavage of laminin-5. *Science* 1997; 277: 225-228.
19. Hiraga A, Kemp BE, Cohen P. Further studies on the structure of the glycogen-bound form of protein phosphatase-1 from rabbit skeletal muscle. *Eur J Biochem* 1987; 163: 253-258.
20. Sambrook J, Fritsch EF, Maniatis T. Molecular Cloning: A Laboratory Manual. New York: Cold Spring Harbor Laboratory Press, 1989.

21. Kohler of pred  
22. Barnes against carbon  
23. Dunca simple specific raised ences.  
24. Murra try of monox  
25. Murra metall-  
Natur

21. Kohler G, Milstein C. Continuous cultures of fused cells secreting antibody of predefined specificity. *Nature* 1975; 256: 495-497.
22. Barnes TS, Shaw PM, Burke MD, Melvin WT. Monoclonal antibodies against human cytochrome P-450 recognising different pregnenolone 16 $\alpha$ -carbonitrile-inducible rat cytochrome P-450. *Biochem J* 1987; 248: 301-304.
23. Duncan ME, McAleese SM, Booth NA, Melvin WT, Fothergill JE. A simple enzyme-linked immunosorbent assay (ELISA) for the neuron-specific  $\gamma$  isozyme of human enolase (NSE) using monoclonal antibodies raised against synthetic peptides corresponding to isozyme sequence differences. *J Immunol Methods* 1992; 151: 227-236.
24. Murray GI, Duncan ME, Melvin WT, Fothergill JE. Immunohistochemistry of neuron specific enolase with gamma-subunit specific anti-peptide monoclonal antibodies. *J Clin Pathol* 1993; 46: 993-996.
25. Murray GI, Duncan ME, O'Neil P, Melvin WT, Fothergill JE. Matrix metalloproteinase-1 is associated with poor prognosis in colorectal cancer. *Nature Med* 1996; 2: 461-462.
26. Shima I, Sasaguri Y, Kusakawa J *et al.* Production of matrix metalloproteinase-2 and metalloproteinase-3 related to malignant behaviour of esophageal carcinoma. *Cancer* 1992; 70: 2747-2753.
27. Watson SA, Morris TM, Robinson G, Crimmin MJ, Brown PD, Hardcastle JD. Inhibition of organ invasion by the matrix metalloproteinase inhibitor batimastat (BB-94) in two human colon carcinoma metastasis models. *Cancer Res* 1995; 55: 3629-3633.
28. Sledge GW, Qulali M, Goulet R, Bone EA, Fife R. Effects of matrix metalloproteinase inhibitor batimastat on breast cancer regrowth and metastasis in athymic mice. *J Natl Cancer Inst* 1995; 87: 1546-1550.
29. Brown PD, Giavazzi R. Matrix metalloproteinase inhibition: a review of anti-tumour activity. *Ann Oncol* 1995; 6: 967-974.
30. Nichifor M, Schact EH, Seymour LW. Macromolecular prodrugs of 5 fluorouracil. 2: Enzymatic degradation. *J Cont Release* 1996; 39: 79-92.

clinical use  
is currently  
it is import  
otentially be  
ost likely to  
collagenase  
ugs<sup>30</sup> could  
ients whose  
us of oeso  
l using im-  
x-embedded

ndowments  
Mr Bryan  
University  
cid sequence

3; Williams GT.  
d edn. Oxford:

1992; 339: 1453-

on: strategies for  
362.

as: and their

ar matrix 6: role  
stasis. *FASEB J*

talloproteases in  
*Cancer Res* 1993;

e IV collagenase  
1991.

gene expression  
neck squamous

sion pattern of  
progression of  
93; 2: 81-89.  
rs in connective

nain of human  
ue reveals the  
263-1269.

atalytic domain  
ence 1994; 263

mm to hemo-  
homolog. *Prot*

orcine synovial  
calcium linked

s (MT-MMPs)

se expressed on  
5.

ses in invasive

evason WG.  
talloprotease-2

structure of the  
skeletal muscle.

A Laboratory  
1989.

256-261 (1998)

# Tryptophan Hydroxylase Antibodies used in the Diagnosis of Carcinoid

Thomas Meyer<sup>1</sup>

Thomas Uher<sup>1</sup>

Giuliano Ramadori<sup>1</sup>

Burckhardt Ringe<sup>2</sup>

Harald Schwoerer<sup>1</sup>

## Corresponding Author:

Thomas Meyer, MD, PhD  
Center for Internal Medicine  
Robert-Koch-Str. 40

D-37075 Goettingen

Germany

Tel: +49-551-398941

Fax: +49-551-398918

Center for Internal Medicine<sup>1</sup> and  
Department of Transplantation  
Surgery<sup>2</sup>, University of  
Goettingen, Goettingen, Germany

**KEY WORDS:** Carcinoid; Serotonin Biosynthesis; Tryptophan Hydroxylase

**ABBREVIATIONS:** Alkaline Phosphatase-Anti-Alkaline Phosphatase (APAAP); Fetal Calf Serum (FCS); 5-Hydroxyindoleacetic Acid (5-HIAA); Sodium Dodecyl Sulfate (SDS)

## SUMMARY

The expression of tryptophan hydroxylase, the rate-limiting enzyme in the biosynthesis of serotonin, is described in a case of a 35 year-old patient with metastatic jejunal carcinoid. Immunohistochemically, monoclonal anti-tryptophan hydroxylase antibodies positively identified liver metastases of a neuroendocrine tumor. The cellular distribution of tryptophan hydroxylase was restricted exclusively to the cytoplasm of carcinoid cells, where it was found in large amounts. By means of immunoblotting, anti-tryptophan hydroxylase antibodies detected in samples from carcinoid tissue two closely migrating polypeptide bands with molecular weights of 26 kDa and 29 kDa, respectively. These two protein bands appear to represent proteolytically degraded polypeptides, since tryptophan hydroxylase is known for its extreme unstability *in vitro*. In our case, the immunohistochemical and biochemical identification of tryptophan hydroxylase in liver lesions of a neuroendocrine tumor permitted the correct diagnosis of a metastatic carcinoid.

## INTRODUCTION

Often, gastrointestinal tumors of neuroendocrine origin are rather easily identified by routine histological examinations, as they are composed of regularly arranged tumor cells with monomorphic nuclei exhibiting a characteristic growth pattern (1-3). In some cases, however, neuroendocrine tumors may be difficult to distinguish from epithelial tumors, especially when they display a low degree of differentiation. In fact, undifferentiated adenocarcinomas with neuroendocrine differentiation or neuroendocrine carcinomas can be misdiagnosed as neuroendocrine tumors, because subpopulations of carcinoma cells may focally display features of neuroendocrine differentiation as well (4). Furthermore, rare types of mixed tumors have been described which share properties of both carcinoid and carcinomatous tissue (5).

Since gastrointestinal carcinoids are defined as solid hormone-producing tumors arising from the diffuse neuroendocrine system of the

gastrointestinal mucosa (1-3,6), the detection of specific neuroendocrine markers, such as chromogranin, synaptophysin and serotonin, helps to discriminate carcinoids from adenocarcinomas (2,3,6-14). However, in carcinoids, the immunohistochemical distribution of tryptophan hydroxylase, the rate-limiting enzyme of the serotonin biosynthetic pathway, thus far has not been demonstrated. Herein, we report on a patient with liver metastases from a neuroendocrine tumor in which the use of anti-tryptophan hydroxylase antibodies permitted the clear diagnosis of carcinoid.

## Laboratory Methods

Tryptophan hydroxylase was immunohistochemically detected by applying the alkaline phosphatase-anti-alkaline phosphatase (APAAP) technique. Antigen retrieval was performed by microwaving the sections for 8 minutes in a commercially available buffer (Dako). Sections of carcinoid tissue were incubated for 45 minutes at

room temperature with anti-tryptophan hydroxylase antibodies (clone WH-3) obtained from Sigma Immunochemicals. The monoclonal antibodies were diluted 1:250 in RPMI 1640 supplemented with 10% fetal calf serum (FCS). Samples were then incubated with rabbit anti-mouse antibodies diluted 1:25 in RPMI + 10% FCS for 30 minutes. After three washes, soluble complexes of calf intestinal alkaline phosphatase and anti-alkaline phosphatase diluted 1:25 in RPMI + 10% FCS were added. Bound immunoreactivity was visualized by the New Fuchsin method using 2-amino-2-methyl-1,3-propanediol, levamisole, naphthol-AS-BI phosphate, New Fuchsin and  $\text{NaNO}_2$ . Sections were exposed to the filtered chromogen reaction solution and counterstained in Mayer's Hematoxylin. Negative controls were carried out by substituting non-immune mouse serum for primary antibody solutions.

For immunoblotting experiments, carcinoid tissue from hepatic metastases (10 mg) was boiled for 5 minutes in a 10 ml SDS sample buffer (5% sodium dodecyl sulfate, 0.025% Bromphenol blue, 10% glycerol, 10% 2-mercaptoethanol, 0.125 M Tris-HCl, pH 6.8). Proteins were separated by SDS electrophoresis on 10% polyacrylamide gels followed by transfer onto nitrocellulose membranes. After blocking with 4% BSA, the membranes were incubated with anti-tryptophan hydroxylase antibodies which were diluted 1:250. As secondary antibodies, peroxidase-labelled rabbit anti-mouse immunoglobulins were used. Visualization of bound immunoreactivity was achieved by using the ECL chemiluminescence reaction (Amersham).

For measuring serum concentrations of gastroenteric hormones, enzyme-linked immunosorbent assays and radioimmunoassays were performed according to the instructions of the manufacturers.

### CASE REPORT

A 35 year-old woman underwent a diagnostic laparotomy and right oophorectomy because of multiple intrahepatic metastases and a mass located in the right ovary. She had been in excellent health until two weeks earlier when she noticed a gradual onset of abdominal pain in the right upper quadrant. Physical examination



FIGURE 1 Computed tomography demonstrated hepatomegaly with multiple liver lesions, which were metastases of jejunal carcinoid.

revealed hepatomegaly with no palpable abdominal mass. The patient had no episodes of paroxysmal flushing, diarrhea or bronchoconstriction.

Histological examination of the surgical biopsies demonstrated a benign follicular cyst in the right ovary and liver metastases of a neuroendocrine tumor. Various attempts to localize the primary tumor were unsuccessful. Gastroduodenoscopic and colonoscopic examinations disclosed no structural disease. Barium contrast studies of the entire small-bowel were unremarkable, with no signs of mucosal irregularity or luminal impingement. Computed tomographic scans revealed multiple liver lesions and massive hepatomegaly (Figure 1). Somatostatin receptor scintigraphy demonstrated enhanced tracer retention in the liver; however, other areas of increased uptake could not be detected.

Endocrinological analysis revealed normal serum levels of free catecholamines (epinephrine 25 ng/l, norepinephrine 294 ng/l). Serotonin was found to be significantly elevated (1794  $\mu\text{g/l}$ ). Serum concentrations of glucagon (103 pg/ml), gastrin (39 pg/ml), pancreatic polypeptide (31 pmol/l), vasoactive intestinal peptide (6 pmol/l) and gastric inhibitory peptide (1048 pg/ml) were normal. Elevated serum concentrations of neuron-specific enolase were measured (45  $\mu\text{g/l}$ ). Urinary excretion of 5-hydroxyindoleacetic acid (45.4 mg/24 h) was far beyond the reference range (up to 7 mg/24 h).

Five months later, the patient was chronically ill and had lost 10 kg in weight. Orthotopic liver

transplantation was performed. During the surgical procedure, a solitary tumor in the proximal jejunum with a diameter of 2cm and regional metastases in mesenteric lymph nodes were discovered and resected. Histological examination confirmed that the jejunal mass was the primary tumor and that it had infiltrated the submucosa.

#### Pathological Findings

Conventional microscopic examination of the liver lesions showed multiple groups of tumor cells which were well demarcated from the surrounding hepatic parenchyma. The neoplastic cells were arranged predominantly in small nests, although foci of trabeculae separated by delicate fibrous septae could be visualized. Signs of necrosis or hemorrhage could not be detected, but a desmoplastic stromal reaction surrounding the tumor nests was frequently pronounced. The mitotic activity of the tumor was low. The monomorphous, polygonal tumor cells had an eosinophilic granular cytoplasm with central nuclei composed of dispersed, coarsely granular chromatin. The packeted groups of neoplastic cells displayed an insular growth pattern, somewhat resembling the histological features of an epithelial neoplasm. Argentaffinity and perinuclear expression of chromogranin, however, classified the tumor as neuroendocrine in origin.

Immunohistochemically, the tumor revealed a positive staining reaction for keratin, somatostatin and vasointestinal peptide. No immunoreactivity could be detected for serotonin, glucagon, gastrin, synaptophysin, insulin, pancreatic polypeptide, adrenocorticotrophic hormone, gastric inhibitory peptide or S100. Staining with anti-tryptophan hydroxylase antibodies revealed strongly positive cytoplasmic immunoreactivity in all tumor cells (Figure 2). Non-neoplastic cells in the vicinity of the tumor nests, such as surrounding hepatocytes and hepatic fibroblasts, were negative for tryptophan hydroxylase. For the biochemical detection of tryptophan hydroxylase, immunoblotting experiments were performed. In samples from the tumor tissue, the tryptophan hydroxylase was identified as two closely migrating polypeptide bands with molecular weights of 26 kDa and 29 kDa, respectively (Figure 3). Total protein extracts from human



**FIGURE 2** Expression of tryptophan hydroxylase in hepatic metastases of carcinoid. The section was immunohistochemically stained with monoclonal anti-tryptophan hydroxylase antibodies using APAAP techniques followed by counterstaining with Mayer's Hematoxylin. Note that positive immunostaining was exclusively restricted to carcinoid cells, which displayed an insular growth pattern.



**FIGURE 3** Immunoblotting analysis of tryptophan hydroxylase expression in carcinoid tissue. Proteins from crude homogenates of hepatic metastases were applied to SDS polyacrylamide gel electrophoresis, and tryptophan hydroxylase was detected with anti-tryptophan hydroxylase antibodies from clone WH-3. Bound immunoreactivity was visualized using the chemiluminescence technique.

blood platelets used as negative controls failed to react with the anti-tryptophan hydroxylase antibodies.

#### DISCUSSION

In the presence of molecular oxygen and the natural cofactor tetrahydrobiopterin, tryptophan hydroxylase catalyzes the hydroxylation of L-tryptophan to 5-hydroxytryptophan (15-18). The formation of 5-hydroxytryptophan is generally considered to be the rate-limiting step in the biosynthesis of the monoamine, serotonin. In an enzymatic reaction requiring aromatic-L-amino acid decarboxylase (16,19), the intermediate 5-hydroxytryptophan further reacts to 5-

hydroxytryptamine (serotonin). Following its release from the tumor, serotonin is inactivated primarily by the enzyme monoamine oxidase (20). The resulting metabolite 5-hydroxyindoleacetaldehyde is rapidly converted to 5-hydroxyindoleacetic acid (5-HIAA) in a reaction catalyzed by aldehyde dehydrogenase. In carcinoids, urinary excretion of the main serotonin metabolite 5-HIAA is significantly elevated, because most of these tumors contain large quantities of aromatic-L-amino acid decarboxylase, which catalyzes the final step in the formation of serotonin (1,19).

Most carcinoids, such as jejunal, ileal, appendiceal and colonic, produce large amounts of serotonin in addition to a number of neuropeptides. Metastatic carcinoids with overproduction of serotonin give rise to the carcinoid syndrome, which is characterized by cutaneous flushing, diarrhea and bronchoconstriction (1,20). Carcinoids derived from the embryonic foregut, however, are frequently deficient in aromatic-L-amino acid decarboxylase, while they release a high amount of 5-hydroxytryptophan in the circulation (20). In these carcinoid subtypes, the synthesis of serotonin as reflected by urinary 5-HIAA production is within the physiologic range. Although many carcinoids derived from the embryonic foregut express tryptophan hydroxylase, as determined by the elevated serum levels of 5-hydroxytryptophan, due to their deficiency in aromatic-L-amino acid decarboxylase, they are unable to synthesize and secrete serotonin (19,20). Thus, the immunohistochemical demonstration of serotonin in tissue sections cannot be regarded as a pathognomonic feature of all carcinoids, since it is missing in certain subtypes.

In this paper, we focused our interest on the expression of tryptophan hydroxylase in a case of metastatic jejunal carcinoid. By means of

immunohistochemical assays, the cellular localization of this enzyme in carcinoid tissue has not yet been studied. Our results clearly showed that the monoclonal anti-tryptophan hydroxylase antibodies positively identified carcinoid cells in the liver metastases as well as the primary tumor. Using APAAP techniques, the cytoplasm of the neoplastic cells was intensely labelled. Surrounding non-tumor cells displayed no specific immunostaining, indicating that the expression of tryptophan hydroxylase was exclusively restricted to the carcinoid cells.

Western immunoblotting experiments were performed to determine the molecular weight of tryptophan hydroxylase in human carcinoid tissue. Samples from crude homogenates of hepatic metastases and the adjacent normal liver were analyzed for the expression of this enzyme. Two closely migrating polypeptide bands with molecular weights of 26 kDa and 29 kDa exhibited a strong immunoreactivity for anti-tryptophan hydroxylase antibodies. Since tryptophan hydroxylase is known to be extremely unstable *in vitro* (17,18), we suggest that the two identified bands represent proteolytically degraded polypeptides. The measured molecular weight is in agreement with the reported molecular weight of tryptophan hydroxylase described by Boularand et al. (22).

In our case of a neuroendocrine tumor, the immunohistochemical identification of tryptophan hydroxylase allowed the correct diagnosis of the hepatic lesions as metastatic carcinoid tissue. Since the studied monoclonal anti-tryptophan hydroxylase antibodies positively labelled carcinoid cells in paraffin-embedded material, we recommend their use in the differential diagnosis of neuroendocrine tumors. A systematic investigation testing the validity of anti-tryptophan hydroxylase antibodies in the diagnosis of carcinoids and related tumors is currently in progress.

## REFERENCES

- 1 Nilsson O: Gastrointestinal carcinoids. Aspects of diagnosis and classification. APMIS 1996; 104:481-492.
- 2 Wilander E: Diagnostic pathology of gastrointestinal and pancreatic neuroendocrine tumours. Acta Oncol 1989; 28:363-369.
- 3 Wilander E, Scheibenpflug L, Eriksson B, Oberg K: Diagnostic criteria of classical carcinoids. Acta Oncol 1991; 30:469-475.
- 4 Gould VE, Jao W, Chejfec G, Banner BF, Bonomi P: Neuroendocrine carcinomas of the gastrointestinal tract. Semin Diagn Pathol 1984; 1:13-18.
- 5 Klappenbach RS, Kurman RJ, Sinclair CF, James LP: Composite carcinoma-carcinoid tumors of the gastrointestinal tract. A morphologic, histochemical, and immunocytochemical study. Am J Clin Pathol 1985; 84:137-143.
- 6 Yang K, Ulich T, Cheng L, Lewin KJ: The neuroendocrine products of intestinal carcinoids. An

- immunoperoxidase study of 35 carcinoid tumors stained for serotonin and eight polypeptide hormones. *Cancer* 1983; 51:1918-1926.
- 7 **Moyana TN, Satkunam N:** A comparative immunohistochemical study of jejunoileal and appendiceal carcinoids. Implications for histogenesis and pathogenesis. *Cancer* 1992; 70:1081-1088.
  - 8 **Lembeck F:** 5-hydroxytryptamine in a carcinoid tumor. *Nature* 1953; 172:910-911.
  - 9 **Burke AP, Federspiel BH, Sobin LH, Shekitka KM, Helwig EB:** Carcinoids of the duodenum. A histologic and immunohistochemical study of 65 tumors. *Am J Surg Pathol* 1989; 13:828-837.
  - 10 **Vyberg M, Horn T, Francis D, Askaa J:** Immunohistochemical identification of neuron-specific enolase, synaptophysin, chromogranin and endocrine granule constituent in neuroendocrine tumours. *Acta Histochemica* 1990; 38 Suppl:179-181.
  - 11 **Wiedenmann B, Franke WW, Kuhn C, Moll R, Gould VE:** Synaptophysin. A novel marker protein for neuroendocrine cells and neoplasms. *Proc Natl Acad Sci USA* 1986; 83:3500-3504.
  - 12 **Weiler R, Feichtinger H, Schmid KW, Fischer-Colbrie R, Grimelius L, Cedermarck B, Papotti M, Bussolati G, Winkler H:** Chromogranin A and B and secretogranin II in bronchial and intestinal carcinoids. *Virchows Arch A Pathol Anat* 1987; 412:103-109.
  - 13 **Eriksson B, Arnberg H, Oberg K, Hellman U, Lundqvist G, Wernstedt C, Wilander E:** Chromogranins. New sensitive markers for neuroendocrine tumors. *Acta Oncol* 1989; 28:325-329.
  - 14 **Kimura N, Sasano N, Yamada R, Satoh J.** Immunohistochemical study of chromogranin in 100 cases of pheochromocytoma, carotid body tumour, medullary thyroid carcinoma and carcinoid tumour. *Virch. Arch. A. Pathol. Anat.* 1988; 413:33-38.
  - 15 **Tipper JP, Citron BA, Ribeiro P, Kaufman S.** Cloning and expression of rabbit and human brain tryptophan hydroxylase cDNA in *Escherichia coli*. *Arch Biochem Biophys* 1994; 315:445-453.
  - 16 **Lovenberg W, Jequier E, Sjoerdsma A.** Tryptophan hydroxylation. Measurement in pineal gland, brainstem, and carcinoid tumor. *Science* 1967; 155:217-219.
  - 17 **Kuhn DM, Rosenberg RC, Lovenberg W.** Determination of some molecular parameters of tryptophan hydroxylase from rat midbrain and murine mast cell. *J Neurochem* 1979; 33:15-21.
  - 18 **D'Sa CM, Arthur RE, Kuhn DM.** Expression and deletion mutagenesis of tryptophan hydroxylase fusion proteins. Delineation of the enzyme catalytic core. *J Neurochem* 1996; 67:917-926.
  - 19 **Gilbert JA, Bates LA, Ames MM.** Elevated aromatic-L-amino acid decarboxylase in human carcinoid tumors. *Biochem Pharmacol* 1995; 50:845-850.
  - 20 **Oates JA, Sjoerdsma A.** A unique syndrome associated with secretion of 5-hydroxytryptophan by metastatic gastric carcinoids. *Am J Med* 1962; 32:333-342.
  - 21 **Thomas RM, Baybick JH, Elsayed AM, Sobin LH.** Gastric carcinoids. An immunohistochemical and clinicopathological study of 104 patients. *Cancer* 1994; 73:2053-2058.
  - 22 **Boularand S, Darmon MC, Ganem Y, Launay JM, Mallet J.** Complete coding sequence of human tryptophan hydroxylase. *Nuclei Acids Res* 1990; 18:4257.

## United States Patent [19]

Srinivasan et al.

[11] Patent Number: 4,988,496

[45] Date of Patent: Jan. 29, 1991

[54] METAL RADIONUCLIDE CHELATING  
COMPOUNDS FOR IMPROVED  
CHELATION KINETICS[75] Inventors: Ananthachari Srinivasan, Kirkland;  
Alan R. Fritzberg, Edmonds; David  
S. Jones, Seattle, all of Wash.

[73] Assignee: NeoRx Corporation, Seattle, Wash.

[21] Appl. No.: 201,134

[22] Filed: May 31, 1988

[51] Int. Cl.<sup>3</sup> ..... A61K 49/02; C07F 13/00[52] U.S. Cl. .... 424/1.1; 534/10;  
534/14

[58] Field of Search ..... 424/1.1; 534/14, 10

## [56] References Cited

## U.S. PATENT DOCUMENTS

- 4,444,690 4/1984 Fritzberg .  
 4,615,876 10/1986 Troutner et al. .  
 4,638,051 1/1987 Burns et al. .... 424/1.1  
 4,666,697 5/1987 Takahashi et al. .  
 4,670,545 6/1987 Fritzberg et al. .  
 4,673,562 6/1987 Davison et al. .  
 4,678,667 7/1987 Meares et al. .  
 4,861,869 8/1989 Nicolotti et al. .

## FOREIGN PATENT DOCUMENTS

- 0188256 7/1986 European Pat. Off. .... 424/1.1  
 2109407 6/1983 United Kingdom .

## OTHER PUBLICATIONS

B. Bubeck et al., "Clinical Comparison of 1-131 o-Iodo-hippurate With Tc-99m CO<sub>2</sub>-DADS-A and Tc-99m MAG<sub>3</sub> By Simultaneous Double Tracer Measurement", *Nuc. Compact* 17:135-138, 1986.

C. Müller-Suur et al., "Clearance and Renal Extraction of a New Renal Scanning Agent: Technetium-99m MAG<sub>3</sub> in Comparison to Hippurate (OIH) and EDTA", *J. Nucl. Med.* 27:572, 1986.

Alan R. Fritzberg et al., "Synthesis and Biological Evaluation of Technetium-99m MAG<sub>3</sub> as a Hippuran Replacement", *J. Nucl. Med.* 27:111-116, 1986.

Ban An Khaw et al., "Technetium-99m Labeling of

Antibodies to Cardiac Myosin Fab and to Human Fibrinogen"; *J. Nucl. Med.* 23:1011-1019, 1982.

D. L. Nosco et al., "Characterization of the New (Tc-99m) Dynamic Renal Imaging Agent (Tc-99m) MAG<sub>3</sub>", *J. Nucl. Med.* 27:939, 1986.

A. Taylor, Jr. et al., "Preliminary Evaluation of Technetium-99m Mercaptoacetyltriglycine (MAG<sub>3</sub>) as a Replacement for Iodine-131 OIH", *J. Nucl. Med.* 27:571-572, 1986.

Primary Examiner—John S. Maples

Attorney, Agent, or Firm—Seed and Berry

## [57] ABSTRACT

The present invention provides metal chelating compounds, to chelates and chelate-targeting agent conjugates formed from the chelating compounds, and to methods for making and using these compositions. The chelating compounds incorporate two nitrogen atoms and three sulfur atoms ("N<sub>2</sub>S<sub>3</sub>"), two nitrogen atoms and four sulfur atoms ("N<sub>2</sub>S<sub>4</sub>"), or three nitrogen atoms and three sulfur atoms ("N<sub>3</sub>S<sub>3</sub>"). Metals, and metal oxides, capable of being chelated by the compounds include those that are radionuclides, such as <sup>99m</sup>Tc and <sup>186/188</sup>Re.

The targeting agent portion of the chelate-targeting agent conjugates provided includes antibodies, peptides, hormones, enzymes and biological response modifiers. Methods for making the conjugates are provided and encompass the addition of a metal, or metal oxide, to a chelating compound prior to attachment to a targeting agent as well as subsequent to the attachment.

Another aspect of the invention provides kits for producing chelate-targeting agent conjugates for radio-pharmaceutical use.

An additional aspect of the invention provides methods for using the chelate-targeting agent conjugates for diagnostic and therapeutic purposes, such as detection of a target site and delivery of a radionuclide to the site, respectively.

13 Claims, No Drawings



# METAL RADIONUCLIDE CHELATING COMPOUNDS FOR IMPROVED CHELATION KINETICS

## DESCRIPTION

### 1. Technical Field

The present invention relates generally to metal chelating compounds, to chelates and chelate-targeting agent conjugates formed from the chelating compounds, and to methods for making and using these compositions. This invention is more particularly related to chelate-targeting agent conjugates in which the metal is a radionuclide and to methods employing the conjugates for diagnostic and therapeutic purposes.

### 2. Background of the Invention

Radiolabeled chelating compounds are useful medical agents. For example, radiolabeled ethylenediamine tetraacetic acid (EDTA), diethylenetetramine-pentaacetate (DTPA) and o-iodohippurate (OIH) have been reported to be useful in evaluating renal functions (Klingensmith et al., *J. Nucl. Med.* 29:377, 1982). Similarly, Kasina et al., *J. Med. Chem.* 29:1933 (1986), report promising renal pharmaceuticals that are technetium (99mTc) chelates of diamide-dimercaptides (N2S2). Other medically useful chelates that have been reported include: tartrate and orthophosphate, Molinski et al., U.S. Pat. No. 3,987,157; propylene amine oxime, Troutner et al., U.S. Pat. No. 4,615,876; poly-hydroxy-carboxylic acids, Adler et al., U.S. Pat. No. 4,615,876; poly-hydroxy-carboxylic acids, Adler et al., U.S. Pat. No. 4,027,005; organo-trisubstituted trivalent phosphorus compounds, Dean et al., U.S. Pat. No. 4,582,700; bis(thiosemicarbazone), Vedeceeta 1., U.S. Pat. No. 4,564,472; mercaptoacetylglucylglycylglycine (MAG3) Fritzberg et al., *J. Nucl. Med.* 27:111-116, 1986; mercapto-carboxylic acids, Winchell et al., U.S. Pat. No. 4,233,285; homocysteine and cysteinamide derivatives, Byrne et al., U.S. Pat. No. 4,571,430; metallothioneine, Tolman, European application 4-10-84 0 137 457 AZ; isonitrile, Jones et al., U.S. Pat. No. 4,452,774; and imidodiphosphonate, Subramaniam et al., U.S. Pat. No. 3,974,268.

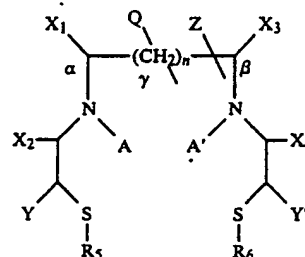
Chelating compounds are useful both as therapeutic and diagnostic agents. They are investigated for the purpose of stably linking the radionuclides to target-specific biological molecules such as antibodies and antibody fragments. Diagnostic imaging of specific target tissue in vivo with a radiometal-chelate-antibody conjugate was reported by Khaw et al., *Science* 209:295, 1980. Similarly, the therapeutic use of radiometal-chelate-antibody conjugates to treat cellular disorders is referred to by Gansow et al., U.S. Pat. No. 4,454,106.

Difficulties associated with the known chelating compounds have limited their usefulness. For example, the rate of chelation of diamide-dimercaptide (N2S2) ligands is relatively low despite the high stability of the Tc and Re complexes formed. An alternative approach, direct attachment of radionuclides to reduced proteins, also results in the formation of a complex in which metal is bound to thiolate and other groups such as amide, amine and carboxylate. However, stability problems have often limited their use in diagnostic and therapeutic applications involving antibody and antibody fragments. The stability problems can be attributed, in part, to the large metal chelate ring sizes required to attain desired donor atom to metal ratios.

Thus, there is a need in the art for metal chelating compounds which are capable of both rapidly complexing a metal and forming a stable chelate. The present invention fulfills this need and further provides other related advantages.

## SUMMARY OF THE INVENTION

Briefly stated, the present invention, in one aspect, provides a compound having the formula (I):



wherein:

X<sub>1</sub> and X<sub>2</sub> are H or =O but both are not =O;

X<sub>3</sub> and X<sub>4</sub> are H or =O, but both are not =O;

A is H, alkyl group of C<sub>6</sub> or less, —CH<sub>2</sub>—CH<sub>2</sub>—S—R<sub>1</sub> or —CO—CH<sub>2</sub>—S—R<sub>1</sub>, with the proviso that when X<sub>1</sub> or X<sub>2</sub> is =O, A is H;

A' is H, alkyl group of C<sub>6</sub> or less, —CH<sub>2</sub>—CH<sub>2</sub>—S—R<sub>2</sub> or —CO—CH<sub>2</sub>—S—R<sub>2</sub>, with the proviso that when X<sub>3</sub> or X<sub>4</sub> is =O, A' is H;

Y is

(a) —CH<sub>2</sub>—S—R<sub>3</sub>, or H, when A is H or an alkyl group of C<sub>6</sub> or less and A' is H or an alkyl group of C<sub>6</sub> or less, or

(b) H;

Y' is

(a) —CH<sub>2</sub>—S—R<sub>4</sub>, or H, when A is H or an alkyl group of C<sub>6</sub> or less and A' is H or an alkyl group of C<sub>6</sub> or less, with the proviso that Y and Y' are not both H, or

(b) H;

R<sub>1</sub>, R<sub>2</sub>, R<sub>3</sub>, R<sub>4</sub>, R<sub>5</sub>, and R<sub>6</sub> are independently selected from sulfur protecting groups;

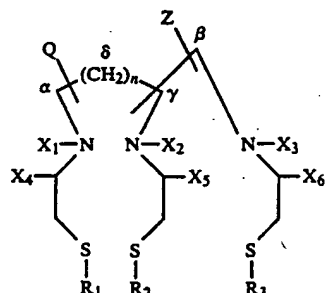
Q is H or a polar group to increase the hydrophilicity of the compound;

n is 0 to 2; and

Z is —(W)<sub>m</sub>—R', where W is —CH<sub>2</sub>—, —CH<sub>2</sub>—O—, —CH<sub>2</sub>—CO—, or combination thereof, m is 0 to 5, and R' is a chemically reactive group, with the provisos that when Z is attached to the carbon designated α there is either no X<sub>1</sub> or no Q at α, that when Z is attached to the carbon designated β there is either no X<sub>3</sub> or no Q at β, that when X<sub>1</sub> is =O there is no Z at α, and that when X<sub>3</sub> is =O there is no Z at β.

Chelates, chelate-targeting agent conjugates, and methods for producing them from compound I are provided. The targeting agent is attached via the reactive group, R', to the chelating compound or the chelate.

In another aspect, the invention provides a compound having the formula (II):



wherein:

R<sub>1</sub>, R<sub>2</sub>, and R<sub>3</sub> are independently selected from sulfur protecting groups;

X<sub>1</sub> and X<sub>2</sub> are independently selected from H and an alkyl group of C<sub>6</sub> or less;

X<sub>3</sub> is H, an alkyl group of C<sub>6</sub> or less, or Z;

X<sub>4</sub>, X<sub>5</sub>, and X<sub>6</sub> are independently selected from H and =O, with the provisos that X<sub>4</sub> is H when X<sub>1</sub> is an alkyl group, that X<sub>5</sub> is H when X<sub>2</sub> is an alkyl group, and that X<sub>6</sub> is H when X<sub>3</sub> is an alkyl group or Z;

Q is H or a polar group to increase the hydrophilicity of the compound;

n is 0 to 4; and

Z is  $-(W)_m-R'$ , where W is  $-CH_2-$ ,  $-CH_2-O-$ ,  $-CH_2-CO-$ , or combinations thereof, m is 0 to 5, and R' is a chemically reactive group.

Chelates, chelate-targeting agent conjugates, and methods for producing them from compound II are provided. The targeting agent is attached via the reactive group, R', to the chelating compound or the chelate.

Another aspect of the present invention provides kits for producing chelate-targeting agent conjugates for radiopharmaceutical use. A metal radionuclide may be added to a chelating compound of formula I or II, either before or after the chelating compound is attached to a targeting agent.

Yet another aspect of the invention provides methods for using the chelate-targeting agent conjugates described above for diagnostic and therapeutic purposes. A diagnostic method is described for detecting the presence or absence of a target site within a mammalian host. This method comprises the steps of administering to a mammal a diagnostically effective dose of the chelate-targeting agent conjugate containing a metal radionuclide, such as <sup>99m</sup>Tc, and detecting the biodistribution of the radionuclide. A therapeutic method is described for delivering a radionuclide, such as <sup>186</sup>Re or <sup>188</sup>Re, to a target site within a mammalian host. This method comprises the step of administering to a mammal a therapeutically effective dose of the chelate-targeting agent conjugate.

Other aspects of the invention will become evident upon reference to the following detailed description.

#### DETAILED DESCRIPTION OF THE INVENTION

Prior to setting forth the invention, it may be helpful to an understanding thereof to set forth definitions of certain terms to be used hereinafter.

Targeting agent—is any molecule that has the capacity to bind to a defined population of cells.

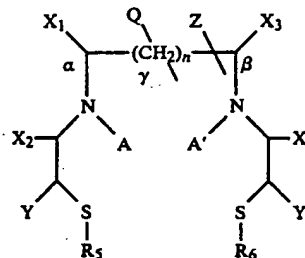
Protein—as used herein, includes proteins, polypeptides, and peptides; and may be an intact molecule, a fragment thereof, or a functional equivalent thereof;

and may be genetically engineered; an example is an antibody.

Antibody—as used herein, includes both polyclonal and monoclonal antibodies; and may be an intact molecule, a fragment thereof, or a functional equivalent thereof; and may be genetically engineered; examples of antibody fragments include F(ab')<sub>2</sub>, Fab', Fab and Fv.

As noted above, the present invention provides compounds of two general formulae that are capable of chelating metals. An advantage of these compounds is that they are capable of rapidly complexing a metal as well as forming a stable chelate. The presence of nitrogen (N) atoms within the chelating compound accelerates complex formation with a metal. This acceleration is due, in part, to the fact that a metal, e.g., Tc, is a soft acid and N, in the form of an amine or amide, is a base. Amines provide a greater increase in chelation rates than amides. The presence of sulfur (S) atoms within the chelating compound, in addition to providing for increased rates of complexation, contribute to the stability of the resulting chelate. Thus, the compounds of the present invention represent a combination of desirable kinetic properties for the formation of a complex with a metal and desirable thermodynamic properties for the retention of the metal. Accordingly, attachment of radionuclides to targeting agent-chelate conjugates formed from the compounds of the present invention which possess increased  $-S-$  (thiolate) groups situated at an appropriate distance alleviates the stability and kinetic problems encountered in both the direct metallation reaction of proteins and protein-chelate conjugates formed from the known chelating compounds.

Compound I has the following formula:

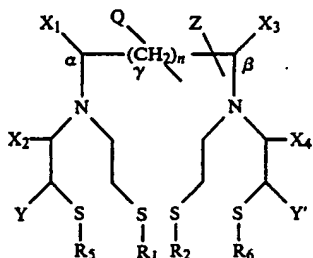
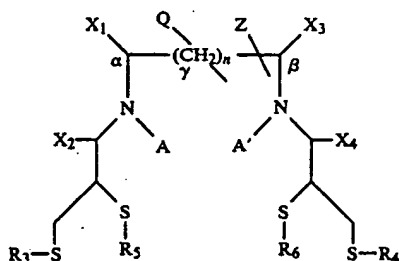


Examples of specific embodiments of the elements of compound I include the following.

X<sub>1</sub> and X<sub>2</sub> may be H or an oxy group (=O), but both are not =O. Likewise, X<sub>3</sub> and X<sub>4</sub> may be H or =O, but both are not =O. By selecting =O for X<sub>1</sub> or X<sub>2</sub>, the N interposed between the carbons to which X<sub>1</sub> and X<sub>2</sub> are bonded will be an amide. Likewise, by selecting =O for X<sub>3</sub> or X<sub>4</sub>, the N interposed between the carbons to which X<sub>3</sub> and X<sub>4</sub> are bonded will be an amide. Thus, a compound with zero, one or two amides may be formed by the appropriate selection of X<sub>1</sub>, X<sub>2</sub>, X<sub>3</sub> and X<sub>4</sub>. Amide nitrogens, relative to amine nitrogens, afford greater stability to the complex formed with a metal, but at the expense of a diminished acceleration of complex formation. Thus, by selection of X<sub>1</sub>, X<sub>2</sub>, X<sub>3</sub> and X<sub>4</sub>, compounds with a wide variety of chelating properties may be formed.

A is a hydrogen (H), alkyl group of C<sub>6</sub> or less,  $-CH_2-$ ,  $-CH_2-S-R_1$  or  $-CO-CH_2-S-R_1$ , except when either X<sub>1</sub> or X<sub>2</sub> is =O, A is H. Similarly, A' is H, alkyl group of C<sub>6</sub> or less,  $-CH_2-$ ,  $-CH_2-S-R_2$  or  $-CO-CH_2-S-R_2$ , except when either X<sub>3</sub> or X<sub>4</sub> is

$=O$ , A' is H. Y is  $-CH_2-S-R_3$ , or H, when A is H or an alkyl group of  $C_6$  or less and A' is H or an alkyl group of  $C_6$  or less. Alternatively, when either A or A' or both are not H or an alkyl group of  $C_6$  or less, then Y is H. Similarly, Y' is  $-CH_2-S-R_4$ , or H, when A is H or an alkyl group of  $C_6$  or less and A' is H or an alkyl group of  $C_6$  or less. However, Y and Y' are both not H when A is H or an alkyl group of  $C_6$  or less and A' is H or an alkyl group of  $C_6$  or less. Alternatively, when either A or A' or both are not H or an alkyl group of  $C_6$  or less, then Y' is H. Thus, compounds of the formula depicted above may be formed containing two nitrogens and three or four sulfurs (" $N_2S_3$ " and " $N_2S_4$ ", respectively). For " $N_2S_4$ " compounds, two of the sulfurs are the sulfurs bearing  $R_3$  and  $R_6$  and the remaining two sulfurs are from A and A' or Y and Y'. The following formulae depict examples of  $N_2S_4$  compounds in which two sulfurs are from Y and Y' (IA) or in which two sulfurs are from A and A' (IB).



$R_1$ ,  $R_2$ ,  $R_3$ ,  $R_4$ ,  $R_5$  and  $R_6$  are independently selected from sulfur protecting groups. Groups which may be used include any of the alkyl, acyl and aryl groups, disulfides and bunte salts known by those skilled in the art. Preferred groups are those that result in the formation of a thioacetal, hemithioacetal, thioester or acetamidomethyl substituent. Particularly preferred groups include p-anisylidene, acetonide, tetrahydrylfuranyl, ethoxyethyl, tetrahydrylpyranyl, acetamidomethyl and derivatives thereof. When conjugated to a targeting agent, the protecting groups may be removed and left as sulfhydryls either during storage or just prior to radiolabeling.

Q may be H or a polar group. One function of a polar group is to increase the hydrophilicity of the compound, e.g., in order to increase its aqueous solubility. Groups which may be used include carboxylates, sulfonates and secondary alcohols. A preferred group is  $-CH_2-COOH$ . Q may be attached to one of the positions designated as  $\alpha$ ,  $\beta$  and  $\gamma$ . Because the number of methylene carbons at the  $\gamma$  position is defined by n which may be greater than one, the Y position includes additional points for attachment of Q.

The distance by which the nitrogen atoms are separated may be increased by interposing methylene ( $-CH_2-$ ) groups between the carbons bonded to the nitrogens. When the number of  $-CH_2-$  groups, repre-

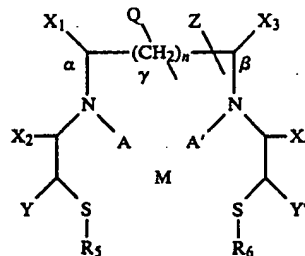
sented by n, is greater than zero, then the number of carbon atoms separating the nitrogen atoms in compound I is increased accordingly. Preferred integers for n are 0 to 2.

Z is  $-(W)_m-R'$ . W is a group that functions as a "spacer arm" and may be useful to distance R' from the chelating portion of the compound. Groups which may be used include methylene ( $-CH_2-$ ), methyleneoxy ( $-CH_2-O-$ ), methylenecarbonyl ( $-CH_2-CO-$ ), or combinations thereof. The number, m, of groups such as these would be typically 0 to 30 and preferably 0 to 5.

Z, or R' when m is 0, may be attached to one of the positions designated as  $\alpha$ ,  $\beta$ , and  $\gamma$ . Because the number of methylene carbons at the  $\gamma$  position is defined by n which may be greater than one, the  $\gamma$  position includes additional points for attachment of a Z or an R'.

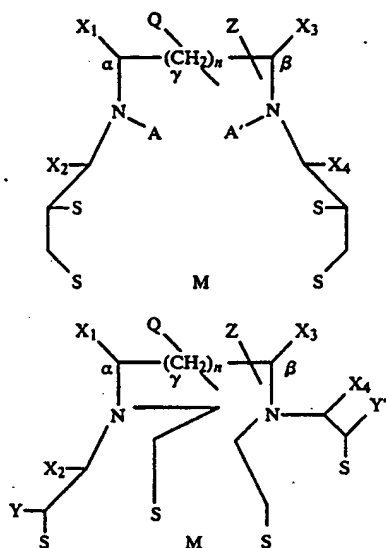
R' is a chemically reactive moiety. The moiety may be strongly electrophilic or nucleophilic and thereby be available for reacting directly with a targeting agent. Alternatively, the moiety may be a weaker electrophile or nucleophile and therefore require activation prior to the conjugation with a targeting agent. This alternative would be desirable where it is necessary to delay activation of R' until a compound has been formed. In either scenario R' is chemically reactive, the scenarios differ by whether following formation of a compound, R' is reacted directly with a targeting agent or is reacted first with one or more chemicals to render R' capable of reacting with a targeting agent. A discussion of reactions illustrative of a direct reaction with R' and of activation of R' is found below.

A metal chelate is formed by addition of a metal or metal oxide to compound I and has the following formula:

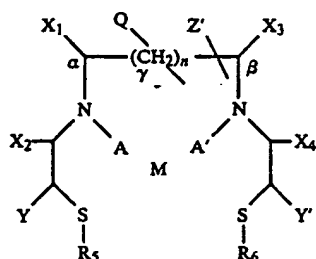


wherein:  $X_1$ - $X_4$ , A, A', Y, Y',  $R_1$ - $R_6$ , Q, n, and Z are defined as described above. M is a metal, or metal oxide, capable of being chelated. Preferred metals and metal oxides are those that are radionuclides. Particularly preferred are  $^{64}Cu$ ,  $^{67}Cu$ ,  $^{97}Ru$ ,  $^{99m}Tc$ ,  $^{105}Rh$ ,  $^{109}Pd$ ,  $^{186}Re$ ,  $^{188}Re$ ,  $^{198}Au$ ,  $^{199}Au$ ,  $^{203}Pb$ ,  $^{212}Pb$ , and  $^{212}Bi$ .

The following formulae depict chelation of M by a compound I in which two of the sulfurs are from Y and Y' (I-M-A) and by a compound I in which two of the sulfurs are from A and A' (I-M-B). The six atoms available for bonding M are shown. Depending on the particular metal or metal oxide, M may be bound to 4-6 of the nitrogen and sulfur atoms of compound 1.



In addition to chelating compound I and the metal chelates therefrom, the invention provides chelate-targeting agent conjugates having the formula:



wherein:  $X_1$ - $X_4$ ,  $A$ ,  $A'$ ,  $Y$ ,  $Y'$ ,  $R_1$ - $R_6$ ,  $Q$ ,  $n$ , and  $M$  are defined as described above.  $Z'$  is  $-(W)_m$ -Targeting agent.

$W$  is a group that functions as a "spacer arm" and may be useful to distance a targeting agent from the compound. Groups which may be used include methylene ( $-\text{CH}_2-$ ), methyleneoxy ( $-\text{CH}_2-\text{O}-$ ), methylenecarbonyl ( $-\text{CH}_2-\text{CO}-$ ), or combinations thereof. The number,  $m$ , of groups such as these would be typically 0 to 30 and preferably 0 to 5.

$Z'$ , or Targeting agent when  $m$  is 0, may be attached to one of the positions designated as  $\alpha$ ,  $\beta$ , and  $\gamma$ . Because the number of methylene carbons at the  $\gamma$  position is defined by  $n$  which may be greater than one, the  $\gamma$  position includes additional points for attachment of a  $Z'$  or a Targeting agent.

The term targeting agent includes any linking group that may be used to join the targeting agent. It will be evident to one skilled in the art that a variety of linking groups, including bifunctional reagents, may be employed within the present invention.

As noted above, a targeting agent has the capacity to bind to a defined population of cells. The targeting agent may bind through a receptor, substrate, antigenic determinant, or other binding site on the target cell population. Preferred targeting agents useful within the present invention include antibody and antibody fragments; peptides, such as bombesin, gastrin-releasing peptide, RGD peptide, substance P, neuromedin-B, neuromedin-C, and metenkephalin; and hormones, such

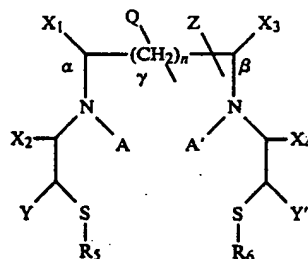
I-M-A

as estradiol, neurotensin, melanocyte stimulating hormone, follicle stimulating hormone, luteinizing hormone, and human growth hormone. Other suitable targeting agents include serum proteins, fibrinolytic enzymes, and biological response modifiers, such as interleukin, interferon, erythropoietin and colony-stimulating factor. Analogs of the above-listed targeting agents that retain the ability to bind to the defined target cell population may also be used within the claimed invention. In addition, synthetic targeting proteins and peptides may be designed and made to "fit" a particular, characterized epitope (binding site). That is, a synthetic targeting protein/peptide would be designed to bind a specific epitope in a "lock and key" fashion. Within the present invention, antibody and antibody fragments, bombesin and gastrin-releasing peptide and their analogs are particularly preferred targeting agents.

I-M-B

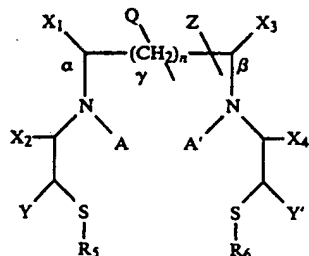
Preferred antibodies are monoclonal antibodies (MAbs). Particularly preferred are MAbs directed against tumor cells. Examples of such MAbs include those designated NR-ML-05, NR-LU-10, NR-CO-02, and NR-CE-01, which are specific for human melanoma, lung, colon, and lung tumor cells, respectively.

Two methods are provided for producing a chelate-targeting agent conjugate having the formula depicted immediately above. In the first method, a chelate is formed which is then joined to a targeting agent to form the conjugate. This method comprises the steps of reacting a compound (I) having the formula:



with a metal or metal oxide capable of being chelated, thereby forming a metal chelate, and combining the metal chelate with a targeting agent under reactive conditions to form the chelate-targeting agent conjugate.  $X_1$ - $X_4$ ,  $A$ ,  $A'$ ,  $Y$ ,  $Y'$ ,  $R_1$ - $R_6$ ,  $Q$ ,  $n$ , and  $Z$  are defined as described above. The preferred, and particularly preferred, metals and metal oxides are also described above. The discussion provided above regarding targeting agent is applicable here as well.

In the second method for producing a chelate-targeting agent conjugate, a chelating compound is joined to a targeting agent to form a conjugate to which a metal or metal oxide is added. This method comprises the steps of combining a compound (I) having the formula:



with a targeting agent under reactive conditions to form a derivatized targeting agent and reacting the derivatized targeting agent with a metal, or metal oxide, capable of being chelated, thereby forming the chelate-targeting agent conjugate.  $X_1$ - $X_4$ ,  $A$ ,  $A'$ ,  $Y$ ,  $Y'$ ,  $R_1$ - $R_6$ ,  $Q$ ,  $n$ , and  $Z$  are defined as described above. The preferred, and particularly preferred, metals and metal oxides are also described above. The discussion provided above regarding targeting agent is applicable here as well.

Thus, the two methods for producing a chelate-targeting agent conjugate have a different order for the addition of the targeting agent. In the first method the targeting agent is joined to the chelate, i.e., after a metal or metal oxide has been added to a chelating compound. Conversely, in the second method the targeting agent is joined to the chelating compound, i.e., before a metal or metal oxide has been added. In both methods, however, a chelate-targeting agent conjugate has a targeting agent joined via  $R'$ . As noted above, a targeting agent may be joined by a direct reaction with  $R'$  or following the activation of  $R'$ .

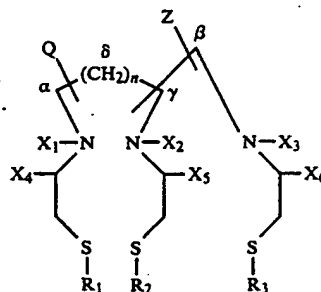
The step of combining a targeting agent with a chelate or chelating compound may be performed by direct reaction of the targeting agent with  $R'$  on the chelate or chelating compound. Alternatively, it may be desirable to include a preparatory step before the step of combining. For example, a targeting agent may be modified in preparation for a direct reaction with  $R'$ . The modification of a targeting agent includes reaction with any of the numerous bifunctional reagents reported in the literature.

A direct reaction with  $R'$  by modified or unmodified targeting agent is intended to mean that  $R'$  is capable of reacting with the modified or unmodified targeting agent. For example,  $R'$  may be an alkyl group containing a good leaving group, e.g., a halide, or a carbonyl-containing group, such as an anhydride, acid halide, or "active ester." The term "active ester" is known to refer to esters which are highly reactive in nucleophilic substitution reactions. In the present invention, the modified or unmodified targeting agent would be the nucleophile. Typically the esters will be activated phenols and cyclic compounds based on hydroxylamine. Examples of commonly used ester groups are tetrafluorophenyl, *N*-hydroxysuccinimidyl, nitrophenyl, isothiocyanate and substituted isothiocyanates. Alternatively,  $R'$  may be a nucleophilic group, such as an amino or sulfhydryl group, which is capable of reacting with a modified targeting agent, e.g., containing a maleimide group.

Another way to perform a step in preparation for the step of combining a targeting agent and a chelate or chelating compound is to convert  $R'$  to a form capable of reacting with the targeting agent. Examples of conversions of  $R'$  include where  $R'$  is a carboxyl group and is then activated. Activation of a carboxyl group includes formation of an "active ester" as defined above.

Another example of a conversion is where  $R'$  is a succinimide derivative containing a protective group, such as phenylsulfonyl. Upon removal of the group, the succinimide is converted to a maleimide which is highly reactive in nucleophilic addition reactions. Alternatively,  $R'$  may be a nucleophilic group, such as an amino or sulfhydryl group, and the conversion comprises reaction with a bifunctional reagent. It will be evident to one skilled in the art that a variety of bifunctional reagents, both homobifunctional and heterobifunctional, may be employed within the present invention.

As noted above, the present invention provides compounds of two formulae that are capable of chelating metals. Compound II, which contains three nitrogens and three sulfurs (" $N_3S_3$ "), has the following formula:



Examples of specific embodiments of the elements of compound II include the following.

$R_1$ ,  $R_2$ , and  $R_3$  are independently selected from sulfur protecting groups. Groups which may be used include any of the alkyl, acyl, aryl groups, disulfides and bunte salts known by those skilled in the art. Preferred groups are those that result in an acyl, a thioacetal or a hemithioacetal. Particularly preferred groups include thioesters, *p*-anisylidene, acetonyl, tetrahydrylfuranyl, ethoxyethyl, tetrahydrylpyranyl, acetamidomethyl, and derivatives thereof.

$X_1$  and  $X_2$  are independently selected from hydrogen (H) and an alkyl group of  $C_6$  or less.  $X_3$  is an H, an alkyl group of  $C_6$  or less, or Z.  $X_4$ ,  $X_5$ , and  $X_6$  are independently selected from H and =O. The selection of =O results in the presence of an amide. Thus, a compound with zero, one, two or three amides may be formed by the appropriate selection of  $X_4$ ,  $X_5$ , and  $X_6$ . Amide nitrogens, relative to amine nitrogens, afford greater stability to the complex formed with a metal, but at the expense of a diminished acceleration of complex formation. Thus, by selection of  $X_4$ ,  $X_5$ , and  $X_6$ , compounds with a wide variety of chelating properties may be formed.

$Q$  may be H or a polar group. One function of a polar group is to increase the hydrophilicity of the compound, e.g., in order to increase its aqueous solubility. Groups which may be used include carboxylates, sulfonates

and secondary alcohols. A preferred group is  $-CH_2-COOH$ .  $Q$  may be attached to one of the positions designated as  $\alpha$ ,  $\beta$ ,  $\gamma$  and  $\delta$ . Because the number of methylene carbons at the  $\delta$  position is defined by  $n$  which may be greater than one, the  $\delta$  position includes additional points for attachment of  $Q$ .

The distance by which the nitrogen atoms are separated may be increased by interposing methylene ( $-CH_2-$ ) groups between the carbons bonded to the nitrogens. When the number of  $-CH_2-$  groups, repre-

11

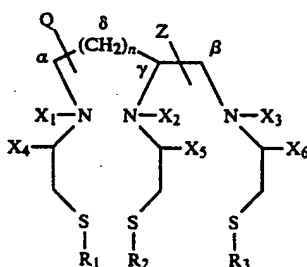
sented by  $n$ , is greater than zero, then the number of carbon atoms separating the nitrogen atoms in compound II is increased accordingly. Preferred integers for  $n$  are 0 to 4.

$Z$  is  $-(W)_m-R'$ .  $W$  is a group that functions as a "spacer arm" and may be useful to distance  $R'$  from the chelating portion of the compound. Groups which may be used include methylene ( $-\text{CH}_2-$ ), methyleneoxy ( $-\text{CH}_2-\text{O}-$ ), methylenecarbonyl ( $-\text{CH}_2-\text{CO}-$ ), or combinations thereof. The number,  $m$ , of groups such as these would be typically 0 to 30 and preferably 0 to 5.

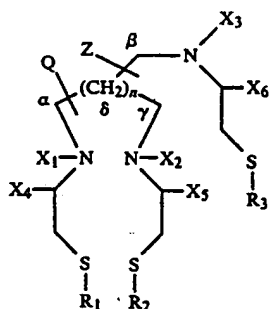
$Z$ , or  $R'$  when  $m$  is 0, may be attached to  $X_3$  or to one of the positions designated as  $\alpha$ ,  $\beta$ ,  $\gamma$ , and  $\delta$ . Because the number of methylene carbons at the  $\delta$  position is defined by  $n$  which may be greater than one, the  $\delta$  position includes additional points for attachment of a  $Z$  or an  $R'$ .

$R'$  is a chemically reactive group and the discussion of it provided above for compound I is applicable here as well.

In compound II, the carbon designated as  $\beta$  may be bonded to any one of the carbons designated as  $\alpha$ ,  $\gamma$  and  $\delta$ . The following formulae depict compounds in which the  $\beta$  carbon is bonded to the  $\gamma$  carbon (IIA) and the  $\beta$  carbon is bonded to the  $\delta$  carbon (IIB).

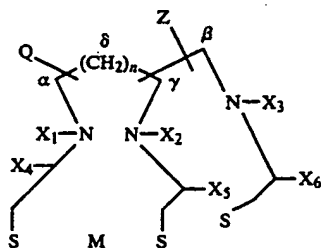


IIA



IIB

A metal chelate is formed by addition of a metal or metal oxide to compound II and has the following formula:

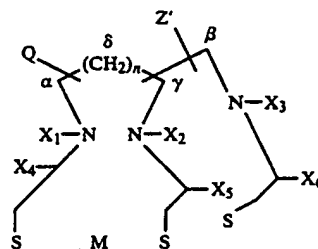


wherein:  $R_1-R_3$ ,  $X_1-X_2$ ,  $X_3$ ,  $X_4-X_6$ ,  $Q$ ,  $n$ , and  $Z$  are defined as described above.  $M$  is a metal, or metal oxide, capable of being chelated. The six atoms avail-

12

able for bonding  $M$  are shown. Depending on the particular metal or metal oxide,  $M$  may be bound to 4-6 of the nitrogen and sulfur atoms of compound II. Preferred metals and metal oxides are those that are radio-nuclides. Particularly preferred are  $^{64}\text{Cu}$ ,  $^{67}\text{Cu}$ ,  $^{97}\text{Ru}$ ,  $^{99\text{m}}\text{Tc}$ ,  $^{105}\text{Rh}$ ,  $^{109}\text{Pd}$ ,  $^{186}\text{Re}$ ,  $^{188}\text{Re}$ ,  $^{198}\text{Au}$ ,  $^{199}\text{Au}$ ,  $^{203}\text{Pb}$ ,  $^{212}\text{Pb}$ , and  $^{212}\text{Bi}$ .

In addition to chelating compound II and the metal chelates therefrom, the invention provides chelate-targeting agent conjugates having the formula:



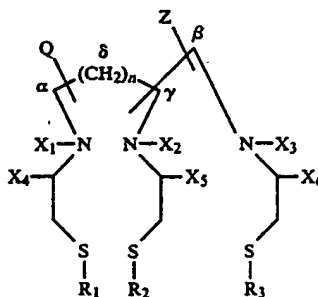
wherein:  $R_1-R_3$ ,  $X_1-X_2$ ,  $X_3$ ,  $X_4-X_6$ ,  $Q$ ,  $n$ , and  $M$  are defined as described above.  $Z'$  is  $-(W)_m$ -Targeting agent.

$W$  is a group that functions as a "spacer arm" and may be useful to distance a targeting agent from the compound. Groups which may be used include methylene ( $-\text{CH}_2-$ ), methyleneoxy ( $-\text{CH}_2-\text{O}-$ ), methylenecarbonyl ( $-\text{CH}_2-\text{CO}-$ ), or combinations thereof. The number,  $m$ , of groups such as these would be typically 0 to 30 and preferably 0 to 5.

$Z'$ , or Targeting agent when  $m$  is 0, may be attached to  $X_3$  or to one of the positions designated as  $\alpha$ ,  $\beta$ ,  $\gamma$  and  $\delta$ . Because the number of methylene carbons at the  $\delta$  position is defined by  $n$  which may be greater than one, the  $\delta$  position includes additional points for attachment of a  $Z'$  or a Targeting agent.

The term targeting agent includes any linking group that may be used to join the targeting agent. It will be evident to one skilled in the art that a variety of linking groups, including bifunctional reagents, may be employed within the present invention. The discussion of targeting agent provided above for compound I-type conjugates is applicable here as well.

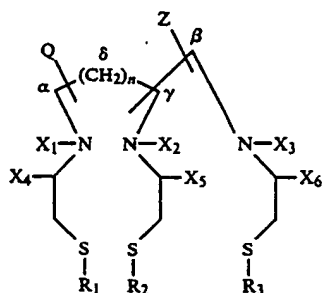
Two methods are provided for producing a chelate-targeting agent conjugate having the formula depicted immediately above. In the first method, a chelate is formed which is then joined to a targeting agent to form the conjugate. This method comprises the steps of reacting a compound (II) having the formula:



with a metal or metal oxide capable of being chelated, thereby forming a metal chelate, and combining the metal chelate with a targeting agent under reactive

conditions to form the chelate-targeting agent conjugate.  $R_1-R_3$ ,  $X_1-X_2$ ,  $X_3$ ,  $X_4-X_6$ ,  $Q$ ,  $n$ , and  $Z$  are defined as described above. The preferred, and particularly preferred, metals and metal oxides are also described above. The discussion provided above regarding targeting agent is applicable here as well.

In the second method for producing a chelate-targeting agent conjugate, a chelating compound is joined to a targeting agent to form a conjugate to which a metal or metal oxide is added. This method comprises the steps of combining a compound (II) having the formula:



with a targeting agent under reactive conditions to form a derivatized targeting agent and reacting the derivatized targeting agent with a metal, or metal oxide, capable of being chelated, thereby forming the chelate-targeting agent conjugate.  $R_1-R_3$ ,  $X_1-X_2$ ,  $X_3$ ,  $X_4-X_6$ ,  $Q$ ,  $n$ , and  $Z$  are defined as described above. The preferred, and particularly preferred, metals and metal oxides are also described above. The discussion provided above regarding targeting agent is applicable here as well.

These two methods for producing a chelate-targeting agent conjugate using compound II are analogous to those provided above for the methods using compound I. The discussion above regarding the difference in the order of joining the targeting agent, the meaning of a direct reaction of a targeting agent with  $R'$ , the modification of a targeting agent before the step of combining, and the conversion of  $R'$  before the step of combining, applies to the methods using compound II as well as those methods using compound I.

Another aspect of the invention provides kits for producing chelate-targeting agent conjugates for radiopharmaceutical use. Two types of diagnostic and therapeutic kits are prepared for use in the administration of chelate-targeting agent conjugates. The first type of kit ("pre-formed") comprises compound I, or compound II, and a targeting agent to be radiolabeled, each in separate containers. The compound is labeled with a metal, or metal oxide, radionuclide and then the resulting chelate is joined to the targeting agent. Thus, the radionuclide is added to the chelating compound prior to the addition of the targeting agent.

The second type of kit ("post-formed") comprises in one container compound I, or compound II, attached to a targeting agent to be radiolabeled and in another container a reducing agent and a complexing agent which in combination are capable of allowing a metal, or metal oxide, radionuclide to form an exchange complex. Thus, the radionuclide is added to the chelating compound after the addition of the targeting agent.

Preferred radionuclides for use in conjunction with a diagnostic kit are  $^{99m}\text{Tc}$ ,  $^{97}\text{Ru}$  and  $^{203}\text{Pb}$  and with a therapeutic kit are  $^{186}\text{Re}$ ,  $^{188}\text{Re}$ ,  $^{67}\text{Cu}$ ,  $^{105}\text{Rh}$ ,  $^{198}\text{Au}$ ,  $^{199}\text{Au}$  and  $^{212}\text{Bi}$ . The discussion provided above regard-

ing targeting agent is applicable here as well. The diagnostic and therapeutic kits, both in a pre-formed and a post-formed type, are described in detail in Example IV.

Yet another aspect of the invention provides methods for using the chelate-targeting agent conjugates described above for diagnostic and therapeutic purposes. The diagnostic method may be used to detect the presence or absence of a target site within a mammalian host. The method comprises the steps of administering to a mammal a diagnostically effective dose of one of the chelate-targeting agent conjugates described above, where the metal or metal oxide is a radionuclide and the conjugate is capable of binding to the target site. This step is followed by a step of detecting the biodistribution of the radionuclide in the mammal to determine the presence or absence of the target site in the host.

A diagnostically effective dose of a chelate-targeting agent conjugate is generally from about 5 to about 35 and typically from about 10 to about 30 mCi per 70 kg body weight. The precise dose for a chelate-targeting agent conjugate is dependent upon the particular targeting agent used because the level of uptake of a conjugate into a tumor is dependent upon the number of receptors for the targeting agent and its affinity for the receptors. The precise dose further depends upon the particular route of administration, e.g., intravenous, intracompartmental, intraarterial or intratumoral. It will be evident to one skilled in the art how to determine the optimal effective dose for a particular chelate-targeting agent conjugate and a particular route of administration. The discussion provided above regarding targeting agent is applicable here as well. Preferred radionuclides are  $^{97}\text{Ru}$ ,  $^{99m}\text{Tc}$  and  $^{203}\text{Pb}$ . A preferred mammal is man.

The therapeutic method may be used for delivering a radionuclide to a target site within a mammalian host. The method comprises the step of administering to a mammal a therapeutically effective dose of one of the chelate-targeting agent conjugates described above, where the metal or metal oxide is a radionuclide and the conjugate is capable of binding to the target site. A therapeutically effective dose is generally from about 20mCi to about 300mCi. The discussion immediately above regarding the precise dose and the targeting agent portion of a chelate-targeting agent conjugate applies here as well. Preferred radionuclides are  $^{186}\text{Re}$ ,  $^{188}\text{Re}$ ,  $^{67}\text{Cu}$ ,  $^{105}\text{Rh}$ ,  $^{198}\text{Au}$ ,  $^{199}\text{Au}$  and  $^{212}\text{Bi}$ . A preferred mammal is man.

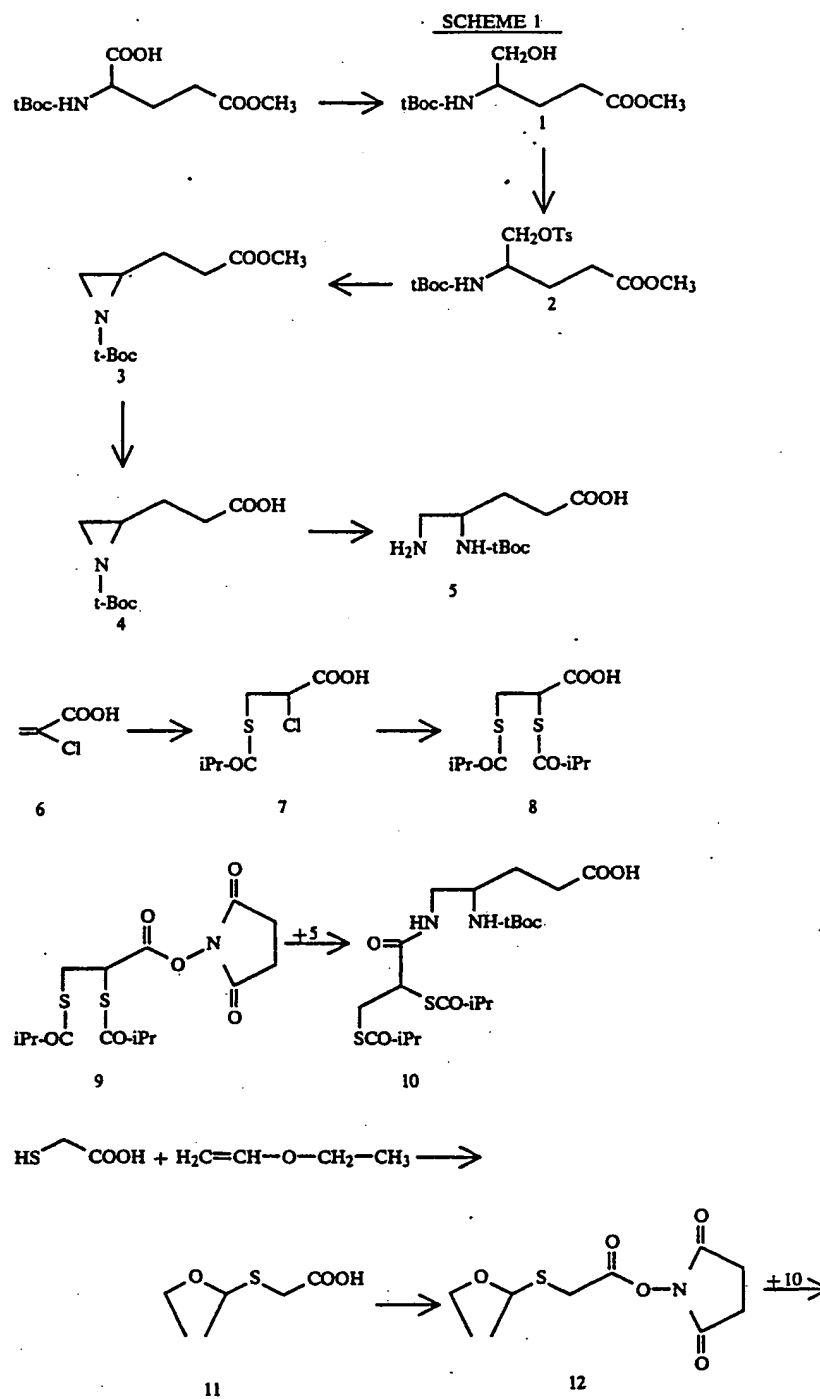
To summarize the examples which follow, Example I provides the preparation of chelating compounds. Example II describes the preparation of radiolabeled chelates and conjugation with targeting agents. Example III describes the preparation of targeting agent-chelating compound conjugates followed by radiolabeling of the conjugates. Example IV discloses kits for producing chelate-targeting agent conjugates. Example V describes biodistribution studies in mice. Example VI provides imaging of tumors in humans.

The following examples are offered by way of illustration and not by way of limitation.

## EXAMPLES

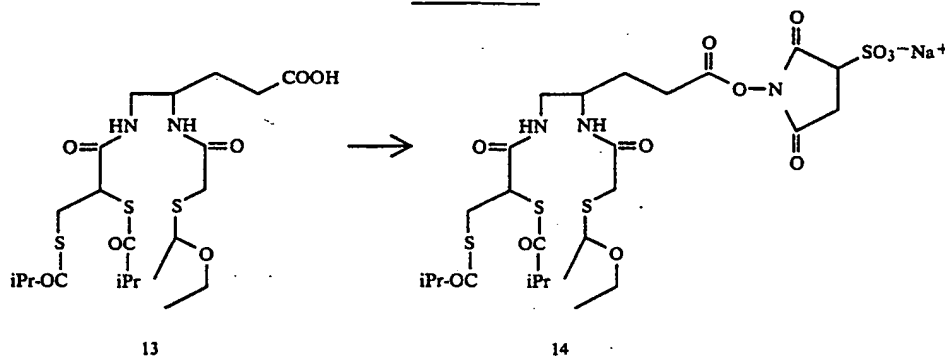
### EXAMPLE 1

#### Preparation of Chelating Compounds





-continued  
SCHEME 1



**N-t-butoxycarbonyl- $\beta$ -carbomethoxyethyl-aziridine 3**

(i) N-t-butoxycarbonyl-L-glutamic acid- $\gamma$ -methyl ester is prepared from L-glutamic acid- $\gamma$ -methyl ester according to the procedure of R. K. Olsen and T. Emery., *J. Org. Chem.* 49:3527, 1984.

(ii) A 1.0 M solution of borane.THF (0.68 mL, 0.68 mmol) is added to a solution of (143 mg, 0.55 mmol) in anhydrous tetrahydrofuran (0.68 mL). The reaction solution is stirred at ambient temperature for one hour and then quenched by the addition of 10 mL of methanol. The reaction solution is then evaporated to give an oil (160 mg). The oil is dissolved in 70 mL of ethyl acetate and washed with saturated  $\text{NaHCO}_3$  (2  $\times$  30 mL). The organic layer is dried over anhydrous  $\text{MgSO}_4$  and evaporated in vacuo to give 1 as a colorless oil (120 mg, 88%).

(iii) p-Toluenesulfonyl chloride (0.85 g, 4.46 mmol) is added to an ice cold (0°–5° C.) solution of 1 (1.00 g, 4.05 mmol) in pyridine (8 mL). The reaction solution is stirred at this temperature overnight. The reaction solution is diluted with methylene chloride (80 mL) and washed with pH 4.0 acetate buffer (3  $\times$  70 mL), then with saturated bicarbonate (40 mL). The organic extract is repeatedly evaporated from toluene (to azeotrope the pyridine) to give the tosylate 2 as a brown viscous oil, which is used in the next step without further purification.

(iv) A solution of the tosylate 2 (1.38 g) in anhydrous dimethylformamide (3.0 mL) to a suspension of NaH (95 mg, 3.78 mmol) in DMF (1.5 mL). The reaction mixture is stirred for 1 hour, diluted with water (40 mL) and extracted with methylene chloride (3  $\times$  40 mL). The combined methylene chloride extracts were dried ( $\text{MgSO}_4$ ) and evaporated to give a yellow oil (0.66 g). The oil is purified by flash chromatography over silica gel (1:1 ethyl acetate:hexanes) to give 3 as a pale yellow oil.

N-t-butoxycarbonylaziridine-3-propionic acid 4: To a solution of 1 mmol of 3 5 mL of ethanol is added 2 mL of 1 N NaOH and the mixture is stirred for 2 hours at ambient temperature. The mixture is partitioned between 25 mL of water and 25 mL of ether. The aqueous layer is acidified to pH 2 and extracted with 2  $\times$  25 mL of ether. The combined ether extracts are washed with brine, dried with anhydrous  $\text{MgSO}_4$ , filtered and concentrated to yield 4.

4-N-t-butoxycarbonylamino-5-amino-pentanoic acid 5: To a solution of 4 (1 mmol) in 5 mL of chloroform is added an excess of hydrazoic acid in chloroform. The mixture is stirred at ambient temperature and concentrated to give the azide. The azide is dissolved in 5 mL

of isopropanol. To the solution is added 5 mmol of sodium borohydride. The mixture is refluxed for 16 hours, allowed to cool to ambient temperature and 5 mL of 1N HCl is added. The mixture is concentrated to give the crude hydrochloride salt of 5.

4-N-t-butoxycarbonylamino-5-(2',3'-bis-S-isobutryl-dimercaptopropionamido)pentanoic acid 10:

(i) 2-Chloro-3-mercaptoisobutryl propionic acid 7: To a solution of  $\alpha$ -chloroacrylic acid 6 (1 mmol) in 10 mL of anhydrous methylene chloride containing 1.2 mmol of trifluoroacetic acid, 1.2 mmol of isothiobutyric acid is added. The solution is stirred for 2–3 hours at room temperature. The solvents are evaporated in vacuo, and the product is isolated by trituration with anhydrous ether. Trituration procedure is repeated several times to ensure complete removal of excess of the reagents that are used in the reaction.

(ii) 2,3-Bis(mercaptoisobutryl)propionic acid 8: A solution of 2-Chloro-3-mercaptoisobutryl propionic acid 7 (1 mmol) in 15–20 mL of i-propanol containing 1% water, 2 mmol of isothiobutyric acid is added and the solution is refluxed for 6–8 hours. The solvents are removed under reduced pressure and the product 3 is isolated by flash chromatography over silica gel. All the above mercapto compounds and derivatives have foul odor and will be handled in a well ventilated hood.

(iii) Succinimidyl 2,3-bis(mercaptoisobutryl) propionate 9. To a solution of 1 mmol of 2,3-bis(mercaptoisobutryl)propionic acid 8 in 10 mL of anhydrous tetrahydrofuran, 1.2 mmol of N-hydroxysuccinimide and 1.2 mmol of N,N'-dicyclohexylcarbodiimide is added and the solution is stirred at ambient temperature for overnight. The precipitated solid is filtered and the solvent is removed in vacuo. The residue is dissolved in ethyl acetate and the organic layer is washed with water. The ethyl acetate layer is dried, the solvent is removed and the product is purified by flash chromatography.

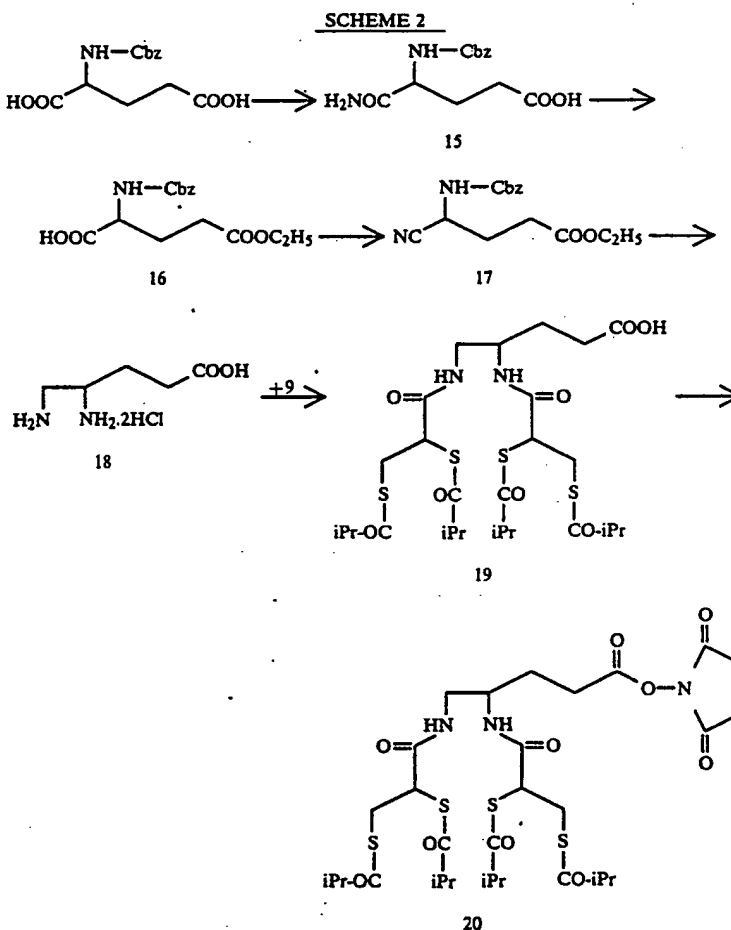
(iv) To a solution of 5 (1 mmol) in 1 mL of dimethylformamide is added 2 mmol of triethylamine followed by 1.1 mmol of the above succinimidate ester 9. The mixture is stirred for 2 hours at ambient temperature and dimethylformamide is removed in vacuo. The residue is partitioned between 1N HCl and ethyl acetate. The organic layer is dried with anhydrous  $\text{MgSO}_4$  and concentrated to give 10.

4-N-(S-1-ethoxyethylmercaptoacetamido)-5-(2',3'-bis-S-isobutryl-dimercaptopropionamido)-pentanoic acid 13

(i) S-(1-ethoxy)ethylmercaptoacetic acid 11: To a solution of 17.38 g of p-toluenesulfonic acid maintained between  $-18^{\circ}\text{C}$ .- $25^{\circ}\text{C}$ ., 23.9 mL of ethylvinyl ether in 125 mL of dichloromethane is added in drops over a period of 1-1.5 hours. When the addition is complete, the mixture is stirred for another 1 hour. To the above cold solution 50 mL of pH 7 phosphate buffer is added and the cold mixture is poured into a mixture of 800 mL of ethyl acetate and 200 mL of water. The organic layer is removed and the aqueous layer is extracted with  $2 \times 200$  mL of ethyl acetate. The combined layers were washed with brine, dried over anhydrous  $\text{MgSO}_4$  and evaporated to give S-(1-ethoxy)ethylmercaptoacetic acid 11 in 100 mL of dry tetrahydrofuran were added 4.85 g of N-hydroxysuccinimide and 8.7 g of N,N'-dicy-

S-1-ethoxyethylmercaptoacetate 12. The mixture is stirred for 2 hours at ambient temperature and the solvent is removed in vacuo. The residue is partitioned between 25 mL of 1N HCl and 25 mL of ethyl acetate. The organic layer is dried with anhydrous  $\text{MgSO}_4$  and concentrated to give 13, which is purified by silica gel chromatography.

Sulfosuccinimidyl-4-N-(S-1-ethoxyethylmercaptoacetamido)-5-(2',3'-bis-S-isobutryl-dimercaptopropionamido) pentanoate 14: A solution of the above acid 13 (1 mmol) in 1  $\text{CH}_3\text{CN}:\text{H}_2\text{O}$  is stirred with N-hydroxysuccinimide and 30 mmol of 1-(3-dimethylamino-propyl)-3-ethylcarbodiimide hydrochloride for overnight at ambient temperature. The solvents are removed in vacuo and the active ester -14 is isolated by HPLC.



clohexycarbodiimide. The mixture is stirred for 2-3 hours. TLC in EtOAc:hexanes:acetic acid 49:50:1 (p-anisaldehyde stain) showed the completion of the reaction. Dicyclohexylurea is removed by filtration and the filtrate is evaporated. The oily residue is dissolved in 50 mL of ethyl acetate and washed with water. The solution is dried over anhydrous  $\text{MgSO}_4$  and evaporated and the product is purified by silica gel flash column chromatography.

(iii) To 1 mmol of 10 in 5 mL of methylene chloride is added 2 mL of trifluoroacetic acid and the mixture is stirred for 1 hour and concentrated in vacuo to a viscous oil. Trituration with either yielded the trifluoroacetate salt as a white solid which is dissolved in 1 mL dimethylformamide. To the solution is added 5 mmol of triethylamine followed by 1.1 mmol of succinimidyl

#### 4,5-Diaminopentanoic acid 18:

(i) N-Benzyloxycarbonyl-L-isoglutamine 15 is prepared from N-Benzyloxycarbonyl-L-glutamic acid according to the procedure of M. Itoh, *Chem. Pharm. Bull.* 17:8, 1986 (1969).

(ii) A suspension of 15.98 g of N-Benzyloxy-carbonyl-L-isoglutamine in 500 mL of absolute ethanol containing 0.54 g of p-toluenesulfonic acid is refluxed for 12 hours until TLC indicated that the reaction is complete. The solution is concentrated to a small volume and addition of ether gave a solid. The solid is filtered and recrystallized to give 16.0 g of N-Benzyloxycarbonyl-L-isoglutamine ethyl ester, 16.

21

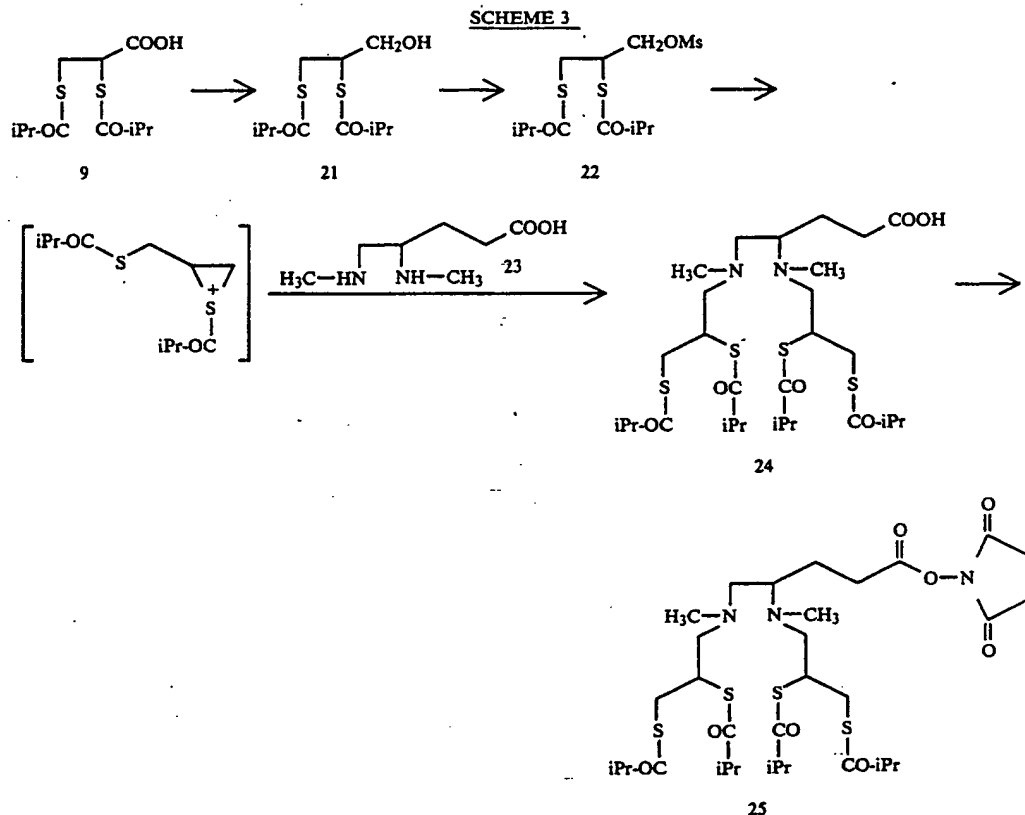
(iii) To a suspension of 21.45 g of N-carbobenzoxycarbonyl-L-isoglutamine ethyl ester in 200 mL of dry tetrahydrofuran kept at 0° C. to -5° C. in an ice-bath 11.82 mL of pyridine is added. To the above solution 9.84 mL of trifluoroacetic anhydride in 100 mL of tetrahydrofuran is added dropwise at such a rate that the bath temperature is maintained. The solution is stirred for 2 hours at this temperature. The solution is evaporated to dryness and the oil is dissolved in ethyl acetate. The organic layer is washed with 1.0 N hydrochloric acid and sterile water. The solution is dried and evaporated in vacuo to give an oil to give 14.8 g of ethyl  $\gamma$ -(N-carbobenzoxycarbonyl)amino- $\gamma$ -cyanobutanoate, 17.

(i v) A solution of 3.0 g of ethyl  $\gamma$ -(N-carbobenzoxycarbonyl)amino- $\gamma$ -cyanobutanoate, 17,

22

water. The organic layer is dried with anhydrous sodium sulfate and evaporated to give 19.

Succinimidyl-bis-4,5-(2',3'-mercaptoisobutyl) propionamido pentanoate 20: To a solution of bis-4,5-(2',3'-mercaptoisobutyl) propionamido pentanoic acid 19 (1 mmol) in 10 mL of anhydrous tetrahydrofuran, N,N'-dicyclohexylhexylcarbodiimide (1.2 mmol) and N-hydroxysuccinimide (1.2 mmol) is added. The mixture is stirred overnight at room temperature. Dicyclohexylurea is filtered and the solution is evaporated to dryness. The residue is dissolved in ethyl acetate and washed with water, dried with anhydrous MgSO<sub>4</sub> and evaporated to give 20. The product is purified by silica gel chromatography followed by HPLC.



y)amino- $\gamma$ -cyanobutanoate in 80 mL of ethanol containing 80 mL of 6N HCl is hydrogenated at 60 psi over 0.5 g of PtO<sub>2</sub> in a Paar apparatus for 14-24 hours. The completion of reaction is checked by NMR and TLC. The catalyst is removed by filtration and the solvent is removed in vacuo. The thick syrup is dissolved in 100 mL of 6N HCl and stirred at 70° C. for approximately four hours. The solution is evaporated under vacuum to a thin oil. Addition of ethanol gave 4,5-diaminopentanoic acid dihydro-chloride 18 as a solid. The solid is recrystallized from ethanol-water and dried in a vacuum desiccator.

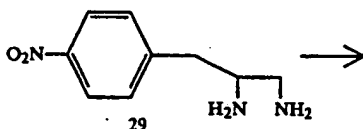
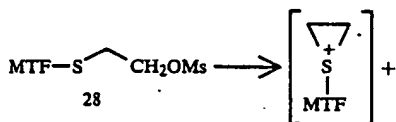
Bis-4,5-(2',3'-mercaptoisobutyl)propionamido pentanoic acid 19: A solution of 4,5-diaminopentanoic acid 18 (1 mmol) in 10 mL of dimethylformamide is treated with 2.2 mmol of triethylamine and stirred for a few minutes. To this suspension 2.2 mmol of succinimidyl 2,3-bis (mercaptoisobutyl) propionate 9 (Scheme 1). The solution is stirred for 2 hours at ambient temperature. Dimethylformamide is removed in vacuo and the residue is dissolved in ethyl acetate and washed with

2,3-Bis(mercaptoisobutyl) propanol 21: To an ice-cold solution of 2,3-bis(mercaptoisobutyl) propionic acid 9 (Scheme 1) (1 mmol) in 10 mL of anhydrous tetrahydrofuran, 1.5 mL of 1M BH<sub>3</sub>.THF is added over a period of 5 minutes (min.). The solution is stirred for another 10 min. and evaporated to dryness. Ten ml of water is added to the residue and the mixture is extracted with ethyl acetate. The organic layer is washed with water, dried and evaporated in vacuo to give the product 21, which is purified by flash column chromatography.

N,N'-Dimethyl-4,5-diaminopentanoic acid 23: To a solution of 4,5-diaminopentanoic acid (18; Scheme 2) (2 mmol) in 30 mL of anhydrous dimethylformamide, 5 mmol of di-t-butyl dicarbonate is added and the solution is stirred overnight at room temperature. The solvent is removed in vacuo and the residue is crystallized to give N,N'-di-t-butoxycarbonylpentanoic acid.

of

Succinimidyl-N,N'-dimethyl-bis-4,5-(2'-3'-mercaptoisobutyryl)-propionyl pentanoate 25: The active ester is prepared by mixed anhydride method. A solution of the acid 24 (1 mmol) in 5 mL of anhydrous tetrahydrofuran and 2 mmol of 4-dimethylaminopyridine is cooled to  $-5^{\circ}\text{C}$ . to  $0^{\circ}\text{C}$ . To this solution is added 1.1 mmol of isobutylchloroformate and stirred at this temperature for 10 min. A pre-cooled solution of N-hydroxysuccinimide (1.1 mmol) in 5 mL is added and the solution is stirred for another hour. Water is added and the mixture is evaporated. The residue is dissolved in 20 mL of methylene chloride and washed with water. The organic layer is dried and evaporated. The product 25 is isolated by reverse phase HPLC.

$$\text{MTF}-\underset{26}{\text{S}-\text{CH}_2-\text{COOH}} \longrightarrow \text{MTF}-\underset{27}{\text{S}-\text{CH}_2-\text{CH}_2\text{OH}} \longrightarrow$$


5  
10  
15  
20  
25  
30  
35

30

31

32

MTF =

**2-Methylsulfonylmethylthio-2-methyltetrahydrofuran**  
**28:** To a solution of **27** (2 mmol) in 10 mL of methylene

25

chloride containing 2 mmol of triethylamine maintained at 0° C. is added methanesulfonylchloride (2 mmol) and the solution is stirred at room temperature for 1 hour. The mesylate 28 is unstable and hence the N-alkylation is carried out in situ without isolating the mesylate as described in the next step.

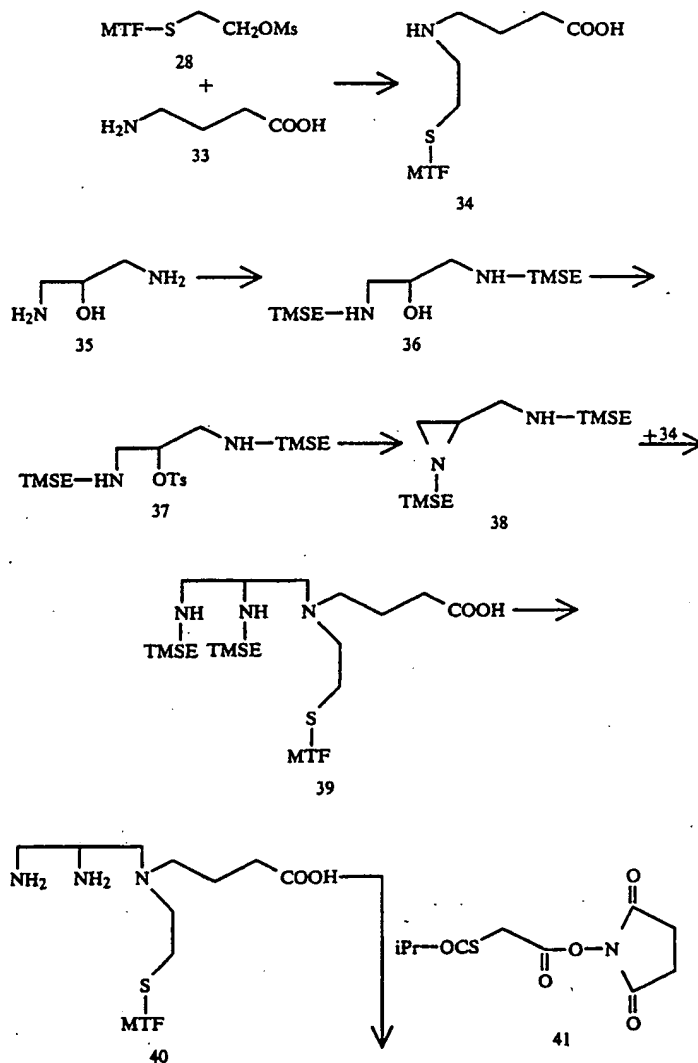
N,N,N',N'-Tetra-(S-2-methyltetrahydrofuran-2-yl)-β-mercaptoethyl-3-p-nitrophenyl-1,2-diaminopropane 30: To the above solution 0.5 mmol of 1,2-diamino-3-p-nitrophenylpropane 29 (prepared according to the procedure of L. H. DeRiemer, C. F. Meares, D. A. Goodwin and C. I. Diamanti, J. of Labelled Compounds and Radiopharmaceuticals 18:1517, 1981) is added and the solution is stirred at room temperature and refluxed for another 2-3 hours. The product is isolated by evaporation purified by silica gel chromatography.

26

N,N,N',N'-Tetra-(S-2-methyltetrahydrofuran-2-yl)-β-mercaptoethyl-3-p-amino-phenyl-1,2-diaminopropane 31: A solution of the nitro compound 30 (1 mmol) in ethanol absolute (mg) (Adams catalyst) is shaken in a Paar hydrogenator for 3 hours. The catalyst is removed by filtration and the solvent is removed in vacuo to yield the amino derivative 31, which is used in the next without further purification.

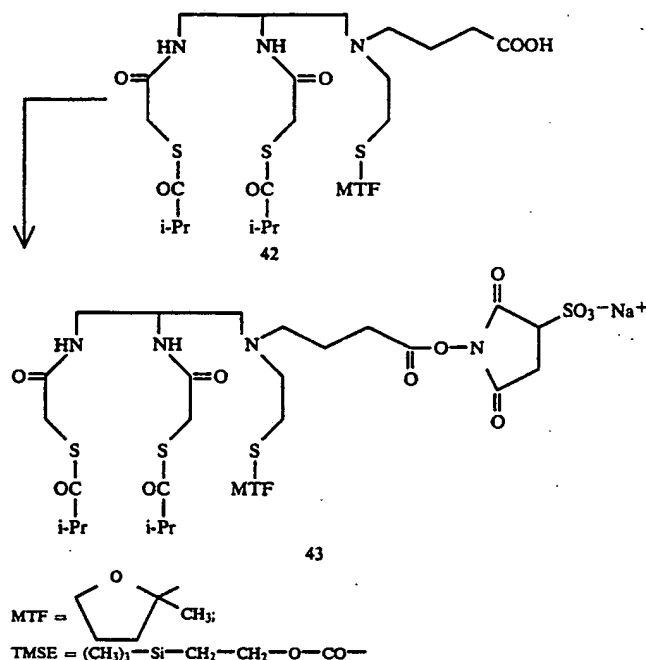
N,N,N',N'-Tetra-(S-2-methyltetrahydrofuran-2-yl)-β-mercaptoethyl-3-p-isothiocyanatophenyl-1,2-diaminopropane 32: To a solution of the above amino compound in 20 mL of methylene chloride is added. 1 mmol of thiocarbonyldiimidazole is added and the mixture is stirred at room temperature overnight. The solution is diluted with methylene chloride and washed with water. Evaporation and purification by liquid chromatography yields the isothiocyanate 32.

SCHEME 5



-continued

SCHEME 5



containing

N-(S-2'-Methyl-tetrahydrofuran-2-yl)- $\beta$ -mercaptoethyl- $\gamma$ -aminobutyric acid 34: A solution of 28 (1 mmol) (see Scheme 4) and  $\gamma$ -aminobutyric acid in 10 mL of methylene chloride and 2 mL pyridine is stirred for 10-15 hours at room temperature. The organic solvent is evaporated and the residue is dissolved in water. Acidification with glacial acetic acid precipitates the product, N-(S-2'-methyl-tetrahydrofuran-2-yl)- $\beta$ -mercaptoethyl  $\gamma$ -aminobutyric acid 34. 30

1,3-(N,N'-Bis-8-trimethylsilylethoxycarbonyl)-diamino-2-propanol 36: To a solution of 10 mmol of 1,3-diamino-2-propanol 35 in 30 mL of 5% sodium bicarbonate and 10 mL of methylene chloride 22 mmol of  $\beta$ -trimethylsilylethoxycarbonyl chloride is added and the mixture is stirred for 6 hours at room temperature. The organic layer is separated and the aqueous layer is extracted with 2  $\times$  50 mL of methylene chloride. The combined organic layer is washed with water, dried and evaporated to give the product 26. 35

1,3-(N,N'-Bis- $\beta$ -trimethylsilylethoxycarbonyl)-diamino-2-O-(p-tosyl)propanol 37: To a solution of the above compound (2 mmol) in 5 mL of pyridine at 0° C., 2 mmol of p-toluenesulfonyl chloride is added and the mixture is stirred at this temperature for 2 hours and kept at 0° C. overnight. The mixture is poured into crushed ice to precipitate the product, which is purified by crystallization. 40

2-N-( $\beta$ -Trimethylsilylethoxycarbonyl)-amnomethyl-1-( $\beta$ -Trimethylsilylethoxycarbonyl)-aziridine 38: To a solution of the above tosyl derivative (1 mmol) 27-, in 5 mL of dry dimethylformamide, 1.1 mmol of sodium hydride is added and the solution is stirred for 2 hours at room temperature. The solvent is removed in vacuo and the residue is dissolved in ethyl acetate. The solution is washed with water, dried with anhydrous sodium sulfate and evaporated to give the aziridine derivative 28. 45

N-(S-2'-Methyl-tetrahydrofuran-2'-yl)- $\beta$ -mercaptoethyl-N-(8,Y-di-trimethylsilylethoxycarbonyl)-aminopropyl- $\gamma$ -butyric acid 39: A solution of the aziridine derivative (1 mmol) 38, in 5 mL of acetonitrile is stirred 60

under reflux with 1 mmol of N-(S-2'-Methyltetrahydrofuran-2-yl)- $\alpha$ -mercaptoethyl- $\beta$ -aminobutyric acid 34 at ambient temperature for 6 hours. Evaporation of the solvent in vacuo and purification of the residue by silica gel chromatography yields the desired product 39. 35

N-(S-2'-Methyl-tetrahydrofuran-2'-yl)- $\beta$ -mercaptoethyl-N-( $\beta$ , $\gamma$ -diaminopropyl)- $\gamma$ -butyric acid 40: To a solution of 1 mmol of 39 in 5 mL of tetrahydrofuran, 2.5 mL of tetra-n-butylammonium fluoride is added and the solution is stirred for 30 minutes at room temperature. The solvent is removed in vacuo, the residue is dissolved in water and acidified to pH = 3.5-4. The precipitated diamino acid 40 is filtered and dried. 40

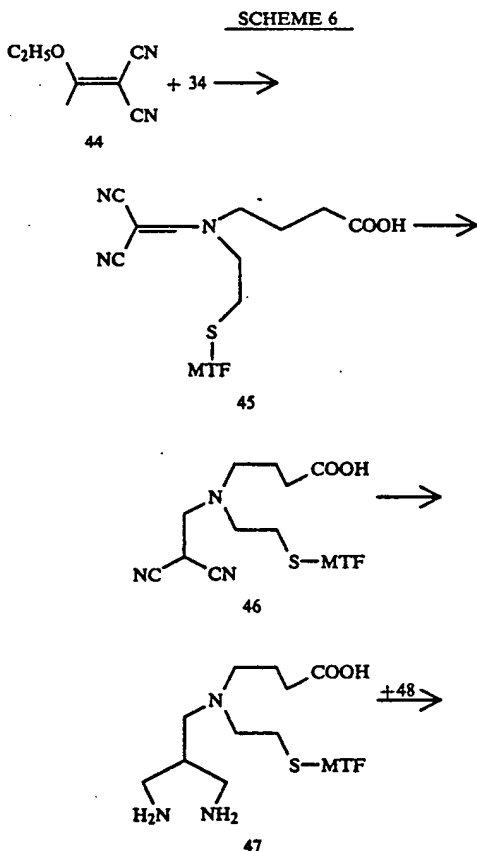
S-Isobutrylmercaptoacetic acid succinimide ester 41: (i) To a solution of 61 mg (0.47 mmol) of  $\text{CoCl}_2$  in 20 mL of acetonitrile under nitrogen atmosphere is added dropwise over 15 minutes, a solution of 4.92 mL (5.0 g, 47 mmol) of isobutryl chloride and 2.97 mL (3.94 g, 43 mmol) of mercaptoacetic acid in 50 mL of acetonitrile. The mixture is stirred at room temperature for 2 hours and worked up by evaporating acetonitrile. The blue oil is partitioned between 50 mL of 0.1 N HCl and 100 mL of ether. The ether layer is washed with brine and concentrated to give an oil. Purification is done by silica gel column chromatography (26% ethyl acetate, 4% acetic acid, 70% hexanes) yielded 3.30 g (47%) of S-isobutrylmercaptoacetic acid as an oil:  $^1\text{H}$  NMR ( $\text{CDCl}_3$ ):  $\delta$  1.23 (d, 6H), 2.84 (m, 1H), 3.85 (s, 2H). 45

(ii) To a solution of 3.30 g (20 mmol) of the above acid in 100 mL of methylene chloride at 0° C. is added 2.53 g (22 mmol) of N-hydroxysuccinimide followed by 4.52 g of N,N'-dicyclohexylcarbodiimide. The mixture is allowed to stir for 16 hours allowing the ice bath to equilibrate to room temperature. The mixture is chilled and filtered through celite. The filtrate is concentrated and purified by silica gel chromatography (50% EtOAc-50% hexanes) to give 4.48 g of 41 as a viscous 65

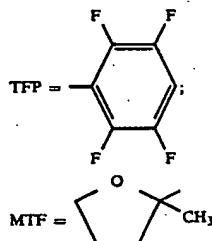
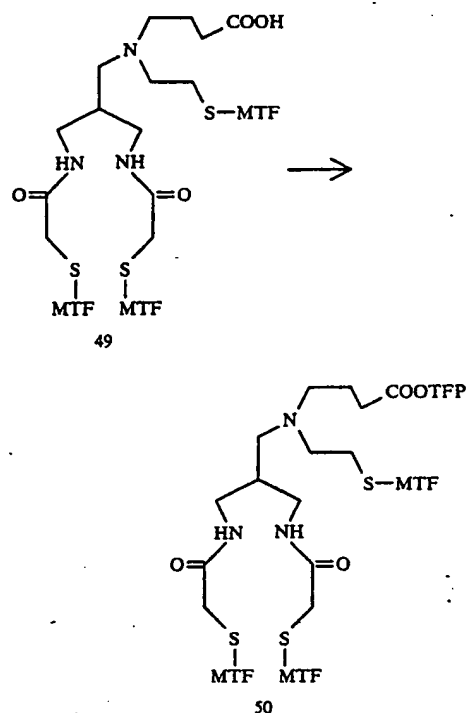
oil:  $^1\text{H}$  NMR ( $\text{CDCl}_3$ ):  $\delta$ 1.23 (d,6H), 2.80 (m,1H), 2.81 (s,4H), 3.98 (s,2H).

N-(S-2'-Methyl-tetrahydrofuran-2'-yl)- $\beta$ -mercapto-ethyl-N-( $\beta$ , $\gamma$ -bis-S-isobutryl-mercaptoacetamido)- $\gamma$ -butyric acid 42: To a solution of 1 mmol of 40 5 mL of dimethylformamide, S-isobutrylmercaptoacetic acid succinimide ester 41 (2 mmol) is added and the solution is stirred for 3 hours at room temperature. The solvent is removed in vacuo and the residue is dissolved in ethyl acetate. The organic layer is washed with water, dried and evaporated to give 42.

N-(S-2'-Methyl-tetrahydrofuran-2'-yl)- $\beta$ -mercapto-ethyl-N-( $\beta$ , $\gamma$ -bis-S-isobutryl-mercaptoacetamido)- $\gamma$ -butyric acid 43: To a solution of the above compound (1 mmol) in 5 mL of tetrahydrofuran containing 1 mmol of 4-dimethylaminopyridine kept at  $0^\circ\text{C}$ ., 1 mmol of isobutylchloroformate is added and the solution is stirred for 20 mins. To this solution a pre-cooled solution of N-hydroxysulfosuccinimide (1 mmol) in 2 mL of anhydrous tetrahydrofuran is added. The solution is stirred for 1 hour and allowed to warm to room temperature. The solvent is removed in vacuo and the residue is dissolved in methylene chloride. The organic layer is washed with water, dried and evaporated to give the ester 43. Final purification is carried out by high pressure liquid chromatography.



-continued  
SCHEME 6



N-( $\beta$ , $\beta$ -Dicyanol)ethylene-N- $\beta$ -(S-2'-methyltetrahydrofuran-2'-yl)mercapto-ethyl- $\gamma$ -butyric acid 45: An equimolar mixture of ethoxyethylenemalononitrile 44 and compound 34 (scheme 5) are heated in an oil bath at  $95^\circ$  to  $100^\circ\text{C}$ . with an air condenser. The mixture is cooled to room temperature and the solidified mass is broken up in ethanol and filtered. The filtered solid is recrystallized.

N- $\beta$ , $\beta$ -Dicyano)ethyl-N- $\beta$ -(S-2'-methyl-tetrahydrofuran-2'-yl)mercapto-ethyl-butyl- $\gamma$ -butyric acid 46: To a solution of the compound 45 (1 mmol) in 10 mL of isopropanol containing 1 gm of silica gel, 3 mmol of sodium borohydride is added and the mixture is stirred for 2-3 hours at room temperature. The silica gel is removed by filtration and the filtrate is evaporated to dryness. The residue is dissolved in ethyl acetate and washed with water, dried and evaporated to give the product. If necessary, the product is purified by silica gel flash chromatography.

N- $\beta$ , $\beta$ -Diaminomethyl)ethyl-N- $\beta$ -(S-2'-methyltetrahydrofuran-2'-yl)mercapto-ethyl- $\gamma$ -butyric acid 47: A solution of the compound 46 (1 mmol) dissolved in 10 mL of ethanol containing 2 mmol of hydrogen chloride is hydrogenated at 50 psi in the presence of sulfided Pd-on carbon. After 10-12 hours the catalyst is removed by filtration and the filtrate is evaporated in vacuo. The product diamine 47 is used in the succeeding step without further purification.

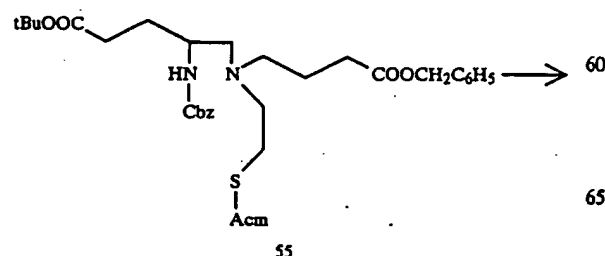
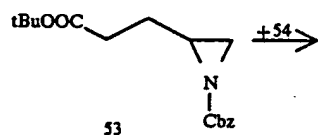
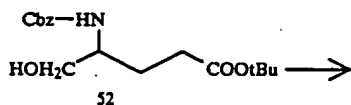
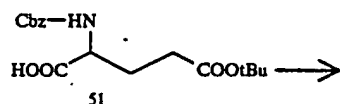
*N*-( $\beta$ , $\beta$ -S-2'-methyltetrahydrofuran-2-yl)mercaptoacetamidomethyl)-ethyl-*N*- $\beta$ -(S-2'-methyltetrahydrofuran-2-yl)mercaptoethyl- $\gamma$ -butyric acid 49

(i) 2-methyl-tetrahydrofuran-2-yl succinimide ester 48: This compound is prepared from 26 (scheme 4) and *N*-hydroxysuccinimide according to the general procedure described for the preparation of 12 (scheme 1).

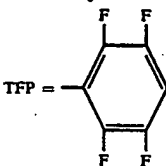
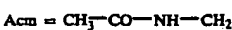
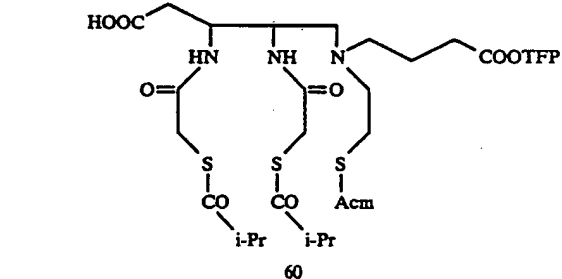
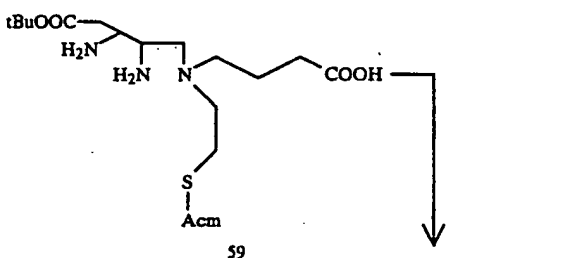
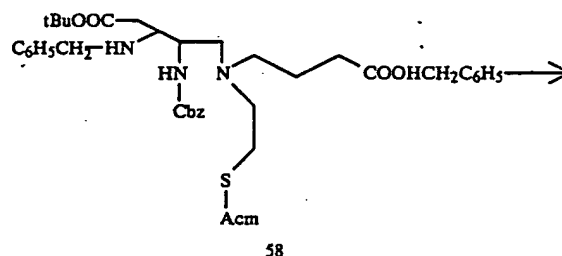
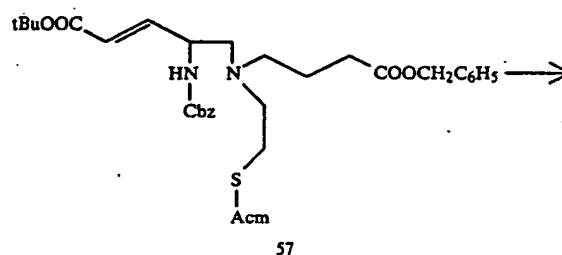
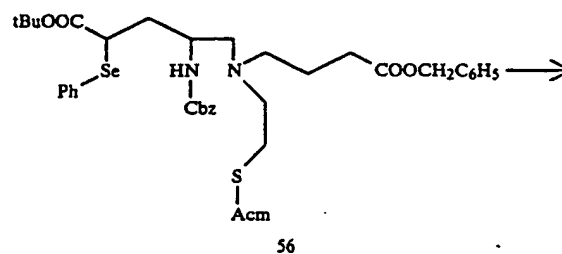
(ii) To a solution of the above diamine 47 (1 mmol) in 5 mL of anhydrous dimethylformamide containing 2.1 mmol of triethylamine, 2.1 mmol of 2-methyl-tetrahydrofuran-2-yl succinimide ester 48 is added and the mixture is stirred for 2-3 hours at room temperature. The solvent is removed in vacuo and the residue is dissolved in 10-15 mL of ethyl acetate. The organic layer is washed with water, dried over anhydrous sodium sulfate and evaporated. The product, 49 is purified by flash column silica gel chromatography.

*N*-( $\beta$ , $\beta$ -S-2'-methyltetrahydrofuran-2-yl)mercaptoacetamidomethyl)-ethyl-*N*- $\beta$ -(S-2'-methyltetrahydrofuran-2-yl)mercaptoethyl- $\gamma$ -butyric acid tetrafluorophenyl ester 50: A solution of the above acid (1 mmol) in 15-20 mL of tetrahydrofuran is stirred with 1.1 mmol of tetrafluorophenol and 1.1 mmol of *N,N'*-dicyclohexylcarbodiimide. After 8 hours at room temperature, the precipitated dicyclohexyl urea is filtered and the filtrate is evaporated to dryness. The residue is dissolved in ethyl acetate and washed with water. The organic layer is dried over anhydrous sodium sulfate and evaporated to dryness. Trituration with ether to remove excess tetrafluorophenol (in any present) gives the product 50. The final purification is carried out in HPLC.

# SCHEME 7



## -continued SCHEME 7



4-Hydroxymethyl-4-(t-butoxycarbonyl)-aminobutanoic acid-t-butyl ester 52: Cbz-Glu-OtBu 51 is converted to 52 via the methyl ester followed by  $\text{LiBH}_4$  reduction according to the procedure of Y. Hamada, M. Shibata, T. Sugiura, S. Kato and T. Shioiri,



*J. Org. Chem.* 52:1242, 1987 used for the conversion of t-Boc-Glu-OtBu to the corresponding alcohol.

N-t-Carbobenzyloxy-aziridine-propionic acid t-butyl ester 53

(i) p-Toluene sulfonyl chloride (1.1 mmol) is added to an ice-cold solution of 52 (1 mmol) in pyridine (5 mL). The reaction is stirred at this temperature overnight. The solution is diluted with 20 mL of methylene chloride and washed with pH 4.0 buffer and then with saturated bicarbonate. The organic extract is repeatedly evaporated with toluene giving the tosylate of 52 which is used in the next step without further purification.

(ii) A solution of the tosylate (1 mmol) in dimethylformamide (1 mL) is added to a suspension of NaH (1.1 mmol) in dimethylformamide (1 mL). The reaction mixture is stirred for one hour, diluted with water and extracted with methylene chloride. The organic layer is washed with water, dried over anhydrous  $MgSO_4$  and evaporated to give 53. Purification is achieved by silica gel flash column chromatography.

5-N-( $\beta$ -S-acetamidomethyl)ethyl-5-N-( $\gamma$ -phenylacetyl)-propyl-4-N'-carbobenzyloxy)-4,5-diaminopentanoic acid-t-butyl ester 55

(i) S-Acetamido-methylmercaptoacetic acid is prepared according to the procedure of J. D. Milkowski, D. Veber, R. Hirschmann, *Org. Syn.* 59:190 using reaction condition similar to the one described for the preparation of S-acetamidomethyl-L-cysteine.

(ii) Reduction of the acid in step (i) to the alcohol, mesylation of the alcohol and displacement of the mesylate with  $\gamma$ -aminobutyric acid benzyl ester are accomplished to give N-( $\beta$ -S-acetamidomethyl)ethyl- $\gamma$ -aminobutyric acid benzyl ester 54 in a procedure similar to the one described in Scheme 4, for the preparation of 34.

(iii) To a solution of N-carbobenzyloxy-aziridine propionic acid t-butyl ester 53 (1 mmol) in anhydrous tetrahydrofuran (5 mL), is added 1 mmol of N-( $\beta$ -S-acetamidomethyl)ethyl- $\gamma$ -aminobutyric acid benzyl ester 54 (from step ii) and the mixture is refluxed for 6-8 hours. The solvent is removed and the product 55 is purified by silica gel chromatography.

5-N-( $\beta$ -S-acetamidomethyl)ethyl-5-N-( $\gamma$ -phenylacetyl)propyl-4-N'-(carbo-benzyloxy)-2-selenophenyl-4, 5-diaminopentanoic acid-t-butyl ester 56: Seleno-phenylation of 55 is carried out to yield 56 according to the procedure of R. B. Silverman, B. J. Invergo and J. Mathew, *J. Med. Chem.* 29(10):1840, 1986, similar to the one used for the preparation of methyl 4-[(benzyloxy-carbonyl)amino]-5-fluoropentanoate.

5-N-( $\beta$ -S-acetamidomethyl)ethyl 5-N-( $\gamma$ -phenylacetyl)propyl 4-N'-(carbo-benzyloxy)-4,5-diamino-2-pentanoic acid-t-butyl ester 57: Oxidation and elimination of selenoxy phenyl group in 56 to yield 57 is carried out according to the procedure of R. B. Silverman, B. J. Invergo and J. Mathew, *J. Med. Chem.* 29(10):1840, 1986, similar to the one used for the preparation of methyl 4-[(benzyloxy-carbonyl)amino]-5-fluoro-2-pentanoate.

5-N-( $\beta$ -S-acetamidomethyl)ethyl-5-N-( $\gamma$ -phenylacetyl)propyl-3-N-benzyl-4-N'-(carbo-benzyloxy)-3,4,5-triamino-pentanoic acid-t-butyl ester 58: The preceding pentenoate 57 (1 mmol) is diluted with methanol (distilled from Mg) and 3 mmol of benzylamine is added. The reaction is stirred in nitrogen atmosphere at

45° to 50° C. for overnight. Evaporation of the solvent is carried out in vacuo and the product is isolated by silica gel chromatography.

5-N-( $\beta$ -S-acetamidomethyl)ethyl-5-N-( $\gamma$ -carboxy)propyl-3,4,5-tri-amino pentanoic acid-t-butyl ester 59: A solution of 58 (1 mmol) in 20 mL of ethanol containing 3 equivalents hydrogen chloride is hydrogenated in a Paar apparatus over pd-C (10%) for 24 hours. The catalyst is removed by filtration through celite and the solvent is removed in vacuo to yield the product.

5-N-( $\beta$ -S-acetamidomethyl)ethyl-5-N-( $\gamma$ -2,3,5,6-tetrafluorophenoxyacetyl)-propyl-3,4-bis-(S-isobutylmercapto actamido)-3,4,5-triamino-pentanoic acid 60

(i) To a solution of the above compound (1 mmol) in 2-3 mL of dimethyl-formamide containing 3 mmol of triethylamine is stirred with S-isobutylmercaptoacetic acid succinimide ester (41: Scheme 5) for 6-8 hours. The solvent is removed by evaporation and the residue is dissolved in ethyl acetate. The organic layer is washed with water, dried and evaporated to give the product, 5-N-( $\beta$ -S-acetamidomethyl)ethyl-5-N-( $\gamma$ -phenoxyacetyl)-propyl-3, 4-bis-(S-isobutyl-mercaptoactamido)-3,4,5-triamino pentanoic acid-t-butyl ester.

(ii) The tetrafluorophenyl ester is of the preceding acid is prepared by mixed anhydride method according to the procedure described earlier for the preparation of 46 (see scheme 6).

(iii) The above mixed ester is dissolved in 20 mL of methylene chloride, to which ethereal hydrogen chloride is added. After few hours the precipitated solid is removed by filtration and washed with ether to yield the final product, 60 as the hydrochloride salt. Final purification is carried out by liquid chromatography.

## EXAMPLE II

### Preparation of Radiolabeled Chelate and Conjugation with Antibody

#### A. Radiolabeling of Chelating Compounds

##### 1. Technetium-99m labeling

Method a: To 100  $\mu$ l of solution containing 5 mg of sodium gluconate and 0.1 mg of  $SnCl_2$  in water, at pH = 6.1, 75-100 mCi of 1 mL  $^{99m}TcO_4$  (pertechnetate) is added. After incubation at room temperature for 10 min. to form a  $^{99m}Tc$ -gluconate complex, 100  $\mu$ g of a chelating compound (see Example I) dissolved in i-propanol:acetic acid, 90:10, at 1 mg/mL, 80  $\mu$ l of 0.2 N HCl and 200  $\mu$ l of i-propanol are added in that order. The reaction mixture is heated to 75° C. for 15 min., then cooled in ice for 5 min.

Method b: Alternatively, 1.0 mL of  $^{99}Mo/^{99m}Tc$  generator eluted pertechnetate (75-100 mCi) is added to a vial containing a lyophilized mixture comprising sodium gluconate, stannous chloride, 0.1 mg; gentisic acid, 0.1 mg; lactose, 25 mg at pH 6.1. The vial is agitated gently to mix the contents by inversion and then incubated at room temperature for 10 mins.

##### 2. Rhenium-188 labeling.

The  $^{188}Re$  chelate of the chelating compound is prepared by a similar procedure. Sodium perrhenate (3 mL, 30 mCi/mL produced from a  $^{188}W/^{188}Re$  generator) is added to a vial containing a lyophilized mixture comprising citric acid, 75 mg; stannous chloride, 0.75 mg; gentisic acid, 0.25 mg and lactose, 100 mg. The vial is agitated gently to mix the contents, then incubated at

room temperature for 10 min. To a separate vial containing 0.50 mg of the chelating compound, 0.50 mL of 2-propanol is added and the vial is agitated for 2 min. to completely dissolve the compound. Then 0.3 mL of this solution is

35 transferred to the vial containing the  $^{188}\text{Re}$ -citrate complex. The reaction mixture is heated to 75° C. for 15 min., then cooled in ice for 5 min.

### 3. Rhenium-186 labeling.

The  $^{186}\text{Re}$  chelate of the chelating compound is prepared by a procedure similar to the  $^{188}\text{Re}$  procedure. Perrhenate  $^{186}\text{ReO}_4$  as sodium, lithium, ammonium or any other suitable counter ion is obtained from irradiation of  $^{185}\text{Re}$  (0.1 to few mg) in a nuclear reactor dissolution and purification of the original solution by previously described procedure (Venderhyden et al., *Inorg. Chem.* 24:1666, 1985) or any other suitable procedure. To the  $^{186}\text{ReO}_4$  vial is added 0.75 mL reconstituted solution made of 1.0 mL of sterile water added to a vial containing a lyophilized mixture comprising citric acid 25 mg, stannous chloride 1 mg, gentisic acid 1 mg and lactose 75 mg.

The vial is agitated gently to mix the contents, then incubated at room temperature of 75° C. To the separate vial containing the chelating compound, 2-propanol is added to obtain a completely dissolved solution. An appropriate amount of this solution to give a ligand to rhenium mole ratio of 1:5 (preferentially between 1 and 1.5 ligand to rhenium mole ratio) is then transferred to the vial containing the  $^{186}\text{Re}$ -citrate complex. The reaction mixture is heated to 75° C. for 20 min. then cooled on ice for 5 min.

### B. Conjugation of Radiolabeled Chelate with Antibody

To the above  $^{99m}\text{Tc}$  chelate, 100  $\mu\text{L}$  of bicarbonate buffer is added so that the pH of the solution is about 6.0. Next, 400  $\mu\text{L}$  of a solution containing antibody (or fragment) at 5 mg/mL is added in the same buffer. The antibody is a monoclonal antibody (or fragments thereof) designated as NR-ML-05, NR-LU-10, NR-CO-02, NR-CE-01 specific for human melanoma, lung, colon and CEA secreting tumor cells, respectively. The reaction mixtures are incubated at room temperature for 15–30 min. as necessary. The ITLC procedure (*Nuclear Medicine Technology and Techniques*, ed. Bernier, D., Longan, J., and Wells, L.: The C. V. Mosby Co., St. Louis, Mo., 1981; pp. 172–174) using 12% trichloroacetic acid is utilized to determine the percentage of chelate attached to the protein.

In the case of radiorheniums, an extra purification step is added depending on the form, e.g.,  $\text{F}(\text{ab}')_2$ , of the antibody to be labeled. This step is designed to guarantee efficient labeling of the  $\text{F}(\text{ab}')_2$  fragment, which is usually more susceptible, to reduction into two Fab' fragments. However, the labeling approach is similar to technetium using the appropriate pH and volume of buffer for conjugation.

In all cases, the final purification of the antibody-chelate complex is achieved by passing the conjugate through an ion exchange (DEAE or QAE Sephadex) or gel permeation column (as sephadex G-25 or acrylamide gel). The purity of the conjugate is over 90% before administration to test animals and to humans. Aseptic techniques are used throughout the radiolabeled monoclonal antibody preparation for human administration.

## EXAMPLE III

### Preparation of Antibody-Chelating Compound Conjugate Followed by Labeling with $^{99m}\text{Tc}$ or $^{188}\text{Re}$

#### A. Preparation of the Conjugate

The antibody conjugation reaction is performed in a final volume of 4.0 mL: 1 mg of the chelating compound (61.67  $\mu\text{mol}$ ), 1.1 mg of a monoclonal antibody (IgG, 7.8 nmol), 1–2 mL of distilled dimethyl formamide (if necessary to solubilize the chelating compound), 0.05 M of borate or 0.5 M bicarbonate buffer at pH 8.5. After stirring for 90 min. at room temperature, 4.4 mL of 5N sodium chloride is added. After an additional 30 min., the reaction mixture is centrifuged to remove any particulates and the supernatant is fractionated by gel filtration column chromatography. The column eluent is monitored at 280 nm and the fractions containing monomeric antibody conjugate are pooled and concentrated in an Amicon stirred cell (30,000 molecular weight cutoff).

#### B. Radiolabeling of the Conjugate

##### 1. Technetium-99m labeling

Stannous tartrate kits were prepared from degassed solutions of 0.5 mL disodium tartrate (10 mg/mL) and 0.1 mL stannous chloride (1.0 mg/mL in ethanol) in an evacuated vial under nitrogen atmosphere. To a stannous tartrate kit at pH 6.0, sodium pertechnetate 0.5 mL (about 15 mCi) is added and allowed to stand at room temperature for 5 min. Quality control for  $^{99m}\text{Tc}$ -tartrate and insoluble  $^{99m}\text{Tc}$  is carried out on Gelman ITLC using methyl ethyl ketone and 0.01 M sodium tartrate pH 7.0 eluents, respectively.  $^{99m}\text{Tc}$ -tartrate formation is typically 98–99% with insoluble  $^{99m}\text{Tc}$  values as  $\text{TcO}_2$  ranging from 0.1 to 0.2%.

In an evacuated vial, 200  $\mu\text{L}$  of sodium phosphate (0.2 M, pH 8.0) and 200  $\mu\text{L}$  of antibody-chelating compound conjugate (1.9 mg/mL) are added successively. Immediately after adding the conjugate, 250  $\mu\text{L}$  of  $^{99m}\text{Tc}$ -tartrate (about 3 to 5 mCi) is added and heated at 37° C for 1 hour. The percent technetium bound to protein and the formation of pertechnetate are determined by ITLC using either 12% TCA or 50% MeOH: 10% ammonium acetate (1:1) and 1-butanol eluents, respectively. Technetium incorporation typically range from 70–90% on a chelating compound-Ab conjugate with a chelating compound per antibody ratio of 1.5 to 3.0.

##### 2. Rhenium-188 labeling.

The  $^{188}\text{Re}$  chelate form of the conjugate is prepared in a procedure similar to that described for  $^{188}\text{Re}$  above. Sodium perrhenate (3 mL, 15 mCi, produced from a  $^{188}\text{W}/^{188}\text{Re}$  generator) is added to a vial containing a lyophilized mixture comprising: citric acid, 75 mg; stannous chloride, 0.75 mg; gentisic acid, 0.25 mg; and lactose, 75 mg. The vial is agitated gently to mix the contents, then incubated at 75° C. for 15 min. to form a activated  $^{188}\text{Re}$ -citrate complex.

Labeling of the conjugate is carried out in a similar procedure described for  $^{99m}\text{Tc}$  above.

##### 3. Rhenium-186 labeling.

The  $^{186}\text{Re}$  chelate form of the conjugate is obtained by a procedure similar to the  $^{186}\text{Re}$  labeling of the chelating compound described above. To the purified perrhenate vial is added 0.75 mL of the reconstituted solu-

tion made of 1.0 mL of sterile water added to a vial containing a lyophilized mixture comprising citric acid 15 mg, stannous chloride 1 mg, gentisic acid 1 mg and lactose 75 mg. The vial is incubated at 75° C. for 15 min. then cooled for 5 min. to field  $^{186}\text{Re}$ -citrate complex ready for labeling of the conjugate. Labeling of the conjugate is carried out in a similar procedure described for Tc-99m with a protein to rhenium mole ratio varying from 0.2 to 10 (preferentially around 1).

#### EXAMPLE IV

##### Kits

Two different types, pre-formed and post-formed, of diagnostic and therapeutic kits are prepared for use in the administration of chelate-protein conjugates: (1) Conjugates from a chelate which is produced by radiolabeling a chelating compound followed by attachment to a protein, e.g., Example II, and (2) Conjugates produced by radiolabeling a chelating compound-protein conjugate, e.g., Example III.

##### A. Diagnostic Kit

1. Pre-formed: Technetium-99m labeling of chelating compound followed by conjugation of the chelate with an antibody

A diagnostic kit containing reagents for preparation of a  $^{99m}\text{Tc}$ -radiolabeled protein conjugate is used as follows. The procedures are conducted under conditions which ensure the sterility of the product (e.g., sterile vials and sterilized reagents are used where possible, and reagents are transferred using sterile syringes). Proper shielding is used once the radioisotope is introduced.

One mL of sterile water for injection is added to a sterile vial containing a stannous gluconate complex (50 mg sodium gluconate and 1.2 mg stannous chloride dihydrate in dry solid form) and the vial is gently agitated until the contents were dissolved. A sterile insulin syringe is used to inject 0.1 mL of the resulting stannous gluconate solution into an empty sterile vial. Sodium pertechnetate (1.0 mL, 75–100 mCi, from a  $^{99}\text{Mo}/^{99m}\text{Tc}$  generator available from DuPont, Mediphsysics, Mallinckrodt or E. R. Squibb) is added, and the vial is agitated gently to mix the contents, then incubated at room temperature for 10 minutes to form a  $^{99m}\text{Tc}$ -gluconate complex.

In an alternative procedure for providing the  $^{99m}\text{Tc}$ -gluconate exchange complex, the kit includes a vial containing a lyophilized preparation comprising 5 mg sodium gluconate, 0.12 mg stannous chloride dihydrate, about 0.1 mg gentisic acid as a stabilizer compound, and about 20 mg lactose as a filler compound. The amount of gentisic acid may vary, with the stabilizing effect generally increasing up to about 0.1 mg. Interference with the desired reactions may occur when about 0.2 mg or more gentisic acid is added. The amount of lactose also may vary, with amounts between 20 and 100 mg, for example, being effective in aiding lyophilization. Addition of stabilizer and a filler compound is especially important when the vial contained these relatively small amounts of sodium gluconate and stannous chloride (compared to the alternative embodiment above). One mL of sodium pertechnetate (about 100 mCi) is added directly to the lyophilized preparation. The vial is agitated gently to mix the contents, then incubated as described above to form the  $^{99m}\text{Tc}$ -gluconate complex.

A separate vial containing 0.3 mg of a chelating agent in dry solid form is prepared by dispensing a solution of 0.3 mg chelating agent in 2-propanol into the vial, then removing the solvent under  $\text{N}_2$  gas, and the resulting vial containing the chelating compound is provided in the kit. To this vial is then added 0.87 mL of 100% isopropyl alcohol, and the vial is gently shaken for about 2 minutes to completely dissolve the chelating agent. Next, 0.58 mL of this solution of the chelating agent is transferred to a vial containing 0.16 mL of glacial acetic acid/0.2 N HCl (2:14), and the vial is gently agitated. Of this acidified solution, 0.5 mL is transferred to the vial containing the  $^{99m}\text{Tc}$ -gluconate complex, described above. After mixing gently by inversion, the vial is incubated in a 75° C.  $\pm$  2° C. water bath for 15 minutes, then immediately transferred to a 0° C. ice bath for 2 minutes.

To a separate vial containing 10 mg of the F(ab) fragment of a monoclonal antibody in 0.5 mL of phosphatebuffered saline, is added 0.37 mL of 1.0 M sodium bicarbonate buffer, pH 10.0. The F(ab) fragment is generated by treating the monoclonal antibody several times with papain according to conventional techniques and dialyzed PBS to eliminate TRIS buffer. The vial is gently agitated.

The vial containing the acidified solution of the  $^{99m}\text{Tc}$ -labeled chelate (see above) is removed from the ice bath, 0.1 mL of the sodium bicarbonate buffer is added, and the vial is agitated to mix. Immediately, the buffered antibody solution (above) is added, gently agitated to mix and incubated at room temperature for 20 minutes to allow conjugation of the radiolabeled chelate to the antibody.

A column containing an anion exchanger, either DEAE-Sephadex or QAE-Sephadex, is used to purify the conjugate. A 5 mL QAE Sephadex column is washed with 5 mL of 37 mM sodium phosphate buffer, pH 6.8. A 1.2  $\mu$  filter (available from Millipore) is attached to the column, and a 0.2u filter is attached to the 1.2 u filter. A 22-gauge sterile, nonpyrogenic needle is attached to the 0.2u filter.

The reaction mixture is drawn up into a 3 mL or 5 mL syringe, and any air bubbles are removed from the solution. After removal of the needle, the syringe is connected to the QAE-Sephadex column on the end opposite the filters. The needle cap is removed from the 22-gauge needle attached to the filter end of the column and the needle tip is inserted into a sterile, nonpyrogenic 10 mL nonevacuated empty vial labeled radio-labeled antibody. Slowly, over 2 minutes, the reaction mixture is injected into the column. The now empty syringe on top of the column is replaced with a 5 mL syringe containing 5 mL of 75 mM (0.45%) sodium chloride solution (from which air bubbles had been removed). Slowly, over 2 minutes, the NaCl solution is injected into the column, and the eluent is collected in the serum vial.

The total radioactivity in the serum vial is measured using a dose calibrator. The yield of the radiolabeled antibody is normally in the 40–60% range. The contents of the serum vial are drawn up into a sterile, pyrogen-free, 30cc syringe and diluted to a total volume of 30 mL with sterile 0.9% NaCl for injection into a human patient. A quality control test is normally performed on a 0.01 mL aliquot before injection by instant thin layer chromatography.

If the radiochemical purity is less than 85%, the material should not be injected into a human patient. Using

this procedure, radiochemical purities generally range from about 90% to 99%. The total amount of radioactivity also is measured prior to injection. In general, from 10 to 30 mCi will be administered to a human patient.

Prior to administering the radiolabeled F(ab) fragment (the diagnostic radiolabeled antibody fragment), an irrelevant antibody and an unlabeled specific antibody are to be administered to the patient to improve the diagnostic images, as described above. The irrelevant antibody, provided in a separate vial in the kit, is a whole murine monoclonal antibody directed against a B-cell lymphoma idiotype. The unlabeled specific antibody, also is in the kit. Both the irrelevant antibody and the unlabeled specific antibody are administered.

The entire 30 mL sample containing the radiolabeled antibody fragment is administered to a patient by intravenous infusion. The infusion is completed in from about 5 min. to about 15 min. The antibody fragment concentration in the sample is 0.33 mg/mL.

## 2. Post-formed: Technetium-99m labeling of antibody-chelating compound conjugate -

Stannous tartrate kits were prepared from degassed solutions of 0.5 mL disodium tartrate (10 mg/mL) and 0.1 mL stannous chloride (1.0 mg/mL in ethanol) in an evacuated vial under nitrogen atmosphere. To a stannous tartrate kit, sodium pertechnetate 0.5 mL (about 15 mCi) is added and heated at 50° C. for 10-15 min. After cooling to room temperature, quality control for <sup>99m</sup>Tc tartrate and insoluble <sup>99m</sup>Tc is carried out on Gelman ITLC using methyl ethyl ketone and 0.01 M sodium tartrate pH 7.0 eluents, respectively. <sup>99m</sup>Tc-tartrate formation is typically 98-99% with soluble <sup>99m</sup>Tc values as Tco<sub>2</sub> ranging from 0.1 to 0.2%.

In an evacuated vial, 200 ul of sodium phosphate (0.2 M, pH 8.0) and 200 ul of antibody-ligand conjugate (1.9 mg/mL) are added successively. Immediately after adding the conjugate, 250 ul of <sup>99m</sup>Tc-tartrate (about 3 to 5 mCi) is added and heated at 37° C. for 1 hour. The percent technetium bound to the protein and the formation of pertechnetate are determined by ITLC using either 12% TCA or 50% MeOH: 10% ammonium acetate (1:1) and 1-butanol eluents, respectively. Technetium incorporation typically ranges from 70-90% on a chelating compound-Ab conjugate with a chelating compound per antibody ratio of 1.5 to 3.0.

## B. Therapeutic Kit

### 1. Pre-formed

a. A therapeutic kit containing reagents for preparation of a <sup>188</sup>Re-radiolabeled protein conjugate is as follows.

Sodium perrhenate (3 mL, 15 to 150 mCi, produced from a <sup>188</sup>W/<sup>188</sup>Re research scale generator) is added to a vial containing a lyophilized mixture comprising citric acid, 75 mg; stannous chloride, 0.75 mg; gentisic acid, 0.25 mg; and lactose, 75 mg. The vial is agitated gently to mix the contents, then incubated at room temperature for 15 minutes to form a <sup>188</sup>Re-citrate exchange complex. To a separate vial containing 0.50 mg of succinimidyl-bis-4,5-(2',3'-mercaptoisobutyl)propionamido pentanoate 20 (an N<sub>2</sub>S<sub>4</sub> chelating agent of the invention comprising isobutyl S-protective groups and a succinimidyl ester group), 0.50 mL of isopropyl alcohol is added and the vial is agitated for 2 min. to completely dissolve the chelating agent. Next, 0.30 mL

of this solution is transferred to the vial containing the <sup>188</sup>Re-citrate complex prepared above.

After gentle mixing, the vial is incubated in a 75° C. +/- 2° C. water bath for 15 min., then immediately transferred to a 0° C. ice bath for 2 min. The yields of <sup>188</sup>Re-labeled chelate then range between 75% and 90%.

A column containing a C<sub>18</sub> reversed phase low-pressure material (Baker C<sub>18</sub> cartridges) is used to purify the <sup>188</sup>Re-labeled chelate. After conditioning of the cartridge with ethanol and water, the sample is loaded and washed with 2 mL of water three times and 2 mL of 20% ethanol/0.01 M phosphate buffer three times. The column is then dried in vacuo and eluted with two times 1.0 mL acetonitrile. About 75% of the <sup>188</sup>Re-radioactivity is normally recovered in greater than 95% purity as the chelate compound.

The chelate is then conjugated to a Fab fragment of a monoclonal antibody directed against an antigen on melanoma cells or small cell lung carcinoma.

A buffered solution of the antibody fragment (5 mg/mL, 0.5 mL) is added to the purified <sup>188</sup>Re-labeled chelate, followed by 0.5 mL of 0.5 M carbonate/bicarbonate buffer pH 9.50. The reaction is kept at room temperature for 15 min., then 25 mg of L-lysine, 0.1 mL, is added and the reaction is pursued at room temperature for 15 min. more.

A column containing Sephadex G-25 material is used to purify the <sup>188</sup>Re conjugate. The reaction mixture is loaded on top of the column, and 1.2 mL aliquots are collected using PBS buffer to rinse the reaction vial and elute the <sup>188</sup>Re conjugate in the third and fourth fractions. The purity of the <sup>188</sup>Re conjugate is usually greater than 97% for about 35% overall radiochemical yields. The conjugate is then further diluted with PBS, and radioactivity is measured prior to injection into the test animals and human subjects.

b. A therapeutic kit containing reagents for preparation of a <sup>186</sup>Re-radiolabeled protein conjugate is as follows. The procedure is conducted under conditions which insure the sterility of the product. Proper shielding is used when a radioisotope is introduced.

A target of Re metal (0.1 to 0.25 mg preferentially 0.15 mg) in quartz vial is irradiated for 15 days in the high core of a nuclear reactor with neutron flux of ca.  $5 \times 10^{14}$  neutrons/cm<sup>2</sup> sec. The target is dissolved with nitric acid and further diluted with sterile water to 5 mL. Upon reception, 0.8 mL of ammonia and 1.0 mL of a tetrabutylammonium solution were added. The stock solution or aliquot thereof is loaded on a C<sub>18</sub> cartridge and washed with water. The Re-186 radioactivity is eluted with 2.0 mL through a sulfonic acid cation exchange column preequilibrated with lithium carbonate solution. The perrhenate solution is dried at 75° C. with a flow of nitrogen. A lyophilized kit comprising 25 mg citric acid, 1 mg stannous chloride, 1 mg gentisic acid and 75 mg lactose is reconstituted with 1.0 mL of sterile water, and 0.75 mL were removed and added to the dry perrhenate. To a separate vial containing 1.2 mg of succinimidyl-bis-4,5-(2',3'-mercaptoisobutyl)propionamido pentanoate 20 (or any appropriate ligand), 0.4 mL of isopropylalcohol is added and 0.2 mL is removed and transferred to the vial containing the <sup>186</sup>Re activity. The vial is incubated at 75° C. for 20 min. then cooled to room temperature using an ice water bath. The yields of <sup>186</sup>Re-labeled chelate ranged between 70 and 90%.

The  $^{186}\text{Re}$  solution is passed through two columns; one made of sulfonic acid cation exchange resin; the second made of  $\text{C}_{18}$  reverse phase material. After water washed and 10% ethanol washes, the  $^{186}\text{Re}$  activity is eluted in another reaction vial with 2.0 mL ethanol. Again, the ethanolic solution is dried at  $75^\circ\text{C}$ . and a flow of nitrogen, then equilibrated at room temperature.

The chelate is then conjugated to a  $\text{F(ab')}_2$  fragment of a monoclonal antibody directed against colon cancer cells. Fifty to 100 mg of antibody fragment (20 mg/mL) is added to the dry  $^{186}\text{Re}$  chelate and 0.5 mL of 1.0M carbonate buffer with pH 9.5 is added. The reaction is kept at room temperature for 15 min; an aqueous solution of lysine (250 mg kit, 0.1 mL) is added and the reaction continued for 5 more min.

A column containing 15 or 30 cc bed volume of an acrylamide gel for gel permeation is used to purify the  $^{186}\text{Re}$  conjugate. The reaction mixture is loaded on top of the column and 8 mL (in the case of the 15 mL column) or 16 mL (for the 30 mL column) were collected using PBS buffer in a vial containing approximately 1% MSA. The conjugate is diluted to 30cc with saline and the  $^{186}\text{Re}$  radioactivity is measured prior to injection into test animals and human subjects. The purity of the conjugate is greater than 97% for about 40% overall radiochemical yields.

## 2. Post-formed

a. The  $^{188}\text{Re}$  chelate form of the conjugate is prepared in a procedure similar to that described for  $^{99\text{m}}\text{Tc}$  above. Sodium perrhenate (3 mL, 15 mCi, produced from a  $^{188}\text{W}/^{188}\text{Re}$  generator) is added to a vial containing a lyophilized mixture comprising: citric acid, 75 mg; stannous chloride, 0.75 mg; gentisic acid, 0.25 mg; and lactose, 75 mg. The vial is agitated gently to mix the contents, then incubated at room temperature for 10 min. to form a  $^{188}\text{Re}$ -citrate complex. The reaction mixture is heated at  $75^\circ\text{C}$ . for 15 min., then cooled on ice for 5 min. to ready the  $^{188}\text{Re}$ -citrate complex for labeling of the conjugate.

Labeling of the conjugate is carried out in a similar procedure described for Tc above.

b. The  $^{186}\text{Re}$  chelate form of the conjugate is prepared in a procedure similar to that described in the Pre-formed procedure.

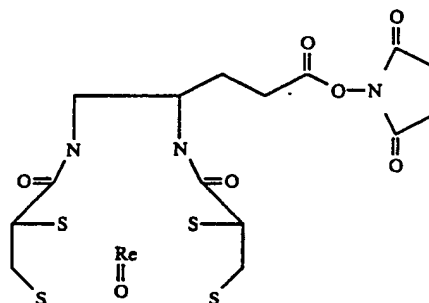
## EXAMPLE V

### Biodistribution Studies in Mice

#### A. With $^{99\text{m}}\text{Tc}$ -labeled Monoclonal Antibody Fragment

Antibody fragments radiolabeled with  $^{99\text{m}}\text{Tc}$  according to the procedures outlined in Examples II and III are injected into mice. The biodistribution of the radionuclide protein conjugate is analyzed for 20 hours after injection according to the method of Hwang et al., *Cancer Res.*, 45: 4150-4155 (1985). The antibody fragment is a Fab fragment of the above-described monoclonal antibodies: NR-ML-05, NR-LU-10, NR-CO-02, NR-Ce-01. The data is collected in terms of the percentage of the injected radioactivity per gram of each specified tissue type and tumor/tissue ratio of injected radioactivity. The tissue types evaluated are as follows tail; tumor, skin; muscle; bone; lung; liver; spleen; stomach; thyroid; kidney; and intestine. Tumor sites effectively identified in each of the mice.

#### B. With $^{188}\text{Re}$ -labeled Monoclonal Antibody Fragment



The chelate  $\text{Re-N}_2\text{S}_4$ , in which the radionuclide metal is  $^{188}\text{Re}$  as shown above, is prepared by the methods described herein. The chelate is conjugated to a Fab fragment of a monoclonal antibody specific for a tumor, e.g., NR-ML-05, NR-LU-10, NR-CO-2, or NR-Ce-1. The Fab fragment is produced by treatment of the monoclonal antibody with papain according to conventional techniques. The conjugation step and purification of the resulting radiolabeled antibody are as described in Example 11. The chelate-antibody conjugate is injected into tumor-bearing mice, biodistribution of the radiolabeled material is analyzed 20 hours after injection according to the method of Hwang et al., *Cancer Res.* 45: 450-4155, 1985, and compared to Tc-99m biodistribution.

#### C. With $^{186}\text{Re}$ -Labeled Monoclonal Antibody Fragment

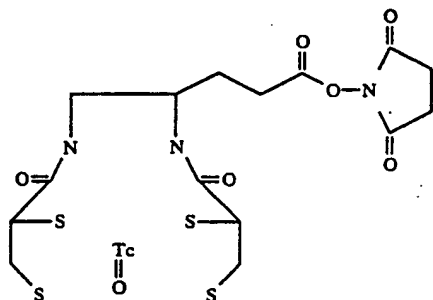
The chelate  $\text{Re-N}_2\text{S}_4$  in which the radionuclide metal is  $^{186}\text{Re}$  is prepared by the methods described herein. To verify tumor uptake, the chelate is conjugated to a Fab fragment of NRMI or antibody. The chelate-antibody conjugate is injected into tumor-bearing mice, biodistribution is analyzed after 20 hours and compared to Re-199 biodistribution.

## EXAMPLE VI

### Imaging of Tumors in Humans

Antibody fragments radiolabeled with  $^{99\text{m}}\text{Tc}$  according to the method of the invention are injected into human patients to detect tumor sites, i.e., melanoma, lung, colon) within the body. The antibody fragments used are  $\text{F(ab')}_2$ , Fab' or Fab fragments of monoclonal antibodies specific for an antigen of the particular tumor. The antibody fragment used may be, for example, a fragment of a monoclonal antibody designated NR-ML-05, NR-LU-10, NR-CE-01 or NR-CO-02, described above. The fragments are generated by standard techniques (i.e., pepsin treatment of the monoclonal antibody to generate the  $\text{F(ab')}_2$  fragment, papain treatment of the monoclonal antibody to generate the Fab fragment, and treatment with a reducing agent such as dithiothreitol or cysteine to generate the Fab' fragment).

The chelate compound ( $\text{Tc-N}_2\text{S}_4$ ):



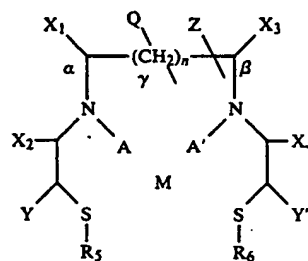
is prepared by one of the methods described herein. A patient receives the chelate prepared and conjugated to the antibody fragment according to the procedures outlined in Examples II and III. The resulting radiolabeled antibody fragment is purified, and a quality control test is performed, as described in Example III. Approximately 40 min. to 1 hour and 30 min. prior to infusion of the radiolabeled antibody, each patient may receive 41 to 50 mg of an irrelevant antibody in 12 to 20 mL of sterile saline by intravenous infusion. In addition, each patient receives 7.5 mg of a non-radiolabeled specific antibody in 20 mL of sterile saline by intravenous infusion either simultaneously with, or approximately 5 min. prior to infusion of the radiolabeled specific antibody. The non-radiolabeled specific antibody is exactly the same as the one used for radiolabeling. The irrelevant antibody is a monoclonal antibody designated NR2AD, which is a murine IgG<sub>2a</sub> immunoglobulin that is designed as an anti-idiotype that bound to a single patient's B-cell lymphoma and to no other human tissue.

Into each patient is injected 20 to 30 mL of sterile saline comprising the radiolabeled antibody fragment, by intravenous infusion. The patients receive from 10 mCi to about 30 mCi of <sup>99m</sup>Tc radioisotope. The desired upper limit of radioisotope administered is 30 mCi, and the minimum for effective imaging of tumors is generally about 10 mCi. The total amount of protein in the administered solutions ranged from 2.5 mg to 10 mg. Imaging with a gamma camera is performed at three time points: immediately following infusion, from 7 to 8 hours post infusion, and from 19 to 20 hours post infusion. The best images of the target sites (tumors) are achieved by imaging at from 7 to 8 hours after completion of infusion of the radiolabeled antibody. Although some accumulation of radioactivity in the kidneys is detected during these imaging procedures, the kidneys generally are not considered to be target sites in the diagnostic procedures of the invention. The percentage of the total injected dose radioactivity (in cpm) which had localized in each of the various tissue types sampled are to be calculated. The ratio of the radioactivity found in tumor site(s) to the radioactivity found in the other types of tissue are also calculated. The value for the percent injected dose per mg for the tumor tissue in a particular patient is divided by the value for the percent injected dose per mg for each non-tumor tissue sample biopsied from the patient to give the tumor:tissue ratio for each non-tumor tissue sample.

From the foregoing, it will be appreciated that, although specific embodiments of the invention have been described herein for purposes of illustration, various modifications may be made without deviating from the spirit and scope of the invention.

We claim:

1. A metal chelate having the formula:



wherein:

M is a metal, or metal oxide, radionuclide which is chelated;

X<sub>1</sub> and X<sub>2</sub> are H or =O, but both are not =O;

X<sub>3</sub> and X<sub>4</sub> are H or =O, but both are not =O;

A is H, alkyl group of C<sub>6</sub> or less, —CH<sub>2</sub>—CH<sub>2</sub>—S—R<sub>1</sub>, or —CO—CH<sub>2</sub>—S—R<sub>1</sub>, with the proviso that when X<sub>1</sub> or X<sub>2</sub> is =O, A is H;

A' is H, alkyl group of C<sub>6</sub> or less, —CH<sub>2</sub>—CH<sub>2</sub>—S—R<sub>2</sub>, or —CO—CH<sub>2</sub>—S—R<sub>2</sub>, with the proviso that when X<sub>3</sub> or X<sub>4</sub> is =O, A' is H;

Y is

(a) —CH<sub>2</sub>—S—R<sub>3</sub>, or H, when A is H or an alkyl group of C<sub>6</sub> or less and A' is H or an alkyl group of C<sub>6</sub> or less, or

(b) H, with the proviso that Y must be selected from (a) when A is H or an alkyl group of C<sub>6</sub> or less and A' is H or an alkyl group of C<sub>6</sub> or less;

Y' is

(a) —CH<sub>2</sub>—S—R<sub>4</sub>, or H, when A is H or an alkyl group of C<sub>6</sub> or less and A' is H or an alkyl group of C<sub>6</sub> or less, with the proviso that Y and Y' are not both H, or

(b) H, with the proviso that Y' must be selected from (a) when A is H or an alkyl group of C<sub>6</sub> or less and A' is H or an alkyl group of C<sub>6</sub> or less;

R<sub>1</sub>, R<sub>2</sub>, R<sub>3</sub>, R<sub>4</sub>, R<sub>5</sub>, and R<sub>6</sub> are independently selected from sulfur protecting groups;

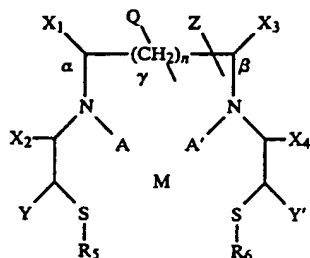
Q is H or a polar group to increase the hydrophilicity of the compound;

n is 0 to 2; and

z is —(W)<sub>m</sub>—R', where W is —CH<sub>2</sub>—, —CH<sub>2</sub>—O—, —CH<sub>2</sub>—CO—, or combinations thereof, m is 0 to 5, and R' is a chemically reactive group, with the provisos that when Z is attached to the carbon designated α there is either no X<sub>1</sub> or no Q at α, that when Z is attached to the carbon designated β there is either no X<sub>3</sub> or no Q at β, that when X<sub>1</sub> is =O there is no Z at β, and that when X<sub>3</sub> is =O there is no Z at β.

2. The metal chelate of claim 1 wherein the metal, or metal oxide, radionuclide is selected from the group consisting of <sup>64</sup>Cu, <sup>67</sup>Cu, <sup>97</sup>Ru, <sup>99m</sup>Tc, <sup>105</sup>Rh, <sup>109</sup>pd, <sup>186</sup>Re, <sup>188</sup>Re, <sup>198</sup>Au, <sup>199</sup>Au, <sup>203</sup>Pb, <sup>212</sup>Pb, and <sup>212</sup>Bi.

3. A chelate-targeting agent conjugate having the formula:



wherein:

M is a metal, or metal oxide, radionuclide which is chelated;

X<sub>1</sub> and X<sub>2</sub> are H or =O, but both are not =O;

X<sub>3</sub> and X<sub>4</sub> are H or =O, but both are not =O;

A is H, alkyl group of C<sub>6</sub> or less, —CH<sub>2</sub>—CH<sub>2</sub>—S—R<sub>1</sub>, or —CO—CH<sub>2</sub>—S—R<sub>1</sub>, with the proviso that when X<sub>1</sub> or X<sub>2</sub> is =O, A is H;

A' is H, alkyl group of C<sub>6</sub> or less, —CH<sub>2</sub>—CH<sub>2</sub>—S—R<sub>2</sub>, or —CO—CH<sub>2</sub>—S—R<sub>2</sub>, with the proviso that when X<sub>3</sub> or X<sub>4</sub> is =O, A' is H;

Y is

(a) —CH<sub>2</sub>—S—R<sub>3</sub>, or H, when A is H or an alkyl group of C<sub>6</sub> or less and A' is H or an alkyl group of C<sub>6</sub> or less, or

(b) H, with the proviso that Y must be selected from (a) when A is H or an alkyl group of C<sub>6</sub> or less and A' is H or an alkyl group of C<sub>6</sub> or less;

Y' is

(a) —CH<sub>2</sub>—S—R<sub>4</sub>, or H, when A is H or an alkyl group of C<sub>6</sub> or less and A' is H or an alkyl group of C<sub>6</sub> or less, with the proviso that Y and Y' are not both H, or

(b) H, with the proviso that Y' must be selected from (a) when A is H or an alkyl group of C<sub>6</sub> or less and A' is H or an alkyl group of C<sub>6</sub> or less;

R<sub>1</sub>, R<sub>2</sub>, R<sub>3</sub>, R<sub>4</sub>, R<sub>5</sub>, and R<sub>6</sub> are independently selected from sulfur protecting groups;

Q is H or a polar group to increase the hydrophilicity of the compound;

n is 0 to 2; and

Z' is —(W)<sub>m</sub>—Targeting agent, where W is —CH<sub>2</sub>—, —CH<sub>2</sub>—O—, —CH<sub>2</sub>—CO—, or combinations thereof, m is 0 to 5, and Targeting agent includes a linking group, with the provisos that when Z' is attached to the carbon designated α there is either no X<sub>1</sub> or no Q at α, that when Z' is attached to the carbon designated β there is either no X<sub>3</sub> or no Q at β, that when X<sub>1</sub> is =O there is no Z' at α, and that when X<sub>3</sub> is =O there is no Z' at β.

4. The chelate-targeting agent conjugate of claim 3 wherein the metal, or metal oxide, radionuclide is selected from the group consisting of <sup>64</sup>Cu, <sup>67</sup>Cu, <sup>97</sup>Ru, <sup>99m</sup>Tc, <sup>105</sup>Rh, <sup>109</sup>Pd, <sup>186</sup>Re, <sup>188</sup>Re, <sup>198</sup>Au, <sup>199</sup>Au, <sup>203</sup>Pb, <sup>212</sup>Pb, and <sup>212</sup>Bi.

5. The chelate-targeting agent conjugate of claim 3 wherein the targeting agent is an antibody.

6. The chelate-targeting agent conjugate of claim 5 wherein the antibody is a monoclonal antibody.

7. The chelate-targeting agent conjugate of claim 6 wherein the monoclonal antibody is directed against an antigen on a tumor cell.

8. A method of detecting the presence or absence of a target site within a mammalian host, comprising the steps of:

administering to a mammal a diagnostically effective dose of the chelate-targeting agent conjugate of claim 3, wherein M is a radionuclide and the conjugate is capable of binding to said target site; and detecting the biodistribution of said radionuclide in said mammal to determine the presence or absence of said target site in said host.

9. The method of claim 8 wherein the mammal is man.

10. The method of claim 8 wherein the radionuclide is selected from the group consisting of <sup>99m</sup>Tc, <sup>97</sup>Ru and <sup>203</sup>Pb.

11. The method of claim 8 wherein the targeting agent of the chelate-targeting agent conjugate is an antibody.

12. The method of claim 11 wherein the antibody is a monoclonal antibody.

13. The method of claim 12 wherein the monoclonal antibody is directed against an antigen on a tumor cell.

\* \* \* \* \*

UNITED STATES PATENT AND TRADEMARK OFFICE  
CERTIFICATE OF CORRECTION

PATENT NO. : 4,988,496 Page 1 of 2  
DATED : January 29, 1991  
INVENTOR(S) : Ananthachari Srinivasan; Alan R. Fritzberg;  
David S. Jones

It is certified that error appears in the above-identified patent and that said Letters Patent is hereby corrected as shown below:

On the title page, item [75] Inventors: please include  
--David W. Wilkening-- as an inventor.

In column 44, claim 1, line 52, please delete "z" and  
substitute therefor --Z--.

In column 44, claim 1, line 54, please delete "R'is" and  
substitute therefor --R' is--.

In column 44, claim 1, line 60, please delete " $\beta$ " and  
substitute therefor -- $\alpha$ --.

In column 44, claim 2, line 64 please delete "<sup>99</sup>mTc" and  
substitute therefor --<sup>99</sup>mTc--.

In column 44, claim 2, line 64, please delete "<sup>109</sup>pd" and  
substitute therefor --<sup>109</sup>Pd--.

In column 45, in the top line of the diagram, please delete  
"Z" and substitute therefor --Z'--.

In column 46, claim 3, line 5, please delete "a" and  
substitute therefor -- $\alpha$ --.



UNITED STATES PATENT AND TRADEMARK OFFICE  
**CERTIFICATE OF CORRECTION**

PATENT NO. : 4,988,496

Page 2 of 2

DATED : January 29, 1991

INVENTOR(S) : Ananthachari Srinivasan; Alan R. Fritzberg; David S. Jones

It is certified that error appears in the above-identified patent and that said Letters Patent is hereby corrected as shown below:

In column 46, claim 4, line 13, please delete "<sup>99</sup>mTc" and substitute therefor --<sup>99</sup>mTc--.

Signed and Sealed this

Twenty-second Day of September, 1992

*Attest:*

DOUGLAS B. COMER

*Attesting Officer*

*Acting Commissioner of Patents and Trademarks*

**United States Patent** [19]**Hawthorne**[11] **Patent Number:** **4,824,659**[45] **Date of Patent:** **Apr. 25, 1989**[54] **ANTIBODY CONJUGATES**[75] **Inventor:** Marion F. Hawthorne, Encino, Calif.[73] **Assignee:** Immunomedics, Inc., Warren, N.J.[21] **Appl. No.:** 742,436[22] **Filed:** Jun. 7, 1985[51] **Int. Cl.<sup>4</sup>** ..... A61N 5/12; A61K 49/02;  
A61K 31/74; A61K 42/02[52] **U.S. Cl.** ..... 424/1.1; 424/9;  
424/78; 424/85.8; 128/1.1; 530/387; 525/54.1;  
600/4[58] **Field of Search** ..... 424/1.1, 9, 78, 85;  
128/1.1[56] **References Cited****U.S. PATENT DOCUMENTS**

4,331,647	5/1982	Goldenberg	424/1.1
4,348,376	9/1982	Goldenberg	424/1.1
4,361,544	11/1982	Goldenberg	424/1.1
4,434,150	2/1984	Azad et al.	424/1.1
4,460,559	7/1984	Goldenberg	424/1.1

4,460,561 7/1984 Goldenberg ..... 424/1.1

4,466,952 8/1984 Hadd ..... 424/1.1

4,665,897 5/1987 Lemelson ..... 128/1.1

4,674,480 6/1987 Lemelson ..... 128/1.1

*Primary Examiner*—John F. Terapane*Assistant Examiner*—J. E. Thomas*Attorney, Agent, or Firm*—Bernhard D. Saxe[57] **ABSTRACT**

An antibody or antibody fragment is modified by chemical linkage to a synthetic poly(amide/urea/thiourea) which contains a plurality of boron atoms or other functional groups, conferring upon the resultant conjugate desirable properties as a diagnostic and/or therapeutic agent. In a preferred embodiment, boron-containing groups are conjugated to the antibody/fragment such that the resultant conjugate contains 50–2000 boron atoms, with about 96% Boron-10 isotope content, to produce conjugates useful for neutron-activated radiotherapy of tumors or pathological lesions.

**17 Claims, No Drawings**

## ANTIBODY CONJUGATES

## BACKGROUND OF THE INVENTION

The present invention relates to an antibody or antibody fragment modified by chemical linkage to a synthetic poly(amide/urea/thiourea) which contains a plurality of boron atoms or other functional groups, conferring upon the resultant conjugate desirable properties as a diagnostic and/or therapeutic agent.

It is known to modify antibodies by chemically linking to them various types of addends. For example, enzymes have been linked to antibodies to make conjugates useful in ELISA immunoassays, boron-containing addends have been linked to antibodies and antibody fragments to produce therapeutic agents, and antibodies have been conjugated to polypeptides such as polylysine. European patent application No. 88,695, to McKearn et al., published 9/14/83, discloses antibodies conjugated to polypeptides made from natural amino acids, which in turn can carry a functional group such as a chelator, drug, toxin and the like.

It would be highly desirable to be able to modify an immunoglobulin to incorporate moieties that contain useful functionality, but in such a way that the addend is precisely defined in terms of its structure. This is particularly useful where it is desired to incorporate a plurality, especially a large number, of added functional groups such as chelating agents, boron-containing groups, radionuclides, spin labels and the like. In the past, it has been troublesome to attempt to characterize such modified antibodies because of the heterogeneity of the conjugates, and this has resulted in difficulties in assuring reproducibility of results. Moreover, it has been difficult to attach sufficient boron atoms to an antibody so that even a low percentage of conjugates localized in tumor or lesion tissue carries a large enough number of boron atoms to be therapeutically significant for neutron activated radiotherapy.

A need therefore continues to exist for chemically modified antibody conjugates having well-defined structures for the modifying groups to minimize the uncertainties in preparing and using these molecular species.

## OBJECTS OF THE INVENTION

One object of the present invention is to provide an antibody conjugate having a sufficiently large number of boron atoms so that it will function as an efficient therapeutic agent for thermal neutron activated radiotherapy of tumors and pathological lesions.

Another object of the present invention is to provide a modified antibody or antibody fragment having a defined, chemically linked addend incorporating useful functional groups for diagnosis and/or therapy.

A further object of the invention is to provide reagents for use in modifying antibodies to confer upon the resultant conjugates desirable properties for diagnosis and/or therapy.

Yet another object of the invention is to provide agents useful for diagnosis and/or treatment of cancer, infectious lesions or other pathological lesions such as myocardial infarctions.

Other objects of the invention will become more readily apparent to those of ordinary skill in the art in light of the following discussion.

## SUMMARY OF THE INVENTION

The foregoing objects can be achieved by providing a modified antibody or antibody fragment, consisting essentially of:

(1) at least one hypervariable region which specifically binds a ligand such that the formation of the resultant immunological complex is of diagnostic or therapeutic utility; and

(2) at least one defined, substantially homogeneous synthetic poly(amide/urea/thiourea) which incorporates residues containing at least one of: (i) a plurality of Boron-10 atoms; (ii) a metal-chelating moiety; (iii) an antineoplastic agent; (iv) a paramagnetic spin label; (v) a radionuclide; (vi) a chemotherapeutic agent; (vii) a photosensitizer; (viii) a magnetic resonance imaging enhancer; (ix) an enzyme; (x) a chromogen; or (xi) a fluorescent marker;

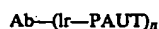
wherein said synthetic poly(amide/urea/thiourea) is chemically bound to said antibody or antibody fragment at one or more sites which do not substantially interfere with the immunological specificity of said hypervariable region; and wherein a plurality of the residues making up said poly(amide/urea/thiourea) are not natural L-amino acids or are natural L-amino acids with modified side chains.

The present invention further provides antibody conjugates carrying functionality other than boron, reagents and methods for preparing the foregoing antibody conjugates, as well as kits containing the conjugates and methods of using the conjugates for diagnosis and therapy.

## DETAILED DESCRIPTION

The modified antibodies and antibody fragments according to the invention contain the hypervariable region, i.e., the region of the immunoglobulin which specifically binds the ligand which defines the specificity of the antibody, and at least one synthetic poly(amide/urea/thiourea) portion having a defined chemical structure, the poly(amide/urea/thiourea) being covalently linked to the immunoglobulin. Each poly(amide/urea/thiourea) portion of the molecule in turn is composed of residues containing the desired useful functionality and/or groups which improve the solubility properties, the separability properties, the conformational properties, or other properties of the resultant conjugate.

Schematically, the modified antibody of the invention can be represented as:



where Ab is an antibody or antibody fragment comprising at least one hypervariable region which specifically binds a ligand of interest, e.g., a marker produced by or associated with a tumor or a pathological lesion; Ir is a linker function, which can simply be, e.g., an ester, amide, urea, carbamate, thiourea, ether or thioether bond, or a multifunctional linker which joins the poly(amide/urea/thiourea) addend to the antibody; "PAUT" is a poly(amide/urea/thiourea) having a defined chemical formula and incorporating the desired functionality; and n is an integer from 1 to 20, preferably from 1 to 10, and more preferably from 1 to 5. It will be appreciated that the addend denoted "Ir-PAUT" may in fact be composed of several polymer chains joined to a multivalent linker, i.e., Ir-(PAUT)<sub>m</sub>, and that within the PAUT there may be one or more branch points.

As used in the context of this disclosure, the term "poly(amide/urea/thiourea)" (hereinafter "PAUT") denotes a sequenced polymer composed of residues, some or all of which contain a plurality of boron atoms or other useful diagnostic or therapeutic groups, the residues being linked by amide, urea and/or thiourea functions. Any single residue in the body of the polymer chain will normally be joined at two points to two adjacent residues, although it will be seen that additional points of attachment for a residue can be envisioned, e.g., for branching. Terminal residues will normally contain a functional group for linking the PAUT to the antibody. This can be a simple function, e.g., an isocyanate or isothiocyanate, a function capable of activation to bind to antibody, e.g., a carboxyl which can be activated by conversion to its anhydride, acid chloride, N-hydroxysuccinimide ester, or a more complex linking function such as one of those disclosed in greater detail hereinafter. Terminal residues not used for linkage to the antibody can be capped or used to bind other useful functions, e.g., chelators, drugs, toxins and the like, or they can be left unmodified.

In a preferred embodiment of the invention, the antibody conjugate would contain a large number of boron atoms, more preferably prepared from reagents enriched in Boron-10 isotope, boron-containing reagents enriched to about 96% Boron-10 being commercially available. Such a conjugate would be of great utility in neutron activated radiotherapy, since it could bring to a tumor site or the site of a pathological lesion a sufficient number of boron atoms to provide a therapeutic dosage of alpha particles to the surrounding tissue upon thermal neutron irradiation, even where the percentage of an injected dose of antibody conjugate which localizes in the target tissue is relatively low, e.g., 1-10%. Such localization percentages are not uncommon for antibody-based diagnostic and therapeutic agents.

Targeted neutron-activated radiotherapy is described, e.g., in Goldenberg et al., *Proc. Natl. Acad. Sci. USA*, 81, 560 (1984); Hawthorne et al., *J. Med. Chem.*, 15, 449 (1972); and in Goldenberg, U.S. Pat. Nos. 4,331,647, 4,348,376, 4,361,544, 4,468,457, 4,444,744, 4,460,459 and 4,460,561, and in related pending applications U.S. Ser. Nos. 609,607 (filed 5-14-84) and 633,999 (filed 7-24-84), the disclosures of all of which are incorporated herein in their entireties by reference.

The aforementioned references disclose, inter alia, methods of incorporating Boron-10-containing addends into antibody conjugates using, e.g., coupling of a carborane (linked to a phenyldiazonium ion) to an antibody, which are suitable for incorporation of an relatively low number of Boron-10 atoms. Typically, between 10 and 120 B-10 atoms have been attached to IgG before the immunoreactivity and yield of recovered product become unacceptably low, using the carboranephenyldiazonium conjugation procedure. However, it would be preferable to be able to conjugate a larger number of B-10 atoms to an antibody so that even a low percentage of tumor accretion of an injected circulating antibody conjugate, e.g., on the order of 1.5%, would nonetheless carry hundreds of B-10 atoms per conjugate to the tumor site.

Several approaches to improving the efficiency of B-10 conjugation have been developed, most of which have related to improving the water solubility of the carborane addend by, e.g., using carborane monoanions or attaching polyhydroxylic tails to the carborane. See, e.g., Sneath et al., *J. Med. Chem.*, 17, 796 (1974); Sneath

et al., *J. Med. Chem.*, 19, 1920 (1976); Hawthorne et al., *J. Am. Chem. Soc.*, 90, 862 (1968); and Mizusawa et al., *Proc. First Internatl. Symp. Neutron Capture Therapy*, Cambridge, MA., Oct. 12-14, 1983, pp 215-224. Other variants involve use of other functional groups instead of diazonium ions to effect conjugation to the antibody. The present method and reagents go well beyond these earlier approaches.

The boron-loaded antibody conjugates according to the present invention have a number of boron atoms per antibody molecule normally ranging from at least about 50 up to about 10,000, preferably from about 200 to about 2,000. To reiterate, these are preferably about 96% Boron-10 enriched, although it may be more cost-effective to use a conjugate having a larger number of boron atoms with the 20% natural abundance of Boron-10 isotope.

The boron-containing PAUT is conjugated to an antibody, which may be any type of immunoglobulin molecule having at least one hypervariable region, i.e., a region which specifically binds to an antigen of diagnostic and/or therapeutic interest. These include whole immunoglobulin, e.g., IgM, IgG, IgA, IgD, IgE and the like, or an immunoglobulin fragment, e.g., F(ab')<sub>2</sub>, F(ab)<sub>1</sub>, Fab, Fab' and the like, or a hybrid antibody or fragment. In this discussion, the term "antibody" will be used to signify any of the foregoing, unless otherwise specified.

The principal types of building blocks for the PAUT according to the invention are selected from amino acids, diamines, diacids, diisocyanates and diisothiocyanates containing boron functions therein, principally boron cage functions which have the advantage of high boron content and attractive chemical properties. The individual residues making up the synthetic PAUT are linked by amide(peptide) bonds, urea or thiourea functions. The amide bonds can be formed either by successive coupling of amino acids, e.g., alpha-amino acids or amino acids wherein the amine and carboxyl groups are farther removed from one another, or successive coupling of diamino groups to dicarboxylic acid groups in a "nylon 66" manner, i.e., with alternating senses of the amide bonds, viz., —NHCO—CONH—NH—CO—CONH—, or a mixture of such couplings. The urea and thiourea functions can be formed by condensation of a chain terminating in an amine function with an isocyanate or isothiocyanate, normally a diisocyanate or diisothiocyanate, used in excess to minimize cross-linking, and the reverse linkage of chains terminating with isocyanate/isothiocyanate functions to amine building blocks.

Examples of monomers which can be condensed to form amide linkages include: the natural L-amino acids, their enantiomers, and mixtures thereof (alpha-amino acids); conjugates of the natural amino acids with boron-containing groups or other groups of interest, e.g., lysine wherein the epsilon-amine function is used to link a boron-containing moiety, and/or a drug, chelator, enzyme, radionuclide carrier moiety, fluorescent marker, chromogen, nmr imaging agent or enhancer or the like; aspartic or glutamic acid wherein the beta- or gamma-carboxyl function is used to link one of the foregoing moieties; tyrosine, phenylalanine or histidine wherein the aromatic ring is substituted with such moieties; serine, threonine, tyrosine or hydroxyproline wherein the hydroxyl group is used to link the moieties, e.g., through an ether function; or cysteine wherein the thiol is used to form a thioether with another function of

interest; other natural and synthetic amino acids with amine and carboxyl groups adjacent or farther removed from one another, and optionally conjugated to one or more of the foregoing types of moieties, examples of which are shown hereinafter; as well as diamines and dicarboxylic acids which can be linked by amide bonds in a "Nylon 66" fashion, the foregoing also optionally carrying additional functionality and/or being conjugated to the moieties mentioned above and further exemplified hereinafter. Examples of monomers which can form urea or thiourea functions include diamines, diisocyanates and diisothiocyanates.

It will be understood that the polymer chain can contain residues which do not contain boron, or which contain boron and other useful functions, e.g., a radio-nuclide, especially I-123, I-125 or I-131, or functions such as chelators, chelates with metal ions, drugs, toxins, chromophores, chromogens, fluorescent markers, and the like. The chain may also incorporate intrachain brancher residues, about which more will be said hereinafter. Finally, the chain may incorporate residues whose primary purpose is to improve the solubility and/or separability of the resultant conjugate.

As presently envisioned, the PAUT addends according to the invention are most advantageously synthesized by using a Merrifield-type solid phase synthesis, e.g., one using one of the currently available automated protein synthesizers. The individual component amino acid, diamino or dicarboxylic acid, diisocyanate or diisothiocyanate building blocks, suitably protected where necessary with groups that can be removed selectively in the course of automated synthesis, will be prepared in advance and coupled in a preselected sequence according to the desired properties of the resultant polymer.

Solid phase peptide synthesis is well known in the art, and the types of solid supports, protecting groups and coupling reactions used with the various naturally occurring amino acids are well documented, e.g., in Garland et al., "Biochemical Aspects of Reactions on Solid Supports", Chapter 3, pp 111-162, Stark, Ed. (Academic Press, New York, 1971); and Stewart et al., "Solid Phase Peptide Synthesis" (Pierce Chemical Corp., Rockford, IL., 1984); and the many specific references therein, all of which are well known to those engaged in the synthesis of polyamides of defined sequence and structure.

These techniques are readily adapted to the synthesis of polyureas and/or polythioureas, and the foregoing linkages can also be incorporated in polypeptide chains by minor modification of the conventional process steps. The standard methods will be modified for use with some of the new building blocks described herein. To the extent that such modifications are not familiar to one of ordinary skill in the art of solid phase peptide synthesis, they will be described in more detail hereinafter. It will also be appreciated that conventional solu-

tion phase reactions may be used to synthesize the PAUT addends, but that the yield, uniformity and purity of the resultant polymer are likely to be significantly lower than those obtainable using a solid phase synthesis technique.

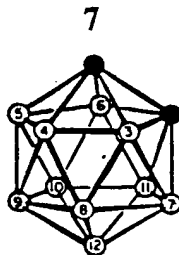
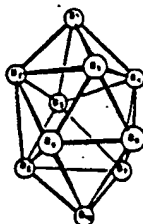
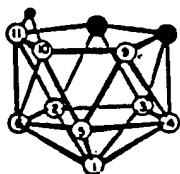
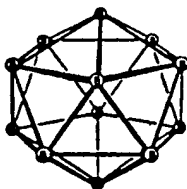
The following discussion will present a more detailed treatment of certain preferred embodiments of the invention to illustrate the methods and utility of the generic invention, without limiting the scope thereof. In light of this discussion, it will become readily apparent how the invention can be practiced to achieve other embodiments.

It will be useful at this juncture to discuss boron cage compounds in a general way, to lay the groundwork for their use in synthesizing building blocks containing these compounds. The reader is referred to general references in this field for most of the reactions to be discussed hereinafter, the best and most comprehensive reference being Muetterties et al., "Polyhedral Boranes", (Dekker, New York, 1968); Muetterties, Ed., "Boron Hydride Chemistry", (Academic Press, New York, 1975); and Grimes, "Carboranes", (Academic Press, New York, 1970). These references contain copious bibliographies on specific topics within the broad subject range.

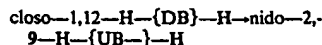
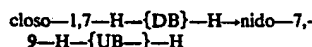
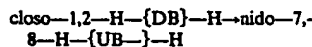
The most common and readily available kinds of boron cage compounds are the carboranes, especially the isomers of dicarba-closo-dodecaborane, having an icosahedral cage structure, and represented hereinafter by the symbol "H-{DB}-H". This cage compound can have any of three isomeric structures, viz., 1,2-, 1,7-, and 1,12-, wherein the two carbon atoms are on adjacent vertices, vertices separated by one boron atom, or vertices separated by two boron atoms (opposite poles) of the icosahedron, respectively. The symbol "H-{D-B}-H" will refer to any of these three isomers, each of which can be used for nearly all of the reactions shown herein, except where noted.

The most common of the carborane cage compounds, and the most useful for further elaboration, is the 1,2-dicarba-closo-dodecaborane, which is readily synthesized by the classic reaction of an acetylene with  $B_{10}H_{14}$ . For example, 1-phenyl-1,2-dicarba-closo-dodecaborane is made by reacting phenylacetylene with  $B_{10}H_{14}$  in acetonitrile solution, and is denoted by the symbol, H-{DB}-C<sub>6</sub>H<sub>5</sub>. A further useful property of these carboranes is their relative inertness to the conditions for many common organic reactions, e.g., aromatic halogenation, aromatic nitration, hydride reduction, catalytic hydrogenation, alkylation, acylation and the like. The carboranes can be converted to anions with one less boron vertex, by reaction with strong base, e.g., ethoxide, in protonic solvents, e.g., ethanol. They are also sensitive to primary and secondary amines, but not tertiary amines.

The structures of 1,2-dicarba-closo-dodecaborane and three cage borane carborane anions are shown below.

H-(DB)-H (1,2-C<sub>2</sub>B<sub>10</sub>H<sub>12</sub>)H-(10B-2)-H (B<sub>10</sub>H<sub>10</sub><sup>-2</sup>)H-(UB)-H (7,8-C<sub>2</sub>B<sub>9</sub>H<sub>12</sub><sup>-</sup>)H-(12B-2)-H (B<sub>12</sub>H<sub>12</sub><sup>-2</sup>)

Conversions of the three isomeric dicarba-closo-dodecaboranes to their respective corresponding dicarba-nido-undecaborane anions, by reaction with base, is shown below.



The nido carborane anions shown above are denoted hereinafter by the symbol "H-{UB}-H", representing a dicarba-nido-undecaborane monoanion.

Other readily available borane cages include the icosahedral closo-dodecaborane (B<sub>12</sub>H<sub>12</sub><sup>-2</sup>) dianion, hereinafter denoted by the symbol "H-{12B-2}-H", or the hexadecahedral closo-decaborane (B<sub>10</sub>H<sub>10</sub><sup>-2</sup>) dianion, hereinafter denoted by the symbol "H-{10B-2}-H", whose structures are shown above. These can be modified to facilitate attachment to PAUT chains. Other less available borane and carborane cage compounds include carba-closo-dodecaboranes, lower boranes having, e.g., 6-9 and 11 boron atoms in the cage, heteroboranes, metalloboranes, and metallocarboranes. The metalloboranes are known, and their chemistry is described by Leyden et al, *J. Am. Chem. Soc.*, 100, 3758 (1978). The other classes of boron cage compounds are relatively rare, although known, and are described in the above-cited Muetterties references. The metallocarboranes, about which not a great deal of organic chemistry is known, are potentially of considerable use in the invention, as will be shown hereinafter.

Illustrative of one type of born containing antibody conjugate according to the present invention is the class wherein, in the formula Ab-(Ir-PAUT)<sub>n</sub>, the polymer moiety, PAUT, is a polypeptide having the formula -(NH-Q-CO)-OH, wherein each NH-Q-CO is a residue derived from (i.e., resulting from condensation of) a natural alpha-L-amino acid, or its enantiomer, or a mixture thereof, or a residue derived from an amino acid having the amine and carboxyl groups more remote than geminal, a plurality of which amino acids have a pendant amine, carboxyl, hydroxyl or thiol to which is bound a carborane-containing group, or a carborane to which are linked an amine and a carboxyl, optionally in positions more remote than geminally. Specific representative examples of carborane-linked amino acids, NH<sub>2</sub>-Q-COOH from which such residues can be derived include, but are not limited to, those having the formula 1-14:

40	H-{DB}-C <sub>6</sub> H <sub>4</sub> NHC(S)NH(CH <sub>2</sub> ) <sub>4</sub> CH(NH <sub>2</sub> )COOH	1
	H-{DB}-(CH <sub>2</sub> ) <sub>3</sub> C(O)NH(CH <sub>2</sub> ) <sub>4</sub> CH(NH <sub>2</sub> )COOH	2
	H-{DB}-C <sub>2</sub> H <sub>4</sub> NHC(S)OCH <sub>2</sub> CH(NH <sub>2</sub> )COOH	3
	H-{DB}-C <sub>6</sub> H <sub>4</sub> NHC(O)(CH <sub>2</sub> ) <sub>2</sub> CH(NH <sub>2</sub> )COOH	4
	M <sup>+</sup> H-{UB}-C <sub>6</sub> H <sub>4</sub> NHC(S)NH(CH <sub>2</sub> ) <sub>4</sub> CH(NH <sub>2</sub> )COOH	5
	M <sup>+</sup> H-{IUB}-C <sub>6</sub> H <sub>4</sub> NHC(S)NH(CH <sub>2</sub> ) <sub>4</sub> CH(NH <sub>2</sub> )COOH	6
45	M <sup>+</sup> H-{UB}-(CH <sub>2</sub> ) <sub>4</sub> C(O)NH(CH <sub>2</sub> ) <sub>4</sub> CH(NH <sub>2</sub> )COOH	7
	H-{DB}-C <sub>6</sub> H <sub>4</sub> N=N-(OH)C <sub>6</sub> H <sub>3</sub> CH <sub>2</sub> CH(NH <sub>2</sub> )COOH	8
	H-{DB}-(CH <sub>2</sub> ) <sub>3</sub> S(CH <sub>2</sub> ) <sub>2</sub> CH(NH <sub>2</sub> )COOH	9
	H-{DB}-(CH <sub>2</sub> ) <sub>3</sub> OC <sub>6</sub> H <sub>4</sub> CH <sub>2</sub> CH(NH <sub>2</sub> )COOH	10
	H-{DB}-(CH <sub>2</sub> ) <sub>3</sub> CH(NH <sub>2</sub> )COOH	11
	M <sup>+</sup> H-{UB}-(CH <sub>2</sub> ) <sub>4</sub> CH(NH <sub>2</sub> )COOH	12
50	H <sub>2</sub> N(CH <sub>2</sub> ) <sub>3</sub> -{DB}-(CH <sub>2</sub> )COOH	13
	M <sup>+</sup> H <sub>2</sub> N(CH <sub>2</sub> ) <sub>3</sub> -{UB}-(CH <sub>2</sub> ) <sub>3</sub> COOH	14

The iodo-substituted ion in compound 6 has one BH vertex replaced by a BI in the cage structure, and is denoted by the symbol "H-{IUB}-H. M<sup>+</sup> in the formulas for compounds 5, 6, 7, 12 and 14 represents one equivalent of a convenient cation, e.g., an alkali metal, especially Na<sup>+</sup> and K<sup>+</sup>, an alkali earth metal, especially Mg<sup>+2</sup> and Ca<sup>+2</sup> or a quaternary ammonium ion, especially (CH<sub>3</sub>)<sub>4</sub>N<sup>+</sup> and the like.

As noted above, the synthesis of linker peptides according to the invention can be achieved by conventional non-automated peptide synthesis routes which are lengthy, tedious and not easily applied to the rapid synthesis of many different members of a new class of peptides containing 2-50 amino acid residues. Indeed, the number of separation and purification steps required in non-automated synthesis makes the method unattractive.

tive from the viewpoint of time spent, synthesis control and quantity of peptide produced. In order to make gross, as well as finely tuned, adjustments in peptide linker sequences, and at the same time provide a sufficiently high throughput of material, it is preferable to use a Merrifield-type automated peptide synthesis machine, e.g., the Beckman Instruments 990 Peptide Synthesizer, and an associated Beckman 340 Series HPLC peptide purification system for the detection and separation of faulty peptide products formed during linker peptide synthesis.

Reagent chemicals such as amine-protected and/or carboxyl-protected amino acids are commercially available and generally usable without prior purification. Amino- and carboxyl-protected derivatives of B-10-containing amino acids or amino acid coupling reagents are new compounds which, after preliminary testing, are preferably prepared with Boron-10-enriched reagents for linker peptide synthesis and synthesis of linker-conjugated antibody for neutron irradiation therapy protocols.

The bonding of boron to a linker peptide may be accomplished in several ways, e.g., by using an amino acid containing a boron moiety integral to its structure, or by attaching a boron-containing moiety to a functional group on a side-chain of an amino acid. As an example of the former approach, synthesis of a bifunctional carborane derivative having an amino group on one arm attached to the cage and a carboxyl group attached to a second arm would allow the cage to be incorporated within the linker peptide chain. Acylation of the epsilon-NH<sub>2</sub> group in lysine using a carborane-containing carboxylic acid would provide an example of the latter tactic. One could also incorporate boron by both methods simultaneously.

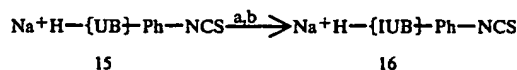
A second factor to be considered is the charge type presented to the linker peptide molecule by the boron-containing residue. Electrically neutral carborane derivatives containing the hydrophobic icosahedral —{D-B}— substituent (derivatization at carborane C-atoms) are advantageously used in the presence of strongly hydrophilic groups or replaced altogether by the related anionic —{UD}— group, which has been incorporated in antibody conjugates and renders them significantly more water soluble (e.g., as Na<sup>+</sup> salts. In general, the desired anionic —{UD}— species can readily be formed from the corresponding neutral —{DB}— icosahedral intermediate. The anionic carboranes are introduced during conjugating reagents which are themselves rendered more water soluble and often more compatible with the reaction medium.

Other charged boron-containing building blocks are available which made use of simple functional groups attached to the H—{12B-2}—H dianion (H—{1-2B-2}—SH is an example), or to the H—{10B-2}—H dianion. Such reagents are less adaptable in synthesis than similar carborane species since the polyhedral borane cages provide their own characteristic reactions reflecting strong electron-releasing properties and organic reactions often proceed in an unpredictable fashion.

The reagents used in the selected peptide syntheses must be compatible with the boron-containing species employed in linker synthesis. The H—{DB}—H icosahedral cage and its C-substituted derivatives are sensibly inert to chemical reagents except strong bases in the presence of an available proton source (OH<sup>-</sup>/ethanol or certain primary and secondary amines). The generation

of bases under conditions which occur during routine peptide synthesis, such as terminal —NH<sub>2</sub> groups, would not be important since the amino groups, when available, are sterically substantially inaccessible to neutral —{DB}— groups in the growing peptide chain and the amine reaction is normally slow.

On the other hand, the 11-vertex carborane anion —{UB}—, in its derivatives, functions as an anion derived from a very strong acid (C<sub>2</sub>B<sub>9</sub>H<sub>13</sub>). This anion is reversibly protonated with strong acids in nonaqueous media and is inert toward reagents other than reactive electrophiles. As an example, radioiodination of the —{UB}— cage is used as a means of radiolabeling compound 15 to form protein conjugation reagent 16, according to the following equation.



(a) Chloramine-T/NaI-125

(b) Na<sub>2</sub>S<sub>2</sub>O<sub>5</sub>

Note that reagent 15 is prepared from the anionic aminophenyl derivative by reaction with thiophosgene, CSCI<sub>2</sub>. Consequently, no serious difficulty is expected in the utilization of reagents based upon the H—{D-B}—H and H—{UB}—H carborane cages in automated linker peptide syntheses.

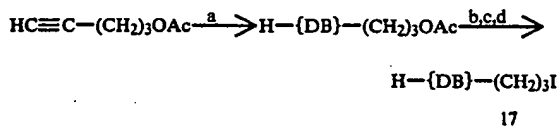
Attractive boron-containing reagents for attachment to side-chains of amino acids would include compounds for alkylation, acylation, amidation, carbamation/ureidation, thiocarbamation/thioureidation and diazonium coupling. They could bear uncharged/hydrophobic groups, e.g., —{DB}—, or charged/hydrophilic groups, e.g., —{UB}—.

Alkylation could be effected, e.g., on the thiol or sulfide groups of cysteine or methionine, on the hydroxyl groups of serine, threonine, hydroxyproline, hydroxylysine or tyrosine, or on the amine groups of lysine or histidine. Acylation could be effected on the epsilon-amine group of lysine or on the aromatic amine group of histidine. It is normally considered disadvantageous to use conjugates linked with ester functions, since they are often readily cleaved by the many esterases in the blood and tissues. Nevertheless, it will be apparent to the skilled worker that the hydroxyl groups of the aforementioned amino acids can be acylated to form esters with boron-containing acylating agents.

Carbamation/ureidation and thiocarbamation/thioureidation are readily effected by reacting pendant amine and/or hydroxyl groups with boron-containing reagents bearing isocyanate or isothiocyanate functions. Amidation can be effected by reaction of pendant amine functions with boron-containing carboxylic acids, or by reacting pendant carboxyl groups such as those on aspartic or glutamic acids with boron-containing amines, conveniently by using a condensing agent, e.g., dichlorohexylcarbodiimide (DCC). Diazonium coupling is effected by reaction of a diazonium salt, prepared by diazotization of a boron-containing amine, e.g., by reaction of the amine with sodium nitrate and acid, with an aromatic amino acid, e.g., tyrosine, histidine or phenylalanine.

Boron-containing alkylating agents 17-21, bearing carborane or borane anion groups, can be synthesized by the following pathways, which are meant to be illus-

trative of the various methods available, and which can be modified and adapted to produce analogous reagents with minor structural differences. Alkylating agents containing carborane anion groups can be most easily produced by base treatment of the corresponding carborane precursors at convenient branch points in their synthesis. Metallocarboranes can be made by adapting syntheses for producing analogous acylating agents, but these are somewhat cumbersome.



(a)  $\text{B}_{10}\text{H}_{14}$ /acetonitrile, reflux

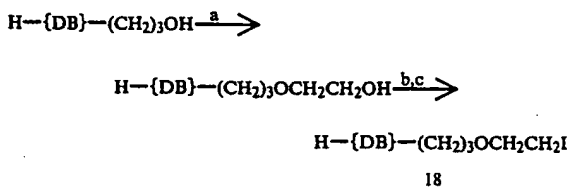
(b)  $\text{LiAlH}_4$ /ether, or aqueous acid hydrolysis ( $\text{OAc} \longrightarrow \text{OH}$ )

(c) toluenesulfonyl chloride/pyridine ( $\text{OH} \longrightarrow \text{OTs}$ )

(d) sodium iodide/acetone ( $\text{OTs} \longrightarrow \text{I}$ )

Zakharkin et al., Zh. Obshch. Khim., 35, 2160(1965)

It will be apparent that either iodide 17 or its precursor tosylate can be used for alkylation of amines, hydroxyls or phenoxides and thiols. Moreover, the chain length can be varied merely by using a starting acetylene of shorter or longer chain length, or by homologating the product by, e.g., conversion of the iodide to a Grignard reagent, followed by addition to formaldehyde, other aldehydes, ketones or epoxides, or the like. Similarly, alkyl-substituted acetylenes can be used initially, as can acetylenes substituted with other groups which do not interfere with subsequent reactions, e.g., ether, aryl, nitro, cyano or fluoro groups, and the like.

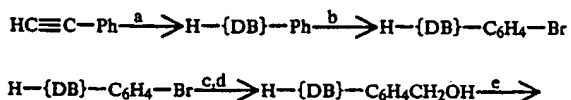


(a) ethylene oxide,  $\text{BF}_3$  (separate oligomers)

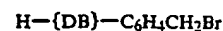
(b)  $\text{TsCl}$ /pyridine ( $\text{OH} \longrightarrow \text{OTs}$ )

(c)  $\text{NaI}$ /acetone ( $\text{OTs} \longrightarrow \text{I}$ )

The length of the chain in the starting acetylenic alcohol, which is an intermediate in the synthesis of 17, can readily be varied as noted above. The resultant alcohol can be homologated, and/or a different epoxide can be used to make the ether-alcohol, to achieve variant structures of this general type.



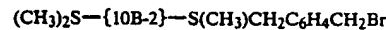
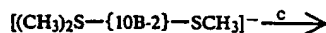
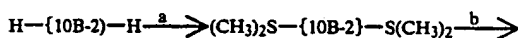
-continued



19

- (a)  $\text{B}_{10}\text{H}_{14}$ /acetonitrile, reflux  
(b)  $\text{Br}_2$   
(c)  $\text{Mg}$ /ether  
(d)  $\text{CH}_2\text{O}$   
(e)  $\text{SOBr}_2$

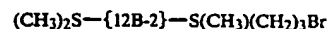
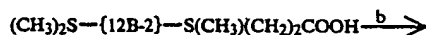
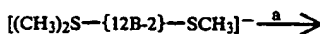
The benzylic alcohol intermediate in the above scheme can be prepared by hydride reduction of the corresponding benzoic acid,  $\text{H}-(\text{DB})-\text{C}_6\text{H}_4\text{COOH}$ , whose preparation is shown hereinafter. Further variants of the general class of alkylating agents represented by compound 19 can be readily envisioned, e.g., ring-substituted derivatives having alkyl, aryl, fluoro, alkoxy, aryloxy, nitro groups, and the like; substituents at the benzylic carbon; and/or homologs and isomers thereof.



20

- (a) dimethylsulfoxide (DMSO)/ $\text{H}^+$   
(b) potassium phthalimide, heat  
(c)  $\text{BrCH}_2\text{C}_6\text{H}_4\text{CH}_2\text{OAc}$   
(d)  $\text{HBr}$   
Sneath, et al., J. Med. Chem., 17, 796(1974)

The tosylate corresponding to bromide 20 can be readily made by base-catalyzed hydrolysis of the acetate intermediate above, and reaction of the resultant alcohol with  $\text{TsCl}$ /pyridine. Structural and isomeric variants of bromide 20 are easily envisioned by the skilled artisan, and these include but are not limited to ring isomers, alkyl, aryl, alkoxy, aryloxy, fluoro, nitro substituents, other alkyl, aryl, aralkyl and aralkyl substituents on the sulfonium group, and the like.



- (a)  $\text{Br}(\text{CH}_2)_2\text{COOH}$   
(b)  $\text{LiAlH}_4$   
(c)  $\text{PBr}_3$  or  $\text{SOBr}_2$  (or  $\text{TsCl}$ /py for tosylate)  
Sneath, et al., J. Med. Chem., 17, 796(1974)

The starting material for this sequence is obtained analogously to the corresponding intermediate in the previous sequence, except that  $\text{H}-(\text{12B-2})-\text{H}$  is used instead of  $\text{H}-(\text{10B-2})-\text{H}$  to react with the DMSO. It will be apparent that other haloacids and/or esters can be used instead of the beta-bromopropionate, e.g., alpha-bromoacetate or other alpha-haloalkanoic acids of esters, methyl alpha-bromophenylacetate or



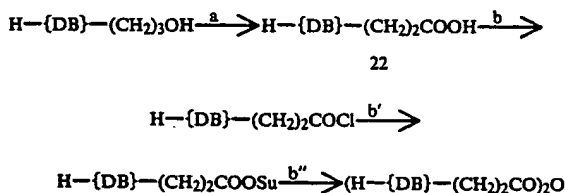
other alpha-haloaralkanoic acids or esters, gamma-haloacids or esters, delta-haloacids or esters, and the like.

Representative examples of the use of these alkylating agents to produce amino acid building blocks for peptide synthesis follow.

It is seen that alkylating agent 17 can be used to convert the thiol of cysteine of a thioether, resulting in compound 9. (The skilled artisan will recognize that the cysteine will normally be in the form of an N- and C-protected derivative, and that one or the other of the protecting groups will normally be removed by conventional means before the boron-containing amino acid is joined to a growing peptide chain under standard solid phase reaction conditions.)

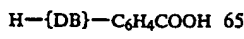
Similarly, compound 17 can alkylate the phenolic oxygen of a suitably protected tyrosine, resulting in the production of boron-containing amino acid 10, again suitably protected. In an analogous fashion, alkylating agents 18-21 can be used to attach other types of boron cage structures to pendant amine, hydroxyl or thiol functions of suitably protected amino acids. In addition, these alkylating agents and their precursors and/or derivatives are also useful as intermediates in various classical amino acid synthesis schemes, examples of which will be shown hereinafter.

Representative acylating agents 22-29, incorporating carborane, carborane anion and borane anion moieties, are shown below, together with illustrative synthetic sequences by which they can be produced. Again, it will be appreciated that many structural and isomeric variants of these compounds may be made by varying the structure of the reactants and by minor modifications of the reaction conditions in ways that are familiar to the skilled artisan. The types of permissible substitution and/or isomerization correspond to those mentioned above for synthesis of related structures.



- (a) chromic acid  
(b) thionyl chloride  
(b') N-hydroxysuccinimide (HOSu)/DCC  
(b'') acetic anhydride

Acid 22 can be condensed with a pendant amine group, e.g., on a lysine residue suitably protected at the alpha-amino and -carboxyl termini, using DCC as an illustrative carbodiimide-type condensing agent. More rapid condensation, which can dispense with the need for a condensing agent, can be effected with any of the activated acid derivatives shown, viz., the acid chloride, the N-hydroxysuccinimide ester or the anhydride, among other known carboxyl derivatives.



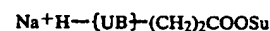
23

- (a) butyl lithium (lithiates phenyl and removes carborane)

-continued

- methylene proton)  
(b) carbon dioxide  
(c) acidification  
(d) ethanol reflux (decarboxylates carborane)  
Hawthorne et al., J. Am. Chem. Soc., 87, 4746(1965)

An intermediate from the synthesis of compound 19 is the starting point for the foregoing sequence, which readily produces 1,2- and 1,7-carboranyl-p-benzoic acids. These can be converted to activated carboxyl derivatives by analogous methods to those used on compound 22.



24

- (a) ethoxide/ethanol (1,2- and 1,7-dicarba-closodode-

carboranes  $\longrightarrow$  corresponding nido-undecaboranes,

1,12-isomer uses Busby et al. method shown earlier)

- (b) acidify, e.g., with HCl  
(c)  $(\text{CH}_3)_4\text{NCl}$   
(d) HOSu/DCC  
(e) ion exchange  
(f) lyophylization  
Hawthorne et al., J. Am. Chem. Soc., 90, 862(1968).

Any of the isomeric carboranes, e.g., carboranyl propionic acid 22 illustrated above, can be degraded with base to the corresponding anion with one less boron vertex, by the procedures shown above, acidified, and the product isolated as the quaternary ammonium ion. The OSu ester is conveniently prepared, and can be optionally converted to the sodium salt by ion exchange and (also optional) lyophylization.



25

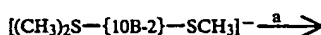
- 50 (a) ethoxide/ethanol (1,2- and 1,7-dicarba-closododeca-

boranes  $\longrightarrow$  corresp. nido-undecaboranes;

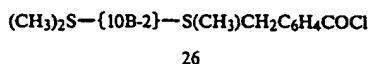
1,12-isomer uses Busby et al. method shown earlier)

- (b) acidify, e.g., with HCl  
(c)  $(\text{CH}_3)_4\text{NCl}$   
(d) HOSu/DCC  
(e) ion exchange  
(f) lyophylization

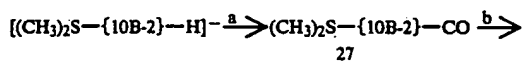
Carboxylic acid 23 can be degraded by a similar sequence and converted to the activated carborane anion acylating agent 25.



-continued

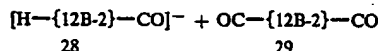
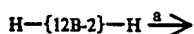
(a)  $\text{BrCH}_2\text{C}_6\text{H}_4\text{COOH}$ (b)  $\text{SOCl}_2$ Sneath et al., *J. Med. Chem.*, 19, 1920(1976)

An intermediate in the synthesis of compound 20 can be S-alkylated with the readily available alpha-bromotoluic acid to produce a neutral toluic acid derivative, which can be converted to acid chloride 26. The reaction sequence can be effected with 1,6- or 1,10-decaboranyl and with 1,12-dodecaboranyl starting materials. It will be appreciated that acid chloride 26 is only one of several possible activated acid derivatives useful for acylation under mild conditions, and that the acid itself can be used for acylation, e.g., with an amine, in the presence of DCC.

a  $(\text{COCl})_2$ b  $\text{RNH}_2$  (e.g., lysine epsilon-amino group)Wong et al., *J. Med. Chem.*, 17, 785(1974)

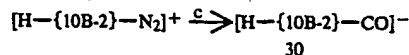
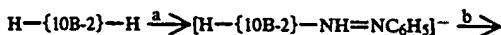
Muettterties et al., "Polyhedral Boranes", op. cit.

The monoaddition product of closo-decaborane dianion and DMSO reacts with oxaloyl chloride to form 1,6-acylium derivative 27, which is reactive with amines to form amide linkages.

a  $\text{CO}/\text{H}^+$ , pressure

Muettterties et al., "Polyhedral Boranes", op. cit.

Closo-dodecaborane dianion adds carbon monoxide to form a monoacylium or 1,7- and 1,12-diacylium derivatives, both of which react with amines to form amides similarly to compound 27.

a  $\text{C}_6\text{H}_5\text{N}_2^+\text{BF}_4^-$ 

b acetonitrile, reflux

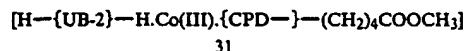
c  $\text{CO}$ , pressure,  $120^\circ\text{C}$ .Leyden et al., *Inorg. Chem.*, 14, 2444(1975)Hawthorne et al., *J. Am. Chem. Soc.*, 87, 2366(1965)

Closo-decaborane dianion reacts with phenyl-diazonium tetrafluoroborate to form an intermediate which loses benzene upon heating, resulting in a diazonium derivative which can be carbonylated under pressure, with loss of nitrogen. The resultant acylium compound, 30, reacts with amines to form amides.

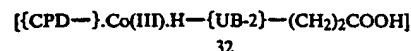
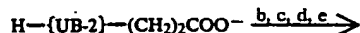
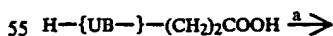
Metallocarborane reagents for modifications of amino acid side chains, or for direct incorporation into PAUTs, can be prepared using reactions which are known to those skilled in the art of boron chemistry. Useful general references for the types of reactions envisaged include, e.g., Muettterties, Ed., "Boron Hydride Chemistry", op. cit., Chapter 11; Hawthorne et

al., *Science*, 78, 462 (1972); Hawthorne et al., *Accts. Chem. Res.*, 1, 281 (1966); and references cited therein. The following examples and reaction sequences are, therefore, merely illustrative of the types of compounds and the types of metal ions which can be incorporated into addends for preparing antibody conjugates. Nearly every type of metal ion has been incorporated or can be incorporated into these metallocarboranes, so that the use of  $\text{Co(III)}$  as a model is clearly not limiting and metals such as  $\text{In(III)}$ -111,  $\text{Ga(III)}$ -67,  $\text{Gd(III)}$ ,  $\text{Y(III)}$ -90, and the like can be substituted therefor. The complexes are of the "sandwich" type similar to ferrocenes and can incorporate substituted or unsubstituted cyclopentadienide rings, hereafter denoted by the symbol " $\{\text{CPD}-\}$ ", as well as  $\{\text{UB}-2\}$  moieties, prepared by treatment of  $\{\text{UB}-\}$  rings with strong base, e.g.,  $\text{NaH}$ , to remove the bridge hydrogen and product the "dicarbollide" dianion.

The cyclopentadienide anion is conventionally produced by cracking cyclopentadiene dimer and reacting the monomer with base, e.g.,  $\text{NaH}$ . The carborane dianion is normally produced by treating the monoanion with strong base, e.g.,  $\text{NaH}$ , to remove the bridge hydrogen. It is common for several isomers to be produced by this procedure, and these may be separated if desired or used as a mixture. Either anion may bear a substituent for later attachment to an amino acid side chain, substituted cyclopentadienides being readily prepared, and substituted dicarbollides having already been shown, either as such or as their monoanion precursors.

a  $\text{H}-\{\text{UB}-2\}-\text{H}$  solution in tetrahydrofuran(THF)b  $\text{CoCl}_2$  in THFc workup in air ( $\text{Co(II)} \rightarrow \text{Co(III)}$ )

It will be recognized that the ester function in compound 31 can be readily hydrolyzed to a carboxylic acid, which can then be converted to an acid halide, anhydride or OSu ester by methods already shown hereinabove. Alternatively, a Schmidt reaction, or analogous degradation, can convert the acid or ester to an isocyanate, which can be further hydrolyzed to an amine. Thus, the metallocarborane sandwich complex can be linked to amino acid side chains by a variety of methods and can form a variety of bonds thereto.

a  $\text{NaH}/\text{THF}$ b  $\{\text{CPD}-\}/\text{THF}$ c  $\text{CoCl}_2/\text{THF}$ 

d workup in air

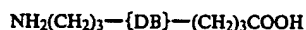
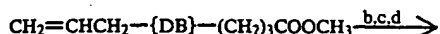
e acidify

The starting carborane anion and the intermediate dicarbollide dianion are both chiral, and can be used as pure enantiomers or as a mixture, e.g., a racemic mix-





metal ion, using a procedure analogous to the following.

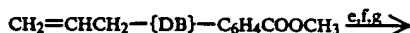


13

- (a)  $\text{B}_{10}\text{H}_{14}/\text{CN}_3\text{CN}$   
 (b)  $\text{B}_2\text{H}_6$   
 (c)  $\text{H}_2\text{NOSO}_3\text{H}$   
 (d)  $\text{H}_3\text{O}^+$

A disubstituted acetylene, prepared by sequential alkylation of acetylide by allyl bromide and methyl gamma-bromobutyrate, is condensed with decaborane tetradecahydride to form the closo-carborane cage. Conventional hydroboration/amination, followed by hydrolysis of the ester, produces an amino acid having a boron cage in the chain which has the amine and carboxyl functions as chain termini. It will be understood that suitable protecting groups, e.g., BOC, will normally be introduced to prepare residues for automated solid phase peptide synthesis.

Analogously to earlier examples, compound 13 can be treated with ethoxide/ethanol to produce anionic boron cage compound 14. It will normally be convenient to isolate this compound as its tetramethylammonium salt.

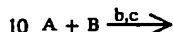


41

- (a) butyl lithium (2 equivalents)/THF  
 (b) allyl bromide (2 equivalents)  
 (c) hydrolysis ( $\text{H}_3\text{O}^+$ , neutralize)  
 (d) diazomethane  
 (e)  $\text{B}_2\text{H}_6$   
 (f)  $\text{H}_2\text{NOSO}_3\text{H}$   
 (g)  $\text{H}_3\text{O}^+$

Compound 23 can be transformed into an in-chain amino acid by alkylation with an allyl group at the remaining carbon vertex of the carborane, followed by conventional hydroboration/amination. By analogy to earlier procedures, treatment of compound 41 with ethoxide/ethanol will produce the corresponding amino acid, 42, with a nido-carborane anion cage. Also by analogy to earlier discussions, the many structural variants of carboxyl and amine compounds can be elaborated by similar schemes to in-chain amino acids.

Metallocarborane sandwich complexes with an amine terminus and a carboxyl terminus on opposite boron anion cages represent one illustration of the type of in-chain species envisioned for this type of boron-containing moiety. It will be apparent that in-chain anionic amino acids such as compound 42 can be further elaborated into metallocarboranes by reaction with strong base and combination with another dianion cage and a



43

- 15 (a) NaH/THF (2 eqvts.)  
 (b)  $\text{CoCl}_2/\text{THF}$   
 (c) workup in air, acidify

The amine anion used to generate Solution A can be produced from acid 22 by Schmidt Reaction, hydrolysis of the resultant isocyanate, and base treatment to generate the nido-carborane anion. Treatment of compound 22 with strong base directly produces the starting material for generation of Solution B. Each of these starting materials can be a mixture of enantiomers or a single enantiomer. Accordingly, the resultant sandwich complex can either be a single chiral product or a mixture of four enantiomeric or diastereomeric products, which can be separated by conventional means or used as a mixture. It will also be appreciated that the reaction can produce byproducts, i.e., the complexes having an amine on both dicarbollide groups or having a carboxyl on both dicarbollide groups. These byproducts can be separated from the desired amino acid complexes by virtue of their differences in acidity/basicity, and they will be useful in other contexts, as will be shown herein after.

It is presently anticipated that synthesis of PAUTS from amino acid residues will be most conveniently effected by means of an automated solid phase peptide synthesizer. The first residue is normally attached to beads of a polymer resin, e.g., polystyrene, suitably functionalized to accept substitution of a carboxylate anion for a labile substituent, e.g., by halomethylation. Standard machine conditions ordinarily involve attachment of the C-terminal residue to the resin, e.g., by attack of its carboxylate on a benzylic carbon of a halomethylated polystyrene. The C-terminal residue and subsequently added residues have their alpha-amino functions protected by BOC groups, which are cleaved by  $\text{CF}_3\text{COOH}$  in  $\text{CH}_2\text{Cl}_2$  after each successive addition of a residue. Condensation of the deblocked N-terminus with the carboxyl group of the next (N-protected) residue is effected with DCC, and excess residue and DCC are washed out with triethylamine. The finished peptide is cleaved from the solid support with liquid HF.

For more sensitive residues, milder conditions can be used, e.g., the use of Bpoc ( $-\text{COOC}(\text{CH}_3)_2-\text{C}_6\text{H}_4-\text{C}_6\text{H}_5$ ) as an N-protecting group, which can be cleaved with dilute  $\text{CF}_3\text{COOH}/\text{CH}_2\text{Cl}_2$ , binding of the C-terminal group to the resin through a readily cleaved ether linkage, or use of a base-cleavable N-blocking group, e.g., the Fmoc (fluorenyl-methoxycarbonyl) group, which can be cleaved by piperidine. Use of the latter protecting group must take cognizance of the fact that it will affect chains where a carborane cage is incorporated, since the piperidine will convert the carborane to its corresponding nido-anion. In certain cases, it

may be useful to achieve this transformation in the course of peptide synthesis, rather than by earlier treatment of the residue with strong base.

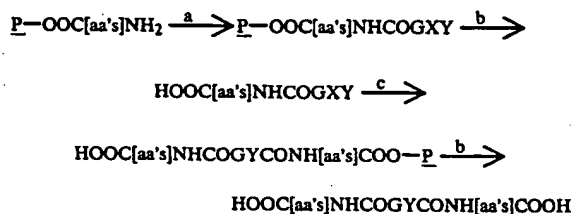
The foregoing are merely suggestive of the procedures which will be familiar to one of ordinary skill in solid phase peptide synthesis, in view of the many excellent and comprehensive references generally available in the art, and Garland et al. and Stewart et al. references noted hereinabove being among the most useful. Once the sequence of amino acid residues is selected, it will normally be a routine matter to choose the proper protecting groups for the individual residues and to choose the proper automated conditions for their linkage.

Further structural variety may be achieved by the use of chain branchers, either at the beginning of a chain or at one or more intermediate points in the chain. These may be residues uniquely designed for this purpose or they may be natural or synthetic amino acids or other related functionally substituted groups which can serve the purpose of accepting branch chains or addends. Representative illustrations of the types of compounds envisioned will show the nature and scope of these components.

The simplest type of brancher is a natural amino acid with a pendant functional group, to which can be attached another preformed PAUT chain. For example, the epsilon-amino group of a lysine residue can be protected with a selectively cleavable group which survives cleavage of the BOC group, e.g., a benzyl group which can be hydrogenolyzed at a point when branching is desired, or e.g., a Bpoc group which can be cleaved without cleaving the chain-terminal N-BOC. In either case, the epsilon-amino group can be linked to a branch chain either prior to or subsequent to further elaboration of the trunk chain. Similarly, an aspartic or glutamic acid residue can be used as a brancher, protected by a selectively cleavable group.

The protecting group also can be cleaved either prior to or subsequent to chain extension of the trunk peptide.

Another type of brancher is a molecule of the general type YG(X)<sub>2</sub>, wherein G is any central structure, Y is a function reactive with an antibody, and X is a more reactive function that will kinetically favor reaction with, e.g., the amine terminus of a growing polymer chain. As an illustration, such a brancher could be 3,5-di(bromocarbonyl)phenylisothiocyanate, wherein G is the benzene ring, Y is the NCS group, and each X is a COBr group. Branching could be effected as follows;



- (a) YG(X)<sub>2</sub>  
 (b) HF or CF<sub>3</sub>COOH  
 (c) H<sub>2</sub>N...COO-P

Here, a first completed polymer chain (deblocked) is reacted with an excess of the brancher, so that each amine terminus bears a brancher with one acyl bromide and one isothiocyanate. The intermediate is cleaved from the resin (P) and the free polymer is reacted with a second completed polymer bound at the C-terminus to resin. A kinetic preference for reaction with the acyl

bromide over the isothiocyanate will result in linkage to form an amide bond. Cleavage again from the resin produces a group having two polymer chains attached to the phenylisothiocyanate by amide bonds, which can then be linked to antibody through the NCS group.

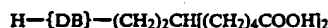
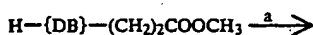
The foregoing examples are merely a suggestion of the manifold possibilities for branchers, which are limited only by the caveat that they have selectively reactive groups thereon which can react first with the terminus or a pendant group of a polymer chain and later with a pendant function on an antibody. Other variants within the scope of the present invention will be apparent to those of ordinary skill in this art.

It should be noted that another type of "brancher" can be used to link together two Fab or Fab' functions, using their free SH groups. This could be done by growing polymer chains and capping the terminal amines with an alkylating group, e.g., COCH<sub>2</sub>Br, cleaving the C-terminal carboxyl from the resin, and reacting the cleaved polymer with p-phenylenediamine/DCC, to produce a longer joined polymer having a bromoacetamide at each end. This could then be reacted with Fab or Fab' fragments, under reducing conditions, to bridge the two fragments. A further option is to include yet a third function on the joining moiety to which additional functional groups can be added. A lysine with two BOC protecting groups on the two amine functions can be added to the end of a polymer chain still attached to the solid phase, the BOC groups cleaved, the two amines acylated with bromoacetyl chloride, and Fab/Fab' fragments reacted with the resultant polymer. Selective protective groups and sequential deblocking/acylation/alkylation with different Fab/Fab' fragments would produce a hybrid divalent immunoreactive agents. The possibility of multivalent hybrids should be recognized, using this technique. The resin-bound product can be cleaved and the C-terminal group further modified if desired.

Additional branching and capping groups will be disclosed hereinafter, in connection with methods of forming PAUTs using homodifunctional residues.

Although automated solid phase peptide synthesis effects great improvement in the production of defined sequenced polymers, the method still requires the use of protecting groups in each step, by virtue of the fact that both an amine and a carboxyl group are present in each residue to be linked. In contrast to McKearn et al., the object of the present invention is not necessarily to conjugate to an antibody a polypeptide made of natural amino acids. Accordingly, this invention envisages the use of homodifunctional residues to build PAUTs, preferably also on a solid phase, but without some of the inconvenience entailed by the use of amino acids as building blocks. The simplest such approach is the use of alternating diamine and diacid building blocks to produce a "nylon 66" type polymer. Another approach is to use diamines with diisocyanates and or/diisothiocyanates to form poly(urea/thiourea) chains, again in the "nylon 66" sense. It will be apparent that any combination of the foregoing can also be used. Moreover, this approach can be combined with the conventional approach, using amino acids, either for construction of the trunk PAUT, or for modification of side chains, branching or linking to particular types of functional groups. More specific representative illustrations of each of these approaches will be disclosed hereinbelow, although it will be appreciated by the ordinary skilled

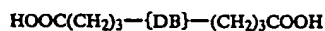
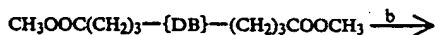
artisan that many other species can be envisaged, all of which fall within the clear scope of the invention.



44

(b) trace  $\text{H}^+$ , heat(c)  $\text{H}_2/\text{Pt}$ (d)  $\text{H}_2\text{O}^+$ (e)  $\text{H}_2\text{CrO}_4$ 

Starting with the methyl ester of compound 22, Grignard reaction with 2 equivalents of the reagent produced by reacting Mg with the ethylene acetal of 5-bromovaleraldehyde results in a tertiary alcohol. The alcohol can be dehydrated under mild conditions, and the resultant olefin is hydrogenated. Hydrolysis of the acetals and oxidation of the aldehyde groups to carboxyls completes the synthesis. It will be recalled that carboxyl groups can be converted to isocyanates by the Schmidt Reaction, and this can be done with the diacid to produce a diisocyanate. Similarly, hydrolysis of the isocyanates produces a diamine, which can be reacted with thiophosgene to give a diisothiocyanate. All of these homodifunctional residues will be useful in the ensuing techniques for chain formation.



45

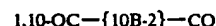
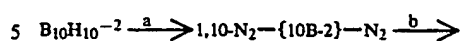
(a)  $\text{B}_{10}\text{H}_{14}/\text{CH}_3\text{CN}$ (b)  $\text{H}_3\text{O}^+$ 

The disubstituted acetylene obtained by reaction of 50 acetylide with two equivalents of methyl 4-bromobutyrate is then reacted with decaborane tetradecahydride to form a carborane cage in a now-familiar reaction. The resultant diester is hydrolyzed to the diacid, which can then be converted by familiar sequences to the diisocyanate, the diamine and the diisothiocyanate, all of which will be useful for chain construction.

Diacids 44 and 45 can each be treated with strong base to form the corresponding carbonate anion derivatives. The diamines can be similarly degraded with strong base to form the anion cage diamines, which can then be treated with phosgene or thiophosgene to form diisocyanates or diisothiocyanates.

The polyhedral borane dianion chemistry shown above offers even more attractive possibilities here for facile generation of homodifunctional chain forming reagents. Compound 29,  $\text{OC}-\{12\text{B}-2\}-\text{CO}$ , will be a particularly versatile intermediate, as will its  $-\{1-$

$\text{OB}-2\}$ — counterpart, whose synthesis is shown below.



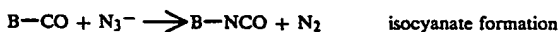
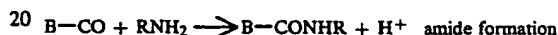
46

10 (a) HONO

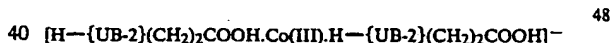
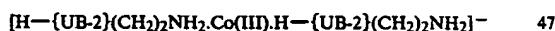
(b) CO, heat

Knoth et al., J. Am. Chem. Soc., 89, 4842(1967) Muetterties et al., "Polyhedral Boranes", op. cit.

15 The borane dicarbonyls are remarkably easy to transform into other useful molecules, as seen below, wherein B-CO denotes one end of the borane dicarbonyl function, both ends behaving similarly.



It has been noted earlier that attempts to form amino acids with metallocarboranes often produce "by-products" having diacid or diamine groups, as shown in the synthesis of compound 43. Where the homodifunctional compound is the desired product, it can be produced in high yield by analogy to the earlier procedures. Thus, compounds 47 and 48 are readily produced from treating Solution A, alone, or Solution B, alone, with cobaltous chloride, with air workup.



Compound 44 can be converted to its carborane dianion by successively stronger base treatments, and combined with unsubstituted dicarbollide and  $\text{CoCl}_2$ , with air workup, to produce diacid 49.



49

It will be recalled that diacids such as 48 and 49 can readily be converted to diisocyanates, diamines and diisothiocyanates.

Prior to cleavage of the PAUT from the polymer resin support, it is useful to cap the N-terminus of the chain with a linker group which, after cleavage of the chain, will serve to link the polymer to the antibody. The linker will preferably have at least one function capable of reacting with a (deblocked) amine and another function which is sufficiently stable to cleavage conditions to survive, while being reactive with pendant groups on the antibody molecule for formation of a covalent bond. The antibody-linking function can be present as such on the linker or as a precursor of masked function.

One advantageous function for antibody linkage is the isothiocyanate group, the isocyanate and the activated acid being useful as well. Amine-reactive groups include benzyl halides, acid halides, anhydrides, OSu

esters, and the like. Typical capping groups include, e.g., p-isothiocyanatobenzyl bromide, p-isothiocyanatobenzoyl bromide, p-isothiocyanatophenacyl bromide, and the like.

Alternatively, the N-terminal amine can be de-blocked and capped with a group that renders it unreactive, after which the C-terminal carboxyl is cleaved and activated so that it functions as the antibody-linking group. One approach would be to cap the N-terminal amine (deblocked) with an acetyl group, then cleave the C-terminal carboxyl, and convert the acid to an OSu ester by reaction with HOSu/DCC. This ester could bind to the antibody, or it could be reacted with excess diamine, and the resultant amine converted to an isothiocyanate with thiophosgene. Other permutations will occur to the ordinary skilled artisan.

Without further elaboration, it is believed that one skilled in the art can, using the preceding description, utilize the present invention to its fullest extent. The following preferred specific embodiments are, therefore, to be construed as merely illustrative, and not limitative of the remainder of the disclosure in any way whatsoever. In the following examples, all temperatures are set forth uncorrected in degrees Celsius; unless otherwise indicated, all parts and percentages are by weight.

The polymers prepared in the following examples are made using a Beckman Model 990 Automated Peptide Synthesizer, and purified using a Beckman Model 340 HPLC system. The basic reagents and procedures are taken from Stewart et al., "Solid Phase Peptide Synthesis, 2nd. Ed.", except where noted. Boron-containing compounds are prepared using 96% B-10-enriched B<sub>10</sub>H<sub>14</sub> (Callery Chemical Co., Callery, Pa.), and reagents derived therefrom by conventional reactions shown herein. Resin beads, BOC-protected natural amino acids and beta-alanine, and standard reagents are all available commercially and can be prepared by conventional means, should commercial sources no longer be available.

The following abbreviations are used in the examples:

Symbol	Meaning
[P]	Merrifield resin of polystyrene crosslinked with 1% divinylbenzene (DVB)
[P]-O-gly-BOC	Above resin (hydroxymethylated) containing 0.4 meq/g esterified BOC-glycine (Peninsula Labs., Inc., Belmont, CA.)
[P]-O-Bal-BOC	Above resin (hydroxymethylated) containing 0.4 meq/g esterified BOC-beta-alanine (Peninsula)
TFA	trifluoroacetic acid
TEA	triethylamine
DCC	dicyclohexylcarbodiimide
DCM	dichloromethane (solvent)
CA-T	Chloramine-T
AddRes	Standard sequence for addition of an amino acid residue (see below)
Weld	Sequence for joining shorter oligomers to form longer oligomer (see below)
Ab	Antibody or antibody fragment
S-Y	Stewart et al., op. cit

## EXAMPLE 1

### Synthesis of a Boron-Loaded Polypeptide

#### (a) Synthesis of reagents.

Compounds 1, 2, 5, and 11-14 are separately reacted with BOC-Cl under standard conditions (see, e.g., S-Y, pp. 61-4) to produce the N-BOC derivative of each. Each BOC-amino acid (1-BOC, 2-BOC, etc.) is supplied to the appropriate reservoir of the synthesizer as a 0.10M solution in DCM. DCC is supplied as a 1M solution in DCM. TFA is supplied as a 1:3 v:v TFA:DCM mixture with 1 mg/ml indole added. TEA is supplied as a 1:9 v:v reagent grade TFA:DCM solution. Resin is supplied as 2.0 g (0.8 meq) [P]-O-gly-BOC.

#### (b) Synthesis of Building Block (BB) decapeptide.

The starting resin is charged to the reaction flask of the peptide synthesizer, and subjected to an AddRes sequence with 2-BOC (in step 8A) as follows:

Step	Reagent	Vol (ml)	Time (min)
1	DCM wash (x3)	30	1.5
2	TFA/DCM/indole	30	1.5
3	TFA/DCM/indole	30	30
4	DCM wash (x6)	30	1.5
5	TEA/DCM	30	1.5
6	TEA/DCM	30	1.5
7	DCM wash (x6)	30	1.5
8A	BOC-aa/DCM	20	1.5
9B	DCC/DCM	2	120*
9	DCM wash (x3)	30	1.5

\*Each coupling reaction is monitored after about 120 min. reaction, by withdrawal of a small portion of resin, which is subjected to the Kaiser ninhydrin qualitative color test. A blue color signifies incomplete coupling, and requires repeating steps 4-8, with a 160 min. coupling time.

The resultant [P]-O-gly-2-BOC is subjected to successive AddRes sequence with 12-BOC, 1-BOC, 13-BOC, 5-BOC, 11-BOC, 14-BOC, 2-BOC, 12-BOC and 13-BOC, respectively to produce the BOC-BB peptide, [P]-O-gly-2-12-1-13-5-11-14-2-12-13-BOC, as its glycyl-resin conjugate.

After successful completion of the synthetic sequence, the resin conjugate is deblocked (steps 1-7 of the AddRes sequence), and the resin is transferred to an HF cleavage apparatus, e.g., HF Reaction Apparatus Type I (Peninsula). The cleavage reaction is conducted with 4 ml of anisole per 0.8 meq of resin. Cleavage with liquid HF (40 ml) is carried out at 0° C. for 45 min. and then pumped down to dryness under vacuum. The resin is immediately transferred to a fritted glass funnel using 20 ml of dry ethyl acetate (EtOAc), washed with 3x20 ml of EtOAc, and the washings discarded. The resin is then extracted with 4x60 ml of 1M aqueous acetic acid (HOAc), followed by 3x30 ml glacial HOAc. The extracts are combined, treated with 0.5 ml of TEA, and immediately lyophilized. The solid residue is the resultant BB peptide, HO-gly-2-12-1-13-5-11-14-2-12-13-NH<sub>2</sub>, as the triethylammonium salts of the anionic residues 5, 12 and 14. Final purification is achieved by HPLC, typically using an Altech/Beckman Ultrasphere ODS column, operated with a 240 nm uv detector, eluted with 50:50 v:v CH<sub>3</sub>CN:H<sub>2</sub>O, with 0.1M HOAc/TEA buffer, pH 4.5. The purified BB peptide is recovered by lyophilization of peptide-rich eluate, which also removes the volatile buffer, and stored at -30° C. Yields are about 80% of purified peptide (m.w., 3588 daltons); as the tetrakis(triethylammonium) salt.

#### (c) Synthesis of 50-residue peptide.



The reaction flask of the peptide synthesizer is charged with 0.5 g (0.2 meq) of [P]—O—Bal—BOC. The BB peptide is prepared as a 0.027M solution in DCM, such that 15 ml of the solution contains 1.44 g (0.4 mmol) of the peptide. Diacid 45 is converted to the corresponding diamine, 45a, by conventional Schmidt degradation, and thence to the corresponding bis-isocyanate, 45b, with phosgene. These are supplied to the peptide synthesizer as 0.1M solutions in DCM, and TEA and TFA/indole are supplied as in part (a) hereof. The Weld sequence is effected on the esterified resin as follows:

Step	Reagent	Vol (ml)	Time (min)
1	DCM wash (×3)	15	1.5
2	TFA/DCM/indole	15	1.5
3	TFA/DCM/indole	15	30
4	DCM wash (×6)	15	1.5
5	TEA/DCM	15	1.5
6	TEA/DCM	15	1.5
7	DCM wash (×6)	15	1.5
8	45b/DCM	15	120
9	DCM wash (×6)	15	1.5
10	BB peptide/DCM	15	180
11	DCM wash (×6)	15	1.5
12	DCC/DCM	1.5	1.5
13	45a/DCM	15	180
14	DCM wash (×6)	15	1.5

The foregoing Weld sequence results in attachment of a bis-isocyanate linker to the resin, to which the glycyl-BB peptide is then bound through another urethane linkage. The free carboxyl terminus of the BB peptide is then condensed with one amine of a diamine linker, preparatory to iteration of steps 8–14 of the Weld sequence with another portion of BB peptide solution to attach another glycyl-decapeptide to the resin-bound chain. Three more iterations of steps 8–14 of the Weld sequence are performed to grow a urethane-bridge 50-residue chain on the resin, incorporating 5 BB peptide segments.

The resultant Large Peptide is capped with a selective sequential bifunctional linker, e.g., bis(p-isothiocyanato)benzoic anhydride (IBA). The latter compound is prepared by reacting p-isothiocyanatobenzoic acid (Fairfield Chemical Co., Blythewood, S.C.) with an excess of thionyl chloride in benzene, azeotropically removing water, e.g., with a Dean-Stark trap, cooling the resultant solution, and collecting the crystalline IBA. The end capping is effected by adding 15 ml of a 0.1M solution of IBA anhydride to the resin-bound Large Peptide, and allowing the reaction to proceed for 120 min. The resin is then washed with 6×15 ml DCM, and the capped Large Peptide is cleaved from the resin under the HF cleavage conditions of part (b) hereof, using proportionally smaller amounts of reagents. The combined HOAC extracts from the cleavage step are lyophilized, and the resultant capped peptide is further purified by HPLC.

The product contains 580 boron atoms per molecule, has a molecular weight of about 22,000 Daltons, and is represented by the condensed structure



It will be appreciated that many other combinations of amino acids disclosed herein can be prepared by minor and conventional modifications of the foregoing procedures, to produce a broad array of polymers fall-

ing within the generic scope of the invention. The peptide chains can be grown by addition of individual residues, short oligopeptide sequences, or longer oligopeptides, optionally linked with Weld sequence-type residues. The type of polymer illustrated by this Example, containing mostly polypeptide chains, optionally linked by a minor proportion of urethane or thiocarbamate junctions, represents a subclass of polymeric conjugate formers according to the invention generally referred to as "predominantly polypeptide".

## EXAMPLE 2

### Production of Boron-Loaded Antibody Conjugate

A sample of NP-2 murine monoclonal anti-CEA IgG (U.S. Ser. No. 609,607) is reacted with a threefold molar excess of capped Large Peptide, prepared according to Example 1(c) hereof, in a buffered aqueous solution, at pH 6 (phosphate buffer). The pH is raised to 7.5 by cautious addition of NaOH, preferably using a pH meter and/or pH-Stat. The reaction is allowed to proceed overnight, at 0° C. The resultant conjugate is freed of unreacted Large Peptide by brief passage through a sizing column, e.g., PD-10 Sephadex G-25, pre-equilibrated with 1% normal human serum albumin in phosphate-buffered saline (PBS), and eluted with the same medium.

The recovered conjugate is stored as a sterile solution containing, per ml:

- (1) 10 mg Human Serum Albumin (HSA) (1%, USP, Parke-Davis)
- (2) 0.01M phosphate buffer, pH7.5 (Bioware)
- (3) 0.9% NaCl
- (4) 100 ug conjugate

## EXAMPLE 3

### Production of Radioiodinated Boron/Antibody Conjugate

The capped Large Peptide prepared according to Example 1(c) hereof is radioiodinated by reaction with CA-T, at 0° C., using carrier-free Na<sup>131</sup>I (Amersham-Searle), by the procedure of Example 1(f) of U.S. Pat. No. 4,348,376, except that the amount of capped Large peptide per mCi of <sup>131</sup>I is adjusted so that iodination results in introduction of about 1–10 iodine atoms per Large Peptide. Iodination occurs substantially only on the carborane anions, of which there are 20 per Large Peptide. The product can be freed of iodination by-products by washing on a 10K-pass Millipore filter, using 0.01M phosphate buffer at pH 6. The final concentration of iodinated Large Peptide should be about 1 mg/ml.

The iodinated Large Peptide is conjugated to antibody according to the procedure of Example 2, and the conjugate, having an average of one Large Peptide per antibody and a specific activity of about 100 uCi/ug, is purified and stored analogously.

It will be appreciated that radioiodination can also be effected with <sup>125</sup>I, for production of antibody conjugates for in vitro or in vivo (i.e., normally animal) studies, or with <sup>123</sup>I, for radioimmunoassay or other uses. Similarly, it will be appreciated that the many other antibodies and antibody fragments which specifically bind markers produced by or associated with tumors or pathological lesions, disclosed in the above-referenced patents and patent applications, as well as those known to the art and those yet to be discovered,

can all be conjugated to predominantly polypeptide polymers according to the invention.

The resultant conjugates include conjugates containing large numbers of boron atoms and/or, in the case where other diagnostically or therapeutically useful addends are bound to side chains of the polypeptide, conjugates containing chelates of radiometal ions or of paramagnetic metal ions (optionally high loadings, e.g., of paramagnetic ions for magnetic resonance image enhancement, or of radioisotopes for therapy), conjugates containing drugs or toxins, conjugates containing markers useful for in vitro assays (e.g., fluorescent groups, enzymes, chromophores and/or chromogens, and the like), conjugates containing photosensitizers, and the like.

#### EXAMPLE 4

##### Production of Boron-Loaded Antibody Conjugate

The BB peptide prepared according to Example 1 hereof, as its tetrakis(triethylammonium) salt, is dissolved in 50% by volume aqueous methanol and passed through a short column of sodium-loaded Dowex 50 cation exchange resin, to produce the sodium salt. The methanol is taken off under aspirator pressure, 0.02M phosphate buffer is added, to adjust the pH to 8.5, with cautious addition of NaOH if necessary, and the resultant solution, containing about 1 mg/ml of peptide, is treated with a tenfold molar excess of IBA, as a 1M solution in benzene, in the presence of 0.1 g Et<sub>4</sub>NI as a phase transfer agent. The mixture is vigorously agitated at room temperature for 1 hr., and the benzene layer is then separated and discarded. The aqueous layer is filtered through a 1K-pass Millipore filter to remove small soluble impurities, and the residue is redissolved at 1 mg/ml, in 0.01M phosphate buffer, pH 6.5, at 0° C.

The resultant isothiocyanate-capped BB peptide is radioiodinated with Na <sup>125</sup>I, according to the procedure of Example 3 hereof, except that the capped Large Peptide is replaced by capped BB peptide. Conditions are adjusted so that 1-4 iodine atoms per BB peptide are introduced (substantially only on carborane anions). The resultant labeled peptide, optionally further purified by Millipore filtration or column gel chromatography, is reacted with anti-CEA monoclonal antibody according to the procedure of Example 3 hereof, except that a tenfold excess of labeled capped BB peptide is used, and the resultant conjugate contains an average of about 5 peptide addends per antibody.

The conjugate is produced in a yield of about 70-80%, with an immunoreactivity of at least about 85% of that of the initial antibody. It is purified and stored analogously to the conjugates of Examples 2 and 3.

#### EXAMPLE 5

##### Synthesis of "Nylon-66-type" polyamide

A 21-residue polyamide, with alternating orientations of the amide linkage, produced by condensation of homodifunctional diamines and dicarboxylates or diacylium components, is constructed using the automated peptide synthesizer and a solid phase resin support, but with a simplified condensation sequence which obviates the need for protecting groups/deprotection steps in the chain building process. The polyamide is chosen so that it has short hydrophilic (anionic) and short hydrophobic (carborane) segments interspersed with one another.

The constituent residues are: diacid 45; related diamine 45a; the carborane anion corresponding to 45a produced by treatment thereof with base, viz., H<sub>2</sub>N(CH<sub>2</sub>)<sub>3</sub>-{UB}- (CH<sub>2</sub>)<sub>3</sub>NH<sub>2</sub>, denoted 45c; and diacylium compound 46. They are supplied to the reaction system as 0.1M solutions in DCM. DCC is supplied as a 1M solution in DCM. TFA is supplied as a 1:3 v:v TFA:DCM mixture with 1 mg/ml indole added. TEA is supplied as a 1:9 v:v reagent grade TFA-DCM solution, except when used to liberate a free amine group in a coupling step, in which case it is supplied as a 1M solution in DCM and denoted 1M TEA.

A 2 g quantity of esterified Merrified resin, [P]-O-gly-BOC, as in Example 1 hereof, is charged to the reaction vessel of a peptide synthesizer. The following sequence of steps is effected to produce the polyamide:

Step	Reagent	Vol (ml)	Time (min)
1	DCM wash (×3)	30	1.5
2	TFA/DCM/indole	30	1.5
3	TFA/DCM/indole	30	30
4	DCM wash (×6)	30	1.5
5	TEA/DCM	30	1.5
6	TEA/DCM	30	1.5
7	DCM wash (×6)	30	1.5
8A	45/DCM	20	1.5
8B	DCC/DCM	2	120
9	DCM wash (×3)	30	1.5
10A	45c/DCM	20	1.5
10B	DCC/DCM	2	120
11	DCM wash (×3)	30	1.5
12	TEA/DCM	30	1.5
13	DCM wash (×3)	30	1.5
14A	45/DCM	20	1.5
14B	DCC/DCM	2	120
15	DCM wash (×3)	30	1.5
16A	45c/DCM	20	1.5
16B	DCC/DCM	20	120
17	DCM wash (×3)	30	1.5
18A	46/DCM	20	1.5
18B	1M TEA	8	120
19	DC wash (×3)	30	1.5
20A	45a/DCM	20	1.5
20B	1M TEA	8	1.5
20C	DCC/DCM	2	120
21	DCM wash (×3)	30	1.5

Repeat steps 14A, 14B and 15 (add 45).  
Repeat steps 20A, 20B, 20C and 21 (add 45a).  
Repeat steps 18A, 18B and 19 (add 46).  
Repeat steps 10A through 19 (add 45c-45-45c-46).  
Repeat steps 20A, 20B, 20C and 21 (add 45a).  
Repeat steps 14A, 14B and 15 (add 45).  
Repeat steps 20A, 20B, 20C and 21 (add 45a).  
Repeat steps 18A, 18B and 19 (add 46).  
Repeat steps 10A, 10B and 11 (add 45c).  
Repeat steps 14A, 14B and 15 (add 45).  
Repeat steps 20A, 20B, 20C and 21 (add 45a).

Upon completion of the polyamide assembly sequence, the cations associated with the anionic residues are converted to lithium ions by treatment of the resin-bound polymer with 100 ml of 0.1M LiOCCF<sub>3</sub> in DCM, the treatment being repeated twice more, followed by 3×30 ml DCM washes for 1.5 min each. Next, the resin beads are dried in a stream of dry nitrogen, and suspended in 30 ml of dry, peroxide-free tetrahydrofuran (THF). After swelling of the beads is complete, 4 mmol (106 mg) of LiBH<sub>4</sub> are added in small portions to the stirred resin suspension, and stirring is continued at 25° C. for about 1 hr. The polyamide is thereby cleaved from the resin under mild conditions, as the terminal alcohol (reduction of the ester-resin linkage to CH<sub>2</sub>OH). This precaution is taken to avoid cleavage

of the somewhat labile amide linkages to residue 46, which can revert to acylium groups if subjected to strong acid conditions such as the HF or TFA used to cleave protecting groups or ester-resin bonds.

Addition of 1 ml of glacial HOAc destroys excess borohydride, and the resin is then extracted with 6×15 ml portions of glacial HOAc. The combined extracts and the THF filtrate are lyophilized. The recovered Li<sup>+</sup> polyamide is dissolved in 50 ml (0.1M) phosphate buffer, pH 8, and shaken vigorously at 0° C. with a tenfold molar excess of IBA, supplied as a 1M solution in benzene, in the presence of 0.1 g of Et<sub>4</sub>NI as a phase transfer agent. After 1 hr, the aqueous capped polyamide phase is separated and concentrated to 20 ml by Micropore filtration. A 50 ml portion of 0.1M phosphate buffer, pH 7.5, is added, and the solution is again concentrated to 20 ml, whereby the cations associated with the anionic residues are exchanged for Na<sup>+</sup> ions.

### EXAMPLE 6

#### Production of Antibody Conjugates

(a) The capped polyamide produced according to Example 5 hereof is conjugated to a F(ab')<sub>2</sub> fragment from affinity purified goat anti-CEA (produced according to Example 1 of U.S. Pat. No. 4,331,647). The conjugation reaction is effected using the procedure of Example 2 hereof, with a fivefold molar excess of capped polyamide over antibody fragment. The resultant conjugate has an average of 2.5 polyamide addends per antibody fragment. Purified conjugate can be stored as a lyophilizate or in sterile solution, analogously to Example 2.

(b) The capped polyamide can be radioiodinated prior to conjugation, using the procedure of Example 3 hereof, to introduce up to 5 <sup>131</sup>I atoms per polyamide chain, thus, up to about 12.5 <sup>131</sup>I atoms per fragment molecule after conjugation under conditions which introduce about 2.5 iodopolyamides per antibody fragment.

It will be appreciated that other antibodies and other fragments can be used instead of those illustrated herein, e.g., antibodies to AFP, HCG or its beta-subunit, CSAP, PAP, other tumor-associated markers and pathological lesion-associated markers. Other diacid/diacylium and diamine residues can be used in the polyamide assembly sequence, taken from the other representative classes and types disclosed hereinabove, and obvious variants thereof. It is also possible to use residues which need not contain boron, and which carry other addends of diagnostic or therapeutic interest, as noted hereinabove.

### EXAMPLE 7

#### Synthesis of Branched Poly(amide/urea/thiourea)

A hybrid polymer is prepared, having amide, urea and thiourea linkages, and illustrating a chain branching option using selectively protected lysine. The resultant polymer also contains metallocarborane residues and easily iodinated residues. Two terminal amino protecting groups are used, BOC and Bpoc, having widely different acid lability. The Bpoc group can be cleaved in 0.2% TFA/DCM, the BOC group being about 120,000 times less reactive under those conditions. The BOC group requires concentrated TFA/DCM for cleavage. The synthesis proceeds by construction of a linear portion containing epsilon-BOC-protected lysine residues, onto which is built a polyurea segment having a temporarily capped terminal amine residue. Next, the

lysine protecting groups are cleaved, and polyurea branches are grown and capped with a thiourea. Finally, the temporary amine cap is removed and the polymer is cleaved from the resin. A linker is used to cap the free polymer, after which it is optionally iodinated and conjugated to antibody.

Residues used for this sequence include: amino acids 11, 12 and 14, each in the form of its Bpoc derivative prepared by conventional procedures, and supplied as 0.1M solutions in DCM; alpha-Bpoc-epsilon-BOC-L-lysine Et<sub>4</sub>N salt (Chemical Dynamics Corp., South Plainfield, N.J.), also as a 0.1M solution in DCM; diamine 45c, as its inner salt (zwitterion of protonated amine and carborane anion), as a 0.1M solution in DCM; zwitterionic diamine 45c-ClZ (o-chlorobenzylzoxycarbonyl protecting group on the unprotected amine of 45c (prepared from 45c and o-chlorobenzyl chloroformate, by standard S-Y procedures), as a 0.1M solution in DCM; metallocarborane diamine 47, as its neutral inner salt, as a 0.1M solution in DCM; diisocyanate 45b, as a 0.1M solution in DCM; isocyanate 46, as a 0.2M solution in DCM; and isothiocyanate 16, as a 0.2M solution in DCM. The Bpoc-protected reagents are stored at dry ice/ethanol bath temperature and allowed to warm to room temperature only when introduced into the synthesizer reaction vessel. TEA and TFA are supplied as in Example 1(a) hereof, the latter solution being denoted herein as TFA (conc.). A TFA (dil.) solution is also used, which contains 0.2% by volume TFA in DCM, with the same amount of added indole.

A 2 g (0.8 meq) sample of esterified Merrifield resin, [P]-O-gly-BOC, as in Example 1 hereof, is charged to the reaction vessel of a peptide synthesizer. The following sequence of steps is effected to produce the branched poly(amide/urea):

Step	Reagent	Vol (ml)	Time (min)
1	DCM wash (×3)	30	1.5
2	TFA (conc.)	30	1.5
3	TFA (conc.)	30	30
4	DCM wash (×6)	30	1.5
5	TEA/DCM	30	1.5
6	TEA/DCM	30	1.5
7	DCM wash (×6)	30	1.5
8A	Bpoc-aa/DCM (11 Bpoc)	20	1.5
8B	DCC/DCM	2	120*
9	DCM wash (×6)	30	1.5
10	TFA (dil.)	30	1.5
11	TFA (dil.)	30	30
12	DCM wash (×6)	30	1.5
13	TEA/DCM	30	1.5
14	TEA/DCM	30	1.5
15	DCM wash (×6)	30	1.5
16	Repeat steps 8A through 15 ten more times, using as Bpoc-aa in step 8A, respectively, 12-Bpoc, BOC-lys-Bpoc, 11-Bpoc, 12-Bpoc, BOC-lys-Bpoc, 11-Bpoc, 14-Bpoc.		
17	45b/DCM	20	120
18	DCM wash (×6)	30	1.5
19A	45c/DCM	20	1.5
19B	TEA/DCM	8	120
20	DCM wash (×6)	30	1.5
21	45b/DCM	20	120
22	DCM wash (×6)	30	1.5
23A	45c-ClZ/DCM	20	1.5
23B	TEA/DCM	8	120
24	DCM wash (×6)	30	1.5
25	TFA (conc.)	30	1.5
26	TFA (conc.)	30	30
27	DCM wash (×6)	30	1.5
28	TEA/DCM	30	1.5

-continued

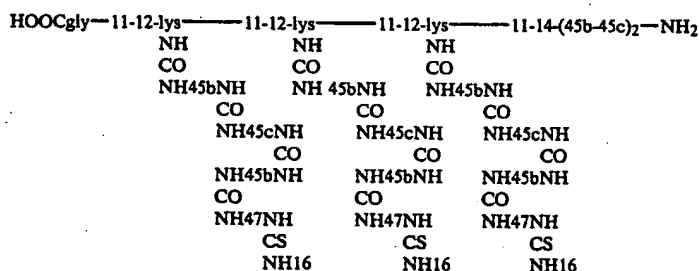
Step	Reagent	Vol (ml)	Time (min)
29	TEA/DCM	30	1.5
30	DCM wash (×6)	30	1.5
31	45b/DCM	60	120
32	DCM wash (×6)	30	1.5
33A	45c/DCM	60	1.5
33B	TEA/DCM	24	120
34	DCM wash (×6)	30	1.5
35	45b/DCM	60	120
36	DCM wash (×6)	30	1.5
37A	47/DCM	60	1.5
37B	TEA/DCM	24	120
38	DCM wash (×6)	30	1.5
39	16/DCM	50	120
40	DCM wash (×6)	30	1.5

\*Each coupling reaction is monitored after about 120 min. reaction, by withdrawal of a small portion of resin, which is subjected to the Kaiser ninhydrin qualitative color test. A blue color signifies incomplete coupling, and requires repeating steps 4-8, with a 160 min. coupling time.

Following step 40, the resin is dried under a stream of dry nitrogen, transferred to the liquid HF reactor, and cleaved with 40 ml of liquid HF containing 4 ml of anisole, at 0° C. for 45 min. This removes the ClZ protecting group from the terminal amine on the main chain and cleaves the resin-polymer ester bond, liberating the C-terminal carboxylate. The resin is then worked up and the poly(amide/urea) recovered and purified as in Example 1(b) hereof. The HPLC-purified polymer, as its Et<sub>3</sub>NH salt, is lyophilized and stored at -30° C.

It will be of interest to note that the chromophore in residues derived from 47 permits determination of concentration by visible spectroscopy, while the phenylthiourea group derived from capping with 16 permits uv monitoring.

The resultant polymer has the schematic structure:



The polymer is capped with IBA by the procedure of Example 5 hereof, at close to 0° C., and optionally iodinated on the carborane anion residues by the procedure of Example 3 hereof.

### EXAMPLE 8

#### Production of Antibody Conjugates

The capped polymer produced in Example 7 hereof is conjugated to whole IgG or F(ab')<sub>2</sub> fragments which specifically bind tumor or lesion markers, according to the procedures of Examples 2, 3, or 6 hereof. Alternatively, conjugation to a hybrid fragment having one arm which binds AFP and one which binds HCG (prepared according to Example 2(b) of U.S. Pat. No. 4,331,647) is effected by the procedure of Example 6 hereof, except that the hybrid fragment is used instead of the anti-CEA F(ab')<sub>2</sub>. The iodinated conjugates are stored analogously to Example 3 hereof.

### EXAMPLE 9

#### Synthesis of a Chelate-Loaded Polythiourea

A polythiourea is prepared, using chain branching groups as a means of functional group amplification. In this example, the highly branched chains are capped with diethylenetriaminepentaacetate (DTPA) chelators. Several readily iodinated carborane anion-containing residues are also included, which can facilitate dual tracer studies comparing the relative stabilities of radioiodine and radiometal in antibody conjugates. The nature of the chelator-loaded polythiourea is such that the metal ion can be incorporated prior to conjugation of the polymer with antibody, thereby avoiding many problems of current radiolabeling methods.

The synthesis uses as the chain splitter 3,5-diaminobenzoic acid, with both amino groups converted to their BOC-beta-alanyl amide derivatives. This species is made by conventional reaction of the 3,5-diaminobenzoic acid starting material with an excess of BOC-beta-alanine N-hydroxysuccinimide ester, which in turn is prepared from BOC-beta-alanine U.S. Biochemical Corp., Cleveland, OH.) and N-hydroxysuccinimide, with DCC/DMF at 0° C. The chain splitter is denoted CS(BOC)<sub>2</sub>. A variant of this structure is made as a point for attaching a final capping function. This is the mixed diamine of 3,5-diaminobenzoic acid with BOC-beta-alanine and ClZ-beta-alanine, denoted CS(BOC)(ClZ), and prepared by reacting 3,5-diaminobenzoic acid with a mixture of BOC-beta-alanine N-hydroxysuccinimide ester and ClZ-beta-alanine N-hydroxysuccinimide ester [made from ClZ-beta-alanine (U.S. Biochem.) and HOSu, as above]. These are supplied to the reaction as 0.1M solutions in DCM.

Diisothiocyanate 45d is prepared from diamine 45a,

as described hereinabove, and provided as a 0.1M solution in DCM. Diamine 45c is provided as an inner salt, as a 0.1M solution in DCM. Diamine 45a is provided as its TFA salt, as a 0.1M solution in DCM. TEA, TFA and DCC are supplied as in Example 1(a) hereof.

A 2 g (0.8 meq) sample of esterified Merrifield resin, [P]-O-gly-BOC, as in Example 1 hereof, is charged to the reaction vessel of a peptide synthesizer. The following sequence of steps is effected to produce the branched polythiourea:

Step	Reagent	Vol (ml)	Time (min)
1	DCM wash (×3)	30	1.5
2	TFA (conc.)	30	1.5
3	TFA (conc.)	30	30
4	DC wash (×6)	30	1.5
5	TEA/DCM	30	1.5
6	TEA/DCM	30	1.5
7	DCM wash (×6)	30	1.5
8A	CS(BOC)(ClZ)	20	1.5

-continued

Step	Reagent	Vol (ml)	Time (min)
8B	DCC/DCM	2	120
9	DCM wash (×6)	30	1.5
10	TFA (conc.)	30	1.5
11	TFA (conc.) 30	30	
12	DCM wash (×6)	30	1.5
13	TEA/DCM	30	1.5
14	TEA/DCM	30	1.5
15	DCM wash (×6)	30	1.5
16	45d/DCM	20	120
17	DCM wash (×6)	30	1.5
18A	45c/DCM	20	1.5
18B	1M TEA/DCM	8	120
19	DCM wash (×6)	30	1.5
20	45d/DCM	20	120
21	DCM wash (×6)	30	1.5
22A	45a/DCM	20	1.5
22B	1M TEA/DCM	8	120
23	DCM wash (×6)	30	1.5
24A	CS(BOC) <sub>2</sub>	20	1.5
24B	DCC/DCM	2	120
25	DCM wash (×6)	30	1.5
26-31	Repeat steps 2-7		
32-47	Repeat steps 16-31, using doubled amounts of reagents		
48-63	Repeat steps 16-31, using quadrupled amounts of reagents		
64-79	Repeat steps 1-31, using octupled amounts of reagents		

After completion of step 79, eight polythiourea chains have been elaborated in a tree-like configuration stemming from one of the two amine functions on the initial chain splitter, viz., the one with the BOC-beta-alanyl amide. The remaining amine is preserved as the ClZ-beta-alanyl amide, which survives the conditions used up to this point. The eight terminal amine functions are now capped with (HOOCCH<sub>2</sub>)<sub>2</sub>NCH(CH<sub>2</sub>C<sub>6</sub>H<sub>4</sub>NCS)CH<sub>2</sub>N-(COOH)CH<sub>2</sub>CH<sub>2</sub>N(CH<sub>2</sub>COOH)<sub>2</sub>, as the dry sodium salt, 12 mmol/50 ml dry dimethylformamide (DMF), used in excess, at room temperature. The isothiocyanatobenzyl-DTPA (DTPA-NCS) is described by Chang et al., "Applications of Nuclear and Radiochemistry", Lambrecht et al, Ed., Chap. 10 (Pergamon Press, New York, NY, 1982). The resin is freed of DCM and swelled with DMF prior to reaction with the DTPA-NCS. Following the capping reaction, the resin is washed with 6×30 ml of DMF, and then washed, swollen and washed again with 6×30 ml of DCM. The resin is then dried under a stream of dry nitrogen and treated with 100 ml of liquid HF containing 10 ml of anisole, at 0° C., for 1 hr. This removes the ClZ protecting group from the second amine on the chain splitter and cleaves the resin-polymer ester bond, liberating the C-terminal carboxylate. The resin is then worked up and the polythiourea is recovered and purified as in Example 1(b) hereof. The HPLC-purified polymer, as its Et<sub>3</sub>NH salt, is lyophilized and stored at -30° C.

The polymer is capped with IBA by the procedure of Example 5 hereof, at close to 0° C., and optionally iodinated on the carborane anion residues by the procedure of Example 3 hereof. The capped polythiourea, either radioiodinated or not, is incubated with an excess of either a radiometal, e.g., <sup>67</sup>GaCl<sub>3</sub>, <sup>111</sup>InCl<sub>3</sub>, <sup>90</sup>YCl<sub>3</sub>, <sup>65</sup>SnCl<sub>2</sub>-reduced <sup>99m</sup>TcO<sub>4</sub>—, or the like, under standard conditions, to chelate the radiometals, or with paramagnetic ions, e.g., solutions of GdCl<sub>3</sub>, EuCl<sub>3</sub>, or the like.

## EXAMPLE 10

## Production of Chelate-Loaded Antibody Conjugates

The capped polymer produced in Example 9 hereof, either iodinated or not, and carrying a radiometal or a paramagnetic ion, is conjugated to whole IgG or F(ab')<sub>2</sub> fragments which specifically bind tumor or lesion markers, according to the procedures of Examples 2, 3, or 6 hereof. Alternatively, conjugation to a hybrid fragment having one arm which binds AFP and one which binds HCG (prepared according to Example 2(b) of U.S. Pat. No. 4,331,647) is effected by the procedure of Example 6 hereof, except that the hybrid fragment is used instead of the anti-CEA F(ab')<sub>2</sub>. The conjugates are stored analogously to Example 3 hereof.

## EXAMPLE 11

## Production of Highly Chelate-Loaded Polymer

Amplification of the chelate loading achieved in Examples 9 and 10 hereof can readily be achieved using the same components, but combining the steps. Thus, the capped polythiourea produced in Example 9 hereof can be substituted for the Meares DTPN-NCS after the last iteration of the branching sequence, to load each of the eight terminal amines with eight chelates, rather than just one, resulting in 64 chelate groups on the resin-bound polymer prior to cleavage and final capping with IBA. Several of these 64-chelate addends can be conjugated to antibody, after loading with radiometal ions or paramagnetic ions, either with or without iodination of the reactive carborane anion groups. It will be appreciated that further iterations of the sequence and/or further branching of the chains can be effected to increase the amplification. More highly branched chain splitters can also be used, as disclosed hereinabove, to achieve this result.

Antibody fragments, especially Fab and Fab' fragments, can be linked to bivalent polymers carrying chelates, through thioether linkages to a pair of haloamide caps, or through, e.g., urea or thiourea linkages to a pair of isocyanate or isothiocyanate caps. Bivalent polymers are easily prepared, e.g., by using a BOC/ClZ-lysine residue, terminating the chain with an amine, cleaving with HF, and reacting the liberated epsilon-NH<sub>2</sub> and the terminal amine with IBA. Many other variants will be apparent to the skilled artisan, in light of the copious disclosure hereinabove.

## EXAMPLE 12

## Neutron Activated Tumor Radiotherapy

The procedure of Example 7 of U.S. Pat. No. 4,348,376 is used to effect therapy by injection of a patient with a radioiodinated, boron-loaded anti-CEA antibody, scanning with a gamma camera to locate the site or sites of uptake of the labeled antibody, and then directing a beam of thermal neutrons at the tumor site. The present example differs from that in the referenced patent by substitution of the conjugate prepared according to Example 3 hereof for the conjugate used in the reference. This offers the advantage that a much higher boron loading is achieved, both because of the use herein of 96% Boron-10 starting materials, and because 580 boron atoms per antibody are carried to the tumor site. Injection of 0.9 mg of conjugate, preferably as three injections of 300 ng each, spaced 3-6 hrs apart, will carry about 1.22 ug of Boron-10 to a 1 g tumor,

even if only 4% of the injected antibody is localized in the tumor. This is within the therapeutic range of 1-30 ug <sup>10</sup>B/g tumor which is considered adequate for this therapy.

It will be appreciated that the boron-loaded conjugates disclosed in the other Examples herein can also be used for analogous therapeutic treatments such as those disclosed in the other herein referenced Goldenberg patents and patent applications. Highly radiolabeled conjugates can also be used for therapy, according to the teachings of the referenced patents and patent applications, or according to art-recognized methods of others in this field.

### EXAMPLE 13

#### Radioimmunodetection of Tumors and Lesions

Tumor localization is effected according to the procedure of Example 7 of U.S. Pat. No. 4,361,544, except that the labeled antibody is the radioiodinated conjugate of Example 6(b) hereof, the antibody being an anti-HCG affinity-purified goat IgG or a monoclonal anti-HCG IgG. Imaging results are comparable. Alternatively, <sup>67</sup>Ga-labeled antibody prepared according to the procedures of Examples 9 and 10 hereof, using anti-CEA IgG, and <sup>111</sup>In-labeled irrelevant IgG can be used in place of the specific and irrelevant IgGs of Example 10 of U.S. Pat. No. 4,444,744 to achieve imaging of colorectal tumors with high resolution.

Example 2 of U.S. Ser. No. 633,999, U.S. Pat. No. 4,624,846, can be effected using the conjugate according to Example 3 herein, except that the antibody is the same murine monoclonal anti-HSV-1 F(ab')<sub>2</sub> in the reference example. Results are comparable.

The preceding examples can be repeated with similar success by substituting the generically or specifically described reactants and/or operating conditions of this invention for those used in the preceding examples.

From the foregoing description, one skilled in the art can easily ascertain the essential characteristics of this invention and, without departing from the spirit and scope thereof, can make various changes and modifications of the invention to adapt it to various usages and conditions.

What is claimed is:

1. A modified antibody or antibody fragment, consisting essentially of:

(1) at least one hypervariable region which specifically binds a ligand such that the formation of the resultant immunological complex is of diagnostic or therapeutic utility; and

(2) at least one defined, substantially homogeneous synthetic sequenced polymer whose constituent residues are linked by amide or urea or thiourea linkages or a combination thereof, and which incorporates residues containing a plurality of Boron-10 atoms;

wherein said synthetic sequenced polymer is chemically bound to said antibody or antibody fragment at one or more sites which do not substantially interfere with the immunological specificity of said hypervariable region.

2. The modified antibody or antibody fragment of claim 1, wherein said synthetic sequenced polymer is a polyamide.

3. The modified antibody or antibody fragment of claim 2, wherein said polyamide has a "Nylon 66" structure along substantially all of its backbone.

4. The modified antibody or antibody fragment of claim 1, wherein said synthetic sequenced polymer is a polythiourea.

5. The modified antibody or antibody fragment of claim 1, wherein said ligand is a marker which is produced by or associated with a tumor or a pathological lesion.

6. The modified antibody or antibody fragment of claim 3, containing 50-2000 boron atoms per antibody/-fragment.

7. The modified antibody or antibody fragment of claim 6, containing 200-2000 boron atoms per antibody or antibody fragment.

8. The modified antibody or antibody fragment of claim 7, wherein said boron atoms are about 96% enriched with Boron-10 isotope.

9. The modified antibody or antibody fragment of claim 2, wherein said polyamide is formed of condensed amino acids a major portion of which contain boron cage structures.

10. The modified antibody or antibody fragment of claim 9, wherein said condensed amino acids are natural amino acids or their enantiomers having pendant amine, hydroxyl, carboxyl or thio groups to which are bound at least one carborane-containing group.

11. The modified antibody or antibody fragment of claim 9, wherein said condensed amino acids are selected from those having the formulas

H—{DB}—C <sub>6</sub> H <sub>4</sub> NHC(S)NH(CH <sub>2</sub> ) <sub>4</sub> CH(NH <sub>2</sub> )COOH	1
H—{DB}—(CH <sub>2</sub> ) <sub>3</sub> C(O)NH(CH <sub>2</sub> ) <sub>4</sub> CH(NH <sub>2</sub> )COOH	2
H—{DB}—C <sub>6</sub> H <sub>4</sub> NHC(S)OCH <sub>2</sub> CH(NH <sub>2</sub> )COOH	3
H—{DB}—C <sub>6</sub> H <sub>4</sub> NHC(O)CH <sub>2</sub> CH(NH <sub>2</sub> )COOH	4
M <sup>+</sup> H—{UB—}—C <sub>6</sub> H <sub>4</sub> NHC(S)NH(CH <sub>2</sub> ) <sub>4</sub> CH(NH <sub>2</sub> )COOH	5
M <sup>+</sup> H—{UB—}—C <sub>6</sub> H <sub>4</sub> NHC(S)NH(CH <sub>2</sub> ) <sub>4</sub> CH(NH <sub>2</sub> )COOH	6
M <sup>+</sup> H—{UB—}—(CH <sub>2</sub> ) <sub>4</sub> C(O)NH(CH <sub>2</sub> ) <sub>4</sub> CH(NH <sub>2</sub> )COOH	7
H—{DB}—C <sub>6</sub> H <sub>4</sub> N=N—(OH)C <sub>6</sub> H <sub>3</sub> CH <sub>2</sub> CH(NH <sub>2</sub> )COOH	8
H—{DB}—(CH <sub>2</sub> ) <sub>3</sub> S(CH <sub>2</sub> ) <sub>2</sub> CH(NH <sub>2</sub> )COOH	9
H—{DB}—(CH <sub>2</sub> ) <sub>3</sub> OC <sub>6</sub> H <sub>4</sub> CH <sub>2</sub> CH(NH <sub>2</sub> )COOH	10
H—{DB}—(CH <sub>2</sub> ) <sub>3</sub> CH(NH <sub>2</sub> )COOH	11
M <sup>+</sup> H—{UB—}—(CH <sub>2</sub> ) <sub>4</sub> CH(NH <sub>2</sub> )COOH	12
H <sub>2</sub> N(CH <sub>2</sub> ) <sub>3</sub> —{DB}—(CH <sub>2</sub> ) <sub>3</sub> COOH	13
M <sup>+</sup> H <sub>2</sub> N(CH <sub>2</sub> ) <sub>3</sub> —{UB—}—(CH <sub>2</sub> ) <sub>3</sub> COOH	14

wherein {DB} is a dicarba-closo-dodecaborane group; {UB—} is a dicarba-nido-undecaborane anionic group; and {IUB—} is an iodo-dicarba-nido-undecaborane anionic group having one vertex of the {UB—} group replaced by a BI in the cage structure; and M<sup>+</sup> represents one equivalent of an alkali metal, an alkali earth metal or a quaternary ammonium cation.

12. In a method of tumor or pathological lesion radiotherapy, which comprises injecting a human subject parenterally with an antibody or antibody fragment which specifically binds a marker produced by or associated with said tumor or lesion and which is conjugated to an addend comprising a plurality of atoms of Boron-10 isotope, permitting said antibody or antibody fragment to accrete in said tumor or lesion or its immediate vicinity by binding to said marker, and directing a beam of thermal neutrons at said patient,

the improvement wherein said boron-labeled antibody or antibody fragment is a modified antibody/-fragment according to claim 1.

13. A kit for use in neutron-activated radiotherapy of a tumor or pathological lesion, comprising a sterile preparation of a boron-labeled modified antibody or antibody fragment according to claim 1, suitable for

preparing an injectable composition for parenteral injection in a human subject.

14. The modified antibody or antibody fragment of claim 2, wherein said ligand is a marker which is produced by or associated with a tumor or a pathological lesion.

15. The modified antibody or antibody fragment of claim 1, containing 50-2000 boron atoms per antibody or antibody fragment.

16. In a method of tumor or pathological lesion radiotherapy, which comprises injecting a human subject parenterally with an antibody or antibody fragment which specifically binds a marker produced by or associated with said tumor or lesion and which is conjugated to an addend comprising a plurality of atoms of

Boron-10 isotope, permitting said antibody or antibody fragment to accrete in said tumor or lesion or its immediate vicinity by binding to said marker, and directing a beam of thermal neutrons at said patient,

the improvement wherein said boron-labeled antibody or antibody fragment is a modified antibody or antibody fragment according to claim 2.

17. A kit for use in neutron-activated radiotherapy of a tumor or pathological lesion, comprising a sterile preparation of a boron-labeled modified antibody or antibody fragment according to claim 2, in a suitable container, suitable for preparing an injectable composition for parenteral injection in a human subject.

\* \* \* \* \*

20

25

30

35

40

45

50

55

60

65



US005877289A

EXHIBIT 2

## United States Patent [19]

Thorpe et al.

[11] Patent Number: 5,877,289

[45] Date of Patent: Mar. 2, 1999

[54] TISSUE FACTOR COMPOSITIONS AND  
LIGANDS FOR THE SPECIFIC  
COAGULATION OF VASCULATURE[75] Inventors: Philip E. Thorpe, Dallas, Tex.;  
Thomas S. Edgington, La Jolla, Calif.[73] Assignees: The Scripps Research Institute, La  
Jolla, Calif.; Board of Regents, The  
University of Texas System, Austin,  
Tex.

[21] Appl. No.: 479,733

[22] Filed: Jun. 7, 1995

## Related U.S. Application Data

[63] Continuation-in-part of Ser. No. 273,567, Jul. 11, 1994,  
which is a continuation-in-part of Ser. No. 205,330, Mar. 2,  
1994, Pat. No. 5,855,866, which is a continuation-in-part of  
Ser. No. 846,349, Mar. 5, 1992.[51] Int. Cl.<sup>6</sup> ..... A61K 39/395[52] U.S. Cl. .... 530/387.1; 530/387.3;  
530/387.7; 530/387.9; 530/388.1; 530/388.22;  
530/388.85; 530/391.7; 530/391.9; 530/381[58] Field of Search ..... 424/136.1, 135.1,  
424/134.1, 69.7; 514/2, 12, 834; 530/387.3,  
350, 381, 387.1, 387.7, 387.9, 388.1, 388.22,  
388.85, 391.7, 391.9

## [56] References Cited

## U.S. PATENT DOCUMENTS

4,456,550	6/1984	Dvorak et al. ....	260/112 R
4,472,509	9/1984	Gansow et al. .	
4,536,387	8/1985	Sakamoto et al. ....	424/14
4,785,077	11/1988	Kornbluth et al. ....	530/351
4,975,369	12/1990	Beavers et al. ....	435/69.1
5,017,556	5/1991	O'Brien et al. ....	514/2
5,021,236	6/1991	Gries et al. .	
5,081,034	1/1992	Bevilacqua et al. .	
5,110,730	5/1992	Edgington et al. ....	435/69.6
5,183,756	2/1993	Schlom ....	435/240.27
5,202,253	4/1993	Esmon et al. ....	435/240.27
5,223,427	6/1993	Edgington et al. ....	435/240.27
5,242,813	9/1993	Pastan et al. ....	435/70.21
5,298,599	3/1994	Rezaie et al. ....	530/350
5,314,695	5/1994	Brown ....	424/450
5,342,757	8/1994	Garin-Chesa et al. ....	435/7.21
5,345,991	9/1994	Roy et al. ....	530/350
5,374,617	12/1994	Morrissey et al. ....	514/8
5,403,713	4/1995	Bevilacqua et al. ....	435/7.1
5,437,864	8/1995	Edgington et al. ....	424/145.1
5,504,064	4/1996	Morrissey et al. ....	514/8
5,504,067	4/1996	Morrissey et al. ....	514/8
5,589,173	12/1996	O'Brien et al. ....	424/145.1
5,589,363	12/1996	Roy et al. ....	435/69.6
5,632,991	5/1997	Gimbrone, Jr. ....	424/178.1
5,726,147	3/1998	Ruf et al. ....	514/2
5,739,101	4/1998	Roy et al. ....	514/2

## FOREIGN PATENT DOCUMENTS

WO 81/01145	4/1981	WIPO ....	C07C 103/52
WO 90/03801	4/1990	WIPO ....	A61K 49/00
WO 90/05539	5/1990	WIPO .	
WO 90/12585	11/1990	WIPO ....	A61K 37/00
WO 90/13300	11/1990	WIPO ....	A61K 31/70

WO 92/12729	8/1992	WIPO ....	A61K 37/22
WO 92/16558	10/1992	WIPO ....	C07K 15/00
WO 92/19646	11/1992	WIPO ....	C07K 7/08
WO 93/08210	4/1993	WIPO .	
WO 93/08473	4/1993	WIPO .	
WO 93/09803	5/1993	WIPO ....	A61K 37/02
WO 93/17715	9/1993	WIPO .	
WO 93/23074	11/1993	WIPO .	
WO 94/05328	3/1994	WIPO ....	A61K 39/395
WO 94/07515	4/1994	WIPO ....	A61K 37/00
WO 04/10202	5/1994	WIPO .	
WO 94/11499	5/1994	WIPO .	
WO 94/28017	12/1994	WIPO ....	C07K 13/00

## OTHER PUBLICATIONS

Osborn et al., "Leukocyte Adhesion to Endothelium in  
Inflammation," *Cell*, 62:3-6, 1990.June et al., "Role of the CD28 Receptor in T-Cell Activa-  
tion," *Immunology Today*, 11(6):211-216, 1990.Denekamp, "Vascular Attack as a Therapeutic Strategy for  
Cancer," *Cancer and Metastasis Reviews*, 9:267-282, 1990.Scott et al., "Anti-CD3 Antibody Induces Rapid Expression  
of Cytokine Genes In Vivo," *The Journal of Immunology*,  
145(7):2183-2188, 1990.O'Connell and Edidin, "A Mouse Lymphoid Endothelial  
Cell Line Immortalized by Simian Virus 40 Binds Lympho-  
cytes and Retains Functional Characteristics of Normal  
Endothelial Cells," *The Journal of Immunology*,  
144(2):521-525, 1990.Ledbetter et al., "CD 28 Ligation in T-Cell Activation:  
Evidence for Two Signal Transduction," Abstract only,  
*Blood*, 75(7):1531-1539, 1990.Watanabe et al., "Exogenous Expression of Mouse Inter-  
feron  $\gamma$  cDNA in Mouse Neuroblastoma C1300 Cells Results  
in Reduced Tumorigenicity by Augmented Anti-Tumor  
Immunity," *Proceedings of the National Academy of Scien-  
tists*, 86:9456-9460, 1989.Schütt et al., "Human Monocyte Activation Induced by an  
Anti-CD14 Monoclonal Antibody," *Immunology Letters*,  
19:321-328, 1988.Thorpe et al., "Improved Antitumor Effects of Immunotox-  
ins Prepared with Deglycosylated Ricin A-Chain and Hin-  
dered Disulfide Linkages," *Cancer Research*,  
48:6396-6403, 1988.Glennie et al., "Preparation and Performance of Bispecific  
(F(ab' $\gamma$ )<sub>2</sub> Antibody Containing Thioether-Linked Fab' $\gamma$   
Fragments," *The Journal of Immunology*,  
139(7):2367-2375, 1987.Bevilacqua et al., "Identification of an Inducible Endothe-  
lial-Leukocyte Adhesion Molecule," *Proceedings of the  
National Academy of Scientists*, 84:9238-9242, 1987.

(List continued on next page.)

Primary Examiner—Lila Feisee

Assistant Examiner—Geetha P. Bansal

Attorney, Agent, or Firm—Arnold White &amp; Durkee L.L.P.

## [57] ABSTRACT

Disclosed are various compositions and methods for use in  
achieving specific blood coagulation. This is exemplified by  
the specific in vivo coagulation of tumor vasculature, caus-  
ing tumor regression, through the site-specific delivery of a  
coagulant using a bispecific antibody.

100 Claims, 8 Drawing Sheets



## OTHER PUBLICATIONS

- Cotran et al., "Induction and Detection of a Human Endothelial Activation Antigen In Vivo," Abstract only, *The Journal of Experimental Medicine*, 164(2):661-666, 1986.
- Groenewegen et al., "Lymphokine Dependence of In Vivo Expression of MHC Class II Antigens by Endothelium," *Nature*, 316:361-263, 1985.
- Moretta et al., Abstract only, *The Journal of Experimental Medicine*, 162(3):823-838, 1985.
- Vaickus and Foon, "Overview of Monoclonal Antibodies in the Diagnosis and Therapy of Cancer," *Cancer Investigation*, 93(2):295-209, 1991.
- Hagemeier et al., "A Monoclonal Antibody Reacting with Endothelial Cells of Budding Vessels in Tumors and Inflammatory Tissues, and Non-Reactive with Normal Adult Tissues," *International Journal of Cancer*, 38:481-488, 1986.
- Duijvestijn et al., "Lymphoid Tissue- and Inflammation-Specific Endothelial Cell Differentiation defined by Monoclonal Antibodies," *The Journal of Immunology*, 138(3):713-719, 1987.
- Murray et al., "Vascular Markers for Murine Tumours," *Radiotherapy and Oncology*, 16:221-234, 1989.
- Schlingemann et al., "Monoclonal Antibody PAL-E Specific for Endothelium," *Laboratory Investigation*, 52(1):71-76, 1985.
- Bruland et al., "New Monoclonal Antibodies Specific for Human Sarcomas," *International Journal of Cancer*, 38:27-31, 1986.
- Reisfeld et al., "Human Tumor-Associated Antigens Defined by Monoclonal Antibodies," *CRC Critical Reviews in Immunology*, 5(1):27-53, 1984.
- Schlom et al., "Monoclonal Antibodies Reactive with Breast Tumor-Associated Antigens," *Advances in Cancer Research*, 43:143-173, 1985.
- Kaplan, "The Diagnostic and Therapeutic Use of Monoclonal Antibodies in Colorectal Cancer," *Hematology/Oncology Clinics of North American*, 3(1):125-134, 1989.
- Smith and Teng, "Clinical Applications of Monoclonal Antibodies in Gynecologic Oncology," *Cancer*, 60:2068-2074, 1987.
- Stavrou, "Monoclonal Antibodies in Neuro-Oncology," *Neurosurgery Review*, 13:7-18, 1990.
- Shepard et al., "Monoclonal Antibody Therapy of Human Cancer: Taking the Her2 Protooncogene to the Clinic," *Journal of Clinical Immunology*, 11(3):117-127, 1991.
- Szymendera, "Clinical Usefulness of Three Monoclonal Antibody-Defined Tumour Markers: CA 19-9, CA 50, and CA 125," *Tumor Biology*, 7:333-342, 1986.
- Catane and Longo, "Monoclonal Antibodies for Cancer Therapy," *Israel Journal of Medical Sciences*, 24:471-476, 1988.
- Greiner et al., "Applications of Monoclonal Antibodies and Recombinant Cytokines for the Treatment of Human Colorectal and Other Carcinomas," *Journal of Surgical Oncology Supplement*, 2:9-13, 1991.
- Thor and Edgerton, "Monoclonal Antibodies Reactive with Human Breast or Ovarian Carcinoma: In Vivo Applications," *Seminars in Nuclear Medicine*, 19(4):295-308, 1989.
- Thorpe et al., "Selective Killing of Proliferating Vascular Endothelial Cells by an Anti-Fibronectin Receptor Immunotoxin," *16th LH Gray Conference*, Sep. 17-21, 1990.
- Ghose et al., "Preparation of Antibody-Linked Cytotoxic Agents," *Methods in Enzymology*, 93:280-333, 1983.
- Thorpe et al., "Targeting to proliferating vascular endothelium," *Int. Symp. on Angio.*, Mar. 13-15, 1991.
- Knowles and Thorpe, "Purification of Immunotoxins Containing Ricin A-Chain and Abrin A-Chain Using Blue Sepharose CL-6B," *Analytical Biochemistry*, 160:440-443, 1987.
- Wang et al., "Photoreactive In-Cyclodextrin Inclusion Complex: a New Heterobifunctional Reagent for Antibody Labeling," *Nuclear Medicine and Biology*, 19(8):897-902, 1992.
- PCT Search Report mailed Jun. 25, 1993.
- Alvarez et al., "Localization of Basic Fibroblast Growth Factor and Vascular Endothelial Growth Factor in Human Glial Neoplasms," *Modern Pathology*, 5(3):303-307, 1992.
- Brown et al., "Expression of Vascular Permeability Factor (Vascular Endothelial Growth Factor) and Its Receptors in Adenocarcinomas of the Gastrointestinal Tract," *Cancer Research*, 53:4727-4735, 1993.
- Kim et al., "Inhibition of vascular endothelial growth factor-induced angiogenesis suppresses tumor growth in vivo," *Nature*, 362:841-843, 1993.
- Dvorak et al., "Distribution of Vascular Permeability Factor (Vascular Endothelial Growth Factor) in Tumors: Concentration in Tumor Blood Vessels," *J. Exp. Med.*, 174:1275-1278, 1991.
- Gerlach et al., "Enhanced Responsiveness of Endothelium in the Growing/Motile State to Tumor Necrosis Factor/Cachectin," *J. Exp. Med.*, 170:913-931, 1989.
- Gougos et al., "Identification of distinct epitopes of endoglin, and RGD-containing glycoprotein of endothelial cells, leukemic cells, and syncytiotrophoblasts," *International Immunology*, 4(1):83-92, 1991.
- Gougos et al., "Identification of a Human Endothelial Cell Antigen with Monoclonal Antibody 44G4 Produced Against a Pre-B Leukemic Cell Line," *The Journal of Immunology*, 141:1925-1933, 1988.
- Gougos et al., "Biochemical Characterization of the 44G4 Antigen from the Hoon Pre-B Leukemic Cell Line," *The Journal of Immunology*, 141:1934-1940, 1988.
- Hagemeier et al., "A Monoclonal Antibody Reacting with Endothelial Cells of Budding Vessels in Tumors and Inflammatory Tissues, and Non-Reactive with Normal Adult Tissues," *Int. J. Cancer*, 38:481-488, 1986.
- Jakeman et al., "Binding Sites for Vascular Endothelial Growth Factor Are Localized on Endothelial Cells in Adult Rat Tissues," *J. Clin. Invest.*, 89:244-253, 1992.
- Nabel et al., "Recombinant fibroblast growth factor-1 promotes intimal hyperplasia and angiogenesis in arteries in vivo," *Nature*, 362:844, 1993.
- O'Connell et al., "Endoglin: a 180-kD endothelial cell and macrophage restricted differentiation molecule," *Clin. Exp. Immunol.*, 90:154-159, 1992.
- Plate et al., "Up-Regulation of Vascular Endothelial Growth Factor and Its Cognate Receptors in a Rat Glioma Model of Tumor Angiogenesis," *Cancer Research*, 53(23):5822-5827, 1993.
- Plate et al., "Vascular endothelial growth factor is a potential tumour angiogenesis factor in human gliomas in vivo," *Nature*, 359:845-848, 1992.
- Rettig et al., "Identification of endosialin, a cell surface glycoprotein of vascular endothelial cells in human cancer," *Proc. Natl. Acad. Sci. USA*, 89:10832-10836, 1992.

- Sarma et al., "Cloning of a Novel Tumor Necrosis Factor- $\alpha$ -Inducible Primary Response Gene that is Differentially Expressed in Development and Capillary Tube-Like Formation in vitro," *The Journal of Immunology*, 148:3302-3312, 1992.
- Senger et al., "Vascular permeability factor (VPF, VEGF) in tumor biology," *Cancer and Metastasis Reviews*, 12:303-324, 1993.
- Shweiki et al., "Vascular endothelial growth factor induced by hypoxia may mediate hypoxia-initiated angiogenesis," *Nature*, 359:843-845, 1992.
- Wang et al., "A Monoclonal Antibody Detects Heterogeneity in Vascular Endothelium of Tumours and Normal Tissues," *Int. J. Cancer*, 54:363-370, 1993.
- Westphal et al., "A New 180-kDa Dermal Endothelial Cell Activation Antigen: In Vitro and In Situ Characteristics," *The Journal of Investigative Dermatology*, 100(1):27-34, 1993.
- Yeo et al., "Vascular Permeability Factor (Vascular Endothelial Growth Factor) in Guinea Pig and Human Tumor and Inflammatory Effusions," *Cancer Research*, 53:2912-2918, 1993.
- Büring et al., "Endoglin is expressed on a subpopulation of immature erythroid cells of normal human bone marrow," *Leukemia*, 5(10):841-847, 1991.
- Dvorak et al., "Structure of Solid Tumors and Their Vasculature: Implications for Therapy with Monoclonal Antibodies," *Cancer Cells*, 3(3):77-85, 1991.
- Gougos and Letarte, "Primary Structure of Endoglin, an RGD-containing Glycoprotein of Human Endothelial Cells," *The Journal of Biological Chemistry*, 265(15):8361-8364, 1990.
- Bach et al., "Factor VII Binding to Tissue Factor in Reconstituted Phospholipid Vesicles: Induction of Cooperativity by Phosphatidylserine," *Biochemistry*, 25:4007-4020, 1986.
- Brennan et al., "Preparation of Bispecific Antibodies by Chemical Recombination of Monoclonal Immunoglobulin GI Fragments," *Science*, 229:81-83, 1985.
- Bruland et al., "Expression and Characteristics of a Novel Human Osteosarcoma-associated Cell Surface Antigen," *Cancer Res.*, 48:5302, 1983.
- Burrows and Thorpe, "Eradication of Large Solid Tumors in Mice With an Immunotoxin Directed Against Tumor Vasculature," *Proc. Natl. Acad. Sci (USA)*, 90:8996-9600, 1993.
- Burrows et al., "A Murine Model for Antibody-Directed Targeting of Vascular Endothelial cells in solid tumors," *Cancer Res.*, 52:5954-5962, 1992.
- Burrows et al., "Influence of Tumor-derived Interleukin-1 on Melanoma-endothelial Cell Interactions in Vitro," *Cancer Res.*, 51:4768-4755, 1991.
- Carnemolla et al., "A Tumor-associated Fibronectin Isoform Generated by Alternative Splicing of Messenger RNA Precursors," *J. Cell. Biol.*, 108:1139, 1989.
- Carnemolla et al., "The Inclusion of the Type III Repeat ED-B in the Fibronectin Molecule Generates Conformational Modifications That Unmask a Cryptic Sequence," *Journal of Biological Chemistry*, 267(34):24689-24692, 1992.
- Denekamp and Hobson, "Endothelial Cell Proliferation in Experimental Tumours," *Brit. J. Cancer*, 46:711-720, 1982.
- Dewerchin et al., "Effect of Chemical Conjugation of Recombinant Single-Chain Urokinase-Type Plasminogen Activator With Monoclonal Antiplatelet Antibodies on Platelet Aggregation and on Plasma Clot Lysis In Vitro and In Vivo," *Blood*, 78(4):1005-1018, 1991.
- Edgington et al., "The Structural Biology of Expression and Function of Tissue Factor," *Thrombosis and Haemostasis*, 66(1):67-79, 1991.
- Epenetos et al., "Limitations of Radiolabeled Monoclonal Antibodies for Localization of Human Neoplasms," *Cancer Res.*, 46:3183-3191, 1986.
- Fiore et al., "The biochemical basis for the apparent defect of soluble mutant tissue factor in enhancing the proteolytic activities of factor VIIa," *J. Biol. Chem.*, 269:143-149, 1994.
- Fisher et al., "Cloning and Expression of Human Tissue Factor cDNA," *Thrombosis Research*, 48:89-99, 1987.
- Folkman, Tumor Angiogenesis, *Adv. Cancer Res.*, 43:175-230, 1985.
- Frelinger et al., "Monoclonal Antibodies to Ligand-occupied Conformers of Integrin  $\alpha_{IIb}\beta_3$  (Glycoprotein IIb-IIIa) Alter Receptor Affinity, Specificity, and Function," *Journal of Biological Chemistry*, 266(26):17106-17111, 1991.
- Frelinger et al., "Selective Inhibition of Integrin Function by Antibodies Specific for Ligand-occupied Receptor Conformers," *Journal of Biological Chemistry*, 265(11):6346-6352, 1990.
- Hayward et al., "p-155, a Multimeric Platelet Protein That Is Expressed on Activated Platelets," *Journal of Biological Chemistry*, 266(11):7114-7120, 1991.
- Heynen et al., "Absence of Ligands Bound to Glycoprotein IIb-IIIa on the Exposed Surface of a Thrombus May Limit Thrombus Growth in Flowing Blood," *J. Clin. Invest.*, 94:1098-1112, 1994.
- Jain, Vascular and Interstitial Barriers to Delivery of Therapeutic Agents in Tumors. *Cancer Meta. Rev.*, 9(3):253-266, 1990.
- Kim et al., "The Vascular Endothelial Growth Factor Proteins: Identification of Biologically Relevant Regions by Neutralizing Monoclonal Antibodies," *Growth Factors*, 7:53-64, 1992.
- Kondo et al., "Significance of Vascular Endothelial Growth Factor/Vascular Permeability Factor for Solid Tumor Growth, and Its Inhibition by the Antibody," *Biochemical and Biophysical Research Communications*, 194(3):1234-1241, 1993.
- Krishnaswamy et al., "Role of the Membrane Surface in the Activation of Human Coagulation Factor X," *J. Biol. Chem.*, 267:26110-26120, 1992.
- Martin et al., "Tissue factor: Molecular recognition and cofactor function," *FASEB J.*, 9:852:859, 1995.
- Morrissey et al., "Molecular Cloning of the cDNA for Tissue Factor, the Cellular Receptor for the Initiation of the Coagulation Protease Cascade," *Cell*, 50:129-135, 1987.
- Morrissey et al., "Monoclonal Antibody Analysis of Purified and Cell-Associated Tissue Factor," *Thrombosis Research*, 52:247-261, 1988.
- Morrissey et al., "Quantitation of activated factor VII levels in plasma using a tissue factor mutant selectively deficient in promoting factor VII activation," *Blood*, 81:734-744, 1993.
- Murray et al., "Tumor-derived Factors Which Induce Endothelial Tissue Factor and Enhance the Procoagulant Response to TNF," *Intl. J. Rad. Biology*, 60:273-277, 1991.

- Nawroth et al., "Tumor necrosis factor/cachectin-induced intravascular fibrin formation in meth A fibrosarcomas," *J. Exp. Med.*, 168:637-647, 1988.
- Nemerson, "Tissue Factor and Hemostasis," *Blood*, 71(1):1-8, 1988.
- Neuenschwander and Morrissey, "Roles of the membrane-interactive regions of factor VIIa and tissue factor. The factor VIIaGla domain is dispensable for binding to tissue factor but important for activation of factor X," *J. Biol. Chem.*, 269:8007-8013, 1994.
- Paborsky et al., "Lipid Association, but Not the Transmembrane Domain, Is Required for Tissue Factor Activity," *J. Biol. Chem.*, 266:21911-16, 1991.
- Paborsky et al., "Purification of Recombinant Human Tissue Factor," *American Chemical Society*, 1989.
- Rehemtulla et al., "High Level Expression of Recombinant Human Tissue Factor in Chinese Hamster Ovary Cells as a Human Thromboplastin," *Thrombosis and Haemostasis*, 65(5):521-527, 1991.
- Rucco et al., "Cytokine Production (IL- $\alpha$ , IL- $\beta$ , and TNF  $\alpha$ ) and Endothelial Cell Activation (ELAM-1 and HLA-DR) in Reactive Lymphadenitis, Hodgkin's Disease, and in Non-Hodgkin's Lymphomas," *Am. J. Pathol.*, 137(5):1163-1171, 1990.
- Ruf and Edgington, "An Anti-Tissue Factor Monoclonal Antibody Which Inhibits TF-VIIa Complex is a Potent Anticoagulant in Plasma," *Thrombosis and Haemostasis*, 66(5):529-533, 1991.
- Ruf and Edgington, "Structural biology of tissue factor, the initiator of thrombogenesis in vivo," *The FASEB Journal*, 8:385-390, 1994.
- Ruf and Edgington, "Two sites in the tissue factor extracellular domain mediate the recognition of the ligand factor VIIa," *Proc. Natl. Acad. Sci. USA*, 88:8430-8434, 1991.
- Ruf et al., "Phospholipid-independent and -dependent Interactions Required for Tissue Factor Receptor and Cofactor Function," *Journal of Biological Chemistry*, 266(4):2158-2166, 1991.
- Ruf et al., "Tissue Factor Residues 157-167 are Required for Efficient Proteolytic Activation of Factor X and Factor VII," *Journal of Biological Chemistry*, 267(31):22206-22210, 1992.
- Scarpati et al., "Human Tissue Factor: cDNA Sequence and Chromosome Localization of the Gene," *Biochemistry*, 26:5234-5238, 1987.
- Schlingemann et al., "Leukocyte Antigen CD34 is Expressed by a Subset of Cultured Endothelial Cells and on Endothelial Albimial Microprocesses in the Tumor Stroma," *Laboratory Investigation*, 62:690-696, 1990.
- Sioussat et al., "Inhibition of Vascular Permeability Factor (Vascular Endothelial Growth Factor) with Antipeptide Antibodies," *Archives of Biochemistry and Biophysics*, 301(1):15-20, 1993.
- Spicer et al., "Isolation of cDNA clones coding for human tissue factor: Primary structure of the protein and cDNA," *Proc. Natl. Acad. Sci. USA*, 84:5148-5152, 1987.
- ten Cate et al., "The activation of factor X and prothrombin by recombinant factor VIIa is mediated by tissue factor," *J. Clin. Invest.*, 92:1207-1212, 1993.
- Thieme et al., "Comparative Analysis of Vascular Endothelial Growth Factor Receptors on Retinal and Aortic Vascular Endothelial Cells," *Diabetes*, 44:98, 1995.
- Tomiyama et al., "The Arg-Gly-Asp (RGD) Recognition Site of Platelet Glycoprotein IIB-IIIa on Nonactivated Platelets is Accessible to High-Affinity Macromolecules," *Blood*, 79(9):2303-2312, 1992.
- Ugarova et al., "Conformational Changes in Fibrinogen Elicited by its Interaction with Platelet Membrane Glycoprotein GPIIb-IIIa," *Journal of Biological Chemistry*, 268(28):21080-21087, 1993.
- Zacharski et al., "Tumor Cell Procoagulant and Urokinase Expression in Carcinoma of the Ovary," *J. Natl. Cancer Inst.*, 85:1225-1230, 1993.
- Zamarron et al., "A Receptor-induced Binding Site in Fibrinogen Elicited by its Interaction with Platelet Membrane Glycoprotein IIB-IIIa," *Journal of Biological Chemistry*, 266(24):16193-16199, 1991.
- UTSD:419; Serial No. 08/273,567, filed Jul. 11, 1994.
- UTSD:433; Serial No. 08/482,369, filed Jun. 7, 1995; C.I.P. of UTSD:419.
- UTSD:456; Serial No. 08/485,482, filed Jun. 7, 1995; C.I.P. of UTSD:419.
- UTSD:457; Serial No. 08/487,427, filed Jun. 7, 1995; C.I.P. of UTSD:419.
- UTSD:460; Serial No. 08/472,631, filed Jun. 7, 1995; C.I.P. of UTSD:419.
- UTSD:461; Serial No. 08/479,727, filed Jun. 7, 1995; C.I.P. of UTSD:419.
- UTSD:462; Serial No. 08/481,904, filed Jun. 7, 1995; C.I.P. of UTSD:419.
- Burrows and Thorpe, "Targeting the Vasculature of Solid Tumors," *Journal of Controlled Release*, 28:195-202, Jan. 1994.
- Clauss et al., "A Polypeptide Factor Produced by Fibrosarcoma Cells That Induces Endothelial Tissue Factor and Enhances the Procoagulant Response to Tumor Necrosis Factor/Cachectin," *The Journal of Biological Chemistry*, 265(12):7078-7083, Apr. 1990.
- Thorpe and Burrows, "Antibody-Directed Targeting of the Vasculature of Solid Tumors," *Breast Cancer Research and Treatment*, 36(2):237-251, 1995.
- Yamazaki et al., "Bispecific Monoclonal Antibodies with Specificities for Activated Platelets and Thrombolytic Agents, Their Production and Use," Abstract for Canadian Patent Application CA 2039259; Chem Abstracts, 117(11), Abstract #109988.
- Lapierre et al., "Three Distinct Classes of Regulatory Cytokines Control Endothelial Cell MHC Antigen Expression," *J. Exp. Med.*, 167:794-804, 1988.
- Qian et al., "Human Peripheral Blood Lymphocytes Targeted with Bispecific Antibodies Release Cytokines That Are Essential for Inhibiting Tumor Growth," *J. Immunol.*, 146(9):3250-3256, 1991.
- Waldman, Thomas A., "Monoclonal Antibodies in Diagnosis and Therapy," *Science*, 252: 1657-1662, 1991.
- Wen et al., "Effects of  $\gamma$ -Interferon on Major Histocompatibility Complex Antigen Expression and Lymphocytic Infiltration in the 9L Gliosarcoma Brain Tumor Model: Implications for Strategies of Immunotherapy," *J. Neuroimmunol.*, 36:57-68, 1992.
- Songsivilai & Lachmann, "Bispecific antibody: a tool for diagnosis and treatment of disease," *Clin. exp. Immunol.*, 79, 315-321 (1990).
- Dermer, "Another Anniversary for the War on Cancer," *Biototechnology*, 12, 320 (1994).

Pober and Cotran, "What Can Be Learned From the Expression of Endothelial Adhesion Molecules in Tissues?", *Laboratory Investigation*, 64(3), 301-305 (1991).

Allowed Claims of U.S. Serial No. 08/327,709, Dvorak.

Osband and Ross, "Problems in the Investigational Study and Clinical Use of Cancer Immunotherapy," *Immunotherapy*, 11:193-195, 1990.

Chatterjee, et al., "Idiotypic antibody immunotherapy of cancer," *Cancer Immunol. Immunotherapy*, 38:75-82, 1994.

European Application Serial No. 93 906 289.9 Office Action dated Sep. 25, 1997.

European Application Serial No. 93 923 817.1 Office Action dated Sep. 25, 1997.

Wellicome et al., A Monoclonal Antibody That Detects A Novel Antigen On Endothelial Cells That Is Induced By Tumor Necrosis Factor, IL-1, Or Lipopolysaccharide, *J. Immunol.*, 144(7):2558-2565, Apr. 1, 1990.

Lazar, E. et al. *Mol. Cell. Biol.* 8(3):1247-1252, Mar. 1988.

Burgess, W.H. et al. *J. Cell Biol.* 111:2129-2138, Nov. 1990.

Tao, M. et al. *J. Immunol.* 143:2595-2601, Oct. 1989.

Gillies, S.D. et al. *Hum. Antibod. Hybridomas* 1(1):47-54, 1990.

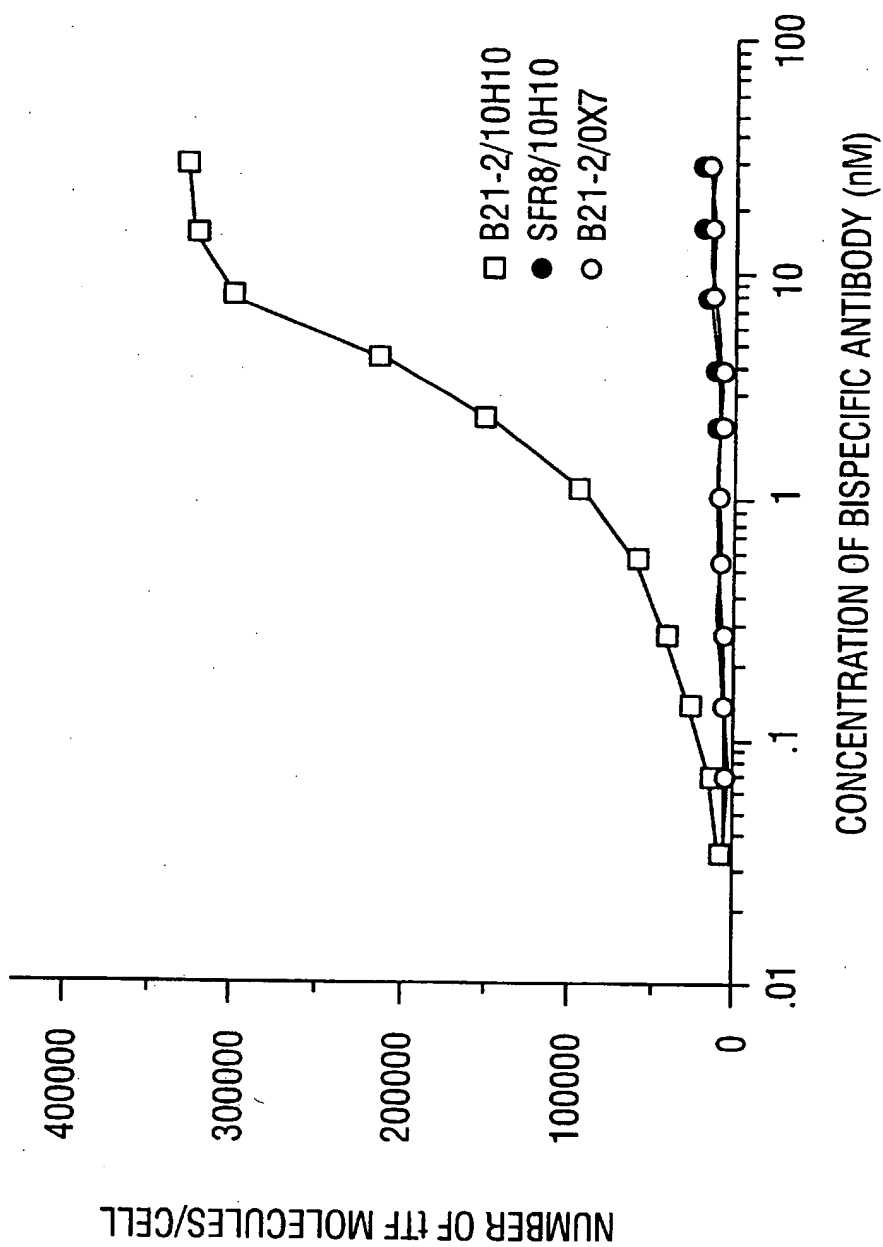


FIG. 1

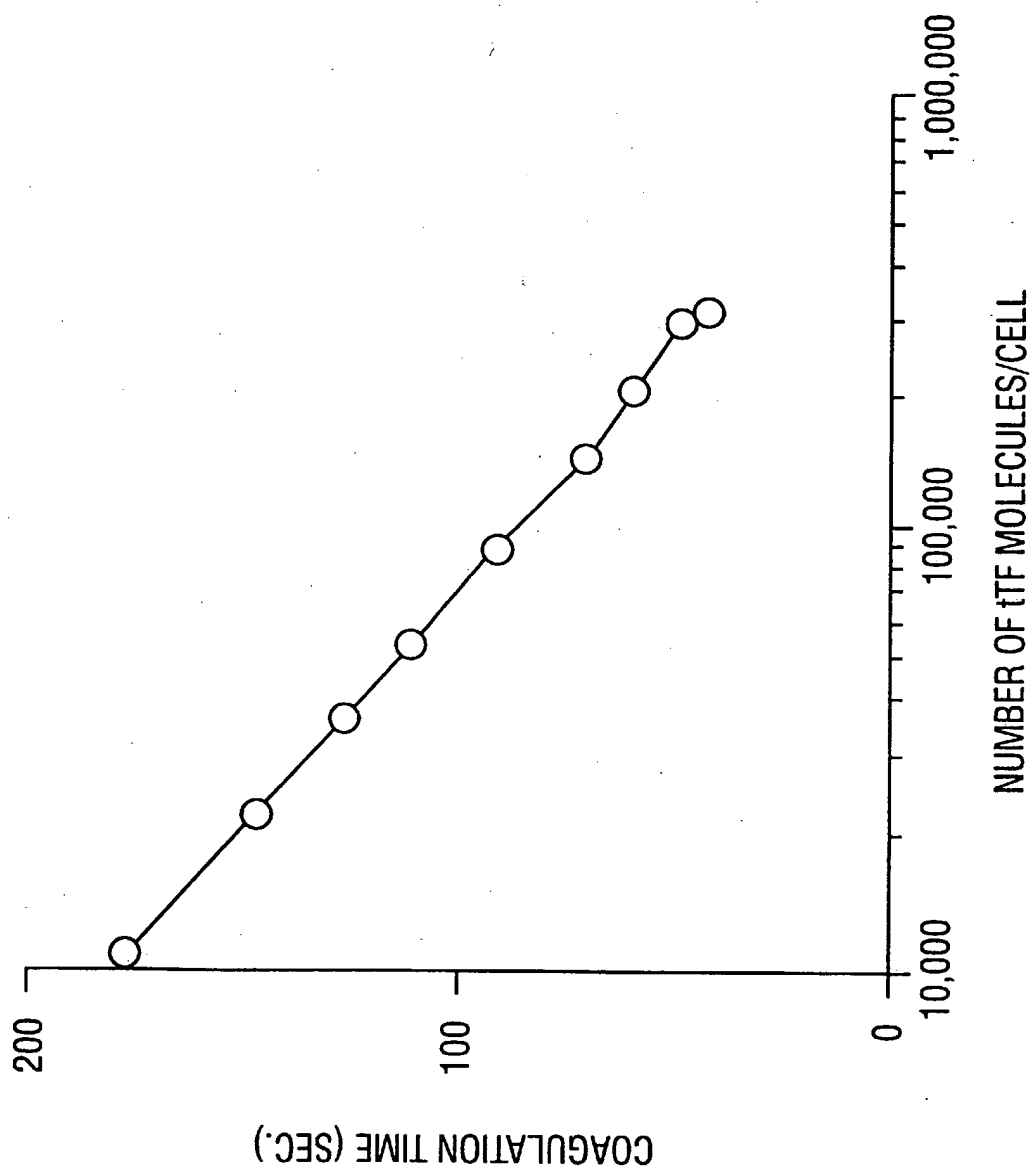


FIG. 2

FIG. 3A

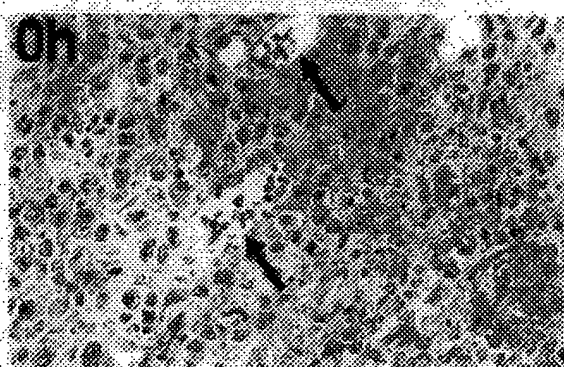


FIG. 3B

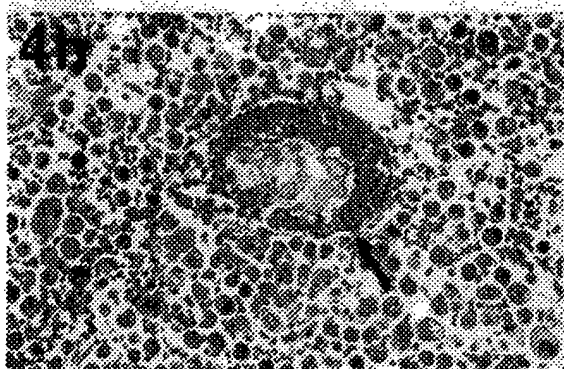
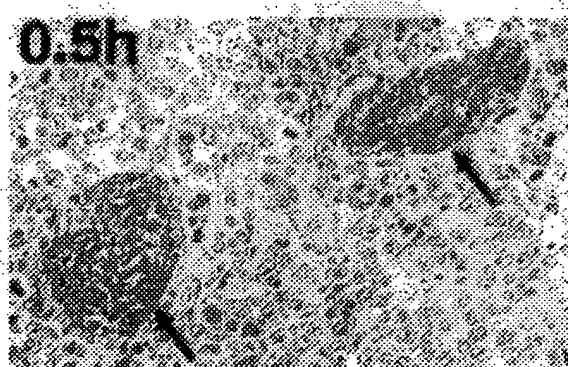


FIG. 3C

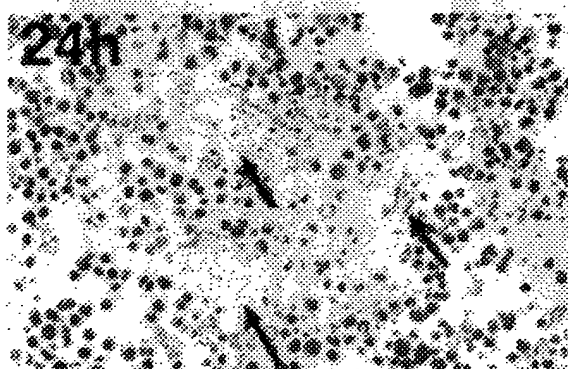


FIG. 3D

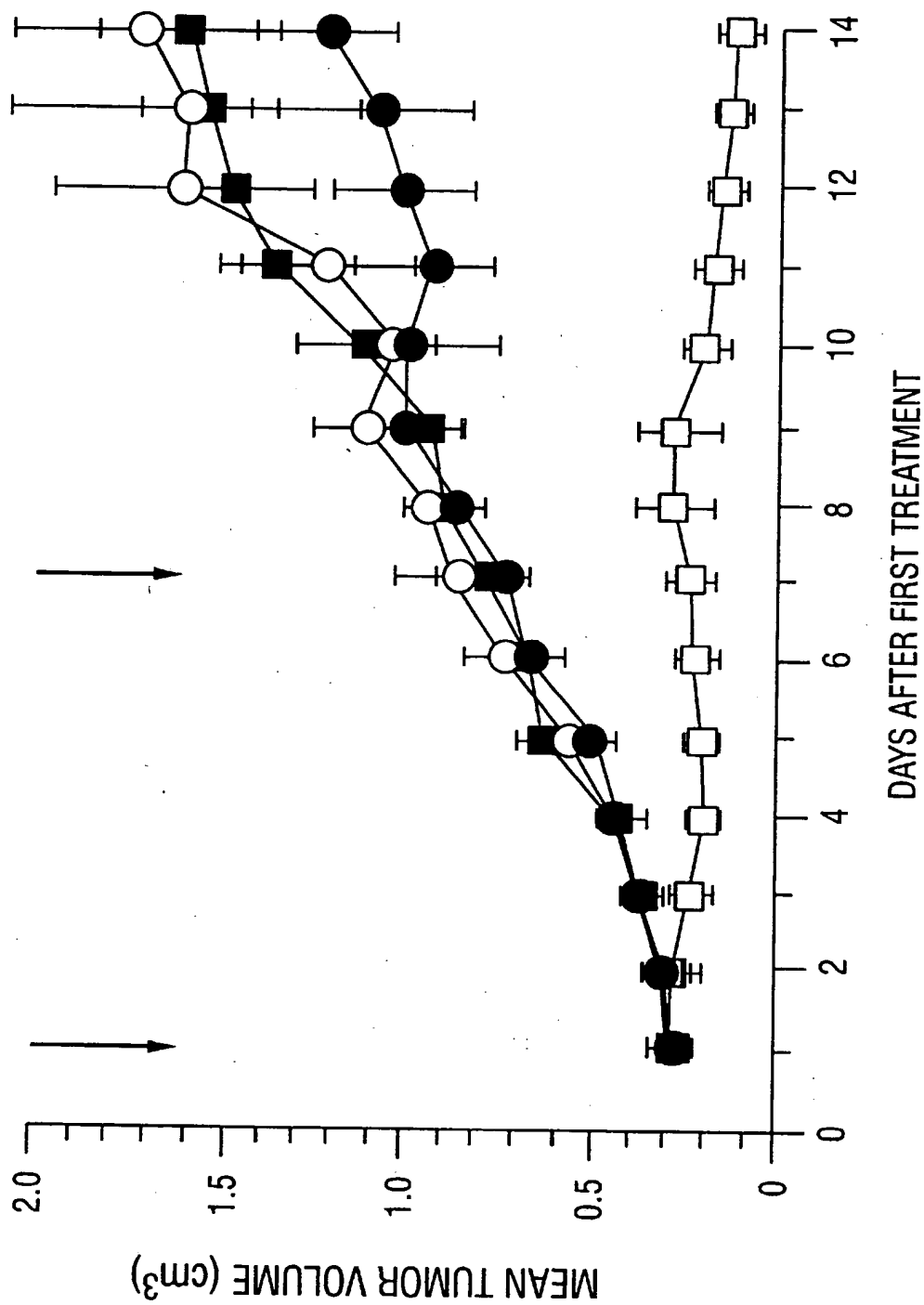


FIG. 4



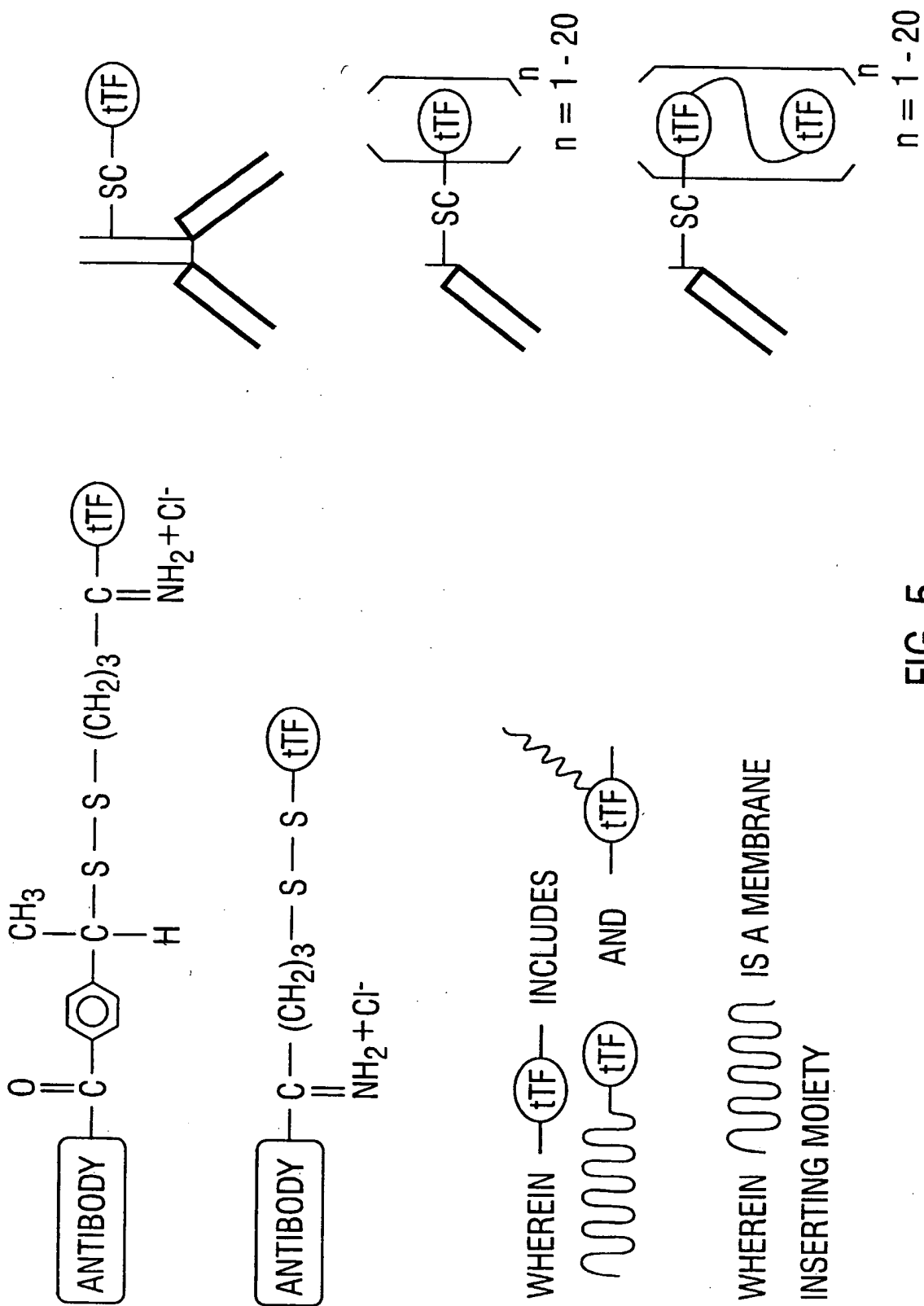


FIG. 5

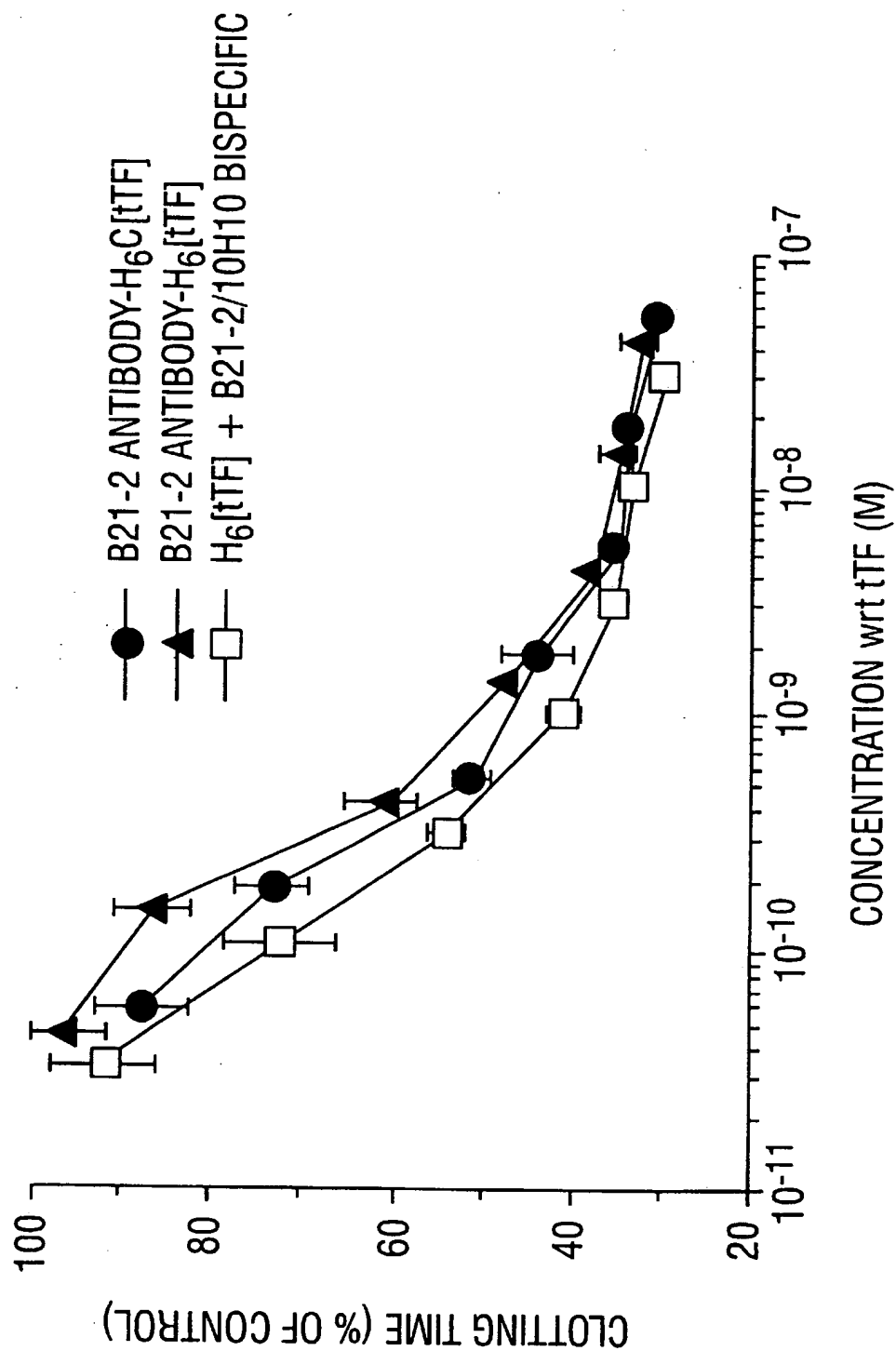


FIG. 6

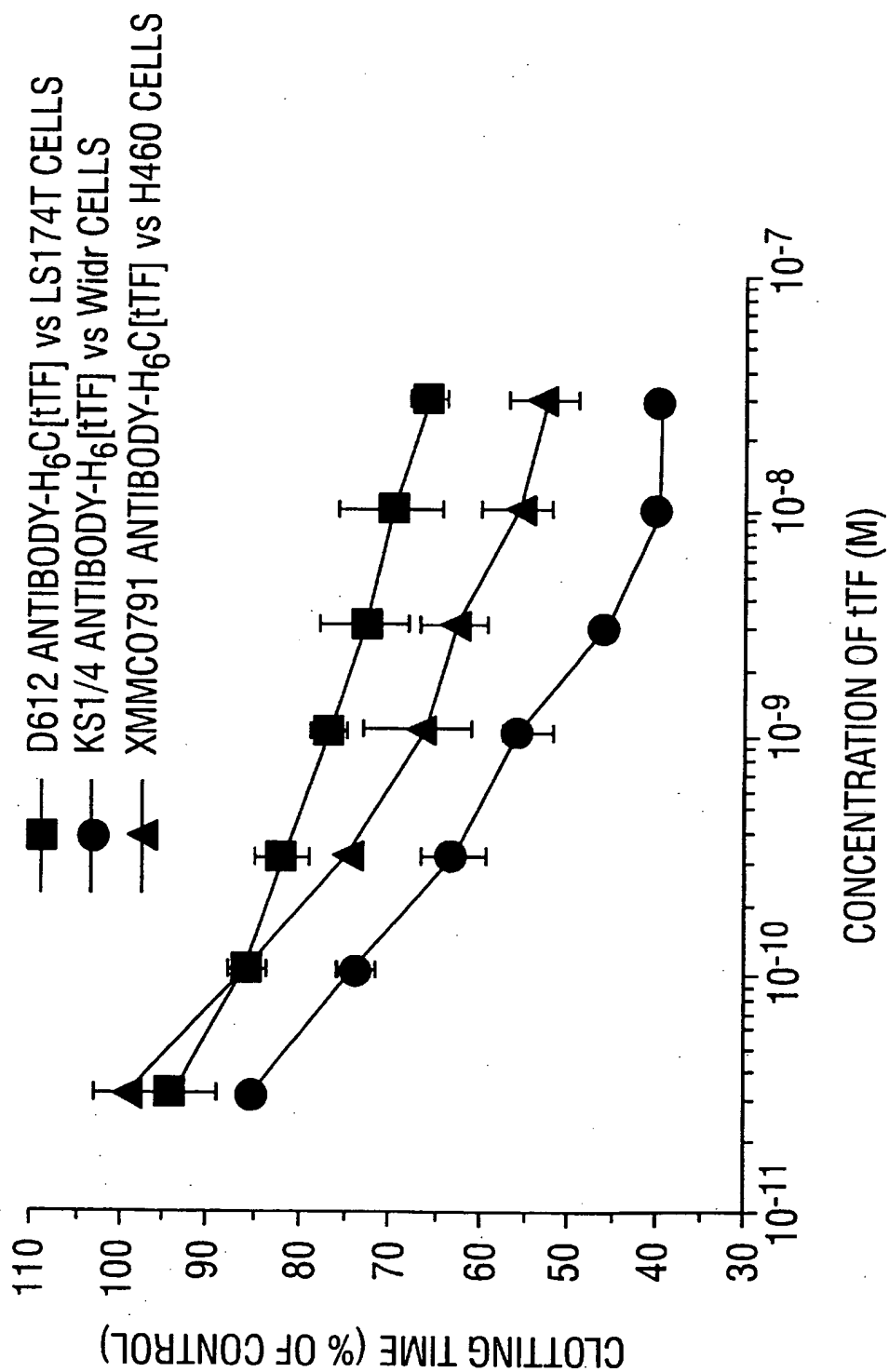


FIG. 7

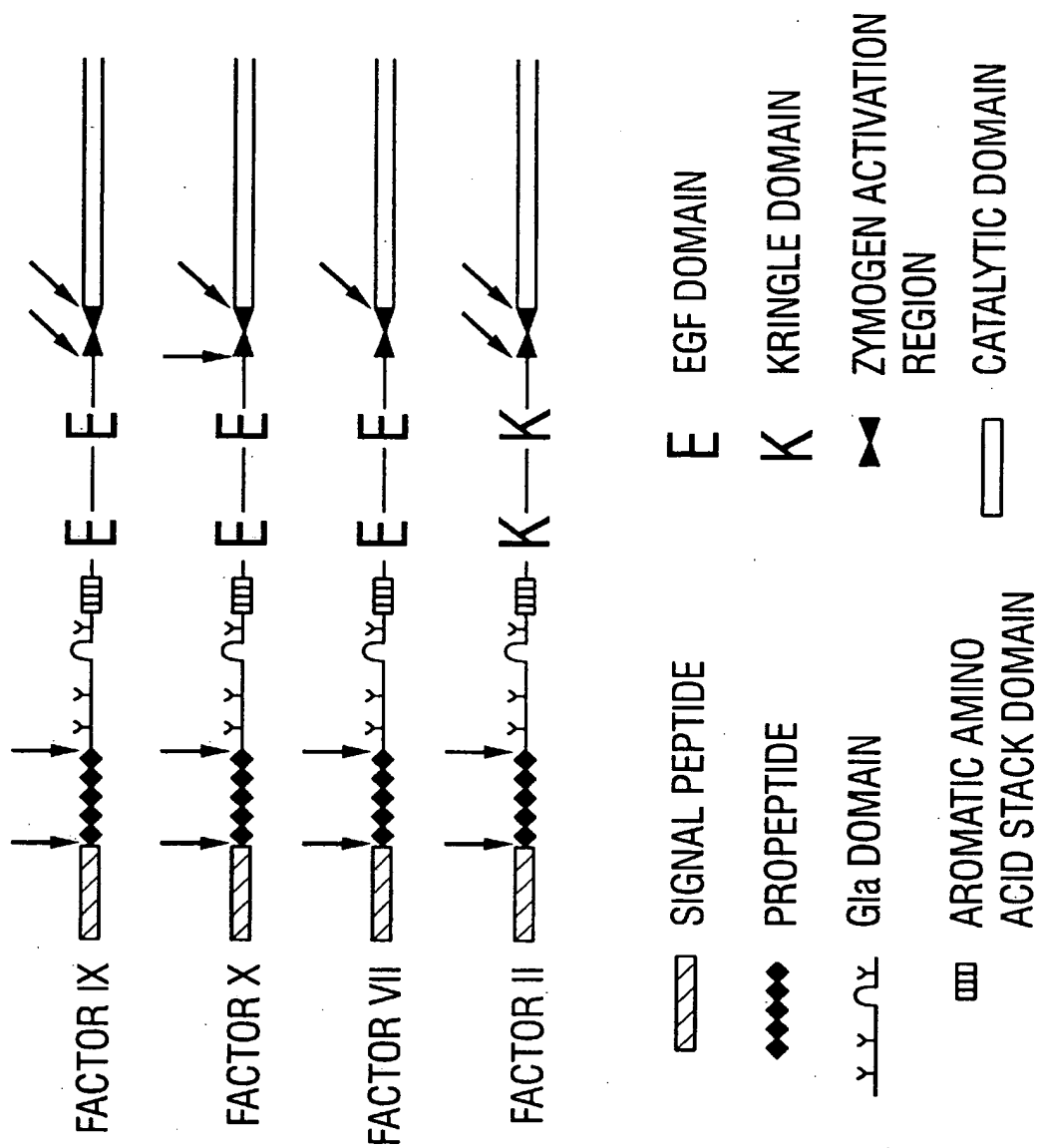


FIG. 8

## TISSUE FACTOR COMPOSITIONS AND LIGANDS FOR THE SPECIFIC COAGULATION OF VASCULATURE

The present application is a continuation-in-part of co-pending U.S. patent application Ser. No. 08/273,567, filed Jul. 11, 1994; which is a continuation-in-part of U.S. patent application Ser. No. 08/205,330, filed Mar. 2, 1994, now U.S. Pat. No. 5,855,866; which is a continuation-in-part of U.S. Ser. No. 07/846,349, filed Mar. 5, 1992. The entire text and figures of the above-referenced disclosures are specifically incorporated herein by reference without disclaimer.

This invention was made with government support under Contract No. P01 HL 16411 by NIH. The government has certain rights in the invention.

### BACKGROUND OF THE INVENTION

#### 1. Field of the Invention

The present invention relates generally to the fields of blood vessels and of coagulation. More particularly, it provides a variety of growth factor-based and immunological reagents, including bispecific antibodies, for use in achieving specific coagulation.

#### 2. Description of the Related Art

Advances in the chemotherapy of neoplastic disease have been realized during the last 30 years. This includes some progress in the development of new chemotherapeutic agents and, more particularly, the development of regimens for concurrent administration of drugs. A significant understanding of the neoplastic processes at the cellular and tissue level, and the mechanism of action of basic antineoplastic agents, has also allowed advances in the chemotherapy of a number of neoplastic diseases, including choriocarcinoma, Wilm's tumor, acute leukemia, rhabdomyosarcoma, retinoblastoma, Hodgkin's disease and Burkitt's lymphoma. Despite the advances that have been made in a few tumors, though, many of the most prevalent forms of human cancer still resist effective chemotherapeutic intervention.

A significant underlying problem that must be addressed in any treatment regimen is the concept of "total cell kill." This concept holds that in order to have an effective treatment regimen, whether it be a surgical or chemotherapeutic approach or both, there must be a total cell kill of all so-called "clonogenic" malignant cells, that is, cells that have the ability to grow uncontrolled and replace any tumor mass that might be removed. Due to the ultimate need to develop therapeutic agents and regimens that will achieve a total cell kill, certain types of tumors have been more amenable than others to therapy. For example, the soft tissue tumors (e.g., lymphomas), and tumors of the blood and blood-forming organs (e.g., leukemias) have generally been more responsive to chemotherapeutic therapy than have solid tumors such as carcinomas.

One reason for the susceptibility of soft and blood-based tumors to chemotherapy is the greater physical accessibility of lymphoma and leukemic cells to chemotherapeutic intervention. Simply put, it is much more difficult for most chemotherapeutic agents to reach all of the cells of a solid tumor mass than it is the soft tumors and blood-based tumors, and therefore much more difficult to achieve a total cell kill. Increasing the dose of chemotherapeutic agents most often results in toxic side effects, which generally limits the effectiveness of conventional anti-tumor agents.

The strategy to develop successful antitumor agents involves the design of agents that will selectively kill tumor

cells, while exerting relatively little, if any, untoward effects against normal tissues. This goal has been elusive to achieve, though, in that there are few qualitative differences between neoplastic and normal tissues. Because of this, much research over the years has focused on identifying tumor-specific "marker antigens" that can serve as immunological targets both for chemotherapy and diagnosis. Many tumor-specific, or quasi-tumor-specific ("tumor-associated"), markers have been identified as tumor cell antigens that can be recognized by specific antibodies. Unfortunately, it is generally the case that tumor specific antibodies will not in and of themselves exert sufficient antitumor effects to make them useful in cancer therapy.

More recently, immunotoxins have been employed in an attempt to selectively target cancer cells. Immunotoxins are conjugates of a specific targeting agent, typically a tumor-directed antibody or fragment, with a cytotoxic agent, such as a toxin moiety. The targeting agent is designed to direct the toxin to cells carrying the targeted antigen and to kill such cells. "Second generation" immunotoxins have now been developed, for example, those that employ deglycosylated ricin A chain to prevent entrapment of the immunotoxin by the liver and reduce hepatotoxicity (Blakey et al., 1987a,b), and those with new crosslinkers to endow the immunotoxins with higher in vivo stability (Thorpe et al., 1988).

Immunotoxins have proven effective at treating lymphomas and leukemias in mice (Thorpe et al., 1988; Ghetie et al., 1991; Griffin et al., 1988a,b) and in man (Vitetta et al., 1991). However, lymphoid neoplasias are particularly amenable to immunotoxin therapy because the tumor cells are relatively accessible to blood-borne immunotoxins. Also, it is possible to target normal lymphoid antigens because the normal lymphocytes, which are killed along with the malignant cells during therapy, are rapidly regenerated from progenitors lacking the target antigens.

In contrast with their efficacy in lymphomas, immunotoxins have proved relatively ineffective in the treatment of solid tumors (Weiner et al., 1989; Byers et al., 1989). The principal reason for this is that solid tumors are generally impermeable to antibody-sized molecules: specific uptake values of less than 0.001% of the injected dose/g of tumor are not uncommon in human studies (Sands et al., 1988; Epenetos et al., 1986). Another significant problem is that antigen-deficient mutants can escape being killed by the immunotoxin and regrow (Thorpe et al., 1988).

Furthermore, antibodies that enter the tumor mass do not distribute evenly for several reasons. Firstly, the dense packing of tumor cells and fibrous tumor stromas present a formidable physical barrier to macromolecular transport and, combined with the absence of lymphatic drainage, create an elevated interstitial pressure in the tumor core which reduces extravasation and fluid convection (Baxter et al., 1991; Jain, 1990). Secondly, the distribution of blood vessels in most tumors is disorganized and heterogeneous, so some tumor cells are separated from extravasating antibody by large diffusion distances (Jain, 1990). Thirdly, all of the antibody entering the tumor may become adsorbed in perivascular regions by the first tumor cells encountered, leaving none to reach tumor cells at more distant sites (Baxter et al., 1991; Kennel et al., 1991).

Thus, it is quite clear that a significant need exists for the development of novel strategies for the treatment of solid tumors. One approach involves the targeting of agents to the vasculature of the tumor, rather than to tumor cells. Solid tumor growth is highly dependent on the vascularization of

the tumor and the growth of tumor cells can only be maintained if the supply of oxygen, nutrients and other growth factors and the efflux of metabolic products are satisfactory. Indeed, it has been observed that many existing therapies may already have, as part of their action, a vascular-mediated mechanism of action (Denekamp, 1990).

The present inventors propose that targeting the vasculature will likely deprive the tumor of life sustaining events and result in reduced tumor growth rate or tumor cell death. This approach is contemplated to offer several advantages over direct targeting of tumor cells. Firstly, the target cells are directly accessible to intravenously administered therapeutic agents, permitting rapid localization of a high percentage of the injected dose (Kennel et al., 1991). Secondly, since each capillary provides oxygen and nutrients for thousands of cells in its surrounding 'cord' of tumor, even limited damage to the tumor vasculature could produce an avalanche of tumor cell death (Denekamp, 1990; Denekamp, 1984). Finally, the outgrowth of mutant endothelial cells, lacking a target antigen, is unlikely because they are normal cells.

At the present time, it is generally accepted that for tumor vascular targeting to succeed, antibodies are required that recognize tumor endothelial cells but not those in normal tissues. Although several antibodies have been raised (Duijvestijn et al., 1987; Hagemeier et al., 1986; Bruland et al., 1986; Murray et al., 1989; Schlingemann et al., 1985), none have shown a high degree of specificity. Also, there do not appear to be reports of any particular agents, other than the aforementioned toxins, that show promise as the second agent in a vascular targeted antibody conjugate. Thus, unfortunately, while vascular targeting presents certain theoretical advantages, effective strategies incorporating these advantages have yet to be developed.

### SUMMARY OF THE INVENTION

The present invention overcomes the limitations of the prior art by providing novel compositions and methods for use in achieving specific coagulation, for example, coagulation in tumor vasculature, with limiting side-effects. The invention, in a general and overall sense, concerns various novel immunological and growth factor-based bispecific compositions capable of stimulating coagulation in disease-associated vasculature, and methods for their preparation and use.

The invention provides binding ligands that may generally be described as "bispecific binding ligands". Such ligands comprise a "first binding region" that typically binds to a disease-related target cell, such as a tumor cell, or to a component associated with such a cell; to some component associated with disease-related vasculature, e.g., tumor vasculature; or to a component of, or associated with, disease-associated stroma. The first binding region is operatively associated with or linked to a "coagulating agent", which may be either a coagulation factor itself or may be a second binding region that is capable of binding to a coagulation factor.

The binding ligands of the invention are described as "bispecific" as they are "at least" bispecific, i.e., they comprise, at a minimum, two functionally distinct regions. Compositions and methods using other constructs, such as trispecific and multispecific binding ligands, are also included within the scope of the invention. Combined compositions, kits and methods of using the bispecific coagulating ligands described herein in conjunction with other effectors, such as other immunological- and growth-

factor-based compositions, antigen-inducing agents, immunostimulants, immunosuppressants, chemotherapeutic drugs, and the like, are also contemplated.

The first binding regions, and any second binding regions, may be antibodies or fragments thereof. As used herein, the term "antibody" is intended to refer broadly to any immunologic binding agent such as IgG, IgM, IgA, IgD and IgE. Generally, IgG or IgM are preferred because they are the most common antibodies in the physiological situation and because they are most easily made in a laboratory setting. Monoclonal antibodies (MAbs) are recognized to have certain advantages, e.g., reproducibility and large-scale production, and their use is generally preferred. Engineered antibodies, such as recombinant antibodies and humanized antibodies, also fall within the scope of the invention.

Where antigen binding regions of antibodies are employed as the binding and targeting agent, a complete antibody molecule may be employed. Alternatively, a functional antigen binding region may be used, as exemplified by Fv, scFv (single chain Fv), Fab', Fab, Dab or F(ab')<sub>2</sub> fragment of an antibody. The techniques for preparing and using various antibody-based constructs are well known in the art and are further described herein.

The coagulation factor portion of the binding ligands is formed so that it maintains significant functional capacity, i.e., it is in a form so that, when delivered to the target region, it still retains its ability to promote blood coagulation or clotting. However, in certain embodiments, the coagulation factor portion of the binding ligands will be less active than, for example, the natural counterpart of the coagulant, and the factor will achieve the desired level of activity only upon delivery to the target area. One such example is a vitamin K-dependent coagulation factor that lacks the Gla modification, which will nonetheless achieve significant functional activity upon binding of the first binding region of the bispecific ligand to a membrane environment.

Where a second binding region is used to bind a coagulation factor, it is generally chosen so that it recognizes a site on the coagulation factor that does not significantly impair its ability to induce coagulation. Likewise, where a coagulation factor is covalently linked to a first binding agent, a site distinct from its functional coagulating site is generally used to join the molecules.

The "first binding region" of the bispecific ligands of the invention may be any component that binds to a designated target site, i.e., a site associated with a tumor region or other disease site in which coagulation is desired. The target molecule, in the case of tumor targeting, will generally be present at a higher concentration in the tumor site than in non-tumor sites. In certain preferred embodiments, the targeted molecules, whether associated with tumor cells, tumor vascular cells, tumor-associated stroma, or other components, will be restricted to such cells or other tumor-associated entities, however, this is not a requirement of the invention.

In this regard, it should be noted that tumor vasculature is 'prothrombotic' and is predisposed towards coagulation. It is thus contemplated that a targeted coagulant is likely to preferentially coagulate tumor vasculature while not coagulating normal tissue vasculature, even if other normal cells or body components, particularly, the normal endothelial cells or even stroma, express significant levels of the target molecule. This approach is therefore envisioned to be safer for use in humans, e.g., as a means of treating cancer, than that of targeting a toxin to tumor vasculature.

In certain embodiments, the first binding regions contemplated for use in this invention may be directed to a tumor

cell component or to a component associated with a tumor cell. In targeting generally to a tumor cell, it is believed that the first binding ligand will cause the coagulation factor component of the bispecific binding ligand to concentrate on those perivascular tumor cells nearest to the blood vessel and thus trigger coagulation of tumor blood vessels, giving the bispecific binding ligand significant utility.

A first binding region may therefore be a component, such as an antibody or other agent, that binds to a tumor cell. Agents that "bind to a tumor cell" are defined herein as ligands that bind to any accessible component or components of a tumor cell, or that bind to a component that is itself bound to, or otherwise associated with, a tumor cell, as further described herein.

The majority of such tumor-binding ligands are contemplated to be agents, particularly antibodies, that bind to a cell surface tumor antigen or marker. Many such antigens are known, as are a variety of antibodies for use in antigen binding and tumor targeting. The invention thus includes first binding regions, such as antigen binding regions of antibodies, that bind to an identified tumor cell surface antigen, such as those listed in Table I, and first binding regions that preferentially or specifically bind to an intact tumor cell, such as binding to a tumor cell listed in Table II.

Currently preferred examples of tumor cell binding regions are those that comprise an antigen binding region of an antibody that binds to the cell surface tumor antigen p185<sup>HER2</sup>, milk mucin core protein, TAG-72, Lewis x or carcinoembryonic antigen (CEA). Another group of currently preferred tumor cell binding regions are those that comprise an antigen binding region of an antibody that binds to a tumor-associated antigen that binds to the antibody 9.2.27, OV-TL3, MOv18, B3, KS1/4, 260F9 or D612.

The antibody 9.2.27 binds to high M<sub>r</sub> melanoma antigens, OV-TL3 and MOv18 both bind to ovarian-associated antigens, B3 and KS1/4 bind to carcinoma antigens, 260F9 binds to breast carcinoma and D612 binds to colorectal carcinoma. Antigen binding moieties that bind to the same antigen as D612, B3 or KS1/4 are particularly preferred. D612 is described in U.S. Pat. No. 5,183,756, and has ATCC Accession No. HB 9796; B3 is described in U.S. Pat. No. 5,242,813, and has ATCC Accession No. HB 10573; and recombinant and chimeric KS1/4 antibodies are described in U.S. Pat. No. 4,975,369; each incorporated herein by reference.

In tumor cell targeting, where the tumor marker is a component, such as a receptor, for which a biological ligand has been identified, the ligand itself may also be employed as the targeting agent, rather than an antibody. Active fragments or binding regions of such ligands may also be employed.

First binding regions for use in the invention may also be components that bind to a ligand that is associated with a tumor cell marker. For example, where the tumor antigen in question is a cell-surface receptor, tumor cells *in vivo* will have the corresponding biological ligand, e.g., hormone, cytokine or growth factor, bound to their surface and available as a target. This includes both circulating ligands and "paracrine-type" ligands that may be generated by the tumor cell and then bound to the cell surface.

The present invention thus further includes first binding regions, such as antibodies and fragments thereof, that bind to a ligand that binds to an identified tumor cell surface antigen, such as those listed in Table I, or that preferentially or specifically binds to one or more intact tumor cells. Additionally, the receptor itself, or preferably an engineered

or otherwise soluble form of the receptor or receptor binding domain, could also be employed as the binding region of a bispecific coagulating ligand.

In further embodiments, the first binding region may be a component that binds to a target molecule that is specifically or preferentially expressed in a disease site other than a tumor site. Exemplary target molecules associated with other diseased cells include, for example, PSA associated with Benign Prostatic Hyperplasia (BPH) and FGF associated with proliferative diabetic retinopathy. It is believed that an animal or patient having one of the above diseases would benefit from the specific induction of coagulation in the disease site.

This is the meaning of "diseased cell" in the present context, i.e., it is a cell that is connected with a disease or disorder, which cell expresses, or is otherwise associated with, a targetable component that is present at a higher concentration in the disease sites and cells in comparison to its levels in non-diseased sites and cells. This includes targetable components that are associated with the vasculature in the disease sites.

Exemplary first binding regions for use in targeting and delivering a coagulant to other disease sites include antibodies, such as anti-PSA (BPH), and GF82, GF67 3H3, that bind to FGF. Biological binding ligands, such as FGF, that bind to the relevant receptor, in this case the FGF receptor, may also be used. Antibodies against vascular targets may also be employed, as described below. The targeting of the stroma or endothelial cells provides a powerful means of treating other diseases where the "diseased cell" itself may not be associated with a strong or unique marker antigen.

In further embodiments, the first binding regions of the invention will be components that are capable of binding to a component of disease-associated vasculature, i.e., a region of vasculature in which specific coagulation would be advantageous to the animal or patient. First binding regions capable of binding to a component specifically or preferentially associated with tumor vasculature are currently preferred. "Components of tumor vasculature" include both tumor vasculature endothelial cell surface molecules and any components, such as growth factors, that may be bound to these cell surface receptors or molecule. These include markers found, expressed, accessible to binding or otherwise localized on the cell surfaces of tumor-associated vascular endothelium as compared to normal vasculature.

Certain preferred binding ligands are antibodies, and fragments thereof, that bind to cell surface receptors and antibodies that bind to the corresponding biological ligands of these receptors. Exemplary antibodies are those that bind to MHC Class II proteins, VEGF/VPF receptors, FGF receptors, TGF $\beta$  receptors, a TIE (tyrosine kinase-immunoglobulin-epidermal growth factor-like receptor, including TIE-1 and TIE-2), VCAM-1, P-selectin, E-selectin,  $\alpha_v\beta_3$  integrin, pleiotropin, endosialin and endoglin.

First binding regions that comprise an antigen binding region of an antibody that binds to endoglin are one group of preferred agents. These are exemplified by antibodies and fragments that bind to the same epitope as the monoclonal antibody TEC-4 or the monoclonal antibody TEC-11, deposited Mar. 12, 1997 with the American Type Culture Collection, 12301 Parklawn Drive, Rockville, Md. 20852, and given the ATCC Accession numbers ATCC HB-12312 and ATCC HB-12311, respectively.

Antigen binding region of antibodies that bind to the VEGF receptor are another group of preferred agents. These

are particularly exemplified by antibodies and fragments that bind to the same epitope as the monoclonal antibody 3E11, 3E7, 5G6, 4D8, 10B10 or TEC-110. Anti-VEGF antibodies with binding specificities substantially the same as any one of the antibodies termed 1B4, 4B7, 1B8, 2C9, 7D9, 12D2, 12D7, 12E10, 5ES, 8E5, 5E11, 7E11, 3F5, 10F3, 1F4, 2F8, 2F9, 2F10, 1G6, 1G11, 3G9, 9G11, 10G9, GV97, GV39, GV97 $\gamma$ , GV39 $\gamma$ , GV59 or GV14 may also be used. Further suitable anti-VEGF antibodies include 4.6.1., A3.13.1, A4.3.1 and B2.6.2 (Kim et. al., 1992); SBS94.1 (Oncogene Science); G143-264 and G143-856 (Pharmingen).

Further useful antibodies are those that bind to a ligand that binds to a tumor vasculature cell surface receptor. Antibodies that bind to VEGF/VPF, FGF, TGF $\beta$ , a ligand that binds to a TIE, a tumor-associated fibronectin isoform, scatter factor, hepatocyte growth factor (HGF), platelet factor 4 (PF4), PDGF (including PDGF $\alpha$  and PDGF $\beta$ ) and TIMP (a tissue inhibitor of metalloproteinases, including TIMP-1, TIMP-2 and TIMP-3) are therefore useful in these embodiments, with antibodies that bind to VEGF/VPF, FGF, TGF $\beta$ , a ligand that binds to a TIE or a tumor-associated fibronectin isoform often being preferred.

In still further embodiments, it is contemplated that markers specific for tumor vasculature may be those that have been first induced, i.e., their expression specifically manipulated by the hand of man, allowing subsequent targeting using a binding ligand, such as an antibody.

Exemplary inducible antigens include those inducible by a cytokine, e.g., IL-1, IL-4, TNF- $\alpha$ , TNF- $\beta$  or IFN- $\gamma$ , as may be released by monocytes, macrophages, mast cells, helper T cells, CD8-positive T-cells, NK cells or even tumor cells. Examples of the induced targets are E-selectin, VCAM-1, ICAM-1, endoglin and MHC Class II antigens. When using MHC Class II induction, the suppression of MHC Class II in normal tissues is generally required, as may be achieved using a cyclosporin, such as Cyclosporin A (CsA), or a functionally equivalent agent.

Further inducible antigens include those inducible by a coagulant, such as by thrombin, Factor IX/IXa, Factor X/Xa, plasmin or a metalloproteinase (matrix metalloproteinase, MMP). Generally, antigens inducible by thrombin will be used. This group of antigens includes P-selectin, E-selectin, PDGF and ICAM-1, with the induction and targeting of P-selectin and/or E-selectin being generally preferred.

Antibodies that bind to epitopes that are present on ligand-receptor complexes, but absent from both the individual ligand and receptor may also be used. Such antibodies will recognize and bind to a ligand-receptor complex, as presented at the cell surface, but will not bind to the free ligand or uncomplexed receptor. A "ligand-receptor complex", as used herein, therefore refers to the resultant complex produced when a ligand, such as a growth factor, specifically binds to its receptor, such as a growth factor receptor. This is exemplified by the VEGF/VEGF receptor complex.

It is envisioned that such ligand-receptor complexes will likely be present in a significantly higher number on tumor-associated endothelial cells than on non-tumor associated endothelial cells, and may thus be targeted by anti-complex antibodies. Anti-complex antibodies include those antibodies and fragments thereof that bind to the same epitope as the monoclonal antibody 2E5, 3E5 or 4E5.

In further embodiments, the first binding regions contemplated for use in this invention will bind to a component of disease-associated stroma, such as a component of tumor-associated stroma. This includes antigen binding regions of

antibodies that bind to basement membrane components, activated platelets and inducible tumor stroma components, especially those inducible by a coagulant, such as thrombin. "Activated platelets" are herein defined as a component of tumor stroma, one reason for which being that they bind to the stroma when activated.

Preferred targetable elements of tumor-associated stroma are currently the tumor-associated fibronectin isoforms. Fibronectin isoforms are ligands that bind to the integrin family of receptors. Tumor-associated fibronectin isoforms are available, e.g., as recognized by the MAb BC-1. This Mab, and others of similar specificity, are therefore preferred agents for use in the present invention. Fibronectin isoforms, although stromal components, bind to endothelial cells and may thus be considered as a targetable vascular endothelial cell-bound ligand in the context of the invention.

Another group of preferred anti-stromal antibodies are those that bind to RIBS, the receptor-induced binding site, on fibrinogen. RIBS is a targetable antigen, the expression of which in stroma is dictated by activated platelets. Antibodies that bind to LIBS, the ligand-induced binding site, on activated platelets are also useful.

One further group of useful antibodies are those that bind to tenascin, a large molecular weight extracellular glycoprotein expressed in the stroma of various benign and malignant tumors. Antibodies such as those described by Shrestha et. al. (1994) and 143DB7C8, described by Tuominen & Kallioinen (1994), may thus be used as the binding portions of the coagulgands. "Components of disease- and tumor-associated stroma" include various cell types, matrix components, effectors and other molecules or components that may be considered, by some, to be outside the narrowest definition of "stroma", but are nevertheless targetable entities that are preferentially associated with a disease region, such as a tumor.

Accordingly, the first binding region may be an antibody or ligand that binds to a smooth muscle cell, a pericyte, a fibroblast, a macrophage, an infiltrating lymphocyte or leukocyte. First binding regions may also bind to components of the connective tissue, and include antibodies and ligands that bind to, e.g., fibrin, proteoglycans, glycoproteins, collagens, and anionic polysaccharides such as heparin and heparin-like compounds.

In other preferred embodiments, the vasculature and stroma binding ligands of the invention will be binding regions that are themselves biological ligands, or portions thereof, rather than an antibody. "Biological ligands" in this sense will be those molecules that bind to or associate with cell surface molecules, such as receptors, that are accessible in the stroma or on vascular cells; as exemplified by cytokines, hormones, growth factors, and the like. Any such growth factor or ligand may be used so long as it binds to the disease-associated stroma or vasculature, e.g., to a specific biological receptor present on the surface of a tumor vasculature endothelial cell.

Suitable growth factors for use in these aspects of the invention include, for example, VEGF/VPF (vascular endothelial cell growth factor/vascular permeability factor), FGF (the fibroblast growth factor family of proteins), TGF $\beta$  (transforming growth factor B), a ligand that binds to a TIE, a tumor-associated fibronectin isoform, scatter factor, hepatocyte growth factor (HGF), platelet factor 4 (PF4), PDGF (platelet derived growth factor), TIMP or even IL-8, IL-6 or Factor XIIIa. VEGF/VPF and FGF will often be preferred.

Targeting an endothelial cell-bound component, e.g., a cytokine or growth factor, with a binding ligand construct



based. on a known receptor is also contemplated. Generally, where a receptor is used as a targeting component, a truncated or soluble form of the receptor will be employed. In such embodiments, it is particularly preferred that the targeted endothelial cell-bound component be a dimeric ligand, such as VEGF. This is preferred as one component of the dimer will already be bound to the cell surface receptor in situ, leaving the other component of the dimer available for binding the soluble receptor portion of the bispecific coagulating ligand.

The use of bispecific, or tri- or multi-specific, ligands that include at least one targeting region capable of binding to a component of disease-associated vasculature has the advantage that vascular endothelial cells, and disease-associated agents such as activated platelets, are similar in different diseases, and particularly in different tumors. This phenomenon makes it feasible to treat numerous diseases and types of cancer with one pharmaceutical, rather than having to tailor the agent to each individual disease or specific tumor type.

The compositions and methods of the present invention are thus suitable for use in treating both benign and malignant diseases that have a vascular component. Such vasculature-associated diseases include benign growths, such as EPH, diabetic retinopathy, vascular restenosis, arteriovenous malformations (AVM), meningioma, hemangioma, neovascular glaucoma and psoriasis. Also included within this group are synovitis, dermatitis, endometriosis, angiofibroma, rheumatoid arthritis, atherosclerotic plaques, corneal graft neovascularization, hemophilic joints, hypertrophic scars, osler-weber syndrome, pyogenic granuloma retrolental fibroplasia, scleroderma, trachoma, and vascular adhesions. Each of the above diseases are known to have a common angio-dependent pathology, it is thus contemplated that achieving coagulation in the disease site would prove beneficial.

The bispecific binding ligand-coagulation factor conjugates of the present invention may be conjugates in which the two or more components are covalently linked. For example, by using a biochemical crosslinker and, preferably, one that has reasonable stability in blood, as exemplified by SMPT. The components may also be linked using the well-known avidin (or streptavidin) and biotin combination. Various cross-linkers, avidin:biotin compositions and combinations, and techniques for preparing conjugates, are well known in the art and are further described herein.

Alternatively, such bispecific coagulating agents may be fusion proteins prepared by molecular biological techniques, i.e., by joining a gene (or cDNA) encoding a binding ligand or region to a gene (or cDNA) encoding a coagulation factor. This is well known in the art and is further described herein. Typically, an expression vector is prepared that comprises, in the same reading frame, a DNA segment encoding the first binding region operatively linked to a DNA segment encoding the coagulation factor and expressing the vector in a recombinant host cell so that it produces the encoded fusion protein.

Coagulation factors for use in the invention may comprise one of the vitamin K-dependent coagulant factors, such as Factor II/IIa, Factor VII/VIIa, Factor IX/IXa or Factor X/Xa. Factor V/Va, VIII/VIIIa, Factor XI/XIa, Factor XII/XIIa and Factor XIII/XIIIa may also be used.

Particular aspects concern the vitamin K-dependent coagulation factors that lack the Gla modification. Such factors may be prepared by expressing a vitamin K-dependent coagulation factor-encoding gene in a procary-

otic host cell (which cells are unable to effect the Glu to Gla modification). The factors may also be prepared by making an engineered coagulation factor gene that encodes a vitamin K-dependent coagulation factor lacking the necessary or "corresponding" Glutamic acid residues, and then expressing the engineered gene in virtually any recombinant host cell. Equally, such a coagulation factor may be prepared by treating the vitamin K-dependent coagulation factor protein to remove or alter the corresponding Glutamic acid residues.

Preferred coagulation factors for use in the binding ligands of the invention are Tissue Factor and Tissue Factor derivatives. One group of useful Tissue Factors are those mutants deficient in the ability to activate Factor VII. A Tissue Factor may be rendered deficient in the ability to activate Factor VII by altering one or more amino acids from the region generally between about position 157 and about position 167 in the amino acid sequence. Exemplary mutants are those wherein Trp at position 158 is changed to Arg; wherein Ser at position 162 is changed to Ala; wherein Gly at position 164 is changed to Ala; and the double mutant wherein Trp at position 158 is changed to Arg and Ser at position 162 is changed to Ala.

Further preferred Tissue Factor derivatives are truncated Tissue Factors, dimeric or even polymeric Tissue Factors and dimeric, or even polymeric, truncated Tissue Factors.

The present invention further provides novel Tissue Factor constructs that comprise a Tissue Factor or derivative operatively linked to at least one other Tissue Factor or derivative. Truncated Tissue Factors are preferred, with truncated Tissue Factors that have been modified to comprise a hydrophobic membrane insertion moiety being particularly preferred. "A hydrophobic membrane insertion moiety", as defined herein, is one or more units that direct the insertion or functional contact of the Tissue Factor with a membrane. The hydrophobic membrane insertion moieties of the invention are exemplified by stretches of substantially hydrophobic amino acids, such as between about 3 and about 20 hydrophobic amino acids; and also by fatty acids.

The hydrophobic amino acids may be located either at the N- or C-terminus of the truncated Tissue Factor, or appended at another point of the molecule. Where hydrophobic amino acids are used, they may be advantageously incorporated into the molecule by molecular biological techniques. Equally, hydrophobic amino acids or fatty acids may be added to the Tissue Factor using synthetic chemistry techniques.

In the Tissue Factor dimers, trimers and polymers of the present invention, each of the Tissue Factors or derivatives may be operatively linked via, e.g., a disulfide, thioether or peptide bond. In certain embodiments, the Tissue Factor units will be linked via a bond that is substantially stable in plasma, or in the physiological environment in which it is intended for use. This is based upon the inventors' concept that the dimeric form of Tissue Factor may prove to be the most biologically active. However, there is no requirement for a stable linkage as Tissue Factor monomers are known to be active in the methods of the invention.

One or more of the Tissue Factors or truncated Tissue Factors in the dimers and multimers may also be modified to contain a terminal cysteine residue or another moiety that is suitable for linking the Tissue Factor construct to a second agent, such as a binding region.

Tissue Factor monomers, truncated Tissue Factors, and Tissue Factor dimers and multimers that contain a peptide that includes a selectively-cleavable amino acid sequence therefore form another aspect of the invention. Peptide

linkers that include a cleavage site for urokinase, plasmin, Thrombin, Factor IXa, Factor Xa or a metalloproteinase, such as an interstitial collagenase, a gelatinase or a stromelysin, are particularly preferred.

The Tissue Factor monomers, truncated Tissue Factors, Tissue Factor dimers and multimers, and indeed any coagulant, may therefore be linked to a second agent, such as an antibody, an antigen binding region of an antibody, a ligand or a receptor, via a biologically-releasable bond. The preference for peptide linkers that include a cleavage site for the above listed proteinases is based on the presence of such proteinases within, e.g., a tumor environment. The delivery of a bispecific agent or ligand to the tumor site is expected to result in cleavage, resulting in the relatively specific release of the coagulation factor.

Particular constructs of the invention are those comprising an operatively linked series of units in the sequence: a cysteine residue, a selectively cleavable peptide linker, a stretch of hydrophobic amino acids, a first truncated Tissue Factor and a second truncated Tissue Factor; or in the sequence: a first cysteine residue, a selectively cleavable peptide linker, a first stretch of hydrophobic amino acids, a first truncated Tissue Factor, a second truncated Tissue Factor and a second stretch of hydrophobic amino acids; wherein each construct may or not be linked to a second agent such as an antibody, ligand or receptor.

Other suitable coagulation factors are Russell's viper venom Factor X activator; platelet-activating compounds, such as thromboxane A<sub>2</sub> and thromboxane A<sub>2</sub> synthase; and inhibitors of fibrinolysis, such as α<sub>2</sub>-antiplasmin.

Also encompassed by the invention are binding ligands in which the coagulation factor is not covalently linked to the conjugate, but is non-covalently bound thereto by means of binding to a second binding region that is operatively linked to the targeting agent of the construct. Suitable "second binding regions" include antigen combining sites of antibodies that have binding specificity for the coagulation factor, including functional portions of antibodies, such as scFv, Fv, Fab', Fab and F(ab')<sub>2</sub> fragments.

Binding ligands that contain antibodies, or fragments thereof, directed against the vitamin K-dependent coagulant Factor II/IIa, Factor VII/VIIa, Factor IX/IXa or Factor X/Xa; a vitamin K-dependent coagulation factor that lacks the Gla modification; Tissue Factor, a mutant Tissue Factor, a truncated Tissue Factor, a dimeric Tissue Factor, a polymeric Tissue Factor, a dimeric truncated Tissue Factor; Prekallikrein; Factor V/Va, VIII/VIIIa, Factor XI/XIa, Factor XII/XIIa, Factor XIII/XIIIa; Russell's viper venom Factor X activator, thromboxane A<sub>2</sub> or α<sub>2</sub>-antiplasmin are therefore contemplated.

The non-covalently bound coagulating agents may be bound to, or "precomplexed", with a coagulation factor, e.g., so that they may be used to deliver an exogenous coagulation factor to a disease site, e.g., the tumor vasculature, of an animal upon administration. Equally, binding ligands that comprise a second binding region that is specific for a coagulation factor may also be administered to an animal in an "uncomplexed" form and still function to achieve specific coagulation; in which instance, the agent would garner circulating (endogenous) coagulation factor and concentrate it within the disease or tumor site.

In terms of the "coagulation factors" or coagulating agents, these may be endogenous coagulation factors and derivatives thereof, or exogenously added version of such factors, including recombinant versions. Coagulants (in the present "coaguligands") have the distinct advantage over

toxins (in immunotoxins) as they will not produce significant adverse side effects upon targeting to a marker that proves to be less than 100% disease-restricted. Furthermore, the coagulants used will most often be of human origin, and will therefore pose less immunogenicity problems than foreign toxins, such as ricin A chain.

Although not limited to such compositions, important examples of compositions in accordance with this invention are bispecific antibodies, which antibodies comprise a first antigen binding region that binds to a disease cell or component of disease-associated vasculature marker and a second antigen binding region that binds to a coagulation factor. The invention also provides scFv, Fv, Fab', Fab and F(ab')<sub>2</sub> fragments of such bispecific antibodies. One currently preferred example of such a bispecific antibody is an antibody comprising one binding site directed against an MHC Class II antigen and another binding site directed against Tissue Factor.

In further embodiments, the present invention provides pharmaceutical compositions of, and therapeutic kits comprising, any or a combination of the above binding ligands and bispecific antibodies in pharmacologically acceptable forms. This includes pharmaceutical compositions and kits where the binding ligand has a first binding region that is covalently linked to a coagulation factor, and also binding ligands in which the first binding region is covalently linked to a second binding region that, in turn, binds to the coagulation factor—whether binding occurs prior to, or subsequent to, administration to an animal.

Pharmaceutical compositions and therapeutic kits that include a combination of bispecific, trispecific or multispecific binding ligands in accordance with the invention are also contemplated. This includes combinations where one binding ligand is directed against a diseased cell or a tumor cell and where another is directed against a vasculature endothelial cell marker or component of disease-associated stroma. Other distinct components may also be included in the compositions and kits of the invention, such as antibodies, immunotoxins, immunoeffectors, chemotherapeutic agents, and the like.

The kits may also include an antigen suppressor, such as a cyclosporin, for use in suppressing antigen expression in endothelial cells of normal tissues; and/or an "inducing agent" for use in inducing disease-associated vascular endothelial cells or stroma to express a targetable antigen, such as E-selectin, P-selectin or an MHC Class II antigen. Exemplary inducing agents include T cell clones that bind disease or tumor antigens and that produce IFN-γ, although it is currently preferred that such clones be isolated from the animal to be treated using the kit.

Preferred inducing agents are bispecific antibodies that bind to disease or tumor cell antigens, or even stromal components, and to effector cells capable of producing cytokines, coagulants, or other factors, that induce expression of desired target antigens. Currently, one preferred group of bispecific antibodies are those that bind to a tumor antigen and to the activation antigens CD14 or CD16, to stimulate IL-1 production by monocytes, macrophages or mast cells; and those that bind to a tumor antigen and to the activation antigens CD2, CD3 or CD28, and preferably CD28, to stimulate IFN-γ production by NK cells or preferably by T cells.

A second preferred group of bispecific antibodies are those that bind to a tumor antigen or to a component of tumor stroma, and to Tissue Factor, a Tissue Factor derivative, prothrombin, Factor VII/VIIa, Factor IX/IXa,

Factor X/Xa, Factor XI/XIa or Russell's viper venom Factor X activator, to stimulate thrombin production. Kits comprising such bispecific antibodies as a first "inducing" composition will generally include a second pharmaceutical composition that comprises a binding ligand that comprises a first binding region that binds to P-selectin or E-selectin.

The bispecific ligands of the invention, and other components as desired, may be conveniently aliquoted and packaged, using one or more suitable container means, and the separate containers dispensed in a single package. Pharmaceutical compositions and kits are further described herein.

Although the present invention has significant clinical utility in the delivery of coagulants and in disease treatment, it also has many *in vitro* uses. These include, for example, various assays based upon the binding ability of the particular antibody, ligand or receptor, of the bispecific compounds. The bispecific coagulating ligands of invention may thus be employed in standard binding assays and protocols, such as in immunoblots, Western blots, dot blots, RIAs, ELISAs, immunohistochemistry, fluorescent activated cell sorting (FACS), immunoprecipitation, affinity chromatography, and the like, as further described herein.

In still further embodiments, the invention concerns methods for delivering a coagulant to disease-associated vasculature, as may be used to treat diseases such as diabetic retinopathy, vascular restenosis, AVM, hemangioma, neovascular glaucoma, psoriasis and rheumatoid arthritis, and tumors that have a vascularized tumor component. Such methods generally comprise administering to an animal, including a human subject, with a disease that has a vascular component, a pharmaceutical composition comprising at least one bispecific binding ligand in accordance with those described above.

The compositions are administered in amounts and by routes effective to promote blood coagulation in the vasculature of the disease site, e.g., in the intratumoral vasculature of a solid tumor. Effective doses will be known to those of skill in the art in light of the present disclosure, such as the information in the Preferred Embodiments and Detailed Examples. Parenteral administration will often be suitable, as will other methods, such as, e.g., injection into a vascularized tumor site.

The methods of the invention provide for the delivery of exogenous coagulation factors, by means of both administering a binding ligand that comprises a covalently-bound coagulation factor and by means of administering a binding ligand that comprises a non-covalently bound coagulation factor that is complexed to a second binding region of the bispecific ligand or antibody.

Further methods of the invention include those that result in the delivery of an endogenous coagulation factor to disease or tumor vasculature. This is achieved by administering to the animal or patient a binding ligand that comprises a second binding region that binds to endogenous coagulation factor and concentrates the factor at the disease-associated or tumor vasculature.

In yet still further methodological embodiments, it is contemplated that markers of tumor vasculature or stroma may be specifically induced and then targeted using a binding ligand, such as an antibody. Exemplary inducible antigens include E-selectin, P-selectin, MHC Class II antigens, VCAM-1, ICAM-1, endoglin, ligands reactive with LAM-1, vascular addressins and other adhesion molecules, with E-selectin and MHC Class II antigens being currently preferred.

When inducing and subsequently targeting MHC Class II proteins, the suppression of MHC Class II in normal tissues is generally required. MHC Class II suppression may be achieved using a cyclosporin, or a functionally equivalent agent. MHC Class II molecules may then be induced in disease-associated vascular endothelial cells using cyclosporin-independent means, such as by exposing the disease-associated vasculature to an effector cell, generally a Helper T cell or NK cell, of the animal that releases the inducing cytokine IFN- $\gamma$ .

Activated monocytes, macrophages and even mast cells are effector cells capable of producing cytokines (IL-1; TNF- $\alpha$ ; TNF- $\beta$ ) that induce E-selectin; whereas Helper T cells, CD8-positive T cells and NK cells are capable of producing IFN- $\gamma$  that induces MHC Class II. Activating monocyte/macrophages in the disease site to produce IL-1, or activating disease-associated Helper T cells or NK cells to produce IFN- $\gamma$ , may be achieved by administering to the animal an activating antibody that binds to an effector cell surface activating antigen. Exemplary activating antigens include CD14 and CD16 (FcR for IgE) for monocytes/macrophages; and CD2, CD3 and CD28 for T cells; with CD14 and CD28, respectively, being preferred for use in certain embodiments.

To achieve specific activation and induction, one currently preferred method is to use a bispecific antibody that binds to both an effector cell activating antigen, such as CD14 or CD28, and to a disease or tumor cell antigen. These bispecific antibodies will localize to the disease or tumor site and activate monocyte/macrophages and T cells, respectively. The activated effector cells in the vicinity of the targeted disease or tumor component will produce inducing cytokines, in this case, IL-1 and IFN- $\gamma$ , respectively.

MHC Class II suppression in normal tissues may also be achieved by administering to an animal an anti-CD4 antibody; this functions to suppress IFN- $\gamma$  production by T cells of the animal resulting in inhibition of MHC Class II expression. MHC Class II molecules may again be specifically induced in disease-associated vascular endothelial cells by exposing only the disease site to IFN- $\gamma$ . One means by which to achieve this is by administering to the animal an IFN- $\gamma$ -producing T cell clone that binds to an antigen in the disease site. The IFN- $\gamma$ -producing T cells will preferably be infiltrating leukocytes obtained from the disease site of the animal, such as tumor infiltrating leukocytes (TILs) expanded *in vitro*.

Methods using bispecific antibodies to induce coagulant, such as thrombin, production, only in a local environment, such as in a tumor site, are also provided. Again, this will generally be achieved by administering to an animal a pharmaceutical composition comprising a bispecific antibody that binds to a tumor cell or a component of tumor stroma and to Tissue Factor, a Tissue Factor derivative, prothrombin, Factor VII/VIIa, Factor IX/IXa, Factor X/Xa, Factor XI/XIa or Russell's viper venom Factor X activator. Antibodies that bind to E-selectin or P-selectin are then linked to a coagulation factor or a second binding region that binds to a coagulation factor and are introduced into the bloodstream of an animal.

More conventional combination treatment regimens are also possible where, for example, a tumor coagulating element of this invention is combined with an existing antitumor therapy, such as with radiotherapy or chemotherapy, or through the use of a second immunological reagent, such as an antitumor immunotoxin. The novel treatment methods for benign diseases can also be combined with other presently used therapies.

## BRIEF DESCRIPTION OF THE DRAWINGS

The following drawings form part of the present specification and are included to further demonstrate certain aspects of the present invention. The invention may be better understood by reference to one or more of these drawings in combination with the detailed description of specific embodiments presented herein.

FIG. 1. Tethering of tTF to A20 cells via B21-2/10H10 bispecific antibody. A20 cells were incubated with varying concentrations of B21-2/10H10 (□), SFR8/10H10 (●) or B21-2/OX7 (○) plus an excess of  $^{125}$ I-tTF for 1 h at 4° C. in the presence of sodium azide. The number of  $^{125}$ I-tTF associated with the cells was determined as described in Example II.

FIG. 2. Relationship between number of tethered tTF molecules per A20 cell and ability to induce coagulation of plasma. A20 cells were incubated with varying concentrations of B21-2/10H10 plus an excess of tTF for 1 h at 4° C. in the presence of sodium azide. The cells were washed, warmed to 37° C., calcium and mouse plasma were added and the time for the first fibrin strands to form was recorded (abscissa). An identical study was performed in which the A20 cells were incubated for 1 h at 40C with bispecific antibody plus  $^{125}$ I-tTF and the number of tTF specifically bound to the cells was determined as described in Example II (ordinate). Plasma added to untreated A20 cells (i.e. zero tTF molecules/cell) coagulated in 190 seconds.

FIG. 3A, FIG. 3B, FIG. 3C and FIG. 3D. Time course of vascular thrombosis and tumor necrosis after administration of coaguligand. Groups of 3 mice bearing 0.8 cm diameter C1300 (Muy) tumors were given an intravenous injection of a coaguligand composed of 14  $\mu$ g B21-2/10H10 and 11  $\mu$ g tTF. FIG. 3A; Before injection: blood vessels are intact and tumor cells are healthy. FIG. 3B; 0.5 hours: blood vessels throughout the tumor are thrombosed; tumor cells are healthy. FIG. 3C; 4 hours: dense thrombi are present in all tumor vessels and tumor cells are separating and developing pyknotic nuclei. Erythrocytes are visible in the tumor interstitium. FIG. 3D; 24 hours: advanced tumor necrosis throughout the tumor. Arrows indicate blood vessels.

FIG. 4. Solid tumor regression induced by tumor-vasculature directed coaguligand therapy. Nu/nu mice bearing approximately 0.8 cm diameter C1300 (Muy) tumors were given two intravenous injections of B21-2/10H10 (14  $\mu$ g) mixed with tTF (11  $\mu$ g) spaced 1 week apart (arrows) (□). Mice in control groups received equivalent doses of tTF alone (●), B21-2/10H10 alone (○) or diluent (■). Other control groups which received equivalent doses of isotype-matched control bispecific antibodies (SFR8/10H10, OX7/10H10 or B21-2/OX7) and tTF had similar tumor responses to those in animals receiving tTF alone. The number of mice per group was 7 or 8.

FIG. 5. Exemplary antibody-tTF constructs. This figure shows both the conjugates synthesized by the linkage of chemically derivatized antibody to chemically derivatized tTF via a disulfide bond, and also the linkage of various TF or TF dimers to antibodies and fragments thereof.

FIG. 6. Clotting activity of tTF conjugates when bound to A20 cells. A20 cells were incubated with varying concentrations of B21-2/10H10 bispecific+H<sub>6</sub>[tTF] in a 1:1 molar ratio, premixed for one hour (□), B21-2 antibody-H<sub>6</sub> C[tTF] (●), and B21-2 antibody-H<sub>6</sub>[tTF] (▲) for 1 hour at 4° C. in the presence of sodium azide. The cells were washed, warmed to 37° C., calcium and mouse plasma were added and the time for the first fibrin strands to form was recorded. The results are expressed as clotting time as a % of the clotting time in the absence of tTF.

FIG. 7. Clotting activity of anti-tumor cell tTF conjugates. LS174T cells (■), Widr cells (●) and H460 cells (▲), preincubated with TF9-6B4 and TF8-5G9 antibodies, were incubated with varying concentrations of D612 antibody-H<sub>6</sub>C[tTF] (■), KS1/4 antibody-H<sub>6</sub>[tTF] (●), and XMMC0791 antibody-H<sub>6</sub>[tTF] (▲) for 1 hour at 4° C. in the presence of sodium azide. The cells were washed, warmed to 37° C., calcium and mouse plasma were added and the time for the first fibrin strands to form was recorded. The results are expressed as clotting time as a % of the clotting time in the absence of tTF.

FIG. 8. Gla domains ( $\gamma$ -carboxyglutamic acid) of Factor II/IIa, Factor VII/IIa, Factor IX/IXa and Factor X/Xa. The arrows represent signal peptide and pro-peptide cleavage sites and activating cleavage sites (slanted arrows).

## DETAILED DESCRIPTION OF THE PREFERRED EMBODIMENTS

Although they show great promise in the therapy of lymphomas and leukemias (Lowder et al., 1987; Vitetta et al., 1991), monoclonal antibodies (MAbs) and immunotoxins (ITs) have thus far proved relatively ineffective in clinical trials against carcinomas and other solid tumors (Byers & Baldwin, 1988; Abrams & Oldham, 1985), which account for more than 90% of all cancers in man (Shockley et al., 1991). A principal reason for this is that macromolecules do not readily extravasate into solid tumors (Sands, 1988; Epenetos et al., 1986) and, once within the tumor mass, fail to distribute evenly due to the presence of tight junctions between tumor cells (Dvorak et al., 1991), fibrous stroma (Baxter et al., 1991), interstitial pressure gradients (Jain, 1990) and binding site barriers (Juweid et al., 1992).

In developing new strategies for treating solid tumors, the methods that involve targeting the vasculature of the tumor, rather than the tumor cells themselves, therefore seem to offer certain advantages. Inducing a blockade of the blood flow through the tumor, e.g., through tumor vasculature specific fibrin formation, would interfere with the influx and efflux processes in a tumor site, thus resulting in anti-tumor effect. Arresting the blood supply to a tumor may be accomplished through shifting the procoagulant-fibrinolytic balance in the tumor-associated vessels in favour of the coagulating processes by specific exposure to coagulating agents.

The present invention provides various means for effecting specific blood coagulation, as exemplified by tumor-specific coagulation. This is achieved using bispecific or multispecific binding ligands in which at least one component is an immunological- or growth factor-based targeting component, and at least one other component is provided that is capable of directly, or indirectly, stimulating coagulation.

## A. Targetable Disease Sites

The compositions and methods provided by this invention are broadly applicable to the treatment of any disease, such as a benign or malignant tumor, having a vascular component. Such vasculature-associated diseases include BPH, diabetic retinopathy, vascular restenosis, arteriovenous malformations (AVM), meningioma, hemangioma, neovascular glaucoma and psoriasis; and also angiofibroma, arthritis, atherosclerotic plaques, corneal graft neovascularization, hemophilic joints, hypertrophic scars, osler-weber syndrome, pyogenic granuloma retrolental fibroplasia, scleroderma, trachoma, vascular adhesions, synovitis, dermatitis and even endometriosis.

Typical vascularized tumors are the solid tumors, particularly carcinomas, which require a vascular component for

the provision of oxygen and nutrients. Exemplary solid tumors that may be treated using the invention include, but are not limited to, carcinomas of the lung, breast, ovary, stomach, pancreas, larynx, esophagus, testes, liver, parotid, biliary tract, colon, rectum, cervix, uterus, endometrium, kidney, bladder, prostate, thyroid, squamous cell carcinomas, adenocarcinomas, small cell carcinomas, melanomas, gliomas, neuroblastomas, and the like.

One binding region of the bispecific agents of the invention will be a component that is capable of delivering the coagulating agent to the tumor region, i.e., capable of localizing within a tumor site, such as those described above. As somewhat wider distribution of the coagulating agent will not be associated with severe side effects, such as is known to occur with a toxin moiety, there is a less stringent requirement imposed on the targeting element of the bispecific ligand. The targeting agent may thus be directed to components of tumor cells; components of tumor vasculature; components that bind to, or are generally associated with, tumor cells; components that bind to, or are generally associated with, tumor vasculature; components of the tumor extracellular matrix or stroma; and even cell types found within the tumor vasculature.

The burden of very stringent targeting, e.g., as imposed when using immunotoxins, is also lessened due to the fact that tumor vasculature is 'prothrombotic' and is predisposed towards coagulation. Therefore, to achieve specific targeting means that coagulation is promoted in the tumor vasculature relative to the vasculature in non-tumor sites. Thus, specific targeting is a functional term rather than a purely physical term relating to the biodistribution properties of the targeting agent, and it is not unlikely that useful targets may be not be entirely tumor-restricted, and that targeting ligands which are effective to promote tumor-specific coagulation may

nevertheless be found at other sites of the body following administration.

#### 1. Tumor Cell Targets

The malignant cells that make up the tumor may be targeted using a bispecific ligand that has a region capable of binding to a relatively specific marker of the tumor cell. In that binding to tumor cells will localize the associated coagulating agent to the tumor, specific coagulation will be achieved. Furthermore, it is expected that this would be a particularly effective means of promoting coagulation as, due to the physical accessibility of perivascular tumor cells, the bispecific agents will likely be concentrated around the tumor cells that are nearest to a blood vessel.

Many so-called "tumor antigens" have been described, any one which could be employed as a target in connection with the present invention. A large number of exemplary solid tumor-associated antigens are listed herein in Table I. The preparation and use of antibodies against such antigens is well within the skill of the art, and exemplary antibodies are also listed in Table I.

Another means of defining a targetable tumor is in terms of the characteristics of a tumor cell itself, rather than describing the biochemical properties of an antigen expressed by the cell. Accordingly, Table II is provided for the purpose of exemplifying human tumor cell lines that are publically available (from ATCC Catalogue).

The information presented in Table II is by means of an example, and not intended to be limiting either by year or by scope. One may consult the ATCC Catalogue of any subsequent year to identify other appropriate cell lines. Also, if a particular cell type is desired, the means for obtaining such cells, and/or their instantly available source, will be known to those of skill in the particular art. An analysis of the scientific literature will thus readily reveal an appropriate choice of cell for any tumor cell type desired to be targeted.

TABLE I

#### MARKER ANTIGENS OF SOLID TUMORS AND CORRESPONDING MONOCLONAL ANTIBODIES

Tumor Site	Antigen Identity/ Characteristics	Monoclonal Antibodies	Reference
A: Gynecological	'CA 125' >200 kD mucin GP	OC 125	Kabawat et al., 1983; Szymendera, 1986
GY	80 Kd GP	OC 133	Masuko et al, Cancer Res., 1984
ovarian	'SGA' 360 Kd GP	OMI	de Kresten et al., 1986
ovarian	High M <sub>r</sub> mucin	Mo v1	Miotti et al, Cancer Res., 1985
ovarian	High M <sub>r</sub> mucin/ glycolipid	Mo v2	Miotti et al, Cancer Res., 1985
ovarian	NS	3C2	Tsuji et al., Cancer Res., 1985
ovarian	NS	4C7	Tsuji et al., Cancer Res., 1985
ovarian	High M <sub>r</sub> mucin	ID <sub>3</sub>	Gangopadhyay et al., 1985
ovarian	High M <sub>r</sub> mucin	DU-PAN-2	Lan et al., 1985
GY	7700 Kd GP	F 36/22	Croghan et al., 1984
ovarian	'gp 68' 48 Kd GP	4F <sub>7</sub> /7A <sub>10</sub>	Bhattacharya et al., 1984
GY	40, 42kD GP	OV-TL3	Poels et al., 1986
GY	'TAG-72' High M <sub>r</sub> mucin	B72.3	Thor et al., 1986
ovarian	300-400 Kd GP	DF <sub>3</sub>	Kufe et al., 1984
ovarian	60 Kd GP	2C <sub>8</sub> /2F <sub>7</sub>	Bhattacharya et al., 1985
GY	105 Kd GP	MF 116	Mattes et al., 1984
ovarian	38-40 kD GP	MOv18	Miotti et al., 1987
GY	'CEA' 180 Kd GP	CEA 11-H5	Wagener et al., 1984
ovarian	CA 19-9 or GICA	CA 19-9 (1116NS 19-9)	Atkinson et al., 1982
ovarian	'PLAP' 67 Kd GP	H17-E2	McDicken et al., 1985
ovarian	72 Kd	791T/36	Perkins et al., 1985
ovarian	69 Kd PLAP	NDOG <sub>2</sub>	Sunderland et al., 1984
ovarian	unknown M <sub>r</sub> PLAP	H317	Johnson et al., 1981
ovarian	p185 <sup>HER2</sup>	4D5, 3H4, 7C2, 6E9,	Shepard et al., 1991

TABLE I-continued

MARKER ANTIGENS OF SOLID TUMORS AND CORRESPONDING MONOCLONAL ANTIBODIES			
Tumor Site	Antigen Identity/ Characteristics	Monoclonal Antibodies	Reference
uterus ovary GY B: BREAST	HMFG-2	2C4, 7F3, 2H11, 3E8, 5B8, 7D3, SB8	Epenetos et al., 1982
	HMFG-2	HMFG2	Butchell et al., 1983
	330-450 Kd GP	3.14.A3	Hayes et al., 1985
	NS	DF3	Ellis et al., 1984
	37kD	NCRC-11	Mandeville et al., 1987
	NS	3C6F9	Teramoto et al., 1982
	NS	MBE6	Glassy et al., 1983
	NS	CLNH5	Kjeldsen et al., 1986
	47 Kd GP	MAC 40/43	Sloane et al., 1981
	High M <sub>r</sub> GP	EMA	Arklie et al., 1981
	High M <sub>r</sub> GP	HMFG1 HFMG2	Arklie et al., 1981
	NS	3.15.C3	Foster et al., 1982
	NS	M3, M8, M24	Foster et al., 1984
	1 (Ma) blood group Ags	M18	Rasmussen et al., 1982
	NS	67-D-11	Kinsel et al., 1989
	oestrogen receptor	D547Sp, D75P3, H222	Sainsbury et al., 1985
	EGF Receptor	Anti-EGF	Horan Hand et al., 1985
	Laminin Receptor	LR-3	Gusterson et al., 1988
	erb B-2 p185	TA1	Hendler et al., 1981
	NS	H59	Soule et al., 1983
	126 Kd GP	10-3D-2	Imam et al., 1984; Schlom et al., 1985
	NS	HmAB1,2	Menard et al., 1983
	NS	MBR 1,2,3	Thompson et al., 1983
	95 Kd	24.17.1	Croghan et al., 1983
	100 Kd	24.17.2 (3E1.2)	Croghan et al., 1984
	NS	F36/22.M7/105	Adams et al., 1983
	24 Kd	C11, G3, H7	Colcher et al., 1981
	90 Kd GP	B6.2	Colcher et al., 1983
	CEA & 180 Kd GP	B1.1	Imperial Cancer Research Technology MAb listing
	colonic & pancreatic mucin similar to Ca 19-9	Cam 17.1	Imperial Cancer Research Technology MAb listing
	milk mucin core protein	SM3	Imperial Cancer Research Technology MAb listing
	milk mucin core protein	SM4	Imperial Cancer Research Technology MAb listing
	affinity-purified milk mucin	C-Mul (566)	Imperial Cancer Research Technology MAb listing
	p185 <sup>HER2</sup>	4D5 3H4, 7C2, 6E9, 2C4, 7F3, 2H11, 3E8, 5B8, 7D3, 5B8	Shepard et al., 1991
	CA 125 > 200 Kd GP	OC 125	Kabawat et al., 1985
	High M <sub>r</sub> mucin/glycolipid	MO v2	Miotti et al., 1985
	High M <sub>r</sub> mucin 'gp48' 48 Kd GP	DU-PAN-2	Lan et al., 1984
	300-400 Kd GP	4F <sub>7</sub> /7A <sub>10</sub>	Bhattacharya et al., 1984
	'TAG-72' high M <sub>r</sub> mucin	DF <sub>3</sub>	Kufe et al., 1984
	'CEA' 180 Kd GP	B72.3	Thor et al., 1986
	'PLAP' 67 Kd GP	ccccCEA 11	Wagener et al., 1984
	HMFG-2 > 400 Kd GP	H17-E2	McDicken et al., 1985
	NS	3.14.A3	Burchell et al., 1983
C: COLORECTAL	NS	FO23C5	Riva et al., 1988
	TAG-72 High M <sub>r</sub> mucin	B72.3	Colcher et al., 1987
	GP37	(17-1A) 1083-17-1A	Paul et al., 1986
	Surface GP	CO17-1A	LoBuglio et al., 1988
	CEA	ZCE-025	Patt et al., 1988
	CEA	AB2	Griffin et al., 1988a
	cell surface AG	HT-29-15	Cohn et al., 1987
	secretory epithelium surface	250-30.6	Leydem et al., 1986
	glycoprotein	44 x 14	Gallagher et al., 1986
	NS	A7	Takahashi et al., 1988

TABLE I-continued

MARKER ANTIGENS OF SOLID TUMORS AND CORRESPONDING MONOCLONAL ANTIBODIES			
Tumor Site	Antigen Identity/ Characteristics	Monoclonal Antibodies	Reference
	NS	GA73.3	Munz et al., 1986
	NS	791T/36	Farrans et al., 1982
	cell membrane & cytoplasmic Ag	28A32	Smith et al., 1987
	CEA & vindesine gp72	28.19.8	Corvalen, 1987
	high M <sub>r</sub> mucin	x MMCO-791	Byers et al., 1987
	high M <sub>r</sub> mucin	DU-PAN-2	Lan et al., 1985
	CEA 180 Kd GP	ID <sub>3</sub>	Gangopadhyay et al., 1985
	60 Kd GP	CEA 11-H5	Wagener et al., 1984
	CA-19-9 (or GICA)	2C <sub>9</sub> /2F <sub>7</sub>	Bhattacharya et al., 1985
	Lewis a	CA-19-9 (1116NS 19-9)	Atkinson et al., 1982
	Lewis a	PR5C5	Imperial Cancer Research Technology Mab Listing
	colonic mucus	PR4D2	Imperial Cancer Research Technology Mab Listing
		PR4D1	Imperial Cancer Research Technology Mab Listing
D: MELANOMA	p97 <sup>a</sup>	4.1	Woodbury et al., 1980
	p97 <sup>a</sup>	8.2 M <sub>17</sub>	Brown, et al., 1981a
	p97 <sup>b</sup>	96.5	Brown, et al., 1981a
	p97 <sup>c</sup>	118.1, 133.2, (113.2)	Brown, et al., 1981a
	p97 <sup>c</sup>	L <sub>11</sub> , L <sub>10</sub> R <sub>10</sub> (R <sub>12</sub> )	Brown et al., 1981b
	p97d	I <sub>12</sub>	Brown et al., 1981b
	p97e	K <sub>5</sub>	Brown et al., 1981b
	p155	6.1	Loop et al., 1981
	G <sub>D3</sub> disialoganglioside	R24	Dippold et al., 1980
	p210, p60, p250	5.1	Loop et al., 1981
	p280 p440	225.28S	Wilson et al., 1981
	GP 94, 75, 70 & 25	465.12S	Wilson et al., 1981
	P240-P250, P450	9.2.27	Reisfeld et al., 1982
	100, 77, 75 Kd	F11	Chee et al., 1982
	94 Kd	376.96S	Imai et al., 1982
	4 GP chains	465.12S	Imai et al., 1982; Wilson et al., 1981
	GP 74	15.75	Johnson & Reithmuller, 1982
	GP 49	15.95	Johnson & Reithmuller, 1982
	230 Kd	Mel-14	Carrel et al., 1982
	92 Kd	Mel-12	Carrel et al., 1982
	70 Kd	Me3-TB7	Carrel et al. 1:387, 1982
	HMW MAA similar to 9.2.27 AG	225.28SD	Kantor et al., 1982
	HMW MAA similar to 9.2.27 AG	763.24TS	Kantor et al., 1982
	GP95 similar to 376.96S 465.12S	705F6	Stuhlmiller et al., 1982
	GP125	436910	Saxton et al., 1982
	CD41	M148	Imperial Cancer Research Technology Mab listing
E: GASTROINTESTINAL	high M <sub>r</sub> mucin	ID3	Gangopadhyay et al., 1985
pancreas, stomach	high M <sub>r</sub> mucin	DU-PAN-2	Lan et al., 1985
gall bladder, pancreas, stomach	NS	OV-TL3	Poels et al., 1984
pancreas, stomach, oesophagus	'TAG-72' high M <sub>r</sub> mucin	B72.3	Thor et al., 1986
stomach	'CEA' 180 Kd GP	CEA 11-H5	Wagener et al., 1984
pancreas	HMF-2 > 400 Kd GP	3.14.A3	Burchell et al., 1983
G.I pancreas, stomach	NS	C COLI	Lemkin et al., 1984
	CA 19-9 (or GICA)	CA-19-9 (1116NS 19-9) and CA50	Szymendera, 1986
pancreas	CA125 GP	OC125	Szymendera, 1986
F: LUNG non-small cell lung carcinoma	p185 <sup>HER2</sup>	4D5 3H4, 7C2, 6E9, 2C4, 7F3, 2H11, 3E8, 5B8, 7D3, SB8	Shepard et al., 1991
	high M <sub>r</sub> mucin/ glycolipid	MO v2	Miotti et al., 1985
	'TAG-72' high M <sub>r</sub> mucin	B72.3	Thor et al., 1986

TABLE I-continued

MARKER ANTIGENS OF SOLID TUMORS AND CORRESPONDING MONOCLONAL ANTIBODIES			
Tumor Site	Antigen Identity/ Characteristics	Monoclonal Antibodies	Reference
Malignant Gliomas	high M <sub>r</sub> mucin	DU-PAN-2	Lan et al., 1985
	'CEA' 180 kD GP	CEA 11-H5	Wagener et al., 1984
	cytoplasmic antigen from 85HG-22 cells	MUC 8-22	Stavrou, 1990
	cell surface Ag from 85HG-63 cells	MUC 2-63	Stavrou, 1990
	cell surface Ag from 86HG-39 cells	MUC 2-39	Stavrou, 1990
G: MISCELLANEOUS	cell surface Ag from 86HG-39 cells	MUC 7-39	Stavrou, 1990
	p53	PAb 240 PAb 246 PAb 1801	Imperial Cancer Research Technology MaB Listing
	small round cell tumors	ERIC.1	Imperial Cancer Research Technology MaB Listing
	medulloblastoma	M148	Imperial Cancer Research Technology MaB Listing
	neuroblastoma	FMH25	Imperial Cancer Research Technology MaB Listing
renal cancer & glioblastomas	p155	6.1	Loop et al., 1981
bladder & laryngeal cancers	"Ca Antigen" 350-390 kD	CA1	Ashall et al., 1982
neuroblastoma	GD2	3F8	Cheung et al., 1986
Prostate	gp48 48 kD GP	4F <sub>7</sub> /7A <sub>10</sub>	Bhattacharya et al., 1984
Prostate	60 kD GP	2C <sub>8</sub> /2F <sub>7</sub>	Bhattacharya et al., 1985
Thyroid	'CEA' 180 kD GP	CEA 11-H5	Wagener et al., 1984

abbreviations: Abs, antibodies; Ags, antigens; EGF, epidermal growth factor; GI, gastrointestinal; GICA, gastrointestinal-associated antigen; GP, glycoprotein; GY, gynecological; HMFG, human milk fat globule; Kd, kilodaltons; Mabs, monoclonal antibodies; M<sub>r</sub>, molecular weight; NS, not specified; PLAP, placental alkaline phosphatase; TAG, tumor-associated glycoprotein; CEA, carcinoembryonic antigen.

footnotes: the CA 19-9 Ag (GICA) is sialosylfucosylactotetraosylceramide, also termed sialylated Lewis pentaglycosyl ceramide or sialylated lacto-N-fucopentaose II; p97 Ags are believed to be chondroitin sulphate proteoglycan; antigens reactive with Mab 9.2.27 are believed to be sialylated glycoproteins associated with chondroitin sulphate proteoglycan; unless specified, GY can include cancers of the cervix, endocervix, endometrium, fallopian tube, ovary, vagina or mixed Mullerian tumor; unless specified GI can include cancers of the liver, small intestine, spleen, pancreas, stomach and oesophagus.

TABLE II

## HUMAN TUMOR CELL LINES AND SOURCES

ATTC HTB NUMBER	CELL LINE	TUMOR TYPE
1	J82	Transitional-cell carcinoma, bladder
2	RT4	Transitional-cell papilloma, bladder
3	ScaBER	Squamous carcinoma, bladder
4	T24	Transitional-cell carcinoma, bladder
5	TCCSUP	Transitional-cell carcinoma, bladder, primary grade IV
9	5637	Carcinoma, bladder, primary
10	SK-N-MC	Neuroblastoma, metastasis to supra-orbital area
11	SK-N-SH	Neuroblastoma, metastasis to bone marrow
12	SW 1088	Astrocytoma
13	SW 1783	Astrocytoma
14	U-87 MG	Glioblastoma, astrocytoma, grade III
15	U-118 MG	Glioblastoma
16	U-138 MG	Glioblastoma
17	U-373 MG	Glioblastoma, astrocytoma, grade III
18	Y79	Retinoblastoma
19	BT-20	Carcinoma, breast
20	BT-474	Ductal carcinoma, breast
22	MCF7	Breast adenocarcinoma, pleural effusion



TABLE II-continued

HUMAN TUMOR CELL LINES AND SOURCES		
ATTC HTB NUMBER	CELL LINE	TUMOR TYPE
23	MDA-MB-134-VI	Breast, ductal carcinoma, pleural effusion
24	MDA-MD-157	Breast medulla, carcinoma, pleural effusion
25	MDA-MB-175-VII	Breast, ductal carcinoma, pleural effusion
27	MDA-MB-361	Adenocarcinoma, breast, metastasis to brain
30	SK-BR-3	Adenocarcinoma, breast, malignant pleural effusion
31	C-33 A	Carcinoma, cervix
32	HT-3	Carcinoma, cervix, metastasis to lymph node
33	ME-180	Epidermoid carcinoma, cervix, metastasis to omentum
34	MS751	Epidermoid carcinoma, cervix, metastasis to lymph node
35	SiHa	Squamous carcinoma, cervix
36	JEG-3	Choriocarcinoma
37	Caco-2	Adenocarcinoma, colon
38	HT-29	Adenocarcinoma, colon, moderately well-differentiated grade II
39	SK-CO-1	Adenocarcinoma, colon, ascites
40	HuTu 80	Adenocarcinoma, duodenum
41	A-253	Epidermoid carcinoma, submaxillary gland
43	FaDu	squamous cell carcinoma, pharynx
44	A-498	Carcinoma, kidney
45	A-704	Adenocarcinoma, kidney
46	Caki-1	Clear cell carcinoma, consistent with renal primary, metastasis to skin
47	Caki-2	Clear cell carcinoma, consistent with renal primary
48	SK-NEP-1	Wilms' tumor, pleural effusion
49	SW 839	Adenocarcinoma, kidney
52	SK-HEP-1	Adenocarcinoma, liver, ascites
53	A-427	Carcinoma, lung
54	Calu-1	Epidermoid carcinoma grade III, lung, metastasis to pleura
55	Calu-3	Adenocarcinoma, lung, pleural effusion
56	Calu-6	Anaplastic carcinoma, probably lung.
57	SK-LU-1	Adenocarcinoma, lung consistent with poorly differentiated, grade III
58	SK-MES-1	Squamous carcinoma, lung, pleural effusion
59	SW 900	Squamous cell carcinoma, lung
60	EB1	Burkitt lymphoma, upper maxilla
61	EB2	Burkitt lymphoma, ovary
62	P3HR-1	Burkitt lymphoma, ascites
63	HT-144	Malignant melanoma, metastasis to subcutaneous tissue
64	Malme-3M	Malignant melanoma, metastasis to lung
66	RPMI-7951	Malignant melanoma, metastasis to lymph node
67	SK-MEL-1	Malignant melanoma, metastasis to lymphatic system
68	SK-MEL-2	Malignant melanoma, metastasis to skin of thigh
69	SK-MEL-3	Malignant melanoma, metastasis to lymph node
70	SK-MEL-S	Malignant melanoma, metastasis to axillary node
71	SK-MEL-24	Malignant melanoma, metastasis to node
72	SK-MEL-28	Malignant melanoma
73	SK-MEL-31	Malignant melanoma
75	Caov-3	Adenocarcinoma, ovary, consistent with primary
76	Caov-4	Adenocarcinoma, ovary, metastasis to subserosa of fallopian tube
77	SK-OV-3	Adenocarcinoma, ovary, malignant ascites
78	SW 626	Adenocarcinoma, ovary
79	Capan-1	Adenocarcinoma, pancreas, metastasis to liver
80	Capan-2	Adenocarcinoma, pancreas
81	DU 145	Carcinoma, prostate, metastasis to brain
82	A-204	Rhabdomyosarcoma
85	Saos-2	Osteogenic sarcoma, primary
86	SK-ES-1	Anaplastic osteosarcoma versus Ewing sarcoma, bone
88	SK-LMS-1	Leiomyosarcoma, vulva, primary
91	SW 684	Fibrosarcoma
92	SW 872	Liposarcoma
93	SW 982	Axilla synovial sarcoma
94	SW 1353	Chondrosarcoma, humerus
96	U-2 OS	Osteogenic sarcoma, bone primary

TABLE II-continued

HUMAN TUMOR CELL LINES AND SOURCES		
ATTC HTB NUMBER	CELL LINE	TUMOR TYPE
102	Malme-3	Skin fibroblast
103	KATO III	Gastric carcinoma
104	Cate-1B	Embryonal carcinoma, testis, metastasis to lymph node
105	Tera-1	Embryonal carcinoma, malignancy consistent with metastasis to lung
106	Tera-2	Embryonal carcinoma, malignancy consistent with, metastasis to lung
107	SW579	Thyroid carcinoma
111	AN3 CA	Endometrial adenocarcinoma, metastatic
112	HEC-1-A	Endometrial adenocarcinoma
113	HEC-1-B	Endometrial adenocarcinoma
114	SK-UT-1	Uterine, mixed mesodermal tumor, consistent with leiomyosarcoma grade III
115	SK-UT-1B	Uterine, mixed mesodermal tumor, consistent with leiomyosarcoma grade III
117	SW 954	Squamous cell carcinoma, vulva
118	SW 962	Carcinoma, vulva, lymph node metastasis
119	NCI-H69	Small cell carcinoma, lung
120	NCI-H128	Small cell carcinoma, lung
121	BT-483	Ductal carcinoma, breast
122	BT-549	Ductal carcinoma, breast
123	DU4475	Metastatic cutaneous nodule, breast carcinoma
124	HBL-100	Breast
125	Hs 578Bst	Breast, normal
126	Hs 578T	Ductal carcinoma, breast
127	MDA-MB-330	Carcinoma, breast
128	MDA-MB-415	Adenocarcinoma, breast
129	MDA-MB-435S	Ductal carcinoma, breast
130	MDA-MB-436	Adenocarcinoma, breast
131	MDA-MB-453	Carcinoma, breast
132	MDA-MB-468	Adenocarcinoma, breast
133	T-47D	Ductal carcinoma, breast, pleural effusion
134	Hs 766T	Carcinoma, pancreas, metastatic to lymph node
135	Hs 746T	Carcinoma, stomach, metastatic to left leg
137	Hs 695T	Amelanotic melanoma, metastatic to lymph node
138	Hs 683	Glioma
140	Hs 294T	Melanoma, metastatic to lymph node
142	Hs 602	Lymphoma, cervical
144	JAR	Choriocarcinoma, placenta
146	Hs 445	Lymphoid, Hodgkin's disease
147	Hs 700T	Adenocarcinoma, metastatic to pelvis
148	H4	Neuroglioma, brain
151	Hs 696	Adenocarcinoma primary, unknown, metastatic to bone-sacrum
152	Hs 913T	Fibrosarcoma, metastatic to lung
153	Hs 729	Rhabdomyosarcoma, left leg
157	FHs 738Lu	Lung, normal fetus
158	FHs 173We	Whole embryo, normal
160	FHs 738B1	Bladder, normal fetus
161	NIH:OVCA-3	Ovary, adenocarcinoma
163	Hs 67	Thymus, normal
166	RD-ES	Ewing's sarcoma
168	ChaGo K-1	Bronchogenic carcinoma, subcutaneous metastasis, human
169	WERI-Rb-1	Retinoblastoma
171	NCI-H446	Small cell carcinoma, lung
172	NCI-H209	Small cell carcinoma, lung
173	NCI-H146	Small cell carcinoma, lung
174	NCI-H441	Papillary adenocarcinoma, lung
175	NCI-H82	Small cell carcinoma, lung
176	H9	T-cell lymphoma
177	NCI-H460	Large cell carcinoma, lung
178	NCI-H596	Adenosquamous carcinoma, lung
179	NCI-H676B	Adenocarcinoma, lung
180	NCI-H345	Small cell carcinoma, lung
181	NCI-H820	Papillary adenocarcinoma, lung
182	NCI-H520	Squamous cell carcinoma, lung
183	NCI-H661	Large cell carcinoma, lung
184	NCI-H510A	Small cell carcinoma, extra-pulmonary origin, metastatic
185	D283 Med	Medulloblastoma
186	Daoy	Medulloblastoma
187	D341 Med	Medulloblastoma

TABLE II-continued

HUMAN TUMOR CELL LINES AND SOURCES		
ATTC HTB NUMBER	CELL LINE	TUMOR TYPE
188	AML-193	Acute monocyte leukemia
189	MV4-11	Leukemia biphenotype

## (a) Anti-Tumor Cell Antibodies

A straightforward means of recognizing a tumor antigen target is through the use of an antibody that has binding affinity for the particular antigen. An extensive number of antibodies are known that are directed against solid tumor antigens. Certain useful anti-tumor antibodies are listed above in Table I. However, as will be instantly known to those of skill in the art, certain of the antibodies listed in Table I will not have the appropriate biochemical properties, or may not be of sufficient tumor specificity, to be of use therapeutically. An example is MUC8-22 that recognizes a cytoplasmic antigen. Antibodies such as these will generally be of use only in investigational embodiments, such as in model systems or screening assays.

Generally speaking, antibodies for use in these aspects of the present invention will preferably recognize antigens that are accessible on the cell-surface and that are preferentially, or specifically, expressed by tumor cells. Such antibodies will also preferably exhibit properties of high affinity, such as exhibiting a  $K_d$  of <200 nM, and preferably, of <100 nM, and will not show significant reactivity with life-sustaining normal tissues, such as one or more tissues selected from heart, kidney, brain, liver, bone marrow, colon, breast, prostate, thyroid, gall bladder, lung, adrenals, muscle, nerve fibers, pancreas, skin, or other life-sustaining organ or tissue in the human body. The "life-sustaining" tissues that are the most important for the purposes of the present invention, from the standpoint of low reactivity, include heart, kidney, central and peripheral nervous system tissues and liver. The term "significant reactivity", as used herein, refers to an antibody or antibody fragment, that, when applied to the particular tissue under conditions suitable for immunohistochemistry, will elicit either no staining or negligible staining with only a few positive cells scattered among a field of mostly negative cells.

Particularly promising antibodies from Table I contemplated for use in the present invention are those having high selectivity for the solid tumor. For example, antibodies binding to TAG 72 and the HER-2 proto-oncogene protein, which are selectively found on the surfaces of many breast, lung and colorectal cancers (Thor et al., 1986; Colcher et al., 1987; Shepard et al., 1991); MOv18 and OV-TL3 and antibodies that bind to the milk mucin core protein and human milk fat globule (Miotti et al., 1985; Burchell et al., 1983); and the antibody 9.2.27 that binds to the high M<sub>r</sub> melanoma antigens (Reisfeld et al., 1982). Further useful antibodies are those against the folate-binding protein, which is known to be homogeneously expressed in almost all ovarian carcinomas; those against the erb family of oncogenes that are over-expressed in squamous cell carcinomas and the majority of gliomas; and other antibodies known to be the subject of ongoing pre-clinical and clinical evaluation.

The antibodies B3, KS1/4, CC49, 260F9, XMMCO-791, D612 and SM3 are believed to be particularly suitable for use in clinical embodiments, following the standard pre-clinical testing routinely practiced in the art. B3 (U.S. Pat.

No. 5,242,813; Brinkmann et al., 1991) has ATCC Accession No. HB 10573; KS1/4 can be made as described in U.S. Pat. No. 4,975,369; and D612 (U.S. Pat. No. 5,183,756) has ATCC Accession No. HB 9796.

Another means of defining a tumor-associated target is in terms of the characteristics of the tumor cell, rather than describing the biochemical properties of an antigen expressed by the cell. Accordingly, the inventors contemplate that any antibody that preferentially binds to a tumor cell listed in Table II may be used as the targeting component of a bispecific ligand. The preferential tumor cell binding is again based upon the antibody exhibiting high affinity for the tumor cell and not having significant reactivity with life-sustaining normal cells or tissues, as defined above.

The invention therefore provides several means for generating an antibody for use in the targeted coagulation methods described herein. To generate a tumor cell-specific antibody, one would immunize an animal with a composition comprising a tumor cell antigen and, as described more fully herein below, select a resultant antibody with appropriate specificity. The immunizing composition may contain a purified, or partially purified, preparation of any of the antigens in Table I; a composition, such as a membrane preparation, enriched for any of the antigens in Table I; any of the cells listed in Table II; or a mixture or population of cells that include any of the cell types listed in Table II.

Of course, regardless of the source of the antibody, in the practice of the invention in human treatment, one will prefer to ensure in advance that the clinically-targeted tumor expresses the antigen ultimately selected. This is achieved by means of a fairly straightforward assay, involving antigenically testing a tumor tissue sample, for example, a surgical biopsy, or perhaps testing for circulating shed antigen. This can readily be carried out in an immunological screening assay such as an ELISA (enzyme-linked immunosorbent assay), wherein the binding affinity of antibodies from a "bank" of hybridomas are tested for reactivity against the tumor. Antibodies demonstrating appropriate tumor selectivity and affinity are then selected for the preparation of bispecific antibodies of the present invention.

Due to the well-known phenomenon of cross-reactivity, it is contemplated that useful antibodies may result from immunization protocols in which the antigens originally employed were derived from an animal, such as a mouse or a primate, in addition to those in which the original antigens were obtained from a human cell. Where antigens of human origin are used, they may be obtained from a human tumor cell line, or may be prepared by obtaining a biological sample from a particular patient in question. Indeed, methods for the development of antibodies that are "custom-tailored" to the patient's tumor are known (Stevenson et al., 1990) and are contemplated for use in connection with this invention.

## (b) Further Tumor Cell Targets and Binding Ligands

In addition to the use of antibodies, other ligands could be employed to direct a coagulating agent to a tumor site by binding to a tumor cell antigen. For tumor antigens that are

over-expressed receptors (oestrogen receptor, EGF receptor), or mutant receptors, the corresponding ligands could be used as targeting agents.

In an analogous manner to endothelial cell receptor ligands, there may be components that are specifically, or preferentially, bound to tumor cells. For example, if a tumor antigen is an over-expressed receptor, the tumor cell may be coated with a specific ligand *in vivo*. It seems that the ligand could then be targeted either with an antibody against the ligand, or with a form of the receptor itself. Specific examples of these type of targeting agents are antibodies against TIE-1 or TIE-2 ligands, antibodies against platelet factor 4, and leukocyte adhesion binding protein.

## 2. Other Disease Targets

In further embodiments, the first binding region may be a component that binds to a target molecule that is specifically or preferentially expressed in a disease site other than a tumor site.

Exemplary target molecules associated with other diseased cells include, for example, leukocyte adhesion molecules, that are associated with psoriasis; FGF, that is associated with proliferative diabetic retinopathy; platelet factor 4, that is associated with the activated endothelium of various diseases; and VEGF, that is associated with vascular proliferative disease. It is believed that an animal or patient having any one of the above diseases would benefit from the specific induction of coagulation in the disease site.

Diseases that are known to have a common angiogenic dependent pathology, as described in Klagsburn & Folkman (1990), may also be treated with bispecific ligand as described herein. In particular, a vascular endothelial cell-targeted ligand or a stroma-targeted ligand will be used to achieve coagulation in the disease site. The treatment of BPH, diabetic retinopathy, vascular restenosis, vascular adhesions, AVM, meningioma, hemangioma, neovascular glaucoma, rheumatoid arthritis and psoriasis are particularly contemplated at the present time.

## 3. Disease-Associated Vasculature Cell Targets

The cells of the vasculature are intended as targets for use in the present invention. In these cases, one binding region of the bispecific ligand will be capable of binding to an accessible marker preferentially expressed by disease-associated vasculature endothelial cells. The exploitation of the vascular markers is made possible due to the proximity of the vascular endothelial cells to the disease area and to the products of the local aberrant physiological processes. For example, tumor vascular endothelial cells are exposed to tumor cells and tumor-derived products that change the phenotypic profile of the endothelial cells.

Tumor cells are known to elaborate tumor-derived products, such as lymphokines, monokines, colony-stimulating factors, growth factors and angiogenic factors, that act on the nearby vascular endothelial cells (Kandel et al., 1991; Folkman, 1985a,b) and cytokines (Burrows et al., 1991; Ruco et al., 1990; Borden et al., 1990). The tumor products bind to the endothelial cells and serve to selectively induce expression of certain molecules. It is these induced molecules that may be targeted using the tumor endothelium-specific coagulant delivery provided by certain aspects of the present invention. Vascular endothelial cells in tumors proliferate at a rate 30-fold greater than those in miscellaneous normal tissues (Denekamp et al., 1982), suggesting that proliferation-linked determinants could also serve as markers for tumor vascular endothelial cells.

In certain embodiments of the invention, the targeting component of the bispecific ligands will be a component that has a relatively high degree of specificity for tumor vascu-

lature. These targeting components may be defined as components that bind to molecules expressed on tumor endothelium, but that have little or no expression at the surface of normal endothelial cells. Such specificity may be assessed by the standard procedures of immunostaining of tissue sections, which are routine to those of skill in the art.

However, as stated above, an advantage of the present invention is that the requirement for selectivity is not as stringent as previously needed in the prior art methods, especially those employing immunotoxins, because any side effects associated with the mis-targeting of the coagulating agent will be minimal in comparison to those resulting from the mis-targeting of a toxin.

Therefore, it is generally proposed that the molecules to be targeted using the bispecific ligands or antibodies of this invention will be those that are expressed on tumor vasculature at a higher level than on normal endothelial cells.

## (a) Vascular Endothelial Cell Markers in Disease

Molecules that are known to be preferentially expressed at the surface of vascular endothelial cells in a disease site or environment are herein termed "natural disease-associated vascular endothelial cell markers". This term is used for simplicity to refer to the endothelial cell components that are expressed in diseases connected with increased or inappropriate angiogenesis or endothelial cell proliferation. One particular example are the tumor endothelial cell components that are expressed *in situ* in response to tumor-derived factors. These components are also termed "naturally-induced tumor endothelial cell markers".

Both VEGF/VPF (vascular endothelial cell growth factor/vascular permeability factor) and components of the FGF (fibroblast growth factor) family are concentrated in or on tumor vasculature. The corresponding receptors therefore provide a potential target for attack on tumor vasculature. For example, VEGF receptors are known to be upregulated on tumor endothelial cells, as opposed to endothelial cells in normal tissues, both in rodents and man (Thieme et al., 1995). Possibly, this is a consequence of hypoxia—a characteristic of the tumor microenvironment (Leith et al., 1992). FGF receptors are also upregulated three-fold on endothelial cells exposed to hypoxia, and so are believed to be upregulated in tumors (Bicknell and Harris et al., 1992).

The TGF  $\beta$  (transforming growth factor  $\beta$ ) receptor (endoglin) on endothelial cells is upregulated on dividing cells, providing another target. One of the present inventors found that endoglin is upregulated on activated and dividing HUVEC in culture, and is strongly expressed in human tissues on endothelial cells at sites of neovascularization, including a broad range of solid tumors and fetal placenta. In contrast, endothelial cells in the majority of miscellaneous non-malignant adult tissues, including preneoplastic lesions, contain little or no endoglin. Importantly, endoglin expression is believed to correlate with neoplastic progression in the breast, as shown by benign fibroadenomas and early carcinomas binding low levels of TEC-4 and TEC-11 antibodies (ATCC HB-12312 and ATCC HB-12311, respectively), and late stage intraductal carcinomas and invasive carcinomas binding high levels of these antibodies.

Other natural disease-associated vascular endothelial cell markers include a TIE, VCAM-1, P-selectin, E-selectin,  $\alpha_v\beta_3$  integrin, pleiotropin and endosialin, each of which may be targeted using the invention.

## (b) Cytokine-Inducible Vascular Endothelial Markers

Due to the nature of disease processes, which often result in localized dysfunction within the body, methods are available to manipulate the disease site whilst leaving other tissues relatively unaffected. This is particularly true in

malignant and benign tumors, which exist as distinct entities within the body of an animal. For example, the tumor environment may be manipulated to create additional markers that are specific for tumor vascular endothelial cells. These methods generally mimic those that occur naturally in solid tumors, and also involve the local production of signalling agents, such as growth factors or cytokines, that induce the specific expression of certain molecules at the surface of the nearby vascular endothelial cells.

The group of molecules that may be artificially induced to be expressed at the surface of vascular endothelial cells in a disease or tumor environment are herein termed "inducible endothelial cell markers", or specifically, inducible tumor endothelial cell markers. This term is used to refer to those markers that are artificially induced, i.e., induced as a result of manipulation by the hand of man, rather than those that are induced as part of the disease or tumor development process in an animal. The term "inducible marker", as defined above, is chosen for simple reference in the context of the present application, notwithstanding the fact that "natural markers" are also induced, e.g., by tumor-derived agents.

Thus, although not required to practice the invention, techniques for the selective elicitation of vascular endothelial antigen targets on the surface of disease-associated vasculature are available that may, if desired, be used in conjunction with the invention. These techniques involve manipulating the antigenic expression, or cell surface presentation, such that a target antigen is expressed or rendered available on the surface of disease-associated vasculature and not expressed or otherwise rendered accessible or available for binding, or at least to a lesser extent, on the surface of normal endothelium.

Tumor endothelial markers can be induced by tumor-derived cytokines (Burrows et al., 1991; Ruco et al., 1990) and by angiogenic factors (Mignatti et al., 1991). Examples of cell surface markers that may be specifically induced in the tumor endothelium and then targeted using a bispecific coagulating ligand, as provided by the invention, include those listed in Table III (Bevilacqua et al., 1987; Dustin et al., 1986; Osborn et al., 1989; Collins et al., 1984).

The mechanisms for the induction of the proposed markers; the inducing, or "intermediate cytokine", such as IL-1 and IFN- $\gamma$ ; and the leukocyte cell type and associated cytokine-activating molecule, whose targeting will result in the release of the cytokine, are also set forth in Table III. In the induction of a specific marker, a bispecific "cytokine-inducing" or "antigen-inducing" antibody is generally required. This antibody will selectively induce the release of the appropriate cytokine in the locale of the tumor, thus selectively inducing the expression of the desired target antigen by the vascular endothelial cells. The bispecific antibody cross-links cells of the tumor mass and cytokine-producing leukocytes, thereby activating the leukocytes to release the cytokine.

The preparation and use of bispecific antibodies such as these is predicated in part on the fact that cross-linking antibodies recognizing CD3, CD14, CD16 and CD28 have previously been shown to elicit cytokine production selectively upon cross-linking with the second antigen (Qian et al., 1991). In the context of the present invention, since only successfully tumor cell-crosslinked leukocytes will be activated to release the cytokine, cytokine release will be restricted to the locale of the tumor. Thus, expression of the desired marker, such as E-selectin, will be similarly limited to the endothelium of the tumor vasculature.

TABLE III

## POSSIBLE INDUCIBLE VASCULAR TARGETS

INDUCIBLE ENDOTHELIAL CELL MOLECULES	ACRONYM	SUBTYPES/ALIASES (MOLECULAR FAMILY)	INDUCING CYTOKINES	LEUKOCYTES WHICH PRODUCE THOSE CYTOKINES	LEUKOCYTE MOLECULES WHICH, WHEN CROSSLINKED BY MONOCLONAL ANTIBODIES ACTIVATE THE CELLS TO PRODUCE CYTOKINES
Endothelial- Leukocyte Adhesion Molecule-1	ELAM-1 E- select- in	— (Selectin)	IL-1, TNF- $\alpha$ , (TNF- $\beta$ ) (Bacterial Endotoxin)	monocytes macrophages mast cells	CD14 CD14 FcR for IgE
Vascular Cell Adhesion Molecule-1	VCAM-1	Inducible Cell Adhesion Molecule-110 (INCAM-110) (Immunoglobulin Family)	(Bacterial Endotoxin) IL-1, TNF- $\alpha$ TNF- $\beta$ , IL-4	monocytes macrophages mast cells helper T cells	CD14 CD14 FcR for IgE CD2, CD3, CD28
Intercellular Adhesion Molecule-1	ICAM-1	— (Immunoglobulin Family)	TNF IL-1, TNF $\alpha$ (Bacterial Endotoxin) TNF- $\beta$ , IFN $\gamma$	NK cells monocytes macrophages mast cells T helper cells	FcR for IgG (CD16) CD14 CD15 FcR for IgE CD2, CD3, CD28
The Agent for Leukocyte Adhesion Molecule-1	LAM-1 Agent	MEL-14 Agent (Mouse)	IL-1, TNF $\alpha$ (Bacterial Endotoxin)	NK cells monocytes macrophages mast cells	FcR for IgG (CD16) CD14 CD14 FcR for IgE
Major Histocompatibi- lity Complex Class II Antigen	MHC Class II	HLA-DR - Human HLA-DP HLA-DQ  I-A - Mouse I-E	IFN- $\gamma$	helper T cells   NK cells	CD2, CD3, CD28   FcR for IgG (CD16)

It is important to note that, from the possible inducible markers listed in Table III, E-selectin and MHC Class II antigens, such as HLA-DR, HLA-DP and HLA-DQ (Collins et al., 1984), are by far the most preferred targets for use in connection with clinical embodiments. The other adhesion molecules of Table III appear to be expressed to varying degrees in normal tissues, generally in lymphoid organs and on endothelium, making their targeting perhaps appropriate only in animal models or in cases where their expression on normal tissues can be inhibited without significant side-effects. The targeting of E-selectin or an MHC Class II antigen is preferred as the expression of these antigens will likely be the most direct to promote selectively in tumor-associated endothelium.

#### E-selectin

The targeting of an antigen that is not expressed on the surfaces of normal endothelium is the most straightforward form of the induction methods. E-selectin is an adhesion molecule that is not expressed in normal endothelial vasculature or other human cell types (Cotran et al., 1986), but can be induced on the surface of endothelial cells through the action of cytokines such as IL-1, TNF, lymphotoxin and bacterial endotoxin (Bevilacqua et al., 1987). It is not induced by IFN- $\gamma$  (Wu et al., 1990). The expression of E-selectin may thus be selectively induced in tumor endothelium through the selective delivery of such a cytokine, or via the use of a composition that causes the selective release of such cytokines in the tumor environment.

Bispecific antibodies are one example of a composition capable of causing the selective release of one or more of the foregoing or other appropriate cytokines in the tumor site, but not elsewhere in the body. Such bispecific antibodies are herein termed "antigen-inducing antibodies" and are, of course, distinct from any bispecific antibodies of the invention that have targeting and coagulating components. Antigen-inducing antibodies are designed to cross-link cytokine effector cells, such as cells of monocyte/macrophage lineage, T cells and/or NK cells or mast cells, with tumor cells of the targeted solid tumor mass. This cross-linking would then effect a release of cytokine that is localized to the site of cross-linking, i.e., the tumor.

Effective antigen-inducing antibodies recognize a selected tumor cell surface antigen on the one hand (e.g., those in Table I) and, on the other hand, recognize a selected "cytokine activating" antigen on the surface of a selected leukocyte cell type. The term "cytokine activating" antigen is used to refer to any one of the various known molecules on the surfaces of leukocytes that, when bound by an effector molecule, such as an antibody or a fragment thereof or a naturally-occurring agent or synthetic analog thereof, be it a soluble factor or membrane-bound counter-receptor on another cell, promotes the release of a cytokine by the leukocyte cell. Examples of cytokine activating molecules include CD14 (the LPS receptor) and FcR for IgE, which will activate the release of IL-1 and TNF $\alpha$ ; and CD16, CD2 or CD3 or CD28, which will activate the release of IFN $\gamma$  and TNF $\beta$ , respectively.

Once introduced into the bloodstream of an animal bearing a tumor, such an antigen-inducing bispecific antibody will bind to tumor cells within the tumor, cross-link those tumor cells with effector cells, e.g., monocytes/macrophages, that have infiltrated the tumor, and thereafter effect the selective release of cytokine within the tumor. Importantly, however, without cross-linking of the tumor and leukocyte, the antigen-inducing antibody will not effect the release of cytokine. Thus, no cytokine release will occur in parts of the body removed from the tumor and, hence,

expression of cytokine-induced molecules, e.g., E-selectin, will occur only within the tumor endothelium.

A number of useful "cytokine activating" antigens are known, which, when cross-linked with an appropriate bispecific antibody, will result in the release of cytokines by the cross-linked leukocyte. The generally preferred target for this purpose is CD14, which is found on the surface of monocytes and macrophages. When CD14 is cross linked it stimulates monocytes/macrophages to release IL-1 (Schutt et al., 1988; Chen et al., 1990), and possibly other cytokines, which, in turn stimulate the appearance of E-selectin on nearby vasculature. Other possible targets for cross-linking in connection with E-selectin induction and targeting include FcR for IgE, found on Mast cells; FcR for IgG (CD16), found on NK cells; as well as CD2, CD3 or CD28, found on the surfaces of T cells. Of these, CD14 targeting is generally preferred due to the relative prevalence of monocyte/macrophage infiltration of solid tumors as opposed to the other leukocyte cell types.

In an exemplary induction embodiment, an animal bearing a solid tumor is injected with bispecific (Fab'-Fab') anti-CD14/anti-tumor antibody (such as anti-CEA, 9.2.27 antibody against high Mr melanoma antigens OV-TL3 or MOv 18 antibodies against ovarian associated antigens). The antibody localizes in the tumor, by virtue of its tumor binding activity, and then activates monocytes and macrophages in the tumor by crosslinking their CD14 antigens (Schutt et al., 1988; Chen et al., 1990). The activated monocytes/macrophages have tumoricidal activity (Palleroni et al., 1991) and release IL-1 and TNF which rapidly induce E-selectin antigens on the tumor vascular endothelial cells (Bevilacqua et al., 1987; Pober et al., 1991).

#### MHC Class II Antigens

The second preferred group of inducible markers contemplated for use with the present invention are the MHC Class II antigens (Collins et al., 1984), including HLA-DR, HLA-DP and HLA-DQ. Class II antigens are expressed on vascular endothelial cells in most normal tissues in several species, including man. Studies in vitro (Collins et al., 1984; Daar et al., 1984; O'Connell et al., 1990) and in vivo (Groenewegen et al., 1985) have shown that the expression of Class II antigens by vascular endothelial cells requires the continuous presence of IFN- $\gamma$  which is elaborated by T<sub>H1</sub> cells and, to a lesser extent, by NK cells and CD8<sup>+</sup> T cells.

MHC Class II antigens are not unique to vascular endothelial cells, and are also expressed constitutively on B cells, activated T cells, cells of monocyte/macrophage lineage and on certain epithelial cells, both in mice (Hammerling, 1976) and in man (Daar et al., 1984). Due to the expression of MHC Class II antigens on "normal" endothelium, their targeting is not quite so straightforward as E-selectin. However, the induction and targeting of MHC Class II antigens is made possible by using in conjunction with an immunosuppressant, such as Cyclosporin A (CsA), that has the ability to effectively inhibit the expression of Class II molecules in normal tissues (Groenewegen et al., 1985). The CsA acts by preventing the activation of T cells and NK cells (Groenewegen et al., 1985; DeFranco, 1991), thereby reducing the basal levels of IFN- $\gamma$  below those needed to maintain Class II expression on endothelium.

There are various other cyclosporins related to CsA, including cyclosporins A, B, C, D, G, and the like, that also have immunosuppressive action and are likely to demonstrate an ability to suppress Class II expression. Other agents that might be similarly useful include FK506 and rapamycin.

Thus, the practice of the MHC Class II induction and targeting embodiment requires a pretreatment of the tumor-bearing animal with a dose of CsA or other Class II immunosuppressive agent that is effective to suppress Class II expression. In the case of CsA, this will typically be on the order of about 10 to about 30 mg/kg body weight. Once suppressed in normal tissues, Class II antigens can then be selectively induced in the tumor endothelium, again through the use of a bispecific antibody.

In this case, the antigen-inducing bispecific antibody will have specificity for a tumor cell marker and for an activating antigen found on the surface of an effector cell that is capable of inducing IFN- $\gamma$  production. Such effector cells will generally be helper T cells ( $T_H$ ) or Natural Killer (NK) cells. In these embodiments, it is necessary that T cells, or NK cells if CD16 is used, be present in the tumor to produce the cytokine intermediate in that Class II antigen expression is achieved using IFN- $\gamma$ , but is not achieved with the other cytokines. Thus, for the practice of this aspect of the invention, one will desire to select CD2, CD3, CD28, or most preferably CD28, as the cytokine activating antigen for targeting by the antigen-inducing bispecific antibody.

The T cells that should be activated in the tumor are those adjacent to the vasculature since this is the region most accessible to cells and is also where the bispecific antibody will be most concentrated. The activated T cells should then secrete IFN- $\gamma$  which induces Class II antigens on the adjacent tumor vasculature.

The use of a bispecific (Fab'-Fab') antibody having one arm directed against a tumor antigen and the other arm directed against CD28 is currently preferred. This antibody will crosslink CD28 antigens on T cells in the tumor which, when combined with a second signal (provided, for example, by IL-1 which is commonly secreted by tumor cells (Burrows et al., 1991; Ruco et al., 1990), has been shown to activate T cells through a  $CA^{2+}$ -independent non-CsA-inhibitable pathway (Hess et al., 1991; June et al., 1987; Bjorndahl et al., 1989).

The preparation of antibodies against various cytokine activating molecules is also well known in the art. For example, the preparation and use of anti-CD14 and anti-CD28 monoclonal antibodies having the ability to induce cytokine production by leukocytes has now been described by several laboratories (reviewed in Schutt et al., 1988; Chen et al., 1990, and June et al., 1990, respectively). Moreover, the preparation of monoclonal antibodies that will stimulate leukocyte release of cytokines through other mechanisms and other activating antigens is also known (Clark et al., 1986; Geppert et al., 1990).

In still further embodiments, the inventors contemplate an alternative approach for suppressing the expression of Class II molecules, and selectively eliciting Class II molecule expression in the locale of the tumor. This approach, which avoids the use of both CsA and a bispecific activating antibody, takes advantage of the fact that the expression of Class II molecules can be effectively inhibited by suppressing IFN- $\gamma$  production by T cells, e.g., through use of an anti-CD4 antibody (Street et al., 1989). Using this embodiment, IFN- $\gamma$  production is inhibited by administering anti-CD4, resulting in the general suppression of Class II expression. Class II is then induced only in the tumor site, e.g., using tumor-specific T cells which are only activatable within the tumor.

In this mode of treatment, one will generally pretreat an animal or human patient with a dose of anti-CD4 that is effective to suppress IFN- $\gamma$  production and thereby suppress the expression of Class II molecules. Effective doses are

contemplated to be, for example, on the order of about 4 to about 10 mg/kg body weight. After Class II expression is suppressed, one will then prepare and introduce into the bloodstream an IFN- $\gamma$ -producing T cell clone (e.g.,  $T_H1$  or cytotoxic T lymphocyte, CTL) specific for an antigen expressed on the surface of the tumor cells. These T cells localize to the tumor mass, due to their antigen recognition capability and, upon such recognition, then release IFN- $\gamma$ . In this manner, cytokine release is again restricted to the tumor, thus limiting the expression of Class II molecules to the tumor vasculature.

The IFN- $\gamma$ -producing T cell clone may be obtained from the peripheral blood (Mazzocchi et al., 1990), however, a preferred source is from within the tumor mass (Fox et al., 1990). The currently preferred means of preparing such a T cell clone is to remove a portion of the tumor mass from a patient; isolate cells, using collagenase digestion, where necessary; enrich for tumor infiltrating leukocytes using density gradient centrifugation, followed by depletion of other leukocyte subsets by, e.g., treatment with specific antibodies and complement; and then expand the tumor infiltrating leukocytes in vitro to provide the IFN- $\gamma$  producing clone. This clone will necessarily be immunologically compatible with the patient, and therefore should be well tolerated by the patient.

It is proposed that particular benefits will be achieved by further selecting a high IFN- $\gamma$  producing T cell clone from the expanded leukocytes by determining the cytokine secretion pattern of each individual clone every 14 days. To this end, rested clones will be mitogenically or antigenically-stimulated for about 24 hours and their culture supernatants assayed, e.g., using a specific sandwich ELISA technique (Cherwinski et al., 1989), for the presence of IL-2, IFN- $\gamma$ , IL-4, IL-5 and IL-10. Those clones secreting high levels of IL-2 and IFN- $\gamma$ , the characteristic cytokine secretion pattern of  $T_H1$  clones, will be selected. Tumor specificity will be confirmed using proliferation assays.

Furthermore, one will prefer to employ as the anti-CD4 antibody an anti-CD4 Fab, because it will be eliminated from the body within 24 hours after injection and so will not cause suppression of the tumor-recognizing T-cell clones that are subsequently administered. The preparation of T cell clones having tumor specificity is generally known in the art, as exemplified by the production and characterization of T cell clones from lymphocytes infiltrating solid melanoma tumors (Maeda et al., 1991).

In using either of the MHC Class II suppression-induction methods, additional benefits will likely result from the fact that anti-Class II antibodies injected intravenously do not appear to reach the epithelial cells or the monocytes/macrophages in normal organs other than the liver and spleen. Presumably this is because the vascular endothelium in most normal organs is tight, not fenestrated as it is in the liver and spleen, and so the antibodies must diffuse across basement membranes to reach the Class II-positive cells. Also, any B cell elimination that may result, e.g., following cross-linking, is unlikely to pose a significant problem as these cells are replenished from Class II negative progenitors (Lowe et al., 1986). Even B cell killing, as occurs in B lymphoma patients, causes no obvious harm (Vitetta et al., 1991).

In summary, although the tumor coagulating compositions and antibodies of the present invention are elegantly simple, and do not require the induction of antigens for their operability, the combined use of an antigen-inducing bispecific antibody with this invention is also contemplated. Such antibodies would generally be administered prior to the bispecific coagulating ligands of this invention.

Generally speaking, the more "immunogenic" tumors would be more suitable for the MHC Class II approach involving, e.g., the cross-linking of T cells in the tumor through an anti-CD28/anti-tumor bispecific antibody, because these tumors are more likely to be infiltrated by T cells, a prerequisite for this method to be effective. Examples of immunogenic solid tumors include renal carcinomas, melanomas, a minority of breast and colon cancers, as well as possibly pancreatic, gastric, liver, lung and glial tumor cancers. These tumors are referred to as "immunogenic" because there is evidence that they elicit immune responses in the host and they have been found to be amenable to cellular immunotherapy (Yamaue et al., 1990). In the case of melanomas and large bowel cancers, the most preferred antibodies for use in these instances would be B72.3 (anti-TAG-72) and PRSC5/PR4C2 (anti-Lewis a) or 9.2.27 (anti-high Mr melanoma antigen).

For the majority of solid tumors of all origins, an anti-CD14 approach that employs a macrophage/monocyte intermediate would be more suitable. This is because most tumors are rich in macrophages. Examples of macrophage-rich tumors include most breast, colon and lung carcinomas. Examples of preferred anti-tumor antibodies for use in these instances would be anti-HER-2, B72.3, SM-3, HMFG-2, and SWA11 (Smith et al., 1989).

#### (c) Coagulant-Inducible Markers

Coagulants, such as thrombin, Factor IX/IXa, Factor X/Xa, plasmin and metalloproteinases, such as interstitial

collagenases, stromelysins and gelatinases, also act to induce certain markers. In particular, E-selectin, P-selectin, PDGF and ICAM-1 are induced by thrombin (Sugama et al., 1992; Shankar et al., 1994).

Therefore, for this induction, an anti-coagulant/anti-tumor bispecific antibody will be utilized. The antibody will localize in the tumor via its tumor binding activity. The bispecific will then concentrate the coagulant, e.g., thrombin, in the tumor, resulting in induction of E-selectin and P-selectin on the tumor vascular endothelial cells (Sugama et al., 1991; Shankar et al., 1994).

Alternatively, targeting of truncated tissue factor to tumor cells or endothelium will induce thrombin deposition within the tumor. As the thrombin is deposited, E-selectin and P-selectin will be induced on the tumor vascular endothelial cells.

#### (d) Antibodies to Vascular Endothelial Cell Markers

A straightforward means of recognizing a disease-associated vasculature target, whether induced in the natural environment or by artificial means, is through the use of an antibody that has binding affinity for the particular cell surface receptor, molecule or antigen. These include antibodies directed against all cell surface components that are known to be present on, e.g., tumor vascular endothelial cells, those that are induced or over-expressed in response to tumor-derived factors, and those that are induced following manipulation by the hand of man. Table IV and Table V summarize useful antibodies and their properties.

TABLE IV

SUMMARY OF VASCULATURE STAINING PATTERNS OF CERTAIN ANTIBODIES TO HUMAN TUMOR VASCULATURE					
Antibody	Antigen	Reference	% Tumor types stained	% tumor vessels stained	normal vessel reactivity
anti-vWF	VIII R Ag		100	100	strong on all
FB5	endostatin	Rettig & old	30	10-20	lymphoid organs
TP3	80 kDa osteosarcoma related antigen protein	Bruland	50	10-30	strong on small
BC-1	fibronectin isoform	Zardi	60	10-30	none
TV-1	fibronectin	Epstein	100	100	strong on all
LM 609	$\alpha_v\beta_3$ vitronectin receptor	Cheneoh	85	70-80	medium on all
TEC 11	endoglin	Thorpe;	100	100	weak on most
TEC 110	VEGF	Thorpe;	100	100	weak on most

TABLE V

COMPARISON OF ANTI-EC mAbs ON HUMAN TUMORS								
TUMOR TYPE	n	TEC 110	TEC 11	FB-5	TP-3	BC-1	TV-1	LM 609
<u>DIGESTIVE</u>								
Gastrointestinal	9	++	++	+	++	+	++	++
Parotid	3	++	++	-	++(SMALL)	-	ND	ND
<u>REPRODUCTIVE</u>								
Breast	1	+	++	-	ND	++	++	-
Ovary	4	++	++	-	++(SMALL)	++	++	+
Uterus	2	++	++	-		++	++	+
<u>RESPIRATORY</u>								
Lung	3	++	++	+	ND	++	++	+
<u>LYMPHOID</u>								
Hodgkins	2	++	++	-	+	-	+++	+



Two further antibodies that may be used in this invention are those described by Rettig et al. (1992) and Wang et al. (1993) that are directed against unrelated antigens of unknown function expressed in the vasculature of human tumors, but not in most normal tissues.

The antibody described by Kim et al. (1993) may also be used in this invention, particularly as this antibody inhibited angiogenesis and suppressed tumor growth in vivo.

Antibodies that have not previously been shown to be specific for human tumors may also be used. For example, Venkateswaran et al. (1992) described the production of anti-FGF MABs. Xu et al. (1992) developed and characterized a panel of 16 isoform and domain-specific polyclonal and monoclonal antibodies against FGF receptor (flg) isoforms. Massaglia et al. (1987) also reported MABs against FGF.

#### (e) Generation of Antibodies to Disease Vasculature

In addition to utilizing a known antibody, such as those described above and others known and published in the scientific literature, one may also generate a novel antibody using standard immunization procedures, as described in more detail hereinbelow. To generate an antibody against a known disease-associated vascular marker antigen, one would immunize an animal with an immunogenic composition comprising the antigen. This may be a membrane preparation that includes, or is enriched for, the antigen; a relatively purified form of the antigen, as isolated from cells or membranes; a highly purified form of the antigen, as obtained by a variety of purification steps using, e.g., a native antigen extract or a recombinant form of the antigen obtained from a recombinant host cell.

The present invention also provides yet further methods for generating an antibody against an antigen present on disease-associated vasculature endothelial cells, which methods are suitable for use even where the biochemical identity of the antigen remains unknown. These methods are exemplified through the generation of an antibody against tumor vasculature endothelial cells. A first means of achieving antibody generation in this manner uses a preparation of vascular endothelial cells obtained from the tumor site of an animal or human patient. One simply immunizes an experimental animal with a preparation of such cells and collects the antibodies so produced. The most useful form of this method is that where specific antibodies are subsequently selected, as may be achieved using conventional hybridoma technology and screening against tumor vascular endothelial cells.

A development of the above method is that which mimics the tumor vasculature phenomenon in vitro, and where cell purification is not necessary. In using this method, endothelial cells are subjected to tumor-derived products, such as might be obtained from tumor-conditioned media, in cell culture rather than in an animal. This method generally involves stimulating endothelial cells with tumor-conditioned medium and employing the stimulated endothelial cells as immunogens to prepare a collection of antibodies. Again, specific antibodies should be selected, e.g., using conventional monoclonal antibody technology, or other techniques such as combinatorial immunoglobulin phagemid libraries prepared from RNA isolated from the spleen of the immunized animal. One would select a specific antibody that preferentially recognizes tumor-stimulated vascular endothelium and reacts more strongly with tumor-associated endothelial cells than with normal adult human tissues.

Stimulated endothelial cells contemplated to be of use in this regard include, for example, human umbilical vein

endothelial cells (HUVE), human dermal microvascular endothelial cells (HDEMC), human saphenous vein endothelial cells, human omental fat endothelial cells, other human microvascular endothelial cells, human brain capillary endothelial cells, and the like. It is also contemplated that endothelial cells from another species may be stimulated by tumor-conditioned media and employed as immunogens to generate hybridomas to produce an antibodies in accordance herewith, i.e., to produce antibodies that crossreact with tumor-stimulated human vascular endothelial cells, and/or antibodies for use in pre-clinical models.

"Tumor-conditioned medium or media" are defined herein as compositions or media, such as culture media, that contain one or more tumor-derived cytokines, lymphokines or other effector molecules. Most typically, tumor-conditioned medium is prepared from a culture medium in which selected tumor cells have been grown, and will therefore be enriched in such tumor-derived products. The type of medium is not believed to be particularly important, so long as it at least initially contains appropriate nutrients and conditions to support tumor cell growth. It is also, of course, possible to extract and even separate materials from tumor-conditioned media and employ one or more of the extracted products for application to the endothelial cells.

As for the type of tumor used for the preparation of the medium or media, one will, of course, prefer to employ tumors that mimic or resemble the tumor that will ultimately be subject to analysis or treatment using the present invention. Thus, for example, where one envisions the development of a protocol for the treatment of breast cancer, one will desire to employ breast cancer cells such as ZR-75-1, T47D, SKBR3, MDA-MB-231. In the case of colorectal tumors, one may mention by way of example the HT29 carcinoma, as well as DLD-1, HCT116 or even SW48 or SW122. In the case of lung tumors, one may mention by way of example NCI-H69, SW2, NCI H23, NCI H460, NCI H69, or NCI H82. In the case of melanoma, good examples are DX.3, A375, SKMEL-23, HMB-2, MJM, T8 or indeed VUP. In any of the above cases, it is further believed that one may even employ cells produced from the tumor that is to be treated, i.e., cells obtained from a biopsy.

Once prepared, the tumor-conditioned media is then employed to stimulate the appearance of tumor endothelium-specific marker(s) on the cell surfaces of endothelial cells, e.g., by culturing selected endothelial cells in the presence of the tumor-conditioned media (or products derived therefrom). Again, it is proposed that the type of endothelial cell that is employed is not of critical importance, so long as it is generally representative of the endothelium associated with the vasculature of the particular tumor that is ultimately to be treated or diagnosed. The inventors prefer to employ human umbilical vein endothelial cells (HUVE), or human dermal microvascular endothelial cells (HDEMC, Karasek, 1989), in that these cells are of human origin, respond to cytokine growth factors and angiogenic factors and are readily obtainable. However, it is proposed that any endothelial cell that is capable of being cultured in vitro may be employed in the practice of the invention and nevertheless achieve beneficial results. One may mention, by way of example, cells such as EA.hy9.2, ECV304, human saphenous vein endothelial cells, and the like.

Once stimulated using the tumor-derived products, the endothelial cells are then employed as immunogens in the preparation of monoclonal antibodies (MABs). The technique for preparing MABs against antigenic cell surface markers is quite straightforward, and may be readily carried

out using techniques well known to those of skill in the art, as exemplified by the technique of Kohler & Milstein (1975), and further described hereinbelow.

Generally speaking, a preferred method of preparing MAbs using stimulated endothelial cells involves the following procedures: Cells or cell lines derived from human tumors are grown in tissue culture for  $\geq 4$  days. The tissue culture supernatant ("tumor-conditioned medium") is removed from the tumor cell cultures and added to cultures of HUVEC at a final concentration of 50% (v/v). After 2 days culture the HUVEC are harvested non-enzymatically and  $1-2 \times 10^6$  cells injected intraperitoneally into mice. This process is repeated three times at two-weekly intervals, the final immunization being by the intravenous route. Three days later the spleen cells are harvested and fused with SP2/0 myeloma cells by standard protocols (Kohler & Milstein, 1975) and hybridomas producing antibodies with the appropriate reactivity are cloned by limiting dilution.

From the resultant collection of hybridomas, one will then desire to select one of more hybridomas that produce an antibody that recognizes the activated vascular endothelium to a greater extent than it recognizes non-activated vascular endothelium. One goal is the identification of antibodies having virtually no binding affinity for normal endothelium. However, in contrast to the prior art, in the present invention this property is not critical. In any event, one will generally identify suitable antibody-producing hybridomas by screening using, e.g., an ELISA, RIA, IRMA, IIF, or similar immunoassay, against one or more types of tumor-activated endothelial cells. Once candidates have been identified, one will desire to test for the absence of reactivity for non-activated or "normal" endothelium or other normal tissue or cell type. In this manner, hybridomas producing antibodies having an undesirably high level of normal cross-reactivity for the particular application envisioned may be excluded.

#### (f) Anti-Endoglin Antibodies

Using the technique described above, antibodies having relative specificity for tumor vascular endothelium have been prepared and isolated. In one particular example, HT29 carcinoma cells were employed to prepare the conditioned medium, which was then employed to stimulate HUVE cells in culture. The resultant HT29-activated HUVE cells were then employed as immunogens in the preparation of a hybridoma bank, which was ELISA-screened using HT29-activated HUVE cells and by immunohistologic analysis of sections of human tumors and normal tissues. From this bank, antibodies that recognized a tumor vascular endothelial cell antigen were selected.

The MAbs termed tumor endothelial cell antibody 4 and tumor endothelial cell antibody 11 (TEC4 and TEC11) were obtained using the above method. The antigen recognized by TEC4 and TEC11 was ultimately determined to be the molecule endoglin. The epitopes on endoglin recognized by TEC4 and TEC11 are present on the cell surface of stimulated HUVE cells, and only minimally present (or immunologically accessible) on the surface of non-stimulated cells. MAbs have previously been raised against endoglin. However, analyzing the reactivity with HUVEC or TCM-activated HUVEC cell surface determinants by FACS or indirect immunofluorescence shows the epitopes recognized by TEC-4 and TEC-11 to be distinct from those of a previous antibody termed 44G4 (Gougos & Letarte, 1988).

Although any of the known anti-endoglin antibodies (e.g., Gougos & Letarte, 1988; Gougos et al., 1992; O'Connell et al., 1992; Bühring et al., 1991) may be used in connection with the present invention, the TEC-4 and TEC-11 mAbs are envisioned to be particularly suitable. This is because they

label capillary and venular endothelial cells moderately to strongly in a broad range of solid tumors (and in several chronic inflammatory conditions and fetal placenta), but display relatively weak staining of vessels in the majority of normal, healthy adult tissues. TEC-11 is particularly preferred as it shows virtually no reactivity with non-endothelial cells. Furthermore, both TEC-4 and TEC-11 are complement-fixing, which imparts to them the potential to also induce selective lysis of endothelial cells in the tumor vascular bed.

Antibodies that are cross-reactive with the MAbs TEC-4 and TEC-11 (ATCC HB-12312 and ATCC HB-12311, respectively), i.e., those that bind to endoglin at the same epitope as TEC-4 or TEC-11, are also contemplated to be of use in this invention. The identification of an antibody or antibodies that bind to endoglin at the same epitopes as TEC-4 or TEC-11 is a fairly straightforward matter. This can be readily determined using any one of variety of immunological screening assays in which antibody competition can be assessed. For example, where the test antibodies to be examined are obtained from a different source to that of TEC-4 or TEC-11, e.g., a rabbit, or are even of a different isotype, for example, IgG1 or IgG3, a competition ELISA may be employed. In one such embodiment of a competition ELISA one would pre-mix TEC-4 or TEC-11 with varying amounts of the test antibodies prior to applying to the antigen-coated wells in the ELISA plate. By using either anti-murine or anti-IgM secondary antibodies one will be able to detect only the bound TEC-4 or TEC-11 antibodies—the binding of which will be reduced by the presence of a test antibody that recognizes the same epitope as either TEC-4 or TEC-11.

To conduct an antibody competition study between TEC-4 or TEC-11 and any test antibody, one may first label TEC-4 or TEC-11 with a detectable label, such as, e.g., biotin or an enzymatic or radioactive label, to enable subsequent identification. In these cases, one would incubate the labelled antibodies with the test antibodies to be examined at various ratios (e.g., 1:1, 1:10 and 1:100) and, after a suitable period of time, one would then assay the reactivity of the labelled TEC-4 or TEC-11 antibodies and compare this with a control value in which no potentially competing antibody (test) was included in the incubation.

The assay may be any one of a range of immunological assays based upon antibody binding and the TEC-4 or TEC-11 antibodies would be detected by means of detecting their label, e.g., using streptavidin in the case of biotinylated antibodies or by using a chromogenic substrate in connection with an enzymatic label or by simply detecting the radiolabel. An antibody that binds to the same epitope as TEC-4 or TEC-11 will be able to effectively compete for binding and thus will significantly reduce TEC-4 or TEC-11 binding, as evidenced by a reduction in labelled antibody binding. In the present case, after mixing the labelled TEC-4 or TEC-11 antibodies with the test antibodies, suitable assays to determine the remaining reactivity include, e.g., ELISAs, RIAs or western blots using human endoglin; immunoprecipitation of endoglin; ELISAs, RIAs or immunofluorescent staining of recombinant cells expressing human endoglin; indirect immunofluorescent staining of tumor vasculature endothelial cells; reactivity with HUVEC or TCM-activated HUVEC cell surface determinants indirect immunofluorescence and FACS analysis. This latter method is most preferred and was employed to show that the epitopes recognized by TEC-4 and TEC-11 are distinct from that of 44G4 (Gougos & Letarte, 1988).

The reactivity of the labelled TEC-4 or TEC-11 antibodies in the absence of any test antibody is the control high value.

The control low value is obtained by incubating the labelled antibodies with unlabelled antibodies of the same type, when competition would occur and reduce binding of the labelled antibodies. A significant reduction in labelled antibody reactivity in the presence of a test antibody is indicative of a test antibody that recognizes the same epitope, i.e., one that "cross-reacts" with the labelled antibody. A "significant reduction" in this aspect of the present application may be defined as a reproducible (i.e., consistently observed) reduction in binding of at least about 10%–50% at a ratio of about 1:1, or more preferably, of equal to or greater than about 90% at a ratio of about 1:100.

The use of "cross-reactivity assays", as described above in the context of TEC-4 and TEC-11 antibodies, may be applied to any antibody for use in the present invention. Therefore, antibodies that bind to a component of a tumor cell, a component of tumor vasculature, a tumor cell-associated component, a tumor vasculature-associated component, a tumor extracellular matrix component, or to any cell type listed herein, at the same epitope as any of the antibodies listed herein, as determined by an antibody competition assay, will be an antibody that falls under the scope of this invention when combined with a coagulating agent to form a bispecific ligand.

#### (g) Use of Vascular Endothelial Cell Binding Ligands

Biological ligands that are known to bind or interact with endothelial cell surface molecules, such as growth factor receptors, may also be employed as a targeting component.

The growth factors or ligands contemplated to be useful as targets in this sense include VEGF/VPF, FGF, TGF $\beta$ , ligands that bind to a TIE, tumor-associated fibronectin isoforms, scatter factor, hepatocyte growth factor (HGF), platelet factor 4 (PF4), PDGF and TIMP.

Particularly preferred targets are VEGF/VPF, the FGF family of proteins and TGF $\mu$ . Abraham et al. (1986) cloned FGF, which is therefore available as a recombinant protein. As reported by Ferrara et al. (1991), four species of VEGF having 121, 165, 189, and 206 amino acids have been cloned.

#### (h) Targeting of Bound Ligands

Antibodies or specific targeting ligands may also be directed to any component that binds to the surface of vascular endothelial cells in a disease site, such as a tumor. Such components are exemplified by tumor-derived ligands and antigens, such as growth factors, that bind to specific cell surface receptors already present on the endothelial cells, or to receptors that have been induced, or over-expressed, on such cells in response to the tumor environment. Tumor vasculature-associated targets may also be termed tumor-derived endothelial cell binding factors.

A level of specificity required for successful disease targeting will be achieved partly because the local endothelial cells will be induced to express, or reveal, receptors that are not present, or are under-expressed or masked, on normal endothelial cells. With tumors, further specificity will result due to the fact that endothelial cells in the tumor will capture the tumor-derived factors, and bind them to the cell surface, reducing the amount of ligand available for other tissues. When combined with the further dilution of the factor or ligand by distribution in the blood and tissue fluid pool, endothelial cells in normal tissues will be expected to bind relatively little of such factors. Thus, operationally, cell-surface bound ligands or factors will be able to be used as a tumor endothelial cell marker.

In addition to manufacture by the tumor cells themselves, tumor endothelial cell binding factors may also originate from other cell types, such as macrophages and mast cells,

that have infiltrated tumors, or may be elaborated by platelets that become activated within the tumor.

Further growth factors or ligands contemplated to be useful as tumor vasculature-associated targets include EGF, FGF, VEGF, TGF $\beta$ , HGF (NaKamura, 1991), angiotropin, TGF- $\alpha$ , TNF- $\alpha$ , PD-ECGF and TIE binding ligands (Bicknell and Harris, 1992). The currently preferred targets are VEGF/VPF, the FGF family of proteins, transforming growth factor- $\beta$  (TGF- $\beta$ ); TGF- $\alpha$ ; tumor necrosis factor- $\alpha$  (TNF- $\alpha$ ); angiotropin; platelet-derived endothelial cell growth factor (PD-ECGF); TIE binding ligands; pleiotropin.

Another aspect of the present invention is the use of targeting antibodies, or binding regions therefrom, that are specific for epitopes present only on ligand-receptor complexes, which epitopes are absent from both the individual (free) ligand and the receptor in its unbound form. These antibodies recognize and bind to the unique conformation that results when a ligand, such as a growth factor, binds to its receptor, such as a growth factor receptor, to form a specifically bound complex. Such epitopes are not present on the uncomplexed forms of the ligands or receptors.

The inventors contemplate that the ligand-receptor complexes to which these antibodies bind are present in significantly higher number on tumor-associated endothelial cells than on non-tumor associated endothelial cells. Such antibodies will therefore be useful as targeting agents and will serve to further increase the specificity of the bispecific coagulants of the invention.

#### (i) Receptor Constructs

Soluble binding domains of endothelial cell surface receptors are also contemplated for use as targeting ligands in the present invention. This concept is generally based upon the well-known sandwich binding phenomena that has been exploited in a variety of *in vitro* and *in vivo* binding protocols. Basically, as the endothelial cells express specific receptors, the cells bind to and adsorb the corresponding ligands, the ligands are then available for binding to further receptor constructs should they be introduced into the system.

A range of useful endothelial cell receptors has been identified in the foregoing sections, with VEGF/VPF, FGF, TGF $\beta$ , TIE-1 and TIE-2 being particularly preferred targets. Each of these receptors could be manipulated to form a soluble binding domain for use as a targeting ligand.

#### 4. Disease-Associated Stromal Cell Targets

##### (a) Extracellular Matrix/Stromal Targets

The usefulness of the basement membrane markers in tumoral pathology was described by Birembaut et al. (1985). These studies showed that the distribution of basement membrane (BM) markers, type IV collagen, laminin (LM), heparan sulphate proteoglycan (HSP) and fibronectin (FN) were disrupted in tumoral pathology. Burtin et al. (1983) also described alterations of the basement membrane and connective tissue antigens in human metastatic lymph nodes.

A preferred target for use with the invention is RIBS. Ugarova et al. (1993) reported that conformational changes occur in fibrinogen and are elicited by its interaction with the platelet membrane glycoprotein GPIIb-IIIa. The binding of fibrinogen to membrane glycoprotein GPIIb-IIIa on activated platelets leads to platelet aggregation. This interaction results in conformational changes in fibrinogen as evidenced by the expression of receptor-induced binding sites, RIBS, epitopes which are expressed by the bound but not the free ligand.

Two RIBS epitopes have been localized by Ugarova et al. (1993). One sequence resides at  $\gamma$ 112–119 and is recognized

by MAb 9F9; the second is the RGDF sequence at A $\alpha$  95–98 and is recognized by mAb 155B16. These epitopes are also exposed by adsorption of fibrinogen onto a plastic surface and digestion of the molecule by plasmin. Proteolytic exposure of the epitopes coincides with cleavage of the carboxyl-terminal aspects of the A $\alpha$ -chains to form fragment X<sub>2</sub>. The inaccessibility of the RGDF sequence at A $\alpha$  95–98 in fibrinogen suggests that this sequence does not participate in the initial binding of the molecule to GPIIb-IIIa.

Binding of fibrinogen to its receptor alters the conformation of the carboxyl-terminal aspects of the A $\alpha$ -chains, exposing the sequences which reside in the coiled-coil connector segments between the D and E domains of the molecule, generating the RIBS epitopes. In practical terms, the RIBS sequences are proposed as epitopes for use in targeting with a coagulant. The MAbs 9F9 and 155B16 may thus be advantageously used, as may the antibodies described by Zamarron et al. (1991).

#### (b) Additional Cellular Targets

The present invention has the further advantage that it may be used to direct coagulants to disease-associated vasculature by targeting them to cell types found within the disease region.

Platelets participate in hemostasis and thrombosis by adhering to injured blood vessel walls and accumulating at the site of injury. Although platelet deposition at sites of blood vessel injury is responsible for the primary arrest of bleeding under physiologic conditions, it can lead to vascular occlusion with ensuing ischemic tissue damage and thrombus embolization under pathologic conditions.

Interactions of platelets with their environment and with each other represent complex processes that are initiated at the cell surface. The surface membrane, therefore, provides a reactive interface between the external medium, including components of the blood vessel wall and plasma, and the platelet interior.

p-155, a multimeric platelet protein that is expressed on activated platelets (Hayward et al., 1991), may be targeted using the invention. Platelets respond to a large number of stimuli by undergoing complex biochemical and morphological changes. These changes are involved in physiological processes including adhesion, aggregation, and coagulation. Platelet activation produces membrane alterations that can be recognized by monoclonal antibodies. The monoclonal antibody JS-1 (Hayward et al., 1991) is one such antibody contemplated for use as part of a coagulant.

Ligand-induced binding sites (LIBS) are sites expressed on cell surface receptors only after ligand binding causes the receptor to change shape, mediate subsequent biological events. These may be seen as counterparts to RIBS and are also preferred targets for use with the present invention.

13 anti-LIBS antibodies have been developed by Frelinger et al. (1990; 1991), any one of which may be used to deliver a coagulant to a disease or tumor site in accordance herewith. The murine monoclonal antiplatelet antibodies MA-TSPI-1 (directed against human thrombospondin) and MA-PMI-2, MA-PMI-1, and MA-LIBS-1 (directed against LIBS on human platelet glycoprotein IIb/IIIa) of Dewerchin et al. (1991) may also be used, as may RUU 2.41 and LIBS-1 of Heynen et al. (1994); OP-G2 of Tomiyama et al. (1992); and Ab-15.

Many other targets, such as antigens on smooth muscle cells, pericytes, fibroblasts, macrophages and infiltrating lymphocytes and leukocytes may also be used.

#### B. Coagulating Agents

The second arm or element of the bispecific agents of the invention will be a component that is capable of promoting

coagulation. "Coagulation promoting agents" may be coagulation factors, factors that indirectly stimulate coagulation, or they may be in the form of a second binding region that is capable of binding and releasing a coagulation factor or factor that indirectly stimulates coagulation.

#### 1. Coagulation Factors

A variety of coagulation factors may be used in connection with the present invention, as exemplified by the agents set forth below. Where a coagulation factor is covalently linked to a first binding agent, a site distinct from its functional coagulating site is used to join the molecules. Appropriate joining regions distinct from the active sites, or functional regions, of the coagulation factors are also described in each of the following sections.

#### (a) Tissue Factor

Tissue factor (TF) is one agent capable of initiating blood coagulation. TF is the activator of the extrinsic pathway of blood coagulation and is not in direct contact with the blood under physiologically normal conditions (Osterud et al., 1986; Nemerson, 1988; Broze, 1992; Ruf & Edington, 1994). In vascular damage or activation by certain cytokines or endotoxin, however, TF will be exposed to the blood, either by the (sub)endothelial cells (Weiss et al., 1989) or by certain blood cells (Warr et al., 1990). TF will then complex with factor VIIa, which under normal conditions circulates at low concentrations in the blood (Wildgoose et al., 1992), and the TF/factor VIIa complex will start the coagulation cascade through the activation of factor X into factor Xa. The cascade will ultimately result in the formation of fibrin.

For this sequence of events to occur, the TF:VIIa complex has to be associated with a phospholipid surface upon which the coagulation-initiation complexes with factors IX or X can assemble (Ruf et al., 1991; Paborsky et al., 1991; Bach et al., 1986). For this reason, truncated TF (or tTF), from which the transmembrane and cytoplasmic regions have been removed by truncating the gene, is a soluble protein having one hundred-thousandth of the factor X-activating activity of native TF (Ruf et al., 1991).

#### (b) Clotting Factors

Thrombin, Factor V/Va and derivatives, Factor VIII/VIIIa and derivatives, Factor IX/IXa and derivatives, Factor X/Xa and derivatives, Factor XI/XIa and derivatives, Factor XII/XIIa and derivatives, Factor XIII/XIIIa and derivatives, Factor X activator and Factor V activator may also be used in the present invention.

#### (c) Venom Coagulants

Russell's viper venom was shown to contain a coagulant protein by Williams and Esnouf in 1962. Kiesel (1979) isolated a venom glycoprotein that activates Factor V; and Di Scipio et al. (1977) showed that a protease from the venom activates human Factor X. The Factor X activator is the component contemplated for use in this invention.

Monoclonal antibodies specific for the Factor X activator present in Russell's viper venom have also been produced (e.g., MP1 of Pukrittayakamee et al., 1983), and could be used to deliver the agent to a specific target site within the body.

#### (d) Prostaglandins and Synthetic Enzymes

Thromboxane A<sub>2</sub> is formed from endoperoxides by the sequential actions of the enzymes cyclooxygenase and thromboxane synthetase in platelet microsomes. Thromboxane A<sub>2</sub> is readily generated by platelets and is a potent vasoconstrictor, by virtue of its capacity to produce platelet aggregation (Whittle et al., 1981).

Both thromboxane A<sub>2</sub> and active analogues thereof are contemplated for use in the present invention. A synthetic protocol for generating thromboxane A<sub>2</sub> is described by

Bhagwat et al. (1985). The thromboxane A<sub>2</sub> analogues described by Ohuchida et. al. (1981) (especially compound 2) are particularly contemplated for use herewith.

It is possible that thromboxane synthase, and other enzymes that synthesize platelet-activating prostaglandins, may also be used as "coagulants" in the present context. Shen and Tai (1986a;b) describe monoclonal antibodies to, and immunoaffinity purification of, thromboxane synthase; and Wang et. al. (1991) report the cDNA for human thromboxane synthase.

#### (e) Inhibitors of Fibrinolysis

$\alpha$ 2-antiplasmin, or  $\alpha$ 2-plasmin inhibitor, is a proteinase inhibitor naturally present in human plasma that functions to efficiently inhibit the lysis of fibrin clots induced by plasminogen activator (Moroi & Aoki, 1976).  $\alpha$ 2-antiplasmin is a particularly potent inhibitor, and is contemplated for use in the present invention.

$\alpha$ 2-antiplasmin may be purified as first described by Moroi and Aoki (1976). Other purification schemes are also available, such as using affinity chromatography on plasminogen-Sepharose, ion-exchange chromatography on DEAE-Sephadex and chromatography on Concanavalin-A-Sepharose; or using affinity chromatography on a Sepharose column bearing an elastase-digested plasminogen formulation containing the three N-terminal triple-loop structures in the plasmin A-chain (LBSI), followed by gel filtration (Wiman & Collen, 1977; Wiman, 1980, respectively).

As the cDNA sequence for  $\alpha$ 2-antiplasmin is available (Tone et al., 1977), a preferred method for  $\alpha$ 2-antiplasmin production will be via recombinant expression.

Monoclonal antibodies against  $\alpha$ 2-antiplasmin are also available that may be used in the bispecific binding ligand embodiments of the invention. For example, Hattey et al. (1987) described two MAbs against  $\alpha$ 2-antiplasmin, MPW2AP and MPW3AP. As each of these MAbs were reported to react equally well with native  $\alpha$ 2-antiplasmin, they could both be used to deliver exogenous  $\alpha$ 2-antiplasmin to a target site or to garner endogenous  $\alpha$ 2-antiplasmin and concentrate it within the targeted region. Other antibodies, such as JTPI-2, described by Mimuro and colleagues, could also be used.

#### 2. Agents that Bind Coagulation Factors

Another group of bispecific coagulating ligands of this invention are those in which the targeting region is not directly linked to a coagulation factor, but is linked to a second binding region that binds to a coagulating factor.

Where a second binding region is used to bind and deliver a coagulation factor, the binding region is chosen so that it recognizes a site on the coagulation factor that does not significantly impair its ability to induce coagulation. The regions of the coagulation factors suitable for binding in this manner will generally be the same as those regions that are suitable for covalent linking to the targeting region, as described in the previous sections.

However, in that bispecific ligands of this class may be expected to release the coagulation factor following delivery to the tumor site or region, there is more flexibility allowed in the regions of the coagulation factor suitable for binding to a second binding agent or antibody. Another advantage is that bispecific antibodies can be pre-localized before infusion of tTF which may reduce the amount of tTF required and hence toxicity.

Suitable second binding regions for use in this manner, will generally be antigen combining sites of antibodies that have binding specificity for the coagulation factor, including functional portions of antibodies, such as scFv, Fv, Fab', Fab and F(ab')<sub>2</sub> fragments.

Bispecific binding ligands that contain antibodies, or fragments thereof, directed against Tissue Factor, Thrombin, Prekallikrein, Factor V/Va, Factor VIII/VIIIa, Factor IX/IXa, Factor X/Xa, Factor XI/XIa, Factor XII/XIIa, Factor XIII/XIIIa, Russell's viper venom, thromboxane A<sub>2</sub> or  $\alpha$ 2-antiplasmin are exemplary embodiments of this aspect of the invention.

#### C. Linkage Means

The first, targeting region and second, coagulating region will be operatively linked to allow each region to perform its intended function without significant impairment. Thus, the targeting region is capable of binding to the intended target, as selected from the range of tumor environment targets, and the coagulating region is capable of directly or indirectly, e.g., through the release of a bound factor, promoting blood coagulation or clotting.

To assess the targeting region binding function, all that is required is to conduct a binding assay to ensure that the bispecific ligand still binds to the targeted component in substantially the same manner as the uncomplexed first binding region. The suitable binding assays are of the type usually seen in immunological binding assays, where the first targeting region is an antibody, and/or other biochemical binding assays, e.g., those using <sup>125</sup>Iodine labeled proteins or other radiolabeled components, as used to assess ligand-receptor binding, to generate Scatchard plots, and the like.

The target antigen or component in such assays may be provided in many forms, including proteins purified from natural or recombinant sources, membrane enriched preparations, intact cells and tissue sections. Generally, where protein compositions are used, they will be immobilized on a solid support, such as a microtitre plate, a membrane, or even on a column matrix. It is also generally preferred to use a target composition that reflects the physiological target, therefore as the target will usually be cell-associated, the use of compositions that include intact cells, including tissues and the cells themselves, is also preferred.

The various immunological assays available to confirm the functional binding of a bispecific complex include, e.g., Western blots, ELISAS, ELISAs using fixed cells, immunohistochemistry, and fluorescent activated cell sorting (FACS). The execution of all such assays is generally known to those of skill in the art, and is further disclosed herein.

Assessing the targeting region binding function of a bispecific compound in any of the above or other binding assays is a straightforward matter, where the bispecific ligand and the uncomplexed first binding region will most usually be run in a parallel assay, under the same conditions, to enable ready comparison. Effective bispecific ligands will bind to the target without significant impairment, i.e., in substantially the same manner as the uncomplexed first binding region. Taking the uncomplexed binding region assay result as the 100% reference value, "substantial binding" of the bispecific ligand, as used herein, means that the bispecific ligand exhibits at least about 50% binding, and more preferably, between about 50% and about 80% binding, and most preferably, between about 80% and about 100% binding.

Where the bispecific ligand includes a second binding region that binds to a coagulant, e.g., it is a bispecific antibody, further useful assays are those of the type that allow the binding functions of both arms of the bispecific ligand to be assessed at the same time. For example, this may be achieved by assessing the binding of a radiolabeled coagulant to a target cell via bridging with the bispecific

ligand or antibody. Such an assay is exemplified by the binding of tTF to target cells using the B21-2/10H10 bispecific antibody, as described in Example II.

Determining the coagulating agent function of the bispecific ligand is also a straightforward matter. All that is required here is to conduct a coagulation assay using the bispecific ligand and ensure that it functions to promote coagulation in substantially the same manner as the uncomplexed coagulating agent. This is true for "coagulating agents" that are both coagulation factors themselves and those that are second binding regions that bind to a coagulation factor. Naturally, in the latter case, in an *in vitro* or *ex vivo* assay, the bispecific ligand will be precomplexed with the coagulation factor to allow binding to the second binding region.

One suitable coagulation assay is that in which the bispecific ligands, pre-complexed with coagulant if necessary, are admixed with a plasma sample. The appearance of fibrin strands is indicative of coagulation in this assay. Effective bispecific ligands would thus be expected to reduce the time taken for fibrin strands to appear, and particularly, to significantly reduce the elapsed time in comparison to control levels.

A variation of the above assay involves first exposing appropriate target cells to the bispecific ligand under conditions effective, and for a time sufficient, to allow binding, washing the cells to remove non-specifically bound components and then resuspending the washed cells in plasma. Only cells effectively coated with the bispecific ligand would be expected to reduce the time taken for fibrin strands to appear in the assay. This type of assay is preferred in that it is, in itself, an assay that assesses both of the functions of the bispecific construct, i.e., initial targeting to the cell and subsequent localized coagulation.

To compare the coagulating function of a bispecific compound to that of an uncomplexed coagulating agent, parallel assays may again be conducted. Effective bispecific ligands will function to promote coagulation without significant impairment, i.e., will function in substantially the same manner as the uncomplexed coagulating agent. Taking the uncomplexed coagulant assay result as the 100% reference value, "substantial function", as used herein, means that the bispecific ligand exhibits at least about 50% coagulation, and more preferably, between about 50% and

about 80% coagulation, and most preferably, between about 80% and about 100% coagulation.

The two functional regions of the bispecific ligands may be joined using synthetic chemistry techniques or recombinant DNA techniques. Each of these techniques are routinely employed and well known to those of skill in the art, and are further exemplified in Example I and by the details set forth below.

#### 1. Biochemical Cross-linkers

The joining of an antibody, or other targeting component, to a coagulating agent will generally employ the same technology as developed for the preparation of immunotoxins. However, considerable advantages are apparent in the present technology, as the consequences of a certain amount of uncomplexed coagulating agent becoming available physiologically are not contemplated to be particularly severe. Thus, the stability requirements for any cross-linkers are not so stringent as for linkers employed in other constructs, such as immunotoxins. Therefore, it can be considered as a general guideline that any biochemical crosslinker that is appropriate for use in an immunotoxin will also be of use in the present context, and additional linkers may also be considered.

In addition to toxins, a variety of other chemotherapeutic and pharmacological agents have been linked to antibodies to form conjugates that have been shown to function pharmacologically (see, e.g., Vaickus et al., 1991). Exemplary antineoplastic agents that have been investigated include doxorubicin, daunomycin, methotrexate and vinblastine, amongst others (Dillman et al., 1988; Pietersz et al., 1988). Moreover, the attachment of other agents such as neocarzinostatin (Kimura et al., 1983), macromycin (Manabe et al., 1984), trenimon (Ghose, 1982) and  $\alpha$ -amanitin (Davis & Preston, 1981) has been described. The linking technology described in each of the foregoing scientific papers is also contemplated for use in connection with the present invention.

Cross-linking reagents are used to form molecular bridges that tie together functional groups of two different molecules, e.g., a binding and coagulating agent. To link two different proteins in a step-wise manner, heterobifunctional cross-linkers can be used that eliminate unwanted homopolymer formation (Table VI).

TABLE VI

HETEROBIFUNCTIONAL CROSS-LINKERS			
linker	Reactive Toward	Advantages and Applications	Spacer Arm Length/after cross-linking
SMPT	Primary amines Sulphydryls	Greater stability	11.2 Å
SPDP	Primary amines Sulphydryls	Thiolation Cleavable cross-linking	6.8 Å
LC-SPDP	Primary amines Sulphydryls	Extended spacer arm	15.6 Å
Sulfo-LC-SPDP	Primary amines Sulphydryls	Extended spacer arm Water-soluble	15.6 Å
SMCC	Primary amines Sulphydryls	Stable maleimide reactive group Enzyme-antibody conjugation Hapten-carrier protein conjugation	11.6 Å
Sulfo-SMCC	Primary amines Sulphydryls	Stable maleimide reactive group Water-soluble Enzyme-antibody conjugation	11.6 Å
MBS	Primary amines Sulphydryls	Enzyme-antibody conjugation Hapten-carrier protein conjugation	9.9 Å
Sulfo-MBS	Primary amines Sulphydryls	Water-soluble	9.9 Å
SIAB	Primary amines Sulphydryls	Enzyme-antibody conjugation	10.6 Å

TABLE VI-continued

HETEROBIFUNCTIONAL CROSS-LINKERS			
linker	Reactive Toward	Advantages and Applications	Spacer Arm Length\after cross-linking
Sulfo-SIAB	Primary amines Sulphydryls	Water-soluble	10.6 Å
SMPB	Primary amines Sulphydryls	Extended spacer arm Enzyme-antibody conjugation	14.5 Å
Sulfo-SMPB	Primary amines Sulphydryls	Extended spacer arm Water-soluble	14.5 Å
EDC/Sulfo-NHS	Primary amines Carboxyl groups	Hapten-Carrier conjugation	0
ABH	Carbohydrates Nonselective	Reacts with sugar groups	11.9 Å

An exemplary heterobifunctional cross-linker contains two reactive groups: one reacting with primary amine group (e.g., N-hydroxy succinimide) and the other reacting with a thiol group (e.g., pyridyl disulfide, maleimides, halogens, etc.). Through the primary amine reactive group, the cross-linker may react with the lysine residue(s) of one protein (e.g., the selected antibody or fragment) and through the thiol reactive group, the cross-linker, already tied up to the first protein, reacts with the cysteine residue (free sulphydryl group) of the other protein (e.g., the coagulant).

It can therefore be seen that the preferred coagulants or coagulant binding regions will generally have, or be derivatized to have, a functional group available for cross-linking purposes. This requirement is not considered to be limiting in that a wide variety of groups can be used in this manner. For example, primary or secondary amine groups, hydrazide or hydrazine groups, carboxyl alcohol, phosphate, or alkylating groups may be used for binding or cross-linking. For a general overview of linking technology, one may wish to refer to Ghose & Blair (1987).

The spacer arm between the two reactive groups of a cross-linker may have various lengths and chemical compositions. A longer spacer arm allows a better flexibility of the conjugate components while some particular components in the bridge (e.g., benzene group) may lend extra stability to the reactive group or an increased resistance of the chemical link to the action of various agents (e.g., disulfide bond resistant to reducing agents). The use of peptide spacers, such as L-Leu-L-Ala-L-Leu-L-Ala, is also contemplated.

It is preferred that a cross-linker having reasonable stability in blood will be employed. Numerous types of disulfide-bond containing linkers are known that can be successfully employed to conjugate targeting and coagulating agents. Linkers that contain a disulfide bond that is sterically hindered may prove to give greater stability in vivo, preventing release of the coagulant prior to binding at the site of action. These linkers are thus one preferred group of linking agents.

One of the most preferred cross-linking reagents for use in immunotoxins is SMPT, which is a bifunctional cross-linker containing a disulfide bond that is "sterically hindered" by an adjacent benzene ring and methyl groups. It is believed that steric hindrance of the disulfide bond serves a function of protecting the bond from attack by thiolate anions such as glutathione which can be present in tissues and blood, and thereby help in preventing decoupling of the conjugate prior to the delivery of the attached agent to the tumor site. It is contemplated that the SMPT agent may also be used in connection with the bispecific coagulating ligands of this invention.

The SMPT cross-linking reagent, as with many other known cross-linking reagents, lends the ability to cross-link functional groups such as the SH of cysteine or primary amines (e.g., the epsilon amino group of lysine). Another possible type of cross-linker includes the heterobifunctional photoreactive phenylazides containing a cleavable disulfide bond such as sulfosuccinimidyl-2-(p-azido salicylamido) ethyl-1,3'-dithiopropionate. The N-hydroxy-succinimidyl group reacts with primary amino groups and the phenylazide (upon photolysis) reacts non-selectively with any amino acid residue.

In addition to hindered cross-linkers, non-hindered linkers can also be employed in accordance herewith. Other useful cross-linkers, not considered to contain or generate a protected disulfide, include SATA, SPDP and 2-iminothiolane (Wawrzynczak & Thorpe, 1987). The use of such cross-linkers is well understood in the art.

Once conjugated, the bispecific agent will generally be purified to separate the conjugate from unconjugated targeting agents or coagulants and from other contaminants. It is important to remove unconjugated targeting agent to avoid the possibility of competition for the antigen between conjugated and unconjugated species. A large number of purification techniques are available for use in providing conjugates of a sufficient degree of purity to render them clinically useful. Purification methods based upon size separation, such as gel filtration, gel permeation or high performance liquid chromatography, will generally be of most use. Other chromatographic techniques, such as Blue-Sepharose separation, may also be used.

## 2. Recombinant Fusion Proteins

The bispecific targeted coagulants of the invention may also be fusion proteins prepared by molecular biological techniques. The use of recombinant DNA techniques to achieve such ends is now standard practice to those of skill in the art. These methods include, for example, in vitro recombinant DNA techniques, synthetic techniques and in vivo recombination/genetic recombination. DNA and RNA synthesis may, additionally, be performed using an automated synthesizers (see, for example, the techniques described in Sambrook et al., 1989; and Ausubel et al., 1989).

In general, to prepare a fusion protein one would join a DNA coding region, such as a gene or cDNA, encoding a binding ligand or other targeting region to a DNA coding region (i.e., gene or cDNA) encoding a coagulation factor or coagulant binding region. This typically involves preparing an expression vector that comprises, in the same reading frame, a first DNA segment encoding the first binding region operatively linked to a second DNA segment encoding the



coagulation factor. The sequences are attached in a manner such that translation of the total nucleic acid yields the desired bispecific compounds of the invention. Expression vectors contain one or more promoters upstream of the inserted DNA regions that act to promote transcription of the DNA and to thus promote expression of the encoded recombinant protein. This is the meaning of "recombinant expression".

Should a particular binding region or coagulant be preferred, and the encoding DNA not instantly available, it may be obtained using the techniques of "molecular cloning" in which a DNA molecule encoding the desired protein is obtained from a DNA library (e.g., a cDNA or genomic library). In such procedures, an appropriate DNA library is screened, e.g., using an expression screening protocol employing antibodies directed against the protein, or activity assays. Alternatively, screening may be based on the hybridization of oligonucleotide probes, designed from a consideration of portions of the amino acid sequence of the protein, or from the DNA sequences of genes encoding related proteins. The operation of such screening protocols are well known to those of skill in the art and are described in detail in the scientific literature, for example, in Sambrook et al. (1989).

When produced via recombinant DNA techniques, the targeting agent/coagulating agent compounds of the invention are referred to as "fusion proteins". It is to be understood that such fusion proteins contain, at least, a targeting agent and a coagulating agent as defined in this invention, and that the agents are operatively attached. The fusion proteins may also include additional peptide sequences, such as peptide spacers which operatively attach the targeting agent and coagulating agent compounds, as long as such additional sequences do not appreciably affect the targeting or coagulating activities of the resultant fusion protein.

It will be understood that the recombinant bispecific protein ligands may differ from those bispecific constructs generated by chemically cross-linking the so-called naturally-produced proteins. In particular, the degree of post-translational modifications, such as, for example, glycosylation and phosphorylation may be different between recombinant fusions and chemical fusions of the same two proteins. This is not contemplated to be a significant problem, however, those of skill in the art will know to confirm that a recombinant fusion protein functions as intended, and expected from other data, before use in a clinical setting.

One advantage of recombinant expression is that the linking regions can be readily manipulated so that, e.g., their length and/or amino acid composition is readily variable. Non-cleavable peptide spacers may be provided to operatively attach the two agents of the invention, if desired. Equally, peptides with unique cleavage sites could be inserted between the two components.

If desired in a specific instance, it is possible to provide a peptide spacer operatively attaching the targeting agent and coagulating agent which is capable of folding into a disulfide-bonded loop structure. Proteolytic cleavage within the loop would then yield a heterodimeric polypeptide wherein the targeting agent and the coagulating agent are linked by only a single disulfide bond (see, for example, Lord et al., 1992).

Many standard techniques are available to construct expression vectors containing the appropriate nucleic acids and transcriptional/translational control sequences in order to achieve protein expression in a variety of host-expression systems. The cell types available for expression include, but

are not limited to, microorganisms such as bacteria (e.g., *E. coli*, *B. subtilis*) transformed with recombinant bacteriophage DNA, plasmid DNA or cosmid DNA expression vectors containing targeting agent/coagulating coding sequences; yeast (e.g., *Saccharomyces*, *Pichia*) transformed with recombinant yeast expression vectors containing targeting agent/coagulating agent coding sequences; insect cell systems infected with recombinant virus expression vectors (e.g., baculovirus) containing the targeting agent/coagulating agent coding sequences; plant cell systems infected with recombinant virus expression vectors (e.g., cauliflower mosaic virus, CaMV; tobacco mosaic virus, TMV) or transformed with recombinant plasmid expression vectors (e.g., Ti plasmid) containing the targeting agent/coagulating coding sequence; and mammalian cell systems (e.g., COS, CHO, BHK, 293, 3T3) harboring recombinant expression constructs containing promoters derived from the genome of mammalian cells (e.g., metallothionein promoter) or from mammalian viruses (e.g., the adenovirus late promoter; the vaccinia virus 7.5K promoter).

In bacterial systems a number of expression vectors may be advantageously selected depending upon the use intended for the targeting agent/coagulating agent construct being expressed. For example, when large quantities of bispecific agent are to be produced, vectors that direct the expression of high levels of fusion protein products that are readily purified may be desirable. Such vectors include, but are not limited to, the *E. Coli* expression vector pUR278 (Ruther et al., 1983), in which the targeting agent/coagulating agent coding sequence may be ligated individually into the vector in frame with the lac Z coding region so that a fusion protein additionally containing a portion of the lac Z product is provided; pIN vectors (Inouye et al., 1985; Van Heeke et al., 1989); and the like. pGEX vectors may also be used to express foreign polypeptides, such as the targeting agent/coagulating agent combinations as fusion proteins additionally containing glutathione S-transferase (GST). In general, such fusion proteins are soluble and can easily be purified from lysed cells by adsorption to glutathione-agarose beads followed by elution in the presence of free glutathione. The pGEX vectors are designed to include thrombin or factor Xa protease cleavage sites so that the binding agent/coagulant protein of the overall fusion protein can be released from the GST moiety.

In a useful insect system, *Autograph californica* nuclear polyhidrosis virus (AcNPV) is used as a vector to express foreign genes. The virus grows in *Spodoptera frugiperda* cells. The targeting agent/coagulating agent coding sequences may be cloned into non-essential regions (for example the polyhedrin gene) of the virus and placed under control of an AcNPV promoter (for example the polyhedrin promoter). Successful insertion of the bispecific ligand coding sequences will result in inactivation of the polyhedrin gene and production of non-occluded recombinant virus (i.e., virus lacking the proteinaceous coat coded for by the polyhedrin gene). These recombinant viruses are then used to infect *Spodoptera frugiperda* cells in which the inserted gene is expressed (e.g., see Smith et al., 1983; \*U.S. Pat. No. 4,215,051, Smith).

In mammalian host cells, a number of viral based expression systems may be utilized. In cases where an adenovirus is used as an expression vector, the targeting agent/coagulating agent coding sequences may be ligated to an adenovirus transcription/translation control complex, e.g., the late promoter and tripartite leader sequence. This chimeric gene may then be inserted in the adenovirus genome by *in vitro* or *in vivo* recombination. Insertion in a non-



essential region of the viral genome (e.g., region E1 or E3) will result in a recombinant virus that is viable and capable of expressing bispecific proteins in infected hosts (e.g., see Logan et al., 1984).

Specific initiation signals may also be required for efficient translation of inserted targeting agent/coagulating agent coding sequences. These signals include the ATG initiation codon and adjacent sequences. Exogenous translational control signals, including the ATG initiation codon, may additionally need to be provided. One of ordinary skill in the art would readily be capable of determining this and providing the necessary signals. It is well known that the initiation codon must be in phase (or in-frame) with the reading frame of the desired coding sequence to ensure translation of the entire insert. These exogenous translational control signals and initiation codons can be of a variety of origins, both natural and synthetic. The efficiency of expression may be enhanced by the inclusion of appropriate transcription enhancer elements, transcription terminators, etc. (see Bittner et al., 1987).

In addition, a host cell strain may be chosen which modulates the expression of the inserted sequences, or modifies and processes the gene product in the specific fashion desired. Such modifications (e.g., glycosylation) and processing (e.g., cleavage) of protein products may be important for the function of the protein. Different host cells have characteristic and specific mechanisms for the post-translational processing and modification of proteins. Appropriate cells lines or host systems can be chosen to ensure the correct modification and processing of the foreign protein expressed. To this end, eukaryotic host cells which possess the cellular machinery for proper processing of the primary transcript, glycosylation, and phosphorylation of the gene product may be used. Such mammalian host cells include, but are not limited to, CHO, VERO, BHK, HeLa, COS, MDCK, 293, 3T3, WI38, etc.

For long-term, high-yield production of recombinant proteins, stable expression is preferred. For example, cell lines that stably express constructs encoding the targeting agent/coagulant ligands may be engineered. Rather than using expression vectors that contain viral origins of replication, host cells can be transformed with targeting agent/coagulant DNA controlled by appropriate expression control elements (e.g., promoter, enhancer, sequences, transcription terminators, polyadenylation sites, etc.), and a selectable marker. Following the introduction of foreign DNA, engineered cells may be allowed to grow for 1-2 days in an enriched media, and then are switched to a selective media. The selectable marker in the recombinant plasmid confers resistance to the selection and allows cells to stably integrate the plasmid into their chromosomes and grow to form foci which in turn can be cloned and expanded into cell lines.

A number of selection systems may be used, including, but not limited to, the herpes simplex virus thymidine kinase (Wigler et al., 1977), hypoxanthine-guanine phosphoribosyltransferase (Szybalska et al., 1962), and adenine phosphoribosyltransferase genes (Lowy et al., 1980) can be employed in tk-, hgp<sup>r</sup>t- or ap<sup>r</sup>t-cells, respectively. Also, antimetabolite resistance can be used as the basis of selection for dhfr, which confers resistance to methotrexate (Wigler et al., 1980; O'Hare et al., 1981); gpt, which confers resistance to mycophenolic acid (Mulligan et al., 1981); neo, which confers resistance to the aminoglycoside G-418 (Colberre-Garapin et al., 1981); and hyg<sup>r</sup>, which confers resistance to hygromycin (Santerre et al., 1984).

#### D. Antibodies

Where antibodies are used as one or both portions of the bispecific ligand, the choice of antibody will generally be dependent on the type tumor and coagulating ligand chosen. However, certain advantages may be achieved through the application of particular types of antibodies. For example, while IgG based antibodies may be expected to exhibit better binding capability and slower blood clearance than their Fab' counterparts, Fab' fragment-based compositions will generally exhibit better tissue penetrating capability.

#### 1. Monoclonal Antibodies

Means for preparing and characterizing antibodies are well known in the art (See, e.g., \*Antibodies: A Laboratory Manual, Cold Spring Harbor Laboratory, 1988).

The methods for generating monoclonal antibodies (MAbs) generally begin along the same lines as those for preparing polyclonal antibodies. Briefly, a polyclonal antibody is prepared by immunizing an animal with an immunogenic composition in accordance with the present invention, either with or without prior immunotolerizing, depending on the antigen composition and protocol being employed (e.g., tolerizing to a normal cell population and then immunizing with a tumor cell population), and collecting antisera from that immunized animal. A wide range of animal species can be used for the production of antisera. Typically the animal used for production of anti-antisera is a rabbit, a mouse, a rat, a hamster, a guinea pig or a goat. Because of the relatively large blood volume of rabbits, a rabbit is a preferred choice for production of polyclonal antibodies.

As is well known in the art, a given composition may vary in its immunogenicity. It is often necessary therefore to boost the host immune system, as may be achieved by coupling a peptide or polypeptide immunogen to a carrier. Exemplary and preferred carriers are keyhole limpet hemocyanin (KLH) and bovine serum albumin (BSA). Other albumins such as ovalbumin, mouse serum albumin or rabbit serum albumin can also be used as carriers. Means for conjugating a polypeptide to a carrier protein are well known in the art and include glutaraldehyde, m-maleimidobenzoyl-N-hydroxysuccinimide ester, carbodiimide and bis-biazotized benzidine.

As is also well known in the art, the immunogenicity of a particular immunogen composition can be enhanced by the use of non-specific stimulators of the immune response, known as adjuvants. Exemplary and preferred adjuvants include complete Freund's adjuvant (a non-specific stimulator of the immune response containing killed *Mycobacterium tuberculosis*), incomplete Freund's adjuvants and aluminum hydroxide adjuvant.

The amount of immunogen composition used in the production of polyclonal antibodies varies upon the nature of the immunogen as well as the animal used for immunization. A variety of routes can be used to administer the immunogen (subcutaneous, intramuscular, intradermal, intravenous and intraperitoneal). The production of polyclonal antibodies may be monitored by sampling blood of the immunized animal at various points following immunization. A second, booster injection, may also be given. The process of boosting and titering is repeated until a suitable titer is achieved. When a desired titer level is obtained, the immunized animal can be bled and the serum isolated and stored, and/or the animal can be used to generate MAbs.

MAbs may be readily prepared through use of well-known techniques, such as those exemplified in \*U.S. Pat. No. 4,196,265, incorporated herein by reference. Typically, this technique involves immunizing a suitable animal with a selected immunogen composition, e.g., a purified or partially

purified tumor cell or vascular endothelial cell protein, polypeptide, peptide, or intact cell composition. The immunizing composition is administered in a manner effective to stimulate antibody producing cells. Rodents such as mice and rats are preferred animals, however, the use of rabbit, sheep frog cells is also possible. The use of rats may provide certain advantages (\*Goding, 1986, pp. 60-61), but mice are preferred, with the BALB/c mouse being most preferred as this is most routinely used and generally gives a higher percentage of stable fusions.

Following immunization, somatic cells with the potential for producing antibodies, specifically B lymphocytes (B cells), are selected for use in the MAB generating protocol. These cells may be obtained from biopsied spleens, tonsils or lymph nodes, or from a peripheral blood sample. Spleen cells and peripheral blood cells are preferred, the former because they are a rich source of antibody-producing cells that are in the dividing plasmablast stage, and the latter because peripheral blood is easily accessible. Often, a panel of animals will have been immunized and the spleen of animal with the highest antibody titer will be removed and the spleen lymphocytes obtained by homogenizing the spleen with a syringe. Typically, a spleen from an immunized mouse contains approximately  $5 \times 10^7$  to  $2 \times 10^8$  lymphocytes.

The antibody-producing B lymphocytes from the immunized animal are then fused with cells of an immortal myeloma cell, generally one of the same species as the animal that was immunized. Myeloma cell lines suited for use in hybridoma-producing fusion procedures preferably are non-antibody-producing, have high fusion efficiency, and enzyme deficiencies that render them incapable of growing in certain selective media which support the growth of only the desired fused cells (hybridomas).

Any one of a number of myeloma cells may be used, as are known to those of skill in the art (\*Goding, pp. 65-66, 1986; \*Campbell, pp. 75-83, 1984). For example, where the immunized animal is a mouse, one may use P3-X63/Ag8, X63-Ag8.653, NS1/1.Ag 4 1, Sp210-Ag14, FO, NSO/U, MPC-11, MPC11-X45-GTG 1.7 and S194/5XXO Bul; for rats, one may use R210.RCY3, Y3-Ag 1.2.3, IR983F, 4B210 or one of the above listed mouse cell lines; and U-266, GM1500-GRG2, LICR-LON-HMy2 and UC729-6, are all useful in connection with human cell fusions.

One preferred murine myeloma cell is the A63-A68, 653 myeloma cell line, which is readily available from the ATCC. Another mouse myeloma cell line that may be used is the 8-azaguanine-resistant mouse murine myeloma SP2/0 non-producer cell line.

Methods for generating hybrids of antibody-producing spleen or lymph node cells and myeloma cells usually comprise mixing somatic cells with myeloma cells in a 4:1 proportion, though the proportion may vary from about 20:1 to about 1:1, respectively, in the presence of an agent or agents (chemical or electrical) that promote the fusion of cell membranes. Fusion methods using Sendai virus have been described by Kohler & Milstein (1975; 1976), and those using polyethylene glycol (PEG), such as 37% (v/v) PEG, by Geftter et al. (1977). The use of electrically induced fusion methods is also appropriate (\*Goding pp. 71-74, 1986).

Fusion procedures usually produce viable hybrids at low frequencies, about  $1 \times 10^{-6}$  to  $1 \times 10^{-8}$ . However, this does not pose a problem, as the viable, fused hybrids are differentiated from the parental, unfused cells (particularly the unfused myeloma cells that would normally continue to divide indefinitely) by culturing in a selective medium. The selective medium is generally one that contains an agent that

blocks the de novo synthesis of nucleotides in the tissue culture media. Exemplary and preferred agents are aminopterin, methotrexate, and azaserine. Aminopterin and methotrexate block de novo synthesis of both purines and pyrimidines, whereas azaserine blocks only purine synthesis. Where aminopterin or methotrexate is used, the media is supplemented with hypoxanthine and thymidine as a source of nucleotides (HAT medium). Where azaserine is used, the media is supplemented with hypoxanthine.

The preferred selection medium is HAT. Only cells capable of operating nucleotide salvage pathways are able to survive in HAT medium. The myeloma cells are defective in key enzymes of the salvage pathway, e.g., hypoxanthine phosphoribosyl transferase (HPRT), and they cannot survive. The B cells can operate this pathway, but they have a limited life span in culture and generally die within about two weeks. Therefore, the only cells that can survive in the selective media are those hybrids formed from myeloma and B cells.

This culturing provides a population of hybridomas from which specific hybridomas are selected. Typically, selection of hybridomas is performed by culturing the cells by single-clone dilution in microtiter plates, followed by testing the individual clonal supernatants (after about two to three weeks) for the desired reactivity. The assay should be sensitive, simple and rapid, such as radioimmunoassays, enzyme immunoassays, cytotoxicity assays, plaque assays, dot immunobinding assays, and the like.

The selected hybridomas would then be serially diluted and cloned into individual antibody-producing cell lines, which clones can then be propagated indefinitely to provide MABs. The cell lines may be exploited for MAB production in two basic ways. A sample of the hybridoma can be injected (often into the peritoneal cavity) into a histocompatible animal of the type that was used to provide the somatic and myeloma cells for the original fusion. The injected animal develops tumors secreting the specific monoclonal antibody produced by the fused cell hybrid. The body fluids of the animal, such as serum or ascites fluid, can then be tapped to provide MABs in high concentration. The individual cell lines could also be cultured in vitro, where the MABs are naturally secreted into the culture medium from which they can be readily obtained in high concentrations. MABs produced by either means may be further purified, if desired, using filtration, centrifugation and various chromatographic methods such as HPLC or affinity chromatography.

The inventors also contemplate the use of a molecular cloning approach to generate monoclonals. For this, combinatorial immunoglobulin phagemid libraries are prepared from RNA isolated from the spleen of the immunized animal, and phagemids expressing appropriate antibodies are selected by panning using cells expressing the antigen and control cells e.g., normal-versus-tumor cells. The advantages of this approach over conventional hybridoma techniques are that approximately 104 times as many antibodies can be produced and screened in a single round, and that new specificities are generated by H and L chain combination which further increases the chance of finding appropriate antibodies.

Where MABs are employed in the present invention, they may be of human, murine, monkey, rat, hamster, chicken or even rabbit origin. The invention contemplates the use of human antibodies, "humanized" or chimeric antibodies from mouse, rat, or other species, bearing human constant and/or variable region domains, and other recombinant antibodies and fragments thereof. Of course, due to the ease of prepa-

ration and ready availability of reagents, murine monoclonal antibodies will typically be preferred.

## 2. Functional Antibody Binding Regions

The origin or derivation of the targeting agent antibody or antibody fragment (e.g., Fab', Fab, F(ab')<sub>2</sub>, Fv or scFv) is not believed to be particularly crucial to the practice of the invention, so long as the antibody or fragment that is actually employed for the preparation of the bispecific ligand exhibits the desired binding properties.

It may be necessary use antibody preparations in which the Fc portion has been removed. Fragmentation of immunoglobulin molecules can be achieved by controlled proteolysis, although the conditions will vary considerably with species and immunoglobulin class or subclass. Bivalent F(ab')<sub>2</sub> fragments are usually preferable over the univalent Fab or Fab' fragments.

## Fab

Fab fragments can be obtained by proteolysis of the whole immunoglobulin by the non-specific thiol protease, papain. Papain must first be activated by reducing the sulphhydryl group in the active site with cysteine, 2-mercaptoethanol or dithiothreitol. Heavy metals in the stock enzyme should be removed by chelation with EDTA (2 mM) to ensure maximum enzyme activity. Enzyme and substrate are normally mixed together in the ratio of 1:100 by weight. After incubation, the reaction can be stopped by irreversible alkylation of the thiol group with iodoacetamide or simply by dialysis. The completeness of the digestion should be monitored by SDS-PAGE and the various fractions separated by protein A-Sepharose or ion exchange chromatography.

## F(ab')<sub>2</sub>

The usual procedure for preparation of F(ab')<sub>2</sub> fragments from IgG of rabbit and human origin is limited proteolysis by the enzyme pepsin (Protocol 7.3.2). The conditions, 100xantibody excess w/w in acetate buffer at pH 4.5, 37° C., suggest that antibody is cleaved at the C-terminal side of the inter-heavy-chain disulfide bond. Rates of digestion of mouse IgG may vary with subclass and it may be difficult to obtain high yields of active F(ab')<sub>2</sub> fragments without some undigested or completely degraded IgG. In particular, IgG<sub>2b</sub> is highly susceptible to complete degradation. The other subclasses require different incubation conditions to produce optimal results.

Digestion of rat IgG by pepsin requires conditions including dialysis in 0.1M acetate buffer, pH 4.5, and then incubation for four hours with 1% w/w pepsin; IgG<sub>1</sub> and IgG<sub>2a</sub> digestion is improved if first dialysed against 0.1M formate buffer, pH 2.8, at 4° C., for 16 hours followed by acetate buffer. IgG<sub>2b</sub> gives more consistent results with incubation in staphylococcal V8 protease (3% w/w) in 0.1M sodium phosphate buffer, pH 7.8, for four hours at 37° C.

## 3. Bispecific Antibodies

In general, the preparation of bispecific antibodies is also well known in the art, as exemplified by Glennie et al. (1987). Bispecific antibodies have been employed clinically, for example, to treat cancer patients (Bauer et al., 1991). One method for the preparation of bispecific antibodies involves the separate preparation of antibodies having specificity for the targeted tumor cell antigen, on the one hand, and the coagulating agent (or other desired target, such as an activating antigen) on the other.

Bispecific antibodies have also been developed particularly for use as immunotherapeutic agents. As mentioned earlier in conjunction with antigen-induction, certain of these antibodies were developed to cross-link lymphocytes and tumor antigens (Nelson, 1991; Segal et al., 1992).

Examples include chimeric molecules that bind T cells, e.g., at CD3, and tumor antigens, and trigger lymphocyte-activation by physically cross-linking the TCR/CD3 complex in close proximity to the target cell (Staerz et al., 1985; Perez et al., 1985; 1986a; 1986b; Ting et al., 1988).

Indeed, tumor cells of carcinomas, lymphomas, leukemias and melanomas have been reported to be susceptible to bispecific antibody-mediated killing by T cells (Nelson, 1991; Segal et al., 1992; deLeij et al., 1991). These type of bispecific antibodies have also been used in several Phase I clinical trials against diverse tumor targets. Although they are not novel compositions in accordance with this invention, the combined use of bispecific cross-linking antibodies along with the bispecific coagulating ligands described herein is also contemplated. The bispecific cross-linking antibodies may be administered as described in references such as deLeij et al. (1991); Clark et al. (1991); Rivoltini et al. (1992); Bolhuis et al. (1992); and Nitta et al. (1990).

While numerous methods are known in the art for the preparation of bispecific antibodies, the Glennie et al. (1987) method involves the preparation of peptic F(ab')<sub>2</sub> fragments from the two chosen antibodies, followed by reduction of each to provide separate Fab'YSH fragments. The SH groups on one of the two partners to be coupled are then alkylated with a cross-linking reagent such as o-phenylenedimaleimide to provide free maleimide groups on one partner. This partner may then be conjugated to the other by means of a thioether linkage, to give the desired F(ab')<sub>2</sub> heteroconjugate.

Due to ease of preparation, high yield and reproducibility, the Glennie et al. (1987) method is often preferred for the preparation of bispecific antibodies, however, there are numerous other approaches that can be employed and that are envisioned by the inventors. For example, other techniques are known wherein crosslinking with SPDP or protein A is carried out, or a trispecific construct is prepared (Titus et al., 1987; Tutt et al., 1991).

Another method for producing bispecific antibodies is by the fusion of two hybridomas to form a quadroma (Flavell et al., 1991, 1992; Pimm et al., 1992; French et al., 1991; Embleton et al., 1991). As used herein, the term "quadroma" is used to describe the productive fusion of two B cell hybridomas. Using now standard techniques, two antibody producing hybridomas are fused to give daughter cells, and those cells that have maintained the expression of both sets of clonotype immunoglobulin genes are then selected.

A preferred method of generating a quadroma involves the selection of an enzyme deficient mutant of at least one of the parental hybridomas. This first mutant hybridoma cell line is then fused to cells of a second hybridoma that had been lethally exposed, e.g., to iodoacetamide, precluding its continued survival. Cell fusion allows for the rescue of the first hybridoma by acquiring the gene for its enzyme deficiency from the lethally treated hybridoma, and the rescue of the second hybridoma through fusion to the first hybridoma. Preferred, but not required, is the fusion of immunoglobulins of the same isotype, but of a different subclass. A mixed subclass antibody permits the use if an alternative assay for the isolation of a preferred quadroma.

In more detail, one method of quadroma development and screening involves obtaining a hybridoma line that secretes the first chosen MAb and making this deficient for the essential metabolic enzyme, hypoxanthine-guanine phosphoribosyltransferase (HGPRT). To obtain deficient mutants of the hybridoma, cells are grown in the presence of increasing concentrations of 8-azaguanine (1x10<sup>-7</sup>M to 1x10<sup>-5</sup>M).

The mutants are subcloned by limiting dilution and tested for their hypoxanthine/aminopterin/thymidine (HAT) sensitivity. The culture medium may consist of, for example, DMEM supplemented with 10% FCS, 2 mM L-Glutamine and 1 mM penicillin-streptomycin.

A complementary hybridoma cell line that produces the second desired MAb is used to generate the quadromas by standard cell fusion techniques (Galfre et al., 1981), or by using the protocol described by Clark et al. (1988). Briefly,  $4.5 \times 10^7$  HAT-sensitive first cells are mixed with  $2.8 \times 10^7$  HAT-resistant second cells that have been pre-treated with a lethal dose of the irreversible biochemical inhibitor iodoacetamide (5 mM in phosphate buffered saline) for 30 minutes on ice before fusion. Cell fusion is induced using polyethylene glycol (PEG) and the cells are plated out in 96 well microculture plates. Quadromas are selected using HAT-containing medium. Bispecific antibody-containing cultures are identified using, for example, a solid phase isotype-specific ELISA and isotype-specific immunofluorescence staining.

In one identification embodiment to identify the bispecific antibody, the wells of microtiter plates (Falcon, Becton Dickinson Labware) are coated with a reagent that specifically interacts with one of the parent hybridoma antibodies and that lacks cross-reactivity with both antibodies. The plates are washed, blocked, and the supernatants (SNs) to be tested are added to each well. Plates are incubated at room temperature for 2 hours, the supernatants discarded, the plates washed, and diluted alkaline phosphatase-anti-antibody conjugate added for 2 hours at room temperature. The plates are washed and a phosphatase substrate, e.g., P-Nitrophenyl phosphate (Sigma, St. Louis) is added to each well. Plates are incubated, 3N NaOH is added to each well to stop the reaction, and the OD<sub>410</sub> values determined using an ELISA reader.

In another identification embodiment, microtiter plates pre-treated with poly-L-lysine are used to bind one of the target cells to each well, the cells are then fixed, e.g. using 1% glutaraldehyde, and the bispecific antibodies are tested for their ability to bind to the intact cell. In addition, FACS, immunofluorescence staining, idiotype specific antibodies, antigen binding competition assays, and other methods common in the art of antibody characterization may be used in conjunction with the present invention to identify preferred quadromas.

Following the isolation of the quadroma, the bispecific antibodies are purified away from other cell products. This may be accomplished by a variety of protein isolation procedures, known to those skilled in the art of immunoglobulin purification. Means for preparing and characterizing antibodies are well known in the art (See, e.g., \*Antibodies: A Laboratory Manual, 1988).

For example, supernatants from selected quadromas are passed over protein A or protein G sepharose columns to bind IgG (depending on the isotype). The bound antibodies are then eluted with, e.g. a pH 5.0 citrate buffer. The elute fractions containing the BsAbs, are dialyzed against an isotonic buffer. Alternatively, the eluate is also passed over an anti-immunoglobulin-sepharose column. The BsAb is then eluted with 3.5M magnesium chloride. BsAbs purified in this way are then tested for binding activity by, e.g., an isotype-specific ELISA and immunofluorescence staining assay of the target cells, as described above.

Purified BsAbs and parental antibodies may also be characterized and isolated by SDS-PAGE electrophoresis, followed by staining with silver or Coomassie. This is possible when one of the parental antibodies has a higher

molecular weight than the other, wherein the band of the BsAbs migrates midway between that of the two parental antibodies. Reduction of the samples verifies the presence of heavy chains with two different apparent molecular weights.

Furthermore, recombinant technology is now available for the preparation of antibodies in general, allowing the preparation of recombinant antibody genes encoding an antibody having the desired dual specificity (Van Duk et al., 1989). Thus, after selecting the monoclonal antibodies having the most preferred binding characteristics, the respective genes for these antibodies can be isolated, e.g., by immunological screening of a phage expression library (Oi & Morrison, 1986; Winter & Milstein, 1991). Then, through rearrangement of Fab coding domains, the appropriate chimeric construct can be readily obtained.

#### E. Binding Assays

Although the present invention has significant utility in animal and human treatment regimens, it also has many other practical uses. These uses are generally related to the specific binding ability of the bispecific compounds. In that all the compounds of the invention include at least one targeting and binding component, e.g., an antibody, ligand, receptor, or such like, the resultant bispecific construct may be used in virtually all of the binding embodiments that the original antibody, ligand or receptor, etc., may be used. The presence of the coagulant, or other binding regions, does not negate the utility of the first binding regions in any binding assay.

As such, the bispecific coagulating ligands may be employed in standard binding assays, such as in immunoblots, Western blots, and other assays in which an antigen is immobilized onto a solid support matrix, e.g., nitrocellulose, nylon or a combination thereof. They may be employed simply as an "antibody substitute" or may be used to provide a more-specific detection means for use in detecting antigens against which standard secondary reagents cause an unacceptably high background. This is especially useful when the antigens studied are themselves immunoglobulins or other antibodies are used in the procedure, as exemplified below in the case of ELISAs.

The bispecific binding ligands may also be used in conjunction with both fresh-frozen and formalin-fixed, paraffin-embedded tissue blocks in immunohistochemistry; in fluorescent activated cell sorting, flow cytometry or flow microfluorometry; in immunoprecipitation to separate a target antigen from a complex mixture, in which case, due to their potential to form molecular lattices, they may even achieve precipitation without a secondary matrix-coupled reagent; in antigen or cell purification embodiments, such as affinity chromatography, even including, in certain cases, the one-step rapid purification of one or more cell populations at the same time; and in many other binding assays that will be known to those of skill in the art given the information presented herein.

As an example, the bispecific ligands of the invention may be used in ELISA assays. Many types of ELISAs are known and routinely practiced in the art. The bispecific ligands may be employed in any of the binding steps, depending on the particular type of ELISA being performed and the "antigen" (component) to be detected. The ligands could therefore be used to coat the plate, to compete for binding sites, as an antigen to provide a standard curve, as a primary binding ligand, as a secondary binding ligand or even as a tertiary or other binding ligand. The many modes of conducting ELISAs will be known to those of skill in the art, in further light of the exemplary mode discussed below.

In one form of an ELISA, binding targets, generally antibodies themselves, are immobilized onto a selected

surface, preferably a surface exhibiting a protein affinity such as the wells of a polystyrene microtiter plate. After washing to remove incompletely adsorbed material, it is desirable to bind or coat the assay plate wells with a nonspecific protein that is known to be antigenically neutral with regard to the test antisera such as bovine serum albumin (BSA), casein or solutions of milk powder. This allows for blocking of nonspecific adsorption sites on the immobilizing surface and thus reduces the background caused by nonspecific binding of antisera onto the surface.

In these types of ELISAs, generally termed sandwich ELISAs, the plate-bound antibody is used to "trap" the antigen. After binding of the first antibody to the well, coating with a non-reactive material to reduce background, and washing to remove unbound material, the immobilizing surface is contacted with, in the present exemplary embodiment, a test sample containing the antigenic material to be detected and/or titrated in a manner conducive to immune complex (antigen/antibody) formation. These embodiments are particularly useful for detecting ligands in clinical samples or biological extracts. The samples are preferably diluted with solutions of BSA, bovine gamma globulin (BGG) and phosphate buffered saline (PBS) and a detergent, e.g. Tween.

The layered antisera is then allowed to incubate for from 2 to 4 hours, at temperatures preferably on the order of 25° to 37° C. Following incubation, the antisera-contacted surface is washed so as to remove non-immunocomplexed material. A preferred washing procedure includes washing with a solution such as PBS/Tween, or borate buffer.

Following formation of specific immunocomplexes between the bound antigen and the test sample, and subsequent washing, the occurrence and amount of immunocomplex formation may be determined by subjecting same complex to a secondary specific binding component, which is generally an antibody-based component. In a particular embodiment, the bispecific ligands of the invention are proposed for use in this step. Further specific binding and washing steps are then conducted.

To provide a detecting means, in the present exemplary embodiment, a third antibody is used that is linked to a detectable label, such as an associated enzyme that will generate a color development upon incubating with an appropriate chromogenic substrate. The third, or tertiary, labeled antibody has binding affinity for a component of the bispecific ligand. The ultimate immunocomplex is determined, after appropriate binding and washing steps, by detecting the label, e.g., by incubating with a chromogenic substrate, such as urea and bromocresol purple or 2,2'-azino-di-(3-ethyl-benzthiazoline-6-sulfonic acid [ABTS] and H<sub>2</sub>O<sub>2</sub>. Quantification is then achieved by measuring the degree of color generation, e.g., using a visible spectra spectrophotometer.

Using a bispecific coagulating ligand as a secondary detection reagent in conjunction with the type of ELISA described above has distinct advantages. For example, it allows the use of a tertiary, labeled antibody that is specific for a portion of the bispecific ligand that is distinct from the typical antibody constant regions usually targeted. In particular, a tertiary binding ligand that is specific for the coagulant portion (or coagulant binding region) of the bispecific construct may be employed. This novel means of detecting immune complex formation imparts improved specificity, which is particularly useful in sandwich ELISAs where the tertiary antibody may cross-react with, and bind to, the original material used to coat the plate, i.e., the original antibody, rather than just binding to the intended

secondary antibody. By directing the labelled tertiary component to a non-antibody portion, or even to a novel antigen combining region, of a bispecific ligand, the problem of non-specific binding, and unusually high background, will be avoided.

Further practical uses of the bispecific ligands are evident by exploiting their coagulating ability. As all of the proposed compounds are capable of inducing coagulation, they may be employed, e.g., as a control, in any assay that involves coagulation as a component. The presence of the targeting component does not negate the utility of the coagulant in such assays, as each component functions independently of the other.

#### F. Effective Use of Tissue Factor-Binding Bispecific Antibodies

As mentioned earlier, tissue factor (TF) is one agent capable of initiating blood coagulation. TF is exposed to the blood in vascular damage or following activation by certain cytokines. Available TF then complexes with factor VIIa to initiate the coagulation cascade that ultimately results in fibrin formation.

In one exemplary embodiment, the inventors have synthesized a bispecific antibody with specificity for antigens on tumor vasculature endothelial cells on one antigen combining site and specificity for the extracellular domains of human TF on the other antigen combining site. The antibody with specificity for human TF was previously shown to bind TF with high affinity without interfering with the factor VIIa complexing event or the TF/VIIa activity (Morrissey et al., 1988). Instead of using full length human TF, the inventors used a truncated form (tTF), which is devoid of the cytoplasmic as well as the transmembrane domain. Truncated TF lacks coagulation inducing activity, while still being able to complex factor VIIa, probably because it is not able to complex with a membrane surface upon which the coagulation-initiation complexes, including Factor X, could assemble.

The mouse model used for analyzing the effectiveness of this tumor vasculature endothelial cell specific targeting construct was a recently established model in which MHC class II antigens, that are absent from the vasculature of normal tissues, are expressed on the tumor vasculature through induction by IFN- $\gamma$  that is secreted by the tumor cells (Burrows et al., 1992; Burrows & Thorpe, 1993). It has been demonstrated that anti-class II antibody administered intravenously localizes rapidly and strongly to the tumor vasculature (Burrows et al., 1992).

The present inventors herein demonstrate that, in a C1300 (Muy) tumor bearing mouse, the anti-MHC Class II/anti-TF bispecific antibody is able to induce coagulation specifically in the vasculature of the tumor when administered together with tTF. Indeed, intravenous administration of the antibody:tTF complex induced rapid thrombosis of tumor vasculature and complete tumor regressions in 70% of animals. Neither the bispecific antibody alone, nor tTF alone, nor any of the isotype matched control antibodies in the presence or absence of tTF, was able to elicit the same effect. This indicates that the B21-2/10H10 bispecific antibody acts as a "coaguligand" that is capable of bridging target cells and tTF so that tTF can activate factor X and start the coagulation cascade. It also shows the evident success of the coaguligand in treating solid tumors.

#### G. Pharmaceutical Compositions and Kits

Pharmaceutical compositions of the present invention will generally comprise an effective amount of the bispecific coagulating ligand dissolved or dispersed in a pharmaceutically acceptable carrier or aqueous medium.

The phrases "pharmaceutically or pharmacologically acceptable" refer to molecular entities and compositions that do not produce an adverse, allergic or other untoward reaction when administered to an animal, or a human, as appropriate. As used herein, "pharmaceutically acceptable carrier" includes any and all solvents, dispersion media, coatings, antibacterial and antifungal agents, isotonic and absorption delaying agents and the like. The use of such media and agents for pharmaceutical active substances is well known in the art. Except insofar as any conventional media or agent is incompatible with the active ingredient, its use in the therapeutic compositions is contemplated. Supplementary active ingredients can also be incorporated into the compositions.

#### 1. Parenteral Formulations

The bispecific ligands of the present invention will often be formulated for parenteral administration, e.g., formulated for injection via the intravenous, intramuscular, subcutaneous or other such routes, including direct instillation into a tumor or disease site. The preparation of an aqueous composition that contains a tumor-targeted coagulant agent as an active ingredient will be known to those of skill in the art in light of the present disclosure. Typically, such compositions can be prepared as injectables, either as liquid solutions or suspensions; solid forms suitable for using to prepare solutions or suspensions upon the addition of a liquid prior to injection can also be prepared; and the preparations can also be emulsified.

Solutions of the active compounds as free base or pharmacologically acceptable salts can be prepared in water suitably mixed with a surfactant, such as hydroxypropylcellulose. Dispersions can also be prepared in glycerol, liquid polyethylene glycols, and mixtures thereof and in oils. Under ordinary conditions of storage and use, these preparations contain a preservative to prevent the growth of microorganisms.

The pharmaceutical forms suitable for injectable use include sterile aqueous solutions or dispersions; formulations including sesame oil, peanut oil or aqueous propylene glycol; and sterile powders for the extemporaneous preparation of sterile injectable solutions or dispersions. In all cases the form must be sterile and must be fluid to the extent that easy syringability exists. It must be stable under the conditions of manufacture and storage and must be preserved against the contaminating action of microorganisms, such as bacteria and fungi.

The bispecific ligands or antibodies can be formulated into a composition in a neutral or salt form. Pharmaceutically acceptable salts, include the acid addition salts (formed with the free amino groups of the protein) and which are formed with inorganic acids such as, for example, hydrochloric or phosphoric acids, or such organic acids as acetic, oxalic, tartaric, mandelic, and the like. Salts formed with the free carboxyl groups can also be derived from inorganic bases such as, for example, sodium, potassium, ammonium, calcium, or ferric hydroxides, and such organic bases as isopropylamine, trimethylamine, histidine, procaine and the like.

The carrier can also be a solvent or dispersion medium containing, for example, water, ethanol, polyol (for example, glycerol, propylene glycol, and liquid polyethylene glycol, and the like), suitable mixtures thereof, and vegetable oils. The proper fluidity can be maintained, for example, by the use of a coating, such as lecithin, by the maintenance of the required particle size in the case of dispersion and by the use of surfactants. The prevention of the action of microorganisms can be brought about by various antibacterial ad-

antifungal agents, for example, parabens, chlorobutanol, phenol, sorbic acid, thimerosal, and the like. In many cases, it will be preferable to include isotonic agents, for example, sugars or sodium chloride. Prolonged absorption of the injectable compositions can be brought about by the use in the compositions of agents delaying absorption, for example, aluminum monostearate and gelatin.

Sterile injectable solutions are prepared by incorporating the active compounds in the required amount in the appropriate solvent with various of the other ingredients enumerated above, as required, followed by filtered sterilization. Generally, dispersions are prepared by incorporating the various sterilized active ingredients into a sterile vehicle which contains the basic dispersion medium and the required other ingredients from those enumerated above. In the case of sterile powders for the preparation of sterile injectable solutions, the preferred methods of preparation are vacuum-drying and freeze-drying techniques which yield a powder of the active ingredient plus any additional desired ingredient from a previously sterile-filtered solution thereof.

Upon formulation, solutions will be administered in a manner compatible with the dosage formulation and in such amount as is therapeutically effective. Formulations are easily administered in a variety of dosage forms, such as the type of injectable solutions described above, but drug release capsules and the like can also be employed.

Suitable pharmaceutical compositions in accordance with the invention will generally include an amount of the bispecific ligand admixed with an acceptable pharmaceutical diluent or excipient, such as a sterile aqueous solution, to give a range of final concentrations, depending on the intended use. The techniques of preparation are generally well known in the art as exemplified by Remington's Pharmaceutical Sciences, 16th Ed. Mack Publishing Company, 1980, incorporated herein by reference. It should be appreciated that endotoxin contamination should be kept minimally at a safe level, for example, less than 0.5 ng/mg protein. Moreover, for human administration, preparations should meet sterility, pyrogenicity, general safety and purity standards as required by FDA Office of Biological Standards.

The therapeutically effective doses are readily determinable using an animal model, as shown in the studies detailed herein (see, e.g., Example III). Experimental animals bearing solid tumors are frequently used to optimize appropriate therapeutic doses prior to translating to a clinical environment. Such models are known to be very reliable in predicting effective anti-cancer strategies. For example, mice bearing solid tumors, such as used in Example III, are widely used in pre-clinical testing.

The inventors have used mice with C1300 (Mo8) tumors to determine toxicity limits and working ranges of bispecific that give optimal anti-tumor effects with minimal toxicity.

It is currently proposed that effective doses for use in the treatment of cancer will be between about 0.1 mg/kg and about 2 mg/kg, and preferably, of between about 0.8 mg/kg and about 1.2 mg/kg, when administered via the IV route at a frequency of about 1 time per week. Some variation in dosage will necessarily occur depending on the condition of the subject being treated. The person responsible for administration will, in any event, determine the appropriate dose for the individual subject. Such optimization and adjustment is routinely carried out in the art and by no means reflects an undue amount of experimentation.

It should be remembered that one aspect of the present invention concerns the delivery of a coagulating agent to a



tumor site by administering an uncomplexed bispecific binding ligand that garners an endogenous coagulation factor from the circulation and concentrates it within the tumor site. In these cases, the pharmaceutical compositions employed will contain a ligand having a targeting and coagulant binding region, but will otherwise generally be the same as those described above.

In addition to the compounds formulated for parenteral administration, such as intravenous or intramuscular injection, other pharmaceutically acceptable forms are also contemplated, e.g., tablets or other solids for oral administration, time release capsules, liposomal forms and the like. Other pharmaceutical formulations may also be used, dependent on the condition to be treated. For example, topical formulations that are appropriate for treating pathological conditions such as dermatitis and psoriasis; and ophthalmic formulations for diabetic retinopathy.

## 2. Ingestible Formulations

In certain embodiments, active compounds may be administered orally. This is contemplated for agents that are generally resistant, or have been rendered resistant, to proteolysis by digestive enzymes. Such compounds are contemplated to include chemically designed or modified agents; dextrorotatory peptidyl agents; liposomal formulations; and formulations in time release capsules to avoid peptidase and lipase degradation.

For oral administration, the active bispecific compounds may be administered, for example, with an inert diluent or with an assimilable edible carrier, or they may be enclosed in hard or soft shell gelatin capsule, or compressed into tablets, or incorporated directly with the food of the diet. For oral therapeutic administration, the active compounds may be incorporated with excipients and used in the form of ingestible tablets, buccal tables, troches, capsules, elixirs, suspensions, syrups, wafers, and the like. Such compositions and preparations should contain at least 0.1% of active bispecific coagulant. The percentage of the compositions and preparations may, of course, be varied and may conveniently be between about 2 to about 60% of the weight of the unit. The amount of active compounds in such therapeutically useful compositions is such that a suitable dosage will be obtained.

The tablets, troches, pills, capsules and the like may also contain the following: a binder, as gum tragacanth, acacia, cornstarch, or gelatin; excipients, such as dicalcium phosphate; a disintegrating agent, such as corn starch, potato starch, alginic acid and the like; a lubricant, such as magnesium stearate; and a sweetening agent, such as sucrose, lactose or saccharin may be added or a flavoring agent, such as peppermint, oil of wintergreen, or cherry flavoring. When the dosage unit form is a capsule, it may contain, in addition to materials of the above type, a liquid carrier.

Various other materials may be present as coatings or to otherwise modify the physical form of the dosage unit. For instance, tablets, pills, or capsules may be coated with shellac, sugar or both. A syrup of elixir may contain the active compounds sucrose as a sweetening agent methyl and propylparabens as preservatives, a dye and flavoring, such as cherry or orange flavor. Of course, any material used in preparing any dosage unit form should be pharmaceutically pure and substantially non-toxic in the amounts employed. In addition, the active compounds may be incorporated into sustained-release preparation and formulations.

## 3. Liposomal Formulations

The bispecific coagulating ligands of the present invention may also be formulated in liposomal preparations if desired. The following information may be utilized in gen-

erating liposomal formulations incorporating the present coagulants. Phospholipids form liposomes when dispersed in water, depending on the molar ratio of lipid to water. The physical characteristics of liposomes depend on pH, ionic strength and the presence of divalent cations. Liposomes can show low permeability to ionic and polar substances, but at elevated temperatures undergo a phase transition which markedly alters their permeability. The phase transition involves a change from a closely packed, ordered structure, known as the gel state, to a loosely packed, less-ordered structure, known as the fluid state. This occurs at a characteristic phase-transition temperature and results in an increase in permeability to ions, sugars and drugs.

In addition to temperature, exposure to proteins can alter the permeability of liposomes. Certain soluble proteins such as cytochrome c bind, deform and penetrate the bilayer, thereby causing changes in permeability. Cholesterol inhibits this penetration of proteins, apparently by packing the phospholipids more tightly. It is contemplated that the most useful liposome formations for use with the present invention will contain cholesterol, or even PEG.

The ability to trap solutes varies between different types of liposomes. For example, multilamellar vesicles (MLVs) are moderately efficient at trapping solutes, but small unilamellar vesicles (SUVs) are inefficient. SUVs offer the advantage of homogeneity and reproducibility in size distribution, however, and a compromise between size and trapping efficiency is offered by large unilamellar vesicles (LUVs). These are prepared by ether evaporation and are three to four times more efficient at solute entrapment than MLVs.

In addition to liposome characteristics, an important determinant in entrapping compounds is the physicochemical properties of the compound itself. Polar compounds are trapped in the aqueous spaces and nonpolar compounds bind to the lipid bilayer of the vesicle. Polar compounds are released through permeation or when the bilayer is broken, but nonpolar compounds remain affiliated with the bilayer unless it is disrupted by temperature or exposure to lipoproteins. Both types show maximum efflux rates at the phase transition temperature.

Liposomes interact with cells via four different mechanisms: Endocytosis by phagocytic cells of the reticuloendothelial system such as macrophages and neutrophils; adsorption to the cell surface, either by nonspecific weak hydrophobic or electrostatic forces, or by specific interactions with cell-surface components; fusion with the plasma cell membrane by insertion of the lipid bilayer of the liposome into the plasma membrane, with simultaneous release of liposomal contents into the cytoplasm; and by transfer of liposomal lipids to cellular or subcellular membranes, or vice versa, without any association of the liposome contents. It often is difficult to determine which mechanism is operative and more than one may operate at the same time.

The fate and disposition of intravenously injected liposomes depend on their physical properties, such as size, fluidity and surface charge. They may persist in tissues for hours or days, depending on their composition, and half lives in the blood range from minutes to several hours. Larger liposomes, such as MLVs and LUVs, are taken up rapidly by phagocytic cells of the reticuloendothelial system, but physiology of the circulatory system restrains the exit of such large species at most sites. They can exit only in places where large openings or pores exist in the capillary endothelium, such as the sinusoids of the liver or spleen. Thus, these organs are the predominate site of

uptake. On the other hand, SUVs show a broader tissue distribution but still are sequestered highly in the liver and spleen. In general, this *in vivo* behavior dictates that liposomes concentrate only in those organs and tissues accessible to their large size. As this clearly includes the blood, this is not a limitation to their combined use with the present invention.

In other embodiments, the bispecific components of the invention may be admixed with the liposome surface to direct the drug contents to the specific antigenic receptors located on the target cell surface. Carbohydrate determinants (glycoprotein or glycolipid cell-surface components that play a role in cell-cell recognition, interaction and adhesion) may also be used as recognition sites as they have potential in directing liposomes to particular cell types. Mostly, it is contemplated that intravenous injection of liposomal preparations would be used, but other routes of administration are also conceivable.

#### 4. Topical Formulations

The formulation of bispecific coagulants for topical use, such as in creams, ointments and gels is also contemplated. The preparation of oleaginous or water-soluble ointment bases is also well known to those in the art. For example, these compositions may include vegetable oils, animal fats, and more preferably, semisolid hydrocarbons obtained from petroleum. Particular components used may include white ointment, yellow ointment, cetyl esters wax, oleic acid, olive oil, paraffin, petrolatum, white petrolatum, spermaceti, starch glycerite, white wax, yellow wax, lanolin, anhydrous lanolin and glyceryl monostearate.

Various water-soluble ointment bases may also be used, including glycol ethers and derivatives, polyethylene glycols, polyoxyl 40 stearate and polysorbates. Even delivery through the skin may be employed if desired, e.g., by using transdermal patches, iontophoresis or electrotransport.

#### 5. Ophthalmic Formulations

The bispecific coagulating ligands of the present invention may also be formulated into pharmaceutical compositions suitable for use as ophthalmic solutions. Such ophthalmic solutions are of interest, for example, in the treatment of diabetic retinopathy. Thus, for the treatment of diabetic retinopathy a bispecific conjugate of this invention would be administered to the eye of the subject in need of treatment in the form of an ophthalmic preparation prepared in accordance with conventional pharmaceutical practice, see for example "Remington's Pharmaceutical Sciences" 15th Edition, pages 1488 to 1501 (Mack Publishing Co., Easton, Pa.).

The ophthalmic preparation will contain a novel bispecific coagulant or a pharmaceutically acceptable salt thereof in a concentration from about 0.01 to about 1% by weight, preferably from about 0.05 to about 0.5% in a pharmaceutically acceptable solution, suspension or ointment. Some variation in concentration will necessarily occur, depending on the particular compound employed, the condition of the subject to be treated and the like, and the person responsible for treatment will determine the most suitable concentration for the individual subject. The ophthalmic preparation will preferably be in the form of a sterile aqueous solution containing, if desired, additional ingredients, for example preservatives, buffers, tonicity agents, antioxidants and stabilizers, nonionic wetting or clarifying agents, viscosity-increasing agents and the like.

Suitable preservatives for use in such a solution include benzalkonium chloride, benzethonium chloride, chlorobutanol, thimerosal and the like. Suitable buffers include boric acid, sodium and potassium bicarbonate,

sodium and potassium borates, sodium and potassium carbonate, sodium acetate, sodium biphosphate and the like, in amounts sufficient to maintain the pH at between about pH 6 and pH 8, and preferably, between about pH 7 and pH 7.5. Suitable tonicity agents are dextran 40, dextran 70, dextrose, glycerin, potassium chloride, propylene glycol, sodium chloride, and the like, such that the sodium chloride equivalent of the ophthalmic solution is in the range 0.9 plus or minus 0.2%.

Suitable antioxidants and stabilizers include sodium bisulfite, sodium metabisulfite, sodium thiosulfite, thiourea and the like. Suitable wetting and clarifying agents include polysorbate 80, polysorbate 20, poloxamer 282 and tyloxapol. Suitable viscosity-increasing agents include dextran 40, dextran 70, gelatin, glycerin, hydroxyethylcellulose, hydroxymethylpropylcellulose, lanolin, methylcellulose, petrolatum, polyethylene glycol, polyvinyl alcohol, polyvinylpyrrolidone, carboxymethylcellulose and the like. The ophthalmic preparation will be administered topically to the eye of the subject in need of treatment by conventional methods, for example in the form of drops or by bathing the eye in the ophthalmic solution.

#### 6. Therapeutic Kits

The present invention also provides therapeutic kits comprising the bispecific coagulating ligands described herein. Such kits will generally contain, in suitable container means, a pharmaceutically acceptable formulation of at least one bispecific ligand in accordance with the invention. The kits may also contain other pharmaceutically acceptable formulations, such as those containing additional bispecific coagulating ligands, generally those having a distinct targeting component; extra uncomplexed coagulation factors; bispecific antibodies, T cells, or other functional components for use in, e.g., antigen induction; components for use in antigen suppression, such as a cyclosporin; distinct anti-tumor site antibodies or immunitoxins; and any one or more of a range of chemotherapeutic drugs.

Preferred agents for use in combination kits are inducing agents capable of inducing disease-associated vascular endothelial cells to express a targetable antigen, such as E-selectin or an MHC Class II antigen. Inducing agents can include T cell clones that bind disease or tumor antigens and that produce IFN- $\gamma$ . Preferred inducing agents include bispecific antibodies that bind to disease or tumor cell antigens and to effector cells capable of inducing target antigen expression through the elaboration of cytokines.

As such, the present invention further includes kits that comprise, in suitable container means, a first pharmaceutical composition comprising a bispecific antibody that binds to an activating antigen on an effector cell surface, i.e., a monocyte/macrophage, mast cell, T cell or NK cell, and to an antigen on the cell surface of disease cell; and a second pharmaceutical composition comprising a bispecific ligand that comprises a first binding region that binds to an endothelial cell antigen induced by an activated effector cell, or cytokine therefrom, where the first binding region is operatively linked to a coagulation factor or a second binding region that binds to a coagulation factor.

Kits including a first pharmaceutical composition that comprises a bispecific antibody that binds to the activating antigen CD14, CD16 (FcR for IgE), CD2, CD3, CD28 or the T-cell receptor antigen are preferred, with CD14 or CD28 binding bispecific antibodies being more preferred. Activation of monocyte/macrophages or mast cells via CD14 or CD16 binding results in IL-1 production that induces E-selectin; whereas activation of T cells via CD2, CD3 or CD28 binding results in IFN- $\gamma$  production that induces MHC



class II. Kits that include a second pharmaceutical composition that comprises a bispecific ligand that comprises a first binding region that binds to E-selectin or to an MHC Class II antigen are therefore also preferred.

The kits may have a single container means that contains the bispecific coagulating ligand, with or without any additional components, or they may have distinct container means for each desired agent. Kits comprising the separate components necessary to make a bispecific coagulating ligand are also contemplated.

When the components of the kit are provided in one or more liquid solutions, the liquid solution is an aqueous solution, with a sterile aqueous solution being particularly preferred. However, the components of the kit may be provided as dried powder(s). When reagents or components are provided as a dry powder, the powder can be reconstituted by the addition of a suitable solvent. It is envisioned that the solvent may also be provided in another container means.

The container means of the kit will generally include at least one vial, test tube, flask, bottle, syringe or other container means, into which the bispecific coagulating ligand, and any other desired agent, may be placed and, preferably, suitably aliquoted. Where additional components are included, the kit will also generally contain a second vial or other container into which these are placed, enabling the administration of separated designed doses. The kits may also comprise a second/third container means for containing a sterile, pharmaceutically acceptable buffer or other diluent.

The kits may also contain a means by which to administer the bispecific ligand to an animal or patient, e.g., one or more needles or syringes, or even an eye dropper, pipette, or other such like apparatus, from which the formulation may be injected into the animal or applied to a diseased area of the body. The kits of the present invention will also typically include a means for containing the vials, or such like, and other component, in close confinement for commercial sale, such as, e.g., injection or blow-molded plastic containers into which the desired vials and other apparatus are placed and retained.

The following examples are included to demonstrate preferred embodiments of the invention. It should be appreciated by those of skill in the art that the techniques disclosed in the examples that follow represent techniques discovered by the inventors to function well in the practice of the invention, and thus can be considered to constitute preferred modes for its practice. However, those of skill in the art should, in light of the present disclosure, appreciate that many changes can be made in the specific embodiments that are disclosed and still obtain a like or similar result without departing from the spirit and scope of the invention.

#### EXAMPLE I

##### SYNTHESIS OF A BISPECIFIC COAGULATING ANTIBODY

The present example describes the synthesis of a bispecific antibody capable of specifically directing a coagulant to a tumor site, i.e., a "coaguligand".

##### A. Materials and Methods

##### 1. Reagents

Pepsin (A; EC 3.4.23.1), Ellmans reagent (ER; 5,5'-dithio-bis(2-nitrobenzoic acid, DNTB), 2-mercaptoethanol (2-ME), sodium arsenite (NaAsO<sub>2</sub>) and rabbit brain thromboplastin (acetone powder) were obtained from Sigma Chemical Co., St. Louis Mo. Sephadex G-25 and G-100 were obtained from Pharmacia LKB (Piscataway, N.J.).

##### 2. Human Truncated Tissue Factor (tTF)

Recombinant human truncated TF (tTF) was prepared by one of two different methods.

Method I: Construction of the *E. coli* Expression Vector. The cDNA coding for tTF (residues 1-218) was amplified by PCR using the primers 5'-GAAGAAGGGATCCTGGTGCCTCGTGGTTCTGGCACTACAAATACT-3' (5'-primer; SEQ ID NO:28) and 5'-CTGGCCTCAAGCTTAACGGAATTCACCTTT-3' (3'-primer; SEQ ID NO:29) which allowed the addition of the coding sequence for a thrombin cleavage site upstream of the cDNA. The PCR products were cleaved using BamHI and HindIII and ligated between the BamHI and HindIII sites of the expression vector pTrcHisC (Invitrogen).

DH5 $\alpha$  cells were transformed with the ligation mixture and recombinant plasmids were isolated after selection in the presence of ampicillin. The *E. coli* strain BL21 was transformed with the recombinant plasmid pTrcHisC-tTF and the resultant transformants were used for protein expression.

Method I: Expression, Refolding and Purification of tTF from *E. coli*. The poly(his)-tTF fusion protein was expressed using BL21 cells transformed with pTrc-HisC-tTF. Inoculant cultures (10 ml in LB medium) were grown overnight shaking at 37° C.

Inoculant cultures were added to growth medium which were then grown shaking at 37° C. When the optical density at 550 nm had reached ca. 0.5, 10 ml of 100 mM isopropyl- $\beta$ -D-thiogalactopyranoside was added. Shaking was continued at 37° C. for ca. 20 h (to stationary phase).

The cells were harvested by centrifugation (10,000 $\times$ g, 20 min.) and the inclusion bodies were isolated as follows (quantities of reagents are per gram of cell paste). The cell paste was suspended in 4 ml of 10 mM Tris, pH 7.5, 150 mM NaCl, 1 mM MgCl<sub>2</sub>, 0.17 mg/ml PMSE, 2 mg/ml hen egg white lysozyme (Sigma). Benzonase (250 units, EM Science) was added the suspension was mixed gently at room temperature for 1.5 h then centrifuged at 12,000 g for 15 min.

The pellet was resuspended in 10 mM Tris, pH 7.5, 1 mM EDTA, 3% NP40 (2 ml), sonicated for 1 min at 50% power and centrifuged at 12,000 $\times$ g for 20 min. The pellet was resuspended in water, sonicated for 20-30 seconds at 50% power and centrifuged at 12,000 $\times$ g for 20 min. The water wash was repeated and the final pellet, highly enriched for the inclusion bodies, was suspended in 6M guanidinium chloride, 0.5M NaCl, 20 mM phosphate, 10 mM  $\beta$ -mercaptoethanol, pH 8.0 (9 ml per gram of inclusion bodies) by gentle mixing at room temperature overnight.

The suspension was centrifuged at 12,000 $\times$ g for 20 min and the supernatant was loaded onto a nickel nitriloacetic acid (Ni-NTA, Qiagen) column. The column was washed successively with the same 6M guanidinium chloride buffer at pH 8 then pH 7, then the protein was eluted by decreasing the pH to 4.

Ni-NTA column fractions containing the fusion protein were combined and dithiothreitol was added to 50 mM. The solution was held at room temperature overnight then diluted to a protein concentration of ca. 1 mg/ml in 6M urea, 50 mM Tris, 0.02% sodium azide, pH 8.0 and dialyzed at 4° C. overnight against 10-20 volumes of the same buffer. The buffer was changed to 2M urea, 50 mM Tris, 300 mM NaCl, 2.5 mM reduced glutathione, 0.5 mM oxidized glutathione, 0.02% sodium azide, pH 8.0 (folding buffer). Dialysis was continued for 2 more days, the buffer was replaced by fresh folding buffer and dialysis was continued for 2 more days.

The solution was then dialyzed extensively against 20 mM TEA (pH 7.5), removed from the dialysis bag, treated

with human thrombin (ca. 1 part per 500 parts recombinant protein w/w) overnight at room temperature, and loaded onto a HR-10/10 mono-Q anion exchange column. tTF protein was eluted using a 20 mM TEA buffer containing NaCl in a concentration increasing linearly from 0 to 150 mM over 30 minutes (flow rate 3 ml/min).

Method II: Preparation of tTF complimentary DNA (cDNA). RNA from J-82 cells (human bladder carcinoma) was used for the cloning of tTF. Total RNA was isolated using the GlassMax™ RNA microisolation reagent (Gibco BRL). The RNA was reverse transcribed to cDNA using the GeneAmp RNA PCR kit (Perkin Elmer). tTF cDNA was amplified using the same kit with the following two primers:

5' primer: 5'

GTC ATG CCA TGG CCC TGG TGC CTC GTG CT

CTG GCA CTA CAA ATA CT

3' primer: 5'

TGA CAA GCT TAT TCT CTG AAT TCC CCC TTT CT

(SEQ ID NO:2)

The underlined sequences codes for the N-terminus and C-terminus of tTF. The rest of the sequence in the 5' primer is the restriction site for NcoI allowing the cloning of tTF into the expression vector and codes for a cleavage site for thrombin. The sequence in the 3' primer is the HindIII site for cloning tTF into the expression vector. PCR amplification was performed as suggested by the manufacturer. Briefly, 75  $\mu$ M dNTP; 0.6  $\mu$ M primer, 1.5 mM MgCl<sub>2</sub> were used and 30 cycles of 30" at 95° C., 30" at 55° C. and 30" at 72° C. were performed.

Method II. Vector Constructs. *E. coli* expression vector H<sub>6</sub> pQE-60 was used for expressing tTF (Lee et al., 1994). The PCR amplified tTF cDNA was inserted between the NcoI and HindIII site. H<sub>6</sub> pQE-60 has a built-in (His)<sub>6</sub> encoding sequence such that the expressed protein has the sequence of (His)<sub>6</sub> at the N-terminus, which can be purified on the Ni-NTA column.

Method II. tTF Purification. tTF containing H<sub>6</sub> pQE-60 DNA was transformed to *E. coli* TG-1 cells. The cells were grown to OD<sub>600</sub> = 0.5 and IPTG was added to 30  $\mu$ M to induce the tTF production. The cells were harvested after shaking for 18 h at 30° C. The cell pellet was denatured in 6M Gu-HCl and the lysate was loaded onto a Ni-NTA column (Qiagen). The bound tTF was washed with 6M urea and tTF was refolded with a gradient of 6M-1M urea at room temperature for 16 h. The column was washed with wash buffer (0.05 Na H<sub>2</sub> PO<sub>4</sub>, 0.3M NaCl, 10% glycerol) and tTF was eluted with 0.2M Imidazole in wash buffer.

The eluted tTF was concentrated and loaded onto a G-75 column. tTF monomers were collected and treated with thrombin to remove the H<sub>6</sub> peptide. This was done by adding 1 part of thrombin (Sigma) to 500 parts of tTF (w/w), and the cleavage was carried out at room temperature for 18 h. Thrombin was removed from tTF by passage of the mixture through a Benzamidine Sepharose 6B thrombin affinity column (Pharmacia).

The tTF had identical ability to recombinant tTF from yeast or Chinese hamster ovary cells to bind factor VIIa and to enhance the catalytic activity of VIIa (Ruf et al., 1991). When analyzed by polyacrylamide gel electrophoresis in sodium dodecyl sulfate, it ran as a single component having a molecular weight of approximately 24 kD.

### 3. Monoclonal Antibodies

B21-2 (TIB-229) hybridoma and SFR8-B6 hybridoma (HB-152, hereafter referred to as SFR8) were obtained from the ATCC. Both hybridomas secreted rat IgG2b antibodies, which were purified from culture supernatant by protein G affinity chromatography. The B21-2 antibody reacts with I-A<sup>d</sup> antigen expressed on A20 cells as well as on the vasculature of the C1300 (Muy) transfectant tumors grown in BALB/c/nu/nu mice. SFR8 antibody is directed against the HLA-Bw6 epitope and serves as an isotype matched negative control for the B21-2 antibody.

TF9/10H10 (referred to as 10H10), a mouse IgG1, is reactive with human TF without interference of TF/factor VIIa activity and was produced as described by Morrissey et al. (1988).

The cell line MRC OX7 (referred to as OX7) was obtained from Dr. A. F. Williams (MRC Cellular Immunology Unit, University of Oxford, Oxford, England). It secretes the OX7 antibody, a mouse IgG1 antibody that recognizes the Thy 1.1 antigen on T lymphocytes. It was used as an isotype matched negative control for TF9/10H10.

All antibodies were purified from culture supernatant by protein G affinity chromatography.

#### 4. Synthesis of Bispecific Antibodies

F(ab')<sub>2</sub> fragments were obtained by digesting their respective IgGs with 2% (w/v) pepsin for 5-9 hrs at 37° C. and purification of the fragments by Sephadex G100 chromatography. Synthesis of the bispecific antibodies B21-2/10H10, SFR8/10H10 and B21-2/OX7 was carried out according to the method of Brennan et al. (1985) with minor modifications.

The bispecific antibodies B21-2/10H10, SFR8/10H10, OX7/10H10 and B21-2/OX7 were synthesized according to the method of Brennan et al. (1985) with minor modifications. In brief, F(ab')<sub>2</sub> fragments were obtained from the IgG antibodies by digestion with pepsin and were purified to homogeneity by chromatography Sephadex G100. F(ab')<sub>2</sub> fragments were reduced for 16 h at 20° C. with 5 mM 2-mercaptoethanol in 0.1M sodium phosphate buffer, pH 6.8, containing 1 mM EDTA (PBSE buffer) and 9 mM NaAsO<sub>2</sub>. Ellman's reagent (ER) was added to give a final concentration of 25 mM and, after 3 h at 20° C., the Ellman's-derivatized Fab' fragments (Fab'-ER) were separated from unreacted ER on columns of Sephadex G25 in PBSE.

To form the bispecific antibody, Fab'-ER derived from one antibody was concentrated to approximately 2.5 mg/ml in an ultrafiltration cell and was reduced with 10 mM 2-mercaptoethanol for 1 h at 20° C. The resulting Fab'-SH was filtered through a column of Sephadex G25 in PBSE and was mixed with equal molar quantities of Fab'-ER prepared from the second antibody. The mixtures were concentrated by ultrafiltration to approximately 3 mg/ml and were stirred for 16 h at 20° C. The products of the reaction were fractionated on columns of Sephadex G100 and the fractions containing the bispecific antibody (110 kDa) were concentrated to 1 mg/ml, and were stored at 4° C. in 0.02% sodium azide.

#### B. Results

##### 1. Analysis of Bispecific Antibodies

The molecular weight of the F(ab')<sub>2</sub> fragments and bispecific preparations were determined by SDS-Page electrophoresis with 4-15% gradient gels using the Pharmacia LKB-Phastsystem (Pharmacia LKB, Piscataway, N.J.). Bispecificity as well as the percentage of heterodimer vs homodimer was determined by FACS analysis (Example II).

Analysis of the bispecific antibodies by SDS-Page electrophoresis (and by FACS, Example II) demonstrated that the B21-2/10H10 bispecific contained less than 4%

homodimer of either origin and <10% fragments with a molecular weight of 140 kD or 55 kD. Approximately 10% of the preparation consisted of 140 kD fragments, probably being a F(ab')<sub>2</sub> construct with an extra light chain (of either origin) attached.

### EXAMPLE II

#### COAGULATING ANTIBODY BINDING AND FUNCTION IN VITRO

The present example shows the bispecificity of the coagulating antibody (coaguligand) and demonstrates that specific binding, cellular delivery and coagulation is achieved in vitro using the coaguligand.

##### A. Materials and Methods

##### 1. Cells

The A20 cell line, which is an I-A<sup>d</sup> positive BALB/c B-cell lymphoma, was purchased from the American Type Culture Collection (ATCC; Rockville, Md.; TIB-208). A20 cells were grown in DMEM supplemented with 10% (v/v) fetal calf serum (FCS), 0.2 mM L-glutamine, 200 units/ml penicillin and 100 µg/ml streptomycin, 18 mM Hepes, 0.1 mM non-essential amino acids mix and 1 mM sodium pyruvate (medium hereafter referred to as complete DMEM; all reagents obtained from Life Technologies, Gaithersburg, Md.). 2-ME is added to complete DMEM to a final concentration of 0.064 mM for A20 cells. Cultures were maintained at 37° C. in a humidified atmosphere of 90% air/10% CO<sub>2</sub>.

J82, a human gall bladder carcinoma expressing TF, was obtained from the ATCC (HTB-1). The cells grew adherently in complete DMEM.

The C1300 neuroblastoma cell line was established from a spontaneous tumor, which arose in an A/Jax mouse (Dunham & Stewart, 1953). The C1300 (Muy) 12 line, hereafter referred to as C1300 (Muy) was derived by transfection of C1300 neuroblastoma cells with the murine IFN-γ gene using the IFN-γ expression retrovirus pSVX (Muy ΔAs) (Watanabe et al., 1989). The IFN-γ expression retrovirus was obtained from Dr. Y. Watanabe (Department of Molecular Microbiology, Kyoto University, Japan).

C1300(Muy)12 cells were maintained in Dulbecco's modified Eagle Medium (DMEM) supplemented with 10% (v/v) fetal calf serum (FCS), 2.4 mM L-glutamine, 200 units/ml penicillin, 100 µg/ml streptomycin, 100 µM non-essential amino acids, 1 µM sodium pyruvate, 18 µM HEPES and 1 mg/ml G418 (Geneticin; Sigma). Cultures were maintained at 37° C. in a humidified atmosphere of 90% air/10% CO<sub>2</sub>.

The Thy 1.1-expressing AKR-A mouse T lymphoma cell line was obtained from Prof. Dr. I. MacLennan (Department of Experimental Pathology, Birmingham University, Birmingham, England) and were grown in complete DMEM.

##### 2. Indirect immunofluorescence

A20 cells were resuspended in PBS/0.2% BSA/0.02% Na-azide (hereafter referred to as FACS buffer) at 4×10<sup>6</sup> cells/ml. J82 cells were released from the flask under mild conditions using PBS/EDTA (0.2% w/v) and resuspended at 4×10<sup>6</sup> cells/ml in FACS buffer. 50 µl of cell suspension was added to 50 µl of optimal serial dilutions of the primary antibody in wells of a round-bottomed 96 well plate. After incubation at RT for 15 min, the cells were washed with FACS buffer 3 times. After removing the final supernatant, 50 µl of the secondary antibody conjugated to fluorescein isothiocyanate (FITC), in a 1 in 20 dilution in FACS buffer, was added to the cells. The cells were incubated for a further 15 min at RT and washed 3 times with FACS buffer. Cell

associated fluorescence was measured on a FACScan (Becton Dickinson, Fullerton, Calif.). Data were analyzed using the Lysis II program. When FITC-anti-rat immunoglobulin was used as the secondary antibody, normal mouse serum (10% v/v) was added to block non-specific cross reactivity with the mouse cells.

##### 3. Radiolabeling of Proteins

Proteins were labeled with <sup>125</sup>Iodine according to the chloramine T protocol described by Mason & Williams (1980), (protocol 2). The iodinated product was purified on G25 and stored at -70° C. in the presence of 5% DMSO and 5 mg/ml bovine IgG in the case of the monoclonal fragments and 5% DMSO and 5 mg/ml BSA in the case of tTF. Specific activity ranged between 2.5 µCi/µg and 4.8 µCi/µg.

##### 15 4. Binding studies

Human tTF was labelled with <sup>125</sup>I to a specific activity of 2.5-4.8 µCi/µg using the chloramine T procedure (Protocol 2) described by Mason and Williams (1980). A suspension of A20 cells at 2×10<sup>6</sup> cells/ml in PBS containing 2 mg/ml BSA and 0.02% sodium azide was distributed in 50 µl volumes into the wells of 96 well round-bottomed microtiter plates. To the wells were added 25 µl of bispecific antibodies prepared over a range of concentrations (8 to 0.02 µg/ml) in the same buffer.

25 µl of <sup>125</sup>I-tTF at 8 µg/ml in the same buffer were added to each well, giving a molar excess of tTF. The plates were shaken and incubated for 1 hr at 4° C. The cells were then washed 3× in the plates with 0.9% (w/v) NaCl containing 2 mg/ml BSA. The contents of the wells were pipetted over a 10:11 (v/v) mixture of dibutyl phthalate and bis(2-ethylhexyl)phthalate oils in microcentrifuge tubes. The tubes were centrifuged for 1.5 min at 7500 g and were snap frozen in liquid nitrogen. The tips containing the cells were cut off. The radioactivity in the cell pellet and in the supernatant was measured in a gamma counter.

##### 5. Coagulation Assay

An identical microplate to that used for the binding assay above was set up on the same occasion, except that non-labelled tTF was added instead of <sup>125</sup>I-tTF. After the 1 h incubation at 4° C., the cells were washed 3× as before and were resuspended in 75 µl of 0.9% NaCl containing 2 mg/ml BSA and 12.5 mM CaCl<sub>2</sub>. The contents of the wells were transferred to 5 ml clear plastic tubes and were warmed to 37° C. To each tube was added 30 µl of citrated mouse plasma at 37° C. The time for the first fibrin strands to form was recorded.

##### B. Results

##### 1. Antibody Bispecificity

For SFR8/10H10 bispecificity was shown by FACS using J82 cells (TF positive) as target cells and FITC-anti-mouse immunoglobulin to demonstrate 10H10 presence. FITC-anti-rat immunoglobulin was used to demonstrate the presence of SFR8. The mean fluorescence intensity-versus-concentration curves were coincident for both stains, demonstrating that both the mouse and the rat arm are present in the bispecific preparation.

##### 2. Antibody Binding

Binding studies with <sup>125</sup>Iodine labeled B21-2 Fab' and SFR8 Fab' showed that the concentration at which saturation of binding of B21-2 Fab' to A20 cells is reached is 21.5 nM. The SFR8 Fab' bound non-specifically to A20 cells, with the number of molecules bound per cell being less than 50,000 at 21.5 nM versus 530,000 for B21-2 Fab'.

##### 3. Coagulant Delivery and Tethering

To study the capability of bridging tTF to A20 cells through the B21-2/10H10 bispecific antibody as compared to the control bispecific antibodies, A20 cells were incubated

with bispecific antibody and a  $^{125}\text{I}$ -tTF concentration range as indicated. Saturation was attained at concentrations of bispecific antibody of 10 nM (1  $\mu\text{g}/\text{ml}$ ) or more, when an average of 310,000 molecules of tTF were bound to each A20 cell. The binding was specific since no tTF binding was mediated by either of the isotype-matched control bispecific antibodies, SFR8/10H10 or B21-2/OX7, which had only one of the two specificities needed for tethering tTF (FIG. 1).

#### 4. Coagulation

To investigate whether tTF bound to A20 cells through a bispecific antibody was able to induce coagulation, the inventors first incubated A20 cells with 21.5 nM bispecific antibody and 69 nM tTF. The resulting effect on the coagulation time is shown in Table VII. These first studies showed that A20 cells coated with a complex of B21-2/10H10 and tTF were capable of inducing fibrin formation: it shortened coagulation time from 140 sec (the time for mouse plasma in  $\text{CaCl}_2$  to coagulate in the absence of added antibodies or TF under the specific conditions used) to 60 sec. In contrast, the control bispecific antibodies did not induce activation of coagulation: in these cases coagulation time was 140 sec.

Later studies confirmed and extended the initial results. Mouse plasma added to A20 cells to which tTF had been tethered with B21-2/10H10 coagulated rapidly. Fibrin strands were visible 36 seconds after adding the plasma as compared with 164 seconds in plasma added to untreated A20 cells (Table VII). Only when tTF had been tethered to the cells was coagulation induced: no effect on coagulation time was seen with cells incubated with of tTF alone, homodimeric  $\text{F}(\text{ab})_2$ , Fab' fragments or bispecific antibodies having only one of the two specificities needed for tethering tTF.

A linear relationship existed between the logarithm of the average number of tTF molecules tethered to each A20 cell and the rapidity with which those cells induced coagulation of mouse plasma (FIG. 2). Cells bearing 300,000 molecules of tTF per cell induced coagulation in 40 secs but even with 20,000 molecules per cell coagulation was significantly faster (140 secs) than it was with untreated cells (190 secs).

TABLE VII

Coagulation of mouse plasma induced by tethering tTF to A20 cells with bispecific antibody.	
Reagents added <sup>1</sup>	Coagulation time <sup>2</sup> (sec)
None	164 $\pm$ 4
B21-2/10H10 + tTF	36 $\pm$ 2
B21-2/10H10	163 $\pm$ 2
tTF	163 $\pm$ 3
B21-2/OX7 + tTF	165 $\pm$ 4
SFR8/10H10 + tTF	154 $\pm$ 5
10H10 $\text{F}(\text{ab})_2$ + tTF	160 $\pm$ 3
10H10 Fab' + tTF	162 $\pm$ 2
B21-2 $\text{F}(\text{ab})_2$ + tTF	168 $\pm$ 4
B21-2 Fab' + tTF	165 $\pm$ 4

<sup>1</sup>Bispecific antibodies  $\text{F}(\text{ab})_2$  and Fab' fragments (0.33  $\mu\text{g}/10^5$  cells/100  $\mu\text{l}$ ) and tTF (0.17  $\mu\text{g}/10^5$  cells/100  $\mu\text{l}$ ) were incubated with A20 cells for 1 h at 4° C. in 0.2% w/v sodium azide. The cells were washed, warmed to 37° C., calcium and plasma were added and the time for the first fibrin strands to form was recorded.

<sup>2</sup>Arithmetic mean of triplicate determinations  $\pm$  standard deviation

#### EXAMPLE III

##### SPECIFIC TUMOR VASCULATURE SPECIFIC COAGULATION IN VIVO

The present example describes the specific coagulation of tumor vasculature in vivo that results following the admin-

istration of the bispecific antibody coagulant as a delivery vehicle for human tissue factor.

#### A. Materials and Methods

##### 1. Reagents

Mouse blood was obtained by heartpuncture and collected in 1/10 volume of 3.8% buffered citrate. The blood was centrifuged for 10 min at 3000 g and the plasma snap frozen in small aliquots and stored at -70° C.

##### 2. Animals

BALB/c nu/nu mice were obtained from Simonsen (Gilroy, Calif.) and maintained under SPF conditions.

##### 3. C1300 (Muy) Mouse Model and Treatment

The tumor model was as previously described (Burrows et al., 1992; Burrows & Thorpe, 1993) with three refinements. First, a different antibody, B21-2, was used. This antibody recognizes I-A<sup>d</sup> but not I-E<sup>d</sup>, unlike the previously used M5/114 antibody which recognizes both molecules. The B21-2 antibody has an approximately 10-fold better affinity than M5/114. Second, a subline of the previously used C1300(Muy)12 line was used which grew continuously in BALB/c nu/nu mice. The C1300(Muy) 12 cells used previously had to be mixed with untransfected C1300 cells in order to form continuously growing tumors. The new subline, designated C1300(Muy) t1P3, will be referred to hereafter as C1300(Muy). Third, it was unnecessary to add tetracycline to the mice's drinking water to prevent gut bacteria from inducing I-A<sup>d</sup> on the gastrointestinal epithelium. Unlike immunotoxins, coagulants do not damage I-A<sup>d</sup>-expressing intestinal epithelium.

For establishment of solid tumors,  $1.5 \times 10^7$  C1300 (Muy) cells were injected subcutaneously into the right anterior flank of BALB/c nu/nu mice. When the tumors had grown to 0.8 cm in diameter, mice were randomly assigned to different treatment groups each containing 7-8 mice.

Coagulants were prepared by mixing bispecific antibodies (140  $\mu\text{g}$ ) and tTF (110  $\mu\text{g}$ ) in a total volume of 2.5 ml of 0.9% NaCl and leaving them at 4° C. for one hour. Mice then received intravenous injections of 0.25 ml of this mixture (i.e. 14  $\mu\text{g}$  of bispecific antibody plus 11  $\mu\text{g}$  of tTF). Other mice received 14  $\mu\text{g}$  of bispecific antibodies or 11  $\mu\text{g}$  of tTF alone. The injections were performed slowly into one of the tail veins over approximately 45 sec and were followed with a second injection of 200  $\mu\text{l}$  of saline into the same vein. This injection procedure was adopted to prevent thrombosis of the tail vein which was seen if mice were rapidly injected (1-2 sec). Seven days later, the treatments were repeated.

Perpendicular tumor diameters were measured at regular intervals and tumor volumes were estimated according to the following equation:

$$\text{volume} = \text{smaller diameter}^2 \times \text{larger diameter} \times \pi / 6$$

Differences in tumor volume were tested for statistical significance using the Mann-Whitney-Wilcoxon nonparametric test for two independent samples (Gibbons, 1976).

For histopathological analyses, animals were anesthetized with metofane at various times after treatment and were exsanguinated by perfusion with heparinized saline. 500 IU of heparin were i.v. injected, the animal anesthetized with metofane and the systemic circulation perfused with PBS at a flow rate of 0.6 mls/min until the liver had been cleared of blood. The tumor and normal tissues were excised and formalin fixed (4% v/v). Paraffin sections of the tissues were cut and stained with the standard Martius Scarlet Blue (MSB) trichrome technique for detection of fibrin, and with hematoxylin and eosin stain for cell morphology.

## B. Results

### 1. Improved Tumor Model

To improve the C1300 (Muy) tumor model as described before (Burrows et al., 1992), the inventors subcloned the C1300 (Muy) cell line into a cell line that can grow without being mixed with its parental cell, C1300, but still express the I-A<sup>d</sup> MHC Class II antigen on the endothelial cells of the tumor. The inventors used an anti-I-A<sup>d</sup> antibody (B21-2) that has a 5–10 fold higher affinity for its antigen than the initial anti-I-A<sup>d</sup> antibody (M5/114.15.2) used in this model as determined by FACS. In vivo distribution studies with this new anti-I-A<sup>d</sup> antibody showed the same tissue distribution pattern as did M5/114.15.2. Intense staining with B21-2 was seen in tumor vascular endothelium, light to moderate staining in Kupffer cells in the liver, the marginal zones in the spleen and some areas in the small and large intestines. Vessels in other normal tissues were unstained.

### 2. Determination of Suitable In Vivo Doses

The maximum tolerated dose was 16  $\mu$ g B21-2/10H10 plus 11  $\mu$ g tTF injected intravenously into the tail vein of mice. At this dose, mice lost no weight and had normal appearance and activity levels. At a higher dose of 20  $\mu$ g B21-2/10H10 plus 16  $\mu$ g tTF, two of ten mice developed localized dermal hemorrhages which eventually resolved. The lower dose was adopted for in vivo studies. Truncated tTF itself was not toxic at 50  $\mu$ g, given intravenously.

### 3. Specific Coagulation and Infarction in Tumor Vasculature

Intravenous administration of a coaguligand composed of B21-2/10H10 (20  $\mu$ g) and tTF (16  $\mu$ g) to mice bearing solid C1300 (Muy) tumors caused tumors to assume a blackened, bruised appearance within 30 minutes. A histological study of the time course of events within the tumor revealed that 30 minutes after injection of coaguligand all vessels in all regions of the tumor were thrombosed (FIG. 3B). Vessels contained platelet aggregates, packed red cells and fibrin. At this time, tumor-cells were healthy, being indistinguishable morphologically from tumor cells in untreated mice (FIG. 3A).

By 4 hours, signs of tumor cell distress were evident. The majority of tumor cells had begun to separate from one another and had developed pyknotic nuclei (FIG. 3C). Erythrocytes were commonly observed in the tumor interstitium. By 24 hours, advanced tumor necrosis was visible throughout the tumor (FIG. 3D). By 72 hours, the entire central region of the tumor had compacted into morphologically indistinct debris.

In one of three of the tumors examined, a viable rim of tumor cells 5–10 cell layers thick was visible on the outskirts of the tumor where it was infiltrating into surrounding normal tissues. Immunohistochemical examination of serial sections of the same tumor revealed that the vessels in the regions of tumor infiltration lacked class II antigens.

Tumors from control mice which had received B21-2/10H10 bispecific antibody (20  $\mu$ g) alone 30 minutes or 24 hours earlier showed no signs of infarction. Tumors from mice which received tTF (16  $\mu$ g), alone or in combination with B21-2/OX7 or SFR8/10H10, showed no signs of infarction 30 min after injection but 24 hours after injection, occasional vessels (about 20% of vessels overall) in the tumor were infarcted. These appeared to be most prevalent in the core of the tumor.

No thrombi or morphological abnormalities were visible in paraffin sections of liver, kidney, lung, intestine, heart, brain, adrenals, pancreas and spleen taken from tumor-bearing mice 30 minutes, 4 hours and 24 hours after administration of coaguligand or tTF.

### 4. Tumor Regressions of Solid Tumors

FIG. 4 shows the results of a representative anti-tumor study in which a coaguligand composed of B21-2/10H10 and tTF was administered to mice with 0.8 cm diameter tumors. The tumors regressed to approximately half their pretreatment size. Repeating the treatment on the 7th day caused the tumors to regress further, usually completely. In 5/7 animals, complete regressions were obtained. Two of the mice subsequently relapsed four and six months later. These anti-tumor effects are statistically highly significant ( $P < 0.001$ ) when compared with all other groups.

Tumors in mice treated with tTF alone or with tTF mixed with the isotype-matched control bispecific antibodies, SFR8/10H10 or B21-2/OX7, grew more slowly than those in groups receiving antibodies or diluent alone. These differences were statistically significant ( $P < 0.05$ ) on days 12–14. Thus, part of the anti-tumor effects seen with the B21-2/10H10 coaguligand are attributable to a slight non-specific action of tTF itself.

At the end of the study, two mice which had been treated with diluent alone and which had very large tumors of 2.0 cm<sup>3</sup> and 2.7 cm<sup>3</sup> (i.e. 10–15% of their body weight) were given coaguligand therapy. Both had complete remissions although their tumors later regrew at the original site of tumor growth.

### C. Discussion

The present studies show that soluble human tTF, possessing practically no ability to induce coagulation, became a powerful thrombogen for tumor vasculature when targeted by means of a bispecific antibody to tumor endothelial cells. In vitro coagulation studies showed that the restoration of thrombotic activity of tTF is mediated through its cross-linking to antigens on the cell surface.

tTF binds factors VII and VIIa with high affinity and enhances the catalytic activity of VIIa but does not induce coagulation of plasma because the tTF:VIIa complex has to be associated with a membrane surface for efficient activation of factors IX and X (Ruf et al., 1991; Krishnaswamy et al., 1992). Tethering of tTF:VIIa to the cell surface by means of a bispecific antibody restores its ability to induce coagulation by bringing the tTF:VIIa into close proximity to the membrane: the membrane phospholipid provides the surface on which the coagulation-initiation complexes with factors IX or X can assemble and efficiently produce intermediates in the clotting process.

Administration of a coaguligand directed against class II to mice having tumors with class II-expressing vasculature caused rapid thrombosis of blood vessels throughout the tumor. This was followed by infarction of the tumor and complete tumor regressions in a majority of animals. In those animals where complete regressions were not obtained, the tumors grew back from a surviving rim of tumor cells on the periphery of the tumor where it had infiltrated into the surrounding normal tissues. The vessels at the growing edge of the tumor lacked class II antigens, thus explaining the lack of thrombosis of these vessels by the coaguligand. It is likely that these surviving cells would have been killed by coadministering a drug acting on the tumor cells themselves, as was found previously (Burrows & Thorpe, 1993).

The anti-tumor effects of the coaguligand were similar in magnitude to those obtained in the same tumor model with an immunotoxin composed of anti-class II antibody and deglycosylated ricin A-chain (Burrows & Thorpe, 1993). One difference between the two agents is their rapidity of action. The coaguligand induced thrombosis of tumor vessels in less than 30 minutes whereas the immunotoxin took 6 hours to achieve the same effect. The immunotoxin acts

more slowly because thrombosis is secondary to endothelial cell damage caused by the shutting down of protein syntheses.

A second and important difference between the immunotoxin and the coaguligand is that they have different toxic side effects. The immunotoxin caused a lethal destruction of class II-expressing gastrointestinal epithelium unless antibiotics were given to suppress class II induction by intestinal bacteria. The coaguligand caused no gastrointestinal damage, as expected because of the absence of clotting factors outside of the blood, but caused coagulopathies in occasional mice when administered at high dosage.

The findings described in this report demonstrate the therapeutic potential of targeting human coagulation-inducing proteins to tumor vasculature. For clinical application, antibodies or other ligands are needed that bind to molecules that are present on the surface of vascular endothelial cells in solid tumors but absent from endothelial cells in normal tissues. Tumor endothelial markers could be induced directly by tumor-derived angiogenesis factors (Folkman, 1985) or cytokines (Burrows et al., 1991; Ruco et al., 1990), or could relate to the rapid proliferation (Denekamp & Hobson, 1982) and migration (Folkman, 1985) of endothelial cells during neovascularization.

Several candidate antibodies have been described. The antibody TEC-11, against endoglin is a particular example that binds selectively to human tumor endothelial cells.

Other antibodies include FB5, against endosialin (Rettig et al., 1992), E-9, against an endoglin-like molecule (Wang et al., 1993), BC-1, against a fibronectin isoform (Carnemolla et al., 1989) and TP-1 and TP-3, against an osteosarcoma-related antigen (Bruland et al., 1988). CD34 has been reported to be upregulated on migrating endothelial cells and on the abluminal processes of budding capillaries in tumors and fetal tissues (Schlingemann et al., 1990). The receptors for vascular endothelial cell growth factor (VEGF) become upregulated in tumor blood vessels (Plate et al., 1993; Brown et al., 1993) probably in response to hypoxia (Thieme et al., 1995), and selectively concentrate VEGF in tumor vessels (Dvorak et al., 1991).

The induction of tumor infarction by targeting coagulation-inducing proteins to these and other tumor endothelial cell markers is proposed as a valuable new approach to the treatment of solid tumors. The coupling of human (or humanized) antibodies to human coagulation proteins to produce wholly human coaguligands is particularly contemplated, thus permitting repeated courses of treatment to be given to combat both the primary tumor and its metastases.

#### EXAMPLE IV

##### SYNTHESIS OF TRUNCATED TISSUE FACTOR (tTF) CONSTRUCTS

tTF is herein designated as the extracellular domain of the mature tissue factor protein (amino acid 1-219 of the mature protein; SEQ ID NO:23). SEQ ID NO:23 is encoded by, e.g., SEQ ID NO:22.

##### A. H<sub>6</sub>[tTF]

H<sub>6</sub> Ala Met Ala[tTF]. The tTF complimentary DNA (cDNA) was prepared as follows: RNA from J-82 cells (human bladder carcinoma) was used for the cloning of tTF. Total RNA was isolated using the GlassMax™ RNA microisolation reagent (Gibco BRL). The RNA was reverse transcribed to cDNA using the GeneAmp RNA PCR kit (Perkin Elmer). tTF cDNA was amplified using the same kit with the following two primers:

5' primer: 5'  
GTC ATG CCA TGG CCT CAG GCA CTA CAA

(SEQ ID NO:1)

3' Primer: 5'  
TGA CAA GCT TAT TCT CTG AAT TCC CCC TTT CT

(SEQ ID NO:2)

The underlined sequences codes for the N-terminus of tTF. The rest of the sequence in the 5' primer is the restriction site for NcoI allowing the cloning of tTF into the expression vector. The sequence in the 3' primer is the HindIII site for cloning tTF into the expression vector. PCR amplification was performed as suggested by the manufacturer. Briefly, 75 μM dNTP; 0.6 μM primer, 1.5 mM MgCl<sub>2</sub> were used and 30 cycles of 30" at 95° C., 30" at 55° C. and 30" at 72° C. were performed.

The *E. coli* expression vector H<sub>6</sub> pQE-60 was used for expressing tTF (Lee et al., 1994). The PCR amplified tTF cDNA was inserted between the NcoI and Hind3 site. H<sub>6</sub> pQE-60 has a built-in (His)<sub>6</sub> encoding sequence such that the expressed protein has the sequence of (His)<sub>6</sub> at the N terminus, which can be purified on a Ni—NTA column.

To purify tTF, tTF containing H<sub>6</sub> pQE-60 DNA was transformed to *E. coli* TG-1 cells. The cells were grown to OD<sub>600</sub>=0.5 and IPTG was added to 30 μM to induce the tTF production. The cells were harvested after shaking for 18 h at 30° C. The cell pellet was denatured in 6M Gu-HCl and the lysate was loaded onto a Ni—NTA column (Qiagen). The bound tTF was washed with 6M urea and tTF was refolded with a gradient of 6M—1M urea at room temperature for 16 h. The column was washed with wash buffer (0.05 Na H<sub>2</sub> PO<sub>4</sub>, 0.3M NaCl, 10% glycerol) and tTF was eluted with 0.2M Imidazole in wash buffer. The eluted tTF was concentrated and loaded onto a G-75 column. tTF monomers were collected.

##### B. tTF

Gly[tTF]. The GlytTF complimentary DNA (cDNA) was prepared the same way as described in the previous section except the 5' primer was replaced by the following primer in the PCR.

5' primer: 5'  
GTC ATG CCA TGG CCC TGG TGC CTC GTG CTT CTG  
GCA CTA CAA ATA CT (SEQ ID NO:3)

The underlined sequence codes for the N-terminus of tTF. The remaining sequence encodes a restriction site for NcoI and a cleavage site for thrombin.

The H<sub>6</sub> pQE60 expression vector and the procedure for protein purification is identical to that described above except that the final protein product was treated with thrombin to remove the H<sub>6</sub> peptide. This was done by adding 1 part of thrombin (Sigma) to 500 parts of tTF (w/w), and the cleavage was carried out at room temperature for 18 h. Thrombin was removed from tTF by passage of the mixture through a Benzamidine Sepharose 6B thrombin affinity column (Pharmacia).

##### C. Cysteine-modified tTFS

tTF constructs were modified with an N or C-terminal cysteine to allow for easier conjugation to derivatized antibody through a disulfide bond.

H<sub>6</sub> C[tTF]. (His)<sub>6</sub> Ala Met Ala Cys-[tTF]. The DNA was made as described in the previous section except that the 5' primer was replaced by the following primer in the PCR.

5' primer: 5'  
GTC ATG CCA TGG CCT GCT CAG GCA CTA CAA ATA  
CTG TG (SEQ ID NO:4)

All of the procedures were the same as described above, except the N-terminal cys was protected with an exchangeable oxidizing/reducing reagent.

C[tTF]. Gly Ser Cys [tTF2-219]. The DNA was made as described in the previous section except that the 5' primer was replaced by the following primer in the PCR.

5' primer: 5'  
GTC ATG CCA TGG CCC TGG TGC CTC GTG GTT CTT  
GCG GCA CTA CAA ATA CT (SEQ ID NO:5)

The vector construct and protein purification is the same as described for the (His)<sub>6</sub> Ala Met Ala Cys [tTF] construct, except that thrombin treatment was used to remove the (His)<sub>6</sub> as described above.

H<sub>6</sub> [tTF]C. (His)<sub>6</sub> Ala Met Ala [tTF] Cys. The DNA was made the same way as described in the (His)<sub>6</sub> AMA [tTF] sections, except that the 3' primer was replaced by the following primer.

3' primer: 5'  
TGA CAA GCT TAG CAT TCT CTG AAT TCC CCC TTT CT  
(SEQ ID NO:6)

The underlined sequence encodes the C-terminus of tTF. The rest of the sequence contains the HindIII restriction site for cloning tTF in to the expression vector.

All of the procedures are the same as described in the tTF section except that 10 mM  $\mu$ -ME was used in the 6M Gu-HCl denaturing solution and the C-terminal cysteine was protected with an exchangeable oxidizing/reducing reagent.

Other [tTF] Cys monomers, such as [tTF 1-220] Cys, [tTF 1-221] Cys and [tTF 1-222] Cys are also made (and conjugated) using the same methodology.

D. C Linker [tTF]  
The C Linker [tTF], Gly-Ser-Cys-(Gly)<sub>4</sub>-Ser-(Gly)<sub>4</sub>-Ser-(Gly)<sub>4</sub>-Ser-[tTF], was also constructed. The cDNA was made using a two step PCR procedure as follows:

PCR 1: amplification of linker DNA  
cDNA encoding the NcoI site, the thrombin cleavage site, cysteine, linker and the N-terminus of tTF was amplified using the following primers:

5' primer: 5'  
GTC ATG CCA TGG CCC TGG TGC CTC GTG GTT GCG  
GA GGC GGT GGA TCA GGC (SEQ ID NO:7)  
3' primer: 5'  
AGT ATT TGT AGT GCC TGA GGA TCC GCC ACC TCC  
ACT (SEQ ID NO:8)

The underlined sequences encode the linker peptide. The DNA template used in the PCR was double strand DNA encoding the following linker.

Sequence:  
GGA GGC GGT GGA TCA GGC GGT GGA GGT AGT GGA GGT  
5 GGC GGA TCC (SEQ ID NO:9)

The same PCR conditions were used as described in the tTF section. The 95 b.p. amplified product was linked to tTF DNA in the PCR2.

PCR 2: Linking the Cys-linker DNA to tTF DNA. DNA templates used in the PCR were two overlapping DNA: The 95 b.p. DNA from PCR 1 as described above and tTF DNA. The primers used were the following:

5' primer: 5'  
GTC ATG CCA TGG CCC TG (SEQ ID NO:10)

3' primer: 5'  
TGA CAA GCT TAT TCT CTG AAT TCC CCC TTT CT  
(SEQ ID NO:11)

The final PCR product of 740 b.p. was digested with NcoI and HindIII and inserted into the H<sub>6</sub> pQE 60 as described in the tTF section.

The vector constructs and protein purification procedures are all the same as described in the C[tTF] section.

## EXAMPLE V

### SYNTHESIS OF DIMERIC TISSUE FACTOR

The inventors' reasoned that tissue factor dimers may be more potent than monomers at initiating coagulation. It is possible that native tissue factor on the surface of J82 bladder carcinoma cells may exist as a dimer (Fair et al., 1987). The binding of one factor VII or VIIa molecule to one tissue factor molecule may also facilitate the binding of another factor VII or VIIa to another tissue factor (Fair et al., 1987; Bach et al., 1986). Furthermore, tissue factor shows structural homology to members of the cytokine receptor family (Edgington et al., 1991) some of which dimerize to form active receptors (Davies and Wlodawer, 1995). The inventors therefore synthesized TF dimers, as follows.

#### A. [tTF] Linker [tTF].

The Gly [tTF] Linker [tTF] with the structure Gly[tTF] (Gly)<sub>4</sub> Ser (Gly)<sub>4</sub> Ser (Gly)<sub>4</sub> Ser [tTF] was made. Two pieces of DNA were PCR amplified separately and were ligated and inserted into the vector as follows:

PCR 1: Preparation of tTF and the 5' half of the linker DNA. The primer sequences in the PCR are as follows:

5' primer: 5' GTC ATG CCA TGG CCC TGG TGC CTC GTG GTT  
CTT GCG GCA CTA CAA ATA CT (SEQ ID NO:12)  
3' primer: 5' CGC GGA TCC ACC GCC ACC AGA TCC ACC GCC  
TCC TTC TCT GAA TTC CCC TTT CT (SEQ ID NO:13)

Gly[tTF] DNA was used as the DNA template. Further PCR conditions were as described in the tTF section.

PCR 2: Preparation of the 3' half of the linker DNA and tTF DNA. The primer sequences in the PCR were as follows:



5' primer: 5' CGC GGA TCC GGC GGT GGA GGC TCT TCA GGC  
ACT ACA AAT ACT GT (SEQ ID NO:14)  
3' primer: 5' TGA CAA GCT TAT TCT CTG AAT TCC CCT TTC T  
(SEQ ID NO:15)

tTF DNA was used as the template in the PCR. The product from PCR 1 was digested with NcoI and BamH. The product from PCR 2 was digested with HindIII and BamH1. The digested PCR1 and PCR2 DNA were ligated with NcoI and HindIII-digested H<sub>6</sub> pQE 60 DNA.

For the vector constructs and protein purification, the procedures were the same as described in the Gly [tTF] section.

#### B. Cys [tTF] Linker [tTF]

The Cys [tTF] Linker [tTF] with the structure Ser Gly Cys [tTF 2-219] (Gly)<sub>4</sub> Ser (Gly)<sub>4</sub> Ser (Gly)<sub>4</sub> Ser [tTF] was also constructed. DNA was made by PCR using the following primers were used:

5' primer: 5' GTC ATG CCA TGG CCC TGG TGC CTC GTG GTT  
CTT GCG GCA CTA CAA ATA CT (SEQ ID NO:16)  
3' primer: 5' TGA CAA GCT TAT TCT CTG AAT TCC CCT TTC T  
(SEQ ID NO:17)

[tTF] linker [tTF] DNA was used as the template. The remaining PCR conditions were the same as described in the tTF section. The vector constructs and protein purification were all as described in the purification of H<sub>6</sub>C[tTF].

#### C. [tTF] Linker [tTF]cys

The [tTF] Linker [tTF]cys dimer with the protein structure [tTF] (Gly)<sub>4</sub> Ser (Gly)<sub>4</sub> Ser (Gly)<sub>4</sub> Ser [tTF] Cys was also made. The DNA was made by PCR using the following primers:

5' primer: 5' GTC ATG CCA TGG CCC TGG TGC CTC GTG GTT  
GCA CTA CAA ATA CT (SEQ ID NO:18)  
3' primer: 5' TGA CAA GCT TAG CAT TCT CTG AAT TCC CCT  
TTC T (SEQ ID NO:19)

[tTF] linker [tTF] DNA was used as the template. The remaining PCR conditions were the same as described in the tTF section. The vector constructs and protein purification were again performed as described in the purification of [tTF]cys section.

#### D. Chemically Conjugated Dimers

[tTF] Cys monomer are conjugated chemically to form [tTF] Cys-Cys [tTF] dimers. This is done by adding an equal molar amount of DTT to the protected [tTF] Cys at room temperature for 1 hr to deprotect and expose the cysteine at the C-terminus of [tTF] Cys. An equal molar amount of protected [tTF] Cys is added to the DTT/[tTF] Cys mixture and the incubation is continued for 18 h at room temperature. The dimers are purified on a G-75 gel filtration column.

The Cys [tTF] monomer is conjugated chemically to form dimers using the same method.

### EXAMPLE VI

#### SYNTHESIS OF TISSUE FACTOR MUTANTS

Two tTF mutants are described that lack the capacity to convert tTF-bound factor VII to factor VIIa. There is 300-fold less factor VIIa in the plasma compared with factor VII (Morrissey et al., 1993). Therefore, circulating mutant tTF should be less able to initiate coagulation and hence exhibit very low toxicity. In coaguligands, once the mutant tTF has

localized through the attached antibody to the tumor site, Factor VIIa will be injected to exchange with the tTF-bound Factor VII. The mutants are active in the presence of factor VIIa.

#### 5 A. [tTF]G164A

The "[tTF]G164A" has the mutant protein structure with the amino acid 164 (Gly) of tTF being replaced by Ala. The Chameleon double-stranded site directed mutagenesis kit (Stratagene) is used for generating the mutant. The DNA template is Gly[tTF] DNA and the sequence of the mutagenizing primer is:

5' CAA GTT CAG CCA AGA AAAC (SEQ ID NO:20)

15 The vector constructs and protein purification procedures described above are used in the purification of Gly[tTF].

#### B. [tTF] W158R S162A

The [tTF]W158R S162A is a double mutant in which amino acid 158 (Trp) of tTF is replaced by Arg and amino acid 162 (Ser) is replaced by Ala. The same mutagenizing method is used as described for [tTF] G164A. The mutagenizing primer is:

25 5' ACA CTT TAT TAT CGG AAA TCT TCA GCT TCA GGA AAG  
(SEQ ID NO:21)

The foregoing vector constructs and protein purification procedures are used for purifying Gly[tTF].

### EXAMPLE VII

#### SYNTHESIS OF TISSUE FACTOR CONJUGATES

##### A. Chemical Derivatization and Antibody Conjugation

35 Antibody tTF conjugates were synthesized by the linkage of chemically derivatized antibody to chemically derivatized tTF via a disulfide bond (as exemplified in FIG. 5).

Antibody was reacted with a 5-fold molar excess of succinimidyl oxycarbonyl- $\alpha$ -methyl  $\alpha$ -(2-pyridyldithio) toluene (SMPT) for 1 hour at room temperature to yield a derivatized antibody with an average of 2 pyridyldisulphide groups per antibody molecule. Derivatized antibody was purified by gel permeation chromatography.

A 2.5-fold molar excess of tTF over antibody was reacted with a 45-fold molar excess of 2-iminothiolane (2IT) for 1 hour at room temperature to yield tTF with an average of 1.5 sulphhydryl groups per tTF molecule. Derivatized tTF was also purified by gel permeation chromatography and immediately mixed with the derivatized antibody.

50 The mixture was left to react for 72 hours at room temperature and then applied to a Sephacryl S-300 column to separate the antibody-tTF conjugate from free tTF and released pyridine-2-thione. The conjugate was separated from free antibody by affinity chromatography on a anti-tTF column. The predominant molecular species of the final conjugate product was the singly substituted antibody-tTF conjugate (Mr approx. 176,000) with lesser amounts of multiply substituted conjugates (Mr  $\geq$  approx. 202,000) as assessed by SDS-PAGE.

##### 60 B. Conjugation of Cysteine-Modified tTF to Derivatized Antibody

Antibody-C[tTF] and [tTF]C conjugates were synthesized by direct coupling of cysteine-modified tTF to chemically derivatized antibody via a disulfide bond (as exemplified in FIG. 5).

Antibody was reacted with a 12-fold molar excess of 2IT for 1 hour at room temperature to yield derivatized antibody



with an average of 1.5 sulfhydryl groups per antibody molecule. Derivatized antibody was purified by gel permeation chromatography and immediately mixed with a 2-fold molar excess of cysteine-modified tTF. The mixture was left to react for 24 hours at room temperature and then the conjugate was purified by gel permeation and affinity chromatography as described above.

The predominant molecular species of the final conjugate was the singly substituted conjugate ( $M_r$  approx. 176,000) with lesser amounts of multiple substituted conjugates ( $M_r \geq$  approx. 202,000) as assessed by SDS-PAGE.

#### C. Conjugation of Cysteine-Modified tTF to Fab' Fragments

Antibody Fab'-C[tTF] and [tTF]C conjugates are prepared. Such conjugates may be more potent *in vivo* because they should remain on the cell surface for longer than bivalent conjugates due to their limited internalization capacity. Fab' fragments are mixed with a 2-fold molar excess of cysteine-modified tTF for 24 hours and then the conjugate purified by gel permeation and affinity chromatography as described above.

#### D. Clotting Activity of tTF Conjugates

tTF conjugates were prepared with the B21-2 monoclonal antibody which binds to Class II antigens expressed on the surface to A20 cells. The conjugates were prepared with chemically derivatized tTF and cysteine-modified tTF and the ability of the conjugates to clot mouse plasma in  $\text{CaCl}_2$  was determined after their binding to the surface of A20 cells.

Both B21-2 conjugates shortened the clotting time of mouse plasma in  $\text{CaCl}_2$  (control) in a dose-dependent manner. The tTF conjugates displayed a similar enhancement in coagulation as occurred when tTF was tethered to the surface of A20 cells with the bispecific antibody B21-2/10H10 (FIG. 6).

#### E. Anti-tumor Cell tTF Conjugates

It has already been established that when tTF is targeted to tumor vascular endothelial cells it induces coagulation within the tumor vessels (Examples I through III). The inventors' contemplated that coagulation would be induced in tumor vessels if tTF was targeted to the surface of tumor cells.

Three anti-tumor cell antibodies, KS1/4, D612, and XMMCO-791, were conjugated to tTF as described in the "Preparation of tTF conjugates" section above. KS1/4 was obtained from Dr. R. Reisfeld at the Scripps Research Institute, Department of Immunology, La Jolla, Calif., and is also described in U.S. Pat. No. 4,975,369; D612 was obtained from Dr. J. Schlom at the NCI, Laboratory of Tumor Immunology and Biology, Bethesda, Md., is described in U.S. Pat. No. 5,183,756 and can be obtained from culture supernatants from the ATCC hybridoma cell line Accession No. HB 9796; XMMCO-791 was purified from tissue culture supernatant from the hybridoma cell line purchased from the ATCC.

The human colon carcinoma cell line Widr was used as a target cell for KS1/4. Widr cells were purchased from the ATCC and were maintained in DMEM supplemented with 10% (v/v) fetal calf serum, L-glutamine and antibiotics in an atmosphere of 10% (v/v)  $\text{CO}_2$  in air. The human colon carcinoma cell line LS147T was used as a target cell for D612. LS147T cells were purchased from the ATCC and were maintained in RPMI supplemented with 10% (v/v) fetal calf serum, L-glutamine and antibiotics in an atmosphere of 5% (v/v)  $\text{CO}_2$  in air. The human non small cell lung cancer cell line H460 was used as a target cell for XMMCO-791. H460 cells were obtained from Dr. Adi Gazdar, Simmons Cancer Center, University of Texas South-

western Medical Center, Dallas, Tex. and were maintained in DMEM supplemented with 10% (v/v) fetal calf serum, L-glutamine and antibiotics in an atmosphere of 10% (v/v)  $\text{CO}_2$  in air. All three cell lines grew as adherent monolayers.

The conjugates were tested for their ability to enhance the clotting time of mouse plasma in  $\text{CaCl}_2$  when bound to tumor cells expressing the relevant target antigens. Tumor cells were removed from tissue culture flasks with 0.05% (w/v) EDTA in PBS. The cells were preincubated with TF9-6B4 and TF8-5G9 antibodies to neutralize any native tissue factor activity (Morrissey et. al., 1988) and then the coagulation assay was performed as described for A20 cells.

When bound to their target cell line, all three conjugates shortened the clotting time of mouse plasma in  $\text{CaCl}_2$  (control) in a dose-dependent manner (FIG. 7), indicating that coagulation was accelerated at the surface of tumor cells when tTF was targeted to the cell surface.

### EXAMPLE VIII

#### SYNTHESIS OF TISSUE FACTOR PRODRUGS

Exemplary tTF prodrugs have the following structures: tTF<sub>1-219</sub>(X)<sub>n2</sub>(Y)<sub>n2</sub>Z Ligand, where tTF<sub>1-219</sub> represents TF minus the cytosolic and transmembrane domains; X represents a hydrophobic transmembrane domain n1 amino acids (AA) in length (1-20 AA); Y represents a hydrophilic protease recognition sequence of n2 AA in length (sufficient AA to ensure appropriate protease recognition); Z represents a disulfide thioester or other linking group such as (Cys)<sub>1-2</sub>; Ligand represents an antibody or other targeting moiety recognizing tumor-cells, tumor EC, connective tissue (stroma) or basal lamina markers

The tTF prodrug is contemplated for injection intravenously allowing it to localize to diseased tissue (i.e. tumor). Once localized in the diseased tissue, endogenous proteases (i.e., metalloproteinases, thrombin, factor Xa, factor VIIa, factor IXa, plasmin) will cleave the hydrophilic protease recognition sequence from the prodrug which will allow the hydrophobic transmembrane sequence to insert into a local cell membrane. Once the tail has inserted into the membrane, the tTF will regain its coagulation-inducing properties resulting in clot formation in the vasculature of the diseased tissue.

### EXAMPLE IX

#### SYNTHESIS OF COAGULATION FACTORS LACKING THE Gla MODIFICATION

The vitamin-K-dependent coagulation factors (Factor II/IIa, Factor VII/VIIa, Factor IX/IXa and Factor X/Xa) lacking the Gla ( $\gamma$ -carboxyglutamic acid) modification are contemplated to be useful for the formation of coaguligands. Coagulation factors lacking the Gla modification are poor coagulants because the unmodified factors associate inefficiently with lipid membranes: targeting the factor via a ligand to the vasculature of tumors or other sites should bring the factor back into proximity to the cell surface and enable coagulation to proceed in that site.

"Gla" is made post-translationally by modifying the existing Glu (Glutamic acid) residues. Vitamin-K-dependent coagulation factors (Factor II/IIa, Factor VII/VIIa, Factor IX/IXa and Factor X/Xa) lacking the Gla modification may be made by expressing the genes that encode them in a host, such as bacteria, that does not modify Glu to Gla. The DNA sequences encoding each of Factor II/IIa, Factor VII/VIIa, Factor IX/IXa and Factor X/Xa are included herein as SEQ

ID NO:24, SEQ ID NO:25, SEQ ID NO:26 and SEQ ID NO:27, respectively. Prokaryotic expression is therefore straightforward.

Such Gla-lacking factors may also be made by mutating any of the sequences described above (SEQ ID NO:24, SEQ ID NO:25, SEQ ID NO:26 and SEQ ID NO:27) to change the corresponding Glu residues to another amino acid before expressing the genes, this time in virtually any host cell. The codon to be changed is the GAG codon (GAA also encodes Glu and is to be avoided). Using Factor VII as an example, the Gla "domain" is located generally in the 216-325 region. The first Gla-encoding triplet occurs at 231 of SEQ ID NO:25, and the last extends through 318 of SEQ ID NO:25. The GAG codons may readily be changed using molecular biological techniques.

FIG. 8 shows that the Gla domains of each of the above vitamin-K-dependent coagulation factors lie in an analogous region. Therefore, mutation of the so-called "corresponding" Glu residues in any one of SEQ ID NO:24, SEQ ID NO:26 and SEQ ID NO:27 will also be straightforward.

The following Table of codons is provided to enable ready mutation choices to be made in modifying a given Gla-encoding codon or sequence.

Amino Acids		Codons					
Alanine	Ala	A	GCA	GCC	GCG	GCU	
Cysteine	Cys	C	UGC	UGU			
Aspartic acid	Asp	D	GAC	GAU			
Glutamic acid	Glu	E	GAA	GAG			
Phenylalanine	Phe	F	UUC	UUU			
Glycine	Gly	G	GGA	GGC	GGG	GGU	
Histidine	His	H	CAC	CAU			
Isoleucine	Ile	I	AUA	AUC	AUU		
Lysine	Lys	K	AAA	AAG			
Leucine	Leu	L	UUA	UUG	CUA	CUC	CUG CUU
Methionine	Met	M	AUG				
Asparagine	Asn	N	AAC	AAU			
Proline	Pro	P	CCA	CCC	CCG	CCU	
Glutamine	Gln	Q	CAA	CAG			
Arginine	Arg	R	AGA	AGG	CGA	CGC	CGG CGU
Serine	Ser	S	AGC	AGU	UCA	UCC	UCG UCU
Threonine	Thr	T	ACA	ACC	ACG	ACU	
Valine	Val	V	GUA	GUC	GUG	GUU	
Tryptophan	Trp	W	UGG				
Tyrosine	Tyr	Y	UAC	UAU			

Site-specific mutagenesis is the technique contemplated for use in the preparation of individual vitamin-K-dependent coagulation factors lacking the Gla modification, through specific mutagenesis of the underlying DNA and the introduction of one or more nucleotide sequence changes into the DNA.

Site-specific mutagenesis allows the production of mutants through the use of specific oligonucleotide sequences which encode the DNA sequence of the desired mutation, as well as a sufficient number of adjacent nucleotides, to provide a primer sequence of sufficient size and sequence complexity to form a stable duplex on both sides of the deletion junction being traversed. Typically, a primer of about 17 to 25 nucleotides in length is preferred, with about 5 to 10 residues on both sides of the junction of the sequence being altered.

In general, the technique of site-specific mutagenesis is well known in the art, as exemplified by publications such as Adelman et al. (1983) and by the TF mutant studies described above. The technique typically employs a phage vector which exists in both a single stranded and double stranded form. Typical vectors useful in site-directed mutagenesis include vectors such as the M13 phage (Messing et al., 1981). These phage are readily commercially available and their use is generally well known to

those skilled in the art. Double stranded plasmids are also routinely employed in site directed mutagenesis which eliminates the step of transferring the gene of interest from a plasmid to a phage.

In general, site-directed mutagenesis in accordance herewith is performed by first obtaining a single-stranded vector or melting apart the two strands of a double stranded vector which includes within its sequence a DNA sequence which encodes the vitamin-K-dependent coagulation factor. An oligonucleotide primer bearing the desired mutated sequence is prepared, generally synthetically, for example by the method of Crea et al. (1978). This primer is then annealed with the single-stranded vector, and subjected to DNA polymerizing enzymes such as *E. coli* polymerase I Klenow fragment, in order to complete the synthesis of the mutation-bearing strand. Thus, a heteroduplex is formed wherein one strand encodes the original non-mutated sequence and the second strand bears the desired mutation. This heteroduplex vector is then used to transform appropriate cells, such as *E. coli* cells, and clones are selected which include recombinant vectors bearing the mutated sequence arrangement.

## EXAMPLE X

### FURTHER ANTI-TUMOR VASCULATURE ANTIBODIES

This example describes the generation of antibodies directed against tumor-derived endothelial cell "binding factors" for use in distinguishing between tumor vasculature and the vasculature of normal tissues. Particularly described is the generation of antibodies directed against vascular permeability factor (VPF), also termed vascular endothelial cell growth factor (VEGF), and against bFGF (basic fibroblast growth factor).

For further details concerning FGF one may refer to Gomez-Pinilla and Cotman (1992); Nishikawa et al. (1992), that describe the localization of basic fibroblast growth factor; Xu et al. (1992), that relates to the expression and immunochemical analysis of FGF; Reilly et al. (1989), that concerns monoclonal antibodies; Dixon et al. (1989), that relates to FGF detection and characterization; Matsuzaki et al. (1989), that concerns monoclonal antibodies against heparin-binding growth factor; and Herblin and Gross (1992), that discuss the binding sites for bFGF on solid tumors associated with the vasculature.

In the present studies, rabbits were hyperimmunized with N-terminal peptides of human VEGF, mouse VEGF, guinea pig VEGF, human bFGF, mouse bFGF or guinea pig bFGF coupled to tuberculin (purified protein derivative, PPD) or thyroglobulin carriers. The peptides were 25 to 26 amino acids in length and were synthesized on a peptide synthesizer with cysteine as the C-terminal residue. Antisera were affinity purified on columns of the peptides coupled to Sepharose matrices.

Antibodies to VEGF were identified by ELISA and by their staining patterns on frozen sections of guinea pig tumors and normal tissues. Polyclonal antibodies to guinea pig VEGF and human VEGF reacted with the majority of vascular endothelial cells on frozen sections of guinea pig L10 tumors and a variety of human tumors (parotid, ovarian, mammary carcinomas) respectively. The anti-human VEGF antibody stained mesangial cells surrounding the endothelial cells in normal human kidney glomerulae and endothelial cells in the liver, but did not stain blood vessels in normal human stomach, leg muscle and spleen. The anti-guinea pig VEGF antibody did not stain endothelial cells in any normal tissues, including kidney, brain, spleen, heart, seminal vesicle, lung, large intestine, thymus, prostate, liver, testicle and skeletal muscle.

Polyclonal antibodies to human FGF stained endothelial cells in parotid and ovarian carcinomas, but not those in mammary carcinomas. Anti-human FGF antibodies stained glomerular endothelial cells in human kidney, but not endothelial cells in normal stomach, leg muscle and spleen.

Monoclonal antibodies to guinea pig VEGF, human VEGF and guinea pig bFGF were prepared by immunizing BALB/c mice with the N-terminal sequence peptides (with cysteine at the C-terminus of the peptide) coupled to PPD or to thyroglobulin. The synthetic peptides immunogens of defined sequence are shown below and are represented by SEQ ID NO:30, SEQ ID NO:31 AND SEQ ID NO:32, respectively:

guinea pig VEGF	APMAEGEQKPREVVVKFMDVYKRSYC
human VEGF	APMAEGGGQNHHEVVVKFMDVYQRSYC
guinea pig bFGF	MAAGSITTLPALPEGGDGGAFAPGC

The peptides were conjugated to thyroglobulin or to PPD by derivatizing the thyroglobulin with succinimidyl 4-(N-maleimidomethyl)cyclohexane-1-carboxylate (SMCC) and reacting the derivative with the peptide. This yields a conjugate having one or more peptide sequences linked via a thioether bond to thyroglobulin.

Specifically, the generation of monoclonal antibodies against the above sequences was achieved using the following procedure: BALB/c mice were immunized by serial injections with peptide-PPD or peptide-thyroglobulin into several sites. Four or five days after the last injection, the spleens were removed and splenocytes were fused with P3xG3Ag8.653 myeloma cells using polyethyleneglycol according to the procedures published in Morrow, et al. (1991).

Individual hybridoma supernatants were screened as follows:

First screen: ELISA on peptide-thyroglobulin-coated plates.

Second screen: ELISA on cysteine linked via SMCC to thyroglobulin.

Third screen: Indirect immunoperoxidase staining of frozen sections of guinea pig line 10 tumor or human parotid carcinoma.

Fourth screen: Indirect immunoperoxidase staining of frozen sections of miscellaneous malignant and normal guinea pig and human tissues.

Antibodies were selected that bound to peptide-thyroglobulin but not to cysteine-thyroglobulin, and which

bound to endothelial cells in malignant tumors more strongly than they did to endothelial cells in normal tissues (Table VIII).

TABLE VIII

Reactivity of Monoclonal Antibodies					
MoAB	Immunogen*	Class	Reactivity with Tumor Endothelium		Tumor Reactivity Pattern*
			g. pig	human	
GV14	gp VEGF	IgM	+	+	BV + some tumor cells
GV35	gp VEGF	IgM	+	+	Tumor cells, weak on BV
GV39	gp VEGF	IgM	+	+	BV and some tumor cells
GV59	gp VEGF	IgM	+	+	BV and some tumor cells
GV97	gp VEGF	IgM	+	+	BV, weak on tumor cells
HV55	hu VEGF	IgG	?	+	Basement membrane, some BV
GF67	gp FGF	IgM	+	+	BV and tumor cells
GF82	gp FGF	IgM	+	+	BV and tumor cells

\*BV = blood vessels

\*gp = guinea pig

hu = human

#### A. GV97 Staining of Human and Guinea Pig Tissue Sections

The GV97 antibody against guinea pig VEGF N-terminus bound to endothelial cells in miscellaneous human malignant (Table IX) and normal (Table X) tissues. The GV39 and GV97 antibodies were deposited Dec. 12, 1997, with the American Type Culture Collection (ATCC), 12301 Parklawn Drive, Rockville, Md. 20852, U.S.A. and given the ATCC Accession numbers ATCC HB 12450 and ATCC HB 12451, respectively. Effective Mar. 23, 1998, the address of the ATCC is: 10801 University Boulevard, Manassas, Va., 20110-2209, U.S.A.

Binding to endothelial cells in malignant tumors tended to exceed that to endothelial cells in normal tissues.

The staining of endothelial cells in guinea pig tumor (line 10 hepatocellular carcinoma) and normal tissues was similar in distribution and intensity to that observed with human tissues (Table XI).

In the Tables, + indicates a positive, as opposed to a negative, result. The numbers 2+, 3+ and 4+ refer to a positive signal of increasing strength, as is routinely understood in this field of study.

TABLE IX

Anti-GPVEGF on Human Tumors										
Tumor	TISSUE	Purified GV97			1 ug/ml or		GV97 supt.	GV14	GV39	GV59 supt.
		20 ug/ml	10 ug/ml	5 ug/ml	2 ug/ml	0.5 ug/ml				
DIGESTIVE TRACT										
92-01-A073	esophagus carcinoma		2+	1+	+/-	-ve			4+	4+
M4 Parotid							4+			
87-07-A134	Parotid carcinoma		3+	2+	+/-	-ve			3+	4+
M5 Parotid							4+			
88-04-A010	parotid adenoca.		1-2+	1+	-ve	-ve				1-3+



TABLE X

Anti-GPVEGP on Human Normal Tissues										
Tumor	TISSUE	Purified GV97			1 ug/ml or		GV97 supt.	GV14	GV39	GV59 supt.
		20 ug/ml	10 ug/ml	5 ug/ml	2 ug/ml	0.5 ug/ml				
<u>DIGESTIVE SYSTEM</u>										
91-01-A128	Bladder w/		3+	2+	1+	-ve			2-3+	2-3+
94-02-B020	cystitis									
92-01-A292 N.	uninvolved colon						2-3+		2-3+	
93-10-A116 N.	Colon	4+	4+	4+	3-4+		4+			3-4+
90-06-A116 N.	Colon	2-4+	1-4+	1-3+	-ve-2+	-ve	3-4+		2-3+	3-4+
93-02-A350 N.	colon						3+ of many		2+	
93-05-A503 N.	esophagus		3-4+	3+	1+	+/-			4+	4+
94-03-A244 N.	Ileum		4+	1-3+	-ve-1+	-ve	4+			4+
90-02-B132 N.	Liver	1+ of a	+/-	-ve	-ve	-ve	1-3+	2-3+	2-3+	2-3+
94-01-A181 N.	Pancreas	few	1-4+	1-3+	1-3+ of a	-ve				3-4+
90-05-D008 N.	Pancreas		2-4+	1-3+	+/-	-ve			2-3+	2-3+
93-05-A174 N.	Parotid		2+ of a few	1-2+ of a few	1+ of a few	-ve	-ve		3+ of a few	2-3+
94-04-A391 N.	Small bowel		1-3+	-ve-2+	-ve	-ve				3+
88-06-107 N.	Stomach	3+	2+	+/-	-ve		3-4+			3+
101-84b N.	Stomach (101 = 84a pair)		3-4+ in main and periphery	2-3+ in main and 3-4+ in periphery	+/- in main and 2+ in periphery	-ve in main and 1+ in periphery	3+			3-4+
90-11-B337 N.	Stomach		2-3+	+/-1+	-ve	-ve			3+	3+
<u>REPRODUCTIVE TRACT</u>										
93-04-A041 N.	Breast						4+		3+	
94-02-A197 N.	Breast w/fibrocystic change						4+		3+	
93-02-A051	Breast w/fibrocystic change		-ve-1+	-ve	-ve	-ve			+/-	+/-2+
93-02-A103	Breast w/fibrocyst. change	4+	3+	2+	1+					
92-11-A006 N.	ectocervix	2+ of most	1-2+ of most	0.5+	-ve	-ve	1-2+ of some			3+ of most
91-03-A207 N.	ectocervix		2.5+	1.5+	1+	.5+				2-3+
92-02-A139 N.	ovary w/corp. luteum	1+ in most but 2+ in one area	-ve in most but 1+ in one area	-ve	-ve		-ve in most but 3-4+ in one area			-ve in most bet 3-4 in one area
93-06-A11B N.	Prostate		1+ of a few	-ve	-ve	-ve				3+
93-11-A317d	Prostate chip		3-4+	2-3+	-ve-3+	-ve-1+			3-4+	3-4+
93-02-A315	Seminal Vesicle		0.5-1+	0.5+	-ve	-ve			1+	1.2+
92-04-A069 N.	testis		1+	+/-	+/-	+/-			1-2+	
91-04-A117	Ureter w/inflammation		1+	+/-	-ve	-ve			+/-1+	3-4+
<u>MUSCLE</u>										
94-01-A065 N.			3-4+	2+	+/-	-ve			3-4+	4+

TABLE X-continued

Anti-GPVEGP on Human Normal Tissues										
Tumor	TISSUE	Purified GV97			1 ug/ml or		GV97 supt.	GV14	GV39	GV59
		20 ug/ml	10 ug/ml	5 ug/ml	2 ug/ml	0.5 ug/ml				supt.
Heart										
91-07-D007 N.		1-4+	1-3+	1-2+	-ve	-ve	1-3+			1-3+
skeletal muscle										
95-03-A395 N.			4+	3-4+	1-2+	0.5-1+			4+	4+
Skeletal muscle										
IMMUNE SYSTEM										
90-01-A077 N.		2-3+	2+	1+ of some	-ve	-ve	2-3+			3-4+
lymph node										
90-08-A022 N.			most 1+ but	most 0.5+	most -ve but	most -ve			3+	3+
lymph node			a few 4+	but a few	a few 2+	but a few				
				2+		0.5-1+				
91-03-A057 N.			2+	1+	+/-	-ve			3-4+	3-4+
lymph node										
91-09-B017E			3+	2+	+/-1+	-ve			2-3+	2-3+
uninvolved lymph										
node										
93-07-A236 N.			3-4+	3-4+	-ve-3+	-ve				2-4+
Spicen										
93-07-252 N.			3+	1+	+/-	-ve			2-3+	
spicen										
ENDOCRINE SYSTEM										
94-04-A252 N.		4+	4+	3-4+	1-2+		4+			3+
adrenal w/										
medulia and										
cortex										
93-05-A086 N.			most -ve a	most -ve a	-ve	-ve			2-3+	3-4+
Adrenal medulla			few 1-2+	few 1-2+						
92-03-A157			1+	+/-	+/-	-ve			4+	4+
Hyperplastic										
thyroid										
91-03-B019 N.			-ve-3+	-ve-2+	-ve-1+	-ve			2-3+	2-3+
Thyroid										
URINARY SYSTEM										
93-09-A048 N.							4+			2-3+
Kidney										
91-11-A075 N.			4+	3+	2+	1+	4+ on	4+ on	4+ on	
Kidney							glomeruli	glomeruli	glomeruli	
93-10-B001 N.			4+	3+	+/-	-ve	4+ on	4+ on	4+ on	
Kidney							glomeruli	glomeruli	glomeruli	
INTEGUMENTARY SYSTEM										
92-08-A029 N.			+/- to 4+	+/- to 3+	+/- to 1+	+/-			2+	2+
Breast skin										
89-02-257			4+	3-4+	2-3+	1-2+			1+	3-4+
Cartilage										
marches 2SS										
RESPIRATORY SYSTEM										
93-05-A203 N.			-ve-2+	-ve-1+	+/-	-ve			2+	3+
Lung										
92-12-A263 N.			2-3+ w/ducts	1-2+ w/	-ve	-ve				2-3+
Bronchus			staining 3-4+	ducts staining 2-3+						

TABLE XI

Staining Pattern of 9F7 anti-VEGF by direct immunohistochemical staining on 6-8 week old GP tissues

TISSUE	Purified GV97			1 ug/ml or		9F7 supt.	3F9 supt.	5F9 supt.
	20 ug/ml	10 ug/ml	5 ug/ml	2 ug/ml	0.5 ug/ml			
<u>DIGESTIVE SYSTEM</u>								
LIVER		2+	1-2+	+/-	+/-		1-2+	1-2+
INTESTINE	4+	3+	2+	1+			4 + m	4 + m

TABLE XI-continued

Staining Pattern of 9F7 anti-VEGF by direct immunohistochemical staining on 6-8 week old GP tissues								
TISSUE	Purified GV97				1 ug/ml or			
	20 ug/ml	10 ug/ml	5 ug/ml	2 ug/ml	0.5 ug/ml	9F7 supt.	3F9 supt.	5F9 supt.
PANCREAS	1+ of many and 3+ in islands of cells						lymphoid, rest diff. than	lymphoid, rest diff. than
SMALL INTESTINE	4+ of many and 4+ in lymphoid	2-3+ of many and 4+ in lymphoid, rest diff. than fVIII	1-2+ of many and 4+ in lymphoid, rest diff. than fVIII	+/- of many and 4+ in lymphoid, rest diff. than fVIII			3+ of some and 4+ in lymphoid	3+ of some and 4+ in lymphoid
STOMACH	3-4+	1-2+ on most occasional 3+	+/- on most occasional 2+	+/- on most occasional 1+			3-4+ (some fVIII -ve)	3-4+ (some fVIII -ve)
<u>REPRODUCTIVE SYSTEM</u>								
TESTIS								
MUSCLE AND INTRIGUMENTARY SYSTEM								
HEART	-ve	-ve	-ve	-ve			3-4+ (some fVIII -ve)	3-4+ (some fVIII -ve)
MUSCLE SKIN	1-2+ in fatty layer and 3-4+ in cellular layer	1+ in fatty layer and 3-4+ in cellular layer	+/- in fatty layer and 3-4+ of a few in cellular layer	+/- in fatty layer and 1-2+ of a few in cellular layer			3+	3+
<u>IMMUNE SYSTEM</u>								
SPLEEN	4+	3+	2+	-ve			4+	4+
THYMUS								
<u>URINARY SYSTEM</u>								
KIDNEY	glomeruli 4+	glomeruli 3-4+	glomeruli 2-3+	glomeruli 1-2+			glomeruli 3-4+	glomeruli 3-4+
<u>ENDOCRINE SYSTEM</u>								
ADRENAL								
<u>RESPIRATORY SYSTEM</u>								
LUNG								
<u>NERVOUS SYSTEM</u>								
CEREBELLUM	4+	2+	+/- of most and 1+ of a few	+/- of most and 1+ of a few			4+	4+
<u>TUMORS</u>								
TUMOR	4+	4+	3-4+	2-3+ (2)		4+		3+

#### B. Lack of Reactivity of GV97 With Soluble Human VEGF

To identify antibodies that are specific for VEGF, the VEGF receptor (Flk-1) or VEGF bound (or complexed) to the receptor, an ELISA screening protocol was developed. The procedure is as follows:

Initially, a 96 well ELISA plate (round bottom) was coated (outside wells left blank) with 100  $\mu$ l/well of FLK/seap at 10  $\mu$ g/ml in sensitizing buffer. After overnight incubation, the plate was washed twice with PBS overnight at 4° C. Next the FLK/Seap coated plate was blocked with 250  $\mu$ l/well of PBS+CAH (5%) solution for 1 h at 37° C. The blocking solution was removed and the plate was vigorously tapped on paper towels.

The blocked plates were then incubated with 100  $\mu$ l/well of VEGF-165 (VEGF 165 aa form produced in yeast

obtained from Dr. Ramakrishnan, University of Minnesota) at 2  $\mu$ g/ml in binding plus 0.1  $\mu$ g/ml heparin for 4 h at room temperature or overnight at 4° C. The VEGF solution was collected and the plate washed 2 times with PBS-tween (0.10%). Next, 100  $\mu$ l/well of hybridoma fusion supernatant was added to the wells and incubated for 1 h at 32° C. Following this supernatant incubation, the plate was washed 3 times with PBS tween and then incubated with 100  $\mu$ l/well of secondary antibody (KPL, Gt anti-mouse IgG at 1:1000 in PBS tween+CAH (5%) for 1 hour at 37° C.

Following secondary antibody incubation, the plates were washed 4 times with PBS tween, incubated with 100  $\mu$ l/well of substrate (Substrate Sigma OPD dissolved in citrate buffer+H<sub>2</sub>O<sub>2</sub>) for 20 minutes and read at 490 nm on a Cambridge Technology Microplate Reader (Model

7520). Wells with an absorbance above appropriate control wells were selected as positives and further characterized.

It was found that GV97 did not bind to recombinant VEGF-coated ELISA plates, nor did recombinant human VEGF bind to GV97 coated ELISA plates. Soluble recombinant human VEGF did not block the binding of 5  $\mu$ g/ml GV97 to tumor endothelium in histological sections even when added at 50  $\mu$ g/ml.

These data suggest that GV97 recognizes an epitope of VEGF that is concealed in recombinant human VEGF but which becomes accessible when VEGF binds to its receptor on endothelial cells.

#### C. GV97 Localization in Line 10-Bearing Guinea Pigs

In contrast with staining data obtained from histological sections, GV97 antibody localized selectively to tumor endothelial cells after injection into line 10 tumor-bearing guinea pigs (see Table XII). Staining of endothelial cells in the tumor was moderately strong whereas staining of normal endothelium in miscellaneous organs was undetectable.

#### D. Anti-bFGF Selectively Bind to Tumor Endothelial Cells

GV97 and GF82, which had been raised against guinea pig bFGF N-terminus, bound strongly to endothelial cells in frozen reactions of guinea pig line 10 tumor and to endothelial cells in two types of human malignant tumors (Table XIII). By contrast, relatively weak staining of endothelial cells in miscellaneous guinea pig normal tissues was observed.

TABLE XII

GV97 injected into tumor bearing GP		
TISSUE	GV97 10 ug/ml	GV 97 20 ug/ml serum volume injected
<u>DIGESTIVE SYSTEM</u>		
LIVER	2+	-ve
INTESTINE	3+	possible 0.5-1+ of a few
PANCREAS	+/- of many and 2+ in islands of cells	possible 0.5-1+ of a few
SMALL INTESTINE	2-3+ of many and 4+ in lymphoid, rest diff. than fVIII	+/-
STOMACH	1-2+ on most occasional 3+	possibly 0.5+ of a few
<u>REPRODUCTIVE SYSTEM</u>		
TESTIS	+/-	
<u>MUSCLE AND INTEGUMENTARY SYSTEM</u>		
HEART	-ve	-ve
MUSCLE		-ve
SKIN	1+ in fatty layer and 3-4+ in cellular layer	
<u>IMMUNE SYSTEM</u>		
SPLEEN	3+	possibly a few 1+
THYMUS		
<u>URINARY SYSTEM</u>		
KIDNEY	glomeruli 3-4+	
<u>ENDOCRINE SYSTEM</u>		
ADRENAL	4+	-ve
<u>RESPIRATORY SYSTEM</u>		
LUNG	2+	-ve

TABLE XII-continued

GV97 injected into tumor bearing GP		
TISSUE	GV97 10 ug/ml	GV 97 20 ug/ml serum volume injected
<u>NERVOUS SYSTEM</u>		
CEREBELLUM	2+	-ve
<u>TUMORS</u>		
TUMOR	4+	2-3+

TABLE XXII

Anti-GP FGF Antibody Staining on GP Tissues			
GP TISSUE	GF 67	GF 82	
<u>DIGESTIVE SYSTEM</u>			
LIVER	ND	ND	
INTESTINE	+/-	+/-	
PANCREAS	2-3+	2+	
SMALL INTESTINE	+/-	+/-	
STOMACH	ND	ND	
<u>REPRODUCTIVE SYSTEM</u>			
TESTIS	ND	ND	
<u>MUSCLE AND INTEGUMENTARY SYSTEM</u>			
HEART	2-3+	1+	
MUSCLE	+/-	1+	
SKIN	ND	ND	
<u>IMMUNE SYSTEM</u>			
SPLEEN	3+	-ve	
THYMUS			
<u>URINARY SYSTEM</u>			
KIDNEY	1-2+	-ve	
<u>ENDOCRINE SYSTEM</u>			
ADRENAL	1-2+	+/-	
<u>RESPIRATORY SYSTEM</u>			
LUNG	1-2+	2-3+	
<u>NERVOUS SYSTEM</u>			
CEREBELLUM	1+	-1+	
<u>TUMORS</u>			
LINE 1 TUMOR	4+	4+	
<u>HUMAN TUMORS</u>			
PHEOCHROMO CYTOMA	4+	4+	
SCHWANOMA	4+	4+	

#### EXAMPLE XI

##### HUMAN TREATMENT PROTOCOLS

This example is concerned with human treatment protocols using the bispecific binding and coagulating ligands of the invention. These ligands are contemplated for use in the clinical treatment of various human cancers and even other disorders, such as benign prostatic hyperplasia and rheumatoid arthritis, in which the intermediate or longer term arrest of blood flow would be advantageous.

The bispecific ligands are considered to be particularly useful tools in anti-tumor therapy. From the data presented herein, including the animal studies, and the knowledge in



the art regarding treatment of Lymphoma (Glennie et al., 1988), T-Cell targeting (Nolan & Kennedy, 1990) and drug targeting (Paulus, 1985) appropriate doses and treatment regimens may be straightforwardly developed.

Naturally, before wide-spread use, further animal studies and clinical trials will be conducted. The various elements of conducting a clinical trial, including patient treatment and monitoring, will be known to those of skill in the art in light of the present disclosure. The following information is being presented as a general guideline for use in establishing such trials.

It is contemplated that patients chosen for the study would have failed to respond to at least one course of conventional therapy and had to have objectively measurable disease as determined by physical examination, laboratory techniques, or radiographic procedures. Where murine monoclonal antibody portions are employed, the patients should have no history of allergy to mouse immunoglobulin. Any chemotherapy should be stopped at least 2 weeks before entry into the study.

In regard to bispecific ligand administration, it is considered that certain advantages will be found in the use of an indwelling central venous catheter with a triple lumen port. The bispecific ligands should be filtered, for example, using a 0.22  $\mu$ m filter, and diluted appropriately, such as with saline, to a final volume of 100 ml. Before use, the test sample should also be filtered in a similar manner, and its concentration assessed before and after filtration by determining the  $A_{280}$ . The expected recovery should be within the range of 87 to 99%, and adjustments for protein loss can then be accounted for.

The bispecific ligands may be administered over a period of approximately 4–24 hours, with each patient receiving 2–4 number of infusions at 2–7 day intervals. Administration can also be performed by a steady rate of infusion over a 7 day period. The infusion given at any dose level should be dependent upon any toxicity observed. Hence, if Grade II toxicity was reached after any single infusion, or at a particular period of time for a steady rate infusion, further doses should be withheld or the steady rate infusion stopped unless toxicity improved. Increasing doses of bispecific coagulating ligands should be administered to groups of patients until approximately 60% of patients showed unacceptable Grade III or IV toxicity in any category. Doses that are  $\frac{2}{3}$  of this value could be defined as the safe dose.

Physical examination, tumor measurements, and laboratory tests should, of course, be performed before treatment and at intervals up to 1 month later. Laboratory tests should include complete blood counts, serum creatinine, creatine kinase, electrolytes; urea, nitrogen, SGOT, bilirubin, albumin, and total serum protein. Serum samples taken up to 60 days after treatment should be evaluated by radioimmunoassay for the presence of the intact bispecific ligand or components thereof and antibodies against any or both portions of the ligand. Immunological analyses of sera, using any standard assay such as, for example, an ELISA or RIA, will allow the pharmacokinetics and clearance of the therapeutic agent to be evaluated.

To evaluate the anti-tumor responses, it is contemplated that the patients should be examined at 48 hours to 1 week and again at 30 days after the last infusion. When palpable disease was present, two perpendicular diameters of all masses should be measured daily during treatment, within 1 week after completion of therapy, and at 30 days. To measure nonpalpable disease, serial CT scans could be performed at 1-cm intervals throughout the chest, abdomen,

and pelvis at 48 hours to 1 week and again at 30 days. Tissue samples should also be evaluated histologically, and/or by flow cytometry, using biopsies from the disease sites or even blood or fluid samples if appropriate.

Clinical responses may be defined by acceptable measure. For example, a complete response may be defined by the disappearance of all measurable tumor 1 month after treatment. Whereas a partial response may be defined by a 50% or greater reduction of the sum of the products of perpendicular diameters of all evaluable tumor nodules 1 month after treatment, with no tumor sites showing enlargement. Similarly, a mixed response may be defined by a reduction of the product of perpendicular diameters of all measurable lesions by 50% or greater 1 month after treatment, with progression in one or more sites.

All of the compositions and methods disclosed and claimed herein can be made and executed without undue experimentation in light of the present disclosure. While the compositions and methods of this invention have been described in terms of preferred embodiments, it will be apparent to those of skill in the art that variations may be applied to the composition, methods and in the steps or in the sequence of steps of the method described herein without departing from the concept, spirit and scope of the invention. More specifically, it will be apparent that certain agents which are both chemically and physiologically related may be substituted for the agents described herein while the same or similar results would be achieved. All such similar substitutes and modifications apparent to those skilled in the art are deemed to be within the spirit, scope and concept of the invention as defined by the appended claims.

## REFERENCES

- The following references, to the extent that they provide exemplary procedural or other details supplementary to those set forth herein, are specifically incorporated herein by reference.
- Abbassi et al., *J Clin Invest*, 92(6):2719–30, 1993.
  - Abraham et al., *Science*, 233:545–548, 1986.
  - Abrams & Oldham, *Monoclonal antibody therapy of human cancer*, Foon & Morgan (Eds.), Martinus Nijhoff Publishing, Boston, pp. 103–120, 1985.
  - Adams et al., *Cancer Res.*, 43:6297, 1983.
  - Adelman et al., *DNA* 2:183, 1983.
  - Alvarez et al., *Modern Pathology*, 5(3):303–307, 1992.
  - Antibodies: A Laboratory Manual, Cold Spring Harbor Laboratory, 1988.
  - Arklie et al., *Int. J. Cancer*, 28:23, 1981.
  - Ashall et al., *Lancet*, 2(8288):7–10, 1982.
  - Atkinson et al., *Cancer Res.*, 62:6820, 1982.
  - Ausubel et al., *Current Protocols in Molecular Biology*, Greene Publishing Associates and Wiley Interscience, N.Y., 1989.
  - Bach et al., *Biochemistry*, 25, 4007–4020, 1986.
  - Bauer et al., *Vox Sang*, 61:156–157, 1991.
  - Baxter et al., *Micro. Res.*, 41(1):5–23, 1991.
  - Bevilacqua et al., *Proc. Natl. Acad. Sci. USA*, 84:9238–9242, 1987.
  - Bhagwa et al., *Nature*, 316:511–513, 1985.
  - Bhattacharya et al., *Hybridoma*, 4:153, 1985.
  - Bhattacharya et al., *Cancer Res.*, 44:4528, 1984.
  - Bicknell and Harris, *Seminars in Cancer Biology*, 3:399–407, 1992.
  - Bikfalvi et al., *Exp. Cell Res.*, 181:75–84, 1989.
  - Birembaut et al., *J. Pathology*, 145:283–296, 1985.
  - Bitner et al., *Methods in Enzymol.*, 153:516–544, 1987.
  - Bjorn Dahl et al., *Eur. J. Immunol.*, 19:881–887, 1989.

- Blakey et al., *Biochem Biophys ACTA*, 923Y(1) :59-65, 1987b.
- Blakey et al., *Cancer Res.*, 47:947-952, 1987a.
- Bolhuis et al., *J. Immunol.*, 149:1840-1846, 1992.
- Borden et al., *Cancer*, 65:800-814, 1990.
- Brennan et al., *Science*, 229:81-83, 1985.
- Brinkmann et al., *Proc. Natl. Acad. Sci.*, 88(19):8616-20, 1991.
- Brooks et al., *Cell*, 79:1157-1164, 1994.
- Brooks et al., *Science*, 264:569-571, 1994.
- Brown et al., *J. Exp. Med.*, 176:1375-1379, 1992.
- Brown et al., *PNAS*, 78:539, 1981a.
- Brown et al., *J. Immunol.*, 127:539, 1981b.
- Brown et al., *Cancer Res.*, 53:4727-4735, 1993.
- Broze, *Seminars in Hematol.*, 29:159-169, 1992.
- Bruland et al., *Cancer Research*, 48:5302-5309, 1988.
- Bruland et al., *Int. J. Cancer*, 38(1):27-31, 1986.
- Bühning et al., *Leukemia*, 5:841-847, 1991.
- Burchell et al., *J. Immunol.*, 131(1) :508-13, 1983.
- Burrows, & Thorpe, *PNAS*, 90:8996-9000, 1993.
- Burrows et al., *Cancer Res.*, 52:5954-5962, 1992.
- Burrows et al., *Cancer Res.*, 51:4768-4775, 1991.
- Burrows et al., *Clin. Cancer Res.*, 1995 (in press)
- Burtin et al., *Cancer*, 31:719-726, 1983.
- Byers & Baldwin, *Immunol.*, 65:329-335, 1988.
- Byers et al., *Cancer Res.*, 49:6153-6160, 1989.
- Byers et al., 2nd Int. Conf. Mab Immunocon., *Cancer*, 41:1987.
- Campbell, In: *Monoclonal Antibody Technology, Laboratory Techniques in Biochemistry and Molecular Biology*, Vol. 13, Burden & Von Knippenberg (Eds.), Elsevier, Amsterdam, pp. 75-83, 1984
- Carnemolla et al., *J. Cell Biol.*, 108:1139-1148, 1989.
- Carnemolla et al., *J. Biol. Chem.*, 267(34):24689-24692, 1992.
- Carrel et al., *Hybridoma*, 1:387, 1982.
- Cavenagh et al., *Br J Haematol*, 85(2) :285-91, 1993.
- Chapman et al., *Arthritis Rheum*, 37(12):1752-6, 1994.
- Chee et al., *Cancer Res.*, 43:3142, 1982.
- Chen et al., *J. Immunol.*, 145:8-12, 1990.
- Cherwinski et al., *J. Exp. Med.*, 166:1229-1244, 1989.
- Cheung et al., *Proc. AACR*, 27:318, 1986.
- Clark et al., *Biochim. Biophys. ACTA*, 867:244-251, 1986.
- Clark et al., *Cancer Res.*, 51:944-948, 1991.
- Clark et al., *Int. J. Cancer*, 2:15-17, 1988.
- Clauss et al., *J. Exp. Med.*, 172:1535-1545, 1990.
- Cohn et al., *Arch. Surg.*, 122:1425, 1987.
- Colberre-Garapin et al., *J. Mol. Biol.*, 150:1, 1981.
- Colcher et al., *Cancer Invest*, 1:127, 1983.
- Colcher et al., *Cancer Res.*, 47:1185 and 4218, 1987.
- Colcher et al., *PNAS*, 78:3199, 1981.
- Collins et al., *Proc. Natl. Acad. Sci. U.S.A.*, 81:4917-4921, 1984.
- Conn et al., *Proc. Natl. Acad. Sci. USA*, 87:2628-2632, 1990.
- Connolly et al., *J. Biol. Chem.*, 264(33) :20017-20024, 1989.
- Corgon-Cardo et al., *Laboratory Investigation*, 63(6) :832-840, 1990.
- Corvalen, *Cancer Immuno.*, 24:133, 1987.
- Cotran et al., *J. Exp. Med.*, 164:661-666, 1986.
- Crea et al., *Proc. Natl. Acad. Sci. U.S.A* 75:5765, 1978.
- Croghan et al., *Cancer Res.*, 43:4980, 1983.
- Croghan et al., *Cancer Res.*, 44:1954, 1984.
- Daar et al., *Transplantation*, 38(3):293-298, 1984.
- Davies and Wlodawer, *FASEB J.*, 9:50-56, 1995.
- Davis & Preston, *Analytical Biochemistry*, 116(2) :402-407, 1981.

- de Krestet et al., *Int. J. Cancer*, 37:705, 1986.
- De Vries et al., *Science*, 255:989-991, 1992.
- DeFranco, *Nature*, 352:754-755, 1991.
- deLeij et al., *Bispecific antibodies and targeted cellular cytotoxicity*, Romet-Lemonne et al., p. 249, 1991.
- Denekamp, et al., *Brit. J. Cancer*, 461:711-720, 1982.
- Denekamp, *Cancer Meta. Rev.*, 9:267-282, 1990.
- Denekamp, *Prog. Appl. Microcirc.*, 4:28-38, 1984.
- Detmar et al., *J. Exp. Med.*, 180:1141-1146, 1994.
- Dewerchin et al., *Blood*, 78(4):1005-1018, 1991.
- Di Scipio et al., *Biochemistry*, 16:5253-5260, 1977.
- Dillman et al., *Antibody, Immunocon. Radiopharm.*, 1:65-77, 1988.
- Dippold et al., *PNAS*, 77:6115, 1980.
- Dixon et al., *Mol. & Cell Biol.*, 7:4896-4902, 1989.
- Duijvestijn et al., *J. Immunol.*, 138:713-719, 1987.
- Dunham & Stewart, *J. Natl. Cancer Inst.*, 13:1299-1377, 1953.
- Dustin et al., *J. Immunol.*, 137:245-254, 1986.
- Dvorak et al., *J. Exp. Med.*, 174:1275-1278, 1991.
- Dvorak et al., *Cancer Cells*, 3(3):77-85, 1991.
- Edelman et al., *Proc. Natl. Acad. Sci. USA*, 90:1513-1517, 1993.
- Edgington et al., *Thrombosis and Haemostasis*, 66(1) :67-79, 1991.
- Ellis et al., *Histopathol.*, 8:501, 1984.
- Embleton et al., *Br. J. Cancer*, 63(5):670-674, 1991.
- Epenetos et al., *Cancer Res.*, 46:3183-3191, 1986.
- Epenetos et al., *Lancet*, Nov. 6, 2:1000-1004, 1982.
- Fair et al., *J. Biol. Chem.*, 262, 11692-11698, 1987.
- Farrans et al., *Lancet*, 2:397, 1982.
- Febbraio and Silverstein, *J. Biol. Chem.*, 265(30) :18531-18537, 1990.
- Ferrara et al., *J. Cell. Biochem.*, 47:211-218, 1991.
- Ferrara et al., *Endocrine Reviews*, 13(1):18-32, 1992.
- Fisher et al., *Thrombosis Research*, 48:89-99, 1987.
- Flavell et al., *Br. J. Cancer*, 65:545-551, 1992.
- Flavell et al., *Br. J. Cancer*, 64(2):274-280, 1991.
- Folkman, *Adv. Cancer Res.*, 43:175-230, 1985a.
- Folkman et al., *Ann. Surg.*, 214(4):414-427, 1991.
- Folkman, In: *Important Advances in Oncology, Part I*, DeVita et al. (Eds.), JB Lippincott, Philadelphia, pp. 42-62, 1985b.
- Foster et al., *Virchows Arch. (Pathol. Anat. Histopathol.)*, 394:295, 1982.
- Foster et al., *Human Pathol.*, 15:502, 1984.
- Fox, et al., *J. Biol. Resp.*, 9:499-511, 1990.
- Frelinger III et al., *J. Biol. Chem.*, 266(26):17106-17111, 1991.
- Frelinger III et al., *J. Biol. Chem.*, 265(11):6346-6352, 1990.
- French et al., *Cancer Res.*, 51:2358-2361, 1991.
- Gailani and Broze, Jr., *Science*, 253:909-912, 1991.
- Galfre et al., *Methods Enzymol.*, 73:1-46, 1981.
- Gallagher et al., *J. Surg. Res.*, 40:159, 1986.
- Galland et al., 1233-1240, 1993.
- Gangopadhyay et al., *Cancer Res.*, 45:1744, 1985.
- Gefter et al., *Somatic Cell Genet.*, 3:231-236, 1977.
- Geppert et al., *Immunological Reviews*, 117:5-66, 1990.
- Ghetie et al., *Cancer Res.*, 51:5876-5880, 1991.
- Ghose, *CRC Critical Review in Therapeutic Drug Carrier Systems*, 3:262-359, 1982.
- Ghose & Blair, *CRC Critical Reviews in Therapeutic Drug Carrier Systems*, 3:262-359, 1987.
- Gibbons, In: *J. D. Gibbons (ed.), "Nonparametric methods for quantitative analysis,"* pp. 160, New York: Holt, Rinehart and Winston. 1976.
- Gitoy-Goren et al., *Biochem. Biophys. Res. Comm.*, 190:702-, 1993

- Glassy et al., *PNAS*, 80:63227, 1983.
- Glennie et al., *J. Immunol.*, 141(10):3662-3670, 1988.
- Glennie et al., *J. Immunol.*, 139:2367-2375, 1987.
- Goding, In: *Monoclonal Antibodies: Principles and Practice*, 2d ed., Academic Press, Orlando, Fla., pp. 60-61, 65-66, 71-74, 1986.
- Gomez-Pinilla and Cotman, *Neuroscience*, 49:771-780, 1992.
- Gosset et al., *Int Arch Allergy Immunol*, 106(1):69-77, 1995.
- Gougos et al., *Int. Immunol.*, 4:83-92, 1992.
- Gougos & Letarte, *J. Immunol.*, 141:1925-1933, 1988.
- Griffin et al., *Treat. Res.*, 37:433-455, 1988b.
- Griffin et al., *Proc. 2nd Conf. on Radioimmuno-detection & Therapy of Cancer*, 82, 1988a.
- Groenewegen et al., *Nature*, 316:361-363, 1985.
- Groves et al., *Br J Dermatol*, 124(2):117-23, 1991.
- Gusterson et al., *Br. J. Cancer*, 58:453, 1988.
- Hagemeyer et al., *Int. J. Cancer*, 38:481-488, 1986.
- Hakkert et al., *Blood*, 78(10):2721-6, 1991.
- Hammerling, *Transplant. Rev.*, 30:64-82, 1976.
- Hattey et al., *Thrombosis Research*, 45(5):485-495, 1987.
- Hayes et al., *J. Clin. Invest.*, 75:1671, 1985.
- Hayward et al., *Biological Chemistry*, 266(11):7114-7120, 1991.
- Hendler et al., *Trans. Assoc. Am. Physicians*, 94:217, 1981.
- Herblin and Gross, *Angiogenesis: Key Principles—Science—Technology—Medicine*, 214-218, 1992.
- Hess et al., *Transplantation*, 6:1232-1240, 1991.
- Heynen et al., *J. Clin. Invest.*, 94:1098-1112, 1994.
- Horan Hand et al., *Cancer Res.*, 45:2713, 1985.
- Howard et al., *Developmental Biology*, 146:325-338, 1991.
- Huang et al., *Anticancer Research*, 13:887-890, 1993.
- Imai et al., *JNCI*, 68:761, 1982.
- Imam et al., *J. Immunobiol.*, 1984.
- Inouye et al., *Nucleic Acids Res.*, 13:3101-3109, 1985.
- Jain, *Cancer Meta. Rev.*, 9(3):253-266, 1990.
- Jakeman et al., *J. Clin. Invest.*, 89:244-253, 1992.
- Johnson & Reithmuller, *Hybridoma*, 1:381, 1982.
- Johnson et al., *Am. J. Reprod. Immunol.*, 1:246, 1981.
- June et al., *Molecular Cell Biology*, 12:4472-4481, 1987.
- June et al., *Immunology Today*, 11(6):211-216, 1990.
- Jutila et al., *J Exp Med*, 175(6):1565-73, 1992.
- Juweid et al., *Cancer Res.*, 52:5144-5153, 1992.
- Kabawat et al., *Int. J. Gynecol. Pathol.*, 4:245, 1985.
- Kabawat et al., *Int. J. Gynecol. Pathol.*, 4:265, 1983.
- Kandel et al., *Cell*, 66:1095-1104, 1991.
- Kantor et al., *Hybridoma*, 1:473, 1982.
- Karasek, *J. Invest. Derm.*, 93(2):335-385, 1989.
- Keelan et al., *Am J Physiol*, 266(1 Pt 2) pH278-90, Jan 1994a.
- Keelan et al., *J Nucl Med*, 35(2):276-81, Feb 1994b.
- Kennel et al., *Cancer Res.*, 51:1529-1536, 1991.
- Kim et al., *Growth Factors*, 7:53-64, 1992.
- Kim et al., *Nature*, 362:841-844, 1993.
- Kimura et al., *Immunogenetics*, 11:373-381, 1983.
- Kinsel et al., *Cancer Res.*, 49:1052, 1989.
- Kishimoto et al., *Blood*, 78(3):805-11, 1991.
- Kisiel, *J. Biol. Chem.*, 254(23):12230-12234, 1979.
- Kjeldsen et al., *2nd Int. Wkshop of MAbs & Breast Cancer*, San Fran., Nov., 1986.
- Klagsbrun & Folkman, *Angiogenesis Handook of Experimental Pharmacology*, Vol. 95, Sporn & Roberts, Springer-Verlag, Berlin, pp. 549-586, 1990.
- Kohler & Milstein, *Nature*, 256:495-497, 1975.
- Kohler & Milstein, *Eur. J. Immunol.*, 6:511-519, 1976.
- Kondo et al., *Biochem. and Biophys. Res. Comm.*, 194(3):1234-1241, 1993.

- Krishnaswamy et al., *J. Biol. Chem.*, 267(36):26110-26120, 1992.
- Krishnaswamy et al., *J. Biol. Chem.*, 267(33):23696-23706, 1992.
- Kufe et al., *Hybridoma*, 3:223, 1984.
- Lan et al., *Cancer Res.*, 44:1954, 1984.
- Lan et al., *Cancer Res.*, 45:305, 1985.
- Lee et al., *Methods in Enzymology*, 237:146-164, 1994.
- Leith et al., *British J. Cancer*, 66(2):345-8, 1992.
- 10 Lemkin et al., *Proc. Am. Soc. Clin. Oncol.*, 3:47, 1984.
- Leung et al., *Science*, 246:1306-1309, 1989.
- Leydem et al., *Cancer*, 57:1135, 1986.
- LoBuglio et al., *JNCI*, 80:932, 1988.
- Logan et al., *Proc. Natl. Acad. Sci. USA*, 81:3655-3659, 1984.
- 15 Loop et al., *Int. J. Cancer*, 27:775, 1981.
- Lord et al., In: *Genetically Engineered Toxins*, Frank (Ed.), M. Dekker Publ., p. 183, 1992.
- Lowder et al., *Blood*, 69:199-210, 1987.
- 20 Lowe et al., *Immunol Lett.*, 12:263-269, 1986.
- Lowy et al., *Cell*, 22:817, 1980.
- Maeda et al., *J. Invest. Derm.*, 97:183-189, 1991.
- Manabe et al., *J. Lab. Clin. Med.*, 104(3):445-454, 1984.
- Mandeville et al., *Cancer Detect. Prev.*, 10:89, 1987.
- 25 Mann, *TIBS* 12, 229-233, 1987.
- Mason & Williams, *Biochem J*, 187:1-20, 1980.
- Massaglia et al., *J. Cell. Phys.*, 132:531-537, 1987.
- Masuko et al., *Cancer Res.*, 44:2813, 1984.
- Mattes et al., *PNAS*, 81:568, 1984.
- 30 Mazzocchi et al., *Cancer Immunol. Immunother.*, 32:13-21, 1990.
- McDicken et al., *Br. J. Cancer*, 52:59, 1985.
- Menard et al., *Cancer Res.*, 63:1295, 1983.
- Messing et al., *Third Cleveland Symposium on Macromolecules and Recombinant DNA*, Editor A. Walton, Elsevier, Amsterdam, 1981.
- Metzelaar et al., *Blood*, 79(2):372-379, 1992.
- Metzelaar et al., *J. Biol. Chem.*, 266(5):3239-3245, 1991.
- Mignatti et al., *J. Cell. Biol.*, 113:1193-1201, 1991.
- 40 Millauer et al., *Cell*, 72:835-846, 1993.
- Miotti et al., *Cancer Res.*, 65:826, 1985.
- Miotti et al., *Int. J. Cancer*, 39:297, 1987.
- Montefort et al., *Eur Respir J*, 5(7):815-23, 1992.
- Moroi and Aoki, *J. Biol. Chem.*, 251(19):5956-5965, 1976.
- 45 Morrissey et al., *Blood*, 81:734-744, 1993.
- Morrissey et al., *Cell*, 50:129-135, 1987.
- Morrissey et al., *Thrombosis Res.*, 52:247-261, 1988.
- Moughal et al., *J Periodontal Res*, 27(6):623-30, 1992.
- Mulligan et al., *Proc. Natl. Acad. Sci. USA*, 78:2072, 1981.
- 50 Mulligan et al., *J. Clin. Invest.*, 88:1396-1406, 1991.
- Munz et al., *J. Nucl. Med.*, 27:1739, 1986.
- Murray et al., *Radio. Onc.*, 16:221-234, 1989.
- Nabel et al., *Nature*, 362:844-846, 1993.
- Nakamura, *Prog. Growth Factor Res.*, 3:67-86, 1991.
- 55 Nelson, 1991.
- Nemerson, *Blood*, 71(1):1-8, 1988.
- Neumann et al., *Arch Dermatol*, 130(7):879-83, 1994.
- Nieuwenhuis et al., *Blood*, 70(3):838-845, 1987.
- Nishikawa et al., *Advances in Experimental Medicine and Biology*, 324:131-139, 1992.
- 60 Nitta et al., *Lancet*, 335:368-371, 1990.
- Nolan & Kennedy, *Biochemica et Biophysica Acta*, 1040:1-11, 1990.
- Norton et al., *Biochem Biophys Res Commun*, 195(1):250-8, 1993.
- 65 O'Connell et al., *Clin. Exp. Immunol.*, 90:154-159, 1992.
- O'Connell et al., *J. Immunol.*, 144(2):521-525, 1990.

O'Hare et al., *Proc. Natl. Acad. Sci. USA*, 78:1527, 1981.  
 Ogawa et al., *British J. Haematology*, 75:517-524, 1990.  
 Ohuchida et al., *J. Am. Chem. Soc.*, 103(15):4597-4599, 1981.  
 Oi & Morrison, *Mt. Sinai J. Med.*, 53(3):175-180, 1986.  
 Olander et al., *Biochem. and Biophys. Res. Comm.*, 175(1):68-76, 1991.  
 Olofsson et al., *Blood*, 84(8):2749-58, 1994.  
 Osborn et al., *Cell*, 59:1203-1211, 1989.  
 Osterud et al., *Thrombosis Res.*, 42:323-329, 1986.  
 Paborsky et al., *J. Biol. Chem.*, 266(32):21911-21916, 1991.  
 Palleroni et al., *Int. J. Cancer*, 49:296-302, 1991.  
 Patt et al., *Cancer Bull.*, 40:218, 1988.  
 Paul et al., *Hybridoma*, 5:171, 1986.  
 Paulus, *Behrini Inst. Mitt.*, 78:118-132, 1985.  
 Perez et al., *J. Exp. Med.*, 163:166-178, 1986.  
 Perez et al., *J. Immunol.*, 137:2069-2072, 1986.  
 Perez et al., *Nature*, 316:354-356, 1985.  
 Perkins et al., *Eur. J. Nucl. Med.*, 10:296, 1985.  
 Pietersz et al., *Antibody, Immunoconj. Radiopharm.*, 1:79-103, 1988.  
 Pimm et al., *J. Cancer Res. Clin. Oncol.*, 118:367-370, 1992.  
 Plate et al., *Cancer Res.*, 53:5822-5827, 1993.  
 Plate et al., *Nature*, 359:845-848, 1992.  
 Pober et al., *J. Exp. Med.*, 157:1339-1353, 1991.  
 Poels et al., *J. Natl. Cancer Res.*, 44:4528, 1984.  
 Poels et al., *J. Natl. Cancer*, 76:781, 1986.  
 Pukrittayakamee et al., *Mol. Biol. Med.*, 1:123-135, 1983.  
 Qian et al., *Cancer Res.*, 140:3250, 1991.  
 Rao and Rapaport, *Biochemistry*, 85:6687-6691, 1988.  
 Rasmussen et al., *Breast Cancer Res. Treat.*, 2:401, 1982.  
 Rehemtulla et al., *Thrombosis and Haemostasis*, 65(5):521-527, 1991.  
 Reilly et al., *Biochem. Biophys. Res. Commun.*, 35:164:736-743, 1989.  
 Reisfeld et al., *Melanoma Antigens and Antibodies*, p. 317, 1982.  
 Remington's *Pharmaceutical Sciences*, 16th Ed., Mack Publishing Company, 1980.  
 Rettig et al., *Proc. Natl. Acad. Sci. USA*, 89:10832-10836, 1992.  
 Riva et al., *Int. J. Cancer*, 2:114, 1988.  
 Rivoltini et al., 3rd *Int. Conf. Bispecific Antibodies and Targeted Cellular Cytotoxicity*, 1992.  
 Rowinsky, *Clinical Investigation*, Abstracts from Chemotherapy foundation symposium X. Innovative cancer chemotherapy for tomorrow, pp. 6-9, 1992.  
 Ruco et al., *Am. J. Pathol.*, 137(5):1163-1171, 1990.  
 Ruf and Edgington, *Thrombosis and Haemostasis*, 66(5):529-533, 1991.  
 Ruf et al., *J. Biol. Chem.*, 266(24):15719-15725, 1991.  
 Ruf et al., *J. Biol. Chem.*, 266(4):2158-2166, 1991.  
 Ruf et al., *JBC*, 266:2158-2166, 1991.  
 Ruf & Edgington, *FASEB J.*, 8:385-390, 1994.  
 Ruther et al., *EMBO J.*, 2:1791, 1983.  
 Safran et al., *Oncogene*, 5:635-643, 1990.  
 Sainsbury et al., *Lancet*, 1:364, 1985.  
 Sambrook et al., *Molecular Cloning, A Laboratory Manual*, Cold Spring Harbor Laboratory, N.Y., 1989.  
 Sands, *Immunoconjugates and Radiopharmaceuticals*, 1:213-226, 1988.  
 Santerre et al., *Gene*, 30:147, 1984.  
 Saxton et al., *Hybridoma*, 1:433, 1982.  
 Scarpati et al., *Biochemistry*, 26:5234-5238, 1987.  
 Schlingemann et al., *Lab. Invest.*, 52:71-76, 1985.  
 Schlingemann et al., *Lab. Invest.*, 62:690-696, 1990.

Schlom et al., *Adv. Cancer Res.*, 43:143, 1985.  
 Schutt et al., *Immunol. Lett.*, 19:321-328, 1988.  
 Schweigerer et al., *Nature*, 325:257-259, 1987.  
 Sedmak et al., *Transplantation*, 58(12):1379-85, 1994.  
 Segal et al., 1992.  
 Senger et al., *Cancer and Metastasis Reviews*, 12:303-324, 1993.  
 Senger et al., *Cancer Research*, 50:1774-1778, 1990.  
 Shankar et al., *J. Biol. Chem.*, 269(19):13936-13941, 1994.  
 Shen and Tai, *J. Biol. Chem.*, 261(25):11585-11591, 1986.  
 Shepard et al., *J. Clin. Immunol.*, 11:117-127, 1991.  
 Shockley et al., *Ann. N.Y. Acad. Sci.*, 617:367-382, 1991.  
 Shrestha et al., *Eur. J. Cancer B. Oral. Oncol.*, 30B(6):393-9, 1994.  
 Shweiki et al., *Nature*, 359:843-847, 1992.  
 Silber et al., *J. Clin. Invest.*, 93(4):1554-63, 1994.  
 Silverstein and Febbraio, *Blood*, 80(6):1470-1475, 1992.  
 Sioussat et al., *Arch. Biochem. Biophys.*, 301(1):15-20, 1993.  
 Sloane, *Cancer*, 17:1786, 1981.  
 Smith et al., *J. Virol.*, 46:584, 1983.  
 Smith et al., 1989.  
 Smith et al., *Proc. Am. Soc. Clin. O. col.*, 6:250, 1987.  
 Soule et al., *PNAS*, 80:1332, 1983.  
 Span et al., *Immunology*, 72(3):355-60, 1991.  
 Spicer et al., *Proc. Natl. Acad. Sci. USA*, 84:5148-5152, 1987.  
 Sporn et al., *Blood*, 81(9):2406-12, 1993.  
 Staerz et al., *Nature*, 314(6012):628-631, 1985.  
 Stavrou, *Neurosurg. Rev.*, 13:7, 1990.  
 Stefanik et al., *Cancer Research*, 51:5760-5765, 1991.  
 Steinberg et al., *J. Heart Lung Transplant*, 13(2):306-18, Mar-Apr 1994.  
 Stern et al., *Proc. Natl. Acad. Sci. USA*, 80:4119-4123, 1982.  
 Stern et al., *J. Biol. Chem.*, 260(11):6717-6722, 1985.  
 Stevenson et al., *Chem. Immunol.*, 48:126-166, 1990.  
 Street et al., *Cell. Immunol.*, 120:75-81, 1989.  
 Stuhlmiller et al., *Hybridoma*, 1:447, 1982.  
 Sugama et al., *J. Cell Biol.*, 119(4):935-944, 1992.  
 Sunderland et al., *Cancer Res.*, 44:4496, 1984.  
 Szybalska et al., *Proc. Natl. Acad. Sci. USA*, 48:2026, 1962.  
 Szymendera, *Tumour Biology*, 7:333, 1986.  
 Takahashi et al., *Cancer*, 61:881, 1988.  
 Teramoto et al., *Cancer*, 50:241, 1982.  
 Tessier et al., *J. Biol. Chem.*, 269(17):12456-12461, 1994.  
 Thieme et al., *Diabetes*, 44(1):98-103, 1995.  
 Thompson et al., *J. Natl. Cancer Inst.*, 70:409, 1983.  
 Thor et al., *Cancer Res.*, 46:3118, 1986.  
 Thorpe et al., *Cancer Res.*, 48:6396-6403, 1988.  
 Ting et al., *J. Immunol.*, 141:741-748, 1988.  
 Tischer et al., *Biochem. and Biophys. Res. Comm.*, 165(3):1198-1206, 1989.  
 Tischer et al., *J. Biol. Chem.*, 266(18):11947-11954, 1991.  
 Titus et al., *J. Immunol.*, 138:4018-4022, 1987.  
 Tomiyama et al., *Blood*, 79(9):2303-2312, 1992.  
 Tone et al., *J. Biochem.*, 102(5):1033-1941, 1987.  
 Tsuji et al., *Cancer Res.*, 45:2358, 1985.  
 Tuominen and Kallioinen, *J. Cutan. Pathol.* 21(5):424-9, 1994.  
 Tutt et al., *Eur. J. Immunol.*, 21:1351-1358, 1991.  
 Ugarova et al., *J. Biol. Chem.*, 268(28):21080-21087, 1993.  
 Ulich et al., *Inflammation*, 18(4):389-98, 1994.  
 Vaickus et al., *Cancer Invest.*, 9:195-209, 1991.  
 Vaisman et al., *J. Biol. Chem.*, 265(32):19461-19466, 1990.  
 Van Heeke et al., *J. Biol. Chem.*, 264:5503-5509, 1989.  
 Van Duk et al., *Int. J. Cancer*, 43:344-349, 1989.

- Veale et al., *Arthritis Rheum*, 36(7):893-900, 1993.  
 Venkateswaran et al., *Hybridoma*, 11(6):729-739, 1992.  
 Vitetta et al., *Cancer Res.*, 15:4052-4058, 1991.  
 von Asmuth et al., *Eur J Immunol*, 22(10):2519-26, 1992.  
 Wagener et al., *Int. J. Cancer*, 33:469, 1984.  
 Wang et al., *Int. J. Cancer*, 54:363-370, 1993.  
 Wang et al., *Biochem. and Biophys. Res. Comm.*, 177(1):286-291, 1991.  
 Warr et al., *Blood*, 75:1481-1489, 1990.  
 Watanabe et al., *Proc. Natl. Acad. Sci. USA*, 86:9456-9460, 1989.  
 Wawrzynczak & Thorpe, "Methods for preparing immunotoxins: effect of the linkage on activity and stability", in: *Immunoconjugates: Antibody conjugates in radioimaging and therapy of cancer*, Vogel (ed), New York, Oxford University Press, pp. 28-55, 1987.  
 Weiner et al., *Cancer Res.*, 49:4062-4067, 1989.  
 Weiss et al., *Blood*, 73:968-975, 1989.

- Whittle et al., *Nature*, 292:472-474, 1981.  
 Wigler et al., *Proc. Natl. Acad. Sci. USA*, 77:3567, 1980.  
 Wigler et al., *Cell*, 11:223, 1977.  
 Wildgoose et al., *Blood*, 80:25-28, 1992.  
 Williams and Esnouf, *Biochem. J.*, 84:52-62, 1962.  
 Wilson et al., *Int. J. Cancer*, 28:293, 1981.  
 Wiman and Collen, *Eur. J. Biochem.*, 78:19-26, 1977.  
 Wiman, *Biochem. J.*, 191:229-232, 1980.  
 Winter & Milstein, *Nature*, 349:293-299, 1991.  
 Woodbury et al., *PNAS*, 77:2183, 1980.  
 Wu et al., *Int. J. Pharm.*, 12:235-239, 1990.  
 Xu et al., *J. Biol. Chem.*, 267(25):17792-17803, 1992.  
 Yamaguchi et al., *Proc. Natl. Acad. Sci. USA*, 91:484-488, 1994.  
 Yamaue et al., *Biotherapy*, 2:247-259, 1990.  
 Zamarron et al., *J. Biol. Chem.*, 266(24):16193-16199, 1991.  
 Zhang et al., *Int J Cancer*, 59(6):823-9, 1994.

## SEQUENCE LISTING

## ( 1 ) GENERAL INFORMATION:

( i i i ) NUMBER OF SEQUENCES: 32

## ( 2 ) INFORMATION FOR SEQ ID NO:1:

## ( i ) SEQUENCE CHARACTERISTICS:

- ( A ) LENGTH: 27 base pairs  
 ( B ) TYPE: nucleic acid  
 ( C ) STRANDEDNESS: single  
 ( D ) TOPOLOGY: linear

## ( i i ) MOLECULE TYPE: other nucleic acid

( A ) DESCRIPTION: /desc = "DNA"

## ( x i ) SEQUENCE DESCRIPTION: SEQ ID NO:1:

GTCATGCCAT GGCCTCAGGC ACTACAA

2 7

## ( 2 ) INFORMATION FOR SEQ ID NO:2:

## ( i ) SEQUENCE CHARACTERISTICS:

- ( A ) LENGTH: 32 base pairs  
 ( B ) TYPE: nucleic acid  
 ( C ) STRANDEDNESS: single  
 ( D ) TOPOLOGY: linear

## ( i i ) MOLECULE TYPE: other nucleic acid

( A ) DESCRIPTION: /desc = "DNA"

## ( x i ) SEQUENCE DESCRIPTION: SEQ ID NO:2:

TGACAAGCTT ATTCTCTGAA TTCCCCCTTT CT

3 2

## ( 2 ) INFORMATION FOR SEQ ID NO:3:

## ( i ) SEQUENCE CHARACTERISTICS:

- ( A ) LENGTH: 47 base pairs  
 ( B ) TYPE: nucleic acid  
 ( C ) STRANDEDNESS: single  
 ( D ) TOPOLOGY: linear

## ( i i ) MOLECULE TYPE: other nucleic acid

( A ) DESCRIPTION: /desc = "DNA"

## ( x i ) SEQUENCE DESCRIPTION: SEQ ID NO:3:

GTCATGCCAT GGCCCTGGTG CCTCGTGCTT CTGGCACTAC AAATACT

4 7

## ( 2 ) INFORMATION FOR SEQ ID NO:4:

-continued

---

( i ) SEQUENCE CHARACTERISTICS:  
    ( A ) LENGTH: 38 base pairs  
    ( B ) TYPE: nucleic acid  
    ( C ) STRANDEDNESS: single  
    ( D ) TOPOLOGY: linear

( i i ) MOLECULE TYPE: other nucleic acid  
    ( A ) DESCRIPTION: /desc = "DNA"

( x i ) SEQUENCE DESCRIPTION: SEQ ID NO:4:

GTCATGCCAT GGCCTGCTCA GGCCTACAA ATACTGTG 38

( 2 ) INFORMATION FOR SEQ ID NO:5:

( i ) SEQUENCE CHARACTERISTICS:  
    ( A ) LENGTH: 50 base pairs  
    ( B ) TYPE: nucleic acid  
    ( C ) STRANDEDNESS: single  
    ( D ) TOPOLOGY: linear

( i i ) MOLECULE TYPE: other nucleic acid  
    ( A ) DESCRIPTION: /desc = "DNA"

( x i ) SEQUENCE DESCRIPTION: SEQ ID NO:5:

GTCATGCCAT GGCCTGGTG CCTCGTGGTT CTTGCGGCAC TACAAATACT 50

( 2 ) INFORMATION FOR SEQ ID NO:6:

( i ) SEQUENCE CHARACTERISTICS:  
    ( A ) LENGTH: 35 base pairs  
    ( B ) TYPE: nucleic acid  
    ( C ) STRANDEDNESS: single  
    ( D ) TOPOLOGY: linear

( i i ) MOLECULE TYPE: other nucleic acid  
    ( A ) DESCRIPTION: /desc = "DNA"

( x i ) SEQUENCE DESCRIPTION: SEQ ID NO:6:

TGACAAGCTT AGCATTCTCT GAATTCCTCC TTTCT 35

( 2 ) INFORMATION FOR SEQ ID NO:7:

( i ) SEQUENCE CHARACTERISTICS:  
    ( A ) LENGTH: 50 base pairs  
    ( B ) TYPE: nucleic acid  
    ( C ) STRANDEDNESS: single  
    ( D ) TOPOLOGY: linear

( i i ) MOLECULE TYPE: other nucleic acid  
    ( A ) DESCRIPTION: /desc = "DNA"

( x i ) SEQUENCE DESCRIPTION: SEQ ID NO:7:

GTCATGCCAT GGCCTGGTG CCTCGTGGTT GCGGAGGCGG TGGATCAGGC 50

( 2 ) INFORMATION FOR SEQ ID NO:8:

( i ) SEQUENCE CHARACTERISTICS:  
    ( A ) LENGTH: 36 base pairs  
    ( B ) TYPE: nucleic acid  
    ( C ) STRANDEDNESS: single  
    ( D ) TOPOLOGY: linear

( i i ) MOLECULE TYPE: other nucleic acid  
    ( A ) DESCRIPTION: /desc = "DNA"

( x i ) SEQUENCE DESCRIPTION: SEQ ID NO:8:

AGTATTTGTA GTGCCTGAGG ATCCGCCACC TCCAAT 36

( 2 ) INFORMATION FOR SEQ ID NO:9:

-continued

- ( i ) SEQUENCE CHARACTERISTICS:  
 ( A ) LENGTH: 45 base pairs  
 ( B ) TYPE: nucleic acid  
 ( C ) STRANDEDNESS: single  
 ( D ) TOPOLOGY: linear

- ( i i ) MOLECULE TYPE: other nucleic acid  
 ( A ) DESCRIPTION: /desc = "DNA"

- ( x i ) SEQUENCE DESCRIPTION: SEQ ID NO:9:

GGAGGCGGTG GATCAGGCGG TGGAGGTAGT GGAGGTGGCG GATCC

45

- ( 2 ) INFORMATION FOR SEQ ID NO:10:

- ( i ) SEQUENCE CHARACTERISTICS:  
 ( A ) LENGTH: 17 base pairs  
 ( B ) TYPE: nucleic acid  
 ( C ) STRANDEDNESS: single  
 ( D ) TOPOLOGY: linear

- ( i i ) MOLECULE TYPE: other nucleic acid  
 ( A ) DESCRIPTION: /desc = "DNA"

- ( x i ) SEQUENCE DESCRIPTION: SEQ ID NO:10:

GTCATGCCAT GGCCCTG

17

- ( 2 ) INFORMATION FOR SEQ ID NO:11:

- ( i ) SEQUENCE CHARACTERISTICS:  
 ( A ) LENGTH: 32 base pairs  
 ( B ) TYPE: nucleic acid  
 ( C ) STRANDEDNESS: single  
 ( D ) TOPOLOGY: linear

- ( i i ) MOLECULE TYPE: other nucleic acid  
 ( A ) DESCRIPTION: /desc = "DNA"

- ( x i ) SEQUENCE DESCRIPTION: SEQ ID NO:11:

TGACAAGCTT ATTCTCTGAA TTCCCCCTTT CT

32

- ( 2 ) INFORMATION FOR SEQ ID NO:12:

- ( i ) SEQUENCE CHARACTERISTICS:  
 ( A ) LENGTH: 50 base pairs  
 ( B ) TYPE: nucleic acid  
 ( C ) STRANDEDNESS: single  
 ( D ) TOPOLOGY: linear

- ( i i ) MOLECULE TYPE: other nucleic acid  
 ( A ) DESCRIPTION: /desc = "DNA"

- ( x i ) SEQUENCE DESCRIPTION: SEQ ID NO:12:

GTCATGCCAT GGCCCTGGTG CCTCGTGGTT CTTGCGGCAC TACAAATACT

50

- ( 2 ) INFORMATION FOR SEQ ID NO:13:

- ( i ) SEQUENCE CHARACTERISTICS:  
 ( A ) LENGTH: 53 base pairs  
 ( B ) TYPE: nucleic acid  
 ( C ) STRANDEDNESS: single  
 ( D ) TOPOLOGY: linear

- ( i i ) MOLECULE TYPE: other nucleic acid  
 ( A ) DESCRIPTION: /desc = "DNA"

- ( x i ) SEQUENCE DESCRIPTION: SEQ ID NO:13:

CGCGGATCCA CCGCCACCAG ATCCACCGCC TCCTTCTCTG AATTCCCCTT TCT

53

- ( 2 ) INFORMATION FOR SEQ ID NO:14:

-continued

## ( 1 ) SEQUENCE CHARACTERISTICS:

- ( A ) LENGTH: 44 base pairs
- ( B ) TYPE: nucleic acid
- ( C ) STRANDEDNESS: single
- ( D ) TOPOLOGY: linear

## ( i i ) MOLECULE TYPE: other nucleic acid

- ( A ) DESCRIPTION: /desc = "DNA"

## ( x i ) SEQUENCE DESCRIPTION: SEQ ID NO:14:

CGCGGATCCG GCGGTGGAGG CTCTTCAGGC ACTACAAATA CTGT

4 4

## ( 2 ) INFORMATION FOR SEQ ID NO:15:

## ( i ) SEQUENCE CHARACTERISTICS:

- ( A ) LENGTH: 31 base pairs
- ( B ) TYPE: nucleic acid
- ( C ) STRANDEDNESS: single
- ( D ) TOPOLOGY: linear

## ( i i ) MOLECULE TYPE: other nucleic acid

- ( A ) DESCRIPTION: /desc = "DNA"

## ( x i ) SEQUENCE DESCRIPTION: SEQ ID NO:15:

TGACAAGCTT ATTCTCTGAA TTCCCCTTTC T

3 1

## ( 2 ) INFORMATION FOR SEQ ID NO:16:

## ( i ) SEQUENCE CHARACTERISTICS:

- ( A ) LENGTH: 50 base pairs
- ( B ) TYPE: nucleic acid
- ( C ) STRANDEDNESS: single
- ( D ) TOPOLOGY: linear

## ( i i ) MOLECULE TYPE: other nucleic acid

- ( A ) DESCRIPTION: /desc = "DNA"

## ( x i ) SEQUENCE DESCRIPTION: SEQ ID NO:16:

GTCATGCCAT GGCCCTGGTG CCTCGTGGTT CTTGCGGCAC TACAAATACT

5 0

## ( 2 ) INFORMATION FOR SEQ ID NO:17:

## ( i ) SEQUENCE CHARACTERISTICS:

- ( A ) LENGTH: 31 base pairs
- ( B ) TYPE: nucleic acid
- ( C ) STRANDEDNESS: single
- ( D ) TOPOLOGY: linear

## ( i i ) MOLECULE TYPE: other nucleic acid

- ( A ) DESCRIPTION: /desc = "DNA"

## ( x i ) SEQUENCE DESCRIPTION: SEQ ID NO:17:

TGACAAGCTT ATTCTCTGAA TTCCCCTTTC T

3 1

## ( 2 ) INFORMATION FOR SEQ ID NO:18:

## ( i ) SEQUENCE CHARACTERISTICS:

- ( A ) LENGTH: 44 base pairs
- ( B ) TYPE: nucleic acid
- ( C ) STRANDEDNESS: single
- ( D ) TOPOLOGY: linear

## ( i i ) MOLECULE TYPE: other nucleic acid

- ( A ) DESCRIPTION: /desc = "DNA"

## ( x i ) SEQUENCE DESCRIPTION: SEQ ID NO:18:

GTCATGCCAT GGCCCTGGTG CCTCGTGGTT GCACTACAAA TACT

4 4

## ( 2 ) INFORMATION FOR SEQ ID NO:19:



-continued

## ( i ) SEQUENCE CHARACTERISTICS:

- ( A ) LENGTH: 34 base pairs
- ( B ) TYPE: nucleic acid
- ( C ) STRANDEDNESS: single
- ( D ) TOPOLOGY: linear

## ( i i ) MOLECULE TYPE: other nucleic acid

- ( A ) DESCRIPTION: /desc = "DNA"

## ( x i ) SEQUENCE DESCRIPTION: SEQ ID NO:19:

TGACAAGCTT AGCATTCTCT GAATTCCTTCT TTCT

3 4

## ( 2 ) INFORMATION FOR SEQ ID NO:20:

## ( i ) SEQUENCE CHARACTERISTICS:

- ( A ) LENGTH: 19 base pairs
- ( B ) TYPE: nucleic acid
- ( C ) STRANDEDNESS: single
- ( D ) TOPOLOGY: linear

## ( i i ) MOLECULE TYPE: other nucleic acid

- ( A ) DESCRIPTION: /desc = "DNA"

## ( x i ) SEQUENCE DESCRIPTION: SEQ ID NO:20:

CAAGTTCAGC CAAGAAAAAC

1 9

## ( 2 ) INFORMATION FOR SEQ ID NO:21:

## ( i ) SEQUENCE CHARACTERISTICS:

- ( A ) LENGTH: 36 base pairs
- ( B ) TYPE: nucleic acid
- ( C ) STRANDEDNESS: single
- ( D ) TOPOLOGY: linear

## ( i i ) MOLECULE TYPE: other nucleic acid

- ( A ) DESCRIPTION: /desc = "DNA"

## ( x i ) SEQUENCE DESCRIPTION: SEQ ID NO:21:

ACACTTTATT ATCGGAAATC TTCAGCTTCA GGAAAG

3 6

## ( 2 ) INFORMATION FOR SEQ ID NO:22:

## ( i ) SEQUENCE CHARACTERISTICS:

- ( A ) LENGTH: 657 base pairs
- ( B ) TYPE: nucleic acid
- ( C ) STRANDEDNESS: single
- ( D ) TOPOLOGY: linear

## ( x i ) SEQUENCE DESCRIPTION: SEQ ID NO:22:

TCAGGCACTA CAAATACTGT GGCAGCATAT AATTTAACTT GGAAATCAAC TAATTTCAAG 60

ACAATTTTGG AGTGGGAACC CAAACCCGTC AATCAAGTCT ACACTGTTCA AATAAGCACT 120

AAGTCAGGAG ATTGGAAAAAG CAAATGCTTT TACACAACAG ACACAGAGTG TGACCTCACC 180

GACGAGATTG TGAAGGATGT GAAGCAGACG TACTTGGCAC GGGTCTTCTC CTACCCGGCA 240

GGGAATGTGG AGAGCACCGG TTCTGCTGGG GAGCCTCTGT ATGAGAACTC CCCAGAGTTC 300

ACACCTTACC TGGAGACAAA CCTCGGACAG CCAACAATTC AGAGTTTTGA ACAGGTGGGA 360

ACAAAAGTGA ATGTGACCGT AGAAGATGAA CGGACTTTAG TCAGAAGGAA CAACACTTTC 420

CTAAGCCTCC GGGATGTTTT TGGCAAGGAC TTAATTTATA CACTTTATTA TTGGAAATCT 480

TCAAGTTCAG GAAAGAAAAAC AGCCAAAAACA AACACTAATG AGTTTTTGAT TGATGTGGAT 540

AAAGGAGAAA ACTACTGTTT CAGTGTTCAG GCAGTGATTC CCTCCCGAAC AGTTAACCGG 600

AAGAGTACAG ACAGCCCGGT AGAGTGTATG GGCCAGGAGA AAGGGGAATT CAGAGAA 657

-continued

## ( 2 ) INFORMATION FOR SEQ ID NO:23:

## ( i ) SEQUENCE CHARACTERISTICS:

- ( A ) LENGTH: 219 amino acids
- ( B ) TYPE: amino acid
- ( C ) STRANDEDNESS:
- ( D ) TOPOLOGY: linear

## ( x i ) SEQUENCE DESCRIPTION: SEQ ID NO:23:

```

Ser Gly Thr Thr Asn Thr Val Ala Ala Tyr Asn Leu Thr Trp Lys Ser
1          5          10          15
Thr Asn Phe Lys Thr Ile Leu Glu Trp Glu Pro Lys Pro Val Asn Gln
20          25          30
Val Tyr Thr Val Gln Ile Ser Thr Lys Ser Gly Asp Trp Lys Ser Lys
35          40          45
Cys Phe Tyr Thr Thr Asp Thr Glu Cys Asp Leu Thr Asp Glu Ile Val
50          55          60
Lys Asp Val Lys Gln Thr Tyr Leu Ala Arg Val Phe Ser Tyr Pro Ala
65          70          75          80
Gly Asn Val Glu Ser Thr Gly Ser Ala Gly Glu Pro Leu Tyr Glu Asn
85          90          95
Ser Pro Glu Phe Thr Pro Tyr Leu Glu Thr Asn Leu Gly Gln Pro Thr
100         105         110
Ile Gln Ser Phe Glu Gln Val Gly Thr Lys Val Asn Val Thr Val Glu
115         120         125
Asp Glu Arg Thr Leu Val Arg Arg Asn Asn Thr Phe Leu Ser Leu Arg
130         135         140
Asp Val Phe Gly Lys Asp Leu Ile Tyr Thr Leu Tyr Tyr Trp Lys Ser
145         150         155         160
Ser Ser Ser Gly Lys Lys Thr Ala Lys Thr Asn Thr Asn Glu Phe Leu
165         170         175
Ile Asp Val Asp Lys Gly Glu Asn Tyr Cys Phe Ser Val Gln Ala Val
180         185         190
Ile Pro Ser Arg Thr Val Asn Arg Lys Ser Thr Asp Ser Pro Val Glu
195         200         205
Cys Met Gly Gln Glu Lys Gly Glu Phe Arg Glu
210         215

```

## ( 2 ) INFORMATION FOR SEQ ID NO:24:

## ( i ) SEQUENCE CHARACTERISTICS:

- ( A ) LENGTH: 1947 base pairs
- ( B ) TYPE: nucleic acid
- ( C ) STRANDEDNESS: single
- ( D ) TOPOLOGY: linear

## ( x i ) SEQUENCE DESCRIPTION: SEQ ID NO:24:

```

TGCAGCTGCC TGGCTGCCTG GCCCTGGCTG CCCTGTGTAG CTTGTGTCAC AGCCAGCATG      60
TGTTCTCTGGC TCCTCAGCAA GCACGGTCGC TGCTCCAGCG GGTCCGGCGA GCCAACACCT      120
TCTTGGAGGA GGTGCGCAAG GGCAACCTAG AGCGAGAGTG CGTGGAGGAG ACGTGCAGCT      180
ACGAGGAGGC CTTGAGGGCT CTGGAGTCCT CCACGGCTAC GGATGTGTTC TGGGCCAAGT      240
ACACAGCTTG TGAGACAGCG AGGACGCCTC GAGATAAGCT TGCTGCATGT CTGGAAGGTA      300
ACTGTGCTGA GGGTCTGGGT ACGAACTACC GAGGGCATGT GAACATCACC CGGTCAGGCA      360
TTGAGTGCCA GCTATGGAGG AGTCGCTACC CACATAAGCC TGAAATCAAC TCCACTACCC      420
ATCCTGGGGC CGACCTACAG GAGAATTTCT GCCGCAACCC CGACAGCAGC AACACGGGAC      480
CCTGGTGCTA CACTACAGAC CCCACCGTGA GGAGGCAGGA ATGCAGCATC CCTGTCTGTG      540

```

-continued

GCCAGGATCA	AGTCACTGTA	GCGATGACTC	CACGCTCCGA	AGGCTCCAGT	GTGAATCTGT	600
CACCTCCATT	GGAGCAGTGT	GTCCCTGATC	GGGGGCAGCA	GTACCAGGGG	CGCCTGGCGG	660
TGACCACACA	TGGGCTCCCC	TGCCTGGCCT	GGGCCAGCGC	ACAGGCCAAG	GCCCTGAGCA	720
AGCACCAGGA	CTTCAACTCA	GCTGTGCAGC	TGGTGGAGAA	CTTCTGCCGC	AACCCAGACG	780
GGGATGAGGA	GGGCGTGTGG	TGCTATGTGG	CCGGGAAGCC	TGGCGACTTT	GGGTACTGCG	840
ACCTCAACTA	TTGTGAGGAG	GCCGTGGAGG	AGGAGACAGG	AGATGGGCTG	GATGAGGACT	900
CAGACAGGGC	CATCGAAGGG	CGTACCGCCA	CAAGTGAGTA	CCAGACTTTC	TTCAATCCGA	960
GGACCTTTGG	CTCGGGAGAG	GCAGACTGTG	GGCTGCGACC	TCTGTTCGAG	AAGAAGTCGC	1020
TGGAGGACAA	AACCGAAAGA	GAGCTCCTGG	AATCCTACAT	CGACGGGCGC	ATTGTGGAGG	1080
GCTCGGATGC	AGAGATCGGC	ATGTCACCTT	GGCAGGTGAT	GCTTTTCCGG	AAGAGTCCCC	1140
AGGAGCTGCT	GTGTGGGGCC	AGCCTCATCA	GTGACCGCTG	GGTCCTCACC	GCCGCCCACT	1200
GCCTCCTGTA	CCCGCCCTGG	GACAAGAACT	TCACCGAGAA	TGACCTTCTG	GTGCGCATTG	1260
GCAAGCACTC	CCGCACCAGG	TACGAGCGAA	ACATTGAAAA	GATATCCATG	TTGAAAAAGA	1320
TCTACATCCA	CCCCAGGTAC	AACTGGCGGG	AGAACCTGGA	CCGGGACATT	GCCCTGATGA	1380
AGCTGAAGAA	GCCTGTTGCC	TTCAGTGACT	ACATTACCCC	TGTGTGTCTG	CCCGACAGGG	1440
AGACGGCAGC	CAGCTTGCTC	CAGGCTGGAT	ACAAGGGGCG	GGTGACAGGC	TGGGGCAACC	1500
TGAAGGAGAC	GTGGACAGCC	AACGTTGGTA	AGGGGCAGCC	CAGTGTCCTG	CAGGTGGTGA	1560
ACCTGCCCAT	TGTGGAGCGG	CCGGTCTGCA	AGGACTCCAC	CCGGATCCGC	ATCACTGACA	1620
ACATGTTCTG	TGCTGGTTAC	AAGCCTGATG	AAGGGAAACG	AGGGGATGCC	TGTGAAGGTG	1680
ACAGTGGGGG	ACCCTTTGTC	ATGAAGAGCC	CCTTTAACAA	CCGCTGGTAT	CAAATGGGCA	1740
TCGTCTCATG	GGGTGAAGGC	TGTGACCGGG	ATGGGAAATA	TGGCTTCTAC	ACACATGTGT	1800
TCCGCCTGAA	GAAGTGGATA	CAGAAGGTCA	TTGATCAGTT	TGGAGAGTAG	GGGGCCACTC	1860
ATATTCTGGG	CTCCTGGAAC	CAATCCCCTG	AAAGAATTAT	TTTTGTGTTT	CTAAAACTAT	1920
GGTTCCCAAT	AAAAAGTGACT	CTCAGCG				1947

## ( 2 ) INFORMATION FOR SEQ ID NO:25:

## ( i ) SEQUENCE CHARACTERISTICS:

- ( A ) LENGTH: 2462 base pairs
- ( B ) TYPE: nucleic acid
- ( C ) STRANDEDNESS: single
- ( D ) TOPOLOGY: linear

## ( x i ) SEQUENCE DESCRIPTION: SEQ ID NO:25:

TCAACAGGCA	GGGGCAGCAC	TGCAGAGATT	TCATCATGGT	CTCCCAGGCC	CTCAGGCTCC	60
TCTGCCTTCT	GCTTGGGCTT	CAGGGCTGCC	TGGCTGCAGG	CGGGGTCGCT	AAGGCCTCAG	120
GAGGAGAAAC	ACGGGACATG	CCGTGGAAGC	CGGGGCCTCA	CAGAGTCTTC	GTAACCCAGG	180
AGGAAGCCCA	CGGCGTCTCT	CACCGGCGCC	GGCGCGCCAA	CGCGTTCTCT	GAGGAGCTGC	240
GGCCGGGCTC	CCTGGAGAGG	GAGTGCAAGG	AGGAGCAGTG	CTCCTTCGAG	GAGGGCCGGG	300
AGATCTTCAA	GGACGCGGAG	AGGACGAAGC	TGTTCTGGAT	TTCTTACAGT	GATGGGGACC	360
AGTGTGCCTC	AAGTCCATGC	CAGAATGGGG	GCTCCTGCAA	GGACCAGCTC	CAGTCCTATA	420
TCTGCTTCTG	CCTCCCTGCC	TTCGAGGGCC	GGAAGTGTGA	GACGCACAAAG	GATGACCAGC	480
TGATCTGTGT	GAACGAGAAC	GGCGGCTGTG	AGCAGTACTG	CAGTGACCAC	ACGGGCACCA	540
AGCGCTCCTG	TCGGTGCCAC	GAGGGGTACT	CTCTGCTGGC	AGACGGGGTG	TCCTGCACAC	600

-continued

CCACAGTTGA	ATATCCATGT	GGAAAAATAC	CTATTCTAGA	AAAAAGAAAT	GCCAGCAAAC	660
CCCAAGGCCG	AATTGTGGGG	GGCAAGGTGT	GCCCCAAAGG	GGAGTGTTCA	TGGCAGGTCC	720
TGTTGTTGGT	GAATGGAGCT	CAGTTGTGTG	GGGGGACCCT	GATCAACACC	ATCTGGGTGG	780
TCTCCGCGGC	CCACTGTTTC	GACAAAATCA	AGAACTGGAG	GAACCTGATC	GCGGTGCTGG	840
GCGAGCACGA	CCTCAGCGAG	CACGACGGGG	ATGAGCAGAG	CCGGCGGGTG	GCGCAGGTCA	900
TCATCCCCAG	CACGTACGTC	CCGGGCACCA	CCAACCACGA	CATCGCGCTG	CTCCGCCTGC	960
ACCAGCCCGT	GGTCCTCACT	GACCATGTGG	TGCCCCCTCTG	CCTGCCCCGAA	CGGACGTTCT	1020
CTGAGAGGAC	GCTGGCCTTC	GTGCGCTTCT	CATTGGTCAG	CGGCTGGGGC	CAGCTGCTGG	1080
ACCGTGGCGC	CACGGCCCTG	GAGCTCATGG	TGCTCAACGT	GCCCCGGGCTG	ATGACCCAGG	1140
ACTGCCTGCA	GCAGTCACGG	AAGGTGGGAG	ACTCCCCAAA	TATCACGGAG	TACATGTTCT	1200
GTGCCGGCTA	CTCGGATGGC	AGCAAGGACT	CCTGCAAGGG	GGACAGTGGG	GGCCCACATG	1260
CCACCCACTA	CCGGGGCACG	TGGTACCTGA	CGGGCATCGT	CAGCTGGGGC	CAGGGCTGCG	1320
CAACCGTGGG	CCACTTTGGG	GTGTACACCA	GGGTCTCCCA	GTACATCGAG	TGGCTGCAAA	1380
AGCTCATGCG	CTCAGAGCCA	CGCCCAGGAG	TCCTCTGCG	AGCCCCATTT	CCCTAGCCCA	1440
GCAGCCCTGG	CCTGTGGAGA	GAAAGCCAAG	GCTGCGTCGA	ACTGTCCTGG	CACCAAATCC	1500
CATATATTCT	TCTGCAGTTA	ATGGGGTAGA	GGAGGGCATG	GGAGGGAGGG	AGAGGTGGGG	1560
AGGGAGACAG	AGACAGAAAC	AGAGAGAGAC	AGAGACAGAG	AGAGACTGAG	GGAGAGACTC	1620
TGAGGACATG	GAGAGAGACT	CAAAGAGACT	CCAAGATTCA	AAGAGACTAA	TAGAGACACA	1680
GAGATGGAAT	AGAAAAGATG	AGAGGCAGAG	GCAGACAGGC	GCTGGACAGA	GGGGCAGGGG	1740
AGTGCCAAGG	TTGTCTTGGG	GGCAGACAGC	CCAGCTGAGC	CTCCTTACCT	CCCTTCAGCC	1800
AAGCCCCACC	TGCACGTGAT	CTGCTGGCCC	TCAGGCTGCT	GCTCTGCCTT	CATTGCTGGA	1860
GACAGTAGAG	GCATGAACAC	ACATGGATGC	ACACACACAC	ACGCCAATGC	ACACACACAG	1920
AGATATGCAC	ACACACGGAT	GCACACACAG	ATGGTCACAC	AGAGATACGC	AAACACACCG	1980
ATGCACACGC	ACATAGAGAT	ATGCACACAC	AGATGCACAC	ACAGATATAC	ACATGGATGC	2040
ACGCACATGC	CAATGCACGC	ACACATCAGT	GCACACGGAT	GCACAGAGAT	ATGCACACAC	2100
CGATGTGCGC	ACACACAGAT	ATGCACACAC	ATGGATGAGC	ACACACACAC	CAAGTGCGCA	2160
CACACACCGA	TGTACACACA	CAGATGCACA	CACAGATGCA	CACACACCGA	TGCTGACTCC	2220
ATGTGTGCTG	TCCTCTGAAG	GCGGTTGTTT	AGCTCTCACT	TTTCTGGTTC	TTATCCATTA	2280
TCATCTTCAC	TTCAGACAAT	TCAGAAAGCAT	CACCATGCAT	GGTGGCGAAT	GCCCCCAAAC	2340
TCTCCCCCAA	ATGTATTTCT	CCCTTCGCTG	GGTGCCGGGC	TGCACAGACT	ATTCCCCACC	2400
TGCTTCCAG	CTTCACAATA	AACGGCTGCG	TCTCCTCCGC	ACACCTGTGG	TGCCTGCCAC	2460
CC						2462

## ( 2 ) INFORMATION FOR SEQ ID NO:26:

## ( i ) SEQUENCE CHARACTERISTICS:

- ( A ) LENGTH: 1437 base pairs
- ( B ) TYPE: nucleic acid
- ( C ) STRANDEDNESS: single
- ( D ) TOPOLOGY: linear

## ( x i ) SEQUENCE DESCRIPTION: SEQ ID NO:26:

ATGCAGCGCG	TGAACATGAT	CATGGCAGAA	TCACCAAGCC	TCATCACCAT	CTGCCTTTTA	60
GGATATCTAC	TCAGTGCTGA	ATGTACAGTT	TTTCTTGATC	ATGAAAACGC	CAACAAAATT	120
CTGAATCGGC	CAAAGAGGTA	TAATTCAGGT	AAATTGGAAG	AGTTTGTTC	AGGGAACCTT	180

-continued

GAGAGAGAAT	GTATGGAAGA	AAAGTGTAGT	TTTGAAGAAC	CACGAGAAGT	TTTTGAAAAC	240
ACTGAAAAGA	CAACTGAATT	TTGGAAGCAG	TATGTTGATG	GAGATCAGTG	TGAGTCCAAT	300
CCATGTTTAA	ATGGCGGCAG	TTGCAAGGAT	GACATTAATT	CCTATGAATG	TTGGTGTCCC	360
TTTGGATTTG	AAGGAAAAGAA	CTGTGAATTA	GATGTAACAT	GTAACATTAA	GAATGGCAGA	420
TGCGAGCAGT	TTTGTA AAAA	TAGTGCTGAT	AACAAGGTGG	TTTGCTCCTG	TACTGAGGGA	480
TATCGACTTG	CAGAAAACCA	GAAGTCCTGT	GAACCAGCAG	TGCCATTTCC	ATGTGGAAGA	540
GTTTCTGTTT	CACAAACTTC	TAAGCTCACC	CGTGCTGAGG	CTGTTTTTCC	TGATGTGGAC	600
TATGTAAATC	CTACTGAAGC	TGAAACCATT	TTGGATAACA	TCACTCAAGG	CACCCAATCA	660
TTTAATGACT	TCACTCGGGT	TGTTGGTGGA	GAAGATGCCA	AACCAGGTCA	ATTCCCTTGG	720
CAGGTTGTTT	TGAATGGTAA	AGTTGATGCA	TTCTGTGGAG	GCTCTATCGT	TAATGAAAAA	780
TGGATTGTAA	CTGCTGCCCA	CTGTGTTGAA	ACTGGTGTTA	AAATTACAGT	TGTCGCAGGT	840
GAACATAATA	TTGAGGAGAC	AGAACATACA	GAGCAAAAAGC	GAAATGTGAT	TCGAGCAATT	900
ATTCCTCACC	ACAACTACAA	TGCAGCTATT	AATAAGTACA	ACCATGACAT	TGCCCTTCTG	960
GAACCTGGACG	AACCCTTAGT	GCTAAACAGC	TACGTTACAC	CTATTTGCAT	TGCTGACAAG	1020
GAATACACGA	ACATCTTCCT	CAAATTTGGA	TCTGGCTATG	TAAGTGGCTG	GGCAAGAGTC	1080
TTCCACAAAAG	GGAGATCAGC	TTTAGTTCTT	CAGTACCTTA	GAGTTCCACT	TGTTGACCGA	1140
GCCACATGTC	TTCGATCTAC	AAAGTTCACC	ATCTATAACA	ACATGTTCTG	TGCTGGCTTC	1200
CATGAAGGAG	GTAGAGATTG	ATGTCAAGGA	GATAGTGGGG	GACCCCATGT	TACTGAAGTG	1260
GAAGGGACCA	GTTTCTTAAC	TGGAATTATT	AGCTGGGGTG	AAGAGTGTGC	AATGAAAGGC	1320
AAATATGGAA	TATATACCAA	GGTATCCCGG	TATGTCAACT	GGATTAAAGGA	AAAAACAAAG	1380
CTCACTTAAT	GAAAGATGGA	TTTCCAAGGT	TAATTCATTG	GAATTGAAAA	TTAACAG	1437

## ( 2 ) INFORMATION FOR SEQ ID NO:27:

## ( i ) SEQUENCE CHARACTERISTICS:

- ( A ) LENGTH: 1126 base pairs
- ( B ) TYPE: nucleic acid
- ( C ) STRANDEDNESS: single
- ( D ) TOPOLOGY: linear

## ( x i ) SEQUENCE DESCRIPTION: SEQ ID NO:27:

GGATTGGAAG	GCAAAAACCTG	TGAATTATTG	ACACGGAAGC	TCTGCAGCCT	GGACAACGGG	60
GACTGTGACC	AGTTCTGCCA	CGAGGAACAG	AACCTCTGTG	TGTGCTCCTG	CGCCCGCGGG	120
TACACCCTGG	CTGACAACGG	CAAGGCCTGC	ATTCCCACAG	GGCCCTACCC	CTGTGGGAAA	180
CAGACCCTGG	AACGCAGGAA	GAGGTCAGTG	GCCCAGGCCA	CCAGCAGCAG	CGGGGAGGCC	240
CCTGACAGCA	TCACATGGAA	GCCATATGAT	GCAGCCGACC	TGGACCCAC	CGAGAACCCC	300
TTGACCTGTC	TTGACTTCAA	CCAGACGCAG	CCTGAGAGGG	GCGACAACAA	CCTCACCAGG	360
ATCGTGGGAG	GCCAGGAATG	CAAGGACGGG	GAGTGTCCCT	GGCAGGCCCT	GCTCATCAAT	420
GAGGAAAACG	AGGGTTTCTG	TGGTGGAACC	ATTCTGAGCG	AGTTCTACAT	CCTAACGGCA	480
GCCCACTGTC	TCTACCAAGC	CAAGAGATTG	GAAAGGGACC	GGAACACGGA	GCAGGAGGAG	540
GGCGGTGAGG	CGGTGCACGA	GGTGGAGGTG	GTCTCAAGC	ACAACCGGTT	CACAAAGGAG	600
ACCTATGACT	TCGACATCGC	CGTGCTCCGG	CTCAAGACCC	CCATCACCTT	CCGCATGAAC	660
GTGGCGCCTG	CCTGCCTCCC	CGAGCGTGAC	TGGGCCGAGT	CCACGCTGAT	GACGCAGAAG	720
ACGGGGATTG	TGAGCGGCTT	CGGGCGCACC	CACGAGAAGG	GCCGGCAGTC	CACCAGGCTC	780

-continued

AAGATGCTGG	AGGTGCCCTA	CGTGGACCGC	AACAGCTGCA	AGCTGTCCAG	CAGCTTCATC	840
ATCACCCAGA	ACATGTTCTG	TGCCGGCTAC	GACACCAAGC	AGGAGGATGC	CTGCCAGGGG	900
GACAGCGGGG	GCCCCGACGT	CACCCGCTTC	AAGGACACCT	ACTTCGTGAC	AGGCATCGTC	960
AGCTGGGGAG	AGGGCTGTGC	CCGTAAGGGG	AAGTACGGGA	TCTACACCAA	GGTCACCGCC	1020
TTCCTCAAGT	GGATCGACAG	GTCCATGAAA	ACCAGGGGCT	TGCCCAAGGC	CAAGAGCCAT	1080
GCCCCGGAGG	TCATAACGTC	CTCTCCATTA	AAGTGAGATC	CCACTC		1126

## (2) INFORMATION FOR SEQ ID NO:28:

## (i) SEQUENCE CHARACTERISTICS:

- (A) LENGTH: 45 base pairs
- (B) TYPE: nucleic acid
- (C) STRANDEDNESS: single
- (D) TOPOLOGY: linear

## (ii) MOLECULE TYPE: other nucleic acid

- (A) DESCRIPTION: /desc = "DNA"

## (xi) SEQUENCE DESCRIPTION: SEQ ID NO:28:

GAAGAAGGGA	TCCTGGTGCC	TCGTGGTTCT	GGCACTACAA	ATACT	45
------------	------------	------------	------------	-------	----

## (2) INFORMATION FOR SEQ ID NO:29:

## (i) SEQUENCE CHARACTERISTICS:

- (A) LENGTH: 30 base pairs
- (B) TYPE: nucleic acid
- (C) STRANDEDNESS: single
- (D) TOPOLOGY: linear

## (ii) MOLECULE TYPE: other nucleic acid

- (A) DESCRIPTION: /desc = "DNA"

## (xi) SEQUENCE DESCRIPTION: SEQ ID NO:29:

CTGGCCTCAA	GCTTAACGGA	ATTACCTTT	30
------------	------------	-----------	----

## (2) INFORMATION FOR SEQ ID NO:30:

## (i) SEQUENCE CHARACTERISTICS:

- (A) LENGTH: 25 amino acids
- (B) TYPE: amino acid
- (C) STRANDEDNESS: single
- (D) TOPOLOGY: linear

## (ii) MOLECULE TYPE: peptide

## (xi) SEQUENCE DESCRIPTION: SEQ ID NO:30:

Ala	Pro	Met	Ala	Glu	Gly	Glu	Gln	Lys	Pro	Arg	Glu	Val	Val	Lys	Phe
1				5				10						15	
Met	Asp	Val	Tyr	Lys	Arg	Ser	Tyr	Cys							
			20					25							

## (2) INFORMATION FOR SEQ ID NO:31:

## (i) SEQUENCE CHARACTERISTICS:

- (A) LENGTH: 26 amino acids
- (B) TYPE: amino acid
- (C) STRANDEDNESS: single
- (D) TOPOLOGY: linear

## (ii) MOLECULE TYPE: peptide

## (xi) SEQUENCE DESCRIPTION: SEQ ID NO:31:

Ala	Pro	Met	Ala	Glu	Gly	Gly	Gly	Gln	Asn	His	His	Glu	Val	Val	Lys
1				5				10							15
Phe	Met	Asp	Val	Tyr	Gln	Arg	Ser	Tyr	Cys						

-continued

20

25

## (2) INFORMATION FOR SEQ ID NO:32:

## (i) SEQUENCE CHARACTERISTICS:

- (A) LENGTH: 25 amino acids
- (B) TYPE: amino acid
- (C) STRANDEDNESS: single
- (D) TOPOLOGY: linear

## (ii) MOLECULE TYPE: peptide

## (xi) SEQUENCE DESCRIPTION: SEQ ID NO:32:

Met	Ala	Ala	Gly	Ser	Ile	Thr	Thr	Leu	Pro	Ala	Leu	Pro	Glu	Gly	Gly	
1				5				10						15		
Asp	Gly	Gly	Ala	Phe	Ala	Pro	Gly	Cys								
			20					25								

20

What is claimed is:

1. A binding ligand comprising:

(a) a first binding region that binds to a tumor cell, a component of tumor-associated vasculature or a component of tumor-associated stroma; the first binding region operatively linked to

(b) a Tissue Factor construct or a second binding region that binds to a Tissue Factor construct, wherein said second binding region comprises an antibody or an antigen binding region of an antibody.

2. The binding ligand of claim 1, wherein said Tissue Factor construct comprises a mutant Tissue Factor deficient in the ability to activate Factor VII.

3. The binding ligand of claim 2, wherein said Tissue Factor construct includes a mutation in the amino acid region between about position 157 and about position 167.

4. The binding ligand of claim 3, wherein, within said Tissue Factor construct, Trp at position 158 is changed to Arg; wherein Ser at position 162 is changed to Ala; wherein Gly at position 164 is changed to Ala; or wherein Trp at position 158 is changed to Arg and Ser at position 162 is changed to Ala.

5. The binding ligand of claim 1, wherein said Tissue Factor construct comprises a truncated Tissue Factor.

6. The binding ligand of claim 5, wherein said truncated Tissue Factor comprises amino acids 1 to about 219 of the mature Tissue Factor protein.

7. The binding ligand of claim 5, wherein said truncated Tissue Factor has the amino acid sequence of SEQ ID NO:23.

8. The binding ligand of claim 1, wherein said Tissue Factor construct comprises a first Tissue Factor or truncated Tissue Factor construct operatively linked to a second Tissue Factor or truncated Tissue Factor construct.

9. The binding ligand of claim 8, wherein said Tissue Factor construct comprises two truncated Tissue Factors.

10. The binding ligand of claim 9, wherein said Tissue Factor construct comprises three truncated Tissue Factors.

11. The binding ligand of claim 10, wherein said Tissue Factor construct comprises five truncated Tissue Factors.

12. The binding ligand of claim 8, wherein said Tissue Factor construct comprises a first and second Tissue Factor construct operatively linked via a disulfide, thioether or peptide bond.

13. The binding ligand of claim 1, wherein said Tissue Factor construct comprises a Tissue Factor construct with a hydrophobic membrane insertion moiety, and wherein said

Tissue Factor construct is linked to said first binding region via a biologically-releasable bond.

14. The binding ligand of claim 1, comprising a first binding region operatively linked to said Tissue Factor construct.

15. The binding ligand of claim 14, wherein said first binding region is linked to said Tissue Factor construct via a biologically-releasable bond.

16. The binding ligand of claim 15, wherein said first binding region is linked via a biologically-releasable bond to a Tissue Factor construct that comprises a hydrophobic membrane insertion moiety.

17. The binding ligand of claim 16, wherein said Tissue Factor construct comprises a truncated Tissue Factor that includes a hydrophobic membrane insertion moiety comprising a stretch of between about 3 and about 20 hydrophobic amino acids.

18. The binding ligand of claim 17, wherein said hydrophobic membrane insertion moiety comprises a stretch of hydrophobic amino acids located at the N- or C-terminus of the truncated Tissue Factor.

19. The binding ligand of claim 16, wherein said Tissue Factor construct comprises a truncated Tissue Factor that includes a hydrophobic membrane insertion moiety comprising a fatty acid.

20. The binding ligand of claim 16, wherein said Tissue Factor construct comprises two truncated Tissue Factors, each of which includes a hydrophobic membrane insertion moiety.

21. The binding ligand of claim 15, wherein said first binding region is linked to said Tissue Factor construct via a selectively-cleavable peptide bond.

22. The binding ligand of claim 21, wherein said first binding region is linked to said Tissue Factor construct via a peptide linker that includes a cleavage site for urokinase, plasmin, Thrombin, Factor IXa, Factor Xa or a metalloproteinase.

23. The binding ligand of claim 22, wherein said first binding region is linked to said Tissue Factor construct via a peptide linker that includes a cleavage site for an interstitial collagenase, a gelatinase or a stromelysin.

24. The binding ligand of claim 1, comprising a first binding region operatively linked to a second binding region that binds to said Tissue Factor construct, said second binding region comprising an antibody or an antigen binding region of an antibody.

25. The binding ligand of claim 24, wherein said first binding region is an antibody or an antigen binding region of an antibody.

26. The binding ligand of claim 24, wherein said second binding region comprises an IgG antibody or an IgM antibody.

27. The binding ligand of claim 24, wherein said second binding region comprises an scFv, Fv, Fab', Fab or F(ab')<sub>2</sub> fragment of an antibody.

28. The binding ligand of claim 24, further comprising a Tissue Factor construct bound to said second antibody or antigen binding region of an antibody.

29. The binding ligand of claim 1, wherein said first binding region comprises an antibody or an antigen binding region of an antibody.

30. The binding ligand of claim 25, wherein said first binding region comprises an IgG antibody or an IgM antibody.

31. The binding ligand of claim 29, wherein said first binding region comprises an scFv, Fv, Fab', Fab or F(ab')<sub>2</sub> fragment of an antibody.

32. The binding ligand of claim 29, wherein said first binding region comprises an antigen binding region of an antibody that binds to the tumor cell surface antigen p185<sup>HER2</sup>, milk mucin core protein, TAG-72, Lewis a, carcinoembryonic antigen (CEA) or a tumor-associated antigen that binds to an antibody selected from the group consisting of B3 (ATCCHB10573), KS1/4 (NRRLB/18536 and NRRLB/18537), 260F9 (ATCCHB8488) and D612 (ATCCHB9796).

33. The binding ligand of claim 29, wherein said first binding region comprises an antigen binding region of an antibody that binds to a surface-expressed, surface-accessible or surface-localized component of intratumoral blood vessels of a vascularized tumor.

34. The binding ligand of claim 33, wherein said first binding region comprises an antigen binding region of an antibody that binds to a tumor vasculature cell surface receptor.

35. The binding ligand of claim 34, wherein said first binding region comprises an antigen binding region of an antibody that binds to an MHC Class II protein, a VEGF/VPF receptor, an FGF receptor, a TGF $\beta$  receptor, a TIE, VCAM-1, ICAM-1, P-selectin, E-selectin,  $\alpha_v\beta_3$  integrin, pleiotropin, endosialin or endoglin.

36. The binding ligand of claim 35, wherein said first binding region comprises an antigen binding region of an antibody that binds to an MHC Class II protein.

37. The binding ligand of claim 35, wherein said first binding region comprises an antigen binding region of an antibody that binds to a VEGF/VPF receptor.

38. The binding ligand of claim 35, wherein said first binding region comprises an antigen binding region of an antibody that binds to VCAM-1.

39. The binding ligand of claim 35, wherein said first binding region comprises an antigen binding region of an antibody that binds to ICAM-1.

40. The binding ligand of claim 35, wherein said first binding region comprises an antigen binding region of an antibody that binds to P-selectin.

41. The binding ligand of claim 35, wherein said first binding region comprises an antigen binding region of an antibody that binds to E-selectin.

42. The binding ligand of claim 35, wherein said first binding region comprises an antigen binding region of an antibody that binds to endoglin.

43. The binding ligand of claim 42, wherein said first binding region comprises an antigen binding region of an antibody that binds to the same epitope as the monoclonal antibody TEC-4 (ATCC HB 12312).

44. The binding ligand of claim 43, wherein said first binding region comprises an antigen binding region of the monoclonal antibody TEC-4 (ATCC HB 12312).

45. The binding ligand of claim 42, wherein said first binding region comprises an antigen binding region of an antibody that binds to the same epitope as the monoclonal antibody TEC-11 (ATCC HB-12311).

46. The binding ligand of claim 45, wherein said first binding region comprises an antigen binding region of the monoclonal antibody TEC-11 (ATCC HB-12311).

47. The binding ligand of claim 33, wherein said first binding region comprises an antigen binding region of an antibody that binds to a ligand or growth factor that binds to a tumor vasculature cell surface receptor.

48. The binding ligand of claim 47, wherein said first binding region comprises an antigen binding region of an antibody that binds to VEGF/VPF, FGF, TGF $\beta$ , a ligand that binds to a TIE, a tumor-associated fibronectin isoform, scatter factor, hepatocyte growth factor (HGF), platelet factor 4 (PF4), PDGF or TIMP.

49. The binding ligand of claim 48, wherein said first binding region comprises an antigen binding region of an antibody that binds to VEGF/VPF.

50. The binding ligand of claim 49, wherein said first binding region comprises an antigen binding region of an antibody that binds to the same epitope as the monoclonal antibody GV39 (ATCC HB 12450).

51. The binding ligand of claim 50, wherein said first binding region comprises an antigen binding region of the monoclonal antibody GV39 (ATCC HB 12450).

52. The binding ligand of claim 49, wherein said first binding region comprises an antigen binding region of an antibody that binds to the same epitope as the monoclonal antibody GV97 (ATCC HB 12451).

53. The binding ligand of claim 52, wherein said first binding region comprises an antigen binding region of the monoclonal antibody GV97 (ATCC HB 12451).

54. The binding ligand of claim 48, wherein said first binding region comprises an antigen binding region of an antibody that binds to FGF.

55. The binding ligand of claim 48, wherein said first binding region comprises an antigen binding region of an antibody that binds to TGF $\beta$ .

56. The binding ligand of claim 33, wherein said first binding region comprises an antigen binding region of an antibody that binds to a ligand:receptor complex or a growth factor:receptor complex, but does not bind to the ligand or growth factor or to the receptor when the ligand or growth factor or the receptor is not in the ligand:receptor complex.

57. The binding ligand of claim 29, wherein said first binding region comprises an antigen binding region of an antibody that binds to a basement membrane component, tenascin, an activated platelet or an antigen inducible on a basement membrane component or activated platelet.

58. The binding ligand of claim 33, wherein said first binding region is operatively linked to a second antibody or antigen binding region thereof that binds to a Tissue Factor construct.

59. The binding ligand of claim 1, wherein said first binding region comprises a ligand or receptor that binds to a tumor cell, a component of tumor vasculature or a component of tumor stroma.

60. The binding ligand of claim 59, wherein said first binding region comprises VEGF/VPF, FGF, TGF $\beta$ , a ligand that binds to a TIE, a tumor-associated fibronectin isoform, scatter factor, hepatocyte growth factor (HGF), platelet factor 4 (PF4), PDGF, TIMP or a soluble binding domain of a VEGF/VPF receptor.



61. The binding ligand of claim 60, wherein said first binding region comprises VEGF/VPF.

62. The binding ligand of claim 1, comprising a first antibody or antigen binding region of an antibody that binds to a tumor cell, a component of tumor-associated vasculature or a component of tumor-associated stroma; the first binding region operatively linked to a second antibody or antigen binding region of an antibody that binds to a Tissue Factor construct.

63. The binding ligand of claim 1, wherein said first binding region is operatively linked to said Tissue Factor construct or said second binding region via a covalent bond.

64. The binding ligand of claim 10, wherein said first binding region is operatively linked to said Tissue Factor construct or said second binding region via a cross-linker.

65. The binding ligand of claim 10, wherein said binding ligand is a fusion protein prepared by expressing a recombinant vector in a host cell, wherein the vector comprises, in the same reading frame, a DNA segment encoding said first binding region operatively linked to a DNA segment encoding said Tissue Factor construct or said second binding region.

66. The binding ligand of claim 1, dispersed in a pharmacologically acceptable medium.

67. A binding ligand comprising a first antibody or antigen binding region of an antibody that binds to a tumor cell, a component of tumor-associated vasculature or a component of tumor-associated stroma; the first binding region operatively linked to a Tissue Factor construct.

68. A binding ligand comprising a first antibody or antigen binding region of an antibody that binds to a tumor cell, a component of tumor-associated vasculature or a component of tumor-associated stroma; the first binding region operatively linked to a second antibody or antigen binding region of an antibody that binds to a Tissue Factor construct.

69. A bispecific antibody comprising:

(a) a first antibody or antigen binding region of an antibody that binds to a tumor cell, a component of tumor-associated vasculature or a component of tumor-associated stroma; the first antibody or antigen binding region operatively linked to

(b) a second antibody or antigen binding region of an antibody that binds to a Tissue Factor construct.

70. A binding ligand comprising a first binding region that binds to a surface-expressed, surface-accessible or surface-localized marker of intratumoral blood vessels of a vascularized tumor, the first binding region operatively linked to a Tissue Factor construct or to an antibody, or antigen binding region thereof, that binds to a Tissue Factor construct.

71. A binding ligand comprising a first antibody, or antigen binding region thereof, that binds to a surface-expressed surface-accessible or surface-localized marker of intratumoral blood vessels of a vascularized tumor, the first antibody or antigen binding region operatively linked to a Tissue Factor construct or to a second antibody, or antigen binding region thereof, that binds to a Tissue Factor construct.

72. The binding ligand of claim 71; wherein said first antibody, or antigen binding region thereof, is linked to a Tissue Factor construct.

73. The binding ligand of claim 71, wherein said first antibody, or antigen binding region thereof, is linked to a second antibody, or antigen binding region thereof, that binds to a Tissue Factor construct.

74. A Tissue Factor construct comprising an operatively linked first, second and third Tissue Factor construct or truncated Tissue Factor construct.

75. The Tissue Factor construct of claim 74, comprising about five operatively linked Tissue Factor or truncated Tissue Factor constructs.

76. The Tissue Factor construct of claim 75, comprising about ten operatively linked Tissue Factor or truncated Tissue Factor constructs.

77. The Tissue Factor construct of claim 76, comprising about twenty operatively linked Tissue Factor or truncated Tissue Factor constructs.

78. The Tissue Factor construct of claim 74, comprising at least one truncated Tissue Factor.

79. The Tissue Factor construct of claim 78, wherein said truncated Tissue Factor comprises amino acids 1 to about 219 of the mature Tissue Factor protein.

80. The Tissue Factor construct of claim 78, wherein said truncated Tissue Factor has the amino acid sequence of SEQ ID NO:23.

81. The Tissue Factor construct of claim 78, comprising a truncated Tissue Factor that includes a hydrophobic membrane insertion moiety.

82. The Tissue Factor construct of claim 81, comprising a truncated Tissue Factor that includes a stretch of between about 3 and about 20 hydrophobic amino acids.

83. The Tissue Factor construct of claim 82, comprising a truncated Tissue Factor that includes a stretch of hydrophobic amino acids located at the N- or C-terminus of the truncated Tissue Factor.

84. The Tissue Factor construct of claim 81, comprising a truncated Tissue Factor that includes a fatty acid.

85. The Tissue Factor construct of claim 81, comprising two truncated Tissue Factors, each of which includes a hydrophobic membrane insertion moiety.

86. The Tissue Factor construct of claim 78, comprising a truncated Tissue Factor modified to contain a terminal cysteine residue.

87. The Tissue Factor construct of claim 86, comprising two truncated Tissue Factors, each of which is modified to contain a terminal cysteine residue.

88. The Tissue Factor construct of claim 86, further comprising an antibody or an antigen binding region of an antibody operatively linked to said cysteine residue.

89. The Tissue Factor construct of claim 78, comprising a truncated Tissue Factor modified to contain a selectively cleavable peptide linker.

90. The Tissue Factor construct of claim 89, wherein said selectively cleavable peptide linker includes a cleavage site for urokinase, plasmin, Thrombin, Factor IXa, Factor Xa or a metalloproteinase.

91. The Tissue Factor construct of claim 90, wherein said selectively cleavable peptide linker includes a cleavage site for an interstitial collagenase, a gelatinase or a stromelysin.

92. The Tissue Factor construct of claim 89, further comprising an antibody or an antigen binding region of an antibody operatively linked to said selectively cleavable peptide linker.

93. The Tissue Factor construct of claim 67, comprising an operatively linked series of units in the sequence: a cysteine residue, a selectively cleavable peptide linker, a stretch of hydrophobic amino acids, a first truncated Tissue Factor, a second truncated Tissue Factor, and a third truncated Tissue Factor.

94. The Tissue Factor construct of claim 93, further comprising an antibody or an antigen binding region of an antibody operatively linked to said cysteine residue.

95. The Tissue Factor construct of claim 93, comprising an operatively linked series of units in the sequence: a

139

cysteine residue, a selectively cleavable peptide linker, a first stretch of hydrophobic amino acids, a first truncated Tissue Factor, a second truncated Tissue Factor, a third truncated Tissue Factor and a second stretch of hydrophobic amino acids.

96. The Tissue Factor construct of claim 95, comprising an operatively linked series of units in the sequence: a first cysteine residue, a selectively cleavable peptide linker, a first stretch of hydrophobic amino acids, a first truncated Tissue Factor, a second truncated Tissue Factor, a third truncated Tissue Factor, a second stretch of hydrophobic amino acids and a second cysteine residue or a second a selectively cleavable peptide linker.

97. The Tissue Factor construct of claim 96, comprising an antibody or an antigen binding region of an antibody operatively linked to said first or second cysteine residue.

140

98. A Tissue Factor construct comprising a first Tissue Factor or truncated Tissue Factor construct operatively linked to a second Tissue Factor or truncated Tissue Factor construct wherein at least one of said Tissue Factor or truncated Tissue Factor constructs is a mutant Tissue Factor deficient in the ability to activate Factor VII.

99. The Tissue Factor construct of claim 98, comprising a Tissue Factor that includes a mutation in the amino acid region between about position 157 and about position 167.

100. The Tissue Factor construct of claim 99, comprising a mutant Tissue Factor wherein Trp at position 158 is changed to Arg; wherein Ser at position 162 is changed to Ala; wherein Gly at position 164 is changed to Ala; or wherein Trp at position 158 is changed to Arg and Ser at position 162 is changed to Ala.

\* \* \* \* \*

UNITED STATES PATENT AND TRADEMARK OFFICE  
**CERTIFICATE OF CORRECTION**

PATENT NO. : 5,877,289

DATED : March 2, 1999

INVENTOR(S) : Philip E. Thorpe and Thomas S. Edgington

It is certified that error appears in the above-identified patent and that said Letters Patent is hereby corrected as shown below:

Claim 30, column 135, line 13, delete --25-- and insert "29" therefor.  
Claim 32, column 135, line 25, delete --18536-- and insert "18356" therefor.  
Claim 32, column 135, line 26, delete --18537-- and insert "18357" therefor.  
Claim 64, column 137, line 13, delete --10-- and insert "63" therefor.  
Claim 65, column 137, line 16, delete --10-- and insert "63" therefor.  
Claim 93, column 138, line 57, delete --67-- and insert "74" therefor.

Signed and Sealed this

Twenty-fourth Day of August, 1999

Attest:



Q. TODD DICKINSON

Attesting Officer

Acting Commissioner of Patents and Trademarks

## United States Patent [19]

Woodle et al.

[11] Patent Number: 5,013,556

[45] Date of Patent: May 7, 1991

## [54] LIPOSOMES WITH ENHANCED CIRCULATION TIME

[75] Inventors: Martin C. Woodle, Menlo Park; Francis J. Martin, San Francisco; Annie Yau-Young, Los Altos; Carl T. Redemann, Walnut Creek, all of Calif.

[73] Assignee: Liposome Technology, Inc., Menlo Park, Calif. .

[21] Appl. No.: 425,224

[22] Filed: Oct. 20, 1989

[51] Int. Cl.<sup>5</sup> ..... A61K 37/22

[52] U.S. Cl. .... 424/450; 424/1.1; 264/4.3

[58] Field of Search ..... 424/450, 1.1; 264/4.3

## [56] References Cited

## U.S. PATENT DOCUMENTS

4,534,899 8/1985 Sears .  
4,837,028 6/1989 Allen ..... 424/450  
4,885,172 12/1989 Bally et al. .... 424/450  
4,904,479 2/1990 Illum .  
4,920,016 4/1990 Allen et al. .

## OTHER PUBLICATIONS

"Targeting of Colloidal Particles to the Bone Marrow", Illum et al., Life Sciences, vol. 44, pp. 1553-1560, (1987).

"Effect of the Nonionic Surfactant Poloxamer 338 on the Fate and Deposition of Polystyrene Microspheres

Following Intravenous Administration", Illum et al., J. Pharm. Sci., vol. 72, No. 9, (Sep. 83).

"The Organ Distribution and Circulation Time of Intravenously Injected Colloidal Carriers Sterically Stabilized with a Blockcopolymer-Poloxamine 908", Illum et al., Life Sciences, vol. 40, pp. 367-374, (1987).

"The Organ Uptake of Intravenously Administered Colloidal Particles Can Be Altered Using a Non-Ionic Surfactant (Poloxamer 338)", Illum et al., Federation of European Biochem. Soc's, (Elsevier Science Publishers B.V.), vol. 167, No. 1, (Feb. 1984).

Primary Examiner—Thurman K. Page

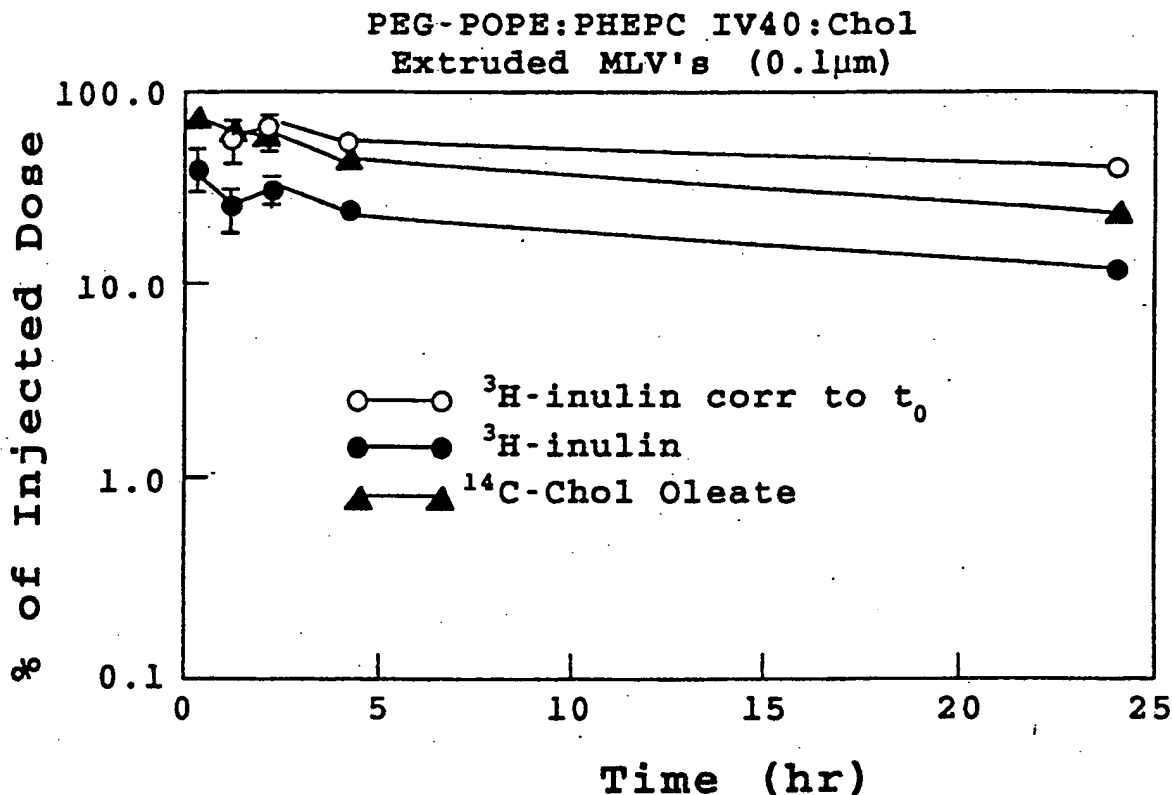
Assistant Examiner—P. L. Prater

Attorney, Agent, or Firm—Peter J. Dehlinger

## [57] ABSTRACT

A liposome composition which contains between 1-20 mole percent of an amphipathic lipid derivatized with a polyalkylether, as exemplified by phosphatidylethanolamine derivatized with polyethyleneglycol. The derivatized lipid enhances the circulation time of the liposomes severalfold, and this enhancement is achieved with either fluid or membrane-rigidifying liposome components. Also disclosed are methods for delivering a drug for slow release from the bloodstream, and for targeting a selected tissue or cells with liposomes, via the bloodstream.

34 Claims, 4 Drawing Sheets



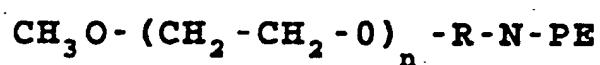
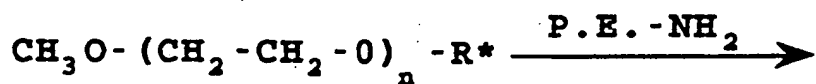
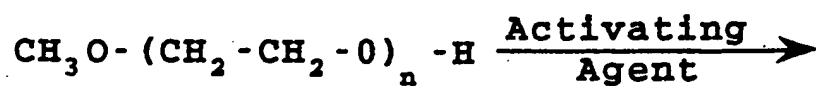


Fig. 1

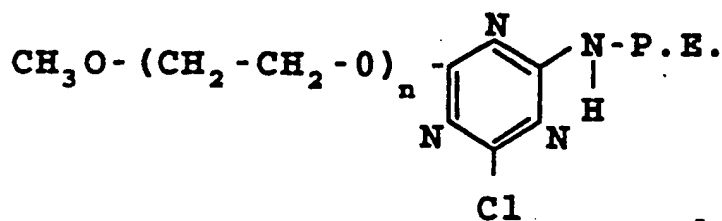
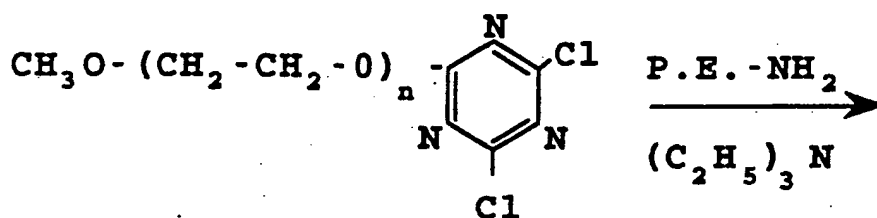
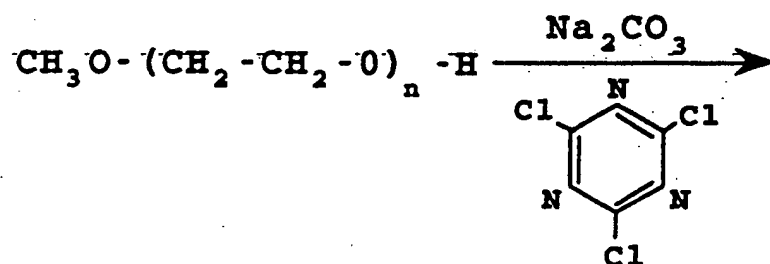
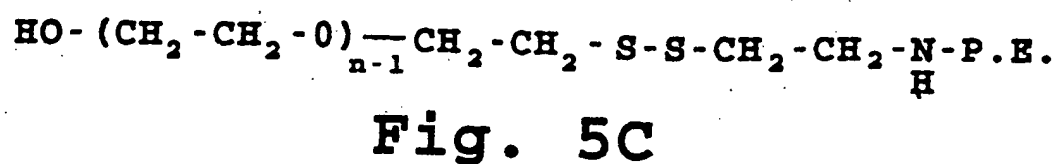
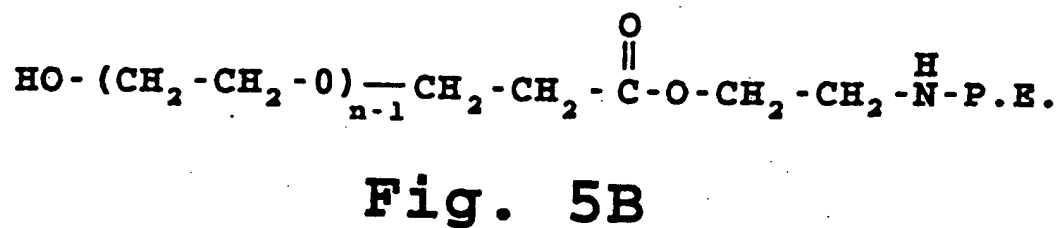
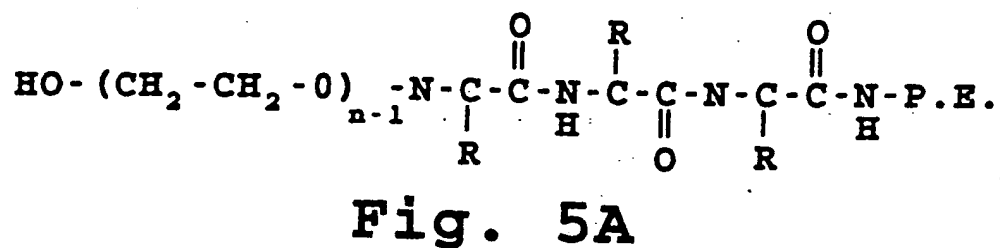
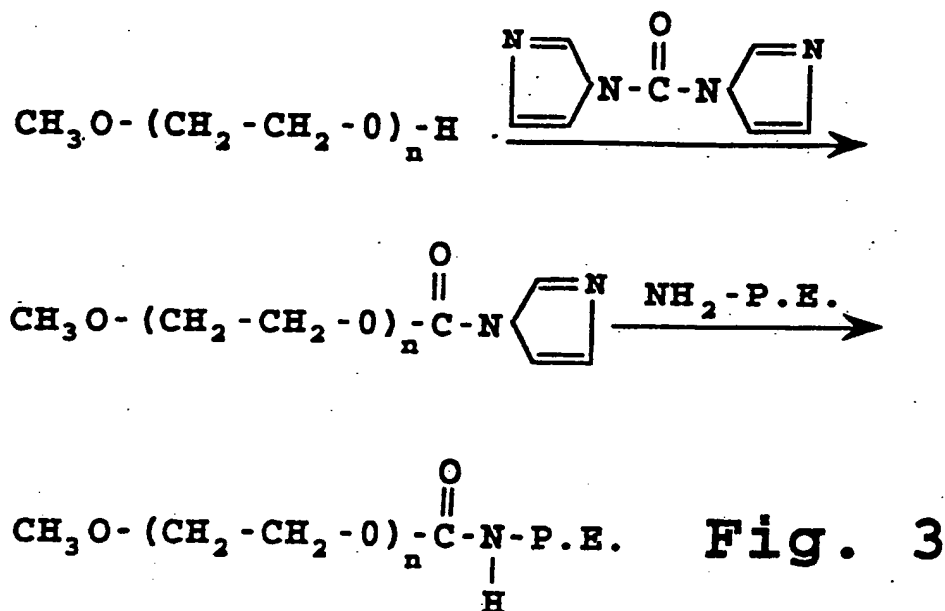


Fig. 2



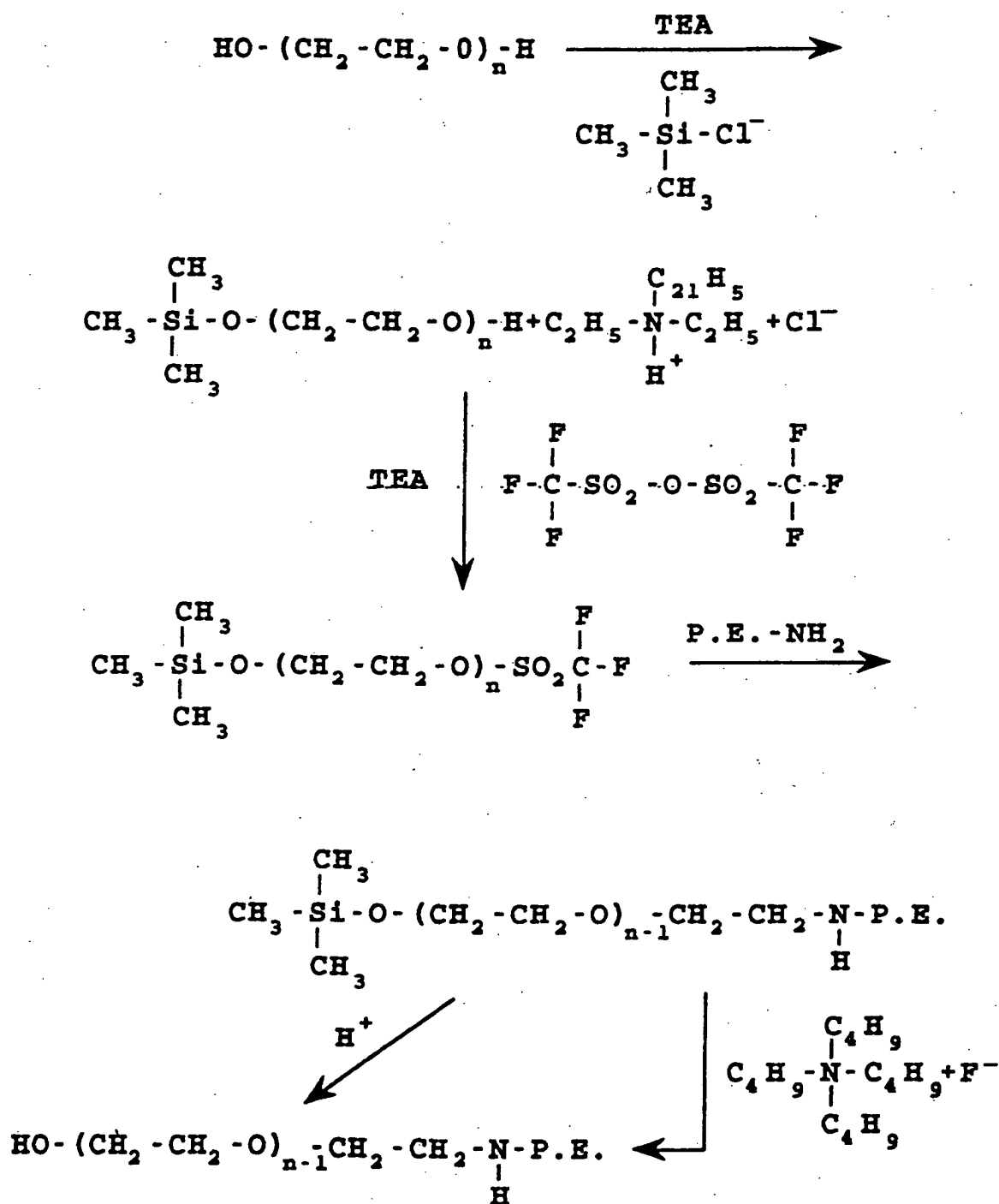
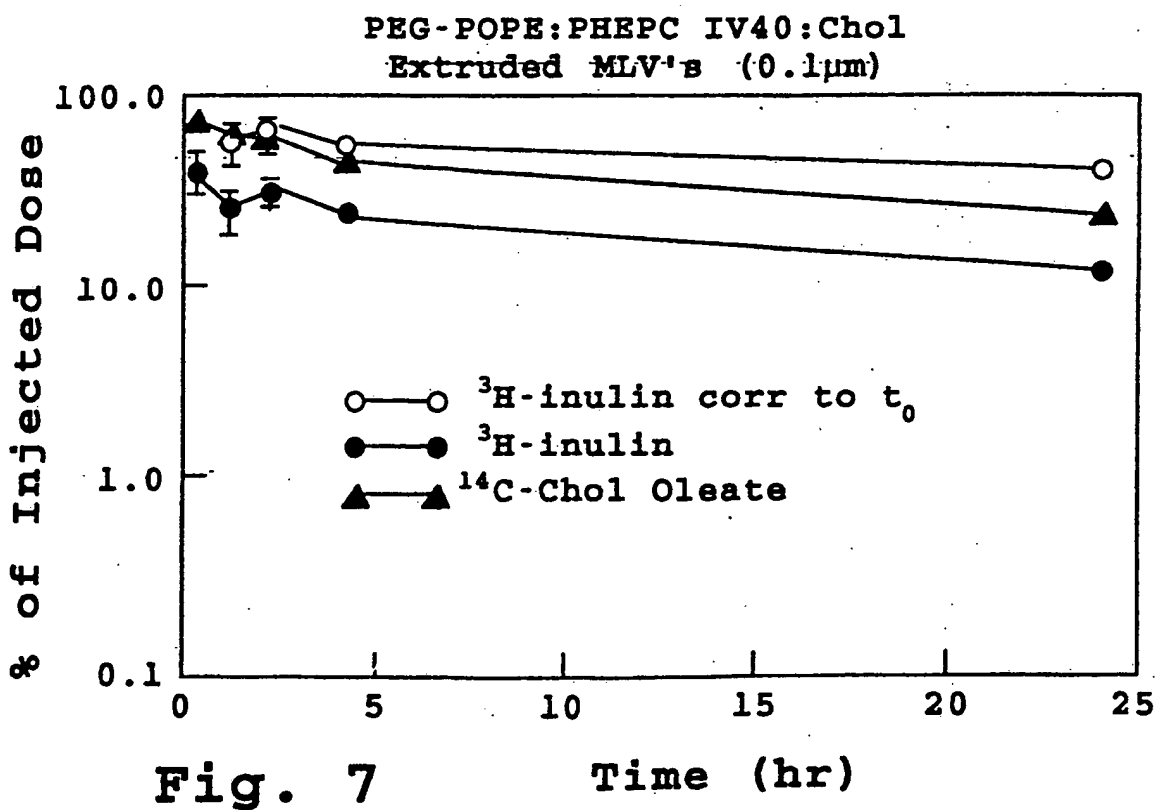
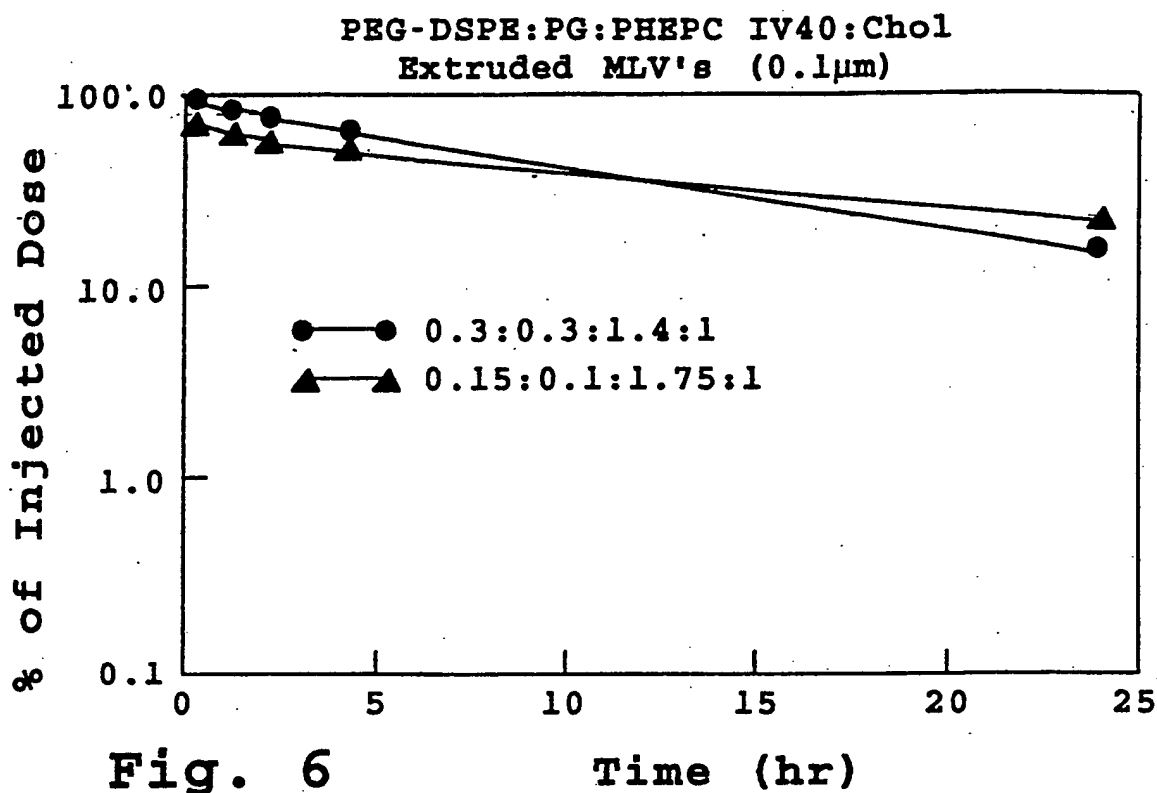


Fig. 4





# LIPOSOMES WITH ENHANCED CIRCULATION TIME

## 1. FIELD OF THE INVENTION

The present invention relates to liposome therapeutic compositions, and, more particularly, to liposome compositions which have enhanced circulation time when administered intravenously.

## 2. REFERENCES

- Allen, T. M., (1981) *Biochem. Biophys. Acta* 640: 385397.
- Allen, T. M., and Everest, J. (1983) *J. Pharmacol. Exp. Therap.* 226: 539-544.
- Altura, B. M. (1980) *Adv. Microcirc.* 9, 252-294.
- Alving, C. R. (1984) *Biochem. Soc. Trans.* 12: 342344.
- Ashwell, G., and Morell, A. G. (1974) *Adv. Enzymology* 41, 99-128.
- Czop, J. K. (1978) *Proc. Natl. Acad. Sci. USA* 75:3831.
- Durocher, J. P., et al. (1975) *Blood* 45:11.
- Ellens, H., et al. (1981) *Biochim. Biophys. Acta* 674: 10-18.
- Gabizon, A., et al., *J. Liposome Research* 1:123 (1988).
- Gregoriadis, G., and Ryman, B. E. (1972) *Eur. J. Biochem.* 24, 485-491.
- Gregoriadis, G., and Neerunjun, D. (1974) *Eur. J. Biochem.* 47, 179-185.
- Gregoriadis, G., and Senior, J. (1980) *FEBS Lett.* 119, 43-46.
- Greenberg, J. P., et al (1979) *Blood* 53:916.
- Hakomori, S. (1981) *Ann. Rev. Biochem.* 50, 733-764.
- Hwang, K. J., et al. (1980) *Proc. Natl. Acad. Sci. USA* 77:4030.
- Jonah, M. M., et al. (1975) *Biochem. Biophys. Acta* 401, 336-348.
- Juliano, R. L., and Stamp, D. (1975) *Biochem. Biophys. Res. Commun.* 63, 651-658.
- Karlsson, K. A. (1982) In: *Biological Membranes*, Vol. 4, D. Chapman (ed.) Academic Press, N.Y., pp. 1-74.
- Kimelberg, H. K., et al. (1976) *Cancer Res.* 36, 2949-2957.
- Lee, K. C., et al., *J. Immunology* 125:86 (1980).
- Lopez-Berestein, G., et al. (1984) *Cancer Res.* 44, 375-378.
- Okada, N. (1982) *Nature* 299:261.
- Poznansky, M. J., and Juliano, R. L. (1984) *Pharmacol. Rev.* 36, 277-336.
- Richardson, V. J., et al. (1979) *Br. J. Cancer* 40, 3543.
- Saba, T. M. (1970) *Arch. Intern. Med.* 126, 1031-1052.
- Schaver, R. (1982) *Adv. Carbohydrate Chem. Biochem.* 40:131.
- Scherphof, T., et al. (1978) *Biochim. Biophys. Acta* 542, 296-307.
- Senior, J., and Gregoriadis, G. (1982) *FEBS Lett.* 145, 109-114.
- Senior, J., et al. (1985) *Biochim. Biophys. Acta* 839, 1-8.
- Szoka, F., Jr., et al. (1978) *Proc. Natl. Acad. Sci. USA* 75:4194.

Szoka, F., Jr., et al. (1980) *Ann. Rev. Biophys. Bioeng.* 9:467.

Woodruff, J. J., et al. (1969) *J. Exp. Med.* 129:551.

## 3. BACKGROUND OF THE INVENTION

Liposome delivery systems have been proposed for a variety of drugs. For use in drug delivery via the bloodstream, liposomes have the potential of providing a controlled "depot" release of a liposome-entrapped drug over an extended time period, and of reducing toxic side effects of the drug, by limiting the concentration of free drug in the bloodstream. Liposome/drug compositions can also increase the convenience of therapy by allowing higher drug dosage and less frequent drug administration. Liposome drug delivery systems are reviewed generally in Poznansky et al.

One limitation of intravenous liposome drug delivery which has been recognized for many years is the rapid uptake of blood-circulating liposomes by the mononuclear phagocytic system (MPS), also referred to as the reticuloendothelial system (RES). This system, which consists of the circulating macrophages and the fixed macrophages of the liver (Kupffer cells), spleen, lungs, and bone marrow, removes foreign particulate matter, including liposomes, from blood circulation with a half life on the order of minutes (Saba). Liposomes, one of the most extensively investigated particulate drug carriers, are removed from circulation primarily by Kupffer cells of the liver and to a lesser extent by other macrophage populations.

A variety of studies on factors which effect liposome uptake by the RES have been reported. Early experiments, using heterogeneous preparations of multilamellar liposomes (MLV) containing phosphatidylcholine (PC) and cholesterol (CH) as their principal lipid constituents, demonstrated that these liposomes are rapidly removed from circulation by uptake into liver and spleen in a biphasic process with an initial rapid uptake followed by a slow phase of uptake (Gregoriadis, 1974; Jonah; Gregoriadis, 1972; Juliano). Half-time for removal of MLV from circulation was on the order of 5-15 min. following intravenous (IV) injection. Negatively charged liposomes are removed more rapidly from circulation than neutral or positively charged liposomes. Small unilamellar liposomes (SUV) are cleared with half-lives approximately three-to four-fold slower than MLV (Juliano; Allen, 1983). Uptake of liposomes by liver and spleen occurs at similar rates in several species, including mouse, rat, monkey, and human (Gregoriadis, 1974; Jonah; Kimelberg, 1976; Juliano; Richardson; Lopez-Berestein).

Liposomes which are capable of evading the RES would have two important benefits. One is the increased liposome circulation time in the blood, which would both increase the pharmacokinetic benefits of slow drug release in the bloodstream, and also provide greater opportunity for tissue targeting where the liver, spleen, and lungs are not involved. The second benefit is decreased liposome loading of the RES. In addition to the role of the RES in removing foreign particles, the RES is involved in several other functions, including host defense against pathogenic microorganisms, parasites, and tumor cells, host responses to endotoxins and hemorrhagic shock, drug response, and responses to circulating immune complexes (Saba, Altura). It is important, therefore, in liposome administration via the bloodstream, to avoid compromising the RES seriously, by massive short-term or accumulated liposome uptake.

One approach which has been proposed is to increase liposome circulation time by increasing liposome stability in serum. This approach is based on studies which have shown that factors which decrease leakage of liposome contents in plasma also decrease the rate of uptake of liposomes by the RES (Allen, 1983; Gregoriadis, 1980; Allen, 1981; Senior, 1982). One factor contributing to this effect appears to be bilayer rigidity, which renders the liposomes more resistant to the destabilizing effects of serum components, in particular high density lipoproteins (Allen, 1981; Scherphof). Thus, inclusion of cholesterol in the liposomal bilayer can reduce the rate of uptake by the RES (Gregoriadis, 1980; Hwang; Senior, 1985), and solid liposomes such as those composed of distearoylphosphatidylcholine (DSPC) or containing large amounts of sphingomyelin (SM) show decreased rate and extent of uptake into liver (Allen, 1983; Ellens; Senior, 1982; Hwang). However, this approach appears to have a limited potential for increasing liposome circulation times in the bloodstream.

Efforts designed to enhance liposome circulation time, by modifying the liposome outer surface to mimic that of the red blood cell, have also been reported. The role of cell surface carbohydrates in cellular recognition phenomena is widely appreciated (Ashwell, Hakomori, Karlsson). The chemistry, metabolism, and biological functions of sialic acid have been reviewed (Schauer). Surface sialic acid, which is carried by gangliosides, and glycoproteins such as glycophorin, plays an important role in the survival of erythrocytes, thrombocytes, and lymphocytes in circulation. Enzymatic removal of sialic acid, which exposes terminal galactose residues, results in rapid removal of erythrocytes from circulation, and uptake into Kupffer cells of the liver (Durocher). Desialylation of thrombocytes (Greenberg) and lymphocytes (Woodruff) also results in their rapid removal by the liver.

Although desialylated erythrocytes will bind to Kupffer cells or peritoneal macrophages in vitro in the absence of serum, serum must be added in order for significant phagocytosis to occur. The nature of the serum components mediating endocytosis is speculative, but immunoglobulin[globulin?] and complement (C3b) are thought to be involved. Czop et al. (Czop) have shown that sheep erythrocytes, which are not normally phagocytosed by human monocytes, will bind C3b and be phagocytosed upon desialylation. Okada et al. (Okada) have demonstrated that sialoglycolipids on liposome membranes restrict activation of the alternative complement pathway and that removal of the terminal sialic acid from the glycolipids abolishes this restricting capacity and results in activation of the alternative complement pathway. Sialic acid, therefore, may be functioning as a nonrecognition molecule on cell membranes partly through its ability to prevent binding of C3b, thus preventing phagocytosis via the alternative complement pathway. Other immune factors may also be involved in liposome phagocytosis. Alving has reported that 50% of the test sera from individual humans contain naturally occurring "anti-liposome" antibodies which mediated complement-dependent immune damage to liposomes.

The observations reported above suggest that surface sialic acid, and/or other red-cell surface agents, incorporated into liposomes, for example, in the form of ganglioside or glycophorin, may lead to increased circulation half-lives of liposomes. This approach is pro-

posed, for example, in U.S. Pat. No. 4,501,728 for "Masking of Liposomes from RES Recognition."

Co-owned U.S. Pat. No. 4,837,028 discloses a liposome composition which shows significantly enhanced circulation half-life, as measured by blood/RES ratios 2 hours after intravenous administration. Two factors were required for achieving high blood/RES ratios. The first was the presence of the specific ganglioside GM<sub>1</sub>, which produced blood/RES ratios significantly greater than those seen with a variety of other glycosides and/or negatively charged lipids which were examined. Secondly, high blood/RES ratios were only observed in the liposomes composed predominantly of membrane-rigidifying lipids, such as sphingomyelin or phospholipids with saturated acyl chains.

The results reported in the above-cited patent suggest that a combination of specific surface molecules, such as GM<sub>1</sub>, and rigid membrane lipid components, may be required for achieving effective liposome evasion of the RES. However, it is not known from these studies whether other surface molecules would be effective in enhancing liposome blood circulation times, and, if so, whether such molecules would be practical for use in liposomes designed for intravenous injection in humans. Further, the requirement for membrane-rigidifying membrane components may present limitations in liposome formulation methods, and also limit the ability to control the rate of drug release from circulating liposomes, by varying the "fluidity" of the lipids making up the liposomes.

#### 4. SUMMARY OF THE INVENTION

One general object of the invention is to provide a liposome composition characterized by enhanced circulation time in the bloodstream.

Another object of the invention is to provide such a composition in liposomes composed of either fluid or rigid vesicle-forming lipids.

Still another object of the invention is to provide a method which utilizes the liposome composition to deliver drugs to a target tissue accessible via the bloodstream.

The invention includes, in one aspect, a liposome composition for administering a drug via the bloodstream. The composition includes liposomes containing the drug in liposome-entrapped form, and between 1-20 mole percent of an amphipathic lipid derivatized with a polyalkylether. One preferred amphipathic lipid is a phospholipid, such as phosphatidylethanolamine, derivatized with polyethyleneglycol. The liposomes in the composition preferably have a selected average size in the size range between about 0.05 and 0.5 microns.

The vesicle-forming lipids making up the liposomes may be predominantly rigid lipid components, such as sphingomyelin, or fluid lipids, such as phospholipids with predominantly unsaturated acyl chains.

In one embodiment, the polyalkylether is derivatized to the amphipathic lipid through an esterase- or peptidase-sensitive linkage. The rate of clearance of the liposomes from the bloodstream can then be modulated according to the rate of release of polyalkylether groups from the liposome surface.

In another embodiment, the liposomes are formulated to contain surface-bound ligand molecules which are effective to bind specifically and with high affinity to ligand-binding molecules carried on the surface of specific target tissue or cells.

In another aspect, the invention includes a method of enhancing the blood-circulation time of liposomes administered intravenously. The enhanced circulation time is achieved by adding to the liposomes, in an amount between about 1-20 mole percent, an amphipathic lipid derivatized with a polyalkylether. The method is preferably effective to enhance the blood/RES ratio, 24 hours after intravenous administration, by up to tenfold or more over that observed with the same liposomes in the absence of the derivatized amphipathic lipid.

In still another aspect, the invention includes a method of administering a drug intravenously, for delayed drug release into the bloodstream. A suspension of liposomes containing the drug in liposome-entrapped form, and between about 1-20 mole percent of an amphipathic lipid derivatized with a polyalkylether, is administered parenterally, in an amount of the suspension containing a pharmacologically acceptable amount of the drug.

Also included in the invention is a method for delivering a drug selectively to a target tissue or cell type characterized by surface-bound tissue-specific ligand-binding molecules. A suspension of liposomes containing a surface-bound ligand effective to bind specifically and with high affinity to said ligand-binding molecule, and between 1-20 mole percent of an amphipathic lipid derivatized with a polyalkylether is administered parenterally. The target tissue may be a disease-related tissue, such as a solid tumor, or a circulating cell type, such as a virus-infected blood cell having virus-specific surface antigens.

A related aspect of the invention embraces a method of enhancing the uptake, by the reticuloendothelial system, of cells carrying surface-specific ligand-binding molecules which are characteristic of a disease state. The method is based on ligand-specific binding of liposomes containing between 1-20 mole percent of an amphipathic lipid derivatized with a polyalkylether, and a surface-bound ligand to the ligand-binding molecules on the cells.

These and other objects and features of the invention will become more fully apparent when the following detailed description of the invention is read in conjunction with the accompanying drawings.

#### BRIEF DESCRIPTION OF THE DRAWINGS

FIG. 1 illustrates a general reaction scheme for derivatizing an amphipathic lipid amine with a polyalkylether;

FIG. 2 is a reaction scheme for preparing phosphatidylethanolamine (PE) derivatized with polyethyleneglycol via a cyanuric chloride linking agent;

FIG. 3 illustrates a reaction scheme for preparing phosphatidylethanolamine (PE) derivatized with polyethyleneglycol by means of a carbonyl diimidazole activating reagent;

FIG. 4 illustrates a reaction scheme for preparing phosphatidylethanolamine (PE) derivatized with polyethyleneglycol by means of a trifluoromethane sulfonate reagent;

FIG. 5 illustrates an amphipathic lipid derivatized with polyethyleneglycol through a peptide (A), ester (B), and disulfide (C) linkage;

FIG. 6 is a plot of liposome retention time on the blood, expressed in terms of percent injected dose as a function of hours after IV injection, for PEG-PE liposomes containing different amounts of phosphatidylglycerol; and

FIG. 7 is a plot similar to that of FIG. 6, showing retention time in liposomes composed of predominantly unsaturated phospholipid components.

#### DETAILED DESCRIPTION OF THE INVENTION DEFINITIONS

As used herein, the term:

"Polyalkylether" refers to polyethyleneglycol and related homopolymers, such as polymethylethyleneglycol, polyhydroxypropyleneglycol, polypropyleneglycol, polymethylpropyleneglycol, and polyhydroxypropyleneoxide, and to heteropolymers of small alkoxy monomers, such as a polyethyleneglycol/polypropyleneglycol, such polymers having a molecular weight of at least about 120 daltons, and up to about 20,000 daltons.

"Amphipathic lipid" refers to any lipid having an amphipathic hydrophobic group, typically including two acyl hydrocarbon chains or a steroid group by which the lipid can be anchored in the outer lipid layer of a lipid bilayer, and a polar group which contains a reactive chemical group, such as an amine, acid, ester, aldehyde, or alcohol group by which the lipid can be derivatized to a polyalkylether.

"Amphipathic lipid derivatized with a polyalkylether" and "polyalkylether lipids" refers to an amphipathic lipid which is covalently joined, at its polar group, to a polyalkylether.

#### I. PREPARATION OF POLYALKYLETHER LIPIDS

FIG. 1 shows a general reaction scheme for forming polyalkyl ethers. The polyalkylether which is employed, such as the polyethyleneglycol (PEG) molecule shown, is preferably capped by a methoxy, ethoxy or other unreactive group at one end. The polymer is activated at its other end by reaction with a suitable activating agent, such as cyanuric acid, carbonyl diimidazole, anhydride reagent, or the like, as described below. The activated compound is then reacted with a suitable amphipathic lipid, such as the phosphatidylethanolamine (PE) shown, to produce the derivatized lipid. Alternatively, the lipid group may be activated for reaction with the polyalkylether, or the two groups may be joined in a concerted coupling reaction, according to known coupling methods.

The polyalkylether, such as polyethyleneglycol or polypropyleneglycol, or the methoxy- or ethoxy-capped analogs, can be obtained commercially in a variety of polymer sizes, e.g., 120-20,000 dalton molecular weights. Alternatively, the homo- or heteropolymer can be formed by known polymer synthesis methods to achieve a desired monomeric composition and size. One preferred polyalkylether is PEG having a molecular weight between about 1,000 and 5,000 daltons.

The amphipathic lipid is preferably a vesicle-forming lipid having two hydrocarbon chains, typically acyl chains, and a polar head group. Included in this class are the phospholipids, such as phosphatidylcholine (PC), PE, phosphatidic acid (PA), phosphatidylinositol (PI), and sphingomyelin (SM), where the two hydrocarbon chains are typically between about 14-22 carbon atoms in length, and have varying degrees of unsaturation. Also included in this class are the glycolipids, such as cerebroside and gangliosides.

Another amphipathic lipid which may be employed is cholesterol and related sterols. In general, cholesterol may be less tightly anchored to a lipid bilayer membrane, particularly when derivatized with a high molecular weight polyalkylether, and therefore be less effective in promoting liposome evasion of the RES in the bloodstream. Similarly, single-chain lipids, such as long-chain fatty acids, may be derivatized with a polyalkylether, but provide less effective anchoring to the bilayer membrane than a lipid having two or more hydrocarbon chains.

According to one important feature of the invention, the amphipathic lipid may be a relatively fluid lipid, typically meaning that the lipid phase has a relatively low lipid melting temperature, e.g., at or below room temperature, or relatively rigid lipid, meaning that the lipid has a relatively high melting temperature, e.g., up to 50° C. As a rule, the more rigid, i.e., saturated lipids, contribute to greater membrane rigidity in a lipid bilayer structure and also contribute to greater bilayer stability in serum. Other lipid components, such as cholesterol, are also known to contribute to membrane rigidity and stability in lipid bilayer structures. Phospholipids whose acyl chains have a variety of degrees of saturation can be obtained commercially, or prepared according to known methods.

FIG. 2 shows a reaction scheme for producing a PE-PEG lipid in which the PEG is derivatized to PE through a cyanuric chloride group. Details of the reaction are provided in Example 1. Briefly, methoxy-capped PEG is activated with cyanuric chloride in the presence in sodium carbonate under conditions which produced the activated PEG compound shown at the top in the figure. This material is purified to remove unreacted cyanuric acid. The activated PEG compound is reacted with PE in the presence of triethyl amine to produce the desired PE-PEG compound shown at the bottom in the figure. The yield is about 8-10% with respect to initial quantities of PEG.

The method just described may be applied to a variety of lipid amines, including PE, cholesteryl amine, and glycolipids with sugar-amine groups.

A second method of coupling a polyalkylether, such as capped PEG to a lipid amine is illustrated in FIG. 3. Here the capped PEG is activated with a carbonyl diimidazole coupling reagent, to form the activated imidazole compound shown at the center in FIG. 3. Reaction with a lipid amine, such as PE, leads to PEG coupling to the lipid through a carbamate linkage, as illustrated in the PEG-PE compound shown at the bottom in the figure. Details of the reaction are given in Example 2.

A third reaction method for coupling a capped polyalkylether to a lipid amine is shown in FIG. 4. Here a polyalkylether, as exemplified by PEG is first protected at its free OH. The end-protection reaction is shown at the top in the figure, and involves the reaction of trimethylsilylchloride with PEG in the presence of triethylamine. The protected PEG is then reacted with the anhydride of trifluoromethyl sulfonate to form PEG activated with trifluoromethyl sulfonate. Reaction of the activated compound with a lipid amine, such as PE, in the presence of triethylamine, gives the desired derivatized lipid product, such as the PEG-PE compound, in which the lipid amine group is coupled to the polyether through the terminal methylene carbon in the polyether polymer. The trimethylsilyl protective group can be released by acid treatment, as indicated at the

lower left in the figure, or by reaction with a quaternary amine fluoride salt, such as the fluoride salt of tetrabutylamine.

It will be appreciated that a variety of known coupling reactions, in addition to those just described, are suitable for preparing polyalkyletheramine lipid derivatives for use in the liposome composition of the invention. For example, the sulfonate anhydride coupling reagent illustrated in FIG. 4 can be used to join an activated polyalkylether to the hydroxyl group of an amphipathic lipid, such as the 5'OH of cholesterol. Other reactive lipid groups, such as an acid or ester lipid group may also be used for coupling, according to known coupling methods. For example, the acid group of phosphatidic acid can be activated to form an active lipid anhydride, by reaction with a suitable anhydride, such as acetic anhydride, and the reactive lipid can then be joined to a protected polyalkylamine, e.g., by reaction in the presence of an isothiocyanate reagent.

In another embodiment, the derivatized lipid components are prepared to include a labile lipid-polymer linkage, such as a peptide, ester, or disulfide linkage, which can be cleaved under selective physiological conditions, such as in the presence of peptidase or esterase enzyme present in the bloodstream. FIG. 5 shows exemplary lipids which are linked through (A) peptide, (B), ester, and (C), disulfide containing linkages. The peptide-linked compound can be prepared, for example, by first coupling a polyalkylether with the N-terminal amine of the tripeptide shown, e.g., via the reaction shown in FIG. 3. The peptide carboxyl group can then be coupled to a lipid amine group through a carbodiimide coupling reagent conventionally. The ester linked compound can be prepared, for example, by coupling a lipid acid, such as phosphatidic acid, to the terminal alcohol group of a polyalkylether, using alcohol via an anhydride coupling agent. Alternatively, a short linkage fragment containing an internal ester bond and suitable end groups, such as primary amine groups, can be used to couple the polyalkylether to the amphipathic lipid through amide or carbamate linkages. Similarly, the linkage fragment may contain an internal disulfide linkage, for use in forming the compound shown at C in FIG. 5.

## II. PREPARATION OF LIPOSOME COMPOSITION

The liposome composition of the invention is designed for use in delivering a drug via the bloodstream, i.e., via a parenteral route in which the liposomes are accessible to clearance mechanisms involving the reticuloendothelial system (RES). Section IIA below describes the general procedure employed for determining liposome clearance times from the bloodstream, and Section IIB, lipid component parameters which effect blood retention times, in accordance with the invention, and procedures for producing the liposome composition of the invention.

### A. Measuring liposome uptake by the RES in vivo

One method used for evaluating liposome circulation time in vivo measures the distribution of intravenously injected liposomes in the bloodstream and the primary organs of the RES at selected times after injection. In the standardized model which is used, RES uptake is measured by the ratio of total liposomes in the bloodstream to total liposomes in the liver and spleen, the principal organs of the RES. In practice, age and sex matched mice are injected intravenously (IV) through

the tail vein with a radiolabeled liposome composition, and each time point is determined by measuring total blood and combined liver and spleen radiolabel counts. Experimental methods are detailed in Example 5.

Since the liver and spleen account for nearly 100% of the initial uptake of liposomes by the RES, the blood/RES ratio just described provides a good approximation of the extent of uptake from the blood to the RES *in vivo*. For example, a ratio of about 1 or greater indicates a predominance of injected liposomes remaining in the bloodstream, and a ratio below about 1, a predominance of liposomes in the RES. For most of the lipid compositions of interest, blood/RES ratios were determined at selected intervals of between 15 minutes and 24 hours. A related method which is also used herein measures blood circulation lifetime, as determined from the decrease in percent dose in the bloodstream over time.

The data obtained with the model animal system can be reasonably extrapolated to humans and veterinary animals of interest. This is because, as mentioned above, uptake of liposomes by liver and spleen has been found to occur at similar rates in several mammalian species, including mouse, rat monkey, and human (Gregoriadis, 1974; Jonah; Kimelberg, 1976; Juliano; Richardson; Lopez-Berestein). This result likely reflects the fact that the biochemical factors which appear to be most important in liposome uptake by the RES—including opsonization by serum lipoproteins, size-dependent uptake effects, and cell shielding by surface moieties—are common features of all mammalian species which have been examined.

#### B. Lipid Components

The lipid components used in forming the liposomes of the invention may be selected from a variety of vesicle-forming lipids, typically including phospholipids and sterols. According to one important aspect of the invention, it has been discovered that the lipids making up the bulk of the vesicle-forming lipids in the liposomes may be either fluidic lipids, e.g., phospholipids whose acyl chains are relatively unsaturated, or more rigidifying membrane lipids, such as highly saturated phospholipids. This feature of the invention is seen in Example 6, which examines blood/RES ratios in liposomes formed with PEG-PE, cholesterol, and PC having varying degrees of saturation. As seen from the data in Table 4 in Example 6, high blood/RES ratios were achieved in substantially all of the liposome formulations, independent of the extent of lipid unsaturation in the bulk PC phospholipid, and no systematic trend, as a function of degree of lipid saturation, was observed.

Accordingly, the vesicle-forming lipids may be selected to achieve a selected degree of fluidity or rigidity, to control the stability of the liposomes in serum and the rate of release of entrapped drug from the liposomes in the bloodstream. The vesicle-forming lipids may also be selected, in lipid saturation characteristics, to achieve desired liposome preparation properties. It is generally the case, for example, that more fluidic lipids are easier to formulate and size by extrusion than more rigid lipid components, and can be readily formulated in sizes down to 0.05 microns.

Similarly, it has been found that the percentage of cholesterol in the liposomes may be varied over a wide range without significant effect on observed blood circulation lifetime. The studies presented in Example 7A show virtually no change in blood circulation lifetime in the range of cholesterol between 0–30 mole percent.

It has also been found, in accordance with the invention that blood circulation lifetime is also relatively unaffected by the percentage of charged lipid components, such as phosphatidylglycerol (PG). This can be seen from FIG. 6, which plots percent loss of encapsulated marker for PEG-PE liposomes containing either 4.7 mole percent PG (triangles) or 14 mole percent PG (circles). Virtually no difference in liposome retention in the bloodstream over a 24 hour period was observed. It is noted here that the PEG-PE lipid is itself negatively charged and thus the PG represents additional negative charge on the liposome surface.

Thus, according to one feature of the invention, total liposome charge may be varied to modulate liposome stability, to achieve desired interactions with or binding to drugs. The concentration of charged lipid may be about percent or higher.

As an example, in preparing liposomes containing entrapped doxorubicin or epirubicin, additional charged lipid components may be added to increase the amount of entrapped drug, in a lipid-film hydration method of forming liposomes.

The polyalkylether lipid employed in the liposome composition is present in an amount preferably between about 1–20 mole percent, on the basis of moles of derivatized lipid as a percentage of total total moles of vesicle-forming lipids. As noted above, the polyalkylether moiety of the lipid preferably has a molecular weight between about 120–20,000 daltons, and more preferably between about 1,000–5,000 daltons. Example 7B, which examines the effect of very short ethoxy ether moieties (120 daltons) on blood circulation lifetime ratios indicates that polyether moieties of at least about 5 carbon atoms are required to achieve significant enhancement of blood/RES ratios.

#### C. Preparing the Liposome Composition

The liposomes may be prepared by a variety of techniques, such as those detailed in Szoka et al, 1980. One preferred method for preparing drug-containing liposomes is the reverse phase evaporation method described by Szoka et al and in U.S. Pat. No. 4,235,871. In this method, a solution of liposome-forming lipids is mixed with a smaller volume of an aqueous medium, and the mixture is dispersed to form a water-in-oil emulsion, preferably using pyrogen-free components. The drug or other pharmaceutical agent to be delivered is added either to the lipid solution, in the case of a lipophilic drug, or to the aqueous medium, in the case of a water-soluble drug.

After removing the lipid solvent by evaporation, the resulting gel is converted to liposomes, with an encapsulation efficiency, for a water-soluble drug, of up to 50%. The reverse phase evaporation vesicles (REV's) have typical average sizes between about 2–4 microns and are predominantly oligolamellar, that is, contain one or a few lipid bilayer shells. The REV's may be readily sized, as discussed below, by extrusion to give oligolamellar vesicles having a maximum selected size preferably between about 0.05 to 0.5 microns.

To form MLV's, a mixture of liposome-forming lipids of the type detailed above dissolved in a suitable solvent is evaporated in a vessel to form a thin film, which is then covered by an aqueous medium. The lipid film hydrates to form MLV's, typically with sizes between about 0.1 to 10 microns. These vesicles, when unsized, show relatively poor blood/RES ratios, as seen in Table 9, for the unextruded MLV composition. Typically, MLV's are sized down to a desired size range of 0.5 or

less, and preferably between about 0.05 and 0.2 microns by extrusion.

One effective sizing method for REV and MLV involves extruding an aqueous suspension of the liposomes through a polycarbonate membrane having a selected uniform pore size, typically 0.05, 0.08, 0.1, 0.2, or 0.4 microns (Szoka). The pore size of the membrane corresponds roughly to the largest sizes of liposomes produced by extrusion through that membrane, particularly where the preparation is extruded two or more times through the same membrane. This method of liposome sizing is used in preparing homogeneous-size REV and MLV compositions described in Examples 4A and 4B below. A more recent method involves extrusion through an asymmetric ceramic filter. The method is detailed in U.S. patent application for Liposome Extrusion Method, Ser. No. 829,710, filed Feb. 13, 1986.

Alternatively, the REV or MLV preparations can be treated to produce small unilamellar vesicles (SUVs) which are characterized by sizes in the 0.04–0.08 micron range. SUVs may be useful, for example, in targeting a tumor tissue which permits selective passage of small particles, typically than about 0.1 micron, through the capillary walls supplying the tumor. As noted above, SUVs may be formed readily from fluid vesicle-forming lipids.

After final sizing, the liposomes can be treated, if necessary, to remove free (non-entrapped) drug. Conventional separation techniques, such as centrifugation, diafiltration, and molecular-sieve chromatography are suitable. The composition can be sterilized by filtration through a conventional 0.45 micron depth filter.

### III. UTILITY

The significantly increased circulation half life of liposomes constructed as above can be exploited in several types of therapeutic applications. In one application, the liposome composition is designed for sustained release of a liposome-associated drug into the bloodstream by long-life circulating liposomes. As seen above, liposomes constructed according to the invention can be maintained predominantly in the bloodstream up to 24 hours, and therefore sustained release of the drug at physiologically effective levels for up to about 1 day or more can be achieved. As noted above, the liposomes can be prepared from vesicle-forming lipids having a wide range of rigidifying properties, to achieve selected liposome stability and drug release rates from the liposomes in the bloodstream.

A variety of drugs or other pharmacologically active agents are suitable for delivery by the liposome composition. One general class of drugs include water-soluble, liposome-permeable compounds which are characterized by a tendency to partition preferentially into the aqueous compartments of the liposome suspension, and to equilibrate, over time, between the inner liposomal spaces and outer bulk phase of the suspension. Representative drugs in this class include terbutaline, albuterol, atropine methyl nitrate, cromolyn sodium, propranolol, flunisolide, ibuprofen, gentamycin, tobermycin, pentamidine, penicillin, theophylline, bleomycin, etoposide, captopril, n-acetyl cysteine, verapamil, vitamins, and radio-opaque and particle-emitter agents, such as chelated metals. Because of the tendency of these agents to equilibrate with the aqueous composition of the medium, it is preferred to store the liposome composition in lyophilized form, with rehydration

shortly before administration. Alternatively, the composition may be prepared in concentrated form, and diluted shortly before administration. The latter approach is detailed in U.S. patent application for "Liposome Concentrate and Method", Ser. No. 860,528, filed May 7, 1986.

A second general class of drugs are those which are water-soluble, but liposome-impermeable. For the most part, these are peptide or protein molecules, such as peptide hormones, enzymes, enzyme inhibitors, apolipoproteins, and higher molecular weight carbohydrates characterized by long-term stability of encapsulation. Representative compounds in this class include calcitonin, atriopeptin,  $\alpha$ -1 antitrypsin (protease inhibitor), interferon, oxytocin, vasopressin, insulin, interleukin-2, superoxide dismutase, tissue plasminogen activator (TPA), plasma factor 8, epidermal growth factor, tumor necrosis factor, lung surfactant protein, interferon, lipocortin,  $\alpha$ -interferon, macrophage colony stimulating factor, and erythropoietin.

A third class of drugs are lipophilic molecules which tend to partition into the lipid bilayer phase of the liposomes, and which are therefore associated with the liposomes predominantly in a membrane-entrapped form. The drugs in this class are defined by an oil/water partition coefficient, as measured in a standard oil/water mixture such as octanol/water, of greater than 1 and preferably greater than about 5. Representative drugs include prostaglandins, amphotericin B, progesterone, isosorbide dinitrate, testosterone, nitroglycerin, estradiol, doxorubicin, epirubicin, beclomethasone and esters, vitamin E, cortisone, dexamethasone and esters, and betamethasone valerate.

For sustained drug-release via the bloodstream, the liposome composition is administered intravenously in an amount which provides a suitable drug dosage over the expected delivery time, typically 12–24 hours. The injection may be given as a single bolus or slowly by i.v. drip, to allow gradual dispersal of the liposomes from the site of injection.

In another application, the liposome composition is designed for targeting to a specific target tissue or organ. The extended lifetime of the liposomes in the bloodstream makes it possible for a significant fraction of the injected liposomes to reach the target site before being removed from the bloodstream by the RES. For example, this feature allows for targeting a tumor tissue, for drug treatment by intravenous administration to a tumor-bearing subject. For targeting to a tumor site, the liposomes may be prepared as SUVs, for extravasation into the tumor site through capillaries supplying the tumor.

As another example, the liposomes may be prepared with surface-bound ligand molecules, such as antibodies, which are effective to bind specifically and with high affinity to ligand-binding molecules, such as antigens, which are localized specifically on target cells. As an example, the ligand molecules may be tumor-specific antibodies, for binding to tumor-specific antigens on tumor cells. As another example, the ligand may be a CD4 peptide, effective to bind specifically to HIV-infected T cells.

A variety of methods for coupling ligands to the surface of liposomes are known, including incorporation of ligand-derivatized lipid components into liposomes or coupling of ligands to activated liposome surface components.



The targeted liposomes may be prepared to include cancer chemotherapeutic agents, such as those listed above. In one preferred embodiment, the liposomes are prepared to include PEG-PE and PG, to a final concentration of charged lipids up to 40 mole percent, doxorubicin, and remainder neutral phospholipids or neutral phospholipids and cholesterol.

In a liposome composition which is useful for radio-imaging of solid tumor regions, the liposomes are prepared with encapsulated radio-opaque or particle-emission metal, typically in a chelated form which substantially prevents permeation through the liposome bilayer.

In still another application, the liposome composition is designed to enhance uptake of circulating cells or other blood-borne particles, such as bacteria, virus-infected blood cells and the like. Here the long-life liposomes are prepared to include surface-bound ligand molecules, as above, which bind specifically and with high affinity to the selected blood-borne cells. Once bound to the blood-borne particles, the liposomes can enhance uptake by the RES.

Polyalkylether moieties on the liposomes may be derivatized the associated anphipathic lipid by an ester, peptide, or disulfide bond which can be cleaved, after liposome binding, to the target cell, to further enhance RES particle clearance.

Studies performed in support of the present invention indicate that the liposome composition of the invention provides an enhancement in blood circulation lifetime which is equal, and in some cases superior, to the most effective RES-evading rigid-lipid liposomes which have been reported heretofore, including liposomes containing GM<sub>1</sub>, and membrane-rigidifying lipids.

The blood circulation lifetimes achieved in the present invention are substantially greater than any other fluid-lipid liposomes which were examined.

The following examples illustrate methods of preparing liposomes with enhanced circulation times, and for accessing circulation times in vivo and in vitro. The examples are intended to illustrate specific liposome compositions and methods of the invention, but are in no way intended to limit the scope thereof.

### MATERIALS

Cholesterol (Chol) was obtained from Sigma (St. Louis, Mo). Sphingomyelin (SM), egg phosphatidylcholine (lecithin or PC), partially hydrogenated PC having the composition IV40, IV30, IV20, IV10, and IV1, phosphatidylglycerol (PG), phosphatidylethanolamine (PE), dipalmitoyl-phosphatidyl glycerol (DPPG), dipalmitoyl PC (DPPC), dioleoyl PC (DOPC) and distearoyl PC (DSPC) were obtained from Avanti Polar Lipids (Birmingham, Ala).

[<sup>125</sup>I]-tyraminyl-inulin was made according to published procedures. <sup>67</sup>Gallium-8-hydroxyquinoline was supplied by NEN Neoscan (Boston, Mass).

### EXAMPLE 1

#### Preparation of PEG-PE Linked by Cyanuric Chloride

##### A. Preparation of activated PEG

2-O-Methoxypolyethylene glycol 1900-4,6-dichloro-1,3,5 triazine previously called activated PEG was prepared as described in *J. Biol. Chem.*, 252:3582 (1977) with the following modifications.

Cyanuric chloride (5.5 g; 0.03 mol) was dissolved in 400 ml of anhydrous benzene containing 10 g of anhydrous sodium carbonate, and PEG-1900 (19 g; 0.01 mol)

was added and the mixture was stirred overnight at room temperature. The solution was filtered, and 600 ml of petroleum ether (boiling range, 35°-60°) was added slowly with stirring. The finely divided precipitate was collected on a filter and redissolved in 400 ml of benzene. The precipitation and filtration process was repeated several times until the petroleum ether was free of residual cyanuric chloride as determined by high pressure liquid chromatography on a column (250×3.2 mm) of 5-μm "LiChrosorb" (E. Merck), developed with hexane, and detected with an ultraviolet detector. Titration of activated PEG-1900 with silver nitrate after overnight hydrolysis in aqueous buffer at pH 10.0, room temperature, gave a value of 1.7 mol of chloride liberated/mol of PEG.

TLC analysis of the product was effected with TLC reversed-phase plates obtained from Baker using methanol-water, 4:1; v/v, as developer and exposure to iodine vapor for visualization. Under these conditions, the starting methoxy polyglycol 1900 appeared at  $R_f$ =0.54 to 0.60. The activated PEG appeared at  $R_f$ =0.41. Unreacted cyanuric chloride appeared at  $R_f$ =0.88 and was removed.

The activated PEG was analyzed for nitrogen and an appropriate correction was applied in selecting the quantity of reactant to use in further synthetic steps. Thus, when the product contained only 20% of the theoretical amount of nitrogen, the quantity of material used in the next synthetic step was increased by 100/20, or 5-fold. When the product contained 50% of the theoretical amount of nitrogen, only 100/50 or a 2-fold increase was needed.

##### B. Preparation of N-(4-Chloro-polyglycol 1900)-1,3,5-triazinyl egg phosphatidylethanolamine.

In a screw-capped test tube, 0.74 ml of a 100 mg/ml (0.100 mmole) stock solution of egg phosphatidylethanolamine in chloroform was evaporated to dryness under a stream of nitrogen and was added to the residue of the activated PEG described in section A, in the amount to provide 205 mg (0.100 mmole). To this mixture, 5 ml anhydrous dimethyl formamide was added. 27 microliters (0.200 mmole) triethylamine was added to the mixture, and the air was displaced with nitrogen gas. The mixture was heated overnight in a sand bath maintained at 110° C.

The mixture was then evaporated to dryness under vacuum and a pasty mass of crystalline solid was obtained. This solid was dissolved in 5 ml of a mixture of 4 volumes of acetone and 1 volume of acetic acid. The resulting mixture was placed at the top of a 21 mm×240 mm chromatographic absorption column packed with silica gel (Merck Kieselgel 60, 70-230 mesh) which had first been moistened with a solvent composed of acetone acetic acid, 80/20; v/v.

The column chromatography was developed with the same solvent mixture, and separate 20 to 50 ml aliquots of effluent were collected. Each portion of effluent was assayed by TLC on silica gel coated plates, using 2-butanone/acetic acid/water; 40/25/5; v/v/v as developer and iodine vapor exposure for visualization. Fractions containing only material of  $R_f$ =about 0.79 were combined and evaporated to dryness under vacuum. Drying to constant weight under high vacuum afforded 86 mg (31.2 micromoles) of nearly colorless solid N-(4-chloro-polyglycol 1900)-1,3,5-triazinyl egg phosphatidylethanolamine containing phosphorous.

The solid compound was taken up in 24 ml of ethanol/chloroform; 50/50 chloroform and centrifuged to remove insoluble material. Evaporation of the clarified solution to dryness under vacuum afforded 21 mg (7.62 micromoles) of colorless solid.

#### EXAMPLE 2 Preparation of the Carbamate-Linked PEG-PE

A. Preparation of the imidazole carbamate of polyethylene glycol methyl ether 1900.

9.5 grams (5 mmoles) of polyethylene glycol methyl ether 1900 obtained from Aldrich Chemical Co. was dissolved in 45 ml benzene which has been dried over molecular sieves. 0.89 grams (5.5 mmoles) of pure carbonyl diimidazole was added. The purity was checked by an infra-red spectrum. The air in the reaction vessel was displaced with nitrogen. Vessel was enclosed and heated in a sand bath at 75° C. for 16 hours.

The reaction mixture was cooled and the clear solution formed at room temperature. The solution was diluted to 50.0 ml with dry benzene and stored in the refrigerator as a 100 micromole/ml stock solution of the imidazole carbamate of PEG ether 1900.

B. Preparation of the phosphatidylethanolamine carbamate of polyethylene glycol methyl ether 1900.

10.0 ml (1 mmol) of the 100 mmol/ml stock solution of the imidazole carbamate of polyethylene glycol methyl ether 1900 (compound X) was pipetted into a 10 ml pear-shaped flask. The solvent was removed under vacuum. 3.7 ml of a 100 mg/ml solution of egg phosphatidyl ethanolamine (V) in chloroform (0.5 mmol) was added. The solvent was evaporated under vacuum. 2 ml of 1,1,2,2-tetrachloroethylene and 139 microliters (1.0 mmol) of triethylamine VI was added. The vessel was closed and heated in a sand bath maintained at 95° C. for 6 hours. At this time, thin-layer chromatography was performed with fractions of the above mixture to determine an extent of conjugation on SiO<sub>2</sub> coated TLC plates, using butanone/acetic acid/water; 40/5/5; v/v/v; was performed as developer. I<sub>2</sub> vapor visualization revealed that most of the free phosphatidyl ethanolamine of R<sub>f</sub>=0.68, had reacted, and was replaced by a phosphorous-containing lipid at R<sub>f</sub>=0.78 to 0.80.

The solvent from the remaining reaction mixture was evaporated under vacuum. The residue was taken up in 10 ml methylene chloride and placed at the top of a 21 mm×270 mm chromatographic absorption column packed with Merck Kiesel-gel 60 (70–230 mesh silica gel), which has been first rinsed with methylene chloride. The mixture was passed through the column, in sequence, using the following solvents.

TABLE 1

ml	Volume % of Methylene Chloride	Volume % Methanol With 2% Acetic Acid
100	100%	0%
200	95%	5%
200	90%	10%
200	85%	15%
200	60%	40%

50 ml portions of effluent were collected and each portion was assayed by TLC on SiO<sub>2</sub> - coated plates, using I<sub>2</sub> vapor absorption for visualization after development with chloroform/methanol/water/concentrated ammonium hydroxide; 130/70/8/0.5%; v/v/v/v. Most of the phosphates were found in fractions 11, 12, 13 and 14.

These fractions were combined, evaporated to dryness under vacuum and dried in high vacuum to constant weight. They yielded 669 mg of colorless wax of phosphatidyl ethanolamine carbamate of polyethylene glycol methyl ether. This represented 263 micromoles and a yield of 52.6% based on the phosphatidyl ethanolamine.

An NMR spectrum of the product dissolved in deuterio-chloroform showed peaks corresponding to the spectrum for egg PE, together with a strong singlet due to the methylene groups of the ethylene oxide chain at Delta=3.4 ppm. The ratio of methylene protons from the ethylene oxide to the terminal methyl protons of the PE acyl groups was large enough to confirm a molecular weight of about 2000 for the polyethylene oxide portion of the molecule of the desired product polyethylene glycol conjugated phosphatidylethanolamine carbamate, M. W. 2,654.

#### EXAMPLE 3 Preparation of Ethylene-Linked PEG-PE

A. Preparation of I-trimethylsilyloxy-polyethylene glycol is illustrated in Reaction Scheme 3A.

15.0 gm (10 mmoles) of polyethylene glycol (M.Wt. 1500, (Aldrich Chemical)) was dissolved in 80 ml benzene. 1.40 ml (11 mmoles) of chlorotrimethyl silane (Aldrich Chemical Co.) and 1.53 ml (1 mmole) of triethylamine was added. The mixture was stirred at room temperature under an inert atmosphere for 5 hours.

The mixture was filtered with suction to separate crystals of triethylammonium chloride and the crystals were washed with 5 ml benzene. Filtrate and benzene wash liquids were combined. This solution was evaporated to dryness under vacuum to provide 15.83 grams of colorless oil which solidified on standing.

TLC of the product on Si-C<sub>18</sub> reversed-phase plates using a mixture of 4 volumes of ethanol with 1 volume of water as developer, and iodine vapor visualization, revealed that all the polyglycol 1500 (R<sub>f</sub>=0.93) has been consumed, and was replaced by a material of R<sub>f</sub>=0.82. An infra-red spectrum revealed absorption peaks characteristic only of polyglycols.

Yield of I-trimethylsilyloxypolyethylene glycol, M. W. 1500 was nearly quantitative.

B. Preparation of trifluoromethane sulfonyl ester of I-trimethylsilyloxy-polyethylene glycol.

15.74 grams (10 mmol) of the crystalline I-trimethylsilyloxy polyethylene glycol obtained above was dissolved in 40 ml anhydrous benzene and cooled in a bath of crushed ice. 1.53 ml (11 mmol) triethylamine and 1.85 ml (11 mmol) of trifluoromethanesulfonic anhydride obtained from Aldrich Chemical Co. were added and the mixture was stirred over night under an inert atmosphere until the reaction mixture changed to a brown color.

The solvent was then evaporated under reduced pressure and the residual syrupy paste was diluted to 100.0 ml with methylene chloride. Because of the great reactivity of trifluoromethane sulfonic esters, no further purification of the trifluoromethane sulfonyl ester of I-trimethylsilyloxy polyethylene glycol was done.

C. Preparation of N-1-trimethylsilyloxy polyethylene glycol 1500 PE. 10 ml of the methylene chloride stock solution of the trifluoromethane sulfonyl ester of I-trimethylsilyloxy polyethylene glycol was evaporated to dryness under vacuum to obtain about 1.2 grams of residue (approximately 0.7 mmoles). To this residue, 3.72 ml of a chloroform solution containing 372 mg (0.5 mmoles) egg PE was added. To the resulting solution,



139 microliters (1.0 mmole) of triethylamine was added and the solvent was evaporated under vacuum. To the obtained residue, 5 ml dry dimethyl formamide and 70 microliters (0.50 mmoles) triethylamine (VI) was added. Air from the reaction vessel was displaced with nitrogen. The vessel was closed and heated in a sand bath at 110° C. for 22 hours. The solvent was evaporated under vacuum to obtain 1.58 grams of brownish colored oil. A 21×260 mm chromatographic absorption column filled with Kieselgel 60 silica 70–230 mesh, was prepared and rinsed with a solvent composed of 40 volumes of butanone, 25 volumes acetic acid and 5 volumes of water. The crude product was dissolved in 3 ml of the same solvent and transferred to the top of the chromatography column. The chromatogram was developed with the same solvent and sequential 30 ml portions of effluent were assayed each by TLC.

The TLC assay system used silica gel coated glass plates, with solvent combination butanone/acetic acid/water; 40/25/5; v/v/v. Iodine vapor absorption served for visualization. In this solvent system, the N-1-trimethylsilyloxy polyethylene glycol 1500 PE appeared at  $R_f=0.78$ . Unchanged PE appeared at  $R_f=0.68$ .

The desired N-1-trimethylsilyloxy polyethylene glycol 1500 PE was a chief constituent of the 170–300 ml portions of column effluent. When evaporated to dryness under vacuum these portions afforded 111 mg of pale yellow oil of compound.

D. Preparation of N-polyethylene glycol 1500: phosphatidyl-ethanolamine acetic acid deprotection.

Once-chromatographed, PE compound was dissolved in 2 ml of tetrahydrofuran. To this, 6 ml acetic acid and 2 ml water was added. The resulting solution was let to stand for 3 days at 23° C. The solvent from the reaction mixture was evaporated under vacuum and dried to constant weight to obtain 75 mg of pale yellow wax. TLC on Si-C18 reversed-phase plates, developed with a mixture of 4 volumes ethanol, 1 volume water, indicated that some free PE and some polyglycol-like material formed during the hydrolysis.

The residue was dissolved in 0.5 ml tetrahydrofuran and diluted with 3 ml of a solution of ethanol water; 80:20; v/v. The mixture was applied to the top of a 10 mm×250 mm chromatographic absorption column packed with octadecyl bonded phase silica gel and column was developed with ethanol water 80:20% by volume, collecting sequential 20 ml portions of effluent. The effluent was assayed by reversed phase TLC. Fractions containing only product of  $R_f=0.08$  to 0.15 were combined. This was typically the 20–100 ml portion of effluent. When evaporated to dryness, under vacuum, these portions afforded 33 mg of colorless wax PEG-PE corresponding to a yield of only 3%, based on the starting phosphatidyl ethanolamine.

NMR analysis indicated that the product incorporated both PE residues and polyethylene glycol residues, but that in spite of the favorable-appearing elemental analysis, the chain length of the polyglycol chain has been reduced to about three to four ethylene oxide residues. The product prepared was used for a preparation of PEG-PE liposomes.

E. Preparation of N-Polyethylene glycol 1500 P. E. by fluoride deprotection.

500 mg of crude N-1-trimethylsilyloxy polyethylene glycol PE was dissolved in 5 ml tetrahydrofuran and 189 mg (0.600 millimoles) of tetrabutyl ammonium fluoride was added and agitated until dissolved. The reac-

tants were let to stand over night at room temperature (20° C.).

The solvent was evaporated under reduced pressure and the residue was dissolved in 10 ml chloroform, washed with two successive 10 ml portions of water, and centrifuged to separate chloroform and water phases. The chloroform phase was evaporated under vacuum to obtain 390 mg of orange-brown wax, which was determined to be impure N-polyethylene glycol 1500 PE compound.

The wax was re-dissolved in 5 ml chloroform and transferred to the top of a 21×270 mm column of silica gel moistened with chloroform. The column was developed by passing 100 ml of solvent through the column the following solvents in sequence were used.

TABLE 2

Volume % Chloroform	Volume % Methanol Containing 2% Conc. Ammonium Hydroxide/methanol
100%	0%
95%	5%
90%	10%
85%	15%
80%	20%
70%	30%
60%	40%
50%	50%
0%	100%

Separated 50 ml fractions of column effluent were saved. The fractions of the column were separated by TLC on Si-C18 reversed-phase plates. TLC plates were developed with 4 volumes of ethanol mixed with 1 volume of water. Visualization was done by exposure to iodine vapor.

Only those fractions containing an iodine-absorbing lipid of  $R_f$  about 0.20 were combined and evaporated to dryness under vacuum and dried in high vacuum to constant weight. In this way 94 mg of waxy crystalline solid was obtained of M. W. 2226. The proton NMR spectrum of this material dissolved in deuteriochloroform showed the expected peaks due to the phosphatidyl ethanolamine portion of the molecule, together with a few methylene protons attributable to polyethylene glycol. ( $\Delta=3.7$ ).

#### EXAMPLE 4 Preparation of REVs and MLVs

##### A. Sized REVs

A total of 15  $\mu$ moles of the selected lipid components, in the mole ratios indicated in the examples below, were dissolved in chloroform and dried as a thin film by rotary evaporation. This lipid film was dissolved in 1 ml of diethyl ether washed with distilled water. To this lipid solution was added 0.34 ml of an aqueous buffer solution containing 5 mM Tris, 100 mM NaCl, 0.1 mM EDTA, pH 7.4, and the mixture was emulsified by sonication for 1 minute, maintaining the temperature of the solution at or below room temperature. Where the liposomes were prepared to contain encapsulated [125I] tyraminyl-inulin, such was included in the phosphate buffer at a concentration of about 4  $\mu$ Ci/ml buffer.

The ether solvent was removed under reduced pressure at room temperature, and the resulting gel was taken up in 0.1 ml of the above buffer, and shaken vigorously. The resulting REV suspension had particle sizes, as determined by microscopic examination, of between about 0.1 to 20 microns, and was composed predominantly of relatively large (greater than 1 micron) vesicles having one or only a few bilayer lamellae.

The liposomes were extruded twice through a polycarbonate filter (Szoka, 1978), having a selected pore size of 0.4 microns or 0.2 microns. Liposomes extruded through the 0.4 micron filter averaged  $0.17 \pm (0.05)$  micron diameters, and through the 0.2 micron filter,  $0.16 (0.05)$  micron diameters. Non-encapsulated [125I] tyraminyl-inulin was removed by passing the extruded liposomes through Sephadex G-50 (Pharmacia).

#### B. Sized MLVs

Multilamellar vesicle (MLV) liposomes were prepared according to standard procedures by dissolving a mixture of lipids in an organic solvent containing primarily  $\text{CHCl}_3$  and drying the lipids as a thin film by rotation under reduced pressure. In some cases a radioactive label for the lipid phase was added to the lipid solution before drying. The lipid film was hydrated by addition of the desired aqueous phase and 3 mm glass beads followed by agitation with a vortex and shaking above the phase transition temperature of the phospholipid component for at least 1 hour. In some cases a radioactive label for the aqueous phase was included in the buffer. In some cases the hydrated lipid was repeatedly frozen and thawed three times to provide for ease of the following extrusion step.

The size of the liposome samples was controlled by extrusion through defined pore polycarbonate filters using pressurized nitrogen gas. In one procedure, the liposomes were extruded one time through a filter with pores of  $0.4 \mu\text{m}$  and then ten times through a filter with pores of  $0.1 \mu\text{m}$ . In another procedure, the liposomes were extruded three times through a filter with  $0.2 \mu\text{m}$  pores followed by repeated extrusion with  $0.05 \mu\text{m}$  pores until the mean diameter of the particles was below  $100 \text{ nm}$  as determined by DLS. Unencapsulated aqueous components were removed by passing the extruded sample through a gel permeation column separating the liposomes in the void volume from the small molecules in the included volume.

#### C. Loading $^{67}\text{Ga}$ Into DF-Containing Liposomes

The protocol for preparation of  $\text{Ga}^{67}$ -DF labeled liposomes as adapted from known procedures (Gabizon). Briefly, liposomes were prepared with the ion chelator desferal mesylate encapsulated in the internal aqueous phase to bind irreversibly Ga transported through the bilayer by hydroxyquinoline (oxine).

#### D. Dynamic Light Scattering

Liposome particle size distribution measurements were obtained by DLS using a NICOMP Model 200 with a Brookhaven Instruments BI-2030AT autocorrelator attached. The instruments were operated according to the manufacturer's instructions. The NICOMP results were expressed as the mean diameter and standard deviation of a Gaussian distribution of vesicles by relative volume.

### EXAMPLE 5

#### Kinetics of Liposome Clearance from the Bloodstream

##### A. Measuring Blood Circulation Time and Blood/RES Ratios

In vivo studies of liposomes were performed in two different animal models: Swiss-Webster mice at 25 g each and laboratory rats at 200–300 g each. The studies in mice involved tail vein injection of liposome samples at  $1 \mu\text{M}$  phospholipid/mouse followed by animal sacrifice after a defined time and tissue removal for label quantitation by gamma counting. The weight and percent of the injected dose in each tissue were determined. The studies in rats involved establishment of a chronic catheter in a femoral vein for removal of blood samples at defined times after injection of liposome samples in a catheter in the other femoral artery at  $3\text{--}4 \mu\text{M}$  phospholipid/rat. The percent of the injected dose remaining in the blood at several time points up to 24 hours was determined.

##### B. Time Course of Liposome Retention in the Bloodstream

PEG-PE composed of methoxy PEG, molecular weight 1900 and 1-palmitoyl-2-oleyl-PE (POPE) was prepared as in Example 2. The PEG-POPE lipid was combined with and partially hydrogenated egg PC (PHEPC) in a lipid:lipid mole ratio of about 0.1:2, and the lipid mixture was hydrated and extruded through a  $0.1 \mu\text{m}$  polycarbonate membrane, as described in Example 4, to produce MLV's with average size about  $0.1 \mu\text{m}$ . The MLV lipids included a small amount of radio-labeled lipid marker  $^{14}\text{C}$ -cholesteryl oleate, and the encapsulated marker  $^3\text{H}$ -inulin.

The liposome composition was injected and the percent initial injected dose in mice was determined as described in Example 4, at 1, 2, 3, 4, and 24 after injection. The time course of loss of radiolabeled material is seen in FIG. 7 which is a plot of percent injected dose for encapsulated inulin (solid circles), inulin marker corrected to the initial injection point of 100% (open circles), and lipid marker (closed triangles), over a 24-hour period post injection. As seen, both lipid and encapsulated markers showed greater than 10% of original injected dose after 24 hours.

### EXAMPLE 6

#### Effect of Phospholipid Acyl-Chain Saturation on Blood/RES Ratios in PEG-PE Liposomes

PEG-PE composed of methoxy PEG, molecular weight 1900 and distearylPE (DSPE) was prepared as in Example 2. The PEG-PE lipids were formulated with selected lipids from among sphingomyelin (SM), fully hydrogenated soy PC (PC), cholesterol (Chol), partially hydrogenated soy PC (PHSPC), and partially hydrogenated PC lipids identified as PC IV1, IV10, IV20, IV30, and IV40 in Table 3. The lipid components were mixed in the molar ratios shown at the left in Table 4, and used to form MLV's sized to  $0.1 \mu\text{m}$  as described in Example 4.

TABLE 3

Egg PC Form	Phase Transition Temp.(°C.)		Mole % Fatty Acid Comp.							
	Range	Midpoint	18:0	18:1	18:2	20:0	20:1-4	22:0	22:1-6	
Native	<20		12	30	15	0	3	0	5	
IV 40		<20	14	32	4	0	3	0	4	
IV 30	<20-30		20	22	0	1	2	1	3	
IV 20	23-45	41	30	10	0	2	1	2	3	

TABLE 3-continued

Egg PC Form	Phase Transition Temp.(°C.)		Mole % Fatty Acid Comp.						
	Range	Midpoint	18:0	18:1	18:2	20:0	20:1-4	22:0	22:1-6
IV 10	37-50	46	42	4	0	3	1	4	2
IV 1	49-54	52	56	0	0	5	0	6	0

TABLE 4

	Blood	L + S (RES)	B/RES	% Rec
PEG-PE:SM:PC:Chol	19.23	6.58	2.92	49.23
0.2:1:1:1				
PEG-PE:PHSPC:Chol	20.54	7.17	2.86	55.14
0.15:1.85:1				
PEG-PE:PC IV1:Chol	17.24	13.71	1.26	60.44
0.15:1.85:1				
PEG-PE:PC IV1:Chol (Two animals)	19.16	10.07	1.90	61.87
0.15:1.85:1				
PEG-PE:PC IV10:Chol (Two animals)	12.19	7.31	1.67	40.73
0.15:1.85:1				
PEG-PE:PC IV10:Chol	2.4	3.5	0.69	12.85
0.15:1.85:1				
PEG-PE:PC IV20:Chol	24.56	7.52	3.27	62.75
0.15:1.85:1				
PEG-PE:PC IV20:Chol	5.2	5.7	0.91	22.1
0.15:1.85:1				
PEG-PE:PC IV40:Chol	19.44	8.87	2.19	53.88
0.15:1.85:1				
PEG-PE:PC IV40:Chol	17.2	9.35	1.84	58.09
0.15:1.85:1				
PEG-PE:PC IV40:Chol	20.3	8.8	2.31	45.5
0.15:1.85:0.5				
PEG-PE:EPC:Chol	15.3	9.6	1.59	45.9
0.15:1.85:1				

24 hours after injection, the percent material injected (as measured by percent of <sup>57</sup>Ga-desferal) remaining the blood and in the liver (L) and spleen (S) were deter-

ponents (IV40), and intermediate-saturation components (e.g., IV20).

In addition, a comparison of blood/RES ratios obtained using the relatively saturated PEG-DSPE compound and the relatively unsaturated PEG-POPE compound (Example 5) indicates that the degree of saturation of the derivatized lipid is itself not critical to the ability of the liposomes to evade uptake by the RES.

## EXAMPLE 7

## Effect of Cholesterol and Ethoxylated Cholesterol on Blood/RES Ratios in PEG-PE Liposomes

## A. Effect of added cholesterol

PEG-PE composed of methoxy PEG, molecular weight 1900 and was derivatized DSPE as described in Example 6. The PEG-PE lipids were formulated with selected lipids from among sphingomyelin (SM), fully hydrogenated soy PC (PC), and cholesterol (Chol), as indicated in the column at the left in Table 5 below. The three formulations shown in the table contain about 30, 15, and 0 mole percent cholesterol. Both REV's (0.3 micron size) and MLV's (0.1 micron size) were prepared, substantially as in Example 4, with encapsulated tritium-labeled inulin.

The percent encapsulated inulin remaining in the blood 2 and 24 hours after administration, given at the right in the table, show no measurable effect of cholesterol, in the range 0-30 mole percent.

TABLE 5

	% Injected Dose In Blood			
	2 HR. <sup>3</sup> H Aqueous Label (Leakage)	24 HR. <sup>3</sup> H Aqueous Label (Leakage)	2 HR. <sup>14</sup> C - Lipid Label	24 HR. <sup>14</sup> C - Lipid Label
(1) SM:PC:Chol:PEG-DSPE 1:1:1:0.2				
100 nm MLV	19	5	48	24
300 nm REV	23	15	67	20
(2) SM:PC:Chol:PEG-DSPE 1:1:0.5:0.2				
300 nm REV	23	15	71	17
(3) SM:PC:PEG-DSPE 1:1:0.2				
100 nm MLV	19	6	58	24
300 nm REV	32	23	76	43

mined, and these values are shown in the two data columns at the left in Table 4. The blood and L + S (RES) values were used to calculate a blood/RES value for each composition. The column at the right in Table 4 shows total amount of radioactivity recovered. The two low total recovery values in the table indicate anomalous clearance behavior.

The results from the table demonstrate that the blood/RES ratios are largely independent of the fluidity, or degree of saturation of the phospholipid components forming the liposomes. In particular, there was no systematic change in blood/RES ratio observed among liposomes containing largely saturated PC components (e.g., IV1 and IV10 PC's), largely unsaturated PC com-

## B. Effect of ethoxylated cholesterol

Methoxy-ethoxy-cholesterol was prepared by coupling methoxy ethanol to cholesterol via the trifluorosulfonate coupling method described in Section I. PEG-PE composed of methoxy PEG, molecular weight 1900 and was derivatized DSPE as described in Example 6. The PEG-PE lipids were formulated with selected lipids from among distearylPC (DSPC), partially hydrogenated soy PC (PHSPC), cholesterol, and ethoxylated cholesterol, as indicated at the right in Table 6. The data show that (a) ethoxylated cholesterol, in combination with PEG-PE, gives about the same degree of enhancement of liposome lifetime in the blood as PEG-PE alone. By itself, the ethoxylated cholesterol pro-

vides a moderate degree of enhancement of liposome lifetime, but substantially less than that provided by PEG-PE.

TABLE 6

Formulation	% Injected Dose In Blood <sup>14</sup> C-Chol-Oleate	
	2 HR.	24 HR.
HSPC:Chol:PEG-DSPE 1.85:1:0.15	55	9
HSPC:Chol:PEG-DSPE:PEG <sub>5</sub> -Chol 1.85:0.85:0.15:0.15	57	9
HSPC:Chol:HPG:PEG <sub>5</sub> -Chol 1.85:0.85:0.15:0.15	15	2
HSPC:Chol:HPG 1.85:1:0.15	4	1

## EXAMPLE 8

## Effect of Charged Lipid Components on Blood/RES Ratios in PEG-PE Liposomes

PEG-PE composed of methoxy PEG, molecular weight 1900 and was derivatized DSPE as described in Example 6. The PEG-PE lipids were formulated with lipids selected from among egg PG (PG), partially hydrogenated egg PC (PHEPC), and cholesterol (Chol), as indicated in the FIG. 6. The two formulations shown in the figure contained about 4.7 mole percent (triangles) or 14 mole percent (circles) PG. The lipids were prepared as MLV's, sized to 0.1 micron as in Example 4.

The percent of injected liposome dose present 0.25, 1, 2, 4, and 24 hours after injection are plotted for both formulations in FIG. 6. As seen, the percent PG in the composition had little or no effect on liposome retention in the bloodstream. The rate of loss of encapsulated marker seen is also similar to that observed for similarly prepared liposomes containing no PG.

Although the invention has been described and illustrated with respect to particular derivatized lipid compounds, liposome compositions, and use, it will be apparent that a variety of modifications and changes may be made without departing from the invention.

It is claimed:

1. A liposome composition for use in delivering a compound via the bloodstream comprising liposomes composed of vesicle-forming lipids and between 1-20 mole percent of an amphipathic, vesicle-forming lipid derivatized with a polyethyleneglycol, and containing the compound in liposome-entrapped form, and characterized by a blood level, 24 hours after intravenous injection, which is severalfold times that of the liposomes in the absence of the derivatized lipid.

2. The composition of claim 1, wherein the liposomes have a selected average size in the size range between about 0.05 and 0.5 microns.

3. The composition of claim 2, wherein the polyethyleneglycol has a molecular weight is between about 1,000 to 5,000 daltons.

4. The composition of claim 2, wherein the amphipathic lipid is a phospholipid having a polar head group at which the polyethyleneglycol is derivatized, and the liposomes are characterized by a blood circulation lifetime, as measured by the percent liposome marker retained in the blood 24 hours after intravenous injection of the liposomes, which is greater than about 5 percent of the total amount administered.

5. The composition of claim 4, wherein the amphipathic lipid is a phospholipid and the liposomes are characterized by a blood circulation lifetime, as measured by the percent liposome marker retained in the blood 24 hours after intravenous injection of the liposomes, which is greater than about 10 percent of the total amount administered.

6. The composition of claim 4, wherein the phospholipid is phosphatidylethanolamine, and the polyethyleneglycol is coupled to the phospholipid through a lipid amine group.

7. The composition of claim 5, wherein the phospholipid contains acyl chains which are predominantly 18-carbon acyl chains with at least one unsaturated bond.

8. The composition of claim 7, wherein the phospholipid is a phosphatidylethanolamine, and the polyethyleneglycol is coupled to the phospholipid through a lipid amine group.

9. The composition of claim 1, wherein the liposomes contain 10-40 mole percent cholesterol, 40-85 mole percent neutral phospholipid, and 5-15 mole percent phospholipid derivatized with polyethyleneglycol.

10. The composition of claim 1, which is characterized by a blood/RES ratio, 24 hours after intravenous administration, which is at least about tenfold greater than that of the same liposomes in the absence of the derivatized amphipathic lipid.

11. The composition of claim 10, wherein the vesicle-forming lipids making up the liposomes are selected to produce a selected rate of release of the drug from the liposomes circulating in the bloodstream.

12. The composition of claim 11, for the treatment of malignancy, wherein the drug is an amphipathic anti-tumor compound.

13. The composition of claim 12, wherein the drug is doxorubicin or a pharmacologically acceptable analog or salt thereof.

14. The composition of claim 1, wherein the polyalkylether is linked to the amphipathic lipid through an esterase-or peptidase-sensitive linkage.

15. The composition of claim 1, wherein the liposomes include a surface-bound ligand which is effective to bind specifically and with high affinity to ligand-binding molecules carried on the surface of specific cells circulating in the bloodstream.

16. The composition of claim 15, wherein the surface-bound ligand is an antibody effective to bind specifically and with high affinity to an antigen which is expressed in a cell in the bloodstream in a disease state.

17. The composition of claim 15, wherein the surface-bound ligand is CD4 peptide which is effective to bind to HIV-infected T cell or B cells.

18. A method of producing a severalfold increase in the blood-circulation time of intravenously administered liposomes formed of vesicle-forming lipids and containing an entrapped compound, as measured by the percent liposome marker retained in the blood 24 hours after intravenous injection, substantially independent of the degree of saturation of said vesicle-forming lipids, comprising

forming the liposomes to include between about 1-20 mole percent an amphipathic, vesicle-forming lipid derivatized with a polyethyleneglycol.

19. The method of claim 18, wherein the liposomes have a selected average size in the size range between about 0.05 and 0.5 microns.

20. The method of claim 18, for increasing the blood-circulation time of intravenously administered liposomes, as measured by the percent liposome marker retained in the blood 24 hours after intravenous injection of the liposomes, to a level which is greater than about 10 percent of the total amount of lipid administered, wherein the amphipathic lipid is a phospholipid, and the polyethyleneglycol has a molecular weight between about 1,000 to 5,000 daltons.

21. The method of claim 18, wherein adding is effective to enhance the blood circulation lifetime 24 hours after intravenous administration, by at least about ten-fold over that observed with the same liposomes in the absence of the derivatized amphipathic lipid.

22. A method of administering a compound intravenously, to achieve a level of compound in the bloodstream, 24 hours after drug administration, which is at least about 5 percent of the total amount of compound administered, comprising

preparing a suspension of liposomes composed of vesicle-forming lipids and between 1-20 mole percent of an amphipathic, vesicle-forming lipid derivatized with a polyethyleneglycol, and the compound, in liposome-entrapped form, and intravenously administering an amount of the suspension containing a pharmacologically acceptable amount of the drug.

23. The method of claim 22, wherein the polyethyleneglycol has a molecular weight of between about 1,000 and 5,000 daltons.

24. The method of claim 22, wherein the vesicle-forming lipid is a phospholipid, and the level of compound in the bloodstream, 24 hours after liposome administration, is at least about 10 percent of the total compound administered.

25. A method of delivering a drug selectively to a target tissue containing surface-bound tissue-specific ligand-bind molecules, comprising

preparing a suspension of liposomes containing between 1-20 mole percent of an vesicle-forming lipid derivatized with a polyethyleneglycol, a surface-bound ligand effective to bind specifically and with high affinity to said ligand-binding molecule, and the drug, in liposome-entrapped form, and intravenously administering an amount of the suspension containing a pharmacologically acceptable amount of the drug.

26. The method of claim 25, wherein the polyethyleneglycol has a molecular weight of between about 1,000 and 5,000 daltons.

27. The method of claim 26, wherein the vesicle-forming lipid is a phospholipid.

28. The method of claim 25, wherein the target tissue is a solid tumor carrying a tumor specific antigen, and the ligand is an antibody specific against such antigen.

29. The method of claim 25, wherein the target tissue is a solid tumor, and the drug is doxorubicin or a pharmacologically acceptable analog or salt thereof.

30. A method of enhancing the uptake, by the reticuloendothelial system, of cells carrying surface-specific ligand-binding molecules which are characteristic of a disease state, comprising

preparing a suspension of liposomes containing between 1-20 mole percent of an vesicle-forming lipid derivatized with a polyethyleneglycol, and a surface-bound ligand effective to bind specifically and with high affinity to said ligand-binding molecule, and

administering said suspension intravenously.

31. The method of claim 30, wherein the polyethyleneglycol has a molecular weight of between about 1,000 and 5,000 daltons.

32. The method of claim 30, wherein the vesicle-forming lipid is a phospholipid.

33. The method of claim 30, wherein the cells are HIV-infected T-cells or B cells and the surface-bound D4 peptide.

\* \* \* \* \*

45

50

55

60

65

## Conjugation of an Anti-B-cell Lymphoma Monoclonal Antibody, LL2, to Long-circulating Drug-carrier Lipid Emulsions

BO B. LUNDBERG, GARY GRIFFITHS\* AND HANS J. HANSEN\*

*Department of Biochemistry and Pharmacy, Abo Akademi University, BioCity P. O. Box 66, FIN-20521 Abo, Finland and \*Immunomedics Inc, Morris Plains, NJ 07950, USA*

### Abstract

Long-circulating submicron lipid emulsions, stabilized with poly(ethylene glycol)-modified phosphatidylethanolamine (PEG-PE), are promising drug carriers with substantial capacity for solubilization of lipophilic anticancer agents. This study describes the conjugation of the anti-B-cell lymphoma monoclonal antibody LL2 to the surface of lipid-emulsion globules by use of a novel poly(ethylene glycol)-based heterobifunctional coupling agent.

The efficiency of coupling of LL2 to the lipid emulsion was 85% (approx.) and essentially independent of the LL2/emulsion particle ratio and amount of surface-bound PEG-PE. Results from sucrose-gradient centrifugation and Sepharose CL-4B gel filtration indicated stable binding of the antibody to the emulsion. The immunoreactivity of the emulsion-LL2 conjugates was tested with alkaline phosphatase-conjugated LL2 against a monoclonal anti-idiotypic antibody, WN. The binding of the conjugates to WN increased with increasing surface density of LL2 up to 40 monoclonal antibodies/emulsion particle, and exceeded that for the free monoclonal antibody (approx. 20 molecules/particle). Results from competitive-binding ELISA were indicative of similar displacement curves for free LL2 and emulsion-LL2 conjugates. Direct cellular ELISA revealed similar binding of emulsion-LL2 complexes to three types of Burkitt's lymphoma cell lines, Raji, Ramos and Daudi.

The results from this study indicate that emulsion-LL2 complexes might be a useful drug-carrier system for more specific delivery of anticancer drugs to B-cell malignancy.

Antibody-based targeting of antineoplastic drugs is a promising approach to the development of therapy for cancer (Vingerhoeds et al 1994; Vitetta & Uhr 1994). Haematological malignancy, in which the immunoconjugates have unrestricted access to cancer cells, should be particularly amenable to this approach.

LL2 is a murine IgG2a anti-B-cell lymphoma monoclonal antibody raised against the Raji Burkitt lymphoma cell line (Pawlak-Byczkowska et al 1989). It has been proven of clinical importance in the radioimmunodetection and radioimmunotherapy of non-Hodgkin's B-cell lymphoma (Goldenberg et al 1991; Murthy et al 1992). That LL2 is internalized into antigen-bearing cells (Shih et al 1994) makes it potentially useful for

intracellular delivery of cytotoxic agents. In this study LL2 has been conjugated to the surface of submicron lipid-emulsion drug carriers by use of a heterobifunctional coupling agent.

Submicron lipid emulsions have many appealing properties as drug carriers—they are biocompatible, biodegradable and easy to prepare and handle (Lundberg 1993; Wheeler et al 1994; Liu & Liu 1995; Lundberg et al 1996). The emulsions comprise two major components, an oil core (i.e. triglyceride) stabilized by emulsifiers (i.e. phospholipids). The hydrophobic cores of such emulsions can solubilize considerable amounts of lipophilic drugs (Lundberg 1994, 1997, 1998). The poor emulsifying properties of phospholipids can be enhanced by adding a biocompatible coemulsifier such as polysorbate 80 (Lundberg 1994). A severe problem with particulate drug carriers is rapid uptake by the mononuclear phagocyte system (Poste et al 1982). Although this problem can be

Correspondence: B. B. Lundberg, Department of Biochemistry and Pharmacy, Abo Akademi University, BioCity P. O. Box 66, FIN-20521 Abo, Finland.

overcome by engrafting poly(ethylene glycol) (PEG) chains on to the particle surfaces (Woodle & Lasic 1992; Lundberg et al 1996), higher molecular-weight PEGs mask antibody recognition and weaken the targeting capability of immunoconjugates (Blume et al 1993). A successful strategy for solving this problem is to link the monoclonal antibody to the distal PEG terminus (Song et al 1996; Kirpotin et al 1997; Lopes de Menezes et al 1998). An obvious problem with particulate drug carriers such as liposomes and emulsions is slow and non-specific uptake by cells. The conjugation, to the surface of the drug carrier, of an internalizing ligand for cellular receptors would greatly enhance the feasibility of this concept of drug delivery. This paper reports the successful conjugation of an internalizing ligand, monoclonal antibody LL2, to a long-circulating submicron lipid emulsion by means of a heterobifunctional coupling agent.

## Materials and Methods

### Materials

Dipalmitoylphosphatidylcholine (DPPC) was obtained from Alexis (Läufelfingen, Switzerland). Dipalmitoylphosphatidylethanolamine (DPPE), distearoylphosphatidylethanolamine, triolein, polyoxyethylenesorbitan monooleate (polysorbate 80), carbonyl diimidazole, maleimide-activated alkaline phosphatase, and 2-mercaptoethanol were from Sigma (St Louis, MO). Poly(ethylene glycol)vinylsulphone-*N*-hydroxysuccinimide ester (VS-PEG-NHS) was purchased from Shearwater Polymers Europe (Enschede, The Netherlands). [ $^{14}\text{C}$ ]DPPC and  $^{125}\text{I}$  were from Amersham International (Amersham, UK). 1,11-Dioctadecyl-3,3,3',3'-tetramethylindocarbocyanine perchlorate (DiI) was from Molecular Probes (Eugene, OR) and 4-methylumbelliferyl phosphate (MUP) from Koch-Light (Suffolk, UK). Poly(ethylene glycol)-modified phosphatidylethanolamine (PEG-PE) was synthesized by reaction of PEG 2000 with carbonyl-diimidazole then addition of DPPE (Allen et al 1991). Finally PEG-DPPE was dialysed against water by means of a Spectra/Por CE 300 000 MWCO dialysis bag (Spectrum Medical Industries, Houston, TX) and then lyophilized (Maruyama et al 1992). A poly(ethylene glycol) derivative of phosphatidylethanolamine with a vinylsulphone group at the distal terminus of the poly(ethylene glycol) chain (DSPE-PEG-VS) (Figure 1) was synthesized by reacting NHS-PEG-VS (25  $\mu\text{mol}$ ) with DSPE (23  $\mu\text{mol}$ ) and triethylamine (50  $\mu\text{mol}$ ) in chloroform (1 mL) for 6 h at 40°C. The product

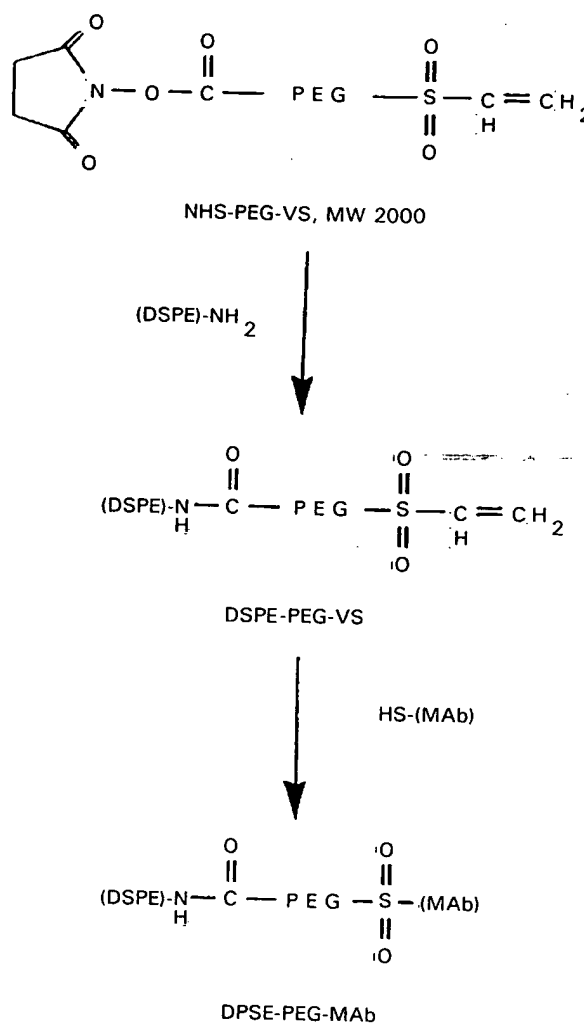


Figure 1. Synthesis of a PEG-DSPE derivative with a vinylsulphone (VS) function at the end of the poly(ethylene glycol) chain, and its reaction with thiol groups on a monoclonal antibody.

was purified by preparative silica gel thin-layer chromatography (TLC) and gave a single spot in analytical TLC when visualized with iodine vapour and molybdate spray.

### Cell lines and monoclonal antibody

Cultured cells from man included Burkitt's lymphoma lines Raji, Daudi and Ramos. The cells were grown in RPMI 1640 medium with 10% foetal calf serum; they were maintained at 37°C and aerated with 5% CO<sub>2</sub> in air.

Murine monoclonal antibody LL2, an I7G (Pawlak-Byczkowska et al 1989) specific for the epitope B of CD22 (Stein et al 1993) raised by immunization of BALB/c mice with an extract of Raji cells, and WN, a rat monoclonal anti-idiotypic

antibody to LL2 (Losman et al 1995) were obtained from Immunomedics. The molecular weight of LL2 was found to be 154 kD by mass-analysed laser-desorption ionization-time-of-flight (MALDI-TOF) mass spectrometry (Mass Consortium, San Diego, CA).  $^{125}\text{I}$  labelling was performed by the chloramine-T procedure. For alkaline phosphatase conjugation of LL2, the monoclonal antibody was first reduced with 50 mM 2-mercaptoethanol for 10 min at 4°C in 0.2 M Tris buffer (pH 8.7) and then reacted with maleimide-activated phosphatase (2 mol enzyme (mol LL2) $^{-1}$ ) in 0.15 M NaCl and 0.1 M sodium phosphate (pH 7.0) for 3 h at room temperature. Remaining maleimide groups were blocked with 1.5 mM 2-mercaptoethanol.

#### *Preparation of emulsion*

Submicron lipid emulsions were prepared and characterized as described in detail elsewhere (Lundberg 1993; Lundberg et al 1996). The basic composition of the lipid emulsions was triolein-DPPC-polysorbate 80:2:1:0.4 (w/w). When indicated, 2–8 mol% PEG-DPPE (calculated relative to DPPC) was added into the lipid mixture. For antibody conjugation, 2 mol% DSPE-PEG-VS (calculated relative to DPPC) was included. The components were dispensed into vials from stock solutions at –20°C and the solvent was evaporated to dryness under reduced pressure. Phosphate-buffered saline (PBS) was added and the mixture was heated to 50°C, vortex mixed for 30 s, and sonicated with an MSE probe sonicator for 1 min. Emulsions were stored at 4°C and used for conjugation within 1 day.

#### *Conjugation of LL2 to lipid emulsions*

Coupling of LL2 to emulsion globules was performed by reaction of the vinylsulphone group at the distal PEG terminus on the surface of the globules with the free thiol groups on the monoclonal antibody (Figure 1). Before conjugation LL2 was reduced by reaction with 2-mercaptoethanol (50 mM) for 10 min at 4°C in Tris buffer (pH 8.7; 0.2 M). The reduced monoclonal antibody was separated from excess 2-mercaptoethanol by use of Sephadex G-25 spin-columns, equilibrated in sodium acetate (50 mM)-buffered 0.9% saline (pH 5.3). After this procedure the antibody exposed 8–10 free thiol groups. The product was assayed for protein concentration by measurement of its absorbance at 280 nm (it was assumed that a 1 mg mL $^{-1}$  monoclonal antibody solution has an absorbance of 1.4) or by quantitation of  $^{125}\text{I}$ -labelled monoclonal antibody. Thiol groups were

determined with Aldrithiol, by monitoring the change in absorbance at 343 nm, with cysteine as standard. The coupling reaction was performed overnight, at room temperature under argon, in HEPES-buffered saline (pH 7.4). Excess vinylsulphone groups were quenched with 2 mM 2-mercaptoethanol for 30 min (Kirpotin et al 1997), excess 2-mercaptoethanol and antibody were removed by gel chromatography on a Sepharose CL-4B column. The immunoconjugates were collected near the void volume of the column, passed through a 0.45- $\mu\text{m}$  sterile filter, and stored at 4°C. Coupling efficiency was calculated by use of  $^{125}\text{I}$ -labelled monoclonal antibody. Recovery of emulsions was estimated by measurement of [ $^{14}\text{C}$ ]DPPC in parallel experiments. The number of monoclonal antibody per emulsion globule was calculated assuming a droplet size of 50 nm (Lundberg 1993) and a molecular weight of 150 kD for LL2.

The integrity of the emulsion-LL2 conjugates was checked by sucrose density-gradient centrifugation and gel filtration. The protein fraction was quantified by  $^{125}\text{I}$  counting and the emulsion by DiI fluorescence (excitation and emission wavelengths 520 and 578 nm, respectively). Centrifugation (50 000 rev min $^{-1}$ , 24 h at 10°C) was performed in a Beckman SW-60 Ti rotor. After centrifugation the tubes were punctured and fractions were collected. Gel filtration was performed on a 30 cm  $\times$  2 cm Sepharose CL-4B column eluted with PBS (0.25 mL min $^{-1}$ ).

#### *ELISA assay and cell binding*

The immunoreactivity of the emulsion-LL2 conjugates was assessed by determining their binding affinities to the anti-idiotypic antibody WN IgG. ELISA plates were coated with WN, 50  $\mu\text{L}$ /well of a solution (10  $\mu\text{g}$  mL $^{-1}$ ) in carbonate buffer (pH 9.6; 50 mM), at 4°C overnight. The wells were washed with 1% Triton X-100 in PBS and additional binding sites blocked with dilution buffer containing 1% bovine serum albumin (BSA) and 1% Triton X-100 in PBS. Alkaline phosphatase-conjugated free and emulsion-associated LL2 with different monoclonal antibody/emulsion particle ratios in dilution buffer were then added to the plates. After incubation for 1 h at room temperature, unbound antibody was removed by washing three times with 1% BSA in PBS. Binding of alkaline phosphatase-conjugated LL2 was then determined by measuring hydrolysis of MUP (0.1 mg mL $^{-1}$ ) in Tris buffer (pH 8.0) by means of a microtitre plate spectrofluorimeter with a 365-nm excitation filter and a 450-nm emission filter. The competitive blocking assays were performed with



the same protocol as above, but the WN-coated wells were incubated with alkaline phosphatase-conjugated free and liposome-associated LL2 in the presence of excess unconjugated LL2 ( $0.1-10 \mu\text{g mL}^{-1}$ ).

The binding of emulsion-LL2 complexes to target cells was measured by use of alkaline phosphatase-conjugated monoclonal antibody. Cells ( $2 \times 10^6$ ) in growth medium were incubated with alkaline phosphatase-conjugated LL2 and its emulsion conjugates for 30 min with shaking at  $4^\circ\text{C}$ . The cells were thoroughly washed with ice-cold PBS and the alkaline phosphatase activity was measured.

## Results and Discussion

### Conjugation

A serious problem associated with the use of particulate lipid and lipid-protein drug-carriers is their very rapid elimination from the bloodstream by the cells of the mononuclear phagocyte system. Although the development of long-circulating dose-independent lipid drug-carrier formulations with engrafted PEG on their surface is a major breakthrough in this field (Woodle & Lasic 1992), surface-attached PEG groups have been shown to interfere with the efficient binding of targeted liposomes to their cellular targets (Klibanov et al 1991; Park et al 1995). With liposomes this problem has recently been tackled by attachment of the targeting antibody to the termini of the surface-grafted PEG chains (Kirpotin et al 1997; Lopes de Menezes et al 1998). In this study a similar approach has been applied to long-circulating lipid emulsions. A novel heterobifunctional coupling agent, NHS-PEG-VS, is used for the conjugation process. The coupling procedure depicted in Figure 1 starts with reaction of the NHS ester group of NHS-PEG-VS, with the amino group of DSPE. The NHS ester is highly reactive toward amino groups, but hydrolytically unstable. Under the conditions used, reaction in chloroform in the presence of triethylamine, the yield was very high (approx. 90%). The next step was reaction of the vinylsulphone (VS) with thiol groups on the monoclonal antibody. Vinylsulphone is an attractive derivative for selective coupling to thiol groups. At near neutral pH VS will couple with a half-life of 15–20 min to proteins containing thiol groups (Morpurgo et al 1996). The reactivity of VS is a little lower than that of maleimide, but the VS group is more stable in water and a stable linkage is produced by reaction with thiol groups. The con-

jugation of reduced LL2 to the VS group of the surface-grafted DSPE-PEG-VS during 16 h at room temperature was very reproducible with an typical efficiency of 85% (approx.) The quenching of excess active groups after the conjugation reaction seems to be important, because in the presence of free thiols or hydrazide groups at the PEG termini immunoliposomes bind appreciably to cells lacking the target antigen (Allen et al 1995; Hansen et al 1995), probably by covalent attachment to cell surface molecules.

### Coupling efficiency

To explore the proper conditions for the conjugation process the starting ratio of LL2 to emulsion globules was varied. The results showed that the coupling process was essentially independent of the starting ratio in the range 5–40 monoclonal antibodies per emulsion particle (Figure 2A). Kirpotin

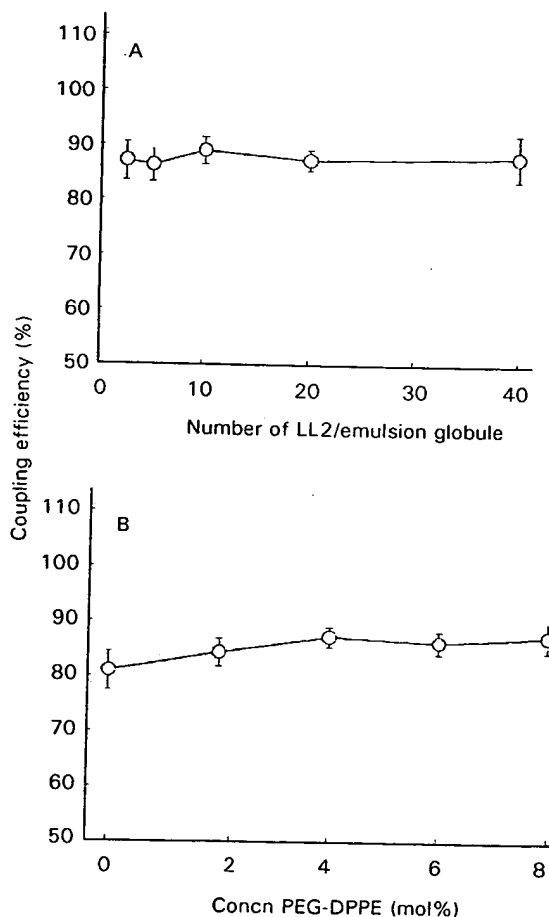


Figure 2. Efficiency of coupling of LL2 to vinyl sulphone-activated lipid emulsions as a function of A. LL2/emulsion particle ratio (4% PEG-DPPE) and B. amount of PEG-DPPE (LL2/emulsion particle ratio 20 : 1).

[ $^{125}\text{I}$ ]LL2  $\times 10^3$  and Dil fluorescence  $\times 10$

Figure 2A  
filtrate  
by m  
core  
emul:

et al (1997) showed that the number of monoclonal antibodies per liposome could be increased to 100–120 without loss of coupling efficiency, although the amount of total cell-associated immunoliposomes reached a plateau at (approx.) 40 monoclonal antibodies/liposome suggesting that there is no need to increase the amount of liposome-conjugated protein beyond this value. It has been shown that high antibody densities on liposomes induce rapid clearance from plasma (Allen et al 1995). Another factor which had to be considered was the effect of the steric stabilizer PEG–DPPE. It has been shown that surface-grafted PEG reduces the conjugation efficiency of short spacer linkers, especially when the PEG–PE content is increased to 3.5% and more, corresponding to the transition from “mushroom” to “brush” conformation of the surface-grafted PEG (Kenworthy et al 1995). In this study, with PEG chains of  $M_r=2000$  for both PEG–DPPE and DSPE–PEG–VS, the coupling was essentially unaffected by PEG–DPPE content (Figure 2B). This result is in agreement with that obtained with long PEG-spacer linkers for the conjugation of monoclonal antibody to liposomes (Kirpotin et al 1997).

### Characterization of conjugates

A previous study showed that a combination of phosphatidylcholine and the non-ionic surfactant polysorbate 80 enables the preparation of stable lipid emulsions with a particle diameter of (approx.) 50 nm (Lundberg 1993). Coating of such emulsion particles with PEG–DPPE results in a prolonged circulation time after parenteral administration (Lundberg et al 1996). These submicron lipid emulsions have been shown to be excellent drug carriers for solubilization of lipophilic anticancer drugs (Lundberg 1994, 1997, 1998). The stable association of LL2 with the drug-carrier emulsions was determined by gel chromatography on a Sepharose CL-4B column and sucrose density-gradient centrifugation (Figure 3). The gel filtration profile contained a symmetrical peak where the  $^{125}\text{I}$ -labelled protein component coeluted with the emulsion fraction labelled with the lipophilic fluorescence marker DiI. In sucrose density-gradient centrifugation components labelled in the same way appeared as peaks at densities of  $1.07 \text{ g mL}^{-1}$  (approx.)

### Immunoreactivity of LL2–emulsion conjugates

The monoclonal anti-idiotype antibody, WN, to LL2 was used to determine LL2 immunoreactivity. WN is exquisitely specific for LL2 and reacts with no other monoclonal antibody and inhibits the binding of LL2 to Raji cells (Losman et al 1995). The binding values presented in Table 1 clearly show that binding increases with the number of LL2 molecules per emulsion globule and exceeds that for free LL2 at ca 20 monoclonal antibody molecules/globule. The result is, however, obscured because binding of one emulsion-conjugated LL2 results in association with WN of the rest of the monoclonal antibody molecules on the same particle. Despite this complication the

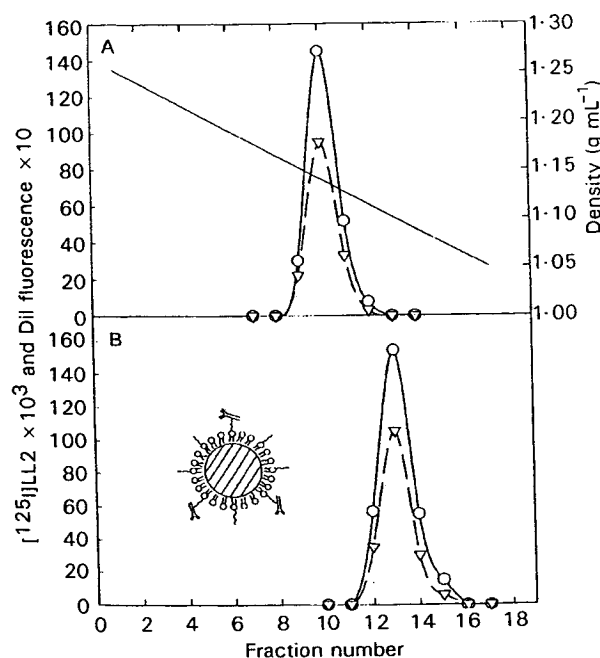


Figure 3. Characterization of lipid emulsion–LL2 complexes by A. sucrose density-gradient centrifugation and B. gel filtration on a Sepharose CL-4B column. LL2 was quantified by measurement of  $^{125}\text{I}$  radioactivity (○) and the emulsion core by DiI fluorescence (▽). Insert. Schematic diagram of emulsion–LL2 globule.

Table 1. Evaluation of the immunoreactivity of emulsion–LL2 conjugates by ELISA.

Monoclonal antibody/emulsion particle ratios	LL2 binding
5:1	$31.1 \pm 3.8$
10:1	$77.5 \pm 1.8$
20:1	$112.2 \pm 5.9$
40:1	$123.2 \pm 3.2$

The plates were coated with the anti-idiotype monoclonal antibody, WN, and alkaline phosphatase-conjugated free and emulsion-associated LL2 with different monoclonal antibody/emulsion particle ratios were added to the plates. After 1 h incubation the binding of alkaline phosphatase-conjugated LL2 was measured (free LL2 = 100). Values are means  $\pm$  standard deviations,  $n=4$ .

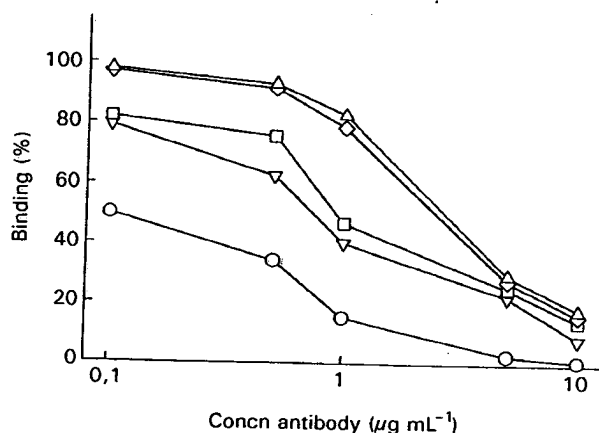


Figure 4. Competitive binding ELISA with WN IgG-coated plates of alkaline phosphatase-conjugated free ( $\Delta$ ) and emulsion-associated LL2 with monoclonal antibody/emulsion particle ratios of 5:1 ( $\circ$ ), 10:1 ( $\nabla$ ), 20:1 ( $\square$ ), and 40:1 ( $\diamond$ ).

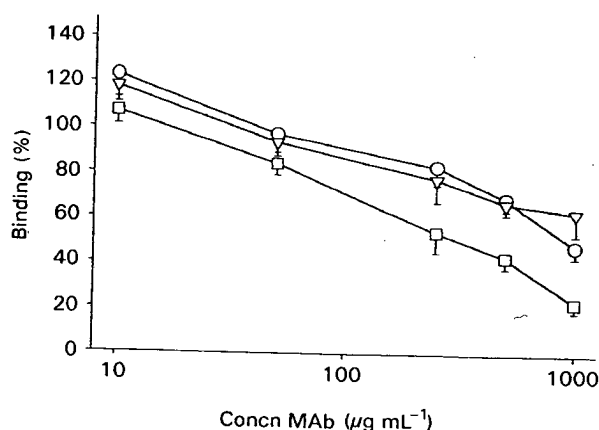


Figure 5. Cell-binding assay of emulsion-alkaline phosphatase-conjugated LL2 complexes (20 monoclonal antibodies/emulsion particle) with Raji ( $\circ$ ), Ramos ( $\square$ ), and Daudi ( $\nabla$ ) cells. The binding is given as percentage of free LL2.

results strongly indicate that the immunoreactivity of the conjugated monoclonal antibody is preserved. The immunoreactivity of conjugated LL2 was further tested with competitive binding ELISA. The results, presented in Figure 4, show that displacement curves were similar for free and emulsion-bound alkaline phosphatase-conjugated LL2, coincubated with excess free LL2. The immunoreactivity of the emulsion-LL2 conjugates was further verified by a cell-binding assay with alkaline phosphatase-conjugated LL2 preparations. The results presented in Figure 5 show that at low concentrations the binding of LL2-emulsion complexes and free LL2 was similar, but the relative binding affinities of the complexes decreased with increasing concentration.

Previous papers from this laboratory have described the preparation, drug incorporation, antineoplastic activity and in-vivo behaviour of drug-carrier lipid emulsions. This study is a further step towards a more specific delivery system whereby drug-carriers can be supplied with a homing device in the form of a monoclonal antibody against an internalizing antigen on cancer cells. We believe that lipid emulsion-LL2 conjugates are a potential targeting system for more specific delivery of anticancer agents to neoplastic cells.

## References

- Allen, T. M., Hansen, C., Martin, F., Redeman, C., Yau-Young, A. (1991) Liposomes containing synthetic lipid derivatives of poly(ethylene glycol) show prolonged circulation half-lives in vivo. *Biochim. Biophys. Acta* 1066: 29-36
- Allen, T. M., Brandeis, E., Hansen, C. B., Kao, G. Y., Zalipsky, S. (1995) A new strategy for attachment of antibodies to sterically stabilized liposomes resulting in efficient targeting to cancer cells. *Biochim. Biophys. Acta* 1237: 99-108
- Blume, G., Cevc, G., Crommelin, M. D. J. A., Baker-Woudenberg, I. A. J. M., Kluft, C., Storm, G. (1993) Specific targeting with poly(ethylene glycol)-modified liposomes: coupling of homing devices to the ends of the polymeric chains combines effective target binding with long circulation times. *Biochim. Biophys. Acta* 1149: 180-184
- Goldenberg, D. M., Horowitz, J. A., Sharkey, R. M., Hall, T. C., Murthy, S., Goldenberg, M., Lee, R. E., Stein, R., Siegel, J. A., Izon, D. O., Burger, K., Swayne, L., Belisle, E., Hansen, H. J., Pinsky, C. M. (1991) Targeting, dosimetry and radioimmunotherapy of B-cell lymphomas with iodine-131-labeled LL2 monoclonal antibody. *J. Clin. Oncol.* 9: 548-564
- Hansen, C. B., Kao, G. Y., Moase, E. H., Zalipsky, S., Allen, T. M. (1995) Attachment of antibodies to sterically stabilized liposomes: evaluation, comparison and optimization of coupling procedures. *Biochim. Biophys. Acta* 1239: 133-144
- Kenworthy, A. K., Hristova, K., Needham, D., McIntosh, T. J. (1995) Range and magnitude of the steric pressure between bilayers containing phospholipids with covalently attached poly(ethylene glycol). *Biophys. J.* 68: 1921-1936
- Kirpotin, D., Park, J. W., Hong, K., Zalipsky, S., Li, W.-L., Carter, P., Benz, C. C., Papahadjopoulos, D. (1997) Sterically stabilized anti-HER2 immunoliposomes: design and targeting to human breast cancer cells in vitro. *Biochemistry* 36: 66-75
- Klibanov, A. L., Maruyama, K., Beckerleg, A. M., Torchilin, V. P. (1991) Activity of amphipathic poly(ethylene glycol) 5000 to prolong the circulation time of liposomes depends on the liposome size and is unfavorable for immunoliposome binding to target. *Biochim. Biophys. Acta* 1062: 142-148
- Liu, F., Liu, D. (1995) Long-circulating emulsions (oil-in-water) as carriers for lipophilic drugs. *Pharm. Res.* 12: 1060-1064
- Lopes de Menezes, D. L., Pilarski, L. M., Allen, T. M. (1998) In vitro and in vivo targeting of immunoliposomal doxorubicin to human B-cell lymphoma. *Cancer Res.* 58: 3320-3330

- Losman, M. J., Leung, S., Shih, L., Shevitz, J., Shukla, R., Haraga, L., Goldenberg, D. M., Hansen, H. J. (1995) Development and evaluation of the specificity of a rat monoclonal anti-idio-type antibody, WN, to an anti-B-cell lymphoma monoclonal antibody, LL2. *Cancer Res (Suppl.)* 55: 5978s
- Lundberg, B. (1993) Preparation of drug-carrier emulsions stabilized with phosphatidylcholine-surfactant mixtures. *J. Pharm. Sci.* 83: 72-75
- Lundberg, B. (1994) The solubilization of lipophilic derivatives of podophyllotoxins in submicron sized lipid emulsions and their cytotoxic activity against cancer cells in culture. *Int. J. Pharm.* 109: 73-81
- Lundberg, B. (1997) A submicron lipid emulsion coated with amphipathic polyethylene glycol for parenteral administration of paclitaxel (Taxol). *J. Pharm. Pharmacol.* 49: 16-21
- Lundberg, B. (1998) Biologically active camptothecin derivatives for incorporation into liposome bilayers and lipid emulsions. *Anticancer Drug Design* 13: 453-461
- Lundberg, B., Mortimer, B.-C., Redgrave, T. G. (1996) Submicron lipid emulsions containing amphipathic polyethylene glycol for use as drug-carriers with prolonged circulation time. *Int. J. Pharm.* 134: 119-127
- Maruyama, K., Yuda, T., Okamoto, A., Kojima, S., Suganaka, A., Iwatsuru, M. (1992) Prolonged circulation time in vivo of large unilamellar liposomes composed of distearoyl phosphatidylcholine and cholesterol containing amphipathic poly(ethylene glycol). *Biochim. Biophys. Acta* 1128: 44-49
- Morpurgo, M., Veronese, F. M., Kachensky, D., Harris, J. M. (1996) Preparation and characterization of poly(ethylene glycol) vinyl sulfone. *Bioconjugate Chem.* 7: 363-368
- Murthy, S., Sharkey, R. M., Goldenberg, D. M., Lee, R. E., Pinsky, C. M., Hansen, H. J., Burger, K., Swayne, L. C. (1992) Lymphoma imaging with a new technetium-99m labeled antibody, LL2. *Europ. J. Nucl. Med.* 19: 394-401
- Park, J. W., Hong, K., Carter, P., Asgari, H., Guo, L. Y., Keller, G. A., Wirth, C., Shalaby, R., Kotts, C., Wood, W. I., Papahadjopoulos, D., Benz, C. C. (1995) Development of anti-p185HER2 immunoliposomes for cancer therapy. *Proc. Natl Acad. Sci. USA* 92: 1327-1331
- Pawlak-Byczkowska, E. J., Hansen, H. J., Dion, A. S., Goldenberg, D. M. (1989) Two new monoclonal antibodies, EPB-1 and EPB-2, reactive with human lymphoma. *Cancer Res.* 49: 4568-4577
- Poste, G., Bucana, C., Raz, A., Bugelski, P., Kirsh, R., Fidler, I. J. (1982) Analysis of the fate of systemically administered liposomes and implications for their use in drug delivery. *Cancer Res.* 42: 1412-1422
- Shih, L. B., Lu, H. H.-Z., Xuan, H., Goldenberg, D. M. (1994) Internalization and intracellular processing of an anti-B-cell lymphoma monoclonal antibody, LL2. *Int. J. Cancer* 56: 538-545
- Song, Y. K., Liu, D., Maruyama, K. Z., Takizawa, T. (1996) Antibody mediated lung targeting of long-circulating emulsions. *PDA. J. Pharm. Sci. Technol.* 50: 372-377
- Stein, R., Belisle, E., Hansen, H., Goldenberg, D. M. (1993) Epitope specificity of the anti-(B cell lymphoma) monoclonal antibody, LL2. *Cancer Immunol. Immunother.* 37: 293-298
- Vingerhoeds, M. H., Storm, G., Crommelin, D. J. (1994) Immunoliposomes in vivo. *Immuno. Methods* 4: 259-272
- Vitetta, E. S., Uhr, J. W. (1994) Monoclonal antibodies as agonists: an expanded role for their use in cancer therapy. *Cancer Res.* 54: 5301-5309
- Wheeler, J. J., Wong, K. F., Ansell, S. M., Masin, D., Bally, M. B. (1994) Polyethylene glycol-modified phospholipids stabilize emulsions prepared from triacylglycerol. *J. Pharm. Sci.* 83: 1558-1564
- Woodle, M. C., Lasic, D. D. (1992) Sterically stabilized liposomes. *Biochim. Biophys. Acta* 1113: 171-199

Journal of nuclear medicine : official  
publ. (IM)  
v. 41, no. 5, suppl. (May 2000)  
General Collection  
W1 JO796  
Received: 05-09-2000

MENT TO

EXHIBIT 30

# The Journal of Nuclear Medicine

# JNM

PROPERTY OF THE  
NATIONAL  
LIBRARY OF  
MEDICINE



## ABSTRACT BOOK

Scientific Abstracts of  
the 47th Annual Meeting of  
the Society of Nuclear Medicine  
St. Louis, Missouri • June 3-7, 2000

association to BSA than the remaining six <sup>99m</sup>Tc complexes. The six <sup>99m</sup>Tc complexes exhibited selective accumulation in hypoxic CHO cells (2.2 to 7.5 fold increases in accumulation at 6 h vs. 5 min) compared to aerobic cells (1.0 to 2.6 fold increases). **Conclusion:** These complexes show promise for imaging tumor hypoxia. The amine-dioxime class of chelator is flexible and convenient for varying the lipophilicity of a <sup>99m</sup>Tc complex, in loading different functional groups in place of 2-nitroimidazole, and in the preparation of mixed-ligand complexes.

# No. 1025

**[<sup>18</sup>F]FLUOROCHOLINE (FCH) AS AN ONCOLOGIC PET TRACER: EVALUATION IN MURINE PROSTATE CANCER XENOGRAFT MODEL.** T. R. DeGrado\*, R. E. Coleman, S. W. Baldwin, M. D. Orr, C. N. Robertson, and D. T. Price, Duke University Medical Center, Durham, NC. (100405)

**Objectives:** [<sup>18</sup>F]Choline (CH) has shown utility for PET imaging of prostate cancer metastases and brain tumors. An <sup>18</sup>F-labeled analog of CH may have utility for clinical PET scanning if the tracer is similarly taken up by malignancies. **Methods:** No-carrier-added [<sup>18</sup>F]FCH was synthesized by a two-step procedure through the intermediate, BrCH<sub>2</sub><sup>18</sup>F. BrCH<sub>2</sub><sup>18</sup>F was isolated by gas chromatography and reacted with dimethylethanolamine in acetone. The FCH was isolated on a cation-exchange SEP-PAK and eluted with sterile 0.9% NaCl. Biodistributions of FCH and [<sup>14</sup>C]choline were evaluated simultaneously in athymic nude mice bearing subcutaneous PC-3 prostate cancer xenografts. **Results:** FCH was synthesized in ~20% radiochemical yield and >98% radiochemical purity in a synthesis time of ~40 min. The biodistribution of FCH and CH were similar in normal tissues and PC-3 tumor with the exceptions of slower clearance of FCH from the kidneys. At 60-min p.i., FCH uptake by tumor was greater than for CH (p<0.05), and tumor:blood ratio was on average 40% higher for FCH relative to CH. The urinary bladder contained ~10% and ~1% of the injected dose with FCH and CH, respectively, at 30 min. **Conclusion:** A practical synthesis of FCH has been achieved. FCH may prove useful as a prostate cancer imaging agent for PET. Further evaluation of FCH in human patients with prostate cancer and brain tumors is ongoing.

Uptake (%dose/kg/100g) of [<sup>18</sup>F]FCH/[<sup>14</sup>C]CH in PC-3 Xenograft Mouse Model

Time (min) (n)	Tumor	Blood	Kidney
10 (5)	3.4±0.4/2.3±0.9	2.6±0.9/2.2±0.4	120±30/107±6
30 (3)	7.1±2.1/4.8±1.6	3.3±0.2/1.5±0.9	116±17/53±7.3
60 (5)	7.9±5.0/6.7±4.3	1.5±0.6/2.2±1.0	94±31/41±15

# No. 1026

**BIODISTRIBUTION OF <sup>111</sup>IN AND <sup>131</sup>I LABELED ADENOVIRAL FIBER KNOB (AdFK) PROTEIN IN MICE.** S. C. Srivastava\*, G. E. Meinken, and P. Freimuth, Brookhaven National Laboratory, Upton, NY. (101199)

**Objectives:** We have studied the biodistribution in mice of <sup>111</sup>In and <sup>131</sup>I labeled AdFK protein to determine the effect of radiolabeling and the molecular size of sub-viral components on the natural binding to the coxsackievirus and adenovirus receptor (CAR)-expressing tissues. **Methods:** Recombinant AdFK (rod-shaped fiber proteins on the virus capsid contact CAR through a distal globular subdomain - the fiber knob) was synthesized in *E. coli* as a trimeric molecule of 60kD. Conjugation with DTPA at 2 or 10 fold molar ratios of DTPA to AdFK, and labeling of the conjugates with <sup>111</sup>In or <sup>131</sup>I were carried out under various conditions. Binding activity of the DTPA conjugates was determined using reaction with biotinylated CAR followed by chemiluminescent detection. Biodistribution was studied following i.v. injection into mice. **Results:** In-vitro assays showed that the binding specificity to CAR was maintained only if the 6-Histidine extension on the AdFK (used for purification) was not removed prior to conjugation with DTPA. <sup>111</sup>In-6-His-AdFK-DTPA was more preferentially taken up (%IDg at 6h) into lungs (6.0%) and liver (12.8%), indicating specific binding to CAR expressing organs. There was some uptake into other tissues as expected, but much less than the liver and the lungs. When the 6-HIS-AdFK-DTPA labeled with <sup>131</sup>I (Iodogen method) was injected into mice, a similar trend was observed. Results with the 2X and 10X DTPA preparations were not statistically different. **Conclusion:** 6-HIS-AdFK-DTPA labeled with <sup>111</sup>In and <sup>131</sup>I retains specificity of binding to CAR as shown from our in-vitro and in-vivo studies. There appears to be a protective effect of histidine without which the CAR binding specificity of both <sup>111</sup>In and <sup>131</sup>I labeled AdFK-

DTPA is compromised. Work supported by USDOE under Contract No. DE-AC02-98CH10886.

# No. 1027


**SYNTHESIS, BIODISTRIBUTION AND IMAGING OF MAMMARY TUMORS USING <sup>99m</sup>Tc-EC-POLYGLUTAMATE: A GLUTAMATE RECEPTOR PEPTIDE.** E. E. Kim\*, D. J. Yang, J.-G. Choe, A. Azhdarinia, D.-F. Yu, F. Zaré, N. Nair, and D. A. Podoloff, M.D. Anderson Cancer Center, Houston, TX; Korea University Hospital, Seoul, South Korea. (101181)

**Objectives:** Glutamic acid is a major excitatory neurotransmitter in the mammalian central nervous system. The mechanism of action of glutamate and polyglutamate peptide is via glutamate receptors. Glutamate and polyglutamate peptide bind to glutamate receptors. The receptors are overexpressed in certain tumors. We have developed <sup>99m</sup>Tc-labeled polyglutamate (MW. 750-1000) peptide using ethylenedicycysteine (EC) as a chelator. This study aimed to evaluate its biodistribution and tumor imaging potential. **Methods:** EC was conjugated to an amino analogue of polyglutamate using N-hydroxysuccinimide and 1-ethyl-3-dimethylaminopropyl carbodiimide as coupling agents. After dialysis and lyophilization, yield was 80%. EC-polyglutamate was labeled with <sup>99m</sup>Tc in the presence of tin (II) chloride. Stability assay was performed in dog serum. Tissue distribution and planar imaging of <sup>99m</sup>Tc-EC-polyglutamate were performed in breast tumor-bearing rats at 0.5-4 h. The data was compared to that using <sup>99m</sup>Tc-EC (control). **Results:** The labeling efficiency of <sup>99m</sup>Tc-EC-polyglutamate was 95-99%. No degradation product of <sup>99m</sup>Tc-EC-polyglutamate in dog serum was observed at up to 4 hours. *In vivo* biodistribution of <sup>99m</sup>Tc-EC-polyglutamate peptide in breast tumor-bearing rats showed increased tumor-to-blood, tumor-to-lung, tumor-to-brain and tumor-to-muscle ratios as a function of time. Conversely, tumor-to-blood values showed time-dependent decrease with <sup>99m</sup>Tc-EC in the same time period. Planar images confirmed that the tumors could be visualized clearly with <sup>99m</sup>Tc-EC-polyglutamate from 0.5 to 4 hours. **Conclusion:** The results indicate that <sup>99m</sup>Tc-EC-polyglutamate, a glutamate receptor peptide, may be useful in oncology imaging.

# No. 1028

**LABELING ANTISENSE DNA WITH <sup>99m</sup>Tc LEAVES HYBRIDIZATION UNAFFECTED BUT CAN HINDER CELL MEMBRANE TRANSPORT.** Y. M. Zhang\*, Y. Wang, N. Liu, Z. Zhu, M. Rusckowski, and D. J. Hnatowich, University of Massachusetts Medical School, Worcester, MA; University of Massachusetts, Worcester, MA. (500220)

One outstanding question concerning antisense targeting is whether the chemical modifications of DNA to permit radiolabeling interferes with hybridization and target cell accumulation. **Objectives:** The influence of chemical modifications to an antisense DNA in connection with <sup>99m</sup>Tc labeling was investigated. **Methods:** An 18-mer phosphorothioate DNA antisense to the mRNA of the R1a subunit of PKA was conjugated with NHS-MAG3 via a primary amine/linker. **Results:** By surface plasmon resonance, the association kinetics between "native" (i.e. without amine/linker) DNA and MAG3-amide/linker-DNA were identical. Melting temperatures were also identical for native DNA, amine/linker-DNA and MAG3-amide/linker-DNA. Thus these chemical modifications had no influence on hybridization. Cellular uptake was tested in ACHN tumor cells. An antisense effect was suggested by consistently higher cellular accumulation of antisense DNA than sense (control) DNA when both were labeled with <sup>35</sup>S. The cellular accumulation of this label was found to be identical when cells were incubated with amine/linker-DNA or MAG3-amide/linker-DNA (although native DNA showed significantly lower accumulation). These chemical modifications therefore had no negative effects on cellular accumulation. After radiolabeling with <sup>99m</sup>Tc, size exclusion HPLC analysis showed immediate protein binding in serum, however even after 24 hrs in cytosol, radiolabeled and viable DNA was still detectable. Significantly increased cellular accumulation was again observed following incubation of cells with antisense DNA relative to sense DNA, now labeled with <sup>99m</sup>Tc. However, cellular accumulation of <sup>99m</sup>Tc was lower than that seen under identical conditions with <sup>35</sup>S. By demonstrating identical egress of both labels from cells, the lowered accumulation was determined to be due to decreased cell membrane ingress of <sup>99m</sup>Tc labeled DNA. **Conclusion:** Radiolabeling of antisense DNA with <sup>99m</sup>Tc had no influence on hybridization, however cell mem-

 Annual Reviews  
[www.annualreviews.org/aronline](http://www.annualreviews.org/aronline)  
*Annu. Rev. Nutr.* 1996. 16:501-21  
 Copyright © 1996 by Annual Reviews Inc. All rights reserved

## FOLATE RECEPTORS

*Asak C. Antony*

Division of Hematology-Oncology, Department of Medicine, Indiana University  
 School of Medicine, Indianapolis, Indiana 46202-5121

**KEY WORDS:** folate-binding proteins, transplacental maternal-to-fetal transfer,  
 cellular-transcellular folate uptake/transport, reduced-folate carrier,  
 antifolates, cell proliferation

### ABSTRACT

Glycosyl-phosphatidylinositol-anchored folate receptors (FR) have physiologic and pharmacologic relevance in mediating cellular and transcellular folate/anti-folate transport. Three FR isoforms with differing relative affinities for folates and expression patterns in normal and malignant cells/tissues are recognized, but the precise mechanism of cellular entry of folate via FR remains controversial. Although FR expression allows previously FR-deficient cells to survive a reduced folate milieu, an inverse relationship between FR expression and cell proliferation has been established in some cells. The inverse regulation of FR expression by the extracellular folate concentration suggests heterogeneity in underlying mechanisms. Whereas reduced FR expression is yet another mechanism for acquiring antifolate resistance, overexpression of FR does not invariably render cells more sensitive to antifolates. The exploitation of FRs as Trojan horses to deliver folate-tagged liposomes bearing diverse cargo represents a novel therapeutic strategy to target FR-expressing cells. Finally, a critically important role of human placental FR in mediating maternal-to-fetal transplacental transport of folates has been established. Thus, FR appear to have a major impact on several aspects of human physiology and medicine.

### CONTENTS

INTRODUCTION .....	502
STRUCTURE OF FOLATE RECEPTORS .....	503
<i>Molecular and Biochemical Aspects</i> .....	503
<i>Ligand Binding by FR</i> .....	503
TRANSCELLULAR FOLATE TRANSPORT VIA FOLATE RECEPTORS .....	505
<i>Maternal-to-Fetal Transplacental Folate Transport</i> .....	505
<i>Renal Folate Conservation</i> .....	507
CELLULAR TRANSPORT OF FOLATES VIA FOLATE RECEPTORS .....	507
EXPRESSION AND REGULATION OF FOLATE RECEPTORS .....	510
<i>Expression of FR</i> .....	510
<i>Regulators of FR Expression</i> .....	511
<i>Regulation by the EFC</i> .....	512
FOLATE RECEPTORS AND CONTROL OF CELL PROLIFERATION .....	513
	501

EXPLOITATION OF FOLATE RECEPTORS AS TROJAN HORSES .....	514
FUTURE DIRECTIONS .....	516

## INTRODUCTION

The shutdown of DNA synthesis and one-carbon metabolism arising from folate deficiency perturbs the cell cycle and results in megaloblastosis, which, if uncorrected, leads to premature cell death, with characteristic clinical presentations (5). Acquisition of folate, therefore, is critically important to the viability of proliferating cells (4, 28). In general, folate transport involves translocation of the ligand into cells from the extracellular compartment (i.e. cellular uptake mechanisms) and across cellular barriers from one compartment to another (i.e. transcellular mechanisms). Since the last comprehensive review on the biological chemistry of folate receptors (FR) (4), several studies have provided new insights into their biological function. This review highlights these issues, with an emphasis on nutritional aspects of FR-mediated cellular and transcellular folate transport. [Due to space limitations, the bibliography has been generally restricted (with the exception of molecular biology-related data) to those papers published in the past five years. The reader is referred to previous reviews (4, 28) for important references of historical interest.]

The basis for separate classification of the components and mechanisms for cellular folate transport was outlined previously (4). The reduced-folate carrier (RFC) is a low-affinity, high-capacity system that mediates the uptake of reduced folates into cancer cells, predominantly at pharmacologic (micromolar) extracellular folate concentrations (EFC). A RFC cDNA (22) that restores sensitivity to a methotrexate transport-resistant cell line functionally deficient in RFC encodes a 58-kDa polypeptide and resembles the mammalian glucose transporter (GLUT 1), a member of the 12 transmembrane domain-spanning membrane transporter family. Although RFC systems have not been definitively shown to exist in normal human cells through functional studies, this deficiency in data should be rectified shortly. Cellular folate transport can also be mediated by 38- to 44-kDa membrane-associated folate-binding proteins (FBP) or FR (these terms are used synonymously throughout), which bind physiologic folates with high affinity in the nanomolar range. The third pathway for cellular folate transport via passive diffusion was only documented as a pharmacologic effect (4). However, new data indicate that it is an integral part of transplacental folate transport occurring in concert with FR (29).

Transcellular folate transport systems include transport across the placenta, renal tubular cells, and the blood-brain barrier/blood-cerebrospinal fluid barrier. Although these barriers overexpressed FR (4), their functional role has been unclear until recently.



## STRUCTURE OF FOLATE RECEPTORS

### *Molecular and Biochemical Aspects*

Three human FR cDNA isoforms, FR- $\alpha$  (14, 19, 24, 37, 65), FR- $\beta$  (53, 58), and FR- $\gamma$  (69, 70), and two related cDNAs from murine L1210 cells (12) have been cloned. Although the open reading frames and the 3'-untranslated regions of the reported FR- $\alpha$  cDNA are identical, their 5'-untranslated regions are heterogeneous in length and sequence. The genomic organization of human FR genes (14, 57) has been identified in chromosome 11q13.2→q13.5, where four FR-related genes were found within a 140-kilobase (kb) region. The FR- $\alpha$  and FR- $\beta$  genes were in sequence (< 23 kb apart), with two additional FR-related genes or pseudogenes located upstream of the FR- $\alpha$  gene. Genomic clones containing FR- $\beta$  have been independently isolated by Elwood's and Rothenberg's laboratories (53, 64). The FR- $\beta$  gene is ~5 kb long and has five exons and four introns. The promoter lacks TATA and CAAT elements but contains sequences recognized by the *ets* oncogene-encoded transcription factor and SP1, which may regulate expression of FBPs (64). The genomic DNA sequence of the FR- $\alpha$  gene is not yet published, but its structure is more complex than FR- $\beta$ . Although the number of exons and introns were different in two preliminary studies (53, 63), a recent report indicates that FR- $\alpha$  contains at least two independent, tissue/cell-specific functional promoters. Interestingly, one promoter is located within an intron and contains three clustered SP1 binding sites and an initiator region, all of which are necessary for basal promoter activity (67).

With possible exceptions, FR are glycosyl-phosphatidylinositol (GPI) anchored (43, 73, 77). [Although FR- $\gamma$  was originally believed to be GPI anchored (69), further analysis (70) revealed it was a secretory form predominantly expressed in hematopoietic cells.] The  $\omega$  locus is the amino acid to which a preformed GPI anchor is added following posttranslational cleavage of a carboxyl-terminal domain of the nascent polypeptide by a GPI transamidase (8). Although data from the cDNA and amino acid analysis of a GPI-anchored protein can predict the  $\omega$  locus with ~100% accuracy (8), this locus has not been ascertained directly from mature FR. Now, recent molecular studies on FR- $\alpha$  and FR- $\beta$  suggest Ser-234 and Asn-230, respectively, as the preferred sites of GPI-anchor attachment (85).

### *Ligand Binding by FR*

Analysis by circular dichroism has identified conformational changes following folate binding to FBP (35), and the increase in folding stability induced by ligand binding is derived from ligand-induced aggregation of these proteins.

There are diverse intracellular folate-dependent enzymes with little homol-

ogy in their primary structure to FR/FBP that interact with folates (5). Although human saliva contained species with low epitope relatedness to FBP, only a minor fraction of these FBP specifically bound folate with high affinity. The major fraction did not contain bound endogenous folate and did not bind radiolabeled folates (i.e. nonfunctional FBP) (76). Other mutant FBPs have subsequently been described (51). In general, however, nonfunctional FBPs can be mimicked in numerous trivial ways: These relate to prior occupancy of the ligand-binding site by folate (21), the presence of potential inhibitors of folate binding (72), destruction of the ligand-binding site of FBPs shortly after synthesis by potential proteases, cross-reacting species with a different preferred ligand than folates (86), or aglycosylated forms not yet posttranslationally processed to acquire functionally active ligand-binding sites (46). Thus, it is imperative to subject putative nonfunctional proteins to rigorous biochemical tests (ideally, after their isolation) before a FBP can confidently be assigned nonfunctional status. For example, in the instance that a nonfunctional FBP binds endogenous folate with a higher affinity than normal folate, there is the possibility that bound endogenous folate may not be dissociated by low pH (the method conventionally used). Naturally, this FBP will not bind exogenous radiolabeled folate, leading to the erroneous conclusion that the FBP is a nonfunctional species. Denaturation of FBPs will release endogenous-bound folates, with restoration of ligand-binding capacity on subsequent renaturation (76). Therefore, at a minimum, any putative nonfunctional species must withstand this degree of experimental scrutiny to eliminate trivial explanations. No less unusual are dominant negative phenotypes of mutant FR (52), but here additional controls are necessary. Clearly, demonstration that isolated mutant FR also confer a dominant negative phenotype to endogenous FR and assurance that transfected plasmids did not alter the regulation of endogenous FR, or sequester them into subcellular compartment(s) inaccessible to radiolabeled folate applied to the cell surface, would reduce ambiguity. Such studies could also provide an intellectual framework for understanding the functional basis of these mutant phenotypes. This concept (52) is nevertheless intriguing and again highlights a relationship between aggregation of FR and changes in affinity for folate. Finally, it would be of exceptional interest if dominant negative FR were actually identified *in vivo*.

Ratnam's laboratory has determined that FR- $\alpha$  are predominantly expressed in most normal and malignant epithelial tissues (with the exception of sarcomas) (60). This is significant because FR- $\alpha$  and FR- $\beta$  exhibit differences in relative affinities (compared with folic acid) for the (6S) (physiologic) and (6R) (unphysiologic) diastereoisomers of various folates (80). For example, (6S)5-methyltetrahydrofolate, (6S)5-formyltetrahydrofolate, and methotrexate bound FR- $\alpha$  with ~50-, ~100-, and ~20-fold more affinity, respectively. However, (6R) forms bound FR- $\alpha$  only ~2- and 4-fold more avidly. In contrast,

FR-B bound (6*R*) forms ~7 and 12 times more tightly than (6*S*) forms. Such data have been confirmed with murine FR (11). The newer antifolate, (6*S*)5,10-dideazatetrahydrofolate, which is preferentially transported at nanomolar concentrations via FR (54), showed ~10-fold greater affinity for FR- $\alpha$  than for FR-B; these (6*S*) forms also had ~3-fold higher affinity for FR- $\alpha$  than (6*R*) forms had. Conversely, (6*S*) and (6*R*) forms had comparable affinity for FR-B. Thus, pending direct experiments, a reasonable assumption is that the net efficiency of transport of various folates into cells would depend on the relative expression of one FR isoform over the other. Such data may eventually be important in optimizing efficient delivery of antifolates to effect maximal cytotoxicity of target cells while protecting normal cells.

Although limited site-specific mutagenesis has not yet characterized the ligand-binding site of FR (16), some unusual issues related to this domain in salivary FBPs (76), in different FR isoforms (11, 80), and in nonfunctional/mutant FBPs may only be resolved by analysis of the crystal structure of these proteins, which will shortly be reported on.

## TRANSCELLULAR FOLATE TRANSPORT VIA FOLATE RECEPTORS

### *Maternal-to-Fetal Transplacental Folate Transport*

Pregnancy is the most common cause of megaloblastic anemia in adults worldwide; and with lactation, folate requirements increase 5- to 10-fold more than in nonpregnant women (to 300–400 g/day), for growth of the fetus, placenta, and maternal tissues (5). This demand for folate, which is further aggravated by increased folate catabolism during pregnancy (50), must be met by adequate dietary intake. Since folate deficiency during pregnancy leads to decreased placental weight and premature, low-birth-weight infants, administration of folate supplements from the outset of pregnancy diagnosis has been routine (5, 6). However, the landmark study from Hungary indicates the necessity of periconceptional folate supplementation for healthy women to reduce the incidence of neural-tube defects (spina bifida, meningocoele, anencephaly) in their babies (20). In addition to demonstrating that periconceptional folic acid in higher doses (4 mg/day) protects ~75% of fetuses of women at risk (50a), such data highlight the importance of folates in neurologic development. But how do folates traverse the placenta from mother to fetus?

The clinical observations (5) that folate-deficient mothers deliver babies with normal folate stores invariably recall the metaphor of the fetus as a parasite. But this fact is also a vivid, physiologically relevant “experiment of nature” (and thank God for such reproducible and successful experiments!) that proves there exists a clearly defined mechanism to protect the fetus from

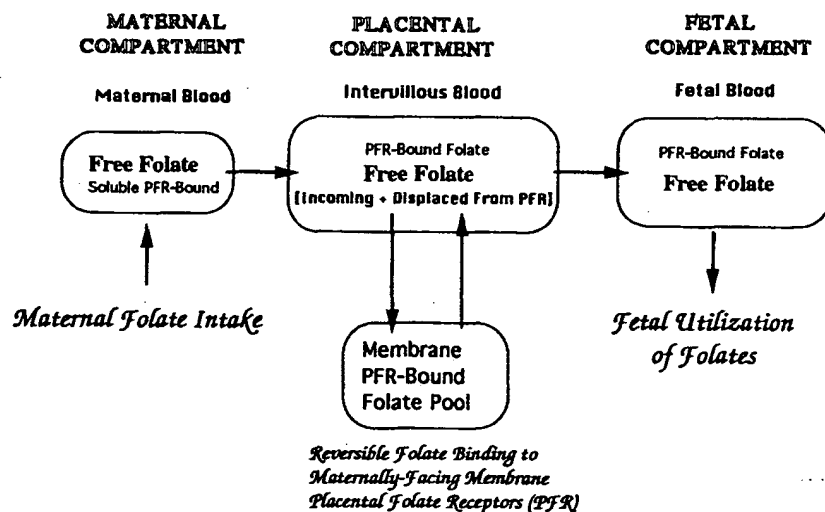


Figure 1 Diagrammatic representation of maternal-to-fetal transplacental folate transport involving folate receptors. (Adapted from Reference 29.)

the consequences of folate deficiency during critical stages in its growth and development. Curiously, although this system is concentrative and resistant to decreased maternal folate, it is sensitive to maternal folate loads such that, when presented with higher-than-normal folate levels, transport to the fetus is enhanced. So why has such a remarkable homeostatic system that favors fetal folate acquisition not been mechanistically defined? A major stumbling block has been the paucity of good models. Accordingly, with the collective experience of GI Henderson and S Schenker, acknowledged leaders in this field, an *ex vivo* placental cotyledon perfusion model was used to test the hypothesis that under physiologic conditions, placental FRs played a major functional role in transplacental folate transport. This model had a decided advantage in allowing individual perfusion and sampling of maternal and fetal compartments in studies that lasted ~4 h per freshly delivered placenta.

The results of these collaborative studies (29) indicate that net maternal-to-fetal folate transfer is a process consisting of two steps. The first step is the concentrative component in which circulating 5-methyltetrahydrofolate is bound to (captured by) placental FR on the maternally facing chorionic surface. Although kinetics favor binding, a dynamic state exists wherein a gradual release of 5-methyltetrahydrofolate from this pool adds to incoming circulating folates to generate an intervillous blood level approximately three times that in the maternal blood. In the second step, folates are transferred to the fetal

circulation along a downhill concentration gradient. Thus, it turns out that the prodigious, reversible, high-affinity binding of maternal folates by placental FR (77) is the key to mediation of transplacental folate transport. In fact, once captured, placental FR-bound folates are predestined for transplacental folate transport, since incoming (dietary) folates displace placental FR-bound folates that then passively diffuse down a concentration gradient to the fetus. And so this elegant cycle goes on, assuring continued unidirectional transplacental folate transport (Figure 1). As only FR- $\alpha$  was identified in normal trophoblasts (56), this form likely mediates this process. [FR- $\beta$  may have derived (4, 58) from sheared maternal decidua during delivery.]

### *Renal Folate Conservation*

Selhub and colleagues have accumulated data that strongly support the conclusion that folate transport across proximal renal tubular cells involves FR-mediated endocytosis (briefly reviewed in 68). Significantly, electron microscopy and autoradiography following infusion of radiolabeled folate revealed movement of the label as a function of time from proximal tubule brush borders to endocytotic vesicles and lysosomes (30). Thus, a likely scenario is that after glomerular filtration, the luminal folate binds FR in the brush-border membranes of proximal renal tubular cells and is internalized rapidly via FR-mediated endocytosis; in the low pH of endocytotic vesicles, there is dissociation of the folate and slow transport across the basolateral membranes into the blood with recycling of apo-FR back to the luminal brush-border membrane (68).

## CELLULAR TRANSPORT OF FOLATES VIA FOLATE RECEPTORS

As highlighted earlier (4), the pathway(s) for entry of folates and antifolates is likely to be distinct in different cells, depending on the relative efficiency of FR- and RFC-mediated mechanisms, as well as on the intra- and extracellular concentration of folates and antifolates.

Is there anatomic or functional coupling between the FR and RFC? Earlier studies had established that FR-mediated uptake was quite independent of, and did not require the participation of, the RFC (4). Independent data from a variety of models, including transplacental folate transport (29), cloning of RFC cDNA (22), and transfection of RFC-defective cells with FR cDNA (23, 72), have come to similar conclusions. However, this ignores earlier data from Kamen and Anderson's group, which spawned the concept of linkage of FR and the RFC/(anion channels) in potocytosis, the paradigm for receptor-mediated uptake of small molecules via caveolae (caveolae are invaginations in the

plasma membrane and are distinct from classic clathrin-coated pits, which are involved in receptor-mediated endocytosis) (2, 3, 61). In this hypothetical model, folates bind to GPI-anchored FR, which then moves into caveolae. The mouths of caveolae then transiently seal, and the enclosed FR-bound folate is dissociated by acidification followed by transport of the released folate into the cytoplasm via anion channels, while apo-FRs are recycled to bind more folate.

The finding that probenecid-inhibited uptake of folate suggested that anion channels were involved in *trans*-caveolar translocation of the ligand to the cytosol (36). Moreover, while activators of protein kinase C did not inhibit endocytosis via clathrin-coated pits, they inhibited the internalization of folate coincident with demonstration of a reduction in the number of invaginations of caveolae (71). Furthermore, lowering the cholesterol content of cells inhibited FR-mediated folate transport coincident with disruption of the clustered organization of FR and the integrity of caveolae (15). However, Goldman's laboratory recently reported (72) that probenecid inhibits folate interaction with FR in a dose-dependent manner. These data have indirectly raised questions about the validity of earlier conclusions from studies with probenecid (36) and have also served to highlight the importance of the electron microscope demonstration of movement of directly labeled folate or FR into caveolae.

Now a new revelation (49) in the form of additional control experiments formally questions the validity of the entire concept of potocytosis and the role of caveolae in FR-mediated folate uptake (2, 3). This controversy is dramatized by the fact that the protagonists involve the lead and senior author of the original report describing the potocytosis model (62). At issue is the surprising identification (49) that sequestration of FR (and other GPI-anchored proteins) into discrete clusters is dependent on cross-linking by a second antibody. Thus, when the primary anti-FR antibody was directly labeled, there was no clustering in the absence or presence of folate (49). These authors concluded that their data "[argue] strongly against the potocytosis model of folate uptake." Moreover, the earlier data that "GPI-anchored proteins are excluded from coated pits may be explained by the ability of GPI-anchored proteins to redistribute to caveolae artifactually during the process of immuno-localization, thereby apparently depleting coated pits of GPI-anchored proteins" (49). Anderson's group have countered that the primary antibody to FR *per se* may have prevented clustering (59). They generated additional data pointing to a differential regulatory role of wild-type (GPI-anchored) FR versus chimeric FR targeted to clathrin-coated pits; this provides some more support for a role of caveolae in regulating FR-mediated folate uptake (59). However, since net uptake of folate was equally good when folate was internalized by wild-type and chimeric FR, it is still a matter of debate whether or not the differential

behavior observed "formally establishes that coated pits are not normally used for the endocytosis of folate" (59). Thus, although there has been substantial (albeit mostly indirect) support for involvement of caveolae in GPI-anchored, FR-mediated folate transport via potocytosis, direct demonstration of FR within these organelles has remained elusive. Notwithstanding, there is independent support for a probenecid-sensitive folate transporter in choriocarcinoma cells that is driven by a transmembrane H<sup>+</sup> gradient generated by a membrane-associated vacuolar type H<sup>(+)</sup>-pump (55). Although studies on transcellular folate transport have ruled out a role for anion channels, such channels could be uniquely required for cellular folate transport into malignant/immortalized cells. Thus, it is entirely plausible that FR may interact with this (non-RFC) pump in some cells to explain the earlier data (36). However, as of now, we are still some way from resolving this charged controversy.

Is there an interrelationship between FR and the RFC? Both methotrexate and 5,10-dideazatetrahydrofolate utilize both RFC and FR for transport into cells (4, 54). However, the major determinants of net antifolate transport are the prevailing EFC, the concentration of antifolate, and the extent of RFC and FR expression (4). Cell lines have been isolated for primary resistance to methotrexate through defective RFC, but which also overexpress FR (10). Because this mutation in overexpression of FR in these cells allows for continued growth in folate-depleted media, the expression of FR clearly had a salutary effect for these neoplastic cells in that it compensated for defective RFC expression.

Do the RFC- and FR-mediated folate-transport systems communicate with one another? Apparently not. Thus, beginning with wild-type breast cancer cells, which only exhibited RFC-mediated folate transport, and a methotrexate-resistant mutant cell line, Cowan's laboratory studied the potential interaction of the RFC and FR after transfection of FR- $\alpha$  cDNA (23). After transfection, both wild-type and methotrexate transport-resistant cells that previously required >100 nM of folic acid for growth were able to grow in 1 nM folic acid. Furthermore, methotrexate transport-resistant cells, which were unable to grow in 1  $\mu$ M 5-formyltetrahydrofolate were now also able to grow in 1 nM 5-formyltetrahydrofolate. Since FR expression allowed both cell types to accumulate similar (albeit increased) amounts of folic acid, 5-formyltetrahydrofolate, and methotrexate, these data allowed for the conclusion that the FR functioned independently of RFC expression, and vice versa (i.e. alteration of RFC function failed to affect FR function). Parenthetically, in contrast to data from Elwood's laboratory (17), these cells did not exhibit an increased sensitivity to methotrexate. Moreover, their apparently paradoxical resistance to the lipophilic antifolate, trimetrexate, suggests that these cells were rescued by FR-mediated uptake of 5-formyltetrahydrofolate. These contradictory results (17, 23) from different breast cancer cell lines are examples where additional



variables likely play a role. Thus, the sensitivity of cells to antifolates may not be invariably enhanced by transfection or transduction of FR genes, and specific studies with several malignant and normal cells will be required to comprehensively test this hypotheses in vitro and in vivo. Recently, Schornagel and Jansen's group have also independently arrived at a similar conclusion (84).

How efficient are the two systems in transport of methotrexate? Goldman's laboratory compared the transport of methotrexate in L1210 cells, which expressed only RFC, and a mutant L1210 cell line with a defective RFC that was transfected with FR cDNA. The conclusion of this study was significant in that the RFC and FR functioned essentially independently of one another (72). More importantly, however, when enough FR were expressed, these proteins mediated the uptake of methotrexate and 5-methyltetrahydrofolate with comparable rates to cells expressing only the RFC. Thus, FR have both physiologic and pharmacologic importance, directly confirming several earlier studies (4). Once again, this may not be the case with all malignant human cells; for example, despite high FR expression, the RFC was recently found to be the preferential carrier of antifolates in some cells (84).

Is there a role for FR in antifolate resistance? Yes. Methotrexate resistance can be due to alterations in dihydrofolate reductase (gene amplification or diminished affinity), reduced intracellular polyglutamation, increased efflux, or reduced transport via the RFC. Recent studies in cells that primarily depend on FR for folate uptake now also implicate a reduction in expression of FR (66). Thus, if similar mechanisms operate in vivo, it could likewise adversely influence methotrexate and 5,10-dideazatetrahydrofolate uptake (23, 27) into tumors that mainly depend on FR-mediated transport, and negatively impact therapy.

## EXPRESSION AND REGULATION OF FOLATE RECEPTORS

### *Expression of FR*

Polyclonal and monoclonal antibodies used against FR from a variety of sources demonstrated cross-reacting proteins in several normal and malignant human cells/tissues (Table 1). However, without confirmatory data with molecular and other biochemical methods (60), it may be premature to make definitive conclusions on the extent of expression of FR, especially in cells/tissues that apparently do not have cross-reactive FR-like species on cell surfaces. This relates to the fact that FR-negative tissues can be generated in vitro even from tissues that overexpress FR. A good example is human placenta, where a time-dependent release of hydrophilic FR from placental membranes medi-



**Table 1** Folate receptor (FR) expression in normal and malignant human tissues

Cells/tissues	Determinants	Expression
<b>Normal</b>		
	Genitourinary system	Placenta, chorionic villus, trophoblastic cells (29, 56, 75, 77, 83); fallopian tube, uterus, ovary (83); vas deferens, epididymis, semen (83); kidney (proximal tubules) (83)
	Central nervous system	Choroid plexus epithelial cells, CSF (31, 83)
	Hematopoietic system	Hematopoietic progenitor cells [CFU-GEMM, CFU-GM, BFU-E, CFU-E] (7)
	Gastrointestinal system	Salivary (submandibular) (76, 83); colon (32)
	Respiratory system	Bronchial glands and alveolar lining (type-I and-II pneumocytes) (83)
	Endocrine systems	Breast (acinar cells) (83) and human milk (4); thyroid, pancreas (83)
	Miscellaneous	Fibroblasts (4)
<b>Malignant</b>		
	Consistently high and uniform expression	Nasopharyngeal carcinoma (4); cervical carcinoma (73); ovarian carcinoma (19, 26, 74); choriocarcinoma (56)
	Relatively lower, inconsistent expression	Endometrial carcinoma (26); breast carcinoma (4); primary brain tumors (81, 82); colorectal carcinoma (26, 37); sarcomas (60); renal cell carcinoma (26)

ated by an EDTA-sensitive endogenous metalloprotease was demonstrated (77). Similar activation of the metalloprotease may also occur with apparently innocuous agents/buffers used in cell culture (25, 75). Hydrophobic FR can also be cleaved off the cell surface by GPI-specific phospholipases present in media (77) and trypsin (4). Furthermore, there may be FR isoform-specific differences in affinity for various antibodies (an unknown variable) or other intrinsic nuances in detecting FR expression (e.g. use of monoclonal versus polyclonal antibodies, or cells in suspension versus frozen/fixed tissues, etc). Thus, it is quite possible that additional tissues (not listed in Table 1) may be found to express FR.

### *Regulators of FR Expression*

Conversion of hydrophobic GPI-anchored FR to hydrophilic FR as mediated by a metalloprotease (25, 75) or by GPI-specific phospholipases C or D (43,



77) can potentially be an important mechanism for posttranslational regulation of the expression of FR. However, no probes are available to directly study these hydrophobic FR-directed enzymes. We have recently isolated a FR-directed hydrophobic metalloprotease (85a) and should eventually be able to determine the potential significance of this protein in the regulation of FR expression and net folate transport. Although a major role for the metalloprotease was not identified in the placenta at term (29), its activity could easily determine the extent of acquisition of folates by FR on trophoblasts, thereby influencing placental growth and development. The extent of contribution of hematopoietic cell FR- $\gamma$  (70), and the relative role of GPI-phospholipases versus metalloprotease in generating hydrophilic FBPs in serum, also awaits clarification.

### *Regulation by the EFC*

The EFC inversely regulates FR expression (4, 28). In human nasopharyngeal carcinoma (KB) cells, when FR was increased in response to low EFC, there was an increase in FR mRNA (65) as a result of increased mRNA stability (33). Conversely, with excess EFC of folates and antifolates, FRs were down-regulated with a reduction in FR mRNA (34). Although low-EFC-adapted L1210 cells exhibited a rearrangement in the locus upstream from the start codon of the FR gene (involving insertion of an intracisternal A particle) (13), this retrovirus-like sequence was unresponsive to the folate status of the cell. Thus, the reversible, physiologic mechanism(s) for transcriptional FR regulation by the EFC remains undiscovered.

In general, steady-state up-regulation of FR accompanied by an increase in FR mRNA can result from increased rates of transcription of FR genes and/or increased stability of FR mRNA. In addition, FR up-regulation may involve independent changes in the translational or posttranslational pathways involving FR metabolism (i.e. increased rate of FR synthesis, decreased rate of degradation of FR, or reduced activity of potential regulators of cell surface FR membrane association). Conversely, down-regulation of FR could be a function of independent or combined alterations in these parameters in the opposite sense, all of which constitute cellular FR metabolism. Thus far, however, studies on up- or down-regulation of FR have not comprehensively investigated each of these parameters of FR metabolism in response to low and high EFC. And whether one or more of the steps in the biosynthesis and/or degradation of FR is a dominant responsive parameter to changes in the EFC also remains to be determined. We have recently determined that in cervical carcinoma cells, regulation of FR expression by the EFC is primarily controlled at the translational level through dominant alterations in FR synthetic rates (45a). In addition, we have identified an 18-base *cis*-element in the 5' untrans-

lated region of FR- $\alpha$  mRNA that specifically binds a 46-kDa cytosolic (*trans*-factor) protein (72a). Therefore, our immediate challenge is to determine the functional basis of this interaction in the regulation of FR, and specifically in response to changes in the EFC.

## FOLATE RECEPTORS AND CONTROL OF CELL PROLIFERATION

Interaction of anti-FR immunoglobulin (Ig) G with FR on hematopoietic progenitors earlier led to increased cell proliferation that was independent of induction of megaloblastosis and intracellular folate deficiency (7). However, it was unclear whether anti-FR IgG perturbed a normally inhibitory role of FR or accentuated a stimulatory function of FR in cell proliferation (4). Furthermore, was there a similar constitutive role for FR in control of cell proliferation in malignant cells?

Recent studies have documented that transfection of FR cDNA into various cells that do not constitutively express FR (9, 17, 47, 48) led to greater proliferation and survival when compared with controls cultured in low EFC. Thus, FR clearly have an overall growth-promoting function. However, it is unclear whether these findings were due to independent effects of (a) a greater concentration of intracellular folates accumulated by FR cDNA-transfected cells (which prevented folate-deficient cell death at low EFC), (b) a proliferative signal generated at the level of FR per se, or (c) a combination of both. To sort out these possibilities, we encapsidated FR cDNA in the sense/antisense orientation into infectious adeno-associated virions, transduced cervical carcinoma cells, and determined the functional consequences of over- and under-expression of FR on cell proliferation at high (micromolar) EFC (73). This latter issue was crucial to eliminate the variable of intracellular folates on cell proliferation among various cohorts studied, since micromolar EFC led to passive diffusion of folic acid into cells (4). When compared with antisense FR cDNA-transduced and untransduced cells, sense FR cDNA-transduced cells exhibited statistically significant increases in total FR, smaller colonies, lowered cell proliferation *in vitro*, and less tumor volumes with dramatic prolongation of tumor doubling times (225 versus 96 h) after transplantation into nude mice. In addition, with single cell-derived transduced clones, an inverse relationship between cell proliferation and FR expression was formally established (Figure 2) (73).

Can these apparently opposing [e.g. growth-promoting (9, 17, 47, 48) and growth-inhibiting (73)] functions of FR be unified into a hypothesis linking folate deficiency, FR expression, and cell proliferation? That malignant cells, which constitutively overexpress FR, can inversely regulate FR in response to EFC (4) is well documented. However, in some (but not all) cell lines, up-

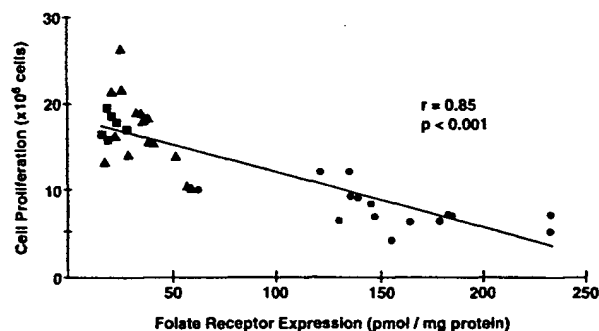


**Figure 2** Relationship between cell proliferation and folate receptor expression. A total of 36 randomly isolated, single cell clone-derived cell lines, 15 from sense FR cDNA-transduced cells (circles), 15 from antisense FR cDNA-transduced cells (triangles), and 6 from untransduced control cells (squares), were analyzed for cell proliferation and FR expression. (From Reference 73.)

regulation of FR is also accompanied with a prolongation in doubling time, and vice versa. Our recent data (73) therefore allow us to propose a simple hypothesis wherein the up-regulated FR in response to low EFC could serve to check proliferation of cells by moving them into the resting phase of the cell cycle—a beneficial way to reduce folate requirements under the stress of nutrient deficiency. Conversely, with nutrient excess, the ensuing down-regulation of FR could concomitantly serve to release the normal inhibitory influence of FR on cell proliferation, thereby leading to a permissive state for cell proliferation. If there is a similar inverse relationship between FR expression and hematopoietic progenitor cell proliferation, this could have other clinical significance. For example, clonally derived hematopoietic cells from patients with paroxysmal nocturnal hemoglobinuria, and which lack GPI-anchored proteins (including FR), have a selective proliferative advantage over normal cells—this results in excess hemolysis and impacts on the severity of clinical presentation. So it is not entirely unreasonable to ask if the lack of FR in affected cells has any role in determining their proliferative advantage over normal cells.

## EXPLOITATION OF FOLATE RECEPTORS AS TROJAN HORSES

Colnaghi's group have used chimeric murine-human anti-FR antibodies to mediate cell kill of ovarian carcinoma cells in vitro (18); demonstration of similar data in vivo would indeed be an important and welcome addition to the oncologist's meager therapeutic armamentarium.

By covalently attaching folic acid via one of its free carboxyls to toxic proteins or liposomes containing biologically active agents, Low's laboratory exploited FR as Trojan horses to mediate the cellular uptake of these folate conjugates for therapeutic and diagnostic use. Of significance, the rate and the extent of endocytosis of internalized folate-conjugates was independent of the conjugated moiety but was dependent on the expression of apo-FRs (38, 40). Equally important, folate-conjugated proteins also retained their function once internalized via FRs (39). Thus, although the ribosome-inactivating protein, momordin, was nontoxic at micromolar concentrations, conjugation with folate rendered it cytotoxic at nanomolar concentrations (through high affinity interaction with FRs). Actual translocation into the cytoplasm was also shown by using a translocation-defective (from endosomes to cytoplasm) *Pseudomonas* exotoxin coupled to folate that was internalized via FR into the cytoplasm, where it was lethal (42). Furthermore, since internalization was dependent on expression of FR, malignant cells that overexpressed FR were selectively targeted (41).

The capacity to conjugate liposomes to folate by using polyethylene glycol (PEG, as a spacer) has significantly expanded the potential repertoire of this technology (44). When compared with conventional drug delivery, encapsulation of substances into liposomes (drugs, toxins, oligonucleotides) significantly protects this cargo from premature plasma degradation and retards their renal disposition. The generation of several-hundred folate-PEG tethers built into each liposome led to multiple simultaneous attachments to cell surface FRs. This fortuitously led to an increase in the binding affinity to FR by six orders of magnitude. Selective targeting to FR-expressing cells has also been demonstrated with liposome-entrapped Doxorubicin (45) by using co-cultures of FR-overexpressing cancer cells and low-FR expressing normal cells. Interestingly, whereas free Doxorubicin entered both normal and cancer cells equally nonselectively, the folate-PEG-liposomes containing Doxorubicin exclusively entered, and thereby selectively killed, only cancer cells. FR-targeted liposomes have also been successfully employed for targeted cytoplasmic delivery of antisense oligodeoxynucleotides against the human epidermal growth factor receptor in KB cells (78). This technology is therefore ripe for clinical exploitation because agents of various molecular sizes, composition, and metabolism can be targeted for delivery to cells that express FR.

Folate conjugated to  $^{67}\text{Ga}$ -Deferoxamine has also shown promise in nuclear medicine and could replace  $^{67}\text{Ga}$ -citrate, which is clinically employed as a tumor-specific imaging agent. Normally, tumor selectivity (usually >5:1 tumor:blood ratio) arises from transfer of  $^{67}\text{Ga}$ -citrate to transferrin with subsequent binding of  $^{67}\text{Ga}$ -transferrin to cancer cells that express transferrin receptors. With  $^{67}\text{Ga}$ -Deferoxamine-folate (79) used to image FR-expressing tumors in nude mice (when compared with  $^{67}\text{Ga}$ -Deferoxamine or  $^{67}\text{Ga}$ -cit-

rate), by 4 and 45 h postintravenous injection, the tumor:blood ratio of the  $^{67}\text{Ga}$ -Deferoxamine-folate had exceeded 400:1 and 1400:1, respectively (P Low, personal communication). Aside from the tumor, significant uptake was seen only in the liver and kidney through non-FR-mediated and FR-mediated mechanisms, respectively. Preclinical studies are underway and it may only be a matter of time before clinical trials are initiated.

## FUTURE DIRECTIONS

Recent research on FRs has widened their scope and interest in several branches of biology and medicine. Because cellular folate/antifolate transport is a major determinant of sensitivity and/or resistance to cell proliferation, studies on transport of these ligands via FR into normal and malignant cells are of continued importance to hematology and oncology. Extension of studies on transduction of FR cDNA to modulate cell proliferation and their sensitivity to antifolates, combined with the exploitation of FR as Trojan horses, could have a major diagnostic and therapeutic impact in nuclear medicine, pharmacology, and therapeutics. Discovery of the mechanism of placental FR in maternal-to-fetal folate transfer impacts on reproductive physiology and human development within the context of nutrition, as well as on obstetrics and perinatology. This mechanism may be a paradigm for the transplacental transport of other small  $M_r$  ligands that bind cognate placental receptors with high affinity. Together with data implicating FR in renal conservation of folates, these studies will be a beacon for future investigations on folate transport into the central nervous system. The studies with GPI-anchored FR-mediated folate uptake system as a paradigm for potocytosis (fueled by the recent controversy) will undoubtedly continue and, it is hoped, will resolve into a clearer understanding of the underlying mechanism(s). The independent role of FR in constitutive control of cell proliferation has now evolved into a testable hypothesis that potentially places FR within the circuitry of the cell cycle. However, the domain of the FR molecule responsible for the generation, as well as the type, path, and target, of the signal(s) transduced remains undiscovered. The molecular basis of regulation of FR by the EFC and selective tissue expression is still unclear, but the recent isolation of promoters for FR- $\alpha$  and FR- $\beta$  genes and identification of *cis*-elements in FR mRNA and the 46-kDa *trans*-factors promise significant discoveries ahead. Such investigations will likely provide comprehensive information on the molecular mechanisms controlling regulation of FR at the transcriptional and posttranscriptional level. Moreover, having isolated the metalloprotease, we are also in a position to identify its regulatory role in FR expression. In summary, based on the sustained interest generated in the recent past along multiple fronts, the next few years will likely prove a period of intense activity and excitement arising from

new discoveries related to FR and FR metabolism. This would likely stem from advances developing at the molecular, biochemical, and cell biological realm, with subsequent translation to the area of diagnostics and experimental therapy encompassing various areas of clinical medicine.

#### ACKNOWLEDGMENTS

This review on the state of the art is dedicated to all the investigators referenced below. It has been my honor and pleasure to analyze your work within the context of The Big Picture. However, the words from Paul's interpretation of (agape) love (naturally taken completely out of context) is worth recalling: "But when that which is perfect is come, then that which is in part shall be done away" (1 Cor. 13:10, King James Version). So I hope that future reviews will be able to highlight how little we really knew in 1995!

Any *Annual Review* chapter, as well as any article cited in an *Annual Review* chapter, may be purchased from the Annual Reviews Preprints and Reprints service.  
1-800-347-8007; 415-259-5017; email: arpr@class.org

#### Literature Cited

1. Deleted in proof.
2. Anderson RG. 1993. Caveolae: where incoming and outgoing messengers meet. *Proc. Natl. Acad. Sci. USA* 90: 10909-13
3. Anderson RG, Kamen BA, Rothberg KG, Lacey SW. 1992. Potocytosis: sequestration and transport of small molecules by caveolae. *Science* 255:410-11
4. Antony AC. 1992. The biological chemistry of folate receptors. *Blood* 79:2807-20
5. Antony AC. 1995. Megaloblastic anemias. In *Hematology. Basic Principles and Practice*, ed. R Hoffman, EJ Benz Jr, SJ Shattil, B Furie, HJ Cohen, LE Silberstein, pp. 552-86. New York: Churchill Livingstone. 2nd ed.
6. Antony AC. 1996. Pernicious anemia and other megaloblastic anemias. In *Conn's Current Therapy—1996*, ed. RE Rakel, pp. 350-53. Philadelphia: Saunders
7. Antony AC, Briddell RA, Brandt JE, Straneva JE, Verma RS, et al. 1991. Megaloblastic hematopoiesis in vitro. Interaction of anti-folate receptor antibodies with hematopoietic progenitor cells leads to a proliferative response independent of megaloblastic changes. *J. Clin. Invest.* 87:313-25
8. Antony AC, Miller ME. 1994. Statistical prediction of the locus of endoproteolytic cleavage of the nascent polypeptide in glycosylphosphatidylinositol-anchored proteins. *Biochem. J.* 298:9-16
9. Bottero F, Tomassetti A, Canevari S, Miotti S, Menard S, Colnaghi MI. 1993. Gene transfection and expression of the ovarian carcinoma marker folate binding protein on NIH/3T3 cells increases cell growth in vitro and in vivo. *Cancer Res.* 53:5791-96
10. Brigle KE, Seither R, Westin EH, Goldman ID. 1994. Increased expression and genomic organization of a folate-binding protein homologous to the human placental isoform in L1210 murine leukemia cell lines with a defective reduced folate carrier. *J. Biol. Chem.* 269:4267-72
11. Brigle KE, Spinella MJ, Westin EH, Goldman ID. 1994. Increased expression and characterization of two distinct folate binding proteins in murine erythroleukemia cells. *Biochem. Pharmacol.* 47:337-45
12. Brigle KE, Westin EH, Houghton MT, Goldman ID. 1991. Characterization of two cDNAs encoding folate-binding proteins from L1210 murine leukemia cells. Increased expression associated with a genomic rearrangement. *J. Biol. Chem.* 266:17243-49
13. Brigle KE, Westin EH, Houghton MT, Goldman ID. 1992. Insertion of an in-

- tracisternal A particle within the 5'-regulatory region of a gene encoding folate-binding protein in L1210 leukemia cells in response to low folate selection. Association with increased protein expression. *J. Biol. Chem.* 267: 22351-55
14. Campbell IG, Jones TA, Foulkes WD, Trowsdale J. 1991. Folate-binding protein is a marker for ovarian cancer. *Cancer Res.* 51:5329-38
15. Chang WJ, Rothberg KG, Kamen BA, Anderson RG. 1992. Lowering the cholesterol content of MA104 cells inhibits receptor-mediated transport of folate. *J. Cell Biol.* 118:63-69
16. Chung KN, Paik TH, Roberts S, Kim CH, Kirassova M, et al. 1994. Site-directed mutagenesis of tryptophan residues to conserved hydrophobic residues inhibits the processing of human KB cell folate receptor. *Arch. Biochem. Biophys.* 315:407-14
17. Chung KN, Saikawa Y, Paik TH, Dixon KH, Mulligan T, et al. 1993. Stable transfectants of human MCF-7 breast cancer cells with increased levels of the human folate receptor exhibit an increased sensitivity to antifolates. *J. Clin. Invest.* 91:1289-94
18. Coney LR, Mezzanzanica D, Sanborn D, Casalini P, Colnaghi MI, Zurawski VR Jr. 1994. Chimeric murine-human antibodies directed against folate binding receptor are efficient mediators of ovarian carcinoma cell killing. *Cancer Res.* 54:2448-55
19. Coney LR, Tomassetti A, Carayannopoulos L, Frasca V, Kamen BA, et al. 1991. Cloning of a tumor-associated antigen: MOv18 and MOv19 antibodies recognize a folate-binding protein. *Cancer Res.* 51:6125-32
20. Czeizel AE, Dudas I. 1992. Prevention of the first occurrence of neural-tube defects by periconceptional vitamin supplementation. *N. Engl. J. Med.* 327: 1832-35
21. da Costa M, Rothenberg SP. 1995. Purification and characterization of folate binding proteins from rat placenta. *Biochim. Biophys. Acta*. In press
22. Dixon KH, Lanpher BC, Chiu J, Kelley K, Cowan KH. 1994. A novel cDNA restores reduced folate carrier activity and methotrexate sensitivity to transport deficient cells. *J. Biol. Chem.* 269:17-20
23. Dixon KH, Mulligan T, Chung KN, Elwood PC, Cowan KH. 1992. Effects of folate receptor expression following stable transfection into wild type and methotrexate transport-deficient ZR-75-1 human breast cancer cells. *J. Biol. Chem.* 267:24140-47
24. Elwood PC. 1989. Molecular cloning and characterization of the human folate-binding protein cDNA from placenta and malignant tissue culture (KB) cells. *J. Biol. Chem.* 264:14893-901
25. Elwood PC, Deutsch JC, Kolhouse JF. 1991. The conversion of the human membrane-associated folate binding protein (folate receptor) to the soluble folate binding protein by a membrane-associated metalloprotease. *J. Biol. Chem.* 266: 2346-53
26. Garin-Chesa P, Campbell I, Saigo PE, Lewis J Jr, Old LJ, Rettig WJ. 1993. Trophoblast and ovarian cancer antigen LK26. Sensitivity and specificity in immunopathology and molecular identification as a folate-binding protein. *Am. J. Pathol.* 142:557-67
27. Habeck LL, Leitner TA, Shackelford KA, Gossett LA, Schultz RM, et al. 1994. A novel class of monoglutamated antifolates exhibits tight-binding inhibition of human glycylamide ribonucleotide formyltransferase and potent activity against solid tumors. *Cancer Res.* 54:1021-26
28. Henderson GB. 1990. Folate binding proteins. *Annu. Rev. Nutr.* 10:319-35
29. Henderson GI, Perez T, Schenker S, Mackins J, Antony AC. 1995. Maternal-to-fetal transfer of 5-methyltetrahydrofolate by the perfused human placental cotyledon: evidence for a concentrative role by placental folate receptors in fetal folate delivery. *J. Lab. Clin. Med.* 126:184-203
30. Hjelle JT, Christensen EI, Carone FA, Selhub J. 1991. Cell fractionation and electron microscope studies of kidney folate-binding protein. *Am. J. Physiol.* 260:C338-46
31. Holm JS, Hansen SI, Hoier-Madsen M, Bostad L. 1991. High-affinity folate binding in human choroid plexus. Characterization of radioligand binding, immunoreactivity, molecular heterogeneity and hydrophobic domain of the binding protein. *Biochem. J.* 280:267-71
32. Holm JS, Hansen SI, Hoier-Madsen M, Sondergaard K, Bzorek M. 1994. The high-affinity folate receptor of normal and malignant human colonic mucosa. *Acta Pathol. Microbiol. Immunol. Scandinavica* 102:828-36
33. Hsueh CT, Dolnick BJ. 1993. Altered folate-binding protein mRNA stability in KB cells grown in folate-deficient medium. *Biochem. Pharmacol.* 45: 2537-45



34. Hsueh CT, Dolnick BJ. 1994. Folate-binding protein (FBP) is responsible for the cellular transport of folate and methotrexate (MTX) in human KB (nasopharyngeal epidermoid carcinoma) cells. *Biochem. Pharmacol.* 47:1019-27
35. Kaarsholm NC, Kolstrup AM, Danielson SE, Holm J, Hansen SL. 1993. Ligand-induced conformation change in folate-binding protein. *Biochem. J.* 292: 921-25
36. Kamen BA, Smith AK, Anderson RG. 1991. The folate receptor works in tandem with a probenecid-sensitive carrier in MA104 cells in vitro. *J. Clin. Invest.* 87:1442-49
37. Lacey SW, Sanders JM, Rothberg KG, Anderson RG, Kamen BA. 1989. Complementary DNA for the folate binding protein correctly predicts anchoring to the membrane by glycosyl-phosphatidylinositol. *J. Clin. Invest.* 84:715-20
38. Leamon CP, Low PS. 1991. Delivery of macromolecules into living cells: a method that exploits folate receptor endocytosis. *Proc. Natl. Acad. Sci. USA* 88:5572-76
39. Leamon CP, Low PS. 1992. Cytotoxicity of momordin-folate conjugates in cultured human cells. *J. Biol. Chem.* 267:24966-71
40. Leamon CP, Low PS. 1993. Membrane folate-binding proteins are responsible for folate-protein conjugate endocytosis into cultured cells. *Biochem. J.* 291: 855-60
41. Leamon CP, Low PS. 1994. Selective targeting of malignant cells with cytotoxin-folate conjugates. *J. Drug Target* 2:101-12
42. Leamon CP, Pastan I, Low PS. 1993. Cytotoxicity of folate-*Pseudomonas* exotoxin conjugates toward tumor cells. Contribution of translocation domain. *J. Biol. Chem.* 268:24847-54
43. Lee HC, Shoda R, Krall JA, Foster JD, Selhub J, Rosenberry TL. 1992. Folate binding protein from kidney brush border membranes contains components characteristic of a glycosylphosphatidylinositol anchor. *Biochemistry* 31:3236-43
44. Lee RJ, Low PS. 1994. Delivery of liposomes into cultured KB cells via folate receptor-mediated endocytosis. *J. Biol. Chem.* 269:3198-204
45. Lee RJ, Low PS. 1995. Folate-mediated tumor cell targeting of liposome-entrapped doxorubicin in vitro. *Biochim. Biophys. Acta* 1233:134-44
- 45a. Li Q-J, Sun X-L, Antony AC. 1996. Regulation of folate receptors in human cervical carcinoma cells by the extracellular folate concentration: evidence for dominant modulation at the translational level associated with homeostatic changes. *J. Invest. Med.* 44:203A (Abstr.)
46. Luhrs CA. 1991. The role of glycosylation in the biosynthesis and acquisition of ligand-binding activity of the folate-binding protein in cultured KB cells. *Blood* 77:1171-80
47. Luhrs CA, Raskin CA, Durbin R, Wu B, Sadasivan E, et al. 1992. Transfection of a glycosylated phosphatidylinositol-anchored folate-binding protein complementary DNA provides cells with the ability to survive in low folate medium. *J. Clin. Invest.* 90:840-47
48. Matsue H, Rothberg KG, Takashima A, Kamen BA, Anderson RG, Lacey SW. 1992. Folate receptor allows cells to grow in low concentrations of 5-methyltetrahydrofolate. *Proc. Natl. Acad. Sci. USA* 89:6006-9
49. Mayor SK, Rothberg G, Maxfield FR. 1994. Sequestration of GPI-anchored proteins in caveolae triggered by cross-linking. *Science* 264:1948-51
50. McPartlin J, Halligan A, Scott JM, Darling M, Weir DG. 1993. Accelerated folate breakdown in pregnancy. *Lancet* 341:148-49
- 50a. MRC Vitamin Study Research Group. 1991. Prevention of neural tube defects: results of the Medical Research Council Vitamin Study. *Lancet* 338:131-37
51. Orr RB, Kamen BA. 1994. UMSCC38 cells amplified at 11q13 for the folate receptor synthesize a mutant nonfunctional folate receptor. *Cancer Res.* 54: 3905-11
52. Orr RB, Kamen BA. 1995. Identification of a point mutation in the folate receptor gene that confers a dominant negative phenotype. *Cancer Res.* 55: 847-52
53. Page ST, Owen WC, Price K, Elwood PC. 1993. Expression of the human placental folate receptor transcript is regulated in human tissues. Organization and full nucleotide sequence of the gene. *J. Mol. Biol.* 229:1175-83 [Erratum. 1994. *J. Mol. Biol.* 238(4):639]
54. Pizzorno G, Cashmore AR, Moroson BA, Cross AD, Smith AK, et al. 1993. 5,10-Dideazatetrahydrofolic acid (DDATHF) transport in CCRF-CEM and MA104 cell lines. *J. Biol. Chem.* 268:1017-23
55. Prasad PD, Mahesh VB, Leibach FH, Ganapathy V. 1994. Functional coupling between a bafilomycin A1-sensitive proton pump and a probenecid-sensitive folate transporter in human

- placental choriocarcinoma cells. *Biochim. Biophys. Acta* 1222:309-14
56. Prasad PD, Ramamoorthy S, Moe AJ, Smith CH, Leibach FH, Ganapathy V. 1994. Selective expression of the high-affinity isoform of the folate receptor (FR- $\alpha$ ) in the human placental syncytiotrophoblast and choriocarcinoma cells. *Biochim. Biophys. Acta* 1223:71-75
57. Ragoussis J, Senger G, Trowsdale J, Campbell IG. 1992. Genomic organization of the human folate receptor genes on chromosome 11q13. *Genomics* 14:423-30
58. Ratnam M, Marquardt MH, Duhring JL, Freisheim JH. 1989. Homologous membrane folate binding proteins in human placenta: cloning and sequence of a cDNA. *Biochemistry* 28:8249-54
59. Ritter TE, Fajardo O, Matsue H, Anderson RG, Lacey SW. 1995. Folate receptors targeted to clathrin-coated pits cannot regulate vitamin uptake. *Proc. Natl. Acad. Sci. USA* 92:3824-28
60. Ross JF, Chaudhuri PK, Ratnam M. 1994. Differential regulation of folate receptor isoforms in normal and malignant tissues in vivo and in established cell lines. Physiologic and clinical implications. *Cancer* 73:2432-43
61. Rothberg KG, Ying YS, Kamen BA, Anderson RG. 1990. Cholesterol controls the clustering of the glycosphospholipid-anchored membrane receptor for 5-methyltetrahydrofolate. *J. Cell Biol.* 111:2931-38
62. Rothberg KG, Ying YS, Kolhouse JF, Kamen BA, Anderson RG. 1990. The glycosphospholipid-linked folate receptor internalizes folate without entering the clathrin-coated pit endocytic pathway. *J. Cell Biol.* 110:637-41
63. Sadasivan E, Cedeno MM, Rothenberg SP. 1992. Genomic organization of the gene and a related pseudogene for a human folate binding protein. *Biochim. Biophys. Acta* 1131:91-94
64. Sadasivan EM, Cedeno M, Rothenberg SP. 1994. Characterization of the gene encoding a folate-binding protein expressed in human placenta. Identification of promoter activity in a G-rich SPI site linked with the tandemly repeated GGAAG motif for the ets encoded GA-binding protein. *J. Biol. Chem.* 269:4725-35
65. Sadasivan E, Rothenberg SP. 1989. The complete amino acid sequence of a human folate binding protein from KB cells determined from the cDNA. *J. Biol. Chem.* 264:5806-11 [Erratum. 1990. *J. Biol. Chem.* 265(3):1821]
66. Saikawa Y, Knight CB, Saikawa T, Page ST, Chabner BA, Elwood PC. 1993. Decreased expression of the human folate receptor mediates transport-defective methotrexate resistance in KB cells. *J. Biol. Chem.* 268:5293-301
67. Saikawa Y, Price K, Hance KW, Chen TY, Elwood PC. 1995. Structural and functional analysis of the human KB cell folate receptor gene P4 promoter: cooperation of three clustered Sp1-binding sites with initiator region for basal promoter activity. *Biochemistry* 34:9951-61
68. Selhub J. 1994. Folate binding proteins: mechanisms for placental and intestinal uptake. In *Nutrient Regulation During Pregnancy, Lactation and Infant Growth*, ed. L Allen, J King, B Lonnerdahl, pp. 141-49. New York: Plenum
69. Shen F, Ross JF, Wang X, Ratnam M. 1994. Identification of a novel folate receptor, a truncated receptor, and receptor type beta in hematopoietic cells: cDNA cloning, expression, immunoreactivity, and tissue specificity. *Biochemistry* 33:1209-15
70. Shen F, Wu M, Ross JF, Miller D, Ratnam M. 1995. Folate receptor type gamma is primarily a secretory protein due to lack of an efficient signal for glycosylphosphatidylinositol modification: protein characterization and cell type specificity. *Biochemistry* 34:5660-65
71. Smart EJ, Foster DC, Ying YS, Kamen BA, Anderson RG. 1994. Protein kinase C activators inhibit receptor-mediated potocytosis by preventing internalization of caveolae. *J. Cell Biol.* 124:307-13
72. Spinella MJ, Brigle KE, Sierra EE, Goldman ID. 1995. Distinguishing between folate receptor-alpha-mediated transport and reduced folate carrier-mediated transport in L1210 leukemia cells. *J. Biol. Chem.* 270:7842-49
- 72a. Sun X-L, Antony AC. 1996. Identification of an 18-base cis-element in the 5'-untranslated region of human folate receptor- $\alpha$  mRNA which specifically binds 46-kDa cytosolic (trans-factor) proteins. *J. Invest. Med.* 44:203A (Abstr.)
73. Sun X-L, Murphy BR, Li Q-J, Gullapalli S, Mackins J, et al. 1995. Transduction of folate receptor cDNA into cervical carcinoma cells using recombinant adeno-associated virions delays cell proliferation in vitro and in vivo. *J. Clin. Invest.* 96:1535-47
74. Tomassetti A, Coney LR, Canevari S, Miotti S, Facheris P, et al. 1993. Isola-

- tion and biochemical characterization of the soluble and membrane forms of the folate binding protein expressed in the ovarian carcinoma cell line IGROV1. *FEBS Lett.* 317:143-46
75. Verma RS, Antony AC. 1991. Kinetic analysis, isolation, and characterization of hydrophilic folate-binding proteins released from chorionic villi cultured under serum-free conditions. *J. Biol. Chem.* 266:12522-35
76. Verma RS, Antony AC. 1992. Immunoreactive folate-binding proteins from human saliva. Isolation and comparison of two distinct species. *Biochem. J.* 286:707-15 [Erratum. 1993. *Biochem. J.* 289(3):927]
77. Verma RS, Gullapalli S, Antony AC. 1992. Evidence that the hydrophobicity of isolated, in situ, and de novo-synthesized native human placental folate receptors is a function of glycosyl-phosphatidylinositol anchoring to membranes. *J. Biol. Chem.* 267:4119-27
78. Wang S, Lee RJ, Cauchon G, Gorenstein DG, Low PS. 1995. Delivery of antisense oligodeoxyribonucleotides against the human epidermal growth factor receptor into cultured KB cells with liposomes conjugated to folate via polyethylene glycol. *Proc. Natl. Acad. Sci. USA* 92:3318-22
79. Wang SR, Lee J, Mathias CJ, Green MA, Low PS. 1995. Synthesis, purification and tumor cell uptake of <sup>67</sup>Ga-deferoxamine-folate, a potential radiopharmaceutical for tumor imaging. *Bioconj. Chem.* In press
80. Wang X, Shen F, Freisheim JH, Gentry LE, Ratnam M. 1992. Differential stereospecificities and affinities of folate receptor isoforms for folate compounds and antifolates. *Biochem. Pharmacol.* 44:1898-901
81. Weitman SD, Frazier KM, Kamen BA. 1994. The folate receptor in central nervous system malignancies of childhood. *J. Neurooncol.* 21:107-12
82. Weitman SD, Lark RH, Coney LR, Fort DW, Frasca V, et al. 1992. Distribution of the folate receptor GP38 in normal and malignant cell lines and tissues. *Cancer Res.* 52:3396-401
83. Weitman SD, Weinberg AG, Coney LR, Zurawski VR, Jennings DS, Kamen BA. 1992. Cellular localization of the folate receptor: potential role in drug toxicity and folate homeostasis. *Cancer Res.* 52:6708-11
84. Westerhof GR, Rijnboutt S, Schornagel JH, Pinedo HM, Peters GJ, Jansen G. 1995. Functional activity of the reduced folate carrier in KB, MA104, and IGROV-I cells expressing folate-binding protein. *Cancer Res.* 55:3795-802
85. Yan W, Ratnam M. 1995. Preferred sites of glycosylphosphatidylinositol modification in folate receptors and constraints in the primary structure of the hydrophobic portion of the signal. *Biochemistry* 34:14594-600
- 85a. Yang XY, Mackins J, Li Q-J, Antony AC. 1996. Isolation and characterization of a novel folate receptor (FR)-directed metalloprotease from human placenta: evidence for plasma membrane localization in several human tumor cell lines. *Proc. Am. Assoc. Cancer Res.* 37:3379 (Abstr.)
86. Zheng DB, Lim HM, Pene JJ, White H. 1988. Chicken riboflavin-binding protein. cDNA sequence and homology with milk folate-binding protein. *J. Biol. Chem.* 263:11126-29

## Folate receptor of human mammary adenocarcinoma

JAN HOLM,<sup>1</sup> STEEN I. HANSEN,<sup>3</sup> MIMI HØIER-MADSEN,<sup>4</sup> KNUD SØNDERGAARD<sup>2</sup> and  
 MICHAEL BZOREK<sup>2</sup>

<sup>1</sup>Department of Clinical Chemistry and <sup>2</sup>Department of Pathology, Central Hospital Nykøbing Falster,  
 Nykøbing Falster, <sup>3</sup>Department of Clinical Chemistry, Central Hospital Hillerød, Hillerød and  
<sup>4</sup>Laboratory for Autoimmune Serology, Statens Seruminstitut, Copenhagen, Denmark

Holm, J., Hansen, S. I., Høier-Madsen, M., Søndergaard, K. and Bzorek, M. Folate receptor of human mammary adenocarcinoma. *APMIS* 102: 413-419, 1994.

Binding of <sup>3</sup>H-folate to human mammary tumor homogenate was of a high-affinity type ( $K = 10^{10}$  M<sup>-1</sup>) and displayed apparent positive cooperativity. Radioligand dissociation was slow at pH 7.4, but rapid at pH 3.5. As compared to methotrexate, 5-formyltetrahydrofolate acted as a strong inhibitor of radioligand binding. Gel chromatography of radioligand-labeled homogenate of tumor tissue revealed three peaks: a small  $\geq 110$  kDa peak and two major peaks of folate-binding activity ( $M_r \sim 25$  kDa and  $M_r \sim 100$  kDa). Mammary tumor tissue showed immunostaining with rabbit antibodies against human milk folate binder. A parallel elevation in the concentrations of folate-binding protein and triglyceride in tumor tissue as compared to normal tissue adjacent to the tumor was compatible with the localization of folate-binding protein in the triglyceride-rich fraction of mammary gland homogenate.

**Key words:** Folate binding; high-affinity; mammary tumor; human.

Jan Holm, Department of Clinical Chemistry, Central Hospital Nykøbing Falster, 4800 Nykøbing F., Denmark.

The intracellular level of folates is of crucial importance for one-carbon transfer processes mediated by enzyme systems involved in DNA synthesis (2). The folate-binding protein (FBP), a high-affinity glycopospholipid-linked folate receptor, resides in the plasmalemmal vesicles of many eukaryotic cells and internalizes folates by a process known as potocytosis (3, 1, 19). FBPs exist in both membrane-bound and soluble forms (2). A soluble FBP purified from bovine milk has been characterized as to primary and secondary structure, polymerization phenomena, and ligand-binding mechanism (5, 16, 21, 25, 27). Extensive homology existed between the amino acid sequence of the bovine FBP and FBPs in human milk (26) and membranes of certain human cancer cells and placenta (4, 17, 22, 24). High-affinity FBPs in several normal human tissues, e.g. cho-

roid plexus and proximal kidney tubules, shared antigenic determinants with human milk FBP (10, 11). FBPs with glycopospholipid domains susceptible to cleavage by glycosylphosphatidyl inositol-specific phospholipase C were found in human milk, semen, and choroid plexus (7).

We have recently characterized a high-affinity FBP or folate receptor in homogenized human mammary gland tissue; the receptor was associated with a triglyceride-rich fraction of the homogenate (12). The present work deals with the folate receptor in human mammary tumor tissue and describes its radioligand-binding characteristics, ligand dissociation, substrate specificity, molecular size, and immunologic properties.

### METHODS

#### *Tissue preparation*

Malignant tissue and adjacent normal mammary

Received September 27, 1993.

Accepted March 14, 1994.

gland tissue obtained from women undergoing surgery for mammary adenocarcinoma were processed separately. The tissue was homogenized with a Braun homogenizer (5 strokes at 1000 rev/min) in 5 mmol/l Tris/HCl buffer (pH 7.4, 4°C) containing 5 mmol/l mannitol (5 ml of buffer/g of tissue). Homogenate solubilized (2 h, 4°C) with Triton X-100 (20 g/l) was centrifuged (1000 g, 30 min) and the supernatant analyzed. The proteinase inhibitor phenylmethane sulphonyl fluoride (PMSF) (1 mmol/l; BDH) was added to all preparations.

The concentration of protein was determined by a commercial assay (Bio-Rad Protein Assay Kit 500-0001) and the concentration of triglyceride by a commercial assay (Boehringer-Mannheim; Triglycerides GPO-PAP 701882), according to the instructions given by the manufacturer.

#### *Radioligand binding and inhibition*

Tissue preparations were dialyzed against 0.2 mol/l acetate buffer of pH 3.5 at 4°C to remove endogenous folate.

Equilibrium dialysis experiments were performed as described previously (10, 11) for periods of 20 h in 0.17 mol/l Tris/HCl buffer of pH 7.4 (37°C) with the tissue sample in the internal (1000 µl) and <sup>3</sup>H-folate (<sup>3</sup>H-pteroylglutamate with a specific activity of 24–31 Ci/mmol from Amersham International Ltd, Amersham, UK) in the external solution (100 ml). Triton X-100 at a concentration of 10 g/l was added to both sides of the dialysis membrane. Radioactivity measurements were performed as previously described (10, 11). In inhibition experiments folate analogues was always added to the external solution (cf above) together with the radiolabel. The following analogues were used: methotrexate (Lederle, 4587-24) purified as previously described (9) and 5-formyl-tetrahydrofolate (6).

#### *Radioligand dissociation*

Aliquots (1000 µl) of tissue predialysed to equilibrium (pH 7.4, 7°C) against <sup>3</sup>H-folate (1.0 nmol/l) were subjected to dialysis in 1000 ml volumes of folate-free buffer according to a previously published procedure (10, 11).

#### *Enzyme-linked immunosorbent assay (ELISA) for FBP in mammary tissue*

Low-molecular-weight FBP was purified from human milk and used for immunization of rabbits (15). Rabbit antisera were pooled, the immunoglobulins precipitated and employed in a previously described ELISA for quantitation of human FBP (10, 11, 15).

#### *Gel filtration*

The molecular size of FBP in mammary tissue was estimated by chromatography on a column (5.3 cm<sup>2</sup> × 94 cm) of Ultrogel® AcA 44 (IBF) run and calibrated as previously reported (10, 11). Triton X-

100 (1 g/l) was added to the elution buffer 0.17 mol/l Tris/HCl of pH 7.4 (5°C). The tissue sample was incubated with <sup>3</sup>H-folate (10 nmol/l) for 3 h (25°C) prior to column application.

#### *Immunohistochemistry*

Immunohistochemistry on paraffin-embedded 5–8 µm sections of formalin-fixed mammary tumor tissue was performed by a standard procedure (14) as recently described (10, 11). The primary antibody, rabbit immunoglobulin (cf above) against human milk FBP, was diluted 1:100 with 12.5% (w/v) bovine serum albumin (BSA). Parallel controls were performed using non-immune rabbit immunoglobulin (Dakopatts X 936) at a protein concentration equal to that of the primary antibody solution. The secondary antibody, HRP-conjugated swine anti-rabbit immunoglobulin (DAKO P-217), was diluted 1:50 with 12.5% BSA. The chromogen 1-diaminobenzidine (Merck 2924) was dissolved (1 tablet) in 10 ml distilled water containing 40 µl 3% H<sub>2</sub>O<sub>2</sub>.

## RESULTS

#### *Mechanism of radioligand binding and dissociation*

Saturation curves for radioligand binding in mammary tumor tissue at two FBP concentrations are shown in Fig. 1 (Scatchard plots inserted). Binding data analyzed in Scatchard and Hill plots (not shown) are summarized in Table 1. The binding displayed apparent positive cooperativity as indicated by a Hill coefficient significantly higher than 1.00 and an upward convex Scatchard plot (Fig. 1) at FBP concen-

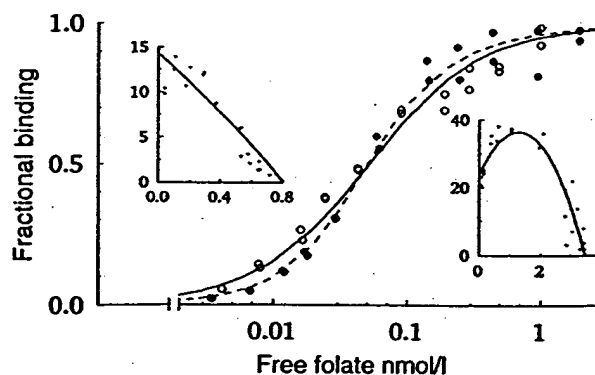


Fig. 1. High-affinity binding of <sup>3</sup>H-folate in solubilized mammary tumor homogenate (●) and a 5-fold dilution (○). Equilibrium dialysis experiments in 0.17 mol/l Tris-HCl buffer (pH 7.4, 37°C). Scatchard plots of binding data (abscissa, bound folate nmol/l; ordinate, bound/free) are given as insets (right, undiluted samples; left, diluted samples).

TABLE 1. Parameters of high-affinity binding of  $^3\text{H}$ -folate to mammary tumor tissue and non-malignant tissue adjacent to tumor in equilibrium dialysis experiments (pH 7.4, 37°C). Binding data were analyzed by Scatchard and Hill plots.  $N$ , maximum  $^3\text{H}$ -folate bound;  $S_{0.5}$ , the concentration of free folate at half saturation of folate binding. 'Overall' affinity expressed as  $1/S_{0.5}$

	$N$ (nmol/l)	$S_{0.5}$ (nmol/l)	$1/S_{0.5}$ (l/mol)	$h$ (SD)
Tumor, undiluted	3.5	0.053	$1.9 \times 10^{10}$	1.36 (0.074)*
Tumor, 5-fold diluted	0.77	0.046	$2.2 \times 10^{10}$	0.98 (0.049)
Tissue adjacent to tumor, undiluted	1.3	0.049	$2.1 \times 10^{10}$	0.99 (0.06)

The Hill coefficient ( $h$ ) is significantly higher than 1.00:  $P < 0.001$  (calculation of  $h$  based on 16 observations).

trations of 3.5 nmol/l. The concentration of FBP had no or only a slight effect on binding affinity (Table 1). At 0.77 nmol/l FBP the binding became non-cooperative, i.e. the Hill coefficient did not differ significantly from 1.00 (Table 1), and the Scatchard plot appeared rectilinear (Fig. 1). As can be seen (Table 1), the binding data for FBP in normal adjacent tissue were very similar; the binding was non-cooperative. No dissociation of  $^3\text{H}$ -folate from mammary tumor tissue occurred at pH 7.4 after dialysis for 24 h (data not shown). Dissociation was rapid at pH 3.5, however, with a residual binding of 5% (data not shown). The effect of

the folate analogues, methotrexate and 5-formyltetrahydrofolate, on binding was studied (Fig. 2). Methotrexate was a weak inhibitor as compared to 5-formyltetrahydrofolate.

#### Molecular size of FBP in mammary tumor tissue

The relative molecular mass of FBP in mammary tumor tissue was estimated by gel filtration. Tissue samples were pre-exposed to an excess of  $^3\text{H}$ -folate prior to Ultrogel® AcA 44 gel chromatography (Fig. 3). The elution dia-

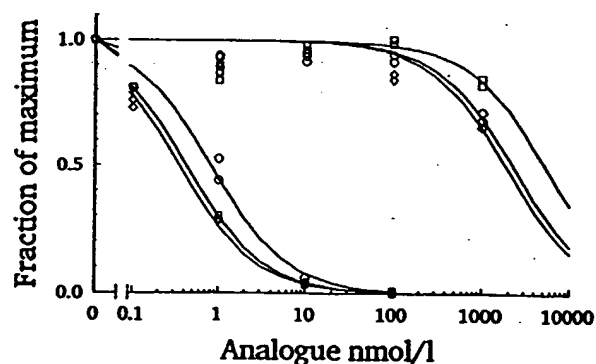


Fig. 2. Effect of methotrexate (upper curve) and 5-formyltetrahydrofolate (lower curve) on  $^3\text{H}$ -folate binding in mammary tissue. Equilibrium dialysis experiments (cf Fig. 1) with 0.1 nmol/l  $^3\text{H}$ -folate in the external solution. The analogue was added to the external solution (abscissa, concentration of analogue) together with radiolabeled folate. Normal mammary gland ( $\circ$ ), non-malignant tissue adjacent to tumor ( $\square$ ), and tumor tissue ( $\diamond$ ). The curves were fitted to the following equation (13):  $f = (1 + F \cdot K) / (1 + F \cdot K + I \cdot M)$ ;  $f$  is the fraction of maximum bound folate,  $F$  is the free folate concentration (constant = 0.1 nmol/l),  $K$  is the apparent association constant for folate binding,  $I$  is the apparent association constant for analogue binding, and  $M$  is the analogue concentration. Estimated  $K/I$  ratios were 10–30,000 for methotrexate and 2–5 for 5-formyltetrahydrofolate.

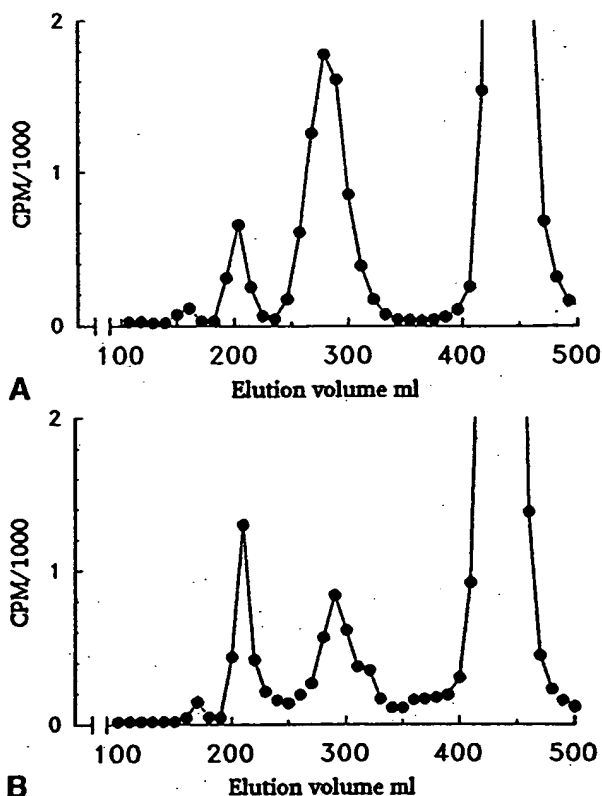


Fig. 3. Ultrogel AcA 44 chromatography of mammary tumor tissue (A) and non-malignant tissue adjacent to tumor (B). Both preparations were incubated with  $^3\text{H}$ -folate before column application. The column was calibrated as previously described (10, 11).

grams of both malignant and non-malignant tissue samples contained a very small peak in void volume at 160–170 ml ( $\geq 110$  kDa) as well as two major peaks of  $^3\text{H}$ -folate FBP, one at a position of 200–210 ml ( $M_r \sim 100$  kDa), and one at a position of 280–290 ml ( $M_r \sim 25$  kDa). The latter peak represented the main fraction of  $^3\text{H}$ -folate FBP in malignant tissue.

#### *Immunoreactivity of FBP in mammary tumor tissue*

A two-site ELISA was used for quantification of FBP in mammary tumor and normal mammary gland; FBP expressed as maximum  $^3\text{H}$ -folate binding was used as the reference. The titration curves in Fig. 4 show that malignant tissue contains a higher amount of immunoreactive FBP in comparison with adjacent normal tissue and normal mammary gland tissue.

#### *Immunohistochemistry*

Fig. 5A shows immunostaining of sections of mammary tumor tissue exposed to rabbit anti-(human milk FBP) immunoglobulin (1:100 dilution). No staining reaction (Fig. 5B) occurred with non-immune rabbit immunoglobulin.

#### *Concentration of FBP and triglyceride in malignant tissue and adjacent normal tissue*

The FBP concentration, expressed as maximum  $^3\text{H}$ -folate binding, was determined in ma-

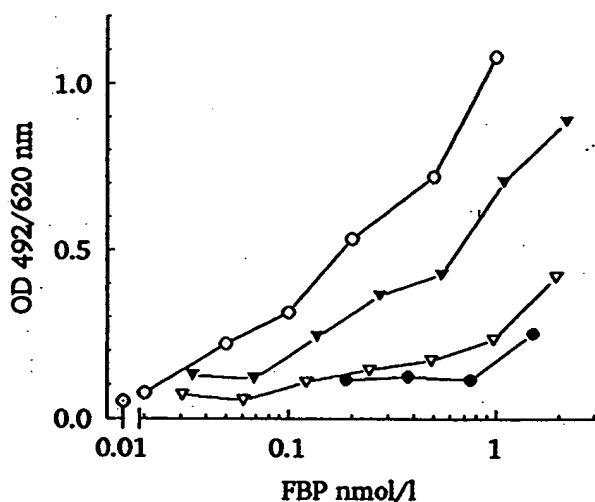


Fig. 4. Relationship between maximum  $^3\text{H}$ -folate binding (abscissa) and immunoreactive FBP determined by ELISA in human milk FBP (○), mammary tumor tissue (▼), non-malignant tissue adjacent to tumor (▽), and normal mammary gland tissue (●).

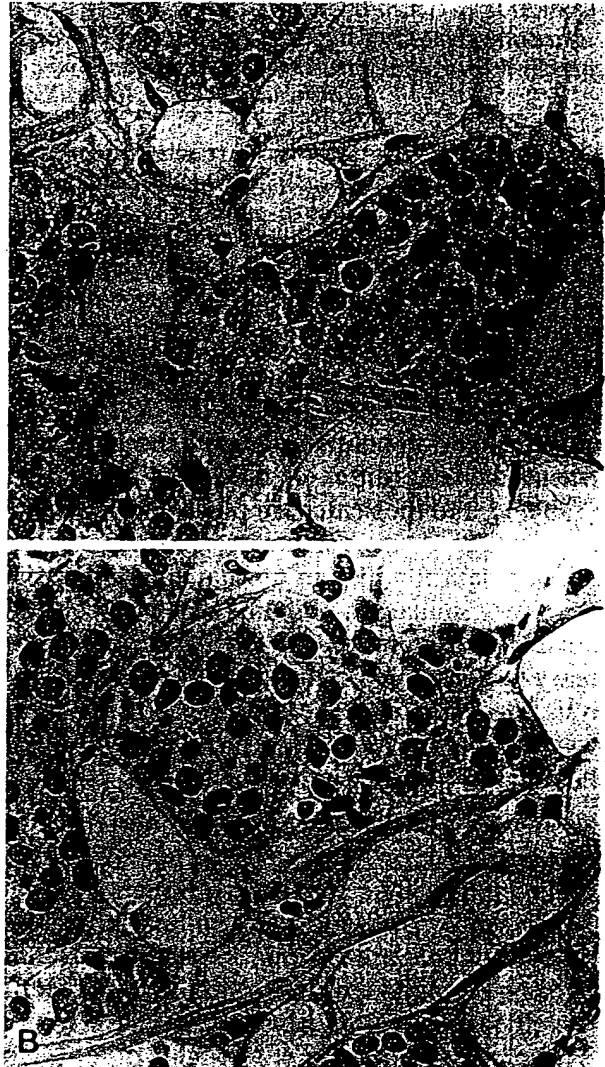


Fig. 5. Immunostaining of sections of mammary tumor after exposure to rabbit anti-(human milk FBP) immunoglobulin (1:100 dilution). B. Control sections exposed to non-immune rabbit immunoglobulin.

lignant and adjacent tissue of mammary adenocarcinoma from 11 patients (Fig. 6A). The FBP concentration was higher in malignant tissue than in normal tissue. The difference was statistically significant. A statistically significant difference was also found between the triglyceride concentrations in malignant tissue and adjacent normal tissue (Fig. 6B).

## DISCUSSION

The present report describes the presence of a high-affinity folate-binding protein (FBP) or

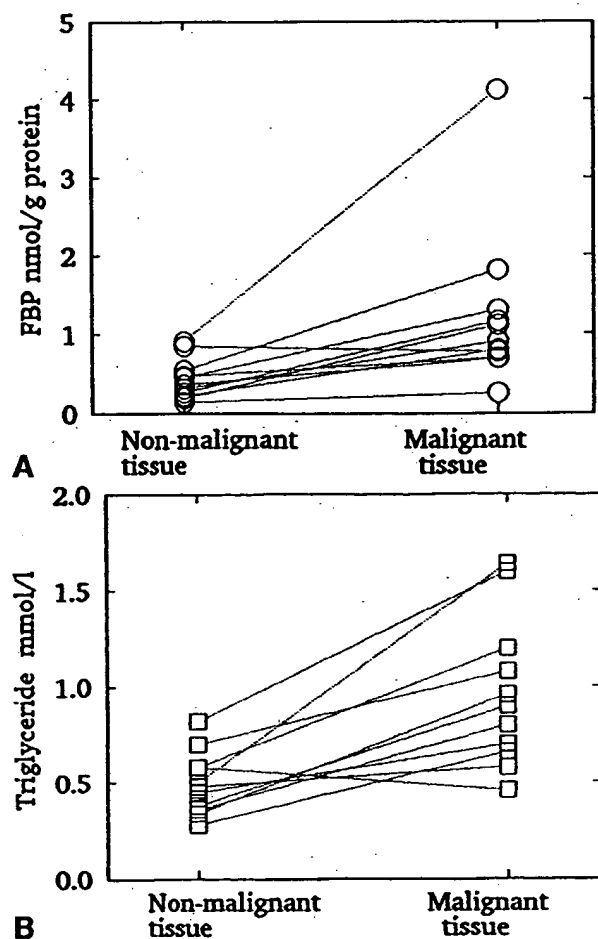


Fig. 6. A. Concentration of FBP expressed as maximum  $^3\text{H}$ -folate binding/g protein (median values with ranges in parentheses) in mammary tumor tissue, 0.90 (0.25–4.12) and normal tissue adjacent to tumor, 0.36 (0.14–0.90). Adenocarcinomas were taken from 11 women. Dotted lines connect paired values from each patient (paired comparisons). A non-parametric paired test, Wilcoxon signed-rank test, was performed on all differences; each patient served as her own reference,  $P < 0.005$ . B. Concentration of triglyceride, mmol/l, in mammary tumor tissue, 0.48 (0.28–0.82), and normal tissue adjacent to tumor, 0.90 (0.46–1.64),  $P < 0.01$ . For details, cf Fig. 6A.

folate receptor in human mammary tumor tissue. The concentration of FBP in terms of maximum radioligand binding is significantly higher in tumor tissue as compared to adjacent normal mammary gland tissue from the same patient, and so is the concentration of triglyceride (Fig. 6). However, it remains to be clarified whether the higher concentration of FBP in tumor tissue is due to overexpression of FBP, as recently observed in some malignant epithelial

cells (29), or merely to a higher density of epithelial cells per g protein in malignant tissue. The parallel increase in the content of FBP and triglyceride in malignant mammary tissue is in fair agreement with our recent study in which the highest folate-binding activity per g protein was associated with the upper triglyceride-rich layer of the 1000 g supernatant of normal mammary gland homogenate (12). The concentration of FBP per 1 tumor homogenate (Table 1) is close to the value previously reported for nmol folate bound per 1 cytosol in 25 estrogen receptor-positive primary breast cancer tumors (23).

High-affinity folate-binding systems, e.g. in milk, choroid plexus and kidney, display the following characteristics: apparent positive cooperativity which changes into a non-cooperative binding type at relatively low FBP concentrations, a binding affinity that seems to increase with decreasing concentrations of FBP, and an extremely slow ligand dissociation at pH 7.4, which, however, becomes rapid at pH 3.5 (10, 11). High-affinity folate binding in mammary tumor tissue exhibits similar properties (Table 1) with the exception that dependence of binding affinity on FBP concentration is uncertain as compared to e.g. in normal mammary gland tissue (12). Furthermore, the acid dialysis-resistant fraction of bound radioligand was only 5% as compared to 20% in normal mammary gland (12).

The displacement of labeled folate by folate analogues (Fig. 2) shows that 5-formyltetrahydrofolate has a  $\leq 5$ -fold lower affinity for FBP than has oxidized folate, while the affinity of the antifolate drug methotrexate is 10–30,000-fold lower than that of oxidized folate. This affinity profile is basically similar to that of other folate receptors in malignant cells and placenta (28).

The FBP in mammary tumor tissue shares antigenic determinants with human milk FBP as demonstrated by immunohistochemistry (Fig. 5) and ELISA (Fig. 4). Data obtained with the latter technique seem to indicate a higher amount of immunoreactive material in tumor tissue.

As was the case in human milk and normal mammary gland (7, 12), two molecular forms of FBP were found in mammary tumor tissue: a 25 kDa FBP predominant as compared to normal mammary gland tissue (12) and a 100



kDa FBP. By analogy with human milk, the size of the latter could be due to interaction between a hydrophobic moiety on the 25 kDa FBP and Triton X-100 micelles (7).

Detailed knowledge of the nature of folate receptors in normal and malignant cells is of crucial importance for our understanding of the processes which on the molecular level mediate transfer of natural folates across cell membranes. Folate plays an important role in DNA synthesis and chromosome repair, which is in fair agreement with the growing body of evidence suggesting a relationship between folate deficiency and cancer initiation (8). Another point of interest is the observation that excess of intracellular reduced folate increases the cytotoxic effect of fluorinated pyrimidines through an optimal inhibition of thymidylate synthetase (20). Furthermore, the use of receptor-mediated uptake of folic acid to facilitate entry of a folate-toxin conjugate into cultured HeLa and KB cells was shown to inhibit cellular protein synthesis (18).

We appreciate the valuable technical assistance of *Jytte Rasmussen* and *Tove Enggaard Dorph-Jensen*. The study received financial support from *Bryde Nielsen Fonden* and *Johs. M. Klein og Hustrus Mindelegat*.

## REFERENCES

1. Anderson, R. G. W., Kamen, B. A., Rothberg, K. G. & Lacey, S. W.: Potocytosis: Sequestration and transport of small molecules by caveolae. *Science* 255: 410-411, 1992.
2. Antony, A. C.: The biological chemistry of folate receptors. *Blood* 79: 2807-2820, 1992.
3. Elwood, P. C., Kane, M. A., Portillo, R. M. & Kolhouse, J. F.: The isolation, characterization and comparison of the membrane-associated and soluble folate binding proteins from human KB cells. *J. Biol. Chem.* 261: 15416-15423, 1986.
4. Elwood, P. C.: Molecular cloning and characterization of the human folate-binding protein cDNA from placenta and malignant tissue culture (KB) cells. *J. Biol. Chem.* 264: 14893-14901, 1989.
5. Hansen, S. I., Holm, J., Lyngbye, J., Pedersen, T. G. & Svendsen, I.: Dependence of aggregation and ligand affinity on the concentration of the folate-binding protein from cow's milk. *Arch. Biochem. Biophys.* 226: 636-642, 1983.
6. Hansen, S. I., Holm, J. & Nexø, E.: Immobilized purified folate-binding protein. Binding characteristics and use for quantifying folate in erythrocytes. *Clin. Chem.* 33: 1360-1363, 1987.
7. Hansen, S. I. & Holm, J.: Conversion of an apparent 100 kDa folate binding protein from human milk, choroid plexus and semen to a 25 kDa molecular species by phosphatidylinositol-specific phospholipase C. *Biosci. Rep.* 12: 87-93, 1992.
8. Herbert, V.: The role of vitamin B<sub>12</sub> and folate in carcinogenesis. *Adv. Exp. Med. Biol.* 206: 293-311, 1986.
9. Holm, J., Hansen, S. I. & Lyngbye, J.: An impurity, N<sup>10</sup>-methylfolate, associated with methotrexate inhibits folate binding in milk and serum. *Biochem. Pharmacol.* 29: 3109-3112, 1980.
10. Holm, J., Hansen, S. I., Høier-Madsen, M. & Bostad, L.: High-affinity folate binding in human choroid plexus. Characterization of radioligand binding, immunoreactivity, molecular heterogeneity and hydrophobic domain of the binding protein. *Biochem. J.* 280: 267-271, 1991.
11. Holm, J., Hansen, S. I., Høier-Madsen, M. & Bostad, L.: A high-affinity folate binding protein in proximal tubule cells of human kidney. *Kidney Int.* 41: 50-55, 1992.
12. Holm, J., Hansen, S. I. & Høier-Madsen, M.: High-affinity folate binding in human mammary gland. *Biosci. Rep.* 13: 1-7, 1993.
13. Horovitz, A. & Levitzki, A.: An accurate method for determination of receptor-ligand and enzyme-inhibitor dissociation constants from displacement curves. *Proc. Natl. Acad. Sci. USA* 84: 6654-6658, 1987.
14. Hsu, S. & Raine, L.: Protein A, avidin and biotin in immunohistochemistry. *J. Histochem. Cytochem.* 29: 1349-1353, 1981.
15. Høier-Madsen, M., Hansen, S. I. & Holm, J.: Rabbit antibodies against the low molecular weight folate binding protein from human milk. Use for immunological characterization of human folate binding proteins in an enzyme-linked immunosorbent assay (ELISA). *Biosci. Rep.* 7: 553-557, 1987.
16. Kaarsholm, N. C., Kolstrup, A., Danielsen, S. E., Holm, J. & Hansen, S. I.: Ligand-induced conformation change in folate-binding protein. *Biochem. J.* 292: 921-925, 1993.
17. Lacey, S. W., Sanders, J. M., Rothberg, K. G., Anderson, R. G. W. & Kamen, B. A.: Complementary DNA for the folate-binding protein correctly predicts anchoring to the membrane by glycosyl-phosphatidylinositol. *J. Clin. Invest.* 84: 715-720, 1989.
18. Leamon, C. P. & Low, P. S.: Membrane folate-binding proteins are responsible for folate-protein conjugate endocytosis into cultured cells. *Biochem. J.* 291: 855-860, 1993.
19. Luhrs, C. A., Pitiranggon, P., da Costa, M.,

- Rothenberg, S. P., Slomiany, B. L., Brink, L., Tous, G. I. & Stein, S.: Purified membrane and soluble folate-binding proteins from cultured KB cells have similar amino acid compositions and molecular weights but differ in fatty acylation. *Proc. Natl. Acad. Sci. USA* 84: 6546-6549, 1987.
20. Mandelbaum-Shavit, F.: Folinic acid enhanced cytotoxicity of fluoropyrimidines in human breast cancer cells. *Pteridines* 4: 51-55, 1993.
  21. Pedersen, T. G., Svendsen, I., Hansen, S. I., Holm, J. & Lyngbye, J.: Aggregation of a folate-binding protein from cow's milk. *Carlsberg Res. Commun.* 45: 161-166, 1980.
  22. Ratnam, M., Marquardt, H., Duhring, J. L. & Freisheim, J. H.: Homologous membrane folate binding proteins in human placenta. Cloning and sequence of a cDNA. *Biochemistry* 28: 8249-8254, 1989.
  23. Rochman, H., Selhub, J. & Karrison, T.: Folate binding protein and the estrogen receptor in breast cancer. *Cancer Detect. Prev.* 8: 71-75, 1985.
  24. Sadasivan, E. & Rothenberg, S. P.: The complete amino acid sequence of a human folate binding protein from KB cell determined from the cDNA. *J. Biol. Chem.* 264: 5806-5811, 1989.
  25. Svendsen, I., Martin, B., Pedersen, T. G., Hansen, S. I., Holm, J. & Lyngbye, J.: Isolation and characterization of the folate binding protein from cow's milk. *Carlsberg Res. Commun.* 44: 89-99, 1979.
  26. Svendsen, I., Hansen, S. I., Holm, J. & Lyngbye, J.: Amino acid sequence homology between human and bovine low molecular weight folate binding protein isolated from milk. *Carlsberg Res. Commun.* 47: 371-376, 1982.
  27. Svendsen, I., Hansen, S. I., Holm, J. & Lyngbye, J.: The complete amino acid sequence of the folate binding protein from cow's milk. *Carlsberg Res. Commun.* 49: 123-131, 1984.
  28. Wang, X., Shen, F., Freisheim, J. H., Gentry, L. & Ratnam, M.: Differential stereospecificities and affinities of folate receptor isoforms for folate compounds and antifolates. *Biochem. Pharmacol.* 44: 1898-1901, 1992.
  29. Weitman, S. D., Lark, R. H., Coney, L. R., Fort, D. W., Frasca, V., Zurawski, V. R. & Kamen, B. A.: Distribution of the folate receptor GP38 in normal and malignant cell lines and tissues. *Cancer Res.* 52: 3396-3401, 1992.

# Membrane Transport of Natural Folates and Antifolate Compounds in Murine L1210 Leukemia Cells: Role of Carrier- and Receptor-mediated Transport Systems<sup>1</sup>

G. Robbin Westerhof,<sup>2</sup> Gerrit Jansen, Nancy van Emmerik, Ietje Kathmann, Gert Rijksen, Ann L. Jackman, and Jan H. Schornagel

Department of Oncology, [G. R. W., G. J., N. v. E., I. K.], Free University Hospital, P.O. Box 7057, 1007 MB, Amsterdam, Department of Internal Medicine, Netherlands Cancer Institute [J. H. S.], Amsterdam, and Laboratory of Medical Enzymology, Department of Haematology, University Hospital Utrecht, Utrecht [G. R.], The Netherlands; and Drug Development Section, Institute of Cancer Research, Sutton, Surrey, United Kingdom [A. L. J.]

## ABSTRACT

L1210-B73 cells, variants of L1210 cells grown in medium containing nanomolar concentrations of folates, express a membrane associated folate binding protein (mFBP) in addition to the classical reduced folate/methotrexate carrier (RF/MTX-carrier) present in L1210 cells grown in standard high folate medium (G. Jansen *et al.*, Cancer Res., 49: 1959-1963, 1989). In this study we used L1210-B73 and L1210 cells as a model system to study the affinity of the RF/MTX-carrier and the mFBP for the natural folate compounds folic acid and 5-formyltetrahydrofolate (5-CHO-THF), as well as a number of antifolate compounds. Furthermore we studied the contribution of the RF/MTX-carrier and the mFBP in membrane transport of these (anti)folates, and finally we analyzed the role of the mFBP and RF/MTX-carrier in the cytotoxic effects of the antifolates. The antifolates used were either inhibitors of dihydrofolate reductase, including methotrexate (MTX) and 10-ethyl-10-deazaaminopterin (10-EdAM), or two folate-based inhibitors of thymidylate synthase, *N*<sup>10</sup>-propargyl-5,8-dideazafolic acid (CB3717) and 2-deamino-2-methyl-*N*<sup>10</sup>-propargyl-5,8-dideazafolic acid (ICI-198,583).

The affinity of the RF/MTX-carrier for natural and antifolate compounds declined in the order 10-EdAM ≥ ICI-198,583 ≥ 5-CHO-THF > MTX > CB3717 > folic acid. The mFBP exhibited a high binding affinity for CB3717 and ICI-198,583 but a poor binding affinity for MTX and 10-EdAM. Binding affinities of the mFBP decreased in the order CB3717 ≥ folic acid = ICI-198,583 ≥ 5-CHO-THF > MTX = 10-EdAM.

Over 24 h, at 25 nM, [<sup>3</sup>H]folic acid uptake in L1210-B73 cells was found to proceed for more than 98% via the mFBP. Uptake of [<sup>3</sup>H]-5-CHO-THF, at 50 nM extracellular concentration, occurred via both the mFBP (81%) and the RF/MTX-carrier (19%). With respect to antifolates, the mFBP in L1210-B73 cells contributed for less than 30% in the uptake of [<sup>3</sup>H]MTX but was the predominant route (92%) in the uptake of [<sup>3</sup>H]ICI-198,583.

Results from affinity and membrane transport observations were consistent with growth inhibition studies on L1210-B73 cells demonstrating that the mFBP played only a minor role in the cytotoxic effects of MTX or 10-EdAM. On the other hand, L1210-B73 cells were significantly more sensitive to CB3717 (220-fold) and ICI-198,583 (10-fold) than parental L1210 cells. The putative role of the mFBP in the uptake of CB3717 and ICI-198,583 in L1210-B73 cells was further supported by the fact that protection from growth inhibition could be achieved by folic acid rather than by 5-CHO-THF. In L1210 cells, expressing only the RF/MTX carrier, no protection with folic acid was observed.

These results suggest that multiple transport systems may play a role in the uptake of natural folates and nonclassical folate analogues with targets other than dihydrofolate reductase. The possible clinical relevance of these observations will be further discussed.

Received 11/6/90; accepted 8/8/91.

The costs of publication of this article were defrayed in part by the payment of page charges. This article must therefore be hereby marked *advertisement* in accordance with 18 U.S.C. Section 1734 solely to indicate this fact.

<sup>1</sup> This study was supported by the Dutch Cancer Society (Grant IKA 89-34). The authors are very grateful to ICI Pharmaceuticals, Alderly Park, Cheshire, United Kingdom, for their generous funding of the synthesis of the [<sup>3</sup>H]-ICI-198,583.

<sup>2</sup> To whom requests for reprints should be addressed.

## INTRODUCTION

A high affinity/low capacity carrier system is one of the proteins involved in the membrane transport of natural reduced folate compounds and folate analogues like MTX<sup>3</sup> (1-4). This RF-carrier system has been widely characterized in a variety of normal and especially neoplastic cells (2, 4-10). Recent studies have suggested that another class of proteins, mFBP, can mediate the uptake folate compounds as well (reviewed in Refs. 4, 11, and 12). This was supported by *in vitro* observations that: (a) folic acid and 5-CHO-THF could promote growth of cells expressing mFBP, which is consistent with the high affinity of the mFBP for these compounds (13, 14); (b) folate analogues for which the mFBP has a high affinity were potent growth inhibitors of these cells (Refs. 15 and 16; present study); (c) following incubation of cells expressing mFBP with natural and antifolate compounds, these compounds could be identified intracellular as polyglutamate forms (Refs. 16-18; present study), which is the result of a cytoplasmic process (19); and finally (d) anti-mFBP antibodies and chemically activated esters of folic acid/MTX inhibited the uptake of reduced folate compounds in cells expressing mFBP (20, 21).

Recently we have demonstrated the expression of mFBP in a variant of murine L1210 leukemia cells (L1210-B73) which were adapted to grow in folate-conditioned medium containing nanomolar levels of folic acid (22). In addition to mFBP, L1210-B73 cells also expressed the same level of the RF-carrier system, which is present in parental L1210 cells. Parental L1210 cells, grown in standard medium containing 2 μM folic acid, did not express detectable levels of mFBP.

In the present study we have used L1210-B73 cells as a model system to establish the role of the mFBP and/or the RF/MTX-carrier in membrane transport of natural folates and antifolate compounds on the basis of (a) affinities of the mFBP and the RF/MTX-carrier for these compounds, (b) uptake studies with radiolabeled (anti)folates, and (c) cytotoxicity studies. The results indicate that membrane transport in L1210-B73 cells of two folate-based inhibitors of dihydrofolate reductase, MTX and 10-EdAM, mainly proceeds via the RF/MTX-carrier since the mFBP has a poor affinity for these compounds. On the other hand, the mFBP can be an important route in the uptake of folic acid and 5-CHO-THF as well as of two folate-based inhibitors of thymidylate synthase; *N*<sup>10</sup>-propargyl-5,8-dideaza-

<sup>3</sup> The abbreviations used are: MTX, methotrexate; CB 3717, *N*<sup>10</sup>-propargyl-5,8-dideazafolic acid; ICI-198,583; 2-deamino-2-methyl-*N*<sup>10</sup>-propargyl-5,8-dideazafolic acid; 10-EdAM; 10-ethyl-10-deazaaminopterin; TMQ, trimetrexate; 5-CHO-THF, 5-formyltetrahydrofolate; 5-CH<sub>3</sub>-THF, 5-methyltetrahydrofolate; HBSS, HEPES buffered saline solution; HEPES, 4-(hydroxyethyl)-1-piperazine-ethanesulfonic acid; mFBP, membrane-associated folate binding protein; RF/MTX-carrier, reduced folate/methotrexate carrier; TS, thymidylate synthase; DHFR, dihydrofolate reductase; IC<sub>50</sub>, the concentration of inhibitor necessary to inhibit [<sup>3</sup>H]folic acid binding by 50%; DDATHF, 5,10-dideaza-5,6,7,8-tetrahydrofolic acid.

folic acid (CB3717) and ICI-198,583 (23–27). The role of the mFBP in the uptake of the thymidylate synthase inhibitors correlated with the high affinity of the mFBP for these compounds.

## MATERIALS AND METHODS

**Materials.** RPMI 1640, with and without folic acid, fetal calf serum (dialyzed and nondialyzed), and dialyzed horse serum were obtained from Gibco, Grand Island, NY. Folic acid and DL-5-CHO-THF were purchased from Sigma Chemical Co., St. Louis, MO. Digitonin, dinonylphthalate, and dibutylphthalate were purchased from Merck, Darmstadt, Germany. MTX was a gift from Pharmachemie, Haarlem, The Netherlands. 10-EdAM was a gift from Ciba Geigy, Basel, Switzerland. *N*<sup>10</sup>-Propargyl-5,8-dideazafolic acid (CB3717) and ICI-198,583 were provided by ICI-Pharmaceuticals Division, Alderly Park, Macclesfield, Cheshire, United Kingdom. TMQ was obtained from Warner Lambert, Park Davis, Ann Arbor, MI. [<sup>3</sup>H]Folic acid (35 Ci/mmol), [<sup>3</sup>H]MTX (20 Ci/mmol), and L-[<sup>3</sup>H]-5-CHO-THF (50 Ci/mmol) were purchased from Moravsek Biochemicals, Brea, CA. Radiolabels were repurified as described previously (10, 14, 22). [<sup>3</sup>H]ICI-198,583 (25.6 Ci/mmol) was prepared as the diethyl ester in a custom synthesis by Amersham, Amersham, United Kingdom. The compound was hydrolyzed and then purified by high performance liquid chromatography as described before (16).

**Cell Cultures.** Murine leukemic L1210 cells, expressing the RF/MTX-carrier, were grown in RPMI 1640 containing 2  $\mu$ M folic acid, supplemented with 5% fetal calf serum, 2 mM L-glutamine, 100 units/ml of both penicillin and streptomycin, and 50  $\mu$ M 2-mercaptoethanol. L1210-B73 cells, expressing both the RF/MTX-carrier and mFBP, were grown in folate free RPMI 1640 as described previously (22), supplemented with 10% dialyzed fetal calf serum, glutamine, antibiotics, and 2-mercaptoethanol as described above. A 1 nM concentration of either folic acid or 5-CHO-THF was added as the sole folate source. Cells were kept at 37°C in a humidified atmosphere containing 5% CO<sub>2</sub>.

**Growth Inhibition Assay.** L1210 and L1210-B73 cells in the logarithmic phase of cell growth were plated at an initial density of  $7.5 \times 10^4$ /ml into the individual wells of a 24-well tissue culture plate. The medium for both cell lines was folate free RPMI 1640 supplemented with 10% dialyzed fetal calf serum and either 1 nM 5-CHO-THF, 20 nM 5-CHO-THF, or 20 nM folic acid as the sole folate source. Appropriate concentrations of drug were added at the time of plating. After 72 h of drug exposure, cell concentration was determined with a Sysmex CC-110 microcell counter and cell viability was determined microscopically by trypan blue exclusion.

**DHFR Activity Measurement.** Specific activity of DHFR was determined according to the method described by Mini *et al.* (28).

**Binding Studies.** Binding of radiolabeled (anti)folates was performed in HBSS buffer (107 mM NaCl, 20 mM HEPES, 26.2 mM NaHCO<sub>3</sub>, 5.3 mM KCl, 1.9 mM CaCl<sub>2</sub>, 1.0 mM MgCl<sub>2</sub>, and 7.0 mM D-glucose adjusted to pH 7.4 with NaOH) at 4°C, as described previously (22). In short, L1210-B73 cells ( $1 \times 10^6$ /15 ml HBSS) were incubated with [<sup>3</sup>H]folic acid, [<sup>3</sup>H]-5-CHO-THF, [<sup>3</sup>H]ICI-198,583 or [<sup>3</sup>H]MTX (all with a specific activity of 0.5 Ci/mmol) in increasing concentrations. After 10 min, the cells were collected by centrifugation (5 min, 800  $\times$  g) at 4°C. The supernatant was removed by suction and residual fluid using cotton tissues. Pellets were resuspended in water and analyzed for radioactivity in Optifluor scintillation fluid (United Technologies, Packard, Brussels, Belgium) using an Isocap/300 (Searle, Nuclear Chicago) with a counting efficiency for <sup>3</sup>H of 51%. Nonspecific binding of label (usually <2%) was determined by measuring bound radioactivity in the presence of a 1000-fold molar excess of unlabeled folic acid. The relative affinity of mFBP for natural folate and folate analogues was analyzed by a slightly different procedure. L1210-B73 cells ( $3 \times 10^6$  in 1 ml HBSS, pH 7.4) were incubated for 10 min at 4°C with 100 pmol [<sup>3</sup>H]folic acid in the absence or presence of increasing concentrations of natural folate and antifolate compounds. Cells were then centrifuged and the radioactivity in the cell pellet was determined as described above. Relative affinities

are defined as the inverse molar ratio of compound required to displace 50% of [<sup>3</sup>H]folic acid from mFBP.

**Transport Measurements.** L1210 and L1210-B73 cells ( $5 \times 10^6$ ) in the logarithmic phase of growth were suspended in 10 ml folate free RPMI supplemented with 10% dialyzed fetal calf serum and transferred into 25-cm<sup>2</sup> tissue culture flasks. [<sup>3</sup>H]MTX, [<sup>3</sup>H]folic acid, [<sup>3</sup>H]-5-CHO-THF, or [<sup>3</sup>H]ICI-198,583 (all with a specific activity of 0.5 Ci/mmol) were added to final concentrations of 100, 25, 50, and 25 nM, respectively. Control experiments contained the same amounts of <sup>3</sup>H-labeled (anti)folate in the presence of 1  $\mu$ M folic acid. Incubations were performed at 37°C in a humidified atmosphere containing 5% CO<sub>2</sub>. Cells were harvested after 1, 4, and 24 h and checked for cell concentration and viability as described above. After centrifugation (800  $\times$  g, 5 min, 4°C), the supernatant was removed by suction and the residual fluid was removed with cotton tissues. To distinguish between surface bound and intracellular <sup>3</sup>H-labeled (anti)folate in L1210-B73 cells, the cells were rinsed with 1 ml ice-cold acidic saline buffer (137 mM NaCl, 20 mM HEPES, 5.3 mM KCl, 1.0 mM MgCl<sub>2</sub>, 1.9 mM CaCl<sub>2</sub>, and 7.0 mM D-glucose, adjusted to pH 3.5 with acetic acid) to remove surface bound ligand from the mFBP. After centrifugation for 1 min at 13,000  $\times$  g the total cell associated radioactivity was divided in the supernatant fraction (containing cell surface bound ligand) and the pellet fraction (containing intracellular ligand). As a control experiment to establish whether radioactivity found in the acid resistant fraction is still associated with the membrane or transferred to the cytoplasm, a rapid separation of cytosol and particulate fractions was performed by controlled digitonin induced lysis as described by Rijkse *et al.* (29). In short, the procedure is as follows. In an Eppendorf microfuge tube the following gradient was established: lower layer, 100  $\mu$ l HBSS, pH 7.4, containing 10% (v/v) glycerol; middle layer, 500  $\mu$ l of a 3:2 (v/v) mixture of dibutylphthalate and dinonylphthalate; and upper layer, 500  $\mu$ l cell suspension containing  $10^7$  L1210-B73 cells. The upper layer was mixed with 50  $\mu$ l 2 mM digitonin for 30 s, followed by centrifugation in an Eppendorf centrifuge (45 s, 13,000  $\times$  g). The lower layer (containing the particulate fraction) and the upper layer (containing the cytosolic fraction, as checked by the release of the cytosolic marker enzyme lactate dehydrogenase) were collected and analyzed for radioactivity (see "Binding Studies"). From L1210-B73 cells that were incubated for 24 h with <sup>3</sup>H-labeled (anti)folates at concentrations indicated above, more than 85% of the radioactivity in the acid resistant fraction was recovered in the cytosolic fraction (results not shown).

**Analysis of Polyglutamates.** L1210-B73 cells were incubated for 24 h with concentrations of [<sup>3</sup>H]MTX, [<sup>3</sup>H]folic acid, [<sup>3</sup>H]-5-CHO-THF, or [<sup>3</sup>H]ICI-198,583 as indicated above. Cells were harvested by centrifugation and washed once with ice-cold HBSS, pH 7.4, followed by an acidic wash at pH 3.5 (see above) to remove surface bound ligand. The final pellet was resuspended in 50 mM sodium phosphate buffer, pH 5.5, and boiled for 5 min. After centrifugation for 1 min at 13,000  $\times$  g, the clear supernatant was applied to a DE52 minicolumn to separate monoglutamate from polyglutamate forms as described by McGuire *et al.* (30). Monoglutamates were eluted by washing the column with 35 ml, 10 mM Tris-HCl, 125 mM NaCl, and 2.5 mM dithiothreitol, pH 7.5. Polyglutamates were eluted with 3 ml, 0.1 N HCl. The conversion of [<sup>3</sup>H]folic acid to folylpolyglutamate forms could not be analyzed by the DE52 anion-exchange method since the elution of [<sup>3</sup>H]folic acid from this column started at a NaCl concentration (250 mM) at which folylpolyglutamates were eluted as well (not shown).

## RESULTS

**Affinities of RF/MTX-Carrier and mFBP for (Anti)folate Compounds.** The relative affinity of the RF/MTX-carrier for a series of natural and antifolate compounds was studied by inhibition of [<sup>3</sup>H]MTX and [<sup>3</sup>H]-5-CHO-THF transport in L1210 cells (Table 1). The RF/MTX-carrier has a high affinity for 5-CHO-THF, 10-EdAM, MTX, and ICI-198,583, a low affinity for CB3717, and a poor affinity for folic acid. The affinities of the mFBP in L1210-B73 cells for these compounds

Table 1 Inhibition of [ $^3$ H]-5-CHO-THF and [ $^3$ H]MTX transport via the RF/MTX-carrier and displacement of [ $^3$ H]-folic acid binding to the mFBP by folate derivatives

Inhibitor	IC <sub>50</sub> ( $\mu$ M)		
	RF/MTX-carrier <sup>a</sup> (L1210)		mFBP <sup>b</sup>
	[ $^3$ H]MTX (5 $\mu$ M)	[ $^3$ H]-5-CHO-THF (2 $\mu$ M)	(L1210-B73; [ $^3$ H]folic acid, 0.1 $\mu$ M)
10-EdAM	2.1	1.3	3.33 (0.03)
ICI-198,583	3.5	2.9	0.145 (0.69)
5-CHO-THF	5.7	3.8	0.53 (0.19)
MTX	10.3	9.0	3.33 (0.03)
CB3717	114	80	0.063 (1.6)
Folic acid	890	540	0.10 (1.0)

<sup>a</sup> L1210 cells ( $30 \times 10^6$ /ml in HBSS, pH 7.4) were incubated at 37°C with either 5  $\mu$ M [ $^3$ H]MTX or 2  $\mu$ M [ $^3$ H]-5-CHO-THF in the absence or presence of increasing concentrations of the indicated inhibitors. After 3 min uptake was terminated by the addition of ice-cold HBSS, pH 7.4. Cells were washed with ice-cold HBSS buffer, resuspended in 0.5 ml water, and analyzed for radioactivity. Actual influx rates under these conditions were 5.7 pmol/min/10<sup>7</sup> cells for [ $^3$ H]MTX and 3.6 pmol/min/10<sup>7</sup> cells for [ $^3$ H]-5-CHO-THF. Results are the mean of two experiments done in duplicate and expressed as concentration of inhibitor required to inhibit influx of controls by 50% (IC<sub>50</sub>).

<sup>b</sup> L1210-B73 cells ( $3 \times 10^6$  in 1 ml HBSS, pH 7.4) were incubated for 10 min at 4°C with 100 pmol [ $^3$ H]folic acid in the absence or presence of increasing concentrations of inhibitors. Relative affinities (given in parentheses) are defined as the inverse molar ratio of compound required to displace 50% of [ $^3$ H]folic acid from the mFBP. Relative affinity of the mFBP for folic acid is set to 1. Results are the means of at least 3 separate experiments (SD < 15%).

were considerably different. Table 1 shows that the affinity of the mFBP for the TS inhibitors CB3717 and ICI-198,583 is in the same range as for folic acid. The relative affinity for 5-CHO-THF is about 5-fold lower than for folic acid, whereas the affinity for MTX and 10-EdAM is more than 30-fold lower. Consistent with these results were the cell surface binding studies of [ $^3$ H]folic acid, [ $^3$ H]ICI-198,583, [ $^3$ H]-5-CHO-THF and [ $^3$ H]MTX to L1210-B73 cells. Concentrations at which half-maximal binding was observed were 0.9, 2.0, 4.2, and 30–35 nM, respectively, and the total cell surface binding capacity was approximately 100 pmol/10<sup>7</sup> cells (results not shown).

**Membrane Transport of (Anti)folates in L1210/L1210-B73 Cells.** Uptake over a 24-h time period of the antifolates [ $^3$ H]-MTX and [ $^3$ H]ICI-198,583 and the natural folates [ $^3$ H]folic acid and [ $^3$ H]-5-CHO-THF by L1210 and L1210-B73 cells is shown in Fig. 1. To discriminate between internalization via the RF/MTX-carrier or the mFBP in L1210-B73 cells, experiments were carried out in either the absence or presence of 1  $\mu$ M folic acid. Since at this concentration the mFBP is fully saturated and folic acid is poorly transported by the RF/MTX-carrier (Table 1), uptake of  $^3$ H-labeled compounds under this condition represents the accumulation via the latter transport system. The concentrations of [ $^3$ H]folic acid (25 nM), [ $^3$ H]-5-CHO-THF (50 nM), and [ $^3$ H]ICI-198,583 (25 nM) were chosen as being approximately 10-fold above the concentration for half-maximal binding to the mFBP. At the same time these concentrations were well below the  $K_m$  for transport via the RF/MTX-carrier. To compromise for these conditions [ $^3$ H]-MTX was used at a concentration of 100 nM.

Fig. 1 shows that the uptake of [ $^3$ H]folic acid by L1210-B73 cells is significantly higher than by L1210 cells. Furthermore, in the presence of 1  $\mu$ M unlabeled folic acid, uptake of [ $^3$ H]folic acid was reduced by more than 95%, which suggests that folic acid is internalized predominantly via the mFBP in L1210-B73 cells. Both the mFBP and the RF/MTX-carrier in L1210-B73 cells seem to be functional in the uptake of [ $^3$ H]-5-CHO-THF. The mFBP and RF/MTX-carrier contributed for approximately 80 and 20%, respectively, in the uptake of [ $^3$ H]-5-CHO-THF by L1210-B73 cells over a 24-h period of incubation.

Uptake of [ $^3$ H]MTX was only slightly influenced by the presence of 1  $\mu$ M folic acid, which suggests that the RF/MTX-carrier rather than the mFBP plays a major role in the uptake of [ $^3$ H]MTX. In contrast, the main route for uptake of [ $^3$ H]ICI-198,583 in L1210-B73 cells seems to be the mFBP. Although L1210 cells and L1210-B73 cells accumulated significant amounts of [ $^3$ H]ICI-198,583 in the presence of folic acid, indicating uptake via the RF/MTX carrier, more than 85% of [ $^3$ H]ICI-198,583 uptake in L1210-B73 cells occurred via the mFBP.

After 24 h incubation of L1210-B73 cells with 25 nM [ $^3$ H]ICI-198,583, cells were analyzed for the presence of polyglutamate forms of the internalized drug. Separation of [ $^3$ H]ICI-198,583 monoglutamates from polyglutamate forms showed that 67% of total intracellular [ $^3$ H]ICI-198,583 had been converted into polyglutamate forms. Similarly, after incubating L1210-B73 cells for 24 h with 50 nM [ $^3$ H]-5-CHO-THF more than 85% was present as folylpolyglutamate forms.

**Growth Inhibition Studies.** Table 2 shows the growth inhibitory effects of two folate based inhibitors of DHFR (MTX, 10-EdAM) and two folate based inhibitors of TS (CB3717, ICI-198,583) on L1210 and L1210-B73 cells. In order to establish to what extent the RF/MTX-carrier or the mFBP in L1210-B73 plays a role in membrane transport of these compounds, growth inhibition studies were performed in the presence of 20 nM folic acid or 20 nM 5-CHO-THF. In case of transport via

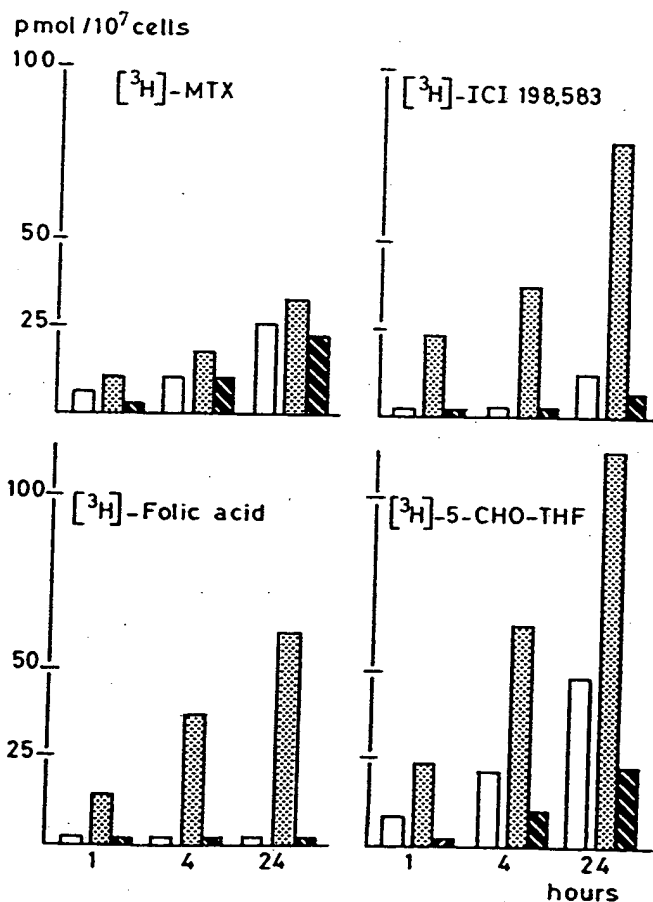


Fig. 1. Uptake of [ $^3$ H]MTX, [ $^3$ H]ICI-198,583, [ $^3$ H]folic acid, and [ $^3$ H]-5-CHO-THF by L1210 cells (□) and L1210-B73 cells over a 1-, 4-, and 24-h time period. Extracellular concentrations of (anti)folate compounds were 100, 25, 25, and 50 nM, respectively. Uptake by L1210-B73 cells was determined either in the absence (□) or presence (▨) of 1  $\mu$ M folic acid to discriminate between internalization via the RF/MTX-carrier or mFBP. Further details are described in "Materials and Methods." Results are the mean of at least 3 separate experiments (SD  $\leq$  21%).

Table 2 Growth inhibition of L1210 and L1210-B73 cells by MTX, 10-EdAM, TMQ, CB3717 and ICI-198,583 in the absence or presence of 20 nM folic acid or 5-CHO-THF as putative protective agents<sup>a</sup>

Inhibitor	Addition	IC <sub>50</sub> (nM) <sup>b</sup>	
		L1210	L1210-B73
MTX	1 nM 5-CHO-THF	2.2 ± 1.0	3.4 ± 1.1
	20 nM 5-CHO-THF	4.9 ± 1.4	15.2 ± 8.6
	20 nM folic acid	2.4 ± 1.1	10.3 ± 3.6
10-EdAM	1 nM 5-CHO-THF	0.98 ± 0.19	2.9 ± 0.6
	20 nM 5-CHO-THF	2.6 ± 1.4	11.3 ± 3.1
	20 nM folic acid	0.99 ± 0.12	4.9 ± 2.0
TMQ	1 nM 5-CHO-THF	2.9 ± 0.9	8.9 ± 3.8
	20 nM 5-CHO-THF	19.2 ± 10.8	131 ± 25
	20 nM folic acid	1.7 ± 0.6	15.6 ± 7.9
CB3717	1 nM 5-CHO-THF	395 ± 32	2.8 ± 0.4
	20 nM 5-CHO-THF	790 ± 60	4.0 ± 0.4
	20 nM folic acid	300 ± 65	28.7 ± 4.5
ICI-198,583	1 nM 5-CHO-THF	9.1 ± 5.0	0.92 ± 0.42
	20 nM 5-CHO-THF	23.0 ± 5.2	5.9 ± 1.4
	20 nM folic acid	6.6 ± 2.3	56.8 ± 16.9

<sup>a</sup> Growth inhibition was determined after 72 h continuous exposure to the drugs.

<sup>b</sup> IC<sub>50</sub> is defined as the drug concentration resulting in 50% inhibition of cell growth compared to controls. Results are the mean of at least 3 separate experiments ± SD.

the mFBP, high affinity binding of folic acid could provide protection from growth inhibition via this route. Likewise, addition of 5-CHO-THF, for which the RF/MTX-carrier has a high affinity, could result in protection from growth inhibition at the level of this carrier. Table 2 also shows the growth inhibitory effects of TMQ, an inhibitor of DHFR which, unlike MTX or 10-EdAM, enters the cell via a process distinct from the RF/MTX carrier (31).

L1210-B73 cells, grown at 1 nM 5-CHO-THF, were found to be less sensitive (1.5- to 3-fold) to MTX, 10-EdAM, and TMQ compared to parental L1210 cells. This difference might be partially explained by a 2.7-fold higher activity of DHFR in L1210-B73 cells compared to L1210 cells (specific activity, 0.32 versus 0.12  $\mu$ mol dihydrofolate/h/mg protein, respectively). The addition of 20 nM 5-CHO-THF to L1210-B73 cells resulted in a 4.5-fold protection from growth inhibition by MTX and 3.9-fold protection from growth inhibition by 10-EdAM. To a lower extent 20 nM folic acid also provided a partial protection against growth inhibition of L1210-B73 cells by MTX and 10-EdAM. 5-CHO-THF (20 nM), but not folic acid, gave a significant protection (15-fold) against TMQ cytotoxicity in L1210-B73 cells. This protection factor was 2-fold higher than for parental L1210 cells. Table 2 demonstrates that L1210-B73 cells were highly sensitive to CB3717 compared to parental cells (IC<sub>50</sub>, 2.8 versus 395 nM, respectively). In addition, significant protection from growth inhibition of L1210-B73 cells by CB3717 was observed by folic acid (10-fold) rather than by 5-CHO-THF (1.6-fold). Although L1210 cells were found to be sensitive for ICI-198,583 (IC<sub>50</sub> 9.1 nM), L1210-B73 cells were even 10-fold more sensitive for ICI-198,583 (IC<sub>50</sub> 0.92 nM). Similarly as for CB3717, protection from ICI-198,583 induced growth inhibition of L1210-B73 cells was more effective with folic acid (65-fold) than with 5-CHO-THF (6.4-fold). No protection from growth inhibition induced by the listed antifolates is observed when L1210 cells were plated in the presence of 20 nM folic acid.

## DISCUSSION

Although mFBPs have been identified in various normal and neoplastic cells and tissues (4, 11, 12, 14, 32-47), their physiological and/or pharmacological role *in vivo* is less well established and is a subject of ongoing discussion: (a) it is evident that in cells or tissues obtained under physiological conditions, the cellular expression of mFBP may not be as high as has been observed in established cell lines maintained *in vitro* in folate conditioned medium (13, 14, 20, 22, 32, 33, 44); (b) when mFBPs are present on the cell surface they will likely be saturated with 5-CH<sub>3</sub>-THF (the predominant circulating reduced folate compound) for which the mFBP has a high binding affinity (4, 11, 12, 17). This may hamper the identification of mFBPs via binding studies with radiolabeled folate compounds; (c) since the mFBP has a high binding affinity for natural reduced folates and is therefore able to internalize these compounds very efficiently (17, 18, 48), cells may not necessarily have to express high levels of mFBP to meet their folate requirements for cell growth; (d) it requires sensitive affinity probes to detect very low cellular levels of mFBP (34, 49). For these reasons, the number of studies regarding the identification and functioning of mFBPs in (non)malignant cellular material obtained *in vivo* or maintained *in vitro* in folate conditioned cell culture medium has been limited at this time.

One of the possible physiological roles of the mFBP may be in the renal retention of folates. There is evidence that mFBP on the brush border membrane of kidney proximal tubules plays a decisive role in maintaining the folate status in mammals (50, 51). The mFBP has also been reported to mediate the cellular folate accumulation in human hematopoietic progenitor cells, a process which was found to be directly related to cell proliferation (35, 36).

It has not been established whether mFBPs, as compared to the RF-carrier, represent a pharmacologically important route for uptake of antifolate drugs. In the present study we were able to address this question by using L1210-B73 cells as a model system. L1210-B73, a subline of murine L1210 leukemia cells adapted to grow at nanomolar concentrations of 5-CHO-THF, expresses the RF-carrier as well as mFBP within one cell (22). The affinities of both proteins for natural folate compounds, folate based inhibitors of DHFR, and folate based inhibitors of TS were analyzed in Table 1. The mFBP exhibited a low affinity for MTX and 10-EdAM as compared to folic acid and 5-CHO-THF. In contrast, the mFBP demonstrated a high affinity for the folate based TS inhibitors which is nearly identical (ICI-198,583) or even higher (CB3717) than for folic acid. On the other hand, the RF-carrier has a high affinity for MTX, 10-EdAM, and ICI-198,583 but a poor affinity for CB3717. Table 2 illustrated that the affinities of the RF-carrier and mFBP for the antifolate compounds correlated with the uptake studies (Fig. 1) and growth inhibitory effects on L1210 and L1210-B73 cells. In addition, the degree of protection from folic acid and 5-CHO-THF against the growth inhibitory effects of the folate based inhibitors of DHFR and TS were consistent with the relative affinities of the mFBP and RF-carrier for these natural folate compounds. Fig. 1 also showed that over a period of 24 h the accumulation of [<sup>3</sup>H]-5-CHO-THF in L1210-B73 cells is higher than for [<sup>3</sup>H]folic acid, even though the affinity of mFBP for folic acid is higher than for 5-CHO-THF. It is reasonable to assume that this difference is explained by a slower release of [<sup>3</sup>H]folic acid from the mFBP and/or reflects a more efficient metabolism and retention of polyglutamate



forms of [ $^3\text{H}$ ]-5-CHO-THF. In this respect, higher rates of entry of 5-CHO-THF and/or folic acid in L1210-B73 cells may also contribute to interactions with antifolates within the cell. In the case of MTX and 10-EdAM, competition at the level of polyglutamylation (52, 53) or transformylation (53, 54) may result in a better protective effect of 5-CHO-THF on growth inhibition. The protective effect of 20 nM 5-CHO-THF on TMQ growth inhibition cannot be accounted for on the basis of effects on polyglutamylation, transport, or inhibition of the above enzymes. Rather, the competition of 5-CHO-THF and its metabolites with TMQ for binding to DHFR, to result in a reactivation of the enzyme (55–57), may form the basis for a diminished growth inhibitory effect of TMQ on L1210-B73 cells (Table 1).

These results with L1210-B73 cells, as well as other studies reported by our laboratory for human CCRF-CEM cells (16), suggest that mFBP is unlikely to play an important role in the membrane transport of folate based DHFR inhibitors. The low affinity of the mFBP for MTX/10-EdAM and the fact that under physiological conditions 5-CH<sub>3</sub>-THF will strongly compete for binding to the mFBP are unfavorable conditions for binding and transport via the mFBP. On the other hand, there can be a role for the mFBP in the uptake of a new series of folate analogues with target enzymes other than DHFR. The TS inhibitors CB3717 and related compounds like ICI-198,583 have been designed in light of the development of cellular resistance to MTX due to increased levels of DHFR (23, 24). Another novel antifolate, DDATHF, has been identified as a potent inhibitor of glycinamide ribonucleotide transformylase, one of the folate dependent enzymes in purine biosynthesis *de novo* (58, 59). These newly synthesized antifolate drugs have been tested in preclinical models and in patients (60–64). In phase I clinical trials with some of these new antifolates some rather unexpected severe side effects have been observed which might be related to the high affinity binding and transport via the mFBP. In a recent study, Grindey *et al.* (65) have shown that toxicity of DDATHF was increased 100-fold when mice were placed on a folate free diet for 2 weeks prior to treatment with this compound. High doses of folic acid in the drinking water completely reversed this toxicity but also the antitumor effects, whereas low doses of folic acid prevented the dietary induced toxicity while maintaining the growth inhibitory effects on the xenograft carcinomas. Since the binding affinity of the mFBP for DDATHF, CB3717, and ICI-198,583 is very high and folic acid (rather than 5-CHO-THF) is able to provide protection against growth inhibition by these drugs (Table 2; Ref. 66), these results may be compatible with the involvement of mFBP in membrane transport of these type of antifolate compounds. Further studies must establish whether the presence of mFBP in a variety of normal cells and tissues is an important factor in toxicity of normal cells to folate based inhibitors of TS and glycinamide ribonucleotide transformylase. Based on the high affinities of the RF-carrier for ICI-198,583 (Table 1; Ref. 66) and DDATHF (66, 67), uptake of these compounds in tumor cells can also proceed via the this carrier system which is expressed in a great number of neoplastic cells (2, 4). The nanomolar concentrations of radiolabeled compounds used in Fig. 1 were selected to be saturating for the mFBP but not for the RF-carrier in L1210-B73 cells. It can be expected that at higher extracellular concentrations (micromolar range) the contribution of the RF-carrier in the uptake of (anti)folate compounds in L1210-B73 cells may proportionally increase due to more favorable transport kinetic conditions for

this carrier system, whereas the saturation of mFBP will be unchanged.

The mechanism of (anti)folate uptake via the mFBP is not well understood. Immunofluorescence studies with anti-mFBP antibodies on MA104 cells (68) indicated that the mFBP-folate complex itself may not be internalized via a classical receptor-mediated endocytosis mechanism. It has been hypothesized (18, 69) that the mFBP serves as a concentrator of folate compounds which are then translocated over the membrane via a second carrier system (*e.g.*, the RF-carrier). In L1210-B73 cells, which express both mFBP and RF-carrier, we did not find evidence for coupling the action of the RF-carrier to the mFBP. Both transport systems seem to operate independently from each other. This can be concluded from the fact that, despite the presence of mFBP in L1210-B73 cells, there is almost no difference in growth inhibition by MTX for L1210 and L1210-B73 cells (Table 2). Furthermore, if the RF-carrier in L1210-B73 cells would be coupled to mFBP, it is difficult to explain the potent growth inhibitory effect of CB3717 on L1210-B73 cells (Table 2) when the RF-carrier has only a poor affinity for this compound (Table 1). Also, the RF-carrier also has a very low affinity for folic acid (Table 1), which results in a very low cellular uptake of this compound in L1210 cells but not in L1210-B73 cells, suggesting that uptake of [ $^3\text{H}$ ]folic acid predominantly proceeds via the mFBP. Finally, in human CCRF-CEM leukemia cells which express mFBP and have no functional RF-carrier, uptake of folate-based TS inhibitor can proceed solely via mFBP (16). Currently, studies are under way to investigate in more detail the molecular events in (anti)folate uptake via mFBP by using a photoaffinity analogue of folic acid (70).

In summary, this study has evaluated the role of the RF-carrier and mFBP in membrane transport of natural folates and folate analogues that are inhibitors of DHFR and TS. The results suggest that the mFBP plays a minor role in the membrane transport of folate based DHFR inhibitors but could be an important transport route for folate based TS inhibitors. The presence of mFBP in various normal tissues and the high affinity of mFBP for these types of antifolates indicate that there may be a pharmacological role for mFBP, *e.g.*, in dealing with the toxic effects to normal cells by nonclassical antifolates.

## REFERENCES

1. Goldman, I. D. The characteristics of the membrane transport of amethopterin and the naturally occurring folates. *Ann. NY Acad. Sci.*, 186: 400–422, 1971.
2. Sirotnak, F. M. Obligate genetic expression in tumor cells of a fetal membrane property mediating "folate" transport: biological significance and implications for improved therapy of human cancer. *Cancer Res.*, 45: 3992–4000, 1985.
3. Sirotnak, F. M. Correlates of folate analog transport, pharmacokinetics and selective antitumor action. *Pharmacol. Ther.*, 8: 71–104, 1980.
4. Ratnam, M., and Freisheim, J. H. Proteins involved in the transport of folates and antifolates by normal and neoplastic cells. In: *Folic Acid Metabolism in Health and Disease*, pp. 91–120. New York: Wiley-Liss, Inc., 1990.
5. Price, E. M., Ratnam, M., Rodeman, K. M., and Freisheim, J. H. Characterization of the methotrexate transport pathway in murine L1210 leukemia cells: involvement of a membrane receptor and a cytosolic protein. *Biochemistry*, 27: 7853–7858, 1988.
6. Jansen, G., Westerhof, G. R., Jarmuszewski, M. J. A., Kathmann, I., Rijkssen, G., and Schornagel, J. H. Methotrexate transport in variant human CCRF-CEM leukemia cells with elevated levels of the reduced folate carrier. *J. Biol. Chem.*, 265: 18272–18277, 1990.
7. Sirotnak, F. M., Goutas, L. J., Jacobsen, D. M., Mines, L. S., Barrueco, J. R., Gaumont, Y., and Kisliuk, R. L. Carrier-mediated transport of folate compounds in L1210-cells. *Biochem. Pharmacol.*, 36: 1659–1667, 1987.
8. Henderson, G. B., Suresh, M. R., Vitols, K. S., and Huennekens, F. M. Transport of folate compounds in L1210 cells: kinetic evidence that folate influx proceeds via the high affinity transport system for 5-methyltetrahydro-

- folate and methotrexate. *Cancer Res.*, 46: 1639-1643, 1986.
9. Sirotak, F. M., Schmid, F. A., Samuels, L. L., and DeGraw, J. I. 10-Ethyl-10-deaza-aminopterin: structural design and biochemical pharmacology and antitumor properties. *Natl. Cancer Inst. Monogr.*, 5: 127-131, 1987.
  10. Henderson, G. B., Tsuji, J. M., and Kumar, H. P. Characterization of the individual transport routes that mediate the influx and efflux of methotrexate in CCRF-CEM human lymphoblastic cells. *Cancer Res.*, 46: 1633-1638, 1986.
  11. Kane, M. A., and Waxman, S. Role of folate binding protein in folate metabolism. *Lab. Invest.*, 60: 737-746, 1989.
  12. Henderson, G. B. Folate binding proteins. *Annu. Rev. Nutr.*, 10: 319-335, 1990.
  13. Henderson, G. B., Tsuji, J. M., and Kumar, H. P. Mediated uptake of folate by a high affinity binding protein in sublines of L1210 cells adapted to nanomolar concentrations of folate. *J. Membr. Biol.*, 101: 247-258, 1988.
  14. Jansen, G., Westerhof, G. R., Kathmann, I., Rademaker, B. C., Rijkse, G., and Schornagel, J. H. Identification of a membrane associated folate binding protein in human leukemic CCRF-CEM cells with transport-related methotrexate resistance. *Cancer Res.*, 49: 2455-2459, 1989.
  15. Henderson, G. B., and Strauss, B. P. Growth inhibition by homofolate in tumor cells utilizing a high-affinity folate binding protein as a means for folate internalization. *Biochem. Pharmacol.*, 39: 2019-2025, 1990.
  16. Jansen, G., Schornagel, J. H., Westerhof, G. R., Rijkse, G. R., Newell, D. R., and Jackman, A. L. Multiple membrane transport systems for the uptake of folate-based thymidylate synthase inhibitors. *Cancer Res.*, 50: 7544-7548, 1990.
  17. Kamen, B. A., Wang, M. T., Streckfuss, A. J., Peryea, X., and Anderson, R. G. W. Delivery of folates to the cytoplasm of MA104 cells is mediated by a surface membrane receptor that recycles. *J. Biol. Chem.*, 263: 13602-13609, 1988.
  18. Kamen, B. A., Johnson, C. A., Wang, M. T., and Anderson, R. G. W. Regulation of the cytoplasmic accumulation of 5-methyltetrahydrofolate in MA104 cells is independent of folate receptor regulation. *J. Clin. Invest.*, 84: 1379-1386, 1989.
  19. Moran, R. G., Colman, P. D., Rosowsky, A., Forsch, R. A., and Chan, K. K. Structural features of 4-amino antifolates required for substrate activity with mammalian folypolyglutamate synthetase. *Mol. Pharmacol.*, 27: 156-166, 1984.
  20. Antony, A. C., Kane, M. A., Portillo, R. M., Elwood, P. C., and Kolhouse, J. F. Studies of the role of a particulate folate binding protein in the uptake of 5-methyltetrahydrofolate by cultured human KB cells. *J. Biol. Chem.*, 260: 14911-14917, 1985.
  21. Deutsch, J. C., Elwood, P. C., Portillo, R. M., Macey, M. G., and Kolhouse, J. F. Role of the membrane-associated folate binding protein (folate receptor) in methotrexate transport in human KB cells. *Arch. Biochem. Biophys.*, 274: 327-337, 1989.
  22. Jansen, G., Kathmann, I., Rademaker, B. C., Braakhuis, B. J. M., Westerhof, G. R., Rijkse, G., and Schornagel, J. H. Expression of a folate binding protein in L1210 cells grown in low folate medium. *Cancer Res.*, 49: 1959-1963, 1989.
  23. Jones, T. R., Calvert, A. H., Jackman, A. L., Brown, S. J., Jones, M., and Harrap, K. R. A potent antitumor quinazoline inhibitor of thymidylate synthase: synthesis, biological properties and therapeutic results in mice. *Eur. J. Cancer*, 17: 11-19, 1981.
  24. Harrap, K. R., Jackman, A. L., Newell, D. R., Taylor, G. A., Hughes, L. R., and Calvert, A. H. Thymidylate synthase: a target for anticancer drug design. *Adv. Enzyme Regul.*, 29: 161-179, 1989.
  25. Jackman, A. L., Taylor, G. A., O'Connor, B. M., Bishop, J. A., Moran, R. G., and Calvert, A. H. Activity of the thymidylate synthase inhibitor 2-desamino-*N*<sup>10</sup>-propargyl-5,8-dideazafofolic acid and related compounds in murine (L1210) and human (W1L2) systems *in vitro* and in L1210 *in vivo*. *Cancer Res.*, 50: 5212-5218, 1990.
  26. Jackman, A. L., Newell, D. R., Jodrell, D. I., Taylor, G. A., Bishop, J. A. M., Hughes, L. R., and Calvert, A. H. *In vitro* and *in vivo* studies with 2-desamino-2-CH<sub>2</sub>-*N*<sup>10</sup>-propargyl-5,8-dideazafofolic acid (ICI 198583), an inhibitor of thymidylate synthase. *In: H. C. Curtius, S. Gishla, and N. Blau (eds.), Chemistry and Biology of Pteridines 1989*, pp. 1023-1026. Berlin: Walter de Gruyter & Co., 1990.
  27. Patil, S. D., Jones, C., Nair, M. G., Galivan, J., Maley, F., Kisliuk, R. L., Gaumont, Y., Duch, D., and Ferone, D. Folate analogues. 32. Synthesis and biological evaluation of 2-desamino-2-methyl-*N*<sup>10</sup>-propargyl-5,8-dideazafofolic acid and related compounds. *J. Med. Chem.*, 32: 1284-1289, 1989.
  28. Mini, E., Moroson, B. A., Franco, C. T., and Bertino, J. R. Cytotoxic effects of folate antagonists against methotrexate-resistant human leukemic lymphoblast CCRF-CEM cell lines. *Cancer Res.*, 45: 325-330, 1985.
  29. Rijkse, G., Staal, G. E. J., Beks, P. J., Streefkerk, M., and Akkerman, J. W. Compartmentation of hexokinase in human blood cells; characterization of soluble and particulate enzymes. *Biochim. Biophys. Acta*, 719: 431-437, 1982.
  30. McGuire, J. J., Mini, E., Hsieh, P., and Bertino, J. R. Role of methotrexate polyglutamates in methotrexate- and sequential methotrexate-5-fluorouracil-mediated cell kill. *Cancer Res.*, 45: 6395-6400, 1985.
  31. Fry, D. W., and Besserer, J. A. Characterization of trimetrexate transport in human lymphoblastoid cells and development of impaired influx as a mechanism of resistance to lipophilic antifolates. *Cancer Res.*, 48: 6986-6991, 1988.
  32. McHugh, M., and Cheng, Y.-C. Demonstration of a high-affinity folate binder in human cell membranes and its characterization in cultured KB cells. *J. Biol. Chem.*, 254: 11312-11318, 1979.
  33. Kamen, B. A., and Capdevila, A. Receptor-mediated folate accumulation is regulated by the cellular folate content. *Proc. Natl. Acad. Sci. USA*, 83: 5983-5987, 1986.
  34. Antony, A. C., Kincade, R. S., Verma, R. S., and Kriehnen, S. R. Identification of high affinity folate binding proteins in human erythrocyte membranes. *J. Clin. Invest.*, 80: 711-723, 1987.
  35. Antony, A. C., Bruno, E., Briddell, R. A., Brandt, J. E., Verma, R. S., and Hoffman, R. Effect of perturbation of specific folate receptors during *in vitro* erythropoiesis. *J. Clin. Invest.*, 80: 1618-1623, 1987.
  36. Antony, A. C., Briddell, R. A., Brandt, J. E., Straneva, J. E., Verma, R. S., Miller, M. E., Kalasinski, L. A., and Hoffman, R. Megaloblastic hematopoiesis *in vitro*. Interaction of anti-folate receptor antibodies with hematopoietic progenitor cells leads to a proliferative response independent of megaloblastic changes. *J. Clin. Invest.*, 87: 313-325, 1991.
  37. Selhub, J., and Franklin, W. A. The folate binding protein of rat kidney: purification, properties, and cellular distribution. *J. Biol. Chem.*, 259: 6601-6606, 1984.
  38. Deutsch, J. C., and Kolhouse, J. F. Folate and methotrexate interactions in the rat kidney. *Cancer Res.*, 49: 5858-5862, 1989.
  39. Hansen, S. I., Holm, J., Huseby, N. E., and Hoier-Madsen, M. High-affinity folate binding proteins in brush-border membranes from human kidney. *Eur. J. Clin. Invest.*, 20: A32, 1990.
  40. Holm, J., Hansen, S. I., Nuseby, N. E., and Hoier-Madsen, M. High affinity folate binding proteins in human choroid plexus. *Eur. J. Clin. Invest.*, 20: A33, 1990.
  41. Ratnam, M., Marquardt, H., Duhring, J. L., and Freisheim, J. H. Homologous membrane folate binding proteins in human placenta: cloning and sequence of a cDNA. *Biochemistry*, 28: 8249-8254, 1989.
  42. Antony, A. C., Utley, C., Van Horne, K. C., and Kolhouse, J. F. Isolation and characterization of a folate receptor from human placenta. *J. Biol. Chem.*, 256: 9684-9692, 1981.
  43. Sadasivan, E., da Costa, M., Rothenberg, S. P., and Brink, L. Purification, properties, and immunological characterization of folate-binding proteins from human leukemia cells. *Biochim. Biophys. Acta*, 925: 36-47, 1987.
  44. Elwood, P. C., Kane, M. A., Portillo, R. M., and Kolhouse, J. F. The isolation, characterization, and comparison of the membrane-associated and soluble folate binding proteins from human KB cells. *J. Biol. Chem.*, 261: 15416-15423, 1986.
  45. Reisenauer, A. M. Affinity labeling of the folate-binding protein in pig intestine. *Biochem. J.*, 267: 249-252, 1990.
  46. Selhub, J., and Rosenberg, I. H. Folate transport in isolated brush border membrane vesicles from rat intestine. *J. Biol. Chem.*, 256: 4489-4493, 1981.
  47. da Costa, M., and Rothenberg, S. P. Characterization of the folate-binding proteins associated with the plasma membrane of rat liver. *Biochem. Biophys. Acta*, 939: 533-541, 1988.
  48. Westerhof, G. R., Jansen, G., Kathmann, G. A. M., Rijkse, G., and Schornagel, J. H. Characterization of receptor-mediated (anti)folate uptake in human CCRF-CEM cells. *In: H. C. Curtius, S. Gishla, and N. Blau (eds.), Chemistry and Biology of Pteridines 1989*, pp. 1284-1287. Berlin: Walter de Gruyter & Co., 1990.
  49. Holm, J., Hansen, S. I., and Hoier-Madsen, M. A high affinity folate binding protein in human amniotic fluid. Radioligand binding characteristics, immunological properties and molecular size. *Biosci. Rep.*, 10: 79-85, 1990.
  50. Selhub, J., Emmanouel, D., Stavropoulos, T., and Arnold, R. Renal folate absorption and the kidney folate binding protein. I. Urinary clearance studies. *Am. J. Physiol.*, 252: F750-F756, 1987.
  51. Selhub, J., Nakamura, S., and Carone, F. A. Renal folate absorption and the kidney folate binding protein. II. Microinfusion studies. *Am. J. Physiol.*, 252: F757-F760, 1987.
  52. Allegra, C. J., Chabner, B. A., Drake, J. C., Lutz, R., Rodbard, D., and Jolivet, J. Enhanced inhibition of thymidylate synthase by methotrexate polyglutamates. *J. Biol. Chem.*, 260: 9720-9726, 1985.
  53. Matherly, L. H., Barlowe, C. K., Phillips, V. M., and Goldman, I. D. The effects on 4-aminoantifolates on 5-formyltetrahydrofolate metabolism in L1210 cells. A biochemical basis of the selectivity of leucovorin rescue. *J. Biol. Chem.*, 262: 710-717, 1987.
  54. Allegra, C. J., Drake, J. C., Jolivet, J., and Chabner, B. A. Inhibition of phosphoribosylaminoimidazolecarboxamide transformylase by methotrexate and dihydrofolic acid polyglutamates. *Proc. Natl. Acad. Sci. USA*, 82: 4881-4885, 1985.
  55. Matherly, L. H., Fry, D. W., and Goldman, I. D. Role of methotrexate polyglutamylation and energy metabolism in inhibition of methotrexate binding to dihydrofolate reductase by 5-formyltetrahydrofolate in Ehrlich ascites tumor cells *in vitro*. *Cancer Res.*, 43: 2694-2699, 1983.
  56. Matherly, L. H., Anderson, L. A., and Goldman, I. D. Role of cellular oxidation-reduction state in methotrexate binding to dihydrofolate reductase and dissociation induced by reduced folates. *Cancer Res.*, 44: 2325-2330, 1984.
  57. Matherly, L. H., Barlowe, C. K., and Goldman, I. D. Antifolate polyglutamylation and competitive drug displacement at dihydrofolate reductase as important elements in leucovorin rescue in L1210 cells. *Cancer Res.*, 46: 588-593, 1986.
  58. Beardsley, G. P., Moroson, B. A., Taylor, E. C., and Moran, R. G. A new folate antimetabolite, 5,10-dideaza-5,6,7,8-tetrahydrofolate is a potent inhibitor of *de novo* purine synthesis. *J. Biol. Chem.*, 264: 328-333, 1989.



59. Moran, R. G., Baldwin, S. W., Taylor, E. C., and Shih, C. The 6*S*- and 6*R*-diastereomers of 5,10-dideza-5,6,7,8-tetrahydrofolate are equiactive inhibitors of *de novo* purine synthesis. *J. Biol. Chem.*, 264: 21047-21051, 1989.
60. Calvert, A. H., Newell, D. R., Jackman, A. L., Gumbrell, L. A., Sikora, E., Grzelakowska-Sztabert, G., Bishop, J. A. M., Judson, I. R., Harland, S. J., and Harrap, K. R. Recent preclinical and clinical studies with the thymidylate synthase inhibitor *N*<sup>10</sup>-propargyl-5,8-dideazafolic acid (CB-3717). *Natl. Cancer Inst. Monogr.*, 5: 213-218, 1987.
61. Vest, S., Bork, E., and Hansen, H. H. A phase I evaluation of *N*<sup>10</sup>-propargyl-5,8-dideazafolic acid. *Eur. J. Cancer Clin. Oncol.*, 24: 201-204, 1988.
62. Cantwell, B. M. J., Macaulay, V., Harris, A. L., Kaye, S. B., Smith, I. E., Milsted, R. A. V., and Calvert, A. H. Phase II study of the antifolate *N*<sup>10</sup>-propargyl-5,8-dideazafolic acid (CB3717) in advanced breast cancer. *Eur. J. Cancer Clin. Oncol.*, 24: 733-736, 1988.
63. Muggia, F., Martin, T., Ray, M., Leichman, C. G., Grunberg, S., Gill, L., Moran, R. G., Dyke, R., and Grindey, G. Phase I study of weekly 5,10-dideazatetrahydrofolate (LY-264618, DDATHF-B). *Proc. Am. Soc. Clin. Oncol.*, 9: 74, 1990.
64. Fergusson, K., Boschelli, D., Hoffman, P., Oronsky, A., Whiteley, J., Galivan, J., Freisheim, J., Hynes, J., and Kerwar, S. S. Synergy between 5,10-dideaza-5,6,7,8-tetrahydrofolic acid and methotrexate in mice bearing L1210 tumors. *Cancer Chemother. Pharmacol.*, 25: 173-176, 1989.
65. Grindey, G. B., Alati, T., and Shih, C. J. Reversal of the toxicity but not the antitumor activity of lometrexol by folic acid. *Proc. Am. Assoc. Cancer Res.*, 32: 324, 1991.
66. Jansen, G., Westerhof, G. R., Kathmann, I., Rijkssen, G., and Schornagel, J. H. Growth inhibitory effects of 5,10-dideazatetrahydrofolic acid (DDATHF) on variant murine L1210 and human CCRF-CEM leukemia cells with different membrane-transport characteristics for (anti)folate compounds. *Cancer Chemother. Pharmacol.*, 28: 115-117, 1991.
67. Pizzorno, G., Moroson, B. A., Cashmore, A. R., Cross, A. D., and Beardsley, G. P. Transport of 5,10-dideazatetrahydrofolic acid (DDATHF) in CCRF-CEM sensitive and methotrexate resistant cell lines. In: H. C. Curtius, S. Gishla, and N. Blau (eds.), *Chemistry and Biology of Pteridines 1989*, pp. 1284-1287. Berlin: Walter de Gruyter & Co., 1990.
68. Rothberg, K. G., Ying, Y., Kolhouse, J. F., Kamen, B. A., and Anderson, R. G. W. The glycopospholipid-linked folate receptor internalizes folate without entering the clathrin-coated pit endocytic pathway. *J. Cell Biol.*, 110: 637-649, 1990.
69. Kamen, B. A., Smith, A. K., and Anderson, R. G. W. The folate receptor works in tandem with a probenecid-sensitive carrier in MA104 cells *in vitro*. *J. Clin. Invest.*, 87: 1442-1449, 1991.
70. Westerhof, G. R., Jansen, G., McAlinden, T. P., Schornagel, J. H., Hynes, J. B., and Freisheim, J. H. A photoaffinity analogue of folic acid as probe for identification and functioning of a membrane-associated folate binding protein in human CCRF-CEM leukemia cells. *Proc. Am. Assoc. Cancer Res.*, 32: 328, 1991.



# Targeted drug delivery via the folate receptor

Jennifer Sudimack B.A., Robert J. Lee PhD\*

*Division of Pharmaceutics and Pharmaceutical Chemistry, College of Pharmacy, The Ohio State University, Rm 542 LM Parks Hall,  
500 W. 12th Ave., Columbus, OH 43210, USA*

Received 19 July 1999; accepted 15 October 1999

## Abstract

The folate receptor is a highly selective tumor marker overexpressed in greater than 90% of ovarian carcinomas. Two general strategies have been developed for the targeted delivery of drugs to folate receptor-positive tumor cells: by coupling to a monoclonal antibody against the receptor and by coupling to a high affinity ligand, folic acid. First, antibodies against the folate receptor, including their fragments and derivatives, have been evaluated for tumor imaging and immunotherapy clinically and have shown significant targeting efficacy in ovarian cancer patients. Folic acid, a high affinity ligand of the folate receptor, retains its receptor binding properties when derivatized via its  $\gamma$ -carboxyl. Folate conjugation, therefore, presents an alternative method of targeting the folate receptor. This second strategy has been successfully applied in vitro for the receptor-specific delivery of protein toxins, anti-T-cell receptor antibodies, interleukin-2, chemotherapy agents,  $\gamma$ -emitting radiopharmaceuticals, magnetic resonance imaging contrast agents, liposomal drug carriers, and gene transfer vectors. Low molecular weight radiopharmaceuticals based on folate conjugates showed much more favorable pharmacokinetic properties than radiolabeled antibodies and greater tumor selectivity in folate receptor-positive animal tumor models. The small size, convenient availability, simple conjugation chemistry, and presumed lack of immunogenicity of folic acid make it an ideal ligand for targeted delivery to tumors. © 2000 Elsevier Science B.V. All rights reserved.

**Keywords:** Drug delivery systems; Folate receptor; Endocytosis; Immunotherapy; Gene therapy; Protein toxins; Radioimaging; Liposomes

## Contents

1. Introduction .....	148
2. Overexpression of folate receptors in human tumors .....	148
3. Delivery of radiopharmaceuticals .....	150
3.1. Delivery of radionuclides utilizing MOv18 .....	150
3.2. Delivery of radionuclides utilizing low molecular weight folate conjugates .....	151
4. Delivery of liposomal drug carriers .....	153
5. Delivery of gene transfer vectors .....	154
5.1. Viral vectors .....	154
5.2. Non-viral vectors .....	155
5.3. Anionic liposome-entrapped polyplexes (LPDII) .....	155

\*Corresponding author. Tel.: +1-614-292-4172; fax: +1-614-292-7766.

E-mail address: lee.1339@osu.edu (R.J. Lee)

6. Delivery of protein toxins .....	157
6.1. Delivery of immunotherapy agents .....	158
7. Summary .....	158
References .....	159

## 1. Introduction

Targeted drug delivery systems promise to expand the therapeutic windows of drugs by increasing delivery to the target tissue as well as the target–non-target tissue ratio. This will in turn lead to a reduction in the minimum effective dose of the drug and the accompanying drug toxicity, and an improvement in therapeutic efficacy at equivalent plasma concentrations. Given the often limited number of targeted receptor sites on any given target tissue, targeted delivery is a particularly attractive approach for agents with narrow therapeutic windows and/or are active at very low concentrations.

For targeted delivery to tumor, the cellular target often consists of a membrane-bound tumor-associated antigen (TAA). The receptor for vitamin folate has been identified as a marker for ovarian carcinomas and has also been found to be frequently overexpressed in a wide range of other types of tumors, therefore, presents an attractive target for tumor-selective drug delivery [1–9].

## 2. Overexpression of folate receptors in human tumors

Folate receptor (FR), also known as the high affinity membrane folate-binding protein, is a glycosylphosphatidylinositol (GPI)-linked membrane glycoprotein with an apparent molecular weight of 38–40 kDa [10]. Two membrane-bound isoforms of FR have been identified in humans, designated  $\alpha$  and  $\beta$ . FRs bind folic acid (an oxidized form of folate) with high affinity. FR  $\alpha$ -isoform has a dissociation constant ( $K_d$ ) for folic acid of  $\sim 0.1$  nM, which is approximately 10-fold lower than its  $K_d$  for reduced folates (e.g., 5-methyltetrahydrofolate) [11,12]. The role of FR in cellular folate transport is not well understood, although a “potocytosis” model has been proposed [13]. FRs were found to be clustered in non-coated membrane regions called caveolae.

Localization of FRs in caveolae and receptor internalization can be induced by receptor crosslinking and is regulated by cholesterol [13,14]. Rather than the FR, an anion transporter with a  $K_i$  in the micromolar range and sensitivity to the anion transporter inhibitor probenecid appeared to be responsible for the transmembrane cellular transport of physiological forms of the folate coenzyme, 5-methyltetrahydrofolate [15].

While elevated expression of FR has frequently been observed in various types of human cancers, the receptor is generally absent in most normal tissues with the exceptions of choroid plexus, placenta, and low levels in lung, thyroid and kidney [8]. Although FR type  $\beta$  has been found on CD34+ cells, the receptor curiously lack affinity for [ $^3$ H] folic acid and various folate derivatives [9]. FR type  $\alpha$  is frequently overexpressed in tumor cells in culture and epithelial lineaged tumors such as ovarian carcinomas. Several studies show that over 90% of ovarian carcinomas overexpress the FR [4,7]. Expression of the receptor is mostly homogeneous in ovarian cancer tissue samples [4]. In a recent study, a monoclonal antibody against the type  $\alpha$  receptor, LK26, was used to determine the frequency of FR overexpression in human tumors by indirect immunohistochemical staining [4]. High frequencies of receptor overexpression were found in many types of tumors, including ovarian (52 of 56 cases tested), endometrial (10 of 11), colorectal (6 of 27), breast (11 of 53), lung (6 of 18), renal cell (9 of 18) carcinomas, brain metastases derived from epithelial cancers (4 of 5), and neuroendocrine carcinomas (3 of 21) [4]. In a separate study, quantitative reverse transcription polymerase chain reaction (RT-PCR) analysis was used to determine the mRNA transcript levels of both subtypes of the FR in various human tumor tissues, and [ $^3$ H] folic acid binding was also used to determine the FR ligand binding capacity in these tissues [7]. Highly elevated levels of the FR were detected in choriocarcinomas, meningiomas, uterine sarcomas, osteosarcomas, non-Hodgkin's

lymphomas, and promyelocytic leukemias [7]. FR type  $\beta$  is frequently overexpressed in non-epithelial lineaged tumors such as sarcomas and acute myeloid leukemias but not in established cell lines of the same origin [16]. The causes of FR overexpression in cancers are unclear. Transfection and expression of FR on NIH/3T3 cells provides cells with the ability to survive in low folate medium and increased cell growth both *in vitro* and *in vivo* [17,18]. However, another study showed that transfection of cervical carcinoma cells with FR cDNA led to a

decrease in the rate of cellular proliferation rather than an increase, suggesting FR expression may not provide a growth advantage to rapidly dividing cells in all cases [19]. Studies also show that high levels of FR expression are associated with increased biological aggressiveness of ovarian carcinomas as shown by a higher percentage of S-phase cells and increased resistance to chemotherapeutic agents [20]. Thus FR elevation may be a useful prognostic factor.

The prevalence of FR overexpression among human tumors makes it a good marker for targeted drug delivery to these tumors. Two strategies have been developed for FR-specific drug targeting: (1) coupling to monoclonal antibodies (e.g., MOv18) against the FR; and (2) coupling to folic acid, in which folic acid functions as the targeting ligand. High affinity FR binding is retained when folate (Fig. 1) is covalently linked via its  $\gamma$ -carboxyl group to a foreign molecule. The general model for the cellular uptake of drug conjugates targeted to the FR is illustrated in Fig. 2.

This review summarizes recent studies on the

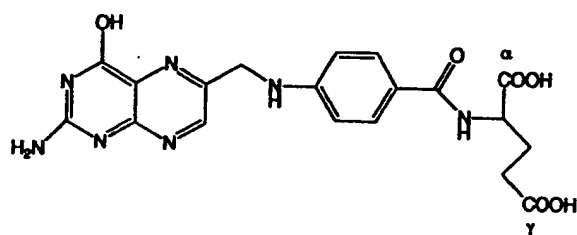


Fig. 1. The structure of folic acid. The  $\alpha$  and  $\gamma$  carboxyl groups are labeled.

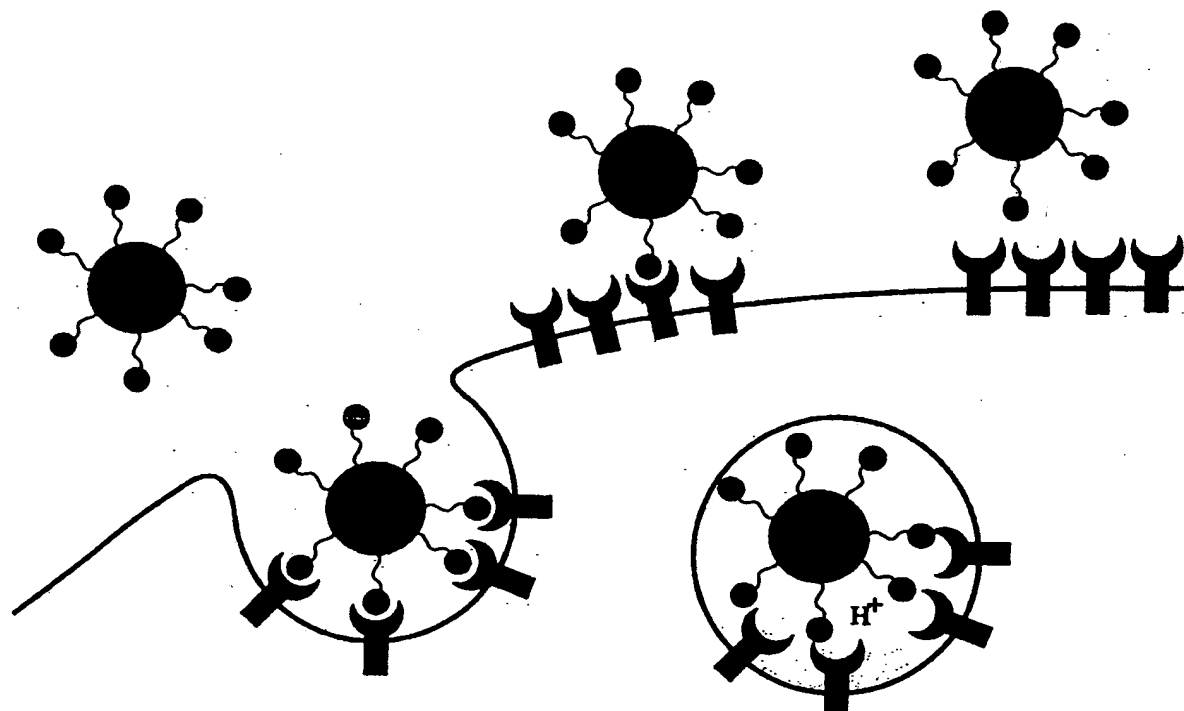


Fig. 2. A schematic diagram of the folate receptor-mediated endocytosis pathway.

diagnostic and therapeutic applications of targeting the FR in vitro and in vivo using either folate or monoclonal antibodies against the FR. The drugs or drug carriers evaluated include liposomes, protein toxins, plasmid DNA complexes, imaging, chemotherapeutic, and immunotherapeutic agents [27,28]. Targeted drug delivery via the FR has been reviewed in several recent articles [21–26].

### 3. Delivery of radiopharmaceuticals

Radioactive tracer techniques are widely used in the diagnostic imaging of tumors due to their ability to non-invasively probe for tissue pathophysiology. The development of new and improved tumor-selective radiopharmaceuticals is clinically desirable as a means of: (i) detecting and/or confirming the presence and location of primary and metastatic lesions; (ii) probing biochemical features of neoplastic tissue that have implications for tumor staging and/or subsequent treatment planning; and (iii) monitoring tumor response to treatment. Photon emitting radiopharmaceuticals that can be used to generate planar and/or tomographic (SPECT) images comprise the cornerstone of current nuclear medicine practice due to the widespread availability of appropriate radionuclides (e.g.,  $^{99m}\text{Tc}$ ,  $^{123}\text{I}$ ,  $^{67}\text{Ga}$ , and  $^{111}\text{In}$ ), FDA-approved radiopharmaceuticals, and the required imaging equipment. Actively targeted  $\gamma$ -emitting radiopharmaceuticals promise to greatly improve the specificity and sensitivity of scintigraphy imaging procedures. If sufficient tumor specificity can be achieved, radiopharmaceuticals labeled with an appropriate  $\alpha$ - or  $\beta$ -emitting radionuclide can also provide an attractive means for site-selective radiation therapy. Criteria for radionuclide selection in the development of diagnostic or therapeutic radiopharmaceuticals include the physical and biological half-lives of the radionuclide, presence or absence of particulate emissions and conversion electrons, as well as the pharmacokinetic and biodistribution properties of the radiopharmaceutical.

Monoclonal antibodies have been evaluated clinically for the tumor-selective delivery of radionuclides for both therapeutic and diagnostic purposes through techniques including radioimmunoscinigraphy (RIS), single-photon-emission computed

tomography (SPECT) and radioimmunotherapy (RIT). Radiolabeled MOv18, a monoclonal antibody against the FR, and its fragments were used in clinical studies in ovarian cancer patients.

#### 3.1. Delivery of radionuclides utilizing MOv18

Radiolabeled antibodies against the FR have been used in the immunohistochemical detection of tissue FR expression, in planar or tomographic (SPECT) imaging, as well as in radioimmunotherapy treatment of ovarian carcinomas.

In a recent clinical study,  $^{131}\text{I}$ -MOv18 was administered either intravenously (i.v.) or intraperitoneally (i.p.) to 30 patients with ovarian carcinoma. Radioimmunoscinigraphy (RIS) was carried out in this study to compare the two routes of administration. A more favorable tumor to non-target (T/NT) ratio (2.8 vs. 1.9) and tumor uptake (1.3% vs. 0.8%) resulted when the  $^{131}\text{I}$ -MOv18 was delivered intraperitoneally. For diagnostic applications, the i.p. route of administration was not very practical. However, the significant increase in targeting ratio achieved via the i.p. route compared to the i.v. route suggests that it may be more appropriate for certain therapeutic applications. The average sensitivity of this method was shown to be 73% (55 tumors detected out of a total of 75 tumors) and the specificity was 100% [29].

In a separate clinical study, 16 patients with minimal residual disease of ovarian cancer were treated by radioimmunotherapy (RIT) with a single i.p. dose of  $^{131}\text{I}$ -MOv18. Complete response (CR) was observed in five patients, no change (NC) in six patients, and progressive disease (PD) in five patients [30]. Furthermore, one patient exhibited long-term CR in a follow-up exam [30].

In single-step radioimmunoimaging protocols, patients are exposed to radiation for a relatively long period of time since it was shown to take approximately 48–72 h for the optimal T/NT ratios to be reached following radiotracer administration [29]. In order to minimize patient radiation exposure, a two-step method was developed. In a two-step protocol, an initial i.p. injection of biotinylated MOv18 was followed by a waiting period, which allows the MOv18 to localize in tumors, and then an i.p. injection of  $^{111}\text{In}$ -streptavidin was administered.

SPECT was then performed for tumor imaging. The mean T/NT ratio obtained was higher (9 vs. 2.8) than when the conventional one-step method was utilized [31]. The improvement in tumor targeting was due to the reduced size and accelerated systemic clearance of the radiotracer  $^{111}\text{In}$ -streptavidin in comparison with the radiolabeled whole antibody. However, this method has limited appeal for clinical imaging applications due to the requirement for repeated i.p. injections at various time intervals and the potential immunogenicity of the streptavidin.

Finally, a three-step method was developed where patients were administered biotinylated MOv18, avidin, followed by  $^{111}\text{In}$ -labeled biotin. The T/NT ratio obtained was 1.7, in contrast to 9 for the two-step method. The relatively poor contrast of this procedure was due to the internalization of the antibody/antigen complexes induced by avidin crosslinking [32]. The receptor-bound avidin, therefore, is no longer accessible to the radiolabeled biotin derivative. While detrimental to tumor imaging, this mechanism of cellular internalization may be exploited for FR-mediated delivery of certain therapeutic agents.

### 3.2. Delivery of radionuclides utilizing low molecular weight folate conjugates

Radiolabeled low molecular weight folate conjugates compared to radiolabeled antibody have greatly reduced size, therefore, much faster systemic clearance. This in turn leads to increased tumor to background ratios. The radionuclides which have been evaluated as folate conjugates include  $^{67}\text{Ga}$ ,  $^{111}\text{In}$ , and  $^{99\text{m}}\text{Tc}$ . The results are summarized as follows:

$^{67}\text{Ga}$  and  $^{111}\text{In}$  are  $\gamma$ -emitting radionuclides commonly used in medical imaging procedures with half-lives of 78 h and 68 h, respectively. When administered as a citrate complex,  $^{67}\text{Ga}$ , forms a high affinity complex with circulating transferrin. Since the transferrin receptor is frequently overexpressed in various types of tumors, the  $^{67}\text{Ga}$ -transferrin complex preferentially localizes in the tumor, which allows for tumor imaging [33–35]. Deferoxamine is a commonly used chelator that forms a stable complex with Ga.  $^{67}\text{Ga}$ -labeled deferoxamine (DF) conjugates have been frequently used in positron

emission tomography (PET) and gamma scintigraphy [36–38]. For FR imaging, folate was conjugated to deferoxamine via its amino group [39]. The resulting conjugate, deferoxamine-folate (DF-folate), was efficiently labeled with  $^{67}\text{Ga}$  [39].  $^{67}\text{Ga}$ -DF-folate was shown to have 100 times greater uptake in FR-positive oral carcinoma KB cells than the non-targeted  $^{67}\text{Ga}$ -DF [39]. Further, KB cell binding was completely blocked by excess free folate, indicating that binding was specific for the FR [39].  $^{67}\text{Ga}$ -DF-folate was then evaluated for its tumor localizing properties in athymic mice, on a folate free diet, carrying xenograft implants derived from subcutaneously injected KB cells [40,41]. The tumor to blood ratio obtained at 4 h post i.v. injection reached 409 to 1, which was far superior than various controls including  $^{67}\text{Ga}$ -DF and  $^{67}\text{Ga}$ -citrate. Only, the tumor and the kidneys accumulated high levels of the radionuclide conjugate. Radioactivity clearance from the tumor and the kidneys was slower than from other organs, resulting in even higher tumor to blood ratios ( $> 1\,000$ ) at 24 h post injection [40]. The undesirable radionuclide accumulation in the kidneys was likely due to the presence of FRs in the kidney proximal tubules. Targeting efficacy was much poorer in mice on the folate-enriched regular rodent diet or when excess free folate was pre-administered as a receptor blocking agent [40]. In addition, the superb imaging property exhibited by  $^{67}\text{Ga}$ -DF-folate was primarily attributable to its rapid blood clearance kinetics.

An  $^{111}\text{In}$ -labeled diethylenetriaminepentaacetic acid (DTPA)-folate was also synthesized and evaluated both in vitro and in vivo using the KB xenograft tumor model, as described for  $^{67}\text{Ga}$ -DF-folate [42]. The tumor to blood ratios obtained at 4 h post i.v. administration was 82 to 1 [43]. Overall the data obtained with  $^{111}\text{In}$ -DTPA-folate was very similar to those for  $^{67}\text{Ga}$ -DF-folate. There was, however, a significant reduction in hepatobiliary clearance of this agent compared to  $^{67}\text{Ga}$ -DF-folate. The overall clearance kinetics of this agent, therefore, was more rapid and more favorable for tumor imaging.  $^{111}\text{In}$ -DTPA-folate is currently being developed as a clinical imaging agent. A phase I/II radioimaging clinical study on  $^{111}\text{In}$ -DTPA-folate is being conducted at the University of Texas MD Anderson Cancer Center in ovarian cancer patients.

Compared to  $^{111}\text{In}$  and  $^{67}\text{Ga}$ ,  $^{99\text{m}}\text{Tc}$  is considered to be a more favorable radionuclide for radioimaging applications due to its short half-life of 6 h, a 140 keV  $\gamma$ -radiation energy, which is optimal for available imaging equipment, and low cost. A novel folate conjugate of a Tc-chelating ligand, 6-hydrazinonicotinamido-hydrazido (HYNIC)-folate, was recently synthesized in our laboratory (Fig. 3). HYNIC-folate was radiolabeled with  $^{99\text{m}}\text{Tc}$  using tricine and trisodium triphenylphosphine-3,3',3"-trisulfonate (TPPTS) as co-ligands. The receptor binding property of  $^{99\text{m}}\text{Tc}$ -HYNIC-folate was studied in cultured KB cells. FR-mediated uptake was  $\sim 300$  times the non-specific binding in the presence of 1 mM free folic acid (Fig. 4).  $^{99\text{m}}\text{Tc}$ -HYNIC-folate was further evaluated in a C57BL/6 mouse model carrying syngeneic solid tumor grafts derived from 24JK-FBP cells, a methylcholanthrene-induced sarcoma

cell line transfected with the human FR type alpha [44]. Tumor to blood ratios reached 55 and 81 at 4 h and 24 h post i.v. injection of the radiotracer, respectively [45]. Tumor uptake of the radioconjugate was blocked by the co-injection of 100  $\mu\text{g}$  of free folic acid, indicating the role of the FR in tumor localization. Tumors were clearly identifiable in gamma-camera images (Fig. 5). Two other  $^{99\text{m}}\text{Tc}$ -labeled folate conjugates have been synthesized and evaluated for gamma-imaging, including  $^{99\text{m}}\text{Tc}$ -DTPA-folate and  $^{99\text{m}}\text{Tc}$ -ethylenedicysteine-folate, each showing good tumor selectivity [46,47].

Regardless of the specific radionuclide chelate-folate conjugate used, high levels of the radiotracers were consistently found in the kidneys besides the tumors. This poses a potential challenge for application of low molecular weight folate conjugates in targeted radiotherapy. However, the high selectivity

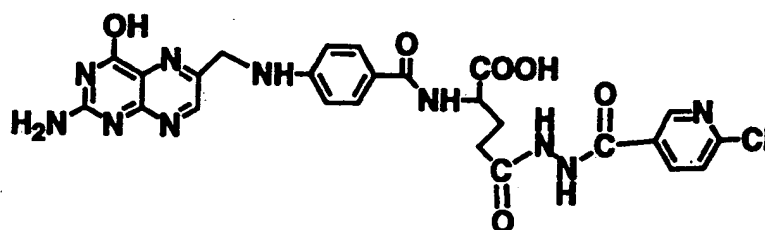


Fig. 3. Structure of 6-hydrazinonicotinamido-hydrazido (HYNIC)-folate.

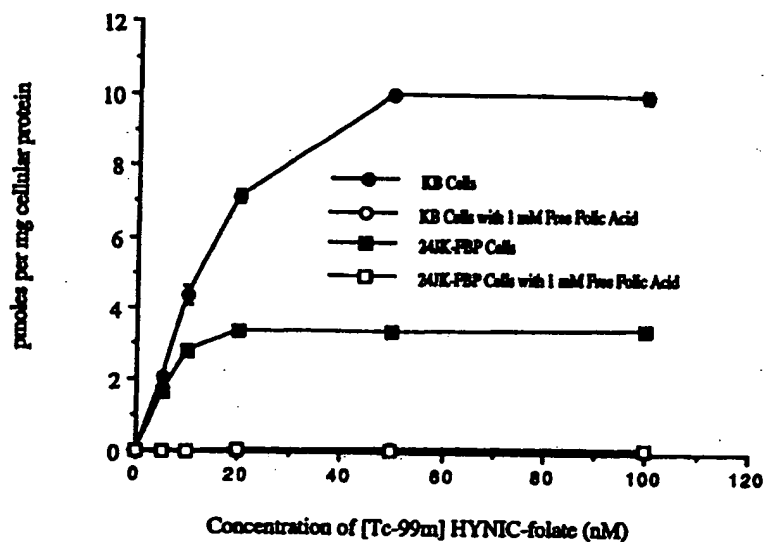


Fig. 4.  $^{99\text{m}}\text{Tc}$ -HYNIC-folate uptake by culture tumor cells.

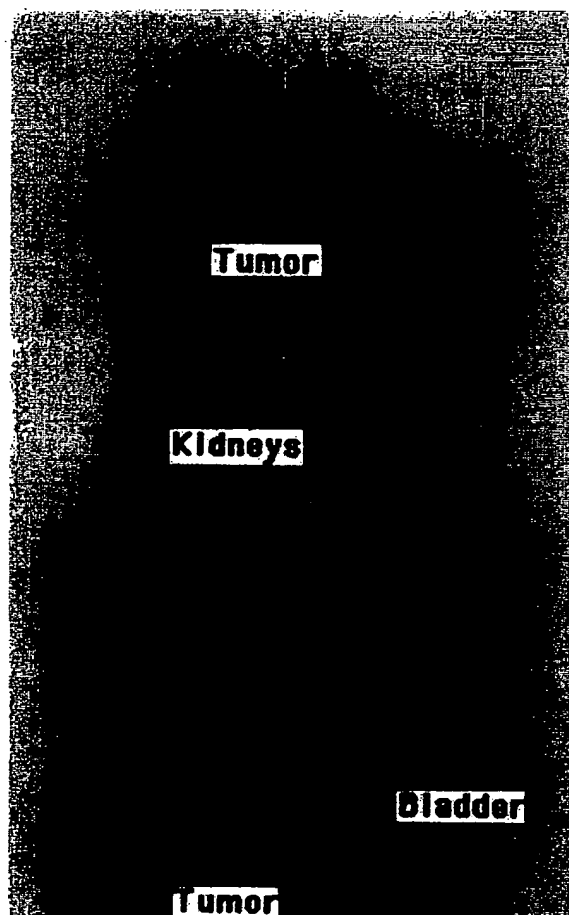


Fig. 5. Gamma camera image of a mouse treated with  $^{99m}\text{Tc}$ -HYNIC-folate.

and the rapid clearance kinetics of these conjugates make them ideal candidates for development as imaging agents for the detection of FR positive tumors.

#### 4. Delivery of liposomal drug carriers

Liposomes are phospholipid bilayer vesicles. As drug carriers, liposomes possess the following properties: (1) the ability to entrap hydrophilic drug molecules in its aqueous interior and/or incorporate hydrophobic molecules in its bilayer(s); (2) long systemic circulation time; (3) efficient uptake by the reticuloendothelial system (RES); and (4) preferen-

tial accumulation in solid tumors due to increased endothelial permeability and reduced lymphatic drainage [48–51]. Low liposome encapsulation efficiency is a limiting factor for delivery of hydrophilic drugs and has been addressed in the delivery of an antitumor agent doxorubicin through the recent development of the “remote-loading” method [52]. Modification of the liposome surface with polyethyleneglycol (PEG) has resulted in reduced RES uptake and further prolonged circulation time [53–60].

The therapeutic efficacy of drug carrying liposomes can potentially be greatly improved if they could be targeted selectively to the tumor. Monoclonal antibodies and their fragments have been attached to the liposome surface to construct immunoliposomes [54–57]. The clinical potential of immunoliposomes is limited because: (1) the targeting ligand is immunogenic. The elicitation of a human-antimouse IgG antibody (HAMA) response precludes repeated administration of immunoliposomes; (2) covalent attachment of a protein to a liposome is technically challenging. The conjugation chemistry for attaching antibodies to lipids is cumbersome and may result in partial denaturation of the targeting ligand; (3) proteinaceous ligands are prone to denaturation upon exposure to organic solvent, limiting the methods available for liposome preparation; (4) immunoliposomes are often unstable and tend to lose immunoreactivity upon storage and/or become rapidly cleared upon injection via  $F_c$  receptor-mediated RES uptake; and (5) few tumor-specific antibodies are available in quantities needed for drug targeting.

For effective targeting of liposomes, folate has to be attached via a long PEG spacer (e.g., PEG  $M_r$  3350) to overcome the steric hindrance encountered at the cell surface [61]. In cultured KB cells, liposome uptake appeared to saturate at  $\sim 2.5 \times 10^5$  sites/cell [61]. The cellular uptake of folate-PEG-liposomes was saturable and could be blocked with a high concentration (1 mM) of free folic acid [60]. The requirement for high concentrations of free folate for effective receptor blocking indicated that folate-targeted liposomes had very high affinity for receptor-bearing tumor cells, possibly due to its capacity to interact with cellular FRs via multivalent interaction [61,62]. Folate-targeted liposomes encap-



sulating a fluorescent dye, calcein, were shown to be taken up by cultured KB cells via receptor-mediated endocytosis and displayed punctate fluorescence pattern when examined under a fluorescence microscope [61]. Folate-PEG-liposomes entrapping doxorubicin were evaluated in cultured KB cells for its uptake and cytotoxicity [63]. Cellular doxorubicin uptake following incubation with these liposomes was 45-fold higher than that of non-targeted liposomes and 1.6 times higher than free doxorubicin, and the cytotoxicity of these liposomes was 86 times and 2.7 times higher, respectively [63]. The cellular uptake of the folate-PEG-liposomes was unaffected by the presence of physiological concentrations of folate in the culture medium [63].

Folate-targeted liposomes have also been used to deliver an antisense oligodeoxyribonucleotide, which inhibits the expression of epidermal growth factor receptor (EGFR) [64]. The main obstacles to the therapeutic application of antisense oligodeoxyribonucleotides were poor cellular uptake, short plasma half-life, and lack of tissue specificity. Folate-PEG-liposome-encapsulated oligonucleotides were efficiently delivered as indicated by increased cellular uptake. These liposomal oligos were also shown to effectively suppress the expression of EGFR in KB cells and to inhibit cell growth [64].

Folate conjugates and folate-targeted liposomes were shown to be internalized into a low-pH endosomal compartment by FR-bearing cells via receptor-mediated endocytosis. The rates of liposome content release following endocytosis and cytosolic drug delivery are effected by the environmental pH and intraliposomal buffer strength [65]. Further, the rate of endosomal release of liposome-entrapped drug molecules could be greatly increased by the utilization of a pH-sensitive lipid composition or attachment of pH-sensitive fusogenic peptides to the surface of liposomes [66,67].

Folate offers many unique advantages as a targeting ligand for liposomes over antibodies. It is non-immunogenic, is not prone to denaturation, has good stability, has simple and defined conjugation chemistry, is highly specific for tumors, is available in large quantities, and is compatible with the use of organic solvent during preparation. Due to the relative large size (50–200 nm in diameter) of liposomes and their tendency to passively accumulate in tumor tissues, it

is difficult to predict whether the incorporation of a targeting ligand could further improve liposome uptake by solid tumors in terms of overall tumor accumulation. Previous studies with immunoliposomes were sparse and results have been mixed. While there was generally very limited increase in tumor accumulation due to targeting based on percent injected dose per gram of tumor tissue, significantly improved therapeutic efficacy has been observed in some cases. For example, intravenously administered anti-HER2 immunoliposomes carrying doxorubicin have shown significantly improved tumor penetration, intracellular accumulation, and antitumor activity compared with non-targeted control liposomes, which primarily accumulated in the interstitial space [57]. Therefore, beneficial effects of liposome targeting are likely found at the cellular and subcellular levels.

## 5. Delivery of gene transfer vectors

Gene therapy presents a promising approach for the treatment of human diseases. A series of potential therapeutic DNA constructs for cancer gene therapy have been developed including those coding for suicide genes, cytokines, tumor-suppressor genes, antisense genes/oligonucleotides, and ribozymes. The clinical application of gene therapy, however, has been limited by the availability of suitable gene transfer vectors. An ideal gene transfer vector should be safe, stable, cost-effective to produce in clinically relevant quantities, and capable of efficient and tissue-specific gene delivery.

### 5.1. Viral vectors

Most of the gene transfer vectors currently under clinical evaluation are based on genetically engineered replication-defective viruses, e.g., retroviral vectors, adenoviral vectors, and adeno-associated viral vectors. While often quite efficient in gene transfer, viral vectors suffer from oncogenic risks associated with random insertion into the host genome (for retro- and adeno-associated viruses) and elicitation of a host immune response, resulting in the elimination of the transduced cells and preventing repeated use of the vector due to induction of

neutralizing antibodies (for adenoviruses). There is also the risk of genetic recombination inside the cell that leads to the generation of infectious viral particles. Viral vectors are also limited in gene-carrying capacity and are challenging to manufacture and purify in clinically relevant quantities. Due to these limitations, there has been considerable interest in the development of non-viral vectors based on synthetic components. Viral vectors can be targeted through attachment of a ligand. Douglas et. al. showed that folate coupled to F<sub>ab</sub> fragments against the adenoviral fiber was able to redirect the viral vector to specifically transfect cells that are positive for the FR [80].

### 5.2. Non-viral vectors

Existing synthetic non-viral vectors often consist of DNA complexes of cationic liposomes and/or cationic polymers [68,69]. They have the common advantages of being non-immunogenic, easy to produce, and non-restrictive on the size of the DNA molecule it carries. The structure and gene transfer activity of these complexes is dependent on both vector composition and the formulation method. Monovalent cationic lipids form a different type of DNA complex (lipoplexes) than cationic lipids with a multivalent cationic head group or when cationic lipid is used in conjunction with a polycation (lipopolyplexes). Under freeze-fracture electron microscopy, monovalent cationic lipid/DNA complexes (lipoplexes) often appears as “spaghetti-like” structures consisting of lipid-coated DNA double helix strands. The multivalent cationic lipid/DNA complexes and lipopolyplexes are often more compact in size and more active in gene transfer (in the absence of serum) [70]. However, the transfection activity of these complexes is usually highly sensitive to the presence of serum in the culture media. The gene transfer efficiencies of non-viral vectors are often much lower than viral vectors, especially when administered in vivo. Also, the performance of these vectors is quite variable depending on the route of injection. Major problems with existing non-viral vectors are vector aggregation, non-specific tissue uptake, rapid systemic clearance, and undesirable organ distribution patterns determined by the first-pass effect.

A common flaw in the design of positively charged DNA complexes for gene transfer is that the formulations are usually optimized for gene transfer in vitro. In tissue culture, cellular uptake of the DNA complexes is mediated by charge interaction between the positively charged DNA complexes and the negatively charged cellular membrane. This interaction further induces cellular internalization via endocytosis of the DNA complexes. However, when administered into the blood stream, the DNA complexes are placed in an environment rich in negatively charged plasma proteins and circulating blood cells. The positive charge of the complex is instantly neutralized and the complexes aggregated and accumulate in the lung by pulmonary embolism and/or by the liver due to first pass effect. Since the positive charge of the DNA complexes is primarily contributing to the extent of vector aggregation and is not likely to be available for target cell interaction, negatively charged DNA complexes and naked DNA are often found to be more active than the in vitro optimized gene transfer formulations, which invariably are positively charged. The fate of the DNA complexes is also highly dependent on the route of administration. Intranasal, intraperitoneal, and intratumoral administration expose the vector to different biological environments, therefore, different vector formulations may be needed for optimal gene delivery efficiency for differing methods of injection.

Attachment of a targeting ligand and/or components that promote endosome escape has shown to greatly improve the gene transfer efficiency of nonviral vectors [71–76]. In addition, studies showed that folate-conjugated polylysine coupled to inactivated viral particles mediated efficient receptor-specific gene delivery in vitro [75,76].

### 5.3. Anionic liposome-entrapped polyplexes (LPDII)

Neutral or anionic liposomes have also been evaluated for plasmid DNA delivery. However, they suffer from low DNA entrapment efficiency (usually less than 20%) due to the large molecular size and heavy negative charge of plasmid DNA. Protocols for DNA entrapment into these liposomes are often cumbersome and require the use of high lipid concentrations for high DNA entrapment, which also

leads to the generation of a large number of empty vesicles. Although anionic pH-sensitive immunoliposomes have been shown to deliver DNA into lymphoma ascites tumors, their practical usefulness in gene therapy has yet to be demonstrated.

In the LPDII system, DNA is first complexed to polylysine to form a cationic complex and then mixed with anionic pH-sensitive liposomes carrying a receptor targeting ligand to form liposome-entrapped polyplex particles by a charge-mediated self-assembly process [77]. Folic acid has been used as the targeting ligand for the receptor-mediated gene delivery to tumor cells.

Folate-targeted pH-sensitive liposomes entrapping polyplexes (folate-LPDII) were capable of highly efficient and receptor-specific gene transfer. Folate-LPDII particles were prepared by mixing anionic liposomes composed of dioleoylphosphatidylethanolamine (DOPE)/cholesteryl hemisuccinate (CHEMS)/folate-PEG-DOPE (60:40:0.1, m/m) and the cationic DNA/polylysine (1:0.75, w/w) complexes. Vector self-assembly was mediated by charge interactions. The resulting vector particles were spherical and had a mean diameter of 70–80 nm as determined by negative-stain electron microscopy. The vector particles could be formulated at a variety of anionic lipid/DNA polyplex charge ratios. At low lipid/polyplex ratios, the overall charge of the vector was positive, cellular uptake and transfection were mediated by non-specific charge interaction. Meanwhile, at high lipid/polyplex ratios, the vector was negatively charged and required the presence of a targeting ligand and transfected only cells that express the corresponding receptor. The negatively charged particles were particularly interesting due to their potential for improved compatibility with blood components and tissue-specific targeted gene delivery.

Folate-targeted LPDII vectors carrying a firefly luciferase reporter gene driven by the Rous sarcoma viral promoter (pRSVL) have been evaluated for their *in vitro* gene transfer activity in cultured KB cells. DNA/polylysine polyplexes alone showed very little transfection activity. High transfection activities were observed with folate-LPDII vectors formed at lipid/DNA ratios of 4, 6, 10, and 12 [77]. But the transfection activity of only vectors formed at high lipid/DNA ratios (10 and 12) could be

partially blocked by 1 mM free folic acid [77]. Complete free folate blocking was not expected since these vectors, similar in size to large unilamellar liposomes, are likely to interact with FR-bearing cells via multivalent binding, resulting in much greater cellular affinity. These data suggest that tumor cell transfection by folate-LPDII is mediated by the FR at lipid/DNA ratios that give anionic particles but not at ratios that produce cationic particles, due to the presence of overriding charge mediated cellular uptake. The transfection activity correlates well with the level of  $^{125}\text{I}$ -labeled DNA uptake by these same cells [77]. The role of the FR was further confirmed by duplicating the above studies in the receptor-negative CHO cells, where transfection was only observed with cationic folate-LPDII vectors where uptake is mediated by charge interaction [77].

The study further showed that the pH-sensitive liposomal composition was essential for the observed transfection pattern. pH-sensitive liposomes are generally composed of a fusogenic lipid, usually DOPE, and a pH-sensitive component that is anionic at extracellular pH but becomes charge neutral at the acidic endosomal pH, such as CHEMS. DOPE is a cone-shaped lipid molecule that favors the transition from bilayer to hexagonal II phase thereby facilitating membrane fusion and/or disruption. This lipid phase transition is blocked by the presence of the negatively charged CHEMS. Upon protonation at endosomal pH, CHEMS becomes uncharged, therefore, can no longer stabilize the bilayer structure and allows for DOPE-mediated membrane fusion. Replacing DOPE with the cylindrical lipid DOPC completely abolishes transfection activity of the folate-LPDII vectors [77]. Also, replacing CHEMS with DOPS, a lipid that does not become extensively protonated at endosomal pH, eliminates transfection activity at high lipid/DNA ratios where negatively charged vectors formed [77].

The structure of folate-targeted LPDII has been studied by negative-stain electron microscopy. The vector particles appeared spherical and consist of a high electron density core representing the DNA polyplex, and a low electron density coat representing lipidic components. When dual isotopically labeled folate-LPDII particles were fractionated on a sucrose gradient, most of the lipid (labeled with  $^3\text{H}$ )

co-migrates with the plasmid DNA (labeled with  $^{125}\text{I}$ ) as an intermediate density band (DNA polyplexes have high density and liposomes have low density).

Under optimal in vitro conditions, negatively charged folate-LPDII vectors are more efficient in transfection than lipoplexes and are specific for receptor-positive tumor cells. The plasmid DNA in LPDII particles is also more optimally condensed compared to cationic liposome lipoplexes resulting in the formation of smaller and colloiddally more stable particles. The negatively charged LPDII particles should also be more compatible with the in vivo environment, which is abundant with negatively charged components. Compared to anionic liposomes containing passively entrapped DNA, LPDII formulation has the advantage of quantitative DNA incorporation and having high transfection activity without the contamination of empty lipid vesicles. The main limitation of existing LPDII formulation is the high level of serum sensitivity. A possible explanation is that the fusogenic activity of DOPE is inhibited by the presence of serum. Further improvements are needed for LPDII formulations to be used for in vivo gene transfer. For in vivo applications, a potential limitation is clearance by the reticuloendothelial system (RES); however, this may be partially overcome by coating vector particles with polyethyleneglycol (PEG). This strategy has previously been applied to produce longcirculating sterically stabilized liposomes.

Folate has also been conjugated to polyethylenimine (PEI, branched polymer,  $M_r \sim 60$  kDa) via a PEG linker. Polyethylenimine (PEI), linear or branched, is a cationic polymer ideally suited for the formation of compact charge complexes with plasmid DNA. In addition to its DNA condensing properties, this polymer also possess endosomallytic activities due to its strong buffering capacity at endosomal acidic pH. In this study, folate conjugates of polyethylenimine were synthesized and evaluated for their ability to mediate receptor-specific gene transfer in vitro. The transfection efficiency of the folate-PEG-PEI/DNA complexes was highly dependent on the PEI nitrogen to DNA phosphate (N/P) ratio, and was partially receptor-dependent [78,79]. This conjugate is simpler than the LPDII system and produces DNA complexes of smaller sizes, therefore,

may be potentially useful for in vivo tumor cell-specific gene delivery.

Furthermore, antisense oligodeoxynucleotides have been specifically delivered to tumor cells in vitro via direct conjugation to folate [81]. Folate was attached to the 3' terminus of an anti-c-fos oligodeoxynucleotide. The cellular uptake in cells, which overexpress the FR, was determined to be approximately eightfold higher with the folate-conjugated oligo compared to the oligo alone. The folate-conjugated oligo also exhibited a much greater tumor inhibitory effect.

## 6. Delivery of protein toxins

Protein toxin, including plant ribosome inactivating proteins and bacterial toxins, have been conjugated to folate and shown to be effectively kill cells overexpressing the FR without damaging the surrounding normal cells [82]. This approach is attractive due to the extreme potency of these toxins to cause cell death. Usually, delivery of a few hundred molecules per cell is sufficient to ensure cellular death. This is very important for targeted delivery systems where the capacity for targeting is limited by the number of receptors on the target cell.

Momordin, a ribosome-inactivating toxin, was conjugated to folate and was utilized in a co-culture with malignant and normal cell lines in vitro [83,84]. The momordin-folate treatment resulted in the selective killing of the malignant cells without damaging the normal cells. The  $\text{IC}_{50}$  for the folate conjugates was reduced to  $10^{-9}$  M. In addition, the momordin-folate did not significantly affect the rate of proliferation of the normal cells at the concentrations tested [84].

Other folate-conjugates, including folate-truncated *Pseudomonas* exotoxin and folate-truncated diphtheria toxin, have also been shown to selectively kill malignant cell lines in co-cultures [85]. LysPE38-folate (a truncated *Pseudomonas* exotoxin-folate) conjugate killed malignant cells 6 times faster and 10 times more potent than the momordin-folate conjugate [85]. This is due to the presence of a translocation domain, which allows for the efficient endosomal escape of the folate conjugates following receptor binding and endocytosis.

Folate conjugated protein toxins are significantly smaller than the corresponding immunotoxins. This should lead to more favorable pharmacokinetics and reduced immunogenicity.

### 6.1. Delivery of immunotherapy agents

Immunotherapy via receptor targeting presents yet another promising approach for the treatment of tumors. A number of strategies are currently being explored, including the use of humanized anti-FR antibody, chimeric anti-FR transfected tumor-infiltrating lymphocytes, bispecific antibodies against the T-cell receptor, and interleukin-2 fusion protein.

Monoclonal antibodies directed against tumor-associated antigens have been shown to mediate lysis of tumor cells by effector immunocytes, such as macrophages, natural killer cells or monocytes. Humanized chimeric antibodies are often used instead of murine antibodies due to the variable Fc receptor affinity and undesirable human anti-mouse antibody (HAMA) response associated with the use of murine antibodies.

Humanized chimeric MOv18 and MOv19 monoclonal antibodies were generated and evaluated for lytic activity against FR-positive tumor cells [86]. An equal amount of lysis of the target ovarian cancer cell line (IGROV1) resulted when murine MOv19 was compared to the chimeric MOv19. Chimeric MOv18 resulted in higher levels and more consistent tumor lysis than murine MOv18. The chimeric analogs were found to bind FR with similar affinity and only one chimeric antibody was required per FR to achieve effective cell kill [86].

A chimeric MOv18 antibody/T-cell receptor construct, which consists of T-cell receptor-transmembrane and signaling chains fused to the variable domains from the MOv18 monoclonal antibody, was also evaluated for tumor immunotherapy [44]. C57BL6 mice carrying FR transfected 24JK-FBP cells were treated with tumor-infiltration lymphocytes transfected with the above chimeric construct [44]. A significant increase in survival resulted in mice treated with MOv-TIL (tumor-infiltrating lymphocytes) over those treated with saline, nontransduced TIL, or TIL transduced with a control antitrinitrophenol chimeric receptor gene. MOv-TIL

treatment also resulted in fewer lung metastases in mice injected intravenously with tumor cells [44].

MOv18-derived bispecific antibodies have also been investigated for potential use in tumor immunotherapy. Bispecific antibody OC/TR were constructed using MOv18 (recognizing the FR) and a monoclonal antibody against the T cell receptor (recognizing CD3). T lymphocytes retargeted using  $F_{(ab')_2}$  fragments of the bispecific monoclonal antibody OC/TR have been shown to lyse ovarian carcinoma cells [87,88]. In a clinical trial, the treatment of in vitro-activated autologous peripheral blood T lymphocytes retargeted with OC/TR combined with IL-2 were evaluated in 19 patients with ovarian cancer for potential therapeutic efficacy. Complete response, complete intraperitoneal response, stable disease, and progressive disease was shown in 3, 1, 7, and 5 patients, respectively. Complete responses lasted from 18 up to 26 months. In addition, the HAMA response was evident at the end of treatment in 21 of 25 patients; however, tumor regression was evident in this study when the bi-specific antibody-retargeted T lymphocytes were used [88].

Folate conjugated anti-T-cell receptor antibody fragment has been evaluated as an alternative to bispecific antibodies. The folate conjugate is smaller in size, easier to prepare, and is highly potent in mediating the lysis of tumor cells, which express either FR isoform [89,90]. The affinity of these folate/anti-T-cell receptor conjugates is found to be only one-tenth of the affinity of free folate [90].

Finally, interleukin 2 (IL-2) has been fused to a single-chain Fv of MOv19. This construct has been shown to specifically accumulate in tumors in a mouse tumor model and exhibit significant antitumor activity [91]. This approach provides local delivery of IL-2 without causing systemic toxicity.

## 7. Summary

In addition to the above mentioned areas, folate has been used in the targeting of chemotherapeutic agents [92] and paramagnetic magnetic resonance imaging contrast agents [91] with very promising results.

Efficacy of targeted drug delivery is greatly affected by the size of the drug conjugate or drug carrier. Larger constructs are often immunogenic, prone to RES uptake, have prolonged systemic circulation time, slow to extravasate, and exhibit significant passive targeting effects in solid tumors. Therefore, in order to achieve high tumor to normal tissue ratios, low molecular weight conjugates are greatly preferred. For the targeted delivery of large particles such as liposomes and gene transfer vectors, it is often difficult to demonstrate a significant increase in overall tumor accumulation. Targeting nonetheless may be beneficial at the cellular and/or subcellular level.

Folate as a targeting ligand offers many potential advantages over macromolecules such as monoclonal antibodies. These include: (1) small size of the targeting ligand, which often leads to favorable pharmacokinetic properties of the folate conjugates and reduced probability of immunogenicity thus allowing for repeated administration; (2) convenient availability and low cost; (3) relatively simple and defined conjugation chemistry; (4) high receptor affinity and lack of normal tissue receptor expression, thus high tumor tissue specificity; (5) the receptor/ligand complex can be induced to internalize via endocytosis, which may facilitate the cytosolic delivery of therapeutic agents, and (6) high frequency of overexpression among human tumors thus a wide range of tumor targets. Therefore, folate-based targeting systems show great potential for future clinical diagnostic and therapeutic applications.

## References

- [1] I.G. Campbell, T.A. Jones, W.D. Foulkes, J. Trowsdale, Folate-binding protein is a marker for ovarian cancer, *Cancer Res.* 51 (1991) 5329–5338.
- [2] L.R. Coney, A. Tomaselli, L. Carayannopoulos et al., Cloning of a tumor-associated antigen: MOv18 and MOv19 antibodies recognize a folate-binding protein, *Cancer Res.* 51 (1991) 6125–6132.
- [3] W.A. Franklin, M. Waintrub, D. Edwards et al., New anti-lung-cancer antibody cluster 12 reacts with human folate receptors present on adenocarcinoma, *Int. J. Cancer* 8 (1994) 89–95.
- [4] P. Garin-Chesa, I. Campbell, P. Saigo, J. Lewis, L. Old, W. Rettig, Trophoblast and ovarian cancer antigen LK26. Sensitivity and specificity in immunopathology and molecular identification as a folate-binding protein, *Am. J. Path.* 142 (1993) 557–567.
- [5] J. Holm, S.I. Hansen, M. Hoier-Madsen, K. Sondergaard, M. Bzorek, Folate receptor of human mammary adenocarcinoma, *APMIS* 102 (1994) 413–419.
- [6] W. Rettig, P. Garin-Chesa, H. Beresford, H. Oettgen, M. Melamed, L. Old, Cell-surface glycoproteins of human sarcomas: differential expression in normal and malignant tissues and cultured cells, *Proc. Natl. Acad. Sci. USA* 85 (1988) 3110–3114.
- [7] J.F. Ross, P.K. Chaudhuri, M. Ratnam, Differential regulation of folate receptor isoforms in normal and malignant tissues in vivo and in established cell lines – Physiologic and clinical applications, *Cancer* 73 (1994) 2432–2443.
- [8] S.D. Weitman, R.H. Lark, L.R. Coney et al., Distribution of the folate receptor GP38 in normal and malignant cell lines and tissues, *Cancer Res.* 52 (1992) 3396–3401.
- [9] J.A. Reddy, L.S. Haneline, E.F. Srour, A.C. Antony, D.W. Clapp, P.S. Low, Expression and functional characterization of the beta-isoform of the folate receptor on CD34+ cells, *Blood* 93 (1999) 3940–3948.
- [10] A.C. Antony, Folate receptors, *Ann. Rev. Nutr.* 16 (1996) 501–521.
- [11] X. Wang, F. Shen, J.H. Freisheim, L.E. Gentry, M. Ratnam, Differential stereospecificities and affinities of folate receptor isoforms for folate compounds and antifolates, *Biochem. Pharmacol.* 44 (1992) 1898–1901.
- [12] K.M. Maziarz, H.L. Monaco, F. Shen, M. Ratnam, Complete mapping of divergent amino acids responsible for differential ligand binding of folate receptors alpha and beta, *J. Biol. Chem.* 274 (1999) 11086–11091.
- [13] R.G.W. Anderson, B.A. Kamen, K.G. Rothberg, S.W. Lacey, Potocytosis: sequestration and transport of small molecules by caveolae, *Science* 255 (1992) 410–411.
- [14] E.J. Smart, C. Mineo, R.G. Anderson, Clustered folate receptors deliver 5-methyltetrahydrofolate to cytoplasm of MA104 cells, *J. Cell Biol.* 134 (1996) 1169–1177.
- [15] S. Miotti, M. Bagnoli, F. Ottone, A. Tomasetti, M.I. Colnaghi, S. Canevari, Simultaneous activity of two different mechanisms of folate transport in ovarian carcinoma cell lines, *J. Cell. Biochem.* 65 (1997) 479–491.
- [16] J.F. Ross, H. Wang, F.G. Behm et al., Folate receptor type beta is a neutrophilic lineage marker and is differentially expressed in myeloid leukemia, *Cancer* 85 (1999) 348–357.
- [17] F. Bottero, A. Tomasetti, S. Canevari, S. Miotti, S. Menard, M.I. Calnagi, Gene transfection and expression of the ovarian carcinoma marker folate binding protein on NIH/3T3 cells increases cell growth in vitro and in vivo, *Cancer Res.* 53 (1993) 5791–5796.
- [18] C.A. Luhrs, C.A. Raskin, R. Durbin et al., Transfection of a glycosylated phosphatidylinositol-anchored folate-binding protein complementary DNA provides cells with the ability to survive in low folate medium, *J. Clin. Invest.* 90 (1992) 840–847.
- [19] X.L. Sun, B.R. Murphy, Q.J. Li et al., Transduction of folate receptor cDNA into cervical carcinoma cells using recombi-

- nant adeno-associated virions delays cell proliferation in vitro and in vivo, *J. Clin. Invest.* 96 (1995) 1535–1547.
- [20] G. Toffoli, C. Cerniglio, A. Russo, A. Gallo, M. Bagnoli, M. Boiocchi, Overexpression of folate binding protein in ovarian cancers, *Int. J. Cancer* 74 (1997) 193–198.
  - [21] R.J. Lee, P.S. Low, Folate-targeted liposomes for drug delivery. Forum on liposome targeting, *J. Liposome Res.* 7 (1997) 455–466.
  - [22] R.J. Lee, P.S. Low, Folate as a targeting device for protein utilizing folate receptor-mediated endocytosis, drug targeting, in: G.E. Francis, C. Delgado (Eds.), *Series on Methods in Molecular Medicine*, 25 (1999).
  - [23] S. Wang, P.S. Low, Folate-mediated targeting of antineoplastic drugs, imaging agents, and nucleic acids to cancer cells, *J. Control. Rel.* 53 (1998) 39–48.
  - [24] J.A. Reddy, P.S. Low, Folate-mediated targeting of therapeutic and imaging agents to cancers, *Crit. Rev. Ther. Drug Carrier Syst.* 15 (1998) 587–627.
  - [25] B.A. Gruner, S.D. Weitman, The folate receptor as a potential therapeutic anticancer target, *Invest. New Drugs* 16 (1998) 205–219.
  - [26] T.M. Trippett, J.R. Bertino, Therapeutic strategies targeting proteins that regulate folate and reduced folate transport, *J. Chemother.* 11 (1999) 3–10.
  - [27] C.P. Leamon, P.S. Low, Delivery of macromolecules into living cells: a method that exploits folate receptor endocytosis, *Proc. Natl. Acad. Sci. USA* 88 (1991) 5572–5576.
  - [28] C.P. Leamon, P.S. Low, Membrane folate-binding proteins are responsible for folate-protein conjugate endocytosis into cultured cells, *Biochem. J.* 291 (1993) 855–860.
  - [29] F. Crippa, G.L. Buraggi, E. Di Re et al., Radioimmunoscinigraphy of ovarian cancer with the MOv18 monoclonal antibody, *Eur. J. Cancer* 27 (1991) 724–729.
  - [30] F. Crippa, G. Bolis, E. Seregni et al., Single-dose intraperitoneal radioimmunotherapy with the murine monoclonal antibody 1-131 MOv18: clinical results in patients with minimal residual disease of ovarian cancer, *Eur. J. Cancer* 31A (1995) 686–690.
  - [31] G. Paganelli, C. Belloni, P. Magnani et al., Two-step tumour targeting in ovarian cancer patients using biotinylated monoclonal antibodies and radioactive streptavidin, *Eur. J. Nucl. Med.* 19 (1992) 322–329.
  - [32] P. Casalini, E. Luisson, S. Menard, M.I. Colnaghi, G. Paganelli, S. Canevari, Tumor pretargeting: role of avidin/streptavidin on monoclonal antibody internalization, *J. Nucl. Med.* 38 (1997) 1378–1381.
  - [33] D. Front, O. Israel, The role of Ga-67 scintigraphy in evaluating the results of therapy of lymphoma patients, *Semin. Nucl. Med.* 25 (1995) 60–71.
  - [34] A.E. van Leeuwen-Stok, A.M. Drager, G.J. Schuurhuis, A.W. Platier, G.J. Teule, P.C. Huijgens, Gallium 67 in the human lymphoid cell line U-715: Uptake, cytotoxicity, and intracellular localization, *Int. J. Radiat. Biol.* 64 (1993) 749–759.
  - [35] M.H. Sohn, B.J. Jones, J.H.J. Whiting, F.L. Datz, R.E. Lynch, K.A. Morton, Distribution of gallium-67 in normal and hypotransferrinemic tumor-bearing mice, *J. Nucl. Med.* 34 (1993) 2135–2143.
  - [36] D.R. Vera, Gallium-labeled deferoxamine-galactosyl-neoglycoalbumin: A radiopharmaceutical for regional measurement of hepatic receptor biochemistry, *J. Nucl. Med.* 33 (1992) 1160–1166.
  - [37] M.A. Green, Metal radionuclides in diagnostic imaging by positron emission tomography (PET), *Adv. Metals Med.* 1 (1993) 75–114.
  - [38] P.M. Smith-Jones, B. Stolz, C. Bruns et al., Gallium-67/gallium-68-[DFO]-octreotide – a potential radiopharmaceutical for PET imaging of somatostatin receptor-positive tumors: Synthesis and radiolabeling in vitro and preliminary in vivo studies, *J. Nucl. Med.* 35 (1994) 317–325.
  - [39] S. Wang, R.J. Lee, C.J. Mathias, M.A. Green, P.S. Low, Synthesis, purification, and tumor cell uptake of <sup>67</sup>Ga-deferoxamine-folate, a potential radiopharmaceutical for tumor imaging, *Bioconj. Chem.* 7 (1996) 56–62.
  - [40] C.J. Mathias, S. Wang, R.J. Lee, D.J. Waters, P.S. Low, M.A. Green, Tumor-selective radiopharmaceutical targeting via receptor-mediated endocytosis of gallium-67-deferoxamine-folate, *J. Nucl. Med.* 37 (1996) 1003–1008.
  - [41] C.J. Mathias, S. Wang, D.J. Waters, P.S. Low, M.A. Green, Receptor-mediated targeting of Ga-67-deferoxamine-folate to folate receptor positive human KB tumor xenografts, *Nucl. Med. Biol.* 26 (1999) 23–25.
  - [42] S. Wang, J. Luo, D.A. Lantrip et al., Design and synthesis of In-111-DTPA-folate for use as a tumor-targeted radiopharmaceutical, *Bioconj. Chem.* 8 (1997) 673.
  - [43] C.J. Mathias, S. Wang, D.J. Waters, J.J. Turek, P.S. Low, M.A. Green, Indium-111-DTPA-folate as a potential folate-receptor-targeted radiopharmaceutical, *J. Nucl. Med.* 39 (1998) 1579–1585.
  - [44] P. Hwu, J.C. Yang, Y.R. Cowherd et al., In vivo antitumor activity of T cells redirected with chimeric antibody/T-cell receptor genes, *Cancer Res.* 55 (1995) 3369–3373.
  - [45] W. Guo, G.H. Hinkle, R.J. Lee, <sup>99m</sup>Tc-HYNIC-folate a novel receptor-based targeted radiopharmaceutical for tumor imaging, *J. Nucl. Med.* 40 (1999) 1563–1569.
  - [46] S. Ilgan, D.J. Yang, T. Higuchi et al., Tc-99m-ethyl-enedicysteine-folate: a new tumor imaging agent. Synthesis, labeling and evaluation in animals, *Cancer Biother. Radiopharm.* 13 (1998) 427–435.
  - [47] C.J. Mathias, D. Hubers, D.P. Trump, P.S. Low, M.A. Green, Synthesis of Tc-99m-DTPA-folate and preliminary evaluation as a folate receptor-targeted radiopharmaceutical, in: *Soc. Nucl. Med. 44th Ann. Meeting*, San Antonio, TX, 1997.
  - [48] D. Lichtenberg, Liposomes: Preparation, characterization, and preservation, *Methods Biochem. Anal.* 33 (1988) 337–462.
  - [49] G. Gregoriadis, A.T. Florence, Liposomes in drug delivery-clinical, diagnostic and ophthalmic potential, *Drugs* 45 (1993) 15–28.
  - [50] N. Garelli, P. Vierling, Incorporation of new amphiphilic perfluoroalkylated bipyridine platinum and palladium complexes into liposomes: Stability and structure-incorporation relationships, *Biochim. Biophys. Acta* 1127 (1992) 41–48.
  - [51] D.C. Litzinger, L. Huang, Phosphatidylethanolamine liposomes: Drug delivery, gene transfer and immunodiagnostic applications, *Biochim. Biophys. Acta* 1113 (1992) 201–227.

- [52] L.D. Mayer, L.C.L. Tai, D.S.C. Ko et al., Influence of vesicle size, lipid composition, and drug-to-lipid ratio on the biological activity of liposomal doxorubicin in mice, *Cancer Res.* 49 (1989) 5922–5930.
- [53] A. Gabizon, R. Catane, B. Uzieli et al., Prolonged circulation time and enhanced accumulation in malignant exudates of doxorubicin encapsulated in polyethylene-glycol coated liposomes, *Cancer Res.* 54 (1994) 987–992.
- [54] L.D. Leserman, J.N. Weinstein, R. Bhumenthal, W.D. Terry, Receptor-mediated endocytosis of antibody-opsonized liposomes by tumor cells, *Proc. Natl. Acad. Sci. USA* 77 (1980) 4089–4093.
- [55] N. Berinstein, K.K. Matthay, D. Papahadjopoulos, R. Levy, B.I. Sikic, Antibody-directed targeting of liposomes to human cell lines: Role of binding and internalization on growth inhibition, *Cancer Res.* 47 (1987) 5954–5959.
- [56] P.G. Milhaud, P. Machy, B. Lebleu, L. Leserman, Antibody targeted liposomes containing poly(rl)-poly(rc) exert a specific antiviral and toxic effect on cells primed with interferons alpha/beta or gamma, *Biochim. Biophys. Acta* 987 (1989) 15–20.
- [57] J.W. Park, K. Hong, D.B. Kirpotin, O. Meyer, D. Papahadjopoulos, C. Benz, Anti-HER2 immunoliposomes for targeted therapy of human tumors, *Cancer Lett.* 118 (1997) 153–160.
- [58] D.C. Litzinger, L. Huang, Biodistribution and immunotargetability of ganglioside-stabilized dioleoylphosphatidylethanolamine liposomes, *Biochim. Biophys. Acta* 1104 (1992) 179–187.
- [59] A.L. Klivanov, K. Maruyama, A.M. Beckerleg, V.P. Torchilin, L. Huang, Activity of amphipathic poly(ethylene glycol)5000 to prolong the circulation time of liposomes depends on the liposome size and is unfavorable for immunoliposome binding to target, *Biochim. Biophys. Acta* 1062 (1991) 142–148.
- [60] D. Liu, L. Huang, pH-sensitive, plasma-stable liposomes with relatively prolonged residence in circulation, *Biochim. Biophys. Acta* 1022 (1990) 348–354.
- [61] R.J. Lee, P.S. Low, Delivery of liposomes into cultured KB cells via folate receptor-mediated endocytosis, *J. Biol. Chem.* 269 (1994) 3198–3204.
- [62] A. Gabizon, A.T. Horowitz, D. Goren et al., Targeting folate receptor with folate linked to extremities of poly(ethylene glycol)-grafted liposomes: in vitro studies, *Bioconj. Chem.* 10 (1999) 289–298.
- [63] R.J. Lee, P.S. Low, Folate-mediated tumor cell targeting of liposome-entrapped doxorubicin in vitro, *Biochim. Biophys. Acta* 1233 (1995) 134–144.
- [64] S. Wang, R.J. Lee, G. Cauchon, D.G. Gorenstein, P.S. Low, Delivery of antisense oligodeoxynucleotides against the human epidermal growth factor receptor into cultured KB cells with liposomes conjugated to folate via polyethylene glycol, *Proc. Natl. Acad. Sci. USA* 92 (1995) 3318–3322.
- [65] R.J. Lee, P.S. Low, Delivery of liposomes into cultured KB cells via folate receptor-mediated endocytosis, *J. Biol. Chem.* 269 (1994) 3198–3204.
- [66] R.J. Lee, S. Wang, M.J. Turk, P.S. Low, The effects of pH and intraliposomal buffer strength on the rate of liposome content release and intracellular drug delivery, *Biosci. Rep.* 18 (1998) 69–78.
- [67] N.K. Subbarao, R.A. Parente, F.C. Szoka, L. Nadasdi, K. Pongracz, pH-dependent bilayer destabilization by an amphipathic peptide, *Biochemistry* 26 (1987) 2964–2972.
- [68] K. Vogel, S. Wang, R.J. Lee, J. Chmielewski, P.S. Low, Peptide-mediated release of folate-targeted liposome contents from endosomal compartments, *J. Am. Chem. Soc.* 118 (1996) 1581–1586.
- [69] P.L. Felgner, T.R. Gadek, M. Holm et al., Lipofection: A highly efficient, lipid-mediated DNA-transfection procedure, *Proc. Natl. Acad. Sci. USA* 84 (1987) 7413–7417.
- [70] E. Wagner, M. Zenke, M. Cotten, H. Beug, M.L. Birnstiel, Transferrin-polycation conjugates as carriers for DNA uptake into cells, *Proc. Natl. Acad. Sci. USA* 87 (1990) 3410–3414.
- [71] J.P. Behr, B. Demeneix, J.P. Loeffler, J.P. Mutul, Efficient gene transfer into mammalian primary endocrine with lipopolyamine-coated DNA, *Proc. Natl. Acad. Sci. USA* 86 (1989) 6982.
- [72] E. Wagner, K. Zatloukal, M. Cotten, H. Kirkappos, K. Mechtler, D.T. Curiel, Coupling of adenovirus to transferrin-polylysine/DNA complexes greatly enhances receptor-mediated gene delivery and expression of transfected genes, *Proc. Natl. Acad. Sci. USA* 89 (1992) 6099–6103.
- [73] D.T. Curiel, E. Wagner, M. Cotten, M.L. Birnstiel, S. Agarwal, C.M. Li, High-efficiency gene transfer mediated by adenovirus coupled to DNA-polylysine conjugates, *Hum. Gene Ther.* 3 (1992) 147–154.
- [74] R.J. Cristiano, L.C. Smith, S.L.C. Woo, Hepatic gene therapy: Adenovirus enhancement of receptor-mediated gene delivery and expression in primary hepatocytes, *Proc. Natl. Acad. Sci. USA* 90 (1993) 2122–2126.
- [75] R.J. Cristiano, L.C. Smith, M.A. Kay, B.R. Brinkley, S.L. Woo, Hepatic gene therapy: Efficient gene delivery and expression in primary hepatocytes utilizing a conjugated adenovirus-DNA complex, *Proc. Natl. Acad. Sci. USA* 90 (1993) 11548–11552.
- [76] K.A. Mislick, J.D. Baldeschwieler, J.F. Kayyem, T.J. Meade, Transfection of folate-polylysine DNA complexes: Evidence for lysosomal delivery, *Bioconj. Chem.* 6 (1995) 512–515.
- [77] S. Gottschalk, R.J. Cristiano, L.C. Smith, S.L.C. Woo, Folate receptor mediated DNA delivery into tumor cells: perosomal disruption results in enhanced gene expression, *Gene Ther.* 1 (1994) 185–191.
- [78] R.J. Lee, L. Huang, Folate-targeted, anionic liposome-entrapped polylysine-condensed DNA for tumor cell-specific gene transfer, *J. Biol. Chem.* 271 (1996) 8481–8487.
- [79] R.J. Lee, L. Huang, Lipidic vector systems for gene transfer, *Crit. Rev. Ther. Drug Carrier Syst.* 14 (1997) 173–206.
- [80] W. Guo, R.J. Lee, Targeted gene delivery via the folate receptor, in: *Annu. Natl. Meeting of Am. Chem. Soc., Anaheim, CA, March, 1999, Abstract.*
- [81] J.T. Douglas, B.E. Rogers, M.E. Rosenfeld, S.I. Michael, M. Feng, D.T. Curiel, Targeting gene delivery by tropism-modified adenoviral vectors, *Nat. Biotech.* 14 (1996) 1574–1578.



- [82] S. Li, H.M. Deshmukh, L. Huang, Folate-mediated targeting of antisense oligodeoxynucleotides to ovarian cancer cells, *Pharm. Res.* 15 (1998) 1540–1545.
- [83] A.E. Frankel, Immunotoxin therapy of cancer, *Oncology* 7 (1993) 69–78.
- [84] C.P. Leamon, P.S. Low, Selective targeting of malignant cells with cytotoxin-folate conjugates, *J. Drug Targeting* 2 (1994) 101–112.
- [85] C.P. Leamon, P.S. Low, Cytotoxicity of momordin-folate conjugates in cultured human cells, *J. Biol. Chem.* 267 (1992) 24966–24971.
- [86] C.P. Leamon, I. Pastan, P.S. Low, Cytotoxicity of folate-pseudomonas exotoxin conjugates toward tumor cells, *J. Biol. Chem.* 268 (1993) 24847–24854.
- [87] L.R. Coney, D. Mezzananza, D. Sanborn, P. Casalini, M.I. Colnaghi, V.R. Zurawski, Chimeric murin-human antibodies directed against folate binding receptor are efficient mediators of ovarian carcinoma cell killing, *Cancer Res.* 54 (1994) 2448–2455.
- [88] S. Canevari, G. Stoter, F. Arienti et al., Regression of advanced ovarian carcinoma by intraperitoneal treatment with autologous T lymphocytes retargeted by a bispecific monoclonal antibody, *J. Natl. Cancer Inst.* 87 (1995) 1463–1469.
- [89] S. Canevari, D. Mezzananza, A. Mazzoni et al., Bispecific antibody targeted T cell therapy of ovarian cancer: Clinical results and future directions, *J. Hematother.* 4 (1995) 423–427.
- [90] D.M. Kranz, T.A. Patrick, K.E. Brigle, M.J. Spinella, E.J. Roy, Conjugates of folate and anti-T-cell-receptor antibodies specifically target folate receptor-positive tumor cells for lysis, *Proc. Natl. Acad. Sci. USA* 92 (1995) 9057–9061.
- [91] C.A. Ladino, R.V. Charm, L.A. Bourret, N.L. Kedersha, V.S. Goldmacher, Folate-maytansinoids: target-selective drugs of low molecular weight, *Int. J. Cancer* 73 (1997) 859–864.
- [92] C. Melani, M. Figini, D. Nicosia et al., Targeting of interleukin 2 to human ovarian carcinoma by fusion with a single-chain Fv of antifolate receptor antibody, *Cancer Res.* 58 (1998) 4146–4154.

## **$^{99m}\text{Tc}$ -Ethylenedicysteine-Folate: A New Tumor Imaging Agent. Synthesis, Labeling and Evaluation in Animals**

Seyfettin Ilgan, MD, David J. Yang, PhD, Tetsuya Higuchi, MD, PhD, Fereshteh Zareneyrizi, MD, Hikmet Bayhan, MD,<sup>1</sup> Dongfang Yu, MS, E. Edmund Kim, MD, and Donald A. Podoloff, MD  
Division of Diagnostic Imaging, Department of Nuclear Medicine, The University of Texas M.D. Anderson Cancer Center, Houston, Texas; and <sup>1</sup>Department of Nuclear Medicine, Gülhane Military Medical Academy and Medical Faculty, Ankara, Turkey.

*It is known that membrane folic acid receptors are responsible for cellular accumulation of folate and folate analogs such as methotrexate and overexpressed on various tumor cells. However, these receptors are highly restricted in normal differentiated tissues. Results of limited in vitro and in vivo animal studies suggest that folate receptors could be a potential target for tumor imaging. This study aimed to develop a  $^{99m}\text{Tc}$ -labeled folic acid using ethylenedicysteine (EC) as a chelator and evaluate its labeling efficiency and potential use as a tumor seeking agent. Tissue distribution of  $^{99m}\text{Tc}$ -EC-folate was determined in breast tumor-bearing rats at 20 min, 1, 2, and 4 h ( $n=3$ /time interval, 370 KBq/rat, i.v.). Blocking study was employed to determine receptor-mediated process;  $^{99m}\text{Tc}$ -EC-folate was co-administrated with 50 and 150  $\mu\text{mol/kg}$  of cold folic acid to tumor-bearing rats. Planar imaging and whole-body autoradiograms were performed. The data was compared to that using  $^{99m}\text{Tc}$ -EC (control). In animal studies, tumor/blood count density ratios at 20 min-4 h increased from  $0.81 \pm 0.09$  to  $1.23 \pm 0.13$  with  $^{99m}\text{Tc}$ -EC-folate. Conversely, these values showed time-dependent decrease from  $0.77 \pm 0.32$  to  $0.65 \pm 0.01$  with  $^{99m}\text{Tc}$ -EC in the same time period. Tumor/muscle and tumor/blood count density ratios significantly decreased with folic acid co-administrations. Planar images and autoradiograms confirmed that the tumors could be visualized clearly with  $^{99m}\text{Tc}$ -EC-folate.*

**Key Words:** tumor imaging, folate receptor, ethylenedicysteine,  $^{99m}\text{Tc}$

### **INTRODUCTION**

Improvement of scintigraphic tumor imaging is extensively determined by development of more tumor specific radiopharmaceuticals. Due to greater tumor

specificity, radiolabeled ligands as well as radiolabeled antibodies have opened a new era in scintigraphic detection of tumors and undergone extensive preclinical development and evaluation<sup>1</sup>. The radiolabeled ligands, such as pentetate and vasoactive intestinal peptide, bind to cell receptors some of which are overexpressed on tumor cells.<sup>2-6</sup> Since these ligands are not immunogenic and are cleared quickly from the plasma, receptor imaging would seem to be more promising compared to antibody imaging.

Address reprint requests to David J. Yang, Ph.D., The University of Texas MD Anderson Cancer Center, Department of Nuclear Medicine, Box 59, 1515 Holcombe Blvd., Houston, TX 77030 (Tel. 713-745-3368, Fax. 713-745-3372) E-mail Address: dyang@rpimail.mdacc.tmc.edu

Folic acid as well as antifolates such as methotrexate enter into cells via high affinity folate receptors (glycosylphosphatidylinositol-linked membrane folate-binding protein) in addition to classical reduced-folate carrier system.<sup>7-9</sup> Folate receptors (FRs) are overexpressed on many neoplastic cell types (e.g. lung, breast, ovarian, cervical, colorectal, nasopharyngeal, renal adenocarcinomas, malign melanoma and ependymomas), but primarily expressed only several normal differentiated tissues (e.g. choroid plexus, placenta, thyroid and kidney).<sup>8,10-16</sup> FRs have been used to deliver folate-conjugated protein toxins, drug/antisense oligonucleotides and liposomes into tumor cells overexpressing the folate receptors.<sup>17-22</sup> Furthermore, bispecific antibodies that contain anti-FR antibodies linked to anti-T cell receptor antibodies have been used to target T cells to FR-positive tumor cells and are currently in clinical trials for ovarian carcinomas.<sup>23-27</sup>

Similarly, this property has also been inspired to develop radiolabeled folate-conjugates, such as <sup>67</sup>Ga-deferoxamine-folate and <sup>111</sup>In-DTPA-folate, for imaging of folate receptor positive tumors.<sup>28-31</sup> Results of limited in vitro and in vivo studies with these agents suggest that folate receptors could be a potential target for tumor imaging.

Due to favorable physical characteristics as well as extremely low price, <sup>99m</sup>Tc have been preferred to label radiopharmaceuticals. Although it has been reported that DTPA-folate conjugate could be labeled with <sup>99m</sup>Tc effectively,<sup>32</sup> DTPA moiety does not chelate with <sup>99m</sup>Tc as stable as with <sup>111</sup>In.<sup>1</sup>

Bis-aminoethanethiol tetradentate ligands, also called diaminodithiol compounds, are known to form very stable Tc(V)O-complexes on the basis of efficient binding of the oxotechnetium group to two thiolsulphur and two amine nitrogen atoms.<sup>33,34</sup> <sup>99m</sup>Tc-L,L-ethylenedicysteine (<sup>99m</sup>Tc-EC) is the most recent and successful example of N<sub>2</sub>S<sub>2</sub> chelates.<sup>34-36</sup> EC, a new renal imaging agent, can be labeled with <sup>99m</sup>Tc easily and efficiently with high radiochemical purity and stability and is excreted through kidney by active tubular transport.<sup>34-40</sup>

This study aimed to develop an <sup>99m</sup>Tc-labeled folic acid using EC as a chelator and evaluate its labeling efficiency and potential use as a tumor seeking agent. Breast tumor-bearing rats were used for tissue distribution, gamma scintigraphy and whole-body autoradiograms, and results were compared to those <sup>99m</sup>Tc-EC (standard).

## MATERIALS AND METHODS

The NMR and mass spectral analysis were conducted at the University of Texas Health Science Center (Houston, TX). Nuclear magnetic resonance (NMR) spectra were recorded on a GE GN-500 Spectrometer. The mass data were obtained by fast atom bombardment on a Kratos MS 50 instrument (England). Elemental analysis was performed at Galbraith Laboratories, Inc. (Knoxville, TN). N-Hydroxysulfosuccinimide (Sulfo NHS) and 1-ethyl-3-(3-dimethylaminopropyl) carbodiimide-HCl (EDC) were purchased from Pierce Chemical Co (Radford, IL). All other chemicals were purchased from Aldrich Chemical Co (Milwaukee, WI). <sup>99m</sup>Tc-pertechnetate was obtained from a commercial <sup>99</sup>Mo/<sup>99m</sup>Tc generator (Ultratechnekow FM™, Mallinckrodt Diagnostica, Holland).

### Synthesis of EC

EC was prepared in a two-step synthesis according to the previously described methods.<sup>41,42</sup> The precursor, L-thiazolidine-4-carboxylic acid, was synthesized (m.p. 195°, reported 196-197°). EC was then prepared (m.p. 237°, reported 251-253°). The structure was confirmed by <sup>1</sup>H-NMR and fast-atom bombardment mass spectroscopy (FAB-MS).

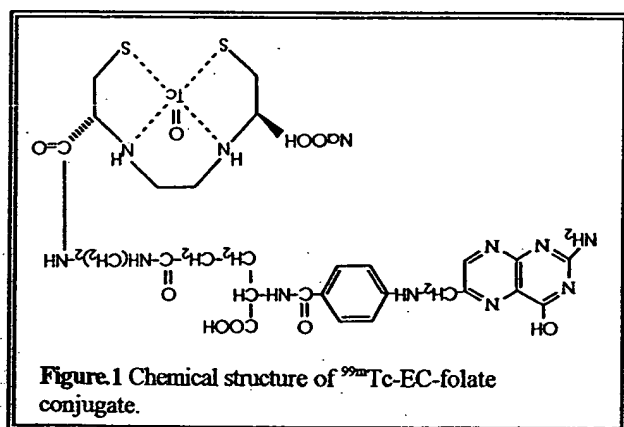
### Synthesis of Aminoethylamido Analogue of Folate (Folate-NH<sub>2</sub>)

Folic acid dihydrate (1 g, 2.0 mmol) was added in 10 ml of water. The pH value was adjusted to 2 using HCl (2 N). To this stirred solution, N-ethoxycarbonyl-2-ethoxy-1,2-dihydroquinoline (EEDQ, 1 g in 10 ml methanol, 4.0 mmol) and ethylenediamine (EDA, 1.3 ml, 18 mmol) were added slowly. The reaction mixture was stirred overnight at room temperature. The solvent was evaporated in vacuo. The product was precipitated in methanol (50 ml) and further washed with acetone (100 ml) to remove the unreacted EEDQ and EDA. The product was then freeze-dried and used without further purification. Ninhydrin (2% in methanol) spray indicated the positivity of amino group. The product weighed 0.6 g (yield 60%) as a yellow powder. m.p. of product: 250° (dec). <sup>1</sup>H-NMR (D<sub>2</sub>O) δ 1.97-2.27 (m, 2H, -CH<sub>2</sub> glutamate of folate), 3.05-3.40 (d, 6H, -CH<sub>2</sub>CONH(CH<sub>2</sub>)<sub>2</sub>NH<sub>2</sub>), 4.27-4.84 (m, 3H, -CH<sub>2</sub>-

pteridinyl, NH-CH-COOH glutamate), 6.68-6.70 (d, 2H, aromatic-CO), 7.60-7.62 (d, 2H, aromatic-N), 8.44 (s, 1H, pteridinyl). FAB MS  $m/z$  calcd for  $C_{21}H_{25}N_9O_5(M)^+$  483, found 483.21.

### Synthesis of Ethylenedicysteine-Folate Conjugate (EC-Folate)

To dissolve EC, NaOH (2N, 0.1 ml) was added to a stirred solution of EC (114 mg, 0.425 mmol) in water (1.5 ml). To this colorless solution, sulfo-NHS (92.3 mg, 0.425 mmol) and EDC (81.5 mg, 0.425 mmol) were added. Folate-NH<sub>2</sub> (205 mg, 0.425 mmol) was then added. The mixture was stirred at room temperature for 24 hours. The mixture was dialyzed for 48 hours using Spectra/POR molecularporous membrane with molecule cut-off at 500 (Spectrum Medical Industries Inc., Houston, TX). After dialysis, the product was freeze dried. The product weighed 116 mg (yield 35%). m.p. 195° (dec); <sup>1</sup>H-NMR (D<sub>2</sub>O) δ 1.98-2.28 (m, 2H, -CH<sub>2</sub> glutamate of folate), 2.60-2.95 (m, 4H and -CH<sub>2</sub>-SH of EC), 3.24-3.34 (m, 10H, -CH<sub>2</sub>-CO, ethylenediamine of folate and ethylenediamine of EC), 4.27-4.77 (m, 5H, -CH<sub>2</sub>-pteridinyl, NH-CH-COOH glutamate of folate and NH-CH-COOH of EC), 6.60-6.62 (d, 2H, aromatic-CO), 7.58-7.59 (d, 2H, aromatic-N), 8.59 (s, 1H, pteridinyl). Anal. calcd for  $C_{29}H_{37}N_{11}S_2O_8 Na_2(8H_2O)$ , FAB MS  $m/z$  (M)<sup>+</sup> 777.3 (free of water). C, 37.79; H, 5.75; N, 16.72; S, 6.95. Found:  $m/z$  (M)<sup>+</sup> 777.7 (20), 489.4 (100). C, 37.40; H, 5.42; N, 15.43; S, 7.58. The chemical structure of EC-folate is shown in Fig. 1.



### Radiolabelling of EC-Folate and EC with <sup>99m</sup>Tc

Radiosynthesis of <sup>99m</sup>Tc-EC-folate was achieved by adding required amount of <sup>99m</sup>Tc-pertechnetate into home-made kit containing the lyophilised residue of

TABLE.1  
Rf Values Determined by Radio-TLC (ITLC-SG) Studies

	System A*	System B†
<sup>99m</sup> Tc-EC-folate	0	1(>95%)
<sup>99m</sup> Tc-EC	0	1(>95%)
Free <sup>99m</sup> Tc	1	1
Reduced <sup>99m</sup> Tc	0	0

\* Acetone

† Ammonium Acetate (1M in water):Methanol (4:1)

EC-folate (3 mg), SnCl<sub>2</sub> (100 µg), Na<sub>2</sub>HPO<sub>4</sub> (13.5 mg), ascorbic acid (0.5 mg) and NaEDTA (0.5 mg). Final pH of preparation was 7.4. <sup>99m</sup>Tc-EC was also obtained by using home-made kit containing the lyophilised residue of EC (3 mg), SnCl<sub>2</sub> (100 µg), Na<sub>2</sub>HPO<sub>4</sub> (13.5 mg), ascorbic acid (0.5 mg) and NaEDTA (0.5 mg) at pH 10. Final pH of preparation was then adjusted to 7.4. Radiochemical purity was determined by TLC (ITLC SG, Gelman Sciences, Ann Arbor, MI) eluted with, respectively, acetone (system A) and ammonium acetate (1M in water):methanol (4:1) (system B). From radio-TLC (Bioscan, Washington, DC) analysis, the radiochemical purity was >95% for both radiopharmaceuticals. Radio-TLC data were summarized in Table.1.

### Stability Assay of <sup>99m</sup>Tc-EC-Folate

Stability of labeled <sup>99m</sup>Tc-EC-folate was tested in serum samples. Briefly, 740 KBq of 1 mg <sup>99m</sup>Tc-EC-folate was incubated in dog serum (200 µl) at 37 °C for 4 hours. The serum samples was diluted with 50% methanol in water and radio-TLC repeated at 20 min, 1, 2 and 4 hours as described above.

### Tissue Distribution Studies

The animal experiments were carried out in compliance with the relevant national laws relating to the conduct of animal experimentation. The animal protocol was approved by The University of Texas M. D. Anderson Institutional Animal Care and Use Committee (IACUC). Female Fischer 344 rats (150±25 g) (Harlan Sprague-Dawley, Indianapolis, IN) were inoculated subcutaneously with 0.1 ml of mammary tumor cells from the 13762 tumor cell line suspension (10<sup>6</sup> cells/rat, a tumor cell line specific to Fischer rats) into the hind legs using 25-gauge needles. Studies performed 14 to 17 days after

implantation when tumors reached approximately 1 cm diameter. Animals were anesthetized with ketamine (10-15 mg/rat, intraperitoneally) before each procedure.

In tissue distribution studies, each animal injected intravenously with 370-550 KBq of  $^{99m}\text{Tc}$ -EC-folate or  $^{99m}\text{Tc}$ -EC ( $n=3$ /time point). The injected mass of  $^{99m}\text{Tc}$ -EC-folate was 10  $\mu\text{g}$  per rat. At 20 min, 1, 2 and 4 h following administration of the radiopharmaceuticals, the anesthetized animals were sacrificed and the tumor and selected tissues were excised, weighed and counted for radioactivity by a gamma counter (Packard Instruments, Downers Grove, IL). The biodistribution of tracer in each sample was calculated as percentage of the injected dose per gram of tissue wet weight (%ID/g). Counts from a diluted sample of the original injectate were used for reference. Tumor/nontarget tissue count density ratios were calculated from the corresponding %ID/g values. Student-t test was used to assess the significance of differences between two groups.

In a separate experiment, blocking studies were performed to determine receptor-mediated process. In blocking studies,  $^{99m}\text{Tc}$ -EC-folate was co-administered (i.v.) with 50 and 150  $\mu\text{mol/kg}$  folic acid to tumor bearing rats ( $n=3$ /group). Animals were killed 1 h post-injection and data was collected in the same way as previously described.

### Scintigraphic Imaging and Autoradiography Studies

Scintigraphic images, using a gamma camera (Siemens Medical Systems, Inc., Hoffman Estates, IL)

equipped with medium-energy, parallel-hole collimator, were obtained 20 min, 1, 2 and 4 h after i.v. injection of 18.5 MBq of each radiotracer.

Whole-body autoradiogram were obtained by a quantitative image analyzer (Cyclone Storage Phosphor System, Packard, Meriden, CT). Following i.v. injection of 37 MBq of  $^{99m}\text{Tc}$ -EC-folate, animal killed at 1 h and body was fixed in carboxymethyl cellulose (4%). The frozen body was mounted onto a cryostat (LKB 2250 cryomicrotome) and cut into 100  $\mu\text{m}$  coronal sections. Each section was thawed and mounted on a slide. The slide was then placed in contact with multipurpose phosphor storage screen (MP, 7001480) and exposed for 15 h. The phosphor screen was excited by a red laser and resulting blue light that is proportional with previously absorbed energy was recorded.

## RESULTS

### Chemistry and Stability of $^{99m}\text{Tc}$ -EC-Folate

A simple, fast and high yield aminoethylamido and EC analogues of folate were developed. The structures of these analogues were confirmed by NMR and mass spectroscopic analysis. Radiosynthesis of EC-folate with  $^{99m}\text{Tc}$  was achieved with high (>95%) radiochemical purity.

$^{99m}\text{Tc}$ -EC-folate was found to be stable at 20 min, 1, 2 and 4 hours in dog serum samples.

### Biodistribution Study

Biodistribution studies showed that tumor/blood count density ratios at 20 min-4 h gradually increased for

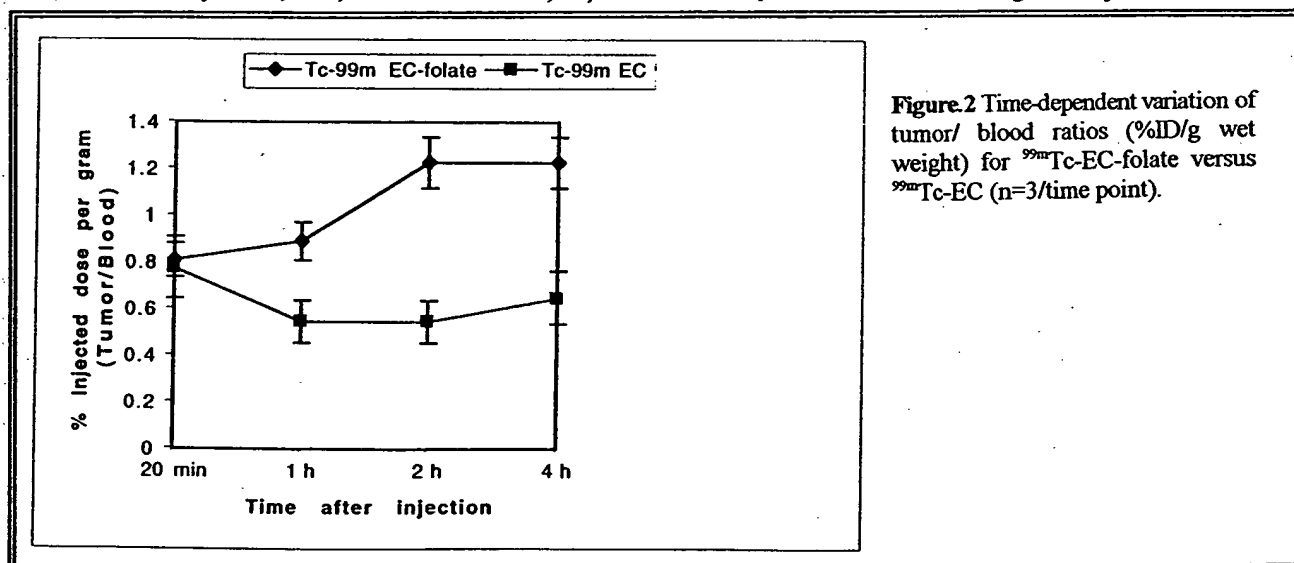


Figure 2 Time-dependent variation of tumor/ blood ratios (%ID/g wet weight) for  $^{99m}\text{Tc}$ -EC-folate versus  $^{99m}\text{Tc}$ -EC ( $n=3$ /time point).

$^{99m}\text{Tc}$ -EC-folate, whereas these values decreased for  $^{99m}\text{Tc}$ -EC in the same time period (Fig.2). %ID/g uptake values, tumor/blood and tumor/muscle ratios for  $^{99m}\text{Tc}$ -EC-folate and  $^{99m}\text{Tc}$ -EC were given in Table 2 and 3, respectively.

## DISCUSSION

The development of new tumor seeking agents is clinically desirable for detecting primary and metastatic lesions as well as monitoring tumor response

**TABLE.2**  
Biodistribution of  $^{99m}\text{Tc}$ -EC-folate in Breast Tumor-Bearing Rats

	% of injected $^{99m}\text{Tc}$ -EC-folate dose per organ or tissue			
	20 min	1 h	2 h	4 h
Blood	0.370±0.049	0.165±0.028	0.086±0.005	0.058±0.002
Lung	0.294±0.017	0.164±0.024	0.092±0.002	0.063±0.003
Liver	0.274±0.027	0.185±0.037	0.148±0.042	0.105±0.002
Stomach	0.130±0.002	0.557±0.389	0.118±0.093	0.073±0.065
Kidney	4.328±0.896	4.052±0.488	5.102±0.276	4.673±0.399
Thyroid	0.311±0.030	0.149±0.033	0.095±0.011	0.066±0.011
Muscle	0.058±0.004	0.0257±0.005	0.016±0.007	0.008±0.0005
Intestine	0.131±0.013	0.101±0.071	0.031±0.006	0.108±0.072
Urine	12.637±2.271	10.473±3.083	8.543±2.763	2.447±0.376
Tumor	0.298±0.033	0.147±0.026	0.106±0.029	0.071±0.006
Tumor/Blood	0.812±0.098	0.894±0.069	1.229±0.325	1.227±0.129
Tumor/Muscle	5.157±0.690	5.739±0.347	6.876±2.277	8.515±0.307

Values shown represent the mean±standart deviation of data from 3 animals.

**TABLE.3**  
Biodistribution of  $^{99m}\text{Tc}$ -EC in Breast Tumor-Bearing Rats

	% of injected $^{99m}\text{Tc}$ -EC dose per organ or tissue			
	20 min	1 h	2 h	4 h
Blood	0.435±0.029	0.273±0.039	0.211±0.001	0.149±0.008
Lung	0.272±0.019	0.187±0.029	0.144±0.002	0.120±0.012
Liver	0.508±0.062	0.367±0.006	0.286±0.073	0.234±0.016
Stomach	0.136±0.060	0.127±0.106	0.037±0.027	0.043±0.014
Kidney	7.914±0.896	8.991±0.268	9.116±0.053	7.834±1.018
Thyroid	0.219±0.036	0.229±0.118	0.106±0.003	0.083±0.005
Muscle	0.060±0.006	0.043±0.002	0.028±0.009	0.019±0.001
Intestine	0.173±0.029	0.787±0.106	0.401±0.093	0.103±0.009
Urine	9.124±0.808	11.045±6.158	13.192±4.505	8.693±2.981
Tumor	0.342±0.163	0.149±0.020	0.115±0.002	0.096±0.005
Tumor/Blood	0.776±0.322	0.544±0.004	0.546±0.010	0.649±0.005
Tumor/Muscle	5.841±3.253	3.414±0.325	4.425±1.397	5.093±0.223

Values shown represent the mean±standart deviation of data from 3 animals.

In blocking studies, tumor/muscle and tumor/blood count density ratios were significantly decreased ( $p<0.01$ ) with folic acid co-administrations (Fig.3).

### Scintigraphic Imaging and Autoradiography Studies

Scintigraphic images obtained at different time points showed visualization of tumor in  $^{99m}\text{Tc}$ -EC-folate injected group. Contrary, there was no apparent tumor uptake in  $^{99m}\text{Tc}$ -EC injected group (Fig.4). Both radiotracer showed evident kidney uptake in all images. Autoradiograms performed at 1 h after injection of  $^{99m}\text{Tc}$ -EC-folate clearly demonstrated tumor activity (Fig.5).

to therapy. None of the contemporary imaging modalities provides complete diagnostic capability because the diagnosis of cancer requires pathologic examination.<sup>43</sup> Therefore, in designing new tumor agents primary concern should be differentiation of benign pathologies from malign ones in order to help clinician for screening asymptomatic patients as well as staging and monitoring therapy. In this aspect, both radiolabeled ligands to specific receptors on cell surfaces and radiolabeled antibodies to specific cell surface epitopes seem to provide new opportunities to oncological nuclear medicine. Immunogenicity and relatively poor target/nontarget ratio because of prolonged circulation are disadvantages for antibody

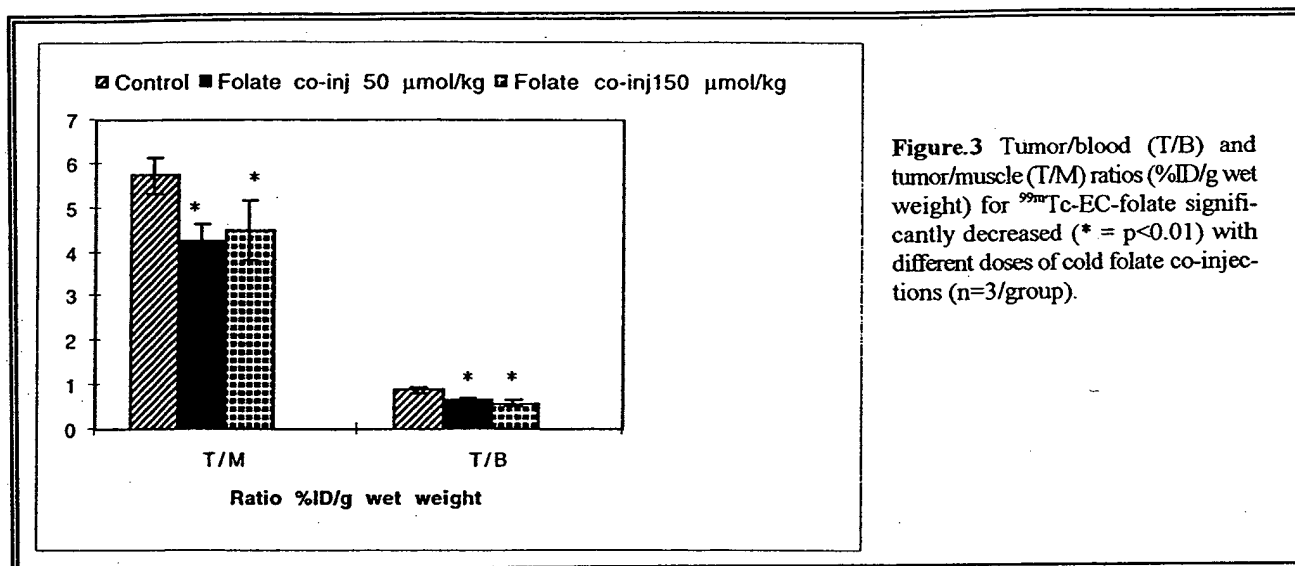


**Figure 3** Tumor/blood (T/B) and tumor/muscle (T/M) ratios (%ID/g wet weight) for  $^{99\text{m}}\text{Tc}$ -EC-folate significantly decreased (\* =  $p < 0.01$ ) with different doses of cold folate co-injections ( $n=3/\text{group}$ ).

imaging. Limited experience with available radio-labeled ligands, such as  $^{111}\text{In}$ -pentetreotide and  $^{123}\text{I}$ -VIP, indicate that receptor imaging would offer solutions to these problems.<sup>1-6</sup>

Folic acid, an essential vitamin (Vitamin M), serves as carbon donors for purine and thymidine synthesis and enters into cells through high-affinity FRs ( $K_D \approx 1 \text{ nM}$ ) in addition to classical low capacity carrier system.<sup>7-9</sup> The classical low affinity/low capacity carrier system (reduced folate carrier system,  $K_D \approx 1\text{--}100 \mu\text{M}$ ) is capable to meet metabolic requirements of normal cells.<sup>25</sup> Although their roles remain unclear, high affinity FRs are overexpressed on many neoplastic cell types.<sup>8,10-16</sup> A number of folic acid conjugates that are directly cytotoxic or that deliver cytotoxic agents as well as anti-FRs antibodies have been suggested to treat the cancers overexpressing FRs.<sup>17-27</sup> Likewise, radiolabeled antibodies which recognize different epitops of FRs have been used for imaging ovarian cancers.<sup>44,45</sup>

It has been reported that when folate is covalently linked to a macromolecule via its  $\gamma$ -carboxylate moiety, its affinity for the cell surface receptors remains essentially unaltered.<sup>30</sup> Results of limited in vitro and in vivo studies with radiolabeled folate analogues, such as  $^{67}\text{Ga}$ -deferoxamine-folate and  $^{111}\text{In}$ -DTPA-folate, suggest that folate receptors could be a potential target for tumor imaging.<sup>28-32</sup> Our biodistribution and imaging studies also support this hypothesis.

However, introducing new imaging modalities into clinical practice depend on, to some extent, other factors such as easy availability and cost. Besides,

offered imaging modality will not be helpful unless it significantly contributes the management of patients and also cost-effective to solve the diagnostic problems at hand. Certainly, less expensive and more chemically stable receptor imaging agents would be most desirable.

Due to better imaging characteristics and lower price attempts are made to replace the  $^{123}\text{I}$ ,  $^{131}\text{I}$ ,  $^{67}\text{Ga}$  and  $^{111}\text{In}$  labeled compounds with corresponding  $^{99\text{m}}\text{Tc}$  labeled compounds when possible. Verbruggen et al. reported that, EC can be labeled with  $^{99\text{m}}\text{Tc}$  very easily and efficiently at room temperature with high radiochemical purity and the preparation remains stable for at least 8 hours.<sup>34</sup> Because of reported labeling capacity and rapid renal clearance EC was selected to synthesize a new  $^{99\text{m}}\text{Tc}$ -labeled folate conjugate. EC-folate was successfully prepared by using relatively simple and fast chemistry. A labeling kit was also developed to make its use in clinical practice easier. This kit formulation consists of a 10 ml vial containing the lyophilisate of EC-folate (5 mg),  $\text{SnCl}_2$  (100  $\mu\text{g}$ ),  $\text{Na}_2\text{HPO}_4$  (13.5 mg), ascorbic acid (0.5 mg) and NaEDTA (0.5 mg). Radio-TLC results with  $^{99\text{m}}\text{Tc}$ -EC-folate kit confirms reported high radiochemical purity and stability of  $^{99\text{m}}\text{Tc}$ -EC. We believe that, due to labeling efficiency and relatively small molecular size (168 d) EC could be an alternative chelator to make new and more stable  $^{99\text{m}}\text{Tc}$ -labeled ligands.

In a study with athymic mice that were inoculated with KB cell line (nasopharyngeal epidermal carcinoma) and fed with folate-free rodent chow, tumor/blood ratio for  $^{67}\text{Ga}$ -deferoxamine-folate was found to be more than 400. Reportedly, this ratio

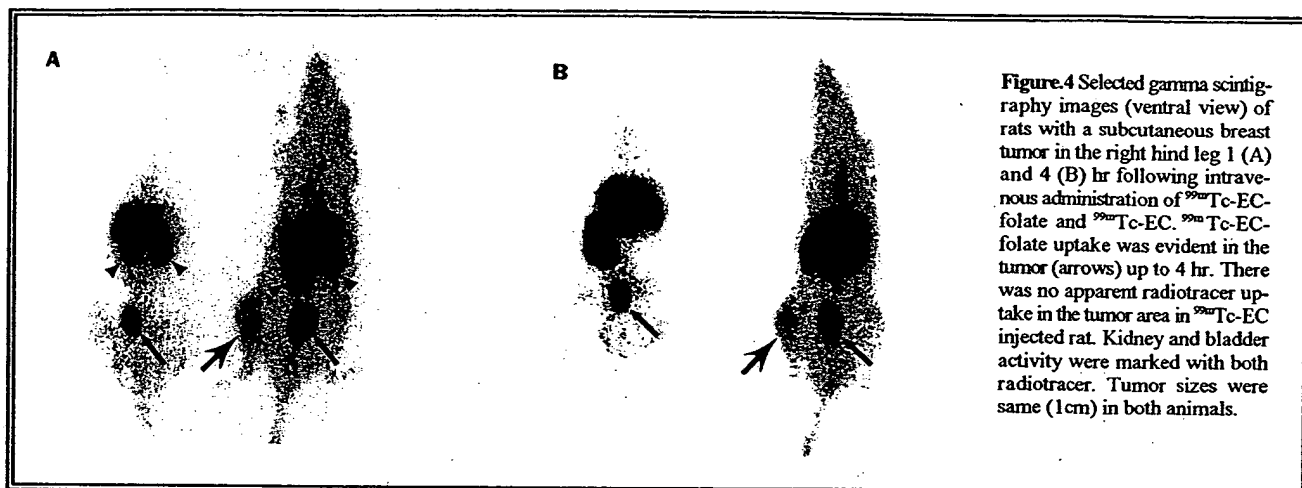


**Figure 4** Selected gamma scintigraphy images (ventral view) of rats with a subcutaneous breast tumor in the right hind leg 1 (A) and 4 (B) hr following intravenous administration of  $^{99m}\text{Tc}$ -EC-folate and  $^{99m}\text{Tc}$ -EC.  $^{99m}\text{Tc}$ -EC-folate uptake was evident in the tumor (arrows) up to 4 hr. There was no apparent radiotracer uptake in the tumor area in  $^{99m}\text{Tc}$ -EC injected rat. Kidney and bladder activity were marked with both radiotracer. Tumor sizes were same (1 cm) in both animals.

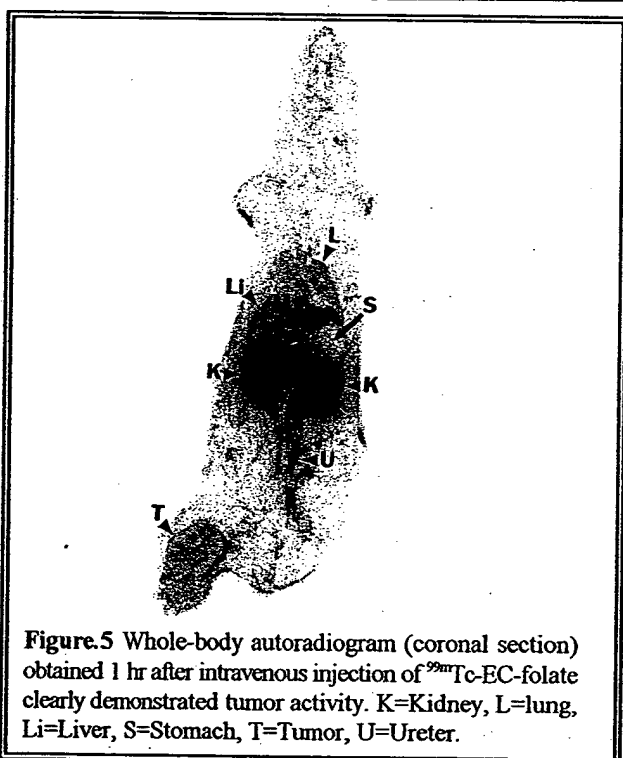


**Figure 5** Whole-body autoradiogram (coronal section) obtained 1 hr after intravenous injection of  $^{99m}\text{Tc}$ -EC-folate clearly demonstrated tumor activity. K=Kidney, L=lung, Li=Liver, S=Stomach, T=Tumor, U=Ureter.

dropped to around 40 in animals receiving regular (folate-supplemented) rodent chow.<sup>28</sup> This high ratio could be due to known anti-tumor activity of  $^{67}\text{Ga}$  as well as greatly overexpressed FRs on studied tumor cells. On the other hand, since serum folate from normal dietary sources directly competes with the labeled folic acid control of animals' dietary intake of folate would be a reasonable intervention to reach human serum folate levels before radiotracer studies. Mathias et al. reported that serum folate level in mice receiving regular (folate-supplemented) rodent chow is about 700 times more than normal human serum folate level.<sup>28</sup>

The other studies conducted in same animal and tumor model also indicate that DTPA-folate conjugate ( $^{99m}\text{Tc}$  or  $^{111}\text{In}$  labeled) could be used for tumor imaging.<sup>29,31,32</sup> Final results of these studies have not been published yet. To use different tumor models which express different levels of FRs would be helpful to investigate the correlation between uptake of labeled-ligand and FRs levels.

In this preliminary study, we used regular (folate-supplemented) rodent chow receiving rats inoculated with available rat tumor model. Therefore, it could be expected to reach better tumor/nontarget ratios with tumor models that are known to be overexpress FRs and by controlling the dietary intake of folate.

High renal uptake seen in imaging studies could be due to reabsorption of folate by the proximal renal tubular cells in addition to the high renal excretion of EC. Hydration of the animals between injection and imaging might decrease the kidney uptake. According to our biodistribution and imaging data best imaging time seems to be between 1 and 2 hours.

Another potential use of folate receptor imaging could be prediction of therapeutic effectiveness of anti-folates. In an in-vitro study, Chung et al. reported that increased expression of FRs by human mammary carcinoma and Chinese hamster ovary cells resulted in an increased folic acid binding, and increased methotrexate uptake and cytotoxicity.<sup>46</sup> It is known that folic acid and antifolates, such as methotrexate, share same transport systems.<sup>7,47-50</sup> Thus, folate receptor imaging could possibly be used to predict therapeutic effectiveness of anti-folates in cancer patients that will be treated with anti-folates.



## CONCLUSION

Our results suggest that  $^{99m}\text{Tc}$ -EC-folate could be a good candidate for imaging folate receptor positive tumors. Its potential value to predict therapeutic effectiveness of antifolates requires further investigation.

## ACKNOWLEDGMENTS

The animal research is supported by M.D. Anderson Cancer Center (CORE) Grant NIH NCI CA-16672.

The authors wish to thank William C. Liu for his excellent technical support in animal studies and Dianne Perez for her clerical support.

## REFERENCES

1. Goldsmith SJ. Receptor imaging: Competitive or complementary to antibody imaging. *Semin Nucl Med* 1997; 27: 85-93.
2. Britton KE, Granowska M. Imaging of tumors, in tomography in nuclear medicine. Proceedings of an International Symposium, Vienna, Austria, IAEA, 1996, pp 91-105.
3. Krenning EP, Kwekkeboom DJ, Bakker WH, et al. Somatostatin receptor scintigraphy with [ $^{111}\text{In}$ -DTPA-D-Phe] and [ $^{111}\text{In}$ -Tyr]-octreotide: The Rotterdam experience with more than 1000 patients. *Eur J Nucl Med* 1995; 7:716-731.
4. Reubi JC, Krenning EP, Lamberts SWJ, et al. In vitro detection of somatostatin receptors in human tumors. *Metabolism* 1992; 41:104-110 (suppl 2).
5. Goldsmith SJ, Macapinlac H, O'Brien JP. Somatostatin receptor imaging in lymphoma. *Semin Nucl Med* 1995; 25:262-271.
6. Virgolini I, Raderer M, Kurtaran A. Vasoactive intestinal peptide (VIP) receptor imaging in the localization of intestinal adenocarcinomas and endocrine tumors. *N Eng J Med* 1994; 331:1116-1121.
7. Westerhof GR, Jansen G, Emmerik NV, Kathmann I, Rijksen G, Jackman AL, Schornagel JH. Membrane transport of natural folates and antifolate compounds in murine L1210 leukemia cells: Role of carrier- and receptor-mediated transport systems. *Cancer Res* 1991; 51:5507-5513.
8. Orr RB, Kreisler AR, Kamen BA. Similarity of folate receptor expression in UMSSC 38 cells to squamous cell carcinoma differentiation markers. *J Natl Cancer Inst* 1995; 87:299-303.
9. Hsueh CT, Dolnick BJ. Altered folate-binding protein mRNA stability in KB cells grown in folate-deficient medium. *Biochem Pharmacol* 1993; 45:2537-2545.
10. Weitman SD, Lark RH, Coney LR, et al. Distribution of folate GP38 in normal and malignant cell lines and tissues. *Cancer Res* 1992; 52:3396-3400.
11. Campbell IG, Jones TA, Foulkes WD, Trowsdale J. Folate-binding protein is a marker for ovarian cancer. *Cancer Res* 1991; 51:5329-5338.
12. Weitman SD, Weinberg AG, Coney LR, Zurawski VR, Jennings DS, Kamen BA. Cellular localization of the folate receptor: potential role in drug toxicity and folate homeostasis. *Cancer Res* 1992; 52:6708-6711.
13. Holm J, Hansen SI, Hoier-Madsen M, Sondergaard K, Bzorek M. Folate receptor of human mammary adenocarcinoma. *APMIS* 1994; 102:413-419.
14. Ross JF, Chaudhuri PK, Ratnam M. Differential regulation of folate receptor isoforms in normal and malignant tissue in vivo and in established cell lines. *Cancer* 1994; 73:2432-2443.
15. Franklin WA, Waintrub M, Edwards D, Christensen K, Prendegast P, Woods J, Bunn PA, Kolhouse JF. New anti-lung-cancer antibody cluster 12 reacts with human folate receptors present on adenocarcinoma. *Int J Cancer-Supplement* 1994; 8:89-95.
16. Weitman SD, Frazier KM, Kamen BA. The folate receptor in central nervous system malignancies of childhood. *J Neuro-Oncology* 1994; 21:107-112.
17. Ginobbi P, Geiser TA, Ombres D, Citro G. Folic acid-polylysine carrier improves efficacy of c-myc antisense oligonucleotides on human melanoma (M14) cells. *Anticancer Res* 1997; 17:29-35.
18. Leamon CP, Low PS. Delivery of macromolecules into living cells: a method that exploits folate receptor endocytosis. *Proc Natl Acad Sci* 1991; 88:5572-5576.
19. Leamon CP, Low PS. Cytotoxicity of momordin-folate conjugates in cultured human cells. *J Biol Chem* 1992; 267:24966-24971.
20. Leamon CP, Pastan I, Low PS. Cytotoxicity of folate-pseudomonas exotoxin conjugates toward tumor cells. *J Biol Chem* 1993; 268:24847-24854.
21. Lee RJ, Low PS. Delivery of liposomes into cultured KB cells via folate receptor-mediated endocytosis. *J Biol Chem* 1994; 269:3198-3204.
22. Ginobbi P, Geiser TA, Ombres D, Citro G. Folic acid-polylysine carrier improves efficacy of c-myc antisense oligodeoxynucleotides on human melanoma (M14) cells. *Anticancer Res* 1997; 17:29-35.
23. Canevari S, Miotti S, Bottero F, Valota O, Colnaghi MI. Ovarian carcinoma therapy with monoclonal antibodies. *Hybridoma* 1993; 12:501-507.
24. Bolhuis RLH, Lamers CHJ, Goey HS, et al. Adoptive immunotherapy of ovarian carcinoma with Bs-MAb targeted lymphocytes. A multicenter study. *Int J Cancer* 1992; 7:78-81.
25. Patrick TA, Kranz DM, van Dyke TA, Roy EJ. Folate receptors as potential therapeutic targets in choroid plexus tumors of SV40 transgenic mice. *J Neurooncol* 1997; 32:111-123.
26. Coney LR, Mezzanzanica D, Sanborn D, Casalini P, Colnaghi MI, Zurawski VR. Chimeric murine-human antibodies directed against folate binding receptor are efficient mediators of ovarian carcinoma cell killing. *Cancer Res* 1994; 54:2448-2455.

27. Kranz DM, Patrick TA, Brigle KE, Spinella MJ, Roy EJ. Conjugates of folate and anti-T-cell-receptor antibodies specifically target folate-receptor-positive tumor cells for lysis. *Proc Natl Acad Sci* 1995; 92:9057-9061.
28. Mathias CJ, Wang S, Lee RJ, Waters DJ, Low PS, Green MA. Tumor-selective radiopharmaceutical targeting via receptor-mediated endocytosis of Gallium-67-deferoxamine-folate. *J Nucl Med* 1996; 37:1003-1008.
29. Wang S, Luo J, Lantrip DA, Waters DJ, Mathias CJ, Green MA, Fuchs PL, Low PS. Design and synthesis of [<sup>111</sup>In]DTPA-folate for use as a tumor-targeted radiopharmaceutical. *Bioconjugate Chem* 1997; 8:673-679.
30. Wang S, Lee RJ, Mathias CJ, Green MA, Low PS. Synthesis, purification, and tumor cell uptake of Ga-67 deferoxamine-folate, a potential radiopharmaceutical for tumor imaging. *Bioconjugate Chem* 1996; 7:56-62.
31. Mathias CJ, Wang S, Waters DJ, Turek JJ, Low PS, Green MA. Indium-111-DTPA-folate as a radiopharmaceutical for targeting tumor-associated folate binding protein (Abstract). *J Nucl Med* 1997 (Supplement); 38:133P.
32. Mathias CJ, Hubers D, Trump DP, Wang S, Luo J, Waters DJ, Fuchs PL, Low PS, Green MA. Synthesis of Tc-99m-DTPA-folate and preliminary evaluation as a folate-receptor-targeted radiopharmaceutical (Abstract). *J Nucl Med* 1997 (Supplement); 38:87P.
33. Davison A, Jones AG, Orvig C, Sohn M. A new class of oxotechnetium(+5) chelate complexes containing a TcON<sub>2</sub>S<sub>2</sub> Core. *Inorg Chem* 1980; 20:1629-1632.
34. Verbruggen AM, Nosco DL, Van Nerom CG, et al. Tc-99m-L,L-ethylenedicycysteine: A renal imaging agent. I. Labelling and evaluation in animals. *J Nucl Med* 1992; 33:551-557.
35. Van Nerom CG, Bormans GM, De Roo MJ, et al. First experience in healthy volunteers with Tc-99m-L,L-ethylenedicycysteine, a new renal imaging agent. *Eur J Nucl Med* 1993; 20:738-746.
36. Surma MJ, Wiewiora J, Liniecki J. Usefulness of Tc-99m-N,N'-ethylene-1-dicycysteine complex for dynamic kidney investigations. *Nucl Med Comm* 1994; 15:628-635.
37. Verbruggen A, Nosco D, Van Nerom C, Bormans G, Adriaens P, De Roo M. Evaluation of Tc-99m L,L-ethylenedicycysteine as a potential alternative to Tc-99m MAG3. *Eur J Nucl Med* 1990; 16:429.
38. Van Nerom C, Bormans G, Bauwens J, Vandecruys A, De Roo M, Verbruggen A. Comparative evaluation of Tc-99m L,L-ethylenedicycysteine and Tc-99m MAG3 in volunteers. *Eur J Nucl Med* 1990; 16:417.
39. Jamar F, Stoffel M, Van Nerom C, et al. Clinical evaluation of Tc-99m L,L-ethylenedicycysteine, a new renal tracer, in transplanted patients. *J Nucl Med* 1993; 34:129P.
40. Jamar F, Van Nerom C, Verbruggen A, et al. Clearance of the new tubular agent Tc-99m L,L-ethylenedicycysteine: Estimation by a simplified method. *J Nucl Med* 1993; 34:129P.
41. Ratner S, Clarke HT. The action of formaldehyde upon cysteine. *J Am Chem Soc* 1937; 59:200-206.
42. Blondeau P, Berse C, Gravel D. Dimerization of an intermediate during the sodium in liquid ammonia reduction of L-thiazolidine-4-carboxylic acid. *Can J Chem* 1967; 45:49-52.
43. Gucalp R, Dutcher JP, Wiernik. Overview by an oncologist: What are the imaging needs of the oncologist and oncological surgeon. *Semin Nucl Med* 1997; 27:3-9.
44. Crippa F, Buraggi GL, Di Re E, et al. Radioimmuno-scintigraphy of ovarian cancer with the MOv18 monoclonal antibody. *Eur J Cancer* 1991; 27:724-729.
45. Paganelli G, Belloni C, Magnani P, et al. Two-step tumour targeting in ovarian cancer patients using biotinylated monoclonal antibodies and radioactive streptavidin. *Eur J Nucl Med* 1992; 19:322-329.
46. Chung KN, Saiwaka Y, Paik TH, et al. Stable transfectants of human MCF-7 breast cancer cells with increased levels of the human folate receptor exhibit an increased sensitivity to antifolates. *J Clin Invest* 1993; 91:1289-1294.
47. Deutsch JC, Elwood PC, Portillo RM, Macey MG, Kolhouse JF. Role of membrane-associated folate binding protein (folate receptor) in methotrexate transport by human KB cells. *Arch Biochem Biophysics* 1989; 274:327-337.
48. Kane MA, Portillo RM, Elwood PC, Antony AC, Kolhouse JF. The influence of extracellular folate concentration on methotrexate uptake by human KB cells. *J Biol Chem* 1986; 261:44-49.
49. Wang X, Shen F, Freisheim JH, Gentry LE, Ratnam M. Differential stereospecificities and affinities of folate receptor isoforms for folate compounds and antifolates. *Biochem Pharmacol* 1992; 44:1898-1901.
50. Sierra EE, Brigle KE, Spinella MJ, Goldman ID. pH dependence of methotrexate transport by the reduced folate carrier and the folate receptor in L1210 leukemia cells. Further evidence for a third route mediated at low pH. *Biochem Pharmacol* 1997; 53:223-231.

59. J. Wu *et al.*, *Proc. Natl. Acad. Sci. U.S.A.* **91**, 2344 (1994).
60. H. von Boehmer, *Cell* **76**, 219 (1994); G. J. V. Nossal, *ibid.*, p. 229.
61. R. G. Scollay, E. C. Butcher, I. L. Weissman, *Eur. J. Immunol.* **10**, 210 (1980); M. Egerton, R. Scollay, K. Shortman, *Proc. Natl. Acad. Sci. U.S.A.* **87**, 2579 (1990).
62. S. R. Webb, J. Hutchinson, K. Hayden, J. Sprent, *J. Immunol.* **152**, 586 (1994); B. Rocha and H. von Boehmer, *Science* **251**, 1225 (1991); S. Webb, C. Morris, J. Sprent, *Cell* **63**, 1249 (1990); J. E. McCormack, J. E. Callahan, J. Kappler, P. C. Marrack, *J. Immunol.* **150**, 3785 (1993); H. R. MacDonald, S. Baschieri, R. K. Lees, *Eur. J. Immunol.* **21**, 1963 (1991).
63. D. Kabelitz, T. Pohl, K. Pechhold, *Immunol. Today* **14**, 338 (1993).
64. C. L. Sidman, J. D. Marshall, H. von Boehmer, *Eur. J. Immunol.* **22**, 499 (1992); L. R. Herron *et al.*, *J. Immunol.* **151**, 3450 (1993).
65. I. N. Crispe, *Immunity* **1**, 347 (1994); P. Musette, C. Pannetier, G. Gachelin, P. Kourilsky, *Eur. J. Immunol.* **24**, 2761 (1994); G. G. Singer and A. K. Abbas, *Immunity* **1**, 365 (1994); M. R. Alderson *et al.*, *J. Exp. Med.* **181**, 71 (1995).
66. J. H. Russell, B. Rush, C. Weaver, R. Wang, *Proc. Natl. Acad. Sci. U.S.A.* **90**, 4409 (1993); J. H. Russell and R. Wang, *Eur. J. Immunol.* **23**, 2379 (1993).
67. F. Vignaux and P. Golstein, *Eur. J. Immunol.* **24**, 923 (1994); I. Gillette-Ferguson and C. L. Sidman, *ibid.*, p. 1181.
68. J. Dhein, H. Walczak, C. Bäumler, K.-M. Debatin, P. H. Krammer, *Nature* **373**, 438 (1995).
69. D. Watanabe, T. Suda, H. Hashimoto, S. Nagata, *EMBO J.* **14**, 12 (1995); J. L. Chu *et al.*, *J. Exp. Med.* **181**, 393 (1995).
70. M. Papiernik, C. Pontoux, P. Golstein, in preparation.
71. J. C. Rathmell and C. C. Goodnow, *J. Immunol.* **153**, 2831 (1994).
72. K. Rajewsky, *Curr. Opin. Immunol.* **4**, 171 (1992).
73. P. T. Daniel and P. H. Krammer, *J. Immunol.* **152**, 5624 (1994).
74. P. A. Henkart, *Annu. Rev. Immunol.* **3**, 31 (1985); E. R. Podack, *Immunol. Today* **6**, 21 (1985); J. W. Shiver, L. Su, P. A. Henkart, *Cell* **71**, 315 (1992); J. W. Heusel, R. L. Wesselschmidt, S. Shresta, J. H. Russell, *Cell* **76**, 977 (1994); D. Kägi *et al.*, *Nature* **369**, 31 (1994).
75. F. Ramsdell *et al.*, *Int. Immunol.* **6**, 1545 (1994).
76. S. Hanabuchi *et al.*, *Proc. Natl. Acad. Sci. U.S.A.* **91**, 4930 (1994).
77. I. C. M. MacLennan, F. M. Gotch, P. Golstein, *Immunology* **39**, 109 (1980); R. Tirosh and G. Berke, *Cell. Immunol.* **95**, 113 (1985); H. L. Ostergaard, K. P. Kane, M. F. Mescher, W. R. Clark, *Nature* **330**, 71 (1987); G. Trenn, H. Takayama, M. V. Sitko, *ibid.*, p. 72; J. D.-E. Young, W. R. Clark, C.-C. Liu, Z. A. Cohn, *J. Exp. Med.* **166**, 1894 (1987).
78. E. R. Podack, J. D.-E. Young, Z. A. Cohn, *Proc. Natl. Acad. Sci. U.S.A.* **82**, 8629 (1985); J. D.-E. Young, A. Damiano, M. A. DiNome, L. G. Leong, Z. A. Cohn, *J. Exp. Med.* **165**, 1371 (1987); S. Ishiura *et al.*, *Mol. Immunol.* **27**, 803 (1990).
79. D. Kägi *et al.*, *Science* **265**, 528 (1994); B. Lowin, M. Hahne, C. Mattmann, J. Tschopp, *Nature* **370**, 650 (1994).
80. T. R. Mosmann *et al.*, *Immunol. Rev.* **123**, 209 (1991).
81. C. M. Walsh, A. A. Glass, V. Chiu, W. R. Clark, *J. Immunol.* **153**, 2506 (1994); H. Kojima *et al.*, *Immunity* **1**, 357 (1994).
82. F. Ramsdell *et al.*, *Eur. J. Immunol.* **24**, 928 (1994).
83. J. Ogasawara *et al.*, *Nature* **364**, 806 (1993).
84. M. C. Sneller *et al.*, *J. Clin. Invest.* **90**, 334 (1992).
85. F. Rieux-Laucat, F. Le Deist, K. M. Debatin, A. Fischer, J. P. De Villartay, *Abstracts of the 12th European Immunology Meeting*, Barcelona, Spain, June 1994 (European Federation of Immunological Societies, 1994).
86. J. Cheng *et al.*, *Science* **263**, 1759 (1994).
87. M. L. Watson *et al.*, *J. Exp. Med.* **176**, 1645 (1992).
88. J. B. Weinberg *et al.*, *ibid.* **179**, 651 (1994).
89. J. H. Lowrance, F. X. O'Sullivan, T. E. Caver, W. Waegell, H. D. Gresham, *ibid.* **180**, 1693 (1994).
90. K. Hiramatsu *et al.*, *Eur. J. Immunol.* **24**, 2446 (1994).

91. N. Oyaizu *et al.*, *Blood* **84**, 2622 (1994).
92. Z.-Q. Wang *et al.*, *Eur. J. Immunol.* **24**, 1549 (1994).
93. K. Ando *et al.*, *J. Exp. Med.* **178**, 1541 (1993).
94. R. Ni *et al.*, *Exp. Cell Res.* **215**, 332 (1995).
95. N. Hiramatsu *et al.*, *Hepatology* **19**, 1354 (1994).
96. D. Watanabe and S. Nagata, unpublished observations.
97. A. N. Theofilopoulos *et al.*, *J. Exp. Med.* **162**, 1 (1985).
98. K.-M. Debatin, C. K. Goldmann, R. Bamford, T. A. Waldmann, P. H. Krammer, *Lancet* **335**, 497 (1990).
99. We thank the members of our laboratories in

Osaka and in Marseille, and collaborators from other laboratories, for dedicated participation to the work quoted in this article. We thank M. Raff for critical reading of the manuscript. S.N. is grateful to O. Hayaishi and C. Weissmann for encouragement and discussion. Supported in part by Grants-in-Aid from the Ministry of Education, Science and Culture of Japan (to S.N.), and the Centre National de la Recherche Scientifique, the Institut National de la Santé et de la Recherche Médicale and l'Association pour la Recherche contre le Cancer (to P.G.).

# Apoptosis in the Pathogenesis and Treatment of Disease

Craig B. Thompson

In multicellular organisms, homeostasis is maintained through a balance between cell proliferation and cell death. Although much is known about the control of cell proliferation, less is known about the control of cell death. Physiologic cell death occurs primarily through an evolutionarily conserved form of cell suicide termed apoptosis. The decision of a cell to undergo apoptosis can be influenced by a wide variety of regulatory stimuli. Recent evidence suggests that alterations in cell survival contribute to the pathogenesis of a number of human diseases, including cancer, viral infections, autoimmune diseases, neurodegenerative disorders, and AIDS (acquired immunodeficiency syndrome). Treatments designed to specifically alter the apoptotic threshold may have the potential to change the natural progression of some of these diseases.

The survival of multicellular organisms depends on the function of a diverse set of differentiated cell types. Once development is complete, the viability of the organism depends on the maintenance and renewal of these diverse lineages. Within vertebrates, different cell types vary widely in the mechanisms by which they maintain themselves over the life of the organism. Blood cells, for instance, undergo constant renewal from hematopoietic progenitor cells. In addition, lymphocytes and cells within the reproductive organs undergo cyclical expansions and contractions as they participate in host defense and reproduction, respectively. In contrast, neural cells have at best a limited capacity for self-renewal, and most neurons survive for the life of the organism.

Within each lineage, the control of cell number is determined by a balance between cell proliferation and cell death (Fig. 1). Cell proliferation is a highly regulated process with numerous checks and balances. For example, growth factors and proto-oncogenes are positive regulators of cell cycle progression (1). In contrast, tumor suppressor genes act to oppose uncontrolled cell

proliferation (1, 2). Tumor suppressors can prevent cell cycle progression by inhibiting the activity of proto-oncogenes. In the last 15 years there has been a rapid increase in our understanding of the mechanisms that control cell proliferation.

Biologists are now beginning to appreciate that the regulation of cell death is just as complex as the regulation of cell proliferation (3). The differentiated cells of multicellular organisms all appear to share the ability to carry out their own death through activation of an internally encoded suicide program (4). When activated, this suicide program initiates a characteristic form of cell death called apoptosis (5, 6). Apoptosis can be triggered by a variety of extrinsic and intrinsic signals (7) (Fig. 2). This type of regulation allows for the elimination of cells that have been produced in excess, that have developed improperly, or that have sustained genetic damage. Although diverse signals can induce apoptosis in a wide variety of cell types, a number of evolutionarily conserved genes regulate a final common cell death pathway that is conserved from worms to humans (8) (Fig. 3).

Apoptotic cell death can be distinguished from necrotic cell death (4-6). Necrotic cell death is a pathologic form of cell death resulting from acute cellular injury, which is typified by rapid cell swelling and lysis. In contrast, apoptotic cell death is

The author is in the Howard Hughes Medical Institute, Departments of Medicine and Molecular Genetics and Cell Biology, Gwen Knapp Center for Lupus and Immunology Research, University of Chicago, Chicago, IL 60637, USA.

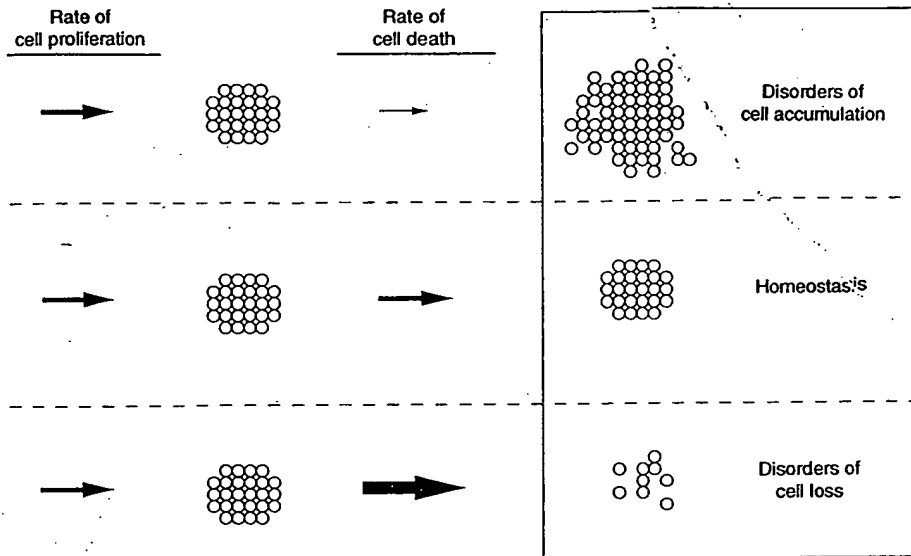


**Fig. 1.** The effect of different rates of cell death on homeostasis. In mature organisms, cell number is controlled as a result of the net effects of cell proliferation and cell death. Here, the rates of cell proliferation and cell death are indicated by the size of the arrows. In the absence of compensatory changes in the rate of cell proliferation, changes in the rate of cell death can result in either cell accumulation or cell loss.

### Inhibitors of Apoptosis

#### Physiologic inhibitors

1. Growth factors
2. Extracellular matrix
3. CD40 ligand
4. Neutral amino acids
5. Zinc
6. Estrogen
7. Androgens

#### Viral genes

1. Adenovirus *E1B*
2. Baculovirus *p35*
3. Baculovirus *IAP*
4. Cowpox virus *cma*
5. Epstein-Barr virus *BHRF1*, *LMP-1*
6. African swine fever virus *LMW5-HL*
7. Herpesvirus  $\gamma 1$  34.5

#### Pharmacological agents

1. Calpain inhibitors
2. Cysteine protease inhibitors
3. Tumor promoters  
PMA  
Phenobarbital  
 $\alpha$ -Hexachlorocyclohexane

### Inducers of Apoptosis

#### Physiologic activators

1. TNF family  
Fas ligand  
TNF
2. Transforming growth factor  $\beta$
3. Neurotransmitters  
Glutamate  
Dopamine  
N-methyl-D-aspartate
4. Growth factor withdrawal
5. Loss of matrix attachment
6. Calcium
7. Glucocorticoids

#### Damage-related inducers

1. Heat shock
2. Viral infection
3. Bacterial toxins
4. Oncogenes  
*myc*, *rel*, *E1A*
5. Tumor suppressors  
*p53*
6. Cytolytic T cells
7. Oxidants
8. Free radicals
9. Nutrient deprivation—antimetabolites

#### Therapy-associated agents

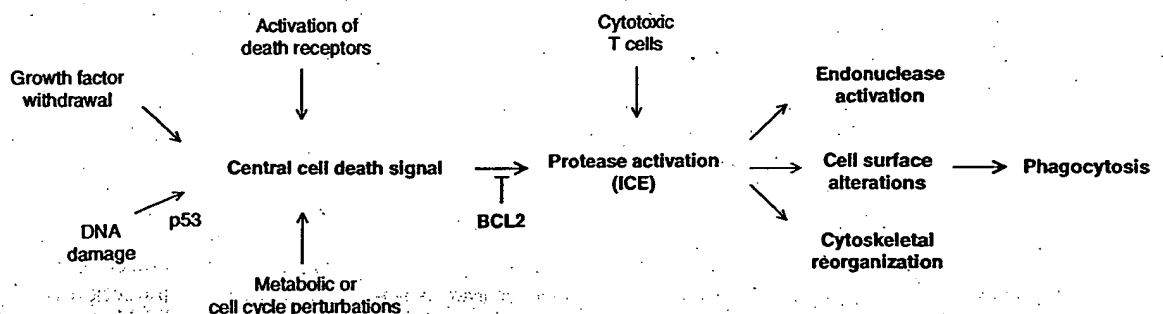
1. Chemotherapeutic drugs  
Cisplatin, doxorubicin, bleomycin, cytosine arabinoside, nitrogen mustard, methotrexate, vincristine
2. Gamma radiation
3. UV radiation

#### Toxins

1. Ethanol
2.  $\beta$ -amyloid peptide

**Fig. 2.** A partial list of the agents that have been reported to induce or inhibit apoptosis.

**Fig. 3.** A hypothetical model for the regulation of apoptotic cell death. As diagrammed, the major end point of apoptotic cell death is the removal of the dying cell by phagocytosis. One of the difficulties in determining the contribution of apoptosis to the pathogenesis of disease is the rapidity with which the phagocytosis of apoptotic cells occurs in vivo. Both the death repressor *BCL2* and ICE are members of larger gene families.



characterized by controlled autodigestion of the cell. Cells appear to initiate their own apoptotic death through the activation of endogenous proteases. This results in cytoskeletal disruption, cell shrinkage, and membrane blebbing. Apoptosis also involves characteristic changes within the nucleus. The nucleus undergoes condensation as endonucleases are activated and begin to degrade nuclear DNA. In many cell types, DNA is degraded into DNA fragments the size of oligonucleosomes, whereas in others larger DNA fragments are produced. Apoptosis is also characterized by a loss of mitochondrial function. This has led to speculation that mitochondria may have an important function in regulating apoptosis; however, data to support this hypothesis are currently unavailable. The dying cell maintains its plasma membrane integrity. However, alterations in the plasma membrane of apoptotic cells signal neighboring phagocytic cells to engulf them and thus to complete the degradation process (9). Cells not immediately phagocytosed break down into smaller membrane-bound fragments called apoptotic bodies. An important feature of apoptosis is that it results in the elimination of the dying cell without induction of an inflammatory response. In contrast, necrotic cell death is associated with an early loss of cell membrane integrity, resulting in leakage of cytoplasmic contents and the induction of an inflammatory response.

In most tissues, cell survival appears to depend on the constant supply of survival signals provided by neighboring cells and the extracellular matrix (10). Cells from most organs will undergo apoptosis if cultured individually in the absence of exogenous survival factors. Death in these cases appears to occur even in the absence of new protein synthesis, which suggests that the proteins that mediate apoptosis are constitutively expressed in many cell types (4). One interpretation of these results is that most cells are programmed to commit suicide if survival signals are not received from the environment, either constantly or at regular intervals (4). Viewed in this way, apoptotic cell death can be thought of as a

default pathway. However, some types of physiologic cell death involve the induction of apoptosis through mechanisms that require new protein synthesis.

Recent evidence suggests that the failure of cells to undergo apoptotic cell death might be involved in the pathogenesis of a variety of human diseases, including cancer, autoimmune diseases, and viral infections (6). In addition, a wide number of diseases characterized by cell loss, such as neurodegenerative disorders, AIDS (acquired immunodeficiency syndrome), and osteoporosis, may result from accelerated rates of physiologic cell death (Fig. 4). Specific therapies designed to enhance or decrease the susceptibility of individual cell types to undergo apoptosis could form the basis for treatment of a variety of human diseases.

### Disorders Associated with Increased Cell Survival

Diseases characterized by the accumulation of cells include cancer, autoimmune diseases, and certain viral illnesses. Cell accumulation can result from either increased proliferation or the failure of cells to undergo apoptosis in response to appropriate stimuli (Fig. 1). Although much attention has focused on the potential role of cell proliferation in these disorders, increasing evidence suggests that alterations in the control of cell survival are important in the pathogenesis of these so-called proliferative disorders.

**Cell death in cancer.** Cells from a wide variety of human malignancies have a decreased ability to undergo apoptosis in response to at least some physiologic stimuli (11). This is most apparent in metastatic tumors. Most normal cells depend on environment-specific factors to maintain their viability (10). This dependence may serve to prevent normal cells from surviving in nonphysiologic sites. Metastatic tumor cells have circumvented this homeostatic mechanism and can survive at sites distinct from the tissue in which they arose. To do this,

tumor cells must develop some degree of independence from the survival factors that restrict the distribution of their nontransformed counterparts. Recent advances are beginning to shed some light on the molecular bases for the increased resistance of tumor cells to undergo apoptosis, and several genes that are critical in the regulation of apoptosis have been defined.

The gene *BCL2* was first discovered as a result of its location at the site of a translocation between chromosomes 14 and 18 and is present in most human follicular lymphomas (12). Initially viewed as an oncogene, *BCL2* was found to have little or no ability to promote cell cycle progression or cell proliferation. Instead, overexpression of *BCL2* specifically prevents cells from initiating apoptosis in response to a number of stimuli (13). Furthermore, the introduction of genes that inhibit *BCL2* can induce apoptosis in a wide variety of tumor types, which suggests that many tumors continually rely on *BCL2* or related gene products to prevent cell death (14). Consistent with this hypothesis, *BCL2* expression has been associated with a poor prognosis in prostatic cancer, colon cancer, and neuroblastoma (15).

Recently, it has been demonstrated that *BCL2* is only one member of a family of genes that can control the apoptotic threshold of a cell (16). The roles of these other *BCL2* family members in the pathogenesis of human malignancies are just beginning to be examined. In tumor cell lines, overexpression of *BCL2* or of the related gene *BCLx* has been found to confer resistance to cell death in response to chemotherapeutic agents such as cytosine arabinoside, methotrexate, vincristine, and cisplatin (17). These results are surprising because chemotherapy was previously thought to kill cells by inducing irreversible metabolic damage that results in target cell necrosis. It now appears that the primary mechanism by which most chemotherapeutic agents induce cell death is through creating aberrations in cellular physiology that result in

the induction of apoptosis. Consistent with this hypothesis, overexpression of *BCL2* or related genes can result in a multidrug resistance phenotype in vitro. The role of the *BCL2* family in the development of multidrug resistance in vivo has not yet been evaluated.

A wide variety of chemotherapeutic agents work by initiating DNA damage. Cell death in response to DNA damage in most instances has been shown to result from apoptosis. The p53 gene product is required for cells to initiate apoptosis in response to genotoxic damage (18). It is also fundamental in the pathway that leads from the sensing of DNA damage to the initiation of apoptosis. The inability of cells to undergo apoptosis in response to DNA damage may underlie the enhanced resistance to chemotherapeutic agents and radiation observed in tumors that are deficient in p53 (19). The failure of cells to die in response to DNA damage may also underlie the high rate of gene amplification observed in p53-deficient cells (20). Cells unable to undergo apoptosis in response to DNA damage may be more prone to acquire genetic alterations than normal cells. Errors in the repair of DNA damage that might otherwise induce apoptosis could contribute to the high mutation rate observed in many human cancers.

For years investigators have used chemicals referred to as tumor promoters to induce experimental malignancies. The exact role of tumor promoters in the pathogenesis of cancer is not clear. Most tumor promoters cannot induce cell proliferation on their own. Recently, it has been shown that tumor promoters such as phorbol myristate acetate (PMA) and  $\alpha$ -hexachlorocyclohexane can act as specific survival factors for the cells in which they promote tumor development (21). These data suggest that inhibition of apoptosis is more important in the development of malignancy than previously believed.

A critical question in cancer biology is why two or more cooperative transforming events are usually required to induce a full neoplastic lesion. One potential explanation is that oncogene transformation leads to a dysregulation of genes that control cell division, such as cyclins and cyclin-dependent kinases (22). Cells normally appear to be able to detect such an imbalance and respond by undergoing apoptosis. Apoptosis may represent a mechanism for protecting the organism from cells that have acquired genetic alterations that predispose them to cell proliferation. For example, in the absence of other transforming events, dysregulation of the *myc* oncogene leads to the induction of apoptosis in serum-starved fibroblasts (23). However, simultaneous overexpression of *BCL2* prevents this apoptotic

#### Diseases Associated with the Inhibition of Apoptosis

1. Cancer
  - Follicular lymphomas
  - Carcinomas with p53 mutations
  - Hormone-dependent tumors
  - Breast cancer
  - Prostate cancer
  - Ovarian cancer
2. Autoimmune disorders
  - Systemic lupus erythematosus
  - Immune-mediated glomerulonephritis
3. Viral infections
  - Herpesviruses
  - Poxviruses
  - Adenoviruses

#### Diseases Associated with Increased Apoptosis

1. AIDS
2. Neurodegenerative disorders
  - Alzheimer's disease
  - Parkinson's disease
  - Amyotrophic lateral sclerosis
  - Retinitis pigmentosa
  - Cerebellar degeneration
3. Myelodysplastic syndromes
  - Aplastic anemia
4. Ischemic injury
  - Myocardial infarction
  - Stroke
  - Reperfusion injury
5. Toxin-induced liver disease
  - Alcohol

Fig. 4. Diseases associated with the induction or inhibition of apoptotic cell death.

response. Cooperation between *myc* and *BCL2* in the pathogenesis of experimental tumors has also been demonstrated (24).

**Cell death and autoimmunity.** Physiologic regulation of cell death is essential for the removal of potentially autoreactive lymphocytes during development and for the removal of excess cells after the completion of an immune response. Failure to remove autoimmune cells that arise during development or that develop as a result of somatic mutation during an immune response can result in autoimmune disease. Recent work in animal model systems has clearly demonstrated the importance of dysregulated apoptosis in the etiology of autoimmune diseases. For example, one molecule critical in regulating cell death in lymphocytes is the cell surface receptor Fas, a member of the tumor necrosis factor (TNF) receptor family (25). Stimulation of Fas on activated lymphocytes can induce apoptosis. Two forms of hereditary autoimmune disease have been attributed to alterations in Fas-mediated apoptosis (25, 26). MRL-lpr mice, which develop fatal systemic lupus erythematosus by 6 months of age, have a mutation in the Fas receptor. In contrast, the GLD mouse, which develops a similar illness, has a mutation in the Fas ligand (26). In humans, a secreted form of Fas has been identified (27). Patients with systemic lupus erythematosus have elevated levels of soluble Fas, which may competitively inhibit Fas ligand-Fas interactions. The resulting decrease in Fas-mediated apoptosis may contribute to the accumulation of autoimmune cells in this disorder. A lupuslike autoimmune disease has also been reported in transgenic mice constitutively overexpressing *BCL2* in their B cells (28). Finally, linkage analysis has established an association between the *BCL2* locus and autoimmune diabetes in nonobese diabetic (NOD) mice (29).

To date, no autoimmune diseases in humans have been directly linked to genes involved in the control of apoptosis. However, investigations into the role of apoptosis in the development of autoimmune diseases such as systemic lupus erythematosus, rheumatoid arthritis, psoriasis, inflammatory bowel disease, and autoimmune diabetes mellitus are just beginning. Alterations in the susceptibility of lymphocytes to die by apoptosis *in vitro* have been reported in several of these diseases (30).

**Cell death in viral infection.** The disruption of cell physiology as a result of viral infection can cause an infected cell to undergo apoptosis (31). The suicide of an infected cell may be viewed as a cellular defense mechanism to prevent viral propagation. Cytotoxic T cells also act to prevent viral spread (32) by recognizing and killing

cells that present viral peptides in association with cell surface major histocompatibility complex (MHC) class I molecules. Recent evidence has demonstrated that T cells can induce cell death by activating the target cell's endogenous cell death program. Cytotoxic T cells induce apoptosis either by activation of the Fas receptor on the surface of the target cell or by introduction of proteases, such as granzyme B, which activate the cell death program from within the cytoplasm (33).

To circumvent these host defenses, a number of viruses have developed mechanisms to disrupt the normal regulation of apoptosis within the infected cell. For example, establishment of an effective adenoviral infection depends on the function of the E1B 19-kD protein (34). The E1B 19-kD protein has been shown to block apoptosis directly, and its function can be replaced in adenovirus by *BCL2*. Primary sequence and mutational analyses suggest that there may also be structural similarity between these two genes (35). The *BHRF1* gene of Epstein-Barr virus and the *LMW5-HL* gene of African swine fever virus both have sequence and functional similarity to *BCL2* (36).

Other viral genes that can inhibit apoptosis have been reported that show no similarity to *BCL2*. For example, both the p35 gene and the inhibitor of apoptosis gene (IAP) found in baculoviruses can inhibit apoptosis in response to a wide variety of stimuli (37). The ability of p35 to inhibit apoptosis is not dependent on the expression of any other viral proteins. Poxviruses appear to inhibit apoptosis by producing an inhibitor of the death effector molecule interleukin-1 $\beta$  (IL-1 $\beta$ )-converting enzyme (ICE). ICE is a cysteine protease closely related to the protein encoded by the *Caenorhabditis elegans* cell death gene, *ced-3*. The *ced-3* product is required for cells to undergo programmed cell death during development in *C. elegans* (38). The cowpox gene *crmA* is a member of the serpin family of protease inhibitors and acts as a specific inhibitor of ICE (39). The *crmA* gene can inhibit apoptosis in response to a number of stimuli and has also been shown to be required to inhibit the development of an inflammatory response to virally infected cells (39, 40).

The prevention of apoptosis is also important for the establishment of viral latency. Epstein-Barr virus establishes a latent infection in B cells. The viral gene *LMP-1*, which is produced during latency, specifically up-regulates the expression of *BCL2*, potentially providing a survival advantage to latently infected cells (41). Chronic Sindbis virus infection has also been reported to be dependent on the host cell's expression of *BCL2* (31).

## Disorders Associated with Excess Cell Death

Excessive cell death can result from acquired or genetic conditions that enhance the accumulation of signals that induce apoptosis or that decrease the threshold at which such events induce apoptosis. Although increased apoptotic cell death has been observed in many of the diseases discussed below, in most degenerative disorders an underlying defect in cell death control has not been defined.

**Virus-induced lymphocyte depletion: AIDS.** Perhaps the most dramatic example of virus-associated cell depletion is AIDS, which is induced by the human immunodeficiency virus (HIV) (42). The development of AIDS has been directly correlated with the depletion of CD4<sup>+</sup> T cells, the cellular targets of viral infection. It has been shown that CD4 acts as a receptor for viral attachment, thus facilitating HIV infection of CD4<sup>+</sup> T cells. Surprisingly, most T cells that die during HIV infections do not appear to be infected with HIV. Although a number of explanations have been proposed, recent evidence suggests that stimulation of the CD4 receptor, by its binding to the soluble viral product gp120, results in the enhanced susceptibility of uninfected T cells to undergo apoptosis (43). In several models of cell death, it has been suggested that disordered signal transduction can result in the induction of apoptosis, perhaps by inducing an abortive cell cycle. CD4<sup>+</sup> T cells are normally activated by simultaneous engagement of the T cell receptor and CD4 by antigen-MHC class II complexes on the surface of an antigen-presenting cell. Both CD4<sup>+</sup> T cells from normal individuals as well as from individuals with HIV undergo apoptosis *in vitro* if cell-surface CD4 is crosslinked before engagement of T cell receptors (44). Thus, it is possible that gp120 promotes apoptotic cell death by its interaction with CD4.

One important question concerning this model is why the virus would develop a mechanism to selectively deplete its host cell. The answer perhaps reflects the fact that CD4<sup>+</sup> T cells have an important function in establishing protective immunity against a wide variety of viral infections. The establishment of a chronic HIV infection may therefore depend on virally mediated depletion of CD4<sup>+</sup> T cells and the concomitant loss of a protective cell-mediated immune response. Viral replication itself may not be limited by this form of CD4-dependent cell death because the viral protein Nef specifically down-regulates the CD4 receptor on infected T cells (45). This down-regulation has been thought to be involved in preventing viral reinfections. However, it may also help to prevent apop-



tosis in response to dysregulated CD4 stimulation. Immunodepletion as a result of viral infection is not restricted to HIV. Viruses in birds, cats, and mice have all been reported to induce immune cell depletion during systemic infection (46).

**Cell death in neurodegenerative disorders.** A wide variety of neurological diseases are characterized by the gradual loss of specific sets of neurons (47). Such disorders include Alzheimer's disease, Parkinson's disease, amyotrophic lateral sclerosis (ALS), retinitis pigmentosa, spinal muscular atrophy, and various forms of cerebellar degeneration. In these diseases, cell death results in specific disorders of movement and central nervous system function. The cell loss in these diseases does not induce an inflammatory response, and apoptosis appears to be the mechanism of cell death. Oxidative stress, calcium toxicity, mitochondrial defects, excitatory toxicity, and deficiency of survival factors have all been postulated to contribute to the pathogenesis of these disorders (48). Each of these pathways predisposes neurons to apoptosis, either in vitro or in vivo. Overexpression of *BCL2* decreases the neurotoxicity of each of these potential inducers of cell death (49). Neurotrophic growth factors and the extracellular matrix also alter the apoptotic threshold of neural cells (50). Together, these data suggest a model in which the threshold for cell death is dynamically regulated. The apoptotic threshold of a cell is thus determined by the combined effects of external and internal survival factors.

One form of hereditary ALS results from mutations in the gene encoding copper-zinc superoxide dismutase (51). Patients with this form of ALS have a mutation that results in a decrease in the ability of a cell to detoxify free radicals. The cell injury caused by free radicals has been shown to induce cells to undergo apoptosis in vitro. Superoxide-induced death can be specifically inhibited by treatment with survival growth factors or antioxidants (52).

Retinal degeneration associated with retinitis pigmentosa occurs as a result of mutations in any one of three photoreceptor-specific genes: rhodopsin, the  $\beta$  subunit of cyclic guanosine monophosphate phosphodiesterase, and the peripherin gene. All three mutations lead to photoreceptor apoptosis (53). Apoptosis may be initiated in response to the accumulation of mutant proteins or as a result of the altered functional properties of the mutant proteins (54). In a hereditary rat model of light-induced retinal degeneration, intraocular injections of eight distinct neurotrophic and growth factors enhanced photoreceptor survival, whereas seven others displayed no beneficial effects (55). These data suggest that treatment of such disorders may be possible with specific neurotrophic

factors either alone or in combination.

Alzheimer's disease is associated with the progressive accumulation of  $\beta$ -amyloid peptide in plaques. Mutations in the  $\beta$ -amyloid precursor protein are associated with some forms of familial Alzheimer's disease. Recently, several groups have shown that  $\beta$ -amyloid peptide induces neurons to undergo apoptosis (56). This effect can be reversed by antioxidants (57).

The spinal muscular atrophies are a group of recessive neurodegenerative disorders of childhood. These disorders are characterized by progressive spinal cord motor neuron depletion. One of the genes recently linked to these disorders, neuronal apoptosis inhibitory protein (*NAIP*), is homologous to the baculovirus inhibitor of apoptosis protein (*IAP*) (58). Baculovirus *IAP* genes have been shown to inhibit apoptosis in insect cells independent of other viral proteins. These data suggest that mutations in the *NAIP* gene may result in motor neurons being more susceptible to apoptosis in patients with spinal muscular atrophy.

**Cell death in blood cell disorders.** Mature blood cells are constantly being produced from hematopoietic stem cells located in the bone marrow. The regulation of hematopoiesis is influenced by a number of growth factors, including stem cell factor, erythropoietin, colony-stimulating factors, and thrombopoietin (59). In addition to stimulating the proliferation of hematopoietic progenitors, hematopoietic growth factors are required to support the survival of their target cells (60). Hematopoietic progenitors rapidly undergo apoptosis in vitro if deprived of growth factors. In fact, hematopoietic growth factors are also important in regulating the survival of postmitotic blood cells such as neutrophils.

It has been suggested that hematopoietic differentiation is primarily determined intrinsically within the precursor cell rather than as a result of the inductive effects of hematopoietic growth factors (61). Consistent with this view, hematopoietic stem cells in which apoptosis is suppressed by overproduction of *BCL2* can differentiate in the absence of extracellular growth factors or cell division. Together, these data suggest that hematopoietic growth factors control blood cell production at least in part by inhibiting apoptosis during the expansion and differentiation of intrinsically committed progenitors.

A number of hematologic diseases are associated with a decreased production of blood cells. Such disorders include anemia associated with chronic disease, aplastic anemia, chronic neutropenia, and the myelodysplastic syndromes. Disorders of blood cell production, such as myelodysplastic syndrome and some forms of aplastic anemia, are associated with increased apoptotic cell

death within the bone marrow (62). These disorders could result from the activation of genes that promote apoptosis, acquired deficiencies in stromal cells or hematopoietic survival factors, or the direct effects of toxins and mediators of immune responses.

Several hematopoietic growth factors are now in widespread clinical use because of their ability to increase the net production of individual types of blood cells (59). For example, erythropoietin can be used to augment red blood cell production in patients with anemia secondary to renal failure and other chronic illnesses. Granulocyte-macrophage colony-stimulating factor (GM-CSF), macrophage CSF, and granulocyte CSF have all been used to promote the recovery of granulocytes and macrophages after systemic chemotherapy for cancer.

### Additional Disorders in Which Apoptosis May Function

Two common disorders associated with cell death are myocardial infarctions and stroke. These diseases arise primarily as a result of an acute loss of blood flow (ischemia). In both disorders, cells within the central area of ischemia appear to die rapidly as a result of necrosis. However, outside the central ischemic zone, cells die over a more protracted time period and morphologically appear to die by apoptosis (63). Ischemia of both neurons and cardiac myocytes in culture results in the induction of apoptosis (64). Agents known to be inhibitors of apoptosis in vitro have been shown to limit infarct size in these disorders (65). However, the most effective method of limiting infarct size is restoration of blood flow. Advances in medicine have allowed for the development of a number of techniques to restore blood flow rapidly in acutely occluded blood vessels. Unfortunately, further tissue injury frequently occurs during establishment of reperfusion. Reperfusion is associated with acute increases in free radical production and increases in intracellular calcium, both potent inducers of apoptosis. The death of cardiomyocytes that occurs during reperfusion bears all the hallmarks of apoptosis (66). Whether agents that alter the apoptotic threshold can prevent reperfusion injury remains to be determined.

Relatively little is known about the mechanisms underlying the two major degenerative disorders of the musculoskeletal system: osteoporosis and degenerative arthritis. To date, no evidence exists that the genes involved in the control of apoptosis are involved in the pathogenesis of these disorders. Nevertheless, the progressive cell death of chondrocytes in osteoarthritis and osteocyte cell death in osteoporosis have morphological features suggestive of apoptosis (67).

Liver cells also undergo programmed cell death. In fact, the term apoptosis was originally used to describe the cell death that occurred outside the zone of central necrosis resulting from ligation of the portal vein (5). Since that time, various toxins (including alcohol) that are associated with acute fatty degeneration of the liver have been shown to induce apoptosis in hepatocytes (68).

### Regulation of Cell Death: Therapeutic Potential

A number of effective methods that induce target cells to undergo apoptosis already exist. Both chemotherapeutic agents and radiation induce tumor cell death primarily by causing damage that induces the cell to commit suicide (17, 69). In addition, many tumors retain some of the same physiologic controls for cell death as the cells from which they arise. For example, tumors arising in reproductive organs are responsive to hormonal manipulation that results in apoptosis (6, 70). Prostate cancers can be treated with androgen-ablation therapy. Moreover, breast cancers often undergo regression when treated with estrogen receptor antagonists. Treatments that restore the ability to properly regulate apoptosis could also be of considerable benefit in some malignancies. For example, it has recently been shown that the growth of human B cell lymphomas bearing *BCL2* translocations can be specifically inhibited in vitro by antisense oligonucleotides targeted against the *BCL2* gene (71).

Autoimmune diseases are characterized by the proliferative expansion of lymphocytes reactive to self-antigens. Several groups have been exploring methods to induce selective apoptosis in the autoreactive cells that cause disease. Recently, it has been shown that repetitive treatment with antigen can result in the selective death of antigen-reactive lymphocytes in vivo. Although the exact mechanisms by which such treatments induce apoptosis are unclear, the treatments may prime cells for Fas-mediated death (72). Specific deletion of lymphocytes by repetitive treatment with a disease-associated autoantigen has been shown to be effective in the treatment of experimental autoimmune encephalitis in mice (73). Similar treatment strategies may prove effective in human autoimmune disease if the specific antigens involved in the autoimmune reaction can be identified.

Conversely, treatments that increase a cell's resistance to undergo apoptosis may be of benefit in degenerative disorders. These treatments may be of benefit even in the absence of specific alterations in the genes involved in cell death regulation. Current evidence suggests that the susceptibility of cells to undergo apoptosis is regulated continuously. For example, enhanc-

ing the expression of *BCL2* can increase the resistance of cells to almost all apoptotic stimuli (13, 17). Thus, treatments that can increase the apoptotic thresholds of specific cells may be beneficial in the treatment of disorders associated with cell loss. Such treatments include the use of growth factors to promote hematopoietic cell recovery after cancer chemotherapy (56), trials of neurotrophic survival factors to enhance the survival of neurons in neurodegenerative disorders or trauma (50, 55), and treatments with antioxidants such as *n*-acetyl cysteine to prevent the death of CD4<sup>+</sup> T cells in response to HIV infection (74). Agents that alter calcium metabolism are currently being tested for the treatment of ischemic injuries (75).

It may also be possible to alter the apoptotic threshold by inhibiting the action of cell surface death effectors. For example, treatment with soluble Fas receptor or TNF antibodies may limit cell death in vivo by preventing deaths induced by Fas ligand and TNF, respectively (27, 76). Although the use of cell surface receptors and second messenger systems to regulate cell death responses in vivo has much appeal, it should be reemphasized that these agents can have pleiotropic effects. Under some circumstances Fas activation has been reported to stimulate lymphocyte proliferation instead of cell death (77). IL-12 treatment in vivo has recently been shown to protect bone marrow cells from gamma irradiation; however, it also potentiates cell death within the gastrointestinal tract in response to the same stimulus (78).

In principle, the genes involved in central cell death control, such as members of the *BCL2* and *ICE* families, could provide ideal targets for therapeutic intervention. However, most diseases are not characterized by a generalized increase in the susceptibility or resistance to apoptosis. There may be relatively little benefit in a therapy that enhances the survival of all neural cells at the expense of an increase in autoimmune disease or the enhancement of tumor progression through the prevention of apoptotic cell death.

Several observations suggest that the central mediators of apoptosis may still be pharmacologically manipulated in a cell-specific fashion. Individual tissues in the body can vary significantly in the expression of individual members of the *BCL2* and *ICE* gene families (79). Furthermore, specific inhibitors of individual members of the *ICE* family exist. The gene *cma* inhibits *ICE* but not the related *Ich-1* cysteine protease (80). This suggests that cysteine protease inhibitors may be developed that are specific for individual members of the *ICE* family. There is also evidence that alternative spliced forms of members of

both the *BCL2* family and cysteine protease family of death effectors can act as dominant inhibitors, perhaps by forming multimers that inhibit the function of active family members (80, 81). Pharmacologic agents that mimic the inhibitors or prevent specific protein-protein interactions within the *BCL2* or *ICE* families may have relative specificity for individual family members or heteromers formed from them. Finally, there is evidence that both the expression and function of individual members of the *BCL2* and *ICE* families are themselves regulated by lineage-specific signal transduction events. *BCL2* has been shown to undergo specific modulation in response to cytokines, cell-cell contact, or cell contact with the extracellular matrix (82). In addition, certain growth factors may function by inducing posttranslational modification of *BCL2* (83). Recent data analyzing mice deficient in *BCL2* expression suggest that the function of *BCL2* is absolutely necessary only in a limited number of normal cell types or, alternatively, that there is significant redundancy within the *BCL2* family such that specific loss of *BCL2* is relatively well tolerated outside of the immune and renal systems (84). Therefore, systemic inhibition of *BCL2* may not be as toxic as might have been expected initially.

One future application of our knowledge concerning cell death may be in designing safer, more effective vectors for gene therapy or vaccination. That many DNA viruses require survival genes to establish persistent viral infection may allow for the generation of vaccines consisting of attenuated viruses that do not have the ability to establish latent infections. Similarly, engineering gene therapy vectors to incorporate specifically regulated cell survival genes may help facilitate the establishment and removal of genetically altered cells in vivo.

### REFERENCES AND NOTES

1. T. Hunter, *Curr. Opin. Gen. Dev.* 3, 1 (1993); E. Rozengurt, *Curr. Opin. Cell Biol.* 4, 161 (1992).
2. A. J. Levine, *Annu. Rev. Biochem.* 62, 623 (1993).
3. R. E. Ellis, J. Yuan, H. R. Horvitz, *Annu. Rev. Cell Biol.* 7, 663 (1991).
4. M. C. Raff, *Nature* 356, 397 (1992); M. D. Jacobson, J. F. Burne, M. C. Raff, *EMBO J.* 13, 1899 (1994).
5. A. H. Wyllie, J. F. R. Kerr, A. R. Currie, *Int. Rev. Cytol.* 68, 251 (1980); J. F. R. Kerr, A. H. Wyllie, A. R. Currie, *Br. J. Cancer* 26, 18 (1972).
6. D. L. Vaux, G. Haeccker, A. Strasser, *Cell* 76, 777 (1994); W. Bursch, F. Oberhammer, R. Schulte-Hermann, *Trends Pharmacol. Sci.* 13, 245 (1992).
7. L. Sachs and J. Lotem, *Blood* 82, 15 (1993); T. M. Buttke and P. A. Sandstrom, *Immunol. Today* 15, 7 (1994); J. C. Reed, *J. Cell Biol.* 124, 1 (1994); D. L. Vaux, I. L. Weissman, S. K. Kim, *Science* 258, 1955 (1992).
8. M. O. Hengartner and H. R. Horvitz, *Cell* 76, 665 (1994); J. Yuan, S. Shaham, S. Ledoux, H. M. Ellis, H. R. Horvitz, *ibid.* 75, 641 (1993).
9. R. E. Ellis, D. M. Jacobson, H. R. Horvitz, *Genetics* 129, 79 (1991); V. A. Fadok et al., *J. Immunol.* 148, 2207 (1992); V. A. Fadok et al., *ibid.* 149, 4029 (1992); S. E. Hall, J. S. Savill, P. M. Henson, C.



- Haslett, *ibid.* 153, 3218 (1994).
10. M. C. Raff *et al.*, *Science* 262, 695 (1993); G. T. Williams, C. A. Smith, E. Spooncer, T. M. Dexter, D. R. Taylor, *Nature* 343, 76 (1990); P. E. Neiman, S. J. Thomas, G. Loring, *Proc. Natl. Acad. Sci. U.S.A.* 88, 5857 (1991); N. Boudreau, C. J. Simpson, Z. Werb, M. J. Bissell, *Science* 267, 891 (1995); J. G. Cyster, S. B. Hartley, C. C. Goodnow, *Nature* 371, 389 (1994); S. Cohen, *Proc. Natl. Acad. Sci. U.S.A.* 46, 302 (1960).
11. B. Hoffman and D. A. Liebermann, *Oncogene* 9, 1807 (1994).
12. Y. Tsujimoto, J. Gorham, J. Cossman, E. Jaffe, C. M. Croce, *Science* 229, 1390 (1985); A. Bakhshi *et al.*, *Cell* 41, 899 (1985); M. L. Cleary and J. Sklar, *Proc. Natl. Acad. Sci. U.S.A.* 82, 7439 (1985).
13. D. M. Hockenbery, G. Nuñez, C. Millman, R. D. Schreiber, S. J. Korsmeyer, *Nature* 348, 334 (1990); G. Nuñez *et al.*, *J. Immunol.* 144, 3602 (1990); D. L. Vaux, S. Cory, J. M. Adams, *Nature* 335, 440 (1988); D. M. Hockenbery, Z. N. Oltvai, X.-M. Yin, C. L. Millman, S. J. Korsmeyer, *Cell* 75, 241 (1993).
14. M. F. Clarke *et al.*, unpublished results.
15. T. J. McDonnell *et al.*, *Cancer Res.* 52, 6940 (1992); A. Hague, M. Moorghen, D. Hicks, M. Chapman, C. Parakeva, *Oncogene* 9, 3367 (1994); V. P. Castle *et al.*, *Am. J. Pathol.* 143, 1543 (1993).
16. L. H. Boise *et al.*, *Cell* 74, 597 (1993); E. Y. Lin, A. Orloffsky, M. S. Berger, M. B. Prystowsky, *J. Immunol.* 151, 1979 (1993); K. M. Kozopas, T. Yang, H. L. Buchan, P. Zhou, R. W. Craig, *Proc. Natl. Acad. Sci. U.S.A.* 90, 3516 (1993); Z. N. Oltvai, C. L. Millman, S. J. Korsmeyer, *Cell* 74, 609 (1993).
17. T. Ohmori *et al.*, *Biochem. Biophys. Res. Commun.* 192, 30 (1993); J. Lotem and L. Sachs, *Cell Growth Differ.* 4, 41 (1993); T. Miyashita and J. C. Reed, *Blood* 81, 151 (1993); A. Minn, C. Rudin, C. B. Thompson, unpublished observations.
18. S. W. Lowe, E. M. Schmitt, S. W. Smith, B. A. Osborne, T. Jacks, *Nature* 362, 847 (1993); A. R. Clarke *et al.*, *ibid.*, p. 849; J. M. Lee and A. Bernstein, *Proc. Natl. Acad. Sci. U.S.A.* 90, 5742 (1993).
19. S. W. Lowe *et al.*, *Science* 266, 807 (1994).
20. X. Lu and D. P. Lane, *Cell* 75, 765 (1993).
21. W. Bursch *et al.*, *Carcinogenesis* 11, 847 (1990); D. McConkey *et al.*, *J. Biol. Chem.* 264, 13399 (1989).
22. L. Shi *et al.*, *Science* 263, 1143 (1994); R. S. Freeman, S. Estus, E. M. Johnson Jr., *Neuron* 12, 343 (1994); L. L. Rubin, K. L. Philpott, S. F. Brooks, *Curr. Opin. Cell Biol.* 3, 391 (1993).
23. G. I. Evan *et al.*, *Cell* 69, 119 (1992).
24. A. Strasser, A. W. Harris, M. L. Bath, S. Cory, *Nature* 348, 331 (1990).
25. R. Watanabe-Fukunaga, C. I. Brannan, N. G. Copeland, N. A. Jenkins, S. Nagata, *ibid.* 356, 314 (1992).
26. T. Suda, T. Takahashi, P. Golstein, S. Nagata, *Cell* 75, 1169 (1993).
27. J. Cheng *et al.*, *Science* 263, 1759 (1994).
28. A. Strasser *et al.*, *Proc. Natl. Acad. Sci. U.S.A.* 88, 8661 (1991).
29. H. J. Garchon, J. J. Luan, L. Eloy, P. Bedossa, J. F. Bach, *Eur. J. Immunol.* 24, 380 (1994).
30. J. D. Mountz, J. Wu, J. Cheng, T. Zhou, *Arthritis Rheum.* 37, 1415 (1994); W. Emlen, J. Niebur, R. Kadera, *J. Immunol.* 152, 3685 (1994).
31. B. Levine *et al.*, *Nature* 361, 739 (1993).
32. P. A. Henkart, *Immunity* 1, 343 (1994).
33. D. Kägi *et al.*, *Science* 265, 528 (1994); D. Kägi *et al.*, *Nature* 369, 31 (1994); J. W. Heusel, R. L. Wesselschmidt, S. Shrestha, J. H. Russell, T. J. Ley, *Cell* 76, 977 (1994).
34. L. Rao *et al.*, *Proc. Natl. Acad. Sci. U.S.A.* 89, 7742 (1992).
35. J. M. Boyd *et al.*, *Cell* 79, 341 (1994).
36. J. G. Neilan *et al.*, *J. Virol.* 67, 4391 (1993); S. Henderson *et al.*, *Proc. Natl. Acad. Sci. U.S.A.* 90, 8479 (1993).
37. R. J. Clem, M. Fechtmeier, L. K. Miller, *Science* 254, 1388 (1991); A. Sugimoto, P. D. Friesen, J. H. Rothman, *EMBO J.* 13, 2023 (1994); S. Rabizadeh, D. J. LaCount, P. D. Friesen, D. E. Bredesen, *J. Neurochem.* 61, 2318 (1993); R. J. Clem and L. K. Miller, *Mol. Cell Biol.* 14, 5212 (1994).
38. M. Miura, H. Zhu, R. Rotello, E. A. Hartwig, J. Yuan, *Cell* 75, 653 (1993).
39. C. A. Ray *et al.*, *ibid.* 69, 597 (1992).
40. V. Gagliardini *et al.*, *Science* 263, 826 (1994).
41. S. Henderson *et al.*, *Cell* 65, 1107 (1991).
42. L. Meygaard *et al.*, *Science* 257, 217 (1992).
43. J. C. Ameisen and A. Capron, *Immunol. Today* 12, 102 (1991); H. Groux *et al.*, *J. Exp. Med.* 175, 331 (1992); M.-L. Gougeon and L. Montagnier, *Science* 260, 1269 (1993).
44. M. K. Newell, L. J. Haughn, C. R. Maroun, M. H. Julius, *Nature* 347, 286 (1990); N. K. Banda *et al.*, *J. Exp. Med.* 176, 1099 (1992).
45. D. R. Littman, *Curr. Biol.* 4, 618 (1994).
46. A. L. Guiot *et al.*, *C. R. Acad. Sci. Ser. III* 316, 1297 (1993); A. C. Vasconcelos and K. M. Lam, *J. Gen. Virol.* 75, 1803 (1994); D. A. Cohen *et al.*, *Cell Immunol.* 151, 392 (1993).
47. O. Isacson, *Trends Neurosci.* 16, 306 (1993); N. Heintz, *Trends Biochem. Sci.* 18, 157 (1993).
48. D. W. Choi, *J. Neurobiol.* 23, 1261 (1992); I. Ziv *et al.*, *Neurosci. Lett.* 170, 136 (1994).
49. L.-T. Zhong *et al.*, *Proc. Natl. Acad. Sci. U.S.A.* 90, 4533 (1993).
50. M. T. Herrero *et al.*, *Neuroscience* 56, 965 (1993); M. Okamoto, S. Mori, H. Endo, *Brain Res.* 637, 57 (1994); E. Arenas and H. Persson, *Nature* 367, 368 (1994).
51. D. R. Rosen *et al.*, *Nature* 362, 59 (1993); H.-X. Deng *et al.*, *Science* 261, 1047 (1993).
52. C. M. Troy and M. L. Shelanski, *Proc. Natl. Acad. Sci. U.S.A.* 91, 6384 (1994).
53. G.-Q. Chang, Y. Hao, F. Wong, *Neuron* 11, 595 (1993).
54. V. R. Rao, G. B. Cohen, D. D. Oprian, *Nature* 367, 639 (1994).
55. M. M. LaVail *et al.*, *Proc. Natl. Acad. Sci. U.S.A.* 89, 11249 (1992).
56. D. T. Loo *et al.*, *ibid.* 90, 7951 (1993); A. Takashima, K. Noguchi, K. Sato, T. Hoshino, K. Imahori, *ibid.*, p. 7789.
57. C. Behl, J. Davis, G. M. Cole, D. Schubert, *Biochem. Biophys. Res. Commun.* 186, 944 (1992).
58. N. Roy *et al.*, *Cell* 80, 167 (1995).
59. R. A. Fleischman, *Am. J. Med. Sci.* 305, 248 (1993); S. Blackwell and J. Crawford, *Pharmacotherapy* 12, 20S (1992); D. Haase and C. Fonatsch, *Blut* 60, 192 (1990).
60. K. Muta and S. B. Krantz, *J. Cell. Physiol.* 156, 264 (1993); L. L. Kelley *et al.*, *Blood* 82, 2340 (1993).
61. L. J. Fairbairn, G. J. Cowling, B. M. Reipert, T. M. Dexter, *Cell* 74, 823 (1993).
62. Y. Yoshida, *Leukemia* 7, 144 (1993).
63. J. J. Cohen, *Hosp. Pract.* 28, 35 (1993).
64. M. Tanaka *et al.*, *Circ. Res.* 75, 426 (1994); D. M. Rosenbaum, J. Kalberg, J. A. Kessler, *Stroke* 25, 857 (1994).
65. O. Uyama, T. Matsuyama, H. Michishita, H. Nakamura, M. Sugita, *Stroke* 23, 75 (1992).
66. R. A. Gottlieb, K. O. Burleson, R. A. Kloner, B. M. Babior, R. L. Engler, *J. Clin. Invest.* 94, 1621 (1994).
67. C. R. Dunstan, N. M. Somers, R. A. Evans, *Calcif. Tissue Int.* 53, S113 (1993); A. M. Parfitt, *ibid.*, p. S82; W. Mohr and H. Lehmann, *Z. Rheumatol.* 51, 35 (1992); Y. Ishizaki, J. F. Burne, M. C. Raff, *J. Cell Biol.* 126, 1069 (1994).
68. R. D. Goldin, N. C. Hunt, J. Clark, S. N. Wickramasinghe, *J. Pathol.* 171, 73 (1993).
69. D. E. Fischer, *Cell* 78, 539 (1994).
70. M. Colombel, C. A. Olsson, P.-Y. Ng, R. Buttyan, *Cancer Res.* 52, 4313 (1992).
71. J. C. Reed *et al.*, *ibid.* 50, 6565 (1990).
72. G. G. Singer and A. K. Abbas, *Immunity* 1, 365 (1994).
73. J. M. Critchfield *et al.*, *Science* 263, 1139 (1994).
74. M. Roederer, F. J. T. Staal, S. W. Elia, L. A. Herzenberg, L. A. Herzenberg, *Pharmacology* 46, 121 (1993).
75. J. Sharkey and S. P. Butcher, *Nature* 371, 336 (1994); M. P. Mattson, R. E. Rydel, I. Lieberburg, V. L. Smith-Swintosky, *Ann. N.Y. Acad. Sci.* 679, 1 (1993).
76. M.-V. Clement and I. Stamenkovic, *J. Exp. Med.* 180, 557 (1994).
77. M. R. Alderson *et al.*, *ibid.* 178, 2231 (1993).
78. R. Neta, S. M. Stiefel, F. Finkelman, S. Herrmann, N. Ali, *J. Immunol.* 153, 4230 (1994).
79. M. González-García *et al.*, *Development* 120, 3033 (1994); D. M. Hockenbery, M. Zutter, W. Hickey, M. Nahm, S. J. Korsmeyer, *Proc. Natl. Acad. Sci. U.S.A.* 88, 6961 (1991).
80. L. Wang, M. Miura, L. Bergeron, H. Zhu, J. Yuan, *Cell* 78, 739 (1994); S. Kumar, M. Kinoshita, M. Noda, N. G. Copeland, N. A. Jenkins, *Genes Dev.* 8, 1613 (1994).
81. X.-M. Yin, Z. N. Oltvai, S. J. Korsmeyer, *Nature* 369, 321 (1994).
82. A. M. Genaro, J. A. Gonzalo, L. Bosea, C. Martinez-A., *Eur. J. Immunol.* 24, 2515 (1994); Y. Levy and J.-C. Brouet, *J. Clin. Invest.* 93, 424 (1994); M. Dancescu *et al.*, *J. Exp. Med.* 176, 1319 (1992).
83. W. S. May *et al.*, *J. Biol. Chem.* 269, 26865 (1994).
84. D. J. Veis, C. M. Sorenson, J. R. Shutter, S. J. Korsmeyer, *Cell* 75, 229 (1993).
85. I wish to thank J. Leiden, S. Reiner, C.-R. Wang, T. Lindsten, and the members of my laboratory for their thoughtful discussions and careful review of the manuscript, and T. Conway for her editorial assistance.

## *In vivo* detection and imaging of phosphatidylserine expression during programmed cell death

FRANCIS G. BLANKENBERG\*†, PETER D. KATSIKIS‡, JONATHAN F. TAIT§, R. ERIC DAVIS¶, LOUIS NAUMOVSKI||, KATSUICHI OHTSUKI†, SUSAN KOPIWODA†, MICHAEL J. ABRAMS\*\*, MARILYN DARKES\*\*, ROBERT C. ROBBINS††, HOLDEN T. MAECKER‡‡, AND H.W. STRAUSS†

†Department of Radiology, ‡Department of Genetics, §Department of Pathology, ¶Department of Pediatrics (Hematology/Oncology), ††Department of Cardiothoracic Surgery, ‡‡Department of Medicine/Oncology, Stanford University School of Medicine, 300 Pasteur Drive, Stanford, CA 94305-5105; §Department of Laboratory Medicine, University of Washington, Health Sciences, Room NW-120, Box 357110, Seattle, WA 98195-7110; and \*\*Anor MED Incorporated, 20353 64th Avenue, Suite #100, Langley, British Columbia, Canada 3A7R3

Communicated by Victor A. McKusick, Johns Hopkins University, Baltimore, MD, March 6, 1998 (Received for review January 27, 1998)

**ABSTRACT** One of the earliest events in programmed cell death is the externalization of phosphatidylserine, a membrane phospholipid normally restricted to the inner leaflet of the lipid bilayer. Annexin V, an endogenous human protein with a high affinity for membrane bound phosphatidylserine, can be used *in vitro* to detect apoptosis before other well described morphologic or nuclear changes associated with programmed cell death. We tested the ability of exogenously administered radiolabeled annexin V to concentrate at sites of apoptotic cell death *in vivo*. After derivatization with hydrazinonicotinamide, annexin V was radiolabeled with technetium 99m. *In vivo* localization of technetium 99m hydrazinonicotinamide-annexin V was tested in three models: fulminant hepatic apoptosis induced by anti-Fas antibody injection in BALB/c mice; acute rejection in ACI rats with transplanted heterotopic PVG cardiac allografts; and cyclophosphamide treatment of transplanted 38C13 murine B cell lymphomas. External radionuclide imaging showed a two- to sixfold increase in the uptake of radiolabeled annexin V at sites of apoptosis in all three models. Immunohistochemical staining of cardiac allografts for exogenously administered annexin V revealed intense staining of numerous myocytes at the periphery of mononuclear infiltrates of which only a few demonstrated positive apoptotic nuclei by the terminal deoxynucleotidyltransferase-mediated UTP end labeling method. These results suggest that radiolabeled annexin V can be used *in vivo* as a noninvasive means to detect and serially image tissues and organs undergoing programmed cell death.

Programmed cell death (apoptosis) plays a crucial role in the pathogenesis of a number of disorders including AIDS and other viral illnesses, cerebral and myocardial ischemia, autoimmune and neurodegenerative diseases, organ and bone marrow transplant rejection, and tumor response to chemotherapy and radiation (1–3). Since the original description of apoptosis by Wyllie in 1972, its assessment *in vivo* has required direct examination of biopsied or aspirated material (4). An imaging technique capable of localizing and quantifying apoptosis *in vivo* would permit assessment of disease progression or regression and similarly define the efficacy of therapy designed to inhibit or induce cell death (5–6).

Cells undergoing apoptosis redistribute phosphatidylserine (PS) from the inner leaflet of the plasma membrane lipid bilayer to the outer leaflet (7, 8). The externalization of PS is a general feature of apoptosis occurring before membrane bleb formation and DNA degradation (7, 8). Annexin V, a human

protein with a molecular weight of 36,000 has a high affinity for cell or platelet membranes with exposed PS *in vitro* and *in vivo* (9–13). This observation has led to testing radiolabeled annexin V in animal models of acute thrombosis and imaging of atrial thrombi in patients with atrial fibrillation (14, 15). In the current study, annexin V was derivatized with hydrazinonicotinamide (HYNIC) and coupled to technetium 99m (<sup>99m</sup>Tc) (16) before i.v. administration in animal models of apoptosis. HYNIC, an nicotinic acid analog, is a bifunctional molecule capable of bonding to lysine residues of proteins on one moiety and conjugates of <sup>99m</sup>Tc on the other. The agent forms stable complexes with proteins (16) without affecting bioactivity. We performed scintigraphic imaging studies with derivatized annexin V to determine its ability *in vivo* to detect sites of apoptotic cell death occurring in Fas-mediated hepatocyte apoptosis, acute cardiac allograft rejection, and cyclophosphamide treatment of B cell lymphoma. Such *in vivo* imaging may prove useful in the clinical setting for noninvasive diagnosis, monitoring of disease progression or regression, and determining efficacy of treatment.

### MATERIALS AND METHODS

**Preparation of <sup>99m</sup>Tc HYNIC-Annexin V.** Human annexin V was produced by expression in *Escherichia coli* as described (13, 17, 18); this material retains PS-binding activity equivalent to that of native annexin V (18). Concentrations were determined using E<sub>280</sub> = 0.6 ml/mg<sup>-1</sup> cm<sup>-1</sup> and molecular weight was taken as 35, 806. HYNIC-derivatized annexin V was produced by the gentle mixing of 5.6 mg/ml of annexin V in 20 mM Hepes, pH 7.4, and 100 mM NaCl for 3 hr shielded from light with succinimidyl 6-HYNIC (Anor Med, Langley, British Columbia) [222 µg in 18.5 µl (42 mM solution) of *N,N*-dimethyl formamide] at room temperature. The reaction was quenched with 500 µl of 500 mM glycine in PBS, pH 7.4, and then dialyzed at 4°C against 20 mM sodium citrate, pH 5.2, and 100 mM NaCl overnight. Precipitate was then removed by centrifugation at 15,000 × *g* for 10 min. Then, 100 µl (100 µg) aliquots of HYNIC-annexin V were stored at –70°C. Incorporation of HYNIC into annexin V was found to be 0.9 mol/mol of annexin V by using the methods of King *et al.* (19). Membrane-binding activity of HYNIC-annexin V and decayed <sup>99m</sup>Tc HYNIC-annexin V was determined by a modified competition assay in which 5 nmol/liter fluorescein isothiocyanate (FITC)-annexin V was substituted for <sup>125</sup>I-annexin V (12, 17). After incubation for 15 min at room temperature, cells

The publication costs of this article were defrayed in part by page charge payment. This article must therefore be hereby marked "advertisement" in accordance with 18 U.S.C. §1734 solely to indicate this fact.

© 1998 by The National Academy of Sciences 0027-8424/98/956349-6\$2.00/0 PNAS is available online at <http://www.pnas.org>.

Abbreviations: TUNEL, terminal deoxynucleotidyltransferase-mediated UTP end labeling; PS, phosphatidylserine; HYNIC, hydrazinonicotinamide; <sup>99m</sup>Tc, technetium 99m; FITC, fluorescein isothiocyanate; HSA, human serum albumin; ROI, region of interest.

\*To whom reprint requests should be addressed. e-mail: MA.FRB@Forsythe.Stanford.Edu.

were centrifuged, the FITC-annexin V bound to the pelleted cells was released with EDTA, and the released FITC-annexin V was measured by fluorometry. In this assay system, unmodified annexin V, HYNIC-annexin V, and decayed  $^{99m}\text{Tc}$  HYNIC-annexin V inhibited 50% of the binding of FITC-annexin V at concentrations of 8 nmol/liter, 10.5 nmol/liter, and 12.3 nmol/liter, respectively.

To bind  $^{99m}\text{Tc}$  to the HYNIC-annexin conjugate 80  $\mu\text{l}$  of stannous chloride (50 mg/ml in 0.1 M HCl purged for 2 hr with  $\text{N}_2$  gas) was first added to 50 ml of a 20 mM tricine solution (pH 7.1, purged for 1 hr with  $\text{N}_2$  gas; tricine = *N*-[tris(hydroxymethyl)methyl]glycine). Two hundred microliters of the Sn-tricine solution was then added to 100  $\mu\text{l}$  of  $^{99m}\text{Tc}$   $\text{O}_4$  (4–20 mCi (1 Ci = 37 GBq) activity in 0.9% NaCl) previously mixed with a 100  $\mu\text{l}$  (100  $\mu\text{g}$ ) aliquot of HYNIC-annexin V according to the methods described by Abrams *et al.* (20). Specific activity was 10–200  $\mu\text{Ci}/\mu\text{g}$  protein (depending on desired activity) with a radiopurity of 92–97% determined with instant thin layer chromatography using 0.9% saline solution as a solvent.

**Scintillation Well Counting.** Samples were counted in a Packard Cobra II gamma counter (Packard). The energy window was set at a lower level of 120 keV and an upper level of 170 keV for  $^{99m}\text{Tc}$ . When  $^{125}\text{I}$  was counted, samples were allowed to decay for at least 24 hr. The samples were then recounted using both the technetium window and an  $^{125}\text{I}$  setting with a lower level of 20 keV and an upper level of 50 keV. Samples were corrected for any residual cross talk.

**Radionuclide Imaging.** A Technicare 420 mobile camera (Technicare, Solon, OH) equipped with a low energy high resolution parallel hole collimator was used to record the radionuclide distribution in mice and rats sedated with a mixture of 80 mg/kg ketamine and 4 mg/kg acepromazine injected i.m. Data were recorded by using a 20% window centered on the 140 keV photopeak of technetium into a 128  $\times$  128 matrix of a dedicated computer system for digital display and analysis (ICON, Siemens, Hoffman Estates, IL). All images were recorded for a preset time of 10–15 min.

**Murine Model of Fas-Mediated Apoptosis.** Massive hepatic apoptosis can be induced within 1–2 hr in mice following i.v. injection of anti-Fas antibody (21). We used this well described model of *in vivo* programmed cell death to test the specific localization of  $^{99m}\text{Tc}$  HYNIC-annexin to an organ undergoing apoptosis *in vivo*. Four- to five-wk-old BALB/c mice were injected i.v. with purified hamster anti-Fas mAb (Jo2, 10  $\mu\text{g}$ /animal, PharMingen, San Diego, CA) using the model proposed by Ogasawara *et al.* (21). Mice were then injected i.v. with 25–50  $\mu\text{g}$ /kg of  $^{99m}\text{Tc}$  HYNIC-annexin V (10–25  $\mu\text{Ci}$ /animal for biodistribution study and 100–150  $\mu\text{Ci}$ /animal for imaging studies) 1 or 2 hr after antibody treatment. Animals were killed 1 hr after administration of radiopharmaceutical followed by organ removal for scintillation counting of radioactivity and for histologic and immunohistochemical analyses.

Control studies with  $^{99m}\text{Tc}$  labeled human serum albumin (HSA) also were performed in untreated and anti-Fas treated mice. Although other proteins were considered as controls, albumin was selected because distinguishing the potential vascular disruption and protein leakage associated with acute apoptosis was a major goal of this control experiment. The animals were injected with 100–150  $\mu\text{Ci}$  of  $^{99m}\text{Tc}$  labeled HSA (25 mg/animal) and imaged at 1 and 2 hr, in similar fashion to the mice receiving  $^{99m}\text{Tc}$  HYNIC-annexin.

**Rodent Model of Cardiac Transplantation.** Adult male ACI rats (250–350 g) received heterotopic cardiac allografts from PVG donors (obtained from Harlan–Sprague–Dawley) anastomosed to the hosts' abdominal aorta and inferior vena cava according to a modification of the technique of Ono and Lindsey (22). Syngeneic cardiac isografts from ACI donors also were transplanted to the abdomens of host ACI rats. PVG cardiac allografts in ACI recipients using the model above begin to undergo rejection between 4 and 5 days post-

transplantation as assessed by decreased pulsation to palpation. Five days after transplantation all of the animals received 700–900  $\mu\text{Ci}$  of  $^{99m}\text{Tc}$  HYNIC-annexin V (10–20  $\mu\text{g}$  protein/kg) via tail vein and were imaged 1 hr later. Animals were then killed, and native and transplanted hearts underwent scintillation counting and histopathologic studies.

**Murine Model of Lymphoma.** 38C13 murine B cell lymphomas (23) were grown in C3H.HeN mice (Harlan Breeders, Indianapolis) following s.c. injection of 400 tumor cells suspended in 200  $\mu\text{l}$  of RPMI medium 1640 (without serum) into the left flank. Fourteen days after implantation mice underwent treatment with 100 mg/kg of cyclophosphamide injected i.p. Mice were injected i.v. with 25–50  $\mu\text{g}$ /kg of  $^{99m}\text{Tc}$  HYNIC-annexin V (100–150  $\mu\text{Ci}$ /animal) 20 hr after cyclophosphamide administration. Animals were then imaged and killed 1 hr after injection of radiopharmaceutical after tumor removal for scintillation counting and histopathologic studies.

**Immunostaining for Bound Human Annexin V and Apoptotic Nuclei.** Formalin-fixed paraffin-embedded tissues were sectioned at 5  $\mu\text{m}$  for staining with hematoxylin/eosin or other techniques. Immunostaining for bound human annexin V was performed with a rabbit anti-serum raised against human placental annexin V and affinity purified with recombinant annexin V coupled to Affi-Gel (Bio-Rad). Immunohistochemical detection then was completed by sequential incubations with biotin-labeled goat anti-rabbit antibody and avidin-horseradish peroxidase complex (Jackson Immuno Research), followed by reaction with 3,3'-diaminobenzidine as described by Bindl and Warnke (24).

For the detection of apoptotic nuclei, sections were stained using a modification of the terminal deoxynucleotidyltransferase-mediated UTP end labeling (TUNEL) method described by Gavrieli *et al.* (25). After inhibition of endogenous peroxidase, deparaffinized sections were digested with proteinase K (20  $\mu\text{g}$ /ml) for 15 min at room temperature. Sections were then incubated with  $\lambda$  exonuclease (Life Technologies, Gaithersburg, MD) at 5 unit/ml for 30 min at 37°C followed by equilibration with terminal deoxynucleotidyltransferase reaction buffer (0.2 M potassium cacodylate, 25 mM Tris-HCl, 0.25 mg/ml BSA, 1.5 mM  $\text{CaCl}_2$ , 20 mg/ml polyvinylpyrrolidone, and 20 mg/ml Ficoll) and 5  $\mu\text{M}$  dATP. The end-labeling reaction then was performed in terminal deoxynucleotidyltransferase reaction buffer also containing a final concentration of 75 unit/ml of terminal deoxynucleotidyltransferase and 100  $\mu\text{M}$  of 1,N-6-ethenol-dATP (Sigma). After a 60-min incubation at 37°C, the reaction was quenched via rinsing with 1 $\times$  SSC (standard saline citrate). Sections were then incubated with murine 1G4 mAb (gift from Regina Santella, Columbia University), which recognizes the ethenoadenine moiety (26). Subsequent immuno-histochemical detection was as described above, using a biotin-labeled goat anti-mouse antibody.

## RESULTS

**Biodistribution of Radiolabeled Annexin V in Fulminant Hepatic Apoptosis.** There was a 134% and 304% increase in the hepatic uptake of  $^{99m}\text{Tc}$  HYNIC-annexin V above controls at 1 and 2 hr after anti-Fas antibody injection, respectively, as determined by biodistribution studies (Table 1). Hepatic uptake was inversely proportional to renal uptake in treated mice with a 75% decrease in renal activity 2 hr after treatment. Of note, there was <5% excretion of administered radiopharmaceutical into the urine in control or treated animals. Splenic uptake was 108% and 54% above control values in the 1- and 2-hr treatment groups, respectively.

Subgroups of mice were co-injected with  $^{125}\text{I}$ -HSA to control for nonspecific uptake of inert protein from the circulation caused by hepatic endothelial cell breakdown (27). Hepatic uptake was 120% above control values at 1 hr after anti-Fas antibody injection and remained unchanged in contrast to the

Table 1. Biodistribution study of radiolabeled annexin V after anti-Fas antibody treatment

A)	<sup>99m</sup> Tc	Controls	1-hr anti-Fas	2-hr anti-Fas
	% ID	(n = 9)	(n = 15)	(n = 12)
	Liver	12.2 ± 1.4	28.6 ± 9.4**	49.3 ± 12.7***
	Kidneys	55.9 ± 8.9	35.2 ± 14.4**	14.0 ± 10.0***
	Spleen	1.6 ± 0.25	3.34 ± 1.42*	2.46 ± 1.22(ns)
B)	<sup>125</sup> I	Controls	1-hr anti-Fas	2-hr anti-Fas
	% ID	(n = 4)	(n = 6)	(n = 5)
	Liver	3.98 ± 1.09	8.77 ± 3.53*	8.4 ± 1.92*
	Kidneys	1.37 ± 0.35	1.88 ± 0.37(ns)	1.82 ± 0.38(ns)
	Spleen	0.39 ± 0.09	0.47 ± 0.15(ns)	0.37 ± 0.041(ns)
C)	Weight	Controls	1-hr anti-Fas	2-hr anti-Fas
	(grams)	(n = 9)	(n = 15)	(n = 12)
	Liver	1.06 ± 0.097	1.29 ± 0.32(ns)	1.37 ± 0.22*
	Kidneys	0.31 ± 0.061	0.32 ± 0.079(ns)	0.37 ± 0.072(ns)
	Spleen	0.12 ± 0.022	0.12 ± 0.02(ns)	0.11 ± 0.014(ns)

% injected dose (ID) per organ corrected for background, decay, and tail infiltration are listed for mice injected with 100–150  $\mu$ Ci (radiopurity >95%, specific activity 150–200  $\mu$ Ci/ $\mu$ g protein) of <sup>99m</sup>Tc HYNIC-annexin co-injected with 0.6  $\mu$ Ci (25 mg) of <sup>125</sup>I radiolabeled HSA. A) Biodistribution of <sup>99m</sup>Tc HYNIC-annexin V, B) <sup>125</sup>I-HSA, and C) Organ weight. Data are expressed as mean  $\pm$  standard error of the mean. P-values are shown in parenthesis ( ) for Dunnett's test for multiple comparison of means of the 1- or 2-hr post-treatment groups compared with control. ns, not significant (i.e., P-value > 0.05); \*, P < 0.05; \*\*, P < 0.001; \*\*\*, P < 0.0001.

progressive rise in annexin V uptake. There was a 29% increase in liver weight at 2 hr. Renal and splenic weight and uptake of <sup>125</sup>I-HSA did not change significantly after treatment.

Sections of livers from mice treated with anti-Fas antibody showed a spectrum of nuclear changes characteristic of apoptosis (margination of chromatin, pyknosis, and karyorrhexis) as early as 1 hr after injection; changes were more pronounced and focally associated with hemorrhage (peliosis) 2 hr after treatment (Fig. 1A). Immunostaining for <sup>99m</sup>Tc HYNIC-annexin V was observed at the cytoplasmic border of apoptotic hepatocytes; although this result was focal, the localization pattern is consistent with PS externalization, and staining never was observed in normal hepatocytes (Fig. 1B) or in anti-Fas antibody-treated mice not injected with <sup>99m</sup>Tc HYNIC-annexin V (data not shown).

**In Vivo Imaging of Fas-Mediated Fulminant Hepatic Apoptosis.** A high concentration of radiolabeled annexin V activity was observed by scintillation camera imaging in the kidneys of control animals with minimal concentration in other organs (Fig. 2). Hepatic uptake in control mice [12% of injected dose (% ID)] did not permit clear delineation of the liver. In mice treated with anti-Fas antibody, there was a diffuse increase in the intensity of hepatic uptake of <sup>99m</sup>Tc HYNIC-annexin V observed at 1 hr, which continued to rise at 2 hr after treatment. The transient increase in splenic uptake and the fall in renal activity found in the biodistribution studies both were visualized readily with external imaging following anti-Fas treatment. A total of 19 mice (six control, seven 1-hr, and six 2-hr anti-Fas-treated animals) underwent biodistribution study after imaging with <sup>99m</sup>Tc HYNIC-annexin V. The percentage of whole body activity per organ determined by region of interest (ROI) image analysis correlated well with the percentage of injected dose per organ determined by biodistribution (linear correlation coefficients for the liver, kidney, and spleen of  $r^2 = 0.853, 0.860,$  and  $0.979$ , respectively.)

There was no perceptible difference in liver, renal, or splenic uptake on the <sup>99m</sup>Tc-HSA images between the treated mice and controls (images not shown). There also was a direct correlation of observed uptake of <sup>99m</sup>Tc-HSA as seen by ROI image analysis and the biodistribution of <sup>99m</sup>Tc-HSA (data not shown), which mirrored the biodistribution of <sup>125</sup>I-HSA.

**In Vivo Imaging of Cardiac Allograft Rejection.** All of the PVG cardiac allografts (n = 4) were visualized easily with <sup>99m</sup>Tc HYNIC-annexin V 5 days after transplantation (Fig. 3).

ACI syngeneic cardiac isografts (n = 3) had no visible activity after injection of <sup>99m</sup>Tc HYNIC-annexin with uptakes of

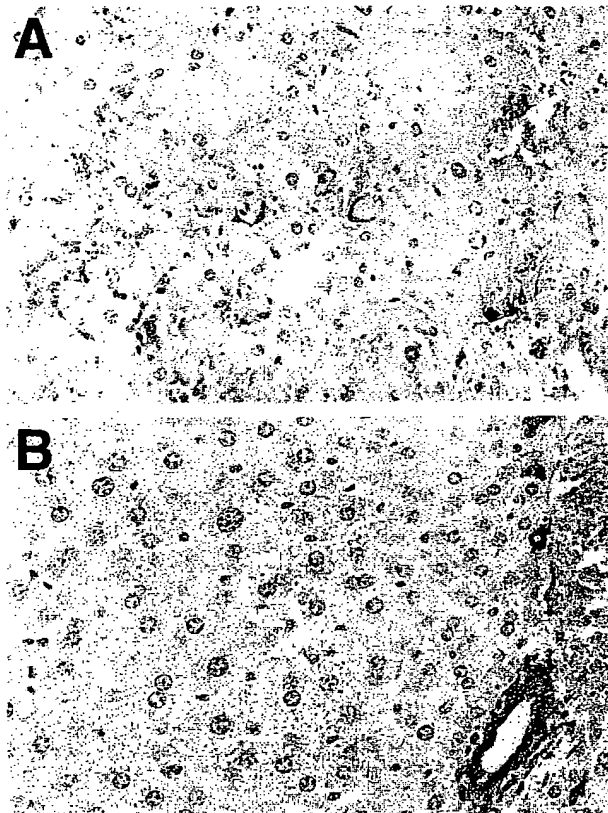


FIG. 1. Histologic sections of murine liver immunostained for exogenously administered human annexin V. (A) Two hours after anti-Fas antibody treatment there is extensive apoptotic nuclear change, slight cytoplasmic retraction, and interstitial hemorrhage. Annexin V staining (brown immunostaining product) is focally present at the cytoplasmic border of apoptotic hepatocytes. (B) No hepatocyte staining was observed in untreated mice. Staining of bile duct epithelium was caused by antibody cross-reactivity because it also was seen in the absence of exogenously administered human annexin V (data not shown). (Diaminobenzidine immunostain with hematoxylin counterstain,  $\times 40$  objective magnification.)

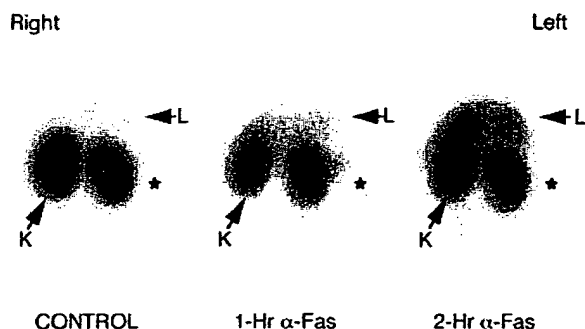


FIG. 2. Imaging Fas-mediated fulminant hepatic apoptosis with radiolabeled annexin V. One hour after injection of 150  $\mu$ Ci of radiopharmaceutical (50  $\mu$ g/kg of protein) mice were imaged in the prone anterior projection. There was a progressive increase in  $^{99m}$ Tc annexin V uptake of the liver of mice at 1 and 2 hr after anti-Fas antibody injection. Liver activity (L) was 111% and 239% above control values in the 1- and 2-hr mice, respectively, as shown by region of interest image analysis. Kidney activity (K) was 70% and 64% below control values in the 1- and 2-hr mice, respectively. Splenic activity (\*) was 168% and 45% above control values in the 1- and 2-hr mice, respectively.

radiopharmaceutical identical to native cardiac activity as confirmed by scintillation well counting (data not shown). The percentage of whole body activity of PVG allografts was 213% above ACI isograft activity ( $P < 0.005$ ; using a two-tailed student's  $t$  test) determined by ROI image analysis. Scintillation well-counting assay revealed a  $>11$ -fold increase in  $^{99m}$ Tc HYNIC-annexin V uptake in PVG allografts as compared with native heart activity.

Sections of PVG cardiac allografts 5 days after transplantation showed a marked mononuclear inflammatory cell infiltrate in all animals; no infiltrate was observed in syngeneic or native hearts. The infiltrate surrounded areas of myocardial injury and was associated with thrombosis of myocardial vessels. In the center of these areas, there was frank necrosis, with no staining by hematoxylin, but at the periphery, there were nuclei with changes of apoptosis as confirmed by TUNEL

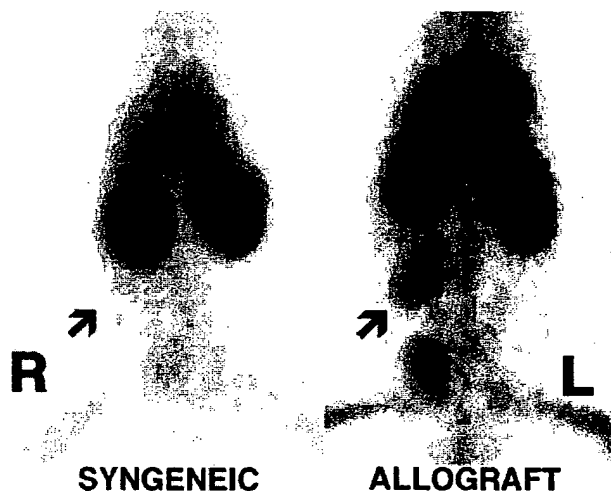


FIG. 3. Imaging cardiac allograft rejection with radiolabeled annexin V. Representative images of abdominal cardiac syngeneic ACI isograft and PVG allograft in ACI host rats 5 days after transplantation. Rats were imaged in the prone anterior projection 1 hr after injection with 900  $\mu$ Ci of  $^{99m}$ Tc-annexin V. Location of transplanted hearts are marked by arrows. Intense uptake of  $^{99m}$ Tc HYNIC-annexin V was observed in the cardiac allograft animal (Right) as compared with the lack of visualization of the syngeneic cardiac isograft (Left).

staining (Figs. 4A and B). Immunostaining for  $^{99m}$ Tc HYNIC-annexin V was observed in a granular pattern in cardiac myocytes at the junction of inflamed and necrotic areas; the nuclei of these cells were stained still by hematoxylin, further suggesting that they were apoptotic rather than necrotic (Fig. 5A). Anti-annexin V staining was far more extensive in terms of the number of positive myocytes and intensity compared with TUNEL. Anti-annexin staining was heavy and clumped in frankly necrotic areas as expected (Fig. 5A) but was specific; no staining was observed in syngeneic or native hearts or in staining of allografted hearts in which the primary antibody was omitted (Fig. 5B).

**In Vivo Imaging of Treated Murine Lymphoma.** Untreated flank tumor implants ( $n = 8$ ) were seen easily by scintillation camera imaging (Fig. 6) and had an annexin V uptake 365% above normal soft tissue activity as shown by ROI image analysis. Treated flank tumors ( $n = 6$ ) showed readily visualizable increases in  $^{99m}$ Tc HYNIC annexin V activity of 78% above control values expressed as whole body activity per gram of tumor ( $P < 0.05$  using a two-tailed student's  $t$  test for significance). This result was confirmed by scintillation well counting in which treated tumors demonstrated a 132% increase in annexin V uptake expressed as percentage of injected dose per gram of tumor ( $P < 0.05$ ) with a 58% fall in weight ( $P < 0.05$ ) compared with the control. The whole body activity per gram of tumor as seen by ROI image analysis linearly correlated to percentage of injected dose per gram of tumor determined on biodistribution study ( $r^2 = 0.831$ ). Histologic

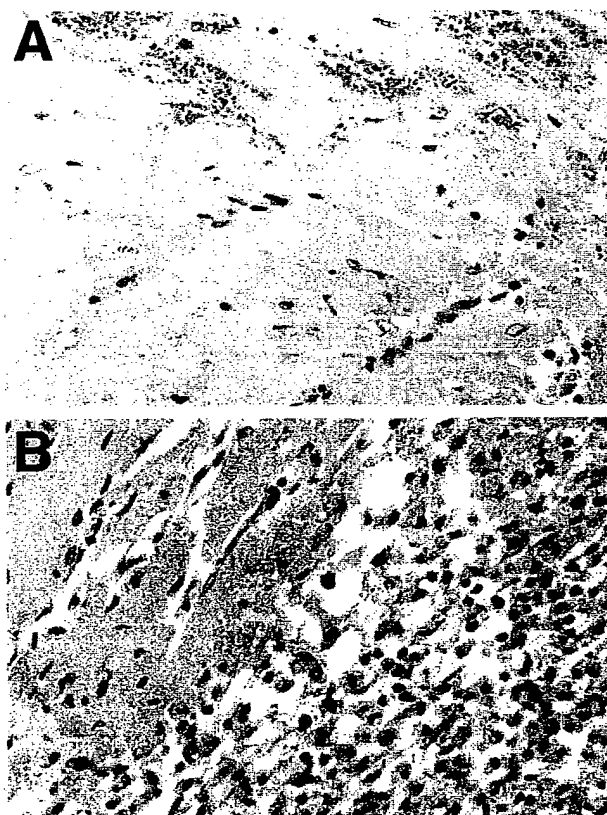


FIG. 4. Staining for apoptotic nuclei in allografted rodent heart 5 days after transplantation. (A) TUNEL staining showing apoptotic nuclei and fragments in some myocytes bordering areas of necrosis (myocytes without visible nuclei in upper half of field). (B) TUNEL positive nuclei and fragments within inflammatory infiltrate (right half of field) and in some myocytes bordering regions of inflammation. (Diaminobenzidine immunostain with hematoxylin counterstain,  $\times 40$  objective magnification.)

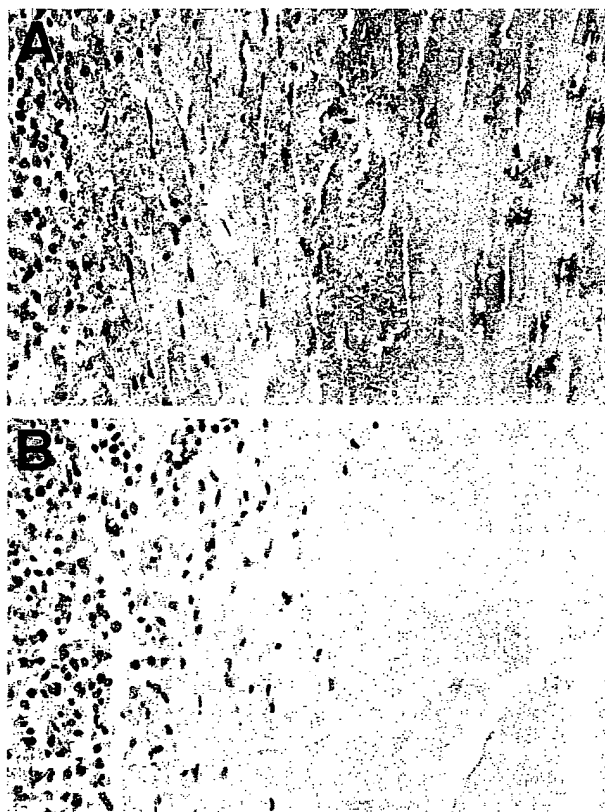


FIG. 5. Immunostaining for exogenously administered human annexin V in allografted rodent heart 5 days after transplantation. (A) Immunostaining with an antibody to human annexin V shows dense, granular staining of apoptotic myocytes at the periphery of the inflammatory infiltrate. Staining of necrotic myocytes (myocytes without visible nuclei) was clumped heavily and central. (B) Immunostaining of area similar to that shown in A omitting the primary antibody, shows no reaction product. (Diaminobenzidine immunostain with hematoxylin counterstain,  $\times 40$  objective magnification.)

analysis demonstrated virtually complete ( $>95\%$ ) apoptosis of all lymphoblasts in treated tumors with  $<5\%$  apoptotic cells in controls (data not shown).

## DISCUSSION

These experiments indicate that exposure of PS on the surface of cells undergoing apoptosis can be detected *in vivo* with radiolabeled annexin V in animal models including Fas-mediated fulminant hepatitis, cardiac allograft rejection, and tumor response to treatment.  $^{99m}\text{Tc}$  HYNIC-labeled annexin V radionuclide imaging demonstrated clear and specific localization to regions of apoptotic cell death. As has been shown for annexin V reagents *in vitro*, annexin V radionuclide imaging can provide a tool which can directly assess for early stages of programmed cell death, before membrane vesicle formation and DNA degradation particularly as measured by the TUNEL method (7, 8). Imaging of tissues undergoing apoptosis could be helpful in monitoring the efficacy of therapy of diseases associated with abnormal induction or inhibition of programmed cell death. Apoptosis appears to play an important role in autoimmune and neurodegenerative diseases, cardiomyopathy, myocarditis, cerebral and myocardial ischemia, infectious diseases, cancer, viral induced hepatitis, and organ and bone marrow transplant rejection (1).

The numerous anti-annexin V positive-staining myocytes found in rejecting rodent heart transplants with nuclei which



FIG. 6. Imaging treated murine lymphoma with radiolabeled annexin V. CH3.HeN mice 14 days after implantation of 38C13 murine B cell lymphoma s.c. into the left flank were treated with 100 mg/kg of cyclophosphamide injected i.p. Twenty hours after treatment mice were injected with 150  $\mu\text{Ci}$  of  $^{99m}\text{Tc}$  HYNIC annexin V (50  $\mu\text{g/kg}$  of protein). One hour after administration of  $^{99m}\text{Tc}$  HYNIC annexin V mice were imaged in the prone anterior projection. Treated tumor demonstrated uptakes of 363% and 454% above control seen by region of interest analysis and biodistribution assay, respectively. Control tumor weight = 1.29 grams, treated tumor weight = 0.82 grams. L, left; R, right.

were only occasionally TUNEL positive implies that radiolabeled annexin V imaging may be superior to standard histopathologic assessments of apoptosis. These data suggests a far greater role for programmed cell death in cardiac allograft rejection than previously reported (28–32). Anti-annexin V staining of apoptotic myocytes (with or without TUNEL stained nuclei) was diffusely granular in appearance in contrast to the peripheral pattern of apoptotic hepatocytes. This pattern of exogenous annexin V localization may relate to the unique cellular morphology of myocardial tissue; the extensive sarcoplasmic reticulum, which communicates with the extracellular space, also may be capable of externalizing PS during apoptosis.

The ability of annexin V to bind to necrotic cells *in vivo* and bind to PS located in the inner leaflet of the plasma membrane is confirmed by finding heavy and clumped anti-annexin V staining in frankly necrotic areas in cardiac allografts. As a result, annexin V localization *in vivo* does not appear to be entirely specific for apoptosis. In the clinical setting, however, the ability of radiolabeled annexin V to noninvasively image both apoptosis and necrosis may prove useful in reducing the need for routine surveillance through endomyocardial biopsy after cardiac transplantation, which currently is the only reliable clinical means to diagnose acute transplant rejection (33, 34). Furthermore, radiolabeled annexin V imaging of the entire myocardium may provide diagnostic information superior to endomyocardial biopsy, which necessarily can only sample a limited region within the right ventricle.

These studies also demonstrate that radiolabeled annexin V imaging can detect an increase in PS exposure associated with apoptosis of implanted murine flank lymphomas after cyclophosphamide treatment. Estimates of the degree of cell death



during the first week of induction therapy using bone marrow aspirates has been shown to provide prognostic information in childhood leukemia (35, 36). Other investigators have shown a direct relationship between the degree of apoptotic cell death and subsequent tumor growth delay in murine models of lymphoma (37, 38). To date, the only noninvasive imaging method shown to detect apoptosis *in vivo* has been lipid proton NMR spectroscopy (5, 6). Lipid proton NMR spectroscopy, however, has inherent problems with magnetic susceptibility outside the central nervous system and has relatively low sensitivity.

Kidneys in control animals have marked uptake of  $^{99m}\text{Tc}$  HYNIC annexin V. The high renal concentration did not preclude the imaging of other major organs undergoing apoptosis. The cellular site of binding is uncertain, but preliminary autoradiographs suggest the renal distribution of annexin V is cortical. The specific mechanism of renal cortical binding is uncertain but may relate to the intrinsic lipid profile of the kidney, in which there is a significantly higher concentration of PS in the cortex as compared with the papillary regions (39).

The initial increase of  $^{125}\text{I}$ -HSA hepatic uptake after anti-Fas treatment is most likely caused by an expanded extracellular fluid volume from the early breakdown of hepatic endothelial cells as described by Lacronique *et al.* (27) and is confirmed by an increased hepatic weight of these treated animals. The initial increase of  $^{125}\text{I}$ -HSA hepatic uptake, which subsequently remained unchanged, is in marked contrast to the progressive rise of radiolabeled annexin V hepatic uptake, which was specific for increasing numbers of apoptotic hepatocytes.

In summary, this study demonstrates the utility of  $^{99m}\text{Tc}$ -radiolabeled annexin V for *in vivo* imaging of PS expression associated with apoptosis. Serial noninvasive assessments of PS externalization with radiolabeled annexin V may provide a more sensitive and rapid means of monitoring disease progression, determining treatment efficacy, and diagnosing a number of human disorders than is currently possible in the clinical setting.

This work was supported in part by the Child Health Research Fund, Lucile Salter Packard Children's Hospital at Stanford, and by the National Institutes of Health Grant HL-47151. The authors also gratefully acknowledge Dr. Regina Santella for the gift of 1G4 antibody.

- Thompson, B. C. (1995) *Science* **267**, 1456–1462.
- Steller, H. (1995) *Science* **267**, 1445–1449.
- Darzynkiewicz, Z. (1995) *J. Cell. Biochem.* **58**, 151–159.
- Kerr, J. F., Wyllie, A. H. & Currie, A. R. (1972) *Brit. J. Cancer* **26**, 239–257.
- Blankenberg, F. G., Storrs, R. W., Naumovski, L., Goralski, T. & Spielman, D. (1996) *Blood* **87**, 1951–1956.
- Blankenberg, F. G., Katsikis, P. D., Storrs, R. W., Bealieu, C., Spielman, D., Chen, J. Y., Naumovski, L. & Tait, J. F. (1997) *Blood* **89**, 3778–3786.
- Martin, S. J., Reutelingsperger, C. P. M., McGahon, A. J., Rader, J. A., van Schie, R. C. A. A., La Face, D. M. & Green, D. R. (1995) *J. Exp. Med.* **182**, 1545–1556.
- Zwaal, R. F. A. & Schroit, A. (1997) *Blood* **89**, 1121–1132.
- Koopman, G., Reutelingsperger, C. P. M., Kuijten, G. A. M., Keehnen, R. M. J., Pals, S. T. & van Oers, M. H. J. (1994) *Blood* **84**, 1415–1420.
- Verhoven, B., Schlegel, R. A. & Williamson, P. (1995) *J. Exp. Med.* **182**, 1597–1601.
- van Heerde, W. L., de Groot, P. G. & Reutelingsperger, C. P. M. (1995) *Thromb. Haemostasis* **73**, 172–179.
- Tait, J. F. & Gibson, D. (1994) *J. Lab. Clin. Med.* **123**, 741–748.
- Wood, B. L., Gibson, D. F. & Tait, J. F. (1996) *Blood* **88**, 1873–1880.
- Tait, J. F., Cerqueira, M. D., Dewhurst, T. A., Fujikawa, K., Ritchie, J. L. & Stratton, J. R. (1994) *Thromb. Res.* **75**, 491–501.
- Stratton, J. R., Dewhurst, T. A., Kasina, S., Reno, J. M., Cerqueira, M. D., Baskin, D. G. & Tait, J. F. (1995) *Circulation* **92**, 3113–3121.
- Abrams, M. J., Juweid, M., tenKate, C. I., Schwartz, D. A., Hauser, M. M., Gaul, F. E., Fuccello, A. J., Rubin, R. H., Strauss, H. W. & Fischman, A. J. (1990) *J. Nucl. Med.* **31**, 2022–2028.
- Tait, J. F., Engelhardt, S., Smith, C. & Fujikawa, K. (1995) *J. Biol. Chem.* **270**, 21594–21599.
- Tait, J. F. & Smith, C. (1991) *Arch. Biochem. Biophys.* **288**, 141–144.
- King, T. P., Zhao, S. W. & Lam, T. (1986) *Biochemistry* **25**, 5774–5779.
- Larsen, S. K., Solomon, H. F., Caldwell, G. & Abrams, M. J. (1995) *Bioconjugate Chem.* **6**, 635–638.
- Ogasawara, J., Watanabe-Fukunaga, R., Adachi, M., Matsuzawa, A., Kasugai, T., Kitamura, Y., Itoh, N., Suda, T. & Nagata, S. (1993) *Nature (London)* **364**, 806–809.
- Woodley, S. L., Gurley, K. E., Hoffman, S. L., Nicolls, M. R., Hagberg, R., Clayberger, C., Holm, B., Wang, X., Hall, B. M. & Strober, S. (1993) *Transplantation* **56**, 1443–1447.
- Maloney, D. G., Kaminski, M. S., Burosowski, D., Haimovich, J. & Levy, R. (1985) *Hybridoma* **4**, 191–209.
- Bindl, J. M. & Warnke, R. A. (1986) *Am. J. Clin. Pathol.* **85**, 490–493.
- Gavrieli, Y., Sherman, Y. & Ben-Sasson, S. (1992) *J. Cell Biol.* **119**, 493–501.
- Young, T. L. & Santella, R. M. (1988) *Carcinogenesis* **9**, 589–592.
- Lacronique, V., Mignon, A., Fabre, M., Viollet, B., Rouquet, N., Molina, T., Porteu, A., Henrion, A., Bouscary, D., Varlet, P., *et al.* (1996) *Nat. Med.* **2**, 80–86.
- Seino, K., Nobuhiko, K., Bashuda, H., Okumura, K. & Yagita, H. (1996) *Int. Immunol.* **8**, 1347–1354.
- Laguens, R. P., Cabeza Meckert, P. M., San Martino, J., Perrone, S. & Favaloro, R. (1996) *J. Heart Lung Transplant.* **15**, 911–918.
- Bergese, S. D., Klenotic, S. M., Wakely, M. E., Sedmak, D. D. & Orosz, C. G. (1997) *Transplantation* **63**, 320–325.
- Jollow, K. C., Sundstrom, J. B., Gravanis, M. B., Kanter, K., Herskowitz, A. & Ansari, A. A. (1997) *Transplantation* **63**, 1482–1489.
- Matiba, B., Mariana, S. M. & Krammer, P. H. (1997) *Immunology* **9**, 59–68.
- Mannaerts, H. F., Simoons, M. L., Balk, A. H., Tijssen, J., van der Borden, S. G., Zondervan P. E., Mochtar, B., Weimer, W. & Roelandt, J. R. (1993) *J. Heart Lung Transplant.* **12**, 411–421.
- Angermann, C. E., Nassau, K., Stempfle, H.-U., Krüger, T. M., Drewello, R., Phys, D., Junge, R., Ing, D., Überfuhr, P., Weib, M., *et al.* (1997) *Circulation* **95**, 140–150.
- Asselin, B. L., Ryan, D., Frantz, C. N., Bernal, S. D., Leavitt, P., Sallan, S. E. & Cohen, H. J. (1989) *Cancer Res.* **49**, 4363–4368.
- Niemeyer, C. M., Gelber, R. D., Tarbell, N. J., Donnelly, M., Clavell, L. A., Blattner, S. R., Donahue, K., Cohen, H. J. & Sallan, S. E. (1991) *Blood* **78**, 2514–2519.
- Stephens, L. C., Hunter, N. R., Ang, K. K., Milas, L. & Meyn, R. E. (1993) *Radiat. Res.* **135**, 75–80.
- Mirkovic, N., Meyn, R. E., Hunter, N. R. & Milas, L. (1994) *Radiother. Oncol.* **33**, 11–16.
- Sterin-Speziale, N., Kahane, V. L., Setton, C. P., del Carmen Fernandez, M. & Speziale, E. H. (1992) *Lipids* **27**, 10–14.

# Quantification of Apoptotic Cells With Fluorescein Isothiocyanate-Labeled Annexin V in Chinese Hamster Ovary Cell Cultures Treated With Cisplatin

Antonius W.M. Boersma, Kees Nooter, Robert G. Oostrum, and Gerrit Stoter

Department of Medical Oncology, University Hospital Rotterdam and Rotterdam Cancer Institute (Daniel den Hoed Kliniek), Rotterdam, The Netherlands

Received for publication October 25, 1995; accepted February 4, 1996

Plasma membrane binding of annexin V was used to detect and quantitate apoptotic cells induced by cytotoxic drug treatment in epithelial cell cultures. Chinese hamster ovary (CHO) cells were incubated for 2 h with the ID90 concentration of Cisplatin (20  $\mu$ M), and 24, 48, 72, and 96 h later the unfixed cells were stained with fluorescein isothiocyanate (FITC)-conjugated annexin V. The fluorescence signal was quantitated by flow cytometry (FCM). During the early phase of the apoptotic response, the annexin V-binding frequency histograms showed two separate cell populations, a dimly and a brightly fluorescent one. At  $t = 96$  h after drug incubation, when the process of apoptosis was completed, only the brightly fluorescent population was present. A dose-effect relationship could be established between the Cisplatin concentration used in the 2 h incubation and the binding of annexin V on the cell membrane, as estimated by FITC fluorescence. The dimly and brightly fluorescent populations were sorted on the basis of annexin V binding, and assayed for 1) DNA

breaks by *in situ* nick translation assay and DNA content by DNA-propidium iodine fluorescence in a bivariate analysis, 2) membrane integrity by dye exclusion, and 3) morphological characteristics of apoptosis. The dimly fluorescent cell population appeared to represent apoptotic cells in the early phase of the death process, as demonstrated by intact cell membranes, normal DNA content, few DNA breaks, and chromatin condensation. The brightly fluorescent cells predominantly had sub-G<sub>1</sub> DNA content, nuclear fragmentation, leaky cell membranes, and probably represent late apoptotic cells. These results demonstrate that cytotoxic drug-induced apoptosis can be quantitated by annexin V binding and that by using this assay early and late apoptotic cells can be identified. © 1996 Wiley-Liss, Inc.

**Key terms:** Cisplatin-induced apoptosis, annexin V, quantification of early and late apoptotic cells by flow cytometry

Apoptosis is the normal physiological way of cell death during, e.g., embryogenesis and tissue homeostasis (24,25), and can also be induced by a large variety of external stimuli, like viral infections and toxic insults, including anticancer drug treatment (5,6,10,21). Apoptosis is a specific form of programmed cell death that is characterized by condensation of cytoplasm and chromatin, nuclear fragmentation, and ultimate sequestration of cellular contents into membrane-bound apoptotic bodies (10,25). Typically, the integrity of organelles and cell membrane is maintained during the early phases of the death pathway. The importance of studying the process of apoptosis is nowadays readily appreciated in medical biology. Defective regulation of programmed cell death may play a role in the etiology of cancer, acquired immunodeficiency syndrome (AIDS), autoimmune diseases, and degenerative diseases of the central nervous system (3). It is believed that the pharmacological manipulation

of apoptosis might offer new possibilities for the prevention and treatment of these diseases.

Several biochemical methods have been described for the detection of apoptotic cells, based on the various characteristics of the apoptotic response (20,25). The hallmark of apoptosis is endonucleolysis, a process whereby nuclear DNA is initially degraded at the nucleosomal linker regions (2). Electrophoresis of such degraded DNA reveals a so-called ladder pattern of nucleosome-sized fragments of 180 base pairs (bp) or a multiple of that. The DNA-ladder technique is commonly used for the detection of apoptotic cells. Unfortunately, this assay system is difficult to quantitate and cannot be

Address reprint requests to Dr. Kees Nooter, Department of Medical Oncology, University Hospital Rotterdam, Room D337, Dr. Molewaterplein 40, 3015 GD, Rotterdam, The Netherlands.



used to evaluate apoptosis in individual cells. Another technique for the detection of single-stranded DNA nicks in individual cells uses in situ labeling of DNA breaks by a reporter molecule, either by in situ nick translation (ISNT) in the presence of a DNA polymerase or by in situ end labeling with terminal deoxynucleotidyl transferase (9). This technique of in situ labeling of DNA breaks can be applied both on formalin-fixed, paraffin-embedded tissue sections (23) and on single cell suspensions, allowing flow cytometric analysis (9). The aforementioned assays for apoptosis rely heavily on DNA breaks as the indicator of the apoptotic process. However, the absolute requirement for multiple DNA breaks during apoptosis has been questioned seriously (4,22). DNA fragmentation during apoptosis proceeds through an ordered series of stages commencing with the production of 300 kbp DNA fragments, which are then degraded to fragments of 50 kbp (22). The oligonucleosomes that form the characteristic DNA ladder are released upon further degradation of the 50 kbp fragments, a process that appears to be cell type specific (16).

It was recently shown that membrane alterations in apoptotic lymphocytes can be used to detect and quantify the apoptotic process (11). Cells undergoing apoptosis lose membrane phospholipid asymmetry and expose phosphatidylserine on the outer leaflet of the plasma membrane (7). Annexin V [formerly called vascular anticoagulant  $\alpha$  (8)] is a member of the annexin family of calcium and phospholipid binding proteins, and binds preferentially to negatively charged phospholipids like phosphatidylserine (1). Upon conjugation with fluorescein isothiocyanate (FITC), annexin V can label Burkitt lymphoma cell lines and freshly isolated germinal center B cells, cultured under apoptosis inducing conditions (11). In the present work we show that annexin V also binds to the membrane of epithelial cells that have been triggered into apoptosis by treatment with cytotoxic drug and that this method can be used for the quantification of early and late apoptotic cell populations.

## MATERIALS AND METHODS

### Cell Lines and Culture Conditions

Chinese hamster ovary (CHO) cells were maintained in monolayer culture in Dulbecco's modified culture medium, supplemented with 10% fetal calf serum, 100 units/ml penicillin, 100  $\mu$ g/ml streptomycin, and 2 mM L-glutamine. The cells were cultured at 37°C in a humidified incubator with 8.5% CO<sub>2</sub> and passaged by trypsinization. To obtain single cell suspensions, cells were trypsinized, washed once with RPMI culture medium containing 10% fetal calf serum, and thereafter washed twice with RPMI culture medium without phenol red. For induction of apoptosis, exponentially growing  $1 \times 10^6$  CHO cells were seeded per 75 cm<sup>2</sup> flask and 24 h later incubated for 2 h with Cisplatin (*cis*-diamminedichloroplatinum II) at various concentrations (5, 10, and 20  $\mu$ M), diluted in culture medium. Thereafter, the cells were washed with culture medium and further cultured in drug-free medium for either 24, 48, 72, or 96 h.

### Annexin V Binding

Labeling of cells with FITC-conjugated annexin V was performed in essence as described (11). Cells were incubated for 1 h at 37°C with 0.5  $\mu$ g/ml FITC-conjugated annexin V (BioWhittaker, Verviers, Belgium) in HEPES-buffered (10 mmol/l HEPES/NaOH, pH 7.4) RPMI culture medium (without phenol red). Thereafter, the cells were washed 2 times in culture medium, and kept on ice until further processing.

### ISNT Assay

The ISNT assay was performed as described previously (9,15). Briefly, at different time points (24, 48, 72, and 96 h) after Cisplatin incubation, cells were fixed in 1% formaldehyde in phosphate-buffered saline (PBS) (pH 7.4) for 30 min on ice. After washing with PBS, the cells were resuspended in 70% ice-cold ethanol in PBS and stored at -20°C until further processing. For ISNT the fixed cells were washed in PBS and resuspended in buffer containing 5 mM MgCl<sub>2</sub>, 10 mM  $\beta$ -mercaptoethanol, 50 mM Tris pH 7.8, 1 unit/ml *Escherichia coli* DNA polymerase, 0.2 nmol biotin-11-dUTP, and 0.2 nmol unlabeled dATP, dCTP, and dGTP. After incubation for 90 min at 15°C, the cells were washed with PBS supplemented with 0.1% Triton X-100 and resuspended in staining buffer consisting of 2.5  $\mu$ g/ml avidin-FITC in  $4 \times$  saline sodium citrate buffer ( $1 \times$  SSC = 0.15 M NaCl, 0.015 M Na-citrate), 0.1% Triton X-100, and 5% (w/v) nonfat dry milk. Staining was performed for 30 min at 37°C. Thereafter, the cells were washed with PBS. DNA was counterstained for 30 min on ice with propidium iodide (PI) (5  $\mu$ g/ml) in PBS.

For sorting of cells labeled by FITC-conjugated annexin V and subsequent ISNT assay, the cells were labeled as described above. After sorting, the cells were washed 2 times with PBS and fixed in 1% formaldehyde in PBS (pH 7.4) for 30 min on ice. After washing with PBS, the cells were resuspended in 70% ice-cold ethanol in PBS and stored at -20°C for ISNT. The formaldehyde fixation removed all annexin V from the cell membrane, excluding interference of FITC bound to annexin in the fluorescence signal obtained in the ISNT assay.

### Flow Cytometry (FCM) and Sorting

FCM was performed on a FACScan flow cytometer (Becton Dickinson, Mountain View, CA) with excitation at 488 nm. The following parameters were measured: forward light scatter (FLS), perpendicular light scatter (PLS), FITC fluorescence (515–545 nm), and fluorescence of the DNA-PI complex (563–607 nm). Compensation was used wherever necessary. Sorting experiments were performed on a FACS Vantage flow cytometer (Becton Dickinson). For annexin V staining, FLS and PLS were measured in linear (lin) mode and FITC in logarithmic (log) mode. For the measurement of ISNT, FLS, PLS, and PI were set in the lin mode and FITC in the log mode. Cell debris was excluded from analysis by appropriate FLS threshold setting.

Fig. 1. FITC-conjugated annexin V staining of CHO cells after 24 h drug-treatment.

After treatment, cells were pelleted by centrifugation at 200  $\times$  g for 5 min. The supernatant was removed and the pellet was resuspended in 200  $\mu$ l of 0.1% Triton X-100 in PBS. The cells were then fixed in 1% formaldehyde in PBS for 30 min on ice. After washing with PBS, the cells were resuspended in 70% ice-cold ethanol in PBS and stored at -20°C for ISNT.

We have shown that the ISNT assay can be used to detect and quantify the apoptotic process in CHO cells.

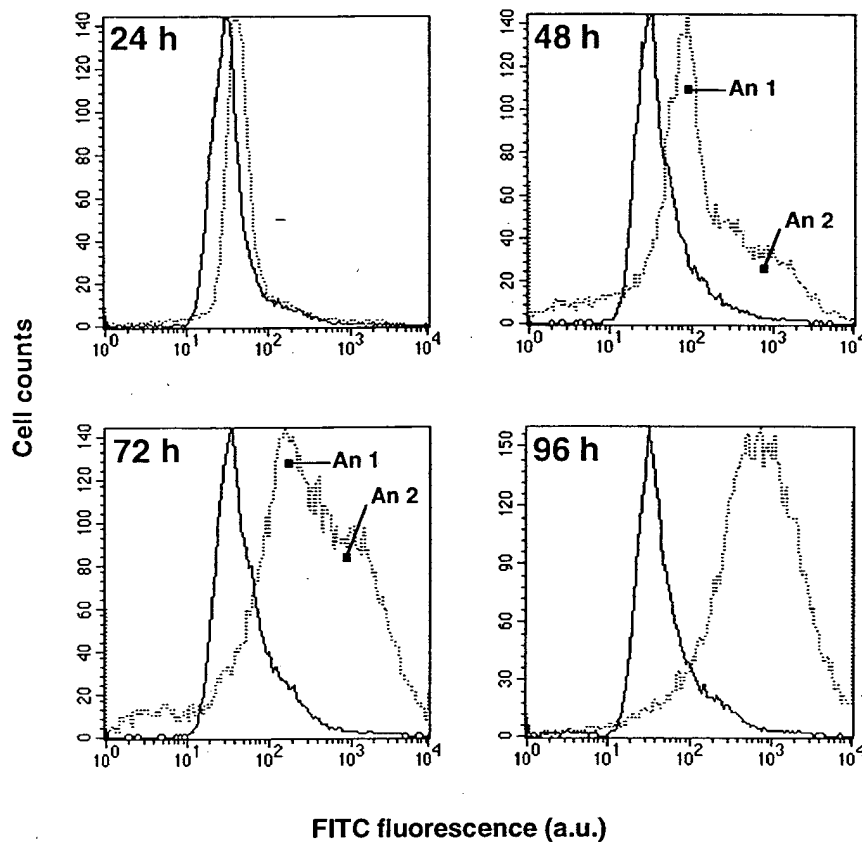


Fig. 1. Fluorescence intensity, expressed in arbitrary units (a.u.), of FITC-conjugated annexin V bound to Cisplatin-treated ( $20 \mu\text{M}$ , 2 h at  $37^\circ\text{C}$ ) CHO cells. At 24, 48, 72, and 96 h after drug incubation, the cells were stained with FITC-conjugated annexin V and the binding of annexin V was quantified by FCM. Solid line: control CHO cells; dotted line: drug-treated CHO cells. At  $t = 48$  h and  $t = 72$  h after drug incubation,

the annexin V-binding frequency histograms of the Cisplatin-treated CHO cells show two distinct cell populations, An1 and An2, with a low and a high capacity, respectively, to bind annexin V. At  $t = 96$  h, all drug-treated cells have a high annexin V-binding capacity. Data from a representative experiment.

### Gel Electrophoresis

After trypsinization  $2.10^6$  cells were collected in a cell pellet. The pellet was resuspended in 400  $\mu\text{l}$  lysis buffer [200 mM Tris pH 8.5, 100 mM EDTA, 1% sodium dodecyl sulfate (SDS), and 100  $\mu\text{g}/\text{ml}$  proteinase K] and incubated overnight at  $37^\circ\text{C}$ . DNA was obtained by phenol extraction and precipitated overnight at  $-20^\circ\text{C}$  with sodium acetate and ethanol. The precipitated DNA was spun down, washed with ethanol (70%), and dried. The pellet was dissolved in 100  $\mu\text{l}$  TE containing 50  $\mu\text{g}/\text{ml}$  RNase A and incubated for 30 min at  $37^\circ\text{C}$ . Twenty microliters of DNA was transferred onto a 1.8% agarose gel and run for 2 h at 50 V in TBE buffer in the presence of 0.5  $\mu\text{g}/\text{ml}$  ethidium bromide.

## RESULTS

### FITC-Conjugated Annexin V Stains Cisplatin-Induced Apoptotic Cells

We have previously shown that incubation of tissue culture cell lines with cytotoxic drugs can trigger an apoptotic response that increases in time, with a maximal

response at about 96 h after drug incubation, and whose extent is concentration dependent (15). In order to determine whether cytotoxic drug-induced apoptosis can also be detected by FITC-conjugated annexin V, we treated CHO cells with a Cisplatin protocol which we had previously shown will induce apoptosis (17). The CHO cells were incubated for 2 h with the ID90 concentration (estimated by MTT cytotoxicity assay), i.e.,  $20 \mu\text{M}$  Cisplatin, and 24, 48, 72, and 96 h later the cells were stained with FITC-conjugated annexin V (Fig. 1). The mean fluorescence signal of the drug-treated cells increased in time, compared with untreated control CHO cells. At  $t = 48$  h, the FITC frequency histogram of the drug-treated cells clearly differed from that of the control cells, and comparison of the histograms obtained at  $t = 48$  h,  $t = 72$  h, and  $t = 96$  h suggests that in the drug-treated cultures, at  $t = 48$  h and  $t = 72$  h, 2 separate cell populations are stained by annexin V (referred to as An1 and An2). At  $t = 48$  h, the annexin V-binding histogram shows one distinct cell population (An1) with a mean fluorescence intensity of about 100 arbitrary units (a.u.)

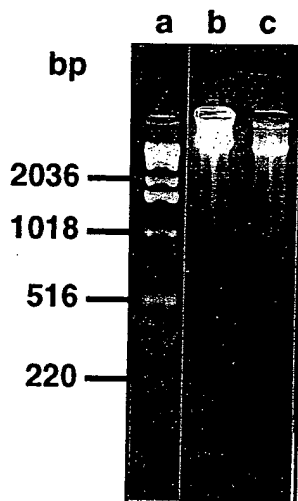


Fig. 2. Agarose gel analysis of DNA fragmentation in Cisplatin-treated ( $20 \mu\text{M}$ , 2 h at  $37^\circ\text{C}$ ) CHO cells 96 h after drug incubation. DNA was electrophoresed in a 1.8% gel containing  $0.5 \mu\text{g/ml}$  ethidium bromide. Lane a: molecular weight standards (Gibco, Grand Island, NY); lane b: DNA isolated from untreated, control CHO cells; lane c: DNA isolated from Cisplatin-treated CHO cells. DNA degradation in nucleosome-sized fragments is evident.

and suggests another, broader population (An2) with a higher fluorescence intensity. The latter clearly increased in time probably due to increased annexin V binding of the cell population (An1) with the weaker fluorescence signal. At  $t = 96 \text{ h}$ , the cells had a typical apoptotic feature with condensed chromatin and nuclear fragmentation (data not shown). DNA degradation in nucleosome-sized fragments could be detected by qualitative gel electrophoresis (Fig. 2), a finding that correlates the annexin V binding with the presence of a typical DNA-ladder pattern, which is the hallmark of apoptosis. A dose-effect relationship could be established between the Cisplatin concentration used in the 2 h incubation period and the binding of annexin V on the cell membrane, as estimated by FITC fluorescence (Fig. 3). A decrease in drug concentration leads to a decrease in the number of cells staining positive for annexin V binding.

#### Annexin V Binding Vs. ISNT Assay

Subsequently, we compared annexin V labeling with ISNT assay for their ability to detect apoptotic cells (Fig. 4). At the indicated time points the Cisplatin-treated samples were split into two: one sample for ISNT and the other sample for annexin V labeling (Fig. 4, inset). Prior to drug incubation, the CHO cells showed hardly any spontaneous apoptosis (Fig. 4, control). At 24 h after drug incubation, cells accumulated in  $G_2$  phase of the cell cycle, and only a small increase in annexin V labeling is observed. At  $t = 48 \text{ h}$ , apoptotic cells can be distinguished with the ISNT assay on the basis of DNA content (DNA-PI fluorescence) and biotin-dUTP labeling (FITC fluorescence). One cluster of apoptotic cells (Ap1) is only shifted on the vertical axis due to incorporation of

biotin-dUTP, and has a normal DNA content. The other cluster of apoptotic cells (Ap2) has a reduced DNA content, probably as a result of loss of diffusible DNA of low molecular weight [200–1,000 bp; mono- and short oligonucleosomes (9)], and the shedding of apoptotic bodies, containing fragments of nuclei. The annexin V histogram at  $t = 48 \text{ h}$  also shows 2 cell populations, a brightly and a dimly fluorescent population. At  $t = 72 \text{ h}$ , the apoptotic cell population Ap2 is strongly increased, relative to Ap1. At  $t = 96 \text{ h}$ , the vast majority of cells is apoptotic, as estimated by both assays.

#### Sorting of Annexin V-Labeled Cells

Comparison of the results obtained with ISNT and annexin V binding as shown in Figure 4 suggests that the apoptotic cells clusters Ap1 and Ap2 correspond, respectively, to the dimly and brightly fluorescent populations An1 and An2, identified by annexin V binding. In order to determine more precisely where the two different apoptotic cell populations in Cisplatin-treated CHO cell cultures identified by ISNT are located in the FITC-conjugated annexin V histograms, we performed cell sorting experiments. The most straightforward approach would be to sort the Ap1 and Ap2 populations and label them with annexin V. However, for the ISNT assay it is an absolute requirement that the cells are fixed in formaldehyde, a condition that does not allow binding of annexin V anymore (data not shown). However, the opposite approach, i.e., sorting on the basis of annexin V binding and thereafter ISNT, indeed appeared to be possible. We had noticed previously that at high Cisplatin concentration ( $100 \mu\text{M}$ ), drug-treated cells start to detach from the tissue culture surface about 1 day after incubation, and that this process proceeds in time till all apoptotic cells are floating and finally fall apart into apoptotic bodies and form cell debris. Therefore, CHO cells were treated with Cisplatin ( $20 \mu\text{M}$ ) and 2 days later the cultures were separated into floating cells, which were simply pipetted off the culture, and adherent cells, obtained by trypsinization. The FITC-conjugated annexin V histogram of the total cell population, obtained by mixing the adherent cells with the floating cells, clearly shows two separate cell populations (Fig. 5b), identical in fluorescence intensity with the previously identified cell populations An1 and An2. These two separate populations (Fig. 5b) are therefore also referred to as An1 and An2. The annexin V-binding histograms of the adherent cells (Fig. 5c) and the floating cells (Fig. 5d) show that An1 represents the adherent cells and An2 the floating cells. Subsequently, we sorted adherent cells (sort I) and floating cells (sort II) on the basis of fluorescence intensity (Fig. 5c,d). These sorted cells were used for ISNT. Fixation of the cells with formaldehyde completely removed the bound annexin V (data not shown). In the ISNT assay, the An1 sorted cells (sort I) primarily consist of cells with normal DNA content and that partly have incorporated biotin-dUTP (Fig. 5e), while the floating cells (sort II) with the highest annexin V binding predominantly have sub- $G_1$  DNA content (Fig. 5f). Cytospin slides of the

FITC fluorescence (a.u.)  
(DNA strand breaks)

Cell counts

Fig. 4. untreated CHO cell incubation fluorescence expression position

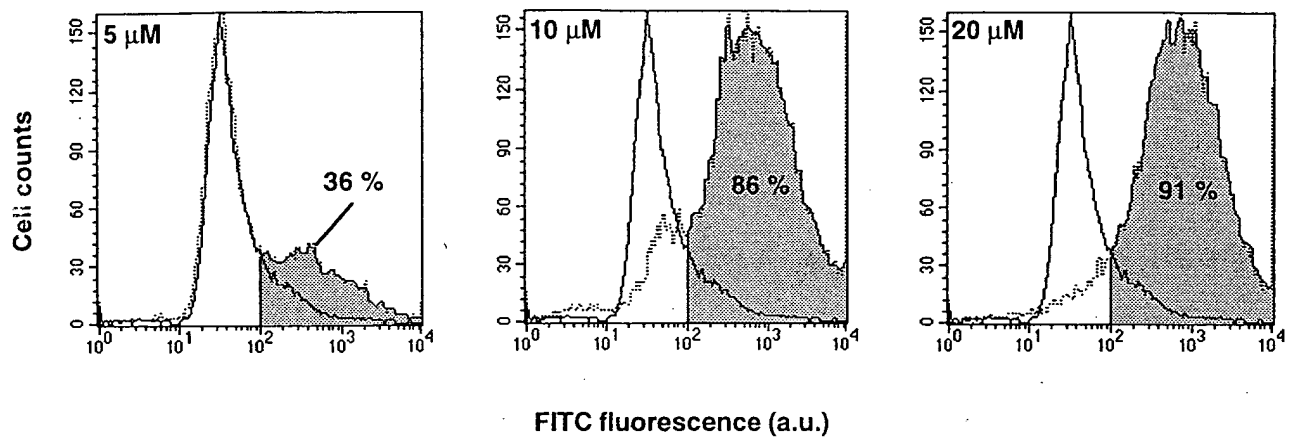


Fig. 3. Fluorescence intensity, expressed in arbitrary units (a.u.), of FITC-conjugated annexin V bound to CHO cells treated for 2 h with different concentrations of Cisplatin (5, 10, and 20  $\mu$ M). The data are representative univariate histograms taken at 96 h after drug incubation. Solid line: control CHO cells; dotted line: drug-treated CHO cells. In each panel the number of apoptotic cells, expressed as percentage of the total number of cells analyzed, is indicated.

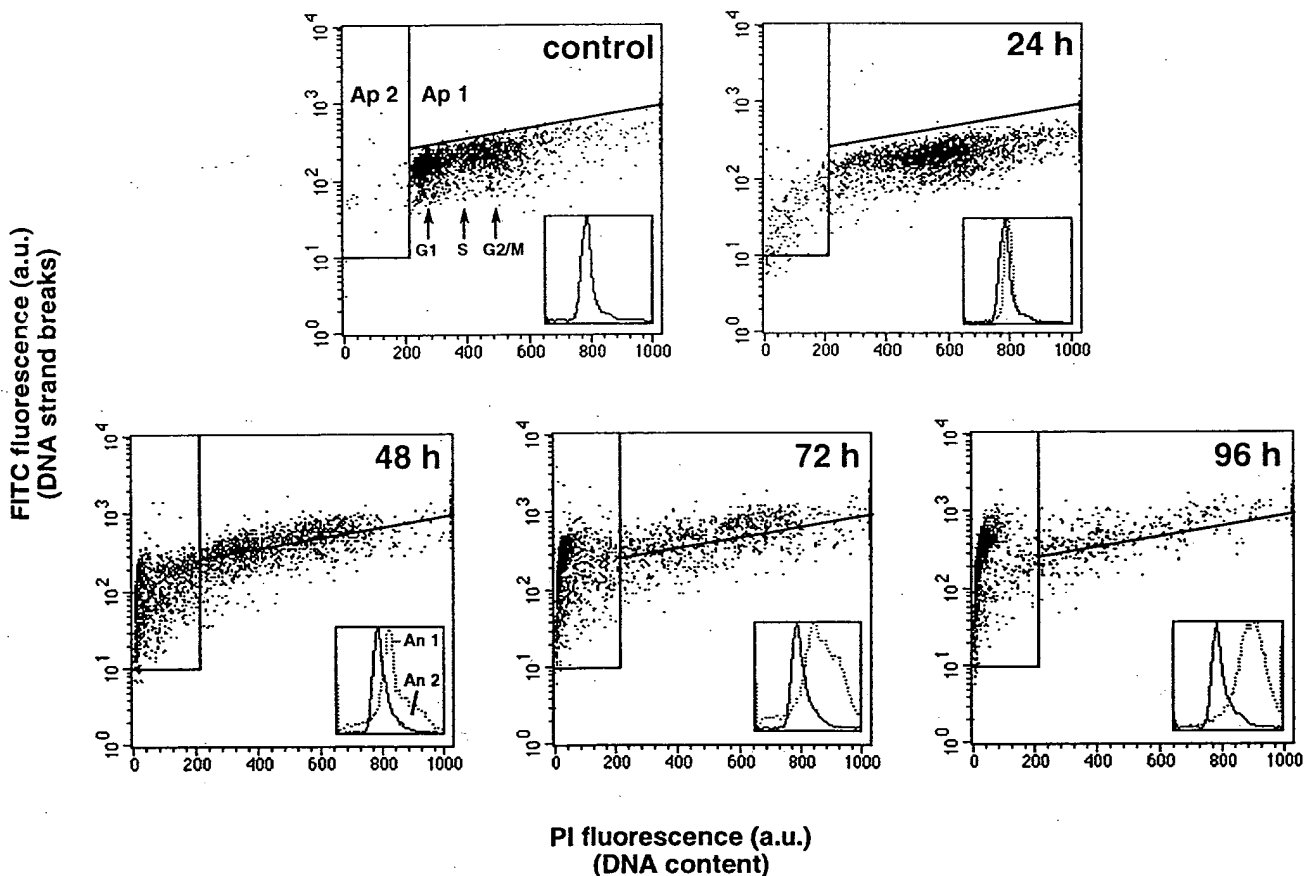


Fig. 4. Labeling of DNA strand breaks with biotin-dUTP by ISNT in untreated, control CHO cells and Cisplatin-treated (20  $\mu$ M, 2 h at 37°C) CHO cells at different time intervals (24, 48, 72, and 96 h) after drug incubation. The extent of DNA strand breaks is estimated by avidin-FITC fluorescence, and cellular DNA content by DNA-PI fluorescence, both expressed in arbitrary units (a.u.). Control, untreated CHO cells. The position of cells in  $G_1$ , S, or  $G_2 + M$  is indicated. Two apoptotic cell

populations are identified: Ap1 and Ap2. Cluster Ap1 is only shifted on the vertical axis due to incorporation of biotin-dUTP and has a normal DNA content, as shown at  $t = 48$  h and  $t = 72$  h. Cluster Ap2 is mainly characterized by sub- $G_1$  DNA content. At  $t = 96$  h, the apoptotic cells are predominantly present in cluster Ap2. The data are representative bivariate histograms of 20,000 events and are displayed as dot plots. Insets: Annexin V binding of the same samples.

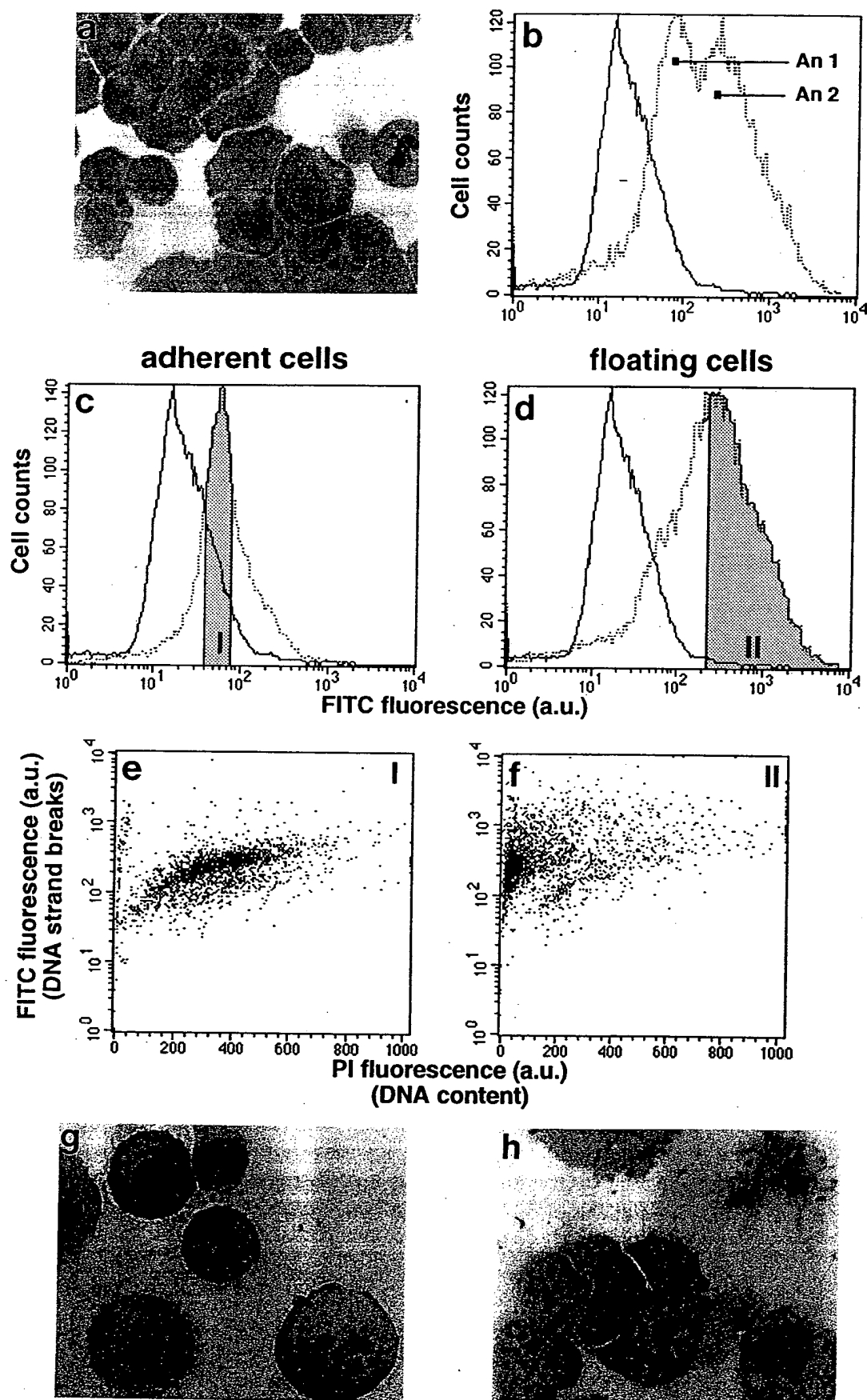


FIG. 5.

sorted cell  
clear frag  
cells with  
fragmenta  
dye exclu  
the sort I  
13% of th  
sort II ce  
cells had  
membran  
X-100 (fi  
permeabi  
crease in  
brightly f

It is ve  
toxic act  
program  
Recent e  
apoptotic  
(5,12,14,  
apoptosis  
genes and  
modulate  
are the t  
gene bcl-  
cellular c  
clinic, it  
cytotoxic  
consequ  
leads to c

The ea  
ized by a  
gination  
plasm (1  
and cons  
into mul  
size and  
siderably  
whereas  
mic orga  
well pre

FIG. 5. S  
basis of FI  
the ISNT a  
2 h at 37°  
population  
optotic cel  
the floatin  
were sorte  
ures. In the  
incorporat  
by a sub-G  
treated Cl  
with the b  
cells from  
from one

sorted cells stained with hematoxylin clearly show nuclear fragmentation in sort II fraction (Fig. 5h), and only cells with the beginning of nuclear condensation and fragmentation in sort I fraction (Fig. 5g). As estimated by dye exclusion assay with trypan blue, the vast majority of the sort I cells had an intact cell membrane: only about 13% of the sort I cells stained with trypan blue. For the sort II cells the opposite was found: about 74% of the cells had taken up the dye, and apparently had a leaky cell membrane. Treatment of adherent cells with Triton X-100 (final concentration 0.03%) for 10 min (100% permeability established by dye exclusion) led to an increase in fluorescence to the intensity shown by the brightly fluorescent cells (data not shown).

### DISCUSSION

It is very likely that anticancer drugs exert their cytotoxic action by triggering a conserved, gene-activated program for cell death, referred to as apoptosis (5,6,21). Recent evidence strongly suggests that inhibition of the apoptotic pathway can lead to cytotoxic drug resistance (5,12,14,18). Although the molecular mechanism of apoptosis is yet unknown, several tumor suppressor genes and oncogenes have been shown to mediate and modulate the apoptotic cell response. Among these genes are the tumor suppressor gene p53 and the protooncogene bcl-2 (12,14,18). Since chemotherapy failure due to cellular drug resistance is still a major problem in the clinic, it is worthwhile to study how cells are killed by cytotoxic drugs and to unravel the events that occur as a consequence of the drug-target interaction that finally leads to cell death (5).

The early phase of the apoptotic response is characterized by an intact cell membrane, compaction and margination of nuclear chromatin, and condensation of cytoplasm (10). At a later stage there is membrane blebbing and constriction of both the nucleus and the cytoplasm into multiple, membrane-bound apoptotic bodies. The size and composition of these apoptotic bodies vary considerably; many contain several nuclear fragments, whereas others lack a nuclear component. The cytoplasmic organelles of newly formed apoptotic bodies remain well preserved (10). Probably, the final goal of this step-

wise breakdown of dying cells is to make them consumable for phagocytic cells. Apoptotic cells are recognized by macrophages and other phagocytic cells before they rupture, which prevents a potentially damaging inflammatory response (25). Apoptotic cells have been shown to lose membrane phospholipid asymmetry and expose phosphatidylserine on the outer leaflet of the plasma membrane (7). Macrophages which specifically recognize phosphatidylserine would then phagocytose apoptotic cells (19).

Koopman et al. (11) have used B-lymphocytes to establish the applicability of annexin V binding for the detection of apoptosis. Martin et al. (13) showed that early redistribution of membrane-bound phosphatidylserine is involved in the apoptosis process, regardless of the initiating stimulus. In this study we show that epithelial cells undergoing apoptosis as a consequence of cytotoxic drug exposure can be labeled with FITC-conjugated annexin V and quantified by FCM.

We identified two distinct apoptotic cell populations, one dimly and one brightly fluorescent one, in Cisplatin-treated CHO cell cultures. The dimly fluorescent cells apparently have a low capacity to bind annexin V, probably due to limited phosphatidylserine exposure on the outer surface of the intact cell membrane. It appears that this cell population represents apoptotic cells in the early phase of the process. In addition to membrane integrity, they show only the beginning of nuclear condensation and fragmentation and only the beginning of DNA breaks, with a normal DNA content. In contrast, the brightly fluorescent apoptotic cells predominantly have sub-G<sub>1</sub> DNA content and strongly fragmented nuclei. Since An2 cells have a disrupted cell membrane, the increased annexin V binding of the late apoptotic cells is probably caused by increased accessibility of annexin V to the inner leaflet of the plasma membrane. It seems very likely that there is a progressive shift from An1 toward An2.

In conclusion, compared to other techniques, the annexin V labeling technique is strongly recommended as an assay for the detection and quantification of especially early apoptotic cell populations. The assay has the advantage that it is rapid and is applied on unfixed cells. This enables FCM cell sorting of the early apoptotic cells which can be used for future studies requiring cells with an intact cell membrane.

### LITERATURE CITED

Fig. 5. Sorting of adherent and floating drug-treated CHO cells on the basis of FITC-conjugated annexin V staining, and subsequent analyses in the ISNT assay. The CHO cells had been treated with Cisplatin (20  $\mu$ M, 2 h at 37°C) 2 days earlier. The annexin V binding of the total cell population shows two separate cell populations (b: An1 and An2). Apoptotic cell population An1 represents the adherent cells (c) and An2 the floating cells (d). Adherent cells (sort I) and floating cells (sort II) were sorted on the basis of the FITC fluorescence indicated in the figures. In the ISNT assay, sort I cells have a normal DNA content and partly incorporate biotin-dUTP (e), while sort II cells are mainly characterized by a sub-G<sub>1</sub> DNA content (f). Morphological appearance of normal, untreated CHO cells stained with hematoxylin (a), cells from sort I (g) with the beginning of chromatin condensation and fragmentation, and cells from sort II (h) with nuclear fragmentation are shown. The data from one representative experiment out of three are shown.

1. Andree HAM, Reutelingsperger CPM, Hauptmann R, Hemker HC, Hermens WTh, Willems GM: Binding of vascular anticoagulant  $\alpha$  (VAC $\alpha$ ) to planar phospholipid bilayers. *J Biol Chem* 265:4923-4928, 1990.
2. Arends MJ, Morris RG, Wyllie AH: Apoptosis: The role of the endonuclease. *Am J Pathol* 136:593-608, 1990.
3. Carson DA, Ribeiro JM: Apoptosis and disease. *Lancet* 341:1251-1254, 1993.
4. Cohen GM, Sun XM, Snowden RT, Dinsdale D, Skilleter DN: Key morphological features of apoptosis may occur in the absence of internucleosomal DNA fragmentation. *Biochem J* 286:331-334, 1992.
5. Dive C, Hickman JA: Drug-target interactions: Only the first step in the commitment to a programmed cell death? *Br J Cancer* 64:192-196, 1991.

6. Eastman A, Barry MA: The origins of DNA breaks: A consequence of DNA damage, DNA repair, or apoptosis? *Cancer Invest* 10:229-240, 1992.
7. Fadok VA, Voelker DR, Campbell PA, Cohen JJ, Bratton DL, Henson PM: Exposure of phosphatidylserine on the surface of apoptotic lymphocytes triggers specific recognition and removal by macrophages. *J Immunol* 148:2207-2216, 1992.
8. Geisow MJ: Common domain structure of  $Ca^{2+}$  and lipid-binding proteins. *FEBS Lett* 203:99-103, 1986.
9. Gorczyca W, Gong J, Darzynkiewicz Z: Detection of DNA strand breaks in individual apoptotic cells by the in situ terminal deoxynucleotidyl transferase and nick translation assays. *Cancer Res* 53:1945-1951, 1993.
10. Kerr JFR, Winterford CM, Harmon BV: Apoptosis: Its significance in cancer and cancer chemotherapy. *Cancer* 73:2013-2026, 1994.
11. Koopman G, Reutelingsperger CPM, Kuijten GAM, Keehnen RMJ, Pals ST, van Oers MHJ: Annexin V for flow cytometric detection of phosphatidylserine expression on B cells undergoing apoptosis. *Blood* 84:1415-1420, 1994.
12. Lowe SW, Rulcy HE, Jacks T, Housman DE: P53-dependent apoptosis modulates the cytotoxicity of anticancer agents. *Cell* 74:957-967, 1993.
13. Martin SJ, Reutelingsperger CPM, McGahon AJ, Rader JA, vanSchie RCAA, LaFace DM, Green DR: Early redistribution of plasma membrane phosphatidylserine is a general feature of apoptosis regardless of the initiating stimulus: Inhibition by overexpression of Bcl-2 and Abl. *J Exp Med* 182:1545-1556, 1995.
14. Miyashita T, Reed JC: Bcl-2 gene transfer increases relative resistance of S49.1 and WEH17.2 lymphoid cells to cell death and DNA fragmentation induced by glucocorticoids and multiple chemotherapeutic drugs. *Cancer Res* 52:5407-5411, 1992.
15. Nooter K, Boersma AWM, Oostrum RG, Burger H, Jochemsen AG, Stoter G: Constitutive expression of the c-H-ras oncogene inhibits doxorubicin-induced apoptosis and promotes cell survival in a rhabdomyosarcoma cell line. *Br J Cancer* 71:556-561, 1995.
16. Oberhammer F, Wilson JW, Dive C, Morris ID, Hickman JA, Wakeling AE, Walker PR, Sikorska M: Apoptotic death in epithelial cells: Cleavage of DNA to 300 and/or 50 kb fragments prior to or in the absence of internucleosomal fragmentation. *EMBO J* 12:3679-3684, 1993.
17. Olie RA, Boersma AWM, Dekker MC, Nooter K, Looijenga LHJ, Oosterhuis JW: Apoptosis of human seminoma cells upon disruption of their micro-environment. *Br J Cancer* (in press).
18. Reed JC: Bcl-2 and the regulation of programmed cell death. *J Cell Biol* 124:1-6, 1994.
19. Sambrano GR, Steinberg D: Recognition of oxidatively damaged and apoptotic cells by an oxidized low density lipoprotein receptor on mouse peritoneal macrophages: Role of membrane phosphatidylserine. *Proc Natl Acad Sci USA* 92:1396-1400, 1995.
20. Schwartz LM, Osborne BA: *Methods in Cell Biology: Cell Death*. Academic Press, San Diego, 1995.
21. Sen S, D'Incalci M: Apoptosis: Biochemical events and relevance to cancer chemotherapy. *FEBS Lett* 307:122-127, 1992.
22. Walker PR, Kokileva L, LeBlanc J, Sikorska M: Detection of the initial stages of DNA fragmentation in apoptosis. *BioTechniques* 15:1032-1040, 1993.
23. Wijsman JH, Jonker RR, Keijzer R, van de Velde CJH, Cornelisse CJ, van Dierendonck JH: A new method to detect apoptosis in paraffin sections: In situ end-labeling of fragmented DNA. *J Histochem Cytochem* 41:7-12, 1993.
24. Wyllie AH: Apoptosis. *Br J Cancer* 67:205-208, 1993.
25. Wyllie AH, Kerr JFR, Currie AR: Cell death: The significance of apoptosis. *Int Rev Cytol* 68:251-306, 1980.

Ea  
 their  
 pose  
 while  
 intact  
 penic  
 a C  
 with  
 here  
 associ  
 tated  
 during  
 In  
 desc  
 phos

Ap  
 death  
 mova  
 that a  
 as pa  
 tosis  
 the a  
 tion c  
 respo  
 over,  
 their  
 of ne  
 impai  
 Sever  
 been  
 trans  
 thoug  
 many  
 the b  
 apopt  
 nanci  
 The  
 degr  
 plas

**Annexin V, the regulator of phosphatidylserine-catalyzed inflammation and coagulation during apoptosis**C. P. M. Reutelingsperger<sup>a,\*</sup> and W. L. van Heerde<sup>a,b</sup><sup>a</sup>*Department of Biochemistry, Cardiovascular Research Institute Maastricht, University of Maastricht (The Netherlands), Fax +31 43 3670988, e-mail: c.reutelingsperger@bioch.unimaas.nl*<sup>b</sup>*INSERM Unité 143, Paris (France)*

**Abstract.** Annexin V belongs to a family of phospholipid binding proteins, the Annexins. It binds in the presence of  $\text{Ca}^{2+}$ -ions with high affinity to negatively charged phospholipids like phosphatidylserine (PS). On the basis of its protein structure and biological activity Annexin V is considered as a protein exhibiting its hitherto unknown function within the intracellular environment. One argument comes from the understanding that PS is predominantly located in membrane leaflets, which face the cytosol. However, recent findings show that each cell type has the molecular machinery to expose PS at its cell surface. This machinery is activated during the execution of apoptosis. Once PS is exposed at the cell surface it exhibits procoagulant and proinflammatory activities. Annexin V will bind to the PS-exposing apoptotic cell and can inhibit thereby the procoagulant and pro-inflammatory activities of the dying cell. These findings together with the presence of Annexin V in the extracellular space depict a novel (patho)physiological significance for Annexin V in vivo.

**Key words.** Annexin V; phosphatidylserine; apoptosis; inflammation; coagulation.

Annexins are a class of proteins that share structural and functional features. To date this family comprises thirteen members whose primary structure has been resolved.

The criteria for being a member of the Annexin family are structural and functional. The Annexin primary structure is characterized by tandem homologous domains, each of which contains the so-called endonexin loop. This conserved amino acid motif harbours the phospholipid binding site, which conveys the functional property of binding to phospholipids. Most Annexins behave as extrinsic membrane proteins which bind reversibly to phospholipid membranes in a manner that depends on  $\text{Ca}^{2+}$ -ions. Annexins also bind preferentially to the negatively charged phospholipid species.

During the past decade a great deal of information about the structure and biological activity of Annexins has been elaborated without, however, solving the enigma of the (patho)physiological significance of the individual Annexin or the whole family. Most of the biological data on Annexins arise from in vitro studies and point to roles in interfacial processing occurring at or involving phospholipid membrane structures. These processes include membrane trafficking, modulation of membrane architecture, transmembrane transport of compounds, membrane receptor function, generation of membrane-derived second messengers, regulation of membrane-dependent enzymes, and so forth (for recent reviews see refs 1 and 2).

Since Annexins lack a secretory signal sequence they are supposed to be intracellular proteins and act as such. This concept fits very well with the Annexin structure and ability to bind to phospholipid, because the intracellular cytoplasmic environment is constitutively surrounded by phospholipid membrane leaflets bearing negatively charged phospholipid species. Some Annexins, like Annexin V, have, however, been reported to have extracellular localization. From the point of view of an Annexin the extracellular space is surrounded by membrane leaflets which are devoid of negatively charged phospholipids. What kind of functions can the extracellular Annexin fulfil if binding to negatively charged phospholipids is mandatory? Novel insights into the regulation of cell surface exposure of phosphatidylserine (PS) shed light on this question and stimulate a line of reasoning embedding a (patho)-physiological significance of Annexins in the extracellular space. This essay uses the paradigm of Annexin V to depict a concept and stimulate discussion and investigations into the significance of the extracellular Annexin.

**Annexin V binding to phospholipid model membranes**

Annexin V is also known by various synonyms, indicating widespread interest and reflecting its abundant presence in the organism as well as its activity in diverse biological systems [3]. Annexin V was isolated from the human umbilical cord artery by virtue of its anticoagulant activity [4], which could be explained by its binding to negatively charged phospholipids [5, 6]. In the presence of  $\text{Ca}^{2+}$ , Annexin V binds to most phospholipid

\* Corresponding author.



species in model systems [5–9]. Whereas Annexin V hardly associates with phosphatidylcholine (PC) and sphingomyelin (at  $<5$  mM  $\text{Ca}^{2+}$ ) [6] it binds with high affinity to negatively charged phospholipids like phosphatidylserine (PS), probably because Annexin V bears a binding pocket specific for the phosphoserine headgroup [10]. Binding to a PC model membrane containing PS occurs with a  $K_d$  of less than  $0.1$  nM [5, 6]. Its interaction with the membrane is cooperative and depends on both the phospholipid composition and the  $\text{Ca}^{2+}$  concentration [11]. The fraction of PS in such membranes, together with the  $\text{Ca}^{2+}$  level, determines the number of Annexin V binding sites [6, 9]. Bound to the phospholipid surface Annexin V forms two-dimensional lattices, which are stabilized by protein-protein interactions [12, 13]. Probably, the first Annexin V molecule associates with its binding site comprising PS and acts as an initiator from which crystallization on the surface may proceed without the necessity for PS at high  $\text{Ca}^{2+}$  levels [13]. Binding of Annexin V to phospholipid membrane is reversible and the rates of association and dissociation are very rapid, suggesting that Annexin V does not penetrate the membrane [6, 14]. Taking these data together, the following picture emerges: Annexin V associates rapidly and reversibly with PS-containing membranes under the influence of  $\text{Ca}^{2+}$ . It then starts to crystallize two-dimensionally and may cover the whole phospholipid surface with triskelions of Annexin molecules. This process depends on phospholipid composition and  $\text{Ca}^{2+}$  level.

Cells treat PS in a specific manner which has consequences for the perception of the (patho)physiological significance of Annexin V (see below).

#### Phosphatidylserine localization and (patho)physiological significance

Phosphatidylserine (PS) belongs to the aminophospholipids and carries a phosphoserine headgroup, which gives this phospholipid a negative charge at pH 7.4. As was first shown for erythrocytes and platelets, PS localizes predominantly in those membrane leaflets facing the cytosol. It is now generally accepted that this PS asymmetry is ubiquitous. It is not a fixed situation but requires generation and maintenance. In 1984 Seigneuret and Devaux demonstrated that the cell uses energy to generate and maintain the phospholipid asymmetry of its membranes [15]. A model exists in which various membrane-associated proteins are directly responsible for the distribution of the phospholipid species between the two leaflets of the membrane [16]. These proteins, which have not yet been identified, transport PS from the outer to the inner leaflet (aminophospholipid translocase) or vice versa (floppase), or bidirectionally (scramblase) [17]. The aminophospholipid translocase selectively transports aminophospholipids whereas the

floppase and scramblase exhibit less specificity and also translocate cholinephospholipids. Under viable and nonperturbing conditions the aminophospholipid translocase activity dominates by creating a situation in which PS is exclusively localized to the inner leaflets. Blood platelets were the first cells for which it was demonstrated that a pathophysiological change in PS asymmetry is invoked by the action of agonists like thrombin and collagen [18, 19]. Stimulation of these cells results in a rise of cytosolic  $\text{Ca}^{2+}$ , which causes on the one hand inhibition of the aminophospholipid translocase, and on the other hand activation of the scramblase [20]. Within minutes the architecture of the plasma membrane is changed such that the cell exposes significant amounts of PS at its surface. Comparable mechanisms operate in erythrocyte membranes and the plasma membranes of nucleated cells [17]. Erythrocytes have  $\text{Ca}^{2+}$ -controlled regulation of phospholipid asymmetry and show an age/density-dependent accumulation of PS in the outer leaflet of the plasma membrane [21]. As was demonstrated for the lymphocyte, the nucleated cell type exposes PS at its surface during apoptosis, which is a well-organized process of cell suicide [22]. It was demonstrated that during apoptosis by lymphocytes the aminophospholipid translocase is inhibited while concomitantly a scramblase is activated [23]. Obviously the cell uses energy to maintain its surface devoid of PS and as soon as termination of existence is precluded the cell transports PS to the outer leaflet of the plasma membrane with a speed that is orders of magnitude faster than the rate of passive diffusion of phospholipids between the membrane leaflets. Hence, the PS topology seems to be of major physiological importance under viable as well as dying conditions.

The platelet plays an active role in coagulation if its PS asymmetry is perturbed by the action of agonists like thrombin and collagen. The PS, which becomes surface-exposed, catalyzes reactions of the coagulation cascade [24]. The physiological significance of this phenomenon resides in the effects of accelerating and localizing thrombin formation at the site of the activated platelet. Thrombin generated at those sites exerts diverse humoral and cellular responses of the inflammatory and haemostatic system [25]. The physiological significance of adequate catalysis of thrombin formation, e.g. cell surface exposure of PS, is underscored by Scott syndrome, which is characterized by an impaired  $\text{Ca}^{2+}$ -induced phospholipid scrambling and a moderately severe bleeding disorder [26, 27].

Ageing of erythrocytes is associated with an accumulation of PS at the cell surface [21]. This surface-exposed PS triggers the reticuloendothelial system, which probably carries an as yet unidentified receptor recognizing the PS ligand at the surface of blood cells [28]. This mechanism scavenges aged cells from the circulation

and thereby prevents PS-exposing and hence procoagulant cells continuing to circulate in the blood.

A similar mechanism of removal of unwanted cells operates in the tissues, where tissue macrophages recognize and engulf PS-exposing cells through receptor-mediated processes. Various tumour cells exhibit aberrant phospholipid asymmetry with cell surface-exposed PS, which is recognized by monocyte-derived macrophages [29]. Fadok and coworkers recognized that cell surface exposure of PS is connected with apoptosis, entailing recognition and engulfment of the dying cell by phagocytes [22]. Among other plasma membrane structures, cell surface-exposed PS appears to signal the termination of viability of the cell. This signal is picked up by phagocytes, probably through a receptor-ligand type of mechanism eliciting phagocytosis [30]. The functionality of this recognition-based removal of cells resides in the physiological need to prevent the dying cell from spilling its pro-inflammatory contents into the environment. Studies employing Annexin V as a tool have revealed that a cell in apoptosis exposes PS at its surface well before plasma membrane integrity becomes compromised (see the section below). Hence, cell surface-exposed PS is physiologically employed to entomb the dying cell before it disintegrates and is able to provoke unnecessary inflammatory responses.

#### Annexin V and cell surface-exposed PS, a revealing *pas de deux* of apoptosis

Over the last five years apoptosis has enjoyed a steep increase of interest, mainly because it represents a new concept of how multicellular organisms from worms to mammals regulate their cell number. Paradoxically, this concept depicts this form of cell death to be crucial for life in many ways. It became clear that apoptosis is a process which is accurately orchestrated and organized inside the cell by gene products. It is now accepted that every cell type carries the machinery to commit suicide by apoptosis. The molecular biology and biochemistry of this death machinery are starting to be unravelled and already show great diversity in the various cell types and the manner in which apoptosis is induced. Beyond this diversity three functionally distinct phases of apoptosis can be distinguished [31, 32]. The initiation phase is the most heterogeneous one in which death-inducing signals like Fas ligand and tumour necrosis factor alpha (TNF $\alpha$ ), a lack of growth and survival signals, or DNA damage may induce the cell to prepare for suicide. This preparation results in the activation of a more general effector phase, in which the cell is able to make the decision to die. This phase is characterized by the activation of proteases of the ICE/ICE-like family (the executioner), which form a cascade amplifying the death signals [33]. The death signals probably target the mitochondrion which subsequently releases the

Table 1. Ubiquity of cell surface exposure of PS during apoptosis.

Cell type	Apoptosis initiating stimulus
Leukocytes	Plasma membrane receptor/ligand
neutrophil	lack of growth factor
T lymphocyte	Fas/Fas ligand interaction
B lymphocyte	TNFR/TNF $\alpha$ interaction
monocyte	Intracellular receptor/ligand
Tissue cells	glucocorticoid
endothelial cell	Intracellular signalling
smooth muscle cell	C2-ceramide
fibroblast	staurosporine
neuron	olomoucine
Tumours	Macromolecular synthesis
leukemic cell	actinomycin D
carcinoma cell	cycloheximide
Mouse tissue	DNA
all embryonic cell types	etoposide
Plant cells	camptothecin
<i>Nicotiana plumbaginifolia</i>	UV irradiation

apoptosis inducing factor (AIF), a protease which is inhibited by Z-VAD.fmk just like the ICE-like proteases. This event marks the point of no return; the cell has entered the degradation phase in which "death" of cytoplasm and nucleus occurs by a thousand cuts, in a way that seems common to all cells [33, 34].

In 1992 Fadok and coworkers reported that apoptotic leukocytes expose PS at their surface, probably to serve the physiological need to remove the dying cell by phagocytosis [22]. At that time Annexin V was known as a PS-binding protein (see section above) and appreciated for its ability to bind to PS-exposing cells like activated platelets [35] and ovarian tumour cells [36]. The publication of Fadok and coworkers triggered us to investigate the binding of Annexin V to apoptotic cells. Using leukocytes it was demonstrated that Annexin V exhibits low affinity for the cell surface of the leukocyte unless apoptosis is being executed [37–39]. Combination of the vital dye propidium iodide with fluoresceinated Annexin V revealed that the apoptotic cell generates Annexin V binding sites at its surface while maintaining the plasma membrane integrity [37–39]. Competition experiments using phospholipid vesicles demonstrated that the binding site for Annexin V on the apoptotic cell comprises PS [40]. The Annexin V assay to measure cell surface exposure of PS [41] rapidly increased our knowledge of the regulation of PS exposure during apoptosis. Apoptosis-associated cell surface exposure of PS happens during the effector phase, probably downstream of the point where the mitochondrion gets involved [42] and releases AIF into the cytoplasm [43]. Indirect evidence for this notion comes from experiments with Bcl-2, which is an anti-apoptotic protein. Bcl-2 inhibits both the release of AIF from mitochondria [43] and cell surface PS-exposure of cells treated with pro-apoptotic agonists [40, 42, 44]. Studies with Jurkat cells showed that Fas-mediated apoptosis activates the executioner, which subsequently turns on the

machinery for exposing PS at the cell surface [44]. This PS-exposing machinery is probably a scramblase [23], which resides constitutively in the plasma membranes of the viable cell [44] as is the case for platelets and erythrocytes. As with platelets and erythrocytes, activation of the scramblase during apoptosis does not require the involvement of the nucleus [42, 44]. Whether the scramblase of nucleated cells is identical to the scramblase of platelets and erythrocytes remains to be shown. Using Annexin V it turned out that cell surface exposure of PS is a general phenomenon of apoptosis occurring in hemopoietic [40, 41] and tissue-embedded cells [45, 46] regardless of the initiating stimulus (table 1). This ubiquitous phenomenon also appeared to be part of apoptosis in vivo, as was shown by van den Eijnde and coworkers by injecting Annexin V-Biotin into the bloodstream of living mouse embryos [47].

A recent study showed that plant cells expose PS at their cell surface during execution of apoptosis indicating that, just like apoptosis itself, the mechanism of regulating PS asymmetry during life and death is conserved through evolution and is apparently an absolute necessity for multicellular life forms as we know them [48].

#### Annexin V, a potential regulator of the biological activity of PS on the surface of apoptotic cells

Annexin V has been detected in extracellular space such as blood plasma [49, 50], seminal plasma [51], amniotic fluid [50] and cell conditioned medium [52, 53]. Since the prevailing  $\text{Ca}^{2+}$  levels are around 1 mM, the pres-

ence of Annexin V in the extracellular space implies that plasma membranes containing PS in their outer leaflet are covered by Annexin V if its concentration is in the nM range or higher. As has been shown in vitro for platelets [54], endothelial cells [55], and tumour cells [36, 56] this binding to the PS membrane results in an inhibition of coagulation reactions, which depend on the catalytic activity of PS.

In vivo the platelet is the classic provider of these catalytic sites for the coagulation system. The novel insights into the regulation of PS asymmetry by nucleated cells open up the possibility that cells in apoptosis express this platelet type of function in the coagulation cascade. Apoptotic cells indeed catalyze coagulation [22, 57]. Moreover this procoagulant activity of apoptotic cells is inhibited by Annexin V [57], indicating that, in vivo, extracellular Annexin V can regulate the catalytic activity of both providers and, consequently, regulates the participation of these cells in coagulation and inflammation [25]. Under physiological conditions apoptotic cells hardly play a role in those systems because of their efficient removal by phagocytes. Pathological conditions with a high incidence of apoptotic cells have been described [58]. In this case, the phenotype of apoptosis, e.g. cell surface-exposed PS, may contribute to coagulation and inflammation and extracellular Annexin V may regulate this contribution (summarized in fig. 1). The Annexin V shielding of PS on the surface of apoptotic cells could produce an adverse effect since PS functions as a recognition signal for phagocytes. Phagocytes have developed redundancy in

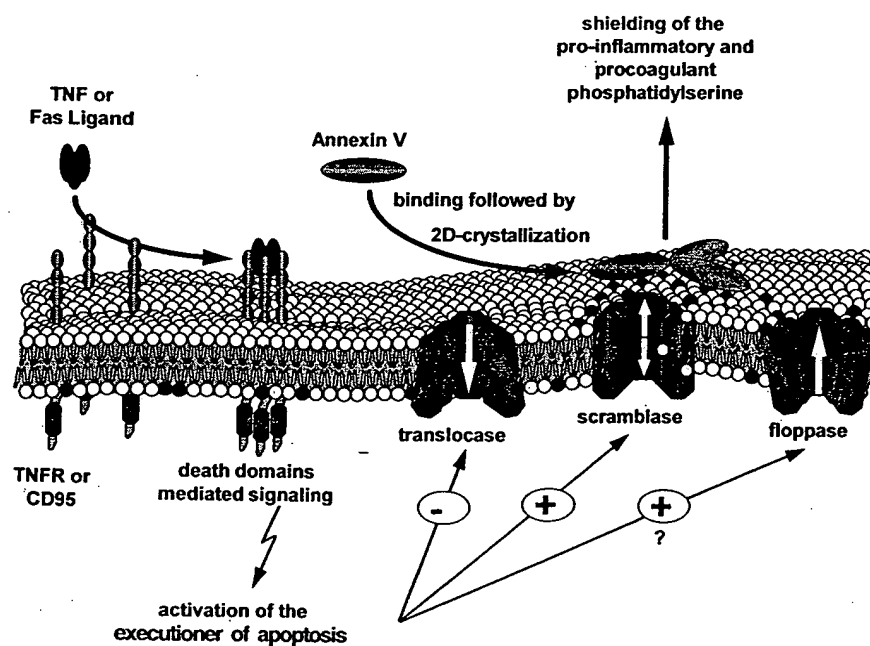


Figure 1. Schematic presentation of the regulation of PS asymmetry of the plasma membrane during life and death, and the role of Annexin V if PS (closed symbol) is exposed at the cell surface. For a detailed explanation see text.

the mechanisms by which they recognize dying cells [30]. Recently it was shown that Annexin V could not completely block phagocytosis of apoptotic bodies [46], indicating selective anticoagulant and anti-inflammatory potential of Annexin V in the interplay between PS-exposing cells and the extracellular environment.

Acknowledgement. WLvH is a research fellow of Netherlands Heart Foundation supported by grant D96-025.

- 1 Raynal P. and Pollard H. B. (1994) Annexins: the problem of assessing the biological role for a gene family of multifunctional calcium- and phospholipid-binding proteins. *Biochim. Biophys. Acta* 1197: 63–93
- 2 Seaton B. A. (ed.) (1996) Annexins: molecular structure to cellular function. Book series: Molecular Biology Intelligence Unit, R. G. Landes Company, Austin, USA
- 3 Van Heerde W. L., Degroot P. G. and Reutelingsperger C. P. M. (1995) The complexity of the phospholipid binding protein annexin V. *Thromb. Haemost.* 73: 172–179
- 4 Reutelingsperger C. P. M., Hornstra G. and Hemker H. C. (1985) Isolation and partial purification of a novel anticoagulant from arteries of human umbilical cord. *Eur. J. Biochem.* 151: 625–629
- 5 Tait J. F., Gibson D. and Fujikawa K. (1989) Phospholipid binding properties of human placental anticoagulant protein-I, a member of the lipocortin family. *J. Biol. Chem.* 264: 7944–7949
- 6 Andree H. A., Reutelingsperger C. P. M., Hauptmann R., Hemker H. C., Hermens W. T. and Willems G. M. (1990) Binding of vascular anticoagulant alpha (VAC alpha) to planar phospholipid bilayers. *J. Biol. Chem.* 265: 4923–4928
- 7 Blackwood R. A. and Ernst J. D. (1990) Characterization of  $\text{Ca}^{2+}$ -dependent phospholipid binding, vesicle aggregation and membrane fusion by annexins. *Biochem. J.* 266: 195–200
- 8 Meers P., Daleke D., Hong K. and Papahadjopoulos D. (1991) Interactions of annexins with membrane phospholipids. *Biochemistry* 30: 2903–2908
- 9 Tait J. F. and Gibson D. (1992) Phospholipid binding of annexin V: effects of calcium and membrane phosphatidylserine content. *Arch. Biochem. Biophys.* 298: 187–191
- 10 Swairjo M. A., Concha N. O., Kaetzel M. A., Dedman J. R. and Seaton B. A. (1995)  $\text{Ca}^{2+}$ -bridging mechanism and phospholipid head group recognition in the membrane-binding protein annexin V. *Nature Structural Biology* 2: 968–974
- 11 Schlaepfer D. D. and Haigler H. T. (1987) Characterization of  $\text{Ca}^{2+}$ -dependent phospholipid binding and phosphorylation of lipocortin I. *J. Biol. Chem.* 262: 6931–6937
- 12 Mosser G., Ravanat C., Freyssinet J. M. and Brisson A. (1991) Sub-domain structure of lipid-bound annexin-V resolved by electron image analysis. *J. Molec. Biol.* 217: 241–245
- 13 Andree H. A., Stuart M. C., Hermens W. T., Reutelingsperger C. P. M., Hemker H. C., Frederik P. M. et al. (1992) Clustering of lipid-bound annexin V may explain its anticoagulant effect. *J. Biol. Chem.* 267: 17907–17912
- 14 Meers P. and Mealy T. (1993) Calcium-dependent annexin V binding to phospholipids: stoichiometry, specificity, and the role of negative charge. *Biochemistry* 32: 11711–11721
- 15 Seigneuret M. and Devaux P. F. (1984) ATP-dependent asymmetric distribution of spin-labeled phospholipids in the erythrocyte membrane: relation to shape change. *Proc. Natl. Acad. Sci. USA* 81: 3751–3755
- 16 Diaz C. and Schroit A. J. (1996) Role of translocases in the generation of phosphatidylserine asymmetry. *J. Membr. Biol.* 151: 1–9
- 17 Zwaal R. F. A. and Schroit A. J. (1997) Pathophysiologic implications of membrane phospholipid asymmetry in blood cells. *Blood* 89: 1121–1132
- 18 Bevers E. M., Comfurius P., van Rijn J. L. M. L., Hemker H. C. and Zwaal R. F. A. (1982) Generation of prothrombin converting activity and the exposure of phosphatidylserine at the outer surface of platelets. *Eur. J. Biochem.* 122: 429–436
- 19 Bevers E. M., Comfurius P. and Zwaal R. F. A. (1983) Changes in membrane phospholipid distribution during platelet activation. *Biochim. Biophys. Acta* 736: 57–66
- 20 Williamson P., Bevers E. M., Smeets E. F., Comfurius P., Schlegel R. A. and Zwaal R. F. A. (1995) Continuous analysis of the mechanism of activated transbilayer lipid movement in platelets. *Biochemistry* 34: 10448–10455
- 21 Connor J., Pak C. C. and Schroit A. J. (1994) Exposure of phosphatidylserine in the outer leaflet of human red cells. Relationship to cell density, cell age and clearance by mononuclear cells. *J. Biol. Chem.* 269: 2399–2404
- 22 Fadok V. A., Voelker D. R., Campbell P. A., Cohen J. J., Bratton D. L. and Henson P. M. (1992) Exposure of phosphatidylserine on the surface of apoptotic lymphocytes triggers specific recognition and removal by macrophages. *J. Immunol.* 148: 2207–2216
- 23 Verhoven B., Schlegel R. A. and Williamson P. (1995) Mechanism of phosphatidylserine exposure, a phagocyte recognition signal on apoptotic T lymphocytes. *J. Expl. Med.* 182: 1597–1601
- 24 Rosing J., Van Rijn J. L. M. L., Bever E. M., Van Dieijen G., Comfurius P. and Zwaal R. F. A. (1985) The role of activated human platelets in prothrombin and factor X activation. *Blood* 65: 319–332
- 25 Esmon C. T. (1993) Cell mediated events that control blood coagulation and vascular injury. *Ann. Rev. Cell Biol.* 9: 1–26
- 26 Rosing J., Bevers E. M., Comfurius P., Hemker H. C., Van Dieijen G., Weiss H. J. et al. (1985) Impaired factor X and prothrombin activation associated with a decreased phospholipid exposure in platelets from a patient with a bleeding disorder. *Blood* 65: 1557–1561
- 27 Weiss H. J. (1994) Scott syndrome: a disorder of platelet coagulant activity. *Semin. Hematol* 31: 312–319
- 28 Schroit A. J., Madsen, J. W. and Tanaka Y. (1985) In vivo recognition and clearance of red blood cells containing phosphatidylserine in their plasma membranes. *J. Biol. Chem.* 260: 5131–5138
- 29 Connor J., Bucana C., Fidler I. J. and Schroit A. J. (1989) Differentiation dependent expression of phosphatidylserine in mammalian plasma membranes: quantitative assessment of outer leaflet lipid by prothrombinase complex formation. *Proc. Natl. Acad. Sci. USA* 86: 3184–3188
- 30 Savill J. (1995) The innate immune system: recognition of apoptotic cells. In: *Apoptosis and the Immune Response*, pp. 341–369, Gregory C. D. (ed.), Wiley-Liss Inc, New York
- 31 Thompson C. B. (1995) Apoptosis in the pathogenesis and treatment of disease. *Science* 267: 1465–1462
- 32 Kroemer G., Petit P. X., Zamzami N., Vayssiere J.-L. and Mignotte B. (1995) The biochemistry of apoptosis. *FASEB J.* 9: 1277–1287
- 33 Martin S. J. and Green D. R. (1995) Protease activation during apoptosis: death by a thousand cuts. *Cell* 82: 349–352
- 34 Susin S. A., Zamzami N. and Kroemer G. (1996) The cell biology of apoptosis: evidence for the implication of mitochondria. *Apoptosis* 1: 231–242
- 35 Thiagarajan P. and Tait J. F. (1990) Binding of annexin V/placental anticoagulant protein I to platelets. Evidence for phosphatidylserine exposure in the procoagulant response of activated platelets. *J. Biol. Chem.* 265: 17420–17423
- 36 Rao L. V., Tait J. F. and Hoang A. D. (1992) Binding of annexin V to a human ovarian carcinoma cell line (OC-2008). Contrasting effects on cell surface factor VIIa/tissue factor activity and prothrombinase activity. *Thromb. Res.* 67: 517–531
- 37 Koopman G., Reutelingsperger C. P. M., Kuijten G. A. M., Keehnen R. M. J., Pals S. T. and Vanoers M. H. J. (1994) Annexin V for flow cytometric detection of phosphatidylserine expression on B cells undergoing apoptosis. *Blood* 84: 1415–1420
- 38 Homburg C. H. E., Dehaas M., Vondemborne A. E. G. K., Verhoeven A. J., Reutelingsperger C. P. M. and Roos D. (1995) Human neutrophils lose their surface Fc gamma RIII and acquire annexin V binding sites during apoptosis in vitro. *Blood* 85: 532–540

39. Vermes I., Haanen C., Steffens-Nakken H. and Reutelingsperger C. P. M. (1995) A novel assay for apoptosis: flow cytometric detection of phosphatidylserine expression on early apoptotic cells using fluorescein labelled Annexin V. *J. Immunol. Methods* 184: 39–52
40. Martin S. J., Reutelingsperger C. P. M., McGahon A. J., Rader J., van Schie C. A. A., LaFace D. M. et al. (1995) Early redistribution of plasma membrane phosphatidylserine is a general feature of apoptosis regardless of the initiating stimulus: inhibition by overexpression of Bcl-2 and Abl. *J. Expl Med.* 182: 1545–1557
41. Martin S. J., Reutelingsperger C. P. M. and Green D. R. Annexin V, a specific probe for apoptotic cells. In: *Techniques in Apoptosis. A User's Guide*, pp. 107–120, Cotter T. G. and Martin S. J. (eds), Portland Press Ltd, London
42. Castedo M., Hirsch T., Susin S. A., Zamzami N., Marchetti P., Macho A. et al. (1996) Sequential acquisition of mitochondrial and plasma membrane alterations during early lymphocyte apoptosis. *J. Immunol.* 157: 512–521
43. Susin S. A., Zamzami N., Castedo M., Hirsch T., Marchetti P., Macho A. et al. (1996) Bcl-2 inhibits the mitochondrial release of an apoptogenic protein. *J. Expl Med.* 184: 1331–1341
44. Martin S. J., Finucane D. M., Amarantemendes G. P., O'Brien G. A. and Green D. R. (1996) Phosphatidylserine externalization during CD95-induced apoptosis of cells and cytoplasts requires ICE/CED-3 protease activity. *J. Biol. Chem.* 271: 28753–28756
45. Van Engeland M., Ramaekers F. C. S., Schutte B. and Reutelingsperger C. P. M. (1996) A novel assay to measure loss of plasma membrane asymmetry during apoptosis of adherent cells in culture. *Cytometry* 24: 131–139
46. Bennett M. R., Gibson D. F., Schwartz S. M. and Tait J. F. (1995) Binding and phagocytosis of apoptotic vascular smooth muscle cells is mediated in part by exposure of phosphatidylserine. *Circulation Res.* 77: 1136–1142
47. van den Eijnde S. M., Boshart L., Reutelingsperger C. P. M., De Zeeuw C. I. and Vermeij-Keers C. (1997) Phosphatidylserine plasma membrane asymmetry in vivo: a pan-cellular phenomenon which alters during apoptosis. *Cell Death Diff.* In press
48. O'Brien I., Reutelingsperger C. P. M. and Holdaway K. (1997) The use of Annexin V and TUNEL to monitor the progression of apoptosis in plants. *Cytometry*. In press
49. Flaherty M. J., West S., Heimark R. L., Fujikawa K. and Tait J. F. (1990) Placental anticoagulant protein-I: measurement in extracellular fluids and cells of the hemostatic system. *J. Lab. Clin. Med.* 115: 174–181
50. Romisch J., Schuler E., Bastian B., Bürger T., Dunkel F. G., Schwinn A. et al. (1992) Annexins I to VI: quantitative determination in different human cell types and in plasma after myocardial infarction. *Blood Coag. Fibrinol.* 3: 11–17
51. Christmas P., Callaway J., Fallon J., Jones J. and Haigler H. T. (1991) Selective secretion of annexin I, a protein without a signal sequence, by the human prostate gland. *J. Biol. Chem.* 266: 2499–2507
52. Koster J. J., Boustead C. M., Middleton C. A. and Walker J. H. (1993) The sub-cellular localization of annexin V in cultured chick-embryo fibroblasts. *Biochem. J.* 291: 595–600
53. Solito E., Raugei G., Melli M. and Parente L. (1991) Dexamethasone induces the expression of the mRNA of lipocortin 1 and 2 and the release of lipocortin 1 and 5 in differentiated, but not undifferentiated U-937 cells. *FEBS Lett.* 291: 238–244
54. Thiagarajan P. and Tait J. F. (1991) Collagen-induced exposure of anionic phospholipid in platelets and platelet-derived microparticles. *J. Biol. Chem.* 266: 24302–24307
55. Vanheerde W. L., Poort S., Vantveer C., Reutelingsperger C. P. M. and Degroot P. G. (1994) Binding of recombinant annexin V to endothelial cells: Effect of annexin V binding on endothelial-cell-mediated thrombin formation. *Biochem. J.* 302: 305–312
56. Sugimura M., Donato R., Kakkar V. V. and Scully M. F. (1994) Annexin-V as a probe of the contribution of anionic phospholipids to the procoagulant activity of tumour cell surfaces. *Blood Coag. Fibrinol.* 5: 365–373
57. Casciola-Rosen L., Rosen A., Petri M. and Schlissel M. (1996) Surface blebs on apoptotic cells are sites of enhanced procoagulant activity: Implications for coagulation events and antigenic spread in systemic lupus erythematosus. *Proc. Natl Acad. Sci. USA* 93: 1624–1629
58. Holmgren L., O'Reilly M. S. and Folkman J. (1995) Dormancy of micrometastasis: balanced proliferation and apoptosis in the presence of angiogenesis suppression. *Nature Med.* 1: 149–153

A  
S.  
D  
F  
A  
pr  
fo  
of  
ex  
ai  
re  
KIt  
It  
co  
ci  
th  
P  
si  
b  
li  
c  
re  
b  
v  
in  
n  
t  
a  
F  
t  
t  
F  
t  
c  
c  
s  
l  
t  
l  
l  
i  
v  
l  
i  
c

## Differential Apoptosis Gene Expression in Pediatric Tumors of the Kidney

By Shigeru Takamizawa, Shinya Okamoto, Warren Bishop, Judy Wen, Ken Kimura, and Anthony Sandler  
Iowa City, Iowa

**Background/Purpose:** Apoptosis, or programmed cell death, is essential in maintaining normal homeostasis of tissues. The process of apoptosis is controlled by numerous pro- and antiapoptotic factors. Variations in expression of such factors may account for some variations in tumor behavior. This study evaluates the expression of apoptotic mRNA species in pediatric renal tumors to determine whether a pattern of differential apoptosis gene expression correlates with tumor grade and type.

**Methods:** Twenty-five frozen tissue specimens were obtained from patients undergoing biopsy or resection of pediatric renal tumors before chemotherapy: Wilms' tumor stage II (WT-II,  $n = 4$ ); Wilms' tumor stage III/IV (WT-III/IV,  $n = 4$ ); clear cell sarcoma of the kidney stage III (CCSK,  $n = 2$ ); rhabdoid tumor of the kidney stage III/IV (RTK,  $n = 4$ ); and normal kidney (NK,  $n = 11$ ). An RNase Protection Assay (RPA) was performed for 19 pro- and antiapoptotic mRNA species to detect and quantify expression (percentage of GAPDH expressed). Expression of specific mRNAs of interest were confirmed by Western Blot (WB).

**Results:** The expression of apoptotic mRNA species varied markedly between tumors. WT-II expressed greater amounts

of proapoptotic receptor mRNA than CCSK or RTK. (Fas,  $17.0 \pm 2.7\% \vee 2.5 \pm 0.5\% \vee 3.3 \pm 0.9\%$ ;  $P < .02$ ; DR5,  $77.0 \pm 8.8\% \vee 13.5 \pm 0.5\% \vee 27.0 \pm 4.8\%$ ;  $P < .001$ ; TNF-R,  $71.3 \pm 17.0\% \vee 21.0 \pm 4.0\% \vee 29.0 \pm 5.0\%$ ;  $P < .07$ , respectively). Surprisingly, antiapoptotic factors (eg, *bcl-2* and *bcl-xl*) were not overexpressed in poor prognostic tumors (CCSK, RTK) compared with those with good prognosis (WT). Expression of TRAIL (a ligand for DR4 and DR5) was significantly lower in CCSK and RTK than in normal kidney ( $9.5 \pm 1.5\% \vee 56.1 \pm 10.1\%$ ;  $P = .01$ ).

**Conclusions:** Proapoptotic receptors are expressed at greater levels in good prognostic tumors, and this finding is compatible with their clinical behavior. Knowledge of differential apoptotic gene expression is of potential value in predicting prognosis and treating such tumors with targeted ligands. *J Pediatr Surg* 35:390-395. Copyright © 2000 by W.B. Saunders Company.

**INDEX WORDS:** Wilms' tumor, clear cell sarcoma of the kidney, rhabdoid tumor of the kidney, apoptosis, pediatric renal tumors.

**W**ILMS' TUMOR is the most common primary malignant renal tumor of childhood and accounts for 5% to 6% of all childhood cancers in the United States. The survival rate of Wilms' tumor stage II and stage III/IV are 92.2% and 73%, respectively.<sup>1</sup> Clear cell sarcoma of the kidney (CCSK) and rhabdoid tumor of the kidney (RTK) are other malignant pediatric renal tumors that show aggressive behavior and poor prognoses. The 6-year relapse-free survival rate of CCSK is about 60%,<sup>2</sup> and only 10% of patients with RTK survive despite aggressive antitumor therapy.<sup>3</sup>

Apoptosis, or programmed cell death, is the process by which activated cells undergo a suicide program that

results in individual cell death. This is a highly orchestrated process in which cells neatly commit suicide by destroying themselves in a regulated fashion. Apoptosis is a normal physiological process that occurs in the developing embryo as well as in mature animals during tissue turnover and during down-regulation of an immune response. Proper regulation of this process is essential for normal homeostasis and tissue development.<sup>4,5</sup> An aberration in the process of apoptosis may contribute to the pathogenesis of cancer.

A depletion of proapoptotic (death) factors or an abundance of antiapoptotic (survival) mediators, could result in failure of dividing cells to undergo apoptosis and contribute to tumorigenicity. Proapoptotic proteins such as Fas, Fas-L, TNFR, TRAIL, DR4, DR5, Bax, Bix, Bak, and Bcl-xs induce apoptosis by either signaling for the activation of proteolytic enzymes called caspases that destroy the cell, or by blocking inhibitors of apoptosis.<sup>6</sup> Antiapoptotic proteins such as Bcl-2, Bcl-xl, and mcl-1 inhibit adapter molecules needed for activation of caspases during apoptosis and hence prolong cell survival.<sup>7</sup>

The balance between pro- and antiapoptotic genes may be critical to the behavior and survival of tumor cells.

From the Department of Surgery and Pediatrics, University of Iowa Hospitals & Clinics, Iowa City, IA.

Presented at the 30th Annual Meeting of the American Pediatric Surgical Association, Rancho Mirage, California, May 16-19, 1999.

This work was supported by a grant from the Children's Miracle Network, sponsored by The University of Iowa.

Address reprint requests to Anthony D. Sandler MD, Department of Surgery, Section of Pediatric Surgery, The University of Iowa Hospitals and Clinics, 200 Hawkins Dr, Iowa City, IA 52242.

Copyright © 2000 by W.B. Saunders Company  
0022-3468/00/3502-0047\$03.00/0

GENE E

Variati  
some  
clini  
totic n  
mine  
expres

Tissue

Twen  
obtain  
at the  
Wilms  
were gr  
Wilms'  
III/IV,  
tumor  
kidney  
by our l

RNase

RNA:  
procedu  
multipl  
differ  
probe s  
tion ass  
include  
bik, ba  
proapo  
namely  
TNFRp

After  
probe v  
and no  
Phosph  
polyme  
Englan  
Life Te  
with th  
or hAp  
by digi  
mixture  
unhybr  
protect  
μL of l  
on 5%  
was dr  
then q  
BIO M  
20 hou

Radi

For  
a perc  
in the  
expres  
fied di  
4000,  
Softw  
each t  
each n

Variations in expression of such factors may account for some of the variations in tumor behavior observed clinically. This study evaluates the expression of apoptotic mRNA species in pediatric renal tumors to determine whether a pattern of differential apoptosis gene expression correlates with tumor stage and type.

## MATERIALS AND METHODS

### Tissue Collection

Twenty-five frozen tissue kidney biopsy or resection specimens were obtained from pediatric patients with renal tumors before chemotherapy at the University of Iowa Hospitals & Clinics and from the National Wilms Tumor Study Group (NWTSG) tissue bank. Tissue specimens were grouped according to clinical stage of disease and tumor type: Wilms' tumor stage II (WT-II,  $n = 4$ ), Wilms' tumor stage III/IV (WT III/IV,  $n = 4$ ), clear cell sarcoma stage III (CCSK,  $n = 2$ ), rhabdoid tumor of the kidney stage III/IV (RTK,  $n = 4$ ), and normal adjacent kidney (NK,  $n = 11$ ). All protocols and tissues harvested were approved by our Institutional Review Board.

### RNase Protection Assay

RNase Protection Assay (RPA) is a highly sensitive and specific procedure that allows for simultaneous detection and quantification of multiple mRNA species. RPA was used to detect and quantify 19 different mRNA apoptotic species expression with 2 human template probe sets, hApo-2 and hApo-3c. (The RiboQuant Multi-probe protection assay system; Pharmingen, San Diego, CA). The probe set hApo-2 includes 8 *bcl-2*-related gene templates including *bcl-xl*, *bcl-xs*, *bfl-1*, *bik*, *bak*, *bax*, *bcl-2*, and *mcl-1*. The hApo-3c probe set includes 11 proapoptotic and tumor necrosis factor family-related gene templates, namely, *caspase-8*, *Fas-L*, *Fas*, *DCR1*, *DR3*, *DR5*, *DR4*, *TRAIL*, *TNFRp55*, *TRADD*, and *RIP*.

After isolating RNA from the tissues of interest, the antisense RNA probe was hybridized in excess to target RNA in-solution. Free probe and nonhybridized single stranded RNA are digested with RNases. Phosphorus P32-labeled antisense RNA was transcribed using T7 RNA polymerase (Pharmingen) and [ $\alpha$ - $^{32}$ P]UTP (Amersham Life Science, England). Total RNA was extracted from tissue using TRIzol (Gibco Life Technologies, MD). Fourteen to 16  $\mu$ g of total RNA was hybridized with the  $^{32}$ P-labeled RNA probes, which were transcribed from hApo-2 or hApo-3c multiprobes (DNA templates) at 56°C overnight, followed by digestion with a 1:417 dilution of RNase "cocktail" (RNase A:T1 mixture; Pharmingen) for 45 minutes at 30°C. Single-stranded and unhybridized excess mRNA was digested by the RNase cocktail. The protected double-stranded RNA pellets were dried and resuspended in 5  $\mu$ L of 1 $\times$  loading buffer (Pharmingen), and electrophoretically resolved on 5% polyacrylamide, 8 mol/L urea gel. The polyacrylamide-urea gel was dried on blotting paper for 1 hour at 80°C. The labeled probes were then quantified by autoradiography by exposing the blotting paper to BIO MAX FILM (Kodak, NY) with an intensifying screen (Kodak) for 20 hours at 80°C.

### Radioanalytic Imaging

For comparative analysis, we quantified mRNA species expression as a percentage of mRNA GAPDH expression. Radioactivity of each band in the sample was quantified, standardized, and compared with GAPDH expression of that sample. Radioactivity of each template was quantified directly from the gel by a radioanalytic imaging system (AMBIS 4000, AMBIS Inc, San Diego, CA) equipped with AMBIS QuantProbe Software Version 3.0 for 1,000 minutes. Net counts were obtained from each template (band), including GAPDH, and the radioactive ratio of each mRNA to GAPDH was calculated.

### Western Blot for Fas Receptor Protein Expression

The standard technique of Western Blot (WB) was performed.<sup>8</sup> Briefly, tissue lysate proteins from WT stage II ( $n = 2$ ), RTK ( $n = 1$ ), and NK ( $n = 2$ ) were isolated by solubilizing in RIPA buffer (1% Triton X-10, 1% Deoxycholate [DOC], 0.1% sodium dodecyl sulfate [SDS], 50 mmol/L Tris-HCl [pH 7.4], 150 mmol/L NaCl, 0.5 mmol/L Na<sub>3</sub>VO<sub>4</sub>, 5 mmol/L EDTA), and protease inhibitors; leupeptin (20  $\mu$ g/mL RIPA), phenylmethylsulfonyl fluoride (PMSF 20  $\mu$ g/mL RIPA). The protein content was equilibrated between samples by using the Lowry protein assay to quantify protein isolated.<sup>9</sup> Subsequently, 120  $\mu$ g of total protein from each specimen was electrophoretically resolved on SDS-containing 8% polyacrylamide gels. Separated proteins were then transferred to a nitrocellulose membrane at 210 mAmps for 4 hours. Membranes were blocked using 5% skim milk in Tris-buffered saline (TBS), supplemented with 0.1% Tween-20 (TBS-T), overnight at 4°C. The nitrocellulose membrane was rinsed with TBS-T and incubated for 1 hour at room temperature in a sealed bag with 1.0  $\mu$ g/mL of the antihuman Fas rabbit polyclonal antibody (Santa Cruz Biotechnology Inc, Santa Cruz, CA) in 5 mL of 5% dry milk in TBS-T. Bound antibody was detected with a 1:2500 dilution of horseradish peroxidase (HRP)-labeled goat antirabbit IgG secondary antibody (SIGMA, MO). Bands denoting Fas expression were viewed after developing on radiographic plates by enhanced chemiluminescence (ECL; Amersham, Arlington Heights, IL).

### Data Analysis

Percent gene expression was compared between the groups using one-way analysis of variance (ANOVA) for *Fas*, *DR4*, *DR5*, *TNFR*, *TRAIL* and *Bcl-2*. The square root transformation was applied to *Fas* and *TNFR*, and the natural logarithm transformation was applied to *Bcl-2* and *TRAIL* before analysis to stabilize the variance among the groups or to normalize the data distribution. A nonparametric test (Kruskal-Wallis test) was applied to *Bax* and *Bcl-xL* because no suitable transformation was found. If the one-way ANOVA F-test or the Kruskal-Wallis test was significant, pairwise comparisons between the groups were performed. To adjust for the multiple tests, Bonferroni's method was used, and the adjusted *P* values less than .05 were considered statistically significant.

## RESULTS

To determine if an association between apoptosis genes and tumor stage and type existed, we categorized the apoptosis mRNA species studied into 2 groups, namely proapoptosis and antiapoptosis species. Comparisons were made between the different tumor types and clinical stages of disease (WT II [ $n = 4$ ] v WT III/IV [ $n = 4$ ] v CCSK III [ $n = 2$ ] v RTK III/IV [ $n = 4$ ] v NK [ $n = 11$ ]) and between groups of tumors (WT [ $n = 8$ ] v CCSK/RTK [ $n = 6$ ] v NK [ $n = 11$ ]).

### Proapoptosis Genes

Concerning the proapoptosis mRNA species, all 15 (*bcl-xs*, *bik*, *bak*, *bax*, *caspase-8*, *Fas-L*, *Fas*, *DCR1*, *DR3*, *DR5*, *DR4*, *TRAIL*, *TNFRp55*, *TRADD*, and *RIP*) were detected in all samples at different intensities (Fig 1). Six species of interest reflecting the proapoptotic pathways were selected for statistical analysis based on their gross differences in expression (*bax*, *Fas*, *DR5*, *DR4*, *TRAIL*, and *TNFRp55*).

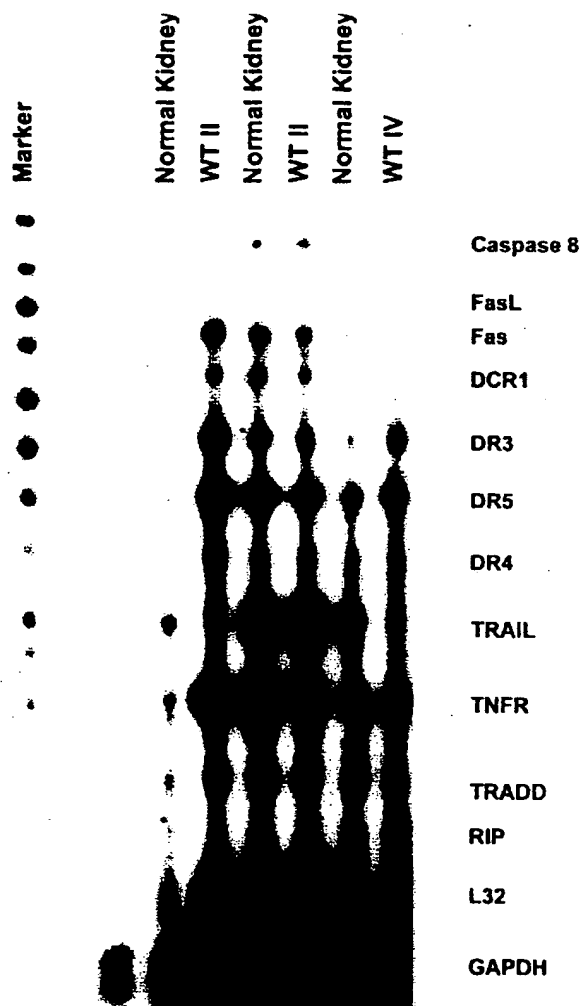


Fig 1. Sample RPA of tissues evaluating proapoptotic (TNF related family) mRNA species. The radioactivity of each band (mRNA specie) is calculated and quantified as a percent of GAPDH expressed.

**Fas.** WT stage II/III/IV showed greater expression ( $13.1 \pm 2.8\%$ ) compared with CCSK/RTK ( $3.0 \pm 0.6\%$ ;  $P = .01$ ) and tended to be greater than NK ( $5.6 \pm 0.9\%$ ;  $P = .09$ ). WT-II, had the greatest expression of Fas mRNA ( $17.0 \pm 2.7\%$ ) compared with WT III/IV ( $9.3 \pm 4.3\%$ ;  $P = .2$ ), CCSK ( $2.5 \pm 0.5\%$ ;  $P = .015$ ), RTK ( $3.3 \pm 0.9\%$ ;  $P = .004$ ) and NK ( $5.6 \pm 0.9\%$ ;  $P = .008$ ).

**DR5.** WT stage II/III/IV expressed greater amounts ( $59.1 \pm 8.1\%$ ) compared with CCSK/RTK ( $22.5 \pm 4.2\%$ ;  $P = .008$ ) and NK ( $25.8 \pm 4.3\%$ ;  $P = .004$ ). WT-II had the greatest expression of DR5 mRNA ( $77.0 \pm 8.8\%$ ) compared with WT-III/IV ( $41.3 \pm 3.6\%$ ;  $P = .019$ ), CCSK ( $13.5 \pm 0.5\%$ ;  $P = .0003$ ), RTK ( $27.0 \pm 4.8\%$ ;  $P = .0005$ ) and NK ( $25.8 \pm 4.3\%$ ;  $P < .0001$ ).

**TNFRp55.** WT-II tended to have the greatest expres-

sion ( $71.3 \pm 16.9\%$ ) compared with CCSK ( $21.0 \pm 4.0\%$ ;  $P = .058$ ) and RTK ( $29.0 \pm 5.0\%$ ;  $P = .07$ ).

**TRAIL.** The expression of TRAIL mRNA (proapoptotic ligand) was significantly lower in CCSK/RTK ( $9.5 \pm 1.5\%$ ) compared with NK ( $56.1 \pm 10.1\%$ ;  $P = .01$ ). Normal kidney adjacent to benign mesoblastic nephroma or normal kidney with unrelated disease had lower TRAIL expression ( $13.7 \pm 3.7\%$ ) than normal kidney adjacent to CCSK and RTK ( $74.0 \pm 13.0\%$ ;  $P = .02$ ).

**Bax.** CCSK/RTK had greater expression of Bax ( $39.8 \pm 6.7\%$ ) compared with NK ( $12.9 \pm 2.0\%$ ;  $P = .003$ ). WT-II ( $32.3 \pm 5.4\%$ ;  $P = .049$ ) and RTK ( $41.8 \pm 10.2\%$ ;  $P = .009$ ) had significantly greater expression of Bax mRNA compared with NK ( $12.9 \pm 2.0\%$ ).

**DR4.** There was no difference in mRNA DR4 expression. (WT stage II,  $19.0 \pm 2.1\%$ ; WT stage III/IV,  $15.8 \pm 1.5\%$ ; CCSK,  $6.0 \pm 1\%$ ; RTK,  $12.8 \pm 3.0\%$ ; and NK,  $13.8 \pm 2.1\%$ ;  $P = .1$ ).

In general, these results show that proapoptotic mediators are more abundantly expressed in tumors with a better stage and prognosis. These findings imply that such tumors have the machinery in place that will allow for the process of apoptosis (Fig 2).

#### Antiapoptosis Genes

All 4 antiapoptosis gene mRNA species (*bcl-xl*, *bfl-1*, *bcl-2* and *mcl-1*) were detected in all samples at different intensities and of those, *bcl-xl* and *bcl-2* were compared (Fig 3).

**bcl-2.** Surprisingly, this inhibitor of apoptosis was expressed at significantly lower levels in poor prognostic tumors (CCSK/RTK  $8.5 \pm 2.1\%$ ) compared with NK ( $14.5 \pm 0.5\%$ ;  $P = .03$ ). RTK also had significantly lower expression of *bcl-2* mRNA ( $5.3 \pm 0.9\%$ ) compared with WT II ( $15.0 \pm 3.6\%$ ;  $P = .02$ ), WT III/IV

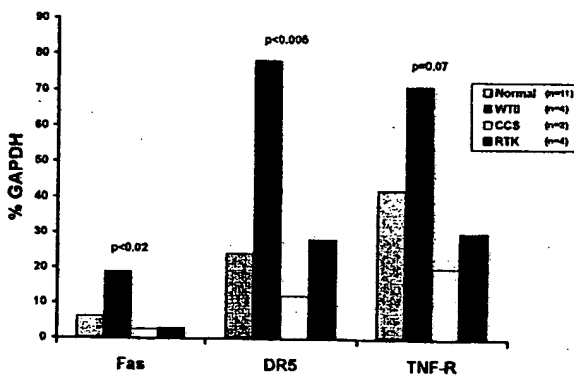


Fig 2. Differences in Fas, DR5 and TNF-R mRNA expression in normal kidney (Normal), Wilms' tumor Stage II (WTII), Clear cell Sarcoma Stage III (CCSK), and Rhabdoid tumor of the kidney stage III/IV (RTK). Note that in each case, WT has the greatest expression of the mRNA of interest.



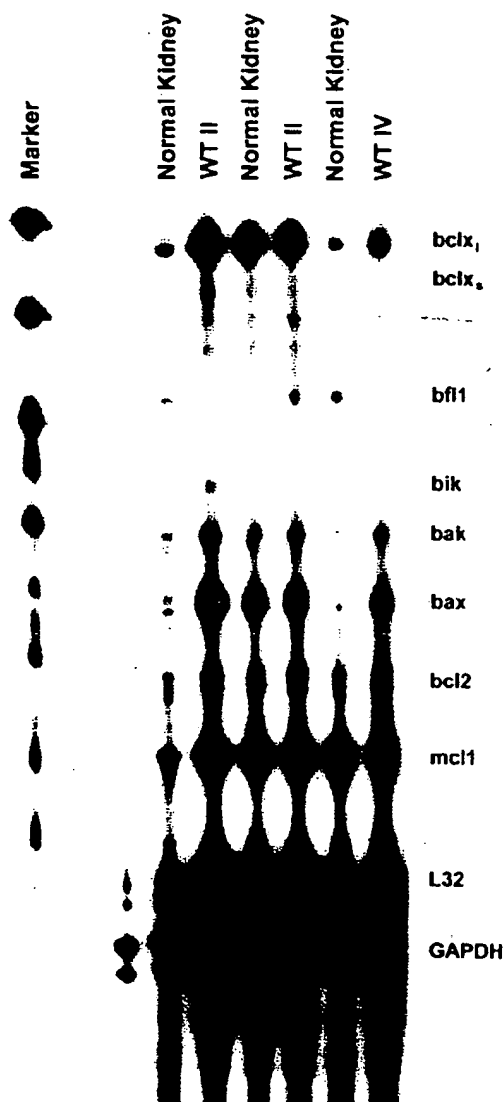


Fig 3. Sample RNase Protection Assay (RPA) of tissues evaluating *bcl-2*-related family mRNA species. The radioactivity of each band (mRNA specie) is calculated and quantified as a percent of GAPDH expressed.

( $13.8 \pm 2.3\%$ ;  $P = .024$ ), CCSK ( $15.0 \pm 0.0\%$ ;  $P = .04$ ), and NK ( $14.5 \pm 0.5\%$ ;  $P = .001$ ).

*bcl-xl*. There was no difference in *bcl-xl* mRNA expression between the various stages or type of renal tumors ( $P = .2$ ). The lower expression of the antiapoptotic factor Bcl-2 in RTK (which carries the worst prognosis) was initially surprising considering previous literature reports.<sup>10</sup> However, in the absence of significant levels of proapoptotic gene expression, the need for abundant expression of antiapoptotic factors may be redundant.

#### Western Blot for Fas and Bcl-xl Proteins

To determine if greater mRNA expression detected by RPA translated into greater protein expression, we selec-

tively performed WB of Fas expression from NK, WTII, and RTK. WB showed a positive Fas band at 45 kDa in WTII, which was far brighter than expression in NK or RTK. This helped in verifying the accuracy of RPA analysis (Fig 4).

#### DISCUSSION

Apoptosis gene expression may contribute to the viability of tumors and may account for their varied clinical behavior. If such a concept were true, predicting the prognosis of tumors would be dependent on their biology, and treatment could be tailored to block or stimulate specific apoptotic factors of interest. The current study was undertaken to explore whether variations in apoptotic gene expression correlate with stage and type of pediatric renal tumors.

Despite the relatively small numbers in this study, it was clear that WT-stage II (in general a good prognostic tumor) expressed proapoptotic mRNA species more abundantly than CCSK or RTK, 2 tumors of worse prognosis. Specifically, Fas, DR5 and TNF-R, representing a family of "death receptors," were all expressed at greater levels in Wilms' tumor stage II. These cell surface receptor proteins bind to specific ligands (Fas-L, TRAIL, and TNF, respectively) that induce activation of proteolytic enzymes called caspases. The caspase cascade disassembles and ultimately destroys the cell.<sup>6</sup> Relating prognosis to expression of proapoptotic receptors is an appealing theory, because both cytotoxic T lymphocytes (CTL) and natural killer (NK) immune surveillance cells use such ligands for killing of target cells.<sup>11,12</sup> Furthermore, TNFR-1, Fas, DR3, and DR4 are activated on overexpression in a ligand-independent manner and may spontaneously induce apoptosis.<sup>13-16</sup>

The mRNA of DR5 is detected in several normal human tissues, and the amount of DR5 transcription is reported to be 100-fold more in most tumor cell lines than in normal tissues.<sup>17</sup> The expression of DR4 or DR5 in tumors of poor prognosis was no different to that of normal kidney in the current study, whereas expression of DR5 in WT II was about 3-fold greater. The ligand for DR4 and DR5 (TRAIL, TNF related apoptosis-inducing

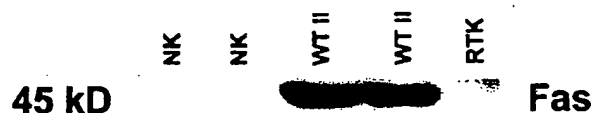


Fig 4. Western Blot (WB) analysis of selected samples looking at Fas protein expression. The differential expression of protein detected by WB correlated with the differential expression of mRNA detected by RPA. Note the absence of Fas bands in the normal kidney (NK) and rhabdoid tumor of the kidney (RTK) lanes, with bright bands in the Wilms tumor stage II (WTII) lanes. This observation verifies the accuracy of RPA results.

ligand) is shown to induce killing of several tumor cell lines, thus expression of these receptors may have therapeutic implications.<sup>18</sup>

The balance between expression of apoptosis-inducing receptors and their ligands may regulate cell susceptibility to undergoing apoptosis.<sup>19</sup> We have shown that overexpression of Fas-L induces apoptosis in Fas-expressing HepG2/C3A hepatoblastoma cell lines by inducing cell suicide (Unpublished data). Fas-L was barely detectable in any of the tumor specimens examined, thus, this suicide effect is probably inconsequential. However, TRAIL, along with its receptors, was expressed in many of the tumors at relatively high levels. The balance between TRAIL and DR4/DR5 receptors potentially could have a regulatory effect on apoptosis in these tumors. It is of interest to note that normal kidney had a nearly 10-fold greater expression of TRAIL than adjacent CCSK or RTK. Although purely conjectural, this phenomenon may be a defensive response of the normal kidney to invasion of the adjacent tumor. Comparatively high levels of expression were not seen in normal kidney biopsied from unrelated disease or when benign mesoblastic nephroma was the adjacent tumor.

Bcl-2 and Bcl-xL are antiapoptosis proteins localized to the outer mitochondrial membrane, endoplasmic reticulum, and nuclear membranes of cells. These factors suppress apoptosis and allow proliferation and prolonged survival that may explain tumor cell viability. Although *bcl-2* is one of the most noted antiapoptosis genes, the correlation between *bcl-2* overexpression and tumor behavior is uncertain. Conflicting studies are reported in neuroblastoma, a childhood malignancy of neurogenic origin. Overexpression of *bcl-2* is said to correlate with tumor progression, poor prognosis, and unfavorable histology,<sup>10,20</sup> whereas another study suggests that *bcl-2* expression is associated with favorable histology.<sup>21</sup> Despite these reports, the expression of *bcl-2* or *bcl-xL* mRNA did not show any correlation between renal tumor

type, stage of disease or normal kidney in our study. The lower expression of the antiapoptotic factor Bcl-2 in RTK (which carries the worst prognosis) seems inconsistent, but in the absence of significant levels of proapoptotic gene expression, the need for abundant expression of antiapoptotic factors may be redundant.

Proapoptosis (*bax*, *bik*, *bak* and *bcl-xs*) and antiapoptosis (*bcl-2*, *bcl-xL*, *bfl-1*, *mcl-1*) activity is different among *bcl-2* gene-related family members.<sup>22</sup> However, there was no association between the ratio of pro- to antiapoptotic *bcl-2*-related mRNA species in the tumors studied. Bcl-2 inhibits apoptosis induced by the tumor suppressor gene *p53*.<sup>23,24</sup> Consequently, the role of *bcl-2* in such tumors cannot be completely understood without studying the associated expression of *p53*.

To determine whether differences in mRNA expression detected by RPA translated into differences in actual protein expression, we examined Fas protein expression by WB and compared its expression with RPA results for several tumors and normal kidney. The differences noted between tumors and normal tissue by RPA were confirmed in that we found Fas followed the same differential pattern of protein expression. This finding helped verify the accuracy of the results obtained by RPA analysis.

In general, these findings show that proapoptosis genes are expressed at greatest levels in good prognostic renal tumors, whereas expression is less in normal kidney and lowest in poor prognostic tumors. This suggests that good prognostic tumors may readily undergo apoptosis, whereas diminished expression of apoptosis genes in normal mature tissue may reflect a state of senescence. Poor prognostic tumors are rapidly proliferating, independent of proapoptotic mediators.

## ACKNOWLEDGMENTS

The authors thank Paul Grundy and the National Wilms Tumor Study Group (NWTSG) for supplying many of the specimens used in this study.

## REFERENCES

1. D'Angio GJ, Breslow N, Beckwith JB, et al: Treatment of Wilms' tumor. Results of the third National Wilms' Tumor Study. *Cancer* 64:349-360, 1989
2. Green DM, Breslow N, Beckwith JB, et al: Treatment of children with clear-cell sarcoma of the kidney: A report from national Wilms' Tumor Study Group. *J Clin Oncol* 12:212-217, 1994
3. Palmer NF, Sutow W: Clinical aspect of the rhabdoid tumor of the kidney: A report of the National Wilms' Tumor Study Group. *Med Pediatr Oncol* 11:242-245, 1983
4. Miller L, Marx J: Apoptosis. *Science* 281:1301, 1998
5. Steller H: Mechanisms and genes of cellular suicide. *Science* 267:1445-1449, 1995
6. Ashkenazi A, Dixit VM: Death receptors: Signaling and modulation. *Science* 281:1305-1308, 1998
7. Adams JM, Cory S: The Bcl-2 protein family: Arbiters of cell survival. *Science* 281:1322-1326, 1998
8. Fogh J, Fogh JM, Orfeo T: One hundred and twenty-seven cultured human tumor cell lines producing tumors in nude mice. *J Natl Cancer Inst* 59:221-226, 1977
9. Lowry O, Rosebrough NJ, Farr AL, et al: Protein measurement with folinphenol reagent. *J Biol Chem* 193:265, 1951
10. Castle VP, Heidelberger KP, Bromberg J, et al: Expression of the apoptosis-suppressing protein *bcl-2*, in neuroblastoma is associated with unfavorable histology and N-myc amplification. *Am J Pathol* 143:1543-1550, 1993
11. Liston P, Roy N, Tamal K, et al: Suppression of apoptosis in mammalian cells by NAIP and a related family of IAP genes. *Nature* 379:349-353, 1996
12. Deveraux QL, Takahashi R, Salvesen GS: X-linked IAP is a direct inhibitor of cell-death proteases. *Nature* 388:300-304, 1997
13. Muzio M, Chinnaiyan AM, Kischkel FC, et al: FLICE, a novel FADD-homologous ICE/CED-3-like proteins, is recruited to the CD95(Fas/Apo-1) death-inducing signaling complex. *Cell* 85:817-827, 1996

14. Chinnaiyan AM, O'Rourke, Yu GL, et al: Signal transduction by DR3, a death domain-containing receptor related to TNFR-1 and CD95. *Science* 274:990-992, 1996
15. Kitson J, Raven T, Jiana YP, et al: A death-domain-containing receptor that mediates apoptosis. *Nature* 384:372-375, 1996
16. Pan G, O'Rourke K, Chinnaiyan AM, et al: The receptor for the cytotoxic ligand TRAIL. *Science* 276:1111-1113, 1997
17. MacFarlane M, Ahmad M, Srinivasula SM, et al: Identification and molecular cloning of two novel receptors for the cytotoxic ligand TRAIL. *J Biol Chem* 272:25417-25420, 1997
18. Walczak H, Miller RE, Ariail K, et al: Tumoricidal activity of tumor necrosis factor-related apoptosis-inducing ligand in vivo. *Nat Med* 5:157-163, 1999
19. Muller M, Strand S, Hug H, et al: Drug-induced apoptosis in hepatoma cells is mediated by the CD95(APO-1/Fas) receptor/ligand system and involves activation of wild-type p53. *J Clin Invest* 99:403-413, 1997
20. Hoehner J, Hedborg F, Wiklund HJ, et al: Cellular death in Neuroblastoma: In situ correlation of apoptosis and bcl-2 expression. *Int J Cancer* 62:19-24, 1995
21. Krajewski S, Chatten J, Handa H, et al: Immunohistochemical analysis of the Bcl2 oncoprotein in human neuroblastoma. *Lab Invest* 72:42-54, 1995
22. D'sa-Eipper C, Subramanian T, Chinnadurai G, et al: bfl-1, a bcl-2 homologue, suppresses p53-induced apoptosis and exhibits potent cooperative transforming activity. *Cancer Res* 56:3879-3882, 1996
23. Miyashita T, Krajewski S, Krajewski M, et al: Tumor suppressor p53 is a regulator of bcl2 and bax gene expression in vitro and in vivo. *Oncogene* 9:1799-1805, 1994
24. Brambilla E, Negoescu A, Grazzini S, et al: Apoptosis-related factors p53, bcl2, and Bax in neuroendocrine lung tumors. *Am J Pathol* 149:1941-52, 1996

## PK11195, a Ligand of the Mitochondrial Benzodiazepine Receptor, Facilitates the Induction of Apoptosis and Reverses Bcl-2-Mediated Cytoprotection

Tamara Hirsch,<sup>1</sup> Didier Decaudin,<sup>1</sup> Santos A. Susin, Philippe Marchetti, Nathanael Larochette, Michèle Resche-Rigon,\* and Guido Kroemer<sup>2</sup>

Centre National de la Recherche Scientifique, Unité Propre de Recherche 420, 19 rue Guy Môquet, F-94801 Villejuif, France; and \*Hoechst-Marion Roussel, 102 rue de Noisy, F-93230 Romainville, France

One critical step of the apoptotic process is the opening of the mitochondrial permeability transition (PT) pore leading to the disruption of mitochondrial membrane integrity and to the dissipation of the inner transmembrane proton gradient ( $\Delta\Psi_m$ ). The mitochondrial PT pore is a polypeptide structure which is inhibited by the apoptosis-inhibitory oncoprotein Bcl-2 and which is closely associated with the mitochondrial benzodiazepine receptor (mBzR). Here we show that PK11195, a prototypic ligand of the 18-kDa mBzR, facilitates the induction of  $\Delta\Psi_m$  disruption and subsequent apoptosis by a number of different agents, including agonists of the glucocorticoid receptor, chemotherapeutic agents (etoposide, doxorubicin), gamma irradiation, and the proapoptotic second messenger ceramide. Whereas PK11195 itself has no cytotoxic effect, it enhances apoptosis induction by these agents. This effect is not observed for benzodiazepine diazepam, whose binding site in the mBzR differs from PK11195. PK11195 partially reverses Bcl-2 mediated inhibition of apoptosis in two different cell lines. Thus, transfection-enforced Bcl-2 overexpression confers protection against glucocorticoids and chemotherapeutic agents, and this protection is largely reversed by the addition of PK11195. This effect is observed at the level of  $\Delta\Psi_m$  dissipation as well as at the level of nuclear apoptosis. To gain insights into the site of action of PK11195, we performed experiments on isolated organelles. PK11195 reverses the Bcl-2-mediated mitochondrial retention of apoptogenic factors which cause isolated nuclei to undergo apoptosis in a cell-free system. Mitochondria from control cells, but not mitochondria from Bcl-2-overexpressing cells, readily release such apoptogenic factors in response to atractyloside, a ligand of the adenine nucleotide translocator. However, control and Bcl-2-overexpressing mitochondria respond equally well to a combination of

atractyloside and PK11195. Altogether, these findings indicate that PK11195 abolishes apoptosis inhibition by Bcl-2 via a direct effect on mitochondria. Moreover, they suggest a novel strategy for enhancing the susceptibility of cells to apoptosis induction and, concomitantly, for reversing Bcl-2-mediated cytoprotection.

© 1998 Academic Press

**Key Words:** mitochondrial transmembrane potential; permeability transition; programmed cell death.

### INTRODUCTION

The mitochondrial permeability transition (PT)<sup>3</sup> pore, also called megachannel or multiple conductance channel, participates in the regulation of matrix  $\text{Ca}^{2+}$ , pH,  $\Delta\Psi_m$ , and volume and functions as a  $\text{Ca}^{2+}$ -, voltage-, pH-, and redox-gated channel with several levels of conductance and little if any ion selectivity [1–4]. Recent evidence suggests that opening of the PT pore, which is regulated by Bcl-2, is a critical event in the process leading to apoptosis [5, 6]. Opening of the PT pore can cause the dissipation of the inner mitochondrial transmembrane potential ( $\Delta\Psi_m$ ) and culminates in the disruption of outer membrane integrity leading to the liberation of intermembrane proteins from the mitochondrion [7–10]. Indeed, the liberation of intermembrane proteins such as cytochrome c and/or the dissipation of the  $\Delta\Psi_m$  are common events of early apoptosis [5, 6, 11–14]. Depending on the experimental system and the cell type, an increase in the matrix volume causing physical disruption of the outer mitochondrial membrane precedes the dissipation of the  $\Delta\Psi_m$  [12, 13, 15] or both the disruption of the outer membrane and the dissipation of the inner membrane

<sup>3</sup> Abbreviations used:  $\Delta\Psi_m$ , mitochondrial transmembrane potential; DiOC<sub>6</sub>(3), 3,3'-dihexyloxycarbocyanine iodide; Eth, ethidium; HE, hydroethidine; mBzR, mitochondrial benzodiazepine receptor; PK11195, 1-(2-chlorophenyl)-N-methyl-N-(1-methylpropyl)-3-isoquinoline-carboxamide; PS, phosphatidylserine; PT, permeability transition; ROS, reactive oxygen species.

<sup>1</sup> T.H. and D.D. contributed equally to this paper.

<sup>2</sup> To whom correspondence and reprint requests should be addressed at 19 rue Guy Môquet, B.P. 8, F-94801 Villejuif, France. Fax: 33-1-49 58 35 09. E-mail: kroemer@infobiogen.fr.

$\Delta\Psi_m$  occur in a near-to-simultaneous fashion [7, 8]. On theoretical grounds [1–4], both the increase in matrix volume preceding  $\Delta\Psi_m$  reduction and the dissipation of the  $\Delta\Psi_m$  may be mediated by opening of the PT pore, which can operate at a reversible low conductance level (which would cause a net inflow of ions and water into the mitochondrial matrix) and at an irreversible high conductance level (which would lead to  $\Delta\Psi_m$  disruption).

The PT pore is a multiprotein complex formed at the contact site between the mitochondrial inner and outer membranes, exactly at the same localization at which the oncoprotein Bcl-2 is particularly abundant [16]. Its pharmacological inhibition prevents apoptosis in a number of different models [5, 6, 17], whereas opening of the PT pore induces apoptosis [18–21]. The exact molecular composition of the pore is not known, although proteins from the cytosol (hexokinase), the outer membrane [mitochondrial benzodiazepine receptor (mBzR); mitochondrial porin, also called voltage-dependent anion channel], the intermembrane space (creatine kinase), the inner membrane (adenine nucleotide translocator, ANT), and the matrix (cyclophilin D) have been implicated in PT pore formation and/or regulation [1, 22–27]. In accord with its complex composite architecture, the PT pore is regulated by multiple endogenous effectors including local ion and pH gradients, ADP/ATP, NAD(P)H, and proapoptotic signal transduction molecules such as  $\text{Ca}^{2+}$  or reactive oxygen species [1–4, 26, 27]. Moreover, several of the components in the PT pore may constitute pharmacological targets for apoptosis modulation [5, 6, 17].

Based on these considerations, we decided to investigate the apoptosis-modulatory effect of 1-(2-chlorophenyl)-*N*-methyl-*N*-(1-methylpropyl)-3-isoquinolinecarboxamide (PK11195), a prototypic ligand of the 18-kDa mBzR, which is one of the molecules associating with the PT pore complex [23, 24]. Here we show that PK11195, which itself is not toxic, facilitates the induction of apoptosis by a number of different stimuli. More importantly, we report that PK11195 can reverse apoptosis inhibition by Bcl-2.

## MATERIALS AND METHODS

**Cells and culture conditions.** Thymocytes from 4- to 6-week-old Balb/c mice, 2B4.11 T cell hybridoma cell lines stably transfected with a SFFV.neo vector containing the human *bcl-2* gene or the neomycin resistance gene (Neo) only [28] (kindly provided by J. Ashwell, NIH, Bethesda, MA), B cell leukemia WEHI231 transfected with the human *bcl-2* gene or a control Neo vector [29] (gift from C. Martínez-A., National Center of Biotechnology, Madrid, Spain), or human CEM-C7.H2 T lymphoblastic leukemia cells [30] (gift from R. Kofler, University of Innsbruck, Austria) were cultured in RPMI 1640 supplemented with 10% FCS, antibiotics, and L-glutamine.

**Induction of apoptosis.** Cells ( $5\text{--}10 \times 10^5/\text{ml}$ ) were cultured in the presence of the indicated amount of PK11195, diazepam (Sigma),

dexamethazone (1  $\mu\text{M}$ , Sigma), RU24858 (1  $\mu\text{M}$ , synthesized by Roussel Uclaf) [31], the glucocorticoid receptor antagonist RU38486 (1  $\mu\text{M}$ , Roussel Uclaf), doxorubicin (1  $\mu\text{g}/\text{ml}$ ; Pharmacia), etoposide (10  $\mu\text{M}/\text{ml}$ ; Sigma), cyclosporin A (10  $\mu\text{M}$ ; Sandoz), or  $\text{C}_8$  ceramide (25  $\mu\text{M}$ ; Biomol, Plymouth Meeting, PA) or treated by gamma irradiation (10 Gy). After the indicated interval, cells were recovered and tested for apoptosis-associated features.

**Cytofluorometric quantitation of apoptosis-associated parameters in intact cells.** Following published protocols [18, 32, 33], the following fluorochromes were employed to determine different apoptosis-associated changes: 3,3'-dihexyloxacarbocyanine iodide ( $\text{DiOC}_6(3)$ , 20 nM) for  $\Delta\Psi_m$  determination; hydroethidine (HE, 4  $\mu\text{M}$ ) for the determination of superoxide anion generation; or annexin V-FITC conjugates (1  $\mu\text{g}/\text{ml}$ ; Nexins Research, Hoeven, The Netherlands) for determination of phosphatidylserine (PS) exposure on the outer plasma membrane. The frequency of hypoploid cells was determined by propidium iodide (PI) staining of ethanol-permeabilized cells.

**Cell-free system of apoptosis.** Mitochondria from 2B4.11 T cell hybridoma cell lines were purified on a Percoll (Pharmacia, Uppsala, Sweden) gradient [34] and were resuspended in CFS buffer: 220 mM mannitol; 68 mM sucrose, 2 mM NaCl, 2.5 mM  $\text{PO}_4\text{H}_2\text{K}$ , 0.5 mM EGTA, 2 mM  $\text{MgCl}_2$ , 5 mM pyruvate, 0.1 mM phenylmethylsulfonyl fluoride (PMSF), 1 mM dithiothreitol, 10 mM Hepes-NaOH, pH 7.4, as described [7, 8]. Mitochondria from  $5 \times 10^6$  cells were incubated in a total volume of 15  $\mu\text{M}$  CFS buffer in the presence or absence of atractyloside (5 mM; Sigma), *tert*-butylhydroperoxide (*t*-BHP; 300  $\mu\text{M}$ ; Sigma), PK11195 (1  $\mu\text{M}$ ), cyclosporin A (10  $\mu\text{M}$ ), and/or bongkreic acid (BA; 25  $\mu\text{M}$ ; kindly provided by Dr. Hans J. Duine, Delft University, Delft, The Netherlands) for 30 min at 4°C, followed by spinning down of mitochondria ( $5 \times 10^3$  g; 20 min) and recovery of the supernatant and ultracentrifugation ( $1.5 \times 10^5$  g, 1 h, 4°C). HeLa cell nuclei ( $10^3$  nuclei/ $\mu\text{l}$ ) purified on a sucrose gradient [35] were incubated for 90 min in the presence of mitochondrial supernatant, stained with PI (10  $\mu\text{g}/\text{ml}$ ; Sigma; minimum 5 min at room temperature), and analyzed in an Epics Profile II cytofluorometer (Coulter, Hialeah, FL) to assess the frequency of hypoploid nuclei, as described [36].

**Experimental design and statistical analysis.** All experiments were performed at least three times yielding similar results, and typical results are shown. Statistical significance was calculated using the paired Student's *t* test.

## RESULTS AND DISCUSSION

**PK11195 facilitates the induction of apoptosis by a variety of stimuli.** PK11195 is the prototypic ligand of the 18-kDa subunit of the mBzR [23, 37–39]. Up to doses of 50 to 100  $\mu\text{M}$ , PK11195 had no toxic effects on a variety of cell types including thymocytes (Fig. 1), acute T cell leukemia CEM-C7 cells (Fig. 2), 2B4.11 T cell hybridoma cell (Fig. 3), and WEHI231 B cell leukemia cells (Fig. 4). As shown in Fig. 1, a dose of cell-permeable  $\text{C}_8$  ceramide which itself did not induce thymocyte apoptosis (25  $\mu\text{M}$ ) did become apoptogenic in the presence of the isoquinoline carboxamide PK11195. In contrast, the benzodiazepine diazepam, a molecule which binds to another subunit of the mBzR [23] or to another binding site within the same molecules [40], had no major coapoptogenic effect (Figs. 1, 3, and 4). Among the different mBzR ligands which we have tested, PK11195 was the most efficient coinducer of apoptosis (relative potency: PK11195 > 4'-chlordi-azepam  $\geq$  diazepam > Ro-5-4864; not shown), corre-

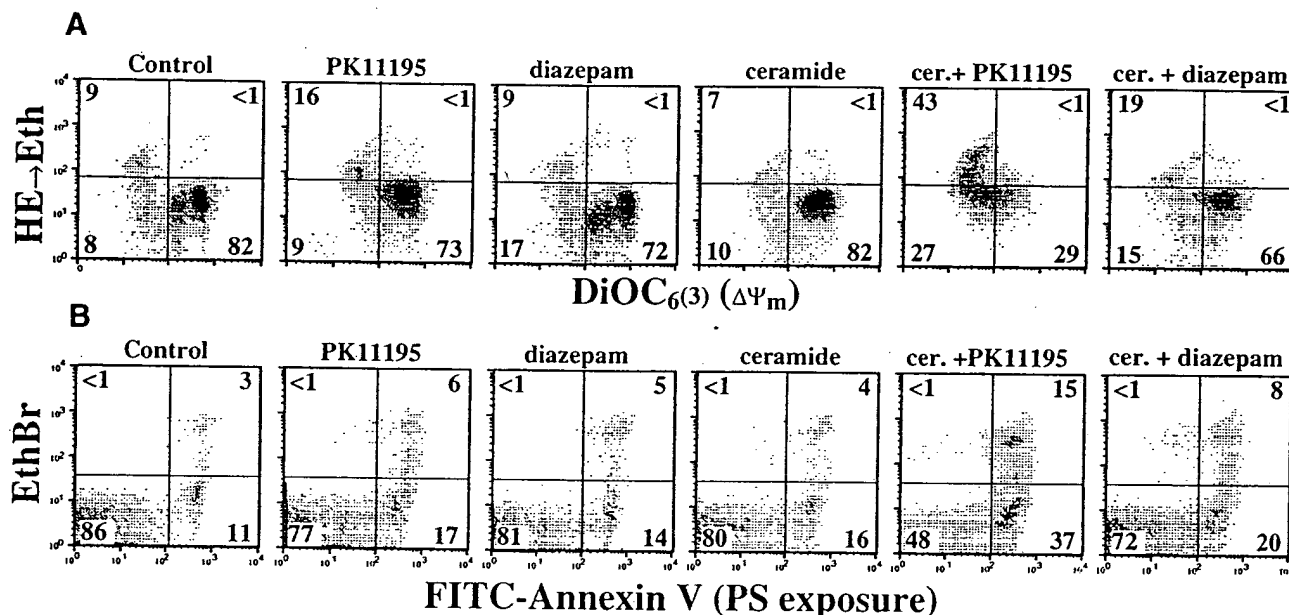


FIG. 1. Synergism between ceramide and PK11195 in the induction of thymocyte apoptosis. Thymocytes were cultured for 4 h in the presence of C8 ceramide (25  $\mu$ M), diazepam (100  $\mu$ M), and/or PK11195 (100  $\mu$ M), followed by determination of several apoptosis-associated parameters, namely, disruption of the  $\Delta\Psi_m$  (determined by means of DiOC<sub>6</sub>(3)), generation of superoxide anion (determined with HE) (A), phosphatidylserine exposure on the plasma membrane surface (measured with FITC-annexin V), and cell viability (EthBr exclusion) (B). Numbers refer to the percentage of cells found in each quadrant.

lating with its antagonist potential on neuromuscular transmission [41, 42]. Synergic effects with PK11195 extended to a variety of different apoptosis inducers including the topoisomerase II inhibitor etoposide (Fig. 2), gamma irradiation (Fig. 4), the intercalating agent doxorubicin (Fig. 4), and, in the case of WEHI231 cells, cyclosporin A (Fig. 4). The apoptosis-inducing effect of cyclosporin A is probably linked to its immunosuppressive function, because a nonimmunosuppressive cyclo-

sporine A derivative (which still binds and inhibits mitochondrial cyclophilin D) does not induce apoptosis, neither alone, nor in combination with PK11195 (Ref. [43] and data not shown). In addition, PK11195 (but not diazepam) facilitated the induction of apoptosis by glucocorticoid receptor agonists including dexamethasone (Fig. 2) and the prototypic "dissociated" glucocorticoid receptor agonist RU24858 (Fig. 2), an agent that has lost its transactivating function yet preserves its

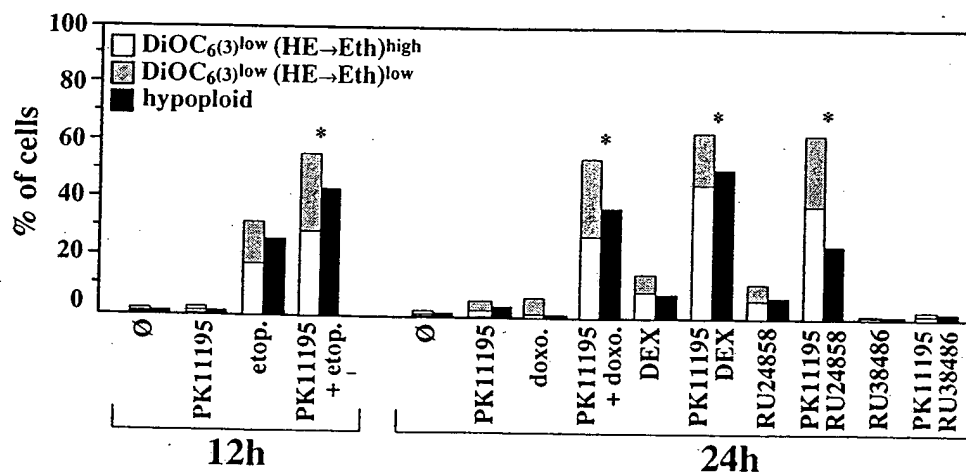


FIG. 2. PK11195 facilitates apoptosis induction in CEM-C7 acute T cell leukemia cells. Cells were cultured with 10  $\mu$ M etoposide, 1  $\mu$ M dexamethasone (DEX), RU24858, RU38486, and/or 75  $\mu$ M PK11195 during the indicated period, followed by determination of the frequency of DiOC<sub>6</sub>(3)<sup>low</sup> (HE→Eth)<sup>low</sup>, DiOC<sub>6</sub>(3)<sup>low</sup> (HE→Eth)<sup>high</sup>, and hypoploid cells as described under Materials and Methods. Asterisks indicate a significant ( $P < 0.01$ ) enhancement of apoptosis induction by PK11195 as compared to control cultures kept in the absence of PK11195.

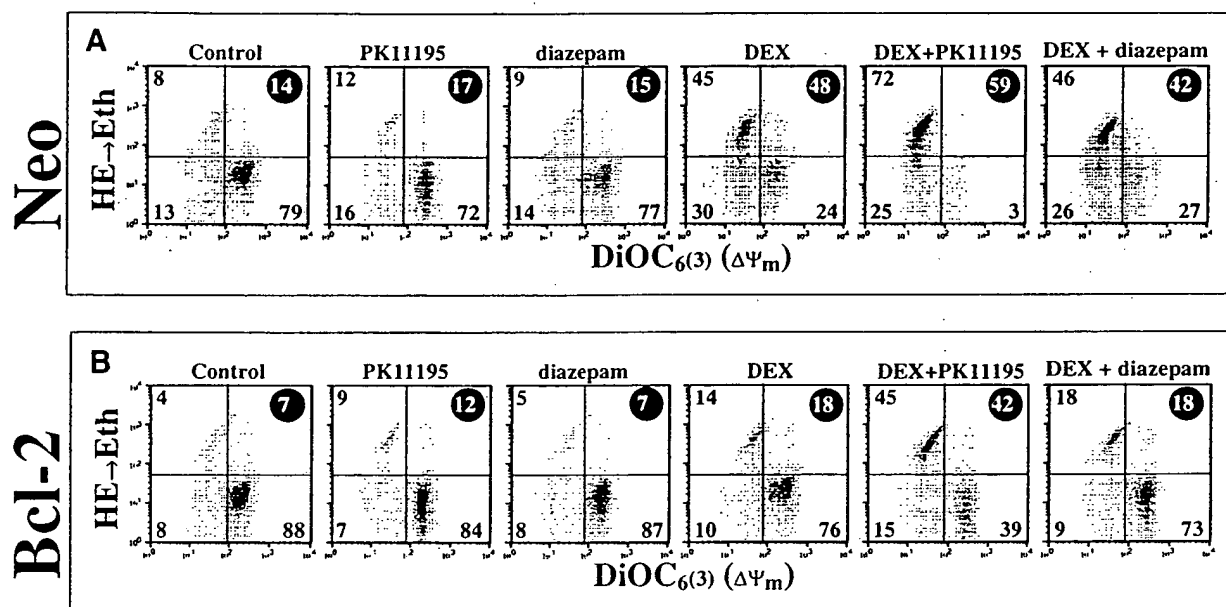


FIG. 3. PK11195 reverses Bcl-2-mediated cytoprotection in T cell hybridoma cells. 2B4.11 T cell hybridoma cell lines stably transfected with a SFFV.neo vector containing the human *bcl-2* gene (B) or the neomycin resistance gene (Neo) only (A) were cultured for 12 h in the presence of dexamethasone (1  $\mu$ M), PK11195 (50  $\mu$ M), and/or diazepam (50  $\mu$ M), followed by determination of the indicated apoptosis-associated parameters. Numbers in black circles indicate the frequency of subdiploid cells. The synergistic effect of PK11195+DEX was highly significant ( $P < 0.01$ ) compared to controls treated with DEX or PK11195 alone. Similar results are obtained when etoposide instead of dexamethasone is used as apoptosis inducer.

transrepressive gene-regulatory activity [31]. As to be expected, no effect of the glucocorticoid receptor antagonist RU38486 was revealed by PK11195 (Fig. 2). In conclusion, PK11195 facilitates the induction of apoptosis in response to a wide array of agents and in very different cell types, including primary cells (Fig. 1) and transformed cells lines of human and murine origin (Figs. 2–4).

*PK11195 facilitates the induction of both mitochondrial and postmitochondrial changes associated with apoptosis.* The synergism between PK11195 and several proapoptotic agents extended to all hallmarks of apoptosis, namely, the early loss of the mitochondrial transmembrane potential (measured by means of the potential-sensitive dye DiOC<sub>6</sub>(3)), the increase in the generation of reactive oxygen species (measured by the superoxide anion-driven conversion of hydroethidine into ethidium; Figs. 1–4), the aberrant exposure of phosphatidylserine residues on the plasma membrane surface (measured by means of FITC–Annexin V conjugate; Fig. 1), and nuclear DNA fragmentation (hypoploidy determined by propidium iodine staining of ethanol-fixed cells; Figs. 2–4). These findings are compatible with the idea that PK11195 acts on a mitochondrial target to facilitate apoptosis induction [19] and confirm the strong association between mitochondrial, redox, plasma membrane, and nuclear features of apoptosis.

*PK11195 partially reverses Bcl-2-mediated apoptosis inhibition in several different cell lines.* Bcl-2 has cytoprotective effects with a wide spectrum of activities [6, 43]. Thus, transfection enforced Bcl-2 overexpression largely prevented the  $\Delta\Psi_m$  disruption, superoxide anion production, and nuclear apoptosis induced by dexamethasone in T cell hybridoma cells (Fig. 3). Again, the simultaneous treatment with PK11195 had a hyperadditive apoptosis-facilitating effect, even in the presence of Bcl-2. Thus, PK11195 restored apoptosis induction in Bcl-2-overexpressing cells at least partially. This effect has been observed in two different cell types, namely, 2B4.11 T cell hybridoma cells (Fig. 3B) and WEHI231 B cell leukemia cells (Fig. 4B). PK11195 largely reversed the Bcl-2-conferred protection against glucocorticoids (Fig. 3B), gamma irradiation, doxorubicin, cyclosporin A (Fig. 4B), and etoposide (not shown). This effect is again observed at the levels of the mitochondrion, cellular redox potentials, and the nucleus (Figs. 3 and 4).

*PK11195 reverses the Bcl-2-mediated block of apoptosis induction in a cell-free system.* Bcl-2 stabilizes the mitochondrial membrane barrier function via a direct local effect [7, 8, 12–15]. Thus, as previously described [7, 8], isolated mitochondria from Bcl-2-overexpressing cells failed to release apoptogenic factors when they were incubated for 10 min in the presence of atractyloside, a ligand of the adenine nucleotide translocator [7]

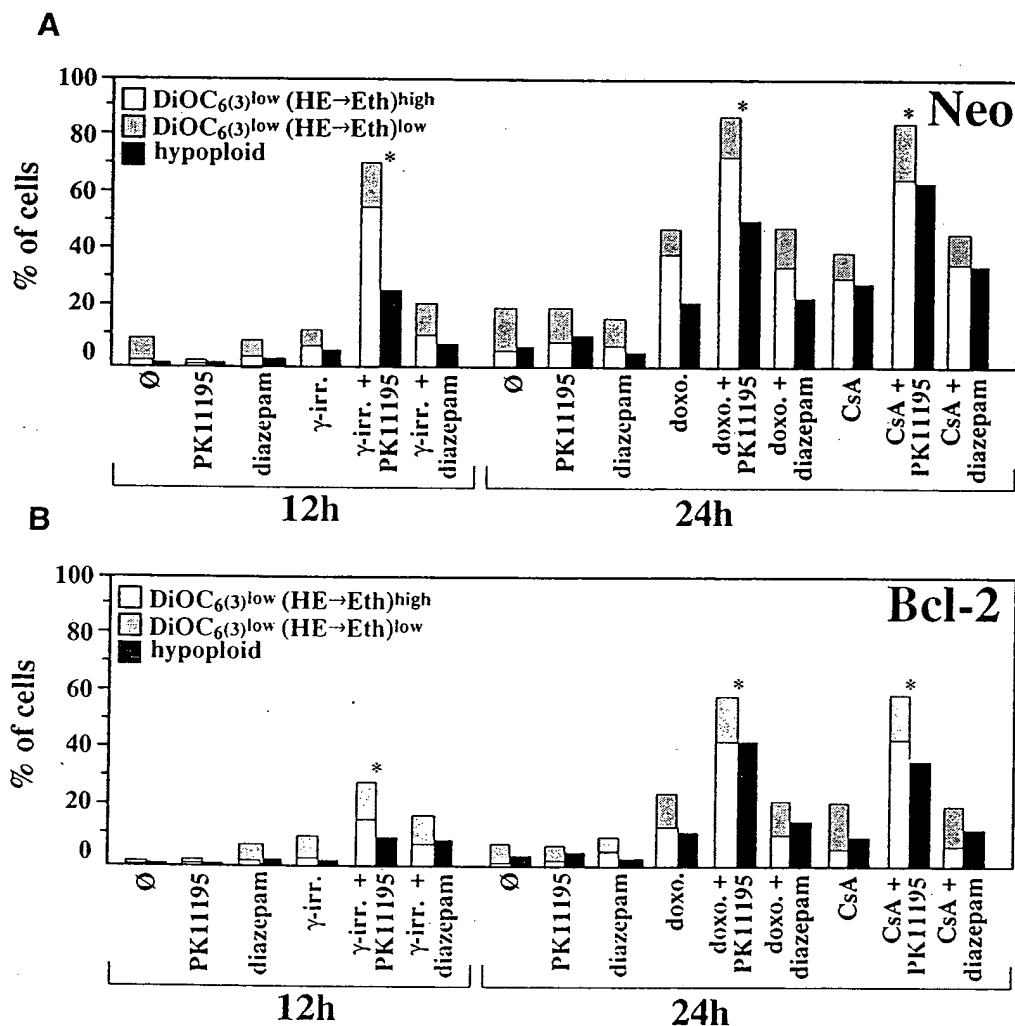


FIG. 4. PK11195 enhances apoptosis susceptibility in WEHI 231 B cell leukemia cells overexpressing Bcl-2. WEHI 231 cells transfected with a neomycin control vector (Neo, A) or the human *bcl-2* gene (B) were treated with gamma irradiation, doxorubicine (doxo), or cyclosporin A (CsA), alone or in combination with PK11195 (40  $\mu$ M) or diazepam (40  $\mu$ M), followed by cytofluorometric determination of the indicated parameters. Asterisks indicate significant ( $P < 0.001$ ) effects of PK11195.

(Fig. 5A). Control mitochondria treated with atractyloside readily released apoptogenic factors, as quantified by an *in vitro* assay in which isolated nuclei are induced to undergo DNA fragmentation and to become hypoploid (Fig. 5A). PK11195 alone had no effect on isolated mitochondria (Fig. 5) nor did it affect the structure of isolated nuclei (not shown). PK11195 did not enhance the effect of atractyloside in control mitochondria (which is probably already optimal, Ref. [7]) from Neo-transfected cells.

In strict contrast to the data obtained with mitochondria from Neo-transfected cells, the combination of PK11195 and atractyloside but neither of these agents alone induced the release of apoptogenic factors from mitochondria purified from Bcl-2-transfected cells. Together, PK11195 and atractyloside were equally efficient in releasing apoptogenic factors from Bcl-2-over-

expressing and control mitochondria (Fig. 5A). Thus, PK11195 can overcome the resistance of Bcl-2-over-expressing mitochondria to the release of apoptogenic factors induced by atractyloside (Fig. 5A) or the prooxidant *tert*-butylhydroperoxide (Fig. 5B). Atractyloside and *tert*-butylhydroperoxide act on mitochondria to open the PT pore [1], and this effect is thought to account for the release of apoptogenic factors [7]. To understand the mechanism of the PK11195-facilitated liberation of apoptogenic factors, we therefore determined the effect of two inhibitors of the PT pore, cyclosporin A and bongkreikic acid (Fig. 5b). Either of these two agents abolishes the effect of PK11195+atractyloside or that of PK11195+*t*-BHP on mitochondria from Bcl-2-over-expressing cells (Fig. 5B). Altogether, these results indicate that (i) PK11195 neutralizes the capacity of



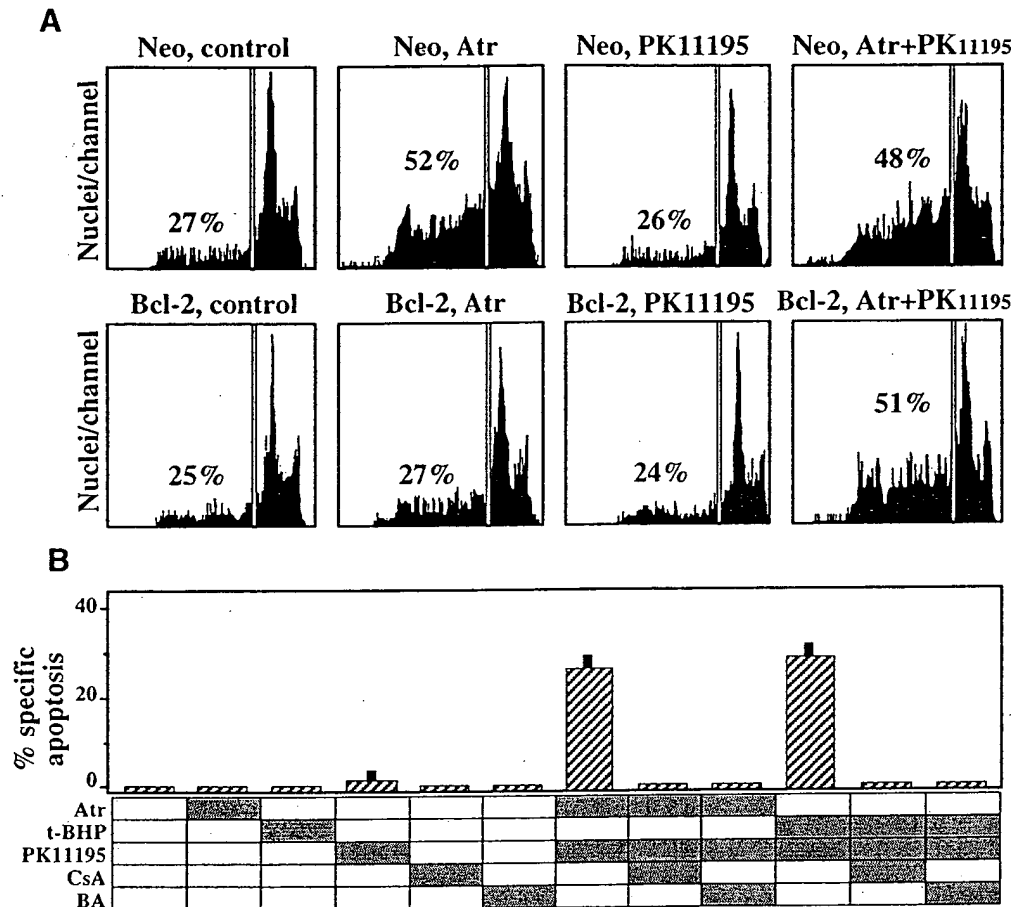


**FIG. 5.** PK11195 overcomes the Bcl-2-mediated mitochondrial retention of apoptogenic factors. (A) Effect of PK11195 and Atr on mitochondria from 2B4.11 T cell hybridoma cells expressing the human *bcl-2* gene or the control vector (Neo). Isolated mitochondria were incubated for 30 min in the presence of atractyloside (5 mM) and/or PK11195 (1  $\mu$ M). The supernatant of mitochondria was then added to purified HeLa nuclei. After a culture period of 90 min the percentage of hypoloid nuclei was determined by PI staining and cytofluorometric analysis. The background value of isolated nuclei cultured in the absence of mitochondrial supernatants was  $22 \pm 2\%$ . (B) Effect of different agents on mitochondria purified from Bcl-2-overexpressing cells. Isolated mitochondria were incubated with the indicated combination of atractyloside (Atr), *tert*-butylhydroperoxide (*t*-BHP), PK11195, cyclosporin A (CsA), and/or bongkreikic acid (BA). Inhibitors (CsA, BA) were added 5 min before inducers (Atr, *t*-BHP, PK11195). The apoptogenic activity contained in the supernatants of mitochondria was then tested on purified HeLa nuclei as in A. Background values were subtracted from experimental values.

Bcl-2 to retain apoptogenic factors in isolated mitochondria and (ii) it acts on PT pores to facilitate apoptosis induction.

**Concluding remarks.** In this work we describe a novel strategy for enhancing the susceptibility of cells to the induction of apoptosis. PK11195, a specific ligand of the 18-kDa mBzR, facilitated the induction of  $\Delta\Psi_m$  disruption by a variety of different apoptosis triggers, including DNA damage (gamma irradiation, etoposide, doxorubicin), ligation of the glucocorticoid receptor (dexamethasone, RU24858), and the proapoptotic second messenger ceramide. Concomitantly, it enhanced the induction of classical signs of apoptosis such as phosphatidylserine exposure on the cell surface and nuclear DNA fragmentation. The mBzR has been previously shown to interact with a number of proteins involved in

the formation and/or regulation of the PT pore complex [23, 24]. Moreover, the PK11195 has been shown to facilitate PT pore opening induced by tumor necrosis factor (TNF- $\alpha$ ) in L929 cells [44]. In that model, TNF induces necrosis [45], and necrosis induction is enhanced by PK11195 [44]. In contrast, we show here that PK11195 can facilitate the induction of apoptosis, correlating with the induction of PT pore-mediated  $\Delta\Psi_m$  dissipation. These findings add to the notion that PT pore opening may be a rate-limiting step of any type of cell death (apoptosis and necrosis) [5] and that postmitochondrial events culminating in the activation of catabolic enzymes (caspases, noncaspase proteases, nucleases) and/or the availability of extramitochondrial ATP sources dictate the modality of cell death [21, 46, 47].

Bcl-2 is the prototypic representative of an apopto-

sis-inhibitory oncogene family which contributes both to the genesis of cancer and to the difficulties in treating it. Most of the cytoprotective effect of Bcl-2 may be attributed to its capacity to protect the integrity of mitochondrial membranes [6–8, 12, 13, 43, 48, 49]. We have shown that Bcl-2 stabilizes mitochondrial membranes in a variety of different models of apoptosis [32, 43]. However, it appears that Bcl-2 fails to protect isolated mitochondria against thiol-crosslinking by diamide [7, 27] and the proteolytic attack mediated by caspases [14], correlating with the fact that Bcl-2 does not inhibit apoptosis induced by diamide [7, 27] and direct caspase activation [14, 50–52]. The Bcl-2 effect is also overcome by treatment with paclitaxel (Taxol), an agent which causes hyperphosphorylation of Bcl-2 [53, 54] and favors opening of the PT pore [55]. Here we demonstrate another possibility to overcome Bcl-2-mediated chemo- or radioresistance. Treatment of cells with PK11195, a ligand of the mBzR, largely reversed cytoprotection mediated by Bcl-2. A quasi-stoichiometric relationship between the expression of Bcl-2 and that of the mBzR, at least in lymphoid cell lines, has been reported [56]. Moreover, Bcl-2 protects isolated mitochondria against opening of the PT pore induced by low doses of protoporphyrin IX, a ligand of the MBzR, and this inhibition is overcome by high doses of protoporphyrin IX [19], suggesting a functional interaction between Bcl-2 and the mBzR. In contrast, the Bcl-2-mediated protection against PT pore opening is not overcome by increasing the doses of other PT pore-targeted agents such as atractyloside, a ligand of the adenine nucleotide translocator [7, 8].

In contrast to protoporphyrin IX, PK11195 itself has no PT-inducing effect and fails to release apoptogenic factors from control or Bcl-2-overexpressing mitochondria. However, it does act in synergy with atractyloside or the prooxidant *t*-BHP to overcome the Bcl-2-mediated retention of apoptogenic factors in isolated mitochondria, and this effect is blocked by two inhibitors of the PT pore, bongkreikic acid and cyclosporin A (Fig. 5). Since ligation of the mBzR does not cause a down-regulation of Bcl-2 expression (Ref. [56] and data not shown), it thus appears probable that specific PK11195-driven conformational changes in the complex composed by the mBzR and the PT pore [1, 22–25] indirectly affect the mitochondrial membrane-stabilizing and antiapoptotic function of Bcl-2. In this context, it appears intriguing that the purified PT pore is under the direct regulatory influence of proteins of the Bcl-2 family [26, 27]. Thus, the components of the PT pore, the mBzR, and the Bcl-2/Bax complex could form higher order molecular complexes which regulate the permeability of the inner and/or outer mitochondrial membranes. This scenario would explain how Bcl-2 can inhibit the atractyloside-induced release of apoptogenic factors and how PK11195 can neutralize this

inhibitory effect. Future studies addressing the putative physical interaction between the mBzR, the proteins composing the PT pore, and Bcl-2-related proteins should elucidate the mechanism via which mBzR and Bcl-2 exert antagonistic effects on mitochondrial membrane integrity.

In conclusion, our present data suggest a novel strategy for enhancing the susceptibility of cells to apoptosis induction, namely, ligation of the mBzR. Ligation of the mBzR with PK11195 may be a valuable strategy for reversing chemoresistance mediated by Bcl-2.

This work has been supported by grants from ANRS, ARC, CNRS, FRM, INSERM, LFC, and Hoechst-Marion-Roussel (to G.K.). We thank Dr. Pierre Carayon (Sanofi-Elf, Montpellier, France) for helpful suggestions.

## REFERENCES

1. Zoratti, M., and Szabò, I. (1995). The mitochondrial permeability transition. *Biochem. Biophys. Acta Rev. Biomembr.* **1241**, 139–176.
2. Kinnally, K. W., Lohret, T. A., Campo, M. L., and Mannella, C. A. (1996). Perspectives on the mitochondrial multiple conductance channel. *J. Bioenerg. Biomembr.* **28**, 115–123.
3. Bernardi, P., and Petronilli, V. (1996). The permeability transition pore as a mitochondrial calcium release channel: A critical appraisal. *J. Bioenerg. Biomembr.* **28**, 129–136.
4. Ichas, F., Jouavill, L. S., and Mazat, J.-P. (1997). Mitochondria are excitable organelles capable of generating and conveying electric and calcium currents. *Cell* **89**, 1145–1153.
5. Kroemer, G., Zamzami, N., and Susin, S. A. (1997). Mitochondrial control of apoptosis. *Immunol. Today* **18**, 44–51.
6. Kroemer, G. (1997). The proto-oncogene Bcl-2 and its role in regulating apoptosis. *Nature Med.* **3**, 614–620.
7. Zamzami, N., Susin, S. A., Marchetti, P., Hirsch, T., Gómez-Monterrey, I., Castedo, M., and Kroemer, G. (1996). Mitochondrial control of nuclear apoptosis. *J. Exp. Med.* **183**, 1533–1544.
8. Susin, S. A., Zamzami, N., Castedo, M., Hirsch, T., Marchetti, P., Macho, A., Daugas, E., Geuskens, M., and Kroemer, G. (1996). Bcl-2 inhibits the mitochondrial release of an apoptogenic protease. *J. Exp. Med.* **184**, 1331–1342.
9. Kantrow, S. P., and Piantadosi, C. A. (1997). Release of cytochrome c from liver mitochondria during permeability transition. *Biochem. Biophys. Res. Commun.* **232**, 669–671.
10. Ellerby, H. M., Martin, S. J., Ellerby, L. M., Naiem, S. S., Rabizadeh, S., Salvese, G. S., Casiano, C. A., Cashman, N. R., Green, D. R., and Bredesen, D. E. (1997). Establishment of a cell-free system of neuronal apoptosis: Comparison of premitochondrial, mitochondrial, and postmitochondrial phases. *J. Neurosci.* **17**, 6165–6178.
11. Liu, X., Kim, C. N., Yang, J., Jemmerson, R., and Wang, X. (1996). Induction of apoptotic program in cell-free extracts: Requirement for dATP and cytochrome C. *Cell* **86**, 147–157.
12. Kluck, R. M., Bossy-Wetzel, E., Green, D. R., and Newmeyer, D. D. (1997). The release of cytochrome c from mitochondria: A primary site for Bcl-2 regulation of apoptosis. *Science* **275**, 1132–1136.
13. Yang, J., Liu, X., Bhalla, K., Kim, C. N., Ibrado, A. M., Cai, J., Peng, T.-I., Jones, D. P., and Wang, X. (1997). Prevention of apoptosis by Bcl-2: release of cytochrome c from mitochondria blocked. *Science* **275**, 1129–1132.

14. Susin, S. A., Zamzami, N., Castedo, M., Daugas, E., Wang, H.-G., Geley, S., Fassy, F., Reed, J., and Kroemer, G. (1997). The central executioner of apoptosis: Multiple links between protease activation and mitochondria in Fas/Apo-1/CD95- and ceramide-induced apoptosis. *J. Exp. Med.* **186**, 25–37.
15. vander Heiden, M. G., Chandal, N. S., Williamson, E. K., Shcunacker, P. T., and Thompson, C. B. (1997). Bcl-XL regulates the membrane potential and volume homeostasis of mitochondria. *Cell* **91**, 627–637.
16. de Jong, D., Prins, F. A., Mason, D. Y., Reed, J. C., van Ommen, G. B., and Kluin, P. M. (1994). Subcellular localization of the Bcl-2 protein in malignant and normal lymphoid cells. *Cancer Res.* **54**, 256–260.
17. Polyak, K., Xia, Y., Zweier, J. L., Kinzler, K. W., and Vogelstein, B. (1997). A model for p53-induced apoptosis. *Nature* **389**, 300–305.
18. Marchetti, P., Castedo, M., Susin, S. A., Zamzami, N., Hirsch, T., Haeflner, A., Hirsch, F., Geuskens, M., and Kroemer, G. (1996). Mitochondrial permeability transition is a central coordinating event of apoptosis. *J. Exp. Med.* **184**, 1155–1160.
19. Marchetti, P., Hirsch, T., Zamzami, N., Castedo, M., Decaudin, D., Susin, S. A., Masse, B., and Kroemer, G. (1996). Mitochondrial permeability transition triggers lymphocyte apoptosis. *J. Immunol.* **157**, 4830–4836.
20. Hortelano, S., Dallaporta, B., Zamzami, N., Hirsch, T., Susin, S. A., Marzo, I., Bosca, L., and Kroemer, G. (1997). Nitric oxide induces apoptosis via triggering mitochondrial permeability transition. *FEBS Lett.* **410**, 373–377.
21. Hirsch, T., Marchetti, P., Susin, S. A., Dallaporta, B., Zamzami, N., Marzo, I., Geuskens, M., and Kroemer, G. (1997). The apoptosis–necrosis paradox: Apoptogenic proteases activated after mitochondrial permeability transition determine the mode of cell death. *Oncogene* **15**, 1573–1582.
22. Beutner, G., Rück, A., Riede, B., Welte, W., and Brdiczka, D. (1996). Complexes between kinases, mitochondrial porin, and adenylate translocator in rat brain resemble the permeability transition pore. *FEBS Lett.* **396**, 189–195.
23. McEnery, M. W., Snowman, A. M., Trifiletti, R. R., and Snyder, S. H. (1992). Isolation of the mitochondrial benzodiazepine receptor: Association with the voltage-dependent anion channel and the adenine nucleotide carrier. *Proc. Natl. Acad. Sci. USA* **89**, 3170–3174.
24. Kinnally, K. W., Zorov, D. B., Antonenko, Y. N., Snyder, S. H., McEnery, M. W., and Tedeschi, H. (1993). Mitochondrial benzodiazepine receptor linked to inner membrane ion channels by nanomolar actions of ligands. *Proc. Natl. Acad. Sci. USA* **90**, 1374–1378.
25. O’Gorman, E., Beutner, G., Dolder, M., Koretsky, A. P., Brdiczka, D., and Wallimann, T. (1997). The role of creatine kinase in inhibition of mitochondrial permeability transition. *FEBS Lett.* **414**, 253–257.
26. Marzo, I., Brenner, C., Zamzami, N., Susin, S. A., Beutner, G., Brdiczka, D., Rémy, R., Xie, Z.-H., Reed, J. C., and Kroemer, G. (1998). The permeability transition pore complex: a target for apoptosis regulation by caspases and Bcl-2 related proteins. *J. Exp. Med.*, in press.
27. Zamzami, N., Marzo, I., Susin, S. A., Brenner, C., Larochette, N., Marchetti, P., Reed, J., Kofler, R., and Kroemer, G. (1998). The thiol-crosslinking agent diamide overcomes the apoptosis-inhibitory effect of Bcl-2 by enforcing mitochondrial permeability transition. *Oncogene*, **16**, 1055–1064.
28. Green, D. R., Mahboubi, A., Nishioka, W., Oja, S., Echeverri, F., Shi, Y., Glynn, J., Yang, Y., Ashwell, J., and Bissonnette, R. (1994). Promotion and inhibition of activation-induced apoptosis in T-cell hybridomas by oncogenes and related signals. *Immunol. Rev.* **142**, 321–342.
29. Cuende, E., Alés-Martínez, J. E., Ding, L., González-García, M., Martínez-A., C., and Nuñez, G. (1993). Programmed cell death by Bcl-2-dependent and -independent mechanisms in B cell lymphoma cells. *EMBO J.* **12**, 1555–1560.
30. Strasser-Wozak, E., Hattmannstorfer, R., Hala, M., Hartmann, B. L., Fiegl, M., Geley, S., and Kofler, R. (1995). Splice site mutation in the glucocorticoid receptor gene causes resistance to glucocorticoid-induced apoptosis in a human acute leukemic cell line. *Cancer Res.* **55**, 348–353.
31. Vayssière, B. M., Dupont, S., Choquart, A., Petit, F., Garcia, T., Marchandeu, C., Gronemeyer, H., and Resche-Rigon, M. (1997). Synthetic glucocorticoids that dissociate transactivation and AP-1 transrepression exhibit anti-inflammatory activity in vivo. *Mol. Endocrinol.* **11**, 1245–1255.
32. Zamzami, N., Marchetti, P., Castedo, M., Decaudin, D., Macho, A., Hirsch, T., Susin, S. A., Petit, P. X., Mignotte, B., and Kroemer, G. (1995). Sequential reduction of mitochondrial transmembrane potential and generation of reactive oxygen species in early programmed cell death. *J. Exp. Med.* **182**, 367–377.
33. Kroemer, G., Lisardo, B., Zamzami, P., Hortelano, S., and Martinez-A., C. (1997). Detection of apoptosis and apoptosis associated alterations. In “The Immunology Methods Manual” (R. Lefkowitz, Ed.), Chapter 14.2, pp. 1111–1125, Academic Press, San Diego.
34. Petit, P. X., O’Connor, J. E., Grunwald, D., and Brown, S. C. (1990). Analysis of the membrane potential of rat- and mouse-liver mitochondria by flow cytometry and possible applications. *Eur. J. Biochem.* **220**, 389–397.
35. Wood, E. R., and Earnshaw, W. C. (1990). Mitotic chromatin condensation in vitro using somatic cell extracts and nuclei with variable levels of endogenous topoisomerase II. *J. Cell Biol.* **111**, 2839–2850.
36. Susin, S. A., Zamzami, N., Larochette, N., Dallaporta, B., Marzo, I., Brenner, C., Hirsch, T., Petit, P. X., Geuskens, M., and Kroemer, G. (1997). A cytofluorometric assay of nuclear apoptosis induced in a cell-free system: Application to ceramide-induced apoptosis. *Exp. Cell Res.* **236**, 397–403.
37. Ripond, J., Mattei, M. G., Kaghad, M., Dumont, X., Guillemot, J. C., Lefur, G., Caput, D., and Ferrara, P. (1991). Molecular cloning and chromosomal localization of a human peripheral type benzodiazepine receptor. *Eur. J. Biochem.* **2**, 305–311.
38. Joseph-Liauzun, E., Farges, R., Delmas, P., Ferrara, P., and Loison, G. (1997). The M-r 18,000 subunit of the peripheral-type benzodiazepine receptor exhibits both benzodiazepine and isoquinoline carboxamide binding sites in the absence of the voltage-dependent anion channel or of the adenine nucleotide carrier. *J. Biol. Chem.* **272**, 28102–28106.
39. Yeliseev, A. A., Krueger, K. E., and Kaplan, S. (1997). A mammalian mitochondrial drug receptor functions as a bacterial “oxygen” sensor. *Proc. Natl. Acad. Sci. USA* **94**, 5101–5106.
40. Farges, R., Joseph-Liauzun, E., Shire, D., Caput, D., Le Fur, G., and Ferrara, P. (1994). Site-directed mutagenesis of the peripheral-type benzodiazepine receptor: Identification of amino acids implicated in the binding site of Ro5-4864. *Mol. Pharmacol.* **46**, 1160–1167.
41. Chiou, L. C., Ling, J. Y., and Chang, C. C. (1995). Enhancement by benzodiazepines of the inhibitory effect of adenosine on skeletal neuromuscular transmission. *Br. J. Pharmacol.* **116**, 1870–1874.
42. Zisterer, D. M., and Williams, D. C. (1997). Peripheral-type benzodiazepine receptors. *Gen. Pharmacol.* **29**, 305–314.

43. Decaudin, D., Geley, S., Hirsch, T., Castedo, M., Marchetti, P., Macho, A., Kofler, R., and Kroemer, G. (1997). Bcl-2 and Bcl-XL antagonize the mitochondrial dysfunction preceding nuclear apoptosis induced by chemotherapeutic agents. *Cancer Res.* **57**, 62–67.
44. Pastorino, J. G., Simbula, G., Yamamoto, K., Glascott, P. A. J., Rothman, R. J., and Farber, J. L. (1996). The cytotoxicity of tumor necrosis factor depends on induction of the mitochondrial permeability transition. *J. Biol. Chem.* **271**, 29792–29799.
45. Schulze-Osthoff, K., Krammer, P. H., and Dröge, W. (1994). Divergent signalling via APO-1/Fas and the TNF receptor, two homologous molecules involved in physiological cell death. *EMBO J.* **13**, 4587–4596.
46. Leist, M., Single, B., Castoldi, A. F., Kühnle, S., and Nicotera, P. (1997). Intracellular adenosine triphosphate (ATP) concentration: A switch in the decision between apoptosis and necrosis. *J. Exp. Med.* **185**, 1481–1486.
47. Nicotera, P., and Leist, M. (1997). Energy supply and the shape of death in neurons and lymphoid cells. *Cell Death Differ.* **4**, 435–442.
48. Boise, L. H., and Thompson, C. B. (1997). Bcl-XL can inhibit apoptosis in cells that have undergone Fas-induced protease activation. *Proc. Natl. Acad. Sci. USA* **94**, 3759–3764.
49. Reed, J. C. (1997). Double identity for proteins of the Bcl-2 family. *Nature* **387**, 773–776.
50. Yasuhara, N., Sahara, S., Kamada, S., Eguchi, Y., and Tsujimoto, Y. (1997). Evidence against a functional site for Bcl-2 downstream of caspase cascade in preventing apoptosis. *Oncogene* **15**, 1921–1928.
51. Strasser, A., Harris, A. W., Huang, D. C. S., Krammer, P. H., and Cory, S. (1995). Bcl-2 and Fas/APO-1 regulate distinct pathways to lymphocyte apoptosis. *EMBO J.* **14**, 6136–6147.
52. Huang, D. C. S., Cory, S., and Strasser, A. (1997). Bcl-2, Bcl-XL, and adenovirus protein E1B19kD are functionally equivalent in their ability to inhibit cell death. *Oncogene* **14**, 405–414.
53. Haldar, S., Jena, N., and Croce, C. M. (1995). Inactivation of Bcl-2 by phosphorylation. *Proc. Natl. Acad. Sci. USA* **92**, 4507–4511.
54. Haldar, S., Chintapalli, J., and Croce, C. M. (1996). Taxol induces bcl-2 phosphorylation and death of prostate cancer cells. *Cancer Res.* **56**, 1253–1255.
55. Evtodienki, Y. V., Teplova, V. V., Sidashi, S. S., Ichas, F., and Mazat, J.-P. (1996). Microtubule-active drugs suppress the closure of the permeability transition pore in tumour mitochondria. *FEBS Lett.* **393**, 86–88.
56. Carayon, P., Portier, M., Dussossoy, D., Bord, A., Petitpretre, G., Canat, X., Le Fur, G., and Casellas, P. (1996). Involvement of peripheral benzodiazepine receptors in the protection of hematopoietic cells against oxygen radical species. *Blood* **87**, 3170–3178.

Received December 12, 1997

Revised version received February 12, 1998

# In Situ Detection of Apoptosis During Embryogenesis With Annexin V: From Whole Mount to Ultrastructure

Stefan M. van den Eijnde,<sup>1\*</sup> Antonius J.M. Luijsterburg,<sup>3</sup> Lenard Boshart,<sup>1</sup> Chris I. De Zeeuw,<sup>2</sup> Jan Hein van Dierendonck,<sup>4</sup> Chris P.M. Reutelingsperger,<sup>5</sup> and Christl Vermeij-Keers<sup>2,3</sup>

<sup>1</sup>MGC Department of Clinical Genetics, Erasmus University Medical School, Rotterdam, The Netherlands

<sup>2</sup>Department of Anatomy, Erasmus University Medical School, Rotterdam, The Netherlands

<sup>3</sup>Department of Plastic and Reconstructive Surgery, Erasmus University Medical School, Rotterdam, The Netherlands

<sup>4</sup>Department of Surgery, Leiden University Medical Center, Leiden, The Netherlands

<sup>5</sup>Department of Biochemistry, Cardiovascular Research Institute, University Maastricht, The Netherlands

Received 6 November 1996; Accepted 4 August 1997

Apoptosis is of paramount importance during embryonic development. This insight stems from early studies which correlated cell death to normal developmental processes and now has been confirmed by linking aberrant cell death patterns to aberrant development. Linking apoptosis to the phenotype of a developing organism requires spatial information on the localization of the dying cells, making *in situ* detection essential. This prerequisite limits the tools available for such studies (1) to vital dyes, which can be detected at the whole mount level only; (2) to detection based upon apoptotic morphology by routine light microscopy and electron microscopy; and (3) to staining for apoptosis associated DNA fragmentation via, e.g., the TUNEL procedure, which marks cells in a relative late phase of apoptosis. New apoptosis markers need to be specific and should preferably detect cells early during this process.

In the present study we show that the recently discovered *in vitro* marker of apoptosis, Annexin V meets these requirements for *in vivo* detection. Through intracardiac injections of biotin labeled Annexin V, a  $\text{Ca}^{2+}$  dependent phosphatidylserine binding protein, we were able to visualize apoptotic cells derived from each germ layer in the developing mouse embryo from the whole mount level up to the ultrastructural level. Double-labeling on paraffin sections for both this method and TUNEL revealed that cells become Annexin V-biotin labeled early during the process of apoptosis. Cytometry 29:313-320, 1997. © 1997 Wiley-Liss, Inc.

**Key terms:** cell death; morphogenesis; mouse embryo; phagocytosis; phosphatidylserine; phospholipids; TUNEL

Cell death as a part of life was first recognized in studies of embryonic development from over a 150 years ago (5). In a thorough review on this subject, Glücksmann listed many of the spatiotemporally changing and species-specific cell death patterns that are present during development (13). In addition, he described the changes in cell morphology accompanying this type of cell death, which consists of nuclear and cytoplasmic condensation, and fragmentation into membrane bound vesicles, sometimes containing dense nuclear material. Similar morphological changes, which were observed in a model of atrophy of adult liver, formed the basis for the definition of apoptosis (17). This specific morphology not only enabled microscopical detection of apoptotic cells but also allowed their distinction from necrotic cells, which are characterized by loss of staining of the nucleus and early degenerative changes of the mitochondria (50).

A functional difference between necrotic and apoptotic cells is that the latter are removed by phagocytes and degraded in phagolysosomes, without eliciting an inflammatory response (6,35,50). To be removed, the apoptotic cell has to signal its death to the environment. Phagocytes pick up this signal and respond by engulfing the apoptotic cell before it loses the integrity of its plasma membrane (35,50). Recent *in vitro* studies have indicated that the aminophospholipid phosphatidylserine (PS), which normally resides in the cytoplasm facing leaflet of the plasma membrane (9), serves as such a signal when it becomes

Contract grant sponsor: Rotterdam Foundation of Clinical Genetics.

\*Correspondence to: Stefan M. van den Eijnde, MGC Department of Clinical Genetics, Erasmus University Medical School, P.O. Box 1738, 3000DR Rotterdam, The Netherlands.

E-mail: vandeneijnde@ikg.fgg.eur.nl

expressed on the outer surface of the apoptotic cell (2,10,11,37).

The PS exposed by the plasma membrane of apoptotic cells can be detected by using Annexin V. This 35 kDa protein is a member of the Annexin family (31,33) and has a high affinity for PS containing membranes after binding  $\text{Ca}^{2+}$ -ions (1,36,39,43). Probing for apoptotic cells with Annexin V-*in vitro* has shown that the cell surface exposure of PS is an early event preceding nuclear changes (4,23), occurring while the integrity of the plasma membrane is still uncompromised (16,20,47). Furthermore, PS exposure appears to be ubiquitous among hematopoietic lineages, occurring irrespective of the apoptosis initiating stimulus (23). Recently it has been demonstrated that apoptotic adherent cell types in culture (3,42) and tissue embedded cells (40) also expose PS at their cell surface.

Reliable means to detect apoptosis are necessary to study the (patho)physiology of this process during development. Appropriate *in situ* markers should facilitate both the identification of the spatial patterns and the cytological/histological characteristics of the apoptotic cells in a selective and sensitive manner. In the present study we have tested the feasibility of Annexin V as an apoptosis marker in embryonic tissues both at the whole mount level and in paraffin and ultrathin sections. Using biotinylated Annexin V (AnxV-biotin) apoptosis was measured in the intact living mouse embryo. Day 11-13 mouse embryos were the model of choice, since these carry spontaneous, highly consistent spatiotemporal apoptosis patterns that have been documented extensively, especially for the limbs (18,19,24,26,41,51).

## MATERIALS AND METHODS

### Embryos

Pregnant FVB-mice, from 11-13 days PC (plug = day 0), were sacrificed by cervical dislocation after ether anesthesia. The uterus was taken out and embryos were collected and temporarily cultured for detection of apoptosis using Nile blue sulfate ( $n = 35$ ) or for detection of cell surface exposed PS using AnxV-biotin [whole mount,  $n = 32$ ; light microscopy (LM),  $n = 95$ ; electron microscopy (EM),  $n = 37$ ]. Eight of the AnxV-biotin injected paraffin-sectioned embryos were used for double labeling experiments, consisting of *in situ* visualization of both AnxV-biotin binding and apoptosis associated DNA fragmentation via the TUNEL assay for 3'-hydroxyl DNA ends (12). Embryos injected with heat inactivated AnxV-biotin ( $n = 16$ ) served as controls.

### Nile Blue Sulfate

After removal of the extra embryonic membranes, embryos were stained *in toto* for 30 minutes at 37°C in a Nile blue sulfate solution (1:20000 w/v) (34). After incubation, the specimens were rinsed twice with phosphate buffered saline (PBS), put on ice, and immediately photographed under a microscope equipped with a video camera connected to a computer (Leica DM-RB, Hitachi HV-C20, PowerMacintosh 8100/80).

### AnxV-biotin

AnxV-biotin (APOPTEST-BIOTIN<sup>®</sup>, product B500) was obtained from NeXins Research B.V. (Hoeven, The Netherlands). For control experiments the phospholipid binding property of AnxV-biotin was irreversibly destroyed by heating the protein for 10 minutes at 56°C (32).

### Microinjection AnxV-biotin

Embryos were injected into the ventricle of the heart using a Hamilton-Syringe based pipette system using glass pipettes with a tip diameter of 15-25  $\mu\text{m}$ . A volume of approximately 3  $\mu\text{l}$  of the AnxV-biotin solution was injected under a surgical microscope while the embryo was kept in HEPES buffer of 37°C. When successfully injected, a temporary blanching of the umbilical vein could be seen. After 30 minutes of incubation, the embryos were examined for heart activity. Successfully injected embryos with positive heart activity were fixed and processed for visualization of bound AnxV-biotin.

### AnxV-biotin; Whole Mounts

After overnight fixation in 4% Formalin/HEPES buffer at 4°C, embryos were washed in PBS and in 0.3% Triton X 100 in PBS, followed by digestion with 0.01% proteinase K (Boehringer-Mannheim, Mannheim, Germany) for 10 minutes. Endogenous peroxidase activity was blocked by incubation in 1%  $\text{H}_2\text{O}_2$  in Tris/EDTA for 60 minutes. After washing with PBS, bound AnxV-biotin was visualized in the embryos at room temperature using the avidin-biotin complex method with horseradish peroxidase conjugated avidin (Vector ABC Elite kit, Brunschwig, Germany), with 3,3'-Diaminobenzidine tetrahydrochlorid (DAB) (0.05%) as a substrate. Specimens were stored in Tris/EDTA at 4°C until examination under a microscope.

### AnxV-biotin; LM

Following overnight fixation in 4% Formalin/HEPES buffer at 4°C, embryos were dehydrated, embedded in paraffin, and serially sectioned at 3  $\mu\text{m}$ . Endogenous peroxidase was blocked by incubation in methanol/ $\text{H}_2\text{O}_2$  (9:1 v/v) for 20 minutes. Sections were washed in PBS and bound AnxV-biotin was visualized as described above. Sections were counterstained with Hematoxylin.

### AnxV-biotin; EM

Day 13 embryos were microinjected with AnxV-biotin as described above and subsequently perfused intracardially with 0.5 ml 2% glutaraldehyde and 2% paraformaldehyde in 0.1 M cacodylate buffer. The limbs were removed, postfixed overnight in the same fixative, and cut on a Vibratome into 50  $\mu\text{m}$  sections, which were processed to visualize the biotinylated Annexin V as described for LM. After the DAB reaction, the sections were subsequently postfixed in 1.5%  $\text{OsO}_4$  in a 8% glucose solution, rinsed in distilled water, stained en bloc in 3% uranyl acetate, dehydrated in dimethoxypropane, and embedded in Dur-

cupan (Reichert, Arnhem, The Netherlands) (CM100).

Don

Major labelling: relative marked totic bo morphic positivit above transfer cedure. the pro preserv: specim at 55°C temper: 20  $\mu\text{g/l}$ : Science washed The lab section: followi 2'-deox ringer calve-th Boehrin cacodyl albumin step wi were in fragmen Mannhe nitro bi indolyl minute-staining with aq

Di

In vi AnxV-b intact a V is the system surface specific proper with he with a bind to

cupan (8). Ultrathin sections were cut on an ultratome (Reichert Ultracut S, Leica, Germany), stained with lead citrate, and examined under a Philips electron microscope (CM100).

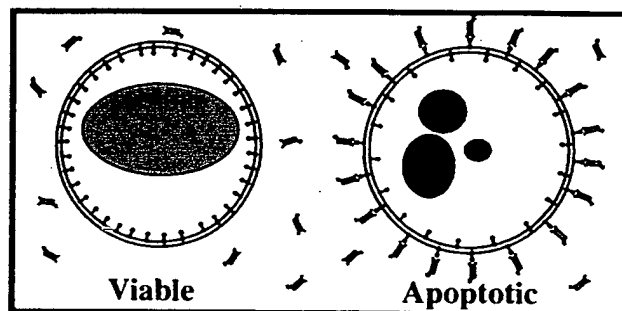
### Double Labeling With AnxV-biotin and TUNEL

Major DNA fragmentation as detected by in situ end-labelling procedures (27,49) has been described as a relatively late event in the process of apoptosis and is a marked feature of DNA containing phagocytosed apoptotic bodies (7). To evaluate whether cells with apoptotic morphology and fragmented DNA indeed showed AnxV positivity, sections stained for AnxV-biotin as described above were subjected to a terminal deoxynucleotidyl transferase-mediated dUTP nick end-labeling (TUNEL) procedure. Based on previous experience (21) we optimized the procedure in terms of signal-enhancement and tissue preservation: best results were obtained by preheating the specimens in 10 mM citrate buffer (pH 6.0) for 10 minutes at 55°C, followed by a slow cooling down to room temperature. Subsequently the sections were treated with 20 µg/ml DNase free proteinase K (Gibco, BRL Life Sciences, Merelbeke, Belgium) for 45 minutes at 37°C and washed 3 times for 5 minutes in Tris buffered saline (TBS). The labeling reaction was performed by incubating the sections under coverslips for one hour at 37°C with the following reaction mixture: 0.016 nmol/µl digoxigenin-11-2'-deoxyuridine-5'-tri-phosphate (DIG-11-dUTP, Boehringer Mannheim, Mannheim, Germany) and 0.135 U/µl calve-thymus terminal deoxynucleotidyl transferrase (TdT, Boehringer Mannheim) in a buffer containing 0.2 M cacodylate, 0.025 M Tris/HCL, 0.24 ng/ml bovine serum albumine, and 1 mM CoCl<sub>2</sub> (pH 6.6). After a preincubation step with block buffer (Boehringer Mannheim), specimens were incubated with alkaline phosphatase-conjugated Fab fragments from sheep raised against DIG (Boehringer Mannheim) for 1 hour. The reaction was developed with nitro blue tetrazolium chloride and 5-bromo-4-chloro-3-indolyl phosphate (NBT-PCIP) in Tris buffer (pH 9.5) for 5 minutes, giving a dark blue reaction product. After the staining for DNA fragmentation, the sections were mounted with aqueous mountant, without counterstaining.

## RESULTS

### Distribution of Intracardially Administered AnxV-biotin in the Viable Embryo

In vivo detection of cell surface exposed PS using AnxV-biotin requires the protein to be administered to the intact and living embryo by intracardiac injection. Annexin V is thus distributed by the specimen's own circulatory system and the protein can reach only the outer cell surface (Fig. 1). To verify whether the staining reflected specific binding that was dependent on the PS binding property of Annexin V, control embryos were injected with heat inactivated AnxV-biotin (32). This AnxV-biotin with a destroyed phospholipid binding activity did not bind to embryonic cells (Fig. 2); hence the observed



⌘: Annexin V-biotin ⌘: Phosphatidylserine

FIG. 1. A schematic representation of AnxV-biotin present in the interstitial compartment of viable mouse embryos after intracardiac administration of the protein. In viable cells, the PS molecules are predominantly facing the cytoplasm and cannot be reached by AnxV-biotin. The surface exposure of PS by apoptotic cells provides binding sites for the AnxV-biotin molecules.

staining with intact protein indicates specific interaction of AnxV-biotin with the plasma membranes.

### Annexin V Binding Cells Are Located in Regions of Developmental Cell Death

An accurate spatiotemporal correlation was found between AnxV-biotin binding patterns in the limbs and the apoptosis patterns known from literature and with those observed using the vital dye Nile blue sulphate (18,19,24,26,41,51) (Fig. 3). Despite the differences in morphology of the fore and hind limbs in day 11-13 embryos, the cell death patterns present were essentially similar. On 11 days of gestation, cells were labeled both in the apical ectodermal ridge (AER) and preaxially and postaxially in the underlying mesoderm (Fig. 3A1-A4). At day 12, labeled cells were still present in the AER, but their numbers were decreased compared to day 11 (Fig. 3B4). Intense labeling was present in the narrow band of mesodermal cells in between the AER and the marginal sinus. In this so-called progress zone, labeling was observed at the pre- and postaxial margins of the autopod in early day 12 embryos (Fig. 3B1 and 3B3-3B4), whereas in late day 12 embryos labeling was most prominently present in the distal parts of the interdigital areas (3B2) (18). Finally, at day 13, labeled cells were virtually absent from the AER, but present in large numbers preaxially, postaxially, and between the digits 1 and 5 (Fig. 3C1-3C4). Also at sites of joint formation in the stylopod, and in between the zeugopod and autopod, AnxV-biotin marked cells were present (Fig. 3C3 and 3C4).

Also at other sites where cell death is known to be present during embryogenesis (13), cells were AnxV-biotin labeled. Staining was distributed left-right symmetrically in the embryos and was present in cells derived from each germ layer. Examples are shown of ectoderm derived cells in the facial processes (Fig. 4A1-A2) and ganglia (Fig. 4B), of endoderm derived cells in the developing lung (Fig. 4C), and of cells from mesodermal origin, i.e., somitic cells



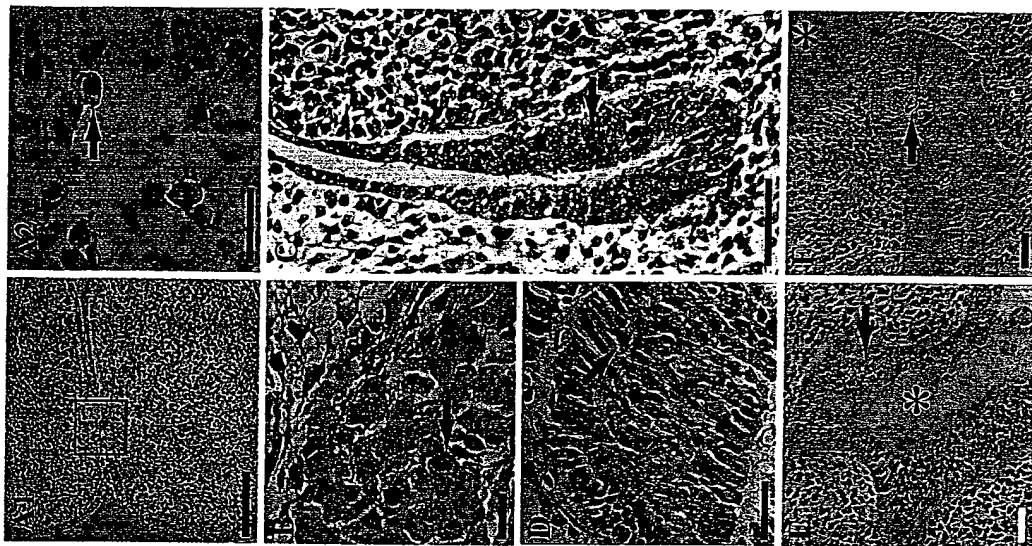


Figure 4

(Fig. 3A and mi  
Occur  
unlabel  
such u  
cytes.  
cells w  
unlabel  
perfus

Ear

For  
binding  
mesod  
AnxV-l  
cal diff  
cells,  
apopto  
conden  
rounde  
and cy  
this ce



Figure 2

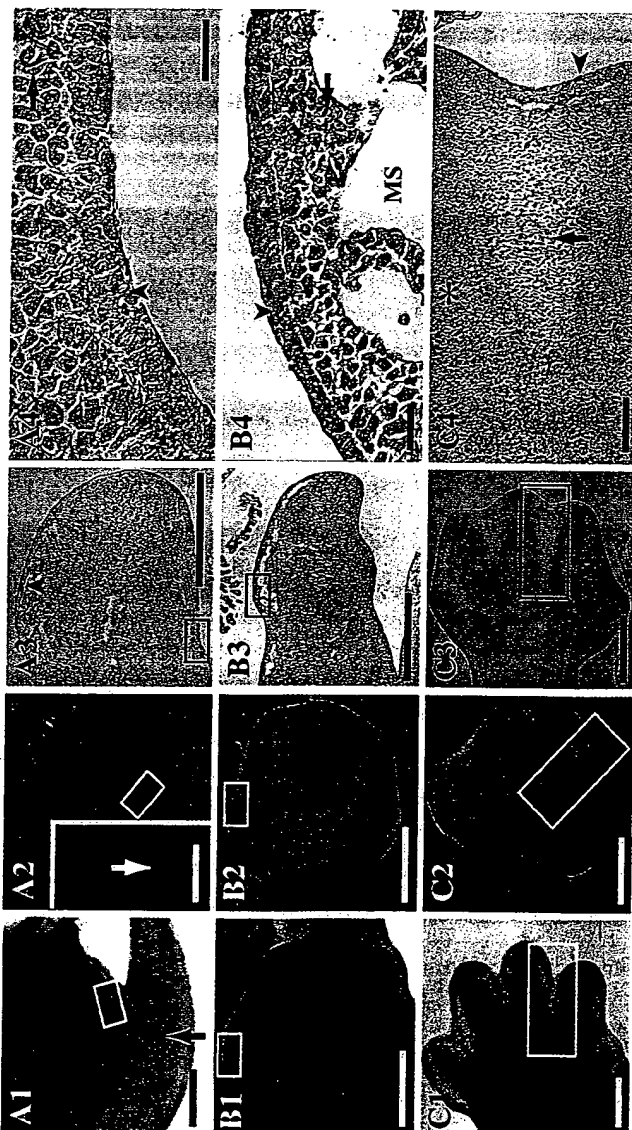


Figure 3

FIG. 2  
biotin in  
in the in  
Figure A  
apoptoti  
the emb  
Scale bar

FIG. 3.  
13 (C) m  
a marke  
(A3-C3)  
r. preser  
Annexin  
the area  
marked  
postaxia  
sulfate  
labeling  
the mar  
arrow).  
autopod  
to the d  
cells we  
to day 1  
virtually  
pre- and  
and C4:  
positive  
100  $\mu$ m

FIG. 4  
serially  
embryo:  
maxillar  
area in  
fusion o  
showing  
(arrow).  
(arrows,  
observe  
the pres  
abundant  
wolfian  
bound t  
(B,D), 2

FIGURES 2-4.



(Fig. 3A1-A2 and Fig. 4D) and cells of the wolffian (Fig. 4E) and müllerian ducts (Fig. 4F).

Occasionally, pyknotic cells were observed that were unlabeled for AnxV-biotin (see Fig. 4E). At the EM level, such unlabeled cells proved to be located within phagocytes. Since phagocytes containing AnxV-biotin positive cells were also present in the material (see below), the unlabeled cells presumably were phagocytosed before perfusion of the specimens with AnxV-biotin.

### Early and Late Apoptotic Cells Bind Annexin V

For the EM study on the morphology of AnxV-biotin binding cells, we used sections through the interdigital mesodermal tissue from day 13 embryos. Some of the AnxV-biotin binding cells showed only subtle morphological differences with vital non-labeled cells. These labeled cells, which supposedly represent the early stages of apoptosis, showed signs of chromatin and cytoplasmatic condensation (Fig. 5A). An AnxV-biotin labeled cell with a rounded-off appearance, and more profound chromatin and cytoplasmatic condensation, is shown in Figure 5B; this cell is located in a phagocyte. The AnxV-biotin binding

cells at later stages of apoptosis were clearly recognizable by their advanced chromatin condensation or by nuclear pyknosis (Fig. 5C). The surrounding viable cells did not show labelling at the plasma membrane.

The labeling for AnxV-biotin and TUNEL was revealed at the light microscopical level as a staining at the plasma membrane and nucleus, respectively. Cells in earlier stages of apoptosis were only AnxV-biotin positive (Fig. 6A1-A2), whereas cells showing both features were all in later stages of apoptosis, i.e., with profound chromatin condensation (Fig. 6A2-B). The pyknotic cell fragments were often only TUNEL-labeled (Fig. 6A1-A2).

### DISCUSSION

The study of apoptotic cell death during embryogenesis not only assists in the understanding of normal development (13,25,26,28,44,45,48), but also aids in understanding of a variety of congenital malformations (14,15,18,19,24,29,46,51). At present, apoptotic cells are detected mostly in the (serially sectioned) specimens on the basis of cell morphology, through the microscope, as it was done 150 years ago (5,13). Though widely applicable, this method is very time consuming, and at the LM level it permits the detection of only the condensed chromatin structure of late apoptotic cells. Alternatively, one may use vital dyes, like Nile blue sulfate (18,19,24,26,41,51), but the use of such dyes is restricted to visualization of cell death in whole mounts. In addition, biochemical markers for apoptosis like TUNEL (12) and ISEL are available (49). These markers detect apoptotic cells at the LM (25,49) and EM (30) level, but they can not be applied to whole mounts.

Studies of developmental cell death may benefit from early detection methods that are selective and can be applied to sections and whole mounts. The method for the in situ detection of apoptotic cell death that is presented in this study is based upon the injection of AnxV-biotin intracardially into viable mouse embryos. The apoptosis patterns in the limbs as visualized in whole specimens using the vital dye Nile blue sulphate (this study and 18,19,24,26,41, and 51) closely match with the AnxV-biotin staining in whole specimens and tissue sections. In subsequent stages of development, cell labeling was observed at various locations, e.g., in the AER, pre- and postaxially, where apoptosis serves the shaping of the hand/footplate; interdigitally, where it is required to separate the digits from each other, and in the presumptive joint-areas, where it is involved in cavity formation (26). AnxV-biotin labeling of apoptotic cells was not restricted to limb tissue, but was also present at other sites in the embryos. Staining was observed at sites in the embryo (1) where cell death serves fusion, e.g., in the facial processes (44,46); (2) where it occurs as degeneration of individual cells, e.g., neurons (22,38) and somitic cells (13); or (3) where it affects whole cell regions, e.g., wolffian duct and müllerian duct (13). In addition, it was observed at sites where the function of apoptosis is still enigmatic, e.g., the lung (13).

Fig. 2. Paraffin section through limb tissue of a heat inactivated-AnxV-biotin injected day 13 mouse embryo showing an absence of DAB staining in the interdigital degenerating tissue (Fig. A1; compare to Fig. 3C3-3C4). Figure A2 depicts a higher magnification of the boxed area in A1, showing apoptotic/pyknotic cells that are unlabeled for AnxV-biotin (arrows). Also, the embryonic erythroblasts were unlabeled (Fig. A1 and A3, arrowheads). Scale bars equal 200  $\mu$ m (A1) or 25  $\mu$ m (A2, A3).

Fig. 3. Apoptosis patterns in limbs from day 11 (A), day 12 (B), and day 13 (C) mouse embryos, visualized in whole limbs using Nile blue sulfate as a marker (A1-C1), and in whole mounts (A2-C2) and paraffin sections (A3-C3 and A4-C4) using Annexin V. Within one age group, boxed areas represent similar regions in Nile blue sulfate treated embryos and in Annexin V treated embryos. In A4-C4 higher magnifications are shown of the areas boxed in A1-C1, A2-C2, and A3-C3. At day 11, cells were marked in the limbs in both the AER (A3-A4: arrowhead) and pre- and postaxially in the underlying mesoderm (A4: arrow). Notice the Nile blue sulfate and AnxV-biotin stained somites (A1-A2: arrow). At day 12, labeling was observed in the narrow band of mesodermal cells in between the marginal sinus (B4: MS) and the AER, i.e., the progress zone (B4: arrow). This labeling was present at the pre- and postaxial margins of the autopods of early day 12 embryos (B1 and B3-B4), whereas it has shifted to the distal interdigital regions in late day 12 embryos (B2). Also, marked cells were still present in the AER but in decreased numbers with respect to day 11 (B4: arrowhead). In day 13 mouse embryos, labeled cells were virtually absent in the AER (C4: arrowhead), but present in large numbers pre- and postaxially and in between the digits 1-5 (C1-C3: boxed areas, and C4: arrow). Also, at sites of joint formation in the stylopod, Annexin V positive cells were found (C4: asterix). Scale bars equal 20  $\mu$ m (A4, B4), 100  $\mu$ m (C4), or 500  $\mu$ m (A1-C1, A2-C2, and A3-C3).

Fig. 4. General presence of Annexin V labeling in paraffin embedded serially sectioned day 11 (A,C,D), day 12 (B) and day 13 (E,F) mouse embryos. In A1, sagittal section showing fusion of the lateral nasal and maxillary processes. In A2, a higher magnification is shown of the boxed area in A1, depicting AnxV-biotin labeled cells (arrow) in the center of fusion of the facial processes. (B) Section through the trigeminal ganglion showing labeled cells with a pyknotic and often also fragmented nucleus (arrow). (C) Labeled cells in the endoderm derived bronchial epithelium (arrows). In transverse sections through the tail region cells were observed labeled in the degenerating tailgut and in the somites at site of the presumptive somitocoel (D, arrow). Annexin V labeled cells were also abundantly present in the urogenital system. Examples are shown of the wolffian (E) and müllerian ducts (F), in the region where the ducts are bound to orifice into the urogenital sinus (asterix). Scale bars equal 10  $\mu$ m (B,D), 25  $\mu$ m (A2, C, E, and F), or 100  $\mu$ m (A1).

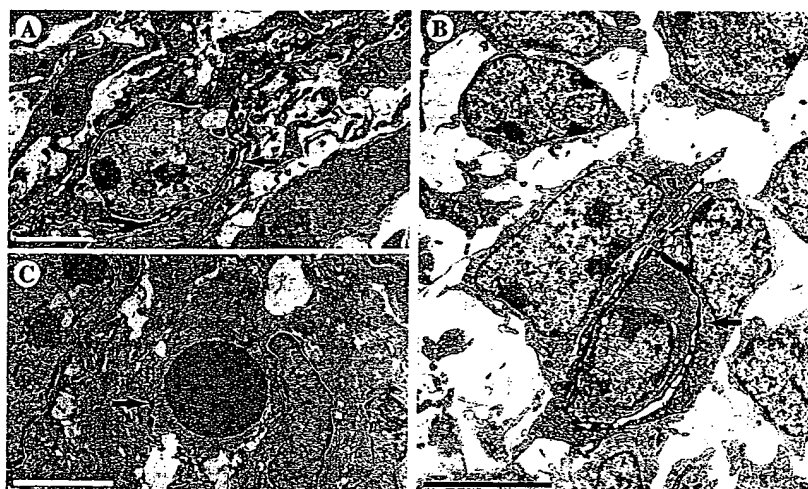


Figure 5

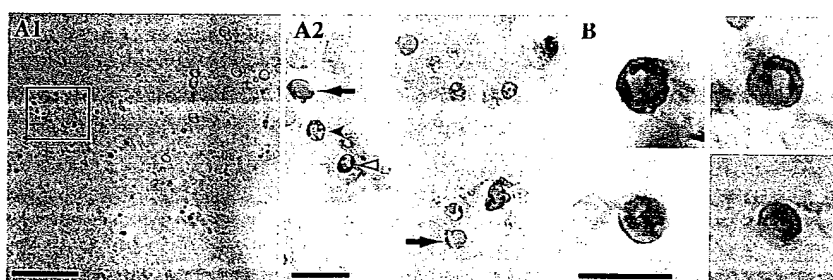


Figure 6

FIG. 5. Electron micrographs, showing AnxV-biotin labeled cells located in the interdigital region of a day 13 mouse embryo. Cells were found labeled at early stages of apoptosis, when showing first signs of chromatin condensation (A), ingested by a phagocyte (B), and up to the later stages of apoptosis when clearly pyknotic (C). Viable cells were unlabeled (asterisk). Scale bar equals 2  $\mu$ m.

FIG. 6. Paraffin sections through day 13 limbs of AnxV-biotin injected mouse embryos that have been stained both for PS exposure at the plasma membrane via AnxV-biotin and for DNA fragmentation via the TUNEL method; no counterstaining was applied. In figure A2 a higher magnifica-

tion is shown of the boxed area in figure A1, showing in one field the three types of labeled cells that were observed: (i) cells that showed AnxV-biotin labeling at the plasma membrane only (arrows), (ii) pyknotic cells that were double labeled for AnxV-biotin and TUNEL (arrowhead), and (iii) pyknotic cells and cell fragments that appeared only TUNEL-positive (open arrowhead). In B, four AnxV+/TUNEL+ cells are depicted in subsequent stages of apoptosis. Such cells were having chromatin margination (upper left and upper right) or nuclear fragmentation (lower left), or were clearly pyknotic (lower right). Scale bar equals 50  $\mu$ m (A1) or 10  $\mu$ m (A2) or 5  $\mu$ m (B).

AnxV-biotin can also be used to detect apoptotic cells at the ultrastructural level. These cells were characterized by their typical morphology (50); their appearance ranged from early stages of apoptosis, where the cells show the first signs of cytoplasmatic and nuclear changes to the later stages, with advanced cytoplasmatic and chromatin condensation and ultimate pyknosis. Additional evidence for the association between apoptosis and PS exposure at the outer layer of the plasma membrane came from double labeling experiments, applying the TUNEL protocol for detection of apoptosis associated internucleosomal DNA fragmentation (12,21) subsequent to the Annexin V protocol. The double labeled cells were all in the late, pyknotic phase of apoptosis. In contrast, the apoptotic cells in relatively early stages of apoptosis were only AnxV-biotin labeled at the plasma membrane. The presence of these AnxV-biotin-positive and TUNEL negative

cells suggests that loss of PS plasma membrane asymmetry precedes the stages when DNA fragmentation can be detected by TUNEL. A similar sequence of events was observed for hematopoietic cells entering apoptosis *in vitro* (4,23). The double labelling experiments also showed that some of the pyknotic cells and cell fragments were only TUNEL positive. At the EM level, the pyknotic cells without AnxV-biotin labeling at the plasma membrane were shown to be located within phagocytes. We hypothesize that these apoptotic cells were already ingested by phagocytes before the embryos were injected with the AnxV-biotin, and therefore could not be reached by the circulating protein.

In conclusion, we demonstrated the feasibility of Annexin V *in vivo* labeling of apoptotic cells in whole mounts and tissue sections of mouse embryos at the light- and ultrastructural level.

and  
photo  
DIG  
tase,  
to fir  
Finar  
Gene

1. A  
H  
to  
2. B  
si  
ex  
3. B  
ap  
cl  
2  
4. C  
K  
m  
1  
5. C  
o  
9  
6. C  
1  
C  
D  
C  
8. E  
si  
in  
C  
1  
9. E  
d  
10. F  
H  
v  
a  
11. F  
F  
h  
F  
12. C  
C  
13. C  
C  
14. C  
C  
15. I  
C  
16. I  
F  
F  
17. I  
C  
18. F  
C  
19. J  
C  
20. J

and Tom de Vries-Lentsch, Mirko Kuit, and Ed Dalm, for photography. We thank Hans Baelde for providing anti DIG Fab fragments and the substrate for alkaline phosphatase, and Rob Keijzer for technical assistance with regard to finding the optimal conditions for the TUNEL procedure. Financial support by the Rotterdam Foundation of Clinical Genetics (S.vdE., L.B.) is gratefully acknowledged.

#### LITERATURE CITED

- Andree HAM, Reutelingsperger CPM, Hauptman R, Hemker HC, Hermens WT, Willems GM: Binding of vascular anticoagulant (VACo) to planar phospholipid bilayers. *J Biol Chem* 265:4923-4928, 1990.
- Bennet MR, Gibson DF, Schwartz SM, Tait JF: Binding and phagocytosis of apoptotic vascular smooth muscle cells is mediated in part by exposure of phosphatidylserine. *Circ Res* 77:1136-1142, 1995.
- Boersma AWM, Nooter K, Oostrum RG, Stoter G: Quantification of apoptotic cells with fluorescein isothiocyanate-labeled Annexin V in chinese hamster ovary cell cultures treated with cisplatin. *Cytometry* 24:123-130, 1996.
- Castedo M, Hirsch T, Susin SA, Zamzami N, Marchetti P, Macho A, Kroemer G: Sequential acquisition of mitochondrial and plasma membrane alterations during early lymphocyte apoptosis. *J Immunol* 157:512-521, 1996.
- Clarke PGH, Clarke S: Nineteenth century research on naturally occurring cell death and related phenomena. *Anat Embryol* 193:81-99, 1996.
- Cohen JJ: Apoptosis: physiologic cell death. *J Lab Clin Med* 761-765, 1994.
- Collins JA, Scandel CA, Young KK, Vessely J, Willing HAMC: Major DNA fragmentation is a late event in apoptosis. *J Histochem Cytochem* 45:923-934, 1997.
- De Zeeuw CI, Holstege JC, Ruigrok TJH, Voogd J: An ultrastructural study of the GABAergic, the cerebellar and the mesodiencephalic innervation of the cat medial accessory olive: Anterograde tracing combined with immunocytochemistry. *J Comp Neurol* 284:12-35, 1989.
- Diaz C, Schroit AJ: Role of translocases in the generation of phosphatidylserine asymmetry. *J Membrane Biol* 151:1-9, 1996.
- Fadok VA, Savill JS, Haslett C, Bratton DL, Doherty DE, Campbell PA, Henson PM: Different populations of macrophages use either the vitronectin receptor or the phosphatidylserine receptor to recognize and remove apoptotic cells. *J Immunol* 149:4029-4035, 1992.
- Fadok VA, Voelker DR, Campbell PA, Cohen JJ, Bratton DL, Henson PM: Exposure of phosphatidylserine on the surface of apoptotic lymphocytes triggers specific recognition and removal by macrophages. *J Immunol* 148:2207-2216, 1992.
- Gavrieli Y, Sherman Y, Ben-Sasson SA: Identification of programmed cell death in situ via specific labelling of nuclear DNA fragmentation. *J Cell Biol* 119:493-501, 1992.
- Glücksman A: Cell deaths in normal vertebrate ontogeny. *Biol Rev Camb Philos Soc* 26:59-86, 1951.
- Goldman AS, Herold R, Piddington R: Inhibition of programmed cell death in the fetal palate by cortisol. *Proc Soc Exp Biol Med* 166:418-424, 1981.
- Hamburger V: Cell death in the development of the lateral motor column of the chick embryo. *J Comp Neurol* 160:535-546, 1975.
- Homburg CHE, de Haas M, von dem Borne AEGK, Verhoeven AJ, Reutelingsperger CPM, Roos D: Human neutrophils lose their surface FcγRIII and acquire Annexin V binding sites during apoptosis in vitro. *Blood* 85:532-540, 1995.
- Kerr JFR, Wyllie AH, Currie AR: Apoptosis: a basic biological phenomenon with wide-ranging implications in tissue kinetics. *Br J Cancer* 26:239-257, 1972.
- Kimura S, Shiota K: Sequential changes of programmed cell death in developing fetal mouse limbs and it possible roles in limb morphogenesis. *J Morphol* 229:337-346, 1996.
- Knudson TB, Kocher DM: The role of morphogenetic cell death during abnormal limb-bud outgrowth in mice heterozygous for the dominant mutation *Hemimelia-extra toe (Hm<sup>+</sup>)*. *J Embryol Exp Morphol* 65 (Supplement):289-307, 1981.
- Koopman G, Reutelingsperger CPM, Kuijten GAM, Keehnen RMJ, Pals ST, van Oers MHJ: Annexin V for flow cytometric detection of phosphatidylserine expression on B cells undergoing apoptosis. *Blood* 84:1415-1420, 1994.
- Lucassen PJ, Chung WCJ, Vermeulen JP, van Lookeren-Campagne M, van Dierendonck JH, Swaab DF: Microwave-enhanced in situ end-labelling of fragmented DNA: Parametric studies in relation to postmortem delay and fixation on rat and human brain. *J Histochem Cytochem* 43:1163-1171, 1995.
- Martin D, Johnson E: Neuronal death and the role of apoptosis. In: *Apoptosis: The Molecular Basis of Cell Death*, Tomei L, Cope F (eds). Cold Spring Harbor Laboratory, Cold Spring Harbor, NY, 1991, pp 263-277.
- Martin SJ, Reutelingsperger CPM, McGahon AJ, Rader J, van Schie RCAA, LaFace DM, Green DR: Early redistribution of plasma membrane phosphatidylserine is a general feature of apoptosis regardless of the initiating stimulus: Inhibition by overexpression of Bcl-2 and abl. *J Exp Med* 182:1545-1556, 1995.
- Milaire J, Rooze M: Hereditary and induced modifications of the normal necrotic patterns in the developing limb buds of the rat and mouse: Facts and hypotheses. *Arch Biol* 94:459-490, 1983.
- Mori C, Nakamura N, Okamoto Y, Osawa M, Shiota K: Cytochemical identification of programmed cell death in the fusing fetal mouse palate by specific labelling of DNA fragmentation. *Anat Embryol* 190:21-28, 1994.
- Mori C, Nakamura N, Kimura S, Irie H, Takigawa T, Shiota K: Programmed cell death in the interdigital tissue of the fetal mouse limb is apoptosis with DNA fragmentation. *Anat Rec* 242:103-110, 1995.
- Negoesu A, Lorieimer P, La Bat-Moleur F, Drouet C, Robert C, Guillerme C, Brambilla C, Brambilla AE: In situ apoptotic cell labeling by the TUNEL method: Improvement and evaluation on cell preparations. *J Histochem Cytochem* 44:959-968, 1996.
- Nievelstein RAJ, Hartwig NG, Vermeij-Keers C, Valk J: Embryonic development of the mammalian caudal neural tube. *Teratology* 48:21-31, 1993.
- Norman DJ, Feng L, Cheng SS, Gubay J, Chan J, Heintz N: The lurcher gene induces apoptotic cell death in cerebellar Purkinje cells. *Development* 121:1183-1193, 1995.
- Pellier V, Astic L: Detection of apoptosis by electron microscopy and in situ labelling in the rat olfactory pit. *Neuroreport* 5:1429-1432, 1994.
- Raynal P, Pollard HB: Annexins: The problem of assessing the biological role for a gene family of multifunctional calcium- and phospholipid-binding proteins. *Biochim Biophys Acta* 1197:63-93, 1994.
- Reutelingsperger CPM, Hornstra G, Hemker HC: Isolation and partial purification of a novel anticoagulant from arteries of human umbilical cord. *Eur J Biochem* 151:625-629, 1985.
- Romisch J, Paques EP: Annexins: Calcium-binding proteins of multifunctional importance? *Med Microbiol Immunol* 180:109-126, 1991.
- Saunders Jr JW, Gasseling MT, Saunders LC: Cellular death in morphogenesis of the avian wing. *Dev Biol* 5:147-178, 1962.
- Savill J, Fadok V, Henson P, Haslett C: Phagocyte recognition of cells undergoing apoptosis. *Immunol Today* 14:131-136, 1993.
- Schlaepfer DD, Mehlman T, Burgess WH, Haigler HT: Structural and functional characterization of endonexin II, a calcium- and phospholipid-binding protein. *Proc Natl Acad Sci USA* 84:6078-6082, 1987.
- Shiratsuchi A, Umeda M, Ohba Y, Nakanishi Y: Recognition of phosphatidylserine on the surface of apoptotic spermatogenic cells and subsequent phagocytosis by Sertoli cells of the rat. *J Biol Chem* 272:2354-2358, 1997.
- Sohal GSP: Embryonic development of nerve and muscle (sixth annual Stuart Reiner memorial lecture). *Muscle & Nerve* 18:2-14, 1995.
- Tait JF, Gibson D, Fujikawa K: Phospholipid binding properties of human placental anticoagulant protein-1, a member of the lipocortin family. *J Biochem* 264:7944-7949, 1989.
- van den Eijnde SM, Boshart L, Reutelingsperger CPM, de Zeeuw CI, Vermeij-Keers C: Phosphatidylserine plasma membrane asymmetry in vivo: A pan-cellular phenomenon which alters during apoptosis. *Cell Death and Differentiation* 4:311-317, 1997.
- van der Hoeven F, Schimmang T, Volkman A, Mattei M-G, Kyewski B: Programmed cell death is affected in the novel mouse mutant *Fused toes (Ft)*. *Development* 120:2601-2607, 1994.
- van Engeland M, Ramaekers FCS, Schutte B, Reutelingsperger CPM: A novel assay to measure loss of plasma membrane asymmetry during apoptosis of adherent cells in culture. *Cytometry* 24:131-139, 1996.
- van Heerde WL, de Groot PG, Reutelingsperger CPM: The complexity of the phospholipid binding protein annexin V. *Thromb Haemost* 73:172-179, 1995.
- Vermeij-Keers C: Degeneration in the epithelial plate of Hochstetter in the mouse; a light and electron microscopic study. *Acta Morph Neerl Scand* 9:386-387, 1972.

45. Vermeij-Keers C, Poelmann RE: The neural crest: A study on cell degeneration and the improbability of cell migration in mouse embryos. *Neth J Zool* 30:74-81, 1980.
46. Vermeij-Keers C, Mazzola RF, van der Meulen JC, Stricker M: Cerebrocraniofacial and craniofacial malformations: An embryological analysis. *Cleft Palate J* 20:128-145, 1983.
47. Vermes I, Haanen C, Steffens-Nakken H, Reutelingsperger CPM: A novel assay for apoptosis. Flow cytometric detection of phosphatidylserine expression on early apoptotic cells using fluorescein labelled Annexin V. *J Immunol Methods* 184:39-51, 1995.
48. White K: Cell death returns to its roots. *Current Biol* 5:371-372, 1995.
49. Wijsman JH, Jonker RC, Keijzer R, van de Velde CJH, Cornelisse CJ, van Dierendonck JH: A new method to detect apoptosis in paraffin sections: In situ end-labelling of fragmented DNA. *J Histochem Cytochem* 41:7-12, 1993.
50. Wyllie A, Kerr J, Currie A: Cell death: The significance of apoptosis. *Int Rev Cytol* 68:251-306, 1980.
51. Zakeri Z, Quaglini D, Ahuja HS: Apoptotic cell death in the mouse limb and its suppression in the hammetoe mutant. *Dev Biol* 165:294-297, 1994.

Ge.  
affec  
have  
differ  
if the  
MCF-  
cells  
trans  
other  
flow  
block  
epiru  
actio  
the o

It is  
exhib  
drugs  
kineti  
respo  
under  
At  
mour  
geneti  
of coi  
tumov  
the co  
would  
under  
p53 is  
comm  
cies, a  
cancer  
The  
Farmit  
of a vr  
The c  
clines  
mecha  
inhibit  
ase II

# The CD95/CD95L ligand system is not the major effector in anticancer drug-mediated apoptosis

Manlio Tolomeo<sup>1</sup>, Luisa Dusonchet<sup>2</sup>, Maria Meli<sup>2,3</sup>,  
 Stefania Grimaudo<sup>4</sup>, Natale D'Alessandro<sup>2</sup>, Giuliana Papoff<sup>5</sup>,  
 Giovina Ruberti<sup>5,6</sup> and Luciano Rausa<sup>3</sup>

<sup>1</sup> Chair of Hematology, University of Palermo, Italy

<sup>2</sup> Institute of Pharmacology, University of Palermo, Italy

<sup>3</sup> Institute of Oncology, University of Palermo, Italy

<sup>4</sup> Institute of Pharmacological Chemistry, University of Palermo, Italy

<sup>5</sup> Department of Immunobiology, Institute of Cell Biology, National Research Council, Roma, Italy

<sup>6</sup> corresponding author: Department of Immunobiology, Institute of Cell Biology, National Research Council, Via E. Ramarini, 32 - 00016 Monterotondo Scalo (Roma) Italy. tel. +39-6-90091263; fax +39-6-90091260; e.mail: giovina@biocell.irmkant.rm.cnr.it

Received 5.1.98; revised 30.3.98; accepted 10.4.98

Edited by R.A. Knight

## Abstract

Many anticancer drugs are able to induce apoptosis in tumor cells but the mechanisms underlying this phenomenon are poorly understood. Some authors reported that the p53 tumor suppressor gene may be responsible for drug-induced apoptosis; however, chemotherapy-induced apoptosis can also be observed in p53 negative cells. Recently, doxorubicin (DXR) was reported to induce CD95L expression to mediate apoptosis through the CD95/CD95L system. Thus, an impairment of such a system may be involved in drug resistance. We evaluated the *in vitro* antitumor activity of several cytotoxic drugs on two human p53-negative T-cell lymphoma cell lines, the HUT78-B1 CD95L-resistant cell line and the HUT78 parental CD95L-sensitive cell line. We demonstrated by Western blotting assay that DXR and etoposide (VP-16) were able to induce CD95L expression after 4 h of treatment. In contrast, they were unable to induce the expression of p53. DXR, at concentrations ranging from 0.001–1 µg/ml, and VP-16, at concentrations ranging from 0.05–1 µg/ml, were equally cytotoxic and induced apoptosis in both cell lines as assessed by fluorescence microscopy and flow cytometry analyses. Although we observed a slightly reduced percentage of apoptotic cells in HUT78B1 when compared with the parental HUT78 cells after few hours of drug exposure, this difference was no longer evident at 48 or 72 h. Similarly, the exposure of HUT78 cells to a CD95-blocking antibody partially reduced early apoptosis (24 h) without affecting the long-term effects of the drugs including cytotoxicity. Furthermore, as observed with DXR and VP-16, both the CD95L-sensitive and the CD95L-resistant cell lines resulted equally sensitive to the cytotoxic effects of a number of different cytotoxic drugs (vincristine, camptothecin, 5-fluorouracil and methotrexate). The treatment with the

Caspase-3 tetrapeptide aldehyde inhibitor, Ac-DEVD-CHO, did not affect the DXR-induced apoptosis whereas it only modestly inhibited apoptosis and cytotoxicity of VP-16, while Z-VAD.FMK, a Caspase inhibitor that prevents the processing of Caspase-3 to its active form, was able to block DXR-induced apoptosis at 24 h but not at 48 h. Thus, our results do not confirm a crucial role for the CD95/CD95L system in drug-induced apoptosis and suggest the involvement of alternative p53-independent pathways at least in this experimental model system.

**Keywords:** apoptosis; anticancer drugs; CD95; CD95L; caspases

**Abbreviations:** CD95L, CD95 Ligand; DXR, Doxorubicin; VP-16, Etoposide; VCR, vincristine

## Introduction

Programmed cell death or apoptosis is a genetically encoded process involved in the homeostasis of multicellular organisms and in carcinogenesis (Kerr *et al*, 1972; Williams and Smith, 1993; Martin and Green, 1995a; Williams, 1991). Several cytotoxic drugs employed in the chemotherapy of malignancies cause apoptosis in target cells (Fisher, 1994; Lennon *et al*, 1991; Collins *et al*, 1991; Walker *et al*, 1991), but the mechanisms by which these drugs induce apoptosis in neoplastic cells are not well understood at the molecular level. Several studies indicate that wild-type p53, a tumor suppressor gene which regulates both cell cycle and cell survival, plays a critical role in triggering cell death by apoptosis upon DNA damage caused by radio- and chemotherapy (Lowe *et al*, 1993a,b; Kinzler and Vogelstein, 1994). Recently, however, further evidence suggests that the p53 status does not necessarily correlate with chemo- or radio-resistance (Del Bufalo *et al*, 1996; Jung *et al*, 1992), and inactivation or mutation of p53 can even render cells more sensitive to cytotoxic agents (Fan *et al*, 1995; Xu *et al*, 1995). CD95 (also known as Fas or APO-1) is a cell surface protein belonging to the TNF receptor family which induces apoptosis upon interaction with agonistic antibodies or with the CD95 Ligand (CD95L). The CD95/CD95L system plays an important role in the immune response (Nagata, 1997; Krammer *et al*, 1994; Nagata and Golstein, 1995) and the expression of CD95L by tumor cells has been reported to be a possible determinant of tumor immunosurveillance and/or invasion *in vivo* (Strand *et al*, 1996; O'Connel *et al*, 1996; Hahne *et al*, 1996; Niehans *et al*, 1997; Saas *et al*, 1997). Crosslinking of CD95 results in rapid receptor aggregation and formation of the Death Inducing Signaling Complex (DISC) (Kischkel *et al*, 1995). This is composed of CD95, FADD or MORT-1 (Chinnaiyan *et al*, 1995; Boldin *et al*, 1995), a death domain-containing adaptor protein and Caspase 8 (FLICE/MACH protein) (Muzio *et al*, 1996; Boldin *et al*, 1996),

a member of the ICE-like family of cysteine proteases also known as Caspases (Alnemri *et al*, 1996), which play important roles in the execution stage of apoptosis (Martin and Green, 1995b; Kumar and Lavin, 1996). Moreover, CD95 crosslinking can also lead to the hydrolysis of sphingomyelin to form ceramide, which can then act as a second messenger to initiate multiple downstream pathways and several biological functions including apoptosis (Testi, 1996; Skowronski *et al*, 1996; Hannun, 1996). Recently, an increased expression of CD95L messenger RNA has been shown to occur in the lymphoblastic T cell CCRF-CEM leukemia exposed to doxorubicin or methotrexate (Friesen *et al*, 1996). Moreover, synthesis of ceramide, has been observed in murine leukemia cells treated with doxorubicin (Bose *et al*, 1995). These studies indicate that the CD95/CD95L system may be involved in apoptosis triggered by cytotoxic drugs. To understand the relationship between CD95 and drug-induced apoptosis, we have therefore studied the effects of doxorubicin (DXR) and etoposide (VP-16), two topoisomerase II inhibitors able to induce apoptosis in several tumor cell lines, in a T cell lymphoma clone resistant to CD95-mediated apoptosis (HUT78B1) as well as in its parental, CD95L-sensitive, counterpart (HUT78). HUT78B1 cells were selected by treatment of the parental HUT78 cell line with a CD95-specific monoclonal antibody, CH-11 and express both wild-type CD95 and a truncated form of the receptor lacking the intracellular death-signaling domain (Cascino *et al*, 1996).

## Results

### Effects of a CD95-agonistic antibody on HUT78 and HUT78B1 cells

HUT78 cells underwent apoptosis when exposed to increasing concentrations of the CD95-agonistic antibody, CH-11. Apoptosis was already observed after 4 h of treatment and reached a plateau at 24 h (90% of apoptotic cells). The CD95 IgG1 antibody, DX2, almost completely blocked the CH-11-induced apoptosis in HUT78 cells at 24 h (Figure 1) and to a similar extent at 48 and 72 h (data not shown). HUT78B1 cells were resistant to CH-11 treatment even at high concentra-

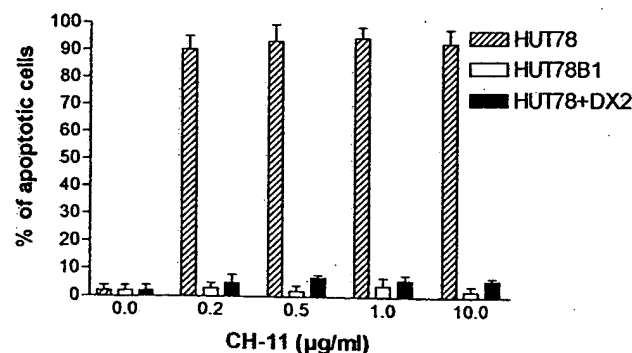


**Figure 1** Percentage of apoptotic cells, evaluated by morphological analysis, after 24 h of exposure to the CD95-agonistic mAb CH11 in HUT78, HUT78B1, or HUT78 cells pretreated with the CD95-blocking Ab DX2. Data are the mean  $\pm$  S.D. of four independent experiments. Flow cytometry analysis of apoptosis gave very similar results

tions, as previously reported (Cascino *et al*, 1996) (Figure 1).

### Expression of p53 and bcl-2 protein in HUT78 and HUT78B1 cells

The expression of wild-type p53 and bcl-2 proteins was evaluated by Western blotting in HUT78 and HUT78B1 cells (Figure 2a and b). Similar levels of bcl-2 protein were observed in both cell lines while p53 protein was undetectable even upon treatment with DXR or VP-16 drugs for 12 or 24 h (Figure 2a).

### Drug-induced apoptosis

DXR- and VP-16-induced apoptosis in HUT78 cells was concentration- and time-dependent (Figure 3a and b). About

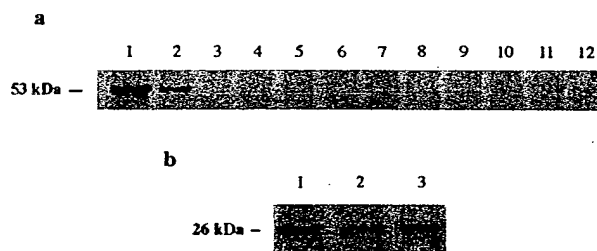


**Figure 2** Expression of p53 (a) and bcl-2 protein (b) in HUT78 and HUT78B1 cells. (a) As a control, the retinoblastoma cell line Y79 was incubated for 24 h in the presence (lane 1) or absence (lane 2) of camptothecin 0.5  $\mu$ M. HUT 78 cells (lanes 3–7) or HUT78B1 cells (lanes 8–12) were exposed to 0.9  $\mu$ g/ml of DXR for 12 (lanes 4 and 9) or 24 h (lanes 5 and 10) or to 1.5  $\mu$ g/ml of VP-16 for 12 (lanes 6 and 11) or 24 h (lanes 7 and 12). (b) Expression of bcl-2 in HUT78 (lane 1), HUT78B1 (lane 2) and Y79 cells (lane 3)

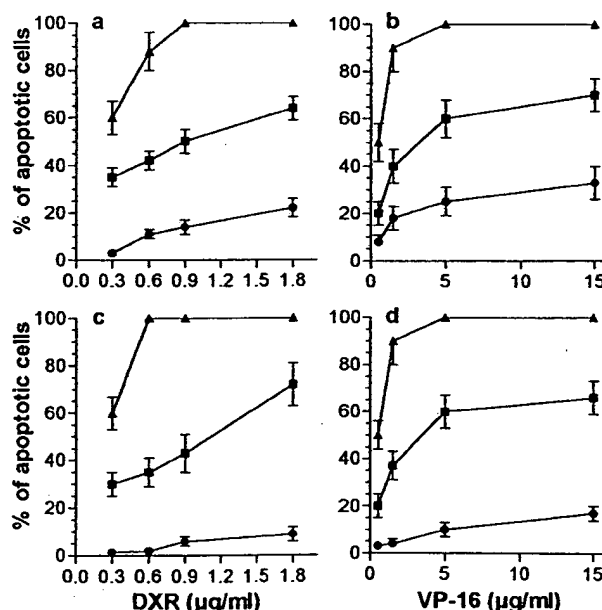


**Figure 3** Percentage of apoptotic cells, evaluated by morphological analysis, after 24 (●), 48 (■) or 72 (▲) h of exposure to DXR (a,c) or VP-16 (b,d) in HUT78 (a,b) and in HUT78B1 cells (c and d). Data are the mean  $\pm$  S.D. of five independent experiments. Flow cytometry analysis of apoptosis gave very similar results

10% of the cells were apoptotic after 24 h of treatment with 0.6  $\mu$ g/ml of DXR or VP-16, and this percentage increased to 22% or 33% at 1.8  $\mu$ g/ml of DXR or 1.5  $\mu$ g/ml of VP-16, respectively. Finally DXR at 0.9  $\mu$ g/ml and VP-16 at 1.5  $\mu$ g/ml induced apoptosis almost in all cells at 72 h. Therefore, in spite of the absence of p53 and the presence of Bcl-2 proteins, HUT78 cells undergo apoptosis upon chemotherapeutic treatment. In the HUT78B1 CD95-resistant cells, a slightly lower percentage of apoptotic cells was observed at 24 h of drug exposure when compared to that of the wild-type HUT78 cells (Figure 3c and d). However, at 48 and 72 h the percentage of apoptotic cells in HUT78B1 was superimposable to that of HUT78 cells (Figure 3c and d).

### Role of the CD95/CD95L system in drug-induced apoptosis in HUT78 and HUT8B1 cells

HUT78 cells express the CD95 receptor and are sensitive to apoptosis; thus we investigated the possible role of the CD95/

CD95L system in drug induced apoptosis. First the expression of CD95L in drug-treated HUT78 cells was evaluated by cytofluorimetric and Western blotting analyses. Since doubts have been raised about the specificity of some anti-CD95L antibodies COS-7 and 293T mock- or human CD95L- transiently transfected cells and NIH3T3 fibroblast transfected with the murine CD95L (Hughes and Crispe, 1995) were used along with the experimental samples. CD95L was detected in all transfectants as well as in the HUT78 cells treated with VP-16 and DXR by both cytofluorimetric (NOK-1 antibody) (Figure 4A and B) and Western blot (G247-4 and clone 33 antibodies) (Figure 4C and D) analyses but not in the mock transfected COS-7, 293T, NIH3T3 fibroblasts and in the untreated HUT78 cells (Figure 4). CD95L was induced at 4 h upon treatment with both VP-16 and DXR and slightly decreased at 8 h as detected by FACS analysis (Figure 4B), such decrease however was barely and only occasionally detectable on total cell lysates in Western blot (Figure 4D). Similar results were obtained with the CD95-

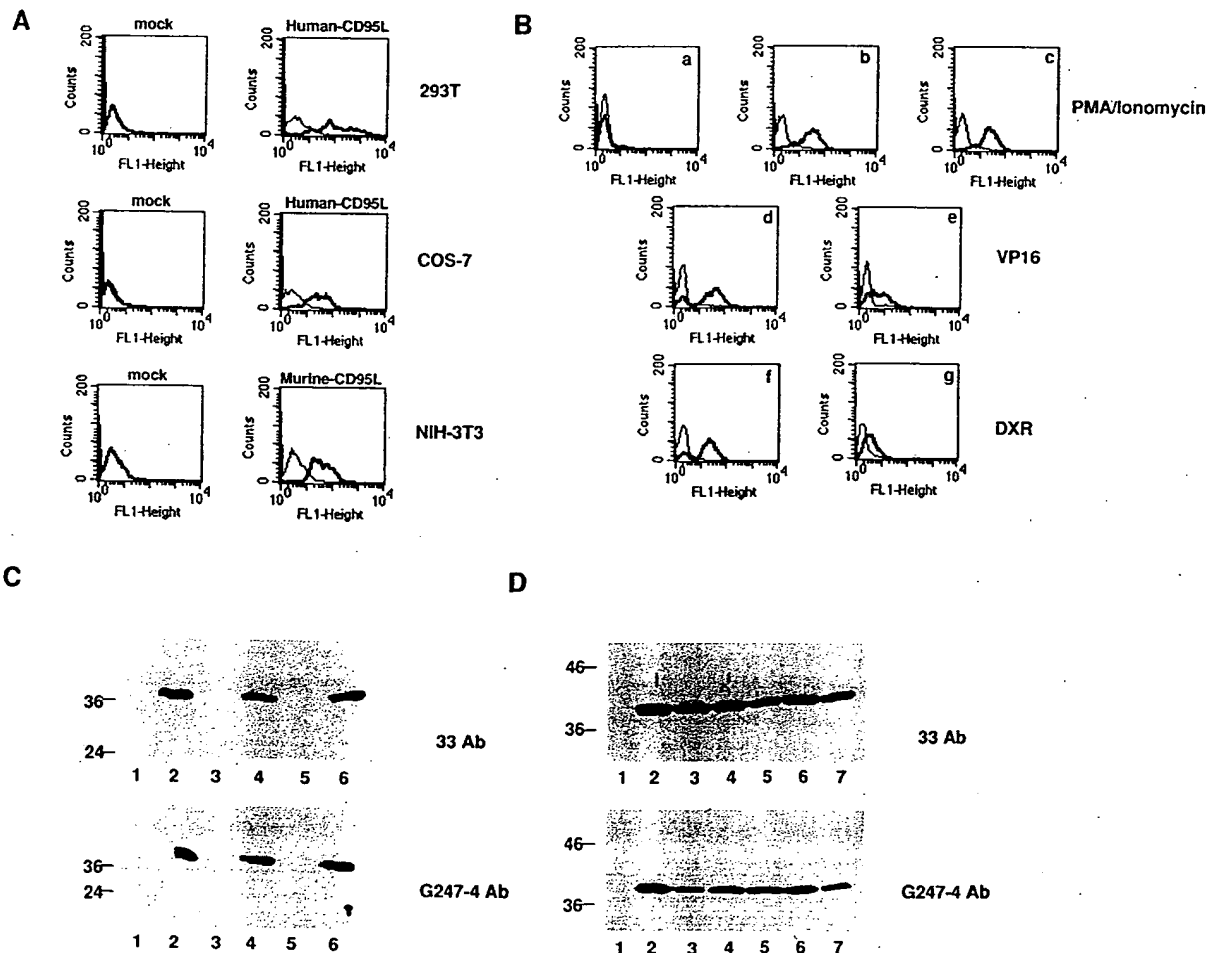


**Figure 4** Expression of CD95L by cytofluorimetric and immunoblotting analyses. Surface CD95L expression detected with the NOK-1 or a isotype-matched control antibody by cytofluorimetric analysis (A, B) in mock or CD95L transfected 293T, COS-7, and NIH3T3 cells as indicated (A) and in HUT78 cells (B): untreated (a), treated with PMA (10 ng/ml and ionomycin (400 ng/ml) for 4 (b) and 8 (c) h, treated with 1.5  $\mu$ g/ml of VP-16 for 4 (d) and 8 (e) h or with 0.5  $\mu$ g/ml of DXR for 4 (f) and 8 (g) h. Immunoblotting analysis with the CD95L antibodies clone G247-4 and clone 33 as indicated (for details see Materials and Methods). (C) 293T, mock-transfected (lane 1); 293T, human CD95L-transfected (lane 2); COS-7 mock transfected (lane 3); COS-7 human CD95L-transfected (lane 4); NIH3T3 mock-transfected (lane 5); NIH3T3 murine CD95L-transfected (lane 6). (D): untreated HUT78 (lane 1), HUT78 treated with PMA and ionomycin for 4 (lane 2) and 8 h (lane 3), HUT78 treated with VP16 for 4 (lane 4) and 8 h (lane 5), HUT78 cells treated with DXR for 4 (lane 6) and 8 (lane 7) h

resistant HUT78B1 cells (data not shown). Next we evaluated the susceptibility to drug-induced apoptosis in HUT78 cells treated with a CD95-blocking antibody (DX2) and we compared the results to that obtained in HUT78B1. Likewise to that observed in HUT78B1, at 24 h of drug exposure a slightly lower percentage of apoptotic cells in the DX2-treated HUT78 than in the HUT78 cells was observed. (Figure 5a and b). However, at 48 (Figure 5c and d) and at 72 h (Figure 5e and f) a similar percentage of apoptotic cells in HUT78, HUT78 exposed to DX2 and in HUT78B1, was detected.

### Drug-induced cytotoxicity

To test whether the CD95/CD95L system may influence antitumoral effects other than apoptosis we evaluated the cytotoxicity of DXR and VP-16 in HUT78 and in HUT78B1 cells by the trypan blue dye exclusion test. Both drugs produced similar cytotoxic effects in the two cell lines (Figure 6). In addition, the treatment with the DX2 antibody did not affect the cytotoxicity of DXR or VP-16 in HUT78 cells (data not shown). Moreover the cytotoxic effects of other

chemotherapeutic drugs, which differ in structure and mechanism of action from DXR and VP-16, were tested in HUT78 and HUT78B1 cells (Table 1). No significant differences in cytotoxicity were detected in the sensitive and in the resistant cell lines.

### Role of Caspases in drug-induced apoptosis

Caspase-3 (CPP32, Yama, apopain) is activated through a protease cascade in response to several apoptotic stimuli, including CD95 crosslinking, and cleaves specific intracellular substrates during apoptosis (Martin and Green, 1995b; Kumar and Lavin, 1996). To understand whether Caspase-3 activation was directly involved in drug-mediated apoptosis, we studied the effects of DXR and VP-16 in HUT78 cells treated with the caspase 3 inhibitor Ac-DEVD-CHO (Acetyl Asp-Glu-Val-Asp aldehyde). While Ac-DEVD-CHO was able to inhibit, almost completely, the CH-11-induced apoptosis (86%, data not shown), it had no effect on apoptosis induced by DXR and only a partial inhibitory effect on apoptosis and cytotoxicity was observed in HUT78 cells exposed to Ac-DEVD-CHO and VP-16 (Figure 7). The

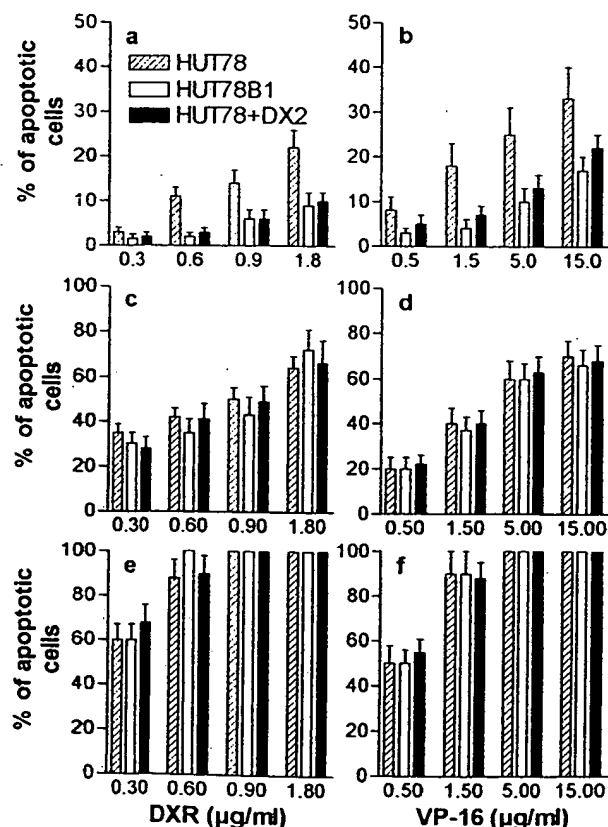


**Figure 5** Comparison between the percentages of apoptosis, evaluated by morphological analysis, induced by DXR or VP-16 in HUT78, HUT78B1, or HUT78 cells exposed to the blocking anti-CD95 Ab DX2; (a) after 24 h of exposure to DXR; (b) after 24 h of exposure to VP-16; (c) after 48 h of exposure to DXR; (d) after 48 h exposure to VP-16; (e) after 72 h of exposure to DXR; (f) after 72 h exposure to VP-16. Data are the mean  $\pm$  S.D. of five independent experiments. Flow cytometry analysis of apoptosis gave very similar results

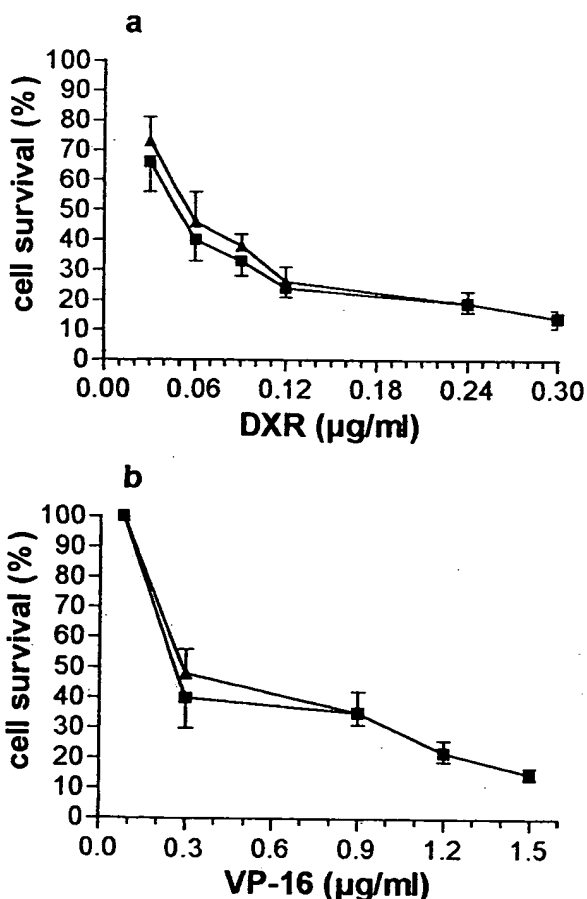


**Figure 6** Cytotoxicity of DXR and VP-16 in HUT78 (■) or HUT78B1 (▲) cells after 72 h of exposure to the agents. Cytotoxicity was evaluated by the trypan blue dye exclusion test. Data are the mean  $\pm$  S.D. of five independent experiments



Caspase inhibitor Z-VAD.FMK (benzyloxycarbonyl-Val-Ala-Asp (OMe) fluoromethylketone) (Slee *et al*, 1996) markedly inhibited DXR-induced apoptosis at 24 hours but not at 48 h and failed to inhibit apoptosis at 48 h when VP-16 was used at 5  $\mu$ g/ml (Figure 7). Z-VAD.FMK was however able to block CH-11-induced apoptosis both at 24 and 48 h (95%, data not shown).

**Table 1** Cytotoxicity of anticancer drugs in HUT78 and HUT78B1 after 72 h of exposure

Drugs	HUT78	HUT78B1	RI*
	IC <sub>50</sub> (ng/ml)	IC <sub>50</sub> (ng/ml)	
DXR	48.0	57.0	1.2
VCR	5.3	9.2	1.7
VP-16	270.0	290.0	1.1
Camptothecin	4.9	5.6	1.1
Methotrexate	27.3	25.0	0.9
5-fluorouracil	650.5	260.2	0.4

RI: Resistance Index

## Discussion

To examine the role of the CD95/CD95L system in the drug sensitivity/resistance of tumor cells, we studied the effects of DXR and VP-16, as well as of other agents, on the T cell lymphoma line HUT78 and on the CD95-resistant derived clone HUT78B1. HUT78 cells express CD95 and undergo apoptosis when treated with CH-11 agonistic antibody; moreover, apoptosis can be blocked by the addition of the DX2 antibody at 24 h (Figure 1) and to a similar extent at 48 and 72 h (data not shown). HUT78B1 cells express both a wild-type and a truncated receptor lacking the intracellular death domain and are completely resistant to the CH-11 antibody. Furthermore, we studied the expression of p53 in HUT78 and B1 clone, employing a monoclonal antibody specific for a sequence at the NH<sub>2</sub>-terminus of the protein (aa 18–30). Wild-type p53 protein in both cell lines even upon treatment with DXR and VP-16 was not detectable by Western blot analysis. DXR and VP-16 induce apoptosis in HUT78 and HUT78B1 cells in a dose- and time-dependent manner. The DX2 antibody was able to interfere with DXR-

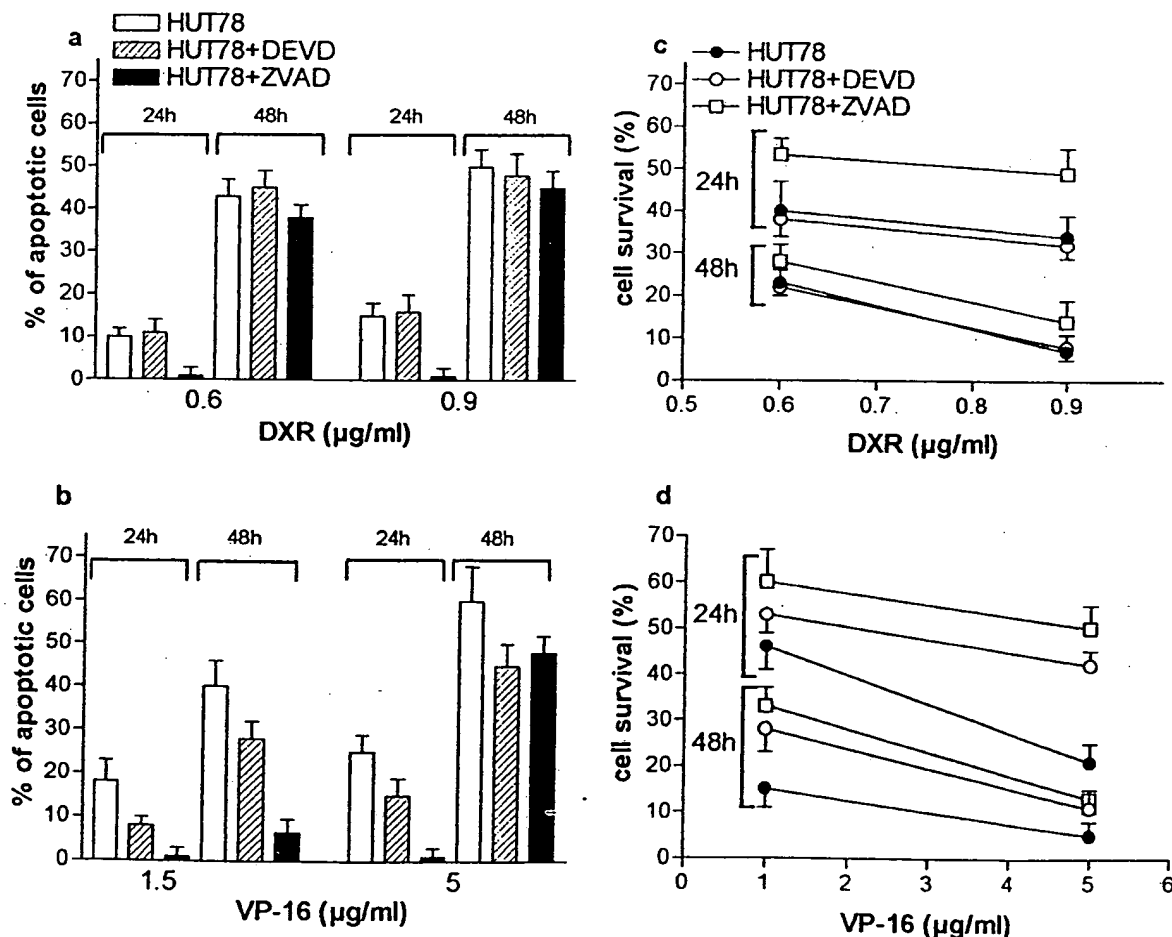


**Figure 7** Effect of the Caspase inhibitors Ac-DEVD-CHO and Z-VAD.FMK on DXR- and VP16-induced apoptosis and cytotoxicity in HUT78 cells. Cells were exposed to 200  $\mu$ M of Ac-DEVD-CHO or 50  $\mu$ M of Z-VAD.FMK and after 90 min DXR or VP16 were added. (a) DXR induced apoptosis in HUT78 cells in the presence or absence of Ac-DEVD-CHO or Z-VAD.FMK; evaluation after 24 and 48 h; (b) VP16 induced apoptosis in HUT78 cells in the presence or absence of caspase inhibitors; evaluation after 24 and 48 h. (c) DXR induced cytotoxicity in HUT78 cells in the presence or absence of caspase inhibitors; evaluation after 24 and 48 h; (d) VP16 induced cytotoxicity in HUT78 cells in presence or absence of caspase inhibitors; evaluation after 24 and 48 h

and VP16-induced apoptosis in HUT78 cells only at 24 h, while it did not influence the percentage of apoptotic cells at 48 or 72 h of treatment. In other words, the addition of the CD95-blocking monoclonal antibody caused only a modest slow down of the apoptotic effects of DXR and VP-16 in HUT78. However, this was not due to the lack of CD95L, in fact a clear increase in CD95L expression shortly after the application of DXR or VP-16 was observed in HUT78 cells as assessed by cytofluorimetric and Western blot analyses (Figure 4). These results suggest that the CD95/CD95L system might play some role only in the early stages of drug treatment while it does not appear to be involved in the apoptosis observed after longer periods (48 or 72 h) of exposure to DXR and VP-16. This conclusion is further supported by the experiments with the HUT78B1 clone. In fact, while a lower percentage of apoptotic cells was observed at 24 h of treatment with DXR or VP-16 in HUT78B1 cells in comparison with the parental cell line, this difference was no longer evident at 48 or 72 h of treatment.

Moreover, the CD95/CD95L system did not influence the cytotoxic effects of other antineoplastic drugs, such as camptothecin, vincristine, 5-fluorouracil and methotrexate in this experimental system.

Remarkably the two cell lines do not express p53, thus this protein is not involved in the apoptotic process. It is tempting to speculate that new p53 independent mechanisms are responsible for the drug-induced apoptosis in this model system.

The drugs might act at a different step of the apoptotic process, such as at the level of the activation of the Caspase cascade. Interestingly, Ibrado *et al.* have shown that Ara-C, mitoxantrone and VP-16 induce activation of Caspase 3, which results in the cleavage of poly-(ADP-ribose) polymerase (PARP) and apoptosis (Ibrado *et al.*, 1996). However, the precise mechanism by which these drugs cause activation of Caspase-3 is still not clear. In order to understand the role of Caspase-3 in drug-induced apoptosis and cytotoxicity in our model system we treated HUT78 cells with DXR and VP-16 in the presence of the specific Caspase-3-like inhibitor Ac-DEVD-CHO. Although Ac-DEVD-CHO treatment almost completely blocked CH-11-induced apoptosis, non univocal results were observed with the antineoplastic drugs. In fact, whereas DXR-induced apoptosis was not affected, Ac-DEVD-CHO induced a partial inhibition of apoptosis and cytotoxicity induced by VP-16. These results are in agreement with recent reports indicating that the activation of Caspase-3 or other ICE-like cysteine proteases may not be a rate-limiting step in the chemotherapy-induced apoptotic process. In fact, cells transfected by CrmA, a cowpox protein which inhibits the apoptotic proteases, became resistant to CD95-mediated apoptosis but remained sensitive to the apoptotic effects of chemotherapy (Decaudin *et al.*, 1997). However, we observed that Z-VAD.FMK, a Caspase inhibitor acting upstream to Caspase-3 activation, was able to markedly inhibit DXR and VP-16 induced apoptosis. This inhibition was evident only in the first 24 h of treatment but not after 48 h. When a moderately cytotoxic concentration of etoposide was used, the apoptotic inhibitory activity of Z-VAD.FMK was evident also at 48 h (data not shown). Z-

VAD.FMK was able to block completely CH-11-induced apoptosis at 24 and 48 h. The complete inhibition of DXR-induced apoptosis by Z-VAD.FMK but not by Ac-DEVD-CHO observed after 24 h support the hypothesis that Caspases different from Caspase-3 may be involved in the early phases of DXR-induced apoptosis in this experimental model.

In conclusion, we think that the mechanisms underlying drug-induced apoptosis may involve several different molecular determinants which can be different depending on the experimental cellular model and the drug employed. Further studies may lead to the identification of new molecular targets for chemotherapeutic drugs.

## Materials and Methods

### Cell culture

HUT78 and HUT78B1 cells were grown in RPMI 1640 (Gibco Grand Island, NY, USA) containing 10% FCS (Gibco) supplemented with 100 U/ml penicillin (Gibco), 100 mg/ml streptomycin (Gibco), and 2 mM L-glutamine (Sigma Chemical Co, St Louis, MO, USA) in a 5% CO<sub>2</sub> atmosphere at 37°C. Monkey COS-7 cells (American Type Culture Collection, Rockville, MD; CRL 1651) murine fibroblast, 293T cells (kindly provided by Dr. R. Beyaert, Laboratory for Molecular Biology, University of Gent, Belgium) were grown in DMEM containing 10% FCS. NIH3T3 transfected cells (kindly provided by Dr. N. Crispe, Yale University School of Medicine, New Haven, USA) were grown in presence of 0.5 mg/ml of G418-supplemented medium.

### Chemicals and antibodies

DXR, VP-16, camptothecin, vincristine, methotrexate and 5-fluorouracil were from Sigma Chemical Co. The Caspase inhibitors Ac-DEVD-CHO and Z-VAD.FMK were purchased from Alexis Biochemicals (Laufellingen, Switzerland). The following antibodies were used: the CD95 monoclonal antibody, DX2, kindly provided by Dr. R. Testi (Department of Experimental Medicine and Biochemical Sciences, Tor Vergata University, Rome, Italy); the CD95-agonistic antibody, CH-11, Upstate Biotechnology (Lake Placid, NY, USA); the CD95L antibodies: clone NOK-1, (Lot N. M021271) PharMingen (San Diego, CA, USA), clone G247-4 (Lot N. M021163) PharMingen and clone 33, (Lot N. 2) Transduction Laboratories (Lexington, KY, USA); the p53, clone DO1, and the Bcl2 monoclonal antibodies from Santa Cruz Biotechnology (Santa Cruz, CA, USA); the Fluorescein-linked or horseradish peroxidase (HPRP)-coupled sheep anti-mouse Ig from Amersham (Bucks, UK) and the Alkaline Phosphatase (AP)-linked anti-mouse IgG from Promega Corporation (Madison, USA).

### Transient transfection

A cDNA coding for a full length CD95L receptor was obtained by RT-PCR using the synthetic oligonucleotides: GR142 GGGGGTACCATGCAATTA and GR115 GGC GGATCCTTAGAGCTTATATAAGCCGAAA and then cloned into the *KpnI* and *BamHI* sites of the pcDNA3 eukaryotic expression vector (Invitrogen Corp., San Diego, CA). The integrity of the insert was confirmed by sequencing analysis. COS-7 or 293T cells respectively by the DEAE-dextran and the Calcium-phosphate methods were transfected with pcDNA3 or with pcDNA3CD95L plasmids. After 48 h, the transfected cells were analyzed by Flow cytometry and immunoblotting.

## Cytotoxicity assays

To evaluate the number of live and dead cells, the cells were treated with trypan blue and counted on a hemocytometer. Cells which showed trypan blue uptake were interpreted as non viable. To determine the growth inhibitory activity of the drugs tested,  $2 \times 10^5$  cells were plated into 25 mm wells (Costar, Cambridge, UK) in 1 ml of complete medium and treated with different concentrations of each drug. After 72 h of incubation, the number of viable cells was determined and expressed as percent of the number of viable control cells. Resistance index (R.I.) for each drug was calculated from the ratio: IC50 in HUT78B1/IC50 in HUT78.

## Flow cytometry analysis

The cells were washed once in ice-cold PBS and resuspended at  $1 \times 10^6$ /ml in a hypotonic fluorochrome solution containing propidium iodide (Sigma) 50  $\mu$ g/ml in 0.1% sodium citrate plus 0.03% (v/v) Nonidet P-40 (Sigma). After 30 min of incubation in this solution, the samples were filtered through nylon cloth, 40 mm mesh, and their fluorescence was analyzed as single-parameter frequency histograms using a FACScan flow cytometer (Becton Dickinson, San Jose, CA, USA). Apoptosis was determined by evaluating the percentage of hypoploid nuclei accumulated in the sub-G<sub>0</sub>-G<sub>1</sub> peak after labeling with propidium iodide (Darziynkiewicz *et al*, 1992). For CD95L expression analysis cells were incubated at 4°C for 30 min with the NOK-1 (5  $\mu$ g/ml) or an isotype matched control antibody, washed and treated with FITC-conjugated sheep anti-mouse Ig. Relative fluorescent intensities of individual cells were analyzed using a FACS Calibur flow cytometer (Becton Dickinson).

## Morphological evaluation of apoptosis

The morphological effects of the drugs were studied by fluorescent microscopy after labeling with acridine orange and ethidium bromide (Duke and Cohen, 1992). Cells ( $2 \times 10^5$ ) were centrifuged (300 g) and the pellet was resuspended in 25  $\mu$ l of the dye mixture. Thereafter 10  $\mu$ l of the cell suspension was placed on a microscope slide, covered with a 22 mm<sup>2</sup> coverslip and examined in oil immersion with a 100 $\times$  objective using a fluorescent microscope. Live cells were identified by the uptake of acridine orange (green fluorescence) and exclusion of ethidium bromide (red fluorescence) stain. Live and dead apoptotic cells were identified by perinuclear condensation of chromatin stained by acridine orange or ethidium bromide, respectively, and by the formation of apoptotic bodies.

## Western blotting analysis of p53 and bcl-2

Cells were lysed for 30 min at 4°C with a solution (15  $\mu$ l/10<sup>6</sup> cells) consisting of 1% NP-40, 0.5% sodium deoxycolate, 0.1% SDS in phosphate buffer saline, pH 7.4, containing inhibitors of proteases (25  $\mu$ g/ml aprotinin, 1 mM phenylmethylsulfonyl fluoride (PMSF), 10 mM sodium orthovanadate, 10 mM NaF, 25  $\mu$ g/ml leupeptin, 0.2 mM sodium pyrophosphate) and sonicated three times for 10 s. Equivalent amounts of protein (40  $\mu$ g) of the supernatants, obtained after centrifugation at 15000 g for 20 min at 4°C, were resolved in SDS-polyacrylamide gel electrophoresis (10% acrylamide). After electroblotting on nitrocellulose filters, proteins were immunoreacted for 2 h with p53 monoclonal antibody, DO1, (dilution 1:1000), or bcl-2 monoclonal antibody (dilution 1:500) followed by a 30-min incubation with anti-mouse IgG AP-linked antibody. Visualization was performed using nitroblue tetrazolium and bromochloro-indoyl-phosphate.

## Western blotting analysis of CD95L

Cells were lysed in 50 mM Tris pH 7.6, 150 mM NaCl, 0.5% NP-40, 2  $\mu$ g/ml aprotinin, 2  $\mu$ g/ml leupeptin, 1 mM PMSF and an equal amount of proteins (30  $\mu$ g) for each sample was loaded on a 12% SDS-PAGE under reducing conditions and transferred to nitrocellulose. CD95L was detected with the CD95L antibodies clone 33 (0.3  $\mu$ g/ml) or clone G247-4 (2  $\mu$ g/ml) using HRPO-coupled sheep anti-mouse Ig and the enhanced chemoluminescence (ECL) system (Amersham).

## Acknowledgements

This work was supported by CNR (Applied Project ACRO) and MURST. ND and GR were supported by grants from Associazione Italiana per la ricerca sul cancro (AIRC). GP was supported by a fellowship from the Fondazione Italiana Ricerca sul Cancro. The authors thank Dr R Testi for the DX2 antibody, Dr R Beyaert for the 293T cells, Dr N Crispe for the NIH3T3 transfectants and Dr R Butler for critical reading of the manuscript. The technical help of E Lancia and I Pauselli is gratefully acknowledged.

## References

- Alnemri ES, Livingston DJ, Nicholson DW, Salvesen G, Thornberry NA, Wong WW and Yuan J (1996) Human ICE/CED-3 protease nomenclature. *Cell* 87: 171
- Boldin MP, Varfolomeev EE, Pancer Z, Mett IL, Camonis JH and Wallach DJ (1995) A novel protein that interacts with death domain of Fas/APO-1 contains a sequence motif related to death domain. *Biol Chem* 270: 7795–7798
- Boldin MP, Goncharov TM, Goltsev YV and Wallach D (1996) Involvement of Mach, a novel MORT1/FADD-interacting protease, in Fas/APO-1- and TNF receptor-induced cell death. *Cell* 85: 803–815
- Bose R, Vermeij M, Haimovitz-Friedman A, Scotto K, Funks Z and Kolesnick R (1995) Ceramide synthase mediates daunorubicin-induced apoptosis: An alternative mechanism for generating death signal. *Cell* 82: 405–414
- Cascino I, Papoff G, De Maria R, Testi R and Ruberti G (1996) Fas/Apo-1 (CD95) receptor lacking the intracytoplasmic signaling domain protects tumor cells from Fas-mediated apoptosis. *J Immunol* 156: 13–17
- Chinnaiyan AM, O'Rourke K, Tewari M and Dixit VM (1995) FADD, a novel death domain-containing protein, interacts with the death domain of Fas and initiates apoptosis. *Cell* 81: 505–512
- Collins RJ, Harmon BV, Souvils T, Pope JH and Kerr JFR (1991) Effects of cycloheximide on B-chronic lymphocytic leukaemic and normal lymphocytes in vitro: induction of apoptosis. *Br J Cancer* 64: 518–522
- Darziynkiewicz Z, Bruno S, Del Bino G, Gorczyca W, Holz MA, Lassota P and Traganos F (1992) Features of apoptotic cells measured by flow cytometry. *Cytometry* 13: 795–798
- Decaudin D, Geley S, Hirsch T, Castedo M, Marchetti P, Macho A, Kofler R and Kroemer G (1997) Bcl-2 and Bcl-xL antagonize the mitochondrial dysfunction preceding nuclear apoptosis induced by chemotherapeutic agents. *Cancer Res* 57: 62–67
- Del Bufalo D, Biroccio A, Soddu S, Laudonio N, D'Angelo C, Sacchi A and Zupi G (1996) Lonidamine induces apoptosis in drug-resistant cells independently of the p53 gene. *J Clin Invest* 98: 1165–1173
- Duke RC and Cohen JJ (1992) Morphological and biochemical assays of apoptosis. In: *Current Protocols in Immunology*, Coligan JE, Kruisbeek AM, (eds) John Wiley & Sons: New York pp. 3.17.1
- Fan S, Smith M.L, Rivet DJ, Duba D, Zhan Q, Kohn KW, Fornace AJ Jr and O'Connor PM (1995) Disruption of p53 function sensitizes breast cancer MCF-7 cells to cisplatin and pentoxifyline. *Cancer Res* 55: 1649–1654
- Fisher DE (1994) Apoptosis in cancer therapy: crossing the threshold. *Cell* 78: 539–542
- Friesen C, Herr I, Krammer PH and Debatin K-M (1996) Involvement of the CD95 (APO-1/Fas) receptor/ligand system in drug-induced apoptosis in leukemia cells. *Nature Med* 5: 574–577

- Hahne M, Rimoldi D, Schroter M, Romero P, Schreier M, French LE, Schneider P, Bornand T, Fontana A, Lienard D, Cerottini J-C and Tschopp J (1996) Melanoma cell expression of Fas (Apo-1/CD95) ligand: implication in tumor immune escape. *Science* 274: 1363–1366
- Hannun JA (1996) Functions of Ceramide in coordinating cellular responses to stress. *Science* 274: 1855–1859
- Hughes DPM and Crispe IN (1995) A naturally occurring soluble isoform of murine Fas generated by alternative splicing. *J Exp Med* 182: 1395–1401
- Ibrado AM, Huang Y, Fang G, Liu L and Bhalla KM (1996) Overexpression of Bcl-2 or Bcl-xL inhibits Ara-C-induced CPP32/Yama protease activity and apoptosis of human acute myelogenous leukemia HL-60 cells. *Cancer Res* 56: 4743–4748
- Jung M, Notario V and Dritschilo A (1992) Mutation in the p53 gene in radiation-sensitive and -resistant human squamous carcinoma cells. *Cancer Res* 52: 6390–6393
- Kerr JFR, Wyllie AH and Currie AR (1972) Apoptosis: a basic biological phenomenon with wide-ranging implications in tissue kinetics. *Br J Cancer* 26: 239–257
- Kinzler KW and Vogelstein B (1994) Clinical implications of basic research: cancer therapy meets p53. *New Eng J Med* 331: 49–50
- Kischkel FC, Hellbardt S, Behrmann I, Germer M, Pawlita M, Krammer PH and Peter ME (1995) Cytotoxicity-dependent APO-1 (FAS/CD95) associated protein form a death-inducing signaling complex (DISC) with the receptor. *EMBO J* 14: 5579–5588
- Krammer PH, Dhein Y, Valczak H, Behrmann I, Mariani S, Matiba B, Fath M, Daniel PT, Knipping E, Westendorp MO, Stricker K, Baumler C, Hellbardt S, Germer M, Peter ME and Debatin K-M (1994) The role of APO-1-mediated apoptosis in the immune system. *Immunol Rev* 142: 175–191
- Kumar S and Lavin MF (1996) The ICE family of cysteine proteases as effectors of cell death. *Cell Death Differ* 3: 255–267
- Lennon SV, Martin SJ and Cotter TG (1991) Dose-dependent induction of apoptosis in human tumor cell lines by widely diverging stimuli. *Cell Prolif* 24: 203–214
- Lowe SW, Schmitt EM, Smith SW, Osborne BA and Jacks T (1993a) p53 is required for radiation-induced apoptosis in mouse thymocytes. *Nature* 362: 847–849
- Lowe SW, Ruley HE, Jacks T, and Housman DE (1993b) p53-dependent apoptosis modulates the cytotoxicity of anticancer agents. *Cell* 74: 957–967
- Martin SJ and Green DR (1995a) Apoptosis and cancer: the failure of controls on cell death and cell survival. *Critical Reviews in Oncology/Hematology* 18: 137–153
- Martin SJ and Green DR (1995b) Protease activation during apoptosis: death by a thousand units? *Cell* 82: 349–352
- Muzio M, Chinnaiyan AM, Kischkel FC, O'Rourke K, Shevchenko A, Ni J, Scaffidi C, Bretz JD, Zhang M, Gentz R, Mann M, Krammer PH, Peter ME and Dixit VM (1996) FLICE, a novel FADD-homologous ICE-CED-3-like protease is recruited to the CD95 (Fas-APO1) death-inducing signaling complex. *Cell* 85: 817–827
- Nagata S (1997) Apoptosis by death factor. *Cell* 88: 355–365
- Nagata S and Golstein P (1995) The Fas death factor. *Science* 267: 1449–1455
- Niehans GA, Brunner T, Frizelle SP, Liston JC, Salerno CT, Knapp DJ, Green DR and Kratzke RA (1997) Human lung carcinomas express Fas ligand. *Cancer Res* 57: 1007–1012
- O'Connell J, O'Sullivan GC, Collins JK and Shanahan F (1996) The Fas counterattack: Fas-mediated T cell killing by colon cancer cells expressing Fas Ligand. *J Exp Med* 184: 1075–1082
- Saas P, Walker P R, Hahne M, Quiquerez AL, Schnuriger V, Perrin G, French L, Van Meir EG, deTribolet N, Tschopp J and Dietrich PY (1997) Fas Ligand expression by astrocytoma in vivo: Maintaining Immune privilege in the brain. *J Clin Invest* 99: 1173–1178
- Skowronski EW, Kolesnick RN and Green DR (1996) Fas-mediated apoptosis and sphingomyelinase signal transduction: the role of ceramide as a second messenger for apoptosis. *Cell Death Differ* 3: 171–176
- Slee EA, Zhu H, Chow SC, MacFarlane M, Nicholson DW and Cohen GM (1996) Benzoyloxycarbonyl-Val-Ala-Asp (Ome) fluoromethylketone (Z-VAD.FMK) inhibits apoptosis by blocking the processing of CPP32. *Biochem J* 315: 21–24
- Strand S, Hofman WJ, Hug H, Muller M, Otto G, Strand D, Mariani SM, Stremmel W, Krammer PH and Galle PR (1996) Lymphocyte apoptosis induced by CD95 (Apo1-/Fas) ligand-expressing tumor cells – a mechanism of immune evasion? *Nature Medicine* 2: 1361–1366
- Testi R (1996) Sphingomyelin breakdown and cell fate. *TIBS* 21: 468–471
- Walker PR, Smith C, Youdale T, Leblanc J, Whitfield LF and Sikorska M (1991) Topoisomerase II-reactive drugs induce apoptosis in thymocytes. *Cancer Res* 51: 1078–1098
- Williams GT (1991) Programmed cell death: apoptosis and oncogenesis. *Cell* 65: 1097–1098
- Williams GT and Smith CA (1993) Molecular regulation of apoptosis: genetic controls on cell death. *Cell* 74: 777–779
- Xu C, Meikrantz W, Schlegel R and Sager R (1995) The human papilloma virus 16 E6 gene sensitizes human mammary epithelial cells to apoptosis induced by DNA damage. *Proc Natl Acad Sci* 92: 7829–7833

# Chemotherapeutic drug-induced apoptosis in human leukaemic cells is independent of the Fas (APO-1/CD95) receptor/ligand system

ANNE J. MCGAHON, ANA P. COSTA PEREIRA, LISA DALY AND THOMAS G. COTTER  
 Tumour Biology Laboratory, Department of Biochemistry, University College, Cork, Ireland

Received 15 October 1997; accepted for publication 13 March 1998

**Summary.** The potential role of the Fas (CD95/APO-1) receptor/ligand system in chemotherapeutic drug-induced apoptosis was examined in a number of human leukaemic cell lines. Flow cytometric profiles of doxorubicin-treated HL-60, K562, U937 and Jurkat cells failed to show any significant increase in Fas or Fas ligand expression over 24 h, despite the induction of significant levels of apoptosis in these cells. Although preincubation of human leukaemic cells with a neutralizing anti-Fas IgG antibody blocked anti-Fas IgM-induced apoptosis, this strategy failed to inhibit chemotherapeutic drug-induced apoptosis. To determine whether recruitment of the Fas/Fas ligand complex during drug-induced apoptosis was a cell-specific event we utilized the CEM cell line. Doxorubicin treatment of CEM cells over 24 h failed to show any up-regulation in Fas or Fas ligand protein levels as detected by flow cytometry. Furthermore,

neutralizing anti-Fas IgG Ab failed to inhibit chemotherapeutic drug-induced apoptosis in CEM cells. The present studies do, however, demonstrate a role for anti-Fas IgM Ab in producing a cytotoxic synergistic effect when used in combination with chemotherapeutic drugs. Low-dose anti-Fas IgM treatment in combination with doxorubicin, methotrexate, camptothecin and etoposide produced an augmented cytotoxicity in CEM cells. Taken together these observations demonstrate that although recruitment of the Fas/APO-1/CD95 receptor/ligand system is not a necessary requirement for chemotherapeutic drug-induced apoptosis, combination of anti-Fas IgM and drug treatment produces a synergistic cytotoxic effect which may prove useful in the treatment of human leukaemias.

**Keywords:** apoptosis, leukaemia, Fas, cytotoxic.

Apoptosis is an active form of cell death which occurs largely under physiological conditions (Kerr *et al*, 1972; Wyllie *et al*, 1980). It is characterized morphologically by such cellular features as membrane blebbing, cell shrinkage and chromatin condensation (Cohen *et al*, 1992). Biochemical events include various types of DNA fragmentation (Bortner *et al*, 1995), cytoskeletal alterations and protease activation (reviewed in Martin & Green, 1995; Zhivotovsky *et al*, 1996). The observation that cytotoxic chemotherapeutic drugs kill their target cells by apoptosis has provided a valuable insight into the treatment of human leukaemias (Hannun, 1997). Chemotherapeutic drugs which have been identified as apoptosis-inducing agents include etoposide, doxorubicin, methotrexate, camptothecin and vincristine (Hannun, 1997). The mechanism by which these

chemotherapeutic drugs induce apoptosis remains to be fully elucidated. Several studies have identified the activation of caspase 3 as a common signalling event in apoptosis induced by chemotherapeutic drugs and other agents (Kaufmann *et al*, 1993; Lazebnik *et al*, 1994). Studies on the interactions of chemotherapeutics with modulators of apoptosis have provided further insight into the mechanism by which these drugs induce apoptosis. Modulators of apoptosis that have been shown to interact with chemotherapy-induced death include *p53* (Fan *et al*, 1995; Eliopoulos *et al*, 1995), *bcl-2* (Miyashita & Reed, 1993; Kamesaki *et al*, 1993), *bcr-abl* (McGahon *et al*, 1994; Bedi *et al*, 1995) and *ras* (Nooter *et al*, 1995). The recent evidence suggests a role for Fas/CD95/APO-1 receptor/ligand system in drug-induced apoptosis (Friesen *et al*, 1996; Mitzutani *et al*, 1997; Nakamura *et al*, 1997).

In the present study we sought to determine if recruitment of the Fas receptor/ligand system is a common mechanism involved in apoptosis induced by chemotherapeutic drugs. To

Correspondence: Professor Thomas G. Cotter, Department of Biochemistry, University College, Lee Maltings, Prospect Row, Cork, Ireland.

determine the role (if any) of the Fas/Fas ligand system in chemotherapeutic drug-induced apoptosis we adopted a number of approaches. Flow cytometric analysis of a variety of human leukaemic cell lines treated with chemotherapeutic drugs failed to show any up-regulation of Fas or Fas ligand in these cells. Although preincubation with an anti-Fas IgG antibody prevented anti-Fas IgM-induced apoptosis in the leukaemic cell lines studied, this strategy failed to prevent chemotherapeutic drug-induced apoptosis. Incubation of CEM cells with anti-Fas IgM antibody and chemotherapeutic drugs did, however, augment the apoptotic response in these cells. Taken together, our observations demonstrate that chemotherapeutic drug-induced apoptosis in human leukaemic cells is independent of Fas/Fas ligand activation. Our results do, however, demonstrate a synergy between chemotherapeutic drugs and anti-Fas IgM Ab which may have useful consequences in the treatment of human leukaemias.

## MATERIALS AND METHODS

**Cell culture and reagents.** The human cell lines K562, HL-60, Jurkat, U937 and CEM were grown in RPMI 1640 (GIBCO, U.K.) supplemented with 10% FCS (GIBCO, U.K.) and 2 mM L-glutamine (GIBCO, U.K.). Cells were grown at 37°C in a humidified CO<sub>2</sub> atmosphere and were routinely subcultured every 2–3 d. All cytotoxic drugs used in this study were purchased from Sigma, U.K. Stock solutions of actinomycin D, camptothecin and etoposide were prepared in DMSO (Sigma, U.K.). Stock solutions of doxorubicin and methotrexate were freshly prepared in sterile ddH<sub>2</sub>O and 0.01 M NaOH, respectively, before each experiment to ensure reproducibility of results.

For the induction of apoptosis by cytotoxic drugs, cells ( $2.5 \times 10^5$ /ml) were seeded in 96-well plates and incubated in varying concentrations of drugs and cell death (%) was assessed at various time points. Similarly, for the induction of apoptosis by Fas ligation, cells ( $2.5 \times 10^5$ /ml) were seeded in 96-well plates and incubated for 6 h with 20 µl of anti-human Fas IgM mAb (Upstate Biotechnology) at a dilution of 1:50 (0.2 µg/ml final concentration) in RPMI 1640. For blocking Fas, cells were preincubated for 30 min with 2 µg/ml anti-Fas IgG, clone SM1/1 (Bender MedSystems, U.K.) and treated as described.

**Assessment of cell death and apoptosis.** Cell death was quantitated by morphological assessment of stained cytospun preparations and also by flow cytometry. Rapi-diff II (Paramount Reagents Ltd, U.K.) stained cytocentrifuged cell preparations were examined for the morphological characteristics of apoptosis using previously defined criteria (Wyllie *et al*, 1980; Gorman *et al*, 1996). Typical identifiable apoptotic features included membrane blebbing and chromatin condensation. Apoptosis was quantitated by scoring triplicate fields of cytospun samples with a minimum of 100 cells per field.

The criteria for cell death as measured by flow cytometry was based on the following parameters: changes in light scattering properties of dead cells due to cell shrinkage and increased granularity (Cotter *et al*, 1992; McGahon *et al*, 1994).

**Flow cytometry and detection of Fas/Fas ligand expression.** For the detection of Fas ligand expression,  $5 \times 10^5$  cells were harvested and fixed in PBS, 1% (w/v) *p*-formaldehyde for 30 min at room temperature. Cells were washed in PBS/0.1 M glycine to quench any remaining formaldehyde groups. Following a further wash in PBS, 0.1% (w/v) BSA, cells were permeabilized in PBS/0.1% (v/v) Triton X-100, for 5 min at room temperature. Cells were stained for 1 h on ice using 20 µl of a polyclonal anti-human IgG Fas ligand, N-20, (Santa Cruz Inc.) at a 1:50 dilution in PBS/1% BSA. Cells were subsequently washed twice with PBS/0.1% BSA and incubated for 30 min with 20 µl of a 1:100 dilution of FITC-conjugated goat anti-rabbit IgG (Sigma, U.K.). Following a further wash in PBS/0.1% BSA, then PBS, samples were read on a FACS flow cytometer equipped with CellQuest software.

For the detection of Fas protein levels, cells ( $5 \times 10^5$ ) were harvested, washed in PBS and incubated for 1 h in 20 µl of PBS/1% BSA containing a 1:50 dilution of anti-human Fas mAb (Upstate Biotechnology, U.S.A.). Following the series of washing steps as described above, cells were incubated for 30 min with 20 µl of a 1:100 dilution of FITC-conjugated goat anti-mouse IgM (Sigma, U.K.). Cells were subsequently washed and fluorescence measured on a FACScan flow cytometer as described above.

## RESULTS

### *Doxorubicin-induced apoptosis occurs independently of Fas/Fas ligand activation in human leukaemic cell lines*

To determine the role (if any) of the Fas/Fas ligand complex in chemotherapeutic drug-induced apoptosis in human leukaemic cells, we adopted a flow cytometric approach. Flow cytometric analysis of HL-60, a human promyelocytic leukaemic cell line, U937, a human monoblastoid line, and Jurkat, a T lymphoblastoid cell line, demonstrated that these cells were positive for both Fas and Fas ligand expression (not shown). K562, a cell line derived from a patient with CML, stained negative for Fas expression (not shown). These cells, however, did express Fas ligand.

We reasoned therefore that if Fas or Fas ligand is indeed involved in chemotherapeutic drug-induced apoptosis we should be able to detect an increase in either of these proteins levels following drug treatment of cells. Fig 1(A) shows a dose response of doxorubicin on the human leukaemic cell lines studied. The susceptibility to apoptosis following an overnight incubation in doxorubicin was measured using previously defined morphological criteria (Wyllie *et al*, 1980; Gorman *et al*, 1996). Each of the cell lines varied in its susceptibility to doxorubicin, reflecting different abilities to cope with toxic insult.

Monitoring of both Fas and Fas ligand levels in human leukaemic cells by flow cytometry at T4, T8 and T24 hours following doxorubicin treatment failed to show any significant change in either of the proteins levels, irrespective of the drug concentration used (Fig 1B). Similar results were obtained with the well-documented chemotherapeutic drugs: methotrexate, camptothecin, etoposide and actinomycin D (data not shown).

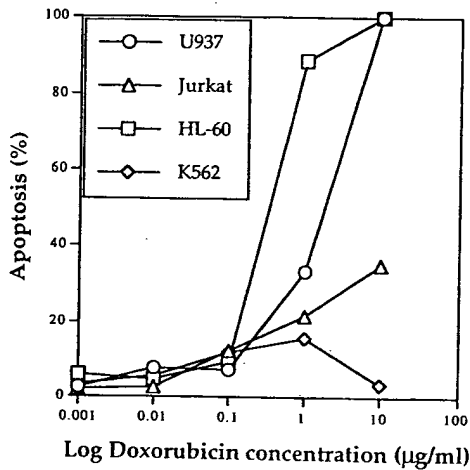
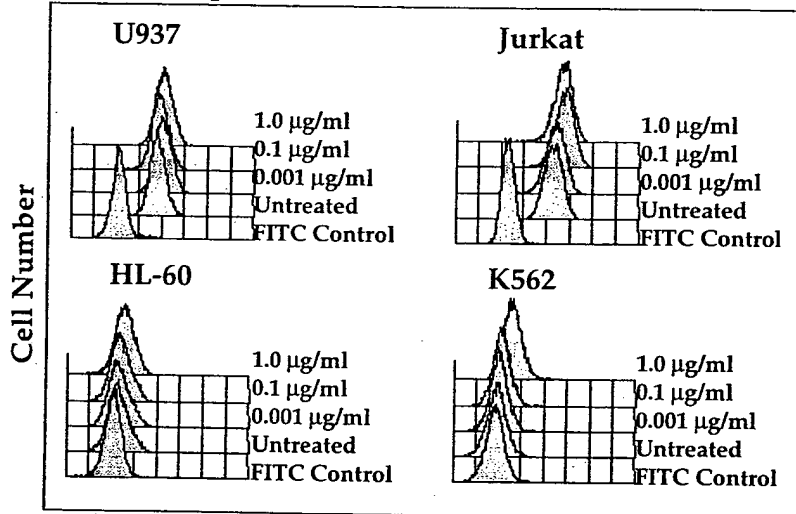


Fig 1(A). Dose-dependent susceptibility of human leukaemic cell lines to doxorubicin-induced apoptosis. Cells ( $2.5 \times 10^5$ /ml) were seeded in 96-well plates and incubated overnight (18 h) in varying concentrations of doxorubicin. Apoptosis was assessed by morphological criteria as described in Materials and Methods. Results are shown as mean apoptosis of triplicate fields of cytopun samples with a minimum of 100 cells per field  $\pm$  standard deviation.

### Fas expression in Dox-treated cells T8hrs



### Fas ligand expression in Dox-treated cells T8hrs

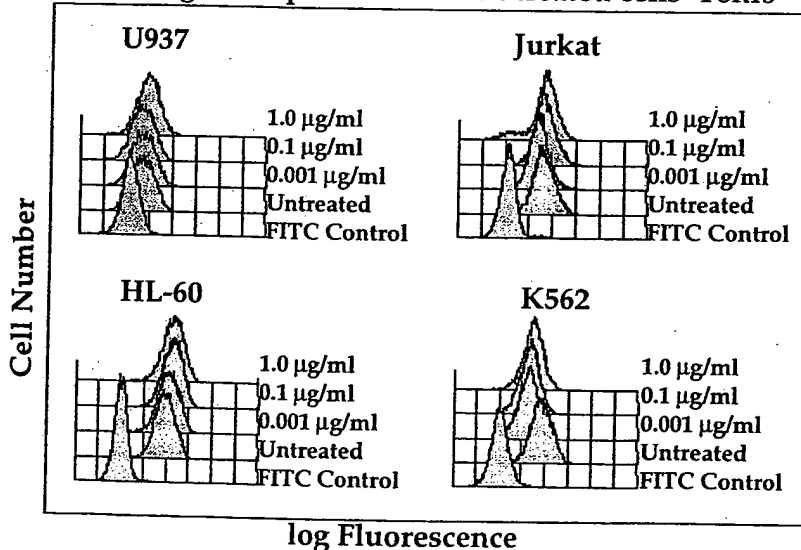


Fig 1(B). Flow cytometric profiles of Fas and Fas ligand levels in doxorubicin-treated human leukaemic cell lines. Cells ( $2.5 \times 10^5$ /ml) were seeded in 96-well plates and incubated overnight in varying concentrations of doxorubicin. Cells were subsequently stained for Fas and Fas ligand expression as described in Materials and Methods. Untreated cells were stained with an FITC-conjugated secondary antibody alone ('control'), or with both primary and secondary antibodies ('untreated'). Data are for the 8 h time point and are similar to those seen for the 4 and 24 h time point except for HL-60 cells, where extensive apoptosis had taken place.

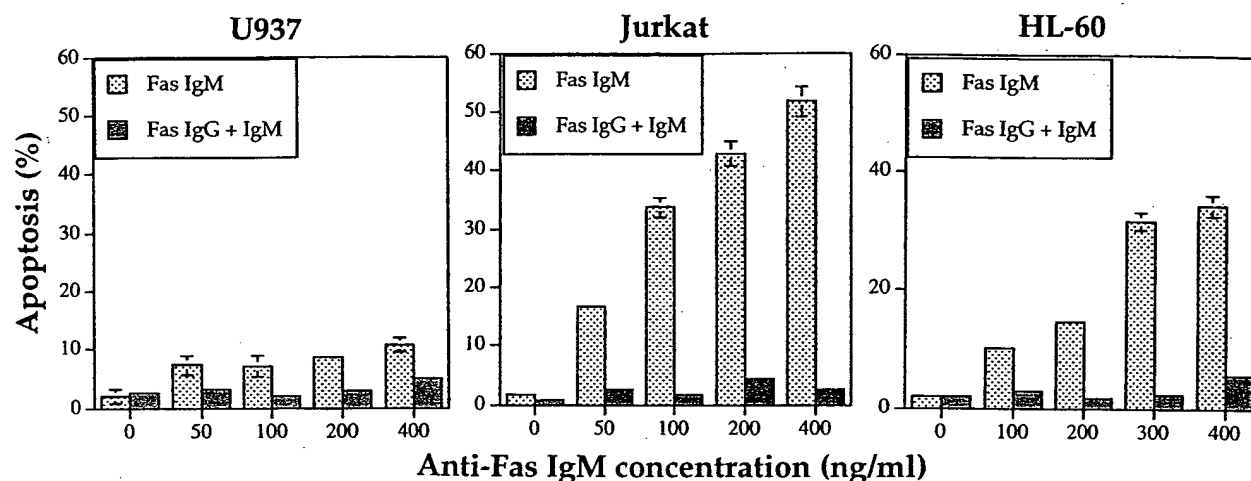


Fig 2. Inhibition of Fas-induced apoptosis in human leukaemic cell lines by anti-human Fas IgG Ab. The human leukaemic cell types indicated were preincubated with an anti-human Fas IgG antibody (1:50 dilution) for 30 min. U937, Jurkat and HL-60 cells were then subjected to a further 4, 6 and 24 h incubation respectively in the presence of anti-human Fas IgM mAb. Apoptosis was assessed by morphological criteria as described in Fig 1A.

#### *Inhibition of Fas-induced apoptosis in human leukaemic cell lines*

Several research groups have demonstrated the ability of a neutralizing anti-Fas IgG antibody to inhibit apoptosis induced by anti-Fas IgM Ab (Liles *et al*, 1996; Uslu *et al*, 1996). We reasoned, therefore, that if the Fas pathway was involved in chemotherapeutic drug-induced apoptosis, then effective blocking of this pathway using a neutralizing anti-Fas IgG Ab should inhibit the drug-induced death.

Fig 2 shows that preincubation of HL-60, U937 and Jurkat cells with neutralizing anti-Fas IgG mAb showed a significant inhibition of anti-Fas IgM-induced apoptosis in these cells.

#### *Chemotherapeutic drug-induced apoptosis in human leukaemic cells occurs independently of the Fas receptor/ligand complex*

Preincubation of the human leukaemic cell lines studied with neutralizing anti-Fas IgG Ab failed to inhibit their susceptibility to both Doxorubicin and Etoposide-induced apoptosis (Figs 3A and 3B), further negating a role for the Fas pathway in drug-induced death in these cells. Similar results were obtained for methotrexate, camptothecin, etoposide and actinomycin D (data not shown).

#### *Involvement of the Fas/Fas ligand complex is not a necessary requirement for doxorubicin-induced apoptosis in CEM cells*

To determine whether the involvement of the Fas receptor/ligand system during chemotherapeutic drug-induced apoptosis is cell type specific, we made use of the CEM cell line. This acute T-ALL cell line has been previously demonstrated to recruit the Fas/Fas ligand complex during drug-induced apoptosis (Friesen *et al*, 1996).

Flow cytometric monitoring of CEM cells over a 24 h period following doxorubicin treatment failed to show any significant change in Fas or Fas ligand protein levels (Fig 4), despite the use of therapeutic concentrations of this drug. Similar results were obtained for methotrexate,

camptothecin, etoposide and Actinomycin D (data not shown).

#### *Inhibition of Fas-induced apoptosis in CEM cells by anti-human Fas IgG antibody, and failure of this neutralizing Ab to inhibit chemotherapeutic drug-induced apoptosis*

The above observations led us to further question the role of the Fas receptor/complex system in chemotherapeutic drug-induced apoptosis in CEM cells. Using the same rationale as that described for the other human leukaemic cell lines studied, we sought to block drug-induced apoptosis in CEM cells with a neutralizing anti-Fas IgG Ab. Anti-Fas IgG antibody significantly inhibited anti-Fas IgM-induced apoptosis in CEM cells (Fig 5).

Preincubation of CEM cells with anti-Fas IgG Ab, however, did not inhibit apoptosis induced by a variety of chemotherapeutic agents (Fig 6). These observations are suggestive of a Fas-independent pathway operating in these cells upon chemotherapeutic drug treatment.

#### *Synergistic cytotoxic effect of anti-Fas IgM and chemotherapeutic drugs in CEM cells*

There have been a number of recent publications documenting a synergistic effect of anti-Fas IgM and cytotoxic drugs (Morimoto *et al*, 1993; Mitutani *et al*, 1997; Nakamura *et al*, 1997). In order to determine if such a synergistic effect was operating in CEM cells, we titrated a number of chemotherapeutic drugs  $\pm$  anti-Fas IgM in these cells. Low-dose anti-Fas IgM treatment in combination with a number of chemotherapeutic drugs resulted in an augmented cytotoxic activity which was strongly suggestive of synergy (Fig 7). The synergy obtained with anti-Fas IgM antibody and chemotherapeutic drugs was specific as anti-Fas IgG, or a number of other irrelevant antibodies resulted in no synergistic or additive effects (data not shown). Taken together, these observations demonstrate



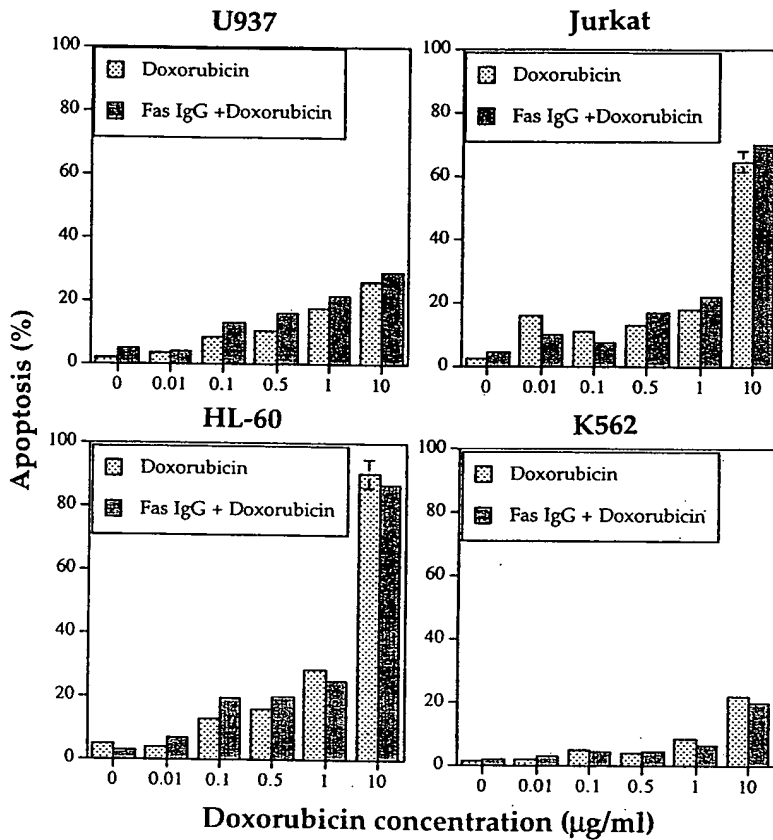


Fig 3(A). Preincubation of human leukaemic cell lines with neutralizing anti-Fas IgG antibody does not inhibit susceptibility to doxorubicin-induced apoptosis. The human leukaemic cell types indicated were preincubated with anti human Fas IgG antibody (1:50 dilution) for 30 min. The cells were then subjected to a further 18 h incubation in the presence of varying concentrations of doxorubicin. Apoptosis was assessed by morphological criteria as described previously. Results are shown as mean apoptosis of triplicate fields of cytopun samples with a minimum of 100 cells per field  $\pm$  standard deviation.

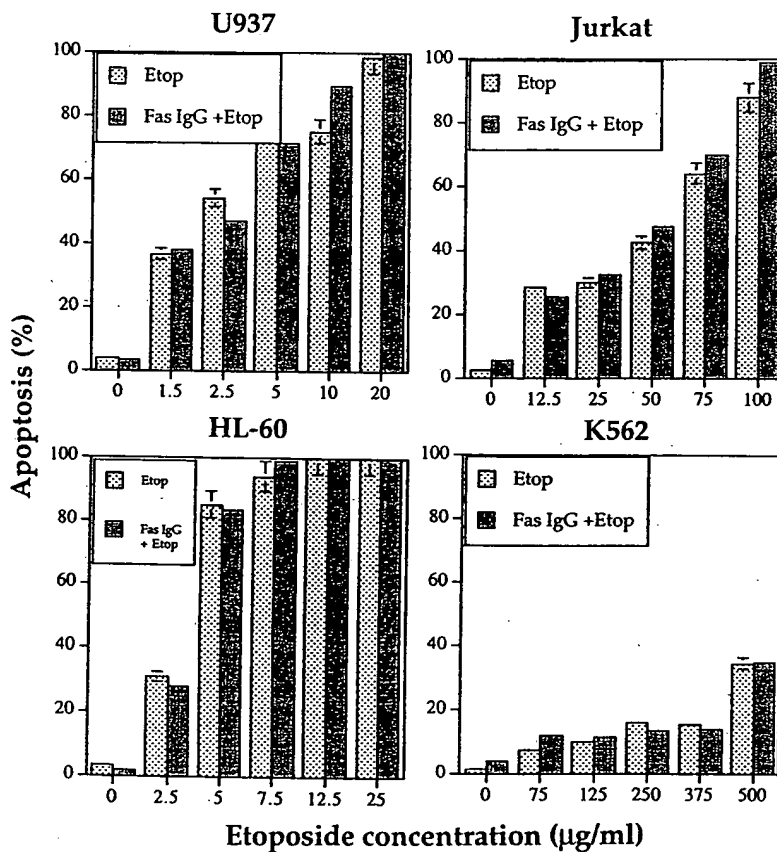


Fig 3(B). Preincubation of human leukaemic cell lines with neutralizing anti-Fas IgG antibody does not block etoposide-induced apoptosis. The human leukaemic cell types indicated were preincubated with anti-human Fas IgG Ab as in Fig 3(A), and subjected to a further 18 h incubation in the presence of varying concentrations of etoposide. Apoptosis was assessed as previously described.

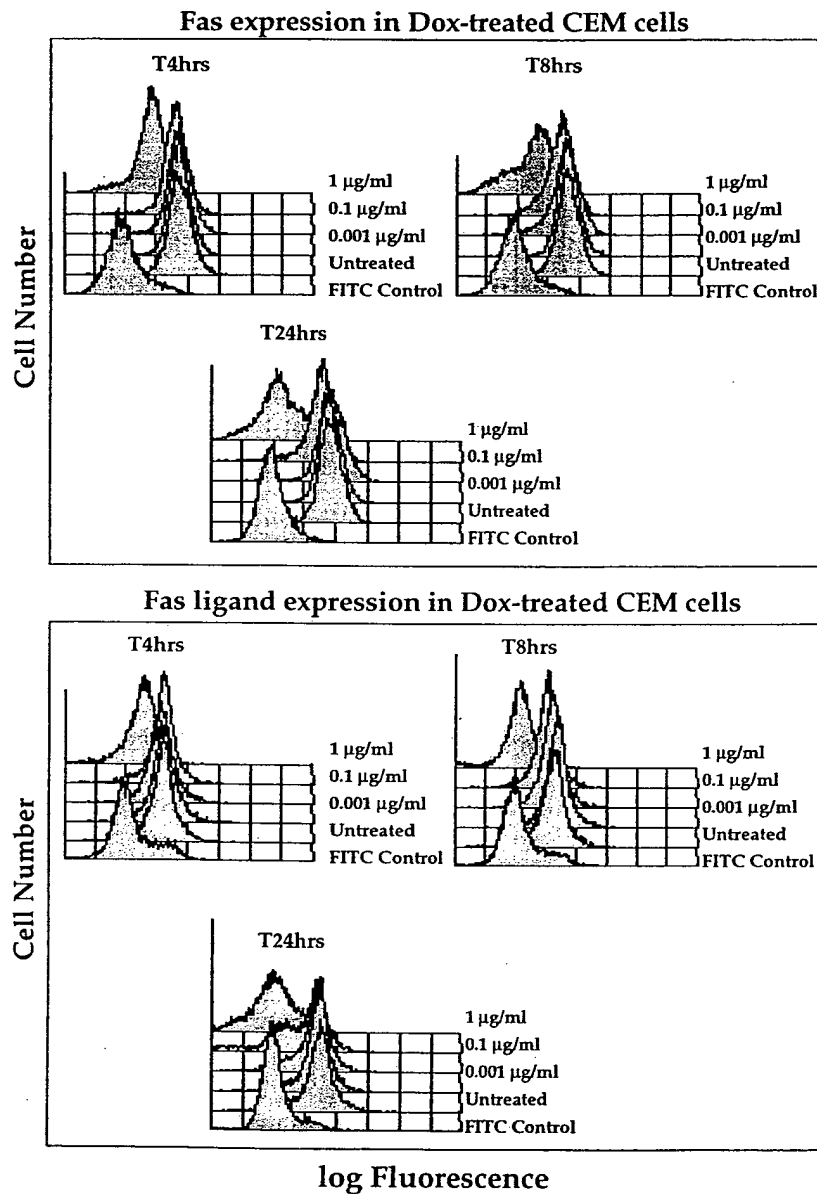


Fig 4. Flow cytometric profiles of Fas and Fas ligand levels in doxorubicin-treated CEM cells. Cells ( $2.5 \times 10^5/\text{ml}$ ) were seeded in 96 well plates and incubated for 24 h in varying concentrations of doxorubicin. Untreated CEM cells were stained with an FITC-conjugated secondary antibody alone ('control'), or with both primary and secondary antibodies ('untreated') and analysed by flow cytometry as described in Materials and Methods.

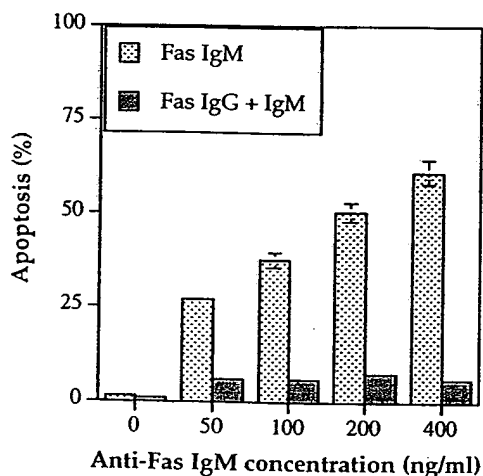


Fig 5. Inhibition of Fas-induced apoptosis in CEM cells by anti-human Fas IgG Ab. CEM cells were preincubated with an anti-human Fas IgG antibody (1:50 dilution) for 30 min. The cells were then subjected to a further 6 h incubation in the presence of anti-human Fas IgM mAb. Apoptosis was assessed by morphological criteria as previously described. Results are shown as mean apoptosis of triplicate fields of cytopun samples with a minimum of 100 cells per field  $\pm$  standard deviation.

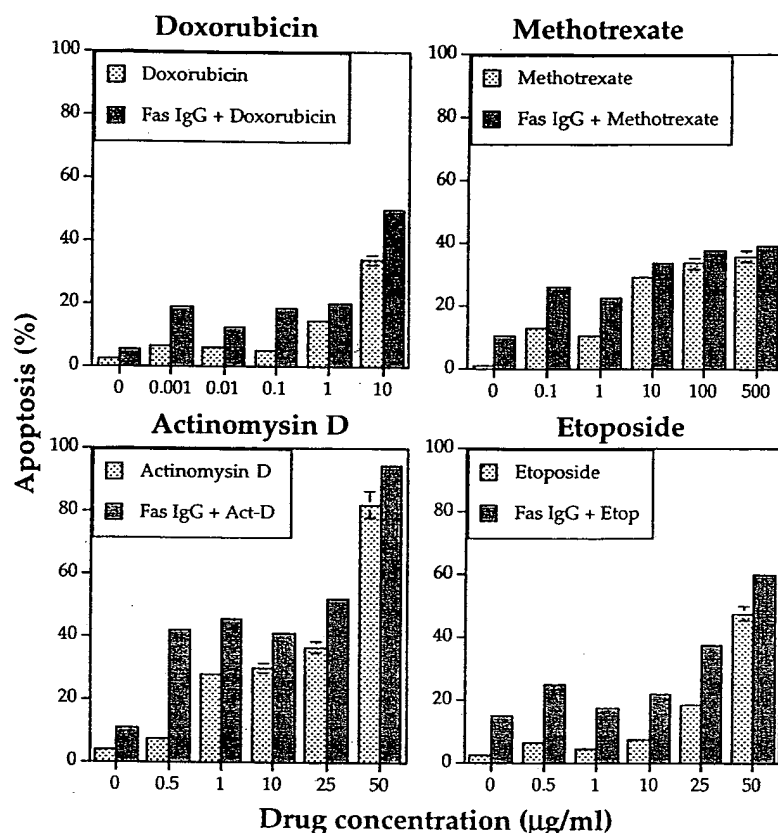


Fig 6. Preincubation of CEM cells with neutralizing anti-Fas IgG Ab does not inhibit susceptibility to cytotoxic drug-induced apoptosis. CEM cells were preincubated with an anti-human Fas IgG antibody (1:50 dilution) for 30 min. Cells were then subjected to a further 18 h incubation in the presence of the drugs indicated, after which apoptosis was assessed by morphological criteria. Results are shown as mean apoptosis of triplicate fields of cytopun samples with a minimum of 100 cells per field  $\pm$  standard deviation.

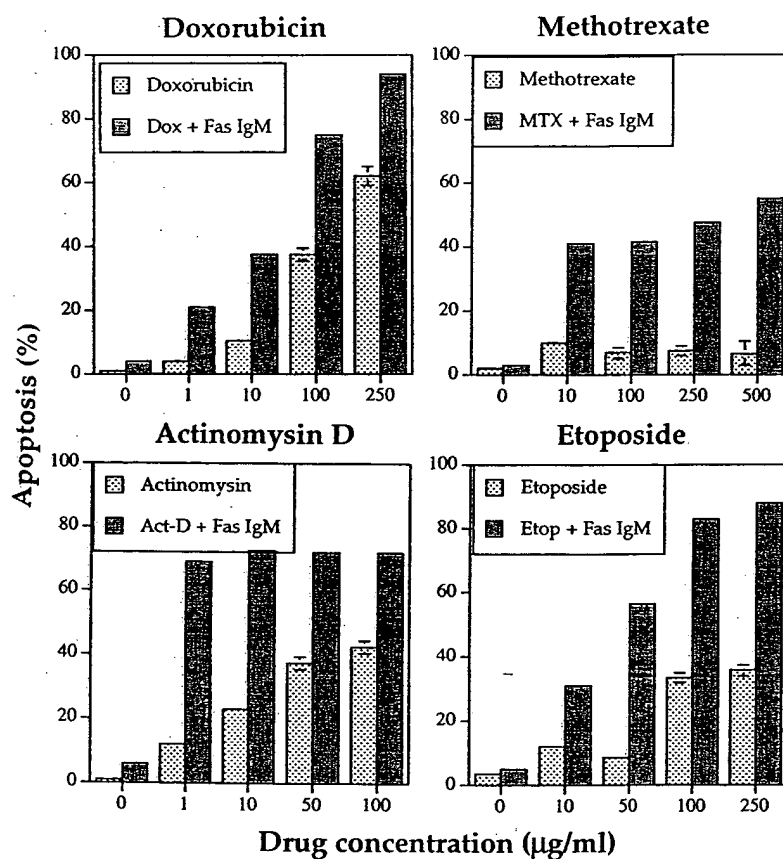


Fig 7. Synergistic effect of anti-Fas IgM Ab on cytotoxic drug-induced apoptosis in CEM cells. CEM cells ( $2.5 \times 10^5$ /ml) were either incubated in the presence varying concentrations of the drugs indicated  $\pm$  anti-human Fas IgM at a concentration of 10 ng/ml for a 6 h period. Apoptosis was assessed as previously described.

that chemotherapeutic drug-induced apoptosis in human leukaemic cells can occur in the absence of Fas receptor/ligand recruitment. A combination of chemotherapeutic drugs and anti-Fas IgM Ab can, however, exert a synergistic cytotoxic effect in leukaemic cells.

## DISCUSSION

There are a growing number of recent publications which document a role for the Fas (CD95/APO-1) receptor/ligand complex in drug-induced apoptosis (Friesen *et al.*, 1996; Uslu *et al.*, 1996; Mitzutani *et al.*, 1997; Muller *et al.*, 1997). In the present study we examined a potential role for the recruitment of the Fas receptor/ligand complex as a common mechanism in chemotherapeutic drug-induced apoptosis. Using flow cytometric analysis of the human leukaemic cell lines HL-60, K562, Jurkat, U937 and CEM, we have shown that apoptosis induced by chemotherapeutic drugs can occur independently of Fas/Fas ligand involvement. Treatment of these leukaemic cells with such diverse chemotherapeutic drugs as doxorubicin, actinomycin D, camptothecin, etoposide and methotrexate failed to induce any up-regulation in Fas or Fas ligand levels. Furthermore, the observation that although anti-Fas IgG neutralizing antibody effectively blocked anti-Fas IgM-induced apoptosis in human leukaemic cells, but failed to block chemotherapeutic drug-induced apoptosis, provides further evidence that drug-induced apoptosis may occur independently of the Fas/Fas ligand system in these cells.

Muller *et al.* (1997) have recently demonstrated that the up-regulation of the Fas/Fas ligand system in hepatoma cells following drug treatment is preceded and directed by p53 up-regulation. Furthermore, transfection of K562 cells (Owen-Shaub *et al.*, 1995; unpublished observations) and HL-60 cells with a temperature-sensitive p53 mutant induced Fas expression and subsequent apoptosis in these cells (Ronen *et al.*, 1996). In light of these observations, it has been suggested that the p53 status of the cell may determine the recruitment of the Fas/Fas ligand during drug-mediated apoptosis (Krammer, 1997). It is of particular significance therefore that the human leukaemic cell lines used in our studies have been proved to be either p53 null (HL-60, U937, Jurkat) (Wolf & Rotter, 1985; Danova *et al.*, 1990) or synthesize negligible p53 (K562) (Danova *et al.*, 1990). It is possible therefore that their inherent lack of p53 expression results in an inability to induce Fas/Fas ligand up-regulation upon drug treatment. CEM cells do, however, possess compound heterozygous mutations in p53 at codons 175/248, but retain the ability to produce p53 which can complex with DNA as well as transactivate (Park *et al.*, 1994). The present observations involving an apparent lack of Fas/Fas ligand up-regulation in CEM cells following drug treatments suggest that the residual p53 activity is insufficient to regulate Fas/Fas ligand up-regulation in our cells.

The intracellular mechanisms responsible for transducing the apoptotic signals generated by chemotherapeutic agents have yet to be fully elucidated. The cytolytic action of chemotherapeutic agents may involve both p53 dependent (Lowe *et al.*, 1993a, b) and p53-independent pathways (Donehower *et al.*, 1992; Clarke *et al.*, 1993). Moreover, this

cytolytic action may involve several levels of interference with endogenous apoptosis pathways. The current observations involving a number of p53 null leukaemic cell lines represent a formal demonstration that chemotherapeutic drug-induced apoptosis can occur in the absence of both p53 expression and Fas/Fas ligand up-regulation. It remains a possibility however, that although chemotherapeutic drug-induced apoptosis and Fas-mediated apoptotic cell death involve two distinct signalling pathways, they may converge or share a common component downstream in the apoptotic pathway. Such common components may include mitochondrial depolarization (Kroemer, 1997), cytochrome c release (Krippner *et al.*, 1996) and the activation of ICE-like proteases (Kaufman *et al.*, 1993; Lazebnik *et al.*, 1994).

The present observation that chemotherapeutic drug-induced apoptosis in a human leukaemic cell line is in fact augmented by anti-Fas IgM treatment lends support to the above hypothesis. Preincubation of CEM cells with low-dose anti-Fas IgM antibody in combination with chemotherapeutic drugs resulted in a synergistic cytolytic effect. We have recently extended our observations to a number of other tumour cell types (unpublished observations). These results are of particular importance given the increasing incidence of multidrug resistance in human leukaemias (for recent review see Preisler, 1995). Combination therapy involving the use of low-dose anti-Fas IgM and chemotherapeutic drugs may prove a useful tool in overcoming such resistance. Furthermore, low-dose combination therapy may avoid some of the potentially deleterious side-effects associated with a high-dose regimen.

## ACKNOWLEDGMENTS

This work was supported by grants from The Children's Leukaemia Research Project, The Irish Cancer Society and The Health Research Board of Ireland. The authors thank Dr Ken Mills, Pre-leukaemia Laboratory, Cardiff, Wales, for the provision of the CEM cell line and Drs Rosemary O'Connor, Adrian McGowan and Sharon McKenna for valuable discussions.

## REFERENCES

- Bedi, A., Zehnauer, A., Barber, J., Sharkis, S. & Jones, R.J. (1990) Inhibition of apoptosis by BCR-ABL in chronic myeloid leukemia. *Blood*, **83**, 2038–2044.
- Bortner, C.D., Oldenburg, N.B.E. & Cidlowski, J.A. (1995) The role of DNA fragmentation in apoptosis. *Trends in Cell Biology*, **5**, 21–26.
- Clarke, A.R., Purdie, C.A., Harrison, D.J., Morris, R.G., Bird, C.C., Hooper, M.L. & Wyllie, A.H. (1993) Thymocyte apoptosis induced by p53-dependent and independent pathways. *Nature*, **362**, 849–852.
- Cohen, J.J., Duke, R.C., Fadok, V.A. & Sellins, K.S. (1992) Apoptosis and programmed cell death in immunity. *Annual Reviews in Immunology*, **10**, 267–293.
- Cotter, T.G., Lennon, S.V., Glynn, J.M. & Green, D.R. (1992) An intact microfilament network is necessary for the formation of apoptotic bodies in cells undergoing apoptosis. *Cancer Research*, **52**, 997–1005.
- Danova, M., Giordano, M., Giuliano, M. & Riccardi, A. (1990) Expression of p53 protein during the cell cycle measured by flow cytometry in human leukemia. *Leukemia Research*, **14**, 417–422.
- Donehower, L.A., Harvey, M., Slagle, B.L., McArthur, M.J.,

- Montgomery, C.A., Butel, J.S. & Bradley, A. (1992) Mice deficient for p53 are developmentally normal but susceptible to spontaneous tumours. *Nature*, 356, 215–221.
- Eliopoulos, A.G., Derr, D.J., Herod, J., Hodgkins, L., Krajewski, S., Reed, J.C. & Young, L.S. (1995) The control of apoptosis and drug resistance in ovarian cancer: Influence of p53 and Bcl-2. *Oncogene*, 11, 1217–1228.
- Fan, S., Smith, M.L., Rivet, D.J.II., Duba, D., Zhan, Q., Kohn, K.W., Fornace, A.J.Jr & O'Connor, P.M. (1995) Disruption of p53 function sensitizes breast cancer MCF-7 cells to cisplatin and pentoxifylline. *Cancer Research*, 55, 1649–1654.
- Friesen, C., Herr, I., Krammer, P.H. & Debatin, K.M. (1996) Involvement of the CD95 (APO-1/Fas) receptor/ligand system in drug-induced apoptosis in leukaemia cells. *Nature Medicine*, 2, 574–577.
- Gorman, A., McCarthy, J., Finucane, D., Reville, W. & Cotte, T.G. (1996) Morphological assessment of apoptosis. *Techniques in Apoptosis: a Users Guide* (ed. by T. G. Cotter and S. M. Martin), pp. 1–21. Portland Press, London.
- Hannun, Y.A. (1997) Apoptosis and the dilemma of cancer chemotherapy. *Blood*, 9, 1845–1853.
- Kamesaki, S., Kamesaki, H., Jorgensen, T.J., Tanizawa, A., Pommier, Y. & Cossman, J. (1993) Bcl-2 protein inhibits etoposide-induced apoptosis through its effects on events subsequent to topoisomerase II-induced DNA strand breaks and their repair. *Cancer Research*, 53, 4251–4256.
- Kaufmann, S.H., Desnoyers, S., Ottaviano, Y., Davidson, N.E. & Poirier, G.G. (1993) Specific proteolytic cleavage of poly(ADP-ribose) polymerase: an early marker of chemotherapy-induced apoptosis. *Cancer Research*, 53, 3976–3985.
- Kerr, J.F.R., Wyllie, A.H. & Currie, A.R. (1972) Apoptosis: a basic biological phenomenon with wide-ranging implications in tissue kinetics. *British Journal of Cancer*, 26, 239–257.
- Krammer, P.H. (1997) The tumour strikes back: new data on the expression of the CD95 (APO-1/Fas) receptor/ligand system may cause paradigm changes in our view on drug treatment and tumour immunology. *Cell Death and Differentiation*, 4, 362–364.
- Kroemer, G. (1997) Mitochondrial implication in apoptosis. Towards an endosymbiont hypothesis of apoptosis evolution. *Cell Death and Differentiation*, 4, 443–456.
- Krippner, A., Matsuno-Yagi, A., Gottlieb, R.A. & Babior, B.M. (1996) Loss of function of cytochrome c in Jurkat cells undergoing Fas-mediated apoptosis. *Journal of Biological Chemistry*, 271, 21629–21636.
- Lazebnik, Y.A., Kaufmann, S.H., Desnoyers, S., Poirier, G.G. & Earnshaw, W.C. (1994) Cleavage of poly(ADP-ribose) polymerase by a proteinase with properties like ICE. *Nature*, 371, 346–347.
- Liles, W.C., Kiener, P.A., Ledbetter, J.A., Aruffo, A. & Klebanoff, S.J. (1996) Differential expression of Fas (CD95) and Fas ligand on normal human phagocytes: implications for the regulation of apoptosis in neutrophils. *Journal Experimental Medicine*, 184, 429–440.
- Lowe, S.W., Ruley, H.E., Jacks, T. & Huosman, D.E. (1993a) P53-dependent apoptosis modulates the cytotoxicity of anticancer agents. *Cell*, 74, 957–967.
- Lowe, S.W., Schmitt, E.M., Smith, S.W., Osborne, B.A. & Jacks, T. (1993b) p53 is required for radiation-induced apoptosis in mouse thymocytes. *Nature*, 362, 847–849.
- Martin, S.J. & Green, D.R. (1995) Protease activation during apoptosis: death by a thousand cuts? *Cell*, 82, 349–352.
- McGahon, A., Bissonette, R.P., Schmitt, M., Cotter, K., Green, D.R. & Cotter, T.G. (1994) Bcr-Abl maintains resistance of chronic myelogenous leukemia cells to apoptotic cell death. *Blood*, 83, 1179–1187.
- Mizutani, Y., Okada, Y., Yoshida, O., Fukumoto, M. & Bonavida, B. (1997) Doxorubicin sensitizes bladder carcinoma cells to Fas-mediated cytotoxicity. *Cancer*, 79, 1180–1189.
- Miyashita, T. & Reed, J.C. (1993) Bcl-2 oncoprotein blocks chemotherapy-induced apoptosis in a human leukemia cell line: *Blood*, 81, 151–157.
- Morimoto, H., Yonehara, S. & Bonavida, B. (1993) Overcoming tumor necrosis factor and drug resistance of human tumor cell lines by combination treatment with anti-Fas antibody and drugs or toxins. *Cancer Research*, 53, 2591–2596.
- Muller, M., Strand, S., Hug, H., Heinemann, E., Walczal, H., Hofmann, W., Strand, W., Krammer, P.H. & Galle, P.R. (1997) Drug-induced apoptosis in hepatoma cells is mediated by the CD95(APO-1/Fas) receptor/ligand system and involves activation of wild-type p53. *Journal of Clinical Investigation*, 99, 403–413.
- Nakamura, S., Takeshima, M., Nakamura, Y., Ohtake, S. & Matsuda, T. (1997) Induction of apoptosis in HL-60 leukemic cells by anticancer drugs in combination with anti-Fas monoclonal antibody. *Anticancer Research*, 17, 173–179.
- Nooter, K., Boersma, A.W.M., Oostrum, R.G., Burger, H., Jochemsen, A.G. & Stoter, G. (1995) Constitutive expression of the c-H-ras oncogene inhibits Doxorubicin-induced apoptosis and promotes cell survival in a rhabdomyosarcoma cell line. *British Journal of Cancer*, 71, 556–561.
- Owen-Shaub, L.B., Zhang, W., Cusack, J.C., Angelo, L.S., Santee, S.M., Fujiwara, T., Roth, J.A., Deiseroth, A.B., Zhang, W.W., Kruzel, E. & Radinsky, R. (1995) Wild-type human p53 and a temperature sensitive mutant induce Fas/APO-1 expression. *EMBO Journal*, 15, 3032–3040.
- Park, D.J., Nakamura, H., Chumakov, A.M., Said, J.W., Miller, C.W., Lin Chen, D. & Koefler, H.P. (1994) Transactivational and DNA binding abilities of endogenous p53 in p53 mutant cell lines. *Oncogene*, 9, 1899–1906.
- Preisler, H.D. (1995) Multidrug resistance is more than MDR1 activity. *Leukemia Research*, 19, 429–431.
- Ronen, D., Schwartz, D., Teitz, Y., Goldfinger, N. & Rotter, V. (1996) Induction of HL-60 cells to undergo apoptosis is determined by high levels of wild-type p53 protein whereas differentiation of the cells is mediated by lower p53 levels. *Cell Growth and Differentiation*, 7, 21–30.
- Uslu, R., Jewett, A. & Bonavida, B. (1996) Sensitization of human ovarian tumour cells by subtoxic CDDP to anti-Fas antibody-mediated cytotoxicity and apoptosis. *Gynecological Oncology*, 62, 282–291.
- Wolf, D. & Rotter, V. (1985) Major deletions in the gene encoding the p53 tumor antigen cause lack of p53 expression in HL-60 cells. *Proceedings of the National Academy of Sciences of the United States of America*, 82, 790–794.
- Wyllie, A.H., Kerr, J.F.R. & Currie, A.R. (1980) Cell death: the significance of apoptosis. *International Reviews in Cytology*, 68, 251–306.
- Zhivotovsky, B., Burgess, D.H. & Orrenius, S. (1996) Proteases in apoptosis. *Experientia*, 52, 968–978.

## Hypoxia-Selective Antitumor Agents. 8. Bis(nitroimidazolyl)alkanecarboxamides: A New Class of Hypoxia-Selective Cytotoxins and Hypoxic Cell Radiosensitisers

Michael P. Hay,<sup>†</sup> William R. Wilson,<sup>‡</sup> John W. Moselen,<sup>†</sup> Brian D. Palmer,<sup>†</sup> and William A. Denny<sup>\*†</sup>

Cancer Research Laboratory and Section of Oncology, Department of Pathology, University of Auckland School of Medicine, Private Bag 92019, Auckland, New Zealand

Received August 27, 1993\*

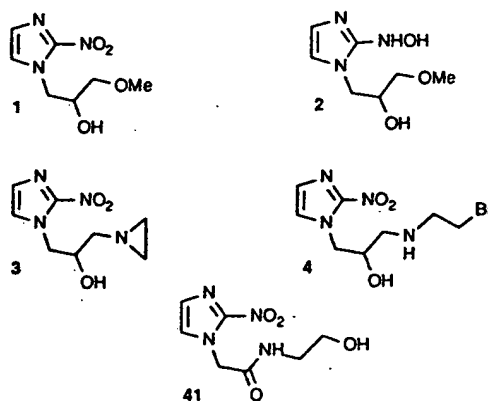
A series of novel bis(nitroimidazolyl)alkanecarboxamides has been prepared and evaluated for hypoxia-selective cytotoxicity and hypoxic cell radiosensitisation *in vitro* and *in vivo*. The compounds were prepared by direct coupling of preformed side chain acid and amine components, using diethyl phosphorocyanidate at room temperature. Although designed to be bis-bioreductive prodrugs of DNA cross-linking agents, none of the compounds showed evidence of DNA cross-linking activity, being equally potent against cell lines deficient and proficient in repair of cross-links. However, one of these compounds, *N*-[2-(2-methyl-5-nitro-1*H*-imidazolyl)ethyl]-4-(2-nitro-1*H*-imidazolyl)butanamide (10; SN 24699), showed high hypoxic selectivity as a cytotoxin (rising to 200-fold after exposure to the drug for several hours) in the repair-proficient Chinese hamster cell line AA8. This selectivity was greater than observed for the alkylating 2-nitroimidazole (4; RB 6145) (40-fold) or simple mononitroimidazoles (5–25-fold). Investigation of structure–activity relationships for hypoxic selectivity of bis(nitroimidazoles) was restricted by their low aqueous solubility, but a certain minimum separation of the two nitroimidazole units (by more than five atoms) appears desirable. All the compounds radiosensitized hypoxic cells *in vitro* but were little more potent as radiosensitizers than the corresponding monomeric nitroimidazoles. Compound 10 caused additional cell killing in the KHT tumor when multiple drug doses were administered in combination with a single dose of radiation. It is not yet clear whether this activity reflects hypoxic cell radiosensitization or cytotoxicity toward hypoxic cells, but this new class of bis-bioreductive agent clearly warrants further investigation.

The existence of hypoxic cells in tumors<sup>1</sup> has long been recognized as a major problem in radiotherapy<sup>2</sup> and is also a potential problem in the chemotherapy<sup>3</sup> of cancer. The development of drugs which combat this problem, using hypoxia as a basis for achieving tumor selectivity,<sup>4</sup> focused first on compounds (oxygen-mimetic radiosensitisers) capable of sensitising hypoxic cells to radiation.<sup>5</sup> More recently, there has been an increasing interest<sup>4,6,7</sup> in the development of drugs (hypoxia-selective cytotoxins, HSCs) which act indirectly as radiosensitizers by themselves killing radioresistant hypoxic cells.

To be effective, such drugs need to penetrate to the hypoxic regions of solid tumors by extravascular diffusion, to undergo selective activation in these regions, and to generate cytotoxic metabolites following activation. This activation is usually by metabolic reduction, and most HSCs can thus be described as bioreductive drugs. One major class of HSCs are the 2-nitroimidazoles, which undergo enzymatic reduction of the nitro group via the one-electron reduction product. This initial step in nitroreduction can be efficiently reversed by oxygen, resulting in preferential metabolism in hypoxic cells.<sup>8</sup>

Thus the 2-nitroimidazole misonidazole (1) shows an hypoxic selectivity of ca. 20-fold in AA8 cells in culture,<sup>10,30</sup> and is known to undergo 4-electron reduction to the unstable<sup>11</sup> hydroxylamine 2, but has low cytotoxic potency. In comparison, the 2-nitroimidazole aziridine analogue (3; RSU-1069)<sup>12</sup> not only has much higher cytotoxicity than misonidazole, but also shows enhanced selectivity for hypoxic cells (ca. 50–100-fold).<sup>10,13</sup> While the predominant mechanism of cytotoxicity of this compound

under aerobic conditions is DNA monoalkylation by the aziridine, reductive metabolism converts it into a much more toxic bifunctional alkylating agent capable of cross-linking DNA.<sup>14</sup> This compound received clinical trial, but severe emetic side effects (attributed to the aziridine moiety) were found.<sup>15</sup> More recently, interest has centered on a prodrug of 3, the 2-bromoethyl compound (4; RB 6145).<sup>16</sup> This compound is rapidly converted to 3 *in vitro* and *in vivo* and shows equivalent activity as a radiosensitizer and an HSC, but is less emetic and has pronounced oral activity.<sup>17</sup>



However, neither aziridines nor 2-haloethyl precursor moieties have selectivity for hypoxic cells, being direct DNA-alkylating functions. Further gains in hypoxic selectivity might, in principle, be achieved by replacing this oxygen-insensitive DNA alkylating moiety with a bioreductive electrophile, thus restricting activation of the electrophilic center to hypoxic cells. Such a compound could be termed a "bis-bioreductive" agent, in that oxygen-

<sup>†</sup> Cancer Research Laboratory.

<sup>‡</sup> Section of Oncology, Department of Pathology.

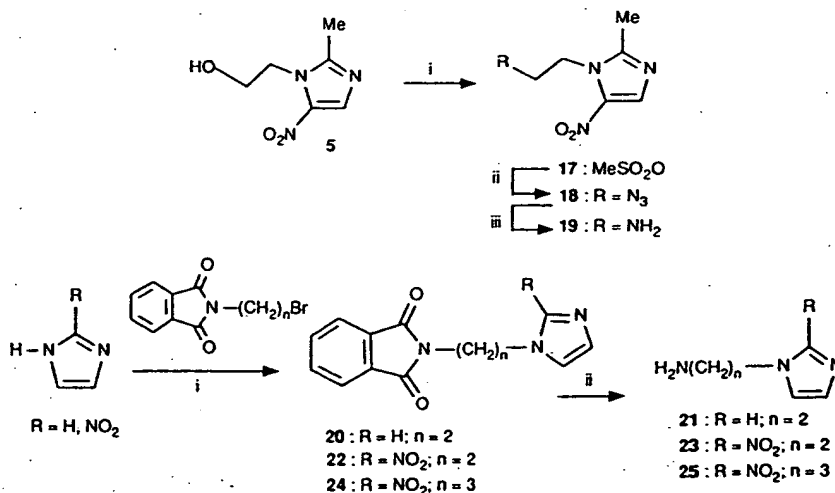
\* Abstract published in *Advance ACS Abstracts*, December 15, 1993.

Table 1. Structural and Physicochemical Data for Bis(nitroimidazolyl) Carboxamides

$R_1-(CH_2)_nCONH(CH_2)_m-R_2$									
no.	$R_1$	$n$	$m$	$R_2$	mp, °C	formula	anal.	log $P^a$	sol <sup>b</sup>
1		misonidazole							>120
4		RB 6145							-0.79
5		metronidazole							-0.80
6	A	3	2	A	149.5–150.5	$C_{12}H_{15}N_7O_5$	$C, H, N^d$	-1.55	4.2
7	A	2	3	A	124–125	$C_{12}H_{15}N_7O_5$	$C, H, N$	-1.55	21
8	A	1	2	B	nc <sup>e</sup>	$C_{11}H_{13}N_7O_5$	$C, H, N$	-1.03	59
9	A	2	2	B	144.5–145.5	$C_{12}H_{15}N_7O_5$	$C, H, N$	-0.99	13
10	A	3	2	B	129	$C_{13}H_{17}N_7O_5$	$C, H, N$	-1.28	20
11	A	4	2	B	136–137.5	$C_{14}H_{19}N_7O_5$	$C, H, N^h$	-0.79	8.6
12	A	5	2	B	133–134	$C_{15}H_{21}N_7O_5$	$C, H, N$	-0.22	2.1
13	A	3	2	C	nc <sup>e</sup>	$C_{12}H_{17}N_6O_3$	HRMS <sup>i</sup>	1.32	408
14	A	3	2	D	175.5–177	$C_{12}H_{15}N_7O_5$	$C, H, N^i$	-1.55	2.3
15	A	3	2	E	152.5–153	$C_{12}H_{15}N_7O_5$	$C, H, N$	-1.55	5.5
16	B	1	2	B	nc <sup>e</sup>	$C_{12}H_{15}N_7O_5$	$C, H, N$	-0.76	36

<sup>a</sup> Calculated using the program CLOGP (version 3.51, BioByte Corp., Claremont, CA 91711). <sup>b</sup> Solubility in millimolar in αMEM + 5% FCS, measured by UV spectrophotometry. <sup>d</sup> N: calcd, 29.07; found, 29.74. <sup>e</sup> Noncrystalline. <sup>f</sup> N: calcd 29.07; found, 29.90. <sup>g</sup> N: calcd 27.91; found 28.46. <sup>h</sup> N: calcd 26.84; found 27.43. <sup>i</sup> High-resolution mass spectrometry. <sup>j</sup> N: calcd 29.07; found 28.32.

## Scheme 1



<sup>a</sup> (i) MsCl/CH<sub>2</sub>Cl<sub>2</sub>/20 °C; (ii) NaN<sub>3</sub>/DMF/100 °C; (iii) Ph<sub>3</sub>P; concentrated HCl/100 °C. <sup>b</sup> (i) NaH/DMF (20) or K<sub>2</sub>CO<sub>3</sub>/DMF (22, 24); (ii) NH<sub>2</sub>NH<sub>2</sub>.

inhibitable reduction of two centers would be required for full cytotoxicity. We have recently shown<sup>18</sup> that another bis-bioreductive agent can achieve very high levels of hypoxic selectivity (>1000-fold).

In this paper we report the synthesis and evaluation as HSCs and hypoxic cell radiosensitizers of a series of bis-(nitroimidazolyl) compounds (6–16) (Table 1), linked by an alkanecarboxamide chain. Nitroimidazoles were selected as the nitroarene units, since examples of 2- and 5-nitroimidazoles have been shown to have hypoxic selectivity due to the generation of reactive intermediates following nitro reduction in cells.

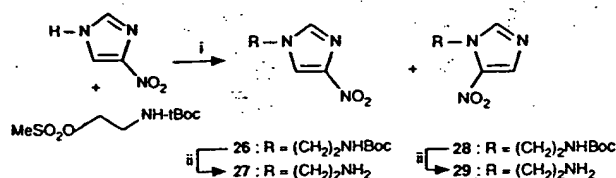
Despite ring fragmentation during nitro reduction under some conditions,<sup>19</sup> the N-1 side chain of misonidazole is known to be retained during covalent binding to macromolecules.<sup>20</sup> This suggests that linkage of bis(nitroimidazoles) via the N-1 positions might be stable to reduction, at least in the case of bis(2-nitroimidazoles), and that reactive bifunctional molecules could thus be generated under hypoxic conditions. In the present study, linkage of the two nitroarene units was effected at the

1-positions through N-alkyl chains. These linkers ensure electronic isolation of the two nitroimidazole units, avoiding significant perturbation of nitro group reduction potentials. A carboxamide linking functionality was chosen for its high hydrophilicity (fragment constant  $f = -2.71$ )<sup>21</sup> and for synthetic flexibility.

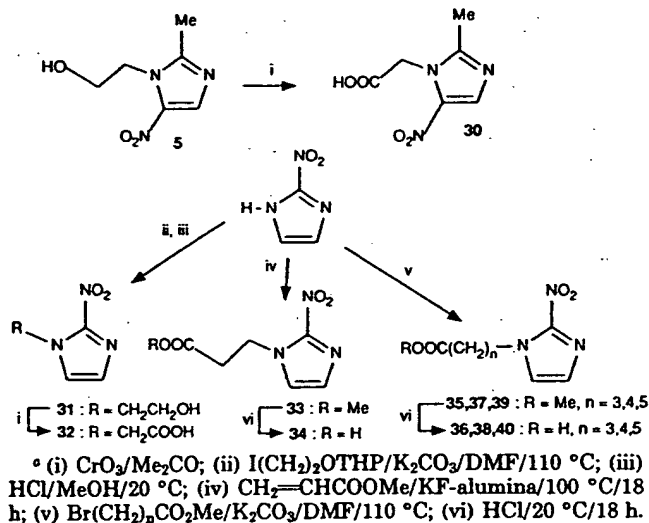
## Chemistry

The carboxamide-linked bis(nitroimidazoles) were prepared by coupling of preformed side chain acid and amine components. A key amine intermediate, 2-(2-methyl-5-nitro-1H-imidazolyl)ethylamine (19), was prepared by nucleophilic displacement of metronidazole mesylate 17 by NaN<sub>3</sub>, and subsequent reduction of the azide 18 to the amine 19 (Scheme 1a). Alkylation of imidazole with (2-bromoethyl)phthalimide gave the phthalimide 20, and phthalimide exchange with hydrazine monohydrate gave 2-(1H-imidazolyl)ethylamine (21) (Scheme 1b). 2-Nitroimidazole was similarly elaborated with (2-bromoethyl)phthalimide and (3-bromopropyl)phthalimide to the amines (23 and 25). Amines 27 and 29 were prepared

## Scheme 2\*



## Scheme 3\*



more conveniently by alkylation of 4-nitroimidazole with *N*-[(*tert*-butoxycarbonyl)mesyl]ethylamine under basic conditions (Scheme 2). This procedure afforded a 6:1 mixture of the 4-nitro and 5-nitro isomers of *N*-Boc-2-(nitro-1*H*-imidazolyl)ethylamine, 26 and 28, which were separated by flash chromatography, and hydrolyzed to the amines under acid conditions.

2-(2-Methyl-5-nitro-1*H*-imidazolyl)acetic acid (30) was prepared by Jones' oxidation of metronidazole (5) (Scheme 3). 2-(2-Nitro-1*H*-imidazolyl)acetic acid (32) was prepared by alkylation of 2-nitroimidazole with the tetrahydropyranyl ether of 2-iodoethanol under basic conditions, followed by deprotection to the alcohol 31 and Jones' oxidation. 4-(2-Nitro-1*H*-imidazolyl)butanoic acid (36) and the higher homologues (38 and 40) were prepared by alkylation of 2-nitroimidazole with the appropriate  $\omega$ -haloalkyl esters, followed by mild acid hydrolysis of the resulting esters (35, 37, 39). Attempts to hydrolyze corresponding nitriles to the acids under more vigorous conditions (AcOH/HCl mixtures) resulted in partial substitution of the imidazole nitro group by chlorine.

3-(2-Nitro-1*H*-imidazolyl)propionic acid (34) could not be prepared by alkylation of 2-nitroimidazole with 3-halopropionic acid esters under basic conditions. Coupling of the preformed 2-nitroimidazole salt with either 3-halopropionic acid esters or methyl acrylate, using 18-crown-6 in acetonitrile, was also unsuccessful. Presumably the nitroimidazolyl anion is sufficiently basic to dehydrohalogenate the reagents, giving the acrylic acid ester. Reaction of 2-nitroimidazole with a large excess of methyl acrylate with 18-crown-6 and  $\text{K}_2\text{CO}_3$ <sup>22</sup> gave mostly starting material and only poor yields (5–10%) of the ester 33, which was hydrolyzed to give the desired propionic acid 34. The yield of ester could be raised to 35% by using KF/alumina<sup>23</sup> as a catalyst.

Coupling of the various amine and acid fragments was best achieved using diethyl phosphorocyanidate (DEPC)<sup>24</sup>

(Scheme 4): Reaction at room temperature for 16 h, followed by chromatographic purification and crystallization, gave moderate to good yields of the amides, free of starting materials. Several other condensation methods, including carbonyldiimidazole, acyl halide, and mixed anhydride, were significantly inferior.

## Biological Studies

The cytotoxicities of the compounds against a panel of four cell lines (the Chinese hamster lines AA8 and UV4, the murine mammary carcinoma EMT6, and the human melanoma FME) were determined under aerobic conditions using a growth inhibition microassay which has been described in detail previously.<sup>25</sup> The UV4 cell line, a repair-defective mutant derived from AA8, is hypersensitive to agents whose cytotoxicity is due to bulky DNA adducts or cross-links<sup>26</sup> and was thus used to provide initial information on mechanisms of cytotoxicity.

The cytotoxic potencies of the compounds were compared under aerobic and hypoxic conditions by clonogenic assay of stirred plateau-phase AA8 cultures, continuously gassed with 5%  $\text{CO}_2$  in air or  $\text{N}_2$ , as described previously.<sup>27,28</sup> Detailed studies of selected compounds in this series show a complex relationship between cell killing, drug concentration, and duration of exposure.<sup>29</sup> While the parameter  $\text{CT}_{10}$  (concentration of drug  $\times$  time for 10% survival) was essentially constant under aerobic conditions, for some drugs this parameter decreased progressively under hypoxia (see Figure 2 for an example) so that hypoxic selectivity was greater using low drug concentrations and long exposure times. Hypoxic selectivity was assessed as the ratio (aerobic  $\text{CT}_{10}$ /hypoxic  $\text{CT}_{10}$ ) at the same time, and ranges of this ratio over the drug exposure period of 1–8 h are shown in Table 3.

Radiosensitization was also examined in stirred AA8 cultures, under the same conditions as for the toxicity assays. Briefly, suspensions of hypoxic AA8 cells were exposed to drug for 30 min and then irradiated with a  $^{60}\text{Co}$   $\gamma$  source at  $37^\circ\text{C}$ . Radiation dose-response curves were generated at a range of drug concentrations to define the concentration required to give a sensitizer enhancement ratio (SER; ratio of radiation doses for 10% survival with and without drug) of 1.6 ( $\text{C}_{1.6}$ ), and these results are given in Table 3. The *in vitro* therapeutic index (IVTI = aerobic  $\text{IC}_{50}$ /hypoxic  $\text{C}_{1.6}$ ) was calculated as a measure of hypoxic cell radiosensitizing potency relative to aerobic cytotoxicity (Table 3).

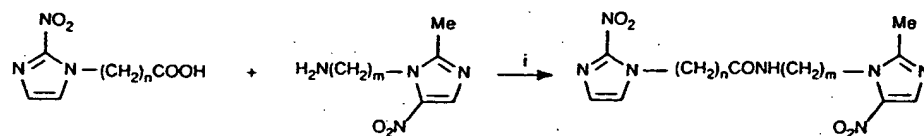
Drug uptake was assessed by HPLC, after exposing the cells to drugs at the  $\text{C}_{1.6}$  concentration for 30 min at  $37^\circ\text{C}$ . Efficiencies of drug recovery from the cellular and extracellular compartments were determined in separate experiments by spiking cell pellets and medium at concentrations close to those estimated in the uptake experiments, and average intracellular concentrations at the  $\text{C}_{1.6}$  ( $\text{C}_{1.6(0)}$ ) were calculated.

Compound 10 was compared with misonidazole (1) in its ability to kill or radiosensitize hypoxic cells in KHT tumors growing subcutaneously in  $\text{C}_3\text{H}/\text{HeN}$  mice. The compounds were administered using single or multiple doses of 2.5 mmol/kg, this being the maximum ip dose of 10 which could be administered due to solubility limitations.

## Results and Discussion

**Physicochemical Properties.** The structures and physicochemical properties of the bis(nitroimidazoles)



Scheme 4<sup>a</sup>

compounds of Table 1

<sup>a</sup> (i) DEPC/Et<sub>3</sub>N/DMF/20 °C/18 h.

Table 2. Aerobic Toxicity of the Bis(nitroimidazole) Derivatives of Table 1 As Determined by Growth Inhibition in Four Cell Lines

no.	IC <sub>50</sub> <sup>a</sup> (mM) AA8	hypersensitivity factor <sup>b</sup>		
		UV4	EMT6	FME
1	12.1 ± 1.1 <sup>c</sup>	1.4 ± 0.1	3.6 ± 0.9	1.9 ± 0.2
4	0.15 ± 0.02	5.9 <sup>d</sup> ± 0.9	1.6 ± 0.1	1.0 ± 0.1
5	23 ± 2	1.0 ± 0.1	1.0 ± 0.1	1.0 ± 0.2
6	ca. 3 <sup>e</sup>			
7	6.1 ± 0.7	1.2 ± 0.1	3.5 ± 0.1	3.9 ± 0.1
8	4.7 ± 0.4	1.0 ± 0.1	2.2 ± 0.5	2.1 ± 0.2
9	5.5 ± 0.1	0.9 ± 0.2	2.5 ± 0.4	2.9
10	7.2 ± 0.8	1.4 ± 0.2	1.3 ± 0.2	4.6 ± 1.2
11	3.8 ± 0.2	1.2 ± 0.1	1.7 ± 0.1	3.5 ± 0.4
12	ca. 1 <sup>e</sup>	ca. 1	ca. 1	ca. 1
13	24 ± 5	1.3 ± 0.1	4.2 ± 0.7	3.0 ± 1.3
14	ca. 2 <sup>e</sup>			
15	>4.2 <sup>f</sup>		>1.7	>2.1
16	7.7 ± 1.5	1.0 ± 0.1	4.4	2.3

<sup>a</sup> IC<sub>50</sub>: the concentration of drug required to reduce cell numbers to 50% of controls in a growth inhibition assay (see text). <sup>b</sup> Hypersensitivity factor = IC<sub>50</sub> for AA8/IC<sub>50</sub> for the indicated cell line. <sup>c</sup> Errors are SEM for two to eight independent determinations. <sup>d</sup> Hypersensitivity factor 30 ± 8 after 18-h exposure under hypoxic conditions. <sup>e</sup> Tested near the solubility limit with variable results. <sup>f</sup> Nontoxic at the solubility limit.

Table 3. Hypoxia-Selective Cytotoxicity, Cellular Uptake, and Radiosensitization by Bis(nitroimidazole) Derivatives in AA8 Cell Cultures

no.	cytotoxicity		radiosensitization			IVTI <sup>f</sup>
	hypoxic CT <sub>10</sub> <sup>a</sup> (mM-h)	air/N <sub>2</sub> <sup>b</sup>	uptake C <sub>i</sub> /C <sub>e</sub> <sup>c</sup>	C <sub>1.6</sub> <sup>d</sup> (mM)	C <sub>1.6</sub> <sup>e</sup> (mM)	
1	8.3–16 <sup>g</sup>	18–25	0.90	0.43	0.40	28
4	0.18–0.38	20–40		0.13		1.1
5	100–135	5–7	1.3	13.3	17.3	1.7
6	3.4	>6 <sup>h</sup>	0.50	1.54	0.77	1.7
7	2.5–5.2	6.5–14				
8	11	2.4	0.50	1.08	0.54	4.3
9	12	>7 <sup>h</sup>	0.60	0.70	0.42	7.9
10	0.37–12	8–200	0.33	0.63	0.21	11
11	6	>7 <sup>h</sup>	0.52	0.93	0.48	4.0
12	1.5	>17 <sup>h</sup>	0.55	0.65	0.36	1.2
13	26–39	8–11	0.33	4.00	1.32	6.0
14	>15 <sup>i</sup>		0.33	>1.1	>0.36	<1.6
15	0.8–4.2	>30 <sup>h</sup>	0.30	0.90	0.27	>4.7
16	50	2.0	1.5	2.7	4.1	2.8

<sup>a</sup> Drug concentration × time to reduce cell survival to 10% of control values under hypoxic conditions. <sup>b</sup> Ratio aerobic CT<sub>10</sub>/hypoxic CT<sub>10</sub>. <sup>c</sup> Ratio of mean intracellular to extracellular drug concentration, determined under hypoxic conditions 30 min after exposure to the drug at the C<sub>1.6</sub> concentration. <sup>d</sup> Drug concentration at which the sensitizer enhancement ratio (SER) = 1.6 under hypoxia. <sup>e</sup> Average intracellular drug concentration when the hypoxic SER = 1.6. <sup>f</sup> IVTI (in vitro therapeutic index) = aerobic IC<sub>50</sub>/hypoxic C<sub>1.6</sub>. <sup>g</sup> Ranges indicate that values changed with time (see text). Where ranges are not given, toxicity was not assessed over a sufficient range of concentrations to estimate changes in CT<sub>10</sub> with time. <sup>h</sup> Not cytotoxic under oxic conditions at the solubility limit. <sup>i</sup> Not cytotoxic under hypoxic or oxic conditions at the solubility limit.

6–16 are shown in Table 1. The majority of the compounds possess a misonidazole-like (2-nitroimidazole) unit (R<sub>1</sub>), linked through the N-1 position via an alkanecarboxamide chain to a second nitroimidazole unit (R<sub>2</sub>) of varying

reduction potential. The *E*(1) values for these various nitroimidazoles are estimated from literature values<sup>30–32</sup> as –390 mV for *N*-alkyl-2-nitro, –490 mV for *N*-alkyl-2-methyl-5-nitro, –560 mV for *N*-methyl-4-nitro, and –470 mV for *N*-methyl-5-nitro isomer and assume complete electronic isolation by the linker chain. The solubilities of the compounds in the buffer used for *in vitro* studies (αMEM with 5% fetal calf serum) were determined by spectrophotometry.

Relative lipophilicities (as log *P*<sub>octanol</sub>) were computed using the program CLOGP.<sup>33</sup> Previous work<sup>34,35</sup> has shown clear relationships between the therapeutic indices of 2-nitroimidazole radiosensitisers and measured log *P* values, with an optimal value for log *P* of ca. –1.4. While the calculated log *P* for misonidazole (–1.25; Table 1) is seriously at variance with the measured value (–0.37),<sup>34</sup> possibly due to unallowed interactions of the side chain OH group, the correspondence is much better for compounds bearing alkylamide side chains of the type discussed here (e.g., for etanidazole (41); measured<sup>34</sup> –1.34; calculated –1.57).

Over the whole dataset, no statistically-significant correlation was observed between CLOGP and aqueous solubility, suggesting that other factors (possibly crystal packing forces) are more important determinants of solubility than is lipophilicity. While the isomeric bis-nitro compounds 6, 14, and 15 all had similar solubilities, addition of a 2-methyl group to 15 to give 10 increased solubility 4-fold, while removal of the (hydrophilic) nitro group altogether (compound 13) increased solubility enormously. However, within the homologous series 8–12, aqueous solubilities did trend as expected with chain length and showed a correlation with CLOGP values.

**Aerobic Cytotoxicity *in Vitro*.** The cytotoxicities of the compounds against AA8 cells, measured as IC<sub>50</sub> values following an 18-h exposure, are given in Table 2. For the bis(2-nitroimidazoles) (6 and 7), IC<sub>50</sub> values were 3–6 mM, indicating cytotoxic potencies 2–4-fold greater than for misonidazole (1), and about 4–8-fold greater than that of the more closely analogous mononitro bisimidazole 13. The mixed bis(nitroimidazoles) with both 2-nitro and 5-nitroimidazole units had IC<sub>50</sub> values in the range 1–7.2 mM, similar to those of the bis(2-nitroimidazoles). There was no obvious dependence on carboxamide chain length within the homologous series 8–12, although the two more lipophilic compounds (11, 12) appeared to be the most cytotoxic. The one example (14) of a 2-nitroimidazole linked to a 4-nitroimidazole was not sufficiently soluble to determine an IC<sub>50</sub> value. The bis(5-nitroimidazole) 16 was about 3-fold more potent than the mono-5-nitroimidazole metronidazole (5). Overall, the carboxamide-linked bis(nitroimidazoles) are therefore not greatly more cytotoxic under aerobic conditions than would be expected for the molar equivalent of the mononitro compounds.

All of the bis(nitroimidazoles) were much less cytotoxic than the alkylating 2-nitroimidazole 4. The latter compound was more active against UV4 than AA8 cells, with

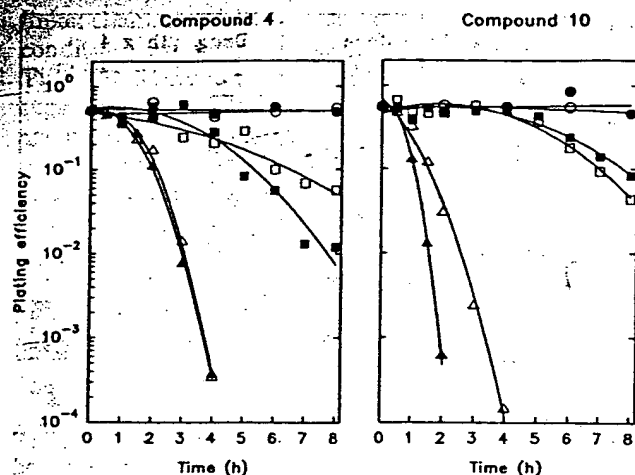


**Figure 1.** Rate of killing of AA8 cells by compound 4 and 10 under aerobic (open symbols) and hypoxic (filled symbols) conditions. Left panel: drug concentrations 0 (○, ●), 0.03 (■), 0.13 (▲), 0.75 (□), and 3.0 (Δ) mM. Right panel: drug concentrations 0 (○, ●), 0.05 (■), 1.0 (▲), 10 (□), and 30 (Δ) mM.

a hypersensitivity factor ( $HF = IC_{50}(AA8)/IC_{50}(UV4)$ ) of 5.9, consistent with a major mechanism of cytotoxicity being DNA interstrand cross-links, as previously suggested for the active aziridinyll form of this agent.<sup>10,14</sup> In contrast, the bis(nitroimidazoles), like the nonalkylating mononitro compounds (1, 5, 13), gave HF values close to unity. This observation suggests that the bis(nitroimidazoles) do not act as DNA cross-linking agents, at least under aerobic conditions. Subsequent comparisons of AA8 and UV4 cells under hypoxic conditions have shown larger HF values for 4 (ca. 20-fold), consistent with increased DNA cross-linking due to nitroreduction. However, 10 was no more toxic to UV4 than AA8 cells, suggesting that it is not a DNA cross-linking agent, even under hypoxic conditions.<sup>29</sup>

All of the compounds tested showed similar aerobic cytotoxic potencies in the AA8, EMT6, and FME cell lines (Table 2). Thus there do not appear to be major species or cell line differences in aerobic cytotoxic potency in this series.

**Hypoxia-Selective Cytotoxicity *in Vitro*.** The hypoxia-selective cytotoxicities of the compounds were determined by clonogenic assay, using stirred suspensions of AA8 cells (Table 3). In each case, the kinetics of killing were assessed at several different drug concentrations which gave widely different rates of killing. Representative data (for compounds 4 and 10) are illustrated in Figure 1.  $CT_{10}$  values were calculated for each survival curve and were in all cases essentially independent of time under aerobic conditions (Figure 2). However, under hypoxia  $CT_{10}$  values often decreased with time. This trend was very marked for compound 10 (Figure 2), and apparent hypoxic selectivities were thus time-dependent. Of the mononitro compounds, 4 was the most selective for hypoxic conditions, with a  $CT_{10}(\text{air})/CT_{10}(\text{N}_2)$  ratio which increased from 20 to 40 between 1 and 8 h. Hypoxic selectivity was less for misonidazole (1) (18–25-fold), metronidazole (5) (5–7-fold) and the mononitro bis(imidazolyl) carboxamide bearing only one nitro group (13) (8–11-fold).

Evaluation of the hypoxic selectivity of the bis(nitroimidazoles) was limited by the low aqueous solubility of many of these compounds, which often precluded measurement of aerobic cell killing under the conditions of the clonogenic assay. However, hypoxic cell killing could be quantitated for all compounds except the bis(nitro-

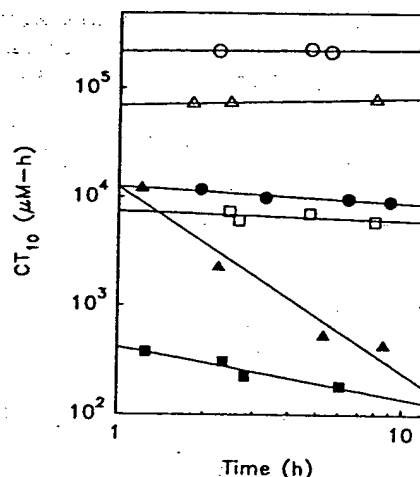


**Figure 2.** Cytotoxic potency of nitroimidazoles ( $CT_{10}$  values) assessed at a range of drug exposure times. Point were derived by interpolating the time for 10% survival from curves of the type shown in Figure 1. Open symbols: aerobic. Filled symbols: hypoxic. Circles: misonidazole (1). Squares: RB 6145 (4). Triangles: compound 10.

imidazole) with a 4-nitro unit 14, which had both a low reduction potential and low solubility. The bis(2-nitroimidazole) 6 and its reversed amide isomer 7 had potencies under hypoxic conditions which were only about 3-fold greater than that of misonidazole (1). The solubility of 7 allowed determination of its hypoxic selectivity, which was less than that of misonidazole (1). Similar results were obtained for the bis(5-nitroimidazole) 16 which was 2–3-fold more potent than metronidazole (5) under hypoxia, but was less hypoxia-selective.

All of the members of the homologous series of mixed 2-nitroimidazole/5-nitroimidazole compounds 8–11 were also selectively toxic under hypoxic conditions, but only two were sufficiently soluble for their aerobic toxicities to be determined in the clonogenic assay. The compound of shortest chain length (8) showed only weak selectivity (2.4-fold). Its higher homologue 9 was more selective (>7-fold), but the C-3 homologue 10 was sufficiently potent and soluble to allow measurement of both aerobic and hypoxic cytotoxicity over a wide time range. Its hypoxic selectivity increased markedly from 8-fold at 1 h to 200-fold by 8 h (Figure 2 and Table 3). At the early times its hypoxic potency was similar to that of misonidazole (1), while at late times its potency approached that of the alkylating analogue 4 (Figure 2). This is consistent with its slow metabolic conversion to a bis-functional species. The corresponding compound without the 2-methyl substituent on the 5-nitroimidazole ring (15) showed biological properties similar to 10, with a potency under hypoxia which also increased markedly with time (Table 3). While this compound was 3.6-fold less soluble than compound 10, and cell killing could not be detected under aerobic conditions, its hypoxic selectivity was >30-fold at late drug exposure times.

**Radiosensitization *in Vitro*.** All of the nitroimidazoles, including the bis compounds, radiosensitized hypoxic AA8 cells in culture as expected. Representative data showing the relationship between SER and concentration are illustrated for misonidazole (1), the aziridine (4), and the bis(nitroimidazole) (10) in Figure 3. The drug concentrations required to provide SER values of 1.6 ( $C_{1.6}$  values) are given in Table 3. The values for the bis(nitroimidazoles) 6–15, containing one or more 2-nitroim-

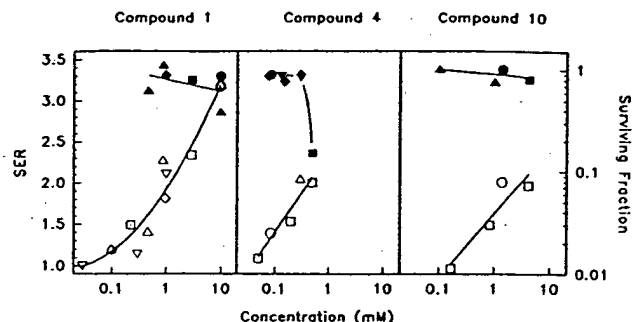


**Figure 3.** Sensitizer enhancement ratios (SER) for radiosensitization of hypoxic A48 cells by compounds 1, 4, and 10 following incubation at 37 °C for 30 min (open symbols). Surviving fractions for unirradiated cultures exposed to drugs under identical conditions are shown as filled symbols.

idazole units, were at least 2-fold lower than the value of 430  $\mu$ M for misonidazole, with no obvious structure-activity relationships. Compound 16, containing two 5-nitroimidazole units, was also more potent (by a factor of 5) than the mono-5-nitroimidazole 5 (metronidazole). Uptake factors (the ratio of average intracellular to extracellular drug concentrations,  $C_i/C_e$ ) were measured at the  $C_{1.6}$  after incubation with the drug for 30 min under hypoxic conditions. The value of 0.9 for misonidazole agrees well with that reported previously.<sup>36</sup> Uptake factors for the bis(nitroimidazoles) 6–15 were significantly lower than this, ranging from 0.33 to 0.6. Again, no relationships could be discerned between uptake and either drug structure or overall lipophilicity, although the compounds span a range of log  $P$  values from –0.22 to –1.55. The bis(5-nitroimidazole) 16 had a somewhat higher uptake factor of 1.5.

When these uptake factors are taken into account, some of the bis(nitroimidazoles) appear to be marginally more efficient radiosensitizers than their monomeric counterparts. Comparing  $C_{1.6}$  values (Table 3), most members of the homologous series 8–11 were more efficient than misonidazole, with the best compound being 10 (shown above to also have the greatest hypoxia-selectivity). The higher potency of the bis(5-nitroimidazole) 16 than metronidazole (5) was also still observed when cellular uptake was taken into account ( $C_{1.6}$  values of 4.1 and 17.3 mM respectively; Table 3). All of the bis(nitroimidazoles) had *in vitro* therapeutic indices (IVTI = aerobic  $IC_{50}$ /hypoxic  $C_{1.6}$ ) greater than that of the very toxic alkylating analogue 4, with the highest index (11) being obtained with compound 10. However, even this is only about half of the IVTI of misonidazole (1) (although interpretation of these data is complicated by the observation that the IVTI for the other mononitroimidazolyl-carboxamide 13 is less than that of misonidazole). Overall, the bis compounds appear to be broadly similar to monomeric nitroimidazoles as hypoxic cell radiosensitizers with respect to potency and radiosensitizing selectivity relative to aerobic toxicity.

**In Vivo Studies.** Because of its high hypoxia-selective cytotoxicity *in vitro*, and its efficient radiosensitizing properties, 10 was selected for *in vivo* evaluation against KHT tumors growing subcutaneously in C<sub>3</sub>H/HeN mice. The maximum dose which could be administered (because of solubility limitations) was 2.5 mmol/kg, using solution in either phosphate-buffered saline (PBS) (50 mM, 0.05 mL/g body weight) or in dimethylacetamide/polyethylene glycol 400/water, 1:3:6 v/v/v (250 mM, 0.01 mL/g body

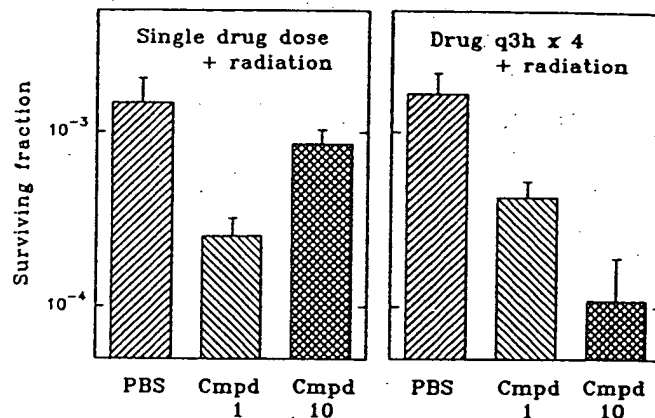


**Figure 4.** Activity of compounds 1 and 10 against the KHT tumor in combination with radiation (15 Gy). Mice were treated with either a single dose of 2.5 mmol/kg (left panel) or four doses of 2.5 mmol/kg at 3 hourly intervals (right panel) and were irradiated whole-body 45 min after the last drug dose. The injection volume was 0.05 mL/g per dose for both compounds and for the controls, which were irradiated 45 min after the last injection of PBS. Each value is the geometric mean  $\pm$  range for two experiments with two to four pooled tumors in each experimental group.

weight). Initial studies with the latter formulation indicated no additional cell killing in irradiated KHT tumors when the drug was administered 90, 60, or 30 min before radiation or 5 min after irradiation (data not shown). Subsequent studies confirmed that 10 is inactive and 1 is active at this dose when given in a large volume of PBS 45 min before irradiation. However, four such doses of 10 at 3-h intervals (with irradiation 45 min after the last dose) gave greater tumor cell killing than radiation alone (Figure 4). No killing was observed with either drug or schedule in the absence of radiation (data not shown). In contrast to the bis(nitroimidazole), misonidazole (1) was no more active in the multidose schedule than in a single dose (Figure 4). This is as expected for "electron-affinic" radiosensitization dependent only on the concentration in the tumor at the time of irradiation, since 1 is cleared with a half-life of 1.5 h at a dose of 2.5 mmol/kg in the mouse,<sup>37</sup> indicating that little accumulation would be expected in tumors with this dosing schedule. The superiority of 10 when administered as multiple doses suggests that its activity in combination with radiation is primarily due to hypoxic cell toxicity rather than direct radiosensitization, although pharmacokinetic studies are required to exclude the possibility that parent drug might accumulate in tumors with the q3h  $\times$  4 schedule. No toxicity was observed in non-tumor-bearing C<sub>3</sub>H/HeN mice treated with 10 using the 4  $\times$  2.5 mmol/kg dose schedule (observation time 30 days). Recent studies have also shown 10 to be active in combination with radiation against the MDAH-MCa-4 mouse mammary tumor in growth delay assays when administered using the above q3h  $\times$  4 schedule (but not as a single dose), while misonidazole (1) was no more active in the multidose schedule.<sup>29</sup>

## Conclusions

The bis(nitroimidazoles) investigated here showed aerobic toxicities quite similar to those of the related mononitro compounds. The potencies of these compounds as hypoxic cell radiosensitizers was also only a little greater than those of analogous mononitroimidazoles. However, compounds 10 and 15, both with a 2-nitro- and a 5-nitroimidazole linked by a seven-atom carboxamide

linker chain, were highly potent cytotoxins under hypoxic conditions using drug exposure times of several hours. The increase in cytotoxic potency with time under hypoxia suggests these compounds may be "bis-bioreductive" agents, with slow reduction at the redox center of lower potential (5-nitroimidazole) generating a bis-reactive molecule under hypoxia. The more soluble of these two compounds, 10, was active as a radiosensitizer of KHT tumors when administered in multiple doses, presumably because of its selective toxicity to hypoxic radioresistant cells. However, the relative contributions of bioreductive toxicity and direct ("electron affinic") radiosensitization to the observed activity have yet to be determined. Evaluation of 10 in combination with fractionated radiation will be of interest; if it is acting primarily as a bioreductive drug there are theoretical reasons to expect it to be more active in a protracted schedule.<sup>4</sup>

One of the possible mechanisms of cytotoxicity considered in the design of bis(nitroimidazoles) was that they might generate DNA cross-linking agents when both nitro groups are reduced to reactive species. The lack of hypersensitivity of the UV4 cell line, which is defective in DNA cross-link repair, suggests that this is not the mechanism of toxicity of these agents under aerobic conditions. Subsequent studies have shown that UV4 is also not hypersensitive to 10 under hypoxic conditions.<sup>29</sup> In addition, alkaline elution studies provide no evidence of interstrand cross-links by 10 under hypoxia using concentrations and exposure times well above those required for cytotoxicity.<sup>29</sup> The lack of cross-linking by 10 is consistent with recent studies showing that metabolic reduction of metronidazole in *E. coli* does not result in significant DNA alkylation, with an upper limit for covalent binding under anoxic conditions of <1 molecule/10<sup>6</sup> base pairs.<sup>38</sup> However, the generation of a highly toxic lesion under hypoxia need not be limited to crosslinking events since other duplex lesions (e.g. a single strand break combined with a monoalkylation site) might also be highly cytotoxic. We have suggested elsewhere that bis(nitroimidazoles) such as 10 might act as bis-bioreductive drugs by generating such locally doubly damaged sites when both nitro groups are reduced.<sup>29</sup>

Despite the use of water-soluble carboxamide linkers, aqueous solubility has limited the evaluation of the present series and structure-activity relationships for hypoxia-selective toxicity are not well defined. The low hypoxic selectivity of 8 suggests that a linker chain length of more than five atoms may be required between the nitroimidazole moieties, but development of more soluble analogues will be required to explore structural requirements further.

## Experimental Section

Analyses indicated by symbols of the elements were within  $\pm 0.4\%$  of theoretical. Analyses were carried out in the Microchemical Laboratory, University of Otago, Dunedin, New Zealand. Melting points were determined on an Electrothermal 2300 melting point apparatus. NMR spectra were obtained on a Bruker AC-200 or AM-400 spectrometer, and are referenced to Me<sub>4</sub>Si for organic solvents, or DSS (2,2-dimethyl-2-silapentane-5-sulfonate) for aqueous solvents. Mass spectra were determined on a Varian VG-70SE mass spectrometer using an ionizing potential of 70 eV at a nominal resolution of 1000. High-resolution spectra were obtained at nominal resolutions of 3000, 5000, or 10000 as appropriate. Spectra were obtained using the ionization mode specified, with PFK as the reference unless otherwise stated. Thin-layer chromatography was carried out on aluminum-backed

silica gel plates (Merck 60 F<sub>254</sub>). Column chromatography was carried out on silica gel (Merck 230–400 mesh). All compounds designated for biological testing were analyzed at >99% purity by reverse-phase HPLC using a Philips PU4100 liquid chromatograph, a Phenomenex BondClone 10-C18 stainless steel column (300 mm  $\times$  3.9-mm i.d.), and a Philips PU4120 diode array detector. Chromatograms were run using various gradients of aqueous (1 M NaH<sub>2</sub>PO<sub>4</sub>, 0.75 M heptanesulfonic acid, 0.5 M dibutylammonium phosphate, and MilliQ water in a 1:1:1:97 ratio) and organic (80% MeOH/MilliQ water) phases.

**2-(2-Methyl-5-nitro-1H-imidazolyl)ethylamine (19).** A solution of methanesulfonyl chloride (5.4 mL, 70 mmol) in CH<sub>2</sub>Cl<sub>2</sub> (10 mL) was added dropwise to a stirred suspension of 2-(2-methyl-5-nitro-1H-imidazolyl)ethanol (5; metronidazole) (10.0 g, 58 mmol) and Et<sub>3</sub>N (12.2 mL, 88 mmol) in CH<sub>2</sub>Cl<sub>2</sub> (200 mL) at 20 °C under N<sub>2</sub>. After being stirred for 4 h, the mixture was filtered, and the filtrate was washed with water (2  $\times$  60 mL), evaporated, and crystallized from CHCl<sub>3</sub> to give 2-(2-nitro-5-nitro-1H-imidazolyl)ethyl methanesulfonate (17) (13.5 g, 92%): mp 153–154 °C; <sup>1</sup>H NMR (CDCl<sub>3</sub>)  $\delta$  8.06 (s, 1H, H-4'), 4.67 (dd, *J* = 5.1, 4.7 Hz, 2 H, H-2), 4.56 (dd, *J* = 5.1, 4.7 Hz, 2 H, H-1), 3.15 (s, 3H, SO<sub>2</sub>CH<sub>3</sub>), 2.46 (s, 3 H, CH<sub>3</sub>); <sup>13</sup>C NMR (CDCl<sub>3</sub>)  $\delta$  151.7 (C-2'), 138.5 (C-5'), 133.0 (C-4'), 45.2 (C-1), 45.0 (C-2), 36.7 (SO<sub>2</sub>CH<sub>3</sub>), 8.3 (CH<sub>3</sub>). Anal. (C<sub>7</sub>H<sub>11</sub>N<sub>3</sub>O<sub>5</sub>S) C, H, N, S. A solution of the mesylate (13.5 g, 54 mmol) and NaN<sub>3</sub> (3.8 g, 59 mmol) in DMF (150 mL) was stirred at 100 °C for 1 h, cooled, poured into brine, and extracted with EtOAc (3  $\times$  200 mL). The combined organic extracts were washed with brine and evaporated to give crude 2-(2-nitro-5-nitro-1H-imidazolyl)ethyl azide (18) (8.26 g, 78%): mp (EtOAc/petroleum ether) 56–58 °C; <sup>1</sup>H NMR (CDCl<sub>3</sub>)  $\delta$  7.98 (s, 1H, H-4'), 4.45 (dd, *J* = 5.7, 5.3 Hz, 2 H, H-2), 3.79 (dd, *J* = 5.6, 5.3 Hz, 2 H, H-1), 2.44 (s, 3 H, CH<sub>3</sub>); <sup>13</sup>C NMR  $\delta$  151.3 (C-2'), 136.7 (C-5'), 133.4 (C-4'), 50.8 (C-1), 45.5 (C-2), 14.5 (CH<sub>3</sub>); HRMS calcd for C<sub>6</sub>H<sub>8</sub>N<sub>4</sub>O<sub>2</sub> 196.0709 (M<sup>+</sup>), found 196.0707. Anal. (C<sub>6</sub>H<sub>8</sub>N<sub>4</sub>O<sub>2</sub>) C, H.

A stirred solution of 18 in dry THF (100 mL) was treated dropwise with a solution of Ph<sub>3</sub>P (14.2 g, 54 mmol) in dry THF (20 mL) at 20 °C and stirred for a further 3 h. Concentrated HCl (150 mL) was then added, and the mixture was heated under reflux for 5 h before being evaporated to dryness. The residue was partitioned between EtOAc and water, and the aqueous layer was evaporated to give 2-(2-methyl-5-nitro-1H-imidazolyl)ethylamine (19) as the dihydrochloride salt (11.0 g, 84%): mp (MeOH) 194–194.5 °C dec; <sup>1</sup>H NMR (D<sub>2</sub>O)  $\delta$  8.50 (s, 1 H, H-4'), 4.86 (t, *J* = 6.9 Hz, 2 H, H-2), 3.58 (t, *J* = 6.9 Hz, 2 H, H-1), 2.78 (s, 3 H, CH<sub>3</sub>); <sup>13</sup>C NMR (D<sub>2</sub>O)  $\delta$  157.2 (C-2'), 140.9 (C-5'), 127.1 (C-4'), 46.5 (C-1), 40.3 (C-2), 14.3 (CH<sub>3</sub>). Anal. (C<sub>6</sub>H<sub>10</sub>N<sub>4</sub>O<sub>2</sub>·2HCl) C, H, N.

**2-(1H-Imidazolyl)ethylamine Dihydrochloride (21·2HCl).** A solution of imidazole (3.0 g, 44.1 mmol) in DMF (30 mL) was added dropwise to a stirred suspension of NaH (1.94 g, 48.5 mmol) in DMF (30 mL) at 0 °C, and the mixture was stirred until homogeneous. A solution of *N*-(2-bromoethyl)phthalimide (11.8 g, 46.3 mmol) in THF/DMF (1:1, 25 mL) was then added, and the mixture was stirred at 100 °C for 2 h, cooled, and poured into brine (200 mL). Extraction with EtOAc, workup of the organic layer, and crystallization from EtOAc/petroleum ether gave *N*-(2-(1H-imidazolyl)ethyl)phthalimide (20) (4.88 g, 46%): mp 162–164 °C; <sup>1</sup>H NMR (CDCl<sub>3</sub>)  $\delta$  7.81–7.84 (m, 2 H, ArH), 7.72–7.75 (m, 2 H, ArH), 7.42 (s, 1H, H-2'), 7.03 (t, *J* = 1.2 Hz, 1 H, H-5'), 6.96 (t, *J* = 1.2 Hz, 1 H, H-4'), 4.29 (t, *J* = 6.5 Hz, 2 H, H-2), 4.05 (t, *J* = 6.5 Hz, 2 H, H-1); <sup>13</sup>C NMR (CDCl<sub>3</sub>)  $\delta$  167.8 (2CO), 137.3 (C-2'), 134.4 (2C<sub>arom</sub>), 131.6 (2C<sub>arom</sub>), 130.0 (C-5'), 123.6 (2C<sub>arom</sub>), 118.9 (C-4'), 44.4 (C-2), 38.3 (C-1). Anal. (C<sub>13</sub>H<sub>11</sub>N<sub>3</sub>O<sub>2</sub>) C, H, N.

A stirred solution of 20 (2.8 g, 11.6 mmol) and hydrazine monohydrate (1.13 mL, 23.2 mmol) in EtOH (100 mL) was heated under reflux for 4 h. The resulting suspension was cooled to 0 °C and filtered, and the filtrate was evaporated to dryness under reduced pressure. The residue was dissolved in 1 N HCl (50 mL) and filtered, and the solvent was removed under reduced pressure to give 2-(1H-imidazolyl)ethylamine dihydrochloride (21·2HCl) (1.49 g, 70%): mp (MeOH/EtOAc) 217–220 °C; <sup>1</sup>H NMR (D<sub>2</sub>O)  $\delta$  8.92 (s, 1 H, H-2'), 7.65 (s, 1 H, H-5'), 7.57 (s, 1 H, H-4'), 4.66 (t, *J* = 6.3 Hz, 2 H, H-2), 3.61 (t, *J* = 6.3 Hz, 2 H, H-1); <sup>13</sup>C NMR (D<sub>2</sub>O)  $\delta$  138.1 (C-2'), 124.5 (C-5'), 123.3 (C-4'), 48.8 (C-1), 4 1.5 (C-1). Anal. (C<sub>6</sub>H<sub>8</sub>N<sub>2</sub>·2HCl) C, H, N, Cl.

**2-(2-Nitro-1*H*-imidazolyl)ethylamine Hydrochloride (23-HCl) and 3-(2-Nitro-1*H*-imidazolyl)propylamine Hydrochloride (25-HCl).** A stirred solution of 2-nitroimidazole (3.0 g, 26.5 mmol), 2-bromoethylphthalimide (7.08 g, 27.9 mmol), and  $K_2CO_3$  (3.85 g, 27.9 mmol) in DMF (75 mL) was heated at 110 °C for 2 h. The solvent was removed under reduced pressure, and the residue was poured into water (200 mL). The precipitate was collected, washed with water (100 mL), and dried to give 2-(2-nitro-1*H*-imidazolyl)ethylphthalimide (22) (5.28 g, 78%): mp 208.5–209 °C (lit.<sup>39</sup> mp 208–210 °C);  $^1H$  NMR ( $(CD_3)_2SO$ )  $\delta$  7.82–7.84 (m, 4 H, ArH), 7.60 (s, 1 H, H-5'), 7.07 (s, 1 H, H-4'), 4.64 (br t, 2 H, H-2), 4.06 (br t, 2 H, H-1);  $^{13}C$  NMR  $\delta$  167.3 (2CO), 144.7 (C-2'), 134.5 (2C<sub>arom</sub>), 131.2 (C-5'), 128.4 (2C<sub>arom</sub>), 127.9 (C-4'), 123.1 (2C<sub>arom</sub>), 48.3 (C-1), 37.1 (C-2). A stirred solution of this phthalimide (3.65 g, 12.8 mmol) and hydrazine monohydrate (1.24 mL, 25.5 mmol) in EtOH (70 mL) was heated under reflux for 2 h. The resulting suspension was cooled to 0 °C and filtered, and the filtrate was evaporated to dryness under reduced pressure. The residue was dissolved in 1 N HCl (50 mL) and filtered, the solvent was removed under reduced pressure, and the residue was crystallized from MeOH/EtOAc to give 2-(2-nitro-1*H*-imidazolyl)ethylamine hydrochloride (23-HCl) (1.49 g, 70%): mp 188.5–189 °C (lit.<sup>40</sup> mp 188–190 °C);  $^1H$  NMR ( $D_2O$ )  $\delta$  7.54 (d,  $J$  = 1.0 Hz, 1 H, H-5'), 7.25 (d,  $J$  = 1.1 Hz, 1 H, H-4'), 4.82 (t,  $J$  = 6.1 Hz, 2 H, H-2), 3.58 (t,  $J$  = 6.1 Hz, 2 H, H-1);  $^{13}C$  NMR ( $D_2O$ )  $\delta$  147.4 (C-2'), 131.1 (C-5'), 130.6 (C-4'), 49.4 (C-2), 41.2 (C-1).

Similar reaction of 2-nitroimidazole with (3-bromopropyl)-phthalimide gave 3-(2-nitro-1*H*-imidazolyl)propylphthalimide (24) (98% yield): mp 203–204 °C;  $^1H$  NMR ( $CD_3Cl$ )  $\delta$  7.85–7.89 (m, 2 H, ArH), 7.74–7.78 (m, 2 H, ArH), 7.37 (s, 1 H, H-4'), 7.16 (s, 1 H, H-5'), 4.48 (t,  $J$  = 7.0 Hz, 2 H, H-3), 3.78 (t,  $J$  = 6.3 Hz, 2 H, H-1), 2.25–2.32 (m, 2 H, H-2);  $^{13}C$  NMR  $\delta$  168.4 (2CO), 144.0 (C-2'), 134.3 (2C-3'), 131.8 (2C-2'), 128.4 (C-4'), 126.3 (C-5'), 123.5 (2C-4'), 47.7 (C-3), 34.7 (C-1), 29.8 (C-2). Anal. ( $C_{14}H_{12}N_4O_4$ ) C, H, N. Reaction of this with hydrazine monohydrate as above gave 3-(2-nitro-1*H*-imidazolyl)propylamine hydrochloride (25-HCl) (23.8 g, 66%): mp (MeOH) 214–214.5 °C;  $^1H$  NMR ( $(CD_3)_2SO$ )  $\delta$  8.26 (br s, 3 H,  $NH_2 \cdot HCl$ ), 7.87 (s, 1 H, H-5'), 7.22 (s, 1 H, H-4'), 4.53 (t,  $J$  = 6.8 Hz, 2 H, H-3), 2.78 (br s, 2 H, H-1), 2.10–2.17 (m, 2 H, H-2);  $^{13}C$  NMR  $\delta$  144.6 (C-2'), 127.9 (C-4'), 127.8 (C-5'), 46.6 (C-3), 35.7 (C-1), 27.5 (C-2). Anal. ( $C_8H_{10}N_4O_2 \cdot HCl$ ) C, H, N, Cl.

**2-(4-Nitro-1*H*-imidazolyl)ethylamine Hydrochloride (27-HCl) and 2-(5-Nitro-1*H*-imidazolyl)ethylamine Hydrochloride (29-HCl).** A stirred solution of 4-nitroimidazole (5.0 g, 44.2 mmol), *N*-(*tert*-butoxycarbonyl)-2-(methylsulfonyl)ethylamine (10.76 g, 48.6 mmol) and  $K_2CO_3$  (6.72 g, 48.6 mmol) in DMF (250 mL) was heated at 110 °C for 4 h. The solvent was removed under reduced pressure, and the residue was partitioned between EtOAc and water (500 mL). The aqueous fraction was washed with EtOAc (2  $\times$  50 mL), and the combined organic fractions were washed with water (2  $\times$  100 mL), brine (150 mL), dried, and evaporated. Chromatography of the residue on silica gel with a gradient (60–100%) of EtOAc/petroleum ether first gave *N*-(*tert*-butoxycarbonyl)-2-(5-nitro-1*H*-imidazolyl)ethylamine (28) (0.78 g, 7%): mp (EtOAc/petroleum ether) 148–149.5 °C;  $^1H$  NMR ( $CDCl_3$ )  $\delta$  8.00 (d,  $J$  = 1.0 Hz, 1 H, H-4'), 7.53 (s, 1 H, H-2'), 4.80 (br t,  $J$  = 5.6 Hz, 1 H, NH), 4.52 (t,  $J$  = 5.6 Hz, 2 H, H-2), 3.51 (dd,  $J$  = 6.0, 5.6 Hz, 2 H, H-1), 1.41 (s, 9 H, *t*-Bu);  $^{13}C$  NMR ( $CDCl_3$ )  $\delta$  155.9 ( $NHCO_2$ ), 142.1 (C-5'), 142.1 (C-2'), 133.8 (C-4'), 80.3 (C-( $CH_3$ )<sub>3</sub>), 47.4 (C-2), 40.6 (C-1), 28.3 (C( $CH_3$ )<sub>3</sub>). Anal. ( $C_{10}H_{16}N_4O_4$ ) C, H, N. Further elution gave *N*-(*tert*-butoxycarbonyl)-2-(4-nitro-1*H*-imidazolyl)ethylamine (26) (4.65 g, 41%): mp 106–107 °C;  $^1H$  NMR ( $CDCl_3$ )  $\delta$  7.80 (d,  $J$  = 1.4 Hz, 1 H, H-5'), 7.41 (d,  $J$  = 1.4 Hz, 1 H, H-2'), 5.33 (br s, 1 H, NH), 4.19 (dd,  $J$  = 5.9, 5.5 Hz, 2 H, H-2), 3.52 (dd,  $J$  = 5.9, 5.6 Hz, 2 H, H-1), 1.43 (s, 9 H, *t*-Bu);  $^{13}C$  NMR ( $CDCl_3$ )  $\delta$  155.9 ( $NHCO_2$ ), 148.0 (C-4'), 136.4 (C-2'), 119.6 (C-5'), 80.4 (C( $CH_3$ )<sub>3</sub>), 47.9 (C-2), 41.2 (C-1), 28.3 (C( $CH_3$ )<sub>3</sub>). Anal. ( $C_{10}H_{16}N_4O_4$ ) C, H, N.

A solution of 28 (0.76 g, 3.0 mmol) in MeOH (20 mL) and 5 N HCl (20 mL) was stirred at 20 °C for 16 h and then evaporated under reduced pressure to give 2-(5-nitro-1*H*-imidazolyl)ethylamine hydrochloride (29-HCl) (0.62 g, 91%): mp (MeOH) 199.5–200 °C dec;  $^1H$  NMR ( $(CD_3)_2SO$ )  $\delta$  8.31 (s, 1 H, H-4'), 8.12 (s, 1

H, H-2'); 7.04 (br s, 1 H, NH), 4.57 (t,  $J$  = 5.8 Hz, 2 H, H-2), 3.15 (q,  $J$  = 5.7 Hz, 2 H, H-1);  $^{13}C$  NMR ( $(CD_3)_2SO$ )  $\delta$  142.8 (C-2'), 138.6 (C-5'), 132.0 (C-4'), 44.8 (C-2), 38.1 (C-1). Anal. ( $C_8H_{10}Cl_2N_4O_2$ ) C, H, N. Similar treatment of 26 gave 2-(4-nitro-1*H*-imidazolyl)ethylamine hydrochloride (27-HCl) (58%): mp (MeOH) 240–241 °C;  $^1H$  NMR ( $(CD_3)_2SO$ )  $\delta$  8.53 (d,  $J$  = 1.4 Hz, 1 H, H-5'), 8.03 (br s, 2 H, NH), 7.95 (d,  $J$  = 1.4 Hz, 1 H, H-2'), 4.44 (d,  $J$  = 6.0, 5.8 Hz, 2 H, H-2), 3.31 (dd,  $J$  = 6.0, 5.8 Hz, 2 H, H-1);  $^{13}C$  NMR ( $(CD_3)_2SO$ )  $\delta$  147.0 (C-4'), 137.7 (C-2'), 121.9 (C-5'), 44.8 (C-2), 38.6 (C-1). Anal. ( $C_8H_{10}Cl_2N_4O_2$ ) C, H, N.

**2-(2-Methyl-5-nitro-1*H*-imidazolyl)acetic Acid (30).** A stirred solution of metronidazole (5) (2.0 g, 11.7 mmol) in  $Me_2CO$  (30 mL) at 0 °C was treated dropwise with  $CrO_3/Me_2CO$  until an orange color persisted. The solvent was removed under reduced pressure and the residue chromatographed on silica. Elution with MeOH/EtOAc (0–10% MeOH) gave 2-(2-methyl-5-nitro-1*H*-imidazolyl)acetic acid (30) (1.05 g, 49%): mp (MeOH/EtOAc) 175–177 °C (lit.<sup>41</sup> mp 179–180 °C);  $^1H$  NMR ( $D_2O$ )  $\delta$  7.96 (s, 1 H, H-4'), 5.05 (s, 2 H, H-2), 2.45 (s, 3 H,  $CH_3$ ).

**2-(2-Nitro-1*H*-imidazolyl)acetic Acid (32).** A stirred suspension of 2-nitroimidazole (2.0 g, 17.1 mmol), 2-iodoethyl tetrahydropyranyl ether (5.0 g, 19.5 mmol), and  $K_2CO_3$  (2.7 g, 19.5 mmol) in DMF (50 mL) was heated at 110 °C for 2 h. The solvent was removed under reduced pressure, and the residue was partitioned between EtOAc and water. The residue from the organic phase was dissolved in MeOH (30 mL) and 6 M HCl (5 mL) and stirred at 20 °C for 18 h and then evaporated under reduced pressure to give 2-(2-nitro-1*H*-imidazolyl)ethanol (31) (1.55 g, 57%): mp (MeOH/EtOAc) 148–150 °C (lit.<sup>42</sup> mp 157 °C);  $^1H$  NMR ( $D_2O$ )  $\delta$  7.47 (s, 1 H, H-5'), 7.19 (s, 1 H, H-4'), 4.62 (t,  $J$  = 5.2 Hz, 2 H, H-2), 3.96 (t,  $J$  = 5.2 Hz, 2 H, H-1);  $^{13}C$  NMR ( $D_2O$ )  $\delta$  147.2 (C-2'), 131.1 (C-5'), 130.4 (C-4'), 62.8 (C-1), 54.6 (C-2).

Oxidation of 31 with Jones' reagent as above, followed by chromatography on silica and elution with a gradient (0–10%) of MeOH/EtOAc gave 2-(2-nitro-1*H*-imidazolyl)acetic acid (32) (0.75 g, 37%): mp (MeOH) 158–159 °C (lit.<sup>43</sup> mp 159–160 °C);  $^1H$  NMR ( $(CD_3)_2SO$ )  $\delta$  7.63 (s, 1 H, H-5'), 7.20 (s, 1 H, H-4'), 5.16 (s, 2 H, H-2);  $^{13}C$  NMR ( $(CD_3)_2SO$ )  $\delta$  168.5 ( $CO_2H$ ), 144.7 (C-2'), 128.3 (C-5'), 127.4 (C-4'), 50.9 (C-2).

**3-(2-Nitro-1*H*-imidazolyl)propionic Acid (34).** A stirred suspension of 2-nitroimidazole (5.0 g, 44.2 mmol), methylacrylate (8 mL, 88.4 mmol), and KF/alumina (0.25 g) was heated at 100 °C for 18 h. The suspension was cooled to 20 °C, the solvent was removed under reduced pressure, and the residue was chromatographed on silica gel. Elution with EtOAc/petroleum ether (1:1) gave methyl 3-(2-nitro-1*H*-imidazolyl)propionate (33) as an oil (3.08 g, 35%) (lit.<sup>22</sup> mp 68–69 °C);  $^1H$  NMR ( $CDCl_3$ )  $\delta$  7.24 (s, 1 H, H-5'), 7.13 (s, 1 H, H-4'), 4.71 (t,  $J$  = 6.2 Hz, 2 H, H-3), 3.69 (s, 3 H,  $OCH_3$ ), 2.93 (t,  $J$  = 6.2 Hz, 2 H, H-2);  $^{13}C$  NMR ( $CDCl_3$ )  $\delta$  170.8 ( $CO_2H$ ), 144.7 (C-2'), 128.4 (C-5'), 127.1 (C-4'), 52.2 ( $OCH_3$ ), 45.6 (C-3), 34.6 (C-2). Hydrolysis of 33 (concentrated HCl/20 °C/4 h) gave 3-(2-nitro-1*H*-imidazolyl)propionic acid (34) (170 mg, 96%): mp ( $H_2O$ ) 162–164 °C;  $^1H$  NMR ( $(CD_3)_2SO$ )  $\delta$  7.66 (s, 1 H, H-5'), 7.16 (s, 1 H, H-4'), 6.33 (br s, 1 H,  $CO_2H$ ), 4.59 (t,  $J$  = 6.9 Hz, 2 H, H-3), 2.85 (t,  $J$  = 6.9 Hz, 2 H, H-2);  $^{13}C$  NMR ( $(CD_3)_2SO$ )  $\delta$  171.1 ( $CO_2H$ ), 144.7 (C-2'), 127.7 (C-5'), 127.6 (C-4'), 44.9 (C-3), 34.2 (C-2). Anal. ( $C_8H_7N_3O_4$ ) C, H, N.

**4-(2-Nitro-1*H*-imidazolyl)butanoic Acid (36): Example of General Method.** A stirred suspension of 2-nitroimidazole (1 equiv), methyl 4-bromobutanoate (1.2 equiv), and  $K_2CO_3$  (1.1 equiv) in DMF (1 mL/3 mmol) was heated at 110 °C for 2 h. Solvent was removed under reduced pressure, and the residue was partitioned between EtOAc and water. The organic layer was worked up, and the residue was chromatographed on silica gel to yield methyl 4-(2-nitro-1*H*-imidazolyl)butanoate (35) as an oil:  $^1H$  NMR ( $CDCl_3$ )  $\delta$  7.16 (s, 1 H, H-5'), 7.15 (s, 1 H, H-4'), 4.53 (t,  $J$  = 7.1 Hz, 2 H, H-4), 3.69 (s, 3 H,  $OCH_3$ ), 2.41 (t,  $J$  = 7.0 Hz, 2 H, H-2), 2.17–2.24 (m, 2 H, H-3);  $^{13}C$  NMR ( $CDCl_3$ )  $\delta$  172.4 ( $CO_2$ ), 144.6 (C-2'), 128.2 (C-5'), 126.1 (C-4'), 51.7 ( $OCH_3$ ), 49.0 (C-4), 30.1 (C-2), 25.3 (C-3). Hydrolysis of 35 (conc. HCl/20 °C/16 h) gave a quantitative yield of 4-(2-nitroimidazol-1*yl*)-butanoic acid (36): mp (water) 114–115 °C;  $^1H$  NMR ( $D_2O$ )  $\delta$  7.50 (s, 1 H, H-5'), 7.22 (s, 1 H, H-4'), 4.54 (t,  $J$  = 7.0 Hz, 2 H, H-4), 2.48 (t,  $J$  = 7.1 Hz, 2 H, H-2), 2.15–2.22 (m, 2 H, H-3);  $^{13}C$  NMR ( $D_2O$ )  $\delta$  179.8 ( $CO_2H$ ), 147.5 (C-2'), 130.7 (C-5'), 130.2



(C-4)\*, 52.0 (C-4), 33.1 (C-2), 27.2 (C-3). (\* Assignments interchangeable.) Anal. (C<sub>7</sub>H<sub>11</sub>N<sub>3</sub>O<sub>4</sub>) C, H, N.

A similar reaction using methyl 5-bromopentanoate gave methyl 5-(2-nitro-1*H*-imidazolyl)pentanoate (37) (87%) as an oil: <sup>1</sup>H NMR (CDCl<sub>3</sub>) δ 7.16 (d, *J* = 1.0 Hz, 1 H, H-5'), 7.15 (d, *J* = 1.0 Hz, 1 H, H-4'), 4.45 (t, *J* = 7.3 Hz, 2 H, H-5), 3.68 (s, 3 H, OCH<sub>3</sub>), 2.39 (t, *J* = 7.2 Hz, 2 H, H-2), 1.88–1.96 (m, 2 H, H-4), 1.66–1.73 (m, 2 H, H-3); <sup>13</sup>C NMR (CDCl<sub>3</sub>) δ 173.2 (CO<sub>2</sub>), 140.5 (C-2'), 128.3 (C-5')\*, 125.9 (C-4')\*, 51.6 (OCH<sub>3</sub>), 49.8 (C-5), 33.0 (C-4), 29.7 (C-3), 21.5 (C-2). Hydrolysis as above gave 5-(2-nitroimidazol-1*H*-yl)pentanoic acid (38), mp (water) 125–126.5 °C. <sup>1</sup>H NMR ((CD<sub>3</sub>)<sub>2</sub>SO) δ 7.71 (s, 1 H, H-5'), 7.19 (s, 1 H, H-4'), 6.25 (br s, 1 H, CO<sub>2</sub>H), 4.40 (t, *J* = 7.0 Hz, 2 H, H-5), 2.26 (t, *J* = 7.3 Hz, 2 H, H-2), 1.75–1.83 (m, 2 H, H-4), 1.54–1.53 (m, 2 H, H-3); <sup>13</sup>C NMR ((CD<sub>3</sub>)<sub>2</sub>SO) δ 174.1 (CO<sub>2</sub>H), 144.6 (C-2'), 127.9 (C-5')\*, 127.8 (C-4')\*, 49.2 (C-5), 33.0 (C-4), 29.1 (C-3), 21.3 (C-2). (\* Assignments interchangeable.) Anal. (C<sub>8</sub>H<sub>11</sub>N<sub>3</sub>O<sub>4</sub>) C, H, N.

A similar reaction using methyl 6-bromohexanoate gave methyl 6-(2-nitro-1*H*-imidazolyl)hexanoate (39) as an oil (92%): <sup>1</sup>H NMR (CDCl<sub>3</sub>) δ 7.14 (s, 2 H, H-4', H-5'), 4.43 (t, *J* = 7.3 Hz, 2 H, H-6), 3.67 (s, 3 H, OCH<sub>3</sub>), 2.39 (t, *J* = 7.3 Hz, 2 H, H-2), 1.85–1.93 (m, 2 H, H-5), 1.65–1.73 (m, 2 H, H-3), 1.37–1.44 (m, 2 H, H-4); <sup>13</sup>C NMR (CDCl<sub>3</sub>) δ 173.6 (CO<sub>2</sub>), 144.7 (C-2'), 128.4 (C-5')\*, 125.9 (C-4')\*, 51.5 (OCH<sub>3</sub>), 49.9 (C-6), 33.5 (C-2), 30.1 (C-4), 25.7 (C-5), 24.0 (C-3). (\* Assignments interchangeable.) Hydrolysis as above gave 6-(2-nitro-1*H*-imidazolyl)hexanoic acid (40): mp (water) 106–108 °C; <sup>1</sup>H NMR (CDCl<sub>3</sub>) δ 7.95 (br s, 1 H, CO<sub>2</sub>H), 7.14 (d, *J* = 0.9 Hz, 1 H, H-5'), 7.10 (d, *J* = 0.9 Hz, 1 H, H-4'), 4.42 (t, *J* = 7.3 Hz, 2 H, H-6), 2.37 (t, *J* = 7.2 Hz, 2 H, H-2), 1.84–1.92 (m, 2 H, H-5), 1.65–1.72 (m, 2 H, H-3), 1.39–1.45 (m, 2 H, H-4); <sup>13</sup>C NMR (CDCl<sub>3</sub>) δ 178.2 (CO<sub>2</sub>H), 144.5 (C-2'), 128.3 (C-5')\*, 125.9 (C-4')\*, 50.0 (C-6), 33.4 (C-2), 30.1 (C-4), 25.7 (C-5), 23.9 (C-3). (\* Assignments interchangeable.) Anal. (C<sub>9</sub>H<sub>13</sub>N<sub>3</sub>O<sub>4</sub>) C, H, N.

*N*-[2-(2-Methyl-5-nitro-1*H*-imidazolyl)ethyl]-4-(2-nitro-1*H*-imidazolyl)butanamide (10): Example of General Method. A stirred suspension of the acid (36) (5.0 g, 25.1 mmol), the amine dihydrochloride (19-2HCl) (6.41 g, 26.3 mmol), and Et<sub>3</sub>N (10.5 mL, 75.3 mmol) in DMF (100 mL) was treated dropwise at 0 °C under N<sub>2</sub> with diethyl phosphorocyanidate (4.57 mL, 30.1 mmol). The suspension was stirred for 2 h at 0 °C and for a further 18 h at 20 °C and then evaporated to dryness under reduced pressure. The residue was chromatographed directly on silica gel, elution with a gradient (0–20%) of MeOH/EtOAc giving *N*-[2-(2-methyl-5-nitro-1*H*-imidazolyl)ethyl]-4-(2-nitro-1*H*-imidazolyl)butanamide (10) (5.5 g, 76%): mp (CHCl<sub>3</sub>/petroleum ether) 129 °C; <sup>1</sup>H NMR (CD<sub>3</sub>CN) δ 7.86 (s, 1 H, H-4''), 7.28 (d, *J* = 1.0 Hz, 1 H, H-5'), 7.07 (d, *J* = 1.0 Hz, 1 H, H-4'), 6.61 (br s, 1 H, CONH), 4.31–4.37 (m, 4 H, H-4, H-2'), 3.47 (2 t, *J* = 6.2 Hz, 2 H, H-1'), 2.38 (s, 3 H, CH<sub>3</sub>), 2.06–2.10 (m, 2 H, H-2), 1.99–2.02 (m, 2 H, H-3); <sup>13</sup>C NMR (CD<sub>3</sub>CN) δ 173.0 (CONH), 152.3 (C-2''), 140.1 (C-2'), 139.1 (C-5'), 133.8 (C-4''), 128.8 (C-5'), 128.1 (C-4')\*, 50.2 (C-2'), 46.5 (C-4), 39.1 (C-1'), 32.8 (C-2), 26.5 (C-3), 14.5 (CH<sub>3</sub>). (\* Assignments interchangeable.) Anal. (C<sub>13</sub>H<sub>17</sub>N<sub>7</sub>O<sub>6</sub>) C, H, N: calcd 27.91; found 28.46.

Similar reaction of 36 and 23 gave *N*-[2-(2-nitro-1*H*-imidazolyl)ethyl]-4-(2-nitro-1*H*-imidazolyl)butanamide (6) (67%): mp (MeOH/iPr<sub>2</sub>O) 149.5–150.5 °C; <sup>1</sup>H NMR ((CD<sub>3</sub>)<sub>2</sub>SO) δ 7.97 (br t, *J* = 5.8 Hz, 1 H, CONH), 7.62 (d, *J* = 1.0 Hz, 1 H, H-5''), 7.52 (d, *J* = 1.0 Hz, 1 H, H-5'), 7.18 (d, *J* = 1.0 Hz, 1 H, H-4''), 7.14 (d, *J* = 1.0 Hz, 1 H, H-4'), 4.43 (t, *J* = 5.8 Hz, 2 H, H-2'), 4.35 (t, *J* = 6.7 Hz, 2 H, H-4), 3.46 (q, *J* = 5.8 Hz, 2 H, H-1'), 1.89–2.08 (m, 4 H, H-2, H-3), 2.35 (s, 3 H, CH<sub>3</sub>); <sup>13</sup>C NMR ((CD<sub>3</sub>)<sub>2</sub>SO) δ 171.4 (CONH), 144.6 (C-2''), 144.5 (C-2'), 128.3, 127.7, 127.6 (C-4', C-4'', C-5', C-5''), 49.0, 48.8 (C-4, C-2'), 38.1 (C-1'), 31.6 (C-2), 25.3 (C-3). Anal. (C<sub>12</sub>H<sub>16</sub>N<sub>7</sub>O<sub>6</sub>) C, H, N: calcd 29.07; found 29.74.

Similar reaction of 34 and 25 gave *N*-[3-(2-nitro-1*H*-imidazolyl)propyl]-3-(2-nitro-1*H*-imidazolyl)propanamide (7) (49% yield): mp (MeOH/iPr<sub>2</sub>O) 124–125 °C; <sup>1</sup>H NMR ((CD<sub>3</sub>)<sub>2</sub>SO) δ 8.02 (br t, *J* = 5.5 Hz, 1 H, CONH), 7.65 (s, 1 H, H-5''), 7.54 (s, 1 H, H-5''), 7.19 (s, 1 H, H-4''), 7.13 (s, 1 H, H-4''), 4.60 (t, *J* = 6.5 Hz, 2 H, H-3), 4.32 (t, *J* = 7.0 Hz, 2 H, H-3'), 3.04 (dt, *J* = 6.5, 6.1 Hz, 2 H, H-1'), 2.67 (t, *J* = 6.6 Hz, 2 H, H-2), 1.57 (quintet, *J* = 6.9 Hz, 2 H, H-2'). (\* Assignments interchangeable.) <sup>13</sup>C NMR δ 169.1 (CONH), 144.6 (C-2'), 127.9, 127.8, 127.7, 127.5

(C-4', C-5', C-4'', C-5''), 47.2 (C-3), 45.8 (C-3'), 35.6 (C-2), 35.5 (C-1'), 29.5 (C-2'). Anal. (C<sub>12</sub>H<sub>16</sub>N<sub>7</sub>O<sub>6</sub>) C, H, N.

Similar reaction of 32 and 19 gave *N*-[2-(2-methyl-5-nitro-1*H*-imidazolyl)ethyl]-2-(2-nitro-1*H*-imidazolyl)ethanamide (8) as a hygroscopic foam (35%): <sup>1</sup>H NMR (CD<sub>3</sub>CN) δ 7.87 (s, 1 H, H-4''), 7.23 (d, *J* = 1.0 Hz, 1 H, H-5'), 7.11 (d, *J* = 1.0 Hz, 1 H, H-4'), 6.96 (br s, 1 H, CONH), 4.97 (s, 2 H, H-1), 4.36 (t, *J* = 6.1 Hz, 2 H, H-2'), 3.58 (2 t, *J* = 6.2 Hz, 2 H, H-1'), 2.41 (s, 3 H, CH<sub>3</sub>); <sup>13</sup>C NMR (CD<sub>3</sub>CN) δ 167.4 (CONH), 152.5 (C-2'), 144.2 (C-2'), 139.9 (C-5''), 133.9 (C-4''), 128.9 (C-5'), 128.8 (C-4'), 57.2 (C-2'), 46.3 (C-2), 39.6 (C-1'), 14.6 (CH<sub>3</sub>); MS (DEI) *m/z* 323 (M<sup>+</sup>, 3), 277 (50%), 231 (85), 97 (100); HRMS (DEI) *m/z* calcd for C<sub>11</sub>H<sub>13</sub>N<sub>5</sub>O<sub>7</sub> 323.0978 (M<sup>+</sup>), found 323.0981. Anal. (C<sub>11</sub>H<sub>13</sub>N<sub>5</sub>O<sub>7</sub>) C, H, N.

Similar reaction of 34 and 19 gave *N*-[2-(2-methyl-5-nitro-1*H*-imidazolyl)ethyl]-3-(2-nitro-1*H*-imidazolyl)propanamide (9) (42%): mp (MeOH/iPr<sub>2</sub>O) 144.5–145.5 °C; <sup>1</sup>H NMR ((CD<sub>3</sub>)<sub>2</sub>SO) δ 8.18 (br t, *J* = 5.7 Hz, 1 H, CONH), 8.00 (s, 1 H, H-4''), 7.51 (s, 1 H, H-5'), 7.13 (d, *J* = 1.0 Hz, 1 H, H-4'), 4.53 (t, *J* = 6.6 Hz, 2 H, H-2), 4.27 (t, *J* = 5.9 Hz, 2 H, H-2'), 3.40 (q, *J* = 5.9 Hz, 2 H, H-1'), 2.62 (t, *J* = 6.6 Hz, 2 H, H-2), 2.35 (s, 3 H, CH<sub>3</sub>); <sup>13</sup>C NMR ((CD<sub>3</sub>)<sub>2</sub>SO) δ 159.5 (CONH), 151.2 (C-2''), 144.5 (C-2'), 138.4 (C-5''), 133.0 (C-4''), 127.9 (C-4'), 127.6 (C-5'), 45.5 (C-3), 45.2 (C-2'), 37.8 (C-1'), 35.3 (C-2), 13.6 (CH<sub>3</sub>). (\* Assignments interchangeable.) Anal. (C<sub>12</sub>H<sub>15</sub>N<sub>7</sub>O<sub>6</sub>) C, H, N: calcd, 29.07; found 29.91.

Similar reaction of 38 and 19 gave *N*-[2-(2-methyl-5-nitro-1*H*-imidazolyl)ethyl]-5-(2-nitro-1*H*-imidazolyl)pentanamide (11) (54%): mp (MeOH/iPr<sub>2</sub>O) 136–137.5 °C; <sup>1</sup>H NMR (CD<sub>3</sub>CN) δ 7.85 (s, 1 H, H-4''), 7.32 (d, *J* = 0.9 Hz, 1 H, H-5'), 7.09 (d, *J* = 0.9 Hz, 1 H, H-4'), 6.55 (br s, 1 H, CONH), 4.32–4.37 (m, 4 H, H-5, H-2'), 3.50 (2 t, *J* = 6.2 Hz, 2 H, H-1'), 2.39 (s, 3 H, CH<sub>3</sub>), 2.04–2.09 (m, 2 H, H-2), 1.72–1.80 (m, 2 H, H-4), 1.45–1.53 (m, 2 H, H-3); <sup>13</sup>C NMR (CD<sub>3</sub>CN) δ 173.7 (CONH), 152.4 (C-2''), 140.1 (C-2'), 139.9 (C-5''), 133.8 (C-4''), 128.8 (C-4'), 128.1 (C-5'), 50.6 (C-2'), 46.6 (C-5), 39.1 (C-1'), 35.8 (C-2), 30.4 (C-4), 22.9 (C-3), 14.6 (CH<sub>3</sub>). (\* Assignments interchangeable.) HRMS *m/z* calcd for C<sub>14</sub>H<sub>19</sub>N<sub>7</sub>O<sub>6</sub> 365.1448 (M<sup>+</sup>), found 365.1452. Anal. (C<sub>14</sub>H<sub>19</sub>N<sub>7</sub>O<sub>6</sub>) C, H, N: calcd 26.84; found 27.43.

Similar reaction of 40 and 19 gave *N*-[2-(2-methyl-5-nitro-1*H*-imidazolyl)ethyl]-6-(2-nitro-1*H*-imidazolyl)hexanamide (12) (53%): mp (MeOH/iPr<sub>2</sub>O) 133–134 °C; <sup>1</sup>H NMR (CD<sub>3</sub>CN) δ 7.88 (s, 1 H, H-4''), 7.33 (d, *J* = 1.0 Hz, 1 H, H-5'), 7.08 (d, *J* = 1.0 Hz, 1 H, H-4'), 6.50 (br s, 1 H, CONH), 4.33–4.38 (m, 4 H, H-6, H-2'), 3.50 (2 t, *J* = 6.2 Hz, 2 H, H-1'), 2.39 (s, 3 H, CH<sub>3</sub>), 2.03 (t, *J* = 7.4 Hz, 1 H, H-2), 1.75–1.83 (m, 2 H, H-5), 1.46–1.54 (m, 2 H, H-4), 1.22–1.28 (m, 2 H, H-3); <sup>13</sup>C NMR (CD<sub>3</sub>CN) δ 173.9 (CONH), 152.4 (C-2''), 140.1 (C-2'), 139.9 (C-5''), 133.9 (C-4''), 128.8 (C-4'), 128.1 (C-5'), 50.7 (C-2'), 46.6 (C-6), 39.1 (C-1'), 36.2 (C-2), 30.7 (C-5), 26.5 (C-4), 25.5 (C-3), 14.6 (CH<sub>3</sub>); HRMS *m/z* calcd for C<sub>15</sub>H<sub>21</sub>N<sub>7</sub>O<sub>6</sub> 379.1604 (M<sup>+</sup>), found 379.1613. Anal. (C<sub>15</sub>H<sub>21</sub>N<sub>7</sub>O<sub>6</sub>) C, H, N.

Similar reaction of 36 and 21 gave *N*-[2-(1*H*-imidazolyl)ethyl]-4-(2-nitro-1*H*-imidazolyl)butanamide (13) (70%) as a hygroscopic gum; <sup>1</sup>H NMR (CD<sub>3</sub>CN) δ 7.42 (s, 1 H, H-2''), 7.29 (d, *J* = 1.0 Hz, 1 H, H-5'), 7.08 (d, *J* = 1.0 Hz, 1 H, H-4'), 7.00 (t, *J* = 1.1 Hz, 1 H, H-5''), 6.90 (s, 1 H, H-4''), 6.62 (br s, 1 H, CONH), 4.37 (t, *J* = 6.9 Hz, 2 H, H-4), 4.02 (t, *J* = 6.1 Hz, 1 H, H-2'), 3.44 (2 t, *J* = 6.0 Hz, 2 H, H-1'), 2.10–2.14 (m, 2 H, H-2), 2.01–2.08 (m, 2 H, H-3); <sup>13</sup>C NMR (CD<sub>3</sub>CN) δ 172.8 (CONH), 141.0 (C-2'), 138.2 (C-2''), 129.7 (C-5''), 128.2 (C-5'), 128.2 (C-4'), 120.4 (C-4''), 50.3 (C-2'), 46.9 (C-4), 40.8 (C-1'), 33.0 (C-2), 26.7 (C-3); MS *m/z* 246 (M<sup>+</sup> – NO<sub>2</sub>, 100); HRMS *m/z* calcd for C<sub>12</sub>H<sub>17</sub>N<sub>6</sub>O<sub>3</sub> 293.1362 (M<sup>+</sup>), found 293.1363.

Similar reaction of 36 and 27 gave *N*-[2-(4-nitro-1*H*-imidazolyl)ethyl]-4-(2-nitro-1*H*-imidazolyl)butanamide (14) (56%): mp (MeOH/iPr<sub>2</sub>O) 175.5–177 °C; <sup>1</sup>H NMR ((CD<sub>3</sub>)<sub>2</sub>SO) δ 8.40 (d, *J* = 1.4 Hz, 1 H, H-5''), 8.08 (t, *J* = 5.6 Hz, 1 H, CONH), 7.81 (d, *J* = 1.4 Hz, 1 H, H-2''), 7.64 (d, *J* = 0.9 Hz, 1 H, H-5'), 7.18 (d, *J* = 0.9 Hz, 1 H, H-4'), 4.35 (t, *J* = 6.7 Hz, 2 H, H-4), 4.12 (dd, *J* = 6.0, 5.2 Hz, 2 H, H-2'), 3.43 (dd, *J* = 6.0, 5.7 Hz, 2 H, H-1'), 1.97–2.09 (m, 4 H, H-2, H-3); <sup>13</sup>C NMR ((CD<sub>3</sub>)<sub>2</sub>SO) δ 171.4 (CONH), 146.9 (C-4'), 144.5 (C-2'), 137.5 (C-2''), 127.7 (C-4', C-5'), 121.7 (C-5''), 48.8 (C-4), 47.0 (C-2'), 45.3 (C-1'), 31.7 (C-2), 25.6 (C-3); MS (DCI) *m/z* 338 (MH<sup>+</sup>, 40), 332 (10), 225 (35); HRMS (DCI) *m/z* calcd for C<sub>12</sub>H<sub>16</sub>N<sub>7</sub>O<sub>6</sub> 338.1213 (MH<sup>+</sup>), found 338.1203. Anal. (C<sub>12</sub>H<sub>16</sub>N<sub>7</sub>O<sub>6</sub>) C, H, N: calcd, 29.07; found 28.32.

Similar reaction of 36 and 29 gave *N*-[2-(5-nitro-1*H*-imidazolyl)ethyl]-4-(2-nitro-1*H*-imidazolyl)butanamide (15) (59%): mp (MeOH/*i*Pr<sub>2</sub>O) 152.5–153 °C; <sup>1</sup>H NMR ((CD<sub>3</sub>)<sub>2</sub>SO) δ 8.07 (s, 1 H, H-4''), 7.07 (br t, *J* = 5.9 Hz, 1 H, CONH), 7.94 (d, *J* = 1.4 Hz, 1 H, H-2''), 7.63 (d, *J* = 0.8 Hz, 1 H, H-5'), 7.18 (d, *J* = 0.8 Hz, 1 H, H-4'), 4.31–4.40 (m, 4 H, H-2'', H-4), 3.43 (dd, *J* = 5.8, 5.3 Hz, 2 H, H-1'), 1.90–2.09 (m, 4 H, H-2, H-3); <sup>13</sup>C NMR ((CD<sub>3</sub>)<sub>2</sub>SO) δ 171.4 (CONH), 144.5 (C-2'), 143.4 (C-2''), 138.5 (C-5''), 133.6 (C-4''), 127.8 (C-5'), 127.7 (C-4'), 48.8 (C-4), 47.0 (C-2'), 38.0 (C-1'), 31.6 (C-2), 25.5 (C-3). (\* Assignments interchangeable.) MS (DCI) *m/z* 338 (MH<sup>+</sup>, 75), 332 (15), 225 (100); HRMS (DCI) *m/z* calcd for C<sub>12</sub>H<sub>15</sub>N<sub>7</sub>O<sub>5</sub> 338.1213 (MH<sup>+</sup>), found 338.1208. Anal. (C<sub>12</sub>H<sub>15</sub>N<sub>7</sub>O<sub>5</sub>) C, H, N.

Similar reaction of 30 and 19 gave *N*-[2-(2-methyl-5-nitro-1*H*-imidazolyl)ethyl]-2-(2-methyl-5-nitro-1*H*-imidazolyl)-ethanamide (16) (55%) as a hygroscopic foam: <sup>1</sup>H NMR (CDCl<sub>3</sub>) δ 7.96 (s, 1 H, H-4''), 7.39 (s, 1 H, H-4'), 6.90 (br s, 1 H, CONH), 4.92 (s, 2 H, H-1), 4.48 (t, *J* = 6.5 Hz, 2 H, H-2'), 3.67 (q, *J* = 6.3 Hz, 2 H, H-1'), 2.50 (s, 6 H, 2CH<sub>3</sub>); <sup>13</sup>C NMR (CDCl<sub>3</sub>) δ 166.2 (CONH), 151.5 (C-2''), 151.2 (C-2'), 142.5 (C-5''), 139.9 (C-5'), 133.6 (C-4''), 133.1 (C-4'), 48.4, 44.6, 39.5 (3CH<sub>2</sub>), 14.2, 14.1 (2CH<sub>3</sub>). (\* Assignments interchangeable.) MS (DEI) *m/z* 337, (M<sup>+</sup>, 4), 291 (35), 245 (20), 211 (45), 53 (100); HRMS (DEI) *m/z* calcd for C<sub>12</sub>H<sub>15</sub>N<sub>7</sub>O<sub>5</sub> 337.1135 (M<sup>+</sup>), found 337.1142. Anal. (C<sub>12</sub>H<sub>15</sub>N<sub>7</sub>O<sub>5</sub>) C, H, N.

**In Vitro Cytotoxicity.** Cell lines were maintained as log-phase monolayers in tissue culture flasks using antibiotic-free Alpha MEM with 10% v/v heat-inactivated (56 °C, 40 min) fetal calf serum. Doubling times were approximately 14 h for AA8, 15 h for UV4, 9 h for EMT6, and 24 h for FME cells. Cultures were tested for mycoplasma contamination frequently, using a cytochemical staining method.<sup>44</sup> Bulk cultures of AA8 cells were prepared in spinner flasks, using the above growth medium plus penicillin (100 IU/mL) and streptomycin (100 µg/mL).

Growth inhibition studies were performed as described in detail elsewhere,<sup>27,45</sup> using 200 AA8, 300 UV4, 50 EMT6, or 1000 FME cells in 0.05 mL per well in 96-well tissue culture dishes. Drugs were added 24 h after initiation of cultures and removed 18 h later. The IC<sub>50</sub> was determined as the drug concentration needed to reduce the cell mass (protein content, measured 72–78 h after drug washout by staining with methylene blue and determining absorbance in a microplate photometer) to 50% of the mean value for eight control cultures on the same 96-well plate.

Clonogenic assays with magnetically-stirred 10-mL suspension cultures (plateau-phase AA8 cells, 10<sup>6</sup>/mL) were performed using continuous gassing with 5% CO<sub>2</sub> in air or N<sub>2</sub>, as detailed elsewhere.<sup>28</sup> Both cell suspensions and drug solutions in growth medium were preequilibrated under the appropriate gas phase for 60 min prior to mixing, to ensure essentially complete anoxia throughout the period of drug contact in hypoxic cultures. Plating efficiency was determined at intervals of 0.5–1 h for up to 8 h, and the concentration × time required to reduce survival to 10% of control values (CT<sub>10</sub>) was estimated at each drug concentration tested. Hypoxic selectivity was determined as the ratio of (interpolated) aerobic and hypoxic CT<sub>10</sub> values at the same time.

**In Vitro Radiosensitization.** Stirred suspensions of AA8 cells were made hypoxic by gassing with 5% CO<sub>2</sub> in N<sub>2</sub> for 60 min using the same conditions as in cytotoxicity assays. Cultures were irradiated at 37 °C (cobalt 60, dose rate ca. 2 Gy/min) 30 min after mixing drug and cells, with the cell cultures, waterbath, and stirrers positioned in the vertical radiation beam. Samples were withdrawn after each radiation dose (typically 6 Gy intervals), and plating efficiency (PE) was determined. The surviving fraction (SF) was determined with respect to unirradiated cells from the same culture, assayed immediately before irradiation. The data was fitted to the linear-quadratic model (ln SF = -αD - βD<sup>2</sup>, where *D* is the radiation dose) to interpolate the dose for 10% survival (D<sub>10</sub>). The sensitizer enhancement ratio (SER = D<sub>10</sub> without drug/D<sub>10</sub> with drug) was determined at a range of drug concentrations to estimate the concentration for an SER of 1.6 (C<sub>1.6</sub>). The SF as determined above corrects for drug toxicity due to preirradiation drug treatment, but not for any additional killing due to drug toxicity during the irradiation period. This was determined separately, using cell suspensions treated identically with drug, in the same waterbath but outside the radiation field, and the SF was calculated relative

to hypoxic controls. The C<sub>1.6</sub> was analyzed using only SER values for drug concentrations where this toxicity was minimal over the irradiation period.

**Drug Uptake Studies.** Intracellular and extracellular drug concentrations were determined under the same conditions as the radiosensitization assays, after a 30-min hypoxic incubation of AA8 cells at a drug concentration equal to the C<sub>1.6</sub>. The culture (10<sup>7</sup> cells) was centrifuged at 140g for 5 min, and samples of the supernatant (50 µL) were diluted into 19 volumes of ice-cold MeCN for determination of extracellular drug concentration. The remaining supernatant was discarded, the tubes centrifuged (13000g for 2 min), aspirated, and centrifuged again to remove residual medium from the walls of the tube. Water (90 µL) was added to lyse the cell pellets, and 9 volumes of MeCN was added. The MeCN extracts were frozen at -80 °C. After thawing, samples were centrifuged (13000g × 5 min), and the supernatant was evaporated to dryness. The residues were dissolved in 0.2 mL of HPLC mobile phase and centrifuged again to remove any particulate matter, and samples (0.17 mL) were analyzed by HPLC using a Waters C18 µ-Bondapak column (8 × 100 mm) at a flow rate of 1.8 mL/min. The initial mobile phase was constructed by mixing an organic phase (MeCN/H<sub>2</sub>O, 4:1, v/v) with formate buffer at pH 4.5 (28 g ammonium formate and 2.55 mL formic acid in 1 L) in the ratio 18:82. After 2 min the organic component was increased linearly to 40% by 12 min. The nitroimidazoles were detected by absorbance at 320 nm using a Hewlett-Packard diode array detector (HP 1040A). All drug concentrations were corrected for recovery (detection efficiency) by spiking culture medium (for extracellular recoveries) or lysed cell pellets (for intracellular recoveries) with known amounts of drug, using concentrations similar to those estimated in the unknown samples. Recoveries were in the range 0.70–0.99 for all compounds. Average intracellular concentrations in cells were calculated assuming a cellular water volume of 11.6 µL/10<sup>7</sup> AA8 cells and an extracellular water volume in the pellet of 1.1 µL in a pellet of 10<sup>7</sup> cells, using [<sup>14</sup>C(U)]sucrose to mark the extracellular space and <sup>3</sup>H<sub>2</sub>O to mark the total water volume as reported elsewhere.<sup>46</sup>

**In Vivo Studies.** Single cell suspensions were prepared from KHT tumors by enzymatic dissociation (0.5 mg/mL, pronase, 0.2 mg/mL collagenase, 0.2 mg/mL DNase I for 40 min). The tumor was passaged in C<sub>3</sub>H/HeN mice by sc inoculation of 2 × 10<sup>5</sup> cells in the inguinal region. Tumors were prepared in the same manner for experiments, and treated when in the size range 0.5–1.0 mL as assessed by caliper measurements. Compounds 1 and 10 were administered ip as solutions in phosphate-buffered saline, using single or multiple doses of 2.5 mmol and an injection volume of 0.01 (1) or 0.04 (10) mL/g body weight per dose. Tumors were irradiated 45 min after the last drug dose, using whole body irradiation (cobalt 60) of unanaesthetised, unrestrained mice at a dose rate of ca 2.5 Gy/min. Tumors were excised 18 h after irradiation, dissociated as above, and the cell yield determined with an electronic cell counter. Clonogenic survival was then assessed, essentially as described,<sup>47</sup> by plating 10–20 replicate 1-mL samples in α MEM containing 0.3% agar, with lethally-irradiated (40 Gy) KHT cells added to give a total of 10<sup>4</sup> cells/mL, in 24-well culture dishes. After growth for 13 days, colonies were stained by adding 0.175 mL of (iodophenyl)(nitrophenyl)-tetrazolium chloride (0.5 mg/mL in H<sub>2</sub>O) to each well. Cultures were incubated at 37 °C overnight, and colonies were counted with a binocular microscope.

**Acknowledgment.** The authors thank Karin Tan, Susan Pullen, Diane Schultz, and Xing Zhi Xu for technical help, Drs. Richard Hill and Stephen Cliffe for advice on the KHT assays, and Wendy Hodgson for preparing the manuscript. This work was carried out under Contract CM-07321-27 from the National Cancer Institute, with further support from the Auckland Division of the Cancer Society of New Zealand and the Health Research Council of New Zealand. We thank Hoffmann-LaRoche (Basel) for a generous gift of 2-nitroimidazole.

## References

- Chapman, J. D. Measurement of tumor hypoxia by invasive and non-invasive procedures: a review of recent clinical studies. *Radiat. Oncol.* 1991, Suppl. 20, 13-19.
- Gatenby, R. A.; Kessler, H. B.; Rosenblum, J. S.; Coia, L. R.; Moldofsky, P. J.; Harz, W. H. Oxygen distribution in squamous cell carcinoma metastases and its relationship to outcome of radiation therapy. *Int. J. Radiat. Oncol. Biol. Phys.* 1988, 14, 831-838.
- Wilson, W. R. Tumor hypoxia; challenges for cancer chemotherapy. In *Cancer Biology and Medicine*; Waring, M. J., Ponder, B. A. J., Eds.; Kluwer Academic: Lancaster, 1992; Vol. 3, pp 87-131.
- Brown, J. M.; Koong, A. Therapeutic advantage of hypoxic cells in tumors: A theoretical study. *J. Natl. Cancer Inst.* 1991, 83, 178-185.
- Adams, G. E.; Stratford, I. J. Hypoxia-mediated nitroheterocyclic drugs in the radio- and chemotherapy of cancer. An overview. *Biochem. Pharmacol.* 1986, 35, 71-76.
- Kennedy, K. A. Hypoxic cells as specific drug targets for chemotherapy. *Anti-Cancer Drug Design* 1987, 2, 181-194.
- Sartorelli, A. C. Therapeutic attack of hypoxic cells of solid tumors: Presidential address. *Cancer Res.* 1988, 48, 775-778.
- Rauth, A. M. Pharmacology and toxicology of sensitizers: mechanism studies. *Int. J. Radiat. Oncol. Biol. Phys.* 1984, 10, 1293-1300.
- Adams, G. E.; Stratford, I. J.; Wallace, R. G.; Wardman, P.; Watts, M. E. Toxicity of nitro compounds towards hypoxic mammalian cells *in vitro*: dependence on reduction potential. *J. Natl. Cancer Inst.* 1980, 64, 555-560.
- Whitmore, G. F.; Guylas, S. Studies on the toxicity of RSU-1069. *Int. J. Radiat. Oncol. Biol. Phys.* 1986, 12, 1219-1222.
- McClelland, R. A.; Fuller, J. R.; Seaman, N. E.; Rauth, A. M.; Battistella, R. 2-Hydroxylaminoimidazoles - unstable intermediates in the reduction of 2-nitroimidazoles. *Biochem. Pharmacol.* 1984, 33, 303-309.
- Stratford, I. J.; O'Neill, P.; Sheldon, P. W.; Silver, A. R. J.; Walling, J. M.; Adams, G. E. RSU-1069, a nitroimidazole containing an aziridine group. *Biochem. Pharmacol.* 1986, 35, 105-109.
- Hill, R. P.; Guylas, S.; Whitmore, G. F. Studies on the *in vivo* and *in vitro* cytotoxicity of the drug RSU 1069. *Br. J. Cancer* 1986, 53, 743-751.
- O'Neill, P.; McNeil, S. S.; Jenkins, T. C. Induction of DNA crosslinks *in vitro* upon reduction of RSU 1069 and RSU 1131. *Biochem. Pharmacol.* 1987, 36, 1787-1792.
- Horwich, A.; Holliday, S. B.; Deacon, J. M.; Peckham, M. J. A toxicity and pharmacokinetic study in man of the hypoxic cell sensitizer RSU-1069. *Br. J. Radiat.* 1986, 59, 1238-1240.
- Jenkins, T. C.; Naylor, M. A.; O'Neill, P.; Threadgill, M. D.; Cole, S.; Stratford, I. J.; Adams, G. E.; Fielden, E. M.; Suto, M. J.; Stier, M. A. Synthesis and evaluation of  $\alpha$ -[[(2-haloethyl)amino]methyl]-2-nitro-1H-imidazole-1-ethanols as prodrugs of  $\alpha$ -[(1-aziridinyl)methyl]-2-nitro-1H-imidazole-1-ethanol (RSU-1069) and its analogues which are radiosensitisers and bioreductively activated cytotoxins. *J. Med. Chem.* 1990, 33, 2603-2610.
- Cole, S.; Stratford, I. J.; Bowler, J.; Nolan, J.; Wright, E. G.; Lormore, S. A.; Adams, G. E. Oral (po) dosing with RSU 1069 or RB 6145 maintains their potency as hypoxic cell radiosensitisers and cytotoxins but reduces systemic toxicity compared with parenteral (ip) administration in mice. *Int. J. Radiat. Oncol. Biol. Phys.* 1991, 21, 387-395.
- Wilson, W. R.; van Zijl, P.; Denny, W. A. Bis-bioreductive agents as hypoxia-selective cytotoxins: nitracrine N-oxide. *Int. J. Radiat. Oncol. Biol. Phys.* 1992, 22, 693-696.
- McClelland, R. A.; Panicucci, R.; Rauth, A. M. Products of the reduction of 2-nitroimidazoles. *J. Am. Chem. Soc.* 1987, 109, 4308-4314.
- Raleigh, J. A. Binding of misonidazole to hypoxic cells in monolayer and spheroid culture: evidence that a sidechain label is bound as efficiently as a ring label. *Br. J. Cancer* 1985, 51, 229-235.
- Hansch, C.; Leo, A. *Substituent constants for correlation analysis in chemistry and biology*; Wiley: New York, 1979.
- Long, A.; Parrick, J.; Hodgkiss, R. J. An efficient procedure for the 1-alkylation of 2-nitroimidazoles and the synthesis of a probe for hypoxia in solid tumours. *Synthesis* 1991, 709-713.
- Bhujanga Rao, A. K. S.; Gundu Rao, C.; Singh, B. B. Formation of N-alkyl-2-methyl-4-nitro-1H-imidazoles via fluoride-ion-mediated Michael additions. *J. Chem. Res. (S)* 1991, 350-351.
- Chen, W.-Y.; Olsen, R. K. Synthesis of di- and tripeptides containing 4-aminocyclohexane carboxylic acids. *J. Org. Chem.* 1975, 40, 350-352.
- Wilson, W. R.; Thompson, L. H.; Anderson, R. F.; Denny, W. A. Hypoxia-selective antitumor agents. 2. Electronic effects of 4-substituents on the mechanisms of cytotoxicity and metabolic stability of nitracrine analogues. *J. Med. Chem.* 1989, 32, 31-38.
- Hoy, C. A.; Thompson, L. H.; Mooney, C. L.; Salazar, E. P. Defective DNA cross-link removal in Chinese hamster cell mutants hypersensitive to bifunctional alkylating agents. *Cancer Res.* 1985, 45, 1737-1743.
- Wilson, W. R.; Anderson, R. F.; Denny, W. A. Hypoxia-selective antitumor agents. 1. Relationships between structure, redox properties and hypoxia-selective cytotoxicity for 4-substituted derivatives of nitracrine. *J. Med. Chem.* 1989, 32, 23-30.
- Wilson, W. R.; Denny, W. A.; Twigg, S. J.; Baguley, B. C.; Probert, J. C. Selective toxicity of nitracrine to hypoxic mammalian cells. *Br. J. Cancer* 1984, 49, 215-223.
- Moselen, J. W.; Hay, M. P.; Denny, W. A.; Wilson, W. R. N-[2-(2-methyl-5-nitroimidazol-1H-yl)ethyl]-4-(2-nitroimidazol-1H-yl)-butanamide (SN 24699), a bis-nitroimidazole with enhanced selectivity for hypoxic cells *in vitro*. Manuscript in preparation.
- Wardman, P.; Clarke, E. D. One-electron reduction potentials of substituted imidazoles measured by pulse radiolysis. *J. Chem. Soc., Faraday Trans. 1* 1976, 72, 1377-1390.
- Adams, G. E.; Flockhart, I. R.; Smith, C. E.; Stratford, I. J.; Wardman, P.; Watts, M. E. Electron-affinic sensitisation. VII. A correlation between structures, one-electron reduction potentials, and efficiencies of 2-nitroimidazoles as hypoxic cell radiosensitisers. *Radiat. Res.* 1976, 67, 9-20.
- Wardman, P. Some reactions and properties of nitro radical anions important in biology and medicine. *Environ. Health Perspect.* 1985, 63, 309-320.
- CLOGP, version 3.51. MedChem Software, Medicinal Chemistry Project, Pomona College, Claremont, CA.
- Brown, D. M.; Parker, E. T.; Brown, J. M. Structure-activity relationships of 1-substituted 2-nitroimidazoles; effect of partition coefficient and side chain hydroxyl groups on radiosensitisation *in vitro*. *Radiat. Res.* 1982, 90, 98-108.
- Brown, J. M.; Lee, W. W. Pharmacokinetic considerations in radiosensitizer development. In *Radiation sensitizers: their use in the clinical management of cancer*; Brady, L. W., Ed.; Masson: New York, 1980; pp 2-13.
- Dennis, M. F.; Stratford, M. R. L.; Wardman, P. A.; Watts, M. E. Cellular uptake of misonidazole and analogues with acid or basic functions. *Int. J. Radiat. Biol.* 1985, 47, 629-643.
- Workman, P. Pharmacokinetics of hypoxic cell radiosensitizers. In *Radiation sensitizers: their use in the clinical management of cancer*; Brady, L. W., Ed.; Masson: New York, 1980; pp 192-206.
- Malliaros, D. P.; Goldman, P. Interaction of metronidazole with *Escherichia coli* deoxyribose nucleic acid. *Biochem. Pharmacol.* 1991, 42, 1739-1744.
- Ahmed, I.; Stratford, I. J.; Jenkins, T. C. Radiosensitizers of hypoxic mammalian cells 1-(hydroxyaminoalkyl)-substituted nitroimidazoles. *Arzneim.-Forsch.* 1985, 35, 1763-1768.
- Threadgill, M. D.; Webb, P. Selective reductions of 1-(carbonyl)-substituted 2-nitroimidazoles with alkali metal borohydrides and borane-tetrahydrofuran. *Synth. Commun.* 1990, 20, 2319-2325.
- Kajfez, F.; Sunjic, V.; Kolbah, D.; Fajdiga, T.; Oklodziga, M. 1-Substitution in 2-methyl-4(5)-nitroimidazole. 1. Synthesis of compounds with potential antitrichromonal activity. *J. Med. Chem.* 1968, 11, 167-169.
- Gallo, G. G.; Pasqualucci, C. R.; Radaelli, P.; Lamcini, G. C. The ionization constants of some imidazoles. *J. Org. Chem.* 1964, 29, 862-865.
- Hofmann LaRoche Co. Br. Pat. 1138529, 1969; Novel imidazole derivatives and a process for the manufacture thereof. *Chem. Abstr.* 1969, 71, 3383d.
- Chen, T. R. *In situ* detection of *Mycoplasma* contamination in cell cultures by fluorescent Hoechst 33258 stain. *Exp. Cell Res.* 1977, 104, 255-262.
- Finlay, G. J.; Baguley, B. C.; Wilson, W. R. A semiautomated microculture method for investigating growth inhibitory effects of cytotoxic compounds on exponentially growing carcinoma cells. *Anal. Biochem.* 1984, 139, 272-277.
- Siim, B. G.; Denny, W. A.; Wilson, W. R. Metabolic and radiolytic reduction of 5-nitroquinoline bioreductive drugs: relationship to selectivity for hypoxic cells. Manuscript in preparation.
- Thomson, J. E.; Rauth, A. M. An *in vitro* assay to measure the viability of KHT tumor cells not previously exposed to culture conditions. *Radiat. Res.* 1974, 58, 262-276.



# Hypoxia-Inducible Factor-1 (HIF-1) Up-Regulates Adrenomedullin Expression in Human Tumor Cell Lines during Oxygen Deprivation: A Possible Promotion Mechanism of Carcinogenesis

Mercedes Garayoa, Alfredo Martínez, Sunmin Lee, Rubén Pío,  
Won G. An, Len Neckers, Jane Trepel, Luis M. Montuenga,  
Heather Ryan, Randall Johnson, Max Gassmann, and  
Frank Cuttitta

Department of Cell and Cancer Biology (M.G., A.M., S.L., R.P.,  
W.G.A., L.N., J.T., F.C.)  
National Cancer Institute  
National Institutes of Health  
Bethesda, Maryland 20892

Department of Histology and Pathology (L.M.M.)  
University of Navarra  
31080 Pamplona, Spain

Department of Biology (H.R., R.J.)  
University of California San Diego  
La Jolla, California 92093

Institute of Physiology (M.G.)  
University of Zürich-Irchel  
CH-8057, Switzerland

Little is known about the molecular mechanisms that control adrenomedullin (AM) production in human cancers. We demonstrate here that the expression of AM mRNA in a variety of human tumor cell lines is highly induced in a time-dependent manner by reduced oxygen tension (1% O<sub>2</sub>) or exposure to hypoxia mimetics such as desferrioxamine mesylate (DFX) or CoCl<sub>2</sub>. This AM expression seems to be under hypoxia-inducible factor-1 (HIF-1) transcriptional regulation, since HIF-1 $\alpha$  and HIF-1 $\beta$  knockout mouse cell lines had an ablated or greatly reduced hypoxia AM mRNA induction. Similarly, inhibition or enhancement of HIF-1 activity in human tumor cells showed an analogous modulation of AM mRNA. Under hypoxic conditions, immunohistochemical analysis of tumor cell lines revealed elevated levels of AM and HIF-1 $\alpha$  as compared with normoxia, and we also found an increase of immunoreactive AM in the conditioned medium of tumor cells analyzed by RIA. AM mRNA

stabilization was shown to be partially responsible for the hypoxic up-regulated expression of AM. In addition, we have identified several putative hypoxia response elements (HREs) in the human AM gene, and reporter studies with selected HREs were capable of enhancing luciferase expression after exposure to DFX. Furthermore, transient co-expression of HIF-1 $\alpha$  resulted in an augmented transactivation of the reporter gene after DFX treatment. Given that most solid human tumors have focal hypoxic areas and that AM functions as a mitogen, angiogenic factor, and apoptosis-survival factor, our findings implicate the HIF-1/AM link as a possible promotion mechanism of carcinogenesis. (Molecular Endocrinology 14:848-862, 2000)

## INTRODUCTION

Adrenomedullin (AM) is a recently discovered hypotensive peptide isolated from a human pheochromocytoma (1). The cDNAs for human, rat, mouse, pig, and cow AM have been cloned and the genomic organi-

zation profile for human and mouse identified (2, 3). This peptide has been shown to mediate a multifunctional response in cell culture and animal systems that includes regulation of cardiovascular tone, bronchodilation, modulation of central brain function, natriuretic and diuretic action, antimicrobial activity, inhibition of hormone release, growth regulation, apoptosis survival, and induction of angiogenesis (see review in Refs. 4–6).

Several prior reports have demonstrated AM and its corresponding receptor (AM-R) to be ubiquitously expressed during embryogenesis and carcinogenesis. Early in both mouse and rat fetal development AM/AM-R are first detected in the heart, and then they appear progressively in other anatomical sites during organogenesis (7, 8). Maternal decidual cells and embryonic cells (fetal cytotrophoblast giant cells) of the ectoplacental cone, a site that mimics the invasion process of carcinogenesis, also show abundant expression of AM/AM-R (8, 9). After its initial identification in a human pheochromocytoma, further studies have demonstrated increased AM expression in tumor tissue of ganglioneuroblastoma, neuroblastoma, and adrenocortical carcinomas (10, 11). In addition, AM plasma levels are elevated in patients with gastrointestinal or lung cancer (12). Our group has shown that AM and AM-R are expressed in human tumor cell lines of the lung, breast, colon, ovary, prostate, brain, cartilage, and blood (13). In several of these lines, AM functioned as an autocrine proliferation factor whose effect could be inhibited by a neutralizing monoclonal antibody (MoAb-G6) causing growth cessation *in vitro* (13). Recently, it has been shown that hypoxic conditions or exposure to  $\text{CoCl}_2$  (a transition metal that mimics hypoxia) induces an increase in AM mRNA expression and protein production in a human colorectal carcinoma cell line, DLD-1 (14).

Focal areas of low oxygen tension ( $\leq 2.0\% \text{ O}_2$ ) are inherent to the biological processes of embryogenesis, wound repair, and carcinogenesis (15–17). A state of diminished free oxygen availability results when regional growth demands exceed the oxygen supply of the capillary bed (15). Under such conditions, an oxygen-sensing mechanism activates a transcription factor known as hypoxia-inducible factor-1 (HIF-1), which in turn up-regulates a series of genes that support the cell to compensate for the potentially lethal microenvironment (18). HIF-1 is a heterodimer composed of HIF-1 $\alpha$  and HIF-1 $\beta$ /ARNT (aryl hydrocarbon receptor nuclear translocator) subunits, both representing members of the PAS (Per, ARNT, Sim) basic-helix-loop-helix family (18). Transcription/translation products of HIF-1 $\alpha$  and HIF-1 $\beta$  are constitutively expressed; however, the HIF-1 $\alpha$  protein contains an oxygen-dependent degradation domain that is rapidly cleaved by the ubiquitin-proteasome pathway under normoxic conditions, thus enabling the modulation of HIF-1 activity in an oxygen-dependent manner (19). Genes transactivated by HIF-1 include aldolase A, enolase 1, erythropoietin (Epo), glucose transporter 1,

heme oxygenase 1, inducible nitric oxide synthase, lactate dehydrogenase A, phosphofructokinase L, phosphoglycerate kinase 1, transferrin (Tf), vascular endothelial growth factor (VEGF), and endothelin-1 (ET-1) (18, 20). Low oxygen tension is known to play a critical role in embryonic development, causes the emergence of drug/radiation-resistant tumor cells, enhances mutagenesis of neoplastic lesions, and elevates metastatic potential of the tumor (15, 21–24).

The way AM gene expression is regulated in human tumors is not yet known, but a decrease in oxygen tension could be a major cause for the induction of this molecule. In our present study we actually demonstrate the ability of hypoxia and hypoxia mimetics to up-regulate the AM message and protein expression in a variety of human tumor cell lines. We also made use of both molecular and biochemical characterization approaches to support that this induction is mediated by transactivation of the AM promoter by HIF-1 transcription factor as well as posttranscriptional mRNA stabilization.

## RESULTS

### AM mRNA Induction in Human Tumor Cell Lines under Hypoxic Treatments

Northern analysis for AM mRNA expression in a variety of human tumor cell lines (cancers of the lung, breast, colon, ovary, prostate, bone, and blood) demonstrated a consistent increase in message induced by exposure to  $1\% \text{ O}_2$ , desferrioxamine (DFX), or  $\text{CoCl}_2$ . All 17 cell lines evaluated in this manner showed inducible AM expression, and Fig. 1 illustrates a representative example of the observed responses to our test conditions (6 h exposure to  $100 \mu\text{M} \text{ CoCl}_2$ , 6 h exposure to  $260 \mu\text{M} \text{ DFX}$  or 12 h exposure to  $1\% \text{ O}_2$ ). Interestingly, although there is variability of expression in the basal AM mRNA levels between cell lines [the two pulmonary cancer cell lines NCI-H1264 (adenocarcinoma) and NCI-H157 (squamous cell carcinoma) being the opposing extremes], all tumor cell lines show increases in AM message expression on exposure to our hypoxic test conditions, with calculated test/basal ratios ranging from 1.3- to 25-fold.

We have used MCF7 (breast adenocarcinoma) as our standard human cancer cell line for all time course studies with exposures to  $\text{CoCl}_2$ , DFX, or  $1\% \text{ O}_2$ . Figure 2, A–C, demonstrates the induction of AM message at different time increments over a 24–48 h exposure series. Note that although  $\text{CoCl}_2$  exposure causes AM mRNA levels to reach a maximum at 8 h, both DFX and  $1\% \text{ O}_2$  induced an AM message zenith at 12 h, indicating a potential mechanistic difference between test reagents. Induced maximum levels of AM message are maintained with all the hypoxia treatments tested at 24 h of exposure, and even elevated levels are still observed at 48 h of exposure to  $1\% \text{ O}_2$ .

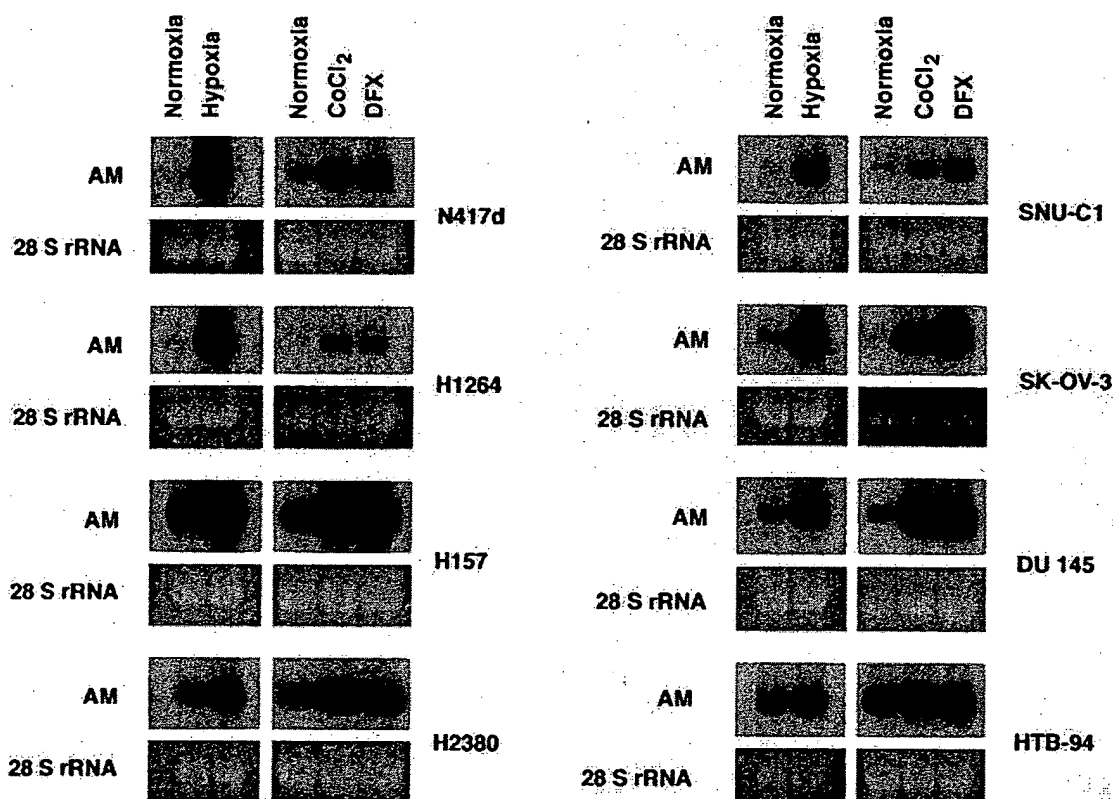


**Fig. 1.** Up-Regulation of AM mRNA in Several Human Tumor Cell Lines under Hypoxic Treatments

Northern blot analysis for AM of cells exposed either to hypoxia mimetics (100  $\mu$ M CoCl<sub>2</sub>, 260  $\mu$ M DFX) for 6 h, or to a hypoxic atmosphere (1% O<sub>2</sub>, 5% CO<sub>2</sub>, 94% N<sub>2</sub>) for 12 h, as compared with untreated cells. Cell lines shown here were selected from a total of 17 cell lines tested and also chosen as representatives of the main human tumor types: carcinomas of the lung (N417d, H1264, H157), breast (H2380), colon (SNUC-1), ovary (K-OV-3), prostate (DU 145), or chondrosarcoma (HTB-94). Fifteen micrograms of total RNA were loaded per lane, and ethidium bromide staining of 28 S rRNA was used to check for equal loading and RNA integrity.

Of the three treatments, exposure to 1% O<sub>2</sub> is the one that shows a steeper induction of AM mRNA over time, and also more dramatic increases between the basal and the maximum induction are observed (>25-fold increase between maximum induction and baseline levels).

We have also performed a parallel analysis for HIF-1 $\alpha$  mRNA in MCF7 cells throughout the hypoxic studies. HIF-1 $\alpha$  transcript levels remained constant or showed a slight decline over time in the CoCl<sub>2</sub> and 1% O<sub>2</sub> time course studies (Fig. 2, A and C). This observation is in accordance with other reports indicating that HIF-1 $\alpha$  is mainly regulated not at the transcriptional level but by protein stabilization in hypoxia, whereas the protein is rapidly degraded by the ubiquitin-proteasome pathway during normoxic conditions (19, 25).

#### Under Hypoxic Conditions, AM Is Also Induced at the Protein Level

To address whether the induction of AM mRNA was accompanied by an increase in the production of AM

protein, the presence and cellular localization of AM and HIF-1 $\alpha$  in tumor cell lines at normoxic or hypoxic conditions were studied using double immunofluorescence followed by confocal microscopy. A typical image is shown in Fig. 3, in which prostate carcinoma DU 145 cells are immunostained for both AM (green fluorescence) and HIF-1 $\alpha$  (red fluorescence). At normoxic conditions (Fig. 3, A and B), both AM and HIF-1 $\alpha$  are moderately expressed in the cytoplasm and nucleus of the cells. After 12 h exposure to 260  $\mu$ M DFX, the cells showed a marked increase of AM staining in the cytoplasm and nucleus (Fig. 3C); in agreement with our previous results (26) HIF-1 $\alpha$  immunoreactivity is primarily elevated in the nucleus of the cells (Fig. 3D). Similar patterns of staining were obtained with H157, MCF7, and SNUC-1 cell lines (data not shown).

Since we and other investigators have reported a rapid secretion of the bioactive processed AM peptide by human tumor cells and endothelial cells (13, 27), we also examined the presence of AM in the conditioned medium of MCF7 under hypoxic conditions. As is shown in Fig. 4, a significant increase in immunoreactive AM (IR-AM) was observed for MCF7 cells treated

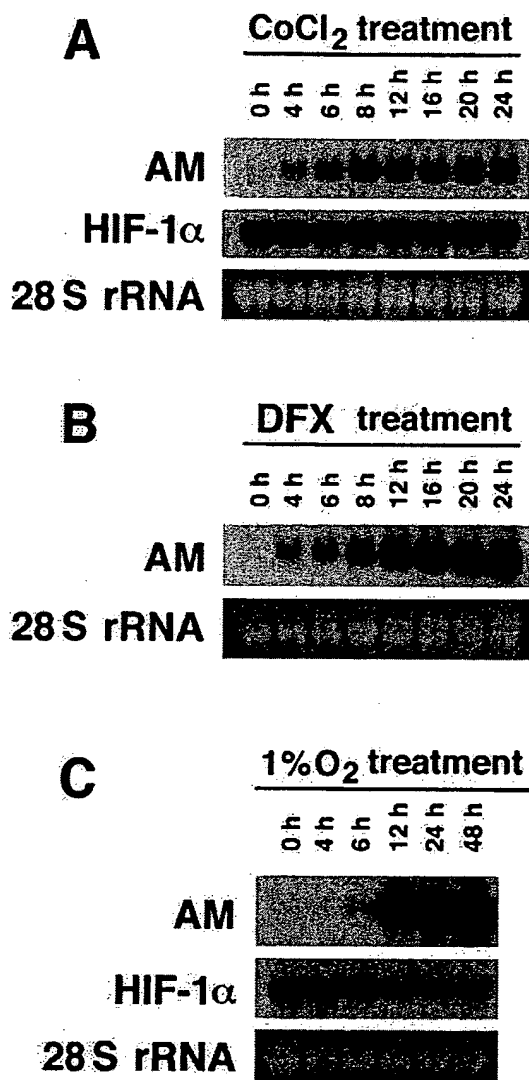


**Fig. 2.** Time Course Analysis of AM Expression  
Northern blot analysis of MCF7 cells cultured under 100  $\mu\text{M}$   $\text{CoCl}_2$  (A), 260  $\mu\text{M}$  DFX (B), or 1%  $\text{O}_2$  (C) for the indicated times. Fifteen micrograms of total RNA were loaded per lane and hybridized subsequently with human AM and human HIF-1 $\alpha$  cDNA probes. Equal loading was monitored by ethidium bromide staining of 28 S rRNA for each blot.

with 1%  $\text{O}_2$  at various times as compared with the cells maintained in normoxic conditions. Increasing values of accumulated IR-AM in the conditioned media of this cell line were also observed for the  $\text{CoCl}_2$  or DFX treatments (data not shown).

#### The Hypoxic Induction of AM mRNA Is Dependent on HIF-1

To determine whether the hypoxic up-regulation of AM mRNA was driven by HIF-1, we used cell lines derived from HIF-1 $\alpha$  or HIF-1 $\beta$  knockout mice to evaluate AM induction capabilities as compared with those of their

wild-type counterparts under hypoxic treatments. Figure 5A illustrates an experiment designed to compare AM mRNA levels in these cell lines when subjected to 6 h treatment of  $\text{CoCl}_2$  or DFX. It is shown that HIF-1 $\alpha$  null (–/–) mouse fibroblast cells failed to induce AM mRNA expression in these conditions, while the wild-type HIF-1 $\alpha$  (+/+) fibroblasts showed an inducible response. Similarly, normal HIF-1 $\beta$  (+/+) mouse embryonic stem (ES) cells demonstrated an inducible response, whereas HIF-1 $\beta$  null (–/–) ES cells showed a 32% and a 60% reduced induction when compared with the wild-type control, depending on the test reagent examined.

In addition, when HIF-1 $\alpha$  +/+ and HIF-1 $\alpha$  –/– cell lines were exposed to a hypoxia (1%  $\text{O}_2$ ) time course study (Fig. 5B), the hypoxic induction of AM mRNA was not detectable on the cells with the null mutation, although it was present in the wild-type cells. We also analyzed the levels of HIF-1 $\alpha$  message expression in this experiment. Note that HIF-1 $\alpha$  mRNA remained constant through the hypoxia treatment; however, HIF-1 $\alpha$  transcripts in HIF-1 $\alpha$  –/– cells present a higher molecular size than in the corresponding wild-type cells, since the null mutation was obtained by replacement of the helix-loop-helix domain of HIF-1 $\alpha$  with a neomycin resistance cassette (28).

Furthermore, artificial manipulation of HIF-1 activity with appropriate biochemical reagents was also used to elucidate the role of this transcription factor in AM message regulation under hypoxia. In this sense, the nitric oxide donor sodium nitroprusside (SNP) as well as genistein (a tyrosine kinase inhibitor), are known to inhibit HIF-1 activity by blocking the synthesis of HIF-1 subunits and/or interfering with HIF-1 DNA binding activity in hypoxia (29, 30). MCF7 cells were cultured for 12 h in normoxic or hypoxic conditions, with or without the appropriate biochemical reagents, and AM mRNA expression was analyzed comparing the treated vs. the nontreated cells (control). As is shown in Fig. 6, addition of 100  $\mu\text{M}$  SNP completely inhibited the induced expression of AM mRNA after 12 h of hypoxia (1%  $\text{O}_2$ ) treatment, while genistein at 100  $\mu\text{M}$  was a less potent suppressor of the AM mRNA induction mediated by low oxygen tension. Thus, the inhibited activity of HIF-1 with SNP and genistein is correlated with a suppressive effect on the AM mRNA hypoxic induction. Conversely, it has been reported that the CO scavenger hemoglobin (Hb) enhances HIF-1 activity by increasing HIF-1 DNA binding (31). Treatment of MCF7 cells with 50  $\mu\text{M}$  Hb was shown to further increase AM mRNA expression under hypoxic conditions by approximately 1.7-fold (Fig. 6).

#### Stabilization of AM Transcripts under Hypoxia

Hypoxia-induced up-regulation of gene expression can be mediated both by *de novo* synthesis of mRNA and by stabilization of the normally labile mRNAs under hypoxic conditions. To test whether the latter possibility was involved in the induced response of AM to

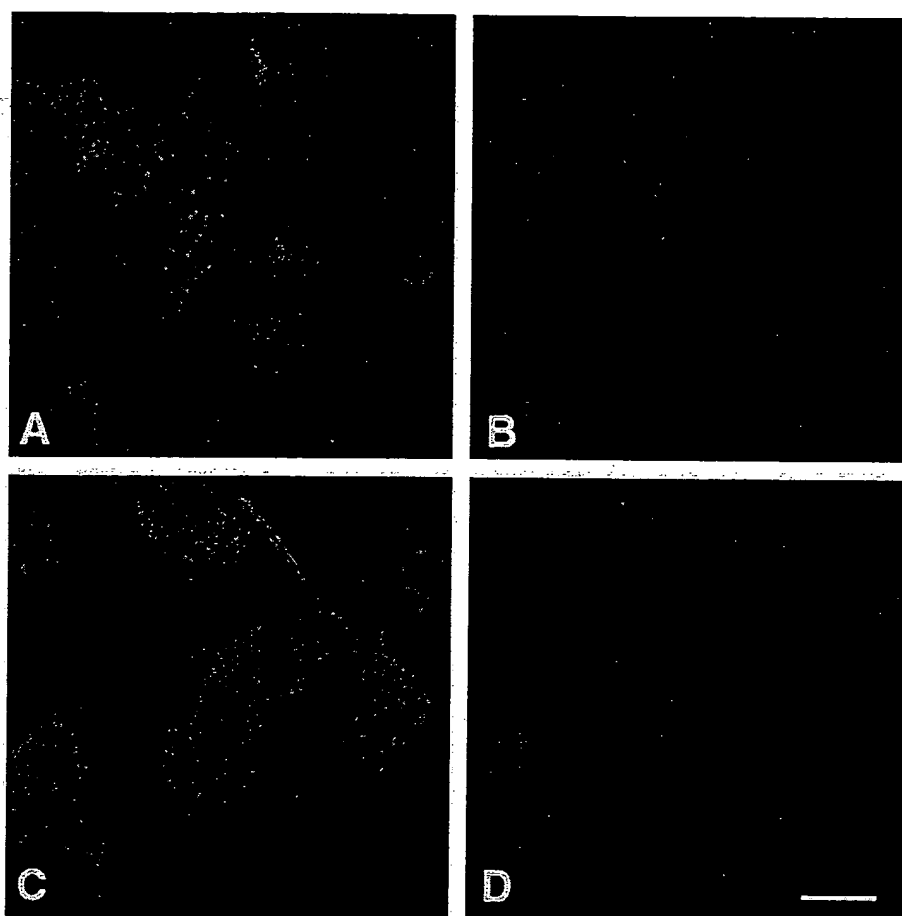


**Fig. 3.** Double Immunostaining for AM and HIF-1 $\alpha$  on DU 145 Cells Analyzed by Confocal Microscopy

Cells were grown on glass slides, left under normoxic conditions (A and B), or treated with 260  $\mu$ M DFX for 12 h (C and D), and then immunostained for AM and HIF-1 $\alpha$ . Equal microscope settings and exposures were maintained on images from normoxic/DFX-treated cells, to compare expression under both conditions. Both AM (A and C) and HIF-1 $\alpha$  (B and D) become markedly overexpressed after 12 h of DFX treatment. Bar = 5  $\mu$ m.

hypoxia, we examined the half-life of AM transcripts under normoxic and hypoxic conditions in the presence of actinomycin D, a compound known to inhibit RNA synthesis. MCF7 cells were maintained under hypoxic (1% O<sub>2</sub>) conditions for 12 h to sufficiently induce the expression of AM transcripts, and AM mRNA level at this point was considered the standard to which the rest of the samples were compared. After the initial hypoxic induction, actinomycin D was added at 4  $\mu$ g/ml, and the cells were further maintained at normoxic or hypoxic (1% O<sub>2</sub>) conditions from 1 to 4 h. As shown in Fig. 7, AM mRNA clearly decayed more rapidly under normoxic than under hypoxic conditions, thus indicating a stabilization process in hypoxia.

Densitometry analysis of the degradation of AM mRNA under normoxia and hypoxia in this experiment was performed, and the pooled data resulted in a calculated half-life of the AM mRNA of 1.7 h under normoxia and of 2.5 h under hypoxia. Our data thus indicate that the hypoxia-induced expression of AM

transcripts is at least partially dependent upon stabilization of AM mRNA.

#### Identification of Putative Hypoxia-Response Element (HRE) Sites in the Human AM Gene

Since it is known that HIF-1 mediated gene transactivation involves its binding to distinct nucleic acid motifs, namely HREs, we used GCG computer software from Genetics Computer Group (Madison, WI) to analyze the human and mouse AM genes (GenBank accession nos. D43639 and D78349, respectively) for appropriate HRE sequences. In this analysis we followed the HRE consensus motif proposed by Wenger and Gassmann (18, 32): (T,G,C) (A,G) CGTG (C,G,A) (G,T,C) (G,T,C) (C,T,G), which has been constructed from the nucleotide sequence of HIF-1 binding sites of 13 oxygen-dependent genes, and allowed for no more than a single base mismatch outside the CGTG core sequence. We have analyzed not only the 5'-promoter region but also the 3'-flanking region, introns/exons,

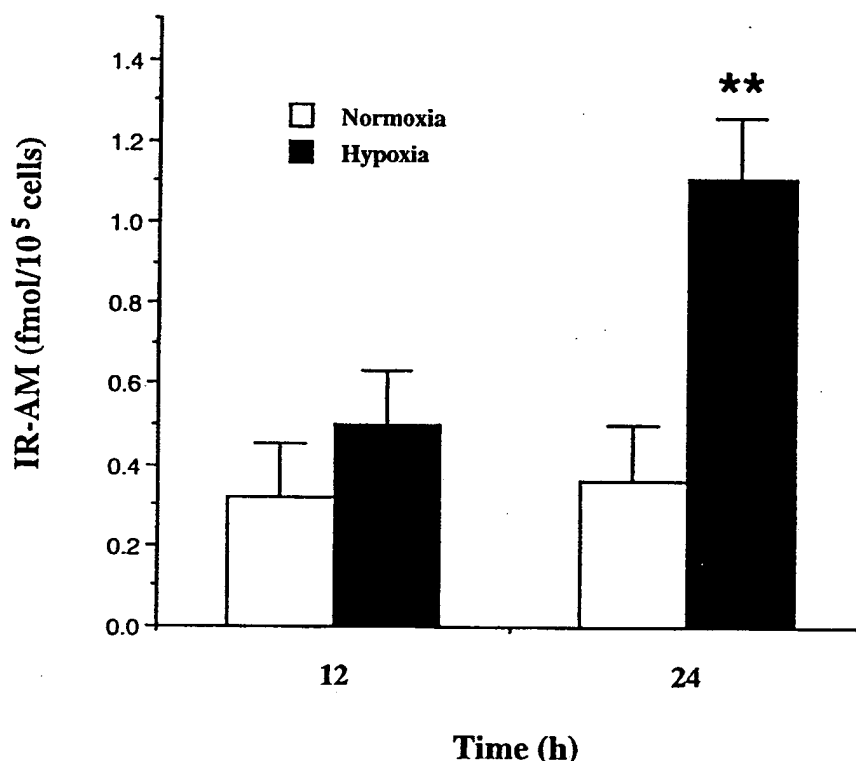


**Fig. 4.** RIA of IR-AM in the Conditioned Media of MCF7 Cells Cultured under Normoxia or 1% O<sub>2</sub> Atmosphere

After 12 h treatment, levels of AM detected in the conditioned medium of cells in both conditions are similar; however, at 24 h, values of accumulated IR-AM in cultured media of 1% O<sub>2</sub> treated cells were significantly higher than those from normoxic cells (\*\*,  $P = 0.004$ ). Values are the mean  $\pm$  SEM.

and looked for consensus motifs in both sense and antisense strands, since these genomic areas have been previously shown to have functional HRE sites in other HIF-1-inducible genes (18, 20, 33). With these premises, eight putative HRE sites at the 5'- and six sites at the 3'-untranslated flanking sequences of the human AM gene were found, together with putative HRE sequences in the first intron and in exon 3 and exon 4 (see Fig. 8). Similar analysis of the mouse AM gene identified three putative HRE sites in the antisense strand of the 5'-promoter region (positions: -1143, [AACTCAGGgA]; -98, [CAAGCAGGct]; and -62, [TGACCAGGCC]), and another three on the sense orientation: one in intron 1 (position 533, [CGCGTGCTGa]), one in intron 2 (position 727, [GCGTGCTTT]), and finally one at exon 4 (position: 1960, [GACGTGAaTG]).

#### Luciferase Reporter Assays for the Human AM Promoter Region under Hypoxia

To determine whether these HRE sites were actually involved in the regulation of AM mRNA expression, luciferase reporter studies were performed for different regions of the 5'-flanking region of the human AM gene. MCF7 cells were transiently transfected with the empty parental plasmid (pGL2basic) or with con-

structs comprising one, two, four, or eight putative HREs of the AM promoter (see Fig. 9A). A cotransfected  $\beta$ -galactosidase expression vector served as internal control for transfection efficiency and extract preparation. After the transfection, cells were left under normoxic conditions or exposed to 260  $\mu$ M DFX for 24 h, and luciferase activity was determined. No significant increase for the luciferase activity in the DFX-treated cells/normoxic cells was obtained when transfections were performed with constructs containing the one or two putative HREs closest to the TATA box (Fig. 9A). However, when cells were transfected with constructs containing four or eight putative HREs sites at the 5'-end of the TATA box, a significant ( $P < 0.01$ ) 1.5- and 1.7-fold increase in luciferase activity was observed when comparing DFX-treated vs. normoxic cells.

To test whether we could potentiate the increase in luciferase activity for the DFX treated/normoxic cells, we performed transient expression experiments using the HIF-1 $\alpha$  expression vector pCMV $\beta$ -HA-HIF-1 $\alpha$  (34). This expression vector was cotransfected into MCF7 cells together with the empty parental vector or plasmid constructs containing four or eight HREs from the AM promoter (pGL2basic, pGL2b-4, or pGL2b-8), and the normalization  $\beta$ -galactosidase plasmid. A repre-

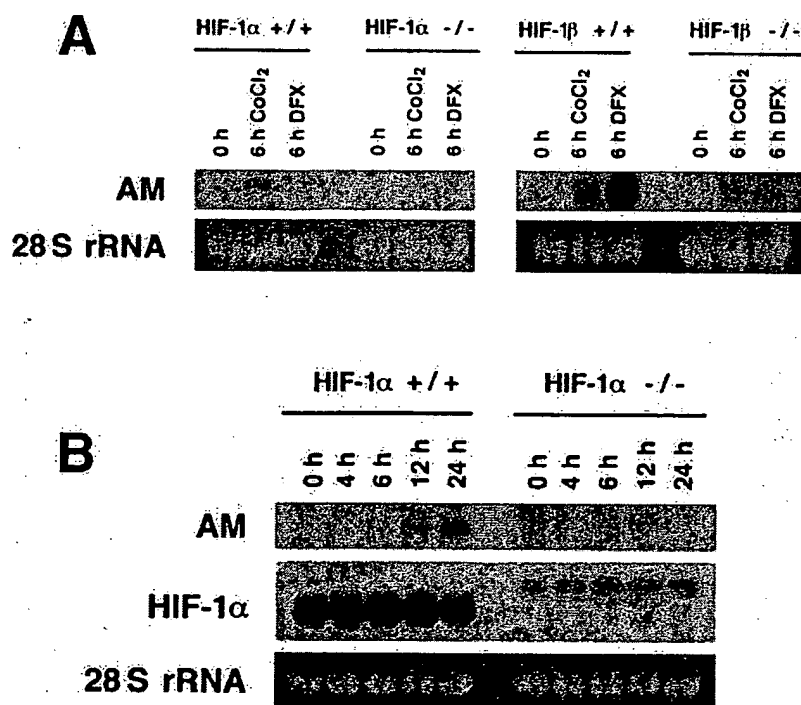


**Fig. 5.** Northern Blot Analysis on HIF-1α and HIF-1β Knockout Mouse Cell Lines

Fifteen micrograms of total RNA were loaded per lane, and equal loading and integrity of RNA were monitored by ethidium bromide staining of 28S rRNA. A, AM mRNA induction is suppressed in fibroblast HIF-1α -/- cells or reduced in ES HIF-1β -/- cells treated with CoCl<sub>2</sub> or DFX for 6 h as compared with their wild-type counterparts. B, Hypoxia (1% O<sub>2</sub>) time course study on HIF-1α wild-type (+/+) and HIF-1α null cells (-/-) probed for mouse AM and HIF-1α. Note that HIF-1α null cells fail to induce AM mRNA expression.

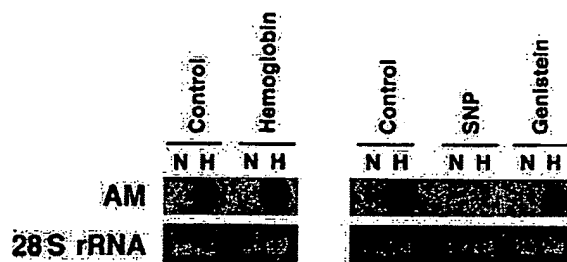


**Fig. 6.** Expression of AM mRNA in MCF7 Cells Treated with Reagents That Modulate HIF-1 Activity

Northern blot analysis was performed on MCF7 cells cultured for 12 h in a normoxic or hypoxic (1% O<sub>2</sub>) fashion with or without 50 μM Hb, 100 μM SNP, or 100 μM genistein. The hypoxic induction of AM transcripts in hypoxia was further augmented with Hb (a reagent that enhances HIF-1 activity), whereas SNP and genistein (known to inhibit HIF-1 activity) had a suppressive effect on that induction.

sentative experiment is shown in Fig. 9B, in which the transient overexpression of HIF-1α augmented the luciferase reporter activity after DFX treatment up to 2.9-fold when four HREs were present, and up to 4.8-fold with eight HREs as compared with the values of transfected cells in normoxic conditions; no significant increase was observed when the HIF-1α expression vector was cotransfected with the pGL2basic empty vector.

## DISCUSSION

Oxygen availability is known to play a key role in the growth-regulatory process underlying carcinogenesis (15). Seminal work by Semenza and collaborators (35, 36) demonstrated the general involvement of HIF-1 in the transcriptional response to hypoxia. Since then, several established growth modulation factors, including Epo, VEGF, Tf, ET-1, and insulin-like growth factor binding protein 1 (IGFBP-1), have been shown to be under HIF-1 transcriptional control (18, 20, 33). Based on previous reports showing that AM functions as an autocrine growth factor for certain human tumor cell lines (13), we began a comprehensive study to determine whether hypoxia could influence the expression of AM via HIF-1 in human tumor cell lines as an *in vitro* approach for similar conditions occurring in solid human cancers.

Our initial analysis by Northern blot in a variety of human tumor cell lines clearly demonstrates that hypoxia increases mRNA levels in these cells as compared with the untreated controls. Interestingly, there is a considerable variation in the basal levels of AM mRNA observed in normoxic conditions. High levels of basal AM mRNA may arise from the constitutive expression of HIF-1α protein in certain cells, a condition that has been previously reported for primary cultures of human pulmonary arterial smooth muscle cells (37).

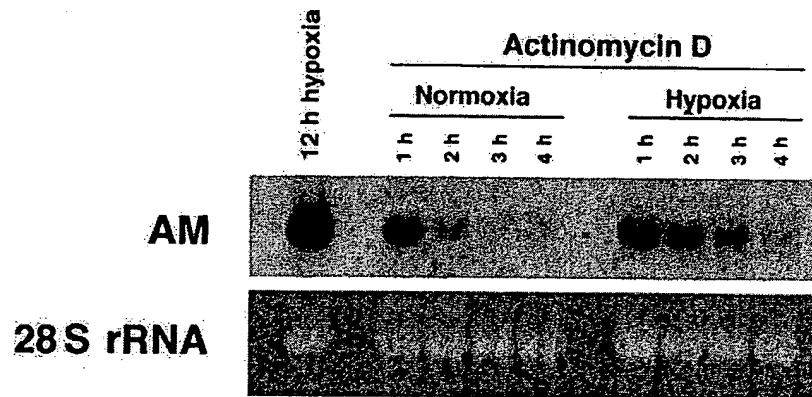


Fig. 7. Stabilization of AM Transcripts under Hypoxia

MCF7 cells were treated with 1%  $O_2$  for 12 h to induce the expression of AM mRNA. After addition of actinomycin D at 4  $\mu g/ml$ , cells were further maintained in normoxic or hypoxic conditions for the indicated times. Fifteen micrograms of total RNA were then loaded in each lane for Northern blot analysis of AM transcripts. AM mRNA levels at each point were compared with levels observed at 12 h hypoxia (previous to the addition of actinomycin D), and the half-life for AM transcripts under normoxic and hypoxic conditions was estimated.

In the time course experiments using MCF7 cells subjected to an hypoxic environment, we also demonstrate that the AM mRNA induction is paralleled by a somewhat delayed increased secretion of AM peptide from the cells to the conditioned media. Given our prior finding that endogenous AM functions as an autocrine growth factor for MCF7 (13), the demonstration that hypoxia augments bioactive AM production and secretion in these cells suggests that a similar scenario may take place in tissue neoplasms. The production and secretion of AM at the hypoxic areas present in tumors (15) could establish an autocrine/paracrine-mediated proliferation event leading to tumor growth. In addition, since AM has angiogenic and vasodilator capabilities (1, 6), the secreted AM could induce neovascularization and facilitate nutritional supplementation to the tumor cells. Finally, AM also has been shown to protect cells from apoptosis (5), and this feature could selectively rescue tumor cells from programmed cell death and might even predispose tumors to a more malignant phenotype (15).

The data obtained with the HIF-1 $\alpha$  and HIF-1 $\beta$  knockout mouse cell lines, together with those from the HIF-1 biochemical modulation studies performed on MCF7 cells, provide consistent evidence supporting the major involvement of HIF-1 in the transcriptional activation of AM by hypoxia and suggest that AM could be considered a new member of the growing family of HIF-1-targeted genes. The absence of inducible AM mRNA expression in HIF-1 $\alpha$  null mouse fibroblast cell line under hypoxia seems to highlight the critical importance of the HIF-1 $\alpha$  subunit in the transactivation of AM mRNA. Recent studies with HIF-1 $\alpha$  knockout mice have shown this genetic deletion to be an embryonic lethal event in the later stages of fetal development (28, 38). In addition, tumors derived from mouse ES cells with HIF-1 $\alpha$  null genotype have retarded growth, reduced VEGF expression, and less angiogenesis than their wild-type counterparts (28).

Given that AM is also highly expressed during embryogenesis (8), it would be interesting to evaluate whether there are modifications in the AM distribution patterns in early HIF-1 $\alpha$  null embryos. HIF-2 $\alpha$ , a hypoxia-inducible transcription factor sharing homology with HIF-1 $\alpha$ , has recently been shown to be essential in embryonic vascularization and catecholamine production (39); we cannot exclude a possible role of HIF-2 $\alpha$  in AM transactivation in endothelial and catecholamines-producing cells of embryos as well as catecholamines-producing tumors. In contrast to HIF-1 $\alpha$  knockout cell lines, ES HIF-1 $\beta$  null cells under hypoxia showed a diminished AM mRNA induction as compared with their wild-type counterparts, which may reflect the ability of other basic helix-loop-helix family members (e.g. ARNT 2 and ARNT 3) to compensate for the loss of HIF-1 $\beta$  in the formation of a functional heterodimer with HIF-1 $\alpha$ , albeit at lower efficiency (40, 41).

Prior studies have demonstrated the ability of reduced oxygen tension to mediate elevations in AM message/protein expression in several animal and cell systems. In this sense, hypoxia was shown to induce AM gene expression and secretion in cultured human umbilical vein endothelial cells (42); focal ischemic regions of the rat brain show high AM mRNA expression (43), and patients with chronic obstructive pulmonary disease involving tissue hypoxia have elevated AM plasma levels (44). Nakayama and colleagues (14) have demonstrated that hypoxia can elevate AM mRNA and protein expression in a single human colorectal carcinoma cell line, DLD-1; however, these investigators did not identify any HRE motifs in the 5'-upstream flanking region of the human AM gene and suggested the possible involvement of AP-1 in the hypoxia elevation they observed. Given that the AM promoter has several AP-1 binding motifs and that hypoxia can elevate *c-fos*, which in turn can activate AP-1 expression (45, 46), their supposition had a log-



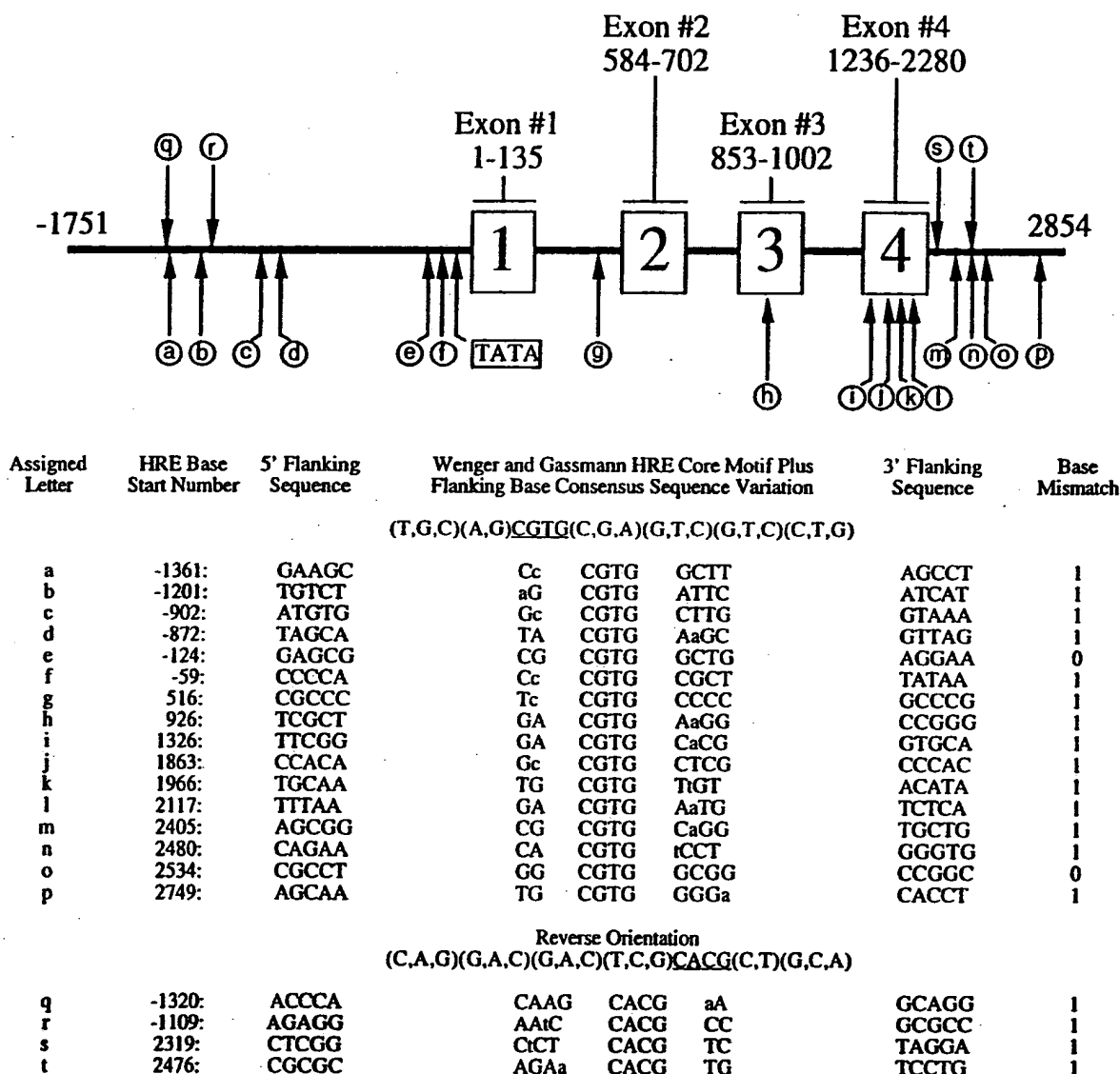


Fig. 8. Schematic Drawing of Potential HRE Motifs in the Human AM Gene

Genomic structure was taken from GenBank accession no. D43639. Identification of putative HIF-1 binding sites is derived from the HRE consensus sequence model of Wenger and Gassmann (18, 32), which represents the deca base region (T,G,C)(A,G)CGTG(C,G,A)(G,T,C)(G,T,C)(C,T,G), and allowing for only one base mismatch outside the CGTG core structure. HRE sites in the schematic drawing are indicated by lowercase letters within circles. GCG analysis was performed in both sense and antisense orientation, and nucleotide positioning of HRE sites was based on the AM transcriptional start site as +1. Accompanying chart identifies numerical positioning of HRE, single mismatched base, and 5'- and 3'-flanking sequences.

ical basis and may in fact work in concert with our observed HIF-1-driven AM expression. Recently, it was also reported that the hypoxic expression of AM in rodent cardiomyocytes is under HIF-1 control (47); although Cormier-Regard and colleagues clearly demonstrate the induction of AM mRNA under hypoxia, no experimental data confirming a similar relationship for AM peptide were shown.

In our luciferase reporter studies, MCF7 cells were transfected with reporter plasmid constructs containing one, two, four, or eight of the putative HRE con-

sensus sequences that we identified in the human AM promoter. Only when four or eight potential HREs were present, a statistically significant fold increase in luciferase expression was observed on exposure to DFX over that of untreated controls. Although the luciferase induction observed in our test conditions is modest, it is within the range observed for the mouse AM gene (47) and human Tf (48). For the human VEGF gene, it has been reported that the increase in transcription rate cannot account for all the observed increase in the steady-state VEGF mRNA levels induced by hypoxia

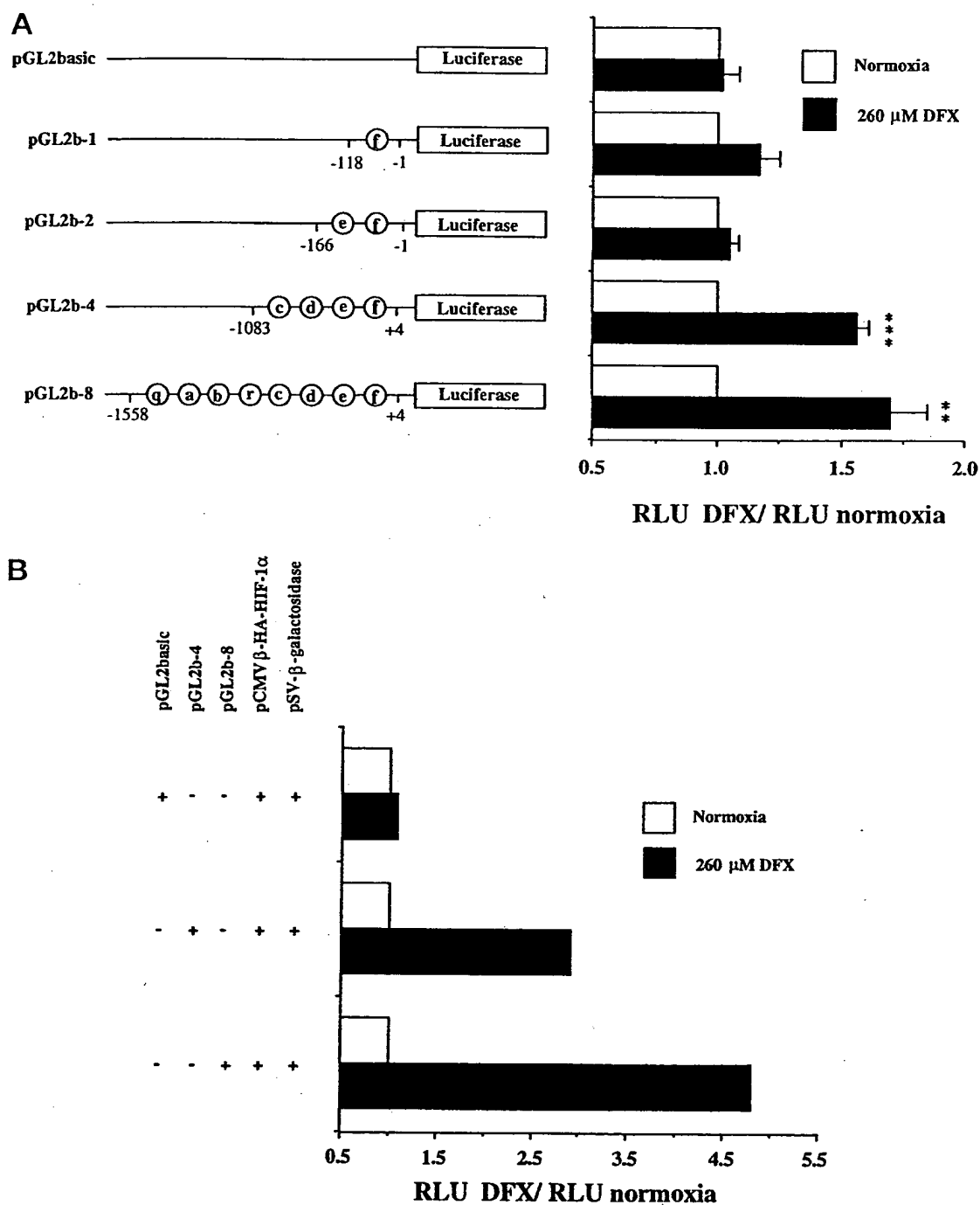


**Fig. 9. Evaluation of HRE Activity by Luciferase Reporter Assay**

**A**, Hypoxia responsiveness of the human AM 5'-flanking region. Schematic diagrams of the luciferase plasmids used in this study, containing one, two, four, or eight putative HREs are shown on the *left*. The HRE sites are named in the same way as in Fig. 8, and numbering refers to the region of the AM promoter inserted into the parental pGL2basic vector relative to the AM transcription start site as +1. MCF7 cells were transiently transfected with one of the mentioned luciferase plasmids and a pSV-β-galactosidase control vector. After normoxic or 260 μM DFX exposure for 24 h, luciferase activity was determined by normalization to the corresponding β-galactosidase values. For each construct tested, fold increase of luciferase activities with 260 μM DFX vs. luciferase values in normoxia (arbitrarily defined as 1) are represented. Means ± SEM of three to five independent experiments are shown; \*\*,  $P < 0.01$ , \*\*\*,  $P < 0.001$ . **B**, Transient expression of HIF-1α potentiates the enhanced luciferase activity after exposure to DFX. MCF7 cells were transiently cotransfected with the HIF-1α expression vector (pCMVβ-HA-HIF-1α) and the plasmid constructs shown at the *left* of the figure. After normoxic or 24 h DFX (260 μM) treatment, the luciferase activity was determined, corrected for transfection efficiency according to the β-galactosidase activity, and in each case normalized to the luciferase value in normoxic conditions arbitrarily defined as 1.

(49), and important posttranscriptional regulation events mediated by mRNA stabilization do, in fact, take place (50). A similar situation could also be depicted for the human AM gene, since not only transcriptional activation but also, as we have shown, RNA stabilization events contribute to the AM mRNA up-regulation under hypoxic conditions. We cannot exclude, however, the possibility of major functional HRE sites at the 3'-flanking region of the human AM gene, a location that has been shown for HREs in the human and mouse Epo gene (51, 52). Furthermore, when MCF7 cells were cotransfected with a HIF-1 $\alpha$  expression vector and plasmid constructs containing four or eight HREs of the 5'-flanking region of the human AM gene, the increase in luciferase activity was remarkably potentiated as compared with the increase obtained with the pGL2-4 or pGL2-8 plasmids alone. This stimulated luciferase reporter activity with the transient overexpression of HIF-1 $\alpha$  has also been reported for the human Tf, VEGF, and Epo genes (48, 53). These data further support that the transcriptional activation of AM in hypoxic conditions is driven by HIF-1 and not through other transcriptional factors activated by hypoxia; additionally, they give stronger evidence that at least some of the selected potential HRE sites in the 5'-flanking region of the human AM gene are functional in the up-regulation of AM transcription under hypoxia.

Based on our actinomycin D studies, we clearly demonstrate AM mRNA stabilization mediated by hypoxic conditions. Recent studies on RNA degradation mechanisms have identified hypoxia-inducible proteins that bind to adenylate-uridylate (AU)-rich elements of the 3'-untranslated region (3'-UTR) of short half-life RNA (*i.e.* VEGF, *c-Myc*, *c-fos*) and suppress ribonuclease degradation (54, 55). One such stabilizing RNA-binding protein, HuR, has been shown to interact with AUUUA or AUUUUA base sequences in the 3'-UTR of the VEGF mRNA and to extend its half-life under hypoxic conditions (55). Interestingly, the 3'-UTR of both human and mouse AM mRNA have AUUUA and AUUUUA sequences that could possibly augment message survival during reduced oxygen tension through a similar HuR or HuR-like interaction. In addition, tumor cell lines that have a mutated von Hippel-Lindau (VHL) tumor suppressor gene contain constitutively stabilized VEGF mRNA and also have constitutively expressed stabilizing RNA-binding proteins (54). Considering these reports and the recent discovery by Ratcliffe and co-workers that the VHL gene product controls the degradation of HIF-1 $\alpha$  protein (25), it will be interesting to determine the status of the VHL suppressor gene in those human tumor cell lines that have an elevated basal expression of AM message under normoxic conditions (*i.e.* H157), to determine whether this feature relates to an increased half-life of AM mRNA mediated by constitutive expression of stabilizing RNA-binding proteins.

In conclusion, we have shown evidence in favor of hypoxia as an inducer of AM mRNA and protein ex-

pression in human tumor cell lines. The data obtained from HIF-1 knockout mouse cell lines, biochemical modulation of HIF-1 activity, and transfection experiments give solid proof for the involvement of HIF-1 in the up-regulation of AM mRNA under hypoxic conditions. In addition to HIF-1 transcriptional activation, increased hypoxic mRNA stability also accounts for AM induction based on our actinomycin D assays. Our collective data, taken together with previous reports that most solid human tumors have common hypoxic regions (15) and that AM can function as a mitogen/angiogenic factor/apoptotic survival factor (5, 6, 13), implicate HIF-1/AM as members of a potential promotion mechanism of carcinogenesis and identify a possible biological target for intervention strategies against malignant disease.

## MATERIALS AND METHODS

### Cell Lines, Hypoxia Treatments, and Reagents

Cell lines used in this study were selected to represent an array of the most widely distributed human cancer types. In particular, we used representatives of carcinomas (CA) or carcinoids of the lung [N417d (small cell CA), H1264 (adenocarcinoma), H157 (squamous cell CA), H720 (carcinoid)], breast (H2380, MCF7, SK-BR-3, ZR-75), colon (H630, H716, SNUC-1), ovary (OVCAR-3, SK-OV-3), prostate (DU 145, PC-3-M), chondrosarcoma (HTB-94) or promyelocytic leukemia (HL-60). All cell lines were obtained from the National Cancer Institute-Navy Medical Oncology Branch or purchased through the American Type Culture Collection (ATCC, Manassas, VA). All tumor cell lines were cultured in RPMI 1640 or DMEM media supplemented with 10% heat inactivated FBS, 2 mM L-glutamine, 10 mM HEPES buffer, 100 U/ml penicillin, and 100  $\mu$ g/ml streptomycin (all tissue culture reagents purchased from Life Technologies, Inc., Gaithersburg, MD). The development, characterization, and maintenance of embryonic stem cell lines from HIF-1 $\beta$  knockout mice have been previously described (56). The HIF-1 $\alpha$  (-/-) fibroblast cell line was generated from HIF-1 $\alpha$  null mice (28) via SV-40 transformation of embryonic fibroblast cells; HIF-1 $\alpha$  (-/-), and (+/+) fibroblast cell lines were maintained with the same media as specified for the human tumor cell lines.

Cells were cultured at 37 C in 20% O<sub>2</sub>, 5% CO<sub>2</sub>, 75% N<sub>2</sub> for normoxic conditions, and new media were added 12 h before the beginning of each hypoxia experiment. The hypoxia induction was achieved either by hypoxia mimetics: 100  $\mu$ M CoCl<sub>2</sub>, 260  $\mu$ M DFX mesylate (both from Sigma, St. Louis, MO), or by culturing cells in a hypoxia chamber at 37 C with 1% O<sub>2</sub>, 5% CO<sub>2</sub>, 94% N<sub>2</sub> atmosphere. The hypoxia chamber was fabricated from a Labconco seamless fiberglass vacuum desiccator (Fisher Scientific, Pittsburgh, PA) fitted with two stainless steel angle ball valves having serrated hose connectors (Washington Valve & Fitting Co., Frederick, MD), which allowed for chamber equilibration to hypoxic environment via venting with gas mixture (Roberts Oxygen Co., Gaithersburg, MD). The chamber was tested for leaks under positive pressure using a bubble-forming agent (SNOOP, Nupro Co., Willoughby, OH) and was shown to hold a 3 psi charge for 48 h.

In the HIF-1 modulating studies, different agents were added to the culture media, and then the cells were incubated under normoxic conditions or in the hypoxia chamber for 12 h at 37 C. SNP (a NO donor), and genistein (a tyrosine kinase inhibitor), were used at 100  $\mu$ M to inhibit HIF-1 activity (29, 30). Hemoglobin (Hb), which acts as a CO scavenger, was

used at a final concentration of 50  $\mu$ M to up-regulate HIF-1 activity (31); Hb was prepared by treatment with excess reducing agent sodium dithionite (57). All reagents were purchased from Sigma.

For the AM mRNA stabilization studies, cells were initially exposed to 12 h hypoxia, after which actinomycin D was added at a final concentration of 4  $\mu$ g/ml (Sigma); cells were subsequently maintained from 1 h to 4 h under normoxic or hypoxic conditions.

#### Northern Blot Analysis

Immediately after treatment for the indicated times, cells were washed once in PBS, and total RNA was extracted using the guanidine isothiocyanate and cesium chloride method (58). Fifteen micrograms of RNA were loaded per lane, run in 1% agarose gels containing 2.2 M formaldehyde, blotted by capillary onto nitrocellulose membranes (Schleicher & Schuell, Inc., Keene, NH), and baked for 2 h at 80°C. Equal loading and integrity of RNA were monitored by ethidium bromide staining of the 28 S subunit of rRNA.

The human AM cDNA probe used in this study was generated as an RT-PCR product (831 bp) obtained using oligonucleotide primers: 5'-TACCTGGGTTTCGCTCGCCTTCTCA-3' (sense, bp 184-207) and 5'-CTCCGGGGGTCTCAGCATTCA-3' (antisense, bp 991-1014). The human HIF-1 $\alpha$  cDNA probe was also produced by RT-PCR (1308-bp product) using oligonucleotide primers: 5'-CGGCGCGAAGCAAGAAAAAGAT-3' (sense, bp 43-66) and 5'-TCGTTGGGTGAGGGGAGCATTACA-3' (antisense, bp 1327-1350). Numbering of the nucleotide base positioning was taken from the GenBank profile accession no. D14874 (human AM mRNA) and U22431 (human HIF-1 $\alpha$  mRNA). All RT-PCR products were sequenced to validate base integrity of the probes. The mouse AM cDNA 550-bp probe was a gift from Dr. Sonia Jakowlew (59).

Probes were labeled with [ $\alpha$ - $^{32}$ P]dCTP (3000 Ci/mmol; NEN Life Science Products, Boston, MA) by random priming, and unincorporated nucleotides were removed by Probe Quant G-50 Micro Columns (Amersham Pharmacia Biotech, Piscataway, NJ). Hybridization was carried out overnight at 42°C in a hybridization buffer containing 40% formamide (58). After stringency washes, blots were exposed to XAR film (Eastman Kodak Co., Rochester, NY) at -80°C for varying times. Densitometry of the autoradiograms was performed using a Chemilmager 4000 (Alpha Innotech Corp., San Leandro, CA). The half-life of the endogenous AM mRNA was calculated using Prism 3.0 software.

#### Confocal Immunofluorescence for AM and HIF-1 $\alpha$

Cells were grown on glass slides, treated with 260  $\mu$ M DFX for 12 h, and fixed in Bouin's fluid (Sigma) for 10 min at room temperature. Slides were blocked with normal goat serum (1:30 in PBS) for 30 min and then incubated overnight at 4°C in a mixture of both antibodies: mgc3 antihuman HIF-1 $\alpha$  monoclonal antibody (60) at 1:500 dilution and rabbit antihuman AM 22-52 antibody (13) at 1:1,000 dilution. The second layer consisted on a mixture of Rhodamine-antimouse and Bodipy-antirabbit IgGs (Molecular Probes, Inc., Eugene, OR) at a final concentration of 1:200 each. The cells were observed with a Carl Zeiss Laser Scanning Microscope 510, equipped with four lasers. Images from cells subjected to DFX treatment and normoxic controls were taken with exactly the same microscope settings and exposures, to compare expression of AM and HIF-1 $\alpha$  in both conditions.

#### RIA of Immunoreactive AM

Concentrations of AM in culture media of MCF7 cells under hypoxia or mimetics treatment were measured by double

antibody RIA. Samples of culture media (1 ml) were mixed with an equal volume of 0.1% alkali-treated casein in PBS, pH 7.4, and applied to reverse-phase Sep-Pak C-18 cartridges (Waters Corp., Milford, MA). The proteins were eluted with 3 ml of 80% isopropanol containing 0.125 N HCl and lyophilized. Extracts were reconstituted in 0.4 ml of RIA buffer (10 mM phosphate, 50 mM EDTA, 135 mM NaCl, 5 mM NaHCO<sub>3</sub>, 0.05% Triton X-100, 0.1% Tween-20, 0.1% alkali-treated casein, 20 mg/l phenol red, pH 7.4), and spun to remove any solid matter. After a 24-h preincubation of 0.1 ml of sample with 0.1 ml of antihuman AM antibody (Phoenix Pharmaceuticals, Inc., Mountain View, CA) at 4°C, 0.1 ml of  $^{125}$ I-labeled AM (Phoenix Pharmaceuticals, Inc.) was added (10,000 cpm) and the mixture was incubated at 4°C overnight. Bound tracer was separated by polyethylenglycol-facilitated precipitation with goat antirabbit IgG and normal rabbit serum. After centrifugation, the supernatant was discarded, and the radioactivity in the pellets was determined in a  $\gamma$ -counter. Data were statistically evaluated by a two-tailed Student's *t* test using Prism 3.0 software. Differences were regarded as significant at a value of *P* < 0.05.

#### Reporter Plasmid Constructs

A PCR product of 118 bp (-118, -1) containing the putative HRE site closest to the transcription start site in the 5'-flanking region of the AM gene (named HRE f in Fig. 8) was generated using human genomic DNA as template and the following oligonucleotide primers: sense, 5'-GCTGAGGAAAGAAAGGAAG-3' and antisense, 5'-TGTCACCAAGAAACCACTGA-3'. Similarly, primers: sense, 5'-AGCCCCAAGGAAGCAATGC-3' and antisense, 5'-TGTCACCAAGAAACCACTGA-3' were used to generate a PCR product of 166 bp (-166, -1) comprising the two potential HREs closest to the transcription start site of the AM promoter (HREs named e and f in Fig. 8). Each of the resulting 118-bp and 166-bp DNA fragments were ligated into the pCR2.1 vector (Invitrogen, Carlsbad, CA) to generate pCR2.1-118 and pCR2.1-166. These plasmids were then digested with *Hind*III and *Xho*I, and the resulting DNA fragments were cloned into the same sites of a promoterless luciferase reporter pGL2basic (Promega Corp., Madison, WI) to generate pGL2b-1 and pGL2b-2, respectively.

The entire 5'-flanking region of the human AM gene was amplified by standard PCR from human genomic DNA using primers: sense, 5'-GAATTCAGGTCCGCTCAGGTGACTCCTTCC-3' and antisense, 5'-GAGCTCGCTAGCCAGTGCACCAAGAAACC-3' (the antisense primer introduced a *Sac*I site [underlined] and an *Nhe*I site [**bolded**]). The resulting 1755 bp (-1751, +4) product was ligated into the pCR2.1 vector to generate pCR2.1-1755. An *Nhe*I/*Nhe*I fragment from pCR2.1-1755 was subcloned into the same site of pGL2basic generating pGL2b-4 (which carries 4 putative HREs from the 5'-end of the AM promoter, namely c, d, e, and f in Fig. 8). In the same way, a *Sac*I/*Sac*I fragment from pCR2.1-1755 was also subcloned into the *Sac*I site of pGL2basic, generating pGL2b-8, which encompasses the 8 putative HREs in the 5'-flanking region of the AM gene (HREs a, b, c, d, e, f, g, and h in Fig. 8). The fidelity of all PCR-derived sequences was verified by sequence analysis. All positions are referred relative to the transcription start site of the AM gene (+1; see Fig. 8).

The HIF-1 $\alpha$  expression vector (pCMV $\beta$ -HA-HIF-1 $\alpha$ ) (34) was generously provided by Dr. D. Livingstone (Dana Farber Cancer Institute).

#### Transient Transfections and Luciferase Reporter Assay

Approximately 20 h before transfection  $1.5 \times 10^5$  MCF7 cells were seeded onto 60-mm plates. Each dish was then transfected for 4 h in the presence of lipofectAMINE and Optimum medium 1 (Life Technologies, Inc.) with 1  $\mu$ g of pSV- $\beta$ -galac-

tosidase control vector (Promega Corp.) and 3 µg of one of the following plasmids: pGL2basic, pGL2b-1, pGL2b-2, pGL2b-4, or pGL2b-8. For the HIF-1α transient overexpression assays, 5 µg of the pCMVβ-HA-HIF-1α vector were cotransfected with an equal amount of one of the following plasmids: pGL2basic, pGL2b-4, or pGL2b-8, together with 1 µg of pSV-β-Galactosidase control vector (quantities referred per dish). All transfections were carried out in duplicate with aliquots of transfection mixture from a single pool. After transfection, cells were incubated in RPMI 1640 medium supplemented with 10% FBS and were either treated with DFX at 260 µM for 24 h or left under normoxic conditions for the same time. Cells were then collected in EBC lysis buffer with protease inhibitors (40 mM Tris, pH 8.0, 120 mM NaCl, 0.5% NP-40, 1 mM AEBSF, 10 µg/ml aprotinin, 1 mM NaVO<sub>4</sub>, 10 µg/ml leupeptin), and luciferase and β-galactosidase activities were determined according to the manufacturer's instructions using a TopCount NXT Packard luminometer and a Bio-Rad Laboratories, Inc. 3550 Microplate Reader. Luciferase readings were normalized by the β-galactosidase values to correct for differences in transfection efficiency and extract preparation. For each construct transfectants, data were expressed as fold increase of the luciferase value obtained with the DFX treatment as compared with the luciferase value obtained in normoxic conditions, which was arbitrarily defined as 1. Data were statistically evaluated by a two-tailed one-sample Student's *t* test using Prism 3.0 software. Differences were regarded as significant at a value of *P* < 0.05.

## Acknowledgments

We thank Dr. J. A. Calera (Georgetown University Medical Center) for his help in the construction of plasmids as well as for useful comments on the manuscript. We are indebted to Dr. G. Camenish for his gift of mgc3 HIF-1α antibody, and to Dr. R. H. Wenger for critical reading of the manuscript (Institute of Physiology, University of Zürich-Irchel). We gratefully acknowledge Dr. Y. Ward (Department of Cell and Cancer Biology, National Cancer Institute) for her expertise in confocal microscopy. Authors are also thankful to Drs. E. Maltepe and C. Simon (Howard Hughes Medical Institute, University of Chicago) for the HIF-1β knockout mouse cell line, and to Dr. D. Livingstone (Dana Farber Cancer Institute) for the pCMVβ-HA-HIF-1α vector.

Received November 23, 1999. Revision received February 1, 2000. Accepted March 1, 2000.

Address requests for reprints to: Dr. Mercedes Garayoa, Cell and Cancer Biology Department, National Cancer Institute, National Institutes of Health, Building 10/12N226, 9000 Rockville Pike, Bethesda, Maryland 20892-1906. E-mail: garayoa@bprb.nci.nih.gov.

M. Garayoa was supported by a postdoctoral fellowship from the Dirección General de Enseñanza Superior, Ministerio de Educación y Cultura, Spain (PF96 0029138440). R. Pio was recipient of a fellowship from the Instituto de Salud Carlos III, Ministerio de Sanidad y Consumo, Spain (Grant 98/9172). This work was also supported in part by the Swiss National Science Foundation (3100-56743.99).

## REFERENCES

- Kitamura K, Kangawa K, Kawamoto M, Ichiki Y, Nakamura S, Matsuo H, Eto T 1993 Adrenomedullin: a novel hypotensive peptide isolated from human pheochromocytoma. *Biochem Biophys Res Commun* 192:553-560
- Barker S, Wood E, Clark AJ, Corder R 1998 Cloning of bovine preproadrenomedullin and inhibition of its basal expression in vascular endothelial cells by staurosporine. *Life Sci* 62:1407-1415
- Kitamura K, Kangawa K, Matsuo H, Eto T 1998 Structure and function of adrenomedullin and PAMP. In: Martínez A, Cuttitta F (eds) *Adrenomedullin*. IOS Press/Ohmsha Ltd., Amsterdam, Tokyo, pp 27-39
- Cuttitta F, Miller MJ, Montuenga LM, Garayoa M, Elsasser T, Walsh T, Unsworth E, Martínez A 1998 Adrenomedullin: *terra incognita*. In: Martínez A, Cuttitta F (eds) *Adrenomedullin*. IOS Press/Ohmsha Ltd., Amsterdam, Tokyo, pp 1-26
- Kato H, Shichiri M, Marumo F, Hirata Y 1997 Adrenomedullin as an autocrine/paracrine apoptosis survival factor for rat endothelial cells. *Endocrinology* 138:2615-2620
- Zhao Y, Hague S, Manek S, Zhang L, Bicknell R, Rees MC 1998 PCR display identifies tamoxifen induction of the novel angiogenic factor adrenomedullin by a non estrogenic mechanism in the human endometrium. *Oncogene* 16:409-415
- Martínez A, Cuttitta F, Teitelman G 1998 Expression pattern for adrenomedullin during pancreatic development in the rat reveals a common precursor with other endocrine cell types. *Cell Tissue Res* 293:95-100
- Montuenga LM, Martínez A, Miller MJ, Unsworth EJ, Cuttitta F 1997 Expression of adrenomedullin and its receptor during embryogenesis suggests autocrine or paracrine modes of action. *Endocrinology* 138:440-451
- Morish DW, Linetsky E, Bhardwaj D, Li H, Dakour J, Marsh RG, Paterson MC, Godbout R 1996 Identification by subtractive hybridization of a spectrum of novel and unexpected genes associated with *in vitro* differentiation of human cytotrophoblast cells. *Placenta* 17:431-441
- Liu J, Kahri A, Heikkilä P, Voutilainen R 1997 Adrenomedullin gene expression and its different regulation in human adrenocortical and medullary tumors. *J Endocrinol* 155:483-490
- Satoh F, Takahashi K, Murakami O, Totsune K, Sone M, Ohneda M, Abe K, Miura Y, Hayashi Y, Sasano H, Ouri T 1995 Adrenomedullin in human brain, adrenal glands and tumor tissues of pheochromocytoma, ganglioneuroblastoma and neuroblastoma. *J Clin Endocrinol Metab* 80:1750-1752
- Ehlenz K, Koch B, Preuss P, Simon B, Koop I, Lang RE 1997 High levels of circulating adrenomedullin in severe illness: correlation with C-reactive protein and evidence against the adrenal medulla as site of origin. *Exp Clin Endocrinol Diabetes* 105:156-162
- Miller MJ, Martínez A, Unsworth EJ, Thiele CJ, Moody TW, Elsasser T, Cuttitta F 1996 Adrenomedullin expression in human tumor cell lines. Its potential role as an autocrine growth factor. *J Biol Chem* 271:23345-23351
- Nakayama M, Takahashi K, Murakami O, Shirato K, Shibahara S 1998 Induction of adrenomedullin by hypoxia and cobalt chloride in human colorectal carcinoma cells. *Biochem Biophys Res Commun* 243:514-517
- Brown JM, Giaccia AJ 1998 The unique physiology of solid tumors: opportunities (and problems) for cancer therapy. *Cancer Res* 58:1408-1416
- Genbacev O, Zhou Y, Ludlow JW, Fisher SJ 1997 Regulation of human placental development by oxygen tension. *Science* 277:1669-1672
- LaVan FB, Hunt TK 1990 Oxygen and wound healing. *Clin Plast Surg* 17:463-472
- Wenger RH, Gassmann M 1997 Oxygen(es) and the hypoxia-inducible factor-1. *Biol Chem* 378:609-616
- Huang LE, Gu J, Schau M, Bunn HF 1998 Regulation of hypoxia-inducible factor 1α is mediated by an O<sub>2</sub>-dependent degradation domain via the ubiquitin-proteasome pathway. *Proc Natl Acad Sci USA* 95:7987-7992

20. Hu J, Discher DJ, Bishopric NH, Webster KA 1998 Hypoxia regulates expression of the endothelin-1 gene through a proximal hypoxia-inducible factor-1 binding site on the antisense strand. *Biochem Biophys Res Commun* 245:894-899
21. Dachs GU, Chaplin DJ 1998 Microenvironmental control of gene expression: implications for tumor angiogenesis, progression, and metastasis. *Semin Radiat Oncol* 8:208-216
22. Gassmann M, Fandrey J, Bichet S, Wartenberg M, Marti HH, Bauer C, Wenger RH, Acker H 1996 Oxygen supply and oxygen-dependent gene expression in differentiating embryonic stem cells. *Proc Natl Acad Sci USA* 93:2867-2872
23. Hasan NM, Adams GE, Joiner MC, Marshall JF, Hart IR 1998 Hypoxia facilitates tumour cell detachment by reducing expression of surface adhesion molecules and adhesion to extracellular matrices without loss of cell viability. *Br J Cancer* 77:1799-1805
24. Yuan J, Glazer PM 1998 Mutagenesis induced by the tumor microenvironment. *Mutat Res* 400:439-446
25. Maxwell PH, Wiesener MS, Chang GW, Clifford SC, Vaux EC, Cockman ME, Wykoff CC, Pugh CW, Maher ER, Ratcliffe PJ 1999 The tumour suppressor protein VHL targets hypoxia-inducible factors for oxygen-dependent proteolysis. *Nature* 399:271-275
26. Chilov D, Camenisch G, Kvietikova I, Ziegler U, Gassmann M, Wenger RH 1999 Induction and nuclear translocation of hypoxia-inducible factor-1 (HIF-1): heterodimerization with ARNT is not necessary for nuclear accumulation of HIF-1 $\alpha$ . *J Cell Sci* 112:1203-1212
27. Isumi Y, Shoji H, Sugo S, Tochimoto T, Yoshioka M, Kangawa K, Matsuo H, Minamino N 1998 Regulation of adrenomedullin production in rat endothelial cells. *Endocrinology* 139:838-846
28. Ryan HE, Lo J, Johnson RS 1998 HIF-1 $\alpha$  is required for solid tumor formation and embryonic vascularization. *EMBO J* 17:3005-3015
29. Sogawa K, Numayama-Tsuruta K, Ema M, Abe M, Abe H, Fujii-Kuriyama Y 1998 Inhibition of hypoxia-inducible factor 1 activity by nitric oxide donors in hypoxia. *Proc Natl Acad Sci USA* 95:7368-7373
30. Wang GL, Jiang BH, Semenza GL 1995 Effect of protein kinase and phosphatase inhibitors on expression of hypoxia-inducible factor 1. *Biochem Biophys Res Commun* 216:669-675
31. Liu Y, Christou H, Morita T, Laughner E, Semenza GL, Kourembanas S 1998 Carbon monoxide and nitric oxide suppress the hypoxic induction of vascular endothelial growth factor gene via the 5' enhancer. *J Biol Chem* 273:15257-15262
32. Wenger RH, Gassmann M 1999 HIF-1 and the molecular response to hypoxia in mammals. In: Storey KB (ed) *Environmental Stress and Gene Regulation*. BIOS Scientific Publishers Ltd., Oxford, UK, pp 25-45
33. Tazuke SI, Mazure NM, Sugawara J, Carland G, Faessen GH, Suen LF, Irwin JC, Powell DR, Giaccia AJ, Giudice LC 1998 Hypoxia stimulates insulin-like growth factor binding protein 1 (IGFBP-1) gene expression in HepG2 cells: a possible model for IGFBP-1 expression in fetal hypoxia. *Proc Natl Acad Sci USA* 95:10188-10193
34. Eckner R, Ewen ME, Newsome D, Gerdes M, DeCaprio JA, Lawrence JB, Livingston DM 1994 Molecular cloning and functional analysis of the adenovirus E1A-associated 300-kD protein (p300) reveals a protein with properties of a transcriptional adaptor. *Genes Dev* 8:869-884
35. Semenza GL, Roth PH, Fang HM, Wang GL 1994 Transcriptional regulation of genes encoding glycolytic enzymes by hypoxia-inducible factor 1. *J Biol Chem* 269:23757-23763
36. Wang GL, Semenza GL 1993 Characterization of hypoxia-inducible factor 1 and regulation of DNA binding activity by hypoxia. *J Biol Chem* 268:21513-21518
37. Yu AY, Frid MG, Shimoda LA, Wiener CM, Stenmark K, Semenza GL 1998 Temporal, spatial, and oxygen-regulated expression of hypoxia-inducible factor-1 in the lung. *Am J Physiol* 275:L818-826
38. Iyer NV, Kotch LE, Agani F, Leung SW, Laughner E, Wenger RH, Gassmann M, Gearhart JD, Lawler AM, Yu AY, Semenza GL 1998 Cellular and developmental control of O<sub>2</sub> homeostasis by hypoxia-inducible factor 1 $\alpha$ . *Genes Dev* 12:149-162
39. Tian H, Hammer RE, Matsumoto AM, Russell DW, McKnight SL 1998 The hypoxia-responsive transcription factor EPAS1 is essential for catecholamine homeostasis and protection against heart failure during embryonic development. *Genes Dev* 12:3320-3324
40. Hirose K, Morita M, Ema M, Mimura J, Hamada H, Fujii H, Saijo Y, Gotoh O, Sogawa K, Fujii-Kuriyama Y 1996 cDNA cloning and tissue-specific expression of a novel basic helix-loop-helix/PAS factor (Arnt2) with close sequence similarity to the aryl hydrocarbon receptor nuclear translocator (Arnt). *Mol Cell Biol* 16:1706-1713
41. Takahata S, Sogawa K, Kobayashi A, Ema M, Mimura J, Ozaki N, Fujii-Kuriyama Y 1998 Transcriptionally active heterodimer formation of an Arnt-like PAS protein, Arnt3, with HIF-1 $\alpha$ , HLF, and clock. *Biochem Biophys Res Commun* 248:789-794
42. Ogita T, Hashimoto E, Nakaoka T, Okabe F, Kira Y, Matsuoka R, Fujita T 1997 Hypoxia induces adrenomedullin gene expression and secretin in cultured human umbilical vein endothelial cells. *Circulation* 96:962
43. Wang X, Yue TL, Barone FC, White RF, Clark RK, Willette RN, Sulpizio AC, Aiyar NV, Ruffolo Jr RR, Feuerstein GZ 1995 Discovery of adrenomedullin in rat ischemic cortex and evidence for its role in exacerbating focal brain ischemic damage. *Proc Natl Acad Sci USA* 92:11480-11484
44. Cheung B, Leung R 1997 Elevated plasma levels of human adrenomedullin in cardiovascular, respiratory, hepatic and renal disorders. *Clin Sci (Colch)* 92:59-62
45. Ishimitsu T, Kojima M, Kangawa K, Hino J, Matsuoka H, Kitamura K, Eto T, Matsuo H 1994 Genomic structure of human adrenomedullin gene. *Biochem Biophys Res Commun* 203:631-639
46. Mishra RR, Adhikary G, Simonson MS, Cherniack NS, Prabhakar NR 1998 Role of c-fos in hypoxia-induced AP-1 cis-element activity and tyrosine hydroxylase gene expression. *Brain Res Mol Brain Res* 59:74-83
47. Cormier-Regard S, Nguyen SV, Claycomb WC 1998 Adrenomedullin gene expression is developmentally regulated and induced by hypoxia in rat ventricular cardiac myocytes. *J Biol Chem* 273:17787-17792
48. Rolfs A, Kvietikova I, Gassmann M, Wenger RH 1997 Oxygen-regulated transferrin expression is mediated by hypoxia-inducible factor-1. *J Biol Chem* 272:20055-20062
49. Levy AP, Levy NS, Wegner S, Goldberg MA 1995 Transcriptional regulation of the rat vascular endothelial growth factor gene by hypoxia. *J Biol Chem* 270:13333-13340
50. Dibbens JA, Miller DL, Damert A, Risau W, Vadas MA, Goodall GJ 1999 Hypoxic regulation of vascular endothelial growth factor mRNA stability requires the cooperation of multiple RNA elements. *Mol Biol Cell* 10:907-919
51. Beck I, Ramirez S, Weinmann R, Caro J 1991 Enhancer element at the 3'-flanking region controls transcriptional response to hypoxia in the human erythropoietin gene. *J Biol Chem* 266:15563-15566
52. Pugh CW, Tan CC, Jones RW, Ratcliffe PJ 1991 Functional analysis of an oxygen-regulated transcriptional enhancer lying 3' to the mouse erythropoietin gene. *Proc Natl Acad Sci USA* 88:10553-10557
53. Blagosklonny MV, An WG, Romanova LY, Trepel J, Fojo T, Neckers L 1998 p53 inhibits hypoxia-inducible factor-stimulated transcription. *J Biol Chem* 273:11995-11998
54. Levy AP, Levy NS, Goldberg MA 1996 Hypoxia-inducible protein binding to vascular endothelial growth factor

- mRNA and its modulation by the von Hippel-Lindau protein. *J Biol Chem* 271:25492-25497
55. Levy NS, Chung S, Furneaux H, Levy AP 1998 Hypoxic stabilization of vascular endothelial growth factor mRNA by the RNA-binding protein HuR. *J Biol Chem* 273: 6417-6423
56. Maltepe E, Schmidt JV, Baunoch D, Bradfield CA, Simon MC 1997 Abnormal angiogenesis and responses to glucose and oxygen deprivation in mice lacking the protein ARNT. *Nature* 386:403-407
57. Martin W, Villani GM, Jothianandan D, Furchgott RF 1985 Selective blockade of endothelium-dependent and glyceryl trinitrate-induced relaxation by hemoglobin and by methylene blue in the rabbit aorta. *J Pharmacol Exp Ther* 232:708-716
58. Davis LG, Kuehl WM, Battey JM 1994 Basic Methods in Molecular Biology, ed. 2. Appleton & Lange, Norwalk, CT
59. Montuenga LM, Mariano JM, Prentice MA, Cuttitta F, Jakowlew SB 1998 Coordinate expression of transforming growth factor- $\beta$ 1 and adrenomedullin in rodent embryogenesis. *Endocrinology* 139:3946-3957
60. Camenisch G, Tini M, Chilov D, Kvietikova I, Srinivas V, Caro J, Spielmann P, Wenger RH, Gassmann M 1999 General applicability of chicken egg yolk antibodies: the performance of IgY immunoglobulins raised against the hypoxia-inducible factor 1 $\alpha$ . *FASEB J* 13:81-88



● Original Contribution

## RADIOLABELED FLUOROMISONIDAZOLE AS AN IMAGING AGENT FOR TUMOR HYPOXIA

JANET S. RASEY, PH.D.,\* WUI-JIN KOH, M.D.,\* JOHN R. GRIERSON, PH.D.,†  
ZDENKA GRUNBAUM, M.S.† AND KENNETH A. KROHN, PH.D.\*†

University of Washington School of Medicine, Seattle, Washington 98195

Fluoromisonidazole labeled with H-3 or F-18 has been tested as a quantitative probe for hypoxic cells *in vitro* and in rodent and spontaneous dog tumors *in vivo*. In V-79, EMT-6(UW), RIF-1, and canine osteosarcoma cells *in vitro*, the binding of 50  $\mu$ M [H-3]Fluoromisonidazole was 50% inhibited by 1000-2000 ppm O<sub>2</sub>, relative to binding under anoxic conditions. After a 3 hr incubation with labeled drug, the anoxic/oxic binding ratios ranged from 12 to 27 for the four cell types. Retention of [H-3]fluoromisonidazole 4 hr after injection was greater in large KHT tumors (400-600 mm<sup>3</sup>) with an estimated hypoxic fraction > 30%, than in smaller tumors (50-200 mm<sup>3</sup>) with an estimated hypoxic fraction of 7-12%. RIF-1 tumors, with an estimated hypoxic fraction of 1.5%, retained the least label, with tumor: blood ratios ranging from 1.7 to 1.9. Spontaneous dog osteosarcomas were imaged with a time of flight positron emission tomograph for up to 5 hr following injection of [F-18] fluoromisonidazole. Analysis of regions of interest in images allowed creation of dynamic tissue time activity curves and calculation of tissue uptake in cpm/gram. These values were compared to radioactivity in plasma. In all cases, retention in some tumor regions exceeded that in plasma and in normal tissue, such as muscle or brain, by 3 to 5 hr post injection. Uptake of fluoromisonidazole in tumors was heterogeneous, with ratios of maximum to minimum uptake as high as 4 in different regions of interest in the same tumor. Tumor:plasma values ranged from 0.28 to 2.02. The oxygen dependency of fluoromisonidazole retention was similar in a variety of cell types and was 50% inhibited by O<sub>2</sub> levels in the transition between full radiobiological hypoxia and partial sensitization. The quantitative regional imaging of [F-18] fluoromisonidazole in spontaneous canine tumors at varying times post-injection lays the basis for imaging and modeling of oxygen-dependent drug retention in different regions of human neoplasms.

Tumor, Hypoxia, Positron emission tomography, Fluoromisonidazole, Tumor predictive assay.

### INTRODUCTION

Radiation resistant hypoxic tumor cells are assumed to be a major cause of local failure in radiotherapy. The existence of radioresistant hypoxic cells in tumors has been inferred from histological studies (30) and radiosensitization of tumors by hyperbaric oxygen (12) or electron affinic nitroimidazole sensitizers (5). Hypoxia has been confirmed by a few direct measurements with oxygen-sensing electrodes in breast cancer (2), cervical cancer (16), and in neck nodes metastatic from head and neck cancers (9). Where low tumor pO<sub>2</sub> has been confirmed with electrode measurements, radioresistance was observed (9). However, hyperbaric oxygen (12) or sensitizing drugs (21) improve radioresponse of only a few tumors, indicating that hypoxia may not be a general cause of treatment

failure. It is important to put the hypoxia problem in perspective on the list of possible causes of failure of radiotherapy (22).

Direct invasive measurements with oxygen electrodes are technically difficult and limited to superficial tumors. An imaging technique that could detect and quantitate hypoxic cells noninvasively and repeatedly would be of value. For this reason, there has been recent interest in some electron affinic drugs, typified by misonidazole, which selectively bind in cells at reduced pO<sub>2</sub> (3, 4, 6, 8, 13, 25, 26). Such drugs, labeled with an appropriate radioisotope, could form the basis for a positive image of hypoxia. A misonidazole congener fluoromisonidazole (FMISO) has been labeled in high yield with the positron emitting isotope F-18 (10).

Studies with tritium labeled FMISO have shown its po-

\* Department of Radiation Oncology.

† Department of Radiology.

Reprint requests to: Janet S. Rasey, Ph.D., Dept. of Radiation Oncology, RC-09, University of Washington, Seattle, WA 98195.

Acknowledgements—The authors wish to thank Thomas Lewellen and Michael Graham for directing the PET imaging, Anthony Shields for referring the tumor bearing dogs, and Robert

Golden for writing the software for performing region of interest analysis of the images. Lay Chin, Norma Nelson, and Barbara Lewellen provided expert technical assistance. Harold Modell and Rod Gronka prepped and monitored the dogs during the studies. This investigation has been supported by NIH research grants 1 P01 CA 42045 and 5 R01 CA34570.

Accepted for publication 17 May 1989.



tential as a quantitative probe for hypoxia in rodent cells and tumor systems (25) and a dog myocardial infarct model (17). This manuscript further quantifies the oxygen dependency of fluoromisonidazole binding in rodent and canine tumor cells *in vitro* and in transplantable mouse tumors and presents the first images of spontaneous animal tumors with [F-18] fluoromisonidazole.

## METHODS AND MATERIALS

### Radiolabeled drugs

[H-3] FMISO was synthesized in our laboratories as described by Grunbaum *et al.* (11) using a method modified from that of Born and Smith (1) for synthesizing [H-3] misonidazole. Briefly, the secondary alcohol in the alkyl side chain of FMISO was oxidized to the corresponding ketone, followed by reduction to the alcohol with [H-3] sodium borohydride. Specific activities as high as 500  $\mu\text{Ci/mg}$  (94.5  $\text{mCi/mMol}$ ) were obtained, but the experiments reported here used a drug with a specific activity of 13 to 25  $\mu\text{Ci/mg}$  (2.46–4.72  $\text{mCi/mMol}$ ).

[F-18] FMISO was synthesized in a two step, two pot reaction (10). Briefly, [F-18] fluoride was reacted with 2R-(–)glycidyl tosylate to prepare [F-18]-epifluorohydrin. Subsequently, the reaction of [F-18] epifluorohydrin with 2-nitroimidazole produced [F-18] FMISO. This synthesis can yield 20–30 millicuries of [F-18] FMISO with a 40% radiochemical yield and a specific activity of greater than 650  $\text{Ci/mmol}$ .

### Cell culture and rodent tumor systems

V-79 1171B Chinese hamster lung fibroblast cells were obtained\* and maintained by seeding  $2 \times 10^5$  cells/25  $\text{cm}^2$  flask in Eagles MEM† plus 10% fetal bovine serum (FBS)‡ and antibiotics. Cells were obtained from a spontaneous dog osteosarcoma and cultured in a 1:1 mixture of Dulbecco's MEM and Ham's F-10 medium† plus 10% FBS. Routine cultures of this line, designated UW CaOs-1, were seeded with  $2.5 \times 10^5$  cells/25  $\text{cm}^2$  flask and fed at weekly intervals.

Two rodent tumor systems having cells capable of growth *in vitro* as monolayers or *in vivo* as solid tumors were used in our studies. The growth characteristics and maintenance of the *in vitro* and *in vivo* forms of the EMT-6(UW) sarcoma of the BALB/c mouse and the RIF-1 sarcoma of the C3H/Km mouse in our laboratories have been described previously (23, 27). RIF-1 tumors were used for biodistributions at 10 to 12 days post transplant. Two additional tumor systems were used for some biodistribution studies, the C3HBA mammary adenocarcinoma (20) or the KHT sarcoma, each growing in the C3H/Km

mouse.§ These two tumors were maintained by mouse-to-mouse passage. Tumors were produced by subcutaneous injection of  $1-2 \times 10^5$  cells in Hanks' balanced salt solution. Cell suspensions were prepared by digestion of minced tumors in 1% neutral protease† dissolved in Waymouth's tissue culture medium plus 15% FBS.

### In vitro drug binding experiments

Binding of FMISO in cells *in vitro* at various oxygen levels was examined in UW CaOs-1, V-79, EMT-6(UW), or RIF-1 cells. The timed cellular uptake of labeled FMISO (50  $\mu\text{mol/L}$ ) as a function of oxygen levels ( $\text{pO}_2$  of 0 to 160 mm Hg; gas mixtures containing 0 to 210,000 ppm) was examined in exponentially growing cells in glass Petri dishes using the thin-film culture technique of Koch (14). Briefly, exponentially growing cell monolayers covering only the central 2.5 cm area of the dish were incubated with 1 ml drug-containing medium/60 mm dish and were subjected to multiple gas exchanges with the desired oxygen level under reduced pressure in aluminum chambers connected to a manifold monitored with a vacuum gauge. This allowed rapid outgassing of  $\text{O}_2$  from the cells and medium and equilibration with the desired  $\text{O}_2$  level. Incubation under slightly reduced pressure (700 mm) for varying time allowed determination of uptake of radiolabeled drug into cells. At the end of incubations, cells were rinsed, trypsinized, and prepared for liquid scintillation counting as described in Rasey *et al.* (24). The gassing procedure and subsequent incubation for up to 3 hr under reduced pressure and anoxia does not damage the cells when viability is tested by colony forming ability.

### Rodent tumor biodistribution experiments

Biodistribution of [H-3] FMISO to tumors and normal tissues in C3H/Km mice was examined after intraperitoneal injection of H-3 labeled drug (5 or 20  $\mu\text{mol/kg}$ ). Mice were sacrificed 4 hr after injection. Drug administration, tissue processing for liquid scintillation counting, and data analysis were as described in Rasey *et al.* (24, 25).

### Imaging studies with [F-18] fluoromisonidazole

Dogs with spontaneous osteosarcomas were referred for imaging, with the owner's written consent.\*\* Preimaging diagnostic tests included, whenever possible, a Tc-99m bone scan and a CT scan, with and without contrast, to verify tumor location, size, and presumptive necrosis. Tumors were imaged continuously with a time of flight positron emission tomograph†† for up to 5 hr after i.v. injection of 5–10 millicuries of [F-18] FMISO. The im-

\* Peggy Olive, British Columbia Cancer Control Agency.

† Sigma Chemical Company, St. Louis.

‡ Flow Laboratories.

§ Radiology Department Stanford University.

\*\* by Dr. Anthony Shields in cooperation with the Canine Tumor Therapy Program of the Fred Hutchinson Cancer Research Center.

†† Scanditronis/PETT Electronics SP-3000 TOF.

aging system includes two computers†† for data acquisition and analysis and a computer§§ for system control and data analysis. The limiting reconstruction resolution was 5 mm and the slice thickness 11.5 mm. Reconstructed time-of-flight images were analyzed with software\*\*\* which allowed definition of regions of interest over tumor and normal tissue and extraction of counts/pixel in the images. After appropriate decay and tomograph efficiency corrections and comparison between gamma well counting and imaging of a bottle of F-18 solution included in the image plane, it was possible to calculate cpm/g of imaged tissue from the images and compare this to plasma samples. Arterial or venous blood samples were taken at precisely timed intervals during imaging and plasma samples were counted in a gamma well counter††† to determine a plasma time-activity curve.

## RESULTS

The time course of [H-3] FMISO uptake by V-79 and RIF-1 cells in monolayer culture is shown in Figure 1a and b, with results expressed as picomoles drug/ $10^5$  cells. For both cell types there was no uptake over time for cells incubated in 95% air/5%  $\text{CO}_2$ . In some experiments, [H-3] FMISO binding after 3 hr in contact with varying  $\text{O}_2$  levels was examined in a single cell type. The results from such a study with EMT-6(UW) cells are shown in Figure 2a. An  $\text{O}_2$  concentration of about 1000 ppm in the gas phase inhibits binding by 50% relative to that obtained in anoxia. Similar results were obtained for RIF-1 and V-79 cells (data not shown). The oxygen dependency of binding in the dog osteosarcoma line, UW CaOs-1, is shown in Figure 2b. The 50% inhibitory level also appears to lie between 1000 and 2000 ppm for this tumor type. In these self-contained experiments, five different gas mixtures were examined with each cell line. Under these conditions the anoxic: oxic binding ratios were: RIF-1,  $27.2 \pm 5.2$ ; EMT-6(UW),  $12.6 \pm 2.2$ ; V-79,  $27.6 \pm 7.1$ ; and CaOs-1,  $21.0 \pm 3.4$ . The values are mean  $\pm$  SEM for replicate dishes in two separate experiments with each cell type.

The results of the biodistribution studies of [H-3] FMISO in tumor-bearing mice are shown in Table 1 for animals sacrificed 4 hr after receiving a single intraperitoneal dose of 5 or 20  $\mu\text{mol/kg}$ . For tumors with sizes ranging from 50–200  $\text{mm}^3$ , the tumor to blood ratios were lowest for the RIF-1 tumor (1.69 to 1.86), which has the lowest estimated hypoxic fraction of the three transplanted mouse neoplasms (19). The values for the C3HBA mammary adenocarcinoma (4.66, 3.96) were higher than for the KHT sarcoma (2.29–2.86), although both tumors are reported to have similar sized fractions of chronically

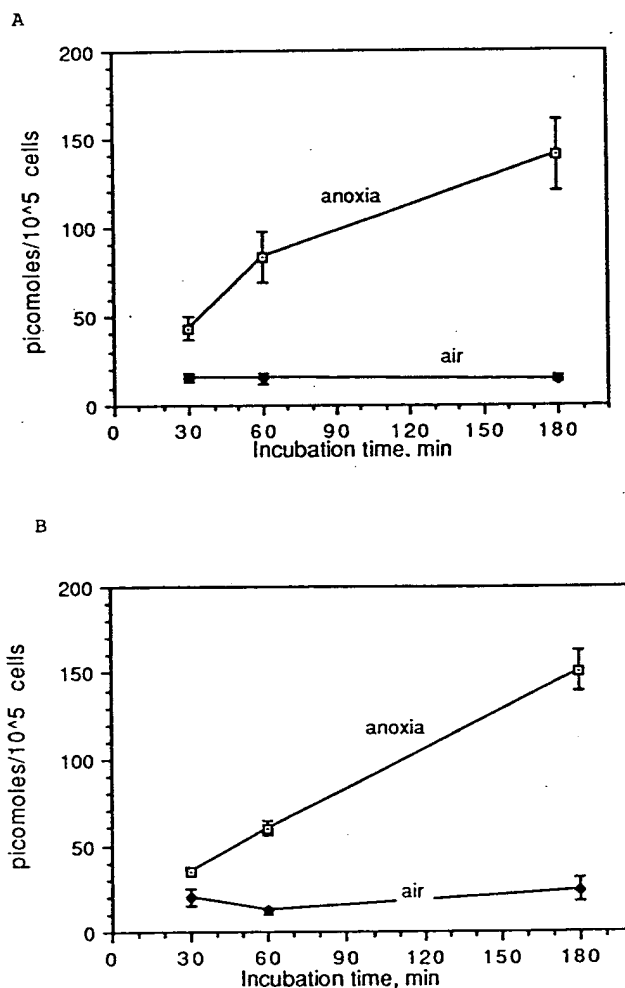


Fig. 1. Uptake of 50  $\mu\text{M}$  [H-3] fluoromisonidazole as a function of time under different oxygen levels. Each point is the mean  $\pm$  SEM for replicate dishes at each time. (a) V-79 cells; (b) RIF-1 cells.

hypoxic cells in this size range (Table 1) (19). Larger KHT tumors, 400–600  $\text{mm}^3$ , take up proportionately more [H-3] FMISO; tumor:blood ratios of 5.8 and 8.3 were measured 4 hr after an i.p. dose of 5  $\mu\text{mol/kg}$  FMISO.

Uptake in tumors relative to other normal tissues is shown in Table 2 for mice bearing small KHT tumors and receiving the lowest dose, 5  $\mu\text{mol/kg}$ . By 4 hr most nonmalignant tissues have nearly equilibrated with blood levels, except kidney and liver, which retain higher levels of parent drug or metabolites (approximately 7 to 9-fold those in blood); retention is also high in gut.

The encouraging results with [H-3] FMISO in cells *in vitro* and in transplanted rodent tumors led to imaging studies in spontaneous dog tumors. Six dogs with osteosarcomas were imaged continuously for 4 to 5 hr after

†† Data General MV4000.

§§ Data General MV10,000SX.

\*\*\* developed at the University of Washington Imaging Research Laboratory.

††† Packard Minaxi- $\gamma$  Autogamma 5000 Series.

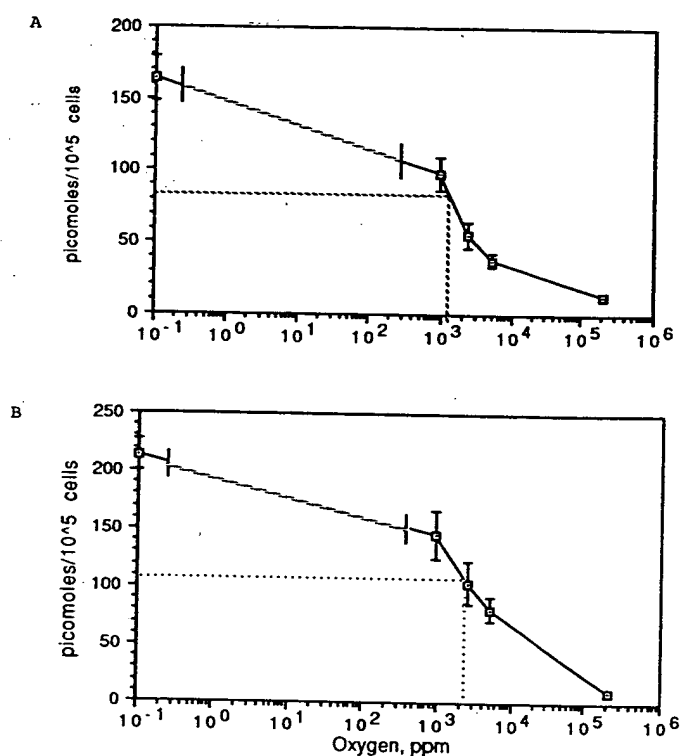


Fig. 2. Oxygen dependency of the uptake of 50  $\mu$ M [H-3] FMISO in cells incubated for 3 hr with labeled drug. The data are combined values from two replicate experiments. Each point is the mean  $\pm$  SEM for six replicate dishes at that  $O_2$  level. The break in the curve below 1000 ppm indicate that the shape of the curve in this region is not known. (a) EMT-6 (UW) mouse sarcoma cells; (b) CaOs-1 (UW) dog osteosarcoma cells.

injection of [F-18] FMISO. For three dogs in which arterial lines were established, arterial plasma time activity curves were obtained (Fig. 3). Plasma values peaked within 2–3 min after beginning the 2 min infusion with a distribution  $T_{1/2}$  of  $7.4 \pm 0.6$  min. This distribution value may be influenced by the FMISO not being injected as a bolus. The  $T_{1/2}$  for clearance has been calculated as  $275 \pm 50$

min and the volume of distribution as  $0.58 \pm 0.21$  L/kg, equivalent to total body water (17).

All tumors contained some areas that intensely concentrated FMISO by 4 hr after injection. However, uptake of this labeled nitroimidazole showed marked heterogeneity over different regions of the tumors (Fig. 4). For each tumor, five to six regions of interest were defined to include the most FMISO-avid regions as well as regions with the least uptake. Normal tissue regions were also sampled. The uptake of F-18 was calculated as cpm/g, as described in Methods and Materials, allowing the creation of comparable plasma and tissue time-activity curves which are shown for one dog with a forelimb osteosarcoma in Figure 5. Highest tissue uptake occurred immediately after injection for both tumor and normal tissue (Fig. 5). The level of activity retained in most tumor regions 3 or 4 hr post injection exceeded that in normal tissue or plasma. Within one tumor, uptake between the different regions varied by a factor of 4 at 3.7 hr post injection. The tumor:plasma ratios in three different tumors at 3 to 4.67 hr post injection ranged from 0.3 to 2.0 (Table 3).

## DISCUSSION

The uptake of [H-3] FMISO by various tumor and V-79 cells *in vitro* is generally consistent with reports of oxygen-dependent binding of [C-14] or [H-3] labeled misonidazole. Franko *et al.* (8) reported that 1000 ppm oxygen inhibited misonidazole binding by 50% relative to anoxia in EMT-6(Ed) monolayer cells *in vitro* incubated in medium containing 50  $\mu$ M radiolabeled drug. Those authors also reported an anoxic:oxic binding ratio of approximately 15 for misonidazole in EMT-6(Ed) cells. This value may be compared with our anoxic:oxic ratio of 12.6 for EMT-6(UW) cells, a variant of the same mouse sarcoma system. Several other tumor types included in that same study showed misonidazole binding to be inhibited by similar or slightly higher  $O_2$  levels. Investigations of misonidazole retention by V-79 cells showed that uptake

Table 1. H-3 fluoromiso biodistribution in mouse tumors: Animals sacrificed 4 hr after single injections

Expt no.	Tumor	Drug dose	Tumor:blood ratios	Tumor volumes, mm <sup>3</sup> *	Estimated hypoxic fractions†
JW894	C3HBA	5 $\mu$ mol/kg	4.66	101 $\pm$ 13	3–12%
JW904	C3HBA	5 $\mu$ mol/kg	3.96	137 $\pm$ 36	
JW1010	KHT	5 $\mu$ mol/kg	2.41	175 $\pm$ 16	7–12%
JW867	KHT	5 $\mu$ mol/kg	2.29	110 $\pm$ 25	
JW1010	KHT	20 $\mu$ mol/kg	2.76	159 $\pm$ 39	
JW867	KHT	20 $\mu$ mol/kg	2.86	123 $\pm$ 37	
JW-1032	KHT	5 $\mu$ mol/kg	5.58	580 $\pm$ 26	>30%
JW-1033	KHT	5 $\mu$ mol/kg	8.34	574 $\pm$ 66	
JW1009	RIF-1	5 $\mu$ mol/kg	1.69	158 $\pm$ 23	~1.5%
JW1009	RIF-1	20 $\mu$ mol/kg	1.76	159 $\pm$ 15	
JW992	RIF-1	20 $\mu$ mol/kg	1.86	136 $\pm$ 37	

\* Tumor volumes are mean  $\pm$  standard deviation for 5 tumors/group.

† The estimated hypoxic fractions are taken from Moulder and Rockwell, (19) and Moulder *et al.*, (18) for tumors of comparable size. Values estimated for C3HBA tumors were those reported for C3H mouse mammary tumors.

Table 2. Biodistribution of H-3 fluoromisonidazole C3H/Km mice with KHT tumors (88–198 mm<sup>3</sup>)\*

Tissue	% ID/gram† (mean ± SEM)	Tissue/blood ratio (mean ± SEM)
KHT tumor	0.80 ± 0.13	2.47 ± 0.30
Liver	2.75 ± 0.40	8.70 ± 1.35
Kidney	2.64 ± 0.80	7.34 ± 1.31
Gut	2.50 ± 1.10	7.48 ± 3.67
Lung	0.40 ± 0.11	1.14 ± 0.31
Heart	0.46 ± 0.45	1.53 ± 0.16
Muscle	0.29 ± 0.03	0.95 ± 0.10
Brain	0.38 ± 0.10	1.05 ± 0.11
Blood	0.34 ± 0.05	1.00

\* Mice received i.p. injections of five  $\mu\text{mol/Kg}$  4 hr before sacrifice. Data are pooled from two experiments, 5 mice/group in each study.

† %ID/g is % injected dose/gram and is calculated as: (dpm/g of tissue/dpm injected)  $\times$  100. For a 25 gram mouse a %ID/g of 4% would be equivalent to uniform distribution of a radiotracer with no excretion.

in that cell type was even more easily inhibited by O<sub>2</sub> than was the case with EMT-6(Ed) cells (7). Those results are not consistent with our findings with [H-3] FMISO binding in V-79 cells, in which the 50% inhibitory level is about 1000 ppm. Different sublines of V-79 cells were used in the two laboratories and this may explain the difference. Alternately, FMISO may be metabolized slightly differently than MISO in some cell lines. The spontaneous dog osteosarcoma CaOs-1 binds substantial amounts of FMISO at somewhat higher O<sub>2</sub> levels than do the rodent cells (Fig. 2b). This is consistent with some human tumors labeled with [C-14] MISO, in which 50% binding inhibition occurred at oxygen levels of 2,000 to 10,000 ppm (8). Taken together, our *in vitro* studies of [H-3] FMISO suggest that 50% binding inhibition occurs over a range of oxygen levels, bracketing that for radiobiological hypoxia, as has been reported for misonidazole (8, 15). This radiopharmaceutical should be useful as a probe for radioresistant hypoxic cells in human neo-

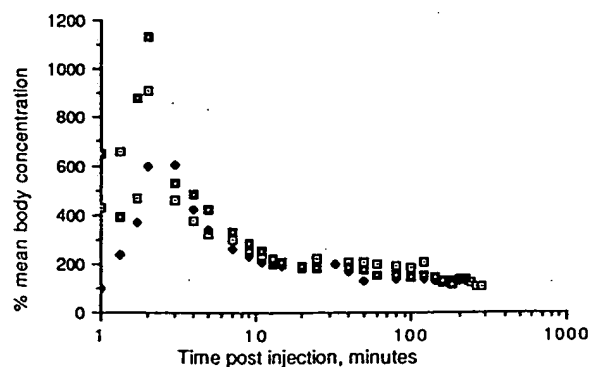


Fig. 3. Arterial plasma time activity curves for three dogs injected intravenously with tracer levels of [F-18] fluoromisonidazole. Data are normalized to % mean body concentration, calculated as: [cpm/gram plasma]/cpm injected  $\times$  body weight, grams  $\times$  100. A % mean body concentration of 100% would be equivalent to uniform distribution with no excretion.

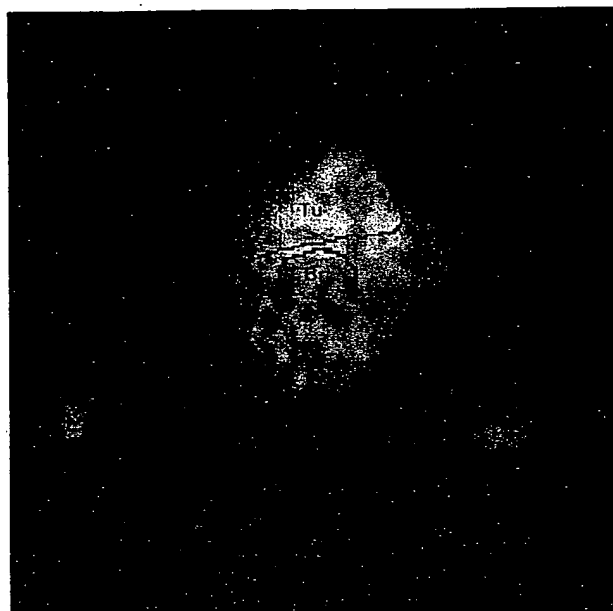


Fig. 4. Positron emission tomograph image of a canine skull osteosarcoma acquired from 60 to 105 min after injection of [F-18] fluoromisonidazole. The image was reconstructed with an 8 mm filter. The outline identifies the tumor and normal tissue structures identified from CT scan and from autopsy after the terminally ill animal received a lethal intravenous injection of KCl.

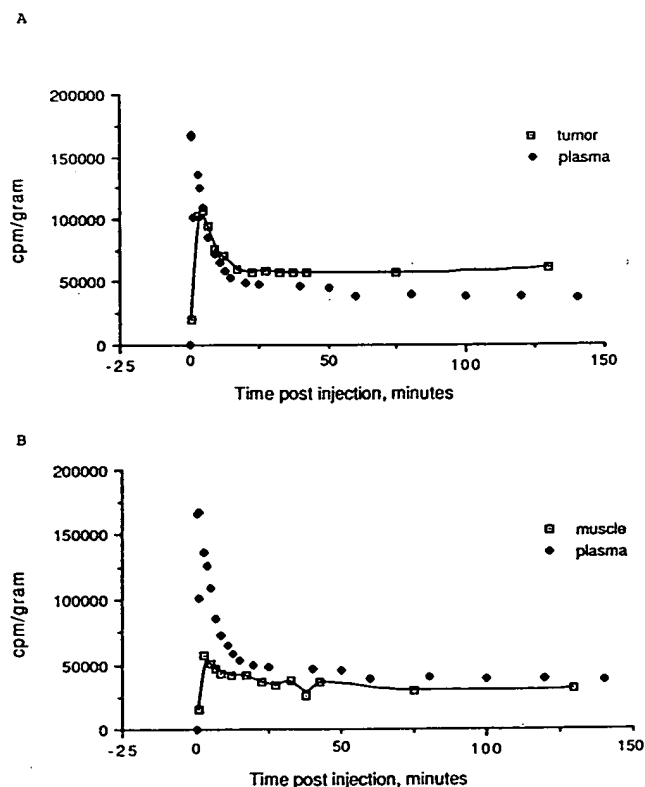


Fig. 5. Tumor and normal tissue time-activity curves extracted from images of a canine forelimb osteosarcoma and adjacent normal muscle. The methods of data extraction and analysis are described in Methods and Materials. (a) Plasma and tumor; (b) Plasma and muscle adjacent to tumor.

Table 3. Tumor and plasma levels of F-18 fluoromisonidazole

Dog	Time post inject.	Plasma, cpm/g ( $\times 10^3$ )	Tumor, cpm/g ( $\times 10^3$ )*	Tumor, max/min
1C2	4.67 hr	1.146	1.155 $\pm$ .3608 (1.178 to 2.269)	1.93
2M	3.08 hr	0.302	0.478 $\pm$ 0.091 (0.360 to 0.610)	1.69
3G	3.67 hr	0.586	0.452 $\pm$ 0.169 (0.164 to 0.655)	4.00

\* Values for tumor are the mean  $\pm$  standard deviation for five or six regions of interest from each tumor. The ranges of values are in parentheses.

plasmas, if it is evaluated carefully in different tumor types and under different conditions.

The results with the biodistribution studies in mouse tumors are supportive of quantitation of tumor hypoxia by imaging the retention of radiolabeled FMISO (Table 1). Small RIF-1 tumors (50–200 mm<sup>3</sup>) had lower tumor:plasma ratios and a smaller proportion of chronically hypoxic cells than either the KHT sarcoma or C3HBA mammary adenocarcinoma (19). In addition, large KHT tumors (400–600 mm<sup>3</sup>) retained proportionately more FMISO than did smaller tumors in animals receiving 5  $\mu$ mol/kg FMISO. The fraction of hypoxic cells in KHT sarcomas increases with tumor growth (18). However, small C3HBA and KHT tumors demonstrated different tumor:plasma ratios at 4 hr, even though the estimated hypoxic fractions are comparable. Reports by others also indicate that fraction of chronically hypoxic tumor cells and nitroimidazole retention do not follow a simple or easily interpreted relationship. Hirst *et al.* (13) measured retention of [C-14] misonidazole in RIF-1 and EMT-6(St) tumors and varied the hypoxic fraction in tumors by making mice anemic or transfusing them to raise the hematocrit. The amount of C-14 label retained 24 hr after misonidazole injection varied less than the tumor cell fraction surviving irradiation.

A limitation of our studies with mice and those reported in the literature is the lack of blood flow information. Flow dominates the tissue input function and the washout of the radiopharmaceutical, although FMISO is very lipophilic and can travel across cell membranes by diffusion. It was not possible, in biodistributions done at one point after drug administration, to estimate drug in non-bound forms equilibrated with plasma. Flow also will vary between tumor regions, leading to heterogeneity in oxygenation and a consequent variation in amount of misonidazole or FMISO retained per unit volume of tumor. In the reported biodistributions, whole or halves of tumors were counted for retention of radiolabel, and so regional variation in oxygen level and nitroimidazole retention could not be accounted for or measured. The relationship between FMISO binding and hypoxic function also would

be more meaningful if individual hypoxic fractions had been determined for each tumor. Hypoxic fractions can vary even in tumors of the same size (19).

Dynamic, regional information about blood flow and FMISO uptake and washout can be obtained with PET, as exemplified by the tissue time-activity curves obtained in the dog tumor imaging studies (Fig. 5). Appropriate modeling of these data can be coupled with data on oxygen dependency of FMISO binding obtained from cell binding studies *in vitro*. This should allow measurement of an FMISO accumulation rate constant attributable to a specific level of oxygenation. Furthermore, FMISO has an octanol:water partition co-efficient of 0.41, high enough to make it easily distributed across capillary membranes. Thus, the initial phase of its uptake after a bolus injection may infer blood flow through the modeling used for freely diffusible tracers such as water.

Dog osteosarcomas were chosen for initial PET imaging studies with [F-18] FMISO because they may have hypoxic cells. These tumors are resistant to radiation treatment, both conventional external beam therapy (28) and treatment with the bone-seeking beta emitter samarium-153 (Anthony Shields, oral communication Sept. 1988). CT examination of osteosarcomas in our studies revealed reduced contrast in some tumor regions, consistent with necrosis. The uptake of FMISO in tumor images shows marked heterogeneity, seen both by visual inspection of the images (Fig. 4) and the range of tumor uptakes calculated from images (Table 3). Regional variation has been seen in autoradiographs of human melanomas labeled with [H-3] misonidazole (31) and the EMT-6(Ed) mouse sarcoma labeled with [C-14] misonidazole (4). However, autoradiography does not allow the quantitation of regional heterogeneity possible with image analysis. The variable uptake of [F-18] FMISO in the spontaneous dog tumors also is compatible with observations of macro- and microheterogeneity of many biochemical and physiological properties in tumors (29).

The utility of [F-18] FMISO imaging ultimately will be tested in human tumors by comparison to direct oxygen measurements with electrodes and by correlation with outcome of radiotherapy under a variety of conditions, either altering tumor oxygenation or using treatments directed towards hypoxic cells, such as hypoxic sensitizers or high LET radiation. Correlative studies in which dog osteosarcomas are treated with radioactive samarium-153 also will allow validation of FMISO as a predictor of response to radiotherapy in an animal model.

In conclusion, the oxygen-dependent binding of labeled fluoromisonidazole has been demonstrated *in vitro*. The studies with [H-3] FMISO in mouse tumors and myocardial infarcts in dogs suggest that labeled FMISO will be a useful hypoxia probe. Imaging tumors and adjacent normal tissues with [F-18] FMISO has been demonstrated, and it is possible to extract quantitative data from these images. Plasma drug levels also can be measured and nonspecific retention of plasma-equilibrated drug can be subtracted. Thus, varying amounts of uptake above

plasma  
The C  
of FM  
confi

1. B  
m  
4.  
2. C  
o:  
p:  
2:  
3. C  
ta  
m  
4. C  
h  
P  
5. L  
c  
S  
6. F  
r  
s  
7.  
8.  
9.  
10.  
11.  
12.  
13  
14  
15

1

plasma levels can be quantified in different tumor regions. The O<sub>2</sub> level associated with partial or complete inhibition of FMISO binding can be measured *in vitro*. If one can confirm that these *in vitro* studies are representative of

the tumor *in situ*, imaging data can be modeled to calculate a proportion of tumor cells at or below a specified oxygen level. This quantification of hypoxia should be a useful predictor in radiotherapy.

## REFERENCES

- Born, J. L.; Smith, B. R. The synthesis of tritium-labeled misonidazole. *J. Labeled Comp. Radiopharmaceut.* 20:429-432; 1983.
- Cater, D. B.; Silver, I. A. Quantitative measurements of oxygen tension in normal tissues and in the tumours of patients before and after radiotherapy. *Acta Radiol.* 53:233-256; 1960.
- Chapman, J. D.; Baer, K.; Lee, J. Characteristics of the metabolism-induced binding of misonidazole to hypoxic mammalian cells. *Cancer Res.* 43:1523-1528; 1983.
- Chapman, J. D.; Franko, A.; Sharplin, J. A. Marker for hypoxic cells in tumors with potential clinical applicability. *Br. J. Cancer* 43:546-550; 1981.
- Dische, S. Chemical sensitizers for hypoxic cells: a decade of experience in clinical radiotherapy. *Radiother. Oncol.* 3: 97-115; 1985.
- Franko, A. J.; Garrecht, B. M. Misonidazole retention by normal tissues: A distinction between label on the ring and side chain. *Int. J. Radiat. Onc. Biol. Phys.* 12:1259-1262; 1986.
- Franko, A. F.; Koch, C. J. Binding of misonidazole to V-79 spheroids and fragments of Dunning rat prostatic and human colon carcinomas *in vitro*: diffusion of O<sub>2</sub> and reactive metabolites. *Int. J. Radiat. Oncol. Biol. Phys.* 10: 1333-1336; 1984.
- Franko, A. J.; Koch, C. J.; Garrecht, B. M.; Sharplin, J.; Hughs, D. Oxygen dependence of binding of misonidazole to rodent and human tumors *in vitro*. *Cancer Res.* 47:5367-5376; 1987.
- Gatenby, R. A.; Kessler, H. B.; Rosenblum, S. J.; Coia, L. R.; Moldofsky, P. J.; Hartz, W. H.; Broder, G. J. Oxygen distribution in squamous cell carcinoma metastases and its relationship to outcome of radiation therapy. *Int. J. Radiat. Oncol. Biol. Phys.* 14:831-838; 1988.
- Grierson, J. R.; Link, J.; Mathis, C. A.; Rasey, J. S.; Krohn, K. A. A radiosynthesis of [F-18] fluoromisonidazole. *J. Nucl. Med.* 10:194-201; 1989.
- Grunbaum, Z.; Freau, S. J.; Krohn, K. A.; Wilbur, D. S.; Magee, S.; Rasey, J. S. Synthesis and characterization of congeners of misonidazole for imaging hypoxia. *J. Nucl. Med.* 28:68-75; 1987.
- Henk, J. M. Does hyperbaric oxygen have a future in radiation therapy? *Int. J. Radiat. Oncol. Biol. Phys.* 7:1125-1128; 1981.
- Hirst, D. J.; Hazlehurst, J. L.; Brown, J. M. Changes in misonidazole binding with hypoxic fraction in mouse tumors. *Int. J. Radiat. Oncol. Biol. Phys.* 11:1349-1355; 1985.
- Koch, C. J. A "thin film" culturing technique allowing rapid gas-liquid equilibration with no toxicity to mammalian cells. *Radiat. Res.* 97:434-442; 1984.
- Koch, C. J.; Stobbe, C. C.; Baer, K. A. Metabolism induced binding of C-14 misonidazole to hypoxic cells: kinetic dependence on oxygen concentration and misonidazole concentration. *Int. J. Radiat. Onc. Biol. Phys.* 10:1327-1332; 1984.
- Kolstad, P. Inter-capillary distance, oxygen tension and local recurrence in cervix cancer. *Scand. J. Clin. Lab. Invest. Suppl.* 106:145-166; 1968.
- Martin, G. V.; Caldwell, J. C.; Rasey, J. S.; Grunbaum, Z.; Cerqueira, M.; Krohn, K. A. Enhanced binding of the hypoxic cell marker [H-3]-fluoromisonidazole in ischemic myocardium. *J. Nucl. Med.* 30:194-201; 1989.
- Moulder, J. E.; Dutreix, J.; Rockwell, S. C.; Siemann, D. W. Applicability of animal tumors to cancer therapy in humans. *Int. J. Radiat. Oncol. Biol. Phys.* 14:913-927; 1988.
- Moulder, J. E.; Rockwell, S. Hypoxic fractions of solid tumors: experimental techniques, methods of analysis, and a survey of existing data. *Int. J. Radiat. Oncol. Biol. Phys.* 10: 695-712; 1984.
- Nelson, J. S. R.; Carpenter, R. E.; Parker, R. G. Response of mouse skin and the C3HBA mammary carcinoma of the C3H mouse to X rays and cyclotron neutrons: effect of mixed neutron-photon fractionation schemes. *Eur. J. Cancer* 11:891-901; 1975.
- Overgaard, J.; Andersen, A. P.; Jensen, R. H.; Hjelm-Hansen, M.; Jorgensen, K.; Petersen, M.; Sandberg, E.; Sand-Hansen, H. Misonidazole combined with split-course radiotherapy in the treatment of invasive carcinoma of the larynx and pharynx: a preliminary report of the Danish Head and Neck Cancer Study (DAHANCA), Protocol 2. *Acta Otolaryngol.* 386(Suppl.):215-220; 1982.
- Peters, L. J.; Withers, H. R.; Thames, H. D. Keynote address: the problem: Tumor adioresistance in clinical radiotherapy. *Int. J. Radiat. Oncol. Biol. Phys.* 8:101-108; 1982.
- Rasey, J. S.; Carpenter, R. E.; Nelson, N. J. Response of EMT-6 tumors to single fractions of X rays and cyclotron neutrons: evaluation of multiple endpoints of response. *Radiat. Res.* 71:430-446; 1977.
- Rasey, J. S.; Grunbaum, A.; Krohn, K. A.; Nelson, N.; Chin, L. Comparison of binding of H-3 misonidazole and C-14 misonidazole in multicellular spheroids. *Radiat. Res.* 101: 473-479; 1985.
- Rasey, J. S.; Grunbaum, Z.; Magee, S.; Nelson, N. J.; Olive, P. L.; Durand, R. E.; Krohn, K. A. Characterization of radiolabeled fluoromisonidazole as a probe for hypoxic cells. *Radiat. Res.* 111:292-304; 1987.
- Rasey, J. S.; Krohn, K. A.; Freau, S. Bromomisonidazole: Synthesis and characterization of a new radiosensitizer. *Radiat. Res.* 91:542-554; 1982.
- Rasey, J. S.; Nelson, N. J. Discrepancies between patterns of potentially lethal damage repair in the RIF-1 tumor system *in vitro* and *in vivo*. *Radiat. Res.* 93:157-174; 1983.
- Silver, I. J. Use of radiotherapy for treatment of malignant neoplasms. *J. Small Anim. Pract.* 13:351-358; 1972.
- Sutherland, R. M. Cell and environment interactions in tumor microregions: the multicell spheroid model. *Science* 240: 177-184; 1988.
- Thomlinson, R. H.; Gray, L. H. The histological structure of some human lung cancers and the possible implications for radiotherapy. *Br. J. Cancer* 58:262-276; 1955.
- Urtason, R. C.; Chapman, J. D.; Raleigh, J. A.; Franko, A. J.; Koch, C. J. Binding of [H-3] misonidazole to solid tumors as a measure of tumor hypoxia. *Int. J. Radiat. Oncol. Biol. Phys.* 12:1263-1267; 1986.

## Characteristics of the Binding of Labeled Fluoromisonidazole in Cells *in Vitro*

JANET S. RASEY,\* NORMA J. NELSON,\* LAY CHIN,\* MARGARET L. EVANS,\* AND ZDENKA GRUNBAUM†

Departments of \*Radiation Oncology and †Radiology, University of Washington School of Medicine, Seattle, Washington 98195

RASEY, J. S., NELSON, N. J., CHIN, L., EVANS, M. L., AND GRUNBAUM, Z. Characteristics of the Binding of Labeled Fluoromisonidazole in Cells *in Vitro*. *Radiat. Res.* 122, 301-308 (1990).

Radiolabeled fluoromisonidazole (FMISO) is being investigated as an imaging agent for hypoxia in tumors and nonmalignant tissues in myocardial infarct or stroke. In this study *in vitro* cell cultures were used to characterize the oxygen dependency of FMISO uptake and to examine other modifying factors. The uptake of [<sup>3</sup>H]FMISO was measured in four cell lines *in vitro*: V-79, EMT-6(UW), RIF-1, and CaOs-1. The modifying effects of different O<sub>2</sub> levels as well as cell growth state and concentration of glucose and nonprotein sulfhydryls were examined. In these cell types an O<sub>2</sub> level between 720 and 2300 ppm inhibited FMISO binding by 50%, relative to binding under anoxic conditions. These values bracket the O<sub>2</sub> level which confers full radiobiologic hypoxia, about 1000 ppm. Some bound label was released from cells in the first 1 to 3 h after a 3-h anoxic labeling with [<sup>3</sup>H]FMISO, but this does not represent tritium loss from the parent molecule. Cells from unfed plateau-phase cultures took up less [<sup>3</sup>H]FMISO than did exponentially growing cells incubated at comparable O<sub>2</sub> levels. Reducing glucose to 1/10 or 1/100 of the usual concentration in medium had little effect on binding of micromolar levels of FMISO, except in V-79 cells, where reduced glucose levels were associated with increased FMISO accumulation. Adding cysteamine to the culture medium moderately increased FMISO uptake. We conclude that cell growth state, glucose, and nonprotein sulfhydryl concentrations affect FMISO binding, albeit less than varying O<sub>2</sub> levels: anoxic/oxic binding ratios vary from 12.6 to 28 for the four cell types examined. Nonetheless these factors must be considered in evaluating the oxygen-dependent binding of this nitroimidazole in tumors or tissues. © 1990 Academic Press, Inc.

### INTRODUCTION

The oxygen-dependent covalent binding of the nitroimidazole misonidazole (1-(2-nitroimidazolyl)-2-hydroxy-3-methoxypropane, MISO) in cells, multicellular spheroids, and tumors (1-8) has stimulated interest in using this drug or a congener as an imaging agent for hypoxia in malignant tumors, myocardial infarct, or cerebral ischemia (9-13).

Unlike misonidazole, the fluorinated congener fluoromisonidazole (1-(2-nitroimidazolyl)-2-hydroxy-3-fluoropropane, FMISO) can be labeled with a positron-emitting isotope, <sup>18</sup>F, which has a long enough half-life for measuring this radiopharmaceutical quantitatively with positron emission tomography. Previous studies from this laboratory have reported hypoxia-dependent binding of [<sup>3</sup>H]FMISO. Radiolabeled FMISO localizes in solid animal tumors containing hypoxic cells (14, 15) and in anoxic cells *in vitro* (16). The [<sup>18</sup>F]FMISO can be detected and quantified in spontaneous dog tumors using positron emission tomography (16). However, interpreting FMISO images requires defining O<sub>2</sub> dependency of binding in several cell types and investigating factors in addition to O<sub>2</sub> which may influence uptake and retention of this tracer. Appropriate *in vitro* studies can provide necessary information and are reported here.

### MATERIALS AND METHODS

#### Radiolabeled Drugs

The [<sup>3</sup>H]FMISO was synthesized in our laboratory as reported previously (14), using a modification of the tritium radiolabeling method for MISO (17). After synthesis and purification, quality control was assayed by high-pressure liquid chromatography (HPLC), using a C<sub>18</sub> column eluted with a 10-80% acetonitrile/water gradient or by thin-layer chromatography (TLC) using C<sub>18</sub> F254 plates developed in methanol/0.5 M NaCl and viewed under uv light. A low specific activity preparation of 22 mCi/mg (4.68 mCi/mmol) was used in these experiments. The [<sup>3</sup>H]FMISO was stored at 4°C and dissolved in ethanol to prevent radiolysis. Absorbance at 325 nm was used to determine the concentration of drug in our preparation by comparison to a standard curve. The [<sup>18</sup>F]FMISO (670 Ci/mmol) was also synthesized in our laboratory as described by Grierson *et al.* (18).

#### Cell Culture Systems

Four cell lines were used to examine uptake and retention of [<sup>3</sup>H]- or [<sup>18</sup>F]FMISO. Cells were used while growing exponentially or were allowed to reach an unfed plateau phase of growth and were treated for 3 h under anoxia (gas mixture of 95% N<sub>2</sub>-5% CO<sub>2</sub>, certified to be no greater than 10 ppm O<sub>2</sub>) or various low oxygen levels to allow incorporation of radiolabeled FMISO. In some experiments cells were labeled under anoxic conditions, rinsed, and then reincubated in drug-free medium for 1 to 6 h under oxic or anoxic conditions to study retention of label.

Chinese hamster lung fibroblasts (V-79-171B) were obtained from Dr. Peggy Olive, British Columbia Cancer Control Agency, and maintained in



Eagle's MEM (Sigma, St. Louis, MO) supplemented with 10% fetal bovine serum (FBS, Flow Laboratories, McLean, VA). A spontaneous dog osteosarcoma (CaOs-1) was established in culture in our laboratory and is grown in BioRich medium (Flow Laboratories) with 10% FBS. Two mouse tumor lines having the capability to grow both *in vitro* and *in vivo* were also used in these investigations; EMT-6(UW), a sarcoma of BALB/c mice, and RIF-1, a sarcoma of C3H/Km mice. Both cell lines grow in Waymouth's MB752/1 medium with 15% FBS and were originally obtained from Robert Kallman, Stanford University. All media contain penicillin/streptomycin and for hypoxia experiments, all contain 25 mM Hepes buffer.

To prepare tissue culture cells for anoxic or hypoxic incubation a spot technique developed by Koch (4) was used. Glass petri dishes (60 mm diameter, with notched edges to allow free exchange of gases) were filled with 3 ml of medium and, using a pipettor, 0.2 ml of medium containing the desired number of cells was carefully spotted in the center of the dish producing a disc of cells about 2.5 cm in diameter. The dishes were allowed to sit undisturbed for 2 h to allow cells to attach, before transfer to the incubator. When experiments involved exponentially growing cells, cultures were begun with  $10^5$  cells and used after 2 days' growth. Fresh medium was used to introduce the labeled drug. When experiments involved plateau-phase cells, cultures were begun with  $2 \times 10^5$  cells and were allowed to grow for 3 days. Depleted medium was used for uptake of [ $^3\text{H}$ ]FMISO and was prepared by filtration of medium from 6-day-old cultures of the same cell type, using a sterile fiberglass filter to remove cells.

To determine uptake of labeled FMISO under various conditions, culture dishes were removed from the incubator, growth medium was aspirated, and 1 ml of medium, typically containing 9.45  $\mu\text{g}/\text{ml}$  (50  $\mu\text{M}$ ) [ $^3\text{H}$ ]FMISO (or a combination of [ $^3\text{H}$ ] and [ $^{18}\text{F}$ ]FMISO), was used to rinse the culture medium from the monolayer disc of cells centered in the dish. This medium was aspirated and replaced with 1 ml of fresh labeled medium for incubation under the designated gas mixture. The cell monolayers then were subjected to multiple gas exchanges with the desired oxygen level under reduced pressure in aluminum chambers connected to a manifold and monitored with a vacuum gauge. This allowed rapid diffusion of  $\text{O}_2$  from the cells and medium and equilibration with the desired  $\text{O}_2$  level. Incubation under slightly reduced pressure for varying time allowed determination of uptake of radiolabeled drug into cells.

Uptake of the radiolabeled drug was accomplished by incubation for 3 h at 37°C after complete exchange of gas to 95%  $\text{N}_2$ -5%  $\text{CO}_2$  (certified to be no greater than 10 ppm  $\text{O}_2$ ) or an oxygen level ranging from 900 to 2500 ppm, with the balance  $\text{N}_2$  plus 5%  $\text{CO}_2$ , or 95% air plus 5%  $\text{CO}_2$  (210,000 ppm  $\text{O}_2$ ). Each aluminum cannister incubated under anoxia included an open dish of sodium dithionite prepared just before closing the chambers to scavenge oxygen molecules. A drop of 0.1 mM methylene blue was added to the dithionite when the chamber was opened to assure the anoxia of the system. If the dithionite is still capable of reduction, the blue disappears.

Sizes of exponentially growing and unfed plateau-phase cells were compared to allow FMISO uptake data to be corrected for cell size differences. Cell diameters were measured from projection slides of photomicrographs of trypsinized exponentially growing and plateau-phase cells, suspended in medium on a slide. All photographs were taken at the same magnification and volumes were calculated using the formula for a sphere:  $V = \frac{4}{3}\pi r^3$ .

In some experiments, cells were harvested at the end of the labeling period. In other experiments, retention of label was studied. Radiolabeled medium was removed from the cultures, which were rinsed twice and reincubated with drug-free medium. In some experiments, in which the replacement medium was sampled for analytic chemistry, it also was serum-free. The cultures were again placed in the aluminum chambers, gases were exchanged, and dishes were reincubated under either oxic or anoxic conditions for 1 to 6 h.

Cells were harvested by trypsinization, and a proportion of the total sample was counted in a Packard Model 3380 liquid scintillation spectrophoto-

meter in 10 ml of Instagel XF (United Technologies, Packard, Downer's Grove, IL). Uptake of the [ $^3\text{H}$ ]FMISO was calculated as dpm/ $10^5$  cells and converted to pmol FMISO/ $10^5$  cells. The activity of [ $^{18}\text{F}$ ]FMISO was measured by counting a proportion of the total cell pellet in the MINAXI g auto gamma counter (United Technologies, Packard). Uptake of the [ $^{18}\text{F}$ ]FMISO was calculated as cpm/ $10^5$  cells.

Cysteamine hydrochloride (2-mercaptoethylamine, Sigma, M6500) was dissolved directly in medium before application. Glucose-free Dulbecco's and glucose-free Waymouth's media (Sigma) were used in the glucose modulation experiments. Waymouth's medium, the medium used for RIF-1 and EMT-6 cells, normally contains 25 mM (4.5 g/liter) glucose and was used at this and lower glucose concentrations for studies with these two cell lines. The normal glucose concentration for BioRich medium as used for CaOs-1 cells is 17.5 mM (3.15 g/liter) glucose. The V-79 cells are normally grown in MEM containing 5.6 mM (1 g/liter) glucose. These two cell lines were grown in Dulbecco's medium, in which they also grow well. Medium of origin was not used because it was not routinely available without glucose. Dry glucose was added to these special media to reach desired concentrations (1.0 $\times$ , 0.1 $\times$ , and 0.01 $\times$  the normal glucose level for each cell line). It was determined that the variation in sugar concentration would not significantly alter the osmotic balance of these preparations.

#### Analytic Chemistry in Drug Release Experiments

To determine if FMISO radioactivity was protein bound, protein was precipitated from 400  $\mu\text{l}$  medium after 3 h incubation of cells with [ $^3\text{H}$ ]FMISO, using 1200  $\mu\text{l}$  acetonitrile:MeOH (1:3). The mixture was then centrifuged 3 min at 14,000 rpm. The supernate was drawn off and counted. The pellet was washed twice with 1 ml ethanol, dried, solubilized, bleached, and counted in Instagel (Packard) scintillation fluid in the liquid scintillation counter. The proportion of radioactivity in pellet and supernatant was calculated from total counts.

To determine if label lost from cells during reincubation involved loss of the tritium atom from FMISO or metabolites, four samples (400  $\mu\text{l}$  each) were taken from the medium overlying cells in the reincubation experiments described above. Three samples were allowed to evaporate to dryness, then reconstituted with 400  $\mu\text{l}$  water. Radioactivity of the original and reconstituted samples was compared.

To determine the molecular form of radiolabel released from cells, normal and reverse-phase TLC was done on samples of deproteinized, [ $^3\text{H}$ ]FMISO-containing medium at the end of a typical 3-h anoxic incubation and on samples of serum-free medium used in the reincubation studies described above. Normal-phase TLC used 5  $\times$  20-cm aluminum-backed silica gel 60F<sub>254</sub> plates (EM Science 5534) in a solvent system of chloroform:methanol (93:7). The lanes were cut into 1  $\times$  2.5-cm sections and counted in the liquid scintillation counter. An unlabeled FMISO standard was run on each plate and visualized with uv light. Reverse-phase TLC employed 5  $\times$  20-cm KC<sub>18</sub> plates (Whatman 4801-600) in a 0.5 M NaCl:methanol (1.3:1) solvent system. FMISO standards were included on each plate and sections (1  $\times$  2.5 cm) were cut and counted as described above for normal-phase TLC.

## RESULTS

The effect of oxygen level on the binding of FMISO is similar in the four cell lines examined. Increased oxygen levels inhibit binding in every cell line, with RIF-1 appearing to be the most sensitive. The oxygen level which inhibits FMISO binding by 50% relative to the anoxic binding level was calculated using a linear regression between the two appropriate adjacent data points and expressed to two significant figures. The 50% inhibitory level ranged from 720 to



TABLE I  
Inhibition of [ $^3\text{H}$ ]FMISO Binding in *in Vitro* Exponentially Growing Cells

Cell line	Oxygen level producing 50% inhibition (ppm) relative to anoxia
RIF-1	720
V-79	1400
EMT-6	1500
CaOs-1	2300

Note. Data obtained from  $n = 6$  plates per data point; data from EMT-6 and CaOs-1 have been published previously (16).

2300 ppm for four cell lines (Table I). Similar data for EMT-6(UW) and CaOs-1 cells have been published previously (16).

The effect of oxygen level on the binding of FMISO was also examined in nutrient-deprived plateau-phase cells. Because of size differences between log and plateau-phase cells these results are corrected for cell size with all data normalized to cell volume. The volume ratio of plateau to exponentially growing cells used to correct the data was 0.84 for RIF-1, 0.94 for EMT-6, 0.89 for V-79, and 1.14 for CaOs-1. Plateau-phase cells did not take up as much FMISO as log-phase cells under anoxic conditions, with the exception of V-79 cells (Figs. 1a–1d). However, FMISO uptake by plateau-phase cells shows an inhibition by oxygen similar to that for exponentially growing cells.

To examine retention of bound FMISO, cells were labeled with  $50\ \mu\text{M}$  [ $^3\text{H}$ ]FMISO for 3 h and then rinsed twice and reincubated in drug-free medium for various times up to 6 h in contact with 5%  $\text{CO}_2$ –95% air or under anoxic conditions (95%  $\text{N}_2$ –5%  $\text{CO}_2$ ). Varying amounts of radioactivity were gradually released from the cells during reincubation. A typical pattern of release is shown for CaOs-1 cells (Fig. 2). More activity was released from each of the four cell types when reincubated under oxic conditions than when reincubated in the absence of oxygen (Table II). At the end of 1 h, cells reincubated with 95%  $\text{N}_2$ –5%  $\text{CO}_2$  retained 69–88% of the label incorporated during the 3-h anoxic labeling period. After 3 h in anoxia, these values ranged from 57 to 73% of the label initially incorporated. Comparable values for oxic reincubation were 41 to 55% of initially incorporated label retained at 3 h.

In one FMISO retention experiment, V-79 cells were incubated for 3 h under anoxic conditions in medium containing both [ $^3\text{H}$ ]FMISO and [ $^{18}\text{F}$ ]FMISO to determine if the two labels were lost at the same rate during the reincubation phase of the experiment. If the two labels tracked each other, it would suggest that the [ $^3\text{H}$ ] label was not being lost from the parent molecule and appearing as tritiated water. Both labels were later released at the same rate. There was no significant difference in the relative amounts of  $^3\text{H}$  vs  $^{18}\text{F}$  retained after 1 or 3 h (Fig. 3).

Protein was precipitated from the medium after a 3-h incubation of cells with [ $^3\text{H}$ ]FMISO. Supernatant and protein pellets were counted in the liquid scintillation counter. The supernatant contained 98% of the radioactivity and the pellet 1% of the counts. This indicated that radioactivity was not bound to protein in the medium.

V-79 cells labeled with [ $^3\text{H}$ ]FMISO ( $50\ \mu\text{M}$  for 3 h in contact with 95%  $\text{N}_2$ –5%  $\text{CO}_2$ ) were rinsed and reincubated in drug-free, serum-free medium under anoxic or oxic conditions for 1 or 3 h. Samples of the reincubation medium were evaporated, reconstituted, and counted for radioactivity as described under Materials and Methods. Radioactivity in the reconstituted medium was essentially identical to that in medium aliquots counted directly after removal from the cells (Fig. 4). Since activity was not lost during evaporation, this suggested that the label was not released from the cells as [ $^3\text{H}$ ]H $_2\text{O}$ .

Medium from the four postlabeling reincubation conditions (1 and 3 h under normoxic or anoxic conditions) also was subjected to TLC to provide further information about the form of released radioactivity. The normal-phase TLC results were essentially the same for each of the four reincubation conditions. There was a peak at the origin, corresponding to polar metabolites, constituting roughly 75% of the total counts. A second peak, which corresponded to the unlabeled FMISO standard run on each plate, constituted approximately 25% of the counts (Table III). However, these medium analysis experiments provide no information about the form of the radioactivity retained in the cells. The FMISO in the medium may represent incomplete rinsing at the end of the labeling period, or it may represent parent drug released from the cells. These results also support previously described evidence that [ $^3\text{H}$ ] label was not being lost as [ $^3\text{H}$ ]H $_2\text{O}$ . With reverse-phase TLC, [ $^3\text{H}$ ]H $_2\text{O}$  would move with the solvent front and ionic molecules not far behind. There were essentially no counts at the solvent front, which is consistent with the evaporation/reconstitution findings of no counts associated with water.

The effect of reduced glucose level on the uptake of [ $^3\text{H}$ ]FMISO under anoxic conditions was also examined. When CaOs-1 cells were incubated under anoxic conditions, a reduced glucose concentration of 1.75 or 0.175 mM in the medium had no significant effect on the amount of [ $^3\text{H}$ ]FMISO taken up during the 3-hr incubation period relative to that accumulated in presence of 17.5 mM glucose, the normal level of glucose in Biorich medium. Results for EMT-6 and RIF-1 cells were similar. The V-79 cells bound significantly *more* FMISO when glucose concentrations were reduced. Table IV lists the percentage uptake of FMISO relative to normal glucose levels in all cell lines examined.

The effect of nonprotein sulfhydryl concentration on FMISO binding was examined by addition of three levels of

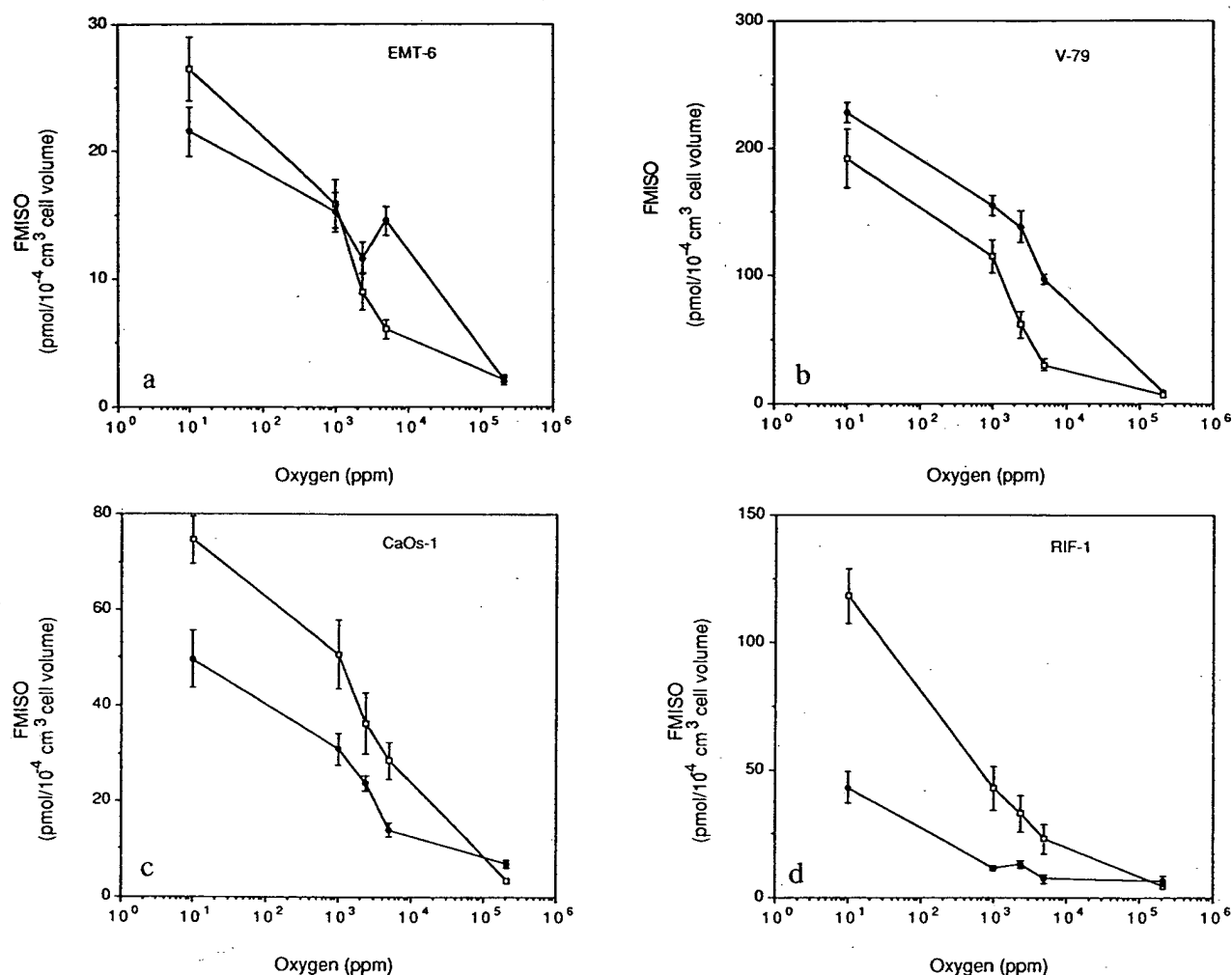


FIG. 1. Oxygen-dependent binding of  $[^3\text{H}]$ FMISO in four exponentially growing ( $\square$ ) and plateau-phase ( $\bullet$ ) cell cultures. Because of size differences between growth phases, binding is expressed relative to cell volume. Results are expressed as mean  $\pm$  SEM for  $n = 6$  plates per data point.

cysteamine to the incubation medium. Increasing levels of cysteamine resulted in significantly increased uptake of FMISO in V-79, RIF-1, and EMT-6 cell lines. Table V lists

the results for all cell lines examined. Results are expressed as percentage change in uptake relative to lowest concentration (0.2 mM).

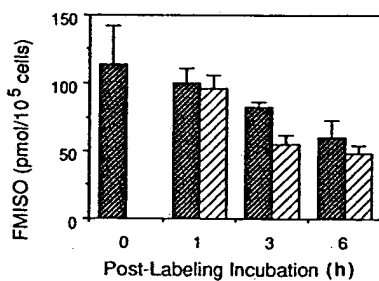


FIG. 2. Retention of  $^3\text{H}$  label in CaOs-1 cells following a 3-h anoxic incubation with  $[^3\text{H}]$ FMISO. Postlabeling incubation conditions were either anoxic (dark hatched) or oxic (light hatched). Results are expressed as mean  $\pm$  SEM for  $n = 6$  plates per data point.

## DISCUSSION

The uptake of  $[^3\text{H}]$ FMISO by tumor and V-79 cells *in vitro* is generally consistent with reports of oxygen-dependent binding of  $^{14}\text{C}$ - or  $^3\text{H}$ -labeled MISO. Franko *et al.* (8) reported that 1000 ppm oxygen inhibited MISO binding by 50% relative to anoxia in EMT-6(Ed) monolayer cells *in vitro* incubated in medium containing 50  $\mu\text{M}$  radiolabeled drug. Those authors also reported an anoxic:oxic binding ratio of approximately 15 for MISO in EMT-6(Ed) cells. These values may be compared to our measurement of a 50% inhibitory level of 1500 ppm for binding of 50  $\mu\text{M}$  FMISO and an anoxic:oxic ratio of 12.6 for EMT-6(UW)

TABLE II  
Retention of [ $^3\text{H}$ ]FMISO in Cells *in Vitro*

Cell line (Postlabeling incubation condition)	Drug level at end of labeling period (pmol/ $10^5$ cells) <sup>a</sup>	Percentage retention at different times from end of labeling period <sup>b</sup>		
		1 h	3 h	6 h
CaOs-1				
(Anoxic)	114.0 $\pm$ 28.6	88.0%	72.6%	52.9%
(Oxic)		84.2	48.4*	42.4*
EMT-6				
(Anoxic)	109.4 $\pm$ 15.6	81.9	56.7*	31.2**
(Oxic)		108.0	55.0*	19.3**
V-79				
(Anoxic)	215.0 $\pm$ 14.2	76.1*	69.4**	65.4**
(Oxic)		59.7**	41.3**	31.1**
RIF-1				
(Anoxic)	176.9 $\pm$ 7.8	68.9**	71.8**	51.6**
(Oxic)		70.8**	53.4**	37.3**

<sup>a</sup> Data expressed as mean  $\pm$  SEM for 6–12 plates per data point.

<sup>b</sup> Data expressed as percentage of label still found in cells relative to the amount found at end of labeling period (second column),  $n = 6$  plates per data point.

\*  $P < 0.05$ ; \*\*  $P < 0.01$ .

cells (16), a variant of the same mouse sarcoma system. Several other tumor types included in that same study (8) showed MISO binding to be inhibited by similar or slightly higher  $\text{O}_2$  levels. Investigations of misonidazole retention by V-79 cells showed that uptake in that cell type was even more easily inhibited by  $\text{O}_2$  than was the case with EMT-6(Ed) cells (5). Those results are not consistent with our

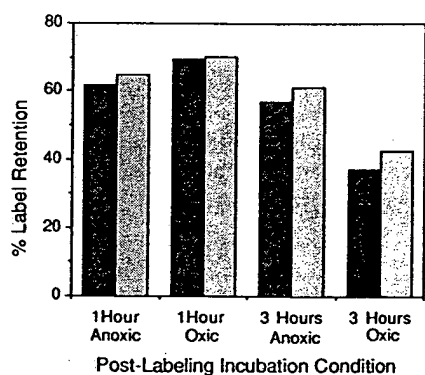


FIG. 3. Comparison of retention of [ $^3\text{H}$ ]FMISO (dark stipple) and [ $^{18}\text{F}$ ]FMISO (light stipple) in V-79 cell cultures. Because isotopes were counted in two different counters results are expressed as percentage retention of label for  $n = 6$  plates per data point. Immediately after the initial 3-h anoxic incubation,  $^3\text{H}$  uptake was  $391 \pm 20$  dpm/ $10^5$  cells and  $^{18}\text{F}$  uptake was  $992 \pm 16$  cpm/ $10^5$  cells. These values were taken as 100% for each isotope and subsequent retention was expressed as a percentage of these values.

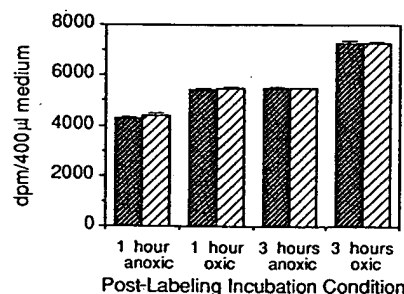


FIG. 4. V-79 cells were reincubated in unlabeled medium after a 3-h incubation in medium containing [ $^3\text{H}$ ]FMISO. Samples of the reincubation medium were counted immediately (dark hatch) or evaporated and reconstituted (light hatch) before counting to verify absence of [ $^3\text{H}$ ]H $_2\text{O}$ .

findings with [ $^3\text{H}$ ]FMISO binding in V-79 cells, in which the 50% inhibitory level is about 1400 ppm, very close to the value obtained for EMT-6(UW). Different sublines of V-79 cells were used in the two laboratories, and this may explain the difference. For the four cell lines studied the amount of oxygen which inhibits binding by 50% ranges from 700 to 2300 ppm, comparable to the 50% inhibitory level for MISO at comparable drug concentrations ( $50 \mu\text{M}$ ) in several tumor types (8). Given the limits of our *in vitro* studies, at one drug concentration, our data suggest that 50% binding inhibition occurs over a range of oxygen levels bracketing that for radiobiological hypoxia, as has been reported for MISO. This range will likely vary as a function of drug concentration (4). Thus FMISO should be useful as a probe for radioresistant hypoxic cells in human neoplasms provided that its binding is dominated by oxygen and less influenced by other factors in the intracellular or extracellular environment.

The growth state of a cell may influence its redox balance. This and the availability of reducing equivalents may determine the oxygen level which is capable of inhibiting FMISO

TABLE III  
Normal-Phase TLC of Medium in FMISO  
Release Experiments

Reincubation	Peak 1	Peak 2
1 h Anoxic	72%	27%
1 h Oxic	74%	25%
3 h Anoxic	76%	22%
3 h Oxic	70%	28%
Initial labeling medium	1%	98%
FMISO standard	2%	96%

Note. Normal-phase thin-layer chromatography analysis of the reincubation medium of V-79 cells previously incubated for 3 h in medium containing [ $^3\text{H}$ ]FMISO (designated initial labeling medium in table above) revealed activity in two major peaks. Peak 2 migrated with the same  $R_f$  as parent drug FMISO.

TABLE IV  
Effect of Glucose on FMISO Binding in Anoxic Cells *in Vitro*

Cell line	Control glucose level (mM)	FMISO binding at control glucose level (mean $\pm$ SEM) (pmol/ $10^5$ cells)	FMISO binding at different glucose levels (% of control)	
			1/10 Normal	1/100 Normal
V-79	5.6	83.9 $\pm$ 21.6	168*	235**
EMT-6	25	231.8 $\pm$ 44.7	84	102
RIF-1	25	156.3 $\pm$ 18.4	76	72**
CaOs-1	17.5	154.2 $\pm$ 12.2	112	101

Note.  $n = 6$  plates per data point.

\*  $P < 0.05$ ; \*\* $P < 0.01$ .

binding. Tumors *in vivo* contain both actively proliferating and quiescent cells (19). Exponentially growing and nutrient-deprived plateau-phase cells in culture model some of the characteristics of these cytokinetic populations and thus were chosen for comparison of uptake of FMISO at various oxygen levels. When uptake over a range of oxygen concentrations is compared for CaOs-1, V-79, RIF-1, and EMT-6 cells, plateau-phase cells take up less FMISO than do exponentially growing cells when data are corrected for cell size with the exception of V-79 cells (Figs. 1a-1d). The largest difference was seen for RIF-1 cells. However, both growth stages show similar  $O_2$  levels for 50% inhibition of binding (Table I and Figs. 1a-1d). Oxygen consumption by plateau-phase cells may be different, and possibly less, than that by cells in exponential growth, indicative of an overall lower metabolic rate. This could be a factor in less FMISO binding at intermediate  $O_2$  levels (a few mm Hg) but likely would not be important in anoxic cultures ( $<10$  ppm  $O_2$ ). Nutritionally inhibited plateau cells in depleted medium also have less glucose available, and this too could cause less binding of FMISO. Such a glucose effect has been reported for misonidazole (20). Some of the differences between exponential and plateau cells may be due to different proportions of cells in the  $G_1$  or  $G_0$  portion of the cell cycle, a difference which could easily be studied using flow cytometry and cell sorting. However, there are so many other differences between plateau and log-phase cells that cell sorting alone is unlikely to explain the observed differences, and for this reason these studies were not pursued. Overall these results and observations indicate that variation in growth state of tumor cells *in vivo* must be considered in interpreting uptake of labeled FMISO as a measure of hypoxic fraction.

Radiolabeled MISO has been reported to be covalently bound to cellular macromolecules including DNA, protein and, principally, RNA (1). After anoxic labeling with [ $^{14}C$ ]-MISO, radioactivity remaining in aerobic, growing EMT-6

and V-79 cells was measured over a period of several days. The  $t_{1/2}$  for loss of TCA-precipitable, bound radioactivity was 55 to 60 h (3). Other investigations using autoradiography to study localization of bound MISO adducts in spheroids have reported that the bound forms of the drug do not migrate to adjacent cells (7). These data, if applicable to FMISO, are very encouraging for PET imaging studies. Modeling the uptake and retention of an essentially irreversibly bound (metabolically trapped) tracer would be much simpler than dealing with a tracer with reversible binding. However, the above results with MISO were obtained with acid-precipitable bound radioactivity or radiolabel that survived the fixation which precedes autoradiography, whereas in an image all retained radioactivity, regardless of form, will be detected. Nonbound tracer equilibrated with plasma can easily be accounted for, but tracer that is bound by various mechanisms but slowly released would dictate a more complicated analysis. For these reasons the retention of drug by cells after *in vitro* labeling was examined by reincubating labeled cells in drug-free medium to determine the time course of release of label and to gain some understanding of the form of any released radioactivity. The FMISO label is lost gradually from each of the four cell types during postlabeling incubation, with greater loss in aerobic than anoxic cells (Table II). The loss rate ranged from 0 to 40% of the bound label within the first hour and up to 60% by 3 h under aerobic reincubation conditions. The greater loss under aerobic conditions in all four cell lines suggests a metabolic reaction occurring more rapidly in the presence of oxygen.

In all tracer studies it is essential to know that one is following the molecule of interest and not some other form of the isotope. Loss of tritium as [ $^3H$ ]H $_2$ O from labeled MISO has been reported (21), but this does not appear to be the explanation for loss of  $^3H$  label during cell reincubation after labeling with [ $^3H$ ]FMISO. Radioactivity is not lost when

TABLE V  
Effect of Cysteamine on FMISO Binding in Anoxic Cells *in Vitro*

Cell line	FMISO binding at 0.2 mM cysteamine (mean $\pm$ SEM, pmol/ $10^5$ cells)	FMISO binding at different cysteamine levels (% of 0.2 mM level)	
		2.0 mM	10.0 mM
V-79	71.2 $\pm$ 3.7	129**	148**
RIF-1	228.4 $\pm$ 16.3	125*	117
CaOs-1	288.9 $\pm$ 33.0	120	135
EMT-6	269.9 $\pm$ 34.4	124	141*

Note.  $n = 6$  plates per data point.

\*  $P < 0.05$ ; \*\* $P < 0.01$ .

reincubation medium is evaporated and reconstituted (Fig. 4), as would occur if tritium were released as tritiated water. Label from [ $^{18}\text{F}$ ]FMISO is lost from V-79 cells at the same rate as is label from [ $^3\text{H}$ ]FMISO (Fig. 3), providing indirect evidence that tritium is not lost from the molecule. Reverse-phase TLC revealed no activity migrating at the solvent front, as would occur if [ $^3\text{H}$ ]H $_2\text{O}$  were present.

TLC provided some information on the form of the released label. Normal-phase TLC of samples of reincubation medium indicates that about 25% of the released radioactivity was in unaltered FMISO, which may be a result of inadequate rinsing, while about 75% was in metabolites. The nature of these metabolites has not been determined but their migration pattern is consistent with at least some activity in the amine of FMISO. The hydroxylamine of MISO is suggested as the form which binds actively in hypoxic cells and disproportionation of two hydroxylamine molecules could give rise to the amine (22). The nitrosoamine has also been suggested as a biologically active form of 2-nitroimidazoles (23). At this time no information is available on the number and type of FMISO metabolites remaining in the cells. These analyses of cell extracts require HPLC, which is in progress.

Both glucose and nonprotein sulfhydryl concentration have been reported to influence MISO uptake by cells (3, 20, 24). Absence of the necessary reducing equivalents at low glucose levels could inhibit the reductive binding of nitroimidazoles (20). Alternatively, oxygen consumption by thiol reduction in medium (25) could increase binding. The requirement for reducing equivalents should be less stringent with the tracer levels of FMISO needed for imaging studies than for millimolar levels of MISO used in sensitization or cytotoxicity studies, and it was predicted (16) that binding of micromolar or lower levels of FMISO should not be much influenced by glucose levels. This is generally borne out by the studies summarized in Table V. In three of four cell types examined (EMT-6, RIF-1, and CaOs-1) glucose level had little effect on FMISO binding in anoxic log-phase cells, while in V-79 cells reduced glucose increased FMISO uptake. High levels of cysteamine increased FMISO uptake by cells. This indicates that excess sulfhydryls are not scavenging nitro radicals produced by reduction of FMISO. The increased uptake was statistically significant in V-79, RIF-1, and EMT-6 cells. However, the use of cysteamine may have led to other complicating factors in the interpretation of these results. Reduction of MISO by thiols in the presence of reduced metal ions should not be a problem when using medium containing serum, as was done in these experiments. Thiol auto-oxidation may also lead to H $_2\text{O}_2$  generation and oxygen depletion in the medium, resulting in lower oxygen concentrations than would otherwise be expected. This could increase FMISO binding at intermediate

oxygen levels but is not a likely explanation for the results obtained with incubations performed in 95% N $_2$ -5% CO $_2$ .

From these studies we conclude that the oxygen dependency of binding is similar for the four cell lines, with 50% inhibition of FMISO binding, relative to anoxia, at O $_2$  levels of 700-2300 ppm. This may be compared to the full hypoxic protection against radiation achieved at 1000 ppm. The anoxic:oxic binding ratios range from 12.6 for EMT-6 to 28 for V-79 and are high enough to allow detection of small foci of hypoxic cells surrounded by well-oxygenated tissue. Cell age coupled with poor nutrient conditions, and, to a lesser extent, nonprotein sulfhydryls do influence uptake. This means that the interpretation of FMISO binding in terms of hypoxic fraction will require careful consideration of other factors. However, the effect of other factors in most cases is small relative to the difference between fully anoxic vs oxic cells (12- to 28-fold difference in binding).

#### ACKNOWLEDGMENT

This work was supported by National Institutes of Health Grants CA34570 and CA42045.

RECEIVED: July 14, 1989; ACCEPTED: February 2, 1990

#### REFERENCES

1. A. VARGHESE and G. WHITMORE, Binding to cellular macromolecules as a possible mechanism for the cytotoxicity of misonidazole. *Cancer Res.* **40**, 2165-2169 (1980).
2. J. D. CHAPMAN, A. FRANKO, and J. A. SHARPLIN, Marker for hypoxic cells in tumors with potential clinical applicability. *Br. J. Cancer* **43**, 546-550 (1981).
3. J. D. CHAPMAN, K. BAER, and J. LEE, Characteristics of the metabolism-induced binding of misonidazole to hypoxic mammalian cells. *Cancer Res.* **43**, 1523-1528 (1983).
4. C. KOCH, A "thin film" culturing technique allowing rapid gas-liquid equilibration with no toxicity to mammalian cells. *Radiat. Res.* **97**, 434-442 (1984).
5. A. J. FRANKO and C. J. KOCH, Binding of misonidazole to V-79 spheroids and fragments of Dunning rat prostatic and human colon carcinomas *in vitro*: Diffusion of O $_2$  and reactive metabolites. *Int. J. Radiat. Oncol. Biol. Phys.* **10**, 1333-1336 (1984).
6. A. J. FRANKO, Hypoxic fraction and binding of misonidazole in EMT6/Ed multicellular tumor spheroids. *Radiat. Res.* **103**, 89-97 (1985).
7. A. J. FRANKO, Misonidazole and other hypoxia markers: Metabolism and applications. *Int. J. Radiat. Oncol. Biol. Phys.* **12**, 1195-1202 (1986).
8. A. J. FRANKO, C. KOCH, B. GARRECHT, J. SHARPLIN, and D. HUGHES, Oxygen dependence of binding of misonidazole to rodent and human tumors *in vitro*. *Cancer Res.* **47**, 5367-5376 (1987).
9. J. D. CHAPMAN, Current concepts in cancer. Hypoxic sensitizers—implications for radiation therapy. *N. Engl. J. Med.* **301**, 1429-1432 (1979).
10. J. D. CHAPMAN, The detection and measurement of hypoxic cells in solid tumors. *Cancer* **54**, 2441-2449 (1984).

11. J. HOFFMAN, J. S. RASEY, A. J. SPENCE, and K. A. KROHN, Binding of the hypoxia tracer H-3 misonidazole in cerebral ischemia. *Stroke* **18**, 168-176 (1987).
12. G. V. MARTIN, J. CALDWELL, J. S. RASEY, Z. GRUNBAUM, M. CERQUEIRA, and K. A. KROHN, Enhanced binding of the hypoxic cell marker [H-3]fluoromisonidazole in ischemic myocardium. *J. Nucl. Med.* **30**, 194-201 (1989).
13. P. A. JARABEK, D. D. DISCHINO, M. R. KILBOURN *et al.*, Synthesis of a fluorine-18 labeled hypoxic cell sensitizer. *J. Nucl. Med.* **25**, 23 (1984).
14. Z. GRUNBAUM, S. FREAUFF, K. A. KROHN, D. WILBUR, S. MAGEE, and J. S. RASEY, Synthesis and characterization of congeners of misonidazole for imaging hypoxia. *J. Nucl. Med.* **28**, 68-75 (1987).
15. J. S. RASEY, Z. GRUNBAUM, S. MAGEE, N. J. NELSON, P. OLIVE, R. DURAND, and K. A. KROHN, Characterization of radiolabeled fluoromisonidazole as a probe for hypoxic cells. *Radiat. Res.* **111**, 292-304 (1987).
16. J. S. RASEY, W. J. KOH, J. G. GRIERSON, Z. GRUNBAUM, and K. A. KROHN, Radiolabeled fluoromisonidazole as an imaging agent for tumor hypoxia. *Int. J. Radiat. Oncol. Biol. Phys.* **17**, 985-991 (1989).
17. J. L. BORN and B. R. SMITH, The synthesis of tritium-labeled misonidazole. *J. Labelled Compd. Radiopharm.* **20**, 429-432 (1983).
18. J. GRIERSON, J. LINK, C. MATHIS, J. S. RASEY, and K. A. KROHN, A. radiosynthesis of [F-18]fluoromisonidazole. *J. Nuclear Med.* **30**, 342-350 (1989).
19. L. A. DETHLEFSEN, In quest of the quaint quiescent cells. In *Radiation Biology in Cancer Research* (R. E. Meyn and H. R. Withers, Eds.), pp. 415-435. Raven Press, New York, 1980.
20. L. LING and R. G. SUTHERLAND, Modulation of the hypoxic toxicity and binding of misonidazole by glucose. *Br. J. Cancer* **54**, 911 (1986).
21. A. J. FRANKO, J. A. RALEIGH, R. G. SUTHERLAND, and K. J. SODERLIND, Metabolic binding of misonidazole to mouse tissues: Comparison between labels of the ring and side chain, and the production of tritiated water. *Biochem. Pharmacol.* **15**, 665-670 (1989).
22. A. J. VARGHESE, S. GULYAS, and J. K. MOHENDRA, Hypoxia-dependent reduction of 1-(2-nitro-1-imidazole)-3-methoxy-2-propanol by Chinese hamster ovary cells and KHT tumor cells *in vitro* and *in vivo*. *Cancer Res.* **36**, 3761-3765 (1976).
23. R. T. MULCAHY, J. J. GIPP, G. A. UBLACKER, R. RANUICUCCI, and R. A. MCCLELLAND, Cytotoxicity and glutathione depletion by 1-methyl-2-nitrosoimidazole in human colon cancer cells. *Biochem. Pharmacol.* **38**, 1667-1671 (1989).
24. L. LING and R. G. SUTHERLAND, Dependence of misonidazole binding on factors associated with hypoxic metabolism. *Br. J. Cancer* **56**, 389-393 (1987).
25. J. PURDIE, E. INHABER, H. SCHNEIDER, and J. LABELLE, Interaction of cultured mammalian cells with WR-2721 and its thiol, WR-1065: Implications for mechanisms of radioprotection. *Int. J. Radiat. Biol.* **43**, 517-527 (1983).

# Noninvasive Assessment of Tumor Hypoxia with $^{99m}\text{Tc}$ Labeled Metronidazole

David J. Yang,<sup>1</sup> Seyfettin Ilgan,<sup>1</sup> Tetsuya Higuchi,<sup>1</sup>  
Fereshteh Zareneyrizi,<sup>1</sup> Chang-Sok Oh,<sup>1</sup>  
Chun-Wei Liu,<sup>1</sup> E. Edmund Kim,<sup>1</sup> and  
Donald A. Podoloff<sup>1,2</sup>

Received November 23, 1998; accepted February 2, 1999

**Purpose.** The assessment of tumor hypoxia by imaging modality prior to radiation therapy would provide a rational means of selecting patients for treatment with radiosensitizers or bioreductive drugs. This study aimed to develop a  $^{99m}\text{Tc}$ -labeled metronidazole (MN) using ethylenedicysteine (EC) as a chelator and evaluate its potential use to image tumor hypoxia.

**Methods.** EC was conjugated to amino analogue of MN using Sulfo-N-hydroxysuccinimide and 1-ethyl-3-(3-dimethylaminopropyl) carbodiimide-HCl as coupling agents, the yield was 55%. Tissue distribution of  $^{99m}\text{Tc}$ -EC-MN was determined in breast tumor-bearing rats at 0.5, 2, and 4 hrs. Planar imaging and whole-body autoradiograms were performed. The data was compared to that using  $^{99m}\text{Tc}$ -EC (control), [ $^{18}\text{F}$ ]fluoromisonidazole (FMISO) and [ $^{131}\text{I}$ ] iodomisonidazole (IMISO).

**Results.** *In vivo* biodistribution of  $^{99m}\text{Tc}$ -EC-MN in breast tumor-bearing rats showed increased tumor-to-blood and tumor-to-muscle ratios as a function of time. Conversely, tumor-to-blood values showed time-dependent decrease, with  $^{99m}\text{Tc}$ -EC in the same time period. Planar images and autoradiograms confirmed that the tumors could be visualized clearly with  $^{99m}\text{Tc}$ -EC-MN from 0.5 to 4 hrs. There was no significant difference of tumor-to-blood count ratios between  $^{99m}\text{Tc}$ -EC-MN and [ $^{131}\text{I}$ ]IMISO at 2 and 4 hrs postinjection. From 0.5 to 4 hrs, both  $^{99m}\text{Tc}$ -EC-MN and [ $^{131}\text{I}$ ]IMISO have higher tumor-to-muscle ratios compared to [ $^{18}\text{F}$ ]FMISO.

**Conclusions.** It is feasible to use  $^{99m}\text{Tc}$ -EC-MN to image tumor hypoxia.

**KEY WORDS:** metronidazole;  $^{99m}\text{Tc}$ ; tumor hypoxia; imaging; radiosensitizer.

## INTRODUCTION

Tumor cells are more sensitive to conventional radiation in the presence of oxygen than in its absence; even a small percentage of hypoxic cells within a tumor could limit the response to radiation (1–3). Hypoxic radioresistance has been demonstrated in many animal tumors but only in a few tumor types in humans (4–6). The occurrence of hypoxia in human tumors has, in most cases, been inferred from histology findings and from animal tumor studies. *In vivo* demonstration of hypoxia has required tissue measurements with oxygen electrodes, and the invasiveness of these techniques has limited their clinical application.

Misonidazole (MISO) is a hypoxic cell sensitizer, and labeling MISO with different radioisotopes (e.g.,  $^{18}\text{F}$ ,  $^{123}\text{I}$ ,  $^{99m}\text{Tc}$ ) may be useful for differentiating a hypoxic but metabolically active tumor from a well-oxygenated active tumor by positron emission tomography (PET) or planar scintigraphy. Moreover, the assessment of tumor hypoxia with labeled MISO prior to radiation therapy would provide a rational means of selecting patients for treatment with radiosensitizing or bioreductive drugs (e.g. mitomycin C). Such selection of patients would permit more accurate treatment because use of these modalities could be limited to patients with hypoxic tumors. It is also possible to select proper modalities of radiotherapy (neutron vs. photon) by correlating labeled MISO results with tumor response.

[ $^{18}\text{F}$ ]Fluoromisonidazole (FMISO) has been used with PET to evaluate tumor hypoxia. Recent studies have shown that PET, with its ability to monitor cell oxygen content through [ $^{18}\text{F}$ ]FMISO, has a high potential to predict tumor response to radiation (7–12). PET gives a higher resolution without collimation, however, the cost of using PET isotopes in a clinical setting is prohibitive. Although labeling MISO with iodine was the choice, high uptake in thyroid tissue was observed (13). Therefore, it is desirable to develop compounds for planar scintigraphy that the isotope is less expensive and easily available in most major medical facilities.

*In vitro* studies using mammalian cells, metronidazole (MN) was shown to sensitize only anoxic cells in a dose dependent manner, a maximum enhancement ratio of 1.9 being obtained (2.5 for MISO). However, *in vivo* studies showed that this sensitizer plus radiation group had survival equivalent to that of patients given standard fractionated high-dose radiation. The difference in sensitization effect may be due to electron affinity, lipophilic character (to reduce systemic toxicity and not to lose sensitization activity) and glutathione depletion characteristics (14).

Due to favorable physical characteristics as well as extremely low price,  $^{99m}\text{Tc}$  have been preferred to label radiopharmaceuticals. Several nitroimidazole analogues have been labeled with  $^{99m}\text{Tc}$  using nitrogen and sulfur chelates (15–18). Bis-aminoethanethiol tetradentate ligands, also called dithionodithiol compounds, are known to form very stable  $\text{Tc(V)O}$ -complexes on the basis of efficient binding of the oxotechnetium group to two thiolsulphur and two amine nitrogen atoms (19,20).  $^{99m}\text{Tc}$ -L,L-ethylenedicysteine ( $^{99m}\text{Tc}$ -EC) is a recent and successful example of  $\text{N}_2\text{S}_2$  chelates. EC can be labeled with  $^{99m}\text{Tc}$  easily and efficiently with high radiochemical purity and stability and is excreted through kidney by active tubular transport (20–22).

Although radiosensitizing effect using MN was not impressive, MN has been shown to sensitize hypoxic tumors. Thus, in this paper, we present the synthesis of  $^{99m}\text{Tc}$ -labeled metronidazole using EC as a chelator and evaluate its potential use as a tumor hypoxic imaging agent and results were compared to those  $^{99m}\text{Tc}$ -EC (standard), [ $^{18}\text{F}$ ]FMISO and [ $^{131}\text{I}$ ]IMISO.

## MATERIALS AND METHODS

The nuclear magnetic resonance (NMR) and mass spectral analysis were conducted at the University of Texas Health Science Center (Houston, TX). NMR spectra were recorded on

<sup>1</sup> Department of Nuclear Medicine The University of Texas M. D. Anderson Cancer Center, Houston, Texas.

<sup>2</sup> To whom correspondence should be addressed. (e-mail: dyang@rpisun1.mdacc.tmc.edu)

a GE GN-500 Spectrometer. The mass data were obtained by fast atom bombardment on a Kratos MS 50 instrument (England). Sulfo-N-hydroxysuccinimide (Sulfo-NHS) and 1-ethyl-3-(3-dimethylaminopropyl) carbodiimide-HCl (EDC) were purchased from Pierce Chemical Co (Radford, IL). All other chemicals were purchased from Aldrich Chemical Co (Milwaukee, WI). Silica gel coated thin-layer chromatography (TLC) plate was purchased from Whatman (Clifton, NJ).  $^{99m}\text{Tc}$ -pertechnetate was obtained from a commercial  $^{99}\text{Mo}/^{99m}\text{Tc}$  generator (Ultratechnekow FM<sup>TM</sup>, Mallinckrodt Diagnostica, Holland).

### Synthesis of L,L-Ethylenedicysteine (EC)

EC was prepared in a two-step synthesis according to the previously described methods (23,24). The precursor, L-thiazolidine-4-carboxylic acid, was synthesized (m.p. 195°, reported 196–197°). EC was then prepared (m.p. 237°, reported 251–253°C). The structure was confirmed by  $^1\text{H}$ -NMR and mass spectroscopy (FAB-MS)  $m/z$  268 ( $\text{M}^+$ , 100).

### Synthesis of 2-(2-Methyl-5-Nitro-1H-Imidazolyl)Ethylamine (Amino Analogue of Metronidazole, MN-NH<sub>2</sub>)

Amino analogue of metronidazole was synthesized according to the previously described methods (25). Briefly, metronidazole was converted to a mesylated analogue (m.p. 149–150°C, reported 153–154°C, TLC:ethyl acetate,  $R_f$  = 0.45), yielded 75%. Mesylated metronidazole was then reacted with sodium azide to afford azido analogue (TLC:ethyl acetate,  $R_f$  = 0.52), yielded 80%. The azido analogue was reduced by triphenyl phosphine and yielded (60%) the desired amino analogue (m.p. 190–192°C, reported 194–195°C, TLC:ethyl acetate,  $R_f$  = 0.15). Ninhydrin (2% in methanol) spray indicated the positivity of amino group of MN-NH<sub>2</sub>. The structure was confirmed by  $^1\text{H}$ -NMR and mass spectroscopy (FAB-MS)  $m/z$  171 ( $\text{M}^+$ , 100).

### Synthesis of Ethylenedicysteine-Metronidazole (EC-MN)

Sodium hydroxide (2N, 0.2 ml) was added to a stirred solution of EC (134 mg, 0.50 mmol) in water (5 ml). To this colorless solution, sulfo-NHS (217 mg, 1.0 mmol) and EDC (192 mg, 1.0 mmol) were added. MN-NH<sub>2</sub> dihydrochloride salt (340 mg, 2.0 mmol) was then added. The mixture was stirred at room temperature for 24 hours. The mixture was dialyzed for 48 hrs using Spectra/POR molecular porous membrane with cut-off at 500 (Spectrum Medical Industries Inc., Houston, TX). After dialysis, the product was frozen dried using lyophilizer (Labconco, Kansas City, MO). The product weighed 315 mg (yield 55%).  $^1\text{H}$ -NMR ( $\text{D}_2\text{O}$ )  $\delta$  2.93 (s, 6H, nitroimidazole-CH<sub>3</sub>), 2.60–2.95 (m, 4H and -CH<sub>2</sub>-SH of EC), 3.30–3.66 (m, 8H, ethylenediamine of EC and nitromidazole-CH<sub>2</sub>-CH<sub>2</sub>-NH<sub>2</sub>), 3.70–3.99 (t, 2H, NH-CH-CO of EC), 5.05 (t, 4H, metronidazole-CH<sub>2</sub>-CH<sub>2</sub>-NH<sub>2</sub>) (s, 2H, nitroimidazole C=CH). FAB MS  $m/z$  572 ( $\text{M}^+$ , 20). The synthetic scheme of EC-MN is shown in Fig. 1.

### Radiolabeling of EC-MN and EC with $^{99m}\text{Tc}$

Radiosynthesis of  $^{99m}\text{Tc}$ -EC-MN was achieved by adding required amount of  $^{99m}\text{Tc}$ -pertechnetate into home-made kit

containing the lyophilized residue of EC-MN (3 mg),  $\text{SnCl}_2$  (100  $\mu\text{g}$ ),  $\text{Na}_2\text{HPO}_4$  (13.5 mg), ascorbic acid (0.5 mg) and NaEDTA (0.5 mg). Final pH of preparation was 7.4.  $^{99m}\text{Tc}$ -EC was also obtained by using home-made kit containing the lyophilized residue of EC (3 mg),  $\text{SnCl}_2$  (100  $\mu\text{g}$ ),  $\text{Na}_2\text{HPO}_4$  (13.5 mg), ascorbic acid (0.5 mg) and NaEDTA (0.5 mg) at pH 10. Final pH of preparation was then adjusted to 7.4. Radiochemical purity was determined by TLC (ITLC SG, Gelman Sciences, Ann Arbor, MI) eluted with acetone (system A) and ammonium acetate (1M in water):methanol (4:1) (system B), respectively. From radio-TLC (Bioscan, Washington, DC) analysis, the radiochemical purity was >95% for both radiotracers.

### Synthesis of [ $^{18}\text{F}$ ]FMISO and [ $^{131}\text{I}$ ]IMISO

[ $^{18}\text{F}$ ]fluoride was produced by the cyclotron using proton irradiation of enriched  $^{18}\text{O}$ -water in a small-volume silver target. The tosyl MISO (26) (20 mg) was dissolved in acetonitrile (1.5 ml), added to the kryptofix-fluoride complex. After heating, hydrolysis and column purification, A yield of 25–40% (decay corrected) of pure product was isolated with the end of bombardment (EOB) at 60 min. HPLC was performed on a C-18 ODS-120T column, 4.6  $\times$  25 mm (Waters Corp., Milford, Mass), with water/acetonitrile, (80/20), using a flow rate of 1 ml/min. The no-carrier-added product corresponded to the retention time (6.12 min) of the unlabeled FMISO under similar conditions. The radiochemical purity was greater than 99%. Under the UV detector (310 nm), there were no other impurities. The specific activity of [ $^{18}\text{F}$ ]FMISO determined was 1 Ci/ $\mu\text{mol}$  based upon UV and radioactivity detection of a sample of known mass and radioactivity.

[ $^{131}\text{I}$ ]IMISO was prepared using the same precursor (26), briefly, 5 mg of tosyl MISO was dissolved in acetonitrile (1 ml), and  $\text{Na}^{131}\text{I}$  (1 mCi in 0.1 ml IN NaOH) (Dupont New England Nuclear, Boston, MA) was added. After heating and purification, the product (60–70% yield) was obtained. Radio-TLC indicated the  $R_f$  values of 0.01 for the final product using chloroform methanol (7:3) as an eluant.

### Stability Assay of $^{99m}\text{Tc}$ -EC-MN

Stability of labeled  $^{99m}\text{Tc}$ -EC-MN was tested in serum samples. Briefly, 740 KBq of 1 mg  $^{99m}\text{Tc}$ -EC-MN was incubated in dog serum (200  $\mu\text{l}$ ) at 37°C for 4 hours. The serum samples was diluted with 50% methanol in water and radio-TLC repeated at 0.5, 2 and 4 hours as described above.

### Tissue Distribution Studies

The animal experiments were approved by The University of Texas M. D. Anderson Institutional Animal Care and Use Committee (IACUC). Female Fischer 344 rats (150  $\pm$  25 g) (Harlan Sprague-Dawley, Indianapolis, IN) were inoculated subcutaneously with 0.1 ml of mammary tumor cells from the 13762 tumor cell line suspension ( $10^6$  cells/rat, a tumor cell line specific to Fischer rats) into the hind legs using 25-gauge needles. Studies performed 14 to 17 days after implantation when tumors reached approximately 1 cm diameter. Rats were anesthetized with ketamine (10–15 mg/rat, intraperitoneally) before each procedure.



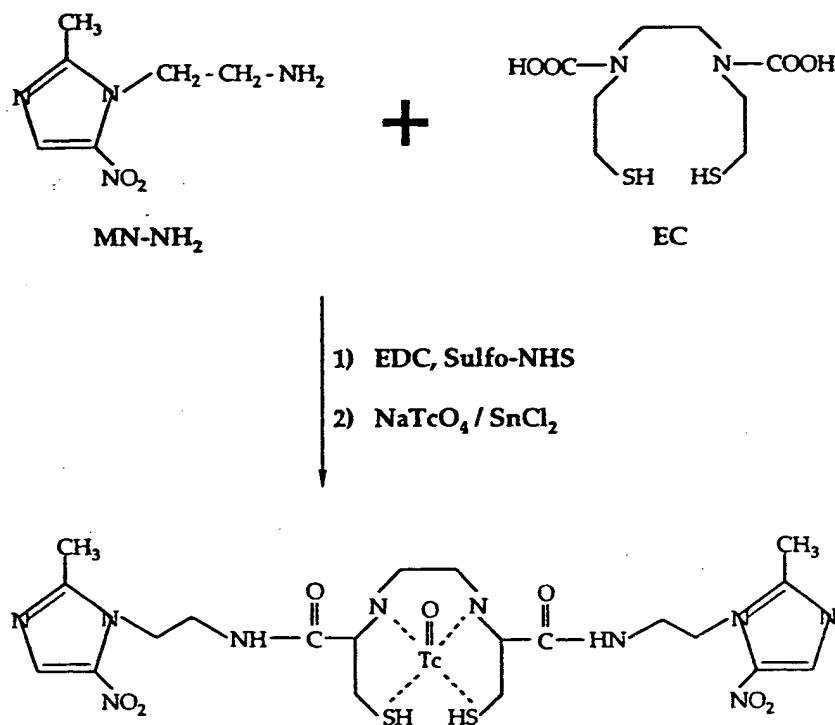


Fig. 1. Radiosynthesis of  $^{99m}\text{Tc}$ -EC-metronidazole (EC-MN).

In tissue distribution studies, each animal was injected intravenously with 370–550 KBq of  $^{99m}\text{Tc}$ -EC-MN or  $^{99m}\text{Tc}$ -EC ( $n = 3/\text{time point}$ ). The injected mass of  $^{99m}\text{Tc}$ -EC-MN was 10  $\mu\text{g}$  per rat. At 0.5, 2 and 4 hrs following administration of the radiotracers, the rats were sacrificed and the selected tissues were excised, weighed and counted for radioactivity. The biodistribution of tracer in each sample was calculated as percentage of the injected dose per gram of tissue wet weight (%ID/g). Tumor/nontarget tissue count density ratios were calculated from the corresponding %ID/g values. The data was compared to [ $^{18}\text{F}$ ]FMISO and [ $^{131}\text{I}$ ]IMISO using the same animal model. Student *t*-test was used to assess the significance of differences between groups.

#### Polarographic Oxygen Microelectrode $\text{pO}_2$ Measurements

To confirm tumor hypoxia, intratumoral  $\text{pO}_2$  measurements were performed using the Eppendorf computerized histographic system. Twenty to twenty-five  $\text{pO}_2$  measurements along each of two to three linear tracks were performed at 0.4 mm intervals on each tumor (40–75 measurements total). Tumor  $\text{pO}_2$  measurements were made on three tumor-bearing rats. Using an on-line computer system, the  $\text{pO}_2$  measurements of each track were expressed as absolute values relative to the location of the measuring point along the track, and as the relative frequencies within a  $\text{pO}_2$  histogram between 0 and 100 mmHg with a class width of 2.5 mm.

#### Scintigraphic Imaging and Autoradiography Studies

Scintigraphic images, using a gamma camera (Siemens Medical Systems, Inc., Hoffman Estates, IL) equipped with low-energy, parallel-hole collimator, were obtained 0.5, 2 and 4 hrs after i.v. injection of 18.5 MBq of each radiotracer.

Whole-body autoradiogram was obtained by a quantitative image analyzer (Cyclone Storage Phosphor System, Packard, Meridian, CT). Following i.v. injection of 37 MBq of  $^{99m}\text{Tc}$ -EC-MN, animal was killed at 1 h and the body was fixed in carboxymethyl cellulose (4%) as previously described (12,13). The frozen body was mounted onto a cryostat (LKB 2250 cryomicrotome) and cut into 100  $\mu\text{m}$  coronal sections. Each section was thawed and mounted on a slide. The slide was then placed in contact with multipurpose phosphor storage screen (MP, 7001480) and exposed for 15 hrs.

Table 1. Biodistribution of  $^{99m}\text{Tc}$ -EC-Metronidazole Conjugate in Breast Tumor Bearing Rats<sup>a</sup>

	30 min	2 hr	4 hr
Blood	$1.46 \pm 0.73$	$1.19 \pm 0.34$	$0.76 \pm 0.14$
Lung	$0.79 \pm 0.39$	$0.73 \pm 0.02$	$0.52 \pm 0.07$
Liver	$0.83 \pm 0.36$	$0.91 \pm 0.11$	$0.87 \pm 0.09$
Spleen	$0.37 \pm 0.17$	$0.41 \pm 0.04$	$0.37 \pm 0.07$
Kidney	$4.30 \pm 1.07$	$5.84 \pm 0.43$	$6.39 \pm 0.48$
Muscle	$0.08 \pm 0.03$	$0.09 \pm 0.01$	$0.07 \pm 0.01$
Intestine	$0.27 \pm 0.12$	$0.39 \pm 0.24$	$0.22 \pm 0.05$
Thyroid	$0.51 \pm 0.16$	$0.51 \pm 0.09$	$0.41 \pm 0.02$
Tumor	$0.34 \pm 0.13$	$0.49 \pm 0.02$	$0.50 \pm 0.09$

<sup>a</sup> Each rat received  $^{99m}\text{Tc}$ -EC-metronidazole (10  $\mu\text{Ci}$ , iv). Each value is percent of injected dose per gram weight ( $n = 3$ )/time interval. Each data represents mean of three measurements with standard deviation.

**Table 2.** Biodistribution of  $^{99m}\text{Tc}$ -EC in Breast Tumor-Bearing Rats<sup>a</sup>

	% of injected $^{99m}\text{Tc}$ -EC dose per organ or tissue		
	30 min	2 hr	4 hr
Blood	0.44 ± 0.03	0.21 ± 0.01	0.15 ± 0.01
Lung	0.27 ± 0.02	0.14 ± 0.01	0.12 ± 0.01
Liver	0.51 ± 0.06	0.29 ± 0.07	0.23 ± 0.02
Stomach	0.14 ± 0.06	0.04 ± 0.03	0.04 ± 0.01
Kidney	7.91 ± 0.90	9.12 ± 0.05	7.83 ± 1.02
Muscle	0.06 ± 0.01	0.03 ± 0.01	0.02 ± 0.01
Intestine	0.17 ± 0.03	0.40 ± 0.09	0.10 ± 0.01
Thyroid	0.22 ± 0.04	0.11 ± 0.00	0.08 ± 0.01
Tumor	0.34 ± 0.16	0.12 ± 0.00	0.10 ± 0.01

<sup>a</sup> Values shown represent the mean ± standard deviation of data from 3 animals.

## RESULTS

### Radiosynthesis and Stability of $^{99m}\text{Tc}$ -EC-MN

Radiosynthesis of EC-MN with  $^{99m}\text{Tc}$  was achieved with high (>95%) radiochemical purity. Radiochemical yield was 100%.  $^{99m}\text{Tc}$ -EC-MN was found to be stable at 0.5, 2 and 4 hrs in dog serum samples. There was no degradation products observed. Radiofluorination and radioiodination of MISO were

achieved easily using the same precursor. In both labeled MISO analogues, the radiochemical purity was greater than 99%.

### In Vivo Tissue Distribution Studies

The tissue distribution of  $^{99m}\text{Tc}$ -EC-MN and  $^{99m}\text{Tc}$ -EC in the tumor-bearing rats is shown in Tables 1 and 2. Due to high affinity for ionic  $^{99m}\text{Tc}$ , there was no significant and consistent thyroid uptake, suggesting the in vivo stability of  $^{99m}\text{Tc}$ -EC-MN (Table 1).

Biodistribution studies showed that tumor/blood and tumor/muscle count density ratios at 0.5-4 hr gradually increased for  $^{99m}\text{Tc}$ -EC-MN, [ $^{18}\text{F}$ ]FMISO and [ $^{131}\text{I}$ ]IMISO, whereas these values did not alter for  $^{99m}\text{Tc}$ -EC in the same time period (Figs. 2 and 3). [ $^{18}\text{F}$ ]FMISO showed the highest tumor-to-blood uptake ratio than those with [ $^{131}\text{I}$ ]IMISO and  $^{99m}\text{Tc}$ -EC-MN at 30 min, 2 and 4 hrs post-injection. Tumor/blood and tumor/muscle ratios for  $^{99m}\text{Tc}$ -EC-MN and [ $^{131}\text{I}$ ]IMISO at 2 and 4 hrs postinjection were not significantly different ( $p < 0.05$ ).

### Scintigraphic Imaging and Autoradiographic Studies

Scintigraphic images obtained at different time points showed visualization of tumor in  $^{99m}\text{Tc}$ -EC-MN group. Contrary, there was no apparent tumor uptake in  $^{99m}\text{Tc}$ -EC injected group (Fig. 4). Autoradiograms performed at 1 hr after injection of  $^{99m}\text{Tc}$ -EC-MN clearly demonstrated tumor activity (Fig. 5).

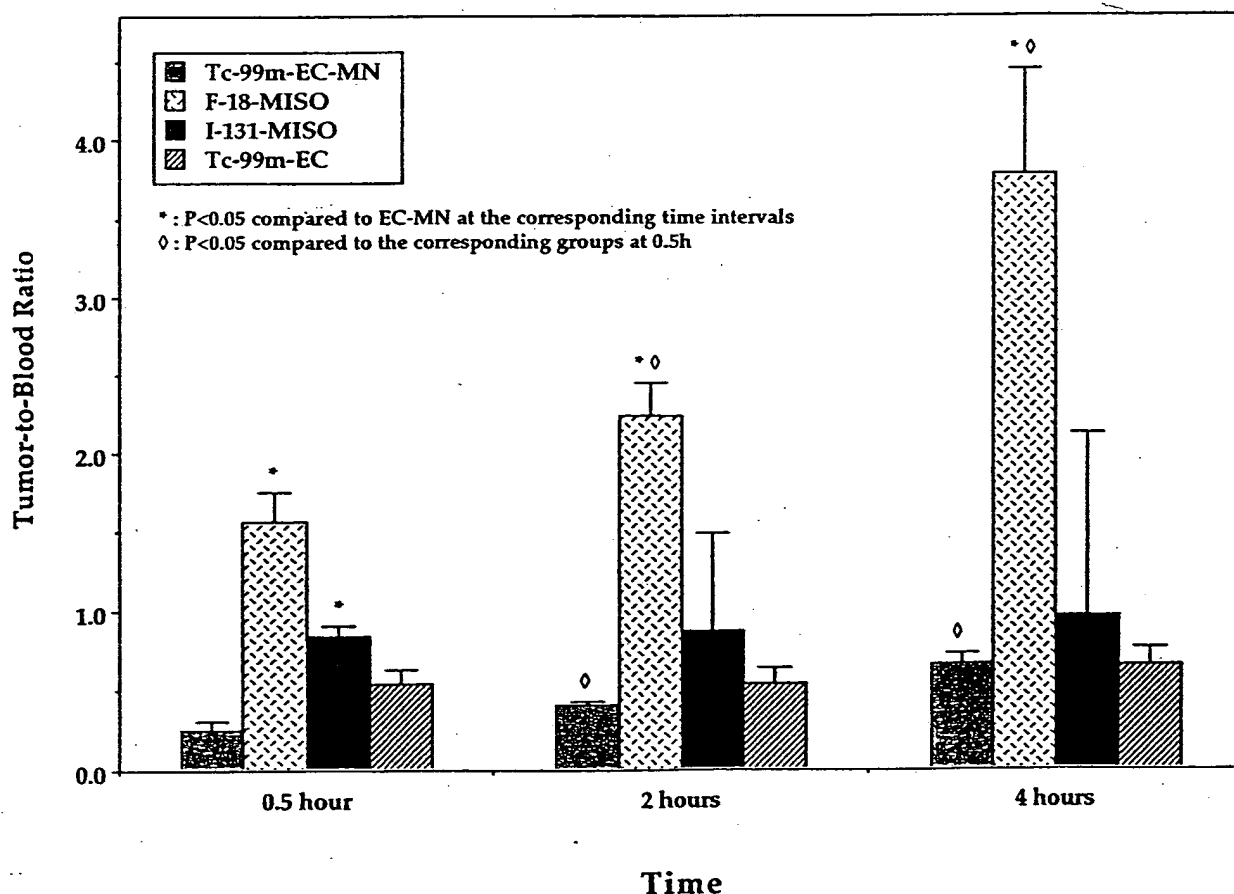


**Fig. 2.** Time-dependent variation of tumor/blood uptake ratios (%ID/g wet weight) with  $^{99m}\text{Tc}$ -EC-MN, [ $^{18}\text{F}$ ]FMISO, [ $^{131}\text{I}$ ]IMISO versus  $^{99m}\text{Tc}$ -EC ( $n = 3/\text{time point}$ ).

### Polarographic Oxygen Microelectrode $pO_2$ Measurements

Intratumoral  $pO_2$  measurements of tumors indicated the tumor oxygen tension ranged  $4.6 \pm 1.4$  mmHg as compared to normal muscle of  $35 \pm 10$  mmHg. The data indicate that the tumors are hypoxic.

### DISCUSSION

The development of new tumor hypoxia agents is clinically desirable for detecting primary and metastatic lesions as well as predicting radioresponsiveness and time to recurrence. None of the contemporary imaging modalities accurately measures hypoxia since the diagnosis of tumor hypoxia requires pathologic examination. It is often difficult to predict the outcome of a therapy for hypoxic tumor without knowing at least the baseline of hypoxia in each tumor treated. Although the Eppendorf polarographic oxygen microelectrode can measure the oxygen tension in a tumor this technique is invasive and needs a skillful operator. Additionally, this technique can only be used on accessible tumors (e.g. head and neck, cervical) and multiple readings are needed. Therefore, an accurate and easy method of measuring tumor hypoxia will be useful for patient selection. However, tumor to normal tissue uptake ratios varies depend upon the radiopharmaceuticals used. Therefore, it would be rational to correlate tumor to normal tissue uptake ratio with the gold standard Eppendorf electrode measures of hypoxia when new radiopharmaceuticals introduced to clinical practice.

$[^{18}F]FMISO$  has been used to diagnose head and neck tumors, myocardial infarction, inflammation, and brain ischemia (27–30). Tumor to normal tissue uptake ratio was used as a baseline to assess tumor hypoxia (29). Although tumor hypoxia using  $[^{18}F]FMISO$  was clearly demonstrated, introducing new imaging agents into clinical practice depends on to some other factors such as easy availability and cost.

Due to better imaging characteristics and lower price attempts are made to replace the  $^{123}I$ ,  $^{131}I$ ,  $^{67}Ga$  and  $^{111}In$  labeled compounds with corresponding  $^{99m}Tc$  labeled compounds when possible. Verbruggen et al. reported that EC can be labeled with  $^{99m}Tc$  very easily and efficiently at room temperature with high radiochemical purity and the preparation remains stable for at least 8 hours (20). Because of reported labeling capacity and rapid renal clearance, EC was selected to synthesize a new  $^{99m}Tc$ -labeled metronidazole. EC-MN was prepared using a relatively simple and fast chemistry. A labeling kit was also developed to make its use in clinical practice easier. Radio-TLC results with  $^{99m}Tc$ -EC-MN kit confirm the high radiochemical purity and stability.

In tissue distribution studies, although no significance difference of tumor-to-tissue uptake between  $^{99m}Tc$ -EC-MN and  $^{99m}Tc$ -EC groups was observed, there was a significantly increased tumor-to-tissue uptake ratio as a function of time in the  $^{99m}Tc$ -EC-MN group. When compared with  $[^{18}F]FMISO$  and  $[^{131}I]IMISO$ , the tumor-to-tissue uptake ratios for  $^{99m}Tc$ -EC-MN is similar to those with  $[^{131}I]IMISO$ .

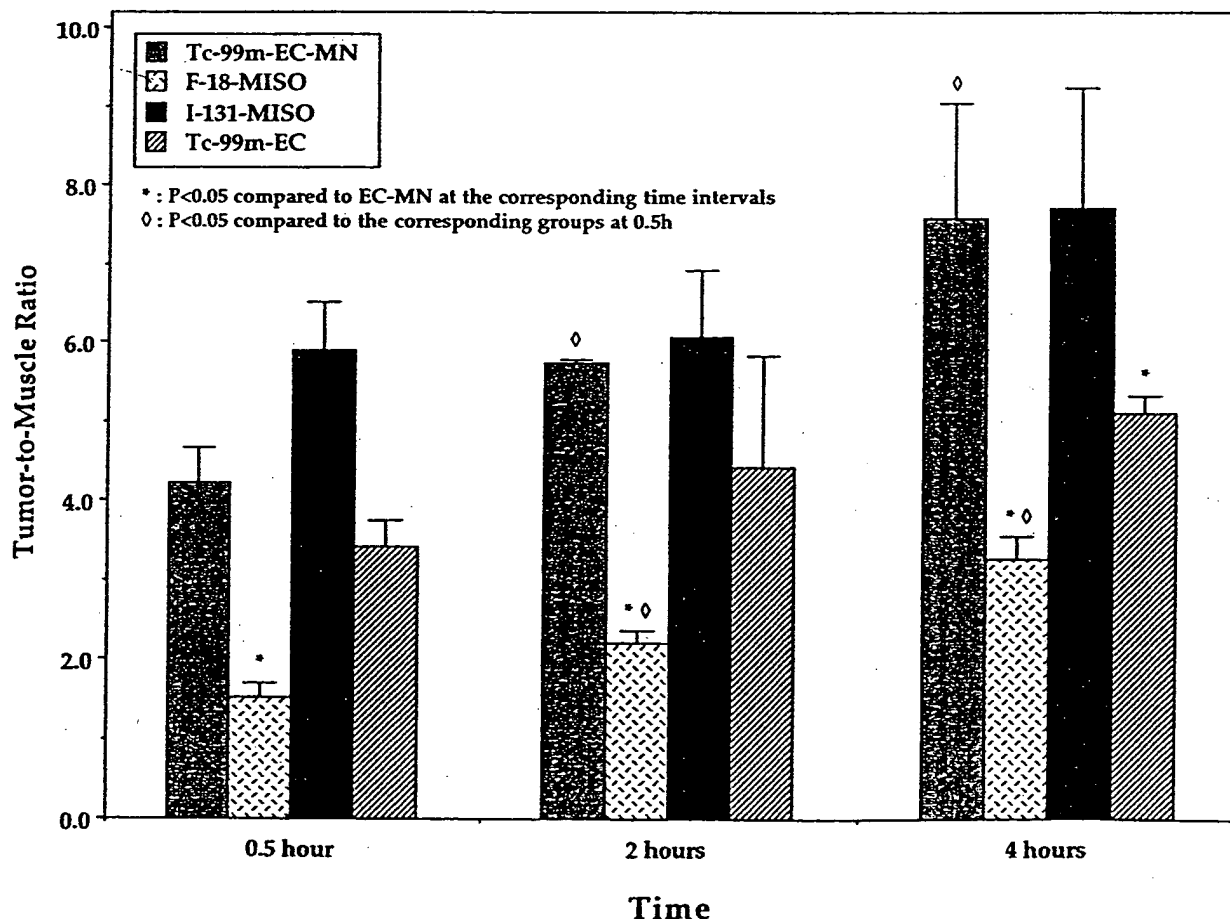


Fig. 3. Time-dependent variation of tumor/muscle uptake ratios (%ID/g wet weight) with  $^{99m}Tc$ -EC-MN,  $[^{18}F]FMISO$ ,  $[^{131}I]IMISO$  versus  $^{99m}Tc$ -EC ( $n = 3$ /time point).

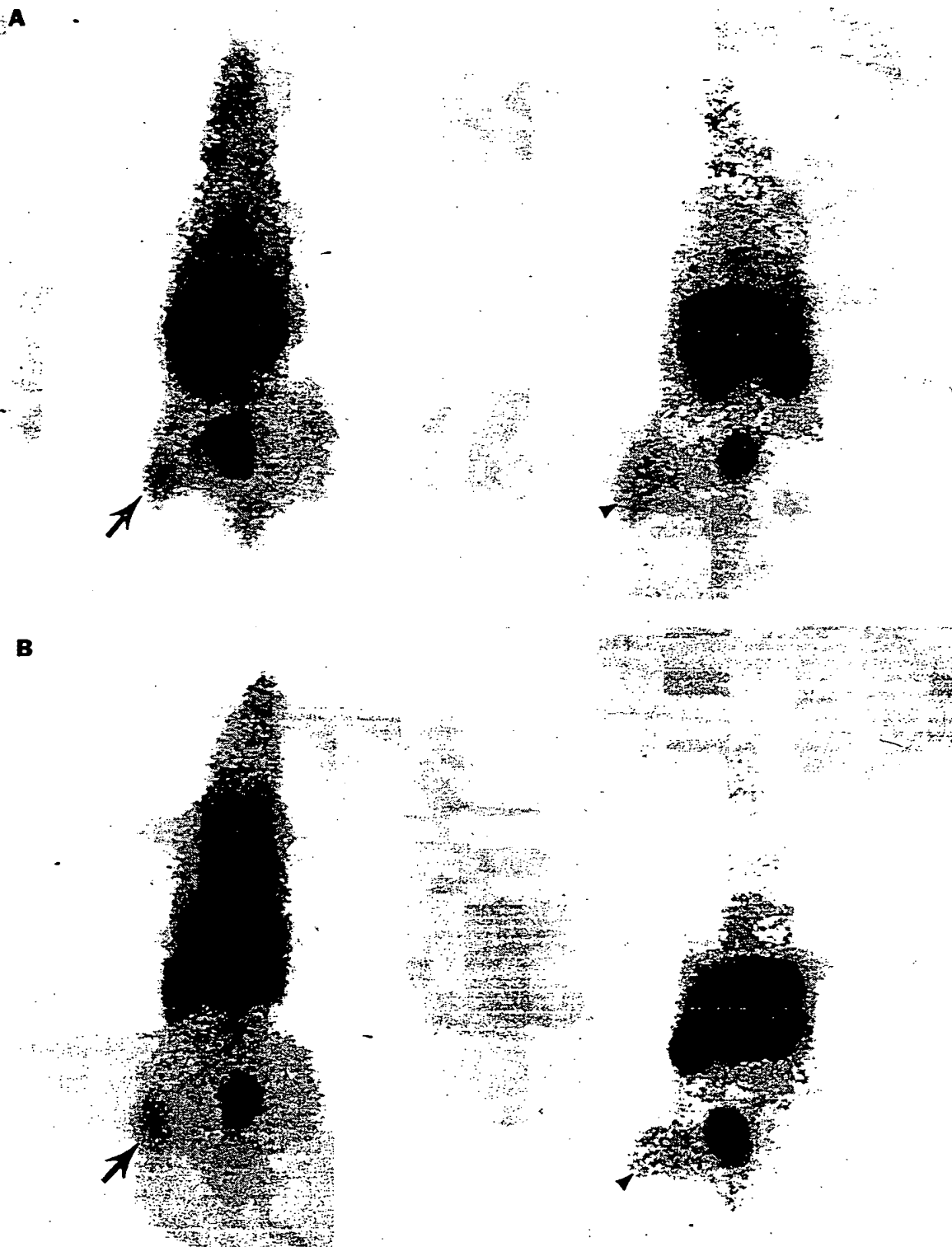


Fig. 4. Selected gamma scintigraphy images (ventral view) of a rat with a subcutaneous breast tumor in the right hind leg at 1 (A) and 4 (B) hrs following intravenous administration of  $^{99m}\text{Tc}$ -EC-MN (left) and  $^{99m}\text{Tc}$ -EC (right).  $^{99m}\text{Tc}$ -EC-MN uptake was evident in the tumor (arrows) up to 4 hr. There was very minimal radiotracer uptake (arrowheads) in the tumor area with  $^{99m}\text{Tc}$ -EC.

Thyroid tissue uptake was not altered after  $^{99m}\text{Tc}$ -EC-MN, whereas thyroid uptake increased with [ $^{131}\text{I}$ ]IMISO. The findings suggest that  $^{99m}\text{Tc}$ -EC-MN is more metabolically stable than [ $^{131}\text{I}$ ]IMISO. Tumor oxygen tension was determined to be 3.2 to 6.0 mm-Hg, whereas normal muscle tissue had 30 to

40 mmHg. Although another factor such as anemia that may influence the level of tumor hypoxia, there was no attempt in identifying this factor. Autoradiograms of  $^{99m}\text{Tc}$ -EC-MN demonstrated the feasibility to assess tumor hypoxia. The findings support that further studies on determining normal tissue dosim-

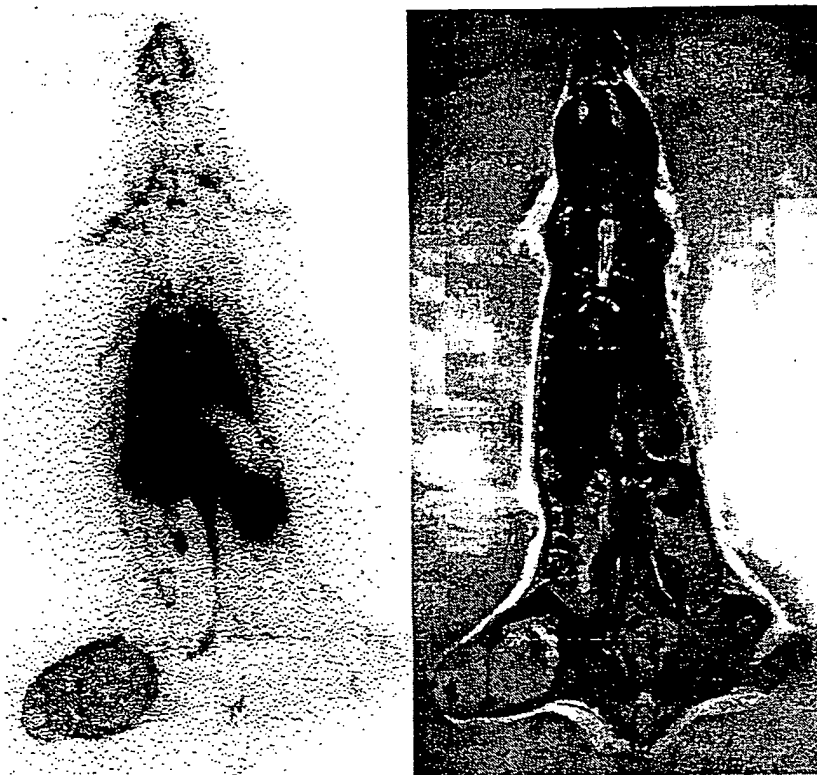


Fig. 5. Whole-body autoradiogram (coronal section) obtained 30 min after intravenous injection of  $^{99m}\text{Tc}$ -EC-MN clearly demonstrated tumor activity. A corresponding sectional image is on the right.

etry, measuring sensitizer enhancement ratio (SER) and identifying whether  $^{99m}\text{Tc}$ -EC-MN can provide a rational means of selecting patients for treatment with radiosensitizing (e.g. SR-2508, Ro-03-8799) or bioreductive agents.

#### ACKNOWLEDGMENTS

The authors wish to thank Dianne Perez for her excellent secretarial assistance in the preparation of this manuscript. This work was supported by the John S. Dunn Foundation and the Cesare Gianturco Fund. The animal research is supported by M. D. Anderson Cancer Center (CORE) Grant NIH NCI CA-16672.

#### REFERENCES

1. E. J. Hall. The oxygen effect and reoxygenation. In E. J. Hall (ed.) *Radiobiology for the radiobiologist*, 3rd edition. J. B. Lippincott Co., Philadelphia, PA, 1988, pp. 137-160.
2. R. S. Bush, R. D. T. Jenkins, W. E. C. Allt, F. A. Beale, H. Bena, A. J. Dembo, and J. F. Pringle. Definitive evidence for hypoxic cells influencing cure in cancer therapy. *Br. J. Cancer* 37 (Suppl. III):302-306 (1978).
3. L. H. Gray, A. D. Conger, M. Elbert, S. Morsney, and O.C.A. Scold. The concentration of oxygen dissolved in tissues at the time of irradiation as a factor in radiotherapy. *Br. J. Radiol.* 26:638-648 (1953).
4. S. Dische. A review of hypoxic-cell radiosensitization. *Int. J. Radiat. Oncol. Biol. Phys.* 20:147-152 (1991).
5. R. A. Gatenby, H. B. Kessler, J. S. Rosenblum, L. R. Coia, P. J. Moldofsky, W. H. Hartz, and G. J. Broder. Oxygen distribution in squamous cell carcinoma metastases and its relationship to outcome of radiation therapy. *Int. J. Radiat. Oncol. Biol. Phys.* 14:831-838 (1988).
6. M. Nordsmark, M. Overgaard, and J. Overgaard. Pretreatment oxygenation predicts radiation response in advanced squamous cell carcinoma of the head and neck. *Radiother. Oncol.* 41:31-39 (1996).
7. W.-J. Koh, J. S. Rasey, M. L. Evans, J. R. Grierson, T. K. Lewellen, M. M. Graham, K. A. Krohn, and T. W. Griffin. Imaging of hypoxia in human tumors with  $^{18}\text{F}$  fluoromisonidazole. *Int. J. Radiat. Oncol. Biol. Phys.* 22:199-212 (1992).
8. P. E. T. Valk, C. A. Mathis, M. D. Prados, J. C. Gilbert, and T. F. Budinger. Hypoxia in human gliomas: Demonstration by PET with  $^{18}\text{F}$  fluoromisonidazole. *J. Nucl. Med.* 33:2133-2137 (1992).
9. G. V. Martin, J. H. Caldwell, J. S. Rasey, Z. Grunbaum, M. Cerqueira, and K. A. Krohn. Enhanced binding of the hypoxic cell marker  $^{18}\text{F}$  fluoromisonidazole in ischemic myocardium. *J. Nucl. Med.* 30:194-201 (1989).
10. J. S. Rasey, W. J. Koh, J. R. Grierson, Z. Grunbaum, and K. A. Krohn. Radiolabeled fluoromisonidazole as an imaging agent for tumor hypoxia. *Int. J. Radiat. Oncol. Biol. Phys.* 17:985-991 (1989).
11. J. S. Rasey, N. J. Nelson, L. Chin, M. L. Evans, and Z. Grunbaum. Characterization of the binding of labeled fluoromisonidazole in cells in vitro. *Radiat. Res.* 122:301-308 (1990).
12. D. J. Yang, S. Wallace, A. Cherif, C. Li, M. B. Gretzer, E. E. Kim, and D. A. Podoloff. Development of F-18-labeled fluoroerythronitroimidazole as a PET agent for imaging tumor hypoxia. *Radiology* 194:795-800 (1995).
13. A. Cherif, S. Wallace, D. J. Yang, R. Newman, V. Wilson, A. Nornoo, T. Inoue, C. Kim, L.-R. Kuang, E. E. Kim, and D. A. Podoloff. Development of new markers for hypoxic cells:  $^{131}\text{I}$ iodomisonidazole and  $^{131}\text{I}$ iodoerythronitroimidazole. *J. Drug Targeting* 4:31-39 (1996).
14. B. A. Teicher and E. A. Sotomayor. Chemical radiation sensitizers and protectors. In W. O. Foye (ed.), *Cancer Chemotherapeutic Agents*, American Chemical Society, Washington, D. C., 1995, pp. 501-527.

15. G. Johnson, K. N. Nguyen, Z. Lui, P. Gao, B. Edwards, C. M. Archer, A. C. King, T. L. North, R. D. Okada, and W. K. Warren. HL91 Technetium-99m: Kinetics of a new hypoxia avid imaging agent in normal and ischemic myocardium as assessed by gamma camera images. *J. Am. Coll. Cardiol.* 407A (1996).
16. K. Fukuchi, H. Kusuoka, K. Yutani, S. Hasegawa, and T. Nishimura. Assessment of reperfused myocardium using new hypoxia avid imaging agent Tc-99m HL91. *J. Nucl. Med.* 37:94 (Abstract) (1996).
17. T. Melo, J. Duncan, J. R. Ballinger, and A. M. Rauth. BMS 194796, a second generation Tc-99m labelled 2-nitroimidazole for imaging hypoxia in tumors. *J. Nucl. Med.* 39:219 (Abstract) (1998).
18. X. Zhang, T. Melo, J. R. Ballinger, and A. M. Rauth. Evaluation of Tc-99m butyleneamino oxime (BnAO), a non-nitroaromatic agent for imaging hypoxia in tumors. *J. Nucl. Med.* 39:216 (Abstract) (1998).
19. A. Davison, A. G. Jones, C. Orvig, and M. Sohn. A new class of oxotechnetium(+5) chelate complexes containing a  $\text{TcON}_2\text{S}_2$  Core. *Inorg. Chem.* 20:1629-1632 (1981).
20. A. M. Verbruggen, D. L. Nosco, C. G. Van Nerom, G. M. Bormans, P. J. Adriaens, and M. J. De Roo. Tc-99m-L,L-ethylenedicycysteine: A renal imaging agent. I. Labelling and evaluation in animals. *J. Nucl. Med.* 33:551-557 (1992).
21. C. G. Van Nerom, G. M. Bormans, M. J. De Roo, and A. M. Verbruggen. First experience in healthy volunteers with Tc-99m-L,L-ethylenedicycysteine, a new renal imaging agent. *Eur. J. Nucl. Med.* 20:738-746 (1993).
22. M. J. Surma, J. Wiewiora, and J. Liniecki. Usefulness of Tc-99m-N,N'-ethylene-1-dicycysteine complex for dynamic kidney investigations. *Nucl. Med. Comm.* 15:628-635 (1994).
23. S. Ratner and H. T. Clarke. The action of formaldehyde upon cysteine. *J. Am. Chem. Soc.* 59:200-206 (1937).
24. P. Blondeau, C. Berse, and D. Gravel. Dimerization of an intermediate during the sodium in liquid ammonia reduction of L-thiazolidine-4-carboxylic acid. *Can. J. Chem.* 45:49-52 (1967).
25. M. P. Hay, W. R. Wilson, J. W. Moselen, B. D. Palmer, and W. A. Denny. Hypoxia-selective antitumor agents. Bis(nitroimidazolyl)alkanecarboxamides: a new class of hypoxia-selective cytotoxins and hypoxic cell radiosensitizers. *J. Med. Chem.* 37:381-391 (1994).
26. A. Cherif, D. J. Yang, W. Tansey, E. E. Kim, and S. Wallace. Synthesis of [ $^{18}\text{F}$ ]fluoromisonidazole. *Pharm. Res.* 11:466-469 (1994).
27. G. V. Martin, J. H. Cardwell, M. M. Graham, J. R. Grierson, K. Kroll, M. J. Xowna, T. K. Lewellen, J. S. Rasey, J. J. Casciari, and K. A. Krohn. Noninvasive detection of hypoxic myocardium using [ $^{18}\text{F}$ ]fluoromisonidazole and PET. *J. Nucl. Med.* 33:2202-2208 (1992).
28. S. H. Yeh, R. S. Liu, H. H. Hu, C. P. Chang, L. S. Chu, K. L. Chou, and L. C. Wu. Ischemic penumbra in acute stroke: demonstration by PET with fluorine-18 fluoromisonidazole. *J. Nucl. Med.* 35:(5)205 (Abstract) (1994).
29. S. H. Yeh, R. S. Liu, L. C. Wu, D. J. Yang, S. H. Yen, C. W. Chang, T. W. Yu, K. L. Chou, and K. Y. Chen. Fluorine-18 fluoromisonidazole tumor to muscle retention ratio for the detection of hypoxia in nasopharyngeal carcinoma. *Eur. J. Nucl. Med.* 23:1378-1383 (1996).
30. R. S. Liu, S. H. Yeh, C. P. Chang, L. S. Chu, M. T. Lui, K. L. Chou, and L. C. Wu. Detection of odontogenic infections by [ $^{18}\text{F}$ ]fluoromisonidazole. *J. Nucl. Med.* 35:113 (Abstract) (1994).



Pergamon

Oncology Research, Vol. 6, No. 4, pp. 405-409, 1994  
Copyright © 1995 Elsevier Science Ltd  
Printed in the USA. All rights reserved  
0961-0477/94 \$9.50 + .00

EXHIBIT 58

0961-0477(94)00063-8

## Glycolysis and Growth Rate in Normal and in Hexokinase-Transfected NIH-3T3 Cells

Maurizio Fanciulli, Marco G. Paggi, Tiziana Bruno, Carlo Del Carlo, Francesco Bonetto,  
Francesco P. Gentile<sup>a</sup>, and Aristide Floridi<sup>b</sup>

Laboratory of Cell Metabolism and Pharmacokinetics, and <sup>a</sup>Laboratory of Medical Physics, Center for Experimental Research,  
Regina Elena Cancer Institute, Via delle Messi d'Oro 156, 00158 Rome, Italy

(Submitted July 15, 1994; sent for revision August 29; received and accepted September 29, 1994)

**Abstract.** The glycolytic enzyme hexokinase plays a key role in regulating cell energy metabolism. Its activity has been associated with cell growth rate and, notably, with neoplastic transformation. NIH-3T3 cells were transfected with a tumor hexokinase cDNA. The transfected cells showed increased hexokinase amount and activity, mainly located in the particulate cellular fraction, increased glycolytic rate evaluated as lactate production, and, finally, enhanced growth rate. These data may suggest that high hexokinase activity might be not merely the consequence of peculiar metabolic demands by actively replicating normal or cancer cells, but also a modification able *per se* to drive, at least partially, a more intense mitotic activity.

**Key words:** hexokinase, transfection, growth rate, NIH-3T3 cells.

Among the most common biochemical characteristics of rapidly growing cells, and particularly of cancer cells, there is the propensity to catabolize glucose at elevated rates, consequently yielding higher lactate production [1-5]. This elevated tumor glycolytic activity has puzzled biochemists for many years [1, 4, 6, 7]; the reason why these cells exhibit such a metabolic transformation is still not clearly understood, although it can be at least partially explained by an increased rate of glucose transport [8] and through some peculiar properties of the glycolytic regulatory enzymes [7]. Singh *et al.* [9] correlate cell transformation with an increase of the HK<sup>c</sup> (EC 2.7.1.1.) activity, the majority of which is found in a particulate form, associated with the outer mitochondrial membrane [10-14]. This peculiar location allows favored access to freshly generated mitochondrial ATP [14] or almost completely abolishes glucose-6-phosphate feedback inhibition [10, 13]; this leads to glucose-6-phosphate overproduction, which is partially utilized by glycolysis and Krebs cycle to increase not only the cellular supply of ATP, but also the accumulation of precursors for the biosynthesis of important metabolites, such as triglycerides and cholesterol, oxidoreductive equivalents for protein biosynthesis, and, by the pentose phosphate pathway, nucleic acids, all of them necessary for cell growth and replication.

Recently, the application of molecular biology techniques shed a new light on the understanding of some

aspects of cancer energy metabolism and, notably, on HK [15-18]. To investigate the role of the HK in supporting high aerobic glycolysis and to define its own influence on cell growth rate, experiments with NIH-3T3 fibroblasts, transfected with an expression construct carrying an entire tumor HK cDNA [16], were carried out.

### MATERIALS AND METHODS

**Cells.** The NIH-3T3 parental cell line was grown at 37°C in Dulbecco's modified Eagle's medium plus 5% fetal bovine serum, 2 mM glutamine (BioWittaker, PBI, Milan, Italy), and antibiotics in a 5% CO<sub>2</sub> atmosphere.

**Transfection.** pSVL-HK, used for transfection, was made by ligating a 2.7-kb *Xba*I-*Xba*I cloned cDNA fragment [16], containing the entire HK cDNA, 4 bp upstream from the transcriptional starting site, into the *Xba*I site of the pSVL vector (Pharmacia, Milan, Italy). Correct orientation of the insert was verified by restriction analysis. Cells were transfected using the calcium phosphate procedure [19], cotransfecting for selection the plasmid pRc/CMV (Invitrogen, SIAL, Rome, Italy) containing a neomycin resistance gene. Another transfection with the pRc/CMV alone was done as a control. Cells were selected in the same medium used for the parental cell line, plus the addition of 0.5 mg/ml neomycin for 3 days, and maintained then at 0.4 mg/ml. Individual lines were derived by isolating single primary colonies.

**Southern and northern blots.** Total genomic DNA was isolated according to Sambrook *et al.* [19], digested with *Bam*HI, and electrophoresed through a 0.8% agarose gel; total RNA was isolated according to Chomczynski and Sacchi [20], subjected to electrophoresed through a 1.2% agarose gel containing formaldehyde [19]. After transfer to a nitrocellulose membrane (BA-85; Schleicher & Schuell, Pabisch, Milan, Italy), hybridizations were carried out using

<sup>a</sup>To whom correspondence should be addressed: Tel. 39-6-4985-2562; FAX 39-6-418-0473.

<sup>b</sup>Abbreviations used: HK, hexokinase; SSC, 150 mM NaCl, 15 mM Na-citrate, pH 7.0; SDS, sodium dodecyl sulphate; PBS, 145 mM NaCl, 10 mM Na-phosphate, pH 7.40; PMSF, phenylmethylsulphonyl fluoride; DTT, DL-dithiothreitol; SDS-PAGE, sodium dodecyl sulfate-polyacrylamide gel electrophoresis; HMW, high molecular weight; LMW, low molecular weight.

probes labeled with the random priming technique [21], using  $\alpha$ -[ $^{32}$ P]-dATP (Amersham, Milan, Italy). Membranes were hybridized at 65°C in the presence of QuikHyb (Stratagene, SIAL, Rome, Italy). After a final high-stringency wash (0.2  $\times$  SSC, 0.1% SDS at 65°C for 30 min), the nitrocellulose was exposed at -70°C using Kodak XAR-5 film with Du Pont Cronex (Florence, Italy) intensifying screens.

**Cell lysis and HK activity.** Cells were washed twice in ice-cold PBS and homogenized in an ice bath using a tight-fitting Potter homogenizer (Thomas Scientific, Swedesboro, NJ, USA) with a Teflon pestle in 0.1  $\times$  PBS, 1 mM PMSF, 1 mM DTT, and 1 mM EDTA. The homogenate was then centrifuged at 1,100 g at 4°C to sediment nuclei and debris. The postnuclear supernatant was centrifuged at 12,000 g for 30 min at 4°C. HK activity was evaluated, according to Parry and Pedersen [12], after a 30-min incubation on ice in the presence of 0.5% Triton X-100, both in the sediment (bound HK) and in the supernatant (free HK).

**Protein determination, SDS-PAGE, and western blot.** Protein concentration in whole-cell extracts was measured according to the bicinchoninic acid method [17] using bovine serum albumin, fraction V, as a standard. SDS-PAGE was done according to Laemmli [22] in a 7.5% acrylamide gel; 100  $\mu$ g of protein was loaded onto each lane. After protein transfer to a nitrocellulose membrane (BA-85; Schleicher & Schuell), HK was visualized using a rabbit anti-AS-30D rat hepatoma HK immune serum [23].

**Glycolysis assay.** Measurements of aerobic glycolysis, as lactate production, were carried out as previously described [24], incubating  $4 \times 10^6$  cells for 60 min.

Lactate in the supernatants was evaluated according to Hohorst [25].

**Growth curves and data analysis.** Growth curves were done by plating  $1 \times 10^5$  cells into 60 mm diameter petri dishes. At daily intervals, cells were removed and counted using a Coulter counter model ZM (Coulter Electronics, Luton, England). The experimental data were fitted by a Gompertzian function [26] and by a previously described computer program [27].

The differences among the fitted growth curves corresponding to the NIH-3T3, 2A, and 4A cell lines have been evaluated by analysis of variance.

## RESULTS AND DISCUSSION

Southern blot in Figure 1A refers to genomic DNA analysis of NIH-3T3 cells, neomycin-resistant transfected 2A cells, and neomycin-resistant and HK cotransfected 4A cells, digested using *Bam*HI as restriction endonuclease, and probed with the HK cDNA. Significantly, in the hybridization pattern of 4A cells shown in Figure 1A, two bands were emphasized, corresponding to the fragments of 1.9 and 0.8 kb, their sum representing the exact size of the transfected HK cDNA (2.7 kb) [16]. Figure 1B is a northern blot showing that the transfected HK cDNA was actively transcribed in a message of 2.7 kb, shorter than the endogenous one (4.3 kb), but strictly in agreement with the size of the transfected sequence.

To evaluate whether the exogenous HK message was translated, an anti-HK serum was utilized to detect the protein quantitatively in western blots of total cell extracts. Both endogenous and exogenous HK were specifically recognized by this immune serum, raised

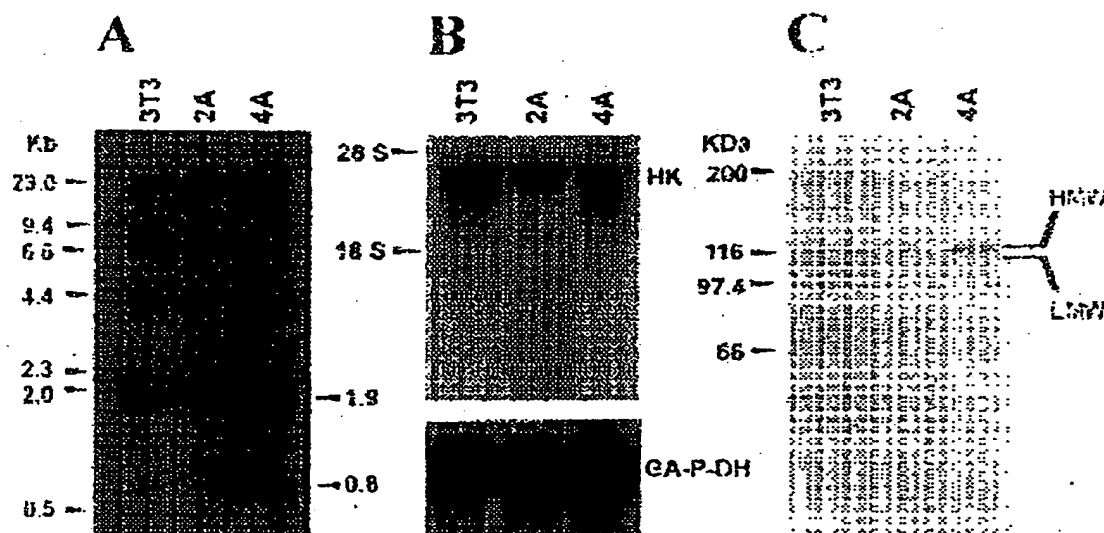


**Figure 1.** The three panels refer to 3T3 (NIH-3T3), 2A, and 4A cells. A) Southern blot of genomic DNA, after *Bam*HI digestion, using the tumor HK cDNA probe [16]. Kilobase pair values represent the molecular size markers migration distances. B) Top: northern blot of total RNA using the tumor HK cDNA probe [16]. The migration distances of 28 S and 18 S rRNA are indicated. Bottom: the same nitrocellulose reprobed with the GAPDH cDNA. C) HK visualized in western blot; HMW and LMW HK are indicated. Kilodalton values represent the molecular weight markers migration distances.



against the AS-30D rat hepatoma HK [23] (Figure 1C); actually, also in these cell lines, two enzymatic forms with slightly different apparent molecular mass, HMW (ca. 117 kDa) and LMW (ca. 111 kDa) HK, were detected. In the NIH-3T3 cell line, an increase of the HMW HK was observed in the 4A but not in the 2A cell line, likely due to the active transcription and translation of the transfected HK cDNA.

In order to verify whether the overexpressed protein was also functionally active, HK activity was measured in extracts from all the above mentioned cell lines (Table 1). The transfected protein was enzymatically active and accounted for a 46% increase of the total HK activity. Interestingly enough, this additive activity could be ascribed to the particulate enzyme, whereas the cytoplasmic activity did not seem to be subject to any change. The effect of this increased level of HK activity influenced the overall glycolytic rate, evaluated as lactate production (Table 1), which raised from 2.4 and 2.3  $\mu\text{mol/mg protein/h}$  for NIH-3T3 and 2A, respectively, to 4.4 for the 4A cell line.

It has been widely observed that tumor cells exhibit increased rates of glycolysis (see [7] for review). This phenomenon is accompanied by an increase of the HK activity and by a change in subcellular distribution of the enzyme from a predominantly cytosolic to a particulate mitochondrially bound form [7, 10, 13]. Our experiments provided data about the correlation between HK activity and glycolytic rate in the NIH-3T3

cell line, showing that the enzyme activity could positively affect the glycolytic rate. Moreover, these results can further support the role of the particulate enzyme in increasing the rate of the Embden-Meyerhof pathway, as observed in tumor cells [14].

Because highly glycolytic cancer cells, such as hepatoma cells, exhibiting a high percentage of mitochondrially bound HK show in addition an elevated cell growth rate [11, 28], we investigated whether a transfected membrane-bound HK activity could affect the NIH-3T3 growth rate. Figure 2 illustrates cell growth rate in NIH-3T3, 2A, and 4A cell lines. The experimental data were fitted by a Gompertzian function [26]. Growth data have been evaluated by modifying a previously described computer program [27]. The data corresponding to the NIH-3T3, 2A, and 4A cell lines have been tested by an analysis of variance, with differences between groups considered significant at  $P < 0.01$ . Using contrasts in an orthogonal comparison, a significant difference between 4A and NIH-3T3 plus 2A cell lines and an insignificant difference between 2A and NIH-3T3 cell lines has been revealed. Data were evaluated either at day 3, where the difference in growth rate was more evident, or at day 6. It also appeared that, after day 6, curves tended to become parallel and eventually to overlap; this may be due to the contact inhibition phenomenon, characteristic of NIH-3T3 cells, which is conserved to some extent in the 4A strain.

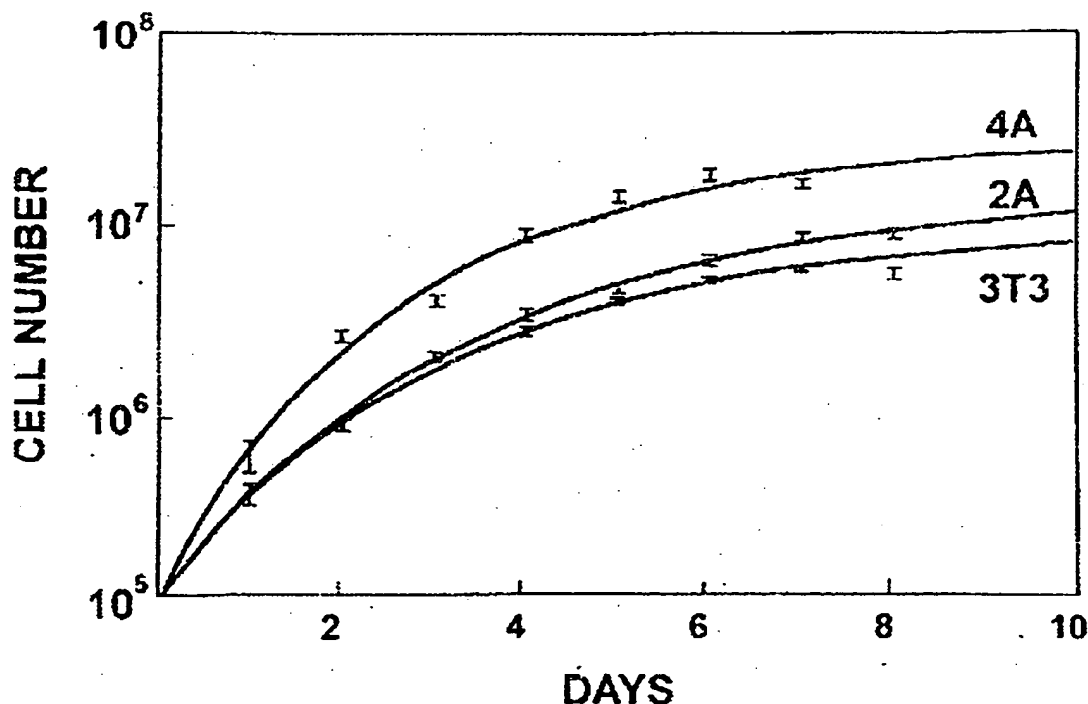


Figure 2. Growth curves of NIH-3T3, 2A, and 4A cells. Points were averaged from three different experiments performed in triplicate.

**Table 1. Total, bound, and free hexokinase activity and aerobic lactate production of normal (3T3), neomycin-(2A), and hexokinase-transfected (4A) NIH-3T3 cells.** HK activity is expressed as nanomoles NADPH formed minute<sup>-1</sup> milligram protein<sup>-1</sup> at 30°C. Lactate production is expressed as micromoles lactate milligram protein<sup>-1</sup> hour<sup>-1</sup> at 30°C. Each value  $\pm$  SD was averaged from five different experiments performed in duplicate.

Cells	Total HK	Bound HK	Free HK	% HK recovery	Lactate production
3T3	120 $\pm$ 4	48 $\pm$ 7	64 $\pm$ 8	93	2.4 $\pm$ 0.1
2A	123 $\pm$ 3	51 $\pm$ 5	64 $\pm$ 6	94	2.3 $\pm$ 0.2
4A	175 $\pm$ 6	93 $\pm$ 4	70 $\pm$ 5	93	4.4 $\pm$ 0.1

These data clearly demonstrated a positive correlation between HK activity and cell growth rate in this cell line. Interestingly, previous works associating these two parameters essentially conclude that the enhanced HK activity, mainly bound, is a required support for rapid cell growth and replication, furnishing elevated concentrations of metabolites [3, 7, 14, 29]; this basically means that enhanced HK synthesis and its shift to the particulate form are seen as an adaptation to the new metabolic requirements of the transformed cell. Our experiments, alternatively, emphasize the possibility that the transfected membrane-bound tumor HK, present in the 4A clone, could be *per se* responsible for the more intense mitotic activity, at least facilitating cell metabolism in some specific conditions, such as during *in vitro* growth.

Tumorigenicity tests on the 4A clone, either *in vivo* or *in vitro*, are underway in an attempt to define accurately the role of HK not only in supporting, but also in eliciting tumor growth.

**ACKNOWLEDGEMENTS:** Work was partially supported by ACKO-CNR, by Associazione Italiana per la Ricerca sul Cancro (AIRC), and by Ministero della Sanità. The authors thank F. Sforza, M. Di Giovanni, and I. Zardin for the graphic and photographic work. Francesco Bonetto is an AIRC fellow.

## REFERENCES

- Goldberg, E. B.; Colowick, S. P. The role of glycolysis in the growth of tumor cells. *J. Biol. Chem.* 240:2786-2790; 1965.
- Wu, R. Control mechanisms of glycolysis in Ehrlich ascites tumor cells. *J. Biol. Chem.* 240:2827-2832; 1965.
- Nakashima, R. A.; Paggi, M. G.; Pedersen, P. L. Contributions of glycolysis and oxidative phosphorylation to adenosine-5'-triphosphate production in AS-30D hepatoma cells. *Cancer Res.* 44:5702-5706; 1984.
- Papaconstantinou, J.; Colowick, S. P. The role of glycolysis in the growth of tumor cells. *J. Biol. Chem.* 236:278-288; 1961.
- Chance, B.; Garfinkel, D.; Higgins, J.; Hess, B. Metabolic control mechanisms. V. A solution for the equations representing interaction between glycolysis and respiration in ascites tumor cells. *J. Biol. Chem.* 235:2426-2439; 1960.
- Warburg, O. Über den Stoffwechsel der Tumoren; arbeiten aus dem Kaiser Wilhelm-Institut für biologie. Berlin: J. Springer; 1926pp. 115-149.
- Pedersen, P. L. Tumor mitochondria and bioenergetics of cancer cell. *Prog. Exp. Tumor Res.* 22:190-274; 1978.
- Flier, J. S.; Mueckler, M. M.; Usher, P.; Lodish, H. F. Elevated levels of glucose transport and transporter messenger RNA are induced by ras or src oncogenes. *Science* 235:1492-1498; 1986.
- Singh, V. M.; Singh, M.; August, J. T.; Horecker, B. L. Alterations in glucose metabolism in chick embryo cells transformed by Rous sarcoma virus: intracellular level of glycolytic intermediates. *Proc. Natl. Acad. Sci. USA* 28:4129-4132; 1974.
- Rose, L. A.; Warren, J. V. B. Mitochondrial hexokinase. Release, rebinding, and location. *J. Biol. Chem.* 242:1635-1645; 1967.
- Dustanante, E.; Pedersen, P. L. High aerobic glycolysis of rat hepatoma cells in culture: role of mitochondrial hexokinase. *Proc. Natl. Acad. Sci. USA* 74:3735-3739; 1977.
- Parry, D. M.; Pedersen, P. L. Intracellular localization and properties of particulate hexokinase in the Novikoff ascites tumor. *J. Biol. Chem.* 258:10904-10912; 1983.
- Nakashima, R. A.; Paggi, M. G.; Scott, L.; Pedersen, P. L. Purification and characterization of a bindable form of a mitochondrial bound hexokinase from the highly glycolytic AS-30D rat hepatoma cell line. *Cancer Res.* 48:913-919; 1988.
- Arora, K. K.; Pedersen, P. L. Functional significance of mitochondrial bound hexokinase in tumor cell metabolism. *J. Biol. Chem.* 263:17422-17428; 1988.
- Arora, K. K.; Filburn, C. R.; Pedersen, P. L. Structure/function relationships in hexokinase. Site-directed mutational analyses and characterization of overexpressed fragments implicate different functions for the N- and C-terminal halves of the enzyme. *J. Biol. Chem.* 268:18259-18266; 1993.
- Arora, K. K.; Fanciulli, M.; Pedersen, P. L. Glucose phosphorylation in tumor cells. Cloning, sequencing, and overexpression in active form of a full-length cDNA encoding a mitochondrial bindable form of hexokinase. *J. Biol. Chem.* 265:6481-6488; 1990.
- Arora, K. K.; Shenbagamurthi, P.; Fanciulli, M.; Pedersen, P. L. Glucose phosphorylation: interaction of a 50-amino acid peptide of yeast hexokinase with trinitrophenyl. *J. Biol. Chem.* 265:5324-5328; 1990.
- Wigley, W. C.; Nakashima, R. A. Evidence for multiple genes coding for the isozymes of hexokinase in the highly glycolytic AS-30D rat hepatoma. *FEBS Lett.* 300:153-156; 1992.
- Sambrook, J.; Fritsch, E. F.; Maniatis, T. *Molecular cloning: a laboratory manual*. Cold Spring Harbor, NY: Cold Spring Harbor Laboratory Press; 1989.
- Chomczynski, P.; Sacchi, N. Single-step method of RNA isolation by acid guanidinium thiocyanate-phenol-chloroform extraction. *Anal. Biochem.* 162:156-159; 1987.
- Feinberg, A. P.; Vogelstein, B. A technique for radiolabeling DNA restriction endonuclease fragments to high specific activity. *Anal. Biochem.* 132:6-13; 1983.
- Laemmli, U. K. Cleavage of structural proteins during the assembly of the head of the bacteriophage T4. *Nature* 227:680-685; 1970.
- Paggi, M. G.; Fanciulli, M.; Del Carlo, C.; Cirio, G.; Bruno, T.; Floridi, A. Glucose utilization by tumor cells: a posttranslational modification of mitochondrial hexokinase may play a regulatory role. *Biochem. Biophys. Res. Commun.* 178:648-655; 1991.
- Floridi, A.; Paggi, M. G.; D'Atri, S.; De Martino, C.; Marcante, M. L.; Silvestrini, B.; Caputo, A. Effect of lonidamine on the energy metabolism of Ehrlich ascites tumor cells. *Cancer Res.* 41:4661-4666; 1981.
- Eikhorst, H. J. Determination with lactic dehydrogenase

- and DPN. In: Bergmeyer, H. U., ed. *Methods of enzymatic analysis*. New York: Academic Press; 1965:pp. 266-270.
26. Gompertz, B. On the nature of the function expressive of the law of human mortality, and on the new mode of determining the value of life contingencies. *Philos. Trans. R. Soc. Lond. Biol.* 115:513-585; 1825.
27. Chiatti, L.; Gentile, F. P.; Schinaia, G.; Carpino, S.; Greco, C.; Floridi, A.; Benassi, M. A simulation model for tumor growth controlled by therapeutic agents. *Anticancer Res.* 11:769-772; 1991.
28. Weinhouse, S. Glycolysis, respiration, and anomalous gene expression in experimental hepatomas. *Cancer Res.* 32:2007-2016; 1972.
29. Nakashima, R. A.; Paggi, M. G.; Arora, K. K.; Pedersen, P. L. Integration of mitochondrial function with high aerobic glycolysis in tumors: role of hexokinase binding to the outer mitochondrial membrane. In: Lemasters, J. J.; Hackenbrock, C. R.; Thurnham, R. O.; Westhoff, H. V., eds. *Integration of mitochondrial function*. New York, NY: Plenum Publishing Company; 1990:pp. 405-411.

# **$^{19}\text{F}$ NMR of 2-Deoxy-2-fluoro-D-glucose for Tumor Diagnosis in Mice. An NDP-Bound Hexose Analog as a New NMR Target for Imaging**

Yoko Kanazawa,<sup>1\*</sup> Keiko Umayahara,<sup>1</sup> Toshiyuki Shimmura<sup>1</sup> and Tsuneo Yamashita<sup>2</sup>

<sup>1</sup> Faculty of Pharmaceutical Sciences, Kyushu University, Fukuoka 812-82, Japan

<sup>2</sup> Daikin Industries, Nishi-ichitsuya, Settsu 566, Japan

A well-known radiopharmaceutical 2-deoxy-2-fluoro-D-glucose widely used for positron emission tomography diagnosis in terms of glucose utilization, was re-evaluated here as a nuclear magnetic resonance pharmaceutical for cancer detection. The uptake and metabolism of FDG in the experimental tumor, MH134, transplanted to the peritoneum of C3H mice as an ascitic tumor was studied extensively by *ex vivo*  $^{19}\text{F}$  NMR. Prolonged retention of FDG and its metabolites over 2 days was confirmed in the tumor cells as well as in the heart. In these tissues, the 6-phosphate of the injected compound was converted reversibly to its epimer 2-deoxy-2-fluoro-D-mannose and further to their NDP bound forms. The metabolites were almost cleared within a day from the other healthy organs where the formation of NDP-2-deoxy-2-fluoro-D-mannose was low. Thus, the  $^{19}\text{F}$  NMR signal of NDP-FDM detected 1 day after the FDG injection could be used as a target signal for tumor detection. Through the use of *in vivo*  $^{19}\text{F}$  NMR spectra and  $^{19}\text{F}$  chemical shift images, the feasibility of this proposal was demonstrated. It was concluded that FDG-NMR has a potential for tumor diagnosis in animals. © 1997 by John Wiley & Sons, Ltd.

*NMR in Biomed.* 10, 35–41 (1997) No. of Figures: 8 No. of Tables: 0 No. of References: 23

**Keywords:** chemical shift imaging; tumour diagnosis; 2-deoxy-2-fluoro-D-glucose; 2-deoxy-2-fluoro-D-mannose;  $^{19}\text{F}$  NMR; mouse

Received 19 December 1996; revised 13 January 1997; accepted 13 January 1997

## **INTRODUCTION**

2-Deoxy-2- $^{18}\text{F}$ fluoro-D-glucose (FDG) has been developed as a radio-pharmaceutical for *in vivo* determination of regional glucose utilization in positron emission tomography (PET),<sup>1</sup> particularly for the measurement of brain activity.<sup>2</sup> Later, cancer has become one of the important research targets<sup>3–5</sup> along with brain activity and cardiac muscles. The metabolic trap of FDG-6 phosphate (FDG-6-P) in tissue has been the established principle of  $^{18}\text{F}$ FDG uptake. Thus, PET-FDG data are analyzed by the model of reversible rate processes of tissue incorporation and 6-phosphorylation.<sup>6</sup> Increased glucose metabolism and diminished activity of glucose-6-phosphatase are thought to explain the image contrast between malignant and healthy tissues in the cancer studies.<sup>3,5</sup> Further metabolic pathways have been less emphasised in the study of  $^{18}\text{F}$  radio-pharmaceuticals which have a lifetime of 110 min.

In nuclear magnetic resonance (NMR) studies of  $^{19}\text{F}$ FDG in mice, the metabolism of FDG beyond FDG-6-P has been observed in most organs.<sup>7–9</sup> The reversible epimerization of FDG-6-P to 2-deoxy-2-fluoro-D-mannose-6 phosphate (FDM-6-P)<sup>8</sup> takes place by the action of phosphoglucose isomerase (PGI), and is observed in almost every tissue.<sup>7–10</sup> The formation of FDM-6-P is fastest in brain, followed by heart<sup>7–9,11</sup> and cancer cells.<sup>10</sup> In basic studies of PET-FDG,<sup>1,3,4</sup> these organs have been found to retain  $^{18}\text{F}$  radioactivity longer than the others and are the subjects of recent FDG-PET studies, and retention of F-compound over

2 days has been confirmed in the heart and tumor using the  $^{19}\text{F}$  NMR method.<sup>7–10</sup> In the proton-coupled tissue spectra obtained 1 day after FDG injection, the signal intensity in the region of FDM relative to that of FDG exceeded the equilibrium ratio between FDM-6-P and FDG-6-P attained by the catalysis of PGI.<sup>8–10</sup> By high-resolution spectroscopy of tissue extracts, we have shown that FDG-6-P and FDM-6-P are metabolized further to their nucleotide-bound forms, NDP-FDG and NDP-FDM, in brain, heart and several other organs as in Fig. 1.<sup>9</sup> We suspected, therefore, that the formation of NDP-bound hexoses could be the source of unusual intensity ratio of FDG and FDM in heart and tumors, and it was proved in the study reported herein.

Chemical shift imaging has long been expected to be an ideal method for visualizing regional tissue characteristics through the metabolism of intrinsic compounds of physiological importance or of specifically designed NMR pharmaceuticals. Due to the inherent low sensitivity of the NMR method, however, metabolic imaging has been applied only to limited systems.<sup>12,13</sup> NMR imaging *in vivo*, by using a stable signal of FDG metabolites beyond FDG-6-P, that is characteristic to tumor cells, was considered to be a powerful technique for the detection and investigation of proliferative tissues. A high field imaging instrument was employed here to observe the unique metabolite of FDG in tumors.

We report here the potential of FDG as an NMR pharmaceutical for cancer diagnosis by *in vivo* NMR measurement. Prolonged retention of FDG metabolites in tumor cells was accompanied by an effective FDG-FDM conversion followed by the synthesis and intensive accumulation of NDP-FDM. The  $^{19}\text{F}$  NMR signals of FDG

\* Correspondence to: Y. Kanazawa.

Contract grant sponsor: Ministry of Education, Japan.

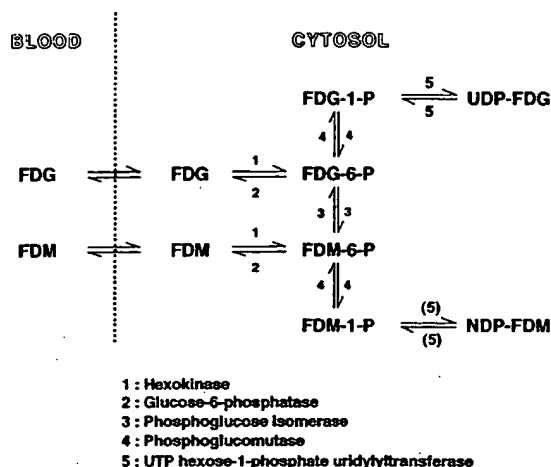


Figure 1. Metabolic pathway of fluorohexoses in tumors and organs.

metabolites were observable in simple *in vivo* NMR spectroscopy and imaging. The feasibility of metabolic imaging of tumor by using NDP-FDM as the target signal was demonstrated.

## MATERIALS AND METHODS

### Materials

FDG was prepared according to the method of Haradahira *et al.*<sup>14</sup> The main impurity, FDM, was determined by  $^{19}\text{F}$  NMR to be below 0.8%.

### Animal experiments

Female C3H mice were supplied from the Animal Center of Kyushu University at 5 weeks of age and kept for 2–4 weeks in the animal room at the Faculty of Pharmaceutical Sciences ( $23 \pm 1^\circ\text{C}$ ). About  $5 \times 10^5$  cells of MH134 hepatoma were transplanted into peritoneal cavities of the mice 7–9 days prior to the NMR experiments. FDG was injected as a saline solution through the tail vein after 16 h of fasting. The dose for *ex vivo* study was 100 mg/kg which was the amount where no apparent sign of behavioral disturbance was observed.<sup>9</sup> It was doubled for *in vivo*  $^{19}\text{F}$  NMR to give a better signal-to-noise ratio.

### Quantification of metabolites

Immediately after the mouse was killed by cervical dislocation, tumor cells were collected from ascitic fluids by repeated centrifugation (400–900 g) and washed three times with ice-cold saline. Healthy organs (brain, heart, liver, muscle, intestine) were excised on an ice bath, washed with cold saline to remove most of the blood, wiped with filter paper, and packed into a 10 mm NMR tube. The intestine was cut into 1–2 cm lengths to remove the contents. The cells and organs in the NMR tubes were heated in boiling water for 3 min for enzyme deactivation, and the air in the tube was replaced with Ar gas to prevent oxidation.

### Metabolite identification

After the NMR measurements of whole organs or cells for quantification at 94 MHz, the metabolites were extracted with water for detailed analysis by high resolution NMR. Tumor cells and organs were homogenized with a teflon homogenizer (WEATON) with distilled and deionized water and centrifuged for 30 min at 18 500 g. The supernatant was added with the aliquot used to rinse the pellet, and with  $\text{D}_2\text{O}$  as the NMR lock signal source. The extracted residue was also packed in a 10 mm NMR tube for the evaluation of extraction efficiency.

### NMR measurements

**Spectral assignments and quantification.** The  $^{19}\text{F}$  NMR spectra of water extracts were obtained by JEOL GSX-270WB operated at 254 MHz under proton decoupling conditions. For the spectral analysis, the conditions were: spectral band width of 20 kHz, pulse width of  $8 \mu\text{s}$  ( $45^\circ$ ),  $TR$  450 ms. Spectral assignment was made by referring to the  $^{19}\text{F}$  NMR data of authentic samples<sup>9,15</sup> measured from an external standard of hexafluorobenzene in benzene (1/400, v/v, abbreviated as HFB) with and without proton decoupling. The concentration of fluorine compounds in organs was determined using the  $^{19}\text{F}$  NMR spectrum of the individual whole organ in a 10 mm NMR tube with a JEOL FX-100 spectrometer operated at 93.7 MHz and  $23 \pm 1^\circ\text{C}$  with a spectral band width of 40 kHz, pulse width of  $16 \mu\text{s}$  ( $45^\circ$ ) and  $TR$  180 ms. The intensities of the three main peaks from whole organs, the FDG-group ( $\alpha$ -,  $\beta$ -FDG, FDG-6-P, FDG-1-P and NDP-FDG) at  $-36$  ppm from HFB, the  $\alpha$ -FDM-group (FDM, FDM-6-P, FDM-1-P and NDP-FDM) at  $-41$  ppm, and the  $\beta$ -FDM-group (FDM and FDM-6-P) at  $-59$  ppm<sup>9</sup> were measured. The quantification was done by the published method<sup>7,9</sup> using an average  $T_1$  determined with deactivated tissues by a standard inversion recovery method using the same spectrometer, a JEOL FX-100: 0.9 s for the FDG group and 0.8 s for the FDM groups in ascitic cells, and 0.7 s for the FDG group and 0.6 s for the FDM group compounds in the other organs, respectively.

***In vivo* spectra.**  $^{19}\text{F}$  spectra of the mice bearing ascitic MH134 tumors were taken with a one-turn surface coil of 12 mm diameter placed on the lower abdomen using a JEOL GSX-270WB spectrometer under halothane anesthesia (0.5% halothane in air). The signal positions of halothane, more than 120 ppm downfield from the FDG-group signals, were too far distant to interfere with the spectral region of interest. The spectra were collected for 15 min under the acquisition conditions of  $8 \mu\text{s}$  pulse ( $22^\circ$  at a depth of 3 mm,  $11^\circ$  at 6 mm) 200 ms pulse repetition time and 80 kHz spectral bandwidth. Spectra were obtained at 1, 6, 24 and 48 h after the injection of 200 mg FDG/kg.

**$^{19}\text{F}$  imaging.** The images of FDG and its metabolites were obtained using a Varian Unity 400plus with a 9.4 T vertical magnet of bore size 89 mm. The image probe, used both for *in vivo* spectra and imaging, was equipped with a  $^1\text{H}/^{19}\text{F}$  tunable bird-cage type rf coil of 40 mm inner diameter and 45 mm height, and shielded gradient coils. FDG (200 mg/kg, i.v.) was injected after 16 h fasting. Thirty minutes before imaging, the mouse was placed in the animal container under pentobarbital anesthesia (50 mg/kg, i.p.).  $^{19}\text{F}$  chemical shift-selected images were obtained at

376 MHz with a simple spin-echo: a chemical shift-selection of 1 kHz band width by a gaussian pulse.  $TR=1$  s,  $TE=4$  ms,  $64 \times 16$  data points, field of vision (FOV) of  $6 \text{ cm} \times 4 \text{ cm}$  without slice selection, and a data accumulation time of 40–160 min. Images were obtained on the first and second days of FDG injection. The mice were fed freely in their cages during the interval between *in vivo* NMR experiments. The ascitic cells and heart were collected immediately after the *in vivo* NMR experiments for quantification.

## RESULTS

### *Ex vivo* $^{19}\text{F}$ spectrum

$^{19}\text{F}$  NMR spectra of packed ascitic cells (93.4 MHz) and a proton decoupled spectrum of the water extracts observed at 254 MHz are shown in Fig. 2. The spectral separation of the FDM groups from the FDG group was sufficient in the whole packed cells without  $^1\text{H}$  decoupling. The increase in the  $\alpha$ -FDM group towards 24 h was clearly shown in a low resolution spectrum at 93.4 MHz. The  $^1\text{H}$  decoupled spectrum of tumor extracts at 254 MHz indicated that NDP-FDM was the main component of the  $\alpha$ -FDM group signal 1 day after FDG injection. The total concentration of fluorine compounds determined from 93.7 MHz NMR spectrum was used as the uptake value of FDG in Fig. 3. In the early period, between 30 and 120 min after the injection

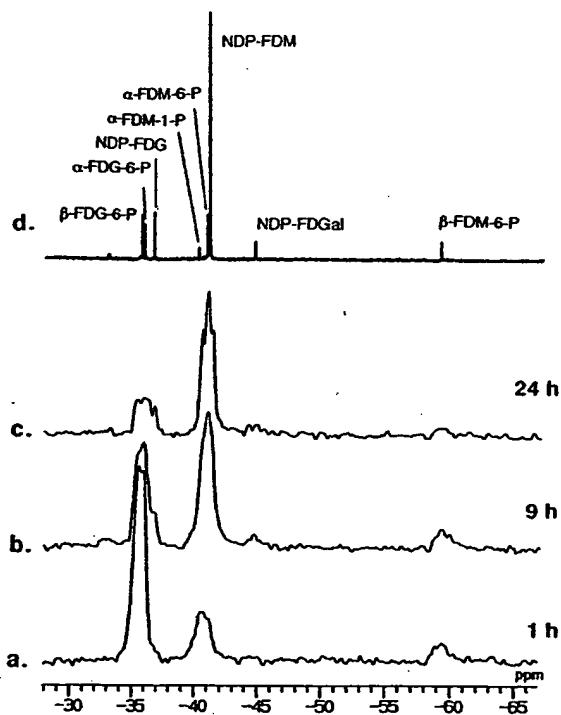


Figure 2.  $^{19}\text{F}$  NMR spectra of MH134 ascitic cells collected at the indicated times after 100 mg/kg i.v. injection. (a)–(c) Packed ascitic cells at 1, 9, and 24 h after injection, observed at 93.4 MHz; (d) proton-decoupled spectrum of water extracts of ascitic cells collected immediately after the observation of (c), at 254 MHz. The chemical shift standard was hexafluorobenzene in benzene (1/400, v/v). The FDG-group (FDG),  $\alpha$ -FDM-group ( $\alpha$ -FDM) and  $\beta$ -FDM-6-P ( $\beta$ -FDM) were distinguishable.

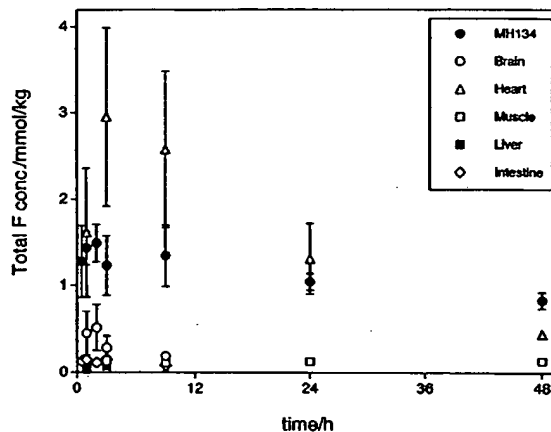


Figure 3. Uptake of FDG in collected ascitic cells and normal organs of 100 mg/kg FDG injected mice. Concentrations were determined from 93.4 MHz  $^{19}\text{F}$  NMR spectra. Most of the points are the averages of  $n$ =two to four points + standard deviation. The data at 48 h are the averages of one to two points.

of 100 mg FDG/kg, uptake was in the order: heart > packed ascite cells > brain  $\gg$  muscle and the other organs. The order of uptake after 9 h was changed as follows: heart = packed ascitic cells  $\gg$  other organs. The remarkably long retention of FDG and its metabolites reported in the previous work, in the heart of healthy male ddY mouse<sup>7,9</sup> and in the ascitic cells of Sarcoma 180 bearing male ddY mice,<sup>10</sup> was reproduced with female C3H mice bearing MH134 tumors in the present study. The contribution from the FDM group to the total uptake is shown in Fig. 4. It increased to 67% of the total uptake value 24 h after and to 72% 48 h after FDG injection in ascitic cells, which is comparable to our previous observation of 73% in the ascitic cells of Sarcoma 180-bearing ddY mice collected 48 h after 200 mg/kg FDG injection.<sup>10</sup> The ratio FDM-group/total uptake was also high in heart, 66–70% at 24 and 48 h, which was similar to the value of 70–74% in the healthy ddY mice.<sup>7</sup> High values were also obtained in the brain and muscle.

The NMR spectra of the extraction residue indicated that the efficiency of the water extraction of metabolites from each organ was higher than 80% of visible signals, and it was nearly constant through the metabolites: FDG,  $\alpha$ -FDM,

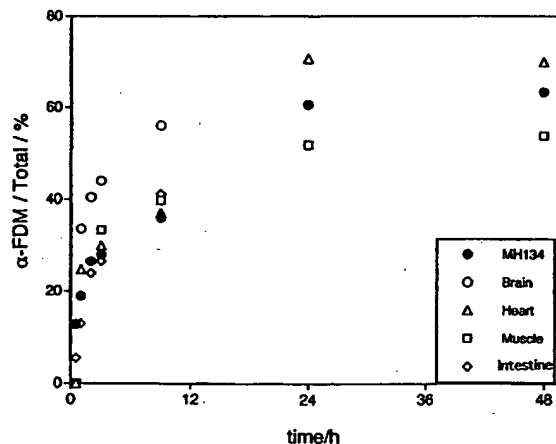


Figure 4. Concentrations of the FDM-group of metabolites found in MH134 ascitic cells and organs of MH134 bearing mice injected with 100 mg/kg FDG, relative to total uptake value. The data of organs without detectable signals were not included.

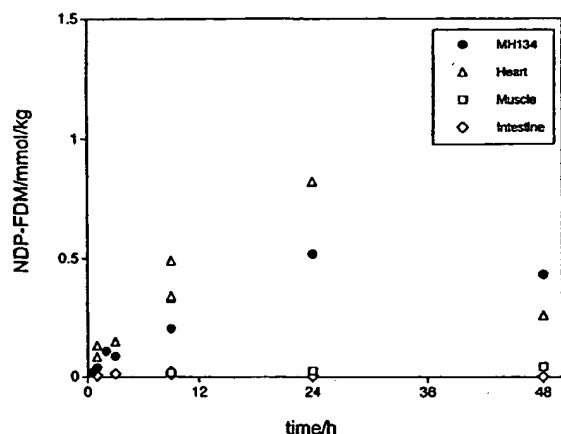


Figure 5. Concentrations of NDP-FDM found in the water extracts of MH134 ascitic cells and organs of 100 mg/kg FDG injected mice.

and  $\beta$ -FDM groups in the phosphates or NDP bound forms. Thus, the composition of metabolites was evaluated from the  $^1\text{H}$  decoupled spectra of water extracts (as in Fig. 2(d)). The contribution of NDP-FDM to the FDM signal in Fig. 4 and consequently to the total uptake was found to be dominant in tumor and heart 1 day after injection, as seen in Fig. 5.

The rate of conversion from FDG to the FDM-group was evaluated in two ways. In the early period after FDG injection, when the reaction was limited to the epimerization from FDG-6-P to FDM-6-P, typically within 1 h, the rate could be estimated by the half time in approaching the equilibrium ratio of these two compounds, when FDM-6-P formed 42.9% of the total metabolites.<sup>11</sup> From the data of Fig. 4, it was evaluated to be 0.6 h for brain and heart, 0.7 h for MH134 cells and 0.5–1 h for muscle, and much slower values for intestine (2 h) and liver (4 h). The next step, the approach to the final state where the dominant metabolite was NDP-FDM, was a very slow process. The half times of approach to the maximum value of NDP-FDM specific to the organs as evaluated from the data of Fig. 5 were of the order of 12 h, e.g. ascitic cells (12 h), heart (10 h) and

muscle (16 h). In the organs such as brain, liver and intestine where the metabolites became almost undetectable in 1 day, the contribution from NDP-FDM was much less. This suggested a correlation between retention and the amount of NDP-FDM formed. Although FDG metabolism in tumor cells were slow, of the order of 0.7 h from FDG-6-P to FDM-6-P and 12 h from FDM-6-P to NDP-FDM at a dose of 100 mg/kg, the rate of excretion from tumor cells was even smaller as seen in Fig. 3. Since the excretion rate was an order of magnitude lower than the rates of these reactions, we were able to measure the time courses of the reactions themselves by the NMR method with low time resolution.

### *In vivo* spectrum

*In vivo* spectra of the mice bearing ascitic hepatomas, taken immediately after the injection of 200 mg/kg of FDG and at some subsequent intervals, are shown in Fig. 6. The time course of FDG dynamics determined from *in vivo* spectra is depicted in Fig. 7. The profile of conversion from the FDG group to the FDM group was in good agreement with the one obtained *ex vivo*. The rate of washout at the initial stage was larger compared to the *ex vivo* data (Fig. 3). The reason is probably the higher dose used for this *in vivo* observation, which was greater by a factor of two than that for the *ex vivo* study. The spectrum of the last *in vivo* observation (in Fig. 6(a)), had essentially same relative intensities as the excised cells (Fig. 5(b)) and the water extract (Fig. 5(c)), which indicated the equal visibility of F signals *in vivo* and in the high resolution NMR probe, and confirms the efficiency of water extraction from tumor cells.

### $^{19}\text{F}$ images

$^{19}\text{F}$  NMR chemical shift selected images were constructed from the signal of the FDG-group, starting at 5 h after the 200 mg FDG/kg injection and accumulated for 107 min,

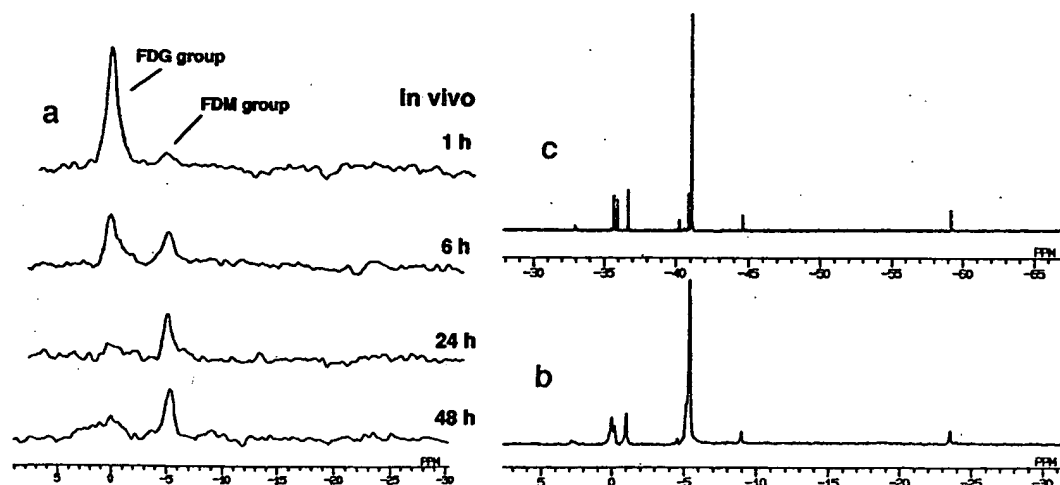
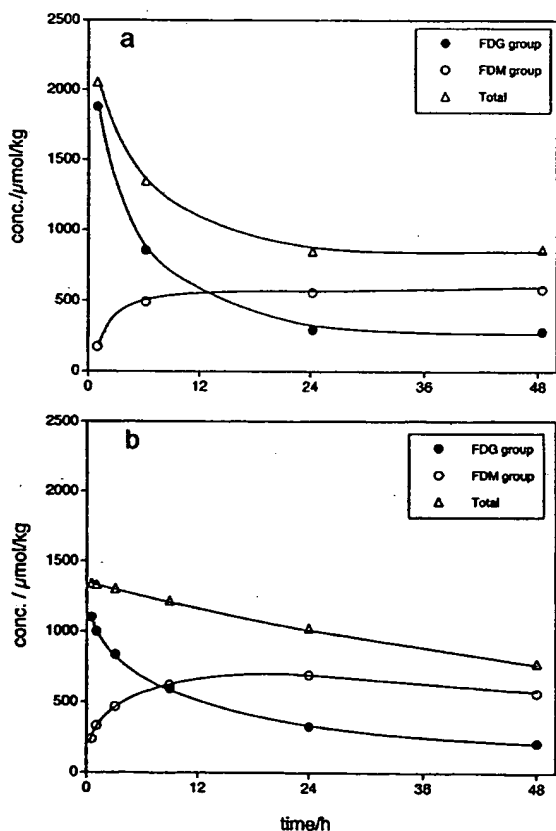


Figure 6.  $^{19}\text{F}$  NMR spectra (254 MHz) of a 200 mg/kg FDG injected mouse. (a) *In vivo* spectra of the lower abdomen, obtained by a 12 mm surface coil under halothane (0.5%) anesthesia, with 15 min data accumulations. The starting time is shown in the figure. (b) Proton-decoupled spectrum of packed ascitic cells immediately after the *in vivo* observation. (c) Proton decoupled spectrum of water extracts of collected cells used for (b).

and of the FDM-group starting at 25 h after the injection and accumulated for 160 min. They are shown in Fig. 8 with the respective  $^1\text{H}$  scout images and  $^{19}\text{F}$  spectra obtained by the same  $^{19}\text{F}/^1\text{H}$  tunable volume coil. In the  $^{19}\text{F}$  FDG-selected image, the signal of the FDG-group was observed mainly at the position in the lower abdomen where ascitic cells were expected. A strong signal was observed at the position of the bladder during this period. The region of tumor cells was visualized in the FDM-group selected image 1 day after FDG injection as well as the position of bladder. A  $^{19}\text{F}$  spectrum taken at 28 h with a 12 mm surface coil as a receiver with a  $43\ \mu\text{s}$  pulse at the lower abdomen was also shown in Fig. 8. The spectral pattern was essentially the same as that which we obtained from the whole body at 25 h. The concentrations of metabolites determined immediately after the last spectral measurement were as follows: FDG-group,  $220\ \mu\text{mol/kg}$ ;  $\alpha$ -FDM-group,  $430\ \mu\text{mol/kg}$ ;  $\beta$ -FDM-group,  $30\ \mu\text{mol/kg}$  in collected ascitic cells; FDG-group,  $210\ \mu\text{mol/kg}$ ; and FDM-group,  $690\ \mu\text{mol/kg}$  in heart. Taking account of the fact that the ascitic cells are in fluid at a concentration of 1/4–1/3, v/v, the *in vivo* concentration of the FDM-group used for the last  $^{19}\text{F}$  image should be below  $150\ \mu\text{mol/kg}$ . No such images were obtained from healthy mice 1 day after FDG injection.



**Figure 7.** (a) The time course of FDG dynamics determined from the data of Fig. 6. The concentrations at 24 h was determined from the spectrum of collected cells, which was used with the relative intensities of *in vivo* spectra to determine the concentration at each time, assuming that the sensitivity in each experiment was the same. (b) The FDG dynamics from the *ex vivo* data of excised ascitic cells in Fig. 3. (a) and (b) are essentially the same except for the initial stage where the effect of the doubled dose used for the *in vivo* observations was significant.

## DISCUSSION

The retention of FDG metabolites in heart and tumor tissue over 2 days was confirmed in female C3H mice by  $^{19}\text{F}$  NMR. It generalized our previous observations of their long retention in heart<sup>7</sup> and tumor<sup>10</sup> using mice of different strains and gender, healthy or with tumor cells of different origin.

The main metabolite found in the ascitic cells 1 day after FDG injection was NDP-FDM, which formed  $0.5\ \text{mmol/kg}$  of packed cells at the dose of  $100\ \text{mg/kg}$  body weight. The formation of NDP-FDG and NDP-FDM in living systems has been reported in yeast and chick-embryo cells using  $^3\text{H}$ -labeled FDG and FDM and  $^{14}\text{C}$ -labeled GTP and UTP by the method of radioactive gas-liquid chromatography.<sup>16</sup> The products of C2-epimerization such as GDP-FDM from FDG have been found in yeast cells.<sup>16</sup> The  $^{18}\text{F}$ -activity found in the nucleotide derivatives of  $^{18}\text{F}$ FDG in rat tumor has been shown to be proportional to that of  $^{18}\text{F}$ FDG-6-P.<sup>17</sup> However, this is probably the first report of the formation of NDP-FDM from FDG as the dominant metabolite in heart and tumor cells.

The slow washout of FDG from cancer cells has been explained by the low activity of glucose 6-phosphatase,<sup>3,5,17</sup> which also accounts for high rate of uptake in brain.<sup>2,6</sup> A decreased activity of glucose-6-phosphatase in Morris hepatomas has been reported.<sup>18</sup> In the present work, however, the half washout time of FDG metabolites in brain of ca. 4 h was much shorter than those of heart of 1 day and tumor which was over 2 days. In spite of very low initial uptake, retention over 2 days was also observed in muscle (Fig. 3), where the formation of the FDM group was not small (Fig. 4). A strong correlation was found between the retention of FDG metabolites and the formation of NDP-FDM. These results suggest the presence of many factors in addition to the modified activity of glucose-6-phosphatase on the glucose analogs FDG-6-P and FDM-6-P as the mechanism of slow FDG clearance. Nor have we any evidence to determine whether the long life of metabolites in these cells was due to the formation of NDP-FDM or whether the regional retention caused the accumulation of this compound. In order to understand the mechanism of retention over 2 days more work will be required, including the determination of the base species in NDP-FDM. The knowledge of such metabolites will contribute to the elucidation of the FDG accumulation mechanism. At least, we can propose here that FDG could be used as an NMR pharmaceutical for tumor diagnosis for both *in vivo* spectroscopy and imaging since the signal of NDP-FDM can be used as a marker of tumor, with almost the only exception being the heart.

A mouse tumor has been visualized by using the unique metabolite of FDG as the target signal for chemical shift selected  $^{19}\text{F}$  NMR imaging. Besides the proof of the new principle of FDG metabolism in tumor, we achieved a  $^{19}\text{F}$  chemical shift image of a metabolite at a concentration below  $150\ \mu\text{mol/kg}$  in a small animal. The success in the chemical shift imaging at such a low concentration in mice was in part due to the slow rate of reaction and even slower rate of clearance of this pharmaceutical, and in part to the use of the high field, 9.4 T. Imaging with a vertical type magnet has the advantage of large  $B_0$  within a limited hardware cost and laboratory space, while being applicable to both *in vivo* study and high-resolution observations.

The use of FDG for tumor diagnosis was originally



proposed using the PET method, and has been established as a standard procedure in that field. Most of the protocols for FDG-PET tumor diagnosis are different from those used for brain activity measurements based on the original principle of FDG-6-P trapping; data acquired 45 min or more after FDG injection are known to have a better tumor to background contrast.<sup>3-5,19</sup> Recently, single photon emission tomography (SPECT) for FDG imaging<sup>20,21</sup> has been seen as a promising method for meeting the wider need for cancer diagnosis due to its better accessibility than PET. It is of interest that the data acquisition periods for the clinical SPECT study are set in the range of 60–150 min after <sup>18</sup>F injection, which is later than the paired PET measurement and the standard FDG-PET protocol.<sup>20</sup> The image contrast for tumors seems to be attained at the latest period allowed for the detection of <sup>18</sup>F because of its limited lifetime. Recent progress in PET technology enables creation of a whole body map<sup>22</sup> which is suitable for searching for metastasis. However, a problem has been found in the accumulation of FDG in healthy muscle which obscures the small target tumor.<sup>22</sup> This result is in good agreement with our finding of low but long muscle retention: a signal source in low concentration but large volume can easily mask a small target with higher

concentration if the imaging method has low spatial resolution. Fukuda *et al.*<sup>23</sup> proposed <sup>18</sup>FDM as a pharmaceutical for PET-tumor imaging. Our results from this NMR study support FDM as a precursor compound for synthesizing NDP-FDM *in vivo*. So far, the results of studies using the radioactive pharmaceutical FDG and those with <sup>19</sup>F NMR are in good agreement, irrespective of the order of magnitude difference in the dose employed, and suggest the importance of elucidating the mechanism of FDG retention in tumors. The combination of molecular information from the NMR study with the abundant clinical and experimental FDG-PET data will lead to that goal.

## CONCLUSION

(1) Prolonged retention of FDG metabolites over 2 days in the heart and in tumors, mainly in the form of NDP-FDM, has been shown for the first time, whereas most metabolites were cleared from the other organs within 1 day.

(2) *Ex vivo* and *in vivo* <sup>19</sup>F NMR spectra of FDG and its products were consistent, confirming *in vivo* NMR detectability of FDG metabolites and the reliability of

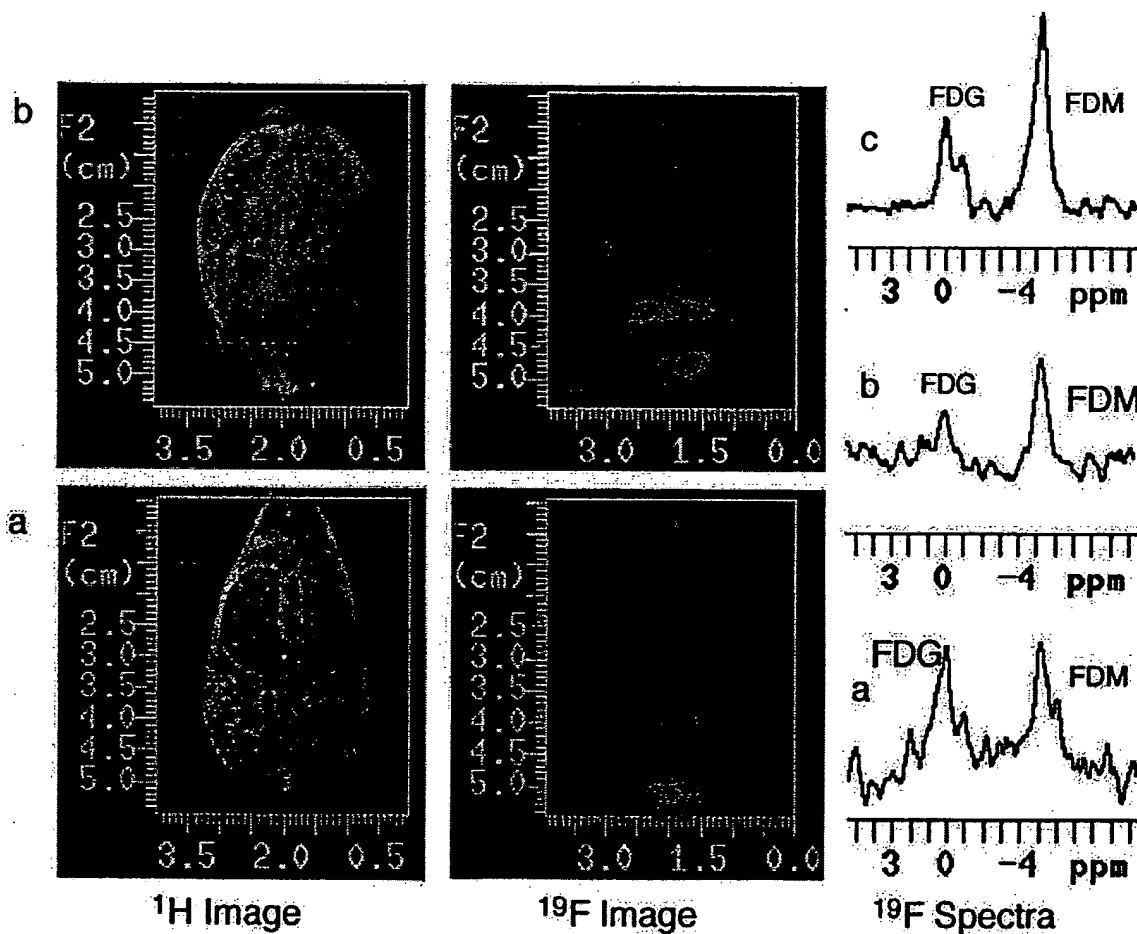


**Figure 8.** Chemical shift selected <sup>19</sup>F coronal images (376 MHz) of a 200 mg/kg FDG injected into an ascites-bearing mouse under pentobarbital anesthesia with corresponding <sup>1</sup>H scout images and the <sup>19</sup>F spectra taken immediately before the <sup>19</sup>F image. (a) Data acquisition started at 5 h after the FDG injection and accumulated for 107 min. The FDG-group was selected for the <sup>19</sup>F image. (b) Data acquisition started at 25 h after the injection of FDG, and accumulated for 160 min. The  $\alpha$ -FDM-group was selected. The image intensity of (b) was doubled compared with that of image (a). <sup>19</sup>F images were processed as follows: zero-filled to 256 × 128 data points, subjected to a gaussian filter of 500 Hz bandwidth, and displayed at 1.2 times intensity steps. (c) <sup>19</sup>F spectrum from the lower abdomen with a 12 mm surface coil.

quantification.

(3) The <sup>19</sup>F NMR signal of the FDM-group of metabolites, mainly from NDP-FDM, was shown to be a good target for *in vivo* spectroscopy and imaging, to assist in tumor detection.

(4) The applicability of chemical shift imaging to the study of metabolites at low concentration in small animals by high field magnetic resonance has been demonstrated.

## Acknowledgements

This work was partly supported by the Grant in Aid for Scientific Research from the Ministry of Education, Japan. We would like to thank Professor Kouji Masuda of Kyushu University, Faculty of Medicine for the use of a GSX-270 spectrometer. MH134 cells were the gift of Taiho Pharmaceutical Co. Ltd. Part of this work was presented at the 2nd International Symposium on PET in Oncology, 1993, Sendai, 12th annual meeting of SMRM (1993) and 2nd meeting of SMR (1994).

## REFERENCES

- Gallagher, B. M., Ansari, A., Atkins, J., Casella, V., Christman, D. R., Fowler, J. S., Ido, T., MacGregor, R. R., Som, P., Wan, C. N., Wolf, A. P., Kuhl, D. E. and Reivich, M. Radiopharmaceuticals XXVII. <sup>18</sup>F-labeled 2-deoxy-2-fluoro-D-glucose as a radiopharmaceutical for measuring regional myocardial glucose metabolism *in vivo*: tissue distribution and imaging studies in animals. *J. Nucl. Med.* **18**, 990-996 (1977).
- Reivich, M., Kuhl, D., Wolf, A., Greenberg, J., Phelps, M., Ido, T., Casella, V., Fowler, J., Hoffman, E., Alavi, A., Som, P. and Sokoloff, L. The [<sup>18</sup>F]fluorodeoxyglucose method for the measurement of local cerebral glucose utilization in man. *Circ. Res.* **44**, 127-137 (1979).
- Yonekura, Y., Benua, R. S., Brill, A. B., Som, P., Yeh, S. D. J., Kemeny, N. E., Fowler, J. S., MacGregor, R. R., Stamm, R., Christman, D. R. and Wolf, A. P. Increased accumulation of 2-deoxy-2-[<sup>18</sup>F]fluoro-D-glucose in liver metastases from colon carcinoma. *J. Nucl. Med.* **23**, 1133-1137 (1982).
- Strauss, R. W. and Conti, P. S. The applications of PET in clinical oncology. *J. Nucl. Med.* **32**, 623-648 (1991).
- Wahl, R. L., Hutchins, G. D., Buchsbaum, D. J., Liebert, M., Grossman, H. B. and Fisher, S. <sup>18</sup>F-2-Deoxy-2-fluoro-D-glucose uptake into human tumor xenographs. *Cancer* **67**, 1544-1550 (1991).
- Sokoloff, L., Reivich, M., Kennedy, C., Des Rosiers, M. H., Patlak, C. S., Pettigrew, K. D., Sakurada, O. and Shinohara, M. The [<sup>14</sup>C]deoxyglucose method for the measurement of local cerebral glucose utilization: theory, procedure, and normal values in the conscious and anesthetized albino rat. *J. Neurochem.* **28**, 897-916 (1977).
- Kanazawa, Y., Momozono, Y., Yamane, H., Haradahira, T., Maeda, M. and Kojima, M. Metabolic pathway of 2-deoxy-2-fluoro-D-glucose studied by F-19 NMR. *Life Sci.* **39**, 737-742 (1986).
- Kanazawa, Y., Momozono, Y., Yamane, H., Haradahira, T., Maeda, M. and Kojima, M. NMR evidence for the unexpected interconversion of 2-deoxy-2-fluoro-D-glucose and 2-deoxy-2-fluoro-D-mannose in mice. *Chem. Pharm. Bull.* **35**, 895-898 (1987).
- Kanazawa, Y., Yamane, H., Shinohara, S., Kuribayashi, S., Momozono, Y., Yamato, Y., Kojima, M. and Masuda, M. 2-Deoxy-2-fluoro-D-glucose as a functional probe for NMR: the unique metabolism beyond its 6-phosphate. *J. Neurochem.* **66**, 2113-2120 (1996).
- Kojima, M., Kuribayashi, S., Kanazawa, Y., Haradahira, T., Maehara, Y. and Endo, H. Metabolic pathway of 2-deoxy-2-fluoro-D-glucose and 2-deoxy-2-fluoro-D-mannose in mice bearing Sarcoma 180 studied by fluorine-19 nuclear magnetic resonance. *Chem. Pharm. Bull.* **36**, 1194-1197 (1988).
- Shinohara, S., Kanazawa, Y. and Kojima, M. Evaluation of energy metabolism in brain using epimerization of 2-deoxy-2-fluoro-D-glucose by <sup>19</sup>F NMR: the effect of anesthesia. *Magn. Reson. Med.* **21**, 191-196 (1991).
- Nakada, T., Kwee, I. L., Card, P. J., Matwiyoff, N. A., Griffey, B. V. and Griffey, R. H. Fluorine-19 NMR imaging of glucose metabolism. *Magn. Reson. Med.* **6**, 307-313 (1988).
- Brix, G., Bellman, M. E., Haberkorn, U., Gerlach, L., Bachert, P. and Lorenz, W. J. Mapping of biodistribution and catabolism of 5-fluorouracil in tumor-bearing rats by chemical-shift selective <sup>19</sup>F imaging. *Magn. Reson. Med.* **34**, 302-307 (1995).
- Haradahira, T., Maeda, M., Kai, Y. and Kojima, M. A new high yield synthesis of 2-deoxy-2-fluoro-D-glucose. *J. Chem. Soc. Chem. Commun.* **1985**, 364-365 (1985).
- Kanazawa, Y., Kuribayashi, S. and Kojima, M. A <sup>19</sup>F NMR study of 2-deoxy-2-fluoro-D-galactose in mice. *Chem. Pharm. Bull.* **36**, 4213-4216 (1988).
- Schmidt, M. F. G., Biely, P., Kratzky, Z. and Schwarz, T. Metabolism of 2-deoxy-2-fluoro-D-[<sup>3</sup>H]glucose and 2-deoxy-2-fluoro-D-[<sup>3</sup>H]mannose in yeast and chick-embryo cells. *Eur. J. Biochem.* **87**, 55-68 (1978).
- Suolinna, E.-L., Haaparana, M., Paul, R., Harkonen, P., Solin, O. and Sipilä, H. Metabolism of 2-[<sup>18</sup>F]fluoro-2-deoxyglucose in tumor bearing rats: chromatographic and enzymatic studies. *Nucl. Med. Biol.* **13**, 577-581 (1986).
- Xiao, Q., Jaspers, I., Matthew, E. and Lea, M. A. Changes in the glucose-6-phosphatase complex in hepatomas. *Mol. Cell. Biochem.* **122**, 17-24 (1993).
- Zasadny, K. R. and Wahl, R. L. Enhanced FDG-PET tumor imaging with correlation-coefficient filtered influx-constant images. *J. Nucl. Med.* **37**, 371-374 (1996).
- Martin, W. M., Delbeke, D., Patton, J. A., Hendrix, B., Weinfeld, Z., Ohara, I., Kessler, R. M. and Sandler, M. P. FDG-SPECT: correlation with FDG-PET. *J. Nucl. Med.* **36**, 988-995 (1995).
- Holle, L.-H., Tranpert, L., Lung-Kurt, S., Villena-Heinsen, C. E., Puschel, W., Schmidt, S. and Oberhausen, E. Investigations of breast tumors with fluorine-18-fluorodeoxyglucose and SPECT. *J. Nucl. Med.* **37**, 615-622 (1996).
- Engel, H., Steinert, H., Berthold, T., Boni, A. H. and von Schulthess, G. K. Whole-body PET: physiological and artifactual fluorodeoxyglucose accumulation. *J. Nucl. Med.* **37**, 441-446 (1996).
- Fukuda, H., Matsuzawa, T., Abe, Y., Endo, S., Yamada, K., Kubota, K., Hatazawa, J., Sato, T., Ito, M., Takahashi, T., Iwata, R. and Ido, T. Experimental study for cancer diagnosis with positron-labeled fluorinated glucose analogs: [<sup>18</sup>F]-2-fluoro-2-deoxy-D-mannose: a new tracer for cancer diagnosis. *Eur. J. Nucl. Med.* **7**, 294-297 (1982).

# AMINOGLYCOSIDE ANTIBIOTICS.

## Structures, Functions, and Resistance

Gerard D. Wright,<sup>1</sup> Albert M. Berghuis,<sup>1</sup> and Shahriar Mobashery<sup>2</sup>

<sup>1</sup>Department of Biochemistry  
McMaster University  
Hamilton, Ontario, Canada L8N 3Z5

<sup>2</sup>Department of Chemistry  
Wayne State University  
Detroit, Michigan 48202

## AMINOGLYCOSIDE DISCOVERY AND STRUCTURES

The aminoglycoside-aminocyclitol antibiotics (hereafter termed aminoglycosides) are a large family of water soluble, cationic molecules which exhibit broad antimicrobial spectra. While the moniker aminoglycoside refers to a vast array of structurally diverse compounds, they all share the incorporation of a six-membered aminocyclitol ring (Fig. 1). The aminoglycosides find use in the treatment of many bacterial infections caused by both Gram-positive and Gram-negative organisms, and are generally administered by injection or intravenously as a result of their relatively poor oral absorption (Edson and Terrell, 1991). Despite some problems of toxicity and bacterial resistance (described in detail below), these antibiotics continue to be a critically important component of our modern antimicrobial arsenal.

The discovery of the first two aminoglycoside antibiotics, streptomycin in 1944 (Schatz et al., 1944) and neomycin in 1949 (Waksman and Lechevalier, 1949), by Selman Waksman (for which he was awarded the Nobel Prize in Physiology and Medicine in 1952) presaged the identification and characterization of a series of clinically useful aminoglycosides over the next 40 years (Table 1). The importance of these initial findings was immediately apparent and its use in the treatment of tuberculosis was reported within one year of the discovery of streptomycin (Hinshaw and Feldman, 1945), and it remains a key component of modern anti-mycobacterial therapy (Musser, 1995).

Aminoglycosides fall into two general structural classes: those that incorporate a 2-deoxystreptamine ring, and those that do not (Table 2). The first group can be subdivided

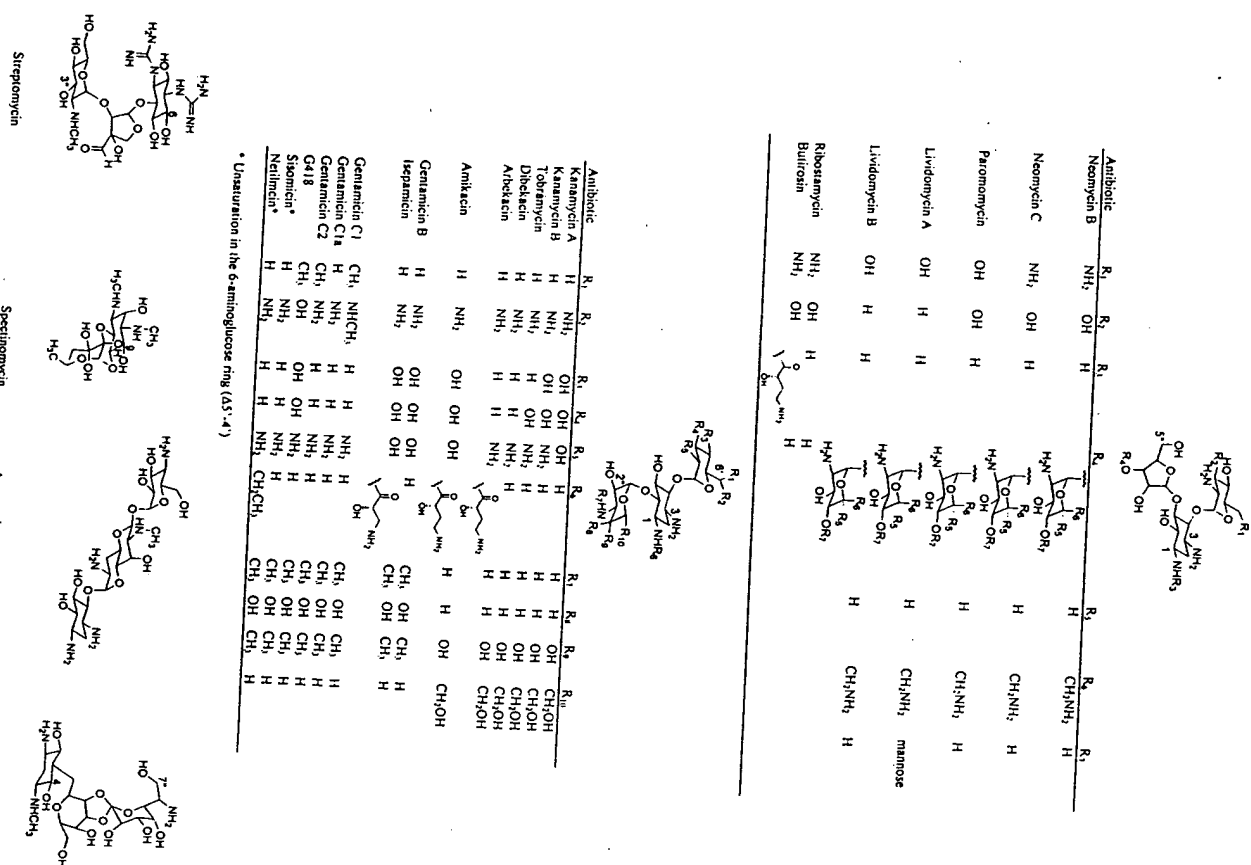


Figure 1. Structures of aminoglycoside antibiotics. Numbers indicate sites of common enzymatic modification.

Antibiotic	R <sub>1</sub>	R <sub>2</sub>	R <sub>3</sub>	R <sub>4</sub>	R <sub>5</sub>	R <sub>6</sub>	R <sub>7</sub>	R <sub>8</sub>	R <sub>9</sub>	R <sub>10</sub>
Neomycin B	NH <sub>2</sub>	OH	H	H	H	H	H	H	CH <sub>2</sub> NH <sub>2</sub>	H
Neomycin C	NH <sub>2</sub>	OH	H	H	H	H	H	H	CH <sub>2</sub> NH <sub>2</sub>	H
Paromomycin	OH	OH	H	H	H	H	H	H	CH <sub>2</sub> NH <sub>2</sub>	H
Lividomycin A	OH	H	H	H	H	H	H	H	CH <sub>2</sub> NH <sub>2</sub>	mannose
Lividomycin B	OH	H	H	H	H	H	H	H	CH <sub>2</sub> NH <sub>2</sub>	H
Ribostamycin	NH <sub>2</sub>	OH	H	H	H	H	H	H	CH <sub>2</sub> NH <sub>2</sub>	H
Butirosin	NH <sub>2</sub>	OH	H	H	H	H	H	H	CH <sub>2</sub> NH <sub>2</sub>	H

Antibiotic	R <sub>1</sub>	R <sub>2</sub>	R <sub>3</sub>	R <sub>4</sub>	R <sub>5</sub>	R <sub>6</sub>	R <sub>7</sub>	R <sub>8</sub>	R <sub>9</sub>	R <sub>10</sub>
Kanamycin A	H	NH <sub>2</sub>	OH	OH	OH	H	H	H	CH <sub>2</sub> OH	CH <sub>2</sub> OH
Kanamycin B	H	NH <sub>2</sub>	OH	OH	OH	H	H	H	CH <sub>2</sub> OH	CH <sub>2</sub> OH
Tobramycin	H	NH <sub>2</sub>	OH	OH	OH	H	H	H	CH <sub>2</sub> OH	CH <sub>2</sub> OH
Dibekacin	H	NH <sub>2</sub>	OH	OH	OH	H	H	H	CH <sub>2</sub> OH	CH <sub>2</sub> OH
Amikacin	H	NH <sub>2</sub>	OH	OH	OH	H	H	H	CH <sub>2</sub> OH	CH <sub>2</sub> OH
Gentamicin B	H	NH <sub>2</sub>	OH	OH	OH	H	H	H	CH <sub>2</sub> OH	CH <sub>2</sub> OH
Isepamicin	H	NH <sub>2</sub>	OH	OH	OH	H	H	H	CH <sub>2</sub> OH	CH <sub>2</sub> OH
Gentamicin C1	CH <sub>3</sub>	NHCH <sub>3</sub>	H	H	H	H	H	H	CH <sub>2</sub> OH	CH <sub>2</sub> OH
Gentamicin C1a	CH <sub>3</sub>	NH <sub>2</sub>	H	H	H	H	H	H	CH <sub>2</sub> OH	CH <sub>2</sub> OH
Gentamicin C2	CH <sub>3</sub>	OH	H	H	H	H	H	H	CH <sub>2</sub> OH	CH <sub>2</sub> OH
G418	CH <sub>3</sub>	OH	H	H	H	H	H	H	CH <sub>2</sub> OH	CH <sub>2</sub> OH
Sisomicin*	H	NH <sub>2</sub>	H	H	H	H	H	H	CH <sub>2</sub> OH	CH <sub>2</sub> OH
Netilmicin*	H	NH <sub>2</sub>	H	H	H	H	H	H	CH <sub>2</sub> OH	CH <sub>2</sub> OH

\* Unsaturation in the 6-aminoglucose ring (Δ<sup>5,6</sup>)

## Aminoglycoside Antibiotics

Table 1. Aminoglycoside antibiotics and their sources

Aminoglycoside	Source	Reference
Streptomycin	<i>Streptomyces griseus</i>	(Schatz et al., 1944)
Spectinomycin	<i>Streptomyces spectabilis</i>	(Mason et al., 1961)
Neomycin	<i>Streptomyces fradiae</i>	(Wakeman and Lechevalier, 1949)
Kanamycin	<i>Streptomyces kanamyceticus</i>	(Umezawa et al., 1957)
Gentamicin <sup>1</sup>	<i>Micromonospora purpurea</i>	(Weinstein et al., 1963)
Tobramycin	<i>Streptomyces tenebrarius</i>	(Higgins and Kasner, 1967)
Ribostamycin	<i>Streptomyces ribosidificus</i>	(Shomura et al., 1970)
Butirosin	<i>Bacillus circulans</i>	(Woo et al., 1971)
Sisomicin	<i>Micromonospora linyocis</i>	(Weinstein et al., 1970)
Amikacin	Semisynthetic derivative of kanamycin B	(Kawaguchi et al., 1972)
Netilmicin	Semisynthetic derivative of sisomicin	(Kabins et al., 1976)
Isepamicin	Semisynthetic derivative of gentamicin B	(Nagebuthan et al., 1978)

<sup>1</sup>Convention has the suffix 'mycin' given to compounds derived from *Streptomyces* while the suffix 'micin' refers to compounds derived from other organisms.

into compounds derivatized at positions 4 and 5, or at positions 4 and 6 of the 2-deoxystreptamine ring (Fig. 1). Convention has the numbering of the 6-aminohexose ring linked to position 4 of the 2-deoxystreptamine designated by prime (') and the hexose or pentose ring linked to position 5 or 6, designated double prime (''). Many of these compounds are natural products produced primarily by bacteria of the group actinomycetes, but several are semisynthetic derivatives of naturally occurring compounds (Table 1, Fig. 1). There are no compounds in current clinical use which are derived from total synthesis.

Aminoglycosides are primarily used for the treatment of Gram-negative and Gram-positive bacterial infections, but some also find use in the treatment of ameboid or protozoal infections (Berman and Fleckenstein, 1991); e.g., paromomycin for treatment of *Cryptosporidium parvum* infections (Fichtenbaum et al., 1994). Aminoglycosides have been used in other contexts as well. They have been shown to inhibit HIV-1 production by blocking the binding of the viral regulatory protein Rev to its response element (Wang et al., 1997; Werstuck et al., 1996; Zapp et al., 1993). In addition, aminoglycoside resistance genes are also extensively used as genetic markers for eukaryotic and prokaryotic molecular biology. For example, the use of the *neo* resistance cassette confers resistance to the aminoglycoside G-418, which is toxic to mammalian and bacterial cells.

Table 2. Representative aminoglycoside antibiotics

2-Deoxystreptamine aminoglycosides	4,6-disubstituted	Other aminoglycosides
Neomycin	Kanamycin	Streptomycin
Ribostamycin	Amikacin	Spectinomycin
Butirosin	Gentamicin	Hygromycin
Lividomycin	Isepamicin	Apramycin
Paromomycin	Tobramycin	Fortimicin
	Netilmicin	
	Sisomicin	
	Dibekacin	

## MODE OF ACTION OF AMINOGLYCOSIDE ANTIBIOTICS

One of the major benefits of the aminoglycosides is that with only a few exceptions such as spectinomycin, which is bacteriostatic, these antibiotics are bactericidal agents. The primary target for aminoglycosides appears to be the ribosome, as point mutations in ribosomal proteins and ribosomal RNA (rRNA), as well as methylation of specific bases of rRNA can confer high-level antibiotic resistance. Chemical footprinting studies have revealed that most aminoglycosides bind to the tRNA binding (A-site) region of the 16S rRNA of the 30S ribosomal subunit, but different bases are protected in the presence of different aminoglycosides (Moez and Noller, 1987; Woodcock *et al.*, 1991). Thus neomycin, paromomycin, gentamicin and kanamycin all protect A1408 and G1494 (*Escherichia coli* 16S rRNA numbering), and spectinomycin protects C1063 and G1064. In contrast, the non-A site directed compound streptomycin, strongly protects A913, A914 and A915.

The NMR structure of paromomycin bound to a 27-nucleotide portion of the 16S rRNA encompassing the conserved A site internal loop region, has recently been reported (Fig. 2; Fourmy *et al.*, 1996). The antibiotic binds within the major groove and makes many contacts to the RNA, either through direct hydrogen bonds, or via intermediary water molecules. In particular, N7 of G1494 binds to the C3 amino group of the 2-deoxystreptamine ring, a common site of acetylation which results in aminoglycoside resistance (*vide infra*). Other common sites of aminoglycoside modification conferring antibiotic resistance e.g. 3'-OH and 6'-OH (which is often an amino group in other aminoglycosides), also make contacts with backbone phosphates of the rRNA.

While it is clear that aminoglycoside affinity for the ribosome is key to antibiotic action, the elucidation of the precise mechanism of cell death has been elusive. Aminoglycoside binding to ribosomes appears to be reversible, with dissociation constants in the  $\mu\text{M}$ - $\text{nM}$  range, which would seemingly suggest the likelihood of a bacteriostatic effect. A key element in this process is the uptake of antibiotic into the cell. Aminoglycosides gain entry into the bacterial cell in a multiphasic fashion (reviewed in Davis, 1987; Hancock, 1981; Taber *et al.*, 1987). The first step is energy independent and involves initial passage through the outer membrane and periplasmic space in Gram-negative organisms, and the cell wall assembly in Gram-positives, which is followed by binding of the cationic aminoglycoside to the exterior of the cell membrane by electrostatic interactions. An energy-dependent phase (EDP-I) then ensues, in which the positively charged molecules gain entry to the cytosol. A protein mediator for this process has remained elusive, though recent

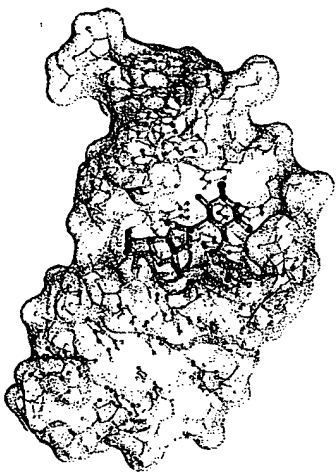


Figure 2. NMR structure of paromomycin bound to a 27-nucleotide portion of the 16S rRNA (Fourmy *et al.*, 1996) (PDB code 1FBR).

work indicates that a single 47 kDa integral inner-membrane protein in *E. coli* binds with high affinity to aminoglycosides, and may prove to be the transporter protein for these antibacterial agents (Roestamadj and Mobashery; unpublished results). The process of import of the aminoglycoside into the cell requires energy derived from the transmembrane electrical potential ( $\Delta\psi$ ) established by the bacterial electron transport system (Bryan and Kwan, 1983; Bryan and Van Den Elzen, 1977; Gilman and Saunders, 1986). Sensitivity of EDP-I to inhibitors of electron transport such as  $\text{CN}^-$ , carbonyl cyanide-*m*-chlorophenylhydrazone (CCCP) and anaerobiosis, provide evidence for the requirement of a threshold  $\Delta\psi$ . This initial process results in modest uptake of the aminoglycoside in the cell. The next step, EDP-II, is rapid and also energy-dependent. This step may occur after aminoglycosides have bound initially to some sensitive ribosomes and accounts for the bulk of the irreversible accumulation of antibiotic in the bacterial cells prior to cell death. The entry of large concentrations of aminoglycoside into the cell has pleiotropic effects. These include mistranslation of mRNA to yield aberrant proteins (Gorini, 1974; Lando *et al.*, 1973), depletion of polyribosomes (Luzzatto *et al.*, 1969), loss of cell membrane integrity resulting in increased permeability and efflux of ions such as  $\text{K}^+$  (Busse *et al.*, 1992; Dubin and Davis, 1961; Hancock, 1961), inhibition of DNA replication (Tanaka *et al.*, 1984), and blockade of the initiation of DNA replication by disruption of *oriC*-membrane interaction (Matsunaga *et al.*, 1986).

Davis has shown that misread proteins can target the cell membrane (Davis *et al.*, 1986) which lead him to propose a unifying theory for the bactericidal action of aminoglycosides (Davis, 1987; Fig. 3). This proposal suggests that a small amount of aminoglycoside antibiotic penetrates the cell during EDP-I and the initial phase of EDP-II and binds to susceptible ribosomes, which results in the misreading of mRNA and the formation of misfolded, non-functional proteins. These proteins can interact with the membrane resulting in loss of membrane integrity causing ion efflux and the formation of pores precipitating additional irreversible influx of antibiotic which saturates all ribosomes in an irreversible fashion, resulting in cell death.

Support for concentration-dependent interactions between ribosomes and aminoglycosides comes from titration of ribosomes with aminoglycosides (Le Goffic *et al.*, 1979) and by photoaffinity labeling of *Escherichia coli* 70S ribosomes with an [ $^3\text{H}$ ]-azidobenzyl derivative of tobramycin (Tangy *et al.*, 1983). The latter experiments showed labeling primarily of ribosomal proteins, principally L6, S4 and S5, rather than rRNA. At high concentrations of label (20  $\mu\text{M}$ ), such as those expected in EDP-II, mRNA misreading is prevalent and virtually all ribosomal proteins were labeled indicating a major, and possibly catastrophic, infiltration of the antibiotic into the ribosomal structure. In addition, Busse and colleagues have suggested that for bactericidal aminoglycoside antibiotics, the degradation products of the misfolded proteins can sequester aminoglycoside molecules within the cell, thus accounting for their irreversible uptake (Busse *et al.*, 1992). Bacteriostatic aminoglycosides do not result in misreading of mRNA and thus do not cause membrane damage (Bakker, 1992).

While it is clear that a precise model which adequately reflects all the experimentally determined effects of aminoglycosides remains elusive, we can nevertheless say that the ribosome is the primary target for aminoglycoside antibiotics and that membrane damage appears to play a role, probably a central one, in cell death. Paradoxically, one report has shown that gentamicin covalently linked to bovine serum albumin, and thus incapable of penetrating the cell, exhibits protein synthesis inhibition, membrane damage, and bactericidal activities in *Pseudomonas aeruginosa* (Kadurugamuwa *et al.*, 1993). Reconciliation

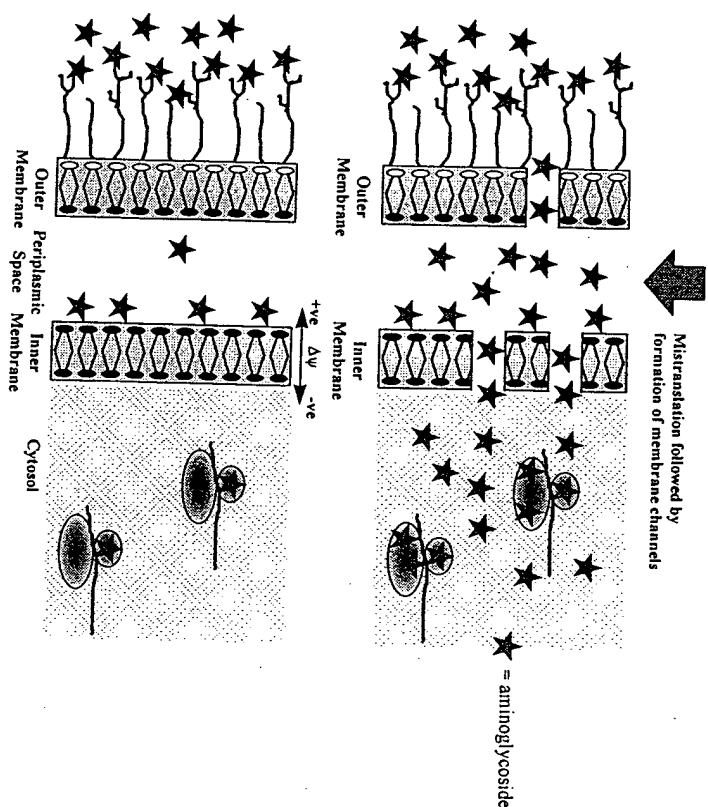


Figure 3. Model for entry and bactericidal action of aminoglycoside antibiotics in Gram-negative bacterial cells.

of these results with the proposed models for aminoglycoside action is not straightforward and points to a need for additional research in this area.

### AMINOGLYCOSIDE RESISTANCE

Resistance to aminoglycosides, like other antibiotics, can be intrinsic or acquired. Of these mechanisms of resistance, two general classes emerge, enzymatic and non-enzymatic. The latter are exclusively intrinsic in nature and, with the exception of a few cases such as streptomycin resistance in *Mycobacterium tuberculosis*, do not play a significant role in clinical resistance. On the other hand, enzymatic resistance, which is generally but not exclusively acquired, is the most prevalent means of aminoglycoside resistance in the clinic. The following sections detail the current knowledge of aminoglycoside resistance mechanisms.

#### Non-Enzymatic Resistance

As noted above, aminoglycoside entry into the bacterial cell requires an intact electron transport chain to establish a sufficient  $\Delta\psi$  for antibiotic transport to occur, thus anaerobic bacteria are in essence intrinsically resistant to aminoglycosides (reviewed in Bryan, 1984; Schlessinger, 1988). Mutations which affect  $\Delta\psi$  are also known to result in

#### Aminoglycoside Antibiotics

Table 3. Aminoglycoside resistance by rRNA methylases

Organism	Gene	Reference
<i>Micromonospora purpurea</i>		
<i>Micromonospora rosea</i>	<i>grrM</i>	(Kleimen <i>et al.</i> , 1991)
<i>Micromonospora zionensis</i>	<i>sgn</i>	(Kojic <i>et al.</i> , 1992)
<i>Micromonospora olivacetivoripora</i>	<i>fmrO</i>	(Ohia and Hasegawa, 1993b)
<i>Streptomyces telyimariensis</i>	<i>kamA (Im-7)</i>	(Ohia and Hasegawa, 1993a)
<i>Streptomyces tenebrarius</i>	<i>kamB</i>	(Skeggs <i>et al.</i> , 1987)
<i>Saccharopolyspora hirsuta</i>	<i>kamC</i>	(Holmes <i>et al.</i> , 1991)
<i>Streptomyces tenebrarius</i>	<i>kamB</i>	(Holmes and Cundliffe, 1991)

aminoglycoside resistance (Miller *et al.*, 1980), and an ATP synthase  $\gamma$ -subunit mutant which shows broad aminoglycoside resistance, may also fall into this category (Humbert and Altendorf, 1989). Another mechanism of aminoglycoside resistance by altered uptake of the drug is operational in some strains of *P. aeruginosa*, where overexpression of OprH saturates the aminoglycoside binding sites on the outer membrane lipopolysaccharide thus preventing the initial energy-independent phase of drug uptake (Young *et al.*, 1992).

Point mutations in rRNA can also confer drug resistance, thus mutation of C1192 of the 16S rRNA results in spectinomycin resistance in *E. coli* (Sigmond *et al.*, 1984). Streptomycin is a first line drug for the treatment of *M. tuberculosis* infection and in this organism, clinical resistance to the aminoglycoside is conferred exclusively by point mutations in the 16S rRNA and ribosomal protein S12 (reviewed in Musser, 1995).

#### Enzymatic Resistance: Ribosomal Modification

Target alteration is a common strategy for resistance to antibiotics. For example, resistance to thiostrepton, macrolide, lincosamide, and streptogramin antibiotics is frequently the result of methylation of specific bases of rRNA (Cundliffe, 1987; Leclercq and Courvalin, 1991). In many aminoglycoside producing organisms, methylation of the 16S rRNA provides high-level resistance to the antibiotics (Beaulieu and Cundliffe, 1987; Matkovic *et al.*, 1984; Thompson *et al.*, 1985) (Table 3). Methylation occurs at N7 of guanine and is S-adenosylmethionine dependent. This target modification results in high-level resistance to aminoglycosides (MIC > 500  $\mu\text{g/mL}$ ), yet unlike the *erm* genes which methylate the 23S rRNA and confer macrolide, lincosamide and streptogramin resistance, the 16S rRNA methylases have not been identified in aminoglycoside resistant clinical isolates thus far, and detailed analysis of the structures and mechanisms of these enzymes is lacking.

#### Enzymatic Resistance: Aminoglycoside Modification

Three distinct mechanisms of covalent modification of aminoglycosides have been observed: O-nucleotidyltransfer, N-acetyltransfer and O-phosphoryltransfer. These reactions are catalyzed by discrete classes of enzymes and are by far the most prevalent and clinically relevant mode of aminoglycoside resistance. The modified aminoglycosides have reduced predilection for the high-affinity sites on the bacterial ribosome, which results in a drug resistance phenotype. The enzyme and gene nomenclature presently used to describe aminoglycoside resistance was largely defined in an excellent review by Shaw and colleagues, which presented a thorough description of the genes identified in each

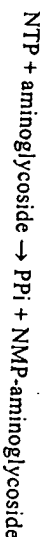
class (Shaw et al., 1993). First, each enzyme is designated by class: ANT for nucleotidyltransferases, AAC for acetyltransferases, and APH for phosphotransferases. The class is followed by a number in parentheses which describes the regioselectivity of group transfer and this is followed by a roman numeral designating a unique aminoglycoside resistance profile. Distinct genes which confer identical resistance phenotypes are further designated by a lower case letter. For example, *ant(6)-Ia* encodes a streptomycin nucleotidyltransferase which modifies position 6 of the drug; *aac(6)-Ic* encodes an acetyltransferase which modifies aminoglycosides at position 6<sup>1</sup>, and has the same resistance profile as *aac(6)-Ia* or *aac(6)-Ib*, but is a unique protein.

The second-substrate requirements of all these enzymes, either ATP or acetyl-CoA, necessitate intracellular localization, and there is no compelling evidence for periplasmic localization of the enzymes in Gram-negative organisms. All these enzymes would appear therefore to be cytosolic.

The aminoglycoside resistance genes are generally found on mobile genetic elements such as transposons and plasmids, but some are chromosomal in origin. The genes found in clinically important Gram-negative organisms tend to be more diverse, while in Gram-positive resistance is generally limited to *aac(6)-aph(2)* (Gent<sup>R</sup>), encoding a unique bifunctional resistance enzyme, *aph(3)-IIIa* (Kan<sup>R</sup>), and *ant(6)* (Strep<sup>R</sup>). A recent survey of resistance patterns has shown that the usage of aminoglycosides in clinical settings over the past several years has resulted in a change in the prevalence of resistance mechanisms (Miller et al., 1997). The previously high prevalence of *ant(2)* (Gent<sup>R</sup>, Tobr<sup>R</sup>) in Gram-negative organisms has now given way to a more complex pattern in which *aac(6)-I* genes are combined with other resistance determinants such as *aac(3)* and *ant(2)* as a result of the introduction of newer aminoglycosides such as netilmicin. Thus the clinical use of aminoglycosides is under constant pressure from an evolving response by target organisms.

### Aminoglycoside Nucleotidyltransferases (ANT)

Several *ant* genes have been cloned which confer resistance to a broad spectrum of aminoglycosides (Table 4). The enzymes catalyze the reaction:



The enzymes in essence activate the aminoglycoside for modification via the  $\alpha$ -phosphoryl of a nucleotide monophosphate (NMP) with concomitant loss of pyrophosphate (PPi). Since ATP is the most prevalent nucleotide triphosphate (NTP) in the cell, these enzymes are no doubt in fact adenylyltransferases. ANT(2<sup>1</sup>) is very common in Gram-negative organisms and is a major cause of clinical drug resistance (Miller et al., 1997), however several other ANT are known and have been cloned from a variety of organisms (Fig. 4).

*Ant(6)*. The streptomycin modifying enzyme ANT(6) has been partially purified from *Bacillus subtilis* Marburg 168 where it is encoded by a chromosomal gene (Kono et al., 1987) and the structure and regioselectivity of the adenylylated product unambiguously assigned by <sup>1</sup>H and <sup>13</sup>C NMR (O'hara et al., 1988). The 53% identical enzyme encoded by *pHI* in *Enterococcus faecalis* (Ounissi and Courvalin, 1987) has not been fully characterized, although the enzyme purified from an *E. coli* overexpression system was found to readily adenylylate streptomycin (Michaels constant ( $K_m$ ) 22  $\mu$ M), but spectinomycin was neither a substrate nor an inhibitor (D. Daigle, S. Clugston, T. Clarke, & G. Wright, unpublished).

### Aminoglycoside Antibiotics

Table 4. Aminoglycoside nucleotidyltransferases

Enzyme	Profile	Source	Phenotype <sup>1</sup>	Reference
ANT(6)	Ia	<i>Enterococcus faecalis</i>	Strep	(Ounissi and Courvalin, 1987)
	Ib <sup>2</sup>	<i>Bacillus subtilis</i>		(Omura et al., 1989)
ANT(9)	Ia	<i>Staphylococcus aureus</i>	Spec	(Murphy, 1985)
	Ib	<i>Enterococcus faecalis</i>		(LeBlanc et al., 1991)
ANT(4)	Ia	<i>Staphylococcus aureus</i>	Kan, Tob, Amik, Neo	(Matsumura et al., 1984)
ANT(2)	Ia	<i>Enterobacteriaceae</i>	Kan, Gent, Tob	(Lee et al., 1987)
ANT(3)	Ia	<i>Enterobacteriaceae</i>	Strep, Spec	(Hollingshead and Vapnek, 1985)

<sup>1</sup> List is not necessarily complete, only reported phenotype given

<sup>2</sup> Chromosomal gene.

Abbreviations: Kan, kanamycin; Amik, amikacin; Tob, tobramycin; Neo, neomycin; Strep, streptomycin; Spec, spectinomycin.

*Ant(3)* and *Ant(9)*. ANT(3) is a 34.6-kDa enzyme encoded by a gene which is widely distributed among several enterobacterial transposons (Hollingshead and Vapnek, 1985). The enzyme is reported to modify streptomycin at position 3<sup>1</sup> and spectinomycin at position 9. Two enzymes with only spectinomycin modification capacity are also known in Gram-positive cocci, ANT(9)-Ia from *Staphylococcus aureus* (Murphy, 1985) and ANT(9)-Ib from *E. faecalis* (LeBlanc et al., 1991). The *S. aureus* gene encodes a protein with a molecular mass of 28.9 kDa and a predicted pI of 8.0, the only aminoglycoside resistance protein thus far reported with a positive charge at neutral pH (in contrast, ANT(9)-Ib and ANT(3) have respective predicted pIs of 6.2 and 4.8). Protein sequence alignment shows that the two ANT(9) enzymes from Gram-positive organisms are 36% identical (57% similar) and that ANT(3) is 28% identical to ANT(9)-Ia and 23% identical to ANT(9)-Ib (51% and 45% similarity, respectively). The molecular basis for the difference in substrate specificity between these enzymes is unknown. We note that streptomycin is neither a substrate nor an inhibitor of the purified ANT(9)-Ia (D. Daigle, G. Wright, unpublished), thus despite the sequence homology with ANT(3), the staphylococcal enzyme does not recognize streptomycin. ANT(3) has an N-terminal extension of roughly 45 amino acids when compared to the ANT(9) enzymes and this may contribute to the ability to adenylylate streptomycin, but no supporting evidence is currently available.

*Ant(2)*. ANT(2) confers resistance to gentamicin C and is among the most highly prevalent aminoglycoside modifying determinants in the *Enterobacteriaceae* (Miller et al., 1997). The enzyme has been purified from an *E. coli* construct and studied in some detail by Northrop and colleagues (Gates and Northrop, 1988a-c; Van Peit and Northrop, 1984).

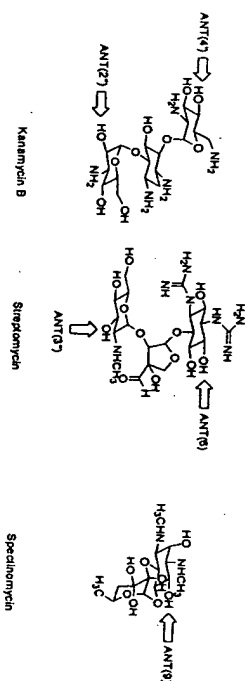


Figure 4. Regioselectivity of ANT.



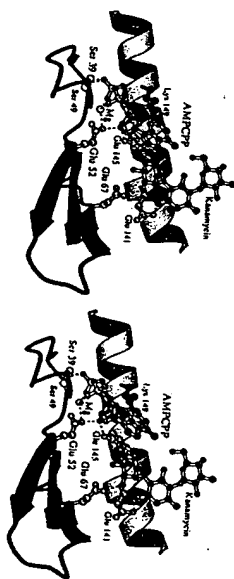
Figure 5. Structure of ANT(4') dimer (Pedersen *et al.*, 1995; PDB code 1KNV).

The 31.5-kDa enzyme shows a broad substrate specificity both for aminoglycosides and NTPs with  $K_m$  in the low to sub  $\mu\text{M}$  range (Gates and Northrop, 1988c). Steady-state kinetic measurements have revealed a Theorell-Chance kinetic mechanism, a special case of the ordered BiBi, where the reaction occurring in the ternary complex does not contribute to the overall rate of catalysis (Gates and Northrop, 1988a). In this case, Mg-ATP binds first and is followed by aminoglycoside. The release of adenylylated aminoglycoside is rate-limiting and preceded by release of pyrophosphate (Gates and Northrop, 1988a,b). The regio- and stereochemistry of adenylyltransfer have also been determined using (Sp)-[ $\alpha$ - $^{18}\text{O}$ ]dATP as substrate (Van Pelt *et al.*, 1986, 1990). The reaction occurs with inversion at the phosphoryl center, consistent with direct attack of the 2'-OH at the  $\alpha$ -phosphate.

**Ant(4').** The three-dimensional structure of ANT(4') from *S. aureus* has been determined in the native state to 3.0 Å (Sakon *et al.*, 1993), and bound to kanamycin and the non-hydrolyzable ATP analogue  $\beta$ - $\gamma$ -methyleneadenosine 5'-triphosphate (AMPCPP) to 2.5 Å (Pedersen *et al.*, 1995) (Fig. 5). The enzyme is a dimer with two distinct heterodimeric catalytic sites. One subunit provides the bulk of the ATP binding residues and the ciliaating its transfer to the aminoglycoside. Both subunits contribute to aminoglycoside binding. Specifically, in the crystal structure, kanamycin forms hydrogen bonds to Glu67 from one subunit and Glu141 and Glu145 from the other subunit (Fig. 6). A further analysis of the aminoglycoside-binding pocket reveals that in addition to these negatively charged residues, several other acidic residues line the wall of the pocket (Glu67 from one subunit, and Asp95 and Glu142 from the other subunit). As a consequence, a highly negative patch is present on the surface of ANT(4'), which is undoubtedly responsible for attracting the positively charged aminoglycosides to its active site (Fig. 7).

As noted above, the stereochemistry of phosphoryl transfer catalyzed by ANT(2'') indicates an associative mechanism where the  $\alpha$ -phosphate of ATP undergoes direct attack

Figure 6. Close-up view of the active site of ANT(4'). Subunits I and II are colored dark and light gray, respectively.



by the nucleophilic hydroxyl group of the aminoglycoside. Based on this precedent, the molecular structure of the ANT(4') ternary complex has been analyzed. In the three-dimensional structure of the dead-end complex of ANT(4')-AMPCPP-kanamycin, kanamycin is positioned such that the 4'-OH approaches the  $\alpha$ -phosphate of ATP in a direct line, though the nucleophilic hydroxyl is quite distant (5.0 Å) from the reactive phosphate (Pedersen *et al.*, 1995). The view of the active site has permitted some speculation on the amino acid side chains which could contribute to adenylyl transfer. With ATP sequestered in the subunit I binding site, Lys149 of subunit II is appropriately placed to polarize the  $\alpha$ -phosphate, rendering it more electrophilic and thus aiding in catalysis by lowering the energy barrier. Glu145 of subunit II is positioned to act as a general base, deprotonating the 4'-OH and increasing its nucleophilicity (Fig. 8). These assignments need to be confirmed by additional studies including site-directed mutagenesis.

Figure 7. Negatively charged patch on the surface of ANT(4'). The surface of ANT(4')-AMPCPP dimer is shown with darker shading corresponding to greater negative charge. Also shown are the two positively charged kanamycin molecules bound to the enzyme.

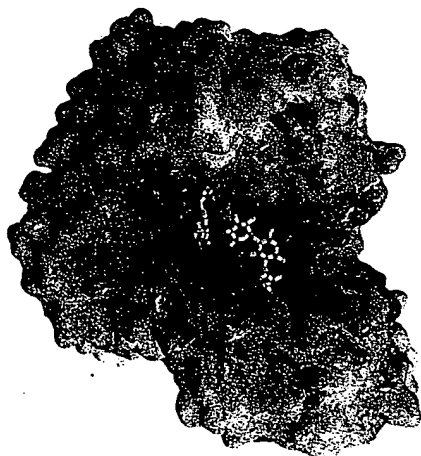
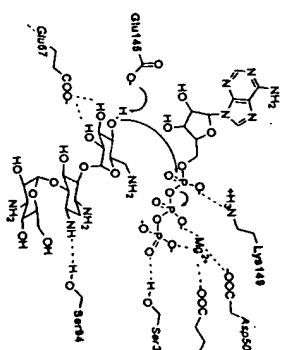


Figure 8. Proposed mechanism of the adenylyl-transfer reaction catalyzed by ANT(4'). Amino acids contributed by the same subunit are differentiated by bold and italic lettering.





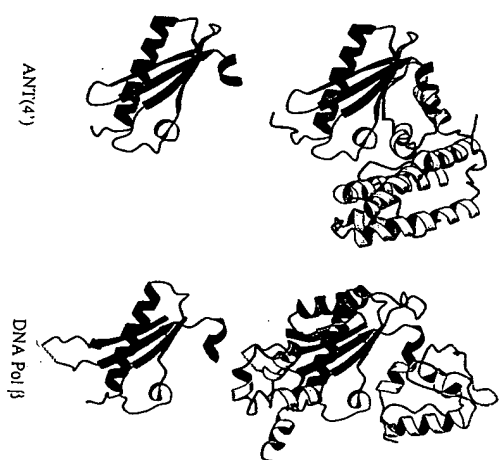


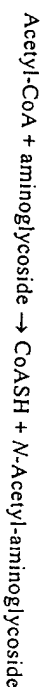
Figure 9. Comparison of ANT(4') and rat DNA polymerase  $\beta$ . Top left and right depicts the ANT(4') monomer and the 31-kD C-terminal domain of DNA polymerase (Sawaya *et al.*, 1994; PDB code 1BPB), respectively. The homologous folding motif is colored in dark gray. The bottom figures highlight the homologous regions between ANT(4') and DNA polymerase  $\beta$  (Holm and Sander, 1995).

Holm and Sander have noted that part of the protein fold of ANT(4') is very similar to that of another NMP transferase, that for the rat DNA polymerase  $\beta$  (Holm and Sander, 1995; Fig. 9). Additionally, the sequence, GS(Xaa)10–12(DE)Xaa(DE) (where X is any amino acid), located in the N-terminus of ANT enzymes is conserved among a variety of NMP transferases (Holm and Sander, 1995). This sequence includes amino acids which are required for positioning of  $Mg^{2+}$ -ATP. The invariant Ser forms a hydrogen bond to the  $\gamma$ -phosphate of ATP and the conserved Asp and/or Glu residues coordinate the  $Mg^{2+}$  ion (Figs. 6 and 8). This suggests that the active site geometry, at least the nucleotide-binding portion, is conserved among ANT enzymes and other NMP transferases which share this motif.

The ANT enzymes are highly interesting, not only because of their importance in clinical aminoglycoside resistance, but also for their structure and mechanism which share similarities with other NMP transferases. The precise mechanism of NMP-transfer, however, remains to be conclusively determined. The solution of additional three-dimensional structures for ANTs, in addition to ANT(4'), along with detailed mechanistic studies which include site-directed mutagenesis are required for a thorough understanding of the enzymes.

### Aminoglycoside Acetyltransferases (AAC)

Modification of aminoglycosides by acetylation is one of the most prevalent mechanisms of clinical aminoglycoside resistance (Miller *et al.*, 1997; Shaw *et al.*, 1993). The AAC enzymes catalyze the reaction:



The AAC family is highly diverse at the gene and protein level (Table 5), though the regiospecificity of aminoglycoside modification is limited to positions 1 and 3 of the 2-deoxystreptamine ring, and positions 6' and 2' of the 6-aminohexose ring (Fig. 10). The enzymes are generally in the size range of 15–22 kDa, though one enzyme, AAC(6')-Ie,

### Aminoglycoside Antibiotics

Table 5. Aminoglycoside acetyltransferases

Enzyme	Profile	Source	Phenotype <sup>1</sup>	Reference
AAC(2')	Ia <sup>2</sup>	<i>Providencia stuartii</i>	Gent, Tob, Amik	(Raither <i>et al.</i> , 1993b)
	Ib-e <sup>2</sup>	<i>Mycobacteria</i>	Gent, Tob	(Ainsa <i>et al.</i> , 1997)
	II	<i>Streptomyces kasugauensis</i>	Gent, Tobek	(Hotta <i>et al.</i> , 1996)
AAC(6')	Ia	<i>Citrobacter diversus</i>	Kan, Tob, Amik, Neo	(Tenover <i>et al.</i> , 1988)
	Ib	<i>Enterobacteriaceae</i>	Kan, Tob, Amik, Neo	(Tran van Nhieu and Collatz, 1987)
	Ic <sup>2</sup>	<i>Serratia marcescens</i>	Kan, Tob, Amik, Neo	(Shaw <i>et al.</i> , 1992b)
	Id	<i>Klebsiella sp. (Tn400)</i>	Kan, Tob, Amik, Neo	(Schmidt <i>et al.</i> , 1986)
	If	<i>Enterobacter cloacae</i>	Kan, Tob, Amik, Neo	(Terán <i>et al.</i> , 1991)
	Ig,h,j,k	<i>Acinetobacter sp.</i>	Kan, Tob, Amik, Neo	(Lambert <i>et al.</i> , 1994a, Rudant, 1994)
	ii <sup>2</sup>	<i>Enterococcus faecium</i>	Kan, Tob, Amik, Neo	(Costa <i>et al.</i> , 1993)
	II	<i>Citrobacter freundii</i>	Kan, Tob, Amik, Neo	(Hannecart-Pokorni <i>et al.</i> , 1997)
	IIm	<i>Escherichia coli</i>	Kan, Tob, Amik, Neo	(Shaw, 1997)
	IIn	<i>Citrobacter freundii</i>	Kan, Tob, Amik, Neo	(Wu <i>et al.</i> , 1997)
	Ie	<i>Enterococci</i>	Kan, Tob, Amik, Neo	(Ferretti <i>et al.</i> , 1986)
		<i>Staphylococci</i>	Fort	(Rouch <i>et al.</i> , 1987)
AAC(1)	II	<i>Pseudomonas aeruginosa</i>	Kan, Tob, Gent, Neo	(Shaw <i>et al.</i> , 1989)
	I	<i>Escherichia coli</i>	Neo, Apra	(Lovering <i>et al.</i> , 1987)
AAC(3)	Ia	<i>Enterobacteriaceae</i>	Gent, Fort	(Tenover <i>et al.</i> , 1989)
		<i>Enterobacteriaceae</i>	Gent, Fort	(Schwocho <i>et al.</i> , 1993)
	Ib	<i>Pseudomonas aeruginosa</i>	Gent, Fort	(Vlieggenhart <i>et al.</i> , 1989)
	Ila	<i>Enterobacteriaceae</i>	Gent, Tob, DibeK, Nel, Siso	(Raither <i>et al.</i> , 1992)
	Ilb	<i>Serratia marcescens</i>	Gent, Tob, DibeK, Nel, Siso	(Vakulenko and Enitina, 1990)
	Ilc	<i>Escherichia coli</i>	Gent, Tob, DibeK	(Vlieggenhart <i>et al.</i> , 1991)
	Illa	<i>Pseudomonas spp.</i>	Gent, Tob, DibeK	(Shaw <i>et al.</i> , 1992a)
	IIlb	<i>Pseudomonas aeruginosa</i>	(Shaw and Leal, 1992)	
	IIlc	<i>Pseudomonas aeruginosa</i>	Gent, Tob, DibeK, Nel, Apra	(Brau <i>et al.</i> , 1984)
	IV	<i>Solimonella spp.</i>	Gent, Tob, Siso, Nel	(Raither <i>et al.</i> , 1993a)
	VI	<i>Enterobacter cloacae</i>	Gent, Kan, Neo, Para, Livid	(Lopez-Cabrera <i>et al.</i> , 1989)
	VII	<i>Streptomyces rimosus</i>	Gent, Kan, Neo, Para, Livid	(Salauze <i>et al.</i> , 1991)
	VIII	<i>Streptomyces fradiae</i>	Gent, Kan, Neo, Para, Livid	(Salauze <i>et al.</i> , 1991)
	IX	<i>Micromonospora chelonea</i>	Gent, Kan, Neo, Para, Livid	(Ishikawa and Hotta, 1991)
	X	<i>Streptomyces griseus</i>	Gent, Kan, Neo, Para, Livid	

<sup>1</sup> Lia is not necessarily complete, only reported phenotype are given

<sup>2</sup> Chromosomal gene

Abbreviations: Kan, kanamycin; Tob, tobramycin; DibeK, dibekacin; Amik, amikacin; Isep, isepamicin; Apra, apramycin; Neo, neomycin; But, butirosin; Ribos, ribostamycin; Para, paromomycin; Livid, lividomycin; Gent, gentamicin; C, Nel, netilmicin; Siso, sisomicin; Apr, apramycin; Fort, fortimicin.

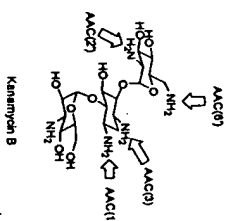


Figure 10. Regiospecificity of AACs.

forms the N-terminal region of a unique bifunctional enzyme which possesses APH(2'') activity as well (described below). Unlike the ANT and APH enzymes, there is no signature protein motif which is common to all members of the family and the amino acid sequences are generally quite diverse.

**AAC(2').** The *aac(2')-I* genes are unusual in that they are integrated into the bacterial genome and not derived from an extrachromosomal element. The genes appear to be universally present in *Providencia stuartii* (Rather *et al.*, 1993b, Clarke *et al.*, 1996) and mycobacteria (Ainsa *et al.*, 1997). The transcriptional activation of *aac(2')-Ia* from *P. stuartii* has been extensively studied by Rather's group. The gene is expressed at low levels in wild-type cells, but mutants were isolated with substantially increased *aac(2')-Ia* mRNA levels (Rather *et al.*, 1993b). This predicted the existence of *trans* activating factors which control gene regulation. A search for regulators of *aac(2')-Ia* expression has resulted in the identification of five genes with the ability to influence gene expression: *aarA*, *aarB*, *aarC*, *aarD* and *aarP*. *AarA*, *B*, *C*, and *D* are negative regulators of *aac(2')-Ia* expression (Macinga and Rather, 1996; Rather and Orosz, 1994; Rather *et al.*, 1993b, 1997b) while *AarP* is a MarA, SoxS homologue with a predicted helix-turn-helix motif *aarP* resulted in decreased levels of *aac(2')-Ia* mRNA while overexpression of *AarP* in *E. coli* conferred a multiple antibiotic resistance (Mar) phenotype and activated *myo*, a SoxS target (Macinga *et al.*, 1995). Recently, expression of *aac(2')-Ia* has been shown to be negatively regulated by a cell-density-dependent extracellular factor, probably a peptide (Rather *et al.*, 1997a).

*P. stuartii*, like many bacteria, has *O*-acetylated peptidoglycan (Clarke, 1993). Mutants which over- or under-express *aac(2')-Ia* show changes in the levels of peptidoglycan (*Payle* and Clarke, 1997; *Payle et al.*, 1995, 1996). AAC(2')-Ia is not restricted to acetyl-CoA as an acyl donor and surprisingly can use *O*-acetyl peptidoglycan components to *N*-acetylate gentamicin (*Payle* and Clarke, 1997). This observation, along with previous results demonstrating a role for AAC(2')-Ia in cell morphology, suggests that this enzyme may be involved in peptidoglycan biosynthesis or degradation, or perhaps lipopolysaccharide acetylation (*Payle* and Clarke, 1997). Thus the aminoglycoside-resistance phenotype conferred by the chromosomally encoded AAC(2') may be a serendipitous secondary effect rather than a primary function.

**AAC(6').** The AAC(6') family of aminoglycoside-modifying enzymes is highly diverse with two phenotypic subfamilies, I and II, all of which have predicted molecular masses of 16–21 kDa. The AAC(6')-I enzymes confer resistance to amikacin, gentamicin C1a and C2 but not gentamicin C1, while all the gentamicin C isoforms are modified by the AAC(6')-II enzymes, but amikacin is not. The *aac(6')-Ib* and *aac(6')-IIa* genes are 74% identical and give rise to proteins with 76% sequence identity. Rather and colleagues, through a series of domain exchange experiments between AAC(6')-Ib and AAC(6')-IIa followed by the isolation and characterization of mutant enzymes, have found that a single point mutation in AAC(6')-Ib, Leu119Ser, is sufficient to convert the resistance profile of the enzyme to that of AAC(6')-IIa (Rather *et al.*, 1992b). A clinical isolate of *Pseudomonas fluorescens*, which exhibited an AAC(6')-II phenotype (Amik<sup>r</sup>, Gent<sup>r</sup>) was found to harbor an *aac(6')-Ib* gene with a single base mutation resulting in a protein with a corresponding Leu83Ser substitution (Lambert *et al.*, 1994b). Thus, this position plays an important role in defining substrate specificity. A complete understanding of the role of this

position in substrate affinity awaits the determination of a high-resolution three-dimensional structure of one of these enzymes.

AAC(6')-Ib (also known as AAC(6')-IV) has been isolated from *E. coli* in two forms which behave differently on dye-ligand and size-exclusion chromatography, and show different activities (Radika and Northrop, 1984c). The more active form appears to be a tetramer based on gel-filtration chromatography. The less active form was non-covalently associated with an entity which possesses a chromophore at 260 nm, the loss of which resulted in conversion of the enzyme to the more active form. The nature of the chromophore is unknown, but could point to possible inhibitors of the enzyme. This enzyme has been well characterized in terms of aminoglycoside and acyl-CoA substrate specificity (Radika and Northrop, 1984a). The enzyme accepts a broad range of both aminoglycoside and acyl-CoA substrates. The  $K_m$  values for aminoglycosides were quite low, generally in the submicromolar range and, like many aminoglycoside-modifying enzymes, AAC(6')-Ib exhibited significant aminoglycoside (but not acyl-CoA) substrate inhibition with  $K_i$  values  $\geq 15xK_m$  (Radika and Northrop, 1984a), and the kinetic mechanism was determined to be rapid equilibrium random BiBi (Radika and Northrop, 1984b). In this mechanism, either the aminoglycoside or acetyl-CoA may bind first and the order of product release, CoASH or acetyl-aminoglycoside, is also random. In addition, the rates of dissociation of substrates and products are rapid compared to the acyl-transfer. Thus, the latter is largely rate-limiting. Amino acid residues which contribute to catalysis have not been determined.

Low-level resistance to many aminoglycosides in *Enterococcus faecium* is the result of the chromosomal *aac(6')-II* gene (Costa *et al.*, 1993). Overexpression of AAC(6')-II in *E. coli* has permitted the rapid purification of this dimeric enzyme for biochemical studies and crystallization. Recently, crystals of AAC(6')-II grown in the presence of cofactor and/or kanamycin have been obtained (L.E. Wybenga and A.M. Beghuis; unpublished results). The quality of these protein crystals is sufficient to allow for a structure determination at atomic resolution. Crystals of AAC(6')-II grown in the presence of the co-substrate acetyl-CoA display a resolution limit of 2.2 Å (measured on the Cornell High-Energy Synchrotron Source F2 beamline), and crystals of the enzyme grown in the presence of kanamycin and CoASH show diffraction beyond 2.8 Å (measured on the Brookhaven National Laboratories National Synchrotron Light Source X8C beamline). Steady-state kinetic analysis has confirmed the broad aminoglycoside specificity of the enzyme predicted by the resistance profile, but revealed low specificity rate constants ( $k_{cat}/K_m \sim 10^{-4} M^{-1}s^{-1}$ ) (Wright and Ladak, 1997). This observation suggests it to be an enzyme which is not optimally evolved for aminoglycoside modification and may point to some other role in cell metabolism, although an *aac(6')-II* deletion mutant of *E. faecium* had no discernible phenotype other than loss of aminoglycoside resistance (Costa *et al.*, 1993). The structures of isepamicin and butirosin bound to the enzyme have recently been determined by NMR techniques (DiGiammarino *et al.*, 1997). These studies demonstrate that the enzyme binds 4,5- and 4,6-disubstituted aminoglycosides differently, as predicted by steady-state kinetic measurements (Wright and Ladak, 1997).

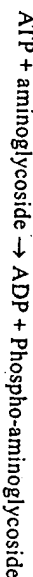
**AAC(3').** Members of the AAC(3') class of enzymes are distributed among many bacterial genera, including the aminoglycoside-producing actinomycetes (Table 5). These enzymes are larger than the AAC(6') proteins (approximately 30 kDa) and confer resistance to the gentamicins and many other clinically important aminoglycoside antibiotics. Unlike the AAC(6') class of modifying enzymes, the AAC(3') family is more homogeneous with significant homology in their N-termini. Two AAC(3') enzymes have been purified and

partially characterized, AAC(3)-I (Williams and Northrop, 1976) and AAC(3)-IV (Bräu and Piepersburg, 1985). The latter was shown to be a monomer by gel filtration methods and showed aminoglycoside  $K_m$  values from 11  $\mu$ M for apramycin to 241  $\mu$ M for kanamycin. The AAC(3)-I has been the most thoroughly studied enzyme of this class. Williams and Northrop have described the purification (Williams and Northrop, 1976), substrate specificity (Williams and Northrop, 1978b) and kinetic mechanism (Williams and Northrop, 1978a) of this enzyme. AAC(3)-I was shown to have aminoglycoside  $K_m$  values ranging from 0.3  $\mu$ M (gentamicin C1) to 25.2  $\mu$ M (gentamicin B), and only acetyl-CoA and propionyl-CoA could serve as acyl-donors (Williams and Northrop, 1978b). Specificity rate constants ( $(V_{max}/E)/K_m$ ) were quite high and, for the best substrates, gentamicin C1a and kanamycin B, were greater than  $10^7$  M<sup>-1</sup>s<sup>-1</sup>, approaching the rate of diffusion of small molecules in solution ( $10^9$  M<sup>-1</sup>s<sup>-1</sup>). The 4,5-disubstituted aminoglycosides such as neomycin, paromomycin and ribostamycin, as well as amikacin and kanamycin A were not substrates but competitive inhibitors of the substrate tobramycin. The kinetic mechanism was determined to be random BiBi, in rapid equilibrium with the good substrates gentamicin C1a and sisomicin, and non-rapid equilibrium with the relatively poor substrate tobramycin (Williams and Northrop, 1978a). This work has not yet been followed up by additional mechanistic or structural studies.

The AAC enzymes have emerged over the past decade as key aminoglycoside resistance elements in the clinic. Unfortunately, our understanding of the structure and mechanism of these diverse enzymes has not kept pace. Three-dimensional structures of representative AAC(6') and AAC(3) enzymes are particularly required. Given the general overall lack of amino acid sequence similarity among the AAC(6')s especially, several structures will no doubt be required in order to adequately compare enzymes. Similarly, the molecular mechanisms of acetyl transfer are not known. Therefore, much additional investigation is required.

### Aminoglycoside Phosphoryltransferases (APH)

Modification of aminoglycosides by phosphorylation is catalyzed by a group of kinases termed APHs which catalyze the following reaction:



Enzymes are known which modify all classes of aminoglycosides (Table 6, Fig. 11). APH(3') are common and representatives are found in both Gram-negative and Gram-positive organisms, but APH(2'') appears to be largely confined to Gram-positives at this time. APHs share amino acid sequence homology in the C-terminal regions of the enzymes of particular significance is the consensus sequence HGD(Xaa)<sub>3</sub>-6N(V/I) which mutagenesis studies and a three-dimensional structure have implicated in phosphoryl transfer.

*APH(3')*. APH(3')s phosphorylate many 2-deoxystreptamine aminoglycosides, notably kanamycin and neomycin. At least seven distinct classes (I-VII) have been identified (Shaw *et al.*, 1993). All are approximately 30 kDa in size and, with the exception of the type III and V classes, found in Gram-negative organisms.

The best studied aminoglycoside kinase is APH(3')-IIIa found primarily in Gram-positive cocci, although it has been detected in the Gram-negative organism *Campylobacter coli* (Papadopoulos and Courvalin, 1988; Taylor *et al.*, 1988). It should be noted that this is a

### Aminoglycoside Antibiotics

Table 6. Aminoglycoside phosphotransferases

Enzyme	Profile	Source	Phenotype <sup>1</sup>	Reference
APH(3')	Ia	<i>Escherichia coli</i>	Kan, Neo, Ribos, Livid	(Oka <i>et al.</i> , 1981)
	Ib	<i>Escherichia coli</i>		(Panssegrau <i>et al.</i> , 1987)
	Ic	<i>Klebsiella pneumoniae</i>		(Lee <i>et al.</i> , 1991)
II	Ic	<i>Escherichia coli</i>	Kan, Amik, Neo, But,	(Beck <i>et al.</i> , 1982)
	II	<i>Escherichia coli</i>	Ribos	
III	Ic	<i>Enterococcus faecalis</i>	Kan, Amik, Isep, Neo, But,	(Trieu-Cuot and
	III	<i>Staphylococcus aureus</i>	Ribos, Livid	Courvalin, 1983) (Gray and
IV	Ic	<i>Bacillus citrullus</i>	Kan, Neo, But, Ribos	Fitch, 1983)
	IV	<i>Streptomyces fradiae</i>	Neo, Ribos	(Thompson and Gray, 1993)
Vb <sup>2</sup>	Vb <sup>2</sup>	<i>Streptomyces rimosus</i>		
	Vc <sup>2</sup>	<i>Microsporium chalcu</i>		
VI	VI	<i>Acinetobacter baumannii</i>	Kan, Amik, Isep, Neo, But,	(Hoshiko <i>et al.</i> , 1988);
	VI	<i>Campylobacter jejuni</i>	Ribos, Livid	(Salauze and Davies, 1991)
VII	VII	<i>Escherichia coli</i>	Kan, Amik, Isep, Neo, But,	(Martin <i>et al.</i> , 1988)
	VII	<i>Streptomyces hygroscopicus</i>	Ribos, Livid	
APH(4)	Ia	<i>Escherichia coli</i>		(Griz and Davies, 1983)
	Ia	<i>Streptomyces hygroscopicus</i>	Hygr	(Zalacain <i>et al.</i> , 1986)
APH(7'')	Ia	<i>Enterococcus faecalis</i>	Gent, Net, Siso, Kan,	(Ferretti <i>et al.</i> , 1986)
	Ic	<i>Staphylococcus aureus</i>	Amik, Isep, Neo, But	(Rouch <i>et al.</i> , 1987)
APH(3'')	Ia	<i>Streptomyces griseus</i>	Ribos, Livid	(Chow <i>et al.</i> , 1997)
	Ib	<i>Escherichia coli</i>		
APH(6)	Ia	<i>Streptomyces griseus</i>		(Heinzel <i>et al.</i> , 1988)
	Ib	<i>Streptomyces glaucus</i>		(Schoiz <i>et al.</i> , 1989)
APH(9)	Ia	<i>Legionella pneumophila</i>		(Distler <i>et al.</i> , 1987)
	Ib	<i>Streptomyces flauoparvus</i>		(Vogtli and Hutter, 1987)
APH(9)	Ia	<i>Streptomyces flauoparvus</i>		(Mazodier <i>et al.</i> , 1985)
	Ib	<i>Streptomyces flauoparvus</i>		(Schoiz <i>et al.</i> , 1989)
APH(9)	Ia	<i>Streptomyces flauoparvus</i>		(Suter <i>et al.</i> , 1997)
	Ib	<i>Streptomyces flauoparvus</i>		(Lyutskanova, <i>et al.</i> , 1997)

<sup>1</sup> List is not necessarily complete, only reported phenotype are given.  
<sup>2</sup> Chromosomal gene.  
 Abbreviations: Kan, kanamycin; Amik, amikacin; Isep, isepamicin; Neo, neomycin; But, butirosin; Ribos, ribostamycin; Livid, lividomycin; Gent, gentamicin; C, Net, netilmicin; Siso, sisomicin; Hygr, hygromycin; Stre, streptomycin; Spec, spectinomycin.

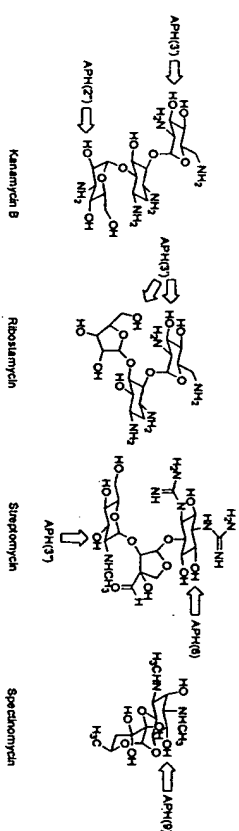


Figure 11. Regiospecificity of APHs.

highly significant observation which demonstrates the potential of gene transfer between Gram-positive and -negative organisms. The *aph(3')-IIIa* gene has been cloned from *E. faecalis* (Trieu-Cout and Courvalin, 1983) and *S. aureus* (Gray and Fitch, 1983) and the protein has been overexpressed and purified in *E. coli* (McKay et al., 1994b). The enzyme was purified as a mixture of monomer and dimer, the latter arising from two inter-molecular disulfide bonds, but both forms are kinetically indistinguishable in the steady state. *APH(3')-IIIa* has a broad substrate profile and will phosphorylate and confer resistance to a wide range of aminoglycosides. Specifically, rate constants for turnover are in the range of  $10^4$ – $10^5$   $M^{-1}s^{-1}$ , turnover numbers ( $k_{cat}$ ) are uniformly in the range of 1.7–4.0  $s^{-1}$  and the enzyme shows substrate inhibition at high concentrations of aminoglycosides (McKay et al., 1994b). Purification of modified aminoglycosides followed by analysis by mass spectrometry,  $^1H$ ,  $^{13}C$  and  $^{31}P$  NMR has confirmed the transfer of phosphate to the 3'-hydroxyl group of kanamycin (McKay et al., 1994b), amikacin, neomycin, and butirosin (Thompson et al., 1996b). Lividomycin A, which lacks the 3'-hydroxyl, is also a good substrate and was found to be phosphorylated at position 5' of the pentose (Thompson et al., 1996b). Similarly, butirosin and neomycin can also be demonstrated (Thompson et al., 1996b). The kinetic mechanism of the enzyme has been determined to be Theorell-Chance (McKay and Wright, 1995). In this mechanism, ATP binds first followed by the aminoglycoside, the phosphoaminoglycoside and ADP are then released sequentially. The mechanism implies that the rate of phosphoryl transfer does not contribute to the steady-state rate and that product release should be rate-limiting. This was confirmed by solvent isotope and viscosity effect experiments, which showed that ADP release was solely rate-limiting (McKay and Wright, 1996), which also accounted for similarity in  $k_{cat}$  values, despite the wide variation in the aminoglycoside structures.

The chemical mechanism of phosphoryl transfer in APHs has been the subject of some speculation, in particular, the presence of an invariant His residue in the conserved N-terminal regions of *APH(3')*s had been suggested to act as a phosphate accepting residue, relaying the phosphoryl group from the  $\gamma$ -position of ATP to the aminoglycoside hydroxyl (Martin et al., 1988). The equivalent His residue in *APH(3')-IIIa*, His 188, was converted to an Ala and similarly, the three additional His residues in the enzyme were also individually mutated to Ala (Thompson et al., 1996a). All His  $\rightarrow$  Ala mutant enzymes were fully active, indicating that they did not play a central role in phosphate transfer. However, much of the activity of the mutant enzyme was insoluble, thus the conservation of this residue is doubtless due to selective pressure for the maintenance of protein structure rather than a direct role in phosphoryl transfer. In addition, positional isotope exchange experiments using  $\gamma$ -[ $^{18}O$ ]-ATP were inconsistent with transfer of the phosphate to the enzyme during catalysis (Thompson et al., 1996a), thus all the evidence to date indicates that the mechanism of phosphoryl transfer is direct attack of the aminoglycoside hydroxyl on the  $\gamma$ -phosphate of ATP.

Affinity labeling of *APH(3')-IIIa* was accomplished using fluorosulfonylbenzoyl adenosine (FSBA; McKay et al., 1994a). FSBA was an irreversible inactivator of the enzyme which could be protected by the addition of ATP, consistent with targeting of the reagent to the nucleotide binding site. This reagent labeled two Lys residues, Lys33 and Lys44, the latter of which is conserved in all *APH(3')*s. Construction of Lys  $\rightarrow$  Ala mutants confirmed the importance of Lys44 but not Lys33 in ATP binding (Hon et al., 1997).

The prediction that Lys44 was important to ATP binding was confirmed with the determination of the X-ray crystal structure of *APH(3')-IIIa* with ADP bound in the nucleotide-binding pocket to 2.2 Å (Hon et al., 1997). The structure revealed two *APH(3')-IIIa*•ADP monomers connected covalently through two intermolecular disulfide

#### Aminoglycoside Antibiotics



Figure 12. Three-dimensional structure of the *APH(3')-IIIa* dimer. The two monomers, which are shaded differently are connected through two disulfide bridges, in a head-to-tail-tail-to-head fashion, the two bound ADP molecules are also depicted.

bonds (Fig. 12). However, the interface between the two monomers did not contain extensive interactions. Furthermore, the active sites on the two monomers were separated by more than 20 Å. These observations suggested that dimer formation is not required for enzyme activity, unlike the situation described earlier for ANT(4') (Perdersen et al., 1995). The suggestion that *APH(3')-IIIa* is active as a monomer is in agreement with steady-state kinetic experiments which revealed no difference between *APH(3')-IIIa* dimer and monomer species (McKay et al., 1994b). Therefore, the remainder of this discussion will focus on the monomer structure of *APH(3')-IIIa*.

The *APH(3')-IIIa* monomer consists of two lobes connected by a tethering segment. The N-terminal lobe is composed of a five stranded anti-parallel  $\beta$ -sheet and two  $\alpha$ -helices, the C-terminal lobe incorporates six helices and four short  $\beta$ -strands. The cleft between the two lobes forms the nucleotide-binding pocket, which harbors in this structure one ADP molecule coordinated to two magnesium ions (see Fig. 13). The specific arrangement of different secondary structure elements into a three-dimensional fold found in

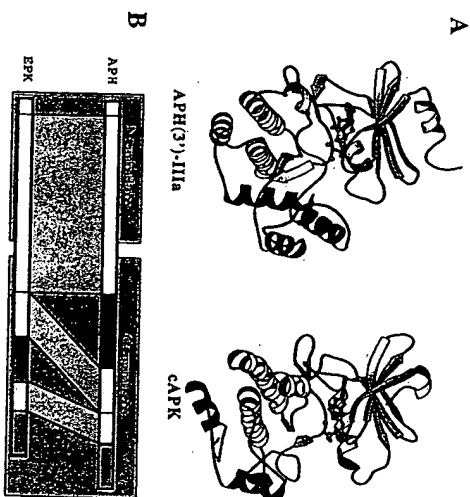


Figure 13. Structural similarity between *APH(3')-IIIa* and eukaryotic protein kinases. A) The structure of *APH(3')-IIIa* and the catalytic subunit of cyclic-AMP-dependent protein kinase (CAPK; Knight et al., 1995; PDB code 1ATP). Regions that differ are shown in darker shaded colors. B) A linear presentation of the enzymes, highlighting the structurally homologous sequences and the location of the insect's APH gene.

APH(3')-IIIa shows strong similarities to the classical eukaryotic protein kinase fold (e.g. Hubbard *et al.*, 1994; Knighon *et al.*, 1991; Owen *et al.*, 1995; Taylor *et al.*, 1992; Xu *et al.*, 1996; Zhang *et al.*, 1994). Specifically, the N-terminal domain and the core of the C-terminal domain, which combine to form the nucleotide-binding pocket, are essentially identical in the two types of structures. To illustrate this, in the N-terminal lobe, defined as residues 16–93, nearly 75% of the residues in APH(3')-IIIa are structurally identical to those in CAPK, with an r.m.s. deviation for main-chain atoms of less than 2 Å. For the core deviation is again less than 2 Å in comparison to CAPK (Fig. 13).

The availability of the three-dimensional structure for APH(3')-IIIa, the sequences of several related APH enzymes, the structures of several eukaryotic protein kinases, and additional sequences of serine/threonine and tyrosine protein kinases, allows for a structure-guided sequence alignment. Analysis of such an alignment will identify conserved residues, which in turn may provide insight into structure-function relationships for APH enzymes. In Fig. 14 and Table 7 such a sequence alignment and analysis are shown.

A few points from the structure-based sequence alignment analysis should be highlighted. The major differences between APHs and eukaryotic protein kinases are confined to the C-terminal lobe. Specifically, two regions can be identified which are fundamentally distinct between the two enzyme classes. First, the C-terminal end of the C-terminal lobe (from residue 233 onwards in both APH(3')-IIIa and CAPK) is folded differently in APH(3')-IIIa and protein kinases. Secondly, with respect to each other, both APHs and

Table 7. Role of strictly conserved residues in aminoglycoside phosphotransferases

Residue	Enzyme class	Role	Interactions observed in APH(3')-IIIa
Gly 23	APH(3') APH	role unknown	—
Ser 27	APH(3')	nucleotide binding	Ser27 OH - ADP O2B
Lys 44	APH(3') APH EPK	nucleotide binding	Lys44 NZ - ADP
Glu 60	APH(3') APH EPK	nucleotide binding	Glu60 OE1 & OE2 - Lys44 NZ
Trp 66	APH(3')	stability	side-chain packs against residue 130
Leu 67	APH(3')	stability	side-chain packs against residue 73
Pro 74	APH(3')	role unknown	—
Cys 130	APH(3')	stability	side-chain packs against residues 66 and 213
Pro 131	APH(3')	stability	—
Asp 153	APH(3')	substrate binding	electrostatic & H-bond (modeled)
His 188	APH(3') APH	stability	His188 NE2 - 207 O (H-bond)
Gly 189	APH(3')	stability	Gly189 CA packs against side-chain of residue 219
Asp 190	APH(3') APH EPK	stability	Asp190 OD1 - 188 N, Asp219 OD2 - 218 N
Asn 195	APH(3') APH EPK	nucleotide binding	Asp195 OD1 - Mg <sup>2+</sup>
Asp 208	APH(3') APH EPK	nucleotide binding	Asp208 OD1 & OD2 - Mg <sup>2+</sup>
Arg 211	APH(3')	nucleotide binding	H-bond (modeled)
Gly 213	APH(3')	substrate binding	Gly213 CA packs against residues 63 and 130
Ala 215	APH(3')	stability	Ala215 CB packs against side-chain of residue 219
Asp 216	APH(3')	stability	Asp219 OD1 - 183 N, Asp219 OD2 - 218 N
Asp 220	APH(3') EPK	stability	Asp220 OD1 - 188 N, Asp220 OD2 - H <sub>2</sub> O - 191 O
Leu 260	APH(3')	stability	side-chain packs against residues 136, 140, and 143
Asp 261	APH(3')	substrate binding	electrostatic & H-bond (modeled)
Glu 262	APH(3')	substrate binding	electrostatic & H-bond (modeled)

The extent of the conserved nature of the residue is indicated by whether it is only conserved in the APH(3') sub-family, or whether it is conserved in all aminoglycoside phosphorylating enzymes (APH), or if the residue is also conserved in eukaryotic protein kinase enzymes (EPK).



Figure 14. Protein sequence alignment of APHs and protein kinases. Boxed residues with white letters are either absolutely conserved (black background) or functionally conserved (grey background) within the APH(3') sub-family, the APH family or the protein kinase family of enzymes. Boxed residues which have a light-grey background are either absolutely or functionally conserved in another (sub-)family, or are frequently (>75%) in more than one (sub-)family. Some inserts are shown as boxes with the number indicating the position of residues in APH(3')-IIIa, and would likely display a different fold. Abbreviations: CAPK, cyclic-AMP-dependent protein kinase; CSK, casein kinase; MAPK, MAP kinase ERK2, Ptk, phosphorylase kinase.

protein kinases possess an insert. In APHs an insert is located in-between helix  $\alpha_4$  and strand  $\beta_6$ , in eukaryotic protein kinases an insert is positioned just before helix  $\alpha_5$  (Figs. 13 and 14). Although the conformation and location in the sequence differs between APHs and Ser/Thr/Tyr protein kinases, the positioning of these segments in the three-dimensional structure is similar. Both inserts are located in front of the nucleotide-binding pocket, ideally positioned to interact with substrates. In fact, it is well established that in eukaryotic protein kinases the insert is responsible for substrate specificity (Johnson *et al.*, 1996), and in many cases this insert also corresponds to the activation segments, i.e., it contains the sites of phosphorylation which transform the kinase from an inactive to an ac-

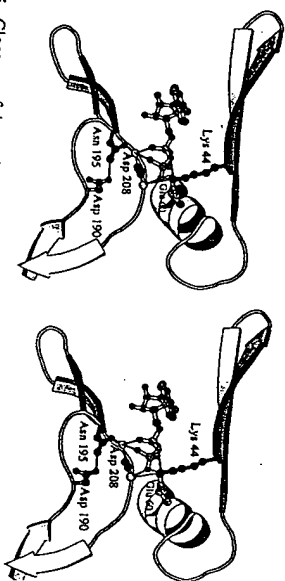


Figure 15. Close up of the active site of APH(3')-IIIa showing the five strictly conserved residues.

tive enzyme. Based on modeling studies (*vide infra*) it is likely that the APH insert is also involved in modulating substrate specificity.

Among APHs and eukaryotic protein kinases there are only five strictly conserved residues: Lys44, Glu60, Asp190, Asn195 and Asp208 (APH(3')-IIIa numbering). These five residues are all directly or indirectly involved in binding of the nucleotide, reflecting the structural similarity about the ATP-binding pocket between APHs and protein kinases (Fig. 15). Of these conserved residues, Asp190 is of particular interest, since this residue has been shown to be critical for catalysis in protein kinases (Cole *et al.*, 1995; Madhusudan *et al.*, 1994; Zhou and Adams, 1997). The importance of the active site Asp residue in APH(3')-IIIa (Hon *et al.*, 1997). The Asp190Ala enzyme was catalytically inactive, supporting a critical role for this residue and, based on precedent in protein kinases studies, it may be the active-site base required for deprotonation of the substrate hydroxyl group (Fig. 16). Thus, protein kinases and APH(3')-IIIa, and by inference all APHs, share a similar chemical mechanism for phosphoryl transfer.

Somewhat surprisingly, only two additional residues (beside the five residues discussed above) are conserved among all aminoglycoside phosphotransferases, namely Glu25 and His188. His188, as mentioned before, was previously postulated to be involved in catalysis, but mutagenesis studies have shown the residue to be important for protein stability (Thompson *et al.*, 1996a). The reason for the conserved nature of residue 25 is unclear from the three-dimensional structure of APH(3')-IIIa and additional studies will be required to elucidate its role.

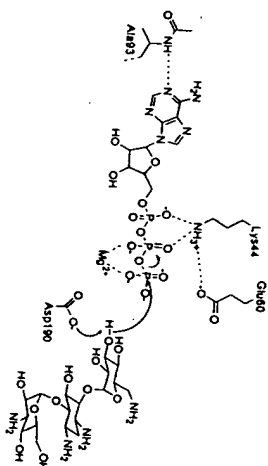
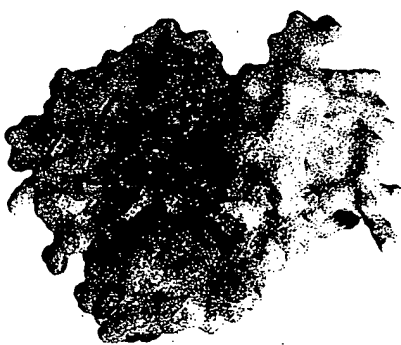


Figure 16. Proposed chemical mechanism of APH(3')-IIIa.

Figure 17. The negatively charged patch on the surface of APH(3')-IIIa. The surface of APH(3')-IIIa is shown. ADP monomer with darker shading corresponding to greater negative charge.



A structure of an aminoglycoside-APH(3')-IIIa complex is of particular interest for understanding the mechanism of aminoglycoside modification by this enzyme. Unfortunately, such a structure has so far remained elusive. The absence of this structural information does not, however, imply that nothing is known about the APH(3')-IIIa-aminoglycoside complex. Based on the required proximity of an aminoglycoside to Asp190 and the  $\gamma$ -phosphate group of ATP for catalysis, a limited area on the surface of APH(3')-IIIa was identified where antibiotic binding site was predicted to be located. This putative antibiotic binding site also corresponds exactly to a surface region with excessive negative charge, so as to provide favorable interactions with the positively charged antibiotics, analogous to what was seen for ANT(4') (Fig. 17). In APH(3')-IIIa the putative antibiotic binding site is lined with nine acidic residues (Asp104, Asp153, Asp155, Glu157, Asp190, Glu230, Asp231, Asp261, and Glu262) and only three basic residues (Arg139, Arg211, and Arg219); most of these residues are functionally highly conserved in the APH(3') family of enzymes (Fig. 14). Studies on modified aminoglycosides which have a reduced positive charge have shown the critical importance of electrostatics in binding of several aminoglycoside phosphorylating enzymes (discussed below; McKay *et al.*, 1996; Roes-tamaji *et al.*, 1995a). Note that several of the residues implicated in aminoglycoside binding are located on the "APH insert", suggesting that this region of the enzyme is involved in determining substrate specificity.

In addition to the location of the antibiotic-binding site, structural information is also available for aminoglycosides when bound to APH(3')-IIIa. The conformations of both amikacin (a 4,6-disubstituted aminoglycoside) and butyrosin A (a 4,5-disubstituted aminoglycoside) complexed to this enzyme have been examined by NMR (Cox *et al.*, 1996; Cox and Serspersu, 1997). The NMR analysis of amikacin suggests that the two torsion angles of the glycosidic linkage between the primed ring and the 2-deoxy streptamine ring of the aminoglycoside can take on a variety of values. This implies that all of the bound conformations are productive in terms of phosphoryl transfer, which might account for the significantly lower  $k_{\text{cat}}/K_m$  for this substrate (McKay *et al.*, 1994b).

The conformation of butyrosin A when bound to APH(3')-IIIa reveals that the primed and double-primed rings are in a stacking arrangement with both the 3'-OH and 5'-OH in close proximity to the  $\gamma$ -phosphate group of ATP. This is intriguing in that APH(3')-IIIa

can phosphorylate both of these hydroxyl groups. Furthermore, it was assumed that phosphorylation of 3' and 5' hydroxyl groups by APH(3')-IIa implied two distinct binding modes for butirosin. However, the NMR structure suggests that only one conformation of butirosin is present when bound to the enzyme and that this conformation allows either hydroxyl group to undergo phosphorylation.

The cumulative information on aminoglycoside binding to APH(3')-IIa is extensive and can be used to model the antibiotic-enzyme-ATP ternary complex. Efforts to achieve this objective are currently in progress (J.D.W. Swartzenhauer and A.M. Berghuis; unpublished results). However, it is clear that these modeling studies require additional mutagenesis studies in order to test specific interactions which are predicted between enzyme and substrate.

APH(3')-I is the most common APH expressed by Gram-negative bacteria. APH(3')-Ia has been purified to homogeneity from *E. coli* using a neomycin-Sepharose affinity column (Siregar et al., 1995). Analogous to APH(3')-IIa, the protein can exist as a dithiothreitol sensitive dimer or as a monomer. Kinetic parameters for a series of aminoglycosides and ATP have been determined and substrates give specificity rate constants,  $k_{cat}/K_m$  of  $10^6$ – $10^8$  M<sup>-1</sup>s<sup>-1</sup>, indicating a highly evolved and efficient catalyst (Siregar et al., 1995). Aminoglycosides yielding  $k_{cat}/K_m$  of  $10^6$  M<sup>-1</sup>s<sup>-1</sup> also showed lower MIC values ( $\leq 8$  µg/mL) while substrates with  $k_{cat}/K_m$  of  $10^7$ – $10^8$  M<sup>-1</sup>s<sup>-1</sup> gave rise to MICs of  $>1024$  µg/mL. This parallels studies with other aminoglycoside-resistance enzymes, notably APH(3')-IIIa (McKay et al., 1994b), ANT(2'') (Bongers and Molendijk, 1984; Dettengrath and Lerner, 1985), and AAC(6')-Ib (Radika and Northrop, 1984d). The biological significance of these observations is that aminoglycoside-modifying enzymes are optimally effective at low concentrations (sub  $K_m$ ) of antibiotic, a scenario which is ideally suited to a detoxifying mechanism. Steady-state kinetic analysis of APH(3')-Ia is consistent with a rapid equilibrium random mechanism and the regioselectivity of phosphoryltransfer to the 3'-hydroxyl of kanamycin was confirmed by <sup>1</sup>H, <sup>13</sup>C and <sup>31</sup>P NMR (Siregar et al., 1995). These efforts indicate that a similar direct-displacement mechanism for the  $\gamma$ -phosphoryl group of ATP to the aminoglycoside hydroxyl moiety is also possible in this case, such as indicated for the APH(3')-IIa, though the details of the mechanisms are slightly different.

In the absence of aminoglycosides, ATP is hydrolyzed with the following kinetic parameters by APH(3')-Ia:  $K_m = 49 \pm 1$  µM,  $k_{cat} = 0.023 \pm 0.002$  s<sup>-1</sup>,  $k_{cat}/K_m = 6.0 \times 10^5$  M<sup>-1</sup>s<sup>-1</sup> (Roestamadj et al., 1995a). The  $K_m$  values for ATP for the ATPase activity are in the same range as those for the phosphotransferase activity in phosphorylation of aminoglycosides. This observation indicates that binding of aminoglycoside does not influence the affinity of the enzyme for ATP. In light of the fact that the concentration of ATP in bacteria is typically 3.0–3.3 mM (Bochner and Ames, 1982; Findly et al., 1983), saturation is seen for this activity at any given time. Since APHs are expressed constitutively, it would appear that APH(3')s are constantly hydrolyzing ATP *in vivo* in the absence of any aminoglycoside [APH(3')-IIa though, does not have significant ATPase activity]. However, the value for  $k_{cat}$  is attenuated by as much as 4000-fold for the ATP hydrolase activity, hence the ATPase activity is not competitive with phosphorylation of aminoglycosides. Therefore, the enzyme phosphorylates amino-glycosides when these drugs are present, and it phosphorylates water ("ATPase" activity) when aminoglycosides are absent.

The APH(3')-Ia and the closely related APH(3')-Ic have also been respectively isolated from *E. coli* and *Klebsiella pneumoniae* and partially characterized (Lee et al., 1991). Enzymes were purified over neomycin-Sepharose and steady-state kinetic constants determined for several aminoglycosides and ATP. The  $K_m$  values were significantly higher than those determined by Siregar et al. (Siregar et al., 1995), but this is most likely

due to the use of the less reliable phosphocellulose binding assay rather than the more robust and accurate spectrophotometric continuous determination of ADP by coupling its release to pyruvate kinase and lactate dehydrogenase. Nevertheless, it is clear from these studies that APH(3')-Ia and Ic are closely related enzymes.

Overexpression of APH(3')-Ia has been implicated in resistance to tobramycin, an aminoglycoside which lacks a 3'-hydroxyl group (McNard et al., 1993). It has been suggested that while tobramycin is definitely not a substrate for APH(3')-I, it can be bound by the enzyme and thus overexpression effectively can act as a sequestering mechanism which results in low-level resistance. However, two facts have yet to be reconciled with this proposal. First, the dissociation constant from APH(3') is at best 0.1 µM, thus the ribosome has comparable or higher affinity for the antibiotic with more than one binding site (Le Goffic et al., 1979), and second, the concentration of tobramycin binding sites provided by APH(3') relative to the binding sites on ribosomes per cell needs to be considered. Should this mechanism prove valid, this augurs poorly for future development of novel aminoglycosides designed to avoid enzymic modification.

APH(3')-II differs from APH(3')-I in its ability to confer resistance to butirosin and lividomycin. The enzyme has been purified from *E. coli* and its substrate specificity determined (Siregar et al., 1994). Specificity rate constants,  $k_{cat}/K_m$ , were on the order of  $10^4$ – $10^5$  M<sup>-1</sup>s<sup>-1</sup> and a mutant enzyme, Glu182Asp, which had previously been reported (Yenofsky et al., 1990), has also been purified and characterized (Siregar et al., 1994). The  $K_m$  for ATP for this mutant was increased nine-fold over the wild-type enzyme implicating this residue in ATP binding. Comparison with the APH(3')-IIa three-dimensional structure shows that Glu182 is actually quite distant from the ATP-binding site, and thus the change in  $K_m$  is unexpected.

APH(3')-II is derived from transposon Tn5 (Beck et al., 1982) and has been the subject of several site-directed mutagenesis experiments which were performed before the availability of the three-dimensional structure of APH(3')-IIa to guide the efforts (Blázquez et al., 1991; Kocablyik and Perlin, 1992a,b, 1994). Most of these studies were confined to the conserved C-terminal region and demonstrated the importance of His188 and Asp190 among other residues. One mutant in the N-terminal region, Val36Met, resulted in a 20-fold decrease in kanamycin resistance, though the enzyme was not purified. Val36 corresponds to Val31 in APH(3')-IIa, which is located in the  $\beta$ -2 strand with the isopropyl side-chain lining the wall of the nucleotide-binding pocket, directly positioned above the ribose and  $\alpha$ -phosphate group. Based on the structure, it is evident that a larger side chain (like a Met) would be predicted to prevent binding of ATP to the enzyme.

Electrostatic effects (e.g., hydrogen bonding and ion pairing) are believed to be significant for interactions of the resistance proteins and aminoglycosides. These interactions, even at sites remote from the seat of the enzymic reaction within the expanded active-site region may have a stabilizing effect on the structure for the transition state for the reaction that the enzyme catalyzes. Based on these observations, we expected that the ammonium/amine functions in aminoglycosides should make relatively strong interactions with the active sites of the resistance enzymes. The exact nature of these interactions remains unknown at the present. However, we decided to prepare a series of individually deaminated analogues of aminoglycosides to evaluate the importance of these interactions with the active sites of APH(3')s. Toward that goal, several compounds were synthesized (Fig. 18). Compounds 1–4 are based on the structure of neamine and compounds 5–7 are based on the structure of kanamycin A, both of which are excellent substrates for APH(3')s. In essence, this was "mutagenesis" on the substrate, instead of the enzyme.



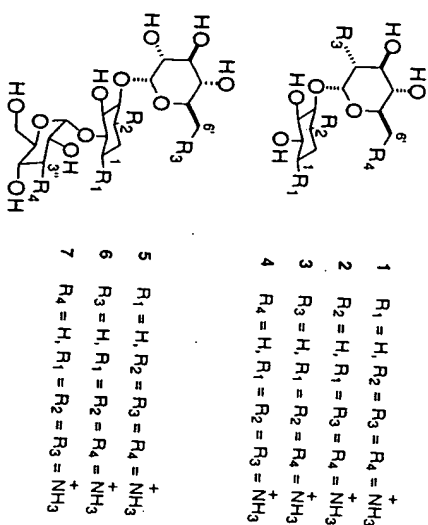


Figure 18. Deaminated aminoglycosides prepared for study of ionic interactions with APH(3')s. Derivatives of neamine 1-4 and kanamycin A 5-7 were prepared.

Turnover of compounds 1-7 was studied with purified APH(3')-IIa, APH(3')-IIa and APH(3')-IIa. Compounds 1-7 were all extremely poor substrates for both APH(3')-IIa and APH(3')-IIa (Roeslamadi et al., 1995a). This was an unexpected finding, which argued for the critical importance of electrostatic interactions with the amino-acid residues in the active site in the course of turnover. In general, the  $K_m$  values increased modestly compared to the corresponding values for the parent compounds (neamine and kanamycin A). Insofar as  $K_m$  may approximate  $K_d$ , this indicated that binding of the compounds to the enzyme active sites had not been affected much. The most significant effects were manifested on  $k_{cat}$  values. These values decreased significantly by as much as  $6 \times 10^5$ -fold. Our results indicate that the binding energies of the enzyme to the transition-state species are within the high range of 6-11 kcal/mol. To our knowledge, these examples are the strongest interactions recorded between an ammonium/amine moiety and a counterpart in an enzyme active site.

Surprisingly, when surveyed against APH(3')-IIa, an enzyme with broader substrate specificity and lower  $k_{cat}/K_m$  than APH(3')-IIa or -IIa, many of these deaminated compounds were relatively good substrates (McKay et al., 1996). Thus these enzymes, which perform similar functions and show significant amino acid sequence homology, interact with these compounds in dramatically different ways, an observation which provides a cautionary note for the development of broad specificity inhibitors of APHs based on aminoglycoside structure.

APH(3')-IV has been cloned from the butirosin producer *Bacillus circulans* (Herbert et al., 1986). The protein has been overexpressed in *E. coli* and purified using neomycin-Sepharose affinity chromatography. The regioselectivity of phosphate transfer to position 3' of ribosamine was confirmed by  $^1H$  and  $^{13}C$  NMR (Sarvar and Akhtar, 1990). The APH(3')-V enzymes have been cloned from aminoglycoside producing actinomycetes such as the neomycin producers *Streptomyces fradiae* (Thompson and Gray, 1993) and *Micromonospora chalybeata* (Saluza and Davies, 1991). The *aph(3')-Va* gene from *S. fradiae* is notable due to the lack of a 5'-leader sequence or ribosome binding site (Jones et al., 1992). The *aph(3')-VI* gene is found primarily in *Acinetobacter* spp. (Martin et al.,

1988) and the encoded protein is 54% similar to APH(3')-IIa, but lacks the capacity to confer resistance to the 3'-deoxyaminoglycoside lividomycin A. APH(3')-IV from *Campylobacter jejuni* shows the highest similarity to APH(3')-IIa (59%) and has a similar resistance phenotype differing only in resistance to amikacin (Tenover et al., 1988).

The findings reported in this section have significant implications for evolution of APH(3')s. At the present, it is not known from what primordial activity APH(3')s have evolved. In response to the challenge of aminoglycosides, the survival needs of bacteria would have favored selection of mutants in a primordial enzyme/protein such that it would have eventually acquired the new aminoglycoside-modifying (phosphorylating) activity. It would appear from our data with the deaminated compounds that evolution may have been geared in selection of mutations that would have recognized the amines of aminoglycosides as important determinants for this new activity. This is intuitively reasonable in light of the fact that the presence of amines in sugars is not so common, and would have permitted the ready specialization of these enzymes in the course of evolution.

*Aph(2')*. Gentamicin resistance in the Gram-positive cocci is almost exclusively the result of a bifunctional enzyme consisting of two domains with AAC(6')-Ie and APH(2')-Ia activities (Hodel-Christian and Murray, 1991; Kauffhold et al., 1992; Thal et al., 1993). The gene has been cloned from both *S. aureus* (Rough et al., 1987) and *E. faecalis* (Ferretti et al., 1986) where it is located on plasmid pIP800 or *Tn4001*, respectively. The predicted protein sequence indicated two distinct domains consisting of AAC(6') in the N-terminus and APH(2') in the C-terminus, a prediction that has been confirmed by truncated gene constructs (Ferretti et al., 1986) and overexpression and purification of the individual domains from *E. coli* constructs (D. Daigle and G. Wright; unpublished results). The enzyme has been purified from *S. aureus* and *S. epidermidis* (Ubukata et al., 1984) as well as from expressing constructs in *E. coli* (Azucena et al., 1997) and *B. subtilis* (D. Daigle and G. Wright; unpublished results). The kinetic mechanisms of both activities have been determined to be random rapid equilibrium (Marlet et al., 1983). The individually acetylated and phosphorylated aminoglycosides kanamycin (Azucena et al., 1997) and arbekacin (Kondo et al., 1993) have been purified and characterized by  $^1H$  and  $^{13}C$  NMR as well as doubly modified products, supporting unequivocally the predicted regioselectivity of group transfer as well as demonstrating that both phosphoryl and acetyl transfer can occur on one aminoglycoside molecule. It is perhaps this fact which is responsible for the very high MIC values ( $>1,000$  mg/mL) regularly determined from clinical isolates. The purified enzyme shows a very broad capacity for aminoglycoside phosphorylation and acetylation with virtually all the 2-deoxystreptamine antibiotics serving as substrates. Among the substrates studied by Azucena et al. (1997) for this enzyme, all showed considerably better ability to undergo phosphorylation than acetylation. Consistent with these determinations, kanamycin A was shown to undergo phosphorylation exclusively in *in vivo* experiments (Azucena et al., 1997).

In addition, the AAC(6')-Ie acetylates fortimicin, a unique feature of this AAC(6'), though this is not a substrate for the APH(2') (Shaw et al., 1993; D. Daigle and G. Wright; unpublished results). The AAC(6') activity is not confined to N-acetylation, and the 6'-hydroxyl aminoglycosides, paromomycin and lividomycin A, are in fact substrates with  $k_{cat}/K_m$  of  $10^3$  M $^{-1}$ s $^{-1}$ , lower than 6'-amino compounds ( $k_{cat}/K_m$  of  $10^4$ - $10^5$  M $^{-1}$ s $^{-1}$ ), but significant nonetheless (D. Daigle and G. Wright; unpublished results). The acetylated products are highly susceptible to base hydrolysis, consistent with 6'-O-acetylation which is an activity which is so far unique to this enzyme.



Initially, AAC(6)-APH(2") was thought to be found only in Gram-positive organisms. However, Ketner *et al.* (1991) have recently detected this enzyme in Gram-negative bacteria as well. This alarming report demonstrates the ability of a plasmid-encoded Gram-positive gene to be transferred and expressed in Gram-negative bacteria, whereby the resistance phenotype is disseminated to other less-related bacterial strains. The fact that this bifunctional enzyme is devastatingly effective at aminoglycoside modification heightens the importance of this observation.

A recently isolated gene from *Enterococcus gallinarum* encodes a protein with high homology (53% similar) to the N-terminus of the bifunctional AAC(6)-APH(2") enzyme and has a resistance profile consistent with APH(2") (Chow *et al.*, 1997). This observation along with the recent isolation of the *aac(6)-I* gene from *E. coli* (Shaw, 1997) which encodes an AAC(6)-Ie homologue, supports the proposal (Ferretti *et al.*, 1986) that the bifunctional enzyme has arisen as a consequence of a gene fusion event.

*Aph(4)* and *Aph(7)*. Resistance to the aminoglycoside hygromycin B is frequently used as a marker for eukaryotic and bacterial cell culture studies. The gene responsible for this resistance is *aph(4)*, which was originally cloned from an *E. coli* isolate (Griz and Davies, 1983). The gene encodes a protein of predicted mass of 39 kDa and the site of hygro-mycin phosphorylation has been determined by <sup>1</sup>H and <sup>13</sup>C NMR (Rao *et al.*, 1983).

The hygromycin producer *Streptomyces hygroscopicus* also produces a phosphorylating enzyme, but the site of modification is the 7"-hydroxyl (Pardo *et al.*, 1985). The gene encoding the enzyme has been cloned (Zalacain *et al.*, 1986), expressed in *E. coli* (Zalacain *et al.*, 1987a), and the protein purified to homogeneity over a hygromycin-Sepharose column (Zalacain *et al.*, 1987b). The *K<sub>m</sub>* for ATP was determined to be 36.4 µM and for hygromycin 0.56 µM. The protein migrates as a 41-kDa monomer by gel filtration (Pardo *et al.*, 1985).

*Aph(3")* and *Aph(6)*. APH(3") and APH(6)s are streptomycin selective kinases. The tandem genes, *strA-strB*, respectively, encode APH(3")-Ib and APH(6)-Id (Shaw *et al.*, 1993). The *strA-strB* cassette is found on Gram-negative broad host range plasmids such as RSF1010 (Scholz *et al.*, 1989) and transposons and is widely distributed in the environment (Sundin and Bender, 1996).

Similarly, the streptomycin-producing organism *Streptomyces griseus*, also encodes both an APH(3") and APH(6) (Distler *et al.*, 1987; Heinzel *et al.*, 1988). The *aphD* gene encodes the APH(6) enzyme and is clustered with aminoglycoside biosynthesis genes in *S. griseus* (Distler *et al.*, 1987) and in *Streptomyces glaucescens* (Vogtli and Hutter, 1987) which also produces streptomycin. On the other hand, the *aphE* gene encodes the APH(3"), which is not associated with streptomycin biosynthetic genes.

*Aph(9)*. A spectinomycin phosphotransferase gene has been cloned from *Legionella pneumophila*, the bacterium responsible for Legionnaire's disease (Suter *et al.*, 1997). Initial enzyme assays have shown that the enzyme is specific to spectinomycin. This has been confirmed with purified enzyme from an *E. coli* overexpression construct (P. Thompson, D.W. Hughes, N.P. Cianciotto, & G. Wright; unpublished results). Spectinomycin is an excellent substrate with *k<sub>cat</sub>/K<sub>m</sub>* of 10<sup>6</sup> M<sup>-1</sup>s<sup>-1</sup>, other aminoglycosides such as phospho-spectinomycin, followed by <sup>1</sup>H, <sup>13</sup>C and <sup>31</sup>P NMR have shown that the hydroxyl group at position 9 is the site of phosphoryl transfer, thus we propose that the enzyme should be designated APH(9)-Ia.

A gene encoding a spectinomycin specific APH, *specN*, has also been cloned from the spectinomycin producer *Streptomyces flavopersicus* (Lyuzkanova *et al.*, 1997). The predicted amino-acid sequence is not similar to APH(9) from *L. pneumophila*. The site of phosphorylation was predicted to be at either one or both hydroxyls at positions 7 or 9, though based on the precedents of adenylation and phosphorylation of position 9 noted above, it is likely that this enzyme is also an APH(9).

### Inhibition of Aminoglycoside-Modifying Enzymes

Inhibition studies of aminoglycoside-modifying enzymes can be divided into two groups, those which are aminoglycoside-based inhibitors, and non-aminoglycoside inhibitors. Inhibition of many modifying enzymes by aminoglycosides is well established. Thus, tobramycin and dibekacin, 3'-deoxy aminoglycosides, are competitive inhibitors of kanamycin modification by APH(3") with *K<sub>i</sub>* < 1 µM (McKay and Wright, 1995). Similarly, paromomycin and lividomycin A, both 6'-hydroxy aminoglycosides, are competitive inhibitors of kanamycin 6'-N-acetyltransfer catalyzed by AAC(6)-II with *K<sub>i</sub>* of 1.06 µM and 0.50 µM, respectively (Wright and Ladak, 1997). 6'-Methyl-derivatives of kanamycin have also been shown to be effective antibiotics against strains bearing *aac(6)* genes (Umezawa *et al.*, 1972). Inhibition of modifying enzymes by aminoglycosides generally has the potential added benefit that the inhibitors themselves may function as antibiotics.

Williams and Northrop prepared 3-N-chloroacetyl-CoA by incubation of β-chloroacetyl-CoA, gentamicin C1a and AAC(3)-I (Williams and Northrop, 1979). The chloroacetylated aminoglycoside was reacted *in situ* with CoASH to form a bisubstrate analogue which was purified, partially characterized, and used in inhibition studies of AAC(3)-I (Fig. 19A). This compound was a time-dependent enzyme inhibitor with a *t<sub>1/2</sub>* for the regain of activity of 34 min and a *K<sub>i</sub>* of 0.5–2 nM, but could not reverse antibiotic resistance in an *E. coli* strain bearing the *aac(3)-I* gene, probably due to difficulty in transport across cell membranes. However, this study did demonstrate the feasibility and potential of the use of compounds with multisubstrate character as potent inhibitors of aminoglycoside-modifying enzymes.

A series of four regioselectively synthesized N-bromoacetylated neamine derivatives have been prepared recently. All these compounds served both as substrates and affinity inactivators for APH(3")-IIa (Roestamadjii and Mobashery; unpublished results). The sites of protein modifications were identified by mass-spectroscopic analyses of the proteolytic fragments in an effort to map the active site.

Mechanism-based inactivation of APH(3")-I and APH(3")-II by synthetic aminoglycoside analogues has been reported (Roestamadjii *et al.*, 1995b). Two compounds were synthesized, 8 and 9 (Fig. 20A), with a nitro group at position 2'. Phosphoryl transfer to the 3'-hydroxyl results in the positioning of a phosphate group β to the 2'-nitro group. This compound can readily undergo elimination of phosphate generating an electrophilic nitroalkene in the active site of the enzyme (Fig. 19B). This highly reactive compound is then postulated to alkylate susceptible amino acid side chains resulting in irreversible enzyme inactivation. Unfortunately, these compounds have not been found to be effective in reversing antibiotic resistance, but they provide the necessary precedent for the synthesis of additional analogues which may be more effective in this regard.

The similarity between APH(3") and protein kinases prompted a survey of known protein kinase inhibitors as potential inhibitors of APHs (Daigle *et al.*, 1997). The indole carbazole, staurosporine, a potent inhibitor of protein kinase C, as well as ebsastin and typhostin analogues, which are known inhibitors of tyrosine protein kinases, did not in-

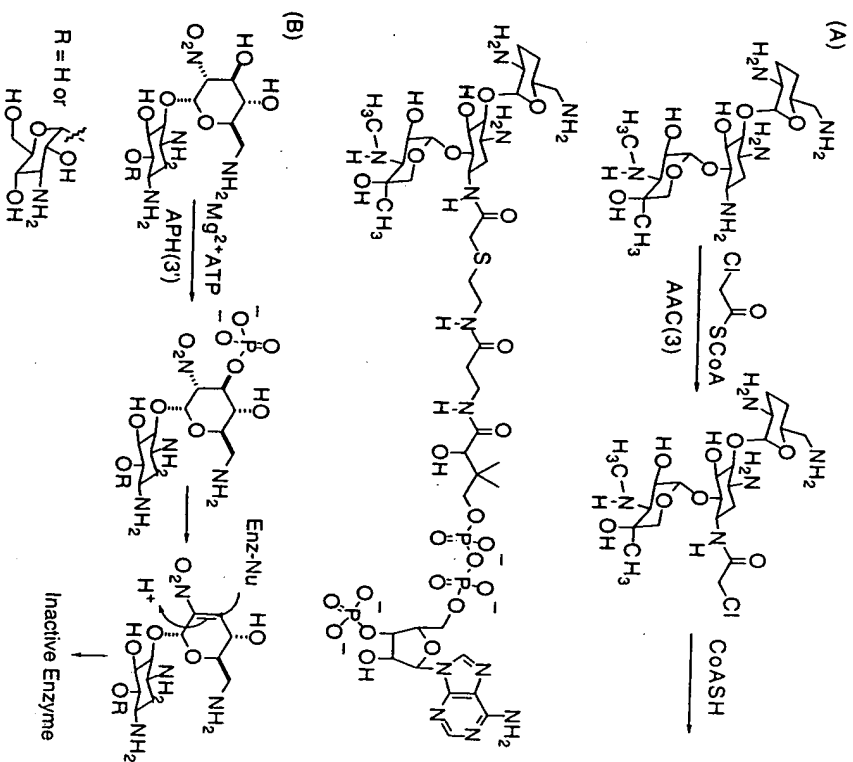


**Figure 19.** Inhibition of aminoglycoside-modifying enzymes. (A) Synthesis of bifunctional inhibitor of AAC(3). (B) Mechanism-based inactivation of APH(3) by 2'-deamino-2'-nitro aminoglycosides.

hibit APH(3)-IIa or AAC(6')-APH(2'') (Daigle *et al.*, 1997; G. McKay, D. Daigle and G. Wright, unpublished results). On the other hand, the protein kinase inhibiting flavonoids, genestein and quercetin (Fig. 20B), were inhibitors of APH(3'), but not AAC(6')-APH(2'') (Daigle *et al.*, 1997). The most potent dual protein kinase/APH inhibitors were the isouinolinesulfonamides of the H and CKI series (Fig. 20B). Several of these compounds gave  $K_i$  values below 100  $\mu$ M for both APH(3')-IIa and AAC(6')-APH(2'') (Daigle *et al.*, 1997). Inhibition was competitive with ATP and non-competitive against kanamycin. None of the compounds tested were able to reverse aminoglycoside resistance in bacterial cells harboring either the *aph(3')-IIa* or *aac(6')-aph(2'')* genes. However, this initial study augurs well for the synthesis of potent APH-directed compounds which incorporate the isouinolinesulfonamide nucleus. The fact that many pharmaceutical companies have been active in the synthesis of protein kinase inhibitors suggests that among these, potent inhibitors of APHs already exist.

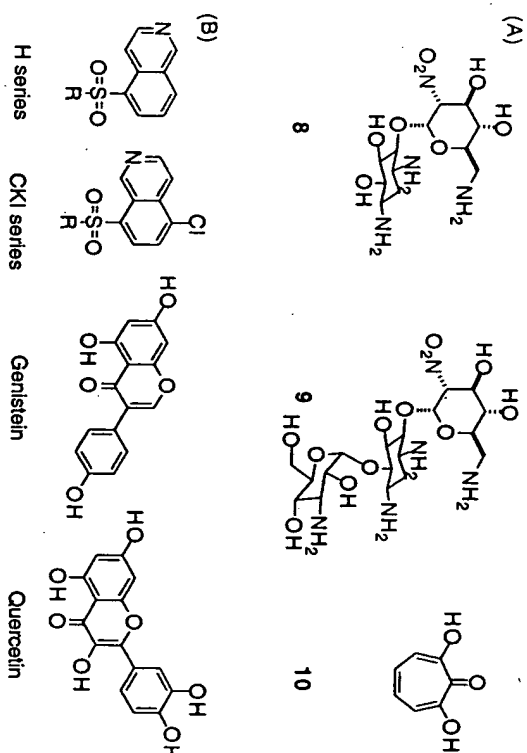


**Figure 20.** Inhibitors of aminoglycoside-modifying enzymes. (A) Compounds which inhibit aminoglycoside-modifying enzymes exclusively. (B) Protein kinase inhibitors which inhibit APHs.

7-Hydroxytropolone (compound 10, Fig. 20A), a natural product produced by *Streptomyces neyagawaensis*, has been shown to be an inhibitor of ANT(2'') (Allen *et al.*, 1982). Inhibition was competitive with ATP ( $K_i = 10 \mu$ M), and either non- or un-competitive with respect to tobramycin. Several analogues of the lead compound were also found to have inhibitory activity, though only one of these, 4-isopropyl-7-hydroxytropolone, was comparable in potency to 7-hydroxytropolone. This compound did reverse tobramycin resistance in *E. coli* harbouring the *ant(2'')* gene, but not in cells with other aminoglycoside-modifying enzymes. This study provides valuable proof of concept for the use of inhibitors of aminoglycoside-modifying enzymes as a means of combating antibiotic resistance, in much the same fashion as  $\beta$ -lactamase inhibitors are clinically used to rescue the usefulness of  $\beta$ -lactam antibiotics (Sutherland, 1991).

## Origin of Aminoglycoside-Modifying Enzymes

The variety and widespread dissemination of aminoglycoside resistance genes suggests that they have arisen from several different sources. Some genes are probably fortuitously resistance determinants; e.g., the chromosomal *aac(2')* from *P. stuartii* and *Mycobacterium* (Table 5), however, the majority of resistance genes are found on mobile genetic elements and undoubtedly have evolved specifically for the detoxification of aminoglycosides. A likely source for these genes are the aminoglycoside-producing organisms, a hypothesis put forth some 25 years ago by Benveniste and Davies who noted the similarities between aminoglycoside resistance enzymes expressed by clinical isolates and those found in antibiotic-producing organisms (Benveniste and Davies, 1973). Indeed, several *aac(3)* and *aph* genes have been cloned and sequenced from aminoglycoside-producing bacteria in the interim (Tables 5 and 6). Thus, these organisms are probably the reservoir for these genes where they are associated with self-resistance, although some of the genes

are not clustered within the biosynthetic gene cluster; e.g. *aac(3)-VIII* from *S. fradiae* (Thompson et al., 1980) and their origins are therefore cryptic.

The origin of other resistance genes such as the members of the *aac(6)* and *ant* families is less obvious in that no aminoglycoside producer has yet been shown to harbor either of them. There are a few known chromosomal *aac(6)*'s e.g. *aac(6)-Ic* and *Ii*, and it is possible that the other *aac(6)* genes have evolved from similar chromosomal elements. The fact that purified *AAC(6)-II* is a relatively poor aminoglycoside acetyltransferase (Wright and Ladak, 1997) suggests another function for this enzyme, and should one be found, it may point to a common origin for these enzymes. Protein sequence analysis has shown modest similarities between AACs and other bacterial acetyltransferases such as Rim I, Rim J, Rim L, CysE and LacA, and one (or several) of these may be an ancestor (Peipersberg et al., 1988, 1991).

The ANTs, as noted above, share a common protein fold with enzymes which catalyze nucleotidyltransfer, and thus such genes may be the origin of *ants*.

The three-dimensional structure of APH(3')-IIIa (Hon et al., 1997) has dramatically expanded on the observations (Brenner, 1987; Martin et al., 1988), most extensively described by Peipersberg's group (Heinzel et al., 1988), that APHs and protein kinases share regions of amino acids sequence similarity (Fig. 13 and 14). The fact that APH(3')-IIIa and protein kinases share a similar chemical mechanism and sensitivity to inhibitors suggests a close evolutionary link between these classes of enzymes. APHs also demonstrate measurable serine protein kinase activity (D. Daigle, G. McKay, G. Wright; unpublished results). Purified APH(3')-IIIa and *AAC(6)-APH(2)* were shown to phosphorylate several common protein kinase substrates including myelin basic protein and protamine. Actinomycetes and other bacteria encode Ser/Thr protein kinases (reviewed in Kennelly and Potts, 1996; Zhang, 1996), thus these are a potential source of APHs.

## SIDE EFFECTS OF AMINOGLYCOSIDE ANTIBIOTICS

From the outset of their use as antibacterial agents, it has been known that aminoglycosides are associated with significant oto and nephrotoxicity (e.g., Hinshaw and Feldman, 1945). The severity of these effects is dependent on the nature of the aminoglycoside structure, and thus less toxic compounds are clinically used in place of for example, neomycin, which shows significant toxicity. In addition, monitoring of serum levels of aminoglycosides and once daily dosing has decreased the incidences of hearing loss as a result of aminoglycoside therapy. The details of the molecular mechanisms of the ototoxic side effects remains elusive despite much activity in the area.

Aminoglycosides are eliminated from the body virtually exclusively by glomerular filtration, thus the kidney is exposed to high levels of these antibiotics (Ali, 1995). The suggestion that a P-450-derived metabolite may be involved in toxicity (Crann et al., 1992) in both the kidney and the ear remains controversial (Sanders et al., 1993). Aminoglycosides are taken up by tubule cells on the brush border of the glomerulus and accumulate in lysosomes (Nasberger et al., 1990). Several studies have demonstrated pleiotropic effects of aminoglycosides, gentamicin in particular, on renal tissue; these include increased production of hydrogen peroxide, increase in the rate of phospholipidosis, inhibition of Na<sup>+</sup>/K<sup>+</sup>-ATPase, injury to organelles such as mitochondria and lysosomes, increase in thromboxane A<sub>2</sub> and inhibition of protein synthesis (reviewed in Ali, 1995). A unifying feature in most of these effects, which parallels the findings in bacteria, is membrane damage.

Ototoxicity appears to be the result of specific toxicity to the outer hair cells (reviewed in Schacht, 1993). It has been proposed that a mechanism of toxicity is related to aminoglycoside affinity for phosphatidylinositol-4,5-bisphosphate and inhibition of ornithine decarboxylase (reviewed in Schacht, 1993) though it is not clear how these effects may result in the specificity of toxic effects. Hypersensitivity to aminoglycoside induced ototoxicity has also been shown to be associated with a A→G transition in the mitochondrial 12S rRNA of susceptible individuals (Coropassi and Hutchin, 1994; Hutchin and Coropassi, 1994). A model has been proposed in which this mutation results in mistranslation of mitochondrially encoded proteins such as complex I, which results in an increase in superoxide production and oxidative damage resulting in apoptosis (Coropassi and Hutchin, 1994; Hutchin and Coropassi, 1994). Aminoglycosides are also known to activate phospholipase C and this activity may also contribute to toxicity (Morris & Mensa-Wilmon, 1997).

Pruska and Schacht (1995) have shown recently that gentamicin has the ability to chelate iron ions and the complex can promote formation of free radicals effectively. These radicals are believed to be involved in adventitious reactions, which lead to adverse oto and renal toxicity. The same group showed subsequently that free-radical scavengers and iron chelators can prevent ototoxicity in experiments performed in guinea pigs, indicating the clinical promise for combination therapy of aminoglycosides in conjunction with these agents to overcome the toxicity of these versatile antibacterials (Song and Schacht, 1996).

## CONCLUSIONS AND FUTURE DIRECTIONS

The rise of resistance to the aminoglycosides over the past several decades and the development of newer broad spectrum antibacterial agents has resulted in the marginalization of these potent antibiotics. The vast array of resistance enzymes and the mobilization of their corresponding genes would appear to prohibit significant new uses for these drugs. However, since there are only three general mechanisms of resistance: adenylation, acetylation and phosphorylation, and given the importance of discovering new antibiotics in the face of the growing crisis of antibiotic resistance, the aminoglycosides should be seriously reconsidered as antibiotics of choice. The development and clinical implementation of inhibitory compounds targeted to modifying enzymes which could rescue the use of aminoglycosides is not unreasonable. The recent advances in the knowledge of the molecular mechanisms and structure of aminoglycoside resistance enzymes has provided the basis for rational inhibitor design and has already resulted in modest success. Continued efforts in this area will provide additional knowledge which is critical for the development of new antibacterial agents and may result in a new era of wide spread use of these potent bactericidal agents.

## ACKNOWLEDGMENTS

The work described from the authors' laboratories was funded by the Medical Research Council of Canada (A.M.B. and G.D.W.) and by the National Institutes of Health (S.M.). We thank members of the Wright laboratory and Lakshmi Kotra of the Mobashery laboratory for critical reading of the manuscript.

## REFERENCES

- Ainsa, J.A., Pérez, E., Pellicio, V., Berthel, F.X., Gicquel, B. and Martin, C., 1997. Aminoglycoside 2'-N-acetyltransferase genes are universally present in mycobacteria: characterization of the *aac(2)-Ic* gene from *Mycobacterium tuberculosis* and the *aac(2)-IId* gene from *Mycobacterium mageritense*. *Mol. Microbiol.* 24:431-441.
- Ali, B.H., 1995. Gentamicin nephrotoxicity in humans and animals: some recent research. *Gen. Pharmacol.* 26:147-1487.
- Allen, N.E., Jr., W.E.A., Jr., J.N.H. and Kirst, H.A., 1982. 7-Hydroxytropolone: An inhibitor of aminoglycoside 2'-O-acetyltransferase. *Antimicrob. Agents Chemother.* 22:824-831.
- Azcuna, E., Grapass, I. and Mobashery, S., 1997. Properties of a bifunctional bacterial antibiotic resistance enzyme that catalyzes ATP-dependent 2'-phosphorylation and acetyl-CoA-dependent 6'-acetylation of aminoglycosides. *J. Am. Chem. Soc.* 119:2317-2318.
- Bakker, E.P., 1992. Aminoglycoside and aminocyclitol antibiotics: hygromycin B is an atypical bactericidal compound that exerts effects on cells of *Escherichia coli* characteristic for bacteriostatic aminocyclitols. *J. Gen. Microbiol.* 138:563-569.
- Beauleck, A.A. and Cundliffe, E., 1987. Sites of action of two ribosomal RNA methylases responsible for resistance to aminoglycosides. *J. Mol. Biol.* 93:661-671.
- Beck, E., Ludwig, G., Auerwald, E.A., Reiss, B. and Schaller, H., 1982. Nucleotide sequence and exact localization of the neomycin phosphotransferase gene from transposon *Tr5*. *Gene* 19:327-336.
- Benveniste, R. and Davies, J., 1973. Aminoglycoside antibiotic-inactivating enzymes in actinomycetes similar to those present in clinical isolates of antibiotic-resistant bacteria. *Proc. Natl. Acad. Sci. U.S.A.* 70:2276-2280.
- Berman, J.D. and Fleckenstein, L., 1991. Pharmacokinetic justification of antiparasitic therapy: A US perspective. *Clin. Pharmacokinet.* 21:479-493.
- Blázquez, J., Davies, J. and Moreno, F., 1991. Mutations in the *aphA-2* gene of transposon *Tr5* mapping within the regions highly conserved in aminoglycoside-phosphotransferases strongly reduce aminoglycoside resistance. *Mol. Microbiol.* 5:1511-1518.
- Bochner, B.R. and Ames, B.N., 1982. Complete analysis of cellular nucleotides by two-dimensional thin layer chromatography. *J. Biol. Chem.* 257:9759-9769.
- Bongaerts, G.P.A. and Molendijk, L., 1984. Relation between aminoglycoside 2'-O-nucleotidyltransferase activity and aminoglycoside resistance. *Antimicrob. Agents Chemother.* 25:224-237.
- Bräu, B. and Piepersberg, W., 1985. Purification and characterization of a plasmid-encoded aminoglycoside 3'-N-acetyltransferase IV from *Escherichia coli*. *FEBS Lett.* 185:43-46.
- Bräu, B., Pilz, U. and Piepersberg, W., 1984. Genes for gentamicin-(3)-N-acetyltransferases III and IV. I. Nucleotide sequence of the *AAC(3)-IV* gene and possible involvement of an IS140 element in its expression. *Mol. Gen. Genet.* 193:179-187.
- Brenner, S., 1987. Phosphotransferase sequence homology. *Nature* 329:21.
- Bryan, L.E. (1984). Aminoglycoside resistance. in *Antimicrobial Drug Resistance* (L. E. Bryan, Ed.) pp 241-277. Academic Press, Orlando.
- Bryan, L.E. and Kwan, S., 1983. Roles of ribosomal binding, membrane potential, and electron transport in bacterial uptake of streptomycin and gentamicin. *Antimicrob. Agents Chemother.* 23:835-845.
- Bryan, L.E. and Van Den Elzen, H.M., 1977. Effects of membrane-energy mutations and cations on streptomycin and gentamicin accumulation by bacteria: a model for entry of streptomycin and gentamicin in susceptible and resistant bacteria. *Antimicrob. Agents Chemother.* 12:163-177.
- Busse, H.-J., Wörmann, C. and Bakker, E.P., 1992. The bactericidal action of streptomycin: membrane permeabilization caused by the insertion of mistranslated proteins into the cytoplasmic membrane of *Escherichia coli* and subsequent caging of the antibiotic inside the cells due to degradation of these proteins. *J. Gen. Microbiol.* 138:551-561.
- Chow, J.W., Zervos, M.J., Lerner, S.A., Thal, L.A., Donabedian, S.M., Jaworski, D.D., Tsai, S., Shaw, K.J. and Clewell, D.B., 1997. A novel gentamicin resistance gene in *Enterococcus faecalis*. *Antimicrob. Agents Chemother.* 41:511-514.
- Clarke, A.J., 1993. Extent of peptidoglycan O acetylation in the ribe-Protease. *J. Bacteriol.* 175:4550-4553.
- Clarke, A.J., Francis, D. and Kienle, W.J., 1996. The prevalence of gentamicin 2'-N-acetyltransferase in the protease and its role in the O-acetylation of peptidoglycan. *FEBS Microbiol. Lett.* 145:201-207.
- Cole, P.A., Grace, M.R., Phillips, R.S., Burn, P. and Walsh, C.T., 1995. The role of the catalytic base in the protein tyrosine kinase Csk. *J. Biol. Chem.* 270:22105-22108.
- Corrassini, G. and Hutchin, T., 1994. A molecular and cellular hypothesis for aminoglycoside-induced deafness. *Hear. Res.* 78:27-30.
- Costa, Y., Galland, M., Leclercq, R., Duval, J. and Courvalin, P., 1993. Characterization of the chromosomal *aac(6)-Ii* gene specific for *Enterococcus faecium*, *Antimicrob. Agents Chemother.* 37:1896-1903.
- Cox, J.R., McKay, G.A., Wright, G.D. and Serepau, E.H., 1996. Arrangement of substrates at the active site of an aminoglycoside antibiotic 3'-phosphotransferase as determined by NMR. *J. Am. Chem. Soc.* 118:1295-1301.
- Cox, J.R. and Serepau, E.H., 1997. Biologically important conformations of aminoglycoside antibiotics bound to an aminoglycoside 3'-phosphotransferase as determined by transferred nuclear Overhauser effect spectroscopy. *Biochemistry* 36:2253-2259.
- Cram, S.A., Huang, M.Y., McLaren, J.D. and Schacht, J., 1992. Formation of a toxic metabolite from gentamicin by a hepatic cytosolic fraction. *Biochem. Pharmacol.* 43:1835-1839.
- Cundliffe, E., 1987. On the nature of antibiotic binding sites in ribosomes. *Biochimie* 69:863-869.
- Daigle, D.M., McKay, G.A. and Wright, G.D., 1997. Inhibition of aminoglycoside antibiotic resistance enzymes by protein kinase inhibitors. *J. Biol. Chem.* 272:24755-24758.
- Davis, B.D., 1987. Mechanism of action of aminoglycosides. *Microbiol. Rev.* 51:341-350.
- Davis, B.D., Chen, L.L. and Tai, P.C., 1986. Mistrad protein creates membrane channels: an essential step in the bactericidal action of aminoglycosides. *Proc. Natl. Acad. Sci. U.S.A.* 83:6164-6168.
- DeHertogh, D.A. and Lerner, S.A., 1985. Correlation of aminoglycoside resistance with  $K_m$  and  $V_{max}/K_m$  ratios of enzymatic modification of aminoglycosides by 2'-O-nucleotidyltransferase. *Antimicrob. Agents Chemother.* 27:670-671.
- DiGiambardino, E.L., Drake, K.A., Wright, G.D. and Serepau, E.H., 1997. Solution studies of isepamicin and conformational comparisons between isepamicin and butirosin A when bound to an aminoglycoside 6-N-acetyltransferase determined by NMR spectroscopy. *Biochemistry* in press.
- Disler, J., Braun, C., Ebert, A. and Piepersberg, W., 1987. Gene cluster for streptomycin biosynthesis in *Streptomyces griseus*: analysis of a central region including the major resistance gene. *Mol. Gen. Genet.* 208:204-210.
- Dubin, D.T. and Davis, B.D., 1961. The effect of streptomycin on potassium flux in *Escherichia coli*. *Biochim. Biophys. Acta* 52:400-402.
- Edson, R.S. and Terrell, C.L., 1991. The aminoglycosides. *Mayo. Clin. Proc.* 66:158-164.
- Ferreit, J.J., Gilmore, K.S. and Courvalin, P., 1986. Nucleotide sequence analysis of the gene specifying the bifunctional 6'-aminoglycoside acetyltransferase 2'-aminoglycoside phosphotransferase enzyme in *Streptococcus faecalis* and identification and cloning of gene regions specifying the two activities. *J. Bacteriol.* 167:631-638.
- Fichtenbaum, C.J., Ritchie, D.J. and Powderly, W.G., 1994. Use of paromomycin for treatment of cryptosporidiosis in patients with AIDS. *Clin. Infect. Dis.* 16:298-300.
- Findly, R.C., Gillies, R.J. and Shulman, R.G., 1983. *In vivo* phosphorus-31 nuclear magnetic resonance reveals lowered ATP during heat shock of *Tetrahymena*. *Science* 219:1223-1225.
- Fourny, D., Reeth, M.L., Blanchard, S.C. and Puglisi, J.D., 1996. Structure of the A site of *Escherichia coli* 16S ribosomal RNA complexed with an aminoglycoside antibiotic. *Science* 274:1367-1371.
- Gates, C.A. and Northrop, D.B., 1988a. Alternative substrate and inhibition kinetics of aminoglycoside nucleotidyltransferase 2'-I in support of a Theorell-Chance kinetic mechanism. *Biochemistry* 27:3826-3833.
- Gates, C.A. and Northrop, D.B., 1988b. Determination of the rate-limiting segment of aminoglycoside nucleotidyltransferase 2'-I by pH- and viscosity-dependent kinetics. *Biochemistry* 27:3834-3842.
- Gates, C.A. and Northrop, D.B., 1988c. Substrate specificities and structure-activity relationships for the nucleotidyltransferase of antibiotics catalyzed by aminoglycoside nucleotidyltransferase 2'-I. *Biochemistry* 27:3820-3825.
- Gilman, S. and Saunders, V.A., 1986. Accumulation of gentamicin by *Staphylococcus aureus*: the role of the transmembrane electrical potential. *J. Antimicrob. Chemother.* 17:37-44.
- Gorini, L. (1974). Streptomycin and misreading of the genetic code. in *Ribosomes* (M. Nomura, A. Tissières and P. Lengyel, Eds) pp 791-803. Cold Spring Harbor Laboratory, Cold Spring Harbor, NY.
- Gray, G.S. and Fitch, W.M., 1993. Evolution of antibiotic resistance genes: The DNA sequence of a kanamycin resistance gene from *Staphylococcus aureus*. *Mol. Biol. Evol.* 10:37-46.
- Gritz, L. and Davies, J., 1983. Plasmid-encoded hygromycin B resistance: the sequence of hygromycin B phosphotransferase gene and its expression in *Escherichia coli* and *Saccharomyces cerevisiae*. *Gene* 25:179-188.
- Hancock, R., 1961. Early effects of streptomycin on *Bacillus megaterium*. *J. Bacteriol.* 88:633-639.
- Hancock, R.E., 1981. Aminoglycoside uptake and mode of action with special reference to streptomycin and gentamicin. I. Antagonists and mutants. *J. Antimicrob. Chemother.* 8:249-276.

- Hannecart-Pokorni, E., Depuydt, F., de Wit, L., van Bossuyt, E., Content, J. and Vanhoof, R., 1997. Characterization of the 6'-N-acetylglucoside acetyltransferase gene *aac(6)-II* associated with a *suII*-type integron. *Antimicrob. Agents Chemother.* 41:314-318.
- Heinzel, P., Werbitzky, O., Distler, J. and Piepersberg, W., 1988. A second streptomycin resistance gene from *Streptomyces griseus* codes for streptomycin-3'-phosphotransferase. Relationships between antibiotic and protein kinases. *Arch. Microbiol.* 150:184-192.
- Herbert, C.J., Sarwar, M., Net, S.S., I.G., G. and Akhtar, M., 1986. Sequence and interspecies transfer of an aminoglycoside phosphotransferase gene (*APH*) of *Bacillus circulans*. Self-defence mechanism in antibiotic-producing organisms. *Biochem. J.* 233:383-393.
- Higgins, C.E. and Kasner, R.E., 1967. Nebamycin, a new broad-spectrum antibiotic complex. II. Description of *Streptomyces tenebrarius*. *Antimicrob. Agents Chemother.* 7:324-331.
- Hinshaw, H.C. and Feldman, W.H., 1945. Streptomycin in treatment of clinical tuberculosis: preliminary report. *Mayo Clin.* 20:313-318.
- Hodel-Christen, S.L. and Murray, B.E., 1991. Characterization of the gentamicin resistance transposon *Tn5281* from *Enterococcus faecalis* and comparison to staphylococcal transposons *Tn4001* and *Tn4031*. *Antimicrob. Agents Chemother.* 35:1147-1152.
- Hollingshead, S. and Vapnek, D., 1985. Nucleotide sequence analysis of a gene encoding a streptomycin-specific, nomycin adenylyltransferase. *Plasmid*, 13:17-30.
- Holm, L. and Sander, C., 1995. DNA polymerase  $\beta$  belongs to an ancient nucleotidyltransferase superfamily. *Trends Biol. Chem.* 20:345-347.
- Holmes, D.J. and Cundliffe, E., 1991. Analysis of a ribosomal RNA methylase gene from *Streptomyces tenebrarius* which confers resistance to gentamicin. *Mol. Gen. Genet.* 229:229-237.
- Holmes, D.J., Drocourt, D., Tiraby, G. and Cundliffe, E., 1991. Cloning of an aminoglycoside-resistance-encoding gene, *kamC*, from *Saccharopolyspora litorea*: comparison with *kamB* from *Streptomyces tenebrarius*. *Gene*, 102:19-26.
- Hon, W.C., McKay, G.A., Thompson, P.R., Sweet, R.M., Yang, D.S.C., Wright, G.D. and Berghuis, A.M., 1997. Structure of an enzyme required for aminoglycoside resistance reveals homology to eukaryotic protein kinases. *Cell*, 89:887-899.
- Hoshiko, S., Nojiri, C., Matsunaga, K., Katsumata, K., Satoh, E. and Nagoka, K., 1988. Nucleotide sequence of the ribosomal phosphotransferase gene and of its control region in *Streptomyces ribosidificus*. *Gene*, 68:285-296.
- Hotta, K., Zhu, C.B., Ogata, T., Sunada, A., Ishikawa, J., Mizuno, S., Ikeda, Y. and Kondo, S., 1996. Enzymatic 2'-N-acetylation of arbekacin and antibiotic activity of its product. *J. Antibiot.* 49:458-464.
- Hubbard, S.R., Wei, L., Ellis, L. and Hendrickson, W.A., 1994. Crystal structure of the tyrosine kinase domain of the human insulin receptor. *Nature*, 372:746-754.
- Humbert, R. and Altendorf, K., 1989. Defective gamma subunit of ATP synthase (F1F0) from *Escherichia coli* leads to resistance to aminoglycoside antibiotics. *J. Bacteriol.* 171:1435-1444.
- Hutchin, T. and Coropassi, G., 1994. Proposed molecular and cellular mechanism for aminoglycoside ototoxicity. *Antimicrob. Agents Chemother.* 38:2517-2520.
- Ishikawa, J. and Hotta, K., 1991. Nucleotide sequence and transcriptional start point of the *kun* gene encoding an aminoglycoside 3'-N-acetyltransferase from *Streptomyces griseus* SS-1198R. *Gene*, 108:127-132.
- Johnson, L.N., Noble, M.E. and Owen, D.J., 1996. Active and inactive protein kinases: structural basis for regulation. *Cell*, 85:149-158.
- Jones, R.L.D., Jaskula, J.C. and Janssen, G.R., 1992. *In vivo* translational start site selection on leaderless mRNA transcribed from the *Streptomyces fradiae* *aph* gene. *J. Bacteriol.* 174:4753-4760.
- Kabins, S.A., Nathan, C. and Cohen, S., 1976. *In vitro* comparison of netilmicin, a semisynthetic derivative of sisomicin, and four other aminoglycoside antibiotics. *Antimicrob. Agents Chemother.* 10:139-145.
- Kadurungamuwa, J.L., Clarke, A.J. and Beveridge, T.J., 1993. Surface action of gentamicin on *Pseudomonas aeruginosa*. *J. Bacteriol.* 174:5798-5805.
- Kaufhold, A., Podbielski, A., Horand, T. and Fentien, P., 1992. Identical genes confer high-level resistance to gentamicin upon *Enterococcus faecalis*, *Enterococcus faecium*, and *Streptococcus agalactiae*. *Antimicrob. Agents Chemother.* 36:1215-1218.
- Kawaguchi, H., Naito, T., Nakagawa, S. and Fujiwara, K., 1972. BBK8, a new semisynthetic aminoglycoside antibiotic. *J. Antibiot.* 25:695.
- Kelmen, G.H., Cundliffe, E. and Finesses, L., 1991. Cloning and characterization of gentamicin-resistance genes from *Micromonospora purpurea* and *Micromonospora rastei*. *Gene*, 98:53-60.
- Kennelly, P.J. and Potts, M., 1996. Fancy meeting you here! a fresh look at "prokaryotic" protein phosphorylation. *J. Bacteriol.* 178:4759-4764.

## Aminoglycoside Antibiotics

- Kettner, M., Maciejek, T. and Kremery, V.J. (1991), in *Antimicrobial Chemotherapy in Immunocompromised Host. International Congress of Chemotherapy* pp 273-275. Berlin.
- Knighton, D.R., Zheng, J.H., Ten Eyck, L.F., Ashford, V.A., Xuong, N.H., Taylor, S.S. and Sowadski, J.M., 1991. Crystal structure of the catalytic subunit of cyclic adenosine monophosphate-dependent protein kinase. *Structure*, 253:407-414.
- Kocabiyik, S. and Petlin, M.H., 1992a. Altered substrate specificity by substitutions at Tyr218 in bacterial aminoglycoside 3'-phosphotransferase. *FEMS Microbiol. Lett.* 93:199-202.
- Kocabiyik, S. and Petlin, M.H., 1992b. Site-specific mutations of conserved C-terminal residues in aminoglycoside 3'-phosphotransferase II: Phenotypic and structural analysis of mutant enzymes. *Biochem. Biophys. Res. Commun.* 185:925-931.
- Kocabiyik, S. and Petlin, M.H., 1994. Amino acid substitutions within the analogous nucleotide binding loop (P-loop) of aminoglycoside 3'-phosphotransferase-II. *Int. J. Biochem.* 26:61-66.
- Kojic, M., Topisirovic, L. and Vasiljevic, B., 1992. Cloning and characterization of an aminoglycoside resistance determinant from *Micromonospora zionensis*. *J. Bacteriol.* 174:7868-7872.
- Kondo, S., Tamura, A., Gomi, S., Ikeda, Y., Takeuchi, T. and Mitsuhashi, S., 1993. Structures of enzymatically modified products of arbekacin by methicillin-resistant *Staphylococcus aureus*. *J. Antibiot.* 46:310-315.
- Kono, M., Ohmura, K., Kanda, T., Noguchi, N. and O'hara, K., 1987. Purification and characterization of chromosomal streptomycin adenylyltransferase from derivatives of *Bacillus subtilis* Marburg 168. *FEMS Microbiol. Lett.* 40:223-228.
- Lambert, T., Gerbaud, G. and Courvalin, P., 1994a. Characterization of the chromosomal *aac(6)-I* gene of *Acinetobacter* sp. J3 and the *aac(6)-Ib* plasmid gene of *Acinetobacter baumannii*. *Antimicrob. Agents Chemother.* 38:1883-1889.
- Lambert, T., Ploy, M.-C. and Courvalin, P., 1994b. A spontaneous point mutation in the *aac(6)-Ib* gene results in altered substrate specificity of aminoglycoside 6'-N-acetyltransferase of a *Pseudomonas fluorescens* strain. *FEMS Microbiol. Lett.* 115:297-304.
- Lando, D., Cousin, M.A. and Privat de Garille, M., 1973. Misreading, a fundamental aspect of the mechanism of action of several aminoglycosides. *Biochemistry*, 12:4528-4533.
- Le Goffic, F., Capman, M.L., Tangy, F. and Baillarge, M., 1979. Mechanism of action of aminoglycoside antibiotics. Binding studies of tobramycin and its 6'-N-acetyl derivative to the bacterial ribosome and its subunits. *Eur. J. Biochem.* 102:73-81.
- LeBlanc, D.J., Lee, L.N. and Inamine, J.M., 1991. Cloning and nucleotide base sequence analysis of a spectinomycin adenylyltransferase *AAD(9)* determinant from *Enterococcus faecalis*. *Antimicrob. Agents Chemother.* 35:1804-1810.
- Leclercq, R. and Courvalin, P., 1991. Bacterial resistance to macrolide, lincosamide, and streptogramin antibiotics by target modification. *Antimicrob. Agents Chemother.* 35:1267-1272.
- Lee, K.-Y., Hopkins, J.D. and Syvonen, M., 1991. Evolved neomycin phosphotransferase from an isolate of *Klebsiella pneumoniae*. *Mol. Microbiol.* 5:2039-2046.
- Lee, S.C., Cleary, P.P. and Gerdling, D.N., 1987. More than one DNA sequence encodes the 2"-O-adenylyltransferase phenotype. *Antimicrob. Agents Chemother.* 31:667-670.
- Lopez-Gabrea, M., Perez-Gonzalez, J.A., Heinzel, P., Piepersberg, W. and Jimenez, A., 1989. Isolation and nucleotide sequencing of an aminocyclitol acetyltransferase gene from *Streptomyces rimosus forma parvimonitus*. *J. Bacteriol.* 171:321-328.
- Lovering, A.M., White, L.O. and Reeves, D.S., 1987. AAC(1), a new aminoglycoside-acetylating enzyme modifying the C1 amino group of apramycin. *J. Antibiot.* 40:803-813.
- Luzzatto, L., Apirion, D. and Schlessinger, D., 1969. Polyribosome depletion and blockage of the ribosome cycle by streptomycin in *Escherichia coli*. *J. Mol. Biol.* 42:315-335.
- Lyuztkanova, D., Distler, J. and Altenbuchner, J., 1997. A spectinomycin resistance determinant from the spectinomycin producer *Streptomyces flavogriseus*. *Microbiology*, 143:2133-2143.
- Macinga, D.R., Parojic, M.M. and Rathner, P.N., 1995. Identification and analysis of *aarP*, a transcriptional activator of the 2'-N-acetyltransferase in *Providencia stuartii*. *J. Bacteriol.* 177:3407-3413.
- Macinga, D.R. and Rathner, P.N., 1996. *aarD*, a *Providencia stuartii* homologue of *cysD*: role in 2'-N-acetyltransferase expression, cell morphology and growth in the presence of an extracellular factor. *Mol. Microbiol.* 19:511-520.
- Madhusudan, T., Trahy, E.A., Xuong, N.-H., Adams, J.A., Ten Eyck, L.F., Taylor, S.S. and Sowadski, J.M., 1994. CAMP-dependent protein kinase: Crystallographic insights into substrate recognition and phosphorylation. *Proc. Sci.* 3:176-187.
- Martel, A., Masson, M., Moreau, N. and Goffic, F.L., 1983. Kinetic studies of aminoglycoside acetyltransferase and phosphotransferase from *Staphylococcus aureus* RPA. *Eur. J. Biochem.* 133:515-521.

- Martin, P., Julien, E. and Courvalin, P., 1988, Nucleotide sequence of *Acinetobacter baumannii* *aphA-6* gene: evolutionary and functional implications of sequence homologies with nucleotide-binding proteins, kinases and other aminoglycoside-modifying enzymes, *Mol. Microbiol.* 2:615-625.
- Mason, D.J., Dietz, A. and Smith, R.M., 1961, Actinospectacin: a new antibiotic. Discovery and biological properties, *Antibiot. Chemother.* 11:118-122.
- Malkovic, B., Pien, W. and Bock, A., 1984, Ribosomal resistance as a widespread self-defence in aminoglycoside-producing *Micromonospora* species, *FEMS Microbiol. Lett.* 24:273-276.
- Matsumura, M., Katakura, Y., Inakura, T. and Aiba, S., 1984, Enzymatic and nucleotide sequence studies of a kanamycin-inactivating enzyme encoded by a plasmid from thermophilic bacilli in comparison with that encoded by plasmid pUB110, *J. Bacteriol.* 160:413-420.
- Matsunaga, K., Yamaki, H., Nishimura, T. and Tanaka, N., 1986, Inhibition of DNA replication initiation by aminoglycoside antibiotics, *Antimicrob. Agents Chemother.* 30:468-474.
- Mazodier, P., Cossart, P., Giraud, E. and Gasser, F., 1985, Completion of the nucleotide sequence of the central region of Tn5 confirms the presence of three resistance genes, *Nucleic Acids Res.* 13:195-205.
- McKay, G.A. and Wright, G.D., 1996, Catalytic mechanism of enterococcal kanamycin kinase (APH(3')-IIIa): Viscosity, pH, and solvent isotope effects support a Theorell-Chance mechanism, *Biochemistry*, 35:8680-8685.
- McKay, G.A., Robinson, R.A., Lane, W.S. and Wright, G.D., 1994a, Active-site labeling of an aminoglycoside antibiotic phosphotransferase (APH(3')-IIIa), *Biochemistry*, 33:14115-14120.
- McKay, G.A., Roesslami, J., Mobashery, S. and Wright, G.D., 1996, Recognition of aminoglycoside antibiotics by enterococcal-staphylococcal aminoglycoside 3'-phosphotransferase type IIIa: Role of substrate amino groups, *Antimicrob. Agents Chemother.* 40:2648-2650.
- McKay, G.A., Thompson, P.R. and Wright, G.D., 1994b, Broad spectrum aminoglycoside phosphotransferase type III from *Enterococcus*: Overexpression, purification, and substrate specificity, *Biochemistry*, 35:6936-6944.
- McKay, G.A. and Wright, G.D., 1995, Kinetic mechanism of aminoglycoside phosphotransferase type IIIa: Evidence for a Theorell-Chance mechanism, *J. Biol. Chem.* 270:24686-24692.
- Ménard, R., Molinas, C., Arthur, M., Duval, J., Courvalin, P. and Lecomte, R., 1993, Overproduction of 3'-amino-glycoside phosphotransferase type I confers resistance to tobramycin in *Escherichia coli*, *Antimicrob. Agents Chemother.* 37:78-83.
- Miller, G.H., Sabatelli, F.J., Hare, R.S., Glupczynski, Y., Mackey, P., Shlaes, D., Shimizu, K., Shaw, K.J. and Aminoglycoside Resistance Study Groups, 1997, The most frequent aminoglycoside resistance mechanisms—changes with time and geographic area: a reflection of aminoglycoside usage patterns?, *Clin. Infect. Dis.* 24:S46-S52.
- Miller, M.H., Edberg, S.C., Mandel, L.J., Behar, C.F. and Steigbigel, N.H., 1980, Gentamicin uptake in wild-type and aminoglycoside-resistant small-colony mutants of *Staphylococcus aureus*, *Antimicrob. Agents Chemother.* 18:722-729.
- Moazed, D. and Noller, H.F., 1987, Interaction of antibiotics with functional sites in 16S ribosomal RNA, *Nature*, 327:389-394.
- Morris, J.C. and Mensa-Wilmot, K., 1997, Role of 2,6-dideoxy-2,6-diaminoglucose in activation of a eukaryotic phospholipase C by aminoglycoside antibiotics, *J. Biol. Chem.* 272:29554-29559.
- Murphy, E., 1985, Nucleotide sequence of a spectinomycin adenyltransferase AAD(9) determinant from *Staphylococcus aureus* and its relationship to AAD(3')-9, *Mol. Gen. Genet.* 200:33-39.
- Musser, J.M., 1995, Antimicrobial agent resistance in mycobacteria: molecular genetic insights, *Clin. Microbiol. Rev.* 8:496-514.
- Nagabushan, T.L., Cooper, A.B., Tsi, H., Daniels, P.J. and Miller, G.H., 1978, The synthetases and biological properties of 1-N-(S-4-amino-2-hydroxybutyl)-gentamicin B and 1-N-(S-3-amino-2-hydroxypropyl)-gentamicin B, *J. Antibiot.* 31:681-687.
- Nassberger, L., Bergstrand, A. and DePierre, J.W., 1990, Intracellular distribution of gentamicin within the rat kidney cortex: a cell fractionation study, *Exp. Mol. Pathol.* 52:212-220.
- O'Hara, K., Ohnishi, K. and Kono, M., 1988, Structure of adenylated streptomycin synthesized enzymatically by *Bacillus subtilis*, *Antimicrob. Agents Chemother.* 32:949-950.
- Ohnishi, K., Tanaka, T., Noguchi, N., O'Hara, K. and Kono, M., 1989, Nucleotide sequence of the chromosomal gene coding for the aminoglycoside 6-adenyltransferase from *Bacillus subtilis* Marburg 168, *Gene*, 78:377-378.
- Ohta, T. and Hasegawa, M., 1993a, Analysis of the nucleotide sequence of *fmrT* encoding the self-defense gene of the streptomycin producer, *Streptomyces tendamensis* ATCC 31602; comparison with the sequences of *kunB* of *Streptomyces tenebrarius* NCIB 11028 and *kamC* of ICL102, *J. Antibiot.* 46:511-517.

## Aminoglycoside Antibiotics

- Ohta, T. and Hasegawa, M., 1993b, Analysis of the self-defense gene (*fmrO*) of a fortimicin A (astromycin) producer, *Micromonospora olivasterospora*: comparison with other aminoglycoside-resistance-encoding genes, *Gene*, 127:63-69.
- Oka, A., Sugisaki, H. and Takamami, M., 1981, Nucleotide sequence of the kanamycin resistance transposon *Tn903*, *J. Mol. Biol.* 147:217-226.
- ounissi, H. and Courvalin, P. (1987), Nucleotide sequences of streptococcal genes, in *Streptococcal Genetics* (J. J. Ferretti and R. Curtiss III, Eds.), pp 275. American Society for Microbiology, Washington, D.C.
- Owen, D.J., Noble, M.E., Garman, E.F., Papageorgiou, A.C. and Johnson, L.N., 1993, Two structures of the catalytic domain of phosphorylase kinase: an active protein kinase complexed with substrate analogue and product, *Structure*, 3:467-482.
- Pansgrau, W., Miele, L., Lutz, R. and Lanka, E., 1987, Nucleotide sequence of the kanamycin resistance determinant of plasmid RP4: Homology to other aminoglycoside 3'-phosphotransferases, *Plasmid*, 18:193-204.
- Papadopoulos, B. and Courvalin, P., 1988, Dispersal in *Campylobacter* spp. of *aphA-3*, a kanamycin resistance determinant from gram-positive cocci, *Antimicrob. Agents Chemother.* 32:945-948.
- Pardo, J.M., Malpartida, F., Rico, M. and Jimenez, A., 1985, Biochemical basis of resistance to hygromycin B in *Streptomyces hygroscopicus*—the producing organism, *J. Gen. Microbiol.* 131:1289-1298.
- Payle, K.G. and Clarke, A.J., 1997, Characterization of gentamicin 2'-N-acetyltransferase from *Providencia stuartii*: its use of peptidoglycan metabolites for acetylation of both aminoglycosides and peptidoglycan, *J. Bacteriol.* 179:4106-4114.
- Payle, K.G., Ratner, P.N. and Clarke, A.J., 1995, Contribution of gentamicin 2'-N-acetyltransferase to the O-acetylation of peptidoglycan in *Providencia stuartii*, *J. Bacteriol.* 177:4303-4310.
- Payle, K.G., Strating, H. and Clarke, A.J., 1996, The role of O-acetylation in the metabolism of peptidoglycan in *Providencia stuartii*, *Microb. Drug Resist.* 2:135-140.
- Pedersen, L.C., Benning, M.M. and Holden, H.M., 1995, Structural investigation of the antibiotic and ATP-binding sites in kanamycin nucleotidyltransferase, *Biochemistry*, 34:13305-13311.
- Piepersberg, W., Disler, J., Heinzel, P. and Perez-Gonzalez, J.-A., 1988, Antibiotic resistance by modification: many resistance genes could be derived from cellular control genes in actinomycetes—A hypothesis, *Actinomycetol.* 2:83-98.
- Piepersberg, W., Heinzel, P., Mansouri, K., Mönighoff, U. and Pissowatzki, K. (1991), Evolution of antibiotic resistance and production genes in streptomycetes, in *Genetics and product formation in Streptomyces* (S. Baumberg, H. Krigel and D. Novack, Eds.), pp. 161-170, Plenum Press, New York.
- Pruska, E.M. and Schacht, J., 1995, Formation of free radicals by gentamycin and iron and evidence for an iron-gentamycin complex, *Biochem. Pharmacol.* 50:1149.
- Radika, K. and Northrop, D.B., 1984a, Substrate specificities and structure-activity relationships for acylation of antibiotics catalyzed by kanamycin acetyltransferase, *Biochemistry*, 23:1118-1122.
- Radika, K. and Northrop, D.B., 1984b, The kinetic mechanism of kanamycin acetyltransferase derived from the use of alternative antibiotics and coenzymes, *J. Biol. Chem.* 259:12343-12346.
- Radika, K. and Northrop, D., 1984c, Purification of two forms of kanamycin acetyltransferase from *Escherichia coli*, *Arch. Biochem. Biophys.* 233:272-285.
- Radika, K. and Northrop, D.B., 1984d, Correlation of antibiotic resistance with  $V_{max}/K_m$  ratio of enzymatic modification of aminoglycosides by kanamycin acetyltransferase, *Antimicrob. Agents Chemother.* 25:479-482.
- Rao, R.N., Allen, N.E., Hobbs, J.N.J., Albom, W.E.J., Kirst, H.A. and Paschal, J.W., 1983, Genetic and enzymatic basis of hygromycin B resistance in *Escherichia coli*, *Antimicrob. Agents Chemother.* 24:689-695.
- Ratner, P.N., Mann, P.A., Mierzwa, R., Hare, R.S., Miller, G.H. and Shaw, K.J., 1993a, Analysis of the *aac(3)-Ia* gene encoding a novel 3'-N-acetyltransferase, *Antimicrob. Agents Chemother.* 37:2074-2079.
- Ratner, P.N., Mierzwa, R., Hare, R., Miller, G. and Shaw, K., 1992a, Cloning and DNA sequence analysis of an *aac(3)-Ib* gene from *Serratia marcescens*, *Antimicrob. Agents Chemother.* 36:2222-2227.
- Ratner, P.N., Munayyer, H., Mann, P.A., Hare, R.S., Miller, G.H. and Shaw, K.J., 1992b, Genetic analysis of bacterial acetyltransferases: Identification of amino acids determining the specificities of the aminoglycoside 6'-N-acetyltransferase Ib and IIa proteins, *J. Bacteriol.* 173:3196-3203.
- Ratner, P.N. and Oroz, E., 1994, Characterization of *aacA*, a pleiotropic negative regulator of the 2'-N-acetyltransferase in *Providencia stuartii*, *J. Bacteriol.* 176:5140-5144.
- Ratner, P.N., Oroz, E., Shaw, K.J., Hare, R. and Miller, G., 1993b, Characterization and transcriptional regulation of the 2'-N-acetyltransferase gene from *Providencia stuartii*, *J. Bacteriol.* 175:6492-6498.
- Ratner, P.N., Parojic, M.M. and Paradise, M.R., 1997a, An extracellular factor regulating expression of the chromosomal aminoglycoside 2'-N-acetyltransferase of *Providencia stuartii*, *Antimicrob. Agents Chemother.* 41:1749-1754.



- Raether, P.N., Solinsky, K., A. Paradise, M.R. and Parojic, M.M., 1997b. *aacC*, an essential gene involved in density-dependent regulation of the 2'-N-acetyltransferase in *Providencia stuartii*. *J. Bacteriol.* 179:2267-2273.
- Reestamadi, J., Grapsas, I. and Mobashery, S., 1995a. Loss of individual electrostatic interactions between aminoglycoside antibiotics and resistance enzymes as an effective means to overcoming bacterial drug resistance. *J. Am. Chem. Soc.* 117:11060-11069.
- Reestamadi, J., Grapsas, I. and Mobashery, S., 1995b. Mechanism-based inactivation of bacterial aminoglycoside 3'-phosphotransferases. *J. Am. Chem. Soc.* 117:80-84.
- Rouch, D.A., Byrne, M.E., Kong, Y.C. and Skurray, R.A., 1987. The *aacA-aphD* gentamicin and kanamycin resistance determinant of *Tn4001* from *Staphylococcus aureus*: Expression and nucleotide sequence analysis. *J. Gen. Microbiol.* 133:3039-3052.
- Sakon, J., Liao, H.H., Kanikula, A.M., Benning, M.M., Rayment, I. and Holden, H.M., 1993. Molecular structure of kanamycin nucleotidyl transferase determined to 3 Å resolution. *Biochemistry*, 32:11977-11984.
- Salauze, D. and Davies, J., 1991a. Isolation and characterization of an aminoglycoside phosphotransferase from neomycin-producing *Micromonospora chateaui*: Comparison with that of *Streptomyces fridley* and other producers of 4,6-disubstituted 3-deoxystreptamine antibiotics. *J. Antibiot.* 44:1432-1443.
- Salauze, D., Perez-Gonzalez, J.-A., Piepersberg, W. and Davies, J., 1991b. Characterization of aminoglycoside acetyltransferase-encoding genes of neomycin-producing *Micromonospora chateaui* and *Streptomyces fridley*. *Gene*, 101:143-148.
- Sanders, T.W.J., Reinhard, M.K., Jollow, D.J. and Holtendorf, G.H., 1993. Lack of *in vivo* evidence of a cytochrome P450 metabolite participating in aminoglycoside nephrotoxicity. *Biochem. Pharmacol.* 45:780-782.
- Sarwar, M. and Akhtar, M., 1990. Cloning of aminoglycoside phosphotransferase (APH) gene from antibiotic-producing strain of *Bacillus circulans* into a high-expression vector, pKK223-3. Purification, properties and location of the enzyme. *Biochem. J.* 268:671-677.
- Sawaya, M.R., Pelletier, H., Kumar, A., Wilson, S.H. and Kraus, J., 1994. Crystal structure of rat DNA polymerase  $\beta$ : evidence for a common polymerase mechanism. *Science*, 264:1930-1933.
- Schacht, J., 1993. Biochemical basis of aminoglycoside ototoxicity. *Otolaryngol. Clin. North. Am.* 26:845-856.
- Schatz, A., Bugie, E. and Waksman, S.A., 1944. Streptomycin, a substance exhibiting antibiotic activity against Gram-positive and Gram-negative bacteria. *Proc. Soc. Exp. Biol. Med.* 55(66-69).
- Schlessinger, D., 1988. Failure of aminoglycoside antibiotics to kill anaerobic, low-pH, and resistant cultures. *Clin. Microbiol. Rev.* 1:54-59.
- Schmidt, F.R., Nücken, E.J. and Henschke, R.B., 1988. Nucleotide sequence analysis of 2'-aminoglycoside nucleotidyl-transferase (ANT2') from *Tn4000*: its relationship to AAD(3') and impact on *Tn21* evolution. *Mol. Microbiol.* 2:709-717.
- Scholz, P., Haring, V., Wittmann-Liebold, B., Ashman, K., Bagdasarian, M. and Scherzinger, E., 1989. Complete nucleotide sequence and gene organization of the broad-host-range plasmid RSF1010. *Gene*, 75(271-288).
- Schwob, L.R., Schaffner, C.P., Miller, G.H., Hare, R.S. and Shaw, K.J., 1995. Cloning and characterization of a 3-N-aminoglycoside acetyltransferase gene, *aac(3)-Ib*, from *Pseudomonas aeruginosa*. *Antimicrob. Agents Chemother.* 39:1790-1796.
- Shaw, K.J., 1997. Personal communication.
- Shaw, K.J., Cramer, C.A., Rizzo, M., Mierzwia, R., Gevwin, K., Miller, G.H. and Hare, R.S., 1989. Isolation, characterization, and DNA sequence analysis of an AAC(6)-II gene from *Pseudomonas aeruginosa*. *Antimicrob. Agents Chemother.* 33:2052-2062.
- Shaw, K.J., Gomez-Lus, S. and Shannon, K.W., 1992a. unpublished sequence. GenBank accession no. L06160.
- Shaw, K.J. and Leal, I., 1992. unpublished sequence GenBank accession no. L06161.
- Shaw, K.J., Raether, P.N., Sabatelli, F.J., Mann, P., Munayyer, H., Mierzwia, R., Petrakios, G.L., Hare, R.S., Miller, G.H., Bennett, P. and Downey, P., 1992b. Characterization of the chromosomal *aac(6)-Ic* gene from *Serratia marcescens*. *Antimicrob. Agents Chemother.* 36:1447-1455.
- Shaw, K.J., Raether, P.N., Hare, R.S. and Miller, G.H., 1993. Molecular genetics of aminoglycoside resistance genes and familial relationships of the aminoglycoside-modifying enzymes. *Microbiol. Rev.* 57:138-163.
- Shomura, T., Ezaki, N., Tsurutoka, T., Niwa, T., Akita, E. and Nida, T., 1970. Studies on antibiotic SF-733, a new antibiotic. I. Taxonomy, isolation and characterization. *J. Antibiot.* 23:155-161.
- Sigmund, C.D., Elayachi, M. and Morgan, E.A., 1984. Antibiotic resistance mutations in 16S and 23S ribosomal RNA genes of *Escherichia coli*. *Nucleic Acids Res.* 12:4653-4663.
- Siregar, J.J., Lerner, S.A. and Mobashery, S., 1994. Purification and characterization of aminoglycoside 3'-phosphotransferase Type IIa and kinetic comparison with a new mutant enzyme, *Antimicrob. Agents Chemother.* 38:641-647.

- Siregar, J.J., Miroshnikov, K. and Mobashery, S., 1995. Purification, characterization, and investigation of the mechanism of aminoglycoside 3'-phosphotransferase Type Ia. *Biochemistry* 34:12681-12688.
- Skeggs, P.A., Holmes, D.J. and Cundliffe, E., 1987. Cloning of aminoglycoside-resistance determinants from *Streptomyces tenebrarius* and comparison with related genes from other actinomycetes. *J. Gen. Microbiol.* 133:915-923.
- Song, B.B. and Schacht, J., 1996. Variable efficacy of radical scavengers and iron chelators to attenuate gentamicin ototoxicity in guinea pig *in vivo*. *Hearing Res.* 94:87.
- Sundin, G.W. and Bender, C.L., 1996. Dissemination of the *strA-strB* streptomycin-resistance genes among commensal and pathogenic bacteria from humans, animals, and plants. *Mol. Ecol.* 5:133-143.
- Suter, T.M., Viswanathan, V.K. and Ciancio, N.P., 1997. Isolation of a gene encoding a novel spectinomycin phosphotransferase from *Legionella pneumophila*. *Antimicrob. Agents Chemother.* 41:1385-1388.
- Sutherland, R., 1991.  $\beta$ -Lactamase inhibitors and reversal of antibiotic resistance. *Trends Pharmacol. Sci.* 12:227-232.
- Taber, H.W., Mueller, J.P., Miller, P.F. and Arrow, A.S., 1987. Bacterial uptake of aminoglycoside antibiotics. *Microbiol. Rev.* 51:439-457.
- Tanaka, N., Matsunaga, K., Yamaki, H. and Nishimura, T., 1984. Inhibition of initiation of DNA synthesis by aminoglycoside antibiotics. *Biochem. Biophys. Res. Commun.* 122:460-465.
- Tangy, F., Capnau, M.-L. and Le Goffic, F., 1983. Photo-induced labelling of *Escherichia coli* ribosomes by a tetracycline analog. *Eur. J. Biochem.* 131:581-587.
- Taylor, D.E., Yan, W., Ng, L.K., Manavathu, E.K. and Courvalin, P., 1988. Genetic characterization of kanamycin resistance in *Campylobacter coli*. *Ann. Inst. Pasteur Microbiol.* 139:665-676.
- Taylor, S.S., Knighon, D.R., Zheng, J., Ten Eyck, L.F. and Sowadski, J.M., 1992. Structural framework for the protein kinase family. *Annu. Rev. Cell Biol.* 8:429-62.
- Tenover, F.C., Filipula, D., Phillips, K.L. and Plorde, J.J., 1988. Cloning and sequencing of a gene encoding an aminoglycoside 6'-N-acetyltransferase from an R factor of *Citrobacter diversus*. *J. Bacteriol.* 170:471-473.
- Tenover, F.C., Gilbert, T. and O'Hara, P., 1988. Nucleotide sequence of a novel kanamycin resistance gene, *aphA-7*, from *Campylobacter jejuni* and comparison to other kanamycin phosphotransferase genes. *Plasmid*, 22:52-58.
- Tenover, F.C., Phillips, K.L., Gilbert, T., Lockhart, P., O'Hara, P.J., 1989. Development of a DNA probe from the deoxyribonucleotide sequence of a 3-N-aminoglycoside acetyltransferase [AAC(3)-I] resistance gene. *Antimicrob. Agents Chemother.* 33:551-559.
- Terán, F.J., Suárez, J.E. and Mendoza, M.C., 1991. Cloning, sequencing, and use as a molecular probe of a gene encoding an aminoglycoside 6'-N-acetyltransferase of broad substrate profile. *Antimicrob. Agents Chemother.* 35:714-719.
- Thal, L.A., Chow, J.W., Patterson, J.E., Perri, M.B., Donabedian, S., Clewell, D.B. and Zervos, M.J., 1993. Molecular characterization of highly gentamicin-resistant *Enterococcus faecalis* isolates lacking high-level streptomycin resistance. *Antimicrob. Agents Chemother.* 37:134-137.
- Thompson, C.J. and Gray, G.S., 1993. Nucleotide sequence of a streptomycin aminoglycoside phosphotransferase gene and its relationship to phosphotransferases encoded by resistance plasmids. *Proc. Natl. Acad. Sci. U S A*, 90:5190-5194.
- Thompson, C.J., Ward, J.M. and Hopwood, D.A., 1980. DNA cloning in *Streptomyces*: resistance genes from antibiotic-producing species. *Nature*, 286:525-527.
- Thompson, J., Skeggs, P.A. and Cundliffe, E., 1985. Methylation of 16S ribosomal RNA and resistance to the aminoglycoside antibiotics gentamicin and kanamycin determined by DNA from the gentamicin-producer, *Micromonospora purpurea*. *Mol. Gen. Genet.* 201:168-173.
- Thompson, P.R., Hughes, D.W. and Wright, G.D., 1996a. Mechanism of aminoglycoside 3'-phosphotransferase type IIIa: His188 is not a phosphate-accepting residue. *Chem. Biol.* 3:747-755.
- Thompson, P.R., Hughes, D.W. and Wright, G.D., 1996b. Regioselectivity of aminoglycoside phosphotransferase from *Enterococci* and *Streptococci* (APH(3)-IIIa). *Biochemistry*, 35:8686-8695.
- Tan van Nieu, G. and Colliatz, E., 1997. Primary structure of an aminoglycoside 6'-N-acetyltransferase AAC(6)-4, fused *in vivo* with the signal peptide of the *TnA*-encoded  $\beta$ -lactamase. *J. Bacteriol.* 169:5708-5714.
- Trieu-Cuot, P. and Courvalin, P., 1983. Nucleotide sequence of the *Streptococcus faecalis* plasmid gene encoding the 3'-aminoglycoside phosphotransferase type III. *Gene*, 23:331-341.
- Ubukata, K., Yamashita, N., Goroh, A. and Komuro, M., 1984. Purification and characterization of aminoglycoside-modifying enzymes from *Staphylococcus aureus* and *Staphylococcus epidermidis*. *Antimicrob. Agents Chemother.* 25:754-759.

- Umezawa, H., Nishimura, Y., Tsuchiya, T. and Umezawa, S., 1972. Syntheses of 6'-N-methylkanamycin and 3',4'-dideoxy-6'-N-methylkanamycin B active against resistant strains having 6'-N-acetylating enzymes. *J. Antibiot.* 25:743-745.
- Umezawa, H., Ueda, M., Maeda, K., Yagishita, K., Kando, S., Okami, Y., Uahara, R., Osato, Y., Nita, K. and Kakeuchi, T., 1957. Production and isolation of a new antibiotic kanamycin. *J. Antibiot.* 10:181-189.
- Vakulenko, S.B. and Entina, E.G., 1990. Nucleotide sequence of *aacC2* gene from a clinical strain of *Escherichia coli*. *Antibiot. Khimioter.* 35:46-50.
- Van Peil, J.E., Iyengar, R. and Frey, P.A., 1986. Gentamicin nucleotidyltransferase. Stereochemical inversion at phosphorus in enzymatic 2'-deoxyadenylyl transfer to tobramycin. *J. Biol. Chem.* 261:15995-15999.
- Van Peil, J.E. and Northrop, D.B., 1984. Purification and properties of gentamicin nucleotidyltransferase from *Escherichia coli*: Nucleotide specificity, pH optimum, and the separation of two electrophoretic variants. *Arch. Biochem. Biophys.* 230:250-263.
- Van Peil, J.E., Mooberry, E.S. and Frey, P.A., 1990. <sup>1</sup>H, <sup>13</sup>C, and <sup>31</sup>P Nuclear magnetic resonance spectral assignments for tobramycin, 2'-(adenosine-5'-phosphoryl)-tobramycin and 2'-(adenosine-5'-thiophosphoryl)-tobramycin. *Arch. Biochem. Biophys.* 280:284-291.
- Vliegeland, J.S., Ketselaar-van Gaalen, P.A. and van de Klundert, J.A., 1989. Nucleotide sequence of the *aacC2* gene, a gentamicin resistance determinant involved in a hospital epidemic of multiply resistant members of the family Enterobacteriaceae. *Antimicrob. Agents Chemother.* 33:1153-1159.
- Vliegeland, J.S., Ketselaar-van Gaalen, P.A. and van de Klundert, J.A., 1991. Nucleotide sequence of the *aacC3* gene, a gentamicin resistance determinant encoding aminoglycoside-(3)-N-acetyltransferase III expressed in *Pseudomonas aeruginosa* but not in *Escherichia coli*. *Antimicrob. Agents Chemother.* 35:892-897.
- Vögeli, M. and Hütner, R., 1987. Characterisation of the hydroxystreptomycin phosphotransferase gene (*spH*) of *Streptomyces glaucus*: nucleotide sequence and promoter analysis. *Mol. Gen. Genet.* 208:195-203.
- Wakaman, S.A. and Lechevalier, H.A., 1949. Neomycin, a new antibiotic active against streptomycin-resistant bacteria, including tuberculosis organisms. *Science*. 109:305-307.
- Wang, Y., Hamasaki, K. and Rando, R.R., 1997. Specificity of aminoglycoside binding to RNA constructs derived from the 16S rRNA decoding region at the HIV-RRE activator region. *Biochemistry*. 36:768-779.
- Weinstein, M.J., Lucdemann, G.M., Oden, E.M., Wagman, G.H., Rossetti, J.P., Marquez, J.A., Coniglio, C.T., Chaney, W., Hetzogl, H.L. and Black, J., 1963. Gentamicin, a new antibiotic complex from *Micromonospora*. *J. Med. Chem.* 6:463-464.
- Weinstein, M.J., Marquez, J.A., Testa, R.T., Wagman, G.H., Oden, E.M. and Waite, J.A., 1970. Antibiotic 6640, a new *Micromonospora*-produced aminoglycoside antibiotic. *J. Antibiot.* 23:551-554.
- Wersuck, G., Zapp, M.L. and Green, M.R., 1996. A non-canonical base pair within the human immunodeficiency virus Rev-responsive element is involved in both Rev and small molecule recognition. *Chem. Biol.* 3:129-137.
- Williams, J.W. and Northrop, D.B., 1976. Purification and properties of gentamicin acetyltransferase I. *Biochem. biophys. Res. Commun.* 71:125-131.
- Williams, J.W. and Northrop, D.B., 1978a. Kinetic mechanism of gentamicin acetyltransferase I. *J. Biol. Chem.* 253:5902-5907.
- Williams, J.W. and Northrop, D.B., 1978b. Substrate specificity and structure-activity relationships of gentamicin acetyltransferase I. *J. Biol. Chem.* 253:5908-5914.
- Williams, J.W. and Northrop, D.B., 1979. Synthesis of a tight-binding, multisubstrate analog inhibitor of gentamicin acetyltransferase. *J. Antibiot.* 32:1147-1154.
- Woo, P.W.K., Dion, H.W. and Bartz, Q.R., 1971. Butirosin A and B, aminoglycoside antibiotics. I. Structural units. *Tet. Lett.* 26:17-2620.
- Woodcock, J., Moazed, D., Cannon, M., Davies, J. and Noller, H.F., 1991. Interaction of antibiotics with A- and P-site-specific bases in 16S ribosomal RNA. *EMBO J.* 10:3099-3103.
- Wright, G.D. and Ladak, P., 1997. Overexpression and characterization of the chromosomal aminoglycoside 6'-N-acetyltransferase from *Enterococcus faecium*. *Antimicrob. Agents Chemother.* 41:956-960.
- Wu, H.Y., Miller, G.H., Guzman Blanco, M., Hare, R.S. and Shaw, K.J., 1997. Cloning and characterization of an aminoglycoside 6'-N-acetyltransferase gene from *Citrobacter freundii* which confers an altered resistance profile. *Antimicrob. Agents Chemother.* 41:2439-2447.
- Xu, R.-M., Carnei, G., Kurt, J. and Cheng, X., 1996. Structural basis for selectivity of the isouquinoline sulfonamide family of protein kinase inhibitors. *Proc. Natl. Acad. Sci. USA*. 93:6308-6313.
- Yerofsky, R.L., Fine, M. and Pellow, J.W., 1990. A mutant neomycin phosphotransferase II gene reduces the resistance of transformants to antibiotic selection pressure. *Proc. Natl. Acad. Sci. USA*. 87:3435-3439.
- Young, M.L., Bains, M., Bell, A. and Hancock, R.E., 1992. Role of *Pseudomonas aeruginosa* outer membrane protein OprM in polymyxin and gentamicin resistance: isolation of an OprM-deficient mutant by gene replacement techniques. *Antimicrob. Agents Chemother.* 36:2566-2568.

## Aminoglycoside Antibiotics

- Zalacain, M., Gonzalez, A., Guerrero, M.C., Mattaliano, R.J., Malpartida, F. and Jimenez, A., 1986. Nucleotide sequence of the hygromycin B phosphotransferase gene from *Streptomyces hygroscopicus*. *Nucleic Acids Res.* 14:1565-1581.
- Zalacain, M., Malpartida, F., Pulido, D. and Jimenez, A., 1987a. Cloning and expression in *Escherichia coli* of a hygromycin B phosphotransferase gene from *Streptomyces hygroscopicus*. *Eur. J. Biochem.* 162:413-418.
- Zalacain, M., Pardo, J.M. and Jimenez, A., 1987b. Purification and characterization of a hygromycin B phosphotransferase from *Streptomyces hygroscopicus*. *Eur. J. Biochem.* 162:419-422.
- Zapp, M.L., Stern, S. and Green, M.R., 1993. Small molecules that selectively block RNA binding of HIV-1 Rev protein inhibit Rev function and viral production. *Cell*. 74:969-978.
- Zhang, C.-C., 1996. Bacterial signalling involving eukaryotic-type protein kinases. *Mol. Microbiol.* 20:9-15.
- Zhang, F., Strand, A., Robbins, D., Cobb, M.H. and Goldsmith, E.J., 1994. Atomic structure of the MAP kinase ERK2 at 2.3 Å resolution. *Nature*. 367:704-11.
- Zhou, J. and Adams, J.A., 1997. Is there a catalytic base in the active site of cAMP-dependent protein kinase? *Biochemistry*. 36:2977-2984.



## Modeling RNA–Ligand Interactions: The Rev-Binding Element RNA–Aminoglycoside Complex

Fabrice Leclerc and Robert Cedergren\*

Département de Biochimie, Université de Montréal, C.P. 6128, Succursale Centre-ville Montréal, Québec H3C3J7, Canada

Received June 6, 1997<sup>§</sup>

An approach to the modeling of ligand–RNA complexes has been developed by combining three-dimensional structure–activity relationship (3D-SAR) computations with a docking protocol. The ability of 3D-SAR to predict bound conformations of flexible ligands was first assessed by attempting to reconstruct the known, bound conformations of phenyloxazolines complexed with human rhinovirus 14 (HRV14) RNA. Subsequently, the same 3D-SAR analysis was applied to the identification of bound conformations of aminoglycosides which associate with the Rev-binding element (RBE) RNA. Bound conformations were identified by parsing ligand conformational data sets with pharmacophores determined by the 3D-SAR analysis. These “bioactive” structures were docked to the receptor RNA, and optimization of the complex was undertaken by extensive searching of ligand conformational space coupled with molecular dynamics computations. The similarity between the bound conformations of the ligand from the 3D-SAR analysis and those found in the docking protocol suggests that this methodology is valid for the prediction of bound ligand conformations and the modeling of the structure of the ligand–RNA complexes.

### Introduction

Research over the past several years has amply demonstrated the importance of RNA–ligand complexes in cellular processes. Consequently, there is a growing interest in targeting RNA complexes for therapeutics. A case in point is the aminoglycoside inhibition of the association between the Rev protein and the Rev-binding element RNA (RBE) of HIV-1, which determines the fate of viral mRNA.<sup>1,2</sup> Although the conformation of the RBE bound to the Rev peptide has been predicted by modeling<sup>3</sup> and subsequently confirmed by two NMR studies,<sup>4,5</sup> this structure offers little indication as to how an aminoglycoside could bind to the RNA in a way to prevent the interaction with the Rev protein.

Modeling and docking a ligand to a receptor is computationally complex in general because of the requirement to find mutually complementary sites in two conformationally flexible molecules. But in the case of RNA complexes, more difficulties arise, because many of the computational tools available for studying the structure of molecular complexes have been developed with proteins in mind. Since NMR and X-ray structures of RNA molecules are becoming more commonplace and a method of predicting bound conformations of RNA from low-resolution chemical data and in vitro selection from random libraries<sup>3,6</sup> has been developed in our laboratory, we have recently focused more on methods which determine the bioactive conformation of the ligand and the structure of the complex rather than the bound RNA conformation. Previously, we showed that structure–activity relationship (SAR) analysis of conformationally rigid ligands can be used to obtain information on the three-dimensional structure of the complex between DNA and quinolones<sup>7</sup> and that a docking

protocol based on electrostatic and van der Waals energies can be applied to modeling of the Rev peptide–RBE complex.<sup>8</sup>

Here, we first assess the validity and reliability of the SAR method to identify bioactive conformations for the case of conformationally flexible inhibitors, the phenyloxazolines, whose bound structures with human rhinovirus 14 (HRV14) have been determined by X-ray crystallography.<sup>9</sup> Then, the same approach is applied to the study of the RBE-binding aminoglycosides where the bioactive conformation is unknown. A docking protocol that incorporates the binding properties of the aminoglycosides inferred from the 3D-SAR study is then used to predict the binding conformation of the aminoglycosides within the RNA binding site. The final model of the complex is supported by the high similarity between the bioactive conformations of the ligands produced by the SAR study and the docking protocol as well as the ability of the model to rationalize available experimental data from the complex.

### Results and Discussion

We have devised a scheme based on a 3D-SAR analysis and a docking protocol to model the bound, bioactive conformation of aminoglycosides and the RBE RNA–aminoglycoside complex (Figure 1). The method involves the prediction of the biologically significant conformations by a 3D-SAR analysis using extensive conformational generation (Figure 1, steps 1–4). The bioactive conformers thus identified are used as starting conformations for a docking and modeling protocol. During docking extensive conformational sampling is used again which, together with molecular mechanics, produces a new series of bioactive conformations (steps 5 and 6). The reliability of models is then evaluated by comparison of the bioactive conformations identified by 3D-SAR and docking (step 7); this step provides a type

\* Corresponding author. Tel: (514) 343-6320. Fax: (514) 343-2177.  
E-mail: ceder@poste.umontreal.ca.

<sup>§</sup> Abstract published in *Advance ACS Abstracts*, December 15, 1997.

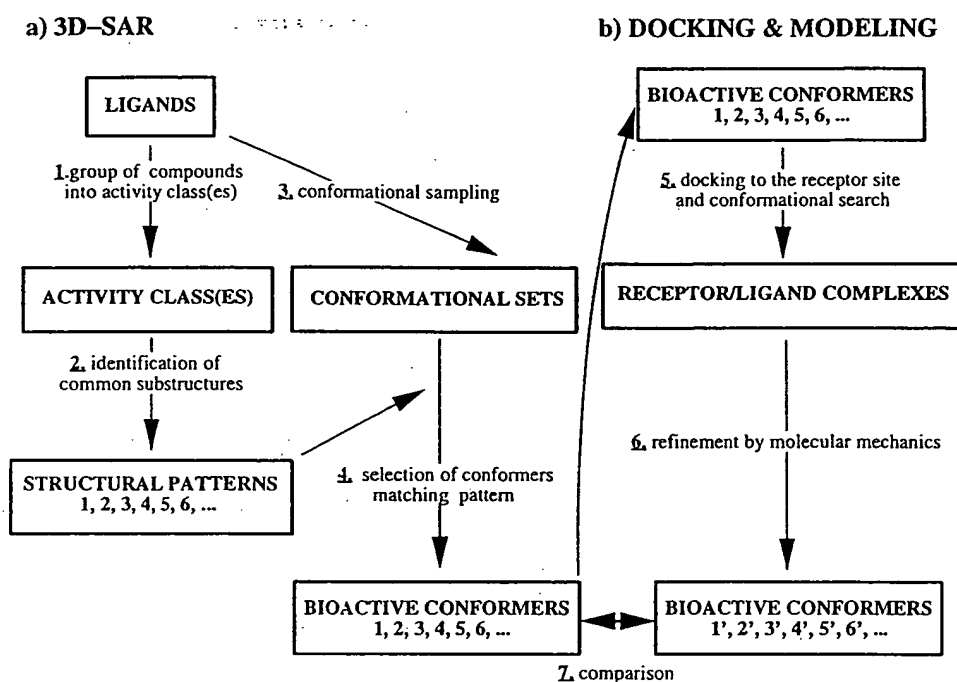
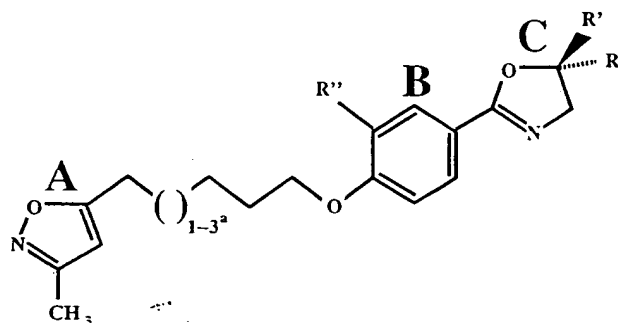


**Figure 1.** Flowchart for the proposed protocol: (a) 3D-SAR approach (steps 1–4), (b) docking and modeling approach (steps 5, 6) and comparison of the bioactive conformations (step 7).



name	R	R'	R''	PDB	MIC (μM)
I1 <sup>a</sup>	Me	H	H	2RS1	0.03
I2 <sup>a</sup>	H	Me	H	2RR1	0.4
I3 <sup>a</sup>	Me	H	Cl	2RM2	0.2
I4 <sup>a</sup>	Et	H	H	2RS3	0.02
I5 <sup>a</sup>	H	H	H	2R04	0.6
I6	Me	H	H	2RS5	0.6
I7	H	H	H	2R06	0.5
I8	H	H	Cl	2R07	2.4

**Figure 2.** WIN compounds and their activities: chemical structures and the respective biological activities. The letter x represents three methylene groups in compounds I1–I5 and one in compounds I6–I8. A represents the oxazole and B, C the phenyloxazole group.

of internal validation of the modeling procedure. The 3D-SAR aspect of the approach was tested first using the inhibitors of HRV14 (the WIN compounds), and subsequently the entire strategy was applied to the study of the RBE-binding aminoglycosides.

**Bioactive Conformations of WIN Compounds.** The antiviral WIN compounds shown in Figure 2 were chosen for testing since the X-ray crystallographic structures revealed two alternate orientations of the compounds, an indication of high flexibility.<sup>10,11</sup> compounds I1–I4 have the isoxazole, ring A, in the “heel” of the binding pocket composed of amino acids T216, L106, C199, and Y197 (Figure 3a), and compounds I5–

I8 have the isoxazole in the “toe” of the binding pocket composed of amino acids P174, V176, and A24 (Figure 3b).

To predict the binding conformation of the WIN compounds, we first combined all eight compounds into a single class in order to find all possible binding orientations and then subsequently determined bioactive conformations for each ligand orientation after classifying them into two groups. The eight WIN compounds produced a number of pharmacophores identified by the APEX-3D program (Table 1); however, the pharmacophores could be divided into two types: one which featured only one ligand orientation with respect to the receptor and the second which allowed two orientations for these groups as found in the crystallographic structures. The statistics for the best pharmacophore of each type are given in Table 1.

The detection of two potential binding orientations led us to separate the compounds into two groups, which in fact corresponded to the higher activity compounds (I1–I4) and the lower activity group, I5–I8 (Figure 2). Table 1 shows the statistically most significant pharmacophores for each group. The bioactive conformation of each compound, shown in Figure 3c,d, was then obtained by parsing the conformational sets generated for each ligand in a group with the pharmacophore identified for the group. These conformations were then compared with the ligand conformation in the crystal structure. The best pharmacophore in group I aligned the ligands very well: the rmsd between the 3D-SAR and crystal structure was 0.0 for compounds I1–I3 and 1.3 Å for I4 (group I, Figure 3c). The best pharmacophore of the group II compounds predicted bioactive conformations of these compounds within a distance of 1.4 Å rmsd from the crystal structure for I6–I8 and 2.0 Å for I5 (Figure 3d).

Thus, the simple qualitative SAR model permitted the identification of pharmacophores that correctly describe

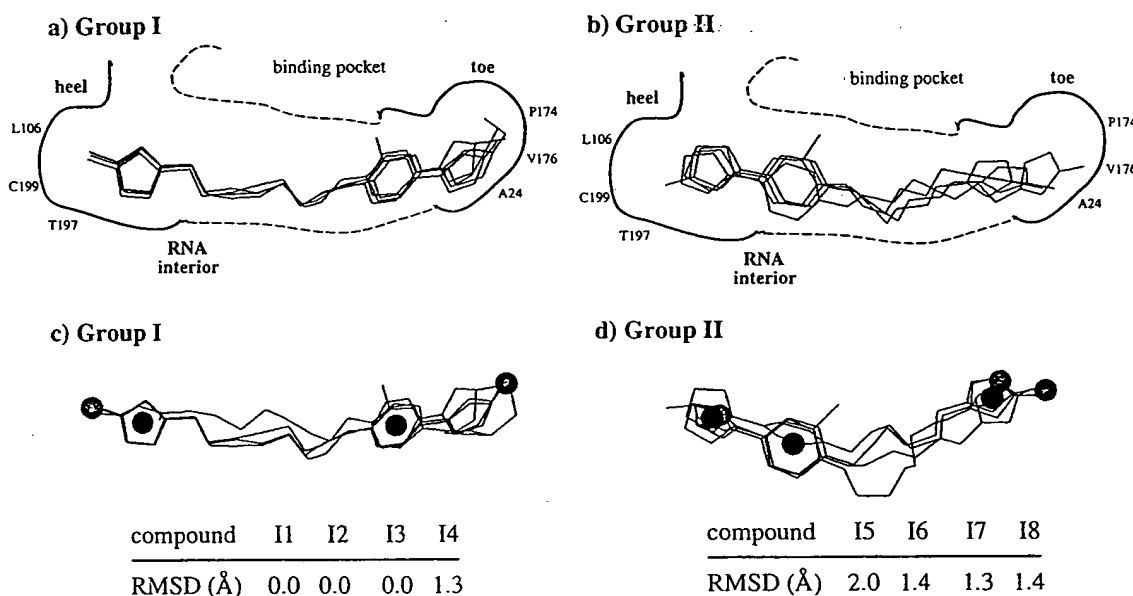


**Figure 3.** Conformations and binding modes of the WIN inhibitors: (a) crystal structures of inhibitors **I1–I4** superimposed according to their position and orientation in the binding pocket, (b) crystal structures of **I5–I8** superimposed according to their position and orientation in the binding pocket, (c) alignment of group I compounds using the pharmacophore of Table 1 (rmsd values refer to the differences between the 3D-SAR structure and that of the crystal), (d) alignment of group II compounds using the pharmacophore of Table 1.

**Table 1.** Pharmacophores of WIN Compounds

data compd	no. of pharmacophores	orientation	probability	reliability	match
all	151 <sup>a</sup>	one	0.90	n/a	0.38
		two	0.90	n/a	0.27
group I	55 <sup>b</sup>	one	0.83	0.94	0.67
group II	6 <sup>b</sup>	one	0.83	0.94	0.36

<sup>a</sup> Number of pharmacophores found for all compounds having a probability  $\geq 0.80$  and match  $\geq 0.20$ . This number included two types of pharmacophores: one having one orientation for all ligands and the other two orientations. <sup>b</sup> Number of pharmacophores found for group I (**I1–I4**) and group II (**I5–I8**) compounds having a probability  $\geq 0.83$ . Among these pharmacophores those having the highest match value are indicated.

the binding orientation and bioactive conformation of seven of the eight WIN compounds within 1.4 Å rmsd, and this result must be viewed in the light of the fact that the receptor structure was not used during the determination.

**Bioactive Conformations of Aminoglycosides.** Ten aminoglycosides which inhibit the Rev-RBE RNA complex formation belong to two structural families: the 4,5-diglycosyl-2-deoxystreptamines (4,5-DOS) including neomycin B, ribostamycin, lividomycin A, and paromomycin (Figure 4a) and the 4,6-diglycosyl-2-deoxystreptamines (4,6-DOS) including tobramycin, kanamycin A and B, and gentamicin C1a (Figure 4b). Thus one of the subordinate goals of this study is to determine whether the two structural classes bind to the RNA receptor (Figure 4c) in the same manner. For this reason our analysis focuses on neomycin and tobramycin, the two most active inhibitors belonging to the two structural classes.

The most significant pharmacophores shared by the highly active compounds, neomycin B, lividomycin A, tobramycin, ribostamycin, kanamycin B, and gentamicin C1a, are shown in Figure 5 and summarized in Table 2. Significantly, these patterns show that the core structure defined by rings A and B binds similarly for

both the 4,5- and 4,6-DOS compounds. The pharmacophores were then used to parse the conformations and align the compounds. The rmsd calculated between the bioactive conformations predicted by pharmacophores 3 and 4 was 2.3 and 2.9 Å for neomycin and tobramycin, respectively, whereas the rmsd between the conformations predicted by pharmacophores 4 and 5 was 1.4 Å for neomycin. The most similar pair of bioactive conformers was produced by pharmacophores 1 and 4 where the difference for neomycin and tobramycin was 1.2 and 0.6 Å, respectively.

**Docking of Aminoglycoside Antibiotics.** Docked models were produced for the neomycin B (high activity), tobramycin (high activity), kanamycin B (low activity), paromomycin (inactive) complexes. The initial structure for each complex, models 1–5, was constructed with the five bioactive conformers produced by the pharmacophores (Figure 5). Models were also built using the energy-minimized conformations of the ligands and were identified as models M1 and M2. In all cases, ligands were bound to the previously suggested G46, G47, and G48 region<sup>1</sup> (Figure 4c) of the bound RBE conformation constructed by Leclerc et al.<sup>3</sup> and supported by NMR data.<sup>4,5</sup> Two orientations of the ligand with respect to the RNA binding site were evaluated during docking (see Methods). Only those initial models whose interaction energies were within 50 kcal/mol of the lowest energy model constructed with the energy-minimized ligand conformation were retained for further study (Table 3). Subsequently, searches of ligand conformational space of the retained models were undertaken by exploring the sterically available torsional angles of the ligand until an optimal value for the interaction energy was obtained for each model (see Methods). The significance of the models was evaluated by comparing them with two control models, C1 and C2, which were constructed by docking the aminoglycoside to the region of nucleotides 50, 51, and 52, instead of

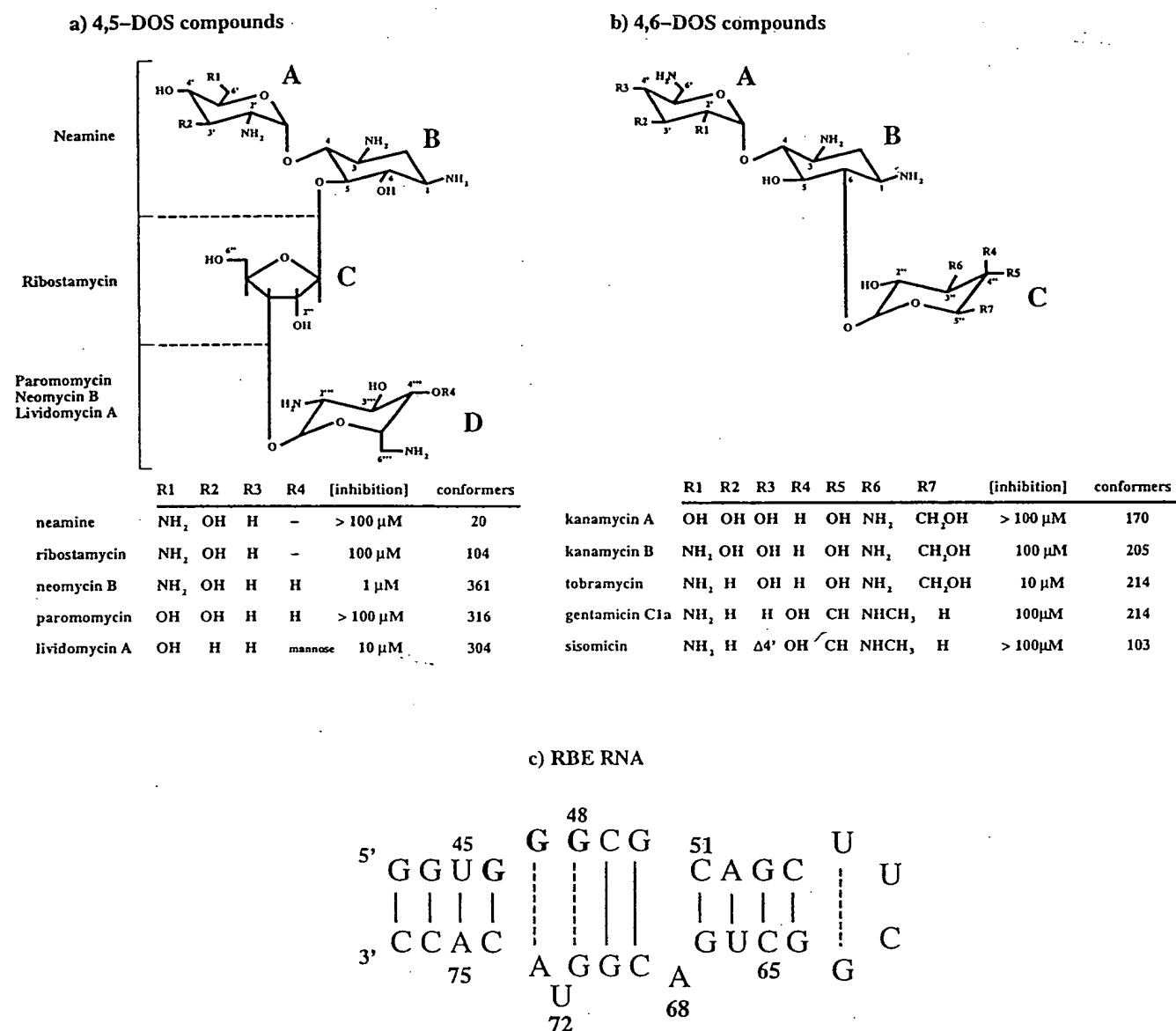


**Figure 4.** Aminoglycoside inhibitors of the RBE RNA: (a) chemical structures and biological activities of the 4,5-DOS compounds, (b) chemical structures and biological activities of the 4,6-DOS compounds, (c) secondary structure of the RBE RNA. Watson-Crick base pairs are indicated by solid lines and the non-Watson-Crick base pairs by dashed lines. The positions protected from chemical modification by neomycin and tobramycin are indicated in bold.

the G46, G47, and G48 region in two opposite orientations (see Methods). Complexes were solvated and energy-optimized; Table 3 shows the association free energies of the models for the four representative aminoglycosides.

In the case of the 4,5-DOS compounds neomycin and paromomycin, the bioactive conformations selected by pharmacophores 4 and 5 converged to the same model 5 during optimization. Similarly, the bioactive conformations of 4,6-DOS compounds (tobramycin and kanamycin B) from pharmacophores 1 and 4 converged to model 1. The three models with the most favorable association free energies (models 2, 5, and M1) were submitted to molecular dynamics (MD) simulations for further refinement. In these cases, an explicit representation of the solvent which allows displacement of the ligand from its binding site by water molecules was used to evaluate their relative stability. After MD, the geometries of the final structures were similarly optimized, and the association free energies were calculated

to determine the degree of accordance between the models and the experimental data. As shown in Table 3, the optimal association free energy is obtained for model 5 in the case of both neomycin and tobramycin supporting the thesis of a common binding mode for 4,5-DOS and 4,6-DOS compounds.

The docking protocol produced bioactive conformations from pharmacophore 2 or the control M1 (models 2 and M1) which significantly deviated from the SAR conformations for both neomycin and tobramycin. However the conformations of model 5 and the SAR-derived structure were quite similar: the heavy atom rmsd calculated between the 3D-SAR bioactive conformation and those obtained after MD is 1.2 Å for both neomycin and tobramycin. We propose model 5 as the best representation of the complex structure based on its consistent results and highest association free energy.

**Model of the RBE-Aminoglycoside Complex.** The docking and modeling strategy used in this study produced model 5 of the neomycin B or tobramycin and

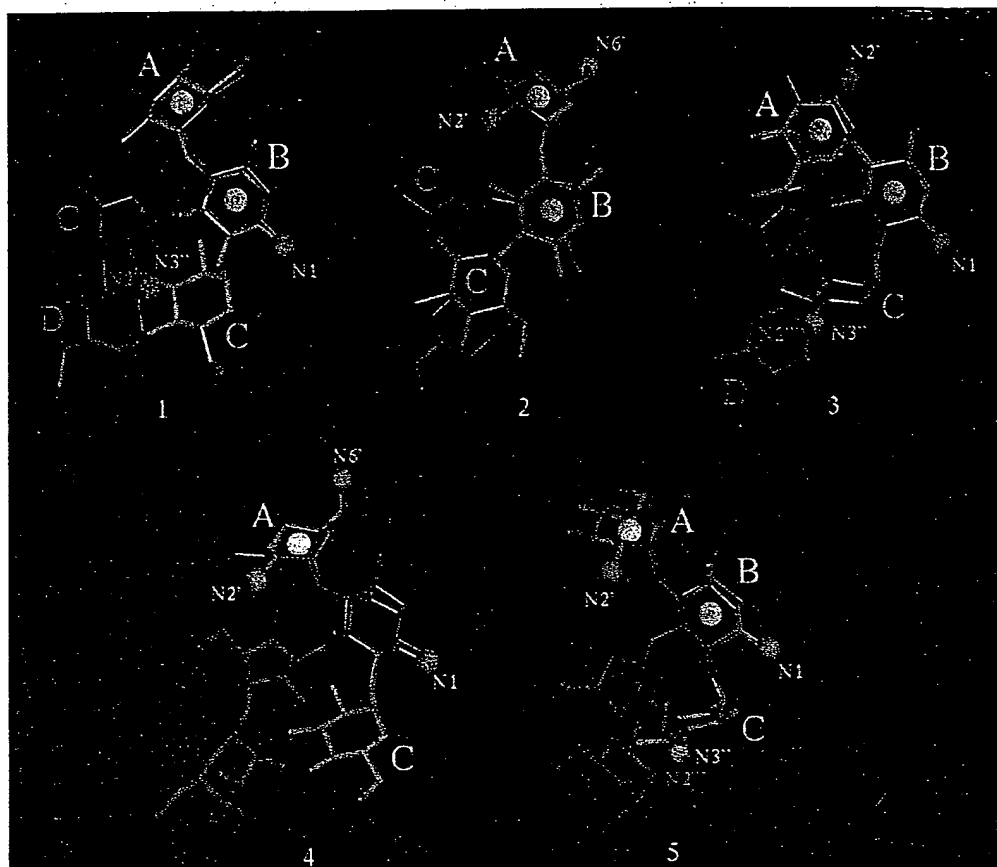


**Figure 5.** Pharmacophores and bioactive conformations of neomycin and tobramycin. Five pharmacophores were used to align inhibitors illustrated with the neomycin (blue) and tobramycin (orange) bioactive conformations. The pharmacophoric centers are indicated by yellow spheres in the case of ring centers and cyan spheres in the case of atomic centers.

**Table 2.** Pharmacophores of Aminoglycoside Antibiotics

data compd	no. of pharmacophores	pharmacophore <sup>a</sup>	probability	reliability	match
active	29 <sup>b</sup>	1	0.88	0.97	0.40
		2	0.86	0.97	0.57
		3	0.86	0.95	0.55
		4	0.86	0.95	0.52
		5	0.86	0.95	0.47

<sup>a</sup> Five best pharmacophores based on probability. <sup>b</sup> Pharmacophores present in at least five of the six highly active compounds identified having a probability  $\geq 0.85$ .

the RBE RNA shown in Figure 6 (top and bottom, respectively). These models reveal that the local interactions between both neomycin and tobramycin and the RBE RNA involve all the atomic centers defined by the patterns of pharmacophores 2 and 5. For example, N2' makes a contact with the Hoogsteen face of G47 and G48 in model 2 and the phosphates of G46 and G47 in model 5. Moreover, the association free energies of this model can rationalize differences in inhibitory strength. The best free energies of complexes reported in Table 3 for the two 4,5-DOS compounds, neomycin B (strong, model 5) and paromomycin (weak, model M1), differ by more than 15 kcal/mol as do the energies between the two 4,6-DOS compounds, tobramycin (strong, model 5) and kanamycin B (weak, model 5).

The models generated for the RBE-aminoglycoside complexes are in agreement with the chemical protection data showing that modifications of the nucleotides G46, G47, and G48 are blocked by neomycin B and tobramycin.<sup>1</sup> The models are also consistent with in

vitro selection experiments,<sup>2</sup> where, for example, a decrease in binding affinity of neomycin is observed by substituting the non-Watson-Crick base pair A48:A71 for G48:G71. This observation suggests a direct contact between these residues and the aminoglycoside,<sup>2</sup> a feature of our model (Figure 6).

Although the binding mode is presently unknown, Zapp et al.<sup>1</sup> have proposed an interaction of aminoglycosides with nucleotides G46, G47, and G48 of the RBE RNA. Also, Robinson et al.<sup>12</sup> suggested that the binding involves formation of a bridge across the major groove. Our model 5 supports both these proposals. Even though docking was initiated in the G46-G48 region, modeling did involve extensive translation of the ligands with respect to the RBE, and only suboptimal models were obtained by binding ligands to other regions of the RNA. Parts of the neomycin and tobramycin (rings B, C, and D for neomycin) aminoglycosides bind the region of G46, G47, and G48, and the key nitrogen atom N6' (ring A) identified in the 3D-SAR study (present in neomycin but absent in the inactive aminoglycoside paromomycin) forms a contact on the opposite side of the major groove with C65 and G66. Recent experimental data demonstrated that aminoglycoside binding to the RBE RNA is stoichiometric and suggested that hydrophobic and/or stacking interactions could occur between the pyrene moieties (ring B; see Figure 6) and the RBE RNA.<sup>13</sup> Although our model did not incorporate this most recent information, model 5 features a B ring buried in the major groove consistent with the experimental data.

**Table 3.** Binding Energy Contributions for the Different Molecular Models of RBE–Aminoglycoside Complexes after Docking and MD

aminoglycosides	model <sup>b</sup>	association free energies (kcal/mol) <sup>a</sup>					
		after docking			after MD		
		$\Delta G_{el}$	$\Delta G_n$	$\Delta G_{total}$	$\Delta G_{el}$	$\Delta G_n$	$\Delta G_{total}$
neomycin B	1	-30	-46	-76			
	2	-35	-56	-91	-31	-41	-72
	3	-23	-46	-69			
	5 (4) <sup>c</sup>	-41	-50	-91	-25	-56	-81
	M1	-43	-48	-91	-31	-30	-61
	C1	-34	-48	-82			
	C2	-27	-50	-77			
tobramycin	1 (4) <sup>c</sup>	-25	-44	-69			
	2	-30	-42	-72	-35	-34	-69
	3	-27	-42	-69			
	5	-35	-46	-81	-32	-48	-79
	M1	-27	-38	-65	-28	-30	-58
	M2	-26	-34	-60			
	C1	-28	-44	-72			
kanamycin B	1 (4) <sup>c</sup>	-23	-42	-65			
	2	-26	-48	-74	-28	-28	-56
	3	-24	-44	-68			
	5	-30	-42	-72	-27	-33	-60
	M1	-34	-42	-76	-30	-29	-59
	M2	-26	-36	-62			
	C1	-26	-42	-68			
paromomycin	C2	-20	-40	-60			
	1	-20	-46	-66			
	2	-20	-50	-68			
	3	-16	-48	-64			
	5 (4) <sup>c</sup>	-23	-45	-69			
	M1	-29	-50	-79	-15	-42	-57
	C1	-25	-42	-67			
	C2	-18	-50	-68			

<sup>a</sup> The association free energy,  $\Delta G_{total}$ , was calculated according to the approach used by King and Barford<sup>22</sup> based on the separation of the electrostatic and hydrophobic contributions. The electrostatic contribution,  $\Delta G_{el}$ , was calculated by the FDPB method as described by Srinivasan et al.<sup>8</sup> The hydrophobic contribution was calculated from the surface-accessible surface area with a proportionality constant of 40 cal/mol Å<sup>2</sup>. <sup>b</sup> The models identified by the same root name correspond to a common superposition mode of the core structure among the different aminoglycosides; in parentheses are the pharmacophores which the bioactive conformations led to the same model. <sup>c</sup> The SAR model indicated in parentheses led to the same docked model.

Finally, it is noteworthy that our modeled structure of the neomycin B–RBE RNA complex shares some common structural features with the structure of the complex formed between the 16S rRNA and paromomycin.<sup>14</sup> Both binding regions include an internal loop, featuring non-Watson–Crick base pair interactions and bulged nucleotides, sandwiched between two stems. The similarities between the two complexes reside in the aminoglycoside bioactive conformation and the specificity of the contacts formed with the RNA receptor. In our model, the aminoglycoside adopts an L-form conformation in which rings B, C, and D form a linear array similar to that observed in the 16S rRNA complex. The aminoglycoside exhibits chair conformations for rings A, B (with the amino and hydroxyl groups in equatorial positions), and D with the amino group N6" in an equatorial position and the other substituents (hydroxyl and amino groups) in axial positions, another structural feature retrieved in our model (Figure 6, top).

Rings A and B establish the more specific contacts. In the 16S rRNA, the amino group N1 interacts with the essential nucleotide U1495,<sup>14</sup> whereas in the RBE RNA, it interacts with the nucleotides G47 and G48 chemically protected by neomycin and tobramycin upon binding.<sup>1</sup> In contrast, the C and D rings form only

contacts with the phosphate backbone. Similarly, in our model, ring C makes direct contacts with the phosphate backbone at G46 and A68, whereas ring D makes contacts mediated through water molecules with the phosphate backbone at U45 and G70 and the Hoogsteen face (O6 and N7 atoms) of the base at the third chemically protected position G46 (Figure 6, top).

## Conclusions

The prediction of bioactive conformations and binding orientations of ligands is not an easy task. Recent X-ray crystallographic studies of ligand–receptor complexes have shown that very similar ligands can adopt different binding modes<sup>15</sup> as in the case of the WIN compounds. Since ligand–receptor interactions may involve high-energy conformations of the individual molecules, bioactive conformations may differ significantly from the unbound conformation. Nevertheless, we show here that it is possible to describe accurately the binding properties of ligands, using a modeling strategy based on 3D-SAR and docking studies, even in the case of small sets of very flexible ligands. The advantage of this protocol is that the computationally complex docking protocol is performed with a greatly reduced, but relevant, conformational library as determined by 3D-SAR. The original conformational space generated for neomycin (maximum rmsd of 5.3 Å) and tobramycin (maximum rmsd of 4.0 Å) was reduced dramatically to rmsd of 2.3 and 2.9 Å for neomycin and tobramycin during docking. Docking and modeling is thus initiated with more likely ligand conformations and refined by an explicit representation of the receptor's geometry. In the final step, MD simulations were used to optimize the interaction with the receptor RNA.

## Methods

**Data.** The data used in this paper were taken from Badger et al.<sup>10</sup> for the phenyloxazolines (the so-called "WIN" compounds) and from Zapp et al.<sup>1</sup> for the aminoglycosides. In the case of the aminoglycosides, since data were collected from experiments carried out at pH 7.9,<sup>1</sup> all amino groups of the 4,5-diglycosyl-substituted 2-deoxystreptamine (4,5-DOS) compounds were assumed to be protonated,<sup>16</sup> with the exception of the 3-amino group of the B ring.

**Conformational Libraries.** Conformational libraries of all compounds were generated by the Search-Compare module (version 2.3.5; Biosym/MSI Technologies, San Diego, CA) which systematically samples free torsion angles (each single bond of the ligand was rotated through 360° in increments of 120°, unless otherwise indicated). Conformers were clustered into subclasses based on the pairwise root-mean-square deviation (rmsd) determined by superimposing the three-dimensional structures of conformers. A conformational "set" of around 200 conformers for each compound was assembled by taking the lowest energy conformer of each subclass.

Conformational generation was initiated for the WIN compounds using conformations found in the crystal structures of their complexes.<sup>10</sup> Pairwise distances among subclasses of the conformational set were from 0.6 to 1.0 Å rmsd. Starting conformations for the aminoglycosides were those found after structure optimization by molecular mechanics calculations using the CFF93.1 set of force-field parameters<sup>17</sup> or the conformations found in the 3D-SAR study presented here. During conformational generation, a 60° increment of rotation around each single bond was used except for the single nonring connecting bonds which were incremented by 120°. The major pucker forms (C2'-endo, O4'-endo, C3'-endo) for the ribose and the two twist conformers for iodopyranose were also represented in the conformational evaluations. The pairwise

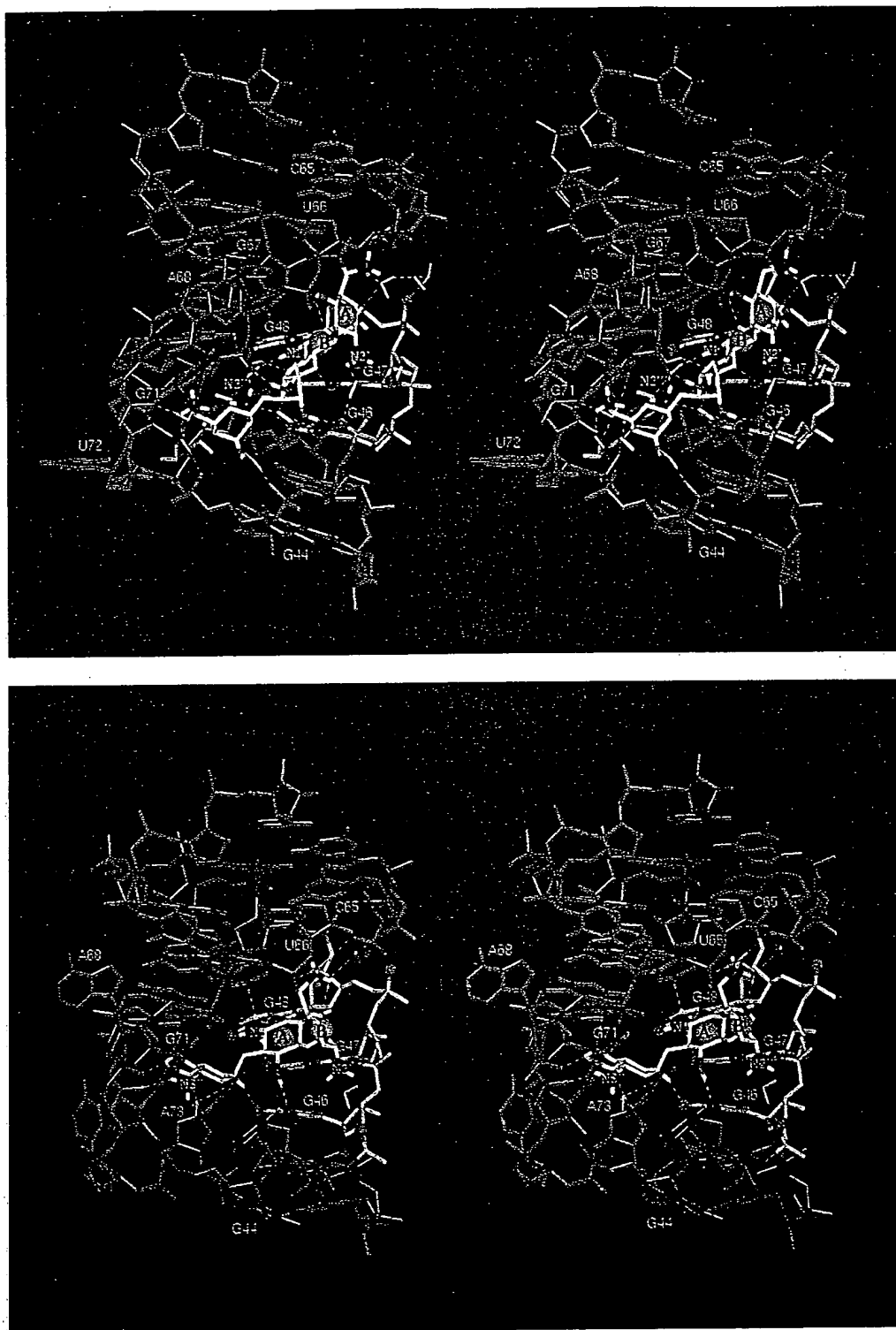


**Figure 6.** RBE RNA-aminoglycoside model: (top) stereoview of the RBE RNA-neomycin B complex (model 5), (bottom) stereoview of the RBE RNA-tobramycin complex (model 5). The neomycin B and tobramycin are bound in the major groove of the RNA. The nucleotides of the region strongly protected upon binding are indicated in gray (nucleotides G46, G47, G48).<sup>1,2</sup> The nitrogen and oxygen atoms of neomycin B and tobramycin forming molecular contacts are indicated in dark blue (N2', N1, N2'', or N3'') and red, respectively. The rings corresponding to pharmacophoric centers are indicated by a sphere in gold placed at the center of mass of the ring. The nitrogen atoms corresponding to pharmacophoric centers are in CPK representation as are the O6, N7, and O1P atoms of G47 and G48. Water molecules or counterion (Na<sup>+</sup>) involved in phosphate or base contacts between the antibiotic and the binding site are in cyan and purple, respectively. Hydrogen bonds are indicated by white dashed lines.

distances among these conformational subclasses were from 1.0 to 2.5 Å rmsd.

**SAR Methodology.** The 3D-SAR studies were carried out using the APEX-3D expert system<sup>18</sup> developed by Golender et al.<sup>19</sup> for the classification of compounds sharing a given biological activity (in this case, binding to a receptor). Cor-

relations among atomic and ring centers of the ligand, their associated physical properties, and their activity were determined. Centers and their associated properties were then organized into coherent substructures, the pharmacophores, which represented structural properties common to the largest number of ligands of the activity class. Bioactive conforma-



tions were estimated by examining every conformer of each compound to identify which conformation(s) permitted the best overall three-dimensional superimposition of the pharmacophore. The congruency of the superimposition was estimated by the "match" value calculated from the proportion of centers which overlap. This value varies from 0 to 1 (with 1 as the best-possible fit). The statistical significance of the pharmacophores was estimated by two criteria: (1) the probability that a novel compound, possessing the pharmacophore, would belong to the same activity class (a Bayesian estimate) and (2) the reliability, a measure of a nonchance occurrence of the pharmacophore (binomial probability). By these definitions, when the entire training set belongs to a single class, the reliability is not applicable and the probability is equal for all pharmacophores.

**Docking of Aminoglycosides.** Aminoglycosides were docked to the Rev-binding RNA in a two-step procedure using starting conformations determined by the SAR analysis or by molecular mechanics calculations of the ligands and the conformation of the Rev-binding RNA previously determined.<sup>3</sup> In the first step, the starting conformations were oriented in either of two ways: one featured the A ring pointing toward the tetraloop and the C and D rings toward the open end of the RBE RNA; the other was oriented in the opposite direction. Different juxtapositions of the ligand with respect to the receptor site were constructed by translations and rotations of the ligand in space with respect to the receptor using increments of 0.1 Å and 0.5°, respectively. All structures were evaluated to find a locally optimal orientation by determination of the van der Waals and electrostatic components of the energy of interaction.<sup>8</sup> In the second step of the procedure, the energy of interaction was optimized by sampling the ligand conformational space within the binding site by rotation about all sterically unhindered single bonds. Final models were obtained after molecular dynamics refinement.

**Computer Simulations of the RBE-Aminoglycoside Complexes.** The RBE-aminoglycoside complexes constructed in the absence of explicit solvent were subjected to energy minimization until the maximum derivative was less than 5.0 kcal/mol Å. Counterions (Na<sup>+</sup>) were placed at 6 Å from the phosphorus atoms along the O-P-O axis. The resulting complex was then solvated with a 6.0-Å thick water layer (approximately 2200 water molecules). To remove the van der Waals conflicts created by hydrating the RNA-aminoglycoside complexes, water molecules were subjected to energy minimization until the maximum derivative was less than 50 kcal/mol Å and then to a 1-ps MD simulation at 300 K. Intermediate evaluations of candidate RBE-aminoglycoside structures were conducted by optimizing their geometry until the maximum derivative was less than 1.0 kcal/mol Å. Models having high binding energies were retained for further analyses. Simulations were completed for these models by first heating the solvent and counterions from 10 to 300 K in steps of 50 K for 3 ps while keeping the RNA-ligand complex fixed in space. In the second heating cycle, the position of the RNA-ligand complex was constrained in space by (1) tethering the first base pair of the RNA stem/loop structure to its initial position with a force constant of 50 kcal/mol Å<sup>2</sup>, (2) imposing distance constraints based on quadratic force constants of 20 and 10 kcal/mol Å<sup>2</sup> for Watson-Crick and non-Watson-Crick base pairings, respectively, (3) imposing an equilibrium distance of 2.9 Å between heavy atoms involved in hydrogen bonding, and (4) constraining the angles between the hydrogen donor and acceptor to 160° using quadratic restraints with a force constant of 2.0 kcal/mol Å<sup>2</sup>. Finally, the system was submitted to 150 ps of MD simulation under distance constraints only. The nonbonded interactions were treated by the Cell Multipole Method.<sup>20,21</sup> All simulations were performed using the Discover package interfaced to the CFF93.1 force field in the constant-temperature, constant-volume ensemble.

**Acknowledgment.** The authors would like to thank Erich Vorpapel for his gracious collaboration and helpful comments. R. Cedergren is a Richard Ivey Fellow of the Evolutionary Biology Group of the Canadian Insti-

tute of Advanced Research. This work was supported by the Medical Research Council of Canada and Biochem Thérapeutique.

## References

- (1) Zapp, M. L.; Stern, S.; Green, M. Small molecules that selectively block RNA binding of HIV-1 Rev protein inhibit Rev function and viral production. *Cell* 1993, 74, 969-978.
- (2) Werstuck, G.; Zapp, M. L.; Green, M. R. A noncanonical base pair within the human immunodeficiency virus Rev-responsive element is involved in both Rev and small molecule recognition. *Chem. Biol.* 1996, 3, 129-137.
- (3) Leclerc, F.; Cedergren, R.; Ellington, A. D. A three-dimensional model of the Rev-binding element of HIV-1 derived from analyses of aptamers. *Nature Struct. Biol.* 1994, 1, 293-300.
- (4) Peterson, R. D.; Bartel, D. P.; Szostak, J. W.; Horvath, S. J.; Feigon, J. <sup>1</sup>H NMR studies of the high-affinity Rev binding site of the Rev responsive element of HIV-1 mRNA: base pairing in the core binding element. *Biochemistry* 1994, 33, 5357-5366.
- (5) Battiste, J. L.; Tan, R.; Frankel, A. D.; Williamson, J. R. Assignment and modeling of the Rev response element RNA bound to a Rev peptide using <sup>13</sup>C-heteronuclear NMR. *J. Biomol. NMR* 1995, 6, 375-389.
- (6) Leclerc, F.; Srinivasan, J.; Cedergren, R. Predicting RNA structures: The model of the RNA element binding Rev meets the NMR structure. *Folding Des.* 1997, 2, 141-147.
- (7) Llorente, B.; Leclerc, F.; Cedergren, R. Using SAR and QSAR analysis to model the activity and structure of the Quinolone/DNA complex. *Bioorg. Med. Chem.* 1996, 61-71.
- (8) Srinivasan, J.; Leclerc, F.; Xu, W.; Ellington, A. D.; Cedergren, R. A docking and modelling strategy for peptide-RNA complexes: applications to BIV Tat-TAR and HIV-RBE. *Folding Des.* 1996, 463-472.
- (9) Diana, G. D.; McKinlay, M. A.; Otto, M. J.; Akullian, V.; Oglesby, C. [(4,5-Dihydro-2-oxazolyl)phenoxy]alkyl]isoxazole inhibitors of picornavirus uncoating. *J. Med. Chem.* 1985, 1906-1910.
- (10) Badger, J.; Minor, I.; Kremer, M. J.; Oliveira, M. A.; Smith, T. J.; Griffith, J. P.; Guerin, D. M. A.; Krishnaswamy, S.; Leo, M.; Rossmann, M. G.; McKinlay, M. A.; Diana, G. D.; Dutko, F. J.; Fancher, M.; Rueckert, R. R.; Heinz, B. A. Structural analysis of a series of antiviral agents complexed with human rhinovirus 14. *Proc. Natl. Acad. Sci. U.S.A.* 1988, 85, 3304-3308.
- (11) Klebe, G.; Abraham, U. On the prediction of binding properties of drug molecules by comparative molecular field analysis. *J. Med. Chem.* 1993, 36, 70-80.
- (12) Robinson, H.; Wang, A. H. J. Neomycin, spermine and hexaaminocobalt(III) share common structural motifs in converting B- to A-DNA. *Nucleic Acid Res.* 1995, 24, 3700-3706.
- (13) Wang, Y.; Hamasaki, K.; Rando, R. R. Specificity of aminoglycoside binding to RNA constructs derived from the 16S rRNA decoding region and the HIV-RRE activator region. *Biochemistry* 1997, 36, 768-779.
- (14) Fourmy, D.; Recht, M. I.; Blanchard, S. C.; Puglisi, J. D. Structure of the A site of *Escherichia coli* 16S ribosomal RNA complexed with an aminoglycoside antibiotic. *Science* 1996, 274, 1367-1371.
- (15) Mattos, C.; Ringe, D. Multiple binding modes. In *3D-QSAR in Drug Design: Theory, Methods and Applications*; Kubinyi, H., Ed.; ESCOM: Leiden, 1993; pp 226-254.
- (16) Botto, R. E.; Coxon, B. Nitrogen-15 nuclear magnetic resonance spectroscopy of neomycin B and related aminoglycosides. *J. Am. Chem. Soc.* 1983, 105, 1021-1028.
- (17) Potential Energy Functions Consortium PEFC 1994 release; Biosym/MSI Technologies, San Diego, CA.
- (18) Golender, V. E.; Vorpapel, E. R. Computer-assisted pharmacophore identification. In *3D-QSAR in Drug Design: Theory, Methods and Applications*; Kubinyi, H., Ed.; ESCOM: Leiden, 1993; pp 137-149.
- (19) Golender, V. E.; Rozenblit, A. B. *Logical and Combinatorial Algorithms in Drug Design*; Research Studies Press: Letchworth, 1983.
- (20) Ding, H.-Q.; Karasawa, N.; Goddard, W. A. Atomic level simulations on a million particles: the cell multipole method for Coulomb and London nonbond interactions. *J. Chem. Phys.* 1992, 97, 4309-4315.
- (21) Mathiowetz, A. M.; Jain, A.; Karasawa, N.; Goddard, W. A. Protein simulations using techniques suitable for very large systems: the cell multipole method for nonbond interactions and the Newton-Euler inverse mass operator method for internal coordinate dynamics. *Proteins* 1994, 20, 227-247.
- (22) King, G.; Barford, R. A. Calculations of association free energies. Separation of electrostatic and hydrophobic contributions. In *Molecular Modeling: From Virtual Tools to Real Problems*; Kumosinski, T. F.; Liebman, M. N., Eds.; ACS Symp. Series 576; American Chemical Society: Washington, DC, 1994; pp 173-184.



advertisement



Introducing Delicious New Ensure Healthy Mom<sup>™</sup> Shakes and Snack Bars!  
Specially Developed for Pregnant and Nursing Moms.

**RxList**

DISCLAIMER

R-BOARD

ALTERNATIVES

TOP 200

ADVANCED SEARCH

ONLINE PHA

## Octreotide

DESCRIPTION	CLINICAL PHARMACOLOGY	INDICATIONS and DOSAGE	SIDE EFFECTS: DRUG INTERACTIONS	WARNINGS: PRECAUTIONS	OVERDOSAGE: CONTRAINDICATIONS	PATIENT INFORMATION
-------------	-----------------------	------------------------	---------------------------------	-----------------------	-------------------------------	---------------------

### DESCRIPTION

 Drug Search

**WebMD**
**Health Source**
[my.webmd.com](http://my.webmd.com)

► **Newly Diagnosed?:**

[Start Here](#)

► **Take A Quiz:**

[Test Your Knowledge](#)

► **Questions Answered:**

[Symptoms, Treatments, More](#)

► **Find it Fast:**

[WebMD Medical Library](#)

☑ **Breaking Health**

**Alerts:**
[Sign Up Here](#)

Can't Find What You Need?

Search WebMD Health:



Octreotide is the acetate salt of a cyclic octapeptide. It is a long-acting octapeptide with pharmacologic properties mimicking those of the natural hormone somatostatin. Octreotide is known chemically as L-Cysteinamide, D-phenylalanyl-L-cysteiny-L-phenylalanyl-D-tryptophyl-L-lysyl-L-threonyl-N-[2-hydroxy-1-(hydroxy-methyl) propyl]-, cyclic (207)-disulfide; [R-(R\*,R\*)].

Sandostatin LAR<sup>®</sup> Depot (octreotide acetate for injectable suspension) is available in a vial containing the sterile drug product, which when mixed with diluent, becomes a suspension that is given as a monthly intragluteal injection. The octreotide is uniformly distributed within the microspheres which are made of a biodegradable glucose star polymer, D,L-lactic and glycolic acids copolymer. Sterile mannitol is added to the microspheres to improve suspendability.

Sandostatin LAR<sup>®</sup> Depot is available as: sterile 5-mL vials in 3 strengths delivering 10 mg, 20 mg or 30 mg octreotide free peptide. Each vial of Sandostatin LAR<sup>®</sup> Depot delivers:

Name of Ingredient	10 mg	20 mg	30 mg
octreotide acetate	11.2 mg*	22.4 mg*	33.6 mg*
D, L-lactic and	188.8 mg	377.6 mg	566.4 mg
glycolic acids copolymer			
mannitol	41.0 mg	81.9 mg	122.9 mg
*Equivalent to 10/20/30 mg octreotide base.			

## Advertisements

## Featured Centers

- [Can't Sleep?](#)
- [Get Vitamins 50% Off](#)
- [Home Defibrillator](#)
- [Having a Baby?](#)
- [Epilepsy Help](#)
- [Heart Failure Device](#)
- [Years of Joint Pain?](#)

advertisement

**ATTENTION PHYSICIANS**

**Need Help?**

Try Medscape.com's Specialty Services

- [Medline Access](#)
- [Conference Coverage](#)
- [Free CME](#)

[click here](#) **Medscape**

## News From WebMD

- [Company Issues](#)  
[Pacemaker Malfunction](#)  
[Warning](#)
- [Deaths Seen With](#)  
[Fentanyl Narcotic Pain](#)  
[Patch](#)
- [FDA Reviews Adult](#)  
[Antidepressant-Suicide](#)  
[Link](#)

Each syringe of diluent contains:	
carboxymethylcellulose sodium	12.5 mg
mannitol	15.0 mg
water for injection	2.5 mL

The molecular weight of octreotide is 1019.3 (free peptide,  $C_{49}H_{66}N_{10}O_{10}S_2$ ) and its amino acid sequence is H-D-Phe-Cys-Phe-D-Trp-Lys-Thr-Cys-Thr-ol•xCH<sub>3</sub>COOH where x = 1.4 to 2.5

For information on ordering Sandostatin LAR Online, please click the "online pharmacy" link on the blue horizontal navigation bar at the top of every page or click the "Get a Price Quote" Badge on the right side of pages like this one for a more direct route to a specific product. Finally you may click [Order Online Here](#).

RxList only refers patients to online pharmacies certified by [VIPPS, Verified Internet Pharmacy Practice Sites](#), a program administered by the National Association of Boards of Pharmacy which ensures that member pharmacies offering online prescription services are bona fide, fully licensed, and demonstrate "competent Internet/interstate pharmacy practices."

This Page Last Updated 12/08/2004

[Return to Top](#) 

[Search Medical Dictionary](#) 

[FAQ/Patient Monograph](#) 

[RxList Home](#) • [Contact RxList](#) • [About RxList](#) • [Terms & Policies](#) • [Privacy Policy](#)

Copyright © 2004 by RxList Inc.

**APPENDIX 3**

**RELATED PROCEEDINGS APPENDIX**

None

**This Page is Inserted by IFW Indexing and Scanning  
Operations and is not part of the Official Record**

**BEST AVAILABLE IMAGES**

Defective images within this document are accurate representations of the original documents submitted by the applicant.

Defects in the images include but are not limited to the items checked:

☐ BLACK BORDERS

☐ IMAGE CUT OFF AT TOP, BOTTOM OR SIDES

☒ FADED TEXT OR DRAWING

☐ BLURRED OR ILLEGIBLE TEXT OR DRAWING

☐ SKEWED/SLANTED IMAGES

☐ COLOR OR BLACK AND WHITE PHOTOGRAPHS

☐ GRAY SCALE DOCUMENTS

☒ LINES OR MARKS ON ORIGINAL DOCUMENT

☒ REFERENCE(S) OR EXHIBIT(S) SUBMITTED ARE POOR QUALITY

☐ OTHER: \_\_\_\_\_

**IMAGES ARE BEST AVAILABLE COPY.**

**As rescanning these documents will not correct the image problems checked, please do not report these problems to the IFW Image Problem Mailbox.**